

# 2011

AMERICAN SOCIETY OF BIOMECHANICS



## 35TH ANNUAL MEETING

August 10 - 13, 2011

Westin Long Beach

Long Beach, CA





# 2011

AMERICAN SOCIETY OF BIOMECHANICS



## TABLE OF CONTENTS

|  |                   |
|--|-------------------|
| Welcome                                  | 5                 |
| The Meeting and Program Committees       | 6                 |
| Meeting Information at a Glance          | 8                 |
| Networking and Professional Development  | 9                 |
| Social Program                           | 9                 |
| Instructions for Presenters              | 10                |
| Tutorials                                | 11                |
| Virtual Lab Tours                        | 11                |
| Plenary and Awards Sessions              | 12                |
| Symposia                                 | 14                |
| Podium Sessions                          | 15                |
| Poster Sessions                          | 22                |
| Podium/Poster Session Presenters         | 52                |
| Westin Long Beach Third Level Floor Plan | 58                |
| Long Beach Area Map                      | Inside back cover |
| Meeting Schedule                         | Back cover        |



# Trigno™ Solutions

...take your research to new heights.

## Physiological monitoring

- Full-bandwidth sEMG sensors
- Accurate EKG sensors
- 3DOF inertial sensors
- Global positioning sensors
- Force sensors
- Angle sensors

## 8 hours of mobile data logging

Trigno™ Mobile supports 8 hours of continuous logging for capturing long term physiological trends.

## 40 meters indoor range

Trigno™ sensors are truly wire-free, allowing completely unrestricted subject motion while still maintaining optimal signal quality and full-bandwidth sampling.

### Trigno™ Mobile



#### Congratulations



2011 James J. Hay Award Lecture  
Professor Joe Hamill, University of Massachusetts



2011 Borelli Award Lecture  
Professor Scott Delp, Stanford University

### Trigno™ Lab



# 35TH ANNUAL MEETING

AUGUST 10 - 13, 2011



## W elcome Fellow Biomechanists

On behalf of the ASB executive board, the University of Southern California, and everyone who has contributed to the planning and execution of this meeting, we would like to enthusiastically welcome you to Long Beach, California. We are excited for the opportunity to host the 35th Annual Meeting of the American Society of Biomechanics.

We are pleased by the continued growth of the ASB annual meeting. In total, 488 abstracts were submitted to this year's meeting from across the United States and the world. Of the submitted abstracts, 100 were selected as podium presentations and 345 as poster presentations. In addition, the meeting will feature informative tutorials and symposia, engaging keynote lectures, award presentations, networking opportunities, and virtual lab tours. These opportunities will surely make for an enlightening, energizing, and productive meeting for all attendees.

The ASB and its Annual Meeting are run exclusively by volunteers. Each year, the tireless efforts of many make it possible for attendees to enjoy a first rate meeting experience. We would like to thank all of those who have contributed to the planning and implementation of this meeting. In particular, the ASB executive board and the representatives at the University of Southern California provided critical guidance and assistance in the planning and organization of the meeting. Abstract reviewers carefully evaluated submissions and many student volunteers donated their time prior to and during the meeting. We greatly appreciate these efforts.

Furthermore, financial support for the meeting has been provided by the following institutions: USC Division of Biokinesiology and Physical Therapy, USC Department of Kinesiology, USC Viterbi School of Engineering, National Skeletal Muscle Research Center, and the National Institute of Biomedical Imaging and Bioengineering at the National Institutes of Health.

And last, but certainly not least, we would like to thank you, the meeting participants, for making this event a worthwhile endeavor. We are confident you will enjoy Long Beach and the planned social activities. We are pleased to welcome you and wish you a wonderful stay.

Sincerely,

**Christopher Powers**  
Meeting Co-Chair

**George Salem**  
Meeting Co-Chair

**Susan Sigward**  
Head Local Organizing Committee

**Wendy Murray**  
Program Chair

# THE MEETING AND PROGRAM COMMITTEES

## ASB Local Committee

Susan Sigward (chair) • Robert Gregor • Kornelia Kulig • Gerald Loeb • Jill McNitt-Gray • Francisco Valero Cuevas

## ASB Program Committee

Robert Gregor • Samuel Ward • Elizabeth Hsiao-Wecksler

## Assistants to the Program Chair

Special thanks to Jen Nichols • Vikram Darbhe • Ben Binder-Macleod • Craig Goehler • Xiao Hu • Jeremy Mogk • Carrie Peterson • Mike Rehorn • Sarah Wohlman for assistance with program organization and website development.

## ASB Review Committee

Mohammad Abdoli-Eramaki

Alaa Ahmed

Don Anderson

Allison Arnold

Anita Bagley

Silvia Blemker

Thomas Burkholder

Robert Catena

John Challis

Young-Hui Chang

Gary Christopher

John De Witt

Ashish Deshpande

Paul DeVita

Jonathan Dingwell

Jon Doan

Janet Dufek

Ahmet Erdemir

Alejandro Espinoza

Margaret Finley

Craig Goehler

Jinger Gottschall

Mark Grabiner

Robert Gregor

Melissa Gross

Kate Hamel

Daniel Herman

Walter Herzog

Brian Higginson

Elizabeth Hsiao-Wecksler

Richard Hughes

Devin Jindrich

Andrew Karduna

Tom Kepple

Jason Kutch

Laurel Kuxhaus

Richard Lauer

William Ledoux

David Lin

Wei Liu

Kurt Manal

Craig McGowan

Scott McLean

Jill McNitt-Gray

Clare Milner

Erika Nelson-Wong

Boris Prilutsky

Jeff Reinbolt

Stacie Ringleb

Marco Santello

Katherine Saul

Michael Schwartz

Jason Scibek

Na Jin Seo

Rob Siston

Kimberly Szucs

Karen Troy

Carole Tucker

Brian Umberger

Anita Vasavada

Samuel Ward

Tishya Wren

Jianhua (Jerry) Wu

Ting Xia

Joseph Zeni

## ASB Executive Committee

**President:** Jill McNitt-Gray, University of Southern California

**President – Elect:** Donald D. Anderson, University of Iowa

**Past-President:** Tom Buchanan, University of Delaware

**Treasurer:** Gary Heise, University of Northern Colorado

**Secretary:** Michael Madigan, Virginia Tech

**Education Committee Chair:** Gerald Smith, Utah State University

**Communications Committee Chair:** Zong-Ming Li, Cleveland Clinic

**Meeting Chairs:** Christopher Powers & George Salem, University of Southern California

**Program Chair:** Wendy Murray, Northwestern University

**Program Chair-Elect:** Elizabeth Hsiao-Wecksler, University of Illinois at Urbana-Champaign

**Newsletter Editor:** Michelle Sabick, Boise State University

**Student Representative:** Meghan Vidt, Wake Forest University

## Meeting Sponsors



*Division of Biokinesiology and Physical Therapy  
Department of Kinesiology  
Viterbi School of Engineering*



The Society gratefully acknowledges the support of the following Corporate Members



## MEETING INFORMATION AT A GLANCE

### Meeting Location

All of the academic meeting events (podium presentations, posters, mentoring sessions, etc.) will be held on the third level of the Westin Long Beach hotel. The welcome reception and banquet will be held off-site.

### Registration

The registration desk is located on the third level of the Westin Long Beach, next to the escalators. The registration desk will be staffed on Wednesday from 12 pm to 6 pm, and Thursday and Friday from 7 am to 5 pm.

### ASB Executive Board/ Exhibitor's Reception

**Wednesday, August 10, 2011**

6:00 - 6:30 pm, *Ocean Terrace West*

Attendance limited to ASB Executive Board, Exhibitor Representatives, and Organizers of the 2011 and 2012 Annual Meetings of the ASB.

### General Opening Reception

**Wednesday, August 10, 2011**

6:30 - 8:30 pm, *Aquarium of the Pacific in Long Beach*

Attendance is open to all meeting delegates, staff and exhibitor representatives. *See Social Program for details.*

### Exhibitor Booths

Exhibitor booths will be located in the Centennial Ballroom foyer and Ballroom A.

### Poster Presentations

**Thursday, from 2:30 pm to 6:30 pm, and  
Saturday, from 8:30 am to 12:30 pm.**

*There will be two formal poster sessions:*

200 posters will be presented in Centennial Ballroom A. Posters scheduled for the Thursday session should be removed from display by 11:30am on Friday, August 12 so that the Saturday posters can be posted. The remaining 141 posters will be displayed in the Barcelona/Casablanca, Melbourne, Odessa, Tokyo/Vancouver and Shanghai meeting rooms. Posters in these rooms will be presented during both poster sessions. At least one named author is required to be present at each poster during its designated poster session. Light refreshments will be served during both poster sessions. A drink ticket for the poster sessions is included in the registration materials and additional drinks may be purchased at the cash bar.

### Podium Presentations

Presenters are allotted 10 minutes for the presentation and 5 minutes for discussion. Due to time constraints speakers will not be allowed to use their own computers for podium presentations. Speakers must upload their presentation to the conference computer in the Naples room on the day prior to their presentation. *Please see Instructions for Presenters for additional information.*

### Breakfasts

**7:00 am Thursday and Friday, 8:00 am Saturday**

A light Continental Breakfast will be served daily.

### Lunches

**12:30 pm (Thursday, Friday and Saturday)**

A choice of box lunches will be provided daily, including a vegetarian option. There will be sandwich boxes on Thursday and Saturday and salad boxes on Friday.

### Banquet

**Friday, August 12, 2011**

6:30 – 10:00 pm, *Queen Mary, Long Beach*

The Meeting Banquet will be held aboard the historic Queen Mary (*see Social Program for more details*). The first bus will leave the Westin Long Beach at 5:45pm. The last bus will leave the Queen Mary at 10pm.

### Internet Access

Free wireless internet access is available in the hotel lobby. You are encouraged to check and download updated meeting proceedings from the ASB 2011 website prior to the presentation sessions.

### Meeting Proceedings

A thumb drive loaded with all meeting proceedings is included in the materials distributed at registration.

## NETWORKING AND PROFESSIONAL DEVELOPMENT

### Student Event

**Wednesday, August 10, 2011, 5:00 - 6:00 pm**

*Tokyo/Vancouver Rooms*

This event will include tips and pointers on how to make the most of this year's ASB meeting. Irene Davis, Ajit Chaudhari, and several of your fellow student members, will be leading discussions about how to effectively network while at the meeting, how to deliver a good poster or podium presentation, and how to become more involved in ASB through regional meetings.

### Diversity Luncheon

**Thursday, August 11, 2011, 12:30 – 1:30 pm**

*Ballroom D*

A discussion led by members of the Diversity Committee. A variety of topics relating to unique issues and opportunities for those of diverse backgrounds will be discussed. The luncheon is open to all students and professionals, but due to room size constraints, reservations will be required. *Please contact the Student Representative, Meghan Vidt (mvidt@wfubmc.edu) for more information.*

### Student Night on the Town

**Thursday, August 11, 2011, 6:30pm - ?**

*Rock Bottom Brewery*

An informal opportunity for students to mix and mingle with other ASB student members. While students are on their own for dinner and drinks this evening, the Brewery provides students with a casual atmosphere to meet fellow ASB students and network with one another over a delicious microbrew. *Please contact the Student Representative, Meghan Vidt (mvidt@wfubmc.edu) for more information.*

### Women in Science Breakfast

**Friday, August 12, 2011, 7:00 – 8:00 am**

*Ballroom D*

A roundtable discussion between students and members of ASB. The informal atmosphere allows students and professionals to network and discuss the experience of being a woman pursuing a career in a scientific field. This has been a very popular event in the past, so reservations are required. *Please contact the Student Representative, Meghan Vidt (mvidt@wfubmc.edu) for more information.*

## SOCIAL PROGRAM

### Opening Reception –

**Wednesday, August 10, 2011 6:30 – 8:30 pm**

*Aquarium of the Pacific, Long Beach*

The Aquarium of the Pacific is one of the largest aquariums in the United States. It features a collection of over 12,500 animals representing over 550 different species. The aquarium overlooks the Rainbow Harbor with beautiful views of the Long Beach Skyline. The Aquarium will be closed to the public during the reception, allowing meeting participants full access to many exhibits on two levels. A buffet-style meal will be served. One free drink is included in meeting registration and further drinks may be purchased at the cash bar. *The Aquarium of the Pacific is located at 100 Aquarium Way, in Long Beach, a 10-15 minute walk from the Westin Long Beach meeting venue (0.6 miles). Transportation will be provided for those who are unable to walk to the Aquarium.*

### Banquet

**Friday, August 12, 2011 6:30 – 10:00 pm**

*Queen Mary, Long Beach*

At the time of her maiden voyage in 1936, the Queen Mary was considered the grandest ship ever built. She is now a Long Beach and Southern California attraction, popular with locals and tourists alike for historic guided and self-guided tours, paranormal experiences and tours, dining events, year-round festivals and entertainment. A buffet-style meal will be served in the Grand and Windsor Salons. One free drink is included in meeting registration and additional drinks may be purchased at the cash bar. *The Queen Mary is located at 1126 Queens Highway, Long Beach, 1 mile from the Westin Long Beach meeting venue. The first bus will leave the Westin Long Beach at 5:45pm. The last bus will leave the Queen Mary at 10pm.*

### Beach Fun Run

**Saturday August 13, 2011 7:00 – 8:00 am**

Join us for an informal fun run. Please meet in the lobby of the Westin Long Beach at 7am. Course to be announced.

### The Long Beach Area

#### Long Beach Restaurants

There are more than 100 restaurants within an 8-block area of downtown Long Beach, catering to all tastes and budgets. *See the visitor guide in the registration materials for more information.*

#### Area Attractions

All ASB meeting attendees can obtain a special \$5 entrance rate to the Aquarium of the Pacific by showing their meeting badge at the Aquarium's ticket window after 2pm, or on the weekend after the meeting. *(see flyer in registration materials).*

# INSTRUCTIONS FOR PRESENTERS

## Poster Presentations

Posters will be mounted on free-standing poster boards with push pins. With the exception of awards posters, all posters can be a maximum of 36" wide x 48" tall.

There are two 4-hour time blocks dedicated to posters: **Poster Session I (Thursday afternoon, from 2:30 pm to 6:30 pm)** and **Poster Session II (Saturday morning, from 8:30 am to 12:30 pm)**.

All posters have been assigned at least one shorter, scheduled time block, during which time at least one named author is required to stand by the poster to interact with meeting attendees.

Logistics for poster display depend on where your poster has been assigned to be displayed.

With the exception of the finalists for the Journal of Biomechanics and Clinical Biomechanics Award, posters assigned to Centennial Ballroom A will be presented either during Poster Session I or Poster Session II, but not both

### Posters assigned to Centennial Ballroom A

- Poster Session I should be mounted by 9:00 a.m. on Thursday, August 11 and removed by 11:30 am on Friday, August 12
- Poster Session II should be mounted by 12:30 pm on Friday, August 12 and removed by 1:00 pm on Saturday, August 13

### The two finalists for the Journal of Biomechanics Award and the two finalists for the Clinical Biomechanics Award

- Presented during both Poster Session I and Poster Session II
- Should be mounted by 9:00 am on Thursday, August 11 and removed by 1:00 pm on Saturday, August 13
- Finalists for the Journal of Biomechanics and Clinical Biomechanics Awards (to be announced) can make posters a maximum of 72" wide x 48" tall

### Posters assigned to the suite of Meeting Rooms (including Barcelona/Casablanca, Melbourne, Odessa, Tokyo/Vancouver, and Shanghai)

- Presented during both Poster Session I and Poster Session II
- Should be mounted by 9:00 am on Thursday, August 11 and removed by 1:00 pm on Saturday, August 13
- Meeting Rooms posters are located in the following rooms:

**Poster #201-220 in Odessa**

**Poster #221-240 in Shanghai**

**Poster #241-280 in Tokyo/Vancouver**

**Poster #281-317 in Barcelona/Casablanca**

**Poster #318-341 in Melbourne**

## Podium Presentations

### Presentation preparation:

- Presentation slides should be prepared with PowerPoint 2007 or higher.
- At the meeting, presentation files will be played with **MS Office 2010 on a Windows 7 PC**. Presenter's responsibility to ensure compatibility of the presentation file with **PowerPoint 2010**.
- Please save the PowerPoint (.pptx) file and all media files (include animation, video, audio, etc.) in a folder. The presentation folder and the PowerPoint file should be named in the format of *[session name]\_[presenting time]\_[first author's last name]*. Please note that the presenting time should be in 24-hour format.
  - Ex. The first author of the talk in Rehabilitation is Wang M at 4:15 PM in the session Rehabilitation. The presentation folder and PowerPoint file should be named as 'Rehabilitation\_1615\_Wang (.pptx)'.
  - Suggestion: **'Publish'** function in PowerPoint is recommended to ensure all media files used in the slides are included.

### Transferring presentation files:

- Please prepare a USB drive with a copy of the presentation FOLDER.
- All talks are to be transferred to the meeting computers in **Naples room**, at the Westin.
- Naples room will be open for 2.5 hour windows for presenters to upload their talks.
  - Thursday 8/11 Presentations:  
Load Wednesday 8/10, between 2:30-5:00pm
  - Friday, 8/12 *morning* presentations:  
Load Thursday 8/11, between 12:30-3:00pm
  - Friday, 8/12 *afternoon* presentations:  
Load Thursday 8/11, between 3:00-5:30pm
  - Saturday, 8/13 presentations:  
Load Saturday, 8/13, between 8:30-11:00am
- After uploading your talks to the meeting computer, you may have **up to 5 minutes** to check/run through your slides on that computer. No editing or other usage is allowed on the meeting computers.
- No internet access is available in Naples room. Please have your materials ready in a USB drive prior to uploading in Naples room.

## TUTORIALS

**Wednesday, August 10**

**1:00pm-3:00pm, Tokyo/Vancouver Room**

**Tutorial 1: Plasticity of Muscle Mechanics**

**Presenter: Richard Lieber, PhD**

**Wednesday, August 10**

**3:15pm-5:00pm, Tokyo/Vancouver Room**

**Tutorial 2: Visual3D: Inside the Black Box**

**Presenter: Tom Kepple, PhD and W. Scott Selbie, PhD**

## VIRTUAL LAB TOURS

**Wednesday, August 10**

**3:00pm-5:00pm, Barcelona Room**

Members of the USC Biomechanics community will be present to discuss the work in their lab and provide "virtual tours". Below is a list of the labs that will be represented:

Applied Mathematical Physiology Lab

Jason Kutch, PhD

[pt.usc.edu](http://pt.usc.edu)

Brain-Body Dynamics Lab

Francisco Valero-Cuevas, PhD

[bbdl.usc.edu](http://bbdl.usc.edu)

Development of Infant Motor Performance Lab

Linda Fetters, PhD, PT, FAPTA

[pt.usc.edu](http://pt.usc.edu)

Engineering, Neuroscience & Health seminar series

[bbdl.usc.edu/ENH](http://bbdl.usc.edu/ENH)

Health, Technology and Engineering program

[hte.usc.edu](http://hte.usc.edu)

Human Performance Lab

Susan Sigward, PhD, PT, ATC

[pt.usc.edu](http://pt.usc.edu)

John C. Wilson, Jr. Motion Analysis Laboratory

Tishya Wren, PhD

[www.chla.org](http://www.chla.org)

Medical Device Development Facility

Gerald Loeb, MD

[mddf.usc.edu](http://mddf.usc.edu)

Motor Behavior and Neurorehabilitation Lab

Carolee Winstein, PhD, PT, FAPTA

[pt2.usc.edu/labs/mbnl](http://pt2.usc.edu/labs/mbnl)

Motor Control Development Lab

Nina S. Bradley, PhD, PT

[pt.usc.edu/labs/mcdl](http://pt.usc.edu/labs/mcdl)

Musculoskeletal Biomechanics Research Lab

Christopher Powers, PhD, PT, FAPTA

George Salem, PhD

Kornelia Kulig, PhD, PT, FAPTA

[www.usc.edu/go/mbrl](http://www.usc.edu/go/mbrl)

Rehabilitation Engineering Program

@ Rancho Los Amigos National Rehabilitation Center

Philip Requejo, PhD

[www.ranchorep.org](http://www.ranchorep.org)

Rehabilitation Engineering Research Center for  
Technologies for Successful Aging with Disability

[www.isi.edu/research/renc](http://www.isi.edu/research/renc)

Sanger Lab

Terrance Sanger, MD, PhD

[sangerlab.org](http://sangerlab.org)

USC Biomechanics Research Lab

Jill McNitt-Gray, PhD

[dornsife.usc.edu/kinesiology](http://dornsife.usc.edu/kinesiology)

# PLENARY AND AWARDS SESSIONS

## Thursday, August 11

### 11:30am-12:30pm

*Ballroom B-D*

#### Keynote Address

Natural Armor: Interdisciplinary Convergence Between Engineering, Evolutionary Biology and Architecture

*Christine Ortiz, PhD, Massachusetts Institute of Technology*

#### About the Speaker

Dr. Ortiz is a prolific scientist with over 100 publications in more than 20 different academic journals. Her research program focuses on the mechanics of structural biological materials, in particular musculoskeletal and exoskeletal tissues with the objective of obtaining a fundamental, mechanistic-based understanding of tissue function, quality, and pathology. Model systems include; articular cartilage, bone, natural flexible armor, transparent armor, and biological armor for extreme conditions (e.g. blast, heat, thermal). Dr. Ortiz's research employs novel experimental and theoretical methodologies across multiple scales, ranging from individual molecules to live animal biomechanics. Her work has relevance to medical and engineering fields, facilitating development of improved medical treatments for musculoskeletal disease and injury as well as providing guidance for improved materials for protective applications, such as armor for biochemical toxin resistance. Dr. Ortiz has numerous national and international honors including, the National Security Science and Engineering Faculty Fellow (NSSEFF) Award and the National Science Foundation Presidential Early Career Award for Scientists and Engineers (NSF-PECASE). In 2009, she was awarded the MIT Martin Luther King Jr. Leadership Award for her important and lasting impact on students, staff and faculty at MIT.

### 2:00pm-2:15pm

*Ballroom B-D*

#### Young Scientist Predoctoral Award

Effects of Crack Morphology on Local Cartilage Stresses  
*Curtis-Goreham-Voss, University of Iowa*

### 2:15pm-2:30pm

*Ballroom B-D*

#### Young Scientist Postdoctoral Award

Effects of Anti-Whiplash Seats on Cervical Facet and Disc Kinematics During Simulated Rear Crashes  
*Paul Ivancic, PhD, Yale University*

## Friday, August 12

### 11:30am-12:30pm

*Ballroom B-D*

#### Borelli Award Lecture

Illuminating Muscle Function  
*Scott Delp, PhD, Stanford University*

#### About the Speaker

Scott Delp graduated Sum Cum Laude with a B.S. in Mechanical Engineering from Colorado State University in 1983. He worked in Hewlett Packard's computer graphics group before beginning graduate school at Stanford University in 1985. Delp received the M.S. and Ph.D. degrees from Stanford and in 1990 joined the faculty of Northwestern University. He returned to Stanford in 1999, and in 2002 became the founding Chairman of Stanford's Bioengineering Department. Professor Delp's work draws on computational mechanics, biomedical imaging, and neuromuscular biology to improve treatments for individuals with physical disabilities. He has led the development of software systems (SIMM and Open-Sim) that enable simulation of human and animal movements; these software systems have become the platform for an international collaboration involving hundreds of research centers. Delp also developed fundamental patents in surgical navigation. Delp has received numerous awards for his work, including a National Young Investigator Award from NSF and a Technology Reinvestment Award for which he was honored by President Clinton at the White House. He is currently the James H. Clark Professor of Bioengineering, Mechanical Engineering, and Orthopaedic Surgery at Stanford.

## Friday, August 12

**5:00pm-6:00pm**

*Ballroom B-D*

### **Keynote Address**

Simulating Human Motion for Graphics and Robotics  
*Jessica Hodgins, PhD, Carnegie Mellon University*

### **About the Speaker**

Dr. Hodgins has had a significant impact on our understanding, simulation, and animation of movement. Her research lab has played a leadership role in the development of new techniques in simulation, control systems, and motion capture. Dr. Hodgins is best known for her work on animating humans; her papers from the early 1990s on legged motion and human athletics laid the groundwork for use of dynamics to simulate complex characters in computer graphics. Hodgins also applied physics to create realistic animations of inanimate objects, including the animation of brittle fracture, explosions, and the motion of complex media like sand, mud, and snow. Her work has resulted in improved techniques for capturing and modeling the deformable elements of human motion and she has made major contributions in the area of user control of complex, synthesized motions. Dr. Hodgins has received a NSF Young Investigator Award, a Packard Fellowship, and a Sloan Fellowship. She was editor-in-chief of ACM Transactions on Graphics from 2000-2002 and ACM SIGGRAPH Papers Chair in 2003. In 2010, she was awarded the ACM SIGGRAPH Computer Graphics Achievement Award.

## Saturday, August 13

**1:15pm-1:45pm**

*Ballroom B-D*

### **James J. Hay Memorial Lecture**

Coordinative Variability: An Indicator of Overuse Injury?

*Joseph Hamill, PhD, University of Massachusetts*

### **About the Speaker**

Dr. Hamill received a B.A. (political science) from York University, Toronto, a B.S. from Concordia University (Science), Montreal, and both an M.S. and Ph.D. (biomechanics) from University of Oregon. Presently, he is a Professor in the Department of Kinesiology at the University of Massachusetts and has been the Director of the Biomechanics Laboratory for the past 25 years. He is also an Honorary Professor at the University of Edinburgh in Scotland, an Adjunct Professor at the university of Limerick, Ireland and at Plymouth State University in New Hampshire, a Distinguished Research Professor at the Republic Polytechnic in Singapore and a Staff Scientist at the Shriners' Hospital for Children in Springfield, MA. He previously served as Chair of the department for 11 years and as Associate Dean of the School of Public Health and Health Sciences for 3 years. His research interests are focused on lower extremity biomechanics during normal and pathological locomotion and he has utilized modeling and dynamical systems to study optimization of human locomotion. He has authored or co-authored over 120 research papers, over 160 research proceedings, several book chapters and three books. During his academic career, Dr. Hamill has mentored over 45 doctoral and Master's students. He has served on the Executive Boards of the International Society of Biomechanics, the Footwear Biomechanics Group, the International Society of Biomechanics in Sports, the New England Chapter of the American College of Sports Medicine and the Canadian Society of Biomechanics.

**3:30pm-4:00pm**

*Ballroom B-D*

### **Closing Ceremony and Awards**

# SYMPOSIUM

Friday, August 12

**9:45am-11:00am**

*Ballroom B*

## **Teaching Biomechanics**

*Organized by Andrew Karduna, PhD,  
University of Oregon*

ASB has traditionally been a venue where researchers can share their research with colleagues. However, for many of us, teaching is also a big part of our jobs. The goal of this symposium is to have faculty who are teaching biomechanics in different ASB disciplines share their experiences and elicit feedback from the audience. Hopefully this will start a conversation that can be continued on in future ASB meetings.

## **9:45 Clinical Biomechanics Instruction Using Active Learning and Context-Rich Laboratory Experiences**

*David Nuckley, PhD, University of Minnesota*

## **10:05 Teaching Biomechanics with Just-in-Time Teaching (JiTT)**

*Jody Riskowski, PhD, University of Texas at El Paso*

## **10:25 Teaching human movement to engineers: experiences from nine institutions**

*Kate Saul, Jeff Reinbolt, Silvia Blemker, Blake Ashby, Scott Delp, Saryn Goldberg, Rob Siston, Darryl Thelen, Joshua Webb, Wake Forest, U. Tennessee, University of Virginia, Grand Valley State University, Stanford University, Hofstra University, Ohio State University, University of Wisconsin, Latournea University*

## **10:45 Panel Discussion**

**1:30pm-3:00pm**

*Ballroom B*

## **Upper Extremity Symposium on Wheelchair Biomechanics**

*Organized by Philip S. Requejo, PhD, Rancho Los Amigos National Rehabilitation Center*

There have been many improvements in the design and function of wheelchairs and seating systems that have maximized independence of wheelchair users. Yet upper extremity pain and dysfunction resulting from wheelchair use are still prevalent. Creation of evidence-based strategies aimed at maintaining a maximal level of independence must address multiple factors related to ergonomics and equipment selection, performance techniques, and load-bearing capability of the musculoskeletal system. This symposium will bring together experts in the field to discuss their recent accomplishments and outline how major challenges can be overcome in the near future. This symposium will complement ongoing research at Rancho Los Amigos National Rehabilitation Center and Rehabilitation Engineering Research Center on Aging with Disability, in collaboration with the University of Southern California

## **1:30 Toward An Understanding of Shoulder Demands in Manual Wheelchair Users**

*Kenton Kaufman, Melissa Morrow, Wendy Hurd, Kristin Zhao, Meegan Van Straaten, Duane Morrow, Brian Kotajarvi, Lan-Yuen Guo, Michelle Sabick, Fong-Chin Su, Jeffrey Basford, Kai-Nan An.*

## **1:45 Insight into Wheelchair Biomechanics Using Musculoskeletal Modeling and Simulation Techniques**

*Richard R. Neptune, Jeffery W. Rankin and W. Mark Richter*

## **2:00 Biofeedback Propulsion Training**

*W. Mark Richter, Ph.D.*

## **2:15 Biomechanical Analysis of Sitting Pivot Wheelchair Transfers**

*Alicia Koontz, Padmaja Kankipati, Chung-Ying Tsai, Yen-Sheng Lin*

## **2:30 Biomechanics of the Shoulder Joint During Manual Wheelchair Propulsion in Persons With Paraplegia**

*Sara Mulroy, Philip Requejo, Puja Ruparel, Patricia Hatchet, Lisa Lighthall Haubert, Valerie Eberly, Carmen Muller-Karger*

## **2:45 Panel Discussion**

# PODIUM SESSIONS

THURSDAY, AUGUST 11, 8:00 AM – 9:15 AM

|                | <b>Bone</b><br>Centennial Ballroom B   | <b>Neuromechanics</b><br>Centennial Ballroom C  | <b>Gait</b><br>Centennial Ballroom D   |
|----------------|--|---|--|
| Session Chair  | <b>Ron Zernicke, PhD</b><br><i>University of Michigan</i>  | <b>Francisco Valero-Cuevas, PhD</b><br><i>USC</i>   | <b>Kenton Kaufman, PhD</b><br><i>Mayo Clinic</i>   |
| <b>8:00 AM</b> | <b>Altering Joint Loading Direction in the Sheep Generates Trabecular Orientation Adjustment</b><br>Barak M, Hublin J, Lieberman D<br><i>Max Planck Institute for Evolutionary Anthropology; Harvard University</i>    | <b>Isokinetic Strength and Power Deficits in the Hand Following Stroke</b><br>Conrad M, Kamper D<br><i>Rehabilitation Institute of Chicago</i>  | <b>Gait Adaptations When Walking on a Destabilizing Rock Surface</b><br>Gates D, Wilken J, Scott S, Sinitski E, Dingwell J<br><i>Brooke Army Medical Center</i>                        |
| <b>8:15 AM</b> | <b>Validation of a 3-Pt Bending Technique for Small Bone Specimens</b><br>Albert C, Jameson J, Smith P, Harris G<br><i>Marquette University</i>  | <b>Variability of Gait is Dependent on Direction of Motion</b><br>Wurdeman S, Huben N, Stergiou N<br><i>Nebraska Biomechanics Core Facility, University of Nebraska at Omaha</i>  | <b>The Effects of Aging on the Metabolic Cost of Supporting Body Weight During Walking</b><br>Musolf S, Ortega J<br><i>Humboldt State University</i>                                   |
| <b>8:30 AM</b> | <b>Age Differences in Femoral Neck Strains During Gait</b><br>Anderson D, Madigan M<br><i>Beth Israel Deaconess Medical Center</i>   | <b>To What Extent Can Posture-Related Changes in Corticomotor Excitability Be Explained by Muscle Biomechanics?</b><br>Mogk J, Rogers L, Murray W, Perreault E, Stinear J<br><i>Rehabilitation Institute of Chicago</i> | <b>Effect of Incline on Walking Mechanics, Energetics and Neuromuscular Control</b><br>Silder A, Delp S, Besier T<br><i>Stanford University</i>  |
| <b>8:45 AM</b> | <b>Effect of Strain Gauge Size and Placement During the Mouse Axial Ulnar Loading Protocol Calibration</b><br>Wagner D, Beaupre G<br><i>VA Palo Alto Health Care System</i>  | <b>Velocity Dependency of Parkinsonian Rigidity Assessed at the Wrist</b><br>Powell D, Muthumani A, Hanson N, Threlkeld A, Xia R<br><i>Creighton University</i>   | <b>Comparison of Automated Event Detection Algorithms in Pathological Gait</b><br>Bruening D, Standifird T, Denning M, Trager Ridge S<br><i>Shriners Hospitals for Children - Erie</i> |
| <b>9:00 AM</b> | <b>Image Segmentation and Registration Algorithm for Quantification of Rib Morphology Across Ages and Genders</b><br>Weaver A, Stitzel J<br><i>Virginia Tech-Wake Forest University Center for Injury Biomechanics</i> | <b>Lower Extremity Joint Moment Asymmetry During Split-Belt Treadmill Walking</b><br>Roemmich R, Hass C<br><i>University of Florida</i>   | <b>BMI, Body Volume Distribution, and Sagittal Plane Gait Parameters</b><br>Blazek K, Asay J, Erhart J, Andriacchi T<br><i>Stanford University</i>                                     |

# PODIUM SESSIONS

THURSDAY, AUGUST 11, 9:45 AM – 11:00 AM

PODIUM SESSIONS

|                 | <b>Imaging</b><br>Centennial Ballroom B   | <b>Tendon and Ligament</b><br>Centennial Ballroom C  | <b>Upper Extremity</b><br>Centennial Ballroom D  |
|-----------------|---|--|--|
| Session Chair   | <b>J. J. Trey Crisco, PhD</b><br><i>Brown University</i>  | <b>Walter Herzog, PhD</b><br><i>University of Calgary</i>  | <b>Kate Saul, PhD</b><br><i>Wake Forest School of Medicine</i>   |
| <b>9:45 AM</b>  | <b>Vastus Lateralis:Vastus Medialis Activation Ratio Correlates with Vastus Medialis Activation Delay and Patellar Maltracking in Patellofemoral Pain Patients</b><br><br>Pal S, Besier T, Draper C, Fredericson M, Gold G, Beaupre G, Delp S<br><i>Stanford University</i> | <b>Achilles Tendon Strain Distributions During Cyclic Inertial Loading of the Plantar Flexors</b><br><br>Chernak L, Bungler D, Thelen D<br><i>University of Wisconsin-Madison</i>                                | <b>Typing Style Affects Arm Kinetics, Kinematics and Muscle Activation</b><br><br>Trudeau M, Asundi K, Dennerlein J<br><i>Harvard School of Public Health</i>  |
| <b>10:00 AM</b> | <b>Short Term Mechanical Loading Increases Trabecular Bone Mineral Content and Moments of Inertia in the Radius of Young Women</b><br><br>Edwards W, Troy K<br><i>University of Illinois at Chicago</i>   | <b>ACL Cross-Sectional Area and Medial Tibial Plateau Geometry Provide Insights on the Gender Difference in Peak ACL Strain</b><br><br>Lipps D, Oh Y, Wojtys E, Ashton-Miller J<br><i>University of Michigan</i> | <b>Multi-Digit Coordination and Adaptation to Object Mass Distribution in Carpal Tunnel Syndrome</b><br><br>Zhang W, Johnston J, Smith A, Ross M, Coakley B, Gleason E, Dueck A, Santello M<br><i>Arizona State University</i> |
| <b>10:15 AM</b> | <b>In Vivo Chondrocyte Mechanics in the Intact Mouse Knee Joint</b><br><br>Abusara Z, Herzog W<br><i>University of Calgary</i>  | <b>Effect of Prior Testing on the Plantar Soft Tissue Shear Properties</b><br><br>Pai S, Vawter P, Ledoux W<br><i>VA Puget Sound and University of Washington</i>  | <b>Changes in the Thumb Carpo-Metacarpal Joint Space During High-Demand Functional Tasks</b><br><br>Halilaj E, Rainbow M, Moore D, Got C, Crisco J<br><i>Brown University</i>  |
| <b>10:30 AM</b> | <b>The Effect of Elevated Vacuum Suspension on Axial Bone-Socket Displacement in Persons with a Traumatic Transtibial Amputation</b><br><br>Darter B, Sinitski K, Wilken J<br><i>Brooke Army Medical Center</i>   | <b>How Flatfoot Deformity Affects Moment Arms</b><br><br>Choisne J, Ringleb S, McCullough M, Bawab S, Kaufman K, Kitaoka H<br><i>Old Dominion University</i>   | <b>Upper Limb Muscle Volume and Strength, and Their Relationship in Older Adults</b><br><br>Vidt M, Daly M, Miller M, Davis C, Marsh A, Saul K<br><i>Wake Forest University</i>  |
| <b>10:45 AM</b> | <b>A Markerless Radiostereometric Analysis (Rsa) System for Measuring Glenohumeral Translation: Details and Validation</b><br><br>Fox A, Kedgley A, Jenkyn T<br><i>The University of Western Ontario</i>  | <b>Identifying Factors That Affect Changes in Peak Achilles Tendon Strain Over 6 Months in Youth 10-14 Years Old</b><br><br>Neugebauer J, Hawkins D<br><i>University of California - Davis</i>                   | <b>Influence of Index Finger Joint Fusion on Precision Pinch Kinematics</b><br><br>Domalain M, Li Z<br><i>Cleveland Clinic</i>   |

# PODIUM SESSIONS

FRIDAY, AUGUST 12, 8:00 AM – 9:15 AM

|                | <b>Joint Mechanics</b>   | <b>Injury</b>  | <b>Muscle</b>   |
|----------------|--|--|---|
|                | <b>Centennial Ballroom B</b>   | <b>Centennial Ballroom C</b>   | <b>Centennial Ballroom D</b>  |
| Session Chair  | <b>Peter Cavanagh, PhD</b><br><i>University of Washington</i>  | <b>Irene Davis, PhD</b><br><i>University of Delaware</i>   | <b>Bob Gregor, PhD</b><br><i>USC</i>  |
| <b>8:00 AM</b> | <b>Validation of Video-Based Motion Analysis of Scapular and Humeral Rotational Kinematics During Simulated Throwing</b><br>Chu Y, Akins J, Lovalekar M, Tashman S, Lephart S, Sell T<br><i>University of Pittsburgh</i> | <b>Mechanical Properties of Human Craniovertebral Ligaments</b><br>Mattucci S, Cronin D, Chandrashekar N, Moulton J<br><i>University of Waterloo</i>   | <b>Sarcomere Behaviour in Myofibrils During Local Deactivation</b><br>Leonard T, Herzog W<br><i>University of Calgary</i>   |
| <b>8:15 AM</b> | <b>The Mechanics &amp; Energetics of Human Walking &amp; Running: A Joint Level Perspective</b><br>Farris D, Sawicki G<br><i>North Carolina State University</i>   | <b>Effects of Stroke-Induced Sensory and Motor Deficit on Phalanx Force Magnitude and Angular Deviation During Power Grip</b><br>Enders L, Seo N<br><i>University of Wisconsin-Milwaukee</i>                   | <b>Automated Methods for Determination of 3D Muscle Fascicle Orientation in Human Muscle Using Free Hand Ultrasound</b><br>Rana M, Wakeling J<br><i>Simon Fraser University</i> |
| <b>8:30 AM</b> | <b>Load Transfer Across the Pelvic Bone During Normal Walking</b><br>Ghosh R, Pal B, Ghosh D, Gupta S<br><i>Indian Institute of Technology Kharagpur</i>   | <b>Tibial Geometry, Joint Compression, and Their Effects on Anterior Cruciate Ligament Strain: An In-Vitro Study</b><br>Breighner R, Hashemi J, Chandrashekar N, Slauterbeck J<br><i>Texas Tech University</i> | <b>Skeletal Muscle Fibrosis in Response to Compliant Muscle Fibers</b><br>Meyer G, Smith L, Lieber R<br><i>University of California, San Diego</i>                              |
| <b>8:45 AM</b> | <b>Influence of a Fixed Ankle on Joint Mechanics and Metabolic Cost of Walking</b><br>Wutzke C, Sawicki G, Lewek M<br><i>University of North Carolina at Chapel Hill</i>   | <b>Do Knee Eccentric Strength and Knee Joint Kinetics Differ Between Jumpers and Non-Jumpers in Landing Activities?</b><br>Wu X, Zhang S, Zhang D, Xie C<br><i>The University of Tennessee</i>                 | <b>Muscle and Fascicle Excursions in Children with Cerebral Palsy</b><br>Matthiasdottir S, Hahn M, Yaraskavitch M, Herzog W<br><i>University of Calgary</i>                     |
| <b>9:00 AM</b> | <b>Transducer and Base Compliance Alter the in Situ 6 Dof Force Measured from Muscle During an Isometric Contraction in a Multi-Joint Limb</b><br>Sandercock T, Yeo S, Pai D, Tresch M<br><i>Northwestern University</i> | <b>Does Foot Strike Pattern Predict Loading Rates During Shod Or Barefoot Running?</b><br>Becker J, Sinsurin K, Pisciotta E, James S, Osternig L, Chou L<br><i>University of Oregon</i>                        | <b>The Mechanical Effect of Rat FCU Muscle After Tendon Transfer</b><br>Maas H, Huijing P<br><i>VU University Amsterdam</i>   |

# PODIUM SESSIONS

FRIDAY, AUGUST 12, 9:45 AM – 11:00 AM

PODIUM SESSIONS

|                 | <b>Teaching Symposium</b><br>Centennial Ballroom B   | <b>Methods</b><br>Centennial Ballroom C  | <b>Sports</b><br>Centennial Ballroom D   |
|-----------------|--|--|--|
| Session Chair   | <b>Andrew Karduna, PhD</b><br><i>University of Oregon</i>  | <b>James Ashton-Miller, PhD</b><br><i>University of Michigan</i>   | <b>Jill McNitt-Gray, PhD</b><br><i>USC</i>   |
| <b>9:45 AM</b>  | <b>9:45 am – 10:05 am<br/>Clinical Biomechanics<br/>Instruction Using Active<br/>Learning and Context-Rich<br/>Laboratory Experiences</b><br>Nuckley D<br><i>University of Minnesota</i>                 | <b>A Method of Normalization<br/>for CT-Based Texture<br/>Analysis in Fracture Severity<br/>Assessment</b><br>Kilburg A, Thomas T,<br>Anderson D, Brown T<br><br><i>University of Iowa</i>   | <b>Biomechanics of Head<br/>Impacts in American Football<br/>Players</b><br>Crisco J, Wilcox B, Beckwith J, Chu<br>J, Duhaime A, Rowson S, Duma S,<br>Maerlander A, Greenwald R<br><br><i>Brown University</i> |
| <b>10:00 AM</b> | <b>10:05 am – 10:25 am<br/>Teaching Biomechanics<br/>with Just-in-Time Teaching<br/>(JiTT)</b><br>Riskowski J<br><i>University of Texas at El Paso</i>   | <b>An Instrumented Split-Belt<br/>Treadmill System Using<br/>Commercial Part</b><br>Rich K, Prince J, Qiao M,<br>Jindrlich D<br><br><i>Arizona State University</i>  | <b>Dynamic Sagittal-Plane Trunk<br/>Control During ACL-Injury</b><br>Sheehan F, Sipprell W, Boden B<br><br><i>National Institute of Health</i>   |
| <b>10:15 AM</b> | <b>10:25 am – 10:45 am<br/>Teaching Human Movement<br/>to Engineers: Experiences<br/>from Nine Institutions</b><br>Reinbolt J, Saul K<br><i>University of Tennessee &amp;<br/>Wake Forest University</i> | <b>Kinematic Methods for<br/>Determining Gait Events<br/>During Level and Slope<br/>Walking in the Cat</b><br>Pantall A, Prilutsky B<br><br><i>Georgia Institute of Technology</i>   | <b>Effects of a Fatiguing Run on<br/>Lower Extremity Mechanics in<br/>Female Runners</b><br>Truebenbach C, Earl-Boehm<br>J, Huddleston W, Swartz A,<br>O'Connor K<br><br><i>UW-Milwaukee</i>                   |
| <b>10:30 AM</b> |  | <b>Reliability of Medial and<br/>Lateral Forefoot Segment<br/>Kinematics During Shod<br/>Treadmill Running</b><br>Ford K, Masters T, Carson D<br><br><i>Cincinnati Children's Hospital<br/>Medical Center</i>                        | <b>Quadriceps Activation Predicts<br/>Knee Kinetics During Single-<br/>Leg Landings</b><br>Brown T, McLean S, Palmieri-<br>Smith R<br><br><i>University of Michigan</i>  |
| <b>10:45 AM</b> | <b>Panel Discussion</b>  | <b>Dynamic Control of Fingertip<br/>Forces: Development in Child-<br/>hood and Decline with Aging</b><br>Dayanidhi S, Hedberg A,<br>Hagg I, Lilja N, Forssberg H,<br>Valero-Cuevas F<br><br><i>University of Southern California</i> | <b>Dynamic Effect of Lacrosse<br/>Stick Shape on Ball Speed<br/>During Throwing</b><br>Sheets A, Hubbard M<br><br><i>The Ohio State University</i>   |

# PODIUM SESSIONS

FRIDAY, AUGUST 12, 1:30 PM – 3:00 PM

|                | Wheelchair Symposium<br>Centennial Ballroom B   | Knee<br>Centennial Ballroom C  | Posture and Balance<br>Centennial Ballroom D   |
|----------------|---|--|--|
| Session Chair  | <b>Phil Requejo, PhD</b><br><i>Rancho Los Amigos</i>  | <b>Ajit Chaudhari, PhD</b><br><i>Ohio State University</i>   | <b>Melissa Gross, PhD</b><br><i>University of Michigan</i>   |
| <b>1:30 PM</b> | <b>Toward an Understanding of Shoulder Demands in Manual Wheelchair Users</b><br>Kaufman K<br><i>Mayo Clinic</i>  | <b>Does Knee Extensor Muscle Imbalance Cause Changes in Patellar Tracking?</b><br>Sawatsky A, Leonard T, Herzog W<br><i>University of Calgary</i>  | <b>Age-Related Changes in Control of Center of Mass in Response to Support Surface Perturbations</b><br>Hsu W, Chou L, Woollacott M<br><i>National Taiwan University</i>                                     |
| <b>1:45 PM</b> | <b>Insight into Wheelchair Biomechanics Using Musculoskeletal Modeling and Simulation Techniques</b><br>Neptune R<br><i>The University of Texas at Austin</i>                   | <b>Differences in External Knee Adduction Moment Between ACL Reconstructed and Contralateral Knees</b><br>Zabala M, Scanlan S, Donahue J, Andriacchi T<br><i>Stanford University</i>   | <b>Altered Neuromuscular Control After Anterior Cruciate Ligament Injury</b><br>MacLeod T, Manal K, Snyder-Mackler L, Buchanan T<br><i>University of Delaware</i>  |
| <b>2:00 PM</b> | <b>Biofeedback Propulsion Training</b><br>Richter WM<br><i>MAX Mobility LLC</i>   | <b>Comparing Knee Joint Kinematics, Kinetics and Cumulative Load Between Healthy-Weight and Obese Young Adults</b><br>MacLean K, Maly M, Callaghan J<br><i>University of Waterloo</i>  | <b>Balance During Rotations in Dance</b><br>Lott M, Laws K<br><i>Bryn Mawr College</i>   |
| <b>2:15 PM</b> | <b>Biomechanical Analysis of Sitting Pivot Wheelchair Transfers</b><br>Koontz A<br><i>University of Pittsburgh</i>  | <b>Knee Osteoarthritis Results in Asymmetric Joint Moment Distribution During Gait</b><br>Richardson T, Higginson J<br><i>University of Delaware</i>   | <b>Postural Responses to Translational and Rotational Perturbations in Young and Older Adults</b><br>Roche J, Redfern M<br><i>University of Pittsburgh</i>   |
| <b>2:30 PM</b> | <b>Biomechanics of the Shoulder Joint During Manual Wheelchair Propulsion in Persons with Paraplegia</b><br>Mulroy S<br><i>Rancho Los Amigos National Rehabilitation Center</i> | <b>Knee Extensor and Flexor Torque - Angle - Angular Velocity Profiles from Maximal Voluntary and Electrically Stimulated Efforts</b><br>Pain M, Kim J, Young F, Forrester S<br><i>Loughborough University</i>                                     | <b>Are Age-Related Modifications During Squatting Task Implemented by Working-Age Men?</b><br>DiDomenico A, McGorry R, Banks J<br><i>Liberty Mutual Research Institute for Safety</i>                        |
| <b>2:45 PM</b> | <b>Panel Discussion</b><br>Special Guests: Jacquelin Perry, MD, Robert Waters, MD; Charles Whitehead (consumer)   | <b>Influence of Axial Rotation Moments on ACL Strain: A Cadaveric Study of Single- and Multi-Axis Loading of the Knee</b><br>Kiapour A, Quatman C, Ditto R, Levine J, Wordeman S, Hewett T, Goel V, Demetropoulos C<br><i>University of Toledo</i> | <b>Weakness in Ankle Dorsiflexors Reduces Balance Recovery Ability During a Stance Disturbance in the Elderly</b><br>Fujimoto M, Hsu W, van Donkelaar P, Woollacott M, Chou L<br><i>University of Oregon</i> |

# PODIUM SESSIONS

FRIDAY, AUGUST 12, 3:15 PM – 4:30 PM

PODIUM SESSIONS

|                | <b>Motor Control</b>   | <b>Orthopedics</b>   | <b>Rehabilitation</b>  |
|----------------|--|--|--|
|                | <b>Centennial Ballroom B</b>   | <b>Centennial Ballroom C</b>   | <b>Centennial Ballroom D</b>   |
| Session Chair  | <b>Mark Grabiner, PhD</b><br><i>University of Illinois-Chicago</i>   | <b>Tom Brown, PhD</b><br><i>University of Iowa</i>   | <b>Margaret Finley, PhD</b><br><i>University of Indianapolis</i>   |
| <b>3:15 PM</b> | <b>Effect of Walking Speed on Inter-Joint Coordination Differs Between Young and Elderly Adults</b><br>Chiu S, Chou L<br><i>University of Oregon</i>   | <b>Dislocation in the Morbidly Obese Total Hip Patient</b><br>Elkins J, Pedersen D, Singh B, Yack J, Callaghan J, Brown T<br><i>University of Iowa</i>                                       | <b>Joint Specific Toy Controller for Pediatric Upper Extremity Rehabilitation</b><br>Wilcox B, Kerman K, Crisco J<br><i>Brown University</i>   |
| <b>3:30 PM</b> | <b>Voluntarily Changing Step Width and Step Length Affects Dynamic Stability of Human Walking</b><br>McAndrew Young P, Dingwell J<br><i>University of Texas at Austin</i>  | <b>Effect of Loading Direction on Force to Dislocate in Reverse Shoulder Arthroplasty</b><br>Clouthier A, Hetzler M, Fedorak G, Bryant T, Deluzio K, Bicknell R<br><i>Queen's University</i> | <b>Finite State Control of a Variable Impedance Knee Mechanism for Restoration of Stance Phase Knee Flexion After Spinal Cord Injury</b><br>Bulea T, Kobetic R, Triolo R<br><i>Case Western Reserve University</i>   |
| <b>3:45 PM</b> | <b>The Human Splenius Capitis Muscle is Primarily a Head-Neck Rotator</b><br>Siegmond G, Vasavada A, Blouin J<br><i>MEA Forensic Engineers &amp; Scientists</i>  | <b>Moment Arms of Middle Deltoid and Rotator Cuff with Alterations in Glenoid and Humeral Head Inclination</b><br>Langenderfer J, Faber N<br><i>Central Michigan University</i>              | <b>Identification and Improvement of Difficult Hand Grip Movement Components for Stroke Survivors Using the Box and Block Test</b><br>Scott J, Brandenburg A, Allard B, Seo N<br><i>University of Wisconsin-Milwaukee</i>  |
| <b>4:00 PM</b> | <b>Fascicle Length Changes in Denervated Feline Soleus During Walking</b><br>Maas H, Gregor R, Prilutsky B<br><i>VU University Amsterdam</i>   | <b>Helical Axis Approach to Aberrant Motion Identification in Patients with Chronic Neck Pain</b><br>Ellingson A, Schulz C, Bronfort G, Nuckley D<br><i>University of Minnesota</i>          | <b>Biomechanical Demands of Therapeutic Hatha Yoga Poses in Older Adults: Modified Chair and Downward Facing Dog</b><br>Wang M, Yu S, Hashish R, Samarawickrame S, Haines M, Mulwitz L, Kazadi L, Greendale G, Salem G<br><i>University of Southern California</i> |
| <b>4:15 PM</b> | <b>Recruitment of Musculature During Extension from Full Trunk Flexion is Altered in People Who Develop Low Back Pain During Prolonged Standing</b><br>Nelson-Wong E, Alex B, Csepe D, Lancaster D, Callaghan J<br><i>Regis University</i> | <b>A Finite Element Simulation of Anterior Cruciate Ligament Reconstruction with a Patella Tendon Graft</b><br>Kwon T, Schroeder M, Dhaher Y<br><i>Rehabilitation Institute of Chicago</i>   | <b>The Influence of Hallux Valgus Surgery on Pelvis and Lower Extremities Movement During Gait</b><br>Kozakova J, Janura M, Sos Z, Svoboda Z<br><i>Palacky University in Olomouc</i>   |

# PODIUM SESSIONS

SATURDAY, AUGUST 13, 2:00 PM – 3:30 PM

|                | <b>Prosthetics</b>  | <b>Computational Modeling</b>   | <b>Ergonomics</b>  |
|----------------|---|---|--|
|                | <b>Centennial Ballroom B</b>  | <b>Centennial Ballroom C</b>  | <b>Centennial Ballroom D</b>   |
| Session Chair  | <b>Gerald Loeb, PhD</b><br><i>USC</i>   | <b>Donald Anderson, PhD</b><br><i>University of Iowa</i>  | <b>Angela DiDomenico, PhD</b><br><i>Liberty Mutual Research Institute for Safety</i>   |
| <b>2:00 PM</b> | <b>Evaluation of the Biomimetic Properties of a New Powered Ankle-Foot Prosthetic System</b><br>Ferris A, Aldridge J, Sturdy J, Wilken J<br><i>Brooke Army Medical Center</i>   | <b>Paretic Muscle Work is Increased in Pre-Swing During Hemiparetic Walking</b><br>Peterson C, Kautz S, Neptune R<br><i>Rehabilitation Institute of Chicago</i>   | <b>Energy Expenditure and Muscular Activation Patterns Through Active Sitting on Compliant Surfaces</b><br>Surowiec R, Wang H, Hite A, Dickin D<br><i>Ball State University</i>  |
| <b>2:15 PM</b> | <b>Bionic Leg Prosthesis Emulates Biological Ankle Joint During Walking</b><br>Grabowski A, D'Andrea S, Herr H<br><i>Dept. of Veterans Affairs &amp; Mass. Institute of Technology</i>                                | <b>Impact of Anatomical Adhesions on Stress Distribution Within the Extensor Hood of the Index Finger</b><br>Ellis B, Lee S, Traylor K, Weiss J, Kamper D<br><i>Illinois Institute of Technology</i>            | <b>Effects of Exercise-Induced Low Back Pain on Intrinsic Trunk Stiffness</b><br>Miller E, Bazrgari B, Nussbaum M, Madigan M<br><i>Virginia Tech - Wake Forest</i>   |
| <b>2:30 AM</b> | <b>Changes to Energy Storage and Return Foot Stiffness Alter the Walking Mechanics of Below-Knee Amputees</b><br>Fey N, Klute G, Neptune R<br><i>The University of Texas at Austin</i>                                | <b>Incorporation of Dynamic X-Ray Based Knee Kinematics Improves Quadriceps Force Prediction in Musculoskeletal Modeling</b><br>Shetye S, Li K, Tashman S, Harner C, Zhang X<br><i>University of Pittsburgh</i> | <b>Joint Loading of the Thumb while Operating a Mechanical Pipette—an Inverse Dynamic Analysis</b><br>Wu J, Sinsel E, Gloekler D, Wimer B, Zhao K, An KN, Buczek F<br><i>National Institute for Occupational Safety and Health</i> |
| <b>2:45 PM</b> | <b>Ankle and Knee Muscle Co-Contraction Differences in Trans-Tibial Amputee Residual and Intact Limbs and Matched Controls During Gait</b><br>Seyedali M, Morgenroth D, Czerniecki J, Hahn M<br><i>VA Puget Sound</i> | <b>Biomechanics to Brain: Unraveling the Complex Neural Connectivity of Multi-Muscle Control</b><br>Kutch J<br><i>University of Southern California</i>   | <b>Ergonomic Application of Hand Model: Tendon Excursion</b><br>Bae S, Armstrong T<br><i>University of Michigan</i>  |
| <b>3:00 PM</b> | <b>Asymmetry in Amputee Gait: The Propagating Effects of Weak Push-Off</b><br>Adamczyk P, Kuo A<br><i>Intelligent Prosthetic Systems, LLC</i>   | <b>Combining Musculoskeletal Modeling and Optimization to Estimate Muscle Forces at the Ankle</b><br>Crowell H, Davis I, Higginson J, Manal K, Wang L<br><i>U.S. Army Research Laboratory</i>                   | <b>Effects of Glove and Ladder Rung Design on Prevention of Ladder Fall</b><br>Hur P, Motawar B, Seo N<br><i>University of Wisconsin-Milwaukee</i>   |
| <b>3:15 PM</b> | <b>A Unified Deformable Segment Model of the Combined Ankle-Foot System That Does Work</b><br>Takahashi K, Razzook A, Guinn L, Schrank E, Kepple T, Stanhope S<br><i>University of Delaware</i>                       | <b>The Effect of Independent Manipulations of Body Weight and Mass on Instantaneous Metabolic Power During Walking</b><br>McGowan C, Neptune R, Kram R<br><i>University of Idaho</i>                            | <b>Local Dynamic Stability of the Lower Limb Kinematic Chain During Symmetric Lifting</b><br>Graham R, Costigan P, Sadler E, Almosnino S, Stevenson J<br><i>Queen's University</i>   |

# POSTER SESSION I

ORGANIZED BY TOPIC – THURSDAY 2:30 PM – 6:30 PM

## Posters 1-100, 201-341

See Poster Listings for Specific Presentation Times

| Topic                            | Poster #      | Location              |
|----------------------------------|---------------|-----------------------|
| J Biomech Award Finalist         | JB1, JB 2     | Centennial Ballroom A |
| Clin Biomech Award Finalist      | CB 1, CB 2    | Centennial Ballroom A |
| Best Computational Paper*        | SBCP          | Odessa                |
| Student Computational Modeling** | 1-16, 51-66   | Centennial Ballroom A |
| Clinical                         | 296-309       | Barcelona/Casablanca  |
| Computational Modeling           | 67-74         | Centennial Ballroom A |
| Ergonomics                       | 75-76         | Centennial Ballroom A |
|                                  | 329-332       | Melbourne             |
| Gait                             | 17-19, 77-78  | Centennial Ballroom A |
|                                  | 268-280       | Tokyo/Vancouver       |
|                                  | 281-295       | Barcelona/Casablanca  |
|                                  | 333-341       | Melbourne             |
| Lower Extremity                  | 20-23, 79-80  | Centennial Ballroom A |
|                                  | 310-317       | Barcelona/Casablanca  |
|                                  | 318-325       | Melbourne             |
| Methods                          | 24-30         | Centennial Ballroom A |
| Motor Control                    | 226-231       | Shanghai              |
| Muscle                           | 81-84         | Centennial Ballroom A |
|                                  | 221-225       | Shanghai              |
| Popular Choice***                | 201-220       | Odessa                |
| Posture and Balance              | 31-34, 85-87  | Centennial Ballroom A |
|                                  | 241-256       | Tokyo/Vancouver       |
| Prosthetics                      | 232-236       | Shanghai              |
| Running                          | 88-89         | Centennial Ballroom A |
|                                  | 326-328       | Melbourne             |
| Spine                            | 35-37, 90-92  | Centennial Ballroom A |
| Sports                           | 38-40, 93-96  | Centennial Ballroom A |
|                                  | 237-240       | Shanghai              |
| Tissue Mechanics                 | 41-45         | Centennial Ballroom A |
| Upper Extremity                  | 46-50, 97-100 | Centennial Ballroom A |
|                                  | 257-267       | Tokyo/Vancouver       |

\*Simulia Best Computational Paper Award. Award winner selected by 2011 Awards Committee before the meeting based on abstract review.

\*\*Simulia Student Poster Competition Session. Award winners to be selected by 2011 Awards Committee during the meeting based on first author student poster presentation.

\*\*\*Interactive session where meeting attendees select award winners from a group of abstracts representative of the highest scored abstracts from the peer-review process.

# POSTER SESSION II

ORGANIZED BY TOPIC – SATURDAY, AUGUST 13, 8:30 AM – 12:30 PM

## Posters 101-341

See Poster Listings for Specific Presentation Times

| Topic                            | Poster #         | Location              |
|----------------------------------|------------------|-----------------------|
| J Biomech Award Finalist         | JB1, JB 2        | Centennial Ballroom A |
| Clin Biomech Award Finalist      | CB 1, CB 2       | Centennial Ballroom A |
| Best Computational Paper*        | SBCP             | Odessa                |
| Student Computational Modeling** | 101-116          | Centennial Ballroom A |
| Clinical                         | 160-162          | Centennial Ballroom A |
|                                  | 296-309          | Barcelona/Casablanca  |
| Computational Modeling           | 151-159          | Centennial Ballroom A |
| Ergonomics                       | 163-165          | Centennial Ballroom A |
|                                  | 329-332          | Melbourne             |
| Gait                             | 117-123, 166-170 | Centennial Ballroom A |
|                                  | 268-280          | Tokyo/Vancouver       |
|                                  | 281-295          | Barcelona/Casablanca  |
|                                  | 333-341          | Melbourne             |
| Lower Extremity                  | 124-128          | Centennial Ballroom A |
|                                  | 310-317          | Barcelona/Casablanca  |
|                                  | 318-325          | Melbourne             |
| Methods                          | 129-137          | Centennial Ballroom A |
| Motor Control                    | 171-174          | Centennial Ballroom A |
|                                  | 226-231          | Shanghai              |
| Muscle                           | 175-176          | Centennial Ballroom A |
|                                  | 221-225          | Shanghai              |
| Popular Choice***                | 201-220          | Odessa                |
| Posture and Balance              | 138-142, 177-179 | Centennial Ballroom A |
|                                  | 241-256          | Tokyo/Vancouver       |
| Prosthetics                      | 232-236          | Shanghai              |
| Running                          | 143-147, 180-188 | Centennial Ballroom A |
|                                  | 326-328          | Melbourne             |
| Spine                            | 148-150, 189-190 | Centennial Ballroom A |
| Sports                           | 191-195          | Centennial Ballroom A |
|                                  | 237-240          | Shanghai              |
| Upper Extremity                  | 196-200          | Centennial Ballroom A |
|                                  | 257-267          | Tokyo/Vancouver       |

\*Simulia Best Computational Paper Award. Award winner selected by 2011 Awards Committee before the meeting based on abstract review.

\*\*Simulia Student Poster Competition Session. Award winners to be selected by 2011 Awards Committee during the meeting based on first author student poster presentation.

\*\*\*Interactive session where meeting attendees select award winners from a group of abstracts representative of the highest scored abstracts from the peer-review process.

# POSTER SESSION I

ORGANIZED BY TIME & LOCATION

## Posters 1-100

Centennial Ballroom A

Thursday: 2:30 pm - 4:00 pm

| Topic                              | Poster # |
|------------------------------------|----------|
| <i>J Biomech</i> Award Finalist    | JB 1     |
| <i>Clin Biomech</i> Award Finalist | CB 1     |
| Student Computational Modeling*    | 1-16     |
| Gait                               | 17-19    |
| Lower Extremity                    | 20-23    |
| Methods                            | 24-30    |
| Posture and Balance                | 31-34    |
| Spine                              | 35-37    |
| Sports                             | 38-40    |
| Tissue Mechanics                   | 41-45    |
| Upper Extremity                    | 46-50    |

\*Simulia Student Poster Competition Session

Thursday: 5:00 pm - 6:30 pm

| Topic                              | Poster # |
|------------------------------------|----------|
| <i>J Biomech</i> Award Finalist    | JB 2     |
| <i>Clin Biomech</i> Award Finalist | CB 2     |
| Student Computational Modeling*    | 51-66    |
| Computational Modeling             | 67-74    |
| Ergonomics                         | 75-76    |
| Gait                               | 77-78    |
| Lower Extremity                    | 79-80    |
| Muscle                             | 81-84    |
| Posture and Balance                | 85-87    |
| Running                            | 88-89    |
| Spine                              | 80-82    |
| Sports                             | 93-96    |
| Upper Extremity                    | 97-100   |

\*Simulia Student Poster Competition Session

## Posters 201-341

Meeting Rooms

“Cardinal”, “Gold”, and “Gray” topics are distributed throughout the meeting rooms so that a comparable number of posters are presented in each room during each hour. Refer to following page for presentation times.

### Cardinal

| Topic                     | Poster # |
|---------------------------|----------|
| Best Computational Paper* | SBCP     |
| Popular Choice            | 201-220  |
| Muscle                    | 221-225  |
| Posture and Balance       | 241-256  |
| Lower Extremity           | 310-325  |

\*Simulia Best Computational Paper Award

### Gold

| Topic           | Poster # |
|-----------------|----------|
| Motor Control   | 226-231  |
| Upper Extremity | 257-267  |
| Clinical        | 296-309  |
| Running         | 326-328  |
| Ergonomics      | 329-332  |

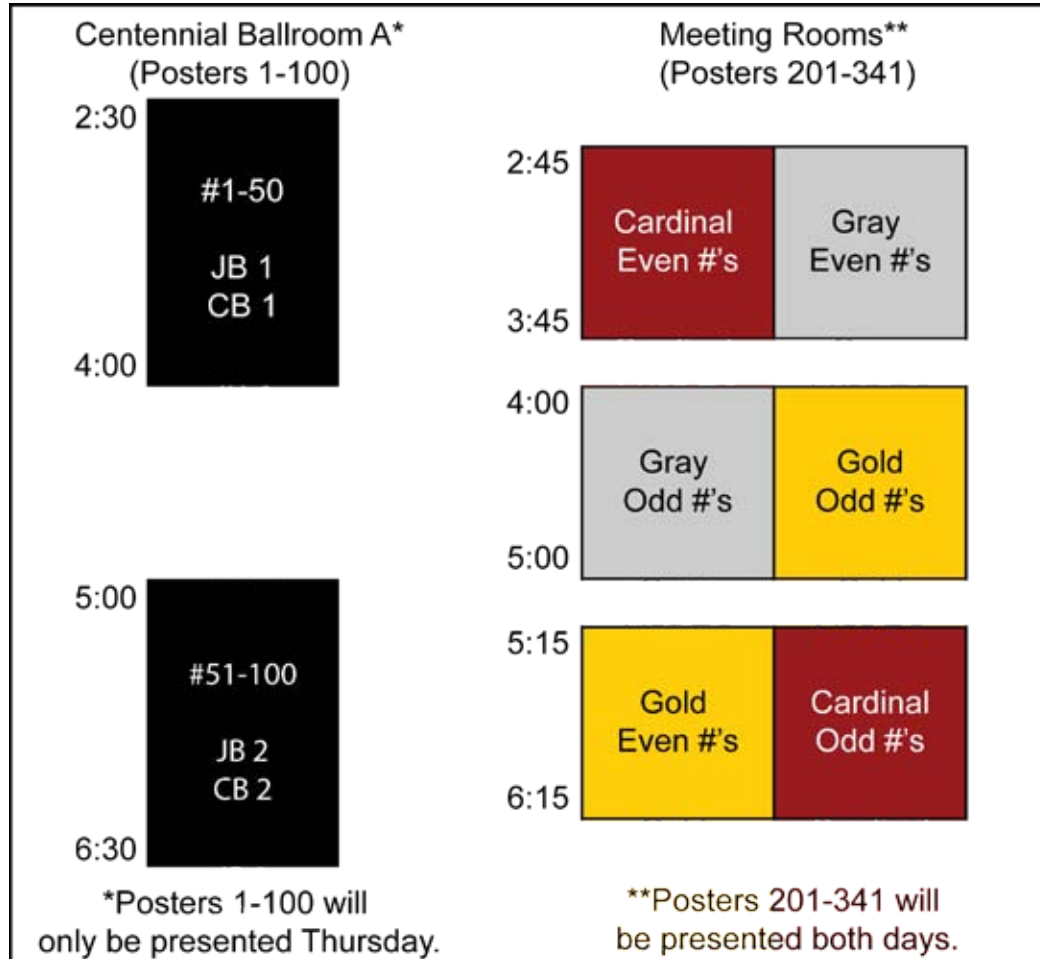
### Gray

| Topic       | Poster # |
|-------------|----------|
| Prosthetics | 232-236  |
| Sports      | 237-240  |
| Gait        | 268-295  |
| Gait        | 333-341  |

# POSTER SESSION I

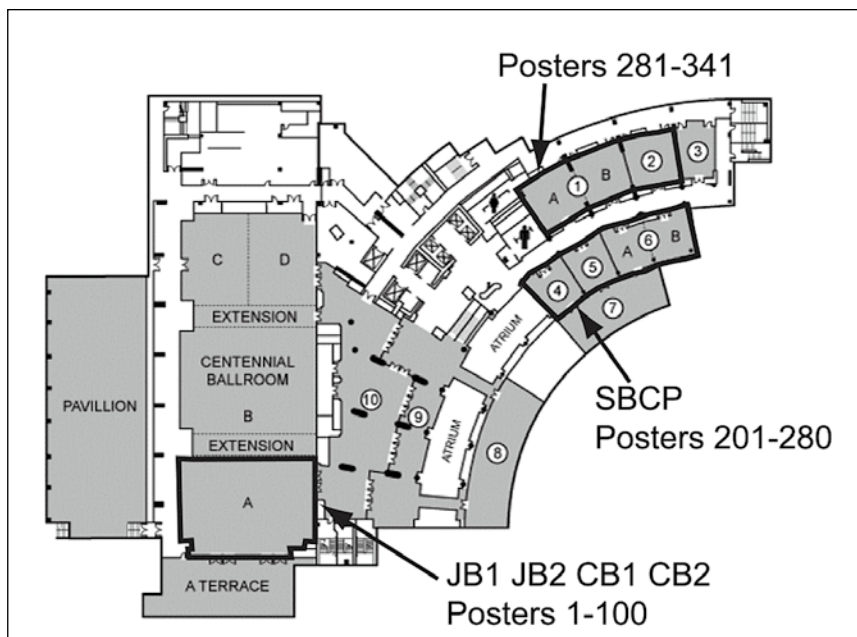
## ORGANIZED BY TIME & LOCATION

Authors will present their posters at the following times:



POSTER SESSIONS

Posters are located on the third level in the following locations:



“Cardinal”, “Gold”, and “Gray” topics are distributed throughout the meeting rooms so that a comparable number of posters are presented in each room during each hour.

**Poster # range in each meeting room:**

- 201-220 in (4) Odessa
- 221-240 in (5) Shanghai
- 241-280 in (6) Tokyo/Vancouver
- 281-317 in (1) Barcelona/Casablanca
- 318-341 in (2) Melbourne

# POSTER SESSION II

## ORGANIZED BY TIME & LOCATION

### Posters 101-200

#### Centennial Ballroom A

Saturday: 8:30 am - 10:00 am

| Topic                              | Poster # |
|------------------------------------|----------|
| <i>J Biomech</i> Award Finalist    | JB 1     |
| <i>Clin Biomech</i> Award Finalist | CB 2     |
| Student Computational Modeling*    | 101-116  |
| Gait                               | 117-123  |
| Lower Extremity                    | 124-128  |
| Methods                            | 129-137  |
| Posture and Balance                | 138-142  |
| Running                            | 143-147  |
| Spine                              | 148-150  |

\*Simulia Student Poster Competition Session

Saturday: 11:00 am - 12:30 pm

| Topic                              | Poster # |
|------------------------------------|----------|
| <i>J Biomech</i> Award Finalist    | JB 2     |
| <i>Clin Biomech</i> Award Finalist | CB 1     |
| Computational Modeling             | 151-159  |
| Clinical                           | 160-162  |
| Ergonomics                         | 163-156  |
| Gait                               | 166-170  |
| Motor Control                      | 171-174  |
| Muscle                             | 175-176  |
| Posture and Balance                | 177-179  |
| Running                            | 180-188  |
| Spine                              | 189-190  |
| Sports                             | 191-195  |
| Upper Extremity                    | 196-200  |

\*Simulia Student Poster Competition Session

### Posters 201-341

#### Meeting Rooms

“Cardinal”, “Gold”, and “Gray” topics are distributed throughout the meeting rooms so that a comparable number of posters are presented in each room during each hour. Refer to following page for presentation times.

#### Cardinal

| Topic                     | Poster # |
|---------------------------|----------|
| Best Computational Paper* | SBCP     |
| Popular Choice            | 201-220  |
| Muscle                    | 221-225  |
| Posture and Balance       | 241-256  |
| Lower Extremity           | 310-325  |

\*Simulia Best Computational Paper Award

#### Gold

| Topic           | Poster # |
|-----------------|----------|
| Motor Control   | 226-231  |
| Upper Extremity | 257-267  |
| Clinical        | 296-309  |
| Running         | 326-328  |
| Ergonomics      | 329-332  |

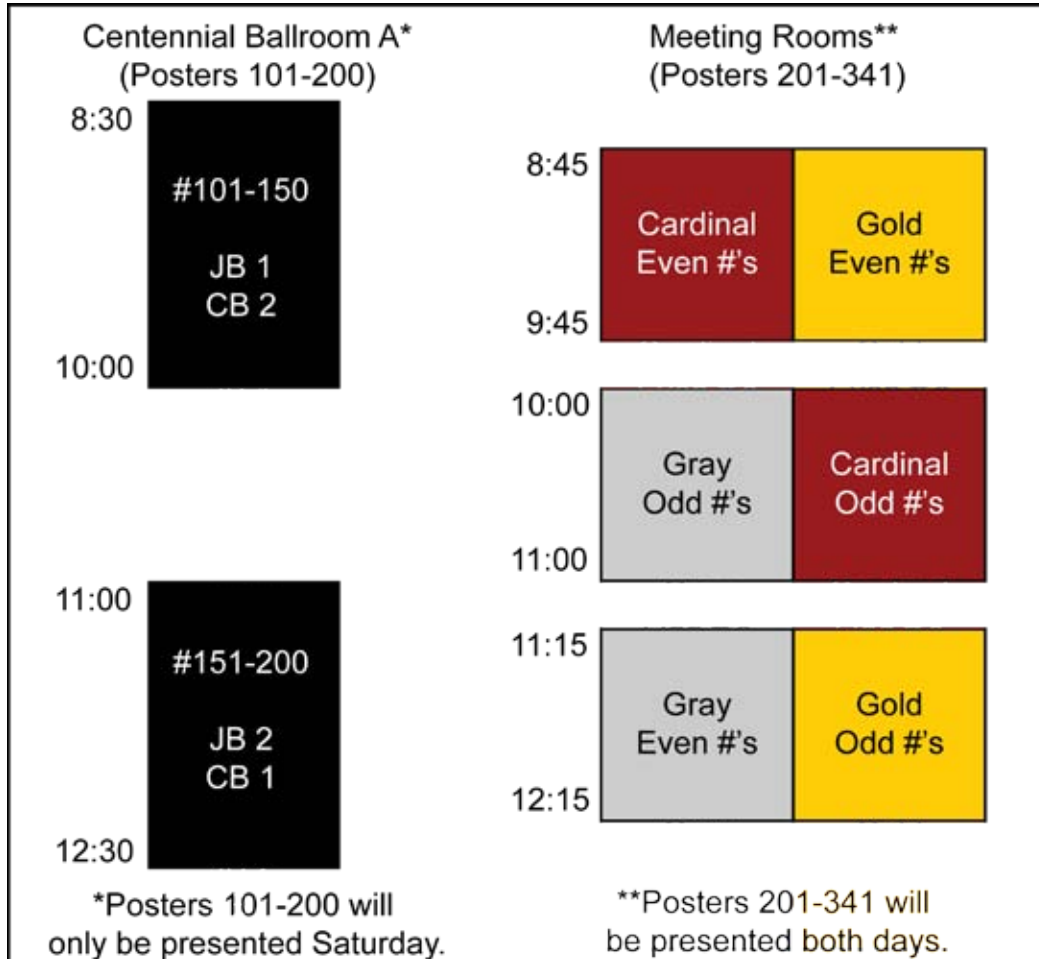
#### Gray

| Topic       | Poster # |
|-------------|----------|
| Prosthetics | 232-236  |
| Sports      | 237-240  |
| Gait        | 268-295  |
| Gait        | 333-341  |

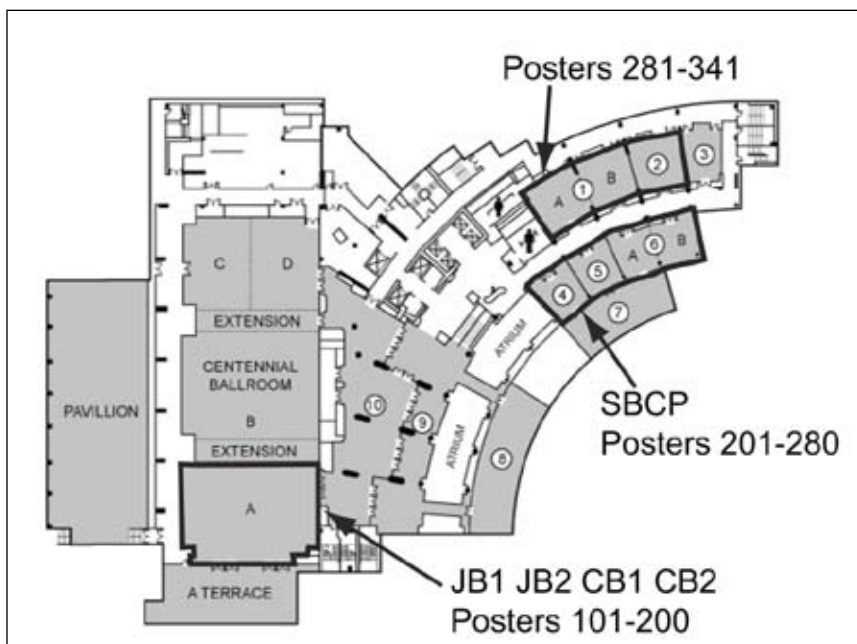
# POSTER SESSION II

## ORGANIZED BY TIME & LOCATION

Authors will present their posters at the following times:



Posters are located on the third level in the following locations:



“Cardinal”, “Gold”, and “Gray” topics are distributed throughout the meeting rooms so that a comparable number of posters are presented in each room during each hour.

**Poster # range in each meeting room:**

- 201-220 in (4) Odessa
- 221-240 in (5) Shanghai
- 241-280 in (6) Tokyo/Vancouver
- 281-317 in (1) Barcelona/Casablanca
- 318-341 in (2) Melbourne

# POSTER SESSION I

THURSDAY 2:30 PM – 6:30 PM

## Posters 1-50 (2:30pm-4:00pm) & Posters 51-100 (5:00pm-6:30pm)

Centennial Ballroom A

Thursday, August 11, 2:30 pm - 4:00 pm

### Award Finalists

**JB1. Measuring Subject Specific Muscle Model Parameters of the First Dorsal Interosseous in Vivo**

Infantolino B, Challis J  
*Penn State University - Berks*

**CB1. Mechanical Properties of Muscle in Hamstring Contractures of Children with Spastic Cerebral Palsy**

Smith L, Lee K, Carr A, Ward S, Chambers H, Lieber R  
*University of California, San Diego*

### Student Computational Modeling

**1. Development and Validation of a Pediatric Head and Neck Musculoskeletal Model**

Cochenour C, Mehta H, Peterson T, Nuckley D  
*University of Minnesota, Twin Cities*

**3. Quantitative Prediction of Grasp Impairment Following Peripheral Neuropathies of the Hand**

Inouye J, Kutch J, Valero-Cuevas F  
*University of Southern California*

**5. Estimation of Articular Contact Loads in Total Knee Replacement Using a Dual-Joint Modeling Paradigm**

Hast M, Piazza S  
*The Pennsylvania State University*

**7. Why Does the Pubovisceral Muscle Fail at Its Entesis, and Not Elsewhere, During the Second Stage of Labor? A Computational Study**

Kim J, DeLancey J, Ashton-Miller J  
*University of Michigan*

**9. Module Control of Walking: A 3D Simulation Study**

Allen J, Kautz S, Neptune R  
*The University of Texas at Austin*

**11. Comparing Filter Cutoff Frequency Effects on Lower Extremity Joint Moments Calculated for Use in Musculoskeletal Modeling**

Laughlin W, Weinhandl J, O'Connor K  
*University of Wisconsin-Milwaukee*

**13. An Optimization Algorithm to Improve Computed Muscle Control**

Weinhandl J, Laughlin W, O'Connor K  
*University of Wisconsin - Milwaukee*

**15. Abstract Withdrawn**

**2. Moving Muscle Points Provide Accurate Curved Muscle Paths in a Model of the Cervical Spine**

Suderman B, Vasavada A  
*Washington State University*

**4. Preliminary Comparisons of Experimental and Computational Knee Loading Conditions Simulating Daily Loading Scenarios**

Hale R, Gonzalez R  
*LeTourneau University*

**6. Motion Analysis of Simulated Minimally Invasive Surgery**

Ohu I, Cho S, Awad M, Matthews B  
*Southern Illinois University Edwardsville*

**8. An Evaluation of Phenomenological Models of the Force-Velocity Relationship of Shortening Muscle**

Yeo S, Lappin A, Nishikawa K, Pai D  
*University of British Columbia*

**10. EMG-Driven Muscle Activations Tune Post-Stroke Computed Muscle Control Simulations**

Ramsay J, Buchanan T, Higginson J  
*University of Delaware*

**12. Derivation of the Equation of Motion for the Alveolar Spring-Hinge Model**

Lee J, Ahn J, Kim D, Park Y, Kim I  
*Hanyang University*

**14. Estimation of Curvature Feature Using a Biomimetic Tactile Sensor**

Su Z, Li Y, Loeb G  
*University of Southern California*

**16. Abstract Withdrawn**

# POSTER SESSION I

THURSDAY 2:30 PM – 6:30 PM

## Posters 1-50 (2:30pm-4:00pm) & Posters 51-100 (5:00pm-6:30pm)

Centennial Ballroom A

### Gait

**17. Gait in Patients with Copd is Mainly Affected in Proximal Musculature**

Yentes J, Rennard S, Stergiou N  
*University of Nebraska at Omaha*

**2010 Grant-in-Aid Recipient**

**18. Heel Height Affects Lower Extremity Frontal Plane Joint Moments During Walking**

Barkema D, Derrick T, Martin P  
*Iowa State University*

**19. Comparison of Objective Measures of Foot Structure and Function in the Population-Based Framingham Foot Study**

Hagedorn T, Riskowski J, Dufour A, Hillstrom H, Lenhoff M, Frey J, Casey V, Hannan M  
*Institute for Aging Research at Hebrew SeniorLife*

### Lower Extremity

**20. Understanding Contact Pressure Distribution in the Ankle and Subtalar Joint During Motion in the Sagittal Plane**

Choisne J, Ringleb S, Paranjape R, Bawab S, Anderson C  
*Old Dominion University*

**22. Effect of a Neuromuscular Dentistry-Designed Mouthguard on Peak Knee Valgus Moments During Single Leg Landing**

Chaudhari A, Cotter J, Jamison S, Mossad D  
*The Ohio State University*

**21. Effects of Towing a Weighted Sled with Different Loads and Attachment Points on Lower Limb Moments**

Lawrence M, Hartigan E, Tu C  
*University of New England*

**23. Sex Differences in Plantar Flexion Strength May Predispose Middle Age Females to Falls**

Chimera N, Manal K  
*Northern Arizona University*

### Methods

**24. A Technique for Dynamic Marker Identification to Locate Occluded Anatomical Landmarks**

Yoo B, Kim S, Merryweather A  
*University of Utah*

**26. Force Platform Center of Pressure Measures Used to Predict Nintendo Wii Fit Balance Scores During Yoga Poses**

Heise G, Smith J, Leich A, Kneisel K, Hoke M  
*University of Northern Colorado*

**28. Experimental Validation of a Finite Element Model of the Composite Pelvis Using Digital Image Correlation**

Ghosh R, Gupta S, Dickinson A, Browne M  
*Indian Institute of Technology, Kharagpur*

**30. Estimating Ground Reaction Forces During Locomotion in Adults from Actigraph Activity Monitor Data**

Collins K, Neugebauer J, Hawkins D  
*University of California - Davis*

**25. Effects of Locomotor Task and Marker Placement on Minimum Foot Clearance**

Loverro K, Greaves N, Hamel K  
*Oak Ridge Institute for Science and Education (ORISE)/NSRDEC*

**27. Markerless Tracking Error of a Bi-Planar X-Ray Motion Capture System**

Miranda D, Schwartz J, Dawson M, Fleming B, Crisco J  
*Brown University*

**29. A Novel Device for Physiologic Mr Imaging of the Patellofemoral Joint Cartilage Under Controlled Loads**

Chehab E, Brown S, Ward S  
*University of California, San Diego*

# POSTER SESSION I

THURSDAY 2:30 PM – 6:30 PM

## Posters 1-50 (2:30pm-4:00pm) & Posters 51-100 (5:00pm-6:30pm)

Centennial Ballroom A

### Posture and Balance

- 
- 31. Obesity Does Not Influence the Ability of Young Adults to Recover Balance from a Forward Fall with a Single Step**  
Matrangola S, Costello K, Madigan M  
*Virginia Tech*
- 32. Incremental Training: Reducing Challenges to Balance Control while Learning a Novel Locomotor Task**  
Sawers A, Hahn M  
*University of Washington*
- 33. Does the Development of Transient Low Back Pain Affect Postural Changes During Prolonged Standing?**  
Gallagher K, Nelson-Wong E, Callaghan J  
*University of Waterloo*
- 34. Wii Fit Training to Improve Balance in Older Adults: a Feasibility Study**  
Bieryla K, Dold N  
*Bucknell University*

### Spine

- 
- 35. Considerations for the Use of C7 Translaminar Screws in Cervicothoracic Instrumentation**  
Gandhi A, Kode S, Ilgenfritz R, Smucker J, Fredericks D, Grosland N  
*University of Iowa*
- 36. Anticipated Walking Turns in People with Recurrent Low Back Pain: A Kinematic Study**  
Armour Smith J, Beneck G, Kulig K  
*University of Southern California*
- 37. Trunk Neuromuscular Control is Reduced in Patients with Clinical Lumbar Instability**  
Silfies S, Cannella M, Sung W, Wattananon P, Mehta R  
*Drexel University*

### Sports

- 
- 38. Cyclic Compressive Loading Facilitates Acute and Accumulated Recovery of Viscoelastic Properties of Skeletal Muscle Following Eccentric Exercise**  
Haas C, Zhao Y, Butterfield T, Best T  
*The Ohio State University*
- 39. Kinetics and Kinematics of Swimming Push-Off Strategies**  
Weimar W, Sumner A, Patel J, Romer B, Fox J, Snead J, Shroyer F  
*Auburn University*
- 40. Improvements in Joint Kinetics in Return to Competition from ACL Injury and Reconstruction: A Case Study**  
Chiu L, Bryanton M, Moolyk A, Newstead L, Kennedy M  
*University of Alberta*

### Tissue Mechanics

- 
- 41. Effects of Bifurcation Angle on the Wall Shear Stress in Stenosed Coronary Artery Bifurcation**  
Molavi Zarandi M, Mongrain R, Bertrand O  
*McGill University*
- 42. Radiolucent Composites Providing High Resistance Against Sterilization Decomposition**  
Sedlacek R, Suchy T, Sochor M, Balik K, Sucharda Z, Benes J  
*Czech Technical University in Prague, Faculty of Mechanical Engineering*
- 43. Passive Elastic Properties of the Rat Ankle**  
Wu M, Tresch M, Pai D, Sandercock T  
*Northwestern University*
- 44. Mechanotransduction of External Load to the Brain: The Effect of Trabecular Architecture**  
Saboori P, Sadegh A  
*The City College of the City University of New York*
- 45. Investigation on Individual Collagen Fibrils of Osteoarthritic Cartilage with Atomic Force Microscopy**  
Wu C, Tang B, Wen C, Lu W, Yan C, Chiu K  
*The University of Hong Kong*

# POSTER SESSION I

THURSDAY 2:30 PM – 6:30 PM

## Posters 1-50 (2:30pm-4:00pm) & Posters 51-100 (5:00pm-6:30pm)

Centennial Ballroom A

### Upper Extremity

- 46. Force Sharing Among Fingers During Multi-Finger Pressing in Different Finger Configurations**  
Martin J, Latash M, Zatsiorsky V  
*Pennsylvania State University*
- 47. Interrater and Intrarater Reliability of the Functional Movement Screen**  
Smith C, Chimera N, Wright N, Warren M  
*Northern Arizona University*
- 48. Humeral Head Translations and Subacromial Pressure After Shrinking the Posterior Glenohumeral Joint Capsule**  
Borstad J, Dashottar A  
*Ohio State University*
- 49. Elbow Extensor Torque As a Function of Vibration Frequency**  
Friesenbichler B, Coza A, Nigg B  
*University of Calgary*
- 50. Reaching Kinematics of the “Less Affected” Upper Extremity in Individuals with Chronic Stroke and Healthy Controls**  
Finley M, Combs S, Carnahan K, Peacock S, Van Buskirk A  
*University of Indianapolis*

### Thursday, August 11, 5:00 pm - 6:30 pm

#### Award Finalists

- JB2. The Viscoelasticity of Chondrocytes in Situ**  
Han S, Herzog W  
*University of Calgary*
- CB2. Loss of Vasti Medialis Function Alters in Vivo Knee Joint Kinematics: Implications for Patellofemoral Pain Syndrome**  
Sheehan F, Behnam A, Borotikar B, Alter K  
*National Institutes of Health*

#### Student Computational Modeling

- 51. Spatiotemporal Contact Properties of the Tibiofemoral Joint Following ACL-Reconstruction**  
Schroeder M, Kwon T, Dhaher Y  
*Northwestern University*
- 52. A Dynamic Simulation Approach to Evaluating Nerve Transfer Strategies Following C5-C6 Brachial Plexus Injury**  
Crouch D, Li Z, Barnwell J, Daly M, Li Z, Saul K  
*Department of Biomedical Engineering, Wake Forest University School of Medicine*
- 53. A Novel Methodology to Compare Grasp Quality: Application to Two Dominant Tendon-Driven Designs**  
Inouye J, Kutch J, Valero-Cuevas F  
*University of Southern California*
- 54. A Comprehensive Experimental Evaluation of Existing Models of the Extensor Mechanism Calls for Novel Data-Driven Models**  
Kurse M, Lipson H, Valero-Cuevas F  
*University of Southern California*
- 55. Evaluating a Biomechanical Model of the Thumb for Simulation of Both Individual and Coordinated Muscle Actions**  
Wohlman S, Murray W  
*Northwestern University*
- 56. Controlling Compliance: Feed-Forward Stimulation Pattern Influences Elastic Tuning During Cyclic Muscle-Tendon Contractions**  
Robertson B, Sawicki G  
*UNC-Chapel Hill/NC State University*
- 57. Mammalian Muscle Model for Predicting Force and Energetics During Physiological Behaviors**  
Tsianos G, Rustin C, Loeb G  
*University of Southern California*
- 58. Simulations of Optimal Reweighting of Muscle Coordination Reveal Important Benefits of Muscle Redundancy**  
Racz K, Valero-Cuevas F  
*University of Southern California*

# POSTER SESSION I

THURSDAY 2:30 PM – 6:30 PM

## Posters 1-50 (2:30pm-4:00pm) & Posters 51-100 (5:00pm-6:30pm)

Centennial Ballroom A

**59. Identifying the Criterion Spontaneously Minimized During Sub-Maximal Movements Through Optimal Synthesis**

Jackson M, Benkhemis I, Thouze A, Sardain P, Begon M  
*Universite de Montreal*

**61. Estimation of Patella Bone Stress: A Comparison of Homogeneous and Heterogeneous Finite Element Models**

Ho K, Mokarram N, Yang N, Vaziri A, Powers C,  
*University of Southern California*

**60. Compensatory Muscle Control Strategies When Walking with a Customized Pd-Afo**

Schrank E, Higginson J, Stanhope S  
*University of Delaware*

**62. Optimal Control and Forward Dynamics of Periodic Forearm Motions Using Fourier Series for Muscle Excitations**

Sharif Shourijeh M, McPhee J, Azad N  
*University of Waterloo*

### Student Computational Modeling Cont'd

**63. Force-Based Index Finger Biomechanical Model**

Qiu D, Kamper D  
*Illinois Institute of Technology*

**64. A Probabilistic Approach to Feedforward Fes Control in the Rat Hindlimb**

Jarc A, Berniker M, Tresch M  
*Northwestern University*

**65. The Measurement Setup for Online Biomechanical Analysis of Rowing on an Ergometer**

Cerne T, Kamnik R, MuniH M  
*Alpineon d.o.o.*

**66. Wrist Kinematics Following Scaphoid-Excision Four Corner Fusion**

Nichols J, Bednar M, Balaram A, Havey R, Murray W  
*Northwestern University*

### Computational Modeling

**67. Load Variation Influences on Joint Work During Squat Exercise in Reduced Gravity**

De Witt J, Fincke R, Logan R, Guilliams M, Ploutz-Snyder L  
*Wyle Integrated Science and Engineering*

**68. Glenohumeral Joint Force Estimations During Shoulder Exertions Using Forward Dynamics Simulations**

Sasaki K  
*Boise State University*

**69. Comparing Surface-Marker Based and X-Ray Based Knee Joint Kinematics During Functional Activities**

Li K, Shetye S, Tashman S, Zhang X  
*University of Pittsburgh*

**70. Surgical Impaction of Ceramic Femoral Resurfacing Heads**

Dickinson A, Taylor A, Browne M  
*University of Southampton*

**71. A Model of Chimpanzee Hindlimb Musculoskeletal Geometry**

Umberger B, O'Neill M, Larson S, Demes B, Stern J  
*University of Massachusetts Amherst*

**72. Hamstring Contributions to Knee Motion During Terminal Swing in Crouch Gait**

Yong J, Steele K, Hicks J, Schwartz M, Delp S  
*Stanford University*

**73. Optimization of Shift Lever Position**

Vilimek M, Horak Z, Kubovy P  
*Czech Technical University in Prague*

**74. A Time-Efficient Method for Analyzing Bone Strain with Large Subject Pools**

Leib D, Dugan E, Wang H  
*Boise State University*

### Ergonomics

**75. Affect of Weight and Type of Jackhammer on Vibration and Grip Pressure**

Singh G, Campbell-Kyureghyan N, Strobel D, Cooper K  
*Department of Industrial Engineering, University of Wisconsin-Milwaukee*

**76. Workday Arm Elevation Exposure, a Comparison Between Two Professions.**

Ettinger L, Kincl L, Karduna A  
*University of Oregon*

# POSTER SESSION I

THURSDAY 2:30 PM – 6:30 PM

## Posters 1-50 (2:30pm-4:00pm) & Posters 51-100 (5:00pm-6:30pm)

Centennial Ballroom A

### Gait

- 
- |   |   |
|---|---|
| <b>77. Leg Stiffness Increases with Speed to Modulate Gait Frequency and Propulsion Energy</b><br>Kim S, Park S<br><i>KAIST</i> | <b>78. Mechanical Impulse During Step-To-Step Transition Balances Propulsion Energy and Collision Loss</b><br>Kim S, Park S<br><i>KAIST</i> |
|---|---|

### Lower Extremity

- 
- |  |  |
|--|--|
| <b>79. Altered Stair Climbing Mechanics in Subjects Wth Femoroacetabular Impingement</b><br>Rylander J, Shu B, Asay J, Safran M, Andriacchi T<br><i>VA Hospital Bone and Joint RR&amp;D, Palo Alto, CA</i> | <b>80. Kinematic Model for Total Knee Replacement Surgical Training and Planing</b><br>Moonjaita P, Suthakorn J<br><i>Mahidol University</i> |
|--|--|

### Muscle

- 
- |  |   |
|--|---|
| <b>81. Effects of Cyclic Compressive Loading on Ed1+ and Ed2+ Macrophages in Healthy Skeletal Muscle in Vivo</b><br>Waters C, Dupont-Versteedgen E, Butterfield T<br><i>University of Kentucky</i> | <b>82. A Nonlinear Model of Passive Skeletal Muscle Viscosity</b><br>Meyer G, McCulloch A, Lieber R<br><i>University of California, San Diego</i>   |
| <b>83. Scaling of Passive Tension in Skeletal Muscle</b><br>Winters T, Takahashi M, Lieber R, Ward S<br><i>University of California, San Diego</i>   | <b>84. Knee Angle-Spastic Gracilis Muscle Force Relationship Measured Intraoperatively Shows No Abnormal Muscular Mechanics</b><br>Ates F, Ayturk O, Temelli Y, Yucesoy C<br><i>Bogazici University</i> |

### Posture and Balance

- 
- |  |  |
|--|--|
| <b>85. Comparison of Trunk Kinematics Between Experimental Tripping Protocols</b><br>Caudle S, Matrangola S, Madigan M<br><i>Virginia Tech</i>   | <b>86. Age-Related Differences in Center of Mass Control During Sit-To-Walk</b><br>Chen C, Chou L<br><i>University of Oregon</i> |
| <b>87. Postural Training in a Non-Threatening Environment Results in Limited Transfer During Induced Postural Anxiety</b><br>Sessford D, Doan J, Weeks D, Brown L<br><i>University of Lethbridge</i> |  |

### Running

- 
- |   |  |
|---|--|
| <b>88. Ground Reaction Forces &amp; Joint Moments in Habitual Versus Converted Forefoot Strike Runners</b><br>Rooney B, Derrick T<br><i>Iowa State University</i> | <b>89. Experimental Knee Joint Pain Affects Certain Running Kinematics</b><br>Seeley M, Park J, King D, Hopkins J<br><i>Brigham Young University</i> |
|---|--|

### Spine

- 
- |  |   |
|--|---|
| <b>90. Adolescent Idiopathic Scoliosis Rib Hump: A First Biomechanical Study</b><br>Berteau J, Lasaygues P, Follet H, Pithioux M, Chabrand P<br><i>Institute of Movement Sciences UMR 6233</i> | <b>91. Influence Lumbar Support Prominece Magnitude on Body Posture and Subjective Comfort During Prolonged Driving.</b><br>De Carvalho D, Callaghan J<br><i>University of Waterloo</i> |
|--|---|

# POSTER SESSION I

THURSDAY 2:30 PM – 6:30 PM

## Posters 1-50 (2:30pm-4:00pm) & Posters 51-100 (5:00pm-6:30pm)

Centennial Ballroom A

### 92. Accurate Prediction of Neck Muscle Volumes

#### Using a Two-Step Process

Zheng L, Siegmund G, Vasavada A

*Washington State University*

### Sports

### 93. Deceleration and Redirection Mechanics During a Cutting Maneuver

Havens K, Sigward S

*University of Southern California*

### 94. Relationship Between Torso Rotation and Gluteal Muscle Group Activation in Baseball and Softball Catchers: Skeletally Immature and Mature

Oliver G, Plummer H, Dwelly P

*University of Arkansas*

### 95. An Improved Method for Quantifying the Stiffness of Running Shoes

Ballun M, Williams B, Goehler C, Sevener K

*Valparaiso University*

### 96. Effects of Cut Angle and Online Processing on Cutting Maneuvers

Cesar G, Havens K, Chang Y, Sigward S

*University of Southern California*

### Upper Extremity

### 97. Force Changes During Passive Finger Movement

Georgeson A, Martin J

*Pennsylvania State University*

### 98. Lack of Modulation of Maximum Pinch Force Depending on Grip Surface in Stroke Survivors

Pounds C, Enders L, Seo N

*University of Wisconsin-Milwaukee*

### 99. A Novel Technique for Measurement of Ulnar Collateral Ligament Strain

Weisenbach C, Rosch J, Corbiere N, Cowgill M,

Miller M, Kuxhaus L

*Clarkson University*

### 100. Abstract Withdrawn



# POSTER SESSION II

SATURDAY 8:30 AM – 12:30 PM

Posters 101-150 (8:30am-10:00am) & Posters 151-200 (11:00am-12:30pm)

Centennial Ballroom A

Saturday, August 13, 8:30 am - 10:00 am

## Award Finalists

**JB1. Measuring Subject Specific Muscle Model Parameters of the First Dorsal Interosseous in Vivo**

Infantolino B, Challis J  
*Penn State University - Berks*

**CB2. Loss of Vasti Medialis Function Alters in Vivo Knee Joint Kinematics: Implications for Patellofemoral Pain Syndrome**

Sheehan F, Behnam A, Borotikar B, Alter K  
*National Institutes of Health*

## Student Computational Modeling

**101. Increased Tibiofemoral Compressive Loads in Females Who Have Undergone Anterior Cruciate Ligament Reconstruction**

Tsai L, McLean S, Colletti P, Powers C  
*University of Southern California*

**103. Evaluating the Accuracy of a Cyberglove Motion Capture Protocol with Computed Tomography Data**

Buffi J, Crisco J, Murray W  
*Northwestern University*

**105. Biomechanical Simulation of the Passive Mechanical Coupling in the Hand and Wrist**

Binder-Macleod B, Dewald J, Murray W  
*Northwestern University*

**107. Simulation of Non-Periodic Gait Optimized for Traversing a Specified Distance in Minimum Time**

Celik H, Piazza S  
*The Pennsylvania State University*

**109. Insights into the Role of Proactive Strategies in Postural Responses to Slips Using Gait Simulations**

Chambers A, Cham R, Mahboobin A  
*University of Pittsburgh*

**111. Achilles Tendon Forces in Forefoot and Rearfoot Running**

Gruber A, Umberger B, Jewell C, Del Pilar S, Hamill J  
*Univeristy of Massachusetts*

**113. Antagonistic Co-Contraction in Optimization Prediction of Knee Contact Forces**

Brandon S, Thelen D, Deluzio K  
*Queen's University*

**115. Predicting Fracture Initiation, Propagation and Diversion in Long Bones Under Impact Using Drucker-Prager Plastic Model and Damage Modeling**

Arun M, Chawla A, Mukherjee S  
*Indian Institute of Technology, Delhi*

**102. A Finite Element Analysis of the Moment Arm Hypothesis for Modulating Ultimate Vertebral Shear Failure Tolerance**

Howarth S, Karakolis T, Callaghan J  
*University of Waterloo, Rochon Engineering*

**104. A Finite Element Model of Two Surgical Procedures for Correcting the Clawed Hallux Deformity**

Isvilanonda V, Dengler E, Ledoux W  
*VA Puget Sound and University of Washington*

**106. Which Muscle Data Set to Use in a Finite Element Model of the Knee? an Rms-Based Method to Identify Mean, Maximum, and Minimum**

Boyd J, Gill H, Zavatsky A  
*University of Oxford, Dept of Engineering Science*

**108. Maximising Post-Flight Height in Gymnastics Vaulting: The Influence of the Table Contact Phase**

Jackson M, Yeadon M, Hiley M  
*Universite de Montreal*

**110. The Influence of Ball Mass on Youth Baseball Injury Potential - a Simulation Study**

Matta P, Myers J, Sawicki G  
*University of North Carolina - Chapel Hill & North Carolina State University*

**112. Expedited Evaluation of Contact Stress in the Human Ankle Joint**

Kern A, Anderson D, Brown T  
*University of Iowa*

**114. Identification of Muscle Contributions to a Forward Reaching Task Using an Induced Acceleration Analysis**

Daly M, Vidt M, Marsh A, Saul K  
*Wake Forest University*

**116. Abstract Withdrawn**

# POSTER SESSION II

SATURDAY 8:30 AM – 12:30 PM

Posters 101-150 (8:30am-10:00am) & Posters 151-200 (11:00am-12:30pm)

Centennial Ballroom A

## Gait

- 117. Are Knee and Hip Joint Motions Affected by a Newly Designed Curved-Bottom Shoe During Level-Walking?**  
Paquette M, Zhang S, Milner C, Westlake C, Byrd E  
*Biomechanics/Sports Medicine Lab, The University of Tennessee, Knoxville*
- 118. Leg Stiffness Increased with Gait Speed in the Elderly**  
Hong H, Kim S, Park S  
*Korea Advanced Institute of Science and Technology*
- 119. Empirical Evaluation of Soleus and Gastrocnemius Function During Walking: Implications for Equinus Gait**  
Lenhart R, Francis C, Lenz A, Thelen D  
*University of Wisconsin - Madison*
- 120. Long-Term Changes in Stair Negotiation and Walking Post-ACL Surgery**  
Hall M, Stevermer C, Gillette J  
*Iowa State University*
- 121. Frontal Joint Dynamics When Initiating Stair Ascent with and Without Gait Speed**  
Vallabhajosula S, Yentes J, Tan C, Siu K, Stergiou N  
*University of Nebraska at Omaha*
- 122. Effects of Obesity on the Biomechanics of Uphill Walking**  
Browning R, Reynolds M, Board W, Massie C  
*Colorado State University*
- 123. Changes in Foot Bony Motion Under Different Loading Conditions Using a Cadaveric Robotic Gait Simulator**  
Whittaker E, Aubin P, Ledoux W  
*VA Puget Sound and University of Washington*

## Lower Extremity

- 124. Longitudinal Changes in Muscle Strength, Flexibility and Knee Laxity During Puberty in Girls**  
Wild C, Steele J, Munro B  
*University of Wollongong*
- 125. Quantitative Comparison of Knee Joint Angles and Moments Between Two Different Marker Representations of the Proximal Shank**  
Petit D, Willson J, Barrios J  
*University of Dayton*
- 126. The Influence of Patellofemoral Kinematics on the Effective Quadriceps Moment Arm: A Dynamic in Vivo Study**  
Goltzer O, Sheehan F  
*National Institutes of Health*
- 127. Cartilage Contact Centers Calculated Using Proximity Weighting Are Insensitive to Threshold Distance Used to Define Contact Region**  
Barrance P, Gade V, Allen J  
*Kessler Foundation Research Center*
- 128. Predicting Structural Properties of the Anterior Cruciate Ligament: A Multiple Linear Regression Approach**  
Hashemi J, Mansouri H, Chandrashekar N, Slauterbeck J, Beynon B  
*Texas Tech University*

## Methods

- 129. The Development of a Method to Induce Injurious Hyperextension of the First Metatarsophalangeal Joint**  
Frimenko R, Lievers W, Riley P, Crandall J, Bolton J, Kent R  
*University of Virginia*
- 130. Assessing Accuracy of a 3D Cancellous Bone Quantifying Algorithm**  
Corbiere N, Sonar A, Issen K, Carroll J, Kuxhaus L  
*Clarkson University*

# POSTER SESSION II

SATURDAY 8:30 AM – 12:30 PM

## Posters 101-150 (8:30am-10:00am) & Posters 151-200 (11:00am-12:30pm)

Centennial Ballroom A

**131. Waveform Consistency-Based Decision Rules for Discriminating Between Types and Levels of Musculature Efforts**

Almosnino S, Dvir Z, Bardana D, Graham R, Stevenson J  
*Queen's University*

**133. A Novel Method to Predict Posture of Human Model When Designing Resistance Training Machines Using Musculoskeletal Analysis**

Jung M, Kim Y, Cho K, Lee K  
*Seoul National University*

**135. Is Humeral Motion More Accurate Using Data from Forearm and Scapular Sensors?**

Lin Y, Karduna A  
*University of Oregon*

**137. Does Tester Experience Influence the Reliability of 3D Gait Analysis? A Comparison of the Functional and Predictive Approaches**

Leigh R, Pohl M, Lloyd C, Ferber R  
*The University of Calgary*

**132. Problem-Based Learning and Interactive White Board Technology Compared to Traditional Lecture for Undergraduate Student Learning in Biomechanics**

Mandeville D, Yun K, Imamura R, Neide J  
*California State University, Sacramento*

**134. Determining Body Segment Pose for a Deformable Marker Configurations**

Challis J  
*Penn State University*

**136. A Sub-Maximal Treadmill Protocol to Assess Vo2**

Tulchin K, Jeans K  
*Texas Scottish Rite Hospital for Children*

### Posture and Balance

**138. Prediction of Frontal Plane Hip & Ankle Kinematics During Uni-Pedal Stance Using a Dual-Segment, Center of Pressure-Based Postural Model**

Lee S, Powers C  
*University of Southern California*

**140. Strength Decreases Postural Variability in Obese Adolescents**

King A, Challis J, Bartok C, Costigan F, Newell K  
*Pennsylvania State University*

**142. Why Do Older Women Utilize Slower Volitional Center of Pressure Movements When Accuracy is Constrained? The Role of the Primary Submovement**

Hernandez M, Ashton-Miller J, Alexander N  
*University of Michigan*

**139. Abstract Withdrawn**

**141. Effects of Deceptive Behavior on Biomechanical Measures of Standing Posture**

Mullin D, King G, Derakshani R, Lovelace C  
*University of Missouri- Kansas City*

### Running

**143. Ground Reaction Forces in Barefoot Running Before and After Exertion**

Hashish R, Samarawickrame S, Salem G  
*University of Southern California*

**145. Association of Overstriding and Injury Status in Runners with and Without Iliotibial Band Syndrome**

Hafer J, Brown A, Maschi R, Kirane Y, Hillstrom H  
*Hospital for Special Surgery*

**144. Center of Pressure Trajectory Differences Between Shod and Barefoot Running**

Pisciotta E, Becker J, Sinsurin K, James S, Osternig L, Chou L  
*University of Oregon*

**146. Human Sprinters Have Longer Forefeet and Shorter Plantarflexor Moment Arms**

Baxter J, Novack T, Pennell D, Piazza S  
*The Pennsylvania State University*

# POSTER SESSION II

SATURDAY 8:30 PM – 12:30 PM

Posters 101-150 (8:30am-10:00am) & Posters 151-200 (11:00am-12:30pm)

Centennial Ballroom A

## Running Cont'd

- 147. The Mechanical Determinants of Energetic Cost in Backward Running**  
Conti C, Musolf S, Ortega J  
*Humboldt State University*

## Spine

- 148. Inter-Rater Reliability of Rating Kinematic Plots of Forward Bend Movement Patterns**  
Wattananon P, Sung W, Biely S, Silfies S, Cannella M  
*Drexel University*
- 149. Biomechanical Effects of Incompleteness and Slackness in Annular Fibers Are Higher in the Tissues of Nucleus than That of Annulus: A Finite Element Model Investigation**  
Hussain M  
*Logan University*
- 150. Neuromuscular Regulation of Reaction Forces During the Golf Swing**  
McNitt-Gray J, Zaferiou A, Munaretto J, Requejo P, Flashner H  
*University of Southern California*

Saturday, August 13, 11:00 am – 12:30 pm

## Award Finalists

- JB2. The Viscoelasticity of Chondrocytes in Situ**  
Han S, Herzog W  
*University of Calgary*
- CB1. Mechanical Properties of Muscle in Hamstring Contractures of Children with Spastic Cerebral Palsy**  
Smith L, Lee K, Carr A, Ward S, Chambers H, Lieber R  
*University of California, San Diego*

## Computational Modeling

- 151. Increase Patella Cartilage Stress with Internal Femoral Rotation: Evaluation Using Finite Element Analysis**  
Yang N, Ho K, Farrokhi S, Powers C  
*University of Southern California*
- 152. Virtual Aging of the Muscular System and Its Effects on Running Biomechanics**  
Miller R, Umberger B, Kent-Braun J, Caldwell G  
*Queen's University*
- 153. Validation of a Real-Time Markerless Tracking System for Clinical Gait Analysis - Ad Hoc Results**  
Oberlander K, Bruggemann G  
*Institute of Biomechanics and Orthopaedics, German Sport University Cologne*
- 154. Improved Mesh for a Finite Element Model of Fracture Risk Assessment in Osteogenesis Imperfecta**  
Fritz J, Grosland N, Smith P, Harris G  
*Marquette University*
- 155. The Influence of Head Weight on the Biomechanical Response of the Cervical Spine Under Applied Moments**  
Mesfar W, Moglo K  
*Royal Military College of Canada, Kingston, ON, Canada*
- 156. A Biomechanical Model of the Rat Hindlimb**  
Wei Q, Jarc A, Yeo S, Sandercock T, Tresch M, Pai D  
*Northwestern University*
- 157. a Continuous Method to Quantify Stress-Strain Behavior of Biologic Materials**  
Kuxhaus L, Weisenbach C, Miller M, Tanaka M  
*Clarkson University*
- 158. Reconfiguration of the Upper Extremity Relative to the Pushrim Affects Load Distribution During Wheelchair Propulsion**  
Munaretto J, McNitt-Gray J, Flashner H, Requejo P  
*University of Southern California*

# POSTER SESSION II

SATURDAY 8:30 AM – 12:30 PM

Posters 101-150 (8:30am-10:00am) & Posters 151-200 (11:00am-12:30pm)

Centennial Ballroom A

## 159. Virtual Prototyping and User Training for

### Neural Prosthetic Systems in Msms

Davoodi R, Loeb G

*University of Southern California*

## Clinical

### 160. Phase Identification of Sitting Pivot Wheelchair Transfers

Kankipati P, Koontz A, Vega A, Lin Y

*University of Pittsburgh*

### 161. Error-Enhancement Gait Training with a Robotic Exoskeleton: A Pilot Study After Stroke

Srivastava S, Kao P, Agrawal S, Scholz J

*University of Delaware*

### 162. Effects of Subthalamic Nucleus Deep Brain Stimulation on Parkinsonian Gait Behavior

Park K, Vallabhajosula S, Roemmich R, Hass C,

Hsiao-Wecksler E

*University of Illinois at Urbana-Champaign*

## Ergonomics

### 163. Validity and Accuracy of a Slip Resistance Measurement Protocol for the Assessment of Slip Potential

Blanchette M, Powers C

*University of Southern California*

### 164. The Impact of Posture on the Transmission of Vibration Across a Functional Spinal Unit.

Gooyers C, McMillan R, Howarth S, Eger T,

Callaghan J

*University of Waterloo*

### 165. Effects of Gloves with Different Coefficients of Friction on Fall Recovery During Simulated Ladder Falls

Motawar B, Hur P, Seo N

*University of Wisconsin*

## Gait

### 166. Mechanics and Energetics of Post-Stroke Walking: Towards a Muscle-Level Understanding

Hampton A, Farris D, Sawicki G

*Joint Department of Biomedical Engineering - North Carolina State University and University of North Carolina - Chapel Hill*

### 167. An Improved Method for Inferring Stability and Other Dynamical Information from Nearly-Periodic Noisy Human Locomotion Data

Wang Y, Srinivasan M

*The Ohio State University*

### 168. A Marker Set-Independent Approach to Joint Translation Measurement of the Knee During Walking

Wang H, Zheng N

*University of North Carolina at Charlotte*

### 169. Adaptations in Joint Kinetics Over Consecutive Steps in Stair Negotiation

Yentes J, Vallabhajosula S, Stergiou N

*University of Nebraska at Omaha*

### 170. The Effects of Shoe Architecture on Impact Forces During Gait

Harmon S, Williams B, Sevener K, Goehler C

*Valparaiso University*

# POSTER SESSION II

SATURDAY 8:30 AM – 12:30 PM

## Posters 101-150 (8:30am-10:00am) & Posters 151-200 (11:00am-12:30pm)

Centennial Ballroom A

### Motor Control

- 
- 171. Multi-Functional Use of the Elongate Hind Foot of the Zebra-Tailed Lizard During Running on Different Substrates**  
*Li C, Hsieh T, Umbanhowar P, Goldman D*  
*Georgia Institute of Technology*
- 172. Biomechanical Constraints on Coordination in Children and Adults**  
*Asmussen M, Przysucha E, Zerpa C*  
*Lakehead University*
- 173. Age-Related Changes in Motor Adaptation to Novel Dynamics**  
*Pienciak A, Ahmed A*  
*University of Colorado*
- 174. Effect of Task Constraints on Limb Stabilization During Human Locomotion**  
*Auyang A, Chang Y*  
*Georgia Institute of Technology*

### Muscle

- 
- 175. Skeletal Muscle Stiffness Across the Adult Lifespan of the Rat**  
*Pauwels L, Eklund K, Breighner R, Domire Z*  
*Texas Tech University*
- 176. Quantitative Description of Throwing from the Knees in Baseball and Softball Catchers**  
*Plummer H, Oliver G*  
*University of Arkansas*

### Posture and Balance

- 
- 177. Use of a Judo Break-Fall Technique During a Lateral Fall**  
*Lehman S, DeGoede K*  
*Elizabethtown College*
- 178. Effects of Whole-Body Vibration Training on Dynamic Postural Stability in Elderly Adults**  
*Wang Y, Lin W, Lin J, Lee A*  
*National HsinChu University of Education*
- 179. Dependency of Spatiotemporal Characteristics of Head Stabilization on Visual and Inertial Stimulation**  
*Rastgar Agah M, Darvish K, Wright W, Keshner E*  
*Temple University*

### Running

- 
- 180. The Influence of Sagittal-Plane Trunk Posture on Patellofemoral Joint Stress During Running**  
*Teng S, Ho K, Powers C*  
*University of Southern California*
- 181. Do Barefoot Runners Display More Variability in Footstrike Mechanics than Shod Runners?**  
*Altman A, Davis I*  
*University of Delaware*
- 182. Correlation of Lower Limb Events After a 45 Minute Run**  
*Hageman E, Derrick T*  
*Iowa State University*
- 183. A Multi-Segment Foot Model Based on In-Vivo and In-Vitro Stereophotogrammetric Studies and Clinical Theories of Dynamic Foot Function: Running Gait Reliability**  
*Bauer R, Joshi M, Klinkner T, Cobb S*  
*University of Wisconsin-Milwaukee*
- 184. Kinematic and Kinetic Differences Between Shod and Barefoot Running**  
*Samarawickrame S, Hashish R, Salem G*  
*University of Southern California*
- 185. Investigating In-Vivo Motion of the Medial Longitudinal Arch with Different Orthotic Types Using Lateral Fluoroscopy Images During Dynamic Gait**  
*Balsdon M, Bushey K, Dombroski C, Jenkyn T*  
*The University of Western Ontario*

# POSTER SESSION II

SATURDAY 8:30 AM – 12:30 PM

## Posters 101-150 (8:30am-10:00am) & Posters 151-200 (11:00am-12:30pm)

Centennial Ballroom A

**186. Ramp Angle, Not Final Plateau Height, Determines Hill Walking Transition Strategies**  
Sheehan R, Gottschall J  
*The Pennsylvania State University*

**188. Limb Asymmetries During a Side-Cutting Task in Adolescent Patients 6-12 Month Following ACL Reconstruction**  
Dai B, Butler R, Garrett W, Queen R  
*Michael W. Krzyzewski Human Performance Lab, Duke University*

**187. Effect of Time Normalizing Gait Data on the Condition Signature of Lower Limb Joint Motions**  
Park K, Morris E, Hsiao-Wecksler E  
*University of Illinois at Urbana-Champaign*

### Spine

**189. The Effect of Whole Body Vibration on Proprioception in Lumbar Spine**  
Solc A, Chopra N, Sylvain G  
*Laurentian University*

**190. Biomechanical Testing of Multi-Level Laminoplasty and Laminectomy Procedures**  
Kode S, Gandhi A, Smucker J, Fredericks D, Grosland N  
*The University of Iowa*

### Sports

**191. Muscle Forces During Single Leg Landing**  
Morgan K, Donnelly J, Reinbolt J  
*University of Tennessee*

**192. Changes in Effort Distribution of American Collegiate Triple Jumpers During the Course of a Season**  
Romer B, Johnson D, Romer T, Sinclair A, Weimar W  
*Auburn University*

**193. The Relationships Between Technique Variability and Performance in Elite Discus Throwers During Competition**  
Dai B, Leigh S, Li H, Yu B  
*The University of North Carolina at Chapel Hill*

**194. The Different Task Demands of a Drop Land and Side-Step Cut**  
Pratt K, Sigward S  
*University of Southern California*

**195. Landing Mechanics During Contextually Relevant Practice Conditions**  
Hamzey R, Uyeda K, Munaretto J, McNitt-Gray J  
*University of Southern California*

### Upper Extremity

**196. A Pilot Study of Biomechanical Factors Affecting Upper Limb Posture During Grasping, Holding, and Placing Cylindrical Object**  
Zhou W, Armstrong T, Wegner D, Reed M  
*University of Michigan*

**197. Multi-Digit Coordination During a Pouring Task That Requires Dynamic Stability**  
Manis R, Santos V  
*Arizona State University*

**198. Effects of Variations in Velocity on Viscoelastic Behaviour in the Metacarpophalangeal (MCP) Joint of the Human Hand**  
Kuo P, Deshpande A  
*University of Maine*

**199. Shoulder Position Impacts the Measurement of Glenohumeral Internal Rotation and Infraspinatus Hardness**  
Dashottar A, Borstad J  
*The Ohio State University*

# POSTER SESSION I & II

## Posters 201-341

Meeting Rooms

**ODD:** **Simulia Best Computational Poster Award** **EVEN:**  
Th, 5:15pm-6:15pm **Room:** Odessa Th, 2:45pm-3:45pm  
Sat, 10:00am-11:00am Sat, 8:45am-9:45am

### SBCP. 2D/3D Hybrid Structural Model of Vocal Folds

Cook D, George P, Julias M  
*New York University Abu Dhabi*

**ODD:** **Popular Choice** **EVEN:**  
Th, 5:15pm-6:15pm **Room:** Odessa Th, 2:45pm-3:45pm  
Sat, 10:00am-11:00am Sat, 8:45am-9:45am

### 201. Ultrasonographic Investigation of Hand Muscle Atrophy in Stroke Survivors

Triandafilou K, Kamper D  
*Sensory Motor Performance Program, Rehabilitation Institute of Chicago*

### 202. Vertebral Fracture Location Influences Risk of Future Vertebral Fracture

Bruno A, Anderson D, D'Agostino J, Bouxsein M  
*Harvard-MIT Division of Health Sciences and Technology*

### 203. Mechanobiology of Alpha-Keratin Using North American Porcupine Quills

Chou S, Overfelt R  
*Auburn University*

### 204. Sparse Control of Force During Human Locomotion: Lessons from Hopscotch

Yen J, Chang Y  
*Georgia Institute of Technology*  
**2010 Grant-in-Aid Recipient**

### 205. Morphological Changes in Skeletal Muscle Endomysial and Perimysial Collagen Networks Subjected to Strain

Gillies A, Inoue N, Lieber R  
*University of California San Diego and VA San Diego Healthcare System*

### 206. Localized Strain Measurements of the Intervertebral Disc During Biaxial Tensile Testing

Karakolis T, Callaghan J  
*University of Waterloo*

### 207. Postural Sway in Patients with Low Back Pain - Association Between Mean Sway Characteristics and Clinical Outcomes

Xia T, Long C, Gudavalli R, DeVocht J, Owens E, Wilder D, Cao Y, Meeker W, Goertz C  
*Palmer College of Chiropractic*

### 208. Effects of a Global Alteration of Running Technique on Chronic Exertional Compartment Syndrome

Gregory R, Diebal A, Alitz C, Gerber J  
*U.S. Military Academy*

### 209. A 3D Extended Inverted Pendulum Model to Simulate the Center of Mass Trajectory During Normal Gait

Hayot C, Sakka S, Fohanno V, Lacouture P  
*Institut Pprime*

### 210. Effect of Footwear on Balance

Rose W, Bowser B, McGrath R, Salerno J, Wallace J, Davis I  
*University of Delaware*

### 211. Age-Related Changes in Gaze Behavior, Center of Mass and End-Point Control During Step Negotiation

Hamel K, Greaves N, Loverro K  
*San Francisco State University*

### 212. Force-Velocity Behaviour of Human Medial Gastrocnemius Shifts at the Walk to Run Transition

Farris D, Sawicki G  
*North Carolina State University*

### 213. Static and Dynamic Optimization Solutions for Wheelchair Propulsion

Morrow M, Rankin J, Neptune R, Kaufman K  
*Mayo Clinic*

### 214. The Mechanics of Sloped Walking Revisited: Mechanical Work Performed by the Individual Limbs

Franz J, Lyddon N, Kram R  
*University of Colorado Boulder*

# POSTER SESSION I & II

## Posters 201-341

### Meeting Rooms

- 215. Response of Below-Knee Amputee Muscle Activity to Changes in Energy Storage and Return Foot Stiffness Using Additive Manufacturing**  
Fey N, Klute G, Neptune R  
*The University of Texas at Austin*
- 216. Moved to Awards**
- 217. Moved to Awards**
- 218. Moved to Awards**
- 219. Moved to Awards**
- 220. Moved to Awards**

| ODD:                                      | Muscle       | EVEN:                                   |
|---|--------------|---|
| Th, 5:15pm-6:15pm<br>Sat, 10:00am-11:00am | Room: Odessa | Th, 2:45pm-3:45pm<br>Sat, 8:45am-9:45am |

- 221. Estimation of in Vivo Force-Velocity Properties in Human Skeletal Type I Muscle with Crossbridge Modeling**  
Gollapudi S, Lin D  
*Washington State University*
- 222. Non-Uniform Upregulation of the Hypertrophic Pathway in Skeletal Muscle Following Lengthening Contractions: Implications for Regional Muscle Adaptations**  
Abshire S, Butterfield T  
*University of Kentucky*
- 223. Alterations in Gene Expression due to Differing Magnitudes of Cyclic Compressive Loads in Healthy Skeletal Muscle**  
Waters C, Dupont-Versteedgen E, Butterfield T  
*University of Kentucky*
- 224. Quantification of Atrophy and Activation Failure in the Plantarflexors Post-Stroke**  
Knarr B, Ramsay J, Buchanan T, Binder-Macleod S, Higginson J  
*University of Delaware*
- 225. The Effects of Electrical Stimulation on Muscle Injected with Botulinum Toxin a (Botox)**  
Fortuna R, Horisberger M, van der Marel R, Herzog W  
*University of Calgary*

| ODD:                                      | Motor Control  | EVEN:                                   |
|---|----------------|---|
| Th, 4:00pm-5:00pm<br>Sat, 11:15am-12:15pm | Room: Shanghai | Th, 5:15pm-6:15pm<br>Sat, 8:45am-9:45am |

- 226. The Relation Between Independent Control of Digit Forces and EMG-EMG Coherence During Precision Grip**  
Jesunathadas M, Shibata D, Laitano J, Santello M  
*Arizona State University, Tempe*
- 227. Minimum Toe Clearance Adaptations to Floor Surface Irregularity and Gait Speed in Older Adults**  
Schulz B, Hart-Hughes S, Bulat T  
*VA HSR&D/RR&D Center of Excellence in Maximizing Rehabilitation Outcomes*
- 228. Contributors to Ankle Proprioception for Static and Dynamic Tasks**  
Floyd L, Holmes T, Dean J  
*Medical University of South Carolina*
- 229. Quantification of Sensory Reweighting for the Directional Motion Perception**  
Yi Y, Park S  
*Korea Advanced Institute of Science and Technology*
- 230. Flexor Muscle Coactivation is Joint Specific**  
Frey Law L, Avin K, Krishnan C  
*The University of Iowa*

# POSTER SESSION I & II

## Posters 201-341

### Meeting Rooms

- |   |   |
|---|---|
| <p><b>231. Measurement of the Aerodynamic Stability and Control Effectiveness of Human Skydivers</b><br/>Cardona G, Evangelista D, Ray N, Tse K, Wong D<br/><i>University of California, Berkeley</i></p> <p><b>233. Influence of a Compliant Artificial Ankle on Mechanics and Energetics of Human Walking</b><br/>Huang T, Adamczyk P, Zelik K, Kuo A<br/><i>University of Michigan</i></p> <p><b>235. A Comparison of the Affect of Soft and Rigid Custom-Made Corrective Orthotics and Over-The-Counter Proprioceptive Feedback Orthotics on Hindfoot Pronation During Walking Gait: A Two-Dimensional Dynamic Fluoroscopic Study</b><br/>Bushey K, Balsdon M, Dombroski C, Jenkyn T<br/><i>University of Western Ontario</i></p> | <p><b>232. The Development of Orthosis in Consideration of Rotation Axis</b><br/>Fukumoto T, Maeoka H, Ando T<br/><i>Kio University</i></p> <p><b>234. Kinematics and Kinetics with a Powered Lower Leg System During Stair Ascent Following Transtibial Amputation</b><br/>Aldridge J, Ferris A, Sturdy J, Wilken J<br/><i>Center for the Intrepid, Department of Orthopedics and Rehabilitation, Brooke Army Medical Center, Fort Sam Houston, TX</i></p> <p><b>236. The Effects of Total Ankle Replacement on Ankle Joint Mechanics During Walking</b><br/>Brown S, Wang H, Frame J, Herbst S<br/><i>Ball State University</i></p> |
|---|---|

#### ODD:

Th, 4:00pm-5:00pm  
Sat, 10:00am-11:00am

#### Sports

Room: Shanghai

#### EVEN:

Th, 2:45pm-3:45pm  
Sat, 11:15am-12:15pm

- |  |   |
|--|---|
| <p><b>237. Dynamic Coordination of Leg Musculature is Associated with Agility in High School Soccer Athletes</b><br/>Lyle M, Tsai L, Valero-Cuevas F, Gregor R, Powers C<br/><i>University of Southern California</i></p> <p><b>239. Peak Times of Muscle Activities During Landing from Rotations Jump</b><br/>Bai D, Kasubuchi K, Tokuda M, Fukumoto T<br/><i>Heisei Memorial Hospital</i></p> | <p><b>238. Miniaturized Wireless Imu Enables Low-Cost Baseball Pitching Training Aid</b><br/>McGinnis R, Perkins N, King K<br/><i>University of Michigan</i></p> <p><b>240. Improvements in the Rate of Force Development-Scaling Factor Following a High Speed-Low Resistance Cycling Exercise Program</b><br/>Bellumori M, Knight C<br/><i>University of Delaware</i></p> |
|--|---|

#### ODD:

Th, 5:15pm-6:15pm  
Sat, 10:00am-11:00am

#### Posture and Balance

Room: Tokyo/Vancouver

#### EVEN:

Th, 2:45pm-3:45pm  
Sat, 8:45am-9:45am

- |  |   |
|--|---|
| <p><b>241. Biodynamics of Stepping Up and Down while Wearing Multifocal Lens Eyeglasses</b><br/>Beschorner K, Tomashek D, Smith R<br/><i>University of Wisconsin-Milwaukee</i></p> | <p><b>242. Effects of Vibration Amplitude and Frequency on Postural Sway in Altered Sensory Environments</b><br/>Dickin D, McClain M, Hubble R<br/><i>Ball State University</i></p> |
|--|---|

# POSTER SESSION I & II

## Posters 201-341

### Meeting Rooms

- 243. Surrogation Analysis Reveals Development of Deterministic Structure in the Control of Posture**  
Haworth J, Kokkoni E, Harbourne R, Stergiou N  
*College of Public Health, University of Nebraska Medical Center*
- 244. Effect of Age on the Threshold of Balance Recovery in Younger, Middle-Aged and Older Adults: Preliminary Results**  
Carbonneau E, Smeesters C  
*Universite de Sherbrooke*
- 245. The Influence of Firefighter Boot Type on Postural Measures**  
Chander H, Wade C, Garner J, Garten R, Acevedo E  
*University of Mississippi*
- 246. Nonlinear Dynamics and Bifurcations in Postural Control with and Without a Wobble Board**  
Chagdes J, Raman A, Rietdyk S, Haddad J, Zelaznik H  
*Purdue University*
- 247. Stochastic Resonance Electrical Stimulation to Improve Postural Control in Knee Osteoarthritis**  
Collins A, Blackburn T, Yu B, Olcott C, Jordan J, Weinhold P  
*The University of North Carolina at Chapel Hill*
- 248. Conventional Wisdom Regarding Yoga Pose Modification May Not Benefit Healthy Older Adults: Examining the Modified Tree Pose**  
Yu S, Wang M, Mulwitz L, Haines M, Samarawickrame S, Hashish R, Kazadi L, Greendale G, Salem G  
*University of Southern California*
- 249. Variations in Posturography Testing Methods: Effect of Talking, Visual Fixation, and Time on Plate on Sway Measurements**  
Sutton E, Kinor D, Denzinger C, Jules A, Bigelow K  
*University of Dayton*
- 250. Time to Contact Measures Demonstrate Modulation of Postural Stability During a Lower Extremity Dynamic Movement Task**  
Schloemer S, Cotter J, Jamison S, Chaudhari A  
*The Ohio State University*
- 251. Human Stabilization of a Bicycle on Rollers**  
Cain S, Perkins N  
*University of Michigan*
- 252. Obesity Increases Body Angular Velocity Immediately After a Trip**  
Matrangola S, Madigan M  
*Virginia Tech*
- 253. Relationships Between Quiet Standing and Limits of Stability Assessments in Cancer Survivors**  
Smith J, Carpenter A, Heise G, Repka C, Challis J  
*University of Northern Colorado*
- 254. The Effects of Balance Training on Obstacle Crossing in Older Adults**  
Muir B, Rietdyk S, Haddad J, Seaman J, Heijnen M  
*Purdue University*
- 255. The Effect of Perturbation Magnitude on Walking Stability**  
Sinitski E, Terry K, Wilken J, Dingwell J  
*Department of Orthopedics and Rehabilitation, Center for the Intrepid*
- 256. Prenatal Motor Development Affects Observed Motor Behavior for Different Incubation Periods in Domestic Chick**  
Racz K, Sindhurakar A, Bradley N, Valero-Cuevas F  
*University of Southern California*

#### ODD:

Th, 4:00pm-5:00pm

Sat, 11:15am-12:15pm

#### Upper Extremity

Room: Tokyo/Vancouver

#### EVEN:

Th, 5:15pm-6:15pm

Sat, 8:45am-9:45am

**257. 3D Orientation of the Distal Phalanges of the Thumb and Index Finger During Pinch**

Mondello T, Domalain M, Li Z  
*Cleveland Clinic*

**258. A Pilot Study of the Effects of Upper Extremity Lymphedema on 3-Dimensional Shoulder Kinematics and Function in Survivors of Breast Cancer**

Biggers L, Bojrab R, Hilts B, Kempson J, Overman Z, Rundquist P  
*University of Indianapolis*

# POSTER SESSION I & II

## Posters 201-341

### Meeting Rooms

- 259. A Comparison Between Dart-Throwing Motion Plane Rom and the Dash Score After Distal Radius Fracture**  
Kasubuchi K, Fukumoto T, Imagita H  
*Heisei Memorial Hospital*
- 260. Bilateral Three-Dimensional Wrist Velocity During Activities of Daily Living: Towards Generating Normative Upper Limb Kinematic Profiles**  
Lulic T, Sravanapudi A, Gonzalez D, Dickerson C, Roy E  
*University of Waterloo*
- 261. A Prototype Video Game System for Studying Rehabilitative Learning**  
Holt B, Reyes A, Valero-Cuevas F  
*University of Southern California*
- 262. Development of Humeral Intramedullary Fixation Nail (Hifn) Based on Korean Cadaveric Tests**  
Chon C, Ko C, Oh J  
*Solco Biomedical Co.*
- 263. Motor Learning Reduces Metabolic Cost of Arm Reaching**  
Huang H, Kram R, Ahmed A  
*University of Colorado, Boulder*
- 264. The Effect of Shoulder Position on Scapular Kinematics in a Traditional Push-Up**  
Suprak D, Donegan J, Morales G, Stroschein J  
*Western Washington University*
- 265. Survivors of Stroke May Achieve Cyclic Reaching: A Biomechanical Analysis of the Hemiparetic and Less-Affected Upper-Extremities.**  
Massie C, Malcolm M, Browning R  
*Colorado State University*
- 266. Design of a 2 Degree of Freedom Upper Limb Prosthetic Controller**  
Barton J  
*University of Maryland*
- 267. Surgery of Trapeziometacarpal Joint Arthritis: Increasing Or Decreasing the Degrees of Freedom?**  
Domalain M, Seitz W, Evans P, Li Z  
*Cleveland Clinic*

#### ODD:

Th, 4:00pm-5:00pm  
Sat, 10:00am-11:00am

#### Gait

**Room:** Tokyo/Vancouver (268-280) &  
Barcelona/Casablanca (281-295)

#### EVEN:

Th, 2:45pm-3:45pm  
Sat, 11:15am-12:15pm

- 268. Altered Walking Performance During Simultaneous Cognitive Tasks**  
Lenz A, Higginson C, Higginson J  
*University of Delaware*
- 269. Biomechanical Characterization of Slipping on Pervious and Traditional Concrete Walking Surfaces**  
Bruetsch A, King G, Kevern J  
*University of Missouri-Kansas City*
- 270. The Effect of Torsion Deformity and Medial Knee Osteoarthritis on Lower Limb Extensor Moments During Gait.**  
Mandeville D, Rachala S, Imamura R, Bayers-Thering M, Krackow K  
*California State University, Sacramento*
- 271. Muscle Co-Activation and Stride Variability: Implications for Walking Economy in People with Parkinson's Disease**  
Christiansen C, Davidson B, Schenkman M, Kohrt W  
*University of Colorado Denver*
- 272. Investigating the Influence of Obesity on Gait Using Support Vector Machine Analysis**  
Milner C, McBride J, Freedman J, Zhao X  
*University of Tennessee*
- 273. Effects of a Passive Elastic Exoskeleton During Walking**  
Dean J  
*Medical University of South Carolina*
- 274. Development of an Experimental Model to Examine the Role of Hip Muscle Impairment on Distal Muscle and Joint Function**  
Dwyer M, Ronan K, Miracle A, Butterfield T  
*University of Kentucky*

# POSTER SESSION I & II

## Posters 201-341

### Meeting Rooms

- 275. Impact Forces When Stepping Off Moving Railroad Equipment**  
Serina E, White K  
*Talas Engineering, Inc.*
- 277. Energetics and Biomechanics of Slow Uphill Vs. Fast Level Walking in Obese and Non-Obese Adults**  
Browning R, Reynolds M, Board W  
*Colorado State University*
- 279. Muscle Activity During Gait Transitions**  
Berg Robertson A  
*University of Houston*
- 281. 3-D Tarsal Kinematics Acquired Using Bi-Planar Videofluoroscopy and a Simple Static Gait Simulator**  
Schwartz J, Dawson M, Blankenhorn B, Bariteau J, Rainbow M, DiGiovanni C, Moore D  
*Rhode Island Hospital / Warren Alpert Medical School of Brown University*
- 283. Changes in Locomotor Adaptations and Aftereffects in Control and Spinal Cord Injury Populations Following Swing Phase Resistance**  
Thajchayapong M, Schmit B, Hornby T  
*Northwestern University*
- 285. A Curved-Bottom Shoe Alters Ground Reaction Forces and Ankle Biomechanics During Walking**  
Zhang S, Paquette M, Milner C, Westlake C, Byrd E, Baumgartner L  
*Biomechanics/Sports Medicine Lab, The University of Tennessee, Knoxville*
- 287. Stride Length Influences Lower Extremity Coupling During Walking**  
Russell E, Hamill J  
*The Andrews-Paulos Research & Education Institute*
- 289. Voluntary Changes in Step Width and Step Length Affect Step-To-Step Stability During Human Walking**  
McAndrew Young P, Dingwell J  
*University of Texas at Austin*  
**2010 Grant-in-Aid Recipient**
- 276. A Multi-Segment Foot Model Based on In-Vivo and In-Vitro Stereophotogrammetric Studies and Clinical Theories of Dynamic Foot Function: Walking Gait Reliability**  
Cobb S, Joshi M, Bauer R, Klinkner T  
*University of Wisconsin-Milwaukee*
- 278. Influences of Load Carriage and Fatigue on Lower Extremity Kinetics During Walking**  
Wang H, Frame J, Ozimek E, Reedstrom C, Leib D, Dugan E  
*Ball State University*
- 280. Effects of Ballistic Extremity Armor on Joint Kinematics During Gait**  
Adams A, Hasselquist L, Schiffman J  
*Natick Soldier Research, Development, and Engineering Center*
- 282. Reduced Visual Input Affects Gait Characteristics During Treadmill Walking in a Virtual Environment**  
Huang C, Chien J, Vallabhajosula S, Siu K  
*Nebraska Biomechanics Core Facility, University of Nebraska at Omaha; College of Public Health, University of Nebraska Medical Center*
- 284. Effects of Obesity on Symmetry and Spatio-Temporal Characteristics of Adolescent Gait**  
Dufek J, Mercer J, Currie R, Gouws P, Candela L, Gutierrez A, Putney L  
*University of Nevada, Las Vegas*
- 286. Ground Reaction Forces During Stair Ascent in Pregnant Fallers and Non-Fallers**  
McCrorry J, Chambers A, Daftary A, Redfern M  
*West Virginia University*
- 288. Effects of Varying Gait Strategy on Metabolic Cost and Stability**  
Franz C, Monsch E, Dean J  
*Medical University of South Carolina*
- 290. Are Running and Sprinting Different Gait Modes? Evidence from Forward Dynamics Simulations**  
Miller R, Deluzio K  
*Queen's University*

# POSTER SESSION I & II

## Posters 201-341

### Meeting Rooms

**291. Preferred Walking Speed in a Virtual Environment**

Bartlett J, Sessoms P  
*Naval Health Research Center*

**293. The Effect of an Unexpected Underfoot Perturbation on Step Kinematics in Subjects with and Without Peripheral Neuropathy**

Kim H, DeMott T, Allet L, Richardson J, Ashton-Miller J  
*University of Michigan*

**295. Whole-Body Angular Momentum while Walking on Sloped Surfaces**

Silverman A, Wilken J, Sinitski E, Neptune R  
*Colorado School of Mines*

**292. Loading Patterns During a Step Task in Individuals with Knee Osteoarthritis**

Winters J, Kumar D, Rudolph K  
*University of Delaware*

**294. Kinematic Changes in Contralateral Knee During Training with Real-Time Biofeedback in Women with Knee Hyperextension**

Teran-Yengle P, Yack H  
*University of Iowa*

**ODD:**

Th, 4:00pm-5:00pm  
Sat, 11:15am-12:15pm

**Clinical**

**Room:** Barcelona/Casablanca

**EVEN:**

Th, 5:15pm-6:15pm  
Sat, 8:45am-9:45am

**296. Wireless Multi-Channel Device to Capture Dynamics of Complex Sensorimotor Tasks**

Reyes A, Valero-Cuevas F  
*University of Southern California*

**297. Polyethylene Wear and Patient Specific Contact Stress in Total Hip Arthroplasty**

Daniel M, Kosak R, Igljic A, Kralj-Igljic V  
*Czech Technical University in Prague*

**298. Removing the Human Factor from Clinical Reflexology**

Bush T, Mukherjee R, Sikorskii A, Wyatt G  
*Michigan State University*

**299. Effect of Decision Making on Landing Mechanics in Women and Men**

Mache M, Hoffman M, Pavol M  
*California State University, Chico*

**300. Variability Measures of Trunk and Pelvis Acceleration During Walking and Quiet Stance Are Related in Patients with Multiple Sclerosis and in Healthy Controls**

Huisinga J, St. George R, Horak F  
*Oregon Health and Science University*

**301. The Role of Experimentally Induced Hip Abductor Muscle Strength Deficits on Frontal Plane Biomechanics During Gait**

Pohl M, Kendall K, Wiley P, Patel C, Emery C, Ferber R  
*University of Calgary*

**302. Relationship Between Neural-Reflex Torque and Muscle Reflex Response in Parkinsonian Rigidity**

Muthumani A, Powell D, Hanson N, Kremer L, Wagner L, Threlkeld A, Xia R  
*Creighton University*

**303. Relationship Between Movement Speed and Regularity of Movement in Parkinson's Disease**

Muthumani A, Powell D, Haider H, Threlkeld A, Xia R  
*Creighton University*

**304. Comparison of Three Methods for Measurement of Foot Progression Angle Magnitude and Asymmetry**

Merriwether E, Hastings M, Bohnert K, Penelton K, Sinacore D  
*Washington University in St. Louis*

**305. Biomechanics of Sit to Stand and Stand to Sit from High and Low Chair After Total Hip Arthroplasty in Obese Subjects**

Singh B, Brown T, Callaghan J, Yack J  
*University of Iowa*

**306. Time-To-Boundary Predictions Based on Other Center of Pressure Measures in Cancer Survivors**

Carpenter A, Smith J, Heise G, Repka C, Challis J  
*University of Northern Colorado*

# POSTER SESSION I & II

## Posters 201-341

### Meeting Rooms

**307. The Effects of Ankle Bracing on Joint Moments and Loading Rates During Jump Landing Tasks**

Stafford E, Gillette J  
*Iowa State University*

**309. Comparison of Five Headless Screws for Fixation of Small Bones**

Assari S, Darvish K, Ilyas A  
*Temple University*

**308. Size of Error Affects Retention of Locomotor Adaptation in Human Sci**

Yen S, Landry J, Wu M  
*Rehabilitation Institute of Chicago*

**ODD:**

Th, 5:15pm-6:15pm  
Sat, 10:00am-11:00am

**Lower Extremity**

**Room:** Barcelona/Casablanca (310-317) & Melbourne (318-325)

**EVEN:**

Th, 2:45pm-3:45pm  
Sat, 8:45am-9:45am

**311. Odds-Ratio and Injury Probability Estimation Based on Tibial Plateau Geometry: Subjects with Multiple ACL Injuries**

Hashemi J, Breighner R, Mansouri H, Slauterbeck J, Beynnon B  
*Texas Tech University*

**313. Joint Moments During Stair Descent: Step-By-Step Versus Step-Over-Step**

Gillette J, Stevermer C, Hall M  
*Iowa State University*

**315. Gender Differences in Lower Extremity Biomechanics During Landing**

Stearns K, Powers C  
*University of Southern California*

**317. Knee Joint Moment Comparison Between Unicompartmental Knee Arthroplasty and Healthy Individuals for Stair Ascent**

Fu Y, Yom J, Mahoney O, Simpson K  
*University of Georgia*

**319. Effects of Gluteus Maximus Fatigue on Jump-Landing Kinematics and Electromyography in Women**

Hollman J, Hohl J, Kraft J, Strauss J, Traver K  
*College of Medicine, Mayo Clinic*

**321. A Method to Detect Individual Muscle Impairments Across the Whole Lower Limb in Patients with Cerebral Palsy**

Handsfield G, Sauer L, Hart J, Abel M, Meyer C, Blemker S  
*University of Virginia*

**310. Quantitative Evaluation of Rotational Knee Joint Stability Using a Mechanical 'Pivot Shift' Device**

Sena M, Coughlin D, Lotz J, Feeley B  
*University of California, San Francisco*

**312. The Search for a Limiting Joint During Lower Extremity Collapse: A Case Study**

Flanagan S, Kulik J, Salem G  
*California State University, Northridge*

**314. Frontal Plane Knee Kinematics in Land-And-Go Tasks with Whole Body Rotation Requirements**

Held L, Mathiyakom W, Flashner H, McNitt-Gray J  
*University of Southern California*

**316. Do Calcaneal Motion and Tibial Torsion Influence Leg Axial Rotation During Weight-Bearing Dorsiflexion?**

Chizewski M, Shewaga K, Porter S, Chiu L  
*University of Alberta*

**318. Knee Mechanics Before and After Perturbation Training in Subjects with ACL Deficiency**

Manal K, Gardinier E, Snyder-Mackler L  
*University of Delaware*

**320. Effects of Increasing Inertia on Sidestep Cutting Turns**

Qiao M, Brown B, Westlake C, Jindrich D  
*Arizona State University*

**322. Lower Extremity Dynamics for Drop Jumps Onto Different Surfaces**

Johnson L, Forrester S  
*Loughborough University*

# POSTER SESSION I & II

## Posters 201-341

### Meeting Rooms

**323. Increased Toe Clearance Accuracy During Obstacle Avoidance: Validation of Cubic Interpolation to Upsample Kinematic Data**

Heijnen M, Muir B, Rietdyk S  
*Purdue University*

**324. Association Between Functional Hip Abductor Strength and Hip Joint Kinematics and Kinetics During a Dynamic Uni-Pedal Drop Landing Task**

Lee S, Powers C  
*University of Southern California*

**325. Foot Type and Falls in Older Adults: The Framingham Foot Study**

Riskowski J, Hagedorn T, Dufour A, Casey V, Hannan M  
*Institute for Aging Research*

**ODD:**

Th, 4:00pm-5:00pm  
Sat, 11:15am-12:15pm

**Running**

**Room:** Melbourne

**EVEN:**

Th, 5:15pm-6:15pm  
Sat, 8:45am-9:45am

**326. Runners with Anterior Knee Pain Utilize a Greater Percentage of Their Available Pronation Range of Motion**

Rodrigues P, TenBroek T, Hamill J  
*New Balance Sports Research Lab*

**327. Forefoot-Rearfoot Kinematics in Recreational Runners with a History of Tibial Stress Injury**

Barnes A, Wheat J, Milner C  
*Sheffield Hallam University*

**328. Alterations in Hip and Pelvis Kinematics During Running in Persons with Femoroacetabular Impingement**

Peterson J, Giordano B, Meyer J, Snibbe J, Powers C  
*University of Southern California*

**ODD:**

Th, 4:00pm-5:00pm  
Sat, 11:15am-12:15pm

**Ergonomics**

**Room:** Melbourne

**EVEN:**

Th, 5:15pm-6:15pm  
Sat, 8:45am-9:45am

**329. Dynamic Loading of Upper Extremity Joints with Sign Language**

Abdoli-Eramaki M, Johnson R, Fischer S, Woodcock K  
*Ryerson University*

**330. Effect of Probe Size on EMG Activity of the Wrist and Hand in Diagnostic Medical Sonographers**

Kuhlman S, Gerard C, Burns J, Sabick M  
*Boise State University*

**331. A Study on Development of a Senior-Friendly Lift Handgrip Through Drivability Tests**

Ko C, Cho D, Chun K  
*Korea Institute of Industrial Technology (KITECH)*

**332. Vertical Affordance for Pulling During Simulated Baggage Handling**

Doan J, Fowler S, Sessford D, Brown L  
*University of Lethbridge*

**ODD:**

Th, 4:00pm-5:00pm  
Sat, 10:00am-11:00am

**Gait**

**Room:** Melbourne

**EVEN:**

Th, 2:45pm-3:45pm  
Sat, 11:15am-12:15pm

**333. Velocity Modulation During Walking by Young Adults**

DeVita P, Sidiropoulos A, Rider P, Taylor A, Roseno S, Manbeck R, Hortobagyi T  
*East Carolina University*

**334. Multiscale Entropy of EMG During Walking in Young and Older Adults**

Dela M, Dingwell J, Kang H  
*California State Polytechnic University, Pomona*

# POSTER SESSION I & II

## Posters 201-341

### Meeting Rooms

**335. External Work is Increased Using Rocker Bottom Shoes**

Henning H, Wurdeman S, Huben N, Stergiou N  
*Nebraska Biomechanics Core Facility, University of Nebraska at Omaha*

**337. Meta-Analysis to Predict Metabolic Cost As a Function of Walking Speed and Added Mass at Different Body Locations**

Scherzter E, Reimer R  
*Ben-Gurion University*

**339. Reconstructing the Takeoff Mechanics of Giant Pterosaurs**

Habib M  
*Chatham University*

**341. Robotic Performance-Based Resistance Versus Assistance for Learning of a Novel Gait Pattern with a Robotic Exoskeleton**

Kao P, Srivastava S, Agrawal S, Scholz J  
*University of Delaware*

**336. Effects of Hand Carried Load on Metabolic Cost and Trunk-Pelvis Coordination During Walking**

Boynton A, Royer T  
*US Army Research Lab/University of Delaware*

**338. Force Running Wheel for Measuring Individual Limb Forces in Mice During Spontaneous Locomotion**

Roach G, Edke M, Griffin T  
*Oklahoma Medical Research Foundation*

**340. Gait Kinematics Change When Emotions Are Felt Vs. Portrayed**

Kang G, Gross M  
*University of Michigan*

**Magnetic Tracking is  
Now Wireless!  
Visit Our Booth to  
Learn About:**

**G<sup>4</sup>**

**POLHEMUS**  
INNOVATION IN MOTION™

[www.polhemus.com/biomechanics](http://www.polhemus.com/biomechanics)  
802-655-3159 / US & Canada 1-800-357-4777

REGISTERED  
**ISO 9001**

G<sup>4</sup> is a trademark of Polhemus

**C-Motion**  
Research Biomechanics

**Visual3D**  
Software for Biomechanics Research

- Kinematics, Inverse Dynamics
- Inverse Kinematics
- Advanced Modeling
- Export to OpenSim
- Motion Capture System Independent
- Process EMG, instrumented treadmills
- And much more...

[www.c-motion.com](http://www.c-motion.com)

# PODIUM/POSTER SESSION PRESENTERS

■ = PODIUM PRESENTATION ■ = POSTER PRESENTATION

| Author           | Podium/Poster # | Author           | Podium/Poster # | Author                | Podium/Poster #               | Author          | Podium/Poster #                 |
|------------------|-----------------|------------------|-----------------|-----------------------|-------------------------------|-----------------|---------------------------------|
| Abdoli-Eramaki M | 329             | Bardana D        | 131             | Bowser B              | 210                           | Chabrand P      | 90                              |
| Abel M           | 321             | Bariteau J       | 281             | Boyd J                | 106                           | Chagdes J       | 246                             |
| Abshire S        | 222             | Barkema D        | 18              | Boynton A             | 336                           | Challis J       | JB1, 134, 140,<br>201, 253, 306 |
| Abusara Z        | 22              | Barnes A         | 327             | Bradley N             | 256                           | Cham R          | 109                             |
| Acevedo E        | 245             | Barnwell J       | 52              | Brandenburg A         | 87                            | Chambers A      | 109, 286                        |
| Adamczyk P       | 233             | Barrance P       | 127             | Brandon S             | 113                           | Chambers H      | CB1, 202                        |
| Adamczyk P       | 106             | Barrios J        | 125             | Breighner R           | 175, 311                      | Chander H       | 245                             |
| Adams A          | 280             | Bartlett J       | 291             | Breighner R           | 38                            | Chandrashekar N | 128                             |
| Agrawal S        | 161, 341        | Bartok C         | 140             | Bronfort G            | 89                            | Chandrashekar N | 32, 38                          |
| Ahmed A          | 173, 263        | Barton J         | 266             | Brown A               | 145                           | Chang Y         | 96, 174, 204                    |
| Ahn J            | 12              | Basford J        | 61              | Brown B               | 320                           | Chaudhari A     | 22, 250                         |
| Akins J          | 31              | Bauer R          | 183, 276        | Brown L               | 87, 332                       | Chawla A        | 115                             |
| Albert C         | 4               | Baumgartner L    | 285             | Brown S               | 29, 236                       | Chehab E        | 29                              |
| Aldridge J       | 234             | Bawab S          | 20              | Brown T               | 112, 305                      | Chen C          | 86                              |
| Aldridge J       | 94              | Bawab S          | 26              | Brown T               | 47, 57, 80                    | Chernak L       | 17                              |
| Alex B           | 91              | Baxter J         | 146             | Browne M              | 28, 70                        | Chien J         | 282                             |
| Alexander N      | 142             | Bayers-Thering M | 270             | Browning R            | 122, 265, 277                 | Chimera N       | 23, 47                          |
| Alitz C          | 208             | Bazgari B        | 99              | Bruening D            | 12                            | Chiu K          | 45                              |
| Allard B         | 87              | Beaupre G        | 10, 16          | Bruetsch A            | 269                           | Chiu L          | 40, 316                         |
| Allen J          | 9, 127          | Becker J         | 144             | Bruggemann G          | 153                           | Chiu S          | 79                              |
| Allet L          | 293             | Becker J         | 44              | Bruno A               | 202                           | Chizewski M     | 316                             |
| Almosnino S      | 131             | Beckwith J       | 48              | Bryant T              | 83                            | Cho D           | 331                             |
| Almosnino S      | 111             | Bednar M         | 66              | Bryanton M            | 40                            | Cho K           | 133                             |
| Alter K          | CB2, 214        | Begon M          | 59              | Buchanan T            | 10, 224                       | Cho S           | 6                               |
| Altman A         | 181             | Behnam A         | CB2, 214        | Buchanan T            | 66                            | Choisne J       | 20                              |
| An K             | 61, 102         | Bellumori M      | 240             | Buczek F              | 102                           | Choisne J       | 26                              |
| Anderson C       | 20              | Beneck G         | 36              | Buffi J               | 103                           | Chon C          | 262                             |
| Anderson D       | 112, 202        | Benes J          | 42              | Bulat T               | 227                           | Chopra N        | 189                             |
| Anderson D       | 7, 47           | Benkhemis I      | 59              | Bulea T               | 84                            | Chou L          | 86, 144                         |
| Ando T           | 232             | Berg Robertson A | 279             | Bunger D              | 17                            | Chou L          | 44, 63, 78, 79                  |
| Andriacchi T     | 79              | Berniker M       | 64              | Burns J               | 330                           | Chou S          | 203                             |
| Andriacchi T     | 15, 65          | Berteau J        | 90              | Bush T                | 298                           | Christiansen C  | 271                             |
| Armour Smith J   | 36              | Bertrand O       | 41              | Bushey K              | 185, 235                      | Chu J           | 48                              |
| Armstrong T      | 196             | Beschorner K     | 241             | Butler R              | 188                           | Chu Y           | 31                              |
| Armstrong T      | 105             | Besier T         | 9, 16           | Butterfield T         | 38, 81, 222,<br>223, 274      | Chun K          | 331                             |
| Arun M           | 115             | Best T           | 38              | Byrd E                | 117, 285                      | Clouthier A     | 83                              |
| Asay J           | 79              | Beynonn B        | 128, 311        | Cain S                | 251                           | Coakley B       | 21                              |
| Asay J           | 15              | Bicknell R       | 83              | Caldwell G            | 152                           | Cobb S          | 183, 276                        |
| Ashton-Miller J  | 7, 142, 293     | Biely S          | 148             | Callaghan J           | 33, 91, 102,<br>164, 206, 305 | Cochenour C     | 1                               |
| Ashton-Miller J  | 20              | Bieryla K        | 34              | Callaghan J           | 68, 80, 91                    | Colletti P      | 101                             |
| Asmussen M       | 172             | Bigelow K        | 249             | Campbell-Kyureghyan N | 75                            | Collins A       | 247                             |
| Assari S         | 309             | Biggers L        | 258             | Candela L             | 284                           | Collins K       | 30                              |
| Asundi K         | 18              | Binder-Macleod B | 105             | Cannella M            | 37, 148                       | Combs S         | 50                              |
| Ates F           | 84              | Binder-Macleod S | 224             | Cao Y                 | 207                           | Conrad M        | 2                               |
| Aubin P          | 123             | Blackburn T      | 247             | Carbonneau E          | 244                           | Conti C         | 147                             |
| Auyang A         | 174             | Blanchette M     | 163             | Cardona G             | 231                           | Cook D          | SBCP                            |
| Avin K           | 230             | Blankenhorn B    | 281             | Carnahan K            | 50                            | Cooper K        | 75                              |
| Awad M           | 6               | Blazek K         | 15              | Carpenter A           | 253, 306                      | Corbiere N      | 99, 130                         |
| Ayturk O         | 84              | Blemker S        | 321             | Carr A                | CB1, 202                      | Costello K      | 31                              |
| Azad N           | 62              | Blouin J         | 85              | Carroll J             | 130                           | Costigan F      | 140                             |
| Bae S            | 105             | Board W          | 122, 277        | Carson D              | 56                            | Costigan P      | 111                             |
| Bai D            | 239             | Boden B          | 51              | Casey V               | 19, 325                       | Cotter J        | 22, 250                         |
| Balaram A        | 66              | Bohnert K        | 304             | Caudle S              | 85                            | Coughlin D      | 310                             |
| Balik K          | 42              | Bojrab R         | 258             | Celik H               | 107                           | Cowgill M       | 99                              |
| Ballun M         | 95              | Bolton J         | 129             | Cerne T               | 65                            | Coza A          | 49                              |
| Balsdon M        | 185, 235        | Borotikar B      | CB2, 214        | Cesar G               | 96                            | Crandall J      | 129                             |
| Banks J          | 75              | Borstad J        | 48, 199         |                       |                               | Crisco J        | 27, 103                         |
| Barak M          | 1               | Bouxsein M       | 202             |                       |                               |                 |                                 |

■ = PODIUM PRESENTATION ■ = POSTER PRESENTATION

| Author          | Podium/Poster # | Author               | Podium/Poster # | Author           | Podium/Poster # | Author        | Podium/Poster # |
|-----------------|-----------------|----------------------|-----------------|------------------|-----------------|---------------|-----------------|
| Crisco J        | 24, 48, 81      | Dingwell J           | 3, 82           | Ford K           | 56              | Graham R      | 131             |
| Cronin D        | 32              | Ditto R              | 77              | Forrester S      | 322             | Graham R      | 111             |
| Crouch D        | 52              | Doan J               | 87, 332         | Forrester S      | 74              | Greaves N     | 25, 211         |
| Crowell H       | 107             | Dold N               | 34              | Forssberg H      | 59              | Greendale G   | 248             |
| Csepe D         | 91              | Domalain M           | 257, 267        | Fortuna R        | 225             | Greendale G   | 90              |
| Currie R        | 284             | Domalain M           | 30              | Fowler S         | 332             | Greenwald R   | 48              |
| Czerniecki J    | 103             | Dombroski C          | 185, 235        | Fox A            | 28              | Gregor R      | 237             |
| Daftary A       | 286             | Domire Z             | 175             | Fox J            | 39              | Gregor R      | 88              |
| D'Agostino J    | 202             | Donahue J            | 65              | Frame J          | 236, 278        | Gregory R     | 208             |
| Dai B           | 188, 193        | Donegan J            | 264             | Francis C        | 119             | Griffin T     | 338             |
| Daly M          | 52, 114         | Donnelly J           | 191             | Franz C          | 288             | Grosland N    | 35, 154, 190    |
| Daly M          | 27              | Draper C             | 16              | Franz J          | 214             | Gross M       | 340             |
| D'Andrea S      | 97              | Dueck A              | 21              | Fredericks D     | 35, 190         | Gruber A      | 111             |
| Daniel M        | 297             | Dufek J              | 284             | Fredericson M    | 16              | Gudavalli R   | 207             |
| Darter B        | 25              | Dufour A             | 19, 325         | Freedman J       | 272             | Guilliams M   | 67              |
| Darvish K       | 179, 309        | Dugan E              | 74, 278         | Frey J           | 19              | Guinn L       | 109             |
| Dashottar A     | 48, 199         | Duhaime A            | 48              | Frey Law L       | 230             | Guo L         | 61              |
| Davidson B      | 271             | Duma S               | 48              | Friesenbichler B | 49              | Gupta S       | 28              |
| Davis C         | 27              | Dupont-Versteedgen E | 81, 223         | Frimenko R       | 129             | Gupta S       | 37              |
| Davis I         | 181, 210        | Dvir Z               | 131             | Fritz J          | 154             | Gutierrez A   | 284             |
| Davis I         | 107             | Dwelly P             | 94              | Fu Y             | 317             | Haas C        | 38              |
| Davoodi R       | 159             | Dwyer M              | 274             | Fujimoto M       | 78              | Habib M       | 339             |
| Dawson M        | 27, 281         | Earl-Boehm J         | 54              | Fukumoto T       | 232, 239, 259   | Haddad J      | 246, 254        |
| Dayanidhi S     | 59              | Eberly V             | 73              | Gade V           | 127             | Hafer J       | 145             |
| De Carvalho D   | 91              | Edke M               | 338             | Gallagher K      | 33              | Hagedorn T    | 19, 325         |
| De Witt J       | 67              | Edwards W            | 19              | Gandhi A         | 35, 190         | Hageman E     | 182             |
| Dean J          | 228, 273, 288   | Eger T               | 164             | Gardinier E      | 318             | Hagg I        | 59              |
| DeGoede K       | 177             | Eklund K             | 175             | Garner J         | 245             | Hahn M        | 32              |
| Del Pilar S     | 111             | Elkins J             | 80              | Garrett W        | 188             | Hahn M        | 42, 103         |
| Dela M          | 334             | Ellingson A          | 89              | Garten R         | 245             | Haider H      | 303             |
| DeLancey J      | 7               | Ellis B              | 98              | Gates D          | 3               | Haines M      | 248             |
| Delp S          | 72              | Emery C              | 301             | George P         | SBCP            | Haines M      | 90              |
| Delp S          | 9, 16           | Enders L             | 98              | Georgeson A      | 97              | Hale R        | 4               |
| Deluzio K       | 113, 290        | Enders L             | 35              | Gerard C         | 330             | Halilaj E     | 24              |
| Deluzio K       | 83              | Erhart J             | 15              | Gerber J         | 208             | Hall M        | 120, 313        |
| Demes B         | 71              | Ettinger L           | 76              | Ghosh D          | 37              | Hamel K       | 25, 211         |
| Demetropoulos C | 77              | Evangelista D        | 231             | Ghosh R          | 28              | Hamill J      | 111, 287, 326   |
| DeMott T        | 293             | Evans P              | 267             | Ghosh R          | 37              | Hampton A     | 166             |
| Dengler E       | 104             | Faber N              | 86              | Gill H           | 106             | Hamzey R      | 195             |
| Dennerlein J    | 18              | Farris D             | 166, 212        | Gillette J       | 120, 307, 313   | Han S         | JB2, 206        |
| Denning M       | 12              | Farris D             | 34              | Gillies A        | 205             | Handsfield G  | 321             |
| Denzinger C     | 249             | Farrokhi S           | 151             | Giordano B       | 328             | Hannan M      | 19, 325         |
| Derakshani R    | 141             | Fedorak G            | 83              | Gleason E        | 21              | Hanson N      | 302             |
| Derrick T       | 18, 88, 182     | Feeley B             | 310             | Gloekler D       | 102             | Hanson N      | 11              |
| Deshpande A     | 198             | Ferber R             | 137, 301        | Goehler C        | 95, 170         | Harbourne R   | 243             |
| DeVita P        | 333             | Ferris A             | 234             | Goel V           | 77              | Harmon S      | 170             |
| DeVocht J       | 207             | Ferris A             | 94              | Goertz C         | 207             | Harner C      | 101             |
| Dewald J        | 105             | Fey N                | 215             | Gold G           | 16              | Harris G      | 154             |
| Dhafer Y        | 51              | Fey N                | 100             | Goldman D        | 171             | Harris G      | 4               |
| Dhafer Y        | 92              | Fincke R             | 67              | Gollapudi S      | 221             | Hart J        | 321             |
| Dickerson C     | 260             | Finley M             | 50              | Goltzer O        | 126             | Hart-Hughes S | 227             |
| Dickin D        | 242             | Fischer S            | 329             | Gonzalez D       | 260             | Hartigan E    | 21              |
| Dickin D        | 96              | Flanagan S           | 312             | Gonzalez R       | 4               | Hashemi J     | 128, 311        |
| Dickinson A     | 28, 70          | Flashner H           | 150, 158, 314   | Gooyers C        | 164             | Hashemi J     | 38              |
| DiDomenico A    | 75              | Fleming B            | 27              | Got C            | 24              | Hashish R     | 143, 184, 248   |
| Diebal A        | 208             | Floyd L              | 228             | Gottschall J     | 186             | Hashish R     | 90              |
| DiGiovanni C    | 281             | Fohanno V            | 209             | Gouws P          | 284             | Hass C        | 162             |
| Dingwell J      | 255, 289, 334   | Follet H             | 90              | Grabowski A      | 97              | Hass C        | 14              |

# PODIUM/POSTER SESSION PRESENTERS

■ = PODIUM PRESENTATION ■ = POSTER PRESENTATION

| Author            | Podium/Poster #    | Author         | Podium/Poster # | Author        | Podium/Poster # | Author         | Podium/Poster #       |
|-------------------|--------------------|----------------|-----------------|---------------|-----------------|----------------|-----------------------|
| Hasselquist L     | 280                | Huisinga J     | 300             | Kennedy M     | 40              | Kutch J        | 104                   |
| Hast M            | 5                  | Hur P          | 165             | Kent R        | 129             | Kuxhaus L      | 99, 130, 157          |
| Hastings M        | 304                | Hur P          | 108             | Kent-Braun J  | 152             | Kwon T         | 51                    |
| Hatchet P         | 73                 | Hurd W         | 61              | Kepple T      | 109             | Kwon T         | 92                    |
| Haubert L         | 73                 | Hussain M      | 149             | Kerman K      | 81              | Lacouture P    | 209                   |
| Havens K          | 93, 96             | Iglic A        | 297             | Kern A        | 112             | Laitano J      | 226                   |
| Havey R           | 66                 | Ilgenfritz R   | 35              | Keshner E     | 179             | Lancaster D    | 91                    |
| Hawkins D         | 30                 | Ilyas A        | 309             | Kevern J      | 269             | Landry J       | 308                   |
| Hawkins D         | 29                 | Imagita H      | 259             | Kiapour A     | 77              | Langenderfer J | 86                    |
| Haworth J         | 243                | Imamura R      | 132, 270        | Kilburg A     | 47              | Lappin A       | 8                     |
| Hayot C           | 209                | Infantolino B  | JB1, 201        | Kim D         | 12              | Larson S       | 71                    |
| Hedberg A         | 59                 | Inoue N        | 205             | Kim H         | 293             | Lasaygues P    | 90                    |
| Heijnen M         | 254, 323           | Inouye J       | 3, 53           | Kim I         | 12              | Latash M       | 46                    |
| Heise G           | 26, 253, 306       | Issen K        | 130             | Kim J         | 7               | Laughlin W     | 11, 13                |
| Held L            | 314                | Isvilanonda V  | 104             | Kim J         | 74              | Lawrence M     | 21                    |
| Henning H         | 335                | Jackson M      | 59, 108         | Kim S         | 24, 77, 78, 118 | Laws K         | 69                    |
| Herbst S          | 236                | James S        | 144             | Kim Y         | 133             | Ledoux W       | 104, 123              |
| Hernandez M       | 142                | James S        | 44              | Kincl L       | 76              | Ledoux W       | 23                    |
| Herr H            | 97                 | Jameson J      | 4               | King A        | 140             | Lee A          | 178                   |
| Herzog W          | JB2, 206, 225      | Jamison S      | 22, 250         | King D        | 89              | Lee J          | 12                    |
| Hetzler M         | 22, 33, 42, 62, 83 | Janura M       | 93              | King G        | 141, 269        | Lee K          | CB1, 133, 202         |
| Hewett T          | 77                 | Jarc A         | 64, 156         | King K        | 238             | Lee S          | 138, 324              |
| Hicks J           | 72                 | Jeans K        | 136             | Kinor D       | 249             | Lee S          | 98                    |
| Higginson C       | 268                | Jenkyn T       | 185, 235        | Kirane Y      | 145             | Lehman S       | 177                   |
| Higginson J       | 10, 60, 224, 268   | Jenkyn T       | 28              | Kitaoka H     | 26              | Leib D         | 74, 278               |
| Higginson J       | 71, 107            | Jesunathadas M | 226             | Klinkner T    | 183, 276        | Leich A        | 26                    |
| Hiley M           | 108                | Jewell C       | 111             | Klute G       | 215             | Leigh R        | 137                   |
| Hillstrom H       | 19, 145            | Jindrich D     | 320             | Klute G       | 100             | Leigh S        | 193                   |
| Hilts B           | 258                | Jindrich D     | 50              | Knarr B       | 224             | Lenhart R      | 119                   |
| Hite A            | 96                 | Johnson D      | 192             | Kneisel K     | 26              | Lenhoff M      | 19                    |
| Ho K              | 61, 151, 180       | Johnson L      | 322             | Knight C      | 240             | Lenz A         | 119, 268              |
| Hoffman M         | 299                | Johnson R      | 329             | Ko C          | 262, 331        | Leonard T      | 33, 62                |
| Hohl J            | 319                | Johnston J     | 21              | Kobetic R     | 84              | Lephart S      | 31                    |
| Hoke M            | 26                 | Jordan J       | 247             | Kode S        | 35, 190         | Levine J       | 77                    |
| Hollman J         | 319                | Joshi M        | 183, 276        | Kohrt W       | 271             | Lewek M        | 40                    |
| Holmes T          | 228                | Jules A        | 249             | Kokkoni E     | 243             | Li C           | 171                   |
| Holt B            | 261                | Julias M       | SBCP            | Koontz A      | 160             | Li H           | 193                   |
| Hong H            | 118                | Jung M         | 133             | Koontz A      | 70              | Li K           | 69                    |
| Hopkins J         | 89                 | Kamnik R       | 65              | Kosak R       | 297             | Li K           | 101                   |
| Horak F           | 300                | Kamper D       | 63, 201         | Kotajarvi B   | 61              | Li Y           | 14                    |
| Horak Z           | 73                 | Kamper D       | 2, 98           | Kozakova J    | 93              | Li Z           | 52, 257, 267          |
| Horisberger M     | 225                | Kang G         | 340             | Krackow K     | 270             | Li Z           | 30                    |
| Hornby T          | 283                | Kang H         | 334             | Kraft J       | 319             | Lieber R       | CB1, 82, 83, 202, 205 |
| Hortobagyi T      | 333                | Kankipati P    | 160             | Kralj-Iglic V | 297             | Lieber R       | 39                    |
| Howarth S         | 102, 164           | Kankipati P    | 70              | Kram R        | 214, 263        | Lieberman D    | 1                     |
| Hsiao-Weckslers E | 162, 187           | Kao P          | 161, 341        | Kram R        | 110             | Lievers W      | 129                   |
| Hsieh T           | 171                | Karakolis T    | 102, 206        | Kremer L      | 302             | Lilja N        | 59                    |
| Hsu W             | 63, 78             | Karduna A      | 76, 135         | Krishnan C    | 230             | Lin D          | 221                   |
| Huang C           | 282                | Kasubuchi K    | 239, 259        | Kubovy P      | 73              | Lin J          | 178                   |
| Huang H           | 263                | Kaufman K      | 213             | Kuhlman S     | 330             | Lin W          | 178                   |
| Huang T           | 233                | Kaufman K      | 26, 61          | Kulig K       | 36              | Lin Y          | 135, 160              |
| Hubbard M         | 60                 | Kautz S        | 9               | Kulig J       | 312             | Lin Y          | 70                    |
| Hubble R          | 242                | Kautz S        | 95              | Kumar D       | 292             | Lipps D        | 20                    |
| Huben N           | 335                | Kazadi L       | 248             | Kuo A         | 233             | Lipson H       | 54                    |
| Huben N           | 5                  | Kazadi L       | 90              | Kuo A         | 106             | Lloyd C        | 137                   |
| Hublin J          | 1                  | Kedgley A      | 28              | Kuo P         | 198             | Loeb G         | 14, 57, 159           |
| Huddleston W      | 54                 | Kempson J      | 258             | Kurse M       | 54              | Logan R        | 67                    |
| Huijing P         | 45                 | Kendall K      | 301             | Kutch J       | 3, 53           |                |                       |

■ = PODIUM PRESENTATION ■ = POSTER PRESENTATION

| Author           | Podium/Poster #    | Author           | Podium/Poster #    | Author           | Podium/Poster #  | Author          | Podium/Poster #                                 |
|------------------|--------------------|------------------|--------------------|------------------|------------------|-----------------|---|
| Long C           | 207                | Mercer J         | 284                | Nelson-Wong E    | 91               | Petit D         | 125   |
| Longworth J      | 200                | Merriweather E   | 304                | Neptune R        | 9, 213, 215, 295 | Piazza S        | 5, 107, 146                                     |
| Lott M           | 69                 | Merryweather A   | 24                 | Neptune R        | 64, 95, 100, 110 | Pienciak A      | 173   |
| Lotz J           | 310                | Mesfar W         | 155                | Neugebauer J     | 30               | Pisciotta E     | 144   |
| Lovalekar M      | 31                 | Meyer C          | 321                | Neugebauer J     | 29               | Pisciotta E     | 44  |
| Lovelace C       | 141                | Meyer G          | 82                 | Newell K         | 140              | Pithioux M      | 90  |
| Loverro K        | 25, 211            | Meyer G          | 39                 | Newstead L       | 40               | Ploutz-Snyder L | 67  |
| Lu W             | 45                 | Meyer J          | 328                | Nichols J        | 66               | Plummer H       | 94, 176   |
| Lulic T          | 260                | Miller E         | 99                 | Nigg B           | 49               | Pohl M          | 137, 301  |
| Lyddon N         | 214                | Miller M         | 99, 157            | Nishikawa K      | 8                | Porter S        | 316   |
| Lyle M           | 237                | Miller M         | 27                 | Novack T         | 146              | Pounds C        | 98  |
| Maas H           | 45, 88             | Miller R         | 152, 290           | Nuckley D        | 1                | Powell D        | 302, 303  |
| Mache M          | 299                | Milner C         | 117, 272, 285, 327 | Nuckley D        | 46, 89           | Powell D        | 11  |
| MacLean K        | 68                 | Miracle A        | 274                | Nussbaum M       | 99               | Powers C        | 61, 101, 138, 151, 163, 180, 237, 315, 324, 328 |
| MacLeod T        | 66                 | Miranda D        | 27                 | Oberlander K     | 153              | Pratt K         | 194   |
| Madigan M        | 31, 85, 252        | Mogk J           | 8                  | O'Connor K       | 11, 13           | Prilutsky B     | 53, 88  |
| Madigan M        | 7, 99              | Moglo K          | 155                | O'Connor K       | 54               | Prince J        | 50  |
| Maeoka H         | 232                | Mokarram N       | 61                 | Oh J             | 262              | Przysucha E     | 172   |
| Maerlander A     | 48                 | Molavi Zarandi M | 41                 | Oh Y             | 20               | Putney L        | 284   |
| Mahboobin A      | 109                | Mondello T       | 257                | Ohu I            | 6                | Qiao M          | 320   |
| Mahoney O        | 317                | Mongrain R       | 41                 | Olcott C         | 247              | Qiao M          | 50  |
| Malcolm M        | 265                | Monsch E         | 288                | Oliver G         | 94, 176          | Qiu D           | 63  |
| Maly M           | 68                 | Moolyk A         | 40                 | O'Neill M        | 71               | Quatman C       | 77  |
| Manal K          | 23, 318            | Moonjaita P      | 80                 | Ortega J         | 147              | Queen R         | 188   |
| Manal K          | 66, 107            | Moore D          | 281                | Ortega J         | 6                | Rachala S       | 270   |
| Mansouri H       | 128                | Moore D          | 24                 | Osternig L       | 144              | Racz K          | 58, 256   |
| Marsh A          | 27                 | Morales G        | 264                | Osternig L       | 44               | Rainbow M       | 281   |
| Martin J         | 46, 97             | Morgan K         | 191                | Overfelt R       | 203              | Rainbow M       | 24  |
| Martin P         | 18                 | Morgenroth D     | 103                | Overman Z        | 258              | Raman A         | 246   |
| Maschi R         | 145                | Morris E         | 187                | Owens E          | 207              | Ramsay J        | 10, 224   |
| Massie C         | 122, 265           | Morrow D         | 61                 | Ozimek E         | 278              | Rana M          | 36  |
| Masters T        | 56                 | Morrow M         | 213                | Pai D            | 8, 43, 156       | Rankin J        | 213   |
| Mathiyakom W     | 314                | Morrow M         | 61                 | Pai D            | 43               | Rankin J        | 64  |
| Matrangola S     | 31, 85, 252        | Mossad D         | 22                 | Pai S            | 16               | Rastgar Agah M  | 179   |
| Matta P          | 110                | Motawar B        | 165                | Pain M           | 74               | Ray N           | 231   |
| Matthews B       | 6                  | Motawar B        | 108                | Pal B            | 37               | Razzook A       | 109   |
| Matthiasdottir S | 42                 | Moulton J        | 32                 | Pal S            | 23               | Redfern M       | 286   |
| Mattucci S       | 32                 | Muir B           | 254, 323           | Palmieri-Smith R | 57               | Redfern M       | 72  |
| McAndrew Young P | 289                | Mukherjee R      | 298                | Pantall A        | 53               | Reed M          | 196   |
| McAndrew Young P | 82                 | Mukherjee S      | 115                | Paquette M       | 117, 285         | Reedstrom C     | 278   |
| McBride J        | 272                | Muller-Karger C  | 73                 | Paranjape R      | 20               | Reimer R        | 337   |
| McClain M        | 242                | Mullin D         | 141                | Park J           | 89               | Reinbolt J      | 191   |
| McCroory J       | 286                | Mulroy S         | 73                 | Park K           | 162, 187         | Reinbolt J      | 52  |
| McCulloch A      | 82                 | Mulwitz L        | 248                | Park S           | 77, 78, 118, 229 | Rennard S       | 17  |
| McCullough M     | 26                 | Mulwitz L        | 90                 | Park Y           | 12               | Repka C         | 253, 306  |
| McGinnis R       | 238                | Munaretto J      | 150, 158, 195      | Patel C          | 301              | Requejo P       | 150, 158  |
| McGorry R        | 75                 | Munih M          | 65                 | Patel J          | 39               | Requejo P       | 73  |
| McGowan C        | 110                | Munro B          | 124                | Pauwels L        | 175              | Reyes A         | 261, 296  |
| McGrath R        | 210                | Murray W         | 55, 66, 103, 105   | Pavol M          | 299              | Reynolds M      | 122, 277  |
| McLean S         | 101                | Murray W         | 8                  | Peacock S        | 50               | Rich K          | 50  |
| McLean S         | 57                 | Musolf S         | 147                | Pedersen D       | 80               | Richardson J    | 293   |
| McMillan R       | 164                | Musolf S         | 6                  | Penelton K       | 304              | Richardson T    | 71  |
| McNitt-Gray J    | 150, 158, 195, 314 | Muthumani A      | 302, 303           | Pennell D        | 146              | Richter W       | 64, 67  |
| McPhee J         | 62                 | Muthumani A      | 11                 | Perkins N        | 238, 251         | Rider P         | 333   |
| Meeker W         | 207                | Myers J          | 110                | Perreault E      | 8                | Rietdyk S       | 246, 254, 323                                   |
| Mehta H          | 1                  | Neide J          | 132                | Peterson C       | 95               | Riley P         | 129   |
| Mehta R          | 37                 | Nelson-Wong E    | 33                 | Peterson J       | 328              |                 |   |
|                  |                    |                  |                    | Peterson T       | 1                |                 |   |

# PODIUM/POSTER SESSION PRESENTERS

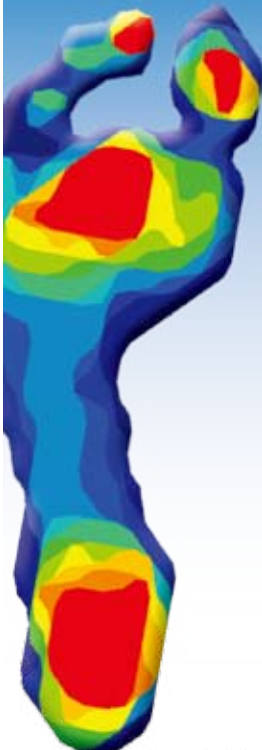
■ = PODIUM PRESENTATION ■ = POSTER PRESENTATION

| Author           | Podium/Poster #    | Author             | Podium/Poster # | Author           | Podium/Poster #        | Author           | Podium/Poster #                   |
|------------------|--------------------|--------------------|-----------------|------------------|------------------------|------------------|-----------------------------------|
| Ringleb S        | 20                 | Scherzter E        | 337             | Sinsurin K       | 144                    | Suthakorn J      | 80                                |
| Ringleb S        | 26                 | Schiffman J        | 280             | Sinsurin K       | 44                     | Sutton E         | 249                               |
| Riskowski J      | 19, 325            | Schloemer S        | 250             | Sipprell W       | 51                     | Svoboda Z        | 93                                |
| Riskowski J      | 49                 | Schmit B           | 283             | Siu K            | 121, 282               | Swartz A         | 54                                |
| Roach G          | 338                | Scholz J           | 161, 341        | Slauterbeck J    | 128, 311               | Sylvain G        | 189                               |
| Robertson B      | 56                 | Schrank E          | 60              | Slauterbeck J    | 38                     | Takahashi K      | 109                               |
| Roche J          | 72                 | Schrank E          | 109             | Smeesters C      | 244                    | Takahashi M      | 83                                |
| Rodrigues P      | 326                | Schroeder M        | 51              | Smith A          | 21                     | Tan C            | 121                               |
| Roemmich R       | 162                | Schroeder M        | 92              | Smith C          | 47                     | Tanaka M         | 157                               |
| Roemmich R       | 14                 | Schulz B           | 227             | Smith J          | 26, 253, 306           | Tang B           | 45                                |
| Rogers L         | 8                  | Schulz C           | 89              | Smith L          | CB1, 202               | Tashman S        | 69                                |
| Rogers M         | 266                | Schwartz J         | 27, 281         | Smith L          | 39                     | Tashman S        | 31, 101                           |
| Romer B          | 39, 192            | Schwartz M         | 72              | Smith P          | 154                    | Taylor A         | 70, 333                           |
| Romer T          | 192                | Scott J            | 87              | Smith P          | 4                      | Temelli Y        | 84                                |
| Ronan K          | 274                | Scott S            | 3               | Smith R          | 241                    | TenBroek T       | 326                               |
| Rooney B         | 88                 | Seaman J           | 254             | Smucker J        | 35, 190                | Teng S           | 180                               |
| Rosch J          | 99                 | Sedlacek R         | 42              | Snead J          | 39                     | Teran-Yengle P   | 294                               |
| Rose W           | 210                | Seeley M           | 89              | Snibbe J         | 328                    | Terry K          | 255                               |
| Roseno S         | 333                | Seitz W            | 267             | Snyder-Mackler L | 318                    | Thajchayapong M  | 283                               |
| Ross M           | 21                 | Sell T             | 31              | Snyder-Mackler L | 66                     | Thelen D         | 113, 119                          |
| Rowson S         | 48                 | Sena M             | 310             | Sochor M         | 42                     | Thelen D         | 17                                |
| Roy E            | 260                | Seo N              | 98, 165         | Solc A           | 189                    | Thomas T         | 47                                |
| Royer T          | 336                | Seo N              | 35, 87, 108     | Sonar A          | 130                    | Thouze A         | 59                                |
| Rudolph K        | 292                | Serina E           | 275             | Sos Z            | 93                     | Threlkeld A      | 302, 303                          |
| Rundquist P      | 258                | Sessford D         | 87, 332         | Sravanapudi A    | 260                    | Threlkeld A      | 11                                |
| Ruparel P        | 73                 | Sessoms P          | 291             | Srinivasan M     | 167                    | Tokuda M         | 239                               |
| Russell E        | 287                | Sevener K          | 95, 170         | Srivastava S     | 161, 341               | Tomashek D       | 241                               |
| Rustin C         | 57                 | Seyedali M         | 103             | St. George R     | 300                    | Trager Ridge S   | 12                                |
| Rylander J       | 79                 | Sharif Shourijeh M | 62              | Stafford E       | 307                    | Traver K         | 319                               |
| Sabick M         | 330                | Sheehan F          | CB2, 126, 214   | Standifird T     | 12                     | Traylor K        | 98                                |
| Sabick M         | 61                 | Sheehan F          | 51              | Stanhope S       | 60                     | Tresch M         | 43, 64, 156                       |
| Saboori P        | 44                 | Sheehan R          | 186             | Stanhope S       | 109                    | Tresch M         | 43                                |
| Sadegh A         | 44                 | Sheets A           | 60              | Stearns K        | 315                    | Triandafilou K   | 201                               |
| Sadler E         | 111                | Shetye S           | 69              | Steele J         | 124                    | Triolo R         | 84                                |
| Safran M         | 79                 | Shetye S           | 101             | Steele K         | 72                     | Troy K           | 200                               |
| Sakka S          | 209                | Shewaga K          | 316             | Stergiou N       | 17, 121, 169, 243, 335 | Troy K           | 19                                |
| Salem G          | 143, 184, 248, 312 | Shibata D          | 226             | Stergiou N       | 5                      | Trudeau M        | 18                                |
| Salem G          | 90                 | Shroyer F          | 39              | Stern J          | 71                     | Truebenbach C    | 54                                |
| Salerno J        | 210                | Shu B              | 79              | Stevenson J      | 131                    | Tsai C           | 70                                |
| Samarawickrame S | 143, 184, 248      | Sidiropoulos A     | 333             | Stevenson J      | 111                    | Tsai L           | 101, 237                          |
| Samarawickrame S | 90                 | Siegmund G         | 92              | Stevermer C      | 120, 313               | Tse K            | 231                               |
| Sandercock T     | 43, 156            | Siegmund G         | 85              | Stinear J        | 8                      | Tsianos G        | 57                                |
| Sandercock T     | 43                 | Sigward S          | 93, 96, 194     | Stitzel J        | 13                     | Tu C             | 21                                |
| Santello M       | 226                | Sikorskii A        | 298             | Strauss J        | 319                    | Tulchin K        | 136                               |
| Santello M       | 21                 | Silder A           | 9               | Strobel D        | 75                     | Umbanhowar P     | 171                               |
| Santos V         | 197                | Silfies S          | 37, 148         | Stroschein J     | 264                    | Umberger B       | 71, 111, 152                      |
| Sardain P        | 59                 | Silverman A        | 295             | Sturdy J         | 234                    | Uyeda K          | 195                               |
| Sasaki K         | 68                 | Simpson K          | 317             | Sturdy J         | 94                     | Valero-Cuevas F  | 3, 53, 54, 58, 237, 256, 261, 296 |
| Sauer L          | 321                | Sinacore D         | 304             | Su F             | 61                     | Valero-Cuevas F  | 59                                |
| Saul K           | 52, 114            | Sinclair A         | 192             | Su Z             | 14                     | Vallabhajosula S | 121, 162, 169, 282                |
| Saul K           | 27, 52             | Sindhurakar A      | 256             | Sucharda Z       | 42                     | Van Buskirk A    | 50                                |
| Sawatsky A       | 62                 | Singh B            | 305             | Suchy T          | 42                     | van der Marel R  | 225                               |
| Sawers A         | 32                 | Singh B            | 80              | Suderman B       | 2                      | van Donkelaar P  | 78                                |
| Sawicki G        | 56, 110, 166, 212  | Singh G            | 75              | Sumner A         | 39                     | Van Straaten M   | 61                                |
| Sawicki G        | 34, 40             | Sinitiski E        | 255, 295        | Sung W           | 37, 148                | Vasavada A       | 2, 92                             |
| Scanlan S        | 65                 | Sinitiski E        | 3               | Suprak D         | 264                    |                  |                                   |
| Schenkman M      | 271                | Sinitiski K        | 25              | Surowiec R       | 96                     |                  |                                   |
|                  |                    | Sinsel E           | 102             |                  |                        |                  |                                   |

PRESENTERS

■ = PODIUM PRESENTATION ■ = POSTER PRESENTATION

| Author       | Podium/Poster #   | Author       | Podium/Poster # | Author         | Podium/Poster # | Author       | Podium/Poster # |
|--------------|-------------------|--------------|-----------------|----------------|-----------------|--------------|-----------------|
| Vasavada A   | 85                | Weinhandl J  | 11, 13          | Wright W       | 179             | Yong J       | 72              |
| Vawter P     | 23                | Weinhold P   | 247             | Wu C           | 45              | Yoo B        | 24              |
| Vaziri A     | 61                | Weisenbach C | 99, 157         | Wu J           | 102             | Young F      | 74              |
| Vega A       | 160               | Weiss J      | 98              | Wu M           | 43, 308         | Yu S         | 193, 247, 248   |
| Vidt M       | 114               | Wen C        | 45              | Wu X           | 41              | Yu S         | 90              |
| Vidt M       | 27                | Westlake C   | 117, 285, 320   | Wurdeman S     | 335             | Yucesoy C    | 84              |
| Vilimek M    | 73                | Wheat J      | 327             | Wurdeman S     | 5               | Yun K        | 132             |
| Wade C       | 245               | White K      | 275             | Wutzke C       | 40              | Zabala M     | 65              |
| Wagner D     | 10                | Whittaker E  | 123             | Wyatt G        | 298             | Zaferiou A   | 150             |
| Wagner L     | 302               | Wilcox B     | 48, 81          | Xia R          | 302, 303        | Zatsiorsky V | 46              |
| Wakeling J   | 36                | Wild C       | 124             | Xia R          | 11              | Zavatsky A   | 106             |
| Wallace J    | 210               | Wilder D     | 207             | Xia T          | 207             | Zelaznik H   | 246             |
| Wang H       | 74, 168, 236, 278 | Wiley P      | 301             | Xie C          | 41              | Zelik K      | 233             |
| Wang H       | 96                | Wilken J     | 234, 255, 295   | Yack H         | 294             | Zerpa C      | 172             |
| Wang L       | 107               | Wilken J     | 3, 25, 94       | Yack J         | 305             | Zhang D      | 41              |
| Wang M       | 248               | Williams B   | 95, 170         | Yack J         | 80              | Zhang S      | 117, 285        |
| Wang M       | 90                | Willson J    | 125             | Yan C          | 45              | Zhang S      | 41              |
| Wang Y       | 167, 178          | Wimer B      | 102             | Yang N         | 61, 151         | Zhang W      | 21              |
| Ward S       | CB1, 29, 83, 202  | Winters J    | 292             | Yaraskavitch M | 42              | Zhang X      | 69              |
| Warren M     | 47                | Winters T    | 83              | Yeadon M       | 108             | Zhang X      | 101             |
| Waters C     | 81, 223           | Wohlman S    | 55              | Yen J          | 204             | Zhang X      | 101             |
| Wattananon P | 37, 148           | Wojtys E     | 20              | Yen S          | 308             | Zhao K       | 61, 102         |
| Weaver A     | 13                | Wong D       | 231             | Yentes J       | 17, 121, 169    | Zhao X       | 272             |
| Weeks D      | 87                | Woodcock K   | 329             | Yeo S          | 8, 156          | Zhao Y       | 38              |
| Wegner D     | 196               | Woollacott M | 63, 78          | Yeo S          | 43              | Zheng L      | 92              |
| Wei Q        | 156               | Wordeman S   | 77              | Yi Y           | 229             | Zheng N      | 168             |
| Weimar W     | 39, 192           | Wright N     | 47              | Yom J          | 317             | Zhou W       | 196             |



## GET A VIEW INSIDE THE SHOE!

Enhance gait analysis with  
*F-Scan*® Pressure Mapping

The new *F-Scan Wireless* allows for complete freedom of movement and more natural shod gait. See in-shoe plantar pressure profiles in real time and record them for later. Analyze pressure and force data for additional insight on foot function and gait disorders.

WELCOME TO THE  
AMERICAN SOCIETY OF BIOMECHANICS  
**2011 ANNUAL MEETING**




Visit us at  
**Booth #16**  
to learn more!



Tekscan, Inc. | 307 West First St., South Boston, MA 02127 | 617.464-4500 / 800.248.3669  
www.tekscan.com

PRESENTERS

# WESTIN LONG BEACH

## FLOORPLAN – THIRD FLOOR



# CITY OF LONG BEACH

## AREA MAP



AREA MAP

# ASB 35TH ANNUAL CONFERENCE

## SCHEDULE AT A GLANCE



Wednesday, August 10

Thursday, August 11

Friday, August 12

Saturday, August 13

|       | Ballroom B   | Ballroom C                            | Ballroom D                                    | Ballroom B   | Ballroom C                 | Ballroom D                 | Ballroom B  | Ballroom C          | Ballroom D                 |                             |      |      |
|-------|--|---------------------------------------|---|--|----------------------------|----------------------------|---|---------------------|----------------------------|-----------------------------|------|------|
| 7:00  | Breakfast<br><i>(food provided)</i>                                    |                                       |   | Past Presidents Breakfast  | Breakfast<br><i>(food)</i> | Women in Science Breakfast | Beach Fun Run   |                     |                            | 7:00                        |      |      |
| 7:15  |  |                                       |   |  |                            |                            |   |                     |                            | 7:15                        |      |      |
| 7:30  |  |                                       |   |  |                            |                            |   |                     |                            | 7:30                        |      |      |
| 7:45  |  |                                       |   |  |                            |                            |   |                     |                            | 7:45                        |      |      |
| 8:00  | Bone   | Neuro-mechanics                       | Gait  | Joint Mechanics  | Injury                     | Muscle                     | Breakfast<br><i>(food provided)</i>   |                     |                            | 8:00                        |      |      |
| 8:15  |  |                                       |   |  |                            |                            |   |                     |                            | 8:15                        |      |      |
| 8:30  |  |                                       |   |  |                            |                            |   |                     |                            | 8:30                        |      |      |
| 8:45  |  |                                       |   |  |                            |                            |   |                     |                            | 8:45                        |      |      |
| 9:00  |  |                                       |   |  |                            |                            |   |                     |                            | 9:00                        |      |      |
| 9:15  | Break and Exhibits   |                                       |   | Break and Exhibits   |                            |                            | Poster Session II<br>Includes display of JoB, Clinical Biomechanics, and Simulia Awards<br><i>(food provided)</i> |                     |                            | 9:15                        |      |      |
| 9:30  |  |                                       |   |  |                            |                            |   |                     |                            | 9:30                        |      |      |
| 9:45  | Imaging  | Tendon and Ligament                   | Upper Extremity                               | Invited Symposium  | Methods                    | Sports                     |   |                     |                            | 9:45                        |      |      |
| 10:00 | Break and Exhibits   |                                       |   | Break and Exhibits   |                            |                            |   |                     |                            | 10:00                       |      |      |
| 10:15 |  |                                       |   |  |                            |                            |   |                     |                            | 10:15                       |      |      |
| 10:30 |  |                                       |   |  |                            |                            |   |                     |                            | 10:30                       |      |      |
| 10:45 |  |                                       |   |  |                            |                            |   |                     |                            | 10:45                       |      |      |
| 11:00 |  |                                       |   |  |                            |                            |   |                     |                            | 11:00                       |      |      |
| 11:15 |  |                                       |   |  |                            |                            |   |                     |                            | 11:15                       |      |      |
| 11:30 |  |                                       |   |  |                            |                            |   |                     |                            | 11:30                       |      |      |
| 11:45 |  |                                       |   |  |                            |                            | 11:45   |                     |                            |                             |      |      |
| 12:00 | Keynote Lecture<br>Christine Ortiz                                     |                                       |   | Borelli Award Lecture<br>Scott Delp  |                            |                            |   |                     |                            | 12:00                       |      |      |
| 12:15 |  |                                       |   |  |                            |                            |   |                     |                            | 12:15                       |      |      |
| 12:30 | Lunch<br><i>(food provided)</i>  |                                       | Diversity Luncheon                            | Lunch<br><i>(food provided)</i>  |                            | Business Meeting           | Lunch<br><i>(food provided)</i>   |                     |                            | 12:30                       |      |      |
| 12:45 |  |                                       |   |  |                            |                            | Hay Award Lecture<br>Joe Hamill   |                     |                            | 12:45                       |      |      |
| 1:00  |  |                                       |   |  |                            |                            |   |                     |                            | 1:00                        |      |      |
| 1:15  |  |                                       |   |  |                            |                            |   |                     |                            | 1:15                        |      |      |
| 1:30  | TUTORIALS I<br>Tokyo/Vancouver Room                                    |                                       | Induction of ASB Fellows                      |  |                            |                            |   |                     |                            | 1:30                        |      |      |
| 1:45  |  |                                       | Young Scientist Awards                        |  |                            | Invited Symposium          | Knee  | Posture and Balance | Break                      |                             | 1:45 |      |
| 2:00  |  |                                       |   |  |                            |                            |   |                     | Gait: Prosthetics          |                             | 2:00 |      |
| 2:15  |  |                                       |   |  |                            |                            |   |                     | Computational Biomechanics |                             | 2:15 |      |
| 2:30  |  |                                       |   |  |                            |                            |   |                     | Ergonomics                 |                             | 2:30 |      |
| 2:45  |  |                                       |   |  |                            |                            |   |                     |                            |                             | 2:45 |      |
| 3:00  |  |                                       |   |  |                            | Break                      |   |                     |                            |                             | 3:00 |      |
| 3:15  |  |                                       |   |  |                            |                            |   |                     |                            |                             | 3:15 |      |
| 3:30  |  |                                       |   |  |                            |                            |   |                     |                            |                             | 3:30 |      |
| 3:45  |  |                                       |   |  |                            | Motor Control              | Orthopaedics  | Rehabilitation      | Break                      |                             | 3:45 |      |
| 4:00  | ASB Executive Board Meeting  | TUTORIALS II<br>Tokyo/Vancouver Room  | VIRTUAL LAB TOUR<br>Barcelona/Casablanca Room | Poster Session I<br>Includes display of JoB, Clinical Biomechanics, and Simulia Awards<br><i>(food provided)</i> |                            |                            | Break and Exhibits<br><i>(food provided)</i>  |                     |                            | Closing Ceremony and Awards |      | 4:00 |
| 4:15  |  |                                       |   |  |                            |                            |   |                     |                            |                             |      | 4:15 |
| 4:30  |  |                                       |   |  |                            |                            |   |                     |                            |                             |      | 4:30 |
| 4:45  |  |                                       |   |  |                            |                            |   |                     |                            |                             |      | 4:45 |
| 5:00  |  | Student Event<br>Tokyo/Vancouver Room |   |  |                            |                            | Keynote Lecture<br>Jessica Hodgins  |                     |                            | ASB Executive Board Meeting |      | 5:00 |
| 5:15  |  |                                       |   |  |                            |                            |   |                     |                            |                             |      | 5:15 |
| 5:30  |  |                                       |   |  |                            |                            |   |                     |                            |                             |      | 5:30 |
| 5:45  |  |                                       |   |  |                            |                            |   |                     |                            |                             |      | 5:45 |
| 6:00  | Exhibitor's Reception<br>Ocean Terrace West                            |                                       |   |  |                            |                            | Break   |                     |                            |                             |      | 6:00 |
| 6:15  |  |                                       |   |  |                            |                            |   |                     |                            |                             |      | 6:15 |
| 6:30  |  |                                       |   |  |                            |                            |   |                     |                            |                             |      | 6:30 |
| 6:45  |  |                                       |   |  |                            |                            |   |                     |                            |                             |      | 6:45 |
| 7:00  | Opening Reception<br>Aquarium of the Pacific<br><i>(food provided)</i> |                                       |   | Night on the Town  |                            |                            | Conference Banquet<br>Queen Mary<br><i>(food provided)</i>  |                     |                            |                             |      | 7:00 |
| 7:15  |  |                                       |   |  |                            |                            |   |                     |                            |                             |      | 7:15 |
| 7:30  |  |                                       |   |  |                            |                            |   |                     |                            |                             |      | 7:30 |
| 7:45  |  |                                       |   |  |                            |                            |   |                     |                            |                             |      | 7:45 |
| 8:00  |  |                                       |   |  |                            |                            |   |                     |                            |                             |      | 8:00 |
| 8:15  |  |                                       |   |  |                            |                            |   |                     |                            |                             |      | 8:15 |
| 8:30  |  |                                       |   |  |                            |                            |   |                     |                            |                             |      | 8:30 |
| 8:45  |  |                                       |   |  |                            |                            |   |                     |                            |                             |      | 8:45 |
| 9:00  |  |                                       |   |  |                            |                            |   |                     |                            |                             |      | 9:00 |
| 9:15  |  |                                       |   |  |                            |                            |   |                     |                            |                             |      | 9:15 |
| 9:30  |  |                                       |   |  |                            |                            |   |                     |                            |                             |      | 9:30 |
| 9:45  |  |                                       |   |  |                            |                            |   |                     |                            |                             |      | 9:45 |

# DYNAMIC LOADING OF UPPER EXTREMITY JOINTS WITH SIGN LANGUAGE

<sup>1</sup>Mohammad Abdoli-E, <sup>1</sup>Ron Johnson, <sup>2</sup>Steve Fischer, and <sup>1</sup>Kathryn Woodcock

<sup>1</sup>Ryerson University, Toronto, ON, Canada. email: [m.abdoli@ryerson.ca](mailto:m.abdoli@ryerson.ca)

<sup>2</sup>Faculty of Kinesiology, University of New Brunswick, Fredericton, NB

## INTRODUCTION

A recent survey of Canadian sign language interpreters (SLI) registered with the Association for Visual Language Interpreters of Canada (AVLIC) revealed that nearly 40% of respondents have been diagnosed with repetitive or cumulative strain type injuries affecting the upper extremities including: carpal tunnel syndrome, thoracic outlet syndrome, tendonitis and arthritis (Fischer & Woodcock, 2007). These findings are not unique; SLI has long been recognized as having a significantly higher rate of repetitive strain disorders (DeCaro et al. 1992; Feuerstein et al. 1997; Scheuerle et al. 2000). Signing involves rapid arm motion incorporating the shoulder, elbow, wrist and hand with the latter three joints moving through a full range of motion. Currently there is little quantitative biomechanics research documenting the magnitude of these motions and the corresponding loading during SLI. Excessive motions have been reported as a risk factor for the development of repetitive strain in other occupations (Marras and Schoenmarklin 1993); it is useful to understand how interpreters work within the context of these findings to understand how SLI become injured. The purpose of this investigation is to quantify upper limb joint motion and loading during sign language interpreting.

## METHODS

To date, a pilot sample of three novice SLI (registered with AVLIC, under 5 years working experience) have participated in this study; 2 females (25 and 27 years old) and 1 male (28 years old). During testing, participants interpreted a pre-recorded lecture under conditions simulating the typical interpreting requirements when working in an institutional setting. Although the lecture was unknown to the participant prior to testing, preparation materials were provided in advance, as is consistent within parameter of a normal interpreting contract. Interpreters completed a trial

involving three twenty minute work session separated by two twenty minute rest periods.

A Fastrak<sup>TM</sup> (Polhemus, Colchester, VT, US) human motion system was used to continuously track the angular orientation of the trunk (sensor overlying T10), and bilateral upper arm, forearm, and hands using sensors strapped to the posterior aspect of each segment. Using the angular orientation data recorded, subsequent angular velocities and accelerations were calculated using central differences. Maximum, minimum and mean angular orientations, velocities and accelerations were then determined for each SLI within each of the three 20 minute interpreting bouts

## RESULTS AND DISCUSSION

The maximum, minimum and mean angular orientations, velocities, and accelerations are shown in tables 1. These values are approximately twice as high as that reported for male industrial workers (Marras and Schoenmarklin 1993).

The maximum and mean acceleration of the wrist (Table 1) are also consistent with those found by Marras and Schoenmarklin (1993).

## CONCLUSIONS

These preliminary results reveal that the kinematic demands of sign language interpreting are greater than those for industrial workers reported to have an elevated risk for cumulative trauma disorders. These excessive motions may provide the context for understanding why SLI have a high prevalence for developing repetitive strain injuries. Unfortunately the task of reproducing language through visual means is not likely to change; interpreters and researchers alike are faced with the challenge of finding alternative solutions to overcoming the problem of excessive motion. Perhaps the use of more optimal work to rest strategies may provide a means to improve any regenerative processes, helping to combat any

fatigue related trauma occurring from this highly demanding task.

## REFERENCES

1. DeCaro JJ, Feuerstein M, Hurwitz TA (1992) Cumulative trauma disorders among educational interpreters. Contributing factors and intervention. *Am Ann Deaf* 137:288–292.
2. Feuerstein M, Burrell LM, Carosella AM, Marshall L, DeCaro JJ (1997) Occupational upper extremity symptoms in sign language interpreters: prevalence and correlates of pain, function, and work disability. *J Occup Rehab* 7:187–205.
3. Fischer SL, Woodcock K. (2007). Interpreting ergonomics: Are ergonomic interventions necessary in the sign language interpreting community? Industrial Accident Prevention Association Conference. Toronto, ON, 2007.
4. Marras WS, Schoenmarklin RW (1993) Wrist motions in industry. *Ergonomics* 36:341–351.
5. Scheuerle J, Guilford AM, Habal MB (2000) Work-related cumulative trauma disorders and interpreters for the deaf. *Appl Occup Environ Hyg* 15:429–434

**Table 1:** Mean and standard deviation values of wrist angle, velocity, and acceleration in the flexion/extension, radial/ulnar, and pronation/supination planes.

|                               | Joint Angle<br>(deg) |             | Joint velocity<br>(deg/sec) |                | Joint Acceleration<br>(deg/sec <sup>2</sup> ) |                |
|-------------------------------|----------------------|-------------|-----------------------------|----------------|---|----------------|
|                               | R wrist              | L wrist     | R wrist                     | L wrist        | R wrist                                       | L wrist        |
| <b>Flexion/<br/>Extension</b> |                      |             |                             |                |   |                |
| <i>Max</i>                    | 75 ± 28.2            | 33 ± 11.5   | 1,791 ± 168.2               | 1,117 ± 105.42 | 20,429 ± 2,546                                | 18,247 ± 5,628 |
| <i>Mean</i>                   | 26.16 ± 12.2         | 14.1 ± 5.2  | 12.48 ± 2.2                 | 9.53 ± 1.9     | 245.36 ± 37.8                                 | 175.24 ± 27.3  |
| <b>Radial/<br/>Ulnar</b>      |                      |             |                             |                |   |                |
| <i>Max</i>                    | 43.24 ± 23.4         | 23.14 ± 7.6 | 221 ± 28.5                  | 117 ± 15.7     | 1,287 ± 147                                   | 1,097 ± 117    |
| <i>Mean</i>                   | 16.55 ± 3.9          | 8.21 ± 1.7  | 6.24 ± 0.7                  | 4.2 ± .8       | 99.21 ± 7.2                                   | 105.12 ± 9.24  |
| <b>Pron/<br/>Supin</b>        |                      |             |                             |                |   |                |
| <i>Max</i>                    | 74.3 ± 14.8          | 17.3 ± 4.1  | 487 ± 64.2                  | 323.42 ± 35.6  | 5,842 ± 612                                   | 4,127 ± 745    |
| <i>Mean</i>                   | 27.81 ± 5.9          | 7.21 ± 2.2  | 25.63 ± 3.5                 | 21.47 ± 4.2    | 121.21 ± 18.23                                | 138.54 ± 27.21 |

# NON-UNIFORM UPREGULATION OF THE HYPERTROPHIC PATHWAY IN SKELETAL MUSCLE FOLLOWING LENGTHENING CONTRACTIONS: IMPLICATIONS FOR REGIONAL MUSCLE ADAPTATIONS

Sarah M. Abshire and Timothy A. Butterfield  
University of Kentucky, Lexington, KY, USA

web: [http://www.mc.uky.edu/athletic\\_training/butterfield](http://www.mc.uky.edu/athletic_training/butterfield)

## INTRODUCTION

Lengthening muscle contractions, also known as eccentric contractions (or eccentric exercise, EEX), produce high forces during concomitant stretching of the muscle-tendon unit (MTU). Although often associated with severe strain-injury, most often EEX results in less severe subcellular damage exhibited as delayed onset muscle soreness or DOMS [1]. Unlike severe strain injuries, DOMS is self-rectifying, and alleviates with time. Interestingly, the recovery following a non-injurious bout of EEX not only enhances the function of the MTU, but also provides resistance to damage during repeated EEX bouts. One proposed mechanism of this 'repeated bout effect' or RBE is the addition of sarcomeres in series within the muscle fibers.

Although we have shown that sarcomere number addition occurs following EEX with controlled MTU lengthening in the rabbit TA, dramatic regional differences in serial sarcomere number adaptations were observed [2]. Although the MTU underwent positive strain during EEX, not all regions of the muscle adapted similarly: the deep fibers of the TA lost sarcomeres, and the superficial fibers exhibited the largest gains. Regional mechanosensitive myocytes had produced disparate responses during EEX of controlled MTU stretch.

Recently, we have demonstrated that blocking stretch-activated ion channels during four weeks of EEX completely abrogated functional adaptations associated with serial sarcomere number addition in the NZW rabbit TA [3]. This lack of adaptation was associated with a reduced phosphorylation of p70s6 kinase (p70s6k), one of three different pathways [phosphatidylinositol-3 kinase (PI-3 kinase), PDK1 and Akt/PKB mTOR] associated with the initiation of translation, protein synthesis, and adaptive hypertrophy following resistance

exercise [4]. All three of these pathways lead to phosphorylation of p70s6 kinase (p70s6k), shown to play a critical role in protein synthesis and muscle hypertrophy [5].

Although not directly associated with serial sarcomere number addition, p70s6k does govern myofibrillogenesis in muscle, and activated by strain and activation. Therefore, we hypothesize that p70 phosphorylation following EEX will be: 1) non-uniform through the muscle; and 2) strain and load dependent.

## METHODS

The dorsiflexors of three female skeletally mature NZW rabbits were subjected to a single bout (5 sets of 10 repetitions) of EEX following tenotomy of one synergist muscle, resulting in four groups with n=3 muscles: (TAS) **TA Shortened** during EEX following tenotomy; (EDLL) **EDL Lengthened** during EEX with tendon intact; (TAL) **TA Lengthened** during EEX with tendon intact; (EDLS) **EDL Shortened** during EEX following tenotomy. Immediately following the exercise bout, the rabbits were euthanized and the muscles were excised, separated into regions and frozen in liquid nitrogen prior to storage at -80°C.

Western blot analyses were performed on regional homogenized samples of the TA muscles. Samples were centrifuged and the supernatant proteins (50ug per well) were loaded onto 7.5% Tris-HCl gels. Proteins were then transferred onto PVDF blotting membranes and blocked with Odyssey blocking buffer at room temperature (RT) for 1h. Membranes were then incubated overnight at 4°C in primary antibodies (rabbit anti-p70s6k, (1:1000) Santa Cruz Biotechnology, Santa Cruz, CA or mouse anti-p70s6k Thr389/412, (1:1000) Cell Signal, Danvers, MA). Blots were washed with PBS then incubated in the appropriate secondary antibody

(donkey anti-rabbit, (1:10,000) Licor, Lincoln, Nebraska or donkey anti-mouse (1:10,000) Licor, Lincoln, Nebraska) for 1h at RT. Blots were then washed in PBS then scanned on a Licor Odyssey system. Protein bands were quantified using software provided with the Licor Odyssey system. The ratio of phosphorylated p70s6k (p-p70s6k) to non-phosphorylated (p-p70s6k/p70s6k) was used for quantification of protein activation.

## RESULTS AND DISCUSSION

The p-p70s6k/p70s6k levels were similar following negative (EDLS) and positive (EDLL) active strain in the EDL ( $p=0.091$ ), and differences in protein expression were found for distal and proximal regions ( $p=0.63$  and  $p=0.54$ ).

Interestingly, p-p70s6k/p70s6k following exercise was higher in the TA Superficial region compared to both the TA deep region and the EDL for both strain conditions ( $p<0.001$ ). The effects of activation and strain on phosphorylation of p70s6k in the deep region of the TA and the EDL were similar in both strain groups ( $p>0.60$ ). This illustrates that the activation of the hypertrophic pathway in fibers of the deep region of the TA and the entire EDL are similar regardless of strain. However, the fibers of the superficial region of the TA respond with a greater upregulation, implicating a greater sensitivity to the same stimulus, or experiencing a stimulus of greater magnitude.

Within the TA muscle itself, there were disparate regional responses to activation and strain (Figure 1). Only the distal region of the Central superficial TA responded differently to strain, with greater p-p70s6k/p70s6k following positive strain (intact TA tendon, lengthening contraction) compared to the TAS group, which did not lengthen during activation,  $p=0.035$ . Within the TAS and TAL muscles, activation of the hypertrophic pathway was not different within the distal and proximal regions of the central superficial and deep regions of the TA ( $p>0.05$ , Figure 1).

## CONCLUSIONS

Previously, we have shown that long term EEX in rabbit TA muscle exhibits disparate regional adaptations in serial sarcomere numbers that serve

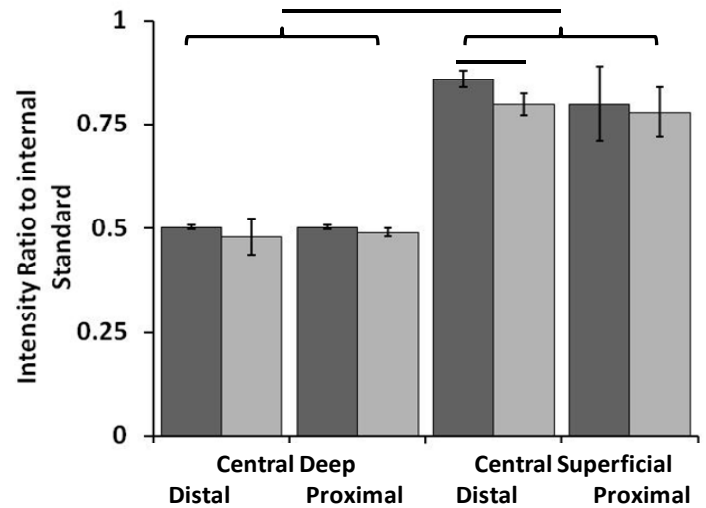


**Figure 1.** p-p70s6k/p70s6k levels in regions of the TA muscle following activation and shortening with minimal load (TAS, light grey bars) and activation and lengthening against high load (TAL, dark grey bars). The central superficial region exhibited greater hypertrophic response compared to the deep region in both conditions, with the central superficial region increasing p-p70s6k/p70s6k activation with positive strain (EEX).

to provide the muscle with altered function and resistance to damaging effects of subsequent EEX bouts. Although the cellular mechanisms for serial sarcomere number adaptations are unknown, activation and strain have been shown to upregulate the hypertrophic, mTOR pathway in skeletal muscle by phosphorylation of the p70s6k protein. Here we have shown the cell's hypertrophic response to mechanical load is non-uniform in and between synergist muscles, and is related to strain in the central superficial region of the TA. These non-uniform cell signaling responses are in close agreement with regional of serial sarcomere number adaptations we have shown previously [2]. Further work is underway to isolate pathways governing serial sarcomere number adaptations to exercise.

## REFERENCES

1. Butterfield TA. *ESSR* **38**(2), 51-60, 2010
2. Butterfield TA and Herzog W. *Pflügers Archiv* **451**(5), 688-700, 2006
3. Butterfield TA and Best TM *MSSE* **41**(2), 351-360, 2009
4. Abshire SM et al., *Proceedings of the ASB*, Providence, RI, 2010
5. Miyazaki M and Esser KA. *J Appl Physiol* **106**, 1367-1373, 2009

# ***In Vivo* Chondrocyte Mechanics In The Intact Mouse Knee Joint**

Ziad Abusara and Walter Herzog

Human Performance Laboratory, University of Calgary, Calgary, Alberta, Canada

Email: zabusara@kin.ucalgary.ca

## **INTRODUCTION**

Mechanical loading of joints deforms articular cartilage, which in turn causes deformation of the matrix embedded cells, the chondrocytes [1]. Chondrocyte deformation has been associated with biosynthetic responses aimed at maintaining the tissue healthy and strong [2]. However, excessive loading of cartilage and cells is thought to lead to cartilage degeneration and osteoarthritis [3]. Much of the work relating mechanical states of cells and their biosynthetic response is based on isolated cells, or cells embedded in explant samples removed from their natural *in situ* environment. Neither the mechanics nor the associated biological responses of chondrocytes have been studied in intact cartilage attached to its native bone or in the intact joint. The purpose of this study was to design and apply methods to study the mechanics of chondrocytes in the intact knee in live animals while loaded physiologically through muscular contraction.

## **METHODS**

In order to achieve the purpose of this study, we developed a novel *in vivo* testing system that allows for quantification of the mechano-biology of chondrocytes in the intact knee of live mice (Figure 1). Mice are fixed in a custom-built jig on the stage of a dual photon microscope. Controlled forces of the knee extensor muscles are produced through direct muscle stimulation. Imaging of the chondrocytes is performed using a Zeiss 40× 0.95 NA water-immersion objective coupled with a Coherent Chameleon IR laser tuned at 780 nm for two-photon excitation.

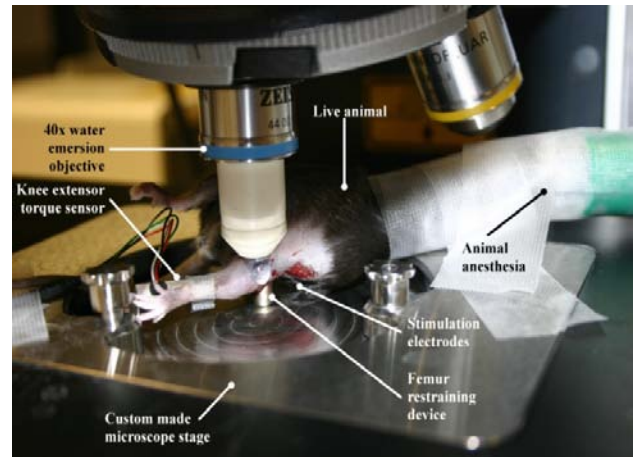


**Figure 1:** In vivo mouse knee preparation for imaging of dynamic chondrocyte deformation.

## **RESULTS**

Chondrocytes and their nuclei deform on average 18-25% for sub-maximal muscular loading in the intact mouse knee. Deformation occurs “instantaneously” upon loading, but requires minutes for full cell shape recovery (Figures 2- 4).

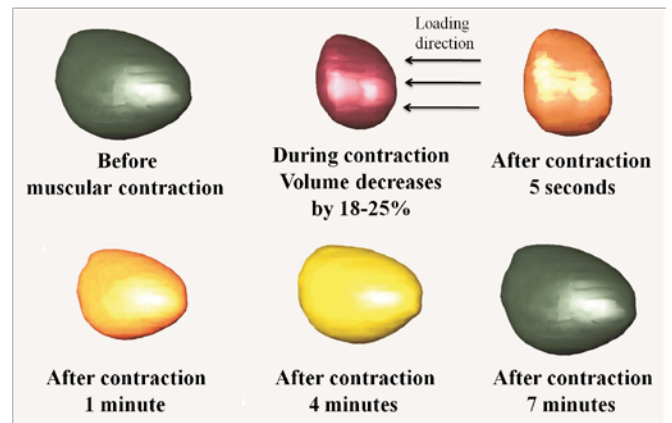


**Figure 2:** Cell deformation in the knee of a live mouse before, during and after muscular contraction.

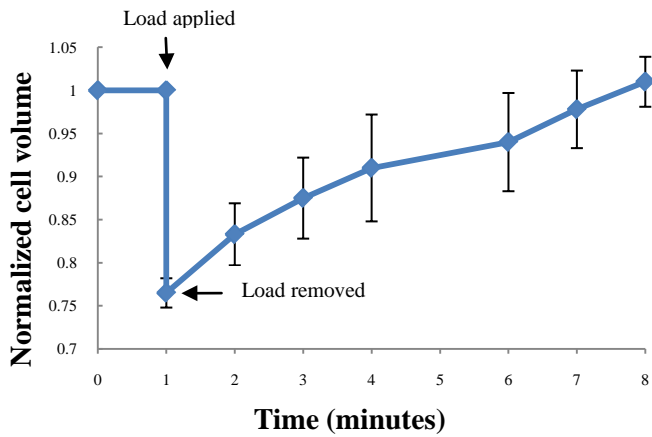


**Figure 3:** Normalized cell volume changes (means  $\pm 1SD$ ;  $n=5$ ) as a function of time. Upon loading, cells immediately loose between 18-25% of volume which is only fully recovered after about 7 minutes following load removal.

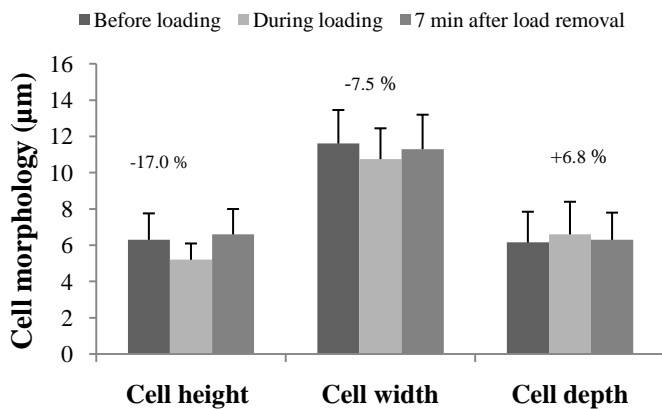


**Figure 4:** Changes in chondrocyte morphology during and after loading of the knee by muscular contraction. Cell height and width decreased during compression while cell depth increased. All morphometric parameters return to the original values after about 7 minutes load removal. Cell height is defined as the diameter perpendicular to the cartilage surface.

Application of muscle force below a certain threshold did not cause cell deformation, while increasing the loading beyond that threshold was associated with a nearly linear decrease in cell volume (Figure 5).

## DISCUSSION

Our results indicate that cell deformations occur “instantaneously” upon muscular loading of the

joint but require minutes to recover their original shape upon unloading. The quick deformation and volume loss during loading is probably a mechanism aimed at limiting pressure build up inside chondrocytes that might be fatal. The loss of volume, the associated cell strains, and the loss of ions during volume regulation upon loading all provide possible pathways for chondrocyte signaling that may result in adaptive or degenerative responses of the tissue to joint loading. These pathways will need careful exploration in future studies.

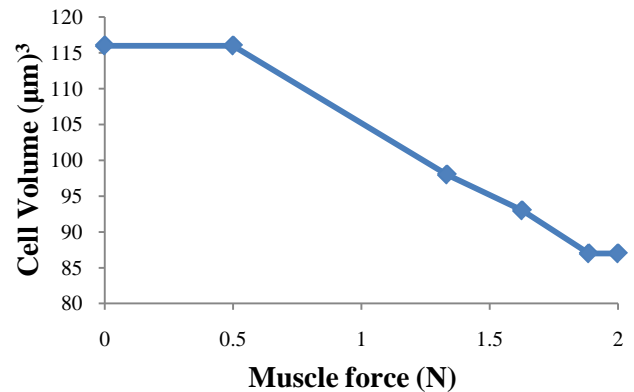


**Figure 5:** Cell volume as a function of muscle force.

## CONCLUSIONS

We developed an accurate and reliable method to measure dynamic cell deformations in the intact knee of live mice. Apart from having the advantage of observing cell mechanics in the functioning joint, it also allows for observations of dynamic (rather than just steady-state) loading conditions and permits repeat measurements on the same cell. Our results suggest that cell deformations upon muscular joint loading are ‘instantaneous’ but take minutes to recover.

## REFERENCES

- [1] Guilak, F., *J. Biomech.* **28**, 1529-1541, 1995.
- [2] Sah, R.L., Kim, et al. *J. Orthop Res* **7**, 619-636, 1989.
- [3] Moskowitz R. Experimental models of OA. 213-232, 1984.

## ACKNOWLEDGEMENTS

Alberta Innovates - Health solutions, AHFMR Team grant on Osteoarthritis, CIHR, CFI, Canada Research Chair Program.

# ASYMMETRY IN AMPUTEE GAIT: THE PROPAGATING EFFECTS OF WEAK PUSH-OFF

<sup>1,2</sup>Peter G. Adamczyk, <sup>1</sup>Arthur D. Kuo

<sup>1</sup>University of Michigan, Ann Arbor, MI, USA

<sup>2</sup>Intelligent Prosthetic Systems, LLC, Ann Arbor, MI, USA

email: [p.g.adamczyk@gmail.com](mailto:p.g.adamczyk@gmail.com)

## INTRODUCTION

Unilateral amputees exhibit a variety of gait asymmetries. Asymmetries in outcome variables such as swing and stance times [1], step length, forward trunk velocity [2], ground reaction forces [1], and joint mechanics [3] are widely attributed to the reduced ankle push-off work of the prosthetic foot. However it is not known whether gait asymmetry is fundamental to impaired push-off, or arises from compensatory adaptations. We employed a dynamic walking model to predict how weak push-off on one leg should affect whole-body center of mass (COM) mechanics. We also modeled possible compensations for this reduced push-off, and their consequences. We compared experimental data from amputees and non-amputees against model predictions, and found that weak push-off causes a cascade of asymmetries that are not prevented by simple adaptations.

## METHODS

We developed a simple dynamic walking model (based on [4] but with asymmetrical power input; Fig 1) to investigate the effects of unilateral weak push-off. The model is powered most economically by symmetric push-off, applied impulsively just before the leading leg's heel-strike collision. Compensation for weak push-off may occur through continuous work on the stance leg, similar to hip joint work in humans. The nominal model has two rigid legs with human-like mass distribution, a pin joint at the hips, and a linear torsional spring across the legs to adjust swing characteristics. Continuous work during single support is modeled by walking down a shallow slope. The magnitude of the push-off impulse and the slope can be different for each leg, and can be varied parametrically to alter the balance of energy supplied by push-off and gravity.

We numerically solved the model for cyclic gait under conditions similar to normal walking (with powering only from push-off), as well as cases with unilateral "prosthesis-like" push-off work (about 63% of normal) and zero push-off work. In the reduced-push-off cases, we simulated three compensations using slopes: during weak leg stance only; during strong leg stance only; and equally during both steps. Speed and stride length were held constant across all parameters by numerically adjusting the initial conditions, compensatory slope, and hip joint spring stiffness. Finally, we computed result metrics including mid-stance COM velocity, step time, push-off work and collision work on both the "strong" and "weak" legs. The model results formed the predictions for our human experiments.

We measured ground reaction forces (GRF) from twelve unilateral transtibial amputees and ten non-amputees walking at a range of speeds (0.7 to 1.6  $\text{m}\cdot\text{s}^{-1}$ ) on a split-belt force treadmill. We integrated GRF to estimate COM velocity and COM work rate, assuming periodic gait [4]. We integrated COM work rate to find total positive and negative COM work performed during push-off and collision phases of gait, and during the whole stride [4]. We compared COM work, COM velocity fluctuations and other metrics from prosthetic and intact steps.

## RESULTS AND DISCUSSION

Model results demonstrated several asymmetries in performance (Fig 1), arising as direct and indirect consequences of unilateral push-off weakness:

- The model's "strong" ("intact") leg experienced dramatically increased heel-strike collisions as compared to the normal, symmetric case. Weak contralateral push-off fails to redirect the COM velocity upward as it should, leaving the COM to fall harder on the landing leg.

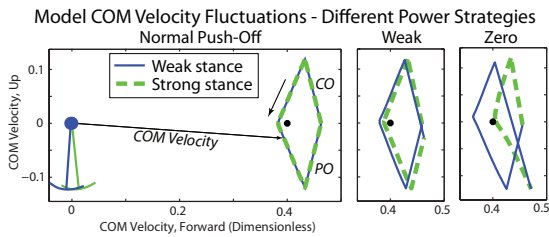


**Fig 1:** A dynamic walking model shows asymmetry in COM velocity trajectories (vertical vs. forward, called a *hodograph*) for weak push-off models with different powering: (a) “Normal,” symmetrical push-off power [4,5]; (b) unilateral “Prosthesis-Like” weak push-off, with bilateral slope; (c) unilateral Zero push-off, with bilateral slope. PO: Push-off; CO: Collision.

- The total energy input to the model is much higher for all weak-push-off models than for normal (~25% for “prosthesis-like”, ~165% for zero push-off), but varies only slightly across compensatory strategies. Thus, if total work drives compensation strategy in humans, there is little incentive to choose one leg preferentially.
- COM speed at mid-stance is lower on the “strong” leg (~2% for “prosthesis-like,” ~10% for zero weak-side push-off), regardless of compensation strategy. The fact that shifting compensatory work from one leg to the other does not influence this result suggests that this asymmetry is unavoidable in cases of impaired push-off.

We also found that adding energy during single stance, even on the “strong” leg, did not lead to large increases in “weak” leg collisions. The strong leg’s normal push-off remained large enough to preempt hard collisions on the weak side. Additionally, the model demonstrated greater stance time on the strong leg (because of lower forward speed), and lower symmetry in COM velocity fluctuations with greater push-off impairment.

Human experiments demonstrated results that are largely parallel to the model predictions. Among statistically significant results ( $P < 0.05$ ), we found:

- Negative collision work per step was 79% higher on the intact side than on the prosthetic side, and 43% higher than in non-amputees.
- Average total COM work rate was 17% higher in amputees than in non-amputees, with roughly equal work per stride but 11% higher stride rate.
- COM speed was lower at intact mid-stance (90% of walking speed) than prosthetic mid-stance (98%). These values surrounded that observed in non-amputees (93% of walking speed).

Unexpectedly, negative collision work was 20% less on the prosthetic side of amputees than in non-

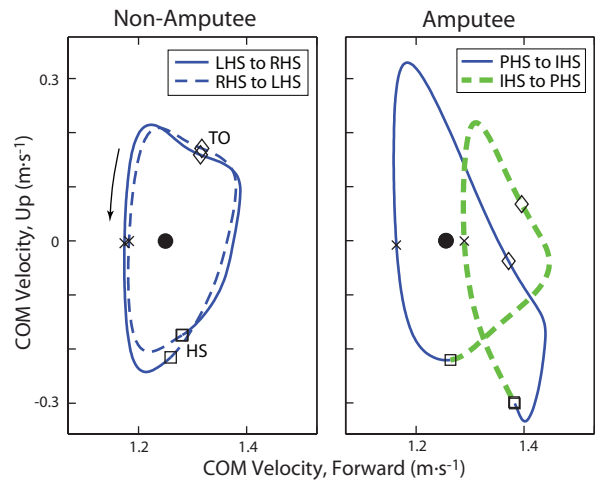


**Fig 2:** COM Hodographs [5] for a typical nonamputee at 1.25 m/s, and an example unilateral transtibial amputee at 1.3 m/s. Normal hodographs are largely symmetrical with respect to Right and Left legs. Unilateral amputees exhibit marked asymmetry in forward speed at mid-stance (x) and other aspects of COM kinetics. HS: Heel Strike, □; TO: Toe-Off, ◇; P: Prosthetic; I: Intact; R: Right; L: Left.

amputees, whereas the model predicted it should be very slightly higher. But as in the model, stance duration was greater on the intact limb of amputees (67% of stride) than on the prosthetic side or in non-amputees (both 64%), and COM velocity fluctuations were less symmetric in amputees than in non-amputees (Fig 2).

## CONCLUSIONS

Push-off impairment and compensation with symmetric single-stance hip work appear sufficient to explain many asymmetries commonly observed in the gait of unilateral transtibial amputees. Weak prosthetic-side push-off leads to a large collision on the intact leg, followed by lower stance-phase speed and higher stance duration. To compensate for the lost push-off work (in order to maintain average speed), work output is increased in both legs during stance phases. The impairment and associated compensation lead to overall reductions in COM motion symmetry. All of these asymmetries can be attributed to the most basic limitation of the prosthetic limb and the requirements of the task, independent of secondary adaptations such as from pain or inertial properties of the prosthesis.

## REFERENCES

1. Nolan L *et al*, *Gait Post*, **17**, 142-151, 2003.
2. Murray MP, *Bull Pros Res*, **17**, 35-45, 1980.
3. Silverman AK *et al*, *Gait Post*, **28**, 602-9, 2008.
4. Adamczyk PG *et al*, *JEB*, **209**, 3553-63, 2006.
5. Adamczyk PG *et al*, *JEB*, **212**, 2668-78, 2009.

# EFFECTS OF BALLISTIC EXTREMITY ARMOR ON JOINT KINEMATICS DURING GAIT

<sup>1,2</sup>Albert A. Adams, <sup>1</sup>Leif Hasselquist, <sup>1</sup>Jeffrey Schiffman

<sup>1</sup> Natick Soldier Research, Development and Engineering Center, Natick, MA, USA

<sup>2</sup> Worcester Polytechnic Institute, Worcester, MA, USA

email: albert.adamsiii@us.army.mil

## INTRODUCTION

In addition to the standard armor vest, the U.S. military has been issuing ballistic armor designed to protect the arms and legs. Some of these extremity armor systems allow for scalable protection, providing soldiers with increased ballistic armor coverage when deemed necessary by adding additional components that protect the forearms and shanks to the upper arm and thigh components with hook and loop straps. Few studies have investigated the effects of extremity armor on gait, and none have included joint kinematics in their analysis. Hasselquist et.al (2008), previously reported that in both walking and running,  $VO_2$  increased significantly when any extremity armor was worn, as compared to a no armor condition. Researchers have also shown that walking with added mass reduces the stability of the leg kinematics and possibly the overall balance of the walking pattern [2]. Existing research on limb loading provides clues as to what gait effects may be expected with varying levels of armor applied to the limbs. Researchers have found loading the legs increases stride length and swing time [3]. It has also been found that in addition to the mass, the distribution of the load applied to the limbs has an effect on gait kinematics, with more distal loading resulting in greater increases to stride length and swing time [4]. The purpose of the current study was to characterize the joint kinematics of a scalable extremity armor system on gait, minimize its impact on gait and aid in the design of future armor systems. It was hypothesized that the wearing of the distal extremity armor components would alter joint kinematics during gait, as compared to both wearing no armor and wearing only the proximal armor components.

## METHODS

The extremity armor system tested composed of a standard military helmet and armor vest (21.2 kg), upper arm and thigh components (3.6 kg), and removable forearm and shank components (2.0 kg). Twelve U.S. Army enlisted men participated in the study (mean 21.7 yrs; 1.78 m, 85.1 kg). The study was completed in accordance with Army Regulation 70-25 (Use of Volunteers as Subjects in Research). Subjects were asked to walk (1.34 m/s) and run (2.46 m/s) on a level treadmill (AMTI, Watertown, MA, USA) with each of three different levels of extremity armor coverage: a no armor (NA) condition (2.0 kg) that consisted of minimal clothing, combat boots, and a helmet; a partial extremity armor (PEA) configuration (24.9 kg) that consisted of an armor vest and extremity armor on the upper arms and thighs in addition to clothing worn in the NA condition; and a full extremity armor (FEA) configuration (26.9 kg) that consisted of forearm and shank armor in addition to the PEA configuration. After 5 min on the treadmill, 20 sec of kinematic data was collected (Qualisys Medical AB, Gothenburg, Sweden). From the kinematic data collected, trunk, hip, knee and ankle angles, as well as temporal gait measures, were calculated for 10 consecutive strides and averaged for each trial (Visual3D, C-Motion Inc., Germantown, MD, USA). Joint angles were normalized to each participant's anatomical neutral standing position. One-way repeated measures ANOVAs ( $\alpha=0.05$ ) were performed for all variables.

## RESULTS AND DISCUSSION

In walking, PEA and FEA conditions resulted in significant changes to hip, knee, and ankle ranges of motion (ROM), compared to NA (Table 1). The PEA and FEA conditions resulted in a decrease in mean maximal plantar flexion per step, and an

increase in maximal dorsiflexion, maximum knee flexion, maximum hip flexion. No statistically significant differences were found in walking between the effects of the PEA and FEA. This may indicate that the forearm and shank components of the FEA were not heavy enough to elicit effects on gait when added. The increases in hip and knee ROM, as well as an observed increase in double support time in walking, are similar to standard backpack load carriage [5]. The volunteers may have adopted a gait strategy based on the torso armor load which weighed 20 kg and the extremity loading may have been negligible after that weight point. In running, hip flexion, hip extension, dorsiflexion at the ankle, and trunk ROM were increased by use of armor in the PEA and FEA conditions, while plantar flexion at the ankle decreased. Such a decrease in plantar flexion could not be found in any previous load carriage or extremity loading literature, and warrants further investigation.

When looking at total joint ROM in running (Table 1), the reduction in maximum plantar flexion nullified the increased dorsiflexion, preventing the ankle ROM from reaching a significant difference. Only the hip and trunk displayed a significant increase in total ROM resulting from the PEA and FEA, as compared to running with the NA condition. Such an increase in hip ROM is also typical of torso loading during running [6], and points to the mass of the vest overpowering potential effects of the extremity armor. No changes in temporal running kinematics were found between armor conditions.

## CONCLUSIONS

Wearing of the extremity armor system used in this study was found to alter joint kinematics of walking and running, compared to walking and running unarmored. Contrary to our hypothesis, no significant changes in the joint kinematics were found between the effects of the PEA and FEA conditions, which may be partly due to the low mass of the distal armor components. Other researchers have shown that added body mass of up to 30% of body weight had only small changes on sagittal plane joint kinematics [2]. However, that study only addressed total body mass changes.

For soldiers, this study indicates that there would be no biomechanical benefit to removing the distal components of the extremity armor system. The altered joint kinematics may interact with the impact of the energy cost of weight while wearing the FEA. Stability and balance during ambulation may also be affected due to the added mass and changes in the joint kinematics. The results of the current study are limited to the specific extremity armor system tested, but demonstrate the need for further investigation into the biomechanical effects of load placement on the limbs and the interaction effects of limb loading and torso loading.

## REFERENCES

1. Hasselquist L, et al. *Proceedings of NACOB'08*, Ann Arbor, MI, USA, 2008.
2. Arellano AJ, et al. *JEB* **212**, 1965-1970, 2009.
3. Browning RC, et al. *MSSE* **39**(3), 515-25, 2007.
4. Royer TD, Martin PE. *MSSE* **37**(4), 649-56 2005.
5. Kinoshita H. *Ergonomics* **28**, 1347-1362, 1985.
6. LaFiandra M, et al. *J Biomech* **36**(1), 87-95. 2003.

**Table 1.** Mean (SD) sagittal plane range of motion of the joints during walking and running (degrees).

|  | Walking           |                    |                    |                    | Running           |                   |                    |                   |
|--|-------------------|--------------------|--------------------|--------------------|-------------------|-------------------|--------------------|-------------------|
|  | ROM Lean          | ROM Ankle          | ROM Hip            | ROM Knee           | ROM Lean          | ROM Ankle         | ROM Hip            | ROM Knee          |
| No Armor   | 3.588*<br>(0.806) | 27.965*<br>(3.390) | 37.999*<br>(2.573) | 62.780*<br>(3.367) | 6.643*<br>(1.505) | 34.987<br>(5.485) | 43.247*<br>(3.650) | 74.759<br>(8.511) |
| Partial Armor  | 4.721<br>(1.542)  | 23.374<br>(2.814)  | 40.679<br>(2.250)  | 72.743<br>(5.042)  | 9.082<br>(1.847)  | 32.498<br>(5.113) | 46.099<br>(4.383)  | 74.268<br>(8.294) |
| Full Armor   | 4.015<br>(0.935)  | 24.698<br>(2.322)  | 38.985<br>(2.760)  | 71.584<br>(2.948)  | 8.037<br>(2.351)  | 34.011<br>(5.168) | 44.655<br>(4.257)  | 75.223<br>(5.800) |
| Asterisks (*) indicates significant difference from other armor conditions ( $\alpha < 0.05$ ) |                   |                    |                    |                    |                   |                   |                    |                   |

# VALIDATION OF A 3-PT BENDING TECHNIQUE FOR SMALL BONE SPECIMENS

<sup>1</sup>Carolyn Albert, <sup>1</sup>John Jameson, <sup>2</sup>Peter Smith and <sup>1,2</sup>Gerald Harris

<sup>1</sup>Orthopaedic and Rehabilitation Engineering Center (OREC), Marquette University  
and the Medical College of Wisconsin, Milwaukee WI, USA

<sup>2</sup>Shiners Hospitals for Children - Chicago, IL, USA

email: [carolyne.albert@marquette.edu](mailto:carolyne.albert@marquette.edu) web: [www.orec.org](http://www.orec.org)

## INTRODUCTION

Limited information is currently available to describe the material properties of pediatric bones. This limited data is largely due to a scarcity of pediatric specimens available for testing, as studies of bone material properties generally use cadaveric specimens. Small bone specimens can be obtained from biopsies or during routine orthopaedic surgery such as those for fracture repair or corrective osteotomies. While such specimens could be used to characterize the material behavior of pediatric bone, their small size renders them unsuitable for most mechanical test protocols, in which specimens are typically a few millimeters in width and thickness, and a few centimeters in length [e.g., 1].

Microspecimens (e.g., 100 x 100 x 1500  $\mu\text{m}$ ) have been used in some studies, however, these specimens are too small to capture the heterogeneous microstructure and composition of cortical bone; and they result in moduli (4-6 GPa [2]) that are far lower than those generally accepted for human cortical bone, e.g., 17 GPa [3]. Nanoindentation has also been used to measure the modulus in such small pediatric specimens [e.g., 4], however, this technique does not provide a measure of strength.

The first objective of this study was to develop and validate a method for mechanical characterization of small cortical bone specimens, such as those obtained by biopsy or routine surgery, without underestimating the modulus. A secondary objective was to examine the effect of specimen thickness (dimension) on the measured modulus ( $E$ ) and yield strength ( $\sigma_y$ ) of bone in bending.

## METHODS

Bending tests were performed on 48 cortical bone specimens obtained from the mid-femoral diaphysis

of a year-old female cow. Rectangular beams were machined using a diamond saw (IsoMet™ Low Speed Saw, Buehler®) with a 0.3 mm-thick blade. The beams were divided into four groups (Table 1), with each group (n=12) having a different thickness ( $t$ ) range. The beams were at least 5 mm long and approximately 1 mm wide (0.816-1.042 mm). The long axes were parallel to the long axis of the source femur.

**Table 1:** Beam thicknesses, mean (SD), and loading displacement rates ( $d_{\text{rate}}$ ).

| Group                      | 1           | 2           | 3           | 4           |
|----------------------------|-------------|-------------|-------------|-------------|
| $t$ ( $\mu\text{m}$ )      | 976<br>(28) | 810<br>(20) | 726<br>(21) | 506<br>(34) |
| $d_{\text{rate}}$ (mm/min) | 1.00        | 0.80        | 0.75        | 0.60        |

The beams were loaded in 3-point bending on an electromechanical testing machine (Model 3345, Instron®), using a custom-built jig (Figure 1) and a 50N load cell. A constant span length of 4.0 mm was used. This span was chosen as the maximum appropriate length on the basis of a prior study of small bone specimens collected during routine orthopaedic surgeries [4].

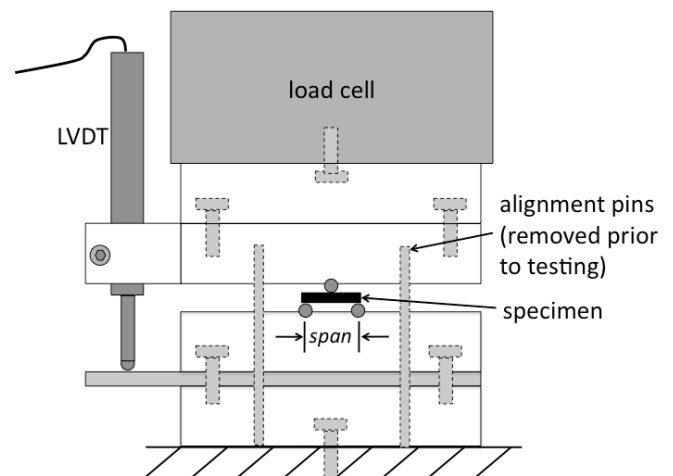


**Figure 1:** Diagram of testing set-up.

Loading consisted of five cycles of pre-conditioning (<50MPa), followed by a ramp to failure. For each group, a fixed displacement rate ( $d_{rate}$ , Table 1) was chosen to achieve a strain rate of approximately 0.15%/s. The displacement of the top platen relative to the bottom platen was measured with a linear variable displacement transducer (LVDT, Model 2601-092, Instron®).

Stress and strain were obtained from the load and LVDT displacement data using beam theory equations. The material properties were calculated from the stress-strain data. The results were compared among the four thickness groups using ANOVA with a significance level of 0.05. SNK tests were used for post-hoc comparisons.

## RESULTS AND DISCUSSION

A typical stress-strain curve is shown in Figure 2. Results for each group are summarized in Table 2.

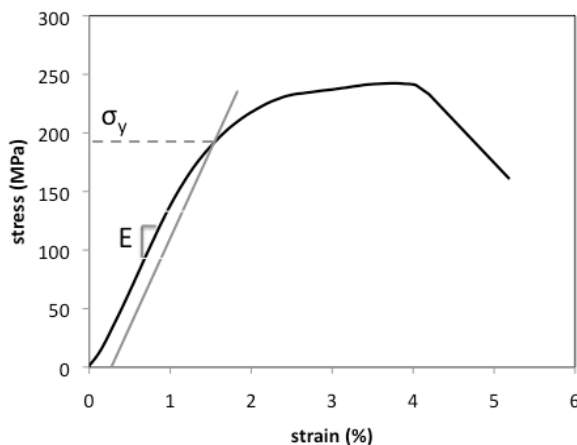


**Figure 2:** Typical stress-strain curve.

**Table 2:** Bone properties by group. Mean (SD).

| Group | E (GPa)    | $\sigma_y$ (MPa)      |
|-------|------------|-----------------------|
| 1     | 14.7 (1.7) | 194 (27)              |
| 2     | 16.1 (1.2) | 192 (18)              |
| 3     | 15.6 (1.8) | 186 (20)              |
| 4     | 15.0 (1.4) | 163 (15) <sup>a</sup> |

<sup>a</sup>  $p < 0.01$  compared to the other groups

For all specimens, E was within the range of values previously reported for bovine bone in bending, e.g., 10-22 GPa [1], while  $\sigma_y$  was somewhat higher than values reported from tensile tests, e.g., 154 MPa [3]. These differences in  $\sigma_y$  may be attributed to differences in loading configuration.

While group (thickness) did not affect E ( $p=0.11$ ), it affected  $\sigma_y$  ( $p < 0.002$ ). Specifically,  $\sigma_y$  was lower

for group 4 (the smaller thickness) than for the other groups, but it did not vary among groups 1-3.

During the study, four important sources of experimental error were identified: improper load cell calibration; jig/load cell compliance; jig misalignment; and non-parallel beam surfaces. These error sources, which can result in gross underestimation of E, were addressed as follows:

- Load cell calibration was validated with precision-calibrated weights.
- Flexion displacement was measured with an external LVDT (Figure 1), for which the calibration was validated with gage blocks.
- The platens were aligned carefully using dowel pins.
- The diamond saw blade was fastened tightly and no added weights were used during beam machining to minimize bending of the blade.

Further analysis also revealed that the strain rate ranged 0.12-0.16%/s, and a small negative correlation was observed between E and strain rate ( $R^2=0.36$ ). Thus, variance in E may be reduced by controlling strain rate rather than using a fixed displacement rate.

## CONCLUSIONS

The mechanical testing protocol developed in this study will enable the accurate measurement of pre-yield material properties of small cortical bone specimens obtained by biopsy or during routine orthopaedic surgery. The measured properties were not significantly affected by beam thickness for beam thickness greater than 700  $\mu\text{m}$ .

## REFERENCES

- Martin and Boardman. *J Biomech* **26**, 1047-54, 1993.
- Choi K, et al. *J Biomech* **23**, 1103-13, 1990.
- Currey JD. *J Biomech* **37**, 549-56, 2004.
- Fan et al. *Connect Tissue Res* **48**, 70-5, 2007.

## ACKNOWLEDGEMENTS

This work was supported by US Department of Education NIDRR grant H133P080005. The contents of this abstract were developed under a grant from the Department of Education, NIDRR grant H133E100007. However, these contents do not necessarily represent the policy of the Department of Education, and you should not assume endorsement by the Federal Government.

# KINEMATICS AND KINETICS WITH A POWERED LOWER LEG SYSTEM DURING STAIR ASCENT FOLLOWING TRANSTIBIAL AMPUTATION

Jennifer M. Aldridge, Abbie E. Ferris, Jordan T. Sturdy and Jason M. Wilken

Department of Orthopedics and Rehabilitation, Center for the Intrepid, Brooke Army Medical Center

Fort Sam Houston, TX, USA

email: Jennifer.aldridge@us.army.mil

## INTRODUCTION

Persons with unilateral transtibial amputation (TTA) commonly demonstrate significant between limb asymmetries and deviations from normal gait when ascending stairs [1]. Deviations include significantly increased involved side hip flexion and joint power, and significantly increased hip joint moments and reduced knee joint powers bilaterally [1]. These deviations are thought to result, in part, from a reduction of ankle motion and power generation on the involved side as compared to intact ankles.

Conventional energy storing and returning (ESR) feet allow motion through deformation of a carbon fiber keel, but are unable to replicate the ankle motion and power provided by the intact ankle. Recently, however, powered prosthetic devices which provide the ability to restore ankle push-off power have been developed. The first of these devices to reach the clinical market uses a series-elastic actuator to provide powered push-off [2]. The effect that such a device will have on stair ascent performance in individuals with TTA is unknown. Therefore, the purpose of the current study was to determine if ankle push-off power improves lower extremity kinematics and kinetics during stair ascent in individuals with TTA.

## METHODS

Eleven individuals with unilateral TTA and eleven height and weight matched controls were recruited for the study. Individuals with TTA participated in two biomechanical gait analysis testing sessions: 1) using an ESR foot, and 2) using the powered BiOM device (Powerfoot BiOM, iWalk). Subjects were provided a three week acclimation period to the BiOM device

prior to testing. Control subjects (CONT) participated in a similar gait analysis session.

Lower extremity kinematic data were recorded using an optoelectronic motion capture system (Motion Analysis Corp., Santa Rosa, CA) collecting at 120 Hz. Ground reaction force data were collected for four steps (AMTI Inc., Watertown, MA) at 1200 Hz as subjects ascended a 16-step staircase at a cadence of 80 steps per minute. Sagittal plane ankle, knee, and hip angles, moments and powers were calculated for five cycles per side and normalized to 100% gait cycle. Peak values were extracted using a custom MatLab program (Mathworks Incorporated, Natick, MA).

A 2x2 repeated measures ANOVA was used to determine limb (involved and uninvolved) and condition (ESR and BiOM) differences. A one-way ANOVA was used to determine significant differences between the BiOM (involved and uninvolved) and CONT.

## RESULTS AND DISCUSSION

Mean peak kinematic and kinetic values at the ankle, knee, and hip joints for the ESR condition (uninvolved and involved limb) were similar to previously published results [1]. The mean values, standard deviation and significance levels of the statistical tests for ankle peak values are presented in Table 1.

### *Ankle*

Condition dependent differences (ESR vs. BiOM) were observed at the ankle (Figure 1). An increase in involved limb peak plantarflexion (PF) angle ( $p < 0.001$ ) resulted in a larger ankle range of motion ( $p < 0.001$ ) when using the BiOM ( $17.5 \pm 3.7^\circ$ ) as compared to ESR ( $8.9 \pm 2.6^\circ$ ). However, these increases

failed to completely normalize ankle kinematics while using the BiOM (ROM:  $p < 0.001$ , Peak PF:  $p = 0.002$ ). Participants experienced a 167% increase in involved side peak ankle push-off power ( $p < 0.001$ ) from ESR to BiOM. Further, no significant difference between BIOM and CONT were observed, indicating successful normalization of ankle power generation.

### Knee and Hip

Limb asymmetries including greater involved side hip flexion throughout the gait cycle, greater involved side hip power during stance, and decreased involved side knee power during stance were observed in both the BIOM and ESR conditions ( $p < 0.05$ ). Despite changes in ankle ROM and power no significant kinematic or kinetic changes were observed at the knee or hip between conditions.

### CONCLUSIONS

The results of the study indicate that the PowerFoot BiOM device was successful in restoring ankle power during stair ambulation. Further investigation is under way to determine

why changes in ankle range of motion and power did not significantly alter function of proximal and contralateral joints. Additional training may be necessary for patients to fully utilize the device during stair ambulation.

### REFERENCES

1. Alimusaj, M., et al., *Gait & Posture*, **30**, 2009.
2. Eilenberg, M.F., et al., *IEEE Trans Neural Syst Rehabil Eng*, **18**, 2010.

### ACKNOWLEDGEMENTS

Support provided by the U.S. Army Telemedicine & Advanced Technology Research Center (to JMW).

The view(s) expressed herein are those of the author(s) and do not reflect the official policy or position of Brooke Army Medical Center, the U.S. Army Medical Department, the U.S. Army Office of the Surgeon General, the Department of the Army, Department of Defense or the U.S. Government.

**Table 1:** Mean  $\pm$  standard deviation for ankle peak kinematic and kinetic values.

<sup>+</sup> $p < 0.05$  significantly different from controls, <sup>\*</sup> $p < 0.05$  significantly different from ESR

<sup>1</sup>Positive value = dorsiflexion, Negative value = plantarflexion

| Parameter                          | Controls        | Uninvolved Limb |                   | Involved Limb   |                     |
|------------------------------------|-----------------|-----------------|-------------------|-----------------|---------------------|
|                                    |                 | ESR             | BIOM              | ESR             | BIOM                |
| PF max - stance (deg) <sup>1</sup> | $-14.7 \pm 7.2$ | $-24.2 \pm 3.3$ | $-23.9 \pm 6.6^+$ | $5.8 \pm 2.7$   | $-4.5 \pm 4.4^{+*}$ |
| DF max - swing (deg) <sup>1</sup>  | $17.6 \pm 4.2$  | $15.8 \pm 5.4$  | $14.4 \pm 5.2$    | $7.7 \pm 2.8$   | $5.1 \pm 2.4^*$     |
| PF moment max1 (Nm/kg)             | $0.82 \pm 0.22$ | $1.03 \pm 0.23$ | $1.15 \pm 0.19^+$ | $1.11 \pm 0.27$ | $1.05 \pm 0.14$     |
| PF moment max2 (Nm/kg)             | $1.22 \pm 0.13$ | $1.47 \pm 0.19$ | $1.53 \pm 0.14^+$ | $1.04 \pm 0.29$ | $1.13 \pm 0.17$     |
| PF power gen. max (W/kg)           | $2.12 \pm 0.49$ | $4.09 \pm 0.99$ | $4.5 \pm 0.99^+$  | $0.59 \pm 0.20$ | $1.64 \pm 0.51^*$   |

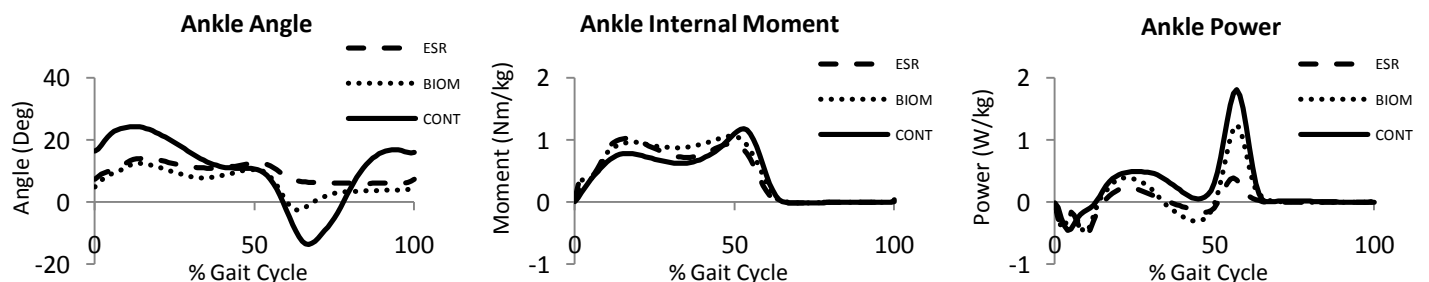


**Figure 1:** Sagittal plane ankle kinematics and kinetics during stair ascent for controls and patient's involved side while using an ESR device and the BiOM

# MODULAR CONTROL OF WALKING: A 3D SIMULATION STUDY

<sup>1</sup>Jessica L. Allen, <sup>2,3</sup>Steven A. Kautz and <sup>2</sup>Richard R. Neptune

<sup>1</sup>Department of Mechanical Engineering, The University of Texas at Austin, Austin, TX, USA

<sup>2</sup>Ralph H Johnson VA Medical Center, Charleston, SC, USA

<sup>3</sup>Department of Health Sciences and Research, Medical University of South Carolina, Charleston, SC, USA

email: [jessica.allen@mail.utexas.edu](mailto:jessica.allen@mail.utexas.edu) web: [www.me.utexas.edu/~neptune](http://www.me.utexas.edu/~neptune)

## INTRODUCTION

Recent studies have suggested that complex locomotor tasks such as walking may be achieved using a reduced set of neural control elements, or modules [1,2]. A previous 2D simulation study analyzed the contributions of identified modules to the biomechanical subtasks of walking (i.e., body support, forward propulsion and leg swing) [3]. However, since the model was constrained to the sagittal plane, the contributions of each module to frontal plane tasks such as control of mediolateral (ML) balance through the ML ground reaction force (GRF) and power transfer between legs could not be assessed. The purpose of this study was to use a 3D musculoskeletal model and forward dynamics simulation of healthy walking to gain a comprehensive view of modular control of human walking. Specifically, we analyzed the module contributions to the 3D GRFs and power generation, absorption and transfer between body segments.

## METHODS

A previously described 3D musculoskeletal model [4] and forward dynamics simulation of walking was generated using SIMM (MusculoGraphics, Inc.). Experimental kinematics, GRFs and electromyography (EMG) were collected from 14 healthy subjects. Four muscle excitation modules were identified from the EMG data using non-negative matrix factorization and used as the simulation muscle control inputs [3]. Within a given module, if the average module weighting for a given muscle was >40% across subjects, then that muscle was considered to be excited by that module. Muscles with similar anatomical function for which EMG data were not recorded were also included in each module. A fifth module was also

included to account for the hip flexors [3] and received a bimodal excitation pattern. All muscles within each module received the same excitation timing but the magnitude was allowed to vary. For those muscles that were not associated with a module, a bimodal excitation pattern was used. To improve optimization convergence speed, torques were applied at each joint to drive them back to their desired experimental kinematics using proportional control. A simulated annealing algorithm was then used to optimize the muscle excitation patterns to eliminate those torques. Ground reaction force decomposition [3] and segmental power [4] analyses were performed to quantify individual muscle contributions to the biomechanical subtasks of walking. The contribution of each module to the subtasks of body support (vertical GRF), forward propulsion (horizontal GRF), ML balance (ML GRF) and power transfer between legs was then found by summing the contributions from those muscles associated with each module.

## RESULTS AND DISCUSSION

The biomechanical functions produced by each module in the sagittal plane were consistent with those previously found [3]. Module 1 (gluteus muscles, vasti and rectus femoris) provided body support and decelerated the body during early stance and accelerated the body medially throughout stance (Fig. 1). Module 1 also transferred energy to the contralateral leg during early stance prior to and during contralateral swing (Fig. 2). This was consistent with previous work showing the gluteus maximus contributes to swing initiation [4]. The primary function of Module 2 (plantarflexors) was to provide body support and forward propulsion in late stance while accelerating

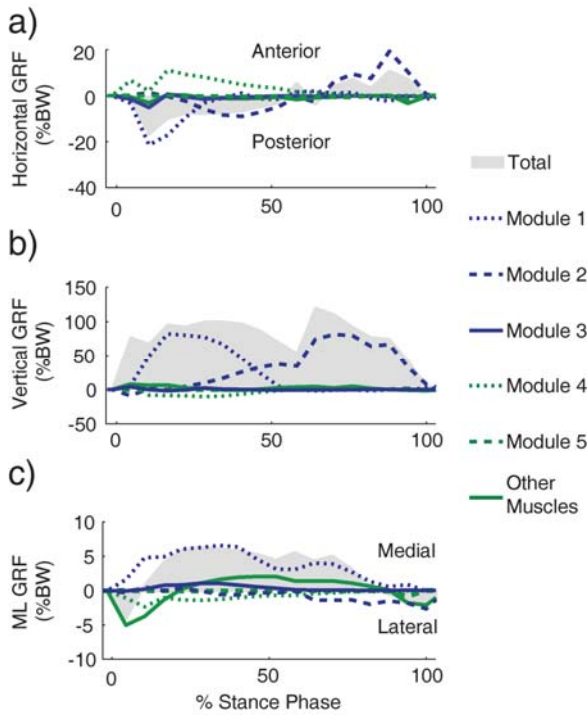


**Figure 1:** Module contributions to the GRFs.

the body laterally (Fig. 1). Module 3 (ankle dorsiflexors and rectus femoris) absorbed power from the ipsilateral leg during early stance and transferred that energy to the trunk (Fig. 2). Module 3 also helped control ipsilateral leg swing by accelerating the leg forward in early swing (i.e., generated power to the leg) and decelerating the leg in late swing (i.e., absorbed power from the leg) (Fig. 2). Module 4 (hamstrings) accelerated the body forward and laterally during early stance (Fig. 1). Module 4 also transferred energy to the contralateral leg during early stance prior to contralateral swing (Fig. 2). This was consistent with previous work showing the hamstrings contribute to contralateral swing initiation [4]. Module 4 also decelerated the ipsilateral leg (absorbed power) during late swing (Fig. 2). The primary function of Module 5 (hip flexors) was to facilitate leg swing by generating positive power to the ipsilateral leg in pre- and early-swing (Fig. 2).

## CONCLUSIONS

The simulation analysis showed a reduced set of neural control elements or modules are sufficient to perform the necessary subtasks of walking. Modules 1 (gluteus muscles, vasti and rectus femoris) and 2 (plantarflexors) combined to provide body support, Modules 1, 2 and 4 (hamstrings)

regulated forward propulsion and provided ML balance. Modules 3 (ankle dorsiflexors and rectus femoris), 4 and 5 (hip flexors) combined to control ipsilateral leg swing while Modules 1 and 4 contributed to contralateral swing initiation and swing control.

These results have important clinical implications for impaired populations. For example, recent work found that some post-stroke hemiparetic subjects are unable to independently activate all modules [1], which will impair their ability to successfully perform the walking subtasks and most likely lead to walking deficiencies.

## REFERENCES

1. Clark DJ, et al., *J Neurophysiol.* **103**, 844-57, 2010.
2. Ivanenko YP, et al., *J Physiol.* **556**, 267-82, 2004.
3. Neptune RR, et al., *J Biomech.* **42**, 1282-7, 2009.
4. Peterson CL, et al., *J Biomech.* **43**, 2348-55, 2010.

## ACKNOWLEDGEMENTS

This work was supported by NIH Grant R01 HD46820 and the NSF GRFP. The contents are solely the responsibility of the authors and do not necessarily represent the official views of the NIH, NICHD or NSF.

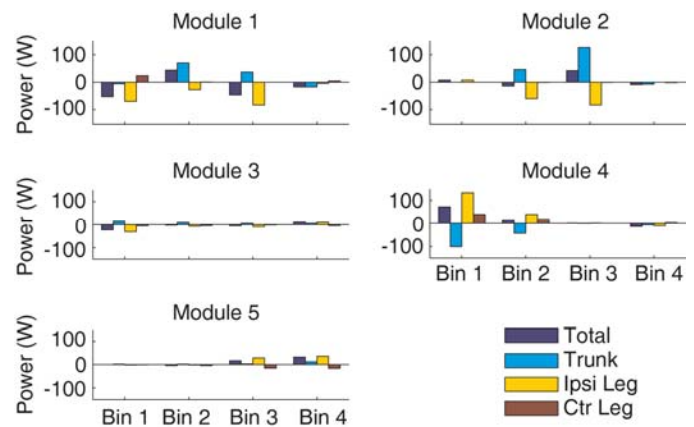


**Figure 2:** Average mechanical power delivered to the trunk and legs during different regions of the gait cycle. Bin 1 is contralateral pre-swing, Bin 2 is contralateral leg swing, Bin 3 is ipsilateral pre-swing, and Bin 4 is ipsilateral swing (Total = power delivered to the body; Trunk = power delivered to the trunk segment; Ipsi Leg = power delivered to the ipsilateral leg, and Ctr Leg = power delivered to the contralateral leg).

# WAVEFORM CONSISTENCY-BASED DECISION RULES FOR DISCRIMINATING BETWEEN TYPES AND LEVELS OF MUSCULATURE EFFORTS

<sup>1</sup>Sivan Almosnino, <sup>1,2</sup>Zeevi Dvir, <sup>1</sup>Davide Bardana, <sup>1</sup>Ryan Graham and <sup>1</sup>Joan Stevenson

<sup>1</sup>Queen's University, Kingston, ON, Canada

<sup>2</sup>Tel-Aviv University, Ramat Aviv, Israel

email: [sivan.almosnino@queensu.ca](mailto:sivan.almosnino@queensu.ca) web: <http://www.skhs.queensu.ca/ergbio/>

## INTRODUCTION

Muscle strength testing is regularly performed in medical, rehabilitative, occupational, and athletic settings. In these contexts, it is essential to determine the type and level of effort exerted by the participant during testing, as these may influence the values of outcome measures upon which decisions are based. In this respect, several factors have been identified that may inhibit maximal effort production during strength testing. These may include the presence of injury or pain; apprehension to perform due to fear of injury or pain; anxiety; low self-efficacy; lack of understanding regarding the importance of the test; and motivation of secondary financial gain [1]. In this latter factor, it is arguable that the intent of the produced effort is different than those obtained in the presence of the former limiting factors. That is, a purposeful attempt may be made to influence test results in a manner that deceives the examiner into concluding the existence of deficiencies in muscular force producing capabilities. Thus, a distinction needs to be made regarding identification of effort level (maximal or submaximal) and effort type (sincere or feigned).

The purpose of this investigation was to examine whether an analysis considering both a measure of isokinetic-based moment curve shape similarity, namely the cross correlation function (CC), and a measure quantifying curve magnitude differences (percent root mean square difference, %RMSD), enables the discrimination between types and levels of effort exerted during testing of the knee. Specifically, this investigation reports on the development of two prediction models utilizing the two aforementioned variables. The purpose of the first model is to establish a cutoff score for differentiating between maximal and submaximal or

feigned efforts. The second model is aimed at establishing a cutoff score for differentiating between effort types; namely between sincere (both maximal and submaximal efforts) and feigned efforts. Both models were subsequently validated using a different sample of participants.

## METHODS

For initial model development, healthy participants (n=37) performed 4 sets of 6 concentric knee extension-flexion repetitions on 2 testing occasions. The sets consisted of: 1) maximal effort; 2) self-perceived 75% of maximal effort; 3) self-perceived 50% of maximal effort, and; 4) a set attempting to feign injury.

Average CC and %RMSD values were computed between moment curves in each direction. Logistic regression was used to derive decision rules for differentiating between maximal and submaximal effort levels; and between sincere and feigned effort types. The cutoff was selected to achieve 100% specificity in the development sample. In other words, the cutoff score for the first model was set such that no maximal score would be classified as either submaximal or feigned. Conversely, the cutoff score for the second model was set such that no sincere maximal or submaximal effort was classified as feigned. As there is no guarantee that these decision rules will achieve 100% specificity in new or larger samples, Monte Carlo simulations were used to estimate the cutoff values required to achieve 99.0% and 99.9% specificity for predicting non-maximal efforts. These cutoffs were then applied to our development sample to obtain the corresponding sensitivities.

The models were subsequently validated using a different sample of 17 participants.

## RESULTS AND DISCUSSION

Figure 1 show exemplar moment curves obtained for maximal, submaximal, and feigned efforts. Readily observed is the within-set shape and magnitude consistency of curves obtained from maximal efforts in comparison to those obtained from all other efforts.

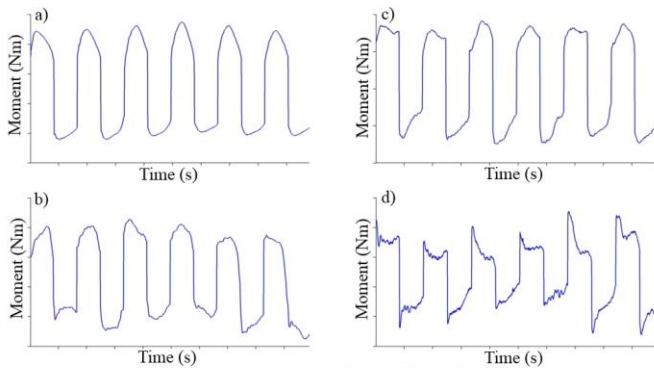


**Figure 1:** Exemplar scale adjusted moment-time curves obtained from a participant in the investigation: a) Maximal effort; b) 50% effort; c) 75% effort; d) Feigned effort.

Receiver operator characteristic curves of the two models are presented in Figure 2. From these models, we derived the decision rules presented in table 1. The first decision rule uses the cutoff required to maintain specificity at 100% within our development sample; the corresponding sensitivity is 96.4%. Using the cutoffs that resulted in decision rules with 99.0% and 99.9% specificity in our simulation study yielded 95.5% and 89.6% sensitivity in development sample, respectively. With respect to the results obtained using the 2<sup>nd</sup> model; at the cutoff value where none of the sincere maximal or submaximal scores are classified as feigned; the sensitivity is 31%.

Lastly, all efforts performed by scores obtained from the validation group were correctly classified as either being maximal or not, but 41% (7/17) of the feigned efforts were misclassified.

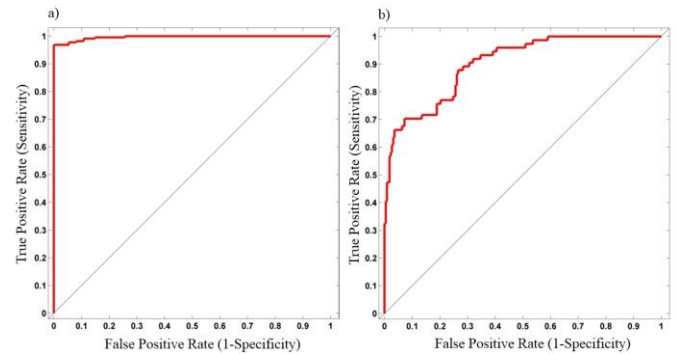


**Figure 2:** Receiver operating characteristics curves for: a) Model identifying submaximal effort, b) Model identifying feigned effort. Area under the curves (95% CI) equaled 0.996 (0.990 to 1.00) and 0.902 (0.853 to 0.949), respectively.

## CONCLUSIONS

This investigation reports upon the use of 2 novel predictor variables in the development and validation of model's meant for differentiating between knee isokinetic musculature effort types and levels. Using the models, clinicians may be able to ascertain, in healthy participants, whether maximal efforts were in fact produced. If this was not the case, evidence regarding the participant's intentions to purposefully attempt to influence test results may be gauged, although to a limited extent.

## REFERENCES

1.Dvir Z. *Isokinetics*, Churchill Livingstone, 2004.

**Table 1:** Performance of decision rules for differentiating between types and levels of effort. **Sn** = Sensitivity.

| # | Decision Rule  | Sn(%) | Number of misclassifications by effort level |      |       |       |         |
|---|--|-------|--|------|-------|-------|---------|
|   |  |       | Overall                                      | Max  | 50%   | 75%   | Feigned |
| 1 | Declare submaximal effort if:<br>67.9(CC) -1.02 (%RMSD) < 53.5 | 96.4  | 8/296  | 0/74 | 3/74  | 5/74  | 0/74    |
| 2 | Declare submaximal effort if:<br>67.9(CC) -1.02 (%RMSD) < 52.2 | 95.5  | 10/296                                       | 0/74 | 3/74  | 7/74  | 0/74    |
| 3 | Declare submaximal effort if:<br>67.9(CC) -1.02 (%RMSD) < 49.2 | 89.6  | 23/296                                       | 0/74 | 11/74 | 12/74 | 0/74    |
| 4 | Declare feigned effort if:<br>0.16(CC) -2.1(%RMSD) ≥ 5.87      | 31.1  | 51/296                                       | 0/74 | 0/74  | 0/74  | 51/74   |

# DO BAREFOOT RUNNERS DISPLAY MORE VARIABILITY IN FOOTSTRIKE MECHANICS THAN SHOD RUNNERS?

<sup>1</sup>Allison R. Altman, <sup>1,2</sup>Irene S. Davis

<sup>1</sup>Biomechanics & Movement Sciences, Physical Therapy, University of Delaware, Newark, DE, USA

<sup>2</sup>Spaulding National Running Center, Department of Physical Medicine and Rehabilitation, Harvard Medical School, Cambridge, MA, USA

email: [aaltman@udel.edu](mailto:aaltman@udel.edu)

## INTRODUCTION

Runners strike the ground thousands of times during a typical run. Excessive impact loading has been associated with several overuse injuries [1]. However, reduced variability in movement has also been hypothesized as a mechanism for overuse injuries [2]. Dynamical systems theory suggests that some degree of variability is evidence of healthy motor control [3]. In the case of running, the variability provided with each footstrike may protect the internal structures from becoming overloaded.

Barefoot running has recently grown in popularity. Barefoot runners often report a reduction of injuries following transition from shod running. These runners naturally adopt a forefoot strike pattern to protect their naked heel [4]. This has been shown to reduce impact loading that can be related to injury. It is also plausible that barefoot runners utilize increased variability with each footstrike due to the increased sensory feedback they receive from their bare feet. This variability may further protect them from injury.

The manner in which runners make initial contact with the ground plays an important role in the way the body is loaded. For example, rearfoot strikers with lower strike indices (SI) tend to have greater vertical instantaneous (VILR) and average (VALR) load rates. They also have greater dorsiflexion (DF@FS) and lower knee flexion angles at footstrike (KF@FS), reducing their potential for attenuating loads. A slight change in these variables with each footstrike will vary the load exposure to the body. This variability may be increased in barefoot runners due to the increased sensory input from their bare feet.

The purpose of this study was to compare the variability of footstrike mechanics between barefoot and shod runners. It was hypothesized that barefoot runners would have increased variability of SI, VILR, VALR, DF@FS, and KF@FS.

## METHODS

This is an ongoing study of which 12 healthy runners (6 shod and 6 barefoot) have been studied to date. Subject characteristics are presented in Table 1.

**Table 1:** Mean (SD) of subject characteristics. \* Indicates a moderate effect size, and \*\* indicates a high effect size.

|                      | <b>Shod</b>      | <b>Barefoot</b>  | <b>Effect</b> |
|----------------------|------------------|------------------|---------------|
|                      | <b>Mean (SD)</b> | <b>Mean (SD)</b> | <b>Size</b>   |
| <b>Male</b>          | 2                | 4                | <i>n/a</i>    |
| <b>Female</b>        | 4                | 2                | <i>n/a</i>    |
| <b>Height (m)</b>    | 1.75 (0.10)      | 1.78 (0.10)      | 0.4           |
| <b>Weight (kg)</b>   | 64.1 (13.6)      | 75.0 (6.8)       | 0.9**         |
| <b>MPW (mi)</b>      | 27.0 (21.2)      | 13.2 (2.2)       | 0.9**         |
| <b>Years Running</b> | 8.2 (4.8)        | 9.2 (11.0)       | 0.4           |

Prior to data collection, markers were placed on the right limb of each subject. Shod runners wore Nike Air Pegasus (Nike, Beaverton, OR) running shoes. Windows were cut into the back such that calcaneal markers could be placed directly on the heel and remain in view of the cameras.

Subjects ran across a force plate (Bertec, Columbus, OH) at 3.7 m/s until 10 good trials were collected. Data were collected using an 8 camera Vicon Nexus system (Vicon, Oxford, UK). Analog data were sampled at 1000 Hz, and marker data were sampled at 200 Hz.

Kinematic and kinetic data were processed using Visual 3D (C-Motion, Rockville, MD). SI was determined by locating the coordinate of the center of pressure along the long axis of the foot at the time of footstrike. It was then calculated as a percentage of foot length, with 0-33% = rearfoot strike, 34-66% = midfoot strike and >66% = forefoot strike. VALR and VILR were calculated based on the initial loading phase of the vertical ground reaction force curve [1].

Effect size (ES) was calculated to determine differences between the barefoot and shod groups. An ES greater than 0.1 was considered small, greater than 0.5 was considered moderate, and greater than 0.8 was considered high [5].

## RESULTS AND DISCUSSION

The means of the variables of interest in Table 2 correspond with the previous literature for barefoot and shod runners, indicating accurate representation of these groups [4,7].

SI was higher in the barefoot group indicating more of an anterior strike pattern (Table 2). Barefoot runners were also less dorsiflexed and in more knee flexion at footstrike than the shod runners, Both VILR and VALR were lower as expected for a forefoot strike pattern [4] (Table 2).

Variability of DF@FS and KF@FS were not different between groups. However, SI and VILR were greater barefoot group (Figure 1). VALR variability was greater as well, but demonstrated a small effect size.

Some degree of variability is considered protective against injury. In fact, it has been noted that injured individuals demonstrate reduced variability compared with healthy controls [2]. However, increased variability has also been associated with

less skilled movements. For example, trained runners have been shown to be less variable than untrained runners [6]. As the barefoot runners ran half the miles of the shod runners, their increased variability may be a result of being less trained. To address this issue, running mileage will be examined as a covariate once additional subjects are added.

**Table 2:** Comparison of footstrike variables. \* Indicates a moderate effect size, and \*\* indicates a high effect size.

|       | Shod  |        | Barefoot |        | Effect Size |
|-------|-------|--------|----------|--------|-------------|
|       | Mean  | (SD)   | Mean     | (SD)   |             |
| SI    | 32.6  | (22.9) | 64.9     | (10.8) | 1.3**       |
| VILR  | 90.3  | (23.2) | 70.9     | (34.3) | 0.6*        |
| VALR  | 81.9  | (20.6) | 55.4     | (31.8) | 1.0**       |
| DF@FS | 8.0   | (7.9)  | -1.2     | (3.6)  | 1.3**       |
| KF@FS | -12.7 | (3.0)  | -21.3    | (4.0)  | 1.5**       |

## CONCLUSIONS

These preliminary data suggest that barefoot runners demonstrate increased variability in some footstrike mechanics. This reduction, combined with reduced load rates, may be protective against overuse injuries in these runners.

## REFERENCES

1. Milner CE, et al. *MSSE* **38(2)**, 323-8, 2006.
2. Hamill J, et al. *Clin Biomech* **14**, 297-308, 1999.
3. Latash ML, et al. *Motor Control* **11(3)**, 276-308, 2007.
4. Lieberman DE et al. *Nature* **463(7280)**, 531-5, 2010.
5. Cohen J. *Psychol Bull* **112(1)**, 155-9, 1992.
6. Nakayama Y, et al. *Gait Post* **31**, 331-5, 2010.
7. Williams DS, et al. *J App Biomech* **16**, 210-8, 2000.

## ACKNOWLEDGEMENTS

NIH 1 S10 RR02239

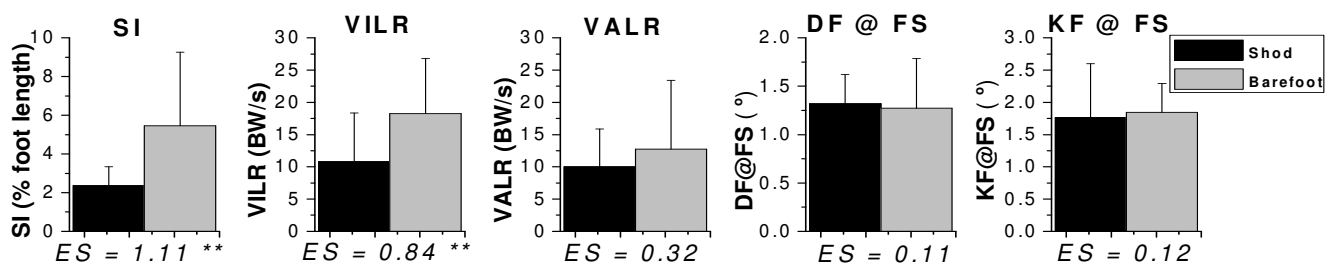


**Figure 1.** Variability of variables of interest in shod and barefoot runners. \* Indicates a moderate and \*\* a high effect size.

# AGE DIFFERENCES IN FEMORAL NECK STRAINS DURING GAIT

<sup>1</sup>Dennis Anderson and <sup>2</sup>Michael Madigan

<sup>1</sup>Beth Israel Deaconess Medical Center, Boston, MA, USA

<sup>2</sup>Virginia Polytechnic Institute and State University, Blacksburg, VA, USA

email: [danders7@bidmc.harvard.edu](mailto:danders7@bidmc.harvard.edu)

## INTRODUCTION

Hip fractures are serious injuries that increase greatly in incidence with age [1], and are associated with increased mortality in older adults [2]. Bone mineral density (BMD) is useful as a predictor of hip fracture risk, but the BMD of fracture patients overlaps that of age-matched individuals without hip fracture [2]. Thus, understanding additional factors that may contribute to hip fractures would be useful in risk evaluation and prevention. One possible factor is the dynamic loading experienced by the femur over extended period of time. This can stimulate remodeling and adaptation, which can strengthen or weaken bone, as well as play a role in the development of material fatigue.

Aging may cause changes in femoral loading and strains during gait, as older adults are known to exhibit differences in gait kinetics as compared to young adults (DeVita and Hortobagyi 2000). As gait is a routinely performed activity, age-related changes in strains in the proximal femur due to altered gait could contribute to bone adaptation or material fatigue in older adults, increasing the risk of hip fracture. Thus, the purpose of this study was to examine age differences in strains in the femoral neck during gait.

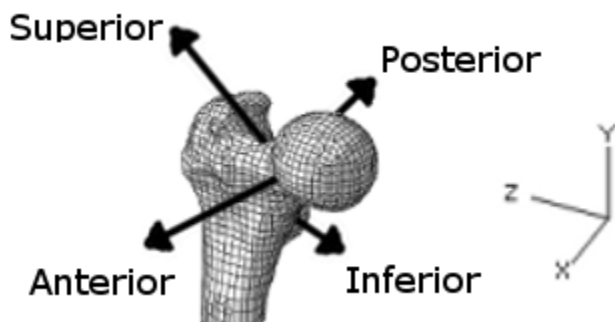


**Figure 1:** Proximal portion of femoral finite element model, indicating locations on the femoral neck where strains were examined.

## METHODS

Five younger (mean  $\pm$  standard deviation age 25.0 $\pm$ 4.3 years) and five older (79.4 $\pm$ 4.6 years) adults participated in gait trials, walking at 1.1 m/s with a step length of 0.65 m. The age groups were similar in that each contained two males and three females, and there were no significant differences in height or mass between groups. The study was approved by the IRB at Virginia Tech, and the participants provided informed consent prior to participation.

Muscle forces during gait were estimated with static optimization and a musculoskeletal model in OpenSim [4]. A finite element model was obtained from the public dataset of the VAKHUM project [5] and geometrically scaled to match the size of each participant. Estimated muscle forces and joint reaction forces were applied to the finite element model. Maximum principal (tensile), minimum principal (compressive) and maximum shear strains were determined at superior, anterior, inferior and posterior locations on the femoral neck (Figure 1). Peak strains occurred in early and late stance, corresponding to peaks in hip joint contact force (Figure 2), and were examined for age differences.

## RESULTS AND DISCUSSION

Peak strains in early and late stance are displayed in Table 1. The largest maximum principal strains occurred in the superior part of the neck in late stance, and the largest minimum principal and maximum shear strains occurred in the inferior part of the neck in late stance. No age differences were found for the largest magnitude shear or tensile strains. The only age differences in peak strains were found in the posterior femoral neck in late stance. Specifically, maximum principal strain was 33% lower, minimum principal strain was 36% lower, and maximum shear strain was 36% lower in

older adults. However, strain magnitudes were relatively low at this location compared to the largest strains.

Peak hip joint contact force magnitude was 18% lower in older adults, ( $435 \pm 51$  % body weight (BW) in older adults,  $529 \pm 39$  %BW in young adults,  $p=0.011$ ). In particular, the downward and posteriorly directed components of hip force were significantly reduced (Figure 2). Interestingly, despite the decrease in total joint contact force in older adults, there was not a corresponding reduction in the largest magnitude strains.

## CONCLUSIONS

Reduced hip contact forces in older adults during gait appear to reduce strains only on the posterior side of the femoral neck. Because the largest strains remain similar between age groups, it cannot be concluded that age differences in gait contribute to the risk of hip fracture in older adults. However, only gait was examined, and it remains possible that other activities may increase the risk of hip fracture by bone adaptation or material fatigue mechanisms.

## REFERENCES

1. Sugarman, JR, et al. *J Am Geriatr Soc* **50**, 1638-1643, 2002.
2. Marks, R, et al. *Ageing Res Rev* **2**, 57-93, 2003.
3. DeVita, P, et al. *J Appl Physiol* **88**, 1804-1811, 2000.

4. Delp, SL, et al. *IEEE Trans Biomed Eng* **54**, 1940-1950, 2007.

5. Van Sint Jan, S. *The VAKHUM Project*, accessed from <http://www.ulb.be/project/vakhum/>, 2008.

## ACKNOWLEDGEMENTS

This work was supported by Award Number F31AG030904 from the National Institute on Aging. The content is solely the responsibility of the authors and does not necessarily represent the official views of the National Institute on Aging or the National Institutes of Health.

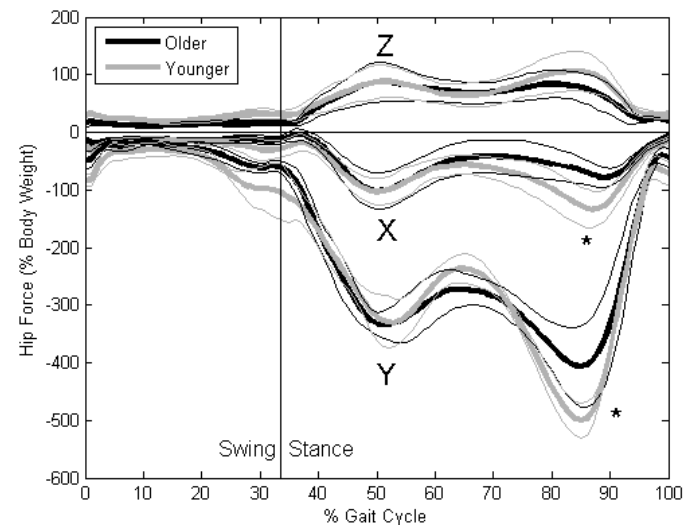


**Figure 2:** Average hip joint contact forces (%BW) in a femur-fixed coordinate frame during gait for young and older age groups. Thick lines indicate mean values, and the thin lines indicate  $\pm 1$  SD. The X axis points anteriorly, Y up, and Z laterally (see Figure 1). \*Significant age difference in peak force.

**Table 1: Mean (SD) values of peak strains ( $\mu\epsilon$ ) in the femoral neck during early stance and late stance.**

| Location  | Strain        | Early Stance |             | Late Stance  |             |
|-----------|---------------|--------------|-------------|--------------|-------------|
|           |               | Older        | Younger     | Older        | Younger     |
| Superior  | Max Principal | 1738 (446)   | 1571 (229)  | 2414 (784)   | 2624 (340)  |
|           | Min Principal | -549 (139)   | -493 (76)   | -774 (252)   | -831 (110)  |
|           | Max Shear     | 1145 (290)   | 1032 (153)  | 1594 (518)   | 1728 (225)  |
| Anterior  | Max Principal | 428 (189)    | 403 (174)   | 308 (110)    | 470 (184)   |
|           | Min Principal | -434 (81)    | -369 (60)   | -505 (159)   | -479 (59)   |
|           | Max Shear     | 426 (116)    | 380 (114)   | 385 (104)    | 462 (113)   |
| Inferior  | Max Principal | 812 (157)    | 742 (116)   | 1057 (300)   | 1140 (112)  |
|           | Min Principal | -2629 (503)  | -2404 (370) | -3392 (958)  | -3668 (354) |
|           | Max Shear     | 1720 (330)   | 1573 (243)  | 2224 (629)   | 2404 (233)  |
| Posterior | Max Principal | 525 (197)    | 501 (150)   | 414 (94)*    | 621 (154)   |
|           | Min Principal | -1420 (552)  | -1367 (436) | -1122 (281)* | -1746 (441) |
|           | Max Shear     | 972 (374)    | 934 (293)   | 758 (189)*   | 1184 (297)  |

\*Peak strain significantly smaller in older adults.

# ANTICIPATED WALKING TURNS IN PEOPLE WITH RECURRENT LOW BACK PAIN: A KINEMATIC STUDY

<sup>1</sup>Jo Armour Smith, <sup>2</sup>George Beneck and <sup>1</sup>Kornelia Kulig

<sup>1</sup>University of Southern California, Los Angeles, USA

<sup>2</sup>California State University, Long Beach, Los Angeles, USA

email: joannesm@usc.edu, web: <http://pt2.usc.edu/labs/mbrl/>

## INTRODUCTION

There is increasing evidence that optimal variability of relative motion between segments (inter-segmental coordination) is an important component of successful motor performance. Treadmill walking studies suggest that there is a decrease in variability of inter-segmental trunk coordination in the axial plane in persons with recurrent low back pain (RLBP) [1]. Walking turns are common functional activities that have greater mechanical demand than straight walking. In particular, turning using an ipsilateral pivot strategy requires greater trunk axial plane displacement and velocity than other turning strategies [2]. The purpose of this study was to compare the magnitude of inter-segmental trunk coordination variability between subjects with RLBP and matched healthy controls during an anticipated walking turn.

## METHODS

Four female subjects participated in this study (mean age 25.3 years). Two (RLBP1 & RLBP2) had a history of unilateral RLBP. They were matched in age, height, weight, and activity level by two healthy controls (CTRL1 & CTRL2). Both RLBP subjects were in symptom remission at the time of data collection. Subjects walked along a 6-meter walkway at a controlled velocity of  $1.5\text{m s}^{-1}$ . For the walking turns, subjects performed a  $90^\circ$  turn midway along the walkway and then continued walking perpendicular to the original direction. The use of an ipsilateral pivot strategy for the walking turns was ensured by defining the turn area with cones (Fig. 1.)

Each subject completed at least 3 successful straight walking trials and three turning trials in both directions. Successful turns were characterized by maintenance of correct approach speed and correct foot placement prior to and during the turn. Markers on the greater trochanters, sacrum, iliac crests, anterior superior iliac spines, sternum,

acromioclavicular joints and C7 were used to construct a two segment trunk model. Kinematics were collected at 250Hz using an 11 camera motion capture system (Qualisys AB, Gothenburg, Sweden). Angular displacement of the thorax and pelvis segments in the axial plane was calculated and each stride cycle was time-normalized to 101 points (Visual 3D software, C-Motion Inc, MD, USA). Gait events were identified using the vertical displacement trajectory of markers on the heels. The vector coding technique was used to quantify the coordination (relative motion) between the thoracic and pelvic segments for both the straight walking and walking turn trials. The variability of the coordination across repeated trials (angular deviation) was calculated using circular statistics (MATLAB, MathWorks, MA, USA) [3].

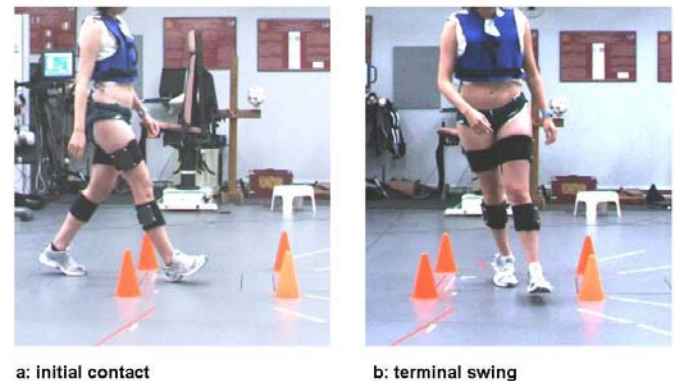


**Figure 1:** The ipsilateral pivot turn: a) ipsilateral initial contact; b) contralateral terminal swing phase

## RESULTS AND DISCUSSION

For clarity, all the data presented here are for turns to the right. Comparable results were seen for left turns. No relationship was observed between side of symptoms and direction of turn in the RLBP subjects. All data are for a complete stride (right foot initial contact to right foot initial contact). Duration of the stride cycle of the turn did not differ

between RLBP subjects and controls (Table 1). There was also no consistent difference in the amplitude of angular displacement of the thorax relative to the pelvis between RLBP subjects and controls either during straight walking or the walking turn (Table 1). This confirms evidence from treadmill walking studies that peak kinematics do not differ between subjects with RLBP and controls [1]. In all subjects, the magnitude of coordination variability was least during the ipsilateral (right) stance phase and greatest just prior to ipsilateral toe off and during the ipsilateral swing phase (Fig. 2). This increase in variability during ipsilateral swing may be a mechanism to adjust momentum and center of mass position during the recovery phase of the turn.

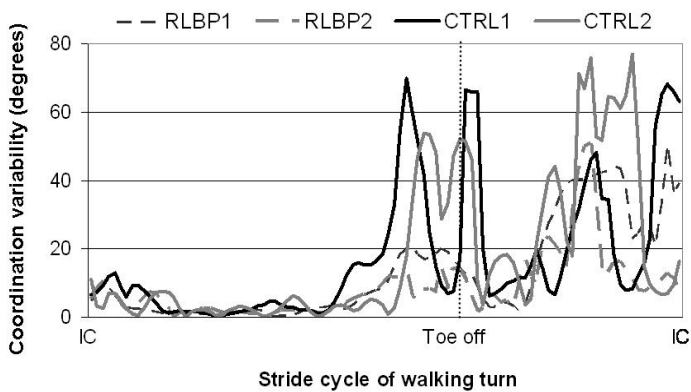


**Figure 2:** Coordination variability across the time-series of the turn stride cycle (IC = initial contact of the right foot, dotted vertical line indicates the average time of right toe off, n=4)

Coordination variability was greater in the controls than in the RLBP subjects during straight walking (Fig. 3: a). This difference was more pronounced in the walking turn (Fig 3: b). The analysis of coordination variability was more sensitive than the other kinematic analyses in detecting differences between groups.

**Table 1:** Mean (SD) kinematics for each study participant

|   | RLBP1        | RLBP2        | CTRL1        | CTRL2        |
|---|--------------|--------------|--------------|--------------|
| <b>Duration of turn stride cycle (s)</b>  | 1.16(0.04)   | 1.20(0.10)   | 1.09 (0.04)  | 1.22(0.03)   |
| <b>Straight walking: total amplitude of thorax axial plane displacement (degrees)</b> | 11.60 (0.57) | 10.84 (0.17) | 6.60 (1.75)  | 15.85 (1.92) |
| <b>Walking turn: total amplitude of thorax axial plane displacement (degrees)</b>     | 14.6 (1.32)  | 14.78(2.31)  | 13.20 (1.95) | 13.43(1.10)  |

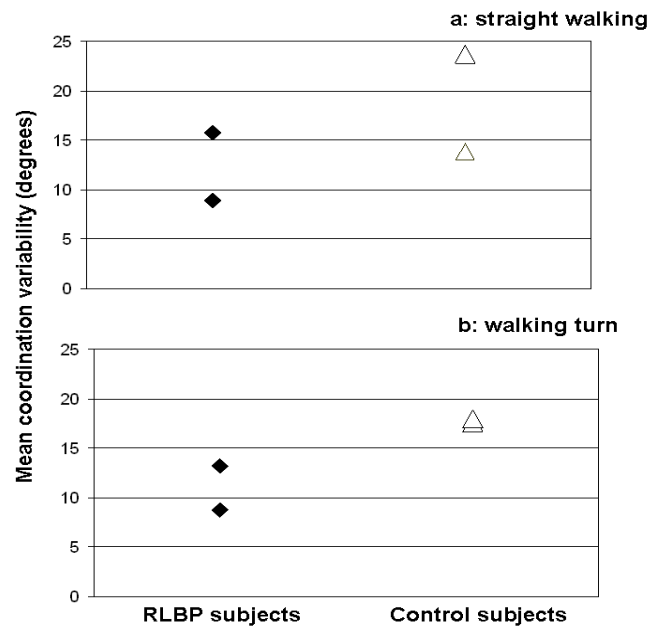


**Figure 3:** Mean coordination variability during a: straight walking, and b: the walking turn.

## CONCLUSIONS

This study is the first to investigate inter-segmental trunk coordination during a walking turn. In this small sample, persons with RLBP had decreased variability of inter-segmental trunk coordination in the axial plane during an anticipated walking turn. This suggests a persistent change in neuromuscular control in these subjects that can be observed between symptomatic episodes. The walking turn is a valuable paradigm for studying adaptations in neuromuscular control in persons with RLBP.

## REFERENCES

1. Lamoth, CJC et al. *European Spine Journal* **15**, 23-40, 2006.
2. Taylor, MJD, Dabnichki, P. & Strike, SC. *Human Movement Science* **24**, 558-573, 2005.
3. Hamill, J, Haddad, JM, McDermott, J. *Journal of Applied Biomechanics* **16**, 407-418, 2000.

# PREDICTING FRACTURE INITIATION, PROPAGATION AND DIVERSION IN LONG BONES UNDER IMPACT USING DRUCKER-PRAGER PLASTIC MODEL AND DAMAGE MODELING

Mike.W.J. Arun, Anoop Chawla and Sudipto Mukherjee  
Indian Institute of Technology, New Delhi, India  
email: [achawla@mech.iitd.ernet.in](mailto:achawla@mech.iitd.ernet.in) web: <http://web.iitd.ac.in/~achawla/>

## INTRODUCTION

For more than four decades, researchers around the world have been trying to decipher both the material and structural behavior of human bones. Many theories at the material level try to predict the quasi-static failure of bones. Even graves were dug to determine fracture patterns in long bones [1]. But, very few attempts have been made to study the fracture behavior of long bones under impact. The objective of this work is to determine the fracture initiation, propagation and diversion in long bones under impact. Drucker-Prager plastic model along with a damage model is used to simulate the fracture behavior. Results are compared with fractures observed in dynamic three-point bending tests on isolated humerus specimens.

## METHODS

Four isolated humeri were tested in three point bending with span width 174 mm in a drop tower setup until failure. The carriage of mass 30 kg, instrumented with a load cell was dropped from a height of 1.5 m. The load cell was sampled at 400 kHz using a digital storage oscilloscope. High speed cameras were used to record the fracture event at a frame rate 30,000 per second. Mesh for finite element simulation was prepared from CT scan data. Material property was assigned for the mesh based on [2]. For a computationally efficient FE model, the bone mesh in the mid-diaphysis where the impact occurs was refined to an average element size of 3.5 mm, whereas it had an average element size of 7mm elsewhere. It was observed that all four fractures were oblique in nature and were reproduced in the FE model using tensile dilatation cut-off stress criterion [3]. In one case, the fracture propagated at approximately 45° and changed direction of propagation when the crack tip approached the impact side. This fracture was not captured by the Von-Mises yield criterion.

An extended linear Drucker-Prager (D-P) plastic model was then used to capture the phenomenon due to the following reasons:

1. Unlike Von-Mises plastic model D-P model includes the effect of dilation of the material in yielding [4].
2. It allows modeling the asymmetry of yielding in tension and compression modes.
3. It is known to be a good predictor of inelastic shearing in porous materials.

In order to capture the initiation and progression of the crack, a strain based damage model which is a function of critical dilatational stress was used.

The calibration of the model parameters for the D-P model was done manually to match the fracture type. The calibrated values are i. Friction angle: 48°, ii. Flow stress ratio: 0.8 and iii. Dilation angle: 0°. The calibrated values are similar to that reported in [5].

## RESULTS AND DISCUSSION

Simulations were done in Abaqus/Explicit™ and the results are discussed below:

1. At the moment of impact, two distinctive zones were formed, one on the convex side of the bending (tension zone) and the other on the concave side of the bending (compression zone) by 0.05 ms (Fig 1.a).

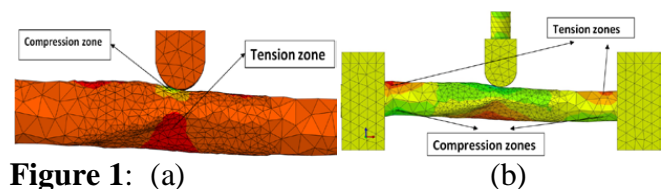
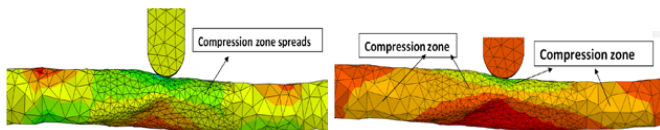


Figure 1: (a)

(b)

2. Additional tensile and compressive zones were formed as characteristic of the three point bending mode (Fig 1.b). Distance of these zones from the impactor location was approximately 70 mm.



**Figure 2:** (a)

(b)

3. It was observed that the compression zone which was originally concentrated in the vicinity of the impactor spreads further at 0.08 ms (Fig 2.a).

4. By the onset of failure at about 0.39 ms, the compression zone expands further to about 70 mm either side of the impact vector (Fig 2.b).

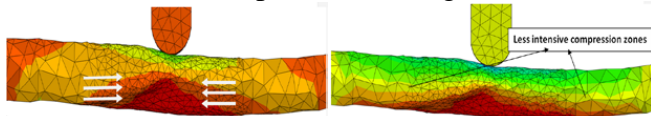


**Figure 3:** (a)

(b)

5. This compression zone may act to resist the failure of elements in the tensile zone (Fig 3.a).

6. The size and magnitude of the compression zone was observed to be a function of impact speed. Fig 3.b shows the state of stress just before failure of the same model with an impact speed of 2.5 m/s. It is observed that the spread of the compression zone is small when compared with an impact speed of 4.4 m/s.

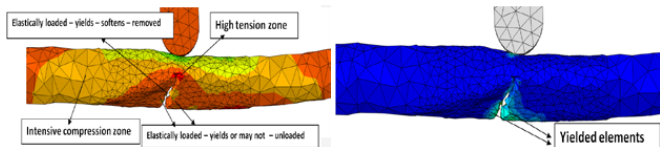


**Figure 4:** (a)

(b)

7. The stiffness of the element deemed to have failed is degraded using a linear evolution law and eventually removed from the mesh. The elements in the fracture line are seen to be first elastically loaded in tension, they then yield, soften and are removed. On the other hand, the elements near but not on the fracture line are elastically loaded, they may or may not yield and are finally unloaded (Fig 4).

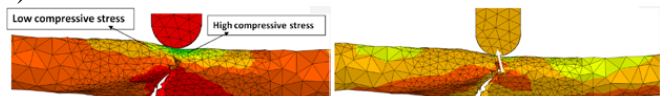


**Figure 5:** (a)

(b)

8. The elements at the crack tip are always loaded in tension (Fig 4.a). If the crack tip elements are loaded only in tension then in principle the crack should progress vertically.

It can be argued that the size of the compression zone on either side of the impact vector plays a vital role in deciding the path of fracture progression. In the 4.4 m/s impact case the left hand side compression zone dominates, which was decided based on the magnitude and spread of compressive

stresses in these elements. The magnitude of compressive stresses varies between 25 – 130 Mpa on the left hand side zone while on the right hand zone had compressive stresses in the range of 18 – 80 Mpa. In addition to this, volume of material with compressive stress is more on the left hand side. Therefore these compressive forces resist the tensile forces at the crack tip.

Due to this phenomenon a complex and triaxial state of stress exists in the crack tip. Therefore the crack path takes the least resistive plane which is the plane of maximum shear stress which is approximately 45 degrees.

As the crack tip nears the vicinity of impact where a high state of compressive stress is present (Fig 5.a), the right side zone dominates. The progression of the fracture is resisted by this high compression zone as bone is stronger in compression, thereby diverting the path towards the left hand side (Fig 5.a).

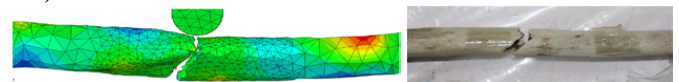


**Figure 6:** (a)

(b)

9. This phenomenon may be justified by considering the 2.5 m/s impact case, where the compressive forces are much lower than the 4.4 m/s case (Fig 3.b). In this case tensile stresses dominate at the crack tip and the fracture was observed to progress 90 degrees to the horizontal. However the fracture initiation point remains the same as in the 4.4 m/s case.

10. Fig 6 shows the comparison between the fracture obtained between simulation and experiment.

## REFERENCES

1. Burrell, L., M. Maas, and D. Van Gerven, *Patterns of long-bone fracture in two nubian cemeteries*. Human Evolution, 1986. **1(6)**: p. 495-506.
2. Schileo, E., et al., *An accurate estimation of bone density improves the accuracy of subject-specific finite element models*. Journal of Biomechanics, 2008. **41(11)**: p. 2483-2491.
3. Chawla, A., S. Mukherjee, and M. Arun. *Predicting fractures in human bones under impact*. in *6th World congress of biomechanics*. 2010. Singapore.
4. Currey, J.D. and K. Brear, *Tensile yield in bone*. Calcified Tissue International, 1974. **15(1)**: p. 173-179.
5. Mullins, L.P., M.S. Bruzzi, and P.E. McHugh, *Calibration of a constitutive model for the post-yield behaviour of cortical bone*. Journal of the Mechanical Behavior of Biomedical Materials, 2009. **2(5)**: p. 460-470.

# BIOMECHANICAL CONSTRAINTS ON COORDINATION IN CHILDREN AND ADULTS

<sup>1</sup>Michael J. Asmussen, <sup>1</sup>Eryk Przysucha, and <sup>1</sup>Carlos Zerpa

<sup>1</sup>Lakehead University, Thunder Bay, ON, CAN  
email: [mjasmuss@lakeheadu.ca](mailto:mjasmuss@lakeheadu.ca)

## INTRODUCTION

Bernstein [1], along with other accomplishments, introduced the seemingly straightforward problem of motor redundancy. Despite kinematic and muscular redundancy, humans tend to exhibit the same movement pattern under similar task constraints. At the intra-limb level, biomechanical constraints represent a prominent factor that the CNS has to account for when planning an action. Bernstein hypothesized that to perform smooth and effective actions, muscular torque must contribute to or oppose interaction torque rather than “fight” or fail to account for its effects on joint movement. Interaction torque is comprised of centripetal, Coriolis, and inertial torque and is produced in all multi-joint actions. It has been shown that the ability to optimally modulate interaction torque represents an important constraint on coordination. Developmental research has focused on how infants modulate/compensate for interaction torques [2], however, relatively little is known about how older children modulate/compensate interaction torques, and at what age torque modulation becomes adult-like. As a result, the purpose of this research was to examine if children and adults exhibit similar torque modulation strategies and coordination patterns during a one-handed interceptive catching task.

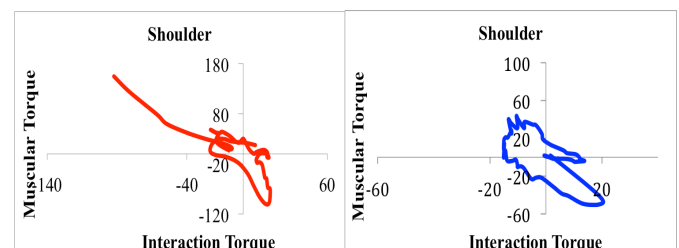
## METHODS

Five children, between the ages of 9 and 12, and five adults, between the ages of 18 and 30, completed the one-handed catching task. Each participant attempted to catch 10 balls that were ejected from a tennis ball machine. The ball travelled to the participant from 9m away at 7m/s (horizontal velocity). A 2D kinematic analysis was completed on the catching action using Vicon Motus. Passive reflective markers were placed on the superior aspect of the iliac crest in line with the

shoulder, one inch below the acromion, lateral epicondyle, styloid process, and distal end of the fifth metacarpal of the participant’s catching arm. In addition, anthropometric data of the catching arm was gathered to estimate the moment of inertia, center of mass (CoM), and CoM location of the upper arm, forearm, and wrist [3].

The 2D kinematic analysis allowed the researcher to examine the nature of coordination between the two groups. Coordination was inferred by the degree (mean) and stability (standard deviation) of correlation coefficients between angular displacements of the shoulder-elbow and elbow-wrist joint pairs. The angular displacement, velocity, and acceleration along with the anthropometric data was used to determine the nature of net, interaction (INT), and muscular (MUS) torque produced at the shoulder, elbow, and wrist. These torques were calculated in 2D using the equation for a planar three link chain presented in past literature [3]. The MUS and INT torque were plotted against each other to determine the relationship between these torques at the shoulder, elbow and wrist pairings. These plots were used to determine if differences in MUS and INT torque relations coincided with differences in coordination patterns. Lastly, movement functionality was examined by comparing the percentage of balls caught between groups. Since there was a small sample size only descriptive statistics were used to analyze the data.

## RESULTS AND DISCUSSION



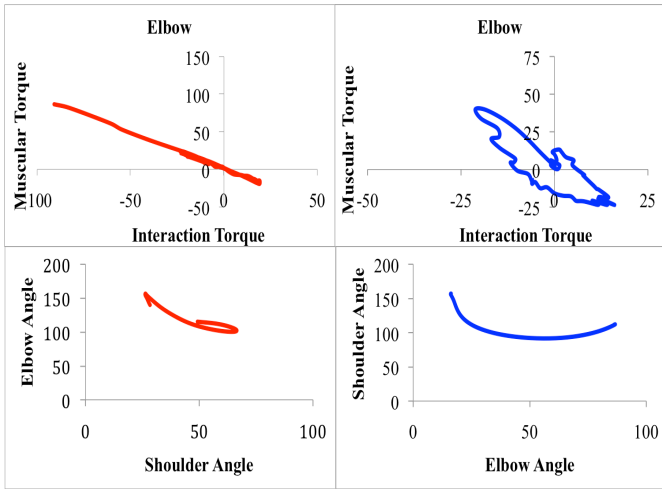


**Figure 1:** Muscular/interaction torque profiles and angle-angle plots. The graphs on the left (red line) represent the typical performance by the adults, while the graphs on the right (blue line) represent the typical performance by the children. The torque profiles (top four) are expressed in Nm ('+' = flexion, '-' = extension) and the angle-angle plots are in degrees. (Note: the torque scales were reduced for the children because they had lower moment of inertias for each segment)

As evident from Table 1, there were differences in the mean correlation coefficient of the shoulder and elbow relations between the adults and children. This difference was also seen at the elbow and wrist pairing because on average the adults had higher correlations compared to the children. This result shows that the adult group exhibited a higher degree of coordination at the shoulder-elbow and elbow-wrist pairing meaning that this sample of children and adults did not organize their actions in the same manner. In terms of variation across trials, the adults had a lower standard deviation at the shoulder-elbow pairing compared to the children, however, both groups had similar variability at the elbow-wrist pairing. This result shows that the children have yet to develop a stable coordination pattern between the shoulder and elbow joint, but the elbow-wrist relations suggest that adults and children have similar stability when organizing this joint pair. It could be that, given the constraints of this task, children develop a stable coordinative structure between the elbow and wrist, before the shoulder and elbow.

**Table 1:** Correlation coefficients of the shoulder-elbow and elbow-wrist joint angular displacements.

| Joint Pair     | Degree (mean, $r$ ) |          | Stability (standard deviation, $r$ ) |          |
|----------------|---------------------|----------|--------------------------------------|----------|
|                | Adults              | Children | Adults                               | Children |
| Shoulder-elbow | 0.85                | 0.57     | 0.06                                 | 0.17     |
| Elbow-wrist    | 0.77                | 0.61     | 0.21                                 | 0.26     |

With regards to torque modulation, the adults showed a strong relationship between MUS and INT torque at both the shoulder and elbow joint that resulted in a high correlation coefficient between shoulder and elbow angular displacement (**Figure 1, left column**). The children, however, exhibited a weaker relationship between MUS and INT torque and consequently, a lower correlation between shoulder and elbow angular displacement (**Figure 1, right column**). The graphs representing the shoulder and elbow relations were also consistent with the elbow-wrist pairing (not shown). These results indicate that the CNS' ability to account for INT torques, or failure to do so, could be an underlying constraint on the degree of coordination expressed at a given joint pair.

Since there were differences in coordination and underlying torque modulation strategies, movement functionality was examined. The adults performed better than the children during the one-handed catch (90% vs. 50% of balls caught) illustrating that, aside from differences in coordination, torque modulation could also be a factor contributing to movement effectiveness. From the information presented, it was concluded that children between the ages of 9 and 12 have yet to develop an "adult-like" torque modulation strategy that accounts for INT torques during multi-joint actions. The children's strategy produced qualitatively different movement patterns (coordination) than that of the adults; as a result, the children had less functional actions during the one-handed catch. This study should be repeated with a different task that does not require a grasp component.

## REFERENCES

1. Bernstein, N. *Co-ordination and regulation of movement*. Pergamon Press, 1967.
2. Zernicke, RF. et al. *Child Development* **4**, 982-1004, 1993.
3. Zatsiorsky, VM. *Kinetics of Human Motion*. Human Kinetics, 2002.

# COMPARISON OF FIVE HEADLESS SCREWS FOR FIXATION OF SMALL BONES

<sup>1</sup>Soroush Assari, <sup>1</sup>Kurosh Darvish and <sup>2</sup>Asif M. Ilyas

<sup>1</sup>Temple University, Philadelphia, PA, USA

<sup>2</sup>Jefferson University Hospital, Philadelphia, PA, USA

email: [kdarvish@temple.edu](mailto:kdarvish@temple.edu) web: [www.temple.edu/engineering/research/labs/tbl](http://www.temple.edu/engineering/research/labs/tbl)

## INTRODUCTION

Headless screws are favored for internal fixation in the treatment of displaced or unstable small bone (e.g., Scaphoid) fractures, because they are embedded below the articular surface of the bone, reducing tissue irritation and immobilization. Compression plays an important role in fracture stability, maintaining gap reduction and also accelerating the healing of cancellous bone [1]. There are several types of screws being used in practice and it is of clinical interest to know how different they are in generating and maintaining the compression force.

Several studies have investigated the compressive forces of headless screws [2,3]. However, little attention has been paid to the fastening torque and the effect of pre-drilling. This study compares the generated compression force and fastening torque and the effect of pre-drilling during the insertion of five frequently used headless compression screws that are typically used for scaphoid fixation.

## MATERIAL AND METHODS

Five cannulated headless bone screws, Herbert-Whipple (Zimmer, Inc.), Mini-Acutrak 2 (Acumed®), Kompressor Mini (Kompressor™), HCS 3.00mm (Synthes) and 3.2mm Twinfix (Stryker®) with nominal size of 3x24 mm were used in this study. Previous studies have shown that the density and elastic modulus of the scaphoid cancellous bone are highly variable and affect the maximum achievable compression [3]. Therefore, in this study solid rigid polyurethane foam (Sawbones®, 0.16 g/cm<sup>3</sup>), commonly used as a cancellous bone surrogate material [2,3], was chosen to make 50 identical bone models. To simulate a 30mm scaphoid with a transverse fracture in the middle, the bone models were cut into two 15mm-thick pieces. The setup was made such that both bone models could freely move along four rods which transferred the fastening torque to a torque cell (QWFK-8M, Sensotec®) (Fig. 1). A washer load cell (LC8200, Omegadyne, Inc.) was placed between the two Sawbones parts to measure the generated compression force. All the screws were applied according to their technical instruction. However, in order to study the risk of loss of

compression due to over-fastening, the fastening continued until compression did not change any more. Since all the screws in this study are self-cutting, in order to study the effect of pre-drilling, the screws were tested once with the suggested pre-drilling method and once without pre-drilling.

For each screw, the maximum generated compression, the stage at which it was generated and the fastening torque at that stage were compared using the Student's *t* Test in JMP software (SAS Institute Inc.). Two-way ANOVA was used to compare the maximum compression between screw types and the effect of pre-drilling method on its magnitude.  $p < 0.05$  was considered significant.

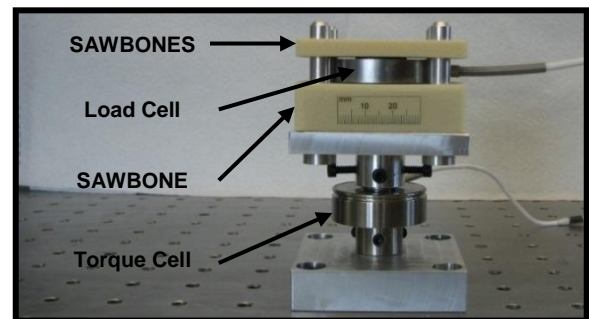


Figure 1: Experimental setup

## RESULTS

**Mini-Acutrak 2 (Acumed)** - The compression generated by Mini-Acutrak 2 and the fastening torque gradually increased with each turn until the compression reached 4.63 kgf (Fig. 2). The generated force did not change by over-fastening. The achieved compression without pre-drilling was higher (5.00 kgf) but was not significantly different. However, the fastening torque at the same stage increased by 87%.

**Twinfix (Stryker)** - Unlike the Mini-Acutrak, the maximum achievable compression was generated immediately after a quarter to half a turn after unlocking the second stage of screwdriver and it reached 3.13 kgf. There was a high risk of loss of compression up to 42% by advancing a quarter of turn more. Without pre-drilling there was no significant increase in the maximum generated force, but the fastening torque increased by 73%.

**Kompressor Mini** - Although the generated compression trend was similar to Twinfix, the compression gradually reached the maximum level of 2.12 kgf one turn after compression stage started, and the compression loss due to more turns was 24%. The fastening torque increased with decreasing of compression due to over-fastening (Fig. 3). Without pre-drilling the maximum compression was 17% higher and there was no significant increase in the fastening torque.

**HCS 3mm (Synthes)** - The maximum achievable compression using Synthes screw was 1.76 kgf which was not significantly different from the without pre-drilling method (1.8 kgf). There was 67% increase in fastening torque without pre-drilling. Over-fastening of the screw did not change the generated compression in both methods.

**Herbet-Whipple** - This screw generated the least compression force equal to 1.37 kgf and it did not change significantly without pre-drilling (1.03 kgf). Unlike the other screws, the self-cutting did not work well without pre-drilling and it was needed to apply extra 2 kgf axial load on the screw to make more advance, which caused 129% increase in fastening torque.

## DISCUSSION

In this study solid rigid polyurethane foam was used as substitution to human cancellous bone to achieve more consistent statistical results. Pre-drilling did not have a significant effect on the average maximum generated compression, although it significantly increased the fastening torque for all the screws except Kompressor Mini. Mini-Acutrak 2 generated the maximum compression and showed the most reliability and sustainability of the generated compression and no risk of losing compression due to over-fastening was observed. This is because of its conical and variable pitch design. Twinfix and Kompressor Mini, contrary to other screws, have a rotating head which generates most of the compression. Twinfix had the second highest generated compression, 31% more than Kompressor Mini which might be the result of its larger thread size. However, since the head of Twinfix is axially fixed, it showed a higher risk of losing compression (Fig. 3). The maximum generated compression by Mini-Acutrak 2 (Acumed), Herbert-Whipple (Zimmer) and HCS 3mm (Synthes) presented in this study are in agreement with results reported in other studies [2,3] and there was no report in the literature on Kompressor Mini and the fastening torques of either screws.

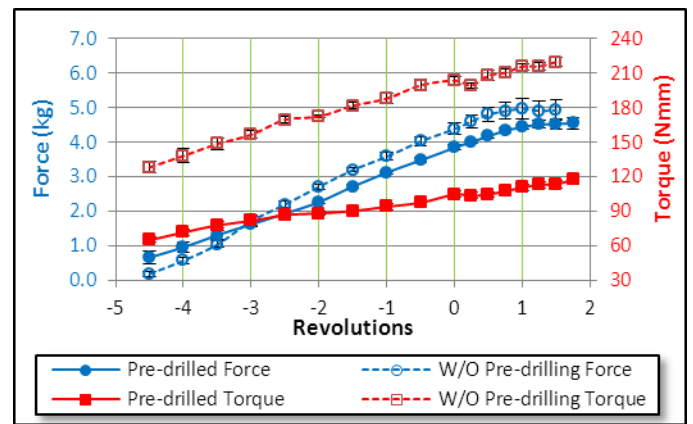


**Figure 2:** Mini-Acutrak 2 (Acumed) results

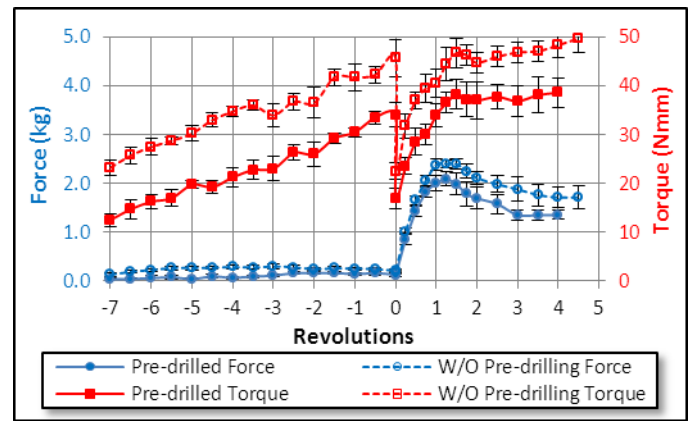


**Figure 4:** Kompressor Mini results

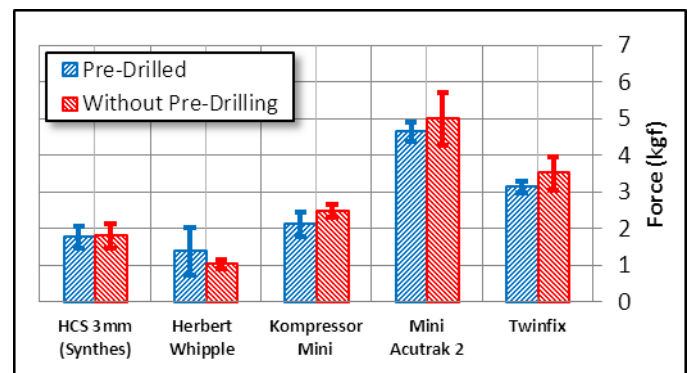


**Figure 3:** Comparison of generated compression.

## REFERENCES

1. Aro HT, Chao EY. "Bone healing patterns affected by loading, fracture fragment stability, fracture type and fracture site compression" *Clin Orthop*, 1993
2. Hausmann JT, et al. "Interfragmentary compression forces of scaphoid screws in a sawbone cylinder model" *Injury*, 2007
3. Adla DN, Kitsis C, "Compression forces generated by Mini bone screws, a comparative study done on bone model" *Injury*, 2005

# KNEE ANGLE-SPASTIC GRACILIS MUSCLE FORCE RELATIONSHIP MEASURED INTRAOPERATIVELY SHOWS NO ABNORMAL MUSCULAR MECHANICS

<sup>1</sup>Filiz Ateş, <sup>1</sup>Oya Aytürk, <sup>2</sup>Yener Temelli and <sup>1</sup>Can A. Yucesoy

<sup>1</sup>Boğaziçi University, Biomedical Eng. Institute, Istanbul, Turkey

<sup>2</sup>Istanbul University, Istanbul Medical School, Istanbul, Turkey

email: [filiz.ates@boun.edu.tr](mailto:filiz.ates@boun.edu.tr) web: <http://www.bme.boun.edu.tr/biomechanics>

## INTRODUCTION

For improved understanding of human muscle functioning, direct measurement of joint angle-muscle force relationship is necessary. However, access to human muscle is limited. Therefore, direct measurements of human muscle forces [e.g., 1-2] are rarely done. The goal of the present study was to measure previously unstudied isometric forces of activated human spastic G muscle as a function of knee joint angle, intraoperatively.

## METHODS

Surgical and experimental procedures [for full details see 3], in strict agreement with the guidelines of Helsinki declaration were approved by a Committee on Ethics of Human Experimentation at Istanbul University, Istanbul. Seven subjects (four male and three female: mean age  $8 \pm 4.6$ ) diagnosed with spastic diplegic cerebral palsy participated. Knee angle-G muscle force data (n=10) were collected intraoperatively (three patients were operated bilaterally) during muscle lengthening surgery after routine incisions to reach the distal G tendon and before any other surgical procedures. Subjects were under general anesthesia and no muscle relaxants or tourniquet was used. Intraoperative experiments were performed. A buckle force transducer (S shape, width, length and height equaling respectively 12, 20 and 9 mm, TEKNOFIL, Turkey) was mounted over the tendon.

Isometric spastic G muscle force was measured at various knee joint angles: from  $120^\circ$  (knee joint at maximal experimentally attainable flexion, as limited by the surgery table) to  $0^\circ$  (full knee extension) with  $30^\circ$  increments. The knee angle as well as the hip angle (to  $0^\circ$  both in the sagittal and frontal planes) was fixed.

A pair of gel-filled skin electrodes (EL501, BIOPAC Systems, CA, USA) were placed on the skin, over G muscle belly. Using a custom made constant current high voltage source (cccVBioS, TEKNOFIL, Istanbul, Turkey) the muscle was stimulated supramaximally (transcutaneous electrical stimulation with a bipolar rectangular signal, 160 mA, 50Hz). After each contraction, the muscle was allowed to recover for 2 minutes at flexed knee posture.

## RESULTS AND DISCUSSION

Peak spastic G muscle forces show a sizable variability: mean peak force =  $41.02 \pm 41.18$  N. No significant correlations were found between peak spastic G muscle force and thigh length ( $27.5 \pm 5.4$  cm) or mid-thigh perimeter ( $32.3 \pm 8.8$  cm): Spearman's rank correlation coefficient equals -0.09 and -0.06, respectively. Therefore, due to inter-subject variability, patient specific planning of remedial surgery may be necessary.

Our results indicate that spastic G muscle is not operating within a narrow length range (Figure 1): (1) For none of the knee angles studied, spastic G muscle was at active slack length showing that this length corresponds to a knee flexion over  $120^\circ$ . Remarkably, (2) 80% of the entire set of data points collected represents muscle forces exerted at muscle lengths corresponding to optimum knee angle or lower: (i) for four of the limbs experimented (IV, VII, VIII, and X), the muscle was active entirely in the ascending limb of its knee joint angle-muscle force characteristics. (ii) For the remainder six, operational range of this curve consisted of parts of both ascending and descending limbs nevertheless, with the exception of V, majority of data points were still in the ascending limb.

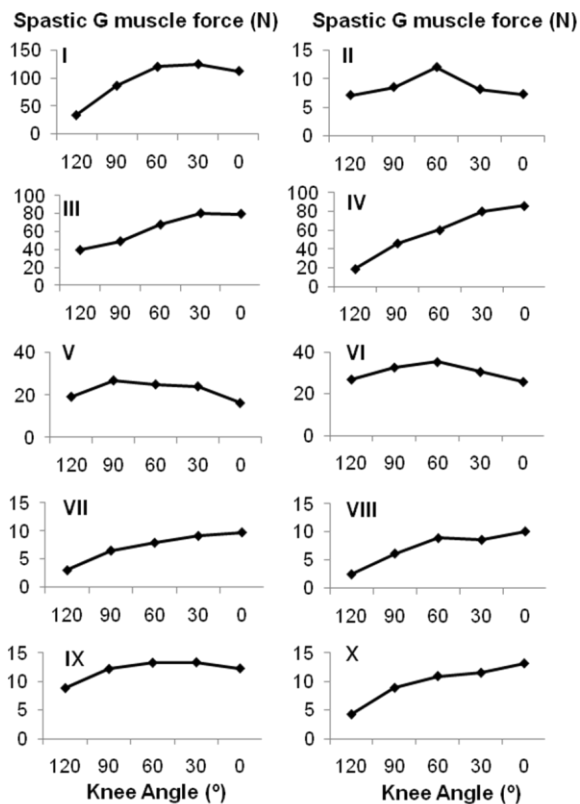


**Figure 1:** Isometric muscle knee angle-force characteristics.

Our present results show that knee angle-spastic G muscle force characteristics are not representative of the pathological condition occurring at the joint and are comparable qualitatively to those measured intra-operatively from healthy subjects in our previous study [3]. The activity of spastic G muscle predominantly in the ascending limb indicates that the greatest resistance of this muscle to knee extension is available only at higher muscle lengths (optimal knee angle equals  $30.0^{\circ} \pm 31.6^{\circ}$ ), attainable closer to full knee extension. This contradicts with an expectation that spastic muscle is a source of high forces causing the apparent movement limitation at the joint. Accordingly, Huijing [4] posed the question “what could be the origin of high forces within the spastic paretic limb?” He suggested that the mechanism should involve epimuscular myofascial force transmission [for a review of key concepts see 5]. After eliminating the synergistic muscles as a plausible source (they are also at low lengths and therefore, should not be capable of exerting very high forces) Huijing developed an hypothesis that high forces within the spastic paretic limb may originate from the antagonistic muscles at lengths favorable for higher force exertion: forces generated within

sarcomeres of antagonistic muscles can be exerted at the distal tendons of a target muscle due to epimuscular myofascial force transmission [e.g., 6].

An important difference of the present experimental conditions to those *in vivo*, is that the target G muscle was activated solely. This suggests in agreement with Huijing’s hypothesis that movement limitation apparent at the joint may originate from an abnormal system of muscular and myofascial structures instead of individually abnormal muscle. New studies are indicated to test the role of epimuscular myofascial force transmission under conditions of simultaneous simulation of antagonistic knee extensor muscle with G muscle.

## CONCLUSIONS

Isometric knee angle-force characteristics of spastic G muscle stimulated alone appears “normal”: G muscle operates within a fairly wide length range of active force exertion and more importantly higher muscle forces are exerted only at higher muscle lengths corresponding to a more extended knee. In agreement with Huijing’s recent hypothesis, lack of epimuscular myofascial force transmission from antagonistic muscles may explain such normal mechanics of spastic G muscle.

## REFERENCES

1. Komi P et al., *Clin Sports Med*, **11**, 521-531, 1992.
2. Smeulders MJ, et al., *Muscle Nerve*, **32**, 208-215, 2005.
3. Yucesoy CA, et al., *J Biomech*, **43**, 2665-2671, 2010.
4. Huijing PA, *J Electromyogr Kinesiol*, **17**, 708-724, 2007.
5. Yucesoy CA, *Exercise Sport Sci R* **38**, 128-134, 2010.
6. Yucesoy CA, et al. *J Electromyogr Kinesiol*, **20**, 118-26, 2010.

## ACKNOWLEDGEMENTS

This work was supported by (1) Bogazici University Research Fund under grant 09HX101D and (2) The Turkish Academy of Sciences (TÜBA) under Distinguished Young Scientist Award to Can A. Yucesoy.

# Effect of Task Constraints on Limb Stabilization During Human Locomotion

Arick Auyang, Young-Hui Chang

Comparative Neuromechanics Lab, School of Applied Physiology, GeorgiaTech, Atlanta, GA, USA

Email: arick.auyang@gmail.com

<http://www.ap.gatech.edu/chang/CNLmission.html>

## INTRODUCTION

Humans can stably locomote in the real world while being constantly subjected to multiple task constraints. The goal of this study was to investigate how stabilization of task level variables leg length and leg orientation changes when presented with locomotor task constraints. Our previous study showed that leg length and leg orientation are task level performance variables that are stabilized through the structuring of segment angle variance during human hopping in place [1]. We also found that as subjects hopped at non-preferred frequencies, there was an increase in the structuring of variance to stabilize leg length [1]. We determined the amount of task variable stabilization by quantifying the Goal-Equivalent Variance (GEV) and Non-Goal Equivalent Variance (NGEV) components of leg segment angle variance using an Uncontrolled Manifold approach [1,2]. The purpose of this study was two-fold. First, to determine if applying a leg orientation constraint through requiring accurate foot placement would elicit an increase in leg orientation stabilization. The second purpose is to determine how stabilization of leg length and leg orientation is affected when both variables are simultaneously constrained by both an accurate foot placement constraint and a toe clearance constraint.

Subjects hopped in place into a square target projected onto the ground. Three target sizes were used to vary task difficulty according to Fitts' Law. We reasoned that decreasing target size should increase the need for leg orientation stabilization, as small errors in leg orientation during the small target task would lead to subjects hopping outside of the target. We hypothesized that as target size decreases, leg orientation stabilization should increase.

To constrain both leg length and leg orientation, we again constrained foot placement using different size targets, but this time during a forward hopping task on a treadmill. During hopping in place, leg length is stabilized during mid-stance while leg

orientation is stabilized during mid-aerial phase [1]. The swing phase of forward locomotion has the added constraint of toe clearance. Consequently, we expect to see stabilization of both leg length and leg orientation in the aerial phase. With smaller targets during forward hopping, we hypothesized that leg orientation stabilization would increase due to the smaller targets while leg length stabilization sees no effect from changes in target size.

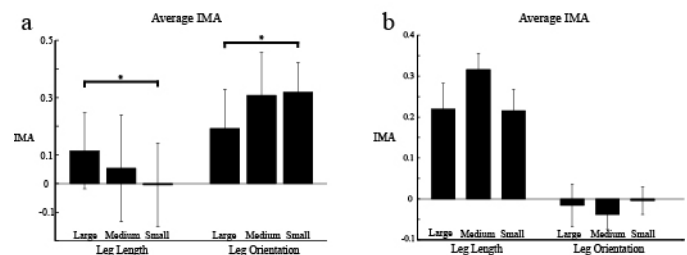


**Fig. 1.** Index of Motor Abundance (IMA) for leg length and leg orientation averaged across hop cycle during (a) hopping in place with three target conditions and (b) forward hopping with three target conditions. \* denotes where IMA was significantly different than 0 ( $p < 0.01$ ).

## METHODS

Eleven subjects hopped in place and forward on a treadmill moving at 0.8 m/s on their dominant leg at 2.2Hz into three different targets (88, 213, and 466mm<sup>2</sup>). 3-D lower body kinematics data were collected (VICON). Target sizes were determined using Fitts' Law which describes a relationship between the distance traveled by the end effector and the target size. Sagittal plane segment angles were calculated using Matlab. An Uncontrolled Manifold (UCM) analysis was performed for each performance variable (leg orientation and leg length) at 1% bins over the entire hopping cycle for all hops (~180 hops per condition). The UCM analysis quantified the amount of kinematic motor redundancy used to stabilize either performance variables leg length or orientation [1,2,3]. The Index of motor abundance was calculated as the difference

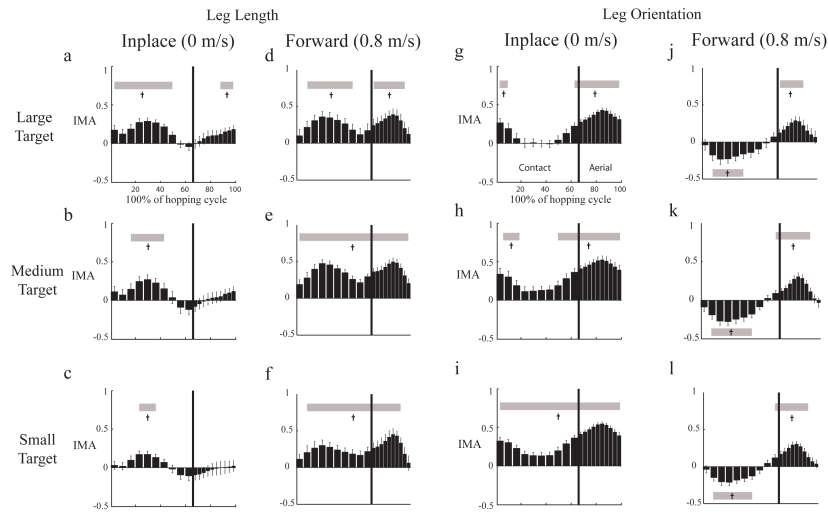


**Fig. 2.** (a-f) Leg length IMA and (g-l) leg orientation IMA for hopping in place and forward hopping across targets. Grey bars above bins denotes bins are significantly greater than zero. Grey bars below bins denotes bins are significantly less than zero.

between GEV and NGEV divided by the sum of GEV and NGEV  $((GEV-NGEV)/(GEV+NGEV))$ . We calculated the IMA at each time point to test whether subjects selectively utilized motor redundancy in the joints to stabilize each performance variable, indicated by an IMA greater than 0. IMA results were further binned into each 10% of the hopping cycle.

## RESULTS

Mean leg orientation stabilization across the entire hopping cycle increased and mean leg length stabilization decreased as target size decreased during hopping in place (**Fig. 1a**). There were no changes in mean leg orientation or leg length stabilization during forward hopping (**Fig. 1b**). Peak leg orientation stabilization was in aerial phase for both hopping in place and forward hopping and all target conditions (**Fig. 2g-l**). Leg length stabilization had a peak at midstance during hopping conditions (**Fig. 2a-f**) and a second peak in swing phase during forward hopping (**Fig. 2d-f**).

## DISCUSSION

The purpose of this study was to investigate the effects of specific constraints on task level performance variables. As we hypothesized, we found that as the target landing area got smaller during hopping in place, the subjects responded by increasing overall stabilization of leg orientation (**Fig. 1a**). This is consistent with the leg length stabilization changes we previously observed when an appropriate leg length constraint was placed on

the task [1]. This suggests that when a constraint is placed on a task critical performance variable, there is increased structuring of kinematic variance to stabilize the appropriate performance variable.

The second purpose of our study was to determine how stabilization of leg length and leg orientation would change when simultaneously constrained through a toe clearance and accurate foot placement constraint. In forward locomotion, the importance of toe clearance requires that leg length also be stabilized during swing phase along with the typical leg orientation stabilization (**Fig. 2d**). With smaller targets during forward hopping, there was no change in leg length or leg orientation IMA. Further analysis reveals that the solution spaces for leg length and leg orientation stabilization are orthogonal to each other. While leg length and leg orientation can be individually stabilized when only one variable is critical to the task, when both need to be stabilized during the aerial phase of forward hopping, variance is appropriately structured to stabilize both leg length or leg orientation. Motor redundancy is maximized when task variables are stabilized only when necessary. This redundancy is then available to respond when additional task constraints are presented, such as with unexpected obstacles or even with neuromuscular injury.

## REFERENCES

1. Auyang A, Yen J, and Chang Y.H. (2009). *Exp Brain Res.* 192, 253-64.
2. Yen J, Auyang A, and Chang Y.H. (2009). *Exp Brain Res.*

# ERGONOMIC APPLICATION OF HAND MODEL: TENDON EXCURSION

Sungchan Bae and Thomas Armstrong

University of Michigan, Ann Arbor, MI, USA  
email: scbae@umich.edu

## INTRODUCTION

Previous studies have shown that tendon loads and excursions in the wrist are associated with the risk of work-related musculoskeletal disorders (WMSDs) of the upper extremities [1-4]. In addition to the wrist, tendon excursions are also caused by finger motion. This study investigates the possible contribution of finger motions to tendon excursions and chronic injuries in the hand.

## METHODS

Bae et al. [5] proposed a model for describing finger motion based on object size and orientation. Hand postures at three specific points (i.e., initial, maximum open, final) are predicted for pinching cylindrical objects by using the empirical model. Those hand postures are adjusted if the object is non-cylindrical shape or the task is power-grip, and then they are transformed into continuous joint angle profiles as a function of time using the finger motion model. The resulting model can be used to predict hand postures and finger motions for each element of a work cycle (e.g., reach, grasp, move), from which tendon excursions at finger joints are calculated using the relationship between hand posture and tendon movement [6]. The cumulative tendon excursions (CTE) are computed to indicate the total distance that each tendon travels, which is then normalized by time to consider a repetition level of a job.

Latko et al. [4] classified jobs based on experts' repetition rating (high, middle, low repetition level). Choi [2] used time-based analysis to calculate normalized CTEs of the flexor digitorum profundus (FDP) and the flexor digitorum superficialis (FDS) tendons at the wrist for those jobs and showed that higher-risk jobs cause greater tendon movement, which can raise the risk of the WMSDs. In this study, we reexamined three jobs (one for each

repetition level) to obtain necessary information about finger motion. For example, time study of the high repetition job presents work elements and their corresponding duration for one cycle (Table 1). One job cycle consists of reaching for and grasping a handle, moving and positioning it for machining, followed by moving it back to release for another cycle. The video analyses provide clues for assumptions needed for finger motion analysis, such as work object size and shape and cycle time ( ).

**Table 1:** Time study of handle assembly job (high repetition) with joint angle predictions of the index finger and corresponding CTEs for one cycle.

| Time | Work Element | $\Delta t$ | Index finger joint angles ( $^{\circ}$ ) |      |      | CTE (mm) |      |
|------|--------------|------------|--|------|------|----------|------|
|      |              |            | MCP                                      | PIP  | DIP  | FDP      | FDS  |
| 0.00 | Reach        | 0.10       | 46.6                                     | 26.1 | 12.0 | 0        | 0    |
| 0.10 | Grasp        | 0.03       | 38.1                                     | 17.9 | 8.0  | 3.5      | 3.1  |
| 0.13 | Move         | 0.24       | 60.9                                     | 21.9 | 14.6 | 10.0     | 9.3  |
| 0.37 | Position     | 0.20       | 60.9                                     | 21.9 | 14.6 | 10.0     | 9.3  |
| 0.57 | Move         | 0.46       | 60.9                                     | 21.9 | 14.6 | 10.0     | 9.3  |
| 1.03 | Release      | 0.14       | 46.6                                     | 26.1 | 12.0 | 14.1     | 13.3 |
| 1.17 | Finish       |            |  |      |      |          |      |

**Table 2:** Summary of assumptions for each job.

| Assumption                        | Handle assembly (high-level)                 | Isostatic machine (mid-level)                                   | Torwegge (low-level)  |
|-----------------------------------|--|---|---|
| Worker                            | 50% Male                                     | 50% Female  | 50% Male  |
| Work object condition             | A cylinder (D=3cm) in horizontal orientation | A cylinder (D=2cm) in horizontal orientation                    | A rectangle (D=3cm) in horizontal orientation               |
| Task                              | Pulp pinch                                   | Pulp pinch  | Pulp pinch  |
| Total time of one cycle (sec)     | 1.17   | 6.77  | 14.78   |
| Duration of work elements (units) | Reach/Grasp (1)<br>Move (7)<br>Release (1)   | Reach/Grasp1 (1)<br>Reach/Grasp2 (1)<br>Move (6)<br>Release (2) | Reach/Grasp (3)<br>Move/Wait (9)<br>Push (1)<br>Release (2) |

## RESULTS AND DISCUSSION

The predicted index finger joint angles for one cycle of a high repetition level job is shown in Figure 1A.

Based on joint angle predictions, tendon excursions of the FDP and FDS tendons at the finger joints (MCP, PIP, DIP) are calculated using the relationship between hand posture and tendon movement [6]. Then, the CTE for each finger joint is computed by integrating absolute values of tendon excursion rate over time to obtain the tendon travel distance and is summed over each finger joint (Table 1); for example, the FDP and FDS tendons of the index finger travels 14.1 and 13.3mm, respectively, for one cycle of high repetition job (Figure 1B). These results are normalized by a cycle time, which generates the normalized CTE of 43.5 and 41.0 m/hr for the FDP and FDS tendons, respectively. Similar procedures are used to estimate tendon excursion for the other two jobs of low and middle level repetitions.

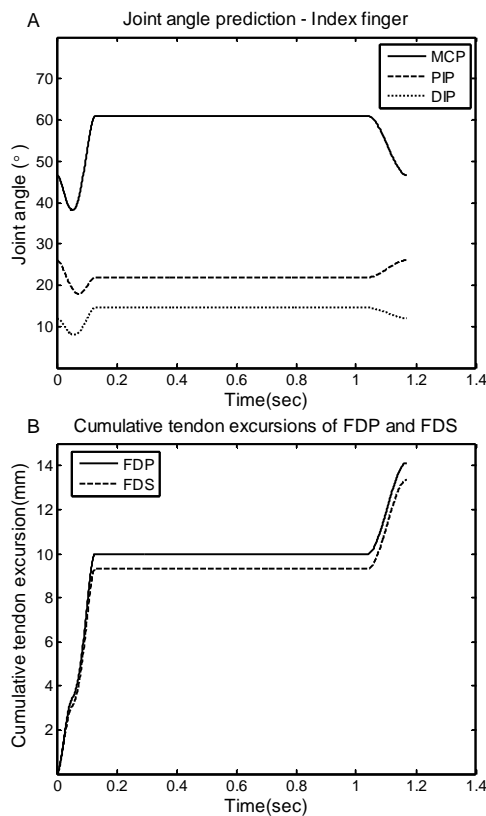


**Figure 1:** (A) Index finger joint angle prediction during reach/grasp, movement, and release for high repetition job, (B) CTEs of the FDP and FDS tendon of the index finger.

Figure 2 presents normalized CTEs of the FDP and FDS tendons at the wrist [2] and at the index finger obtained from the current study. The finger joints generate the normalized CTEs from 41 to 101% of the wrist, to which the MCP joints contribute the most (62 to 81%). When the normalized CTEs at

the finger joints are added to those at the wrist, the difference between three repetition levels becomes even more significant; for the FDP tendon, the difference is 43.4 and 25.6 m/hr between high and middle levels and between middle and low levels, respectively, compared to 14.7 and 17.4 m/hr when only the wrist is considered; for the FDS tendon, the difference is 45.1 and 27.7 m/hr, compared to 21.1 and 24.3 m/hr. The total CTEs are comparable to the previous study [3], in which 18.6 m/hr was observed for low repetition jobs, whereas 71.5 m/hr observed for high repetition jobs.

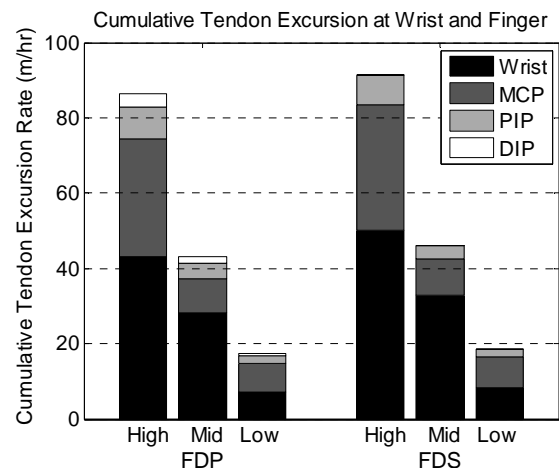


**Figure 2:** CTEs of FDP and FDS tendons at the wrist and the index finger joints – MCP, PIP, DIP – for three jobs of different repetition levels.

## CONCLUSIONS

Finger motion, particularly the MCP joints, contributes nearly as much as the wrist to tendon excursions in the wrist. Tendon excursions due to the fingers and the wrist should be included in future studies of chronic tendon injuries in the wrist.

## REFERENCES

1. Marras WS, et al. *Ergonomics* **36**, 341-351, 1993.
2. Choi J. *Ph.D Dissertation*, University of Michigan, 2008.
3. Moore A, et al. *Ergonomics* **34**, 1433-1453, 1991.
4. Latko WA, et al. *Am J Ind Med* **36**, 248-259, 1999.
5. Bae S, et al. *Int J Ind Ergonomics* **41**, 79-89, 2011.
6. Armstrong TJ, et al. *J Biomech* **11**, 119-128, 1978.

# PEAK TIMES OF MUSCLE ACTIVITIES DURING LANDING FROM ROTATIONS JUMP

<sup>1</sup>Daisuke Bai , <sup>1</sup>Kenji Kasubuchi , <sup>1</sup>Mitsunori Tokuda and <sup>2</sup>Takahiko Fukumoto

<sup>1</sup>Heisei Memorial Hospital, Nara, JPN

<sup>2</sup>University of Kio, Nara, JPN

## INTRODUCTION

Anterior cruciate ligament (ACL) injury is a common and traumatic knee injury. The female athletes have more a risk of the ACL injury. A majority of these injuries are non-contact, many of which occur in response to a cutting maneuver or during an uncontrolled landing from a jump. Therefore, appropriate alignment maintenance during landing from a jump appears pertinent to reducing ACL injury. It is known well that neuromuscular controls lead to prevent ACL injury. Recently it is paid attention that preactivity helps the limits of neuromuscular controls. Underlying the ability of the hamstrings to decrease tibial anterior shear is the time of firing in comparison with the quadriceps. This timing may be aided by neural programming during a planned or expected activity. Most studies have reported landing from a vertical jump or a drop jump but few studies have reported landing from a rotation jump. The purpose of this study was to investigate the peak times of the muscle activities of the hamstrings and quadriceps during about landing from 360 degrees rotations jump.

## METHODS

The subject was eleven healthy female university students (mean age;  $19.8 \pm 1.0$  years, weight;  $50.2 \pm 2.6$  kg, tall;  $157.1 \pm 3.9$  cm). The subject was to jump one right-handed rotation. The subject was instructed to fold their arms across their chest, to land as naturally as possible with both feet on the landing platform and to keep about 2 seconds with landing posture. The electromyography (EMG) signals of the following muscles were determined simultaneously on the left leg of all individuals: the vastus medialis (VM), the vastus lateralis (VL), the semimembranosus (SM) and biceps femoris (BF). EMG activity was captured by an EMG system (SX230; Biometrics Ltd. UK). The sampling

frequency of the EMG was 2000Hz. For this subject, the ground reaction forces generated during landing from rotation jump were recorded using a force platform (MA8000; ANIMA Corp. Japan). These data were measured at the times of initial foot-ground contact(IC). The sampling frequency of the force platform was 125 Hz. We used the data of 0.2 seconds intervals before and after IC.

## RESULTS AND DISCUSSION

The peak mean times of the muscle activities of the hamstrings (BF and SM) resulted in significantly earlier than the quadriceps (VM and VL). There is no significant difference between BF and SM and between VM and VL (Fig. 1).

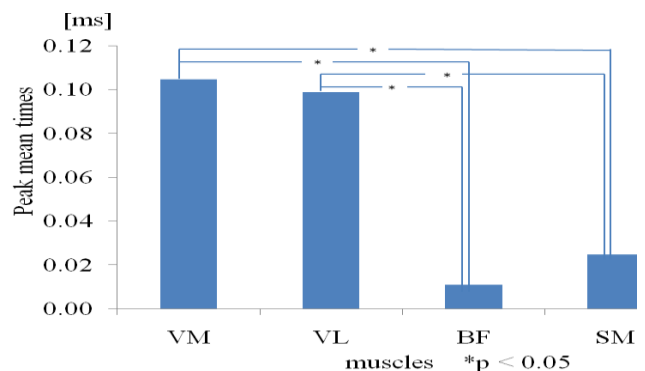


**Figure 1:** The peak mean times of muscle activities

Past researches were reported that preactivities of hamstrings were recorded before IC. And peak muscle activities of hamstrings occurred before IC, whereas peak muscle activities of quadriceps occurred after IC. However, peak muscle activities of hamstrings were recorded after IC in this subject. Rotation jump is more difficult than vertical jump or drop jump. Generally speaking, muscle preactivity is influenced on visual information. This subject may be not so much relied on the visual information. And, it was not possible to expect landing posture because rotation jump is not always

done. So this result is suggested to delay the peak muscle activities of hamstrings.

Even if the rotation stress joins knee joint, there is no significant difference between BF and SM and between VL and VM. The activities of VM and SM lead to internal rotation against the femur as for the tibia and VL and BF lead to external rotation. This result is suggested that the rotation stress is reduced by the activities of BF and SM at the same time. So this result is suggested to prevent the greater knee valgus positions.

## CONCLUSIONS

This subject was 360 degrees rotations jump however the muscle activities of hamstrings and quadriceps were showed the same results that were reported landing from a vertical jump or a drop jump. The peak times of the muscle activities of hamstrings are earlier than the quadriceps during

landing from rotation jump. It is known well that the muscle activities of hamstrings lead to posterior movement of tibia and reduce ACL injury. This result of generating earlier onset times of the antagonistic quadriceps muscles is suggested to lead the greater knee flexion and the more inferior knee valgus. Increased muscle activity before and after IC is important for stabilization. We will report the relationship between the timing of the muscle activities and knee angles during rotation jump.

## REFERENCES

1. Richard G, et al. *Journal of Athletic Training* 34, 115-120, 1999.
2. E J Cowling, et al. *Br J Sports Med* 37, 126-130, 2003.
3. Hewett TE, et al. *AM J Sports Med* 33, 492-501, 2005.

# AN IMPROVED METHOD FOR QUANTIFYING THE STIFFNESS OF RUNNING SHOES

<sup>1</sup>Marjorie Ballun, <sup>2</sup>Bruce Williams, <sup>1</sup>Craig M. Goehler, <sup>1</sup>Kathleen Sevener  
<sup>1</sup>Department of Mechanical Engineering, Valparaiso University, Valparaiso, IN, USA  
<sup>2</sup>Breakthrough Podiatry, Merrillville, IN, USA  
email: kathleen.sevener@valpo.edu

## INTRODUCTION

A running shoe aims to protect a runner's foot from injury by stabilizing motion and cushioning impact. As material technology and product testing develop, shoes can offer more protection through advanced designs. A typical test for running shoes is a flexion test in which the shoe is bent through a fixed angle and the applied force is measured. A popular method for flexion testing consists of bending a shoe that has been fixed such that bending occurs at a particular point in the shoe, usually the forefoot, and then determining the stiffness in that region from the measured force [1,2,3]. While this method provides one measure of shoe stiffness, the method characterizes stiffness over a limited portion of the shoe. In actual use, a running shoe bends over a much larger area during a typical footstep. An improved test would permit shoe bending, and the determination of stiffness, for different sections of the shoe.

The goal of this study is to develop an improved flexion test for evaluating and quantifying the stiffness of running shoes in both the forefoot and mid-foot sections. The results generated with the new test method will be used to better evaluate shoe design and to assess shoe performance for injury prevention. This paper describes the experimental setup and method for the improved test, and also discusses the preliminary data collected for two different shoe architectures.

## METHODS

To facilitate the measurement of shoe flexion at various locations, an apparatus was designed so that the distance between the loading actuator and the shoe fixture column is adjustable (Fig. 1). This distance is adjusted by sliding the apparatus base within the test frame. This adjustability allows testing a range of shoe sizes and allows for a custom bend length. The apparatus also features interchangeable supports, mounted to the shoe

fixture column, that offer a flexible length inner support in the shoe (Fig. 2).



**Figure 1:** Testing rig with adjustable base and experimental setup in the MTS machine

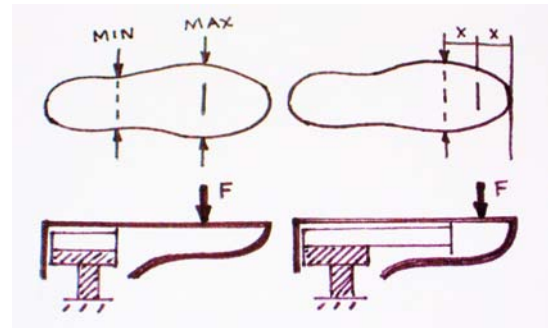


**Figure 2:** Diagram of shoe inserts, bend locations (dotted line), and force application points (solid line)

A cushioned shoe and a stability shoe, with a noticeable tactile difference in stiffness, were chosen for evaluation with the new apparatus in order to determine if the method could be used to quantify the difference in stiffness. Two regions of each shoe sole were tested: the mid-foot, located at the narrowest part of the shoe, and the forefoot, located at the widest part. To keep bend lengths proportional to the shoe size, the actuator was positioned on the forefoot line for the mid-foot test and at a distance halfway from the bend zone to the end of the shoe for the forefoot test.

For the flexion test, the apparatus was mounted in an MTS Q-Test 150 load frame and the shoes were clamped to the shoe fixture column (Fig. 1) For each test, the supports in the shoe extended far enough to keep part of the shoe rigid, and allow it to bend in the desired location. The actuator was positioned at the appropriate bend location and then lowered at a rate of 1 inch per minute until each shoe had been bent to an angle of at least 15 deg. The applied force and actuator displacement were recorded and used for calculating the stiffness. After the desired flexion was achieved, the actuator was raised and load was removed.

Oleson et al. defined stiffness as “the ratio of ground reaction moment to the angular deflection” of the shoe, producing a quantity with the units of lbf-in/deg [3]. Following Oleson’s method, the ground reaction moment was calculated by multiplying the true bend length ( $d_2$ ) by the true force (Fig. 3). The true force was found using the applied force and bend geometry ( $y$  and  $d_1$ ). The stiffness is plotted versus the bend angle and a value was selected based on where the curves leveled off.

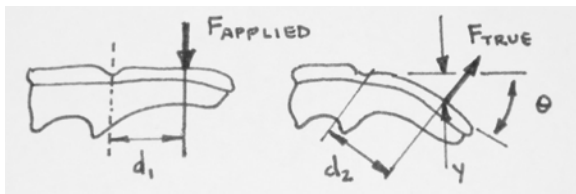


**Figure 3:** Bend geometry of tested shoes

## RESULTS AND DISCUSSION

Figure 4 illustrates the calculated stiffness of both shoes in the mid-foot and forefoot sections. The stability shoe exhibits a higher stiffness than the cushioned shoe in both sections. The cushioned shoe had a measured stiffness of 2.5 lbf-in/deg in the midsole and 0.5 lbf-in/deg in the forefoot while the stability shoe had values of 6 lbf-in/deg and 1.2 lbf-in/deg, respectively.

The stiffness was higher in the stability shoe, regardless of where the bending occurred, supporting the tactile difference that was noticed during shoe selection. A trend seen in both bend locations is that the stability shoe resists the applied force longer, presenting a delayed flex, as shown by the curve leveling off at a higher bend angle. Another interesting outcome of this test is that both

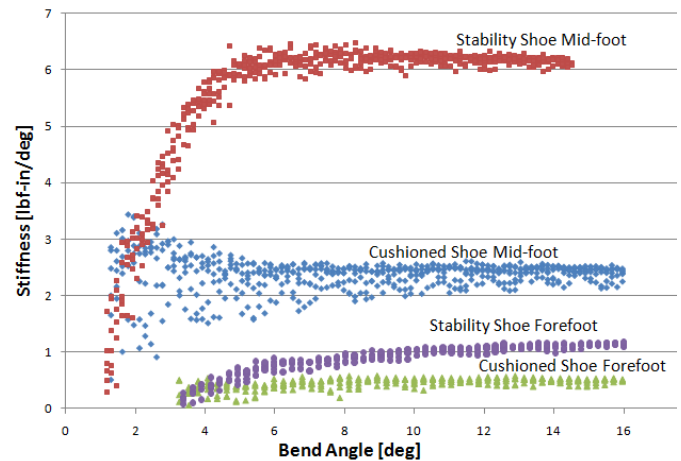


**Figure 4:** Comparison of stiffness vs. bend angle in the midfoot and forefoot sections of a stability shoe and a flexible shoe

shoes differ in stiffness amounts, yet both have a mid-foot / forefoot stiffness ratio of 5.0. Further testing may demonstrate that a certain ratio is a favorable design factor in shoes. Oleson et al. measured values of forefoot stiffness in the range of about 0.8 to 1.7 lbf-in/deg while data from this study range from 0.5 to 1.2 lbf-in/deg, showing that the test concepts remain consistent [3].

The initial results obtained with this new apparatus indicate that shoe stiffness is a function of both the shoe architecture and the location of measurement. Since there is a measurable difference in the stiffness values in the forefoot and mid-foot regions of the shoe, future work will focus on determining the optimal locations for testing to determine the most appropriate measure of shoe stiffness. Eventually, this information will be correlated with impact forces exerted on a foot during the gait cycle to examine the influence of shoe design on injury prevention.

## REFERENCES

1. Cheskin, M., Fredericksen, R. *Podiatry Management* **24**, 107-118, 2005.
2. Drez, D. *The American Journal of Sports Medicine* **8**, 140-141, 1980.
3. Oleson, M. et al. *Journal of Biomechanics* **38**, 1886–1894, 2005.

# Investigating in-vivo motion of the medial longitudinal arch with different orthotic types using lateral fluoroscopy images during dynamic gait

<sup>1</sup>Megan Balsdon, <sup>1</sup>Kristen Bushey, <sup>2</sup>Colin Dombroski and <sup>1,3</sup>Tom Jenkyn

<sup>1</sup>Dept. of Mechanical and Materials Engineering, Faculty of Engineering, The University of Western Ontario, London, ON, Canada

<sup>2</sup>Sole Science, Fowler Kennedy Sports Clinic, The University of Western, Ontario

<sup>3</sup>School of Kinesiology, Faculty of Health Sciences, The University of Western Ontario  
email: mbalsdon@uwo.ca

## INTRODUCTION

Foot orthotics are commonly prescribed as a conservative treatment for many musculoskeletal disorders such as pes cavus and pes planus. It is commonly thought that they mechanically change the positions and motions of the foot bones by applying forces or constraint to the plantar surface. Although there are many studies using fluoroscopic imaging to evaluate the movement of the bones of the medial column of the foot during functional activity [1], there has yet to be a study of the affect of foot orthotics on the physiologically loaded foot.

The motion of the bones of the medial longitudinal arch (MLA) has been examined in static weight bearing conditions. However, these analyses were limited from providing information regarding its dynamic function during gait. Elongation of the arch has been noted to correspond with ground reaction peaks during stance phase of walking. The shortening of the MLA coincided with increased flexor muscle activity [1] during stance. The use of orthotics may change this motion during stance phase, by constraining and supporting the bones of the medial column and limiting the elongation of the arch with loading.

X-ray fluoroscopy has recently been demonstrated to be a feasible method for measuring foot bone motions during in-vivo weight bearing gait [2]. To the authors' knowledge, a fluoroscopic study of the foot during orthotic use has not yet been done. In this study, x-ray fluoroscopy is used to compare the medial longitudinal arch during orthotic use. Four conditions were tested: barefoot walking, soft and rigid orthotic walking and proprioceptive feedback influenced walking during weight bearing gait. It

was hypothesized that the lowest arch would occur during barefoot walking, and the highest during walking with the rigid orthotic.

## METHODS

Eighteen volunteers (6 controls, 6 with diagnosed pes cavus, and 6 pes planus) were fitted for custom-made orthotics by a Canadian Certified Pedorthist using the foam box technique with plastazote (soft) and subortholen (firm) material as per usual clinical practice. Each volunteer walked along a custom-made wooden platform that raised their feet to the height of a single fluoroscope (SIREMOBIL Compact-L; Siemens, Malvern, PA). On the platform, each volunteer was able to walk normally and fully weight bearing past the fluoroscope. The left foot was imaged during stance phase from a sagittal plane view.

Volunteers were first instructed to stand in quiet, full weight bearing double limb stance and a static weight bearing image was taken of the left foot. The volunteers were then instructed to walk along the platform past the fluoroscope at their preferred pace, placing their left foot in the view with the heel aligned with a mark on the platform. The fluoroscope recorded moving images at 30 frames per second. Each trial condition was repeated twice, ensuring that the entire hindfoot, tarsus and first metatarsal were visible at all times. There were four conditions tested: 1) barefoot, 2) shoed with a soft custom-made orthotic, 3) shoed with a rigid custom-made orthotic and 4) shoed with a proprioceptive feedback-type orthotic (PFO, Barefoot Science; Mississauga, ON, Canada). The two custom-made orthoses were constructed with an aggressive support for the medial longitudinal arch.

The PFO device had a soft dimple under the middle of the plantar surface of the foot.

The fluoroscopic images were digitized in the control PC and stored as mpeg format. Each frame was post-processed using custom-written software (Matlab; Mathworks Inc., Natick, MA). In each image two landmarks were identified on the plantar aspect of the calcaneus, at the most posterior and anterior corners (Figure 1). These landmarks were then connected with a line. A line running along the dorsal aspect of the first metatarsal was then identified and the angle between these two lines were determined (Figure 1). This calcaneal-first metatarsal angle (CFMA) defined the convexity of the medial longitudinal arch as described in Murley [3]. A smaller angle indicated a higher arch.

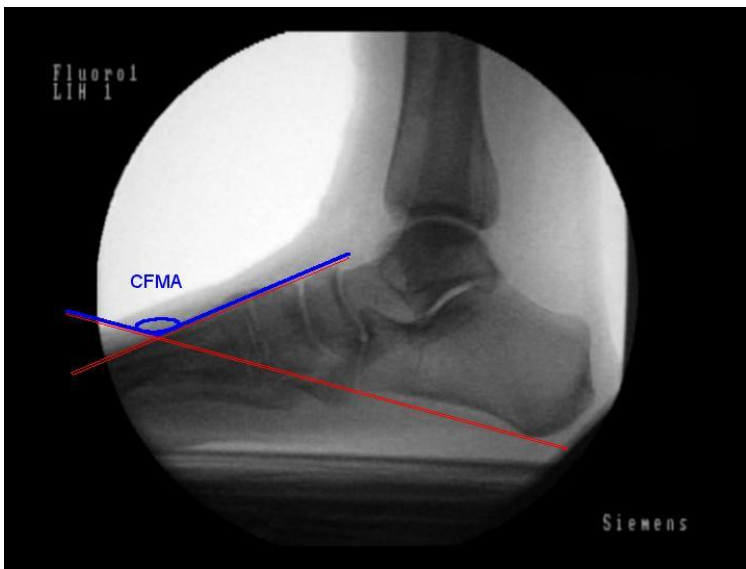


**Figure 1:** Sagittal fluoroscopic image of the left foot showing the lines defining the alignment of the calcaneus and the first metatarsal. The angle between the two defined the convexity of the medial longitudinal arch (calcaneal-first metatarsal angle, CFMA).

The CFMA was measured at midstance and compared between the four test conditions. It was hypothesized that the CFMA would be reduced (i.e. higher arch) with the soft orthotic compared to the barefoot condition. The CFMA was expected to be even less (i.e. even higher arch) with the rigid orthotic. The PFO device was hypothesized to have a slightly higher angle (i.e. lower arch) than the rigid orthotic, but to be similar to the soft orthotic.

## RESULTS

There was a trend of decreased CFMA angle across subjects (mean  $4.63 \pm 2.4$  degrees) when comparing the soft orthotic to the barefoot condition. This is consistent with the hypothesis. The PFO devices showed an increased CFMA compared with the barefoot case (mean  $1.61 \pm 1.3$  degrees). The rigid orthotic did not show a clear trend across the test volunteers.

## DISCUSSION

As was expected, the soft orthotic provided support to the medial longitudinal arch compared to barefoot and restricted the drop of the arch at midstance. However, the affect of the rigid orthotic was less clear, showing no clear trend of either raising or lower the arch compared to barefoot. This was unexpected, but it is anticipated that a trend will appear as more volunteers are recruited into this study. The PFO device showed an unexpected trend of lowering the medial longitudinal arch compared to barefoot at midstance. However this effect was very small and is not statistically significant.

Possible reasons for inconsistent data may be due to slight differences in foot structure of the test volunteers. 'Control' subjects are not classified as normal based on their arch, but because they are asymptomatic. Therefore some controls may actually have an asymptomatic pes cavus or pes planus that respond differently to the orthotics. Despite these results being preliminary, the use of fluoroscopy to measure CFMA during in-vivo gait appears to be feasible. Further analysis, including three-dimensional investigation, needs to be completed before conclusions can be drawn.

## REFERENCES

1. Wearing SC, et al. *Foot and Ankle Int.* **19**:11, 738-742, 1998.
2. Bryant JA. *J American Podiatric Med Association* **91**:5, 234-239, 2001.
3. Murley GS, et al. *J Foot and Ankle Research* **2**:22, 2009.
4. Wearing SC, et al. *Gait and Posture* **21**, 326-332, 2005.

# ALTERING JOINT LOADING DIRECTION IN THE SHEEP GENERATES TRABECULAR ORIENTATION ADJUSTMENT

<sup>1,2</sup>Meir Max Barak, <sup>1</sup>Jean-Jacques Hublin and <sup>2</sup>Daniel Lieberman

<sup>1</sup>Max Planck Institute for Evolutionary Anthropology, Leipzig, Germany.

<sup>2</sup>Harvard University, Cambridge, MA, USA

email: [mbarak@fas.harvard.edu](mailto:mbarak@fas.harvard.edu)

## INTRODUCTION

It has long been postulated that trabecular bone modifies to line up its principle material axes with the trajectory of the principal loads within a joint. This assumption is often known as Wolff's law [1], even though this "law" has not been well tested. Recently, Pontzer et al., 2006 [2] have shown that trabecular bone in the guinea fowl distal femur adjusts its orientation in correspondence to predicted changes in joint angle at peak compressive forces. Yet, to our knowledge, no study has yet tested in vivo the extent to which trabecular orientation matches load orientation in a large mammal.

## METHODS

Twenty sheep, 4 weeks old, were divided into 3 groups. 8 sheep ran daily on a level treadmill (level group), 8 sheep ran daily on an inclined treadmill (6-7°; incline group) and 4 controls did not run (control group). The sheep run for 15min, 6 days a week for 5 weeks. While running, carpal and tarsal joint angles were recorded using a high speed camera synchronized with a force plate embedded in the treadmill. Throughout the treatment period, except while running on the treadmill, the control and incline groups wore platform shoes on their forelimbs. These shoes elevated the forelimbs to maintain the same joint angles as inclined locomotion during running. At the end of the experiment the distal radii and tibiae were scanned at high resolution with microCT. Trabecular properties and orientation were measured in the lateral and medial regions of the bone just below the joint surface and then compared between the groups.

## RESULTS AND DISCUSSION

Carpal joint angle did not differ between the level and incline groups (177.5° and 177.5° respectively) while tarsal joint angle was statistically significant different (124.3° and 127.9° respectively) (Figure 1).

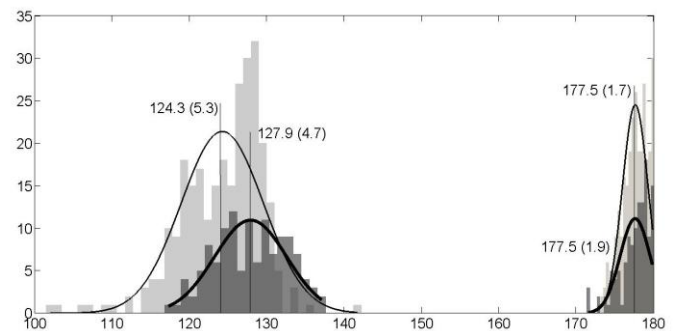


**Figure 1:** tarsal (left) and carpal (right) histograms of joint angles with fitted normal distribution of level group (light grey) and incline group (dark grey).

CT scanning revealed much less trabecular bone in the lateral groove of the distal tibia compared to the medial groove (figure 2a and 2b). Overall, trabecular bone just below the joint surface in the distal tibia was much more scarce compared to the distal radius (figure 2c). In both the distal radius and distal tibia the area between the medial and lateral regions was almost devoid of trabecular tissue (figure 2d), perhaps reflecting the fact that this region of the joint is not loaded directly.

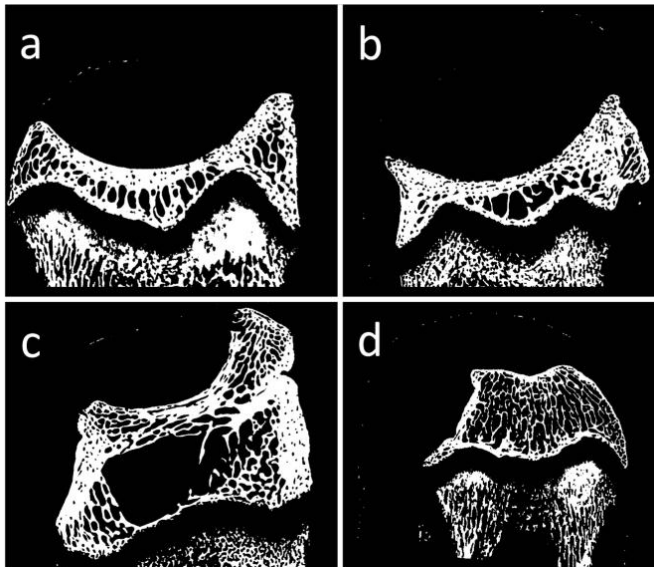


**Figure 2.** Trabecular bone in the medial (a) and lateral (b) grooves and the ridge between them (c) in the distal tibia; compared to the distal radius (d).

Trabecular bone parameter measurements in the lateral region of the distal radius showed a significant increase in trabecular bone volume (BV/TV) and trabecular number (Tb.N) and a significant decrease in trabecular spacing (Tb.Sp) in both exercising groups (level and incline) compared to the control group. These results demonstrate that the exercise effectively induced the formation of new trabecular bone. Interestingly, the main response was to create new trabeculae (increase in Tb.N) rather than to thicken existing struts (increase in Tb.Th).

As predicted from Wolff's law, trabecular orientation in the distal radius did not differ between the 3 groups, while trabecular bone in the distal tibia of the incline group modified itself as predicted to realign the principle material axes with the joint new loading direction (however, only the medial region showed statistically significant different) (Figure 3).

Contrary to our expectations, trabecular orientation in the distal tibia of the control group (which wore platform shoes and by that mirrored the tarsal joint angle of the incline group) did not change. This result may be explained by the fact that the sheep were kept in a pen and spent most of the day sedentary.

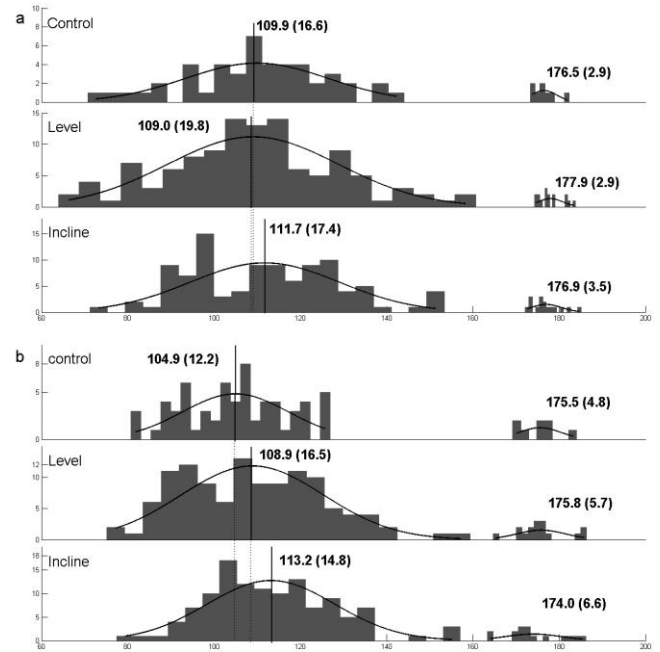


**Figure 3.** tarsal (left) and carpal (right) histograms of trabecular orientations with fitted normal distribution of control, level and incline groups. Figure 3a lateral region; figure 3b medial region.

## CONCLUSIONS

Our results demonstrate for the first time in large mammals that trabecular bone responds in vivo to a change in loading direction by altering its principle material axes and realigning with the trajectory of the new principal loads within a joint.

## REFERENCES

1. Cowin SC. The false premise in Wolff's law. In: *Bone Mechanics Handbook 2<sup>nd</sup> ed*, CRC Press, Boca Raton, FL, USA, 2001.
2. Pontzer H, et al. *J Exp Biol* **209**, 57-65, 2006.

## ACKNOWLEDGEMENTS

Supported by Minerva Stiftung Gesellschaft für die Forschung mbH (a subsidiary of the Max Planck Society).

This work was performed in part at the Center for Nanoscale Systems (CNS), Harvard University

# HEEL HEIGHT AFFECTS LOWER EXTREMITY FRONTAL PLANE JOINT MOMENTS DURING WALKING

Danielle D. Barkema, Timothy R. Derrick, and Philip E. Martin

Iowa State University, Ames, IA, USA  
email: d-barkema@northwestern.edu

## INTRODUCTION

Wearing high heels alters walking kinematics and kinetics and can create potentially adverse effects on the musculoskeletal structures of the lower extremity. Although research is limited, higher external knee adduction moments, which are thought to contribute to larger medial tibiofemoral compartment loads [1], have been shown in shoes of moderate heel height compared to flat shoes [2, 3]. Additionally, little is known about the effects of heel height on the hip and ankle in the frontal plane. Our purpose was to determine how heel height affects frontal plane joint moments at the hip, knee, and ankle, with a specific focus on the external knee moment due to its importance for joint loading and knee osteoarthritis (OA) [1]. It was hypothesized that frontal plane net joint moments of the lower extremity increase systematically as heel height increases.

## METHODS

Fifteen women ( $23.8 \pm 4.4$  yrs,  $165.5 \pm 7.1$  cm,  $60.9 \pm 8.7$  kg) completed two test sessions. In session 1, anthropometric measures were taken and subjects were fitted with three shoes with heel heights of 1, 5, and 9 cm. Heel height was randomly ordered and preferred walking speed was determined for each shoe condition as the average of 10 overground trials. Subjects then practiced overground walking at the experimental speed of  $1.3 \text{ m}\cdot\text{s}^{-1}$  for each of the three heel height conditions.

Session 2 was completed within 7 days after session 1. Fifteen reflective markers were placed on anatomical landmarks of the subject's trunk, pelvis and right lower extremity. Subjects completed shoe conditions in the same randomly determined order as used in session 1. Ten trials for each of the three heel height conditions were completed at each

subject's preferred walking speed ( $\pm 3\%$ ). Subjects then completed 10 trials for each heel height condition at  $1.3 \pm 0.04 \text{ m}\cdot\text{s}^{-1}$ . Marker position and ground reaction force (GRF) data were collected synchronously at 200 Hz and 1000 Hz, respectively.

Net internal three-dimensional joint moments were calculated using inverse dynamics with rigid body assumptions. Because of limited musculature counteracting the external knee adduction moment [1], the frontal plane knee moment was presented as an external knee moment [2, 4], whereas the hip and ankle were expressed as internal joint moments.

A one-way, repeated measures ANOVA was used to assess the effect of heel height on frontal plane net joint moments and walking kinematics for preferred and fixed walking speed conditions.

## RESULTS AND DISCUSSION

Average preferred walking speed was slower for 9 cm heels ( $1.28 \pm 0.15 \text{ m}\cdot\text{s}^{-1}$ ) compared to 1 cm ( $1.35 \pm 0.10 \text{ m}\cdot\text{s}^{-1}$ ) and 5 cm heels ( $1.35 \pm 0.15 \text{ m}\cdot\text{s}^{-1}$ ). Overall, heel height effects on net frontal plane moments of the hip, knee, and ankle were similar for fixed and preferred walking speed conditions; peak joint moments increased as heel height increased (Table 1).

As hypothesized and consistent with previous heel height investigations [2, 3], peak external knee adduction moments early and late in the stance phase increased systematically as heel height increased for fixed speed and preferred speed conditions (Fig 1). Our results demonstrate that the direct relationship between heel height and peak external knee adduction moment can be extended beyond moderate heel heights, which has important implications on how higher heel heights affect medial loading in the knee. Because high external

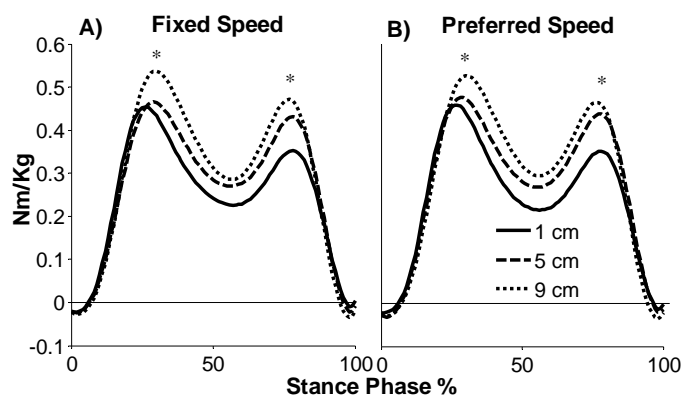


**Figure 1.** Ensemble average external knee adduction moment response to heel height for a) fixed and b) preferred speed conditions. (\*significant heel height effect).

knee adduction moments are believed to be an important contributor to the development of medial compartment knee OA, wearing high heels, especially higher heels, may put individuals at greater risk for developing knee OA.

As expected, net frontal plane ankle moments increased in amplitude as heel height increased. Specifically, peak ankle eversion moment was higher for the 5 and 9 cm heel heights compared to the 1 cm height for both fixed and preferred speed conditions (Table 1). Kinetic changes at the ankle with increasing heel height likely contribute to adverse loading at the knee. Lower peak external knee adduction moments have been associated with lower peak ankle eversion moments [5]. Increasing heel height contributes to an inversion-biased foot position, contributing to higher peak ankle eversion moments and higher peak external knee adduction moments. Therefore, the changes in foot and ankle orientation with higher heel heights may contribute to higher compression on the medial compartment of the knee.

**Table 1.** Mean (SD) frontal plane joint moments ( $N \cdot m \cdot kg^{-1}$ ) in response to heel height at fixed and preferred walking speeds.

|  | 1.3 m·s <sup>-1</sup> |            |            | Preferred speed |            |            |
|--|-----------------------|------------|------------|-----------------|------------|------------|
|  | 1 cm                  | 5 cm       | 9 cm       | 1 cm            | 5 cm       | 9 cm       |
| <b>Peak internal hip abduction moment</b> <sup>a</sup>                   | 0.78(0.07)            | 0.79(0.08) | 0.86(0.09) | 0.79(0.10)      | 0.80(0.09) | 0.84(0.09) |
| <b>Peak external knee adduction moment – early stance</b> <sup>a b</sup> | 0.46(0.11)            | 0.48(0.07) | 0.55(0.08) | 0.47(0.12)      | 0.49(0.07) | 0.53(0.08) |
| <b>Peak external knee adduction moment – late stance</b> <sup>a b</sup>  | 0.38(0.06)            | 0.44(0.09) | 0.49(0.10) | 0.37(0.06)      | 0.45(0.08) | 0.48(0.10) |
| <b>Peak internal ankle eversion moment</b> <sup>a b</sup>                | 0.14(0.08)            | 0.23(0.12) | 0.29(0.10) | 0.13(0.09)      | 0.22(0.13) | 0.27(0.10) |

<sup>a</sup> = significant heel height effect ( $p < 0.05$ ) for fixed speed trials, <sup>b</sup> = significant heel height effect for preferred speed trials

Although the peak frontal plane hip moment slightly increased as heel height increased, only the peak hip abduction moment for the 9 cm heel height in early stance under the fixed speed condition differed significantly from other values (Table 1). A higher peak hip abduction moment during stance would attempt to produce a more varus position at the knee, contributing to medial loading within the knee. However, because differences in hip moments were small with differing heel heights, adaptations within the hip with increasing heel height likely do not contribute substantially to adverse loading at the knee.

## CONCLUSIONS

Frontal plane net joint moments of the lower extremity during the stance phase of walking increase systematically as heel height increases. The observed changes likely contribute to higher compressive loading on the medial aspect of the knee, which is believed to contribute to the development of knee OA. Therefore, wearing high heels may put individuals at greater risk for the development of medial compartment knee OA.

## REFERENCES

1. Schipplein OD & Andriacchi TP. *J Orthopaed Res* **9**, 113-19, 1991.
2. Kerrigan DC, et al. *Arch Phys Med Rehab* **86**, 871-75, 2005.
3. Esenyel M. *J Am Podiatr Med Assoc* **30**, 914-18, 2003.
4. Baliunas AJ, et al. *Osteoarthr Cartilage* **10**, 573-79, 2002
5. Andrews M, et al. *J Orthopaed Res* **14**, 289-95, 1996.

# FOREFOOT-REARFOOT KINEMATICS IN RECREATIONAL RUNNERS WITH A HISTORY OF TIBIAL STRESS INJURY

<sup>1</sup>Andrew Barnes, <sup>1</sup>Jonathan Wheat and <sup>2</sup>Clare E. Milner

<sup>1</sup>Sheffield Hallam University, Sheffield, UK

<sup>2</sup>University of Tennessee, Knoxville, TN, USA

email: [A.Barnes@shu.ac.uk](mailto:A.Barnes@shu.ac.uk)

## INTRODUCTION

There is some evidence to support the notion that those with a history of tibial stress injuries exhibit a different loading pattern compared to an uninjured population [1]. Dynamic foot function during loading may be important in determining injury risk. At the rearfoot, greater peak eversion has been reported in female runners with a history of tibial stress fracture, compared to runners without previous bony injury [2]. However, a link between peak rearfoot eversion and risk of stress fracture was not found during a prospective study on military recruits [3]. Given these contrasting findings, peak rearfoot eversion is worthy of further investigation in injured populations. Forefoot motions during gait have not been investigated previously in those with a history of tibial stress injury. Significant motion occurs between the forefoot and rearfoot during early stance [4]. The foot has been suggested to act as a twisted plate model which produces counter rotations of the forefoot with respect to the rearfoot [5]. Rearfoot eversion is accompanied by both forefoot inversion [5] and forefoot abduction [6]. These motions result in separation at the joints of the midfoot. Ligament laxity and muscle function help to govern not only the magnitude of joint separation, but also the rate of rotation. Therefore, peak joint angles and velocities might be important in determining the loading response of the foot.

The purpose of this study was to investigate forefoot-rearfoot kinematics during running as risk factors for tibial stress injury. Specifically, it aimed to establish if differences exist in forefoot-rearfoot mechanics between recreational runners with a history of tibial stress injury (TSI) and a control group with no previous bony injuries (CON). Variables of interest were peak rearfoot eversion, peak forefoot inversion and peak forefoot

abduction. It was hypothesised that those with a history of TSI would demonstrate greater peak joint angles than a CON group. Peak joint velocities of the selected rotations were also analysed.

## METHODS

After institutional ethics approval, six recreational runners (4 males and 2 females) with a history of TSI were recruited (age  $28.0 \pm 11.2$  years, height  $181.2 \pm 0.12$  cm, mass  $77.2 \pm 15.1$  kg, weekly mileage  $12.8 \pm 2.6$  miles). The TSI group comprised two participants with a previously reported tibial stress fracture, confirmed with bone scans. The remaining four participants were diagnosed as having a TSI by physical assessment. The assessment parameters have been validated previously against diagnostic imaging techniques [7]. The CON group comprised six participants with no history of bone related lower extremity injury (age  $27.8 \pm 7.4$  years, height  $173.4 \pm 0.03$  cm, mass  $71.6 \pm 8.2$  kg, weekly mileage  $14.5 \pm 4.6$  miles). The TSI and CON groups were matched by gender, age and weekly mileage. At the time of testing all participants were free from injury and had been pain free for at least the previous eight weeks.

Participants completed 10 good trials of running ( $3.5\text{m/s} \pm 5\%$ ) wearing gait sandals (Bite, Orca). A three segment model [8] comprising the shank, rearfoot and forefoot was used, with markers fixed directly to the skin. All three dimensional kinematic data were collected using an eight camera motion capture system (Motion Analysis Corporation), sampling at 500Hz. A force platform (Kistler, 9281CA) was sampled simultaneously at 1000Hz. Raw coordinate data were filtered (8 Hz) and cropped to the stance phase of gait using the force data to indicate stance. Rearfoot motion was calculated relative to shank, and forefoot relative to rearfoot, using a joint coordinate system [9]. Peak

rearfoot eversion (RFEV) and peak forefoot abduction (FFABD) were defined as the minimum value during stance, while peak forefoot inversion (FFIN) was defined as the maximum value during stance. Joint velocities were defined as the maximum value between foot strike and peak joint angle, these included peak rearfoot eversion velocity (RFEV<sub>v</sub>), peak forefoot inversion velocity (FFIN<sub>v</sub>) and peak forefoot abduction velocity (FFABD<sub>v</sub>). Cohen's *d* values were calculated as a measure of effect size (ES). The following thresholds were used to interpret effect size: *ES*=.20 small, *ES*=.50 medium, *ES*=.80 large. Only moderate and large effect sizes were considered to be clinically meaningful.

## RESULTS

A large effect for greater RFEV in the TSI group compared to the CON group was found (Table 1). Small effects for group were found for RFEV<sub>v</sub>, FFIN, FFIN<sub>v</sub> and FFABD. FFABD<sub>v</sub> was greater in the TSI compared to the CON group.

**Table 1:** Means (SD) of rearfoot and forefoot variables of interest for TSI and CON groups, plus effect sizes (ES).

| Variables                | CON ( <i>n</i> =6) | TSI ( <i>n</i> =6) | ES   |
|--------------------------|--------------------|--------------------|------|
| RFEV (°)                 | 4.4 (2.9)          | 6.3 (1.3)          | 0.85 |
| RFEV <sub>v</sub> (°/s)  | 224.0 (96.4)       | 245.0 (45.3)       | 0.28 |
| FFIN (°)                 | 8.6 (2.6)          | 7.5 (3.3)          | 0.38 |
| FFIN <sub>v</sub> (°/s)  | 88.1 (29.0)        | 82.1 (11.3)        | 0.27 |
| FFABD (°)                | 11.5 (5.8)         | 13.7 (5.3)         | 0.38 |
| FFABD <sub>v</sub> (°/s) | 71.2 (10.8)        | 103.6 (25.6)       | 1.60 |

## DISCUSSION

The purpose of this study was to compare forefoot-rearfoot kinematics in recreational runners with a history of TSI and a matched CON group. Key differences were found in peak rearfoot eversion angle and peak forefoot abduction velocity between groups, these group differences may provide some insight into potential injury mechanisms. It was hypothesised that individuals with a history of TSI would exhibit greater peak joint angles compared to CON. This hypothesis was supported at the rearfoot, with 1.9° greater peak eversion in the TSI group than the CON group. This finding supports previous research which found 2.7° greater peak

rearfoot eversion in female runners with a history of tibial stress fracture compared to controls [2]. The hypothesis was not supported for peak forefoot inversion and peak forefoot abduction. Both variables were similar between groups. These data do not support the notion of greater separation of the joints of the midfoot in those with a history of TSI.

Both forefoot inversion velocity and rearfoot eversion velocity were similar between groups. Similar findings have been reported previously for the rearfoot [3]. In the present study, greater forefoot abduction velocity was observed in those with a history of TSI compared to a CON group. Similar peak forefoot abduction was found in both groups. However, a greater abduction excursion over a shorter time period in the TSI group resulted in the higher peak forefoot abduction velocity compared to CON. A reduced forefoot abduction excursion time in the TSI group may allow less time for the body's momentum to be reduced and result in higher average forces exerted on the skeletal structures of the lower extremity [3].

## CONCLUSIONS

Peak rearfoot eversion angle and peak forefoot abduction velocity were greater in those with a TSI compared to a CON group. These differences may be important in relation to understanding TSI risk. Findings represent an initial insight into forefoot-rearfoot kinematics in runners with a history of TSI, further investigation in larger scale studies is needed to establish a specific link to TSI risk.

## REFERENCES

1. Milner CE. et al. *Med Sci Sports Exerc* **38**, 323-328, 2006.
2. Pohl M. et al. *J Biomech* **41**, 1160-1165, 2008.
3. Hetsroni I. et al. *Clin J Sports Med* **18**, 18-23, 2008.
4. Arndt A. et al. *J Biomech* **40**, 2672-2678, 2007.
5. Sarrafian SK. *Foot Ankle Int* **8**, 4-18, 1987.
6. Pohl M. et al. *Clin Biomech* **21**, 175-83, 2006
7. Fredericson M. et al. *Am J Sports Med* **23**, 472-481, 1995.
8. Barnes A. et al. *Foot Ankle Int* **In Press**, 2011.
9. Cole GK. et al. *J Biomech Eng* **115**, 344-349, 1993.

# CARTILAGE CONTACT CENTERS CALCULATED USING PROXIMITY WEIGHTING ARE INSENSITIVE TO THRESHOLD DISTANCE USED TO DEFINE CONTACT REGION

Peter Barrance<sup>1,2</sup>, Venkata Gade<sup>1</sup>, and Jerome Allen<sup>1</sup>

<sup>1</sup>Kessler Foundation Research Center, West Orange, NJ, USA

<sup>2</sup>University of Medicine and Dentistry of New Jersey, Newark, NJ, USA

email: pbarrance@kesslerfoundation.org

## INTRODUCTION

In vivo measurement of locations and areas of contact between articular surfaces has the potential to shed light on the etiology of conditions such as patellofemoral pain and tibiofemoral osteoarthritis. Several research groups have developed imaging systems and techniques to provide such measures [1,2]. Cartilage geometry may be represented by surface points developed from digitization of MR images. Considering evenly spaced points on two hypothetical cartilage surfaces A and B, the center of the region of surface A in contact with surface B can be calculated as follows: (i) for each point in A, find the closest neighbor point in B and its associated closest distance; (ii) use the closest distances to define a contact region of points in A for which the distances are below a given threshold value; (iii) find the geometric centroid of the contact region points.

The above method is intuitive but relies on the selection of a proximity threshold value, and the centroid positions calculated necessarily depend on this value. Selection of the threshold may be made to avoid small scale sampling error effects (threshold too low), or biasing caused by asymmetry of the contact geometry (threshold too high). If the selected value is large enough to be above the sampling error range, and if it is consistently used to analyze data within a study, biasing errors may be relatively consistent and have little influence on contrasts of interest (e.g. between-subject differences).

The objectives of the current study were therefore (1) to assess the sensitivity of the tibiofemoral contact location (calculated using the geometric centroid method) to the threshold distance parameter; (2) to compare this sensitivity to that of a method in which the point-to-point distance (proximity) is used as a weighting factor in calculating the center of the contact region. The weighting method has the effect of driving the

centroid location toward the region with the closest distances.

## METHODS

Contact center algorithms: The following algorithms for calculating centers of contact of the medial and lateral femoral condyles on the tibial plateau were implemented using Matlab (The Mathworks, Inc.):

1. Fit surfaces to digitized cartilage points and interpolate to give evenly spaced points ( $\mathbf{T}_g$  : tibial points,  $\mathbf{F}_g$  : femoral points)
2. Closest points calculation: Use a fast sort algorithm to calculate  $d_i$  = distance to closest point in  $\mathbf{F}_g$ , for each point  $\mathbf{T}_{gi}$
3. For each point  $\mathbf{T}_{gi}$ :
  - a. Method 1 (geometric centroid): if  $d_i \leq d_t$  (threshold distance), add  $\mathbf{T}_{gi}$  to vector quantity  $\mathbf{C}_1$ ; add 1 to  $n_C$  (count of points within threshold distance).
  - b. Method 2 (proximity weighted centroid): if  $d_i \leq d_t$ , add  $\mathbf{T}_{gi}/d_i$  to vector quantity  $\mathbf{C}_2$ ; add  $1/d_i$  to scalar quantity  $S_d$
4. Final calculation:
  - a. Geometric centroid location: Vector quantity  $\mathbf{Cent}_1 = \mathbf{C}_1/n_C$ .
  - b. Proximity weighted centroid location:  $\mathbf{Cent}_2 = \mathbf{C}_2/S_d$ .

### Quantification of sensitivity to threshold distance:

Test data, described below, were analyzed for each Method, with the threshold distance  $d_t$  varied between 0.5 mm and 3.0 mm in 0.1 mm steps. The changes in centroid coordinates were calculated for each step and divided by the step size. The absolute values of these changes were then averaged across the above range of  $d_t$ . This yielded a single value characterizing the sensitivity of centroid location to  $d_t$  (mm/mm) for each test condition.

Additionally, the contact center coordinates were averaged over the test range of  $d_t$  to assess overall similarity or difference of the results from the two methods.

**Test data:** Previously acquired tibiofemoral cartilage surface data digitized from 8 MRI scans were used to compare the sensitivity and average results of the methods. The data were from both knees of two subjects, scanned in low and high weightbearing conditions using a vertically open MRI scanner (Upright MRI, Fonar Corp.) and a previously described protocol [3]. Informed consent was acquired from the subjects in accordance with the policies of the Kessler Foundation Research Center's Internal Review Board. A single operator traced the cartilage surfaces on each image using a digitizing screen (Wacom Cintiq), and the surface points were transformed into an anatomical coordinate system referenced to the tibial plateau. Contact centroids for lateral and medial compartments (LC, MC) were calculated.

**Statistical tests:** Paired t-tests with  $\alpha=0.05$  were used to compare (a) sensitivity; (b) average value, for anterior/posterior (A/P) and medial/lateral (M/L) tibiofemoral contact locations between Methods 1 and 2.

## RESULTS AND DISCUSSION

The proximity weighted centroid method (Method 2) was significantly less sensitive to threshold value for all test results (Fig. 1). Method 2 sensitivity values were low and consistent (0.12-0.15 mm/mm), whereas sensitivities for Method 1 were more variable (0.29-0.55 mm/mm).

Average values of the contact center coordinates from each method were similar (Fig. 2). However, Method 2 calculated the MC contact to be 0.44 mm more anterior than Method 1 ( $p<0.05$ ).

## CONCLUSIONS

This study compared the sensitivities of geometric and proximity-weighted contact center calculation methods to threshold distance  $d_t$ . Over a range of  $d_t$  values, the weighted method showed low and consistent sensitivity to the parameter. The results appear to support the use of this method for calculation of articular contact center coordinates.

Nevertheless, the overall differences between the results of the two methods were relatively small. Moreover, it seems likely that small bias effects, such as that observed in the MC A/P coordinate with Method 1, would have a negligible effect on the results of between-joint or between-group comparisons.

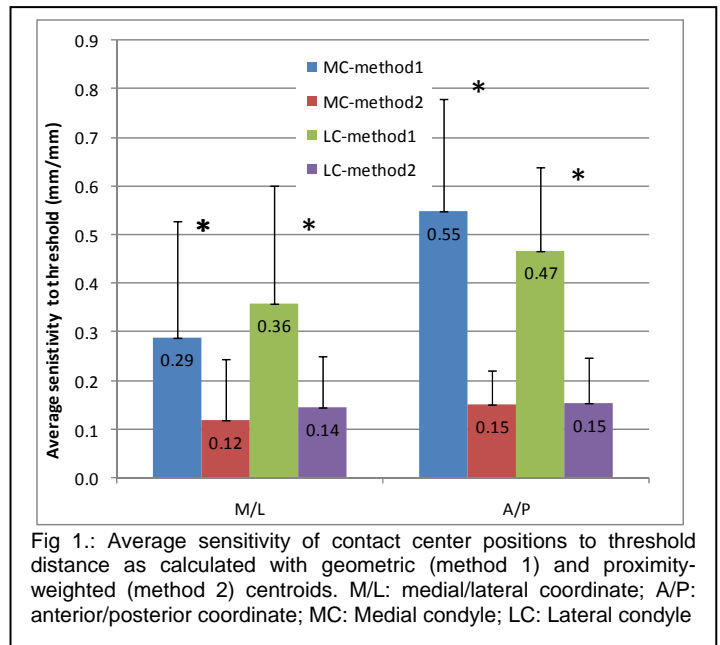


Fig 1.: Average sensitivity of contact center positions to threshold distance as calculated with geometric (method 1) and proximity-weighted (method 2) centroids. M/L: medial/lateral coordinate; A/P: anterior/posterior coordinate; MC: Medial condyle; LC: Lateral condyle

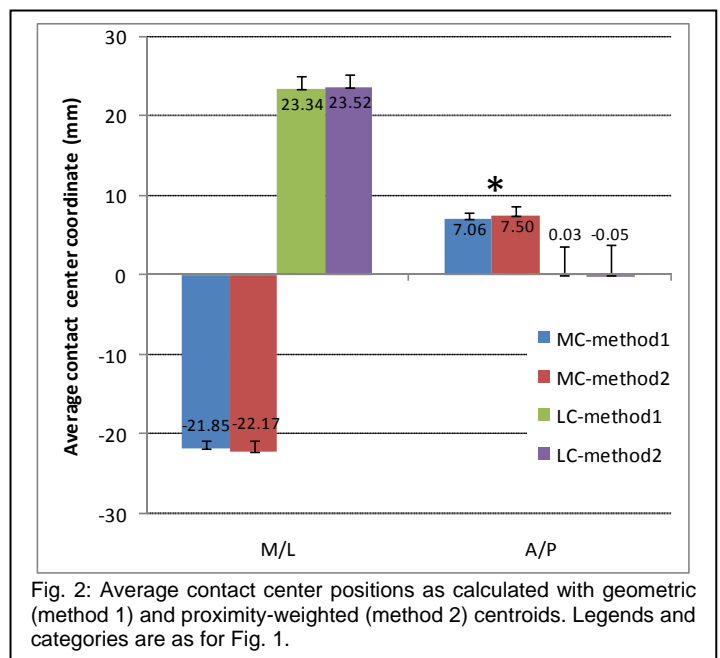


Fig. 2: Average contact center positions as calculated with geometric (method 1) and proximity-weighted (method 2) centroids. Legends and categories are as for Fig. 1.

## REFERENCES

1. Ward SR, et al.. *J Bone Joint Surg Am*, **89**, 1749-55, 2007
2. Van de Velde SK, et al. *Arthritis Rheum*, **60**, 3693-702, 2009
3. Dubowsky SR, et al. *American Society of Biomechanics Conference*, Providence RI, 2010

## ACKNOWLEDGEMENTS

Contents of this abstract were developed under a grant from the Dept of Education, NIDRR H133G080136. However, those contents do not necessarily represent the policy of the Dept of Education, and you should not assume endorsement by the Federal Government. Support for the work was also provided by the Kessler Foundation.

# PREFERRED WALKING SPEED IN A VIRTUAL ENVIRONMENT

Jamie L. Bartlett and Pinata H. Sessoms  
Naval Health Research Center, San Diego, CA, USA  
email: jamie.bartlett@med.navy.mil

## INTRODUCTION

Mechanical differences have been noted between walking overground versus walking on a treadmill [1, 2]. Generally, biomechanical studies will match the subject's average preferred overground walking speed to the speed of the treadmill. However, the influence of the external environment on gait cannot be ignored, particularly when assessing gait abnormalities in clinical populations.

The flow (or lack of flow) of the visual field while walking on a treadmill complements the sensory systems involved in locomotion control. Previous studies have demonstrated the effects of visual flow changes on preferred treadmill walking speeds [3–5].

Emerging technology has led to the creation of the virtual environment (VE) for laboratory testing. These environments can immerse the individual in a realistic scenario that emulates the physics and sensations of the real world. Under such conditions, visual feedback can be coupled with the movement of the subject in real time. This enhances the ability to immerse the subject into the environment. Ideally, subjects will walk similarly in the VE as they walk overground.

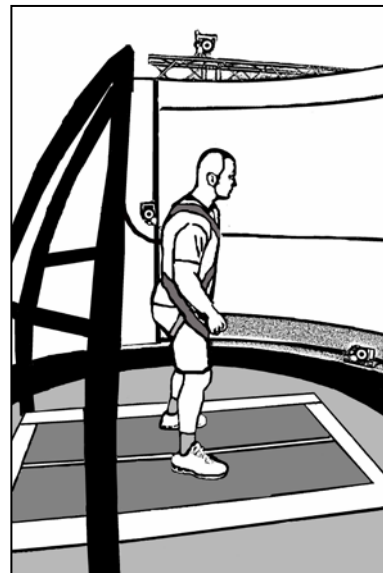
The present study explored the effects of a VE on preferred walking speed (PWS). We hypothesized that PWS on a treadmill in a VE with matched visual flow would be similar to PWS overground. Further, we expected that PWSs on a treadmill in the environment without visual flow would be slower than PWSs overground.

## METHODS

We acquired data from 15 male and 5 female active-duty military volunteers (respective means: age =  $28.0 \pm 6.5$ ,  $24.0 \pm 3.5$  years; height =  $179.3 \pm 5.2$ ,  $159.6 \pm 5.1$  cm; weight =  $85.0 \pm 10.1$ ,  $69.0 \pm$

$12.0$  kg). We first determined overground PWS using a GAITRite walkway system (CIR Systems, Inc., Havertown, PA). Next, we determined PWS while subjects walked in the VE (CAREN Extended System, Motek Medical, The Netherlands) with and without coupled visual flow.

The VE contains a motion platform with a dual-belt motorized treadmill in the center (Figure 1). The platform and treadmill are controlled by the CAREN software and synchronized with the projected video image on the wraparound screen (9 feet high, 180°). Using a wireless handheld device, subjects could control the treadmill speed while walking in the VE. All subjects were familiar with treadmill walking and were given unlimited time to adjust their speed. For the walking condition with coupled visual flow, the surrounding image displayed an “endless hallway” (Figure 2) scene.



This scene was synced with the speed of the treadmill to give the sensation that the person was walking down the hall. For the VE trial without visual flow, the center section of the screen displayed a stationary picture. Trial order was randomized for each subject.

**Figure 1.** Side view of virtual environment. Includes dual-belt instrumented treadmill integrated into a 6-degree of freedom motion platform and 180-degree projection screen. Subject is shown with safety harness attached to safety support system.



**Figure 2.** Endless hallway scene that is displayed during the visual flow walking condition in the virtual environment.

## RESULTS AND DISCUSSION

Mean PWS for all subjects during overground walking was within normal walking speeds ( $1.27 \pm 0.17$  m/s). This was statistically faster than PWS while walking on a treadmill in the VE with visual flow ( $1.03 \pm 0.13$  m/s) and with no visual flow ( $0.93 \pm 0.14$  m/s) ( $p < 0.001$ ). Both treadmill conditions (with and without visual flow) were also significantly different from each other (Figure 3,  $p = 0.002$ ).

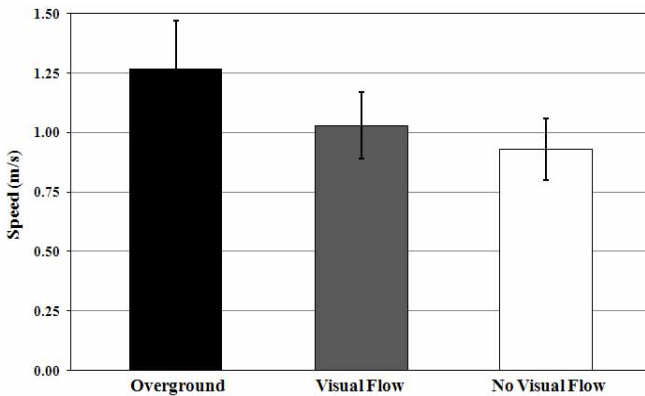


**Figure 3.** Mean speed of 20 subjects at each walking condition. Error bars indicate the standard deviation for each condition.

We hypothesized that adding synchronized visual flow to treadmill walking using a VE would create optical flow similar to that of overground walking. By using realistic visual flow during treadmill walking, we demonstrated an increase in preferred treadmill walking speeds compared with walking with no visual flow. The dramatically slower speeds observed in the treadmill walking in the novel VE to overground walking may be because of the lack of familiarization with the dual-belt instrumented platform. Though subjects were given unlimited time to choose their PWS while on the treadmill, they usually selected their walking speed within 30 to 60 seconds. Previous research has shown that familiarization with walking or running on a treadmill takes 6 to 20 minutes, before characteristics are similar to overground walking [6, 7]. A longer acclimation period while walking in the novel environment may further increase PWSs and reflect closer values to preferred overground walking speeds.

## CONCLUSIONS

PWSs in a VE are more likely to reflect PWSs overground. There is an increased sense of realism compared with treadmill walking without synchronized visual flow.

## REFERENCES

1. Riley, P.O., et al. *Gait and Posture* **26** (1): 17-24, 2007.
2. Lee, S.J. and Hidler, J. *J Appl. Physiol* **104** (3): 747-755, 2008.
3. Warren, W.H., et al. *J Exp Psychol: Hum Percept Perform* **22**: 818-838, 1996.
4. Mohler, B.J., et al. *Exp Brain Res* **181**: 221-228, 2007.
5. Prokop, T., et al. *Exp Brain Res* **114**: 63-70, 1997.
6. Schellenbach, M., et al. *Gait and Posture* **31**: 295-299, 2010.
7. Lavcanska, V., et al. *Human Movement Science* **24** (4): 544-557, 2005.

# DESIGN OF A 2 DEGREE OF FREEDOM UPPER LIMB PROSTHETIC CONTROLLER

Joseph Barton

Baltimore Veterans Administration Medical Center, Baltimore MD, USA

University of Maryland School of Medicine, Baltimore MD, USA

email: [jbarton@som.umaryland.edu](mailto:jbarton@som.umaryland.edu)

## INTRODUCTION

The first goal of this study was to develop a 2 degree of freedom (DOF) upper limb controller utilizing shoulder elevation/depression and protraction/retraction. Its primary purpose is to control powered prosthetic shoulder joints being incorporated into a new generation of prosthetic arms for shoulder disarticulation and very high transhumeral amputees. There is no generally accepted method to objectively and quantitatively evaluate prosthesis and prosthesis control performance, and the second goal of this study was to develop one based on Fitts' Law [1]. The evaluation protocol has quite general applicability and can be used to compare different reaching/pointing devices, or to compare variations in the design or operation of a particular device.

## METHODS

*Goal 1:* Four candidate control assemblies were assessed. The first three (Fig. 1) consisted of a one-piece, machined aluminum base which fixes to a body socket at the base of the neck. Steel rods of varying diameter (and thus stiffness) (Table 1) were then press fit into a hole drilled into the cantilever end of the base. Subjectively, rod stiffness ranged

**Table 1: Controller Characteristics**

| Rod Material        | Stiffness (N/cm-deflection) |
|---------------------|-----------------------------|
| 6.0 mm OD Steel     | 4.1                         |
| 6.7 mm OD Steel     | 6.6                         |
| 7.7 mm OD Steel     | 11.1                        |
| 2 DOF Potentiometer | 0.0                         |

from just-noticeable to very noticeable. Four strain gauges were mounted on each face of the square aluminum cantilever end and arranged in a Wheatstone Bridge to sense bending of the rod. The bridge's output was utilized as the control signal. The fourth assembly, a 2 DOF potentiometer, offered no resistance to motion. We tested these assemblies in a position control scheme (controlled element position is proportional to shoulder position) and a velocity control scheme (direction and velocity are proportional).

Shoulder movement was represented by the corresponding movement at the acromion process. Very little data quantifying the movement or forces ex-

erted at the acromion process exist; so as a first step



**Figure 1: Controller Configuration.**

we quantified the shoulder's motion and the forces it is capable of comfortably exerting in each direction.

Ten able-bodied adults (five men aged 28-56 and five women aged 26-61) gave informed consent according to the guidelines of the Northwestern University Institutional Review Board to participate. Five measurements of movement range in each direction were taken and averaged. The maximum amount of force that could comfortably be applied against a padded load cell in elevation, protraction, and retraction was also measured five times and averaged. (Shoulder depression could not be measured with this particular arrangement.)

*Goal 2:* In pointing tasks Fitts [1] noted a linear relationship between pointing time and pointing difficulty (size and distance to target), given by (see Fig. 2)

$$ID = \log_2 \left( \frac{D}{d} + 1 \right).$$

In our implementation of this test (Fig. 2), subjects pointed from circle 1 to circle 2, to circle 3, and so on until returning to circle 1. 16 different combinations of D and d were employed and for each combination there were 11 different pointing move-

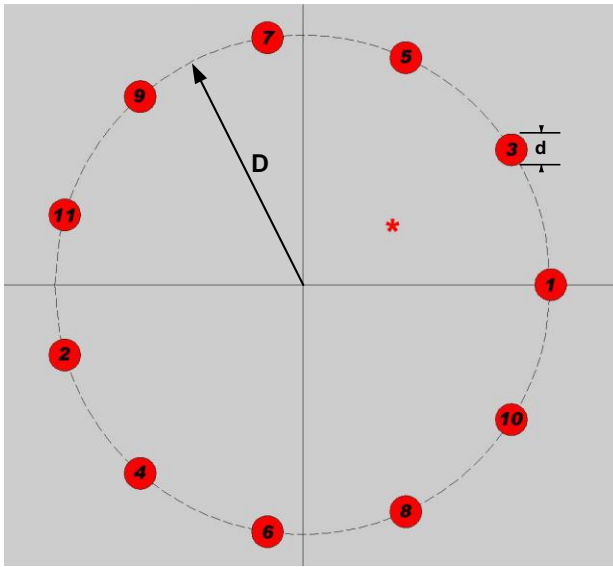


**Figure 2:** Evaluative task based on Fitts Law

ments (Fig. 2). Instead of pointing with their fingers, subjects moved a cursor on a display screen via shoulder movement using each candidate control assembly/scheme.

## RESULTS AND DISCUSSION

Overall performance in the displacement and force evaluations (Table 2) indicated that men and women exhibited similar movement range (~2.0–4.5 cm) and force sensitivity (~24 N). Five of the ten subjects then participated in the controller evaluations. A linear mixed-effects model was used to assess the effect of the different assemblies and schemes on the time to complete the pointing over different indices of difficulties. The model included fixed effect terms for assembly, scheme, index of difficulty, assembly-by-time, scheme-by-time, and assembly-by-scheme-by-index of difficulty and the random effect terms on the intercept and the slope at subject, assembly, and scheme levels. There was no significant difference in performance between the three steel assemblies ( $p=0.53$ ); but all of the steel assemblies performed significantly better than the potentiometer assembly ( $p=0.005$ ). Furthermore, for all of the assemblies, the velocity control scheme was significantly better than the position control scheme ( $p=0.001$ ).

We believe that the resistance to motion offered by the steel assemblies is responsible for their superior performance compared to that of the potentiometer. The steel assemblies constitute a limited implementation of *extended physiological proprioception* (EPP), as proposed by Simpson [2]. According to this concept, if the manner in which a mechanical device is controlled can be such that the operator is able to accurately perceive its static and dynamic characteristics through naturally arising proprioceptive sensations, the device becomes an artificial extension of the operator. By introducing a resistance to shoulder motion we provide the user a "feel" for the task which he/she can use to improve performance. The superiority of the velocity control scheme suggests that it is easier to control direction and speed (i.e., to "push" the controlled element towards the target and make mid-course corrections along the way) than absolute position.

## CONCLUSIONS

Design specifications for a 2 DOF prosthetic shoulder controller were developed, along with a tool to evaluate and compare different designs. Several candidate controllers were then evaluated. Designs based on EPP performed better than those that were not. Here the evaluation task was to move a cursor on a display screen. In actual practice a prosthetic arm would be the controlled element and these results imply that performance would be enhanced if the assembly's resistive characteristics were matched to those of the prosthesis.

## ACKNOWLEDGEMENTS

This study was carried out in the laboratory of Dr. Todd Kuiken of The Rehabilitation Institute of Chicago.

## REFERENCES

1. Fitts PM, *Journal of Experimental Psychology*, 47, 381-391, 1954.
2. Simpson DC, *The Control of Upper-Extremity Prostheses and Orthoses*, Herbert et al, Springfield, IL, 146-150, 1974.

**Table 2: Displacements and Forces Exerted at the Acromion Process**

| Displacement (cm) | Men | Women | Overall Average | Force (N)   | Men  | Women | Overall Average |
|-------------------|-----|-------|-----------------|-------------|------|-------|-----------------|
| Elevation         | 3.9 | 4.7   | 4.3             | Elevation   | 23.5 | 27.6  | 25.5            |
| Protraction       | 4.0 | 3.2   | 3.6             | Protraction | 21.4 | 21.1  | 21.3            |
| Retraction        | 3.0 | 2.5   | 2.7             | Retraction  | 23.2 | 27.9  | 25.5            |
| Depression        | 1.8 | 1.9   | 1.9             |             |      |       |                 |

# A MULTI-SEGMENT FOOT MODEL BASED ON IN-VIVO AND IN-VITRO STEREOPHOTOGAMMETRIC STUDIES AND CLINICAL THEORIES OF DYNAMIC FOOT FUNCTION: RUNNING GAIT RELIABILITY

<sup>1</sup>Robin L Bauer, <sup>1</sup>Mukta N Joshi, <sup>1</sup>Trevor R Klinkner, <sup>1</sup>Stephen C Cobb  
<sup>1</sup>Neuromechanics Laboratory, University of Wisconsin-Milwaukee

## INTRODUCTION

Lower extremity musculoskeletal injuries are prevalent during athletic and recreational activities. Clinically, abnormal foot structure is believed to cause abnormal gait mechanics that result in increased risk for numerous lower extremity injuries. The scientific relationship between abnormal foot structure and gait dysfunction, however, is not clear [1]. A limiting factor in most previous research studies may have been modeling of the entire foot as a single rigid segment [2] or only tracking the rearfoot complex [3]. Both models ignore distal foot motion. Recent in-vitro [4] and invasive in-vivo [5] three-dimensional studies, however, have reported significant motion in the distal foot joints. These data suggest that single-segment foot models may ignore important foot motion during gait.

To date, no studies have applied multi-segment foot models to investigate the effect of foot structure on running gait kinematics [6]. Investigation of the effect of foot structure on motion in the distal foot segments during running may improve our understanding of the relationship between abnormal foot structure and running-related injuries.

A prerequisite step to these investigations, however, is development of a multi-segment model that is reliable during running gait. The purpose of the current study was to examine the reliability of a multi-segment foot model, developed based upon the previously mentioned in-vitro and invasive in-vivo three-dimensional studies and clinical concepts of dynamic foot function.

## METHODS

Three participants (1 f, 2 m, age =  $21.7 \pm 3.8$  yrs; ht =  $184.66 \pm 1.2$  cm; mass =  $94.2 \pm 30.4$  kg) with no history of lower extremity injury within the previous six months, no diagnosed foot pathologies, and “typical” foot structure were recruited. Typical foot structure was determined based on the navicular index (NI) measure (the ratio of navicular height to truncated foot length) assessed using the digital photographic measurement method (DPMM). The digital DPMM computes the NI with moderate-high intra- and inter-tester reliability [7]. To qualify as having typical foot structure, individuals had an NI ratio within 1 SD of the mean of 111 previously collected participants [7]. The typical foot structure criterion was used to reduce foot function variability that may occur with differing foot structures.

Six technical marker clusters (6.4 mm markers) were located either directly on the participant’s skin or on custom built wands, secured to areas of minimal skin movement (Table 1).

Prior to completing the running trials, an anatomical calibration procedure was performed to identify anatomical landmarks and define local coordinate systems within each segment (Figure 1). Participants then completed 7 running trials at  $4.0 (\pm 5\%)$  m/s. Three-dimensional positions of the technical and anatomical marker clusters were collected at 120 Hz with a 10-camera Eagle system (Motion Analysis). A force plate (AMTI) sampling at 960 Hz was used to identify initial contact and toe-off.

Following completion of the running trials, a

custom written Matlab program was used to filter the data, reconstruct the 3D position of each segment using the calibrated



**Figure 1:** Technical and anatomical markers. **Top figure:** Leg ( $x_L, y_L, z_L$ ), calcaneus ( $x_C, y_C, z_C$ ), cuboid ( $x_{CU}, y_{CU}, z_{CU}$ ), lateral rays ( $x_{LR}, y_{LR}, z_{LR}$ ), and hallux ( $x_H, y_H, z_H$ ) anatomical coordinate systems.

**Bottom figure:** Navicular ( $x_N, y_N, z_N$ ), and medial rays ( $x_{MR}, y_{MR}, z_{MR}$ ) anatomical coordinate systems. All of the anatomical coordinate systems were defined using the appropriate anatomical landmarks.

anatomical system technique (CAST) with a single value decomposition optimization procedure, and compute joint angles between adjacent segments (Figure 1).

Five trials were then selected and used to calculate the coefficient of multiple

correlation to determine model reliability. Coefficients of multiple correlation  $> 0.70$  were considered very repeatable.

## RESULTS AND DISCUSSION

Coefficients for the sagittal, frontal and transverse planes were computed (Table 1). Running gait kinematics is very repeatable in all three planes for the rearfoot complex and calcaneocuboid functional articulations (Table 1). Running gait kinematics for the calcaneonavicular and 1<sup>st</sup> metatarsophalangeal functional articulations were very reliable in the sagittal and transverse planes and moderately repeatable in the frontal plane (Table 1). Based on the results of the study, the multi-segment foot model is reliable during running gait. Application of the model in future studies investigating the effect of foot structure on running gait will allow clinicians to better understand the relationship between foot function and lower extremity injury.

## REFERENCES

- [1]Williams DS, et al. *Clinical Biomechanics*, **16**, 341-347, 2001.
- [2]Nigg BM, et al. *J Biomech*, **8**, 909-916, 1993.
- [3]McClay I & Manal K. *J Appl Biomech*, **13**, 109-124, 1997.
- [4]Nester CJ, et al. *J Biomech*, **40**, 1927-1937, 2007.
- [5]Lundgren A. *Acta Orthopaedica Scandinavica Supplementum*. **233**, 1-23, 1989.
- [6]Cobb SC, et al. *Gait and Posture*. **30**, 334-339, 2009
- [7]Cobb SC, et al. *J Athl Train*, **46**, 20-30.

This study was supported by grants from the Wisconsin Athletic Trainers' Association and the UW-Milwaukee Graduate School.

**Table 1. Coefficients of multiple correlations for the six functional articulations**

|                                     | Sagittal | Frontal | Transverse |
|-------------------------------------|----------|---------|------------|
| Rearfoot complex                    | 0.949    | 0.889   | 0.902      |
| Calcaneonavicular                   | 0.775    | 0.692   | 0.836      |
| Calcaneocuboid                      | 0.810    | 0.883   | 0.770      |
| Medial Forefoot                     | 0.659    | 0.742   | 0.448      |
| Lateral Forefoot                    | 0.866    | 0.424   | 0.696      |
| 1 <sup>st</sup> Metatarsophalangeal | 0.876    | 0.601   | 0.772      |

# HUMAN SPRINTERS HAVE LONGER FOREFEET AND SHORTER PLANTARFLEXOR MOMENT ARMS

<sup>1</sup>Josh R. Baxter, <sup>1</sup>Thomas A. Novack, <sup>2</sup>David Pennell, and <sup>1</sup>Stephen J. Piazza

<sup>1</sup>The Pennsylvania State University, University Park, PA, USA

<sup>2</sup>Vanderbilt University, Nashville, TN, USA

email: [piazza@psu.edu](mailto:piazza@psu.edu)

## INTRODUCTION

Effective sprinting, whether performed to win a race or to outrun predator or prey, requires rapid acceleration from rest. The forward impulse that determines this acceleration depends on large forward-directed contact force and contact time sufficient for that force to act. The best animal sprinters have limb structures that are favorable for generating large forward impulses. The cheetah, for example, has longer toes and metatarsals and a shorter plantarflexor moment arm (pfMA) than are found in less capable sprinters of similar size [1]. These differences contribute to the cheetah having a large “gear ratio” (ratio of the ground reaction force moment arm to the moment arm of the plantarflexor about the ankle), which enables the plantarflexors to operate at a lower shortening velocity and thus maintain muscle force production near toe-off [2,3].

It is less clear, however, whether variation in foot and ankle structure within species, and specifically among humans, might explain differences in sprinting ability. Lee and Piazza [4] found that human sprinters’ moment arms estimated from Achilles tendon excursion were significantly smaller than those of height-matched non-sprinters, but it is unclear whether those measurements of tendon excursion were affected by differences in tendon compliance between the two groups. Lee and Piazza [4] also found sprinters to have longer toes as indicated by external measurements made from the first metatarsal head to the end of the great toe, and the extent to which these measurements were affected by errors in identifying bony landmarks or by differences in soft tissue thickness is not clear. Scholz et al. [5] and Raichlen et al. [6] did not study sprinters, but did identify a link between human foot structure and function; both groups reported that running economy negatively

correlates with calcaneal tuber (heel) length in trained distance runners.

The purpose of this study was to use magnetic resonance (MR) imaging of the Achilles tendon and the bones of the foot to determine whether the foot and ankle structure of trained sprinters differs from that of non-sprinters. We hypothesized that sprinters would have longer phalanges and metatarsals but have shorter pfMA than those of non-sprinters.

## METHODS

Achilles tendon moment arms and the lengths of foot bones were measured in seven trained sprinters (mean 100 m time of  $10.82 \pm 0.20$  s,  $6.6 \pm 3.0$  y of sprint training) and seven height-matched non-sprinters (see Table 1 for subject characteristics). Sagittal-plane images of the foot and ankle were made with a 3T Siemens MR scanner (Siemens; Erlangen, Germany) at  $15^\circ$  dorsiflexion, neutral position, and  $15^\circ$  plantarflexion. Subjects were positioned supine on the scanner bed with the knee flexed to  $30^\circ$ . Each scan required 5 s, during which time the subjects isometrically co-contracted their ankle muscles. Moment arm was defined to be the shortest distance between the center of tibiotalar rotation obtained from the  $15^\circ$  dorsiflexion and  $15^\circ$  plantarflexion images using a modified Reuleaux method similar to that implemented by Maganaris et al. [7] (Figure 1). The lengths of the first distal phalanx ( $L_{DP1}$ ), the first proximal phalanx ( $L_{PP1}$ ), and the first metatarsal ( $L_{MT1}$ ) were measured from quasi-sagittal-plane images reconstructed from the three-dimensional MR image data set using OsiriX Viewer (Atlanta, Georgia, USA). The lengths of the phalanges were summed to obtain first toe length and  $L_{MT1}$  was added to first toe length to obtain the length of the first ray ( $L_{R1}$ ).

Differences between sprinter and non-sprinter means were assessed using two-tailed, unpaired t-tests for each variable.

## RESULTS AND DISCUSSION

The phalanges, metatarsals, and first rays of sprinters were longer on average than those of non-sprinters (Table 1). First rays of sprinters were 8 mm, or 6.5%, longer than those of non-sprinters ( $p = 0.018$ ) and this difference was equally attributable to differences in the lengths of the metatarsals and the combined phalanges. Achilles tendon moment arms of sprinters were 4 mm (6.8%) shorter on average than the moment arms of non-sprinters, but this difference was found to be significant only at the  $\alpha=0.10$  level ( $p = 0.096$ ) in our two-tailed tests. The ratio of first ray length to pfMA, a quantity similar to the gear ratio described in previous studies was 14.2% greater for sprinters than non-sprinters ( $p = 0.005$ ). Heel-to-toe foot lengths were nearly identical between the two groups ( $p = 0.960$ ).

These are the first findings of foot and ankle morphology differences between groups with different functional abilities. These differences are similar to the sprinter/non-sprinter differences reported by Lee and Piazza [4], but measurements in the present study are derived from MR images of bony geometry. Computer simulations of sprint push-off performed by Lee and Piazza suggested that even slightly longer toe lengths enhance sprint performance by extending the time of contact and that shorter pfMA permitted maintenance of plantarflexor force in late stance by reducing shortening velocity.

The results presented here raise the question of whether structural differences in sprinters are genetically determined or follow from years of sprint training. Also unclear from the present study is if sprinters' unique foot and ankle structure conveys a functional advantage that is significant compared to advantages resulting from other sprinter characteristics, such as longer muscle fascicles and a higher proportion of fast-twitch muscle fibers.

## CONCLUSIONS

The structure of the foot and ankle in sprinters differs from that of non-sprinters. Shorter pfMA

coupled with a longer forefoot provides sprinters with a higher gear ratio that is likely to provide sprinters with enhanced force generation and longer time of contact that may benefit sprint performance during rapid acceleration.

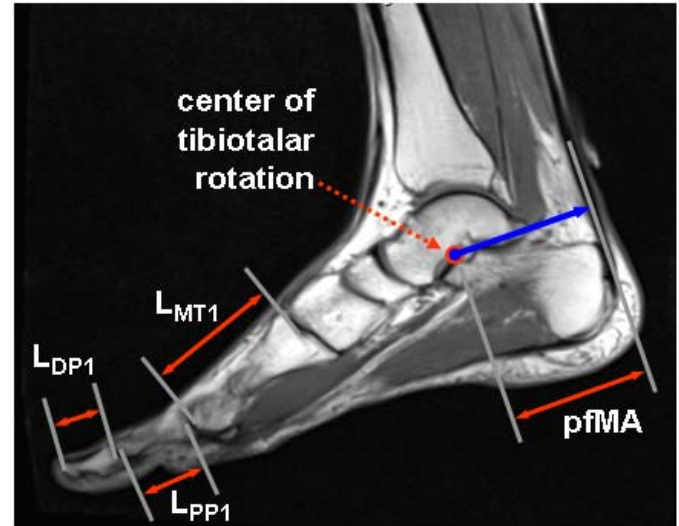


**Figure 1:** Phalangeal lengths, metatarsal lengths, and plantarflexor moment arm were measured from sagittal-plane MR images.

|                        |    | Sprinters   | Non-sprinters | p-value  |
|------------------------|----|-------------|---------------|----------|
| stature                | cm | 175.9 ± 0.6 | 175.6 ± 0.6   | 0.931    |
| body mass              | kg | 76.3 ± 7.9  | 82.0 ± 8.9    | 0.226    |
| age                    | y  | 21.2 ± 2.7  | 23.8 ± 2.7    | 0.099*   |
| foot length            | cm | 27.3 ± 1.2  | 27.3 ± 0.9    | 0.960    |
| $L_{PP1} + L_{DP1}$    | cm | 6.0 ± 2.1   | 5.6 ± 2.7     | 0.007*** |
| $L_{MT1}$              | cm | 7.0 ± 2.2   | 6.6 ± 4.0     | 0.068*   |
| $L_{R1}$               | cm | 13.0 ± 1.2  | 12.2 ± 6.2    | 0.018**  |
| pfMA                   | cm | 5.5 ± 0.4   | 5.9 ± 0.6     | 0.096*   |
| $L_{R1} : \text{pfMA}$ | 1  | 2.4 ± 0.2   | 2.1 ± 0.2     | 0.005*** |

**Table 1.** Mean differences between groups. (\*\*\*  $p < 0.01$ ; \*\*  $p < 0.05$ ; \*  $p < 0.10$ )

## REFERENCES

- Hildebrand M. *Sci Am.* **202**, 148-157, 1960.
- Carrier D.R., et al. *Science.* **265**, 651-653, 1994.
- Nagano A., Komura T. *J Biomech.* **36**, 1675-1681, 2003.
- Lee S.S.M., Piazza S.J. *J Exp Biol*, **212**, 3700-3707, 2009.
- Scholz M.N., et al. *J Exp Biol*, **211**, 3266-3271, 2008.
- Raichlen D.A., et al. *J Human Evol.* **60**, 299-308, 2011.
- Maganaris C.N., et al. *J Physiology*, **510.3**, 977-985, 1998

# DOES FOOT STRIKE PATTERN PREDICT LOADING RATES DURING SHOD OR BAREFOOT RUNNING?

<sup>1</sup>James Becker, <sup>2</sup>Komsak Sinsurin, <sup>1</sup>Eric Pisciotta, <sup>3</sup>Stan James, <sup>1</sup>Louis Osternig, and <sup>1</sup>Li-Shan Chou

<sup>1</sup>Department of Human Physiology, University of Oregon, Eugene OR, USA

<sup>2</sup>Faculty of Physical Therapy, Mahidol University, Thailand

<sup>3</sup>Slocum Center for Orthopedics and Sports Medicine, Eugene, OR, USA

email:chou@uoregon.edu; web: <http://biomechanics.uoregon.edu/MAL/>

## INTRODUCTION

Traditionally, it has been thought that running with a rear foot strike (RFS) pattern results in a distinct impact peak in the vertical ground reaction force (vGRF), with significant attenuation of this peak observed when using a midfoot (MFS) or forefoot (FFS) strike [1]. Based on these findings, it has been suggested that adopting a MFS or FFS pattern may help individuals avoid injuries by reducing impact forces imparted to the body [2]. However, a recent meta-analysis suggests it may be the vertical instantaneous loading rate (VILR), not the magnitude of the impact peak, which is more important in development of running injuries [3]. That there are no differences in VILR in RFS shod runners who are asked to run with a FFS [4] suggests more work is required to clarify relationships between lower limb loading, injury, and foot strike patterns.

Running barefoot or using minimalist shoes is one way individuals can force their body to adopt a MFS or FFS strike pattern. Interestingly, pilot data from our lab showed several individuals who, while running barefoot with a MFS, still displayed significant impact peaks in their vGRF curve. Therefore, one purpose of this study was to examine whether foot strike pattern predicts VILR under both shod and barefoot running conditions.

Since individuals running barefoot usually adopt a MFS or FFS pattern, a second purpose was to examine changes in VILR when individuals switched from shod to barefoot running. Switching from a RFS to a MFS or FFS pattern should result in a different pattern in the center of pressure (COP) trajectory. Therefore, a final purpose of this study was to examine whether changes in foot strike

pattern, as indicated by COP trajectories, from shod to barefoot running were associated with changes in the VILR.

## METHODS

This study is part of a larger, ongoing study examining the relationship between running biomechanics and injury. To date 13 subjects (6 female 7 male) have been analyzed. All subjects were habitually shod, recreational runners currently running at least 20 miles per week. Subjects ran continuous laps around a 25 meter track in the laboratory under both shod and barefoot conditions. Whole body motion data was collected at 200 Hz using an 8 camera motion capture system (Motion Analysis Corp.) Ground reaction forces were recorded at 1000 Hz by three force plates (AMTI) located in series along the 5 meter capture region. Subjects ran at a self selected speed approximating their normal training run pace.

The VILR and COP trajectory were calculated for all trials with a clean force plate strike. Foot strike pattern was identified using the strike index (SI) [1]. Simple linear regression was used to assess the ability of SI to predict VILR under both shod and barefoot conditions. Paired *t*-tests were used to assess changes in VILR between shod and barefoot conditions and to confirm that there were no differences in running speed between conditions within an individual. Left and right feet were analyzed separately for each subject. Since it is highly likely that responses to barefoot running are unique to the individual, the above statistical tests were also performed using a single subject analysis approach.

Changes in COP trajectories between shod and

barefoot conditions were examined qualitatively by plotting the COP trajectory within a rough outline of the individual's foot generated from marker locations during the foot flat phase of stance.

## RESULTS AND DISCUSSION

As a group, foot strike did not significantly predict VILR for the shod condition ( $p = .92$ ,  $R^2 = .01$ ). but did for the barefoot condition ( $p = .03$ ,  $R^2 = .16$ ). However, the single subject analysis suggested the ability of SI to predict VILR was highly variable among individuals for both conditions (Table 1).

Table 1. Ability of SI to predict VILR for each foot under both conditions. Numbers are individual feet.

|                                 | Shod                  |                       | Barefoot              |                       |
|---------------------------------|-----------------------|-----------------------|-----------------------|-----------------------|
|                                 | Yes                   | No                    | Yes                   | No                    |
| SI significantly predicts VILR? | 4                     | 22                    | 4                     | 22                    |
| Average $R^2$                   | .441<br>( $\pm .07$ ) | .121<br>( $\pm .13$ ) | .545<br>( $\pm .22$ ) | .118<br>( $\pm .15$ ) |

The group analysis showed no statistically significant differences in VILR between conditions ( $p = .114$ ), however this could be due to the large inter-individual variations observed in the response to barefoot running (Figures 1 & 2). Visual inspection of the COP trajectories suggested changes in foot strike pattern were not necessarily related to changes in VILR, as large changes in the COP trajectory were observed without corresponding changes in VILR (Figure 3).

These data suggest whether or not VILR changes between shod and barefoot running is entirely dependent on the individual. While SI did predict VILR for a few individuals, for the most part SI was a poor predictor of VILR. The observation that some individuals have drastically different COP trajectories between footwear conditions with no

differences in VILR, suggests other variables such

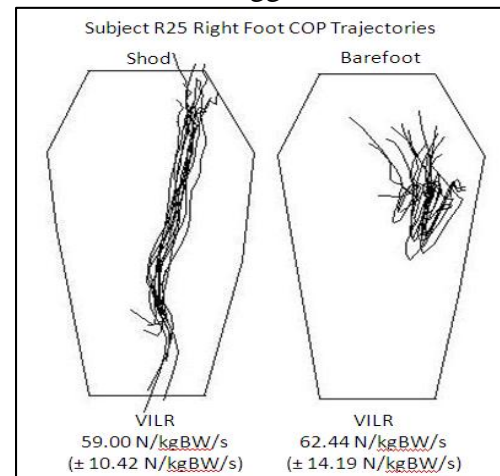


Figure 3. Example from one subject with large differences in SI and COP trajectories but no differences in VILR between shod and barefoot conditions.

as joint kinematics, joint stiffness, or muscle activity, may play a more dominant role in determining the VILR. If VILR is important to consider in relation to injury, then future studies should attempt to clarify relationships between these other variables, foot strike patterns, and loading rates.

## CONCLUSIONS

Based on this small sample, it appears foot strike pattern is a poor predictor of VILR, and changes in VILR when one switches from shod to barefoot, or from RFS to FFS, are highly variable between individuals. Thus, generalizations regarding the benefits of one foot strike pattern compared to another should be interpreted with caution.

## REFERENCES

1. Cavanagh, P., et al. *J. Biomech.* **13**: 397-406, 1980.
2. Lieberman, D., et al. *Nature.* **463**:531-536, 2010.
3. Zadpoor, A., et al. *Clin. Biomech.* **26**: 23-28, 2011.
4. Laughton, C., et al. *J. Applied Biomechanics.* **19**: 153-168, 2003.

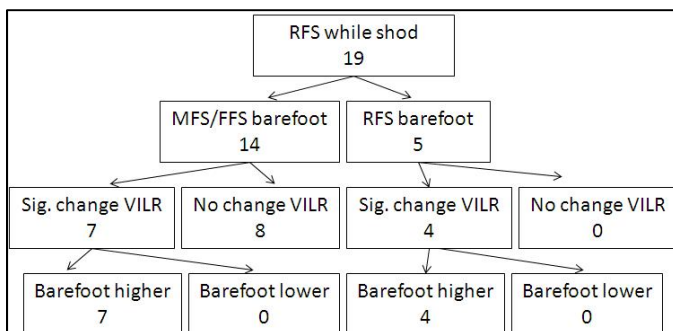


Figure 1. Changes in VILR in subjects with a RFS while running shod.

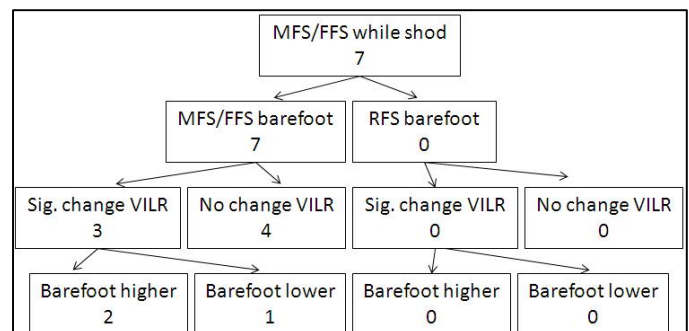


Figure 2. Changes in VILR in subjects with a MFS/FFS while running shod.

# Improvements in the Rate of Force Development-Scaling Factor Following a High Speed-Low Resistance Cycling Exercise Program

Maria Bellumori, MS and Christopher A. Knight, PhD

University of Delaware, Newark, DE, USA

email: [mariab@udel.edu](mailto:mariab@udel.edu)

## INTRODUCTION

Physical quickness is a movement quality of widespread interest in sport, aging, falls, pathology and rehabilitation. Under the instructions to produce isometric muscular force pulses most rapidly and across a range of submaximal amplitudes, there is a positive linear relationship between the peak force (PF) of a pulse and the corresponding rate of force development (RFD) [1]. The slope of this relationship, termed the *rate of force development-scaling factor* (RFD-SF), quantifies the extent to which RFD scales with the amplitude of the contraction. Studies involving maximal power training have shown improvements of this measure in both young and older adults [3].

It has been suggested that maximal force production does not always correlate with functional ability [2] and high resistance exercise may not be advisable for all elderly and patient populations. Therefore, the first aim of this study was to determine whether a six week exercise program that uses high speed-low resistance stationary cycling would improve the quickness of isometric muscular force production in knee extensors (KE) as well as functional measures in older adults. Assuming that improved quickness would be observed, a second aim was to determine if training in the legs (KE) would transfer to increases in quickness in the arms (elbow extensors - EE) indicating a central adaptation.

## METHODS

Participants visited the laboratory for baseline testing. Assessments included quickness testing (to determine RFD-SF) and functional measures including the Timed Up & Go (TUG) test, 6 meter walk test, and nine-hole peg test. Participants included 6 older adults (mean (SD) age = 73(7) years, height = 165.4(11.4) cm, mass = 77.3(14.9) kg) recruited from a local senior center.

To obtain the RFD-SF, participants were instructed to produce each isometric pulse as quickly as possible and then relax instantly. Participants completed five trials consisting of five brief pulses to each of four approximate amplitudes (20, 40, 60, 80 %MVC). Visual feedback of force was provided as a vertical bar graph, on a computer screen placed at eye level. Isometric pulses were performed in the KE and EE while seated in a custom chair.

Similar to the methods used by others [1] the PF-RFD relationship was computed from the sets of rapid isometric contractions (pulses) performed across a full range of amplitudes. Linear regression parameters were calculated for each subject and the slope (RFD-SF) was the main dependent measure of interest. RFD was computed as the first derivative of force pulses across over-lapping .1s intervals.

After baseline testing, participants completed a six week recumbent cycling program supervised by the experimenter (2 days/week = 12 sessions). During the first session, preferred pedaling cadence (PPC) was determined. Fast cycling was initially defined as 20% faster than the PPC. Exercise sessions began with a 5 minute warm up at the PPC. Then participants completed 10 bouts of fast cycling lasting 20 seconds each. There was a 60 second active recovery period, at PPC, between fast bouts. Sessions concluded with a 5 minute cool down at the PPC. As participants progressed through training, their fast cycling cadence was increased in sensible, individually determined increments.

Upon training completion, participants were assessed in the same baseline parameters to test for improvements. They were tested again four weeks after training cessation to determine if such improvements were retained.

## RESULTS AND DISCUSSION

After six weeks of cycling, RFD-SF improved in all cases except one. One individual's RFD-SF decreased slightly in right EE. There were no differences between the left and right limbs within each individual pre- and post-exercise ( $p > .1$ ). There were differences between individuals indicating that some had greater muscular quickness than others. Greater RFD-SF is associated with higher quality function of the nervous system [1,3].

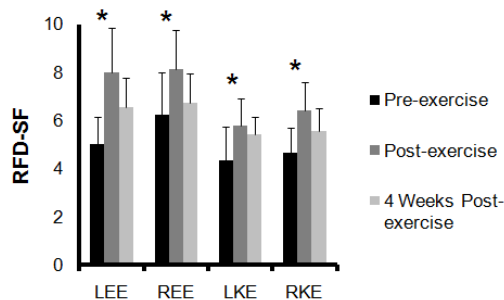


**Figure 1:** Means of RFD-SF before and after cycling intervention. Error bars (SE) indicate between-subjects variability in RFD-SF values. There were significant improvements in RFD-SF in both EE (left and right sides) and KE (left and right sides) with exercise ( $p < .05$ ). Means decreased 4 weeks post-exercise but were not significantly different than post-exercise.

Despite high variability between subjects, this high speed-low resistance cycling program elicited visible improvements in the ability to produce rapid isometric muscle contractions across a full range of forces. Such contractions are especially relevant to fall prevention in the elderly and those with neural impairments as well as activities of daily living including typing, catching an object before it falls, and crossing the street quickly. In conjunction, there were improvements in the TUG and 6 meter walk test which are both standardized measures of walking ability. Along with improved walking speed, most individuals reported increased confidence in walking and ability to take larger steps. That there were improvements in the RFD-SF in EE as well as the 9 hole peg test (a standardized tool to assess hand dexterity) suggests that training one set of muscles may induce adaptations in the central nervous system. Further

analysis of these measures in a control group will elucidate the magnitude of these effects.

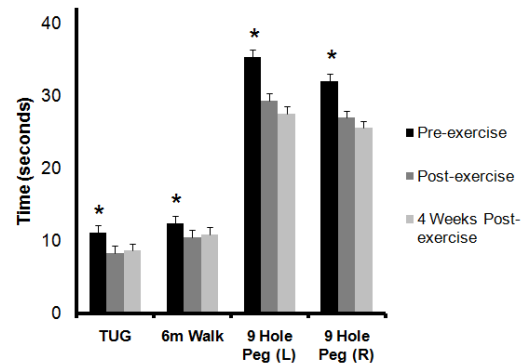


**Figure 2:** There were significant improvements in all functional measures (means presented) pre-post exercise ( $p < .05$ ) and there were no changes 4 weeks following post-exercise testing ( $p > .05$ ).

It is anticipated that the RFD-SF is a measure with high potential to inform rehabilitation researchers and human movement scientists about the quality of movement initiation and the quickness of force production. The RFD-SF measure is appealing because it can be used to quantify the quality of quick force production across the full range of amplitudes, and the resulting units ( $s^{-1}$ ) make it mathematically independent of strength and size of the muscle group of interest. This latter feature facilitates comparisons between individuals and between muscle groups with respect to the underlying neuromuscular determinants of quickness [1].

Interestingly, RFD-SF trended back toward baseline four weeks post-exercise ( $p > .05$ ) while functional measures remained relatively constant. Retention of functional improvements may be suggestive of enhanced self-efficacy in these tasks. In addition, decreases in RFD-SF highlight the importance of remaining active to provide the stimulation necessary to maintain neuromuscular function.

## REFERENCES

1. Freund HJ, Budingen HJ. *Exp Brain Res* **31**, 1-12, 1978.
2. Jaric S. *Sports Med* **32(10)**, 615-631, 2002.
3. Van Cutsem et al. *J Physiol* **513**, 295-305, 1998.

# MUSCLE ACTIVITY DURING GAIT TRANSITIONS

Angela M Berg Robertson

University of Houston, Houston, TX, USA

email: [amrobertson@uh.edu](mailto:amrobertson@uh.edu) web: <http://www.uh.edu/~amrober>

## INTRODUCTION

The triggers underlying gait transitions in humans have received much attention, and explanations related to metabolic cost, bone stress, and muscle function have all been proposed. Most of these studies have analyzed steady walking and running at speeds at or near the preferred walk-run transition speed (PTS). Previous work on the actual realization of gait transitions has generally constrained subjects to a constant acceleration [1], yet transitions executed in daily life are often performed in order to switch suddenly between two different speeds. Moreover, subjects typically walk at speeds much lower than the PTS and run at speeds much higher than the PTS, suggesting that steady gait at the PTS may not typically occur prior to a gait transition. Biomechanical changes during spontaneous transitions between self-selected speeds remain largely unexplored. The objective of this study is to characterize the time-varying activity of important lower extremity muscles during the realization of gait transitions between subjects' self-selected speeds.

There are notable differences in muscle activity patterns during walking and running, even at the same speeds. For example, when walking at the PTS, plantarflexors and dorsiflexors show greater activity than when running at the PTS [2-4]. These observations suggest that increased activity in some muscles is a trigger for gait transitions. This study examined whether peak muscle activities occurred during the step immediately preceding the transition. Although the legs show asymmetry during gait transitions [1], the differences in muscle activity between the leading and trailing legs have not been described. This study also sought to investigate the differences in muscle activity between the legs during gait transitions.

## METHODS

Muscle activations in the rectus femoris (RF), biceps femoris (BF), tibialis anterior (TA), and lateral gastrocnemius (LG) were recorded using surface electromyography (EMG) electrodes (Biometrics). Step parameters (heel strike, toe off) were recorded using a GaitRITE mat and foot switches attached inside subjects' shoes (Biometrics). These data enabled identification of the transition step and the leg used to initiate the transition. Three subjects (one female, two male) were instructed to walk at a comfortable pace and then switch to a comfortable running pace after taking at least one step on the GaitRITE mat. Subjects then performed run-to-walk transitions (RWTs), running at a comfortable pace and then switching to a comfortable walking pace after stepping on the GaitRITE mat. Steady walks were also recorded.

The transition step for WRTs was defined as the step that included the first flight phase. The leading leg for the WRT was defined as the leg that launched into the first flight phase. The transition step for RWTs was defined as the step that included the first double-support phase, with the understanding that the preceding flight phase was part of the transition. The leading leg for the RWT was defined as the leg that landed from the final flight phase. Data from the foot switches were used to determine the transition step and transition leg. EMG signals were band-pass filtered at 20–400Hz, rectified, and then low-pass filtered at 10Hz. The EMG linear envelope was then normalized to the mean EMG activity for each muscle during steady walking (“relative EMG activity”).

## RESULTS AND DISCUSSION

Walk-to-run transition (Fig.1): Results from previous studies suggest that a peak in activation of

the TA and LG during the step just prior to the transition triggers the WRT [2-4]. The activity pattern of the trailing leg TA supports this prediction. By contrast, the leading leg TA increases gradually in activity until the transition, but does not show a notable peak. Also, the LG of the leading leg shows a peak in activity during the actual transition step, while the trailing leg LG shows the greatest activity during the first running step. Activity in the leading leg RF and BF increased the most from the final walking step to the transition step, and then began a slow decline during running. The trailing leg RF and BF showed patterns similar to the leading leg.

Run-to-walk transition: Muscle activity during the RWT showed a generally decreasing trend from the final running steps through the first walking steps. Activity in the leading leg RF, BF, and TA showed slight increases before the final running step. The leading leg RF was the only muscle to show a peak in activity during the step preceding the RWT. However, most muscles showed the greatest decline in activity levels in steps adjacent to the transition.

## CONCLUSIONS

Most muscles do not show peaks in muscle activity during the step just prior to a gait transition. Yet, many muscles do exhibit greater changes in activity at or near the transition step. Humans appear to avoid large peaks in muscle activity during spontaneous gait transitions between self-selected speeds.

## REFERENCES

1. Segers V, Lenoir M, Aerts P and De Clercq D. *Gait & Posture* **26**, 349-361, 2007.
2. Hreljac A. *Gait & Posture* **1**, 217-223, 1993.
3. Neptune RR and Sasaki K. *Journal of Experimental Biology* **208**, 799-808, 2005.
4. Cappellini G, Ivanenko YP, Poppele RE and Lacquaniti F. *Journal of Neurophysiology* **95**, 3426-3437, 2006.

## ACKNOWLEDGEMENTS

Supported in part by the Joe W. King Orthopedic Institute (UH-98166).

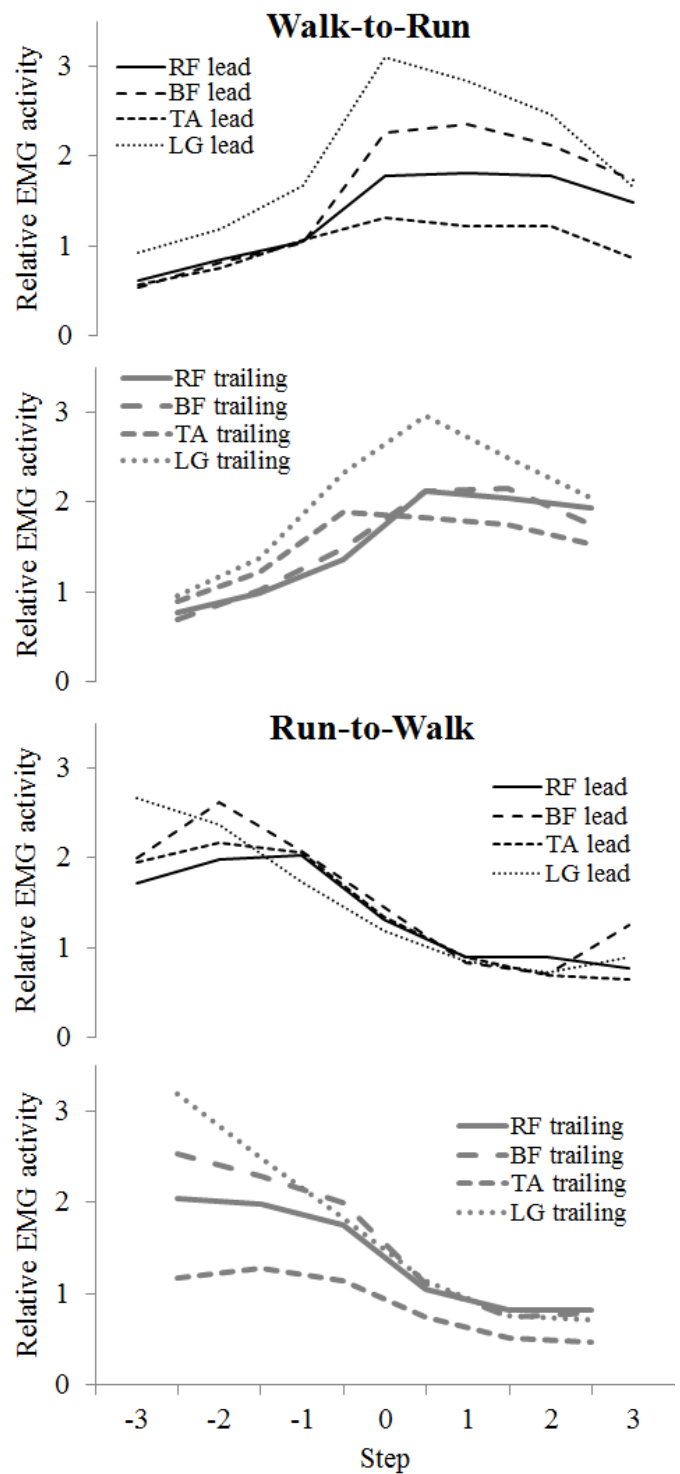


**Figure 1:** Muscle activity during gait transitions, relative to activity during steady walking. Step “0” is the transition step; negative step numbers indicate steps prior to transition; positive step numbers indicate steps after transition. Data shown are grand means.

# ADOLESCENT IDIOPATHIC SCOLIOSIS RIB HUMP: A FIRST BIOMECHANICAL STUDY

<sup>1,2</sup> Jean-Philippe Berateau, <sup>2</sup>Philippe Lasaygues, <sup>3</sup>Hélène Follet, <sup>1</sup>Martine Pithioux and <sup>1</sup>Patrick Chabrand

<sup>1</sup> Institute of Movement Sciences E.J.Marey, (GIBoc team)  
UMR 6233 CNRS/ University of the Méditerranée ; 163, Avenue de Luminy, CP 918  
13288 Marseille Cedex 09, FRANCE

<sup>2</sup> Laboratory of Mechanics and Acoustics (Wave and Propagation team)  
UPR 7051 CNRS 31 ; chemin Joseph-Aiguier 13402 Marseille cedex 20, FRANCE

<sup>3</sup> INSERM UMR 1033, University of Lyon  
7-11 rue G. Paradin 69372 Lyon Cedex 08, FRANCE  
email:jean-philippe.berateau@univmed.fr

## INTRODUCTION

In Adolescent Idiopathic Scoliosis, several investigations [1-2] demonstrated that low bone mineral density (BMD) is a systematic disorder which can be persistent. However, unlike vertebrae, no specific scoliotic ribs data are available in literature neither for internal morphometric data nor for mechanical properties and mineral distribution. To model scoliotic rib cage, realistic data are necessary. Focusing on specific scoliotic's ribs characteristics at the rib hump level is the aim of this paper. Ribs from human surgery wastes (gibbectomy) were studied to assess cross sectional dimensions, BMD and mechanical properties (Young's modulus). A three-step method was developed: firstly, we evaluated the porosity of cortical bone by histology, secondly we processed a Ct-scan evaluation, on whole ribs for cross section dimensions, and on cortical sticks extracted for BMD. Finally, an ultrasonic experimentation provided mechanical values.

## METHODS

On the last two years at the children's hospital, two patients (F15 and F17, respectively female of 15 and 17 years old) without any exclusion criterion (chronic use of medicine, genetic or neuronal disorder, minimum calcium daily amount, ...) and with severe deformities (more than 40° of Cobb angle) were studied. Gibbectomy of ribs 4 to 9 was done, and then the proximal part (1cm length) of each was embedded in methyl metacrylate and

sectionned (8µm thick sections) to process an histomorphometric evaluation with ImageJ®.

A CT-scan (Siemens 64 dual source, Siemens AG, Erlangen, Germany) was carried out to assess the morphology of each rib, cortical thickness was measured at 4 locations (top, bottom, anterior and posterior) and the torsion (alpha angle) of the cortical shell was measured along ribs axis (Fig 1). On cortical sticks, another CT-scan process allowed to relate the CT Hounsfield units (HU) (linear equation) to their own BMD.

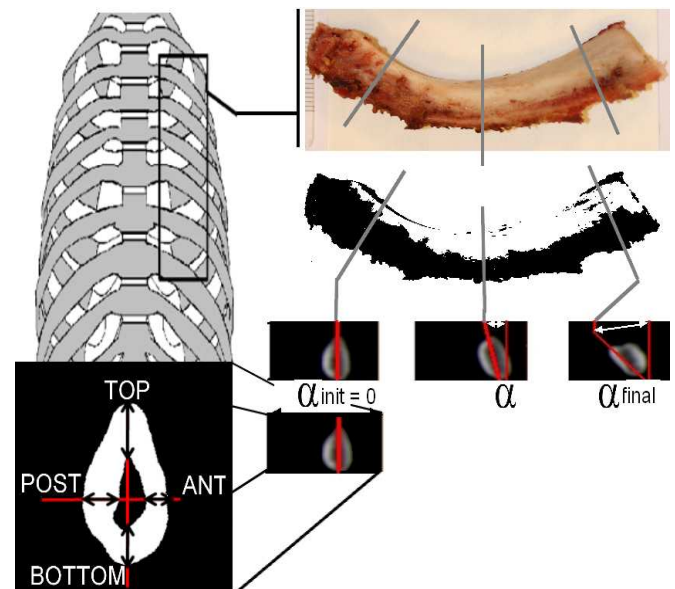


**Figure 1:** morphometric rib analysis

A specific ultrasound device was designed to obtain longitudinal and transversal velocities (VL and VT) using 7 MHz transducer. In longitudinal direction and knowing the density value ( $\rho$ ), Young modulus (E) is obtained.

## RESULTS AND DISCUSSION

Porosity of cortical part is lower than 2.18 %, average value is 1.35 % +/- 0.52 (Results are presented as: mean +/- standard deviation). The histological images show a classical cortical bone organization (lamellar bone with osteon).

Cross sectional dimensions are shown on table1, the three first ribs (R4, R5, R6) got similar alpha rotation angle. The standard deviation does not allow to give normative morphometric data, more subject are expected for.

Because of the curve of each ribs extracted, only 7 rectangular samples were cut from F15's ribs and 8 for F17. The linear equation obtained with HydroxyApatite (HA) phantom, ( $BMD = 0.8565HU + 224.23$ ;  $R^2 = 0.991$ ) lead us to an average value for F15 of  $2204 \text{ mgHA.cm}^{-3}$  and  $2500 \text{ mgHA.cm}^{-3}$  for F17.

Considering condition that the wavelength of the ultrasonic wave (0.22 mm) is ten times lower than slides thickness, we can calculate the longitudinal Young modulus using a law for non-porous material. For the F15's ribs samples, VL is  $2575 \text{ m.s}^{-1}$  (ranged from 2079 to  $3103 \text{ m.s}^{-1}$ ) and VT is  $16601 \text{ m.s}^{-1}$  (ranged from 1598 to  $1746 \text{ m.s}^{-1}$ ). Considering the F17's ribs, VL:  $2711 \text{ m.s}^{-1}$  (ranged from 1799 to  $3516 \text{ m.s}^{-1}$ ) and VT:  $1796 \text{ m.s}^{-1}$  (ranged from 1576 to  $2009 \text{ m.s}^{-1}$ ). In literature, VL values for cortical part of human bone are  $2700 - 3800 \text{ m.s}^{-1}$  [3] and  $3550 - 4180 \text{ m.s}^{-1}$  [4]. To our knowledge up to date, there is no human ribs evaluated using ultrasonic experimentation.

Considering the Young's modulus (E) for F15 and F17 is respectively  $12.1 \pm 4.3 \text{ GPa}$  and  $13.5 \pm 2.5 \text{ GPa}$ . They are different from the range value (5GPa for E) used in most of the finite element models [5]. We cannot compare them because these values are from a global vertebro-costal complex study and models of scoliosis mimics ribs as if it was one entity. Furthermore, we cannot compare our results to 15/17-year-old non scoliotic female

rib due to the lack of reference in pediatric population bone's data.

## CONCLUSIONS

This study is a preliminary histological, Ct-scan and ultrasonic experimental evaluation which provides normative data of cortical sample from scoliotic ribs. In order to provide relevant statistic more samples are necessary. Due to the drastic inclusion criteria, a long term project is planned to study a sufficient number of subjects. Patient specific numerical models of spinal scoliotic deformity optimize brace or surgical treatment, their reliability is an important issue of biomechanical modeling; these new data could improve their biofidelity.

## REFERENCES

1. Lam TP, Hung VW, Yeung HY et al. Abnormal Bone Quality in Adolescent Idiopathic Scoliosis - A Case-control Study on 635 Subjects and 269 Normal Controls with Bone Densitometry and Quantitative Ultrasound. , *Spine*, 2011, Jan 6.
2. Lee WT, Cheung CS, Tse YK et al. Association of osteopenia with curve severity in adolescent idiopathic scoliosis: a study of 919 girls. *Osteoporos Int.*,2005 , Dec16 (12) , 1924-32
3. Katz J.L., Yoon H.S., Lipson S. et al. The effects of remodeling on the elastic properties of bone, *Calcified Tissue International* 1984 36, S31–S36.
4. Yoon H.S., Katz J.L., Ultrasonic wave propagation in human cortical bone - I. Theoretical considerations for hexagonal symmetry; II. Measurements of elastic properties and microhardness, *Journal of Biomechanics*, 1976, 9, 407–412.
5. Describes JL., Aubin CE., Skalli W. et al. Modelling of facet joints in a finite element model of the scoliotic spine and thorax : mechanical aspects *Rachis*, 1995, 7, n°6, 301-314.

| F17 | TOP +/-   | POST +/-  | BOTTOM +/- | ANT +/-   | LENGTH | ALPHA | F15 | TOP +/-   | POST +/-  | BOTTOM +/- | ANT +/-   | LENGTH | ALPHA |
|-----|-----------|-----------|------------|-----------|--------|-------|-----|-----------|-----------|------------|-----------|--------|-------|
| R4  | 0,68 0,20 | 1,11 0,71 | 0,75 0,28  | 0,99 0,20 | 83     | 51    | R4  | 0,84 0,21 | 0,59 0,15 | 0,65 0,14  | 0,63 0,18 | 64,2   | 54    |
| R5  | 1,11 0,35 | 0,95 0,25 | 0,95 0,38  | 0,98 0,44 | 66,6   | 7     | R5  | 0,86 0,18 | 0,60 0,16 | 0,62 0,12  | 0,72 0,29 | 46,8   | 6     |
| R6  | 1,16 0,35 | 0,91 0,18 | 0,84 0,24  | 0,76 0,18 | 62,4   | 18    | R6  | 0,54 0,17 | 0,79 0,15 | 0,90 0,41  | 0,56 0,20 | 49,8   | 16    |
| R7  | 0,99 0,26 | 0,74 0,13 | 0,66 0,08  | 0,82 0,15 | 44     | 0     | R7  | 0,59 0,25 | 0,42 0,19 | 0,59 0,24  | 0,80 0,40 | 40     | 14    |
| R8  | 1,07 0,24 | 0,74 0,24 | 0,61 0,20  | 1,04 0,41 | 28,6   | 3     | R8  | 0,67 0,21 | 0,49 0,16 | 0,61 0,2   | 0,85 0,37 | 27     | 36    |
| R9  | 0,61 0,14 | 1,00 0,22 | 0,75 0,16  | 0,77 0,16 | 13,6   | 2,7   | R9  | 0,46 0,25 | 0,38 0,23 | 0,46 0,24  | 0,53 0,24 | 12,6   | 11    |

**Table 1:** Cortical thickness (mm) of the ribs (Ri) measured at four locations (Top, Post, Bottom and Ant) are presented as mean +/- SD, length of each piece of rib is reported as well as angle alpha (in degrees).

# BIODYNAMICS OF STEPPING UP AND DOWN WHILE WEARING MULTIFOCAL LENS EYEGLASSES

<sup>1</sup>Kurt E. Beschorner, Dennis Tomashek and Roger O. Smith

University of Wisconsin-Milwaukee, Milwaukee, WI, USA

<sup>1</sup>email: [beschorn@uwm.edu](mailto:beschorn@uwm.edu) web: [http://www4.uwm.edu/ceas/faculty\\_profiles/KEBeschorner.html](http://www4.uwm.edu/ceas/faculty_profiles/KEBeschorner.html)

## INTRODUCTION

Bifocal and other multifocal lens (MFL) eyeglasses are commonly prescribed for people with vision deficits that require different corrective eyewear for close and distance viewing. MFL glasses have the side effect of blurring and distorting the lower field of vision during walking, which increases the risk of falling [1]. This distortion makes identifying step edges particularly difficult (Fig. 1). In response to this distortion, MFL wearers typically adapt a cautious approach to stepping up by increasing toe clearance and slowing of the gait [2]. This increased toe clearance is accompanied by an increase of toe clearance variability due to the inability to precisely identify the location of the step edge [2]. Research on stepping down while wearing MFL glasses has suggested a similarly cautious strategy accompanied with higher leg support of the stance leg, increased step execution time and increased knee flexion and ankle plantarflexion [3]. This research however, was collected from a stationary position, which may be a systematically different task than stepping down off of a step while walking, which requires that a person identify the location of the step edge and plan their gait to appropriately approach the step. The aim of this study examines gait changes in stepping down from steps while wearing non-corrective single lens and multifocal lens glasses.



Figure 1: Picture of step through progressive lens glasses

## METHODS

Five college-aged participants were recruited for a single 1.5 hour testing session. The protocol was approved by the University of Wisconsin-Milwaukee Institutional Review Board. Subjects were asked to perform a loop course, which includes walking a 15 m straightaway followed by a modified dynamic gait index tasks. Subjects experienced five walking conditions in random order: baseline walking, walking up a ramp followed by a 75 mm step down, walking up a ramp followed by a 150 mm step down, a 75 mm step up followed by a ramp down and a 150 mm step up followed by a ramp down. Subjects performed at least 3 of each of these trials while wearing single lens (SL) or progressive MFL glasses with no upper lens region correction, and an “add” of +2.75 diopters in the lower region.

The kinematics of the step up and the kinematics and dynamics of the step down were examined. In particular, our analysis focused on the ability of the subjects to identify the location of the lower floor surface. These measures included heel clearance during step down, peak normal force during step down and the vertical heel velocity during step down. Traditional step up measures including toe clearance and toe clearance variability were used to compare the subject population with previously tested populations. Statistical significance was set at 0.05.

## RESULTS AND DISCUSSION

While wearing progressive lens glasses compared with single lens glasses, subjects had increased toe clearance during the step up trials ( $p < 0.05$ ). This effect was exacerbated by the high step up condition as indicated by a toe clearance by step height

interaction ( $p < 0.05$ ). Toe clearance was associated with vertical lifting of the foot ( $r = 0.99$ ), longer distance from the step to the stance foot ( $r = 0.67$ ), smaller distance from the step to the foot placement of the stepping foot ( $r = -0.61$ ) and larger hip flexion angle ( $r = 0.45$ ). The higher toe clearance is indicative of a cautious strategy to reduce trip risk by increasing the safety margin. This effect is consistent with effects reported previously by Elliott & Chapman and indicates that young novice wearers adapt a similar strategy to stepping up while wearing MFL glasses as older adults [2].

Subjects wearing MFL glasses during the step down condition had an increase in maximum normal force ( $p < 0.01$ ). Once again the higher height of the step exacerbated this effect as indicated by the step height by glasses condition effect ( $p < 0.05$ ). The vertical force was correlated with vertical heel velocity ( $r = -0.55$ ). The larger normal force and higher heel vertical velocity indicates that subjects were not able to accurately identify the location of the lower level and were not able to match their heel velocity to the floor. The results are contradictory to previous results, which have shown that subjects cautiously step down off of a step while wearing multifocal lens glasses and “feel” for the lower level while keeping force on the stance leg [3]. In the previous research, subjects stepped down from a standing condition, which may have allowed them to take a longer time during the step down condition. In this study, subjects were walking and their forward walking velocity may have reduced their ability to keep weight on the stance leg while the walking leg was stepping down. In addition, subjects were required to plan the location of their approach step as well as the step down, which might have compromised their ability to determine the location of the step down as compared with Elliott & Chapman [2]. This study indicates that while wearing MFL glasses, people who walk aggressively or those in a hurry who do not terminate gait prior to step down may be at increased risk of losing balance than those who do terminate gait.

Subjects who wore MFL glasses adapt cautious protective strategies that likely reduce fall risk during step up conditions yet are not able to create those same adaptive strategies during step down without terminating gait. This indicates that studies

on MFL glasses and stepping should be particularly interested in the step down conditions. Research by van Linden et al. has shown that an unexpected step down can destabilize the body and require a whole body response to recover balance [4]. A similar yet possibly milder effect should be expected when a person knows that a step down is occurring but is unsure of the height of the step down and therefore is unable to match their heel velocity during step down. In addition, the increased normal forces associated with MFL glasses may lead to buckling of the leg in older adults with weaker leg muscles.

The subjects used in this study were primarily young and healthy subjects and were novel MFL wearers. While this group does not represent the typical subject population wearing MFL glasses, their response to MFL glasses during step up conditions is consistent with previous studies that used experienced older adults [2]. In addition, these data show at a fundamental level, how distorting the lower visual field affects a person’s ability to match heel velocity during step down and properly perceive the height of the step. Our intention is to expand this pilot study to include novice and experienced older adult MFL wearers to isolate differences caused by aging as well as experience in stepping down ability.

## CONCLUSIONS

Subjects wearing MFL glasses during stepping up conditions adapt protective responses that are not possible during step down conditions. Research identifying fall risk and training programs to reduce fall risk should particularly consider stepping down condition. In addition, future research isolating the role of aging, experience and the effect of multiple steps on balance would shed more light on the role of aging and vision during stepping down task.

## REFERENCES

1. Lord SJ et al. *J. Am. Geriatrics Society* **58**, 1760-6, 2002.
2. Elliott DB and Chapman, GJ, *Inv Ophthalmology & Visual Science* **51**, 718-22, 2010.
3. Buckley JK et al. *Gait & Posture* **21**, 65-71, 2005.
4. van der Linden MD et al. *J. Neurophysiology* **97**, 3639-50

# WII FIT TRAINING TO IMPROVE BALANCE IN OLDER ADULTS: A FEASIBILITY STUDY

Kathleen Bieryla and Neil Dold

Bucknell University, Lewisburg, PA, USA

email: [k.bieryla@bucknell.edu](mailto:k.bieryla@bucknell.edu)

## INTRODUCTION

Training using Nintendo's Wii Fit may be a novel way to improve balance in older adults. The Wii Fit is a game for Nintendo's Wii that uses an additional accessory, the Wii Balance Board. The Balance Board is similar to a force platform as it can monitor the center of pressure of a person but is less expensive and requires minimal training [1]. Using the Wii Fit would allow participants to complete training in their own living room with no supervision. This may make it more likely that participants would continue with the training after a study has ended.

The purpose of this study is to investigate the feasibility of training using the Wii Fit and Balance Board to improve clinical measures of balance in older adults. It is hypothesized that older adults who train with the Wii Fit will increase their Berg Balance Scale (BBS) score and Functional Reach (FR), and decrease their Timed Up & Go (TUG) time.

## METHODS

Eleven healthy older adults recruited from a local senior living community ranging in age from 70-92 years old completed the study. The study was approved by Bucknell University's Institutional Review Board and written consent was obtained from all participants prior to participation.

Participants were randomly assigned to either an experimental group (n=5) or control group (n=6). The experimental group completed training on the Wii Fit three times a week for three weeks (Fig. 1). Each training session consisted of a series of strength exercises, yoga poses, and balance games and lasted approximately 30 minutes. The control group continued with their normal daily routine.

Three clinical measures of balance were collected one week before training, one week after training, and one month after training: BBS, FR, and TUG.



**Figure 1:** Older adult completing the half moon yoga pose during training with the Wii Fit.

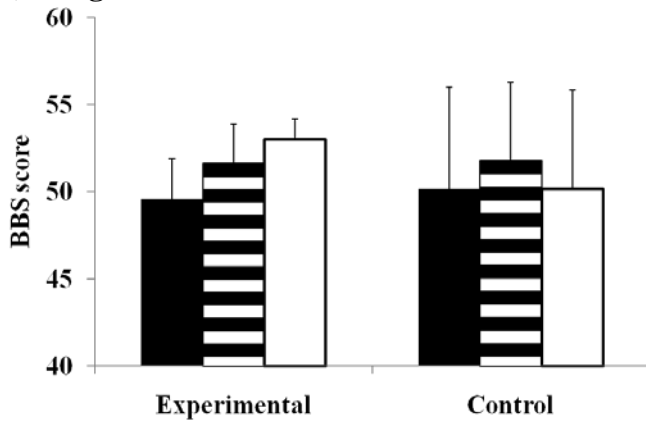
Clinical measures of balance before training were compared to one week and one month after training. An increase in BBS and FR would be considered an improvement in balance as would a decrease in TUG. Paired t-tests were conducted on the control and experimental group to determine if training using the Wii Fit influenced measures of balance. All statistical analysis was completed in JMP with significance set at  $p < 0.05$ .

## RESULTS AND DISCUSSION

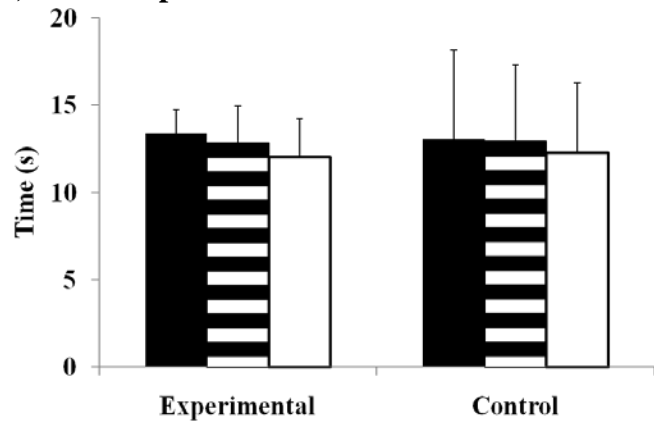
BBS scores significantly increased one week and one month after training when compared to before training for the experimental group ( $p < 0.05$ ) (Fig. 2). There was no significant change in BBS for the control group.

TUG and FR were not significantly different from before training for either the control group or experimental group ( $p > 0.05$ ).

**a.) Berg Balance Scale**



**b.) Timed Up & Go**



**c.) Functional Reach**

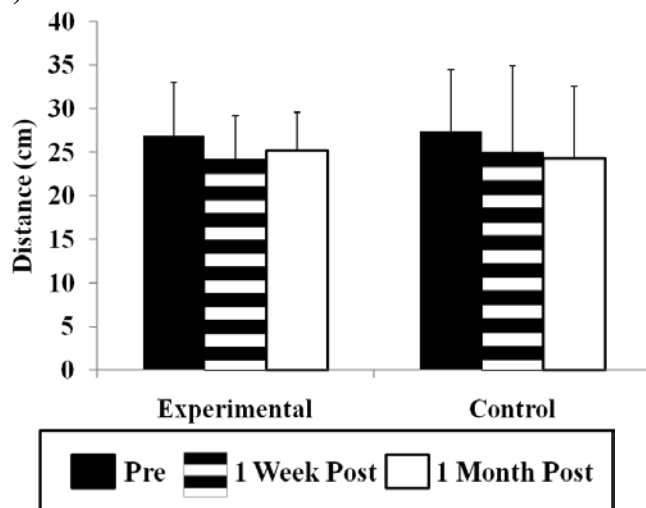


**Figure 2:** BBS (a), TUG (b), and FR (c) results from before training, one week after, and one month after for both the experimental and control group. Error bars represent standard deviation.

Few studies have examined the efficacy of training using the Wii Balance Board to improve measures of balance in older adults. One study examined the effect of four training sessions on a single stroke patient [2]. Although this was only one subject and

not an extended training period, this subject was able to decrease their TUG by 10 seconds and also increase their FR and BBS. These changes may not be directly attributed to the Wii Fit training, but do show promise. Another study involving stroke patients used the Wii Balance Board for training with a custom designed program [3]. Although no quantitative results were given, qualitatively the participants enjoyed the physical therapy and thought it to be more challenging compared to regular therapy. The prior studies examine the effect of training on stroke patients while this is the first to examine the effect on healthy older adults but the results for all studies are promising.

The possibility of using the Wii Fit with Balance Board for balance training is appealing for many reasons. First, participants tend to enjoy what they are doing [3]. Another benefit is the low cost for the entire system. The Wii along with the Wii Balance Board and Wii Fit game can be purchased for under \$300. This low cost would allow people to continue the training at home. With these reasons, the potential for long term adherence to the training program outside of the study is large.

**CONCLUSIONS**

In conclusion, this pilot study provides some evidence that training using the Wii Fit and Balance Board can lead to some improvements in clinical measures of balance in older adults. A larger study is needed to confirm the efficacy of training as a method to improve balance.

**REFERENCES**

1. Clark RA, et al. *Gait & Posture* **31**, 307-310, 2010.
2. Sugarman H, et al. *Virtual Rehabilitation International Conference* 111-116, 2009.
3. Lange B, et al. *Top Stroke Rehabil* **17**, 345-352, 2010.

**ACKNOWLEDGEMENTS**

Neil Dold was supported by The Bucknell Program for Undergraduate Research.

# A PILOT STUDY OF THE EFFECTS OF UPPER EXTREMITY LYMPHEDEMA ON 3-DIMENSIONAL SHOULDER KINEMATICS AND FUNCTION IN SURVIVORS OF BREAST CANCER

Linda Biggers, Ryan Bojrab, Brian Hilts, Justin Kempson, Zach Overman, Peter Rundquist

University of Indianapolis, Indianapolis, IN, USA  
email: [prundquist@uindy.edu](mailto:prundquist@uindy.edu)

## INTRODUCTION

Breast cancer is the most common form of cancer in women [1]. It is estimated that up to one third of breast cancer survivors will be diagnosed with lymphedema [2]. Lymphedema may lead to difficulty performing activities of daily living above 90° elevation, discomfort, and sensation of heaviness [1,3].

There is little research on the effects of lymphedema on shoulder function. Two research hypotheses were developed: 1) Affected upper extremity (UE) range of motion in at least one plane of motion would be significantly less and volume would be significantly greater than the unaffected UE. 2) Participant's demographics (age, months from surgery, months from lymphedema diagnosis), affected UE volume, and shoulder kinematics would be significantly correlated to the Penn Shoulder Score (PSS).

## METHODS

This study included 10 participants with unilateral lymphedema post mastectomy. Shoulder flexion (FLX), abduction (ABD), and elevation in the plane of choice (POC) were assessed using a 3-dimensional electromagnetic motion capture system. Humerus, scapula, and trunk segment locations and rotation sequences were performed as recommended by the International Society of Biomechanics [4]. Data was collected from the unaffected shoulder first. Participants performed each motion three times. The peak value across the trials was utilized for data analysis. The order of motions was randomized for each participant. Arm volume was measured with a volumeter. Shoulder function was assessed using the PSS.

Data analyses included paired t-tests comparing the upper extremities' kinematics and volume and correlations between the factors of interest and PSS. Significance level was  $p \leq 0.05$ .

## RESULTS AND DISCUSSION

All of the variables were normally distributed except for length of time from lymphedema diagnosis. Participants' affected UE volume, demographics, and PSS are outlined in table 1. All participants were right handed, and 5/10 had lymphedema in their right upper extremities.

**Table 1:** Participant demographics

|                         | Mean   | s.d.  |
|-------------------------|--------|-------|
| Affected UE Volume (ml) | 3048.0 | 302.6 |
| Age (years)             | 62.8   | 8.3   |
| Months from surgery     | 48.3   | 35    |
| Penn Shoulder Scale     | 75.1   | 19.7  |
|                         | Median | Range |
| Months from Diagnosis   | 7.0    | 1-109 |

UE volume was the only statistically significant difference found ( $t=4.620$ ,  $p = .001$ ). Scapular upward rotation (UR) during elevation in POC and humerus to trunk (HT) abduction approached significance ( $t = -2.170$ ,  $p = .058$  and  $t = -2.124$ ,  $p = .063$  respectively). The humerus to trunk and scapula to trunk kinematics are outlined in Figure 1.

None of the PSS correlations were statistically significant. The Spearman correlation between months of time from lymphedema diagnosis and the PSS was the closest ( $r = 0.628$ ,  $p = .052$ ). Correlation results are outlined in table 2.

Paired t-test effect size analysis [5] yielded effect sizes of .77 (large) and .70 (medium) for scapular UR during elevation in the POC and HT ABD.

Correlation effect size analysis yielded a .63 (medium) effect size. Power analysis yielded paired t-test sample sizes of 14 and 16 and correlation sample size of 21 to reach significance [6].

The first hypothesis was partially supported. The involved UEs had significantly more volume than the noninvolved. However, none of the kinematics were significantly different between extremities. The second hypothesis was not supported. None of the correlations to the PSS were significant.

The results are limited by sample size. With 22 participants, statistically significant differences may have been found in scapular UR during elevation in the POC, in HT ABD and significant correlation between months from lymphedema diagnosis and the PSS.

Significant differences in HT ABD and scapular UR during elevation in the POC would point to potential rehabilitation emphases in this population. A positive correlation between months since lymphedema diagnosis and PSS indicates the longer someone has lymphedema the better they function. This may point toward compensation.

As none of the correlations to the PSS were significant, an alternative shoulder functional scale may be more appropriate. There is currently no lymphedema specific scale in the literature.

## CONCLUSIONS

Extremity volume is different in participants with lymphedema post-breast cancer surgery. Further study is necessary to determine the effect of lymphedema on upper extremity kinematics and function in this population.

## REFERENCES

1. Morrell RM, et al. *Mayo Clin Proc* **80**, 1480-1484, 2005.
2. Thomas-Maclean R, et al. *Oncol Nurs Forum* **35**, 65 -71, 2008.
3. Kwan W et al. *J Clin Oncol* **20**, 4242-4248, 2002.
4. Wu G, et al. *J Biomech.* **38**, 980-992, 2005.
5. Thalheimer W and Cook S, *How to Calculate Effect Sizes from Published Research: A Simplified Methodology*, Work-Learning Research, 2002.
6. Howell DC. *Statistical Methods for Psychology*, 4<sup>th</sup> ed, Duxbury Press, 1997.

**Table 2:** Correlations Between PSS and Factors of Interest

|       | Volume | HT ABD | ST ABD | HT FLX | ST FLX | ST POC | ST POC | Age   | Dx Mo | Surg Mo |
|-------|--------|--------|--------|--------|--------|--------|--------|-------|-------|---------|
| PSS r | -.151  | .277   | -.096  | .036   | -.066  | -.226  | -.226  | -.193 | .628  | .074    |
| p     | .677   | .438   | .792   | .922   | .856   | .530   | .530   | .593  | .052  | .850    |

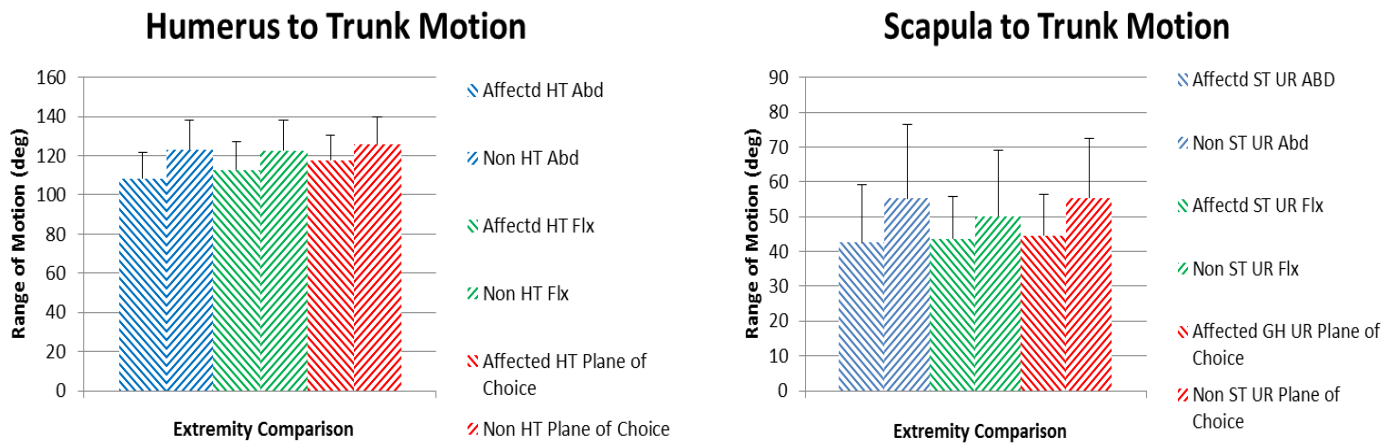


**Figure 1:** Comparative Humerus to Trunk and Scapula to Trunk Motion

# Biomechanical Simulation of the Passive Mechanical Coupling in the Hand and Wrist

<sup>1,2,4</sup>Ben Binder-Macleod, <sup>1,2,3</sup>Jules Dewald, and <sup>1,3,4,5</sup>Wendy Murray

Departments of <sup>1</sup>Biomedical Engineering, <sup>2</sup>PTHMS, and <sup>3</sup>PM&R, Northwestern University, Chicago, IL  
<sup>4</sup>SMPP, Rehabilitation Institute of Chicago, Chicago, IL; <sup>5</sup>Edward Hines Jr. VA Hospital, Hines, IL  
email: [bbinder@u.northwestern.edu](mailto:bbinder@u.northwestern.edu) web: <http://www.bme.northwestern.edu/>

## INTRODUCTION

Many of the muscles that control hand movement cross more than one joint. In particular, the extrinsic muscles of the hand originate in the forearm and cross the wrist. This complex musculoskeletal anatomy creates passive mechanical linkages between joints; the passive moment about a given joint is highly dependent on the position of all of the the joints a multi-articular muscle crosses [1]. In nonimpaired individuals, the passive coupling between the wrist and hand facilitates opening and closing of the fingers during grasping tasks. Because of the passive forces produced by the extrinsic finger muscles, wrist flexion assists opening of the fingers and wrist extension facilitates closing of the fingers. This coupling can be altered in the impaired hand. For example, stroke survivors have difficulty opening their fingers to grasp an object even in flexed wrist postures. Understanding the mechanisms that alter this coupling is imperative to enhancing rehabilitation techniques.

We used a multi-joint musculoskeletal model of the upper limb to evaluate how the passive properties of the multi-articular extrinsic finger muscles affect the resting position of the metacarpophalangeal (MCP) joint of the index finger. The objective of this study was to demonstrate the importance of including the passive coupling between the wrist and the fingers in biomechanical models.

## METHODS

A computer-graphics based kinematic model of the upper-extremity [2] was utilized to facilitate a static equilibrium analysis. The model consists of 3D surface representations of all the bones of the thorax, arm, forearm, wrist, and hand, joint kinematics for 15 degrees of freedom of the upper limb, and muscle-tendon paths and force generating properties of 50 muscles and muscle compartments. We defined the inertial properties of the upper limb

to be consistent with published data describing a 50<sup>th</sup> percentile male [3]. With the exception of the MCP and wrist joints, we constrained all joints within the model. We also defined a “restraining moment” for the MCP joint to enforce the limits of the range of motion. The restraining moment is independent of adjacent joint postures and reflects the elastic moments produced by the joint capsule, ligaments, the intrinsic muscles, and other soft tissues. The restraining moment for the MCP joint was defined based on experimental data [1].

With the model in a posture in which gravity opposes wrist extension (90° elbow flexion, 90° pronation), we calculated the joint angle ( $\theta$ ) at which the net passive moments about the MCP joint equal 0 Nm. That is;

$$M_g(\theta, \varphi) + M_R(\theta) + M_{FDP}(\theta, \varphi) + M_{FDS}(\theta, \varphi) \\ + M_{EI}(\theta, \varphi) + M_{EDC}(\theta, \varphi) = 0$$

Where  $M_g$  is the moment produced by the mass of the distal, middle, and proximal phalanges of the finger,  $M_R$  is the restraining moment, and the remaining terms are the passive moments produced by the extrinsic muscles of the index finger; flexor digitorum profundus (FDP), flexor digitorum superficialis (FDS), extensor indices (EI), and extensor digitorum communis (EDC).

The passive moments calculated for the individual extrinsic muscles were estimated using the model [2]. The kinematic model allows calculations of muscle length, forces, and joint moments as a function of all the joints the muscle crosses. The published model prescribed the optimal length of muscles near the anatomical neutral position of the hand. We adjusted the tendon slack lengths of the extrinsic muscles of the index finger to replicate the passive moments produced by the extrinsic muscles of the index fingers reported experimentally [1].

At each wrist position, we evaluated the work done passively by the individual extrinsic muscles to resist motion of the MCP joint:

$$W_i(\varphi) = \int_{-\frac{5\pi}{18}}^{\frac{\pi}{2}} |M_i| d\theta$$

where  $W_i$  is the work of the  $i$ th extrinsic muscle over the MCP range of motion, -50 to 90 degrees flexion (converted to radians), at wrist angle  $\varphi$ , and  $M_i$  is the moment of the  $i$ th muscle at MCP angle  $\theta$ . The work done by the passive intrinsic structures to resist motion over the MCP range of motion was calculated similarly. To simulate a flexion contracture, the optimal fiber lengths of the extrinsic flexor muscles were decreased to 95% of nominal lengths [4]. The passive work of the flexor muscles was recalculated to assess the potential for a flexion contracture to limit motion.

## RESULTS AND DISCUSSION

Our simulations of the resting position of the MCP joint of the index finger replicate the natural passive coupling observed between the fingers and the wrist in the nonimpaired hand. As the wrist rotates from an extended to a flexed posture, the rest position of the MCP joint moves from a flexed to an extended posture, respectively (Fig. 1). In extended wrist postures, the primary musculoskeletal structures resisting motion at the MCP joint passively are the extrinsic flexors (Fig. 2). This resistance decreases substantially as the wrist moves to neutral, and then is replaced by the actions of the extrinsic extensors when the wrist is flexed. The work done passively by the structures intrinsic to the hand is relatively small.

The work done by the flexors nearly doubled in extended wrist postures when we simulated even a very small adaptation in muscle fiber length. These simulations suggest that even minimal structural changes to the extrinsic muscles of the hand can have a large effect on the passive resistance to motion.

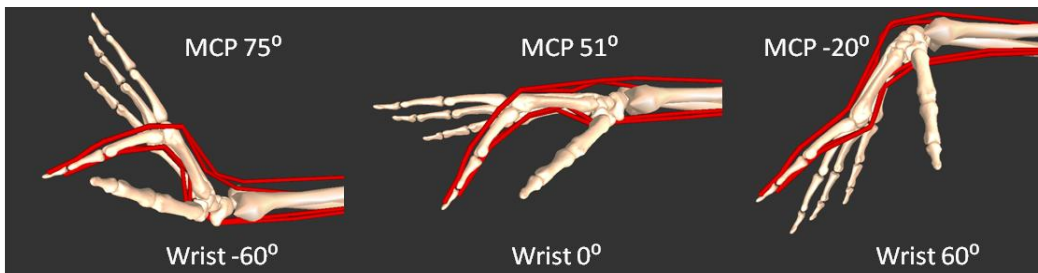


**Figure 1.** Resting position of the MCP joint as a function of wrist position.

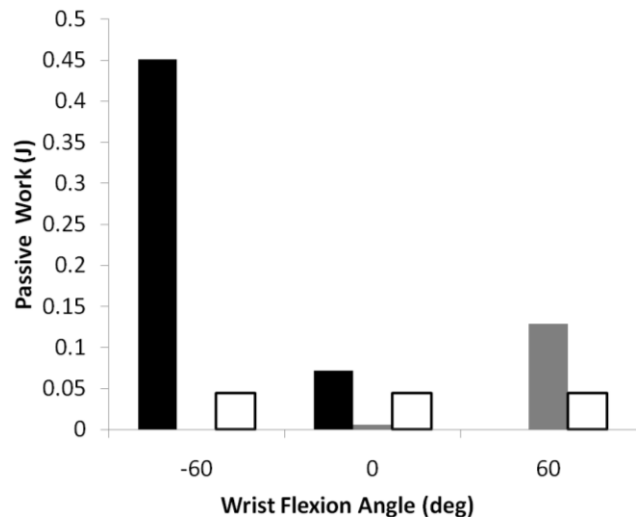


**Figure 2.** The work done passively to resist motion of the MCP by the extrinsic flexor muscles (black bars), extrinsic extensors (gray bars) and structures intrinsic to the hand (open bars).

## CONCLUSIONS

This study describes a musculoskeletal model of the hand that can be used to study the functional consequences of the mechanical couplings that results from the complex musculoskeletal anatomy of the upper limb. Expanding our simulations to incorporate multiple joints of the index finger, as well as including multiple fingers and the thumb should lend insight to the study of neuromuscular control of functional hand motion and its rehabilitation.

## REFERENCES

1. Knutson JS, et al. J Biomech. 33:1675-81. 2000
2. Holzbaur KR, et al. Ann Biomed Eng. 33:829-40. 2005
3. McConville JT, et al. AFAMRL-TR-80-119. 1980
4. Kamper KG, et al. Muscle Nerve 23:954-961. 2000

## ACKNOWLEDGEMENTS

This work is funded by the NIH (T32 EB009406) and The Searle Funds of the Chicago Community Trust.

# Validity and Accuracy of a Slip Resistance Measurement Protocol for the Assessment of Slip Potential

Mark G Blanchette and Christopher M Powers

University of Southern California, Los Angeles, CA, USA  
email: [mgblanch@usc.edu](mailto:mgblanch@usc.edu), web: <http://pt.usc.edu/labs/mbri>

## INTRODUCTION

Slips occur when the utilized friction (uCOF) of an individual exceeds the available friction (COF) provided by the shoe-floor interface [1]. An important issue in preventing slips and slip-related injuries is accurate assessment of the available friction provided by the shoe-floor interface. To date, the current method accepted in the footwear industry as the gold standard (SATRA STM 603) has not been evaluated in the peer-reviewed literature. The purpose of this study was to assess the validity of the SATRA STM 603 whole shoe tester using standard ISO EN 13287 [2] in predicting slip potential. A secondary purpose was to determine the accuracy with which EN 13287 predicts slip outcome.

## METHODS

Five men ( $31.2 \pm 5.2$  years,  $1.8 \pm 0.0$  m,  $81.8 \pm 5.1$  kg) and 5 women ( $28.4 \pm 7.4$  years,  $1.7 \pm 0.1$  m,  $57.7 \pm 5.9$  kg) participated in this study. Each subject was provided with footwear in their respective size. Each shoe was constructed of the same upper design and material. Each outsole was constructed of the same material (styrene butadiene rubber) and hardness (62 A). The footwear tread was standardized with the following groove parameters: 3 mm width, 4 mm depth and perpendicular orientation. Available friction testing of the footwear was performed with the SATRA STM 603 utilizing the EN 13287 protocol with the following test parameters (Normal force 500 N, sliding velocity 30 cm/s, contact angle  $7^\circ$ ) [2]. The COF of the test shoe was assessed to be 0.336.

To ensure safety, subjects wore a fall-arresting safety harness (Miller Model 550-64; Franklin, PA) attached via 8 mm climbing rope (Pigeon Mountain Industries, LaFayette, GA) to an overhead trolley

that moved along an overhead track. A 2' x 4' dry porcelain tile was embedded in the middle of a 10 m walkway. During a single walking trial, subjects were exposed to a potentially slippery condition without their knowledge (distilled water applied to a porcelain tile). Subjects wore goggles with the lower half of the visual field blocked to prohibit awareness of the slip condition. Slips were defined as greater than 4 cm resultant translation of the heel marker while in contact with the contaminated surface [3].

Lower extremity three-dimensional kinematics were recorded at 150 Hz (Qualisys AB, Gothenburg, Sweden) and ground reaction forces were recorded at 1500 Hz (AMTI, Newton, MA, US). Utilized friction was calculated as the ratio of resultant shear force to vertical force. For each trial, subjects' peak uCOF was determined during the first 50% of the stance phase. To avoid spuriously high friction values occurring when minimal body weight is supported by the stance limb, only uCOF data after the first 5% of stance phase was considered. To determine the relation between probability of slip and the difference between available friction and peak uCOF, a logistic regression model was generated. Validity of EN 13287 was assessed by whether the difference between available friction and peak uCOF was a significant predictor of slip outcome. Model significance was determined by a Wald test ( $p < 0.05$ ). Slip prediction accuracy of the EN 13287 test method was determined from the percentage of no slip and slip outcomes that corresponded to the associated positive or negative difference between available friction and peak uCOF [4]. To test for differences in anthropometrics and walking velocity between individuals who experienced a slip and those who did not, an independent t-test was performed ( $p < 0.05$ ).

## RESULTS AND DISCUSSION

Five of the 10 subjects slipped on the contaminated surface (2 women and 3 men). There were no differences in anthropometrics or walking velocity between individuals who experienced a slip and those who did not (Table 1).

The difference between available friction and peak uCOF was not a significant predictor of slip outcome for the EN 13287 protocol (Fig. 1). All 10 subjects had a positive difference between available friction and peak uCOF, indicating no slips should have occurred. However, 5 of the 10 subjects did slip. Overall, assessment of COF with the EN 13287 protocol resulted in only a 50% slip prediction accuracy.

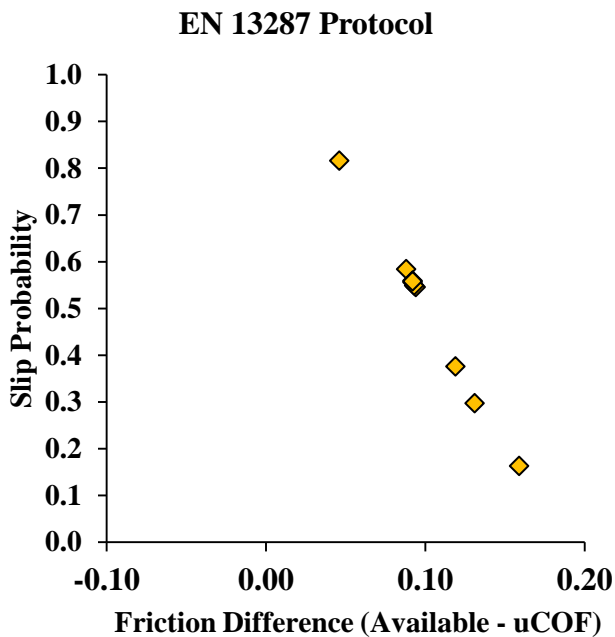


**Figure 1:** The relation between predicted slip outcome and the difference between available and peak uCOF. Available friction measured with EN 13287.

**Table 1:** Characteristics of slip outcome groups. Mean (SD)

| Outcome | N | Age (yrs)  | Height (m) | Weight (kg) | Velocity (m/s) |
|---------|---|------------|------------|-------------|----------------|
| Slip    | 5 | 31.6 (6.6) | 1.82 (0.1) | 73.2 (9.3)  | 1.95 (0.1)     |
| No Slip | 5 | 28.0 (5.9) | 1.68 (0.1) | 66.3 (17.5) | 1.83 (0.1)     |

\* indicates significantly different between groups.

Available friction was assessed with the EN 13287 protocol using the SATRA STM 603. The difference between available friction and peak uCOF was not a significant predictor of slip outcome. These preliminary results are based on a logistic regression model that lacks power due to inadequate sample size. Further data collection is required. Based on the preliminary data, the EN 13287 protocol only predicted 50% of slip trial outcomes. To prevent slip related injuries, a valid test method with a high degree of slip prediction accuracy is essential.

## CONCLUSIONS

The results of our study indicate that the use of the SATRA STM 603 with the EN 13287 protocol may not be a valid method to predict slip potential. Future research is required to determine if altering the parameters of EN 13287 improves model validity and slip prediction accuracy.

## REFERENCES

1. Hanson JP, et al. *Ergonomics* **42**, 1619-33, 1999.
2. ISO EN 13287. *Test Method for Slip Resistance*, 2007
3. Powers CM, et al. *J Forensic Sci* **55**, 366-70, 2010.
4. Burnfield JM, Powers CM. *Ergonomics* **49**, 982-95, 2006.

# BMI, BODY VOLUME DISTRIBUTION AND SAGITTAL PLANE GAIT PARAMETERS

<sup>1,2</sup>Katerina Blazek, <sup>2</sup>Jessica Asay, <sup>2</sup>Jennifer Erhart, <sup>1,2</sup>Thomas Andriacchi

<sup>1</sup>Stanford University, Stanford, CA USA

<sup>2</sup>VA Bone and Joint Rehabilitation R&D Center, Palo Alto, CA USA

email: [kblazek@stanford.edu](mailto:kblazek@stanford.edu)

## INTRODUCTION

Obesity has been shown to be a major risk factor for knee osteoarthritis (OA) incidence, with greater risk for women than men.<sup>4</sup> Recent work<sup>2</sup> has shown that early OA changes in obese individuals are localized to the patello-femoral joint, and are likely linked to knee hyperextension. It has been suggested that differences in adiposity distribution can help explain these gait differences, but a recent study<sup>6</sup> found no relationship between peak knee adduction moment and thigh circumference or waist to thigh circumference ratio (WTR) in a group of obese adults after controlling for weight. Given the relationship between cartilage changes and knee flexion during walking, the link between obesity distribution and changes in sagittal motion at the knee is an important research question. **The purpose of this present study was therefore to address the following hypotheses: 1.) Body mass index (BMI) will be negatively associated with knee flexion angles and moments during normal walking; 2.) Measures of body volume distribution (waist and thigh circumference, waist to thigh ratio, and % lower body volume) will be associated with knee flexion angle and flexion moment during gait after controlling for BMI, gender, age, and walking speed.**

## METHODS

102 subjects between 20 and 60 years old and with a BMI of 18-40 kg/m<sup>2</sup> were enrolled in this study after providing IRB approved informed consent. 55 subjects were normal weight (BMI < 25 kg/m<sup>2</sup>) (23 men, age: 37.4 ± 11.8 years), 31 were overweight (BMI between 25 and 30kg/m<sup>2</sup>) (18 men, age: 38.7 ± 13.7 years), and 16 were obese (BMI > 30 kg/m<sup>2</sup>) (9 men, age: 40.25 ± 10.3 years).

Subjects underwent an MRI scan of both knees using a proton density sequence and were excluded based on the presence of meniscal or ligament injuries, cartilage damage, or bone marrow edema. Subjects were also excluded if they self-reported

chronic pain that prevents them from walking normally or have gross malalignment of the knee. Each subject was tested in the gait lab, using a 9 camera optoelectronic system and force plate to capture gait kinematics and kinetics during walking at self-selected normal speed. A link model<sup>1</sup> was used to calculate intersegmental forces and moments; moments were normalized to % body weight\*height. With gait test markers in place, each subject was also scanned using a whole body laser scanner (Cyberware, CA, USA). From the model, waist circumference was measured at the iliac crest markers, thigh circumference for each leg was measured at 1/3 of the distance between the lateral femoral condyle and greater trochanter markers, and the two quantities were divided to calculate the waist-to-thigh ratio (WTR).<sup>5</sup> % lower body volume was measured as the volume below the iliac crest markers as a percentage of total body volume, corrected for functional residual lung capacity.<sup>3</sup> One side was randomly chosen for gait and anthropometric analysis. Univariate linear regression was first used to analyze the association between BMI and individual gait variables. Because gender and age are associated with BMI and walking speed is a covariate of the knee flexion moment, the association between BMI and gait variables was then corrected for these factors using a multivariate model. Finally, measures of body volume distribution were added to the multivariate model to determine if they provide additional explanatory power.

## RESULTS

As shown in Figure 1, BMI is inversely associated with the heelstrike knee flexion angle (KFA) ( $r^2=.122$ ,  $p<.001$ ), first peak KFA during stance ( $r^2=.073$ ,  $p=.006$ ), maximum KFA during swing ( $r^2=.114$ ,  $p<.001$ ), and first peak knee flexion moment (KFM) during stance ( $r^2=.097$ ,  $p=.001$ ). In the multivariate model (see Table 1), using walking speed, age, gender, and BMI as predictors,

heelstrike KFA is inversely associated with BMI ( $r^2=.127$ ,  $p=.009$ ), first peak KFA during stance and maximum KFA during swing phase are inversely associated with BMI and positively associated with age ( $r^2=.129$ ,  $p=.009$  and  $r^2=.313$ ,  $p<.001$ , respectively), and first peak KFM is inversely associated with BMI and positively associated with walking speed ( $r^2=.254$ ,  $p<.001$ ).

BMI and gender together are very correlated with measures of adiposity: waist circumference ( $r^2=.67$ ,  $p<.001$ ), thigh girth ( $r^2=.8$ ,  $p<.001$ ), WTR ( $r^2=.22$ ,  $p<.001$ ), and % lower body ( $r^2=.53$ ,  $p<.001$ ); therefore when each measure of body volume distribution was added to the multivariate model, as shown in Table 1, no significant improvement in explanatory power, as measured by increase in  $r^2$  and  $p$ , was seen for any gait variable and volume measure. When subjects were stratified by gender, including relative volume measures did not significantly improve the model fit when walking speed, age, and BMI were used as predictors.

## DISCUSSION

The results of the study support the first hypothesis: individuals with higher BMI adopt an overall more extended knee during gait and show reduced quadriceps use during the first part of stance. Muscle moment arms do not scale with BMI, so heavier individuals need to support a greater body mass against gravity with the same mechanical lever arm between muscles and joints. By adopting a more upright posture, more body weight is supported by the skeleton instead of contracting

muscles, so greater extension allows high BMI individuals to maintain upright stature without significantly increased muscle strength.

The second hypothesis is not supported: measures of relative volume distribution are not associated with gait parameters independently of BMI, gender, age, and walking speed. These results are consistent with previous work indicating that relative measures of adiposity distribution are not associated with OA incidence, independent of BMI.<sup>6</sup> Because BMI was the only variable consistently associated with gait parameters linked to OA risk, this study suggests that the distribution of excess weight is not related to the mechanism of increased OA risk in the obese. Similarly, because the results were unchanged when subjects were stratified by gender, the results indicate that female gender increases OA risk only through BMI; however, this finding needs to be confirmed through future studies.

## REFERENCES

- 1.Andriacchi, et al. In: 1997; Mow V.C., Hayes W.C. (Eds.), *Basic Orthopaedic Biomechanics*, 2nd ed, pp. 37-67.
- 2.Blazek, et al. *Proc ORS Annual Meeting*, 2011.
- 3.Crapo. *Bull Eur Phys Resp*. 18:419-425, 1982.
- 4.Felson. *Ann Rheum Dis* 55(9):668-70.
- 5.Li, et al. *Dia Res Clin Pract* 89(1):79-87, 2010.
- 6.Segal, et al. *Am J Phy Med Reh* 88(3): 180-188.

## ACKNOWLEDGEMENTS

Funding was provided by VA #A4861R and the NSF Graduate Fellowship.

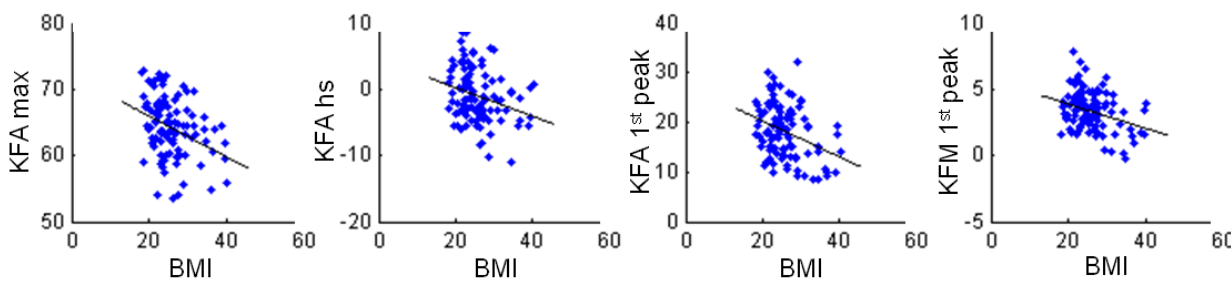


**Figure 1:** Univariate linear regression relationships between gait variables and BMI.

| Predictors                            | KFA hs | KFA 1st peak | KFA swing max | KFM 1st peak |
|---------------------------------------|--------|--------------|---------------|--------------|
| BMI                                   | 0.122  | 0.073        | 0.114         | 0.097        |
| BMI, age, speed                       | 0.127  | 0.123        | 0.283         | 0.252        |
| BMI, gender, age, speed               | 0.127  | 0.129        | 0.313         | 0.254        |
| BMI, gender, age, speed, thigh girth  | 0.156  | 0.144        | 0.334         | 0.259        |
| BMI, gender, age, speed, waist girth  | 0.131  | 0.148        | 0.312         | 0.255        |
| BMI, gender, age, speed, WTR          | 0.136  | 0.148        | 0.335         | 0.267        |
| BMI, gender, age, speed, % lower body | 0.147  | 0.137        | 0.324         | 0.256        |

**Table 1:**  $r^2$  values for multivariate regression analyses using BMI, age, walking speed, and measures of adiposity to predict gait variables; KFA=knee flexion angle, KFM=knee flexion moment

# HUMERAL HEAD TRANSLATIONS AND SUBACROMIAL PRESSURE AFTER SHRINKING THE POSTERIOR GLENOHUMERAL JOINT CAPSULE

<sup>1</sup>John Borstad and <sup>1</sup>Amitabh Dashottar

<sup>1</sup>The Ohio State University, Columbus, OH, USA  
email: [borstad.1@osu.edu](mailto:borstad.1@osu.edu)

## INTRODUCTION

Greater than 20% of the musculoskeletal pain annually reported in the United States is at the shoulder. The pathomechanics for shoulder pain are typically multifactorial, with contracture of the posterior glenohumeral joint (GHJ) capsule an identified mechanism. Harryman et al [1] reported increased anterior and superior humeral head translations after suturing the posterior GHJ capsule, suggesting approximation of bony segments and increased compressive forces on subacromial tissues.

Posterior GHJ capsule contracture develops in throwing athletes in response to high tensile loads on the posterior shoulder during arm deceleration, and Ticker et al [2] have reported posterior GHJ capsule contracture in individuals with refractory shoulder pain. The contracture is believed to include a thickened capsule, a higher ratio of collagen to elastin, and an increased modulus of elasticity. Considering these changes, the application and generalizability of the Harryman et al findings to shoulder pathomechanics may be limited: suturing the capsule reduces the amount of tissue available, but does not change its underlying material or mechanical properties; and the effect of humeral head translations on the subacromial space are unknown. This project aims to address these concerns by changing the posterior GHJ capsule length using a method intended to more closely approximate a tissue contracture, and then quantifying subacromial pressure and humeral head translations.

## METHODS

This project used fresh-frozen cadaver specimens and a within-subject design. Specimens consisted of a scapula, clavicle, and entire upper extremity.

Specimens were thawed and stripped of skin over the scapula and deltoid regions, the deltoid and posterior rotator cuff were removed, and the scapula was secured to a wooden post in anatomical resting position. Data were collected on each specimen during passive arm elevation in the scapular plane.

The dependent variables were humeral head translations, and subacromial pressure. Humeral head translation data in both the Anterior-Posterior (A-P) and Superior-Inferior (S-I) directions were collected with the Flock of Birds electromagnetic motion capture system and MotionMonitor software. Receivers were rigidly secured to both the scapula and humerus to capture segment kinematics. Translations were calculated using the estimated humeral head center relative to the anterior-lateral acromion. Subacromial pressure was quantified with a TekScan pressure sensor secured in the subacromial space.

Independent variables were the humeral elevation angles during passive motion, and the length of the posterior GHJ capsule. Elevation angles were extracted using ISB recommendations. Pressure and translation data were collected with the posterior GHJ capsule in its native condition, and after shrinking the tissue 20% and 40% of its native length using a radiofrequency thermal energy probe (Mitek), a method that contracts the tissue by coagulating collagen.

Mean peak subacromial pressure during arm elevation was determined for each capsule length and compared using a 1 factor (Length) ANOVA. Mean humeral head translations every 10° of elevation were calculated, adjusted to a starting position of zero, and the change in translation between the lengths compared using a 2 factor

(Angle x Length) ANOVA. Statistical significance was set at  $p < 0.05$ .

## RESULTS AND DISCUSSION

Subacromial peak pressure significantly decreased as capsule length decreased, which was not expected (Fig 1). However, the position of the humeral head translated 0.4cm anteriorly and 1.8cm inferiorly after contracture, increasing the distance between the humeral head and acromion. Current testing is adding a compressive force to the GHJ to potentially minimize this effect.

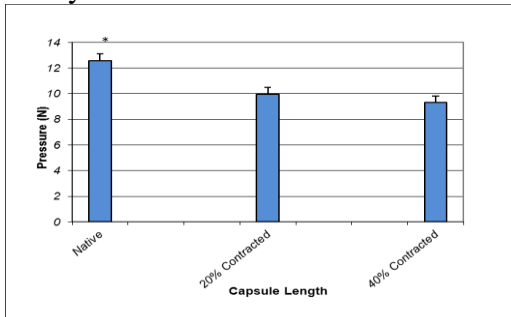


**Figure 1.** Mean peak pressure (N) as the posterior GHJ capsule is contracted.

After adjusting the starting position, there was no statistically significant interaction effect for A-P translations (Fig 2), but there were increased superior translations at higher arm elevation angles that depended on capsule length (significant interaction effect). At  $80^\circ$  superior translations after 40% contracture were greater than at both native and 20%, and at  $90^\circ$  superior translations at 40% were greater than at 20%, which were greater than at native length (Fig 3). In both directions, the 40% contracture resulted in significantly greater anterior and superior translations, respectively, than the native length (significant main effects).

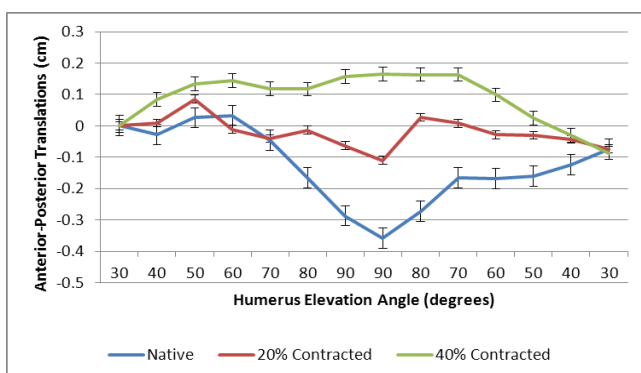


**Figure 2:** Mean A-P translations (SE) as the posterior GHJ capsule is contracted. (+ = Anterior)

Compared to Harryman et al [1], anterior translation changes in this study are similar, yet were not as large or as early in elevation. The differing methods for contracting the capsule are likely responsible for this result. Superior translations in this study were larger in the 40% condition at the highest elevation angles, an effect not previously reported.

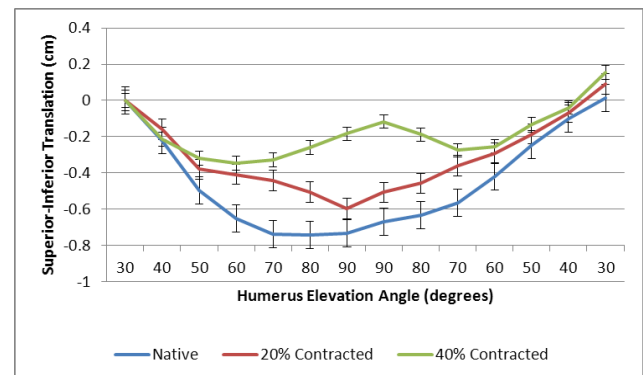


**Figure 3.** Mean S-I translations (SE) as the posterior GHJ capsule is contracted. (+ = Superior)

While Harryman et al [1] did not report the relative amount of capsule shortening, they report using a 2cm suture plication. In our work the native capsule lengths averaged 5cm, so our 40% contracture and the 2 cm suture plication used by Harryman are probably comparable.

Because the scapula did not move in this study, reported arm elevation angles are lower than what would be seen *in vivo*. Therefore, the significant superior translation differences seen at  $80^\circ$  and  $90^\circ$  probably would occur at approximately  $120^\circ$ , which may be too high to be considered a pathomechanism for shoulder pain.

## CONCLUSIONS

Contracting the posterior GHJ capsule increases anterior and superior humeral head translations during arm elevation. A decrease in subacromial pressure also results, probably related to a shift in the starting position of the humeral head after contracture.

## REFERENCES

1. Harryman DT, et al. *J Bone Jt Surg*, **72-A**, 1334-1343, 1990.
2. Ticker JB, et al. *Arthroscopy, J Arthroscopic Rel Surg*, **16**, 27-34, 2000.

# WHICH MUSCLE DATA SET TO USE IN A FINITE ELEMENT MODEL OF THE KNEE? AN RMS-BASED METHOD TO IDENTIFY MEAN, MAXIMUM, AND MINIMUM

<sup>1</sup>Jennifer L. Boyd, <sup>2</sup>Harinderjit S. Gill, and <sup>1</sup>Amy B. Zavatsky

University of Oxford, <sup>1</sup>Department of Engineering Science & <sup>2</sup>NDORMS, Oxford, UK  
email: jennifer.boyd@eng.ox.ac.uk

## INTRODUCTION

Muscle forces contribute significantly to loading within the knee [1]. They can be calculated from motion analysis trials and then applied to finite element (FE) models to understand loading during activity. Multiple motion analysis cycles are usually collected for each subject and activity; peak muscle forces and patterns vary between cycles. This presents a challenge for the selection of the most representative loading for an FE model. It is important to establish an objective, consistent method for selecting the cycle with the most representative mean, maximum, and minimum calculated muscle forces.

This abstract describes a robust procedure for the selection of the most representative cycle for application of multiple muscle forces to an FE model. The proposed method is capable of selecting cycles which are most representative of the forces calculated for individual muscles as well as those cycles which are most representative of all muscles collectively.

## METHODS

Representative cycles were selected based on RMS differences between muscle forces calculated for an individual motion cycle and the mean muscle forces calculated for a set of motion cycles. Each cycle was first normalized to 100 time points per motion cycle. The mean force value at each time point was then calculated for each individual muscle. The individual muscle forces were then compared to the calculated mean values, and RMS differences were determined using the following formula:

$$\text{RMS difference for muscle } m = \sqrt{\frac{\sum_{i=1}^n (F_{mi} - \overline{F}_{mi})^2}{n}}$$

where  $F_{mi}$  represents muscle forces in a given motion cycle,  $\overline{F}_{mi}$  the calculated mean forces, and  $n$

the number of time points in the motion cycle. RMS differences for all muscles ( $j = 1:m$ ) during a cycle were summed to calculate the overall RMS difference in each cycle. The motion cycle with the minimum RMS difference for either an individual muscle (former case) or for all muscles (latter case) was selected as the most representative cycle.

This method was used to analyze motion analysis data from three subjects. Data were collected at the Oxford Gait Laboratory (Nuffield Orthopaedic Centre, Oxford, UK) while subjects performed a minimum of 12 level walking motion cycles (6 left and 6 right force plate heel strikes) and 6 stair descent motion cycles (3 right and 3 left force plate heel strikes) within the capture volume of 12 cameras (Vicon 612, Vicon). Two force plates (OR6 AMTI), located in the floor and just after the last step of the stairs, simultaneously recorded ground reaction forces.

Marker, force plate, and subject limb length data were then used to create and scale a subject-specific lower limb model (AnyBody Version 3.0, AnyBody Technology), which calculated forces generated by lower limb muscles during level walking and stair descent. The calculated forces in 11 different muscles surrounding the knee (gastrocnemius, vastus lateralis, vastus medialis, vastus intermedius, rectus femoris, semitendinosus, semimembranosus, biceps femoris caput longum, biceps femoris caput breve, sartorius, and gracilis) were then investigated for each motion cycle for each activity.

The described RMS method was then used to select the most representative cycle for each individual muscle as well as the overall most representative motion cycle for each subject and activity. Similarly, substituting  $\overline{F}_{mi}$  with 95% confidence interval upper and lower bounds allowed the cycles most representative of these bounds to be identified; muscle forces from these cycles could then be

applied to FE models to represent the upper and lower bounds of muscle forces at the knee.

## RESULTS AND DISCUSSION

Both intra- and inter-subject variability existed in the calculated muscle forces. The variability in 6 cycles of stair descent and the mean  $\overline{F_{mi}}$  (thick black line) of the cycles are shown in Figure 1.

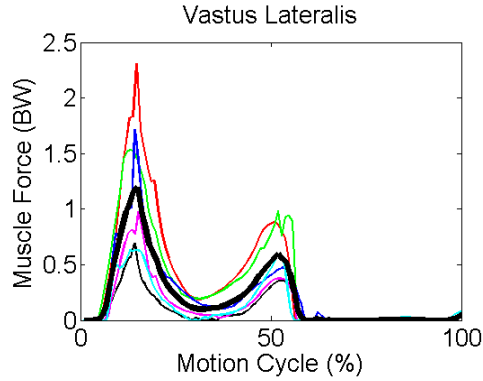


**Figure 1:** Individual (thin lines) and mean  $\overline{F_{mi}}$  (thick black line) vastus lateralis muscle forces during 6 stair descent cycles [BW = body weight]

RMS differences between the mean and individual cycles were compared to determine the most representative cycle for each muscle (Table 1) and for each subject and activity (Table 2). Different representative cycles were commonly selected for different muscles, and comparing RMS differences for the two activities showed that the relative variability between the tasks was subject-dependent.

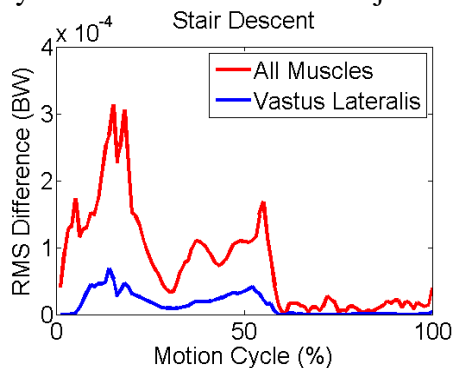


**Figure 2:** RMS differences from mean throughout representative cycle for stair descent

After determining the most representative motion cycles, the RMS differences throughout the cycles were investigated. Figure 2 shows the overall RMS differences from the mean (red) as well as the RMS difference in the vastus lateralis (blue) during the representative cycle for right heel strike stair descent in Subject 1.

**Table 1:** Individual muscle representative cycles and RMS differences from mean during stair descent (Subject 1)

| Muscle                         | Representative Cycle | RMS Difference (BW)    |
|--------------------------------|----------------------|------------------------|
| Gastrocnemius                  | 8                    | $1.5 \times 10^{-3}$   |
| Vastus Lateralis               | 5                    | $0.72 \times 10^{-3}$  |
| Vastus Medialis                | 5                    | $0.71 \times 10^{-3}$  |
| Vastus Intermedius             | 5                    | $0.83 \times 10^{-3}$  |
| Rectus Femoris                 | 8                    | $0.54 \times 10^{-3}$  |
| Semitendinosus                 | 7                    | $0.086 \times 10^{-3}$ |
| Semimembranosus                | 8                    | $0.96 \times 10^{-3}$  |
| Biceps Femoris<br>Caput Longum | 8                    | $0.97 \times 10^{-3}$  |
| Biceps Femoris<br>Caput Breve  | 7                    | $0.20 \times 10^{-3}$  |
| Sartorius                      | 3                    | $0.30 \times 10^{-3}$  |
| Gracilis                       | 2                    | $0.76 \times 10^{-3}$  |
| OVERALL                        | 8                    | $7.6 \times 10^{-3}$   |

**Table 2:** RMS differences from mean in representative cycles for level walking and stair descent

| Subject | RMS Difference (BW) for: |                      |
|---------|--------------------------|----------------------|
|         | Level Walking            | Stair Descent        |
| 1       | $7.8 \times 10^{-3}$     | $7.6 \times 10^{-3}$ |
| 2       | $8.3 \times 10^{-3}$     | $6.1 \times 10^{-3}$ |
| 3       | $6.2 \times 10^{-3}$     | $9.6 \times 10^{-3}$ |

## CONCLUSIONS

Variability exists both between subjects and within subjects between cycles and tasks. The presented method provides an objective way of identifying the most representative mean, maximum, and minimum cycles for each subject and task for input to FE models of the joints.

## REFERENCES

- Sasaki, K & Neptune, R. *J Biomech* **43**, 2780-2784, 2010.

## ACKNOWLEDGEMENTS

J Boyd was funded by the Clarendon Fund, National Science Foundation and Whitaker International Fellowship. Financial support was received from the Furlong Foundation and the NIHR Biomedical Research Unit into Musculoskeletal Disease, Nuffield Orthopaedic Centre and University of Oxford.

# EFFECTS OF HAND CARRIED LOAD ON METABOLIC COST AND TRUNK-PELVIS COORDINATION DURING WALKING

<sup>1,2</sup>Angela Boynton and <sup>3</sup>Todd Royer

<sup>1</sup>U.S. Army Research Laboratory, Aberdeen Proving Ground, MD, USA

<sup>2</sup>Program in Biomechanics and Movement Science, University of Delaware, Newark, DE, USA

<sup>3</sup>Department of Kinesiology & Applied Physiology, University of Delaware, Newark, DE, USA

email: [angela.c.boynton@us.army.mil](mailto:angela.c.boynton@us.army.mil)

## INTRODUCTION

Load carriage is a fundamental task for dismounted Soldiers. In the future, it is likely that in addition to carrying a weapon in their hands, part of their load will be borne on their arms (e.g. body armor, communications equipment, etc.). Because hand carrying loads can involve either swinging the arms naturally or holding them in a fixed position, the effects of arm swing restriction on gait dynamics must be taken into account in addition to the effects of load location. Understanding the relationship between the mechanics and energetics of carrying load in the hands will allow for better prediction of Soldier mobility performance under various load conditions and help developers design manually carried Soldier equipment with a minimal impact on mission performance. It will also provide insight into the mechanics and energetics of gait in general.

It is well-established that the metabolic cost of load carriage increases with more distal placement of the load relative to the body's center of mass. However, conflicting results have been reported for the effect of arm swing restriction on metabolic cost. With respect to the coordination between transverse plane trunk and pelvis rotation during walking, backpack load carriage [1] and arm swing restriction [2] have both been found to result in rotations that are more in phase with one another. However, adding load to the arms [2] and walking with a rifle in both hands [3] have been reported to have no effect on trunk-pelvis coordination.

It seems likely that changes in the normal coordination pattern between the trunk and pelvis might decrease gait efficiency, thus increasing physiologic demand. Therefore, a pilot study was conducted to simultaneously evaluate the effects of

load location and arm swing on metabolic cost and trunk-pelvis coordination during walking.

## METHODS

Data were collected for three young, healthy subjects (1 M, 2 F, age: 21-23 yrs) as part of an ongoing study evaluating the effects of hand carried loads on the mechanics and energetics of gait. Subjects walked on a treadmill at 1.34 m·s<sup>-1</sup> for ten 5-minute periods while carrying loads of 0, 5 and 10% body weight evenly distributed on their trunk or between their hands. For half of the conditions they allowed their arms to swing naturally and for the other half they held them in a fixed position with elbows flexed approximately 90 degrees.

Retroreflective markers were placed on the arms, hands, trunk, pelvis, legs and feet. Cortex software and 9 Eagle cameras (Motion Analysis Corp, Santa Rosa, CA) were used to record 3-D motion data at 60 Hz during the final 30 seconds of each trial. Subject specific models were created in Visual3D (C-Motion Inc, Rockville, MD) and used to calculate trunk and pelvis rotation in the transverse plane. Mean continuous relative phase (CRP) was calculated as a measure of coordination between trunk and pelvis rotations over the gait cycle [4]. A portable cardiopulmonary system (Cosmed USA, Chicago, IL) continuously sampled expired gases throughout each trial and data from the final minute were used to calculate metabolic rate. Given the small sample size to date, at this time only descriptive statistics were calculated for each of the variables of interest.

## RESULTS AND DISCUSSION

Both metabolic cost (Figure 1) and trunk-pelvis

coordination (Figure 2) appear to be affected by load location and arm swing condition, but in different ways. In general, carrying load in the hands had a greater effect on both metabolic cost and trunk-pelvis coordination than carrying the same load on the trunk. The magnitude of the observed differences also seems to depend on the amount of load carried and arm swing condition.

It appears that walking with a trunk load up to 10% BW does not have much effect on metabolic rate, and holding the arms in a fixed position during trunk load carriage tends to increase metabolic rate only slightly (Figure 1). Carrying a 10% BW load in the hands resulted in a greater increase in metabolic rate than carrying the same load on the trunk. Additionally, arm fixation during hand load carriage resulted in greater increases in metabolic rate, with a particularly large effect for the 10% BW load. These results are consistent with previous studies.

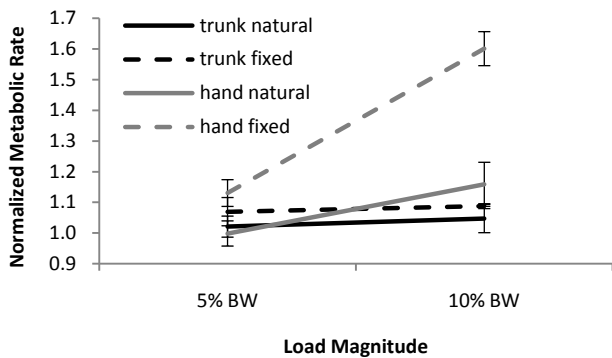


**Figure 1:** The effects of load location (trunk, hands) and arm swing (natural, fixed) on metabolic rate during load carriage. Values are normalized to metabolic rate during the baseline condition (0% BW with natural arm swing).

As with metabolic rate, carrying load on the trunk does not seem to have much effect on CRP in the transverse plane (Figure 2). This result differs from the finding of LaFiandra, et al., however, the largest load in this study was only 10% BW compared to the 40% BW load used in the previous study. Arm fixation during trunk load carriage seems to result in rotations that are more in phase with one another, but not necessarily at the level of significance reported by Pontzer, et al. In contrast to trunk load carriage, hand load carriage appears to have a substantial effect on CRP. This differs from the finding of Pontzer, et al., but the disparity might be explained by the more distal location of the load in

this study. Holding the arms in a fixed position tended to reduce the extent to which trunk-pelvis coordination was affected by carrying load in the hands, but still resulted in a large decrease in CRP. The 5% BW hand carried load with fixed arm condition in this study is comparable to the rifle condition used in the study by Seay, et al., but an effect on CRP was found only in the present study. This discrepancy may be explained by a difference in subjects (Soldiers vs. untrained civilians).

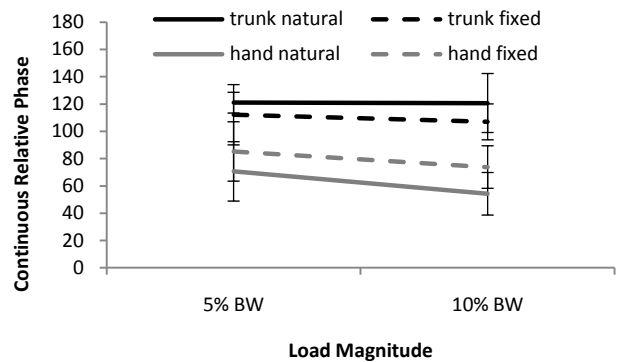


**Figure 2:** The effects of load location (trunk, hands) and arm swing (natural, fixed) on mean continuous relative phase between trunk and pelvis rotation during load carriage. A value of 180 degrees represents rotations that are completely out of phase. Mean CRP for the baseline condition (0% BW, natural arm swing) was  $125.8 \pm 19.5$  degrees.

## CONCLUSIONS

These results appear to support the idea that both load location and arm swing condition need to be taken into account when evaluating the effects of hand carried loads on gait mechanics and energetics. However, additional subjects are needed to determine the significance of the observed differences. Additionally, the differing effects of load location and arm swing condition on metabolic rate and CRP seem to indicate that changes in transverse plane trunk-pelvis coordination alone cannot explain the increases in physiologic demand associated with hand carrying load.

## REFERENCES

1. LaFiandra M, et al. *J Biomech* **36**, 87-95, 2003.
2. Pontzer H, et al. *J Exp Biol* **212**, 523-534, 2009.
3. Seay JF, et al. *Ergonomics* **54**, 187-196, 2011.
4. van Emmerik RE & Wagenaar RC. *J Biomech* **29**, 1175-1184, 1996.

# ANTAGONISTIC CO-CONTRACTION IN OPTIMIZATION PREDICTION OF KNEE CONTACT FORCES

<sup>1</sup>Scott C. E. Brandon, <sup>2</sup>Darryl G. Thelen, and <sup>1</sup>Kevin J. Deluzio

<sup>1</sup>Queen's University, Kingston, ON, Canada

<sup>2</sup>University of Wisconsin-Madison, WI, USA

[brandon@me.queensu.ca](mailto:brandon@me.queensu.ca)

## INTRODUCTION

Joint contact loads depend not only on readily obtainable external kinematics and reaction forces, but also on the forces generated by an indeterminate system of muscle and other soft tissues. Accurate contact predictions, verified using an instrumented knee implant, have been obtained using an optimization approach to resolve the indeterminacy [1]. However, muscles do not always activate in an optimal manner; during gait, both extensor (quadriceps) and flexor (hamstrings and calf) muscles compress the knee joint by activating at the same time [2]. The level of co-contraction of antagonistic knee muscle groups is elevated in subjects with knee osteoarthritis, which may contribute to abnormal joint loading and disease progression [2]. This study presents preliminary results from a musculoskeletal model that was developed to incorporate co-contraction of antagonistic knee muscle groups into a prediction of knee contact forces.

## METHODS

Three-dimensional limb segment trajectories and external ground reaction forces were obtained for a single subject with moderate medial knee osteoarthritis walking at self-selected speed [3]. A detailed, open-source musculoskeletal model including 44 separate heads of 35 muscles of the lower extremity [4] was scaled to the subject and adapted to account for the individual's bow-legged knee alignment using x-ray data. The OpenSim dynamics engine was used to solve the inverse kinematics and inverse dynamics problems, and to compute the muscle moment arms for each muscle about each joint during both gait trials [5]. Muscle forces were estimated using a two-level constrained nonlinear multivariable optimization in Matlab

(Mathworks, Natick MA). The hybrid optimization problem minimizes the sum of squares of muscle stresses [6] while constraining the activation patterns of a subset of muscles to match experimental electromyographic (EMG) data.

$$J(\mathbf{w}_k, \mathbf{F}_i) = \sum_{t=1}^{100} \left( \sum_{i=1}^{36} \left( \frac{F_{i,t}}{PCSA_{i,t}} \right)^2 + \sum_{k=1}^8 \left( \frac{\mathbf{w}_k * Fmax_k * a_{k,t}}{PCSA_{k,t}} \right)^2 \right)$$

$F_{i,t}$  = force generated by muscle,  $i$

$PCSA_{i,t}$  = physiological cross-sectional area for muscle,  $i$

$t$  = instant in gait cycle

$w_k$  = activation pattern weight factor for muscle,  $k$

$Fmax_{k,t}$  = theoretical max force for muscle,  $k$

$a_{k,t}$  = measured activation at instant,  $t$ , for muscle,  $k$

In the inner level, muscle forces,  $F_{i,t}$ , for 36 non-prescribed muscle forces were computed to minimize the sum of squares of muscle stresses at each percent of the gait cycle,  $t$ , given the prescribed forces  $F_{k,t}$ . In the outer level, the patterns of activation throughout the gait cycle,  $[0 \leq a_{k,t} \leq 1]$ , for 8 muscles spanning the knee joint were prescribed from experimental electromyographic (EMG) measurements of muscle activation. Activation patterns were scaled by optimization weight factors,  $w_k$ , and multiplied by the estimated maximum force-generating capacity of each muscle to prescribe the muscle forces at each instant in the gait cycle for these 8 muscles. Then, the activation weight factors,  $w_k$  were optimized to minimize the overall sum of squares of muscle stress throughout the entire gait cycle. Muscle forces were

constrained to balance net joint moments for hip flexion, hip adduction, knee flexion, and ankle flexion. Finally, medial and lateral knee contact forces were computed using a simple static frontal plane model to combine contributions from external forces and internal muscle forces (Figure 1). The distance between contact locations was estimated from a radiograph. The net axial contact force was computed as the sum of medial and lateral contact forces.

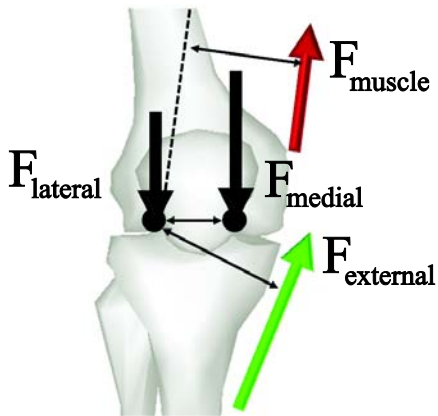


**Figure 1:** Unknown contact forces ( $F_{lateral}$  and  $F_{medial}$ ) are calculated using static moment balance at each contact location

## RESULTS AND DISCUSSION

A peak axial knee joint contact force of 3.8 times body weight was predicted early in the gait cycle using the hybrid objective function (Figure 2). Antagonistic co-contraction of knee flexor and extensor muscle groups was observed in EMG patterns during the early-stance (0-20%) and late-swing (80-100%) phases of the gait cycle for the single subject. This antagonistic activity was incorporated into the hybrid objective function, and accounted for an increase in axial knee contact force of approximately 1.5 times body weight during early-stance and late-swing as compared with the traditional stress-squared criterion.

Throughout the gait cycle, the medial contact force was greater than the lateral contact force. The model did not predict unloading of either compartment at any point during the gait cycle. The magnitude of the predicted axial contact forces is within the range of two to four times body weight reported in literature for recent models of level walking [1,7]. Contact force predictions were

approximately one body weight larger than forces reported for a limited sample of *in vivo* instrumented knee implant measurements [8]. However, the subject in this study was younger and exhibited only moderate radiographic osteoarthritis; these factors may have contributed to an overall higher walking speed and greater axial loading of the knee. The hybrid optimization in this study demonstrated that knee contact forces are highly sensitive to antagonistic muscle co-contraction, even for level walking.

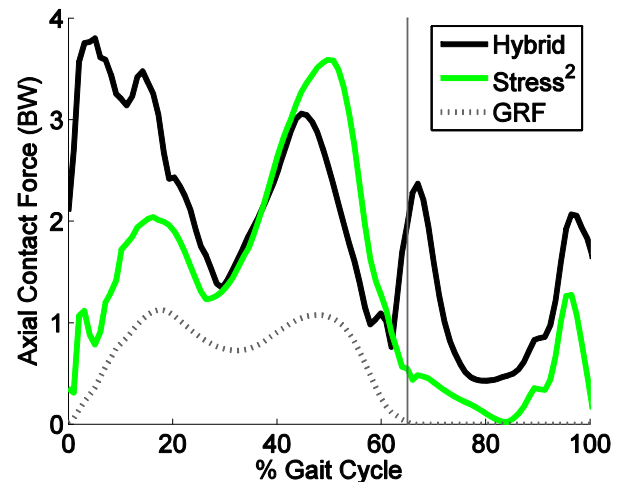


**Figure 1:** Net axial contact force (times body weight) computed using Hybrid (black) and the traditional stress-squared (green) objective functions to resolve muscle forces. The vertical component of the external ground reaction force (dashed) is shown for comparison. Toe-off occurred at 65% of the gait cycle (vertical line).

## REFERENCES

1. Lin, YC et al. *J.Biomech* **43**, 945-952, 2010
2. Zeni JA et al. *J.Electromyogr.Kinesiol.* **20**, 148-154, 2010
3. Brandon SC et al. *Clin.Biomech.* **26**, 65-70, 2011
4. Arnold EM et al. *Ann.Biomed.Eng.* **38**, 269-279, 2010
5. Delp S et al. *IEEE Trans.Biomed.Eng.* **54**, 1940-1950 (2007)
6. Crowninshield RD et al. *J.Biomech* **14**, 793-801, 1981
7. Winby CR et al. *J.Biomech* **42**, 2294-2300, 2009
8. Kutzner I et al. *J.Biomech* IN PRESS, 2011

## ACKNOWLEDGEMENTS

Funding for this study was provided by NSERC.

# TIBIAL GEOMETRY, JOINT COMPRESSION, AND THEIR EFFECTS ON ANTERIOR CRUCIATE LIGAMENT STRAIN: AN IN-VITRO STUDY

<sup>1</sup>Breighner, R; <sup>1</sup>Hashemi, J; <sup>2</sup>Chandrashekar, N; <sup>3</sup>Slauterbeck, J R

<sup>1</sup>Texas Tech University, Lubbock, TX, <sup>2</sup>University of Waterloo, Ontario, CA, <sup>3</sup>University of Vermont, Burlington, VT

email: [javad.hashemi@ttu.edu](mailto:javad.hashemi@ttu.edu), web: <http://www.ttu.edu>

## INTRODUCTION

The physical detriment and economic costs of anterior cruciate ligament (ACL) injury are well documented in the literature. Unfortunately, key risk factors and mechanisms of non-contact ACL injury have yet to be fully identified. A family of risk factors of increasing importance focuses on the geometry of the tibial plateau. One study of tibial geometry showed that depth of the medial plateau (MTD) and slope of the medial and lateral aspects of the plateau (MTS and LTS, respectively) can be used to estimate probability of injury<sup>1</sup>. Additionally, tibial geometry has been shown to affect kinematics of the knee<sup>2</sup>.

Although studies have established that MTD, LTS, and MTS can be used to assess injury risk, the direct effects of these factors on ACL strain have not yet been reported. This study aims to show the effect of tibial geometry on ACL strain. Previous in-vitro studies<sup>3</sup> of joint compression and ACL injury have rigidly constrained angular displacements of the tibia and femur, maintaining constant knee flexion. This approach may obscure any protective effects that joint compression has as the knee flexes. The present study further seeks to assess the influence of tibiofemoral compression on ACL strain in a dynamic activity where knee flexion is present.

It is hypothesized that during a simulated jump landing, steeper tibial slopes (MTS and LTS) will result in increased ACL strain. Further, knees presenting deeper medial tibial plateaus (MTD) will experience lower ACL strain. Additionally, it is hypothesized that increased pre-landing compression of the knee joint will lead to reduced ACL strain under simulated landing conditions. These hypotheses will be evaluated using an accepted in-vitro simulation technique<sup>5</sup> and a purpose-built dynamic knee-loading simulator.

## METHODS

A dynamic knee-loading machine was designed and fabricated for the in-vitro simulation of various tasks with established risk of ACL injury, including jump landing. This apparatus allows for anterior-posterior positioning of the hip and ankle. Additionally, initial knee flexion, and thus ankle and hip flexion, can be adjusted. Stepper motor-driven winches generate tension in drive cables attached to the patella and the proximal-posterior femur to generate muscle/joint forces. The machine also allows for the application of impulsive loads at the ankle to simulate impact and weight acceptance at landing. The machine was also used in conjunction with the Tekscan K-Scan pressure mapping system (Tekscan, Inc., Boston, MA) to measure joint forces arising from the application of muscle forces.

Nine fresh-frozen human cadaver knees were used in this experiment (7 M, 2 F; age: 52.6(12.0)). Magnetic resonance images of the intact knees were obtained using a 1.5-T clinical MRI machine. From the MRIs measurements of MTS, LTS, and MTD were taken for each knee, as reported previously<sup>1,4</sup>. All knee specimens included a minimum of 17.5 cm of bone proximal and distal the joint space. Following MR imaging, the knees were thawed, dissected to the capsule level, and examined for injury. Specimens were stored at -20°C until the evening prior to dissection/testing, when they were thawed overnight at room temperature. Each knee was installed in the machine and its ACL was instrumented with a differential variable reluctance transformer (DVRT) to measure ligament elongation/strain. The knees were then subjected to a series of nine simulated landings. Initial flexion angles (10°, 20°, 30°) and pre-landing joint compression were varied in each of these trials. Joint compression was induced through the application of simulated gluteus muscle forces (SGFs) at levels of 0 N, 100 N, and 200 N coupled

with a constraint on inferior/posterior ankle displacement. The gluteus maximus is a hip extensor that, in conjunction with the imposed ankle constraint resists knee flexion. This antagonism increases joint force, as measured in six knees prior to the landing tests (figure 1). A quadriceps force of 200 N was also applied prior to each test. An impulsive ground reaction force was then applied. Multiple linear regression analyses were conducted to assess the extent of the relationship between ACL strain and MTS, LTS, MTD, and SGF within each flexion angle.

## RESULTS AND DISCUSSION

Multiple regression analysis revealed that tibial geometry and simulated gluteus force were significant regressors for at least one of the tested flexion angles. At 10° of initial knee flexion, medial tibial depth (MTD) and simulated gluteus force (SGF) were both related to significant decreases in ACL strain ( $p = 0.028$  and  $p = 0.009$ ). At 20°, increased MTD also negatively influenced ACL strain ( $p = 0.011$ ) and lateral tibial slope (LTS) was associated with significant increases in ACL strain ( $p = 0.047$ ). Similarly, at 30° of flexion, knees presenting higher MTD experienced lower ACL strain ( $p = 0.001$ ); knees with increased LTS again saw greater ACL strain ( $p = 0.022$ ). The

To the authors' knowledge this is the first study to report the influence of tibial geometry on directly measured strain in the anterior cruciate ligament. The results of this study indicate that greater MTD is protective at all tested flexion angles. The posterior-decreasing slope of the lateral tibial plateau is a factor that exacerbates ACL loading at 20° and 30° of flexion. This may indicate that the protective effect of MTD near full extension overcomes the detrimental effects of LTS. Finally, our results show that at 10° knee flexion, increasing joint compression (via the gluteus in this case) prior to landing also protects the ACL. We believe that this protective mechanism is due to compression-induced increases in joint congruence. The strong relationship between gluteus levels and joint force supports this assertion. We believe that even the mild amounts of pre-landing joint force utilized in this study are protective of the ACL during athletic activities when the knee is near full extension. This is consistent with the findings of another study that posited a similar protective effect due to the quadriceps muscles<sup>5</sup>.

standardized regression coefficients are shown in Table 1. It was also found that a strong relationship exists between increased gluteus force and joint force in the presence of constraints on ankle displacement (figure 1).

**Table 1. Standardized coefficients ( $\beta$ ) and p-values from regression within flexion angles. The  $\beta$ s indicate the change in ACL strain due to one standard deviation change in the regressor. \*denotes significance**

| Variable | 10°     |         | 20°     |         | 30°     |         |
|----------|---------|---------|---------|---------|---------|---------|
|          | $\beta$ | p-value | $\beta$ | p-value | $\beta$ | p-value |
| MTS      | 0.295   | 0.218   | 0.278   | 0.166   | 0.046   | 0.822   |
| LTS      | 0.065   | 0.767   | 0.380   | 0.047 * | 0.464   | 0.022 * |
| MTD      | -0.380  | 0.028 * | -0.375  | 0.011 * | -0.534  | 0.001 * |
| SGF      | -0.415  | 0.009 * | -0.145  | 0.244   | -0.025  | 0.844   |

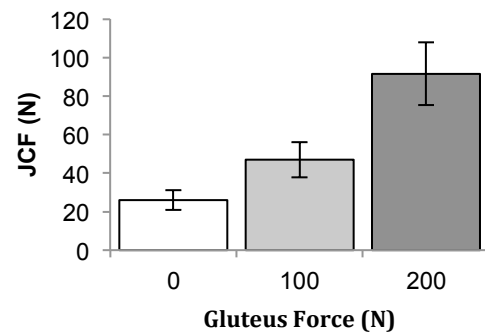


**Figure 1. Increasing joint compressive forces (JCF) under increasing gluteus forces. Mean  $\pm$  SEM.**

Our results show that flexion angle affects the dependence of ACL strain on tibial plateau geometry. We believe that this connection is extremely complex but crucial in understanding the true behavior of the knee. A limitation of our study is that we did not consider the interaction among the covariates. There may exist strong and complex interaction among MTS, LTS, MTD, and muscle forces that could possibly influence these results.

## CONCLUSIONS

This study illustrates the direct influence of various tibial geometries on ACL strain in a dynamic loading scenario. Further, it has been demonstrated that joint compression, at low to moderate levels is protective of the ACL.

## REFERENCES:

1. Hashemi et al. (2010), *Am J Sports Med*, 38(1): 54-62.
2. McLean et al. (2010), *Clin Biomech (Bristol, Avon)*, [Epub AoP].
3. Meyer et al. (2005), *J Biomech*, 38(11): 2311-6.
4. Hashemi et al. (2009), *J Bone Joint Surg*, 90(12): 2724-34.
5. Hashemi et al. (2010), *Knee*, 17(3): 235-41.

# THE EFFECTS OF TOTAL ANKLE REPLACEMENT ON ANKLE JOINT MECHANICS DURING WALKING

<sup>1</sup>Scott Brown, <sup>1</sup>Henry Wang, <sup>1</sup>Jeffery Frame and <sup>2</sup>Steven Herbst

<sup>1</sup>Ball State University, Muncie, IN, USA

<sup>2</sup>Central Indiana Orthopedics Center, Muncie, IN, USA

email: srbrown@bsu.edu web: <http://bsu.edu/biomechanics>

## INTRODUCTION

In the past, ankle arthrodesis (ankle fusion) procedure was considered as the “gold standard” for the surgical treatment of end-stage ankle Osteoarthritis (OA) [1]. However, this method of treatment has been known to induce the development of subtalar and midtarsal degenerative joint disease, decreased ankle’s functional ability and range of motion and increased discomfort in the ankle joint during daily activities [2,4]. In recent years, total ankle replacement (TAR) has become an alternative of arthrodesis for the treatment of severe ankle OA. TAR can alleviate ankle pain due to OA and restore normal ankle joint function [2,3]. The Salto Talaris™ Anatomic Ankle (STAA) (Tornier Inc., France) is a fixed bearing TAR that can mimic the anatomy and flexion/extension movement of the natural ankle joint [3]. Although the previous generation of the Salto Talaris™ TAR had received satisfaction from patients [5], it is unclear if the STAA TAR system could help patients achieve normal ankle strength and restore normal ankle function during daily activities such as walking.

The purpose of this study was to examine the ankle joint function and mechanics during level walking in patients with unilateral ankle OA on the following two occasions: pre and three months post surgery with the STAA TAR. It was hypothesized that the TAR joint would demonstrate improved gait parameters and ankle joint mechanics when compared to the same limb before surgery during level walking.

## METHODS

The study included five subjects (3 males and 2 females; mean age of:  $67 \pm 6$  yrs; body height:  $173 \pm 7$  cm; body mass:  $91 \pm 17$  kg) all previously

diagnosed with unilateral advanced, end-stage ankle OA. All subjects signed informed consent forms prior to participation in the study.

Each subject performed level walking at a self-selected pace on two occasions in a gait laboratory: pre and three months post TAR surgery. Three dimension kinematics and kinetics data were collected using a 12-camera motion capture system (100 Hz) (VICON Inc., Oxford Metric, London, England) and two AMTI force platforms (1000 Hz) (Advanced Mechanical Technologies Inc., Watertown, MA, USA). Spherical retro-reflective markers were placed bilaterally on specific lower extremity anatomical landmarks following the plug-in-gait protocol.

Gait temporo-spatial parameters such as walking speed, stride length, stance time and double support were calculated. In addition, ankle joint mechanics such as ankle joint moment and power were analyzed in the involved limb both pre and post TAR surgery. One-tail paired Student t-tests were used to examine if the TAR system improved gait parameters and ankle joint mechanics after three months of surgery. Significant level was set at 0.05.

## RESULTS AND DISCUSSION

Gait temporo-spatial parameters of pre and three months post TAR surgery were presented in Table 1. All patients showed significant increases in stride length and walking speed and decrease of double support time after three months of surgery ( $P < 0.05$ ). In addition, patients exhibited a trend of decrease in stance time ( $P = 0.055$ ).

The involved ankle joint mechanics were also presented in Table 1. Compared to pre-surgical condition, at three months of post TAR surgery,

four out of five patients showed an increase in peak ankle plantar-flexion ( $P = 0.193$ ); and all patients showed significant increases in ankle range of motion (from peak dorsi-flexion to peak plantar-flexion) during terminal stance ( $P < 0.05$ ). Three months after the surgery, the TAR ankle demonstrated increased power absorption and production during stance ( $P < 0.05$ ) (Figure 1). In addition, three out of five patients demonstrated increased ankle plantar-flexor moment at push-off at three months post TAR surgery.

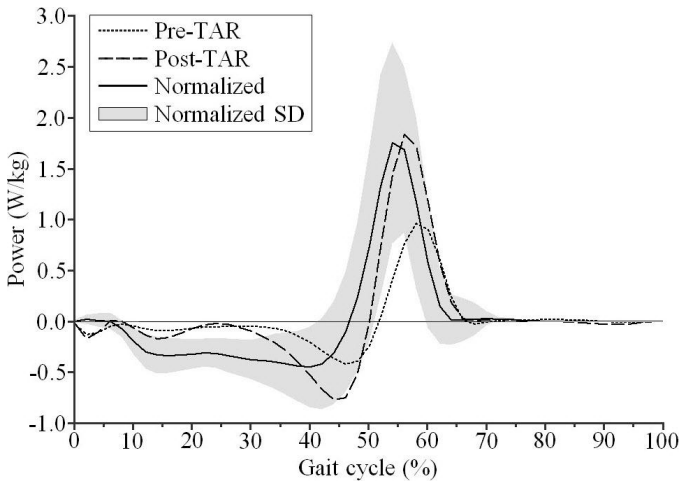


**Figure 1:** Average ankle power for pre and three months post TAR compared to normalized ankle average and standard deviation with respect to the gait cycle (GC).

The pre TAR surgery data indicated that patients had impaired ankle joint function, which limited their ability to perform daily activity such as level

walking. Three months after TAR surgery, patients were able to depend on their TAR ankle to produce increased ankle joint power, stride length, and walking speed. The increased stride length and walking speed appeared to be results of increased TAR ankle range of motion and ankle joint power during stance.

## CONCLUSIONS

The STAA TAR appears to help patients regain ankle range of motion and strength. With a STAA TAR, in as little as three months of surgery, patients were able to increase ankle joint range of motion and joint power and subsequently increase walking speed significantly.

Future research should look into examining the longevity of the STAA TAR in order to eliminate a further revision and to firmly establish its long-term benefits and functionality.

## REFERENCES

1. Gougoulis NE, et al. *Br Med Bull* **89**, 111-151, 2009.
2. Saltzman CL, et al. *J Orthop Sports Phys Ther* **30** (2), 56-67, 2000.
3. www.tornier-us.com
4. Gould JS, *Am J Orthop* **33**, 169-170, 2004.
5. Bonnin M, et al. *Clin Orthop & Rel Res* **424**, 6-18, 2004.

**Table 1:** Gait parameters and involved ankle joint mechanics during walking pre and three months post TAR surgery [mean (standard deviation)].

| Dependent variables                   | Conditions   |              |         |
|---------------------------------------|--------------|--------------|---------|
|                                       | Pre-TAR      | Post-TAR     | P value |
| <b>Temporo-Spatial parameters</b>     |              |              |         |
| Walking speed (m/s)                   | 0.74 (0.12)  | 0.93 (0.11)  | 0.005   |
| Stride length (m)                     | 0.87 (0.11)  | 1.04 (0.08)  | 0.013   |
| Stance time (% GC)                    | 66 (4)       | 63 (3)       | 0.055   |
| Double support (% GC)                 | 34 (5)       | 29 (4)       | 0.044   |
| <b>Involved ankle joint mechanics</b> |              |              |         |
| Peak ankle plantar-flexion (°)        | 3.5 (9.4)    | 1.0 (7.3)    | 0.193   |
| Ankle ROM (°)                         | 15.2 (7.9)   | 19.9 (6.0)   | 0.045   |
| Ankle plantar-flexor moment (Nm/kg)   | 0.85 (0.17)  | 1.04 (0.28)  | 0.075   |
| Ankle absorption power (W/kg)         | -0.43 (0.17) | -0.69 (0.15) | 0.023   |
| Ankle production power (W/kg)         | 1.08 (0.63)  | 1.81 (0.73)  | 0.039   |

# QUADRICEPS ACTIVATION PREDICTS KNEE KINETICS DURING SINGLE-LEG LANDINGS.

Tyler Brown, Scott McLean and Riann Palmieri-Smith  
School of Kinesiology, University of Michigan, Ann Arbor, MI, USA

## INTRODUCTION

Anterior cruciate ligament (ACL) injury prevention programs purportedly combat hazardous knee joint loading through beneficial modification of lower limb neuromuscular control strategies and joint biomechanics. Experimental evidence suggests that quadriceps and hamstrings activation patterns may be related to biomechanical patterns (i.e. knee joint anterior shear force and/or abduction torque) that result in loading of the ACL [1]. During dynamic activities, it has been suggested that preparatory muscle activity plays an essential role in maintaining adequate knee joint stability [2]. How these specific preparatory activation patterns are related to high-risk biomechanical patterns during single-leg landings is unclear. Understanding which neuromuscular parameters predict high-risk knee joint biomechanical patterns may be an important step to improve current prevention strategies and reduce injury risk. With that in mind, the purpose of this study was to examine the relationship between explicit preparatory lower limb neuromuscular control strategies and peak stance knee flexion and abduction moments, and anterior knee joint reaction force elicited during single-leg landings.

## METHODS

Thirty female athletes ( $14.7 \pm 0.6$  years,  $1.64 \pm 0.05$  m and  $55.9 \pm 8.7$  kg) had 3D lower limb (hip, knee and ankle) joint biomechanical and EMG data recorded during a series of single-leg jump landings. Subjects were required to successfully execute five successful single-leg landings off both the right and left limbs. For each landing, subjects jumped a distance equal to their leg length over a 17cm box on to a force platform (AMTI OR6, Advanced Mechanical Technology Inc., Watertown, MA) embedded in the floor, while eight high-speed (240 fps) optical cameras (MX-13, Vicon, Lake Forest, CA) recorded motion data. The jump direction (left or right) after landing was randomly

ordered prior to initiating the jump sequence. Specifically, the subjects were required to land on either their left foot only and immediately jump laterally to the right, or land only on the right foot and rapidly jump to the left [3].

For each landing, knee joint biomechanics were quantified from 3D coordinates of 31 reflective skin markers using Visual 3D (C-Motion, Rockville, MD) to process and solve for lower limb joint rotations, according to our previous work [3]. Filtered kinematic and synchronous GRF data were used to obtain 3D the intersegmental forces and external moments at the knee joint. The external moments at the knee were characterized as flexion-extension, abduction-adduction and internal-external rotation with respect to the cardanic axes of their joint coordinate systems.

During all jump-landing trials, subjects had lower extremity muscle activity recorded at 1200 hertz using a 16 channel EMG system (Delsys, Boston, MA) Surface EMG electrodes were placed over the muscle bellies of the medial (MH) and lateral hamstrings (LH), vastus lateralis (VL), and rectus femoris (RF) during all landings. Prior to collection of the landing trials, EMG data was recorded during a two-second MVIC. Both the dynamic and MVIC EMG data were band-pass (10 – 500 Hz) filtered with a fourth order, zero lag Butterworth filter to attenuate movement artifacts and processed with a 50-millisecond RMS moving window. The dynamic EMG data was normalized to the MVIC activity of each respective muscle before calculating average RMS activity during the pre-activity (100 ms prior to ground contact) phase.

For analysis, peak knee flexion (KFM) and abduction moments (KAM), and peak anterior knee joint reaction force (ANT) were assessed during the first 50% of stance, and normalized to body mass and height, or body mass, respectively. Subject-based means were then subsequently calculated for

the dominant limb from the five single leg landings. Finally, multiple stepwise linear regression analyses ( $P < 0.05$ ) was used to assess the relationship between VL, LH and RF with KFM and ANT, and VL, LH and MH with KAM, respectively.

## RESULTS AND DISCUSSION

During the single-leg landings, RF pre-activity was significantly associated with ANT ( $R^2 = 0.266$ ,  $b = 1.851$  and  $P = 0.004$ ) (Fig. 1A). Specifically, a 1 increase in RF activity predicted 1.8 greater ANT when all other predictors were held constant. Since ANT may be an indicator of ACL load [4], injury prevention programs may be warranted to develop neuromuscular control strategies that limit ANT. To prevent excessive ANT injury prevention programs may want to focus on increased quadriceps strength. In female athletes, strength has been suggested to a significant predictor of preparatory quadriceps activation levels during dynamic landings [5]. The weaker athlete may rely upon greater quadriceps activity to maintain joint stability. Thus, improved quadriceps strength may afford the athlete adequate knee stability with lower activation levels, which may decrease ANT and subsequent ACL load.

Interestingly, both VL and RF pre-activity were associated with KFM ( $R^2 = 0.273$ ,  $b_{vl} = 0.153$ ,  $b_{rf} = -0.525$  and  $P = 0.013$ ) (Fig. 1B). Specifically, a 1 increase in VL activity resulted in 0.15 greater KFM, while a 1 increase in RF activation predicted a 0.53 decrease in KFM. The reason for discrepancy in the relationship between VL and RF pre-activity with KFM is not immediately known. A possible reason for the discrepancy is the fact the RF is bi-articular. Greater RF activity may increase hip flexion posture, which has been shown to reduce KFM during dynamic landings [5]. Although, hip flexion posture was not immediately recorded these findings suggest further study is warranted to determine how RF activation impacts hip posture during dynamic landings.

Finally, no significant association ( $P > 0.05$ ) was evident for any EMG variable and KAM. These findings contradict previous experimental evidence [1]. The reason for the discrepancy is unknown, but future work is warranted to identify neuromuscular control patterns that are associated with KAM to improve injury prevention program effectiveness.

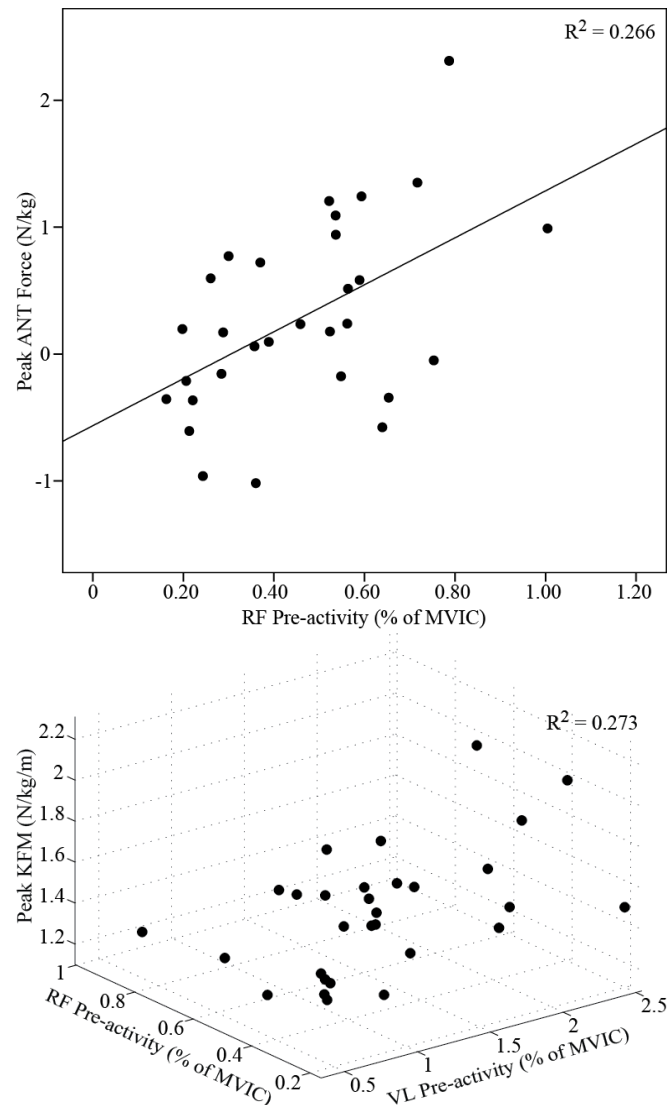


**Figure 1A:** Relation between peak stance ANT and RF pre-activity, and **B:** VL and RF pre-activity with peak KFM during single-legged landings.

## CONCLUSIONS

In conclusion, injury prevention programs may be warranted to focus on improved quadriceps strength as a means to reduce sagittal plane knee joint loading. Future work, however, is needed to identify preparatory activation patterns that are associated with knee abduction moments to provide injury prevention efforts a target for reducing dynamic valgus loading of the knee joint.

## REFERENCES

1. Palmieri-Smith et al. *JAT* **44**, 256-63, 2009
2. Dyhre-Poulsen et al. *J Physiol* **350**, 121-36, 1984
3. Brown et al. *BJSM* **43**, 1049-56, 2009
4. Markolf et al. *AJSM* **32**, 1144-49, 2004
5. Shultz et al. *MSSE* **41**, 857-66, 2009

# ENERGETICS AND BIOMECHANICS OF SLOW UPHILL VS. FAST LEVEL WALKING IN OBESE AND NON-OBESE ADULTS

Raymond Browning, Michelle Reynolds, Wayne Board

Colorado State University, Fort Collins, CO, USA.

email: [ray.browning@colostate.edu](mailto:ray.browning@colostate.edu)

## INTRODUCTION

Brisk walking is a recommended form of exercise for obese individuals. However, walking may be a source of biomechanical loads that link obesity and musculoskeletal injury and pathology, including knee osteoarthritis [1]. In obese adults, lower extremity joint loads and the associated risk of musculoskeletal injury or pathology increase with walking speed on level ground [2], but these individuals may walk with a more extended leg to reduce knee joint loads [3]. Walking uphill at a slower speed may be an alternative form of moderate intensity exercise that reduces joint loading. During uphill walking at the same speed, hip and knee extensor moments are greater than during level walking in non-obese adults [4] but may be smaller in obese adults when walking at a slower speed. To date, no study has compared the energetics and biomechanics of obese and non-obese adults during faster level vs. slower walking. A comprehensive understanding of how obesity and gradients affect the energetics and biomechanics of walking may aid in the development of exercise recommendations that provide adequate physiologic stimulus while reducing the risk of musculoskeletal pathology.

The purpose of this study was to quantify the energetics and biomechanics of level vs. uphill walking in moderately obese vs. non-obese adults. We hypothesized that metabolic rate would be similar while net muscle moments would be smaller during slow, uphill vs. fast, level walking and that there would be no differences between groups.

## METHODS

Fifteen obese, 105.5 (16.7) kg, 35.0 (4.5) kg/m<sup>2</sup>, (mean (SD)) and thirteen non-obese, 64.4 (10.6) kg, 21.6 (2.0) kg/m<sup>2</sup> adult volunteers participated in this

study. We measured metabolic rate, ground reaction forces, three-dimensional lower extremity kinematics while subjects walked for 6 minutes on a dual-belt force measuring treadmill at 1.50 m/s (0°) and 0.75 m/s (6°). Metabolic data was measured continuously via a portable indirect calorimetry system while 30 seconds of biomechanics data was collected during the final minute of the each trial. Kinematic parameters were recorded at 100 Hz using a 7-camera motion capture system. Ground reaction forces and moments were recorded at 1000 Hz by force platforms embedded under each treadmill belt. Body segment parameters were estimated via DEXA and published regression equations [5]. Lower extremity joint centers were determined after adjusting for markers placed over adipose tissue. We calculated gross and net metabolic rate (W/kg) and metabolic cost (J/kg/m) and net muscle moments and powers at the hip, knee and ankle. We calculated the mean of each variable of interest over 10-25 strides at each grade for each subject and the mean across subjects for each trial.

A two-factor (obesity and grade) repeated-measures ANOVA determined how obesity affected metabolic, kinematic, and kinetic variables. Necessary post-hoc comparisons using Holm-Sidak were performed. A criterion of  $p < 0.05$  defined significance.

## RESULTS AND DISCUSSION

Net metabolic rate (gross-standing) was similar during the two walking trials and between groups. When walking at 1.50 m/s, net metabolic rate was 3.74 (0.11) vs. 3.41 (0.21) (mean (SE)) W/kg for the obese and non-obese, respectively. During uphill walking, net metabolic rate was 3.91 (0.06) vs. 4.11 (0.09) W/kg for the obese and non-obese, respectively.

Both groups adjusted temporal-spatial parameters during uphill vs. level walking, as would be expected based on the change in walking speed. At both speed/grade combinations, the obese participants walked with wider steps, shorter strides and spent more time in double support compared to the non-obese participants.

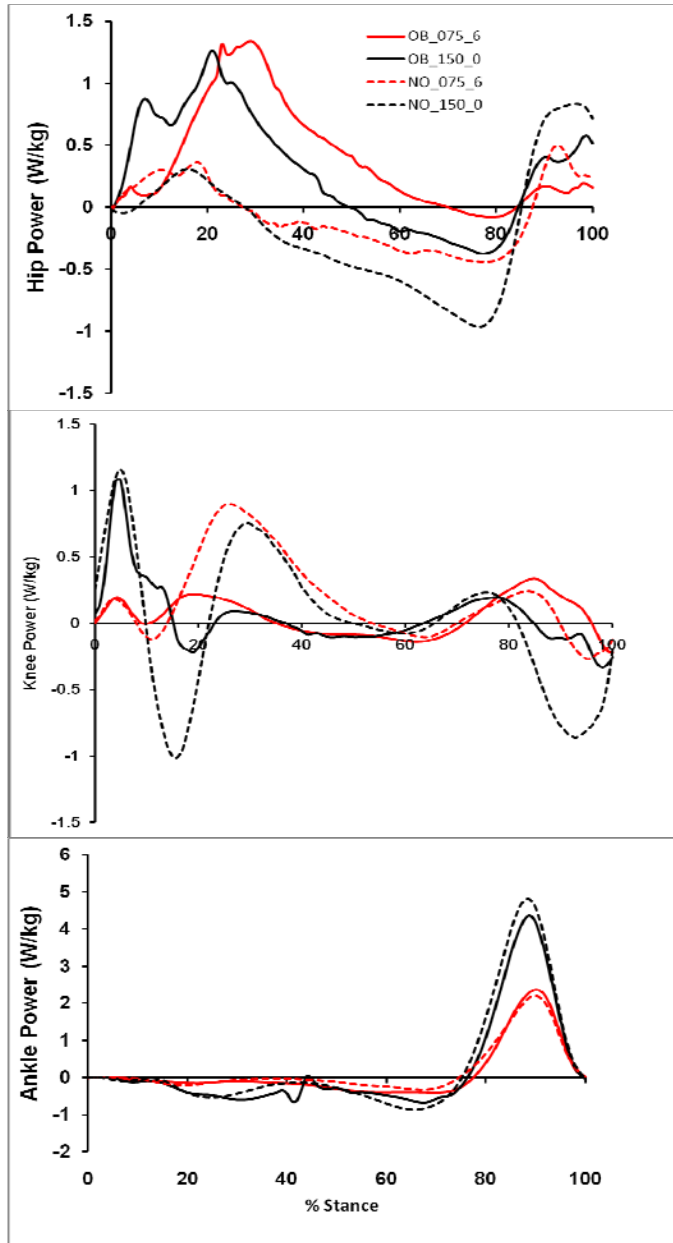


Figure 1. Mean sagittal plane joint power (W/kg) versus percent of stance for obese (OB, solid) and non-obese (NO, dashed).

Both groups walked uphill with a more flexed posture, characterized by greater knee and hip flexion. Peak net muscle moments were smaller during uphill vs. level walking in both groups and peak knee net muscle moments were smaller in obese vs. non-obese adults. As a result, hip joint positive power was much greater during uphill vs. level walking (Figure 1). In addition, knee joint negative power during early stance in obese adults was smaller compared to non-obese adults.

Obese adults performed much more net hip joint work during level and uphill walking compared to non-obese adults. Positive knee joint work was greater during level walking and obese individuals performed much less negative knee joint work compared to non-obese individuals, particularly during early and late stance. Ankle joint work was similar when walking uphill vs. level walking but obese adults performed less net work compared to non-obese adults.

## CONCLUSIONS

These results suggest that slow uphill vs. faster, level walking requires greater net hip joint work in obese but greater net knee joint work in non-obese adults. Thus, different gait strategies result in similar net metabolic rates.

## REFERENCES

1. Felson, D.T., et al. *Ann Intern Med*, **109**, 18-24, 1988.
2. Browning, R.C. et al. *Med Sci Sports Exerc*, **39**(9), 1632-41, 2007.
3. DeVita, P., et al. *J Biomech*, **36**, 1355-62, 2003.
4. Lay, A.N., et al. *J Biomech*, **39**(9), 1621-8, 2006.
5. Durkin, J.L., et al. *J Biomed Eng*, **125**, 515-522, 2003.

## ACKNOWLEDGEMENTS

This research was supported by a grant from the CSU College of Applied Human Sciences and NIH grant R03AR05926

# EFFECTS OF OBESITY ON THE BIOMECHANICS OF UPHILL WALKING

Raymond Browning, Michelle Reynolds, Wayne Board, Crystal Massie

Colorado State University, Fort Collins, CO, USA.

email: [ray.browning@colostate.edu](mailto:ray.browning@colostate.edu)

## INTRODUCTION

Walking is a popular form of exercise for the prevention and treatment of obesity. However, walking may be a source of biomechanical loads that link obesity and musculoskeletal injury and pathology, including knee osteoarthritis [4]. During level walking, moderately obese adults have greater lower extremity net muscle moments (Nm) vs. their non-obese counterparts [1,2]. During uphill walking at the same speed, hip and knee extensor moments are greater than during level walking in non-obese adults [3]. In addition, biarticular hip extensor/knee flexor muscle activity increases during uphill vs. level walking, suggesting that net muscle moments may underestimate knee joint loading when individuals walk uphill [3]. The effects of obesity on lower extremity kinematics, kinetics and muscle activation during uphill vs. level walking are not known. Thus, the relationship between net muscle moments and joint loading in obese adults has not been established. A comprehensive understanding of how gradients affect the biomechanics of walking in obese adults may aid in the development of exercise recommendations that provide adequate cardiovascular stimulus while reducing the risk of musculoskeletal pathology.

The purpose of this study was to quantify the biomechanics of uphill vs. level walking in moderately obese vs. non-obese adults. We hypothesized that hip and knee extensor moments (Nm/kg) and muscle activity would increase during uphill vs. level walking in both groups with no between group differences.

## METHODS

Fifteen obese, 105.5 (16.7) kg, 35.0 (4.5) kg/m<sup>2</sup>, (mean (SD)) and thirteen non-obese, 64.4 (10.6) kg, 21.6 (2.0) kg/m<sup>2</sup> adult volunteers participated in this study. We measured ground reaction forces, three-

dimensional lower extremity kinematics and EMG of five lower extremity muscles (Biceps Femoris (BF), Semimembranosus (SM), Vastus Lateralis (VL), Vastus Medialis (VM) and Lateral Gastrocnemius (GAST)) while subjects walked on a dual-belt force measuring treadmill at 1.25 m/s. Each subject completed 2 or 6 minute trials with the treadmill grade set at 0, 3, 6 and 9°, with 30 seconds of biomechanics data collected during the final minute of the trial. Kinematic parameters were recorded at 100 Hz using seven optoelectric cameras. Ground reaction forces and moments were recorded at 1000 Hz by force platforms embedded under each treadmill belt and EMG data were recorded at 2000 Hz via surface electrodes placed over each muscle. Body segment parameters were estimated via DEXA and published regression equations [5]. We calculated net muscle moments and powers at the hip, knee and ankle via standard inverse dynamics techniques after adjusting for markers placed over adipose tissue. We also determined the timing, duration and mean EMG amplitude of each muscle and normalized these variables to the level walking condition. We calculated the mean of each variable of interest over 10-25 strides at each grade for each subject and the mean across subjects for each trial.

A two-factor (obesity and grade) repeated-measures ANOVA determined how obesity affected kinematic, kinetic and EMG variables. Necessary post-hoc comparisons using Holm-Sidak were performed. A criterion of  $p < 0.05$  defined significance.

## RESULTS AND DISCUSSION

Obese adults had a greater step width and longer period of double support compared to non-obese adults. There were no significant temporal-spatial differences measured in uphill vs. level walking, (i.e. stride length and stride frequency were similar).

Participants walked uphill with a more flexed posture, characterized by greater knee and hip flexion.

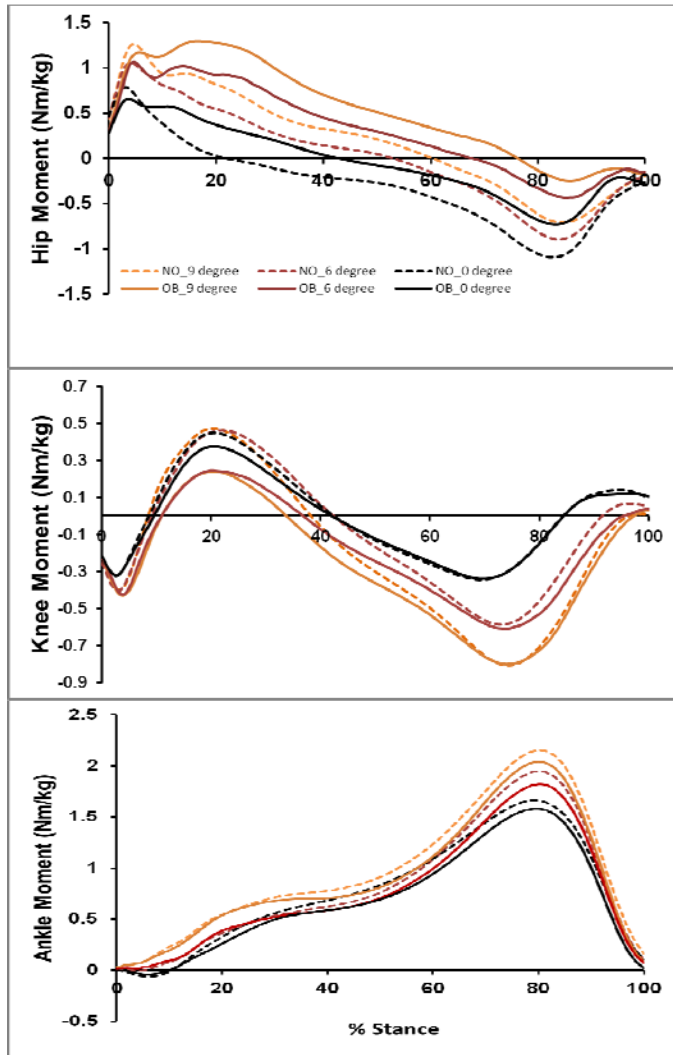


Figure 1. Mean sagittal plane net muscle moments (Nm/kg) versus percent of stance for obese (OB, solid) and non-obese (NO, dashed). Positive moments are extensor/plantarflexor.

Both groups exhibited increased hip extensor and flexor net muscle moments when walking uphill vs. level walking (Fig. 1). Hip extensor angular impulse was much greater in obese vs. non-obese participants at all gradients ( $p < 0.001$ ). Peak knee extensor moments were smaller during uphill vs. level walking in obese but similar in non-obese across the gradients. Ankle plantarflexor moments increased with grade and were smaller in obese vs. non-obese individuals. EMG amplitude was greater during uphill vs. level walking in both groups (Fig. 2), but there were no differences between groups. SM and BF amplitudes increased much more than

the VL, VM and GAST. EMG duration was also greater during uphill vs. level walking in all muscles. As a result, there was greater co-activation of knee flexors and extensors during early stance, coincident with the peak knee extensor moment.

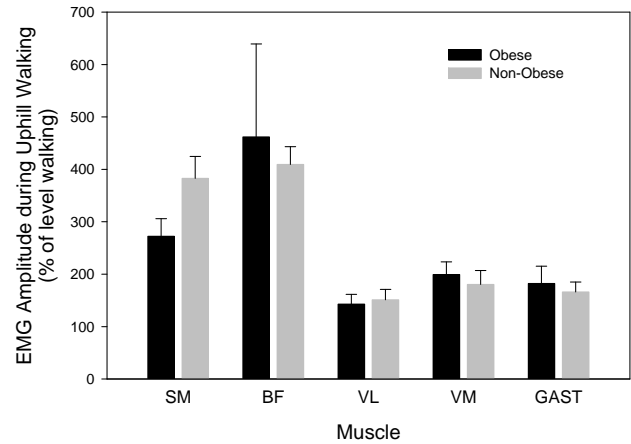


Figure 2. Mean changes in stance phase EMG during uphill walking ( $6^\circ$ ) vs. level walking.

## CONCLUSIONS

These results suggest that obese and non-obese adults walk uphill using a similar strategy that relies more on the hip extensor muscles than during level walking. This strategy results in significant increases in EMG activity and co-contraction of the muscles that cross the knee joint, likely resulting in increased knee joint loading during stance. Thus, while knee net muscle moments decrease in obese adults during uphill vs. level walking at the same speed, this may not be associated with reduced knee joint loads.

## REFERENCES

1. Browning, R.C. et al. *Med Sci Sports Exerc*, **39**(9), 1632-41, 2007.
2. Lai, P.P., et al. *Clin Biomech.*, **23**, S2-6, 2008.
3. Lay, A.N., et al. *J Biomech.*, **39**(9), 1621-8, 2006.
4. Felson, D.T., et al. *Ann Intern Med*, **109**, 18-24, 1988.
5. Durkin, J.L., et al. *J Biomed Eng*, **125**, 515-522, 2003.

## ACKNOWLEDGEMENTS

This research was supported by a grant from the CSU College of Applied Human Sciences and NIH grant R03AR05926.

# COMPARISON OF AUTOMATED EVENT DETECTION ALGORITHMS IN PATHOLOGICAL GAIT

<sup>1</sup>Dustin Bruening, <sup>2</sup>Tyler Standifird, <sup>2</sup>Matt Denning, <sup>2</sup>Sarah Trager Ridge

<sup>1</sup>Shriners Hospitals for Children, Erie, PA

<sup>2</sup>Brigham Young University, Provo, UT

Email: [dbruening@shrinenet.org](mailto:dbruening@shrinenet.org)

## INTRODUCTION

Automated gait event (heel strike, toe off) detection is critical for many applications (e.g. real time biofeedback) and can increase productivity in clinical settings, yet automated event accuracy remains elusive for many complex pathological gait patterns. The handful of kinematic-based algorithms in the literature have had limited evaluation in these populations. While it is unlikely that any one algorithm will have sufficient accuracy for all subjects, it may be possible to choose appropriate algorithms through gait pattern classification. The purpose of this study was to compare published kinematic-based event detection algorithms among several types of involved gait patterns.

## METHODS

Existing gait data (captured at 120 Hz with a Vicon 612 system) from 25 pediatric subjects with cerebral palsy or similar disorders were chosen, based on their event patterns. Subjects were classified in the following five categories:

- 1) *Shuffle*: Patient had a shuffling gait pattern, where the foot slid across the ground just prior to foot strike (focus is on foot strike).
- 2) *Equinus*: Foot strike is made by the mid/forefoot (focus is on foot strike).
- 3) *Steppage*: Subjects used a walker with a marching type of gait (increased vertical motion with decreased horizontal motion).
- 4) *Drag*: Toes/forefoot dragged along the ground after toe off (focus is on toe off).
- 5) *Slow*: A mix of gait patterns with very slow walking speeds. Some subjects used a walker or crutches.

One unilateral stride from each subject was used. Gold standard events were found manually, using force plate data as a guide when available. Seven

kinematic-based algorithms from the literature were then used to calculate comparison events:

- 1) *Zeni* [1]: Position relative to sacrum.
- 2) *Desailly* [2]: High pass filter of position.
- 3) *Ghoussayni* [3]: Sagittal plane velocity threshold.
- 4) *Torres* [4]: Ratio, horizontal/resultant velocity.
- 5) *Hreljac* [5]: Vertical, Horizontal acceleration peaks.
- 6) *Hsue* [6]: Horizontal acceleration peaks.
- 7) *O'Connor* [7]: Vertical velocity peak, position threshold.

A difference threshold of 3 frames (120 Hz) from the manual events was chosen as an acceptable clinical error. The number of subjects in each group within this threshold was tabulated separately for foot strike (Table 1) and toe off (Table 2).

## RESULTS AND DISCUSSION

For the Shuffle group foot strike, Zeni, Desailly, and Hsue performed accurately on all subjects. These three algorithms use horizontal kinematics, which appear most appropriate for a subject sliding into foot strike. For the Equinus group foot strike, several algorithms performed accurately for 4 out of 5 subjects. Event accuracy in this group may be more related to choosing the appropriate evaluation marker (i.e. midfoot for midfoot strike, forefoot for forefoot strike, etc.) than the specific algorithm. For the Steppage group, Hreljac performed best for foot strike (4 out of 5 subjects), while for toe off, Zeni performed best (4 out of 5 subjects). This gait type is characterized primarily by a vertical contact pattern, matching well with the vertical acceleration used in Hreljac. Vertical acceleration might also be considered for toe off, although Zeni performed well using horizontal kinematics. For the Drag group toe off, Zeni again performed best (4 out of 5 subjects). For the Slow group, none of the algorithms were successful for more than 3 out of 5

subjects on foot strike, although Hreljac identified all 5 subjects within 4 frames. Due to the slow walking speeds, the accuracy threshold might arguably be increased. Zeni again performed best (4 out of 5 subjects) on toe off. The Slow group includes some of the most difficult cases, and may need to be more clearly defined to achieve sufficient accuracy.

**Table 1:** *Foot strike.* Number of subjects in each group (n=5) that were within 3 frames of the manual identification.

|            | Shuffle | Equinus | Steppage | Drag | Slow | Total     |
|------------|---------|---------|----------|------|------|-----------|
| Hsue       | 5       | 4       | 3        | 5    | 2    | <b>19</b> |
| Zeni       | 5       | 4       | 0        | 5    | 3    | <b>17</b> |
| Desailly   | 5       | 4       | 0        | 3    | 2    | <b>14</b> |
| Hreljac    | 2       | 2       | 4        | 2    | 3    | <b>13</b> |
| Torres     | 2       | 4       | 0        | 1    | 2    | <b>9</b>  |
| O'Connor   | 1       | 1       | 0        | 0    | 1    | <b>3</b>  |
| Ghoussayni | 0       | 0       | 0        | 0    | 0    | <b>0</b>  |

**Table 2:** *Toe off.* Number of subjects in each group (n=5) that were within 3 frames of the manual identification.

|            | Shuffle | Equinus | Steppage | Drag | Slow | Total     |
|------------|---------|---------|----------|------|------|-----------|
| Zeni       | 5       | 4       | 4        | 4    | 4    | <b>21</b> |
| O'Connor   | 4       | 5       | 0        | 2    | 2    | <b>13</b> |
| Hreljac    | 2       | 3       | 0        | 2    | 0    | <b>7</b>  |
| Hsue       | 2       | 3       | 0        | 2    | 0    | <b>7</b>  |
| Desailly   | 2       | 0       | 0        | 0    | 0    | <b>2</b>  |
| Ghoussayni | 0       | 0       | 0        | 0    | 0    | <b>0</b>  |
| Torres     | 0       | 0       | 0        | 0    | 0    | <b>0</b>  |

Overall, several algorithms performed well on foot strike (Zeni, Desailly, Hreljac, Hsue), and accurate identification of this event appears to be possible using the foot strike pattern to choose the algorithm. Zeni substantially outperformed all other algorithms on toe off, with only one subject outside of 6 frames from the manual identification. With the increased use of multi-segment foot models, toe off events may have increased accuracy in all algorithms if a hallux marker is used instead of a forefoot (metatarsal) marker.

Algorithms that involved specific thresholds did not perform well as employed in this study. These were used as published in the original papers, even though the population in our study had variable and complex pathological gait patterns. Ghoussayni

used a velocity threshold, which the authors admitted may not be accurate for all measurement systems. Using a minimum velocity for foot strike, rather than a velocity threshold, may also have potential for some gait patterns. Torres' ratio was extremely sensitive to subtle changes in motion, which are magnified in pathological populations; although it often found foot strikes just outside of the acceptable range of 3 frames. O'Connor used vertical velocity peaks, along with a position threshold which also may have been too sensitive for these gait patterns. It may be possible to increase the accuracy of these algorithms by adjusting the thresholds to be specific to the gait pattern.

In this study we used manual identification as the gold standard for event detection. While most studies consider force or pressure thresholds as a gold standard, in many pathological cases even these are unreliable (e.g. foot slide or toe drag), and often not available (e.g. assistive devices). In these cases, the most accurate option has been careful manual identification. The 3 frame threshold used to determine accuracy in this study was admittedly somewhat arbitrary, but proved effective in differentiating among algorithms.

## CONCLUSIONS

The results from this study suggest that accuracy can be achieved by classifying subjects by gait pattern, and then choosing the most appropriate algorithm. Possible future directions include expanding the study with additional subjects and gait categories as well as evaluating the algorithms using markers employed in newer multi-segment foot models (e.g. hallux and midfoot).

## REFERENCES

1. Zeni, et al., *Gait Posture* **27**(4), 710-714, 2008.
2. Desailly, et al., *Gait Posture* **29**(1), 76-80, 2009.
3. Ghoussayni, et al., *Gait Posture* **20**(3), 266-272, 2004.
4. Salazar-Torres, *Gait Posture* **24S**, S130-S131, 2006.
5. Hreljac & Marshall, *J Biomech* **33**(6), 783-786, 2000.
6. Hsue, et al., *J Biomech* **40**(S2), S529, 2007.
7. O'Connor, et al., *Gait Posture* **25**(3), 469-474, 2007.

# BIOMECHANICAL CHARACTERIZATION OF SLIPPING ON PERVIOUS AND TRADITIONAL CONCRETE WALKING SURFACES

Adam P. Bruetsch, Gregory W. King, and John T. Kevern

University of Missouri – Kansas City, Kansas City, MO, USA

email: apb2nf@mail.umkc.edu, web: <http://sce.umkc.edu>

## INTRODUCTION

Slips and falls can be frightening and dangerous experiences. Non-ideal surfaces such as ice or rain-covered sidewalks increase the risk of such accidents. Slippery walking surfaces pose a particular danger to older adults, who often suffer from reduced mobility and high fall risk. The use of pervious concrete, a porous material that allows rain and melted ice to pass through its surface and drain elsewhere, could significantly reduce the risk associated with slips and falls during cold weather conditions. Therefore, the purpose of this study was to analyze slip-related biomechanical characteristics during gait on pervious and traditional concrete in dry and icy conditions. We tested the hypothesis that pervious concrete, compared to traditional, would exhibit fewer slip-related characteristics including friction usage, ankle dorsiflexor EMG activity, and stance phase foot velocity.

## METHODS

One healthy adult male participant performed gait trials on traditional and pervious concrete surfaces. Each concrete surface (20" by 18") was placed on top of a force platform (AMTI, Watertown, MA, USA), with rubber tape placed between concrete and force platform to prevent slipping. The participant was instructed to walk such that his right foot contacted the concrete surface. Ten trials were captured during icy conditions for both traditional (TC) and pervious (PC) concrete. To achieve icy conditions, concrete surfaces were frozen to 10 degrees Fahrenheit, then repeatedly misted with water and re-frozen until a 1/8<sup>th</sup> inch layer of ice had accumulated. Frozen samples were allowed to warm up prior to gait trials; initial testing revealed that slips were most likely to occur at a concrete surface temperature of 25 degrees Fahrenheit; therefore all subsequent trials were performed after concrete surfaces had warmed up to 25 degrees.

Data captured during each trial included stance phase ground reaction forces; foot motion measured with motion capture equipment (Vicon, Los Angeles, CA, USA) tracking a reflective marker placed on the heel; and tibialis anterior (TA) EMG activity (Delsys, Boston, MA, USA). Force platform and EMG data were captured at a sampling frequency of 1000 Hz; motion data were captured at a sampling frequency of 100 Hz.

All data analysis was performed in the 100-msec window following heel strike, which is where slips are reported to occur most often [1]. Outcome variables included friction usage, defined as the average ratio of AP to vertical ground reaction force; foot velocity, defined as the minimum AP velocity of the heel marker; and TA activity, defined as the RMS amplitude of the TA EMG signal during heel strike. Outcome variables were compared between TC and PC using standard t-tests.

## RESULTS AND DISCUSSION

Our analysis revealed that PC, compared to TC, was characterized by a larger amount of friction usage in icy conditions. No significant differences were found between PC and TC for foot velocity or TA amplitude; however EMG results revealed marginal significance, with trends toward reduced ankle dorsiflexion in the TC condition.

Our friction usage results suggest that pervious concrete provides a larger amount of traction in comparison to traditional concrete under similar icy conditions. We did not observe a pervious-related decrease in foot velocity during heel strike as expected; this result suggests that, although differences in friction exist, pervious may not provide an overall advantage from a stability

standpoint. On the other hand, reduced stability accompanied by an increase in velocity may only be observed during an actual slip; in our study, slips did not occur in all trials, which may have contributed to variability causing similar foot velocities in TC and PC conditions. Anecdotally, however, we did observe more instances of slipping on TC in comparison to PC, as evidenced by Figures 1 & 2.

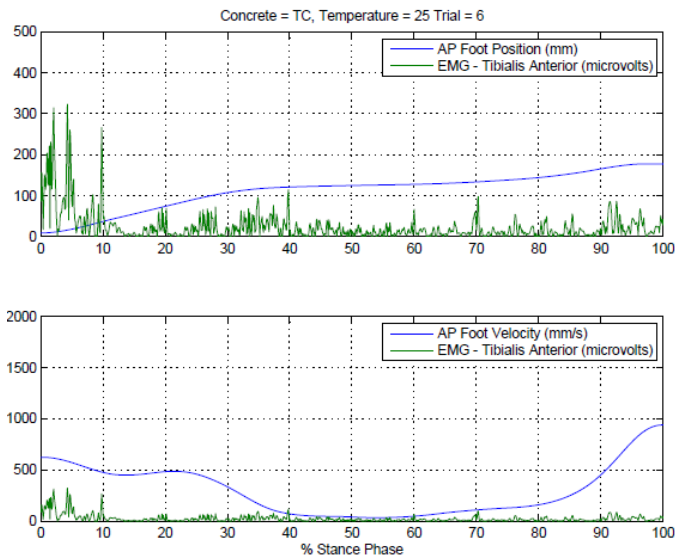


**Figure 1: TC AP foot position/velocity and TA EMG**

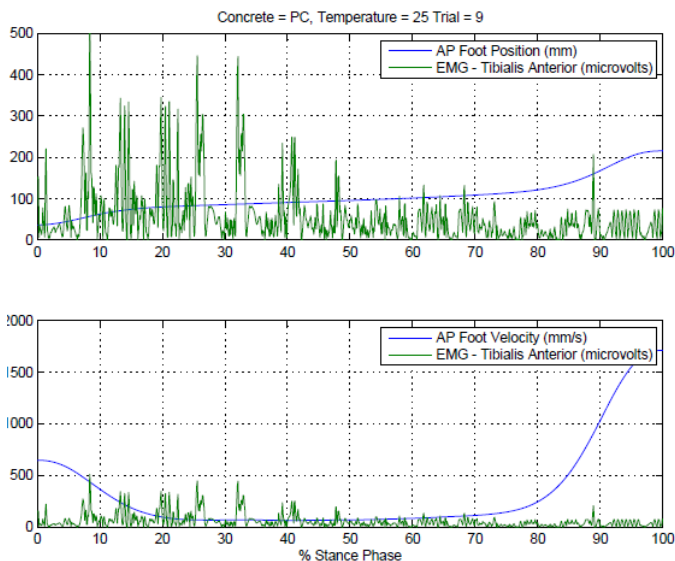


**Figure 2: PC AP foot position/velocity and TA EMG**

Although not significant, our result that TC is associated with reduced TA EMG activity is consistent with studies reporting reduced ankle dorsiflexion during slipping [2]. This trend may suggest marginal improvement of slip performance when walking on pervious concrete.

|                      |    | Mean       | Std. Deviation |
|----------------------|----|------------|----------------|
| Friction Usage       | TC | 0.322086   | 0.0924446      |
|                      | PC | 0.499925   | 0.0871453      |
| EMG Amplitude (mV)   | TC | 0.052929   | 0.0317789      |
|                      | PC | 0.096450   | 0.0637486      |
| Heel Velocity (mm/s) | TC | 287.299711 | 89.3143247     |
|                      | PC | 235.147925 | 57.9425174     |

**Table 1: Statistical evaluation of coefficient of friction**

Taken together, these results suggest a modest improvement in slip performance on pervious concrete in comparison to traditional concrete under similar icy conditions. Measures of stability and muscle activity may not have reached statistical significance due to the small number of samples used in this preliminary study. Further investigation is needed to gain a more complete understanding of their relationship to slipping.

## CONCLUSIONS

We observed larger friction usage on PC, compared to TC. This suggests that PC provides better traction in icy conditions and may be more effective in preventing slips and falls. We also observed trends towards larger ankle dorsiflexion and smaller slip likelihood on PC, compared to TC; these results were not significant in this preliminary study, but may have importance as more samples are captured in future work.

## REFERENCES

- 1) Fong, D., Mao, D.W., Li, J.X., and Hong, Y. (2008). "Greater toe grip and gentler heel strike are the strategies to adapt to slippery surface." *Journal of Biomechanics*, 41, 838-844.
- 2) Gao, C., Oska, J., Rintamäki, H., and Holmér, I. (2008). "Gait muscle activity during walking on an inclined icy surface." *Industrial Health*, 46, 15-22.

## ACKNOWLEDGEMENTS

We gratefully acknowledge the help of Kyle Dunning for his assistance with concrete preparation and preliminary testing. This work was supported by a National Science Foundation EAGER grant (CMMI-0951444).

# VERTEBRAL FRACTURE LOCATION INFLUENCES RISK OF FUTURE VERTEBRAL FRACTURE

<sup>1,2</sup>Alexander Bruno, <sup>1,3</sup>Dennis Anderson, <sup>1</sup>John D'Agostino and <sup>1,3</sup>Mary Bouxsein

<sup>1</sup>Center for Advanced Orthopaedic Studies, Beth Israel Deaconess Medical Center,

<sup>2</sup>Harvard-MIT Division of Health Sciences and Technology,

<sup>3</sup>Department of Orthopedic Surgery, Harvard Medical School, Boston, MA, USA

email: [agbruno@mit.edu](mailto:agbruno@mit.edu)

## INTRODUCTION

Vertebral fractures occur in one-third of women after age 50, leading to marked pain, disfigurement, loss of function, and depression. In addition, the presence of a vertebral fracture significantly increases the risk of incurring subsequent vertebral fractures, and this is evidenced by the fact that 20% of women with a vertebral fracture will incur another fracture within a year [1]. Although the mechanisms underlying this increased fracture risk are unknown, prior work in our laboratory suggests that altered spine biomechanics may play a role. We hypothesized that an initial fracture alters the geometry of the spine such that compressive loading on the non-fractured vertebral bodies is increased, thereby increasing risk of future fractures. The aim of this study is to examine the effect of initial fracture location on the risk of future vertebral fractures during different activities of daily life (ie bending, lifting) using a musculoskeletal model. We compared a fracture in the mid-thoracic region to a fracture in the thoraco-lumbar junction (the two most common sites of vertebral fracture) [2], and hypothesized that the thoraco-lumbar fracture would increase risk of future fracture more than a mid-thoracic fracture.

## METHODS

We used a previously developed quasi-static biomechanical model of the thoracic and lumbar spine [3] to simulate a severe anterior-wedge fracture at T8 (mid-thoracic) and L1 (thoraco-lumbar junction). A severe anterior-wedge fracture was defined as a 40% reduction in the anterior height of the vertebral body, which would result in a forward tilting of the spine. These geometric changes were implemented in a model of a

representative 66-year-old woman (ht = 167 cm, wt = 69.4 kg). The model was used to estimate compressive force on the T6 through L5 vertebrae for three different conditions: 1) a non-fractured control spine; 2) a spine with a fracture at T8; and 3) a spine with a fracture at L1. These conditions were modeled during three different activities: 1) upright standing with a 10 kg weight in each hand; 2) 30° of forward flexion while holding a 10 kg weight in each hand; and 3) forward flexion combined with a twist to the right, each at 30°, with a 10 kg weight in each hand. Vertebral body strength was estimated using 3D QCT scans of the thoracic and lumbar spine taken from 1609 women, aged 35-93, enrolled in the population-based Framingham Heart and Multidetector CT Study. We used an empirically derived relationship that relates vertebral body cross-sectional area and total volumetric BMD (measured on the QCT scans) to vertebral body compressive strength [4], and for each vertebral level chose the 25<sup>th</sup> percentile strength for women between the ages of 60 and 70 (n = 313). Factor of risk for vertebral fracture was then defined as the ratio of applied compressive force to vertebral body strength, with a factor of risk greater than one (when load exceeds strength) corresponding to a significant risk of fracture.

## RESULTS AND DISCUSSION

In general, factor of risk across the spine was greatest for the flexion and twisting task, followed by the pure flexion task, with the lowest values for factor of risk occurring in the upright standing task. The factor of risk along the spine was generally the highest for the case of a fracture at L1, followed by a fracture at T8, with the lowest values of factor of risk observed in the non-fractured spine, and this trend held for each activity (Fig. 1). As vertebral

strength was the same for the different activities and conditions, differences in factor of risk were due to differences in compressive loading.

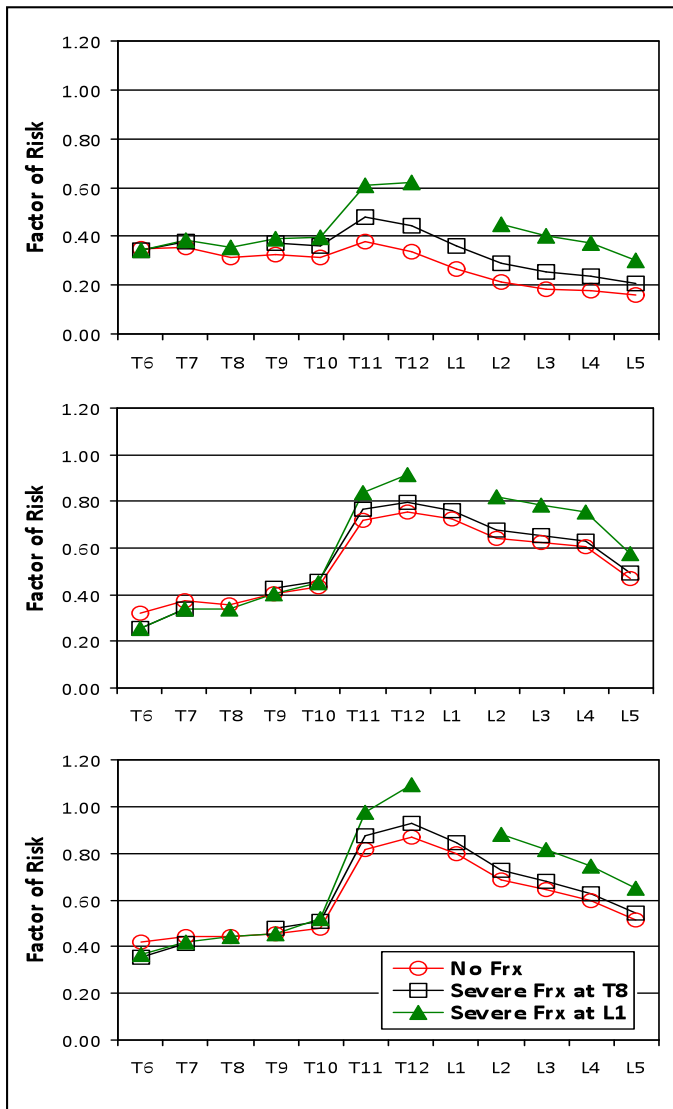


**Figure 1:** Factor of risk at vertebral levels T6-L5 following a fracture at T8, a fracture at L1, and when no fracture is present: top) upright standing; middle) 30° forward flexion; and bottom) forward flexion and twist, each at 30°. Factor of risk was not calculated at the fractured levels.

The presence of a fracture minimally affected factor of risk in the thoracic spine, but resulted in large increases in fracture risk in the thoraco-lumbar junction and lumbar region, with the most dramatic changes occurring at T12. For upright standing with a 10 kg weight in each hand, a fracture at T8 increased the factor of risk at T12 by 31% relative to the non-fractured control spine, and the presence of a fracture at L1 increased the T12 factor of risk by 83% relative to the non-fractured control spine.

For all activities and conditions, there appeared to be a peak in factor of risk in the thoraco-lumbar junction, which is the region in which fractures occur most frequently. However, factor of risk tended to be low in the mid-thoracic region (T6-T8) and was minimally affected by the presence of a fracture, which was an unexpected finding considering that the mid-thoracic region is the second most common sight for fractures [2]. The observation that a fracture at L1 increased the factor of risk more than a fracture at T8 likely results from the fact that L1 is lower in the spine than T8, and so a fracture there will result in a larger percentage of body mass being shifted anteriorly, resulting in higher flexion moments and compressive loading.

## CONCLUSIONS

These results demonstrate that the location of a fracture along the spine can influence the risk of future vertebral fractures, and that a fracture in the thoraco-lumbar junction increases fracture risk more than a fracture in the mid-thoracic region. The results also demonstrate that fractures at both T8 and L1 had a larger effect on factor of risk in the lumbar and thoraco-lumbar junction than in the mid-thoracic spine, which could be due to the mechanical contribution of the ribs and sternum in that region. Altogether these data are consistent with the hypothesis that alterations in spine biomechanics after a first vertebral fracture contribute to increased risk of subsequent fractures.

## REFERENCES

1. Lindsay R, et al. *The Journal of the American Medical Association* **285**, 320-323, 2001.
2. Ismail A, et al. *Osteoporosis International* **9**, 206-213, 1999.
3. Iyer S, et al. *Clinical Biomechanics* **25**, 853-858, 2010.
4. Bouxsein M, et al. *Journal of Bone and Mineral Research* **21** 1475-1482, 2006.

## ACKNOWLEDGEMENTS

This work was supported by NIH R01AR053986, R01AR/AG041398, T32 AG023480, and the National Heart, Lung, and Blood Institute (NHLBI) Framingham Heart Study (NIH/NHLBI Contract N01-HC-25195).

# EVALUATING THE ACCURACY OF A CYBERGLOVE MOTION CAPTURE PROTOCOL WITH COMPUTED TOMOGRAPHY DATA

<sup>1,3</sup>James Buffi, <sup>5</sup>Joseph J. Crisco and <sup>1,2,3,4</sup>Wendy M. Murray

Departments of <sup>1</sup>Biomedical Engineering and <sup>2</sup>PM&R, Northwestern University, Chicago, IL

<sup>3</sup>SMPP, Rehabilitation Institute of Chicago, Chicago, IL; <sup>4</sup>VA Hines, Hines, IL

<sup>5</sup>Department of Orthopaedics, Brown University and Rhode Island Hospital, Providence, RI

email: [jamesbuffi2013@u.northwestern.edu](mailto:jamesbuffi2013@u.northwestern.edu)

web: <http://www.smpp.northwestern.edu/research/arms/index.html>

## INTRODUCTION

The human hand plays a vital role in our ability to interact with our environment. Despite its importance, hand function can be difficult to study quantitatively. Specifically, characterizing hand kinematics during functional tasks can present many challenges.

To study kinematics during human motion, experimental protocols generally link motion capture data to musculoskeletal models. For the hand, optical tracking methods or instrumented gloves are often employed. Optical tracking protocols are usually considered the most accurate. However, set up and execution can be problematic. Marker placement is time-consuming and difficult to repeat without substantial training [1]. During functional tasks, issues also arise involving marker occlusion and skin motion artifact [1]. Instrumented glove protocols mitigate these issues. However, finding transformations relating sensor values to joint angles brings new issues to light [2]. There is also a paucity of information about how accurately instrumented gloves track hand motion.

In this study, kinematic data collected via a Cyberglove (San Jose, CA) was animated using a kinematic model of all five digits of the hand [3]. We compared the animated hand postures to a “gold standard”: hand postures quantified via computed tomography (CT) at the same time the Cyberglove data was collected.

## METHODS

To assess the accuracy of our motion capture protocol, kinematic and CT data were collected

simultaneously. To begin, a single subject donned the Cyberglove and we implemented a previously described calibration process [3]. In brief, voltage offsets were first collected in a baseline posture (a posture in which the longitudinal axes of finger bones are aligned and the thumb lies in the same plane as the palm) and then voltage outputs were recorded from 20 sensors of the Cyberglove during four serial calibration tasks (one for each finger). Each task involved cyclical flexion and extension of the thumb (digit 1) and a single finger (digits 2-5), while contact was maintained between their distal segments.

Once the calibration tasks were completed, the subject was asked to assume three different functional poses as data were simultaneously recorded from the Cyberglove and a GE Lightspeed 16 CT Scanner (Milwaukee, WI). The poses included the baseline posture described above, a grasp posture in which the digits were flexed while grasping a cylindrical object (“jar grasp”), and an opposition posture in which the thumb (digit 1) opposed the little finger (digit 5). Voltage data were collected from the Cyberglove at a rate of 90 Hz. Image data were collected with tube settings of 80 kVp and 40 mA, slice thickness of 0.625 mm, and in-plane resolution of 0.3 x 0.3 mm.

Following data collection, raw voltage data from the Cyberglove were converted to joint angles using Equation (1):

$$(1) \quad [\theta(t)] = [g][v(t) - v_0]$$

Given the voltage offsets recorded in the baseline posture during calibration, the gains for each of the 20 Cyberglove sensors were calculated using an optimization routine that minimized the distance

between the “pad” of digit 1 and the “pad” of the appropriate digit of our kinematic model [3]. The functional hand poses were then recreated and the orientations of the individual bones in the model were compared to the orientations of the bones from the CT scans. Each CT scan was manually segmented and reconstructed. Principal axes were calculated for each bone for both the kinematic model and the 3D reconstructions. In both cases, joint angles were calculated as Euler angles relating the principal axes of neighboring bones. The angle about the principal axis in the ulnar-to-radial direction was defined as flexion/extension.

Joint angle error was defined as the absolute difference between the corresponding Cyberglove and CT angles. Statistical significance was assessed via the signed-rank or Wilcoxon rank-sum test.

Finally, the data analysis protocol was repeated using “gold standard” voltage offsets: the voltage offsets recorded while the baseline posture was produced during the CT scan.

## RESULTS AND DISCUSSION

For the tasks evaluated in this study, the motion capture protocol we implemented had a median accuracy of 9°. The overall precision of the system was 11°. Median accuracy of individual joints ranged from 1° to 23° (Table 1). Precision also varied substantially across joints, with IQRs ranging from 0.4° to 37°. We observed significant differences ( $p < 0.05$ ) among the three postures; accuracy and precision were significantly different in the jar grasp and finger opposition postures compared to baseline (cf., open boxes, Fig. 1).

Using voltage offsets recorded during the CT scan significantly reduced errors (Fig. 1). Median error decreased from 9° to 2° in the baseline posture. For the other two postures, precision improved from 14° to 11° (jar) and from 12° to 7° (opposition). The

absolute maximum error observed at any joint was also reduced by 5° (jar) and 8° (opposition).

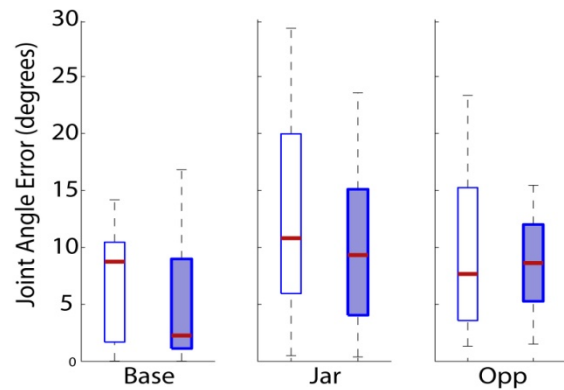


**Figure 1.** Box plots of joint angle errors separated by posture. Open boxes use voltage offsets recorded during calibration, filled boxes use offsets recorded during the CT scans.

The errors associated with our technique were on the same order as those reported by a previous study that calibrated digits 1-3 of an instrumented glove using optical tracking techniques [4]. (Note that error assessment was different between the two studies and we re-calculated our errors using their methods to compare).

## CONCLUSIONS

We have developed a robust motion capture protocol and evaluation technique for conclusively analyzing complex tasks involving the whole hand.

## REFERENCES

1. Metcalf, C.D., et al., *IEEE Trans on BME* **55**, 1199-1210, 2008.
2. Griffin, W.B., et al., *Proceedings of ASME IMECE*, 2000.
3. Buffi, J.H. and W.M. Murray, *Proceedings of the 34<sup>th</sup> Meeting of ASB*, Providence, RI, USA, 2010.
4. Veber, M., et al., *Meccanica* **42**, 451-463, 2007.

## ACKNOWLEDGEMENTS

This work was funded by NIH R01 HD046774.

**Table 1.** Accuracy\* and precision\* of flexion angles of individual joints.

|        | Digit 1 |    |    | Digit 2 |     |     | Digit 3 |     |     | Digit 4 |     |     |     | Digit 5 |     |     |     |         |
|--------|---------|----|----|---------|-----|-----|---------|-----|-----|---------|-----|-----|-----|---------|-----|-----|-----|---------|
| Joint  | cmc     | mp | ip | mcp     | pip | dip | mcp     | pip | dip | cmc     | mcp | pip | dip | cmc     | mcp | pip | dip | Overall |
| Median | 2       | 14 | 1  | 7       | 7   | 19  | 4       | 8   | 11  | 13      | 9   | 9   | 9   | 2       | 15  | 7   | 23  | 9       |
| IQR    | 0.4     | 12 | 21 | 5       | 6   | 7   | 9       | 2   | 5   | 10      | 13  | 16  | 9   | 0.5     | 10  | 5   | 37  | 11      |

\* accuracy was estimated as the median error across all trials, precision was estimated by the interquartile range (IQR).

# FINITE STATE CONTROL OF A VARIABLE IMPEDANCE KNEE MECHANISM FOR RESTORATION OF STANCE PHASE KNEE FLEXION AFTER SPINAL CORD INJURY

<sup>1</sup>Thomas C. Bulea, <sup>2</sup>R. Kobetic, <sup>1,2</sup>Ronald J. Triolo

<sup>1</sup>Case Western Reserve University, Cleveland, OH, USA

<sup>2</sup>Louis Stokes Cleveland Department of Veterans Affairs Medical Center, Cleveland, OH, USA

email: [tcb9@case.com](mailto:tcb9@case.com)

## INTRODUCTION

Functional neuromuscular stimulation (FNS) can be utilized to restore walking function after spinal cord injury (SCI). While excellent at propelling the body forward, the high stimulation duty cycles and limited number of stimulation channels compared to lower extremity degrees of freedom result in unnatural gait patterns and rapid muscle fatigue. Combining a FNS system with a controllable lower extremity orthosis can alleviate these problems by reducing the degrees of freedom during gait. Typically, such hybrid neuroprostheses (HNP) lock the knee during stance phase to support body weight and reduce stimulation; however, these systems retain the stiff-legged stance phase typical of FNS walking systems.

We have developed a novel orthosis capable of regulating knee rotation by providing variable amounts of resistance through the use of MR fluid [1]. A finite state control system has been developed to utilize this mechanism in a HNP to restore and regulate stance phase knee flexion during FNS-driven gait. Such a system has the capability to restore functions which are unattainable with FNS walking systems, including controlled flexion for impact absorbance and forward stair descent.

## METHODS

The advantages of allowing stance phase knee flexion have been previously reported in prosthetics [2]. We seek to effectively restore stance phase knee flexion through the use of a controllable orthosis in combination with FNS walking system. The FNS system will propel the body forward using contractions of the user's muscles, while the orthosis will control the motion of the knee during

stance phase. The controller functions based on feedback from sensors mounted on the lower extremity brace to monitor sagittal plane hip and knee angle and velocity, foot-ground contact at the heel and forefoot, and axial acceleration of the lower leg. A typical gait cycle can be split into six distinct phases: loading response, mid-stance, terminal stance, pre-swing, early swing, and late swing [3]. The distinct knee behavior during these six phases of gait suggests that a finite state machine can be implemented for use as a knee controller (Figure 1). A similar approach has been taken in the development of controllers for prosthetic knees [4].

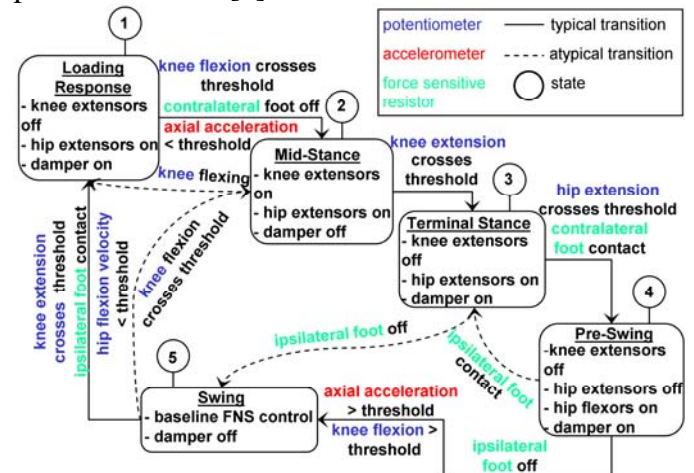


**Figure 1:** Schematic representation of finite state controller for stance phase knee flexion control using a variable impedance orthosis. Conditions for moving between states are indicated along transition lines; colors indicate which sensor will monitor the control variable.

To minimize parasitic losses of limb motion under FNS activity, the VIKM will remain off during both swing phases, enabling them to be lumped into a single state. Transition between the five states will proceed as follows. State 1 begins when the ipsilateral foot contacts the floor; the damper is

turned on to absorb the shock of impact and accept the body weight. As forward progression continues, the damper regulates knee flexion caused by thigh inertia and body weight load at the proximal end of the femur. Once initial knee flexion passes a predetermined threshold (approximately  $15^\circ$  [3]), the controller transitions to state 2. Knee and hip extensors are turned on while the damper is turned off to facilitate transfer of the body weight vector to the anterior side of the knee joint. When the knee reaches near full extension (within  $3^\circ$ ) the FNS is turned off and the damper is turned on to prevent flexion and to rest the muscles as the controller moves to state 3. When the contralateral foot contact is sensed, the transition to state 4 takes place; the damper is active, regulating knee flexion which occurs as the ipsilateral hip flexes under FNS control and the load of weight bearing is transferred to the contralateral side. Once the ipsilateral foot leaves the ground, the damper is turned off to allow unencumbered knee motion during swing, after which the cycle repeats.

The knee damper actively regulates stance flexion during states 1, 3, 4. During these states, a secondary controller is activated which monitors knee angular velocity and adjusts damping proportionally. The level of resistance supplied by the MR damper is controlled by the duty cycle of a high frequency (800 Hz) pulse width modulated signal attached to a MOSFET switch gait. An onboard microcontroller adjusts the values of digital outputs – three for each knee – based on the output from the proportional controller; this enables the damper to have eight distinct damping states with eight different duty cycles ranging from 0% to 90%. At 0%, the damper is off and provides minimal resistance to knee rotation (less than 4 Nm), while at 90% the orthosis provides up to 64.5 Nm of resistance [1]. At any time during stance, if the knee angle flexion velocity or knee angle exceeds a preset threshold, the damper duty cycle is set to 90% to prevent collapse until FNS stimulation can resume to extend the leg.

The controller was validated during level ground walking experiments with able body subjects. Real time assessment of gait phase was performed by the controller based on inputs measured from the sensor set described above. The results from the controller were verified by comparing with data collected

using a Vicon<sup>®</sup> MX40 motion capture system (Vicon Motion Systems, Oxford, UK).

## RESULTS AND DISCUSSION

During able body walking, the controller was able to successfully identify all phases of gait. Over an average of 22 strides, the damper was actively regulating stance phase knee flexion during initial impact/weight acceptance, terminal stance, and pre-swing while turning off to allow stance phase extension during mid-swing (Figure 2). The range of knee angle was slightly diminished compared to normal walking, which is likely due to passive resistance within the orthosis.

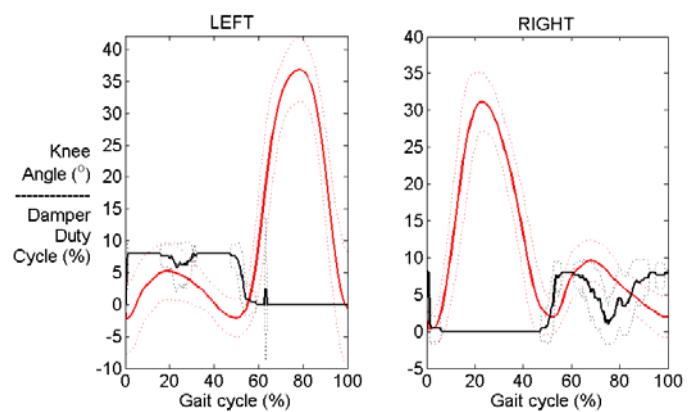


**Figure 2:** Average left and right knee angle (red line) and damper duty cycle (black) for 22 strides of walking with the variable impedance orthosis.

## CONCLUSION

The data presented here indicate the finite state controller is able to appropriately actuate the variable impedance knee mechanism for control of stance phase knee flexion. Stance phase knee flexion is currently non-existent in FNS-only walking systems, and may provide opportunity for increased gait efficiency and expansion of walking functions to include other maneuvers which require controlled knee flexion, such as ramp and stair descent.

## REFERENCES

1. Bulea, TC, et al. *IEEE/ASME Trans Mech*, in press.
2. Johansson, JL, et al. *Am J Phys Med Rehab* **84**, 563-575, 2005.
3. Perry, J. *Gait Analysis*, McGraw-Hill, Inc., 1992.
4. Herr, H, et al. *Ind Robot*, **30**, 42-55, 2003.

# REMOVING THE HUMAN FACTOR FROM CLINICAL REFLEXOLOGY

<sup>1</sup>Tamara Reid Bush, <sup>1</sup>Ranjan Mukherjee, <sup>1</sup>Alla Sikorskii, <sup>1</sup>Gwen Wyatt

<sup>1</sup>Michigan State University, East Lansing, MI, USA  
email: [reidtama@msu.edu](mailto:reidtama@msu.edu) web: <http://www.egr.msu.edu/~reidtama>

## INTRODUCTION

Reflexology is a form of alternative medicine that involves the physical application of pressure to specific body parts by a reflexologist. Human feet, in particular, are mapped with regions called “reflexes,” where each of these reflexes corresponds to specific body parts, including organs and glands (Fig. 1). The underlying theory is that stimulation of a reflex will result in a therapeutic reaction of the corresponding body part – leading to improved function. Studies have produced mixed evidence of the effectiveness of reflexology, and researchers cite that the “human factor” of the reflexologist (e.g. effects of human touch, pleasant conversation with the patient, etc.) confounds the results.

Thus, to evaluate the effects of reflex stimulation without the “human factor,” the need exists for an alternative method to deliver reflexology. The objective of this work was to design and create a robotic device that would provide a clinically based reflexology protocol independent of the human factor. The specific focus for this study was patients with breast cancer.

## METHODS

A protocol specific to breast cancer was designed to stimulate the body regions affected by this disease [1]. This was done in an effort to remove the toxic byproducts of chemotherapy. The following reflexes were stimulated on the foot: breast, chest, lymphatic, spine, lungs, diaphragm, kidneys, adrenals, intestinal and spleen. The associated breast and chest reflexes are located on the top of the foot, near the toes, while the lymphatic reflexes are located around the ankle, and the remaining reflexes are on the sole of the foot. To accomplish the stimulation of these three areas, three mechanical systems were designed and built; two were integrated into a single unit (Fig. 2) while the

third was a separate unit. All three mechanisms were developed to mimic the stimulation techniques used by a reflexologist.

In addition, a semi-automated foot calibration routine was developed for the sole of the foot. This was accomplished by inputting the coordinates of six anatomical related landmarks on the foot so that the robotic device could automatically locate the reflexes.

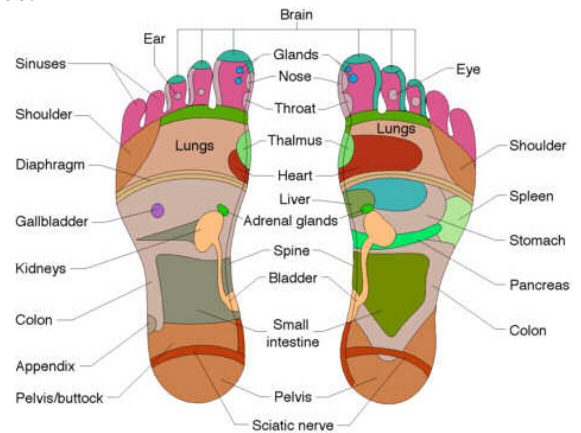


**Figure 1:** Mapping of reflexes on the sole of the feet [http://www.exhalereflexology.com]

## Mechanism for stimulating the sole of the foot:

The robotic reflexology device was designed as a rectangular unit with a calf support. A single opening accommodated either the left or right foot (Fig 2). Reflex stimulation was achieved by a small sphere that applied pressure on the sole of the foot. Position was controlled by two slides (XY axes), and actuation was perpendicular to the plane of the slides (Z axis). Flexible fabric was mounted over the foot contact region which prevented direct contact between the foot and the sphere. The fabric kept friction constant, and prevented pinching or wrinkling of the skin during device interaction. The device had default forces set for each reflex; however the patient could adjust those forces to her comfort level via a hand-held dial. These force data were also recorded.

**Mechanism for stimulating the ankle:** A second mechanism stimulated the lymphatic reflexes around the base of the ankle. This unit consisted of a series of small spheres attached to a flexible cord secured around the ankle by a spring/hook system. Once positioned, the patient initiated reflex stimulation through a remote control device. The remote control turned on a motor that produced a reciprocating motion which, in turn, caused the spheres to roll back and forth over the ankle region, stimulating the reflexes.

**Mechanism for stimulating the top of the foot:** A separate mechanism was used for stimulation of the area that runs across the top of the foot near the toes. Once the foot was positioned in the device, a set of flexible arms with soft rubber wheels at the end of each arm were lowered such that the wheels were located on the soft tissue regions between the toes. A motor and cam mechanism caused the wheels to move back and forth stimulating the breast and chest reflexes. Adjustments of the arms enabled it to adapt to different foot sizes, and to accommodate either the left or right foot. Tension adjustments allowed for various levels of pressure application.

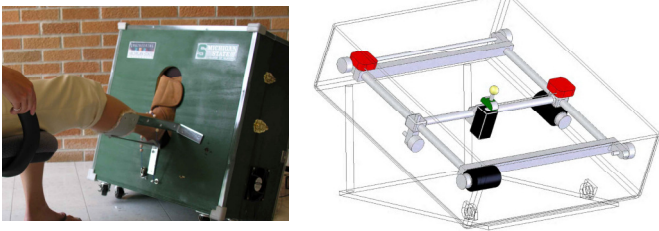


**Figure 2:** Photo and schematic of the device.

**Patient Testing:** Two patient samples were tested, with each participant undergoing 4 weeks of reflexology, with one session per week. Group 1, the feasibility, and acceptability group, consisted of 13 breast cancer survivors not currently undergoing treatment. Feasibility and acceptability tests were conducted in the laboratory to ensure that the device would be accepted as an effective mechanism for delivering reflexology.

The second group of subjects (Group 2) was a sample of women actively undergoing chemotherapy for breast cancer (n=13). This group was tested to evaluate physical function and symptom changes with the use of the device.

Testing occurred in a community-based oncology clinic where the women were receiving chemotherapy.

A symptom inventory [2] was used to evaluate the severity of established symptoms experienced by cancer patients, (i.e., pain, fatigue, nausea, disturbed sleep, distress, shortness of breath, cognitively difficulties, decreased appetite, drowsiness, dry mouth, sadness, numbness/tingling) and the interference of these symptoms with daily life. A separate, established evaluation instrument was used to assess physical function [3].

## RESULTS AND DISCUSSION

Results from Group 1 (the feasibility group) indicated that the robotic device was acceptable to the women. Further, data indicated this technology was an effective means for delivering reflexology with high satisfaction. These results allowed investigation of this device with Group 2, women undergoing chemotherapy.

Data for Group 2 indicated that symptom severity significantly decreased ( $p=0.02$ ) between the initial and the final robotic reflexology sessions. Further, physical function also improved ( $p=0.06$ ). However, our third assessment, interference of symptoms with daily activity, did not show significant improvement.

In conclusion, the team was successful in its goal to design and build a robotic device which could apply a clinically based reflexology protocol to the feet, thus removing the “human factor”. Further, results from patient testing point to the efficacy of the device. The stimulation of reflexes resulted in symptom improvement and an achievement of enhanced physical function for women undergoing chemotherapy.

Further development of this robotic technology will allow for advanced studies of reflexology and its effectiveness.

## REFERENCES

1. Wyatt GK et al. *NIH* 1R01 CA104883-01A1
2. Cleeland CS et al. *Cancer*. 1634-, 2000
3. Ware JE, et al. *Medical Care*. 34(3):220-, 1996

# A COMPARISON OF THE AFFECT OF SOFT AND RIGID CUSTOM-MADE CORRECTIVE ORTHOTICS AND OVER-THE-COUNTER PROPRIOCEPTIVE FEEDBACK ORTHOTICS ON HINDFOOT PRONATION DURING WALKING GAIT: A TWO-DIMENSIONAL DYNAMIC FLUOROSCOPIC STUDY

<sup>1,2</sup>Kristen M. Bushey, <sup>1,2</sup>Megan E.R. Balsdon, <sup>3</sup>Colin Dombroski, <sup>1,2</sup>Thomas R. Jenkyn

<sup>1</sup>Wolf Orthopaedic Biomechanics Laboratory, Fowler Kennedy Sports Medicine Clinic, London, ON, Canada

<sup>2</sup>University of Western Ontario, London, ON, Canada

<sup>3</sup>Sole Science, Fowler Kennedy Sports Medicine Clinic

email: [tjenkyn@uwo.ca](mailto:tjenkyn@uwo.ca) web: <http://www.eng.uwo.ca/people/tjenkyn/>

## INTRODUCTION

Orthotics are commonly prescribed for the conservative treatment of musculoskeletal disorders of the foot and ankle such as pes cavus or pes planus. These devices are thought to alter the motion of the bones of the foot by applying constraint or support to various structures on the plantar surface. Orthotics can be either custom-made by a pedorthist or bought 'off-the-shelf'. Custom-made orthotics can also be constructed of soft, compliant material or with more rigid material, depending on the preference and the clinician and the amount of control desired [1]. A recent development to off-the-shelf orthotics are proprioceptive feedback devices such as the Barefoot Science orthotic (Mississauga, ON, Canada). This device is intended not to mechanically support the foot, but to instead provide a passive stimulus to the plantar surface of the foot to activate intrinsic muscles of the foot [2].

X-ray fluoroscopy has recently been demonstrated to be a feasible method for measuring foot bone motions during in-vivo weight bearing gait [3]. To the authors' knowledge, a fluoroscopic study of the foot during orthotic use has not yet been done. In this study, a x-ray fluoroscopy is used to compare the motion of the calcaneus in the transverse plane (i.e. pronation and supination) during orthotic use. Four conditions were tested: barefoot walking, soft and rigid orthotic walking and proprioceptive feedback influenced walking during weight bearing gait. It was hypothesized that the most pronation of the calcaneus would occur during barefoot walking, and the least during walking with the rigid orthotic.

## METHODS

Eighteen volunteers (6 controls, 6 with diagnosed pes cavus, and 6 pes planus) were fitted for custom-made orthotics by a Canadian Certified Pedorthist using the foam box technique with plastazote (soft) and subortholen (firm) material as per usual clinical practice. Each volunteer walked along a custom-made wooden platform that raised their feet to the height of a single fluoroscope (SIREMOBIL Compact-L; Siemens, Malvern, PA). On the platform, each volunteer was able to walk normally and fully weight bearing past the fluoroscope. The left foot was imaged during stance phase from an oblique, dorsal-medial to plantar-lateral view.

Initially, each volunteer was instructed to stand quietly in double limb support stance and a static weight bearing image was taken of the left foot. They were then instructed to walk along the platform at their preferred pace while the fluoroscope recorded moving fluoroscopic images at 30 frames per second. Only the left foot was imaged, from heel strike until toe off. Each trial condition was repeated twice, ensuring that the entire hindfoot and tarsus was visible at all times. There were four conditions tested: 1) barefoot, 2) shod with a soft custom-made orthotic, 3) shod with a rigid custom-made orthotic and 4) shod with a proprioceptive feedback-type orthotic (PFO, Barefoot Science; Mississauga, ON, Canada). The two custom-made orthoses were constructed with a deep heel box intended to limit the pronation of the calcaneus during stance. The PFO device had a flat heel box.

The fluoroscopic images were digitized in the control PC and stored as mpeg format. Each frame was post-processed using custom-written software (Matlab; Mathworks Inc., Natick, MA). In each image, the most lateral and medial aspects of Chopart's line were identified and a line drawn between the two points (Figure 1). Another line was drawn along the lateral aspect of the calcaneus posteriorly from the lateral aspect of Chopart's line. The angle between these lines was defined as the amount of calcaneus pronation with respect to the midfoot defined by the tarsal bones. An increasing angle indicated increasing pronation.

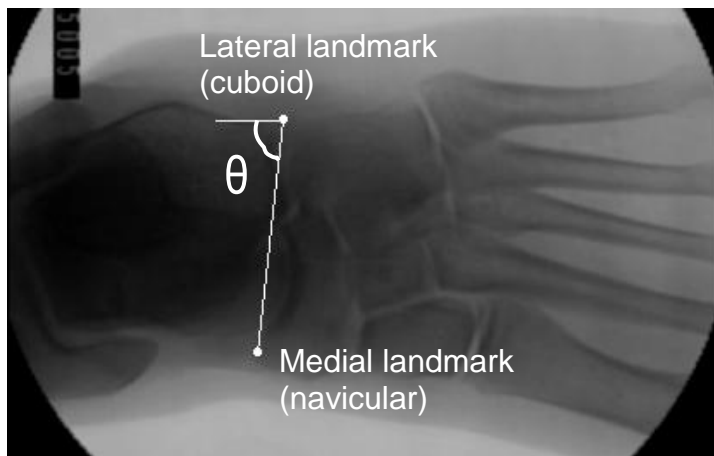


**Figure 1:** Fluoroscopic image including location of bony landmarks of the cuboid and navicular as well as the pronation angle ( $\theta$ ).

Calcaneus pronation angle was compared between two instances of stance phase: at heel strike (HS) and foot-flat (FF). It was assumed that at the instant of HS the foot was non-weight bearing. FF was assumed to be fully weight bearing although not necessarily maximal.

**Table 1:** Preliminary results from two volunteers (both controls) are shown with the calcaneus pronation angle ( $\theta$ ) during static and dynamic (HS and FF) trials.

| Condition      | Subject 1 |       |       |       | Subject 2 |       |       |       |
|----------------|-----------|-------|-------|-------|-----------|-------|-------|-------|
|                | Static    | HS    | FF    | FF-HS | Static    | HS    | FF    | FF-HS |
| Barefoot       | 85.3°     | 90.0° | 97.6° | 7.6°  | 98.4°     | 95.9° | 98.4° | 2.5°  |
| Rigid orthotic | 90.0°     | 91.2° | 95.3° | 4.1°  | 96.1°     | 95.5° | 95.4° | -0.1° |
| Soft orthotic  | 91.5°     | 89.2° | 94.0° | 4.8°  | 98.2°     | 94.0° | 99.4° | 5.4°  |
| PFO            | 95.3°     | 91.7° | 89.0° | -2.7° | 93.2°     | 89.0° | 93.1° | 4.1°  |

## RESULTS AND DISCUSSION

Preliminary results from two subjects are shown in Table 1. The largest difference in calcaneus pronation angle between FF and HS was found during the barefoot and soft orthotic conditions. The firm custom-made orthotic showed a smaller difference in calcaneus pronation angle between HS to FF for both subjects compared to the soft orthotic.

The PFO showed an increase in the calcaneus pronation angle between FF and HS for subject 2, but a decrease for subject 1. During FF with the PFO the calcaneus was observed to change its pronation angle several times and therefore no trend was found in the preliminary results.

## CONCLUSIONS

Preliminary results indicate orthotics generally reduce calcaneus pronation as the foot enters the FF position of stance phase. The PFO device did not show a clear trend between these two subjects, however at this point the analysis is not statistically powered. Despite these results being preliminary, the use of fluoroscopy to measure calcaneus pronation during weight bearing gait appears to be feasible. Further analysis, including three-dimensional investigation, needs to be completed before conclusions can be drawn.

## REFERENCES

- 1.Fields, KB, et al. *Curr. Sports Med. Rep.* **9**, 3, 176-182, 2010.
- 2.Fowler P, et al. *Medical and Scientific advisors.* <http://www.barefoot-science.ca/medicaladvisors.html>, 2009
- 3.Kedgley, AE, et al. *J Biomech* **42**, 1350-1354, 2009.

# HUMAN STABILIZATION OF A BICYCLE ON ROLLERS

Stephen M. Cain and Noel C. Perkins

University of Michigan, Ann Arbor, MI, USA  
email: [smcain@umich.edu](mailto:smcain@umich.edu)

## INTRODUCTION

Bicycles are self-stabilized within a narrow speed range [1] and so rider control effort is required for stability outside this range. While much is known about bicycle self-stability [1], little is known about how human riders induce stability. Herein, we explore rider-induced stabilization through experiments on subjects riding bicycles on rollers, a task requiring significant rider stabilization effort. The goals of this study are: 1) to examine how bicycle speed affects the control behavior of a rider, and 2) to identify differences in the control used by experienced versus novice riders.

## METHODS

Five subjects rode an instrumented bicycle [2] on a set of bicycle rollers (Fig. 1). We classified two subjects as “cyclists” (regularly commute by bicycle and/or ride recreationally) and three subjects as “non-cyclists” (ride only a few times per year); only one of the subjects had previous experience riding on rollers. When riding on rollers, a subject must actively maintain bicycle/rider stability and steer the bicycle to remain on the rollers. Each subject rode in four experimental conditions distinguished by pedaling cadence (via a metronome) and bicycle speed (via gearing). The four conditions were executed in the following order: 1) cadence 80 rpm and speed 5.1 m/sec, 2) cadence 80 rpm and speed 6.8 m/sec, 3) cadence 80 rpm and speed 2.7 m/sec, and 4) cadence 40 rpm and speed 1.6 m/sec. Each subject pedaled for a minimum of five minutes in each condition until s/he could ride for at least 30 seconds without support.

The instrumented bicycle [2] is a standard geometry mountain bike fitted with slick tires. Embedded instruments measure steer torque (load cell), steer angle (optical encoder), bicycle speed (magnetic reed switch), acceleration of the bicycle frame

(three-axis accelerometer), and angular velocity of the bicycle frame (three single-axis angular rate gyros). With the exception of bicycle speed, all measurements are low-pass filtered using a 10 Hz cutoff. Numerical differentiation of steer angle yields steer angle velocity, which when multiplied by steer torque yields the instantaneous power used by the rider to steer the bicycle. Integration of steering power yields the steering work which is further decomposed into positive and negative work components.



**Figure 1:** A subject riding the instrumented bicycle on rollers.

For analysis, we selected the last 30 seconds of continuous riding in each condition. To investigate the steering corrections that a subject used to maintain stability, we calculated the standard deviation of the steer angle for a ten-second window updated every 0.5 seconds, yielding 41 data points per trial. For each ten-second window, we also calculated the steering work and divided by the time (ten seconds) yielding the average steering power. We used a mixed linear model (allowing us to account for repeated measures and unequal variances) to test for significant effects ( $\alpha = 0.05$ ) of bicycle speed and rider type (cyclist versus non-cyclist).

## RESULTS AND DISCUSSION

All subjects were able to learn to ride on the rollers with less than five minutes of practice. Subjects

noted that riding on rollers is more difficult than riding a bicycle on pavement and that increasing bicycle speed made it easier to stabilize the bicycle.

We found that the standard deviation of steer angle (Fig. 2) decreases with bicycle speed for all subjects ( $p < 0.01$ ). This result is similar to the result of Moore et al. [3], who found that the variation of the steer angle decreases with increasing speed for a bicycle ridden on a treadmill. In addition, increasing speed also reduced the variance of the standard deviation of the steer angle ( $p < 0.01$ ), meaning that a rider's control behavior becomes more uniform at higher speeds. The standard deviation of steer angle was significantly less for cyclists than non-cyclists for all conditions ( $p < 0.01$ ), but there was no significant difference between cyclists and non-cyclists in the variance of the standard deviation of the steer angle ( $p = 0.19$ ). These results suggest that increased speed and increased skill allow riders to use smaller steering corrections to maintain stability of a bicycle.

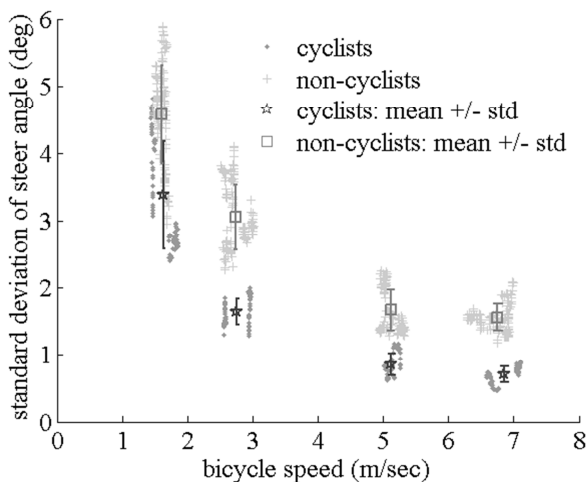


**Figure 2:** Standard deviation of steer angle versus bicycle speed. Individual data points as well as group means and standard deviations are shown. The illustrated standard deviation bars represent the variation of the steer angle standard deviation between ten-second windows for each group.

The average positive steering power (Fig. 3) also decreased significantly with bicycle speed for all subjects ( $p < 0.01$ ). In contrast, the average negative steering power remains very small for all subjects and speeds. The variation of the average positive steering power does not significantly change with increasing speed ( $p = 0.09$ ). Cyclists used significantly less positive steering power than non-cyclists for all conditions ( $p < 0.01$ ) and the

variance of the average positive steering power was significantly less for cyclists than non-cyclists ( $p < 0.01$ ). There were no significant differences in the average negative steering power between cyclists and non-cyclists. These results suggest that average positive steering power is a good measure of steering effort and that increased speed and increased rider skill reduce the steering effort required for stabilization.

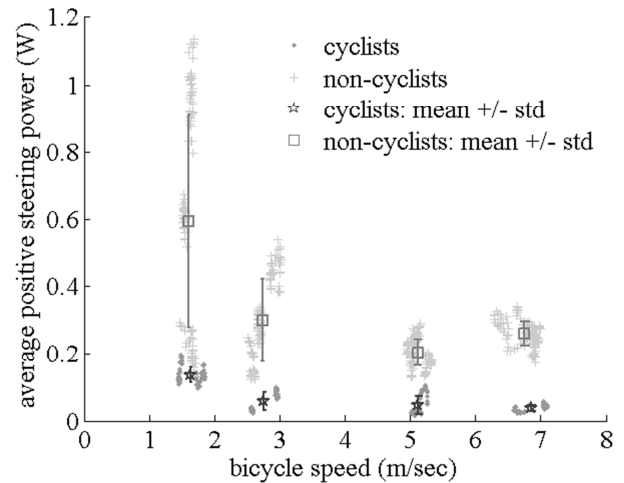


**Figure 3:** Average positive steering power versus bicycle speed. The standard deviation bars represent the variation of the average positive steering power between ten-second windows for each group.

## CONCLUSIONS

We measured the primary control used by a human rider (steering torque) and the resulting motion of a bicycle ridden on rollers. We show that bicycle speed and rider experience have an effect on the steering angle variation and average steering power used to stabilize a bicycle. Increasing speed decreases the variation of the steer angle, decreases the average positive steering power, and increases the uniformity of the control actions. Relative to inexperienced riders, experienced riders exhibit less steering variation and average positive steering power to maintain bicycle/rider stability.

## REFERENCES

1. Meijaard JP, et al. *Proc R Soc Lond A Math Phys Sci* **463**(2084), 1955-1982, 2007.
2. Cain SM and NC Perkins. *Proceedings of Bicycle and Motorcycle Dynamics 2010*, Delft, Netherlands, 2010.
3. Moore JK, et al. *Procedia Engineering* **2**, 2937-2942, 2010.

# EFFECT OF AGE ON THE THRESHOLD OF BALANCE RECOVERY IN YOUNGER, MIDDLE-AGED AND OLDER ADULTS: PRELIMINARY RESULTS

Evelyne Carbonneau and Cécile Smeesters

Research Center on Aging, Sherbrooke QC, Canada

Human Performance and Safety Research Group (PERSEUS), Sherbrooke QC, Canada

Department of Mechanical Engineering, Université de Sherbrooke, Sherbrooke QC, Canada

e-mail: [Cecile.Smeesters@USherbrooke.ca](mailto:Cecile.Smeesters@USherbrooke.ca) web: <http://www.usherbrooke.ca/gmecanique>

## INTRODUCTION

The rate per 100 000 of fatal and nonfatal unintentional injuries due to falls increases exponentially with age above 50yrs [1]. However, the critical age at which balance recovery abilities decrease significantly has not been determined. Doing so could provide guidelines for when to start screening ageing adults to prevent future falls.

Furthermore, case-control studies have shown that side falls, compared to other fall directions, increase hip fracture risk 3 to 5 times [2]. However, to our knowledge, only 2 studies have experimentally explored balance recovery in response to large postural perturbations at the threshold of balance recovery in more than one direction. Both Hsiao and Robinovitch (support translation) [3] and Telonio and Smeesters (initial lean) [4] showed that balance recovery was more difficult for backward falls than sideways and forward falls.

Finally, to our knowledge, no studies at the threshold of balance recovery, where avoiding a fall is not always possible, have included middle-aged adults (35-60yrs). Indeed, Hsiao and Robinovitch, only included younger adults (22-35yrs) [3] and Telonio and Smeesters only compared younger (18-29yrs) and older adults (60-85yrs).

Therefore, the purpose of this study was to determine the effect of age on the forward, sideways and backward threshold of balance recovery, not only in healthy younger and older adults, but also in healthy middle-aged adults.

## METHODS

For these preliminary results, data previously obtained for 16 younger adults (YA:

mean $\pm$ SD=22.9 $\pm$ 3.1yrs, range=18-29yrs) and 16 older adults (OA: 68.1 $\pm$ 5.8yrs, 60-85yrs) was used [4]. As with our YA and OA, we determined the maximum forward, sideways and backward lean angles from which 7 middle-aged adults (MA: 43.4 $\pm$ 9.5yrs, 30-59yrs) could be suddenly released and still recover balance. Balance recovery was successful if participants used no more than one step and less than 20% body weight was supported by the safety harness. Starting at 5deg, the initial lean angle was increased in 5.0-2.5deg increments at each successful trial, until participants failed to recover balance twice at a given initial lean angle.

Using 3 force platforms (OR6-7, AMTI, Newton MA), 2 load cells (FD-2 and MC3A, AMTI, Newton MA) and 4 optoelectronic position sensors (Optotrak, NDI, Waterloo ON) with 24 markers, the following kinematic variables were obtained: maximum lean angle as well as reaction time, weight transfer time, step time, step velocity and step length at the maximum lean angle.

For each lean direction, the effect of age on all our kinematic variables was determined using one-way analyses of variance with 3 age groups: YA vs MA vs OA. For each lean direction, the effect of age on the maximum lean angle was also more finely investigated using one-way analyses of variance with 5 age groups of 15yrs each: 18-24yrs (N=10), 25-39yrs (N=9), 40-54yrs (N=3), 55-69yrs (N=14), 70-85yrs (N=3). Finally, post-hoc paired t-tests with a Bonferroni correction were used.

## RESULTS AND DISCUSSION

With 3 age groups (Table 1), maximum lean angles decreased with age for all 3 lean directions (p<0.001). At the maximum lean angles, age affected reaction time for all 3 lean directions

( $p \leq 0.002$ ) and weight transfer time for sideways and backward leans ( $p \leq 0.033$ ), but not weight transfer time for forward leans or step time for all 3 lean directions. Finally, age decreased step velocity for all 3 lean directions ( $p \leq 0.005$ ) and step length for forward and sideways leans ( $p < 0.001$ ) with a trend for backward leans ( $p = 0.097$ ).

With 5 age groups (Figure 1), maximum lean angles decreased with age for all 3 lean directions ( $p < 0.001$ ). Post-hoc comparisons showed no significant differences among the first 3 (18-24, 25-39 and 40-54yrs) or the last 3 (40-54, 55-69 and 70-85yrs) age groups for all 3 lean directions. However, there were significant differences between the 1<sup>st</sup> and 4<sup>th</sup> (18-24 and 55-69yrs), 1<sup>st</sup> and 5<sup>th</sup> (18-24 and 70-85yrs) and 2<sup>nd</sup> and 5<sup>th</sup> (25-39 and 70-85yrs) age groups for all 3 lean directions, as well as between the 2<sup>nd</sup> and 4<sup>th</sup> (25-39 and 55-69yrs) age groups for forward and sideways leans.

## CONCLUSIONS

We have determined, for the first time, the forward, sideways and backward threshold of balance recovery in middle-aged adults. These preliminary results have allowed us to determine that a sample size of 4 participants per 5 years of age (52 participants aged 18 to 85yrs) should have sufficient power to detect an effect of age and lean direction on the forward, sideways and backward maximum lean angles. Determining the critical age at which balance recovery abilities decrease significantly

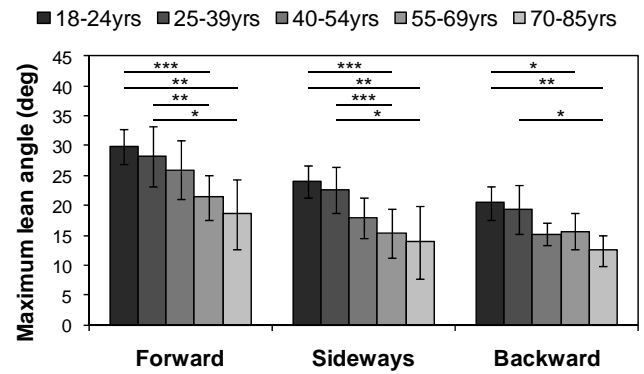


**Figure 1:** Effect of age on the maximum lean angles for each lean direction (mean±SD)  
\*  $p \leq 0.05$ , \*\*  $p \leq 0.01$ , \*\*\*  $p \leq 0.001$

could provide guidelines for when to start screening ageing adults to prevent future falls.

## REFERENCES

1. Web-based Injury Statistics Query and Reporting System (WISQARS), Centers for Disease Control and Prevention, 2007.
2. Greenspan SL, et al. *Am J Med* **104**, 539-545, 1998.
3. Hsiao ET and Robinovitch SN. *J Biomech* **31**, 1-9, 1998.
4. Telonio A and Smeesters C. *31<sup>st</sup> Annu Meet Am Soc Biomech*, Stanford CA, 2007.

## ACKNOWLEDGEMENTS

Mathieu Hamel, Myriam Jbabdi and Geneviève Schoeb for technical assistance and NSERC grant 298229-2009 for financial support.

**Table 1:** Effect of age on kinematic variables at the maximum lean angles for each lean direction (mean±SD)

| Lean Direction | Age            | Maximum Lean Angle (deg) | Reaction Time (ms) | Weight Transfer Time (ms) | Step Time (ms) | Step Velocity (m/s) | Step Length (mm) |
|----------------|----------------|--------------------------|--------------------|---------------------------|----------------|---------------------|------------------|
| Forward        | OA             | 20.7±4.2                 | 90±13              | 163±27                    | 211±37         | 3.79±0.81           | 779±113          |
|                | MA             | 26.0±5.2                 | 79±7               | 159±23                    | 232±44         | 4.20±0.99           | 940±105          |
|                | YA             | 29.6±3.3                 | 72±13              | 150±22                    | 202±18         | 4.86±0.59           | 980±116          |
|                | <b>p-value</b> | <b>0.000</b>             | <b>0.001</b>       | 0.334                     | 0.138          | <b>0.001</b>        | <b>0.000</b>     |
| Sideways       | OA             | 15.1±4.4                 | 91±9               | 181±48                    | 218±52         | 2.72±0.77           | 553±106          |
|                | MA             | 19.4±4.4                 | 72±16              | 135±38                    | 213±36         | 3.29±0.86           | 689±168          |
|                | YA             | 23.6±3.2                 | 87±9               | 134±29                    | 204±30         | 3.64±0.43           | 734±100          |
|                | <b>p-value</b> | <b>0.000</b>             | <b>0.002</b>       | <b>0.004</b>              | 0.632          | <b>0.002</b>        | <b>0.000</b>     |
| Backward       | OA             | 14.8±2.9                 | 103±13             | 112±42                    | 261±43         | 2.66±0.65           | 673±87           |
|                | MA             | 18.0±5.1                 | 80±10              | 137±48                    | 219±43         | 3.36±0.67           | 739±215          |
|                | YA             | 19.9±2.8                 | 88±10              | 92±21                     | 233±54         | 3.41±0.61           | 776±131          |
|                | <b>p-value</b> | <b>0.000</b>             | <b>0.000</b>       | <b>0.033</b>              | 0.121          | <b>0.005</b>        | 0.097            |

OA: Older Adults (N=16), MA: Middle-aged Adults (N=7), YA: Younger Adults (N=16). Significant p-values ( $p \leq 0.05$ ) are **bolded**.

# MEASUREMENT OF THE AERODYNAMIC STABILITY AND CONTROL EFFECTIVENESS OF HUMAN SKYDIVERS

<sup>1</sup>G. Cardona, <sup>1</sup>D. Evangelista, <sup>1</sup>N. Ray, <sup>1</sup>K. Tse, <sup>1</sup>D. Wong

<sup>1</sup>University of California, Berkeley, CA, USA  
email: [gcardona29 at gmail dot com](mailto:gcardona29@gmail.com)

## INTRODUCTION

In comparative biomechanics, understanding the role of maneuvers during high angle of attack flight is critical to understanding the evolution of aerial behaviors like flight. We report the aerodynamic stability and control effectiveness of human skydivers in free fall measured using physical models in a wind tunnel. The effect of posture and movements of the limbs is examined and compared to previously published simulation results and to guidance given during typical skydiving instruction, as well as the experience of human skydivers in a vertical wind tunnel and during actual free fall maneuvers. Comparison will also be made to other animals in free fall and in high angle-of-attack aerial maneuvers.

## METHODS

Physical models of human skydivers (Figure 1) were constructed using six-inch artists' anatomical manikins (Dick Blick; Galesburg, IL) placed in typical human skydiving postures [1]. Aerodynamic forces (lift, drag, and side force) and moments (pitch, roll, and yaw) acting on models in a wind tunnel were measured using a six degree-of-freedom force/torque sensor (ATI Industrial Automation; Apex, NC). Forces and moments were normalized to the planform area of a "flat" resting human. To quantify static aerodynamic stability, models were placed at varying pitch, roll, and yaw angles and the restoring torques acting about the center of gravity were measured and used to obtain static stability coefficients (e.g.,  $dC_m/d\alpha$ ) [2,3,4]. Similarly, control effectiveness was measured by placing limbs in turn or roll positions (see Figure 1) and measuring the resulting yawing or rolling moments to obtain control effectiveness coefficients (e.g.,  $dC_m/d\delta$ ) [2,3,4].

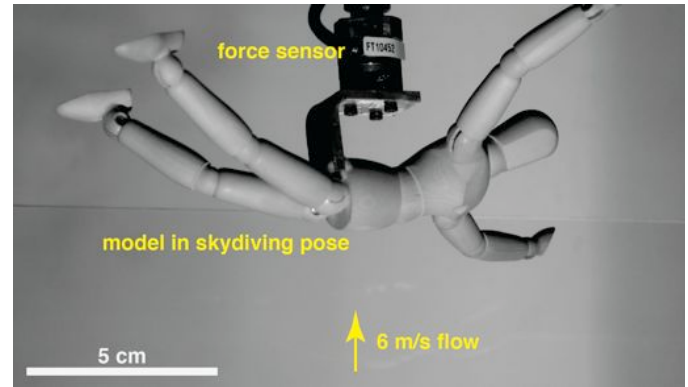


**Figure 1:** Physical model of a human skydiver, mounted on a force/torque transducer in a wind tunnel. Body twist creates a left yaw moment.

We compared stability and control effectiveness observed in model tests to statements in skydiving training literature [1], photo and video of stable positions openly reported on the Internet, and descriptions from interviews with professional skydiving instructors.

## RESULTS AND DISCUSSION

Preliminary results from model tests agree with non-quantitative skydiver self-assessments of

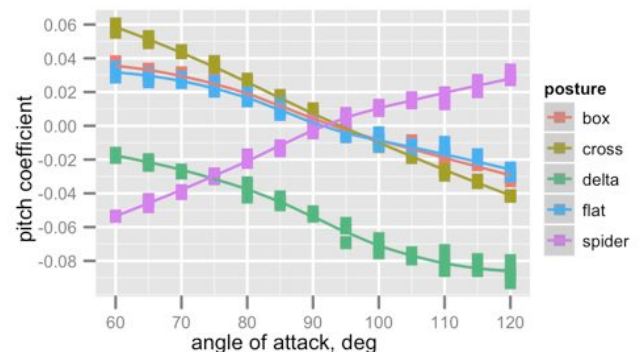


**Figure 2:** Nondimensional pitch coefficient ( $C_M$ ) as a function of angle of attack for typical skydiving postures shows clear differences in static stability; spider position is unstable and track/delta position is only stable at lower angle of attack.

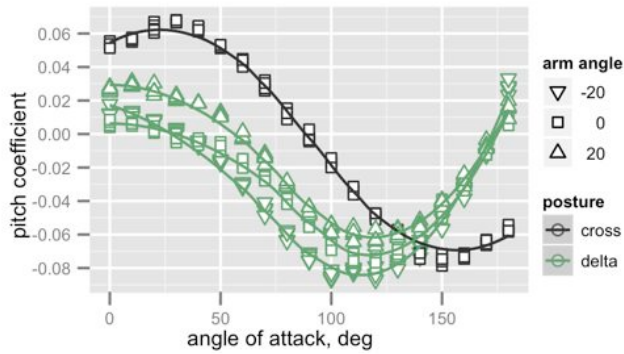


**Figure 3:** Nondimensional pitch coefficient ( $C_M$ ) as a function of angle of attack for track/delta position as arms angle is varied  $20^\circ$  up and down, illustrating pitch control effectiveness.

stability and maneuverability. Different skydiving postures exhibit clear differences in stability and in stable orientation relative to flow (Figures 2 and 3).

These results suggest that skydivers maneuver principally using aerodynamic forces vice inertial reactions. At low speeds, zero angular momentum turns affected by inertia of limb movement, changes in body inertia and body position changes drive changes in body orientation (e.g., gymnastics [5], cliff diving, or other acrobatic maneuvers performed at low speed close to the ground). In contrast, at skydiving speeds (54 m/s, 120 mph), maneuvers are dominated by aerodynamic torques, which scale as  $\frac{1}{2} \rho v^2 \lambda S$ . For example, in track/delta posture, elevation of the arms has sufficient control to create a one-for-one angular pitch change of the body (Figure 3).

As a further test of the relative roles of inertial reactions versus aerodynamic forces, we are currently comparing predicted turn and roll dynamics to those observed in the absence of flow (while statically hanging from a line on the ground), and to maneuvers in a full-scale vertical wind tunnel (iFly; Union City, CA) and during actual skydives (Bay Area Skydiving; Byron, CA). Skydivers have recently adopted miniature GPS loggers originally developed for do-it-yourself unmanned aerial vehicles, and regularly use such tracks to examine their own glide performance and compete with others. Using off-the-shelf components (SparkFun; Boulder, CO), we have ground-tested loggers that record accelerations, angular velocities, and magnetometer readings at 50 Hz and GPS positions

at 4 Hz (example data, Figure 4). A Kalman filter is then applied to estimate full-scale aerodynamic forces and moments during typical maneuvers, such as the turns and rolls required for entry-level skydiving licensing (US Parachuting Association A-level) [1].

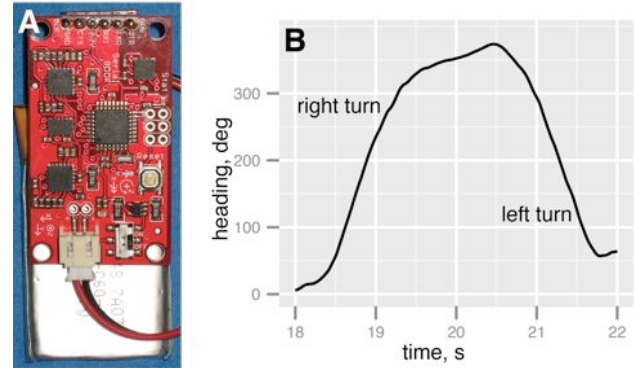


**Figure 4:** Wearable accelerometer (A, width 2.7 cm, mass 30 g) and integrated heading data for series of rapid  $360^\circ$  turns (simulated on the ground) (B).

## CONCLUSIONS

Animals in free fall must maneuver into preferred stable orientations and to affect safe landings. Human free fall is an under-studied, but important, point of comparison, because humans use both inertial and aerodynamic maneuvering mechanisms (depending on speed); skydivers can be asked the rationale behind techniques and can be asked to perform specific test maneuvers; and because of the important practical applications of skydiving.

## REFERENCES

1. Poynter D and Turoff M. *Parachuting: The Skydiver's Handbook*, Para Publishing, 2007.
2. McCay MG. *J exp Biol* **204**, 2817-2826, 2001.
3. Koehl M, et al. *Integ Comp Biol* in prep.
4. McCormick BW. *Aerodynamics, Aeronautics and Flight Dynamics*, John Wiley & Sons, Ltd., 1976.
5. Playter R. *Passive Dynamics in the Control of Gymnastic Maneuvers*, PhD Thesis, 1994.

## ACKNOWLEDGEMENTS

We thank the Berkeley Biomechanics group, esp. Y. Zeng and Y. Munk. We dedicate our work to Alex Lowenstein, who inspired this research and whose loss helped us decide that today is a good day to skydive.

# TIME-TO-BOUNDARY PREDICTIONS BASED ON OTHER CENTER OF PRESSURE MEASURES IN CANCER SURVIVORS

Abigail L. Carpenter<sup>1</sup>, Jeremy D. Smith<sup>1</sup>, Gary D. Heise<sup>1</sup>, Chris P. Repka<sup>1</sup>, John H. Challis<sup>2</sup>

<sup>1</sup>Rocky Mountain Cancer Rehabilitation Institute, University of Northern Colorado, Greeley, CO

<sup>2</sup>The Pennsylvania State University, University Park, PA

email: abigail.carpenter@unco.edu

## INTRODUCTION

Side effects associated with cancer treatments (e.g., peripheral neuropathy and vestibular dysfunction) can lead to postural instability. Balance and posture in cancer survivors has received limited attention in the literature. Previous research, on center of pressure (COP) motion, has focused on a multitude of measures to assess differences in postural steadiness based on age [1]. Using similar COP assessments, postural steadiness was investigated in cancer survivors where surface and vision conditions were altered [2,3]. It was observed that the following time-domain based measures were influenced by surface and vision conditions: root-mean-square (RMS), path lengths, mean velocity, 95% confidence ellipse area [2]. The following frequency-domain measures were also found to be influenced by surface and vision conditions: mean frequency, fractal dimension of the confidence ellipse (FractCE), and total power [3].

Recently, time-to-boundary (TTB) has been utilized to assess postural steadiness. TTB predicts the time it would take the COP to reach the limits of the base of support [4]. Lower TTB measures are associated with greater postural unsteadiness; that is, less time is available to recover from a balance perturbation [5]. TTB has been evaluated in older adults during quiet standing, and the results indicate that TTB is reduced with aging [4]. In addition, TTB has been examined in a young, healthy population during single leg standing to examine how a reduced base of support affects TTB measures [6]. Hertel et al. [6] also investigated relationships between TTB and traditional COP measures; they suggested that TTB provides unique insight into postural steadiness for single leg standing. TTB has not been applied specifically to cancer survivors as a means of assessing postural steadiness.

TTB is a more involved calculation than traditional COP-based measures, but it can be useful when assessing the risk of falling. It is unclear whether TTB provides information beyond the traditional COP-based measures of posture and balance in cancer survivors. Therefore, the purpose of this study was to determine whether TTB could be predicted by traditional COP measures, which were previously found to be sensitive to changes in vision and surface conditions [2,3].

## METHODS

Quiet standing was measured in cancer survivors ( $n=11$ ; mass =  $75.6 \pm 22.1$  kg; height =  $1.60 \pm 0.05$  m; age =  $56 \pm 14$  years) during four different conditions. Participants stood on a rigid surface with eyes open, a rigid surface with eyes closed, a compliant surface with eyes open, and a compliant surface with eyes closed. Force data were collected for 30 s at 1000 Hz. COP data were resampled at 50 Hz for TTB assessments. The TTB algorithm was based on previous literature [4]. The algorithm produced a time series of TTB with multiple minima. The minimum value from each of these local minima was selected as our dependent measure of TTB. A lower TTB is indicative of postural unsteadiness, and these minima illustrate the least amount of time individuals have to recover from a balance disturbance. Because our focus was not on the differences between conditions, but rather on the ability of traditional COP measures to predict TTB, we chose to collapse data across conditions. This decision impacted our statistical analysis, increasing our sample size from 11 to 44, which resulted in a subject to variable ratio of 4.4:1.

Stepwise linear regression was used to determine whether TTB could be predicted from traditional

COP measures which previously showed sensitivity to changes in surface and vision conditions [2,3]. Ten traditional COP measures were used to predict the TTB absolute minima: mean medial/lateral (ML) and anterior/posterior (AP) frequency, ML and AP COP path lengths, fractal dimension of the confidence ellipse, RMS of the ML and AP COP, mean velocity of the ML and AP COP, and the 95% confidence ellipse area.

## RESULTS AND DISCUSSION

Four significant regression models were identified based on the independent variables (Table 1). The first model chosen was based on the mean velocity of the ML COP, indicating that this variable had the highest correlation with TTB. In the second model, RMS of the ML COP was added to the prediction, which increased the explained variance by 9%. In the third model, FractCE was added to the model, which further increased the explained variance by another 5%. A fourth model was also predicted that explained the same amount of variance as model 3 (47%), but eliminated the mean velocity of the ML COP from the prediction. Thus, the mean velocity of ML COP and the RMS of ML COP explain the same amount of variance in TTB when FractCE is also considered. Model 4 was considered the best model for predicting TTB. However, no model explained more than 47% of the variance in TTB, suggesting traditional COP measures are not good predictors of TTB. TTB was independent of the frequency-based COP measures, which was expected, given that TTB is derived from time-domain measures of the COP, specifically velocity and the position of the COP.

Our results are consistent with previous suggestions in the literature that TTB evaluates different aspects of postural steadiness than traditional COP measures [6]. Hertel et al. [6] observed that correlations between TTB measures and traditional COP measures (mean velocities, COP range, and COP standard deviation) ranged from 0.03-0.90 (i.e.,  $r^2 \approx 0.0009 - 0.81$ ). Interestingly, the highest correlations were reported between ML COP velocity and TTB (range  $\approx 0.47-0.90$ ). This is consistent with our predictions in that ML COP velocity was the first variable to enter the stepwise

regression model even though the best model ultimately did not include this measure. Instead, RMS of the ML COP was used to replace ML velocity. As with our previous results [2,3], it appears that ML COP measures are important indicators of postural steadiness. Therefore, ML COP measures should be included when assessing postural steadiness in cancer survivors.

**Table 1.** Regression models for predicting TTB based on traditional COP measures.

| Model | Predictors                        | R <sup>2</sup> | F    | p      |
|-------|-----------------------------------|----------------|------|--------|
| 1     | ML Mean Velocity                  | 0.33           | 20.9 | < .001 |
| 2     | ML Mean Velocity, ML RMS          | 0.42           | 14.6 | < .001 |
| 3     | ML Mean Velocity, ML RMS, FractCE | 0.47           | 11.9 | < .001 |
| 4     | ML RMS, FractCE                   | 0.47           | 18.3 | < .001 |

Note: Regression equation for each model:

$$TTB_1 = -0.037 * \text{ML Mean Velocity} + 0.676$$

$$TTB_2 = -0.025 * \text{ML Mean Velocity} - 0.043 * \text{ML RMS} + 0.720$$

$$TTB_3 = -0.0001 * \text{ML Mean Velocity} - 0.085 * \text{ML RMS} - 1.008 * \text{FractCE} + 2.170$$

$$TTB_4 = -0.85 * \text{ML RMS} - 0.999 * \text{FractCE} + 2.158$$

## CONCLUSIONS

Although TTB was predicted by ML RMS and FractCE, traditional COP based measures did not fully explain variability in TTB. This suggests that TTB provides further insight into mechanisms underlying posture and balance in cancer survivors.

## REFERENCES

- [1] Prieto et al. (1991). *IEEE Trans Biomed Engin*, 43, 956-966.
- [2] Carpenter, A et al. (2011). ACSM abstract C-38-Posture/Balance, Denver, CO.
- [3] Smith, J et al. (2011). ACSM abstract C-38-Posture/Balance, Denver, CO.
- [4] Slobounov et al. (1998). *J Gerontol A Biol Sci Med Sci*. 53, B71-8.
- [5] van Emmerik & van Wegen (2002). *Exerc Sport Sci Rev*, 30, 177-183.
- [6] Hertel, J et al. (2006). *J Appl Biomech*, 22, 67-73.

# COMPARISON OF TRUNK KINEMATICS BETWEEN EXPERIMENTAL TRIPPING PROTOCOLS

<sup>1</sup>Sarah Kate Caudle, <sup>1</sup>Sara Matrangola and <sup>1</sup>Michael Madigan

<sup>1</sup>Virginia Tech, Blacksburg, VA, USA

email: [mlm@vt.edu](mailto:mlm@vt.edu) web: <http://www.biomechanics.esm.vt.edu>

## INTRODUCTION

Forward trips are responsible for up to 53% of all falls among older adults [1]. As such, numerous researchers have investigated how various factors affect the ability to recover balance after tripping in order to prevent a fall. One experimental protocol that has been used in the laboratory is to trip subjects while walking. While this protocol involves movements very similar to real-life trips outside of the laboratory, it can be difficult to control the initial conditions of the trip (body position, velocity, etc.). Another protocol that provides more control over the initial conditions is the so-called lean protocol where subjects are released from a static forward lean. One difference between the lean protocol and tripping while walking is that perturbations start from a static position in the lean protocol, and this may limit the generalization of findings from the lean protocol to trips while walking. To address this, we have developed a novel method to induce trip-like perturbations in the laboratory that do not start from a static position, yet still provides greater control of initial conditions compared to walking while tripping.

The goal of this study was to illustrate differences in trunk kinematics between tripping while walking, the lean protocol, and this new method. Trunk kinematics were investigated because they are important for determining the outcome of a trip [2]. A secondary goal was to investigate the effects of limiting recovery to a single step on trunk kinematics, which is common among studies that employ the lean protocol.

## METHODS

One male subject (21 years old, 179.3 cm tall, 81.7 kg) participated in this study. During his first visit

to the lab, the subject was tripped while walking using established methods [3]. The subject walked at a self-selected speed (2.8 mph-3.0 mph), and when tripped during a randomly selected walk down the walkway, attempted to recover balance with multiple steps and continue walking. During his second visit to the lab, the subject completed multiple trials of the lean protocol over a range of initial lean angles presented in random order using established methods [4]. The subject was leaned forward, folded his arms across his chest, and looked straight ahead. Upon release of the lean cable, the subject fell forward and took multiple steps to attempt to recover balance. These trials were repeated a second time after asking the subject to limit balance recovery to a single step. During his third visit to the lab, the subject completed multiple trials on a TRanslatIng Platform (TRIP). The subject stood upright on the TRIP with arms folded across his chest, head facing forward, eyes closed, and while wearing headphones to prevent audio cues (Fig. 1). A rigid bar on the TRIP behind the subject's lower back provided support to prevent a backward loss of balance. The TRIP was then pushed at a constant speed between 2.6 - 3.2 mph until it impacted the end of a walkway that had the same height as the TRIP. Upon impact, the subject fell forward and took multiple steps to attempt to recover balance. These trials were repeated a second time after asking the subject to limit balance recovery to a single step.

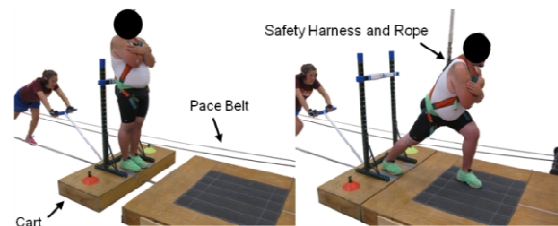


**Figure 1.** Photographs of the TRIP protocol before impact with the walkway (left) and after single step balance recovery (right).

During all trials except for the multistep TRIP trials, the participant wore a harness as a safety precaution. During all trials, the position of reflective markers placed bilaterally on the shoulders and greater trochanters were collected with a Vicon 460 Motion Analysis System. This data was used to determine trunk angle during balance recovery after averaging across the left/right sides of the body. (trunk angle = 0 degrees when vertical and increased as the trunk flexed forward).

## RESULTS AND DISCUSSION

Comparing trunk angle across all three protocols (Fig. 2A) shows trunk angle during the TRIP protocol to be qualitatively more similar to an actual trip than the lean protocol. As such, the TRIP protocol described here may be a viable alternative to the lean protocol that still provides an easy way to manipulate the severity of a perturbation (by controlling how fast the TRIP is pushed), while achieving trunk kinematics more similar to an actual trip compared to the lean protocol.

Limiting balance recovery to a single step in both the TRIP (Fig. 2B) and lean (Fig. 2C) protocols tended to increase the maximum trunk angle. This may be due to single step recovery requiring the trunk kinetic energy to be reduced to zero since a successful recovery requires a near-stationary recovery position. Multistep recovery does not require the trunk kinetic energy to be reduced as much since the subject continued walking after the perturbation. It is important to keep these differences in mind when attempting to generalize findings from single step balance recoveries to balance recoveries with multiple, or unrestricted, stepping.

## CONCLUSIONS

In conclusion, trunk kinematics during the TRIP protocol were qualitatively more similar to an actual trip than the lean protocol. Additionally, maximum trunk angles are increased when recovery is limited to a single step. Future studies should consider these results when establishing protocols to investigate balance recovery after tripping.

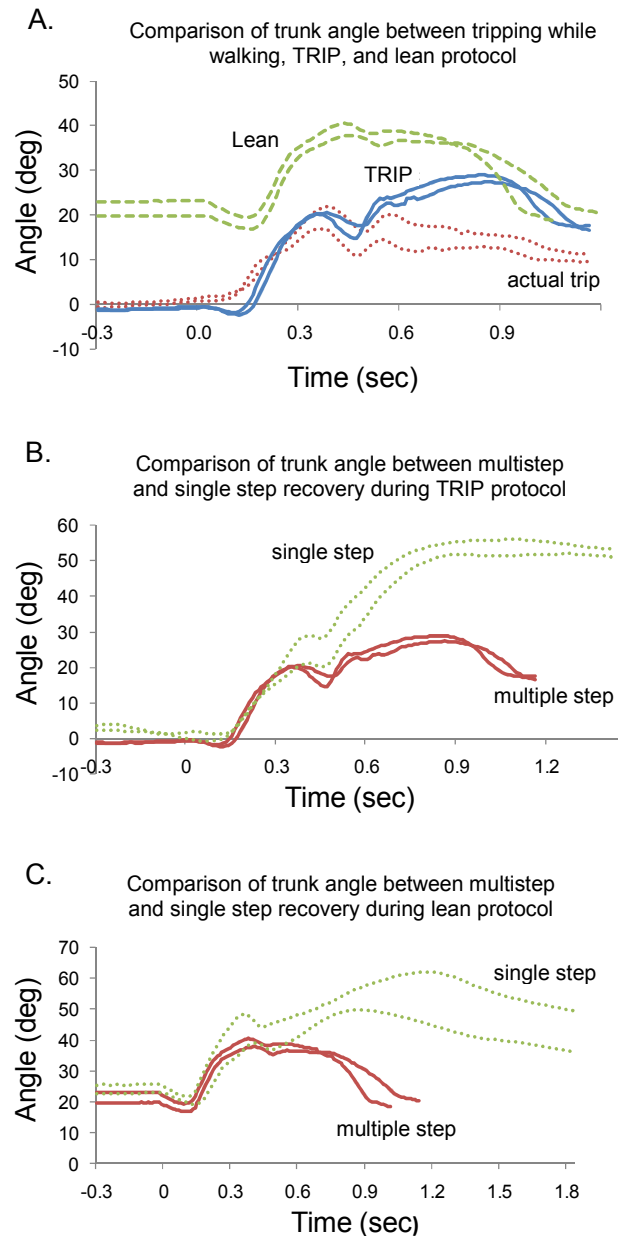


**Figure 2.** Result Graphs (Zero represents the time of contact with either: the walkway in the TRIP protocol, tripping device in the trip protocol, or the time of release in the lean protocol)

## REFERENCES

1. Blake AJM, et al. *Age Ageing* **17**, 365, 1988.
2. Grabiner MD, et al. *Journal of Electromyography and Kinesiology* **18**, 197-204, 2008.
3. Bieryla KA, et al. *Gait & Posture* **26**, 208-213, 2007.
4. Madigan ML, et al. *Journal of Gerontology: Medical Sciences* **60A**, 910-914, 2005.

## ACKNOWLEDGEMENTS

SLM was supported by a National Defense Science and Engineering Graduate (NDSEG) Fellowship.

# SIMULATION OF NON-PERIODIC GAIT OPTIMIZED FOR TRAVERSING A SPECIFIED DISTANCE IN MINIMUM TIME

Huseyin Celik and Stephen J. Piazza

The Pennsylvania State University, University Park, PA, USA  
e-mail: [piazza@psu.edu](mailto:piazza@psu.edu)

## INTRODUCTION

Walking and running have been simulated with a wide variety of models that range from highly complex muscle-driven models [1] to very simple passive models [2]. Common to nearly all of these simulations has been the periodicity of the motion. The periodic nature of steady-state gait permits simulation of a single stride (or half of a stride if right/left symmetry is assumed). There are, however, gaits which are necessarily non-periodic such as sprinting from rest or initiation of a walking gait before a steady state is reached. The purpose of this study is to develop a computer simulation of first steps of a non-periodic gait optimized for traversing a specified distance in minimum time.

## METHODS

The use of spacetime constraints [3,4] may be especially well suited to determination of an optimal solution in a simulation of several non-periodic steps. The problem formulation with spacetime constraints has three main components: (1) mechanical structure that defines geometry, model topology, inertial properties, etc.; (2) constraints on the desired motion, for example, prescribed initial and final conditions, step length, or maximum speed; and (3) constraints that set limits on physical structure, energetics, and Newton's laws that form constraints that specify a physically valid solution [3]. Taking these constraints into account, the generalized positions, velocities  $q(t)$ , and controls  $u(t)$  are determined that minimize an objective function  $\min f(q,u)$ ; with the constraints  $h(q,u)$  as a nonlinear programming problem (NLP). Such an approach was used in the present study to simulate a non-periodic gait with the objective of traversing a specified distance in minimum time.

The model used in the simulation (Figure 1) was composed of the following elements: a point mass at the hip; damped, compliant, and massless legs with telescoping axial actuators; and point feet (each with a mass that was small compared to point mass at hip). Telescoping axial actuators apply compressive forces ( $P_1$  and  $P_2$ ) necessary for foot clearance and the torque ( $T$ ) around the hip is essential for swing of legs. The ground was modeled as a viscoelastic medium.

Using spacetime constraints, the optimal control problem of traversing a specified distance in minimum time from rest was transformed to a NLP problem. The variables of the problem are the generalized positions  $(x, y, \theta, \phi, l_1, l_2)$ , generalized speeds  $(\dot{x}, \dot{y}, \dot{\theta}, \dot{\phi}, \dot{l}_1, \dot{l}_2)$ , and controls  $(F_1, F_2, T)$  discretized at each node (the time span was segmented into  $n$  equal intervals). The final time of simulation is another parameter of the problem and final time served as the objective function to be minimized as well (for a total  $15n + 1$  variables). The initial conditions were imposed as linear constraints and dynamics of the model (equations of motion obtained via Lagrangian method) were imposed as nonlinear constraints. Having formulated the NLP, a gradient-based optimization algorithm (direct interior point) was applied to the problem. MATLAB was the simulation platform and the KNITRO library for solving large scale optimization problems was used to solve the NLP. Outputs of a forward simulation (forward integration with variable time step using MATLAB ode113) in which the controls were edited heuristically were used as an initial guess.

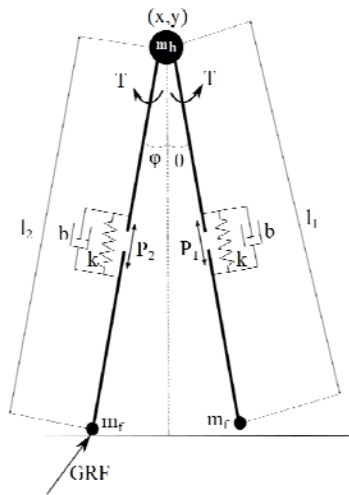


**Figure 1:** The model used in the simulation. The legs were massless and telescoping to permit toe clearance.

### RESULTS AND DISCUSSION

The optimization was successful in that it resulted in a minimum-time solution that traversed the required 2 m distance using seven non-periodic steps. The initial guess required 2.84 s to move 2 m; following optimization the same distance was covered in 2.14 s (Figure 2). Interestingly, the optimal solution included a forward “dive” at the end that was not present in the initial guess (Figure 3). This preliminary simulation of sprinting will be developed into a simulation in which a model incorporating joints is made to sprint a longer

distance so that the influence of joint structure on sprinting ability may be investigated.

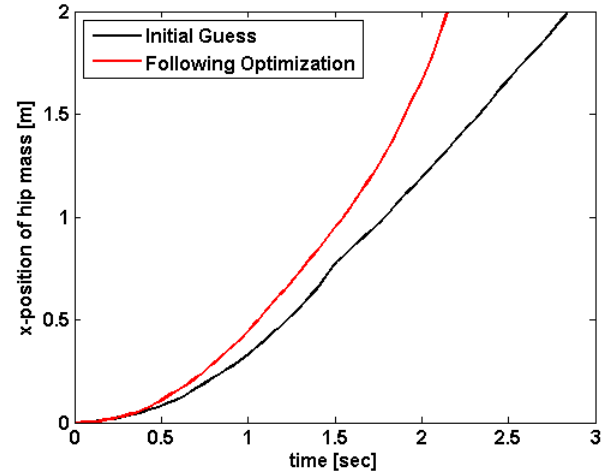


**Figure 2:** The horizontal position of the hip mass before and after optimization

### REFERENCES

1. R.R. Neptune et al., *Comput Method Biomech* **3**, 321-334, 2000.
2. M. Garcia et al., *J Biomech Eng* **120**, 281-288, 1998.
3. A. Witkin et al., *Computer Graphics* **22**, 159-168, 1998.
4. A.J. van den Bogert et al, XII International Symposium of Computer Simulations in Biomechanics. 2009.

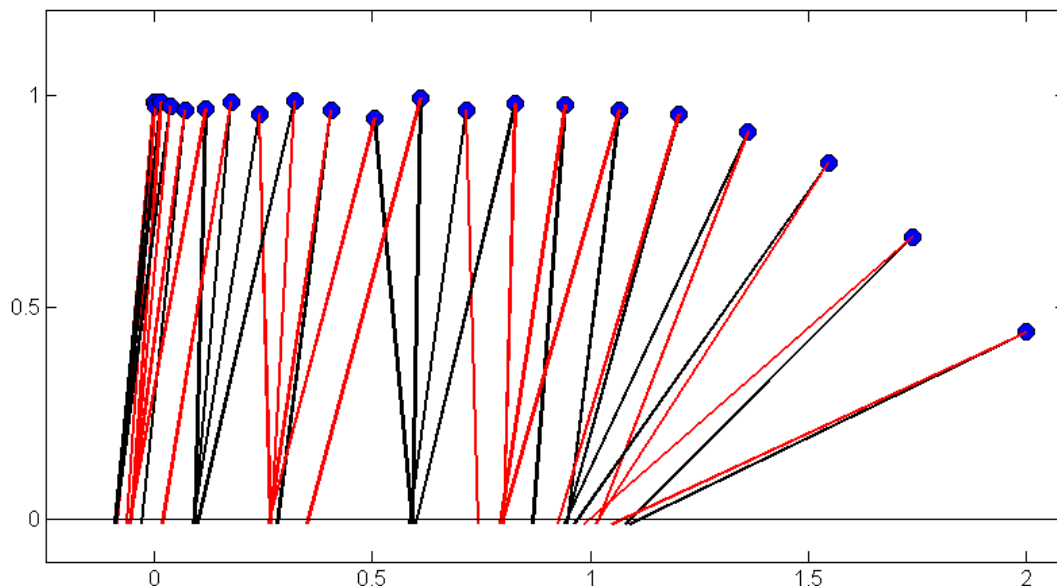


**Figure 3:** Following optimization, the model took seven steps and concluded with a “dive” across the finish line at  $x = 2$  m.

# THE MEASUREMENT SETUP FOR ONLINE BIOMECHANICAL ANALYSIS OF ROWING ON AN ERGOMETER

<sup>1</sup>Tomaž Černe, <sup>2</sup>Roman Kamnik and <sup>2</sup>Marko Munih

<sup>1</sup>Alpineon d.o.o., Ljubljana, Slovenia

<sup>2</sup>University of Ljubljana, Faculty of Electrical Engineering, Ljubljana, Slovenia  
email: [tomaz.cerne@alpineon.si](mailto:tomaz.cerne@alpineon.si) web: <http://www.alpineon.com/>

## INTRODUCTION

Rowing is a technically and physically demanding activity that requires a coordinated and powerful sequence of actions utilizing most of the muscle groups in the body. Rowing simulators can be found in most gyms, but many people who use them have little or no instruction in technique. Non-experts are often not aware of faulty technique, which can lead consequently into injuries. A novel approach for training incorporates real-time feedback providing quantitative information about rowing mechanics, kinematics and kinetic parameters [1]. The purpose of the study was to develop and evaluate a system that measures all kinematic and kinetic parameters, calculates internal forces and joint moments, and provides real-time feedback about these parameters.

## METHODS

Developed measurement setup consists of two computers for data acquisition, an optical system Optotrak Certus with two sets of line infrared cameras and 14 active markers, a video camera and an instrumented rowing simulator Concept2: a load cell (A) mounted between the chain and the handle, a six-axis sensor JR3 (B) mounted under the foot stretcher, an incremental encoder (C) mounted on the axle of a flywheel, a wire incremental encoder (D) mounted on the reverse side of the simulator seat track and beneath the seat (Fig.1).

From the measured data parameters of stroke were determined: the maximum pull force  $f_{p,max}$  (max absolute value of the handle pull force), the max feet reaction force  $f_{r,max}$  (max absolute value of the measured force vector on the foot stretcher), the force ratio  $r_f$  (ratio between  $f_{p,max}$  and  $f_{r,max}$ ), the time delay  $\Delta t$  (difference between the time instant when  $f_{p,max}$  and  $f_{r,max}$  occur), the stroke length  $l$  (difference between the max and min length of the chain pull

and the ratio of the stroke phases  $r_s$  (ratio between the duration of the drive and the recovery phase of the stroke). Joint loads for ankle, knee, hip, LS and shoulder joints were calculated according to the Newton-Euler inverse dynamics approach which is based on the recursive calculation procedure [2]. The rowing maneuver was considered as a planar problem with the assumption of body symmetry regarding the sagittal plane.

For the evaluation of the proposed methodology, ten volunteers (male, Caucasian) participated in the study: five top-level rowers (members of the National Team) and five non-experts (newly introduced to a rowing simulator). The test lasted for two minutes and consisted of three types of activity (the first minute of aerobic type activity at a rate of 20 str/min, followed by 30 seconds of aerobic threshold activity at 26 str/min and 30 seconds of anaerobic activity at 34 str/min). Each participant produced a rowing speed according to his abilities. Before performing the test, the participants warmed up properly.

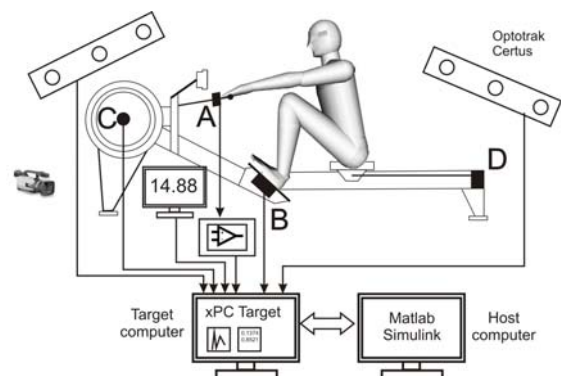


**Figure 1:** Measurement setup.

## RESULTS AND DISCUSSION

The results are presented in Table 1. The stroke length  $l$  was kept constant by the experts in each stroke rate, while non-experts had shorter  $l$  and

increased it with increasing stroke rate. The experts demonstrated a fast drive and a slow recovery, the ratio  $r_s$  lowers with increasing stroke rate. The non-experts achieved a lower ratio of around 1:1, which did not change significantly with increasing stroke rate. The results show that  $f_{p,max}$  and  $f_{r,max}$  of the experts did not change significantly with increasing stroke rate. The forces of the non-experts were significantly lower (the most obvious difference occurred at a rate of 20 str/min, an increase in peak forces was noticed with increasing stroke rate). Figure 2 presents the calculated joint torques for one non-expert subject (left) and one expert subject (right). The repeatable joint loads pattern for the expert at all stroke rates, and the variable pattern of joint loads for the non-expert, demonstrating the lack of technique, can be seen. Large loadings on the LS joint confirm frequent lower back pain and injuries.

## CONCLUSIONS

A measurement environment for detailed on-line biomechanical analysis of rowing was developed. Data processing algorithms provide output data online in real time and allow instantaneous stroke analysis, enabling the coach and the athlete to obtain immediate feedback to their experimentation with rowing technique. The results of the evaluation experiment show noticeable distinctions of the measured parameters between the expert and non-expert rowers. It was demonstrated that the experts use a similar and consistent technique at all stroke rates, while the technique of non-experts varies.

## REFERENCES

1. MacFarlane, et al. *Journal of sports sciences* **15(2)**, 167-173.
2. Kane, T. R., & Levinson, D. A. *Dynamics, theory and applications*. McGraw Hill, 1985

**Table 1:** Results of averaged rowing biomechanical parameters of the evaluation experiment.

| Stroke rate     | Experts       |               |               | Non-experts   |               |               |
|-----------------|---------------|---------------|---------------|---------------|---------------|---------------|
|                 | 20            | 26            | 34            | 20            | 26            | 34            |
| $l$ (m)         | 1.59±0.05     | 1.61±0.07     | 1.57±0.07     | 0.98±0.16     | 1.09±0.12     | 1.16±0.19     |
| $r_s$           | 1 : 2.04±0.15 | 1 : 1.66±0.06 | 1 : 1.31±0.09 | 1 : 1.01±0.18 | 1 : 1.00±0.12 | 1 : 1.04±0.06 |
| $f_{p,max}$ (N) | 1,022±74      | 1,088±67      | 1,162±93      | 145±159       | 238±160       | 448±190       |
| $f_{r,max}$ (N) | 1,232±105     | 1,250±84      | 1,294±92      | 440±97        | 612±97        | 816±89        |
| $r_f$           | 0.83±0.08     | 0.87±0.08     | 0.89±0.05     | 0.29±0.26     | 0.37±0.19     | 0.53±0.17     |
| $\Delta t$      | 0.08±0.03     | 0.08±0.04     | 0.08±0.06     | 0.70±0.38     | 0.47±0.25     | 0.34±0.14     |

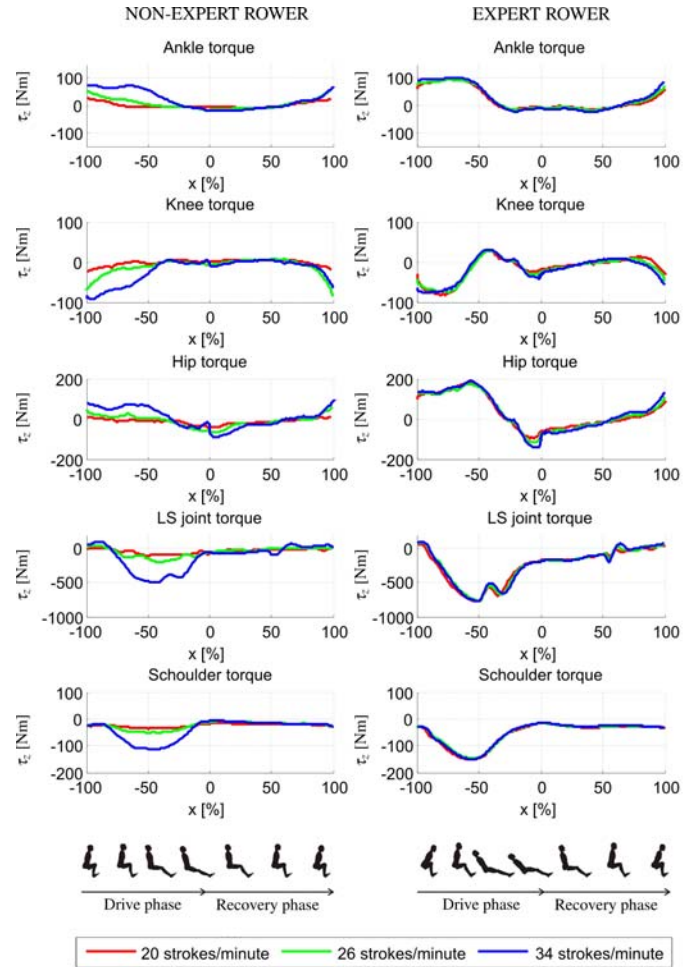


**Figure 2:** Calculated torques in body joints presented for different stroke rates. The beginning of the drive was assigned as value of -100 at the abscissa, the end of the pull and the start of the recovery as value 0 and the end of the recovery as a value of 100.

## ACKNOWLEDGEMENTS

The study was funded by Republic of Slovenia Ministry of Higher Education, Science and Technology. The research work of the first author is part financed by the European Union, European Social Fund.

# EFFECTS OF CUT ANGLE AND ONLINE PROCESSING ON CUTTING MANEUVERS

Guilherme M. Cesar, Kathryn L. Havens, Yu-Jen Chang, Susan M. Sigward

Jacquelin Perry Musculoskeletal Biomechanics Research Laboratory

Division of Biokinesiology and Physical Therapy

University of Southern California, Los Angeles, CA, USA

email: guilhemc@usc.edu, web: www.usc.edu/go/mbrl

## INTRODUCTION

The ability to rapidly change direction, in response to environmental stimuli, is important for successful participation in physical activity and sports [1]. Direction change requires deceleration and re-orientation of the body into the new direction [2]. Factors such as approach velocity and angle of turn affect task demands such that turns performed at greater velocity and to larger degrees require greater forces to reorient forward momentum.

Random directional cues presented as an individual approaches a change of direction task require online postural adjustments to meet the demands of the task. Previous work reported increased lower extremity loading when subjects were required to respond to a random directional cue during change of direction tasks [3]. However, this assessment was limited to changes of direction at small angles ( $<60^\circ$ ). It is not known how random cueing effects loading during more demanding change of direction tasks. Therefore, the purpose of this study was to investigate the influence of random directional cues on loading during running change of direction tasks at angles of  $45^\circ$  and  $110^\circ$  from the original line of progression.

We hypothesized that: (1) a change of direction task performed to a larger angle from the original plane of progression will result in greater loading; and (2) when compared to a change of direction task performed with prior knowledge of angle, a random directional cue presented after task initiation will result in greater loading.

## METHODS

Sixty-three female soccer athletes (average age  $14.4 \pm 3.8$  yrs, height  $156.7 \pm 10.6$  cm, and mass  $50.3 \pm 11.7$  kg) with no history of lower extremity injuries participated. 3D kinematics were collected

(250Hz) using an 8-camera Vicon motion capture system (Oxford Metrics LTD, England). Ground reaction forces (GRF) were quantified (1500 Hz) using AMTI force plate (Newton, MA, USA). Subjects performed change of direction tasks at angles  $45^\circ$  and  $110^\circ$  from the initial plane of progression (Fig. 1) under two conditions; pre-planned (PP) and randomly cued (RC).

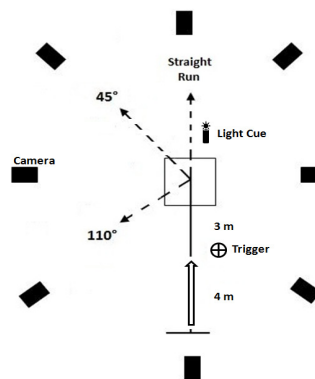


**Figure 1:** Experimental set-up for right dominant subject. Open arrow indicates original plane of progression and dash lines indicate task direction for straight run, CUT45 and CUT110.

For each task, subjects ran at a controlled velocity (4.5-5.5m/s) for 7 meters, planted their dominant foot on the force plate and changed direction to the opposite side. Subjects had knowledge of the change of direction angle prior to initiating the task during the PP condition. During the RC condition, a light cue triggered 3m prior to the force plate indicated one of 3 task directions: straight run, cut to  $45^\circ$  (CUT45) or  $110^\circ$  (CUT110). Task direction was presented in random order.

Vertical and posterior peak GRFs (pkGRF) were analyzed during weight acceptance, defined as the time between initial contact (IC) and first local minima of resultant GRF [4]. Vertical and posterior GRF impulses (GRI) were calculated as the integration of GRF x time curve during the deceleration phase, defined as the time between IC and maximum knee flexion. GRFs were normalized by body mass. Approach velocity was calculated as the average velocity over 3m prior to force plate contact.

An average of four trials was used for statistical analysis. Repeated measures 2x2 ANOVA was used to detect differences between tasks (CUT45, CUT110) and conditions (PP, RC) for each variable. Post-hoc t-tests were performed in the event of a significant interaction at  $p < 0.05$ .

## RESULTS

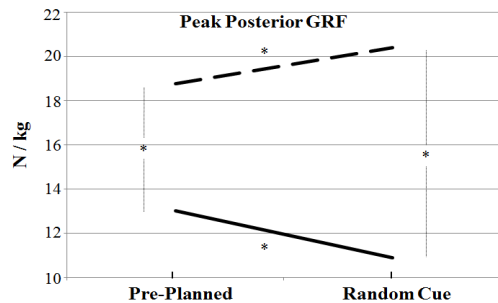


**Figure 2:** Peak posterior GRF. Solid line represents the change of direction at  $45^\circ$  and dash line the change of direction at  $110^\circ$ .  $*=p < 0.001$ .

Main effect of task and a significant task by condition interaction was observed for all GRF variables. CUT110 had greater vertical and posterior pkGRF (Fig. 2) and GRI than CUT45 ( $p < 0.001$ ). When compared to PP, vertical and posterior pkGRFs increased during RC CUT110 ( $p < 0.001$ ) and decreased during RC CUT45 ( $p < 0.001$ ). Larger vertical GRI was observed during RC CUT110 when compared to PP ( $p < 0.001$ ) and smaller posterior GRI was observed during RC CUT45 compared to PP ( $p < 0.001$ ).

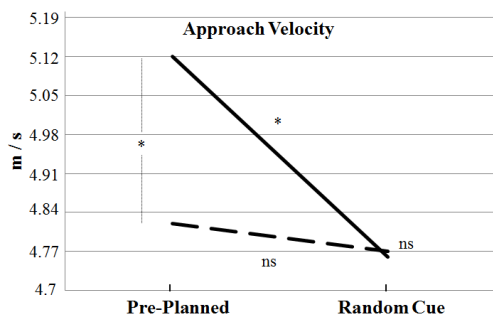


**Figure 3:** Approach velocity. Solid line represents the change of direction at  $45^\circ$  and dash line the change of direction at  $110^\circ$ .  $*=p < 0.001$ . ns=non-significant.

Main effects of task and condition and significant task by condition interactions were observed for approach velocity (CUT110 slower than CUT45,  $p < 0.001$ ; RC slower than PP,  $p < 0.001$ ). When compared to PP subjects decreased their approach

velocity during RC CUT45, but not during RC CUT110 (Fig. 3).

## DISCUSSION

As expected, larger GRFs were observed during CUT110 when compared to CUT45. Together with slower approach speed these data suggest that CUT110 is more challenging than CUT45.

Interestingly, we found that the effect of RC differed between changes of directions performed at different angles. Peak GRFs and GRIs were generally smaller when subjects were randomly cued to perform the CUT45 and greater when cued to perform CUT110.

Despite the fact that approach speed was controlled for, subjects made small adjustments during RC tasks. During PP conditions athletes approached at a slower velocity during the CUT110 compared to CUT45. During the RC condition all tasks were performed at slower velocity (similar to PP CUT110) suggesting that subjects attempted to prepare themselves for the more difficult task.

The decreased loading in RC CUT45 may be attributed to the slower velocity. Increased loading in response to the RC during CUT110, however cannot be attributed to a change in approach velocity and may be the result of online postural adjustments.

## CONCLUSION

RC during demanding tasks result in increased loading. When assessing the effects of RC on performance using a paradigm with tasks of varying demands, interpretation may be limited to the more demanding tasks as subjects will make adjustments to prepare for the potential demands of that task.

## REFERENCES

1. Sheppard JM & Young WB. *J Sports Sci* **24**(9), 919-932, 2006.
2. Jindrich DL, et al. *Chaos* **19**(2), 026105, 2009.
3. Besier TF, et al. *Med Sci Sports Exerc* **33**(7), 1176-1181, 2001.
4. Besier TF, et al. *Med Sci Sports Exerc* **33**(7), 1168-1175, 2001.

# NONLINEAR DYNAMICS AND BIFURCATIONS IN POSTURAL CONTROL WITH AND WITHOUT A WOBBLE BOARD

James Chagdes, Arvind Raman, Shirley Rietdyk, Jeff Haddad, and Howard Zelaznik

Purdue University, West Lafayette, IN, USA

email: [raman@purdue.edu](mailto:raman@purdue.edu) web: <https://engineering.purdue.edu/RamanLab/>

## INTRODUCTION

A single-degree-of-freedom (1-DOF) inverted pendulum has been widely accepted as a valid model for quiet standing human posture sway [1-3]. The simplicity of such a model allows one to capture the nonlinear dynamical behavior and multiple timescales that are known to occur in human posture [4], while describing the motion using a simple equation for postural sway. Previous studies have investigated different neural controllers, mainly linear, to regulate posture [1,2]; whereas few have studied the effects of a nonlinear neural controller, most of which use a Hill muscle model to explore the nonlinearities of the muscles [3].

We aim in this work to study the instabilities and bifurcations inherent these models where the sources of nonlinearity arise from the time delay in proprioceptive or visual feedback, nonlinear muscle stiffness, and geometric nonlinearities from large sway motion. Furthermore, we extend these models to study the dynamics of postural sway when standing on a wobble board. Using this model we have studied the linear and nonlinear stability and bifurcations in simple models of postural sway on rigid surfaces and on a 1-DOF wobble board. In the case of postural sway on a rigid surface we find that increased time delays in neuromuscular feedback can lead to limit cycles as a result of a supercritical Hopf bifurcation, while decreasing feedback gains results in a supercritical pitchfork bifurcation leading unstable posture and a leaning equilibrium. The analysis of postural sway on a 1-DOF wobble board shows a similar result, however the stability of upright equilibrium is also dependent on the stability of the wobble board. As the wobble board stiffness is decreased the region of stability of the upright equilibrium is also decreased.

## METHODS

The equations of motion were determined in the anterior-posterior (AP) direction on a rigid surface by modeling the body as a 1-DOF inverted pendulum with mass  $m_{BODY}$  and height  $h_{BODY}$  to the center of mass (CoM) from the ankle joint and a postural sway angle of  $\theta$  (Fig. 1(a)). Likewise, the equations of motion were determined on a wobble board by modeling the body in the same way and modeling the wobble board as a 1-DOF inverted pendulum with mass  $m_{BOARD}$  and height  $h_{BOARD}$  to the CoM where the wobble board sway angle is  $\phi$  and the postural sway angle is  $\theta$  relative to the board sway angle (Fig. 1(b)).

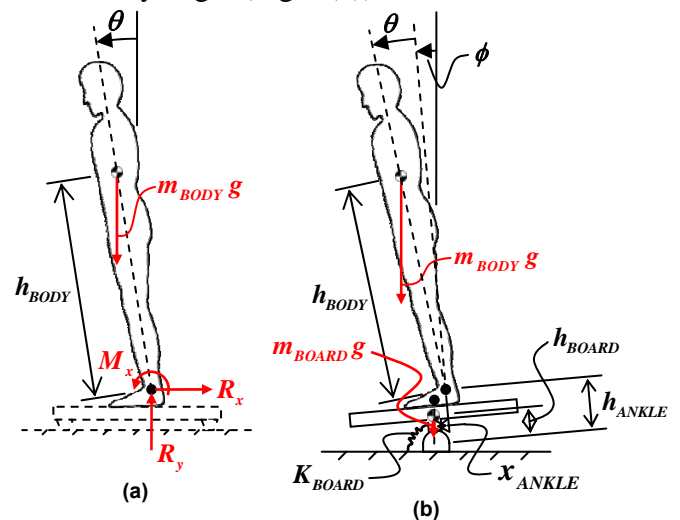


**Figure 1:** Diagram of human posture control on a (a) rigid surface and (b) 1-DOF wobble board.

The corrective ankle torque is a combination of a passive element representing mechanical muscle properties of stiffening and dampening, and an active element representing muscle activity as a result of neuromuscular feedback from the central nervous system with time delay. The passive element is modeled as a nonlinear proportional-derivative (PD) controller with linear  $K_{p,p}$  and

cubic nonlinear stiffness  $K_{p,p}\beta_p$  proportional to the relative sway angle of the body along with linear damping  $K_{d,p}$  proportional to the relative sway angular velocity of the body. The active element is modeled as a nonlinear PD controller with a linear  $K_{p,a}$  and cubic nonlinear stiffness  $K_{p,a}\beta_a$  proportional to the absolute sway angle of the body (and wobble board) at a delayed time  $\tau$  along with linear damping  $K_{d,a}$  proportional to the absolute sway angular velocity of the body (and wobble board) at a delayed time  $\tau$ .

The stability regions of the upright equilibrium were calculated for both models by keeping all parameters constant and varying the active proportional gain  $K_{p,a}$  and the time delay  $\tau$  using MATLAB and MATLAB BIFTOOL.

## RESULTS AND DISCUSSION

In the case of postural sway on a rigid surface the regions of stability were found in the parameters space  $(K_{p,a}, \tau)$  (Fig. 2). The gray region represents the set of parameters that result in a stable upright equilibrium, whereas the white regions represent the set of parameters that result in an unstable upright equilibrium.

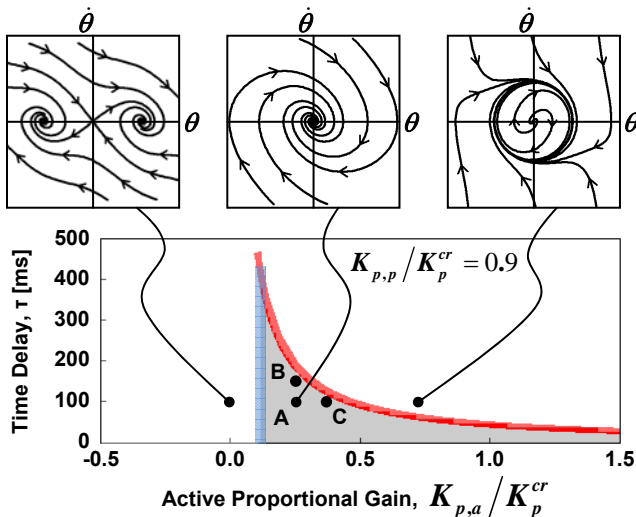


**Figure 2:** Regions of stability for human posture

A decrease in active proportional gain results in a supercritical pitchfork bifurcation (represented in blue in Fig. 2) which leads to an unstable upright equilibrium and two stable equilibriums at angles in the AP directions. An increase in active proportional gain and/or time delay of the neural

feedback system results in a supercritical Hopf bifurcation (represented in red in Fig. 2) which leads to an unstable upright equilibrium and a stable limit cycle reminiscent of those observed in patients with severe neuromuscular disease [5].

In the second case of postural sway on a wobble board the Hopf bifurcation stability boundary found in the parameter space  $(K_{p,a}, \tau)$  for multiple values of wobble board stiffness and can be seen below (Fig. 3).

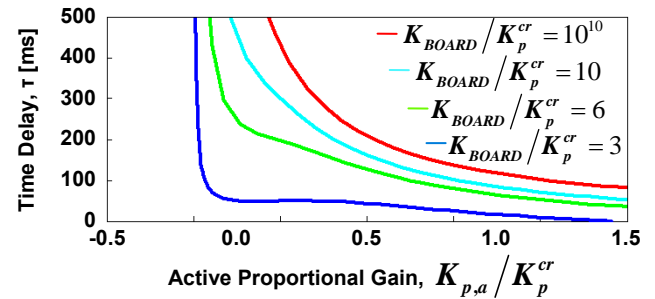


**Figure 3:** Plot of Hopf bifurcation stability boundaries for multiple values of board stiffness for human posture on a 1-DOF wobble board.

As wobble board stiffness is decreased the stability region of the upright equilibrium is also decreased causing a person to actively adjust their feedback gains and possibly lowering their neural feedback system time delay by put a larger cognitive load on the importance of maintaining balance.

## CONCLUSIONS

A simple nonlinear model of postural sway along with a nonlinear feedback controller was used to detect stability boundaries and dynamical behavior about the upright equilibrium. The existences of bifurcations explain some of the postural behavior that has been seen in other works.

## REFERENCES

1. Hur P, et al. *IEEE Trans Neural Syst Rehabil Eng* **18**, 461-467, 2010.
2. Peterka RJ. *Neurophysiol* **88**(3), 1097-1118, 2002.
3. Verdaasenk BW, et al. *Biol Cybern* **91**, 48-62, 2004.
4. Chagdes JR, et al. *Exp Brain Res* **197**, 297-310, 2009.
5. Schmit JM, et al. *Exp Brain Res* **168**, 357-367, 2006.

# DETERMINING BODY SEGMENT POSE FOR A DEFORMABLE MARKER CONFIGURATIONS

John H. Challis

Biomechanics Laboratory, The Pennsylvania State University, PA, USA  
email: [jhc10@psu.edu](mailto:jhc10@psu.edu)

## INTRODUCTION

The determination of the position and orientation, or pose, of human body segments is a fundamental step in kinematic analysis. If, for example, the pose of adjacent segments are determined the kinematics of the joint between the segments can be computed. Using image based motion analysis markers are placed on body segments to permit determination of the segment pose. These markers are placed on the skin they are designed to allow estimation of the underlying bone pose. Studies using bone mounted markers demonstrate, for example during walking, that the markers mounted on the skin have some motion independent of the bones motion [1]. Most methods for determining segment pose are based on least-squares principles [2, 3], but soft tissue deformation may cause a violation of a fundamental assumption of a least squares approach.

Rousseuw and Leroy [4] described a leverage point as a point which has a large effect on a least-squares estimator. If the positions of the markers on a segment are all corrupted by the same magnitude noise then all points will make similar contributions to the residual, but if one point has greater noise for example due to underlying skin motion then it will act as a leverage point. The focus of this study was to present and evaluate a method for determining segment pose from motion analysis data which is not unduly influenced by the type of noise distributions which are caused by soft tissue motion.

It was the purpose of this study to compare two procedures for estimating the pose of a body segment under the noise conditions which can be found in biomechanical studies.

## METHODS

If the position of a point is measured in two reference frames the following relationship exists,

$$y_i = [R]x_i + v$$

Where  $y_i$  - position of a point measured in one reference frame  $\{B\}$ ,  $[R]$  - attitude matrix (sometimes called the rotation matrix),  $x_i$  - position of a point measured in another reference frame  $\{A\}$ , and  $v$  is the position vector of the origin of reference frame  $\{A\}$  measured in frame  $\{B\}$ . The matrix  $[R]$  is a proper orthonormal matrix.

Using least-squares approach the problem of determining  $[R]$  and  $v$  is equivalent to minimizing,

$$\frac{1}{n} \sum_{i=1}^n ([R]x_i + v - y_i)^T ([R]x_i + v - y_i)$$

Where  $n$  is the number of non-collinear points measured in both reference frames ( $n \geq 3$ ). To simplify the problem  $v$  can be eliminated, by computing the mean vectors ( $\bar{x}$  and  $\bar{y}$ ),

$$\bar{x} = \frac{1}{n} \sum_{i=1}^n x_i \quad \bar{y} = \frac{1}{n} \sum_{i=1}^n y_i$$

and defining two new vectors,

$$x'_i = x_i - \bar{x} \quad y'_i = y_i - \bar{y}$$

Appropriate substitution of these vectors into the least-squares equation gives,

$$\frac{1}{n} \sum_{i=1}^n (y'_i - [R]x'_i)^T (y'_i - [R]x'_i)$$

This equation can be solved using a singular value decomposition based procedure [2], here called procedure 1.

If the points have different amounts of noise corrupting them, it can be that a point (marker on the body) acts as a leverage point. Rather than use a least-squares procedure it is potentially a better

option not to square the residuals, but to minimize the following equation,

$$\frac{1}{n} \sum_{i=1}^n |y'_i - [R]x'_i|$$

Matrix  $[R]$  can be decomposed into three parameters [5], so to minimize the preceding equation an optimization algorithm can be used to determine these three parameters [6]. Here this approach is called procedure 2.

Computer simulations were used to assess the accuracy of the two procedures for the determination of  $[R]$  and  $v$ . A segment was defined to have approximately the dimensions of a human limb, with two proximal and two distally. The attitude of the segment was defined using helical angles [5]. The segment was randomly located within a  $1 \text{ m}^3$  volume, with angles varying from  $-180$  to  $180$  degrees. A set of 100 angles and translation vectors were generated.

Marker locations were contaminated with two types of noise,

**Condition 1** -  $\sigma = 1.5$  mm in each coordinate direction.

**Condition 2** -  $\sigma = 1.5$  mm in each coordinate direction, with simulated segment wobble.

Under the segment wobble condition the segment was assumed to dilate and contract as if an impulse was passing along the segment. These cases were randomly generated with the marker locations changed relative to the segmental reference frame resulting in volume changes of  $\pm 5\%$  [7].

The accuracy of each of the two procedures was assessed by computing the mean absolute relative differences between the true angles and the computed angles, and true and computed translation vectors.

## RESULTS AND DISCUSSION

Computationally the second procedure was slower than procedure 1, the singular value based procedure. In the absence of wobble but with noise contaminating the marker locations (Condition 1), the two procedures performed similarly, although procedure 1 was slightly more accurate. The mean absolute relative difference in the estimation of

angles was 0.076 for procedure 1, and 0.081 for procedure 2. The two procedures performed the same for the estimation of the segment position (mean absolute relative difference – 0.015).

Simulated segment wobble, Condition 2, decreased the accuracy of angle and translation computation compared with Condition 1. Under this condition procedure 2 was more accurate than procedure 1. The mean absolute relative difference in the estimation of angles was 0.171 for procedure 1, and 0.162 for procedure 2. The mean absolute relative difference in the estimation of angles was 0.015 for procedure 1, and 0.014 for procedure 2.

## CONCLUSIONS

This study has presented a new method for determining the pose of a rigid body. The procedure produces more accurate result, compared with the normally adopted least-squares procedure, in the presence of segment wobble. Of course segment wobble occurs in many tasks, so this new method reduces the influence of this phenomenon on the estimation of segment pose.

## REFERENCES

1. Manal K, et al. *Clin Biomech* **18**, 126-131, 2003.
2. Challis JH. *J Biomech* **28**, 733-737, 1995.
3. Veldpaus FE, et al. *J Biomech* **21**, 45-54, 1988.
4. Rousseeuw PJ, & Leroy AM. *Robust Regression and Outlier Detection*, Wiley, 1987.
5. Woltring HJ. *Hum Mov Sci*, **10**, 603-616, 1991.
6. Corana A, et al. *ACM Trans Math Soft*, **13**, 262-280, 1987.
7. Pain MTG, & Challis JH. *J Appl Biomech*, **18**, 231-242, 2002.

# INSIGHTS INTO THE ROLE OF PROACTIVE STRATEGIES IN POSTURAL RESPONSES TO SLIPS USING GAIT SIMULATIONS

<sup>1</sup>April Chambers, <sup>1</sup>Rakié Cham and <sup>1</sup>Arash Mahboobin

<sup>1</sup>University of Pittsburgh, Pittsburgh, PA, USA

Email: [arm19@pitt.edu](mailto:arm19@pitt.edu)

## INTRODUCTION

Maintaining balance during walking in challenging environments requires two types of postural strategies: reactive and proactive [1, 2]. Reactive strategies are generated in response to a perturbation, such as a slip or trip. Proactive strategies are generated when expecting the risk of being perturbed. The ability of the motor control system to develop proactive strategies that allow adaptations in challenging environments is crucial to fall prevention [1, 3, 4]. Gait adjustments of proactive strategies can reduce the likelihood of a slip (slip risk) and improve the likelihood of a recovery if a slip occurs (slip severity) [2, 3, 5]. Experimental gait studies alone cannot elucidate the direct effect of an individual component of a proactive strategy, e.g., increased activation of a given muscle or co-contraction, on the effectiveness of reducing slip severity due to the complexity of the musculoskeletal system dynamics. While experimental gait studies provide a valuable description of proactive strategies, computational modeling and simulations are able to provide additional information on how each muscle or muscle group is contributing to a proactive strategy. The objective of this study was to explore, through simulations, the differences in lower extremity muscles utilized during proactive strategies.

## METHODS

Normal walking kinematics and bilateral ground reaction forces were collected from a healthy young subject (age=24 yr, mass=68 kg, height=172 cm) and an older (age=64 yr, mass=56 kg, height=163 cm) subject at the University of Pittsburgh to examine age-related differences in proactive strategies. Following the first set of normal walking trials (baseline dry (BD) condition), a glycerol solution was applied onto the force plate without the

subject's knowledge to generate an unexpected slip at heel contact (HC) of the leading leg (left foot). In the subsequent normal walking trials (anticipation dry (AD) condition), subjects were made aware of the possibility of encountering a slippery floor but no further information was provided. Only the BD trial immediately preceding and the AD trial immediately following the unexpected slip trial were selected for this analysis.

A 3-D musculoskeletal model was developed in OpenSim [6] and used to obtain a kinematically-consistent set of joint angles and muscle excitations using the measured motions and ground reaction forces. The model consisted of 10 segments and 54 Hill-type muscles (24 muscle per leg plus 6 upper body muscles) and 12 degrees-of-freedom. Normal gait was simulated from 50 ms prior to 150 ms after the leading leg HC. This duration was selected due to its importance in evaluating slip risk before any reactive strategies are generated [2, 7].

## RESULTS AND DISCUSSION

The simulated muscle excitations of several lower extremity muscles were different between BD and AD conditions. In both subjects, the inferior gluteus maximus of the leading leg exhibited higher excitation levels in the AD condition. Age-related differences were seen in the left anterior gluteus medius muscle excitations. The older subject had elevated left anterior gluteus medius excitation levels when anticipating a slippery floor (i.e., in the AD condition), while the young subject did not. Both the young and older subjects were found to have a minor burst of left rectus femoris activity before HC during the AD condition that was not present in the BD condition. The most noticeable differences in simulated muscle excitations between BD and AD conditions were observed in the medial gastrocnemius and tibialis anterior muscles before

HC. The young subject had a major burst in the left medial gastrocnemius muscle excitation before HC during anticipation that was not present in the BD condition (Figure 1A). The older subject had a minor burst in the left medial gastrocnemius muscle before HC during the BD condition. However, this excitation was increased and occurred earlier when anticipating a slippery floor (Figure 1B). Both the young and older subjects also had an increased burst in left tibialis anterior muscle excitations before HC during the AD condition (Figure 1C and D).

It is likely that the increased hip extensor muscle excitations observed during anticipation trials, especially inferior gluteus maximus, would be associated with reduced slip risk. The increased knee extensor muscle excitations observed during the anticipation condition before HC might be contributing to increased vertical support, which should be beneficial if a threat to one's balance was present, as was the case during the anticipation trials. Additionally, the increased muscle excitation before HC might contribute to increased co-contraction at the knee. Furthermore, it appears as though the increased medial gastrocnemius excitations observed before HC when anticipating a slippery floor would lead to reductions in slip risk. The increased tibialis anterior excitations before and shortly after HC during the anticipation condition (Figure 1) may also contribute to vertical support, which might be an important component in reducing slip risk. The increased muscle excitations

in tibialis anterior combined with the increased medial gastrocnemius activity when anticipating a slippery floor likely contribute to increased co-contraction at the ankle around HC. Increased ankle co-contraction around HC has been found previously when anticipating a slippery surface and has been associated with less severe slips [2]. In summary, differences found in simulated excitations of the lower extremity muscles likely reduce slip risk when anticipating a slippery floor.

## REFERENCES

1. Pavol MJ, et al. *J Gerontol A Biol Sci Med Sci* **59**, 494-502, 2004.
2. Chambers AJ and Cham R. *Gait Posture* **25**, 565-572, 2007.
3. Cham R and Redfern MS. *Gait Posture* **15**, 159-171, 2002.
4. Lockhart TE, et al. *Gait Posture* **26**, 142-149, 2007.
5. Marigold DS and Patla AE. *J Neurophysiol* **88**, 339-353, 2002.
6. Delp, SL, et al. *IEEE Trans Biomed Eng* **54**, 1940-1950, 2007.
7. Cham R and Redfern MS. *J Biomech* **34**, 1439-1445, 2001.

## ACKNOWLEDGEMENTS

Funding provided by NIOSH (R03 OH007533).

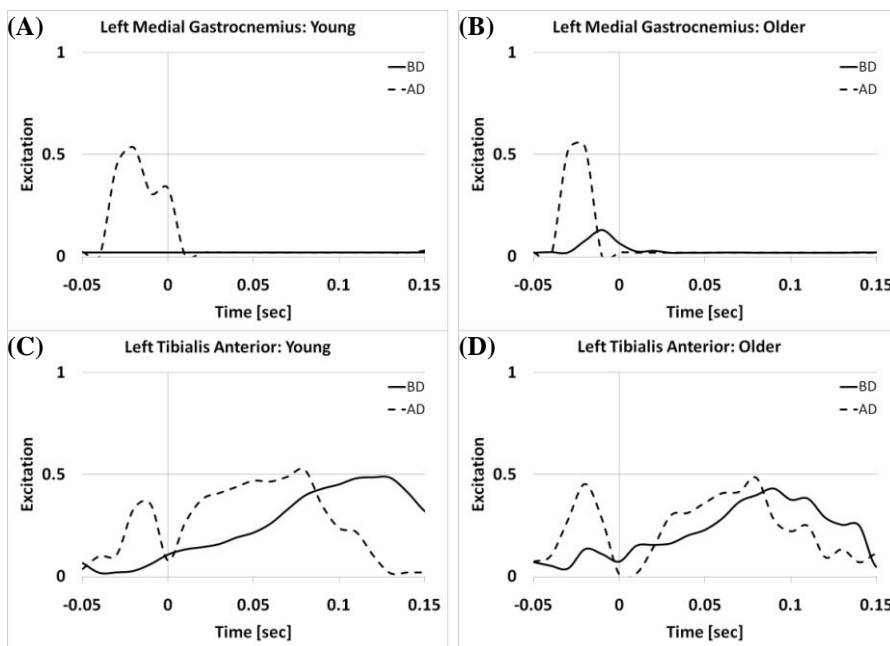


**Figure 1:** Simulated muscle excitations from 50 ms prior to 150 ms after leading leg HC (0 ms) of baseline and anticipation conditions for left medial gastrocnemius (A: Young; B: Older) and left tibialis anterior (C: Young; D: Older).

# THE INFLUENCE OF FIREFIGHTER BOOT TYPE ON POSTURAL MEASURES

Harish Chander<sup>1</sup>, Chip Wade<sup>2</sup>, John C. Garner<sup>1</sup>, Ryan Garten<sup>3</sup>, & Ed Acevedo<sup>3</sup>

<sup>1</sup>Applied Biomechanics and Ergonomics Laboratory, Department of Health, Exercise Science and Recreation Management, University of Mississippi, University, MS. [hchander@olemiss.edu](mailto:hchander@olemiss.edu)

<sup>2</sup>TigErgonomics Laboratory, Department of Industrial and Systems Engineering, Auburn University, Auburn, AL

<sup>3</sup>Department of Health and Human Performance, Virginia Commonwealth University, Richmond, VA

## INTRODUCTION

The occupational hazards and challenges that are presented in the fire protection industry pose a number of potential risks for injuries and illness. The number of general industry non-fatal occupational injuries and illness reported in 2009, declined to 3.3 million cases compared to the 3.7 million cases in 2008 (BLS, 2010). However, the incidence rate in the fire protection industry has risen from 14.8% to 15.3% over the same period (BLS, 2010). The manipulation of relatively large objects was the most commonly encountered application of strength and endurance among firefighters. Further performing work activities in unfamiliar occupational environments while donning mandatory fire protection clothing, footwear, and accessories place extreme demands on the postural control systems. Increased probabilities of falls have been related to decrements in balance control with 45% of these falls attributed to inappropriate footwear. Firefighters use two types of federally approved boots, one made of leather and one made of rubber. Due to the primary safety concern in the design of the boots, the boots may fail to provide appropriate biomechanics that is necessary for a normal gait and maintenance of balance. Based on the previous studies, postural balance was shown to have a decrement with different footwear. Similar decrements in balance measures were also

found in firefighters with protective equipment which included specific fire fighter boots (Punakallio, 2005 Kincl et al, 2002). Currently, there remains a dearth of literature that compares the effects of the two different boot types worn by firefighters on postural control measures. The purpose of the study is to examine the differences in balance in professional fire fighters wearing rubber and leather boots participating in a fire simulation activity.

## METHODS AND PROCEDURES

Twelve professional firefighters ( $33 \pm 6.8$  years; height of  $179 \pm 6.47$  cm; weight of  $95.08 \pm 21.47$  kg), whom received, within the past 8 months a medical evaluation, including resting 12-lead EKG analysis, and clearance by a physician to participate in firefighting participated in this study. Each firefighter participated in two identical testing sessions [leather ( $2.44 \pm 0.20$  kg) and rubber boots ( $2.93 \pm 0.24$  kg)] on two separate days. Firefighters were tested with at least 6 days between the LB and RB sessions. A 22.68 kg weighted vest to simulate their typical personal protective equipment and two 5.67 kg weights on the shoulders to simulate the weight of a high-rise pack (hose bundle) were used. The 5.67 kg weights were only worn during the stair climbs. Balance assessments were done on the NeuroCom Equitest Balance Manager, using the Sensory Organisation Test in the

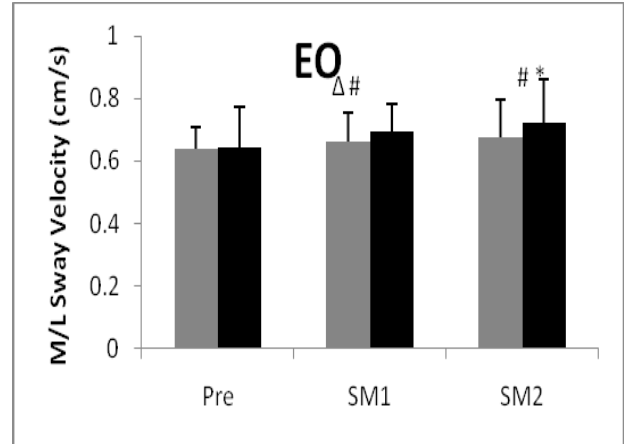
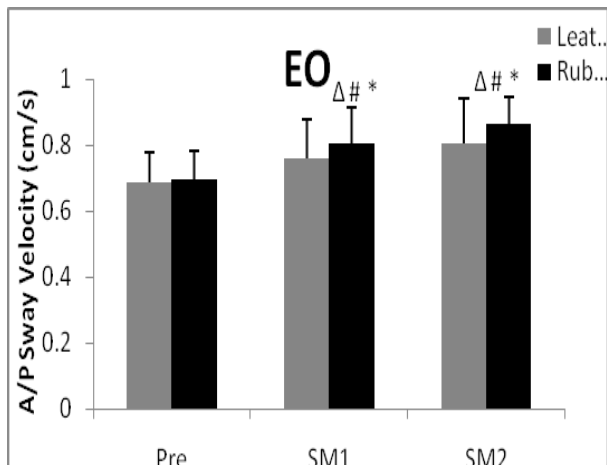
Eyes Open condition. Sway velocity was used as a dependent measure for balance assessments.

Each testing session consisted of three testing sequences: pre test, simulated stair climb-1 (SM1), and simulated stair climb-2 (SM2). Following an initial warm up, firefighters performed the postural stability test. Firefighters then were provided with the weights which simulated the breathing apparatus and hose weight, and conducted a 3-minute simulated stair climb test at 60 steps per min. Following the test, the participant exited the step mill and removed the added weights. Firefighters were then allowed to rest 3 minutes followed by a second simulated stair climb test with the simulated weights, then a final postural stability test.

## RESULTS

Repeated Measures ANOVA revealed a statistically significant difference in sway velocity between the pre and post test measures and among the two different boots.

Fig.1: Eyes open - A/P & M/L sway velocity



## DISCUSSION

An overall increase in sway velocity between the pre and post tests, indicates a diminished postural control in both the anterior/posterior direction and the medial/lateral direction for both conditions. However, the leather boots had a significantly smaller increase in sway velocity in both directions when compared to the rubber boots which indicates a decrement in balance. These results suggest that the heavier rubber boots may elicit greater fatigue in the firefighters, thus impairing balance and postural control measures.

## REFERENCES

Bureau of Labor Statistics: US Department of Labor, 2009.

Punakallio, A. (2005). *Journal of Sports Science and Medicine*, 4, Suppl. 8, 1-47.

Kincl et al. (2002). *Applied Occupational & Environmental Hygiene*, 17, 4, 256-266.

# EFFECT OF A NEUROMUSCULAR DENTISTRY-DESIGNED MOUTHGUARD ON PEAK KNEE VALGUS MOMENTS DURING SINGLE LEG LANDING

<sup>1</sup>Ajit Chaudhari, <sup>2</sup>Joshua Cotter, <sup>1</sup>Steve Jamison and <sup>1</sup>David Mossad

<sup>1</sup>The Ohio State University, Columbus, OH, USA

<sup>2</sup>University of California at Irvine, Irvine, CA, USA

email: chaudhari.2@osu.edu web: <http://sportsmedicine.osu.edu>

## INTRODUCTION

Peak knee valgus moments (pKVM) have been identified as a potential risk factor for ACL injury. Recently, mouthguards developed using principles of neuromuscular dentistry have been touted as being able to enhance balance and strength by promoting optimal jaw alignment. A previous study observed increased vertical jump height when a neuromuscular-dentistry designed mouthguard was used [1]. If wearing such a mouthguard were to improve both balance and strength, it could lead to beneficial effects on dynamic knee loading. Given the prevalence [2], cost [3], and sequelae [4] of ACL injuries in sports where mouthguard use is common such as basketball, improvements in dynamic knee loading that reduce risk of ACL injury may be an important consideration. This study tested the hypothesis that wearing a custom neuromuscular dentistry-based mouthguard reduces pKVM in single-leg landing relative to a low-cost boil-and-bite mouthguard, or no mouthguard.

## METHODS

Forty-six athletes (38M, 8F, 74.8±13.9kg, 1.75±0.09m) participated in this double-blind crossover study after providing IRB-approved informed consent. *A priori* sample size estimation indicated a desired population of 36 for an effect size of 0.25. Inclusion criteria included: (a) 2 or more years of current involvement in a designated sport, (b) an average of 3 or more training sessions per week in the last 3 months, (c) an average of 6 or more hours of total training time per week, (d) 1 or more instances of competition per year in the designated sport, (e) no current pain limiting athletic movement, and (f) no neck or jaw condition that would limit the ability to wear a mouthguard.

Three mouthguard conditions were utilized for the study: NDD - neuromuscular dentistry-designed lower-jaw mouthguard (Pure Power Mouthguard, Makkar Athletics, Inc.); BB - boil-and-bite lower-jaw mouthguard (Gravity 2 STC, Shock Doctor, Inc.); NO - no mouthguard. A fitting session for both mouthguards was performed first by a dentist experienced in fitting both types of mouthguards, followed by a single testing session several weeks later. Fitting for NDD involved 60 min. of transcutaneous electrical nerve stimulation (TENS) to induce jaw muscle relaxation. BB fitting was performed according to package directions.

Subjects performed 3 practice trials of single-leg landing on each leg. Then, for each mouthguard condition, subjects performed 4 test trials on each leg. The condition order was randomly assigned for each subject. Participants dropped off a 48-cm box with both feet, landing with a single leg on a force plate (Bertec, Inc.) and attempting to hold for 2s. An 8-camera optical motion analysis system (Vicon, Inc.) with retro-reflective markers placed on the pelvis and lateral knee, ankle, and foot was used to calculate net external pKVM during the 1<sup>st</sup> 100ms after foot strike (Nm/kg).

1061 out of the 1104 single-leg landing trials collected from the 46 subjects contained usable data for the analysis. One subject only had usable data for the NDD condition, while another only had usable data for the NO condition. An additional 11 randomly-distributed trials were not usable due to marker gaps >100ms.

An unbalanced mixed-effects ANOVA including mouthguard, side, and mouthguard\*side interaction as fixed effects was performed (ANOVAN, Matlab, MathWorks, Inc.), with post-hoc Tukey's HSD comparisons to identify differences between the 3

mouthguard conditions and between sides (MULTCOMPARE, Matlab, MathWorks, Inc.). An *a priori* significance level of  $\alpha=0.05$  was used for all tests.

## RESULTS AND DISCUSSION

Mouthguard condition was a significant main effect ( $p=0.0104$ ), as was side ( $p=0.014$ ). Post-hoc analysis showed that pKVM was significantly lower for NDD than BB, but neither NDD nor BB was significantly different from NO (Figure 1). Participants displayed significantly lower pKVM on their left side than their right side (Figure 2). No significant interaction was observed between mouthguard and side ( $p=0.0879$ ).

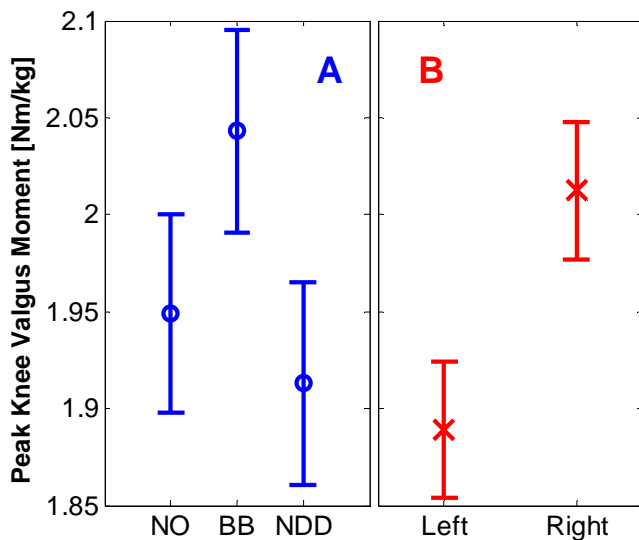


**Figure 1.** Population marginal means for pKVM with 95% confidence intervals. [A] No Mouthguard (NO), Boil-and-Bite (BB), and Neuromuscular Dentistry-Designed (NDD) mouthguards. [B] Left and Right side landings.

The NDD mouthguard appeared to influence neuromuscular control during the single-leg landing task by reducing pKVM relative to the boil-and-bite mouthguard. The reduction was relatively small between mouthguard conditions (6.4%, effect size = 0.15) compared to the previously observed reductions from neuromuscular training in pKVM during a double-leg drop-jump of 10-30% [5]. It should also be noted that the observed difference between BB and NDD was similar in magnitude to the difference between sides (4.4%, effect size = 0.10). Nevertheless, given that an increasing number of sports are requiring or strongly

recommending mouthguards for participation, potential benefits from a more expensive mouthguard, such as a reduction in known biomechanical injury risk factors, may offset increased costs of the mouthguard.

The results of this study should be considered in light of its limitations. First, the single-leg landing test, while clinically relevant, may result in pKVM that is different from other activities such as cutting or stop-jumps. These more dynamic, sport-specific activities could result in a different relationship between the mouthguard conditions. Moreover, it remains unknown whether the results observed during a single testing session would change over time as the wearer grows accustomed to the different mouthguards. Lastly, the boil-and-bite mouthguard is “one size fits all,” which anecdotally resulted in a poor fit for some participants even after multiple attempts at re-fitting. Less than optimal fit in these participants could potentially have contributed to the observed effect on pKVM.

## CONCLUSIONS

This study demonstrated a reduction in pKVM in subjects wearing a custom neuromuscular dentistry-designed lower-jaw mouthguard relative to a standard boil-and-bite lower-jaw mouthguard. Future prospective studies are needed to test the persistence of this phenomenon, whether the results carry over to mouthguards that provide upper-jaw dental protection, and whether these observed differences in pKVM lead to reduced injury rates.

## REFERENCES

1. Arent SM, et al. *Comp Exerc Phys* **7**, 73-79, 2010.
2. Miyasaka KC, et al. *Am J Knee Surg* **4**, 3-8, 1991.
3. Hewett TE, et al. *Am J Sports Med* **33**, 492-501, 2005.
4. Lohmander LS, et al. *Arthritis Rheum* **50**, 3145-3152, 2004.
5. Myer GD, et al. *J Strength Cond Res* **19**, 51-60, 2005.

## ACKNOWLEDGEMENTS

Partial funding for this study was received from Makkar Athletics, Inc.

# A NOVEL DEVICE FOR PHYSIOLOGIC MR IMAGING OF THE PATELLOFEMORAL JOINT CARTILAGE UNDER CONTROLLED LOADS

<sup>1</sup>Eric F. Chehab, <sup>1,2</sup>Stephen H.M. Brown, and <sup>1</sup>Samuel R. Ward

<sup>1</sup>University of California: San Diego, San Diego, CA, USA

<sup>2</sup>University of Guelph, Guelph, ON, Canada

email: [srward@ucsd.edu](mailto:srward@ucsd.edu) web: <http://muscle.ucsd.edu>

## INTRODUCTION

Patellofemoral joint pain (PFP) is a condition affecting up to 30% of active individuals. Although the etiology of this condition is still not well understood, a number of contributing factors have been identified. The natural history of this condition appears to involve abnormal patellofemoral joint kinematics, chondromalacia, and ultimately osteoarthritis. Early detection of cartilage wear is an important component of diagnosis and early treatment for this relatively young group of patients. However, standard morphological MR imaging is not sensitive to early changes in cartilage wear. More recently, MR pulse sequences have been developed to quantify physiological features of cartilage (e.g. water and proteoglycan contents). However, they too, lack sensitivity to early changes in cartilage health. To address this problem, we have proposed a novel method to capture these physiologic properties under known patellofemoral joint loads.

## METHODS

A custom, non-ferromagnetic device was fabricated from a fiberglass-epoxy composite and nylon screws and fitted to a standard knee-foot stack coil (Fig. 1). The device consists of a frame for a PVC pneumatic cylinder and a locking mechanism for the coil. This allows the calibrated cylinder to compress the patella during imaging by controlling air pressure input from the MRI control room. Engineering tests demonstrated that the device could reliably compress a substrate in the range of 5–18 kg with a drift of < 4% over 10 minutes.

10 adult subjects (6 control subjects and 4 subjects with PFP) were recruited under a UCSD approved protocol. After obtaining informed consent, subjects were placed in a 3T

MR system (GE MR750) and the orientation of the compression device plunger was aligned with the anterior surface of the patella.



**Figure 1:** Compression device outside and inside a knee-foot stack coil.

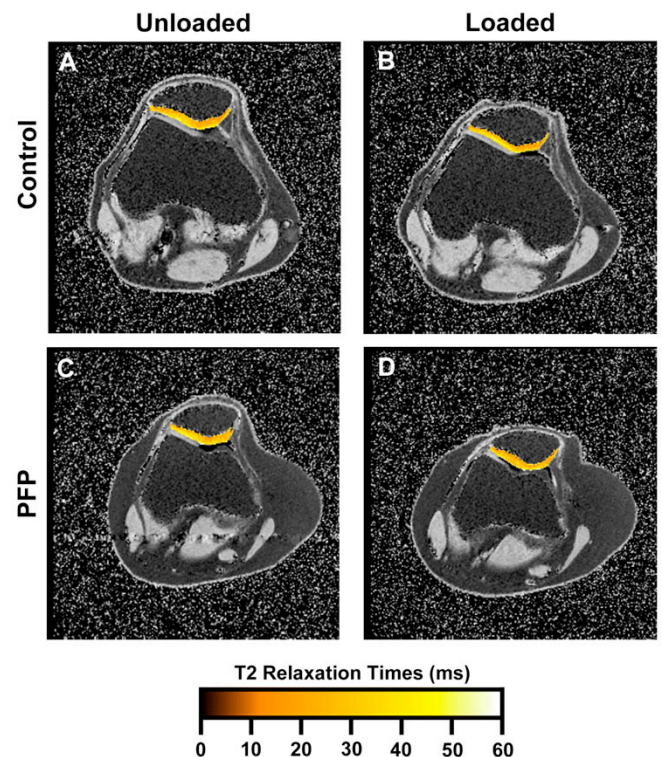


**Figure 2 A-D.** Axial T2 maps of control and PFP patients under unloaded and loaded conditions.

A standard T2 mapping sequence (TR 800ms, TE 10ms, 8 echos) was obtained to quantify regional PFJ cartilage water content with the joint 1) unloaded and 2) under a load of 15% body weight (Fig 2). Note that the knee was axially loaded for 5 minutes prior to the scan and during the scan time of less than 4 minutes.

To quantify T2 values, non-overlapping regions of interest (ROIs) were analyzed on the medial and lateral facets of the patella; the slope of the T2 decay curve (using echos 2-8) was extracted using ImageJ and the MRIAnalysisPak plugin.[1] T2 values were compared using a 2-way repeated measures ANOVA.

## RESULTS AND DISCUSSION

At 15% body weight, the T2 value of the medial facet increased by 19% ( $p < 0.05$ , Fig. 3) and the lateral facet increased by 12% ( $p = 0.13$ , Fig. 4). This indicates that water concentrations in the ROIs were elevated under loading. There were no significant differences between control and PFP subjects at this load and no interactions between group and loading condition. We also found that the cartilage T2 value recovered to its unloaded T2 values within 4 minutes of load removal (data not shown).

These data are directed towards a “proof-of-concept” approach for the device. In our preliminary experience, all but one subject was able to tolerate a load of 15% body weight, and this patient did not tolerate the load because of apprehension about PFJ dislocation, not pain. Furthermore, the device components did not produce any MR artifacts or induce motion-related artifact in the tissues of interest, ensured high spatial resolution and contrast.

Future work with this device is aimed at identifying a critical load for detection of early osteoarthritis by manipulating the load magnitude and load time in a group of patients who have early OA confirmed arthroscopically. Correlating increases in T2 with specific morphological or mechanical measurements of OA will allow for a more precise testing method and the development of a “threshold” between normal cartilage wear and true early OA.

Obviously, this will require a larger group of subjects.

Potential uses for this device are not restricted to those shown in this study. It could also be used to quantify changes in cartilage thickness at a given load in normal and pathological patients. With its wide range of load fidelity, one could envision using it to apply very specific axial loads to other joints or tissues. This device allows us to combine the power of MRI and mechanical loading to analyze the behavior of human tissues in non-resting states.

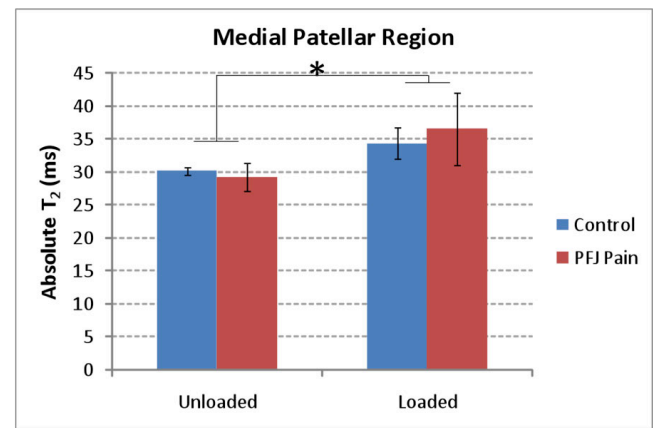


**Figure 3:** Medial patellofemoral joint T2 values. \* indicates statistical significance ( $p < 0.05$ ).

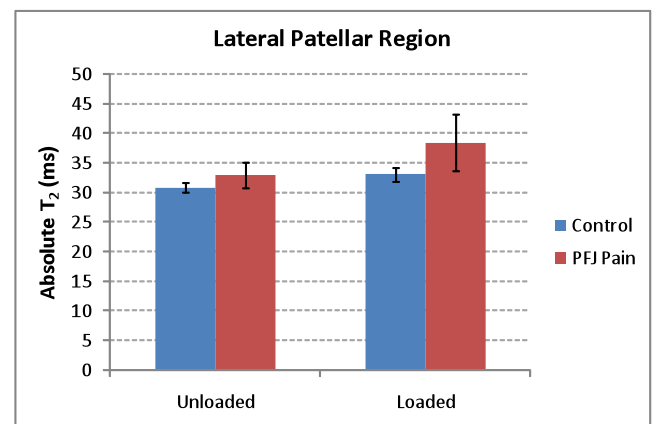


**Figure 4:** Lateral patellofemoral joint T2 values.

## REFERENCES

- [1] Schmidt KF, et al. *J Neurooncol* **68**, 207-215, 2004.

# AGE-RELATED DIFFERENCES IN CENTER OF MASS CONTROL DURING SIT-TO-WALK

Chu Jui Chen and Li-Shan Chou

Department of Human Physiology, University of Oregon, Eugene, Oregon, USA  
E-mail: [chou@uoregon.edu](mailto:chou@uoregon.edu), Web: [biomechanics.uoregon.edu/MAL/index.html](http://biomechanics.uoregon.edu/MAL/index.html)

## INTRODUCTION

Falls are a serious public health problem affecting elderly adults. Approximately one-third of older adults (65 years or older) are reported to have fallen annually. Most falls in elderly adults occur during daily activities [1,2]. Many of these activities require successful movement transitions, such as from sitting to walking. During sit-to-walk motion (STW) elderly adults have been demonstrated to generate a less horizontal center of mass (COM) momentum at seat-off and delay walking in order to maintain a more upright posture when compared to young individuals [3, 4]. There is little information on balance control during STW in older adults with fall histories [5]. Therefore, in this study, control of COM motion during STW was investigated in three subject groups: healthy young adults (YA), elderly adults without fall history in the past year (EA), and elderly adults experienced multiple falls (EF). We hypothesized that elderly adults would have an altered COM motion control when compared to young adults. In addition, EF will demonstrate a different COM control strategy from EA.

## METHODS

Currently, 4 healthy YAs (age =  $29.8 \pm 2.71$  yrs), 8 EAs (age =  $72.0 \pm 7.2$  yrs) and 8 EFs (age =  $74.3 \pm 6.8$  yrs) have been recruited and tested in this study. EFs were those who had reported 2 or more falls in the prior year. Subjects were instructed to stand up from a bench, walk 3 meters, turn around, return to the chair and sit down at a self-selected speed. Subjects were told that they will be timed during the task. Whole body motion data were captured with an 8-camera motion analysis system (Motion Analysis Corp., Santa Rosa, CA). A total of 29 markers were placed on the subject's bony landmarks [6]. The sagittal and frontal plane COM position and velocity were calculated during STW. The data from onset, seat-off, swing leg toe-off

(swing-off), stance leg toe-off (stance-off) during STW were extracted for analysis. Inclusion angle of the line formed by the COM and lateral ankle marker of supporting limb was computed for each frame during STW.

Bilateral hip abductor moments (strength) were measured during isometric maximal voluntary contraction using the Biodex dynamometer (Biodex Medical Systems, Inc., NY). Independent t-test was performed to examine the difference between EF and EA as well as young and all elderly subjects on all variables. The significance levels for all tests were set at 0.05.

## RESULTS AND DISCUSSION

The time required to complete TUG for YA, EA and EF were  $8.33 \pm 1.60$  (STW:  $1.37 \pm 0.36$ ),  $11.37 \pm 2.06$  (STW:  $1.72 \pm 0.28$ ) and  $11.07 \pm 2.01$  (STW:  $1.62 \pm 0.37$ ) seconds, respectively. Average sagittal plane COM velocities at seat-off and swing-off are shown in Figure 1.

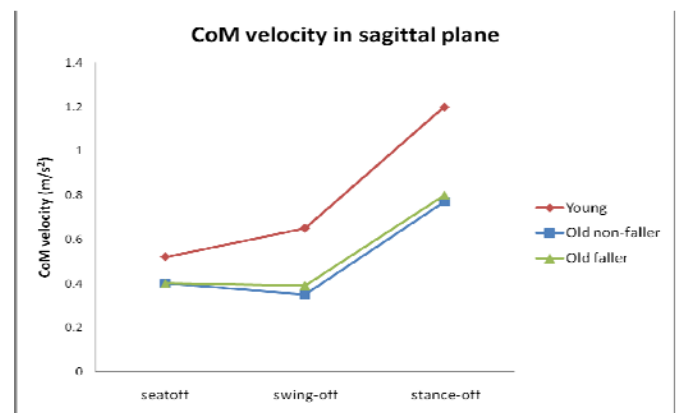


**Figure 1:** Average sagittal plane COM velocities for young, elderly adults, and elderly fallers.

Significant group differences (young vs. elderly) were found in the COM velocity at swing toe-off and stance toe-off ( $p \leq 0.001$ ). In addition,

only YA demonstrated a significant increase in the COM velocity from seat-off to swing-off ( $p = 0.013$ ). No significant group differences were observed in the frontal plane COM velocity at either swing toe-off or stance toe-off. When compared to YA, both elderly groups showed a larger frontal plane COM excursion (Figure 2). No significant differences were found between young and elderly groups in the step width and step length during STW.

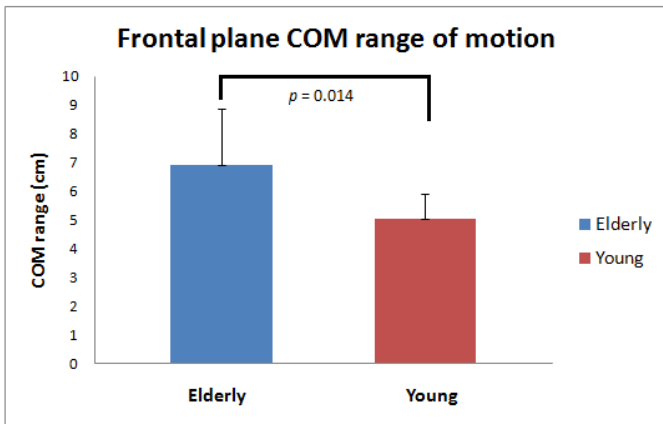


**Figure 2:** Average frontal plane COM range of motion during STW for elderly and young adults.

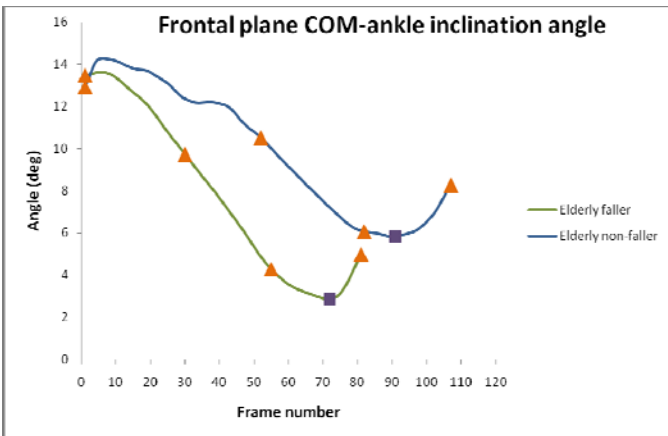


**Figure 3:** Frontal plane COM-ankle inclination angle curve during STW. The four triangles represent the four events during STW: onset, seat-off, swing-off, stance-off. The square represents the minimum angle.

Representative profiles of the frontal plane COM-ankle inclination angles during the STW phase from an elderly non-faller and an elderly faller were shown in Fig. 3. EF showed a smaller frontal plane COM-ankle inclination angle and weaker hip abductor strength than EA. However, no statistical significances were detected (Table1).

Current findings support our first hypothesis that elderly adults demonstrated a reduced forward velocity and increased frontal plane COM motion during STW when compared to young adults. This could imply that elderly adults have a difficulty in controlling the frontal plane COM motion (showing as a greater sway) that diminishes their ability in generating forward COM momentum between the seat-off and swing-off. In addition, EF had a tendency to maintain a smaller frontal plane COM-ankle inclination angle. This might imply that EF were making an effort to position the COM closer to the supporting limb to enhance stability, which could be related to their weaker hip abductor strength and poor balance control.

## REFERENCES

1. Berg, W.P., Alessio H.M. et al. (1997). *Age Ageing*, 26, 261-8
2. Alexander, B.H., Rivara, F.P., and Wolf, M.E. (1992). *Am J Public Health*, 82, 1020-3.
3. Buckley T., Pitsikoulis C. et al. (2009). *J Biomech*, 42, 2318-22.
4. Kouta M., Shinkoda K. (2008). *J Phys Ther Sci*, 20, 185-9.
5. Kerr A., Kerr K.M. et al. (2006). *Gait & Posture*, S262-4.
6. Chou, L. S., Kaufman, K. R., et al. (2003). *Gait & Posture*, 18: 125-33.

## ACKNOWLEDGEMENTS

Assistance from Vipul Lugade, Masahiro Fujimoto, and Shiu-Ling Chiu during data collection is greatly appreciated.

**Table 1:** Minimum COM-ankle inclination angle during STW and hip abductor strength for three groups.

|                            | YA          | EA            | EF           |
|----------------------------|-------------|---------------|--------------|
| Min. COM-ankle angle (deg) | 7.08 ± 2.71 | 6.66 ± 1.91   | 5.35 ± 2.21  |
| Hip abductor strength (Nm) | N/A         | 52.19 ± 15.49 | 38.43 ± 9.81 |

# ACHILLES TENDON STRAIN DISTRIBUTIONS DURING CYCLIC INERTIAL LOADING OF THE PLANTARFLEXORS

Laura Chernak, David Bungler and Darryl Thelen

University of Wisconsin-Madison, Madison, WI, USA  
email: [lchernak@wisc.edu](mailto:lchernak@wisc.edu) web: <http://enr.wisc.edu/groups/nmb1>

## INTRODUCTION

Ultrasonic imaging has provided valuable insight into *in vivo* musculotendon function. For example, cine ultrasound images have been used to describe the synergistic length changes of the Achilles tendon and gastrocnemius muscle fascicles during walking [1]. The analysis of ultrasound images, however, is often based on the motion of a single anatomical landmark, such as the muscle-tendon junction. This approach only allows for an average estimate of overall tissue strain. In contrast, recent computational models suggest that highly nonuniform tissue strain patterns can emerge as a result of muscle architectural factors such as fiber pennation, aponeurosis geometry and moment arms [2]. These strain nonuniformities may be important to consider when assessing the biomechanical factors that contribute to partial tendon tears and tendinopathies [3]. In this study, we investigated the use of ultrasound elastography [4] to assess regional strain patterns in the Achilles tendon in response to cyclic inertial loading of the plantarflexor muscles. We hypothesized that the largest strains would be observed along the superficial edge of the tendon, due to variations in the plantarflexor moment arm across the tendon thickness.

## METHODS

We constructed a mechanical device that induced inertial loading of the Achilles tendon in response to cyclic ankle dorsi- and plantarflexion (Fig. 1). A rigid footplate rotates about a pivot point aligned with the ankle joint, and is connected with a loading assembly by a kevlar belt. The loading assembly has a high overall gear ratio (30.8:1), such that relatively small inertial disks can induce a substantial load on the lengthening plantarflexors. Five healthy adults were recruited and asked to lie prone on an examination table with their knee extended ( $\sim 20^\circ$  of flexion). The foot was then

securely strapped into a rigid soled shoe attached to the footplate. Subjects were instructed to cyclically dorsi- and plantarflex their ankle in time with a metronome set to 0.5 Hz. The ankle range of motion was  $\sim 30^\circ$  resulting in a peak plantarflexion moment of  $\sim 10$  Nm. Raw radiofrequency (RF) ultrasonic data were collected from a 10 MHz linear array transducer (Ultrasonic Corp) at 70 Hz. Data were collected in a 40 by 20 mm image window, positioned such that the superior edge of the calcaneus was visible. Each subject performed three trials, each lasting eight seconds in duration.

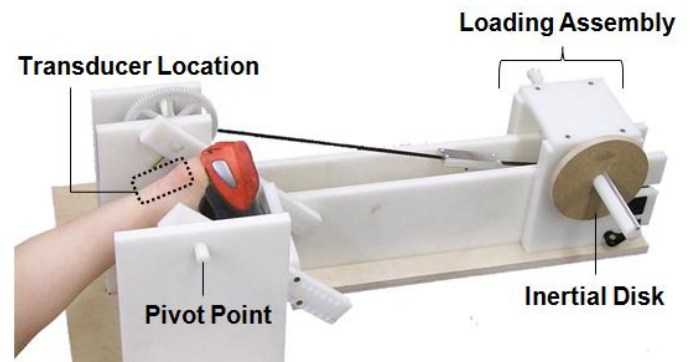


**Figure 1.** Inertial loading device.

Ultrasonic data were analyzed using a custom elastography algorithm. First, the two-dimensional frame-to-frame displacements of small kernels (0.3 by 1.0 mm) were estimated from the RF data using a statistical cross-correlation approach [5]. A triangular element mesh (edge length of 0.5 mm) was then overlaid onto the visible tendon, and nodal displacements were computed by averaging nearby pixel displacements. Nodal displacements were integrated over time in both the forward and backward directions, and the nodal trajectories were taken as the weighted average of the integration results. Small strain analysis of the nodal trajectories was used to estimate cumulative strain in the along-fiber and transverse directions, with the reference nodal positions chosen as those from the most plantarflexed position.

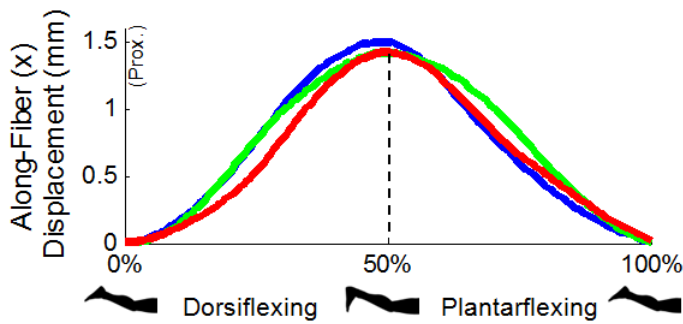


**Figure 2.** Average tendon motion within image window across successive cycles for one subject.

## RESULTS

Highly consistent measures of tissue motion were obtained across repeat cycles in both the along-fiber and transverse directions (Fig. 2). The resulting spatial strain distributions exhibited greater strain along the superficial edge of the tendon at the time of peak dorsiflexion (Fig. 3). When the tendon was equally divided into superficial and deep regions, the average superficial strains were from 1.3 to 3.3 times higher than the average strains in the deeper tissue (Fig. 4).

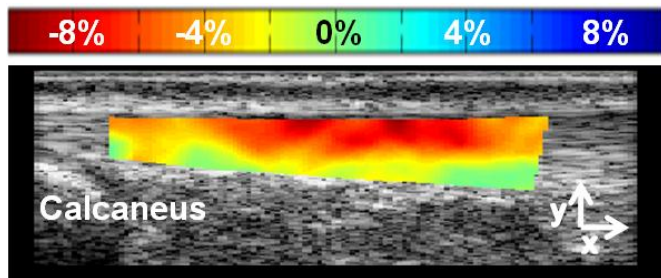


**Figure 3.** Sample image of transverse (y) strain distributions within the Achilles tendon at the time of peak dorsiflexion.

## DISCUSSION

Ultrasound elastography is traditionally used to track tissue motion along the transducer beam direction [4]. High resolution measures of tissue displacement can be obtained by utilizing the phase of raw RF signals to track the movement of speckle patterns. In this study, we leveraged this capability to assess regional variations in tendon strain during cyclic loading of the plantarflexors. As hypothesized, the largest strains were observed along the superficial edge of the tendon. This result could reflect the slightly greater moment arm of the superficial tissue, which requires greater length excursion during dorsiflexion than the deeper tissue. Another potential contributing factor to the strain

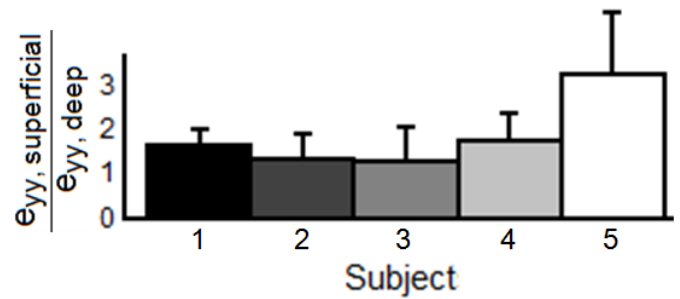


**Figure 4.** Ratio of the average superficial strain normalized to the average deep tissue strain.

variations is the relative loading of the gastrocnemius and soleus muscles, which insert onto the superficial and deep portions of the tendon respectively. Varying knee angles would theoretically modulate the relative loading of the gastrocnemius, and provide a mechanism to assess the possible bimuscular loading contributions to nonuniform strains in the Achilles tendon.

Ultrasound elastography may be useful for assessing biomechanical aspects of tendon damage. For example, Achilles tendinosis is often reported to originate on the deep edge of the tendon [6], proximal to the calcaneal insertion. In our study, this region actually exhibited relatively low strains (Fig. 3). While counter-intuitive, it has recently been suggested that localized tendon tissue damage could arise from a stress shielding phenomenon in which under-loaded tissue is insufficiently conditioned to handle overload conditions [3]. Elastographic analysis provides an innovative means to investigate this conjecture. Further, this quantitative imaging technique may enable the tracking of tissue strain variations that occur with remodeling and treatment following injury.

## REFERENCES

1. Fukunaga, T, et al., *Proc Biol Sci* **268**, 229-33, 2001.
2. Blemker, SS, et al., *J Biomech* **38**, 657-665, 2005.
3. Maganaris, CN, et al., *Sports Med* **34**, 1005-17, 2004.
4. Varghese, T, *Ultrasound Clinics* **4**, 323-338, 2009.
5. Ophir, J, et al., *Ultrasonic Imaging* **13**, 111-134, 1991.
6. Gibbon, WW, et al., *J Clin Ultrasound* **28**, 61-6, 2000.

## ACKNOWLEDGEMENTS

NIH AR056201, Ryan DeWall, Nathan Kleinhans, Kenneth Lee, Ray Vanderby, Tomy Varghese.

# SEX DIFFERENCES IN PLANTAR FLEXION STRENGTH MAY PREDISPOSE MIDDLE AGE FEMALES TO FALLS

<sup>1</sup>Nicole Chimera and <sup>2</sup>Kurt Manal

<sup>1</sup>Northern Arizona University, Flagstaff, AZ, USA

<sup>2</sup>University of Delaware, Newark, DE, USA

email: [Nicole.Chimera@nau.edu](mailto:Nicole.Chimera@nau.edu) web: [www.nau.edu](http://www.nau.edu)

## INTRODUCTION

It is well documented that with increased age there are concomitant decreases in muscular mass and strength [1]. Furthermore, gender appears to significantly influence the ability to produce force, with females generally demonstrating lower absolute strength than males across muscle groups [1]. Additionally, it has been documented that elderly females are weaker than males even when strength is normalized for body weight [2].

The risk for fall related injury increases with age, and older females have an increased rate of falls compared to older males [3]. Strength deficits have been implicated as risk factors for falls, with fallers reportedly exhibiting significant plantar flexion weakness compared to non-fallers [4]. While these contributions to the literature are extremely important and relevant to understand how plantar flexor muscle strength is related to falls, there is a vital part of the literature that is lacking. Plantar flexor muscle strength is almost exclusively tested in full knee extension. In this position we are unable to isolate soleus muscle strength.

The soleus is a postural muscle; therefore strength deficits could have significant implications on balance and stability. Performing ankle plantar flexion with the knee flexed to 90° minimizes the contribution of the gastrocnemius [5], allowing for isolated soleus muscle function. It is important to understand if sex differences occur when looking specifically at the soleus muscle as it may provide insight into the increased rate of falls in females. Further, it is important to understand if this postural muscle exhibits differences between sexes during middle age as this may indicate that females are predisposed to falls at an earlier age.

If middle aged women demonstrate significant weakness compared to middle aged men, perhaps interventions should be implemented earlier in life. Therefore, the purpose of this study was two-fold. First, to investigate if soleus muscle deficits are apparent in middle age females compared to middle aged males. Secondly, to investigate if plantar flexion strength deficits exist between sexes in the middle aged population.

## METHODS

Data was collected from 25 healthy (12 male and 13 female) volunteers (Table 1). Subjects were between 40 and 65 years of age and were free of any unresolved musculoskeletal or neurological disorder by self-report. The test leg was chosen at random (female: 6 right legs, 7 left legs; males: 5 right legs, 7 left legs). Subjects also had to have at least 5° of ankle dorsiflexion with full knee extension as measured with a bi-plane goniometer. This device was used instead of a standard goniometer because it enables proper subtalar joint neutral positioning, which allows for true measurement of talocrural ankle dorsiflexion; and it has higher reliability than a standard goniometer [6].

The Biodex System 3 was used to measure isometric ankle plantar flexion strength with full knee extension (triceps surae) and 90° of knee flexion (soleus). For both measures the ankle position was held constant in maximum available dorsiflexion. Plantar flexion strength data was normalized by body mass to account for differences known to exist in subjects of varying sizes. The Foot and ankle Ability Measure (FAAM) was used to evaluate differences in self-reported function between sexes. Independent sample t-tests were used to compare differences between sexes.

## RESULTS AND DISCUSSION

There were no differences in age; however males were significantly larger than females (Table 1). Females were significantly weaker than males in ankle plantar flexion strength with knee extension (Figure 1). They were also significantly weaker in ankle plantar flexion strength with knee flexion (Figure 1). These differences persisted even though strength data was normalized for body mass (Figure 2). There were no significant differences between sex for self-reported rating of function or global rating of function (Table 1).

### Absolute Isometric Plantar Flexion

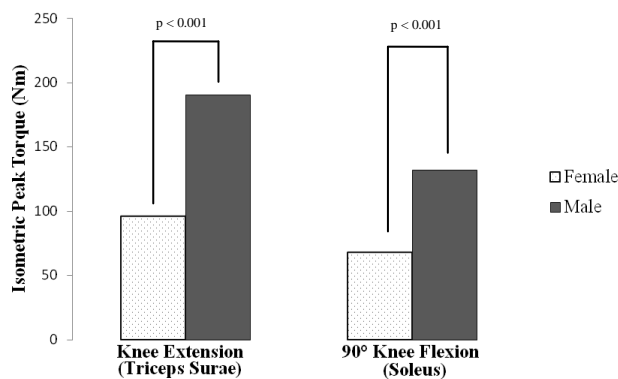


**Figure 1:** Absolute plantar flexion strength with knee flexion and full knee extension.

The difference between middle aged males and females in absolute plantar flexion strength was expected. It was however, interesting to note that these differences persisted even when normalized for body mass. This was contrary to previous reports in this age group, in which plantar flexion strength deficits did not exist between sexes when normalized for body size [1]. However, our results are similar to reports that elderly females were significantly weaker than elderly males in plantar flexion strength when data were normalized for size [2].

We believe this is the first report to demonstrate that middle aged females are significantly weaker than middle aged males in both soleus and triceps

### Normalized Isometric Plantar Flexion

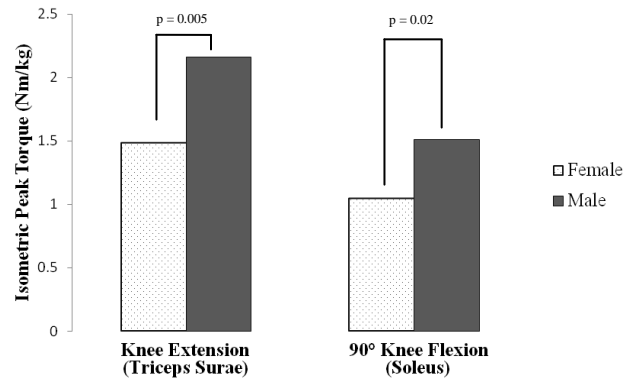


**Figure 2:** Normalized plantar flexion strength with knee flexion and full knee extension.

surae isometric muscle strength. Further, this may indicate that these females are predisposed to falls at an earlier age. However, additional data collection, including isokinetic strength, balance, and posture assessment, is needed to truly assess this risk.

## CONCLUSIONS

Our data indicate that women are weaker than males even when plantar flexion strength is normalized for differences in body size. Further, isolating the soleus muscle revealed significant weakness in females. This has clinical implications for an increased risk of fall in middle aged females, which may be due to postural muscle control deficits.

## REFERENCES

1. Frontera WR, et al. *J Appl Physiol* **71**, 644-650, 1991.
2. Basseij EJ, et al. *Clin Sci (Lond)* **74**, 85-89, 1988.
3. CDC, *NCIPC*, 2008.
4. Pijnappels M, et al. *Eur J Appl Physiol* **102**, 62-69, 2008.
5. Cresswell AG, et al. *Exp Brain Res* **105**, 283-290, 1995.
6. Donnery MS & Spencer RB. *J Am Pod Med Assoc* **78**, 348-351, 1988.

**Table 1:** Gender differences in demographics and self-reported level of function.

|                | Age        | Weight (kg) | Height (m) | FAAM Global (%) | FAAM Function (%) |
|----------------|------------|-------------|------------|-----------------|-------------------|
| <b>Male</b>    | 49.2 ± 7.9 | 90.1 ± 23.2 | 1.8 ± 0.1  | 99 ± 3          | 98 ± 5            |
| <b>Female</b>  | 47.8 ± 8.3 | 66.7 ± 13.3 | 1.6 ± 0.1  | 100 ± 0         | 100 ± 0           |
| <b>p-value</b> | 0.67       | p < 0.001*  | p < 0.01*  | 0.30            | 0.35              |

\* denotes statistical significance between males and females.

# IMPROVEMENTS IN JOINT KINETICS IN RETURN TO COMPETITION FROM ACL INJURY AND RECONSTRUCTION: A CASE STUDY

Loren ZF Chiu, Megan A Bryanton, Amy N Moolyk, Laura Newstead and Michael D. Kennedy

Neuromusculoskeletal Mechanics Research Program, University of Alberta, Edmonton, AB, Canada  
email: [Loren.Chiu@ualberta.ca](mailto:Loren.Chiu@ualberta.ca) web: [www.ualberta.ca/~loren1/NMRP.htm](http://www.ualberta.ca/~loren1/NMRP.htm)

## INTRODUCTION

Anterior cruciate ligament (ACL) injuries present a challenge for rehabilitation professionals. Individuals who incur an ACL injury and return to activity in competitive sports have a higher risk of re-injury [5]. Further, many athletes do not return to the same level of performance as before injury.

The strength of the quadriceps influences successful return to activity and competitive play following ACL reconstruction. It is theorized that a large proportion of individuals, particularly female athletes, develop long-term inhibition of the quadriceps [2,4]. Quadriceps strength has also been associated with jumping performance, where an increase in quadriceps strength has a greater influence on jump height than increasing hip extensor or ankle plantar-flexor strength [3].

These studies clearly indicate the importance of the quadriceps for athletes returning to activity and competitive performance following ACL injury. However, the specific muscular deficits and how they influence the muscles functioning during motor tasks remains unclear. In jumping, performance is not solely dependent on the maximum torque but also the total impulse generated by the knee extensors. The purpose of this report is to describe changes in joint kinetics in an ACL-reconstructed individual training to return to competitive play.

## METHODS

The participant in this case study was an 18 year old female varsity volleyball player. She tore her right ACL in May and had reconstructive surgery using an allograft in September. The initial data collection session was in December, 15 weeks following reconstructive surgery. This data collection was part of a larger study investigating the relation between knee extensor strength and vertical jump performance in volleyball players.

The second data collection was 10 weeks later. In these 10 weeks, she was participating in a strength and conditioning program aimed at improving performance and reducing injury risk. The training program included heavy squatting and weightlifting exercises, common exercises used in performance enhancement training programs for volleyball players. All training was supervised by an experienced weightlifting coach.

Both data collection sessions involved 3D motion capture using a 6-camera optoelectronic system (Qualisys) and two 6-component force platforms (AMTI). The athlete performed 4 maximum height countermovement jumps with 2 hand reach. Retro-reflective tracking and calibration markers were placed on her lower extremity. Calibration markers were used to define proximal and distal ends of segments and tracking markers consisted of clusters of 3 (foot) or 4 (thigh and shank) markers fixed on rigid thermoplastic plates. Data were processed in Visual 3D using rigid body modeling and inverse dynamics. Data were analyzed graphically and numerically. For graphical analysis, time series data was normalized from 0% (initiation of countermovement) to 100% (take-off). Numerically, peak and average net joint moment (NJM) were determined for the hip and knee extensors, and ankle plantar-flexors, as well as the time of the jump and time to peak knee extensor NJM. NJMs were expressed as internal moments. The differences between sessions were compared using effect sizes.

## RESULTS AND DISCUSSION

Vertical jump height increased from 13 inches to 14 inches, while body mass increased from 71.8kg to 73.8kg. The increase in body mass was expected as a result of participation in the strength and conditioning program, where muscle hypertrophy would occur. That she could jump higher although

weighing more suggests she improved the capabilities of her lower extremity to perform work at a high rate.

Graphical analysis of NJM-time curves indicated: 1) an increased area under the curve (i.e. net joint impulse) at the ankle, knee and hip and 2) increased consistency between repetitions.

For session 2 versus 1, peak NJM increased at the right ankle from  $-93\text{N}\cdot\text{m}$  to  $-101\text{N}\cdot\text{m}$  ( $\text{ES}=1.43$ ) and at the right knee from  $99\text{N}\cdot\text{m}$  to  $107\text{N}\cdot\text{m}$  ( $\text{ES}=1.13$ ). Peak hip extensor NJM decreased slightly from  $-100\text{N}\cdot\text{m}$  to  $-96\text{N}\cdot\text{m}$  ( $0.59$ ). Similar changes were observed in the left limb. Peak left ( $107\text{N}\cdot\text{m}$ ) and right ( $111\text{N}\cdot\text{m}$ ) knee extensor NJM were comparable in the second session.

For session 2 versus 1, average NJM increased at the right ankle from  $-40\text{N}\cdot\text{m}$  to  $-56\text{N}\cdot\text{m}$  ( $\text{ES}=4.24$ ), the right knee from  $56\text{N}\cdot\text{m}$  to  $62\text{N}\cdot\text{m}$  ( $\text{ES}=1.21$ ) and the right hip from  $-45\text{N}\cdot\text{m}$  to  $-62\text{N}\cdot\text{m}$  ( $\text{ES}=2.58$ ). Total jump time decreased from  $0.95\text{s}$  to  $0.90\text{s}$  ( $\text{ES}=0.87$ ) and time to peak knee extensor NJM decreased from  $0.46\text{s}$  to  $0.26\text{s}$  ( $\text{ES}=3.53$ ).

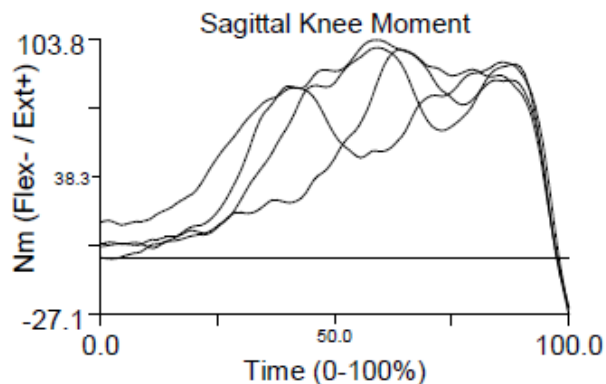


Fig. 1 – Right knee extensor NJM from session 1.

Taken together, this data suggests the athlete's ability to utilize her hip and knee extensors, and ankle plantar-flexors increased following the 10-week training program. Further, training adaptations manifested as an increase in peak and average ankle plantar-flexor and knee extensor NJM, increase in the average hip extensor NJM, and faster time to peak NJM. In combination with the graphical analysis, these data indicate training elicited a change in the manner in which NJM were generated at the ankle, knee and hip. Specifically, the moment-time curves became more "U" shaped. Analysis of the vertical ground reaction force-time curve also indicated a similar change. Proficient

jumpers demonstrate a "U" as opposed to "V" shaped ground reaction force-time curve is [1].

Perhaps the most important adaptation was the increase in consistency in the moment-time curves. In particular at the knee, the pattern of NJM generation was varied across the 4 jumps performed in the first session (Fig. 1), which was not observed in the second session (Fig. 2).

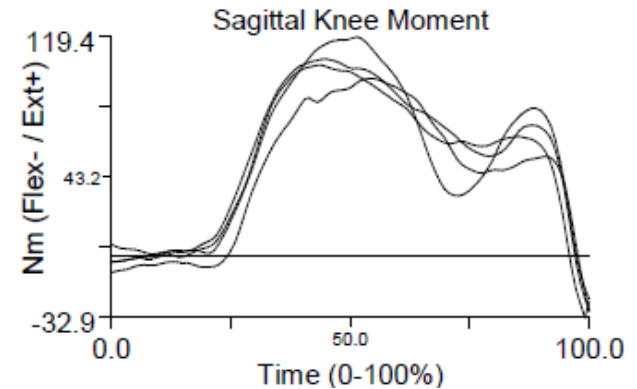


Fig. 2 – Right knee extensor NJM from session 2.

## CONCLUSIONS

We present case study data of a female volleyball player training to return to competitive play. Following 10 weeks of strength and conditioning training her jumping performance increased. Adaptations manifested as improved ability for the hip and knee extensors, and ankle plantar-flexors to generate impulse. These data provide insight into the muscular deficits in an individual with ACL injury and the effects of training. An understanding of these deficits is important for optimizing rehabilitation and return to competition training protocols.

## REFERENCES

1. Garhammer J, and Gregor R. *J Appl Sport Sci Res* **6**, 129-134, 1992.
2. Lewek M, et al. *Clin Biomech* **17**, 56-63, 2002.
3. Nagano A, and Gerritsen KGM. *J Appl Biomech* **17**, 113-128, 2001.
4. Palmieri-Smith RM, et al. *Clin Sports Med* **27**, 405-424, 2008.
5. Shelbourne KD, et al. *Am J Sports Med* **37**, 246-251, 2009.

## ACKNOWLEDGEMENTS

Data collected in this case study was part of an investigation supported by a Sports Science Association of Alberta grant.

# EFFECT OF WALKING SPEED ON INTER-JOINT COORDINATION DIFFERS BETWEEN YOUNG AND ELDERLY ADULTS

Shiu-Ling Chiu and Li-Shan Chou

Department of Human Physiology, University of Oregon, Eugene, Oregon 97403, USA.

email: [chou@uoregon.edu](mailto:chou@uoregon.edu), web: <http://biomechanics.uoregon.edu>

## INTRODUCTION

Human gait requires fine coordination among multiple joints to achieve a precise end point motor control [1]. Walking speed has been identified as a factor influencing individual joint kinematics and kinetics [2]. Significant age-related differences in gait measures are also frequently reported [3]. Further, elderly adults are found to have proprioceptive deficits in position and motion senses, which are critical in planning and updating the inter-joint coordination when performing activities of daily living [4]. However, age-related differences in the inter-joint coordination have not been well examined. A better understanding of the effect of walking speed on the inter-joint coordination may provide insights into the essential modulation of neuromuscular control. The purpose of this study was to investigate the effects of walking speed and age on the pattern and variability of inter-joint coordination.

## METHODS

Twenty adults were recruited and divided into two groups in this study. Ten healthy young subjects (5 men, 5 women, age =  $24.7 \pm 4.1$  yrs, BMI =  $22.1 \pm 1.5$  kg/m<sup>2</sup>) and 10 healthy elderly subjects (5 men, 5 women, age =  $71.6 \pm 5.2$  yrs, BMI =  $26.0 \pm 2.9$  kg/m<sup>2</sup>). An eight-camera motion analysis system (Motion Analysis Corp., Santa Rosa, CA) was used to collect the whole body motion data during level walking. All subjects were asked to walk along a 10-m walkway with three different self-selected walking speeds, including a comfortable (preferred), faster or slower speed. A total of 29 reflective markers were placed on bony landmarks. Joint kinematics of the bilateral lower extremities was calculated by using OrthoTrak kinematic analysis software (Motion Analysis Corp).

Continuous related phase (CRP), derived from the phase portraits of two adjacent joints (hip-knee or knee-ankle), was used to investigate the inter-joint coordination pattern and variability [5]. Walking speed effects on CRP patterns were examined by using cross-correlation measures and root-mean-square (RMS) difference to compare the ensemble mean curves of the faster or slower to preferred speed walking. The variability of coordination for each subject was calculated as the average standard deviation of all points on the ensemble CRP curve over a gait cycle, namely the deviation phase (DP). A mixed-model analysis of variance with repeated measures was used to analyze the effects of groups and speeds on cross correlation, RMS, and DP values. Significance level was set at 0.05.

## RESULTS AND DISCUSSION

All subjects were able to walk significantly slower or faster than their preferred speed (Table 1). No significant group differences were detected at each of the corresponding walking speed. When asked to walk faster, young and elderly adults walked with 126.9% and 126.0%, respectively, of their preferred walking speeds. When walked slower, young and elderly adults walked with 70.8% and 83.0%, respectively, of their preferred walking speeds.

For hip-knee CRP patterns, there was a marginal group by speed change interaction ( $p=0.07$ ). For young subjects, RMS difference between the preferred and slower speeds was significantly greater than that between the preferred and faster speeds (Fig. 1). However, this walking speed induced difference was not observed in the elderly group. When changing from preferred to slower walking speed, the young group also exhibited a significantly greater RMS difference in hip-knee CRP patterns than the elderly group. Cross-correlation measures in both groups were overall strong for hip-knee CPR patterns (average  $r^2=0.93$ ),

but moderate for knee-ankle CRP patterns (average  $r^2=0.63$ ) (Fig. 2). For hip-knee CRP patterns, the elderly group demonstrated significantly greater correlation coefficients between walking speeds than the young group.

Both groups demonstrated greater hip-knee and knee-ankle DP values when walking slower, as compared to the preferred or faster speed (Table 1). In general, when compared to young adults, elderly adults showed greater DP values in slow speed but smaller DP values in preferred and fast speeds. Significant gait velocity effects were detected in hip-knee DP values between slower and faster speeds ( $p < 0.01$ ). No significant group differences were detected for all three walking speeds.

## CONCLUSIONS

Our results suggested that gait velocity has significant effects on the pattern and variability of inter-joint coordination, especially the hip-knee coordination. When asked to walk with different speeds, elderly adults seem to use conservative control strategies by maintaining a similar inter-joint coordination. Such differences in modulation and adaptability between elderly and young adults may be associated with their preferred walking speed and age-related mobility impairments.

## REFERENCES

1. Winter, DA. *Phys Ther*. **72**, 45-53, 1992.
2. Chung, MJ, et al. *Gait Posture* **31**, 131-135, 2010.
3. Winter, DA, et al. *Phys Ther* **70**, 340-347, 1990.
4. Goble, DJ, et al. *Neurosci Biobehav Rev* **33**, 271-278, 2009.
5. Burgess-Limerick, R, et al. *J Biomech* **26**, 91-94, 1993.

**Table 1:** DP values for CRP curves of young and elderly adults.

| Walking speed       | Young           |                 |                 | Elderly         |                 |                 | p values |
|---------------------|-----------------|-----------------|-----------------|-----------------|-----------------|-----------------|----------|
|                     | Slow            | Preferred       | Fast            | Slow            | Preferred       | Fast            |          |
| Gait Velocity (m/s) | 1.01<br>(0.14)  | 1.42<br>(0.12)  | 1.80<br>(0.18)  | 1.08<br>(0.19)  | 1.30<br>(0.17)  | 1.63<br>(0.19)  | < 0.001* |
| Hip-Knee            | 12.34<br>(6.1)  | 11.47<br>(5.36) | 8.72<br>(2.68)  | 12.63<br>(6.34) | 8.87<br>(10.17) | 8.05<br>(2.41)  | < 0.01 * |
| Knee-Ankle          | 20.86<br>(5.33) | 19.57<br>(8.29) | 21.09<br>(7.09) | 23.10<br>(9.38) | 18.99<br>(3.61) | 17.73<br>(7.77) |          |

\* speed effect.

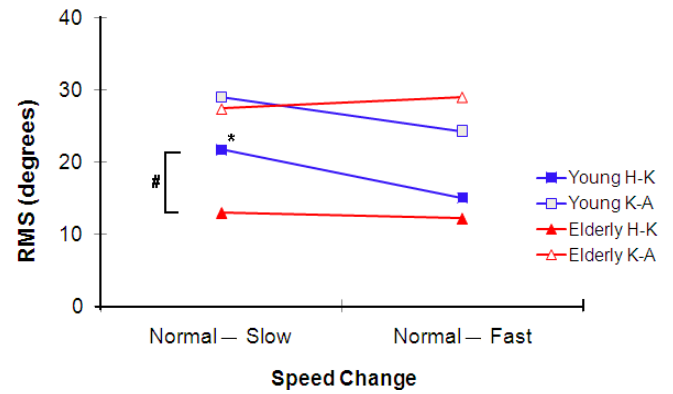


**Figure 1:** RMS difference (degrees) for CRP patterns between different walking speeds (\* speed effect; # group effect).

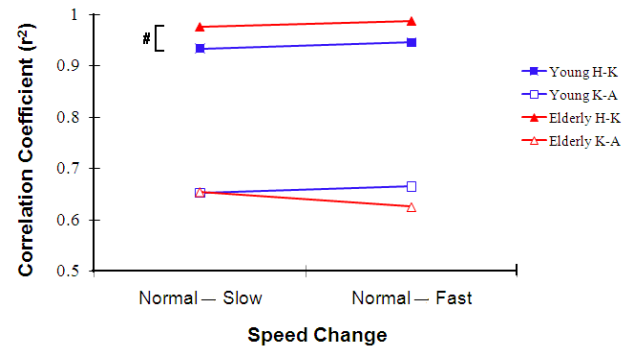


**Figure 2:** Cross-correlation ( $r^2$ ) for CRP patterns between different walking speeds (# group effect).

## ACKNOWLEDGEMENTS

Assistances from Hao-Ling Chen, Vipul Lugade, and Chi-Jui Chen are greatly appreciated.

# DO CALCANEAL MOTION AND TIBIAL TORSION INFLUENCE LEG AXIAL ROTATION DURING WEIGHT-BEARING DORSIFLEXION?

Michael G. Chizewski, Kaylynn S. Shewaga, Samantha N. Porter, and Loren Z. F. Chiu

University of Alberta, Edmonton, AB, Canada  
web: [www.ualberta.ca/~loren1/NMRP.htm](http://www.ualberta.ca/~loren1/NMRP.htm)

## INTRODUCTION

The sub-talar joint is often described as a mitered-hinge. In theory, calcaneal eversion, through the morphology of the talo-crural articulation, would result in internal rotation of the leg. However, our preliminary analyses of the 3D rotation of the leg during squatting and jumping tasks suggest two populations – one where the leg internally rotates and the other which externally rotates. From the mitered-hinge concept, it may be speculated that individuals whose leg externally rotates have calcaneal inversion occurring.

An alternate hypothesis that may explain the difference in leg rotation is tibial torsion angle. Tibial torsion describes the offset between the tibio-femoral and talo-crural joints' flexion-extension axes in the transverse plane (Fig. 1). Differences in tibial torsion have been reported between men and women [1] and may influence gait mechanics [2]. Greater external tibial torsion could theoretically influence the transverse plane rotation of the leg segment.

The purpose of this research was twofold. First, the influence of calcaneal motion in three planes on leg rotation in the transverse plane during weight-bearing dorsiflexion was studied. Second, this research investigated whether differences between internally and externally rotating legs during weight-bearing dorsiflexion could be explained by tibial torsion angle.

## METHODS

Healthy women (n=25; age=25.2±5.3 years) and men (n=23; age=25.1±5.4 years) volunteered to participate in this investigation. Retro-reflective markers in a 6-degree of freedom configuration

were recorded by a 6-camera motion capture system (Qualisys) at 120 Hz sampling frequency.

Markers were placed on the medial and lateral tibial condylar prominences and the medial and lateral malleoli to define the leg segment. A four marker tracking cluster in a square configuration was fixed to the lateral side of the leg. Markers were placed on the medial, lateral, and posterior calcaneus, with additional markers on the distal great toe, the heads of metatarsals I and V, and the dorsum of the foot (at the joint between second and third cuneiforms).

Over a minimum of three trials, participants were asked to maintain a vertical trunk while flexing at the hip and knee, and dorsiflexing at the ankle to a position of maximum voluntary dorsiflexion. The distance between the greater trochanters of the femur was used to align the second toes of each foot in a standardized forward facing position.

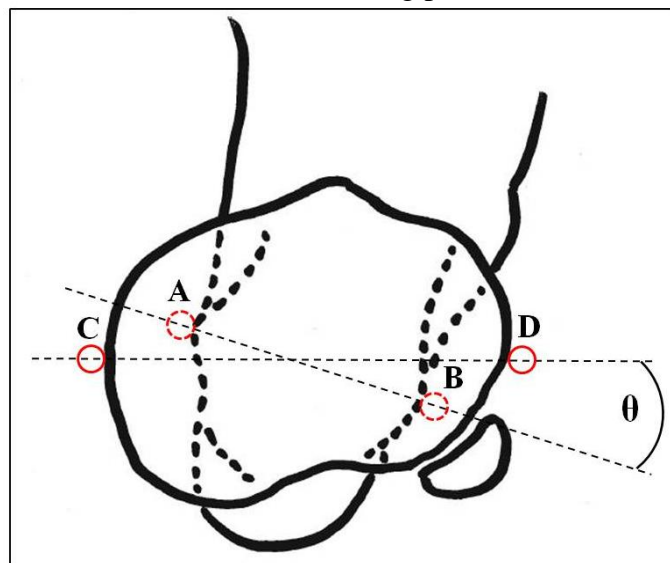


**Fig. 1:** Tibial torsion angle ( $\theta$ ) (superior view) [1]. Markers/anatomic landmarks: A (medial malleolus); B (lateral malleolus); C (medial tibial condyle); D (lateral tibial condyle).

The leg (tibia and fibula) and calcaneus were modeled as rigid segments in Visual3D software. Rotations of the leg and calcaneus were determined relative to the laboratory using a ZYX Cardan sequence [3]. Mean calcaneal range of motion to maximum ankle dorsiflexion was calculated for three planes. Tibial torsion angle was calculated from measuring the offset in the transverse plane between the axis passing through the proximal tibial condyle markers and the axis passing through the distal markers on the malleoli (Fig. 1).

Participants were grouped by whether their leg internally or externally rotated. Participants were grouped for their left and right leg separately, as a small number of participants (n=6) had one leg internally rotate while the other externally rotated. Tibial torsion and calcaneal rotation in the sagittal, frontal, and transverse planes were compared between the internal and external leg rotators using unpaired two-tailed *t* tests.

## RESULTS AND DISCUSSION

Anterior tilt of the calcaneus (sagittal plane) and external rotation of the calcaneus (transverse plane) were not significantly different between internal and external rotators (Table 1). Significant differences ( $p < 0.01$ ) were found for calcaneal eversion (frontal plane), with externally rotating legs demonstrating greater calcaneal eversion than those that internally rotated ( $6.60 \pm 2.47$  versus  $4.66 \pm 2.46$ ). The motion of the calcaneus in the sagittal and transverse planes does not appear to influence axial rotation of the leg. In the frontal plane, calcaneal eversion appears to be a factor in whether the leg internally or externally rotates. However, the greater calcaneal eversion associated with externally rotating legs opposes the mitered-hinge theory.

For the legs that internally rotated during the weighted dorsiflexion task, tibial torsion angles were  $11.56 \pm 6.24$  and  $11.65 \pm 5.56$  in left and right

limbs respectively. For legs that externally rotated, tibial torsion angles were  $19.93 \pm 9.57$  and  $18.89 \pm 4.03$  in left and right limbs respectively. Significant differences were noted for left ( $p < 0.001$ ) and right ( $p < 0.0001$ ) tibial torsion angles when comparing internal versus external leg rotators. This data indicates that tibial torsion angle plays a role in whether a leg internally or externally rotates during weighted dorsiflexion.

## CONCLUSIONS

The direction of axial leg rotation will affect loading on the structures of the knee and potentially the hip [2]. Axial rotation of the tibia has been implicated as a factor in lower extremity injuries, for example, anterior cruciate ligament rupture. Research of injuries where tibial rotation is a factor should consider tibial torsion as a non-modifiable risk factor.

It is not known what causes differences in external tibial torsion. Further study must be devoted to identifying genetic or environmental conditions which may contribute to the magnitude of external tibial torsion. Additionally, it is unclear where in the leg segment the tibial torsion is created.

Our research demonstrates that an anatomical factor influences axial rotation of the leg. The task in this study required the foot to be in contact with the ground. However, it is important to study how tibial torsion influences leg and foot mechanics in non-weight-bearing situations, as well as during the transition from non-weight-bearing to weight-bearing tasks such as during gait.

## REFERENCES

1. Yoshioka Y, et al. *J Orthop Res* **7**, 132-137, 1989.
2. Hicks, J, et al. *Gait Posture* **26**, 546-552, 2007.
3. Baker, R. *Gait Posture* **13**, 1-6, 2001.

**Table 1:** Comparison of calcaneal rotation (in three planes) and tibial torsion angles of internally (IR) and externally (ER) rotating legs. For calcaneal rotation: positive = anterior tilt (X), inversion (Y), and internal rotation (Z). Tibial torsion angle: positive = increasing external tibial torsion.

|       | Calcaneus-X (deg) |          | Calcaneus-Y (deg) |          | Calcaneus-Z (deg) |          | Tibial Torsion (deg) |          | n  |    |
|-------|-------------------|----------|-------------------|----------|-------------------|----------|----------------------|----------|----|----|
|       | IR                | ER       | IR                | ER       | IR                | ER       | IR                   | ER       | IR | ER |
| Left  | 10.3±2.5          | 10.3±2.7 | -4.7±2.7          | -6.4±2.5 | -1.2±0.9          | -1.6±1.6 | 11.6±6.2             | 19.9±9.6 | 29 | 18 |
| Right | 10.7±3.0          | 10.4±2.6 | -4.7±2.7          | -7.1±2.5 | -1.6±1.2          | -2.2±1.4 | 11.6±5.6             | 18.9±4.0 | 27 | 20 |

# UNDERSTANDING CONTACT PRESSURE DISTRIBUTION IN THE ANKLE AND SUBTALAR JOINT DURING MOTION IN THE SAGITTAL PLANE

<sup>1</sup>Julie Choisine, <sup>1</sup>Stacie I. Ringleb, <sup>1</sup>Rajesh Paranjape, <sup>1</sup>Sebastian Y. Bawab, <sup>2</sup>Claude D. Anderson

<sup>1</sup>Mechanical Engineering, Old Dominion University, Norfolk, VA, USA

<sup>2</sup>Department of Orthopaedic Surgery, Naval Medical Center Portsmouth, Portsmouth, VA USA  
email: [SRingleb@odu.edu](mailto:SRingleb@odu.edu)

## INTRODUCTION

Intra-articular contact stress distribution in the ankle is important to understand and prevent osteoarthritis. Data quantifying talocrural joint contact area and pressure will be helpful for the design of total ankle replacement. Also, mean and peak pressure data from a cadaver specimen might help validating finite element models as high inter-specimen variability exist in ankle joint contact distribution [1].

While intra-articular pressure distributions in the ankle and subtalar joint have been measured, more data are needed. Some studies did not apply load on muscles crossing the ankle joint that may alter the contact area as well as the pressure distribution [1-3]. Suckel et al. [4] simulated stance phase gait with tendon loading based on course EMG activation patterns for normal gait [5]. Potthast et al. [6] looked at the contact stress distribution of the talocrural joint with varying axial and extrinsic tendon loading, but did not apply motion to the specimens during the experiment. Anterior and posterior articulation of the subtalar joint pressure distribution were analyzed during plantar - dorsiflexion and inversion-eversion motion applied to the foot [7], but there were no tendon or axial loads applied. Understanding the pressure distribution in the ankle and subtalar joint through the sagittal plane range of motion using tendon and axial loads similar to those used in gait simulation may help to improve our understanding the pathogenesis of joint disorders.

The purpose of this study was to evaluate contact pressure distribution in the ankle and medial subtalar joint for different position of the foot during flexion-extension motion with an axial and extrinsic tendon loads applied.

## METHODS

One left fresh-frozen cadaveric lower extremity was obtained and sectioned at the midpoint of the shank (age 74.3 years). The specimen was placed into a custom six degree-of-freedom positioning and loading device. Two pressure measure pads (Pliance ankle and pliance strip sensors: Novel, Munich, Germany) were inserted into the articular surface of the tibiotalar joint and over the posterior-lateral facet of the subtalar joint. The tendons of the tibialis anterior (TA), the tibialis posterior (TP), the extensor hallucis longus (EHL), the extensor digitorum longus (EDL), the flexor hallucis longus (FHL), the flexor digitorum longus (FDL), the peroneus brevis (PB), the peroneus longus (PL) and the Achilles tendon (AT) were clamped to external weights to simulate scaled forces similar to the stance phase of gait (Table 1). An axial load of 183N was applied to the tibia. Pressure data were collected in neutral, plantarflexion (5°, 10°, 15° and 20°) and dorsiflexion (5° and 10°). Angles were measured using a Goniometer.

**Table 1:** Tendon loading protocol for every position of the foot (in Newton).

| Tendons | Neutral | 5 DF  | 10 DF | 5 PF | 10 PF | 15 PF | 20 PF |
|---------|---------|-------|-------|------|-------|-------|-------|
| TA      | 29.3    | 7.3   | 0     | 7.3  | 0     | 0     | 0     |
| TP      | 11      | 7.3   | 11    | 7.3  | 11    | 11    | 14.65 |
| EHL     | 22      | 14.65 | 7.3   | 14.7 | 7.3   | 7.3   | 3.66  |
| EDL     | 22      | 14.65 | 7.3   | 14.7 | 7.3   | 7.3   | 3.66  |
| PB      | 0       | 0     | 3.66  | 0    | 3.66  | 3.66  | 3.66  |
| PL      | 0       | 0     | 29.3  | 0    | 29.3  | 29.3  | 29.3  |
| FH      | 0       | 0     | 22    | 0    | 22    | 22    | 22    |
| FD      | 0       | 0     | 3.66  | 0    | 3.66  | 3.66  | 3.66  |
| AT      | 73.2    | 73.2  | 73.2  | 73.2 | 73.2  | 73.2  | 73.2  |

## RESULTS AND DISCUSSION

For analysis, the talocrural joint was divided in four zones; anterior-lateral, anterior-medial, posterior-lateral and posterior-medial. The peak pressure was found in the anterior medial side of the ankle joint

for all positions except when the foot was in 10° dorsiflexion, the peak pressure moved to the anterior lateral part of the ankle. The maximum peak pressure was 2550 kPa, which occurred while the foot was in 5, 10 and 15 degrees of plantarflexion. From neutral to 15° plantarflexion, the mean pressure was higher in the anteromedial part and moved to the lateral side of the ankle in 20° plantarflexion and dorsiflexion (Figure 1). However, the majority of the contact area was found mostly in the posterior part of the joint for all positions of the foot.

The peak pressure of 1630 kPa was situated in the medial zone of the ankle joint contact area in neutral position, which is in the same range observed by Potthast et al. [6]. However, it is difficult to compare the other results as Potthast et al. did not apply motion to their foot. The normalized peak pressure in the talocrural joint was consistent with the results found by Suckel et al. [4] throughout their stance phase simulation. However, the non normalized results were not consistent as their ground reaction force were twice as high as the ones used in this study. The tibiotalar joint contact area results were consistent with Matricali et al. [1]. Results show that there is more contact area when the foot is 10° dorsiflexed than when it is 10° plantarflexed.

The force transmitted to the subtalar joint was 30% of the axial load applied to the shank in neutral position. Results showed a decrease in force and pressure during plantarflexion and an increase during dorsiflexion. Wang et al. [7] showed the

same force transmission pattern to the posterior facet of the subtalar joint during plantar-dorsiflexion. However, the subtalar joint contact area was higher in this study than in Wang et al. [7] study, which could explain the difference in pressure results. This difference in joint contact area can be explained with the load of tendon in the present study.

## CONCLUSION

This study showed that it is important to include axial and tendon loads when measuring contact pressure at the ankle and subtalar joints.

## REFERENCES

1. Matricali, G.A., *Clin Biomech* **24**, 117-120, 2009.
2. Rosenbaum, D., E. *J Biomech*, **36**, 81-86, 2003.
3. Michelson, J.D., *Foot Ankle Int*, **22**, 226-233, 2001.
4. Suckel, A., *Knee Surg Sports Traumatol Arthrosc*, **18**, 664-668, 2010.
5. Hurschler, C., *Foot Ankle Int*, **24**, 614-622, 2003.
6. Potthast, W., *Clin Biomech*, **23**, 632-639, 2008.
7. Wang, C.L., *J. Biomech.*, **28**, 269-279, 1995.

## ACKNOWLEDGEMENTS

The views expressed in this article are those of the author(s) and do not necessarily reflect the official policy or position of the Department of the Navy, Department of Defense, or the United States Government.

Research data derived from *Development of a Subject Specific Model of the Hindfoot*, an approved Naval Medical Center, Portsmouth protocol. One author is a military service member. This work was prepared as part of his official duties. Title 17 U.S.C. 105 provides that 'Copyright protection under this title is not available for any work of the United States Government.' Title 17 U.S.C. 101 defines a United States Government work as a work prepared by a military service member or employee of the United States Government as part of that person's official duties.

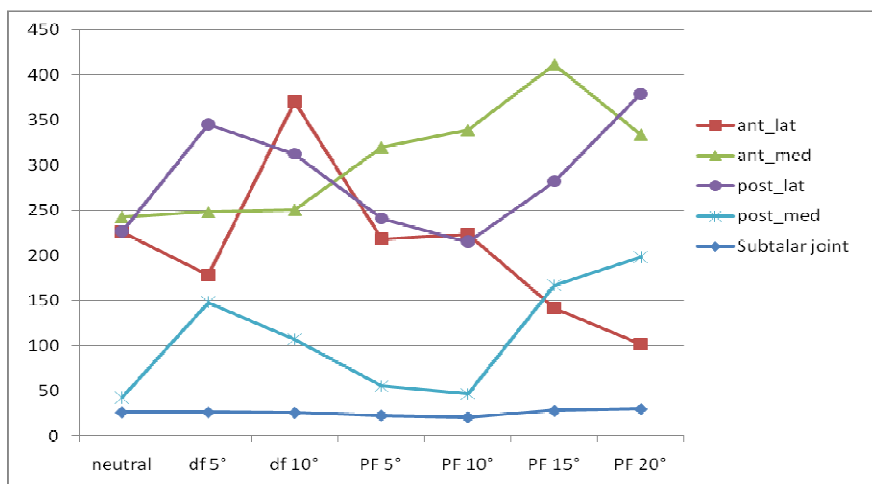


**Figure 1:** Mean pressure in kPa at the subtalar joint and at the ankle joint and in the antero-lateral, antero-medial, postero-lateral and postero-medial part of the joint

## How Flatfoot Deformity Affects Moment Arms

<sup>1</sup>Julie Choisne, <sup>1</sup>Stacie I. Ringleb, <sup>2</sup>Matthew B.A. McCullough, <sup>1</sup>Sebastian Bawab, <sup>3</sup>Kenton R. Kaufman, <sup>3</sup>Harold B. Kitaoka

<sup>1</sup>Old Dominion University, Norfolk, VA, USA

<sup>2</sup>North Carolina A&T State University, Greensboro, NC, USA

<sup>3</sup>Mayo Clinic, Rochester, MN, USA

email: SRingleb@odu.edu

### INTRODUCTION

Flatfoot deformity, also known as pes planus, is characterized by an increase in metatarsal-talar pronation [1] and loss of arch height. Complications of a flatfoot can cause inflammation in ligaments situated in the sole of the feet, Achilles and posterior tibialis tendinitis, shin splints, stress fractures in the lower leg, rigid flatfoot deformities and arthritis. Non congenital flatfoot can be caused by rupture of ligaments or tendons in the foot, a tight Achilles tendon, tarsal coalition or most commonly Posterior Tibial Tendon Dysfunction (PTTD).

Muscle moment arms represent a muscle's ability to produce a moment about a joint [2]. Determining the tendon moment arm in a flatfoot deformity is important in understanding muscle contribution during motion, in planning tendon altering surgery, evaluating treatment and modeling flatfoot behavior.

### METHODS

Five fresh frozen male cadaveric specimens were used (average age, 82 years). Each specimen was placed in a custom made six degree-of-freedom testing device that prescribed specific motions and measured tendon excursions [2]. Kinematics of the tibia, calcaneus, talus and first metatarsal were monitored using an optoelectronic motion tracking system (Optotrak Certus, Northern Digital Inc., Waterloo, Ontario, Canada). Tendon excursions and kinematics were collected with the Motion Monitor (Innovative Sports Training, Chicago, IL, USA) [2].

Data were collected in the intact and flatfoot condition, where the flatfoot deformity was created using the method developed by Kitaoka et al. [1].

In each condition, supination (20° plantarflexion, 20° inversion and 20° internal rotation), pronation

(20° dorsiflexion, 20° eversion and 20° external rotation) and plantarflexion (35°)/ dorsiflexion (25°) were applied in a sequential manner. The tendon excursion method [3] was used to calculate the moment arms of the tibialis anterior (TA), tibialis posterior (TP), the peroneus brevis (PB), the peroneus longus (PL) and the Achilles tendons using a custom program written in Matlab (The Mathworks, Natick, MA). These muscles were selected because they are most affected by flatfoot deformity. The moment arms were calculated with respect to a pre-determined range of motion taken over the midrange of supination-pronation (-13° to 9°) and plantar-dorsiflexion (-20° to 20°).

### RESULTS AND DISCUSSION

The kinematics were examined to ensure that a flatfoot condition occurred. In 4 of the 5 specimen flatfoot kinematics, similar to previously reported work, were observed [1]. Differences were observed in the moment arms between the intact and flatfoot conditions at the Achilles tendon during plantar-dorsiflexion (Figure 1) and in the TP, TA, PB and PL tendon during supination-pronation motion (Figure 2). Data are presented for a representative specimen.

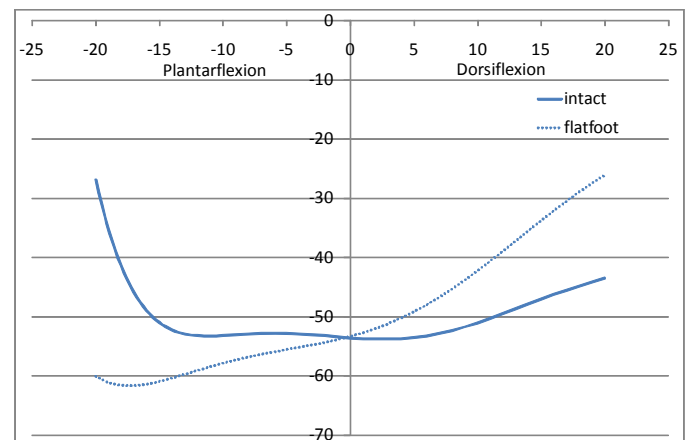


**Figure 1:** Moment arm of the Achilles tendon during plantarflexion-dorsiflexion in one specimen.

In the intact condition, the TA resulted in a pronating moment arm suggesting that it acted more as a dorsiflexor than an invertor during supination-pronation motion. The TP acted as an invertor, while the PB and PL acted as everter. Flatfoot deformity increased the moment arm during supination in the TA, PB and PL tendons, suggesting that they compensate for the changes in foot kinematics when the foot is supinated. Additionally, flatfoot deformity increased the plantarflexor function of the Achilles tendon at maximum plantarflexion.

High intra-specimen variability in the moment arm was observed in both the intact and flatfoot condition, especially in the tendons crossing more than 2 joints in the foot, like the TP, the PB and TL, with insertion sites in the foot bones. When the deformity is created, the variability was greater than the intact condition, suggesting that it may be beneficial to examine these data on a specimen specific basis. This suggests that using changes in moment arms as a tool for surgical decision-making may be difficult do to the fact that these muscles cross multiple joints and some have several insertion sites as well.

## CONCLUSIONS

The present study suggests that flatfoot deformity increases TA, TP, PL and PB effective moment arms during supination-pronation and Achilles tendon moment arm during plantarflexion. Data collected in vivo have shown changes in ankle moments and muscle activity in patients with stage II PTTD [4], which may be effected by these measured changes in effective muscle moment arms. Whenever these effective moment arms are applied to practical situations, we must also consider the fact that there is high inter-specimen variability, and the means may not apply to all cases.

## REFERENCES

1. Kitaoka HB, et al. *Foot & Ankle Int.* **19**, 447-451, 1998.
2. McCullough MBA, et al. *Foot & Ankle Int.* **32**, March 2011.
3. An KN, et al. *J. Biomech.* **16**, 419-425, 1983
4. Ringleb SI, et al. *Gait & Posture* **25**, 555-564, 2007.

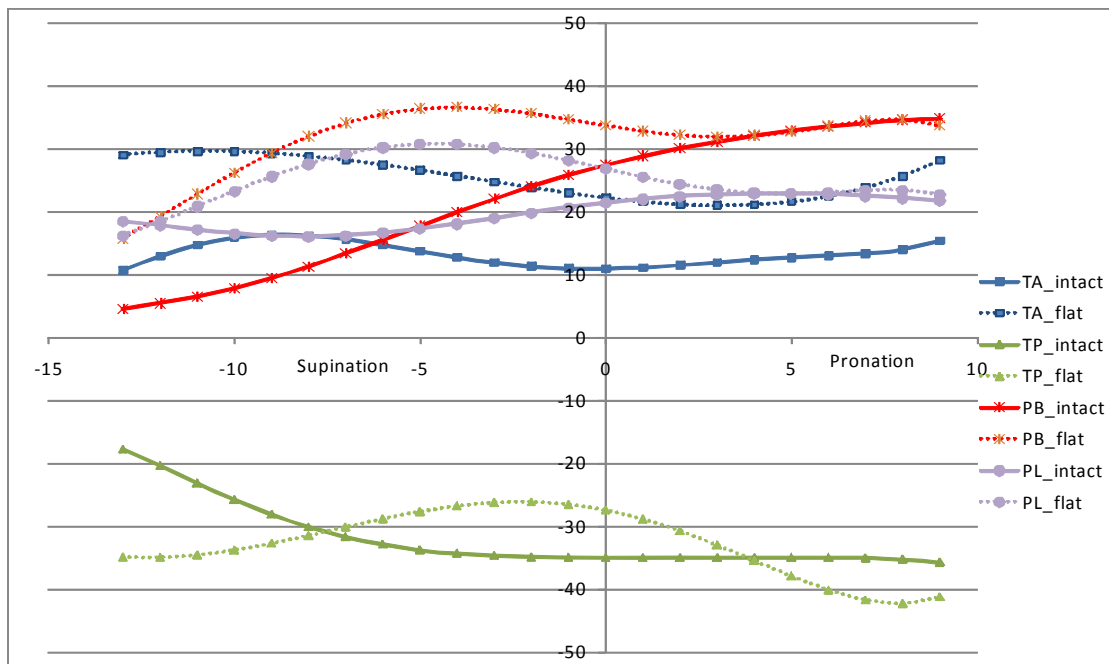


**Figure 2:** Moment arms of the tibialis anterior, tibialis posterior, peroneus brevis and peroneus longus tendons in the intact (solid line) and flatfoot (dashed line) conditions during supination-pronation motion applied at the foot for one specimen.

# DEVELOPMENT OF HUMERAL INTRAMEDULLARY FIXATION NAIL (HIFN) BASED ON KOREAN CADAVERIC TESTS

<sup>1</sup>ChangSoo Chon, <sup>2</sup>CheolWoong Ko and <sup>3</sup>JongKeon Oh

<sup>1</sup>Biomedical Engineering Institute, Solco Biomedical Co., Ltd., Pyungtaek, Korea

<sup>2</sup>Gerontechnology Center, Korea Institute of Industrial Technology, Chonan, Korea

<sup>3</sup>Department of Orthopedic Surgery, Korea University Guro Hospital, Seoul, Korea

email: [suhohoon@solco.co.kr](mailto:suhohoon@solco.co.kr) web: <https://www.solco.co.kr/>

## INTRODUCTION

Due to a wide range of motions and frequent movements of the upper arm, there is a high incidence rate of humeral fractures in human skeleton. Using a humeral intramedullary fixation nail (HIFN) for humeral fractures is one of effective MIS (Minimally Invasive Surgery) methods, and this kind of surgery can usually provide the patient with an early recovery [1,2]. Most of the HIFNs shown in Korea are mainly foreign-made ones developed by the anatomical information of foreigners, reporting that they are not suitable for Koreans [3]. This study developed a HIFN based on Korean cadaveric tests referring to the anatomical features of the Korean humerus. Biomechanical stability was also compared and analyzed with that of a foreign-made product. The convenience and safety of humeral surgery was simultaneously verified through clinical tests.

## METHODS

Total 72 humeral bones were collected from Korean cadavers (Male: 66, Female: 6) to obtain morphological information from the CT images of Korean humeral bones. CT scans were taken after separating the humeral bones from the cadavers, and the Korean humeral model was created by reconstructing 3D cadaveric CT images (Fig. 1). Based on the reconstructed Korean humeral model, design parameters necessary for developing a HIFN such as total dimension (TD) of the medulla, proximal bending angle (PBA), proximal epiphysis diameter (PED), diaphysis diameter (DD), and distal epiphysis diameter (DED) were selected. Also, the measurement values from the 3D reconstruction FE model were analyzed to define a HIFN suitable for Koreans (Fig. 2).

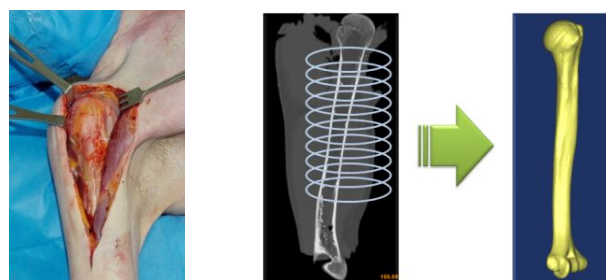


**Figure 1:** Construction of 3D Korean Humeral Model based on Korean Cadaveric CT Images

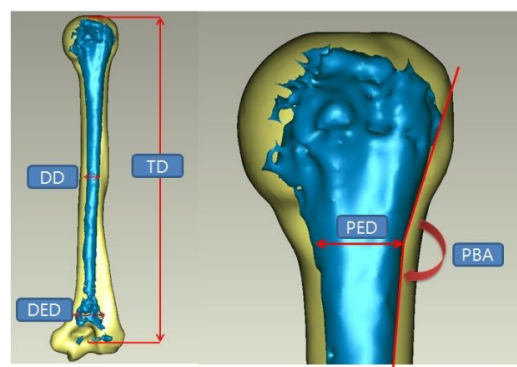


**Figure 2:** Morphological Design Parameters selected from 3D Korean Humeral Model for Development of a HIFN suitable for Koreans

The HIFN prototype (Ti-6Al-4V, 10.0mm×180mm) was developed by applying the measured values of the design parameters. The foreign-made HIFN (Ti-6Al-4V, 11.0mm×200mm, Polarus, ACUMED™, USA) was selected for biomechanical comparison and analysis. Mechanical tests were conducted using the MTS 858 Table Top System, USA. A static 4-point bending test with a loading rate 1 mm/sec and a static torsional with a loading rate 5°/min were carried out based on the ASTM F1264-03 (Fig. 3).

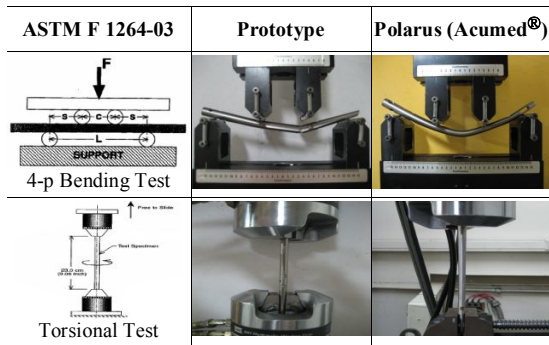


**Figure 3:** Mechanical 4-point Bending and Torsional Tests based on ASTM F1264-03

## RESULTS AND DISCUSSION

According to the static 4-point bending test results, the bending stiffness of the prototype was equivalent to the Polarus, and the maximum fracture load of the prototype resulted to be approximately 83% of the Polarus. On the other hand, static torsional test results showed that the torsional stiffness of the prototype was approximately 140% of the Polarus, and the maximum torsional fracture load of the prototype was approximately 350% of the Polarus, securing excellent performance.

To verify the convenience and safety of the developed HIFN prototype during the humeral surgery, clinical tests using the Korean cadavers were conducted. From the tests, nerve damage due to the interference with the Axillary Nerve was found near the two holes located in the proximal part of the HIFN prototype, when the fixing screws were inserted inside the holes (Fig. 4). As a countermeasure for this, design modification was carried out for the location and inserting direction of the screw holes (Fig. 5), and the stability of the fixation nail was finally secured.

## CONCLUSIONS

In this study, a 3D Korean humeral model was constructed based on the CT images of the Korean cadavers. The HIFN prototype suitable for Koreans was developed referring to the anatomical and morphological information. Static 4-point bending and torsional tests were conducted on the developed prototype, showing that the prototype had the almost equal or superior mechanical performance compared to the foreign-made one. The results of the clinical tests using Korean cadavers also showed

the possibility of Axillary Nerve damage in the proximal part of the humerus. It was possible to secure the performance of the HIFN prototype by modifying the design specifications of the screw holes.

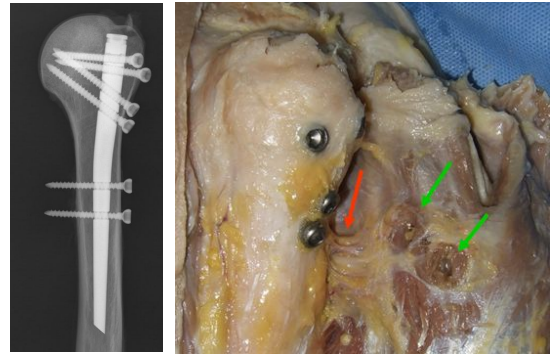


**Figure 4:** Damage Area of the Axillary Nerve due to Fixation Screws of a HIFN Prototype

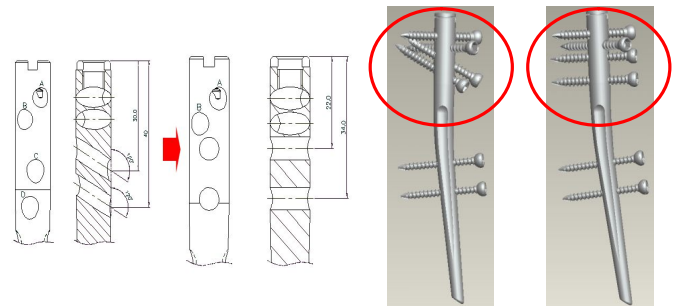


**Figure 5:** Design Modifications of Screw Holes in a HIFN Prototype

## REFERENCES

1. Linn J, "Treatment of Humeral Shaft Fractures with Humeral Locked Nail and Comparison with Plate Fixation", *J Trauma*, 44, 859-864, 1998.
2. Blum J, Janzing H, Gahr R, Langendorff HS, Rommens PM, "Clinical Performance of a New Medullary Humeral Nail: Antegrade versus Retrograde Insertion", *J Orthop Trauma*, 15, 342-349, 2001.
3. Seung Rim Park, M.D., et al., *Journal of the Korean Fracture Society*, Vol. 20, No.2 166-171, 2007.

## ACKNOWLEDGEMENTS

This study was supported by the Advanced Technology Center (ATC) Association at the Ministry of Knowledge Economy in Korea (10014102).

# Mechanobiology of Alpha-Keratin Using North American Porcupine Quills

Shih-Feng Chou and \*Ruel A. Overfelt

Auburn University, Auburn, AL, USA

\*email: [overfra@auburn.edu](mailto:overfra@auburn.edu) web: <http://www.eng.auburn.edu/users/overfra/>

## INTRODUCTION

Keratin biomaterials can be found abundantly in nature and exhibit in the form of either soft keratins (stratum corneum) or hard/structural keratins (e.g., quills). In recent years, studies of hard/structural keratins have drawn increased attention due to potential applications in tissue engineering and drug delivery [1]. Recently, avian feathers/quills have been studied for their application as light weight composite materials whereas hooves and horns have been investigated for their energy-absorption properties [2]. Unfortunately, there is still a considerable lack of literature data on the basic mechanical response of mammalian quills, such as North American porcupine quills.

A porcupine quill can be regarded as a keratin-based biocomposite consisting basically of a strong cylindrical outer shell reinforced with a soft and lightweight inner-foam core. The specific chemical compositions and the microstructural arrangements of the keratin molecules and the other tissue constituents can vary considerably from tissue to tissue and from animal to animal depending upon the particular application for which the tissue is being utilized, e.g., strength with low density or energy absorption. Thus a wide range of mechanical properties would be expected for keratin-based tissues.

## METHODS

North American porcupine quills (40 ~ 50 mm in length and 1.5 ~ 2.0 mm in diameter) were purchased from Spirit Connection Store (Titusville, PA., USA). Tensile testing of porcupine quills was performed with a miniaturized stress-strain apparatus (PASCO, Roseville, CA., USA) automated by attaching a rotary motor and a gear box to provide a constant strain rate of  $4.8 \times 10^{-4} \text{ s}^{-1}$ . For mechanical tests on the quill shell only,

sectioning and foam core removing were performed by a sharp razor blade and custom-made tools.

Compositional analyses on the inner surface as well as the outer surface of North American porcupine quill shell were performed by attenuated total reflection Fourier transform infrared spectroscopy (ATR-FTIR) using a Nicolet 6700 (Thermo Fisher Scientific Inc., USA) spectrometer with a diamond crystal, over a scan range from  $1580 \text{ cm}^{-1}$  to  $1700 \text{ cm}^{-1}$  for amide I band. Each spectrum was obtained by a total number of 32 scans at the resolution of  $4 \text{ cm}^{-1}$ .

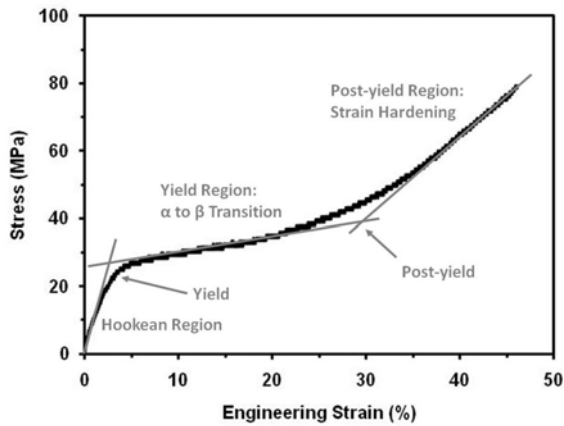
Nanoindentations on both axial and circumferential cross-sectional planes were performed with an MTS NanoIndenter XP system with a Berkovich diamond tip in depth controlled continuous stiffness mode. During the indentation, the Poisson's ratio was set to 0.50, and the allowable drift rate was 0.05 nm/sec with a harmonic displacement target of 2 nm.

## RESULTS AND DISCUSSION

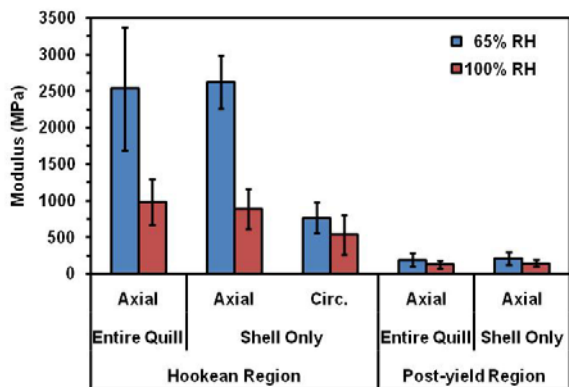
An experimental stress versus strain plot for axially-oriented North American porcupine quill is shown in Fig. 1. The tensile response of keratins typically displays an initial linear viscoelastic region, then a yield region with minimal increase of stress, and finally a post-yield strain-hardening region where significant increases in stress are required to produce additional increments of strain.

Fig. 2 shows the mean moduli in the Hookean and post-yield region for entire quill and shell-only samples at 65% RH and 100% RH (50 specimens each). The 65% RH entire quills show a significant (99% confidence level) higher Hookean modulus (~2500 MPa) than the 100% RH quills (~1000 MPa). In the post-yield region, the mean modulus for 65% RH and 100% RH entire quill samples decreased to values of 190 MPa and 130 MPa with significance, respectively. Also shown in Fig. 2 are the mean Hookean and post-yield moduli for shell-only samples. The mean values of moduli for shell-only

samples in the axial direction are not significantly different from the whole quill; however, the mean Hookean modulus for shell-only samples oriented in the circumferential direction is significantly lower than that in the axial direction.



**Figure 1:** An experimental stress-strain curve for a typical entire North American porcupine quill.



**Figure 2:** Young's modulus of the 65% RH and 100% RH entire quill and shell-only samples (axial and circumferential direction).

The fracture surfaces of the quill samples after tensile testing are investigated. The 65% RH specimens exhibit significant less evidence of plastic deformation than the 100% RH specimens and the fracture surfaces are generally perpendicular to the applied load. High magnification images reveal quill shell consisted of 3 layers with distinct fracture surfaces. The outer layer of the shell exhibits a smooth mirror-like fracture surface due to the presence of lipids. Microfibers ( $\sim 0.5 \mu\text{m}$  in diameter) aligned parallel to the growth direction of the quill are seen.

Nanoindentation on the quill shells shows the average hardness and elastic modulus of the inner layer are higher than the intermediate and outer layer. For indentations on the inner layer, the average hardness and elastic modulus in the axial

direction are higher than the circumferential direction. The results are in agreement with the suggested model proposed by Busson et al. [3]. Further investigation on compositional changes at the amide I band (C=O stretching) due to an applied load is shown in Fig. 3. The deconvolution of the peak involves two major sub-peaks centered at  $1651 \sim 1657 \text{ cm}^{-1}$  for  $\alpha$ -keratin and  $1621 \sim 1631 \text{ cm}^{-1}$  for  $\beta$ -keratin, using a  $15 \sim 17 \text{ cm}^{-1}$  full width at half maximum. In general, increasing strain decreases the composition of  $\alpha$ -keratin and increases the composition of  $\beta$ -keratin.

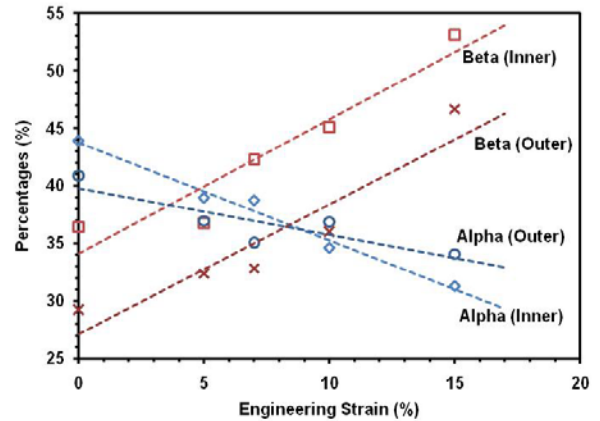


**Figure 3:** Change of average  $\alpha$  phase unfolded into  $\beta$  phase as an increase of strain for outer and inner shell of North American porcupine quills.

## CONCLUSIONS

In this research, we have presented a comprehensive set of mechanobiology data on over a hundred samples of North American porcupine quills. Results of the current research are in agreement with studies of other keratin biomaterials where the unfolding process of  $\alpha$ -keratin into  $\beta$ -keratin is quantitatively measured in this research.

## REFERENCES

1. Katoh K, et al. *Biomater* **25**, 4255-4262, 2004.
2. Meyers MA, et al. *Prog Mater Sci* **53**, 1-206, 2008.
3. Busson B, et al. *J Synchrotron Rad* **6**, 1021-1030, 1999.

# MUSCLE CO-ACTIVATION AND STRIDE VARIABILITY: IMPLICATIONS FOR WALKING ECONOMY IN PEOPLE WITH PARKINSON'S DISEASE

<sup>1</sup>Cory L Christiansen, <sup>1,2</sup>Bradley S Davidson, <sup>1</sup>Margaret L Schenkman and <sup>1</sup>Wendy M Kohrt

<sup>1</sup>University of Colorado Denver, Aurora, CO, USA

<sup>2</sup>University of Denver, Denver, CO, USA

email: [cory.christiansen@ucdenver.edu](mailto:cory.christiansen@ucdenver.edu)

## INTRODUCTION

People with Parkinson's disease (PD) have greater steady-state aerobic demand at sub-maximal walking speeds (i.e., poorer walking economy) than healthy individuals of similar age [1]. Two factors linked to walking economy are stride variability [2] and muscle co-activation [3]. It is also possible that asymmetry in muscle activation, seen in people with PD [4], may contribute to poor walking economy. Taken together, asymmetric and excessive stride variability and muscle co-activation [5] during functional tasks may be primary factors related to poorer walking economy for people with PD.

The purpose of this study was to measure side-to-side differences in muscle co-activation and stride time variability for people in early to mid-stages of PD. Additionally, the association of walking economy with muscle co-activation and stride variability was examined.

## METHODS

Ten participants in early to mid-stage PD (Hoehn and Yahr scale 2.0-3.0) participated (age:  $66.4 \pm 8.5$  years; mass:  $76.8 \pm 8.0$  kg; height:  $1.73 \pm 0.09$  m;  $76.8 \pm 8.0$  kg; sex: 6 men and 4 women). Participants reported which side they experienced the majority of tremor (or other motor symptoms) to allow directional comparison of co-activation and stride symmetry.

Rate of oxygen consumption ( $VO_2$ ) was measured with indirect calorimetry (ParvoMedics, Sandy, UT) during treadmill walking. Measurement of  $VO_2$  was completed during a 5-minute sitting period before walking and across the last 2 minutes of a 5 minute walking period at 2.5 mph. Walking

economy was calculated as net  $VO_2$  ( $VO_{2walk} - VO_{2rest}$ ).

Electromyographic (EMG) signals were collected (Delsys, Boston, MA) at 1000 Hz with bipolar electrodes (Ag-AgCl) attached to 2 sites on each thigh: 1) vastus lateralis (2/3 distance along the line from the anterior superior iliac spine to the lateral mid-patella) and 2) medial hamstring (1/2 distance along the line from the ischial tuberosity to medial tibial epicondyle).

EMG signal energy, calculated using the Teager-Kaiser Energy Operator [6], was low-pass filtered (10Hz cutoff), and normalized to the mean value from the entire walking trial to produce a time-course of muscle activation. Thigh coactivation index (CI) [7] was calculated for 15 consecutive strides (Figure 1). The CIs were averaged across strides to quantify co-activation for both thighs.

Stride time was calculated as the time between subsequent heel contacts using foot switches placed

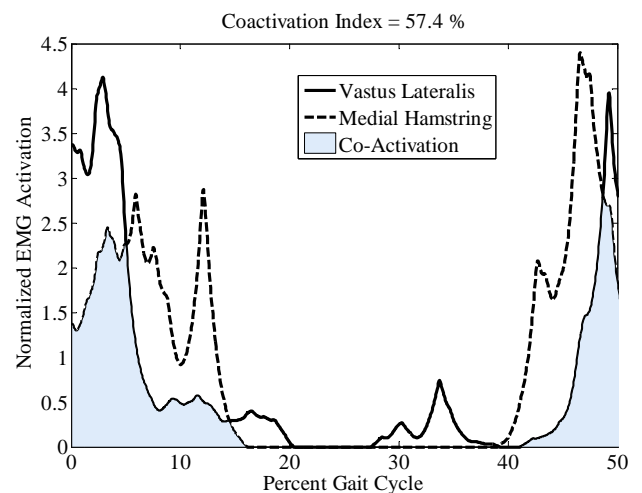


**Figure 1:** Illustrated co-activation index measure over one stride of a representative participant.

at the heel of each shoe (Delsys, Boston, MA). Stride time variability was defined as the standard deviation of the first 200 strides for each limb.

Paired t-tests were used to compare CI and stride time variability between the patient-identified tremor and the contralateral limb. Pearson product-moment correlations were used to measure associations of walking economy with involved side CI and stride variability.

## RESULTS AND DISCUSSION

Table 1 presents CI and stride variability data for each lower limb. Net VO<sub>2</sub> for the group was 8.54 (± 1.84) ml/min/kg. CI was greater on the patient-identified “tremor” side compared to the contralateral side (*p* = 0.051) and there was no difference between sides in stride time variability (*p* = 0.495). There was a moderate association between CI of the “tremor” side and walking economy (*r* = 0.54; 90% Confidence Interval: -0.02 to 0.84) and no association between stride time variability and walking economy (*r* = -0.03; 90% Confidence Interval: -0.53 to 0.57).

These results suggest side-to-side differences in thigh muscle activation patterns for people with PD. This agrees with findings by Miller and colleagues who found people with PD (H&Y 2-3) have asymmetry in lower leg muscle timing and magnitude compared to healthy people of similar age [4].

Additionally, the results indicate thigh muscle co-activation is directly associated with VO<sub>2</sub>, as higher levels of co-activation are associated with higher VO<sub>2</sub>. This finding agrees with a recent study of healthy older adults by Peterson & Martin who found higher thigh muscle co-activation to be linked to poorer walking economy [3].

The lack of difference between sides in stride time variability may be influenced by the treadmill. It has been shown that people with PD have reduced stride variability with treadmill versus over ground walking [8]. However, the walking economy measurements taken during treadmill walking were not related to magnitude of stride variability during the same trial.

Further study is warranted to determine underlying mechanisms related to poor walking economy for people with PD, as there are implications related to physical function and fatigue. This study has identified increased muscle co-activation as one possible mechanism. Other potential mechanisms, such as trunk rigidity, pulmonary dysfunction, and quantified motor symptom severity should be investigated.

## CONCLUSIONS

People in early to mid-stages of PD have asymmetry in thigh muscle co-activation during treadmill walking, having increased co-activation in the limb with more pronounced motor symptoms. Additionally, thigh muscle co-activation is directly related to rate of oxygen consumption, with higher levels of co-activation associated with higher rates of consumption.

## REFERENCES

1. Christiansen CL, et al. *Mov Disord* **24**, 1481-1487, 2009.
2. Dean JC, et al. *IEEE Trans Biomed Eng* **54**, 1919-1926, 2007.
3. Peterson DS & Martin PE. *Gait Posture* **31**, 355-359, 2010.
4. Miller RA, et al. *Electroencephalogr Clin Neurophysiol* **101**, 1-7, 1996.
5. Dimitrova D, et al. *J Neuropysiol* **91**, 489-501, 2004.
6. Solnik S, et al. *Acta Bioeng Biomech* **10(2)**, 65-68, 2008.
7. Winter D, *Biomechanics and motor control of human movement*, John Wiley & Sons, 1990.
8. Frenkel-Toledo, et al. *Mov Disord* **20**, 1109-1114, 2005.

**Table 1:** Co-activation index and stride variability between limbs and correlations with walking economy.

|                                    | “Tremor” Side*  | Contralateral Side |
|------------------------------------|-----------------|--------------------|
| <b>Thigh CI (%)</b>                | 35.64 ± 13.83   | 27.45 ± 15.65      |
| <b>Stride Time Variability (s)</b> | 0.0356 ± 0.0234 | 0.0355 ± 0.0163    |

CI = Co-activation index, VO<sub>2</sub> = Net oxygen consumption (ml/min/kg) at 2.5 mph. \* “Tremor” Side was defined as the patient-identified side of the body with the most tremor. Values mean ± SD.

# VALIDATION OF VIDEO-BASED MOTION ANALYSIS OF SCAPULAR AND HUMERAL ROTATIONAL KINEMATICS DURING SIMULATED THROWING

Yung-chien Chu, Jon Akins, Mita Lovalekar, Scott Tashman, Scott Lephart, and Timothy Sell

University of Pittsburgh, Pittsburgh, PA, USA

email: [yuc24@pitt.edu](mailto:yuc24@pitt.edu)

## INTRODUCTION

Efficient and coordinated scapular kinematics is essential for optimal performance and to minimize risk of shoulder injury in overhead athletes [1]. Altered scapular kinematics during slow-paced arm elevation has been observed in both healthy and symptomatic overhead throwers [2,3], but little is known about scapular kinematics during throwing. Most scapular kinematics studies have been conducted with electromagnetic tracking technology, which requires wired sensors that restrict subjects' movement and may not be optimal for testing complex, multi-plane movements such as throwing due to noise in recorded signals [4]. Video-based motion analysis (VMA) offers greater freedom of movement and is capable of the higher sampling frequency necessary for measurement of high speed movements. VMA has been validated for scapular kinematics in a slow-paced arm elevation task [5]. Humeral angles are involved in throwing analysis for phase defining and inverse kinetic estimation. The validity of skin-based humeral kinematic measurements has been evaluated in slow-paced arm elevation but not in rapid movements like throwing [6]. The purpose of this study was to validate the use of VMA for three-dimensional scapular and humeral kinematics during simulated throwing. If validated, scapular kinematics can be integrated into throwing analysis for future biomechanical studies.

## METHODS

This validation study involved the comparison of a VMA technique against a dynamic stereo x-ray (DSX), a previously established gold-standard for tracking scapular kinematics [7]. Five adult right-hand dominant male subjects (Age=27.8±6.9 yrs; Ht=1.81±4.9 cm; Wt=77.9±9.5 kg) participated in

this study. Reflective markers were attached to anatomical landmarks on each subject's thorax, right humerus, and right scapula, following the ISB recommendations [8]. A custom-made triad with three reflective markers was attached to the flat, broad portion of the acromion process. A static capture of the marker set was taken for each subject, establishing the spatial relationship between the triad and the scapula markers. Markers attached to the scapula other than the AC joint were removed during testing. Subjects were seated and assumed a start position of about 90° shoulder abduction and elbow flexion, followed by a maximum effort overhead throwing movement. The VMA system (Vicon Motion Systems, Inc., Centennial, CO) and DSX system were synchronized to capture the movement at 150Hz during a one second capture. A CT-scan of the subject's humerus and scapula were used to create subject-specific 3D bone models. The anatomical landmarks of the humerus and scapula were marked on the bone models. The 3D trajectories of these anatomical landmarks were reconstructed by matching the bone models to the DSX images. The 3D trajectories of the reflective markers were exported from the VMA system and the virtual trajectories of the anatomical landmarks of the scapula were reconstructed. Humeral and scapular angles were calculated following the ISB recommendations using the 3D trajectories from each system [8]. The initiation of movement was defined as the humeral resultant angular velocity exceeded 10°/s. For each angle, a Pearson's product-moment correlation coefficient was calculated for every subject and averaged to examine the relationships between VMA and DSX data throughout the movement. Root mean-squared (RMS) error for each angle was also calculated. A paired t-test was performed to compare the range of motion of each angle between VMA and DSX data with alpha = 0.05 set *a priori*.

## RESULTS AND DISCUSSION

Figure 1 is a representation of DSX model matching process and the comparison of scapular kinematic between VMA and DSX of one subject. Humeral angles with respect to the thorax measured with VMA were highly correlated to those measured with DSX, with all mean Pearson's R over 0.976. Scapular angles with respect to the thorax measured with VMA had good to excellent correlation with DSX data, with mean Pearson's r ranging between 0.693 to 0.969 (Table 1). RMS errors ranged between 0.97 to 4.13° with the initial angles set at zero (Table 1). VMA overestimated humeral internal rotation and scapular protraction (Table 2), likely due to soft tissue effect. The excellent correlations suggested high pattern similarity between the VMA and DSX data, but the overestimation should be acknowledged for data interpretation.

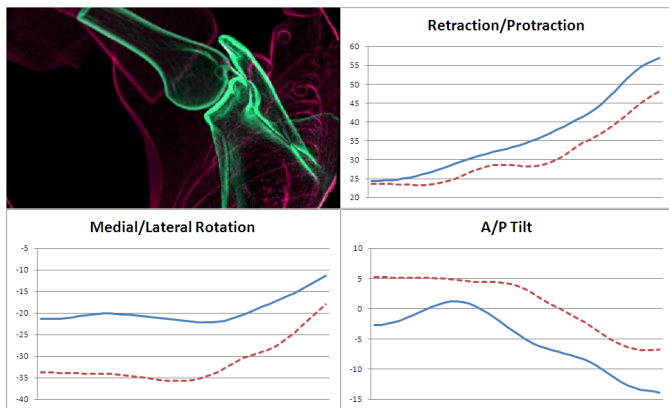


**Figure 1:** DSX scapular model matching and a sample comparison between VMA and DSX. Blue solid line is VMA and red dotted line is DSX data.

The current results suggest that VMA is valid for tracking scapular and humeral rotational movement patterns during a simulated throw. It is noteworthy that the Pearson's r in the current simulated throwing task were comparable to those in the widely-applied, slow-paced arm elevation task [5]. Soft tissue effect, threatening the validity of any skin-based measurement technique, was not further increased due to the rapid nature of the current task. Although the velocity of the current simulated throwing task was not as fast as throwing in sports activities, we consider the proposed VMA technique appropriate for evaluating scapular kinematics during high velocity throwing for overhead athletes.

## REFERENCES

1. Kibler WB. *Am J Sports Med* **26**, 325-337, 1998.
2. Laudner KG, et al. *Am J Sports Med* **35**, 2091-2095, 2007.
3. Laudner KG, et al. *J Orthop Sports Phys Ther* **36**, 485-494, 2006.
4. Meyer KE, et al. *J Appl Biomech* **24**, 24-34, 2008.
5. Sell TC, et al. *Proceedings of 57<sup>th</sup> ORS Annual Meeting*, Long Beach, CA, USA, 2011.
6. Ludewig PM, et al. *J Appl Biomech* **18**, 163-170, 2002.
7. Bey MJ, et al. *J Biomech Eng* **128**, 604-609, 2006.
8. Wu G, et al. *J Biomech* **38**, 981-992, 2005.

## ACKNOWLEDGEMENTS

This study was funded by the Central Research Development Fund, Office of Research, University of Pittsburgh.

**Table 1:** Tables may extend across both columns, and those should be included at the bottom of the abstract

|                      | Humerus            |               |                    | Scapula                  |                    |                 |
|----------------------|--------------------|---------------|--------------------|--------------------------|--------------------|-----------------|
|                      | Plane of Elevation | Elevation     | Int / Ext Rotation | Protraction / Retraction | Med / Lat Rotation | Ant / Post Tilt |
| <b>Pearson's R</b>   | 0.993 ± 0.002      | 0.976 ± 0.052 | 0.988 ± 0.007      | 0.969 ± 0.021            | 0.795 ± 0.212      | 0.693 ± 0.288   |
| <b>RMS Error (°)</b> | 4.09 ± 1.25        | 0.97 ± 0.43   | 3.76 ± 0.56        | 4.13 ± 0.64              | 3.43 ± 1.01        | 2.61 ± 1.37     |

**Table 2:** Humeral and scapular range of motion during the simulated throwing

| Measurement Technique | Range of Motion (°)  |             |                    |              |                 |               |
|-----------------------|----------------------|-------------|--------------------|--------------|-----------------|---------------|
|                       | Humerus              |             |                    | Scapula      |                 |               |
|                       | Horizontal Adduction | Adduction   | Internal Rotation* | Protraction* | Medial Rotation | Anterior Tilt |
| <b>VMA</b>            | 71.1 ± 17.8          | 33.7 ± 11.7 | 72.7 ± 13.9        | 32.9 ± 5.5   | 14.4 ± 4.6      | 14.0 ± 3.6    |
| <b>DSX</b>            | 74.0 ± 20.7          | 30.1 ± 14.9 | 52.6 ± 16.6        | 22.2 ± 5.9   | 17.4 ± 0.7      | 11.4 ± 1.5    |

\* Significant difference between two measurement techniques ( $p < 0.05$ )

# EFFECT OF LOADING DIRECTION ON FORCE TO DISLOCATE IN REVERSE SHOULDER ARTHROPLASTY

<sup>1</sup>Allison Clouthier, <sup>1</sup>Markus Hetzler, <sup>2</sup>Graham Fedorak, <sup>1</sup>Tim Bryant, <sup>1</sup>Kevin Deluzio and <sup>2</sup>Ryan Bicknell

<sup>1</sup>Queen's University, Kingston, ON, Canada  
<sup>2</sup>Kingston General Hospital, Kingston, ON, Canada  
email: [clouthiera@me.queensu.ca](mailto:clouthiera@me.queensu.ca)

## INTRODUCTION

Reverse shoulder arthroplasty is a relatively new surgery that can be used to treat conditions such as massive rotator cuff tear combined with glenohumeral arthritis that are generally not successfully managed using traditional shoulder replacements. This prosthesis, in which the 'ball-and-socket' anatomy of the shoulder is reversed, has been successful in reducing pain and improving function in these patients. However, complication rates are generally around 24% with instability being one of the most common complications [1]. The stability of reverse shoulder arthroplasty has been examined; however, previous investigations have not considered the impact of the muscles or bones of the shoulder. Although it has been observed clinically that the stability of the prosthesis varies with direction [2], the mechanism of dislocation is not well understood for reverse shoulder arthroplasty. Therefore, the objectives of this study were: (1) to develop a shoulder simulator that models the musculature and bony geometry of the shoulder and (2) compare shoulder stability in four primary directions.

## METHODS

A DePuy Delta XTEND™ reverse prosthesis was implanted into artificial bones (Sawbones, Vashon) and the scapula was fixed on a custom designed shoulder simulator (Figure 1). The simulator models the deltoid using three pneumatically actuated cables to represent the muscle as three sections (anterior, middle, and posterior). As a rotator cuff deficient shoulder is the primary indication for this surgery, a worst case scenario of a complete rotator cuff tear was assumed so these muscles were not modelled. Muscle insertion points and lines of

action were based on anatomical studies [3] and a 3.6 kg weight was attached to the humerus to represent the mass of the arm. A displacing force was applied to the humeral head using a cable connected to a material testing machine (Instron, Norwood). Muscle forces and the displacing force were recorded using load cells and a data acquisition unit (ODAU II, NDI, Waterloo).

The muscle forces were configured to position the shoulder in a neutral posture with a moderate amount of abduction (45°). The displacing force was then applied at 30mm/min and the force required to dislocate the prosthesis in the superior, inferior, posterior, and anterior directions was recorded.



**Figure 1:** Mechanical shoulder simulator

## RESULTS AND DISCUSSION

A typical plot of the displacing and muscle forces is shown in Figure 2 for the case of a superior dislocation. The tension in the displacing cable increased until the joint began to sublux at 10s, then as the humerus translated, the force decreased until the joint was fully dislocated at 22s.

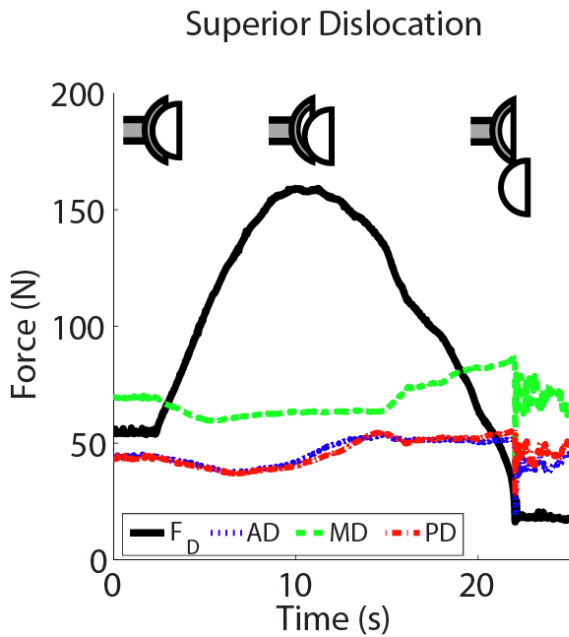


**Figure 2:** Displacing and muscle forces during a superior dislocation trial.  $F_D$  = displacing force, AD = anterior deltoid, MD = middle deltoid, PD = posterior deltoid.

The force required to dislocate the shoulder and the muscle forces at the instance of maximum displacing force are shown in Table 1. The shoulder was most stable in the inferior direction. This was expected as inferior instability is rarely reported with this prosthesis [2] and, mechanically, the upward pull of the muscle forces oppose this motion. The least stable direction was the posterior direction. Posterior instability is also rarely reported; however, there are few studies that indicate the direction of dislocation for reverse shoulder. In addition, the middle deltoid, the muscle with the greatest force, is directed slightly posteriorly. Thus when it opposes a displacement, the force required to dislocate the joint is increased, as seen in Table 1 with the inferior and anterior dislocations. The force in the middle deltoid for the posterior dislocation is lower than these two, indicating that the middle deltoid does not contribute as much to stabilizing the joint in this

direction. It is also possible that the remaining rotator cuff muscles play an important role in posterior stability of the reverse shoulder.

The muscle forces required to maintain the prescribed posture are similar to those found in computer simulations [4]. In addition, the ratio of dislocating to compressive force was found to be  $1.2 \pm 0.2$ , which is in agreement with previously reported values [5].

A computer simulation is being developed concurrently and future work will investigate the effect of posture, component parameters, and component orientations on stability using both physical and software models.

## CONCLUSIONS

A shoulder simulator was developed and was capable of demonstrating that a rotator cuff deficient reverse arthroplasty shoulder is least stable in the posterior and superior directions and most stable in the inferior and anterior directions.

## REFERENCES

1. Zumstein MA, et al. *J Shoulder Elbow Surg* **20**, 146-157, 2011.
2. Cuff D, et al. *J Bone Joint Surg Am* **90**, 1244-1251, 2008.
3. Liu J, et al. *Clin Biomech* **12**, 32-38, 1997.
4. Terrier A, et al. *J Bone Joint Surg Br* **90B**, 751-756, 2008.
5. Favre P, et al. *J Shoulder Elbow Surg* **19**, 550-556, 2010.

## ACKNOWLEDGEMENTS

Funding provided by the NSERC-CREATE Training Program and Queen's University, the prosthesis was supplied by DePuy, and detailed frame design was completed by CPI Automation.

**Table 1:** Force required to dislocate the shoulder and muscle forces at moment of maximum displacement force

| Dislocation Direction | Anterior Deltoid Force (N) | Middle Deltoid Force (N) | Posterior Deltoid Force (N) | Force to Dislocate (N) |
|-----------------------|----------------------------|--------------------------|-----------------------------|------------------------|
| Superior              | 42                         | 63                       | 40                          | 159                    |
| Inferior              | 52                         | 88                       | 58                          | 203                    |
| Anterior              | 38                         | 84                       | 54                          | 201                    |
| Posterior             | 51                         | 74                       | 42                          | 138                    |

# **A MULTI-SEGMENT FOOT MODEL BASED ON IN-VIVO AND IN-VITRO STEREOPHOTOGAMMETRIC STUDIES AND CLINICAL THEORIES OF DYNAMIC FOOT FUNCTION: WALKING GAIT RELIABILITY**

<sup>1</sup>Stephen C Cobb, <sup>1</sup>Mukta N Joshi, <sup>1</sup>Robin L Bauer, <sup>1</sup>Trevor R Klinkner  
<sup>1</sup>Neuromechanics Laboratory, University of Wisconsin-Milwaukee

## **INTRODUCTION**

Studies investigating walking gait have traditionally either modeled the foot as a single rigid segment, or as a rearfoot segment. While these studies have improved the understanding of foot function during gait, they assume the joints distal to the calcaneus do not contribute significantly to foot function. Recent, in-vitro [1] and invasive in-vivo [2] studies, however, suggest that significant motion does occur in the joints distal to the calcaneus during gait.

Several surface based multi-segment foot models have recently been developed [3,4] and applied in a number of clinical and injury related investigations. These studies have further advanced the understanding of the effect of injury and disease on foot function. Absent from the majority of the foot models have been definitions of medial and lateral midfoot and forefoot segments. A recent invasive in-vivo multi-segment foot study [5], however, reported relatively independent motion in the medial and lateral forefoot segments. Although the study suggested that the medial and lateral midfoot may function as a relatively rigid segment in healthy individuals, the coupling may not be rigid in persons with abnormal foot structure or in clinical populations.

The purpose of the current study, therefore, was to investigate the reliability of a six-segment foot model that includes medial and lateral forefoot and midfoot segments during walking gait.

## **METHODS**

Three healthy participants (2 f, 1 m; age:  $20.3 \pm 1.5$  yrs; mass:  $86.9 \pm 38.8$  kg; height:  $177.0 \pm 14.9$  cm) were with typical foot posture were recruited. Typical foot posture was determined using a digital photographic measurement method and previously collected descriptive data [6]. Specifically, typical foot posture was defined as navicular indices (navicular height/truncated foot length) that were within  $\pm 1$  SD of the mean indices from the descriptive data.

The foot model defined 6 functional articulations (rearfoot complex, calcaneonavicular complex, calcaneocuboid joint, medial forefoot, lateral forefoot, 1st metatarsophalangeal complex) from 6 foot segment and a leg segment (Figure 1). Three-dimensional (3D) positions of groups of 6.4 mm reflective markers (technical clusters) located on the leg and foot segments were captured using a 10 camera Motion Analysis Eagle motion capture system sampling at 120 Hz.

Gait analysis consisted of completion 7 successful walking trials at a speed ranging between 1.3 and 1.4 m/s. Prior to the gait analysis trials, an anatomical calibration procedure was performed to identify the positions of additional anatomical reference landmarks and to define local coordinate systems within each segment.

A custom written program (Matlab) was used to filter the data, reconstruct the 3D

position of each segment using the calibrated anatomical system technique with a single value decomposition optimization procedure, and compute joint angles between adjacent segments (Figure 1).

The coefficient of multiple correlation was used to determine the reliability of

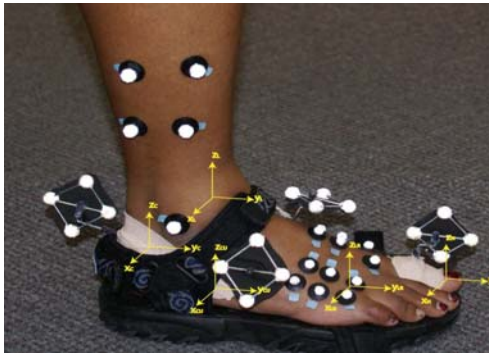


**Figure 1:** Technical and anatomical markers. **Top figure:** Leg ( $x_L, y_L, z_L$ ), calcaneus ( $x_C, y_C, z_C$ ), cuboid ( $x_{CU}, y_{CU}, z_{CU}$ ), lateral rays ( $x_{LR}, y_{LR}, z_{LR}$ ), and hallux ( $x_H, y_H, z_H$ ) anatomical coordinate systems. **Bottom figure:** Navicular ( $x_N, y_N, z_N$ ), and medial rays ( $x_{MR}, y_{MR}, z_{MR}$ ) anatomical coordinate systems. All of the anatomical coordinate systems were defined using the appropriate anatomical landmarks

the model using 5 of the walking trials. Correlation coefficients  $\geq 0.70$  were considered to be very repeatable.

## RESULTS AND DISCUSSION

Walking gait kinematics were very repeatable in all three motion planes for the rearfoot complex, calcaneocuboid, medial forefoot, and 1<sup>st</sup> MTP functional articulations (Table 1). For the calcaneonavicular complex, walking gait kinematics were very repeatable in the sagittal and transverse planes and moderately repeatable in the frontal plane (Table 1). Finally, for the lateral forefoot the gait kinematics very repeatable in the transverse plane and moderately repeatable in the sagittal and frontal planes (Table 1).

The study suggests the six segment foot model is very reliable during walking gait.

## REFERENCES

1. Nester CJ, et al. *J Biomech* **40**, 1927-37, 2007.
2. Lundgren P, et al. *Gait & Posture* **28**, 93-100, 2008.
3. Kidder SM, et al. *IEEE Trans Rehab Eng* **4**, 25-32, 1996.
4. Stebbins J, et al. *Gait & Posture* **4**, 401-410, 2006.
5. Wolf P, et al. *Gait & Posture* **28**, 434-41, 2008.
6. Cobb SC, et al. *Gait & Posture* **46**, 20-30, 2011.

This study was supported by grants from the Wisconsin Athletic Trainers' Association and the UW-Milwaukee Graduate School.

**Table 1. Coefficients of multiple correlations for the six functional articulations**

|                                     | Sagittal | Frontal | Transverse |
|-------------------------------------|----------|---------|------------|
| Rearfoot complex                    | 0.970    | 0.706   | 0.834      |
| Calcaneonavicular                   | 0.746    | 0.695   | 0.714      |
| Calcaneocuboid                      | 0.806    | 0.756   | 0.808      |
| Medial Forefoot                     | 0.935    | 0.752   | 0.914      |
| Lateral Forefoot                    | 0.635    | 0.682   | 0.753      |
| 1 <sup>st</sup> Metatarsophalangeal | 0.806    | 0.756   | 0.808      |

# DEVELOPMENT AND VALIDATION OF A PEDIATRIC HEAD AND NECK MUSCULOSKELETAL MODEL

<sup>1</sup>Carolyn Cochenour, <sup>1</sup>Hitesh Mehta, <sup>2</sup>Travis Peterson and <sup>1</sup>David Nuckley

<sup>1</sup>University of Minnesota, Minneapolis, MN, USA

<sup>2</sup>University of Washington, Seattle, WA, USA

email: [dnuckley@umn.edu](mailto:dnuckley@umn.edu) web: <http://mrbl.umn.edu>

## INTRODUCTION

Neuromuscular control of the head and neck is essential for daily activities and prevention of injury. Understanding dynamic control of the pediatric neck musculoskeletal system enables us to address injury biomechanics in children as well as aid children with neuromuscular disabilities. Maturation of the head and neck involves complex changes in relative head size, ligament elasticity, as well as orientation of the facets and vertebral bone density. These changes make younger children (< 8 y.o.) twice as likely to sustain serious spinal injuries compared with their older counterparts (9-16 y.o.) [1]. Motor accidents are the most common cause of spinal injury to younger children, 72% of which are cervical spine injuries [2].

In spite of the need to understand neck musculoskeletal control for injury prevention, there exists no validated head and neck musculoskeletal model. The objective of this study was to develop an anatomically and biomechanically accurate musculoskeletal model of the pediatric head and neck, then validate its kinematics and muscle activation response.

## METHODS

Our pediatric model was designed after the adult musculoskeletal spine model by Vasavada et al. [3] using the OpenSim (v.2.0.2) platform. The pediatric model was scaled specific to the six year old male by adjusting the following parameters: anatomical dimensions, mass properties, moments of inertia, maximum isometric muscle force, and tendon slack length.

Anatomic scaling of the bones was performed based upon anthropomorphic data [4] (Figure 1). Each bone was linearly scaled in three dimensions using the averages of vertebral body height, sagittal



**Figure 1:** Anatomical scaling of the musculoskeletal model bones and muscles from adult (left) to pediatric (center and right). Additional parameters adjusted in development of the pediatric model include: mass properties, moments of inertia, maximum isometric muscle force, and tendon slack length.

length, and coronal length. Neck length data were used to transform each vertebra to its new position. Next, pediatric vertebral mass properties were ascribed based on from Lowrance's study of adult vertebral mass [5]. The head and vertebral moments of inertia were calculated from mass and geometry:

$$I_{axes} = I_{cg} + m_{segment}r_{axes}^2 [6]$$

In addition to anatomically scaling the adult spine model, the muscle properties were also scaled to reflect the developing pediatric musculoskeletal system. The muscles were categorized into three groups: (1) flexion, (2) extension, and (3) lateral bending. In each direction of bending, the maximum isometric force (as a percent of adult) was measured in a healthy sample [7]. This age based percentage was then applied to each individual muscle in that respective group. Tendon slack length in children is longer relative to muscle length compared with adults and was scaled down for the pediatric model based on calculations from O'Brien et al [8].

Finally the pediatric model range of motion was defined based on human subject data for 6 y.o. males where sagittal plane motion was  $-60.3^\circ$  (flexion) to  $77.2^\circ$  (extension), coronal plane motion equaled  $-51.0^\circ$  to  $51.0^\circ$ , and transverse plane rotation was  $-74.0^\circ$  to  $78.0^\circ$  [9].

Model stability and validity were evaluated using the Static Optimization tool in OpenSim. Pediatric neck EMG data (n=9) was further used to validate the model's muscle response to flexion/extension activities.

## RESULTS AND DISCUSSION

Muscle output for the model was generated using the Static Optimization tool in OpenSim. The model was stable in Static Optimization and generated real muscle forces. These forces and activation patterns of the sternocleidomastoid, trapezius, and splenius capitis muscle groups were plotted over the range of motion for flexion/extension. The muscle activation

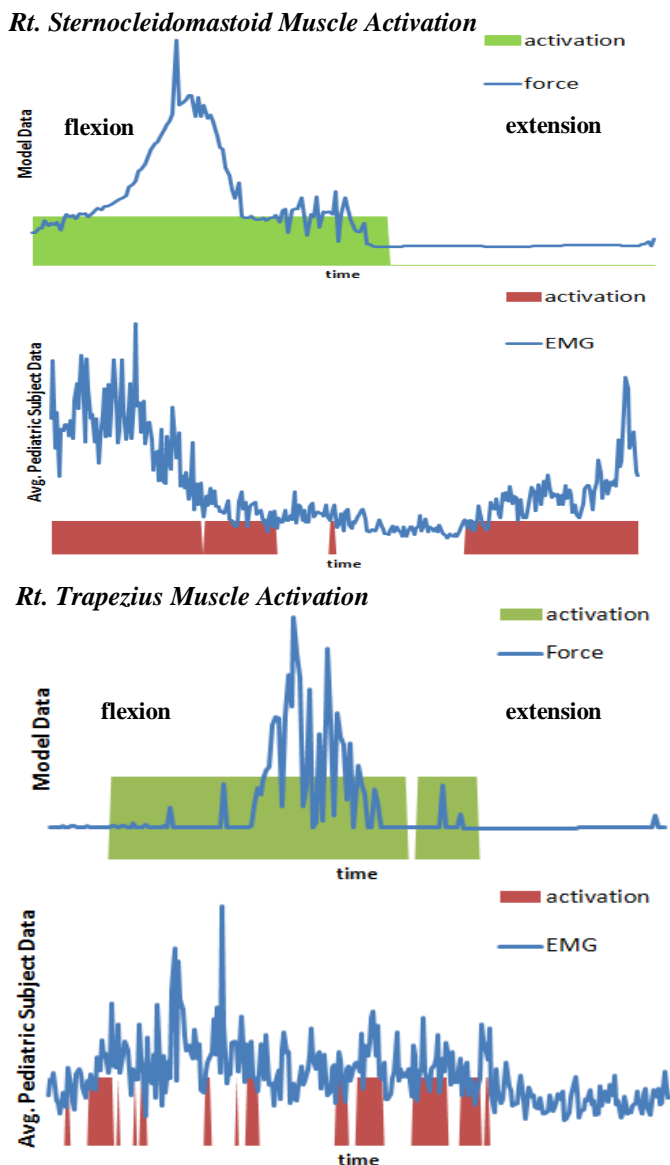


**Figure 2:** Muscle force activation as identified by the model (green) was compared with the average activation of pediatric human subjects (ages 5-7 years) (n=9) as measured with surface EMG. These data demonstrate similar patterns for the flexion extension activity performed.

was computed using singular spectral analysis to distinguish time periods in which the muscle was 'on' versus 'off' (Figure 2).

Assumptions and limitations of the OpenSim pediatric model include right/left symmetry, three degrees of freedom, assuming the TSL scaling factor is the same for all muscle groups as well as assuming that superficial and deep muscle properties are scaled alike. Based on an extensive literature search these assumptions provide for the most accurate model to date in the absence of more data. Currently the model is validated for static optimization of flexion/extension, but future plans include multi-axial static and dynamic validation.

This is the first pediatric musculoskeletal model which is stable and validated for kinematics, muscle forces, and muscle activation from pediatric human subject data. The musculoskeletal model's similar patterns of muscle force and activation make it a valuable tool to understand pediatric neck control.

## CONCLUSIONS

An anatomically accurate pediatric (6 y.o.) head and neck musculoskeletal model was developed and validated for flexion/extension kinematics and muscle response. This model will lead the way in characterizing the unique head and neck biomechanics specific to the pediatric population and potentially aid in injury prevention in children.

## REFERENCES

1. Bilston et al. *SPINE* **32**, 2339-2347, 2007.
2. Brown et al. *J. Pediatric Surgery* **36**, 1107-1114, 2001.
3. Vasavada et al. *SPINE* **23**, 412-422, 1998.
4. Bradtmiller et al. *The Development of a 3-D Data Base of Head and Facial Anthropometry for Children and Youths*, 1-173, 1994.
5. Lowrance et al. *Anat. Rec.* **159**, 83-88.
6. Ahn. *Korean J. Anatomy* **38**, 1-9, 2005.
7. Vincent et al. *J Biomech* (in press).
8. O'Brien et al. *J. Anatomy* **216**, 631-642, 2010.
9. Argogast et al. *SPINE* **10**, E309-E315, 2007.

## ACKNOWLEDGEMENTS

Research funded by NIH (NICHD). We also thank Anita Vasavada for her assistance with this model.

# STOCHASTIC RESONANCE ELECTRICAL STIMULATION TO IMPROVE POSTURAL CONTROL IN KNEE OSTEOARTHRITIS

<sup>1</sup>Amber Collins, <sup>1</sup>J. Troy Blackburn, <sup>1</sup>Bing Yu, <sup>1</sup>Chris Olcott, <sup>1</sup>Joanne Jordan, and <sup>1</sup>Paul Weinhold

<sup>1</sup>The University of North Carolina at Chapel Hill, Chapel Hill, NC, USA  
email: atcollin@udel.edu

## INTRODUCTION

Knee osteoarthritis (OA) is associated with reduced postural control, which may put those with knee OA at greater risk of falling. Adults with knee OA have reduced knee proprioception (joint position sense), suggesting reduced proprioception sensation about the knee [1]. Proprioceptive acuity is a key component of postural control. Stochastic resonance (SR) stimulation has been theorized as a means by which sensory input may be enhanced. Studies have shown improvements in postural control when plantar, trunk, or ankle stimulation (electrical or mechanical) were applied [2,3,4]. Knee sleeves have also shown some ability to improve postural control in knee OA [5]. However, the application of SR stimulation in combination with a knee sleeve in knee OA subjects has not previously been investigated as a means of improving postural control.

The purpose of this study was to determine whether the application of SR electrical stimulation (ES) combined with a knee sleeve would improve measures of static balance in knee OA subjects.

## METHODS

Fifty-two subjects (30F, 22M) with mild to moderate radiographic knee OA (KL grade 1-3) were recruited for participation. After giving their informed consent about the risks of participation, subjects were asked to maintain single leg standing balance for a period of 20 seconds within each trial. Postural control was assessed during 6 conditions with 3 trials within each condition. The first and sixth conditions were control conditions where no ES and no sleeve were applied (NE:NS). The second through fifth conditions were presented in a counterbalanced manner and included: no ES and sleeve (NE:S), 75% ES and sleeve (E75:S), 100%

ES and sleeve (E100:S), 150% ES and sleeve (E150:S).

Prior to testing, a neoprene knee sleeve was fit to each subject and two pairs of SR ES electrodes were placed 2 cm above and below the tibio-femoral joint line on the medial and lateral aspects of the knee. SR stimulation consisted of a Gaussian white noise (zero mean, 0-1000Hz) signal with amplitude based on subject's threshold for SR ES detection. Subject's threshold for detection was determined for both inferior and superior electrode pairs prior to testing. Subsequent testing incorporated these threshold values at 75%, 100%, and 150%.

Postural control outcome measures included Center of Pressure (COP) mean velocity, displacement range, and standard deviation in the medial-lateral (ML) and anterior-posterior (AP) directions. Additionally COP total path length was measured. Periods of non-test leg touchdown were detected and excluded from the subsequent calculation of outcome measures.

A paired t-test assessed differences between the two control conditions (NE:NS1 and NE:NS2,  $p < 0.05$ ). The two control conditions were then averaged (NE:NSave) and used in subsequent analyses. Differences between the remaining five conditions were assessed with a repeated measures analysis of variance (ANOVA,  $p < 0.05$ ).

## RESULTS AND DISCUSSION

A significant effect of the treatment conditions was observed ( $p < 0.05$ ) with significant reductions in the COP total path length for all treatment conditions (NE:S, E75:S, E100:S, E150:S) relative to the control condition (NE:NSave) (Figure 1).

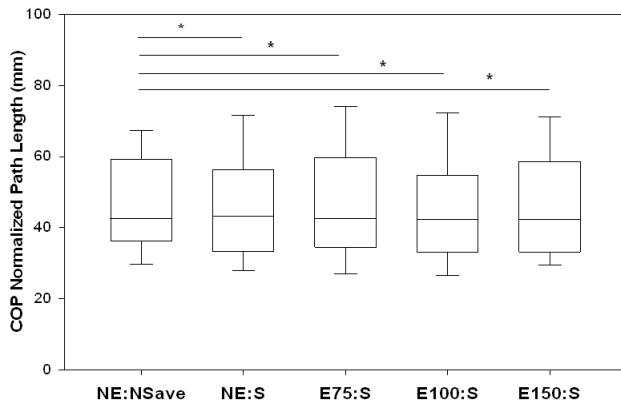


**Figure 1:** Median COP normalized total path length (mm) during all five testing conditions. \*indicates a significant difference between conditions at the end of the horizontal bars.

Additionally, the AP COP velocity was significantly different between the treatment conditions compared to the control condition ( $p < 0.05$ ) (Figure 2).

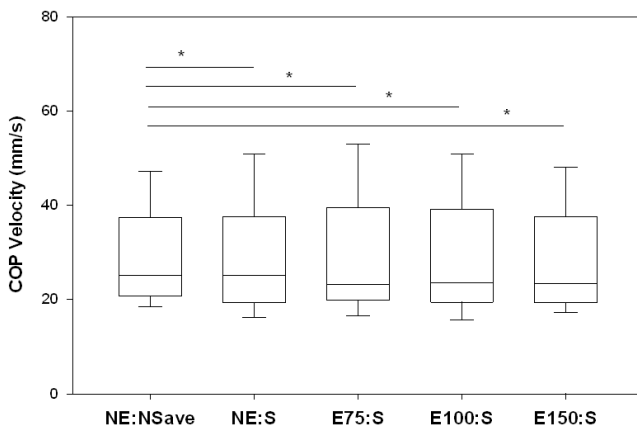


**Figure 2:** Median AP COP velocity (mm/s) during all five testing conditions. \*indicates a significant difference between conditions at the end of the horizontal bars.

However, the COP range and standard deviation in AP and ML directions and the COP mean velocity in the ML direction were not significantly different between the five conditions.

No significant differences were found between the three stimulation conditions or between the sleeve alone and the three stimulation conditions for any outcome measure.

These results are consistent with previous studies showing improved measures of postural control with the use of a knee sleeve. The absence of a significant additive improvement in balance with SR ES in this study may be due to the nature of sensory impairment in knee OA. SR ES aims to improve mechanoreceptor sensitivity. However, in a population with mechanoreceptor degradation resulting from OA, sensitivity improvements may not be possible.

Additionally, it is possible that any improvements with SR were masked by improvements resulting from the knee sleeve. Lastly, it is possible the sensitivity of specific mechanoreceptors necessary for proper postural control was not enhanced due to electrode placement and amplitude of the SR ES signal.

## CONCLUSIONS

The results of our study demonstrate the ability of a neoprene knee sleeve to reduce some static postural sway measures during a single-leg stance task in those with knee OA. However, the addition of SR ES appeared to have no significant added benefit.

Questions remain regarding the clinical significance of small improvements in the COP velocity and normalized total path length while wearing a knee sleeve. Future work should focus on optimization of both the stimulus placement and the detection threshold procedure for knee OA subjects in order to achieve a maximal effect of the SR ES.

## REFERENCES

1. Barret DS, et al. *The Journal of Bone and Joint Surgery* **73(B)**, 53-56, 1991.
2. Priplata AA, et al. *Annals of Neurology* **59**, 4-12, 2005.
3. Reeves P, et al. *Spine* **34**, 316-321, 2009.
4. Ross et al. *British Journal of Sports Medicine* **41**, 656-659, 2007.
5. Chuang et al. *Kaohsiung Journal of Medical Sciences* **23**, 405-410, 2007.

## ACKNOWLEDGEMENTS

This work was supported by a grant from the Arthritis Foundation

# ESTIMATING GROUND REACTION FORCES DURING LOCOMOTION IN ADULTS FROM ACTIGRAPH ACTIVITY MONITOR DATA

<sup>1</sup>Kelsey H. Collins, <sup>2</sup>Jennifer M. Neugebauer, M.S. and <sup>1,2</sup>David A. Hawkins, Ph.D.

<sup>1</sup>Department of Neurobiology, Physiology, and Behavior, UC Davis, CA, USA

<sup>2</sup> Biomedical Engineering Graduate Group, UC Davis, CA, USA

Email: dahawkins@ucdavis.edu

## INTRODUCTION

Physical activity monitors are small devices often worn on a person's hip to quantify the frequency, duration, and intensity of physical activity. These data have been used to estimate the person's energy expenditure. Some activity monitors (AM) provide output data in both units of energy expenditure (counts) and multiples of gravity (g). Recently, efforts have been made to use these devices to estimate the ground reaction forces acting on the body during gait. Neugebauer developed a regression equation to estimate peak vertical ground reaction forces (pVGRF) for children 10-14 years of age during walking and running tasks using a Biotrainer Activity Monitor (IM Systems, Arnold, MD) [1]. The Biotrainer AM utilizes a biaxial accelerometer and provides average peak acceleration information for a specified time epoch, the shortest epoch being 15 seconds. The Biotrainer AM data can be used to estimate average pVGRF during steady state gait, but may miss important force fluctuations that occur within a gait epoch. The ActiGraph GT3X+ monitor (ActiGraph LLC, Pensicola, FL) utilizes a tri-axial accelerometer and can report continuous acceleration data sampled at 100 Hz. This capability provides an opportunity to estimate pVGRF on a step-by-step basis. The purpose of this study was to develop a regression equation to estimate single step pVGRF for young adults during walking and running tasks using the ActiGraph AM.

## METHODS

Ten adults, 2 males and 8 females (age  $20.5 \pm 1.1$  yrs, height  $1.71 \pm 0.07$  m, mass  $70.6 \pm 3.6$  kg, BMI  $24.4 \pm 3.0$  kg/m<sup>2</sup>), wore an ActiGraph GT3X+ AM on a belt over their right hip. A second ActiGraph AM was worn on their right ankle to identify right

foot strike. Each subject completed eight to ten walking and running trials over a designated range of speeds. AM intensities (g) and pVGRF data (N) (Kistler, Amherst, NY) were measured for each trial. Six walking and six running trials were used to develop a mixed effects repeated measures model to predict natural log transformed pVGRF (R, R Foundation for Statistical Computing, Austria). The initial model included hip AM intensity, sex, height, mass, type of activity (run or walk), and intensity-type of activity interaction as fixed effects. Random effects included the subject specific response to increasing intensity. The desired significance level was  $p < 0.05$ . To validate the regression model, predicted pVGRF was compared to measured pVGRF for 2 to 4 of the gait trials per subject that were not used to develop the model.

## RESULTS

There was a positive relationship between the natural log transformed pVGRF and the activity monitor intensity for all subjects. The relationship between pVGRF and intensity differed for running trials compared to walking trials and between subjects (Figure 1).

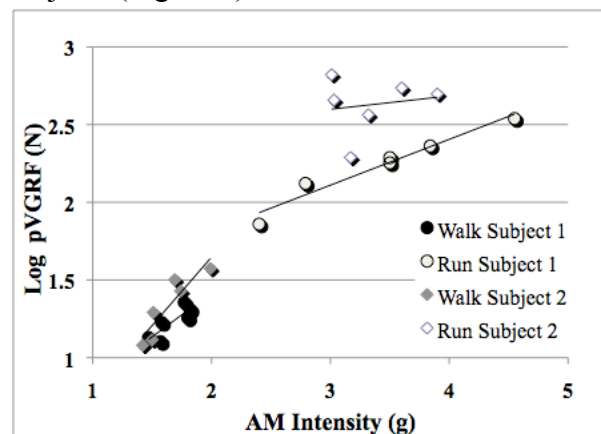


**Figure 1:** pVGRF as a function of AM intensity for two representative subjects included in the model.

Activity monitor intensity, mass, BMI, speed, type of activity (run or walk), and the intensity-type of activity interaction were significant fixed effects ( $p < 0.05$ ). Sex and activity monitor used were not significant fixed effects. The subject specific response to activity monitor intensity was a significant random effect ( $p < 0.001$ ). The coefficients for the derived mixed effects model equation (Equation 1) are listed in Table 1.

$$Y_{ij} = \beta_0 + X_{ij1}\beta_1 + X_{ij2}\beta_2 + X_{ij3}\beta_3 + X_{ij4}\beta_4 + X_{ij5}\beta_5 + X_{ij6}\beta_6 + A_{i0} + A_{i1}\text{intensity} + e_{ij} \quad (1)$$

where

$Y_{ij}$  = log-transformed pVGRF for subject i, trial j (N)

$X_{ij1}$  = hip activity monitor intensity (g)

$X_{ij2}$  = mass (kg)

$X_{ij3}$  = BMI ( $\text{kg}/\text{m}^2$ )

$X_{ij4}$  = speed (m/s)

$X_{ij5}$  = type of activity (run)

$X_{ij6}$  = Intensity-type of activity interaction

$\beta$  = coefficient associated with respective fixed effect

$A_{i0}$  = overall tendency for a subject i to be above or below line

$A_{i1}$ intensity = differential response to increasing intensity for subject i

$e_{ij}$  = error in trial j for subject i

## DISCUSSION

pVGRF depends on body mechanics, mass, and the acceleration at the time when the individual contacts the ground. As mass and height increase, pVGRF generally increases. Also, an individual's gait pattern affects pVGRF. As a result, intensity, mass, speed, and type of activity were expected to be significant fixed effects.

The significance of activity type in the model illustrates the difference in responses for walking

and running trials. The random effects interaction between the individual and the activity monitor intensity further illustrates the subject specific response for running and walking.

On average, the regression equation was able to predict pVGRF within 10.5% of the measured pVGRF. This was determined to be an acceptable accuracy for estimating lower extremity loading of people performing their normal daily gait activities.

A limitation of this investigation is the number of subjects evaluated. A larger subject pool including more male subjects would provide better generalizability to estimate force for a broader population. Additionally, walking and running trials were exclusively included in the model. Future analysis including jumping trials could extend the predictive ability of the model.

## CONCLUSION

A regression equation was developed to estimate single step pVGRF for young adults during walking and running tasks using the ActiGraph AM and person specific characteristics. The fixed effects model used to develop a regression equation should include AM intensity, mass, BMI, speed, type of activity, and the intensity-type of activity interaction. Additionally, the random effects of the subject specific response to increasing activity monitor intensity should be included. The ActiGraph GT3X+ Activity Monitor can be used to estimate single step pVGRF for a young adult population.

## REFERENCES

1. Neugebauer, J., Med. Sci. Sports Exerc. 42(5), 270, 2010.

**Table 1:** Coefficients from fixed effects ActiGraph regression equation.

| Effect      | $\beta_0$ | $\beta_1$ | $\beta_2$ | $\beta_3$ | $\beta_4$ | $\beta_5$ | $\beta_6$ |
|-------------|-----------|-----------|-----------|-----------|-----------|-----------|-----------|
| Coefficient | 5.5       | 0.203     | 0.016     | 1.2       | 0.14      | 0.9       | -0.23     |
| P-Value     | <0.001    | <0.001    | <0.05     | 0.05      | <0.001    | <0.001    | <0.001    |

# ISOKINETIC STRENGTH AND POWER DEFICITS IN THE HAND FOLLOWING STROKE

<sup>1</sup>Megan Conrad and <sup>1,2</sup>Derek Kamper

<sup>1</sup>Rehabilitation Institute of Chicago, Chicago, IL, USA

<sup>2</sup>Illinois Institute of Technology, Chicago, IL, USA

email: [m-conrad@northwestern.edu](mailto:m-conrad@northwestern.edu)

## INTRODUCTION

The ability to grasp and manipulate objects is essential for activities of daily living. Successful object manipulation requires control both of hand posture and of the force applied to the object, often simultaneously. Impairment of this motor control following stroke leads to hand disability. While isometric force or torque generation and velocity of hand movement have been studied independently in stroke survivors, the impact of the stroke on the dynamic interaction of these quantities, or force production during movement, remains relatively unexplored. Thus, the goal of this study was to compare the torque production in paretic and non-paretic hands during isokinetic tasks following stroke. We hypothesized that the paretic hand would produce lower torque when moving at high velocities. Additionally, we expected power deficits to be accentuated at higher velocities and to be greater in finger extension compared to finger flexion.

## METHODS

The maximum flexion and extension torque produced by the MCP joint was measured in the paretic and non-paretic hand of ten moderately impaired (Stage 4 or 5) chronic stroke survivors (as measured on the Stage of Hand Section of the Chedoke-McMaster Stroke Assessment [1]). The subject's wrist was fixed in a neutral posture with a fiberglass cast, which was clamped to a tabletop such that the palm was perpendicular to the table. The fingers were coupled to a servomotor (PMI Motion Technologies, Radford, VA) through a U-shaped shaft. Rotation of the shaft produced identical rotation of the MCP joints of the four fingers. Each trial consisted of a maximum isokinetic flexion (from 0° to 60° flexion) or isokinetic extension (from 60° to 0° flexion) movement. The servomotor controlled movement during each trial at one of four constant rotational

velocities: 0°/s (isometric), 10°/s, 60°/s or 120°/s. The experimenter verbally encouraged subjects to exert maximum torque in opposing the imposed movement of the shaft throughout all trials. A total of 24 trials (3 trials x 2 directions x 3 velocities) were completed, with sufficient rest between trials to minimize fatigue. Position and torque were recorded from the optical encoder (PMI) and torque transducer (Transducer Tech, Temecula, CA) on the servomotor. EMG signals were recorded from the flexor digitorum superficialis (FDS) and extensor digitorum communis (EDC) muscles (Delsys Inc., Boston, MA).

Position, velocity and torque data was low-pass filtered at 20 Hz using a 30<sup>th</sup> order FIR filter. Mean torque recorded from the transducer during each trial was compared between the four movement velocities. Power, a measure of the force production at a given velocity, was calculated according to  $P(t)=\tau(t)\cdot\omega(t)$  where  $\tau$  represents torque and  $\omega$  represents angular velocity at a given time,  $t$ . Power deficits were computed at each movement velocity as the percent decrease in power produced by the paretic hand compared to the non-paretic hand. EMG data was bandpass filtered (10-320 Hz), rectified and low pass filtered (10 Hz) to obtain an envelope. Muscle activation at each movement velocity was evaluated as a percentage of the maximum activity during isometric contractions. A repeated measures ANOVA was performed to explore the effects of velocity and direction on EMG, torque and power production ( $\alpha= 0.05$ , SPSS, Chicago, IL).

## RESULTS AND DISCUSSION

As expected, significantly lower flexion and extension torques were produced with the paretic hand ( $p<0.05$ , Fig.1). During isometric contractions, the mean torque produced by the paretic hand was less during extension (1.69 Nm) compared to flexion (2.05 Nm). However, torque deficits, or the

amount of torque produced in the paretic hand compared to that produced by the non-paretic hand, were considerably less during extension (26% compared to a 41% deficit during flexion). For isokinetic contractions, though, relative deficits were greater for extension torque than flexion torque production (Fig. 1).

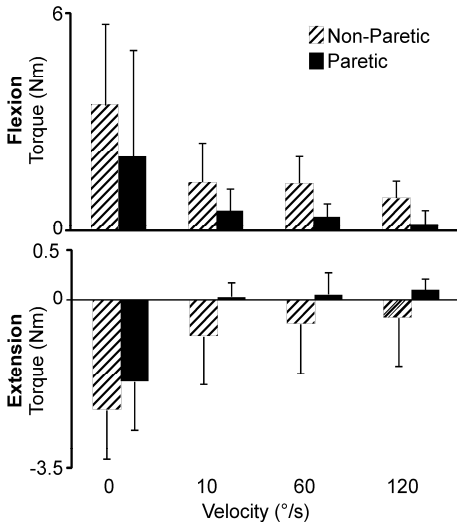


**Figure 1:** Torque production was lower in the paretic hand than the non-paretic hand and was influenced by movement direction (flexion vs extension) and rotational velocity of the MCP joint.

In fact, many subjects were unable to maintain extension torques throughout the duration of isokinetic movement trials, thereby resulting in a mean flexion torque during extension trials. Power deficits in general increased with greater rotational speed (Fig. 2). Extension deficits increased from 26% at the isometric contraction to the maximum value (100%) at 10°/s, and stayed at this level for higher speeds. Flexion deficits jumped from 41% at isometric to 57% at 10°/s and continued to rise to 76% at 120°/s.

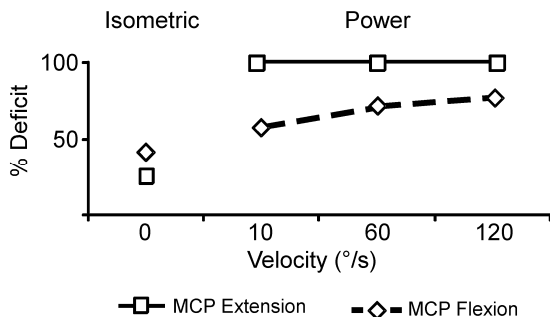


**Figure 2:** Deficits in the amount of force exerted by the stroke hand are greater in extension than during flexion and appear to increase with movement velocity

Thus, strength testing of stroke survivors under isometric conditions may underestimate the level of impairment, as even at very low movement speeds

torque deficits increase substantially. The mechanisms of this power impairment have not been fully elucidated. Co-contraction of agonist and antagonist muscles could contribute, but we actually observed a smaller ratio of antagonist to agonist activity in paretic muscles than in non-paretic muscles during both flexion and extension trials (Fig. 3).

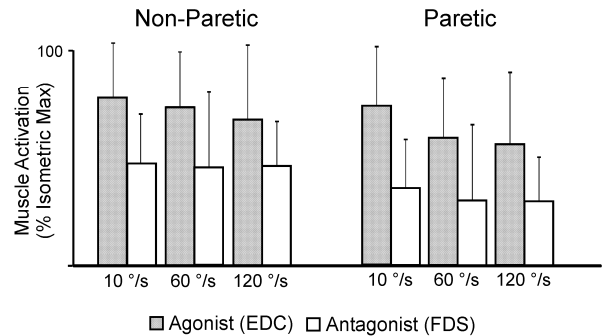


**Figure 3:** Peak muscle activation as a percent peak isometric activity suggests agonist-antagonist co-activation was not greater in paretic muscles.

An ultrasound study recently conducted in our laboratory suggests that muscle atrophy, while present, accounts for only a small percentage of these deficits. A shift toward type I (slow twitch) muscle fibers from type II (fast twitch) fibers would decrease the ability of stroke survivors to generate force, particularly at high movement velocities. Yet, some studies in this area suggest that there is actually a shift from type I to type II fibers [2]. Type II fibers, however, may be more susceptible to atrophy than type I fibers [3]. Additionally, an inability to voluntarily activate all existing muscle fiber or a decrease in the number of active motor units in hand muscle would also affect force production. Our data suggest further investigation into the underlying neuromuscular mechanisms behind isokinetic force production is warranted, especially in respect to extensor versus flexor muscles.

## REFERENCES

- Gowland C, et al. *Stroke* **24**, 58-63, 1993.
- Hafer-Macko CE, et al. *J Rehabil Res Dev*, **45**, 261 – 72, 2008.
- Klein CS, et al. *J Appl Physiol*, **109**, 1337-46, 2010.

## ACKNOWLEDGEMENTS

This research was supported by an American Heart Association Fellowship (#11POST4980024).

# THE MECHANICAL DETERMINANTS OF ENERGETIC COST IN BACKWARD RUNNING

Cynthia Conti, Sarah Musolf and Justus Ortega

Humboldt State University, Arcata, CA USA  
email: jdo1@humboldt.edu, web: <http://www.humboldt.edu/~jdo1>

## INTRODUCTION

Backward running elicits a 30% higher metabolic cost than forward running [4]. Prior research suggests that the greater metabolic cost of backward running results from generating muscle force at a faster rate due to using a faster stride frequency [7]. However, backward running may be energetically more costly as a result of using a more flexed limb posture and thus, a reduction in leg extensor muscle mechanical advantage during the stance phase [3].

In healthy adults, the metabolic cost of running increases with stride frequency [6]. Backward running is associated with a faster stride frequency than forward running [7] and thus, may cause a greater metabolic cost of leg swing. However, the higher metabolic cost of backward running may also be related to an increase in the metabolic cost of supporting body weight as a result of running with a more flex limb posture that reduces the mechanical advantage of the leg extensor muscles [1]. This study tests the hypothesis that backward running increases metabolic energy consumption due to a greater cost of generating force resulting from a decreased time of ground contact and increased flexion of the legs during the stance phase of running and not due to an increase in stride frequency.

## METHODS

Twelve adults ( $31.4 \pm 11.4$  years; six females and six males) ran forward and backward on a treadmill at a speed of 2.24 m/s (5 mph). We examined the effect of stride frequency on metabolic cost and kinematics as subjects performed three seven minute running trials: one forward at preferred stride frequency, one backward at preferred stride frequency and one forward at a prescribed stride frequency matched to the backward stride frequency (Matched SF). Metabolic cost was determined using indirect calorimetry during the last two minutes of

each treadmill trial [2]. We calculated the net metabolic cost (W/kg) by subtracting standing metabolic power from gross metabolic power and dividing by body mass. We measured the kinematics of the lower limbs for 10 strides during the last two minutes of each treadmill trial using a 3-D motion capture system (Vicon, Centennial, CO). We calculated maximum joint flexion angle and average joint flexion angle during the stance phase of each step for the hip, knee and ankle joints. We measured the time of foot-ground contact ( $T_C$ ) and then calculated the cost coefficient ( $c$ ) as the ratio of the net metabolic rate ( $\dot{E}_{met}$ ) to  $1/T_C$ , normalized to body weight ( $W_b$ ). We calculated preferred stride frequency for forward and backward running from the number of steps taken in a 1-minute period.

## RESULTS AND DISCUSSION

At preferred stride frequency, backward running elicits a 38% increase in metabolic cost, compared to forward running ( $P < 0.0001$ ). Moreover, when using the same stride frequency, backward running elicited a 33% greater metabolic cost than forward running ( $P < 0.0001$ ) (Figure 1; Table 1).

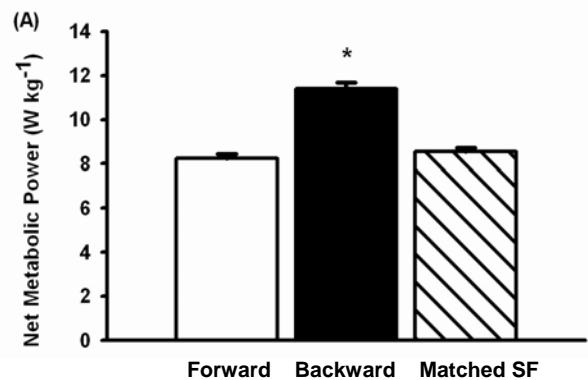


**Figure 1:** Net metabolic power for forward running (preferred stride frequency), backward running (preferred stride frequency), and forward running at a stride frequency matched to backward running.

The cost coefficients of backward and forward running were both 0.26 ( $P=0.424$ ). In backward running, subjects spent approximately 31% less time in contact with the ground ( $P<0.0001$ ) than in forward running ( $P<0.0001$ ). At the same stride frequency, subjects spent an average 26% less time in contact with the ground during backward running ( $P<0.0001$ ). Interestingly, when subjects ran backwards the average knee joint angle during the stance phase was 18% more flexed when compared to forward running ( $P=0.009$ ) (Figure 2; Table 1).

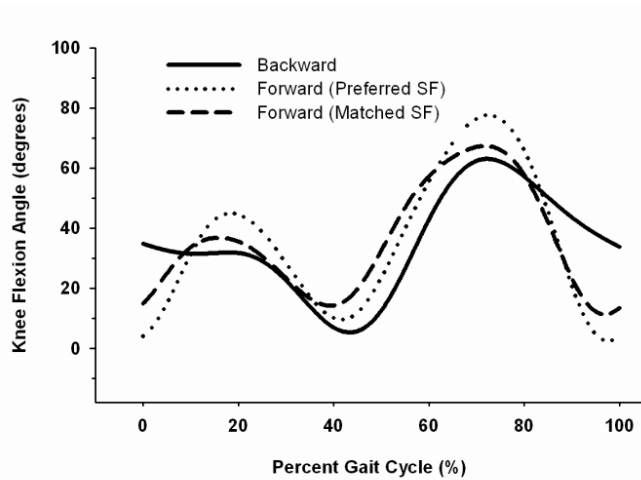


**Figure 2:** Average knee flexion angle as a function of gait cycle for three running conditions: Backward (preferred stride frequency), Forward (preferred stride frequency), and Forward (matched stride frequency).

Whether using preferred or matched stride frequencies, backward running elicits a greater metabolic cost compared to forward running. Thus, in support of our hypothesis, these results suggest the greater metabolic cost of backward running is not the result of using a faster stride frequency. Instead, we found that human runners consume substantially more metabolic energy when running backward primarily due to an increase in the cost of generating force as a result of spending less time in contact with the ground and using greater knee

flexion during the stance phase. Using a shorter time of ground contact increases the rate of muscle force generation [5]. Moreover, using greater stance knee flexion decreases the mechanical advantage of the stance limb extensor muscles and thus requires more force to support body weight [1]. Together these factors increase the metabolic cost of generating force in backward running. Further validation of our findings is present in the cost coefficient data of forward and backward running which suggests the difference in metabolic cost between forward and backward running is directly proportional to the rate of ground force application.

## CONCLUSIONS

In conclusion, the results of our study strongly support the hypothesis that the cost of generating force is a primary determinant of metabolic energy consumption for backward running due to the decreased mechanical advantage of the knee extensor muscles and the increased rate of force generation.

## REFERENCES

1. Biewener AA. *Science*, **245**, 45-48, 1989.
2. Brockway JM. *Human Nutrition: Clinical Nutrition*, **41**, 463-471, 1987.
3. DeVita P & Stribling J. *Medicine and Science in Sport and Exercise*, **23**, 602-610, 1991.
4. Flynn TW, et al. *Journal of Orthopedic and Sports Physical Therapy*, **17**, 108-112, 1993.
5. Kram R & Taylor, CR *Nature*, **346**, 265-267, 1990
6. Taylor CR, et al. *Journal of Experimental Biology*, **219**, 1104-1107, 1982.
7. Wright S & Weyand PG. *The Journal of Experimental Biology*, **204**, 1805-1815, 2001.

**Table 1:** Metabolic and kinematic data for forward, backward, and forward (matched stride frequency) running

|                   | Net Cost<br>(Watt/kg) | $T_C$<br>(seconds) | Cost Coefficient<br>(J/N) | Ave Knee Flexion<br>(deg) | Stride<br>Frequency (Hz) |
|-------------------|-----------------------|--------------------|---------------------------|---------------------------|--------------------------|
| <b>Forward</b>    | 8.23 ± 0.73           | 0.32 ± 0.04        | 0.27 ± 0.04               | 26.2 ± 3.4                | 1.37 ± 0.08              |
| <b>Backward</b>   | 11.40 ± 0.98          | 0.22 ± 0.04        | 0.26 ± 0.05               | 31.0 ± 5.7                | 1.55 ± 0.14              |
| <b>Matched SF</b> | 8.54 ± 0.65           | 0.31 ± 0.04        | 0.26 ± 0.03               | 26.0 ± 2.6                | 1.54 ± 0.14              |

## 2D/3D hybrid structural model of vocal folds

Douglas Cook<sup>\*</sup>, Pradeep George and Margaret Julias

Division of Engineering, New York University, Abu Dhabi, UAE

### INTRODUCTION

The modeling of human phonation presents a formidable challenge since this system involves complex fluid dynamics, structural vibration, acoustic propagation, and active control of the vocal apparatus by the speaker. Models of phonation by necessity thus rely upon simplifying assumptions: the fluid and solid domains have both been approximated as two-dimensional and the acoustic system is commonly approximated as one dimensional [1]. In a series of studies beginning in 1985, Fari Alipour and his collaborators used a modeling scheme in which several thin two-dimensional regions were coupled together using a string model [2]. The discrepancy between the 2D and 3D models have been reported by Cook [3]. This study demonstrates that the shear stresses neglected by plane strain models are indeed responsible for the differences between 2D and 3D vocal fold models [3] by introducing a new model that exhibits the vibratory characteristics of a 3D model with the computational efficiency of a 2D model.

### METHODS

Consider a thin region,  $R$ , of thickness  $w$ , one side of which lies at the center of an idealized vocal fold geometry (see Figure 1). Previous formulations have modeled  $R$  using a plane strain model. When  $R$  is examined in the absence of the remaining vocal fold structure, the stresses acting on this region are  $\sigma_{yy}$ ,  $\sigma_{yx}$ , and  $\sigma_{yz}$  ( $\sigma_{ij}$  represents the stress acting in the  $j$ -direction on the  $i$ -direction face). By including the stress components listed above, we can obtain an improved formulation that more accurately represents the three-dimensional characteristics of the vocal folds.

Following the method of Berry and Titze[4], we assume a vocal fold displacement field that is sinusoidal in the  $y$ -direction, while neglecting displacements in the anterior/posterior direction. The 3D displacement field of the vocal folds can then be expressed as notated in the following equations (1a, 1b, 1c). In these equations,  $u_c$  and  $w_c$  represent the vocal fold displacements at the mid-coronal plane of the vocal folds. To complete the model, we require the values of shear stresses that

act on  $R$ . Assuming a transversely isotropic material, Hooke's Law provides equations for the remaining stress components  $\sigma_{yx}$  and  $\sigma_{yz}$ .  $G'$  indicates the longitudinal shear modulus of the vocal folds and  $\epsilon_{ij}$  represents shear strain. When the assumed forms of  $U$ ,  $V$ , and  $W$  were substituted into displacement strain relationships, equations 2(a) and 2(b) were obtained. The final model (referred to hereafter as the "hybrid" model) uses a 2D computational domain, but produces a 3D vocal fold displacement field.

$$U(x, y, z) = u_c(x, z) \sin\left(\frac{\pi y}{L}\right) \quad 1(a)$$

$$V(x, y, z) = 0 \quad 1(b)$$

$$W(x, y, z) = w_c(x, z) \sin\left(\frac{\pi y}{L}\right) \quad 1(c)$$

$$\tau_{yx} = \frac{G'\pi}{2L} u_c(x, z) \cos\left(\frac{\pi y}{L}\right) \quad 2(a)$$

$$\tau_{yz} = \frac{G'\pi}{2L} w_c(x, z) \cos\left(\frac{\pi y}{L}\right) \quad 2(b)$$

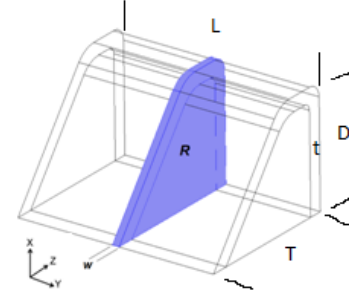
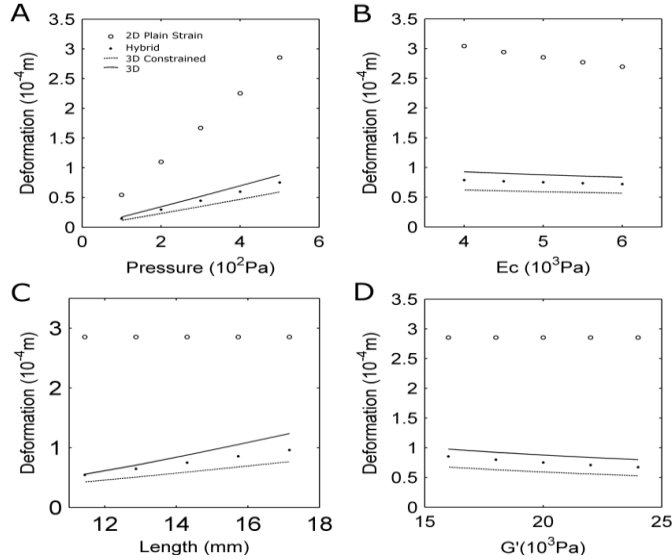


Figure1. 3D view of vocal fold geometry

### RESULTS AND DISCUSSION

The validity of the hybrid model was thoroughly tested using a series of comparisons between four models: a regular 2D plane strain model, a 2D/3D hybrid model as described above, a 3D model in which longitudinal motion was constrained, and a 3D unconstrained vocal fold model. All models possessed the same coronal geometry (cross-section in fig.1). The model dimensions and linearly elastic material properties are given in Table I. All motion was restricted at the anterior, posterior, and lateral boundaries. Static deformation simulations were

used to assess each model's stiffness characteristics, for a given applied pressure loading on the inclined edge while modal analysis is used to assess dynamic characteristics of the models. The response of various models when subjected to static pressure loading is shown in Figure 2. The hybrid model, was found to produce deformations similar to both the three-dimensional models. The average relative errors for plane-strain, constrained, and hybrid models were 222%, 33%, and 14% respectively with respect to the 3D model.



**Figure 2:** Static deformation at the inferior point of a mid-coronal cross-section of the vocal folds. A) static deformation as a function of pressure amplitude. B) static deformation as a function of  $E_c$  ( $P = 500$  Pa); C) static deformation as a function of  $L$  ( $P = 500$  Pa); D) static deformation as a function of  $G'$  ( $P = 500$  Pa).

**Table I: Properties for the models**

| Parameter                             | Nominal value | Applicable models: |        |    |
|---------------------------------------|---------------|--------------------|--------|----|
|                                       |               | Plane strain       | hybrid | 3D |
| Length ( $L$ )                        | 14.3mm        |                    | x      | x  |
| Depth ( $D$ )                         | 8.5mm         | x                  | x      | x  |
| Thickness ( $T$ )                     | 11mm          | x                  | x      | x  |
| Cover thickness ( $t$ )               | 1mm           | x                  | x      | x  |
| Cover stiffness ( $E_c$ )             | 5kPa          | x                  | x      | x  |
| Transverse Young's Modulus ( $E_b$ )  | 10kpa         | x                  | x      | x  |
| Longitudinal Young's Modulus ( $E'$ ) | 30kpa         |                    |        | x  |
| Longitudinal Shear Modulus ( $G'$ )   | 20kpa         |                    | x      | x  |

All results in the modal analysis section were restricted to the x-10 and x-11 modes of vibration [5]. In all modal analyses, the modal frequencies of the hybrid model were found to be more accurate than the plane strain model as shown in Figure 3. The frequencies predicted by the plane strain model are from 16 to 53 Hz lower than those of the three-dimensional model (12% to 34% relative error).

The hybrid model is much more accurate, with relative error ranging from 1.4% to 6.9%.

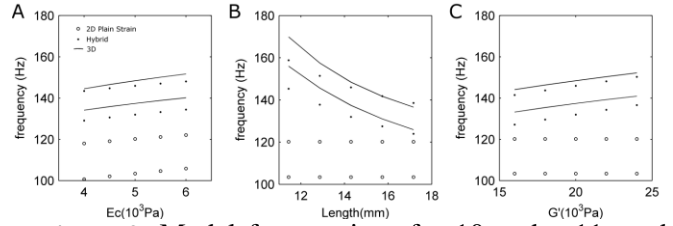


**Figure 3:** Modal frequencies of x-10 and x-11 mode shapes for plane strain, hybrid, and three-dimensional models. For each model, the higher modal frequency represents the x-11 mode while the lower modal frequency represents the x-10 mode.

## CONCLUSIONS

The inclusion of shear stresses (which are neglected in plane strain models) has been shown to account for the discrepancies observed between 2D and 3D vocal fold models. The hybrid model produces a three-dimensional displacement field similar to that of a three-dimensional model. The hybrid model therefore appears to be an excellent alternative to plane strain models since it captures important three-dimensional effects of the vocal folds without the added computational expense of a three-dimensional model.

## REFERENCES

1. Liljencrants, J., 1985. Speech synthesis with a reflection-type line analog. Ph.D. dissertation, Royal Institute of Technology, Stockholm, Sweden.
2. Alipour-Haghighi F., and Titze I.R., 1985. Simulation of particle trajectories of vocal fold tissue during phonation. Vocal Fold Physiology: Biomechanics, Acoustics, and Phonatory Control. Ed. by Titze and Scherer, Denver Center for the Performing Arts, Denver, CO, USA.
3. Cook, D.D., 2009. Systematic structural analysis of human vocal fold models. PhD Dissertation, Purdue University, USA.
4. Berry, D.A., and Titze, I.R., 1996. Normal modes in a continuum model of vocal fold tissues. *J. Acoust. Soc. Am.* 100, pp. 3345–3354.
5. Titze, I.R., and Strong, W.J., 1975. Normal modes in vocal cord tissues. *J. Acoust. Soc. Am.* 57, pp. 736–744.

# ASSESSING ACCURACY OF A 3D CANCELLOUS BONE QUANTIFYING ALGORITHM

Nicole C. Corbiere, Ajay V. Sonar, Kathleen A. Issen, James J. Carroll, and Laurel Kuxhaus

Clarkson University, Potsdam, NY, USA

email: lkuxhaus@clarkson.edu web: http://people.clarkson.edu/~lkuxhaus

## INTRODUCTION

Osteoporosis can lead to vertebral compression fractures and there is currently no method to predict in whom such fractures will occur. Vertebral cancellous bone micro-architecture includes rod-like and plate-like structures of varying sizes and orientations. It is the failure of these structures that leads to vertebral collapse. Identifying fracture origin will help physicians determine which patients are at the highest risk for a fracture. To make this prediction, it is necessary to quantify the micro-architecture of cancellous bone. A bone quantifying algorithm [2] was implemented and validated. This algorithm describes the geometric properties of cancellous bone using images from a micro-computed tomography ( $\mu$ CT) scan [5]. To validate this implementation, models of known geometry were created using computer aided design.

## METHODS

The quantification algorithm was implemented in MATLAB (MathWorks, Natick, MA). Briefly, the algorithm reads  $\mu$ CT images of cancellous bone, creates a voxel file, and outputs descriptive geometric parameters [5]. To assess the accuracy of the algorithm, 3D structures of known size with both regular and bone-like geometry were created. The *regular structures* were created in Pro/ENGINEER (PTC, Needham, MA). A 3D grid of eight parallelepiped cells was created (Figure 1a), with 54 struts. The cells have an aspect ratio of 1.3, similar to cancellous bone [1]. To test the algorithm with a variety of known orientations, this structure was then rotated  $+5^\circ$  and  $-30^\circ$  to create tilted structures (Figures 1b and 1c). The regular structure was perturbed to create the *bone-like structure*. Custom MATLAB code used a Voronoi algorithm to perturb the rectilinear arrangement, creating a cancellous bone-like structure. The parameter of perturbation,  $\alpha$ , was 0.4, similar to that of

cancellous bone [4]. The coordinates of the “trabecula” intersections were then imported into AutoCAD (Autodesk Inc., San Rafael, CA) and used as the corners of the structure. A custom program in AutoLISP (Autodesk Inc., San Rafael, CA) connected these corners with cylindrical struts and spherical joints of the same diameter. When the  $2 \times 2 \times 2$  regular cube structure was perturbed, it became a structure of 27 Voronoi cells. For algorithm validation, one of the perturbed cells (Figure 1d), which had 49 struts, was constructed in AutoCAD.

The geometric files were exported in surface triangulation language (STL) format, and converted to a voxel file, similar to the output of a  $\mu$ CT scanner. The images were then imported into the bone quantifying algorithm and the following geometric properties were computed: rod trabecular thickness (rTb.Th), trabecular spacing (Tb.Sp), bone volume (BV), and trabecular angle (Tb.Ang) which is the angle of the strut from the xy plane.

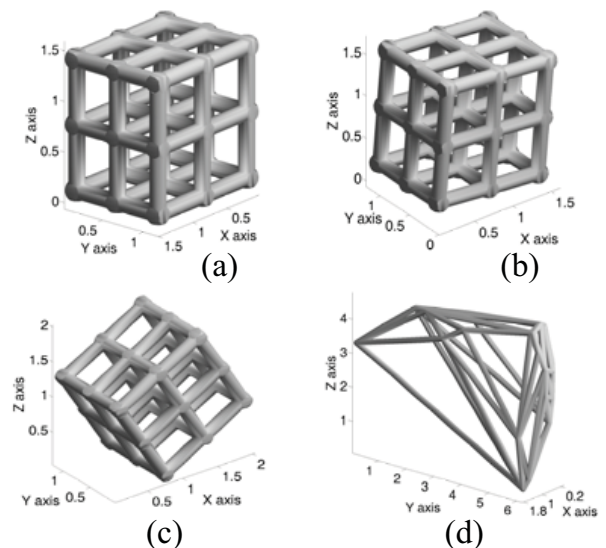


**Figure 1** - (a) Regular structure, (b) Rotated  $+5^\circ$ , (c) Rotated  $-30^\circ$ , (d) Bone-like 1-cell structure (Units are mm.)

The percent error between the known and computed values was determined for rTb.Th, Tb.Sp, and BV. The absolute error was determined for Tb.Ang.

Resolution is an adjustable parameter in this algorithm. The error should be reduced as resolution is increased. The regular structure (Figure 1a) was used to evaluate this hypothesis using four different resolutions.

## RESULTS

Table 1 shows the computed errors. For computational efficiency, these were calculated at a resolution of 0.0167 mm/voxel for structures *a*, *b*, and *c*, and at a resolution of 0.0333 mm/voxel for structure *d*. Tb.Sp was not computed for structure *d*. Figure 2 shows the exponential-like decay of error for Tb.Sp and BV as the resolution becomes finer. The error for rTb.Th does not follow this trend at the smallest voxel sizes.

**Table 1** – Parameter error

| Parameter    | a     | b     | c     | d     |
|--------------|-------|-------|-------|-------|
| rTb.Th (%)   | 4.18  | 4.12  | 1.54  | 2.34  |
| Tb.Sp (%)    | 3.64  | 4.29  | 1.70  | ---   |
| BV (%)       | 1.29  | 0.07  | 0.02  | 0.85  |
| Tb.Ang (abs) | 0.08° | 0.67° | 2.30° | 1.65° |

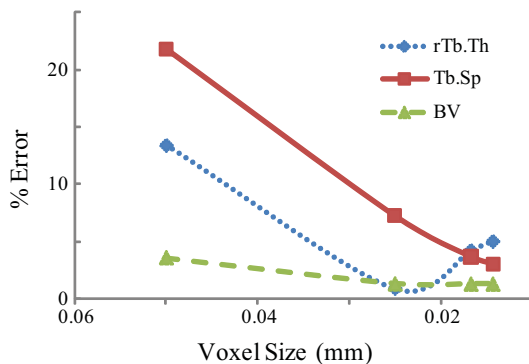


**Figure 2** - Percent error vs. voxel size

## DISCUSSION

A 3D quantification algorithm to describe cancellous bone micro-architecture was validated with bone-like structures of known dimensions. Absolute error of Tb.Ang was low – always less than 3°. A possible source of this error is that the true angles were exported as integers from AutoCAD.

The percent error for rTb.Th, Tb.Sp, and BV could be lower for structure *c* than for structures *a* and *b* because the algorithm creates partially-filled voxels when strut borders do not coincide with voxel boundaries. This results in an overestimate (“pseudo-thickening”) of the rTb.Th, which contributes to the errors in the measured parameters, especially of structure *a*. Structures *b* and *c* are less affected due to their strut orientations. The pseudo-thickening effect is reduced with a finer resolution. For rTb.Th, the error is lowest for a voxel size of 0.025 mm. In this case, the strut thickness was nearly an integer multiple of the voxel size and the strut boundaries most nearly coincided with the voxel boundaries, minimizing the pseudo-thickening effect. This suggests that the most accurate results would be obtained from  $\mu$ CT scans of vertebrae tilted 45°. It is expected that, when using the algorithm to quantify cancellous bone, the error will be comparable to the values shown for structure *d* in Table 1.

The consistency of the bone quantifying algorithm was demonstrated, given that the percent error values are the same order of magnitude. This implementation of the quantifying algorithm had errors of less than 5% for voxel sizes smaller than 0.02 mm. Thus the algorithm is sufficient for use in the development of a clinically-useful tool.

Current work includes measuring Tb.Sp of perturbed structures, quantifying structures with plates, and combining this algorithm with a bone remodeling algorithm [3]. This will ultimately lead to a clinical tool that predicts the micro-architectural initiation of vertebral compression fractures.

## REFERENCES

1. Gilad I and Nissan M *J Anat* **143**, 115-120, 1985.
2. Hildebrand T et al. *JBMR*. **14**, 1167-1174, 1999.
3. Ruimerman R et al. *Comp Meth Biomech Biomed. Eng.* **4**, 433-448, 2001.
4. Silva MJ and Gibson LJ. *Bone* **21**, 191-199, 1997.
5. Sonar AV et al. *ASB*, Providence, RI, USA, 2010.

## ACKNOWLEDGEMENTS

Thanks to Bill Gilliss and Kenneth Willmert for assistance with AutoLISP and AutoCAD.

# BIOMECHANICS OF HEAD IMPACTS IN AMERICAN FOOTBALL PLAYERS

Joseph J. Crisco<sup>1</sup>, Bethany J. Wilcox<sup>1</sup>, Jonathan G. Beckwith<sup>2</sup>, Jeffrey J. Chu<sup>2</sup>, Ann-Christine Duhaime<sup>3</sup>, Steve Rowson<sup>4</sup>, Stefan M. Duma<sup>4</sup>, Arthur C. Maerlender<sup>5</sup> and Richard M. Greenwald<sup>2</sup>

<sup>1</sup>Bioengineering Laboratory, Department of Orthopaedics, Brown University, Providence, RI, USA, <sup>2</sup>Simbex, Lebanon, NH, USA, <sup>3</sup>Pediatric Neurosurgery, Dartmouth Hitchcock Medical School, Lebanon, NH, USA, <sup>4</sup>Virginia Tech-Wake Forest, Center for Injury Biomechanics, Blacksburg, VA, USA <sup>5</sup>Department of Psychiatry, Dartmouth Hitchcock Medical School, Lebanon, NH, USA  
email: [joseph\\_crisco@brown.edu](mailto:joseph_crisco@brown.edu) web: <http://www.brownbiomechanics.org>

## INTRODUCTION

Concussion and subconcussive injuries remain poorly understood in part because the injury mechanism remains elusive. The purpose of this study was to quantify head impact exposures (impact frequency, location on the helmet and magnitude) for individual collegiate football players and to investigate differences in head impact exposure by player position.

## METHODS

A total of 314 players from three National Collegiate Athletic Association (NCAA) football programs (Brown University, Dartmouth College, and Virginia Tech) were recruited in this institutional review board approved observational study after informed consent was obtained. During the 2007, 2008 and 2009 fall football seasons, each player was categorized into one of eight positions: defensive line (DL, n = 49), linebacker (LB, n = 47), defensive back (DB, n = 55), offensive line (OL, n = 75), offensive running back (RB, n = 37), wide receiver (WR, n = 30), quarterbacks (QB, n = 14), and Special Teams (ST, n = 7). ST players were not included in this analysis because of the relative low number of players.

All players wore Riddell (Riddell, Chicago IL) football helmets instrumented with the HIT System, consisting of six linear accelerometers (sampling 1000 Hz) and associated electronics that enable the recording of every head impact and computation of head accelerations and associated severity measures [1]. Laboratory impact tests have determined that the linear and rotational accelerations measured by the HIT System were within  $\pm 4\%$  of those accelerometers measured concurrently with a

Hybrid III dummy fitted with a HIT System helmet [2].

Head impact exposure was defined for each individual player using measures of impact frequency, location and magnitude. Head impact frequency was quantified by *impacts per season*, the total number of head impacts for a player during all team sessions in a single season. *Impact locations* were categorized as front, side (left and right), back, and top. Impact magnitude was quantified by *peak linear acceleration* (g) and *peak rotational acceleration* (rad/s<sup>2</sup>). Additionally, a non-dimensional measure of head impact severity, *HITsp* [3] was computed. HITsp transforms the computed head impact measures of peak linear and peak angular acceleration into a single latent variable using Principal Component Analysis, and applies a weighting factor based on impact location. It thus serves as a measure of impact severity, with weight given to factors shown in previous head injury research to predict increased likelihood of clinical or anatomic injury. Impacts were further reduced for analysis by computing the 95<sup>th</sup> percentile value of all seasonal impacts for each individual player.

Results were expressed as median [25-75% interquartile range]. The significance of the differences among player positions in impact frequency (impacts per season) and in severity measures (95th percentile peak linear acceleration, 95th percentile rotational acceleration, and 95th HITsp) were examined separately using a Kruskal-Wallis one-way ANOVA on ranks with a Dunn's post-hoc test for all pairwise comparisons. Statistical significance was set at  $\alpha = 0.05$ . All statistical analyses were performed using SigmaPlot (Systat Software, Chicago, IL).

## RESULTS AND DISCUSSION

A total of 286,636 head impacts were analyzed in this study. The total number of impacts received by an individual player during a single season was 420 [217-728], with a maximum of 2492.

The number of impacts per season ranged from 149 [96-341] for QB to 718 [468-1012] for DL (Fig. 1). DL, LB and OL received the highest number of impacts per season, and QB and WR the lowest. The number of impacts per season received by DL were significantly ( $P < 0.05$ ) more frequent than QB, WR (157 [114-245]), RB (326 [256-457]), DB (306 [204-419]), but not different than LB (592 [364-815]) or OL (543 [264-948]). LB received significantly ( $P < 0.05$ ) more frequent impacts per season than QB, WR, DB and RB. OL received significantly ( $P < 0.05$ ) more frequent impacts per season than QB, WR and DB.

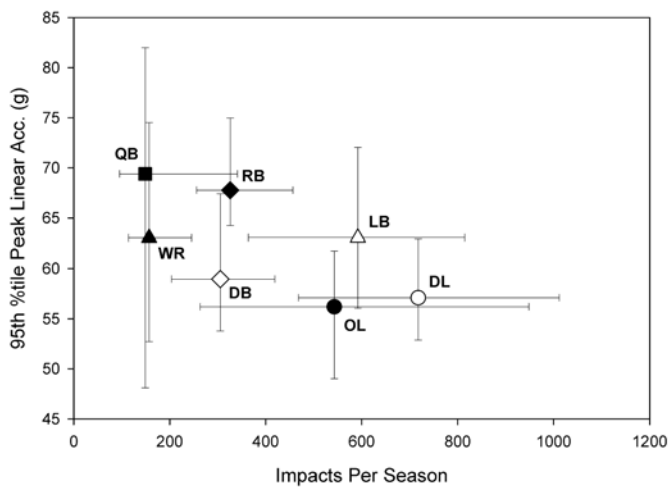


**Figure 1.** Median [25%- 75%] 95<sup>th</sup> percentile of peak linear acceleration (g) as a function of the median [25%- 75%] number of head impacts per season categorized by player position.

RB received the impacts with greatest magnitude accelerations and highest HITsp values. The 95th percentile peak linear and rotational acceleration for RB were significantly ( $P < 0.05$ ) greater than OL, DL and DB. The 95th percentile HITsp for RB and LB were also significantly ( $P < 0.05$ ) greater than OL and DL. Although OL and DL received the most frequent impacts per season, the magnitudes of the impacts were the least of all player positions. The median 95th percentile peak linear and rotational accelerations values were greatest for QB, but these were not significantly different from the other player positions.

The magnitudes of impacts to the front of the helmet were significantly ( $P < 0.05$ ) greater for RB than for OL, DL, WR and DB. LB, which were not different from RB, received significantly ( $P < 0.05$ ) greater magnitude front impacts than OL and DL. Although the magnitudes were the least, OL received significantly ( $P < 0.05$ ) more frequent front impacts than QB, WR, DL, and LB. QB received significantly ( $P < 0.05$ ) less frequent front impacts than all player positions except WR. For all player positions, top impacts were significantly ( $P < 0.05$ ) the least frequent impact location (approximately 13% of all head impacts), but were associated with the greatest ( $P < 0.05$ ) peak linear acceleration magnitudes of all impact locations. In contrast, peak rotational accelerations associated with top impacts had significantly ( $P < 0.05$ ) less magnitude than all locations for all player positions. Impacts to the back of the helmet tended to be the highest magnitude for the QB and WR, and were significantly ( $P < 0.05$ ) more frequent for QB and WR than for all other positions.

## CONCLUSIONS

We have reported head impact exposures for a large cohort of collegiate football players. We found that player position was the largest factor (as opposed to team or session) in determining an individual player's head impact exposure. Concussion injuries are a result of an impact that results in head accelerations. In order to prevent and to help diagnosis concussion and subconcussive injuries an understanding the biomechanics of these impacts is necessary. These impacts are complex events that we are studying by quantifying the head impact exposures measures of frequency, location and severity.

## REFERENCES

1. Crisco J.J. et al. *J Biomech Eng*, **126**(6) 849-54, 2004.
2. Duma S.M. et al., *Clin J Sport Med*, **15**(1) 3-8, 2005.
3. Greenwald R.M. et al. *Neurosurgery*, **62**(4) 789-98, 2008.

## ACKNOWLEDGEMENTS

NIH R01HD048638 and the National Operating Committee on Standards for Athletic Equipment.

# A DYNAMIC SIMULATION APPROACH TO EVALUATING NERVE TRANSFER STRATEGIES FOLLOWING C5-C6 BRACHIAL PLEXUS INJURY

<sup>1,2</sup>Dustin L. Crouch, <sup>3</sup>Zhongyu Li, <sup>3</sup>Jonathan Barnwell, <sup>1,2</sup>Melissa Daly, and <sup>1,2</sup>Katherine R. Saul

<sup>1</sup>Dept. of Biomedical Engineering, Wake Forest University School of Medicine, Winston-Salem, NC, USA

<sup>2</sup>Virginia Tech/Wake Forest School of Biomedical Engineering Sciences, Winston-Salem, NC, USA

<sup>3</sup>Dept. of Orthopaedic Surgery, Wake Forest University School of Medicine, Winston-Salem, NC, USA

email: [dcrouch@wfubmc.edu](mailto:dcrouch@wfubmc.edu)

## INTRODUCTION

Many dynamic musculoskeletal simulation techniques have been developed and validated for the lower limb, and similar development is needed for the upper limb. While dynamic analyses for the upper and lower limbs share similar foundations, lower limb analytical methods must be adapted in order to address clinical questions particular to the upper limb. After upper limb paralysis, important factors for functional ability include whether intact or restored muscles are strong enough to perform a task, how much effort is required to perform the task, and whether compensatory strategies are available. Brachial plexus palsy, a devastating upper limb neuromuscular injury, affects approximately 1% of the multi-trauma population [1]. Following avulsion of the C5-C6 nerve roots, elbow flexion and shoulder function can be restored by nerve transfer. Double nerve transfer to the suprascapular and axillary nerves is preferred to restore shoulder function, but a single nerve transfer to either nerve may be performed due to limited donor nerve availability or surgeon's expertise. In this study, the consequences of different shoulder nerve transfer strategies on joint strength and muscle effort were explored in the context of an elbow flexion movement in order to demonstrate how established dynamic simulation approaches can be extended to address new and important biomechanical questions in the upper limb.

## METHODS

Four scenarios (unimpaired and three common nerve transfer scenarios) were generated using a computational upper limb model [4] implemented for dynamic simulation [5] in OpenSim [6]. For the nerve transfer scenarios, muscles in the model were altered to reflect published descriptions of nerve transfers following C5-C6 avulsion injury for which paralysis would present in the supraspinatus,

infraspinatus, deltoid, teres minor, biceps brachii, brachialis, and brachioradialis muscles (Table 1). Neural activation of unimpaired muscles ranged from passive-only to maximally active. Paralyzed muscles were allowed to generate passive forces only, while reinnervated muscles were limited to 20% of maximal activation based on reported differences in measured elbow flexion strength between the upper limb following nerve transfer and the unimpaired contralateral limb [7]. In all nerve transfer scenarios, the biceps brachii and brachialis muscles were restored, representing concomitant musculocutaneous nerve transfer. The axillary nerve transfer scenario included the associated paralysis of the triceps long head.

**Table 1:** Modeled scenario descriptions.

| Scenario              | Reinnervated Muscles            |
|-----------------------|---------------------------------|
| unimpaired            | none                            |
| axillary              | DELTA, TMIN, BIC, BRA           |
| suprascapular         | SUP, INF, BIC, BRA              |
| double nerve transfer | SUP, INF, DELTA, TMIN, BIC, BRA |

SUP = supraspinatus, INF = infraspinatus, DELTA = deltoid, TMIN = teres minor, BIC = biceps brachii, BRA = brachialis

During a simulated movement representing a characteristic upper limb task, the elbow flexed from full extension (0° flexion) to 120° flexion over one second while the shoulder maintained a functional posture of 25° shoulder elevation (SE) in a plane 25° forward from the abduction plane, and 45° internal shoulder rotation (IR). For each scenario, simulations were performed with 5 hand-held cylindrical weights of the following masses (in kg): 0, 1.1, 2.3, 3.4, and 4.5. A computed muscle control (CMC) algorithm minimizing a cost function related to muscle effort was used to determine the muscle activations required to optimally track the movement [8].

To address factors important for upper limb function, we compared movement performance among the scenarios based on the following outcome measures: error in tracking the desired movement trajectory, total muscle effort, and muscle-generated joint moment. A difference in joint angles between the desired and tracking motion indicated that the model, in a given scenario, was not sufficiently strong to perform the desired movement due to simulated muscle weakness or paralysis. Total effort was calculated as the sum of the cost, based on the CMC cost function, for each muscle over the entire movement. Joint moments generated by muscles crossing the shoulder and elbow were calculated with the 4.5 kg mass.

## RESULTS AND DISCUSSION

All simulations for all scenarios found a successful solution and flexed the elbow, but only the unimpaired and double nerve transfer scenarios had adequate strength to maintain the desired shoulder posture (joint angle errors  $< 0.3^\circ$ ) for all hand weights. The maximum shoulder joint angle errors for the axillary and suprascapular nerve transfer scenarios were  $10.2^\circ$  and  $17.2^\circ$ , respectively.

Of the nerve transfer scenarios, the total muscle effort of the double nerve transfer scenario most closely resembled that of the unimpaired scenario for all hand weights (Fig. 1). The total muscle effort of the suprascapular nerve transfer scenario was  $147 \pm 60\%$  (mean  $\pm$  SD) higher than that of the axillary nerve transfer scenario.

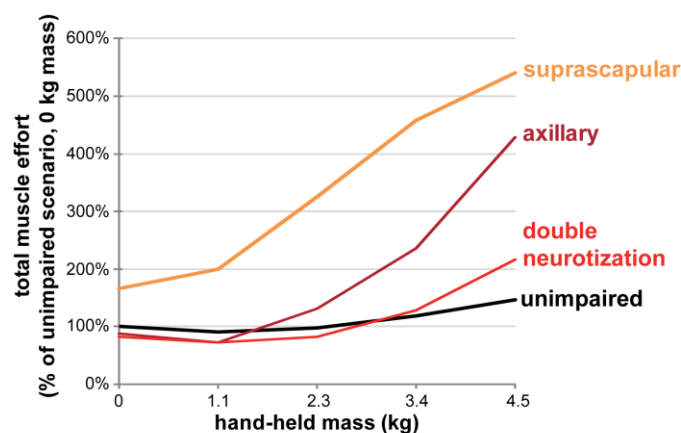


**Figure 1:** Total muscle effort relative to the unimpaired simulation with no hand weight.

Though the net joint moments of the unimpaired and double nerve transfer scenarios were the same, the individual muscle contributions to net joint moment differed. For example, subscapularis (SUB)

contribution to net SE moment increased by  $68 \pm 8\%$  to compensate for medial deltoid weakness. However, as a result of the SUB moment arm for IR in this posture, SUB also generated moments that detracted from the net external rotation (ER) moment. Consequently, infraspinatus contributed an additional  $44 \pm 27\%$  to ER moment simply to overcome the adverse effect of SUB compensation and maintain the desired shoulder posture.

In terms of joint angle error and muscle effort, the double nerve transfer scenario exhibited the best movement performance of the three nerve transfer scenarios, which is in agreement with clinical outcomes [2]. Of the single shoulder nerve transfer scenarios, the axillary scenario more closely resembled the function of the unimpaired upper limb for this movement. Previous biomechanical comparisons of single shoulder nerve transfers have not accounted for complex muscle behavior or interactions among muscles during a multi-joint movement, and clinical outcomes have varied [2,3]. Because the objective of nerve transfer is to restore as much function to the upper limb as possible, we plan to characterize movement performance of nerve transfer scenarios for additional tasks in future studies.

## CONCLUSIONS

This study demonstrated how a dynamic simulation approach can be used to explore important clinical questions related to upper limb function, such as the biomechanical consequence of nerve transfer strategies, in terms of joint strength, effort, and muscle coordination. Evaluating movement performance using dynamic simulations can aid clinicians in achieving surgical or rehabilitative treatment objectives.

## REFERENCES

1. Midha R. *Neurosurg* **40**, 1182-1189.
2. Merrell GA, et al. *J Hand Surg* **26**, 303-314.
3. Leechavengvongs S, et al. *J Hand Surg* **28A**, 633-638.
4. Holzbaur KRS, et al. *Ann Biomed Eng* **33**, 829-840.
5. Daly M, et al. *ASB Conf Proceedings*, State College, PA, 2009.
6. Delp SL, et al. *IEEE Trans Biomed Eng* **54**, 1940-1950.
7. Bertelli JA, Ghizoni MF. *J Hand Surg* **35A**, 769-775.
8. Thelen DG, Anderson FC. *J Biomech* **39**, 1107-1115.

## ACKNOWLEDGEMENTS

National Institutes of Health (NIH 5R24HD050821-02), Wake Forest University School of Medicine.

# COMBINING MUSCULOSKELETAL MODELING AND OPTIMIZATION TO ESTIMATE MUSCLE FORCES AT THE ANKLE

<sup>1</sup>Harrison Philip Crowell, <sup>2</sup>Irene S. Davis, <sup>3</sup>Jill S. Higginson, <sup>3</sup>Kurt Manal and <sup>3</sup>Liyun Wang

<sup>1</sup>US Army Research Laboratory, Aberdeen Proving Ground, MD, USA

<sup>2</sup>Harvard Medical School, Boston, MA, USA

<sup>3</sup>University of Delaware, Newark, DE, USA

email: [harrison.philip.crowell@us.army.mil](mailto:harrison.philip.crowell@us.army.mil)

## INTRODUCTION

It is important to include the muscle forces with the external forces when estimating the stresses and strains on a bone (such as the tibia), which is susceptible to stress fractures. Musculoskeletal models can produce estimates of muscle forces and moments based on data collected during the activity of interest. To assess the accuracy of the model's results, the joint moments computed by the model should be compared to experimentally measured joint moments [1]. The purpose of this work was to develop a method for estimating muscle forces in the lower leg that accurately reproduce the ankle joint moments measured experimentally and can be used to calculate stresses and strains that occur in the tibia early in the stance phase of running.

## METHODS

Kinematic, kinetic, and electromyographic (EMG) data from five subjects participating in an ongoing gait retraining study were used to demonstrate this method. During pre-training (5 trials) and post-training (5 trials) assessments, the subjects ran (3.7 m/s) across a force plate (Bertec Corp., Worthington, OH) while a motion capture system (Vicon, Oxford, UK) recorded their movements. For each subject, kinematic and kinetic data were processed in Visual 3D™ (C-Motion, Inc., Rockville, MD) to determine the ankle joint moments. The EMG data from tibialis anterior, soleus, medial gastrocnemius and lateral gastrocnemius were processed in a custom program. In the program, EMG data from the running trials were full-wave rectified and passed through a recursive, 6 Hz, second order, Butterworth filter. They were then normalized to the highest voltage recorded for each muscle during the running trials.

Then for each trial, a multi-step process was used to determine the forces in the muscles of the lower leg. First, Software for Interactive Musculoskeletal Modeling (SIMM) (MusculoGraphics, Inc., Santa Rosa, CA) was used to calculate the moments about the ankle. These calculations were made with SIMM's Dynamics Tool. The inputs to SIMM were the kinematic and kinetic data and muscle activations based on the EMG data. There were 12 muscles in the model. The activation level of tibialis anterior represented the dorsiflexors. The activation of soleus represented the plantar flexors other than medial and lateral gastrocnemii. The moments calculated with SIMM (Initial Estimate) were compared to the ankle joint moments calculated in Visual 3D (Experimental). All of the muscle activations were then shifted forward in time (4 ms to 21 ms) to account for the muscles' electromechanical delay (EMD), and the ankle joint moment was calculated in SIMM again. This process continued until the timing of the peak positive (i.e., dorsiflexion) and peak negative (i.e., plantar flexion) moments calculated by SIMM matched those of the Experimental moment (Shifted). At this point, the individual muscle moments, muscle orientation vectors and muscle moment arms calculated in SIMM were output.

Next, the Excel tool SOLVER.XLA (Microsoft Corp., Redmond, WA) was used to optimize the individual muscle moments. The objective of the optimization scheme was to minimize the sum of the squared difference between the Shifted and Experimental ankle joint moments. This optimization process focused on the early part of stance – foot strike to peak plantar flexion moment. In the optimization scheme, each muscle moment had its own scale factor throughout the trial. Scale factors for each muscle moment were constrained to

be between 0.5 and 2.0, inclusive. This kept all 12 muscle moments in the solution and prevented the SOLVER.XLA from attributing all of the ankle joint moment to just one or two muscles. The result was the Optimized ankle joint moment. Finally, the individual muscle moments were divided by their moment arms at each time step to determine the individual muscle forces that produced the motion.

## RESULTS AND DISCUSSION

In this study, the mean shift in muscle activations was 46 ms  $\pm$  13 ms. This is within the physiological limits of EMD [2].

For a representative trial, Figure 1 shows the Initial Estimate, Shifted, and Optimized ankle joint moments compared to the Experimental ankle joint moment. The timing and magnitude of the peak dorsiflexion moment and the peak plantar flexion moment of the Optimized moment is a much better match to the Experimental moment during the time period of interest – foot strike to peak plantar flexion moment, than either the Initial Estimate or the Shifted moment.

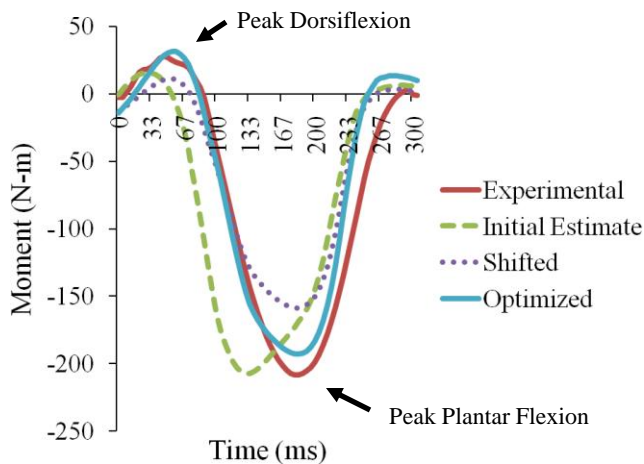


**Figure 1:** Ankle joint moments calculated for a representative trial.

The root mean square (RMS) deviations of the Shifted and Optimized ankle joint moments from the Experimental moments were calculated for 50 trials. The mean RMS deviation of the Optimized ankle joint moments (10.9 N-m  $\pm$  7.7 N-m) was roughly one third of the RMS deviation for the Shifted ankle joint moments (33.5 N-m  $\pm$  17 N-m).

For the representative trial shown in Figure 1, Figure 2 shows the forces in the individual muscles

of the lower leg as calculated with the optimization scheme. From Figures 1 and 2, it can be seen that the peak dorsiflexion moment corresponds to the peak force generated by the tibialis anterior (tib\_ant). Similarly, the peak plantar flexion moment corresponds to the peak forces generated by the plantar flexors such as soleus and medial gastrocnemius (gas\_med). It is important to know the magnitude and timing of the muscle forces at the ankle because stress fractures seem to be related to loading on the tibia in early stance [3].

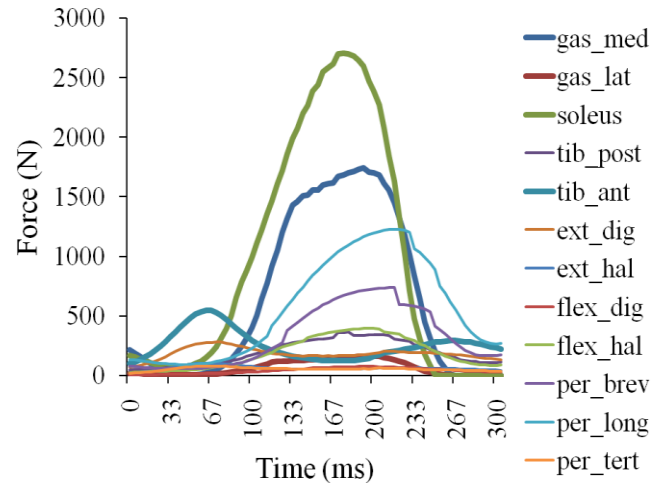


**Figure 2:** Lower leg muscle forces for a representative trial.

## CONCLUSIONS

The method described here for combining musculoskeletal modeling and optimization can produce reasonable estimates of muscle forces at the ankle during the early part of stance phase in running. The close match between the Optimized and Experimental ankle joint moments suggests that the individual muscle forces that produced the Optimized ankle joint moment will provide a better estimate of the magnitude and timing of the muscle forces at the ankle than would be produced by the musculoskeletal modeling program alone.

## REFERENCES

1. Delp SL and Loan JP. *Comput Biol Med*, **25**, 21-34, 1995.
2. Manal K, et al. *Comput Biol Med*, **32**, 25-36, 2004.
3. Milner CE, et al. *Med Sci Sports Exerc*, **38**, 323-328, 2006.

# LIMB ASYMMETRIES DURING A SIDE-CUTTING TASK IN ADOLESCENT PATIENTS 6-12 MONTH FOLLOWING ACL RECONSTRUCTION

<sup>1</sup>Boyi Dai, <sup>1</sup>Robert J. Butler, <sup>1</sup>William E. Garrett, <sup>1</sup>Robin M. Queen

<sup>1</sup>Duke University, Durham, NC, USA

email: bdai@email.unc.edu web: <http://klab.surgery.duke.edu/>

## INTRODUCTION

An estimated 175,000 - 300,000 anterior cruciate ligament reconstructions (ACL-R) are performed annually in the United States. Adolescents have the greatest risk of sustaining an ACL injury. In this patient population there is more than a 20% re-injury rate following return to sports [1].

Conservative rehabilitation programs allow patients to return to sports 9 to 12 months following surgery, while accelerated rehabilitation program allow returning to sports within 4 to 6 months after the operation. Commonly used criteria for patients to return to contact sports include no effusion, full range of motion, good knee stability and strength, and completing running programs [2].

Biomechanical asymmetries between surgical (S) and nonsurgical (NS) limbs have been observed in patients post ACL-R [3]. Use of a functional knee brace has been shown to decrease the biomechanical risk factors of ACL injuries during athletic tasks in a control population [4]. However, little is known about the longitudinal changes in biomechanical limb asymmetries and bracing effects in adolescent patients following ACL-R.

## METHODS

9 subjects (6 men, 3 women,  $1.7 \pm 0.1$  m,  $71.3 \pm 19.7$  kg, and  $16.2 \pm 1.5$  yrs) were tested 6 and 12 month after their primary ACL-R. Three-dimensional kinematic and kinetic data were collected bilaterally during 6 trials of  $35^\circ$  side-cutting tasks while the patients were non-braced (NB) or braced (B) on the surgical side. The knee brace was a custom made functional knee brace that resists knee extension through the terminal  $35^\circ$  of knee extension. NB condition was tested first. Knee flexion angles (KFA), knee flexion velocities

(KFV), internal knee extension moments (KEM), and vertical ground reaction forces (VGRF) from toe touch to toe off during the cutting tasks were calculated. The dependant variables included peak VGRF, peak KFV, KFA at peak KFV, peak KFA, KEM at peak KFV, peak KEM, range of motion (ROM), and joint stiffness. ROM was calculated using peak KFA minus KFA at toe touch. Stiffness was calculated using KEM at peak KFA minus KEM at toe touch then divided by ROM. Data were analyzed using month (6 vs. 12) by side (S vs. NS) repeated measure ANOVAs ( $\alpha=0.05$ ) with Tukey's post-hoc testing. Two ANOVAs were conducted with one for NB condition and one for B condition.

## RESULTS AND DISCUSSION

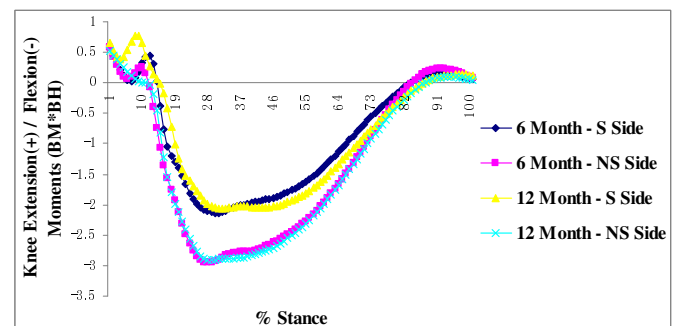


**Figure 1:** Bilateral knee internal extension moments at 6 and 12 month for non-braced condition

For the non-braced condition (Figure 1; Table 1), a significant interaction suggested the S side had less peak KFA than the NS side only at 6 month. Main effects for side demonstrated less ROM, KEM at peak KFV, and peak KEM for the S side compared to the NS side at both 6 and 12 month. No main effects for month were observed. For the braced condition, a significant interaction suggested the S side had decreased peak KFA than the NS side only at 6 month. Main effects for side demonstrated less peak VGRF, peak KFV, KEM at peak KFV, and peak KEM for the S side than the NS side at both 6

and 12 month. No main effects for month were observed.

The results demonstrated that for both non-braced and braced conditions, subjects increased their S side peak KFA from 6 to 12 month. However, the ROM was still less on the S side than the NS side during non-brace condition. No changes in side asymmetries were observed in KEM at peak KFV or peak KEM from 6 to 12 month for both non-brace and braced conditions. The findings of current study were consistent with previous literature which found biomechanical asymmetries between S and NS limbs during athletic tasks in patients post ACL-R [3]. The decrease in KEM on the S side which suggested less use of the knee joint could be the results of decreased strength, changed neuromuscular control, or fear of re-injury [2]. The decreased KFA on the S side suggested a more erect landing pattern compared to the NS side and might place the graft at risk for re-injury [4].

Little improvements were observed for KEM from 6 month and 12 month. These patients have received physical therapy and have all been released from therapy to return to sport prior to the 12 month testing date. In this patient population, return to sport criteria was less than 15% difference in muscle strength and less than 10% deficit at single-leg hop with full range of motion on the surgical side. However, during a side cutting task, our results demonstrated that the S side had 27% less peak KEM at 6 month and 28% less peak KEM at 12 month than the NS side for non-braced condition. The magnitude of asymmetries in KEM

was greater than the strength deficit criteria for return to sport, which suggested that basic strength and a single-leg hop test may not be sensitive enough to detect biomechanical asymmetries and therefore might not be adequate for determining return to play in this patient population.

## CONCLUSIONS

Bilateral knee biomechanical asymmetries persisted during a side-cutting task from 6 to 12 month in adolescent patients following ACL-R. The continued asymmetries are of concern with regards to injuring the graft or the contralateral limb when the patients are allowed to return to sport. The results of the study indicate the importance of examining the current rehabilitation and return to sport criteria for adolescent patients following ACL-R.

## REFERENCES

1. Shelbourne KD, et al. *Sports Health* **1**, 236-241, 2009
2. Kvist J. *Sports Med* **34**, 269-280, 2004
3. Decker MJ, et al. *Med Sci Sports Exerc* **34**, 1408-1413, 2002
4. Yu B, et al. *Am J Sports Med* **32**, 1136-1143

## ACKNOWLEDGEMENTS

The authors would like to thank DonJoy for their support of this project and Mary Russell for her assistance in data collection.

**Table 1:** Means, SD and p values for the bilateral variables at 6 and 12 month for non- braced condition

| Dependant Variables | 6 month S side | 6 month NS side | 12 month S side | 12 month NS side | P value Month | P value Side    | P value Interaction |
|---------------------|----------------|-----------------|-----------------|------------------|---------------|-----------------|---------------------|
| Peak VGRF           | 28.6 ± 6.4     | 31.4 ± 4.8      | 27.3 ± 3.7      | 29.3 ± 5.4       | 0.24          | 0.13            | 0.44                |
| KFA at Peak KFV     | 28.9 ± 4.9     | 31.8 ± 4.1      | 29.5 ± 6.9      | 31.6 ± 4.5       | 0.91          | 0.19            | 0.74                |
| Peak KFA            | 44.3 ± 8.2     | 52.5 ± 5.5      | 48.2 ± 7.8      | 52.4 ± 6.9       | 0.18          | 0.04            | <b>&lt;0.01</b>     |
| ROM                 | 28.0 ± 8.0     | 37.7 ± 6.4      | 32.2 ± 9.0      | 37.3 ± 8.1       | 0.23          | <b>0.02</b>     | 0.17                |
| Peak KFV            | 599 ± 103      | 696 ± 65        | 624 ± 82        | 681 ± 110        | 0.78          | 0.06            | 0.28                |
| KEM at Peak KFV     | 1.1 ± 0.8      | 1.7 ± 0.5       | 0.9 ± 0.6       | 1.7 ± 0.4        | 0.43          | <b>&lt;0.01</b> | 0.24                |
| Peak KEM            | 2.4 ± 0.8      | 3.3 ± 0.5       | 2.3 ± 0.8       | 3.2 ± 0.4        | 0.47          | <b>&lt;0.01</b> | 0.76                |
| Stiffness           | 0.10 ± 0.02    | 0.09 ± 0.02     | 0.09 ± 0.04     | 0.09 ± 0.02      | 0.71          | 0.68            | 0.92                |

\*S: Surgical; NS: Non-surgical; VGRF: Vertical ground reaction forces (Body mass); KFA: Knee flexion angles (Degs); KFV: Knee flexion velocities (Degs/s); ROM: Range of motion (Degs); KEM: Knee extension moments (Body mass\*Body Height); Stiffness (Body mass\*Body Height /Degs).

# THE RELATIONSHIPS BETWEEN TECHNIQUE VARIABILITY AND PERFORMANCE IN ELITE DISCUS THROWERS DURING COMPETITION

<sup>1</sup>Boyi Dai, <sup>1</sup>Steve Leigh, <sup>2</sup>Hanjun Li, <sup>1</sup>Bing Yu

<sup>1</sup>The University of North Carolina at Chapel Hill, Chapel Hill, NC, USA

<sup>2</sup>Beijing Sport University, Beijing, China

email: bdai@email.unc.edu web: <http://www.med.unc.edu/ahs/physical>

## INTRODUCTION

Discus throwing is a physically and technically demanding sport. The goal is to achieve maximum discus release speed with optimal release heights and release angles. Previous studies have demonstrated that discus throwing performance was associated with selected technique variables [1].

Intra-individual variability may affect discus throwing performance. Previous studies assumed the movement patterns of skilled discus throwers were relatively invariant [1]. Research in other sports has shown less variability in skilled athletes compared to unskilled athletes, while some studies suggested a potential increase in functional variability in elite athletes [2]. The relationships between technique variability and performance during discus throwing have not been investigated.

The purpose of this study was to investigate the relationships between technique variability and performance during a discus throwing event. We hypothesized that athletes with better performances would have less variability (better consistency) in technique variables.

## METHODS

18 male and 15 female discus throwers competing in the 2010 USA Outdoor Track & Field Championships were included in this study. Throwers' three throws during the first round were recorded by two S-VHS video camcorders at a frame rate of 60 Hz.

The global reference markers, body landmarks, and the centre of the discus in each camcorders view were manually digitized [1]. The direct linear transformation procedure was used to obtain three-

dimensional coordinates which were then filtered through a Butterworth low-pass filter at 7.14 Hz [1].

The critical instants of maximum backswing and release of the discus were identified for every trial. Considering the key techniques and the major joints contributions to discus delivery, eight joint angles were chosen. Arm-shoulder separation angle (ASS), arm-shoulder elevation angle (ASE), shoulder-hip separation (SHS), right hip flexion angle (RHF), left hip flexion angle (LHF), right knee flexion angle (RKF), left knee flexion angle (LKF), and trunk forward-backward tilt angle (TFBT) were calculated and normalized into 101 points from maximum back swing to release of discus [1]. For each angle, the standard deviation (SD) of three trials of each thrower was calculated at each point. The mean of SDs of all 101 points was calculated for each angle as variability measurements [3].

The best official distance for each thrower was used as the measurement for performance, because this determined their final place in the competition. Pearson correlation coefficients (PCC) between best official distance and mean SD of each angle were calculated with a Type I error rate set at 0.05. Males and females were analyzed separately.

## RESULTS AND DISCUSSION

For males (Table 1), performance was significantly and negatively correlated with mean SDs of ASE, SHS, RHF, LHF, RKF, LKF, and TFBT. For females (Table 2), although most of PCC were negative, no significant correlations were found between performance and any variability measurement.

The results suggested that for males, athletes with better performance had lower variability in their

movement patterns. Performance was associated with variability in shoulder, trunk, hip, and knee joint angles. The results suggested that male throwers with better performance had better consistency across the joints that make a major contribution to discus delivery. For females, although the correlations were negative, a lack of statistical significance suggested these linear correlations were not strong in females.

Inter-individual and intra-individual variability exists widely in sports [2]. Previous studies have demonstrated that during certain sports maneuvers, skilled individuals had lower variability in key techniques compared to less skilled individuals, and that variability decreased with practice and learning [2]. On the other hand, some other studies suggested elite athletes might increase variability to give the body flexibility in response to changes in movement constraint [2]. Considering discus throwing is a closed skill with little perturbation from the environment, the results for male throwers supports the notion of better movement consistency in skilled athletes. In addition, it should be noticed that the data were collected during competition, and the goal of these athletes was to achieve maximum performance instead of obtaining new techniques. Therefore, it appears that whether athletes could replicate their trained techniques during competition is important.

No significant correlation between performance and variability in females suggests variability might be not only sports specific but gender specific. Previous studies found that the magnitude of ASS, SHS, and TFBT angles at critical instants were

associated with performance in females, while only SHS angle was correlated with performance in males. The authors suggested that females tended to rely on effective technique while males may have a relative homogenous technique [1]. The gender disparity might be caused by different throwing styles and physical characteristics between males and females. Based on the postulations that male throwers have a more homogenous technique, it is expected that better male throwers will have better consistency in replicating the technique. Therefore, it is more likely to find negative correlations between variability and performance in males than females.

## CONCLUSIONS

Significantly negative correlations between technique variability and performance were found in elite male but not female discus throwers during competition. The disparity between genders might be caused by different technique patterns and physical capacities. The study suggested reducing motion variability may be an important goal for discus training in males.

## REFERENCES

1. Leigh S, et al. *Sports Biomech* **7**, 173-193, 2008
2. Bartlett R, et al. *Sports Biomech* **6**, 224-243, 2007
3. Li L, et al. *Hum Mov Sci* **24**, 257-267, 2005

## ACKNOWLEDGEMENTS

The authors would like to thank USA Track & Field and the US Olympic Committee for their support.

Table 1. PCC and P values between performance and mean SD of each angle for males

|         | ASS   | ASE   | SHS   | RHF   | LHF   | RKF   | LKF   | TFBT  |
|---------|-------|-------|-------|-------|-------|-------|-------|-------|
| PCC     | -0.44 | -0.63 | -0.59 | -0.58 | -0.57 | -0.65 | -0.47 | -0.59 |
| P Value | 0.07  | <0.01 | 0.01  | 0.01  | 0.01  | <0.01 | 0.05  | 0.01  |

Table 2. PCC and P values between performance and mean SD of each angle for females

|         | ASS   | ASE   | SHS   | RHF   | LHF   | RKF  | LKF   | TFBT  |
|---------|-------|-------|-------|-------|-------|------|-------|-------|
| PCC     | -0.33 | -0.44 | -0.25 | -0.24 | -0.19 | 0.11 | -0.28 | -0.43 |
| P Value | 0.23  | 0.10  | 0.37  | 0.40  | 0.49  | 0.69 | 0.32  | 0.11  |

PCC: Pearson correlation coefficient; ASS: arm-shoulder separation angle; ASE: arm-shoulder elevation angle; SHS: shoulder-hip separation; RHF: right hip flexion angle; LHF: left hip flexion angle; RKF: right knee flexion angle; LKF: left knee flexion angle; TFBT: trunk forward-backward tilt angle.

# IDENTIFICATION OF MUSCLE CONTRIBUTIONS TO A FORWARD REACHING TASK USING AN INDUCED ACCELERATION ANALYSIS

<sup>1</sup>Melissa Daly, <sup>1</sup>Meghan E. Vidt, <sup>2</sup>Anthony P. Marsh, and <sup>1</sup>Katherine R. Saul

<sup>1</sup>Virginia Tech/Wake Forest School of Biomedical Engineering and Sciences, Winston-Salem, NC, USA

<sup>2</sup>Wake Forest University Department of Health and Exercise Science, Winston-Salem, NC, USA

email: mdaly@wfubmc.edu web: <http://www.sbes.vt.edu/kholzbau/MoBL>

## INTRODUCTION

Induced acceleration analysis has been used to identify the individual muscle contributions to healthy and pathological gait, but has not been widely used to characterize upper limb tasks [1;2]. Many common functional activities (e.g. eating, dressing, bathing) require the use of the upper limb and are vital for maintaining independence. Identifying the muscles with the most substantial contributions to a forward reach would provide insight into the dynamics of a common upper limb task, and may provide a foundation for the development of improved interventions that focus on the most important muscles for functional movement production. This may be particularly useful for rehabilitation in impaired individuals, such as older adults or those recovering from stroke or rotator cuff tears. The aim of this study was to determine the contributions of upper limb muscles to the horizontal and vertical acceleration of the hand during a forward reaching task using a simulation approach.

## METHODS

An adult male (5'11", 180 lbs) performed a forward reaching task with his dominant (right) hand, reaching forward from a posture with the elbow flexed to 90° and the shoulder adducted (0% of movement) until the elbow was in 10-20° flexion (50%), and then returning to the starting posture (100%). Torso and wrist movement were restricted by means of a chest strap and wrist brace. Kinematics were recorded over a 3.5 second reach using a 7 camera Hawk system (Motion Analysis Corp., Santa Rosa, CA). EMG data were collected from the triceps, biceps and deltoid muscles using 1cm surface electrodes

(BIOPAC Systems Inc., Goleta, CA), and normalized to EMG collected during a maximum isometric contraction for each muscle.

An upper limb model based on a previously described kinematic model [3] of the upper limb was implemented in OpenSim [4] and used in the analysis, including five degrees of freedom, 32 muscles crossing the shoulder, elbow and forearm, and appropriate inertial parameters for the segments [5,6]. Computed muscle control (CMC) was used to determine the muscle activations necessary to produce the reaching task [7]. To verify that the CMC muscle activations were physiologically reasonable, they were compared to the timings of EMG activity. The muscle activations determined using CMC captured the salient features of the timings of the muscle activations as measured using EMG (e.g. Figure 1).

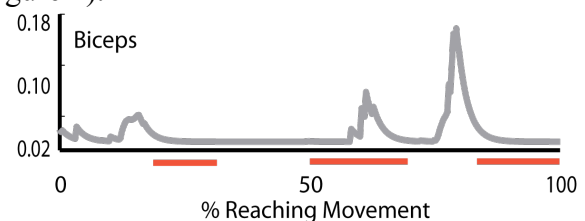


**Figure 1.** Estimated muscle activity for biceps as determined using the CMC algorithm (grey lines) and measured using EMG (red bars). EMG represents the onset and offset times for the study subject (>3SD above resting EMG).

The contributions of individual muscles to the accelerations of the hand in the nominal solution were analyzed using a previously described induced acceleration analysis [8,9]. This analysis set the muscle forces of all muscles but one to zero. The force of the muscle of interest was then applied and the resulting accelerations of the hand were calculated. This process was repeated for each of the 32 muscle-tendon actuators and

required approximately 1 hour of computation time for a 3.5sec reach. To identify the muscles that contribute most to elevating the hand off the table and moving it toward and away from the body, the five muscles with the largest contributions to horizontal and vertical accelerations in the negative and positive directions were identified.

## RESULTS AND DISCUSSION

The CMC algorithm tracked the recorded kinematics with average error of  $0.0003^\circ$  (max  $0.06^\circ$ ). The combined contributions of muscles and gravity from the induced acceleration analysis closely matched those from the nominal simulation. The five muscles with the greatest contribution to the acceleration of the hand away from the body (positive horizontal), toward the body (negative vertical), upward off the table (positive vertical) and downward toward the table (negative vertical) were identified (e.g. Figure 2). Of the 12 muscles and muscle compartments identified as having substantial contributions to the acceleration of the hand during the reaching task, 8 cross the shoulder.

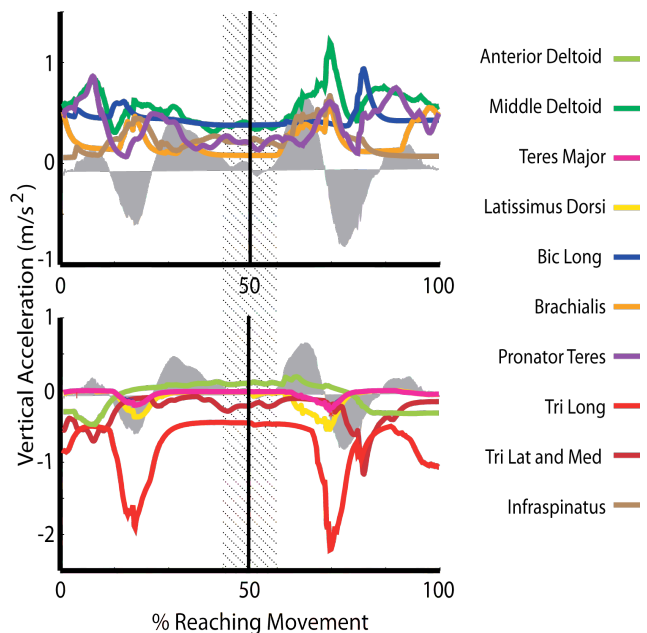


**Figure 2.** The five muscles with the greatest contributions to the positive (top) and negative (bottom) vertical acceleration (dark grey band) of the hand during the reaching task. Diagonal lines represent the region of the movement where subject difficulty is most frequently observed.

From this analysis, we identified interesting features of the muscle contributions to movement. For example, we observed experimentally that the subject was most likely to fail in efforts to perform the movement when the arm is most extended from the body due to inability to elevate the hand (movement region indicated with diagonal lines in Figure 2). Therefore, the muscles we identified that provide positive contributions to vertical accelerations in this region are critical and may be important targets for strengthening. In addition, we note that negative accelerations due to triceps extension of the elbow in this period must be counteracted by these positive contributors.

Muscle contributions may not be the same for other populations or reaching movements; for example, kinematic analysis has shown that the relative activity of muscles, as measured using EMG, changes when the angle of the reach is increased or decreased [10].

## CONCLUSIONS

The results from this analysis indicate that shoulder muscles play an important role in accelerating the hand during functional reaching tasks and may be relatively more important to upper extremity reaching function than elbow and forearm muscle. Targeting these functionally relevant muscles may be beneficial during resistance training interventions aimed to help impaired populations, such as older adults, maintain their independence.

## REFERENCES

- [1] Delp SL and Loan JP. *Comput Biol Med* 1995;25(1):21-34.
- [2] Hicks JL, et al. *J Biomech.* 2008; 41:960-967.
- [3] Holzbaur KR, et al. *Ann Biomed Eng* 2005;33(6):829-40.
- [4] Delp SL, et al. *IEEE Trans Biomed Eng* 2007;54(11):1940-50.
- [5] Harrington MA, Jr., et al. *J Biomech* 1993;26(4-5):417-26.
- [6] McConville JT, et al. *AFAMRL-TR-80-119*. 1980.
- [7] Thelen DG, et al. *J Biomech* 2003;36(3):321-8.
- [8] Hamner, SR, et al. *J Biomech.* 2010; 43: 2709-2716.
- [9] Zajac, FE and Gordon ME. *Exerc. Sci. Rev.* 1989; 17: 187-230.
- [10] Vandenberghe A, et al. *Gait Posture* 2010;32(4):500-7.

## ACKNOWLEDGEMENTS

NIH Award #5R24HD050821-02, NSF CBET-0828115, WFU Science Research Fund, WFU Cross Campus Collaboration Research Fund.

# POLYETHYLENE WEAR AND PATIENT SPECIFIC CONTACT STRESS IN TOTAL HIP ARTHROPLASTY

<sup>1</sup>Matej Daniel, <sup>2</sup>Robert Košak, <sup>3</sup>Aleš Iglič and <sup>3</sup>Veronika Kralj-Iglič

<sup>1</sup>Czech Technical University in Prague, Prague, Czech Republic

<sup>2</sup>University Medical Centre, Ljubljana, Slovenia

<sup>3</sup>University of Ljubljana, Ljubljana, Slovenia

email: [matej.daniel@fs.cvut.cz](mailto:matej.daniel@fs.cvut.cz) web: <http://www.biomechanics.cz>

## INTRODUCTION

Contact stress in total hip arthroplasty (THA) reportedly relates to polyethylene wear in numerical models and THA simulators: long lasting high contact stress is connected to larger volumetric wear. In order to prove clinically relevant, this relation should be tested in vivo by showing larger volumetric wear in patients with higher postoperative contact stress at the prosthesis/cup interface. We therefore asked whether the correlation between stress at the prosthesis head/cup interface and polyethylene wear that was observed in laboratory experiments but not confirmed in a previous clinical study [1] can be proved in long term follow up of THA in vivo.

## METHODS

We retrospectively reviewed the radiographs of 80 patients (43 women and 37 men), who had revision hip arthroplasty for aseptic loosening between 1997 and 2001. The median age at revision was 82 years (range, 57-92 years). The median period between the first arthroplasty and revision was 12 years (range, 4-17 years). To exclude the effect of prosthesis design on wear, the group consisted of patients with identical implanted bearing couples in material and geometry; in all patients, a prosthesis with a CoCrMo head and a UHMWPE polyethylene cup with an inner surface diameter of 32 mm was implanted.

Polyethylene wear was assessed by a treating surgeon. RK assessed polyethylene wear by means of linear penetration  $d$  and volumetric wear  $V$  using the duoradiographic method of Livermore [2]. Two radiographs of each patient were selected for the study; the first of these was made immediately after

the operation, and the second was made before the revision arthroplasty.

The hip reaction force and the contact stress distribution on the inner surface of the acetabular cup in one-legged stance were determined for each patient individually according to the HIPSTRESS method from a postoperative AP radiogram [3]. One-legged stance was taken as a representative body position as it was shown that the contact stress distribution during one-legged stance closely resembled the averaged contact stress distribution during the walking cycle.

The assessment of the hip reaction force  $\mathbf{R}$  was based on the force and the torque equilibrium of the body in one-legged stance [3]. The geometry of the musculoskeletal model of the hip was scaled for each patient individually according to the following geometric parameters measured from an AP radiogram (Fig 1): height of the pelvis  $H$ , width of the pelvis  $C$ , and vertical and horizontal position of the greater trochanter  $x$  and  $z$ , respectively. In addition to the resultant hip force, the input parameters of the mathematical model for calculation of the contact stress [3] were the geometry of the prosthesis given by the radius of the acetabular cup  $r$  and the position of the acetabular cup given by cup inclination  $\alpha$ .

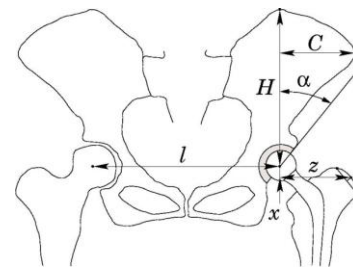


**Figure 1:** The geometric parameters of the hip and pelvis needed for determining the peak contact hip stress ( $p_{max}$ ) within the HIPSTRESS method.

## RESULTS AND DISCUSSION

We observed correlations between linear penetration  $d$  ( $r^2=0.70$ ,  $p<0.001$ ), volumetric wear  $V$  ( $r^2=0.50$ ,  $p<0.001$ ), and the peak contact stress normalized to the body weight  $p_{max}/W_B$  (Table 1). The greater the magnitude of the peak contact stress determined on the basis of postoperative radiograms, the higher the wear determined at followup (Fig 2). Measured wear characteristics  $d$  and  $V$  significantly correlates with the mediolateral position of greater trochanter  $z$  and acetabular cup inclination  $\alpha$  (Fig 1). Higher wear was related to the acetabular cup being opened more laterally, ie, small  $\alpha$ , and to the trochanter being located more medially, ie, small  $z$ . Other geometric parameters of the hip (Fig 1) did not correlate with linear and volumetric wear (Table 1).

**Table 1:** Pearson's correlation coefficients ( $r^2$ ) and p values between radiographic and biomechanical parameters and linear penetration ( $d$ ) and volumetric wear ( $V$ )

| Parameter     | $d$   |         | $V$   |         |
|---------------|-------|---------|-------|---------|
|               | $r^2$ | p       | $r^2$ | p       |
| $p_{max}/W_B$ | 0.70  | < 0.001 | 0.50  | < 0.001 |
| $R/W_B$       | 0.35  | < 0.001 | 0.51  | < 0.001 |
| $l$           | 0.00  | 0.746   | 0.01  | 0.334   |
| $H$           | 0.01  | 0.390   | 0.00  | 0.631   |
| $C$           | 0.10  | 0.003   | 0.11  | 0.002   |
| $x$           | 0.00  | 0.877   | 0.01  | 0.398   |
| $z$           | 0.29  | < 0.001 | 0.39  | < 0.001 |
| $\alpha$      | 0.43  | < 0.001 | 0.06  | < 0.001 |
| $W_B$         | 0.03  | 0.123   | 0.01  | 0.284   |

The role of contact stress in the wear process of THA is manifested by correlations between the values of the peak contact stress determined from postoperative radiograms and both linear penetration  $d$  and volumetric wear  $V$  measured at the last followup before revision of the prosthesis. These results complements previous laboratory measurements which yielded the correlation between the contact stress and polyethylene wear by using idealized loading in joint simulators. The direct relationship between postoperative contact stress and wear at followup presented in this study indicates that the HIPSTRESS method could be used can be used in planning the operation and configuration of a reconstructed hip based on minimizing the contact stress [2]. For this, the

existing software should be upgraded to include a possibility of simulating geometry changes and re-calculation of stress.

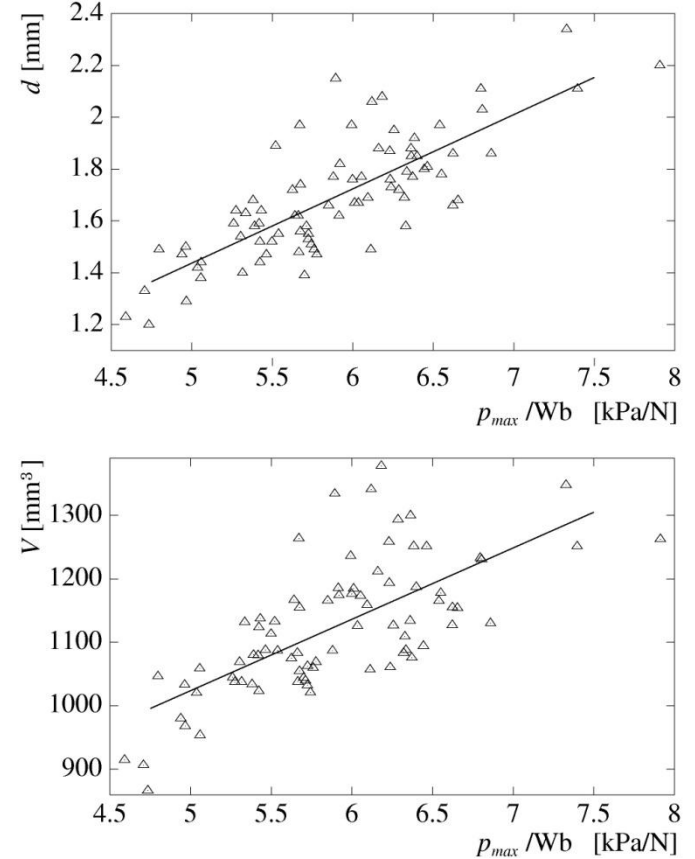


**Figure 2:** (A) Linear penetration  $d$  and (B) volumetric wear  $V$  of the polyethylene cups as functions of the peak contact hip stress normalized to the body weight  $p_{max}/W_B$  in 80 THAs.

## CONCLUSIONS

The relationship between stress and wear of THA has been well established in theoretical models and laboratory measurements, however a 5 year followup study of THA in a group of patients [2] yielded indecisive answers. Designing the study as to assess THA at revision, we decisively show that volumetric wear statistically significantly correlates with peak stress at the prosthesis head/cup interface. We also show that a specific patient geometry of the hip increases polyethylene wear in THA.

## REFERENCES

1. The B, et al. *J Biomech.* **41**,100-5, 2008.
2. Kosak R, et al. *Skeletal Radiol.*; **32**, 679-86, 2003.
3. Igljic A, et al. *Comput Methods Biomech Biomed Eng.* **5**, 185-192, 2002.

# The Effect of Elevated Vacuum Suspension on Axial Bone-Socket Displacement in Persons with a Traumatic Transtibial Amputation

Benjamin J. Darter, Kiril Sinitski and Jason M. Wilken

Center for the Intrepid, Department of Orthopedics and Rehabilitation, Brooke Army Medical Center,  
Ft. Sam Houston, TX 78234, USA  
email: benjamin.darter@amedd.army.mil

## INTRODUCTION

Following transtibial amputation prosthetic sockets must transfer forces from the distal prosthetic components to the residual limb in a way that will not damage the soft tissue. During walking the residual limb is cyclically loaded and unloaded producing axial bone-socket motion and undesirable shear forces on the skin of the residual limb [1]. Commonly referred to as pistoning, in active individuals the axial motion can quickly lead to breakdown of the skin in areas along bony prominences and adjacent to skin grafts [1,2]. Elevated vacuum suspension systems, which use mechanical or electric pumps to draw air from the socket, may maintain bone-socket position better than passive suction sockets [3,4]. However, limitations in the study designs and radiographic techniques make interpreting the results difficult. Digital Video Fluoroscopy (DVF) offers potential advantages over previous techniques and has been shown to be reliable for assessing motion [5]. The objective of this study was to determine the effect of elevated vacuum on axial bone-socket motion in persons with a traumatic transtibial amputation (TTA) using DVF.

## METHODS

Bone-socket motion was assessed in eight male subjects ( $30 \pm 6$  yrs,  $93 \pm 3$  kg,  $1.9 \pm 0.04$  m) with TTA secondary to trauma. Participants were assessed while wearing total surface bearing sockets that accommodated both elevated vacuum and passive suction suspension devices.

In order to replicate the loading conditions experienced during walking, the subjects applied vertical loads through the residual limb within the socket from 0 to 100% body weight (BW) in

increments of 20%. Loading of the limb was controlled using force plate data to provide auditory and visual biofeedback. To ensure consistency of loading between trials, subjects were required to be within 5% of the desired vertical load with shear forces in any direction less than 5% of the total load. Three medial-lateral digital video fluoroscopy images of the residual limb within the socket were collected at each loading condition. The distance between the distal point of the tibia and the superior border of the socket adapter was measured for each BW increment as well as 0%-100% BW (Figure 1). A radiopaque reference ruler was used to account for any inter image variability in magnification. A 2-factor (suspension type, loading condition) ANOVA and follow-up Tukey paired t-tests were used to evaluate axial displacement with the elevated vacuum on and off.



**Figure 1.** Sample fluoroscopy image of residual limb displacement within the socket during loading at 0, 60 and 100% body weight. The contour of tibia and fibula have been digitally enhanced.

## RESULTS AND DISCUSSION

A statistically significant interaction between suspension type and load condition was found ( $p=0.002$ ) so the results reported are based on the paired t-tests for each load condition (figure 2). Total axial displacement between the 0% and 100% BW conditions was significantly lower with the elevated vacuum on (ON 1.3cm, OFF 1.7cm,  $p=0.01$ ). No significant differences were found between elevated vacuum on and off for any loaded

condition, except for a clinically insignificant difference between 80% and 100% BW (ON 0.03cm, OFF 0.13cm,  $p=0.04$ ). In addition, an approximate 0.3cm difference for 0-20% condition approached significance ( $p=0.07$ ) and would likely reach statistical significance with additional subjects. Overall, nearly 80% of the vertical displacement occurred by the 40% BW condition with both suspension types, with less than 0.3cm of displacement occurring with additional loading up to 100% BW.

## CONCLUSIONS

Our results suggest elevated vacuum systems reduce axial motion of the residual limb in the socket by better maintaining position of the limb within the socket during unloaded conditions. It is unlikely the elevated vacuum provides a meaningful improvement in limb-socket motion once 40% BW is applied.

## ACKNOWLEDGEMENTS

Supported by Military Amputee Research Program (JWM)

## DISCLAIMER

The view(s) expressed herein are those of the author(s) and do not reflect the official policy or position of Brooke Army Medical Center, the U.S. Army Medical Department, the U.S. Army Office of the Surgeon General, the Department of the Army, Department of Defense or the U.S. Government.

## REFERENCES

1. Sanders JE, et al. *J Rehabil Res Dev* **34**, 19-43, 1997
2. Ferguson J, et al. *Foot Ankle Clin N Am* **15**, 151-174, 2010
3. Board WJ, et al. *Prosthetic Orthotics International* **25**, 202-209, 2001
4. Soderberg B. *J Prosthetics Orthotics* **15**, 95-99, 2003
5. Teyhen DS, et al. *Spine* **30**, E406-413, 2005

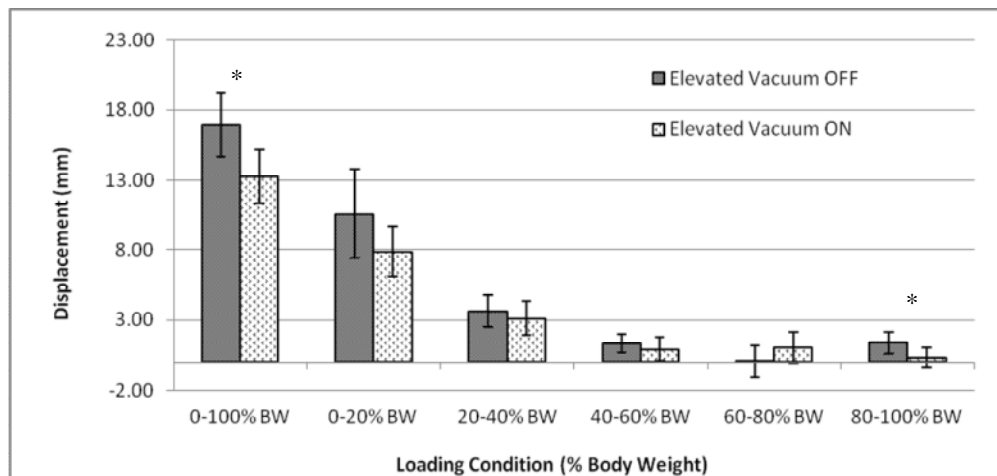


**Figure 2.** Axial bone-socket displacement between each body weight condition with the elevated vacuum on and off. The displacement was calculated as the distance between the distal point of the tibia and the superior border of the socket adapter. Error bars represent the standard deviation for each body weight condition  
\* Indicates a statistically significant difference in axial bone-socket displacement between the suspension types ( $p<0.05$ )

# SHOULDER POSITION IMPACTS THE MEASUREMENT OF GLENOHUMERAL INTERNAL ROTATION AND INFRASPINATUS HARDNESS.

<sup>1</sup>Amitabh Dashottar, <sup>1</sup>John Borstad

<sup>1</sup>The Ohio State University, Columbus, OH, USA

Email: dashottar.1@buckeyemail.osu.edu

## INTRODUCTION

Shoulder pain rates are high for athletes in overhead throwing sports such as baseball, tennis, and volleyball. In most instances, shoulder pain in these athletes is associated with shoulder range of motion (ROM) changes, especially loss of glenohumeral joint (GHJ) internal rotation (IR). This loss of IR may be from increased passive tension in the GHJ external rotators, posterior GHJ capsule contracture, or increased humeral retroversion. However, current clinical measurements cannot differentiate how IR ROM is influenced by the muscles, the capsule, or the amount of retroversion [1].

This project represents pilot data that will be used to develop a larger study that will identify valid and reliable independent clinical measurements for posterior shoulder muscle length, posterior GHJ capsule length, and humeral retroversion. The purpose of this pilot study was to examine several proposed posterior shoulder muscle measurements for their ability to detect a change in IR ROM resulting from an increase in muscle tension. Because eccentric exercise is known to result in an immediate increase in muscle passive tension [4], we used a fatigue protocol that emphasized eccentric contractions to change muscle tension and evaluate the effect on IR ROM. To verify increased muscle tension, we also assessed the change in muscle hardness after fatigue.

## METHODS

The study used a pre-task post-task design to evaluate three potential muscle measurements: 1) Glenohumeral Neutral (GHN) - subject sitting, shoulder joint abducted to 60° in the plane of scapula (POS) and internally rotated; 2) Extension with Internal Rotation (EIR) - subject sitting, shoulder joint abducted to 60° in the POS, horizontally abducted 90° and internally rotated; 3)

Horizontal Adduction (HAD) - subject in sidelying, shoulder and elbow flexed to 90° and neutrally rotated. ROM in each position was quantified with a digital inclinometer (Baseline Evaluation Instruments) both before and after an exercise task. The order of measurements was randomized for both sessions.

In addition to IR ROM, muscle hardness or compliance was quantified in each of the 3 positions using a Myotonometer (Neurogenic). Compliance was also quantified in a control position with the subjects' arm supported in neutral at their side. Hardness measurements were also taken before and after the fatigue task. To ensure reproducibility, a standardized measurement location was marked on each subject and the measurement was taken by the same investigator.

All subjects performed repetitions of concentric and eccentric external rotation in a sidelying position with resistance equal to 5% of their body weight. The repetitions were "controlled" if the eccentric phase lasted 2 seconds. When unable to perform the concentric phase, an investigator assisted the subject and the eccentric phase was continued. Two consecutive failed attempts to lower the weight under control marked the end of the protocol. Measurements for ROM and muscle hardness resumed immediately following the completion of the fatigue task.

The main dependent variable for the study was the change in IR ROM in degrees. Mean IR ROM was determined separately for each position before and after the task. Change was calculated as the *Pre task IR ROM* – *Post task IR ROM*. The secondary dependent variable was the change in infraspinatus muscle hardness. Muscle hardness was determined by calculating the area under the force-displacement curve generated by the Myotonometer. Mean muscle hardness by position and task was

determined, and change in hardness was calculated as *Post task hardness – Pre task hardness*.

## RESULTS AND DISCUSSION

5 males and 6 females (mean age 23 years) volunteered for the study. All were right hand dominant and all but one had the non-dominant shoulder tested. Due to the small sample size, only descriptive statistics were determined.

The fatigue task resulted in decreased IR ROM and increased infraspinatus hardness in all 3 positions (Figs 1 & 2). The largest decrease in IR ROM and increase in muscle hardness was observed in the EIR position. These results were expected and are consistent with the previously reported data [2].

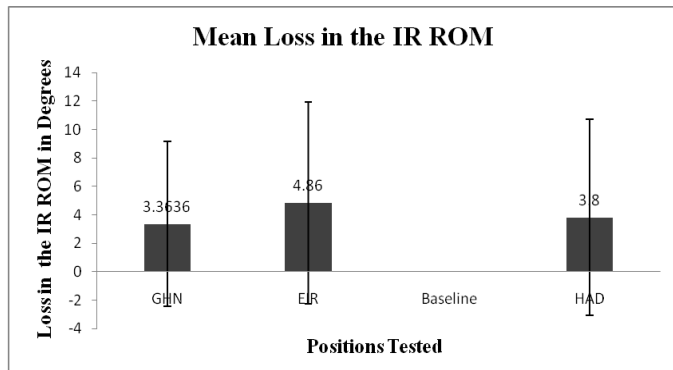


**Figure 1:** Mean loss in the IR ROM across positions after fatigue protocol. ROM was not measured in baseline position.

Several key variables are likely to interact in the effectiveness of a position to measure muscles influence on joint ROM. These include the amount of passive tension in the muscle, the orientation of the line of action of the passive tension and the influence the position has on the joint capsule. We believe that in the EIR position the line of action of passive tension in the infraspinatus muscle may be optimally oriented to influence IR ROM. The infraspinatus attachment on the humeral head will move anterior with extension, and with the addition of IR, moves lateral and inferior, optimally lengthening the muscle so as to efficiently increase passive tension. Furthermore, the EIR position likely approximates the attachments of the posterior capsule attachments on the posterior glenoid and humeral head, creating some laxity in the posterior capsule and decreasing the ability of the capsule to limit GHJ IR.

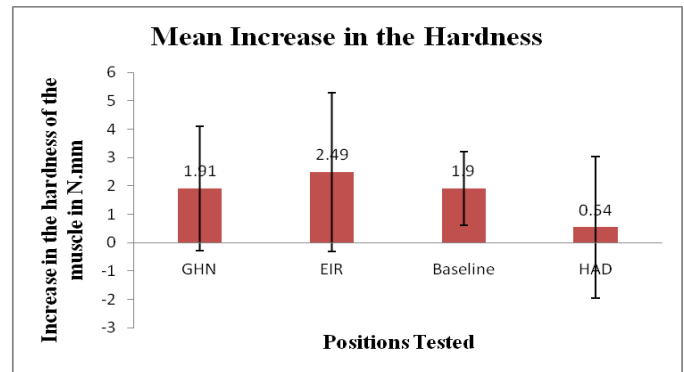


**Figure 2:** Mean increase in the hardness of muscle across the positions.

We quantified muscle hardness as a way to verify that a change in muscle tension was responsible for any change in IR ROM. Muscle hardness increases with the increasing tension in a muscle [3]. In all subjects, there was an increase in hardness immediately following the fatigue task. Repeated eccentric contractions cause acute sarcomere injury and result in increased muscle hardness. HAD is commonly used to measure posterior shoulder tissue tightness. This position had the smallest change in muscle hardness, but the second largest change in ROM. This inconsistency may be from using a side lying position to assess the ROM and hardness in HAD, which is less reliable than supine because scapula movement may influence the ROM measurement. This probably also accounts for the large standard deviations seen with this measurement. However, we chose side lying HAD because the simultaneous quantification of muscle hardness will not be possible in supine lying position.

## REFERENCES

1. Borstad JD, et.al. *J Orthop Sports Phys Ther.* Feb; 41(2):90-9 2011.
2. Muraki T, et.al. *Clin Biomech.* Jun; 21(5):474-80. 2006
3. Murayama M, et.al. *Eur J Appl Physiol.* 93: 489-495. 2005
4. Whitehead NP, et.al. *J Physiol.* Jun 1; 533(Pt 2):593-604. 2001

## ACKNOWLEDGEMENTS

We wish to thank Ashley Hayes, Josh Garza, Megan Anzak and Troy Harmon for their assistance with data collection.

# VIRTUAL PROTOTYPING AND USER TRAINING FOR NEURAL PROSTHETIC SYSTEMS IN MSMS

Rahman Davoodi and Gerald E. Loeb

Department of Biomedical Engineering  
University of Southern California, Los Angeles, CA, USA  
E-mail: [davoodi@usc.edu](mailto:davoodi@usc.edu), Web: <http://mddf.usc.edu>

## INTRODUCTION

Research on control of human movement and development of neural prostheses for restoration and rehabilitation of movement after spinal cord injury and amputation can benefit greatly from modeling and virtual simulation. MSMS is a software tool that can be used to develop models of human or prosthetic limbs and the objects they interact with and simulate their movement in interactive virtual reality environments. Specialized tools and utilities allow users to test and evaluate mechanical characteristics of prosthetic limbs before manufacturing, evaluate their controllability by the patients in interactive virtual environments before clinical application, and train the patient to operate them effectively once they are delivered to the patients. MSMS's modeling and simulation tools are routinely used in a number of research laboratories around the country to study the control of movement and develop and test neural prostheses for patients with paralysis and amputations.

## METHODS

Models of limbs and objects representing specific neural prosthesis systems or rehabilitation and training applications are assembled in MSMS using its interactive graphical modeling tools or imported from other modeling software such as SIMM (Musculographics Inc.) and SolidWorks (SolidWorks Corp.) (Fig. 1). A utility for importing OpenSim models is under development. The MSMS model can be automatically converted to Simulink

(Mathworks Inc.) where an extensive array of toolboxes can be used to add models of prosthetic control systems and drivers to interface with the patient and external devices. The Simulink model simulates the behavior and movement of the system in response to control inputs and external forces. In addition, the Simulink model packages and sends the resulting motion data to MSMS for run-time animation of the virtual model.

The Simulink models created by MSMS can also be compiled and run in xPC Target real-time PCs (Mathworks Inc.) (Fig. 2). The latter allows the user to turn their MSMS models into real-time interactive simulations where the subject (human or non-human primate) can generate voluntary commands (limb movement, EMG, cortical neural activity) to control the movement of the virtual limb in MSMS and at the same time view the resulting movement animated in MSMS and displayed on 2D or 3D stereoscopic displays from the user's point of view. This enables the patient to learn the correct movement based on visual feedback, as he/she would with the real prosthetic system. There are utilities for measuring the execution time of the simulation code in real-time PC and animation rendering times in visualization PC that can facilitate the design of real-time applications.

## RESULTS

The modeling and simulation tools in MSMS and Simulink offer a powerful virtual prototyping environment using

readily available programming expertise and PC hardware and software that are accessible to most academic laboratories. It reduces the time, expense and potential hazards associated with building mechatronic hardware and testing it iteratively with patients.

MSMS has been used to develop and evaluate control systems for prosthetic and functionally stimulated limbs [5]. The subject's voluntary shoulder movements were used to control the movement of a simulated limb in virtual world. The availability of a safe and readily available training environment will become even more important when patients are fitted with multi-degrees of freedom prosthetic limbs and have to learn to produce complex neural commands to operate them.

At Johns Hopkins Applied Physics Laboratory, a virtual integration environment was developed to facilitate the collaborative development of sophisticated neural prostheses for upper limb amputees [1]. MSMS is used to build sophisticated models of neural prostheses for amputees and simulate them in real-time using a PC configuration illustrated in Fig. 2.

In Walter Reed Army Medical Center, Zeher et al. [6] have used MSMS's animation tools to develop a virtual version of "Mirror Therapy" to alleviate amputee phantom limb pain. The animations are built with a MSMS tool that allows the users to assemble primitive movements into complex motion sequences in Microsoft's PowerPoint [3].

MSMS has enabled motor control scientists to perform innovative closed-loop control experiment that are far superior to traditional open-loop methods for development of decode algorithms for neural prosthesis [2]. MSMS is now routinely used in major motor

control laboratories such as Stanford [2], Caltech [4], and Johns Hopkins and Rochester universities [1] to study the control of reach and grasp movements.

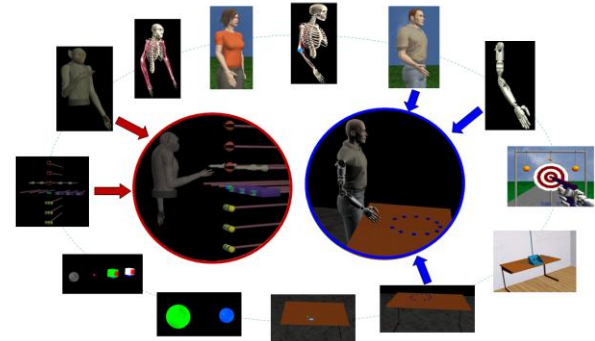


**Figure 1:** Example models of limbs and tasks in MSMS and their combination to build complete virtual models.

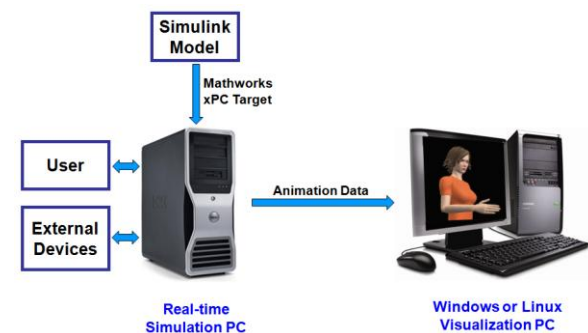


**Figure 2:** Minimal hardware setup for interactive real-time simulations with two PCs. The real-time PC acquires patient inputs, runs the simulation code and application logic, and sends the simulated motion data to visualization PC that animates it in real-time.

## REFERENCES

1. Aggarwal, V. et al. (2011). *Proc. of IEEE-EMBS Conf. on Neural Eng.*
2. Cunningham, J. P. et al. (2010). *J. Neurophysiol.*, in press.
3. Davoodi, R. and Loeb, G.E. (2011). *Stud. Health Technol. Inform.*, **163**:156-162.
4. Hauschild, M. et al. (2009). *Proc. of the SfN.*
5. Kaliki, R. et al. (2010). *IEEE Trans. Biomed. Eng.*, in press.
6. Zeher, M.J. et al. (2011). *Stud. Health Technol. Inform.*, **163**, 730-736.

# DYNAMIC CONTROL OF FINGERTIP FORCES: DEVELOPMENT IN CHILDHOOD AND DECLINE WITH AGING

<sup>1</sup>Sudarshan Dayanidhi, <sup>2</sup>Åsa Hedberg, <sup>2</sup>Isak Hägg, <sup>2</sup>Novalie Lilja, <sup>2</sup>Hans Forssberg, <sup>1</sup>Francisco J Valero-Cuevas

<sup>1</sup> University of Southern California, Los Angeles, CA, USA

<sup>2</sup>Karolinska Institute, Stockholm, Sweden.

email: [dayanidh@usc.edu](mailto:dayanidh@usc.edu) web: <http://bbdl.usc.edu>

## INTRODUCTION

Dexterity, which we define as the dynamic control of fingertip forces for manipulation, improves in typically developing children with practice and neuromaturational [1]. At the other extreme of the lifespan, there is a decline in dexterity with aging related to deterioration of brain function, sensory acuity, and muscle function [2]. Previous studies on both populations have primarily focused on grasp of rigid objects, or on timed pick-and-place tasks, as a means to quantify manual abilities. However, these metrics lack resolution as they saturate upon moderate manipulation ability. As an alternative, we focus on the fact that dexterous manipulation depends on dynamic control of fingertip force direction—and use paradigms centered on grasp of unstable objects to quantify this control [3-6]. Our hypothesis is that a dynamic grasp paradigm can detect changes in dynamic control of fingertip forces at both extremes of the life span.

## METHODS

### *Instrumentation*

We used four custom-made springs (Century Springs Corp., Los Angeles, CA) that require low force for complete compression and have the same stiffness. As each spring is compressed, its slenderness defines its propensity to buckle, thus the hand-spring system acquires different levels of instability. The anatomy of the hand and the sensorimotor control must dynamically regulate fingertip forces to overcome this instability to hold a maximal level of compression for each spring [5]. The longer the spring, the greater the propensity to buckle, and the greater the instability to be controlled. After a brief familiarization with all springs and the tasks, we presented the springs in order, starting with the shortest (Spring 4) to find

the first spring they could not compress fully. This was their ‘minimally impossible-to-compress’ spring. The specifications are in Table 1.

Two compression load cells (ELB4-10, Measurement Specialties, Hampton, VA) were mounted at the spring endcaps (Figure 1). The load cells were connected to a signal-conditioning box and a USB-DAQ (Measurement Computing, Norton, MA) sampled the data at 400 Hz using a custom written MATLAB program (Natick, MA).



**Figure 1:** Dynamic device and spring set.

**Table 1:** Spring Specifications

|                          | Spr 1  | Spr 2 | Spr 3  | Spr 4  |
|--------------------------|--------|-------|--------|--------|
| <b>Free Length (in)</b>  | 1.56   | 1.42  | 1.275  | 1.14   |
| <b>Solid Length (in)</b> | 0.27   | 0.27  | 0.27   | 0.27   |
| <b>Force Range (N)</b>   | 0–2.84 | 0–2.5 | 0–2.19 | 0–1.89 |

### *Experimental Procedure*

90 children (4-16 yrs), 13 young adults (21-35 yrs) and 20 older adults (50-85 yrs) participated in this multi-site study. Subjects were asked to compress their minimally impossible-to-compress spring with their dominant index-thumb to the point beyond which they felt the device would slip out of their hand, and maintain that compression for at least 3 seconds. We collected 3-5 trials such successful trials per subject.

### Data Reduction

A custom written MATLAB<sup>®</sup> (Mathworks, Natick, MA) program was used to visually identify (*ginput*) the hold phases based on the force and force rate. To facilitate this in the presence of high frequency dynamic changes in the force, we used a *loess* smoother with a span of 10% before force rate was computed. We defined a hold phase when the rate was bounded within 1 standard deviation of the mean force rate. The start was identified when the rate was close to zero and the end when the rate went out of bounds & the force dropped towards baseline. The hold phase data were downsampled to 100 Hz, low pass filtered at 25 Hz while maintaining phase (*Butterworth, filtfilt*). The average of the two finger force time series were computed to create a representative force.

The springs were weighted such that for each subject a Dexterity score was computed by summing the maximal force of each spring they could compress fully, plus the maximal force they could hold in their impossible spring, normalized to that maximally possible over the four springs. For most children in our study Spring 1 or 2 were used as the impossible spring (a few of the younger children used Spring 3), while for all adults it was only Spring 1. The variables of interest were the dexterity score during successful 3 s holds, and the three maximal ones per subject were used for analysis.

### RESULTS AND DISCUSSION

Significant differences were seen between the younger and older adults in the dexterity score ( $73.6 \pm 3.3$ ,  $59.6 \pm 3$ ,  $p < 0.5$ ) using a repeated measures

ANOVA (young vs. old age groups). During development we see a steady increase in the dexterity score in children totaling 40%, well approximated with a sigmoid curve and well beyond the age at which other metrics of hand function saturate (Fig 2).

### CONCLUSIONS

The use of a dynamic grasp paradigm presents a unique way of understanding and quantifying development and decline of dexterity, with improving control demonstrated throughout childhood and reduction with aging. Importantly, dynamical analysis reveals similar control at both ends of the lifespan. Therefore this method can provide quantitative means to evaluate rehabilitation and treatment modalities.

### REFERENCES

1. Forsberg, H., et al., *Exp Brain Res*, **85**(2), 451-7, 1991.
2. Cole, K.J., *Exp Brain Res*, **175**(2), 285-91, 2006.
3. Mosier, K.M., et al., *J Neurophysiology*, (**In Press**).
4. Vollmer, B., et al., *Developmental Medicine & Child Neurology*, **52**(10), 948-954, 2010.
5. Venkadesan, M., et al. *J Biomech*, **40**(8), 1653-61, 2007.
6. Valero-Cuevas, F.J., et al., *J Biomech*, **36**(2), 265-70, 2003.

### ACKNOWLEDGEMENTS

This material is based upon work supported by RERC Grant 84-133E2008-8 to FVC.

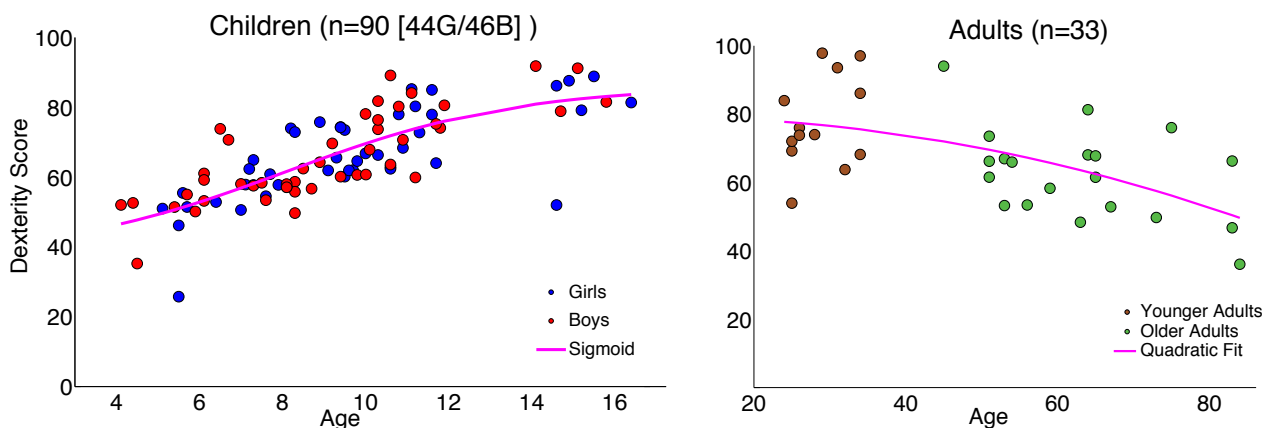


Figure 2: Development and decline of directional control of fingertip forces.

# INFLUENCE LUMBAR SUPPORT PROMINENCE MAGNITUDE ON BODY POSTURE AND SUBJECTIVE COMFORT DURING PROLONGED DRIVING.

Diana E. De Carvalho and Jack P. Callaghan  
University of Waterloo, Waterloo, ON, Canada  
email: ddecarva@uwaterloo.ca

## INTRODUCTION

The use of lumbar supports has been associated with decreased reports of low back pain during driving exposures [1, 2]. However, there is limited work aimed at determining how much support is appropriate to improve both subjective comfort and biomechanical variables. This study examined the impact of self-selected lumbar support prominence magnitudes on subjective and postural responses of the low back and pelvis during two hours of simulated driving. Specific goals of the study were to explore any gender differences in seated posture and to establish preliminary data on lumbar support preferences of male and female subjects (both initial and retrospective).

## METHODS

Seventeen participants, 9 males and 8 females, with no recent history of low back pain were recruited from a university population (males: average age 24.89 years +/- 4.26, height 1.842 cm +/- 0.0795 and mass 90.4 kg +/- 12.3; females: 23.75 years +/- 2.76, height 1.61 cm +/- 0.236 and mass 59.25 kg +/- 5.73).

Lumbar spine flexion and pelvic angles were obtained using tri-axial accelerometers (S2-10G-MF, NexGen Ergonomics, Montreal, Quebec, Canada) placed over the L1 spinous process and the sacrum at S2. Active light emitting diode markers for the collection of kinematic data via an optoelectronic motion analysis system (Optotrak, Certus, Northern Digital Inc., Waterloo, Ontario, Canada) were taped to the right side of the participants. From these markers two-dimensional angles for the shoulder, trunk, hip, elbow and knee were calculated. Prior to commencing the prolonged driving trial, subjects were asked to select one of five lumbar support settings (0 cm, 1

cm, 2 cm, 3 cm, 4 cm) that they felt would be most comfortable for an extended period of time.

Throughout the prolonged driving trial seat pressure, motion analysis, and accelerometer data were collected continuously for the 2-hour test session. For data reduction purposes, data collection was separated into eight 15-minute intervals and the first 2 minutes of each 15 minute trail were analyzed. Ratings of perceived discomfort (RPD) were completed at 15-minute intervals throughout the prolonged driving trial using visual analogue scales (0 - 10 cm) for 7 regions of the low back and pelvis. At the end of the simulated driving period the subjects filled out a final RPD questionnaire and the outcome questionnaire was completed. Two-way mixed model analyses of variance, with time as the within factor and gender as the between factor, were completed to compare dependent variables during the prolonged driving trial. Tukey's Studentized Range Test post hoc was used on all significant effects. In all statistical tests a p-value of less than 0.05 was accepted as statistically significant.

## RESULTS AND DISCUSSION

Females tended to self select larger support levels than males: 2 cm = 1, 3 cm = 4, 4 cm = 3 (females), 1 cm = 1, 2 cm = 3, 3 cm = 4, 4 cm = 1 (males).

Analysis of time varying posture data throughout the simulated driving trial found no differences over time for all subjects ( $p = 0.9985$ ). Both lumbar and pelvic angles remained relatively static throughout the two-hour period (Figure 1). No significant differences were found between genders for lumbar flexion angle (72.80 % ROM  $\pm$  1.28 males, 84.47 % ROM  $\pm$  4.02 females:  $p=0.2882$ ). Significant differences were found between male and female pelvic posture ( $p = 0.0096$ ) with females having

more pelvic flexion relative to upright standing than males ( $20.41^\circ \pm 0.65^\circ$  males,  $15.0^\circ \pm 0.95^\circ$  females).

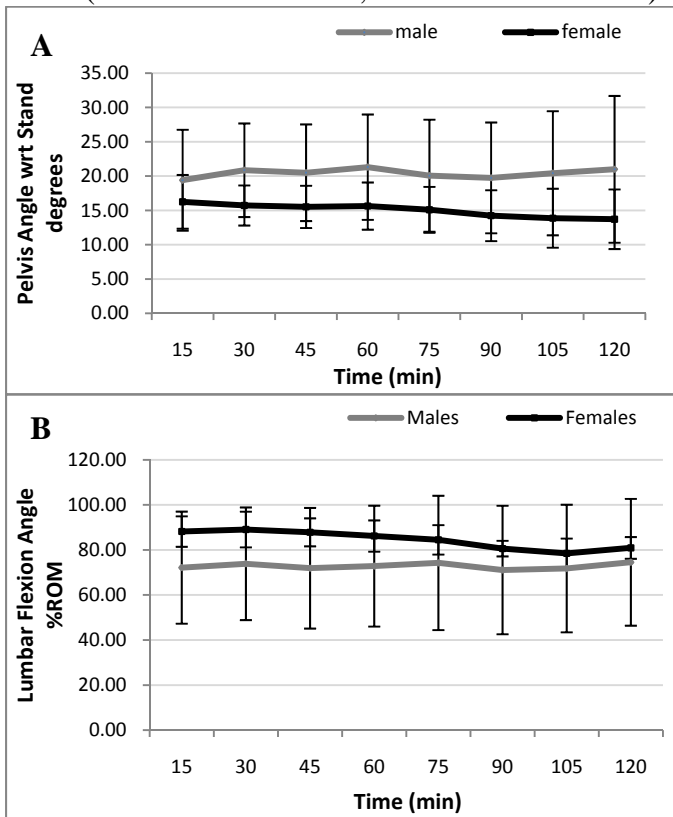


Figure 1: Time varying lumbar flexion angle (A) and pelvic tilt angle (B) throughout the driving trial.

During the time varying driving trial data a main effect of time was found for trunk angle ( $p=0.0007$ ) with increases of  $1.99^\circ$  (SD  $1.48^\circ$ ) for males and  $2.10^\circ$  (SD  $0.961^\circ$ ) for females by the end of the second hour.

Although there was a tendency for female subjects to report lower levels of discomfort than males, these differences were not significant. For the time varying data, significant main effects of time were found for the following body areas: sacrum ( $p=0.003$ ), bilateral iliac crests ( $p<0.0001$ ), left buttock ( $p=0.0002$ ) and right buttock ( $p<0.0001$ ).

When the discomfort of the low back is stratified by the support setting chosen by subjects for the 2 hours of prolonged driving there is a clear trend of a minimum level of discomfort developing in the 3 cm group (Figure 2). Statistical analyses could not be completed on these grouping due to small sample numbers in each group and with some settings not being chosen at all (0 cm).

Outtake questionnaire responses indicated that no subjects would have desired a setting beyond 4cm,

and the majority of respondents who indicated a desire for a change, had it been allowed, would have selected a increased magnitude of support with a setting between 3 and 4 cm.

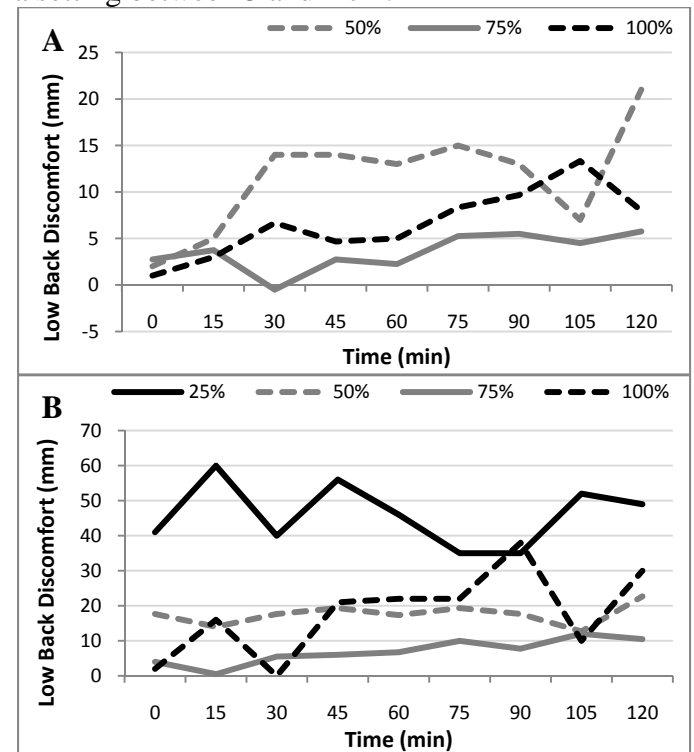


Figure 2: Low back discomfort ratings grouped by lumbar support choice for female (A) and male (B) subjects.

## CONCLUSIONS

The lumbar spine and pelvic angle magnitudes found are consistent with prior work [3]. Self-selected lumbar support, with settings beyond the lumbar support deflections currently available commercially, likely contributed to the lack of gender differences that have been previously reported. The results suggest that increasing the excursion by 150% to 3cm of lumbar support prominence would improve comfort and could have a potentially beneficial impact on low back postures.

## REFERENCES

1. Chen et al. (2005). *Scand J Work Environ Health* 31(4): 258-265.
2. Donnelly et al. (2009). *Int J Occup Saf Ergon* 15(3):295-307.
3. Beach et al. (2005). *Open Erg J* 1(1); p.1-9

## ACKNOWLEDGEMENTS:

NSERC, CIHR, SCHUKRA, FCER

# LOAD VARIATION INFLUENCES ON JOINT WORK DURING SQUAT EXERCISE IN REDUCED GRAVITY

<sup>1</sup>John K. DeWitt, <sup>1</sup>Renita S. Fincke, <sup>2</sup>Rachel L. Logan, <sup>1</sup>Mark E. Williams, and <sup>3</sup>Lori L. Ploutz-Snyder

<sup>1</sup>Wyle Integrated Science and Engineering, Houston, TX, USA; <sup>2</sup>Midwestern University, Downers Grove, IL, USA; <sup>3</sup>Universities Space Research Association, Houston, TX, USA. email: john.k.dewitt@nasa.gov

## INTRODUCTION

Resistance exercises that load the axial skeleton, such as the parallel squat, are incorporated as a critical component of a space exercise program designed to maximize the stimuli for bone remodeling and muscle loading. Astronauts on the International Space Station perform regular resistance exercise using the Advanced Resistive Exercise Device (ARED).

Squat exercises on Earth entail moving a portion of the body weight plus the added bar load, whereas in microgravity the body weight is 0, so all load must be applied via the bar. Crewmembers exercising in microgravity currently add ~70% of their body weight to the bar load as compensation for the absence of the body weight. This level of body weight replacement (BWR) was determined by crewmember feedback and personal experience without any quantitative data.

The purpose of this evaluation was to utilize computational simulation to determine the appropriate level of BWR in microgravity necessary to replicate lower-extremity joint work during squat exercise in normal gravity based on joint work. We hypothesized that joint work would be positively related to BWR load.

## METHODS

Six subjects (3M/3F) completed a squat exercise in normal gravity on the ground-based ARED at NASA Johnson Space Center. Motion-capture data were collected at 250 Hz

with a twelve-camera system (SMART-D, BTS Bioengineering SPA, Milanese, Italy). Ground reaction force (GRF) data were collected bilaterally at 1000 Hz by independent force platforms (Kistler Model 9261, Kistler Instruments AG, Winterthur, Switzerland). Data were collected simultaneously on a single workstation.

OpenSim software (OpenSim 2.2.0, Simbios, Palo Alto, CA) was used to determine lower-extremity kinematics and joint torques at the ankle, knee, and hip [1]. The base model used for the analysis was a generic musculoskeletal model with 23 degrees of freedom that accompanied the OpenSim software [2].

Subject-specific models based on anthropometry were created. The hip joint was modeled as a ball and socket joint (3 dof) while the knees and ankles were modeled as hinge joints (1 dof). For this analysis, we focused on motions in the sagittal plane.

Once inverse kinematic analyses were completed, the joint torques at the ankle, knee, and hips were computed using an inverse dynamics analysis. Instantaneous joint power was computed as the product of torque and angular velocity. Positive work for the concentric (upward) phase was found by integrating the power versus time curve. All computations were performed with custom scripts using MATLAB (version R2010a, MathWorks, Natick, MA).

All simulations were initially completed at 1G and subsequently performed for comparison with a 0G condition with BWR loads of 0%, 30%, 50%, 70%, and 100%. BWR

simulations were completed by reducing the GRF data for a given condition by the appropriate percentage of body weight and assuming that joint kinematics in 0G were the same as in 1G.

Linear regression was used to determine the relationship between joint work and BWR load. The BWR load necessary to replicate the work performed in 1G at each joint was found using the derived regression equations relating work to BWR level. Separate analyses were performed for each subject.

## RESULTS and DISCUSSION

For all joints, net work was related to BWR ( $r^2=0.99\pm 0.01$ ) The mean BWR to replicate 1G net positive work in the lower extremities was  $66.77\pm 4.92\%$ ,  $88.30\pm 4.17\%$ , and  $96.05\pm 1.26\%$  for the hips, knees, and ankles, respectively. Figure 1 illustrates the relationship between net joint work and BWR. Work values were normalized by 50% of the body weight + resistance load.

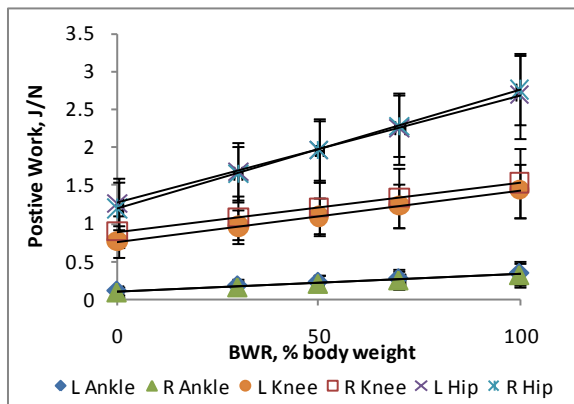


**Figure 1:** Normalized positive work vs. BWR for all subjects (mean $\pm$ s.d.).

Simulation results suggest that with the current BWR of 75% used by crewmembers, musculature at the hip may be loaded sufficiently while the knees and ankles are

underloaded compared to 1G. Using body segment parameters of de Leva [3], about 59%, 88%, and 97% of body mass is above the hips, knees, and ankles respectively. Our results suggest that using net body mass anatomically superior to the joint of interest to guide BWR may be sufficiently load the knees and ankles, but may underload the hips. More study is necessary to determine BWR influences on specific musculature, and if similar relationships occur with other axial loading exercises.

## CONCLUSIONS

Our approach using simulation has allowed us to provide some evidence that current squat exercise prescriptions for crewmembers may be sufficient to load the hips, but may underload the knees and ankles. Simulations were completed using existing data at a fraction of the cost of completing an experiment in actual or simulated 0G.

## REFERENCES

1. Delp SL, et al. *IEEE Transactions on Biomedical Engineering*, **54**, 1940-1950, 2007.
2. Delp SL, et al. *IEEE Transactions on Biomedical Engineering*, **37**, 757-767, 1990.
3. de Leva P. *J Biomech*, **29**, 1223-1230, 1996.

## ACKNOWLEDGEMENTS

This project was funded by the Human Research Program at NASA Johnson Space Center. We thank personnel from the Human Adaptation and Countermeasures Division and Exercise Physiology and Countermeasures Project for their support with this project.

# EFFECTS OF A PASSIVE ELASTIC EXOSKELETON DURING WALKING

Jesse Dean

Medical University of South Carolina, Charleston, SC, USA

email: [deaje@musc.edu](mailto:deaje@musc.edu)

## INTRODUCTION

Locomotor function is often limited following a neurological injury, although the underlying mechanisms are not always clear. While walking appears to be a complex task from a neural control perspective, many aspects of gait may be predicted simply from the passive mechanics of the body, the focus of a field commonly termed dynamic walking.

Following a stroke or spinal cord injury, gait speed is primarily limited by maximal step frequency [1, 2]. Recent dynamic walking model simulations predicted that step frequency is primarily controlled by actuation at the hip and knee joints [3]. This actuation does not require complex active control, but may be provided by passive elastic elements. Such an actuation method can produce human-like gait speeds and leg swing kinematic patterns without the need for energetic input at the hip or knee. These simulation results suggest that neurological patients may have limited maximal step frequencies due to an inability to appropriately activate their proximal leg musculature.

Based on our previous model simulations, we developed a passive exoskeleton which is able to store and return mechanical energy using springs which parallel the users' legs. The springs are situated such that a single spring produces torque at the hip and knee, a configuration our simulations suggest is necessary to produce typical leg swing kinematics. These two-joint springs are similar in concept to bi-articular muscles of the upper leg, specifically the rectus femoris and biceps femoris.

We hypothesized that storage and return of mechanical energy by the exoskeleton's elastic elements would reduce the need for subjects to actively produce joint torques. We expected that the mechanical assistance provided by the springs would allow subjects to reduce the swing phase activity of muscles acting across the hip and knee.

## METHODS

The exoskeleton was lightweight (3.5 kg), consisting of a carbon fiber waist belt attached to adjustable length aluminum segments lateral to the thigh and shank (Fig. 1). Thrust bearing hinges connected the rigid segments, and were aligned with the subjects' hip and knee joints. Padded plastic cuffs around the shanks and thighs mechanically linked the user to the device. Extension springs (stiffness = 2000 N/m) were placed in series with wires running along grooved aluminum sheaves at the hip (moment arm = 7.6 cm) and knee (moment arm = 2.5 cm). The ratio between the hip and knee moment arms was based on earlier simulations [3].

Four young ( $27 \pm 3$  yrs), healthy subjects walked on a treadmill at 1.25 m/s under three conditions: *No Exoskeleton*; *Exoskeleton with No Springs*; *Exoskeleton With Springs*. Trial order was randomized. For each trial, subjects were given 3 minutes to reach a steady state, and data was recorded for the next 30 seconds.

We collected bilateral EMG data from the rectus femoris (RF) and biceps femoris (BF). Electrodes were placed over the muscle bellies, avoiding contact with the exoskeleton. Pressure footswitches were used to quantify stride timing. For analysis, processed EMG data for each muscle were divided



**Figure 1.** We built a passive exoskeleton with two-joint springs crossing the hip and knee. The design of this device was based on previous model simulations, with the goal of providing swing phase gait assistance.

into strides, averaged, and normalized by the peak value across all trials. For one subject, we quantified spring joint torques using load cells placed in series with the springs.

## RESULTS AND DISCUSSION

The net joint torques produced by the springs varied as expected. At the beginning of the swing phase, the springs produced hip flexion and knee extension torques. Later in swing the effects of the springs reversed, producing hip extension and knee flexion torques. This swing phase torque profile is similar to the pattern of active torque production typically seen in human walking [4].

As expected, the hip and knee joint torques produced by the springs late in the swing phase allowed subjects to reduce BF muscle activity (Fig. 2). Averaged across subjects, this effect was significant ( $p=0.010$ ). Donning the exoskeleton slightly increased muscle activity, likely due to the mass of the device. But adding springs decreased BF activity below the level seen during normal walking. This implies that subjects were able to adapt their muscle activation pattern to take advantage of the exoskeleton assistance.

The effects of the exoskeleton on RF activity were less clear (Fig. 3). RF activity was quite low during

the Pre-Swing phase, when we would expect the exoskeleton assistance to be most beneficial. While the springs appeared to slightly decrease RF activity, this change was not significant ( $p=0.52$ ). Unexpectedly, the addition of springs significantly ( $p=0.049$ ) decreased RF activity during early stance, when RF activity was maximal. It is possible that the springs acted to stabilize the knee at heel strike, allowing subjects to decrease co-contraction.

## CONCLUSIONS

A simple passive exoskeleton worn while walking allows users to decrease muscle activity during specific gait phases. Such a device has the potential to provide useful gait assistance during rehabilitation, but future work must investigate effects outside of the sagittal plane.

## REFERENCES

1. Bayat R, et al. *Neurorehabil Neural Repair* **19**, 115-24, 2005.
2. Pepin A, et al. *Spinal Cord* **41**, 271-9, 2003.
3. Dean JC, et al. *J Roy Soc Interface* **6**, 561-73, 2009.
4. Winter DA. *The biomechanics and motor control of human gait: normal, elderly and pathological*. Waterloo Biomechanics, 1991.

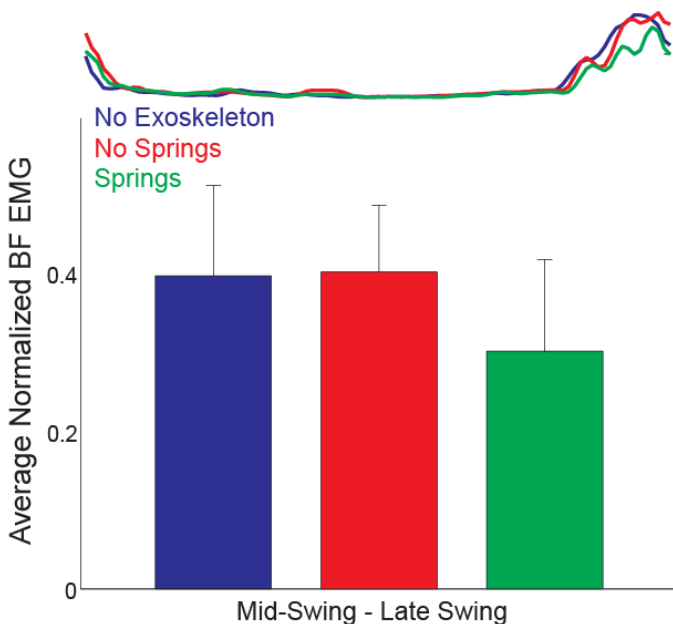


**Figure 2.** Changes in BF activity are illustrated for a single subject (top) and averaged group data (bottom). Single subject data is plotted from heelstrike to heelstrike, while group data is averaged over Mid and Late Swing (73-100% gait cycle).

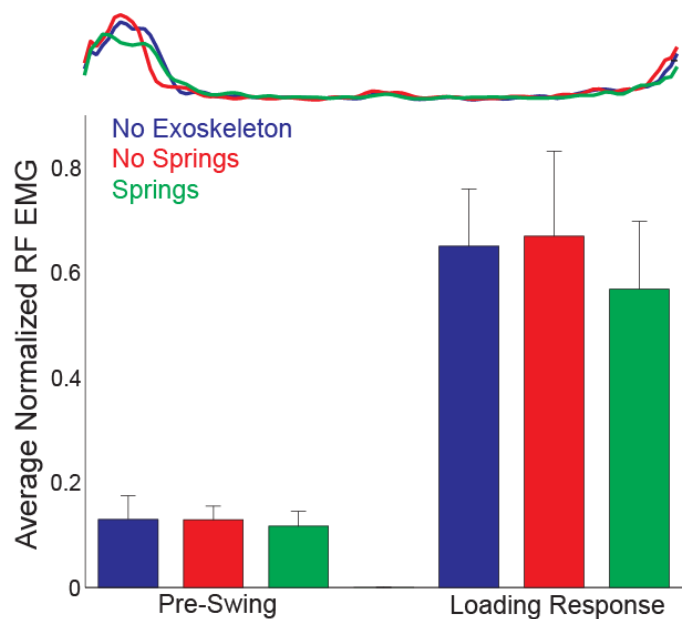


**Figure 3.** Changes in RF activity for a single subject (top) and averaged group data (bottom). Group data is averaged separately over Pre-Swing (50-58% gait cycle) and Loading Response (1-10% gait cycle).

# MULTISCALE ENTROPY OF EMG DURING WALKING IN YOUNG AND OLDER ADULTS

<sup>1</sup>Mark D. Dela, <sup>2</sup>Jonathan B. Dingwell and <sup>1</sup>Hyun Gu Kang

<sup>1</sup>California State Polytechnic University, Pomona, CA, USA

<sup>2</sup>University of Texas at Austin, Austin, TX, USA

email: hgkang@csupomona.edu web: <http://www.csupomona.edu/~hgkang>

## INTRODUCTION

Aging is associated with the accumulation of deficits in the function of the neuromuscular system, which may lead to motor deficits, gait instability, and falls. Aging has been hypothesized to manifest in lower complexity of physiological dynamics, evidenced by heart rate, step time, as described using fractal and other multiscale characteristics<sup>1</sup>. However, others in the biomechanics field have shown that older adults exhibit higher entropy values, rather than lower values, as a measure of complexity<sup>2,3</sup>. This discrepancy seems to arise because different studies have considered different timescales of behaviour. To resolve this inconsistency, we need to compare motor behaviour over a wide range of timescales. To observe the behaviour of the nervous system, we can consider the motor outputs in the form of EMG. Therefore, we tested whether the muscle activation patterns as measured by EMG are more complex in young adults compared to older adults and whether EMG complexity is affected by walking speed.

## METHODS AND PROCEDURES

Eighteen healthy older adults (age 72±6) and 17 height- and weight-matched young adults (23±3), with no orthopedic or neurological conditions, participated with informed consent. Each walked for 5 minutes on a Woodway treadmill at 80%, 90% 100%, 110% and 120% of their preferred speed (PWS)<sup>4</sup>. EMG from the left *gastrocnemius*, were sampled at 1080Hz (Bagnoli-8, Delsys). After bandpass filtering (20-300 Hz), sample entropy of the signal was calculated after each successive coarse-graining (averaging then down-sampling) of the EMG signal<sup>4,5</sup>. Sample entropy values were integrated over 37 time scales, from timescale 4 to timescale 40, to calculate multiscale entropy, or MSE (Figure 1). These timescales represent dynamics of the EMG signal over ~4 to 40 ms. The effect of the age group and walking speed on MSE and on sample entropy values for timescales 4 to 40 inclusive were assessed using a randomized block design (SAS 9.2).

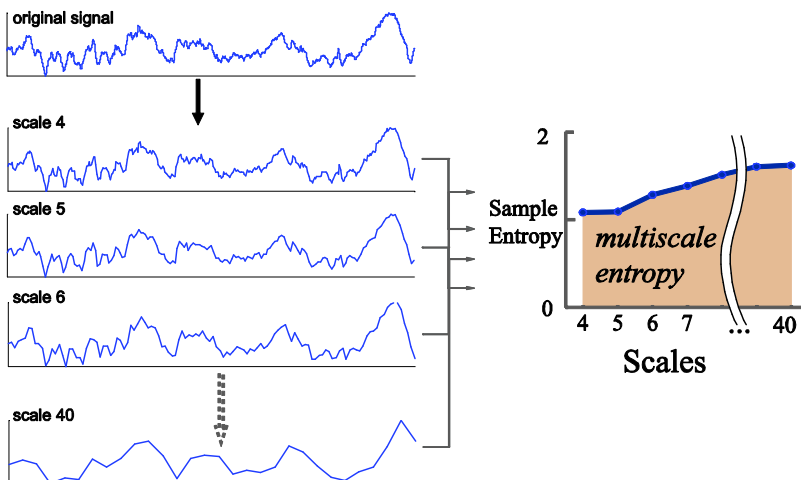


Figure 1. Schematic of Multiscale Entropy Calculations. The signal is coarse grained to isolate the dynamics at a particular timescale, where successive sets of points are averaged. Sample entropy of each coarse grained signal is calculated and combined to determine the multiscale entropy, or MSE.

## RESULTS

The age main effect on MSE was significant ( $p < 0.001$ ). Older adults exhibited an MSE value of  $9.86 \pm 3.31$  compared to  $6.42 \pm 1.37$  in young adults. Walking speed did not influence MSE ( $p = 0.93$ ), and there was no interaction effect between age group and walking speed on MSE ( $p = 0.66$ ).

Results were similar when examining sample entropy values at each individual timescale (Figure 1). Age group differences were significant for all timescales except for scales 33 ( $p = 0.14$ ), 34 ( $p = 0.77$ ), and 35 ( $p = 0.15$ ).

## DISCUSSION

Considering the larger MSE values in older adults alone, our results correspond with other studies in biomechanics<sup>2,3</sup> but not with physiological studies<sup>1</sup>. However, this is not the whole picture: over the timescales studied, older adults exhibit a sample entropy profile more similar to white noise (decaying over timescales) compared to that of young adults who exhibit a more flat profile<sup>5</sup> (Figure 2). It is unclear if at larger timescales, older adults will continue

to exhibit overall higher entropy values or lower ones (i.e., more similar to white noise). A possible future study would be to examine sample entropy values at higher timescales. Our results may be evidence of increased neuromuscular noise in older adults, which takes the characteristic of white noise. Future work could also determine whether muscle activation patterns via EMG signals for other muscles exhibit the type of behaviour described here.

## REFERENCES

1. Lipsitz, L.A. (2002) *J Gerontol A* 57: B115-25
2. Duarte, M. et al. (2008) *Exp Brain Res* 191:265-76
3. Vaillancourt D.E. et al (2005) *J Appl Physiol* 94:903-12
4. Kang, H.G. et al. (2009) *J Biomech* 42:2231-7
5. Kang, H.G. et al. (2009) *J Gerontol A* 64:1304-11

## ACKNOWLEDGEMENTS

Whitaker Foundation; American Society of Biomechanics Grant-in-Aid; Cal Poly Pomona Teacher-Scholar Program.

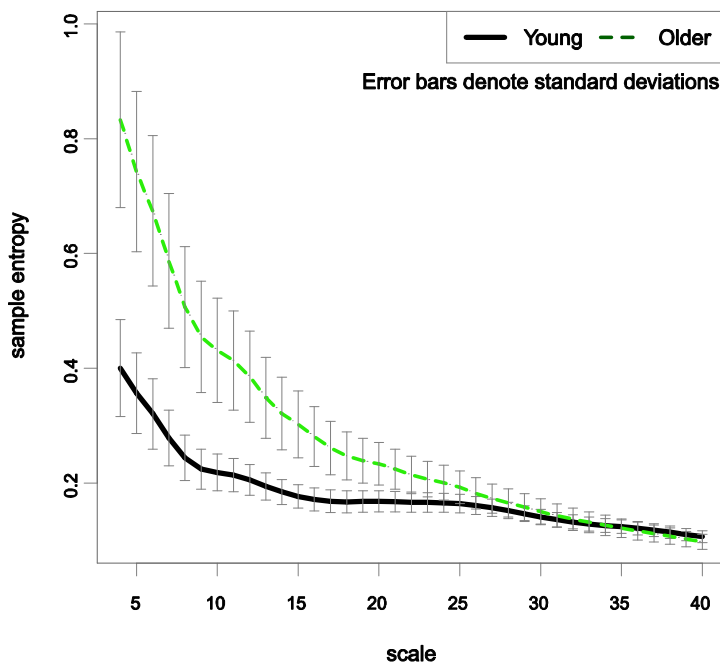


**Figure 2.** Mean sample entropy values vs. timescale for both young and older adult age groups. The sample entropy profile of older adults is similar to that of white noise while young adults have a more flat profile. Error bars denote standard deviations within each timescale.

# VELOCITY MODULATION DURING WALKING BY YOUNG ADULTS

Paul DeVita, Alexis Sidiropoulos, Patrick Rider, Aubrey Taylor, Steven Roseno, Ryan Manbeck & Tibor Hortobagyi, East Carolina University, Greenville, NC email: [devitap@ecu.edu](mailto:devitap@ecu.edu)

## INTRODUCTION

Walking velocity is a fundamental component of locomotion and has been widely used as both a dependent variable when investigating the effects of various conditions or treatments on velocity [eg 1,2] and as an independent variable when investigating the effects of manipulating velocity on other gait biomechanics [eg 3,4]. This later work often investigates the biomechanical processes used to modulate walking velocity. For example, Neptune et al [3] showed the systematic increase in muscle work throughout the lower extremity with discrete increases in walking velocity. This study and others however [eg 4] treated velocity as a categorical variable and have not identified the precise (i.e. mathematical) relationships between walking velocity and its controlling mechanics. In contrast Lelas et al [5] fitted joint torques and powers onto a continuous range of velocity data from 64 adults and reported the equations of best fit, thus precisely quantifying these relationships.

In related work, we previously showed that modulation of stride length while walking was more accurately assessed through discrete, individual participant analyses than through grouped, population analyses [6]. Thus we hypothesize that: 1) walking velocity is modulated by lower extremity joint torques and powers and 2) torque and power values fitted to velocity data within each participant will more accurately assess velocity modulation than the group or population based analyses. The purpose of the study was to identify the relationships among joint torques and powers and walking velocity within individual participants and the pooled participant group through regression analyses.

## METHODS

Walking velocity and joint torques and powers were derived from 3D lower limb kinematics and ground reaction forces from 20 walking trials from each of 22 adults (age:  $20.3 \pm 1.5$  yrs, mass:  $69.1 \pm 12.1$  kg)

after they provided written informed consent. Participants walked at self-selected speeds ranging from very slow to very fast in random sequences. Walking velocities were approximately evenly distributed through the range of velocities for each participant. Observed walking velocities ranged from  $0.81$  to  $2.71 \text{ ms}^{-1}$  and the mean velocity over all participants and trials was  $1.74 \pm 0.36 \text{ ms}^{-1}$ . Relationships between maximum stance phase torques and powers and velocity were derived through linear or curvilinear regression for each participant and for the entire sample as a population based assessment of velocity modulation. Maximum torques and powers were also summed across joints to identify total limb mechanical output and these variables were then regressed onto walking velocity. Individual participant regression coefficients were averaged across participants using Fisher transformation. Coefficients of determination were derived to identify the explained variances between the variables and velocity. Walking velocity was strongly correlated with velocity normalized to height (all subjects,  $r=0.96$ ). Thus, velocity in units of  $\text{ms}^{-1}$  was used.

## RESULTS AND DISCUSSION

The population analysis showed all maximum joint torques contributed to modulating walking velocity. The strength of the contributions were strongest at the hip ( $R^2=0.747$ ) and lower at the knee ( $R^2=0.499$ ) and lower still at the ankle ( $R^2=0.197$ , Table 1). Therefore, we observed a proximal to distal gradient in velocity modulation by lower limb joint torques. All maximum joint powers also contributed to modulating walking velocity. The strength of the contributions were however similar across joints, ranging from  $R^2=0.592$  at the hip to  $R^2=0.462$  at the knee. Most importantly, the summed joint torques and powers most strongly contributed to velocity modulation with  $R^2=0.850$  for summed torque and  $R^2=0.753$  for summed power. We conclude therefore that humans modulate walking velocity by modulating the total torque and power from the

lower limb more so than by modulating individual joint mechanical output.

The individual participant analyses provided greater insight into velocity modulation. These data had regression equations similar to the population equations (i.e. quadratic in nearly all variables) and confirmed the proximal to distal gradient in joint torques and the absence of this gradient in the joint powers. However, they also showed much stronger associations for each variable compared to the population data (Table 1 and Figure 1). *We emphasize that all individual participant results showed stronger associations than the population results.* Therefore, while the population analyses provided a general overview of velocity modulation in walking, these data failed to describe precisely how humans modulate walking velocity. Humans tightly couple joint torque and power magnitude to walking velocity and we manipulate velocity by precisely altering these torques and powers. Finally, the insight provided by the individual participant analyses is most evident in the summed torque and power data. Despite the already strong population-based relationships between the summed variables and velocity, the individual participant data showed even stronger relationships (Figure 2). Both the summed torque and power variables had greater

than 90% explained variance in walking velocity.

## CONCLUSIONS

Walking velocity is partially modulated by selecting appropriate amounts of torque and power at each lower limb joint. Humans more precisely modulate velocity however by controlling the total magnitude of torque and power from all joints more so than by controlling each individual joint. The precise controlling functions for joint torques and powers were most accurately observed on an individual participant basis. All individuals had stronger associations than corresponding population results. Thus, population results were not representative, average assessments but clearly underestimated the precision with which humans manipulate joint torques and powers to modulate walking velocity.

## REFERENCES

1. DeVita P, et al. *J App Phys*, **88**, 1804-1811, 2000.
2. Menant J, et al. *Gait & Post*, **29**, 392-397, 2009.
3. Neptune R, et al. *Gait & Post*, **28**, 135-143, 2008.
4. Arnold A, et al. *J Biomech*, **40**, 3660-3671, 2007.
5. Lelas J et al, *Gait & Post*, **17**, 106-112, 2003.
6. DeVita P et al. *Proc Amer Soc Biomech*, 2009.

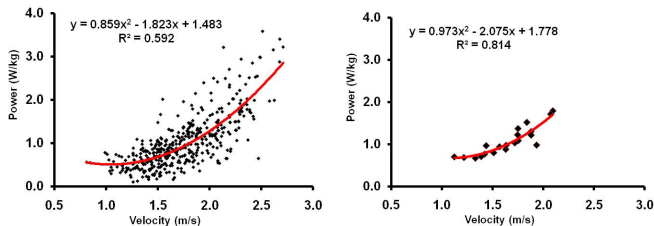


**Figure 1.** Maximum hip power and velocity for population (left) and most representative individual participant (right).

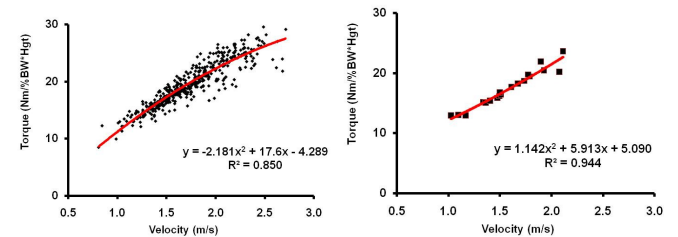


**Figure 2.** Summed torques and velocity for population (left) and most representative individual participant (right).

**Table 1:** Regression equations and squared regression coefficients among walking velocity and torque and power variables. All equations and coefficients statistically significant ( $p < 0.05$ ).

|                    | Torque                            |               | Power                            |               |
|--------------------|-----------------------------------|---------------|----------------------------------|---------------|
| <b>Hip - Pop</b>   | $y = 1.139x^2 + 1.071x + 0.278$   | $R^2 = 0.747$ | $y = 0.859x^2 - 1.823x + 1.483$  | $R^2 = 0.592$ |
| <b>Ind</b>         | $y = 1.375x^2 + 1.768x - 0.348$   | $R^2 = 0.956$ | $y = 0.973x^2 - 2.075x + 1.778$  | $R^2 = 0.814$ |
| <b>Knee - Pop</b>  | $y = -1.228x^2 + 8.241x - 6.170$  | $R^2 = 0.499$ | $y = 1.113x - 0.780$             | $R^2 = 0.462$ |
| <b>Ind</b>         | $y = 4.480x^2 - 12.88x + 12.985$  | $R^2 = 0.870$ | $y = 1.860x - 1.790$             | $R^2 = 0.757$ |
| <b>Ankle - Pop</b> | $y = -2.207x^2 + 8.808x + 1.120$  | $R^2 = 0.197$ | $y = -1.344x^2 + 6.955x - 4.015$ | $R^2 = 0.472$ |
| <b>Ind</b>         | $y = -3.215x^2 + 13.308x - 3.535$ | $R^2 = 0.577$ | $y = -0.263x^2 + 2.843x - 0.676$ | $R^2 = 0.824$ |
| <b>Sum - Pop</b>   | $y = -2.181x^2 + 17.6x - 4.289$   | $R^2 = 0.850$ | $y = -0.972x^2 + 8.093x - 5.045$ | $R^2 = 0.753$ |
| <b>Ind</b>         | $y = 1.142x^2 + 5.913x + 5.090$   | $R^2 = 0.944$ | $y = -0.747x^2 + 5.996x - 2.543$ | $R^2 = 0.917$ |

Pop: Population includes all participants and trials; Ind: data from most representative individual (i.e.  $R^2$  value closest to mean  $R^2$  across all individual participants)

# EFFECTS OF VIBRATION AMPLITUDE AND FREQUENCY ON POSTURAL SWAY IN ALTERED SENSORY ENVIRONMENTS

D. Clark Dickin, Matthew McClain and Ryan Hubble

Biomechanics Laboratory - Ball State University, Muncie, IN, USA

email: [dcDickin@bsu.edu](mailto:dcDickin@bsu.edu) web: <http://www.bsu.edu/biomechanics>

## INTRODUCTION

The application of whole body vibration (WBV) has been shown to elicit positive effects on measures of power, strength, speed, flexibility, bone density, circulation and balance. However, the findings in many of these areas have been equivocal [1]. Although the mechanism(s) contributing to increased performance remain unknown one possible explanation is an alteration or activation of the muscle spindle. In an attempt to elicit an increased level of activation from the stretch reflex through heightened activation of the muscle spindle the frequency range of 25-40 Hz has been used. If WBV can increase the activity level of the muscle spindle, the spindle could then become primed for easier activation in future muscular contractions [2]. Although studies have assessed this specific range of WBV on postural control, the ideal frequency/amplitude combination may differ from the tested levels and has not been determined.

Increased sensitivity and reduced activation threshold levels of the muscle spindle may result in faster or more vigorous activation of the somatosensory system in response to postural sway or perturbations. For individuals with impairments in postural stability this increased level of activation could result in a quicker and more vigorous reflexive response to the postural challenge.

To this end the current study assessed the impact of a broad range of vibration frequencies and amplitudes on postural control; more specifically the effects vibration on sway frequency and regularity/predictability were assessed. If exposure to a vibrating platform alters balance, understanding the degree of active control over postural sway as well as the frequency of postural corrections in response to postural challenges may help to understand how WBV can be used as a training tool.

## METHODS

To assess the impact of both frequency and amplitude of WBV on postural control 12 healthy young adults were assessed in both altered and unaltered sensory environments. Posture was assessed prior to, immediately following, and again at 10 and 20 minutes post vibration. Each participant was exposed to 4-minutes of WBV in each of the six vibration amplitude (low: 2mm; high: 5mm) and frequency (10, 30 or 50Hz) combinations on separate days in a random order (Pro-Vibe, Pneumex; Sandpoint, ID). To minimize any residual effect from the previous WBV exposure a minimum period of 48 hours was imposed between each test session. Postural sway was assessed using the measures of mean power frequency (MPF) and approximate entropy (ApEn) from data collected using a NeuroCom SMART Balance Master in three sensory environments (stable support surface, sway-referenced support surface eyes open, and sway-referenced support surface eyes closed). Each of the three sensory conditions was presented in a random order for each individual but was held constant within a testing session.

*Design:* To determine the effects of vibration on postural sway separate 4 x 6 (Time x Vibration) RM-ANOVA's were used for each of the three sensory conditions for ApEn and MPF. Follow-up pairwise contrasts were performed where appropriate. Significance was set at  $p \leq 0.05$  for all tests.

## RESULTS AND DISCUSSION

Significant changes in postural stability in both altered and unaltered sensory environments were elicited in response to WBV. For the baseline (unaltered) condition significant increases in sway frequency (increased MPF) were found but no

differences in the overall predictability and degree of active control (no change in ApEn). This was not surprising since the postural challenge is small and the need for increased levels of active control may not have been warranted.

Through the use of a sway-referenced support surface somatosensory information was reduced. When combined with visual information the sway-referenced surface elicited a significant increase in sway frequency immediately following the vibration that did not return to baseline until 20 minutes post vibration (Table 2). For the same condition there was a significant increase in ApEn immediately following vibration that returned to baseline levels within 10 minutes of the WBV application.

**Table 1: Approximate Entropy**

| Trial       | Baseline   | Eyes Open   | Eyes Closed |
|-------------|------------|-------------|-------------|
| Pre-Vibe    | .46 (0.04) | *.43 (0.02) | .47 (0.04)  |
| Post-Vibe   | .47 (0.05) | .46 (0.06)  | .48 (0.05)  |
| 10-min post | .45 (0.05) | *.43 (0.05) | *.44 (0.07) |
| 20-min post | .45 (0.07) | *.42 (0.04) | *.45 (0.05) |

(\* indicates significant difference from Post-Vibe)

**Table 2: Mean Power Frequency**

| Trial       | Baseline    | Eyes Open   | Eyes Closed |
|-------------|-------------|-------------|-------------|
| Pre-Vibe    | *.57 (0.04) | *.62 (0.10) | †.65 (0.12) |
| Post-Vibe   | .61 (0.05)  | .65 (0.10)  | †.65 (0.10) |
| 10-min post | *.56 (0.05) | .63 (0.10)  | .62 (0.10)  |
| 20-min post | *.57 (0.05) | *.61 (0.12) | .62 (0.09)  |

(\* indicates significantly lower MPF than Post-Vibe; † indicates significantly greater MPF than 20-min post)

With eyes closed on the sway-referenced surface sway frequency (MPF) was not altered, from baseline levels, until 20 minutes post vibration exposure. A similar effect was seen for sway predictability (ApEn) where a difference from pre- and post-vibration levels occurred at 10 minute post vibration and persisted after 20 minutes.

Postural control was differentially affected depending on the sensory information available to the individual. When all three sensory systems

provided accurate information the active control and predictability of postural sway was not altered following WBV despite increased sway frequency. However, when somatosensory information was reduced sway predictability decreased while sway frequency increased following WBV. When both vision and somatosensory information were altered the effect of WBV was not realized until 10-20 minutes post vibration. At which time both the frequency of sway and sway complexity was reduced below both pre- and post-vibration levels indicating improved postural stability.

Interestingly, the impact of vibration on posture was not dependent upon either the amplitude or frequency of the vibration. In terms of the frequency of postural responses and the overall predictability of postural sway it would appear that the exposure to WBV is more critical than the absolute intensity of the vibration. The effect of varying levels of vibration duration, however, remains to be determined.

Based on the vibration parameters used in this study WBV did have an acute effect on postural control with an elevated effect when visual and/or somatosensory information was altered.

## REFERENCES

- [1] Cochrane DJ. Vibration exercise: the potential benefits. *Int J Sports Med* **32** 75-99, 2011
- [2] Cardinale M, Bosco C. The use of vibration as an exercise intervention. *Exerc Sport Sci Rev* **31** 3-7, 2003

## ACKNOWLEDGEMENTS

The authors would like to thanks Jon Doan and David Sessford for their work in processing the raw data used in this study.

# SURGICAL IMPACTION OF CERAMIC FEMORAL RESURFACING HEADS

<sup>1</sup>Alexander Dickinson, <sup>2</sup>Andrew Taylor and <sup>1</sup>Martin Browne

<sup>1</sup>Bioengineering Research Group, University of Southampton, Southampton UK,  
<sup>2</sup>Aurora Medical Ltd., Chilworth, UK

## INTRODUCTION

Femoral head resurfacing has demonstrated excellent clinical outcomes as an osteoarthritis treatment, particularly for young, male patients [1]. Resurfacing prostheses are implanted by impaction onto the prepared bone, using a polymer tipped impactor instrument and a mallet. Ceramic resurfacing prostheses can be proposed as an alternative to metal implants, combining their bone conserving advantages with the removal of metal ions, mitigating the risk of sensitivity reactions. However, with low wall-thickness required for bone conservation, the strength of new ceramic resurfacing prostheses must be verified, with particular focus on their performance under impact loads. This study aimed to produce a computational model of the impaction of a ceramic resurfacing prosthesis concept to verify its strength under surgical loads. An experimental impact test was conducted to allow representative damping parameters to be applied to the computational model, and the model was used to test a range of implant sizes and loading.

## METHODS

Initially, mechanical tests were conducted to obtain baseline impact data. Ø58mm DeltaSurf prostheses (Finsbury Development Ltd., UK), made from BIOLOX Delta (CeramTec AG, Germany) Zirconia-Toughened Alumina composite were cemented onto 40pcf polyurethane foam stubs (Sawbone AG, Sweden) with Palacos Low Viscosity PMMA bone cement (Heraeus Medical GmbH, Germany) and the stub was attached to the ±25kN capacity load cell from an Instron 8874 (Instron Corp., USA). A rod for a slide hammer was attached to a standard Finsbury Orthopaedics Ltd. femoral head impactor instrument to give repeatable impacts, with the hammer dropped from a measured height to give a  $2\text{ms}^{-1}$  initial velocity. The slide hammer mass was 745g, and the impactor was stabilised by hand. The experimental setup is shown in Figure 1. The prosthesis was impacted ten times, and the axial impact force at the bone stub base was recorded with Measurement and

Automation Explorer software (National Instruments Corp., TX, USA) at 5kHz, the Instron's maximum output sampling frequency. The cumulative impulse was calculated by integrating the impact force with respect to time.

Second, a 3D half-plane symmetry computational model was produced using LS-DYNA (ANSYS Inc., PA, USA) explicit dynamic Finite Element (FE) analysis software. A schematic of the model geometry is shown in Figure 1. The base of the bone stub was constrained against displacement, and the mallet was given an initial velocity of 2.0m/s. Model outputs were the impact reaction force at the base of the bone stub, the duration of the impact and the peak tensile (first principal) stress in the prosthesis.

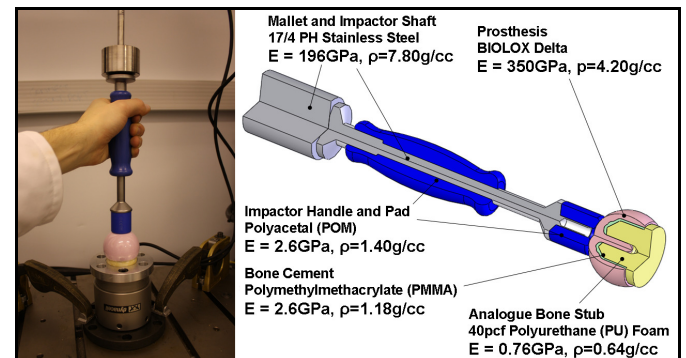


**Figure 1:** Experimental Test Setup (left) and Schematic of FE Model with Materials Properties.

Two versions of the FE model were used. First, a model was solved representing the experimental setup as closely as possible, to attempt to fit damping parameters. The resulting model was solved first with the impactor resting free on the prosthesis ('basic model'), and then with a 2kg mass attached to the impactor handle ('hand damped model'), representing the surgeon's hand and forearm. Then the preferred model was used to predict the peak prosthesis stresses under surgical impaction loads. A 990g surgical mallet was modelled, and the analysis was run with the smallest (Ø40mm) and largest (Ø58mm) prosthesis heads in the size range, with two impaction directions: ideally, with impaction along the prosthesis axis, and more realistically, with the impactor angled at 10° to the prosthesis axis.

## RESULTS AND DISCUSSION

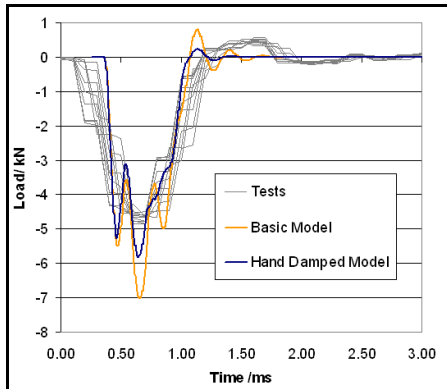


**Figure 2:** Experimental vs. Model Impact Force.

The comparative results from the experimental tests and basic model are included in Table 1. The peak force and impulse results were consistent with instrumented mallet measurements from surgery and cadaveric tests [2,3]. Results from a similar computational analysis [4] suggest that this study's stiff analogue bone stub represents a worse case than a real bone, with a similar overall impulse but a higher peak force and lower impact duration. The basic FE model over-estimated the measured peak impact force by 49% and underestimated the impact duration by 36% (Fig. 2), but was in close agreement with the experimental cumulative impulse (Fig. 3). Including the surgeon's hand and forearm reduced the peak force overestimation to 23% but the impact duration was unchanged, so this led to an underestimate of the cumulative impulse by 16%. Therefore the basic model without the surgeon's hand and forearm mass was used for subsequent investigation, as a worst case.

The results of the investigation into the prosthesis' performance under surgical impact loads are included in Table 2. The peak stresses experienced by the prostheses were higher in the smaller, Ø40mm head, and highest with inclined loading from the impactor tilted off-axis which stressed the prosthesis stem root. The peak tensile stress predicted was 68.7MPa, only 6% of the 1150MPa static strength of the material [5], which indicates that

prosthesis fracture would be highly unlikely during surgical impaction.

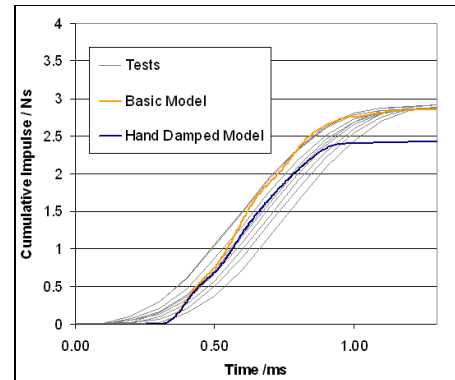


**Figure 3:** Experimental vs. Model Cumulative Impulse.

## CONCLUSIONS

A computational model of femoral head impaction was developed and used to predict the peak stress in a ceramic resurfacing head prosthesis under surgical loading. Predicted peak impact stresses were considerably below the material strength. This is evidence to suggest that the risk of intraoperative fracture of the ceramic resurfacing head would be very low, and that it could be implanted safely following current resurfacing operative techniques.

## REFERENCES

1. AOA NJRR Annual Report 2009.
2. Kohan, L. et al, *Trans ORS*, **32**: 1701, 2007.
3. Schlegel U.J. et al, *J Arthroplasty*, **26**, 2011.
4. Hogg, M. et al, *Trans ORS*, **33**: 1797, 2008.
5. Willmann G., *Adv Eng Mat*, **3**: 153-141, 2001.

## ACKNOWLEDGEMENTS

This research was funded by a European Union 7<sup>th</sup> Framework Programme (Grant No. 232151). The authors would like to thank Finsbury Orthopaedics Ltd. and CeramTec AG for their help in the prosthesis development process and for providing sample prostheses and instruments.

**Table 1:** Model Development: Computationally Predicted and Experimentally Measured Impact Characteristics.

| Test                   |                   | Impact Force /kN | Impact Duration /ms | Total Impulse /Ns |
|------------------------|-------------------|------------------|---------------------|-------------------|
| Computational Results: | Basic Model       | 7.0              | 0.70                | 2.88              |
|                        | Hand Damped Model | 5.8              | 0.72                | 2.43              |
| Experimental Results:  | Mean (st.dev.)    | 4.70 (0.11)      | 1.1 (0.06)          | 2.88 (0.017)      |

**Table 2:** Surgical Impact Model Predictions.

| Test    |              | Impact Force /kN | Impact Duration /ms | Peak Prosthesis Stress /MPa |
|---------|--------------|------------------|---------------------|-----------------------------|
| Axial   | 40mm Head    | 7.6              | 0.77                | 42.5                        |
| Impacts | 58mm Head    | 8.9              | 0.66                | 20.0                        |
|         | 10° Off-Axis | 40mm Head        | 7.7                 | 0.77                        |
| Impacts | 58mm Head    | 8.5              | 0.66                | 27.9                        |

# ARE AGE-RELATED MODIFICATIONS DURING A SQUATTING TASK IMPLEMENTED BY WORKING-AGE MEN?

Angela DiDomenico, Raymond W. McGorry and Jacob J. Banks

Liberty Mutual Research Institute for Safety, Hopkinton, MA, USA

email: [angela.didomenico@libertymutual.com](mailto:angela.didomenico@libertymutual.com)

web: <http://libertymutualgroup.com/researchinstitute>

## INTRODUCTION

Declines in functional capacity related to aging may contribute to decreased postural control, thus leading to an increase in falls and fall-related injuries for older adults. Difficulty performing certain activities of daily living, such as bending down to pick up an object from the floor, is a risk factor for falls in older adults [1]. Modifications in movement patterns during various reaching tasks have been detected in older adults, possibly to compensate for changes in physical abilities [2-4]. This study seeks to determine at what age modifications in reaching movement patterns are initiated during a squatting task.

## METHODS

### *Participants*

Forty-five male volunteers, between 18 and 65 years of age, were recruited from the local community. Mean (SD) age, height and body mass of the participants were 40.5 (14.8) years, 1.77 (0.07) m and 83.6 (14.1) kg, respectively.

### *Experimental procedure*

Participants were instructed to stand comfortably with feet approximately shoulder width apart. When alerted by an auditory signal, participants performed a squat, picked up a 2.5 cm foam cube, and then returned to a standing position (Figure 1). The cube was placed directly in front of the participants. Participants performed three squats at a self-selected speed and squat depth while standing on two 40 cm x 60 cm force plates (Model # 9286AA, Kistler Instruments AG, Winterthur, Switzerland). A 12-camera passive motion capture system (Motion Analysis Corp., Santa Rosa CA) was used to collect whole-body motion data. All data was sampled at 100Hz prior to filtering (zero-

lag fourth-order 6Hz and 8Hz low-pass Butterworth filters, respectively).

Four phases of the task, similar to Kuo [3], were identified. Phase 1 (standing) encompassed the period from the auditory signal to the initiation of knee movement. Phase 2 (accelerating) included the interval from the onset of knee movement to the maximum angular velocity at the knee. Phase 3 (decelerating) continued until the point of maximal knee flexion. Phase 4 (returning) was defined as the time when the individual returned to standing after reaching maximal knee flexion.



Figure 1. Participant performing a typical squat and reaching to pick up foam cube.

### *Dependent measures*

Angular displacements of the knee, thigh, and trunk in the sagittal and frontal planes were determined. Angular displacement of the head in the sagittal plane was also calculated. The minimum distance of the center of pressure (COP) from the edge of the base of support (BOS) was considered as an indicator of balance control.

### *Statistical analyses*

Values for the three trials were averaged for each participant. Pearson correlation coefficients were calculated between age as a continuous variable

and each of the dependent measures. Statistical significance for all tests was determined at  $p < 0.05$ .

## RESULTS AND DISCUSSION

The mean duration of the squatting task was 3.01 (0.51) s measured from standing to standing. The decelerating phase was completed in 0.74 (0.24) s. Table 1 includes the measures of interest for the decelerating phase, which immediately preceded the pick-up of the foam cube and encompassed the most unstable portion of the movement. Although the instructions and task were not identical, the decelerating phases of the two experiments were very similar allowing for comparison of certain measures. Indeed, knee and thigh angular values were similar to those provided by Kuo [3] for young adults even though the current study examined men of a wider age range.

Table 1. Measures for the decelerating phase.

| Measure                       | Mean (St Dev)    |
|-------------------------------|------------------|
| Maximal Knee Flexion          | 131.0 (10.7) °   |
| Maximal Knee Angular Velocity | 138.6 (12.6) °/s |
| Maximal Thigh Sagittal        | 75.4 (6.5) °     |
| Maximal Thigh Frontal         | 20.0 (5.5) °     |
| Maximal Trunk Sagittal        | 76.2 (6.7) °     |
| Maximal Trunk Frontal         | 25.6 (3.1) °     |
| Maximal Head Sagittal         | 60.0 (7.0) °     |
| Minimum Distance COP to BOS   | 100.7 (30.4) mm  |

Correlation values (Table 2) did not indicate any significant changes in technique for the older participants, whereas Kuo [3] identified significant differences in squatting technique between younger adults (mean = 20 (0.9) years) and older adults (mean = 77 (4.6) years).

Table 2. Correlation coefficients between measures and age.

| Measure                       | Correlation |
|-------------------------------|-------------|
| Maximal Knee Flexion          | -0.260      |
| Maximal Knee Angular Velocity | -0.324      |
| Maximal Thigh Sagittal        | -0.103      |
| Maximal Thigh Frontal         | 0.024       |
| Maximal Trunk Sagittal        | 0.158       |
| Maximal Trunk Frontal         | 0.196       |
| Maximal Head Sagittal         | 0.034       |
| Minimum Distance COP to BOS   | 0.121       |

Trends in the current data indicated a slight reduction in maximal angular velocity of knee flexion for older participants (Figure 2). The significant decline found by Kuo [3] either occurs after 65 years of age or is due to other health factors. Levels of activity and conditioning were not indicated in the Kuo [3] paper while only healthy active men were included in the current study.

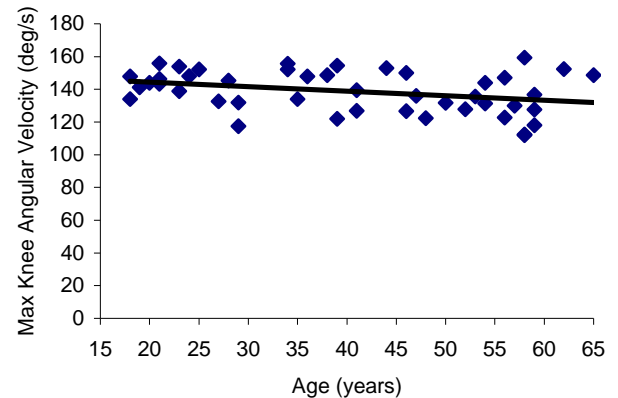


Figure 2. Age versus maximal knee angular velocity.

## CONCLUSIONS

Differences in squatting movement techniques have been found between younger and older adults. The current study examined similar movements in a broader range of adults but found no significant differences in many angular displacement and balance control measures. The onset of differences in squatting movement techniques seems to occur later in life (>65 years) but further research is needed to determine what physical factors lead to the changes.

## REFERENCES

1. O'Loughlin, J.L., et al. *American Journal of Epidemiology* **137**(3), 342-354, 1993.
2. Chateauroux, E. and Wang X. *Human Factors* **50**(2), 211-226, 2008.
3. Kuo, F.C., et al. *Gait and Posture* **33**(1), 124-129, 2011.
4. Row, B.S. and Cavanagh, P.R. *Clinical Biomechanics*. **22**(2), 155-164, 2007.

# VERTICAL AFFORDANCE FOR PULLING DURING SIMULATED BAGGAGE HANDLING

<sup>1</sup>Jon B. Doan, <sup>1</sup>Sam Fowler, <sup>1</sup>K. David Sessford, and <sup>1</sup>Lesley A. Brown

<sup>1</sup>University of Lethbridge, Lethbridge AB Canada – Department of Kinesiology & Physical Education  
email: [jon.doan@uleth.ca](mailto:jon.doan@uleth.ca)

## INTRODUCTION

Gibson's theory of affordance provides a framework for modeling perception-action coupling [1], but it has not been widely employed in the study of occupational biomechanics [2]. Airline baggage handling is an occupation associated with both high musculoskeletal injury incidence and affordance-rich task environments, including highly variable loads and load coupling, confined spaces, and dynamic working postures [3]. The purpose of the current research was to examine affordance, strategy, and mechanics of manual materials handling in a simulated baggage handling task.

## METHODS

42 university students (30 females) provided informed consent to participate in the study, in concordance with research ethics policies at the University of Lethbridge, and participant height, weight, and age were recorded. Each participant was outfitted with large (4 cm diameter) colour contrast markers on the scapula, distal posterior upper arm, distal dorsal forearm, iliac crest, popliteal fold, and shoe heel of their right side. Participants' feet were positioned in a defined workspace 40 cm square, and 25 cm posterior (in the sagittal plane) from the centre of the suitcase (Figure 1). Lateral distance to the centre of the suitcase was individualized to 25% total height for each subject. The case could be securely mounted such that the handle pointed in each of the four cardinal directions, and participants were randomly assigned one of those four orientations. Prior to the mounting, participants hoisted the suitcase (57 L) by the handle with their right hand to obtain a perception of both mass (8 kg) and mass distribution (uniform perimeter weighting).

Participants were read the fixed script of a manual material handling task (adapted from [4]), where that script defined the job (airline baggage handler),

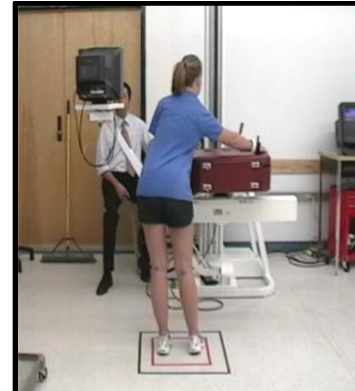


**Figure 1:** Participant delivering isometric horizontal pull. Vertical affordance for suitcase was selected by participant, and coupling strategy, foot movement, and pulling mechanics were recorded for multiple isometric trials.

the task (pulling suitcases horizontally, with vertical support), the task frequency (5 suitcase transfers per minute), and the shift duration (8 hour shift with 1 hour of formal 'break'). At the end of the script, participants were invited to choose the baggage handling height (vertical affordance) that would 'allow them to handle the bags as safely as possible without causing pain or discomfort'. Participants were encouraged to request as many changes to the vertical affordance as appropriate prior to the start of the physical testing. Participants were not allowed to touch the suitcase during vertical affordance setting, but they were permitted to address it to reinforce affordance perceptions [5].

Each participant completed 5 isometric pulling trials at their vertical affordance, and pulling force was recorded through the dynamometer (LIDO WorkSet™), while behaviour in frontal plane was recorded from posterior. Video data were clipped and analyzed in frame of maximum shoulder joint angular posture (DartFish™). Participants completed a validated personality inventory [6] for association with their affordance perceptions.

## RESULTS AND DISCUSSION

No effects of suitcase orientation were observed on affordance perceptions, nor did any participants use the suitcase handle to pull the load, therefore subsequent comparisons were collapsed across suitcase orientation. Perceptions of safe vertical affordance ranged from 0.81 m to 1.23 m. Participants' vertical affordance perceptions were normalized by stature for subsequent comparisons.

Perceptions of vertical affordance were not associated with risk-related personality items (Figure 2). Perceptions of vertical affordance also showed no statistical relationship with pulling force peak or average values.

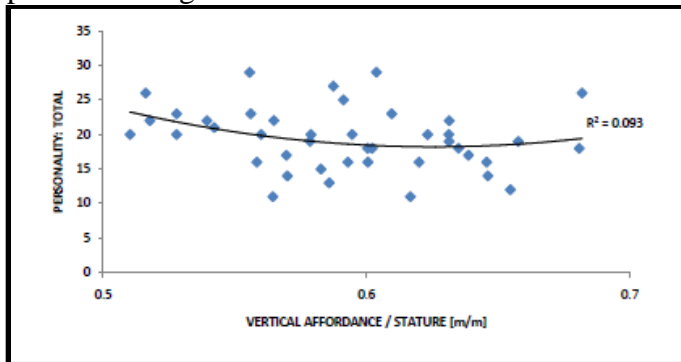


**Figure 2:** Association between risk-taking and perception of vertical affordance. Total risk-taking score and individual risk-taking factor scores (impulsiveness, liveliness, failure to plan) had no relationship with vertical affordance.

Behavioural analysis of the video identified three distinct coupling strategies: TOP edge, where participants grasped the suitcase with a hook grip and a fully pronated right forearm; SIDE, where participants grasped the suitcase with a cupped hook grip and a neutral right forearm position; BOTTOM edge, where participants grasped the suitcase with a hook grip and a partially supinated forearm. Figure 1 is an example of TOP coupling with the right hand. Coupling strategy was highly consistent (0 of 42 participants changed coupling style across their 5 trials) but had no statistical relationship with perceived vertical affordance or with pulling kinetics. Coupling did have a predictable effect on body postures (Figures 3 + 4).

## CONCLUSIONS

Kinematics of manual material handling in this task were more dependent on coupling strategy, specifically hand placement location for pulling action, than they were on the psychophysical

parameter of perceived affordance. Safety efforts amongst new workers should emphasize relationships between work strategies and occupational biomechanics.

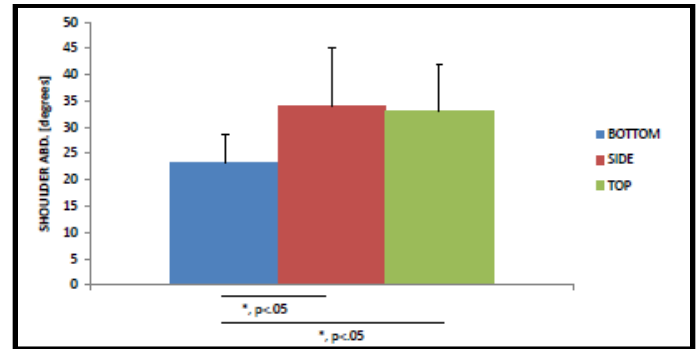


**Figure 3:** Maximum shoulder abduction angle during isometric pull. Shoulder abduction angles were significantly higher for participants who grasped either the SIDE or the TOP edge of the suitcase, compared to those who grabbed the BOTTOM edge.

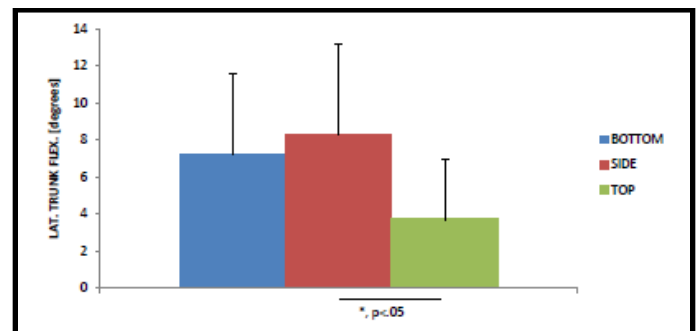


**Figure 4:** Lateral trunk flexion angle during isometric pull. Lateral flexion was significantly higher for participants who grasped either the TOP edge of the suitcase, compared to those who grabbed on the SIDE.

## REFERENCES

- 1.Chemero A. *Eco Psych* **15**, 181-195, 2003.
- 2.Gielo-Perczak K & Karwowski W. *Erg* **46**, 310-326, 2003.
- 3.Korkmaz SV et al. *Int J Ind Erg* **36**, 301-312, 2006.
- 4.Potvin JR et al. *Int J Ind Erg* **26**, 625-637, 2000.
- 5.Stoffregen TA et al. *Eco Psycho* **17**, 75-104, 2005.
- 6.Eysenck SBG & Eysenck HJ. *Br J Soc Clin Psychol* **16**, 57-68, 1977

## ACKNOWLEDGEMENTS

Special thanks to Dr. Robert Marley and Montana State University for the gift of the LIDO WorkSet.



# INFLUENCE OF INDEX FINGER JOINT FUSION ON PRECISION PINCH KINEMATICS

Mathieu Domalain, Zong-Ming Li

Departments of Biomedical Engineering, Physical Medicine and Rehabilitation, and Orthopedic Surgery, Cleveland Clinic, Cleveland, OH 44195, USA; email: [liz4@ccf.org](mailto:liz4@ccf.org)

## INTRODUCTION

Fusion of finger interphalangeal joints is commonly indicated in the treatment of diseases such as osteoarthritis, gout, and scleroderma. The surgery provides a painless stable joint [1] but obviously fails to recover the biomechanics of a healthy finger. Nonetheless proximal interphalangeal (PIP) joint fusion was associated with limited impairment as index finger metacarpophalangeal (MCP) joint's range of motion changed with only a few daily life activities [2]. However a single joint range of motion is not sufficient to appreciate the natural coordination that arises at multiple levels (muscles, joints, fingers) and allows an accurate and reliable precision pinch [3, 4].

The aim of this study was to investigate the effects of index finger PIP fusion on precision pinch kinematics. It was hypothesized that PIP joint fusion would led to 1) decreased maximal pinch aperture, 2) increased variability of joint angles and digit tips location at timing of contact, and 3) decreased joints coordination throughout the movement.

## METHODS

Eleven healthy volunteers participated in this study. Fusion of the PIP joint was experimentally simulated with the adjunction of aluminum splints and adhesive tape following the protocol of [2]. Each subject performed cyclic pinching movements at a frequency of 1Hz. Four conditions were randomly tested: unrestricted (CONTROL), simulated PIP fusion at 30 (PIP30), 40 (PIP40), and 50 (PIP50) deg of flexion. Each condition consisted of 3 trials of 30 cycles.

Hand motion data was obtained by tracking attached reflective markers (4 mm in diameter) with a motion capture system (Vicon MX, Oxford, UK)

(Fig. 1). The trapezium coordinate system was assessed according to [5] and joint angles computed with the Euler angles (rotation sequence of *flexion*, *external rotation*, and *abduction*).

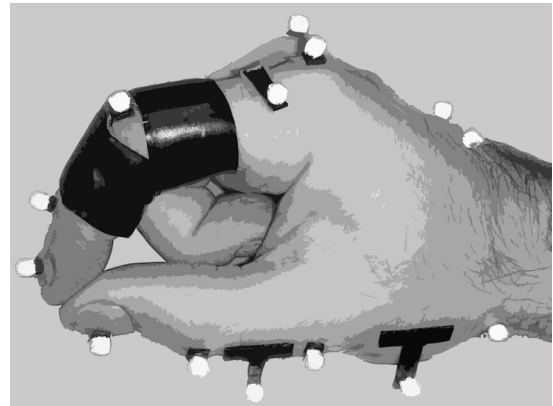


**Figure 1:** PIP joint splinting and marker set-up.

For each pinch cycle, the pinching/closing phase was identified as starting at the maximal opening and ending at pulp contact. Maximal pinch aperture was calculated as the maximal distance between the digit tips marker. At pulp contact, joint angles and dispersion of tip markers were computed. Pearson's coefficients of correlation between joint angles were calculated throughout the closing phases. Statistical significance of the effects of fusion condition was evaluated with one-way repeated measure analyses of variance and Tukey post-hoc tests ( $p < .5$ ).

## RESULTS AND DISCUSSION

Maximal aperture was 163.7, 153.5, 147.7 and 141.5 mm for CONTROL, PIP30, PIP40 and PIP50 respectively. Maximal aperture was significantly restricted with increasing PIP fusion angle by 6.2, 9.8 and 13.6 % for PIP30, PIP40 and PIP50 respectively ( $p < .001$ ).

At the pulp contact, index finger joints compensated for the lost fused PIP joint. Index distal interphalangeal (DIP) joint angle increased with

increasing PIP fusion angle (10.6, 15.1, 16.2 and 17.7 deg for the CONTROL, PIP30, PIP40 and PIP50 conditions respectively). MCP joint angle significantly increased in the PIP30 condition (61.7 deg) in comparison to the CONTROL condition (53.2 deg) ( $p < .01$ ). However, the MCP joint angles were not significantly different among the CONTROL, PIP40 and PIP50 conditions. The natural PIP angle for pinching recorded during the CONTROL condition was 44.1 deg which is close to PIP40 and PIP50. This may explain why the MCP joint angle did not change during those conditions and the PIP joint slightly adjusted. Thumb joint angles did not significantly change ( $p = .14$ ).

PIP fusion did not lead to an increase in the variation (standard deviation) of individual joint angles at pulp contact. However the overall variability of the end effectors, as estimated with the dispersion of tip marker location, was affected. In particular, thumb tip location was significantly more variable ( $p < .01$ ) in PIP50 than in the other the conditions (Fig 2). Thumb tip dispersion was 2.7, 2.6, 2.4 and 3.1 mm for the CONTROL, PIP30, PIP40 and PIP50 conditions respectively. No significant change was observed in index tip dispersion.

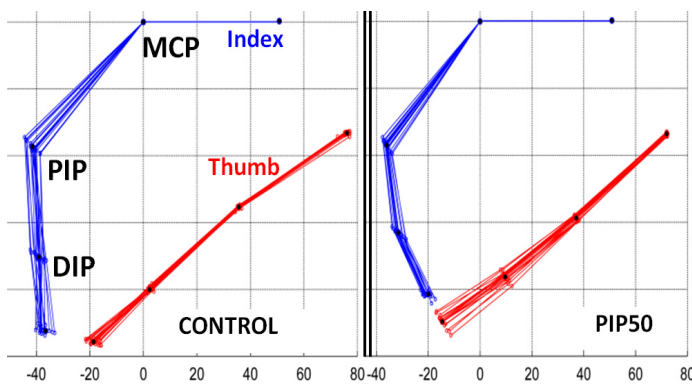


**Figure 2:** 2D representation of joint angles variation and digit tips dispersion (mm) at timing of contact

Pearson's coefficients of correlation between joint angles revealed that both intra-finger (Index distal IP-MCP) and inter-finger (thumb IP- Index distal IP) coordination were affected. Dynamic coordination throughout the pinching phase decreased with PIP arthrodesis (Table 1).

**Table 1:** Pearson's coefficients of correlation among joint flexion angles throughout the pinching movements

|                | Thumb |        | Index   | Both Digits |
|----------------|-------|--------|---------|-------------|
|                | IP-MP | MP-TMC | DIP-MCP | IP-DIP      |
| <b>CONTROL</b> | 0.90  | 0.76   | 0.93    | 0.91        |
| <b>PIP30</b>   | 0.87  | 0.68   | 0.89*   | 0.91        |
| <b>PIP40</b>   | 0.87  | 0.69   | 0.87*   | 0.88        |
| <b>PIP50</b>   | 0.90  | 0.74   | 0.86*   | 0.83*       |

\*indicated a significant difference with CONTROL

## CONCLUSION

This study aimed at analyzing the effects of PIP fusion on pinch kinematics. We first quantified that PIP fusion at 50 deg decreases pinch aperture by 13%, thus restricting the ability to grasp large objects. Furthermore we demonstrated that PIP fusion not only affects MCP joint motion [2] but also the coordination between digit joints. This eventually increases variability in thumb tip location and may lead to an overall impaired precision. Finally, the comparison between angles of fusion would suggest that increasing angle lead to more natural MCP joint angle but also to a more restricted aperture as well as a greater overall variability. As a limitation, this study simulated joint fusion without mimicking the underlying pathological mechanisms that lead to clinical fusion.

## REFERENCES

1. Pellegrini VD et al. *J Hand Surg Am* **15**,194-209, 1990.
2. Woodworth JA, et al. *J Hand Surg* **31**, 940-946, 2006.
3. Cole KJ and Abbs JH. *J Neurophysiol* **55**,1407-1423, 1986.
4. Darling WG et al. *Exp Brain Res* **73**, 225-235, 1988.
5. Cooney W, et al. *J Bone Joint Surg [Am]* **63**,1371-1381, 1981.

# SURGERY OF TRAPEZIOMETACARPAL JOINT ARTHRITIS: INCREASING OR DECREASING THE DEGREES OF FREEDOM?

Mathieu Domalain, William H. Seitz, Peter J. Evans, Zong-Ming Li

Departments of Biomedical Engineering, Physical Medicine and Rehabilitation, and Orthopedic Surgery, Cleveland Clinic, Cleveland, OH 44195, USA; email: [liz4@ccf.org](mailto:liz4@ccf.org)

## INTRODUCTION

The intact TMC joint has 2 DoFs in flexion-extension (F-E) and abduction-adduction (A-A). Because the F-E and A-A axes are not perpendicular or concurrent with each other an automatic pronation-supination (P-S) also naturally occurs [1, 2]. This unique anatomical configuration allows both dexterous motion and forceful grip force, but it also leads to a high prevalence of joint degenerative osteoarthritis [3]. Currently, several surgical methods are available for the treatment, but they affect the natural biomechanics of the joint. After a joint fusion, the joint is frozen and all joint DoFs disappear. Therefore, monoarticular muscles acting at the TMC joint become useless and polyarticular muscles are not obligated to equilibrate the fused joint. When a ball-and-socket arthroplasty is performed the restricted P-S becomes free and the corresponding component of the joint moment which was previously equilibrated by joint boundaries and ligaments has to be equilibrated by muscles. The goal of this study was to examine the influence of freezing or liberating DoFs at the TMC joint on muscle and joint forces reorganization.

## METHOD

The computer simulation developed in this study was adapted from the original *normative model* [4]. Because the kinematic model of [4] considered the TMC joint articulated around 2 orthogonal and crossing rotation axes we incorporated the anthropometric data of axes locations/orientation reported by [1] to account for the automatic P-S motion and model a more anatomically accurate joint (Fig. 1, left). Coordinate system transformations were conducted using the transformation matrix  $[T]$  such that  $O_{5'} = [T] \times O_5$  and  $O_{6'} = [T] \times O_6$  with:

$$T = \begin{bmatrix} cFcA & sFcA & -sA & t_x \\ cFsAsR - sFcR & sFsAsR + cFcR & cAaR & t_y \\ cFsAcR + sFsR & sFsAcR - cFsR & cAcR & t_z \\ 0 & 0 & 0 & 1 \end{bmatrix}$$

c and s standing for the cosinus and sinus functions respectively. F, A, R, rotation angles equal to 6.4, 0, 11.7 degrees and -14.7, 13.6, 0 degrees, for coordinate systems  $O_{5'}$  and  $O_{6'}$  respectively.  $t_x, t_y, t_z$  correspond to the translation coordinates and equal to -6.27, 0, 0 mm and 0, 0, 0 mm for  $O_{5'}$  and  $O_{6'}$  respectively. Rigid body static laws were applied and joint moments were equilibrated by the 9 muscle forces (FPL, *flexor pollicis longus*, FPB, *flexor pollicis brevis*, OPP, *opponent pollicis* APB, *abductor pollicis brevis*, APL, *abductor pollicis longus*, ADPO, *adductor pollicis* oblique head ADPT, *adductor pollicis* transverse head EPL, *extensor pollicis longus* EPB, *extensor pollicis brevis*).

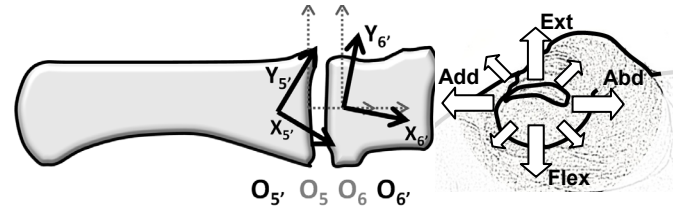


**Figure 1.** Left: Thumb metacarpal and trapezium bone coordinate systems (notations adapted from [1]). Right: Orientations of the simulated thumb tip force.

The thumb assumed a pulp pinch posture [5] and external force was simulated as a unit force vector applied at 75% of the total length of the distal phalanx along 8 directions in the transverse plane (Fig 1, right). Simulated joint angles and thumb tip force were used as input data for the calculation of external joint moments and muscle/joint forces. The underdeterminate problem associated with muscle redundancy was solved with a static non-linear optimization [5].

## RESULTS AND DISCUSSION

OPP and APL muscle forces acting on the TMC joint only were thus appropriately set to 0 N by the simulation for the 0 DoF condition. The 0 DoF condition exhibited an overall decrease of 0.8 N in muscle forces in comparison with the 2 DoFs (intact) condition (average among all 9 muscles and 8 force directions). The 3 DoFs condition resulted in a 9.0 N increase of muscles forces with disparate results: FPL was the less influenced (+2.7N) and APL the most (29.0N) (Fig. 2).

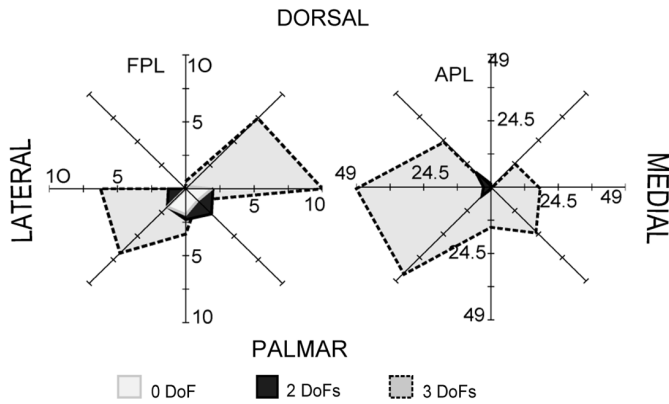


**Figure 2.** Thumb muscle force (N) envelope to equilibrate a 1 N external force exerted at the thumb tip in 8 different orientations.

Comparing to the intact joint, IP, MP and TMC joint forces were generally smaller when TMC is fused (Fig. 3).

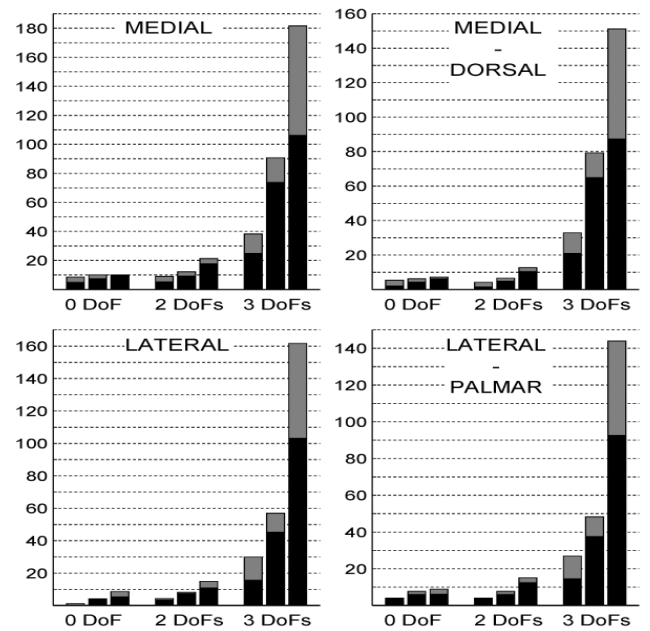
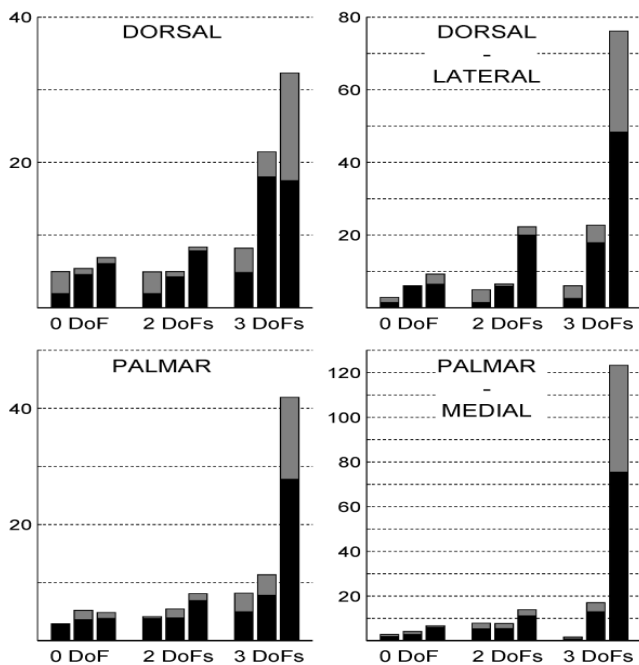


**Figure 3.** Joint forces in the 0, 2, and 3 DoFs conditions. For each condition, the first, second and third columns represent the IP, MP and TMC joints respectively. Normal (black) and shear (grey) force components are shown.

However, IP and MP joint forces were also occasionally greater (e.g. +25.3 and 42.8% respectively in PALMAR-LATERAL direction). On the contrary, excessively large joint forces were observed in the 3 DoFs condition, especially at the TMC joint (88.3 vs. 7.2 N, average across all external force orientations).

## CONCLUSION

This study gains new insights into the biomechanical consequences of two TMC joint osteoarthritis surgeries. Overall, the ball-and-socket arthroplasty condition lead to larger muscle/joint forces but we also pointed out some interesting particularities in the fusion condition such as a potential overuse in the small FPB muscle as well as occasionally greater forces at IP and MP joints.

## REFERENCES

- Hollister A, et al. *J Orthop Res* **3**, 454-460, 1992.
- Li ZM and Tang J. *J Biomech* **40**,502-510. 2007.
- Wilder FV, et al. *Osteoarthr Cartil* **9**, 953-957, 2006.
- An KN, et al. *J Biomech* **10**,775-788, 1979.
- Vigouroux L, et al. *J Biomech* **42**,1172-1177, 2009.

# EFFECTS OF OBESITY ON SYMMETRY AND SPATIO-TEMPORAL CHARACTERISTICS OF ADOLESCENT GAIT

Janet S. Dufek, John A. Mercer, Rayland Currie, Philana-Lee Gouws, Lori Candela, Antonio P. Gutierrez and LeAnn G. Putney

University of Nevada, Las Vegas, Las Vegas, NV, USA  
email: [janet.dufek@unlv.edu](mailto:janet.dufek@unlv.edu) web: <http://kinesiology.unlv.edu/biomechanics.htm>

## INTRODUCTION

Child obesity is becoming all too prevalent as society becomes more sedentary. The percentage of overweight children 12-19 yrs old in the U.S. has increased over 11% since 1980, with the current level reported at 16.1% [1]. In adults, gait characteristics have been shown to vary with increasing adiposity, most notably a slower preferred walking speed, longer stance and double support phases, and greater base of support [2-4]. It is not known if obesity leads to similar locomotor outcomes for adolescents. In addition, the question of symmetry has been raised relative to limb dominance observed in obese children [5]. The purpose of the study was to examine the effects of obesity on bilateral symmetry and spatio-temporal characteristics of adolescent walking.

## METHODS

Institutionally approved written parental permission and child assent was obtained from 111 adolescents between the ages of 12 to 17 years of age ( $14.2 \pm 1.4$  yrs) enrolled in grades 7-10 at a charter school. All participants performed walking trials as part of a regularly scheduled physical activity period during the school day. The height and weight of each participant was obtained by a registered nurse using a digital medical beam scale (HealthOMeter, 500 KL).

Each participant walked twice at their preferred pace over a 4.27 m instrumented walkway (CIR Systems, Haverhill, PA; 120 Hz), which was centered in a 10 m hallway and placed directly over the carpet-over-concrete flooring. All participants started at the same position, walked through the hallway and over the walkway, stopped, turned around, and walked back to the starting position.

Next, each participant was given the verbal instruction: "Walk as fast as you can" in order to elicit a fast walking condition. Approximately two walking strides were completed prior to and following contact with the walkway. There was no attempt to control for footwear or attire that the participants wore during data collection, thus replicating typical school day locomotion for each participant.

Body mass index (BMI) was calculated for each participant following procedures established by the Centers for Disease Control for children and teens. This procedure to determine adiposity level is both age and gender specific and scales the BMI value to age and gender percentile values. All participants with BMI% <85<sup>th</sup> percentile were assigned to the normal weight (NW) group (n = 70) while those with BMI%  $\geq$ 85<sup>th</sup> percentile were assigned to the overweight/obese (OWO) group (n = 41).

The two passes over the walkway at each speed were concatenated producing 8-17 complete walking steps per participant-speed. Six spatio-temporal dependent variables (velocity, Vel; cadence, Cad; step length, SL; percent swing, SW; percent double support, DS; stance width, StWd) and three right-left difference symmetry dependent variables (step time, step length, cycle time) were extracted using custom software (GAITRite, version 4.0, 59). Vel and SL were normalized to leg length.

Two-way mixed model Group x Speed analyses of variance were used to address the study purpose. Level of significance was set at  $\alpha = 0.05$ . The right-left symmetry analysis was conducted first in order to determine whether there was a need to separate limbs for subsequent analyses. All statistical tests were conducted using SAS (version 9.1) software.

## RESULTS AND DISCUSSION

The symmetry analysis resulted in no significant interactions or right-left limb differences (symmetry) in step time, step length or cycle time by group or speed ( $p > 0.05$ ), therefore, data for only one limb was used to assess the spatio-temporal parameters. There were no significant Group x Speed interactions observed for any of the spatio-temporal parameters. With the exception of StWd, all dependent variables were significantly different ( $p < 0.05$ ) for levels of speed. Vel, Cad, SW, DS and StWd were all significantly different ( $p < 0.05$ ) between the NW and OWO groups. Results are summarized in Table 1.

Hills [5] previously commented on the observation of limb asymmetry in children as a result of obesity, but did not specify the age range of the referenced children. Subsequently, Hills et al, [6] reported limb asymmetry in pre-pubescent obese children. In contrast, the current study failed to detect significant limb differences in step length, step time or cycle time at levels of speed or group. It may be that our subjects were older than those in Hills et al [6] and it is not clear if symmetry is a function of skillful locomotion as opposed to adiposity per se.

Differences observed between preferred and fast walking were anticipated per study design. Our interest in incorporating walking speed as a factor in the design was to specifically examine any potential interaction effects between group and speed, which were not found. One can conclude that NW and OWO adolescents achieve a faster walking speed by scaling on similar parameters, none of which influence StWd. The observed increases in StWd

and DS for OWO may be the result of optimizing on stability while decreased SW could be the combined result of stability and lack of core strength to control the inertial characteristics of the swing leg, therefore spending more time in the stance phase of gait.

## CONCLUSIONS

Obesity was not shown to influence bilateral gait symmetry in adolescents. Locomotor differences observed between NW and OWO adolescents were similar to those reported for similarly grouped adults [2-4]. Further research is needed to determine whether such differences in walking patterns precipitating at an early age place OWO adolescents at greater risk earlier in their lives for joint pain or debilitating joint degeneration.

## REFERENCES

1. National Center for Health Statistics. *Health, United States, 2004*. Hyattsville, MD, 2004.
2. Browning RC, et al. *Med Sci Sports Exerc* 39, 1632-1641, 2007.
3. DeVita P, et al. *J Biomech* 36, 1355-1362, 2003.
4. Wearing SC, et al. *Obesity Rev*, 7, 13-24., 2006.
5. Hills AP. *Exercise and Obesity*, Smith-Gordon, 1994.
6. Hills AP, et al. *Arch Phys Med Rehabil* 72, 403-407, 1991.

## ACKNOWLEDGEMENT

Funding provided by a University of Nevada, Las Vegas School of Nursing/School of Allied Health Sciences Obesity-Related Award.

**Table 1:** Main effect mean and standard deviation values by variable.

| Main Effect Level | Vel (m/s)         | Cad (Hz)            | SL (m)      | SW (% cycle) | DS (% cycle) | StWd (m)    |
|-------------------|-------------------|---------------------|-------------|--------------|--------------|-------------|
| <b>Group</b>      |                   |                     |             |              |              |             |
| NW                | <i>1.51 ± 0.3</i> | <i>116.5 ± 14.1</i> | 0.77 ± 0.09 | 38.8 ± 2.0   | 22.5 ± 3.9   | 0.09 ± 0.03 |
| OWO               | <i>1.44 ± 0.3</i> | <i>113.6 ± 12.8</i> | 0.75 ± 0.09 | 36.9 ± 2.3   | 26.3 ± 4.0   | 0.10 ± 0.03 |
| <b>Speed</b>      |                   |                     |             |              |              |             |
| Preferred         | <i>1.28 ± 0.2</i> | <i>107.6 ± 10.0</i> | 0.71 ± 0.07 | 37.2 ± 2.1   | 25.7 ± 4.0   | 0.09 ± 0.04 |
| Fast              | <i>1.70 ± 0.3</i> | <i>123.5 ± 12.1</i> | 0.82 ± 0.08 | 38.9 ± 2.2   | 22.2 ± 4.0   | 0.09 ± 0.04 |

*Italics represents significant ( $p < 0.05$ ) difference.*

# DEVELOPMENT OF AN EXPERIMENTAL MODEL TO EXAMINE THE ROLE OF HIP MUSCLE IMPAIRMENT ON DISTAL MUSCLE AND JOINT FUNCTION

Maureen K. Dwyer, Kerry Ronan, Anna Miracle, and Timothy A. Butterfield  
University of Kentucky, Lexington, KY, USA  
Website: [http://www.mc.uky.edu/athletic\\_training/butterfield](http://www.mc.uky.edu/athletic_training/butterfield)

## INTRODUCTION

Muscles are the primary contributors to mechanical joint loading and determine the force distribution across a joint surface during weight-bearing [1]. As such, weakness of the quadriceps muscle group has been proposed to be a mechanistic contributor to progressive musculoskeletal dysfunction following traumatic joint injury due to altered joint loading [2]. However, in the absence of joint trauma, the contribution of muscle weakness to initiate progressive joint dysfunction is less clear. Recently, experimental models of muscle weakness have been developed to address the role of muscle dysfunction on joint morphology [4]. To date, however, these models have focused on weakening the periarticular muscles surrounding the knee joint.

Recent focus on potential contributors to knee joint pathology has expanded to include the potential role of altered hip joint function. Due to the interdependence of the hip and knee during ambulation, impairment of the hip abductor muscles results in altered pelvic and thigh kinematics, influencing both knee joint position and torque [3]. However, the contribution of hip muscles to knee joint stability is relatively unexplored and may prove pivotal in the initiation of events leading to the development of distal musculoskeletal dysfunction, including knee joint osteoarthritis.

Therefore, the aim of this study was to quantify the alterations in muscle function of the proximal and distal segments of the rat hindlimb for seven days following impairment of gluteus medius (GM) function.

## METHODS

In this pilot study, indwelling bipolar electromyographic (EMG) electrodes were surgically implanted into agonist-antagonist muscle

pairs of the left hindlimb of three Long-Evans rats: vastus lateralis (VL), semimembranosus (SM), tibialis anterior (TA), and gastrocnemius (GS). EMG and video data were collected simultaneously during level treadmill ambulation. Baseline data were collected 7 days post-surgery to assure full recovery. Immediately following data collection, the left GM was identified by manual palpation and received one intramuscular injection of BTX-A (3.5units/kg). EMG and video data were collected immediately following injection and every 24 hours for the next 7 days (Figure 1).

Each rat was recorded during level walking at 15m/min. Gait cycle phases of swing and stance were visually determined and identified with synchronized video, and 5-10 consecutive steps were selected daily. A gait cycle was not included in the analysis if the rat was not walking in a normal manner. The root mean squared amplitude during gait cycle for each muscle was computed. These data were normalized to the daily peak amplitude, which was determined by identifying the highest 100ms RMS amplitude from the selected steps. The RMS amplitude for each step was averaged across the steps and reported as percentage of this daily peak activity. Average muscle activation onset times prior to paw contact were also calculated for each muscle.

## RESULTS AND DISCUSSION

There were no significant changes from baseline to 7 days post injection for any of the muscles. However, there was a trend for reductions in average muscle amplitudes following BTX-A injection into the ipsilateral GM (Figure 2). Seven days following BTX-A injection into the ipsilateral GM, mean EMG values during level treadmill ambulation were reduced for the SM ( $42.3 \pm 6.4\%$ ), TA ( $42.6 \pm 27.7\%$ ), and GS ( $48.6 \pm 9.6\%$ ) when compared to baseline levels ( $50.6 \pm 7\%$ ,  $63.5 \pm$

7.2%, and  $55.3 \pm 6.3\%$ , respectively, Figure 2). These changes illustrate a general reduction in motor unit recruitment in three of the four instrumented muscles in response to proximal muscle dysfunction.

All four distal muscles exhibited earlier activation onset times prior to paw strike at 7 days compared to baseline during ambulation (Table 1). The change in activation times was significant for the VL ( $p = 0.049$ ) and GS ( $p = 0.046$ ) muscles. The earlier muscle activation resulted in co-contraction of the VL and SM during stance phase, and may illustrate a compensatory mechanism to stiffen and stabilize the hindlimb during reduced MU recruitment.

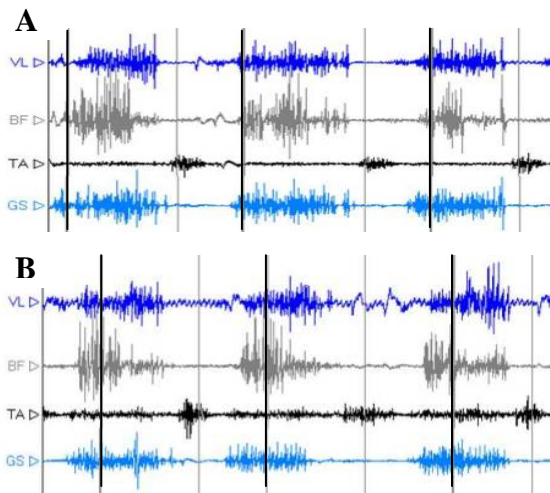


**Figure 1.** Representative EMG tracings for the VL, BF, TA, and GS muscles. prior to (A) and 7 days following (B) BTX-A injection into the ipsilateral GM muscle. (Black line is Paw Strike)

## CONCLUSIONS

Impairment of the GM muscle resulted in dysfunction of distal hindlimb muscles of the leg and shank at 7 days. Reductions in motor unit recruitment in conjunction with the altered timing of muscle activation in two distal limb segments

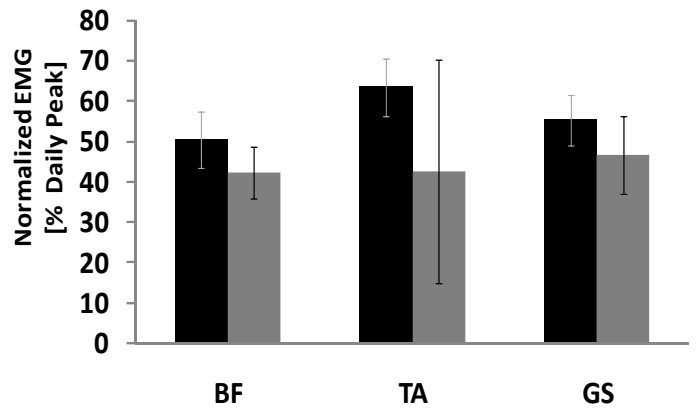


**Figure 2:** Normalized mean EMG amplitude expressed as the percentage of daily peak EMG per step cycle during level treadmill ambulation for the BF, TA, and GS muscles prior to (■) and at 7 days following (■) BTX-A injection into the ipsilateral GM muscle.

during gait illustrates the early compensatory mechanism to proximal muscle weakness. The shift in TA activation and co-contraction of the knee flexor and extensors is indicative of stiffening of the distal joints. GM dysfunction resulted in compensatory activation patterns of the knee and ankle flexor and extensor muscles that may stiffen the hindlimb and predispose the knee and ankle joints to altered loads within 7 days.

## REFERENCES

1. Neumann DA. *JOSPT* **40**, 82-94, 2010.
2. Hurley M. *Osteoarthritis* **25**, 283-298, 1999.
3. Besier T, et al. *J Orthop Res* **26**, 1627-1635, 2008.
4. Youseff RA, et al. *Osteoarth Cartil* **17**, 1128-1235, 2009.

## ACKNOWLEDGEMENTS

We would like to thank Dr. Mauro Giordani for acquiring the botulinum toxin for the completion of this pilot study.

**Table 1:** Average Muscle Activation Prior to Paw Contact during Level Treadmill Ambulation prior to (Pre-Botox) and following (Post-Botox) BTX-A Injection into the Ipsilateral GM Muscle

| Testing Session | Muscle           |                  |                    |                   |
|-----------------|------------------|------------------|--------------------|-------------------|
|                 | VL               | SM               | TA                 | GS                |
| Pre-Botox       | $53.3 \pm 35.9$  | $36.7 \pm 15.7$  | $-160.8 \pm 180.5$ | $62.47 \pm 7.7$   |
| Post-Botox      | $105.0 \pm 21.3$ | $86.19 \pm 33.2$ | $19.14 \pm 276.5$  | $115.88 \pm 41.2$ |
| <i>p</i> -value | 0.049            | 0.080            | 0.200              | 0.046             |

# SHORT TERM MECHANICAL LOADING INCREASES TRABECULAR BONE MINERAL CONTENT AND MOMENTS OF INERTIA IN THE RADIUS OF YOUNG WOMEN

W. Brent Edwards and Karen L. Troy

University of Illinois at Chicago, Chicago, IL, USA  
email: edwardsb@uic.edu, web: <http://www.uic.edu/ahs/biomechanics>

## INTRODUCTION

Bone is a dynamic tissue that can adapt through its (re)modeling response to mechanical loads. Animal loading models have been valuable tools for understanding this process. In an animal, well-controlled mechanical stimuli can be applied to the bone, and the adaptive response directly measured [1]. The remodeling dynamics of bone vary considerably between organisms [2] and it is unclear if loading patterns that are osteogenic in animals may be translated to clinically effective interventions for humans.

To provide a translational link between existing animal loading models and human exercise interventions, we have developed a mechanical loading model for humans in which the non-dominant forearm is cyclically loaded. The purpose of this study was to quantify the effects of a well-controlled mechanical stimulus on the distal radius of young women. We hypothesized that the applied mechanical stimulus would initiate increases in bone mineral density and content in both cortical and trabecular regions of the loaded radius.

## METHODS

Eight healthy young women (age  $19.6 \pm 1.1$  yrs, height  $164.9 \pm 6.5$  cm,  $57.7 \pm 6.9$  kg) were recruited for this institutionally approved study. Following written informed consent, subjects participated in a voluntary mechanical loading intervention targeting the distal radius of the non-dominant forearm. The loading protocol required subjects to lean onto their palm, thereby applying a compressive force, for 50 cycles per day, 3 days per week, for 14 weeks (Fig 1). A load cell device and oscilloscope provided real-time visual feedback of the applied load so that subjects could achieve a target load of 300 N ( $\approx \frac{1}{2}$  bodyweight) every 2 sec (Fig 1).

Cadaveric experimentation suggested that the

applied load of 300 N produced peak principal compressive and tensile strains on the periosteal surface of the distal radial metaphysis of  $-2013 \pm 451 \mu\epsilon$ , and  $1341 \pm 302 \mu\epsilon$ , respectively. Approximately three centimeters proximal in the radial diaphysis, corresponding values were  $-1263 \pm 225 \mu\epsilon$  and  $651 \pm 312 \mu\epsilon$  [3]. Power spectral analysis revealed the frequency of the loading waveform to have major components at 1 and 2 Hz.

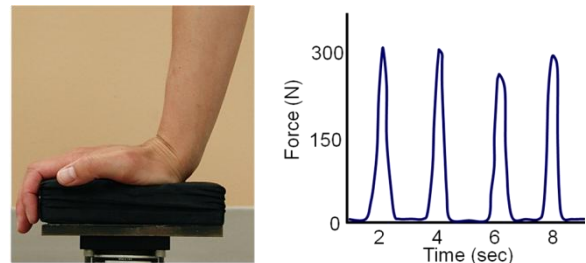


**Figure 1.** Forearm loading and representative force time series.

Computed tomography (CT) data were acquired at weeks 0 and 14 (voxel size:  $625 \times 234 \times 234 \mu\text{m}$ ). Images were reconstructed using a high spatial frequency (bone) algorithm. A calibration phantom was included in each scan to establish a linear relationship between Hounsfield units and hydroxyapatite equivalent density. The CT data were resliced based on bony landmarks to ensure similar coordinate systems between pre- and post-intervention CT scans.

Bone segmentation was performed using Mimics 13.1 (Materialise, Leuven, Belgium). Segmentations were separated into two regions of interest: the ultra distal radius (UDR) and the mid radius (MR). The UDR is comprised primarily of trabecular bone and was defined as the 15-mm transverse section immediately proximal to the subchondral plate. The MR is comprised primarily of cortical bone and was defined as the 30-mm transverse section immediately proximal to the UDR (Fig 2).

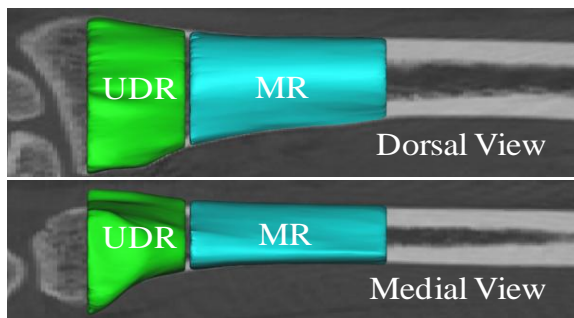


**Figure 2.** Representative dorsal and medial view of the segmented regions of interest UDR and MR.

Dependent variables within each region of interest included cortical (Ct) and trabecular (Tb) specific bone volume (BV), bone mineral content (BMC), bone mineral density (BMD), and maximum (Imax) and minimum (Imin) principal mass moments of inertia. The density thresholds defining bone from marrow and trabecular from cortical bone were 0.1 and 0.48 g/cm<sup>3</sup>, respectively.

Pre- and post-loading dependent variables for each region were compared using paired Student's t-tests. The criterion alpha level was set to 0.05.

## RESULTS AND DISCUSSION

Fourteen weeks of mechanical loading significantly influenced trabecular variables of the UDR. For example, Tb.BMC, Tb.Imin, and Tb.Imax increased by 6.1, 6.6, and 5.0%, respectively (Table 1). No changes were observed for cortical variables of the UDR or any variable of the MR.

The reason that bone adaptive changes were limited to the UDR may be related to the large amount of trabecular bone in this region. Owing, in part, to its lower BMD, the strains in this region are greater than those at the MR, which would be associated with a larger tissue-level mechanical stimulus. Trabecular bone is also more metabolically active and has a higher rate of turnover than cortical bone

due to its large surface/volume ratio. Consequently, trabecular bone is more responsive to mechanical stimuli [4] and pharmacologic [5] intervention than cortical bone.

Despite these arguments, changes in Ct.BMD and Ct.Imin at the MR approached significance (Table 1). It is possible that significant cortical bone apposition took place on the endosteal and/or periosteal surfaces but that our CT resolution was not adequate to capture these changes. If we assume for example, a maximum rate of bone deposition on the periosteal surface of 1 μm/day [2], this would correspond to approximately 100 μm which is still less than half our in-plane resolution. The current study is still ongoing, and perhaps, later time points may illustrate changes in cortical bone.

## CONCLUSIONS

Fourteen weeks of axial compressive mechanical loading is associated with significant increases in trabecular bone mineral content and mass-weighted principal moments of inertia of the ultra distal radius. These increases are likely associated with meaningful improvements in the mechanical competence of the radius, and our future work will investigate this using computational modeling techniques. The current work is ongoing and we have plans to investigate different loading regimens that vary in terms of mechanical stimulus (e.g., magnitude, frequency, and loading cycles).

## REFERENCES

1. Turner CH, et al. *Bone* **23**, 399-407, 1998.
2. Martin RB, et al. *Skeletal Tissue Mechanics*, Springer, 1998.
3. Troy KL, et al. *J Ortho Res*, In Revision.
4. Rubin, C, et al. *Bone* **30**, 445-452, 2002.
5. Keaveny TM, et al. *J Bone Miner Res* **23**, 1974-1982, 2008.

**Table 1.** Mean (SD) percent change in dependent variables and the corresponding *p*-values for paired t-tests. Positive changes correspond to an increase post-loading and significant changes are highlighted in bold.

|     |                 | Ct.BV     | Ct.BMC    | Ct.BMD    | Ct.Imin  | Ct.Imax  | Tb.BV      | Tb.BMC          | Tb.BMD    | Tb.Imin         | Tb.Imax         |
|-----|-----------------|-----------|-----------|-----------|----------|----------|------------|-----------------|-----------|-----------------|-----------------|
| UDR | %Change         | -1.6(4.0) | -2.5(3.7) | -0.9(1.5) | 0.2(5.2) | 0.4(5.9) | 6.9(9.7)   | <b>6.1(4.1)</b> | -0.4(5.6) | <b>6.6(4.5)</b> | <b>5.0(4.0)</b> |
|     | <i>p</i> -value | 0.305     | 0.126     | 0.116     | 0.944    | 0.907    | 0.071      | <b>0.004</b>    | 0.744     | <b>0.002</b>    | <b>0.009</b>    |
| MR  | %Change         | -05(1.6)  | 0.6(1.5)  | 1.1(1.3)  | 2.0(2.3) | 1.0(2.6) | -0.7(10.2) | -1.5(12.5)      | -1.0(3.2) | -0.9(22.9)      | -3.3(19.7)      |
|     | <i>p</i> -value | 0.385     | 0.348     | 0.052     | 0.077    | 0.351    | 0.702      | 0.582           | 0.395     | 0.578           | 0.518           |

# DISLOCATION IN THE MORBIDLY OBESE TOTAL HIP PATIENT

<sup>1,2</sup>JM Elkins; <sup>1</sup>DR Pedersen; <sup>3</sup>B Singh; <sup>3</sup>H. John Yack; <sup>1,4</sup>JJ Callaghan and <sup>1,2</sup>TD Brown

Departments of <sup>1</sup>Orthopaedics; <sup>2</sup>Biomedical Engineering; and <sup>3</sup>Physical Therapy, University of Iowa, Iowa City, IA; <sup>4</sup>Iowa City Veterans Administration Medical Center, Iowa City, IA  
email: jacob-elkins@uiowa.edu

## INTRODUCTION

Obesity places substantial burden on the musculoskeletal system. Obesity demonstrates a dose-effect relationship to development of hip and knee osteoarthritis, and as a result of which obese patients require total hip arthroplasty (THA) more commonly and at a younger age than do non-obese individuals [1]. Additionally, obesity is a significant risk factor for several post-operative complications following THA, including a 4-fold higher risk of dislocation [2,3]. Given that dislocation typically occurs during extremes of hip flexion, the increased dislocation rate in obese patients is perplexing, owing to the decreased habitual hip joint angular excursion in obesity [4]. One possible mechanism is that thigh-thigh impingement can lead to instability ([2], Figure 1). We decided to test this hypothesis with a physically validated [5] finite element (FE) model of THA dislocation.

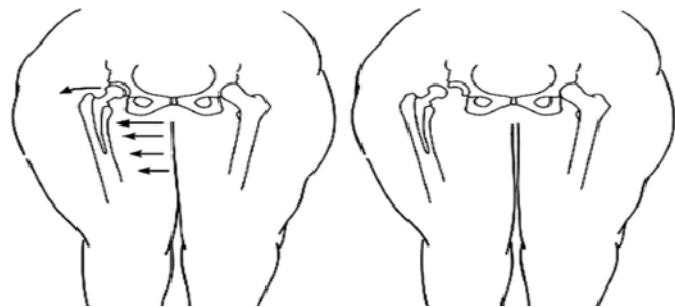


**Figure 1:** During hip adduction, thigh-thigh impingement generates a laterally directed force with possibly sufficient magnitude to cause dislocation. From [2].

## METHODS

The obesity dislocation model (Figure 2) consisted of three parts: (1) THA hardware (2) the hip capsule; (2) and mirrored right and left thighs. The material properties of the thigh soft tissues were assigned values from literature. Thigh morphology was based on anatomical geometric shape functions. Using anthropometric and cadaveric data, these were scaled for eight levels of BMI (Figure 3).

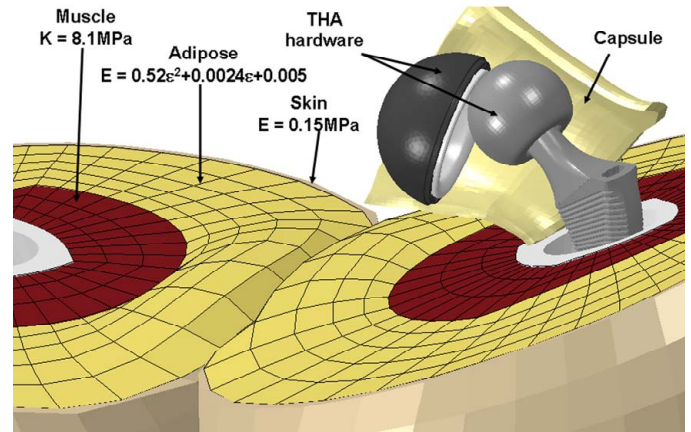


**Figure 2:** The model of thigh-thigh impingement consisted of (1) THA hardware; (2) hip capsule; and (3) mirrored right and left thighs, composed of adipose tissue, muscle, skin and the femur. E=Young's modulus, K=bulk modulus, ε=strain.

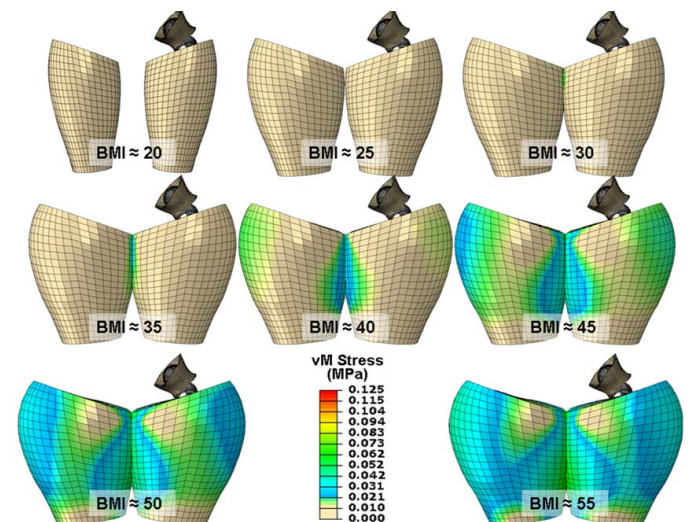


**Figure 3:** Eight levels of BMI were used in the dislocation FE series. Geometric patterns were determined from cadaveric and anthropometric data.

A sit-to-stand maneuver was used as the dislocation challenge. Right-left motion symmetry was assumed. Joint contact forces were scaled for each model's simulated body weight. Three separate THA implants were considered: (1) a standard 28mm implant; (2) a large 36mm implant; and (3) a

36mm implant with a large (8mm) neck offset. Fifteen separate acetabular cup orientations were assessed by varying cup inclination from 30° to 65°, in 2.5° increments.

Physical validation was conducted using a calibrated pressure mat (Tekscan), allowing for real-time collection of thigh impingement loads in obese subjects (Figure 4).

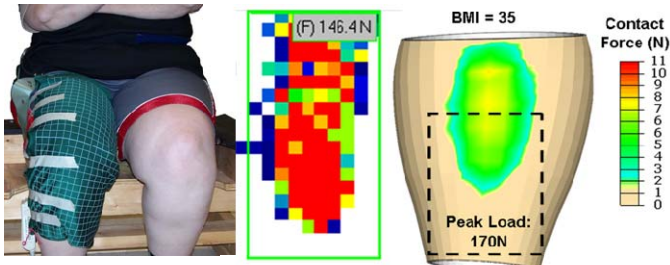


**Figure 4:** Physical validation of the thigh-thigh impingement force was performed using an interface pressure mat monitoring thigh-thigh contact during a sit-to-stand in an obese subject. When registering the area covered by the mat to the FE simulation with the nearest thigh circumference, a 16% error in force agreement was achieved.

## RESULTS AND DISCUSSION

The thigh-thigh impingement was found to deliver a substantial impetus for dislocation in the obese patient models, independent of implant hardware impingement. Dislocation risk was found to be sensitive to both cup orientation and BMI. Femoral head subluxation (instability) did not become appreciable, however, until BMI reached approximately 40 (Figure 5). Increased head diameter resulted in only marginal stability improvement, particularly for the lower cup inclinations (Figure 5A-B). However, the use of a high-offset femoral neck resulted in a significant improvement in stability, with no dislocations occurring in this series. The mechanism for improved stability with an offset is plausibly twofold: (1) applying a neck offset increases capsule tension, resulting in improved stability and (2) offset allows for an increase in initial thigh-thigh spacing, thereby decreasing the magnitude of the impingement force.

## CONCLUSIONS

Obesity has a disproportionately elevated incidence in the general orthopaedic patient population. Of particular concern is the 4-fold increase in dislocation risk for obese THA patients. The present

work corroborates clinical observation [2] that thigh impingement may decrease THA stability. The FE model demonstrated a dose-effect relationship between BMI and instability, with an apparent threshold of 40. An effect onset threshold in this range has been noted clinically [3,6].

The combination of a large head implant, high neck offset and lower cup orientations were shown to substantially reduce dislocation risk in the obese.

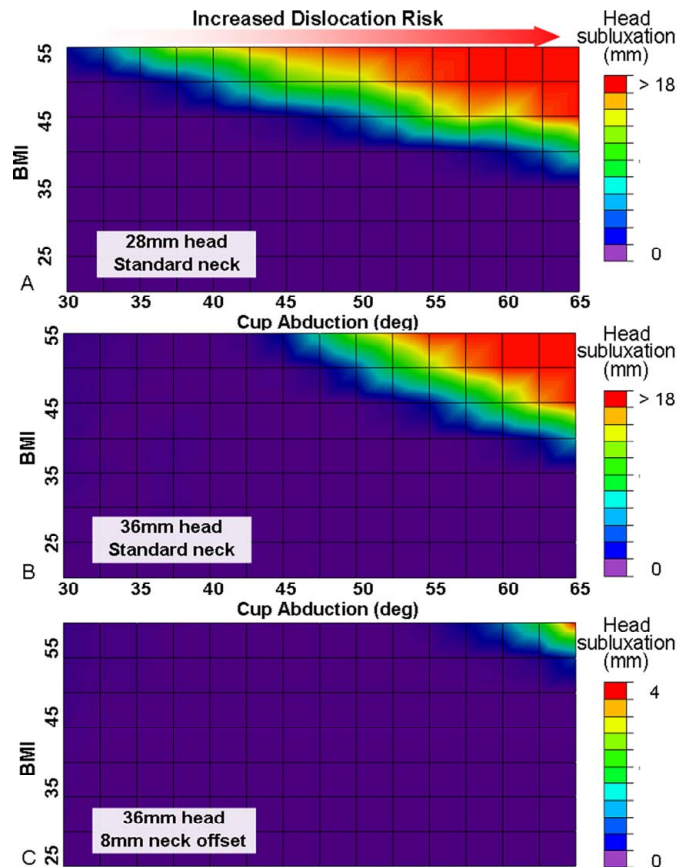


**Figure 5:** Dislocation risk was found to be sensitive to both BMI and cup orientation for the 28mm head (A). An almost similarly strong BMI-orientation relationship was found for the 36mm implant (B). However, dislocation risk was substantially reduced when an offset neck was used (C).

## REFERENCES

1. Changulani M et al. *JBJS Br* **90**(3),360-363, 2008
2. Kim Y et al. *CORR* **453**, 142-146, 2006
3. Andrew JG et al. *JBJS Br* **90**(4), 424-429, 2008
4. Jackson M et al. *JBJS Br* **91**(10):1296-300, 2009
5. Elkins JM et al. *CORR* **469** 454-463 2011
6. Grant JA et al. *Rheum. Int.* **11**, 1105-1109 2008

## ACKNOWLEDGEMENTS

Financial support provided by the NIH (AR53553 and AR46601) and the Veterans Administration.

# Helical Axis Approach to Aberrant Motion Identification in Patients with Chronic Neck Pain

<sup>1</sup>Arin M. Ellingson, <sup>2</sup>Craig Schulz, <sup>2</sup>Gert Bronfort, and <sup>1</sup>David J. Nuckley

<sup>1</sup>University of Minnesota, Minneapolis, MN, USA

<sup>2</sup>Northwestern Health Sciences University, Bloomington, MN, USA

email: [ellin224@umn.edu](mailto:ellin224@umn.edu) web: <http://www.mbrl.umn.edu>

## INTRODUCTION

Chronic neck pain affects approximately one-third of the population in the course of 1 year and 5-10% of these will result in a significant disabling neck problem<sup>1,2</sup>. Often diagnosis relies on planar motion, typically flexion/extension, however this does not effectively examine the complex coupled motion of the cervical spine. Previous groups have aimed to quantify the kinematics and helical axes of healthy individuals<sup>3,4</sup> and those suffering from neck pain<sup>5-7</sup>. However, many of these investigate motion only in the anatomic planes and the few that look at off-axis or coupled motion are still planar, but at an oblique angle. Kinematic analysis of neck circumduction, Figure 1, allows us to explore how helical axes are affected by the coupling nature of the cervical spine.

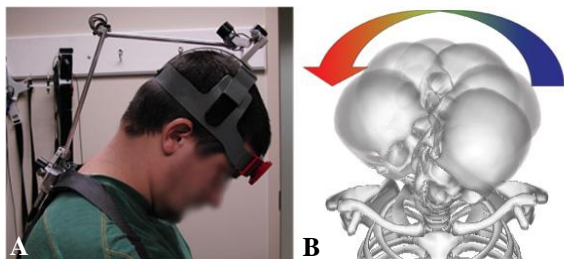


Figure 1 A: Linkage System Set-up B: Head Circumduction.

There are no reliable functional mechanical exams to diagnosis, differentiate, or assess progress of individuals with chronic neck pain. *Therefore, the purpose of this study was to investigate neck function/motion in subjects suffering from chronic neck pain while they perform a circumduction exercise with their head using an instantaneous helical axis (IHA) approach.*

## METHODS

Head-to-torso kinematic data was collected on 22 subjects (age: 45.2±9.5 years, 14 female) with chronic neck pain twice prior to and following a treatment intervention. The two baseline measurements were taken 1-2 weeks apart.

These subjects, a subset of the complete 270 patient sample, were used to examine a motion anomaly algorithm in the current study. Pain intensity, range

from 0-10, and neck disability index (NDI), range from 0-50, values were recorded before each session. Pain was categorized into three equally distributed bins 'low' (n=20), 'medium' (n=37), 'high' (n=12). NDI was categorized in a similar way: 'low' (n=13), 'medium' (n=38), 'high' (n=15). Relative position and orientation of the head with respect to the torso was computed via a CA-6000 Linkage system (OSI, CA) at a frequency of 100 Hz. The inferior end of the linkage system, located over the spinous process of T1, was secured to a harness that was snugly strapped around the torso. The superior end was connected to a helmet (Figure 1A).

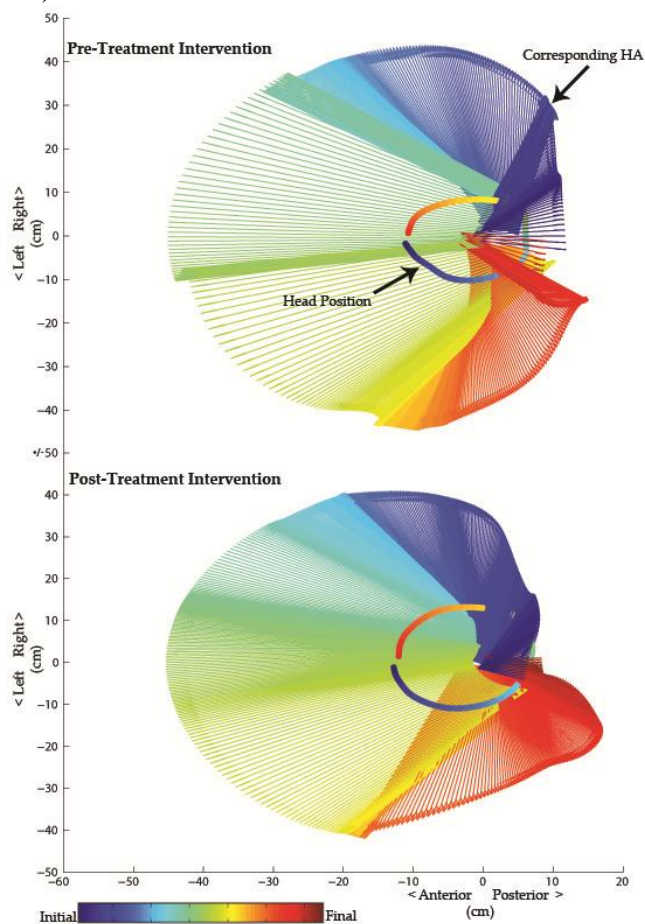


Figure 2- Instantaneous Helical Axes and Head Position. Above: Pre-Treatment Intervention (pain = medium). Below: Post-Treatment Intervention (pain = low). Note the smoothness of the post-treatment IHA compared with that same individual prior to treatment.

Subjects were instructed to perform a circumduction exercise while standing with their arms by their side. Beginning from neutral position the subjects went into full flexion rolled their head to the left and around back to full flexion before returning to neutral position (Figure 1B).

IHA were calculated for each time step between the subject's initial full flexion position and their final full flexion position<sup>8</sup>. Figure 2 illustrates the head position and IHA at each step.

The IHA vector tips were fit to a three-dimensional plane and transformed into spherical coordinates, where theta is the azimuthal angle. Aberrant motion was defined when the numerical derivative of theta was negative, indicating where the IHA folds back upon itself. This is displayed in Figure 3 as red vectors and markings on head position plot. The number of folds, location of folds with respect to head position, as well as percent range of motion and percent time the subject was in the midst of aberrant motion were also analyzed. In an effort to identify if aberrant motion is correlated with pain intensity and NDI, ANOVA techniques were performed with an alpha acceptance of 0.05.

## RESULTS AND DISCUSSION

IHA computation for neck circumduction was found to be correlated with patient outcome measures. Specifically, number of folds ( $p=0.049$ ) and percent time in folds ( $p=0.014$ ) showed a significant increase as pain intensity increased, but percent range of motion did not. NDI was not indicative of any changes with any of the metrics.

Observationally, the smoothness of the IHA seems to be related to pain intensity. Even distribution of IHA vectors as indicative of a more constant velocity of motion. Also, the range of motion of the head seems to increase following treatment.

Limitations of this approach include no a priori knowledge of how IHA relate to neck dysfunction. This coupled with the lack of a healthy control dataset does not allow us to determine a causal relationship between aberrant motion and patient outcome measures.

Further analysis of the 270 patients in this dataset will enable us to draw generalizable conclusions regarding the IHA and chronic neck pain.

## CONCLUSIONS

The circumduction activity is robust for similar pain ratings within an individual, but distinct when the pain levels are different. This analysis allows for the detection of subtle changes in the path of motion

that are not detectable by eye or any classic metrics. Thus, this methodology represents a new way to examine neck pain patients with respect to their aberrant motion so as to develop an assessment and tracking measure for care of these patients.

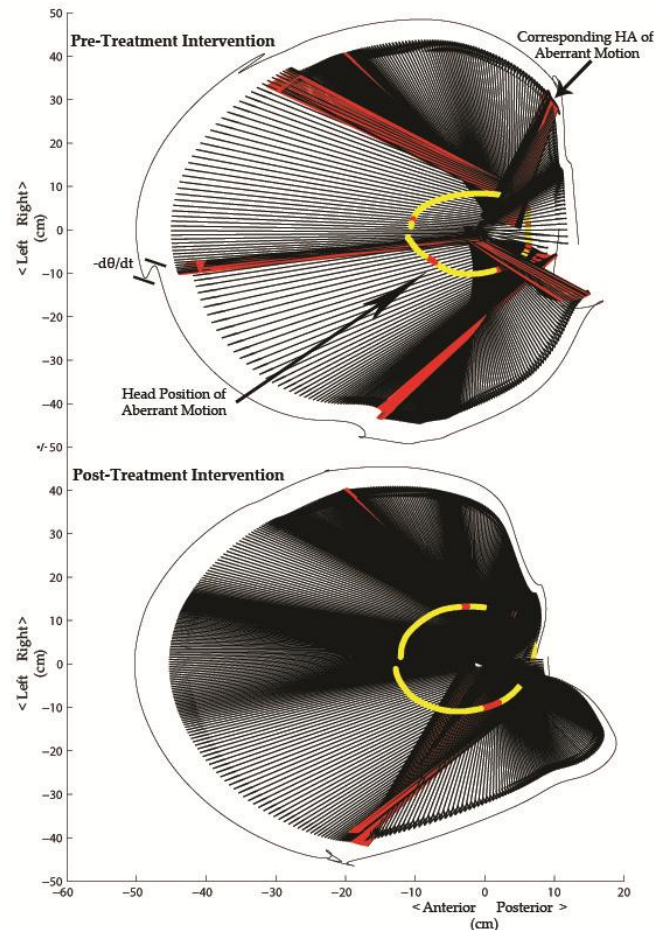


**Figure 3- Instantaneous Axes with Highlighted Aberrant Motion (red).** Notice many folds for the pre-treatment subject and smooth axes for same patient post-treatment.

## REFERENCES

1. Bovim G, et al. *Spine (Phila Pa 1976)*. Jun 15 1994;19(12):1307-1309.
2. Cote P, et al. *Spine (Phila Pa 1976)*. Aug 1 1998;23(15):1689-1698.
3. Greaves LL, et al. *Spine (Phila Pa 1976)*. Jul 15 2009;34(16):1650-1657.
4. Crompton PA, et al. *J Biomech*. Aug 2001;34(8):1091-1096.
5. Osterbauer PJ, et al. *J Manipulative Physiol Ther*. Oct 1992;15(8):501-511.
6. Osterbauer PJ, et al. *J Manipulative Physiol Ther*. May 1996;19(4):231-237.
7. Amevo B, et al. *Spine (Phila Pa 1976)*. Jul 1992;17(7):748-756.
8. Spoor CW, et al. *J Biomech*. 1980;13(4):391-393.

# IMPACT OF ANATOMICAL ADHESIONS ON STRESS DISTRIBUTION WITHIN THE EXTENSOR HOOD OF THE INDEX FINGER

<sup>1</sup>Benjamin Ellis, <sup>2</sup>Sang Wook Lee, <sup>3</sup>Kay Traylor, <sup>1</sup>Jeffrey Weiss, and <sup>3,4</sup>Derek Kamper,

<sup>1</sup>Musculoskeletal Research Laboratories, University of Utah, Salt Lake City, UT, USA

<sup>2</sup>Department of Biomedical Engineering, Catholic University of America, Washington, D.C., USA

<sup>3</sup>Department of Biomedical Engineering, Illinois Institute of Technology, Chicago, IL, USA

<sup>4</sup>Sensory Motor Performance Program, Rehabilitation Institute of Chicago, Chicago, IL, USA

email: u0241427@utah.edu

web: <http://smpp.northwestern.edu/research/hand/research.html>

## INTRODUCTION

The extensor hood is a complex structure which transmits forces from finger muscles to the phalanges. In the index finger alone, four and possibly five tendons are incorporated into this aponeurosis which runs the length of the finger. These tendons arise from the first palmar interosseous (FPI), lumbrical (LUM), extensor digitorum communis (EDC), extensor indicis (EI), and, in some instances, the first dorsal interosseous. While the extensor hood consists of a continuous sheet of collagenous tissue, it is often represented as a network of discrete tendons [1-2], typically with a rhomboid structure [3]. The tendons representing the central slip (CS) and terminal slip (TS) are the two that actually attach to the bones, namely to the middle and distal phalanges, respectively.

Whether modeled as a network of tendons or as a continuous sheet, the question arises as to the need to include further connections, beyond those of CS and TS, between the bones and the extensor mechanism. A number of fibrous adhesions along the extensor mechanism help to reduce translation of the hood with respect to the phalanges. Otherwise, contraction of FPI, for example, which connects to the ulnar edge of the extensor mechanism, might produce medial displacement of the hood. It is not known, however, the role these adhesions play in force transmission.

Thus, the goal of this study was to quantify the impact of these adhesions on the distribution of stresses within the hood. A finite element model (FEM) of the hood was created and simulations with and without certain adhesions were run. We hypothesized that these connections would

substantially impact the stress distribution and need to be included in extensor hood models.

## METHODS

A FEM of the extensor hood and bones (the metacarpal and proximal, middle, and distal phalanges) of the index finger was created (Fig. 1). Anatomical magnetic resonance images of a cadaver hand were obtained; these images were segmented in Amira (Visage Imaging, Inc., San Diego, CA) to generate 3D surfaces of the extensor hood and bones. A deformable shell mesh was created for the extensor hood using the finite element preprocessor, TrueGrid (XYZ Scientific, Livermore, CA), while the surface meshes for the bones were used to generate rigid shell meshes. A mesh convergence study was conducted for the extensor hood to assure proper discretization.

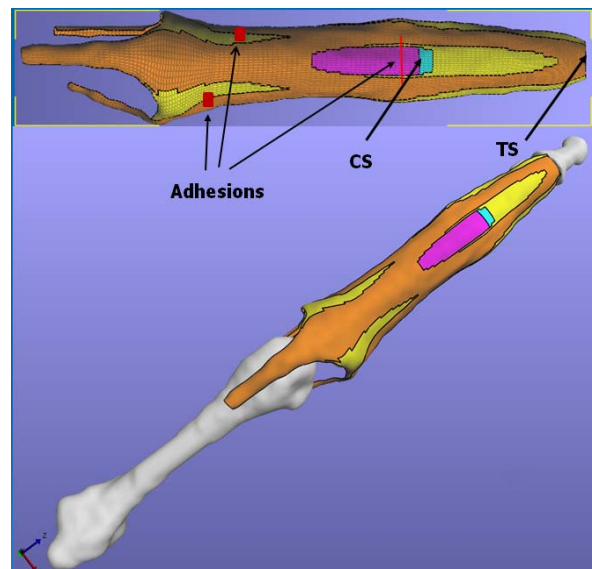


**Figure 1:** Finite element model of the extensor hood. Regions with different colors have different material properties. CS: central slip; TS: terminal slip.

The extensor hood was represented as a homogeneous, isotropic, compressible, St. Venant-Kirchhoff elastic material with a constant thickness of 1.0 mm. The elastic modulus and Poisson's ratio ( $E = 1825.5$  MPa,  $\nu = 0.4$ ) for the banded portions of the extensor hood were obtained from previously published research [4]. As the extensor hood is a heterogeneous structure, different moduli were used for different parts of the hood, in accordance with measured values [4] (see Fig. 1). Rigid attachments between the extensor hood and the bones were created through rigid node sets located at the attachments of the CS and TS with the middle and distal phalanges, respectively. All FE pre-processing (after mesh generation), post-processing, and analysis were conducted with the FEBio Suite of software (<http://mrl.sci.utah.edu/software>).

Locations of major adhesions were determined through dissection of cadaveric fingers. These adhesions were included in the models through the introduction of springs connecting the bone and the hood. The springs exert force only when stretched, not when compressed. Two sets of these adhesions were modeled sequentially for this study.

Thus, three conditions were simulated: no adhesion (NO), two adhesions distal to the MCP joint, one on the radial side and one on the ulnar side (RU), and one adhesion just proximal to the PIP joint, representing a connection between the central slip and the joint capsule (CS). These three conditions were run at two different finger postures (MCP flexion, PIP flexion, DIP flexion):  $(0^\circ, 0^\circ, 0^\circ)$ ,  $(0^\circ, 45^\circ, 30^\circ)$ . The following loading pattern was used: EDC/EI – 12 N, LUM – 0.25 N, FPI – 0.25 N.

## RESULTS AND DISCUSSION

Both finger posture and the presence of the adhesions had a profound impact on stress distribution within the hood. The flexed posture led to localized stresses an order of magnitude greater than those observed in the extended posture for all three conditions (NO, RU, and CS) for loading of EDC/EI.

Inclusion of the adhesions affected magnitude and distribution of the stresses (Fig. 2). The RU adhesions generated larger stresses in the more proximal portion of the hood, while the CS

adhesion produced very high stresses around the PIP joint.

Interestingly, the ratio of the CS:TS insertion forces also changed with the inclusion of certain adhesions. In the flexed posture, the NO and CS models yielded ratios of 3.6:1. In contrast, the RU model produced a ratio of 1.1:1, which is much closer to the 0.6:1 ratio reported from cadaver experiments [5]. Thus, these adhesions may play an important role in force distribution through the hood and warrant further investigation.

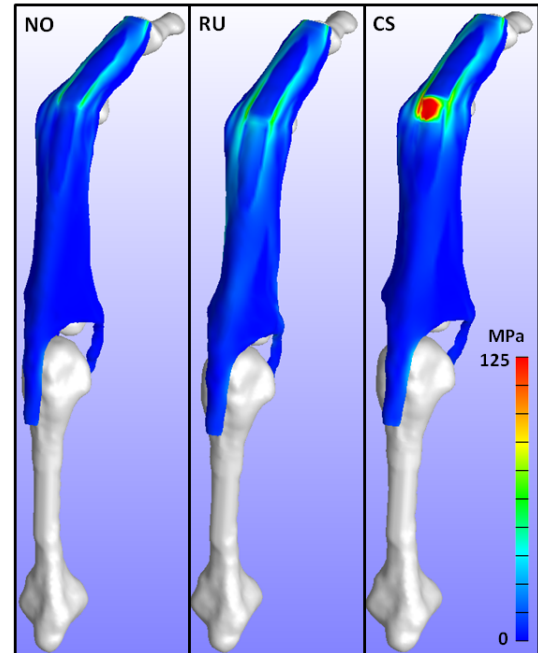


**Figure 2:** Simulation results at the flexed finger posture of (MCP, PIP, DIP) =  $(0^\circ, 45^\circ, 30^\circ)$  for a loading pattern of (EDC, LUMB, FPI) = (12 N, 0.25 N, 0.25 N). NO: no adhesions; RU: adhesions on radial and ulnar sides of MCP. CS: adhesions to joint capsule just proximal to PIP joint.

## REFERENCES

1. Garcia-Elias M, et al. *J Hand Surg Am* **16**, 1130-6, 1991.
2. Valero-Cuevas FJ, et al. *IEEE Trans BME* **54**, 1161-6, 2007.
3. Zancolli E, *Structural and Dynamic Bases of Hand Surgery*, 1979.
4. Garcia-Elias M, et al. *J Hand Surg Am* **16**, 1136-40, 1991.
5. Lee SW, et al. *J Biomech Eng* **130**, 0510141-9, 2008.

## ACKNOWLEDGEMENTS

This work was supported by NINDS of NIH (1R01NS052369).

# EFFECTS OF STROKE-INDUCED SENSORY AND MOTOR DEFICIT ON PHALANX FORCE MAGNITUDE AND ANGULAR DEVIATION DURING POWER GRIP

Leah R. Enders, and Na Jin Seo

University of Wisconsin-Milwaukee, Milwaukee, WI, USA  
email: lrenders@uwm.edu web: <https://pantherfile.uwm.edu/seon/www/>

## INTRODUCTION

More than 6.5 million stroke survivors currently reside in the U.S. [1]. Many stroke survivors suffer from disability in the hands and arms [2]. Loss of hand grip function limits stroke survivors' ability to grasp and manipulate objects required by everyday activities. To grasp an object successfully, a person adapts phalanx force magnitudes and trajectories (phalanx force vector direction relative to the direction normal to the object surface) [3] to an object's characteristics (e.g., weight, coefficient of friction (COF)) using anticipatory control as well as feedback control via sensory feedback [4]. Specifically, to maintain stable contact with a grasped object (i.e. object not slipping against the finger), phalanx force should not be deviated from the normal direction more than an angle equal to the arctangent of COF [5]. Many stroke survivors exhibit reduced tactile sensation in the fingers [6]. This reduced sensation may diminish their feedback control and cause altered grip (reduced phalanx force magnitude and misdirected phalanx force trajectories). This excessive phalanx force angular deviation for stroke survivors can lead to ineffective gripping and object slippage from the hand.

Knowledge regarding stroke survivors' altered grip is sparse for power grip, even though power grip is often required for everyday tasks. In addition, how sensory deficit plays a role in stroke survivors' altered phalanx force magnitudes and force trajectories has not been studied. The first objective of this study was to quantify the extent of altered phalanx force magnitudes and trajectories during power grip for people with stroke compared to age-matched neurologically-intact control subjects. The second objective was to determine if such altered power grip is severer with sensory deficit than without sensory deficit among stroke survivors with similar levels of motor deficit.

## METHODS

Seven chronic stroke survivors with sensory deficit (mean age  $\pm$ SD =  $62 \pm 14$  years), 5 chronic stroke survivors without sensory deficit ( $64 \pm 11$  years), and 6 age-matched healthy control subjects ( $61 \pm 16$  years) participated. Mean motor impairment, quantified by the Chedoke-McMaster Stroke Assessment [7], was stage 4 for both stroke groups.

Subjects performed power grip with maximum and 50% of perceived maximum efforts on a custom-made grip dynamometer (Fig. 1). The grip dynamometer had a rubber surface (COF with finger skin = 0.9 [8]). Normal force and proximal-distal shear force for all phalanges of the 5 fingers were recorded for 3 repetitions to compute mean phalanx normal force and trajectory. The phalanx force trajectory was quantified as the deviation of the phalanx force from the direction normal to the grip surface (arctangent of the absolute ratio of shear to normal force). Two ANOVA determined if normal force magnitude and trajectory varied significantly for subject group, grip effort, and their interaction. Finger and phalanx were blocking factors. Tukey post hoc tests evaluated differences among the 3 subject groups.

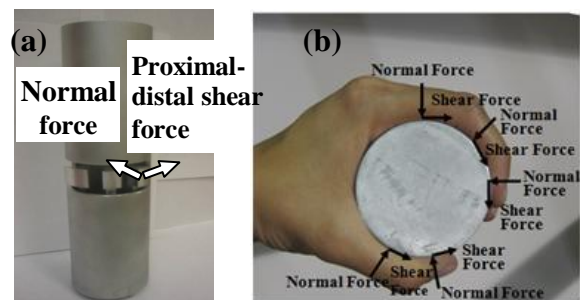


**Figure 1:** The grip dynamometer had 3 adjustable contact pads (a) aligned with a finger to measure each phalanx's proximal-distal shear force (tangential to grip surface) and normal force (normal to grip surface) during power grip (b).

## RESULTS

The mean normal force was 15.9 N (SE=0.8 N), 11.5 N (SE=0.8 N), and 8.6 N (SE=0.6 N) for healthy controls, stroke survivors without sensory deficit, and stroke survivors with sensory deficit, respectively (Fig. 2). Mean normal forces were significantly different among the 3 subject groups ( $p < .01$  for ANOVA and Tukey post-hoc test for all 3 comparisons). The grip effort level and the interaction between grip effort level and subject group significantly affected normal force ( $p < .01$ ).

The mean angular deviation of the phalanx force was 17.1° (SE=0.7°), 20.9° (SE=0.9°), and 25.1° (SE=1.0°) healthy controls, stroke survivors without sensory deficit, and stroke survivors with sensory deficit, respectively (Fig. 3). Mean angular deviations were significantly different among the 3 subject groups ( $p < .01$  for ANOVA and Tukey post-hoc test for all 3 comparisons). The grip effort level and the interaction between grip effort level and subject group did not significantly affect angular deviation ( $p > .05$ ).

## DISCUSSION

The present study demonstrated that stroke survivors gripped with, on average, 37% reduced phalanx normal force and 35% greater phalanx force angular deviation, compared to age-matched healthy controls. More importantly, the present study demonstrated that the stroke survivors with sensory deficit gripped with, on average, 25% less normal force and 21% greater phalanx force angular deviation, compared to stroke survivors without sensory deficit. These results suggest that not only motor deficit, but also sensory deficit following stroke are responsible for impaired hand grip for stroke survivors. Stroke survivors with sensory deficit may have an increased incidence of dropping grasped objects compared to those without sensory deficit and healthy controls, not only due to a greater reduction in normal force, but also due to more altered phalanx force trajectories.

## ACKNOWLEDGEMENTS

The University of Wisconsin-Milwaukee College of Engineering & Applied Science, the University of Wisconsin-Milwaukee Research Growth Initiative, Wisconsin Women's Health Foundation

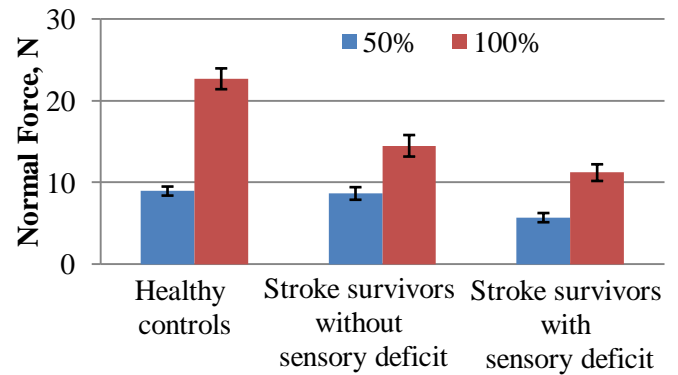


**Figure 2:** Mean  $\pm$  SE phalanx normal force was smallest for stroke survivors with sensory deficit, followed by stroke survivors without sensory deficit and controls ( $p < .01$ ) (averaged across phalanges, fingers, and subjects).

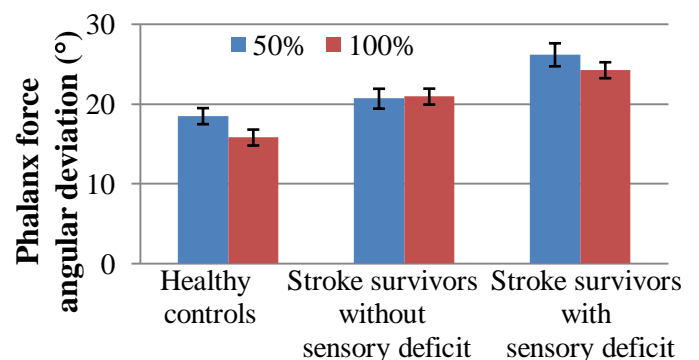


**Figure 3:** Mean  $\pm$  SE phalanx force angular deviation from the direction normal to the grip surface was the greatest for stroke survivors with sensory deficit, followed by stroke survivors without sensory deficit and controls ( $p < .01$ ) (averaged across phalanges, fingers, and subjects).

## REFERENCES

1. Loyd-Jones D., et al. *Circ* **119**, 480-486, 2009.
2. Gray C.S. et al. *Age Ageing* **19**, 179-184, 1990.
3. Zatsiorsky V.M. and Latash M.L. *Exerc Sport Sci Rev* **32**, 2004.
4. Johansson R.S. and Westling G. *Exp Brain Res* **56**, 550-564, 1984.
5. Mackenzie C.L and Iberall T. *The Grasping Hand*, North Holland, 1994.
6. Cary L.M. *Crit Rev Phys Rehabil Med*, **7**, 51-91, 1995.
7. Gowland C. et al. *Chedoke-McMaster Stroke Assessment: Development, Validation and Administration Manual*, Chedoke-McMaster Hospitals and McMaster University, 1995.
8. Seo N.J and Armstrong T.J. *Ergonomics*, **52**, 609-616, 2009.

# Workday Arm Elevation Exposure, a Comparison between Two Professions.

<sup>1</sup>Luke Ettinger, <sup>2</sup>Laurel Kincl and <sup>1</sup>Andrew Karduna

<sup>1</sup>University of Oregon, Eugene, OR, USA

<sup>2</sup>Labor Education and Research Center, Eugene, OR, USA

email: [lettinge@gmail.com](mailto:lettinge@gmail.com)

## INTRODUCTION

Occupations that require repetitive arm motions above 60° and 90° of humeral elevation have been attributed as being potentially injurious professions for the shoulder [4]. 11% - 68% of currently working dental hygienists have shoulder related pain and or dysfunction [1, 3]. Unlike dental hygienists, workers who use computers for the majority of their workday do not share the same risk factors for occupational musculoskeletal injuries of the shoulder [5]. It is hypothesized that because dental hygienists have a greater tendency for shoulder disorders that they will spend a greater percentage of their workday at elevated humeral angles than computer based workers.

## METHODS

Twenty female dental hygienists with an average age of 42.6 years (24 – 56 years) and nineteen female computer workers with an average age of 42.6 years (26-62 years) participated in our study. Computer workers were recruited to match the dental hygienist population as closely as possible for age, arm dominance, number of years employed and total number of hours worked per week. All data were collected on an eight hour workday for both dental hygienists and computer workers (8.8 hours, 8.1 hours, respectively). Before the start of the workday subjects were fit with two tri-axial accelerometers (Virtual Corset) bilaterally at the level of the deltoid tuberosity of the humerus. Virtual Corset data were recorded at 7.6 Hz until the device was removed at the end of the workday. Data were converted from linear accelerations to arm elevation angles using a previously validated equation [2] (Figure 1). The total amount of time participants spent with their arm elevated above 30°, 60° and 90° was summed and then averaged as a percentage of total working hours - this measure is treated as the quantitative dependant variable.

Independent samples t-tests were used to quantify differences between total arm usage above 30°, 60° and 90° for dental hygienists and computer workers.

$$\theta = \tan^{-1} \frac{\sqrt{x^2 + y^2}}{z}$$

**Figure 1:** Equation used to quantify humeral elevation from linear accelerations.

## RESULTS

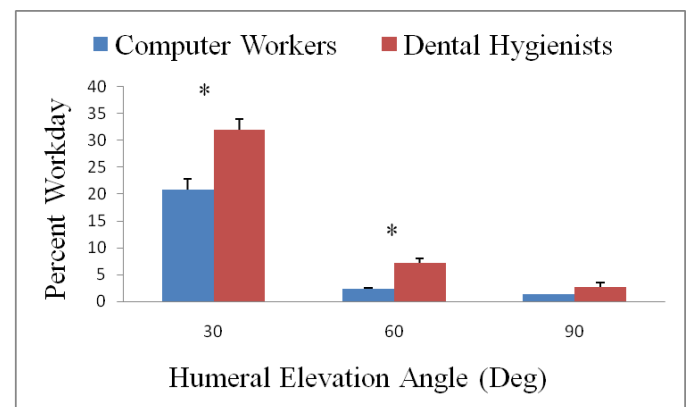


**Figure 2:** Percent of workday with arm elevated above 30°, 60° and 90° for dental hygienists and computer workers. \* Indicates significant differences where p<.05.

On average dental hygienists worked with their arms above 30° for 11% of their workday more than computer workers (p<.001) and above 60° for 5% of their workday more than computer workers (p<.001). No significant differences between groups existed above 90° (p=.07).

## DISCUSSION

Occupational risk factors for shoulder disorders have been attributed to awkward and constrained posture, the intensity and duration of force loads on the shoulder and the repetitious nature of the work being preformed [4]. Svendsen et al., composed a

cross-sectional analysis comparing arm usage in different overhead professions such as painters, machinists and car machinists. From that study it was identified that the greater duration of working hours with the arm elevated above 60° and 90° yields a stronger correlation with shoulder injuries. The results of our study support our hypothesis that dental hygienists spend a significantly greater percentage of their workday with their arm elevated above 30° and 60° degrees when compared to computer workers. Trends in the literature regarding both dental hygienists and computer workers suggest that dental hygienists have a greater tendency for shoulder disorders than computer workers. Our results may help to explain, at least in part, why dental hygienists may be at greater risk for developing shoulder injuries than other occupations. There could be other occupational factors that could be contributing to the differences in injury rates between these two populations.

Dental hygienists did not significantly differ from computer workers above 90° of humeral elevation.

Findings from this study suggests that chronic exposure to humeral elevations angles below 60° may be sufficient to increase the risk of occupational shoulder injuries.

## REFERENCES

1. Akesson I, et al. *Int Archive of Occupation Environ Medicine*, **72**, 395-403, 1999.
2. Amasay T, et al. *Int Journal of Industrial Ergonomics* **39**, 783-789, 2009.
3. Liss G, et al. *American Journal of Industrial Medicine*, **28**, 521-540, 1995.
4. Svendsen S et al. *Occupation Environ Medicine*, **61**, 844-853, 1998.
5. Waersted R, et al. *Journal of Calif Dent Assoc*, **11**, 123-131, 2010.

## ACKNOWLEDGEMENTS

Cameron Carter and Sara Garfinkel for technical assistance.

# FORCE-VELOCITY BEHAVIOUR OF HUMAN MEDIAL GASTROCNEMIUS SHIFTS AT THE WALK TO RUN TRANSITION

<sup>1</sup>Dominic J Farris & <sup>1</sup>Gregory S Sawicki

<sup>1</sup>Joint Dept. of Biomedical Engineering, North Carolina State University & UNC-Chapel Hill, NC, USA  
[djfarris@ncsu.edu](mailto:djfarris@ncsu.edu)

## INTRODUCTION

The human medial gastrocnemius (MG) exhibits considerable stretch and recoil in its series elastic element (SEE) during walking and running. This has two main benefits: (1) The SEE can recycle elastic energy to provide power for push-off that would otherwise have to come from active muscle shortening. (2) It allows the muscle fascicles to operate at lower velocities which favours economical force production. This has been established for typical walking speeds and moderate running speeds but the question remains: Is this optimal behaviour maintained across a wider range of speeds?

Simulations of human walking show that positive fascicle work in the MG increases with walking speed [1] and cat gastrocnemius fascicle velocity increases with walking speed [2]. Conversely, running turkeys exhibit nearly isometric MG fascicle behaviour which is almost constant with varied speed [3]. Increasing fascicle velocity with walking speed might impair the muscle's ability to produce force which has been cited as a reason for transitioning to running gait [4]. If, as in turkey's, the fascicles remain at very low velocities in running than fascicle behaviour might be a factor in determining the preferred walk to run transition speed.

Furthermore, were fascicle velocity to increase with walking speed it might require the MG to recruit a larger volume of muscle to produce sufficient force to keep walking. Also, the intrinsic properties of muscle mean that producing force at faster velocities is less efficient. Thus changes in fascicle velocities might be reflected in the metabolic cost of transport and the efficiency of muscular work.

We aimed to test how MG fascicle dynamics varied with locomotor speed and gait. We hypothesised that fascicle velocity would increase with walking

speed, impairing force production. Also, fascicle velocity would not change across running speeds.

## METHODS

Ten participants (six male, four female) walked at four speeds (0.75, 1.25, 1.75, 2.0 m·s<sup>-1</sup>) and ran at four speeds (2.0, 2.25, 2.75, 3.25 m·s<sup>-1</sup>) on a split-belt treadmill instrumented with bilateral force platforms embedded under the belts (BERTEC, USA). Kinematic data were recorded for the right leg and pelvis using an eight camera motion analysis system (VICON, UK; 120 Hz) and a modified Helen Hayes marker set. Ground reaction forces (980 Hz) and kinematic data were combined in an inverse dynamics analysis of the right leg (symmetry was assumed between legs).

MG fascicle length and pennation angle during walking and running were measured on ultrasound images (50 Hz) taken by a linear transducer (TELEMED, Lithuania) taped over the midbelly of the MG. The length of the whole MG muscle-tendon unit (MTU) was determined from kinematics and SEE length was MTU length minus fascicle length (corrected for pennation angle). Lengths were differentiated to obtain velocities. MG fascicle force was calculated first by dividing the ankle moment by the Achilles tendon moment arm and then multiplying this force by the relative cross sectional area of MG within the triceps surae (this was considered the force in the SEE). This force was then corrected for pennation angle to give fascicle force. Multiplying fascicle and SEE forces with their respective velocities gave fascicle and SEE power which was integrated to estimate fascicle work and SEE energy stored and returned.

Metabolic energy consumption at each speed was determined by indirect calorimetry and cost of transport was calculated. Efficiency of positive work was calculated as average positive mechanical power divided by net metabolic power.

## RESULTS & DISCUSSION

The average positive power output of the MG MTU did not change with walking speed but was significantly greater after switching to running gait (Fig 1). This increase in power output was not due to any change in average fascicle power which did not change with speed or gait (Fig 1). It was actually due to increased storage and return of energy in the SEE which was significantly greater during running but did not change with speed within gait (Fig 1).

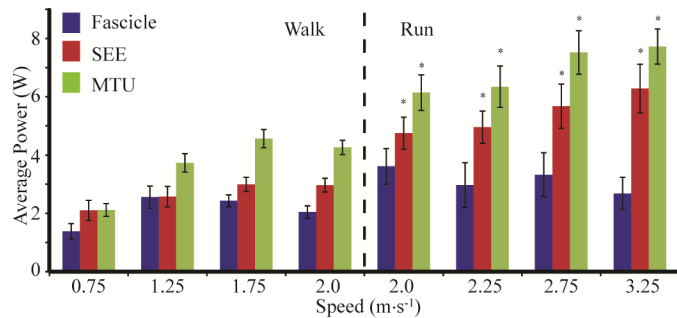


**Fig 1.** Average positive power output of the fascicle, SEE and MTU of MG vs. speed

An increase in storage and return of energy in the tendon implies greater forces being applied to it and this was the case as peak fascicle force ( $F_{MGmax}$ ) increased for all running conditions compared with walking at  $2.0 \text{ m}\cdot\text{s}^{-1}$  (Fig 2). This increase in force coincided with a significant decrease in fascicle velocity at the time of peak force ( $V_{MGmax}$ ) (Fig 2).  $F_{MGmax}$  declined significantly with increasing walking speed and  $V_{MGmax}$  increased significantly as walking speed increased from  $1.25$  to  $2.0 \text{ m}\cdot\text{s}^{-1}$  (Fig 2).

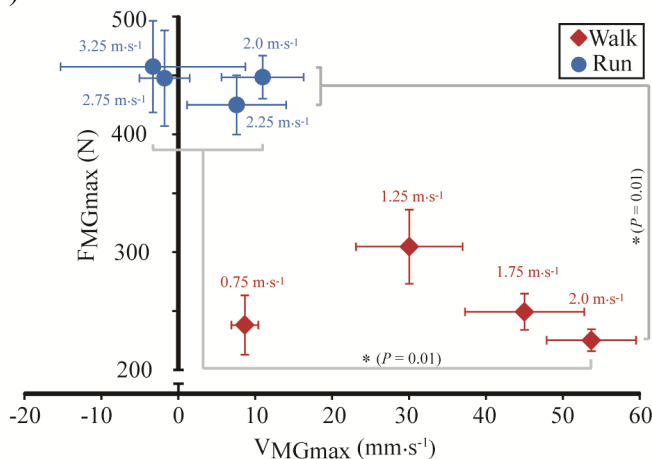


**Fig 2.** Peak MG fascicle force vs. Fascicle velocity at the time of peak MG force

The trends in  $V_{MGmax}$  were mirrored in the efficiency of positive work with higher efficiencies occurring at walking speeds where  $V_{MGmax}$  was less (except for at  $0.75 \text{ m}\cdot\text{s}^{-1}$ ). Efficiency of positive work increased and  $V_{MGmax}$  decreased after switching to running. However linking the two is difficult as there was no data for other muscles.

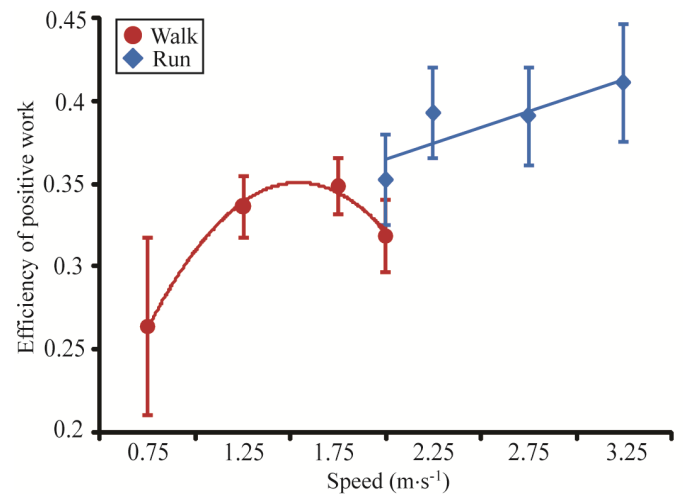


**Fig 3.** The efficiency of positive work vs. walking and running speed

## CONCLUSION

Transitioning from walking to running shifts MG fascicles to a more favourable part of the force-velocity relationship. If other muscles behave similarly this might help to explain trends in efficiency and cost of transport.

## REFERENCES

- [1] Neptune RR et al., *Gait Posture*, **28**(1):135-43 (2008)
- [2] Prilutsky BI et al., *J Exp Biol*, **199**(4):801-14 (1996)
- [3] McGowan CP et al., *J Appl Physiol*, **101**(4):1060-69 (2006)
- [4] Neptune RR & Sasaki K, *J Exp Biol*, **208**(5):799-808 (2005)

## ACKNOWLEDGEMENTS

Dr Michael Lewek (UNC-Chapel Hill) & Phil Matta (NC State University)

# THE MECHANICS & ENERGETICS OF HUMAN WALKING & RUNNING: A JOINT LEVEL PERSPECTIVE

<sup>1</sup>Dominic J Farris & <sup>1</sup>Gregory S Sawicki

<sup>1</sup>Joint Dept. of Biomedical Engineering, North Carolina State University & UNC-Chapel Hill, NC, USA  
email: [djfarris@ncsu.edu](mailto:djfarris@ncsu.edu)

## INTRODUCTION

The links between the metabolic and mechanical demands of human locomotion have been studied extensively. Attempts to explain trends in the metabolic cost of transport (COT) based on the overall positive mechanical work done and the time available for generation of forces applied to the ground have most recently concluded that both factors are similarly important determinants of the COT [1]. However, much of the work contributing to this conclusion calculated positive mechanical work as the energy required to raise and accelerate the body's centre of mass (COM) and limbs. This approach exhibits considerable redundancy as this work is the net result of work done by each of the lower limbs which is, in turn, the net result of work done at individual joints.

Joint level data would reveal how power production is distributed among joints and how this distribution varies with speed and gait. In tasks such as incline running (where net positive work is done), power output is redistributed and a greater contribution to total power output is apparent at the hip [2]. This also occurs when switching from running to sprinting [3]. Steady speed locomotion never requires net work but moving faster involves greater positive work per stride. This may require redistribution of power output among joints.

Muscle groups acting at proximal joints within the leg typically have long fascicles with short tendons and small pennation angles. This may make them less efficient than their distal counterparts that are able to recycle energy in compliant tendons and contract with slow fascicle velocities. Thus, if power output shifts proximally (i.e. to the hip) this might affect the overall efficiency of positive work and might contribute to changes in metabolic COT with speed and gait.

Our study aimed to test the hypothesis that changes in overall mechanical power with locomotion speed would primarily be modulated through adjusting hip power output. We also hypothesised that increasing the hip joint contribution to power output would decrease the efficiency of total positive work.

## METHODS

Ten participants (six male, four female) walked at four speeds (0.75, 1.25, 1.75, 2.0 m·s<sup>-1</sup>) and ran at four speeds (2.0, 2.25, 2.75, 3.25 m·s<sup>-1</sup>) on a split-belt treadmill instrumented with bilateral force platforms embedded under the belts (BERTEC, USA). Kinematic data were recorded for the right leg and pelvis using an eight camera motion analysis system (VICON, UK; 120 Hz) and a modified Helen Hayes marker set. Ground reaction forces (980 Hz) and kinematic data were combined in an inverse dynamics analysis to calculate ankle, knee and hip average power outputs. Individual joint powers were summed to calculate total mechanical power and each joint's percentage contribution to the total was determined. Participants walked or ran for seven minutes at each speed, during which time their oxygen consumption was measured using a portable metabolic system (OXYCON MOBILE, GERMANY) so as to calculate their rate of metabolic energy consumption and COT. Efficiency of positive work was calculated as the ratio of total average mechanical power to metabolic power.

## RESULTS

Individual joint average power as a percentage of total average mechanical power did not change as a function speed for walking or running (Fig 1). Walking at 2.0 m·s<sup>-1</sup> utilised a significantly ( $P=0.02$ , repeated measures ANOVA) greater percentage contribution from hip joint power and lesser contribution from ankle joint power to total

mechanical power than running at the same speed (Fig 1).

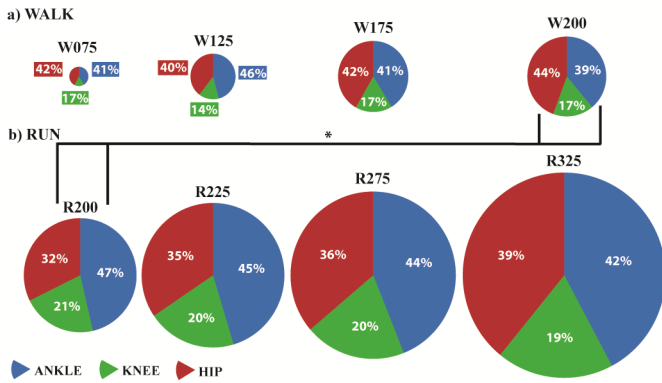


**Fig 1.** Pie charts showing the percentage of total average positive power contributed at the hip (red), knee (green) and ankle (blue) joints. The total area of each pie represents the total average positive power relative to the other conditions. \*Indicates a significant difference ( $P = 0.02$ , repeated measures ANOVA) in ankle and knee joint contributions.

COT was minimised for walking at  $1.25 \text{ m}\cdot\text{s}^{-1}$  and then increased with walking speed, but remained relatively constant across running speeds (Fig 2). Efficiency of positive work decreased at faster walking speeds but increased again after switching to running gait at speeds above  $2.0 \text{ m}\cdot\text{s}^{-1}$  (Fig 2).

## DISCUSSION

The increase in total average positive mechanical power that occurred with speed was achieved by systematically increasing power output at the hip, knee and ankle joints for both walking and running. Thus, the proportional contributions from each joint did not change with speed but, these did change when switching from walking to running gait, with a significant shift in the distribution from the hip to the ankle joint (Fig 1). Interestingly, this redistribution of power output coincided with a change in the trend for efficiency of positive work. Efficiency was decreasing at faster walking speeds but after switching to running at  $2.0 \text{ m}\cdot\text{s}^{-1}$  began to increase again (Fig 2). Therefore, as hypothesised a change in the distribution favouring the use of distal joints over the hip may be linked to increased efficiency. Actually,  $2.0 \text{ m}\cdot\text{s}^{-1}$  is approximately the preferred walk to run transition speed for humans and therefore we propose that switching to running may be a strategy to maximize efficiency of locomotion by utilizing distal muscle groups more than proximal. Such a theory is dependent on the assumption that more distal muscle groups generate positive power more efficiently than proximal muscles. It also assumes that increases in distal joint power outputs represent increased power output of distal muscle groups and not increased transfer of power from proximal groups via biarticular muscles. Therefore, direct measurements of in-vivo muscle fascicle and series elastic component behavior are required to support this hypothesis. This is now possible with ultrasound imaging techniques.

## REFERENCES

- [1] Grabowski, AM. *Arch Phys Med Rehab*, **91**(6): 951-57. 2010.
- [2] Roberts, TJ & Belliveau, RA. *J Exp Biol*, **208** (10): 1963-70. 2005
- [3] Novacheck, TF *Gait Posture*, **7**(1): 77-95. 1998

## ACKNOWLEDGEMENTS

Dr Michael Lewek (UNC-Chapel Hill) & Phil Matta (NC State University)

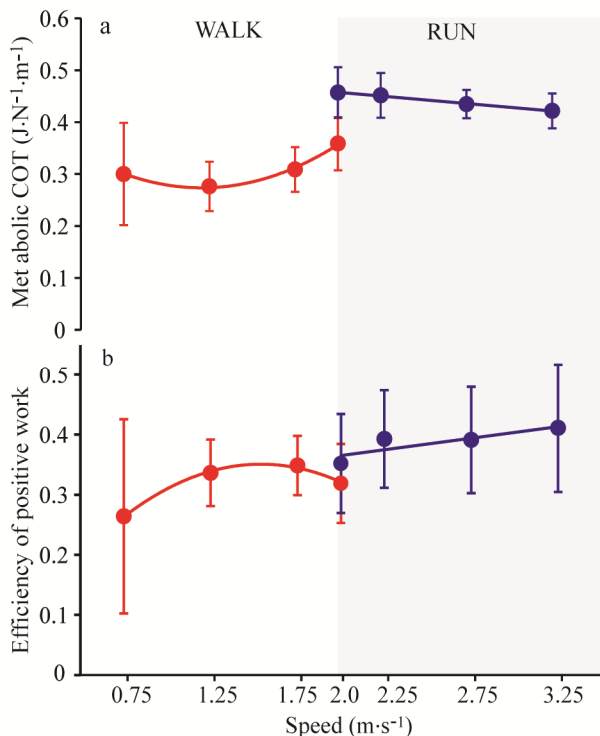


**Fig 2.** COT (a) and efficiency of positive work (b) at all walking (red) and running (blue) speeds.

# EVALUATION OF THE BIOMIMETIC PROPERTIES OF A NEW POWERED ANKLE-FOOT PROSTHETIC SYSTEM

Abbie E. Ferris, MS; Jennifer E. Aldridge, MS; Jordan T. Sturdy, BS; Jason M. Wilken, PhD MPT  
Department of Orthopedics and Rehabilitation, Center for the Intrepid, Brooke Army Medical Center  
Fort Sam Houston, TX, USA

E-mail: [Abbie.E.Ferris.ctr@us.army.mil](mailto:Abbie.E.Ferris.ctr@us.army.mil)

## INTRODUCTION

Following transtibial amputation (TTA) individuals demonstrate gait deviations due to the inability of currently available prosthetic devices to effectively mimic the function of an unimpaired ankle. Deviations include decreased walking velocity and asymmetries in stride length, step length, swing time, and increased stance time [1-3].

Active persons with TTA commonly use energy storing and returning (ESR) prosthetic feet which exhibit significantly reduced ankle motion and provide roughly 50% of peak power generated by an unimpaired ankle. To address the limitations of ESR feet, microprocessor controlled devices which replicate normal motion and power production are in development [4]. The PowerFoot BiOM (iWalk) is the first of these devices to become commercially available. The purpose of the present investigation was to determine if the BiOM more effectively mimics ankle joint motion and power of an unimpaired and the intact ankle during overground walking compared to ESR. We hypothesized the addition of power would aid in restoration in more normal gait characteristics.

## METHODS

Eleven young healthy individuals with TTA underwent biomechanical gait assessment while walking over level ground at a controlled speed using an ESR foot and again with the BiOM. Kinematic data were captured using an optoelectronic motion capture system (Motion Analysis Corp., Santa Rosa, CA) and ground reaction forces were collected using five force plates (AMTI, Inc., Watertown, MA) imbedded in the floor. Weight and height matched control subjects were also assessed. Kinematic and kinetic data were used to calculate ankle angle and joint power using an inverse dynamics approach. Walking speed was controlled and standardized across subjects based on leg length [5]. Feedback

was provided using an auditory cue to ensure the target speed was maintained. A repeated measures 2X2 (condition x limb) ANOVA was used to identify changes between limbs and between devices. A one way ANOVA was used to identify differences between prosthetic devices (ESR and BiOM), intact limbs, and control subjects. Significance was set at the  $P=0.05$  level.

## RESULTS AND DISCUSSION

### *Temporal-Spatial*

An increased swing time (Table 1) was observed in the ESR limb compared to the intact limb ( $P=0.001$ ) and BiOM ( $P=0.004$ ). Further, the ESR limb took shorter steps than the BiOM ( $P=0.001$ ) where the BiOM took longer steps than the intact limb ( $P=0.001$ ). ESR step time was longer than the intact limb ( $P=0.036$ ) and the BiOM ( $P=0.004$ ). Use of the BiOM resulted in temporal-spatial parameters that more closely approximated those of uninjured individuals.

### *Ankle Angle*

Peak ankle dorsiflexion (DF) during mid stance was significantly higher in ESR ( $P=0.004$ ) compared to BiOM (Figure 1). ESR devices return to neutral as it unloads, resulting in significantly reduced plantarflexion (PF) during push-off ( $4.96^{\circ}\pm 2.90^{\circ}$  DF). This resulted in large PF differences between the ESR and control ( $13.79^{\circ}\pm 3.92^{\circ}$  PF,  $P=0.001$ ), BiOM ( $9.75^{\circ}\pm 2.59^{\circ}$  PF;  $P=0.001$ ) and intact limb ( $16.77^{\circ}\pm 5.31^{\circ}$  PF;  $P=0.006$ ). Although the BiOM was able to PF, its maximum PF angle was still smaller than the intact limb ( $P=0.001$ ).

While ankle range of motion (ROM) with the BiOM was larger than ESR ( $P=0.013$ ), ROM was significantly lower with the ESR ( $17.68^{\circ}\pm 3.74^{\circ}$ ,  $P=0.001$ ) and BiOM ( $22.56^{\circ}\pm 3.89^{\circ}$ ,  $P=0.022$ ) as compared to control subjects ( $28.17^{\circ}\pm 3.27^{\circ}$ ) and intact limb.

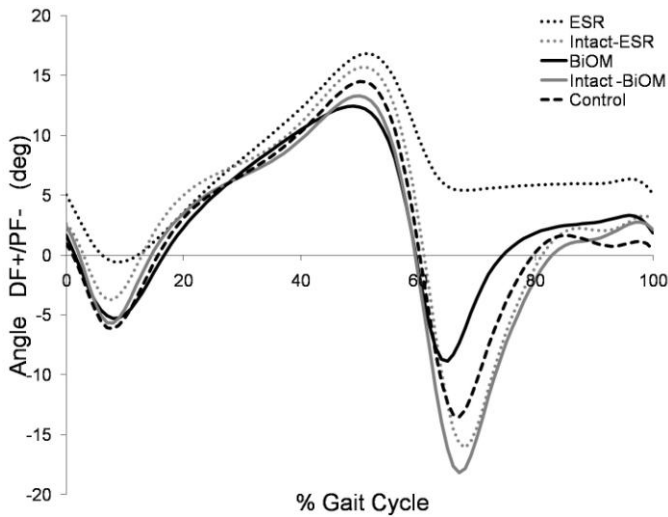


**Figure 1:** Sagittal ankle angle during walking.

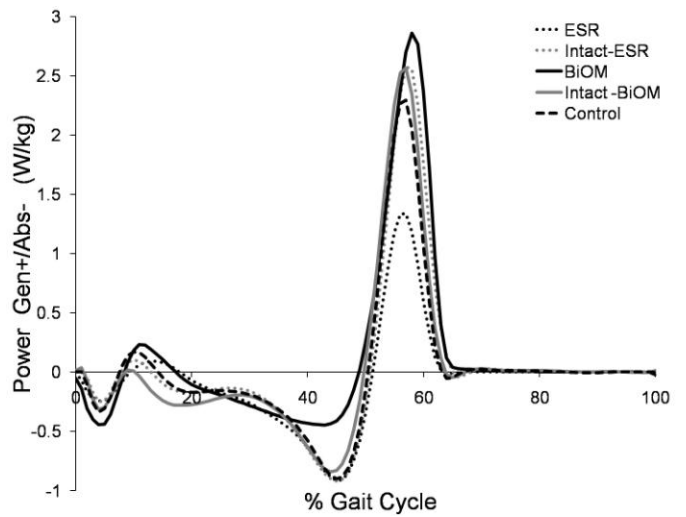


**Figure 2:** Ankle joint power during walking.

### Ankle Power

As seen in previous studies, ESR peak power absorption was similar to intact and control limbs (Figure 2). However, peak absorption at terminal stance was significantly lower in the BiOM than the ESR ( $P < 0.001$ ), intact limb ( $P = 0.025$ ) and controls ( $P = 0.028$ ). At push-off, the ESR behaved as expected, producing 53% and 60% less peak power than the intact and control limbs respectively. However, the BiOM produced 224% more peak power than the ESR and 135% more than the control. No significant differences were seen between the BiOM and intact limb.

### CONCLUSIONS

The PowerFoot BiOM is better able to replicate unimpaired ankle function than conventional ESR feet by providing increased ankle motion and peak power. Patients also stated their preference for the higher power levels provided by the BiOM. Restoring normal ankle motion and peak plantar flexion power may alleviate comorbidities associated with TTA such as lower back pain and contralateral lateral

knee osteoarthritis. Efforts are underway to determine the effect of the increased motion and power on the proximal joints of the involved and uninvolved limbs.

### REFERENCES

1. Barth DG et al., *J Prosthetics Orthotics* **4**, 1992.
2. Sadeghi H et al., *Am.J.Phys.Med.Rehabil.* **80**, 2001.
3. Isakov E et al., *Scand. J. Rehabil. Med.* **29**, 1997.
4. Au S et al., *Neural Netw* **21**, 2008.
5. McAndrew PM et al., *J. Biomech.* **43**, 2010.

### ACKNOWLEDGEMENTS

Support provided by the U.S. Army Telemedicine & Advanced Technology Research Center (JMW).

The view(s) expressed herein are those of the author(s) and do not reflect the official policy or position of Brooke Army Medical Center, the U.S. Army Medical Department, the U.S. Army Office of the Surgeon General, the Department of the Army, Department of Defense or the U.S. Government.

**Table 1:** Temporal-spatial data (mean± standard deviation) for controls and TTA at controlled walking velocity.

| Temporal-spatial Variables |                 |                |                 |               |                  |
|----------------------------|-----------------|----------------|-----------------|---------------|------------------|
| Limb                       | Stance Time (s) | Swing Time (s) | Step Length (m) | Step Time (s) | Stride Length(m) |
| Control                    | 0.74±0.06       | 0.44±0.03      | 0.73±0.06       | 0.59±0.04     | 1.45±0.10        |
| ESR                        | 0.73±0.02       | 0.46±0.02      | 0.71±0.05       | 0.60±0.02     | 1.45±0.10        |
| ESR-Intact                 | 0.75±0.05       | 0.42±0.03†     | 0.73±0.07       | 0.57±0.04†    | 1.43±0.13        |
| BiOM                       | 0.74±0.03       | 0.43±0.03†     | 0.76±0.03†      | 0.58±0.02†    | 1.47±0.07        |
| BiOM-Intact                | 0.74±0.03       | 0.43±0.03      | 0.70±0.05*      | 0.59±0.03     | 1.47±0.07        |

\*Denotes significant difference from BiOM ( $P < 0.05$ ); † Denotes significant difference from ESR ( $P < 0.05$ ).

# RESPONSE OF BELOW-KNEE AMPUTEE MUSCLE ACTIVITY TO CHANGES IN ENERGY STORAGE AND RETURN FOOT STIFFNESS USING ADDITIVE MANUFACTURING

<sup>1</sup>Nicholas P. Fey, <sup>2</sup>Glenn K. Klute and <sup>1</sup>Richard R. Neptune

<sup>1</sup>Department of Mechanical Engineering, The University of Texas at Austin, Austin, TX, USA

<sup>2</sup>Department of Veterans Affairs, Puget Sound Health Care System, Seattle, WA, USA

email: [nfey@mail.utexas.edu](mailto:nfey@mail.utexas.edu) web: <http://www.me.utexas.edu/~neptune>

## INTRODUCTION

Unilateral below-knee amputations often lead to differences in walking characteristics that include bilateral asymmetries, altered muscle activity and higher metabolic cost relative to non-amputees. Many differences in these walking characteristics are attributed to the absence of the ankle muscles, which provide needed body support, forward propulsion and swing initiation during non-amputee walking [1].

To improve amputee walking ability, proper prosthetic foot design and prescription is critical. Carbon fiber energy storage and return (ESAR) feet store and release elastic energy during stance in an attempt to restore some functions of the amputated limb. However, the appropriate ESAR stiffness governing energy storage and release for a given amputee is not evidence-based. Clinicians primarily base prosthetic prescription on a patient's body weight, activity level, and clinical experience rather than objective biomechanical data. Studies are needed to systematically vary foot stiffness to assess its influence on gait characteristics.

One challenge to such studies is the difficulty in creating ESAR feet of varying stiffness levels using traditional manufacturing techniques. One solution to overcome this difficulty is to use an additive manufacturing technology such as selective laser sintering (SLS). We recently developed a SLS-based framework to fabricate ESAR feet that replicated the geometry and dynamic response of a commercially available carbon fiber foot [2]. The purpose of this study was to use this framework to manufacture ESAR feet with a range of stiffness levels to identify the influence of ESAR foot stiffness on lower-limb muscle activity during overground walking.

## METHODS

Three SLS feet were manufactured from Rilsan<sup>TM</sup> D80 (Nylon 11 powder, Arkema, Inc.) using a Vanguard HiQ Sinterstation (3D Systems, Inc.). One closely matched the nominal stiffness of a widely prescribed carbon fiber foot (Highlander<sup>TM</sup>, FS 3000, Freedom Innovations, LLC), one was 50% more stiff, and one was 50% more compliant (Fig. 1). These feet were mechanically tested and later used in the overground walking trials of amputees.



**Figure 1:** ESAR prosthetic feet fabricated using SLS additive manufacturing technology.

Twelve unilateral below-knee amputees (10 traumatic, 2 secondary illness;  $52 \pm 17$  years) walked overground along a 10-meter walkway at  $1.2 \pm 0.06$  m/s with the three different prosthetic feet in a randomized order. A certified prosthetist ensured proper alignment, and subjects were allowed sufficient time to feel comfortable with each foot. Repeated trials were collected at each condition until at least five gait cycles per leg were measured.

Electromyographic (EMG) data were collected at 2160 Hz using surface EMG electrodes (TeleMyo 900, Noraxon U.S.A., Inc.) from eight intact leg muscles and five residual leg muscles. Raw EMG signals were demeaned and then smoothed using a moving 80-ms root-mean-square window. The smoothed data from each gait cycle were time-normalized to represent 100% of the gait cycle. The data for each gait cycle were then integrated within

specific regions of the gait cycle that corresponded to the loading response and mid-stance (0-30% gait cycle), terminal stance and pre-swing (30-60% gait cycle), swing (60-100% gait cycle) in addition to over the entire gait cycle (0-100% gait cycle). These integrated EMG (iEMG) quantities were averaged at each condition and then normalized for each subject by the 0-100% gait cycle iEMG magnitude from the nominal stiffness condition. The iEMG quantities over each phase of the gait cycle were compared across stiffness conditions for each muscle using repeated-measure analysis of variance (ANOVA). For significant main or interaction effects, pairwise comparisons were evaluated using a Bonferroni adjustment for multiple comparisons to determine statistical significance ( $\alpha=0.05$ ).

## RESULTS AND DISCUSSION

From 0-30% of the respective gait cycle, changes in muscle activity were observed in the residual leg gluteus medius (GMED) (compliant to stiff,  $p=0.003$ ) and intact leg vastus medialis (VAS) (compliant to nominal,  $p=0.015$ ) and rectus femoris (RF) (compliant to nominal,  $p=0.026$ ), which all increased activity as prosthetic stiffness decreased (Fig. 2). From 30-60% of the respective gait cycle, changes in muscle activity were observed in the residual leg GMED (compliant to nominal,  $p=0.037$ ; compliant to stiff,  $p=0.007$ ) and VAS (compliant to nominal,  $p=0.030$ ), which increased activity as prosthetic stiffness decreased (Fig. 2). Also from 30-60% of the respective gait cycle, biceps femoris long head (BF) excitation decreased as stiffness decreased (compliant to stiff,  $p=0.016$ ). No differences in muscle activity were found during the swing phase.

The increased activities of residual leg GMED throughout stance and residual leg VAS during the second half of stance as stiffness decreased were consistent with their functional roles to provide needed body support [e.g., 3]. Similarly, during late stance of the residual leg (early stance of the intact leg), the increased activities of the intact leg knee extensors (VAS and RF) were also consistent with their roles to provide body support [e.g., 3]. Thus, as less support was provided by the prosthetic feet as stiffness decreased, these muscles appeared to compensate by increasing their activity. Previously, increased residual leg VAS activity during the first half of stance had been observed in below-knee

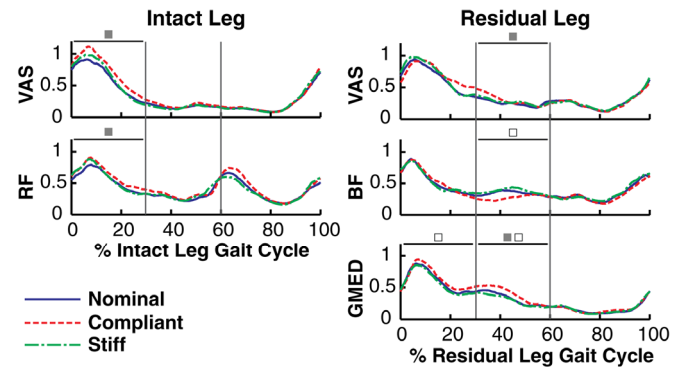


**Figure 2:** Group average smoothed EMG data. In each region (0-30%, 30-60% and 60-100% gait cycle), significant iEMG differences between nominal and compliant (■) and between compliant and stiff (□) conditions are indicated.

amputee walking using clinically prescribed prostheses [e.g., 4]. Our results suggest that decreased prosthetic stiffness prolongs this compensatory mechanism into the second half of residual leg stance.

The energy stored in ESAR feet is primarily returned in late stance of the residual leg, which mimics the function of the ankle plantar flexors during non-amputee walking to deliver energy to the trunk for forward propulsion [1]. Since BF contributes to propulsion throughout stance in non-amputee walking [e.g., 3], the reduced activity of this muscle in the compliant condition suggests that the compliant prosthetic foot is providing increased propulsion during the second half of stance.

## CONCLUSIONS

A tradeoff in prosthetic foot design appears to exist between providing greater body support with increased stiffness and providing increased forward propulsion with decreased stiffness.

## REFERENCES

1. Neptune RR, et al. *J Biomech* **34**(11), 1387-98, 2001.
2. South BJ, et al. *J Biomech Eng* **132**(1), 015001(1-6), 2010.
3. Liu MQ, et al. *J Biomech* **39**(14), 2623-30, 2006.
4. Powers CM, et al. *Gait & Posture* **8**(1), 1-7, 1998.

## ACKNOWLEDGEMENTS

This work was supported by the NSF grant 0346514 and VA grant 1 I01 RX000311.

# CHANGES TO ENERGY STORAGE AND RETURN FOOT STIFFNESS ALTER THE WALKING MECHANICS OF BELOW-KNEE AMPUTEES

<sup>1</sup>Nicholas P. Fey, <sup>2</sup>Glenn K. Klute and <sup>1</sup>Richard R. Neptune

<sup>1</sup>Department of Mechanical Engineering, The University of Texas at Austin, Austin, TX, USA

<sup>2</sup>Department of Veterans Affairs, Puget Sound Health Care System, Seattle, WA, USA

email: [nfey@mail.utexas.edu](mailto:nfey@mail.utexas.edu); web: <http://www.me.utexas.edu/~neptune>

## INTRODUCTION

Unilateral below-knee amputees often develop asymmetrical gait patterns and comorbidities in their intact and residual legs, which is attributed to the loss of the ankle muscles that provide essential biomechanical functions such as body support and forward propulsion during walking [1]. The development and prescription of effective prosthetic devices are needed to improve amputee rehabilitation. Energy storage and return (ESAR) feet have been designed to absorb and release elastic energy in an attempt to restore some functions of the amputated limb. However, selection of the appropriate ESAR stiffness level for a given amputee is a challenge since the influence of foot stiffness on amputee gait remains unclear. Understanding how foot stiffness influences amputee gait mechanics is needed to develop evidence-based rationale for prosthetic foot prescription to improve amputee care.

The purpose of this study was to use additive manufacturing, specifically selective laser sintering (SLS) [2], to manufacture ESAR feet with a range of stiffness levels and identify their influence on overground walking mechanics in below-knee amputees. In addition, we analyzed how changes in stiffness influence prosthetic foot energy stored, returned and mechanical efficiency during walking.

## METHODS

Three SLS prosthetic feet were manufactured from Rilsan<sup>TM</sup> D80 (Nylon 11, Arkema, Inc.) using a Vanguard HiQ Sinterstation (3D Systems, Inc.). One foot closely matched the stiffness level of a commonly prescribed carbon fiber foot (Highlander<sup>TM</sup>, FS 3000, Freedom Innovations, LLC), while one foot was 50% more stiff and the

other was 50% more compliant.

Prosthetic foot order was randomized as 12 unilateral below-knee amputees (10 traumatic, 2 secondary illness;  $52 \pm 17$  years) walked overground at  $1.2 \pm 0.06$  m/s along a 10-meter walkway. Kinematic data were measured using a motion capture system (Vicon Nexus, Oxford Metrics, Inc.) and ground reaction force (GRF) data were measured using four embedded force plates (Advanced Mechanical Technology, Inc. and Bertec Corporation). Repeated trials were collected for each foot condition until at least five gait cycles per leg were measured.

Inverse dynamics was performed to calculate net intersegmental joint moments using Visual3D (C-Motion, Inc.). Kinematic and GRF data were low-pass filtered. GRFs and joint moments were normalized by body weight and body mass, respectively. Prosthetic foot energy storage and return characteristics were estimated by evaluating the negative ankle power (energy stored) and positive ankle power (energy returned) (J/kg) time integrals during stance of the residual leg, respectively. Efficiency was calculated as the ratio of energy returned divided by the energy stored. Across stiffness levels, peak GRFs, sagittal-plane joint angles and intersegment moments, and prosthetic energy quantities were compared using repeated-measure analysis of variance (ANOVA). For significant main or interaction effects, pairwise comparisons were evaluated using a Bonferroni adjustment for multiple comparisons to determine statistical significance ( $\alpha=0.05$ ).

## RESULTS AND DISCUSSION

In both legs, peak braking GRFs were larger in the compliant condition (Table 1). Intact leg first

vertical (V1) GRF peak was larger in the stiff condition. Residual leg second vertical (V2) GRF peak was reduced in the compliant condition. During stance, residual leg dorsiflexion angle systematically increased as foot stiffness decreased and intact leg dorsiflexion angle was larger in the compliant condition (Table 1), consistent with a flexed posture. During swing, the residual knee flexion angle was larger in the compliant condition and may have been needed to provide toe clearance. Also, the residual leg plantarflexion moment in the compliant condition was reduced (Table 1). These results suggest decreased body support was provided as prosthetic foot stiffness decreased.

To compensate, the residual leg knee flexion moment (K2) and knee extension moment in late stance (K3) and intact leg knee extension moment in early stance (K1) and intact leg hip extension moment (H1) became more extensor (Table 1), which is consistent with their roles of providing body support [3]. But, increases in knee moments may have led to the larger braking GRFs observed in the compliant condition in both legs since knee extensor muscles have been shown to contribute to GRF braking [e.g., 4].

Energy stored and returned values increased and mechanical efficiency decreased as stiffness decreased (Fig. 1). The energy stored is primarily returned in late residual leg stance, which mimics ankle plantar flexor function to deliver energy to the trunk and leg for forward propulsion and swing initiation, respectively [1]. Thus, the contributions of the compliant feet to forward propulsion and swing initiation may be greater in comparison. However, the increased energy returned in late stance occurred as a consequence of substantially

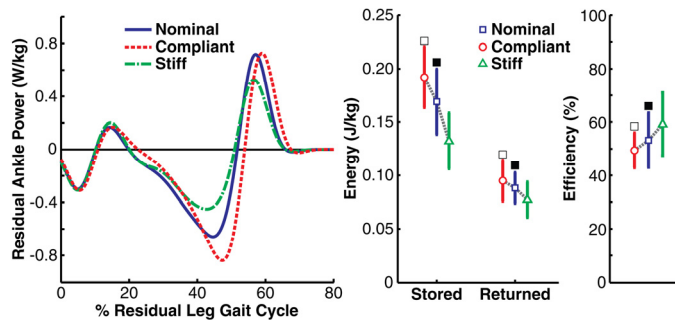


**Figure 1:** Group average residual leg ankle power and group average  $\pm$  standard deviation prosthetic energy quantities. Significant differences between compliant and stiff ( $\square$ ), and nominal and stiff ( $\blacksquare$ ) conditions are indicated.

greater energy storage (negative work) from mid to late stance and resulted in lower mechanical efficiency (Fig. 1).

## CONCLUSIONS

Decreasing ESAR stiffness may improve prosthetic contributions to forward propulsion, but requires compensation to provide necessary body support. In addition, increasing stiffness improves mechanical efficiency, but increases intact leg GRFs.

## REFERENCES

1. Neptune RR, et al. *J Biomech* **34**(11), 1387-98, 2001.
2. South BJ, et al. *J Biomech Eng* **132**(1), 015001(1-6), 2010.
3. Kepple TM, et al. *Gait & Posture* **6**(1), 1-8, 1997.
4. Liu MQ, et al. *J Biomech* **39**(14), 2623-30, 2006.

## ACKNOWLEDGEMENTS

This work was supported by the NSF grant 0346514 and VA grant 1 I01 RX000311.

**Table 1:** Group mean  $\pm$  standard deviation GRF, joint angle and moment data.

|   |                                 | Nominal                            | Compliant                          | Stiff                              |
|---|---------------------------------|------------------------------------|------------------------------------|------------------------------------|
| <b>GRFs (% Body Weight)</b>               |                                 |                                    |                                    |                                    |
| V1 $\circ$                                | Residual $\square$              | 110.3 $\pm$ 4.8                    | 112.0 $\pm$ 3.6                    | 109.7 $\pm$ 5.8                    |
|   | Intact $\blacksquare$           | <b>113.1 <math>\pm</math> 8.2</b>  | 113.0 $\pm$ 5.6                    | <b>117.4 <math>\pm</math> 8.3</b>  |
| V2 $\blacktriangle \circ$                 | Residual $\blacksquare \square$ | <b>102.1 <math>\pm</math> 5.0</b>  | <b>96.5 <math>\pm</math> 4.3</b>   | <b>103.4 <math>\pm</math> 4.6</b>  |
|   | Intact $\square$                | 105.9 $\pm$ 5.8                    | 106.2 $\pm$ 5.3                    | 107.0 $\pm$ 5.1                    |
| Braking $\blacktriangle$                  | Residual $\blacksquare \square$ | <b>-13.9 <math>\pm</math> 3.2</b>  | <b>-15.8 <math>\pm</math> 3.1</b>  | <b>-13.4 <math>\pm</math> 2.5</b>  |
|   | Intact $\blacksquare \square$   | <b>-17.3 <math>\pm</math> 2.6</b>  | <b>-19.3 <math>\pm</math> 3.1</b>  | <b>-17.3 <math>\pm</math> 2.5</b>  |
| <b>Joint Angles (<math>^\circ</math>)</b> |                                 |                                    |                                    |                                    |
| Dorsiflexion $\blacktriangle \circ$       | Residual $\blacksquare \square$ | <b>8.6 <math>\pm</math> 2.5</b>    | <b>13.1 <math>\pm</math> 2.9</b>   | <b>5.7 <math>\pm</math> 2.4</b>    |
|   | Intact $\square$                | 10.2 $\pm$ 2.3                     | <b>11.0 <math>\pm</math> 2.4</b>   | <b>9.2 <math>\pm</math> 3.0</b>    |
| Knee flexion $\blacktriangle$             | Residual $\square$              | -57.2 $\pm$ 6.4                    | <b>-58.8 <math>\pm</math> 6.2</b>  | <b>-56.7 <math>\pm</math> 5.8</b>  |
|   | Intact $\square$                | -60.3 $\pm$ 5.9                    | -60.4 $\pm$ 5.4                    | -59.5 $\pm$ 6.2                    |
| <b>Joint Moments (Nm/kg)</b>              |                                 |                                    |                                    |                                    |
| Plantarflexion $\blacktriangle \circ$     | Residual $\blacksquare \square$ | <b>-1.05 <math>\pm</math> 0.17</b> | <b>-0.85 <math>\pm</math> 0.15</b> | <b>-1.04 <math>\pm</math> 0.13</b> |
|   | Intact $\square$                | -1.32 $\pm$ 0.13                   | -1.33 $\pm$ 0.13                   | -1.34 $\pm$ 0.13                   |
| K1 $\blacktriangle \circ$                 | Residual $\square \blacksquare$ | <b>0.27 <math>\pm</math> 0.24</b>  | <b>0.24 <math>\pm</math> 0.25</b>  | <b>0.33 <math>\pm</math> 0.24</b>  |
|   | Intact $\blacksquare$           | <b>0.44 <math>\pm</math> 0.17</b>  | <b>0.56 <math>\pm</math> 0.19</b>  | 0.48 $\pm$ 0.17                    |
| K2 $\blacktriangle \circ$                 | Residual $\blacksquare \square$ | <b>-0.10 <math>\pm</math> 0.15</b> | <b>0.05 <math>\pm</math> 0.15</b>  | <b>-0.14 <math>\pm</math> 0.16</b> |
|   | Intact $\square$                | -0.20 $\pm$ 0.15                   | <b>-0.16 <math>\pm</math> 0.17</b> | <b>-0.21 <math>\pm</math> 0.14</b> |
| K3 $\blacktriangle \circ$                 | Residual $\blacksquare \square$ | <b>0.28 <math>\pm</math> 0.10</b>  | <b>0.34 <math>\pm</math> 0.12</b>  | <b>0.27 <math>\pm</math> 0.11</b>  |
|   | Intact $\square$                | 0.28 $\pm$ 0.09                    | 0.30 $\pm$ 0.11                    | 0.29 $\pm$ 0.09                    |
| H1 $\blacktriangle$                       | Residual $\square$              | -0.67 $\pm$ 0.18                   | -0.68 $\pm$ 0.21                   | -0.65 $\pm$ 0.18                   |
|   | Intact $\square$                | -0.58 $\pm$ 0.19                   | <b>-0.60 <math>\pm</math> 0.20</b> | <b>-0.54 <math>\pm</math> 0.19</b> |

$\blacktriangle$  significant prosthetic main effect

$\circ$  significant leg\*prosthetic interaction effect

$\blacksquare$  significant nominal to compliant pairwise comparison

$\square$  significant compliant to stiff pairwise comparison

$\blacksquare$  significant nominal to stiff pairwise comparison

# REACHING KINEMATICS OF THE “LESS AFFECTED” UPPER EXTREMITY IN INDIVIDUALS WITH CHRONIC STROKE AND HEALTHY CONTROLS

<sup>1</sup>Margaret Finley, <sup>1</sup>Stephanie Combs, <sup>1</sup>Kristen Carnahan, <sup>1</sup>Sarah Peacock and <sup>1</sup>Ashley Van Buskirk

<sup>1</sup>Krannert School of Physical Therapy, University of Indianapolis, Indianapolis, IN, USA  
email: [finleym@uindy.edu](mailto:finleym@uindy.edu) web: <http://pt.uindy.edu>

## INTRODUCTION

Over 780,000 persons in the United States have a new or recurrent stroke each year.[1] Despite therapeutic efforts, as many as 80% of persons with stroke continue to have residual deficits, particularly within the paretic, affected limbs. Studies have suggested the possibility that in individuals with stroke the upper extremity ipsilateral to the lesion may exhibit deficits, although it has been traditionally considered to be “unaffected”.[2] While reaching movement kinematics have been shown to be different between the affected and unaffected limbs in persons with chronic stroke, greater impairment in the paretic limb was related to altered movement patterns in the unaffected limb.[3] Additionally, greater deficits in movement patterns of the unaffected limb have been reported in individuals with left hemispheric damage.[4] The purpose of this preliminary study was to a) compare reaching kinematics of the “less affected” limb, stratified by side of hemispheric lesion, in persons with chronic stroke and to b) compare reaching kinematics stratified by side of hemispheric lesion to a group of matched, individuals without stroke.

## METHODS

Fifteen individuals with upper extremity impairment from chronic stroke (right hemispheric lesion= 8, left hemispheric lesion = 7) and seven individuals without stroke participated. (Table 1) All participants were right hand dominant. Following informed consent, the upper extremity section of the Fugl-Meyer Motor Assessment (FM-UE) was performed to clinically document level of impairment in the paretic limb in the participants with stroke. While seated with the trunk restrained, participants performed three repetitions of unilateral reaching to targets, level with the top of a table, located ipsilateral and contralateral to the limb. Participants were instructed to reach to the target at a self-selected, comfortable speed as well as a

condition of reaching to the targets as fast as possible. Order of target location, reaching limb and speed condition were randomly presented.

Three-dimensional kinematic data of upper extremities and trunk were collected (MotionMonitor™ Minibirds, 100Hz) during the reaching tasks. International Society of Biomechanics International Shoulder Group recommendations for definition of global and local coordinate systems as well as Euler rotation sequences for segmental and joint motions were followed.[5] Data were exported and processed with custom routines in Excel™ with movement initiation defined as the time when tangential velocity exceeded 5% of maximal velocity and end of movement defined when the velocity dropped below this 5% threshold. Scapulohumeral, trunk and elbow kinematics as well as mean speed, peak speed, smoothness metric (mean speed/peak speed)[4] and movement duration were calculated.

Pearson correlations ( $r$ ,  $p \leq 0.05$ ) determined if relationships existed between the FM-UE and the movement kinematics of the “less affected” limb during ipsilateral and contralateral reaching. Independent t- tests ( $p \leq 0.05$ ) compared right vs. left sided hemispheric lesion groups as well the control group left extremity with left hemispheric lesion group and control group right extremity with right hemispheric lesions for ipsilateral and contralateral reaching during each speed condition. Given the small sample, Cohen's  $d$  was calculated to determine the strength of the comparative relationships with effect size defined as small ( $d \geq 0.2$ ), medium ( $d \geq 0.5$ ) or large ( $d \geq 0.8$ ).

## RESULTS AND DISCUSSION

A moderate inverse relationship ( $r = -0.479$ ,  $p = 0.071$ ) was found between the FM-UE and movement smoothness across the fifteen

participants with impairment from stroke. When compared to controls, the left lesion group had significantly greater ( $p=0.001$ ) shoulder flexion for the contralateral fast speed condition. Overall, shoulder flexion was increased, with large effect sizes, in all four reaching conditions in the left hemispheric lesion group. Medium to large effect sizes were found in both reaching directions at self selected speed with the left hemispheric lesion group demonstrating reduced smoothness, increased shoulder flexion and reduced elbow extension compared with the control group.

Decreased peak velocity ( $p=0.041$ ) of the right lesion group was found in the ipsilateral self selected reaching condition compared with the controls. Additionally, with large effect sizes, this condition revealed the right lesion group to have reduced mean speed, smoothness, movement duration with increased shoulder flexion. The greater shoulder flexion angle with large effect size was demonstrated in the right lesion in all four reaching conditions.

When comparing right vs. left lesion groups, significantly greater smoothness ( $p=0.039$ ) was found in the right hemispheric lesion group compared with left in fast speed ipsilateral reaching condition. Although not statistically different, the right hemispheric lesion group consistently had lower peak speed with greater movement smoothness with medium to large effect sizes

demonstrated across both ipsilateral speed conditions and the contralateral self-selected speed condition. Figure 1.

### CONCLUSIONS

The preliminary findings of this study reveal that differences do exist in reaching kinematics of the “less affected” limb in individuals with chronic stroke as compared with individuals without stroke. Overall, the group with stroke demonstrated reduced movement smoothness with a movement strategy of increased shoulder flexion when reaching to designated targets, regardless of movement speed or hemispheric lesion. In agreement with previous literature[4] the “less affected” extremity of persons with a right side hemisphere stroke demonstrated improved movement smoothness compared with left hemispheric lesions.

### REFERENCES

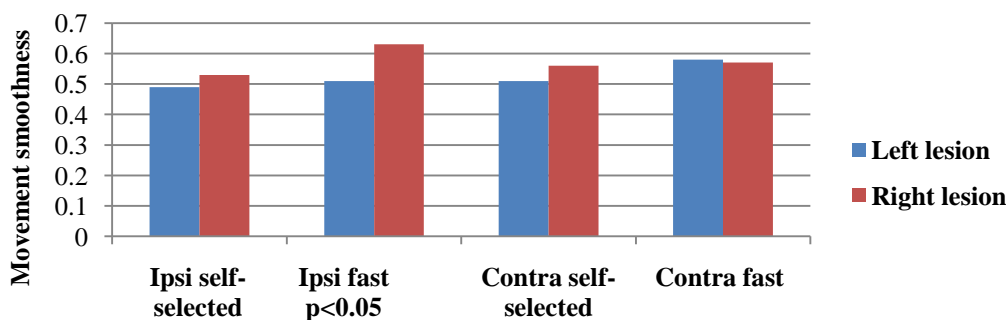
1. Rosamond W, et al *Circulation*. **115**(5):e69-171, 2008
2. Niessen M et al *J Rehabil Med*. **40**(6):482-486, 2008
3. Finley, M. et al, *Proceedings of 34<sup>th</sup> Annual Meeting, ASB*, Aug. 2011.
4. Sugarman, H et al. *Brain Cog*, **48**(2-3), 2002
5. Wu G, et al. I. *J Biomech*. May 2005

**Table 1: Demographic characteristics by group (means  $\pm$  sd)**

|                          | Control<br>(n=7) | Left-sided lesion<br>(n=7) | Right-sided lesion<br>(n=8) |
|--------------------------|------------------|----------------------------|-----------------------------|
| Age (yrs)                | 55.9 $\pm$ 10.8  | 66.6 $\pm$ 5.5*            | 57.9 $\pm$ 8.5              |
| Gender (male/female)     | 2/5              | 5/2                        | 4/4                         |
| Stroke_onset (months)    | n/a              | 59.3 $\pm$ 52.0            | 87.1 $\pm$ 47.9             |
| Fugl-Meyer_UE (max = 66) | n/a              | 50.4 $\pm$ 17.7            | 46.7 $\pm$ 20.1             |

\*Indicates significant difference from other groups ( $p\leq 0.05$ )

**Figure 1: Movement smoothness by groups**



# THE SEARCH FOR A LIMITING JOINT DURING LOWER EXTREMITY COLLAPSE: A CASE STUDY

<sup>1</sup>Sean P. Flanagan, <sup>1</sup>Janelle Kulik and <sup>2</sup>George J. Salem

<sup>1</sup>California State University, Northridge, CA, USA

<sup>2</sup>University of Southern California, Los Angeles, CA, USA

email: sean.flanagan@csun.edu web: <http://www.csun.edu/~sflanagan>

## INTRODUCTION

Winter's [1] concept of the support moment states that collapse of the lower extremity(ties) (LE) requires a simultaneous collapse of all 3 (or 6) joints of the lower extremity(ties). While the resulting collapse of the entire LE system is apparent, the underlying cause of that collapse remains elusive. Can a certain joint (or joints) be the limiting factor, or is there simply a total system failure? The purpose of this investigation was to examine various methodologies used to search for a limiting joint in the case of LE collapse, using a case study to illustrate the advantages of using a mechanical energy analysis approach.

## METHODS

A single subject, who was part of a larger study, was used in this analysis. As part of the protocol, the subject was to complete 3 repetitions of a back squat with a loaded barbell (equivalent to the subject's 3 repetition maximum). However, the subject was unable to complete the third repetition. The second and third repetitions were deemed the "successful" and "failed" repetitions, respectively, for further analysis.

The subject performed the repetitions with a force platform (AMTI, Watertown, MA) under each foot while instrumented for biomechanical analysis. A six camera (Vicon 370, Oxford, UK) motion capture system collected marker coordinate data at a rate of 120 Hz. Ground reaction forces were collected at 2400 Hz. Standard inverse dynamics techniques were used to create a model of the subject and determine kinematic (angle, angular velocity) and kinetic (net joint moment, power, work) joint variables. Visual inspection was used to determine the beginning of the movement and the

time point at which failure occurred on the failed repetition. A corresponding start and time interval was then determined for the successful repetition.

Net joint moment (NJM) data of the six primary joints (left and right ankles, knees, and hips) were compared between repetitions. This data included peak NJM, NJM impulse, NJM power, and NJM work. An additional variable, NJM energy, was calculated by integrating the NJM power curve using a 0.417 msec time interval. NJM energy represents the total amount of energy generated by the NJM up to each point in time. It is equivalent to NJM work at the end of the total time interval.

## RESULTS AND DISCUSSION

Findings were similar for both limbs and the NJMs at the ankles were, on average, 15-18% of the other joints; thus, for brevity and clarity, discussion will be limited to the right hip and knee.

During the failed squat, the peak NJM was slightly larger at the hip (1%) but less (-7%) at the knee (Figure 1). NJM impulse at the knee (-9%) and hip (-6%) were less for the failed squat. Although these findings suggest that the knee was the limiting joint, they may be misleading. NJMs are greatly affected by flexion angles. During the latter half of the time interval (where the NJM is higher for the failed squat), the flexion angles were smaller (the subject was more upright) during the successful repetition. This position required less NJMs at the joints. Additionally, NJM impulse does not infer the joint is actually moving.

NJM power oscillated greatly for both joints during both conditions (Figure 2). This was probably due to the slow movement speed required by the heavy load. Peak NJM power was less for the both the hip

(-90%) and knee (-57%) during the failed attempt, but occurred late in the movement for the successful squat and did not explain the failure.

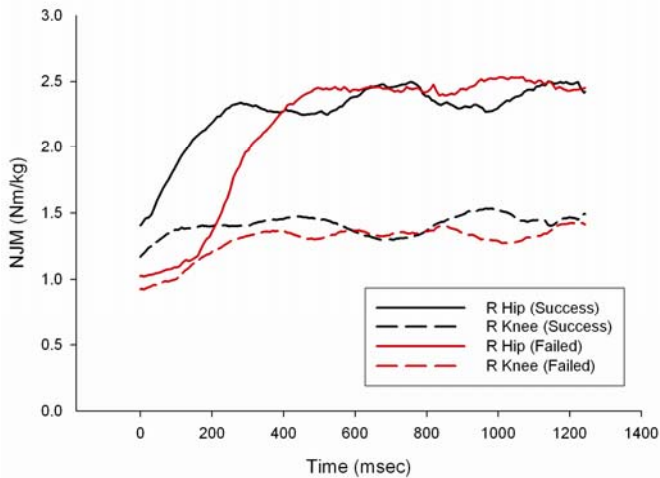


**Figure 1:** NJM as a function of time.

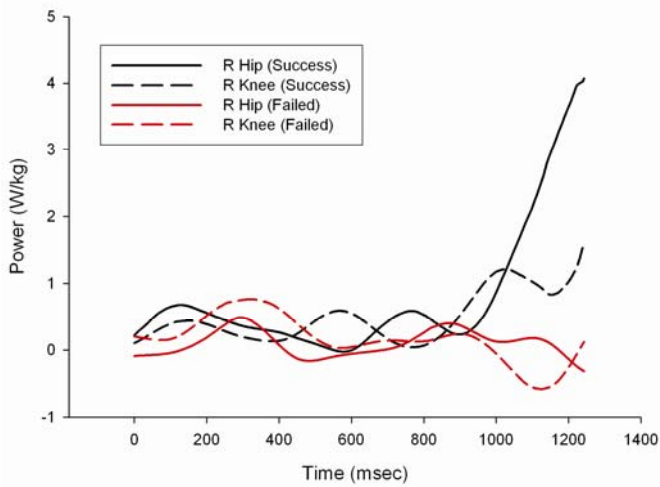


**Figure 2:** NJM power as a function of time.

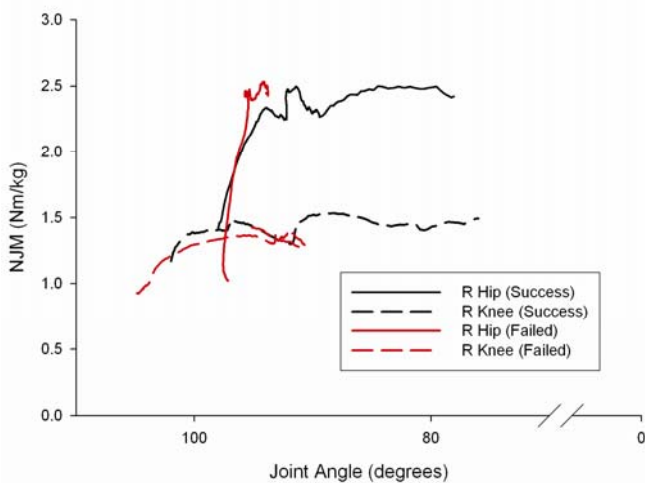


**Figure 3:** NJM as a function of joint angle.

Another possibility was to examine the NJMs as a function of joint angle, as was done in Figure 3. The area under this curve is the NJM work, which was clearly less for the knee (38%) and hip (-77%)

during the failed squat. In contrast to the moment data, these data would suggest that the hip was the limiting joint. Some care must be taken when interpreting these results, for two reasons. First, the temporal characteristics of the movement are no longer evident, and similar joint angles do not imply temporal synchronization. Second, according to the support moment concept, system collapse would eventually require failure at all joints [1]. All joints would be expected to perform less work (a similar argument could be made for impulse).

Mechanical energy analysis solves both of these problems by accounting for changes in both time *and* joint configuration. Figure 4 illustrates the total energy added to the system by each NJM as a function of time. It appears evident that the knee NJM is adding more energy to the system in order to compensate for the lack of energy supplied by the hip NJM (as evidenced by a comparison of the failed squat to the successful one) indicating the hip is the limiting joint. Such a conclusion could not be reached by examining the NJM-time, NJM-joint angle or the NJM power-time curves, independently.

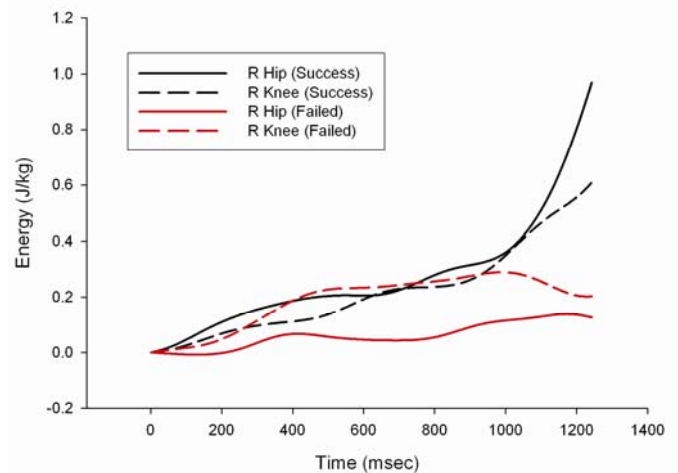


**Figure 4:** Mechanical energy added to the system by the hip and knee NJM as a function of time.

## CONCLUSIONS

Mechanical energy analysis offers promise as a way of detecting the limiting joint in a squat movement during LE collapse. Further and more expanded exploration is warranted.

## REFERENCES

1. Winter DA *J Biomech* **13**, 923-927, 1980.

# CONTRIBUTORS TO ANKLE PROPRIOCEPTION FOR STATIC AND DYNAMIC TASKS

Lisa Floyd, Taylor Holmes and Jesse Dean

Medical University of South Carolina, Charleston, SC, USA

email: [deaje@musc.edu](mailto:deaje@musc.edu)

## INTRODUCTION

Proprioception, the sense of the limbs' position and motion, is a vital element of functional movement. A common proprioception metric is Joint Position Sense (JPS), a measure of the accuracy with which a posture can be recreated. Decreased JPS accuracy has been associated with decreased gait speed in chronic stroke patients [1], presumably due to an inability to accurately produce movement patterns with typical levels of efficiency and stability.

Proprioceptive feedback is traditionally thought to derive from muscle spindles, with a lesser contribution from joint receptors [2]. But this mechanism does not explain the improved JPS accuracy at the elbow when subjects are required to actively support the weight of their forearms against gravity [3]. Active muscle contractions may improve proprioception accuracy by increasing muscle spindle sensitivity through descending fusimotor drive [4]. Alternatively, "sense of effort", a representation of the motor command required to overcome the elbow joint torque produced by gravity, may also contribute to position sense [5].

Previous studies of this topic have primarily focused on matching static elbow positions. In contrast, we investigated proprioception accuracy of the ankle, matching both static positions and rhythmic oscillatory movements, which may be more functionally relevant during tasks such as gait. By placing subjects in a position in which gravity will not exert torque around the ankle joint, we disrupted the link between fusimotor drive and sense of effort required to overcome gravity.

Our experiment tested two competing explanations for the apparent improvement in proprioception accuracy during active muscle contractions. 1) *Increased fusimotor drive* improves spindle sensitivity. This will occur when muscles are active,

independent of positioning with respect to gravity. We would thus expect active positioning and movement trials to be more accurate. 2) *Sense of effort* provides additional proprioceptive feedback based on the effort required to overcome gravity. By operating in the horizontal plane, we eliminate this source of potential feedback, and would no longer expect improved accuracy with active trials.

## METHODS

Five young ( $23 \pm 1$  yrs), healthy subjects participated in this experiment. We quantified left ankle position using a custom-built frame instrumented with a potentiometer aligned with the ankle joint. We also measured tibialis anterior (TA) and soleus (SO) muscle activity using surface EMG electrodes.

For all trials, subjects lay on their right sides (Fig. 1). Foam padding was placed appropriately to ensure comfort and keep the left hip, knee and ankle aligned horizontally. A splint held the left knee in a fully extended position. The subject wore sneakers modified with a rigid aluminum plate in the sole, which was bolted to a rotating footplate with the axis aligned with the ankle joint. Ankle motion was thus restricted to plantarflexion and dorsiflexion, and gravity did not exert a torque around this axis. In some trials, a background dorsiflexion torque was applied by hanging a mass from a wire running over a pulley and attached to the footplate posterior to the ankle joint. The torque produced by this mass ( $\sim 3$  Nm) was nearly constant throughout the range of motion used in this experiment (varying by a maximum of 6%).

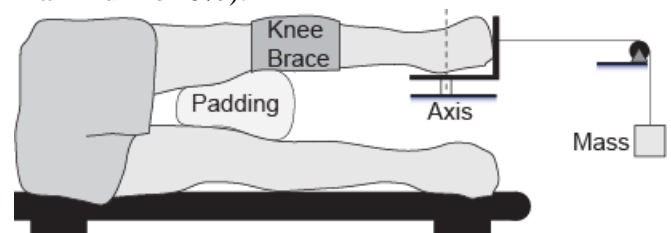


Figure 1. Setup illustrated with background dorsiflexion torque.

In static trials, subjects matched a constant target ankle position (neutral; 10° plantarflexion; 20° plantarflexion). The target position was set using three conditions: *Passive*, for which the experimenter placed the ankle in a position while the subject remained relaxed (monitored using EMG); *Active*, for which the subject positioned the ankle using visual feedback; *Weighted*, which was identical to the *Active* condition, but with background dorsiflexion torque. Once the subject reported awareness of their ankle position, the experimenter moved the ankle back and forth, and the subject then actively recreated the target position without any visual feedback.

In dynamic trials, subjects matched a sine wave trajectory (5° amplitude, 8s period; 5° amplitude, 4s period; 10° amplitude, 4s period). Again, the target trajectory was set under the *Passive*, *Active*, and *Weighted* conditions. Once subjects were aware of the ankle movement pattern, they actively recreated the motion without visual feedback.

For the static trials, we quantified performance as the absolute value of the error between the target position and the subsequent subject-generated position. For the dynamic trials, we quantified performance as the absolute value of the error between the target sine wave amplitude and the amplitude of a sine wave fit to the subsequent subject-generated trajectory. One subject's errors during the dynamic trials were consistently outliers, and were not included in the group calculations.

## RESULTS AND DISCUSSION

For the static position matching task, muscle activity varied as expected between conditions when establishing the target position (Fig 2A). Neither TA nor SO exhibited measurable activity during *Passive* trials; TA activity dominated *Active*

trials; SO activity dominated *Weighted* trials. Despite these differences in muscle activity, and thus fusimotor drive, matching errors did not differ between conditions when subjects attempted to recreate the target position (Fig. 2B;  $p=0.71$ ).

For the dynamic task, the target trajectory was approximately matched for all conditions (Fig. 2C). As with the static trials, muscle activity was not detected during *Passive* trials, dominated by TA during *Active* trials, and dominated by SO during *Weighted* trials. When subjects attempted to match this target trajectory without visual feedback, there was no significant difference in amplitude errors across conditions (Fig. 2D;  $p=0.24$ ).

Substantial changes in muscle activity did not affect subjects' ability to match either static positions or dynamic trajectories, suggesting that increased fusimotor drive alone does not improve proprioception accuracy. These results are consistent with the proposal that sense of effort can provide proprioceptive information, but only if this relationship has previously been learned through development [6]. By removing the effects of gravity, we disrupted this relationship, preventing sense of effort from being used to improve performance. Clinically, it may be important for patients to re-learn the link between sense of effort and peripheral mechanical state in order to return to typical levels of proprioception accuracy.

## REFERENCES

1. Lin SI. *Arch Phys Med Rehab* **86**, 197-203, 2005.
2. Gandevia SC. *Kinaesthesia: Roles for afferent signals and motor commands*. Oxford Press, 1996.
3. Goodwin GM, et al. *Brain* **95**, 705-48, 1972
4. Ansems GE, et al. *J Physiol* **576**, 444-55, 2006.
5. Winter JA, et al. *J Physiol* **568**, 1035-46, 2005.
6. Walsh LD, et al. *J Appl Phys* **100**, 1109-16, 2006.

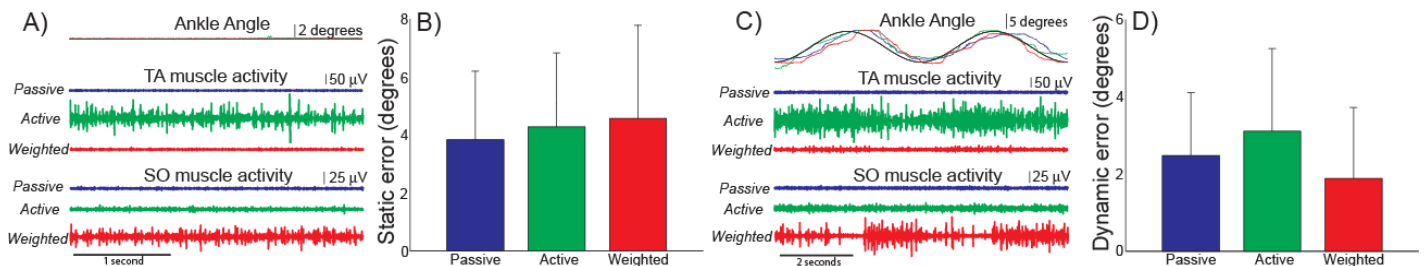


**Figure 2.** Sample position data, sample EMG data and group error data for static trials (A-B) and dynamic trials (C-D). Condition (Passive, Active, or Weighted) had a dramatic effect on muscle activity while the target behavior was set, but did not affect the resultant error when subjects attempted to recreate the position or movement.

# Reliability of Medial and Lateral Forefoot Segment Kinematics during Shod Treadmill Running

<sup>1,2</sup>Kevin R. Ford, <sup>2</sup>Tamara L. Masters and <sup>1</sup>Daniel W. Carson

<sup>1</sup>Cincinnati Children's Hospital Medical Center, Cincinnati, OH, USA

<sup>2</sup>University of Cincinnati, Cincinnati, OH, USA

email: [kevin.ford@cchmc.org](mailto:kevin.ford@cchmc.org) web: <http://research.cchmc.org/hpl>

## INTRODUCTION

Forefoot injuries are common in sports and recreation [1]. Foot plantar loading magnitude and timing differs between the medial and lateral forefoot during athletic movements and may help explain the risk for certain types of injuries. Foot medial/lateral kinetic differences also likely lead to kinematic variations at the foot that, until recently, were not routinely measured with motion analysis.

A variety of multi-segment kinematic foot models have been established to reduce the violation of the rigid body assumption. Nester et al. [2] proposed a multi-segment model that included rearfoot, midfoot, medial forefoot and lateral forefoot segments and reported a reasonable match between the kinematic data from skin, plate and bone pin protocols. The purpose of this study was to determine the reliability of within session and between session 3D kinematic testing from a multi-segment foot model, with separate medial and lateral forefoot segments, during shod treadmill running.

## METHODS

Four recreationally active adult subjects (age: 22.3 (1.0) years; mass: 67.2 (11.4) kg; height: 174.4 (4.8) cm) gave informed consent to participate in the study. Each subject completed a running protocol on a custom high-speed treadmill at a self-selected speed (mean 3.6 (0.2) m/s). Each subject was retested approximately one week later at the same self-selected speed. 12 retroreflective skin markers (9.5 mm diameter) were placed on the right foot defining 4 foot segments: rearfoot, midfoot, medial forefoot, and lateral forefoot [2]. For the shod condition, Newport H2 sport sandals (Keen Inc., Portland, OR) were modified to accommodate the marker set. Retroreflective markers were also attached to the pelvis, thigh and shank as previously described (Figure 1)[3].



**Figure 1:** Lower extremity marker locations.

Kinematic data was collected at 240 Hz using a 10 camera motion capture system (Eagle, Motion Analysis Corp., Santa Rosa, CA). A standing static trial for each subject was collected to define neutral kinematic posture. Kinematic analysis was performed in Visual 3D (C-Motion, Inc. Germantown, MD) and MATLAB (The MathWorks, Natick, MA). A low-pass fourth-order Butterworth filter at a cutoff frequency of 12 Hz was used to filter each 3D marker trajectory trial. Kinematic data was analyzed from initial contact to toe off for the right foot of each subject [4].

Mean and standard deviation range of motion for Session 1 and Session 2 were calculated for the distal/proximal segments for each rotation. Standard error of measurement (SEM) and coefficient of multiple correlations (CMC) values for within and between sessions were calculated.

## RESULTS AND DISCUSSION

Segment range of motion is presented in Table 1. Within session reliability measures were excellent (CMC>0.9, Table 1) for all rotations. Between session CMC (mean 0.86) and SEM (mean 1.6°) are presented in Table 1. Excellent between session reliability was found in medial forefoot dorsiflexion/plantarflexion and inversion/eversion

rotation referenced to the lateral forefoot (CMC>0.9).

During treadmill running forefoot inversion/eversion motion occurs independently in the medial and lateral segments (Figure 2). The lateral forefoot had eversion relative to the midfoot early in stance while the medial forefoot had eversion relative to the midfoot during late stance (Figure 2).

Based on lateral and medial forefoot range of motion, investigations which aim to examine forefoot motion during running would likely violate the assumptions of a rigid body if the medial and lateral forefoot were not separately modeled.

## REFERENCES

1. Matheson GO, et al. *Am J Sports Med* **15**, 46-58, 1987.
2. Nester C, et al. *J Biomech* **40**, 3412-23, 2007.
3. Ford KR, et al. *Med Sci Sports Exerc* **39**, 2021-8, 2007.
4. Fellin, RE, et al. *J Sci Med Sport* **13**, 646-50, 2010.

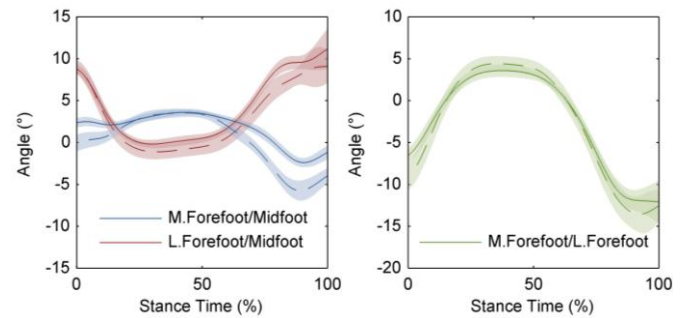


**Figure 2:** Representative subject's angular displacement (mean and standard deviation) over stance time for each test session (Session 1 dashed; Session 2 solid). Left: inversion+/eversion- rotation of the medial forefoot (blue) and lateral forefoot (red) in relation to the midfoot. Right: inversion+/eversion- rotation of the medial forefoot (green) in relation to the lateral forefoot.

## ACKNOWLEDGEMENTS

We acknowledge the generous footwear donation by KEEN Inc., Portland OR.

**Table 1:** Range of motion, standard error of measurement and within and between sessions CMC during shod treadmill running.

| <i>Distal/Proximal Segments</i> | <i>Rotation</i> | <i>Session 1</i> | <i>Session 2</i> | <i>SEM</i> | <i>Within CMC</i> | <i>Between CMC</i> |
|---------------------------------|-----------------|------------------|------------------|------------|-------------------|--------------------|
| Shank/Thigh                     | Ext/Flex        | 27.0 ± 1.6       | 26.5 ± 1.5       | 0.7        | 0.991             | 0.994              |
|                                 | Add/Abd         | 3.5 ± 1.2        | 3.6 ± 1.1        | 0.3        | 0.914             | 0.843              |
|                                 | Int/Ext         | 11.9 ± 5.1       | 11.5 ± 4.2       | 0.7        | 0.979             | 0.790              |
| Rearfoot/Shank                  | DF/PF           | 35.3 ± 4.0       | 32.9 ± 2.9       | 1.9        | 0.993             | 0.992              |
|                                 | Inv/Ev          | 18.3 ± 3.6       | 16.7 ± 3.7       | 1.5        | 0.988             | 0.932              |
|                                 | Add/Abd         | 13.4 ± 4.2       | 12.4 ± 5.4       | 1.1        | 0.963             | 0.921              |
| Midfoot/Shank                   | DF/PF           | 41.0 ± 3.1       | 43.8 ± 1.4       | 1.4        | 0.994             | 0.992              |
|                                 | Inv/Ev          | 13.8 ± 2.4       | 14.9 ± 3.1       | 2.1        | 0.981             | 0.954              |
|                                 | Add/Abd         | 15.6 ± 3.3       | 15.9 ± 5.7       | 2.4        | 0.974             | 0.956              |
| Midfoot/Rearfoot                | DF/PF           | 9.4 ± 1.0        | 12.5 ± 2.0       | 1.6        | 0.971             | 0.784              |
|                                 | Inv/Ev          | 6.5 ± 3.5        | 4.8 ± 0.9        | 2.0        | 0.959             | 0.694              |
|                                 | Add/Abd         | 5.2 ± 0.8        | 5.4 ± 1.5        | 1.4        | 0.959             | 0.694              |
| M.Forefoot/Midfoot              | DF/PF           | 15.7 ± 2.7       | 11.7 ± 2.3       | 1.5        | 0.989             | 0.915              |
|                                 | Inv/Ev          | 8.1 ± 2.3        | 11.0 ± 3.9       | 3.0        | 0.977             | 0.719              |
| L.Forefoot/Midfoot              | DF/PF           | 6.5 ± 2.4        | 5.0 ± 1.6        | 1.3        | 0.945             | 0.659              |
|                                 | Inv/Ev          | 10.1 ± 2.2       | 8.9 ± 3.9        | 1.4        | 0.909             | 0.822              |
| M.Forefoot/L.Forefoot           | DF/PF           | 10.9 ± 2.7       | 9.2 ± 2.1        | 3.0        | 0.984             | 0.909              |
|                                 | Inv/Ev          | 15.2 ± 2.8       | 17.6 ± 2.3       | 2.1        | 0.982             | 0.975              |

*Extension (Ext); Flexion (Flex); Adduction (Add); Abduction (Abd); Dorsiflexion (DF); Plantarflexion (PF); Inversion (Inv); Eversion (Ev).*

# The Effects of Electrical Stimulation on Muscle Injected with Botulinum Toxin A (Botox)

<sup>1</sup>Rafael Fortuna, <sup>1,2</sup>Monika Horisberger <sup>1</sup>Robert van der Marel <sup>1</sup>Walter Herzog

<sup>1</sup>Human Performance Laboratory, University of Calgary, Alberta, Canada

<sup>2</sup>Orthopaedic Department, University Hospital Basel, Switzerland

email: rfortuna@kin.ucalgary.ca

## INTRODUCTION

Botulinum toxin type A (BTX-A) is a frequently used treatment in neuromuscular disorders characterized by increased neuromuscular activity such as in cerebral palsy (CP) and following stroke [1]. BTX-A acts by preventing the release of acetylcholine at the neuromuscular junction, creating a chemical denervation and muscle paralysis [1,2,3]. The beneficial effects of BTX-A injections are well recognized [1]. However, recent works have shown that BTX-A treatment has specific adverse effects causing muscle atrophy, strength loss, fat invasion, and loss of contractile material in target and non-target muscles [2,3]. We speculated that these adverse effects might be prevented if BTX-A injected muscles could be strengthened through regular exercise. However, because of the denervation induced by BTX-A, voluntary exercise is precluded, but direct muscle electrical stimulation (ES) is possible and may offer an opportunity to limit or prevent many of the adverse effects created by BTX-A treatment.

Therefore, the purpose of this study was to determine the effects of direct muscle ES on strength, mass, and contractile material of the quadriceps femoris muscles of New Zealand White (NZW) rabbits.

## METHODS

Seventeen, one year old, female NZW rabbits were divided into three groups as follows: Control ( $n=5$ ), BTX-A ( $n=5$ ), and BTX-A+ES groups ( $n=7$ ). Control group rabbits received saline injections. Rabbits in both BTX-A groups received monthly BTX-A injections (3.5U/Kg) into the left quadriceps femoris for six months. In addition, the BTX-A+ES group was exposed to three weekly ES

training sessions for the BTX-A injected muscles (15min of cyclic activation, 0.5s on and 1.5s off at 20% of maximal muscle activation).

Outcome measures included knee extensor strength, muscle mass and the percentage of contractile material. Mass and strength were assessed by weighing the muscles and measuring the maximal isometric strength across the physiological knee joint range of motion. The percentage of contractile material was determined histologically by quantifying the area fraction of the contractile material compared to the total muscle cross-sectional area.

A 3 way-ANOVA with the main factors leg (injected and non-injected contralateral control) groups (Control, Experimental BTX-A without ES, and Experiment BTX-A with ES Groups) and muscles (vastus lateralis, rectus femoris, and vastus medialis) was performed using a level of significance of 0.05.

## RESULTS AND DISCUSSION

Electrical stimulation partially preserved muscle strength in target and non-target muscles of BTX-A+ES compared to BTX-A group rabbits ( $p<0.05$ ; Fig 1).

Muscle mass in target muscles was significantly greater for the BTX-A+ES compared to BTX-A group rabbits ( $p<0.05$ ). Furthermore, muscle mass for the non-target muscles of the BTX-A+ES group reached control group values ( $p>0.05$ ; Fig 2). Muscle mass preservation was muscle specific, being greater for the vastus lateralis than the remaining muscles (results not shown).

Contractile material was found to be around 96% for Control group rabbits. Contractile material was

significantly decreased  $p < 0.05$ ) for the target ( $43\% \pm 9.7$ ) and non-target vastus lateralis ( $74\% \pm 6.5\%$ ) in BTX-A group rabbits. For BTX-A+ES group, loss of contractile material was significantly greater ( $p < 0.05$ ) in the injected limb (28% loss) compared to the contralateral limb (4% loss) (Figure 3;  $p < 0.05$ ), showing that ES partially and fully preserved the contractile material in target and non-target muscles, respectively.

BTX-A group rabbits. Note that muscle mass on the contralateral side of BTX-A+ES group rabbits was fully preserved and similar to control group values.

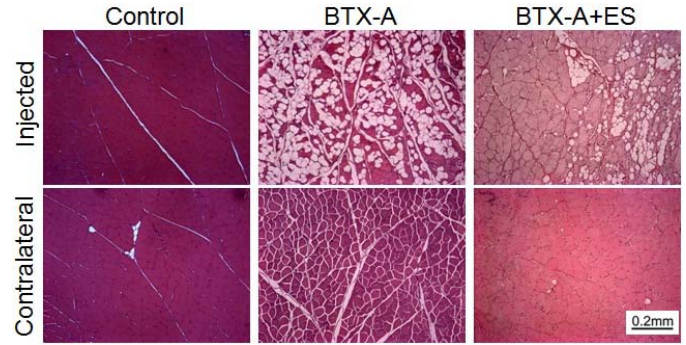


**Figure 3** Muscle histology of the injected (first row) and contralateral (second row) for the Control (left) BTX-A (middle) and BTX\_A+ES group rabbits (right). Percentage contractile material was normalized to Control group values (left column). A significant loss ( $p < 0.05$ ) in contractile material was observed for the BTX-A group rabbits (middle column). However, contractile material was significantly preserved ( $p < 0.05$ ) for BTX-A+ES group rabbits (right column).

## CONCLUSIONS

Direct electrical stimulation of BTX-A injected muscles partially preserves strength, mass and contractile material in target muscles and completely preserves muscle mass and contractile material in non-target muscles far removed from the injection site. These results suggest that low level direct electrical stimulation might be a valuable treatment companion to BTX-A treatments, allowing for the beneficial effects of the treatment while simultaneously limiting adverse effects in target muscles and eliminating adverse effects in non-target muscles.

## REFERENCES

1. Brin, MF. *Muscle & Nerve* **6**, 146-168, 1991.
2. Fortuna R, et al. *J Biomech* **44**, 39-44, 2011.
3. Yaraskavitch M, et al. *J Biomech* **41**, 897-902, 2008.

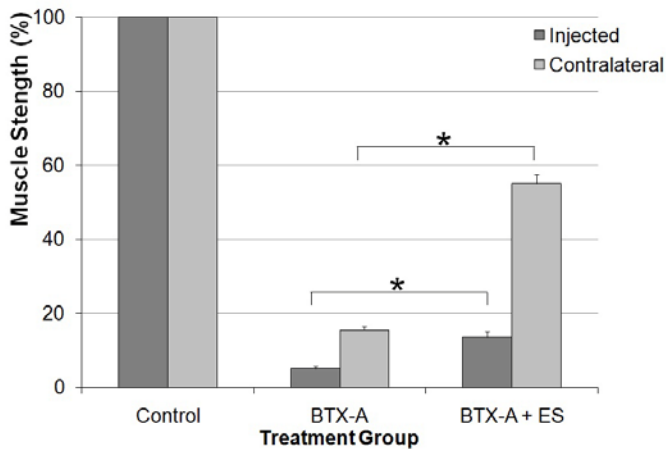


**Figure 1** Normalized muscle strength ( $\pm 1$  SD) for the Control, BTX-A, and BTX-A+ES group rabbits and the injected (dark bars) and contralateral quadriceps muscles (light bars). Muscle strength was normalized relative to control group values. A significant increase in muscle strength ( $p < 0.05$ ) was observed for both injected and contralateral quadriceps femoris muscles of the BTX-A+ES compared to BTX-A group rabbits.

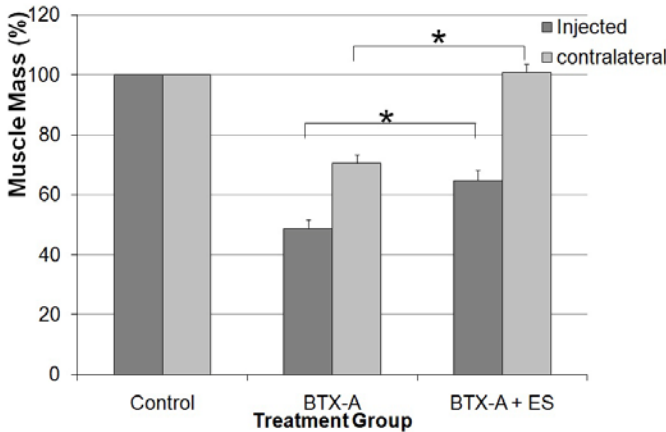


**Figure 2** Muscle mass ( $\pm 1$  SD) for the control, BTX-A, BTX-A+ES group rabbits for injected (dark bars) and contralateral quadriceps muscles (light bars). Values of muscle mass were normalized to control group values. A significant increase in muscle mass ( $p < 0.05$ ) was observed for both injected and contralateral quadriceps femoris muscles in the BTX-A+ES compared to

# A MARKERLESS RADIOSTEREOMETRIC ANALYSIS (RSA) SYSTEM FOR MEASURING GLENOHUMERAL TRANSLATION: DETAILS AND VALIDATION

Anne-Marie V. Fox, Angela E. Kedgley and Thomas R. Jenkyn

The University of Western Ontario, London, ON, Canada, email: AllenAV@orthosurg.ucsf.edu

## INTRODUCTION

Accurately measuring three-dimensional (3D) glenohumeral translation and orientation remains a challenge. Current methods are often two-dimensional (2D) measures, are limited by skin motion artefact errors or are invasive techniques. The markerless radiostereometric analysis (RSA) technique requires no invasive marker beads and is based on aligning models of the bones of interest with their silhouettes on a pair of radiographs. This method is promising, but limited details exist in the literature regarding its implementation. The specific goals of this work were (1) to provide a detailed description of the markerless RSA method, allowing other laboratories to more easily implement their own systems and (2) to assess the accuracy of a markerless RSA method in measuring 3D glenohumeral translations and orientations under ideal contrast conditions.

## METHODS

Bone phantoms of the humerus and scapula (Sawbones; Pacific Research Laboratories, Vashon, WA, USA) were positioned in four relative orientations (Table 1). In each the humerus was translated in 0.500 mm increments using a precision cross-slide table (Model VCT 514; Sowa Tool and Machine Co. Ltd., Kitchener, ON, Canada) and imaged after each increment using two fluoroscopes (Siremobil Compact-L; Siemens Medical Solutions USA Inc., Malvern, USA) (Fig. 1). The cross-slide table served as the “gold standard” to quantify kinematic translation, having an accuracy of  $\pm 1 \mu\text{m}$  and standard, beaded RSA served as the “gold standard” to quantify kinematic orientation, having an accuracy of  $0.121^\circ$  [1].

Images of a calibration frame with beads at known locations were taken prior to the commencement of data collection in order to calibrate the RSA system.

Following testing, images of a grid of stainless steel beads (a distortion grid) were taken by each fluoroscope to correct for image distortion.

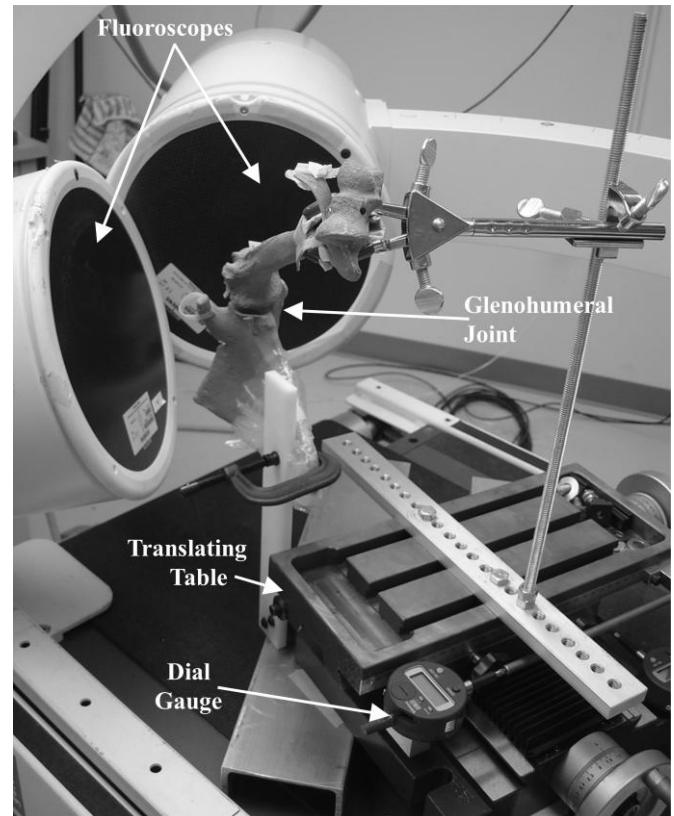


**Figure 1:** Experimental set-up showing the cross-slide table, dial-gauge, stationary scapula bone phantom, moveable humerus bone phantom and relative orientation of the two fluoroscopes.

From the images of the calibration frame, bead locations were digitized and corrected for image distortion. Using these locations, the x-ray foci were found using the standard RSA algorithm [1,2]. The additional calibration parameters (image plane orientation and distance from x-ray source to image plane) were found using custom-written software (MatLab; The MathWorks, Natick, USA) based on the work of Rougée *et al.* [3]. Specifically, each fluoroscope was modeled as a pinhole camera, using a perspective projection model. A relationship

between the 3D calibration points and their 2D projection locations was defined and an optimization routine was employed. An image plane correction based on the rotation and translation of the distortion grid with respect to the coordinate system of the images was required in order to reposition and realign the fluoroscopy image.

The bone phantoms were scanned using computed tomography (CT) (Lightspeed VCT; GE Healthcare, Piscataway, USA). Image segmentation software (Materialise Interactive Medical Image Control System, MIMICS; Materialise, Ann Arbor, USA) was used to create 3D computer bone models on which bony landmarks required to create anatomical reference frames were digitized.

Using the calibration parameters and image plane correction, a virtual experimental set-up was created in a solid modeling program (Rhinoceros; Robert McNeel & Associates, Seattle, USA). For each glenohumeral pose, the bone surface models of the humerus and scapula were manually aligned with their bony outlines on the two fluoroscopic images.

Inter-operator reliability was assessed by having three operators perform the alignment procedure for the same image pair. Intra-operator reliability was assessed by having one operator align the same image pair on three different occasions.

Intraclass correlation coefficients (ICC) evaluated the agreement between the known (cross-slide table) and calculated (markerless RSA) translations and the error in each translation was quantified using the root mean squared error (RMSE) and the standard error of measurement (SEM). RMSE and SD were calculated to assess the accuracy of

measuring glenohumeral orientation. Inter-operator and intra-operator reliability were assessed using the SD of the kinematic parameters.

## RESULTS AND DISCUSSION

Excellent agreement was found between the gold standard and markerless RSA, with all ICCs greater than 0.99 (Table 1). The average SEM and RMSE were calculated to be 0.068 mm and 0.096 mm, respectively. The average RMSE and SD for markerless RSA in determining kinematic orientations were  $1.35^\circ \pm 0.72^\circ$  and  $1.43^\circ$ . The average inter-operator and intra-operator reliability in angular measurement were  $0.75^\circ$  and  $0.53^\circ$ , respectively. The average inter-operator and intra-operator reliability in measuring glenohumeral position were 0.49 mm and 0.58 mm, respectively.

The sub-millimeter accuracies obtained in this study compare well to other existing bi-planar systems [4] and surpass measurement systems currently used such as dynamic ultrasound and electromagnetic tracking via skin markers.

Future work will focus on creating a semi-automated matching procedure and measuring the accuracy of this system in an *in vivo* setting.

## REFERENCES

1. Kedgley AE, et al. *J Biomech* **42**, 1350-1354, 2009.
2. Selvik G. *Acta Orthop Scand Suppl* **232**, 1-51, 1989.
3. Rougée A, et al. *Comput Med Imaging Graph* **17**, 295-300, 1993.
4. Bey MJ, et al. *J Biomech Eng* **128**, 604-609, 2006.

**Table 1:** The orientation number, relative orientation in degrees and translation performed for the humerus phantom relative to the scapula phantom as well as translational accuracy results showing intra-class correlation coefficients (ICC), standard errors of measurement (SEM) and root mean squared errors (RMSE) for all tests.

| Orientation # | Flexion (°) | Abduction (°) | External Rotation (°) | Translation | ICC    | SEM (mm) | RMSE (mm) |
|---------------|-------------|---------------|-----------------------|-------------|--------|----------|-----------|
| 1             | 20          | 20            | 0                     | Anterior    | 0.9997 | 0.046    | 0.063     |
|               | 20          | 20            | 0                     | Posterior   | 0.9991 | 0.079    | 0.11      |
|               | 20          | 20            | 0                     | Inferior    | 0.9993 | 0.077    | 0.11      |
| 2             | 10          | 10            | 20                    | Inferior    | 0.9988 | 0.077    | 0.11      |
| 3             | 10          | 10            | 90                    | Inferior    | 0.9994 | 0.067    | 0.093     |
| 4             | 0           | 90            | 15                    | Anterior    | 0.9988 | 0.067    | 0.096     |
|               | 0           | 90            | 15                    | Posterior   | 0.9995 | 0.065    | 0.091     |

# EFFECTS OF VARYING GAIT STRATEGY ON METABOLIC COST AND STABILITY

Chris Franz, Eric Monsch and Jesse Dean

Medical University of South Carolina, Charleston, SC, USA

email: [deaje@musc.edu](mailto:deaje@musc.edu)

## INTRODUCTION

While it is generally accepted that nondisabled individuals prefer gait patterns which minimize metabolic cost [1], the role stability plays in determining the preferred gait pattern remains unclear. We have recently shown that humans walking down moderate slopes do not prefer a gait pattern minimizing metabolic cost [2]. Downhill walking presents an environment in which humans may voluntarily alter their preferred gait pattern, taking advantage of gravitational potential energy to reduce the metabolic cost of walking. However, downhill slopes also challenge stability. The preference for a gait pattern of non-minimal metabolic cost may be due to an increased focus on maintaining stability, suggesting a potential relationship between metabolic cost and stability.

We investigated this potential relationship between metabolic cost and stability while walking downhill under various conditions. *Careful* and *Relaxed* walking trials were used to investigate humans' ability to voluntarily modulate the amount of active control exerted during gait. A *Threatened* walking trial, in which subjects anticipated mechanical perturbations, was used to investigate the response to an increased fall risk in the absence of specific instructions. For all trials, we quantified basic stride kinematics, metabolic cost, and several previously developed indicators of gait stability.

We hypothesize that a gait strategy continuum exists presenting an inverse relationship between instability and metabolic cost, such that humans are unable to simultaneously optimize both metabolic cost and stability. We predict that voluntary changes to the gait pattern are possible, where increasing or decreasing metabolic costs coincide with an opposing shift of instability. Varying environmental conditions will lead to a subconscious shift along

this continuum, where greater importance is placed on minimizing either metabolic cost or instability.

## METHODS

Seven young ( $25 \pm 2$  years), healthy subjects walked on a treadmill with a 15% downhill slope at 1.25 m/s for a series of trials in randomized order, each lasting either 6 or 9 minutes. A harness prevented falls, but did not provide body weight support. Active kinematic markers were placed on the C7 spinous process, left heel, and right heel. We used an indirect spirometry system to measure oxygen consumption and carbon dioxide production.

Subjects performed walking trials under a series of conditions. To vary voluntary control of gait, they were instructed to walk normally (*Normal* walking), walk carefully keeping their legs underneath them (*Careful* walking), and walk relaxed allowing the downhill slope and gravity do the work (*Relaxed* walking). To investigate subconscious changes in gait strategy, subjects walked while receiving perturbations applied by the experimenters pulling long cords running forward and backward from the subject's pelvis. To avoid anticipation of specific perturbations, the pull direction was randomized (forward/backward), pull timing was randomized (separated by 15-20 seconds), and subject vision of the experimenters was blocked. Subjects were then instructed that a single "maximal perturbation" would be delivered, and continued to walk for an additional 3 minutes (*Threatened* walking). A maximal perturbation was not actually delivered.

Net metabolic cost was quantified during the last 3 minutes of each trial condition to ensure the subject had reached steady-state. While no metrics that directly quantify gait stability currently exist, several indirect indicators have been associated with fall risk, including stride period variability [3] and early local dynamic stability [4]. We calculated

stride period variability as the standard deviation of the stride period values for each subject. We used methods described in detail elsewhere [4] to calculate early local dynamic stability (eLDS) of C7 velocity in the anterior-posterior direction, which quantifies the response to small naturally occurring perturbations during gait. Each of these stability indicators was calculated from the final 150 strides of each trial using the kinematic marker data.

## RESULTS AND DISCUSSION

Gait strategy had a significant ( $p < 0.001$ ) effect on stride period (Fig. 1A). Subjects walked with slower, longer strides when using the *Relaxed* gait pattern. Conversely, subjects walked with faster, shorter strides with the *Careful* gait pattern. During *Threatened* walking, when subjects anticipated perturbations, they preferred to walk with shorter stride periods, similar to *Careful* walking. These results match the predictions of a simple dynamic walking model, for which stability is increased by walking with shorter stride periods [2].

Metabolic cost was also significantly ( $p = 0.004$ ) influenced by gait strategy (Fig. 1B). As expected, the metabolic cost increased as the voluntary gait strategy became more controlled (*Relaxed*  $\rightarrow$  *Normal*  $\rightarrow$  *Careful*). Anticipating perturbations caused subjects to walk with a metabolic cost more similar to the *Careful* gait strategy.

The effects of gait strategy on stability are less clear. Stride period variability was significantly ( $p = 0.04$ ) influenced by gait strategy (Fig. 1C), but did not scale with the expected changes in stability. Instead, variability increased during non-preferred gait patterns, whether subjects walked with less controlled (*Relaxed*) or more controlled (*Careful*) gait strategies. Also, variability did not decrease during *Threatened* walking, when we would expect

subjects to increase stability in anticipation of perturbations. The discrepancy between our expectations and the variability results may be due to the complex non-intuitive relationship between variability and stability [5].

Dynamic stability (eLDS) also varied significantly ( $p = 0.002$ ) with gait strategy (Fig. 1D). However, this metric indicated that increases in voluntary control actually decreased stability, and stability did not improve during *Threatened* walking. While possible, it seems unlikely that healthy subjects would be unable to appropriately modulate their gait stability either voluntarily or in anticipation of perturbations. It is also unclear why subjects would prefer the *Normal* gait strategy to the *Relaxed* gait strategy if the *Relaxed* strategy decreases both metabolic cost and instability.

## CONCLUSIONS

We have previously proposed that the preferred gait pattern is influenced by the dual goals of minimizing metabolic cost and maintaining stability. Our present results indicate that changes in gait strategy (whether voluntary or subconscious) predictably alter average stride period and metabolic cost. On the other hand, existing indicators of gait stability do not reveal the expected changes in stability with various gait strategies.

## REFERENCES

1. Alexander RM. *Am J Hum Biol* 14, 641-8, 2002.
2. Hunter LC, et al. *J Biomech* 43, 1910-5, 2010.
3. Hausdorff JM, et al. *Arch Phys Med Rehabil* 82, 1050-6, 2001.
4. Bruijn SM. *Is stability an unstable concept?* PhD thesis. Ipskamp, Amsterdam. 2010.
5. Li L, et al. *Hum Move Sci* 24, 257-67, 2005.

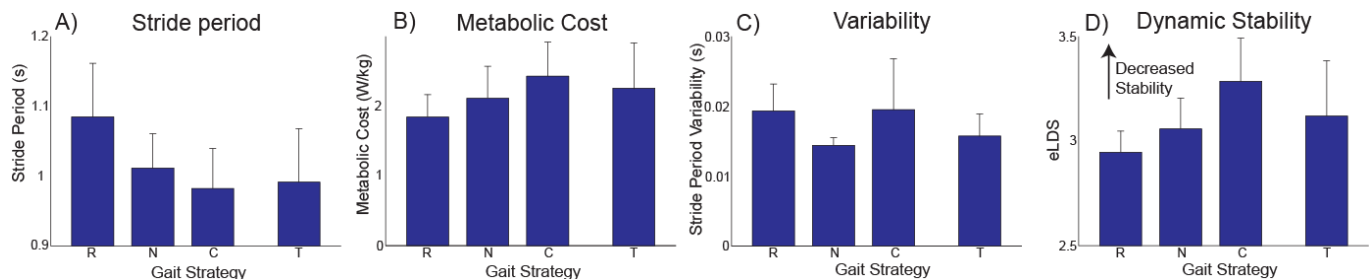


**Figure 1.** Various walking parameters were influenced by changes in gait strategy, including voluntary changes (Relaxed, R; Normal, N; Careful, C) and changes due to anticipation of perturbations (Threatened, T).

# THE MECHANICS OF SLOPED WALKING REVISITED: MECHANICAL WORK PERFORMED BY THE INDIVIDUAL LIMBS

Jason R. Franz, Nicholas E. Lyddon, and Rodger Kram

University of Colorado, Boulder, CO, USA

email: [jason.franz@colorado.edu](mailto:jason.franz@colorado.edu) web: [www.colorado.edu/intphys/research/locomotion.html](http://www.colorado.edu/intphys/research/locomotion.html)

## INTRODUCTION

When walking over level ground, humans perform equal amounts of positive ( $W_{ext}^+$ ) and negative ( $W_{ext}^-$ ) external mechanical work on the body's center of mass (CoM). Clearly, humans perform net  $W_{ext}^+$  to walk uphill and net  $W_{ext}^-$  to walk downhill in order to raise and lower the CoM, respectively.

However, previous studies [e.g. 1-3] of the mechanical work performed during uphill and downhill walking have ignored the simultaneous  $W_{ext}^+$  and  $W_{ext}^-$  performed by the trailing and leading legs during double support. Using the individual limbs method (ILM), Donelan et al. [4] found one-third greater mechanical work than that calculated using the combined forces from both legs. Further, the ILM provides fundamental insight into the distinct functions of the individual legs. Here, we quantified the mechanical work performed by the individual legs during uphill and downhill walking.

We hypothesized that 1) with steeper uphill grade  $W_{ext}^-$  performed by the leading leg becomes negligible as the trailing leg performs progressively greater  $W_{ext}^+$  to raise the CoM, and 2) with steeper downhill grade  $W_{ext}^+$  performed by the trailing leg becomes negligible as the leading leg performs progressively greater  $W_{ext}^-$  to lower the CoM.

## METHODS

11 healthy young adults (6M/5F, mass:  $71.0 \pm 12.3$  kg) walked at  $1.25 \text{ m}\cdot\text{s}^{-1}$  on a dual-belt force measuring treadmill at seven grades (0,  $\pm 3$ ,  $\pm 6$ , and  $\pm 9^\circ$ ) [5]. We collected three-dimensional ground reaction forces (GRF) of the right leg. Assuming symmetry, we phase shifted right leg GRFs by 50% and reversed the polarity of the medio-lateral forces to emulate the forces produced by the left leg. We determined the timing of single and double support within a step-cycle using a 50N threshold for the perpendicular GRF.

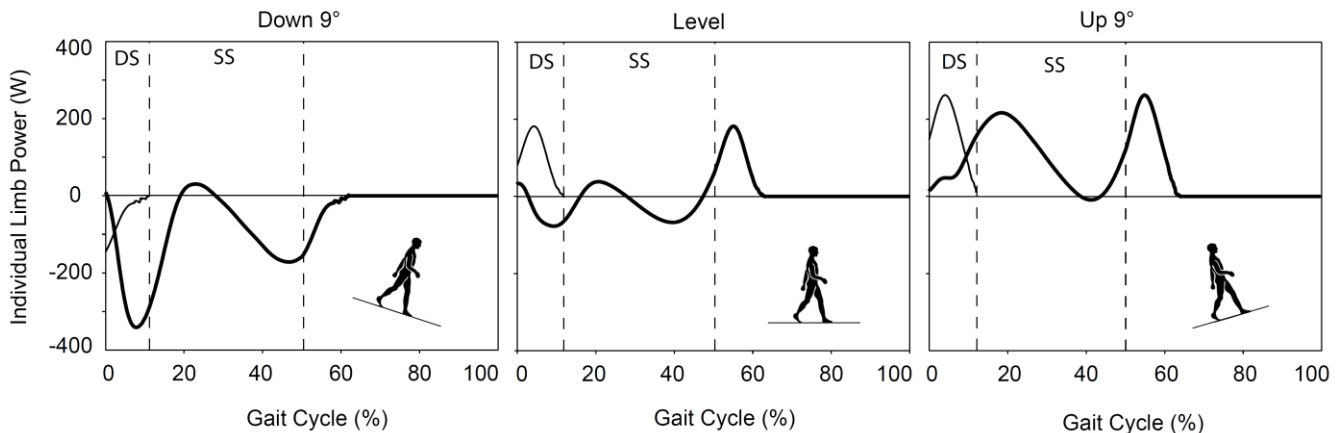


**Figure 1.** Individual limb power over an average stride illustrating the contribution of the leading (thick line) and trailing (thin line) legs during double support. DS: Double Support, SS: Single Support.

We used the individual limb method [4] to calculate the mechanical work performed on the CoM during 15 consecutive strides. This involved determining the CoM velocity by integrating the combined forces from both legs with respect to time. We then computed individual limb power as the dot product of CoM velocity and individual leg GRF, and individual limb work by integrating these power curves with respect to time. An analysis of variance (ANOVA) for repeated measures tested for significant main effects of grade ( $p < 0.05$ ).

## RESULTS AND DISCUSSION

We observed a prominent and progressive shift in the functions of the individual legs with steeper uphill and downhill grade (Fig. 1). Our results confirmed that when walking over level ground the leading and trailing legs simultaneously absorb ( $W_{ext}^-$ ) and generate ( $W_{ext}^+$ ) mechanical power during double support, respectively. In contrast, the leading and trailing legs both contributed progressively more to power generation with steeper uphill grade and to power absorption with steeper downhill grade.

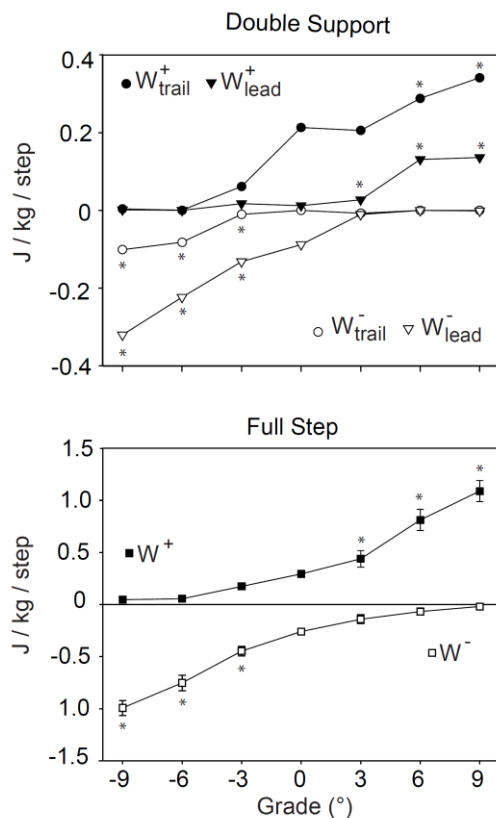


**Figure 2.** Individual limb work performed during double support and over a complete step. Double support (full step) values are means ( $\pm$  SE). \* Significantly different from level walking (All  $p$  values  $< 0.02$ ).

As expected, the  $W_{ext}^-$  performed by the leading leg became negligible with steeper uphill grade as the trailing leg performed progressively greater  $W_{ext}^+$  ( $p < 0.001$ , Fig. 2). Also as expected, the  $W_{ext}^+$  performed by the trailing leg became negligible with steeper downhill grade as the leading leg performed progressively greater  $W_{ext}^-$  ( $p < 0.005$ ). The residual contributions of  $W_{ext}^-$  when walking uphill and  $W_{ext}^+$  when walking downhill decreased to less than 5% of the work performed during a step at  $\pm 9^\circ$ .

More remarkable, the leading leg performed  $W_{ext}^+$  when walking uphill, and the trailing leg performed  $W_{ext}^-$  when walking downhill ( $p < 0.02$ , Fig. 2). In fact, when walking up  $9^\circ$ , the leading leg accounted for 28% of the total  $W_{ext}^+$  performed during double support (12% of the total  $W_{ext}^+$  performed during a step). Further, when walking down  $9^\circ$ , the trailing leg accounted for 24% of the  $W_{ext}^-$  performed during double support (10% of the total  $W_{ext}^-$  performed during a step).

## CONCLUSIONS

As expected, the trailing leg performs progressively greater  $W_{ext}^+$  with steeper uphill grade, and the leading leg performs progressively greater  $W_{ext}^-$  with steeper downhill grade. More remarkable, similar to an all-wheel drive vehicle, both legs simultaneously generate mechanical power to walk uphill and absorb mechanical power to walk downhill.

## REFERENCES

1. Margaria R. *Atti Accademia Nazionale dei Lincei* 7, 299-368, 1938.
2. Cotes JE, Meade F, *Ergonomics* 3, 97-119, 1960.
3. Minetti AE, Ardigo LP, Saibene F, *J Physiol* 471, 725-35, 1993.
4. Donelan JM, Kram R, Kuo AD, *J Biomech* 35, 117-124, 2002.
5. Gottschall JS, Kram R, *J Exp Biol* 209, 4895-900, 2006

## ACKNOWLEDGEMENTS

A grant from NIH (5T32AG000279) and a student Grant-in-Aid Award from the American Society of Biomechanics awarded to J.R.F. supported this study.

# FLEXOR MUSCLE COACTIVATION IS JOINT SPECIFIC

<sup>1</sup>Laura Frey Law, <sup>1</sup>Keith Avin, and <sup>2</sup>Chandramoulli Krishnan

<sup>1</sup>University of Iowa, Iowa City, USA

<sup>2</sup>Rehabilitation Institute of Chicago, Chicago, IL, USA

email: [laura-freylaw@uiowa.edu](mailto:laura-freylaw@uiowa.edu)

## INTRODUCTION

Coactivation, which is the simultaneous activation of the agonist and antagonist, is believed to be an important motor control strategy to improve joint stability during functional activities [1]. Mechanically, coactivation minimizes shear forces, while increasing stiffness and compressive forces, thereby improving knee stability [2]. Interestingly, the extent of coactivation may be sex specific, with females typically exhibiting higher antagonistic activity than males when performing a similar task. However, it is not clear whether these coactivation patterns are systemic (widespread across joints) versus muscle specific as previous investigations have focused predominantly on the knee. Thus, the purpose of this study was to examine flexor coactivation in two hinge joints, the knee and elbow, during maximal isometric and isokinetic strength testing in men and women.

## METHODS

52 healthy volunteers participated in the study: 28 males ( $26 \pm 6.1$  yrs,  $182.7 \pm 5.6$  cm,  $86.3 \pm 6.5$  kg) and 24 females ( $22.6 \pm 3.3$  yrs,  $169.2 \pm 6.1$  cm,  $66.1 \pm 12.3$  kg). Muscle activity was measured during maximal isometric and isokinetic strength testing (see below) using surface electromyography (EMG). Bipolar electrodes (Delsys Bagnoli, Boston, MA) were placed over the biceps femoris during knee extension and the biceps brachii during elbow extension testing. The EMG signals were pre-amplified 10 times locally and further amplified 1k or 10k times and bandpass filtered (20 – 450 Hz) using the Delsys anti-aliasing filter.

Subjects performed a 5-min joint specific warm-up. All isometric and isokinetic strength testing was completed using standard Biodex System 3 Isokinetic Dynamometer test poisoning for knee and elbow joints (Biodex, Biodex Medical Systems,

NY). Subjects were positioned so that the respective joint centers of rotation were aligned with the dynamometer axis of rotation. Range of motion (ROM) limits were set from full extension ( $0^\circ$ ) to approximately  $120^\circ$  of knee flexion or  $140^\circ$  of elbow flexion. *Isometric Testing:* maximal isometric torque was measured at five positions across the available knee or elbow ROM ( $15^\circ, 35^\circ, 55^\circ, 75^\circ$ , and  $100^\circ$  for knee;  $15^\circ, 45^\circ, 60^\circ, 90^\circ$ , and  $110^\circ$  for elbow). *Isokinetic Testing:* Four to seven maximal isokinetic repetitions were performed at five angular velocities of 60, 120, 180, 240, and  $300^\circ/\text{s}$ .

The raw analog signals were sampled at 1000 Hz using a 16-bit data acquisition board (National Instruments, Austin, TX) and recorded using custom Labview 8.0 software (National Instruments, Austin, TX, USA). The digitized data were processed using 200ms linear envelopes (moving average, Labview 8.0 software). Antagonist muscle EMG was standardized using the respective peak concentric muscle contraction (% max) for each test condition (i.e., isometric angle and isokinetic velocity). Baseline noise was accounted for using nonlinear baseline correction techniques [3]. Coactivation was operationally defined as the median antagonist activity (% max EMG) level for each contraction type (5 angle-specific isometric and 5 velocity-specific isokinetic conditions) and each respective joint (knee or elbow).

Mixed, repeated measures analysis of variance (ANOVA) were used to test for differences in coactivation between men and women, between joints, and across contraction conditions (angle or velocity). Correlation coefficients were calculated between coactivation levels for each joint and contraction type (isometric vs. isokinetic). Significance was set at  $\alpha = 0.05$ .

## RESULTS AND DISCUSSION

There were no significant differences in coactivation across the five velocities ( $p=0.38$ ) or the five angles ( $p=0.073$ ). To maximize study power, these data were then collapsed into single mean coactivation levels for each joint and contraction type. During both isometric and isokinetic muscle contractions there were significantly greater coactivation at the knee than the elbow ( $p<0.001$ , see Figure 1a, b and Table 1). Women demonstrated significantly higher flexor coactivation for elbow contractions ( $p<0.001$ ), but not for knee ( $p>0.14$ ).

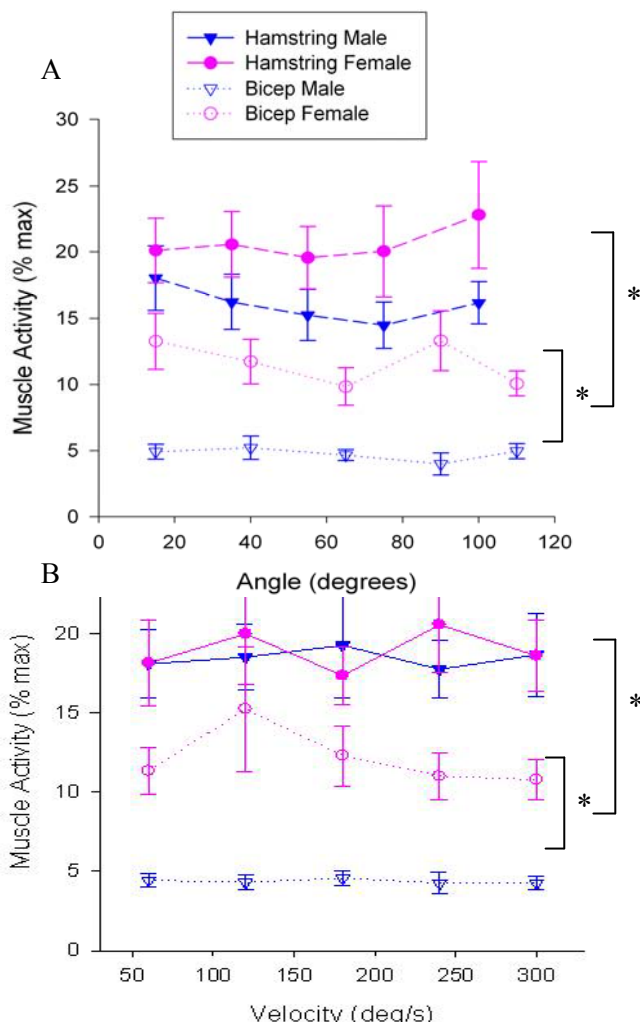


**Figure 1.** Mean (SEM) muscle coactivation for A) isometric and B) isokinetic contractions for knee and elbow joints in men and women. \*  $p \leq 0.05$ .

Coactivation was strongly associated between contraction types ( $r^2 > 0.48$  within joint, Table 2). However, significant moderate correlations between joints also occurred ( $r^2 = 0.06$  to  $0.19$ ).

**Table 1.** Mean (SEM) coactivation (% max) levels.

|       | Male      |           | Female    |           |
|-------|-----------|-----------|-----------|-----------|
|       | IsoM      | IsoK      | IsoM      | IsoK      |
| Knee  | 16.0(1.9) | 18.5(2.4) | 20.6(2.9) | 18.9(2.6) |
| Elbow | 4.7(0.6)  | 4.4(0.5)  | 11.6(1.7) | 12.1(2.0) |

**Table 2.** Spearman's rho (p-value) between mean coactivation (% max) levels.

|            | Knee IsoM          | Elbow IsoM         | Elbow IsoK |
|------------|--------------------|--------------------|------------|
| Elbow IsoM | <b>.44</b> (.001)  | -                  | -          |
| Elbow IsoK | <b>.34</b> (.02)   | <b>.78</b> (<.001) | -          |
| Knee IsoK  | <b>.69</b> (<.001) | .24 (.11)          | .28 (.06)  |

The results of this study indicate flexor coactivation patterns are joint-specific, thus predominantly driven by biomechanical or neuromuscular factors that are region specific. Approximately 50% of variability in coactivation was shared between static and dynamic contractions at each joint; whereas similar contraction types between joints only shared 8 to 19% variability. Accordingly, the systemic (across joint) influences are also present, but to a lesser degree. Surprisingly, muscle coactivation did not vary based upon the angle or velocity at which the contraction occurred; or between the isometric and isokinetic conditions, a finding consistent at both joints. Women demonstrated significantly greater coactivation only at the elbow, suggesting sex differences are not universal strategies, but can be region specific. Therefore, it appears that coactivation is a neuromuscular control response determined foremost by the joint of interest and secondarily by sex.

## REFERENCES

1. Kellis E, Baltzopoulos V. *Med Sci Sports Exerc* **30**:1616-1623, 1998.
2. Baratta R, et al. *Am J Sports Med* **16**:113-122, 1998
3. Frey Law et al. *J Biomechanics* **44**:202-205, 2011

## ACKNOWLEDGEMENTS

The authors were funded in part by the National Institutes for Health, K01AR056134, NRSA F31 AR056175, United States Council for Automotive Research (USCAR), and the Foundation for Physical Therapy.

# ELBOW EXTENSOR TORQUE AS A FUNCTION OF VIBRATION FREQUENCY

<sup>1</sup>Bernd Friesenbichler, <sup>1</sup>Aurel Coza and <sup>1</sup>Benno M. Nigg

<sup>1</sup>University of Calgary, Calgary, AB, Canada  
email: [berndf@kin.ucalgary.ca](mailto:berndf@kin.ucalgary.ca) web: [www.ucalgary.ca/hpl](http://www.ucalgary.ca/hpl)

## INTRODUCTION

Soft tissue vibrations are often the result of impacts during walking, running, skiing and other physical activities. Additionally, industry has developed vibration platforms, which artificially impose vibrations on the body and are used by the public as a workout tool with the aim to improve muscle performance and/or bone strength. Research on the effects of vibrations on muscle tissue addresses a wide range of crucial vibration parameters such as amplitude and frequency. It is, therefore, no surprise that the outcome of many studies varies substantially, so that beneficial [1] but also potentially harmful [2] effects of vibrations were reported with regards to muscle performance and structural integrity. However, the acute effects of vibrations on force generation have rarely been tested and are generally little understood. A systematic study of muscle force production and its dependency on superimposed vibrations could help researchers to tune vibration characteristics individually for their studies. As a first step, the current study investigates the influence of systematically changing vibration frequency on torque production of the elbow extensor muscles.

## METHODS

In order to superimpose vibrations on the triceps brachii muscle, a pneumatic vibrator was mounted onto the crank of a dynamometer. This setup allowed for the superposition of longitudinal vibrations transmitted through the wrist of the subjects. Eight healthy female subjects were instructed to perform a series of maximal voluntary contractions (MVCs) against the crank (elbow-extension). The upper arm to forearm angle (elbow angle) was set at 60, 90 and 120 degrees. At each angle, subjects performed one control MVC without vibrations and three MVCs with vibrations at different frequencies. Muscle torque was quantified

by the dynamometer, vibration frequency and amplitude were quantified using an accelerometer attached to the bony part of the wrist. Root mean square values (RMS) were calculated from electromyographic (EMG) activity of the triceps brachii, which was measured using surface electrodes. The EMG signal was filtered using a band-stop filter (20-40 Hz) in order to minimize mechano-vibratory artifacts in the signal. Vibration frequency was modulated by changing the input pressure to the pneumatic vibrator. All variables were synchronously recorded at 2400 Hz and averaged over a 0.5s period starting at the flat part of the torque-time curve. Torque and RMS values under vibration were compared to control using a paired Student's t-test (significance level:  $p < 0.05$ ) and Pearson correlation coefficients were used to correlate torque and RMS to vibration frequency.

## RESULTS AND DISCUSSION

The vibration frequency was between 20 and 40 Hz at an average vibration amplitude of  $5.9 \text{ mm} \pm 2.25 \text{ mm}$  (peak to peak). At a 60 degree elbow angle, average torque (normalized to control) was unaffected by vibrations ( $101.8 \% \pm 9.2 \%$ ) and was not correlated with respect to frequency ( $r = -0.2$ ). At 90 degrees, average torque was significantly lower with vibrations ( $93.2 \% \pm 11.3 \%$ ) and showed no correlation to vibration frequency ( $r = 0.02$ ). At the largest elbow angle, 120 degrees, average torque was significantly lower ( $86.2\% \pm 7.6\%$ ) and showed moderate correlation with vibration frequency ( $r = 0.64$ ; Fig. 1). At each angle the RMS values were significantly ( $p < 0.01$ ) increased with vibrations. When taking the results from each elbow angle into one dataset, vibration exposure appears in average to slightly suppress torque production, independent from vibration frequency (fig. 2). However, results between the three angles show noteworthy differences. At 60 degrees, torque was not affected by vibrations.

However, a significant torque decrease was observed at 90 degrees and a further decrease at 120 degrees. This indicates that the shorter the initial length of the triceps brachii, the less torque was produced under vibrations compared to control. The effect may be explained by disturbances of cross-bridge bindings within the sarcomeres of the triceps, initiated by the quick fiber stretch under vibration. At 60 degrees, the fibers of the triceps are presumably stretched to a length at which actin and myosin filaments are not fully overlapping anymore (descending limb of the force-length relationship). Since passive forces are increasingly engaged as the sarcomere length increases, disruption of cross-bridges may be partially compensated by passive structural elements. As the sarcomere length decreases, the influence of the passive structures and thus also the compensatory effects would diminish as the elbow angle increases. In addition, the stretch-reflex may be evoked at the position of greatest stretch (60 degrees) as vibrations are superimposed, in order to protect the muscle/tendon. As the muscle length decreases with increasing elbow angle, the Golgi tendon organs may experience lower absolute tension (less pre-stretch) and therefore may not be triggered, leading to no reflex contractions. Unlike the two smaller elbow angles, a correlation between torque and vibration frequency is present at 120 degrees (fig. 1). As the frequency increases, torque production under vibration approaches control values. The reason why this correlation is only present at this angle is unclear, however, it may be speculated that the ascending limb of the force-length relationship is susceptible to changes in vibration frequency for some reason. Significantly increased RMS activity has previously been observed during and immediately after vibration exposure, and was related to muscle spindle activation and additional recruitment of motor units due to the vibratory stimulus. However, the increased RMS values under vibration in this study did not relate to elevated torque. The elevated neural activation does not seem to be translated to torque production and has been reported previously [3].

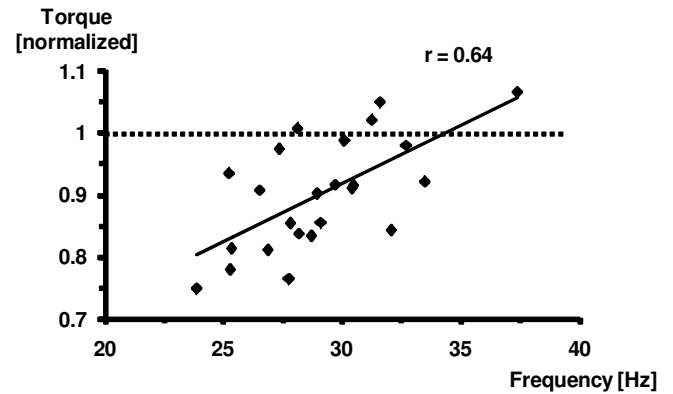


**Figure 1:** Torque as a function of vibration frequency at an elbow angle of 120°

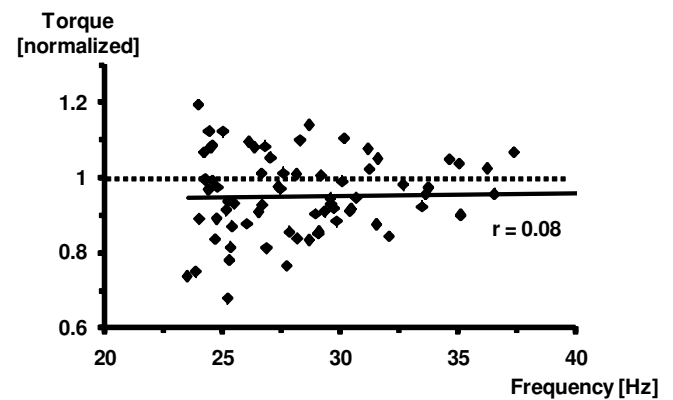


**Figure 2:** Torque as a function of vibration frequency from all three elbow angles.

## CONCLUSIONS

The results of this study showed that (a) elbow torque under vibration exposure decreases as the elbow angle increases, (b) torque development is not frequency dependent in general but (c) is possibly dependent on initial muscle pre-stretch. The frequency band tested in this study is relatively narrow and tests with a significantly wider band as well as systematically changing amplitude need to be conducted in order to understand the complex reactions of muscle during vibration exposure.

## REFERENCES

1. Bosco C, et al. *Eur J Appl Physiol* **79**, 306-311, 1999.
2. Necking LE, et al. *Scand J Plast Reconstr Hand Surg* **30**, 99-103, 1996.
3. Park, HS & Martin, BJ. *Scand J Work Environ Health* **19**, 35-42, 1993.

# THE DEVELOPMENT OF A METHOD TO INDUCE INJURIOUS HYPEREXTENSION OF THE FIRST METATARSOPHALANGEAL JOINT

<sup>1</sup>Rebecca Frimenko, <sup>1</sup>W.B. Lievers, <sup>1</sup>Patrick Riley, <sup>1</sup>Jeff Crandall, <sup>1</sup>Jim Bolton, and <sup>1</sup>Richard Kent

<sup>1</sup>University of Virginia, Charlottesville, VA, USA  
email: ref3jk@virginia.edu

## INTRODUCTION

Injury to the plantar plate (PP) of the first metatarsalphalangeal joint (1MTP), frequently referred to as turf toe (TT), is one of the more common foot injuries in American football. One review of professional football players<sup>1</sup> found that 45% of the 80 players surveyed had been diagnosed with TT during their career. TT can range in severity. In athletes, it is associated with an average time-loss of 6 days, with a range of 0 to 56 days<sup>2</sup>. First-hand accounts from injured athletes and their trainers indicate that TT most commonly occurs through hallux hyperextension<sup>1</sup>, but no *in vitro* studies have been performed to verify and quantify this mechanism. This paper describes the development of a test device capable of reproducing clinically relevant TT in cadaver limbs via hyperextension of the 1MTP.

## METHODS

Based on the available injury reporting, four key design specifications were established for the test device: 1) generate extension of the 1MTP that exceeds the natural range of motion (*viz.* 115° from neutral), 2) generate this extension at a nearly constant angular velocity representative of the rates present when injuries occur in the field, 3) maintain the axis of rotation of the proximal phalanx within the head of the first metatarsal, and 4) minimize noise due to vibrations of the system as the loading is applied. A minimum angular velocity of 8.73 rad/s at the 1MTP was targeted based on a concurrent study of athletes' performance in a range of tasks.

The foot fixture was designed to induce rotation at the metatarsophalangeal joints (Fig 1). This fixture consists of a stationary plate (foot plate) designed to be loaded by the metatarsal heads and a rotating

assembly (toe plate) designed to be loaded by the phalanges. Each of the plates was mounted to a six-axis load cell.

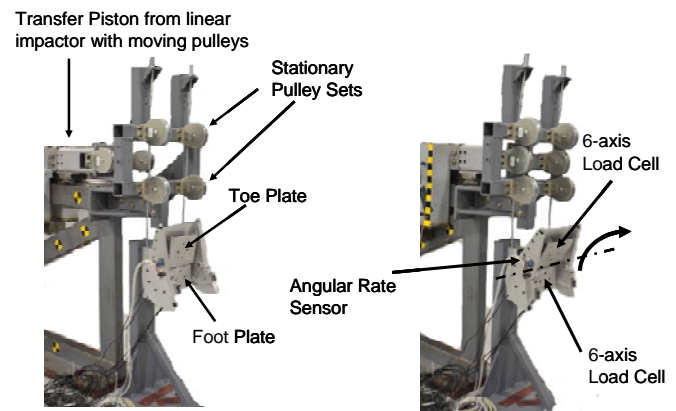


**Figure 1:** Foot fixture showing before and during impact interaction between the sets of pulleys, wire cables, and foot fixture.

Rotation of the toe plate was driven by the interaction of a linear impactor with cables wrapped around a cam mounted to the toe plate. The total angular displacement of the toe plate was controlled by limiting the stroke of the impactor, which was sufficiently massive (91 kg) that its motion could be assumed independent of the characteristics or even the presence of the loaded foot. The toe plate rotated about a fixed axis of rotation nominally passing through the rotation axes of all five proximal phalanges. The angular velocity of the toe plate was varied by changing the initial launch pressure of the linear impactor.

During pre-test preparation, each specimen was amputated immediately distal to the knee and fixed to a positioning tower. Arrays of motion-capture markers were screwed into to the proximal phalanx of the great toe and to the first metatarsal so that 6-degree-of-freedom motion of those structures could be measured. Markers were also mounted to the foot and toe plates. Specimens were dissected after

testing by orthopedic surgeons familiar with turf toe injuries.

Three cadaver feet have been tested to date. Significant compliance of the foot was observed in the first test. This compliance effectively off-loaded the 1MTP as the toe plate rotated and prevented an injurious level of angular displacement at the 1MTP. To reduce this foot compliance and allow for injurious loading of the 1MTP, a platform was added to limit posterior displacement of the calcaneus and an external fixation system was introduced between the tibia and the first metatarsal to limit midfoot compliance. Both subsequent tests used this modified foot mounting scheme. Data from the first test is not included in this analysis.

## RESULTS AND DISCUSSION

The transfer piston traveled at a linear velocity of 1.6 m/s in test 2 and at 1.3 m/s in test 3. In test 2 the angular velocity of the toe plate increased nearly linearly for 0.062 s before reaching a plateau of 20.9 rad/s for a period of 0.051 s (Fig 2). In test 3, which involved a lower launch pressure, the toe plate angular velocity took 0.081 s to reach a plateau of 17.5 rad/s, which was maintained for 0.062 s. The foot fixture rotated through 114° for each test. This rotation occurred over 0.126 s in test 2 and 0.154 s in test 3.

By design, the motion of the first proximal phalanx was not tightly coupled to the motion of the toe plate. Preliminary analysis of the motion capture data indicates that, while the toe plate rotated a total of 114° in all tests, the proximal phalanx of the great toe experienced 101° of rotation during test 2 and 90° during test 3. The loading in test 2 generated a peak 1MTP extension moment of 54.6 Nm, while the loading in test 3 generated 31.4 Nm.

TestS 2 and 3 generated clinically relevant injuries (Table 1) to the 1MTP, as described in Table 1.

Previous *in vitro* studies of lower extremity mechanics have included passive tensioning of intrinsic and extrinsic muscular load paths<sup>3</sup>. The pilot experiments reported here did not include this. Maintaining the structural integrity of the plantar aponeurosis was judged by the authors to be the top priority and the risk of damage by attempting to tension the intrinsic foot muscles was considered too high. Future tests may include passive tensioning of intrinsic and extrinsic tendons of the foot since it is possible that this will change the stress state and thus the injury tolerance of the PP.

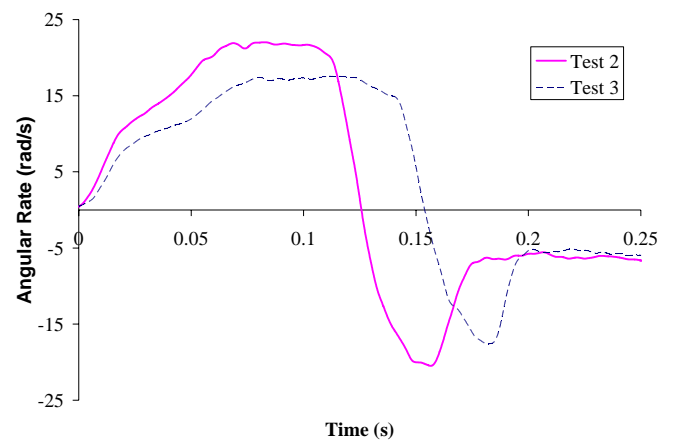


**Figure 2:** Plot of the toe plate angular velocity (rad/s) in tests 2 and 3.

## CONCLUSIONS

A test fixture was designed and built to generate turf toe, or ligamentous 1MTP injury, *in vitro*. Realistic dynamics of the 1MTP and clinically relevant injuries were produced.

## REFERENCES

1. Rodeo SA, et al. *Am. J. Sports Med.* **18**, 280-285, 1990.
2. Clanton TO, et al. *Foot & Ankle.* **7**, 162-176, 1986.
3. Funk JR, et al. *J. Biomech. Eng.* **124**, 750-757, 2002.

**Table 1:** Summary of test conditions and observed injuries in tests 2 and 3.

| Test | Specimen Age (yrs) | Angular Rate (rad/s) | Max Fixture Angle (deg) | Max Toe Angle (deg) | Observed Injury*                                     |
|------|--------------------|----------------------|-------------------------|---------------------|--|
| 2    | 69                 | 20.9                 | 114                     | 100                 | Lateral PP attenuation; medial PP tear; MCL avulsion |
| 3    | 69                 | 17.5                 | 114                     | 90                  | Medial PP tear; MCL avulsion                         |

\*PP – plantar plate; MCL – medial collateral ligament

# IMPROVED MESH FOR A FINITE ELEMENT MODEL OF FRACTURE RISK ASSESSMENT IN OSTEOGENESIS IMPERFECTA

<sup>1</sup>Jessica Fritz, <sup>2</sup>Nicole Grosland, <sup>3</sup>Peter Smith and <sup>1,3</sup>Gerald Harris

<sup>1</sup>Marquette University, Milwaukee, IL, USA

<sup>2</sup>The University of Iowa, Iowa City, IA, USA

<sup>3</sup>Shriners Hospital for Children, Chicago, IL, USA

email: jessica.fritz@marquette.edu

## INTRODUCTION

This study investigates an improved finite element (FE) mesh for long bone fracture risk analysis. Osteogenesis imperfecta (OI) is a heritable bone fragility disorder with several clinical types (I-VIII) which are characterized by skeletal deformity and “brittle” bones. It is estimated that the disorder affects 20,000 to 50,000 persons in the United States (1). OI bones exhibit abnormal mineralization and altered mechanical properties of bone tissue. Across all types, the poor bone quality poses major orthopaedic and rehabilitation challenges. Fractures in OI patients result from numerous factors, including altered bone material properties and geometry as well as loading on the bone. Risk of fracture is a major consideration when prescribing activity restrictions and physical therapy. Quantifying bone fracture risk would be an invaluable clinical tool for treating children with OI. FE models have the potential to provide patient-specific feedback on the effects of fracture risk factors in long bones, such as the femur and humerus. A patient-specific FE model of an OI type I patient’s femur during normal ambulation has been developed and assessed for fracture risk (2). This model was automeshed using tetrahedral elements in Abaqus. Although tetrahedral elements may be readily used to mesh virtually any structure, their behavior tends to be overly stiff. Consequently, hexahedral elements are often preferable. To improve the biofidelity of the fracture risk assessment model, a new all hexahedral mesh was developed using IA-FEMesh (3). The new model comprised a parametric study of the effects of lateral bowing, which included the level of bowing modeled in the original patient-specific FE analysis (Fig. 1).



**Figure 1. Coronal plane x-ray of the right femur with mild bowing from an OI type I patient.**

## METHODS

The current model was meshed in IA-FEMesh and analyzed with Abaqus (3). The femur geometry originated from a surface file of a reconstructed CT scan of an adult femur. Using IA-FEMesh, the femur was meshed with an outer cortical shell, inner cancellous layer and an intermedullary canal. Based on material property data from literature, the cortical and cancellous layers were assigned Young’s modulus values of 17 GPa and 15 GPa, respectively (4). Once the mesh was generated, it was scaled to match that of the original tetrahedral mesh. To introduce the bowing as illustrated in the coronal plane x-ray (Fig. 1) we relied on an FE displacement analysis.

Displacements were applied to a set of nodes corresponding to the apex of bowing and the model was run in Abaqus. The coordinates resulting from the applied displacement were calculated and assigned as the coordinates for the new ‘bowed’ mesh. Figure 2 shows how the loads from the kinetic results of gait and muscle forces were applied to the model (2). The full analytical set consisted of a series of seven models; one without

bowing, a second with 5 mm of lateral bowing and five more models where the bowing was incrementally increased by 10 mm. The FE model was run and analyzed for maximum von Mises stresses.



**Figure 2. FE model of bowed femur (15 mm).**

## RESULTS AND DISCUSSION

As expected, the results show that the maximum von Mises stress values increase with the level of bowing. Interestingly, it exhibits a linear relationship (Fig. 3).

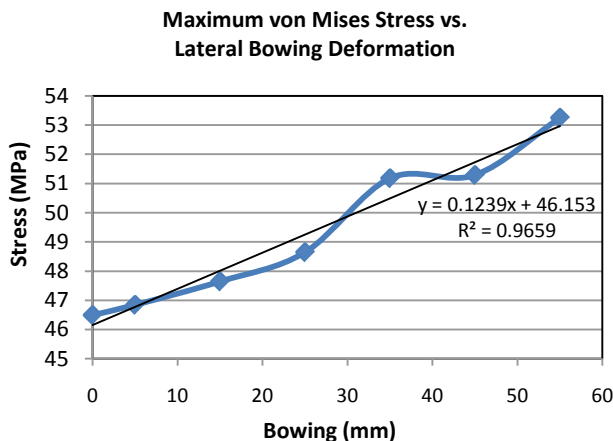


**Figure 3. Scatter plot of von Mises stress results.**

The original model with a tetrahedral mesh exhibited a maximum von Mises stress around 30 MPa for the same loading condition with lateral bowing of 7 mm. The maximum von Mises stress of the model with hexahedral elements is over 50% higher than that of the tetrahedral mesh. This indicates that the tetrahedral elements create a stiffer model than the hexahedral elements. However, the current model also had a cancellous

layer, whereas the original model had a single material with a Young's modulus of 17 GPa. This would account for a portion of the difference in stress levels seen with the same loading conditions.

The all hexahedral mesh resulted in a smoother geometry and mesh for the FE model. It allowed for smooth meshing of complex geometry. Since the model's ultimate goal is to examine femoral fracture risk in patients with OI, having a good mesh is essential to represent the complex and often abnormal geometry of OI femurs. The next step for the fracture risk assessment model is to examine the sensitivity to applied muscle forces and compare those results to the original model (4). Concurrently, studies are being conducted to better characterize the structure of OI bones, which is another contributing factor to fracture risk (6). The overall aim is to create and implement a method for patient-specific FE model to assess fracture risk and predict potential femoral fracture for persons with OI.

## REFERENCES

1. Osteogenesis Imperfecta Foundation, [www.oif.org](http://www.oif.org), March 16, 2011.
2. Fritz JM et al, *Med Eng Phys* **31**, 1043-1048 2009.
3. Groland NM et al, *Comput Methods Programs Biomed* **94**, 96-107, 2009.
4. Fan Z et al, *Connect Tissue Res* **48**, 70-75, 2007.
5. Fritz JM et al, *Biomed Sci Instrum* **45**, 316-321, 2009.
6. Jameson J et al, *Proceedings of SPIE*, Orlando, FL, USA, 2011.

## ACKNOWLEDGEMENTS

The contents of this abstract were developed under a grant from the Department of Education, NIDRR grant number H133E100007. However, the contents do not necessarily represent the policy of the Department of Education, and you should not assume endorsement by the Federal Government. We would also like to thank the MIMX lab members at The University of Iowa for IA-FEMesh training.

# KNEE JOINT MOMENT COMPARISON BETWEEN UNICOMPARTMENTAL KNEE ARTHROPLASTY AND HEALTHY INDIVIDUALS FOR STAIR ASCENT

<sup>1</sup>Yang-Chieh Fu, <sup>1</sup>Jae Pom Yom, <sup>2</sup>Ormonde M. Mahoney, <sup>1</sup>Kathy J. Simpson

<sup>1</sup>University of Georgia, Athens, GA, USA

<sup>2</sup>Athens Orthopedic Clinic, Athens, GA, USA

email: [ycfu@uga.edu](mailto:ycfu@uga.edu) web: <http://www.coe.uga.edu/kinesiology/research-service/biomechanics/>

## INTRODUCTION

Unicompartmental knee arthroplasty (UKA) can be used to replace either the medial (MED) or lateral (LAT) compartment if damaged by severe osteoarthritis. Based on unsatisfactory outcomes of earlier generations of component technology and surgical procedures, some surgeons are reluctant to use UKA and/or have a preconception that LAT-UKA clinical outcomes are not as good as MED-UKA [1]. However, knowledge of knee joint biomechanics of UKA patients for functional tasks, especially of LAT-UKA, is limited to support it. Moreover, whether the clinical outcomes and knee mechanics of LAT-UKA individuals are similar to MED-UKA remain controversial. Therefore, the purpose of the study was to compare the knee joint moments displayed during stair ascent of MED-UKA and LAT-UKA individuals to equivalent, healthy control (CON) individuals.

## METHODS

A total of 26 healthy unilateral UKA participants (20 Align 360<sup>®</sup> Unicompartmental Knee System; Cardo Medical, CA, 6 Zimmer<sup>®</sup> Unicompartmental High Flex Knee System; Zimmer, IN), 17 MED-UKA (14 Cardo and 3 Zimmer), 9 LAT-UKA (6 Cardo and 3 Zimmer), and 26 healthy CON participants who matched pair-wise with the individuals of the two UKA groups were recruited (Table 1). All participants had the UKA performed by the author (O. M. M.) at least 6 months prior to testing. All participants provided informed consent.

Reflective markers placed on the lower extremities and positions of markers were captured using high-speed infrared cameras (120 Hz), and ground reaction forces were collected (1200 Hz) via force platforms mounted in the floor and 1<sup>st</sup> step.

Participants walked up 4 stairs barefoot at a self-selected speed for 5 trials.

The limb of interest was the UKA limb for a UKA individual; and for a CON participant, it was the limb of the same dominance as the matched UKA individual. The stance phase when the limb of interest was on the first step was analyzed. Joint moments were generated followed standard inverse dynamics procedures. Peak knee joint moment magnitudes and times to peak moments common to all participants were compared between each UKA and the corresponding CON group using paired t-tests ( $p < 0.05$ ). Confidence intervals (CIs) were reported, and effect size was generated using Cohen's  $d$  [2].

## RESULTS AND DISCUSSION

No significant differences were found for any peak knee joint moment or time to peak moment values (Table 2). MED-UKA ( $0.38 \pm 0.07$  m/s) and LAT-UKA ( $0.37 \pm 0.05$  m/s) walked slower than their respective CON group (MED-CON =  $0.44 \pm 0.06$  m/s,  $p = 0.012$ ,  $d = 0.689$ ); LAT-UKA =  $0.43 \pm 0.05$ ,  $p = 0.009$ ,  $d = 1.165$ ).

The results of the current study showed that, generally, the MED-UKA, and possibly, the LAT-UKA group demonstrated knee kinetics of stair ascent that were not atypical. This is supported by confidence intervals similar to those of their respective CON groups combined with the lack of statistically-significant differences, and similar moment-time patterns and magnitudes to those reported in previous literature [3-5]. Values for our MED-UKA and LAT-UKA, maximum knee moments for all directions in this current study were within the range of values reported for young and older adults with healthy knees [3, 4].

Based on the CIs for peak joint moment magnitudes and time to peak moments, it is possible that group means of MED-UKA are within the corresponding population means of healthy individuals. However, sample size could also explain the lack of statistical differences. A *post-hoc* power analysis showed that a feasible sample size is 20 per group. As the sample sizes of the MED groups were slightly smaller than 20, there is some chance of Type II error.

For the LAT groups, except for extension moment magnitude, CIs for rest of peak joint moment magnitudes and time to peak moments are within the corresponding population means of healthy individuals. However, the lack statistically significant moment differences may be due, in part, to small sample size, and LAT groups might have higher chance of Type II error compared to MED groups in the study.

Both UKA groups showed slower walking velocities compared to CON groups. The tendency

( $p = 0.08$ ) for the LAT-UKA compared to LAT-CON group to display a lower peak flexion moment may suggest that sagittal knee kinetics affected LAT-UKA stair ascent speed. Flexion/extension kinetics about the hip and ankle joints may also have affected stair ascent speed of both UKA groups, but are not reported here.

In conclusion, it is likely that MED-UKA and, perhaps LAT-UKA individuals may demonstrate typical knee kinetics for stair ascent.

## REFERENCES

1. Verdonk, R., et al., *Knee Surg Sport Tra A*, **13**, 163-166, 2005.
2. Faul, F., et al., *Behav Res Methods*, **39**, 175-191, 2007.
3. Reeves, N. D., et al., *J Electromyog Kines*, **19**, e57-e68, 2009.
4. Lin, H.-C., et al., *J of Mech*, **21**, 41-50, 2005.
5. Novak, A. C. and Brouwer, B., *Gait & Posture*, **33**, 54-60, 2011.

**Table 1:** Participant characteristics (mean  $\pm$  SD).

|         | Gender (n)  | Age (yrs)      | Height (cm)     | Mass (kg)       |
|---------|-------------|----------------|-----------------|-----------------|
| MED-UKA | M: 6; F: 11 | 68.0 $\pm$ 7.4 | 162.7 $\pm$ 7.1 | 74.1 $\pm$ 12.3 |
| MED-CON | M: 6; F: 11 | 67.4 $\pm$ 8.9 | 165.4 $\pm$ 9.3 | 70.3 $\pm$ 14.0 |
| LAT-UKA | M: 3; F: 6  | 63.1 $\pm$ 7.8 | 167.2 $\pm$ 6.4 | 71.1 $\pm$ 13.3 |
| LAT-CON | M: 3; F: 6  | 63.1 $\pm$ 7.0 | 168.7 $\pm$ 8.0 | 70.0 $\pm$ 14.3 |

**Table 2:** Means  $\pm$  SD and 95% CI for peak knee joint moment magnitudes (N·m/body mass/leg length) and times to peak moments (% of stance phase) of all groups,

|                | Extension moment                 |                                 | Abduction moment                 |                                  | External rotation moment         |                                  |
|----------------|----------------------------------|---------------------------------|----------------------------------|----------------------------------|----------------------------------|----------------------------------|
|                | Magnitude                        | Time to peak                    | Magnitude                        | Time to peak                     | Magnitude                        | Time to peak                     |
| MED-UKA        | 1.21 $\pm$ 0.19<br>(1.11 – 1.31) | 30.2 $\pm$ 2.2<br>(29.1 – 31.4) | 0.63 $\pm$ 0.28<br>(0.48 – 0.77) | 71.8 $\pm$ 10.9<br>(66.2 – 77.3) | 0.10 $\pm$ 0.07<br>(0.06 – 0.14) | 78.9 $\pm$ 10.6<br>(73.4 – 84.4) |
| MED-CON        | 1.31 $\pm$ 0.30<br>(1.15 – 1.46) | 29.7 $\pm$ 3.5<br>(27.9 – 31.4) | 0.51 $\pm$ 0.30<br>(0.35 – 0.66) | 71.1 $\pm$ 12.7<br>(64.5 – 77.6) | 0.07 $\pm$ 0.07<br>(0.04 – 0.11) | 80.9 $\pm$ 7.8<br>(76.9 – 84.9)  |
| <i>p</i> value | 0.305                            | 0.305                           | 0.171                            | 0.862                            | 0.225                            | 0.526                            |
| Cohen's d      | 0.257                            | 0.154                           | 0.347                            | 0.043                            | 0.307                            | 0.157                            |
| LAT-UKA        | 1.02 $\pm$ 0.17<br>(0.90 – 1.15) | 30.4 $\pm$ 3.6<br>(27.6 – 33.2) | 0.40 $\pm$ 0.19<br>(0.26 – 0.54) | 68.2 $\pm$ 10.3<br>(60.3 – 76.1) | 0.07 $\pm$ 0.04<br>(0.04 – 0.10) | 81.4 $\pm$ 4.1<br>(78.3 – 84.6)  |
| LAT-CON        | 1.29 $\pm$ 0.31<br>(1.06 – 1.53) | 30.5 $\pm$ 3.2<br>(28.0 – 32.9) | 0.40 $\pm$ 0.20<br>(0.25 – 0.56) | 73.4 $\pm$ 10.3<br>(65.5 – 81.3) | 0.08 $\pm$ 0.04<br>(0.04 – 0.11) | 80.4 $\pm$ 7.0<br>(75.0 – 85.8)  |
| <i>p</i> value | 0.082                            | 0.932                           | 0.976                            | 0.386                            | 0.822                            | 0.710                            |
| Cohen's d      | 0.661                            | 0.029                           | 0.010                            | 0.306                            | 0.079                            | 0.128                            |

# WEAKNESS IN ANKLE DORSIFLEXORS REDUCES BALANCE RECOVERY ABILITY DURING A STANCE DISTURBANCE IN THE ELDERLY

Masahiro Fujimoto, Wei-Li Hsu, Paul van Donkelaar, Marjorie Woollacott and Li-Shan Chou

Department of Human Physiology, University of Oregon, Eugene, OR, USA

email: [chou@uoregon.edu](mailto:chou@uoregon.edu), web: <http://biomechanics.uoregon.edu/MAL/>

## INTRODUCTION

Controlling the center of pressure (COP) by ankle muscles is necessary to keep the center of mass (COM) within a desired region to achieve a stable upright standing. The base of support (BOS) provides such a range for possible COP movement, and the occurrence of stepping has been regarded as a consequence when the horizontal COM movement goes beyond the limits of BOS [1]. However, the functional base of support (FBOS), an effective area for COP movement, decreases with aging [2]. Decreases in FBOS indicate a constriction of the limits of stability, which would reduce an individual's ability to restore balance during a perturbed stance. Enhancement of ankle muscle strength was reported to lead to improvements in balance recovery to perturbations in the elderly [3]. Weakness in ankle muscles would contribute to a decreased FBOS, which could explain increased stepping incidences in the elderly when stance is perturbed. This study investigated the relationship between ankle muscle strength and FBOS as well as perturbation speed threshold that required a heel-rise or step to maintain balance.

## METHODS

Standing posture of 16 healthy young adults [8 men, 8 women; mean age  $25.4 \pm 4.3$  years] and 16 healthy elderly adults [7 men, 9 women; mean age  $74.9 \pm 6.2$  years] was perturbed with a backward support surface translation with the speed ranging from 15 to 70cm/s. Subjects stood with one foot on each of two electronically synchronized force platforms (Institute of Neuroscience, University of Oregon) with their arms folded on their chest and were asked to maintain their balance without moving their feet during perturbations. For all velocities, the platform displaced 15 cm, with different peak accelerations across trials. Motion data were captured with a ten-

camera motion analysis system (Motion Analysis, Santa Rosa, CA) at 120Hz. A total of 29 reflective markers were placed on each subject's bony landmarks. Additional 4 markers were placed on the corners of the moving platform to obtain platform movement. Ground reaction forces were collected at 960 Hz.

Responses to the platform perturbation were classified as in-place, step (STEP), or heel-rise (HR). An in-place response occurred when the feet remained in contact with the supporting surface throughout the trial. A STEP response occurred if a step was observed. A HR response occurred if the heel was raised more than 1% of their body height.

COP positions during sustained maximal forward and backward leaning were measured to determine the forward FBOS (FFBOS), backward FBOS (BFBOS), and total FBOS (TFBOS). FFBOS and BFBOS were calculated from the ankle joint, and TFBOS was the sum of FFBOS and BFBOS. Ankle plantar- and dorsi-flexor strengths (PF and DF, respectively) were measured during maximum voluntary contraction with BIODEX dynamometer (Biodex Medical Systems, NY).

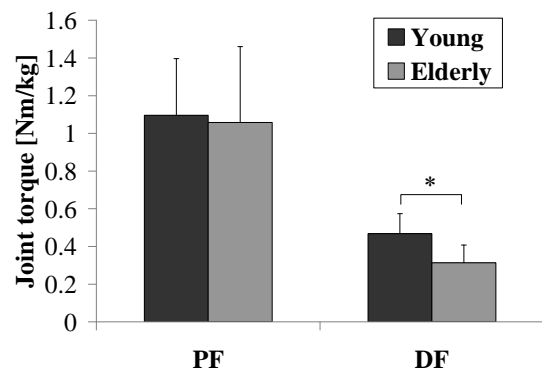


Figure 1: Ankle muscle strength ( $*p < .001$ )

An independent t-test was performed to examine group differences. Linear regression analyses were performed to examine the relationship between ankle muscle strength and FBOS measures as well as threshold perturbation acceleration for STEP and HR responses (TAccSTEP and TAccHR, respectively). Significance level was set at  $\alpha=.05$

## RESULTS AND DISCUSSION

As the perturbation speed increased, the number of STEP/HR responses increased, and 26% and 74% of HR responses were followed by STEP responses for the young and elderly subjects, respectively. Elderly subjects showed significantly smaller DF strength than young subjects, but no significant differences were found in PF strength (Fig.1). They also showed significantly smaller FFBOS, BFBOS, and TFBOS compared to young subjects (Fig.2). DF strength was found to significantly correlate with FFBOS, BFBOS, TFBOS, and TAccHR ( $p < .01$ ) with a moderate effect size ( $R^2 = .24 \sim .41$ ) (Table1).

Individuals with weaker dorsiflexor strength showed smaller FBOS measures and raised their heel during stance perturbations with smaller magnitudes, while plantarflexor strength didn't correlate with any of these measures. Moreover, most of elderly subjects took a step once they raised their heels, while most of the young subjects were able to restore their balance after heel-rise.

A previous study of quadripedal standing on their toes showed that backward translations induced muscle activity on tibialis anterior (TA), suggesting that balance recovery after heel-rise could require dorsiflexor activation [4]. It has been also reported that as the velocity of backward translation increased, muscle activations on the anterior aspect of the body appeared [5]. Dorsiflexor activity could be also important for balance maintenance during backward stance disturbance. Elderly subjects may

not be able to use their toes as effectively as younger subjects to control the COP due to weakness in ankle dorsiflexors, which would limit their ability to restore balance during stance perturbation.

## CONCLUSIONS

Ankle dorsiflexor strength was found to be significantly associated with FBOS measures as well as threshold perturbation speed for heel-rise. Elderly subjects could demonstrate a reduced ability to control the COP while standing on their toes due to ankle dorsiflexor weakness.

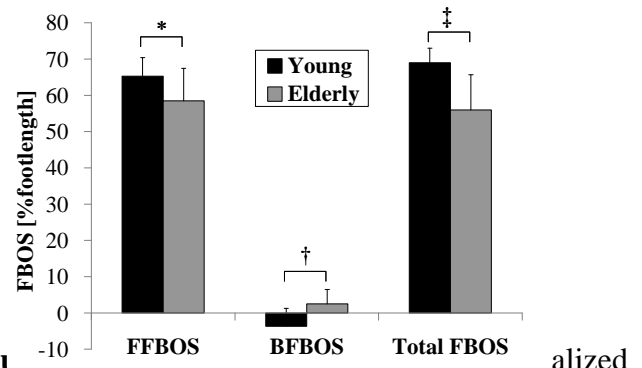


**Fig** 2. FBOS measures normalized by foot length (\* $p=.013$ , † $p=.001$ , ‡ $p<.001$ .)

## REFERENCES

1. Jensen JL, et al. *Exp Aging Res.* **27**(4), 361-376, 2001.
2. King JA, et al. *J Gerontol.* **49**(6), M258-263, 1994.
3. Hess JA, et al. *Aging Clin Exp Res.* **18**(2), 107-115, 2006.
4. Dunbar DC, et al. *Am J Phys Anthropol.* **69**(1), 93-105, 1986.
5. Runge CF, et al. *Gait Posture* **10**(2), 161-170, 1999.

## ACKNOWLEDGEMENTS

This study was supported by NIH Grant #AG05317.

**Table 1:** Results of Linear Regression Analyses

| Variables | FFBOS [m] |       | BFBOS [m] |       | TFBOS [m] |       | TAccSTEP [m/s <sup>2</sup> ] |       | TAccHR [m/s <sup>2</sup> ] |       |
|-----------|-----------|-------|-----------|-------|-----------|-------|------------------------------|-------|----------------------------|-------|
|           | $\beta$   | $R^2$ | $\beta$   | $R^2$ | $\beta$   | $R^2$ | $\beta$                      | $R^2$ | $\beta$                    | $R^2$ |
| PF[Nm/kg] | 0.009     | 0.02  | -0.002    | 0.00  | 0.010     | 0.02  | 0.42                         | 0.01  | -0.31                      | 0.01  |
| DF[Nm/kg] | 0.083*    | 0.24  | -0.060*   | 0.29  | 0.143*    | 0.41  | 3.48                         | 0.04  | 4.90*                      | 0.29  |

\* $p < .01$ .

# THE DEVELOPMENT OF ORTHOSIS IN CONSIDERATION OF ROTATION AXIS

<sup>1</sup>Takahiko Fukumoto, <sup>1</sup>Hiroshi Maeoka, <sup>2</sup>Toshio Ando

<sup>1</sup>Department of Physical Therapy, Faculty of Health Science, Kio University, Nara, Japan

<sup>2</sup>Research and Development Division, Okamoto Corp., Nara, Japan

email: t.fukumoto@kio.ac.jp

web: <http://www.kio.ac.jp>

## INTRODUCTION

A lot of orthoses are developed recently. The orthosis has a purpose to control some articulations. Therefore it applies technique of the taping and put some stays. However, its technique is not often considered about a joint kinematics.

We developed some orthosis in consideration of eversion-inversion rotation axis of ankle joint this time. These orthosis are the ideal form that a rotational axis and a forced ways are perpendicular (Fig. 1). We developed the orthosis which guided an ankle to eversion course for sprain prevention. The purpose of this study was the orthosis effect measurement of during walking.

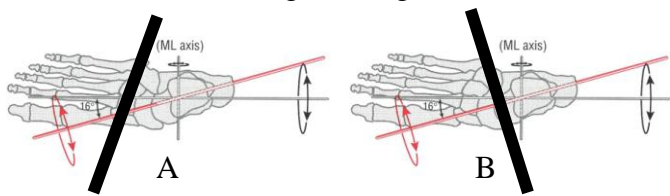


**Figure 1:** In a general way, the compelling force becomes in parallel with toe line (A). However, the compelling force should be a rotational axis and a right angle (B).



**Figure 2:** The position of the general derivation belt (A). The position of the belt which we developed (B).



**Figure 3:** Orthosis wearing. It is guided by figure of eight to eversion course.

## METHODS

Eight healthy young adults (male 4: age  $25.0 \pm 8.1$  years, height  $170.3 \pm 2.3$  cm, weight  $63.0 \pm 7.9$  kg, and female 4: age  $21.7 \pm 2.0$  years, height  $160.3 \pm 2.3$  cm, weight  $50.7 \pm 2.9$  kg) who had provided written informed consent beforehand participated in this study. We prepared 2 types of braces with different forced ways (Fig. 2,3). The participants were tested in three conditions of the "bare foot" "type A" "type B". The participants walked about 10m on floor reaction plate at each comfortable speed ( $3.9$  km/h,  $\pm 5\%$ ). Each participant was required to perform three trials at every type of brace and bare foot. A two axes electro-goniometer was fixed on the lateral ankle joint, and sagittal and frontal angles were measured during walking. The sampling frequency of the floor reaction plate and electro-goniometer was 100 Hz. We knew the heel strike time from a floor reaction plate. We extracted 1 gait cycle and were normalized. We compared the angle every phase.

## RESULTS AND DISCUSSION

These are sagittal and frontal angle of one gait cycle (Fig 4,5).

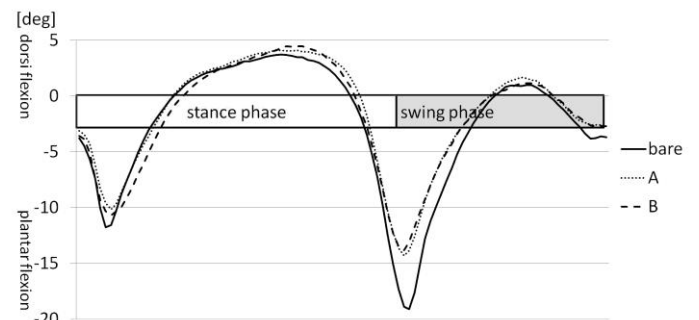


**Figure 4:** Sagittal angle of one gait cycle. The significant difference was not found in the sagittal angle between each group.

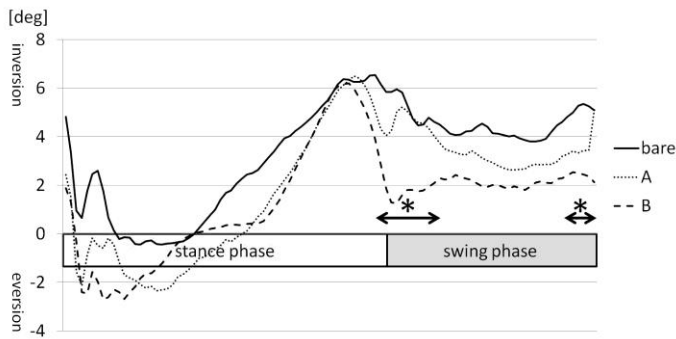


**Figure 5:** Frontal angle of one gait cycle. \*:  $p < 0.05$ . It was significantly different in “Bare foot” and “type B”.

It followed that the angle measurement of a sagittal plane and the frontal plane resembled angle measurement by Perry’s gait analysis very much. Therefore, this mensuration was very accurate.

The significant difference was not found in the sagittal angle between each group. In the frontal plane, it was significantly different from 61% to 73% (gait cycle) and from 89% to 99% in “Bare foot” and “Type B”.

The eversion inductivity of the type B is located in the fifth metatarsal bones basal part, and is right-angled to the rotation axis. There may be the run of

the peroneus group of muscles in the very efficient place.

We ought to develop the orthosis in consideration of an articular rotation axis in future.

## CONCLUSIONS

We developed an orthosis in consideration of a rotation axis. We observed the effect of the orthosis by measuring a walking ankle angle. The brace significantly guided a walking ankle to eversion course. We ought to make all orthoses and taping in consideration of an articular rotation axis.

## REFERENCES

1. Donald A et al: Ankle and Foot. Kinesiology of the musculoskeletal system: Foundations for Physical Rehabilitation. 477-521, Mosby, 2002
2. Donald A et al: Kinesiology of walking. Kinesiology of the musculoskeletal system: Foundations for Physical Rehabilitation. 523-569, Mosby, 2002
3. Jacquelin Perry: Ankle-Foot Complex. Gait Analysis: Normal and Pathological Function. 51-82, Slack Inc., 2010.

# DOES THE DEVELOPMENT OF TRANSIENT LOW BACK PAIN AFFECT POSTURAL CHANGES DURING PROLONGED STANDING?

<sup>1</sup>Kaitlin M. Gallagher, <sup>2</sup>Erika Nelson-Wong and <sup>1</sup>Jack P. Callaghan

<sup>1</sup>University of Waterloo, Waterloo, ON, CA

<sup>2</sup>Regis University, Denver, CO, USA

email: [kgallagh@uwaterloo.ca](mailto:kgallagh@uwaterloo.ca)

## INTRODUCTION

Asymptomatic individuals have been previously shown to clearly separate into low back pain (LBP) developer (PD) and non-pain developer (NPD) groups during a 2-hour bout of prolonged standing, with reports of 40-70% of subjects being characterized as PD[1-3]. Co-contraction of both the bilateral gluteus medius muscles[1-3] and trunk flexor-extensor muscle groups[1] has been shown to be elevated in PD during prolonged standing. This co-contraction may induce a “frozen” posture, which will prevent PD from performing both conscious (body weight shifts) and unconscious (center of pressure patterns) postural changes when standing for extended periods of time. These postural changes have been hypothesized to occur as a mechanism to reduce fatigue and discomfort while standing. The purpose of this study was to examine the relationship between postural changes and the subjective reporting of LBP during a 2-hour prolonged standing occupational simulation. It was hypothesized that PD and NPD would show different amplitudes and frequencies of postural changes and that these would change over time.

## METHODS

Forty-one subjects (20 male, 21 female) were recruited from the University of Waterloo student population. Exclusion criteria included any prior history of LBP requiring medical treatment or resulted in more than three days off work/school, previous hip surgery, inability to stand for greater than two hours, and having an occupation that required prolonged standing.

Participants completed a 2-hour prolonged standing protocol on a level surface. Each participant rated their discomfort on a visual analog scale (VAS) when they entered the lab on collection day and

every 15 minutes during the standing protocol. The VAS score was used to classify each participant as a PD or NPD. Two force plates were used to separately measure the ground reaction forces under the left and right foot (sampled at 1024 Hz) and the center of pressure (COP) was calculated under each foot.

Left foot COP shift, fidget, and drift patterns were defined for both the anterior-posterior and medial-lateral center of pressure using the methods of Duarte and Zatsiorsky[4]. Body weight (BW) shifts were defined using the vertical ground reaction force under the left foot. Symmetrical stance was defined as between 50±15% of their BW supported by the left leg. When the subject placed greater than 65% of their BW on their left leg, the stance was defined as asymmetrical and a shift onto their left leg, while below 35% supported by the left leg signified a shift onto the right leg. A shift was counted each time the subject passed either of the asymmetrical thresholds.

The 2-hour protocol was segmented into eight 15-min blocks. COP (shift, drift, fidget frequency and amplitude) and BW shift (frequency, duration, total time in an asymmetrical stance, and shifts onto the left leg) outcome measures were entered into a three-way linear model with between factors of gender and pain group (PD/NPD) and a repeated measure within factor of time (eight blocks) (significance of  $p<0.05$ ).

## RESULTS AND DISCUSSION

Thirty-two percent of participants developed low back pain in this study (four male, nine female). BW shift frequency increased ( $p<0.0001$ ) and average shift duration decreased ( $p=0.0006$ ) over the 2-hour protocol (Figure 1), which was independent of pain group. Interestingly, the

changes in both of these variables occurred up until the VAS scores of the PD began to increase[1]. After this point, both variables began to level off for the remainder of the protocol.

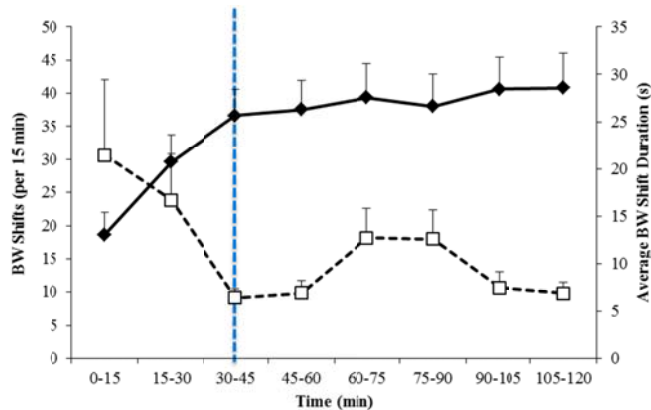


**Figure 1:** BW shift frequency (solid) & duration (dashed). The vertical dashed line represents the time of initial VAS score increase for PD[1].

There were only a few differences found between pain groups, with male PD varying the most from the other three groups. A three-way interaction was found for total BW asymmetry, with male PD spending more of the initial 45 minutes in a symmetrical stance than male NPD (Figure 2). Over time, Male PD increased the amount of time spent in an asymmetrical stance to a similar level of the male NPD. Gender by pain group interactions were found for ML center of pressure drift frequency, AP drift amplitude and percentage of total shifts to the left foot, but no consistent differences were found for each of these variables.

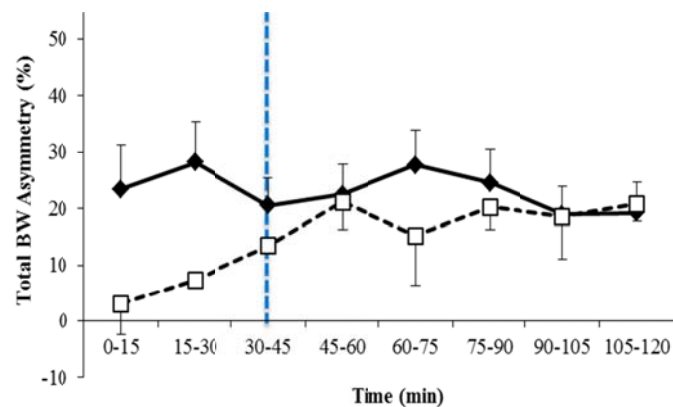


**Figure 2:** Total body weight asymmetry for male PD (dashed) & NPD (solid). The vertical dashed line represents the time of initial VAS score increase for PD[1].

Although it was hypothesized that the increased bilateral gluteus medius co-contraction would prevent PD from shifting during the standing protocol, very few differences were shown between the two groups. This is similar to previous literature looking at chronic low back pain patients and healthy individuals during a 30-min unconstrained standing protocol[5].

Although the two groups show similar postural changes, the mechanisms driving these changes may not be the same between the pain groups. As a result, PD may not receive the fatigue relieving effects that these postural changes potentially provide to NPD. The mechanisms utilized by the PD group resulting in bilateral co-contraction may be an inefficient or an aberrant motor control pattern, and as a result, cause pain and discomfort.

## CONCLUSIONS

Few differences were found between two pain groups, with male PD varying the most from the other three groups. Co-contraction did not prevent the PD from shifting into an asymmetrical stance; however, these subjects might have used an inefficient or aberrant motor control pattern to drive these shifts. Future work should look at how mechanisms during quiet standing are altered before and after a prolonged standing and whether an exercise intervention can alter any of these strategies, especially for the male PD.

## REFERENCES

1. Nelson-Wong E & Callaghan JP. *J Electromyog Kin* **20**, 256-63, 2010.
2. Nelson-Wong E et al. *Clin Biomech* **23**, 545-53, 2008.
3. Marshall P et al. *Hum Mov Sci* **30**, 63-73, 2011.
4. Duarte M & Zatsiorsky VM. *Motor Control* **3**, 12-27, 1999.
5. Lafond D et al. *Gait Posture*, **29**, 421-27, 2009.

## ACKNOWLEDGEMENTS

The authors would like to thank the Natural Sciences and Engineering Research Council (NSERC) of Canada and the Foundation for Physical Therapy for funding this project. Dr. Jack P. Callaghan is supported by a Canadian Research Chair in Spine Biomechanics and Injury Prevention.

# CONSIDERATIONS FOR THE USE OF C7 TRANSLAMINAR SCREWS IN CERVICOTHORACIC INSTRUMENTATION

<sup>1,2</sup>Anup Gandhi, <sup>1,2</sup>Swathi Kode, <sup>3</sup>Ryan Ilgenfritz, <sup>3</sup>Joseph Smucker,  
<sup>3</sup>Doug Fredericks, and <sup>1,2,3</sup>Nicole Grosland

<sup>1</sup>Department of Biomedical Engineering, <sup>2</sup>Center for Computer Aided Design,

<sup>3</sup>Department of Orthopaedics and Rehabilitation

The University of Iowa, Iowa City, IA

email: nicole-grosland@uiowa.edu

web: <http://www.ccad.uiowa.edu/mimx>

## INTRODUCTION

The unique bony anatomy of the C7 vertebrae poses a challenge for instrumentation at the caudal aspect of the cervical spine and cervicothoracic junction. Although widely used at C7, cervical pedicle screws placement is a challenge due to the close proximity of the vertebral artery and neurological structures [1].

Due to similar anatomic constraints, the use of translaminal screw fixation has become popular in the upper cervical spine (at C2) and upper thoracic spine (at T1 and T2) [3, 4]. Biomechanical analyses of such instrumentation has demonstrated the ability to control motion along multiple axes in order to provide a stable mechanical environment for fusion at these highly mobile segments [5]. Extrapolation of this data to clinical use at the C7 level has begun to develop in the literature, however, there is a current lack of objective data to support the safe use of C7 translaminal screws in patients [6].

The objective of this study was to determine experimentally the applicability of C7 translaminal screws in cervicothoracic instrumentation via a biomechanical analysis.

## METHODS

Eight C2 and six C7 vertebrae were harvested from nine human cadaveric spines (4 male and 5 female) for this study. In preparation for biomechanical testing, the specimens were thawed to room temperature and denuded of all soft tissue.

Bilateral crossing translaminal screws were placed in each C2 and C7 vertebrae (Figure 1) using previously described techniques [3, 4]. Based on

radiographic measurements of C7, 3.5mm diameter x 20mm long titanium poly-axial screws (Stryker Orthopaedics, NJ) were selected as the standard screw size and used universally in all specimens.

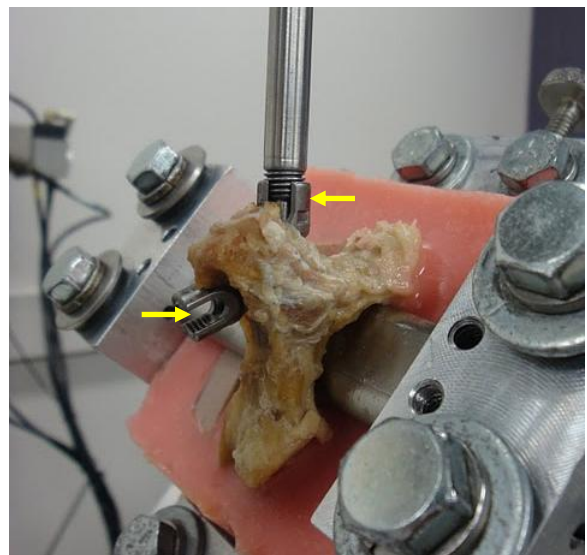


**Figure 1:** C7 vertebra implanted with bilateral translaminal screws axially aligned for pullout.

Each specimen was potted in PMMA and mounted on a material testing machine (858 MTS Mini Bionix II; Eden Prairie, MN). The specimen was cyclically loaded ( $\pm 50$ N) at the rate of 1Hz for 5,000 cycles, parallel to the cranial-caudal axis of the vertebrae using a custom designed fixture. The displacement of the screw head was recorded after the first cycle and every 50 cycles thereafter. After cyclic loading, the screws were pulled in line with their central axis at a rate of 2.5 mm/min until an abrupt change in the slope of the load-displacement curve was noted (Figure 1). The peak load to failure (Newtons) and the mode of failure was recorded.

Following the testing of the C7 translaminar screws, bilateral pedicle screws were placed in each C7 vertebrae under direct visualization[2]. Biomechanical data was then obtained for each C7 pedicle screw using the aforementioned laminar screw protocol.

A student t-test was used to analyze the pullout strength measurements. For all statistical analysis, significance was set at  $p < 0.05$  value.

## RESULTS AND DISCUSSION

A total of twelve C7 crossing laminar screws were placed without complication or laminar cortical breach, in a total of six specimens. Four of the six C7 specimens had failure of the bony lamina-lateral mass junction before failure at the screw-bone interface. In these instances, the fracture occurred during load to failure testing of the first screw, making testing of the second screw not possible. The load at which fracture occurred in these specimens was recorded as “pull-out strength” for the single screw that was tested. Similar occurrences were not encountered during testing of the C7 pedicle screws or the C2 laminar screws. The mean load to failure after cyclic loading was  $452.9 \pm 206.24$  N for the eight C7 laminar screws tested.

A total of sixteen C2 crossing laminar screws were placed without complication or laminar cortical breach, in a total of eight specimens. The mean load to failure after cycling was  $384 \pm 284$  N for the sixteen C2 laminar screws tested.

A total of ten C7 pedicle screws were placed without complication or pedicle cortical breach, in a total of five specimens that had previously undergone testing with C7 laminar screw fixation. The mean load to failure after cycling was  $585 \pm 411.6$  N for the ten C7 pedicle screws tested.

Student t-test showed no statistically significant difference in load to failure values between C7 and C2 laminar screws ( $p = 0.506$ ), or load to failure between C7 laminar screws and C7 pedicle screws ( $p = 0.391$ ).

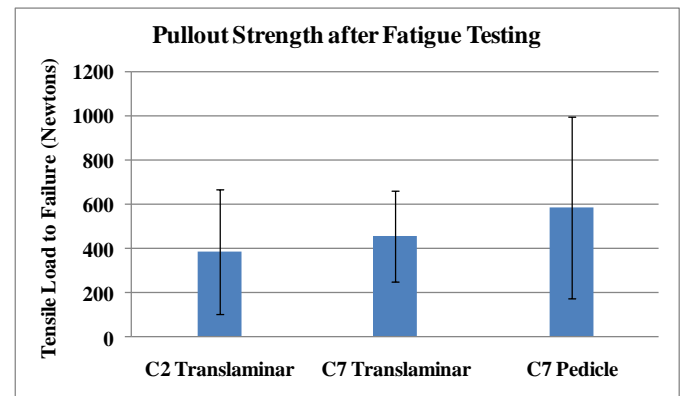


**Figure 2:** Mean screw pullout strength after cyclic loading.

## CONCLUSIONS

Biomechanical analysis performed in this study suggests that C7 translaminar screws are at least as strong as similar screw fixation at C2. According to biomechanical trends in this study, the load to failure for the C7 laminar screws was less than that exhibited by the C7 pedicle screws. However, there was no statistically significant difference between the C7 laminar screws and C7 pedicle screws. Additional work needs to be completed in order to safely apply this data to clinical practice. Hence, we plan to investigate the applicability of this technique by testing multilevel constructs.

## REFERENCES

1. Rhee JM, et al, *Spine*, **30**, E636-40, 2005.
2. Jones EL, et al., *Spine*, **22**, 977-82, 1997.
3. Kretzer RM, et al., *J Neurosurg Spine*, **5**, 527-33, 2006.
4. Wright NM, *J Spinal Disord Tech*, **17**, 158-62, 2004.
5. Cardoso MJ, et al., *Spine*, **33**, 2612-7, 2008.
6. Hong, J.T., et al., *Spine*, **33**, 1739-43, 2008.

## ACKNOWLEDGEMENTS

The authors would like to acknowledge Stryker (Stryker Orthopaedics, NJ) for donation of the screws.

# GAIT ADAPTATIONS WHEN WALKING ON A DESTABILIZING ROCK SURFACE

<sup>1</sup>Deanna H. Gates, <sup>1</sup>Jason M. Wilken, <sup>2</sup>Shawn J. Scott, <sup>1</sup>Emily H. Sinitski, and <sup>3</sup>Jonathan B. Dingwell

<sup>1</sup>Brooke Army Medical Center, Ft. Sam Houston, TX, USA

<sup>2</sup>Moncrief Army Community Hospital, Fort Jackson, SC, USA

<sup>3</sup>University of Texas at Austin, Austin, TX, USA

email: [deanna.h.gates@gmail.com](mailto:deanna.h.gates@gmail.com)

## INTRODUCTION

People frequently encounter a variety of different walking surfaces in their daily lives. The ability to compensate for the destabilizing effects of some of these surfaces is essential to maintain balance and prevent falls. Previous work on challenging walking surfaces primarily focused on changes in temporal-spatial parameters. Depending on the challenge of the walking surface, young adults may [1] or may not [2,3] adapt by decreasing their walking speed. In contrast, when negotiating uneven terrain, older adults typically adopt a more conservative walking pattern characterized by a slower walking speed [4], greater double support time [1] and wider steps [3]. Each of these studies instructed individuals to walk at a self-selected pace [3], which has generally been slower for uneven terrain [1,4]. As such, changes in step parameters may reflect changes in speed more than any differences in movement strategies. To date, no studies have examined what kinematic adaptations healthy adults make to successfully negotiate uneven terrain at controlled walking speeds. The purpose of this study was to quantify lower limb joint kinematics while subjects walked across a level walkway and a destabilizing surface (loose rocks) at four controlled speeds.

## METHODS

Fifteen healthy young adults ( $22 \pm 5$  years) participated. Subjects walked over two ground surfaces: level, over ground ('OG') and rocks ('RO'; Fig. 1) at each of 4 controlled speeds. Five strides for both the right and left foot were collected for each speed. Walking speeds were normalized to scale speed to each subject's leg length.

The motion of 55 reflective markers were tracked at 120 Hz using Motion Analysis (Santa Rosa, CA)

and used to construct a 15 segment rigid body model. Angular motions of the ankle, knee, and hip were calculated using Euler angles. Peak angles were assessed at multiple points in the gait cycle (Fig. 2). Step length (SL), time (ST), and width (SW) were calculated from the positions of the heel markers at heel contact. Foot angle was the sagittal plane angle between the heel and toe markers and horizontal at heel-strike [1]. A series of 2-factor (Surface x Speed) within-subjects ANOVAs were used to identify differences across speeds (1-4) and walking surfaces (OG v RO) for each dependent measure.



**Fig.1** Rock surface ('RO')

## RESULTS

### *Temporal-Spatial*

When walking at faster speeds, subjects increased their SL ( $p < 0.001$ ) and decreased their ST ( $p < 0.001$ ), but maintained constant SW ( $p = 0.634$ ). There were no differences in SL, ST, or SW between walking surfaces ( $p > 0.230$ ).

### *Kinematics – Stance*

Compared to level ground, subjects struck the ground with a relatively flatter foot when walking over the rock surface ( $p < 0.001$ ). Foot angles increased with walking speed ( $p < 0.001$ ). There was an absence of ankle plantarflexion during early stance when walking over the rock surface (Fig.

2A-B;  $p = 0.001$ ). The knee was more flexed during initial stance when subjects walked over the rock surface compared to level ground ( $p < 0.001$ ). Similarly, the hip was also more flexed during early stance over the rock surface ( $p < 0.001$ ). Peak ankle plantarflexion and peak knee and hip flexion all increased with walking speed ( $p < 0.001$ ).

Subjects dorsiflexed their ankles quickly during midstance, when walking over the rocks, such that they reached similar final positions prior to toe off as during level walking. They also reached similar peak extension at the hip and knee in late stance over both surfaces. While the differences at the ankle and hip were statistically significant, they were  $< 1^\circ$  on average.

### Kinematics – Swing

When walking over the rock surface, subjects exhibited increased hip, knee and ankle flexion during swing ( $p < 0.001$ ). Peak knee and hip flexion increased with walking speed ( $p < 0.001$ ), while ankle dorsiflexion decreased ( $p < 0.001$ ). There were significant speed  $\times$  surface interactions for all comparisons ( $p < 0.03$ ). Changes in peak hip and knee angle with speed were greater when subjects walked on the rocks than on level ground. At the ankle, dorsiflexion decreased with speed over level ground, but did not change in the rocks.

## CONCLUSIONS

The subjects in this study successfully negotiated the rock surface without changing their speed, SL, ST, or SW. These results suggest that subjects adapted to the rock surface by making preparatory adjustments to their posture prior to contact with the walking surface.

## REFERENCES

1. Menant JC, et al. *Gait Posture* **29**: 392-7, 2009.
2. Menz HB, et al. *Age Ageing* **32**: 137-42, 2003.
3. Thies SB, et al. *Gait Posture* **22**: 26-31, 2005.
4. Menant JC, et al. *Arch Phys Med Rehabil* **89**: 1970-6, 2008.

## ACKNOWLEDGEMENTS

Supported by Military Amputee Research Program (JWM), US Army Medical Specialty Corps Long-Term Health Education Training Fellowship (SJS) and NIH Grant 1-R01-HD059844 (JBD & JWM). The views expressed herein are those of the authors and do not reflect the official policy or position of Brooke Army Medical Center, the U.S. Army Medical Department, the U.S. Army Office of the Surgeon General, the Department of the Army, Department of Defense or the U.S. Government.

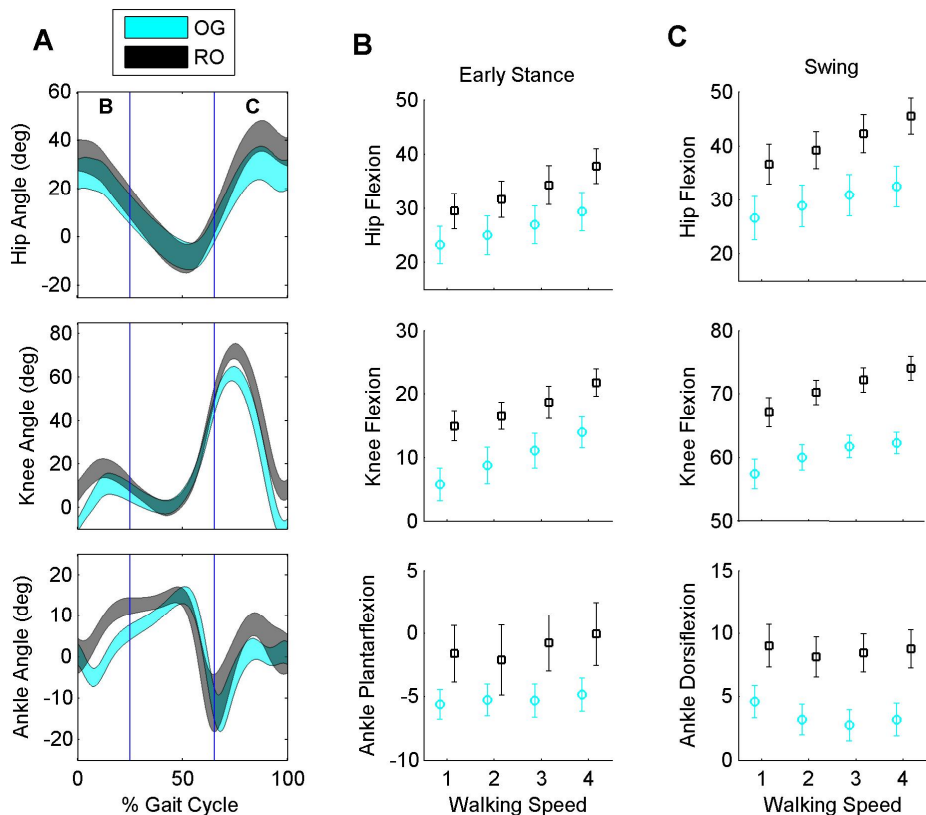


**Figure 1.** A) Bands represent the mean  $\pm$  standard deviation of the average joint angle across subjects. Peaks during early stance (B) were identified between 0 and 25% of the gait cycle. Swing phase peaks (C) were the maximum joint angle between 65 and 100% of the gait cycle. Errorbars represent the 95% confidence intervals about the mean. There were statistically significant main effects for walking speed ( $p \leq 0.001$ ) and walking surface ( $p < 0.001$ ) for all peaks presented in B and C.

# Force Changes During Passive Finger Movement

Andrew Georgeson and Joel Martin  
Pennsylvania State University, University Park, PA, 16802  
email: jrm496@psu.edu

## INTRODUCTION

The net force output of fingers during multi-finger pressing tasks is a product of both active and passive force production. The complex anatomical architecture of the hand causes fingers to unintentionally produce force when other fingers intentionally produce force [1, 2, 3, 4]. This unintentionally force production is partly due to passive properties of muscles, tendons and other tissues connecting the fingers. During object manipulation the CNS must account for the contribution of passive forces of fingers not explicitly involved in the task in order to successfully perform the action. Passive forces can make performing fine movements, requiring low forces, more difficult. The purpose of this study was to measure force changes in fingers as a subset of fingers was passively perturbed at different rates and magnitudes.

## METHODS

Six participants took part in the study (age:  $20.0 \pm 3.0$  yr; height:  $177.7 \pm 4.6$  cm; weight:  $75.4 \pm 12.2$  kg; mean  $\pm$  STD). All subjects were in good health and reported no disease or injury affecting finger/hand function.

The testing equipment consisted of four force transducers mounted on top of linear actuators that produced movement of the transducers in the vertical direction. Subjects sat facing the testing table positioned in approximately  $45^\circ$  of shoulder abduction,  $45^\circ$  of shoulder flexion, and  $45^\circ$  degree of elbow flexion. Subjects were told rest the tips of each finger on top of each transducer in a natural, comfortable finger joint configuration which was generally  $10\text{-}20^\circ$  of MCP flexion,  $45\text{-}60^\circ$  of PIP flexion, and  $15\text{-}30^\circ$  of DIP flexion.

The experimental procedure consisted of 225 trials in which different subsets of finger {I, M, R, L, IM, IR, IL, MR, ML, RL, IMR, IRL, IML, MRL, IMRL} were raised to three different heights (0.5, 1.0, and 2.0 cm) at three different speeds (0.5 cm/s, 1.0 cm/s, and 3.0 cm/s). The one and two finger combinations were performed twice and all other combinations were performed once for all combinations of height and speed. Subjects were instructed to rest their fingers on the sensors and not to react or voluntarily produced any force when the sensors were lifted. No force feedback was shown to the subjects, however; the experimenter was able to view the force changes during the experiment.

The data of interest were the force changes of all fingers during the finger raising. Force changes ( $\Delta F$ ) were computed as force immediately after the finger lifting movement ceased minus the background force prior to finger lifting. Mean and standard error (SE) of  $\Delta F$ 's were computed across subjects. A three-way repeated measures ANOVA was used to test for the effect of FINGER lifted, HEIGHT, and SPEED of  $\Delta F$  of both lifted and non-lifted fingers in *single* finger lifting trials.

## RESULTS AND DISCUSSION

The results presented will be limited to the  $\Delta F$ 's during single finger raising trials. They will be further divided into force changes of lifted and non-lifted fingers.

### *$\Delta F$ 's of Lifted Fingers*

All lifted fingers showed a positive  $\Delta F$ . The  $\Delta F$  was significantly affected by FINGER, HEIGHT, and SPEED ( $p < 0.001$  for all). The largest  $\Delta F$  for all fingers was observed at the 2.0 cm height and 3.0 cm/s speed combination (Fig. 1).

contains the  $\Delta F$ 's of non-lifted fingers for extreme conditions of speed and height of lift.

## CONCLUSIONS

The data exhibited several important features. First, the force changes of the lifted fingers showed a significant effect of height lifted and speed of lifting. The passive, spring-like properties of muscles were expected cause height to affect the force changes. Additionally, the viscous properties of muscles were expected to lead to a speed effect. Perhaps, the force changes of non-lifted fingers are more interesting. If pure mechanics were responsible for the force changes of non-lifted fingers they should have been equal to or less than zero. This was not the case as positive force changes were common. The reason for positive force changes is unknown. This study exemplifies the complexity of finger interaction, even in conditions in which no active force production was present.

## REFERENCES

1. Chao EY, et al. *J Biomech* **9**, 387-396, 1976.
2. Fahrer M. *The Hand*, Saunders, 1998.
3. Magnusson SP, *Scand J Med Sci Spo*, **8(2)**, 65-77, 1998.
4. Zatsiorsky VM, et al. *Biol Cybern* **79**, 139-150, 1998.

## ACKNOWLEDGEMENTS

We would like to thank Dr. Vladimir Zatsiorsky, Dr. Mark Latash, and the late Jim Metzler for their assistance with the study.

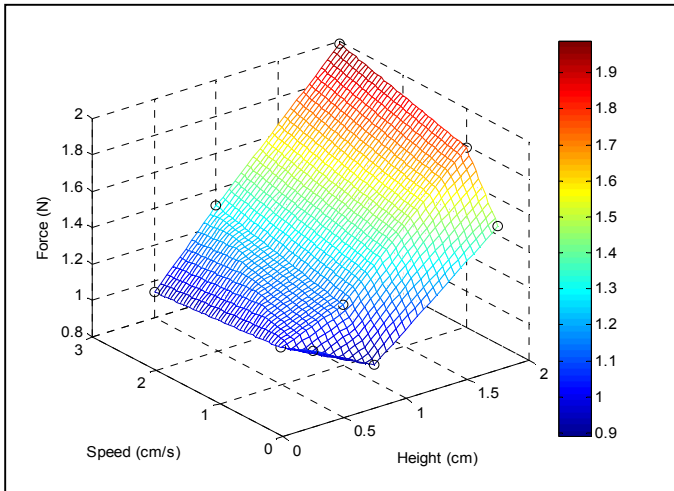


**Figure 1:** Force change of Index finger when raised versus speed and height of raising. Other fingers showed similar patterns. Black open circles represent data points averaged across subjects. Surface was fitted to these points.

### *$\Delta F$ 's of Non-Lifted Fingers*

The majority of  $\Delta F$ 's of non-lifted fingers were negative for single finger lifting trials (81 of 108 instances). Generally, the magnitude of negative  $\Delta F$ 's were small ( $<0.26$  N in all cases). The documented positive force changes were quite small as well. The largest  $\Delta F$  was 0.11 N. The  $\Delta F$  of non-lifted fingers was significantly affected by SPEED for all fingers lifted. The effect of FINGER lifted on non-lifted finger force changes was significant when R- and L-fingers were lifted, but not when I- or M-fingers were lifted. Table 1

**Table 1:** Force changes of fingers for minimum and maximum lifting conditions of single fingers. Mean across subjects with SE in parentheses.

| Finger | Height (cm) | Speed (cm/s) | Mean (SE)      |                |                |                |
|--------|-------------|--------------|----------------|----------------|----------------|----------------|
|        |             |              | I              | M              | R              | L              |
| I      | 0.5         | 0.5          | 1.076 (0.214)  | -0.092 (0.087) | -0.037 (0.082) | -0.005 (0.099) |
| M      | 0.5         | 0.5          | 0.011 (0.085)  | 0.820 (0.134)  | -0.038 (0.054) | -0.013 (0.057) |
| R      | 0.5         | 0.5          | 0.014 (0.119)  | -0.025 (0.143) | 0.633 (0.128)  | -0.020 (0.068) |
| L      | 0.5         | 0.5          | 0.029 (0.113)  | -0.098 (0.110) | 0.056 (0.176)  | 0.713 (0.164)  |
| I      | 2           | 3            | 1.989 (0.240)  | -0.140 (0.122) | -0.015 (0.102) | -0.026 (0.104) |
| M      | 2           | 3            | -0.256 (0.142) | 1.782 (0.216)  | -0.190 (0.144) | -0.141 (0.133) |
| R      | 2           | 3            | -0.044 (0.111) | -0.180 (0.142) | 1.323 (0.170)  | -0.183 (0.095) |
| L      | 2           | 3            | -0.094 (0.126) | -0.257 (0.102) | -0.227 (0.100) | 1.640 (0.183)  |

# EXPERIMENTAL VALIDATION OF A FINITE ELEMENT MODEL OF THE COMPOSITE PELVIS USING DIGITAL IMAGE CORRELATION

<sup>1</sup>Rajesh Ghosh, <sup>1</sup>Sanjay Gupta, <sup>2</sup>Alexander Dickinson and <sup>2</sup>Martin Browne

<sup>1</sup>Department of Mechanical Engineering, Indian Institute of Technology Kharagpur, West Bengal, India

<sup>2</sup>Bioengineering Research Group, School of Engineering Sciences, University of Southampton, UK

email: [sangupta@mech.iitkgp.ernet.in](mailto:sangupta@mech.iitkgp.ernet.in), [doctor@soton.ac.uk](mailto:doctor@soton.ac.uk)

## INTRODUCTION

Finite element (FE) analysis of bone has often been used to test clinical hypotheses. However experimental validation is necessary to assess the quality of the numerical predictions [1-4]. The aim of this study is to experimentally validate a 3D FE model of an analogue composite pelvis under load using the digital image correlation (DIC) technique.

## METHODS

One large left fourth generation composite pelvis (model 3405, Sawbones AG, Sweden) was used to assess strain measurement in the loaded pelvis. Random speckle patterns were applied on the regions of interest with a compressed air brush. Specially designed fixtures were used to hold the specimen in an orientation representing heel contact in a normal walking cycle (Fig. 1). The pelvis was fixed at the sacroiliac joint and the pubis.

The hip contact force was applied vertically downwards through a 46mm diameter steel femoral head (Young's Modulus,  $E=200\text{GPa}$ ) attached to an Instron mechanical testing machine (Instron 8874, Instron Ltd., UK, capacity  $\pm 25\text{ kN}$  load cell). The displacement of the speckle patterns due to load application were recorded using 2MP digital cameras (Limesh GmbH, Germany). Subsequently, VIC 3D correlation software (Correlated Solutions Inc., SC, USA) was used to calculate the strain field. The equivalent 3D FE model of the tested composite pelvis was based on a CAD model obtained from the manufacturer (Fig. 2). The model was meshed with  $\sim 269,000$  ten-node tetrahedral elements using ANSYS v11 (ANSYS Inc., PA, USA). Linear isotropic homogeneous material properties were used for the foam ( $E=155\text{ MPa}$ ) representing the cancellous bone, and the glass fiber filled epoxy ( $E=16.7\text{ GPa}$ ) representing the cortical bone shell of the composite pelvis. The Poisson's ratio for all materials was 0.3. Three-dimensional asymmetric surface-to-surface contact elements were simulated between the femoral head and the acetabular cavity, with friction coefficient 0.1.

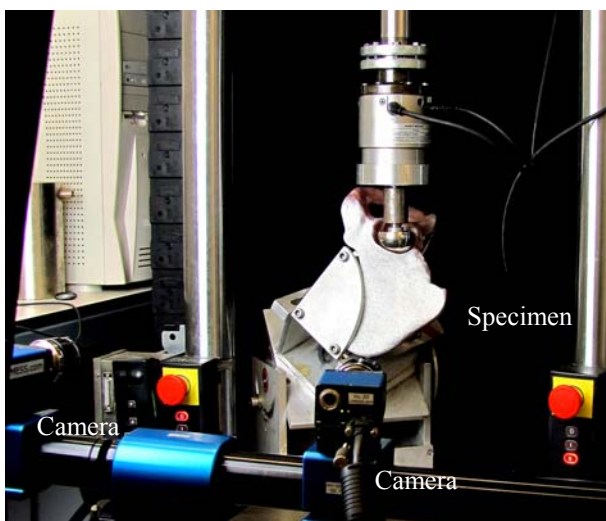


**Figure 1.** Experimental setup for DIC measurement.

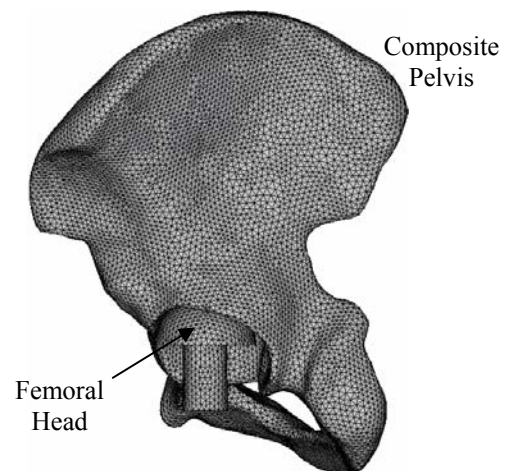


**Figure 2.** FE Model of the Composite Pelvis.

Applied loading and boundary conditions were equivalent to the experiment. Eight load cases with hip contact force varying between 700N and 1400N were chosen to compare FE and experimentally measured strain patterns. For brevity, results corresponding to one such load case (hip contact force=1400N) are presented. Regression analysis of strain values was undertaken to evaluate the quality of agreement between the FE and measured strains at comparable locations on the pelvis surface.

## RESULTS AND DISCUSSION

Quantitative DIC measurements of von Mises strain patterns were found to correlate very well with the FE strain distributions in the region of interest (ROI) as shown in Figures 3 and 4. Measurement repeatability was assessed in five successive experimentations with the same sample. High von Mises strain, ranging between 600 and 1200 microstrain ( $\mu\epsilon$ ), was observed in the ilium (ROI) due to application of hip contact force for the experimental and numerical analyses (Figs. 3 and 4). High correlation coefficient (0.91–0.95), low standard error (110–170  $\mu\epsilon$ ) and low percentage error in regression slope (9–14%) were observed between the FE and measured strain values at similar locations, indicating excellent agreement.

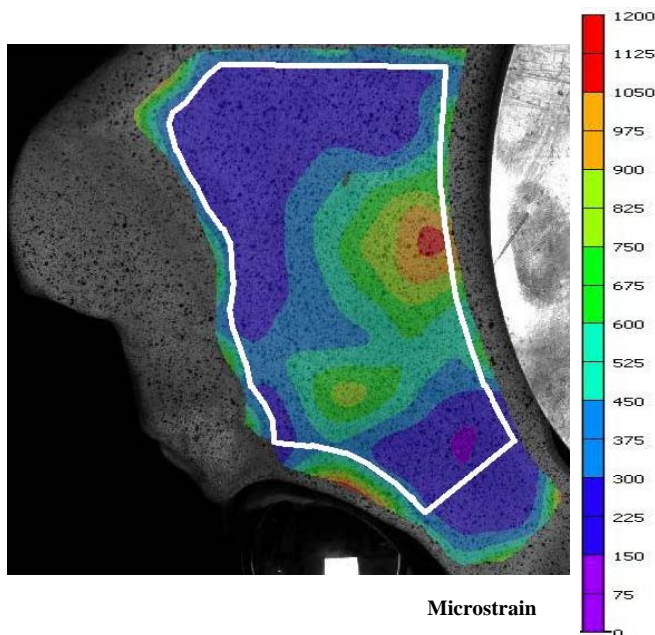


**Figure 3.** Experimental measurement of von Mises strain pattern using DIC technique.

However, some deviations in results were observed at locations around the curved irregular boundaries in the ROI, which may be attributed to the subtended acute angle in the viewing direction of the camera.

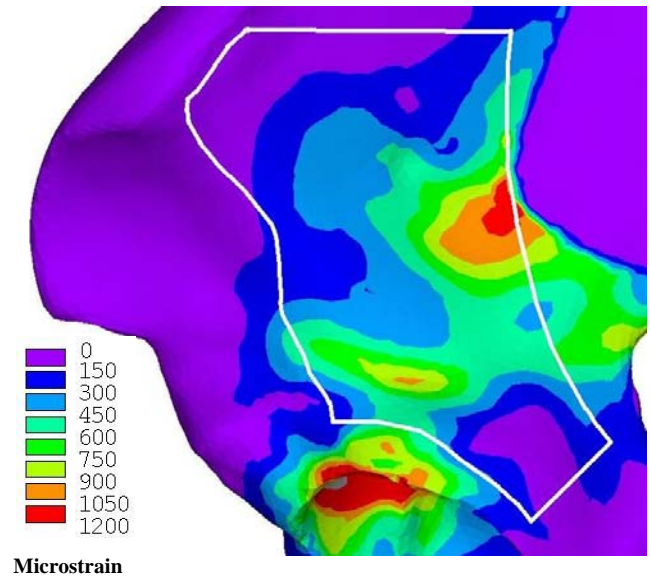


**Figure 4.** Distribution of von Mises strain in the equivalent FE model of the composite pelvis.

## CONCLUSIONS

Calculated FE strain patterns were in good agreement with those measured by the DIC technique. Therefore, the FE model was a valid predictor of the experimentally measured strain in the composite pelvis model, confirming its suitability for further computational investigations.

## REFERENCES

1. Pal B, et al. *J Biomech* **43**, 1923-1930, 2010.
2. Dickinson AS, et al. *J Biomech Engg* **133**, 014504-1-014504-6, 2011.
3. Anderson AE, et al. *J Biomech Engg* **127**, 364-373, 2005.
4. Dalstra M, et al. *J Biomech* **28**, 715-724, 1995.

## ACKNOWLEDGEMENTS

The authors are thankful to IIT Kharagpur, University of Southampton and UKIERI British Council for supporting this study.

# LOAD TRANSFER ACROSS THE PELVIC BONE DURING NORMAL WALKING

Rajesh Ghosh, Bidyut Pal, Debatri Ghosh and Sanjay Gupta

Department of Mechanical Engineering, Indian Institute of Technology Kharagpur, West Bengal, India  
email: [sangupta@mech.iitkgp.ernet.in](mailto:sangupta@mech.iitkgp.ernet.in)

## INTRODUCTION

Pre-clinical evaluations of acetabular prosthesis designs call for an accurate numerical model of the natural pelvis. Stress analysis of the pelvis during physiological loading conditions is necessary to understand the load transfer mechanism, its relation with bone morphology and to analyze the deviations in stress distributions due to implantation of the acetabulum. Despite a few experimental and finite element (FE) studies [1-3], the load transfer in the pelvic bone remains scarcely investigated, quantitatively. The purpose of the study is to develop a realistic 3-D FE model of a hemi-pelvis and to understand the stress distributions across the pelvis during a normal walking cycle.

## METHODS

Presumably, the method of application of the hip-joint reaction force on the acetabulum would have predominant effect on the quantitative values of stress and strain in the pelvis, in particular, the acetabular region. Accordingly, three FE models of the same right hemi-pelvis were developed using the CT scan data of a 62 year old female patient, (1) with a natural femoral head, (2) with a spherical femoral head, and (3) without any femoral head, force vectors directly applied on the acetabular cavity. The images of the pelvis were stored in 500 x 410 pixels, with a pixel size of 0.781 mm, slice thickness of 2.5mm. These models were meshed with ten-noded tetrahedral solid elements with element edge lengths of 0.5 – 3mm using ANSYS v11 FE analysis software (ANSYS Inc., PA, USA). The FE model of natural pelvis contained 183,700 elements. Additional 76,819 and 31,470 elements were generated for the models that included natural femoral head and the spherical femoral head, respectively. One such FE model is shown in Figure 1. The apparent density of each bone element was calculated using linear calibration of CT number of

bone, from which the Young's modulus ( $E$  in MPa) was determined using  $E = 3790 \rho^3$  [4]. Contact elements with a very low friction coefficient of 0.02 were simulated between the acetabular cavity and femoral heads (for natural and spherical). The Augmented Lagrangian contact algorithm was used for the contact simulation, with chosen values of contact stiffness and penetration tolerance required for the convergence of the non-linear solution. Applied loading conditions were based on eight different phases of the normal walking cycle, designated as eight load cases, similar to the study by Dalstra et al. [2]. Data on the musculoskeletal loading conditions that included the action of twenty one muscle forces and hip-joint reaction force were obtained from earlier studies [2,3]. The hip-joint reaction force was applied at the centre of the femoral head (Fig. 1). The muscle ( $m.$ ) forces were applied as distributed loads on the surfaces of those elements which were located in the respective areas of insertion [2,3]. Fixed constraints were applied at the pubis and the sacro-iliac joint (Fig. 1).

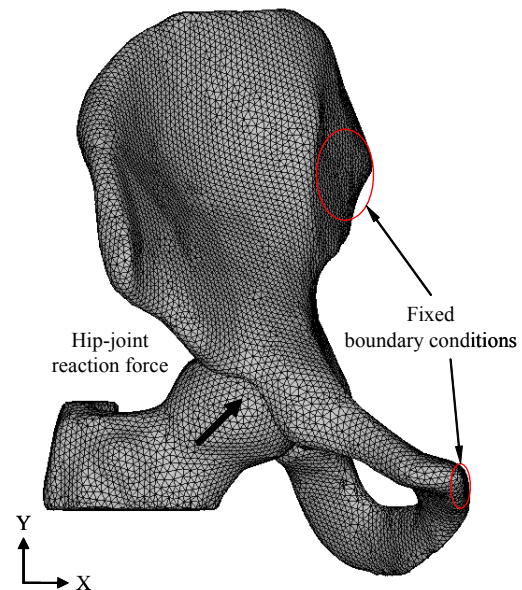


**Figure 1.** Finite element model of pelvis with the proximal femur.

Stress distributions in these three FE models were compared to evaluate the most realistic method of load application for the hip-joint reaction force.

## RESULTS AND DISCUSSION

Stress distributions were obtained for all the load cases. Results for the load case 2 (beginning of single support phase; 13% of gait cycle) was considered, since the magnitude of the hip-joint reaction force is maximum for this load case. Although the von Mises stress distributions at the ilium, ischium and pubis of the pelvic bone were very similar for all the three models, considerable differences were observed around the acetabulum. Maximum von Mises stress of 67 MPa was observed at the anterior rim of the acetabulum for the pelvic bone with the natural femoral head, as compared to ~90 MPa in the similar location for the other two models. This difference may be attributed to the method of load application, which causes differences in the stresses distributions due to bending in a localized region of the acetabulum. Therefore, the FE model of the pelvic bone with a natural femoral head appears to predict stress distributions across the pelvis, realistically.

The muscle forces have a considerable effect on the stress distributions in the pelvic bone. Stress distribution (von Mises) across the pelvic bone is presented in two views (lateral and medial) in Figure 2. High stresses (20–45 MPa) were generated around the posterior and anterior part of the ilium, which is caused due to the action of hip joint reaction force, m. gluteus and the constraint condition at the sacro-iliac joint (Figs. 2a,b). Stresses of 5–20 MPa were generated around ischium, due to the action of forces exerted by m. gemellus superior, m. semimembranosus and semitendinosus (Fig. 2a). Around the acetabulum, the high compressive stresses (20–30 MPa) were observed in the superior acetabular wall. High stresses (20–45 MPa) were also generated in the pubis region due to the action of hip-joint reaction force, m. adductor and constraint condition at the pubis (Figs. 2a,b). Similar results were predicted by earlier studies [2,3]. Moreover, very high stresses (45–67 MPa) were generated at the anterior rim of the acetabulum (Fig. 2a).

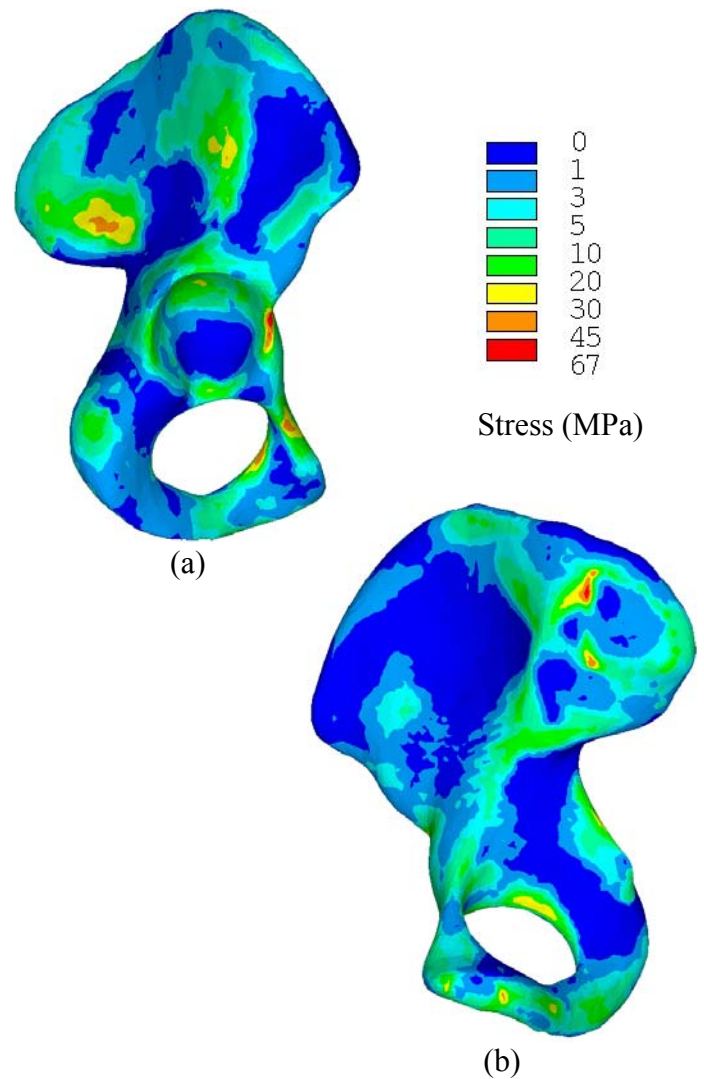


**Figure 2.** The distribution of von Mises stress in the pelvic bone; (a) lateral view, (b) medial view.

## CONCLUSIONS

A realistic FE model of the pelvic bone has been developed, which can be used in combination with the musculoskeletal model of forces to numerically predict stress distributions across the pelvis.

## REFERENCES

1. Anderson AE, et al. *J Biomech Engg* **127**, 364-373, 2005.
2. Dalstra M, et al. *J Biomech* **28**, 715-724, 1995.
3. Phillips ATM, et al. *Med Engg & Physics* **29**, 729-748, 2007.
4. Carter DR and Hayes WC. *J Bone Joint Surg Am* **59**, 954-962, 1977.

# JOINT MOMENTS DURING STAIR DESCENT: STEP-BY-STEP VERSUS STEP-OVER-STEP

<sup>1</sup>Jason Gillette, <sup>2</sup>Catherine Stevermer, and <sup>3</sup>Michelle Hall

<sup>1</sup>Iowa State University, Ames, IA, USA

<sup>2</sup>Des Moines University, Des Moines, IA, USA

<sup>3</sup>University of Melbourne, Victoria, Australia

email: gillette@iastate.edu

## INTRODUCTION

The ability to complete stair descent movements is a common requirement for mobility in public and home environments. Stair descent is mechanically challenging in that it involves controlled lowering of body weight from one step to the next. Numerous populations, including older adults and those with lower extremity pain, may find stair descent to be difficult. Older adults reduce their ankle plantarflexion moments when descending stairs, but still utilize a higher percentage of knee extension moment capacity than young adults [1]. Young women with patellofemoral pain reduce knee angular velocities during stair descent [2], while older adults with knee osteoarthritis display increased impulsive loading as compared to level walking [3]. One compensatory strategy for those who struggle with stair descent is to use a step-by-step instead of a step-over-step technique. Since it involves dual stance on each step, a step-by-step technique would be expected to reduce impulsive loading and likely reduce lower extremity joint moments in the sagittal plane. However, a step-by-step technique would also result in reduced forward momentum, which could increase demands on frontal plane movement control. Increased frontal plane joint moments with the step-by-step technique would be of concern as a potential fall risk.

The purpose of this study was to determine lower extremity joint moments during stair descent when using the step-by-step as compared to the step-over-step technique. Analyzing peak joint moments during the stair descent initiation for step one and the continued descending movement for step two were of interest. It was hypothesized that the step-by-step technique would result in reduced ankle plantarflexion and knee extension moments during stair descent.

## METHODS

Twenty individuals (gender 4/16 M/F, age  $22\pm 2$  yr, height  $1.70\pm 0.06$  m, mass  $67\pm 14$  kg) participated in this study. Twenty-six reflective markers were tracked by an eight-camera system (Vicon). Portable force platforms (AMTI) were located on step one and two of a three step staircase (19 cm step height, 28 cm tread depth). Participants started from rest at the top of the staircase, descended three steps to ground level, and continued walking two meters. The step-over-step technique involved alternating single footfalls on each step, while the step-by-step technique involved dual footfalls on each step. Participants descended the stairs at a self-selected speed with freely swinging arms. Each stair descent technique was performed twice with a right and a left lead for a total of eight trials.

Step initiation and termination were detected when the vertical ground reaction force first reached and fell below 5% body weight. For step-over-step, the weight acceptance phase was defined as the first 50% of single stance and the descent continuance phase as the remaining 50% of single stance. For step-by-step, weight acceptance was defined as step initiation until dual stance initiation and descent continuance as dual stance termination until step termination. Dual stance initiation and termination were detected using heel and toe marker positions. Using inverse dynamics, sagittal and frontal plane joint moments were calculated at the ankle, knee, and hip. Peak joint moments during weight acceptance and descent continuance for steps one and two were normalized by body mass, averaged for left and right leads, and averaged across two trials. Paired t-tests were used to test for significant differences in peak joint moments for step-by-step as compared to step-over-step techniques. Significance levels were set to  $p < 0.05$ .

## RESULTS AND DISCUSSION

Significant differences in peak joint moments as a function of stair descent technique are shown in Table 1. Peak ankle plantarflexion moments were significantly increased with the step-over-step technique during weight acceptance and descent continuance for steps one and two ( $p < 0.02$ ). Peak knee extension moments were significantly increased during weight acceptance ( $p < 0.001$ ) and peak hip flexion moments were significantly greater during descent continuance ( $p < 0.001$ ) with the step-over-step technique for steps one and two. Peak hip abduction moments were also significantly increased with the step-over-step technique during weight acceptance for step one ( $p < 0.03$ ). In contrast, peak external knee varus moments were significantly increased with the step-by-step technique during weight acceptance and descent continuance for step one ( $p < 0.02$ ). In addition, peak knee extension moments were significantly increased during descent continuance of step one ( $p < 0.05$ ) and peak ankle inversion moments were significantly increased during descent continuance of step two ( $p < 0.02$ ) with the step-by-step technique.

The hypothesis that ankle plantarflexion moments would be reduced when using the step-by-step technique was supported by significantly lower peak values during weight acceptance and descent continuance for steps one and two. The hypothesis that knee extension moments would be reduced when using the step-by-step technique was only partially supported by lower peak values during weight acceptance during steps one and two. The

45% reduction in peak knee extension moments during weight acceptance when using step-by-step was the most dramatic difference observed, although this technique did not reduce peak knee extension moments during descent continuance. Distinct reductions in peak ankle plantarflexion and hip flexion moments during descent continuance with step-by-step was likely related to the reduced step length associated with this technique.

Taken together, it appears that using the step-by-step technique may benefit the individual by reducing potentially painful eccentric knee loading during weight acceptance and reducing ankle and hip strength requirements needed for step-over-step propulsion and step clearance. However, it is of concern that the step-by-step technique resulted in increased peak external knee varus moments during step one, since medial knee compression related to this type of loading has been linked to progression of knee osteoarthritis [4]. Further insight into lower extremity loading during stair negotiation would be gained by descending additional steps, analyzing stair ascent, measuring EMG to indicate muscle co-contraction, and studying populations such as older adults and those with lower extremity pain.

## REFERENCES

1. Reeves ND, et al. *J Electromyogr Kinesiol* **18**, 218-227, 2008.
2. Grenholm A, et al. *Clin Biomech* **24**, 88-94, 2009.
3. Liikavainio T, et al. *Knee* **14**, 231-238, 2007.
4. Miyazaki T, et al. *Ann Rheum Dis* **61**, 617-622, 2002.

**Table 1:** The effects of stair descent technique on lower extremity joint moments.

| Step, Phase | Peak Joint Moments (Nm/kg) |                    |                    |                    |                    |                    |
|-------------|----------------------------|--------------------|--------------------|--------------------|--------------------|--------------------|
|             | Ankle Plantarflexion       | Ankle Inversion    | Knee Extension     | Knee Varus         | Hip Flexion        | Hip Abduction      |
| SOS S1, WA  | <b>0.83 ± 0.15</b>         | 0.16 ± 0.05        | <b>0.67 ± 0.19</b> | 0.22 ± 0.09        | 0.27 ± 0.13        | <b>1.02 ± 0.16</b> |
| SBS         | 0.74 ± 0.18                | 0.15 ± 0.04        | 0.36 ± 0.21        | <b>0.25 ± 0.10</b> | 0.28 ± 0.16        | 0.97 ± 0.16        |
| SOS S1, DC  | <b>1.05 ± 0.11</b>         | 0.15 ± 0.06        | 1.15 ± 0.15        | 0.09 ± 0.08        | <b>0.40 ± 0.14</b> | 0.86 ± 0.15        |
| SBS         | 0.93 ± 0.13                | 0.15 ± 0.06        | <b>1.21 ± 0.22</b> | <b>0.13 ± 0.08</b> | 0.31 ± 0.14        | 0.89 ± 0.15        |
| SOS S2, WA  | <b>0.90 ± 0.20</b>         | 0.13 ± 0.05        | <b>0.64 ± 0.24</b> | 0.29 ± 0.10        | 0.19 ± 0.13        | 1.01 ± 0.17        |
| SBS         | 0.82 ± 0.18                | 0.12 ± 0.04        | 0.36 ± 0.25        | 0.31 ± 0.08        | 0.19 ± 0.10        | 0.99 ± 0.17        |
| SOS S2, DC  | <b>1.12 ± 0.12</b>         | 0.14 ± 0.05        | 0.99 ± 0.16        | 0.19 ± 0.11        | <b>0.47 ± 0.14</b> | 0.79 ± 0.14        |
| SBS         | 0.93 ± 0.13                | <b>0.16 ± 0.06</b> | 0.97 ± 0.18        | 0.17 ± 0.08        | 0.34 ± 0.10        | 0.75 ± 0.13        |

Bold type indicates significant differences ( $p < 0.05$ ). SOS: step-over-step, SBS: step-by-step, S1: step one, S2: step two, WA: weight acceptance, DC: descent continuance

# MORPHOLOGICAL CHANGES IN SKELETAL MUSCLE ENDOMYSIAL AND PERIMYSIAL COLLAGEN NETWORKS SUBJECTED TO STRAIN

<sup>1</sup>Allison R. Gillies, <sup>2</sup>Nozomu Inoue and <sup>1,3</sup>Richard L. Lieber

<sup>1</sup>University of California San Diego, La Jolla, CA, USA

<sup>2</sup>Rush University Medical Center, Chicago, IL, USA

<sup>3</sup>VA San Diego Healthcare System, San Diego, CA, USA

email: rlieber@ucsd.edu web: <http://muscle.ucsd.edu>

## INTRODUCTION

The skeletal muscle extracellular matrix (ECM) plays an important role in muscle fiber force transmission [1], however its structure-function relationships are not clearly understood. Some of this uncertainty is due to the lack of studies specifically describing endomysial and perimysial structures and their response to strain. The reorientation of endomysial collagen in highly digested tissue has been described [2], but ECM structures and their changes with strain have not been described in undigested tissue, which was the purpose of this study.

## METHODS

All procedures were performed in accordance with the NIH Guide for the Use and Care of Laboratory Animals. The 5<sup>th</sup> toe of the extensor digitorum longus (EDL) muscle was dissected from wildtype mice for scanning electron microscopy (SEM) analysis. Muscles were formalin-fixed at resting length or longitudinally stretched 30% past resting length. Muscles were then dehydrated in graded ethanol, frozen and lyophilized. Muscles were sputter coated with iridium and viewed with a FEI XL30 SEM.

Endomysial collagen fibril diameter was measured by a custom software program (resting length: n=2 muscles; stretched: n=3 muscles). Each void space of the collagen network was identified by a particle analysis technique. Surfaces of the collagen fibrils were then registered using an edge tracking algorithm. Collagen fibril diameters were determined by the least distance algorithm [3]. Perimysial collagen diameter was measured manually with ImageJ software (resting length: n=2; stretched: n=3). Collagen diameter distributions from resting length and longitudinally stretched muscles were compared by

Mann-Whitney nonparametric tests with  $p < 0.05$  considered significant.

## RESULTS AND DISCUSSION

Surprisingly, SEM observations revealed structures specific either to skeletal muscle endomysium or perimysium. During processing, patches of ECM were separated from muscle fibers (Fig. 1, P). Based on morphology, it appeared that these patches were likely endomysium that pulled away from the muscle fiber surface (Fig. 1, F). Endomysial collagen networks were typically composed of thin fibrils in a mesh-like structure.

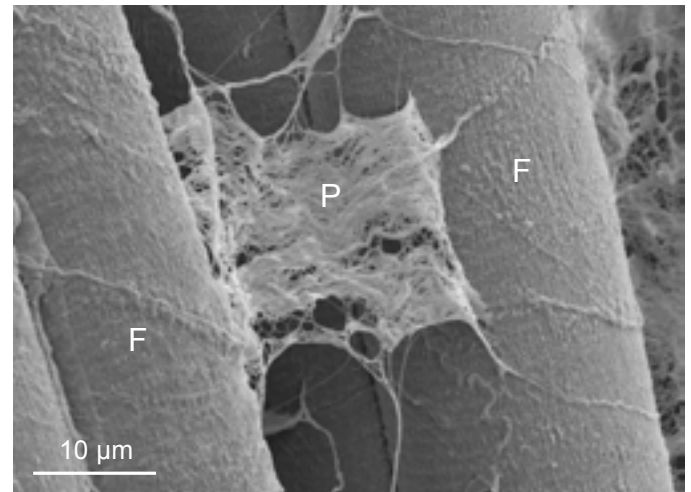


**Figure 1:** Patch (P) of endomysium pulled away from EDL muscle fibers (F) at resting length.

In contrast to the endomysium, perimysial collagen was organized as thick cables of collagen and had no apparent preferential direction in muscle at resting length. However, perimysial collagen cables were preferentially aligned with the axis of strain in stretched muscles (Fig. 2A). These collagen cables were composed of many collagen fibrils bundled together (see close-up in Fig. 2B).

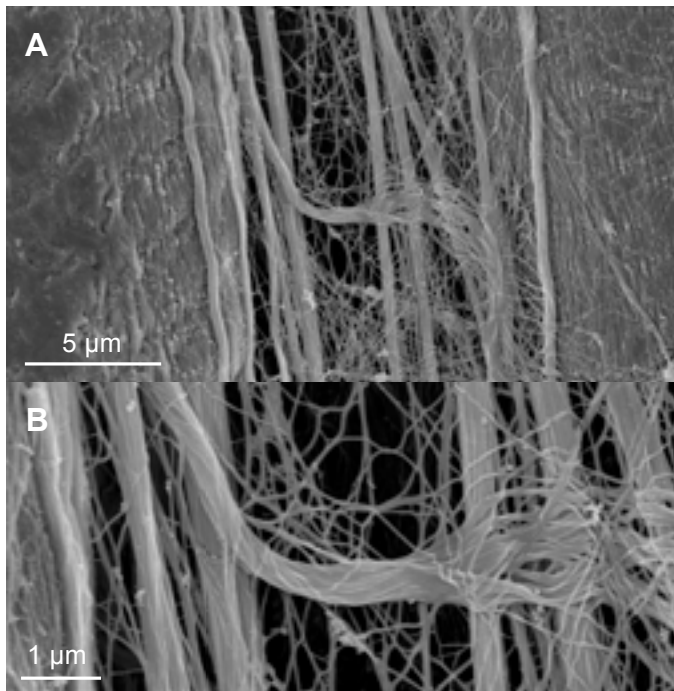


**Figure 2:** Morphology of perimysium in longitudinally stretched EDL muscle. Stretched collagen cables were found between muscle fibers (A). Collagen cables were composed of many collagen fibrils, which was demonstrated by a “frayed” cable (B).

Endomysial collagen diameter distribution in stretched muscle was significantly different from muscle at resting length (Fig. 3;  $p < 0.0001$ ) with a

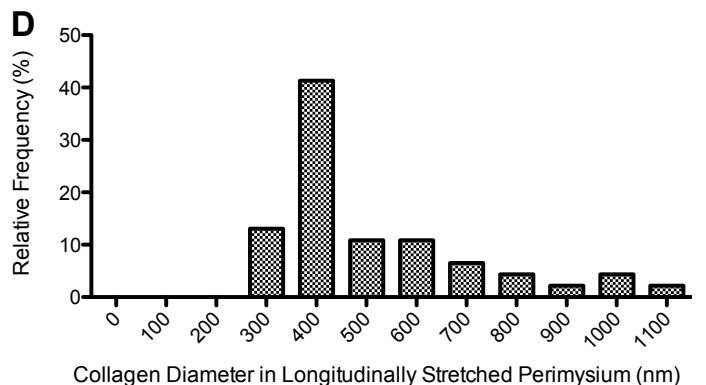
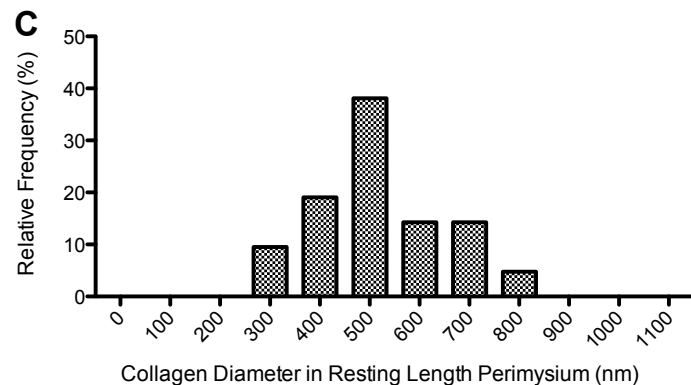
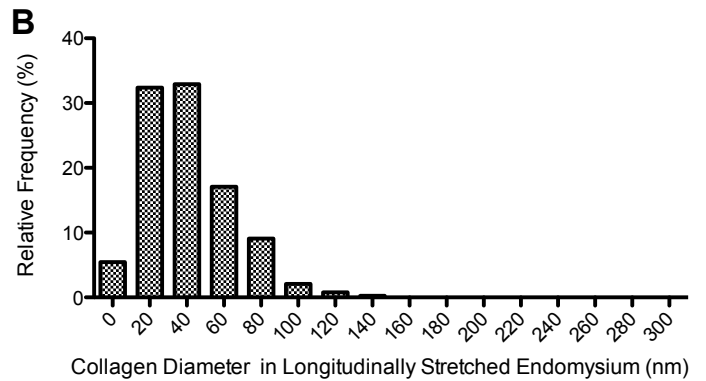
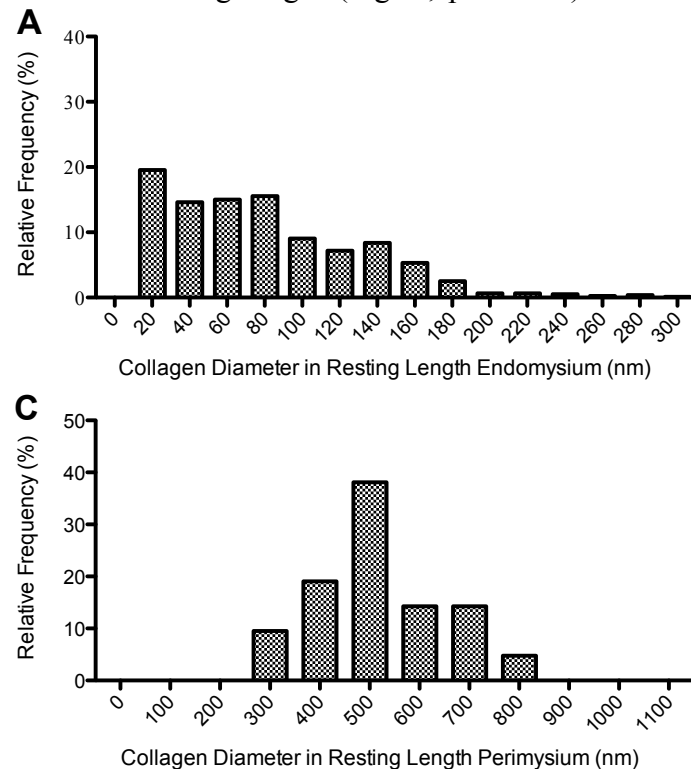


**Figure 3:** Histograms of collagen diameter in endomysium (A, resting length, and B, longitudinally stretched) and perimysium (C, resting length, and D, longitudinally stretched).

shift toward smaller diameters at stretched length, however stretched perimysial collagen diameter was not different from resting length. These results suggest that endomysial and perimysial structures may be distinct and that thin fibrils of the endomysial collagen mesh may be more sensitive to strain than thicker perimysial collagen cables. The different morphologies of endomysial and perimysial collagen may be a result of different functional requirements at each level of ECM organization. Further studies are required to define specific biochemical and biomechanical differences between these important load-bearing ECM components.

## REFERENCES

1. Tidball JG. *J Biomech* **24** (Suppl 1), 43-52, 1991.
2. Purslow PP, et al. *J Muscle Res Cell Motil* **15**, 299-308, 1994.
3. Duan CY, et al. *Osteoarthritis Cartilage* **19**, 96-102, 2010.

## ACKNOWLEDGEMENTS

The authors acknowledge the Department of Veterans Affairs, NIH grant R24HD050837, and NSF for a Graduate Research Fellowship (ARG).

# ESTIMATION OF *IN VIVO* FORCE-VELOCITY PROPERTIES IN HUMAN SKELETAL TYPE I MUSCLE WITH CROSSBRIDGE MODELING

Sampath K. Gollapudi and David C. Lin

Washington State University, Pullman, WA, USA  
Email: davidlin@wsu.edu

## INTRODUCTION

The force-velocity (F-V) relationship of skeletal muscle is important for understanding optimal motor function and is a key element of many muscle models. However, accurate *in vivo* measurement of F-V properties in humans is generally not possible, leading to uncertainty in model parameters and simulation results.

Our objective was to estimate the *in vivo* F-V properties of human type I muscle from measurements in isolated single muscle fibers. A problem with this approach is that temperatures lower than that *in vivo* must be used to avoid sarcomere inhomogeneity (SI), which profoundly changes the contractile properties. To overcome this problem, our approach was to: measure the F-V properties at lower than *in vivo* temperatures; estimate the rate parameters of a crossbridge muscle model from these data; extrapolate the rate parameters to their *in vivo* temperature values using the parameter versus temperature relationships; and predict the F-V relationship with the *in vivo* model parameters.

## METHODS

A biopsy of the soleus muscle was obtained in a healthy human subject. Isolated single fibers were prepared by a chemical skinning solution and mechanical separation. Fibers were maximally activated in a high calcium solution (pCa=4.5) at one of four test temperatures (15, 20, 25, and 30°C). To

measure the F-V properties, we used a force ramp (F-R), which is linear change in force over time, instead of a series of isotonic loads because more consistent shortening and lengthening F-V measurements can be obtained with the F-R method [1]. To minimize the effect of SI in our data, we only analyzed fibers with uniform sarcomere length changes (assessed from laser diffraction measurements). F-V curves were made by plotting the force and velocity at each point in time during the F-R.

Optimization was used to estimate the kinetic rate parameters of a 3-state crossbridge model [2] by fitting the model simulations of the F-R data at each test temperature. Rate parameters were plotted on a semi-log scale as a function of the inverse of temperature to estimate the coefficients of Arrhenius' equation (*i.e.*, the relationship of first-order kinetics to temperature). These coefficients were used to extrapolate each model rate parameter to its value at 37°C. The model with these parameter values was then used to predict the *in vivo* F-V curve by simulating the response to isovelocity length changes.

## RESULTS AND DISCUSSION

Experimental data with minimal SI were obtained at 15 ( $n=11$ ), 20 ( $n=10$ ), 25 ( $n=12$ ), and 30°C ( $n=11$ ) from type I single fibers (type confirmed by electrophoresis). Averaged F-V data for the different test temperatures are shown in Figure 1.

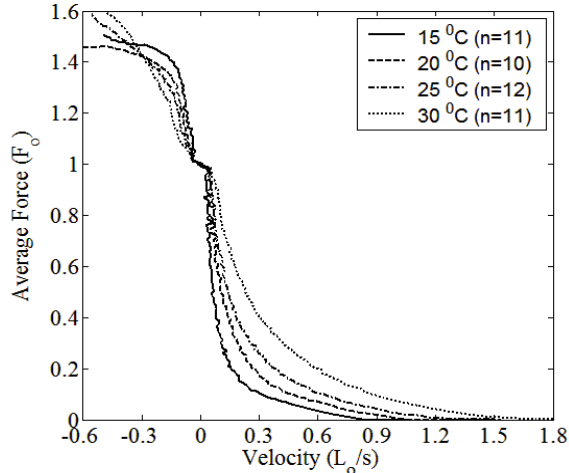


**Figure 1.** Average shortening and lengthening F-V curves for each test temperature.  $L_0$  = initial fiber length and  $F_0$  is initial isometric force.

We had to include an in-series thin-filament stiffness of 25 pN/nm to fit the experimental data. This value is low compared to that of other species (*e.g.*, rat or frog), but is consistent with the longer thin filaments in human muscle [3]. We also found that many model rate parameters had little effect on the F-V simulations and could not be estimated robustly. Based upon sensitivity analysis (not shown), we reduced the

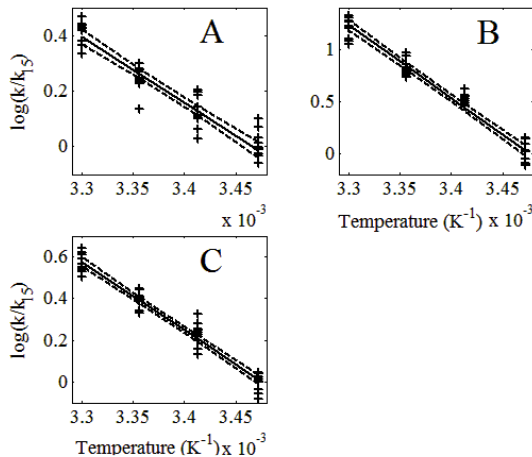


**Figure 2.** Arrhenius plots using the logarithmic ratio of the rate parameters at the test temperatures to rate parameter at 15°C against the reciprocal of absolute temperatures. Regression lines (—) with the 95% confidence intervals (---) are shown for: (A)  $k_{max,1}$  ( $r^2 = 0.9$ ) (B)  $k_{0,2}$  ( $r^2 = 0.96$ ) (C)  $\beta_1$  ( $r^2 = 0.96$ ), which are related to the transition from detached to weakly bound, weakly to strongly bound, and strongly bound to detached states respectively.

parameter space from ten to three parameters, one each representing the transition between the three crossbridge states. Arrhenius' equation described (with high  $r^2$  values) the dependence of these three model parameters on temperature (Figure 2).

With the extrapolated rate parameters, we calculated the *in vivo* F-V relationship for type I fibers. To compare our predictions with *in vivo* experimental measurements, we calculated the maximal shortening velocity ( $V_{max}$ ) to be  $2.26 \pm 0.16 \text{ FL}\cdot\text{s}^{-1}$ , where FL is the fiber length. Experimental estimates of  $V_{max}$  range from 3.56 to 14  $\text{FL}\cdot\text{s}^{-1}$  for the triceps surae [4]-[6]. Given that these estimates were from a muscle group with mixed fiber types and are sensitive to assumptions about musculoskeletal geometry (*e.g.*, fiber length to moment arm ratio), it is not surprising that our prediction of  $V_{max}$  was lower than the experimental estimates.

## CONCLUSIONS

Crossbridge modeling allowed prediction of the *in vivo* F-V curve from measurements at lower temperatures. Our predictions can be used to set muscle model parameters for type I human muscle.

## REFERENCES

- [1] Lin, D.C. and Nichols, T.R. (2003). *ASME J. Biomech. Eng.*, **125**, 132-140.
- [2] Campbell, K.S. and Moss, R.L. (2002). *Biophys J* 82, 929-43.
- [3] Walker, S.M. and Schrodt, G.R. (1974). *Anat Rec* 178, 63-81.
- [4] Sasaki, K. and Ishii, N. (2005). *J Physiol* 567, 1047-56.
- [5] Wickiewicz, T.L., *et al.* (1983). *Clin Orthop Relat Res* 275-83.
- [6] Winters, J.M. and Stark, L. (1988). *J Biomech* 21, 1027-41.

# THE INFLUENCE OF PATELLOFEMORAL KINEMATICS ON THE EFFECTIVE QUADRICEPS MOMENT ARM: A DYNAMIC IN VIVO STUDY

<sup>1,2</sup>Oren Goltzer and <sup>2</sup>Frances T. Sheehan, Ph.D.

<sup>1</sup>University of Miami Miller School of Medicine

<sup>2</sup>Rehabilitation Medicine Department, CC, NIH; email: fsheehan@cc.nih.gov

## INTRODUCTION

The moment arm (**ma**) of a tendon is a crucial quantity for musculoskeletal dynamics as it defines how the linear force within a muscle is transformed into a torque. For the quadriceps this relationship is complicated by the fact that the patella serves as an intermediary (a dynamic fulcrum) between the quadriceps and tibia. Thus, the term *effective quadriceps moment arm (EQma)* was coined to define the quadriceps indirect ability to generate a torque on the tibia [1]. To date, no study has quantified the *EQma* during dynamic *in vivo* movement. Furthermore, the critical question of how patella-femoral (PF) kinematics may influence the *EQma* remains unresolved. Specifically, patella alta has been widely implicated as the source of a reduced *EQma* in patients with cerebral palsy, contributing to an already weakened extensor mechanism [2]. Yet, a recent study demonstrated that individuals with patella alta had a significantly larger *EQma* [3]. Therefore the purpose of this study was to determine the *EQma* during a knee extension exercise in a large group of asymptomatic controls, using *in vivo* dynamic MRI. A secondary goal of the study was to determine if the *EQma* was correlated with PF or tibiofemoral (TF) kinematics.

## METHODS

Forty-one knees (19M/22F, age = 26.2 ±7.9 years, height = 170.9 ± 10.8cm, mass = 69 ±13.4kg) were included within this IRB approved study. All participants were placed supine in an MR imager (1.5T, GE Medical Systems, Milwaukee, WI) and were asked to cyclically flex and extend their knee while a dynamic cine-phase contrast (CPC) MR image set (x,y,z velocity and anatomic image frames) was acquired [4]. Dynamic cine images (anatomic image frames only) were also acquired in three axial planes to establish anatomical coordinate systems. The kinematics of each bone were derived through integration of the velocity data. This enabled the quantification of the 3D PF kinematics

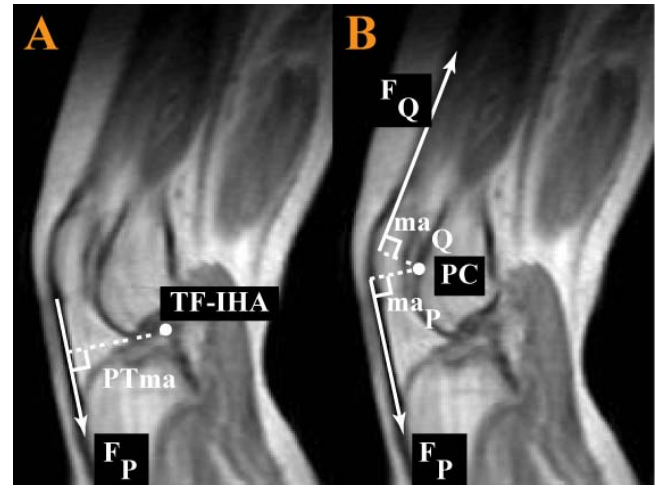


**Figure 1:** A. PTma was quantified by tracking the patellar tendon insertions and quantifying the through integration of the CPC data. B. ma<sub>Q</sub> and ma<sub>P</sub> were defined through direct image-based measures at the time frames representing 10°, 20° (above), and 30° of knee extension.

and TF Instantaneous Helical Axis (IHA), as well as the patellar tendon moment arm (PTma), relative to the IHA, throughout the motion cycle [5]. The *EQma* was quantified based on the ratio of the patellar tendon to the quadriceps force (F<sub>p</sub>/F<sub>q</sub>, Fig 1), calculated using the moment balance equation for the patella relative to the PF point of contact (PC, assumed to be the center of PF line of contact in the mid-patellar image):

$$EQma = PTma * (F_p / F_q) = PTma * (ma_Q / ma_P)$$

ma<sub>P</sub>: **ma** of the patellar tendon, relative to PC

ma<sub>Q</sub>: **ma** of the quadriceps tendon, relative to PC

Since the CPC data were acquired temporally, all kinematic data were interpolated to single knee angle (KA) increments. The *EQma* required a lengthy visual image analysis, thus the analysis was performed at three distinct KAs (10°, 20°, and 30°). If a specific KA fell between two images, both images were analyzed and the *EQma* was

calculated using interpolation. Correlations were calculated between the **ma** variables (the *EQma*,

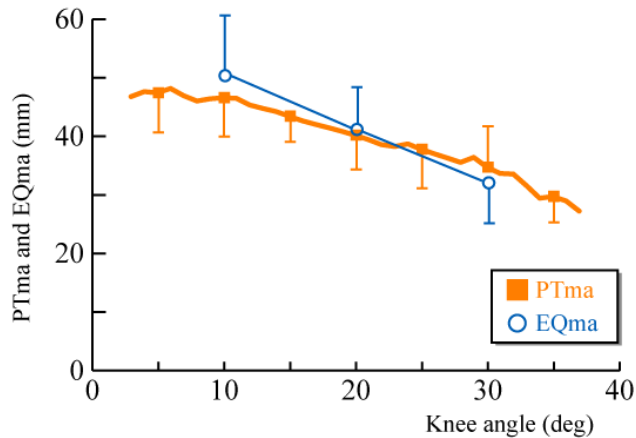


**Figure 2:** PTma and *EQma* with 1 SD bars. Due to variations in subjects' ranges of motion within the MR, not all subjects were represented at the extremes of motion. Average PTma values that did not include at least 11 subjects were eliminated.

$ma_Q/ma_P$  ratio, and PTma) both the PF and the TF kinematics (significance:  $p < 0.05$ ).

## RESULTS AND DISCUSSION

Both the PTma and *EQma* consistently trended up as the KA decreased (Fig 2). The ratio of  $ma_Q/ma_P$  agreed well in terms of shape and value with the results of Yamaguchi et al [1]. In both studies, the ratio increased as the KA decreased and crossed above 1.0 at a KA just greater than 20°. Thus, at KAs less than 20°, the patella improves the mechanical efficiency of the quadriceps, while at higher KAs it detracts from this efficiency. Since Yamaguchi et al [1] used the TF point of contact as the reference for the PTma, the *EQma* cannot be compared directly to this work. In contrast, the *EQma*,  $ma_Q/ma_P$  ratio, and PTma were all different in both shape and value in comparison to the work of Ward et al [3]. One of the largest sources for these differences can be attributed to the TF IHA, which, in the current study was directly calculated from the TF kinematics, whereas in the previous study it was estimated using the crossing points of the anterior and posterior cruciate ligaments. Another potential source of variance was the consistency at which KAs could be measured. In the current study, the KA was directly calculated from bone geometry and tracked using the CPC data, whereas in the previous study the KA was measured externally and the subjects were asked to maintain this static angle throughout the scan.

**Table 1:** Correlations between the inferior-superior (IS) location of patella and the ratio, PTma, and EQma at 10°, 20° & 30°. \*  $p < 0.05$

| Knee angle | IS:Ratio | IS:PTma | IS:EQma |
|------------|----------|---------|---------|
| 10         | 0.56*    | 0.08    | 0.41*   |
| 20         | 0.27     | 0.14    | 0.32*   |
| 30         | 0.43*    | 0.13    | 0.15    |

The PF inferior-superior location was weakly, but significantly correlated with *EQma* at 10° and 20° but not at 30° KA (Table 1). At 10° and 30° KAs, the PF inferior-superior location correlated with the ratio. While the inferior-superior position of the patella appears to play a role in the *EQma* at smaller KAs, its weak correlation indicates that there are other factors involved.

There were two primary limitations to this study. The first is that in order to identify the PF point of contact, subjective visual analysis of the MRIs was required. The excellent inter- and intra-rater reliability for the *EQma*, as evidenced by the intraclass correlation coefficients (0.93-0.94), indicated that this did not likely add imprecision to the data. Second, in order to find a unique relationship between the Fp and Fq, the analysis was forced to remain two-dimensional. Although the 3D quadriceps **ma** has been calculated relative to the patellar center [6], future work will be needed to relate the 3D quadriceps force to the tibial torque.

## CONCLUSIONS

As this is the first study to characterize the *EQma* *in vivo* during dynamic volitional activity in a large group of asymptomatic controls, it will serve as a foundation upon which to explore how pathological conditions such as patellofemoral pain and cerebral palsy affect the *EQma* as compared to asymptomatic controls. In addition it provides fundamental data for future modeling studies.

## REFERENCES

1. Yamaguchi GT, et al., *J Biomech.* **22**,1-10, 1989.
2. Lotman DB, *Dev Med Child Neurol.* **18**,315-9, 1976.
3. Ward SR, et al., *J Biomech.* **38**,2415-2422, 2005.
4. Sheehan FT, et al., *J Biomech.* **31**:21-26, 1998.
5. Sheehan FT, *J Biomech.* **40**,1968-1974, 2007.
6. Wilson NA, et al., *J Biomech.* **42**,1891-97, 2009.



# THE IMPACT OF POSTURE ON THE TRANSMISSION OF VIBRATION ACROSS A FUNCTIONAL SPINAL UNIT

<sup>1</sup>Chad E. Gooyers, <sup>1</sup>Robert McMillan, <sup>1</sup>Samuel J. Howarth,  
<sup>2</sup>Tammy R. Eger, <sup>1</sup>Jack P. Callaghan

<sup>1</sup>Department of Kinesiology, University of Waterloo, Waterloo, ON, Canada

<sup>2</sup>School of Human Kinetics, Laurentian University, Sudbury, ON, Canada

email: [cgooyers@uwaterloo.ca](mailto:cgooyers@uwaterloo.ca)

## INTRODUCTION

Occupational whole-body vibration exposure is a prevalent risk factor for the development of musculoskeletal injury. Conservative estimates have been made that up to 7% of the workforces in North America and Europe are exposed to potentially harmful levels of vibration [1]. However, despite the epidemiological link that exists between vibration exposure and intervertebral disc (IVD) degeneration [2], very little tissue-based evidence exists to show how the risk of injury from vibration exposure is modified by other mechanical factors such as postural or diurnal changes in height.

The International Organization for Standardization (ISO) provides quantitative guidelines for the assessment of health risks associated with human whole-body vibration exposure (ISO2631-1; ISO 2631-5). However, at the present time these standards do not consider the contribution of spinal posture or time dependent changes in their recommendations for acceptable levels of exposure. Therefore, the purpose of the present work was to investigate the influence of static postural deviation combined with cyclic compressive load on: (1) vertebral joint height loss and (2) the transmission of vibration across a functional spinal unit.

## METHODS

Twenty-four fresh-frozen porcine functional spinal units (FSUs) (12 c34, 12 c56), consisting of two adjacent vertebrae and the intervening IVD were excised from twelve porcine cervical spines, leaving only the osteoligamentous components intact. Upon dissection, each FSU was potted into custom aluminum cups with 18 gauge steel wire (placed around the anterior and posterior bony structures) and dental plaster (Denstone, Miles, South Bend, IN, USA). Additionally, two modified 63.5mm

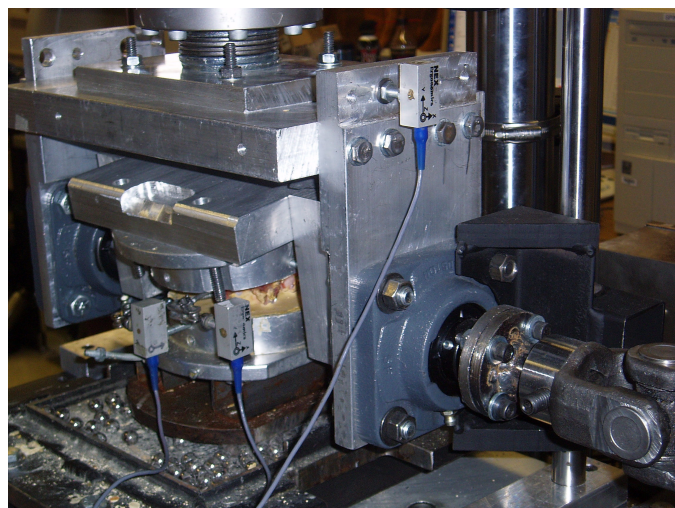


**Figure 1:** Modified servo-hydraulic testing apparatus with three tri-axial accelerometers used for testing.

wood screws were rigidly fixed into the anterior-face of both the inferior and superior vertebrae (at equal depth). These components served as attachment sites for tri-axial accelerometers.

Each FSU was then randomly assigned to one of three posture conditions that were tested in this study (neutral, flexed, or extended). Normalized testing postures were established from a range of motion (ROM) test that applied flexion/extension motion through a brushless servomotor (AKM23D, Kolmorgen/Danaher Motion, Radford, VA, USA) at a constant rate of 0.5 degrees / second [3]. Using the angular-position and applied torque data (T120-106-1K, SensorData Technologies Inc., Sterling Heights, MI, USA) sampled during this test, each specimen's 'neutral zone' could be identified [4]. The 'endpoints' of this neutral zone were used to normalize both the flexed and extended posture conditions respectively. The point of 'zero moment' about the flexion/extension axis was used to define the neutral posture.

After the ROM test, each FSU received a two-hour dose of cyclic compressive loading. Compressive load was applied to each specimen's caudal vertebra using a servo-hydraulic materials testing machine (Figure 1; 8872, Instron Canada, Toronto, ON, Canada) in the form a 5 Hz sinusoidal waveform (1500N ± 1200N). Throughout each test the compressive force (N) and actuator position (mm) were continuously sampled from the Instron® system at a rate of 100 Hz. Additionally, the three-dimensional linear accelerations of the vertebrae were continuously sampled at 256 Hz from three tri-axial accelerometers (S2-10G-MF, NexGen Ergonomics, Montreal, QC, Canada), which were fixed to the 63.5mm wood screw attachment sites and the testing apparatus.

Two dependent measures were considered for analysis in this study using a two-way ANOVA (segment level, posture). These included: (1) temporal changes in FSU height loss; calculated after each 20 minutes of cyclic loading with respect to the initial actuator position recorded at the start of each test (1500 N static compressive load applied) and (2) changes in transmission of vibration across the joint; computed as the amplitude ratio of RMS vertical accelerations recorded from the cranial vertebra (output) to that of the caudal vertebra (input).

## RESULTS AND DISCUSSION

As expected, FSU height loss followed a typical first order response previously reported by Heuer et al. [5], with the majority (~60%) of the loss occurring in the first 20 minutes of testing. Specimens assigned to the flexed posture group experienced significantly greater total height loss than both the neutral ( $p = .0014$ ) and extended postures ( $p < .0001$ ). When considering the temporal changes in height loss, the flexed postured evoked significantly greater amounts of height loss after each 20-minute interval of testing (Table 1).

Based on the accelerometer data, a neutral posture elicited resonance behavior near the start and end of

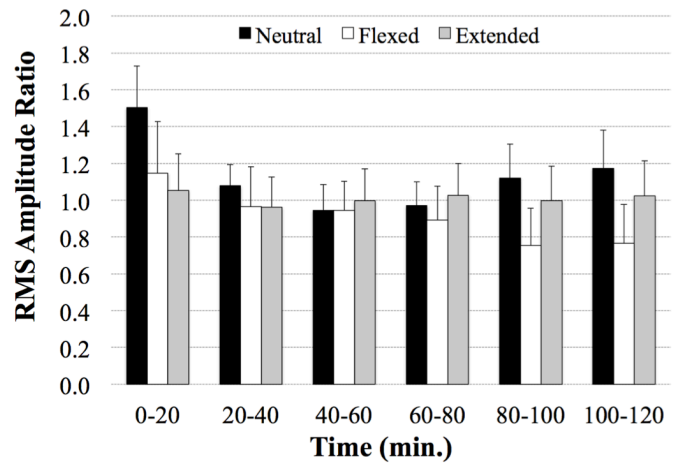


**Figure 2:** Amplitude ratio of RMS vertical accelerations (cranial vertebrae / caudal vertebrae).

testing (Figure 2). Despite what appears to be reduced transmission in flexion at these same periods of testing, due to the high variability within each group there were no significant differences.

## CONCLUSIONS

As evidenced by the results of this investigation, posture is likely an important consideration when assessing the risks of injury to the lumbar spine arising from vibration exposure. Specifically, this study found that flexed postures combined with cyclic compressive load imposed significantly greater specimen height loss, with (potentially) altered transmission of load across the joint. This work may have direct implications for seated whole-body vibration exposure in the workplace.

## REFERENCES

1. C.E.N. Vibration Report #12349. Belgium, 1996.
2. Seidel H. *Ind Health*. 43(3): 361-377, 2005.
3. Callaghan JP, et al. *Clin Biomch*. 16(1): 28-37, 2001.
4. Thompson RE, et al. *Clin Biomch*. 18(2): 89-98, 2003.
5. Heuer F, et al. *Clin Biomch*. 22(7): 737-44, 2007.

## ACKNOWLEDGEMENTS

The authors greatly acknowledge financial support from CRE-MSD and NSERC.

**Table 1:** Temporal changes in vertebral joint height loss (mm).

| Posture         | Time (min.)  |              |              |              |              |              |
|-----------------|--------------|--------------|--------------|--------------|--------------|--------------|
|                 | 0 – 20       | 20 – 40      | 40 – 60      | 60 – 80      | 80 – 100     | 100 - 120    |
| <b>Neutral</b>  | 1.80 (0.27)  | 0.52 (0.03)  | 0.36 (0.02)  | 0.22 (0.02)  | 0.18 (0.01)  | 0.12 (0.01)  |
| <b>Flexed</b>   | *3.43 (0.57) | *0.75 (0.11) | *0.57 (0.10) | *0.40 (0.05) | *0.32 (0.05) | *0.23 (0.04) |
| <b>Extended</b> | 1.46 (0.52)  | 0.43 (0.15)  | 0.28 (0.10)  | 0.19 (0.07)  | 0.12 (0.04)  | 0.11 (0.04)  |

**Note:** Data presented as Mean (SEM); \*Significantly greater height loss within the same interval of time ( $p < .05$ )

# EFFECTS OF CRACK MORPHOLOGY ON LOCAL CARTILAGE STRESSES

<sup>1,2</sup>Curtis Goreham-Voss and <sup>1,2</sup>Thomas Brown

<sup>1</sup>University of Iowa, Dept. of Orthopaedics and Rehabilitation, Iowa City, IA, USA

<sup>2</sup>University of Iowa, Dept. of Biomedical Engineering, Iowa City, IA, USA

email: curtis-voss@uiowa.edu

## INTRODUCTION

Cracks are a recognized feature of degenerating articular cartilage. They can vary from small superficial clefts to full-thickness fissures and/or large-area defects [1]. Lewis et al. have shown localized chondrocyte death in the vicinity of cartilage cracks [2]. It is not clear whether this chondrocyte death occurs at the time of acute injury, or whether it develops with repetitive loading, in response to the altered stress environment around the crack. In this study, finite element models of representative cartilage cracks were used to investigate the effects of the crack on the local stress environment. Perturbations of the crack geometry were then tested to determine which crack morphology characteristics would lead to more deleterious stresses and strains.

## METHODS

A baseline crack model was created using average parameters from previous work quantifying populations of crack morphology in a rabbit OA model [1]. The baseline crack had a single branch, perpendicular to the local articular surface, with an opening width of 0.035 mm and extending to a depth of 38.6% of the cartilage thickness (Figure 1). The crack was sited in idealized cartilage layers 0.67 mm thick, with radii of curvature of 7 mm and 8 mm for the inferior and superior layers, respectively. These layers were representative of rabbit tibial-femoral joints [3]. The FE model was meshed with hexahedral elements except for the region within 0.1 mm of the crack tip, where wedge elements were used to enable localized high mesh resolution. The cartilage layers were one element thick (out of plane), and were constrained to behave in plane-strain. Six perturbations of the baseline geometry were then considered (Figure 2). The opening width was reduced by half and doubled, the crack depth was halved and doubled, and the angle

of the crack relative to the local articular surface was reduced to 45° and to 20°. A model with non-cracked cartilage was created to allow for comparison of stress environments between normal and damaged cartilage.

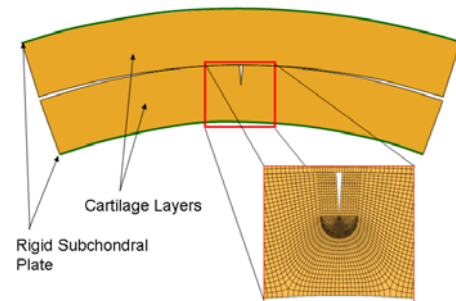


Figure 1. Finite element model of cartilage crack.

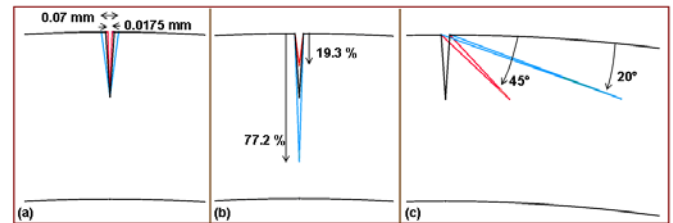


Figure 2. Perturbations in crack (a) width, (b) depth, and (c) angle to articular surface. The baseline crack is shown for reference in all panels.

All models were formulated as poroelastic contact analyses in FEBio. The nodes representing the subchondral plate of the inferior and superior cartilage layers were constrained to be rigid bodies, controlled by reference points located at the layer's center of curvature. A 3 N force was applied to the superior cartilage, resulting in a nominal stress of 2 MPa. Once fully loaded, the inferior cartilage layer was articulated through 4°. Contact was defined between the inferior and superior articular surfaces, between the crack faces, and, when necessary, between crack faces and the superior articular surface. A depth-dependent material model was used for cartilage. The solid matrix of the cartilage was modeled as a non-linear fiber-reinforced Neo-Hookean material [3]. A meta-analysis of depth-wise cartilage properties, each normalized to its own series maximum, was used to derive depth-dependent trends for the material properties. Each

material property had one independent value, and the depth-wise variation was governed by the derived trends. The final material model was found to compare well with studies of through-thickness cartilage strains published in literature.

## RESULTS

The stress results from the uncracked and baseline crack models at 4° of knee flexion are shown in Figure 3. The presence of the crack significantly compromises local load carriage in the fluid phase. Shear strains were increased along part of the crack face, particularly near the point where the crack closed. The crack caused elevated tensile stresses in the superficial zone of the inferior cartilage.

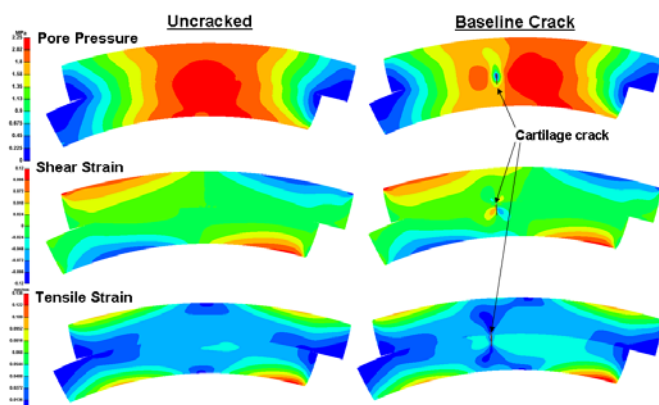


Figure 3. Fluid pore pressure and strains in the uncracked and baseline crack models.

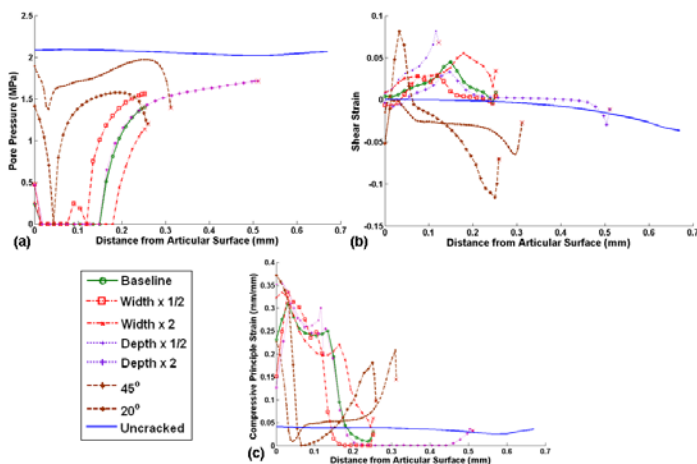


Figure 4. (a) Fluid pore pressure, (b) shear strain, and (c) compressive principle strain along crack faces. Pore pressure and strain through the cartilage depth at the center of the uncracked model are also shown.

The effects of crack morphology on the fluid pressure and strains along the crack face are highlighted in Figure 3. Altering the crack depth had no effect on the resultant fluid pressure, while altering the crack width had only minor effects on the fluid pressure or strains. Changes to the crack angle had a substantial effect on the local strain environment. Fluid pressures were higher (and

compressive strains lower) along the 20° and 45° cracks, due to those cracks closing more completely. Shear strains were also more uniform along the face of the 20° crack.

## DISCUSSION

The results in this study provide a unique opportunity to evaluate the local stress and strain fields around individual cartilage cracks. The most striking results from the baseline crack were the broad reduction in fluid pressure and the increased tensile strains in the superficial zone. Such increased tensile strains could plausibly play a role in superficial fibrillation in degenerating cartilage. Shear stress has often been suggested as the most deleterious of cartilage stresses, but the non-uniform shear strains near the baseline crack do not appear to correlate with the uniform chondrocyte death reported by Lewis et al. This finding has two possible explanations: (1) chondrocyte death occurs acutely, rather than as a response to altered chronic loading, or (2) other chronic mechanical stimuli (perhaps increased fluid flux, or increased compressive strains due to reduced fluid load support) are responsible for the increased chondrocyte death.

The alterations to crack morphology provide insight into the crack characteristics most likely to lead to the propagation of cartilage degeneration. The specific depth or width of a perpendicular crack had little effect on the final results, due to the crack closing when loaded. Cracks that were not perpendicular to the articular surface also closed, but their influence on fluid pressure was spread throughout a larger proportion of the cartilage layers. Future work with these models will investigate the effects of multiple cracks and of alternate loading.

## REFERENCES

1. Goreham-Voss CM, et al. *34th Annual Meeting of the ASB*. Providence, RI, USA, 2010. #345.
2. Lewis et al. *JOR* 21(5):881-7, 2003.
3. Borrelli et al. *JOT* 16(3) :182-8, 2002.
4. Mass et al. <http://mrl.sci.utah.edu/software/febio> 2010.

## ACKNOWLEDGEMENTS

This study was supported by a grant from the NIH (5P50 AR055533).

# BIONIC LEG PROSTHESIS EMULATES BIOLOGICAL ANKLE JOINT DURING WALKING

<sup>1,2</sup>Alena Grabowski, <sup>1</sup>Susan D'Andrea and <sup>1,2</sup>Hugh Herr

<sup>1</sup>Dept. of Veterans Affairs Center for Restorative and Regenerative Medicine, Providence, RI, USA

<sup>2</sup>Massachusetts Institute of Technology, Cambridge, MA, USA

email: [alenag@mit.edu](mailto:alenag@mit.edu) web: <http://media.mit.edu/~alenag>

## INTRODUCTION

Over time, leg prostheses have improved in design, yet until now, prostheses have been incapable of actively adapting to different walking velocities in a manner comparable to a biological limb. People with a leg amputation (PWA) using such conventional prostheses have abnormal biomechanics during walking compared to non-amputees.

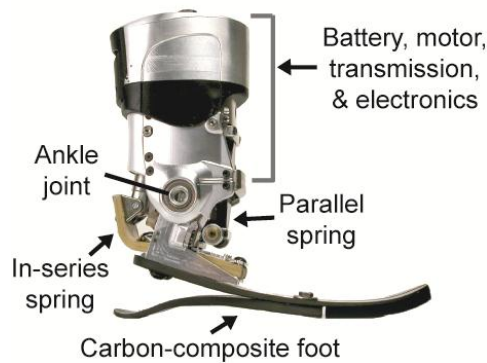


**Figure 1.** The bionic prosthesis' mass of 2.0 kg is equivalent to a biological foot and partial shank of an 80 kg person. The prosthesis includes a carbon-fiber in-series leaf spring, unidirectional parallel leaf spring, and heel and forefoot leaf springs that provide elasticity. A series-elastic actuator performs negative and positive work. The actuator is comprised of a 200-Watt DC brushless motor and ball screw transmission in series with a carbon-composite leaf spring.

To facilitate normative mechanics during walking, the biological leg must support body weight and accelerate body mass [1-3]. During a single stride, the net mechanical work done on the body's center of mass is nearly zero, but the leg muscles perform both negative and positive work. The biological calf muscles typically perform greater positive than negative work during each stance period [4] and

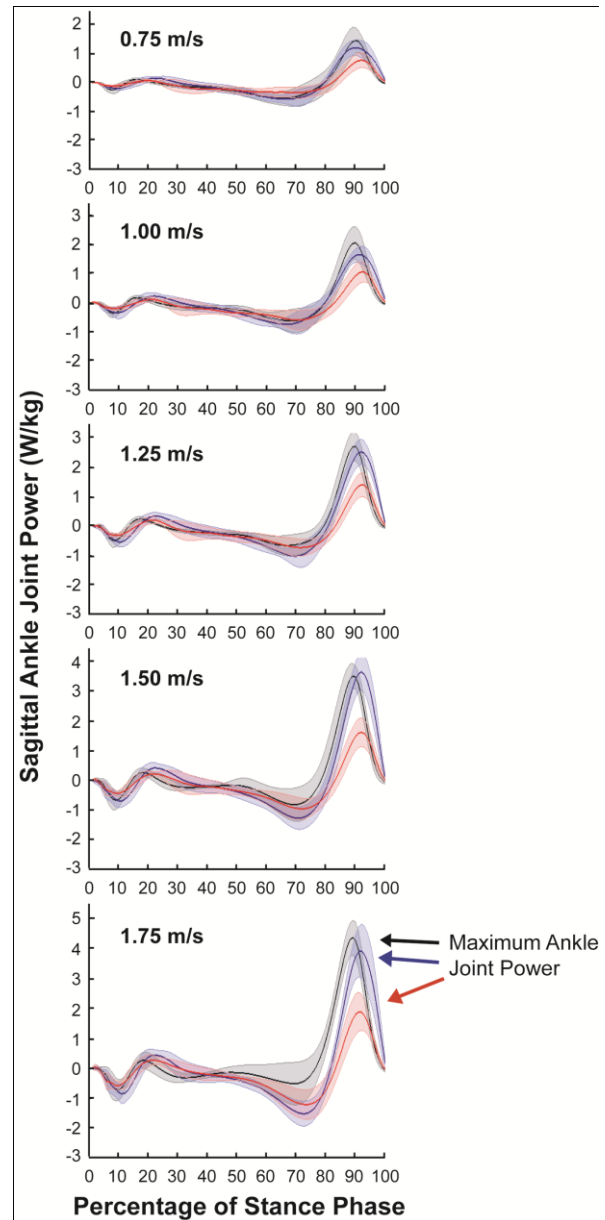


**Figure 2.** Mean (shaded area +/- S.D.) sagittal ankle joint power during the stance phase of walking was nearly equivalent for PWA using the bionic prosthesis (blue line) compared to non-amputees (black line); whereas PWA using a conventional passive-elastic prosthesis (red line) experienced significantly less peak power from their prosthetic ankle joint during late stance phase.

generate ~80% of the mechanical work required to complete a gait cycle [5]. In contrast, conventional passive-elastic prostheses store and release elastic strain energy while in contact with the ground, but cannot generate net positive work. We have developed a bionic prosthesis capable of performing non-conservative positive work and generating a push-off force (Fig. 1). We hypothesized that if biologically-equivalent ankle stiffness, net positive work, and power were supplied by the bionic prosthesis, PWA using the prosthesis would achieve normative joint kinetics and kinematics compared to those of non-amputees.

## METHODS

8 people with unilateral transtibial amputations (PWA) and 8 age-, height- and weight-matched non-amputees participated. PWA completed two experimental sessions; one using the bionic prosthesis (Fig. 1) and one using a conventional prosthesis. Non-amputee participants completed one experimental session. We analyzed ground reaction forces (1000 Hz) and motion (100 Hz) of participants as they walked 0.75, 1.0, 1.25, 1.5 and 1.75 m/s across two force platforms mounted in a 10m level walkway. Then, we calculated joint kinetics using inverse dynamics (Visual 3D, C-Motion, Inc.). We compared results from PWA to non-amputees using one-way ANOVAs and compared results between prosthetic foot conditions using repeated measures ANOVAs.

## RESULTS AND DISCUSSION

Across the full range of walking velocities, PWA using the bionic prosthesis normalized sagittal ankle joint power (Fig. 2) and maximum ankle

joint power compared to non-amputees (Table 1:  $P > 0.13$  at 0.75-1.75 m/s) and substantially increased maximum ankle joint power compared to using a conventional prosthesis ( $*P < 0.01$  at 0.75-1.75 m/s).

## CONCLUSIONS

We show that a bionic prosthesis can restore normative ankle joint mechanics to people with a leg amputation during level-ground walking. We also found differences in knee and hip joint mechanics in PWA compared to non-amputees. A lack of a biological gastrocnemius in likely led to these differences. Future prosthetic leg designs that allow energy to be transferred across the knee may further improve biomechanics for PWA.

## REFERENCES

1. Donelan JM, et al. *J. Exp. Biol.* **205**, 3717-3727, 2002.
2. Grabowski A, et al. *J. Appl. Physiol.* **98**, 579-583, 2005.
3. Kuo AD, et al. *Exerc. Sport Sci. Rev.* **33**, 88-97, 2005.
4. DeVita P, et al. *J. Exp. Biol.* **210**, 3361-3373, 2007.
5. Winter, DA. *Clin. Ortho. Rel. Research*, 147-154, 1983.

## ACKNOWLEDGEMENTS

Sponsored by a Dept of the Veterans Affairs Career Development Award from the RR&D Service, and Providence VAMC CRRM (VA RR&D A3962R). We thank Natalie Wilhelm for her data collection assistance, and iWalk, Inc. for providing prostheses and technical assistance.

**Table 1: Average Maximum Ankle Joint Power (W/kg)  $\pm$  S.D.**

|                                | Walking Velocity (m/s) |                  |                  |                  |                  |
|--------------------------------|------------------------|------------------|------------------|------------------|------------------|
|                                | 0.75                   | 1.00             | 1.25             | 1.50             | 1.75             |
| <b>Conventional Prosthesis</b> | 0.78 $\pm$ 0.25*       | 1.06 $\pm$ 0.35* | 1.40 $\pm$ 0.41* | 1.64 $\pm$ 0.49* | 1.90 $\pm$ 0.65* |
| <b>Bionic Prosthesis</b>       | 1.26 $\pm$ 0.28        | 1.66 $\pm$ 0.29  | 2.51 $\pm$ 0.42  | 3.64 $\pm$ 0.61  | 3.94 $\pm$ 0.87  |
| <b>Non-Amputee</b>             | 1.50 $\pm$ 0.41        | 2.10 $\pm$ 0.53  | 2.71 $\pm$ 0.50  | 3.56 $\pm$ 0.38  | 4.38 $\pm$ 0.58  |

\* indicates a significant difference ( $P < 0.01$ ) between prosthetic feet and when comparing use of a conventional prosthesis to non-amputees.

# LOCAL DYNAMIC STABILITY OF THE LOWER LIMB KINEMATIC CHAIN DURING SYMMETRIC LIFTING

<sup>1</sup>Ryan B. Graham, <sup>1</sup>Patrick A. Costigan, <sup>1</sup>Erin M. Sadler, <sup>1</sup>Sivan Almosnino, and <sup>1</sup>Joan M. Stevenson

<sup>1</sup>Queen's University, Kingston, Ontario, Canada

email: [ryan.graham@queensu.ca](mailto:ryan.graham@queensu.ca) web: <http://www.skhs.queensu.ca/ergbio/>

## INTRODUCTION

During goal-directed tasks, such as lifting low-lying objects, the human motor system regulates the body's centre of mass (CoM) position to maintain equilibrium and prevent falling [1]. During lifting, any voluntary trunk movement will perturb that equilibrium, which will elicit an automatic postural response requiring the coordinated control of several joints [2]. To actively counter perturbations and smoothly incorporate them into movement repertoires while walking, the central nervous system prioritizes the stability of the superior over the inferior segments [3]; however, this relationship is unknown for lifting. Therefore, we examined ankle, knee, and hip joint stability during repetitive lifting under two load conditions. Because the active control of trunk motion is crucial in lifting as in walking, we hypothesized that local dynamic stability would increase when moving up the kinematic chain [3]. Furthermore, because local dynamic spinal stability increases with an increase in load lifted [4], we hypothesized that stability would increase at all joints with increased load.

## METHODS

Thirty healthy volunteers (15M, 15F) performed two trials of 30 continuous, symmetrical, freestyle box lifts (10/min) between targets on a table at 50% of their standing height and the floor, synchronous to a metronome (Fig. 1). The two randomized load conditions were zero load (~0%) and 10% of each participant's maximum back strength [4].

Lower limb joint kinematics were collected using an Optotrak 3020 system (Northern Digital Inc., Waterloo, ON, Canada) at 100Hz. Participants were instrumented with four infrared emitting diode (IRED) marker triads, located laterally on the right foot, shank, and thigh, as well as a fin projecting

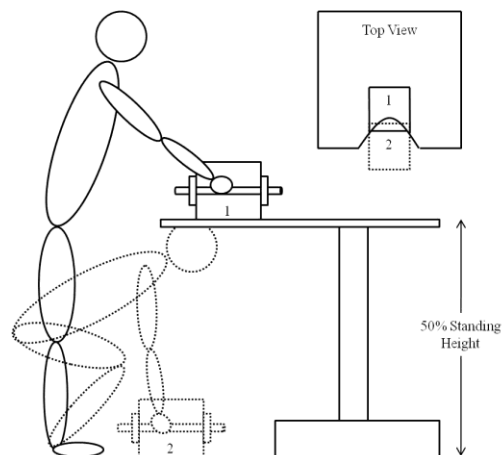


**Figure 1:** Experimental setup used for lifting.

from  $S_1$ . Single IREDs and virtual markers were used to locate the ankle, knee, and hip joint centers and to define segment anatomical coordinate systems with three principal axes: distal-proximal (X), posterior-anterior (Y), and lateral-medial (Z).

Custom Matlab software (The MathWorks, Natick, MA, USA) was used in all processing. Joint angles were calculated using 3D Euler rotations (Z-Y-X), filtered with a 10Hz low-pass 2<sup>nd</sup> order Butterworth filter, and then the last 25 lifts were extracted for each subject and time normalized to 15000 samples. At each joint and for each point in time the Euclidean norm of the three angles was calculated and then, to account for range of motion differences at each joint, standardized to unit variance [3].

For each lower limb joint an attractor was then reconstructed by defining an  $n$ -dimensional state space from the 1D Euclidean norm angles using the method of delays. A time delay of 0.6 seconds (10% of the average lift) ensured all data were processed similarly, while the embedding dimension of five was found using a global false nearest neighbour's analysis [4]. Short- and long-term maximum finite-time Lyapunov exponents ( $\lambda_{\max-s}$  and  $\lambda_{\max-l}$ ) were calculated using standard methods to quantify the

local dynamic stability of each lower limb joint [5]. These were compared across joints, loads, and sexes using mixed-design repeated-measures ANOVAs in SPSS 18 (SPSS Corporation, Chicago, IL, USA).

## RESULTS AND DISCUSSION

Local dynamic stability ( $\lambda_{\max-s}$ ) decreased ( $p < 0.001$ ) when moving up the lower limb kinematic chain (Table 1). Additionally, all three joints were more locally stable when lifting the heavier load ( $p < 0.05$ ). There were no significant effects of sex, or significant interaction effects on  $\lambda_{\max-s}$ , and no significant main or interaction effects on  $\lambda_{\max-l}$ . Under both load conditions, ankle stability ( $\lambda_{\max-s}$ ) was significantly correlated to knee stability, which was correlated to hip stability ( $p < 0.01$ ).

Our findings suggest that local dynamic stability increased when moving down the lower limb kinematic chain during loaded and unloaded repetitive symmetrical lifting. Therefore, inferior (distal) joints can more effectively accommodate small perturbations or neuromuscular control errors that occur naturally during such tasks. These results are contrary to previous results that found local dynamic stability decreased when moving down the kinematic chain during gait [3]; the discrepancy may be because lifting is a fundamentally different motion than walking. During walking the trunk undergoes less angular displacement and is the most stable segment. In lifting it may be necessary to first

ensure a stable ankle joint to control the base of support and accommodate the postural perturbations that occur with trunk flexion. Therefore, controlling the trunk's CoM via lower limb joint stability is accomplished differently for walking and lifting.

Also, lower limb stability appears sequentially dependent since the ankle is correlated to the knee and the knee to the hip. Thus, actively controlling ankle stability will allow for increased stability at the more proximal joints and, ultimately, the trunk. This is important since factors affecting ankle stability, such as the coefficient of friction or an unstable surface, may hinder the ability to produce trunk stability, increasing injury risk. Also, stability increased at all joints when lifting the heavier load, likely due to increased contraction that stiffened the joints to manage the load, or deal with increased postural perturbations when lifting heavier loads.

## REFERENCES

1. Park W, et al. *Comput Biol Med* **38**, 1094-1102, 2008.
2. Kollmitzer J, et al. *J Biomech* **35**, 585-594, 2002.
3. Kang HG, et al. *Gait Posture* **30**, 260-263, 2009.
4. Graham RB, et al. *Hum Mov Sci*, In Revision.
5. Rosenstein MT, et al. *Phys D* **65**, 117-134, 1993.

## ACKNOWLEDGEMENTS

Financial support from NSERC Canada.

**Table 1:** Mixed-design repeated-measures analysis of variance (ANOVA) results.

|                               | Mean (SD) Results |                  |                  | Main Effects (F-Ratio) |               |         | Interaction Effects (F-Ratio) |       |       |       |
|-------------------------------|-------------------|------------------|------------------|------------------------|---------------|---------|-------------------------------|-------|-------|-------|
|                               | 0% Load           | 10% Load         |                  | Joint (J)              | Load (L)      | Sex (S) | J*S                           | L*S   | J*L   | J*L*S |
| $\lambda_{\max-s}$            | Ankle             | 0.249<br>(0.057) | 0.237<br>(0.049) |                        |               |         |                               |       |       |       |
|                               | Knee              | 0.390<br>(0.076) | 0.379<br>(0.080) | <b>183.981**</b>       | <b>4.244*</b> | 0.448   | 0.334                         | 0.102 | 2.997 | 0.844 |
|                               | Hip               | 0.471<br>(0.062) | 0.436<br>(0.076) |                        |               |         |                               |       |       |       |
| $\lambda_{\max-l}$<br>(/1000) | Ankle             | 1.377<br>(3.82)  | 2.294<br>(3.36)  |                        |               |         |                               |       |       |       |
|                               | Knee              | 1.488<br>(4.95)  | 2.623<br>(3.85)  | 0.163                  | 3.205         | 0.07    | 0.309                         | 1.724 | 1.946 | 0.172 |
|                               | Hip               | 0.494<br>(3.86)  | 3.211<br>(5.19)  |                        |               |         |                               |       |       |       |

\*Indicates significance at the  $p < 0.05$  level. \*\* Indicates significance at the  $p < 0.001$  level.

# EFFECTS OF A GLOBAL ALTERATION OF RUNNING TECHNIQUE ON CHRONIC EXERTIONAL COMPARTMENT SYNDROME

<sup>1</sup>Robert Gregory, <sup>2</sup>Angela Diebal, <sup>2</sup>Curtis Alitz and <sup>2</sup>John Gerber

<sup>1</sup>U.S. Military Academy, West Point, NY, USA

<sup>2</sup>Keller Army Community Hospital, West Point, NY, USA

email: [robert.gregory@usma.edu](mailto:robert.gregory@usma.edu) web: <http://www.usma.edu/dpe>

## INTRODUCTION

Chronic exertional compartment syndrome (CECS) is an injury or condition that occurs almost exclusively with running. CECS is defined as reversible ischemia secondary to a noncompliant osseofacial compartment that is unresponsive to the expansion of muscle volume that occurs with exercise [1]. It is most commonly seen in the anterior compartment of the lower leg. The characteristic complaint of patients with CECS is recurrent exercise-induced leg discomfort that occurs at a well-defined and reproducible point in the run and increases if the training persists. Relief of symptoms only occurs with discontinuation of activity.

The mainstay of treatment for CECS is surgery. Either a fasciotomy or fasciectomy is used to release the compartment and to decrease intracompartmental pressure. Conservative treatments such as non-steroidal anti-inflammatory medications, physical therapy, podiatry, or massage are felt to be ineffective since none of these approaches have yielded consistently positive results.

One conservative treatment approach that has not been investigated is the modification of running technique. The purpose of this study was to examine the effectiveness of a global alteration of technique, in which natural rearfoot-strike subjects were instructed in a forefoot-strike movement pattern, on controlling the symptoms associated with CECS during running. It was hypothesized that the instructional program will change running mechanics (decreased step length, contact time, peak vertical ground reaction force, and weight acceptance rate), decrease intracompartmental pressure and pain level, and increase run distance.

## METHODS

Ten individuals (7 M, 3 F; age:  $20.5 \pm 1.5$  yr, height:  $1.74 \pm 0.08$  m, mass:  $84.9 \pm 18.9$  kg) with unilateral or bilateral exercise-induced anterior compartment syndrome participated in this study. All subjects had a history (range: 0.5–4 yr) and physical examination that was consistent with the diagnosis by an orthopedic surgeon of CECS. In addition, all subjects were natural rearfoot-strike runners.

The subjects underwent a pre- and post-instructional program running evaluation. Subjects ran on a Kistler Gaitway instrumented treadmill at a self-selected speed for as long as possible until they reached a pain level of  $\geq 7/10$ . Also, pre- and post-exercise intracompartmental pressures were measured using a Stryker Intracompartmental Pressure Monitor.

The instructional program emphasized a forefoot-strike running technique utilizing specific training drills and exercises as described by Romanov [2]. This program was conducted three times per week for approximately one hour each session and took place over the course of eight weeks.

Kinematic and kinetic data were collected during both the pre- and post-instruction running evaluations for 50 strides at a sampling rate of 500 Hz. The data were filtered using a 4<sup>th</sup> order, low-pass Butterworth filter with a cutoff frequency of 25 Hz. A paired *t* test was used to assess the effects of the running technique instructional program on gait kinematics (step length, step rate, and contact time) and kinetics (peak vertical ground reaction force, impulse, and weight acceptance rate), intracompartmental pressure, pain level, run distance, and running speed.

## RESULTS AND DISCUSSION

There were several notable changes in the gait kinematics as a result of the running technique instructional program. Step length significantly decreased ( $P<0.05$ ; see Table 1), step rate significantly increased ( $P<0.05$ ; see Table 1), and contact time significantly decreased ( $P<0.01$ ; see Table 1). These changes in kinematics are in agreement with previous research in which natural rearfoot-strike runners were instructed in midfoot- or forefoot-strike gaits [3,4].

There were also a number of important changes in the gait kinetics. Peak vertical ground reaction force significantly decreased ( $P<0.05$ ; see Table 1), impulse significantly decreased ( $P<0.05$ ; see Table 1), and weight acceptance rate significantly decreased ( $P<0.05$ ; see Table 1). These changes in peak vertical ground reaction force and weight acceptance rate are also in agreement with previous research comparing runners utilizing a rearfoot-strike versus a midfoot- or forefoot-strike gait [3,4]. Kinematic and kinetic analyses show that midfoot- or forefoot-strike gaits generate smaller collision forces primarily due to a more plantarflexed foot at ground contact [5].

The alterations in gait mechanics due to the running technique instructional program resulted in two key clinical findings. First, post-exercise anterior compartmental pressure significantly decreased from  $66.4 \pm 27.1$  mm Hg to  $39.9 \pm 10.4$  mm Hg ( $P<0.01$ ). Second, post-exercise pain level significantly decreased from  $7.4 \pm 0.5/10$  to  $0.5 \pm 0.9/10$  ( $P<0.0001$ ). In addition, run distance significantly increased from  $1.1 \pm 0.4$  km to  $5.0 \pm 0.0$  km ( $P<0.0001$ ). [NB: All subjects completed a 5.0 km run during the post-instruction evaluation.] Finally, running speed significantly increased from  $3.10 \pm 0.22$  m/s to  $3.30 \pm 0.28$  m/s ( $P<0.005$ ).

## CONCLUSIONS

In an effort to prevent, treat, and/or reduce running injuries, a current trend in rehabilitation medicine has focused on modifying technique. Popular running styles such as ChiRunning and the Pose Method have emerged that advocate a midfoot- or forefoot-strike gait. By avoiding a rearfoot-strike gait with high-impact collisions, it is believed that runners will experience reduced injury rates.

In this study, individuals with CECS who adopted a forefoot-strike running technique experienced a number of changes in gait kinematics (decreased step length, increased step rate, and decreased contact time) and kinetics (decreased peak vertical ground reaction force, impulse, and weight acceptance rate). These changes in running mechanics are hypothesized to reduce the eccentric muscle activity of the anterior leg compartment. This decrease in eccentric muscle activity may limit the increase of anterior compartmental pressure and therefore the symptoms of CECS associated with running. As a result, the subjects were able to increase both their run distance and speed. While more research is required to determine if a forefoot-strike gait can reduce the risk of injuries, adopting such a technique may make runners less prone to repetitive stress injuries.

## REFERENCES

1. Wilder RP, Magrum E. *Clin Sports Med* **29**, 429-435, 2010.
2. Romanov N. *Pose Method of Running*, Pose Tech Press, 2004.
3. Dallam GM, et al. *J Sports Sci* **23**, 757-764, 2005.
4. Arendse RE, et al. *Med Sci Sports Exerc* **36**, 272-277, 2004.
5. Lieberman DE, et al. *Nature* **463**, 531-535, 2010.

**Table 1:** Gait kinematics and kinetics in runners with chronic exertional compartment syndrome (CECS).

|                         | SL<br>(m)       | SR<br>(steps/s) | CT<br>(s)       | vGRF<br>(BW)    | Impulse<br>(BW·s) | WAR<br>(BW/s)  |
|-------------------------|-----------------|-----------------|-----------------|-----------------|-------------------|----------------|
| <b>Pre-Instruction</b>  | $1.14 \pm 0.06$ | $2.75 \pm 0.11$ | $0.30 \pm 0.03$ | $2.39 \pm 0.03$ | $0.38 \pm 0.02$   | $29.7 \pm 5.9$ |
| <b>Post-Instruction</b> | $1.08 \pm 0.07$ | $2.92 \pm 0.17$ | $0.28 \pm 0.03$ | $2.30 \pm 0.03$ | $0.35 \pm 0.02$   | $26.5 \pm 5.4$ |

(SL = step length, SR = step rate, CT = contact time, vGRF = vertical ground reaction force, WAR = weight acceptance rate)

# ACHILLES TENDON FORCES IN FOREFOOT AND REARFOOT RUNNING

Allison H. Gruber, Brian R. Umberger, Carl Jewell, Samuel del Pilar II and Joseph Hamill

Biomechanics Laboratory, University of Massachusetts, Amherst, MA, USA  
email: [agruber@kin.umass.edu](mailto:agruber@kin.umass.edu) web: <http://www.umass.edu/biomechanics/>

## INTRODUCTION

Compared to rearfoot (RF) running, forefoot (FF) running has been suggested to decrease the risk of developing running related injuries due to reduced vertical loading rate and lack of the initial impact peak of vertical ground reaction force [1]. However, impact parameters are not the sole cause of running injuries. Other features of FF running could be protective or harmful with respect to injury compared to RF running.

Previous reports have speculated FF running may place increased stress on the Achilles tendon (AT) because of greater plantar flexor muscle forces associated with this foot fall pattern [2]. Although FF running produces greater plantar flexor moments during stance compared to RF running [3], the force transmitted through the AT for a given joint moment will be affected by the length of the AT moment arm. Static measurements have indicated the AT moment arm is longer when the foot is plantar flexed and shorter when in a dorsiflexed position [4]. Thus, the greater plantar flexor moments in FF running might not necessarily lead to greater AT forces. The purpose of this study was to determine the force in the AT during the stance phase of running with a FF pattern compared to the RF pattern.

## METHODS

Ten natural RF runners (7 males, 3 females; age  $27 \pm 6$  yrs; height  $1.8 \pm 0.1$  m; mass  $71.1 \pm 10.3$  kg) participated in this study. Reflective markers were placed on the right foot and leg of the subjects. A centrally located AMTI force platform (1200 Hz) was surrounded by eight Qualysis Oqus cameras (240 Hz) along a 20m runway. Subjects ran over the force platform at  $3.5 \text{ m} \cdot \text{s}^{-1} \pm 5\%$  while performing the FF and RF running patterns. The FF pattern was defined as making initial contact with the ball of the

foot and preventing the heel from touching the ground. The RF pattern was defined as making initial contact with the heel. Marker position data and GRF data were filtered using a Butterworth low-pass filter with cutoff frequencies of 12Hz and 50Hz, respectively. Sagittal plane ankle joint moments were calculated using a Newton-Euler inverse dynamics approach. Group means of each variable were calculated before determining the AT force generated in each running condition.

A custom MATLAB program was developed to determine the AT force. A second order polynomial was derived to estimate the AT moment arm as a function of ankle joint angle using data from Arnold et al. [5]. An estimate of the passive joint moment [6] was subtracted from the net joint moment to determine the active muscle moment. The active ankle moment was divided by the AT moment arm at each instant of stance to determine the AT force. We assumed the force in the AT was zero whenever the active ankle moment was dorsiflexor. The difference in peak ankle joint moment generated between each footfall pattern was assessed with a student's t-test ( $\alpha = 0.05$ ). The group mean peak AT force was compared between footfall patterns. Differences in ankle joint moment and AT force were also assessed for early (0-33%), mid (34-66%) and late stance (67-100%).

## RESULTS AND DISCUSSION

Peak ankle plantar flexor moment was 226.41 Nm and 194.19 Nm for FF and RF running, respectively ( $p < 0.001$ ) (Figure 1). FF running generated greater ankle plantar flexor moments for early and mid stance ( $p < 0.001$ ) but there was no difference during late stance ( $p = 0.737$ ).

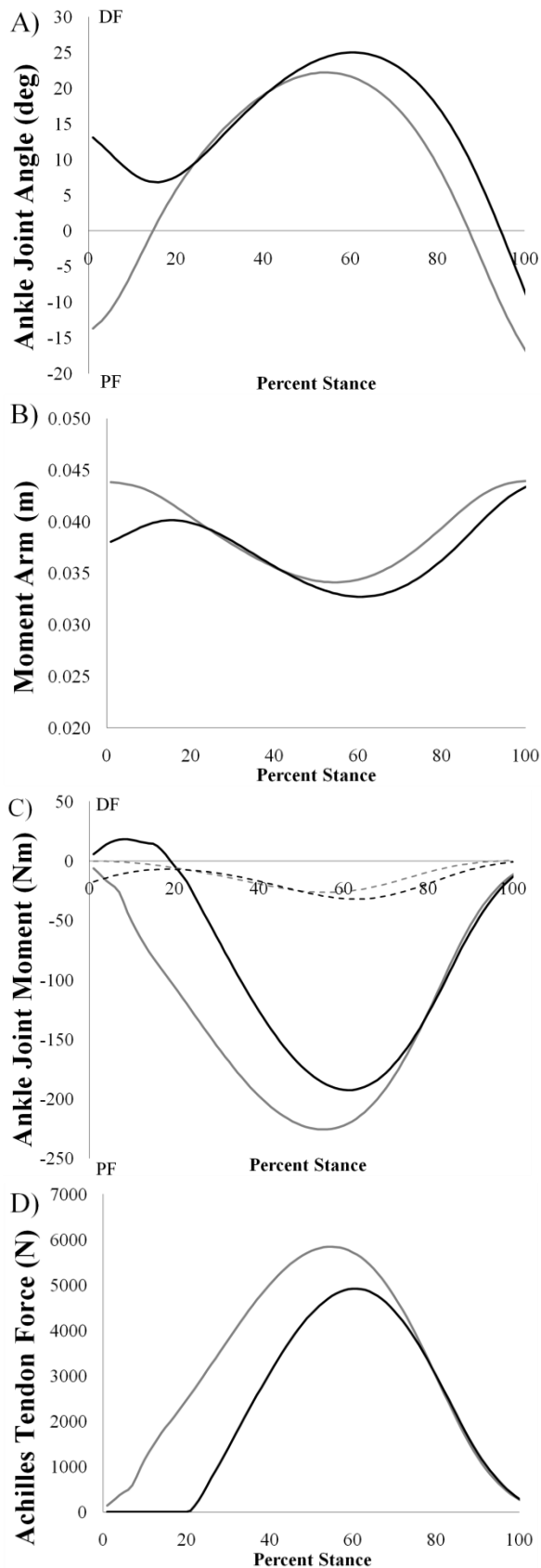


**Figure 1:** Parameter values over the stance phase of FF (gray) and RF (black) running for: A) Ankle joint angle; B) Achilles tendon moment arm length; C) Net (solid line) and passive (dashed line) ankle joint moment; D) Achilles tendon forces.

Peak AT force was 5843.54 N for FF running and 4919.04 N for RF running (Figure 1D). FF running generated greater AT force during early and mid stance but not late stance. The AT force values found in the present study are similar to those found by the plantar flexors in previous studies [7].

Greater AT forces generated during mid stance of FF running may indicate this footfall pattern may increase the risk of soft tissue injury to the plantar flexor muscles or Achilles tendon, including muscle strain, tendonitis or tendon rupture. Consequently, the suggestion that FF running may be protective against running injuries compared to RF running is unsubstantiated. It may be more likely that FF running may be protective against bone injury such as stress fracture due to repeated impact loading whereas RF running may be more protective against some soft-tissue injury such as Achilles tendonitis or plantar fasciitis. Therefore, recommending a runner to alter footfall pattern in order to prevent or treat an injury may not be warranted.

## CONCLUSIONS

Results from the present study indicate the FF running pattern results in greater AT forces during the stance phase compared to RF running. Therefore, FF running may not be protective against all running related injuries as previously suggested [1]. Recommendations to alter footfall pattern to prevent or treat running related injuries should be made with caution.

## REFERENCES

1. Lieberman DE, et al. *Nature* **463**, 531-536.
2. Pratt DJ. *Clin Biomech* **4**, 51-57, 1989.
3. Williams DS, et al. *J App Biomech* **16**, 210-218, 2000.
4. Maganaris CN, et al. *Eur J Appl Physiol* **83**, 363-369, 2000.
5. Arnold EM, et al. *Ann Biomed Eng* **38**, 269-279, 2010.
6. Riener R & Edrich T. *J Biomech* **32**, 529-544, 1999.
7. Hof AL et al. *Acta Physiol Scand* **174**, 17-30, 2002.

# Cyclic Compressive Loading Facilitates Acute and Accumulated Recovery of Viscoelastic Properties of Skeletal Muscle Following Eccentric Exercise

<sup>1</sup>Caroline Haas, <sup>1</sup>Yi Zhao, <sup>2</sup>Timothy A. Butterfield and <sup>1</sup>Thomas M. Best

<sup>1</sup>The Ohio State University, Columbus, OH, USA

<sup>2</sup>University of Kentucky, Lexington, KY, USA

email: [caroline.haas@osumc.edu](mailto:caroline.haas@osumc.edu)

## INTRODUCTION

Although limited evidence exists on the efficacy of massage, Americans make more than 160 million visits annually for relief of musculoskeletal pain and weakness by manipulative or body-based practices. While the majority of experimental work has examined the active and passive responses of skeletal muscle to tensile loading (stretch), both healthy and diseased muscles are also exposed to compressive loads during conditions such as prolonged bed rest, traumatic impact, and manual therapies. The purpose of this study is to determine the effect of reproducible compressive loading on muscle viscoelastic properties in order to understand tolerance levels of human skeletal muscle to manual therapies.

## METHODS

Four skeletally mature New Zealand White rabbits were surgically instrumented with bilateral peroneal nerve cuffs and subcutaneous interfaces for stimulation of the hindlimb tibialis anterior (TA) muscles [1]. Following a bout of eccentric exercise, rabbits were assigned to a protocol with massage frequency of 0.5 Hz at compressive force of 10N for 15 min. The contralateral hindlimb served as the exercised, non-massaged control. Measurements on the contralateral limb occurred one week after those on the initial hindlimb in order to account for cross over effect.

Viscoelastic properties of the TA were evaluated by a ramp and hold protocol with a ramping rate of 75 $\mu$ m/s, compressing the tissue to the depth of 5mm (corresponding to 50% normal strain). Stress relaxation tests were performed prior to one bout of damaging, eccentric exercise, post exercise, and pre and post four consecutive days of massage using a

customized motorized device with a flat tip 6.4mm in diameter. The same device was used for applying massage action with a 12mm flat tip.

A representative set of displacement and loading curves is shown in Figure 1.

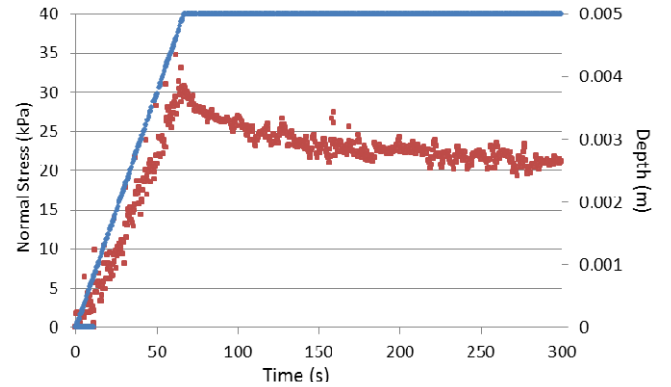


**Figure 1:** The displacement curve (blue) and the loading curve (red) in a representative ramp-and-hold experiment.

The instantaneous elastic response and the time dependent response were separated using the following stress relaxation function:

$$\sigma(t) = G(t) * \sigma^e(\lambda) \quad (1)$$

where the reduced relaxation function  $G(t)$  is expressed by a second order Prony series:

$$G(t) = G_0 \left( 1 - g_1^p \left( 1 - e^{-\frac{t}{\tau_1}} \right) - g_2^p \left( 1 - e^{-\frac{t}{\tau_1}} \right) \right) \quad (2)$$

and the instantaneous response  $\sigma^e(\epsilon)$  has the form:

$$\sigma^e(\epsilon) = A \left( e^{B\epsilon} - 1 \right) \quad (3)$$

where  $A$  is a parameter with the dimension of stiffness and  $B$  is dimensionless. The parameters in equations (2) and (3) were determined from the experimental data using a previously described QLV approach [3].

## RESULTS AND DISCUSSION

Figure 2 shows a group of representative loading curves. In both the control and the massage groups, the loading curves are offset by the eccentric exercise, showing a change in the muscle tissue stiffness. After four days of consecutive massaging, the loading curve approached the pre-exercise reference level, while the loading curve in the control moves in the opposite direction.

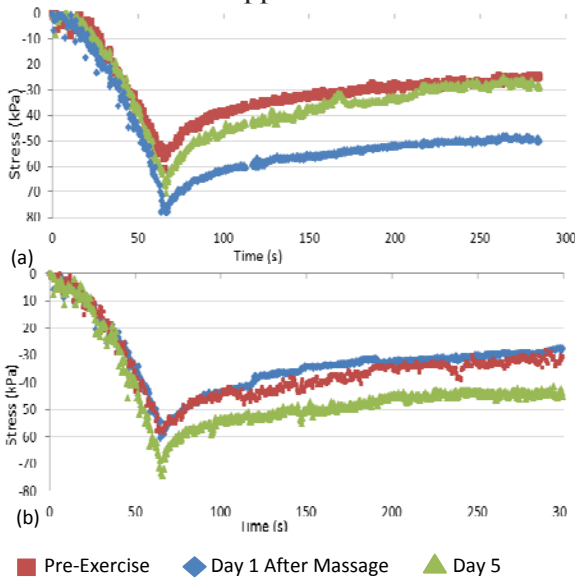


**Figure 2:** Loading curve of muscle tissue prior to eccentric exercise, immediately after exercise and on Day 5: (a) massage group; and (b) control group.

The change of muscle stiffness is best seen from the instantaneous response fitted using the experimental data (Figure 3), where the curves obtained daily prior to the massage exhibited a monotonic decrease, indicating that the massage actions reduces the elastic modulus of the subject tissue. After three days, the elastic modulus reached that of the pre-exercise tissue.

Computation of the reduced relaxation function showed that the coefficient  $g_1^p$  relating to the fast relaxation reduces after each massage, while the time constants did not show a consistent change for the four animals (Figure 4). Further investigation of the viscoelastic data is needed with more experimental data.

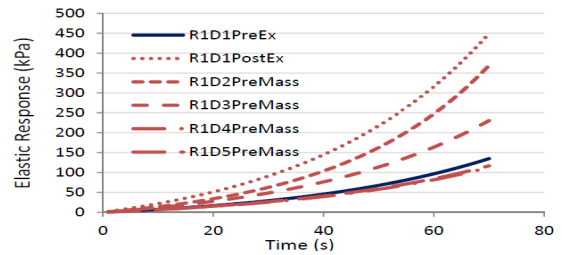


**Figure 3:** The instantaneous elastic response over four days loading period.

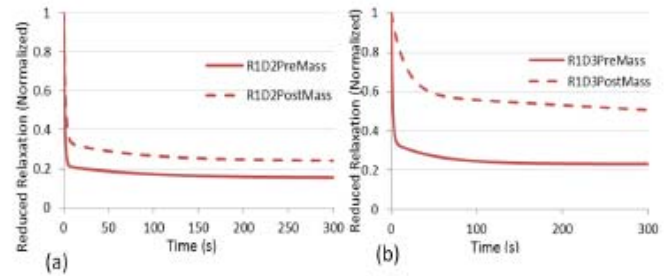


**Figure 4:** Reduced relaxation function shows that massage can decrease  $g_1^p$ , while the effects on the time constants are not clear.

## CONCLUDING REMARKS

This study showed that muscles subjected to cyclic compressive loading following intense eccentric exercise show an acute and accumulated effect of massage on the recovery of viscoelastic properties. Using tolerance levels for skeletal muscle established from animal studies and translating these findings to mathematical models and to human studies may provide an opportunity for researchers to understand how injury and disease alters human muscle function. These data provide a starting point for linking the mechanical properties of skeletal muscle with physical therapies, and may shed light on the design and optimization of therapeutic massage.

## REFERENCES

1. Butterfield, TA, et al. *Med. Sci. Sports Exerc* **40**, 1289–1296, 2008.
2. Zeng, H, et al. *J. Med. Devices* **2**, 027530, 2008.
3. Abramowitch, J, et al., *J Biomech Eng*, **126**, 92–97, 2004.

## ACKNOWLEDGEMENTS

Supported by NIH NCCAM R01AT004922 (TMB)

# RECONSTRUCTING THE TAKEOFF MECHANICS OF GIANT PTEROSAURS

Michael Habib

Chatham University, Pittsburgh, PA, USA  
email: mhabib@chatham.edu

## INTRODUCTION

Reconstructing the behavior and mechanical limits of fossil animals is a challenging biomechanical problem. Fossil species are generally analyzed in a comparative context with modern taxa for which we have more complete information. In some cases, the biomechanical limits of fossil species have been estimated from direct analogy to living groups, but this can lead to inappropriate scaling assumptions and erroneous behavioral inferences. Azhdarchid pterosaurs include the largest known flying animals, with the largest species reaching a potential mass of over 250 kg [1]. This greatly exceeds the maximum size observed in all other flying animals. Prior studies [2,3,4] have suggested that giant pterosaurs would have been incapable of takeoff at realistic body masses. These prior studies have all assumed a bird-like, bipedal launch strategy for pterosaurs. Comparative analyses of long bone structural strength, trabecular bracing, and muscle attachment expansion in pterosaurs, birds, and bats demonstrate that prior assumptions of a bipedal takeoff dynamic in pterosaurs were poorly founded. Instead, it is most likely that pterosaurs were quadrupedal launchers. Here, I review my prior results regarding quadrupedal launch [5,6] and present an expanded model that provides estimates of specific launch times and velocities in pterosaurs, and allows for the consideration of water launch in aquatic pterosaurs. The quadrupedal launch model explains the difference in maximum size observed between pterosaurs and birds, and predicts that giant pterosaurs should have been capable of launching from level ground without need for an initial takeoff run.

## METHODS

Estimates of bone strength in pterosaur long bones were derived from applying a beam model. Exact sections, as derived from CT imaging, were not

available for most of the pterosaur species examined in this study, and an elliptical model was applied where necessary. The taxon *Bennettazhia* was CT scanned at the National Museum of Natural History, and was used to compare the elliptical model to a known, exact section. External measurements of pterosaur long bones were taken at the Smithsonian's National Museum of Natural History (NMNH) in Washington, DC, the American Museum of Natural History in New York City, and the Bavarian State Palaeontological Collection (BSPG) in Munich, Germany. Sections at the midshaft of the humerus and femur of all specimens closely approached a true ellipse. Using a beam model of the femoral and humeral diaphyses, maximum stress in bending is given by  $My/I$  (where  $M$  is the bending moment,  $I$  is the second moment of area about the neutral axis and  $y$  is the maximum distance from the neutral axis to the edge of the section. The moment arm for bending was taken to be proportional to element length.

The section modulus,  $Z$ , in bending is defined as  $I/y$ . If  $M$  and  $T$  are considered to be proportional to the product of body mass ( $B$ ) and bone length ( $L$ ) [7], then structural strength is proportional to  $Z/(B*L)$ . Relative femoral to humeral structural strength is a ratio of  $(Z_{fem}/L_{fem})/(Z_{hum}/L_{hum})$ , and does not require knowledge of animal body mass, which is of great utility in working with fossil taxa. Structural strength in bending was compared for the humerus, femur, and humeral:femoral ratio across 19 pterosaur specimens and 125 specimens of modern birds. The comparative patterns of muscle insertion sites were also examined in four well-preserved pterosaur taxa (*Anurognathus ammoni*, *Anhanguera santanae*, *Pteranodon longiceps*, and *Quetzalcoatlus* sp.)

## RESULTS AND DISCUSSION

The ratio of humeral to femoral strength in pterosaurs far exceeds that measured for birds (Figure 1). The only case in which the structural strength ratios for birds and pterosaurs overlap is in the case of *Anurognathus*, a small (approximately 0.22 meter wingspan) species with a suite of unusual characters in the skull, wing, and hind limb.

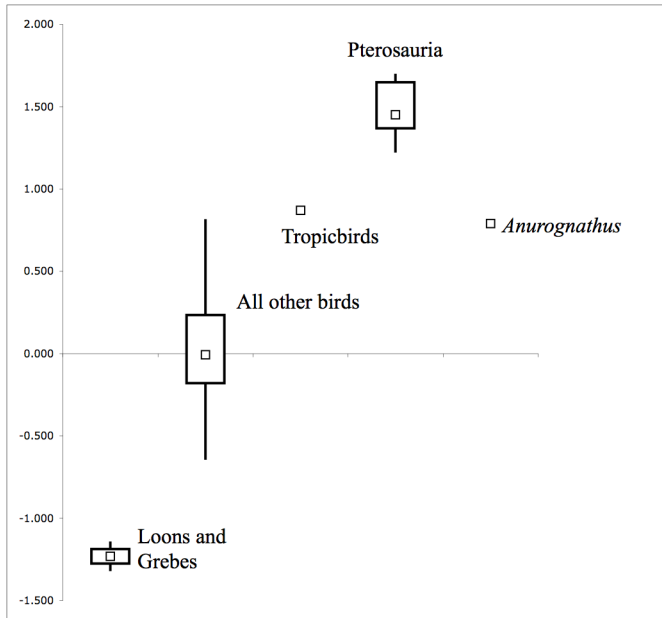


**Figure 1:** Structural strength ratios between the humerus and femur in birds and pterosaurs. Loons, grebes, and tropicbirds are separated as outliers for comparison, as is *Anurognathus ammonii*, a tiny basal pterosaur from central Europe.

The largest pterosaurs show the greatest disparity in strength between the humerus and femur. This is similar to the situation seen in bats, but differs significantly from the allometric relationship measured for birds. This disparity between birds and pterosaurs suggests that, as in ground-launching bats, pterosaur forelimbs acted as the primary power-generation module for all major motion activities: aerial locomotion, terrestrial locomotion, and launch.

Using known patterns of launch time relative to flapping frequency in modern flying animals, along with estimates of burst muscle capability taken from

the closest living relatives of pterosaurs, it is possible to broadly estimate the launch capabilities of giant pterosaurs. For even the largest pterosaurs, a quadrupedal launch model predicts that launch from level ground was possible without special wind conditions. Launch is impossible under a bipedal launch model (femoral failure). This result is robust to uncertainty in body mass and wing proportions. The results for one potential reconstruction are given in Table 1.

## CONCLUSIONS

Prior reconstructions of animal launch, particularly for fossil species, have been consistently confounded by a mistaken assumption that launch forces are primarily lift-based in nature. In reality, animal takeoff is ballistic in nature. Prior estimates of pterosaur launch were likely mistaken in assuming a bipedal launch dynamic in the manner of living birds. Structural strength ratios of the limbs indicate that pterosaurs were quadrupedal launchers. Estimates of launch performance using proper ballistic assumptions and a quadrupedal mode of takeoff indicate that giant pterosaurs were fully launch-capable. Pterosaurs were able to achieve greater maximum sizes than birds because they were quadrupedal launchers; this substantially alters the mechanical limits for flight.

## REFERENCES

1. Witton MP. *Zitteliana* **B28**, 143–159, 2008
2. Chatterjee S, Templin RJ. *Geological Society of America Special Publication*, **376**, 1–64, 2004
3. Sato K, et al. *PLoS ONE* **4**, e5400, 2009
4. Henderson DM. *J. Vert. Paleontology* **30**, 768–785, 2010
5. Habib MB. *Zitteliana* **B28**, 161–168, 2008
6. Witton M, Habib MB. *PLoS ONE* **5**, e13982, 2010
7. Ruff CB. *J. of Human Evolution* **38**, 269–290, 2000

**Table 1:** Estimated launch parameters for *Quetzalcoatlus northropi*. FMF: Flight muscle fraction.

| Body Mass (kg) | Span (m) | FMF  | Wing Area (m <sup>2</sup> ) | Stall Speed (m/s) | Launch time (s) | Flap rate (hrz) | Height gain (m) | Required preload factor |
|----------------|----------|------|-----------------------------|-------------------|-----------------|-----------------|-----------------|-------------------------|
| 259.00         | 10.40    | 0.30 | 9.01                        | 14.43             | 0.63            | 1.19            | 2.00            | 2.02                    |

# ASSOCIATION OF OVERSTRIDING AND INJURY STATUS IN RUNNERS WITH AND WITHOUT ILIOTIBIAL BAND SYNDROME

Jocelyn F. Hafer BS, Allison M. Brown PT PhD, Robert A. Maschi PT DPT CSCS, Yatin Kirane D.Orth, PhD, Howard J. Hillstrom PhD

Hospital for Special Surgery, New York, NY, USA  
email: haferj@hss.edu

## INTRODUCTION

Excessive stride length has been associated with common running injuries. For example, decreases in stride length have been shown to alleviate the symptoms of patellofemoral pain syndrome. [1] Likewise, military recruits with a history of stress fractures had longer marching stride lengths than their healthy counterparts. [2] Iliotibial band syndrome (ITBS) is the second most common overuse running injury [3], and kinematic alterations including increased peak knee flexion [4] have been observed in runners with ITBS. However, the relationship between stride length and ITBS has not been thoroughly examined.

Stride length could be monitored based on the extent of "overstriding" as measured by the horizontal distance from the center of mass to the heel at initial contact (*heel strike distance*, HSD; Figure 1). It was the conviction of this investigational team that injured runners may demonstrate a greater HSD with respect to healthy runners. Therefore, the purpose of this study was to examine whether runners with ITBS demonstrate significant differences in HSD as compared to an uninjured control group. We hypothesized that runners with ITBS would demonstrate a greater HSD as compared to healthy controls.

## METHODS

3-dimensional motion data (Motion Analysis Corporation, Santa Rosa, CA) were collected from 21 healthy female runners and 12 female runners with current symptoms of ITBS as part of a larger study. All runners were rear foot strikers. Participant characteristics are displayed in Table 1.

**Table 1:** Participant characteristics

|         | Age (years) | Leg length (m) | BMI (kg/m <sup>2</sup> ) |
|---------|-------------|----------------|--------------------------|
| Healthy | 29±6        | 0.85±0.05      | 21.8±2.2                 |
| ITBS    | 32±8        | 0.90±0.04      | 21.1±1.3                 |

Participants performed at least 5 acceptable overground running trials at 7.5 mph as measured by photoelectric timer. The horizontal distance of heel strike in front of the center of the pelvis was used as an indicator of overstriding. This was measured as the distance in the sagittal plane between a virtual mid-malleoli marker and a virtual center-of-pelvis marker for both right and left sides (Figure 1).

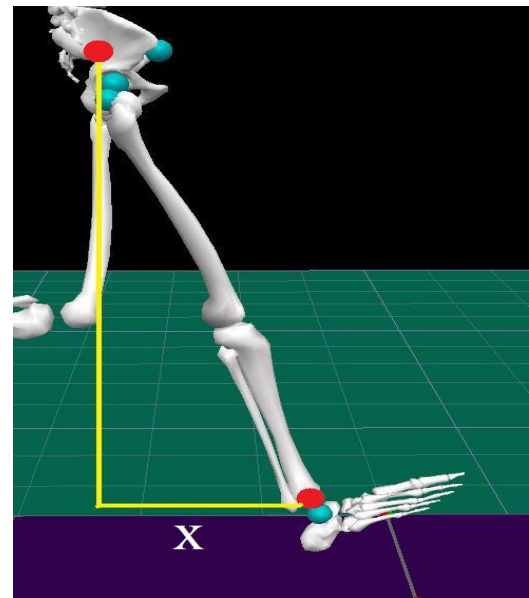


**Figure 1:** Horizontal distance (X) of heel strike in front of the center of the pelvis (HSD).

Leg lengths were measured as the distance between markers on the anterior superior iliac spine and the

medial malleolus for each leg. HSD was not normalized to leg length as previous studies have indicated that leg length and stride length are unrelated. [5] Heel strike distances were averaged by side. Independent t-tests were performed with  $p < 0.05$  considered significant.

## RESULTS AND DISCUSSION

Variables of interest are shown in Table 2.

**Table 2:** Left and right heel strike distances.

|         | Left HSD (cm) | Right HSD (cm) |
|---------|---------------|----------------|
| Healthy | 24.4±2.6      | 24.3±3.0       |
| ITBS    | 25.7±2.3      | 25.6±2.7       |
| P       | 0.17          | 0.22           |

HSD was not significantly different between healthy and ITBS groups in this sample.

## CONCLUSIONS

In this sample of runners, HSD was not significantly different between healthy and ITBS groups. This suggests that overstriding may not be a significant factor in runners who currently have ITBS. A larger sample should be included in future studies to determine if this lack of significance was due to a lack of statistical power. Previous studies

have shown contradictory results regarding kinematics of runners currently experiencing ITBS symptoms [6] and those who have a history of this injury [7] with respect to healthy runners. These differences may be due to the symptomatic runners adopting a "protective" running posture that more closely resembles healthy runners' posture to avoid pain. Therefore, the current results may not be applicable to treating runners with a history of ITBS or for prevention of ITBS. Future studies should compare the HSD of runners with a history of ITBS with that of currently symptomatic runners with ITBS and healthy runners.

## REFERENCES

1. Heiderscheit BC, et al. *Proceedings of CSM 2010*, San Diego, CA, USA, 2010
2. Kelly EW, et al. *Military Medicine* **165**, 142-146, 2000.
3. Taunton JE, et al. *Br J Sports Med* **36**, 95-101, 2002.
4. Miller RH, et al. *Gait Posture* **26**, 407-413, 2007.
5. Cavanagh PR and Kram R. *Med Sci Sports Exerc* **21**, 467-479, 1989.
6. Grau S, et al. *Scand J Med Sci Sports* **21**, 184-189, 2009.
7. Ferber R, et al. *J Orthop Sports Phys Ther* **40**, 52-58, 2010.

# COMPARISON OF OBJECTIVE MEASURES OF FOOT STRUCTURE AND FUNCTION IN THE POPULATION-BASED FRAMINGHAM FOOT STUDY

Thomas J. Hagedorn<sup>1</sup>, Jody L. Riskowski<sup>1,2</sup>, Alyssa B. Dufour<sup>1,3</sup>, Howard J. Hillstrom<sup>4</sup>,  
Mark W. Lenhoff<sup>4</sup>, Jocelyn C. Frey<sup>4</sup>, Virginia A. Casey<sup>1</sup>, Marian T. Hannan<sup>1,2</sup>

1. Institute of Aging Research, Hebrew SeniorLife, Boston, MA, 02131;

2. Harvard Medical School, Boston, MA, 02115;

3. Boston University School of Public Health, Boston, MA, 02118

4. Hospital for Special Surgery, New York City, NY, USA

Email: thomashagedorn@hsl.harvard.edu

## BACKGROUND

Pronation and supination are defined (respectively) as the medial and lateral rolling of the foot and ankle [1]. Objective measures of supination and pronation may provide insights on mechanisms of action and lead to interventions to stabilize the foot and possibly decrease injury and pain.

Currently several methods exist to evaluate excessive pronation and supination, including structural measures like the Arch Index (AI) [2] as well as functional measures such the contact force ratio (CFR) [3] and the center of pressure excursion index (CPEI), which measures the concavity of the center of pressure [4]. Another possible method is compare lateral-to-medial loading of the foot. While both structure and function are important for assessing foot type, it is essential to understand their relationship to one another.

## PURPOSE OF THE STUDY

This study seeks to evaluate the relationship between measures of foot structure and function in a population-based study.

## METHODS

Data were obtained from 1211 subjects enrolled in the Framingham Foot Study, which has been described previously [5].

Foot pressure scans were collected using a Tekscan Matscan pressure mat (Tekscan Inc, Boston, MA), with a resolution of 1.4 sensels/cm<sup>2</sup>. Walking data were collected at 40 Hz while participants walked barefoot at a self-selected pace across a 3.5m walkway, using the two-step method [6]. The dominant foot was defined as having the larger propulsive force. The footprints were masked into their lateral and medial halves using the Novel Automask software (Novel GmbH, Munich, Germany). Lateral-to-medial ratios of pressure-time integrals (PTI) and force-time integrals (FTI) were calculated for each masked region. CPEI, AI and CFR were calculated using custom code in Matlab.

Only dominant feet were analyzed. Correlations between CPEI, each lateral-to-medial-ratio, AI, and CFR were evaluated using Pearson Correlation Coefficients. Alpha was set to 0.05.

## RESULTS

Study participants (57% female) had a mean age of  $64.8 \pm 10.8$  years and body mass index of  $28.3 \pm 5.6$  kg/m<sup>2</sup>. Descriptive statistics for the mechanical measurements are shown in Table 1. Correlation coefficients (table 2) show positive

correlations between all the measured variables.

## DISCUSSION AND CONCLUSIONS

These results suggest that increasing lateral-to-medial mechanical ratios and CPEI correspond to increasing AI and CFR. Given the different constructs of the measures it is not surprising that the correlations vary in magnitude.

Previous studies have shown that AI is negatively correlated to navicular height [2] and that CFR is positively correlated with navicular drop [3]. The positive relation between variables is thus notable, given that arch height is thought to have the opposite relation with pronation and supination. One possible explanation is that parameters measure different planar movements, and may not fully characterize the foot action. It should be noted that none of these parameters are direct measures of structure (e.g., hindfoot alignment, arch height, etc.) or are based upon foot kinematics. While

these results suggest that there is a strong relationship between foot structure and function, the included measures do not appear to fully describe dynamic foot function. Further research is needed to determine the link between these measures and dynamic foot function, pain, and injury.

## ACKNOWLEDGEMENTS

Supported by NIH/NIAMS AR047853

## REFERENCES

1. Cote KP et al. J Athl Train, 2005. 40(1): p. 41-46.
2. Cavanagh, PR and MM Rodgers. J Biomech, 1987. 20(5): p. 547-51.
3. Leung AK et al. Prosthet Orthot Int, 2004. 28: p. 167-174.
4. Song J et al. J Am Pod Med Assoc, 1996. 86(1): p. 16-23.
5. Dufour, AB, et al. Arthritis Rheum, 2009. 61(10): p. 1352-8.
6. McPoil, TG, et al. J Am Pod Med Assoc, 1999. 89(10): p. 495-501.

**Table 1.** Descriptive statistics for the mechanical parameters

|                  | Minimum | Maximum | Mean  | Std. Deviation |
|------------------|---------|---------|-------|----------------|
| <b>AI</b>        | 0.022   | 0.350   | 0.217 | 0.049          |
| <b>CFR</b>       | 0.001   | 0.347   | 0.116 | 0.063          |
| <b>CPEI</b>      | -22.539 | 41.6    | 13.35 | 8.064          |
| <b>PTI ratio</b> | 0.461   | 1.618   | 0.91  | 0.129          |
| <b>FTI ratio</b> | 0.264   | 4.525   | 1.108 | 0.491          |

**Table 2.** Correlations between AI, CFR, CPEI, PTI ratios, and FTI ratios for all dominant feet. All p values were <0.001

|                  | AI    | CFR   | CPEI  | PTI ratio | FTI ratio |
|------------------|-------|-------|-------|-----------|-----------|
| <b>AI</b>        | 1     | 0.763 | 0.134 | 0.093     | 0.238     |
| <b>CFR</b>       | 0.763 | 1     | 0.240 | 0.295     | 0.502     |
| <b>CPEI</b>      | 0.134 | 0.240 | 1     | 0.341     | 0.416     |
| <b>PTI ratio</b> | 0.093 | 0.295 | 0.341 | 1         | 0.729     |
| <b>FTI ratio</b> | 0.238 | 0.502 | 0.416 | 0.729     | 1         |

# CORRELATION OF LOWER LIMB EVENTS AFTER A 45 MINUTE RUN

<sup>1</sup>Elizabeth R. Hageman and <sup>1</sup>Timothy R. Derrick

<sup>1</sup>Iowa State University, Ames, IA, USA

email: [ehageman@iastate.edu](mailto:ehageman@iastate.edu) web: [www.kin.hs.iastate.edu/](http://www.kin.hs.iastate.edu/)

## INTRODUCTION

The coordination of lower limb motion during running has been well researched and proposed as a source of injury. Internal tibial rotation is coupled with eversion and knee flexion during the first half of stance. External tibial rotation is coupled with inversion and knee extension during the second half of stance [1].

A strong correlation ( $r=0.8$ ) exists between calcaneal in/eversion and vertical change in navicular height during static situations [2]. However, during walking, eversion peaks early around 25% of stance while the arch is lowest after heel rise [3]. The collapse of the arch may also influence rearfoot eversion and tibial rotation during running. This mechanism may influence the direction of power flow through the ankle joint and have implications for shoe and orthotic design [4].

Many studies have investigated changes after exhaustive runs, but runners also sustain injuries during regular training. While there were no differences in joint timing after a run at self-selected training speed, eversion, knee internal rotation peak angles, excursions, and peak velocities increased [5]. Therefore, the purpose of this study was twofold: 1) to investigate the relationship between collapse of the medial longitudinal arch and rearfoot eversion and tibial rotation, and 2) to see if the coordination or magnitudes of these events change after a 45 minute run at a comfortable pace.

## METHODS

Healthy recreational runners participated in this study (10 males, 14 females). Participants ran barefoot ( $3.11 \pm 0.36 \text{ m} \cdot \text{s}^{-1}$ ) overground before and after a shod 45 minute treadmill run at the same pace. Reflective markers were placed on the right foot, leg and pelvis. Marker positions were recorded at 200 Hz by 8 Vicon motion analysis cameras.

Cardan joint angles were calculated using the methods of Soderkvist et al. [6] and a medial/lateral - longitudinal axis - anterior/posterior rotation order. In/eversion was defined as the rotation of the rearfoot relative to the tibia about an anterior-posterior axis. Tibial rotation was the rotation of the rearfoot relative to the tibia about the longitudinal axis. Knee flexion was the rotation of the tibia relative to the femur about the mediolateral axis.

Navicular displacement was the change in 3-dimensional distance from the navicular to a line connecting the first metatarsal head and medial calcaneus, relative to sitting navicular position. A positive displacement represents a flattening of the longitudinal arch.

## RESULTS AND DISCUSSION

Peak navicular displacement, eversion, internal tibial rotation, knee flexion and the time to peak are shown in Table 1. Of all the variables, only time to peak internal tibial rotation occurred earlier after the run, indicating that the first of the two peaks was larger more often. All kinematic data are similar to those previously reported [1,5], although we did not observe an increase in eversion or internal tibial rotation reported after a run of similar duration and exertion level [5].

Ensemble curves are shown in Figure 1. Correlations between curves over the entire stance phase were high and did not change much pre- and post-run: navicular displacement-eversion (pre:  $r=0.82$ , post:  $r=0.80$ ) and eversion-tibial rotation (pre:  $r=0.89$ , post:  $r=0.86$ ).

The correlation between peak eversion and tibial rotation increased post-run ( $r=0.56$  to  $r=0.67$ ), while the correlation between peak knee flexion and internal tibial rotation slightly decreased ( $r=0.46$  to  $r=0.42$ ). There was only a weak correlation ( $<0.4$ )

between navicular displacement and eversion or internal tibial rotation.

## CONCLUSIONS

Collapse of the medial longitudinal arch is not strongly correlated to frontal plane rearfoot motion or tibial rotation during barefoot running. After a 45 minute run, peak internal tibial rotation occurred earlier in stance and became more correlated to peak eversion and less correlated to peak knee flexion. This may imply that later in a run, joint motion may be influence more by distal segments, possibly highlighting the importance of footwear and orthotic design to address these issues.

## REFERENCES

1. Pohl MB, Buckley JG. *Clin Biomech* **23**, 334-41, 2008.
2. Mathieson I, et al. *J Am Pod Med Assoc* **94**, 275-281, 2004.
3. Hunt AE, et al. *Clin Biomech* **16**, 592-600, 2001.
4. Bellchamber TL, van den Bogert AJ. *J Biomech* **33**, 1397-1403, 2000.
5. Dierks TA, et al. *J Biomech* **43**, 2993, 2010.
6. Soderkvist I. et al. *J Biomech* **26**, 1473-1477, 1993.

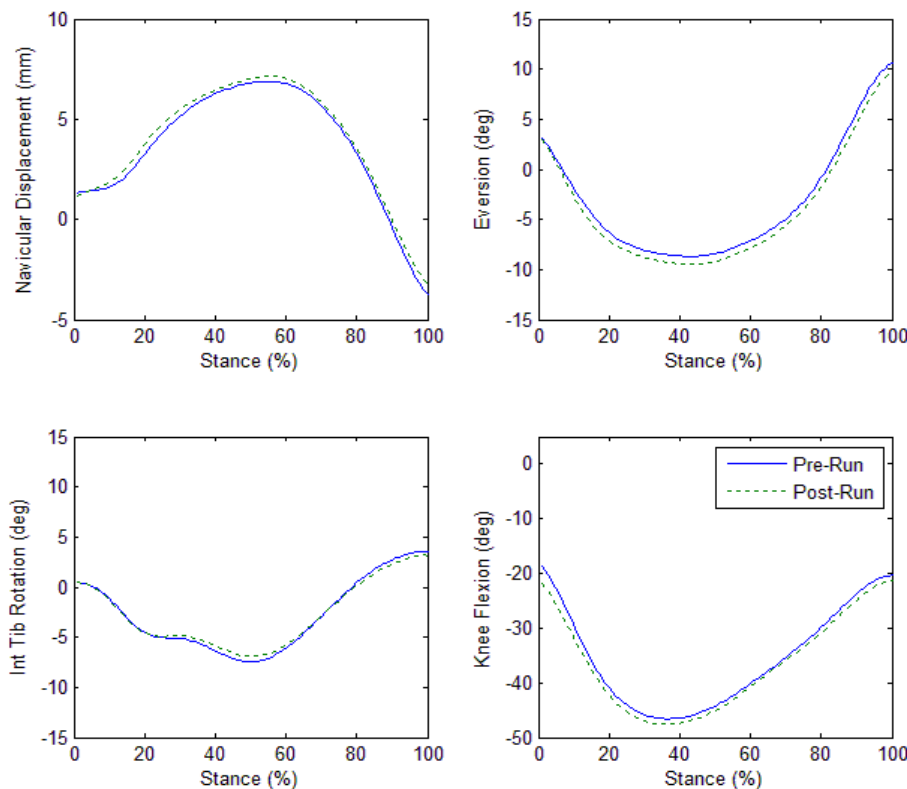


**Figure 1:** Ensemble curves for navicular displacement, eversion, internal tibial rotation and knee flexion before and after 45 minute run.

**Table 1:** Peak displacement/angle and time to peak before and after 45 minute run.

|                 | % Stance  |            |            |             |                 |                 |                 |                 |
|-----------------|-----------|------------|------------|-------------|-----------------|-----------------|-----------------|-----------------|
|                 | ND (mm)   | EV (deg)   | IR (deg)   | KA (deg)    | Time to Peak ND | Time to Peak EV | Time to Peak IR | Time to Peak KA |
| <b>Pre-Run</b>  | 7.1 ± 2.1 | -9.0 ± 3.0 | -8.0 ± 3.6 | -40.3 ± 5.4 | 55±7            | 41±6            | 49±6            | 36±4            |
| <b>Post-Run</b> | 7.2 ± 2.6 | -9.6 ± 3.3 | -7.8 ± 3.6 | -39.8 ± 6.6 | 55±5            | 41±7            | 45±9*           | 35±4            |

ND=navicular displacement; EV=eversion; IR=internal tibial rotation; KA=knee flexion angle

\*Significant from pre-run at p<0.05

# PRELIMINARY COMPARISONS OF EXPERIMENTAL AND COMPUTATIONAL KNEE LOADING CONDITIONS SIMULATING DAILY LOADING SCENARIOS

Rena Hale, Roger Gonzalez  
LeTourneau University, Longview, TX, USA  
email: [Roger.v.gonzalez@gmail.com](mailto:Roger.v.gonzalez@gmail.com)

## INTRODUCTION

Computational models of the human knee are helpful in gaining a greater understanding of joint kinematics and its implications on internal loading conditions. To characterize differences in knee kinematics and internal forces, we have created a prototype specimen specific computational knee model complemented by an experimental specimen testing device to quantify the biomechanical changes within a cadaver knee specimen, given time-varying muscle loading, ground reaction forces, and ACL ligament failure.

## METHODS

A preliminary finite element (FE) model was created in LS-DYNA where the femur, tibia, and patella geometries were segmented from CT images. Model's cartilage elasticity, meniscus cartilage parameters, and Poisson ratio were taken from literature values [1,2]. Ligaments, based on the literature and experimental measurements, were modeled as one-dimensional elements with force-strain relationships.

Two forms of verification were created for the FE model. First, a flexible three dimensional musculoskeletal knee model was made in LifeModular™ (LifeMod) using muscle-tendon parameters based off a previous model [3], with EMG and knee angles [4] used to approximate muscles forces.

An *in-situ* dynamic muscle loading testing device was created to simulate human knee movement, as a second method for FE model validation. Our testing device uses knee subject-data of gait, sit-to-stand, and isotonic muscle trials that were collected from our laboratory and in collaborations with Drs. Lloyd, and Buchanan at the Universities of Western Australia and Delaware, respectively. Muscles included in our analysis were the vastus lateralis,

rectus femoris, semitendinosis, biceps femoris, and gastrocnemius. Tibiofemoral intersegmental pressure was measured with Teckscan™ transducers and ligament strain with MicroStrain M-DVRT-3's for the ACL, PCL, MCL, and LCL.

## RESULTS AND DISCUSSION

Tests to validate our FE model have been conducted using literature, our LifeMod model, and cadaver experiments on our testing device. The FE model was compared to static simulations reported in literature [5] (Fig. 1). Preliminary results demonstrate similar peak stress and center of pressures.

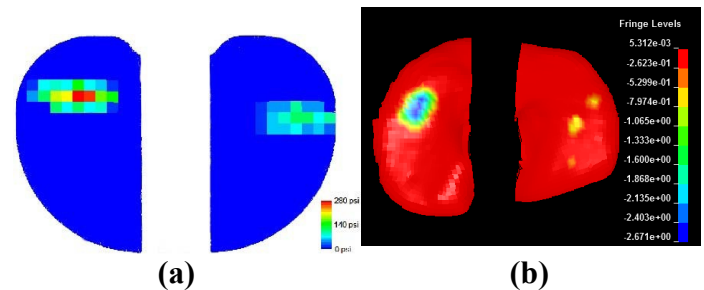


**Figure 1.** Pressure distribution over tibial plateau (a) LifeMod (b) LS\_DYNA

A left leg stance gait simulation was performed on both our specimen knee and our LifeMod knee model (Fig. 2). Results demonstrated that the cadaver run experiment and the model's tibiofemoral contact forces data trended similarly. With LifeMod being a musculoskeletal model, differences in the forces can be accounted for by the simplified geometry of the tibial plateau. Preliminary results indicate our LifeMod knee model is able to replicate the trends of the dynamic loading conditions on the specimen knee.

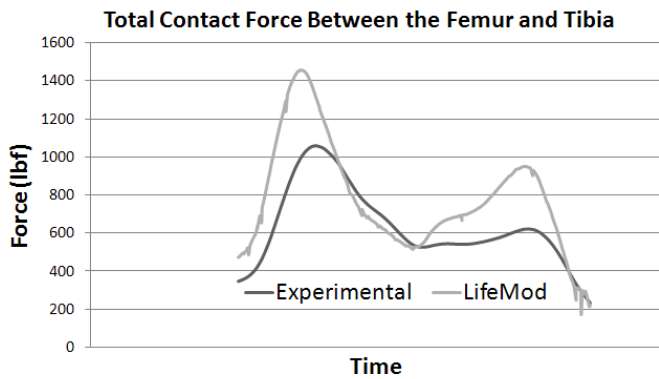


**Figure 2.** LifeMod and experimental knee contact force

Recent advancements with our LifeMod model have included using optimized muscle forces [6] from human gait trials run in our laboratory. LifeMod simulations have resulted in tibial plateau pressure distributions that are comparable to our FE model, and preliminary experimental measurements in our specimen under similar loading conditions.

With regard to our knee specimen experiments, our dynamically loaded cadaver resulted in similar anterior and posterior ground reaction forces that were measured in human trials in our laboratory. Recent developments for our fixture indicate dynamic loading on the ankle with an absolute error of 3.26N with ankle position control with an average absolute error 7.55mm (1.99%). Hip position control can replicate human movement with an absolute error of 5.82mm (0.84%).

Isotonic muscles trials were also run on our knee specimen. Results of our intersegmental measurements (Fig. 3) indicate that during isotonic quadriceps trials the ACL strain increased and PCL strain decreased through approximately 30° flexion. Through the remainder of knee flexion ACL strain decreased and PCL strain increased. Trials in which the hamstrings were activated isotonicly positive PCL strain was noted from 30° to full flexion, where as the ACL exhibited a constant strain reduction. MCL strain was constant during both quadriceps and hamstring trials. However the LCL was not consistent.

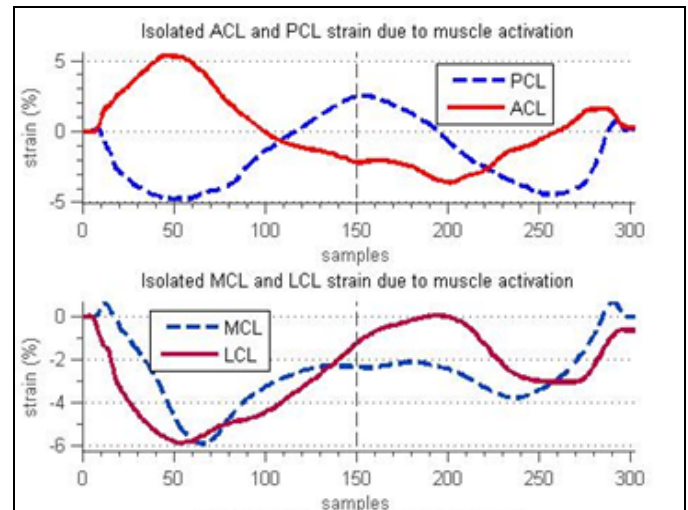


**Figure 2.** Isolated ligament strain due to isotonic activation of quadriceps to 50% peak activation during stance phase of gait.

## CONCLUSIONS

Our general aim is to create subject-specific computational models that quantify intersegmental kinetic differences under varying loading and kinematic knee conditions. Toward that end, we designed an experimental device in which knee specimens can be utilized to evaluate how time-varying muscle loading and ground reaction forces affect intersegmental pressures on the tibial plateau and ligament strain. The data acquired from the knee specimen experiments are then compared to model results under the same loading and kinematic conditions. We believe these results can be used as a resource to further study ligament strain in the knee during various dynamic activities.

## REFERENCES

1. Ramaniraka NA, et al. *Clinical Biomech* **20**, 434-442, 2005.
2. Pena E, et al. *J. Biomech* **39**, 1686-1701, 2006.
3. Delp SL, et al. *IEEE* **37**, 757-767, 1990.
4. Kirkendall DT, et al. *Orthopedic Practice* **403**, S81-S89, 2002.
5. Donahue TL, et al. *J. Biomech* **36**, 19-34, 2003
6. Buchanan TS, et al. *J. Biomech* **118**, 565-575, 1996.

## ACKNOWLEDGEMENTS

This work was funded in part by NSF Grant 0502638 and NIH R15-AR051316



# Changes in the Thumb CMC Joint Space During High-demand Functional Tasks

Eni Halilaj, Michael J Rainbow, Douglas C. Moore, Chris Got, and Joseph J. Crisco  
Department of Orthopaedics, Alpert Medical School of Brown University and Rhode Island Hospital,  
Providence, RI, USA  
email: eni\_halilaj@brown.edu, web: <http://www.brownbiomechanics.org>

## INTRODUCTION

The thumb plays a critical role in many daily tasks that require it to be highly mobile, yet capable of supporting large loads. Much of the thumb's range of motion and support come from the carpometacarpal (CMC) joint, which is a common target for osteoarthritis. Studying the morphology and the biomechanical factors that drive this joint to yield high thumb functionality in normal populations and considerable impairment in pathological ones is an important step in understanding disease progression and developing rational strategies for its treatment.

The purpose of this study was to assess changes in the CMC subchondral joint space areas (JSA) and location of the joint space centroids (JSC) with loading, during three tasks that rely on thumb functionality. We hypothesized that the JSA would increase with loading. Additionally, we set to resolve whether an increase in JSA would be the result of pure compression or sliding by computing displacement of the JSC.

## METHODS

24 volunteers, 12 males (age 25 +/- 3 yr.) and 12 females (age 24 +/- 3 yr.) were scanned with their dominant wrist in a neutral, jar grasp, key pinch, and jar closing position. Mechanical jigs (Fig. 1) were designed to emulate the objects required for these tasks and to standardize wrist positioning across subjects. Image volumes were generated using a 16-slice clinical CT scanner (General Electric, Milwaukee, WI) at tube settings of 80kVp and 80mA, slice thickness of 0.625mm, and in-plane resolution of 0.3mm x 0.3mm or better. Two scans were acquired for each functional task: one while the subjects held their hand relaxed and one while they applied 80% of their maximum load. Wrist bones from the neutral position volume were

segmented with commercial software (Materialise, Ann Arbor, MI), yielding 3-D bone models comprised of polygon meshes.

Bone kinematics for the remaining positions were calculated automatically with a markerless bone registration algorithm<sup>1</sup>. Inter-bone joint spacing between the trapezium and the metacarpal were then computed across the different positions with a previously reported algorithm<sup>2</sup>. The inter-bone joint space area is defined as the subchondral contour area that is less than a prescribed distance from the neighboring bone. The chosen thresholds were 1mm, 2mm, and 3mm. A centroid, weighted by joint space, was calculated for the 3mm areas of both the trapezium and metacarpal subchondral surfaces. Its motion, or the lack thereof, along with changes in the inter-joint space area were used to draw conclusions about what happens at the CMC joint under loading conditions.



**Figure 1.** The three tasks used in this study, from left to right: jar grasp, key pinch, and jar closing.

Paired t-tests were used to assess statistical significance in our outcome measures. To adjust for multiple comparisons, we considered a *p*-value of 0.025 or less to be statistically significant.

## RESULTS AND DISCUSSION

The changes in the 3.0 mm and 2.0 mm JSA, in both the trapezium and the metacarpal, for all three functional tasks, did not reach the level of statistical significance. The 1.0 mm JSA increased with loading during key pinch and jar closing, but not

during jar grasp (Table 1). The JSC of the metacarpal did not move with loading, for all three tasks. The JSC of the trapezium shifted ulnarly and slightly proximally during jar grasp and volarly during key pinch (Table 2).

These results suggest that tasks like key pinch and jar closing, result in increased 1 mm JSA to better support the high load. Pure compression in the joint would have resulted in increased 2mm and probably 3mm JSA. The fact that those areas do not change significantly with loading is suggestive of the bones sliding to a different position to support the load, rather than simply compressing Figure 2 illustrates a volar shift and an increase in the JSA of the trapezium, during key pinch. The fact that an increased JSA was not accompanied by a significant JSC shift in jar closing may result from the high variability in the kinematic data of this task. It is likely that motion of the JSC in the jar grasp task results in very little gain in the 1mm JSA because the load is distributed more evenly across the hand, requiring less demand on the CMC joint.

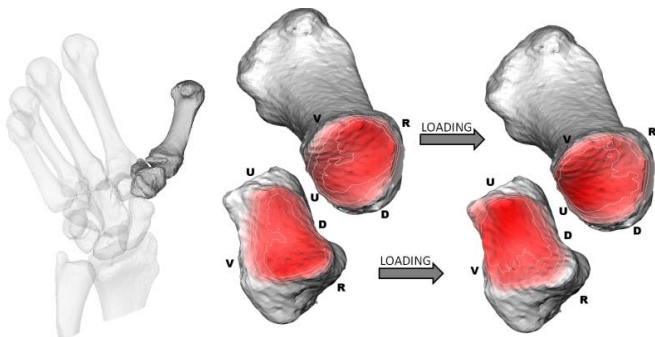


**Figure 2.** The thumb CMC joint in the wrist and joint space areas in both the TPM and MC1, as they go from an unloaded to a loaded state. Gradient represents inter-joint distance, with the reddest parts being the closest.

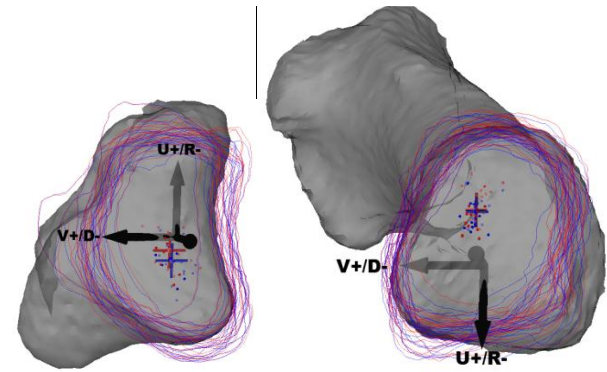


**Figure 3.** 3mm joint space area contours of all the subjects used in the study, with distance-weighted centroids average, and standard deviation, during the jar grasp task. Blue represents unloaded and red loaded. Movement on the TPM centroid in the ulnar direction with loading, during jar grasp, can be observed here.

## CONCLUSIONS

The thumb CMC joint experiences compressive loading that is up to 15% higher than the load required to perform a given task<sup>3</sup> and is highly susceptible to osteoarthritis. Inter-bone joint space area measures in the thumb CMC provide useful insight into the underlying mechanism of load support in this joint. The data presented here suggest that during high demand functional tasks the bones move to a position that maximizes joint contact. Further analysis that combines joint space measurements with kinematic data is required to draw more precise conclusions.

## REFERENCES

1. Marai et al., IEEE Trans. Medical Imaging, 2006
2. Marai et al., IEEE EMBS, 2006
3. Cooney et al., *J. of Bone and Joint Surgery*, 1977

**ACKNOWLEDGMENT:** This work has been funded by ASSH

**Table 1** Changes in the cortical surface area within a 1mm joint space distance, with loading. Statistically significant values are bolded.

|                             | Grasp     |            |         | Pinch            |                  |               | Jar              |                  |                   |
|-----------------------------|-----------|------------|---------|------------------|------------------|---------------|------------------|------------------|-------------------|
|                             | Unloaded  | Loaded     | p-value | Unloaded         | Loaded           | p-value       | Unloaded         | Loaded           | p-value           |
| TPM (JSA) - mm <sup>2</sup> | 52.6±23.4 | 58.6± 24.8 | p=0.03  | <b>30.2±22.0</b> | <b>46.1±38.1</b> | <b>p=0.01</b> | <b>36.2±25.0</b> | <b>59.3±27.5</b> | <b>p&lt;0.001</b> |
| MC1 (JSA) - mm <sup>2</sup> | 50.6±24.2 | 56.0± 26.2 | p=0.04  | <b>30.4±25.4</b> | <b>48.1±38.1</b> | <b>p=0.01</b> | <b>39.4±26.9</b> | <b>62.4±29.1</b> | <b>p&lt;0.001</b> |

**Table 2.** Movement of the inter-joint space area distance-weighted centroids, with loading. Statistically significant values are bolded

|                | Grasp          |          |                 | Pinch      |                |         | Jar        |          |         |
|----------------|----------------|----------|-----------------|------------|----------------|---------|------------|----------|---------|
|                | U+/R-          | V+/D-    | D+/P-           | U+/R-      | V+/D-          | D+/P-   | U+/R-      | V+/D-    | D+/P-   |
| TPM (JSC) - mm | <b>0.8±1.0</b> | 0.2± 0.4 | <b>-0.1±0.1</b> | -0.4.5±2.5 | <b>0.6±1.0</b> | 0.1±0.5 | -0.3.5±0.8 | -0.3±0.8 | 0.0±0.3 |
| MC1 (JSC) - mm | -0.1±.8        | 0.0±.5   | 0.1±0.3         | -0.8±2.5   | -0.2±0.9       | 0.2±0.7 | -0.2.5±1.2 | -1.6±0.8 | 0.2±0.3 |

# LONG-TERM CHANGES IN STAIR NEGOTIATION AND WALKING POST-ACL SURGERY

<sup>1</sup>Michelle Hall, <sup>2</sup>Catherine Stevermer and <sup>3</sup>Jason Gillette

<sup>1</sup>The University of Melbourne, Melbourne, VIC, Australia

<sup>2</sup>Des Moines University, Des Moines, IA, USA

<sup>3</sup>Iowa State University, Ames, IA, USA

email: mhall5@pgrad.unimelb.edu.au

## INTRODUCTION

Individuals with anterior cruciate ligament (ACL) reconstruction are at increased risk to develop knee osteoarthritis (OA) [1]. Knee OA is estimated to develop 5-20 years after initial ACL injury. Gait analysis of functional movements including stair use and walking can provide insight to everyday dynamic loading of the lower extremity.

Individuals 6-12 months post-ACL reconstruction have altered walking patterns as compared to controls, including reduced knee flexion angles at mid-stance and reduced internal knee extension moments during early stance [2]. These gait adaptations may lead to degenerative changes in the articular cartilage by altering the loading patterns on the knee joint. Decreased knee flexion angles and internal knee extension moments have been associated with quadriceps weakness in individuals up to one year post-ACL surgery [3]. Butler et al. observed 21% greater external knee varus moments during walking in individuals five years following ACL reconstruction when compared to a control group, although no changes in frontal hip mechanics were observed [4]. Increased knee varus moments may not be present within the first year of ACL reconstruction, but medial knee loading may increase as time progresses. Further study is required to assess whether dynamic knee joint loading is greater for individuals post-ACL surgery during walking and stair ambulation.

Our objective was to determine if biomechanical factors associated with the development and progression of knee osteoarthritis are present in those >1 yr post-ACL reconstruction. It was hypothesized that those in the post-ACL reconstruction group would exhibit: 1) reduced knee extensor strength, 2) reduced knee flexion angles, 3)

reduced knee extensor moments, and 4) increased knee varus moments as compared to their healthy counterparts.

## METHODS

Fifteen ACL reconstructed individuals (gender 7/8 M/F, age 26±6 yr, 6±4 yr from surgery, height 1.74±0.14 m, mass 75±15 kg) and 17 healthy controls (gender 7/10 M/F, age 26±4 yr, height 1.70±0.12 m, mass 68±12 kg) participated. Knee extensor and flexor strength were assessed using a hand-held dynamometer. Participants performed three maximal voluntary contractions (MVC) to assess strength. A level walkway and a staircase consisting of three steps (step height 18.5cm, tread length 29.5cm) were used. Following a static trial, participants performed three trials leading with each leg for a total of six trials for each task: stair ascent, stair descent, and walking. Individuals descended and ascended the stairs using a step-over-step technique. They wore their preferred shoes and performed all three tasks at a self chosen pace.

Kinematic and kinetic recordings were collected using an 8-camera motion analysis system (Vicon). Portable force platforms (AMTI) were positioned on the first and second stair steps, while an in-ground force platform recorded the walking trials. Reflective markers were placed on the lower extremities and trunk. Using inverse dynamics, hip extension, knee extension and external knee varus moments were calculated during the stance phase of two steps for stair ascent and descent and one step during walking. Joint moments and knee angles were averaged across trials, and joint moments were normalized to body mass. Univariate ANOVA was used to test for main effects of group (ACL vs. control) on maximum joint moments, joint angles, and strength. Significance was set at  $p < 0.05$ .

## RESULTS AND DISCUSSION

Refuting our first hypothesis, knee extensor strength did not differ between the ACL group and the control group ( $369 \pm 166$  N and  $392 \pm 138$  N,  $p = 0.674$ ). Also, no differences were found for knee flexor strength between the ACL and control groups ( $253 \pm 55$  N and  $270 \pm 45$  N,  $p = 0.370$ ). Initial stance knee flexion angles during stair ascent did not differ between the ACL group and the control group on step one ( $58.0 \pm 6.3^\circ$  and  $59.7 \pm 3.3^\circ$ ,  $p = 0.376$ ) or step two ( $61.3 \pm 5.0^\circ$  and  $62.7 \pm 3.1^\circ$ ,  $p = 0.390$ ). However, the ACL group had significantly reduced initial knee flexion angles compared to the control group during stair descent for step one ( $7.8 \pm 4.1^\circ$  and  $11.5 \pm 3.8^\circ$ ,  $p = 0.022$ ) and step two ( $7.9 \pm 4.0^\circ$  and  $11.0 \pm 3.7^\circ$ ,  $p = 0.049$ ), lending partial support to our second hypothesis. During walking, initial stance knee flexion angles were similar when comparing the ACL group to the control group ( $0.7 \pm 6.3^\circ$  and  $-1.0 \pm 3.3^\circ$ ,  $p = 0.328$ ).

Those with ACL reconstruction displayed significantly different joint moments as compared the control group during stair ascent, stair descent, and walking (Table 1). Peak hip extension moments for the ACL group were greater during the second step of stair ascent ( $p = 0.029$ ) and during level walking ( $p = 0.017$ ). In partial support of our third hypothesis, the ACL group displayed lower knee

extension moments on the second step of stair ascent ( $p = 0.024$ ), on step one of stair descent ( $p = 0.035$ ), and on step two of stair descent ( $p = 0.002$ ). Contrary to our fourth hypothesis, external knee varus moments did not differ between the two groups during any of the functional tasks ( $p > 0.05$ ).

## CONCLUSIONS

Long-term changes in lower extremity joint moments during walking and stair ambulation persist even at an average of six years post ACL-reconstruction. Primarily, individuals post-ACL reconstruction compensate for lower knee extension moments by increasing hip extension moments. Collectively these gait adaptations may lead to degenerative changes in the articular cartilage by altering the loading patterns on the knee joint.

## REFERENCES

1. Lohmander LS, et al. *Am J Sports Med*, **35**, 1756-69, 2007.
2. Timoney JM, et al. *Am J Sports Med*, **21**, 887-9, 1993.
3. Lewek M, et al. *Clin Biomech (Bristol, Avon)*, **17**, 56-63, 2002.
4. Butler RJ, et al. *Br J Sports Med*, **43**, 366-370, 2009.

**Table 1:** Maximum Normalized Joint Moments

|                |        | Stair Ascent       |                    | Stair Descent |                    | Walking            |                   |
|----------------|--------|--------------------|--------------------|---------------|--------------------|--------------------|-------------------|
|                |        | ACL<br>n = 14      | Control<br>n = 13  | ACL<br>n = 14 | Control<br>n = 13  | ACL<br>n = 15      | Control<br>n = 17 |
| Hip Extension  | Step 1 | 0.86 ± 0.25        | 0.72 ± 0.26        | 0.25 ± 0.26   | 0.15 ± 0.22        | <b>1.01 ± 0.28</b> | 0.77 ± 0.28       |
|                | Step 2 | <b>0.96 ± 0.25</b> | 0.76 ± 0.19        | 0.37 ± 0.24   | 0.21 ± 0.20        |                    |                   |
| Knee Extension | Step 1 | 1.05 ± 0.22        | 1.22 ± 0.33        | 1.04 ± 0.24   | <b>1.26 ± 0.28</b> | 0.42 ± 0.20        | 0.46 ± 0.13       |
|                | Step 2 | 0.85 ± 0.18        | <b>1.09 ± 0.33</b> | 0.87 ± 0.21   | <b>1.16 ± 0.23</b> |                    |                   |
| Knee Varus     | Step 1 | 0.51 ± 0.17        | 0.52 ± 0.11        | 0.20 ± 0.14   | 0.19 ± 0.10        | 0.50 ± 0.13        | 0.46 ± 0.09       |
|                | Step 2 | 0.57 ± 0.17        | 0.59 ± 0.11        | 0.30 ± 0.17   | 0.30 ± 0.13        |                    |                   |

Bold type indicates significance difference between the post-ACL group and control group ( $p < 0.05$ )

# AGE-RELATED CHANGES IN GAZE BEHAVIOR, CENTER OF MASS AND END-POINT CONTROL DURING STEP NEGOTIATION

Kate Hamel, Nicole Greaves and Kari Loverro

Department of Kinesiology, San Francisco State University, San Francisco, CA  
email: [hamelk@sfsu.edu](mailto:hamelk@sfsu.edu)

## INTRODUCTION

Declines in visual function with age have been linked to decrements in functional mobility and an increased risk of falling in older adults [1, 2]. Despite this knowledge, we know very little about how older adults use visual input to negotiate challenging terrain. Tripping over obstacles, curbs or steps accounts for a large proportion of falls in older adults [3], and may be linked to inadequate or aberrant visual input. The purpose of this study was to characterize the age-related differences in temporal and spatial coupling of gaze behavior with motor output during step negotiation.

## METHODS

Ten young ( $25\pm 3$  yrs) and seven older ( $75\pm 5$  yrs) adults participated in the study. Participants completed tests of cognitive, visual, vestibular and proprioceptive function, balance, self-efficacy and lower extremity power during their first visit to the laboratory. Gaze behavior and 3D whole body kinematics (along with detailed three-dimensional position of the entire shoe sole) were collected as participants negotiated obstacles, steps and stairs. During the step negotiation portion of the study, participants completed 3 trials of level change ascent and descent. The single step ( $17\times 91\times 350$ cm HxWxL) was built to represent a curb or change in level from one room to another. A head-mounted eye-tracking system (ASL 501, Applied Science Laboratories, Bedford, MA) was used to measure gaze location with respect to the environmental scene. The scene camera video with superimposed gaze location was mixed with a video image of the eye and two video images of the whole body and then the mixed video image was synchronized with an 8-camera Vicon MX motion capture system. Gaze fixations and gaze shifts were coded frame-by-frame using the Quite Eye Solutions software

program (QES, Calgary, CAN). Number of fixations and total fixation length on the level change transition region and number of gaze shifts and total gaze shift duration were calculated from the gaze behavior data. Minimum foot clearance, foot placement and center of mass (COM) movement were calculated from the whole body kinematic data set using a custom model in Visual 3D (C-Motion, Inc., Germantown, MD).

A series of three-factor, repeated measures, mixed model ANOVAs were used to examine the effects of age and task (up or down) on the gaze behavior and biomechanical variables. A Pearson product moment correlation matrix was utilized to examine the relationships between gaze and biomechanical variables.

## RESULTS AND DISCUSSION

### *Age differences*

Travel time was significantly longer for older adults compared to younger adults during step ascent, but not step descent ( $p<0.01$ ). Therefore, gaze shift duration and transition region fixation times were normalized to % travel time to account for differences in gait speed.

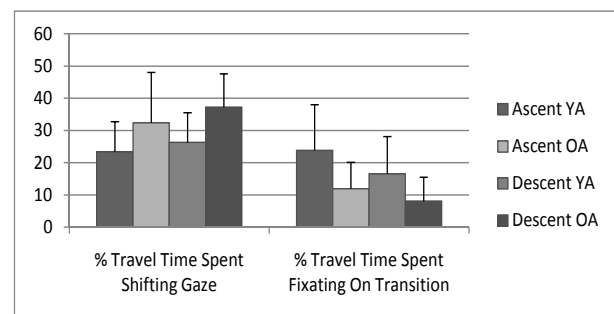


Figure 1: Gaze behavior during step ascent and descent

Older adults spent a smaller percentage of their travel time fixating on the transition region ( $p=0.03$ ) and a greater percentage of their travel time shifting their gaze ( $p = 0.04$ ) during both step ascent and descent compared to young adults (Fig. 1). Older adults also looked away from the transition region sooner than YA by  $\sim 500$ ms (or 1 step) ( $p<.05$ ).

There were no significant age-related differences in lead or trail limb clearance or placement. The only biomechanical difference between young and older adults was significantly larger lead limb medio-lateral (ML) COM displacement in older adults during step ascent (OA =  $6.0\pm 2.1$ cm, YA =  $3.5\pm 1.2$  cm) and step descent (OA= $5.7\pm 2.5$ cm, YA= $4.4\pm 1.5$ cm).

There were no significant correlations between the two gaze behavior measures and the dependent biomechanical variables. The ML COM displacement however, was strongly associated with low-contrast acuity, age and dynamic visual acuity during step ascent ( $R^2 = 83.2\%$ ) and with cognitive status, low-contrast acuity, clinical balance score and dynamic visual acuity during step descent ( $R^2=89.8\%$ ).

#### *Task Differences*

There were no significant differences in travel time between step ascent and descent. Both young and older adults spent a smaller percentage of their travel time fixating on the level change transition region ( $p=0.001$ ) and a greater percentage of their travel time shifting their gaze ( $p= 0.01$ ) during step descent compared to step ascent. Additionally both groups looked away from the transition region significantly sooner during step descent compared to step ascent.

All participants utilized a larger foot clearance during step ascent ( $5.9\pm 2.4$ cm) compared with step descent ( $1.9\pm 1.5$ cm). During step ascent the distance between the trail limb toe and lead limb heel was larger in the anteroposterior direction (40.3cm) compared to step descent (27.7cm). There were no significant differences in lead limb ML

COM displacement between step ascent and descent.

## **CONCLUSIONS**

Although the older adults fixated on the transition region less, shifted their gaze sooner and gaze shifted more frequently, this strategy was adequate for step negotiation under well-lit and high-contrast conditions. Use of this gaze behavior strategy under more typical environmental conditions (poor lighting, cluttered environment, low contrast) may result in inadequate or complete lack of detection of tripping hazards. Inadequate visual identification of a trip hazard coupled with poor balance control in the frontal plane may lead to an increased risk of falling. Future experiments should examine whether these gaze strategies are utilized by older adults under high risk situations, and whether these strategies result in falls.

Both young and older adults spent less time fixating on the transition region, shifted their gaze more frequently and looked away from the transition region sooner during step descent compared to step ascent. These differences in gaze behavior coupled with a smaller AP base of support and much smaller foot clearance may help to explain the much larger incidence of falls while descending steps and stairs compared to step and stair ascent [4]. Further research is needed to identify strategies that would increase the feedforward information provided by the visual system to enable better detection of the transition region during step and stair descent.

## **REFERENCES**

1. West CG. et al. *J Am Ger Soc.* 50:136-45, 2002.
2. Lord SR and Dayhew J. *J Am Ger Soc.* 49:508-15, 2001.
3. Berg WP. et al. *Age Ageing.* 26:261-268, 1997.
4. Svanstrom L. *Scan J Soc Med.* 2:113-120, 1974.

## **ACKNOWLEDGEMENTS**

Funded by NIH grant #1R21AG025865.

# MECHANICS AND ENERGETICS OF POST-STROKE WALKING: TOWARDS A MUSCLE-LEVEL UNDERSTANDING

<sup>1</sup>Austin Hampton, <sup>1</sup>Dominic Farris, and <sup>1</sup>Gregory S. Sawicki

<sup>1</sup>Joint Dept. of Biomedical Engineering, North Carolina State University, Raleigh, NC, USA, and  
University of North Carolina, Chapel Hill, NC, USA  
email: [ashampto@ncsu.edu](mailto:ashampto@ncsu.edu)

## INTRODUCTION

Many stroke survivors have an asymmetrical walking gait that causes altered lower-limb joint mechanics and elevated metabolic energy consumption. By combining center-of-mass (COM) level mechanical analyses with measurements of oxygen consumption, Detrembleur et al. showed that increased total positive mechanical work done by the muscles closely mirrored increased metabolic energy consumption in post-stroke walkers [1]. More recently, Jonkers et al. used inverse dynamics analyses to examine how COM energy is broken down across individual joints during hemiparetic walking. They showed a decrease in positive mechanical work performed by the paretic ankle and a saturation of positive mechanical work done by the paretic hip but did not relate these changes to differences in metabolic cost [2]. It is possible that due to differences in muscle-tendon architecture (i.e. tendon compliance) of the ankle versus hip muscle-tendon units (MTUs), the elevated metabolic cost of asymmetric walking could be explained by a shift in mechanical work from more efficient ankle MTUs to less efficient hip MTUs [3].

Surprisingly, few studies have linked differences in metabolic cost with changes in positive mechanical work performed by the joints (ankle+knee+hip). We hypothesize that when comparing post-stroke walkers to healthy controls at the same speed: (1) the summed total joint positive mechanical work of the paretic plus non-paretic limbs will be higher than in control limbs (2) there will be a shift in positive mechanical work from the ankle joint to the hip joint in the stroke limbs and (3) these mechanical differences will be reflected by an increase in metabolic cost. Furthermore due to weak, uncoordinated force generation, we expect altered length change patterns of medial gastrocnemius (MG) fascicles in stroke versus control muscles during walking.

## METHODS

Thus far, we have recruited one subject with post-stroke hemiparesis (mass=89kg) and one healthy control (mass=90kg). During treadmill walking at 0.75 m/s, we collected kinematic (Vicon Inc. motion capture, 120 Hz), kinetic (Bertec Inc. instrumented treadmill, 980 Hz), real-time muscle fascicle image (Telemed Inc. ultrasound probe, 50 Hz), and oxygen and carbon dioxide flow rate (Jaeger Inc., 1/30 Hz) data. The trials lasted four minutes, which ensured steady-state metabolic measurements. We combined standard inverse dynamics (C-Motion Inc., Visual 3-D) to assess joint mechanical performance and indirect calorimetry to assess metabolic energy expenditure. We calculated the average positive mechanical power (W/kg) for the ankle, knee, and hip joints over a walking stride for both paretic and non-paretic limbs, as well as for both legs in the healthy control. We summed the average powers of the individual joints of each leg to yield total average power (W/kg) performed by the lower-limb joints on the COM. To calculate the net metabolic power (W/kg), we converted oxygen consumption and carbon dioxide production flow rates using standard physiology equations. To examine the length trajectory of the MG during walking, we tracked the origin and insertion points of a single fascicle, frame by frame, in the recorded digital image over a multiple strides.

## RESULTS

As expected, we found a marked increase in net metabolic power when comparing the stroke walker to a size-matched healthy control (Figure 1). At the same walking speed (0.75 m/s), the net metabolic power doubled from 1.56 W/kg in the healthy control to 3.29 W/kg in the hemiparetic walker. The average positive joint mechanical power summed across the paretic and non-paretic joints was 76%

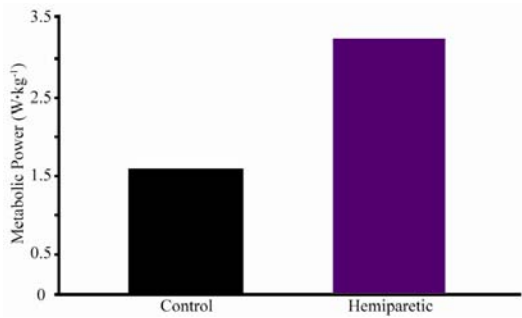


**Figure 1:** Bar graph showing differences in net metabolic power (W/kg) between the healthy control and the stroke walker for treadmill walking at 0.75 m/s.

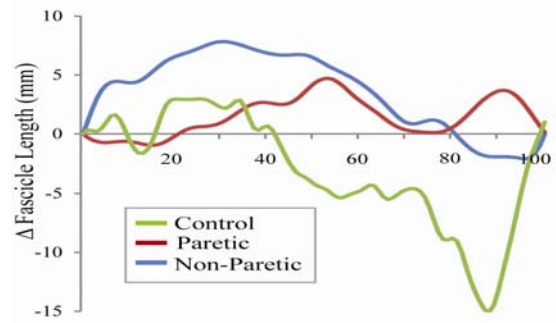


**Figure 3:** Length changes of MG fascicles (mm) during walking at 0.75 m/s. Length changes are shown over a stride (0% heel-strike to 100% heel-strike of same leg) and are taken relative to the recorded length at heel-strike.

higher (0.72 W/kg versus 0.41 W/kg) than the sum across the control joints (Figure 2).

Furthermore, the relative contribution of the total joint positive mechanical work within each limb was altered between control, paretic, and non-paretic limbs (Figure 2). Most notably, the hip joint positive mechanical power output of the paretic plus non-paretic limbs was more than 1.5 times higher than the hip joint mechanical power output of the healthy control limbs (0.34 W/kg versus 0.12 W/kg). Focusing only on the stroke walker, the paretic limb produced ~1/3 of the total joint average mechanical power compared to the non-paretic limb. Within the paretic limb, the hip rather than the ankle produced the majority of the mechanical power (76% vs. 13%).

Figure 3 highlights differences in MG fascicle lengthening and shortening behavior between the stroke and healthy control walkers. As expected, the control MG remained relatively isometric through most of stance before rapidly shortening during push-off (40-60% stride). The non-paretic MG initially lengthened, absorbing energy, before shortening during late-stance. The paretic MG lengthened throughout most of stance and began to shorten well after the transition into swing. These data indicate that the asymmetry in limb mechanics during post-stroke walking may manifest even at the level of the individual muscles.

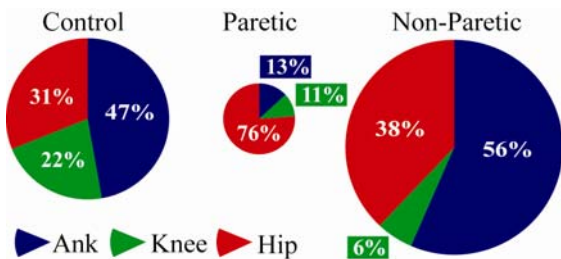


**Figure 2:** Pie charts showing percentage of total average positive mechanical power (W/kg) contributed by the hip, knee, and ankle during walking at 0.75 m/s. The total area of the charts is representative of the total average positive power relative to other conditions. Control pie chart is for both legs combined.

## DISCUSSION AND CONCLUSIONS

As hypothesized, there were increases in both joint positive mechanical work and metabolic cost for the stroke patient when compared to the healthy control. Also, there was a clear shift in mechanical power production from the ankle to the hip in both the non-paretic and paretic limbs.

These findings support the idea that elevated metabolic cost in post-stroke hemiparetic walking is due to (1) increased total workload of lower-limb joints and (2) redistribution of work to proximal MTUs. Redistribution of mechanical work from the ankle to the hip likely requires increased work done by muscle fascicle shortening rather than tendon elastic recoil. This is because hip muscles lack significant series compliant tissues that can be used to store and return elastic energy.

Furthermore, the MG length change patterns we observed in both paretic and non-paretic limbs suggest that the ‘catapult mechanism’ exploited during normal walking may be impaired, significantly reducing the amount of energy recycled in the Achilles’ tendon and aponeurosis.

In future work, we will continue to examine the muscle-level mechanics during post-stroke walking in order to further elucidate the links between mechanics and energetics of asymmetric, hemiparetic walking.

## REFERENCES

1. Detrembleur C et al., *Gait Posture*, **18**, 47-55, 2003.
2. Jonkers I et al., *Gait Posture*, **29**, 129-137, 2008.
3. Sawicki GS et al., *Exerc Sport Sci Rev*, **37**, 130-138, 2009.

## ACKNOWLEDGEMENTS

We thank Dr. Michael Lewek for his help recruiting stroke walkers and the use of his lab facilities in the School of Medicine at UNC-Chapel Hill.

# LANDING MECHANICS DURING CONTEXTUALLY RELEVANT PRACTICE CONDITIONS

<sup>1</sup>Rami Hamzey, <sup>1</sup>Kotaro Uyeda, <sup>1,3</sup>Joseph Munaretto, and <sup>1,2,3</sup>Jill L. McNitt-Gray

USC Biomechanics Research Lab, <sup>1</sup>Departments of Kinesiology, <sup>2</sup>Biological Sciences, and <sup>3</sup>Biomedical Engineering, University of Southern California, Los Angeles, CA, USA

Email: mcnitt@usc.edu

## INTRODUCTION

Recreational and elite athletes perform repetitive landings under both competitive and practice conditions. Many of these landing tasks require that players interact with a ball and make movement-related decisions during the flight phase prior to foot contact. During the contact phase of these sport-specific landings, athletes must also effectively distribute large reaction forces experienced immediately after contact (impact) and convert their vertical momentum at touchdown into horizontal momentum as quickly as possible [1,2,3].

The purpose of this study was to determine if regulation of ground reaction forces during impact and push phases of a land-and-go rebounding task were different between expected and unexpected conditions. We hypothesized that the force-time characteristics during impact and push phases would be different if the individual did (expected) and did not know (unexpected) the direction they needed to go to retrieve a loose ball. We expected that the magnitude or the time of the peak reaction force associated with heel contact would be different under the unexpected condition because of the need to attend to decision-making and last second preparations related to ball retrieval. We also expected that the lateral impulse generation toward the ball would be delayed in the unexpected trials in that more preparation time would be needed to position the body for the push phase of the land-and-go task.

## METHODS

College-age male basketball players with varsity experience at the high school level and currently participating in a recreational basketball league provided informed consent in accordance with the institutional review board for human subjects. Each participant performed a rebound followed by a land-

and-go task. The rebound was performed by jumping for a ball suspended overhead 0.45 m above the player's stand and reach height. After reaching the ball, a chest pass was directed in an expected or unexpected direction (right or left). The chest pass was initiated approximately 6 m in front of the subject to a location approximately 4 m to either side, requiring a quick lateral movement of the whole body immediately following foot contact. The goal of this go-task was to move laterally and retrieve the ball in a ready position as if the player was in a competitive basketball environment. Trials were blocked by experimental condition, and performed at a rate comparable to a practice session. First, passes were made in an expected direction either right (n=10, LGR-E), or left (n=10, LGL-E). Then, passes were made in an unexpected direction (right or left n=22 total, LGL-U, LGR-U).

Ground reaction forces (dual Kistler force plates, 1200 Hz, Amherst, NY) under each foot were recorded at the plate/floor interface. High-speed video (300 Hz, Casio) was acquired simultaneously to confirm each foot was fully supported by one plate and to determine frontal and sagittal segment kinematics. Vertical force-time characteristics were used to determine contact time and lateral force-time characteristics were used to quantify lateral impulse generation. Forces were normalized to body weight for between-subjects comparisons. The maximum push force (P<sub>MAX</sub>) was determined to be the magnitude of the last local maximum lateral force value before plate departure. The push phase was defined as the time between the first local minimum after the peak vertical force associated with heel strike (I<sub>MAX</sub>) and plate departure. The duration between the I<sub>MAX</sub> and P<sub>MAX</sub> was defined as peak-to-peak time (P<sub>2P</sub>) and reflects the duration of the transition between the land and go tasks. Data processing and calculations were performed using custom Matlab scripts (The Mathworks, Inc.).

## RESULTS AND DISCUSSION

During the impact phase, the time to peak vertical force tended to be more variable for the lag leg in the unexpected (LGR-U) as compared to expected (LGR-E) conditions for all five subjects (Figure 1). Mixed results were observed for the LGL trials.

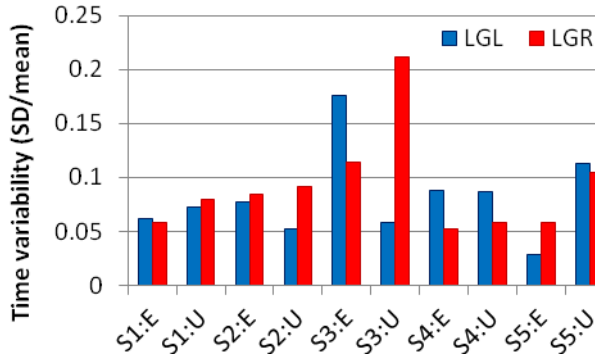


**Figure 1:** IMAX variability for all subjects (S1-S5) between expected and unexpected (E, U) conditions.

Peak vertical force during impact was larger in the unexpected conditions (LGR-U, LGL-U) for 2 and 4 of 5 subjects, respectively (Figure 2).

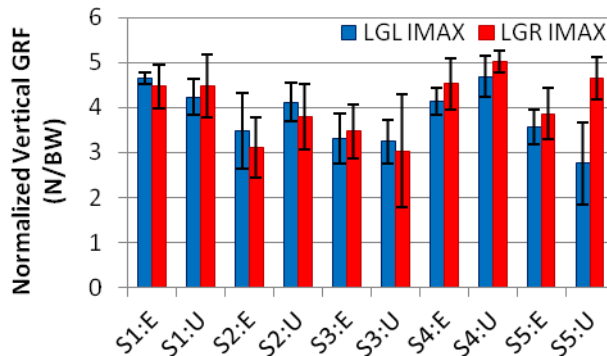


**Figure 2:** Peak vertical ground reaction forces at impact (IMAX) for all subjects (S1-S5) in expected and unexpected (E, U) conditions.

During the push phase, longer P2P times were observed in the unexpected condition than in expected trials for 4 of 5 subjects moving laterally in either direction (Figure 3).

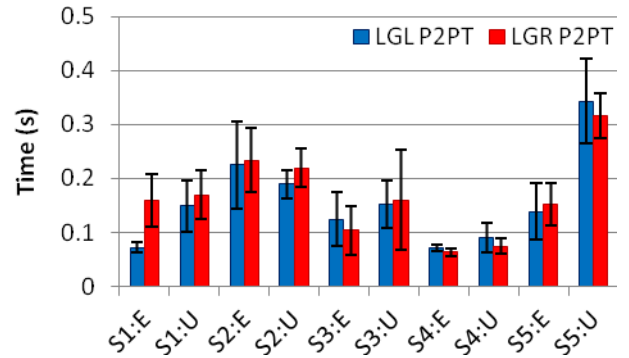


**Figure 3:** P2P times for all subjects (S1-S5) in expected and unexpected (E, U) conditions.

## CONCLUSIONS

Differences between expected and unexpected conditions support the hypothesis that force-time characteristics during both the impact and push phases of land-and-go tasks are affected when athletes are required to make decisions regarding interaction with a ball. The observed differences varied across players and direction of the “go” task. Corresponding kinematics and deviations in landing strategy associated with leg preferences is currently under further investigation.

## REFERENCES

1. Brown, TN et al., *J of Biomech*, **43(13)**,1049-56, 2009.
2. McNitt-Gray, JL et al., *J of Biomech*, **26(9)**,1037-46,1993.
3. Held L et al. *ASB Proceedings*, 2004.

## ACKNOWLEDGEMENTS

Thank you to Dr. Joseph Munaretto, Korkut Brown, and the rest of the Biomechanics Research Lab team. This analysis was funded in part by the SURF and SOAR Undergraduate Research Programs in the USC College of Letters, Arts, and Sciences.

# The Viscoelasticity of Chondrocytes *In Situ*

Sang Kuy Han, and Walter Herzog

The University of Calgary, Calgary, AB, Canada  
email: [shan@ucalgary.ca](mailto:shan@ucalgary.ca) web: <http://www.ucalgary.ca>

## INTRODUCTION

Articular cartilage plays an essential role in joint health through its role in lubricating the articular surfaces and distributing loads. The health and integrity of the cartilage extracellular matrix are maintained by metabolically active cells in cartilage, (chondrocytes) that synthesize the structural macromolecules that make up the tissue's matrix. Viscoelastic responses of cartilage, such as hysteresis under cyclic loading, may provide some hints about the functional demands of the tissue and cells. For instance, strain rate-dependent viscoelastic response of cartilage can substantially reduce periodic alterations of tissue deformations during cyclic compressions [1]. However, previous theoretical and experimental studies have not fully addressed the viscoelastic responses of dynamic chondrocyte deformations *in situ* under dynamic mechanical loadings [2-4]. Especially, previous experimental studies using isolated chondrocytes embedded in agarose gel constructs subjected to static compression likely do not represent the viscoelastic responses of chondrocytes in the intact tissue [2,5]. Therefore, the purpose of this study was to investigate the viscoelastic responses of chondrocytes in their natural environments using a novel *in situ* experimental approach. It was hypothesized that the viscoelastic responses of chondrocytes would help minimize periodic cell deformations that might be expected during cyclic compressive loading of cartilage.

## METHODS

Sample preparations: Articular cartilage and the associated subchondral bone were extracted from the medial femoral groove of skeletally mature bovine knees. Cylindrical cores of osteochondral blocks, 6 mm in diameter, were cut from the knees using an extraction instrument (OATS, Arthrex). Samples were incubated in a dextran solution for 4-

8 hours at 4°C prior to fluorescent confocal imaging. Fluorescein conjugated dextran (excitation: 488nm, emission: 500nm. Molecular Probes, OR, USA) was suspended in DMEM (Dulbecco's Modified Eagle's Medium, Gibco, OR, USA) at a concentration of 4 mg/ml (1.3 mM).

Single static compression test: A single, 20% nominal strain compression, was applied to the intact articular surface of the osteochondral block using a custom-designed indentation system at an average speed of 2%/s (Fig.1, [6]). Once 20% strain was reached, the indenter was returned to its original position at a speed of 3%/s. Confocal image stacks were recorded before loading and at 2 and 4 minutes after loading using a spacing of 0.5  $\mu\text{m}$  in the  $z$  (optical) direction.

Dynamic compression test: A sequence of 2 MPa compressive loading and unloading cycles were applied to the articular surface of the tissue sample (Fig. 3). Cells in the top 50 $\mu\text{m}$  of the superficial zone of the cartilage were quantified for analysis of cell morphology. Compressive local tissue strain, compressive cell strain, and cell volume were analyzed to quantify the viscoelastic responses of the extracellular matrix (ECM) and cells.

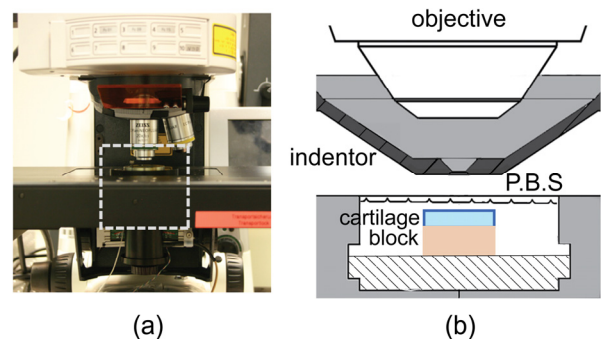


**Figure 1:** Custom-designed indentation system for *in situ* chondrocyte experiments; a: indentation system mounted on confocal microscope, b: schematic illustration for the area marked with the dashed line in a.

## RESULTS AND DISCUSSION

Single static compression test: Following a single 10s static compression, cartilage required approximately four minutes before the local tissue and chondrocytes had recovered to their original pre-load shapes and volumes (Fig. 2). Local ECM and cells appeared to recover at the same rate.

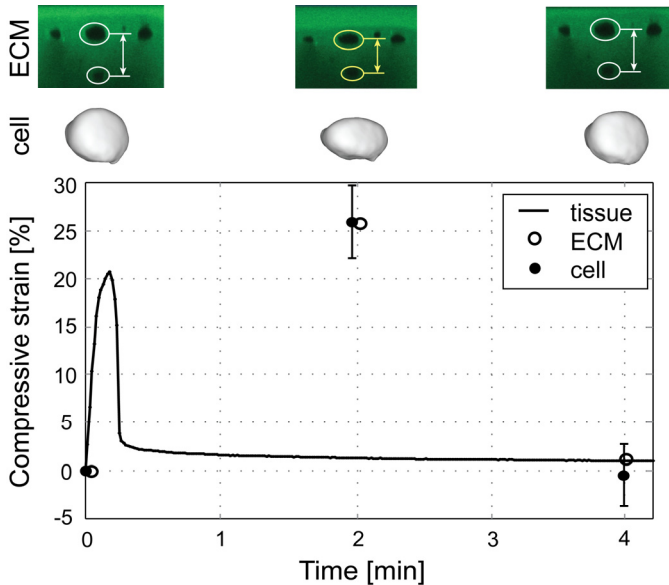


**Figure 2:** ECM: The distance between paired cells was used to determine local tissue deformations and recovery. cell: Three dimensional reconstruction of cell. Compressive strain graph: quantitative analysis of ECM and cell volume recovery after a single static compression.

Dynamic compression test: A sequence of 2 MPa compressive loading and unloading ramps were applied to the articular surface. Compressive cell strains were about  $9 \pm 2\%$  during the first loading cycle. However, compressive cell strains never recovered fully during the unloading phases (Fig. 3).

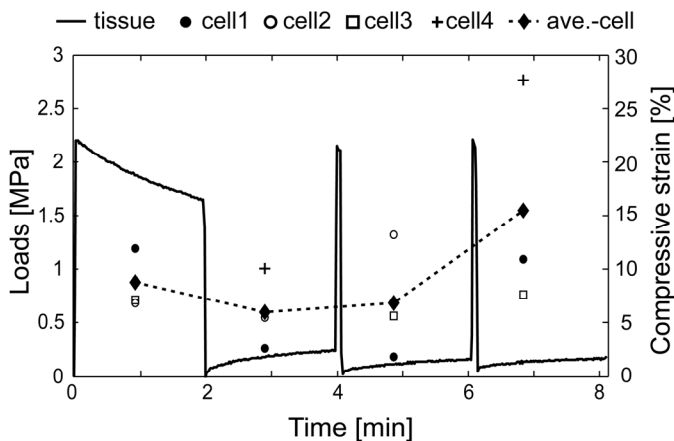


**Figure 3:** Surface contact pressure on the articular surface during dynamic compression testing. Corresponding compressive strains (cell height) in the loading and unloading phases.

Single static compression tests demonstrated the viscoelasticity of chondrocyte *in situ*. These results are consistent with previous findings in the intact mouse tibia-femoral joint [5], where recovery of chondrocyte shape and volume took minutes after a single static compression load. Our results, however, are in contrast with findings in isolated chondrocytes embedded in agarose gel, which recovered immediately and nearly elastically [2]. The extracellular matrix also showed a highly viscoelastic response following a single static compression load. Therefore, we speculate that the viscoelastic response of chondrocytes *in situ* is associated with the viscoelastic behaviour of the extracellular matrix environment.

Based on previous study in the intact mouse tibia-femoral joint [5], it appears that chondrocytes deform rapidly upon loading but take minutes to recover shape and volume upon unloading. This result suggests that cell deformations recover very little (if at all) in the unloading phase of cyclic cartilage compression (Fig. 3), thereby minimizing shape changes and volume fluxes of chondrocytes in cyclic loading conditions that are a common scenario in every day movements, such as in the loading of lower limb joints during locomotion. This result also implies that if cell deformations are related to signaling pathways, such signaling would primarily occur at the beginning of cyclic loading and might be quiescent for subsequent cycles. Pilot results in our lab on calcium signaling in chondrocytes support this idea.

## REFERENCES

1. Suh JK, et al. *J Biomech* **28**, 357-364, 1995.
2. Knight MM, et al. *Med. Eng. & Phys.* **20**, 684-688, 1998.
3. Wu JZ, Herzog W, *J Biomech* **39**, 603-616, 2006.
4. Kim E, et al. *J Biomech Eng.* **130**, 2008
5. Abusara, et al. *J Biomech* **44**, 930-934, 2011.
6. Han S.-K., et al. *Med. Eng. & Phys.* **30**, 684-688, 1998.

## ACKNOWLEDGEMENTS

The AHFMR Team grant on Osteoarthritis. The Canada Research Chair Programm.

# A METHOD TO DETECT INDIVIDUAL MUSCLE IMPAIRMENTS ACROSS THE WHOLE LOWER LIMB IN PATIENTS WITH CEREBRAL PALSY

<sup>1</sup>Geoffrey Handsfield, <sup>2</sup>Lindsay Sauer, <sup>2</sup>Joseph Hart, <sup>2</sup>Mark Abel, <sup>1,3</sup>Craig Meyer, and <sup>1,2,4</sup>Silvia Blemker

Departments of <sup>1</sup>Biomedical Engineering, <sup>2</sup>Orthopaedic Surgery, <sup>3</sup>Radiology, and  
<sup>4</sup>Mechanical and Aerospace Engineering

University of Virginia, Charlottesville, VA, USA

email: [gh8hq@virginia.edu](mailto:gh8hq@virginia.edu), web: <http://www.mae.virginia.edu/muscle/>

## INTRODUCTION

Clinical assessments of gait impairments in patients with cerebral palsy (CP) involve global assessments of movement and function, which include a physical exam, visual observation of the patient's gait, motion capture data, and electromyographic measurements. These types of tests are unable to determine strengths or weaknesses for individual muscles; however, treatments for abnormal gait target individual muscle impairments. Identifying hypertrophy or atrophy of each muscle within a joint is needed to design more tailored treatments intended to improve the gait of CP subjects.

In this study, we designed and implemented a fast, non-invasive imaging technique for assessing the specific muscle volumes in the lower limb of both healthy and CP subjects *in vivo*.

## METHODS

Seven normal, healthy volunteers (three female and four male, age:  $24.6 \pm 3.5$  years, height:  $177.3 \pm 7.7$  cm, weight:  $71.9 \pm 11.1$  kg) and four subjects with cerebral palsy (one female and three male, age:  $12.8 \pm 1.7$  years, height:  $151.2 \pm 11.9$  cm, weight:  $56.2 \pm 13.3$  kg) were scanned feet first in the supine position in a 3T Siemens Trio MRI Scanner. A fast 2D multislice spiral gradient-echo protocol was used with the following imaging parameters: TE/TR/ $\alpha$ : 3.8 ms/800 ms/90°, field of view: 400mm×400mm, slice thickness: 5mm, spatial resolution: 1.1mm×1.1mm. A Chebyshev approximation was used for semi-automatic off-resonance correction [1]. Total imaging time was approximately ten minutes. Axial images were obtained from the iliac crest to the ankle joint.

The muscle bellies of the 34 muscles and muscle groups comprising the lower limb were segmented in axial slices using custom in-house semi-automatic software. Volumes for each structure were determined voxel-wise by rendering structures

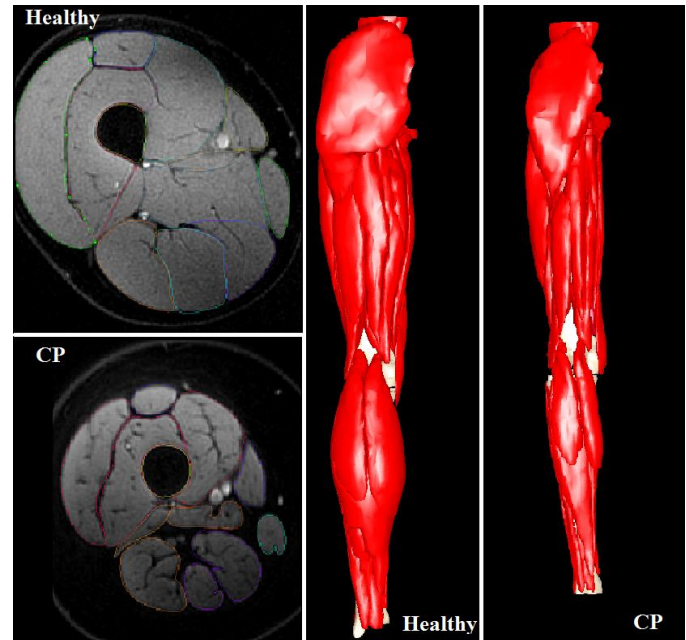


Fig. 1: Illustration of technique: axial images were acquired and segmented for healthy (top left) and CP (bottom left) subjects. 3-D reconstructions (posterior view shown) were generated and volumes calculated for healthy (center) and CP (right) subjects.

in 3-D (Fig. 1). The muscle volume for the entire lower limb was determined by summing over all of the segmented muscle bellies. Muscle volume ratios were calculated for each muscle for the healthy population and for each CP subject:  $R_{mv} = V_i/V_{tm}$ . Muscles were categorized into groups according to the joint that they cross and the action that they perform on that joint (Fig. 2). For each subject colormaps were made which display the number of standard deviations that the individual's muscle volume ratio deviates from the mean healthy muscle volume ratio (Fig. 3).

## RESULTS AND DISCUSSION

There was a high degree of correlation between lower limb muscles grouped by joint and action among both healthy and CP subject groups. Regression lines shown are least squares linear fits to the healthy subjects only, giving a normal line of lower limb volume ratios. The  $R^2$  values reported are for the entire population, illustrating that, with

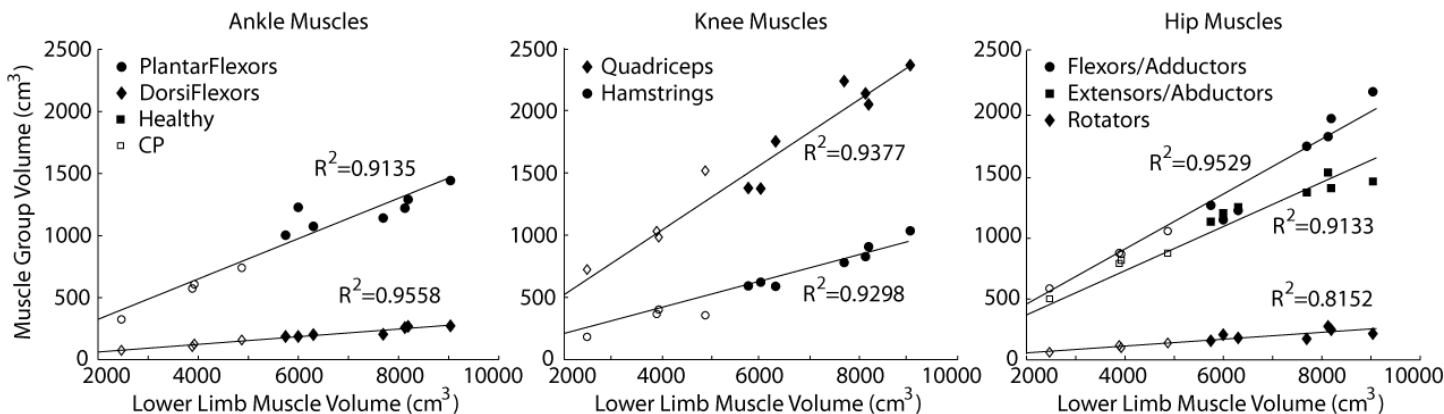


Fig. 2: Volume ratio plots for 7 healthy (filled symbols) and 4 CP (open symbols) subjects for muscles that cross the ankle, hip, and knee. Trendlines were generated using linear regression for the 7 healthy subjects only.  $R^2$  values are for the entire population of 11 subjects with respect to the healthy trendline.

very good correlation, the CP subjects generally have the same volume ratios at each joint as the normal population.

However, colormaps of the CP patients (Fig. 3) illustrate that there is significant atrophy and hypertrophy for specific muscles in a given CP subject compared to the normal population. Thus, despite consistency at the level of joint-crossing muscle groups for CP subjects, there is significant relative weakening and strengthening of individual muscles within those groups that is not detected by assessing joint-crossing groups alone.

## CONCLUSIONS

It is to be expected that abnormal gait patterns will result in changes in musculoskeletal structure as a subject's musculature will optimize for efficiency under an altered walk. However, the level to which muscles within a group compensate for one another

and change in individuals presenting an altered gait is somewhat unknown.

Here we present a non-invasive *in vivo* method for assessing the relative volumes of subjects with impaired gait, specifically CP subjects. Our technique demonstrates reliability in its prediction of a consistent mean muscle volume ratio among healthy subjects and precision in its detecting relative hypertrophy and atrophy at the individual muscle level among CP subjects. Thus, this technique has potential applications as a treatment planning tool for correcting altered gait.

## REFERENCES

1. W Chen, C Sica, and CH Meyer. *Magn. Res. in Med.* **60**,5:1104-1111, 2008.

## ACKNOWLEDGEMENTS

We would like to acknowledge the assistance of Nic Fiorentino, Drew Gilliam, and undergraduate researchers Kelly Anderson, Mary Boyles, and Clara Tran. Funding for this work was provided by the Wallace H. Coulter Foundation.

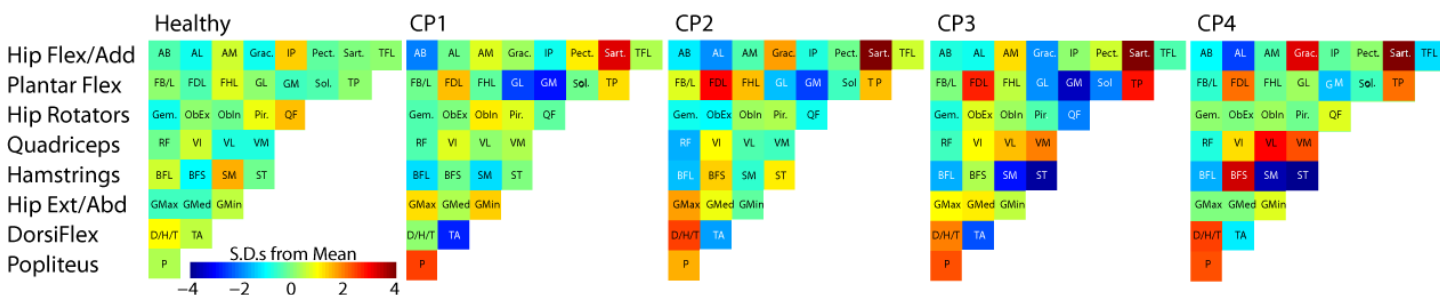


Fig. 3: Colormaps generated for one healthy and four CP subjects. Rows represent joint/action groups while columns represent individual muscles. The colorbar is in units of healthy standard deviations (S.D.) and the scale is -4 S.D. to +4 S.D. The muscles represented in the colorbars are as follows: AB:adductors brevis, AL:adductor longus, AM:adductor magnus, Grac:gracilis, IP:iliopsoas, Pect:pectineus, Sart:sartorius, TFL:tensor fascia latae, FB/L: fibularis brevis/longus, FDL:flexor digitorum longus, FHL:flexor hallucis longus, GL:lateral gastroc, GM:medial gastroc, Sol:soleus, TP:tibialis posterior, Gem:sup/inf gemellus, ObEx:obturator externus, ObIn:obturator internus, Pir:piriformis, QF:quadratus femoris, RF:rectus femoris, VI:vastus intermedius, VL:vastus lateralis, VM:vastus medialis, BFL:biceps femoris longhead, BFS: biceps femoris shorthead, SM:semimembranosus, ST:semitendinosus, GMax:gluteus max, GMed:gluteus medius, GMin:gluteus minimus, D/H/T: extensor digitorum longus/fibularis tertius, TA:tibialis anterior, P:popliteus.

# THE EFFECTS OF SHOE ARCHITECTURE ON IMPACT FORCES DURING GAIT

<sup>1</sup>Stephen Harmon, <sup>2</sup>Bruce Williams, <sup>1</sup>Kathleen Sevenser and <sup>1</sup>Craig M. Goehler

<sup>1</sup>Department of Mechanical Engineering, Valparaiso University, Valparaiso, IN, USA

<sup>2</sup>Breakthrough Podiatry, Merrillville, IN, USA

email: [Craig.Goehler@valpo.edu](mailto:Craig.Goehler@valpo.edu)

## INTRODUCTION

In the current athletic footwear market, there exists a wide range of shoe architectures that offer a variety of options in terms of flexibility and support. The importance of footwear type has proved to be significant in the prevention of an assortment of injuries, including knee osteoarthritis [1, 2]. Footwear type has also been shown to affect the lower extremity kinematics as well as the regulation of leg stiffness for a subject during dynamic activities [3]. An important attribute used to categorize athletic footwear architecture is the inherent flexibility of the shoe. The natural flex observed in the sole of the shoe determines the level of flexibility; a more flexible shoe will flex closer to the mid-foot region while a shoe designed for stability will flex closer to the ball of the shoe.

The main objective of this study is to examine the effect that varying shoe architecture has on the impact forces exerted on the foot during the gait cycle. The results from this study will be used in the future to examine both shoe design as well as injury prevention. This document represents an initial, exploratory study where one subject (a 21 year old male) was examined in order to compare the impact force profiles produced during gait while wearing two different architecture types from the same shoe company.

## METHODS

In order to map the force versus time profile for our subject, we utilized the F-Scan® in-shoe system by Tekscan that consists of in-shoe force sensors which are tethered to a personal computer. These sensors collect the numerical values of the forces exerted on the foot while walking. A force versus time profile was collected for each of two different shoe types while completing a forced walking scenario over a

distance of approximately 30 feet (a metronome was used to dictate when each step should occur). The subject completed three trials in the flexible shoe and three trials in the stability shoe for a total of six forced walking trials. The subject was allowed to rest between trials in order to prevent fatigue. Force measurements were binned for three different regions: the entire foot sole, the ball of the foot, and the heel of the foot. By examining these three regions, we were able to look at the distribution of forces over the entire foot during the gait cycle and were also able to study the forces in the heel and ball of the foot in order to evaluate the interplay (or transition) between the two regions of the foot.

Following the completion of the data acquisition, the force versus time profiles from the three regions for each of the six trials were further analyzed using MATLAB®. The F-Scan® in-shoe system outputs contour maps of the force distribution and files containing the force values. For each of the trials, one period (heel strike to toe off) of the gait cycle was truncated from the remaining data and was normalized to the time associated with that period. This normalization allowed us to compare force profiles across the trials due to varying walking speeds despite the use of the metronome. The truncated and time-normalized data sets for the three associated trials (i.e. Left Foot, Flexible Shoe) were then averaged to obtain a more accurate representation of the force versus time profile. The standard deviation of the three trials was also calculated for each shoe type in order to better observe the variability across trials.

The force versus normalized time curves were individually analyzed for both the heel and ball regions in order to study the variation in slope and compare time periods where the impact force maintained an approximately constant value. These

time periods represent dwells during the gait cycle where the respective region of the foot would endure prolonged contact with the ground. This analysis was achieved by using a paired t-test to determine whether the slope between two neighboring data points was statistically different from zero over the entire range of normalized time.

## RESULTS

The results from our statistical analyses indicate that there existed a significantly larger dwell period in the heel region for the flexible shoe than for the stability shoe ( $p < 0.05$ ), while there were no significant dwells in the ball region for either shoe (Table 1).

**Table 1:** Comparison of time periods maintaining constant force for different shoe types and regions of the foot.

|                | Heel           | Ball           |
|----------------|----------------|----------------|
| Flexible Shoe  | 0.1663 seconds | 0.0000 seconds |
| Stability Shoe | 0.0959 seconds | 0.0000 seconds |

The forces in the heel while the subject was wearing the flexible shoe had a dwell period where the slope was similar to zero for 0.1663 seconds as opposed to 0.0959 seconds while the subject was wearing the stability shoe ( $p < 0.05$ ). There were no time periods in either profile where the forces in the ball region exhibited any dwell.

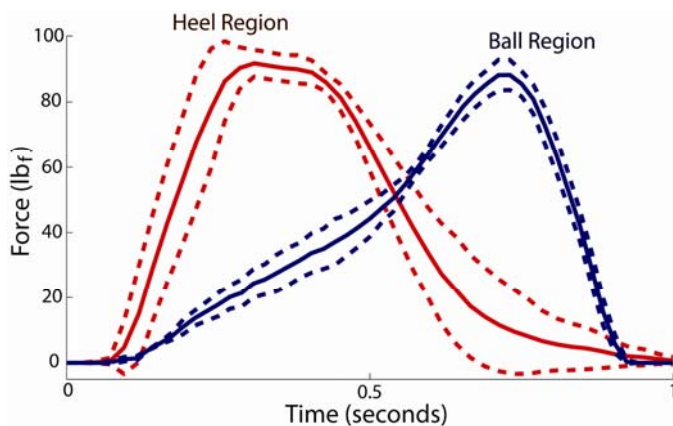


**Figure 1:** Force versus normalized time curves for the left foot of the subject while wearing the flexible shoe (solid: mean; dashed:  $\pm$  s.d.).

The force versus normalized time curves provided an opportunity to qualitatively compare the force profiles for the heel and ball regions. For example, the force curves for the left foot while wearing the flexible shoe demonstrate that the heel profile contains a flat region around the maximum force that remains relatively constant while the ball profile shows the force reaching the maximum and immediately beginning to lessen (Fig.1).

## DISCUSSION

From this preliminary study, we were able to observe a distinct difference between the stability and flexible shoe. In the flexible shoe, the heel of the subject's foot had a longer duration of contact than the stability shoe. This dwell corresponds to a prolonged pronation effect in the foot due to lack of support in the mid-foot region of the shoe. This pronation is compensating for a momentary lack of ankle dorsiflexion and causes the delay in off-loading of the heel that was observed. However, our results also indicate that for this particular subject there was no dwell in the forces on the ball while wearing either shoe type, thus resulting in a smooth toe-off during gait. We expect that this lack of dwell in the ball region will not prove to be the case for all subjects in the future.

The implications of these initial results provide us with a basis for future studies comparing the difference between stability and flexible shoes and the impact they may have in detecting and preventing injury. This work will include looking at stability and flexible shoe types across multiple companies while collecting data from a variety of subjects with varying weight, age, gender, and foot type.

## REFERENCES

1. Kerrigan DC, et al. *Physical Medicine and Rehabilitation* **1**, 1058-1063, 2009.
2. Butler RJ, et al. *Gait & Posture* **26**, 219-225, 2007.
3. Bishop et al. *J Athl Train* **41** (4), 387-392, 2006.

# ODDS-RATIO AND INJURY PROBABILITY ESTIMATION BASED ON TIBIAL PLATEAU GEOMETRY: SUBJECTS WITH MULTIPLE ACL INJURIES

<sup>1</sup>Hashemi, J; <sup>1</sup>Breighner, R; <sup>1</sup>Mansouri, H; <sup>2</sup>Slauterbeck, J R; <sup>2</sup>Beynon, B D

<sup>1</sup>Texas Tech University, Lubbock, TX, <sup>2</sup>University of Vermont, Burlington, VM

email: [javad.hashemi@ttu.edu](mailto:javad.hashemi@ttu.edu), web:<http://www.ttu.edu>

## INTRODUCTION

It is well established that anterior cruciate ligament (ACL) injuries have both short and long term negative consequences pertaining to physical and emotional costs to the injured person as well as significant economic impact on our healthcare system. As with any ailment, prevention of this injury is considered the best treatment. Consequently, the identification of risk factors (RF) and identifying individuals at greatest risk of sustaining this injury, have been the focus of recent research.

Currently, many risk factors have been identified, although none has evolved into a quantitative model that can be applied to predict the probability and relative odds of injury based on the values of the measured risk factors. In a recent publication, Hashemi et al. proposed that increased medial and lateral tibial plateau slopes (MTS, LTS) as well as decreased medial tibial depth (MTD) are associated with increased risk of ACL injury<sup>1</sup>. Logistic models were developed that could be used to predict the odds ratio and probability of an individual suffering ACL injury based on measured values of MTS, LTS, and MTD.

In this work we perform a retrospective study that applies the established logistic model<sup>1</sup> to determine the odds ratio (OR) and the probability of injury for a group of subjects that have suffered multiple ACL injuries (MI) to the same or both knees. We hypothesize that these subjects possess decreased MTDs, and increased MTS and LTS values, leading to very large ORs and probabilities of injury when compared to the uninjured subjects (UI) and single injury (SI) subjects.

## METHODS

Existing knee MRIs of 19 subjects that had suffered multiple ACL injuries, to the same knee or both knees were collected and anonymized. For each subject, the MTS, LTS, and MTD values were measured using the approach previously described by Hashemi et al.<sup>1,2</sup>. The odds-ratio values were

calculated for each subject with respect to the mean values of these risk factors in the uninjured population using the following equation:

$$OR = e^{(-1.12(mtd-\overline{MTD})+0.159(lts-\overline{LTS})+0.169(mts-\overline{MTS})*sex)}$$

where *mtd*, *lts*, and *mts* are individual subject values for each risk factor;  $\overline{MTD}$ ,  $\overline{LTS}$ , and  $\overline{MTS}$  are mean values for the uninjured group; and sex = 0 for female, 1 for male.

Probability of injury, P(inj), was calculated from measured values of the risk factors using the following equation:

$$P(inj) = \frac{e^{1.10-1.121 mtd + 0.159 lts + 0.169 mts*sex}}{1 + e^{1.10-1.121 mtd + 0.159 lts + 0.169 mts*sex}}$$

The calculated ORs and injury probabilities for multiply-injured subjects (MI) were compared to those of the injured subjects (SI) and uninjured controls (UI) presented in Hashemi et al. (2010). Additionally, the risk-factor loci were plotted on a series of ACL injury planes as previously reported<sup>1</sup>. The authors<sup>1</sup> suggest that region IV in the LTS-MTD plane (see Figure 2, lower-right quadrant) represents a ‘super-critical’ region for ACL injuries. To assess the validity of this assertion, the current study superimposes LTS-MTD values for multiply-injured subjects over the existing LTS-MTD plane. The protocol was reviewed and approved by the UVM Institutional Review Board.

## RESULTS AND DISCUSSION

The mean values and standard deviations of P(inj) and OR for the UI, SI, and MI groups are presented in Table 1.

**Table 1. Odds Ratio and Probability of Injury. Mean(SD).**

|                                  | Uninjured (UI) | Single - Injury (SI) | Multiply- Injured (MI) |
|----------------------------------|----------------|----------------------|------------------------|
| <b>Odds Ratio</b>                | 1.6(1.4)       | 8.3(11.6)            | 20.1(30.1)             |
| <b>Probability of Injury (%)</b> | 34(21)         | 61(25)               | 82(13)                 |

Direct application of comparison tests to this data is not easily achieved as the observations in each group are not normally distributed and dependence exists between and within groups. However, if one *were* to compare these data using Welch's t-test, MI and SI subjects would show significantly higher OR than UI subjects. The MI group would present greater mean OR than the SI group, however the difference would not be significant under these tests. Further, the P(inj) of the MI and SI groups would be significantly larger than the UI group. Lastly the P(inj) of the MI group would be significantly larger than that of the SI group. These differences in P(inj) between groups are clearly shown in figure 1.

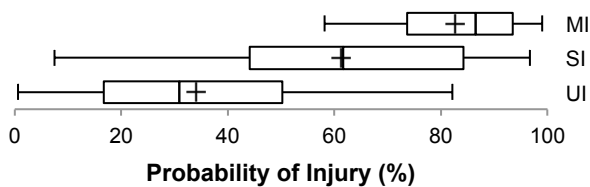


**Figure 1. Box Plot of P(inj) for MI, SI, and UI Subjects.**  
**NOTE: 'whiskers' denote max and min within group, +denotes mean.**

The Normalized LTS-MTD graph showing the uninjured controls (unfilled symbols), single-injured subjects (gray filled), and multiply injured subjects (red filled) is presented in Figure 2. The dark horizontal and vertical lines are the normalized medians of the MTD and LTS values of the uninjured population; they divide the graph into four regions.

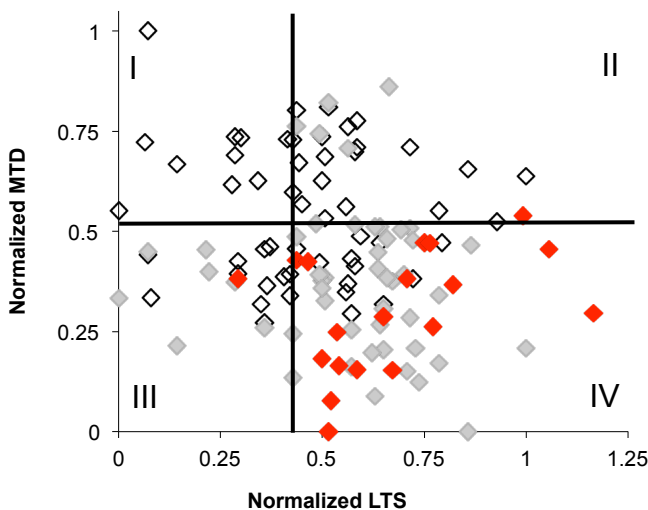


**Figure 2. Location of Multiply-Injured (red), Single Injury (gray), and Uninjured (unfilled) Subjects on the Injury Plane.**

Our results indicate that MI subjects have an extremely large OR (20.1) relative to the uninjured group, and a high probability of ACL injury (82%). The absence of statistical significance for the comparison of ORs between MI and SI groups is likely due to one subject with an extremely high OR value of 136 (resulting in large variance). It is interesting that, in Figure 2, injured subjects (gray-filled) are located in regions II, III, and IV; however, the LTS-MTD positions of the multiply-injured subjects (black-filled) place them primarily in region IV; and this region represents a 'super-critical' region, populated by individuals who may be at greatest risk of suffering ACL injury. Furthermore, not a single MI or SI subject presented with an LTS-MTD locus within region I, which we believe corresponds to the portion of the population that is at decreased risk of ACL injury. Overall, our results reveal that the general population may be partitioned into three categories: those resistant to ACL injury (region I, in Figure 2), those at increased risk (regions II and III in Figure 2), and those at greatest risk (region IV in Figure 2).

## CONCLUSIONS

The findings of this study may be used as a roadmap for the identification of predisposed, hyper-predisposed, or injury resistant populations by sports injury specialists and athletic trainers. Furthermore, this information can be used for patient counseling about return-to-sport and appropriate athletic involvement of multiply ACL-injured/-reconstructed patients.

## REFERENCES

- 1.Hashemi et al. (2010), *Am J Sports Med*, 38(1): 54-62.
- 2.Hashemi et al. (2009), *J Bone Joint Surg*, 90(12): 2724-34.

## ACKNOWLEDGEMENTS

Support: NIAMS R01 AR051477 (BDB)

# PREDICTING STRUCTURAL PROPERTIES OF THE ANTERIOR CRUCIATE LIGAMENT: A MULTIPLE LINEAR REGRESSION APPROACH

+<sup>1</sup>Hashemi, J; <sup>1</sup>Mansouri, H; <sup>2</sup>Chandrashekar, N; <sup>3</sup>Slauterbeck, J R; <sup>3</sup>Beynon, B D

+<sup>1</sup>Texas Tech University, Lubbock, TX, <sup>2</sup>University of Waterloo, Ontario, CA, <sup>2</sup>University of Vermont,  
Burlington, VM

email: [javad.hashemi@ttu.edu](mailto:javad.hashemi@ttu.edu), web: <http://www.ttu.edu>

## INTRODUCTION

Despite noteworthy advances in understanding the mechanobiology as well as various neuromuscular aspects of the anterior cruciate ligament (ACL) injury over the past decades, the exact cause(s) of non-contact ACL injuries still eludes the scientific community. Consequently, the existing sex-based disparity in ACL failure rates also remains inscrutable. There is a need for model-based approaches that produce quantitative insight into the structural properties of the ACL and loads placed upon it during various activities. These models would be more effective if they concurrently incorporated a variety of established risk factors. With this approach one could examine the impact of various risk factors and exclude spurious or redundant ones. Such an approach would guide the community's research efforts in a more efficient manner. In this abstract, we build upon a previously developed model<sup>1</sup> to predict, for the first time, the structural properties of the human anterior cruciate ligament. We focus on development of a linear multivariate regression model to predict linear stiffness of a subject's ACL based on key covariates that are associated with a subject's increased risk of suffering ACL injury. We hypothesize that the linear stiffness of an ACL may be predicted with reasonable accuracy based on age, sex, and anthropometric measurements of the subject and his/her ACL. Aside from its intriguing possibilities of identifying subjects at increased risk of suffering injury, such a model could serve as an important tool for future scientific research in the areas of risk factor analysis, risk management (estimating the probability of ACL injury), tissue engineering, and can be included in inverse dynamics simulations to understand subject-specific responses to ACL loading.

## METHODS

This study was designed to test our hypothesis by performing novel analyses using models presented in our previous publication<sup>1</sup>. A linear model was used to determine whether a general linear relationship exists between the response variables (structural properties) and the explanatory variables (age, sex, height, body mass, BMI, ACL length, minimum area, and volume). The following units were selected for each covariate: age (yrs), body mass (kg), height (m), and BMI (kg/m<sup>2</sup>), ACL length (mm), ACL area (mm<sup>2</sup>), and ACL volume (mm<sup>3</sup>). Although this approach can be applied to all structural properties, due to lack of space, we presently focus only on linear stiffness of the ACL. We devised a new technique to present the predictions from the linear model (with its 8 dimensional nature that accounts for the 8 explanatory variables) and its corresponding 95% prediction intervals. Using Equation 1 (below), we calculated the 17 predicted values (in this application linear stiffness of 17 ACLs) based on the measurements of the covariates obtained from each corresponding donor. The predicted linear stiffness values were ranked (lowest to highest) in ascending order and the percentile for each value was calculated as  $\frac{100 \times (rank - 1)}{n - 1}$  where  $n$  is the number subjects or measurements. Finally, the contributions of both body anthropometry and ACL geometry risk factors to the prediction of linear stiffness were evaluated. This was done by excluding ACL geometry variables, re-evaluating the model, and comparing the reduced model  $R^2$  to the original (geometry included) model  $R^2$ .

## RESULTS AND DISCUSSION

Sex, age, height, and ACL minimum area were found to be significant contributors to the linear stiffness model ( $p < 0.05$ ). The volume of the ACL was not found to be significant. Accordingly, the

estimated regression model for linear stiffness ( $LS$ ) is presented below:

$$LS = 0.925 + 21.2 \cdot sex - 5.3 \cdot age - 16 \cdot m - 119.1 \cdot ht - 105 \cdot bmi - 0.5 \cdot vol + 0.2 \cdot area \quad (1)$$

where  $m$  is mass,  $ht$  is height,  $vol$  is ACL volume and  $area$  is the minimum cross-sectional area of the ACL. The Pearson coefficient of correlation between the experimentally measured values of linear stiffness and their respective predictive values is  $r = 0.87$ . The test for the overall fit of this model is significant with  $p$ -value  $< 0.029$  and  $R^2 = 0.756$  indicating that 75.6% of the variability of the predicted linear stiffness value is explained by the model.

If ACL geometry is removed from the model, the overall fit suffers substantially, as  $R^2$  is reduced to 0.575, the overall model remains significant ( $p = 0.03$ ), but only sex and age remain significant contributors to the model ( $p < 0.05$ ). The prediction curve (Figure 1) for linear stiffness of the ACL (blue) and the corresponding 95% prediction limits (red), are presented in Figure 1. In this figure, the data points represent the actual measured values of linear stiffness. Figure 1 presents the smoothing spline fit to the predicted values of linear stiffness (blue line) and their respective prediction limits (red lines) plotted against rank. In this figure, the vertical axis is the predicted linear stiffness, and the horizontal axis represents the corresponding rank of the predicted value within the full population that was tested.

Figure 1, in conjunction with Equation (1), can be used to obtain the 95% prediction intervals for given values of the explanatory variables (age, sex, body and ACL anthropometric measurements). For example, application of equation (1) to a 30 year old male subject with body mass = 84.4 kg, height = 1.7 m, and BMI = 30.9 kg/m<sup>2</sup>, and ACL-min-area = 70 mm<sup>2</sup>, produces a corresponding linear stiffness of 262.5 N/mm. This value can be identified on the vertical axis of Figure 1 and from that point a horizontal line (dashed) that intersects the blue prediction line can be constructed. Then a perpendicular line that intersects the prediction interval lines (red lines showing lower and upper confidence limits of 41.2 and 483.8 N/mm, respectively) and the horizontal axis (showing the rank of 8.9 out of 17 or approximately the 50<sup>th</sup>

percentile) can be formed. This indicates that the predicted value of 262.5 N/mm falls very close to the middle of the given range in the population that was studied.

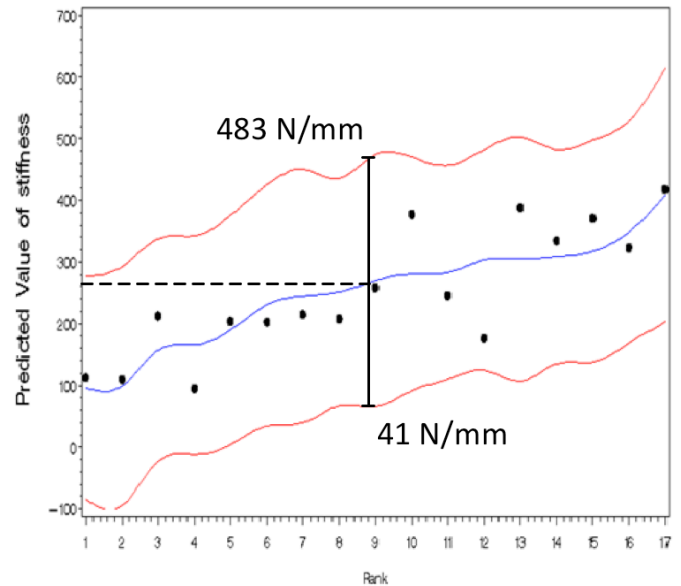


**Figure 1. The smoothing spline predicted values of linear stiffness (blue line) and their respective prediction limits (red lines) plotted against the percentile ranks. Dots indicate observed stiffness values.**

## CONCLUSIONS

The applications for predictive models like the one presented here are myriad, but an example is that one could possibly associate knee laxity with the linear stiffness of subjects. Additionally, this type of model can be utilized in conjunction with other probabilistic techniques to provide a comprehensive method to estimate overall risk of ACL injury. Predictive models like the one presented here are of tremendous importance to the research community including sports injury and athletic training specialists. Other structural properties such as failure load, elongation at failure, and energy at failure can also be determined by similar models. Currently, no other models exist for non-invasively determining structural or material properties of the ACL.

## REFERENCES

Chandrashekar et al. (2006), *J Biomech*, 39(16): 2943-2950.

# GROUND REACTION FORCES IN BAREFOOT RUNNING BEFORE AND AFTER EXERTION

Rami Hashish, Sachithra Samarawickrame and George Salem  
University of Southern California, Los Angeles, CA, USA  
email: [rhashish@usc.edu](mailto:rhashish@usc.edu) web: <http://pt2.usc.edu/labs/mbrl/>

## INTRODUCTION

An increasing number of distance runners are transitioning to barefoot running, spurring research in this field. Barefoot running has been postulated to be potentially less injurious than shod running due to a shift to a more anterior initial contact, thereby reducing the magnitude of the ground reaction force (GRF) passive peak [2] and associated *collision forces* [1]. The purpose of this study was to challenge the prevailing paradigm that promotes barefoot running on the basis of an absence of the passive peak, and to characterize the GRF changes in barefoot running before and after exertion.

## METHODS

Three habitually shod distance runners (Table 1) performed over-ground barefoot running at their self-selected speed, before and after exertion. All subjects included in the study ran a minimum of 12 kilometers (km) per week, and reported no significant injuries over the preceding 12 months. The exertion protocol was a barefoot run of 1.6 km at a self-selected speed, as suggested by Lieberman et al. (2010) when transitioning from shod to minimalistic footwear running [1].

Three-dimensional kinetics were recorded from force platforms (AMTI; Watertown, MA). The amplitude of the passive and active peaks from the vertical force, and braking and pushing peaks from the anterior-posterior force [2] were calculated and normalized to body weight (BW). Loading rate was quantified as the linear slope between initial loading (200 N) [1] and the passive peak, and is reported in body weight per second ( $BWs^{-1}$ ).

Percent change and the associated effect sizes (ES; Cohen's *d*) between the two conditions are reported for the various measures.

## RESULTS AND DISCUSSION

Intra-subject results are presented in Table 1.

### Loading Rate

Following the exertion protocol, despite a reduction in running speed, all subjects demonstrated an increase (92-167%, ES 2.35) in loading rate (Fig. 1).

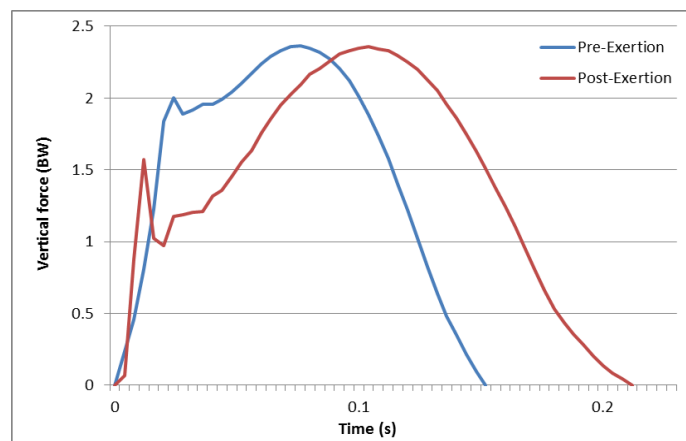


**Figure 1:** Vertical GRF curves of a representative individual pre- and post-exertion running at  $5.1\text{ m s}^{-1}$  and  $3.7\text{ m s}^{-1}$  respectively.

### Vertical Forces

There was a marked decline (20-30%, ES 2.82) in the average passive peak vertical force post-exertion, and a decline in the vertical force subsequent to this passive peak (Fig. 1). There was also a reduction (1-9%, ES 0.93) in the average active vertical peak following the exertion protocol (Figs. 1 and 2).

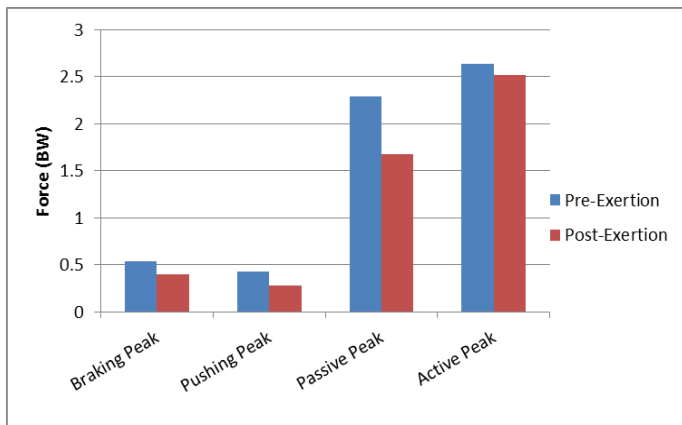


**Figure 2:** Average braking, pushing, passive and active peaks, pre- and post-exertion.

### Anterior-Posterior Forces

Following the exertion protocol, there was a decline in average braking (15-39%, ES 1.47) and pushing peaks (30-40%, ES 5.64) for all subjects (Figs. 2 and 3). This can likely be attributed to the reduction in running speed during the post-exertion condition, which would effectively reduce the magnitude of deceleration of the body at initial contact.

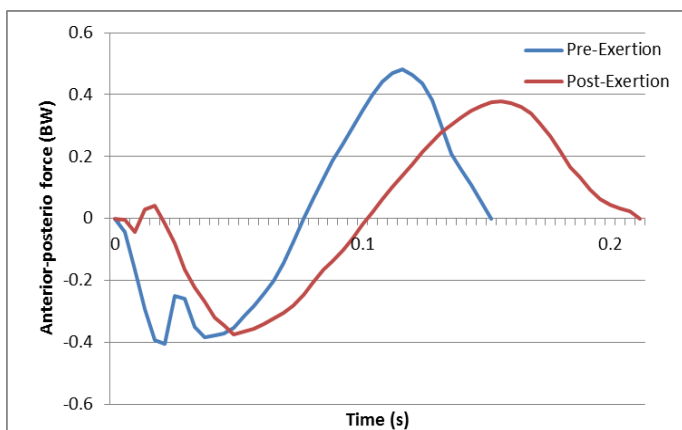


**Figure 3:** Representative anterior-posterior GRF curves pre- and post-exertion running at 5.1m s<sup>-1</sup> and 3.7m s<sup>-1</sup> respectively.

### CONCLUSIONS

The most interesting finding from this preliminary investigation is that despite a reduction in running speed post-exertion, the loading rate increased in all subjects (Table 1). In contrast with previous studies that reported a reduced magnitude in the GRF following the passive peak [2] or elimination of the passive peak all together [1] during barefoot running, all subjects included in this study demonstrated two distinct peaks during the post-exertion condition. These findings will inform the design of expanded, controlled prospective studies, which are needed to better understand the effects of exertion on habitually shod individuals transitioning to barefoot running.

### ACKNOWLEDGEMENTS

We acknowledge the guidance of Dr. Sean Yu in data analysis.

### REFERENCES

- Lieberman DE, et al. *Nature* **463**, 531-535, 2010.
- Divert C, et al. *Int J Sports Med* **26**, 593-598, 2005.

**Table 1:** Demographic and ground reaction force characteristics of each subject included in the study

|           | Age | Weight (kg) | Gender (M/F) | Condition     | Speed (ms <sup>-1</sup> ) | Loading Rate (BWs <sup>-1</sup> ) | Passive Peak (BW) | Active Peak (BW) | Braking Peak (BW) | Pushing Peak (BW) |
|-----------|-----|-------------|--------------|---------------|---------------------------|-----------------------------------|-------------------|------------------|-------------------|-------------------|
| Subject 1 | 40  | 61          | F            | Pre-Exertion  | 3.65                      | 106.1                             | 2.73              | 2.63             | 0.495             | 0.386             |
|           |     |             |              | Post-Exertion | 3.04                      | 283.0                             | 1.92              | 2.60             | 0.397             | 0.27              |
| Subject 2 | 34  | 73          | M            | Pre-Exertion  | 3.73                      | 77.2                              | 2.32              | 2.94             | 0.637             | 0.412             |
|           |     |             |              | Post-Exertion | 2.59                      | 148.2                             | 1.68              | 2.68             | 0.386             | 0.246             |
| Subject 3 | 26  | 65          | F            | Pre-Exertion  | 5.30                      | 79.4                              | 1.82              | 2.34             | 0.490             | 0.476             |
|           |     |             |              | Post-Exertion | 3.62                      | 205.9                             | 1.44              | 2.28             | 0.416             | 0.335             |

# ESTIMATION OF ARTICULAR CONTACT LOADS IN TOTAL KNEE REPLACEMENT USING A DUAL-JOINT MODELING PARADIGM

Michael W. Hast and Stephen J. Piazza

The Pennsylvania State University, University Park, PA, USA  
e-mail: [piazza@psu.edu](mailto:piazza@psu.edu)

## INTRODUCTION

Since the introduction of total knee replacements in the 1970s, prediction of wear characteristics of implants has been a primary concern of clinicians and manufacturers alike. A variety of benchtop tests have been devised to simulate the wear of implants and, while such tests have proven to be effective [1], they are costly to conduct in terms of both time and expense, and often fail to replicate the natural kinematics and kinetics of the knee joint. Instrumented implants circumvent many of the pitfalls of bench-top tests, and have permitted effective direct measurement of implant loads *in vivo* [2]. Current instrumented implants cannot, however, provide a complete characterization of contact mechanics and are not practical for incorporation into the implant design cycle. Computer simulation of human motions is a viable alternative to benchtop and *in vivo* approaches. While faithful recreation of human movements using feedback control of musculoskeletal models has been demonstrated [3], such methods rely on kinematically determined joints (such as revolute and ball joints) and therefore do not permit the determination of articular contact forces.

The purpose of the present work is to develop a novel computer simulation paradigm that predicts the tibiofemoral joint loads that occur during walking while measured knee motions are tracked using feedback control. Results of this simulation will be compared to published load data collected using an instrumented implant during normal gait [2].

## METHODS

Published data (marker coordinates, EMG, and ground reaction forces) from a single male subject (80 y; mass, 67 kg; 1.72 m; 8 months post-TKR) [4] were used to create a simulation of normal gait. OpenSim [5] was used to generate a set of full-body

motions that were consistent with measured marker trajectories from three walking trials. Full-body were used to drive a five-segment model that included the pelvis, the right lower limb, 13 active muscles, and 6 ligaments.

Knee motions and loads were predicted with a *dual-joint modeling* approach with two alternating phases: (1) In the *inverse dynamics* phase a ball-joint was substituted for the knee and was used to compute the muscle forces required to track knee flexion. In this phase, a PD controller computes the desired knee flexion acceleration, inverse dynamics determines the required knee flexion torque, and static optimization is used to distribute muscle activations/forces (Figure 1); (2) In the *forward dynamics* phase, a 12-DOF knee with TF and PF articulations is used to integrate forward in time in 0.005 s increments. During this time, muscle activations determined during the inverse dynamics phase are held constant and ligament and contact forces vary according to the relative positions and velocities of the femur, tibia, and patella (Figure 2).

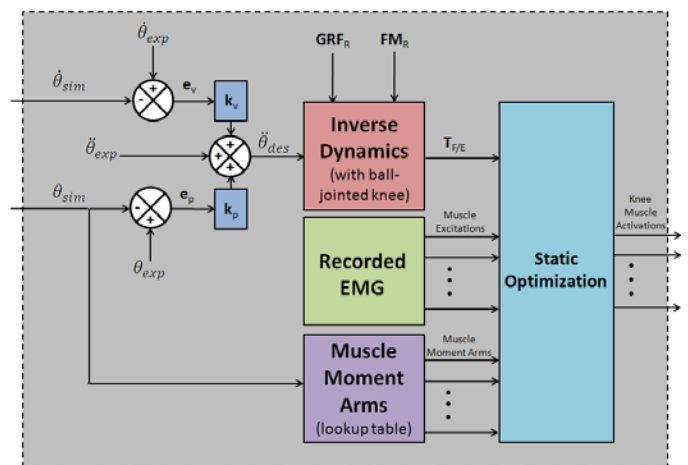


**Figure 1:** Block diagram for inverse dynamics phase in which knee flexion is tracked and required forces for muscles crossing the knee joint are determined.

Inverse dynamics and forward dynamics were performed using SIMM/Dynamics Pipeline (MusculoGraphics, Inc.; Santa Rosa, CA) and SD/FAST (PTC, Inc.; Needham, MA) along with custom-written routines for contact force determination [6]. Muscle activations were selected such that deviation between muscle activations and measured EMG signals were minimized while generating the required torques. Muscle moment arms needed for static optimization were stored in lookup tables created from the output of a simulated ‘Oxford Rig’ test [6]. The procedure was repeated for three walking trials.

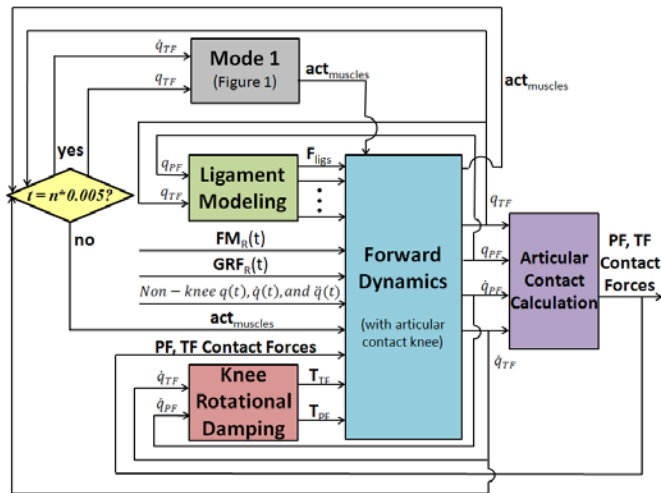


**Figure 2:** Block diagram for forward dynamics phase, in which tibiofemoral and patellofemoral contact forces are calculated.

## RESULTS AND DISCUSSION

Simulated knee flexion and muscle activation were found to track their measured counterparts well. Total tibiofemoral contact force, however, was found to be higher than published values [2] measured using an instrumented tibial implant, especially in early stance (Figure 3). These differences may be attributable to the advanced age of the subject studied by Zhao et al. [2], who was 80 years old and likely had reduced knee muscle strength as a result. We performed a sensitivity study and found that decreasing knee muscle maximum isometric force (while attempting to match the same measured EMG data) led to more realistic tibiofemoral loads. A final estimate of 50% maximum isometric force seems reasonable for an older subject, as Thom et al. [7] showed that peak muscle power of an elderly male population (age:  $73.9 \pm 3.8$  y) is about 45% of that of young men (age:  $26.5 \pm 4.1$  y).

Estimations of medial and lateral tibiofemoral contact forces for three separate gait trials compared favorably to the magnitudes and patterns shown by an instrumented implant used by Zhao et al. [2] although the simulation tended to overestimate medial condyle loads and underestimate lateral condyle loads, differences that may be ascribed to a number of factors, including differences in implant placement between simulation and experiment. The contact forces predicted here are similar to those predicted by Lin et al. [8], who employed an optimization-based approach that incorporated fast contact force computation.

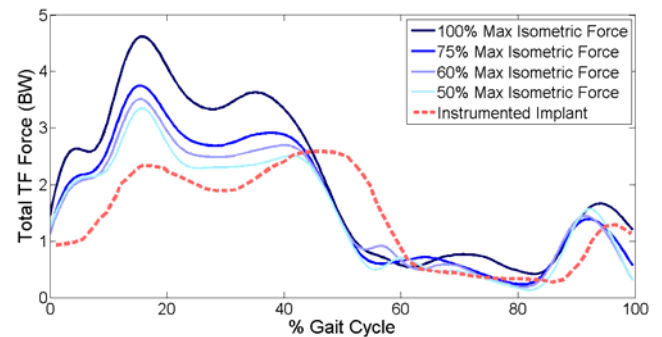


**Figure 3:** TF contact loads plotted vs. %GC. Maximum isometric forces were decreased to simulate an older subject. Experimental contact forces are those reported by Zhao et al. [2].

## CONCLUSIONS

The results of this study demonstrate the potential of dual-joint modeling for estimating articular contact forces using a deformable contact model while using feedback control to track measured kinematics and muscle activity while applying measured ground reaction forces.

## REFERENCES

1. Walker PS et al. *J Biomech* **30**:83-9, 1997.
2. Zhao D et al. *J Orth Res.* **25**:593-602, 2007.
3. Thelen D et al. *J Biomech* **39**:1107-15, 2006.
4. Fregly BJ et al. *J Orth Res.* In preparation.
5. Delp, SL et al. *IEEE Trans Biomed Eng.* **54**:1940-50, 2007.
6. Landon, RL et al. *Comp Meth App Mech Eng* **198**:2339-46, 2009.
7. Thom, JM. *J Gerontol A Biol Sci Med Sci* **60A**:1111-7, 2005.
8. Lin, Y.C. et al. *J Biomech* **43**:945-52, 2010

## ACKNOWLEDGMENTS

This work was supported in part by Stryker Orthopaedics.

# DECELERATION AND REDIRECTION MECHANICS DURING A CUTTING MANEUVER

Kathryn L. Havens, Susan M. Sigward

Jacquelin Perry Musculoskeletal Biomechanics Research Laboratory

Division of Biokinesiology and Physical Therapy

University of Southern California, Los Angeles, CA, USA

email: khavens@usc.edu, web: www.usc.edu/go/mbrl

## INTRODUCTION

Agility or maneuverability is essential for successful participation in multidirectional sports [1]. Maneuverability involves self-generated change of direction from steady state locomotion [2] that requires horizontal deceleration of the body's center of mass (COM) and redirection into the new plane of movement.

When compared to steady state locomotion, greater posterior and medial-lateral ground reaction force impulse (GRI) is needed to decelerate the forward momentum of the body's center of mass and accelerate it into the new direction, respectively [3].

In addition, successful maneuverability requires that the individual adjusts the distance between the COM and center of pressure (COP). Specifically, a more posterior position of the COM with respect to the COP is needed for deceleration of the body, while a more lateral position of the COM with respect to the COP facilitates acceleration in the opposite direction [4, 5].

Mathematical modeling studies suggest that the effective distance between the COM and COP is related to the horizontal COM velocity [4]. While this has been established during walking, it is not known if similar trends exist during running turns performed at much higher velocities.

The purpose of this pilot study was to characterize COM-COP relationships and GRI during sprinting and a cutting task at two speeds.

## METHODS

Three healthy, recreationally active females (25-28 yrs) with no history of previous knee injury participated. Average height and weight was  $164.3 \pm 3.5$  cm and  $62.4 \pm 7.0$  kg, respectively.

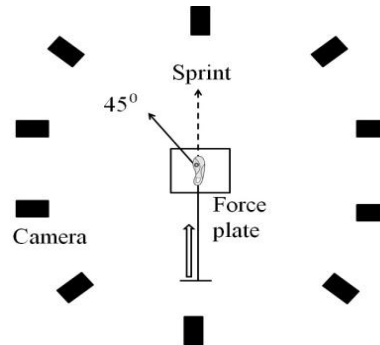


**Figure 1:** Experimental set-up for right dominant subject. Open arrow indicates original line of progression.

Subjects performed a sprinting task and a sidestep cutting task (Scut) under two conditions. For the sprinting task, subjects ran as fast as possible for 10 meters. For the Scut task, subjects ran 7 meters, planted their dominant foot on the force plate and changed direction away from the plant leg at a  $45^\circ$  angle (Fig. 1). Scut tasks were performed as fast as possible (AFAP) and at a speed that was 85% of the AFAP speed (85AFAP).

Three-dimensional kinematics were collected at 250Hz using a 10-camera motion capture system (Qualisys, Inc. Sweden). Ground reaction forces (GRF) were quantified using AMTI force platforms (Newton, MA, USA), 1500 Hz. Whole body COM was calculated as the weighted sum of the COM of all 15 modeled segments (Visual3D™, C-Motion, Inc., Rockville, MD, USA). COP location, the application point of the resultant GRF vector, was determined from force plate recordings.

The distance between the COM and COP was calculated along 3 axes: vertical, anterior-posterior (AP), and medial-lateral (ML) and normalized by height. Peak COM anterior velocity was identified during the approach, 3 meters prior to foot contact on the force plate. AP and ML GRI were calculated as the integration of the GRF-time curves in each direction and normalized by body weight impulse (BWI). GRI was considered during the braking phase of stance, defined as the time in which the AP GRF vector was directed posteriorly. Data were

averaged across three trials. No statistical analysis was performed due to a small sample size.

## RESULTS AND DISCUSSION

Average approach velocity was  $5.6 \pm 0.13$  m/s,  $4.9 \pm 0.1$  m/s and  $4.12 \pm 0.2$  m/s for the sprint, Scut AFAP and Scut 85AFAP, respectively.

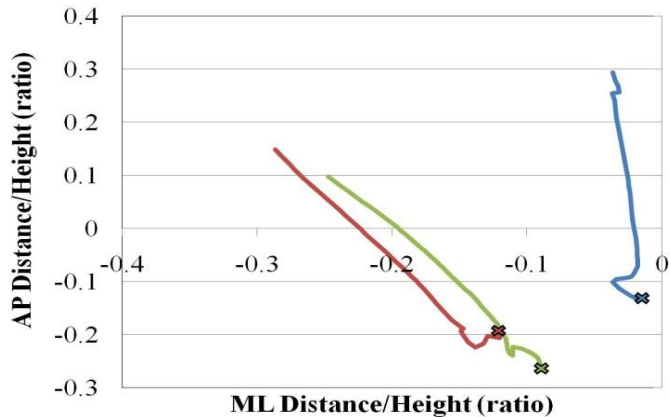


**Figure 2:** COM position relative to COP in AP and ML directions. Initial contact indicated by x. *Blue:* Sprint trial; *Green:* Scut 85AFAP trials; *Red:* Scut AFAP trials.

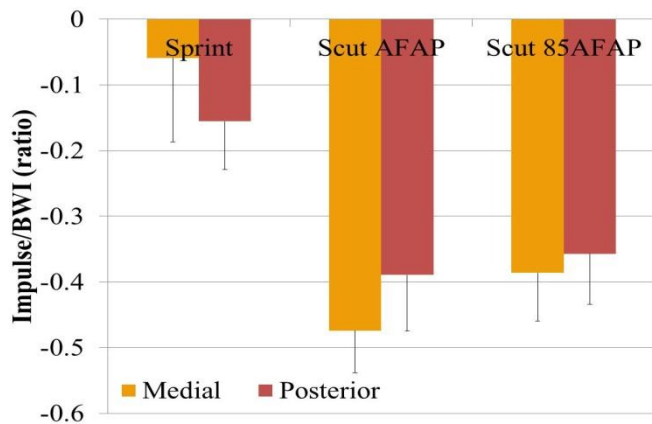


**Figure 3:** GRI during the braking phase

When compared to sprinting, COM relative to COP during Scuts was lower, more posterior, and more medial at initial contact (Fig. 2). When compared to Scut 85AFAP, COM relative to COP during the Scut AFAP was lower and less posterior at initial contact. At toe-off, when compared to sprinting, COM relative to COP during Scuts was less anterior and more medial.

When compared to sprinting, ML GRI remained medial throughout braking, and the posterior and medial GRI was greater during Scuts (Fig. 3). When

compared to Scut 85AFAP, posterior and medial GRI during the braking phase was greater during Scut AFAP.

Subjects performed the Scut AFAP at approximately 87% of their sprint velocity, suggesting that deceleration is required to perform a change of direction task. Consistent with a strategy to decelerate, subjects positioned their COM lower and more posterior to COP during Scuts when compared to sprinting and had an accentuated braking impulse. The lateral position of COP with respect to COM is consistent with a strategy to accelerate the body into a new direction. Greater medial impulse indicates a greater contribution from that plane, as would be expected in a change of direction task [3].

Interesting adjustments were made based on velocity during Scuts. During deceleration, greater braking impulse and lower COM were observed during the Scut AFAP when compared to 85AFAP, but COM was less posterior relative to COP. Subjects also modulated the lateral position of the COP with respect to COM differently.

## CONCLUSIONS

Together, the data suggest that modulation of the distance between an individual's COM and COP as well as GRI gives some indication of deceleration and redirection mechanics, as they are influenced by the direction requirements of the task and the approach velocity. However, additional variables and a greater subject pool would help to determine whether the differences reported here represent real differences in strategy. Thus, further work is needed to characterize change of direction tasks performed at multiple velocities.

## REFERENCES

1. Sheppard JM, et al. *J Sports Sci* **24**, 919-932, 2006.
2. Jindrich DL, et al. *CHAOS* **19**, 026105, 2009.
3. Patla AE, et al. *J Exp Psycho.* **17**, 603-634, 1991.
4. Pai YC, et al. *J Biomech* **30**, 347-353, 1997.
5. Patla AE, et al. *Exp Brain Res* **129**, 626-634, 1999.

# SURROGATION ANALYSIS REVEALS DEVELOPMENT OF DETERMINISTIC STRUCTURE IN THE CONTROL OF POSTURE

Joshua Haworth<sup>1,3</sup>, Elena Kokkoni<sup>1</sup>, Regina Harbourne<sup>2</sup>, Nick Stergiou<sup>1,3</sup>

<sup>1</sup>Nebraska Biomechanics Core Facility, University of Nebraska at Omaha, Omaha, NE, USA

<sup>2</sup>Munroe Meyer Institute, University of Nebraska Medical Center, Omaha, NE, USA

<sup>3</sup>College of Public Health, University of Nebraska Medical Center, Omaha, NE, USA

email: [jlhawort@unmc.edu](mailto:jlhawort@unmc.edu) web: <http://nbcf.unomaha.edu/>

## INTRODUCTION

Surrogation analysis has been used for the evaluation of the deterministic control of posture, performed as a method to evaluate the inherent complexity of this skill. Typically, this analysis is conducted by comparing a characteristic measure of a data series (i.e. approximate entropy) to the same measure of a surrogate time series of that data. While several methods of surrogation exist, generally they are directed at producing a temporally randomized time series from the original, without severely altering its standard properties (i.e. mean and variance). The application of this technique has led to the validation of deterministic structure in biological rhythms such as posture and gait, as well providing justification of the efficacy of nonlinear analysis methods and their subsequent interpretations [1]. An extension of the common interpretations of surrogation analysis includes the quality of information that is brought out of the behavioral data. Report of deterministic structure in postural data suggests, directly, that a considerable control is enacted by the central nervous system in an effort to regulate the position of the body in space. Especially, surrogation may be useful in uncovering the time course of the development of deterministic control of human postural movement. This study seeks to evaluate the emergence of deterministic control of sitting posture in typical infants, via surrogation analysis.

## METHODS

Center of pressure (COP) was recorded (via AMTI force platform, 200Hz) from a group of 20 infants, throughout their development of sitting proficiency (fig. 1); 6 trials collected at each of 3 stages of development for each infant. Surrogated time series

were produced using Theiler's [2] algorithm, while approximate entropy [3] was used to characterize the temporal structure of both the original and surrogate series. Mann-Whitney nonparametric tests were conducted to compare the ApEn values for the 6 original data series against those of the 6 surrogate series. In cases where the ApEn values of these sets were significantly different, the conclusion of the presence of deterministic temporal structure was confirmed.

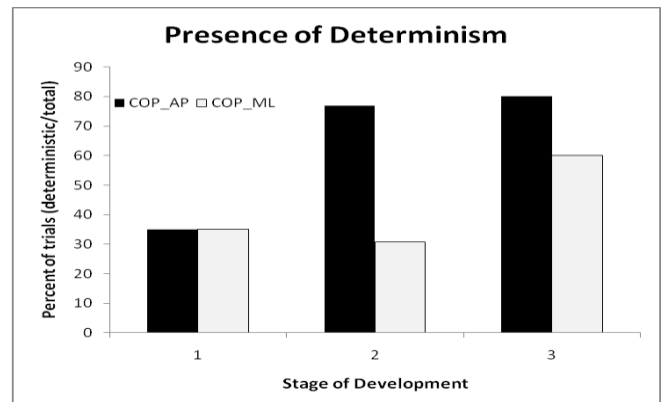


**Figure 2:** Stage-wise comparison of the presence of determinism within the group of infants. Data is plotted as the percent of total trials in which the postural motion was confirmed deterministic. Data is grouped by postural axis (anteroposterior, AP and mediolateral, ML) for each of three sitting Stages.

## RESULTS AND DISCUSSION

Our data (Table 1) suggest that deterministic control of posture is not pervasively present at the initial stages of sitting acquisition, but became more prevalent as the infants accumulated more experience and expressed more advanced postural performance. More specifically, it was shown that deterministic control of posture develops differently for the AP and ML sway axes (see figure 2).

## CONCLUSIONS

This study demonstrates that the evolution of deterministic structure in the control of sitting posture is directly measurable, and changes throughout development. The development of this deterministic structure, as it is uncovered in this evaluation, supports the theoretical perspective of optimal movement variability [4], where we have proposed that motor learning leads to a more organized and deterministic structure of movement variability allowing thus for maximum adaptability and flexibility. Interestingly, the data suggests that deterministic control develops differently for the AP and ML postural axes, indicating that the emergence of control of sitting in the AP direction precedes that of control in the ML direction. This work may prove valuable in the continued assessment of the acquisition of motor skills; particularly those of

postural relevance, but possibly extendable to the general evolution of motor development.

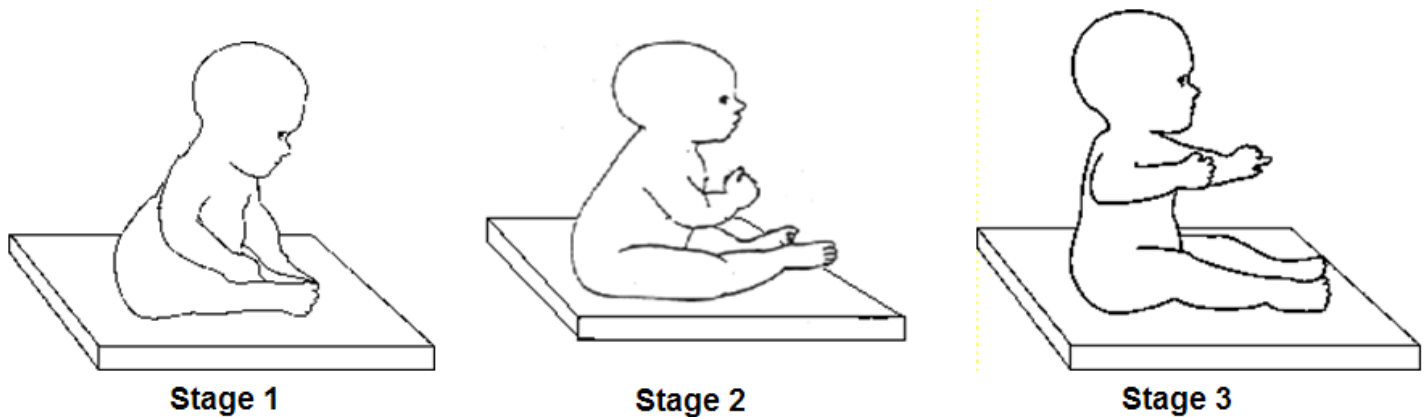
## REFERENCES

1. Stergiou N, ed. *Innovative analyses of human movement*. Champaign, IL: Human Kinetics, 2004
2. Theiler J, et al. *Physica D* **58**, 77–94, 1992
3. Goldberger AL, et al., *PhysioBank, PhysioToolkit, and PhysioNet: Components of a New Research Resource for Complex Physiologic Signals*. *Circulation*, 101(23), e215-e220. Available: <http://circ.ahajournals.org/cgi/content/full/101/23/e215>
4. Stergiou N, et al. *J Neurol Phys Ther*, 2003

## ACKNOWLEDGEMENTS

NIDRR (H133G080023, H133G040118)  
NIH (K25) HD047194  
Nebraska Research Initiative

**Figure 1:** Stages of sitting development. Each stage was described and evaluated by a trained pediatric physical therapist: prop sitting (Stage 1); variable 10s of sitting (Stage 2); and upright without using hands (Stage 3).



# A 3D EXTENDED INVERTED PENDULUM MODEL TO SIMULATE THE CENTER OF MASS TRAJECTORY DURING NORMAL GAIT

<sup>1</sup>Chris Hayot, <sup>2</sup>Sophie Sakka, <sup>1</sup>Vincent Fohanno and <sup>1</sup>Patrick Lacouture

<sup>1</sup>Institut Pprime UPR 3346, CNRS - Université de Poitiers - ENSMA, Poitiers, France

<sup>2</sup>IRCCyn, CNRS - Université de Nantes - ECN - EMN, Nantes, France

email: [chris.hayot@univ-poitiers.fr](mailto:chris.hayot@univ-poitiers.fr)

## INTRODUCTION

The literature about biomechanical modeling of gait commonly focuses on analysis of center of mass (CoM) behavior. In this approach, simplified walking models, such as the inverted pendulum model, are traditionally used. Those models reduce the subject to a point mass linked at a fixed ground contact point by a massless rod of constant length. During single support, the CoM crosses over the rod reaching its maximal height at midstance. Based on this classical model, others simplified mechanical models are dragged from real-time control of biped walking in the robotics field. However, they are based on simplifying assumptions related to the CoM vertical and lateral trajectories [1,2], and the model of double support phase [2].

Thus, even if simplified mechanical models proposed simple and closed-form analytical methods to simulate the CoM trajectory, it is difficult to generate a natural and realistic solution. The aim of the present study was then to propose a spatial mathematical model to simulate realistically the three-dimensional (3D) CoM trajectory during complete gait cycles.

## METHODS

Eight healthy adult subjects were instructed to walk along a 10-m laboratory walkway at three different gait speeds (slow, preferred and fast). Fifty-six reflective markers were placed on bony landmarks of the subjects to compute the reference CoM trajectory. A ten-camera motion analysis system (Vicon, Oxford, UK) was used to collect the 3D marker trajectories sampled at 100 Hz. The center of pressure (CoP) trajectory was measured simultaneously at 1000 Hz from seven staggered force plates (Kistler, Winterthur, Switzerland; Sensix, Poitiers, France) embedded in the walkway.

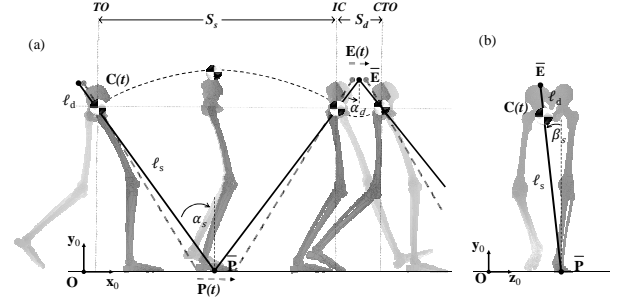


**Figure 1:** Sagittal (a) and frontal (b) representation of EIP3D model.

The inverted pendulum model consisted of a massless rod  $\ell_s$  linking the CoM  $C$  to the fixed CoP  $\bar{P}$  at toe-off instant ( $TO$ ). The predicted CoM sagittal trajectory was computed from a sinusoid portion between  $TO$  and initial contact instant ( $IC$ ) with a pitch angle  $\alpha_s$  during single support (Fig. 1a). We introduced a 3D Extended Inverted Pendulum (EIP3D) model considering the roll angle  $\beta_s$  of the rod (Fig. 1b). The predicted CoM position was defined by:

$$\begin{bmatrix} \overline{OC} \\ 1 \end{bmatrix}_{\mathfrak{R}_0} = T^{0, \bar{P}} \begin{bmatrix} \overline{PC} \\ 1 \end{bmatrix}_{\mathfrak{R}_{\bar{P}}} \quad (1)$$

where  $T^{0, \bar{P}}$  defined the homogeneous matrix from frame  $\mathfrak{R}_0$  to frame  $\mathfrak{R}_{\bar{P}}$  as:

$$T^{0, \bar{P}} = \begin{bmatrix} \cos \alpha_s & \sin \alpha_s \sin \beta_s & \sin \alpha_s \sin \beta_s & x_{\bar{P}} \\ 0 & \cos \beta_s & -\sin \beta_s & y_{\bar{P}} \\ -\sin \alpha_s & \cos \alpha_s \sin \beta_s & \cos \alpha_s \cos \beta_s & 0 \\ 0 & 0 & 0 & 1 \end{bmatrix} \quad (2)$$

We considered that the CoM displacement during double support described a sinusoid and was therefore assimilated to a compound pendulum trajectory [2] (Fig. 1a). Let  $\ell_d$  the constant rod length of the compound pendulum and  $\bar{E}$  its origin. The three points  $\bar{P}$ ,  $C$  and  $\bar{E}$  were aligned at  $IC$  and  $\ell_d$  was computed in proportion to single and double

support repartition as  $\ell_d = S_d/S_s \ell_s$  (Fig. 1a).  $S_d$  and  $S_s$  were respectively the double and single support lengths (Fig. 1a).

The predicted CoM trajectory during successive single and double supports was then computed:

$$\begin{bmatrix} \mathbf{OC} \\ 1 \end{bmatrix}_{\mathfrak{R}_0} = \begin{cases} T^{0,\bar{P}} \begin{bmatrix} \bar{\mathbf{P}}\mathbf{C} \\ 1 \end{bmatrix}_{\mathfrak{R}_{\bar{P}}} ; t \in [TO,IC] \\ T^{0,\bar{E}} \begin{bmatrix} \bar{\mathbf{E}}\mathbf{C} \\ 1 \end{bmatrix}_{\mathfrak{R}_{\bar{E}}} ; t \in [IC,CTO] \end{cases} \quad (3)$$

where  $CTO$  denoted the instant of contralateral toe-off and  $T^{0,\bar{E}}$  the homogeneous matrix from frame  $\mathfrak{R}_0$  to frame  $\mathfrak{R}_{\bar{E}}$  as:

$$T^{0,\bar{E}} = \begin{bmatrix} \cos \alpha_d & \sin \alpha_d \sin \beta_d & \sin \alpha_d \sin \beta_d & x_E \\ 0 & \cos \beta_d & -\sin \beta_d & y_E \\ -\sin \alpha_d & \cos \alpha_d \sin \beta_d & \cos \alpha_d \cos \beta_d & 0 \\ 0 & 0 & 0 & 1 \end{bmatrix} \quad (4)$$

$\alpha_d(t)$  and  $\beta_d(t)$  were the pitch and roll angle of the compound pendulum rod during double support.

Considering that mechanical roll of the stance foot contribute to reduce the CoM vertical [1], we considered the CoP displacement under the stance foot rather than fixed CoP. In substituting  $\bar{P}$  by  $P(t)$  and  $\bar{E}$  by  $E(t)$ , the pivot point of respectively inverted and compound pendulums followed a forward translation and the relation (3) became:

$$\begin{bmatrix} \mathbf{OC} \\ 1 \end{bmatrix}_{\mathfrak{R}_0} = \begin{cases} T^{0,P} \begin{bmatrix} \mathbf{P}\mathbf{C} \\ 1 \end{bmatrix}_{\mathfrak{R}_P} ; t \in [TO,IC] \\ T^{0,E} \begin{bmatrix} \mathbf{E}\mathbf{C} \\ 1 \end{bmatrix}_{\mathfrak{R}_E} ; t \in [IC,CTO] \end{cases} \quad (5)$$

where the rod length of inverted pendulum  $\tilde{\ell}_s$  and compound pendulum  $\tilde{\ell}_d$  were respectively defined during single and double supports with  $\tilde{\ell}_d = S_d/S_s \tilde{\ell}_s$ .

The trajectory of the point E during double support was deduced to a homothetic of center C as

$$\Delta(\mathbf{OE}) = S_d/S_s \Delta(\mathbf{OP}) \text{ at } IC \text{ (Fig. 1a).}$$

A Root Mean Square estimation (RMSe) of CoM trajectory calculation was performed between the reference multibody model and, the EIP3D model considering fixed CoP and CoP translation.

## RESULTS AND DISCUSSION

The results showed that 3D CoM displacements could be accurately predicted by the EIP3D model. As regards to EIP3D model considering both fixed CoP and CoP translation, the approximation in lateral axis was almost exact. The RMSe of both models was minimized in lateral direction during gait cycle for each gait speeds (Table 1).

In horizontal and vertical directions, the EIP3D model considering CoP translation predicted the CoM trajectory with a better accuracy than the model considering fixed CoP. Thus, the introduction of CoP displacement decreased the amplitude of horizontal and vertical displacement during gait cycle (Table 1).

The EIP3D model had the major advantage of realistically generate complete and periodic gait cycles. Thus, it would be very useful in the definition of specific normative data when normal and pathological gait would be compared. Besides, this would be promising in understanding the mechanisms involved in the balance control during physical rehabilitation [2]. This research perspective is supported by the significance taken by the analysis of 3D CoM mechanics as a clinic evaluation tool of pathological gait [3].

## REFERENCES

- Hayot C, et al. *Gait & Posture*, to appear, 2011.
- Zijlstra JG, et al. *Gait & Posture* **6**, 249-262, 1997.
- Detrembleur C. *Gait & Posture*, **12**, 243-250, 2000.

## ACKNOWLEDGEMENTS

The financial support of Région Martinique and Région Poitou-Charentes (CPER2007-2013) are gratefully acknowledged.

**Table 1:** Mean RMSe [mm] of CoM trajectory components computed by EIP3D model considering fixed CoP or CoP translation with gait speeds.

|                   | Mean RMSe [mm] |            |            |            |            |            |
|-------------------|----------------|------------|------------|------------|------------|------------|
|                   | Slow           |            | Preferred  |            | Fast       |            |
|                   | Fixed CoP      | CoP        | Fixed CoP  | CoP        | Fixed CoP  | CoP        |
| <b>Lateral</b>    | 0.16±0.05      | 0.15±0.03  | 0.20±0.16  | 0.15±0.03  | 0.21±0.09  | 0.16±0.05  |
| <b>Horizontal</b> | 2.41±1.07      | 1.58±0.79  | 3.10±0.93  | 2.31±0.84  | 6.27±1.91  | 4.64±1.66  |
| <b>Vertical</b>   | 15.30±5.58     | 11.66±4.59 | 17.79±5.40 | 15.50±5.53 | 26.80±5.14 | 21.71±6.20 |

# INCREASED TOE CLEARANCE ACCURACY DURING OBSTACLE AVOIDANCE: VALIDATION OF CUBIC INTERPOLATION TO UPSAMPLE KINEMATIC DATA

Michel J.H. Heijnen, Brittney C. Muir and Shirley Rietdyk

Purdue University, West Lafayette, IN, USA

Email: [mheijnen@purdue.edu](mailto:mheijnen@purdue.edu)

## INTRODUCTION

Adaptive gait has been extensively examined to provide insight into how the nervous system senses and responds to obstacles in the environment. Starting in 1991 with the first paper [1] examining foot clearance over an obstacle, the number of papers has steadily increased over the years.

Typical sample rates used to capture the kinematic data are fairly low, typically between 50 Hz and 100 Hz [e.g. 1,2]. The sample frequency plays an important role in the accuracy of toe clearance when stepping over an obstacle. This is due to the horizontal and vertical velocity of the limb [3]. The lead and trail limb have similar horizontal toe velocities over the obstacle (3.51 m/s and 2.81 m/s for lead and trail, respectively). The vertical toe velocity over the obstacle is substantially different for both the lead and trail limb (-0.08 m/s and 1.08 m/s for lead and trail, respectively). The vertical toe velocity is especially important since toe clearance is typically measured in this direction. The exact frame when the toe is over the obstacle is not likely to be captured at a typical low sample frequency due to the high velocities. Sampling at a higher frequency could provide a higher spatial resolution, resulting in more accurate toe clearance calculations, especially in the trail limb.

Simply increasing the sample frequency is not always possible. The number of markers that can be tracked by a system can limit the sample frequency. However, sampling at a lower frequency followed by upsampling to a higher frequency might be a solution to increase the accuracy of toe clearance over an obstacle. The purpose of this study was to validate the use of upsampling to increase accuracy of toe clearance measures during obstacle avoidance.

We hypothesized that toe trajectories sampled at 600 Hz signal would provide toe clearance values that were more accurate than the same signals downsampled to 60 Hz; this effect will be greater for the trail limb than the lead limb. We also hypothesized that when the downsampled 60 Hz signal was upsampled to 600 Hz, toe clearance values would be similar to the values from the signal originally sampled at 600 Hz.

## METHODS

Five subjects from a university population participated in this study (3 male, 2 female,  $28.4 \pm 4.4$  years). Two Optotrak 3020 sensors (Northern Digital Inc., Waterloo, ON, Canada) captured the position data of the left and right toe and the obstacle at 600 Hz.

The subjects walked down an eight meter walkway at a self selected speed, stepped over the obstacle (obstacle height was 25% of the subject's leg length) placed at the middle of the walkway, and continued to walk to the end of the walkway. Twenty-five trials per subject were calculated, resulting in a total of 125 trials.

*Data analysis:* Three trials were not included in the analysis due to missing data points. The raw 600 Hz signal was the gold standard (GS 600 Hz). The GS 600 Hz signal was downsampled to 60 Hz (DS 60 Hz) with Matlab 2010a (MathWorks Inc., Natick, MA, USA). These signals were filtered at 8 Hz with a fourth-order zero-phase-shift low-pass Butterworth digital filter [4].

The DS 60 Hz signal was then upsampled to 120 (US 120 Hz), 300 (US 300 Hz) and 600 Hz (US 600 Hz) using the cubic interpolation method from Matlab™ toolbox.

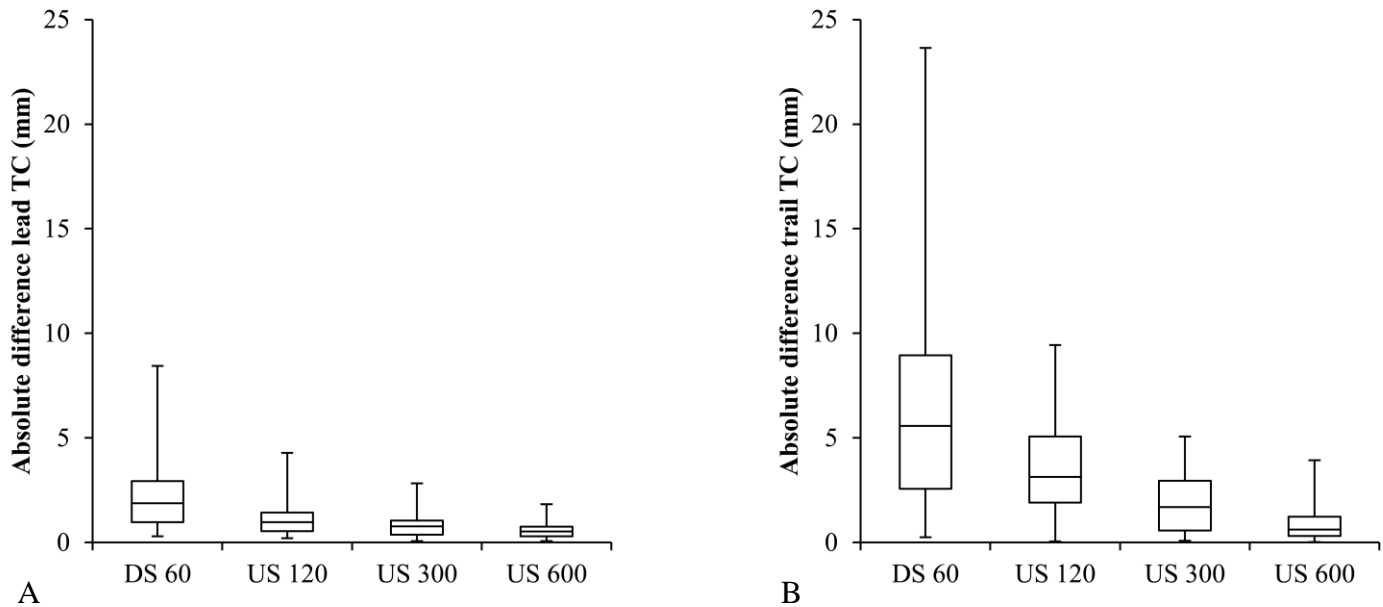


**Figure 1:** Boxplots for the lead (A) and trail (B) toe clearance. Absolute difference between the downsampled and upsampled signals and the gold standard is calculated.

Accuracy was calculated as the absolute difference in toe clearance between GS 600 Hz and each of the remaining signals. To determine if a higher number of trials would improve accuracy for the DS 60 Hz signal, the mean accuracy was calculated as a function of number of trials included in the average, from 2 to 25 trials, for each subject.

## RESULTS AND DISCUSSION

Both lead and trail toe clearance showed more similarities with the GS 600 Hz with a higher upsample rate (Figure 1). As predicted, due to the lower vertical toe velocity, toe clearance was more accurate for the lead toe than the trail toe for all sample rates (Figure 1A versus 1B).

When the 60 Hz signal was upsampled to 600 Hz, the lead and trail toe clearances were only 0.5 mm and 1 mm different, respectively, from the original 600 Hz signal. Therefore, upsampling 60 Hz data to 600 Hz is a valid technique to increase the accuracy of toe clearance. The difference between the GS 600 Hz and the US 600 Hz is probably due to filtering which was completed separately for each signal.

Since it is not likely to capture the exact frame when the toe is over the obstacle, the frame closest to the obstacle is used to calculate toe clearance. If that frame is before the obstacle, toe clearance is

underestimated (toe clearance calculated at 60 Hz is lower than the GS 600 Hz value). If the frame after the obstacle is closer, toe clearance is overestimated. However, these differences will cancel each other out with multiple observations. A comparison of number of trials versus accuracy demonstrated that a minimum of 6 trials for the lead limb and 9 trials for the trail limb are needed to account for under- and overestimation.

A limitation of this study is the fact that only healthy young subjects were measured. The effect on accuracy will likely be reduced in older adults or patients due to lower crossing velocity [1]. However, upsampling to 600 Hz will not result in a less accurate measure of toe clearance.

In summary, upsampling the toe trajectory to 600 Hz with a cubic interpolation is a valid and simple technique to increase accuracy of toe clearance measures during obstacle crossing.

## REFERENCES

- 1.Chen HC, et al. *J Gerontol* **46**, 196-203, 1991.
- 2.Johnson L, et al. *Invest Ophthalmol Vis Sci* **48**, 1466-1471, 2007.
- 3.Patla AE, et al. *J Mot Behav* **28**, 35-47, 1996.
- 4.Winter DA. *Biomechanics and motor control of human movement*, Wiley, 1990.

# FORCE PLATFORM CENTER OF PRESSURE MEASURES USED TO PREDICT NINTENDO Wii FIT BALANCE SCORES DURING YOGA POSES

Heise, G.D., Smith, J.D., Leich, A., Kneisel, K., and Hoke, M.

University of Northern Colorado, School of Sport and Exercise Science, Biomechanics Lab  
gary.heise@unco.edu; www.unco.edu/nhs/ses

## INTRODUCTION

The Nintendo Wii FIT system has become increasingly popular, especially among older adults who wish to improve fitness and balance levels through the balance training components of the software. Little is known about the balance score that the Wii FIT system uses when assessing balance during quiet standing and yoga.

Recent work focusing on the validity of the Wii FIT balance modules found no relation between Wii system balance scores for one-legged and two-legged quiet standing and the mean velocities of the center-of-pressure (COP) in the AP and ML directions [1]. Because yoga poses are popular among Wii system users and because the system presents challenges to users in the form of a game (i.e., earn points for greater stability), the validity of the system was the focus of this investigation.

Prieto et al. [4] suggested multiple stability measures are necessary to characterize differences between groups of subjects based on age and vision and visual input. In other words, to accurately assess balance a single measure is not appropriate. Therefore, the purpose of this study was to use a stepwise regression approach to determine which COP-based stability measures best predict Wii FIT balance scores.

## METHODS

Twenty-nine participants volunteered for this study (age =  $21 \pm 3$  yr; mass =  $71 \pm 15$  kg; ht =  $172 \pm 9$  cm). Each person completed two Wii FIT yoga modules for the half-moon (HM) and tree (TR) poses, both of which required single-leg stance. The tree position required the participants to balance on one leg on a flat foot, pressing the other foot against their inner thigh, as visually

demonstrated by the game software. Arms were raised above the head in a tear drop formation, with hands clasped, pointing upwards. The upper body was expected to remain poised in an upright position, perpendicular to the ground. The half-moon position was similar to the tree position in that the support leg maintained a flat-footed stance, and the other foot was pressed against the inner thigh. Instead of attempting to stand with an upper body orthogonal to the ground, as in the tree position, participants were instructed by the Wii FIT system to maintain an extended support leg while laterally flexing towards the raised leg. Arms once again resembled those of the tree position, and abducted at the shoulder with hands clasped above the head. The tree and half-moon poses were attempted by participants on both right and left support legs.

The Wii FIT platform was placed on top of an AMTI force platform, and during the 30-s long scoring attempts of the participants' efforts to balance in each static yoga pose, ground reaction force data were collected at 100 Hz. COP coordinates were used to calculate the following stability measures in accordance with Prieto et al. [4]: RMS resultant distance; resultant mean velocity; 95% confidence ellipse area; mean frequency; total power; and 95% power frequency. Four stepwise regression models were computed for each condition (HM-right leg; HM-left leg; TR-right leg; TR-left leg). Wii FIT balance scores were the dependent variable and COP-based measures were independent variables. The probability of a Type I error was set at 0.05. As a follow-up to the stepwise regression analysis, a standard intraclass correlation analysis was conducted between Wii FIT balance scores and individual stability measures (critical  $r = 0.35$ ,  $p < .05$ ). Based on the work of Maffiuletti et al. [3], correlations above 0.75 were considered strong.

## RESULTS AND DISCUSSION

Each condition resulted in a statistically significant regression model (see Table 1). RMS, a time domain distance measure [4] was the primary predictor in all models, whereas secondary predictors included another time domain distance measure (mean velocity), a variable from the frequency domain (total power) and an area measure (95% confidence ellipse area). Although all regression models were significant, considerable variability remained unexplained.

From the perspective of instrument validity (i.e., concurrent validity), no individual, COP-based measure demonstrated a Pearson Product moment correlation coefficient greater than 0.78 with the Wii FIT balance scores. Among the six independent variables across the four conditions considered in the regression models, only three correlations exceeded the 0.75, which is indicative of strong concurrent validity [3]. If this criterion correlation is applied to the present study, the Wii Fit system balance platform should not be considered a valid instrument when assessing balance. These findings are consistent with those of Field-Eaton et al. [1], who identified low correlation coefficients (less than 0.35) between Wii system balance scores and COP velocity measures.

The stepwise regression approach used in the present study provides more information than a simple correlation analysis. RMS of the COP resultant distance was the first predictor to enter stepwise regression models of Wii system balance scores across all conditions. In subsequent steps, however, there were different predictors that entered the regression model. It appears that the spatial measure of RMS is one of the best

predictors of Wii system balance score, particularly when considered in combination with a secondary measure that may be from the frequency domain (e.g., total power).

Limitations associated with this study include a data collection duration that exceeds typical durations in postural stability studies. The Wii system's standard yoga attempt lasted 30 s, whereas postural stability experiments contain durations of 20 s or less [4]. Hertel et al. [2] evaluated single-leg stance for only 10 s. The 30 s trials in the present study may have introduced fatigue. Standard postural assessments have subjects stand quietly, whereas subjects in the present study were asked to hold yoga poses for the entire duration of the assessment.

## CONCLUSION

COP stability measures obtained from a force platform predicted Wii FIT system balance scores during yoga poses, with RMS resultant distance being a common predictor across conditions. However, these regression results, coupled with individual correlation coefficients, do not indicate a valid instrument for assessing balance, when evaluated with respect to traditional stability measures.

## REFERENCES

- [1] Field-Eaton, SD, et al. ACSM abstract C-38-Posture/Balance, Denver, CO, 2011
- [2] Hertel J, et al. *J Appl Biomech*, **22**, 67-73, 2006.
- [3] Maffioletti, NA, et al. *Gait & Posture*, **27**, 160-163, 2008.
- [4] Prieto, TE, et al. *IEEE Trans Biomed Engin*, **43**, 956-966, 1991.

**Table 1:** Summary of Regression Models (Wii System Balance Score is dependent variable)

| Condition | Predictors                | R <sup>2</sup> | F-ratio | p-value |
|-----------|---------------------------|----------------|---------|---------|
| HM-right  | RMS, Total Power          | .73            | 35.5    | < .001  |
| HM-left   | RMS, Mean Velocity        | .79            | 47.8    | < .001  |
| TR-right  | RMS, 95%Confidence Ellip. | .60            | 19.4    | < .001  |
| TR-left   | RMS, Total Power          | .65            | 23.6    | < .001  |

Note: HM = half-moon pose; TR = tree pose

# FRONTAL PLANE KNEE KINEMATICS IN LAND-AND-GO TASKS WITH WHOLE BODY ROTATION REQUIREMENTS

<sup>1</sup>Laura Held, <sup>2,5</sup>Witaya Mathiyakom, <sup>4</sup>Henryk Flashner, and <sup>1,2,3</sup>Jill L. McNitt-Gray  
USC Biomechanics Research Lab, Departments of <sup>1</sup>Biomedical Engineering, <sup>2</sup>Kinesiology, <sup>3</sup>Biological Sciences, <sup>4</sup>Aerospace and Mechanical Engineering, University of Southern California;  
<sup>5</sup>Department of Physical Therapy, California State University, Northridge  
E-mail: held@usc.edu

## INTRODUCTION

During landing, multijoint control strategies are implemented prior to and during ground contact. The landing control strategy used by the individual corresponds to the set of mechanical objectives unique to the specific task [1,2,3]. During land-and-go (GO) tasks [2,3], the direction of the horizontal GRF in global space changes based on the GO task direction [3]. This reorientation of the GRF is expected to alter frontal plane moments imposed on the lower extremity. Recent findings, however, indicate that GRF redirection during land-and-go tasks is partially mediated by reorientation of the push leg toward the task direction prior to and/or during ground contact [4]. Still, between-task differences in ankle, knee, and hip frontal plane net joint moments are associated with GO tasks requiring a rotation of the whole body during momentum redirection. How whole body rotation during momentum redirection affects frontal plane knee motion remains unclear.

The purpose of this study was to investigate how GO tasks requiring rotation at the whole body level influence frontal plane knee motion. We hypothesized that GO tasks would result in differences in knee abduction during ground contact compared to land-and-stop tasks (SP). GO tasks with increasing whole body rotation (target located 45° (DG) and 90° (BK) relative to a line parallel to the net) were expected to result in comparable knee angles during impact, with an increase in knee abduction angles during push, as compared to SP.

## METHODS

Five female collegiate Division I volleyball players, medically cleared for participation, provided written informed consent in accordance with the Institutional Review Board. Participants ranged in

age from 19-22 years (mean 20.5 years, SD 1.05 years) with a mean height of 1.89 m (SD 0.03 m) and a mean weight of 775.5 N (SD 43.12 N). Each participant performed a series of SP, DG, and BK tasks using standard three-step footwork at a self-selected speed (Fig. 1). A representative trial of each task was analyzed for each subject.

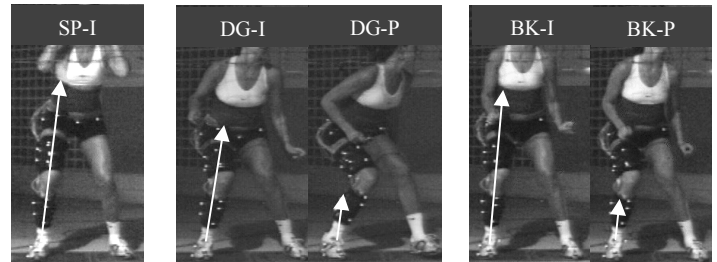


**Figure 1.** GRF and segment orientation in global space during SP, DG, and BK tasks show differences in knee flexion and abduction angle with comparable force magnitudes at peak reaction force during impact (I) and beginning of push (P).

Three-dimensional kinematics (200 Hz, NAC Visual Systems, Burbank, CA, USA) and GRFs (1200 Hz, dual force plates, Kistler, Amhurst, MA) were collected simultaneously during the performance of each task. Anatomic landmarks (ankle, knee, and hip joint centers; lateral femoral condyle; lateral malleolus; heel; and toe) were manually digitized during a standing calibration to define the axes of the foot, shank, and thigh of the push leg. Four reflective tracking markers attached to each segment were digitized (Vicon Motus, Centennial, CO, USA) during standing calibration and all movement trials. Tracking markers coordinates were filtered using a quintic spline (8 Hz). Segment orientation during trials was calculated using a quaternion method [5]. GRF magnitude was normalized to body weight (BW) and used to define the key events during foot contact. Impact (I) phase was defined as the time from initial contact to the first local minimum

following the peak in the vertical GRF. Push (P) phase was defined for DG and BK as the time from foot departure of the lead leg to foot departure of the push leg. Peak resultant GRF (GRFr) during each phase was represented as the average GRFr on the push leg around the time of peak ( $\pm 10$  ms). Calculations were performed using a custom Matlab (The Mathworks Inc, MA) routine.

## RESULTS AND DISCUSSION

No between-task differences in peak GRFr during impact were observed for the push leg (Fig. 2a). Peak GRFr for both DG and BK during the push phase were of comparable magnitude (DG:  $1.49 \pm 0.23$  BW, BK:  $1.67 \pm 0.13$  BW) to peak GRFr during impact phase (SP:  $2.04 \pm 0.44$  BW, DG:  $1.74 \pm 0.56$  BW, BK:  $1.48 \pm 0.47$  BW). Trends in group mean data was not supported by individual subject data (Fig. 2b). However, with the exception of subject 4, the magnitude of peak GRFr during push was comparable or greater than that during impact for DG and BK.

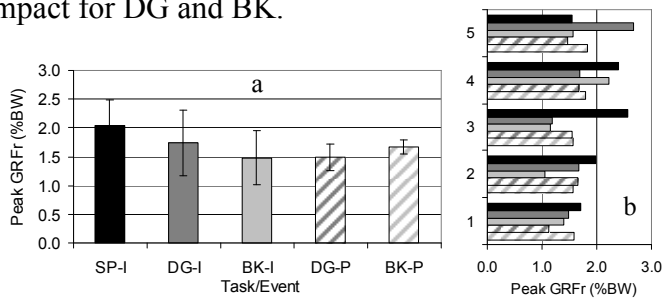


**Figure 2.** a) Mean magnitude of peak GRFr across subjects is comparable during SP, DG, and BK impact (solid) and push (stripes). b) Peak GRFr by subject for each phase shows between-subject differences in redistribution of GRFr between-legs for SP, DG, and BK.

For all subjects, knee abduction angle was greater during push than impact. No between-task differences were observed in mean knee abduction angle at peak GRFr during impact (SP:  $10.3 \pm 3.0^\circ$ , DG:  $11.6 \pm 4.7^\circ$ , BK:  $9.9 \pm 5.4^\circ$ ). Similarly, no between-task differences in mean knee abduction angle at peak GRFr were observed during push (DG:  $18.5 \pm 3.2^\circ$ , BK:  $16.1 \pm 2.5^\circ$ ). Individual subject data demonstrated that knee abduction angle during push was not always greater for BK than DG ( $n=3$ ), contrary to our hypothesis. Examination of the force and kinematic data suggests that these subjects modified the frontal plane knee kinematic control strategy used in DG in order to accommodate the

need to increase the degree of rotation required at the whole body level in BK.

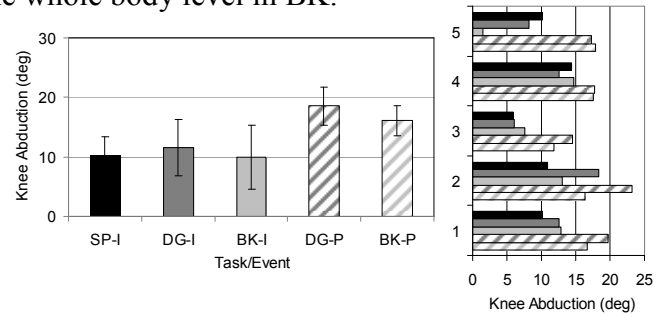


**Figure 3.** a) Mean and b) individual knee abduction angle was greater during push (P) than impact (I).

## CONCLUSIONS

GRFr generated during push are comparable to those experienced during impact phase of realistic GO tasks. GO tasks result in increased knee abduction during push as compared to SP tasks which are often used to screen athletes. The observed increases in knee abduction during GO tasks requiring whole body rotation as part of momentum redirection suggest that the frontal plane moments generated at the ankle, knee, and hip were insufficient for maintaining hinge-like knee behavior. While it is reported that knee injuries typically occur during impact, the repeated exposure to a combination of large GRFr and increased knee abduction excursion during push may create load exposure conditions that predispose athletes to injuries. These results emphasize the need to identify multijoint control strategies that are effective in preserving knee joint integrity in the context of GRFs generated during landings involving momentum redirection.

## REFERENCES

1. McNitt-Gray, JL et al., *J of Biomech*, **34**, 1471–82, 2001.
2. Edwards S, Steele JR, McGhee. *Scand J Med Sci Sports*, **20**, 516-513, 2009.
3. Held L, McNitt JL, Flashner H. *Proceedings of ASB '10*, Providence, RI, WA, USA, 2010.
4. Held L, McNitt JL, Flashner H. *Proceedings of I-FAB '10*, Seattle, WA, USA, 2010.
5. Held L, McNitt JL, Flashner H. Submitted for *Proceedings of ISB '11*, Brussels, Belgium, 2010.
6. Held L, McNitt JL, Flashner H. *Proceedings of ASB '04*, Portland, OR, USA, 2004.

# EXTERNAL WORK IS INCREASED USING ROCKER BOTTOM SHOES

<sup>1</sup>Heather L. Henning, <sup>1</sup>Shane R. Wurdeman, <sup>1</sup>Neil B. Huben, <sup>1</sup>Nicholas Stergiou  
<sup>1</sup>Nebraska Biomechanics Core Facility, University of Nebraska at Omaha, Omaha, NE, USA  
email: swurdeman@unomaha.edu web: http://nbcf.unomaha.edu

## INTRODUCTION

External work is the work performed by external forces (i.e. ground reaction) to move the body's center of mass (COM) through space[1]. External work is decreased when walking with an arc radius attached to the bottom of a walking boot[1]. Decreased external work results in less energy expended in walking, permitting increased activity before fatigue. However, such experimental boots are not practical for every day ambulation due to size. On the other hand, commercial rocker bottom shoes incorporate a "rocker" effect into the shoe's last. Thus, our purpose was to determine if commercial rocker bottom shoes are able to decrease the external work associated with walking like an arc radius. Specifically, we hypothesized that the "rocker" shaped sole will result in decreased negative work for the lead leg during the initial double support period of the stance phase.

## METHODS

Seven healthy young subjects (age:  $23.4 \pm 2.4$  years; height:  $181.6 \pm 3.4$  cm; weight:  $80.5 \pm 9.5$  kg) walked across a 10 meter walkway while kinetics (600Hz; Kistler Instruments) and kinematics were acquired (60Hz; Motion Analysis). Subjects initially walked with a standard sole athletic shoe. Subjects then wore rocker bottom shoes (Masai Barefoot Technology, Roggwil, Switzerland) for a week to allow for acclimation. Each subject then returned to complete a similar data collection with the rocker bottom shoes. External work was calculated as the dot product of ground reaction force and velocity of the body's COM. Velocity of the body's COM was calculated as the first derivative of sacral marker position. External work was normalized to body weight[1]. Stance phase was determined from the vertical GRF. Kinematics was used to divide stance into initial double support, single support, and terminal double support [2]. The three periods and total stance were analyzed for positive and negative external work. The right limb for each shoe was

selected for baseline to rocker bottom comparison using dependent t-tests.

## RESULTS AND DISCUSSION

The rocker bottom shoes resulted in significantly increased magnitude of negative work in the initial double support period of stance (Figure 1; Table 1). The rocker bottom shoes also resulted in a decreased amount of positive work in this initial double support period (Table 1). The positive work of the stance leg in single support period was increased for the rocker bottom shoes (Table 1). For the entire stance phase, subjects performed increased total amounts of positive and negative external work when wearing the rocker bottom shoes (Table 1). Experimental results have shown a rocker shape can reduce the external work associated with locomotion[1]. For this reason, we hypothesized that commercially available shoes that incorporate a rocker shape into the sole would reduce the external work of locomotion. Our hypothesis was not supported. Specifically, individuals wearing rocker bottom shoes had an increased amount of negative work early in stance, when the leg is first coming into contact with the

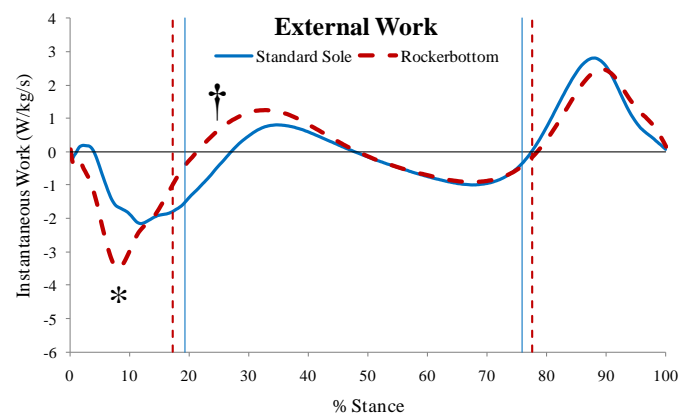


**Figure 1:** Mean ensemble curves for seven subjects. The rocker bottom shoe resulted in an increased amount of negative work in initial double support (\*). As a result, increased positive work was performed in single support (†). Vertical lines denote start and stop of single support.

ground and accepting the body's weight. Although there is also decreased amount of positive work in the rocker bottom shoe during this period, Figure 1 seems to show this is a result of progressing immediately into negative work, or energy absorption, whereas the standard shoe resulted in a small amount of positive work. More importantly, the rocker bottom shoe resulted in increased positive work in single support period. This would likely result in an increased metabolic cost[3]. This period of positive external work in single support coincides with elastic rebound at the knee and work at the hips during stance and swing[3]. Yet, Romkes et al[4] reported increased knee flexion in midstance when subjects walked with rocker bottom shoes, thus decreasing the likelihood of this work coming from knee rebound energy. Furthermore, Nigg et al[5] reported decreased moments at the knee and hip joints through stance as a result of rocker bottom shoes, further decreasing the likelihood of any external work increases occurring at the knee or hip. Romkes et al[4] did report increased gastrocnemius EMG activity in early stance, although they did not distinguish between double support and single support. Thus, it is possible that the increased energy output is from the ankle extensors. Finally, as a result of increased negative work and positive work at different points in the stance phase, subjects expended more total energy during the same gait task. Specifically, the total positive and negative work over the entire stance phase is increased. A limitation to our study is that we did not measure the rollover shape[6] for the rocker bottom shoe. It is likely that the commercial rocker bottom shoes do not provide the optimal rollover shape, which would cause increased mechanical work[1], which equates to an increase in energy expenditure.

## CONCLUSIONS

Our study has the unique aspect of comparing work when wearing standard shoes compared to wearing rocker bottom shoes following an entire week of wear, allowing for adaptation. Our results clearly show subjects are performing increased external work when ambulating in the rocker bottom shoes. It is unclear, however, which muscle groups and mechanisms are responsible for this increased work. Individuals that are interested in increased energy output for purposes such as exercise should consider use of rocker bottom shoes. However, individuals that are utilizing such shoes for other potential benefits, such as rehabilitative purposes, should consider the impact of decreased mechanical efficiency, specifically increased energy cost for walking equal distances. Further research is needed to directly assess the mechanisms responsible for the increased work.

## REFERENCES

1. Adamczyk et al. *J Exp. Biol.* 2006 July;24(209):3953-63.
2. O'Connor et al. *Gait Posture.* 2007 Mar;25(3):469-74.
3. Kuo et al. *Exerc. Sport Sci. Rev.* 2005 Dec;29(33):88-92.
4. Romkes et al. *Clin. Biomech.* 2006 Jan: 21(1):75-81.
5. Nigg et al. *Clin. Biomech.* 2006 Jan: 21(1):82-88.
6. Hansen et al. *Clin. Biomech.* 2004 May;19(4):407-14.

## ACKNOWLEDGEMENTS

This work is supported in part by ASB Grant-in-Aid, NASA Nebraska Space Grant and EPSCoR Fellowship, Golden Key International Honor Society Research Grant, the Nebraska Research Initiative, and NIA (RO1AG034995).

**Table 1.** Group means  $\pm$  standard deviation for right leg of seven subjects in standard sole shoe and rocker bottom shoe during the stance phase of gait. During initial double support, values are reported for the leading stance leg and during terminal double support values are reported for the trailing stance leg.

| Dependent Variable                           | Standard Sole     | Rocker bottom     | p value |
|--|-------------------|-------------------|---------|
| Positive Work during initial double support  | 0.082 $\pm$ 0.06  | 0.023 $\pm$ 0.02  | 0.015*  |
| Negative Work during initial double support  | -1.448 $\pm$ 0.88 | -2.078 $\pm$ 0.83 | 0.026*  |
| Positive Work during single support          | 0.848 $\pm$ 0.75  | 1.503 $\pm$ 0.83  | 0.002*  |
| Negative Work during single support          | -1.965 $\pm$ 0.81 | -1.736 $\pm$ 0.76 | 0.086   |
| Positive Work during terminal double support | 2.113 $\pm$ 0.53  | 1.998 $\pm$ 0.56  | 0.150   |
| Negative Work during terminal double support | -0.068 $\pm$ 0.08 | -0.038 $\pm$ 0.04 | 0.393   |
| Total Positive Work during stance            | 3.044 $\pm$ 0.95  | 3.524 $\pm$ 1.15  | 0.005*  |
| Total Negative Work during stance            | -3.481 $\pm$ 1.12 | -3.851 $\pm$ 1.04 | 0.026*  |

Note: \*  $p < 0.05$ , significant difference between standard sole and rocker bottom  
Units: J/kg \* 10<sup>1</sup>

# WHY DO OLDER WOMEN UTILIZE SLOWER VOLITIONAL CENTER OF PRESSURE MOVEMENTS WHEN ACCURACY IS CONSTRAINED? THE ROLE OF THE PRIMARY SUBMOVEMENT

<sup>1</sup> Manuel Hernandez, <sup>1,2</sup> James Ashton-Miller and <sup>3</sup> Neil Alexander

<sup>1</sup>Department of Biomedical Engineering, <sup>2</sup>Department of Mechanical Engineering, <sup>3</sup>Department of Internal Medicine, University of Michigan, Ann Arbor, MI, USA.  
email: [manueleh@umich.edu](mailto:manueleh@umich.edu) web: [www.med.umich.edu/geriatrics/moblab/](http://www.med.umich.edu/geriatrics/moblab/)

## INTRODUCTION

Older adults are known to have decreased postural control during upright stance or gait [1]. Furthermore, older women have been found to use slower volitional center of pressure (COP) movements in comparison to young women when accuracy is constrained [2]. Given the need for rapid center of pressure (COP) movements to often avoid falls, limited speed provides a mechanism for increased fall risk among older adults.

In this study, we examined the effects of age on the speed and accuracy of primary submovements (SMs) [3] and their corresponding regular COP movements. We hypothesized that in comparison to young women, older women would display a disproportionate decrease of speed and accuracy (e.g., effective target size [ETS] and COP endpoint position) in their overall movements and primary SMs, as the magnitude of COP excursion increases.

## METHODS

*Subjects.* Healthy young (mean±SD, age 23±3, N = 13) and healthy older females (age 76±6, N = 12) were recruited from the local community. Young women were taller (164±6 cm versus 159±5 cm), but did not differ in weight, body mass index, or foot length.

*Protocol.* While standing on a force platform, subjects performed accuracy-constrained COP movements as fast and as accurately as possible. Trials corresponded to varying magnitudes of COP excursion (COP excursion from neutral standing posture to anterior limit of the functional base of support [FBOS] and back [CA<sub>FBOS</sub> trials], or from posterior to anterior limit of the FBOS and back

[AP<sub>FBOS</sub>]), varying target size (2 & 6 cm), and hand support conditions (with or without hand support). A walker placed around the person and set at hip height was provided or removed depending on the hand support condition. A time varying (1-3 sec) auditory tone was used to cue the start and end of movement. Data collection sessions were performed on three separate testing sessions, but only data from the final session is presented at this time.

*Data Analysis.* Repeated measures mixed-model analyses of variance were used to examine the effect of age while controlling for movement direction (i.e., anterior vs. posterior), hand support condition, magnitude of COP excursion (i.e., CA<sub>FBOS</sub> vs. AP<sub>FBOS</sub>), and target size. To account for multiple comparisons, post-hoc tests were carried out using Hochberg's step-up method.  $P < 0.05$  was considered statistically significant.

## RESULTS AND DISCUSSION

Overall, the COP movements of older women were 37% slower than young women while maintaining a similar ETS and COP endpoint position. Posterior movements were slower and less accurate than anterior movements as were those without hand support vs. hand support ( $P < .001$ ). CA<sub>FBOS</sub> trials demonstrated slower speeds vs. AP<sub>FBOS</sub> trials (9±4 vs. 15±6 cm/s) as did 2-cm vs. 6-cm trials ( $P < .001$ ). In comparison to young, older women were unable to increase their mean COP speed at the same rate as young, when going from CA<sub>FBOS</sub> to AP<sub>FBOS</sub> trials ( $P < .001$ , Fig. 1). CA<sub>FBOS</sub> trials had a 14% decrease in ETS, in comparison to AP<sub>FBOS</sub> trials ( $P = .003$ ), whereas 2-cm targets had a 57% decrease in ETS vs. 6-cm targets. No significant interaction with age was observed with other factors in either ETS or COP endpoint position.

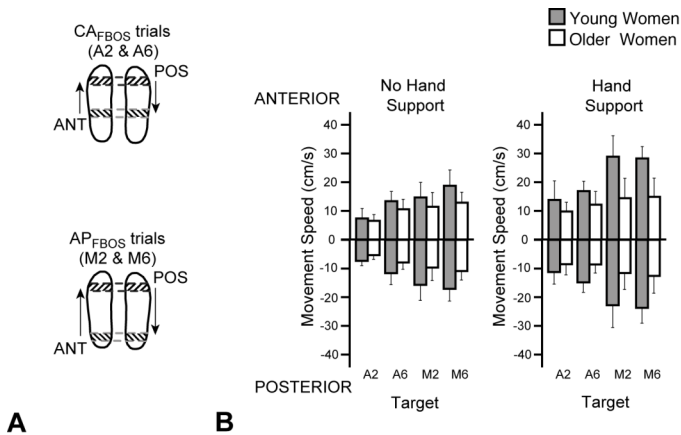


**Figure 1:** (A) Schematic outlining the relative positions of CA<sub>FBOs</sub> and AP<sub>FBOs</sub> trials. (B) Mean  $\pm$  SD COP movement speed of 2-cm (A2,M2) and 6-cm (A6,M6) trials.

*Primary SMs.* Consistent with overall results, older women demonstrated slower primary SMs when compared to young women ( $P < .001$ ). All primary factors were found to significantly affect primary SM speed ( $P < .001$ ). Young women also appeared to disproportionately increase primary SM speed when using hand support vs. no hand support or moving from CA<sub>FBOs</sub> to AP<sub>FBOs</sub> trials ( $P < .001$ ).

The endpoint position of primary SMs demonstrated significant decreases when moving anteriorly, rather than posteriorly, when not using hand support, rather than using it, or decreasing target size ( $P < .001$ ). As the magnitude of COP excursion increased from CA<sub>FBOs</sub> to AP<sub>FBOs</sub> trials, participants arrested their primary SMs well before reaching their desired target, thus, leading to decreased endpoint positions ( $P < .001$ ), particularly among older women ( $P = .003$ ). In particular, older women relied on a more frequent undershooting strategy (67% vs. 57%, Figure 2), when compared to younger women, when moving near the boundary of their FBOS without hand support.

Age-related changes observed in movement speed are consistent with previous studies [2,4]. The slower but similarly accurate movements of older women vs. young women under a wide range of whole body movements appears to have been achieved by age-related changes in the control of the primary SM. Consistent with increases in neuromotor noise due to age, older women are employing increasingly conservative strategies to ensure endpoint accuracy under challenging balance conditions.

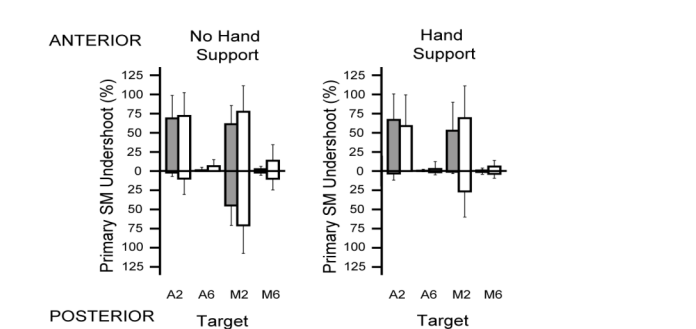
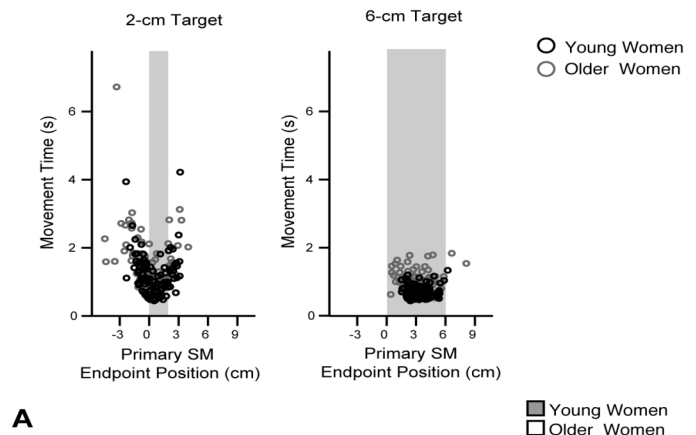


**Figure 2:** (A) Correlations between movement time and primary submovement (SM) endpoint position. (B) Mean (SD) values of the % of primary SMs undershooting target.

## CONCLUSIONS

We conclude that strategic changes in the termination of the primary SM, such as more frequent undershooting of the desired target, provide a rationale for the decreases seen in volitional COP movement speed in older women.

## REFERENCES

1. Prieto TE, et al. *IEEE Trans Biomed Eng* **43**, 956-966, 1996.
2. Hernandez ME, et al. *Annual Meeting of ASB '09*, State College, PA, USA, 2009.
3. Fishbach, et al. *Exp Brain Res* **164**, 442-457, 2005.
4. Ketcham CJ, et al. *J Gerontol* **57B**, P54-P64, 2002.

## ACKNOWLEDGEMENTS

We would like to thank collaborators in the Mobility Research Center for their assistance with data collection and the National Institutes of Health for NRSA Grant Number 1 F31 AG024689-01, which helped support this project.

# ESTIMATION OF PATELLA BONE STRESS: A COMPARISON OF HOMOGENEOUS AND HETEROGENEOUS FINITE ELEMENT MODELS

<sup>1</sup>Kai-Yu Ho, <sup>2</sup>Nazanin Mokarram, <sup>1</sup>Nicholas H. Yang, <sup>2</sup>Ashkan Vaziri, <sup>1</sup>Christopher M. Powers

<sup>1</sup>University of Southern California, Los Angeles, CA, USA

<sup>2</sup>Northeastern University, Boston, MA, USA

email: [kaiyuhoh@usc.edu](mailto:kaiyuhoh@usc.edu), web: <http://pt.usc.edu/labs/mbrl>

## INTRODUCTION

Finite element (FE) analysis is a non-invasive method to estimate subject-specific bone stress. Given the inhomogeneity nature of bone, density-based heterogeneous bone modeling has been considered as the most accurate approach for computing bone stress.<sup>1</sup> Traditionally, voxel-based bone densities can be measured with quantitative computed tomography (QCT), and the average density of several voxels can be assigned to a corresponding element.<sup>1,2</sup> However, as articular cartilage exhibits little signal on QCT, such an approach becomes challenging when studying patellofemoral joint (PFJ) cartilage contact problems. To address this issue, a FE model was developed to acquire subject-specific heterogeneous material property of the patella using water-fat IDEAL magnetic resonance imaging (MRI). As such, the purpose of this pilot study was to compare peak von Mises stress of the patella bone at the cartilage-bone interface among 3 FE patella models (heterogeneous, 2-material consisting of uniform cortical and trabecular bone, and homogeneous). The validity of each model was evaluated by comparing the predicted PFJ contact area to that acquired from MRI.<sup>3</sup>

## METHODS

Subject-specific PFJ geometry of a single female subject with patellofemoral pain was in this study. Input parameters for the FE model included: 1) PFJ geometry, 2) elastic modulus of patella, 3) weight-bearing PFJ kinematics, and 4) quadriceps muscle forces (Fig. 1). PFJ geometry was obtained from sagittal plane MR IDEAL in-phase images acquired with a 3.0 T MR scanner (General Electric Healthcare) and manually segmented (Fig. 1A). The FE mesh of cartilage, femur and tibia was created using FE pre-processor (Hypermesh, Altair Engineering Inc.). Voxel-wise bone density of

patella was estimated from IDEAL IP MRI with the assistance of a calcium hydroxyapatite phantom.<sup>4</sup> The elastic moduli were then calculated based on the density measures. The patella mesh was created with heterogeneous elastic modulus assigned to each element using Mimics software (Materialise) (Fig.1B). The FE mesh of cartilage and bone was then registered to the position of each structure on the weight-bearing MRI (Fig.1C).<sup>3</sup> Quadriceps muscle forces were estimated using a previously described EMG driven model (Fig.1D).<sup>5</sup>

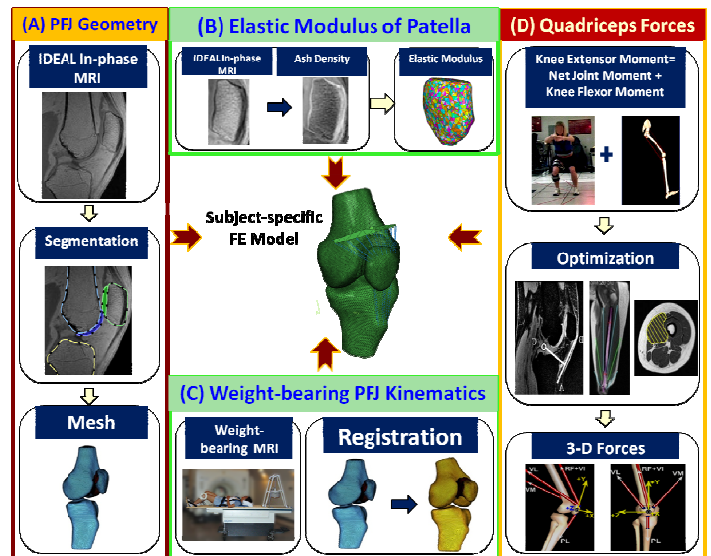


**Fig. 1.** Finite Element Modeling Pipeline.

Quasi-static loading simulations were performed using a nonlinear FE solver (Abaqus, SIMULIA) at 45° of knee flexion. Three assignments of elastic modulus were performed on isotropic tetrahedral continuum elements of patella (i.e., heterogeneous, 2-material, and homogeneous models) with Poisson ratio of 0.3. The heterogeneous patella model was generated as described above with the elastic modulus ranging from 3.9 to 14.8 GPa. The 2-material patella consisted of cortical bone with an elastic modulus 14.8 GPa and trabecular bone with

elastic modulus 3.9 GPa. The homogeneous patella was generated with elastic modulus 14.8 GPa throughout the entire volume of patella. For each model, the femur and tibia were modeled as rigid and the cartilage of the patella and femur was modeled as homogeneous isotropic tetrahedral continuum elements (elastic modulus of 4 MPa<sup>3</sup> and Poisson ratio of 0.47<sup>3</sup>). Quadriceps muscles were divided into 3 functional groups (rectus femoris/vastus intermedius, vastus medialis, and vastus lateralis) made up of 6 equivalent uniaxial connector elements. The patellar tendon was modeled as six uniaxial, tension-only elements with stiffness of 4334 N/mm.<sup>3</sup> The model outputs included peak von Mises stress and PFJ contact area.

## RESULTS AND DISCUSSION

All three models demonstrated similar von Mises stress distribution with the peak stress being located on the lateral facet of patella (Fig. 2). Compared to the heterogeneous model, the difference in peak von Mises stress was 0.21 MPa (8.0%) for the 2-material model and 0.30 MPa (11.5%) for the homogeneous model (Table 1). The predicted contact area of 3 FE models matched well with the contact area measured from MRI (255.16 mm<sup>2</sup>; Table 1).

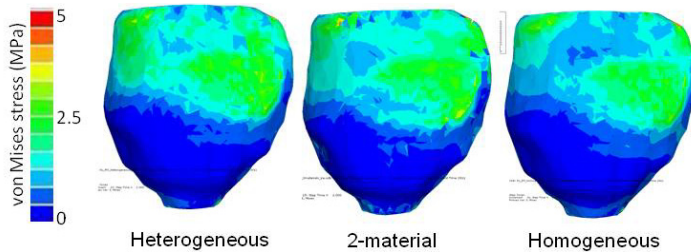


**Fig. 2.** von Mises distribution of patella at the cartilage-bone interface in 3 conditions.

## CONCLUSIONS

In the present study, a method to generate a subject-specific, heterogeneous patella FE model starting from IDEAL MRI was developed. Such an approach was deemed valid as there was excellent agreement in PFJ contact area based on MRI measurements. When comparing the heterogeneous, 2-material, and homogeneous models, meaningful differences in peak von Mises stress were found (8.0 to 11.5%). Therefore, it may be important to consider the heterogeneity of bone when developing bone FE models to assess PFJ cartilage contact problems.

## REFERENCES

1. Taddei F, et al. *J Biomech* **39**, 2457-2467, 2006.
2. Keyak JH, et al. *J Biomed Eng* **15**, 505-509, 1993
3. Farrokhi S, et al. *Osteoarthritis Cartilage* In Press.
4. Ho KY, et al. *Proceedings of ISMRM'11*
5. Chen YJ, et al. *J Appl Biomech* **26**, 415-423, 2010.

**Table 1:** Peak von Mises stress of patella at the cartilage-bone interface and cartilage contact area at 45° of knee flexion with 3 assignments of elastic modulus.

|                      | Peak von Mises stress (MPa) | Contact Area (mm <sup>2</sup> ) |
|----------------------|-----------------------------|---------------------------------|
| <b>Heterogeneous</b> | 2.62                        | 255.96                          |
| <b>2-material</b>    | 2.83                        | 255.97                          |
| <b>Homogeneous</b>   | 2.32                        | 255.99                          |

## ACKNOWLEDGEMENTS

This study is supported by the International Society of Biomechanics Student Dissertation Award.

# EFFECTS OF GLUTEUS MAXIMUS FATIGUE ON JUMP-LANDING KINEMATICS AND ELECTROMYOGRAPHY IN WOMEN

John H. Hollman, Jeffrey M. Hohl, Jordan L. Kraft, Jeffrey D. Strauss and Katie J. Traver

College of Medicine, Mayo Clinic, Rochester, MN, USA

email: [hollman.john@mayo.edu](mailto:hollman.john@mayo.edu)

## INTRODUCTION

The incidence of knee injuries is greater in latter rather than earlier moments of athletic competition [1], leading to speculation that neuromuscular fatigue may contribute to knee injuries. Studies have concluded that fatigue induces mechanical changes during dynamic landing tasks, including decreased flexion angles and increased valgus moments and anterior shear forces at the knee [2,3].

Geiser et al [4] investigated the influence of gluteus medius fatigue on lower extremity (LE) mechanics and concluded that only small increases ( $<2^\circ$ ) in knee valgus occur during side-cutting or jumping post-fatigue. Given that gluteus medius fatigue may have little effect on LE mechanics, it is possible those mechanics may be influenced by impaired gluteus maximus (GMax) function instead. It is unclear whether that may be explained by impaired strength or impaired motor control of the muscle.

The purpose of this study was to examine whether experimentally-induced GMax fatigue alters LE kinematics or EMG recruitment during a jump-landing task in women.

## METHODS

Forty healthy women (age,  $25\pm 3$  years; BMI,  $23\pm 3$   $\text{kg/m}^2$ ) were randomly assigned to two groups. Subjects in the experimental group completed a modified Biering-Sorensen test to fatigue the GMax muscles, whereas subjects in the control group completed repeated push-ups to exhaustion.

Testing consisted of three repeated maximal vertical jumps. Kinematic data were measured at 100 Hz with a Vicon MX motion analysis system. Raw data were smoothed with a Woltring quintic spline filter at a mean square error of 20 mm. Nexus software

was used to quantify LE kinematics in the sagittal, frontal and transverse planes of motion. EMG data were measured with a Bagnoli-16 system and DE-3.1 double-differential surface electrodes. The common mode rejection ratio was 92 dB at 60 Hz, input impedance exceeded  $10^{15}$   $\Omega$  and data were collected through a 16-bit NI-DAQ PCI-6220 analog-to-digital acquisition card. Signals were sampled at 1000 Hz, bandpass filtered from 20 to 450 Hz with a Butterworth filter and processed with EMGworks® 3.7.2.0 data acquisition and analysis software. Data were processed with a root mean square algorithm and normalized to maximum voluntary isometric contractions (MVIC).

Muscle fatigue in the GMax during the Biering-Sorensen test was assessed by examining power density spectra of EMG signals. Spectral analysis was conducted with Hanning window processing and a fast Fourier transformation. Fatigue was represented by the slope of a regression through the median frequency time series. Effects of the intervention were also assessed by measuring pre- and post-fatigue isometric hip extension force production with a microFET2 dynamometer.

We analyzed pre- and post-fatigue ranges of motion at the hip and knee and peak EMG recruitment during the landing phase of the second vertical jump. Data were analyzed with 2-way mixed model ANOVAs ( $\alpha = 0.05$ ) and with post hoc Bonferroni-adjusted tests for multiple comparisons.

## RESULTS AND DISCUSSION

Evidence of Fatigue. Subjects in the experimental group experienced a 0.06 Hz/s decrease in the median EMG frequency during the Biering-Sorensen test (Fig. 1;  $p = 0.020$ ) and a 23% decrease in isometric hip extension strength (Fig. 2;  $p < 0.001$ ). No change in median EMG frequency or

in isometric hip extension strength occurred in the control group.

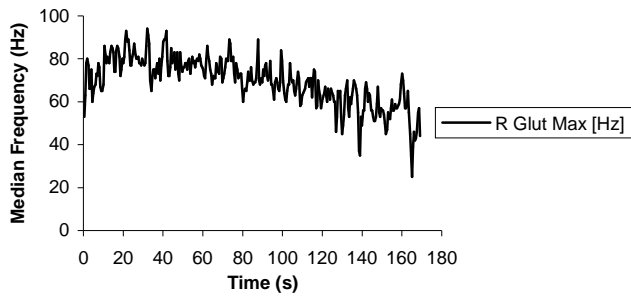


**Fig. 1.** A participant’s EMG power spectrum during the modified Biering-Sorenson test.

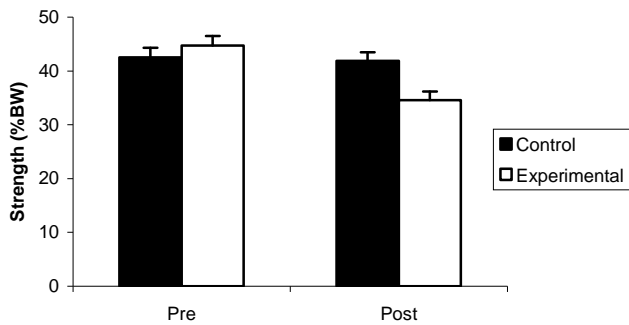


**Fig. 2.** Pre- and post-fatigue isometric gluteus maximus strength (% body weight).

Kinematic Analysis. Hip and knee kinematics differed neither in the experimental group nor in the control group post-fatigue ( $p>0.05$ ).

EMG Analysis. GMax EMG recruitment during the jump-landing task increased by 38% in the experimental group following the fatigue-inducing protocol and changed negligibly in the control group (Fig. 3;  $p = 0.005$ ).

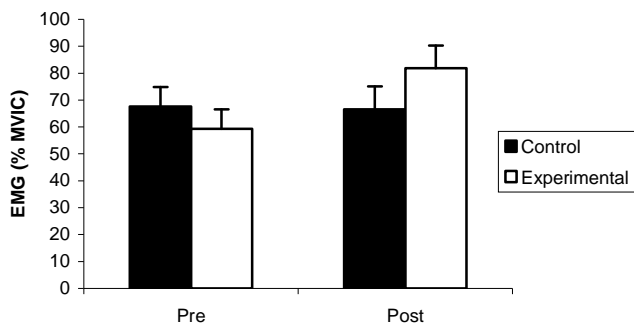


**Fig. 3.** Pre- and post-fatigue EMG recruitment during the landing phase of the jump-landing test.

Despite a 23% reduction in isometric hip extension strength, no change in jump-landing hip or knee kinematics occurred following an intervention that fatigued the GMax muscles. Participants increased their GMax EMG recruitment by 38%. These findings suggest that reduced GMax strength does not appear to cause LE pathomechanics (e.g., increased hip flexion, internal rotation and adduction accompanied by increased knee valgus) during a jump-landing task that may predispose a knee to injury. Rather, participants accommodated for the loss of GMax strength by recruiting more motor units to complete the task. The findings may indicate that in young, active women, GMax motor control (muscle recruitment) may influence LE mechanics during a jump-landing task to a greater extent than does GMax strength.

## CONCLUSIONS

No changes in jump-landing hip or knee kinematics occurred following an intervention that weakened the GMax. The strength reduction in the GMax was compensated for by increased EMG recruitment. Reduced GMax strength may have little effect on hip and knee kinematics during a jump-landing task in women. Impaired motor control of the GMax, rather than impaired strength, may be responsible for pathomechanics that lead to increased knee valgus during a dynamic weightbearing activity.

## REFERENCES

- 1.Hawkins RD, et al. *Br J Sports Med* **35**, 43-47, 2001.
- 2.Chappell JD, et al. *Am J Sports Med* **33**, 1022-1029, 2005.
- 3.Kernozek TW, et al. *Am J Sports Med* **36**, 554-565.
- 4.Geiser CF, et al. *Med Sci Sports Exerc* **42**, 535-545, 2010.

# A PROTOTYPE VIDEO GAME SYSTEM FOR STUDYING REHABILITATIVE LEARNING

Brendan Holt, Alexander Reyes and Francisco Valero-Cuevas

University of Southern California, Los Angeles, CA, USA  
email: [bholt@usc.edu](mailto:bholt@usc.edu) web: <http://bbdl.usc.edu>

## INTRODUCTION

Innovative human-interface devices paired with rich interactive media can enhance neuro-rehabilitation strategies aimed at enabling patients to reach essential skills for daily living. A rehabilitative gaming system could motivate users and provide an appropriate challenge level while they perform the many repetitions required for motor learning. A flexible software framework could enable the investigator to monitor and test the effectiveness of short-term drills or variable practice structures. Testing whether or not gaming and virtual reality in the context of rehabilitation are more than simply aid to repetitive practice requires the ability to deploy low-cost technology into patients' homes and clinics. Therefore, we present the initial stages of the development of an integrated system for in-home gaming for the evaluation and promotion of dexterous manipulation with the fingertips.

## METHODS

Our system has three main components as shown in Figure 1. **(a)** A modified Strength-Dexterity (S-D) input device controlled by the thumb and index fingers. The previously developed S-D test challenges the user to compress an unstable spring with the fingertips. This is a difficult control task especially for patients with dexterity deficits, as the spring is prone to buckling. As a diagnostic tool, it can delineate those aging with a disability, such as osteoarthritis, and individuals with normal hand capability [1,2]. In another recent study, we have demonstrated that the S-D test shows clear engagement of different cortical-striatal-cerebellar brain networks depending on the instability of the spring [3]. Thus, one of our goals is to extend the S-D system from clinical test to dexterity training tool under the guise of a video game device. Load cells on either end of the spring are connected to a microcontroller housed in a small box. A Bluetooth

module broadcasts force data to a computer running the game software. Although the device is not fully wireless, a future miniaturized version could be strapped to the wrist permitting greater freedom of movement during a gaming session. **(b)** A computer with open emulated serial ports receives and optionally filters the data streams, which drive the game mechanics. Currently Microsoft Windows and Apple Mac OS X operating systems are supported for data acquisition. And **(c)**, our work-in-progress software, the main focus of this paper, is a simple side-scrolling arcade game featuring an aircraft whose vertical position is mapped to the compression of the spring controller.

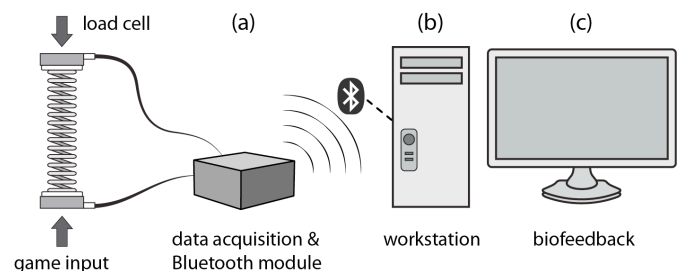


**Figure 1:** Schematic of the prototype game system.

We chose the Unity game design tool (Unity Technologies, San Francisco, CA) for its cross-platform coding and publishing capabilities (Windows, Mac OS X, iOS, Android), rapid prototyping features, modern 3D rendering engine, and C++ plug-in extensibility. The last feature was especially important, because a trade-off of “write-once-run-everywhere” frameworks such as Sun’s Java and Mono (an open source implementation of Microsoft .NET) is that the official APIs have limited access to lower level, operating system-specific components such as serial ports and the Bluetooth stack, both of which are critical for capturing data from lab instrumentation. Writing a native C++ library and an associated wrapper class can circumvent this limitation.

The core game assets including the player's vehicle (Figure 2) and world obstacles were modeled with polygonal geometry in Autodesk Maya 2011 and then exported to the general-purpose Filmbox format (FBX). Backgrounds, textures, and other 2D elements were digitally painted in Adobe Photoshop CS5. The assets were then imported into Unity where a basic game level was assembled and scripts were attached to the interactive entities. Since Unity utilizes the Mono framework for scripting, game logic was written in C#.

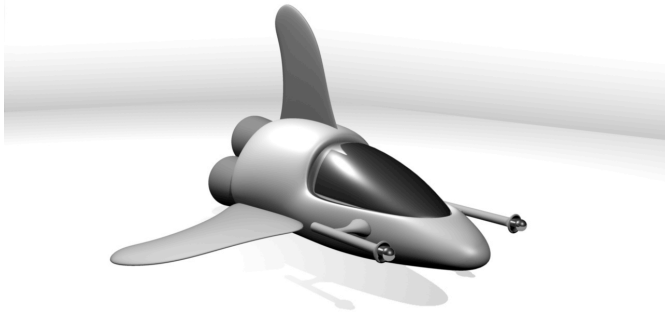


**Figure 2:** The player's avatar, modeled and rendered in Maya.

The structure of a standard game loop listens for user input, updates object and camera transformations, calculates collision detection, and redraws the scene with a real time lighting model. At every frame cycle the ship's vertical screen position will be set to a value proportional to the reported load cell data. The frame of reference will be ship-centric; that is, the view is locked to the ship's horizontal screen position. A combination of obstacles and parallax background traverse the screen from right to left, providing a visual cue that the ship has a velocity in the opposite direction. The user must avoid these obstacles—asteroids, buildings, or terrain depending on the level's environment—by compressing the spring at the appropriate instant and for a proper duration. Collision events will incur a small penalty for an otherwise steadily increasing score.

## RESULTS AND DISCUSSION

We have demonstrated the feasibility of using a Bluetooth spring controller as a new gaming and

data-gathering device for capturing the complex dynamics of dexterous finger manipulation. With only a one-dimensional force input at each sensor, the complexity of games possible is arguably limited, unless one uses a keyboard or some other device (3D load cells are expensive and heavy). Installing 3-axis accelerometers in the S-D system or using a machine vision approach like Microsoft's Kinect will greatly expand the possibilities for intuitive gestures and game control while reducing reliance on unwieldy secondary inputs or expensive force sensors.

For practical therapy, the program must provide enough challenge and variation to motivate the patient for hourly sessions over a span of weeks or months. In order to appeal to all audiences (e.g., children with cerebral palsy, elderly patients with Parkinson's or stroke), we will create several "skins" for the same game or simply a new scenario appropriate for the demographic. For example, a subject who has great difficulty controlling the spring might find the prospect of crashing his or her avatar into asteroids too discouraging. Perhaps a task better suited for that hypothetical individual would be the reverse scenario; instead of dodging obstacles, one must collect trails of energy orbs (a positive reinforcement approach) corresponding to increased control of the instability of the spring.

## REFERENCES

1. Lange BS, et al. *Phys Med Rehabil Clin N Am* **21** (2), 339–56, 2010.
2. Valero-Cuevas FJ, et al. *J Biomech* **36**, 265–270, 2003.
3. Mosier K, et al. *J Neurophysiol*, in Press, 2011, doi:10.1152/jn.00757.2010.

## ACKNOWLEDGEMENTS

This material is funded in part by grants NSF EFRI-COPN 0836042, NIH AR050520, and OPTT-RERC 84-133E2008-8 to FVC, and USC Provost's Ph.D. Fellowship.

# LEG STIFFNESS INCREASED WITH GAIT SPEED IN THE ELDERLY

Hyunhwa Hong, Seyoung Kim and Sukyung Park

Korea Advanced Institute of Science and Technology, Daejeon, Republic of Korea  
email: [sukyungp@kaist.ac.kr](mailto:sukyungp@kaist.ac.kr) web: <http://biomt.kaist.ac.kr>

## INTRODUCTION

Compliant leg models have been widely accepted to explain the basic dynamics of walking and running [1]. Human walking were described as to modulate the apparent stiffness to optimize gait dynamics and energetic. The effective leg stiffness increased with gait speed to build up greater propulsion energy required before collision [2,3]. However, the previous study was demonstrated only on healthy young subjects, thus has not been shown to verify other subjects such as the elderly, who have slower gait speed than the young subjects. In this study, we extend an existing approach to an elderly group to examine how the leg stiffness would be correlated with the gait speed. A damped compliant walking model was used to calculate the leg stiffness of the elderly [2].

## METHODS

### *Subjects*

Seven young ( $22.86 \pm 1.07$  yr) and three elderly ( $68.33 \pm 3.06$  yr) subjects were recruited from the student population, and local community respectively. All subjects had no history of balance disorder and did not experience discomfort while walking. The study was performed in accordance with IRB, ethical approval for procedures obtained from the Korea Advanced Institute of Science and Technology. Each subject provided informed written consent form prior to participation.

### *Protocols*

The subjects walked over-ground with three sets of four different randomly ordered gait speeds, ranging from their self-selected speed to their maximum speed [4]. The subjects were instructed to walk on a straight 12-meter long, 1-meter wide walkway with steady speed guided by metronome's regular beat subsequently analyzed. To avoid intentional stepping on the platform during gait, the force

platform was covered with thin carpet. Trials that stepped consecutive three force platform correctly have been analyzed.

### *Measurement*

Kinetic and kinematic data were collected using three force plates (AMTI, Accugait®) and motion capture cameras (Motion Analysis, Hawk®), respectively. We used platform method to estimate the velocity and position of COM [5]. Optical marker position and GRFs were 5th-order Butterworth low-pass filtered with cutoff frequencies of 10 Hz for motion data and 30 Hz for the force plate data.

### *Analysis*

To calculate the dynamic leg stiffness, we used a damped compliant walking model (Fig.1) [2]. A curved foot was used to consider center of pressure (CoP) excursion. Model parameters (Initial conditions, spring and damping constant) were obtained by optimization that best fit the ground reaction force data using MATLAB®.

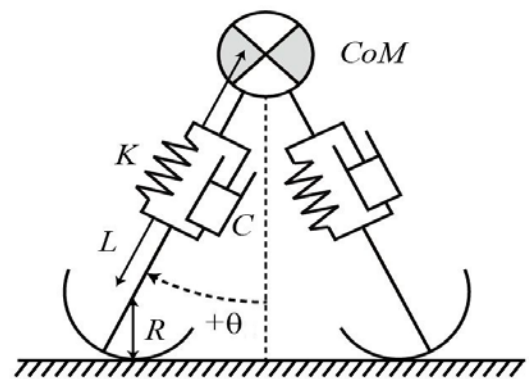


**Figure 1:** Schematic of the damped compliant walking model. The model parameters  $K$ ,  $C$ ,  $\theta$ ,  $L$  and  $R$  are the spring constant, damping constant, leg angle, compliant leg length and radius of the curved foot, respectively.  $K$  and  $C$  were optimization parameters and  $\theta$ ,  $L$  were obtained from the data, and  $R = 0.3$ .

## RESULTS AND DISCUSSION

Model simulations reproduced the trajectories of the GRFs with the goodness of fit ( $R^2 = 0.72 \pm 0.20$ ) for all subjects (Fig.2).

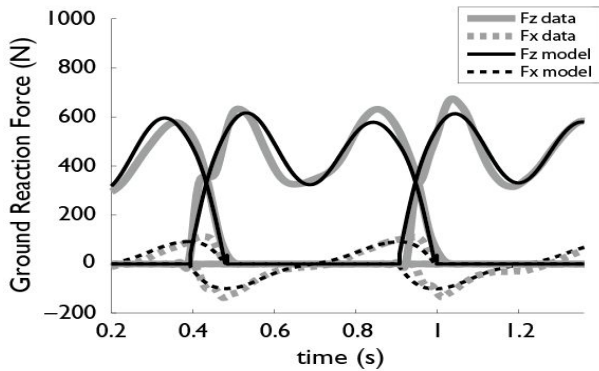


**Figure 2:** GRFs data (gray lines) and model simulation with optimized spring and damping constant (black lines).

The elderly walked in a velocity range between 1.10 m/s and 1.46 m/s, while the young walked between 0.98 m/s and 1.99 m/s. The leg stiffness and damping ratio of the young and the elderly significantly increased as a function of walking speed ( $p < 0.05$ ) (Fig.3), implying gait speed is correlated with leg stiffness as reported previously [2]. The linear regression equations of the normalized stiffness with respect to walking speed in the young and the elderly were  $y = 30.16 * x + 14.93$  and  $y = 32.33 * x + 17.00$ , respectively, showing no significant difference between the two groups. This suggests that the leg stiffness may contribute to determine gait dynamics characteristics, such as gait speed. The damping ratios were very small ( $< 0.08$ ), but necessary to simulate repeated steps robustly that reproduced the human data with various initial conditions.

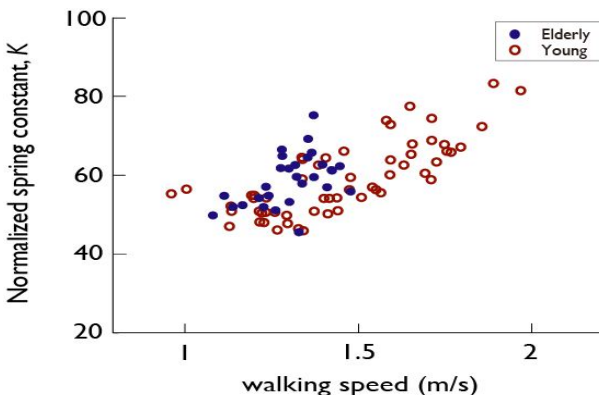


**Figure 3:** Leg stiffness as a function of walking speed for all subjects. Leg stiffness was normalized by the subject's weight divided by height.

Although the average speed of the elderly was slower than that of the young, both groups showed similar leg stiffness at the same walking speed, implying correlation between leg stiffness and walking speed hold similarly for both groups. Leg stiffness could be physiologically achieved by muscle force at each joint. Therefore, slower walking speed of the elderly might be due to the limited increase of leg stiffness by reduced muscle strength with aging.

In conclusion, a damped compliant walking model could explain the human gait dynamics and reproduce one-step gait cycle successfully. Suggested model could quantify gait mechanism in terms of leg stiffness. Increase of leg stiffness with gait speed observed for the elderly similar to those of young implies that there may exist apparent optimal stiffness that minimizes energy expenditure during gait cycle [2].

## REFERENCES

- 1.H.Geyer et al., *Proceedings of the Royal Society B: Biological Sciences*, **273**(1603):2861-2867.
- 2.S.Kim and S. Park, *Journal of Biomechanics*, doi:10.1016/j.jbiomech.2011.02.072, 2011
- 3.J.R. Rebula et al., *Dynamic walking 4<sup>th</sup> Annual Meeting*, 2009
- 4.J.Yeom and S. Park, *Journal of Biomechanics*, 44:59-67, 2011
- 5.S.A.Gard et al., *Human Movement Science*, **22**(2004) 597-610

## ACKNOWLEDGEMENTS

This research was supported by the Happy tech. program through the National Research Foundation of Korea (NRF) funded by the Ministry of Education, Science and Technology (#2010-0020488). The authors thank Heewon Park, Jin Yeom and Juhyung Kim for their contributions to data collection.

# A FINITE ELEMENT ANALYSIS OF THE MOMENT ARM HYPOTHESIS FOR MODULATING ULTIMATE VERTEBRAL SHEAR FAILURE TOLERANCE

Samuel J. Howarth<sup>1,2</sup>, Thomas Karakolis<sup>1</sup>, Jack P. Callaghan<sup>1</sup>

<sup>1</sup>Department of Kinesiology, University of Waterloo, Waterloo, ON, Canada

<sup>2</sup>Rochon Engineering Inc., Bolton, ON, Canada

email: [showarth@rochons.ca](mailto:showarth@rochons.ca)

## INTRODUCTION

Vertebral shear loading during *in vitro* protocols most often leads to failure of the pars interarticularis [1,2]. During shear, a bending moment is generated, that is linked to failure, about the pars by contact between the facets of an inferior and superior vertebra comprising an intervertebral joint[3]. Shear failure tolerance of porcine cervical functional spinal units (FSUs) has been shown to change with applied compressive load and posture [2]. In particular, shear failure tolerance decreased with flexion and increased with extension and compressive force [2]. Based on these findings, and the suggested failure mechanism, it was hypothesized that changes in measured ultimate shear failure tolerance were a direct result of alterations in the moment arm length (MAL) between the centroid of facet contact force and the pars interarticularis failure location. A finite element (FE) model of the porcine C3/C4 FSU was used in this investigation to objectively evaluate the moment arm hypothesis for modulation of measured shear failure tolerances.

## METHODS

Point clouds representing the C3 and C4 vertebral surfaces were obtained using a pair of white light scanners (StarCam FW-3R 3D, VX Technologies Inc, Calgary, AB). A watertight surface was created for each vertebra from the respective point clouds (Geomagic Studio 9, Geomagic, Research Triangle Park, NC). Geometry for the intervertebral disc was generated by interpolating between the surfaces that represented the C3 inferior endplate and the C4 superior endplate.

Vertebra and disc meshes were created using a commercial software package (Hypermesh 10, Altair Engineering, Troy, MI). All materials were considered to have been linear and isotropic. Tetrahedral elements were used to model vertebral trabecular bone ( $E = 229 \text{ MPa}$ ,  $\nu = 0.3$ ). Cortical bone was modeled using triangular shell elements

( $E = 19.4 \text{ GPa}$ ,  $\nu = 0.34$ ) with a constant 0.45 mm thickness. The disc and endplates respectively consisted of hexahedral elements ( $E = 20 \text{ MPa}$ ,  $\nu = 0.49$ ) and quadrilateral shell elements ( $E = 50 \text{ MPa}$ ,  $\nu = 0.3$ ) with a constant thickness of 0.45 mm.

A total of 15 individual simulations were performed, using ABAQUS (ABAQUS CAE 6.9, SIMULIA, Providence, RI). Five different constant compressive forces (0%, 15%, 30%, 45%, or 60%) in combination with three postural positions (extended, neutral, or flexed) comprised the 15 simulations. The absolute compressive load magnitudes were 0, 813.2, 1626.4, 2439.6, and 3252.8 N respectively. The angles of flexion and extension respectively were -5.67 and 3.15 degrees. Boundary conditions assigned to each vertebra in each simulation were representative of boundary conditions that were applied during similar *in vitro* testing [2]. The C4 vertebra was displaced backwards by 3 mm at a constant rate of 0.15 mm/s while the C3 vertebra was held in place for each simulation. Interaction between cortical shell elements for the C3 inferior and C4 superior facets was modeled with frictionless and non-linear surface to node contact.

Stress, strain, and facet contact force profiles were determined throughout the entire 3 mm shear displacement phase for each simulation. The cortical shell element within the C3 pars interarticularis with the highest maximum in-plane principal stress was considered to be the location for initiation of failure. This was verified against fracture patterns from similar *in vitro* testing [2]. The centroid of facet contact force was also calculated for both the left and right inferior C3 facets. Moment arm lengths were calculated between the location of peak stress and the centroid of facet contact force for C3.

## RESULTS AND DISCUSSION

Extension shifted the facet contact centroid superiorly towards the C3 pars interarticularis on

average by 0.55 mm while flexion caused the centroid of facet contact to move inferiorly towards the C3 inferior facet tip by an average of 0.76 mm (Table 1). Each 15% increment in compressive force produced an average 0.18 mm superior migration for the centroid of facet contact force (Table 1). This pattern of changes in facet contact location is similar to previously published data using pressure sensitive film [4].

After 3 mm of shear displacement, extended postures produced a 4.8% decrease in MAL while flexed postures produced a 6.0% increase in MAL (Figure 1). Compressive force also decreased the MAL with the maximum decrement being 2.6% with the 60% compressive load.

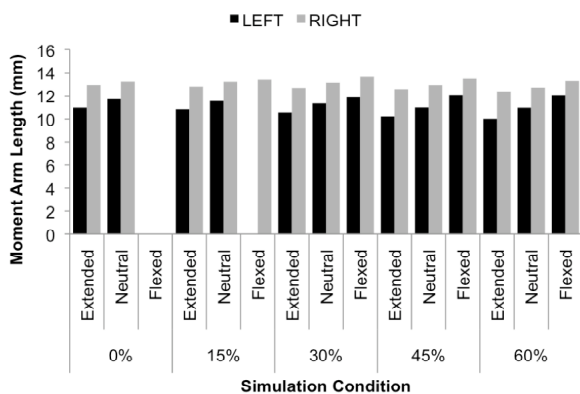


**Figure 1:** Moment arm length at the end of each simulation. The MAL is missing for the flexed posture with 0% compression since the facets did not come into contact during this condition.

Changes in MAL with varying compressive load and postural deviation were able to explain 70% of the variance in measured ultimate shear failure tolerance from comparable *in vitro* failure testing. The demonstrated relationship (Figure 2) indicates that larger MALs are associated with decreasing measured ultimate shear failure tolerances. This finding corresponds with the bending moment mechanism of pars interarticularis failure during shear loading.

**Table 1:** Vertical changes in the centroid of facet contact force relative to the 0% compression and neutral posture simulation. Positive and negative values respectively represent superior and inferior migrations for the centroid of facet contact. All values are reported in millimeters.

|              | 0%   |      |      | 15%  |       |       | 30%  |       |       | 45%  |      |       | 60%  |      |       |
|--------------|------|------|------|------|-------|-------|------|-------|-------|------|------|-------|------|------|-------|
|              | Ext  | Neut | Flex | Ext  | Neut  | Flex  | Ext  | Neut  | Flex  | Ext  | Neut | Flex  | Ext  | Neut | Flex  |
| <b>Left</b>  | 0.76 | 0    |      | 1.02 | 0.38  |       | 1.31 | 0.68  | -0.23 | 1.80 | 1.03 | -0.19 | 2.12 | 1.18 | 0.01  |
| <b>Right</b> | 0.37 | 0    |      | 0.38 | -0.02 | -0.76 | 0.42 | -0.02 | -0.54 | 0.39 | 0.03 | -0.51 | 0.49 | 0.24 | -0.37 |

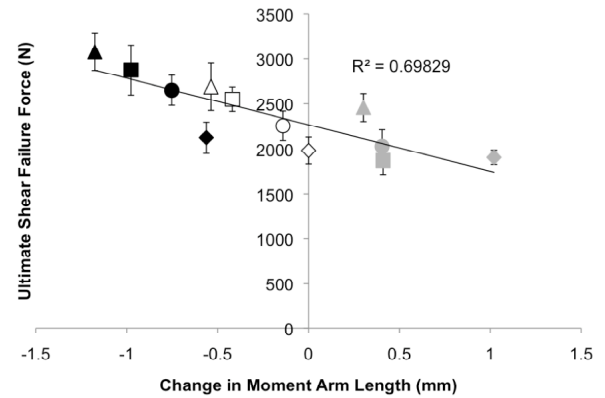


**Figure 2:** Relationship between modeled MAL changes with measured *in vitro* shear failure forces.

## CONCLUSIONS

Current occupational guidelines for low-back shear load exposure, based on *in vitro* shear failure tolerances [5], do not consider the influence of flexed or extended postures, and/or compressive load magnitude. *In vitro* testing [2], and this investigation indicate that compressive load and posture are necessary considerations when assessing occupational low-back shear injury potential. Low-back shear injury potential is modulated with flexion/extension and compressive load through alterations in the MAL between the location of facet contact and pars interarticularis failure. These changes are produced by altered facet interaction caused by flexion/extension and compressive load.

## REFERENCES

1. Yingling VR and McGill SM. *Spine* **24**, 1882-1889, 1999.
2. Howarth SJ. *PhD Thesis*, University of Waterloo, 2011.
3. Cyron BM, et al. *J Bone Joint Surg Br* **58B**, 462-466, 1976.
4. Dunlop RB, et al., *J Bone Joint Surg Br* **66B**, 706-710.
5. McGill SM, et al. *Proc 30<sup>th</sup> Ann Hum Factors Assoc Canada*, Mississauga, 1998.

# AGE-RELATED CHANGES IN CONTROL OF CENTER OF MASS IN RESPONSE TO SUPPORT SURFACE PERTURBATIONS

<sup>1</sup>Wei-Li Hsu, <sup>2</sup>Li-Shan Chou, <sup>2\*</sup>Marjorie Woollacott

<sup>1</sup>National Taiwan University, Taipei, Taiwan

<sup>2</sup>University of Oregon, OA, USA

email: wlhsu@ntu.edu.tw

## INTRODUCTION

Falls represent a significant health risk in the elderly and often result in injuries which require medical attention. Most falls occur after loss of balance stability during daily life activities such as slipping. Motion of the whole body center of mass (CoM) has been shown to identify elderly people who are at risk of falling. To provide effective preventive strategies and interventions, we must understand the mechanisms and factors that to stabilize the CoM. Previous study showed that healthy young adults use multi-joint coordination to stabilize the CoM during both static [1] and dynamic standing activity [2]. The Uncontrolled Manifold (UCM) approach has been used in studying multi-joint coordination in recent motor control research [1,2]. The UCM approach can relate individual joint contributions to the control of CoM. The current study investigated whether healthy older adults use the similar multi-joint coordination control strategy to stabilize their CoM after receiving a balance perturbation.

## METHODS

### Subjects

Sixteen healthy young adults (YA group, mean age:  $26.1 \pm 4.5$  year) and 16 older adults (OA group, mean age:  $74.9 \pm 6.2$  year) participated this study.

### Tasks

Maintain upright posture in response to 15cm backward surface translations randomly applied at the speed 30, 40, 50, and 60 cm/s. Only the trials for 30cm/s perturbation were analyzed here because of a greater tendency to step or lift the heel off the ground for other speeds in OA group.

### Instrumentation

A 8-camera motion capture system was used to record the perturbation response at 120-Hz. The reflective markers placed on the right side of the

body and trunk. The recorded coordinates of each reflective marker were filtered in MATLAB (Mathworks, Version 7.0.1) using a 5-Hz low-pass, bi-directional 2nd order Butterworth digital filter.

### Data reduction

Sagittal plane joint angles: The marker positions were used to calculate the sagittal plane joint angles at the ankle, knee, and hip, between the 12<sup>th</sup> thoracic and 1<sup>st</sup> lumbar vertebrae (LTJ) and the 7<sup>th</sup> cervical and 1<sup>st</sup> thoracic vertebrae (CTJ).

Center of Mass (CoM) position: The segment length of each subject were measured for calculation of each subject's body CoM. Locations of segment CoM and mass proportions were estimated and used to compute the instantaneous position of the body's CoM (Winter 1990). The focus of this report is on control of the anterior-posterior (AP) position of the CoM because the perturbation direction were posteriorly.

Active response phase: Based on CoM trajectory, we defined *onset* as the time of CoM movement reached to 5% of the peak and defined the *offset* as 2 seconds after the onset time (see Fig1 dash line).

Motor Equivalence (ME) Index: The UCM analysis was performed on each trial as following.

- 1) Reference joint configuration (RJC): Computed mean joint configuration during the steady-state baseline period, i.e. over the 120 seconds before the perturbation onset.
- 2) Null-space of Jacobian matrix based on RJC: Derived Jacobian relates changes in CoM position to changes in joint position.
- 3) Joint Deviation Vector (JDV): Compute difference between current joint configuration at each point in the given trial and the RJC.
- 4) Project JDV into the null-space and into its orthogonal (range-space), and compute resultant length, normalizing each projection to the

appropriate DOF. Resulting measures are the lengths of projection of the JDV and categorized as two components:

(a) Motor equivalent (ME) response: Projection into the null-space, indicating the extent to which the difference between the current JC and the RJC, tending to take the CoM back to a pre-perturbation position corresponding to the RJC, i.e. the good coordination.

(b) Non-motor equivalent (NME) response: Projection into the orthogonal-space, indicating the extent to which the JDV tends to lead to a different CoM position, i.e. the bad coordination.

Then we computed the ME-index which is the ratio of the two components (i.e. ME/NME).

## RESULTS AND DISCUSSION

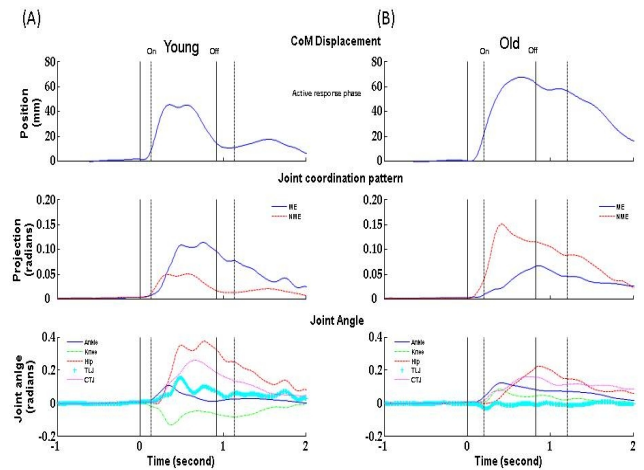
### Joint and center of mass excursion

Most of the joint excursion during the active response phase was not significantly different between YA group and OA group. Only the excursion of thoracic-lumbar junction (TLJ) was significantly lower in OA than those in YA ( $F_{(1,27)}=5.40$ ,  $p<0.05$ ). Although the total joint variance of the five measured joints and the center of mass excursion seems higher in OA than those in YA, this difference did not reach statistical significance.

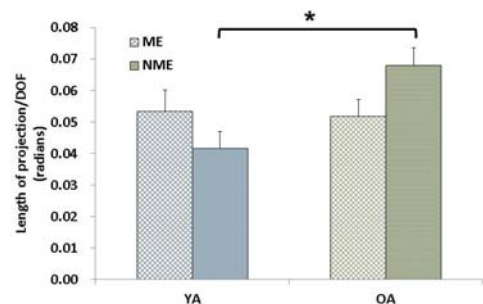
### Motor equivalence index

Fig. 1 shows example perturbation responses of two representative subjects in YA (Fig. 1A) and OA group (Fig. 1B), respectively. The YA had higher ME than NME during the active response phase whereas the OA had higher NME than ME (Fig. 1 middle panel). Moreover, the CoM trajectory returns to close to the pre-perturbation position after the active response phase for the YA while the OA's CoM trajectory did not return to the pre-perturbation state even after 2 seconds.

Fig. 2 presents the average of motor equivalence pattern (ME: good coordination) and non-equivalence pattern (NME: Bad coordination) across the active response phase. A repeated measures analysis of variance revealed a significant main effect on the variance by group ( $F_{(1,27)}=4.43$ ,  $p<0.05$ ). NME was significantly higher in OA than those in YA ( $p<0.01$ ) whereas ME was not significantly different between groups ( $p=0.89$ ).



**Figure 1:** Perturbation responses of one young adult and one older adult resulting from a 15cm support surface translation at 30 cm/s. Figures are the trajectory of CoM position (top), the projections of the joint deviation vector ME(blue line) vs. NME(red line) (middle), and the trajectory of 5 measured joints (bottom). The solid vertical lines indicate the onset/offset of the perturbation, while the vertical-dotted lines indicate the onset/offset of the active response phase.



**Figure 2:** Mean (+SD) of motor equivalent (ME) and non-motor equivalent (NME) pattern for young adults (YA) and older adults (OA).  $*p<0.05$

## CONCLUSIONS

Healthy older adults used a less flexible pattern (NME) compared to the healthy young adults when responded to a backward balance perturbation.

## REFERENCES

1. Hsu, W.L., et al., Control and estimation of posture during quiet stance depends on multijoint coordination. *J Neurophysiol*, 2007. 97: p. 3024-35.
2. Scholz, J., et al., Motor equivalent control of the center of mass in response to support surface perturbations. *Exp Brain Res*, 2007. 180: p. 163-179.

# REDUCED VISUAL INPUT AFFECTS GAIT CHARACTERISTICS DURING TREADMILL WALKING IN A VIRTUAL ENVIRONMENT

<sup>1,2</sup>Chun-Kai Huang, <sup>1,2</sup>Jung Hung Chien, <sup>1</sup>Srikant Vallabhajosula and <sup>1,2</sup>Ka-Chun Siu

<sup>1</sup>Nebraska Biomechanics Core Facility, University of Nebraska at Omaha, Omaha, NE, USA

<sup>2</sup>College of Public Health, University of Nebraska Medical Center, Omaha, NE, USA

email: [chuang@unomaha.edu](mailto:chuang@unomaha.edu) web: <http://nbcf.unomaha.edu/>

## INTRODUCTION

Vision is one of the most important sensory systems in controlling locomotion [1]. Humans rely on visual information from the environment to mediate the foot-placement during walking [1,2]. It has been shown that temporal and spatial features of gait are altered by reducing visual input [3], resulting in an increase of falls. Furthermore, the reduction of lighting was recognized as a contributing factor in falls incidence [4]. However, no research has been conducted to examine the impact of the reduction of visual input on treadmill walking. This is of great interest in gait research since treadmill walking provides a means to study multiple continuous strides.

Another possible way to manipulate the effect of visual input on gait is through the usage of virtual reality (VR) environments [5]. However, the study of the interaction of reduced visual input and virtual reality is also limited in the literature. The aim of this study was to investigate the effect of reduction of visual input on treadmill walking and identify how such decreased visual input interacts with the effect of a simultaneous exposure to a VR environment. We hypothesized that the reduced visual input would change the gait characteristics depending upon the type of VR environment.

## METHODS

Ten healthy adults (mean age= 29.6±4.9 years; height= 174.14±12.45 cm; mass= 76.8±14.82 kg) walked on a treadmill (Bertec Corp. Columbus, OH) for a five-minute familiarization (Fig.1: left). Then they walked on the treadmill with their preferred walking speed for two minutes in four different conditions: 1. in a static VR (with a fixed virtual corridor image projected in front of subjects); 2. wearing a pair of goggles attached with two layers of window film, which reduced the amount of light

from 22 lx to 0.7 lx (Fig.1: right) and walking in the static VR; 3. in a dynamic VR (with a moving virtual corridor at a speed similar to subject's preferred walking speed; 4. wearing the same goggles and walking in the dynamic VR.



**Figure 1:** A subject walking on a treadmill with a safety harness while looking at a virtual corridor (left); a pair of goggles attached with double-layered window films (right).

Three-dimensional kinematics data were collected with an NDI motion capture system at 100 Hz (Northern Digital Inc, Waterloo, Canada). From the kinematics we calculated the average step length and step width. Step length was defined as the distance between two consecutive steps of the heel; step width was defined as the distance between lateral sides of both feet (under the lateral malleolus). In addition, the variability (coefficient of variance, CV) of both step length and step width was evaluated.

A two-way fully repeated measure ANOVA on the VR (static and dynamic conditions) and the visual input (full and dim light environments) as the two within-subject factors was used for all gait characteristics. A multiple comparison test with Bonferroni correction was performed if a significant interaction existed. The significance level was set at 0.05.

## RESULTS AND DISCUSSION

Significant main effect of visual input revealed that the step length was significantly decreased with reduced visual input condition ( $p < 0.001$ ). Significant interactions between VR and visual input conditions were found for both the step length ( $p = 0.037$ , Fig. 2) and the step length variability ( $p = 0.025$ ). Follow-up comparisons indicated that step length was significantly decreased and the step length variability was significantly increased only in reduced visual input condition when dynamic VR was presented in front of the subject (Table 1).

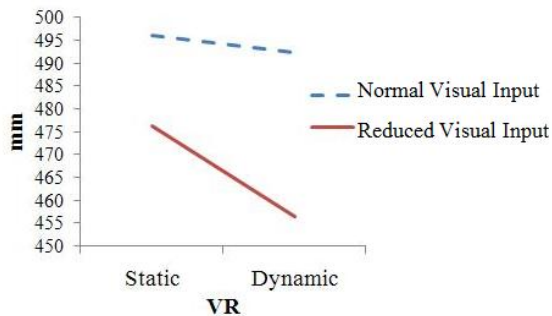


**Figure 2:** The interaction between VR and visual input conditions for the step length.

These results are in line with a previous study which suggested that a dynamic VR environment could induce instability in healthy young subjects, who reduced stride lengths and increased step width [6]. Although subjects increased their step width and step width variability in the reduced visual input condition in our study, no significant effect was found. It is possible that the change of VR was not as dramatic as in previous studies [6,7], since neither a turning nor an expanding VR corridor was presented in this study.

## CONCLUSIONS

The results support our hypothesis in terms of the altered step length but not step width in a dynamic VR environment. In addition, the results of this study suggest that the amount of visual input could influence control during treadmill walking. Such influence is more pronounced when the subject walks on a treadmill in a dynamic VR environment. Overall, the present study provides evidence that vision plays an essential role during not only level walking, but also treadmill walking.

## REFERENCES

1. Patla AE, et al. *Exp Brain Res* **128**, 441-450, 1999.
2. Gibson JJ. *The Ecological Approach to Visual Perception*, Houghton Mifflin, 1979.
3. Torres-Oviedo G, et al. *J Neurosci* **30**, 17015-17022, 2000.
4. Helbostad JL, et al. *Gait Posture* **30**, 233-238, 2009.
5. Adamovich SV, et al. *NeuroRehabilitation* **25**, 29-44, 2009.
6. Hollman JH, et al. *Gait & Posture* **23**, 441-4, 2006.
7. Siu KC, et al. *Program of Neuroscience Meeting Planner*, San Diego, CA, 2010.
8. Dean JC. et al. *IEEE Trans Biomed Eng* **54**, 1919-1926, 2007.

## ACKNOWLEDGEMENTS

This research is supported by the Nebraska Research Initiative and a Graduate Fellowship from the College of Public Health of the University of Nebraska Medical Center.

**Table 1:** Mean $\pm$ SD of gait characteristics in the four conditions.

|            |     | Normal Visual Input              | Reduced Visual Input |
|------------|-----|----------------------------------|----------------------|
| Static VR  | SL  | 496.03 $\pm$ 99.01 <sup>†</sup>  | 476.13 $\pm$ 96.85   |
|            | SLV | 0.02 <sup>*</sup>                | 0.03                 |
| Dynamic VR | SL  | 492.31 $\pm$ 100.09 <sup>†</sup> | 456.39 $\pm$ 86.10   |
|            | SLV | 0.03 <sup>*</sup>                | 0.04                 |

Note: SL: Average step length (mm); SLV: Step length variability; VR: virtual reality;

<sup>†</sup>Significant interaction between visual input and VR on the SL ( $p = 0.037$ );

<sup>\*</sup>Significant interaction between visual input and VR on the SLV ( $p = 0.025$ ).

# MOTOR LEARNING REDUCES METABOLIC COST OF ARM REACHING

<sup>1</sup>Helen J. Huang, <sup>1</sup>Rodger Kram and <sup>1</sup>Alaa Ahmed

<sup>1</sup>University of Colorado, Boulder, CO, USA

email: [helen.huang@colorado.edu](mailto:helen.huang@colorado.edu) web: [http://spot.colorado.edu/~alaa/neuro\\_lab/](http://spot.colorado.edu/~alaa/neuro_lab/)

## INTRODUCTION

The central nervous system is thought to optimize movement performance while minimizing energetic cost. Accordingly, most computational motor control models include minimization of energetic cost in the cost function [1]. While numerous examples of metabolic optimization exist for locomotion [2], only indirect evidence (force, electromyography) of energetic optimization exists for movements such as arm reaching or during motor learning [3]. Previous studies have shown that subjects initially compensate for novel dynamics with metabolically costly muscle co-activation [3]. Co-activation then decreased as an internal model of the task dynamics was developed.

Here, we directly measured metabolic expenditure of subjects learning novel arm reaching dynamics. We hypothesized that 1) metabolic cost would decrease as novel arm reaching tasks are learned and 2) that the reduction of metabolic cost would parallel a reduction in muscle co-activation.

## METHODS

We measured the metabolic rates of 11 subjects using expired gas analysis (Parvomedics) as they performed goal-directed reaching movements using a robotic manipulandum (Interactive Motion Technologies, Shoulder-Elbow Planar Robot). Seated subjects controlled the robot handle to move a cursor from a start circle to a target circle, 20 cm away. On the subsequent trial, the target and home circles switched positions, such that trials alternated between outward and inward movements. The cursor, start, and target circles were displayed on a LCD monitor positioned at eye-level. Visual feedback encouraged subjects to complete movements within 300-600 ms. An auditory metronome helped enforce a constant trial frequency of 0.5 Hz. The experiment began with 10

minutes of quiet sitting to establish a baseline resting metabolic rate. Each subject then performed 200 null trials (no forces, Null 1) and 250 force trials (Force 1). During the force trials, the robot applied a force perpendicular and proportional to the hand velocity, creating a viscous curl field. After a brief rest, subjects completed another 250 force trials (Force 2) and 200 washout null trials (Null 2). Also, one in five trials was catch trial, during which the robot applied a force channel, simulating stiff walls along the straight path between the start and target circles. This allowed us to measure the anticipatory force subjects applied to counter the force field. To calculate the net metabolic rate for the arm movements themselves, we subtracted out the resting metabolic rate and then averaged the net metabolic rate of the last 2 minutes of each phase of trials.

We also collected electromyography (EMG) data (Delsys Trigno) in four subjects from three upper limb muscle pairs: 1) pectoralis major and posterior deltoid (Pec:PD), 2) biceps brachii and triceps long head (BI:TRlg), and 3) brachioradialis and triceps lateral head (BR:TRlat). We identified the minimum normalized EMG (% maximum voluntary contraction, MVC) value within each muscle pair at each time point to generate a co-activation profile curve for each trial. We then calculated the mean co-activation for each muscle pair and trial.

## RESULTS AND DISCUSSION

Subjects exhibited significant learning of the force field (**Fig. 1**). Movement error, the perpendicular deviation of the hand from the straight line path to the target, was  $1.21 \pm 0.25$  cm at late Null 1 (last ten trials). For the first trial in Force 1, movement error increased to  $9.57 \pm 2.0$  cm and decreased significantly to  $1.78 \pm 0.33$  cm at late Force 1 and  $1.34 \pm 0.37$  cm at late Force 2 ( $p$ 's < 0.0001) (**Fig. 1**). The peak applied force during a catch trial

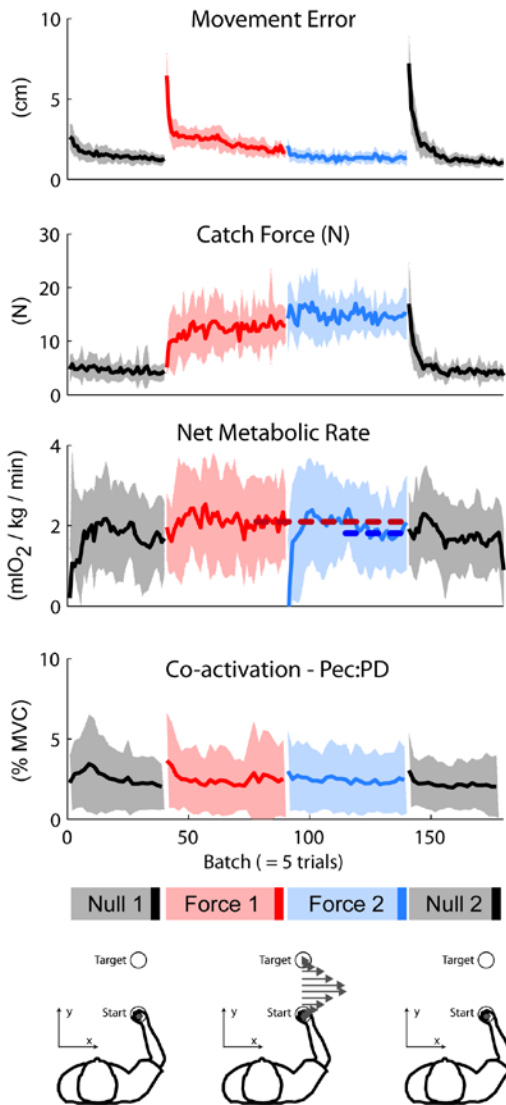


**Fig. 1** Changes in movement error, catch force, net metabolic rate, and co-activation of the pectoralis major and posterior deltoid pair by batch, i.e. the mean of 5 trials (group mean  $\pm$  SD). Note the dashed horizontal lines in the net metabolic rate figure, which highlights the reduction of metabolic cost. Dark bars at the end of each phase indicate “late” in the phase. Co-activation of the BI:TRlg & BR:TRlat muscle pairs were similar to the Pec:PD pair.

increased significantly from the first Force 1 catch trial,  $5.11 \pm 1.3$  N to  $12.9 \pm 3.0$  N at late Force 1 and  $15.11 \pm 3.9$  N at late Force 2 ( $p$ 's  $< 0.0001$ ) (**Fig. 1**). This indicates that subjects developed an internal model of the task dynamics.

The average resting metabolic rate was  $3.78 \pm 0.55$  mlO<sub>2</sub>/kg/min. Net metabolic rate was greatest during Force 1,  $1.64 \pm 0.64$  mlO<sub>2</sub>/kg/min and decreased significantly to  $1.37 \pm 0.58$  by the end of Force 2 ( $p = 0.005$ ), a 16% decrease, i.e.  $1.64/1.37$  (**Fig. 2**).

Muscle co-activation was initially elevated early in Force 1 and rapidly decreased within Force 1 as subjects learned the task dynamics (**Fig. 1**). Further reductions of co-activation were relatively small,  $<1\%$  MVC, from  $2.63 \pm 1.22$  %MVC at late Force 1 to  $2.36 \pm 1.05$  %MVC at late Force 2 for the Pec:PD muscle pair. This suggests that muscle co-activation was unlikely to be the primary mechanism that underlies the decreased metabolic cost observed during late Force 2.

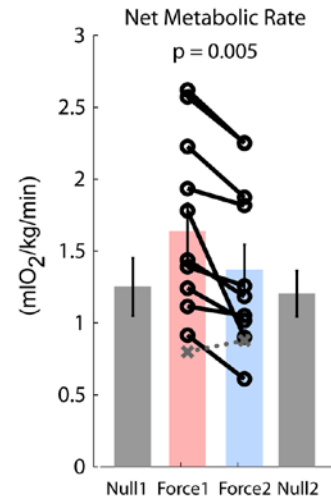


**Fig. 2** Net metabolic rate late in each phase of trials (group mean  $\pm$  SE). Black open circles linked with solid lines are individual subjects who reduced metabolic cost; grey x's linked with dotted lines are individual subjects who did not. P-value is a planned comparison t-test between late Force 1 and late Force 2.

## CONCLUSIONS

These results provide the first evidence that humans reduce metabolic cost when learning novel movement tasks. Further, our data suggest that improved movement efficiency reflected in a reduction of metabolic rate does not necessarily correspond with decreased muscle co-activation and/or decreased force production.

## REFERENCES

1. Todorov, Jordan, *Nature Neurosci*, **5**, 1226-1235, 2002.
2. Alexander, *Physiol. Rev.*, **69**, 1199-1227, 1989.
3. Franklin et al., *J Neurophys*, **92**, 3097-105, 2004.

## ACKNOWLEDGEMENTS

Supported in part by NIH T32 5AG000279. Thanks to Bianca Bzdel and Andrew Kary for help with data collections.

# Influence of a Compliant Artificial Ankle on Mechanics and Energetics of Human Walking

Tzu-wei Huang, Peter G. Adamczyk, Karl E. Zelik and Arthur D. Kuo

Department of Mechanical Engineering, University of Michigan, Ann Arbor, MI, USA

## INTRODUCTION

Elasticity is a feature of the normal Achilles tendon, as well as many prosthetic feet for lower limb amputees. Passive energy storage and return appears to contribute to ankle push-off, but it is unclear why this might be beneficial, as it provides no net energy input. We hypothesize that elasticity-enhanced push-off may lead to a reduced collision of the leading leg with ground, which is largely dissipative. The reduced dissipation might thus explain an energetic benefit from a passive mechanism. This suggests that the stiffness of a passive element at the ankle should influence push-off from that leg and the collision of the other leg. These effects may have consequences for metabolic energy expenditure and may make a particular stiffness optimal. We therefore performed a parametric study of the effect of stiffness in an artificial ankle on walking in normal human subjects.

We studied the effect of stiffness on walking mechanics and metabolic cost. A previous study suggested that trailing leg push-off can reduce the leading leg collision for economical walking [1]. If an elastic ankle contributes to push-off, increasing stiffness should allow for reduced collisions, although too high of a stiffness may be disadvantageous because of an induced hyperextension moment at the knee. We have previously found that long artificial feet induced such a moment, which appeared to contribute to energetic cost. We therefore tested for an optimal stiffness, with increasing stiffness contributing to increasing push-off, but with an energetic trade-off for very high stiffnesses.

## METHODS

Ten intact subjects walked with custom artificial feet with adjustable stiffness, worn bilaterally on prosthesis simulator boots to fixate the intact ankle (Fig. 1). Ankle stiffness was simulated with cantilevered forefoot beams or keels, with four

stiffnesses tested (6.6 - 58.3 kN/m, measured as vertical stiffness at the cantilever tip). Subjects walked on an instrumented treadmill at 1.25 m/s, while ground reaction force (GRF), marker-based motion capture, and oxygen consumption data were collected (Oxycon Mobile, VIASYS). There were 29 markers to track lower limb motion, plus four more markers on each artificial foot to capture the deformation. Powers and other measures were non-dimensionalized using body mass, leg length, and gravitational acceleration as base units.

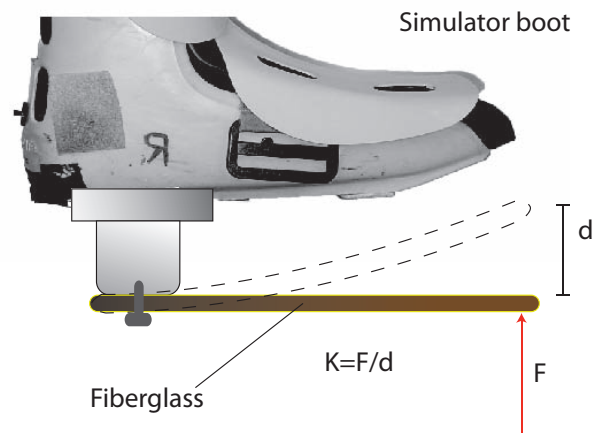


**Figure 1:** Prosthesis simulator boot

The main outcome measures were metabolic power, work performed on the center of mass (termed COM work) through each leg, and instantaneous knee power and artificial foot power. The COM work rate [2] was defined as the dot product of each leg's GRF with velocity of the COM, and was treated in four alternating phases of negative and positive work during stance: Collision, Rebound, Preload and Push-off. We expected push-off to increase with artificial foot stiffness (to a limit), and collision to decrease. We expected there to be an optimum in metabolic rate for a particular value of stiffness, with roughly quadratically increasing cost about the optimum.

## RESULTS AND DISCUSSION

The metabolic power was fit with a significant quadratic trend as a function of stiffness

( $R^2=0.5047$ ,  $p < 0.001$ ). The minimum power was achieved at a stiffness of about 61.7 (dimensionless). This suggests that there exists an optimal stiffness for minimum energy cost.

**Table 1: Sensitivity of COM work to foot stiffness Phases: Collision Rebound Preload Push-off**

| Phase   | Collision | Rebound | Preload | Push-off |
|---------|-----------|---------|---------|----------|
| Slope   | -0.1311   | -0.148  | 0.09    | 0.071    |
| p-value | <0.001    | <0.001  | <0.001  | 0.003    |

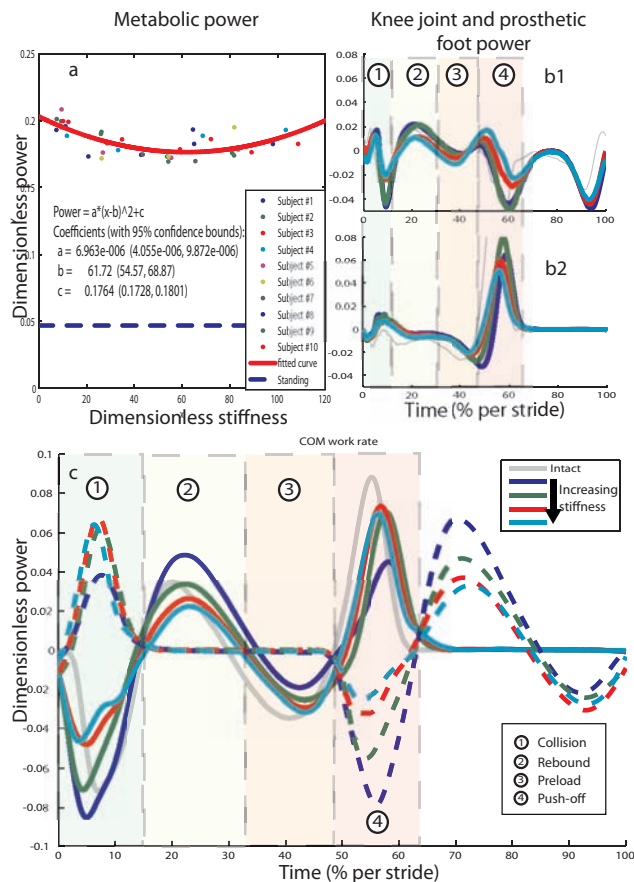


**Figure 2:** (a) Metabolic power versus stiffness, with quadratic fit ( $N = 10$ ). (b.1) Knee joint power. (b.2) Prosthetic foot power. (c) COM work rate vs time (solid lines for right leg, dashed lines for left leg).

The COM work rate changed as a function of stiffness. A linear regression of work per phase vs. stiffness yielded significant slopes for all four phases (Table 1). There was generally increasing push-off with increasing stiffness (possibly with a plateau, see Fig. 2). Collision also decreased with

increasing stiffness, as expected. The Rebound appeared to increase with Collision. Preload tended to increase with stiffness, but greater energy storage did not necessarily result in more push-off, which appeared to vary less at higher stiffnesses.

Ideally, more energy stored in Preload would produce more push-off work, thus reducing collision work. But the return of Preload energy may have been limited by the knee, which must resist a large hyperextension moment with higher stiffnesses. It appears that subjects compensated for that moment by actively producing more knee flexion torque during Preload. This may then have caused the knee to absorb more energy during Push-off instead of allowing Push-off to reduce Collision.

A limitation of the study was that with all of the stiffness conditions, Push-off occurred later than during normal walking. This may have been due to the apparatus design, or perhaps to the fact that no active ankle work could be performed. The late Push-off may have had less result on the simultaneous Collision than might normally occur. Nevertheless, it does appear that stiffness affects Push-off and Collision.

## Conclusion

Metabolic power changed as a function of stiffness, with an intermediate stiffness yielding minimum energy expenditure. Passive stiffness of the ankle or a prosthetic foot appears to affect the mechanics and energetics of walking. The higher peak in Push-off appears to lead to a reduced Collision, thereby reducing the work of walking. A parametric dependence on stiffness might be useful for the design of prosthetic feet with compliant forefoot keels.

## REFERENCES

1. Kuo, A. D. J. *Biomech. Engng*, 124: 113-120, 2002.
2. J. M. Donelan et al. *J. of Experimental Biology*, 205: 3717-3727, 2002.

# Variability measures of trunk and pelvis acceleration during walking and quiet stance are related in patients with multiple sclerosis and in healthy controls

<sup>1</sup>Jessie M. Huisinga, <sup>1</sup>Rebecca J. St. George and <sup>1</sup>Fay B. Horak

<sup>1</sup>Balance Disorder Laboratory, Oregon Health and Science University,  
Beaverton, OR, USA  
email: huisinga@ohsu.edu

## INTRODUCTION

Postural control is essential for any movement task, but postural control strategies during one task in a specific environment may not generalize to another task or situation [1]. Thus, it is difficult to identify common postural control mechanisms across tasks. Control of balance during walking and during quiet standing likely involve both overlapping and independent control systems since walking differs from standing in that the center of mass is constantly moving beyond the base of support [2]. A set of common measures which can be used in gait and in balance tasks to classify postural control across tasks would allow for a better understanding of how postural control is regulated according to task conditions. Thus, the purpose of this study was to apply the same set of variables to measure postural control during steady state walking and during quiet stance. We used body-worn inertial sensors, which could be used in a clinic setting, to identify acceleration measures that reflecting postural control. Both healthy controls and persons with multiple sclerosis (MS) were examined to identify whether the measures are robust enough to identify differences in postural control between controls and very mildly-affected MS subjects. It was hypothesized that variability of the acceleration patterns of the pelvis and the trunk would be related between walking and standing tasks and that there would be differences in variability of acceleration between groups.

## METHODS

Six patients with MS ( $35.8 \pm 8.1$  yrs; 25 foot walk < 5 sec) and 6 healthy, age-matched controls ( $35.0 \pm 7.9$  yrs) performed a walking and a quiet standing task. The walking task consisted of walking up and down a 50-meter hallway at self-selected speed continuously for two minutes. Data was analyzed only for the first 30 seconds of steady-state walking. For the quiet standing task, participants stood quietly, with eyes open for 30 seconds. During both

tasks, the subjects wore 6 MTX Xsens sensors (49A33G15, Xsens, Enschede, NL, USA) sampling at 50 Hz. The sensors contained 3D accelerometers ( $\pm 1.7$  g) and 3D gyroscopes ( $\pm 300^\circ/\text{s}$  range) mounted on: (i) sternum, (ii) sacrum (L5 level), (iii) right and left wrist, (iv) right and left lower leg (Figure 1). Only accelerometer data from the sternum and sacrum were analyzed here. For both tasks, the same variables were



Figure 1: Subject wearing six sensors.

analyzed: range, standard deviation (SD), root mean square (RMS), Lyapunov exponent (LyE), and approximate entropy (ApEn). A 2x2 ANOVA was performed to compare Group (MS v. control) and Sensor location (sacrum v. sternum) effects. Correlations were performed to identify any relationship between variables across the two tasks.

## RESULTS

There were significant correlations between walking and standing M/L acceleration range ( $p=0.001$ ) and SD ( $p=0.036$ ). No other variables were correlated between tasks.

### *A/P direction walking*

Acceleration in the A/P direction showed a significant effect ( $p<0.001$ ) of Sensor location on range, SD, and RMS in which the sacrum sensor values were higher than at the sternum. Also in the A/P direction, there was a significant Group x Sensor interaction for SD ( $p=0.017$ ) and RMS ( $p=0.019$ ) in which the sacrum values were lower in the MS group but there was no difference between groups at the sternum. LyE ( $p=0.000$ ) and ApEn ( $p=0.001$ ) in the A/P direction showed a significant effect of Sensor location in which values were higher at the sternum compared to the sacrum, with no Group by Sensor interaction.

### *M/L direction walking*

Acceleration in the M/L directions showed a significant effect ( $p < 0.01$ ) of Sensor location on range, SD, and RMS in which the sacrum sensor values were higher than the sternum. There was also a significant effect of Sensor location on ApEn in the M/L direction ( $p = 0.001$ ) in which the ApEn value was higher at the sacrum compared to the sternum.

### *Vertical direction walking*

Acceleration in the vertical direction also showed a significant effect of Sensor location for LyE ( $p = 0.019$ ) and ApEn ( $p = 0.000$ ) in which the LyE and ApEn values were higher at the sacrum than at the sternum in both groups. There was also a significant Group x Sensor interaction for LyE ( $p = 0.006$ ) and ApEn ( $p = 0.026$ ) in which the difference between sternum and sacrum values was smaller in the MS group.

### *A/P direction standing*

There was a significant effect ( $p < 0.01$ ) of Sensor location on A/P range, SD, and RMS in which sacrum values were lower than sternum values. LyE of acceleration in the A/P direction showed a significant effect of Sensor location ( $p = 0.037$ ) and a Group x Sensor interaction ( $p = 0.042$ ) in which the LyE value was the same for both sensors in the control group but LyE at the sacrum was lower compared to the sternum in the MS group. There was a significant ( $p = 0.030$ ) effect of Sensor location on ApEn in the A/P direction where the ApEn value was lower at the sacrum compared to the sternum.

### *M/L direction standing*

There was a significant effect ( $p < 0.01$ ) of Sensor location on M/L SD and RMS in which sacrum values were lower than sternum values. There was also a significant effect of Sensor location on LyE ( $p = 0.017$ ) and ApEn ( $p = 0.041$ ) in the M/L direction in which LyE and ApEn values were higher at the sacrum than the sternum in both group.

### *Vertical direction standing*

There was a significant effect ( $p = 0.027$ ) of Sensor on ApEn in the vertical direction where the ApEn value at the sacrum was higher than the sternum.

## **DISCUSSION & CONCLUSIONS**

Lack of differences in variability of trunk accelerations during walking and standing between groups may be due to the very mild gait and balance problems in the MS group. However, the Group x Sensor interaction in the A/P direction during walking for SD and RMS and the interaction in the A/P direction during standing for LyE suggest a difference in trunk control between MS and control subjects.

The Sensor location effects are likely due to the attenuation of accelerations from the pelvis to more proximal segments during gait and stance [3]. This is specifically illustrated by the decrease in the range, SD, and RMS value of the A/P and M/L acceleration components while the vertical acceleration displays negligible variations. Also, differences in LyE and ApEn between the sacrum and sternum during walking and standing could be due to this distal to proximal attenuation of the acceleration signal.

The significant correlations between walking and quiet standing for both acceleration range and SD in the ML direction is consistent with common neural control of M/L body center of mass stability across tasks [4]. Excessive M/L trunk motion during walking has been associated with falls [5]. Larger trunk acceleration range during walking and standing, which can be easily measured with a single accelerometer instead of a complex kinematic laboratory, may be valuable for identifying subjects in a clinical environment who are at risk for falls such as persons with neurological disorders or elderly individuals.

## **REFERENCES**

1. Moe-Nilssen & Helbostad (2002) *Gait Posture*, 16(1).
2. Winters (1991) *The Biomechanics & Motor Control of Human Gait: Normal, Elderly, Pathological*, 2<sup>nd</sup> ed.
3. Mazza et al. (2008) *Gait Posture*, 29(2).
4. Bauby & Kuo (2000) *J Biomech*, 33(11).
5. Maki (1997) *J Am Geriatr Soc*, 45(3).

## **ACKNOWLEDGEMENTS**

This work was supported by the National Multiple Sclerosis Society.

# EFFECTS OF GLOVE AND LADDER RUNG DESIGN ON PREVENTION OF LADDER FALL

Pilwon Hur, Binal Motawar, and Na Jin Seo

Industrial and Manufacturing Engineering, University of Wisconsin-Milwaukee, Milwaukee, WI  
 E-mail: hur@uwm.edu, seon@uwm.edu Web: www4.uwm.edu/ceas/faculty\_profiles/NaJinSeo.html

## INTRODUCTION

Falls from ladders are the leading cause of disabling falls to lower levels and the second leading cause of fatal falls to lower levels [1]. Hands are the only interface available to arrest the body once a fall has been initiated. Persons' physical capability to hold onto a ladder rung before the hand slips off the rung (i.e., breakaway strength) is not well understood. Conventional power grip strength is not an adequate measure of breakaway strength, since it considers only the finger flexion strength, not the frictional coupling between the hand and rung [2]. Improved understanding of the biomechanical coupling between the hand and rung is necessary to prevent falls from ladders and scaffolds.

Biomechanical models for breakaway strength for two representative rung cross-sections have been developed as shown in Fig. 1, based on our previous study [3]. The models assume that people apply the maximum possible shear force at each phalanx (= coefficient of friction, COF  $\times$  phalanx normal force). The models suggest that breakaway strength is affected by the COF between the hand and rung, phalanx force distribution, and rung geometry.

The present study was undertaken to evaluate these biomechanical models by examining the effects of the COF at the hand-rung interface and rung shape on persons' breakaway strength (Experiment 1). In addition, to validate the model assumption that phalanx shear force increases with increased COF, the ratio of shear to normal force was examined for different COF conditions (Experiment 2).

## METHODS

Thirteen right-handed healthy young adults (9 male and 4 female, age=25 $\pm$ 5yrs) participated in this study. Subjects used their non-dominant hand for testing, because people typically use the dominant

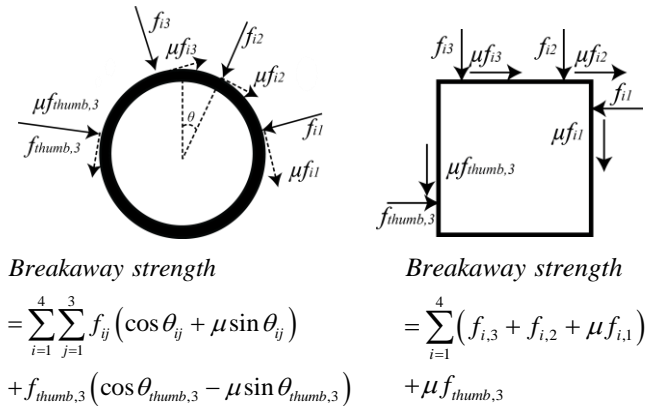


Fig. 1 Biomechanical models of breakaway strength for two rung shapes.  $f_{ij}$  is normal force for  $i$ -th finger and  $j$ -th phalanx,  $\mu$  is COF, and  $\theta_{ij}$  is the angle between a vertical line and  $f_{ij}$ . Shear force can be up to COF  $\times$   $f_{ij}$ . Proximal, middle, and distal phalanges are  $j=1, 2,$  and  $3,$  respectively.

hand for main tasks (e.g., painting, reaching for something) while holding onto a ladder with the non-dominant hand.

For Experiment 1, subjects were seated and strapped down to a fixed chair, with their arm raised to grasp an aluminum rung. They were instructed to hold onto the rung as long as they could, while the rung was raised up at 7 cm/s (Fig. 2). The rung was attached to a pulley whose chain was connected to a winch on one end (to raise the rung) and to a fixed load cell on the other end (to record hand force at 1 kHz). Breakaway strength was determined as the highest hand force recorded (typically occurred immediately before the subject lost the grip of the rung). Three COF conditions simulated by different gloves (COF of 0.33 for a polyester glove, 0.57 for the bare hand, and 1.11 for a latex glove against the aluminum rung) and two rung shapes (a circular cylinder with a radius of 25

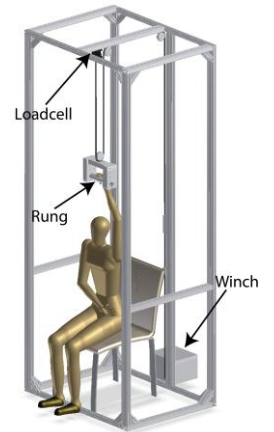


Fig. 2 Experimental setup

mm and a square bar with 38 mm×38 mm cross-section) were tested.

For Experiment 2, subjects performed an isometric pull exertion on a custom-made dynamometer mimicking the circular rung (Fig. 3) using the same posture and holding strategy as in Experiment 1 for 5 seconds, while normal and shear forces for each phalanx of a finger were recorded [4]. Testing was repeated for five fingers and three COF conditions in a randomized order. The ratio of shear force to normal force was computed for each phalanx, finger, and COF condition. Subjects were instructed to apply 50% of their perceived breakaway strength to reduce muscle fatigue and to allow accurate force recording for each phalanx without finger moving across the three measuring contact pads (Fig. 3).



Fig. 3 Custom-made circular dynamometer

For Experiment 1, repeated measures analysis of variance (ANOVA) was performed to determine the main and interaction effects of the COF and rung shape on breakaway strength. For Experiment 2, another repeated measures ANOVA was performed to determine whether the ratio of shear force to normal force significantly varied with COF, fingers and phalanx where fingers and phalanx were blocking factors. The level of significance was  $\alpha=.05$  for both tests (SPSS Inc., Chicago, IL; v17). *Post-hoc* tests were performed to evaluate differences among the three COF conditions.

## RESULTS

The breakaway strength significantly varied for COF, rung shape, and their interaction ( $p<.001$ , Fig. 4a). Increased COF was associated with increased breakaway strength (Fig. 4a). The circular rung resulted in, on average, 12% greater breakaway strength than the square rung (Fig. 4a). The ratio of phalanx shear to normal force significantly varied for COF ( $p=.01$ , Fig. 4b). The two high COF conditions (bare hand and latex) resulted in a significantly greater ratio than the lowest COF condition (polyester glove).

## DISCUSSION

The biomechanical models in Fig. 1 are generally supported by empirical results. Breakaway strength

increased with increased hand-rung COF, as can be predicted by the models (Fig. 1). The models also predict that breakaway strength can be, on average, 7% greater for the circular rung than for the square rung across the three COF conditions, using the phalanx normal forces from Experiment 2 and finger dimensions [5]. This prediction is also consistent with the empirical results (Fig. 4a).

Subjects modulated the phalanx shear to normal force ratio depending on the COF condition. An increased shear to normal force ratio with increased COF may indicate that subjects utilize frictional coupling within available COF to increase breakaway strength. The extent of increase in the ratio with increased COF was less than expected, possibly due to the Experiment 2 task of 50% isometric pull exertion rather than maximum. The greatest mean shear to normal force ratio for the bare hand followed by the latex glove may be related to the bare hand's being most sensitive in detecting COF and the latex glove having the thickest layer hindering detection of COF for submaximum pull [6].

Design of handles and rungs should account for the COF and shape to increase persons' breakaway strength. Optimal design may help prevent future falls from ladders/scaffolds and associated fatalities.

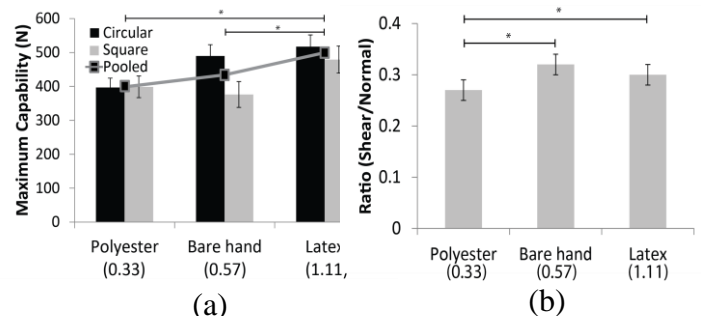


Fig. 4 (a) Breakaway strength for the three COF and rung shapes. (b) The mean ratio of shear to normal force on the phalanges during 50% pull (\* shows  $p<.05$ )

## REFERENCES

1. BLS, *Census of Fatal Occupational Injuries*, 2009
2. Young JG et al. *Human Factors* 51:5, 705-717, 2009
3. Seo NJ et al. *Ergonomics* 53:1, 92-101, 2010
4. Enders LR et al. *JBiomech*, In Press, 2011
5. Wickens CD et al, *Pearson Prentice Hall*, 2004
6. Kinoshita, *Ergonomics* 42:10, 1372-1385, 1999

## ACKNOWLEDGEMENTS

National Institute of Occupational Safety and Health, University of Illinois at Chicago

# BIOMECHANICAL EFFECTS OF INCOMPLETENESS AND SLACKNESS IN ANNULAR FIBERS ARE HIGHER IN THE TISSUES OF NUCLEUS THAN THAT OF ANNULUS: A FINITE ELEMENT MODEL INVESTIGATION

<sup>1</sup>Mozammil Hussain

<sup>1</sup>Logan University, Division of Research, Chesterfield, MO, USA  
email: [mozammil.hussain@logan.edu](mailto:mozammil.hussain@logan.edu)

## INTRODUCTION

Mechanical strength imparted by collagen fibers helps in appropriate functioning of inter-vertebral discs. By acting in tensile mode, these fibers not only aid the discs in transmitting the loads of daily activities from one motion segment to another, but they also contribute to the bulging mechanism of the discs. Biomechanical role played by annular fibers, therefore, is central to overall integrity of the discs.

It is to be noted that the biomechanics of the annular fibers is complex. A biomechanical study noted different class of fibers in the disc annulus, for example, fibers starting from one disc-endplate interface but not reaching to the opposite disc-endplate interface – incomplete annular fibers [1]. Degenerative discs have often been observed with fibers that are slack and loose; thereby affecting the tensile behavior of the fibers [2]. Despite biomechanical studies have reported the tensile behavior of fibers in the disc; it still is not clear how incomplete and lax classes of fibers affect the tissues in annulus fibrosus (AF) and nucleus pulposus (NP).

It would be difficult using *in vivo* and *in vitro* methods to investigate the biomechanical effects of only these classes of fibers on the disc biomechanics. Computational finite element (FE) technique allows such complex modeling by simulating changes only in the spinal structures of interest.

The objective of the current study is to understand the biomechanical effects of incompleteness or laxity in fibers on the tissue response of the annulus and nucleus.

## METHODS

To perform the analysis, an FE model of a C5-C6 disc segment was developed from the anthropometric literature data. This model was previously validated under axial forces [3]. The spinal structures included into the model were: cortical bone, cancellous bone, endplates, AF, NP, and six layers of complete length of collagen fibers. Embedded into AF tissue matrix and running between the superior and inferior disc-endplate interfaces, the fibers were arranged in a zigzag (X) fashion and oriented at an angle of  $\pm 70^\circ$  with respect to the horizontal plane. Two layers of fibers formed each of the outer, middle, and inner AF regions. Tissue material properties of the spinal structures were adopted from the literature.

In a step-by-step manner, morphology or material modifications in fibers were simulated in the outer (Model O), middle (Model M), inner (Model I), outer-middle (Model OM), and middle-inner (Model MI) AF regions. While the morphological modification in annular fibers included a reduction in fiber length (incompleteness), the modification with respect to the material property included a decrease in fiber elasticity (representing slackness and laxity). In a wedge (>) fashion and originating from superior or inferior disc-endplate interface up to mid disc-height, incomplete fibers ran only 50% of the length of complete fibers. By decreasing the fiber elasticity by 30%, slackness in fibers was formulated.

A pressure load was applied on the superior C5 surface of the FE models, equivalent to the upper body weight of the cervical spine – 50 N. The inferior C6 surface was constrained in three perpendicular directions. Using FE software ABAQUS (Dassault Systemes Simulia Corp, Providence, Richmond, USA), stress profiles in AF and NP tissues were investigated followed by stress changes in AF and NP through normalizing with

respect to the healthy AF and NP tissue stresses. Ratio of NP to AF stress changes was calculated.

## RESULTS AND DISCUSSION

For both incompleteness and laxity in annular fibers, a ratio value of greater than unity was found (Figure 1) that indicated the NP stress changes are higher than the AF stress changes. With fiber modifications (incompleteness, laxity), ratio of NP/AF stresses changes were: Model O (2.17, 1.24), Model M (1.68, 1.60), Model I (4.04, 2.46), Model OM (4.55, 2.72), and Model MI (3.25, 2.09). In addition, AF and NP tissues were more affected by incomplete fibers than lax ones. The results also indicate that incompleteness and laxity in more number of fiber layers leads to higher stress changes in AF and NP.

Over a period of time, such changes in fibers may lead to internal tissue failure stresses and strains which further results into rupturing and herniation of the disc. There may be a possible mechanism by which these classes of fibers contribute to the severity of degenerative spinal pathologies. Evidence from past research shows the presence of interrupted, altered, and incomplete collagen fibers in degenerated discs [1].

This model can be further used to explore the effects of degeneration in AF and NP on fiber mechanics or vice versa. Future *in vitro* experimental studies may add insights to this important biomechanical question.

## CONCLUSIONS

Ratio of NP/AF stress changes greater than unity indicates that first signs of degeneration begin in NP, following which load is transferred to the AF tissues. This confirms the clinical results that first signs of degenerative pathology are seen in NP.

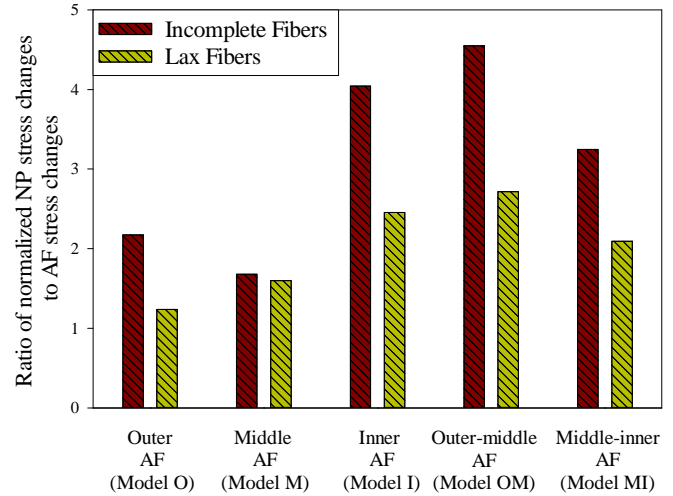


**Figure 1:** Ratio of normalized NP stress changes to AF stress changes for different modifications of fibers in various AF regions

## REFERENCES

1. Tsuji H, et al. *Spine* **18**, 204-210, 1993.
2. Schmidt H, et al. *Medical Engineering & Physics*, **31**, 642-649, 2009.
3. Hussain M, et al. *J Manipulative & Physiological Therapeutics* **33**, 252-260, 2010.

# MEASURING SUBJECT-SPECIFIC MUSCLE MODEL PARAMETERS OF THE FIRST DORSAL INTEROSSEOUS *IN VIVO*

<sup>1</sup>Benjamin W. Infantolino and <sup>2</sup>John H. Challis

<sup>1</sup>Penn State -Berks, Reading, PA, USA

<sup>2</sup>Penn State University, University Park, PA, USA  
email: bwi100@psu.edu

## INTRODUCTION

Many musculoskeletal models rely on cadaveric measurements for some or all of their parameters [1,2]. Many of the model parameters can be measured *in vivo* on live subjects creating a subject-specific musculoskeletal model [3,4]. While many studies have described a methodology which can be used for the measurement of a single parameter, none have demonstrated the combined use of methodologies to obtain completely *in vivo* based subject-specific parameters. The purpose of this study was to demonstrate the use of *in vivo* measurements to generate a completely subject-specific musculoskeletal model of the First Dorsal Interosseous (FDI) muscle.

## METHODS

A custom built finger dynamometer was used to control abduction of the index finger about the second metacarpophalangeal joint and measure the moment generated by the FDI about that joint. Ultrasound (US) was also used in the measurement of parameters of the FDI. Table 1 describes the parameters measured and the equipment used.

**Table 1.** Equipment used to measure FDI muscle model parameters.

| Parameter                             | Equipment       |
|---------------------------------------|-----------------|
| Muscle-tendon length ( $L_{MT,REF}$ ) | US              |
| Pennation Angle ( $\theta$ )          | US              |
| Moment arm ( $r$ )                    | US, dynamometer |
| Tendon length ( $L_{TR}$ )            | US              |
| Tendon stiffness ( $1/K_T$ )          | US, dynamometer |
| Force-length parameters               | US, dynamometer |
| Force-velocity parameters             | US, dynamometer |

Muscle-tendon and tendon length were measured from the US images. Pennation angle was used to determine muscle fascicle length. The moment arm of the muscle was measured using the tendon

excursion method with the dynamometer controlling the joint motion and US measuring tendon travel. Tendon stiffness was measured using a quick-stretch protocol [5]. To determine force-length and force-velocity parameters, measurements from the dynamometer were used to determine the remaining parameters by fitting the remaining parameters to the data in a least-squares sense. The force-length equation used was:

$$F_m = F_{MAX} \cdot \exp \left[ - \frac{\left( \left( \frac{L_F}{L_{F,OPT}} \right)^s - 1 \right)^R}{\omega} \right]$$

Where:  $F_m$  is the muscle force under current conditions,  $F_{MAX}$  is the maximal isometric muscle force,  $L_F$  is the prescribed muscle fascicle length,  $L_{F,OPT}$  is the optimal muscle fascicle length,  $s$  is the skewness parameter,  $R$  is the roundness parameter, and  $\omega$  is the width parameter.

The force-velocity equation used was:

$$F_m = F_{MAX} \cdot F_L(L_F) \cdot \left[ \frac{(V_{F,MAX} - V_F)}{(V_{F,MAX} + k \cdot V_F)} \right]$$

for  $V_F \geq 0$  and

$$F_m = F_{MAX} \cdot F_L(L_F) \cdot \left[ F_{SAT} - 0.5 \left[ \frac{(V_{F,MAX} + V_F)}{(V_{F,MAX} - 2 \cdot k \cdot V_F)} \right] \right]$$

for  $V_F < 0$

Where:  $V_F$  is the prescribed muscle fiber velocity,  $V_{F,MAX}$  is the maximum velocity of muscle fiber shortening,  $F_{SAT}$  is the saturation force under eccentric conditions, and  $k$  is the shape parameter.

Three subjects were used in the study. The subject's characteristics are displayed in table 2.

**Table 2.** Subject characteristics.

| Measurement              | Mean $\pm$ SD   |
|--------------------------|-----------------|
| Age (years)              | 24 $\pm$ 2      |
| Height (m)               | 1.68 $\pm$ 0.04 |
| Mass (kg)                | 67.3 $\pm$ 4.7  |
| Index finger length (cm) | 8.2 $\pm$ 0.8   |

## RESULTS AND DISCUSSION

Variability was seen among all parameters except for the roundness and force-velocity shape parameters (Table 3). Combining some of the parameters to reconstruct the force-length curves for the three subjects shows aspects of this variability (Figure 1). In a similar fashion the force-velocity curves for the three subjects shows variability even when forces and velocity are normalized (Figure 2).

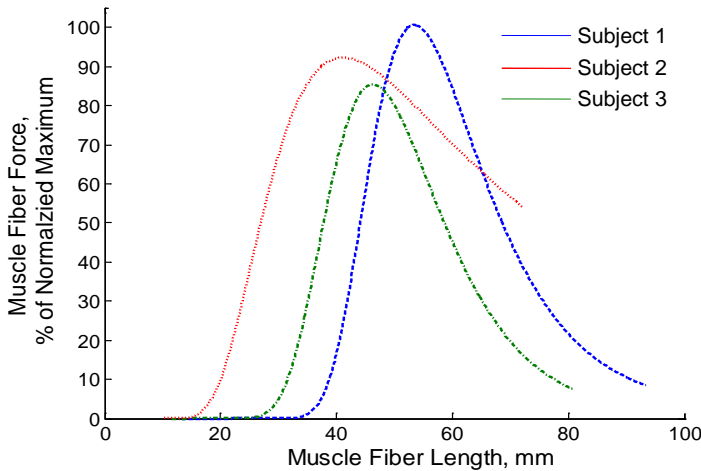


**Figure 1.** Normalized force-length curves of the FDI for the three subjects.

The parameters determined in this study were generally within reported values in the literature [6]. A limitation to the study was the inability of the dynamometer to produce muscle velocities that would be near the maximum velocity of the muscle. This would have only produced faster convergence of the fit for the determination of the remaining parameters, not different parameters.

**Table 3:** Measured subject parameters of the FDI for three subjects

| Subject | $L_{MT, REF}$<br>(mm) | $r$<br>(mm) | $L_{TR}$<br>(mm) | $1/K_T$<br>(mm/N) | $\theta$<br>(deg) | $F_{MAX}$<br>(N) | $L_{F, OPT}$<br>(mm) | $w$<br>(-) | $R$<br>(-) | $S$<br>(-) | $V_{F, MAX}$<br>( $L_{F, OPT}/s$ ) | $k$<br>(-) | $F_{SAT}$<br>(% of $F_{MAX}$ ) |
|---------|-----------------------|-------------|------------------|-------------------|-------------------|------------------|----------------------|------------|------------|------------|------------------------------------|------------|--------------------------------|
| 1       | 68.4                  | 14.8        | 21.8             | 0.0012            | 12.0              | 100.58           | 53.44                | 0.31       | 2          | -1.20      | 9.69                               | 4          | 1.73                           |
| 2       | 55.7                  | 8.9         | 12.9             | 0.0066            | 9.3               | 85.35            | 46.29                | 0.20       | 2          | -0.67      | 4.70                               | 4          | 1.5                            |
| 3       | 49.5                  | 12.1        | 17.5             | 0.0073            | 14.5              | 92.22            | 41.18                | 0.45       | 2          | -0.71      | 5.36                               | 4          | 1.5                            |

**N.B.** –  $L_{MT, REF}$  - reference length of the muscle-tendon complex,  $r$  – moment arm of the FDI about the second metacarpophalangeal joint,  $L_{TR}$  - slack length of the tendon,  $K_T$  - tendon stiffness, and  $\theta$  is the muscle fiber pennation angle. The remaining abbreviations are described in the main text.

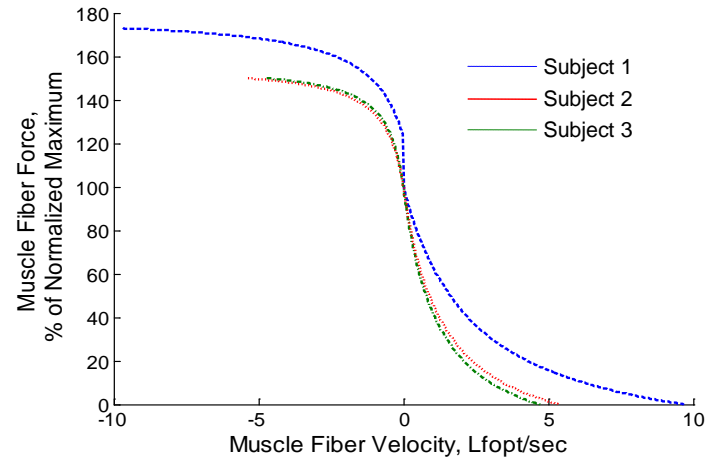


**Figure 2.** Normalized force-velocity curves of the FDI for the three subjects.

## CONCLUSIONS

This study demonstrated that it is feasible to measure all the parameters necessary for a subject-specific musculoskeletal model of the FDI. The measured parameters demonstrated similar high variability as that seen in cadaveric measurements [6], indicating that subject-specific measurements must be used to produce an accurate model of the FDI for a given subject.

## REFERENCES

1. Delp SL et al. *IEEE Trans Biomed Eng* **37**(8), 757-767, 1990.
2. Pierrynowski MR, and Morrison JB, *Math Biosci* **75**(1), 69-101, 1985.
3. Narici M, *J Electromyography Kinesiol* **9**(2), 97-103, 1999.
4. Herzog W et al. *Med Sci Sports Exerc* **23**(11), 1289-1296, 1991.
5. Cook CS, and McDonagh MJ, *E J Appl Physiol* **72**(4), 380-382, 1996
6. Infantolino BW and Challis JH, *J Anat* **216**, 463-469, 2010.

# QUANTITATIVE PREDICTION OF GRASP IMPAIRMENT FOLLOWING PERIPHERAL NEUROPATHIES OF THE HAND

Joshua M. Inouye, Jason J. Kutch, and Francisco J. Valero-Cuevas

University of Southern California, Los Angeles, CA, USA  
email: [jinouye@usc.edu](mailto:jinouye@usc.edu) web: <http://bbdl.usc.edu>

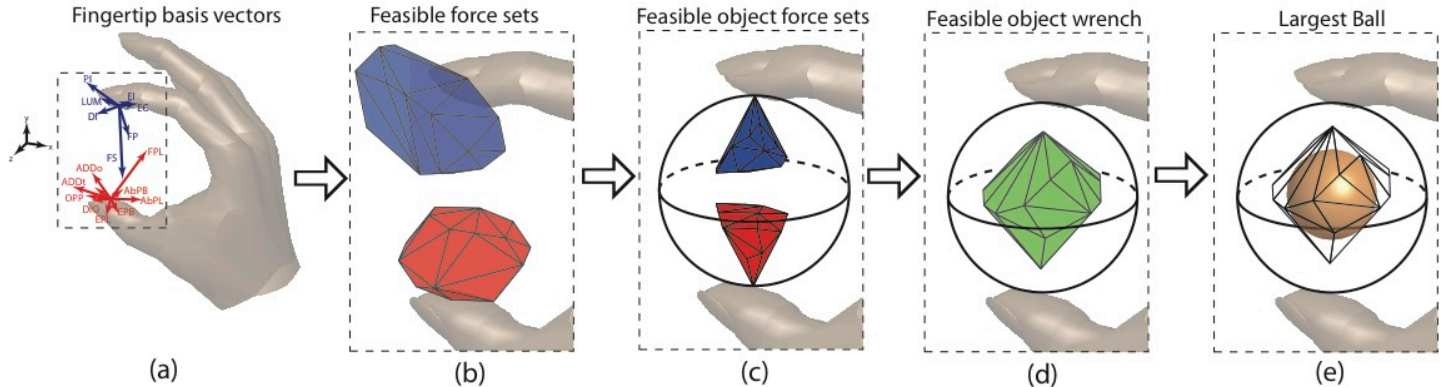


**Figure 1:** Grasp quality calculation steps. (a) Basis vectors. (b) Feasible force sets. (c) Feasible object force sets. (d) Feasible object wrench illustrated in 3-D. (e) Grasp quality metric of radius of largest ball (illustrated in 3-D; actual calculation is in 6-D).

## INTRODUCTION

Grasping is a fundamental hand function that is impaired or eliminated following peripheral neuropathies of the hand [1]. Using a novel computational framework for calculating grasp quality of tendon-driven hands [2], we predicted grasp quality for various degrees of simulated peripheral neuropathies: (i) carpal tunnel syndrome, (ii) low median nerve palsy, (iii) low ulnar nerve palsy, and (iv) low radial nerve palsy.

## METHODS

Calculation of grasp quality for tendon-driven hands involves several steps [2]. The first is determination of the fingertip forces that each tendon produces when tension is applied. We use previously-published cadaveric data from the thumb and index finger [3,4] to determine these “basis vectors” (Fig. 1a), from which the feasible force set (the set of 3-dimensional forces that the fingertip can produce) can be calculated, shown in Fig. 1b. These sets are then intersected with friction cones, producing feasible object force sets: the sets of forces that the fingertip is able to apply to the object, shown in Fig.

1c. From these sets, the set of all forces and torques on the object (i.e., the feasible object wrench) that the grasp can resist may be calculated, shown in Fig. 1d.

The first grasp quality metric we used was the weakest wrench (combination of force and torque) magnitude (in N—torque is scaled to N with the radius of the object) that could be resisted by the grasp. This is equivalent to the radius of the largest ball, centered at the origin, that the feasible object wrench set can contain, and is illustrated in Fig. 1e in 3-D, although the actual measure is in 6-D (3 dimensions for force and 3 for torque). For example, if the grasp quality is 5, then the grasp can resist at least 5N of force or scaled torque in any direction. We call this the *radius of largest ball*.

The second grasp quality metric we used was the radius of the 6-D ball with the same volume as the feasible object wrench, which we call the *characteristic length*.

Using this framework, we simulated various degrees of nerve palsies and carpal tunnel syndrome by progressively “weakening” muscles controlled

by these innervation groups from their maximal force [3,4]. We modeled carpal tunnel syndrome as low median nerve palsy that does not affect extrinsic muscles, since they are innervated proximal to the wrist [5]. The muscles for each innervation group are shown in Table 1.

**Table 1:** Muscles in each nerve pathology group. M: median, R: radial, U: ulnar, CTS: Carpal Tunnel Syndrome.

| Finger | Muscle                               | Innervation group |
|--------|--------------------------------------|-------------------|
| Index  | Flexor digitorum profundus (FDP)     | M                 |
|        | Flexor digitorum superficialis (FDS) | M                 |
|        | Extensor indicis proprius (EIP)      | R                 |
|        | Extensor digitorum communis (EDC)    | R                 |
|        | First lumbrical (LUM)                | M,CTS             |
|        | First dorsal interosseous (FDI)      | U                 |
|        | First palmar interosseous (FPI)      | U                 |
| Thumb  | Abductor pollicis brevis (AbPB)      | M,CTS             |
|        | Abductor pollicis longus (AbPL)      | R                 |
|        | Adductor pollicis oblique (ADDo)     | U                 |
|        | Adductor pollicis transverse (ADDt)  | U                 |
|        | First dorsal interosseous (DIO)      | U                 |
|        | Extensor pollicis brevis (EPB)       | R                 |
|        | Extensor pollicis longus (EPL)       | R                 |
|        | Flexor pollicis brevis (FPB)         | M,CTS             |
|        | Flexor pollicis longus (FPL)         | M                 |
|        | Opponens pollicis (OPP)              | M,CTS             |

## RESULTS AND DISCUSSION

The impairment of grasp quality with simulated advancement of peripheral neuropathy is shown in Fig. 2. We see that low median nerve palsy quantitatively affects both measures of grasp quality most severely. In addition, we observe that complete loss of any innervation group causes the radius of largest ball to be zero. This means that there are some directions of perturbation in 6-D wrench space that the grasp cannot resist, and therefore the grasp does not have *force closure*, which is considered to be a maximally deficient grasp. As expected, carpal tunnel syndrome decreases grasp quality less than full low median nerve palsy. Although low radial nerve palsy affects the extensors of the fingers, it has a comparable effect to carpal tunnel syndrome because they, counterintuitively, also contribute to grasp, as described earlier [6].

## CONCLUSIONS

Our ability to predict grasp quality enables a rigorous comparison of functional deficits across peripheral neuropathies. Comparison of patient outcomes with these quantitative predictions will enable development of efficient treatment modalities

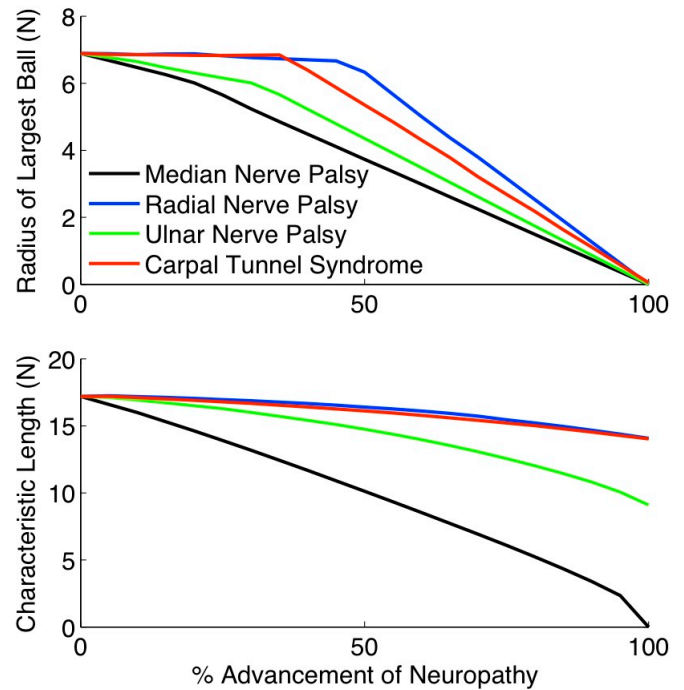


**Figure 2:** Grasp quality deterioration as a function of % advancement of neuropathy.

## REFERENCES

1. Riordan DC. *J Bone Joint Surgery* **50B**, 441, 1968.
2. Inouye JM, et al. *Proceedings of NCM*, San Juan, Puerto Rico, 2011.
3. Pearlman JL, et al. *J Ortho Res*, **22**, 306-312, 2004.
4. Valero-Cuevas FJ, et al. *J Biomech*, **33**, 1601-1609, 2000.
5. Katz JN, et al. *N Engl J Med*, **346**, 1807-1812, 2002.
6. Valero-Cuevas FJ, et al. *J Biomech*, **31**, 693-703, 1998.

## ACKNOWLEDGEMENTS

NSF EFRI 0836042 and NIH AR050520 and AR052345 to FVC.

Thanks to Sudarshan Dayanidhi for helpful discussions

# A NOVEL METHODOLOGY TO COMPARE GRASP QUALITY: APPLICATION TO TWO DOMINANT TENDON-DRIVEN DESIGNS

Joshua M. Inouye, Jason J. Kutch, and Francisco J. Valero-Cuevas

University of Southern California, Los Angeles, CA, USA  
email: [jinouye@usc.edu](mailto:jinouye@usc.edu) web: <http://bbdl.usc.edu>

## INTRODUCTION

The design of biologically-inspired tendon-driven systems for grasping and manipulation is a longstanding problem [1]. Some advantages of tendon-driven over torque-driven systems include light weight, small size, high speed, remote actuation, and significant *design flexibility* in setting moment arms and maximal tendon tensions [2]. This allows optimization of system output capabilities for a particular task.

Previous research on grasp quality for tendon-driven hands has computed a grasp quality metric based on a very specific, pre-defined task wrench space [3]. However, they note that their methodology, which utilizes a linear programming approach, does not generalize to the full set of feasible grasp wrenches.

Here we demonstrate a comprehensive technique for computing the full set of feasible grasp wrenches for any arbitrary tendon-driven finger topology and grasp configuration, allowing the calculation of global grasp quality metrics. To the best of our knowledge, this is the first time that the complete exploration of grasp capabilities is possible for arbitrary tendon-driven hand designs. We present this complete analysis for two- and three-finger grasps performed by 3D fingers, each with four kinematic degrees of freedom (DOFs, one ad-abduction and three flexion-extension joints), with two different tendon routing.

## METHODS

The tendon routings analyzed are shown in Fig. 1. The link lengths were 2cm and all moment arms were 5mm. Fig. 1a shows a “2N” design which has eight tendons (N is the number of DOFs) and Fig. 1b shows an “N+1” design, which has five tendons.

The sum of maximal tendon tensions is 1000N, which is divided up evenly among the tendons for each finger.

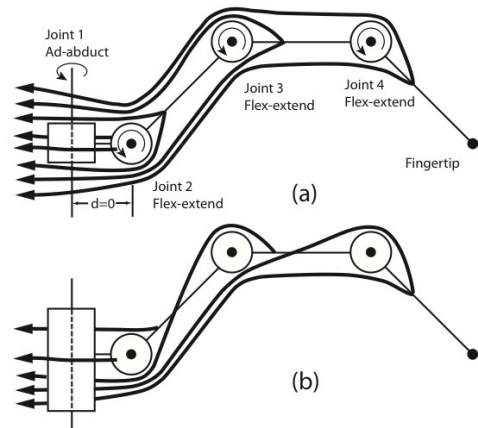


**Figure 1:** Tendon routing designs analyzed. (a) 2N design. (b) N+1 design.

The fingertip force production capabilities for these two designs are determined by calculating the feasible force set, which is a function of tendon routing [4]. After the feasible force sets are calculated, they are intersected with friction cones to produce a feasible object force set. This set represents the forces that can be applied to the object by each fingertip, and it is illustrated in Fig. 2a.

The feasible object force sets are combined to determine the feasible object wrench set, the set of all forces and torques that can be resisted (i.e., in 6-dimensional wrench space: 3 force dimensions and 3 torque dimensions) [4]. The units of the 6-D wrench space are all in N, as torques are scaled to N by the radius of the object.

Two metrics of grasp quality can then be determined from the feasible object wrench set. The first, which we call the *characteristic length*, is

based on the volume of the set, and is calculated using the following formula:

$$\text{Characteristic Length} = \left( \frac{6V}{\pi^3} \right)^{1/6}$$

This is a linear measure that is equal to the radius of the 6-D ball with the same volume as the 6-D set.

The second metric is the *radius of the largest ball*, centered at the origin, that the 6-D set can contain. This is the “weakest wrench magnitude” that can be resisted by the grasp [5].

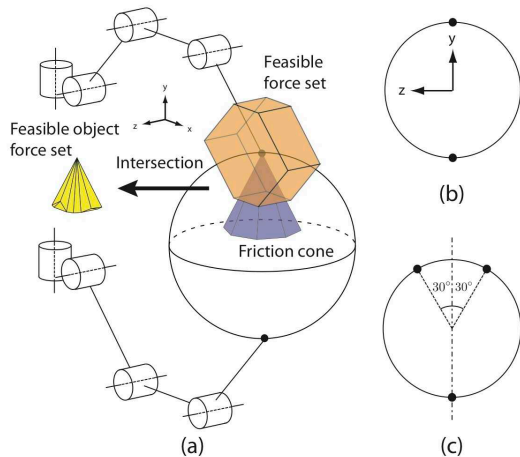


**Figure 2:** (a) Feasible force set intersected with friction cone. Also, isometric view of 2-finger grasp. (b) Front view of 2-finger grasp. (c) Front view of 3-finger grasp.

## RESULTS AND DISCUSSION

The results for each tendon routing and grasp configuration are shown in Fig. 3. For the nominal design, and upon Monte Carlo perturbations of the moment arm lengths, maximal tendon tensions, and link lengths, we see clear trends where the 3-finger grasps outperform 2-finger grasps for these finger placements.

It is not surprising that the 3-finger grasps outperform 2-finger grasps. However, the comparison of 2N vs. N+1 designs, while having the same sum of maximal tendon tensions, was not previously known, nor is it necessarily obvious or intuitive. We see some general advantages to the 2N design, but there exist N+1 designs (which we can identify) that reach high performance with fewer tendons.

This work demonstrates that our method allows calculation of global grasp quality metrics for *any*

tendon routing, maximal tendon tension distribution, moment arm values, and link lengths, which has not been accomplished previously, to the best of our knowledge. This now enables us to use optimization techniques in current studies.

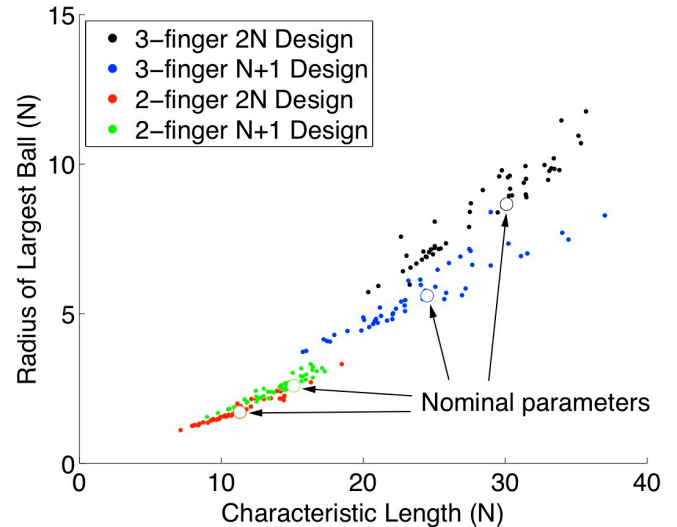


**Figure 3:** Grasp quality results for nominal (large markers) and 50 Monte Carlo simulations (small markers) for uniformly distributed  $\pm 20\%$  perturbations of moment arm, link length, and maximal tendon tension parameters for each design.

In addition, the framework we use in this study can predict the grasp-restoration quality and efficacy of various tendon transfer procedures, which is the subject of current work.

Our method also has very good computational speed and efficiency even if run on a desktop computer. The evaluations took between 1.7 and 39.9 s to complete, depending on hand design and configuration. This enables the use of this methodology with iterative optimization algorithms.

## REFERENCES

1. Salisbury JK, et al. *Int J Robot R* **1:1**, 4, 1982
2. Pons JL, et al. *Robotica*, **17:6**, 674, 1999.
3. Fu JL, et al. *IEEE/RSJ IROS*, 1068-1075, 2006.
4. Valero-Cuevas FJ. *Progress in Motor Control*, 619–633, 2005.
5. Miller AT, et al. *Proc. of IEEE ICRA*. **2**, 1999.

## ACKNOWLEDGEMENTS

This work was supported by NSF EFRI Grant 0836042 and NIH Grants AR050520 and AR052345 to F. J. Valero-Cuevas.

# A FINITE ELEMENT MODEL OF TWO SURGICAL PROCEDURES FOR CORRECTING THE CLAWED HALLUX DEFORMITY

<sup>1,2</sup>Vara Isvilanonda, <sup>1,2</sup>Evan Dengler and <sup>1,2,3</sup>William R. Ledoux

<sup>1</sup>RR&D Center of Excellence for Limb Loss Prevention and Prosthetic Engineering, Department of Veterans Affairs, Seattle, WA, USA; Departments of <sup>2</sup>Mechanical Engineering and <sup>3</sup>Orthopaedics & Sports Medicine, University of Washington, , Seattle, WA, USA  
email: [wrledoux@u.washington.edu](mailto:wrledoux@u.washington.edu) Web: <http://www.amputation.research.va.gov>

## INTRODUCTION

The clawed hallux is a foot deformity characterized by dorsiflexion at the metatarsophalangeal joint (MTPJ) and plantar flexion at the interphalangeal joint (IPJ) of the first ray. This deformity can cause increased pressure under the first metatarsal head (MTH) [1]. Elevated plantar pressure poses risk of diabetic foot ulceration [2] and can lead to lower extremity amputation [3]. The clawed hallux deformity can be caused by imbalanced forces from the extensor hallucis longus (EHL), flexor hallucis longus (FHL) and peroneus longus (PL) muscles [1]. Two surgical techniques, the modified Jones procedure and the FHL transfer, are widely used for treating moderate cases of clawed hallux [4]. In this study, an anatomically detailed finite element (FE) foot model was developed and validated. The model was used to study the clawed hallux deformity resulting from an imbalance of three extrinsic muscles (EHL, FHL and PL). The effectiveness of the modified Jones procedure and the FHL transfer was quantified by correction of abnormal joint angles and restoration of plantar pressures.

## METHODS

The left foot of a 823N, 44-year-old male donor was secured in a loading frame with 70N compressive force on the tibia. The foot was CT and MR scanned at 0.6mm slice thickness. *Multi-Rigid*, a custom software program, and Image-J were used for segmentation of bone, soft tissue, plantar fat and cartilage. ANSYS ICEM CFD was used for linear tetrahedral element generation. Ligaments, tendons, material properties, contacts, constraints and nodal forces were defined in LS-Prepost (Table 1). A total of 27 bones, 7 pairs of anatomically derived cartilages, 19 joints, 6 fat volumes, 8 extrinsic

muscle tendons, 107 ligaments, plantar fascia and an enclosed soft tissue were included in the FE model (Fig. 1). A coefficient of friction of 0.6 was assumed between the foot and ground. Static and dynamic coefficients of friction (0.102 and 0.085) were used for cartilage. Biomechanically realistic forces were applied to the tibia (600N) and Achilles tendon (200N) for quiet stance. The model was validated with data from the literature. The clawed hallux deformity and surgical procedures were simulated at 22% of the stance phase when the tibia-ground angle was 90°. The ground reaction force was maintained at 873N. Loads were applied to the tibia, Achilles tendon (359N) and proximal end of 7 other tendons as in prior work [5]: EHL (4N), FHL (4N), PL (4N), flexor digitorum longus (5.8N), tibialis anterior (37.9N), tibialis posterior (38.9N) and peroneus brevis (5N). FHL and PL overpull (104N and 96N) were chosen from peak force in normal gait. Due to low EHL activity in gait, a tendon subfailure load (200N) was chosen for EHL overpull. The modified Jones procedure was modeled by moving the EHL tendon insertion to the metatarsal neck and fusing the IPJ. The FHL transfer was modeled by inserting the FHL tendon into the base of the proximal phalange [4]. All models were solved in LS-DYNA V971 R5.1.

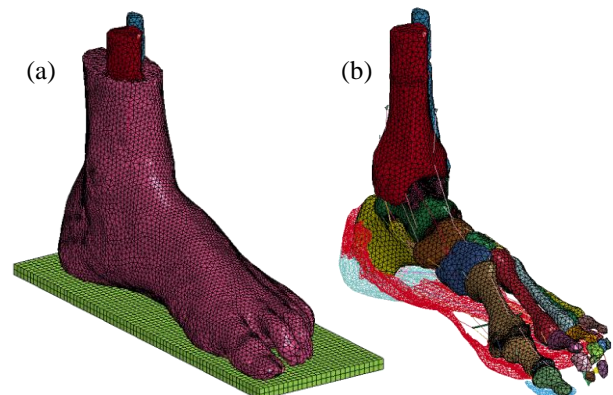


**Figure 1:** (a) FE model (b) structure inside soft tissue showing bone, cartilage, fat, plantar fascia, ligament and tendon.

## RESULTS AND DISCUSSION

The clawed hallux deformity was generated either with severe dorsiflexion at the MTPJ (EHL and PL+EHL overpull), or with large IPJ plantar flexion (EHL+FHL and EHL+FHL+PL overpull) (Fig. 2). The FHL, PL and PL+FHL imbalances did not generate the deformity and will not be discussed further. The modified Jones procedure was found most effective in correcting the clawed hallux deformity from EHL and EHL+PL overpull. In both cases, MTPJ deformity was restored to near normal. Pressure under the MTH was redistributed to other areas and showed reduction below the pre-surgical value. Correction of EHL+FHL and EHL+FHL+PL overpulls by the modified Jones procedure created hallux flexus and led to over pressure at the plantar distal hallux from an unopposed FHL pull. The major shortcoming of the modified Jones procedure was the IPJ immobility. The FHL transfer procedure showed successful correction for the clawed hallux from EHL+FHL and EHL+FHL+PL overpull. In both cases, the MTPJ angles were corrected to within  $\pm 0.5^\circ$  of the normal value. The IPJ angles were reduced to  $1.32^\circ$  to  $2.38^\circ$  dorsiflexion and slightly lifted the distal hallux off the ground. Predicted pressure under the MTH for both cases showed a small increase compared to pre-surgery. However, the magnitudes were still close to or below normal. The FHL transfer procedure failed to correct abnormal angles for EHL and PL+EHL overpull due to insufficient FHL force to counter balance the EHL overpull.

## CONCLUSIONS

The model demonstrates generation of the clawed hallux deformity from four different combinations

of EHL, FHL and PL overpulls. The most severe clawed hallux deformity was caused by overpull of all three muscles. FHL overpull indicated which procedure would be most successful. In the absence of FHL overpull (EHL and PL+EHL overpull), the modified Jones was found most effective; in its presence (EHL+FHL and EHL+FHL+PL overpull), the FHL transfer was ideal.

## REFERENCES

1. Olson SL, et al. *Foot Ankle Int* **24**, 477-485, 2003.
2. Veves A, et al. *Diabetologia* **35**, 660-663, 1992.
3. Pecoraro RE, et al. *Diabetes Care* **13**, 513-521, 1990.
4. Elias FN, et al. *Foot Ankle Int* **28**, 369-376, 2007.
5. Aubin PM. University of Washington, 2011.
6. Dengler E. University of Washington, 2008.
7. Pai S, et al. *J Biomech* **43**, 1754-1760, 2010.
8. Schmidt HK. University of Washington, 2009.
9. Schechtman H. *P I Mech Eng* **208**, 241-248, 1994.

## ACKNOWLEDGEMENTS

This work was supported by the VA Grant A6973R.

**Table 1:** Material models and associated properties.

| Material     | Material Model | Young's Modulus | Poisson's Ratio | Reference |
|--------------|----------------|-----------------|-----------------|-----------|
| Bone         | rigid          | 20,100 MPa      | 0.30            | [6]       |
| Cartilage    | rigid          | 1.1 MPa         | 0.01            | [6]       |
| Fat          | hyperelastic   | †               | 0.49            | [7]       |
| Fat*         | linear elastic | 1.035 MPa       | 0.49            | [7]       |
| Soft tissue  | hyperelastic   | †               | 0.49            | [6]       |
| Soft tissue* | linear elastic | 2.494 MPa       | 0.49            | [6]       |
| Ligament     | nonlinear 1D   | †               | N/A             | [6, 8]    |
| Tendon       | nonlinear 1D   | †               | N/A             | [9]       |

† Force-deformation or stress-strain curve was specified. Ogden hyperelastic was utilized for fat and soft tissue. Ligament and tendon were modeled by tension-only element. 1D = one-dimensional

\* Adjusted properties to account for 70N preload by linear curve fit to the final portion of the stress-strain curve of the hyperelastic material.

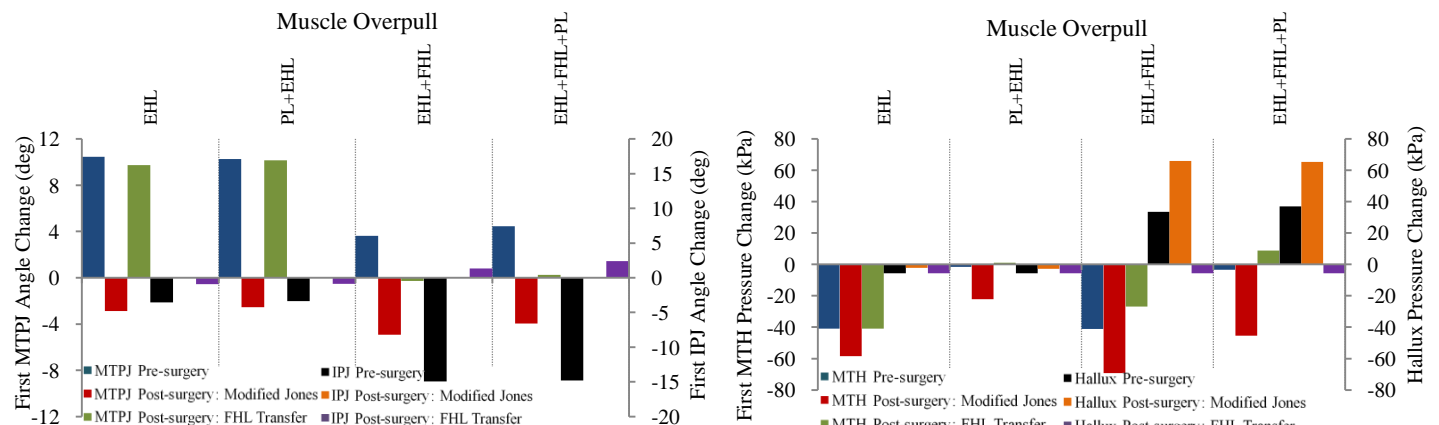


**Figure 2:** Model prediction of joint angle change (left) and plantar pressure change (right) pre- and post-surgery. Positive and negative change indicate values above and below normal, respectively (Positive = dorsiflexion, negative = plantar flexion). Normal absolute angle (MTPJ  $+17.3^\circ$  and IPJ  $-8.37^\circ$ ) and plantar pressure (MTH 114.14 kPa and hallux 5.6 kPa) were taken from foot with no overpull.

# EFFECTS OF ANTI-WHIPLASH SEATS ON CERVICAL FACET AND DISC KINEMATICS DURING SIMULATED REAR CRASHES

Paul C. Ivancic

Biomechanics Research Laboratory, Department of Orthopaedics and Rehabilitation, Yale University School of Medicine, New Haven, CT, USA; email: paul.ivancic@yale.edu

## INTRODUCTION

Automobile rear crashes may cause injury to multiple anatomical structures of the cervical spine including facet joints and intervertebral discs. In attempt to reduce neck injuries during rear crashes, some current automobiles include anti-whiplash seats such as the Whiplash Protection System (WHIPS) or active head restraint (AHR). Occupant momentum pressing into the seatback during the crash activates mechanical-based systems integrated within the seat. The goals of this study were to determine facet joint and disc kinematics and ligaments strains of the lower cervical spine during simulated rear crashes with WHIPS and AHR and to compare these data to those obtained with no head restraint (NHR).

## METHODS

A Human Model of the Neck (**Fig. 1A,B**), consisting of a neck specimen mounted to the torso of BioRID II and carrying a surrogate head and stabilized with muscle force replication, was subjected to simulated rear crashes in a WHIPS seat (**Fig. 1A**; n=6, 12.0 g,  $\Delta V$  11.4 kph) or AHR seat (**Fig. 1B**) and subsequently with NHR (n=6: 11.0 g,  $\Delta V$  10.2 kph with AHR; 11.5 g,  $\Delta V$  10.7 kph with NHR). WHIPS consists of a fixed head restraint, yielding seatback, and a specialized recliner mechanism that contains deformable elements. The goals of WHIPS are to absorb occupant energy, minimize neck motions, and reduce forward rebound into the seatbelt. The AHR rotates forward via a pivoting mechanism between it and the seatback in attempt to contact the head immediately following the crash and minimize head and neck motions. Lower cervical spine facet and disc motions and ligament strains during the crashes were computed (**Fig. 1C**) and average peak values statistically compared ( $P < 0.05$ ) between WHIPS, AHR, and NHR.

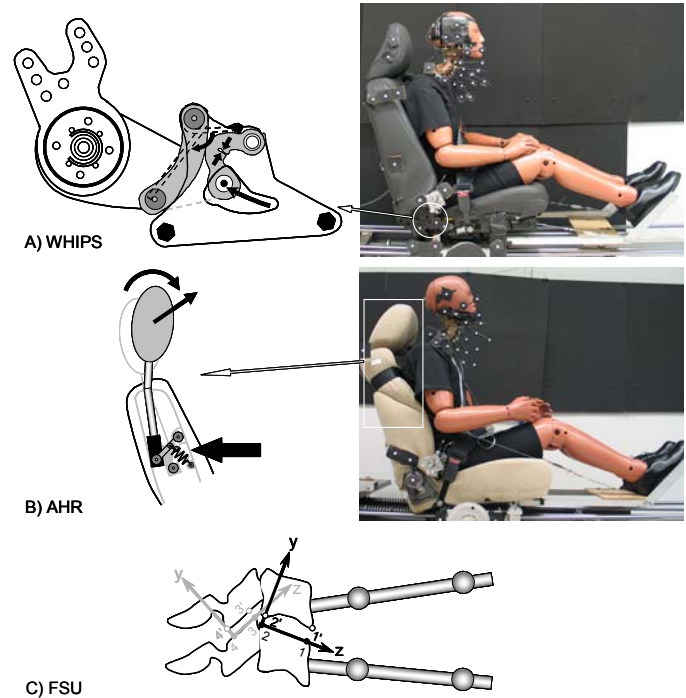


**Figure 1:** Photographs of the Human Model of the Neck and schematic drawings of: **A)** Whiplash Protection System (WHIPS) and **B)** active head restraint (AHR). **C)** Functional spinal unit (FSU) with motion tracking flags and points used to compute facet and disc translations and ligament strains. The facet and endplate coordinate systems (zy) are fixed to and move with the lower vertebra and are used to express the facet and disc translations, respectively: +Tz anterior and -Tz posterior sliding (facet) or shear (disc), +Ty separation, and -Ty compression. Translations are computed at the front (3' relative to 3; 1' relative to 1) and rear (4' relative to 4; 2' relative to 2) facet and endplate.

## RESULTS AND DISCUSSION

Average time-history responses for C6/7 intervertebral rotations, facet and disc translations, and ligament strains (**Fig. 2**) demonstrate temporal differences among WHIPS, AHR, and NHR. Average peak facet and disc translations and ligament strains could not be statistically differentiated between WHIPS and AHR or between AHR and NHR. WHIPS significantly reduced peak capsular ligament strain and peak disc separation at C6/7 as compared with NHR. Facet compression at C6/7 reached 2.9 mm with WHIPS, 1.9 mm with AHR, and 3.2 mm with NHR. Facet joint compression injury may lead to neck pain in some whiplash patients. Our results are supported by a previous *in vivo* simulated rear crash study in which the C5/6 instantaneous center of rotation shifted upward during the crash implying that the facets may forcefully collide leading to impingement injury of the synovial fold or articular cartilage.

## CONCLUSIONS

- We determined the facet joint and disc kinematics and ligament strains of the lower cervical spine during simulated rear crashes with WHIPS, AHR, and NHR. These data could not be statistically differentiated between WHIPS and AHR or between AHR and NHR. WHIPS significantly reduced peak capsular ligament strain (5.3 vs. 32.8%,) and peak axial disc separation (1.8 vs. 5.0 mm) at C6/7 as compared with NHR.
- WHIPS and AHR marginally reduced peak ALL strain as compared to NHR.
- Average peak facet joint compression reached 2.9 mm with WHIPS, 1.9 mm with AHR, and 3.2 mm with NHR.
- WHIPS and AHR effectively limited peak capsular strain below the subfailure threshold but did not protect against potential facet joint compression injuries which may occur during or following contact of the head with the head restraint.
- Future active neck injury prevention systems may be designed to reduce facet joint compression during rear crashes leading to reduced neck pain in whiplash patients.

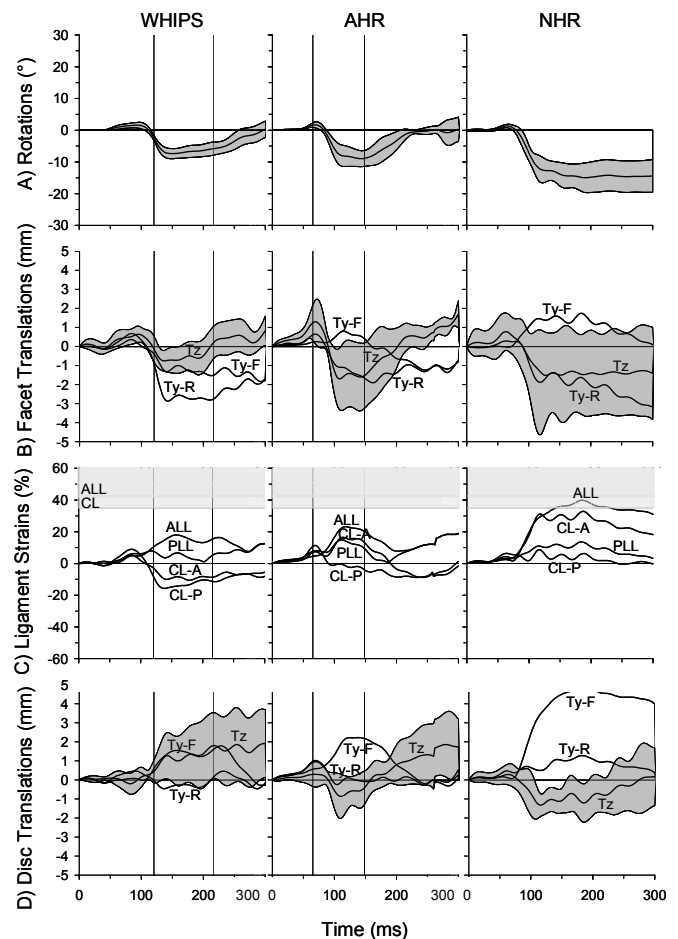


**Figure 2:** Average C6/7 time-history responses during rear crashes with WHIPS, AHR, and NHR: A) intervertebral rotations (+R flexion, -R extension); B) facet translations; C) strains in the anterior longitudinal (ALL), posterior longitudinal (PLL), and anterior capsular (CL-A) and posterior capsular (CL-P) ligaments; and D) disc translations. Facet and disc translations are expressed in the facet and endplate coordinate systems, respectively, of Fig. 1C: +Tz anterior and -Tz posterior sliding (facet) or shear (disc); +Ty separation, -Ty compression; F front and R rear facet/endplate. Shaded regions representing  $\pm 1$  standard deviation are shown only for rotation and Tz. Vertical lines represent the average duration of contact of the head with the HR. Panel C includes shaded regions representing the ALL failure strain threshold of 42.6% and the CL subfailure threshold of 35%.

## ACKNOWLEDGEMENTS

This research was supported by grant 5R01CE001257 from the Centers for Disease Control and Prevention (CDC).

# IDENTIFYING THE CRITERION SPONTANEOUSLY MINIMIZED DURING SUB-MAXIMAL MOVEMENTS THROUGH OPTIMAL SYNTHESIS

<sup>1</sup>M. Jackson, <sup>2,3</sup>I. Benkhemis, <sup>1,2</sup>A. Thouzé, <sup>2</sup>P. Sardain and <sup>1</sup>M. Begon

<sup>1</sup>Département de Kinésiologie, Université de Montréal, Canada

<sup>2</sup>Instiut PPRIMME, Université de Poitiers, France

<sup>3</sup>SENSIX, Poitiers, France

email: monique.jackson@umontreal.ca

## INTRODUCTION

Optimal synthesis, which can be used to predict the kinematics of a movement, requires not only that a model of the system be formulated but that a performance criterion is also specified. For sub-maximal movements the selection of a suitable performance criterion able to generate realistic dynamic behavior is difficult.

The purpose of this study is to identify the criterion which is the closest to that spontaneously minimized by humans during sub-maximal movements. Movement synthesis techniques will be used to evaluate a number of criteria by comparing simulated movements with actual performances. Multi-factorial criteria will be included in the analysis as the literature indicates that it is likely that different criteria are minimized simultaneously [1]. This paper presents the preliminary results for one athlete performing a sub-maximal long jump.

## METHODS

An optoelectronic motion capture system was utilized to collect data from a male athlete who performed a number of sub-maximal long jumps. A chain model that assumed fixed segment lengths was used to process the data and determine the planar motion of the jumper during the take-off phase of each jump. One typical trial was chosen with the data from this trial subsequently analyzed.

The athlete was modeled in planar form using 14 rigid segments, as depicted in Fig. 1. The anthropometric parameters of each segment (length, mass, centre of mass and moment of inertia) were estimated based on the athlete's total mass and segmental lengths.

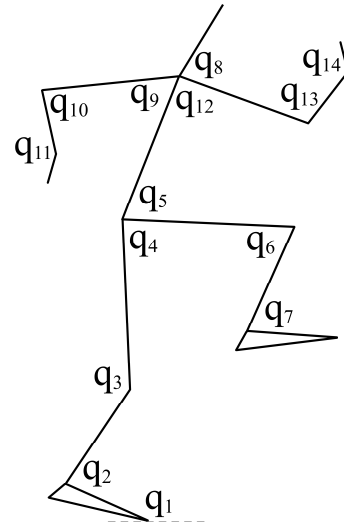


**Figure 1:** Schematic of the 14 segment planar model used to represent the athlete.

The take-off phase was simulated from the beginning of support foot contact  $t^0$  through to the loss of support foot contact  $t^f$ . Throughout this period the joint trajectories were described by a vector of 14 generalized co-ordinates  $q = (q_1, \dots, q_i, \dots, q_n)^T$  as defined in Fig. 1.

The dynamic equations of motion for the movement can be written in the generic form

$$M(q)\ddot{q} + H(q, \dot{q}) = T,$$

where  $M(q)$  is the mass matrix,  $H(q, \dot{q})$  groups Coriolis, centrifugal and gravity terms together and  $T$  represents the torques applied about the joints.

The equations of motion were subject to a number of constraints defined such that the resulting movement was feasible. Firstly, to ensure that joint motions did not exceed human capabilities, anatomical limits were placed on the range of motion of each joint. Secondly, the contact forces exerted by the ground on the foot were constrained

to ensure that the contact was unilateral and that the foot did not slip relative to the ground [2]. Thirdly, in order to avoid collisions of the swing leg with the ground constraints which maintained an adequate clearance distance were defined [2]. Finally, the initial and final joint angular positions and velocities were constrained to be the same as those of the actual performance.

Within this study three criterion factors were considered; the joint intersegmental force, the joint torque and the joint power. Combinations of these factors were also considered as it is likely that the criterion that is spontaneously minimized is multi-factorial due to the compromise between musculoskeletal integrity and energetic economy. Thus in effect, seven different criteria were considered.

The problem consisted of finding the kinematics that satisfied the equations of motion and the constraints, whilst minimizing one of the considered criteria. The non-linear inequality constraint equations made this problem difficult to solve exactly and therefore a parametric optimization technique was employed [2].

Parameterization of the problem involved approximating the generalized co-ordinates by specified functions, defined by a finite set of parameters, and then recasting the equations of motion, constraints and criteria into simple functions of these parameters. Within this study the generalized coordinates were approximated using spline functions of class  $C^3$  obtained by connecting forth order polynomials up to their third derivatives [2]. The resulting problem was solved using the Feasible Sequential Quadratic Programming algorithm.

To compare the results of the different criteria the function  $I_s$  which represents the difference between the actual  $q^a$  and simulated  $q^s$  movement, was utilized:

$$I_s = \frac{1}{14} \sum_{i=1}^{14} \frac{\sum_{t=0}^{t^f} |q_i^a(t) - q_i^s(t)|}{|\max q_i^a - \min q_i^a|}.$$

## RESULTS AND DISCUSSION

The results of this study show synthesis of the take-off phase of a sub-maximal long jump to be sensitive to the chosen criterion (Table 1). A criterion that minimized force resulted in a high degree of similarity with the actual performance; in effect providing the best overall prediction of the joint motion coordination. In contrast a criterion that minimized torque resulted in a low degree similarity with the actual performance.

**Table 1:** Comparison of the seven criteria.

| Criterion          | $I_s$ |
|--------------------|-------|
| Force              | 3.01  |
| Torque             | 10.21 |
| Power              | 3.99  |
| Force-Torque       | 4.83  |
| Force-Power        | 3.31  |
| Power-Torque       | 8.40  |
| Force-Power-Torque | 4.50  |

Criteria used within the literature are generally based on choosing the movement which is the most economical, in terms of the effort (torque) or the energy expenditure (power) [3]. Within this study, a criterion based on ensuring joint integrity by minimizing joint intersegmental forces was introduced and found to be a good overall predictor of joint kinematics.

The multi-factorial criteria assessed within this study did not exhibit as much similarity with the actual data as the criterion that solely minimized forces. However, the weighting of each factor within the multi-factorial criteria was even. A progression of this work would be to introduce criterion weighting factors such that uneven multi-factorial criteria could be obtained. Further work is also required to verify the results for other sub-maximal movements and also for a population.

## REFERENCES

1. Zajac FE, et al. *Gait Posture* **16**, 215-232, 2002.
2. Bessonnet G, et al. *Int J Robot Res* **24**, 523-536, 2005.
3. Leboeuf F, et al. *Multibody Syst Dyn* **16**, 213-236, 2006.

# MAXIMISING POST-FLIGHT HEIGHT IN GYMNASTICS VAULTING: THE INFLUENCE OF THE TABLE CONTACT PHASE

<sup>1</sup>M. Jackson, <sup>2</sup>M.R. Yeadon and <sup>2</sup>M. Hiley

<sup>1</sup>Département de Kinésiologie, Université de Montréal, Canada

<sup>2</sup>School of Sport, Exercise and Health Sciences, Loughborough University, United Kingdom  
email: monique.jackson@umontreal.ca

## INTRODUCTION

Within the literature there is no general consensus about the importance of the table contact phase for vaulting performance. Some sources advocate that vaulting performance is largely determined prior to the table contact phase [1] while others suggest that the gymnast has the ability to change the outcome of the vault during the table contact phase [2].

The purpose of this study was to use a torque-driven simulation model of vaulting to investigate the influence of the table contact phase on vaulting performance, in particular post-flight height. Performance in vaulting can be thought of in terms of the score achieved, with a higher score indicating a better performance. As lack of height in the post-flight receives a specific deduction it has a direct influence on the score, hence the focus on this measure.

## METHODS

An optoelectronic motion capture system was utilized to collect kinematic data from an elite male gymnast who performed three handspring somersault vaults. A chain model that assumed fixed segment lengths was used to process the data and determine the planar motion of the gymnast during the table contact phase of each vault.

Maximal voluntary joint torque data were obtained using an isovelocity dynamometer for flexion and extension of the wrist, shoulder, hip and knee. Gymnast-specific torque surfaces were subsequently fit to the data based on the relationships between torque, angle and angular velocity [3]. Anthropometric measurements were taken from the gymnast and gymnast-specific segmental inertia parameters calculated, while the

inertial parameters of the table were estimated from mass and linear dimensions.

A two-dimensional torque-driven model that simulated the interaction between the gymnast and the vaulting table during the table contact phase was developed. The gymnast was modelled in planar form using seven rigid segments and the table was modelled as a single segment (Fig. 1).

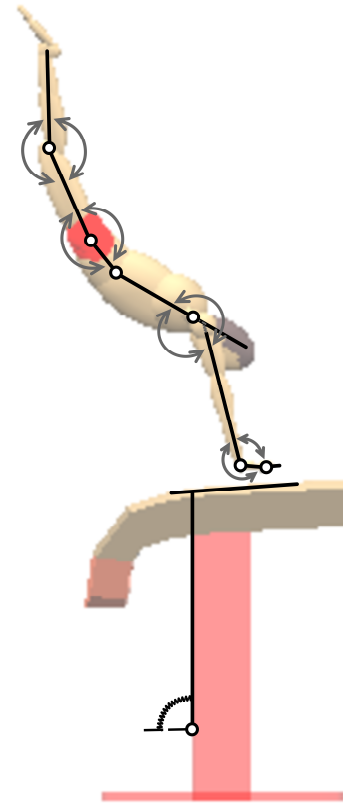


**Figure 1:** Schematic of the torque-driven simulation model.

The contact forces between the gymnast and the table were represented by spring-dampers in the normal direction and a two-state frictional force representation in the tangential direction [4]. Torque generators acted to extend and flex the wrist, shoulder, hip and knee.

The input to the model comprised the gymnast's initial configuration and joint angular velocities, together with the activation time histories of the torque generators. The output from the torque-driven model included the gymnast's configuration, orientation and linear and angular momentum at table take-off.

The torque driven model was evaluated by assessing how closely a simulation matched performance data. A genetic algorithm varied the torque generator activation profiles to minimise an objective function that measured the difference between a simulation and a recorded performance.

The simulation model was then used to determine whether the gymnast's post-flight height could be improved through changes in table contact phase technique and/or configuration at initial table contact. Firstly the torque generator activation profiles were varied in order to determine the potential improvement arising from changes solely to contact phase technique. Secondly the activation profiles were varied along with the initial table contact configuration in order to determine the influence of also changing this aspect of technique. The configuration of the gymnast at table touchdown was defined by three angles: orientation angle of the upper trunk, shoulder angle and hip angle. The gymnast's pre-flight angular momentum and centre of mass trajectory were constrained to be the same as those of the recorded performance; in effect the only difference was the table contact configuration which was assumed to be modifiable by the gymnast during pre-flight.

## RESULTS AND DISCUSSION

Evaluation of the torque-driven model showed that the model adequately simulated the table contact phase of handspring somersault vaults. The three vaulting performances were matched with overall difference scores of 3.1%, 1.8% and 3.5% respectively. Furthermore close agreement was found between the performance and simulation joint angles which indicated that the torque generators included in the model were strong enough to match the performance torques for this vault.

The vault with the best performance was chosen for further analysis. Optimisation of the table contact phase technique showed there was very little potential for improvement in post-flight height with an increase of only 0.05 m.

When the touchdown configuration was varied along with table contact phase technique there was more potential for improvement in post-flight height with an increase of 0.14 m. This increase was achieved through a higher orientation angle at contact and a more open shoulder angle (Fig. 2).

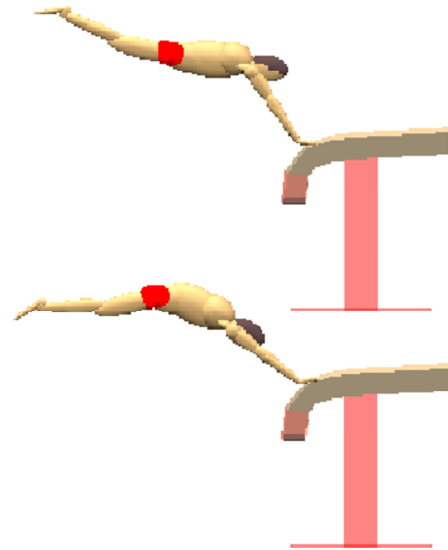


**Figure 2:** Comparison of gymnast's configuration at initial table contact: upper – actual performance, lower – optimised configuration.

While adjustment of the configuration at table contact had the potential to improve performance there was limited scope for the gymnast to alter the performance through technique modifications during the table contact phase. These results suggest that the table contact phase has little influence on vaulting performance, in agreement with [1].

## REFERENCES

1. Prassas & Giankellis. Vaulting Mechanics, *Proceedings of XX Symposium on Biomechanics in Sports*, 2002
2. Smith T. *Gymnastics: A mechanical understanding*, Hodder and Stoughton, 1982
3. Forrester et al. *J. Biomech* doi:10.1016/j.jbiomech.2010.11.024, 2010
4. Jackson et al. Submitted to *J. Biomech*, 2011

# A PROBABILISTIC APPROACH TO FEEDFORWARD FES CONTROL IN THE RAT HINDLIMB

<sup>1</sup>Anthony Jarc, <sup>1</sup>Max Berniker and <sup>1</sup>Matthew Tresch

<sup>1</sup>Northwestern University, Evanston, IL, USA  
email: [m-tresch@northwestern.edu](mailto:m-tresch@northwestern.edu)

## INTRODUCTION

Functional electrical stimulation (FES) is a promising technique to restore behavior to the paralyzed limbs of spinal cord injury patients by artificially stimulating peripheral nerves and/or muscles. However, it is very challenging to design a FES system that continuously modulates behavior using many muscles. So far, FES systems have primarily been successful in restoring either pre-programmed behaviors or relatively simple behaviors with only a few muscles [1]. In this work, we have begun to systematically examine the performance of feedforward FES control of isometric endpoint forces. The results from this research can be used to further improve integrated feedforward-feedback FES control strategies.

We focus our control task on isometric forces because they are an essential component of any complete behavior where the limb interacts with the external environment, e.g. grasping a cup, eating with a fork, etc. The characterization of feedforward isometric force control has been difficult in humans because of internal movements, the comfort of the patient, etc. To overcome these limitations, we developed a test platform using a rat hindlimb model. With this platform, we can co-stimulate over 10 muscles and accurately measure isometric endpoint forces of the hindlimb.

Here, we develop a probabilistic model to optimize commands for desired isometric forces by accounting for the variability of individual recruitment curves. Traditionally, FES control strategies assume a deterministic model to describe the relationship between muscle stimulation commands and force outputs. In other words, these deterministic models assume the isometric muscle force for a given stimulus is known with certainty. However, the recruitment properties of muscles are often variable depending on muscle fatigue,

electrode displacement, and many other factors. Deterministic models are unable to account for this variability and will often lead to inaccurate predictions of isometric force. Our probabilistic model attempts to address this limitation and improve the certainty, and thus accuracy, of feedforward isometric force control.

We compared the certainty of isometric forces predicted assuming our probabilistic model and a deterministic model. We showed that by using a probabilistic model, the certainty of the optimized forces are much higher than when using a deterministic model. This suggests that our probabilistic approach can be used to improve feedforward FES control strategies, especially in real, paralyzed limbs where variability in muscle force properties are expected.

## METHODS

In previous work, we developed a FES test platform to control isometric endpoint forces using the rat hindlimb [2]. All procedures were approved by the Northwestern University animal care and use committee. Adult Sprague Dawley rats were anesthetized. Metal posts were implanted in the pelvis and secured to a stereotaxic frame. A threaded attachment was implanted in the tibia near the ankle and used to connect the hindlimb to a 6 dof force transducer. Monopolar stimulating electrodes were placed in approximately 10 muscles spanning proximal joints. We determined the recruitment curves by stimulating the muscles (0.5s train, 75Hz, biphasic pulses) while the ankle was rigidly attached to the force transducer using a 16-channel stimulator [3]. The average steady-state forces (final 200msec of force plateau) generated at the ankle were recorded for increasing pulse-amplitudes while holding the pulse-width constant at 0.1msec. Forces were measured in the sagittal plane. We collected two sets of recruitment curves separated in time by approximately 1-2 hours.

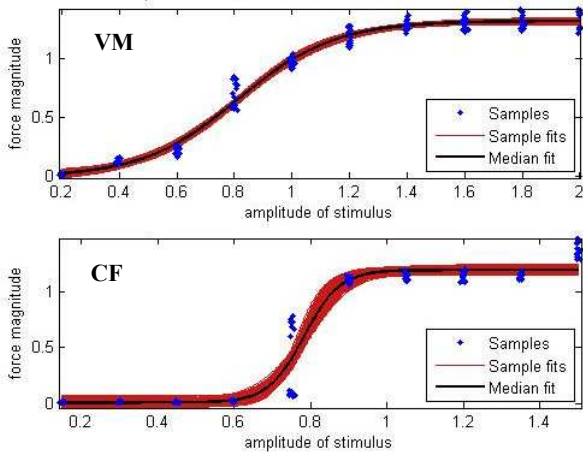


**Figure 1:** Sample recruitment curves parameterized using our probabilistic method. Top: Vastus medialis. Bottom: Caudal femoralis. Force magnitude was measured in N and stimulus amplitude in mA. Red lines are distribution of possible parameterized recruitment curves given the data (blue points).

We fit parameterized functions (sigmoids) to the recruitment data to predict the output isometric force magnitude given a stimulus. For the probabilistic model, we used a sampling method to form a distribution of possible recruitment curves given the force magnitude data (Fig. 1). Uncertainty in the structure of the recruitment curves resulted when the data was variable within a single trial and over time across the two (or more) sets of recruitment curve data. For the deterministic model, we parameterized recruitment curves using maximum likelihood estimation of force magnitude.

We used both models to optimize muscle commands to achieve desired force targets within the feasible force space of the rat hindlimb. We used the same cost function for both models that penalized the sum of the squared activation and expectation of desired forces. For our probabilistic model, the expectation of the desired forces resulted in a penalty on the variability of the force while the deterministic model neglected this variability.

## RESULTS AND DISCUSSION

The goal of this research was to develop a probabilistic method to improve the performance of feedforward FES control strategies. We compared the certainty of optimal forces for targets throughout the feasible force space of the hindlimb using our probabilistic model and a deterministic model. The certainty of the forces produced using

our probabilistic model (Fig. 2A) was much higher than the certainty of the forces produced using the deterministic model (Fig. 2B). This means that we can be confident that we will produce accurate desired forces throughout the workspace when we account for the variability associated with recruitment curves.

## CONCLUSIONS

The results suggest that a probabilistic framework can be used effectively to minimize the reliance on feedback control in more complex FES systems.

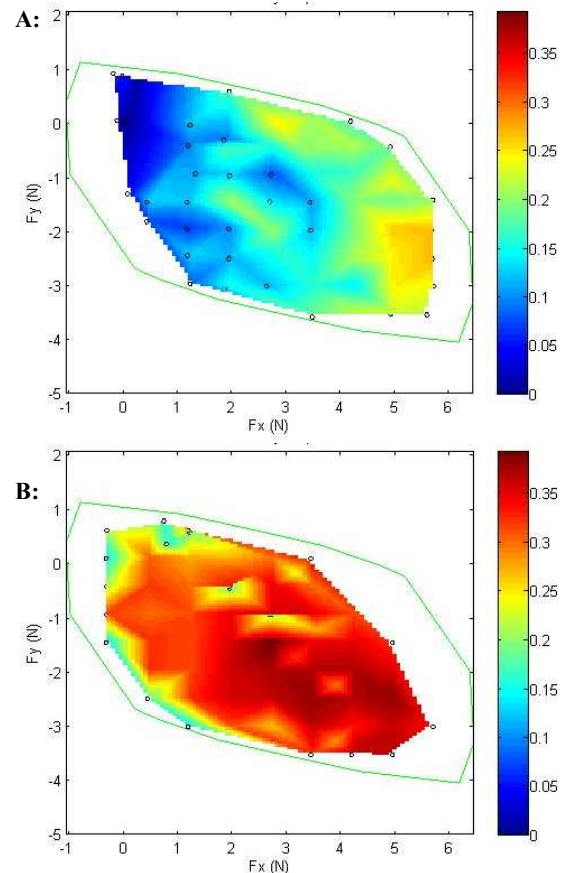


**Figure 2:** Certainty maps of isometric forces in the sagittal plane of the rat hindlimb. A: Probabilistic model. B: Deterministic model. Green outline is the feasible force space of the limb. Certainty was measured in N.

## REFERENCES

1. Peckham PH, et al. *Ann Rev Biomed Eng* **7**, 327-60, 2005.
2. Yeo SH, et al. *J Exp Biol* **214(5)**, 735-46, 2011.
3. Ichihara K, et al. *J Neuro Meth* **176**, 213-24, 2009.

## ACKNOWLEDGEMENTS

NIH R21NS061208 (MCT)  
NIH F31NS068030-01 (AMJ)



# The Relation Between Independent Control of Digit Forces and EMG-EMG Coherence During Precision Grip

<sup>1</sup>Mark Jesunathadas, <sup>1</sup>Daisuke Shibata, <sup>1</sup>Juan Laitano and <sup>1</sup>Marco Santello

<sup>1</sup>Arizona State University, Tempe, AZ, USA  
email: mjesunat@asu.edu

## INTRODUCTION

Much work has been devoted to understanding the mechanisms by which the central nervous system coordinates several hand muscles to perform precision grasp control. One possible mechanism of interest is the correlated activity of muscles, presumably due to synchronous or common inputs from higher centers. Such correlated activity may serve to couple the activity of hand muscles, which are often required to act in conjunction with one another in a stereotypical fashion. For example, both motor unit synchrony and coherence between two electromyographic (EMG) signals (EMG-EMG coherence) are relatively high for the extrinsic muscles of the hand, which often act together to maintain *equal* normal forces of the digits during grasp. In contrast the correlated activity of intrinsic muscles, which often have opposing actions or act independently exhibit relatively weak motor unit synchrony and EMG-EMG coherence [1, 2]. However, it is unknown if this correlated activity can be altered based on the independence of muscle action. Therefore, the purpose of this study was to determine if the EMG-EMG coherence of hand muscles would vary as a function of the degree of independence of digit forces during a precision grip task.

## METHODS

One male subject (26 yrs.) participated in the experimental procedures. The subject sat in an adjustable chair facing a computer monitor ~2.2 m away at eye level. The right forearm was placed on a flat rigid platform with the wrist and hand in a semi-supinated and neutral position, respectively. The hand was positioned in a 2-digit (thumb and index finger) precision grip posture for the experimental task.

The subject performed 2 sets of isometric precision grip contractions. The total target grip force for each set of contractions was set at 25% of the total maximal voluntary grip force (MVF) subjects produced. In set 1 the target forces for each digit were unequal such that the target force for the thumb and index finger was set at 60 and 40% ( $\pm 5\%$ ) of the total target force. In set 2 the target forces were equal for each digit and set at 50% ( $\pm 5\%$ ) of the total target force. Each set of contractions consisted of 10, 10 s trials.

Digit forces were measured with two 3-D force/torque transducers (ATI Nano 17, Apex, NC). The EMG activity of 5 hand muscles was recorded with intramuscular fine wire electrodes comprised of one 50  $\mu\text{m}$  wire inserted into the muscle belly via a 27-gauge hypodermic needle. The EMG signal was amplified 2000x band-pass filtered between 3 Hz and 1 kHz, sampled at 2 kHz, and stored on a computer. The muscles recorded from were the first dorsal interosseus (FDI), flexor pollicis longus (FPL), flexor digitorum superficialis (FDS2), extensor digitorum superficialis (EDS2), and extensor pollicis longus (EPL). EMG data was concatenated for the first three and final three trials separately during the period in which subject's force was within the target force for of each set of contractions. These data were used to compute the integral of the z-transformed EMG-EMG coherence in the range of 0-55 Hz between each possible muscle pair. The coherence values were compared 1) between the beginning three and final three trials for each contraction set and 2) between each set of contractions (unequal and equal digit forces). EMG signal stationarity was tested prior to coherence analysis and all EMG signals exhibited less than 10% of points outside the 95% confidence limits.

## RESULTS AND DISCUSSION

In each trial the subject was able to achieve the required target force. However, the time to reach the target force was greatest for the first trial in which the digit force targets were unequal (4.4 s) compared with the all other trials for the equal and unequal force contractions ( $1.78 \pm 0.51$  s).

The mean amplitude of the rectified EMG signals during the period of time in which digit forces were within the target forces is displayed in Table 1. Each muscle was active except for EDS2. Therefore, coherence analysis was not performed for muscle pairs that included EDS2.

The integral of the z-transformed coherence values for each muscle pair did not seem to differ between the equal (average of all muscle pairs:  $54.8 \pm 30.4$ ) and unequal (average of all muscles pairs:  $56.2 \pm 32.4$ ) digit force contractions (Figure 1).

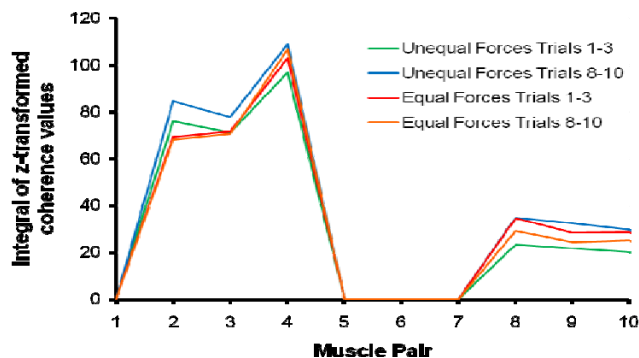


**Figure 1:** Integral of z-transformed coherence values for each muscle pair for the first and last three trials of the two different contraction conditions. Muscle pairs 1-6 are extrinsic-extrinsic pairs and muscle pairs 7-10 are extrinsic-intrinsic pairs. EDS2 was not active so the coherence values for pairs involving this muscle are 0.

Furthermore, similar to previous research [1, 2] the coherence values were larger for the extrinsic-extrinsic muscle pairs ( $83.5 \pm 15.7$ ) than the extrinsic-intrinsic muscle pairs ( $27.6 \pm 4.79$ ).

These findings seem to indicate that the central nervous system coordinates the activity of hand muscles similarly regardless of the task requirements to produce equal or unequal normal forces. This finding may be due to the fact that the EMG activity of muscles did not differ widely for the two different contraction types (Table 1). Another possible reason for this invariant behavior may be that the task still required the digits to produce primarily normal forces, which were relatively close in magnitude (60 vs. 40% of the target force). Tasks, which require the digits to perform actions that are more dissimilar in force magnitude and action (e.g. producing normal and tangential forces that are unequal across the digits) may alter the correlated activity of muscles and give insight into the functional significance of correlated neural activity. However, to date it seems that EMG-EMG coherence during isometric grasp contractions remains invariant across the a number of different task requirements [1, 2]

## REFERENCES

1. Poston B, et al. *J Neurophysiol* **104**, 1141-1154, 2010.
2. Winges SA, et al. *J Neurophysiol* **99**, 1119-1126, 2008.

## ACKNOWLEDGEMENTS

NIAMSD Grant 2R01-AR47301 to Marco Santello.

Table 1. Amplitude of rectified EMG expressed as a % of the amplitude during the MVF contraction

| Muscle | Unequal Forces (Trials 1-3) | Unequal Forces (Trials 8-10) | Equal Forces (Trials 1-3) | Equal Forces (Trials 8-10) |
|--------|-----------------------------|------------------------------|---------------------------|----------------------------|
| EPL    | 28.1                        | 27.3                         | 26.5                      | 22.7                       |
| EDS2   | -                           | -                            | -                         | -                          |
| FPL    | 24.4                        | 23.9                         | 23.4                      | 20.2                       |
| FDS2   | 22.2                        | 21.4                         | 20.5                      | 17.4                       |
| FDI    | 22.7                        | 22.3                         | 22.0                      | 19.0                       |

# LOWER EXTREMITY DYNAMICS FOR DROP JUMPS ONTO DIFFERENT SURFACES

Lewis Johnson and Steph Forrester

Sports Technology Research Group, Loughborough University, UK  
email: s.forrester@lboro.ac.uk, web: www.sports-technology.com

## INTRODUCTION

In many sports activities humans interact with elastic or viscoelastic surfaces, *e.g.* wooden or polymeric indoor sports halls and natural or artificial turf outdoor pitches. It is known that humans adjust their mechanics based on the stiffness of a surface. For submaximal activities (*e.g.* hopping) humans respond to reduce metabolic cost and improve movement economy [1], whilst for maximal activities (*e.g.* drop jumps) the response depends on the specific goal of the task [2]. Sports surfaces often exhibit a spatial variability in properties, for example through localized wear, thereby exposing humans to inconsistent surface conditions [3]. Although humans are adaptable to a known change in surface conditions during submaximal running [4] it is unknown how they respond during maximal activities. The purpose of this study was to investigate how symmetric and asymmetric surface stiffness affected maximal drop jump dynamics.

## METHODS

Ten male athletic subjects ( $21.9 \pm 1.1$  years,  $1.81 \pm 0.06$  m,  $75.9 \pm 7.2$  kg) gave informed consent. Each performed a series of drop jumps from 60 cm onto nine different surface conditions (order randomized). The surfaces comprised three foams of different stiffness (hard-H, medium-M and soft-S) with the foam under each foot controlled independently, *i.e.* S-S, S-M *etc.*. Force-deformation properties of the surfaces were determined in independent tests involving: static loading and unloading using a rigid last; dynamic loading using an Advanced Artificial Athlete; and repeated loadings using a 2.25 kg Clegg hammer.

For each surface condition, familiarization was followed by three drops jumps with the subjects instructed to jump for maximum height. Ground

reaction forces were measured using a force platform under each foot (1000 Hz, Kistler 9281CA), 3D lower body kinematics recorded using a 12 camera motion analysis system (250 Hz, Vicon Nexus) and EMG recorded bilaterally from six lower extremity muscle groups (2000 Hz, Delsys Trigno).

For each surface condition the trial with maximum take-off velocity was analyzed. The following variables were evaluated: take-off velocity, total vertical impulse, centre of mass displacement, leg stiffness, touchdown angle and range of motion for the ankle and knee. Repeated measures ANOVA with Tukey HSD post hoc were used to compare the effect of surface condition on the identified variables ( $p < 0.05$ ).

## RESULTS AND DISCUSSION

The static force-deformation characteristics for the three surfaces are shown in Figure 1. The hard surface was 1.5 to 2 times stiffer than the medium and soft surfaces, with the latter two being of closer stiffness. Similar trends were observed in the AAA results for force reduction and vertical deformation and in Clegg hammer for peak deceleration.

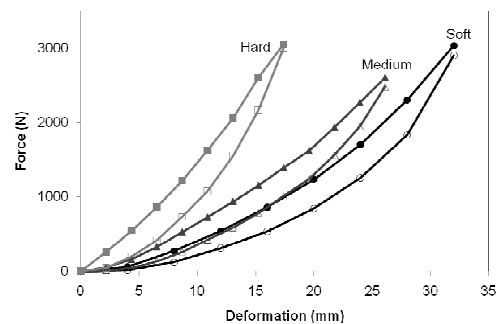


**Figure 1:** Static force-deformation plots for the three surfaces. Filled symbols = loading, outline symbols = unloading.

The performance and biomechanical results for the drop jumps are given in Tables 1 and 2. For the

three consistent surface conditions, jump height performance significantly increased as surface stiffness increased ( $p < 0.05$ ). The hard surface condition (H-H) also showed significantly increased leg stiffness and reduced ankle and knee range of motion compared to the softer surfaces ( $p < 0.05$ ). This trend contrasts submaximal activities where as surface stiffness increases leg stiffness decreases to improve movement economy [5]. However, for maximal activities movement economy is less relevant and the response is dictated by the specific goal of the task [2].

For the asymmetric surface conditions, the main observation relates to the difference between the asymmetric hard - soft condition (H-S / S-H) and symmetric hard (H-H) and soft (S-S) conditions. The hard-soft jump performance and biomechanics were significantly closer to those obtained under the symmetric soft surface conditions suggesting that the human response to asymmetric surface stiffness during a maximal drop jump activity is determined by the softest surface condition encountered. This highlights the need for control over the spatial variability in surface conditions if maximum performance is an important outcome.

## CONCLUSIONS

Surface stiffness has a significant effect on maximum height drop jump performance and biomechanics. Harder surfaces generated better jump performance achieved through a stiffer leg response. For asymmetric surface conditions, the drop jump performance and biomechanics are determined by the softer surface condition.

## REFERENCES

1. Bosco C, et al. *Ergonomics*, **40**, 670–679, 1997.
2. Arampatzis A, et al. *Med Sci Sports Exerc*, **36(3)**, 451–459, 2004.
3. Severn KA, et al. *First Int Conf Sci Tech Res Sport Surf*, 2007.
4. Ferris DP, et al. *J Biomech*, **32**, 787–794, 1999.
5. Ferris DP and Farley CT. *J Appl Physiol*, **82**, 15–22, 1997.

## ACKNOWLEDGEMENTS

The authors would like to thank Recticel (Wetteren, Belgium) for providing the foam surface samples.

**Table 1:** Mean  $\pm$  standard deviation for the main performance and biomechanical variables for the nine surface conditions. The asymmetric results are averaged over the two similar conditions, *i.e.* H-S / S-H is the average of H-S and S-H.

| Surface                         | H-H             | M-M             | S-S             | H-S / S-H       | H-M / M-H       | M-S / S-M       |
|---------------------------------|-----------------|-----------------|-----------------|-----------------|-----------------|-----------------|
| 1 $V_{TO}$ ( $m \cdot s^{-1}$ ) | $2.67 \pm 0.14$ | $2.64 \pm 0.19$ | $2.58 \pm 0.25$ | $2.60 \pm 0.22$ | $2.58 \pm 0.20$ | $2.63 \pm 0.19$ |
| 2 $I_Z$ ( $N \cdot s$ )         | $389 \pm 72$    | $390 \pm 65$    | $392 \pm 68$    | $396 \pm 72$    | $387 \pm 66$    | $390 \pm 64$    |
| 3 $CM_{DIS}$ (cm)               | $34.8 \pm 8.7$  | $34.9 \pm 8.3$  | $36.1 \pm 8.2$  | $36.5 \pm 8.5$  | $34.7 \pm 8.2$  | $35.5 \pm 7.7$  |
| 4 $k_L$ ( $N \cdot m^{-1}$ )    | $12.8 \pm 5.5$  | $12.2 \pm 5.7$  | $11.8 \pm 5.6$  | $11.2 \pm 4.4$  | $12.4 \pm 5.8$  | $12.0 \pm 5.3$  |
| 5 $\theta_A^{TD}$ (deg.)        | $-10.1 \pm 6.1$ | $-11.7 \pm 5.8$ | $-12.1 \pm 7.2$ | $-12.1 \pm 5.4$ | $-11.4 \pm 5.7$ | $-12.0 \pm 5.9$ |
| 6 $\theta_K^{TD}$ (deg.)        | $24.2 \pm 6.7$  | $23.4 \pm 6.4$  | $23.0 \pm 5.7$  | $24.1 \pm 6.2$  | $23.3 \pm 6.1$  | $23.4 \pm 6.5$  |
| 7 $\Delta\theta_A$ (deg.)       | $41.5 \pm 8.3$  | $42.9 \pm 8.2$  | $42.5 \pm 9.8$  | $43.3 \pm 7.0$  | $42.4 \pm 8.5$  | $43.2 \pm 8.2$  |
| 8 $\Delta\theta_K$ (deg.)       | $68.7 \pm 17.4$ | $69.0 \pm 17.1$ | $71.4 \pm 16.0$ | $71.1 \pm 17.0$ | $68.8 \pm 17.6$ | $70.4 \pm 17.0$ |

Notes:  $V_{TO}$  = take-off velocity,  $I_Z$  = vertical impulse;  $CM_{DIS}$  = displacement of the centre of mass;  $k_L$  = leg stiffness,  $\theta_A^{TD}$ ,  $\theta_K^{TD}$  = ankle, knee touchdown angle;  $\Delta\theta_A$ ,  $\Delta\theta_K$  = ankle, knee range of motion.

**Table 2:** Summary of the significant differences ( $p < 0.05$ ) between surface conditions. The numbers refer to the variable reference number given in the first column of Table 1 above.

|     | H-H | M-M   | S-S     | H-S         | H-M | M-S |
|-----|-----|-------|---------|-------------|-----|-----|
| H-H |     | 4,5,7 | 1,4,5,8 | 1,3,4,5,7,8 | 1,5 |     |
| M-M |     |       | 1       |             | 1   | -   |
| S-S |     |       |         | 6           |     | 1   |

# A NOVEL METHOD TO PREDICT POSTURE OF HUMAN MODEL WHEN DESIGNING RESISTANCE TRAINING MACHINES USING MUSCULOSKELETAL ANALYSIS

<sup>1,2,3</sup>Moonki Jung, <sup>1,2</sup>Yeonghun Kim, <sup>1,2</sup>Kilhyun Cho and <sup>1,2</sup>Kunwoo Lee

<sup>1</sup>School of Mechanical and Aerospace Engineering, Seoul National University, Seoul, Korea

<sup>2</sup>Institute of Advanced Machinery and Design, Seoul National University, Seoul, Korea

<sup>3</sup>BK21 Scholl for Creative Engineering Design of Next Generation Mechanical and Aerospace Systems, Seoul National University, Seoul, Korea

email: [mk555@snu.ac.kr](mailto:mk555@snu.ac.kr) web: <http://hccl.snu.ac.kr>

## INTRODUCTION

The focus of product development is shifting from the product to the person using the product. It is now essential to consider both the product and the human body at the same time while designing and analyzing any product that requires close interaction with the human body during usage. In order to analyze human motion when human uses a product, it is effective to use motion capture system. But in design stage which doesn't have a prototype or a real product, it is impossible to use motion capture system. In this case, a method which predicts human posture as using inverse kinematics and optimization, and evaluates a product through simulation. In design stage, the method which creates a human posture is different depending on characteristic and object. Generally an objective function is defined according to an assumption which is human set the most comfort posture. But the product which has a special object, like fitness equipment, it needs to add a constraint to apply the object in posture creation stage. This paper suggests a method creating a human posture with satisfying an additional constraint when human uses incline chest press machine which is one of resistance training machines

## METHODS

In order to predict human posture in design stage and apply the result to a product, the information of the product designed on SolidWorks which is a commercial CAD system is converted to the information which can use on AnyBody which is a musculoskeletal analysis software. And some reference nodes are added for defining the interaction between product and human model.

The constraint which makes the reference node defined on CAD model coincides with end-effector of human model is created in order that human get a posture according the object. For creating the posture which is gotten when human exercise with incline press machine, the interaction between human model and product is defined at hands, foos, pelvis and thorax. The objective function to predict human posture is human body comfort evaluation model used by Marler [1], anyway this research make end-effector coincide with CAD model not only position but also orientation in numerical formula (2).

Objective function:

$$f_{\text{discomfort}} = \sum_{i=1}^n w_i (q_i - q_i^N)^2 \quad (1)$$

End-effector position and orientation constraint:

$$\| X(q) - T_{\text{target}} \| \leq \varepsilon \quad (2)$$

Range of each joint angle:

$$q_i^L \leq q_i \leq q_i^U \quad (i = 1, \dots, n) \quad (3)$$

In case of general products, human postures can be predicted by optimization using the discomfort function. But in case of products have special purpose; e. g. resistance training machines; postures of human model should consider the purpose of products. In this study, we gave additional constraints between the human model and the product when generating human posture which satisfied the purpose of the product. A trend that the position of the elbow joint is placed on the virtual plane that formed with a shoulder joint and a handle of machine can be found when people using incline chest press machine. The reason for this is

counterbalancing moments generated by weights by sustaining handles of incline press machine by lower arms vertically as possible as human can. To consider this trend when generating human postures, we added end-effectors on each elbow joint of human model and gave soft constraints between end-effectors and virtual planes in AnyBody.

By adding additional constraints and using optimization method to minimize  $f_{\text{discomfort}}$ , we can get the posture of the human model performed an incline chest press motion like Figure 1.

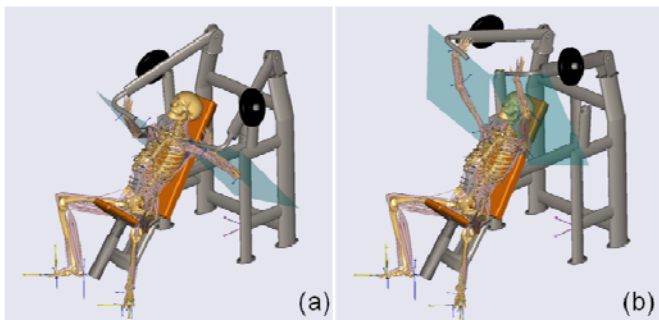


**Figure 1:** Posture of the human model in Anybody satisfied additional constraints on elbow joints (a) initial posture (b) final posture

## RESULTS AND DISCUSSION

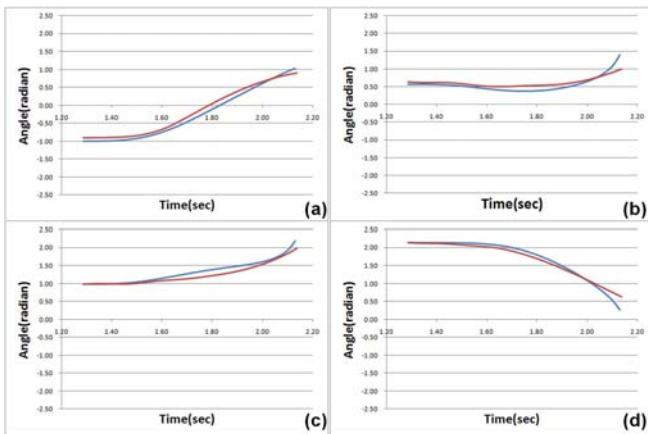


**Figure 2:** Compared result of simulated joint angles (blue lines) with motion capture driven motion (red lines), (a) glenohumeral flexion (b) glenohumeral external rotation (c) glenohumeral abduction (d) elbow flexion

To validate posture of human model considering additional constraints on elbow joints, we compare the simulated human posture with data driven human posture that captured motion of human performed exercise using incline chest press

machine. Figure 2 shows compared results about joint angles of glenohumeral joint and elbow joint of a simulated posture and a motion capture data driven posture. Patterns of joint angles of simulated posture are similar to those of joint angles of motion capture driven posture

## CONCLUSIONS

In this paper, design information of incline chest press machine acquired from CAD system. And musculoskeletal simulation has performed with combined information of product with musculoskeletal human model to generate human posture. And validate results of new algorithm by comparing with experimental results by producing real machine. If the design or structure of training machine that constrain the human posture has changed, the algorithm assumed in this paper that constrains human posture may change. There are many kinds of algorithms to predict a human motion, however one of those algorithms doesn't guarantee that the algorithm can predict every motions successively. If an algorithm that predicting human postures based on acquired motion capture data when we design a new training machine or equipment is developed, human posture can be predicted even if design parameters of that machine have changed, so design of product also can be optimized to maximize its special purpose.

## REFERENCES

1. Marler RT, et al. *Eng. Optimiz* **41**, 925-943, 2008.
2. AnyBody, Anybody Technology.
3. SolidWorks, Dassault Systèmes SolidWorks Corp
4. Engelson V, et al. *Proceeding of SIMS'2003*, Västerås, Sweden, 2003
5. Andersen MS, et al. *Comput Meth Biomech Biomed Eng* **12**, 371-384, 2009

## ACKNOWLEDGEMENTS

This research was supported by Basic Science Research Program through the National Research Foundation of Korea(NRF) funded by the Ministry of Education, Science and Technology(2011-0001147).

# GAIT KINEMATICS CHANGE WHEN EMOTIONS ARE FELT VS. PORTRAYED

Gu Eon Kang and Melissa Gross

University of Michigan, Ann Arbor, MI USA  
email: guekang@umich.edu web: <http://www.umich.edu/~mgross>

## INTRODUCTION

Body movements change when emotions are expressed [1,2]. In studies of emotion-related body movements, emotions are elicited in individuals and encoded in their body movements. Selection of movement trials for analysis is typically based on successful decoding of emotion (i.e., recognition of emotion by observers) without consideration of the emotional experience of encoders. Whether body movements differ when emotions are actually felt rather than just portrayed by the encoders is not known. Further, assessment of the emotional experience of encoders contributes substantially to participant burden in experimental protocols; if emotions can be encoded effectively whether emotions are actually felt or not, methodological efficiency would be increased. The purpose of this study was to test whether gait kinematics differed between trials in which encoders felt or did not feel the decoded emotion. Study outcomes will be useful in designing future studies of emotion kinematics.

## METHODS

Gait data analyzed in this study were generated in two previous studies in our laboratory [3,4]; the methods in both previous studies are described here briefly. Anger, sadness, joy, contentment, and neutral emotion were elicited in 60 young healthy individuals using an autobiographical memories task. After recalling their own emotional memories, participants walked across the lab while kinematic and video data were acquired. To assess the feelings they experienced during walking, participants rated the intensity of eight emotions with a 5-item Likert scale immediately following each gait trial. Trials in which walkers felt an emotion with at least moderate intensity (score  $\geq 3$ ) were considered *felt*.

Whole body motion data were acquired using a video-based, 6-camera system (120 Hz). Marker

coordinate data were filtered at 6 Hz. Gait data were calculated using Visual 3D software. For each gait trial, mean angles were calculated for the neck, trunk, thorax and shoulder girdle. Range of motion (ROM) was calculated for shoulder, elbow, wrist, hip, knee and ankle angles, and for trunk rotation and lateral tilt, and pelvis rotation and lateral tilt.

To determine which emotions were encoded in the body movements during gait, videos of the walkers with faces blurred were shown to 90 observers. After viewing each video, observers selected one of ten feelings that they thought the walker felt. An emotion was *recognized* if the mean observer response rate for an emotion exceeded chance level (10%). A Chi square test was used to test if mean responses differed from chance; all mean response rates exceeded chance level ( $p < .05$ ).

Gait trials were first separated into groups based on which emotion was recognized by observers, and then were separated into two groups based on whether the recognized emotion was felt (F) or not felt (NF) by the walkers. Within each recognized emotion group, data were averaged for the F and NF groups. A mixed model with random walker effects and fixed effects of F/NF group and walker gender was used to test for differences ( $p < .05$ ).

## RESULTS AND DISCUSSION

Mean recognition rates were 16 and 7% greater in F than NF groups for sadness and anger, respectively ( $p < .01$ ) (Table 1). Mean recognition rates were similar between F and NF groups for both joy and contentment.

Mean gait velocity decreased 10% when sadness was felt (F=1.19 m/s; NF=1.32 m/s), and increased 7% when anger was felt (F=1.39 m/s; NF=1.30 m/s), compared to the corresponding NF groups ( $p < .01$ ). Gait velocity was similar between groups for joy

and contentment (1.35 and 1.30 m/s, respectively). Stride length and cadence decreased when sadness was felt (F=1.29 m and 110 steps/min; NF=1.37 m and 114 steps/min;  $p < .01$ ). For anger, joy and contentment, stride length and cadence (1.40, 1.38 and 1.34 m, and 118, 117 and 116 steps/min, respectively) were similar between F/NF groups.

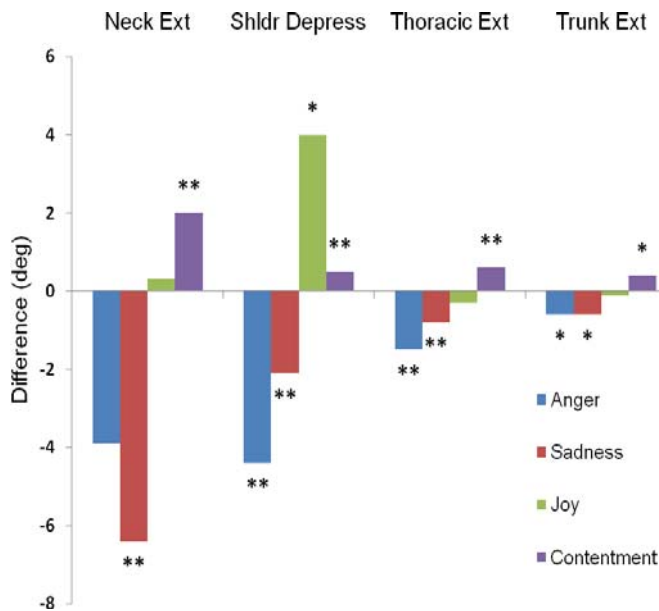


**Figure 1:** Difference in mean angles when emotions were felt by walkers.  $**p < .01$ ,  $*p < .05$ .

Joint ROM differed between F/NF groups for sadness and anger but not for contentment and joy. Shoulder, elbow and wrist ROM decreased 9, 18 and 20%, respectively, when sadness was felt ( $p < .05$ ). Hip ROM decreased 5% for sadness, and increased 5% for anger, in F compared to NF groups ( $p < .05$ ). Trunk rotation ROM decreased 13% ( $p < .01$ ) for sadness and trunk tilt ROM increased 4% for anger ( $p < .05$ ). Knee and ankle ROM was similar between F/NF groups for all emotions.

Mean angles were slightly but significantly different between F and NF groups for all emotions (Fig. 1). The shoulders were more elevated when sadness and anger were felt, and were more depressed when joy and contentment were felt. Mean thorax angles were more flexed when sadness and anger were felt, and were more extended when contentment was felt. Similarly, trunk extension decreased 11% when sadness and anger were felt, and increased 8% when contentment was felt, compared to NF groups.

## CONCLUSIONS

Results of this study indicated that gait kinematics differed between trials in which the recognized emotions were felt rather than just portrayed by the walkers. Mean joint angles seemed to be most sensitive to the emotion experienced by the walker, suggesting that body posture may be a particularly important cue in studies of bodily expression. Further, results suggest that assessment of encoders' subjective emotional experience is an important experimental variable and should be included in studies of emotion encoding in body movement.

## REFERENCES

- Gross MM et al. *J Nonverbal Behavior* **34**, 233-248, 2010.
- Roether CL et al. *J Vision* **9**, 1-32, 2009.
- Crane EA et al. In: England D (Ed.), *Whole Body Interaction*, Springer, 2011.
- Edgeworth R et al. *Proc Amer Soc Biomechanics*, Ann Arbor, MI, USA, 2008.

## ACKNOWLEDGEMENTS

We thank John Berra, Ningyan Chen, Alexandra Rusetzke and Jenna Cooper for help with data analysis.

**Table 1:** Mean emotion recognition rate, number of walking trials, number of walkers generating the trials, and proportion of female walkers included in the Felt and Not Felt groups for each recognized emotion.

| Recognized Emotion | Recognition Rate (%) |      | Trials (n) |      | Walkers (n) |      | Females (%) |      |
|--------------------|----------------------|------|------------|------|-------------|------|-------------|------|
|                    | Not Felt             | Felt | Not Felt   | Felt | Not Felt    | Felt | Not Felt    | Felt |
| Anger              | 23                   | 30   | 45         | 46   | 34          | 40   | 35.6        | 45.0 |
| Sadness            | 34                   | 50   | 67         | 55   | 38          | 48   | 47.4        | 38.7 |
| Joy                | 28                   | 31   | 36         | 48   | 25          | 32   | 64.0        | 59.4 |
| Contentment        | 24                   | 28   | 98         | 69   | 54          | 51   | 53.7        | 47.1 |

## Phase Identification of Sitting Pivot Wheelchair Transfers

<sup>1,2</sup>Padmaja Kankipati, <sup>1,2</sup>Alicia Koontz, <sup>1,2</sup>Alejandra Vega and <sup>1,2</sup>Yen-Sheng Lin

<sup>1</sup>Human Engineering Research Laboratories, Department of Veterans Affairs, Pittsburgh, PA

<sup>2</sup>Department of Rehabilitation Science and Technology, University of Pittsburgh, Pittsburgh, PA

email: [pak33@pitt.edu](mailto:pak33@pitt.edu)

### INTRODUCTION

The ability to perform sitting pivot transfers (SPTs) amongst people with Spinal Cord Injury (SCI) is a crucial factor in the maintenance of an independent and high functioning lifestyle [1]. This high reliance on the upper arms to lift and support the weight of the body throughout the transfer is partially responsible for the high prevalence of shoulder pain [2]. In order to obtain a better clinical understanding of the biomechanics of the upper limbs through the duration of a transfer it is commonly delineated into three distinct phases. The phases being: pre-lift phase (also known as the preparatory phase), lift phase (where the arms are predominantly weight bearing), and the descent/post lift phase. Gagnon et al[3] summarized the various kinematic and kinetic parameters used in delineation of transfer phase and found that no consensus existed as to an optimal technique for phase identification. This is in part due to the different experimental set ups that are currently being used to study SPTs. The purpose of this paper is twofold 1) Describe an identification technique which incorporates force information in combination with marker position data to delineate the different phases of a transfer and 2) Compare peak resultant shoulder forces between phases.

### METHODS

**Subjects:** Eight male participants with paraplegia provided informed consent prior to participation in the study. The inclusion criteria were: SCI at C4 level or below that occurred over one year prior to the start of the study, able to independently transfer to/from a manual wheelchair without human assistance or assistive devices, over 18 years of age, and free from upper extremity pain that influenced their ability to transfer. **Experimental Protocol:** Participants used their personal wheelchairs (WCs) to transfer to and from a bench. For all transfers the wheelchair was positioned and secured at a comfortable angle to an adjustable height tub bench (Figure 1). The bench was adjusted to be level with the subject's wheelchair seat. The platform shown

in Figure 1 contains two force plates (Bertec Corporation, Columbus, OH), one beneath the wheelchair and one beneath the tub bench. The wheelchair and bench were secured to the platform. A steel beam attached to a 6-component load cell (Model MC5 from AMTI, Watertown, MA) was positioned to simulate a wheelchair armrest. A seven camera 3D motion capture system and Nexus 1.6.1 software (Vicon Peak, Lake Forest, CA) measures the position of reflective markers placed on the back, chest, and arms during the transfer. The cameras are positioned around the platform so as to minimize marker drop out. Kinematic and kinetic data were collected at 60 Hz and 360Hz respectively.

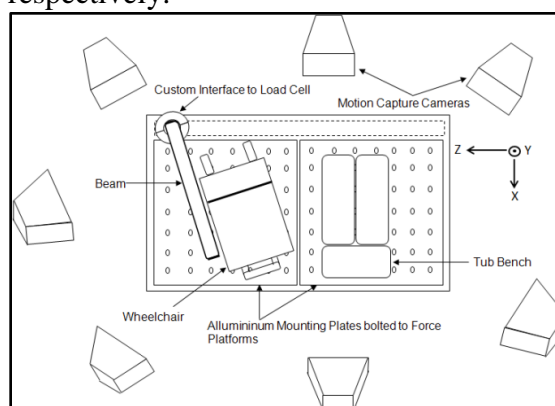


Figure1. Experimental Setup

Participants were instructed to perform a lateral transfer as they normally would from their wheelchair to the adjacent level tub bench and back. Participants were allowed to practice prior to recording three trials.

**Data Analysis:** Kinetic and kinematic data were filtered using a zero-lag low-pass Butterworth, 4<sup>th</sup> order filter with 7 and 5 Hz cut-off frequencies respectively. The vertical forces from the force plate under the tub bench, wheelchair and the force-sensing beam (wheelchair side) were superimposed onto one plot to analyze the phases of transfer. Trunk motion, represented by the C7 and T3 markers, were added to the force data to assist with the delineation of phases of transfer. An inverse

dynamic model [5], was used to calculate peak net shoulder joint resultant force, for both the leading (i.e. arm reaching to the new surface) and trailing arm (i.e. arm behind during move to new surface). Shoulder forces were calculated for each transfer to and from the bench and averaged across the three trials. Differences between the three phases and between the leading and trailing arm, were evaluated using a Two-Way Within subjects ANOVA and a 0.05 level of significance. Main and interaction effects were investigated using simple pair wise comparisons and a post hoc Bonferroni correction. WC to bench and bench to WC transfer were analyzed using two separate models. The statistical tests were performed in SPSS (SPSS Inc., Chicago-IL).

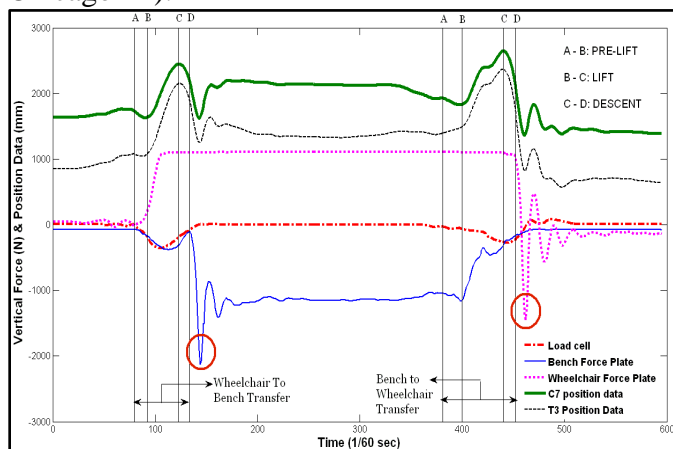


Figure 2 Representative self selected transfer recordings

## RESULTS AND DISCUSSION

Group mean (standard deviation) age, weight and height were 39.5 (11.60) years, 80.80(23.18) kilograms and 1.79 (0.1) meters respectively. The sample had lesion levels varying between T4 – L3. Our definitions of the phases are: Pre-lift (Figure2, A-B) – Begins as soon as force is detected on the grab bar and ends when the buttocks are off the WC/bench as detected by the force plates and a dip in the C7 and T3 marker indicative of trunk flexion; Lift phase (Figure2, B-C)– Begins as soon as the buttocks are off the chair/bench and ends when the trunk is at its highest elevated point (indicated by the peak seen in the C7 and T3 position data); Descent (Figure2, C-D)–begins as soon as the trunk lowers towards either bench/chair and the end of

this phase occurs just prior to the large negative spikes on the WC/bench (circled in Figure 2), which are indicative of the buttocks landing on each surface. Personal style of transferring (e.g. using more of an upright trunk position versus a forward flexed trunk) affected the trajectory of the C7 marker. In these cases we found that the T3 marker provided a more consistent pattern as compared to the C7. As a result both markers should be used for reliable phase identification. This identification method was consistent amongst the participants who varied in self-selected SPT techniques, trunk balance and function. Shoulder forces were significantly higher for the WC to bench lift and descent phases compared to the pre-lift phase in both trailing and leading shoulders ( $p < 0.043$ , Table1). The pre-lift phase had significantly higher forces at the trailing arm as compared to the leading arm for the same transfer ( $p < 0.03$ ). The transfer from the bench to WC imposed higher demands on the shoulders than moving from the WC to bench. Forces in the trailing shoulder were significantly higher for the pre-lift compared to the descent phase ( $p < 0.009$ ) and were higher than the leading shoulder for all phases of transfer ( $p < 0.044$ ). The high forces observed during the pre-lift and descent phases may provide critical information about the dynamic postural control requirements of performing SPTs. Thus prior studies that only analyzed the lift phase of transfer may be missing clinically relevant information concerning transfer technique. A complete analysis of transfer phases will be critical for determining best practices and interventions related to SPT performance.

## REFERENCES

- Nyland, J., et al., Preserving transfer independence among individuals with spinal cord injury. [Review] [70 refs]. *Spinal Cord*, 2000. 38(11): p. 649-657.
- Dalyan, M., D.D. Cardenas, and B. Gerard, Upper extremity pain after spinal cord injury. *Spinal Cord*, 1999. 37(3): p. 191-195.
- Gagnon, D., et al., Biomechanics of Sitting Pivot Transfers Among Individuals with a Spinal Cord Injury: A Review of the Current Knowledge. *Topics in Spinal Cord Injury Rehabilitation*, 2009. 15(2): p. 33-58.

## ACKNOWLEDGEMENTS

Funding for this study was provided by the Department of Veteran Affairs (A4489R) and the National Science Foundation, Project EEC 0552351.

| Variable                   | Wheelchair To Bench Transfer |                             |                             | Bench to Wheelchair Transfer |                             |                             |                            |
|----------------------------|------------------------------|-----------------------------|-----------------------------|------------------------------|-----------------------------|-----------------------------|----------------------------|
|                            | Arm                          | Pre-Lift                    | Lift                        | Pre-Lift                     | Lift                        | Descent                     |                            |
| Peak Resultant Force (%BW) | Trailing Arm                 | ¥13.38(7.97) <sup>a,b</sup> | 23.55(11.25) <sup>a</sup>   | 23.97(5.38) <sup>b</sup>     | &76.15(5.75) <sup>f</sup>   | +68.45(11.95) <sup>Ω</sup>  | 45.08(18.07) <sup>f</sup>  |
|                            | Leading Arm                  | ¥9.88(5.53) <sup>c,d</sup>  | 24.43(12.55) <sup>d,e</sup> | 36.04(15.10) <sup>c,e</sup>  | &10.45(4.64) <sup>g,i</sup> | +18.02(7.01) <sup>h,i</sup> | 26.31(7.55) <sup>g,h</sup> |

Table 1 Mean (SD) of the peak resultant forces represented as % BW (= F (N)/Weight (N)) at both leading and trailing shoulders. Letters a-i and symbols (¥, &, + and Ω) represent pairwise significant differences between phase and arm respectively, at a significance level of  $p < 0.05$ .

# ROBOTIC PERFORMANCE-BASED RESISTANCE VERSUS ASSISTANCE FOR LEARNING OF A NOVEL GAIT PATTERN WITH A ROBOTIC EXOSKELETON

Pei-Chun Kao<sup>1</sup>, Shraddha Srivastava<sup>1</sup>, Sunil K Agrawal<sup>2</sup>, and John P Scholz<sup>1</sup>

<sup>1</sup>Department of Physical Therapy, <sup>2</sup>Department of Mechanical Engineering, University of Delaware, Newark, DE, USA  
Email: [kaop@udel.edu](mailto:kaop@udel.edu)

## INTRODUCTION

Robotic exoskeletons have potential to aid in gait rehabilitation for individuals with neurological dysfunction. To maximize the training effects, it is important to choose control algorithms for the robotic devices that best facilitate motor learning. The principle of performance-based assistance (assist-as-needed), partly derived from the clinical convention, is one method that has been implemented in the control algorithms of some current robotic devices. However, the nature of assist-as-needed limits performance error and may reduce human effort when learning a dynamic motor task (Emken et al, 2007). Error detection is an important stimulus for optimal motor learning.

An alternative control algorithm for robotic training is performance-based resistance. Such error-enhancement training provides additional kinetic and proprioceptive biofeedback to subjects when their gait patterns deviate from a target pattern. The purpose of the current study was to investigate whether robotic performance-based error-enhancement training would better facilitate short-term changes in a person's gait pattern compared to performance-based assistance during treadmill walking, as a basis for future implementations with individuals with gait disability.

Target gait patterns that corresponded to an increased height of the ankle's spatial path were created for training. The amount of robotic resistance or assistance varied based on the amount of deviation between subject's actual ankle positions and the target ankle path. Neither group received visual feedback about the prescribed template for their ankle path, or of their instantaneous ankle positions during training. They

were asked to discover the target gait pattern (virtual path) by attempting to minimize the robotic forces. We hypothesized that the error-enhancement group would exhibit an ankle path closer to the virtual path after single session of training compared to the assist-as-needed group.

## METHODS

We used a robotic leg exoskeleton (Banala et al, 2007) (**Fig 1**) to facilitate changes in subjects' gait patterns while they walked on the treadmill. Ten neurologically intact subjects were assigned to each of two groups: error-enhancement and assist-as-needed. When their instantaneous ankle positions were below the virtual wall of the virtual ankle path, normal forces were applied, either away from or toward the virtual path, respectively (**Fig 2**).

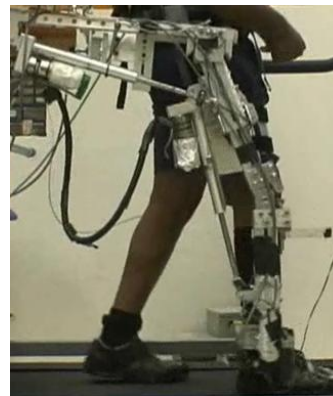


**Fig 1.** The unilateral robotic leg exoskeleton has linear actuators at the hip and knee joints powering the sagittal plane joint movements.

Kinematic data from the right leg were collected while subjects walked with the leg

exoskeleton (1) for 10 minutes without the performance-based force-field (Baseline), (2) for 45 minutes with the force-field turned on (Training), (3) for 10 minutes without the force-field (Post-test). We also collected four 30-second catch trials (i.e., turning off the force-field unexpectedly) during the training. For the post-training sessions, subjects were not informed that the force-field was turned off.

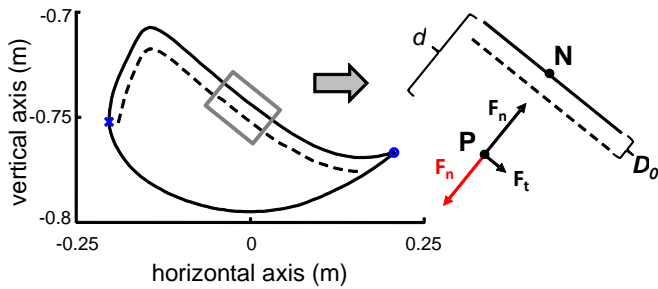


**Fig 2.** Ankle path template with origin set at the hip joint. When subjects' instantaneous ankle position (P) fell below the nearest point on target template (N), the error-enhancement algorithm would tend to take the subject's leg further away from the target (N) while the assist-as-needed algorithm would provide a compliant force to bring subject's leg towards the target (N).

To quantify the deviation between subjects' actual and the virtual ankle path, we computed the area enclosed between the two during the swing phase. We then normalized the area of each trial to the area between baseline and the virtual ankle path.

## RESULTS AND DISCUSSION

While the force-field was on during the training sessions, both groups of subjects walked with an ankle path closer to the virtual ankle path, evidenced by the smaller deviated area between the two paths compared to the baseline (**Fig 3**). By the end of training, both the error-enhancement and assist-as-needed groups showed a significant reduction in the computed area (Tukey's HSD post hoc test,  $p < 0.05$ ) by 33% and 37%, respectively.

While the robotic force was off during the catch and post-training trials, the error-enhancement group maintained an ankle path closer to the prescribed ankle path. In contrast, the assist-as-needed group returned to their baseline performance (**Fig 3**). For error-enhancement group, the deviated area in the catch and post-training trials were all significantly different from the deviated area at the baseline (THSD,  $p < 0.05$ ). There were no significant differences in the deviated area while the force-field was off compared to the baseline (THSD,  $p > 0.05$ ) for the assist-as-needed group. This finding differs from previous results of Kim et al. (2010) who showed a persistent effect with assist-as-needed training. That may have been due to the additional presence of visual feedback provided in that study.

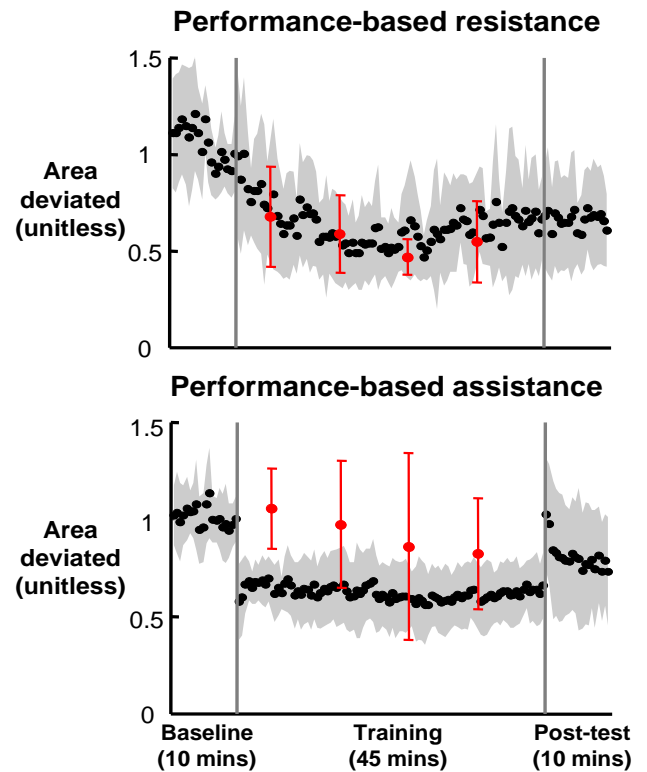


**Fig 3.** Normalized deviated area between subjects' actual and their prescribed ankle paths are shown for each trial. The red dots and associated error bars represent the mean  $\pm$  1SD during the catch trials.

## SUMMARY/CONCLUSIONS

Only the subjects walking with a force field that enhanced ankle path deviations from a prescribed virtual path led to short-term changes in their gait pattern when the force field was removed. Thus, the results of this proof-of-concept study suggest that a robotic training strategy emphasizing an error-enhancement may be more effective for promoting changes in gait patterns of persons with neurological dysfunction than an assist-as-needed paradigm. However, more study is clearly needed with patients before such a conclusion is warranted.

## REFERENCES

1. Emken, et al. JNER, 2007.
2. Banala, et al. IEEE international conference on robotics and automation, 2007.
3. Kim, et al. EBR, 2010.

## ACKNOWLEDGMENTS

Supported by NIH grant HD038582.

# LOCALIZED STRAIN MEASUREMENTS OF THE INTERVERTEBRAL DISC DURING BIAXIAL TENSILE TESTING

Thomas Karakolis, Jack P. Callaghan

Department of Kinesiology, University of Waterloo, Waterloo, ON, Canada  
email: tkarakol@uwaterloo.ca

## INTRODUCTION

Intervertebral disc herniation is defined as the nucleus pulposus breaching the outer margin of the surrounding lamellar structure of the annulus fibrosus[1]. Interlamellar and intralaminar failure of the annulus have both been described as potential modes and contributing factors of disc herniation[2]. Attempts to characterize initial lamellar failure of the annulus have involved tensile testing of small tissue samples[3] to understand the injury initiation mechanics involved in disc herniation. The purpose of this study was to develop a method of measuring local strains (Figure 1) through image analysis of a tensile test conducted on an isolated sample of annular tissue in order to enhance studies of interlamellar and intralaminar annulus tissue failure and injury initiation.

## METHODS

A tissue sample (approx 4 mm x 4 mm x 0.36 mm), consisting of two adjacent layers of the superficial anterior annulus at the C3/C4 level of the porcine spine was biaxial tested to 10% tensile strain (measured from stepper motor actuator displacements) in two orthogonal directions. High resolution images were captured of the tissue surface throughout all testing (1280x690 pixels). Five biaxial tests were collected with no physical markers on the surface of the annulus tissue, and an additional five were collected with small reflective particles acting as physical markers on the surface of the tissue.

### Part A: Strain Estimation Average/Distribution

Surface strains were estimated based on the motion of virtual source points created to track the naturally occurring texture on the tissue surface (using a template matching algorithm previously described

[4]). The number of virtual points used was varied (25 points, 100 points, 400 points) in an attempt to determine an optimal strain mesh resolution. This comprised of three different grids of square strain elements sized: 0.8 mm, 0.4 mm, 0.2 mm. Average strain was calculated for the elements of each mesh resolution, and strain distribution was expressed as the standard deviation of the elemental strains in each mesh. It was hypothesized that average strain distribution would remain constant between the three mesh sensitivities, and strain distribution would increase as mesh sensitivity increased.

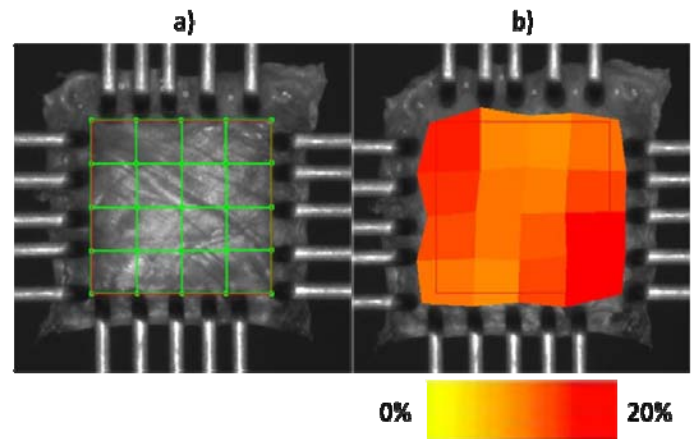


**Figure 1:** a) Tissue sample prior to tensile loading with 25 virtual source points overlaid creating strain elements approximately 0.8 mm x 0.8 mm. b) Tissue sample during tensile testing with local (principal strain map overlaid).

### Part B: Strain Estimation Error

The accuracy of the point tracking was assessed through a comparison of the virtual point tracking method to a method of tracking the motion of physical markers placed on the tissue surface (gold standard or criterion measure). From this, an average tracking error was defined. A local strain estimation error was defined as: average tracking error / initial strain element size. It was hypothesized that average tracking error would

remain constant regardless of the number of tracking points (or mesh sensitivity), and the local strain estimation error would increase as mesh sensitivity increased.

## RESULTS AND DISCUSSION

Increasing the resolution of the local strain grid resulted in an increased distribution of estimated local strains and did not result in an increase in average estimated local strain calculated (Table 1).

Average virtual point tracking error at 10% strain was found to be: 0.028 mm and 0.037 mm (in the x and y-directions respectively) for the 25 point mesh; and 0.023 mm and 0.028 mm for the 100 point mesh. Local strain estimation error was quantified as 3.5% and 3% in the x and y-directions respectively for 25 virtual marker points at 10% biaxial tensile tissue strain and 9.25% and 7% for 100 virtual marker points (Table 2).

**Table 2:** Local strain estimation error of the virtual grid compared to the marker tracked displacements at 10% strain, as determined from the tracking error and initial element size.

| Number of Tracking Points | 25           | 100           |
|---------------------------|--------------|---------------|
| X direction               | 3.5 % strain | 9.25 % strain |
| Y direction               | 3 % strain   | 7 % strain    |

It was previously assumed there is an error associated with tracking each virtual point using the surface texture of porcine annulus tissue [5]. *Part B* of this study is the first known attempt at quantification of this error. The error in tracking the virtual points is the limiting factor when deciding upon the number of tracking points to be used for local strain estimation, and more specifically the spacing between tracking points (or

**Table 1:** Local strain measurements, as calculated by varying parameters using a template matching algorithm, for a bi-layer annulus tissue sample (no markers) biaxially tested to 10% strain. SD - Standard Deviation

| Grid Element Size (mm) | 0.8            |        | 0.4            |        | 0.2            |        |
|------------------------|----------------|--------|----------------|--------|----------------|--------|
|                        | Average Strain | SD     | Average Strain | SD     | Average Strain | SD     |
|                        | 0.0966         | 0.0412 | 0.0876         | 0.0691 | 0.09           | 0.1059 |

strain element size/mesh resolution). It was found that the tracking error for the virtual points remained relatively constant as the number of tracking points increased. Consequently, as the initial mesh element size decreased with the increased tracking points, the strain estimation error increased.

This increasing strain estimation error could explain the increasing distribution of strains as the element size decreased (found in *Part A*). It is likely that the increase in distribution is a result of errors in the tracking rather than the higher resolution grid being able to measure the actual strain distribution in the tissue with a higher level of sensitivity.

## CONCLUSIONS

The findings of this study indicate that low resolution contour tracking local strain grids have a moderately high potential for error. In future, it is recommended that a physical marker technique be used to track point displacement and estimate local strains. In the cases where this is not possible, and use of the naturally occurring surface texture of the annulus tissue must be used to estimate local strain, determination and reporting of average tracking error and local strain error terms is recommended.

## REFERENCES

1. Adams MA and Hutton WC. *Spine* **10**(6), 524-531, 1985
2. Veres et al. *Spine* **33**(25), 2711-2720, 2008
3. Zhu et al. *Clinical Biomechanics* **23**, S74-S82, 2008
4. Veldhuis JH, Brodland GW. *Image and Vision Computing* **17**, 905-911, 1999
5. Karakolis T, et al. *Canadian Society of Biomechanics Biannual Meeting*, Kingston, ON, Canada, 2010

# A COMPARISON BETWEEN DART-THROWING MOTION PLANE ROM AND THE DASH SCORE AFTER DISTAL RADIUS FRACTURE

<sup>1</sup>Kenji Kasubuchi, <sup>2</sup>Takahiko Fukumoto and <sup>2</sup>Hidetaka Imagita

<sup>1</sup>Heisei Memorial Hospital, Nara, Japan

<sup>2</sup>University of Kio, Nara, Japn

## INTRODUCTION

Motion of the midcarpal joint of the wrist extends from radiodorsal to ulnopalmar in radioulnar deviation, in dart-throwing motion (DTM), and in flexion-extension motion. The movement from radiodorsal to ulnopalmar is called DTM.

Radioulnar deviation and flexion-extension motion are combined the DTM of the midcarpal joint and motion of the radiocarpal joint. Motion of the radiocarpal joint approaches zero at wrist positions along DTM. Many ADL require a wrist motion. The movement often used is DTM.

Distal radius fractures are common injuries. There is no relation in the ADL and ROM after a fracture of the distal radius. Only grip strength has relation. However, there is no report about DTM plane ROM after a fracture of the distal radius. The aim of this study was to examine the relationship between dart-throwing motion plane ROM and patient-perceived outcome, measured by the Disabilities of the Arm, Shoulder, and Hand outcome (DASH) score in patients with healed distal radius fractures.

## METHODS

The subject was 18 patients with healed distal radius fractures (AO classification types A(1), B(2), C(15)). Their mean age was  $63.5 \pm 16.4$  years. Twelve patients were treated with volar plate. Six patients were treated with plaster splint. Evaluation criteria were taken as the DASH score, ROM (flexion-extension, radioulnar deviation, pronation-supination, DTM plane), and the grip strength. DTM plane ROM was measured with the developed goniometer (Fig.1). We defined the DTM plane as the movement to the upper and lower sides by the posturing of  $45^\circ$  of pronation (Fig.2). Intra-rater and inter-rater reliability of the developed goniometer exceeded 0.83. Grip strength is expressed as a percentage of the uninjured wrist's value. Statistical

analysis searched for description of liner correlations between DASH score and ROM, grip strength with Pearson's product moment test. Differences were considered significant at p-values $<0.05$ .

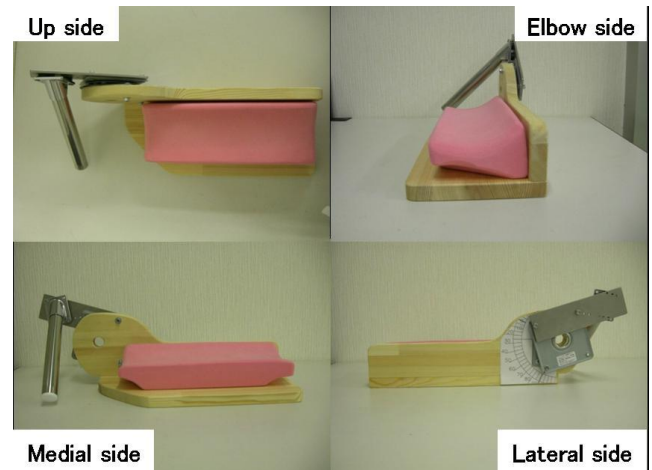


Figure 1: The development of the goniometer which measures DTM plane ROM.

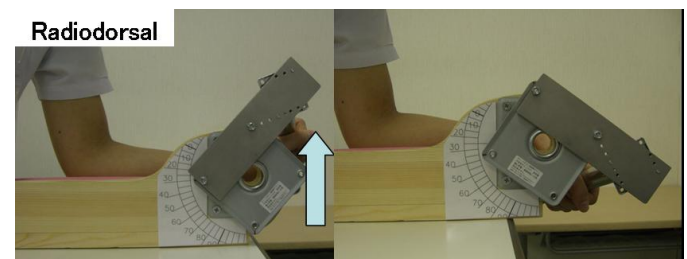


Figure 2: An above movement is the radiodorsal and a down movement is the ulnopalmar. DTM plane ROM was taken as the sum total of radiodorsal and ulnopalmar.

## RESULTS AND DISCUSSION

Table 1 gives the result of the DASH score, ROM, and grip strength.

There were the correlations between DASH score and DTM plane ROM ( $r = -0.65$ ,  $p = 0.004$ ) (Fig.3), grip strength ( $r = -0.49$ ,  $p = 0.040$ ) (Fig.4). We found no statistical relationship between the DASH score and other ROM.

Table 1: The result of the DASH score, ROM, and grip strength.

|                      | n=18       |
|----------------------|------------|
| DASHscore            | 27.5±21.7  |
| flexion-extension    | 131.1±19.8 |
| radioulnar deviation | 56.9±8.5   |
| pronation-supination | 162.2±17.1 |
| DTM plane ROM        | 62.5±16.2  |
| grip strength        | 0.69±0.2   |

grip strength : percentage, ROM : degree

There were the correlations between DASH score and DTM plane ROM ( $r = -0.65$ ,  $p = 0.004$ ) (Fig.3), grip strength ( $r = -0.49$ ,  $p = 0.040$ ) (Fig.4). We found no statistical relationship between the DASH score and other ROM.

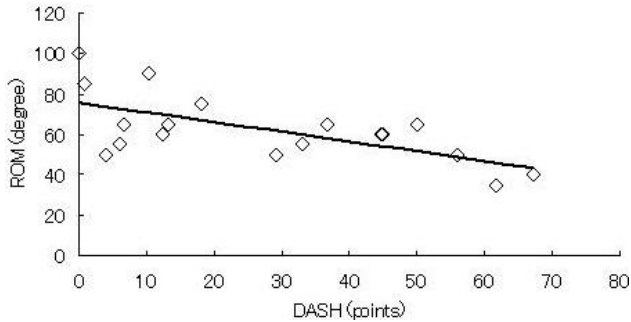


Figure 3: The correlations between DASH score and DTM plane ROM( $r = -0.65$ ,  $p = 0.004$ ).

The movement on a DTM plane is the movement direction often used in ADL, and it is said that DTM evolved in order to use an instrument. Therefore, the significant relationship was acquired by the DASH score and DTM. Moreover, the movement direction which a movement on DTM

plane most often uses after a fracture of the distal radius, and it is an important movement direction.

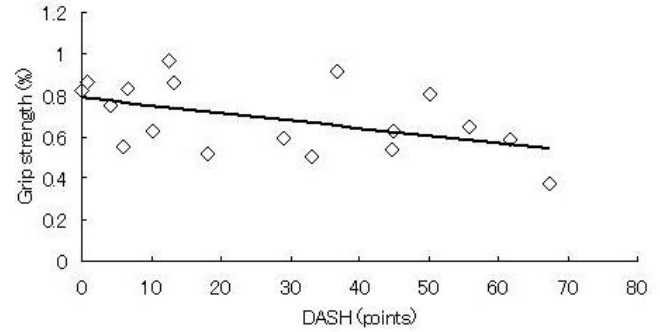


Figure 4: The correlations between DASH score and grip strength ( $r = -0.49$ ,  $p = 0.040$ ).

Furthermore, although the past study has reported that grip strength serves as a parameter of a functional revivification of a wrist, this result is suggested we can grasp a recovery process also by measuring DTM plane ROM.

## CONCLUSIONS

We investigated the relation between the DASH score and DTM plane ROM. There were the correlations between DASH score and DTM plane ROM ( $r = -0.65$ ,  $p = 0.004$ ). The movement direction which a movement on DTM plane most often uses after a fracture of the distal radius, and it is an important movement direction.

## REFERENCES

- 1.Moritomo H, et al. J Bone Joint Surg 88, 611-621, 2006.
- 2.Crisco JJ, et al. J Bone Joint Surg 87, 2729-2740, 2005.
- 3.Wilcke MKT, et al. J Hand Ther 10-11, 290-298, 2007.

# TOWARD AN UNDERSTANDING OF SHOULDER DEMANDS IN MANUAL WHEELCHAIR USERS

Kenton Kaufman, Melissa Morrow, Wendy Hurd, Kristin Zhao, Meegan Van Straaten, Duane Morrow,  
Brian Kotajarvi, Lan-Yuen Guo, Michelle Sabick, Fong-Chin Su, Jeffrey Basford, Kai-Nan An

Mayo Clinic, Rochester, MN, USA

email: kaufman.kenton@mayo.edu

web: <http://mayoresearch.mayo.edu/mayo/research/biomechanics/index.cfm>

## INTRODUCTION

Manual wheelchair users (MWU) rely extensively on their upper extremities for mobility. As a result, MWU experience a high incidence of upper extremity pain and injury [1]. However, the direct link between wheelchair activities and upper extremity (UE) injury has not been established. The overarching goal of our research has been to determine which wheelchair tasks are most likely responsible for upper extremity pain and injury and to design training and rehabilitation programs aimed at reducing injuries.

## METHODS

Over the past 15 years, our research has focused on understanding kinematic and loading mechanisms of MWU. We have progressed from ergometer based studies to the real-world environment to accurately capture the loads experienced during activities of daily living.

Our pursuits began with investigations of the effect of seat position and handrim size on handrim and intersegmental biomechanics [2-3]. These studies were performed using a marker-based motion capture system to measure 3-D UE kinematics and an instrumented handrim to measure applied forces and moments. Additionally, isometric strength production of the shoulder, elbow and wrist in MWU and matched controls was examined [4].

In more recent work, we expanded our methods for studying shoulder pain and pathology [5]. Our musculoskeletal model was changed to include a scapula segment in order to examine impingement [6] during level propulsion, ramp propulsion, and weight relief lifts. Additionally, advanced

optimization modeling was applied to investigate shoulder joint contact forces and muscle force distribution [7].

Our research has now evolved from inside the laboratory into the real-world environment. This began with quantifying the differences between the demands of the traditional laboratory propulsion to that of outdoor and indoor community ambulation [8-10]. Subjects propelled on an ergometer, over level tile, level carpet, inclined carpet, and varying outdoor concrete surfaces. Symmetry, propulsion moment, power, work, and temporal variables were assessed to test the hypothesis that community ambulation differs from laboratory propulsion.

## RESULTS AND DISCUSSION

The results of our earliest work dissipated concerns over seat position and muscle strength imbalances as autonomous contributors to UE injury. The lowest seat position showed improvements in timing variables, but also increased force [2]. Additionally, the UE strength of MWU was not different from matched control subjects [4].

Our modeling work has proven that there is a dramatic difference between joint loading during level propulsion (typical laboratory testing) and higher demand, real-world activities such as ramp propulsion and weight relief lifts [5,7] (Fig. 1). The scapular kinematics of MWU tasks showed detrimental postures for impingement during all tasks with an increased risk during weight relief due to more internal rotation of the humerus [6].

Comparison of laboratory and outdoor community conditions resulted in significant differences in symmetry indexes for all kinetic variables (outdoor

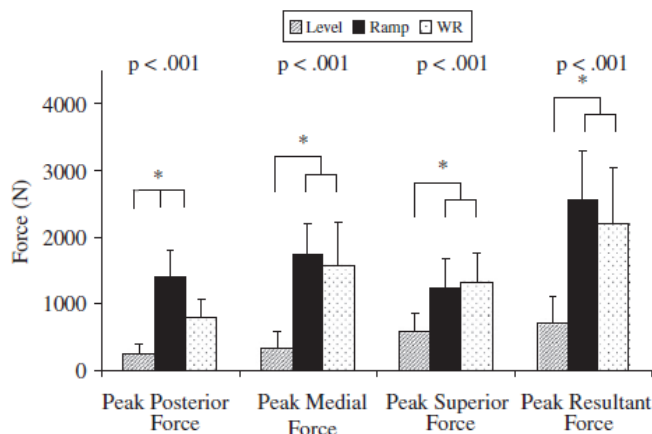


Fig. 1. Model predicted joint contact forces during wheelchair activities

> lab) and the majority of timing variables (moment shown in Fig. 2) [8]. Additionally during outdoor propulsion, greater power generation from the dominant limb occurred during more challenging conditions (Fig. 3) [10]. The presence of asymmetry among manual wheelchair users suggests data collected from one limb or averaging data collected bilaterally may lead to inaccurate interpretations of propulsion biomechanics. The greater asymmetry identified during outdoor versus laboratory conditions emphasizes the need to evaluate wheelchair biomechanics in the user's natural environment.

The average propulsion moment and work were significantly increased from smooth level propulsion to aggregate level, and ramp conditions (Fig. 3) [10]. Effort during outdoor community wheelchair ambulation varies with demands imposed by different ground conditions. These results agree with conclusions drawn from the modeling results.

## CONCLUSIONS

Our recent work has shown that there are large differences between laboratory and community ambulation in terms of handrim biomechanics and shoulder joint contact forces. To accurately capture the relationship between MWU activities and shoulder injuries, it is imperative to collect data in the wheelchair user's natural environment. Our future work will continue to focus on characterizing wheelchair propulsion and joint loading in the real-world setting in order to provide clinically relevant injury prevention strategies and treatment recommendations.

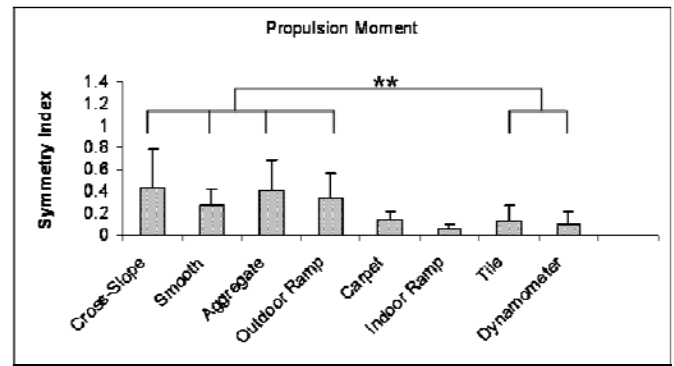


Fig. 2. Propulsion moment symmetry measured during laboratory, indoor, and outdoor community wheelchair propulsion.

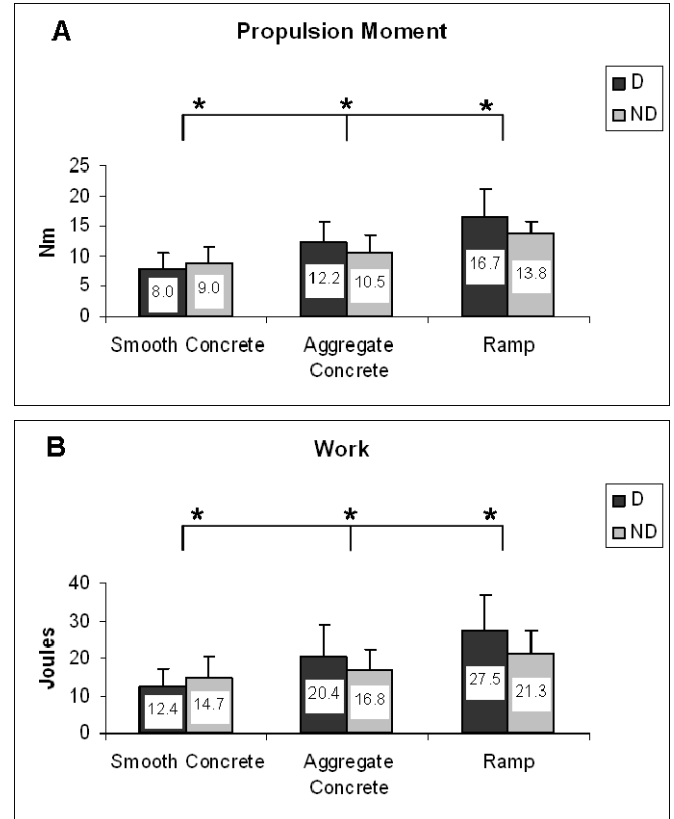


Fig. 3. (A) Propulsion moment and (B) work during outdoor propulsion on smooth concrete, aggregate concrete and a smooth concrete ramp for the dominant (D) and non-dominant (ND) arm.

## REFERENCES

1. Mercer JL et al. Clin Biomech 21:781-9, 2006.
2. Kotajarvi BR et al. JRRD 41:403-14, 2004.
3. Morrow DA et al. Dis & Rehab 25:192-6, 2003.
4. Kotajarvi BR et al. Arch PM&R 83:441-6, 2002.
5. Morrow MM et al. J Elect Kines 20:61-7, 2010.
6. Morrow MM et al. Clin Biomech 26:352-7, 2011.
7. Morrow MM et al. J Biomech 43:2487-92, 2010.
8. Hurd WJ et al. Arch PM&R 89:1996-2002, 2008.
9. Hurd WJ et al. Am J PM&R 87:984-91, 2008.
10. Hurd WJ et al. J Elect Kines 19:942-7, 2009.

## ACKNOWLEDGEMENTS

Funding provided by NIH grants R01HD033806 & R01HD048781.

# EXPEDITED EVALUATION OF CONTACT STRESS IN THE HUMAN ANKLE JOINT

Andrew M. Kern, Donald D. Anderson and Thomas D. Brown

Orthopaedics and Rehabilitation, The University of Iowa, Iowa City, IA, USA

web: <http://poppy.obrl.uiowa.edu> ; e-mail: [andrew-kern@uiowa.edu](mailto:andrew-kern@uiowa.edu)

## INTRODUCTION

Post-traumatic osteoarthritis (PTOA) following an articular fracture is partly explained by contact stress aberrations associated with imperfect fracture reduction [1]. However, the tight association between residual fracture incongruity and acute fracture severity makes it necessary to evaluate large numbers of patients to understand the relative role of these factors in PTOA development.

Prior assessment of contact stress exposure utilized patient-specific finite element analysis (FEA) to study fractured ankles after reconstruction. Promising correlations were made between aberrant contact stress distributions and PTOA development in a relatively small group of patients (n=11) [1]. Additional enrolled patients were not able to be analyzed largely due to numerical convergence issues inherent in contact FEA, suggesting that it is impractical for use in larger studies.

An expedited analysis approach has been developed for evaluating patient-specific articular contact stress distributions from CT. This method involves semi-automated segmentation, automated model alignment to a weight bearing apposition, and use of an elastic contact algorithm.

## METHODS

### *Semi-automated segmentation of tibia and talus*

Ankle joint surface segmentation from the post-reduction CT is difficult due to the relatively low signal contrast between closely opposing surfaces, abrupt fracture incongruities, and fixation hardware metal artifact. To address these challenges, a user-guided segmentation algorithm has been developed using a 3D watershed transform, implemented in MATLAB (Fig. 1).



**Figure 1:** Semi-automated segmentation of ankle joint. CT scan images are first cropped (left), then a 3D watershed segmentation of the tibia and talus bones is performed (middle), with final surface generation and smoothing to produce the ankle model (right).

### *Alignment to weight bearing apposition*

Due to the fact that the patient is supine during CT scan acquisition, the tibia and talus bones need to be aligned to a load-bearing stance. An iterative closest point (ICP) algorithm is used to align the segmented bone surfaces to template surfaces of an intact weight-bearing apposition. This approach is implemented in MATLAB, facilitating direct integration with the segmentation procedure, as well as with subsequent contact stress evaluation. Following the ICP alignment, a vertically oriented settling load is applied to seat the tibia (Fig. 2), using an elastic contact algorithm.

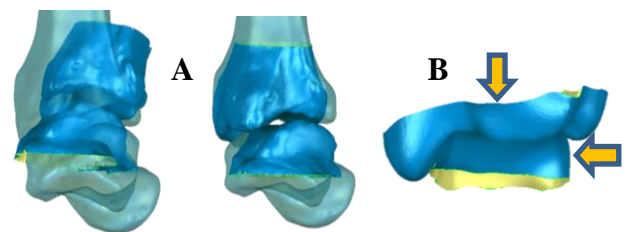


**Figure 2:** Placement of segmented joint into settled load bearing apposition. (A) Iterative closest point algorithm is used to align segmented bone (dark blue) to template (light blue). (B) Functional loading follows to settle the joint into load bearing apposition.

### *Expedited contact stress assessment*

Following alignment and settling, the joint is driven through an expedited contact stress analysis routine, involving a 13-step flexion-extension cycle representing the stance phase of level gait. Contact stresses are calculated using a rigid body spring modeling algorithm implemented in MATLAB. Contact is determined using a pressure over-closure relationship between the talar and tibial cartilage

surfaces, with spring deformation being related to the level of over-closure (Fig. 3) [2]. Engendered loads and moments are then used in a load balancing algorithm on the tibial surface. The simulation is run in load control, scaled to patient body weight, with the tibia constrained in all directions other than superior-inferior translation, and the talus constrained in superior-inferior translation and flexion extension.

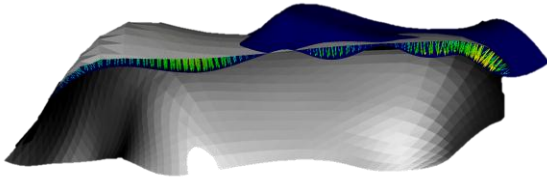


**Figure 3:** Elastic contact algorithm. Springs are created (green) when tibia surface (blue) over closes with the talus surface (gray) thus generating contact stress.

To assess the method’s predictive value, metrics of contact stress-time exposure and of areas of elevated contact stress were compared to PTOA development, judged by a radiographic score (KL grade  $\geq 2$ ) at a minimum 2-year follow-up [3].

## RESULTS AND DISCUSSION

The 3D watershed algorithm performed well, taking approximately 5 minutes to complete. The mean unsigned difference between segmentations obtained using this new method and previous iso-surfaced and hand edited segmentations was  $0.55 \pm 0.22$  mm.

Alignment of the ankle to a neutral loaded apposition using the ICP algorithm required 1-2 minutes of computational time. This alignment was highly reproducible and agreed with prior expert alignments performed on the ankles (Fig. 4).

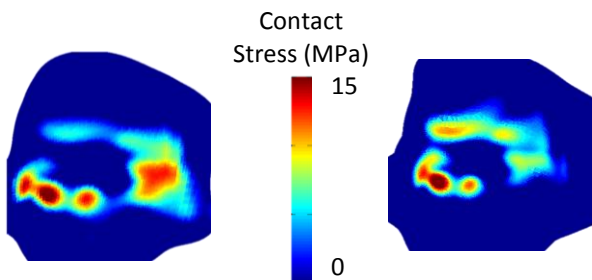


**Figure 4:** Contact stress distributions comparing result from expert alignment (left) and iterative closest point alignment (right)

The elastic contact algorithm provided results for the entire 13-step gait cycle of an ankle within 2-3 minutes of computation time. The difference between the expedited and FEA contact stress-time exposures was  $0.03 (\pm 0.02)$  MPa-s, when evaluated on identical models on a point-by-point basis. Many of the larger differences ( $>1$  MPa) occurred near the edges of contact, at sites where only one methodology predicted contact. Using the previous FEA methods, a contact stress-time-area metric agreed with patient KL grade and OA status (KL  $\geq 2$ ) at concordance rates of 95% and 100%, respectively [1,3]. By comparison, when used on the same ankle models the elastic contact algorithm was able to obtain a 97% KL concordance and 100% OA concordance, thus showing equivalent predictive ability for PTOA development.

When taking into account the time for file processing between steps, the entire expedited process took on the order of 15 minutes per ankle, depending on the user intervention required.

## CONCLUSIONS

These expedited contact stress evaluation methods show promise for use in large studies involving hundreds of patients. The expedited segmentation, alignment, and contact stress analysis components all performed in an equivalent manner compared to the previous FEA study, with a fraction of the required time and user intervention.

## REFERENCES

1. Li W, et al. *J Orthop Res.* 26(8):1039-1045, 2008.
2. Bei Y, Fregly BJ. *Med Eng Phys.* 26(9):777-789, 2004.
3. Anderson DD, et al. *J Orthop Res.* 29(1), 33-39, 2011.

## ACKNOWLEDGEMENTS

This project funded by NIH/NIAMS #AR046601, #AR048939 and #AR055533

# INFLUENCE OF AXIAL ROTATION MOMENTS ON ACL STRAIN: A CADAVERIC STUDY OF SINGLE- AND MULTI-AXIS LOADING OF THE KNEE

<sup>1</sup>Ata Kiapour, <sup>2,3</sup>Carmen Quatman, <sup>1</sup>Richard Ditto, <sup>1</sup>Jason Levine, <sup>2</sup>Samuel Wordeman,  
<sup>2,3</sup>Timothy Hewett, <sup>1</sup>Vijay Goel, <sup>1</sup>Constantine Demetropoulos

<sup>1</sup> Engineering Center for Orthopaedic Research Excellence (ECORE), Department of Bioengineering and Orthopaedic Surgery, Colleges of Engineering and Medicine  
University of Toledo, Toledo, OH, USA

<sup>2</sup>Sports Medicine Biodynamics Center and Human Performance Laboratory, Cincinnati Children's Hospital Research Foundation, Cincinnati, OH, USA

<sup>3</sup>Sports Medicine, The Ohio State University, Columbus, OH, USA

email: [Constantine.Demetropoulos@utoledo.edu](mailto:Constantine.Demetropoulos@utoledo.edu) web: [www.bioe.eng.utoledo.edu](http://www.bioe.eng.utoledo.edu)

## INTRODUCTION

ACL (anterior cruciate ligament) rupture is one of the most common and devastating knee injuries [1]. Many factors influence ACL injury, from anatomical variability to magnitude and direction of loading. Considerable efforts have been made to study ACL behavior under various loading conditions. However, uniplanar and multiplanar mechanisms of ACL injury remain unclear, and more work is needed to characterize the influence of single- versus multi-axis loading on the knee. Previous studies have demonstrated that anterior shear and axial rotation moment may play an important role in the mechanism of ACL injury [2-5]. The purpose of this study was to determine the combined effects of axial rotation and anterior shear on ACL strain. We hypothesized that combined anterior shear and internal rotation result in higher ACL strains compared to internal rotation alone.

## METHODS

Eighteen fresh frozen cadaveric lower extremity specimens (age  $44 \pm 8$  years, 10 female and 8 male, 8 left and 10 right limbs) were used. Specimens were sectioned at the mid-shaft of the femur and potted in polyester resin. The quadriceps (rectus femoris) and hamstrings (semitendinosus, biceps femoris and semimembranosus) tendons were isolated and sutured inside metal tendon grips to allow for the application of simulated muscle loads. In order to estimate strain, displacements were measured across the ACL from full extension through 30 degrees of flexion. A DVRT (Microstrain, Williston, VT) displacement transducer was placed along the ACL (anterior-

medial bundle) arthroscopically. Average strain across the transducer was calculated based on the change in length of the measured segment using following equation:

$$\text{Strain (\%)} = \frac{L - L_0}{L_0} \times 100$$

Where L is the instantaneous length measured across the DVRT, and  $L_0$  is the length measured across the DVRT at the reference length of the ligament. Reference length was calculated based on the method that is described by Howe et al. (1990) [6]. An Optotrak 3020 motion tracking system (Northern Digital Corporation, Waterloo, Ontario, Canada) was used to track the position of the femur, patella and tibia in 3D space using irLED markers. All tests were conducted using a custom designed passive 6-Degree of Freedom Force Couple Testing System (FCTS). This system utilizes servo-electric actuators to drive a cable-pulley system that generates an unconstrained pure moment. An external fixation frame was attached to the tibia such that the centers of the pulleys were located about the knee center of rotation. Simulated muscle loads (quadriceps: 400N and hamstrings: 200N) along with a constant compressive load (150N) were considered as the baseline. The following loading conditions were applied to each specimen in addition to the baseline: 15Nm of internal rotation, 15Nm of external rotation, 134N of anterior shear+15Nm of internal rotation and 134N of anterior shear+15Nm of external rotation. Due to tissue buckling and other phenomena that are not accounted for and may not be linear, these negative values should not be mistaken for compressive strain. This convention has been used in multiple

previous studies including Fleming et al. (2001) [2]. Statistical analyses were conducted on the results using Analysis of Variance (ANOVA) with a post-hoc Bonferroni Correction for multiple comparisons. Differences were considered statistically significant for  $p < 0.05$ .

## RESULTS AND DISCUSSION

Percentage change in ACL length was plotted from 0 to 30 degrees of flexion as shown in Figure 1. Positive values represent percent tensile strain, while reduction in length below the reference length simply indicates ligamentous unloading. At 25 degrees of flexion, the ACL was unloaded in baseline loading ( $\Delta L/L = -1.8 \pm 5.6\%$ ). The ACL was further unloaded in external rotation ( $\Delta L/L = -6.1 \pm 5.1\%$ ). However, ACL laxity was reduced under combined external rotation with anterior shear ( $\Delta L/L = -1.2 \pm 5.9\%$ ). When internal rotation was applied, ACL strain was calculated at  $1.8 \pm 6.4\%$  strain. ACL strain was increased to  $4.4 \pm 6.9\%$  strain when both internal rotation and anterior shear were applied.

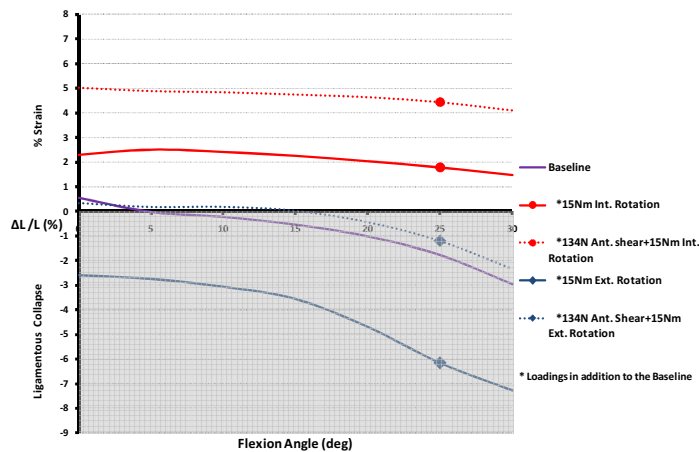


**Figure 1:** Average percent change in ACL AM-bundle length under single- and multi-axis rotation moments.

Internal-external rotation is plotted in Figure 2. At 25 degrees of flexion, baseline loading resulted in a  $2.4 \pm 2.7$  degree internal rotation. Internal rotation moment produced a  $19.2 \pm 5.5$  degrees internal rotation, but only a  $14.5 \pm 7.1$  degrees internal rotation for internal rotation moment with anterior shear. External rotation moment produced a  $16.4 \pm 4.4$  degrees external rotation, but only a  $12.8 \pm 7.5$  degrees external rotation for external rotation moment with anterior shear. Strain calculations were utilized to depict the state of ACL loading. Internal rotation resulted in increased ACL strain, while external rotation unloaded the ACL.

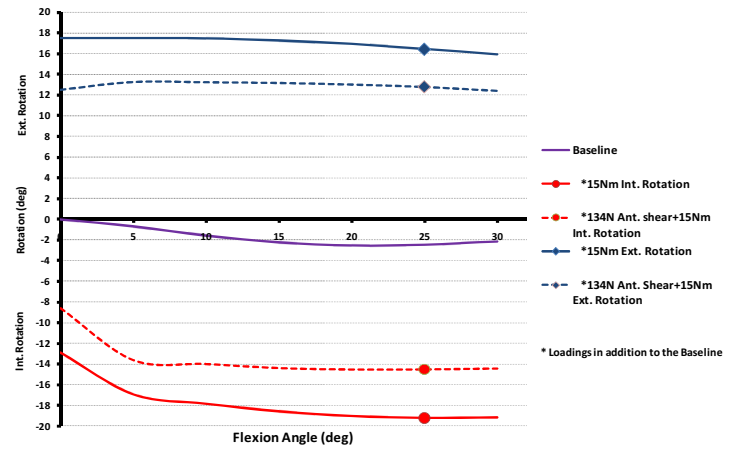


**Figure 2:** Average tibia axial rotation under single- and multi-axis rotation moments.

The combination of anterior shear with internal rotation resulted in higher ACL loading than internal rotation alone. Combined internal rotation and anterior shear resulted in a significant increase in ACL strain relative to the baseline ( $p = 0.031$ ). As expected, internal and external rotation moments resulted in a significant increase in internal and external rotations compared to baseline, with or without anterior shear ( $p < 0.0005$ , all comparisons).

## CONCLUSIONS

This study was conducted to investigate the effects of different axial rotation moments on ACL strain under unconstrained loading. Applied muscle forces were utilized to test the knee under more physiologically relevant conditions. These findings supported our hypothesis that the addition of anterior shear load to internal rotation moment, loads the ACL more than an internal rotation moment alone. Future studies are needed to characterize the effects of abduction and adduction moments (single- and combined-axis) on knee and ACL biomechanics.

## REFERENCES

1. Miyasaka KC, et al. *Am J Knee Surg.* **4**,3-8, 1991.
2. Fleming BC, et al. *J. Biomech* **34**, 163-170, 2001.
3. Koga H, et al. *AJSM* **38**, 2218-2225, 2010.
4. Shin CS, et al. *MSSE*, Epub ahead of print, 2011.
5. Krosshaug T, et al. *AJSM* **35**, 359-367, 2007.
6. Howe JG, et al. *Arthroscopy* **6**, 198-204, 1990.

## ACKNOWLEDGEMENTS

This study was funded by National Institutes of Health (R01 AR056259).

# A Method of Normalization for CT-Based Texture Analysis in Fracture Severity Assessment

Anthony T. Kilburg, Thaddeus P. Thomas, Donald D. Anderson, and Thomas D. Brown

Orthopaedics and Rehabilitation, The University of Iowa, Iowa City, IA, USA

web: <http://poppy.obrl.uiowa.edu> ; e-mail: [anthony-kilburg@uiowa.edu](mailto:anthony-kilburg@uiowa.edu)

## INTRODUCTION

High-energy tibial plafond fractures frequently lead to post-traumatic osteoarthritis (PTOA), with fracture severity a major risk factor. An objective CT-based metric has recently been shown to predict PTOA development based on fracture energy and articular comminution [1]. However, extensive calculation time prevents this method from being clinically utilized. An expedited textural analysis method was subsequently developed to predict PTOA (85% concordance) while requiring less user interaction and calculation time [2].

While effective, both methods were limited by the need to obtain an intact contralateral limb CT for taring purposes. A normative surrogate for the intact limb was subsequently developed for the full severity metric [3]. The objective of the present study was to utilize a similar approach to develop a surrogate for the intact contralateral limb taring value for the expedited textural metric, which would allow study in much larger patient populations without the need to obtain an intact contralateral limb CT.

## METHODS

Prior normalization for the full fracture severity metric relied upon a single scaling according to the patient's height. Different scan settings and field-of-views used while acquiring a CT scan can greatly influence image appearance. Normalizing for textural analysis therefore required the inclusion of two additional parameters: spatial resolution of the CT image acquisition and CT image reconstruction settings. Actual data from intact contralateral tibias, available in the 20 patients previously studied, provided a basis for developing an appropriate normalization procedure.

For a given acquisition, selection of the CT field of view essentially introduces a sampling frequency issue, with sampling bias between otherwise comparable acquisitions. This is because the spatial

resolution of standard CT is well below that of cancellous bone architectural features. For this reason, both slice spacing and in-plane resolutions (mm) were incorporated into a spatial resolution normalization step.

A separate issue involves the convolution kernel chosen during CT image reconstruction, which can significantly influence image texture. Some kernels show greater cancellous bone detail, while others smooth over the details. To obtain uniform images between cases, a 3D anisotropic edge-preserving filter was applied to each CT image set (Figure 1).

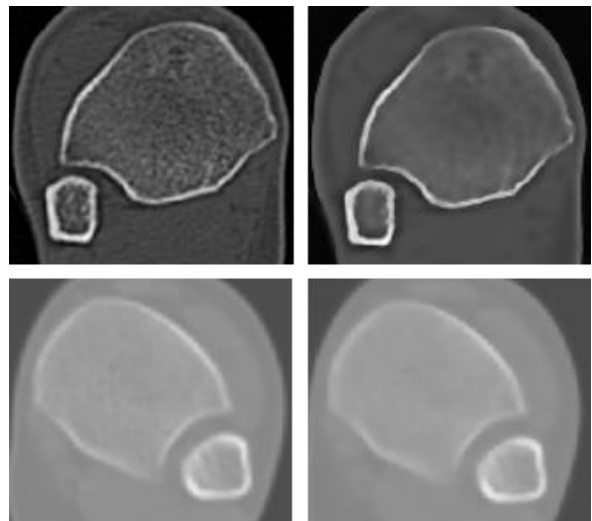


Figure 1: Effect of anisotropic diffusion filter on CT images

With these two additional normalization steps implemented, image heterogeneity (the image textural measure utilized) was plotted versus normalized distance along the tibia from the distal articular surface for the 20 intact tibias. A linear trendline was fit to the data as a basis for developing a surrogate relationship between the textural measure and the distance along the tibia. The fracture severity values obtained using this surrogate were then compared with PTOA development in the ankles of the patients studied.

## RESULTS AND DISCUSSION

When the described procedures were used to normalize the textural metric (image heterogeneity) according to the length along the intact tibia (to provide a surrogate measure), a correlation of 97% between the linear fit and the data was obtained (Figure 2).

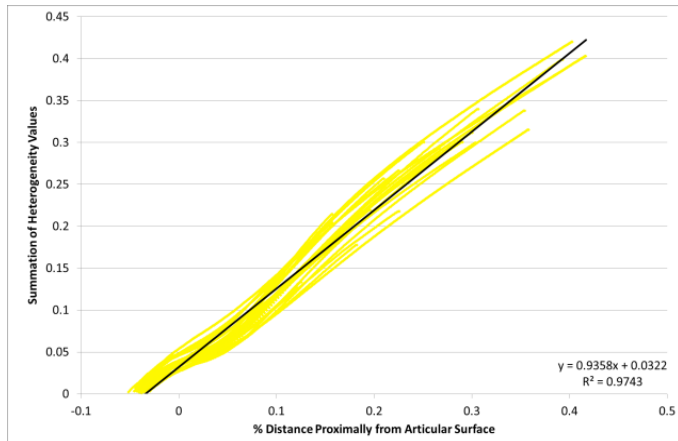


Figure 2: Normalized Heterogeneity Curve Fitting

Image texture-based metrics of fracture energy and articular comminution calculated using the intact surrogate produced a concordance of 63% and 49%, respectively with the KL scores of PTOA development. A fragment dispersion metric calculated using the intact surrogate approach showed a 70% concordance with KL scores.

A combined fracture severity metric was formulated integrating the fracture energy and fragment dispersion metrics. Since fragment dispersion was a stronger predictive metric, it was weighted twice as heavily as the fracture energy in the final metric. Articular comminution was excluded from the final metric due to its poor predictive performance. The final combined severity metric for the initial employment of this method showed a strong 74% concordance with KL score.

## CONCLUSION

Employing normalization adjustments for CT image spatial properties, convolution kernels, and patient height produced a reasonable estimate of intact CT image heterogeneity along the length of the tibia. This surrogate metric, coupled with a fragment displacement metric calculated from surrogate intact areas, proved to be a strong predictor of PTOA, without the use of an intact contralateral limb.

## REFERENCES

1. Thomas TP, et al. J Orthop Trauma 24:764-9, 2010.
2. Haralick RM, et al. IEEE Trans SMC 3:610-21, 1973.
3. Thomas TP, et al. Iowa Orthop J 28:9-13, 2008.

## ACKNOWLEDGEMENTS

This project funded by NIH/NIAMS #AR048939 and #AR055533.

# THE EFFECT OF AN UNEXPECTED UNDERFOOT PERTURBATION ON STEP KINEMATICS IN SUBJECTS WITH AND WITHOUT PERIPHERAL NEUROPATHY

Hogene Kim, Trina DeMott, Lara Allet, James K. Richardson, James A. Ashton-Miller  
Biomechanics Research Laboratory

University of Michigan, Ann Arbor, Michigan

Email: [hogenek@umich.edu](mailto:hogenek@umich.edu), Website: <http://me.engin.umich.edu/brl/>

## INTRODUCTION

Peripheral neuropathy (PN) in older adults has a high risk of falls and fall-related injuries [1]. Many falls in the elderly occur while walking on an irregular surface [2]. Elderly show increased step-time and step-width variability during gait on the irregular surface [3]. Recently a protuberance under the medial aspect of the stance foot, akin to stepping on a pebble, has been shown to cause a cross-over step in order to recover balance [4].

Rather than having patients walk on an irregular surface, which takes up too much storage room in the clinic, a perturbing shoe was developed to simulate the condition in which the swing foot lands on a small medially-located or laterally-located pebble during gait on a flat surface [5].

Since PN show greater variation in gait than healthy old (HO), we tested the null hypothesis that there is no difference in the first post-perturbation step kinematics for a medial perturbation (MP) or lateral perturbation (LP) compared to unperturbed gait, using the perturbing shoe.

## METHODS

We recruited 28 elderly volunteers with diabetic PN and 11 HO without PN (M:20, F:19, age  $69.1 \pm 8.6$  yrs). Each subject wore a pair of custom sandals equipped with hinged flippers concealed within the medial and lateral aspects of the shoe sole, just behind the metatarsal heads. When the medial/lateral flipper was deployed (Figure 1), the resultant sandal sole inversion/eversion inclination angle in the frontal plane was  $\pm 16^\circ$ .



**Figure 1:** The perturbing shoe showing undeveloped fulcrum (middle), medially deployed fulcrum that inverts during midstance (left), and laterally deployed fulcrum that everts during midstance (right).

Subjects performed 60 gait trials walking along a 6 m level walkway at a purposeful speed “as though they were crossing a busy street”. Randomly, in 16 trials, a flipper was covertly deployed during one step cycle under the medial or lateral aspects of forefoot. (8 times on each side)

3-D kinematics of foot, leg, pelvis and trunk, including ankle inversion/eversion angle, step length (SL), step width (SW), step time (ST), were collected at 100 Hz using an optoelectronic Certus system and 28 markers. Two foot switches detected the onset of every heel strike and medial or lateral flipper ground contact was registered by an IR-pair of sensors, sampled at 2kHz.

Statistical comparisons of post-perturbation step kinematics (SW, SL, ST) and their variability (SWV, SLV, STV) were compared to unperturbed gait using a paired T-test and F-test, with  $p < 0.01$  considered significant.

Subjects were divided into two groups (HO vs PN) based on the Michigan Diabetic Neuropathy Score (MDNS). The MDNS has a 0-to 46-point scale (a higher score reflects more severe PN) and correlates well with other neuropathy scores [6]. The MDNS scores of the two groups, HO (MDNS = 0, N=11)

and PN (MDNS = 12.3±6.9, N=28), were also measured.

## RESULTS AND DISCUSSION

Figure 2 plots the first post-perturbation SW against unperturbed SW in the two different subject groups (HO vs PN) and the two different perturbation locations (MP vs LP) with the 95% unperturbed SW range. In the HO group, the paired T-test shows no significant difference between unperturbed and the first post MP/LP SW (Unperturbed:16.1(3.9), MP:15.7(4.2), LP:15.8 (4.6)). Considering all other gait parameters and their variability (SL, ST, SWV, SLV, STV) in the HO group, there were no significant difference between unperturbed and the the post MP/LP gait parameters, using paired T-test and F-test with  $p < 0.01$  considered significant.

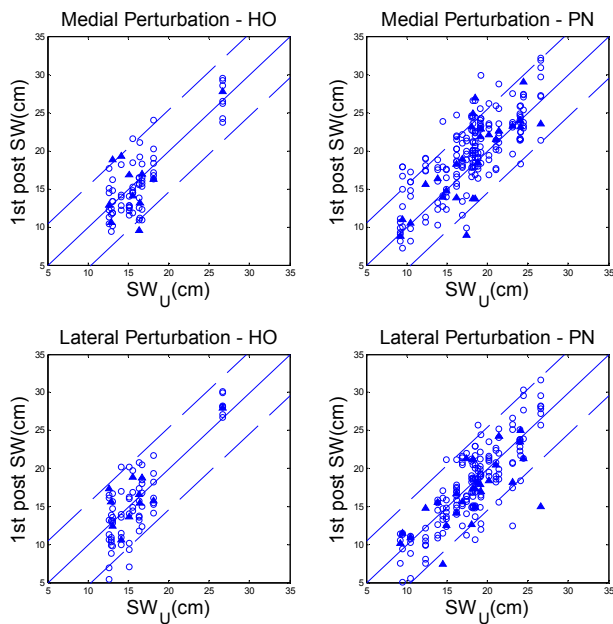


**Figure 2:** Unperturbed vs. first post-perturbation SW in HO (left column) and PN (right column), MP (first row) and LP (second row) (--- lower 5% and upper 95% of unperturbed SW, ▲: the first perturbed trial in each subject, ○: subsequent trials)

However, gait parameters (SW, SL, ST) in the PN group (Table 1) show a significant difference between unperturbed and the first medially or laterally perturbed SW, SL and ST. The medial perturbation significantly increased SW and the lateral perturbation significantly decreased SW,

compared to unperturbed gait. A medial and lateral perturbation significantly decreased SL and ST.

|                 | Unperturbed  | MP            | LP            |
|-----------------|--------------|---------------|---------------|
| <b>SW (cm)</b>  | 18.0 (4.92)  | *19.6 (4.17)  | *17.1 (4.57)  |
| <b>SWV (cm)</b> | 2.79 (0.58)  | 2.93 (1.00)   | 3.27 (2.11)   |
| <b>SL (cm)</b>  | 70.2 (8.88)  | *68.3 (9.28)  | *67.5 (9.48)  |
| <b>SLV (cm)</b> | 3.64 (1.15)  | 4.06 (2.01)   | 4.62 (6.18)   |
| <b>ST (sec)</b> | 0.514 (0.04) | *0.505 (0.04) | *0.502 (0.05) |
| <b>STV(sec)</b> | 0.022 (0.01) | 0.024 (0.01)  | 0.030 (0.04)  |

**Table 1:** PN results: Unperturbed and medially or laterally perturbed step kinematics (\*:  $p < 0.01$  from paired t-test between unperturbed and medially (MP) or laterally (LP) perturbed step kinematics)

This is the evidence that PN alters the ability to reject a sudden medial or lateral underfoot perturbation. HO successfully rejected the perturbation.

## CONCLUSIONS

An unexpected medial or lateral underfoot perturbation causes a significant variation in the SW, SL, ST of diabetic PN subjects, but not healthy subjects.

## REFERENCES

- Richardson JK et al., *J Am Geriatr Soc*, **40**:1008-12, 1992
- Carter SE et al., *Am. J. Phys. Med. Rehabil*, **88** (3):210-5, 2009
- DeMott TK et al., *Am. J. Phys. Med. Rehabil*, **86** (2):125-132
- Thies SB et al. *Gait & Posture*, **26**: 156-160, 2007
- Kim H et al., ASB Annual Meeting, State College PA, 2009
- Feldman EL et al., *Diabetes Care*, **17**:1281-9, 1994

## ACKNOWLEDGEMENTS

PHS grants R01 AG026569 and P30 AG024824

# WHY DOES THE PUBOVISCERAL MUSCLE FAIL AT ITS ENTHESES, AND NOT ELSEWHERE, DURING THE SECOND STAGE OF LABOR? A COMPUTATIONAL STUDY

<sup>1</sup>Jinyong Kim, <sup>2</sup>John O. L. DeLancey and <sup>1</sup>James A. Ashton-Miller

<sup>1</sup>Department of Mechanical Engineering, University of Michigan, Ann Arbor, MI, USA  
<sup>2</sup> Department of Obstetrics & Gynecology, University of Michigan, Ann Arbor, MI, USA  
email: jinyongk@umich.edu web: http://me.engin.umich.edu/brl

## INTRODUCTION

Up to 15 % of the approximately 1.5 million healthy women that deliver their first child vaginally each year sustain an injury to the left and/or right pubovisceral muscle (PVM) [1], part of the pelvic floor muscle. A contributing factor may be the unusually large stretch ratio of 3.26 (i.e., 80 mm → 262 mm) that occurs in the PVM near the end of labor [2]. MRI studies show the location of injury invariably occurs at the enthesis where the PVM takes origin from the pubic bone [1]. Why this should be so is a mystery.

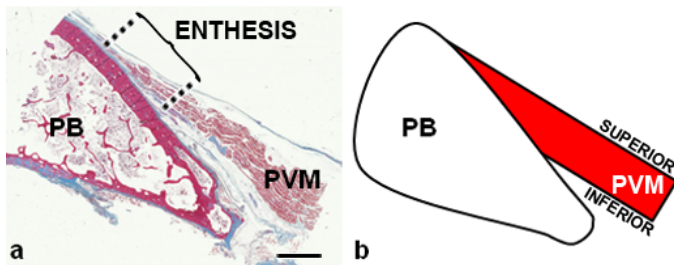


**Figure 1:** The geometry of the PVM model (b) was based on a left medial view of a parasagittal section through the PVM origin on the pubic bone (PB) 1-2 cm from the midline (a, scale bar = 3 mm).

Upon reflection, our histological study of the PVM enthesis [3] reveals that the PVM meets the pubic bone at an oblique angle, a ‘scarf’ junction (Fig. 1). Now it is known that the stress distribution across a scarf joint loaded in tension is not uniform [4]. So we hypothesized that, under the stretch associated with vaginal delivery, the presence of the PVM scarf junction will significantly increase the stress near the inferior margin of the junction more than near its superior margin, and that strain energy (SE) is an appropriate predictor of the PVM failure [5].

The goal of this study was to first model the histology of the PVM at its enthesis, and then to use

the model to conduct a finite element (FE) analysis of the SE distributions of an anisotropic hyperelastic model of the PVM placed under feasible loading scenarios during the second stage of labor. In addition, the sensitivity of the SE concentration to input variable variation was examined.

## METHODS

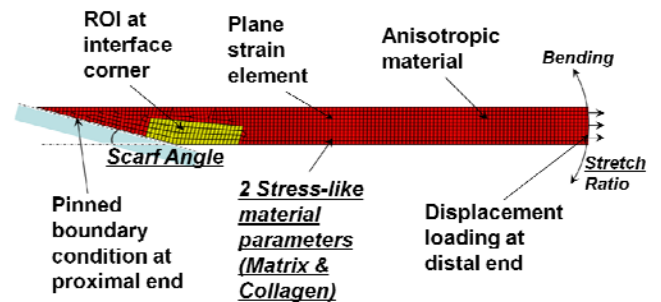


**Figure 2:** Anisotropic hyperelastic FE model of the PVM and its enthesis with model definitions (plain font) and the five input variables used for the sensitivity analysis (underlined italic font).

A planar FE model of the PVM was created based on histological parasagittal cross-sections [3]. The model definitions are given in Fig. 2.

Using Abaqus v.6.9, the FE simulation method was verified by confirming that convergence in SE is achieved within the region of interest (ROI) near the interface corner with mesh refinement [6]. A contour plot analysis of SE was also examined to identify the area of concentrated SE.

Using R v.2.12, a multiple linear regression analysis was performed to model the relationship between an output variable and the five model input variables (Fig. 2) as part of a sensitivity analysis. The output variable was defined as a ratio of the area occupied by the elements containing the largest 5 % of the

element-wise SE per unit area divided by the total area (“Area Ratio”). Therefore, a smaller Area Ratio means a greater PVM SE concentration. The five input variables (each with three plausible values) included PVM stretch ratio (1.25, 2.25, 3.25), scarf angle (10°, 15°, 25°), bending (0°, ±15°), and two stress-like material properties (matrix [0.18, 0.26, 0.35 MPa] and collagen [0.04, 0.06, 0.08 MPa]). To facilitate comparisons, all the variables were converted to standard units (mean 0 and variance 1). We used two-tailed t-tests and ANOVA to test the significance of each variable and its interaction in the regression model, with  $p < 0.05$  considered significant.

## RESULTS AND DISCUSSION

A contour plot (Fig. 3) demonstrates that the inferior margin of the PVM enthesis has significantly greater SE per unit area than the superior margin under the large stretch ratio associated with birth (Fig. 4). This suggests the possible initiation point for the avulsive injury. The location of the SE concentration is consistent with the singular stress field in a linear elastic scarf joint under tension [4]. Neither the mid-section of the PVM nor its distal end (which connects to the perineal body in a butt joint) show any localized SE concentrations. The SE in the ROI shows that little is to be gained by further mesh refinement (Table 1).

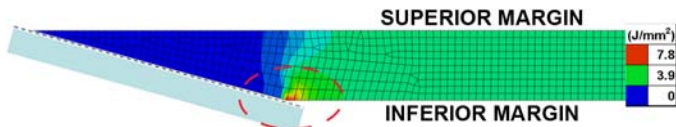


**Figure 3:** Contour plot of the element-wise SE per unit area near the PVM enthesis on the undeformed configuration. Circle contains the area with maximum value on the inferior margin.

**Table 1:** SE and convergence rates at the interface corner ROI.

| Characteristic<br>Mesh<br>Dimension<br>(mm) | SE @ ROI<br>(J x 10 <sup>-3</sup> ) | Incremental<br>% Change in<br>SE (%) |
|---|-------------------------------------|--------------------------------------|
| 2.5   | 25.04                               | N/A                                  |
| 1.25  | 28.33                               | 12.33                                |
| 0.625                                       | 28.63                               | 1.05                                 |
| 0.3125                                      | 28.75                               | 0.42                                 |
| 0.15625                                     | 28.85                               | 0.35                                 |

**Figure 4 (left, vertical orientation):** PVM FE model (9:10 scale) before (at left) and under second stage deformation (at right) at a stretch ratio of 3.25.

The linear regression analysis showed that the five variables explained 53.2% of variation in the output variable, Area Ratio. The Area Ratio was most sensitive to the variations in stretch ratio ( $p < 0.001$ ), followed by scarf angle ( $p = 0.003$ ) and bending ( $p = 0.007$ ). The smaller the scarf angle and the stretch ratio, the greater the degree of PVM enthesis SE concentration. Finally, PVM bending (caused by how far down the fetal head pushes the distal end of the PVM during labor) caused greater concentration of SE (Fig. 5).

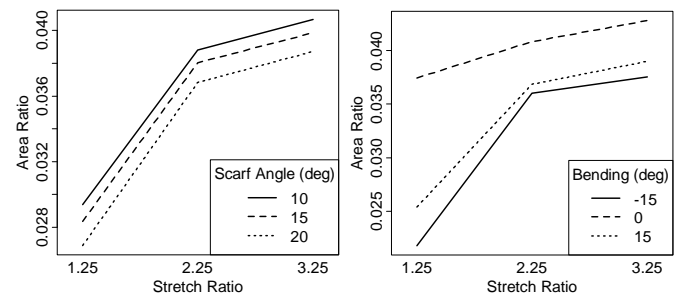


**Figure 5:** Plots of Area Ratio (see Methods) versus Stretch Ratio for variations of Scarf Angle (left) and Bending (right).

The first time that the PVM ever experiences this large a stretch ratio is during the first vaginal birth. We predict that the PVM scarf enthesis fails because of the inherent SE concentration at its inferior margin. An improved understanding of the injury mechanism could lead to improved injury prevention strategies in the future.

## REFERENCES

1. Kearney R, et al. *Obstet Gynecol* **107**, 144-149, 2006.
2. Lien KC, et al. *Obstet Gynecol* **103**, 31-40, 2004.
3. Kim J, et al. *Neurol Urodynam*, in press, 2011.
4. Qian ZQ, et al. *Eur J Mech A-Solid* **18**, 443-463, 1999.
5. Brooks SV, et al. *J Physiol* **488**, 459-469, 1995.
6. Marks LW, et al. *J Biomed Eng* **15**, 474-476, 1993.

## ACKNOWLEDGEMENTS

Funding by NIH grant, SCOR P50 HD044406

# Leg stiffness increases with gait speed to maximize propulsion energy during push-off

Seyoung Kim and Sukyung Park

Korea Advanced Institute of Science and Technology, Daejeon, Korea  
email: sukyungp@kaist.ac.kr

## INTRODUCTION

Compliant walking models have been used to account for the gait dynamics associated with compliant lower limbs [1, 2], and leg compliance has been quantified as a form of vertical lower limb stiffness [3]. However, the vertical stiffness of the lower limb has been defined by the ratio of the force change to the displacement change based on a formulation of  $K_{vert} \approx \Delta F / \Delta x$  without considering a full dynamic equation,  $M\ddot{x}(t) + C\dot{x}(t) + Kx(t) = F(t)$ , thus has a limited ability to represent gait dynamics. As a system parameter, the stiffness of a compliant walking model determines the system characteristics, such as the gait cycle period and the amplitude ratio of center of mass (CoM) oscillations to an external force. Therefore, quantification of the leg stiffness of a compliant walking model and the change in stiffness at different gait speeds would allow a better understanding of the contributions of spring-like leg behavior to gait dynamics.

In this study, we calculated the effective leg stiffness of human subjects walking at four different speeds by simulating a damped compliant walking model that was slightly modified from existing compliant walking models [1, 2]. To examine correlations between leg stiffness and the oscillatory behavior of the CoM during the single support phase, the damped natural frequency of the single compliant leg was compared with the duration of the single support phase. To interpret the change in leg stiffness with gait speed from an energetic perspective, the theoretical leg stiffness that maximized the elastic energy stored in the compliant leg at the end of the single support phase was calculated as a function of leg stiffness and gait speed and was then compared with human leg stiffness data.

## METHODS

Eight subjects walked over-ground at four different gait speeds, ranging from their self-selected speed to

their maximum speed [4]. The dynamic leg stiffness was estimated from a damped compliant walking model (Fig.1) that was optimized to best fit the ground reaction force data (Fig.2). To examine the relationship between leg stiffness and gait dynamics in the view of mechanical resonance, the oscillation period of the compliant walking model was calculated from the damped natural frequency and was compared with the duration of the single support phase. To examine the energetic benefits of leg stiffness changes as a function of gait speed, the propulsion energy indicating the spring potential energy at the end of single support phase was calculated as a function of leg stiffness and gait speed.

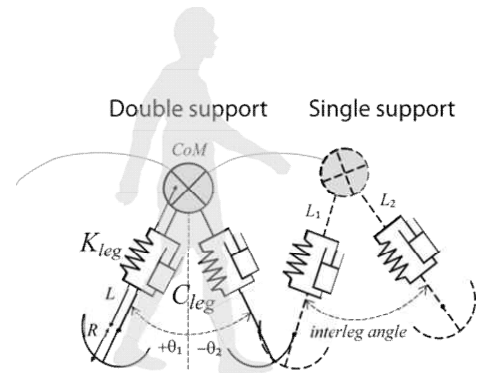


**Figure 1:** A compliant walking model. The human body was modeled with two massless, compliant legs with curved feet. The parameters  $K_{leg}$ ,  $C_{leg}$ ,  $\theta$ ,  $L$  and  $R$  indicate the spring constant, damping constant, leg angle, leg length and curved foot radius, respectively. The subscripts '1' and '2' indicate the trailing leg and the leading leg.

## RESULTS AND DISCUSSION

Model simulations reproduced the trajectories of the GRFs with the goodness of fit ( $R^2 = 0.81 \pm 0.06$ ) for all subjects (Fig. 2). Both the leg stiffness and damping ratio calculated by the model optimization significantly increased as a function of gait speed (Fig.3;  $p < 0.05$ ). The averaged slopes of the dimensionless stiffness (normalized by body weight

divided by height) and the damping ratio with respect to a unit speed change were  $39.82 \pm 12.71$  (s/m) and  $0.036 \pm 0.013$  (s/m), respectively (Fig. 3). Damping ratios ranged from 0.03 to 0.08 and were necessary to robustly generate repeated steps that reproduced the human data with various initial conditions.

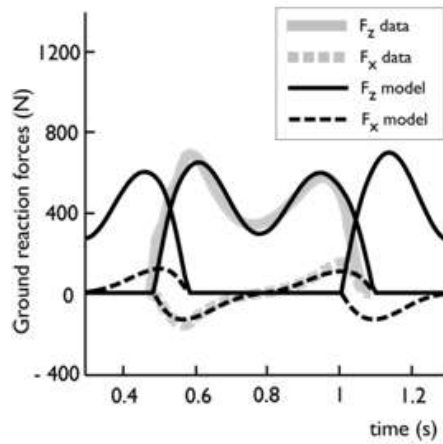


**Figure 2:** Model simulations of the GRFs. The solid lines and the dotted lines represent the vertical and horizontal directions, respectively.

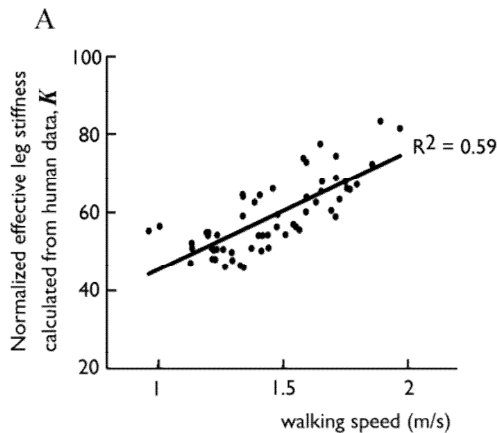


**Figure 3:** The effective leg stiffness as a function of walking speed obtained from the optimization that minimized the data-model fitting error. Leg stiffness was normalized by the subject's weight divided by height. The solid line indicates the linear regression.

The duration of the single support phase correlated well with the period of the damped natural frequency of the single compliant (Fig. 4), suggesting that CoM oscillations during the single support phase may take advantage of resonance characteristics of the spring-like leg. The theoretical leg stiffness that maximized the elastic energy stored in the compliant leg at the end of the single support phase was approximated by the empirical leg stiffness. This result implies that the CoM

momentum change during the double support requires maximum forward propulsion and that an increase in leg stiffness with speed would beneficially increase the propulsion energy.

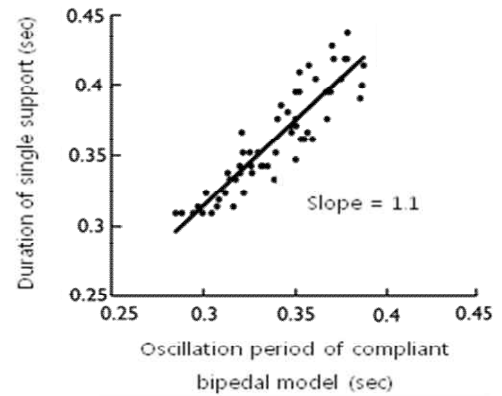


**Figure 4:** The duration of the single support phase and the period of oscillation of the compliant walking model. The single support duration was closely related to the damped natural frequency of the compliant leg.

## CONCLUSIONS

Our results suggest that humans emulate spring-like leg mechanics, and modulate the apparent stiffness to optimize gait dynamics and energetic. The effective leg stiffness increased with gait speed to support the greater propulsion energy required before collision during faster gaits.

**ACKNOWLEDGEMENTS:** This research was supported by the Basic Science Research Program through the National Research Foundation of Korea (NRF) funded by the Ministry of Education, Science and Technology (#2010-0013306) and the Unmanned Technology Research Center (UTRC) at the Korea Advanced Institute of Science and Technology (KAIST), originally funded by DAPA, ADD.

## REFERENCES

1. B.R. Whittington and D.G. Thelen, *Journal of Biomechanical Engineering*, 131(1), 2009.
2. H. Geyer et al., *Proceedings of the Royal Society B: Biological Sciences*, 273(1603):2861-2867, 2006.
3. J.R. Rebular et al., *Dynamic walking 2009*
4. J. Yeom and S. Park, *Journal of Biomechanics*, 44:59-67, 2011.

# Mechanical impulse during step-to-step transition balances propulsion energy and collision loss

Seyoung Kim and Sukyung Park

Korea Advanced Institute of Science and Technology, Daejeon, Korea  
email: sukyungp@kaist.ac.kr

## INTRODUCTION

Studies have suggested that the least costly gait would be achieved when the push-off propulsion fully compensates for the collision loss during the double support [1,2]. Recently the duration of CoM redirection was also defined based on work and peak velocity change reflecting non-rigid human leg and those durations were greater than that of double support [3], which brings an inquiry into the energetic optimality during the step-to-step transition defined differently from double support. The purpose of this study was to examine whether the different definitions of the duration of step-to-step transition would affect energetic balance between push-off propulsion and heel strike loss. We measured the mechanical impulse and work done on the CoM by GRFs during each definition of step-to-step transitions for seven normal human subjects walking at 4 different speeds ranged from self selected to maxim walking speed. Empirical data were then compared with the model predictions that minimize the cost during a single gait cycle.

## METHODS

Seven healthy young subjects (mean age  $22.7 \pm 1.1$  years) participated to the over ground walking experiment after signing informed consent approved by the Institutional Review Board of KAIST prior to the test. Average height and weight of the subjects were  $1.68 \pm 0.06$  m and  $67.7 \pm 11.4$  kg, respectively. Subjects walked on a 10-m long and 1-m wide walkway with three sets of four different randomly ordered gait speeds (1.1 ~ 2.4 m/s). Ground reaction forces for three consecutive steps were measured by force platforms (AMTI, MA, USA) at a 200-Hz sampling frequency. To capture the full step per each platform, we adjusted the location of platforms prior to each data collection. GRF data were 5<sup>th</sup>-order Butterworth low-pass filtered with a cutoff frequency of 30 Hz. Mechanical powers applied by GRFs were calculated by a vector product of external forces and COM velocity. We used three

different definitions of the step-to-step transition as suggested previously [3]: the duration of double support defined by GRFs ( $\tau_{\text{force}}$ ), the duration from the onset of positive push-off work and the end of negative collision work ( $\tau_{\text{work}}$ ), and the time interval from the minimum to the maximum vertical CoM velocities ( $\tau_{\text{vel}}$ ).

$$\begin{cases} W_{\text{push}} = \frac{P}{2m} \{P + 2mv^- \sin(\beta - \alpha) + 2s_{hp}H \cos(\beta + \gamma) - 2s_{gp}G \cos \beta\} \\ W_{\text{heel}} = \frac{H}{2m} \{H - 2mv^- \sin(\alpha + \gamma) + 2s_{ph}P \cos(\beta + \gamma) - 2s_{gh}G \cos \gamma\} \\ W_{\text{S}}|_{P_{\text{opt}}} = -(W_{\text{push}} + W_{\text{heel}})|_{P_{\text{opt}}} = 0 \end{cases} \quad (1)$$

From impulse-momentum relationship, the work done on the CoM by ground reaction forces could be analytically obtained in terms of gait parameters during the step-to-step transition [2] (Fig. 1).

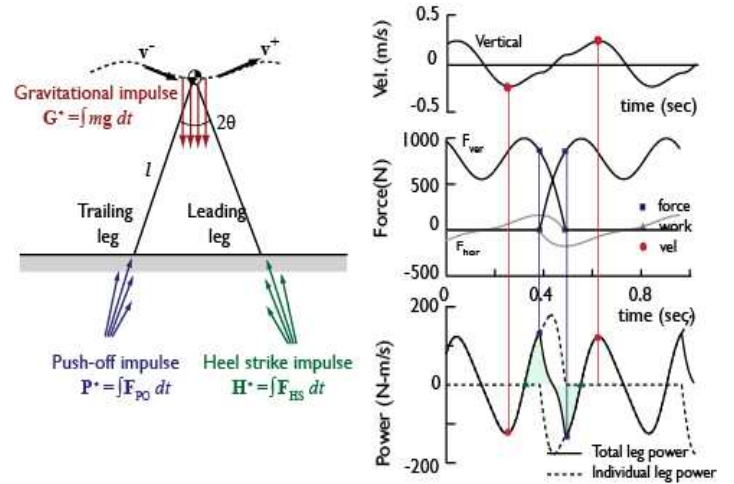


**Figure 1:** Schematics of gait parameters during a step-to-step transition. Push-off ( $P^*$ ), heel strike ( $H^*$ ), and gravitational impulses ( $G^*$ ) generate momentum change of the CoM from  $mv^-$  to  $mv^+$ , where  $v^-$  and  $v^+$  are the pre- and post- step-to-step transition velocities,  $m$  is a body mass, and  $2\theta$  is the inter-leg angle. Three definitions of step-to-step transition based on double support (■), power (▲), and peak velocity (●) were displayed.

## RESULTS AND DISCUSSION

Gait parameters related to the step-to-step transition reflected the exceeded duration of step-to-step

transition defined by work and velocity compared to the GRF and the step transition timing decreased with gait speed for all three definitions. Both linear and reciprocal regression of the step-to-step transition as a function of gait speed showed similar fitting performances, with the best match for the double support data (Fig. 2).

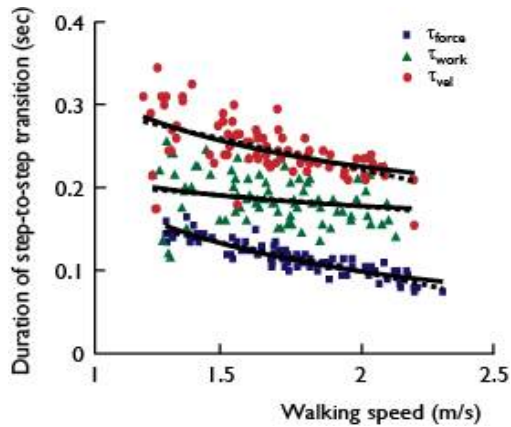


**Figure 2:** The durations of step-to-step transition were regressed as a function of walking speed with both linear (dashed) and reciprocal (solid) function of gait speed.

Mechanical work done on the CoM by the GRF was well approximated by the equations for collisional energy change for the push-off propulsion ( $R^2 > 0.7$ ) but was underestimated for heel strike collision loss ( $R^2 < 0.7$ ). Impulse data were agreed well with the optimal push-off predictions that minimize the energy expenditure during the gait cycle (Eqn. 1, Fig. 3). Gait parameters used for the optimal impulse calculation using Eqn. 1 and 2 were obtained from the data (Fig. 3).

Reasonable match between the data and model prediction of GRF impulses that minimize energy cost during the gait cycle demonstrates that all three definitions of step transition appeared to satisfy energetic optimality. The observed robustness of energetic optimality, regardless of the different definitions of step-to-step transition, may attribute to the almost symmetric oscillatory behavior of the CoM with respect to the double support phase. Recent studies described the excursion of body CoM during gait cycle as the oscillation of an inertia on a compliant leg [4, 5]. Due to the intrinsic symmetry of mechanical power of an oscillatory mechanism around the minimal/maximal position of the CoM (Fig. 1), the mechanical power of the mass before and after the middle of double support duration are approximated to be the same in magnitude but the opposite in sign, showing energetic symmetry.

Therefore, as far as other definitions of step-to-step transition extends the duration of double support in a temporally symmetrical manner, the sum of mechanical power of the CoM during pre- and post-collision would be approximated to be zero, which induces energetic optimality during gait cycle.

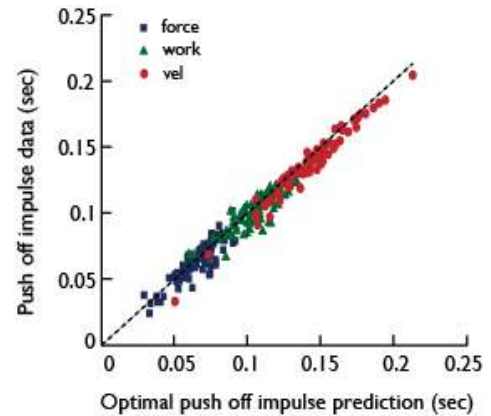


**Figure 3:** Empirical push-off impulse versus to the optimal push off impulse estimation that was obtained by minimizing CoM work throughout the gait cycle (Eqn. 1 and 2). Impulses were normalized by body weight. Dotted lines indicate the equality lines for  $x$  and  $y$  axis.  $R^2 > 0.7$ .

## CONCLUSIONS

The step-to-step transition of human walking occurs in an energetically optimal manner, which may be attributed by the spring-like leg mechanics that generates oscillatory behavior of the CoM.

**ACKNOWLEDGEMENTS:** This research was supported by the Basic Science Research Program through the National NRF of Korea funded by the MEST (#2010-0013306) and the Unmanned Technology Research Center at KAIST originally funded by DAPA, ADD.

## REFERENCES

1. A. Kuo, *Journal of Biomechanical Engineering* 124:113-120, 2002.
2. J. Yeom and S. Park, *Journal of Biomechanics*, 44:59-67, 2011.
3. P. Adamczyk, and A. Kuo, *Journal of Experimental Biology*, 212:2668-2678, 2009
4. H. Geyer, *Proceedings of the Royal Society B: Biological Sciences*, 273:2861, 2006.
5. S. Kim and S. Park, *Journal of Biomechanics*, doi:10.1016/j.jbiomech.2011.02.072, 2011

# STRENGTH DECREASES POSTURAL VARIABILITY IN OBESE ADOLESCENTS

<sup>1</sup>Adam C. King, <sup>1</sup>John H. Challis, <sup>1</sup>Cynthia J. Bartok, <sup>2</sup>F. Aileen Costigan, and <sup>1</sup>Karl M. Newell

<sup>1</sup>Pennsylvania State University, University Park, PA, USA

<sup>2</sup>Cornell University Ithaca, NY, USA

email: [ack196@psu.edu](mailto:ack196@psu.edu)

## INTRODUCTION

The incidence and severity of obesity continues to increase in children and adolescents. An increased body mass can have negative influences on many activities of daily living, including the control of postural stability and locomotion [1]. There is preliminary evidence that increases in body mass index (BMI) interferes with the control of standing posture [2]. However, this negative effect of obesity on postural control may be mediated by the change in other body scale variables (e.g., mechanical and fitness) with changes in BMI. This study investigated the influence of selected body scale, body composition, mechanical and strength variables as predictors of postural motion in obese and non-obese adolescents.

## METHODS

125 healthy adolescents (65 boys, 60 girls) were recruited to fulfill three different ranges of BMI percentile categories for both boys and girls. BMI percentile categories were low (<50<sup>th</sup> percentile), mid (50<sup>th</sup> - 85<sup>th</sup> percentile), and high (> 85<sup>th</sup> percentile). All subjects underwent a battery of tests that assessed body composition (DXA scan), anthropometry (Body segment inertial properties), and muscular strength (Biodex, isometric knee extension).

Additionally, subjects performed three different postural control tasks (two foot quiet standing, dominant leg standing, and sit-to-stand movements) on a force plate. Multiple measures of postural motion variability ( $SD_{ap}$ ,  $SD_{ml}$ ,  $L_{cop}$ ,  $V_{cop}$ ,  $A_{cop}$ ) were derived for analysis with body scale, mechanical and strength parameters separately for boys and girls. For each testing condition, bivariate correlations were run between the parameters collected from the force plate data and physical

dimensions. Individual BMI ratings were used as a continuous variable in the correlation analyses, instead of separate experimental groups. Significant correlations were identified with a value  $p < 0.05$ .

## RESULTS AND DISCUSSION

Table 1 shows the descriptive statistics for the main independent variables used in the correlation analysis. BMI, height and body mass, considered both separately and collectively, were poor and/or inconsistent predictors of variability in all three posture tasks. However, the ratio of strength to whole body moment of inertia showed the highest positive correlation to most postural variability measures in both boys and girls and these effects were strongest in the less stable tasks of single leg and recovery of stance (Table 2).

Table 1. Descriptive statistics of physical dimensions for boys and girls

| Mean (sd) [range]        | Boys                          | Girls                        |
|--------------------------|-------------------------------|------------------------------|
| Age (months)             | 155.9 (6.6)<br>[144.0 -166.0] | 130.1 (7.3)<br>[120.0-143.0] |
| Height (cm)              | 160.1 (9.8)<br>[136.5-188.4]  | 146.7 (8.8)<br>[130.5-169.8] |
| Body mass (kg)           | 52.7 (13.9)<br>[31.9-102.1]   | 40.9 (9.1)<br>[26.4-67.1]    |
| Body fat %               | 26.6 (8.0)<br>[13.1-45.3]     | 32.2 (7.4)<br>[21.3-51.5]    |
| BMI (kg/m <sup>2</sup> ) | 20.3 (3.6)<br>[13.8-31.0]     | 19.0 (3.1)<br>[14.3-25.9]    |
| MI (kg.m <sup>2</sup> )  | 8.4 (2.9)<br>[3.3-18.0]       | 5.3 (2.1)<br>[1.9-11.2]      |
| Knee Strength (N)        | 83.8 (28.0)<br>[35.8-206.4]   | 54.5 (16.0)<br>[6.5-100.8]   |
| S/MI ratio               | 10.5 (3.0)<br>[4.6-21.9]      | 11.6 (4.9)<br>[1.7-26.5]     |

The effects of obesity-related variables on postural control are weakly evident in the standard laboratory task of quiet standing but are more strongly revealed when the system is stressed by narrowing the constraints that define the functional stability boundary. It seems likely that the effects reported here on the predictive role of S/MI in

postural control would be even more manifest if we had had more participants in the extreme ends of the continuum in terms of the body scale obesity-related variables. In general, the influence of obesity related variables on postural control is dependent on the confluence of constraints to action, including those of the environment, the individual and the task [3]

Table 2. Pearson correlations (r) of parameters during the sit-to-stand movements for boys and girls.

|                          | SD <sub>ml</sub> | SD <sub>ap</sub> | L <sub>cop</sub> | V <sub>cop</sub> | A <sub>cop</sub> |
|--------------------------|------------------|------------------|------------------|------------------|------------------|
| <b>BOYS</b>              |                  |                  |                  |                  |                  |
| Height (cm)              | 0.22*            | 0.30**           | 0.22*            | 0.23*            | 0.23*            |
| Body mass (kg)           | 0.20             | 0.23*            | 0.11             | 0.13             | 0.21             |
| BMI (kg/m <sup>2</sup> ) | 0.19             | 0.16             | 0.06             | 0.08             | 0.18             |
| Body Fat %               | 0.16             | 0.00             | -0.05            | -0.03            | 0.03             |
| MI (kg.m <sup>2</sup> )  | 0.21*            | 0.26*            | 0.15             | 0.16             | 0.22*            |
| Knee Strength (N)        | 0.05             | 0.03             | -0.10            | -0.10            | 0.04             |
| S/MI ratio               | -0.27*           | -0.33**          | -0.33**          | -0.35**          | -0.26*           |
| <b>GIRLS</b>             |                  |                  |                  |                  |                  |
| Height (cm)              | 0.32**           | 0.26*            | 0.10             | 0.08             | 0.31*            |
| Body mass (kg)           | 0.08             | 0.29*            | 0.00             | 0.01             | 0.21*            |
| BMI (kg/m <sup>2</sup> ) | -0.07            | 0.19             | -0.02            | 0.00             | 0.09             |
| Body Fat %               | -0.14            | 0.06             | -0.05            | -0.05            | -0.04            |
| MI (kg.m <sup>2</sup> )  | 0.20             | 0.30*            | 0.05             | 0.04             | 0.27*            |
| Knee Strength (N)        | 0.04             | -0.01            | 0.00             | -0.05            | 0.01             |
| S/MI ratio               | -0.26*           | -0.28*           | -0.11            | -0.14            | -0.30*           |

## CONCLUSIONS

The effect of obesity on balance is not merely through changes in the physical properties of body scale that coalesce to determine the mechanical constraints but also through the fitness related

variable of strength that influences the control of body scale as shown in strong predictive properties of the S/MI ratio to postural motion. It is proposed that the findings invite the hypothesis that obesity related variables compromise the robustness of the long established strength to body scale relation and its influence in movement and postural control. Additionally, the role of fitness-related variables, other than strength, and physical activity levels merit further investigations regarding their interaction with obesity across the entire life span [4]. Our findings suggest that there is a need for more comprehensive studies on the influence of obesity and the associated body composition and scale measures on posture and movement and that these may be particularly relevant in the growth spurts of the life span, such as in adolescence.

## REFERENCES

1. Hills AP, Parker AW. *Arch Phys Med Rehabil* **72**:403-7,1991
2. Goulding A, et al. *Gait Posture* **17**:136-145,2003.
3. Newell KM. *Constraints on the development of coordination*. In: Wade M, Whiting H, editors. *Motor skill acquisition in children: Aspects of coordination and control*. p. 341–60, 1986
4. Malina RM et al. *Growth, maturation, and physical activity*. 2004.

## ACKNOWLEDGEMENTS

This project was supported in part by a grant from the American Alliance for Health, Physical Education, Recreation and Dance. We would like to thank the nurses at the GCRC and research assistants who assisted with the data collection

## Quantification of atrophy and activation failure in the plantarflexors post-stroke

<sup>1</sup>Brian A. Knarr, <sup>1</sup>John Ramsay, <sup>1</sup>Thomas S. Buchanan, <sup>1</sup>Stuart A. Binder-Macleod, <sup>1</sup>Jill S. Higginson  
<sup>1</sup>Biomechanics and Movement Science, University of Delaware, Newark, DE, USA  
email: [bknarr@udel.edu](mailto:bknarr@udel.edu)

### INTRODUCTION

Muscle weakness is a common impairment for chronic stroke survivors, and is characterized by lower forces during maximal volitional contraction on the affected side. Weakness in the plantarflexor muscle group is associated with decreased walking speed in stroke subjects (1). Post-stroke muscle weakness is commonly thought to be a result of a combination of central nervous system impairments and muscular atrophy due to disuse. Recent studies have attempted to parse the causes of weakness post-stroke, examining a combination of volitional force, muscle volumes from MRI, and agonist and antagonist EMG (2). While results indicate that activation failure is a primary cause of muscle weakness in persons post-stroke, its contribution to weakness has not been quantified. Muscle atrophy, as well as changes in muscle properties such as specific tension (3) and architecture (4), may also contribute to muscle weakness. The goal of this study is to assess the loss in force generating ability of the plantarflexor muscle group related to activation failure. We hypothesize that activation failure will account for a large portion, but not all, of muscle weakness.

### METHODS

13 subjects post-stroke (Age  $60 \pm 8$  yrs., 2 Female,  $4.2 \pm 3.2$  yrs. post-stroke) were recruited to participate in this study. All subjects were at least 6 months post-stroke and signed informed consent forms approved by the Human Subjects Review Board at the University of Delaware.

Muscle strength was tested using the burst superimposition test. Subjects lay supine on a KIN-COM III dynamometer (Chattecx Corp, Chattanooga, Tennessee) with their knee in extension and ankle at neutral. Velcro straps were used to hold the foot and shank in position. Restraints were placed on the shoulders of the subject to ensure that all forces were directed into the transducer and not lost to body displacement. A

maximal electrical stimulation burst (600  $\mu$ s pulse duration, 100 ms train duration, 135 V, 100 Hz train) (Grass Technologies, Warwick, RI) was delivered while subjects produced their maximum volitional force. Predicted maximum force generating ability (MFGA) using the burst superimposition test (MFGA<sub>burst</sub>) was calculated using the following equation:

$$(1) \text{MFGA}_{burst} = F_{vol} + F_{stim}$$

where  $F_{vol}$  is the volitional force produced by the subject and  $F_{stim}$  is the additional force produced by the stimulation. A cubic adjustment, similar to methods previously used for the quadriceps (5; 6), was applied to the MFGA prediction to account for the incomplete activation of the muscle with the burst. MFGA was converted to torque ( $T_{max}$ ) for comparison to previous studies.

Axial MRI Images were acquired for both legs using a 1.5 T Signa LX scanner (GE Medical, Milwaukee, WI). Two overlapping images were taken for the lower leg using a repetition time of 450 ms, echo time of 10 ms, slice thickness of 10 mm and a space between slices of 11.5 mm. IMOD software was used to manually trace the boundaries of the soleus (SOL), medial gastrocnemius (MG), and lateral gastrocnemius (LG) muscles over the entire muscle length. After adjusting the pixel threshold for fat suppression, volume was calculated by summing the cross-sectional areas multiplied by the slice thickness over the length of the muscle. Difference between interlimb  $T_{max}$  and muscle volume were evaluated using a t-test.

### RESULTS AND DISCUSSION

Average paretic limb MVC plantarflexion torque ( $34.4 \pm 21.3$  Nm) was  $41 \pm 17\%$  of the non-paretic MVC ( $89 \pm 41.5$  Nm) (Figure 1). Predicted max torque of the paretic plantarflexors ( $82.4 \pm 20.2$  Nm) was  $66.5 \pm 9.6\%$  of the non-paretic limb ( $124.9 \pm 30.4$  Nm). The average paretic plantarflexor volume was  $79.8 \pm 9.1\%$  of the non-

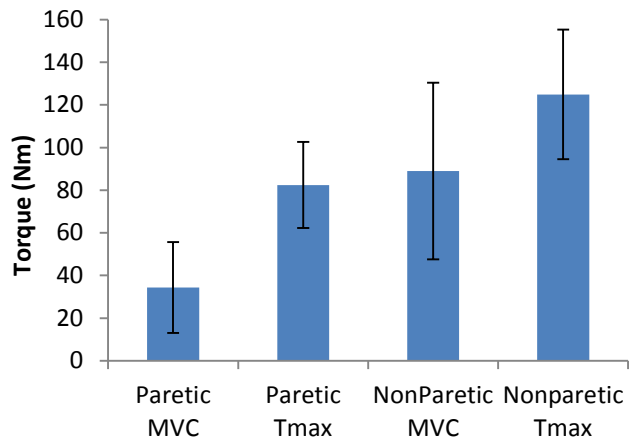


**Figure 1. Maximum voluntary (MVC) and maximum predicted (Tmax) torque for the paretic and non-paretic plantarflexor muscles in thirteen subjects post-stroke.**

paretic limb (Figure 2). Average volitional activation (CAR) of the paretic limb ( $39.9 \pm 15.3\%$ ) was 61% of the non-paretic limb ( $68.4 \pm 16.9\%$ ) (Figure 2).

Relative MVCs for the subjects were consistent with previous studies, showing that paretic plantarflexor muscle strength is 38% of the non-paretic side (2). The paretic side showed ~40% CAR, also consistent with previously reported data (2). Activation impairment was also present on the non-paretic side (~69% CAR). Non-paretic weakness has been previously reported as less than 85% of normal for the lower limb (7) and is likely due to partial innervation by the ipsilateral motor cortex (8).

Activation failure resulted in ~60% loss in volitional (MVC) torque in the paretic limb and ~32% loss in volitional torque (MVC) in the non-paretic limb. With full activation, the paretic limb had a 34% lower maximum torque (Tmax) than in the non-paretic limb (Figure 1). Some of this difference can be accounted for by muscle atrophy (Figure 2), however our results suggest that additional changes in muscle properties such as specific tension, muscle architecture and overall muscle quality are likely the cause of significant (~13%,  $p=0.002$ ) loss in maximum torque of the paretic limb in relation to the non-paretic limb.

#### ACKNOWLEDGEMENTS

NIH NS055383 and NR010786-01

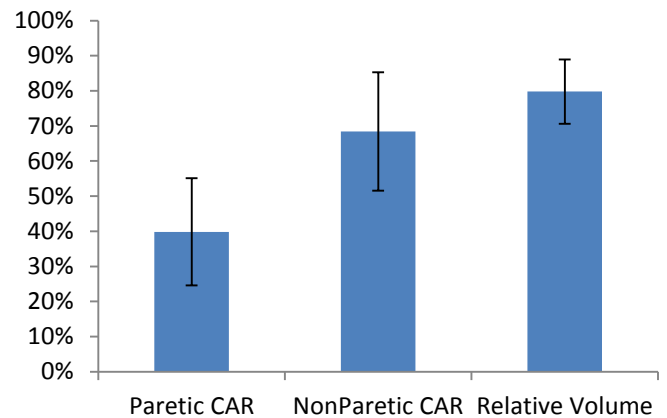


**Figure 2. Paretic and non-paretic side central activation ratio (CAR) and relative (paretic / non-paretic) muscle volume for the plantarflexor muscles in thirteen subjects post-stroke.**

#### CONCLUSIONS

This study assessed the force generating ability of the plantarflexor muscle group related to activation failure and muscle atrophy in patients post-stroke. A modified burst superimposition test was used to predict maximal force generation from a sub-maximally activated muscle. After comparing the maximum muscle force with muscle volumes obtained via MRI, the results suggest that other muscular changes are contributing significantly to post-stroke muscle weakness. Future studies should examine changes in muscle architecture and specific tension bilaterally post-stroke to further quantify their contribution to muscle weakness.

#### REFERENCES

- Nadeau S, Gravel D, Arsenault AB, Bourbonnais D. *Clinical Biomechanics*. 1999 Feb ;**14**(2):125-35.
- Klein CS, Brooks D, Richardson D, McIlroy WE, Bayley MT. *Journal of applied physiology*. 2010 Aug ;(August 2010):1337-1346.
- Frontera WR, Grimby L, Larsson L. *Muscle & nerve*. 1997 Aug ;**20**(8):938-47.
- Gao F, Grant TH, Roth EJ, Zhang L-Q. *Archives of physical medicine and rehabilitation*. 2009 May ;**90**(5):819-26.
- Stackhouse SK, Dean JC, Lee SCK, Binder-MacLeod SA. *Muscle & nerve*. 2000 ;**23**(11):1706-1712.
- Stackhouse SK, Stevens JE, Johnson CD, Snyder-Mackler L, Binder-MacLeod SA. *Muscle & nerve*. 2003 Jan ;**27**(1):40-5.
- Andrews AW, Bohannon RW. *Clinical Rehabilitation*. 2000 Feb ;**14**(1):79-87.
- Adams RW, Gandevia SC, Skuse NF. *Brain*. 1990 Oct ;**113** 51459-76.

# A STUDY ON DEVELOPMENT OF A SENIOR-FRIENDLY LIFT HANDGRIP THROUGH DRIVABILITY TESTS

<sup>1</sup>Cheolwoong Ko<sup>1</sup>, Dukyon Cho, <sup>1</sup>Keyoungjin Chun

<sup>1</sup>Gerontechnology Center, Korea Institute of Industrial Technology (KITECH), Chonan, Korea  
email: [chun@kitech.re.kr](mailto:chun@kitech.re.kr) web: <http://www.kitech.re.kr>

## INTRODUCTION

Recent economic growth and health care development are intensifying global aging. Various R&Ds on senior-friendly products have been taking place in advanced countries in terms of the aging society, such as USA, Europe, and Japan, etc. Generally, with the purpose to improve the Quality of Life (QoL) and effective care for the elderly, mobility assisting devices suitable for indoor movements are actively introduced in care facilities [1]. A multi-purpose lift for indoor movements is one of the representative mobility assisting devices. The optimal development of the lifts considering the physical behaviors of the elderly is in demand. However, studies on an optimal design especially for a lift handgrip, which is one of the major product development factors, are insufficient. In this study, drivability tests of a lift were conducted by selected subjects in developing a senior-friendly multi-purpose lift for indoor movements. An optimal design process for a lift handgrip was also suggested by measuring muscle activity using EMG sensors attached on the subjects.

## METHODS

A prototype of a multi-purpose swivel type lift was developed for drivability tests to obtain optimal design parameters of a lift handgrip. A variable handgrip device that can change or adjust the width, angle, and height of a handgrip was also fabricated (Fig. 1). For drivability tests, three Korean males in their 20s (average age: 27.3, average height: 174cm, average weight: 72.3kg) were selected as subjects. In addition, a human dummy (60kg) was loaded on a bed considering a passenger. An EMG device (Electromyograph, Delsys Inc, USA) was used for measuring the muscle activity in the subject's body while driving the lift. For the EMG sensors, a total of 12 agonist muscles were selected among the

activated ones during the drivability tests (Fig. 2). The drivability tests were conducted on a curved test track (Fig. 3). Total 24 combinations consisting of 4 widths (200mm, 400mm, 600mm, and 800mm), 3 angles (0°, 45°, and 90°), and 2 heights ( $H_1=1,090\text{mm}$ ,  $H_2=1,300\text{mm}$ ) were applied for the lift handgrip specifications during the tests. Each subject was to perform total 8 tests per design specification (192 times\*3 persons). An average of the 6 tests was compared and analyzed, excluding the maximum and the minimum values.

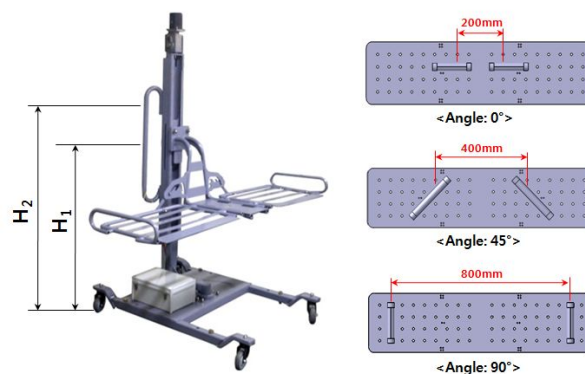
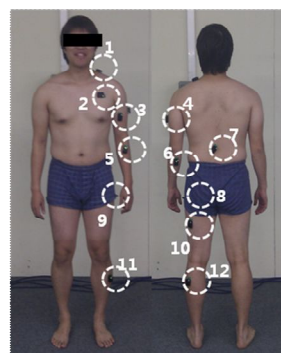


**Figure 1:** Prototype of a Swivel Type Lift and a Variable Handgrip Device



|    |                        |
|----|------------------------|
| 1  | Trapezius              |
| 2  | Pectoralis Major       |
| 3  | Biceps Brachii         |
| 4  | Triceps Brachii        |
| 5  | Pronator Brachii       |
| 6  | Extensor Carpi Ulnaris |
| 7  | Erector Spinae         |
| 8  | Gluteus Medius         |
| 9  | Rectus Femoris         |
| 10 | Biceps Femoris         |
| 11 | Tibialis Anterior      |
| 12 | Gastrocnemius          |

**Figure 2:** Twelve Muscles for Attaching EMG Sensors to Subjects

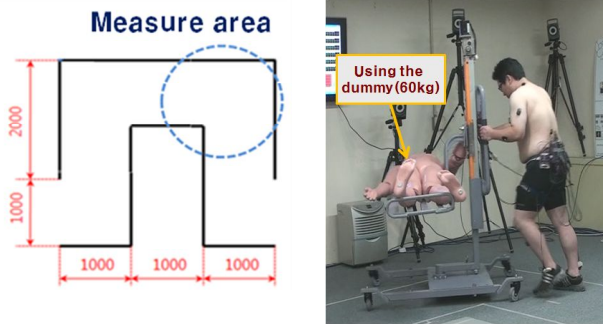


**Figure 3:** Curved Test Track for Drivability Tests of a Lift Loading a Human Dummy

## RESULTS AND DISCUSSIONS

The overall results of the drivability tests showed no significant difference in muscle activity (EMG08~EMG12) in the lower extremity (Fig. 4, Fig. 5). However, there was an obvious difference in muscle activity (EMG03~EMG06) in the upper extremity. The measured muscle activity tended to decrease as the width of a handgrip increased, and the lowest value was obtained at 0° angle. The height of a handgrip  $H_2$  showed a relatively greater muscle activity compared to the  $H_1$  (Fig 6, Fig. 7). The lowest muscular activity (11.49%) was measured when the specifications of a handgrip had 800mm width, 0° angle, and 1,090mm height.

## CONCLUSIONS

In this study, muscle activities of selected subjects were measured through drivability tests on the senior-friendly multi-purpose swivel type lift. The optimal design parameters for a lift handgrip (width: 800mm, angle: 0° angle, height: 1,090mm) were obtained from the tests. The optimal development of a lift handgrip is expected to provide more convenience for caregivers as well as to effectively reduce care costs of caregivers, when drivability tests are performed by female subjects in their 4-50s.

## REFERENCES

1. Kim JH, et al. *Journal of the Ergonomics Society of Korea* **28**, 161-166, 2009.

## ACKNOWLEDGEMENTS

This study was funded by the Ministry of Knowledge Economy in Korea (09-FM-1-0051).

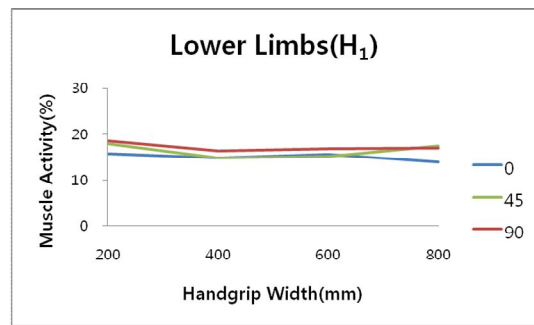


**Figure 4:** Muscle Activities of Lower Limbs at  $H_1$

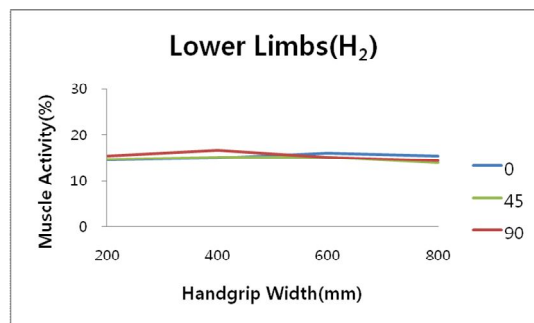


**Figure 5:** Muscle Activities of Lower Limbs at  $H_2$

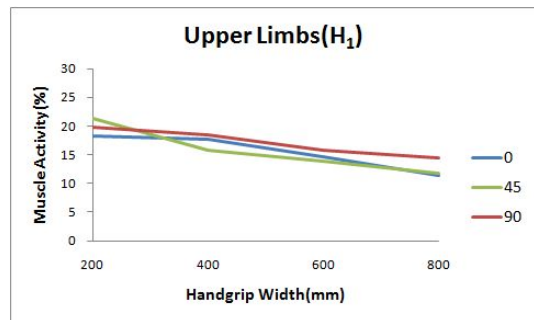


**Figure 6:** Muscle Activities of Upper Limbs at  $H_1$

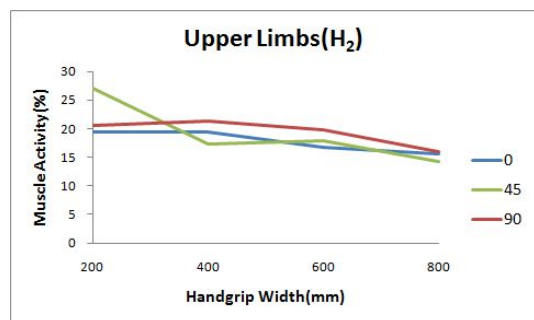


**Figure 7:** Muscle Activities of Upper Limbs at  $H_2$

# BIOMECHANICAL TESTING OF MULTI-LEVEL LAMINOPLASTY AND LAMINECTOMY PROCEDURES

<sup>1,2</sup>Swathi Kode, <sup>1,2</sup>Anup A Gandhi, <sup>3</sup>Joseph D Smucker,  
<sup>3</sup>Douglas C Fredericks, <sup>1,2,3</sup>Nicole M Grosland

<sup>1</sup>Department of Biomedical Engineering, <sup>2</sup>Center for Computer Aided Design,  
<sup>3</sup>Department of Orthopaedics and Rehabilitation

The University of Iowa, Iowa City, IA

Email: nicole-grosland@uiowa.edu, web: <http://www.ccad.uiowa.edu/mimx>

## INTRODUCTION

Cervical spinal stenosis is a medical condition caused by the narrowing of the spinal canal, possibly leading to the compression of the spinal cord or other nerve roots [1]. The traditional posterior method of decompression, laminectomy, involves removal of the lamina and associated ligaments. Laminoplasty, considered an alternative to laminectomy, is a procedure intended to relieve pressure on the spinal cord while maintaining the stabilizing effects of the posterior elements of the vertebrae. Open door laminoplasty (ODL) involves “hinging” one side of the lamina and cutting the other side to form a door. The lamina is then opened and held in place with plates and screws.

The number of lamina to be opened to fully release the spinal cord has always been a question and it depends on the existing pathological conditions. In order to see the longitudinal effects of ODL, a 2-level and 4-level laminoplasty was performed on cervical spinal segments. The current study is an experimental approach, addressing the multidirectional flexibility of the cervical spine in response to both laminoplasty and laminectomy procedures.

## METHODS

A total of 3 fresh-frozen human cadaveric cervical specimens (C2-T1) were used in this study. Specimens were cleaned of all residual musculature and were potted using Bondo (Bondo Corp, Atlanta, GA). The specimens were tested in the following sequential order: (a) Intact (b) Laminoplasty at C5-C6 (LP\_C56) (c) Laminoplasty at C3-C6 (LP\_C3456) (d) Laminectomy at C3-C6 (LT\_C3456)

ODL on C5-C6 levels: After testing the intact specimens, ODL was first performed on the C5 and C6 levels. A 3mm high speed burr was used to create a hinge on the right lamina and lateral mass junction by removing the dorsal cortex and cancellous layer. A cut of approximately 4-5mm was made on the contralateral side by using the same high speed burr. Thereafter, the spinous process of C5 and C6 was resected. Interspinous ligaments (C4-C5, C5-C6 and C6-C7) and unilateral ligamentum flavum on the open side (C4-C5, C6-C7) were resected with a scalpel to aid in laminar opening. The lamina of the involved vertebrae were then opened gently towards the hinge and stabilized with plates and screws (Medtronic Sofamor Danek, Memphis, TN). A 10 mm plate was secured with 2 screws on lateral mass and one on the open end of lamina. Care was taken to preserve the facet capsules.

ODL on C3-C6 levels: After the C5-C6 laminoplasty was tested, the procedure was extended to the C3 and C4 levels. The additional ligaments resected include interspinous ligaments (C2-C3, C3-C4) and unilateral ligamentum flavum on the open side at C2-C3.

Laminectomy on C3-C6 levels: Following the laminoplasty study at C3-C6, a laminectomy was performed (levels, C3-C6) by drilling through the hinge on the right lamina and lateral mass junction. The plates and screws on the contralateral side were removed. The preserved ligamentum flavum at C2-C3 and C6-C7 was then resected for the complete removal of posterior elements.

Experimental Testing Protocol: Specimens were tested using servo hydraulic materials testing

machine (858Mini Bionix II, MTS Corporation, Eden Prairie, MN) retrofitted with 2 spine-loading fixtures. Custom made rigid body sensors consisting of 3 IREDS were rigidly attached to the anterior part of each vertebra and the top and bottom gimbals. The motion of the sensors was then tracked with an optical motion capture system (Optotrak 3020, Northern Digital Inc., Waterloo, Ontario, Canada). The cervical spinal segments were evaluated under a pure moment of 2Nm in flexion/extension, right/left lateral bending and right/left axial rotation at a loading rate of 4Nm/min. To precondition the specimen and to minimize the viscoelastic effects; each test was repeated for two cycles, with the data from the third cycle used for analysis.

## RESULTS AND DISCUSSION

Since the preliminary study is limited to 3 spines, the specimens will be analyzed for statistical significance after testing additional specimens. Figure 1 and Figure 2 show the average range of motion ( $\pm$  standard deviation) data during flexion and extension respectively. During flexion, laminoplasty resulted in 8% increase in the motion while laminectomy resulted in 55% increase in the motion. It can be observed from figure 2 that laminoplasty showed a trend towards decreased range of motion during extension while no major changes were observed after laminectomy.

Both left lateral bending and left axial rotation showed a 13% and 12% increase in the range of motion respectively after open door laminoplasty (LP\_C3456). This inclination towards increased range of motion after left lateral bending and left axial rotation can be attributed to the open door laminoplasty being performed on left side. Laminectomy resulted in profound increase in the motion during left (21%) and right (13%) axial rotation.

Compared to 4-level laminoplasty, 2-level laminoplasty resulted in decrease of motion during flexion and extension. After 2-level laminoplasty, during extension, it was observed that the C4 spinous process touched the opened lamina of C5 thereby resulting in decreased motion at C4-C5.

Lateral bending and axial rotation did not result in any major changes in motion after 2-level laminoplasty.

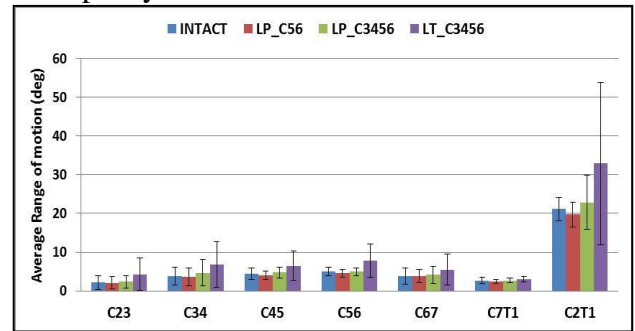


Figure1: Mean Range of motion after laminoplasty and laminectomy (flexion)

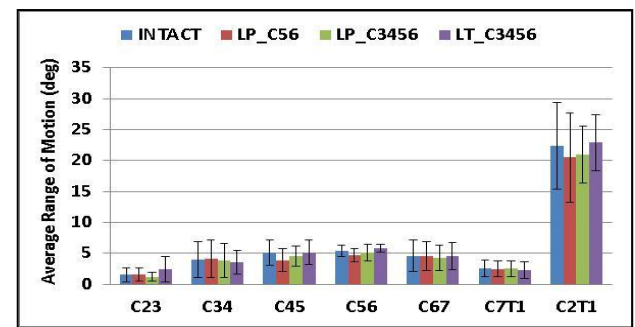


Figure2: Mean Range of motion after laminoplasty and laminectomy (extension)

## CONCLUSION

Earlier *in vitro* studies after ODL show discrepancies in the type of stabilization technique used for holding the lamina in the open position [2]. The plates and screws used in the current study were found to be intact throughout the testing of specimens. The range of motion data shows that laminoplasty resulted in minimal changes while laminectomy resulted in substantial increase during flexion and axial rotation. These results correspond well with existing *in vitro* laminoplasty and laminectomy studies [3]. Our goal is to compare the experimental results to the finite element predictions after ODL and laminectomy.

## REFERENCES

1. Allen et al., *Spine* **12**, 803–808, 1987.
2. Nowinski et al., *Spine* **18**, 1995-2004, 1993.
3. Subramaniam et al., *Spine* **34**, E573-E578, 2009.

# Biomechanical Analysis of Sitting Pivot Wheelchair Transfers

Alicia Koontz, Padmaja Kankipati, Chung-Ying Tsai, Yen-Sheng Lin

Human Engineering Research Laboratories, Department of Veterans Affairs, Pittsburgh, PA  
Department of Rehabilitation Science and Technology, University of Pittsburgh, Pittsburgh, PA  
email: [akoontz@pitt.edu](mailto:akoontz@pitt.edu)

## INTRODUCTION

For individuals who rely on wheelchairs for mobility, performing transfers is essential to achieving independence with activities of daily living (ADL). The most common transfer performed by wheelchair users is the sitting-pivot transfer (SPT) which the arms are predominantly used to move the body from one location to another. Unfortunately SPTs, along with wheelchair propulsion, weight relief and overhead activities are believed to largely contribute to the development of shoulder pain and injury (1). The onset of pain or an overuse injury can be devastating leading to increased healthcare expenses, limitation in activity, depression, decreased societal participation and a reduced quality of life. Despite the importance of transfers for daily living and that transfers are ranked among the most strenuous wheelchair-related activities (2), there is surprisingly a paucity of research on the biomechanics of transfers. This paper describes a measurement system developed to collect kinetics and kinematics of SPTs and a summary of study findings to date.

## METHODS

**Subjects:** The inclusion criteria for the SPT studies are: spinal cord injury (SCI) at C4 level or below that occurred over one year prior to the start of the study, able to independently transfer to/from a manual wheelchair without human assistance or assistive devices, over 18 years of age, and free from upper extremity pain that influence ability to transfer. **Experimental Protocol:** Subjects use their personal wheelchairs (WCs) which are secured at a self-selected angle to a platform as shown in Figure 1. Under each platform are force plates (Bertec Corporation, Columbus, OH), one beneath the wheelchair and one beneath an adjustable height tub bench. A custom steel beam attached to a 6-component load cell (Model MC5 from AMTI, Watertown, MA) is positioned next to the wheelchair to simulate a wheelchair armrest. A seventeen camera 3D motion capture system and

Nexus 1.6.1 software (Vicon Peak, Lake Forest, CA) measures the position of reflective markers placed on the back, chest, and arms during the transfer. Kinematic and kinetic data are collected at 60 Hz and 360Hz respectively. Subjects are asked to perform a SPT as they normally would do and then shown an instructional video on how to perform three other SPTs observed clinically, two which incorporate the head-hips relation (HH) and one that is translational in nature. One of the HH transfers requires the hand be placed on a target on the nearest edge of the bench (HH1), whereas the other HH transfer requires the hand be placed further away (HH2).

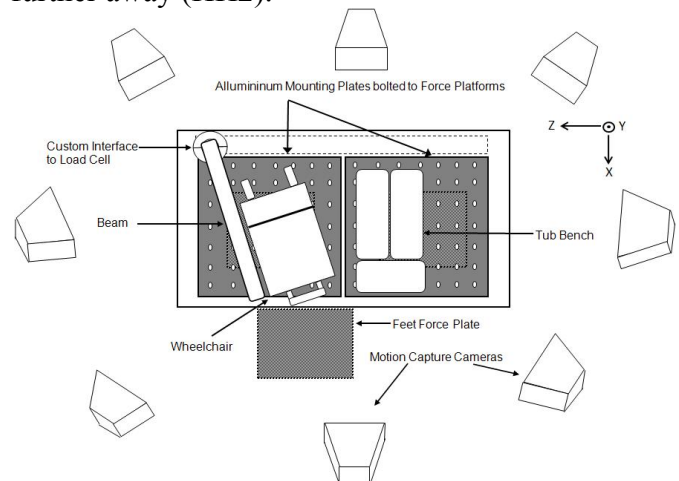


Figure 1 Experimental Setup for collecting biomechanics of SPTs

**Data Analysis:** Vertical forces from the force plate under the tub bench, wheelchair and the force-sensing beam (wheelchair side) and the y coordinate of the C7 and T3 markers are superimposed on one plot to delineate the three phases of SPT: pre-lift, lift and descent. An inverse dynamic model is used to calculate upper limb peak net joint forces, for both the leading (i.e. arm reaching to the new surface) and trailing arm (i.e. arm behind during move to new surface).

## RESULTS AND DISCUSSION

Twenty able bodied and 31 subjects with SCI have been consented to date. A preliminary analysis (n=9 subjects with paraplegia) revealed

that one of the taught transfers (HH1) reduced vertical forces at the shoulder compared to the self-selected transfer ( $p \leq 0.021$ ) (3). While vertical loading decreased, posterior loading at the joint increased but not significantly and was likely due to a shift in the direction of force as the shoulder translated anteriorly with increasing trunk flexion. For approximately half of the subjects however, peak resultant forces at the shoulders were reduced by at least 18% when compared to their self-selected transfer technique, which led us to investigate how much more the legs were being used to support the weight-bearing forces. In a followup study (3) we found forces at the feet were higher for the HH2 technique compared to the translational technique supporting our hypothesis that reduced forces at the shoulder are at least in part due to more lower extremity weight-bearing. The lower limbs in general supported close to 20% body weight averaged across all techniques.

An in depth analysis comparing the SPT techniques was conducted for 14 able-bodied subjects (3). HH techniques while reducing force at the shoulder and elbow alternatively resulted in increased moments at both joints compared to the translational transfer (Table 1). Peak forces at the hand were larger than those measured at the elbow and shoulder suggesting a smaller, more mobile joint is required for weight-bearing. This finding underscores the propensity for transfers to accelerate the development of wrist pain and injuries particularly since the wrist is commonly placed in an extreme position of extension during the weight-bearing portion of the transfer.

Peak resultant shoulder forces were compared across three phases of the SPT for WC to Bench (CB) and Bench to WC (BC) ( $n = 8$ ; subjects with paraplegia) (3). Higher forces were seen during the lift and descent phases compared to pre-lift in both arms for the CB transfer (Fig 2). Shoulder forces reached maximum loading for the the BC transfer suggesting transferring back into the WC was a

more difficult transfer than when transferring to the bench from the wheelchair.

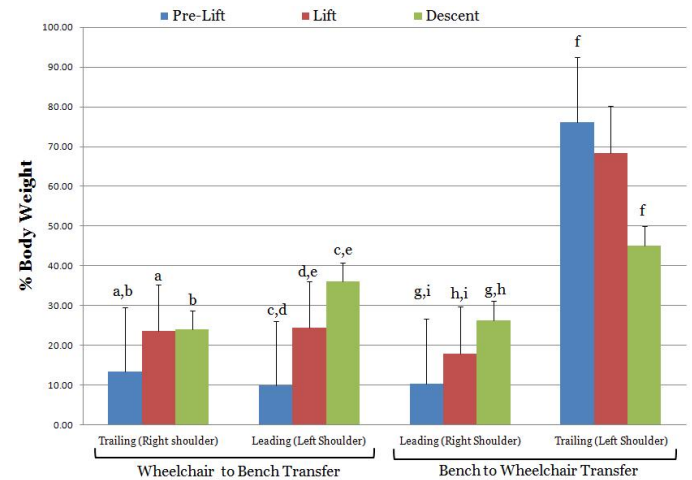


Figure 2 Net resultant forces at the shoulder across three phases of transfers. Letters a- i indicate significant pair-wise comparisons between phases,  $p = 0.05$ .

## CONCLUSIONS

The results collectively suggest that substantial loading occurs at all joints and improvements in SPTs are needed to minimize forces and moments and reduce the prevalence of upper limb pain and injury among WC users with SCI. Determining which strategy may be better requires an individualized approach and future studies that are longitudinal that can prove a reduction in symptoms and pathology overtime after a training intervention.

## REFERENCES

- Nyland, J., et al., Preserving transfer independence among individuals with spinal cord injury. [Review] [70 refs]. Spinal Cord, 2000. 38(11): p. 649-657.
- Gagnon, D., et al., Biomechanics of Sitting Pivot Transfers Among Individuals with a Spinal Cord Injury: A Review of the Current Knowledge. Topics in Spinal Cord Injury Rehabilitation, 2009. 15(2): p. 33-58.
- Seven conference proceedings have been published and two full journal articles have been submitted (one in press and one in review) related to this work.

## ACKNOWLEDGEMENTS

Funding for this study was provided by the Department of Veteran Affairs (A4489R).

Table 1 : Means ( $\pm 1$  standard deviation) of the peak forces experienced at the hand, elbow and shoulder across techniques for each arm. Symbols \*, + and ¥ - represent significant pairwise differences at a significance level of  $p < 0.05$ . IR = internal rotation

| JOINT KINETIC COMPONENT | TRAILING ARM          |                              |                           | LEADING ARM               |                              |                            |                            |
|-------------------------|-----------------------|------------------------------|---------------------------|---------------------------|------------------------------|----------------------------|----------------------------|
|                         | Translational         | HH2                          | HH1                       | Translational             | HH2                          | HH1                        |                            |
| SHOULDER                | Superior Force (N)    | 219.0 (117.6) <sup>*,+</sup> | 73.1 (53.9) <sup>*</sup>  | 88.8 (54.9) <sup>+</sup>  | 162.8 (101.7) <sup>*,+</sup> | 74.8 (84.6) <sup>*</sup>   | 79.1 (87.5) <sup>+</sup>   |
|                         | Resultant Force (N)   | 298.2 (108.4) <sup>*,+</sup> | 200.4 (84.7) <sup>*</sup> | 183.5 (68.5) <sup>+</sup> | 414.3 (244.1)                | 370.6 (267.7)              | 415.1 (240.1)              |
|                         | IR Moment (Nm)        | 23.6 (37.2) <sup>¥</sup>     | 64.7 (58.5) <sup>¥</sup>  | 45.5 (31.7)               | 73.1 (42.5)                  | 93.8 (50.7) <sup>¥</sup>   | 46.5 (23.2) <sup>¥</sup>   |
| ELBOW                   | Posterior Force (N)   | 169.9 (97.9)                 | 147.8 (89.7)              | 170.2 (85.5)              | 102.8 (55.6) <sup>*,+</sup>  | 174.8 (105.0) <sup>*</sup> | 185.5 (102.9) <sup>+</sup> |
|                         | Resultant Force (N)   | 311.7 (110.0) <sup>*,+</sup> | 211.0 (81.8) <sup>*</sup> | 198.9 (75.1) <sup>+</sup> | 318.4 (103.2) <sup>¥</sup>   | 252.5 (108.7) <sup>¥</sup> | 283.86 (86.3)              |
|                         | Extension Moment (Nm) | 23.8 (52.2)                  | 25.9 (48.6)               | 12.8 (21.4)               | 8.5 (10.4) <sup>*</sup>      | 9.1 (16.3) <sup>+</sup>    | 34.5 (20.6) <sup>*,+</sup> |
| HAND                    | Resultant Force (N)   | 320.1 (113.8) <sup>*,+</sup> | 219. (81.2) <sup>*</sup>  | 210.8 (78.9) <sup>+</sup> | 332.0 (105.1)                | 264.0 (113.79)             | 297.8 (89.3)               |

# THE INFLUENCE OF HALLUX VALGUS SURGERY ON PELVIS AND LOWER EXTREMITIES MOVEMENT DURING GAIT

<sup>1</sup>Jitka Kozakova, <sup>1</sup>Miroslav Janura, <sup>2</sup>Zdenek Sos and <sup>1</sup>Zdenek Svoboda

<sup>1</sup> Faculty of Physical Culture, Palacky University, Olomouc, Czech Republic

<sup>2</sup> Department of Orthopaedics, University Hospital, Olomouc, Czech Republic  
email: jitka.kozakova@upol.cz

## INTRODUCTION

Hallux valgus (HV) is a complex progressive triplanar forefoot deformity, it incorporates valgus deviation of the big toe, higher varosity of the first metatarsal and a medial prominentia on its head [1]. The development of this deformity is subsequent. Its risk factors include biomechanical and structural anomalies, systemic diseases, hereditary predispositions, footwear [2]. The hallux and first metatarsophalangeal joint play the main role in a load transmission during walking. The valgus deformity of the big toe is a typical first ray dynamic stabilization failure and loss of contact between the first metatarsophalangeal joint surfaces and sesamoid bones. The centralization and stabilization failure of the first metatarsophalangeal joint in case of the HV deformity doesn't enable to perform the heel-off and toe-off optimally [3]. It could negatively project, especially at the end of the preswing phase. Janura et al. reported that even mild juvenile HV deformity influences kinematic parameters of gait. In people with the juvenile HV greater maximum of hip flexion, greater maximum of knee flexion during swing phase and greater maximum of plantar flexion at the initial contact were found [4].

The aim of this study was to investigate the gait cycle performance after convalescence of the HV surgery, when the patient should be ready to return to work and their normal activities.

## METHODS

The gait cycle performance was compared in eight women ( $53.9 \pm 11.8$  years,  $67.0 \pm 10.2$  kg,  $1.65 \pm 0.06$  m) before and 3.5 months after the HV surgery. For the gait analysis a Vicon MX system (Vicon Motion Systems, Oxford, UK) with 7 infrared cameras and two force platforms (Kistler Instrumente AG Winterthur, Switzerland) were used. The subjects were walking at self-selected

speed. The five trials of each subject were analyzed. The statistical processing was performed by ANOVA for repeated measurement and Fisher's LSD post hoc test (Statistica 8.0, Stat-Soft, Inc., Tulsa, USA).

## RESULTS AND DISCUSSION

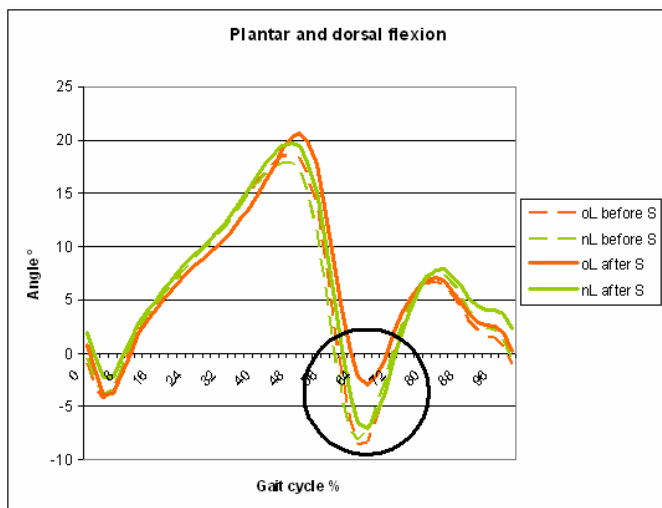
After the HV surgery a smaller plantarflexion ( $p < 0.001$ ) at the end of the preswing phase was found on the operated leg (Fig. 1). Knee flexion decreased during the stance phase on the operated leg ( $p < 0.01$ ) and increased on the non operated leg ( $p < 0.01$ ) after the surgery (Fig. 2). Maximum of the knee extension during stance and swing phase were greater ( $p < 0.01$ ) on operated leg and smaller on non operated leg after the surgery (Fig. 2). Hip flexion decreased and hip extension increased on the operated leg after the surgery ( $p < 0.001$ ). Range of pelvic obliquity was smaller after the surgery ( $p < 0.01$ ).

**Table 1.** Kinematic parameters of gait cycle.

|        | Before surgery |     |        |      | After surgery |     |        |      |
|--------|----------------|-----|--------|------|---------------|-----|--------|------|
|        | oL [°]         |     | nL [°] |      | oL [°]        |     | nL [°] |      |
|        | Mean           | SD  | Mean   | SD   | Mean          | SD  | Mean   | SD   |
| PF St  | 4.1            | 3.5 | 4.2    | 3.1  | 3.4           | 2.3 | 3.0    | 3.5  |
| PF Sw  | 9.2            | 4.2 | 9.6    | 4.9  | 3.4           | 4.0 | 7.9    | 4.8  |
| DF St  | 19.6           | 4.0 | 18.6   | 4.8  | 22.0          | 7.4 | 20.4   | 5.8  |
| DF Sw  | 8.0            | 3.4 | 7.9    | 5.1  | 8.4           | 2.8 | 8.7    | 5.0  |
| KEx St | 6.5            | 5.2 | 4.7    | 6.1  | 2.4           | 4.3 | 6.8    | 4.2  |
| KEx Sw | 5.4            | 5.5 | 3.6    | 5.1  | 3.0           | 3.4 | 5.1    | 3.4  |
| KFI St | 19.7           | 8.1 | 17.1   | 8.3  | 16.1          | 2.5 | 19.8   | 4.1  |
| KFI Sw | 62.2           | 7.0 | 60.6   | 10.2 | 60.7          | 6.6 | 60.2   | 6.2  |
| HFI    | 33.5           | 6.8 | 32.0   | 9.8  | 29.2          | 9.2 | 30.1   | 10.0 |
| HEX    | 9.4            | 7.8 | 11.0   | 7.7  | 12.8          | 7.9 | 11.6   | 8.2  |
| PT     | 3.4            | 0.6 | 3.3    | 0.8  | 3.1           | 0.9 | 3.5    | 0.8  |
| PO     | 7.8            | 3.1 | 8.7    | 3.9  | 8.0           | 2.1 | 7.4    | 3.3  |
| PR     | 9.6            | 2.4 | 11.4   | 5.0  | 12.6          | 1.5 | 9.3    | 2.8  |

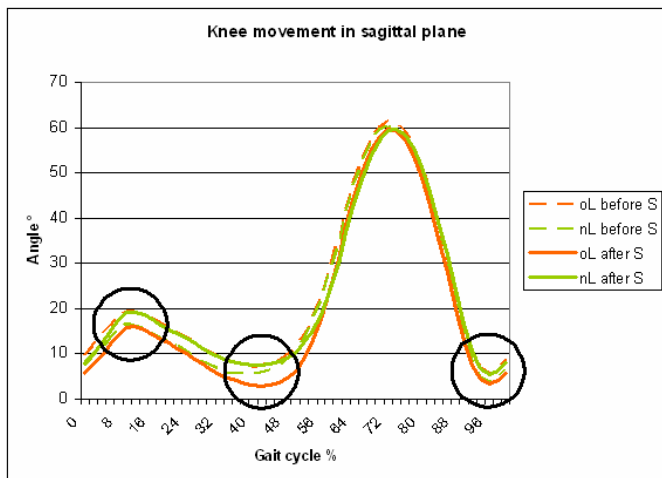
Legend: oL – operated leg, nL – non operated leg; SD – standard deviation; PF – maximum of plantar flexion, DF – maximum of dorsal flexion, KFI – maximum of knee flexion, KEx – minimum of knee flexion (knee extension), HFI – maximum of hip flexion, HEX – maximum of hip extension, PT – range

of pelvic tilt, PO – range of pelvic obliquity, PR – range of pelvic rotation; St – stance phase, Sw – swing phase.



S – surgery, oL – operated leg, nL – non operated leg

**Figure 1.** Ankle movement in sagittal plane before and after surgery during gait cycle.



S – surgery, oL – operated leg, nL – non operated leg

**Figure 2.** Knee movement in sagittal plane before and after surgery during gait cycle.

Costa, et al. reported that the radiographic parameters were improved 3 months after HV surgery, however the loading of the first metatarsal and hallux was still decreased in comparison with increased loading of the central and lateral metatarsal [5]. It probably explains changes in motion at the ankle and knee joint during toe-off.

The pain and difficulty with walking persist after a successful surgery in many cases. Postoperatively it's very important to recover the foot function and physiology gait pattern. Schuh, et al. confirmed that postoperative physical therapy and gait training may lead to improve of function and weight bearing of the first ray after hallux valgus surgery.[6]

It would be appropriate to verify our findings 6 and 12 months after surgery.

## CONCLUSIONS

Our results suggest that the surgery of the HV deformity influences not only foot motion. The surgery could change a kinematic chain of the whole lower extremity and pelvis as well.

Our findings show that convalescence after HV surgery is long-term and the postoperative care is very important to return patients to normal activities.

## REFERENCES

1. Dungal P. *Orthopedics*, Grada, Prague, CZ, 2005.
2. Lorimer DL, et al. *Neale's disorders of the foot* (7th ed.), Edinburgh Churchill Livingstone, 2008.
3. Kolář P. *Rehabilitation and physical medicine* **4**, 152-164, 2001.
4. Janura M, et al. *Journal of Biomechanical Science and Engineering* **3**, 390-398, 2008.
5. Costa JM. et al. *Acta Ortopédica Brasileira* **18**, 191-196, 2010
6. Schuh R, et al. *Physical Therapy* **89**, 934-945, 2009.

## ACKNOWLEDGEMENTS

The study has been supported by the research grant Palacky University in Olomouc FTK\_2010\_017 (No. 43510012) and the research grant from the Ministry of Education, Youth and Sports of the Czech Republic (No. MSM 6198959221).

# EFFECT OF PROBE SIZE ON EMG ACTIVITY OF THE WRIST AND HAND IN DIAGNOSTIC MEDICAL SONOGRAPHERS

Seth Kuhlman<sup>1</sup>, Carly Gerard<sup>1</sup>, Joie Burns<sup>2</sup>, and Michelle Sabick<sup>1</sup>

<sup>1</sup>Center for Orthopaedic & Biomechanics Research

<sup>2</sup>Department of Radiologic Sciences

Boise State University, Boise, ID USA

email: [MSabick@boisestate.edu](mailto:MSabick@boisestate.edu) web: [coen.boisestate.edu/cobr](http://coen.boisestate.edu/cobr)

## INTRODUCTION

Medical sonography covers a broad spectrum of specialty areas including vascular sonography, cardiac sonography, and obstetric sonography. Because medical sonography covers such a broad array of clinical needs without the use of ionizing radiation, it has become essential in the diagnosis of many life-threatening diseases [1].

Although sonography is an indispensable tool, it is not without shortcomings. Every year more than 80% of clinical sonographers experience some form of musculoskeletal related pain, with up to 20% suffering from career ending injuries [1, 2]. These statistics make sonographers among the highest at risk groups for work-related musculoskeletal disorders (WRMSDs).

Current research points to the poor ergonomics of the ultrasound transducer as the main factor in the cause of WRMSDs. The awkward upper extremity positions required, the repetitive nature of the movements and the static aspect of the transducer grip have all been implicated in the development of WRMSDs [3].

The purpose of this study was to quantify wrist range of motion and muscle activation during scanning using two different standard ultrasound transducers. The data will be used to inform design of more ergonomic ultrasound transducers.

## METHODS

Muscle activation and joint angle data were collected from six subjects while using both large and small ultrasound probes. The two probes selected represent a large number of designs

currently on the market. Each trial consisted of scanning a fetal phantom for three different fetal measurements. Subjects performed three trials per probe condition.

Electromyographic (EMG) data were recorded for four wrist/hand muscle groups: extensor carpi group, flexor carpi group, flexor pollicis group, and the flexor digitorum superficialis at 1000 Hz. Wrist flexion/extension and radial/ulnar deviation angles were collected with an electronic goniometer at 50 Hz.

The goniometer used to measure wrist motion was a custom designed device using a high precision joystick potentiometer. The base of the potentiometer was attached to the forearm, proximal to the wrist joint. The joystick of the potentiometer was attached to the backside of the hand, distal to the wrist joint.

Subjects first performed trials to determine the MVIC for each of four muscle groups. A single test which involved gripping a rigid ball at maximal effort was used to quantify the flexor pollicis group and flexor digitorum superficialis MVIC's. Resisted wrist flexion and extension were used to find the MVIC for the flexor and extensor carpi groups. Three trials were performed per muscle group. One static and three dynamic trials were performed for each of two probe sizes (large and small). Each dynamic trial consisted of a fetal ultrasound scan using a fetal phantom.

EMG data from the dynamic trials were bandpass filtered (20-450 Hz), and normalized to maximum voluntary isometric contraction (MVIC). Mean normalized maximum activation values for each condition were determined from group averages. A

paired, two-tailed t-test was performed for each of the muscle groups to determine if any differences were present in muscle activation between small and large probes.

## RESULTS AND DISCUSSION

Muscle activation values were high for both probe conditions, especially in the pollicis group, where mean activations were 70-80% MVIC (Figure 1). There were no statistical differences in muscle activation level between the two probe sizes ( $p > 0.5$  for all conditions). The wrist ranges of motion were only 2-6° for ulnar and radial deviation (Figure 2) and 3-14° for extension and flexion (Figure 3), which indicates a nearly static wrist position during fetal scanning.

During the performance of an ultrasound scan, the demand on the thumb gripping musculature is high, likely due to the relatively narrow waist of the transducers. Sonographers are forced to use an isometric pinching-style grip to stabilize the transducer probe against the patient's body while scanning.

Ultrasound probes should definitely be redesigned to be more ergonomic. To reduce the incidence of wrist pain in sonographers, the primary focus of these efforts should be reducing the amount of muscle activation needed for gripping the device with the wrist in a relatively neutral position.

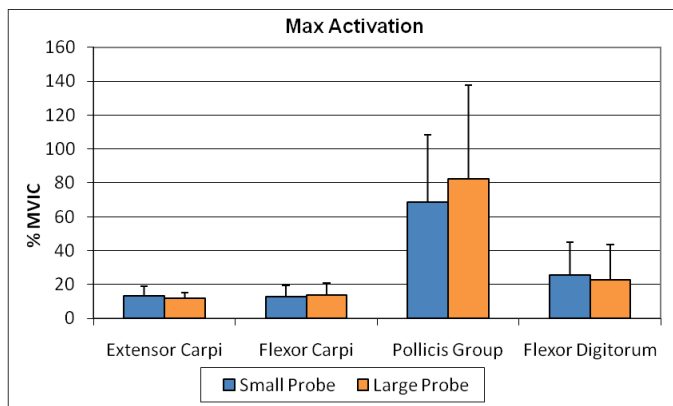


**Figure 1:** Group average of normalized maximum muscle activation during ultrasound scan (as percentage of MVIC for each muscle).

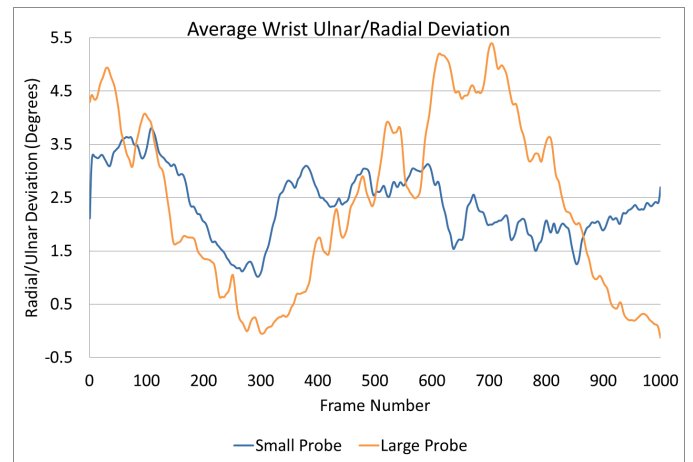


**Figure 2:** Group averages for ulnar and radial deviation of the wrist comparing between the large and small probes. Data was collected over 20s.

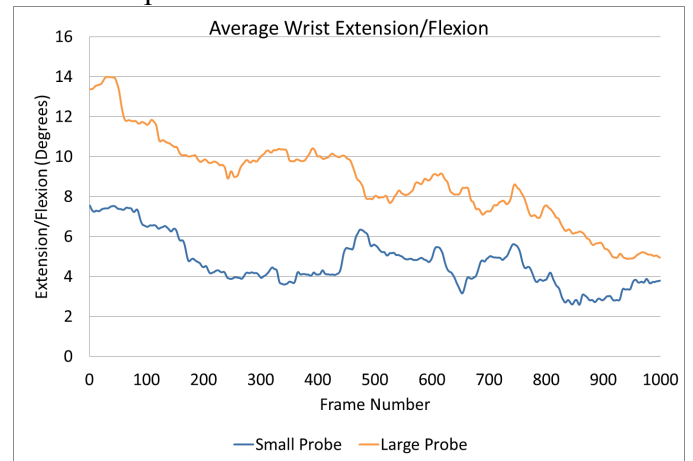


**Figure 3:** Comparison of group averages for wrist flexion and extension between large and small transducer probes. Data was collected over 20s.

## REFERENCES

1. Kroemer K, et al. *Fitting the Task to the Human. A Textbook of Occupational Ergonomics 5th ed.*, Taylor & Francis, Inc., 1997.
2. Murphey SL, et al. U.S. Government Issues Update on WRMSDs in Sonography. *AuntMinnie.com*, December 25, 2006.
3. Pike I, et al. *J Diagnostic Med Sonography* **13(5)**, 219-227, 1997.

## ACKNOWLEDGEMENTS

We would like to acknowledge the students of the Boise State University Department of Radiological Sciences for their involvement in this study.

# EFFECTS OF VARIATIONS IN VELOCITY ON VISCOELASTIC BEHAVIOUR IN THE METACARPOPHALANGEAL (MCP) JOINT OF THE HUMAN HAND

Pei-Hsin Kuo and Ashish Deshpande

Mechanical Engineering Department, University of Maine, Orono, ME, USA  
email: [peihsin.kuo@maine.edu](mailto:peihsin.kuo@maine.edu)

## INTRODUCTION

The soft tissues across a joint and the passive properties of the connected muscle-tendon units (MTUs) lead to viscoelastic behavior in the joint. In the hand joints it is shown that the viscoelastic properties dominate during movements [1]. This study focuses on the MCP joint of the human index finger around its neutral position. Many previous studies assume that the viscoelastic torque in the MCP joint is linearly dependent on the joint angular velocity [2]. Another study shows nonlinear dependency in the dissipative part of the viscoelastic torque which was modeled by a power function of the joint velocity [3]. There is a need to develop a comprehensive understanding of variations in the passive viscoelastic torque in the hand joints as joint angle and velocity change. The purpose of the study is to investigate the effect of variations in velocity on the viscoelastic torque around the neutral position of the MCP joint through experiments with human subject in which the a mechanical device moved the index finger in cyclic movements while the subjects relaxed.

## METHODS

A total of ten right-handed subjects (six male and four females, age = 23 (SD 3.7)) participated in the study in which the index finger was moved in a cyclic motion while the subject relaxed. We designed a mechanism that can generate driving force with various range of motions while precisely measuring the joint angle and external force (using the force sensors) (Fig 1). The mechanism held the index finger from the neutral position defined by the encoder and drove the finger to full extension and then reversed the driving direction to the full flexion cyclically. We defined the range of motion by measuring limit of the subject's index finger in static test. Each subject experienced movements at 14 different cyclic frequencies from 0.1 Hz to 1.0 Hz and at each frequency the movement was carried

out for 40 sec. To identify the precise MCP joint angle we used the VICON motion capture system to capture the kinematic data of 17 markers on the testing finger and predict the instant center of rotation of the MCP joint by using the optimization

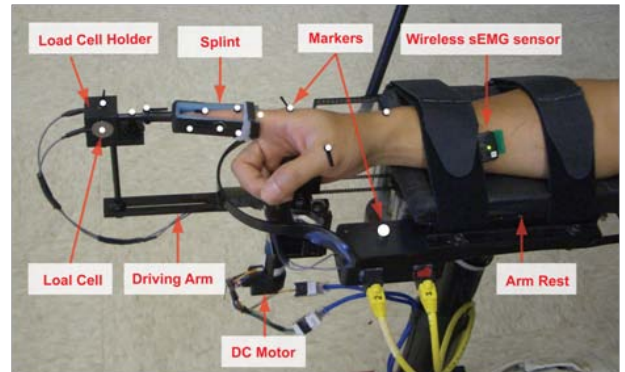


**Figure 1:** A device used to measure the passive forces at the MCP joint of the index finger

method [4]. Then we numerically calculated the velocity ( $\omega$ ) from the estimated MCP joint angle. Here we defined positive and negative velocity as the stretching and flexing velocity respectively. Four of the DELSYS sEMG wireless sensors attaching on the testing hand were also recorded synchronously to monitor undesirable activation of the hand muscles during the experiment. We set up the EMG threshold as 5% of average sEMG for each subject's muscles by proceeding the maximal voluntary contraction test (MVC). We determined the viscoelastic torque ( $\tau_{VE}$ ) by calculating the torques due to the external force ( $\tau_E$ ) and inertia ( $\tau_M$ ) with respect to the MCP joint in the dynamics system, leading to  $\tau_{VE} = \tau_M - \tau_E$ . Analysis of variance (ANOVA) and Turkey's post-hoc were used to evaluate the mean viscoelastic torques across the joint angle and velocity. The critical level of significance in the present study was set as  $P < 0.05$ . Finally we used the piecewise-polynomial functions of the spline fitting in Matlab by choosing the parameter.

## RESULTS AND DISCUSSION

The test generated angular velocities of the MCP joint ranging from 0.1 ~ 200 degrees/s. Fig 2 shows typical variations in angle, velocity and viscoelastic torque during the cyclic test at a low and a high frequency.

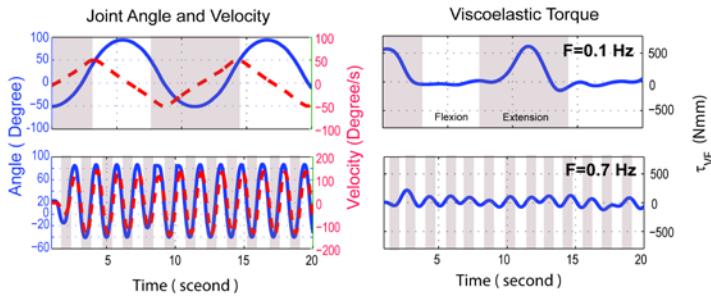


**Figure 2:** The sample results of the angle, velocity and torque in time series. The two upper and bottom figures show the results in frequency 0.1 Hz and 0.7 Hz.

We calculated the passive viscoelastic torque at the neutral angle at various positive and negative velocities. The results for torque-velocity for two subjects are depicted in Fig. 3. The results of viscoelastic torques with respective to the velocity are similar. With the low velocities the MCP joint

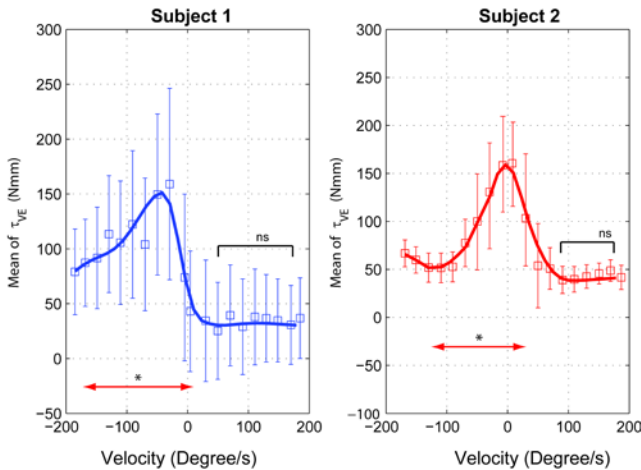


**Figure 3:** The mean torque-velocity for two subjects. \*  $P < 0.05$ , ns:  $P > 0.05$ . The arrow range significantly different from the most of flexing velocities

shows the higher torque values than that at higher velocities. The results also show that the MCP joint has significantly higher viscoelastic torques in stretching velocity than that in flexing direction ( $P < 0.001$ ). It is implied that anatomical structure and components across the MCP joint presented the different viscoelastic ability in different rotational directions and velocities. The other result is that the torques are small while the flexing velocity is over 50 degrees/s. This indicates that the human hands provide the less resistances in close or grasping direction of movement in the high passive velocities. The spline fitting fits the mean torque results very well (Fig 3 and Table 1). It shows that the torque-velocity presents the nonlinear function especially at the low angular velocity range.

## CONCLUSIONS

Our results show that the variations in the passive viscoelastic torque at high flexion velocities is quite different from that at high extension velocities. At low velocities a model depicting nonlinear dependency on the joint velocity fits well. In the future, using this data we plan to develop a comprehensive model of variations in the passive visco-elastic torque as a function of both the joint angle and joint velocities.

## REFERENCES

1. Gialias & Matsuoka, *Proceedings of IEEE EMBS*, 2006
2. A. Z. Hajian and R. D. Howe, *J Biomechanical Engineering*, **119**, 109–114, 1997.
3. Esteki & Mansour. *J Biomechanics* **29**, 443-450, 1996.
4. Halvorsen, et al. *J Biomechanics* **32**, 1221-1227, 1999.

| Parameter | Smoothing Parameter | SEE   | Rsquare | RMSE  |
|-----------|---------------------|-------|---------|-------|
| Subject 1 | 0.0007              | 951.3 | 0.97    | 10.87 |
| Subject 2 | 0.012               | 624.5 | 0.98    | 9.68  |

**Table 1:** The parameters of the spline fitting for the two subjects

# A COMPREHENSIVE EXPERIMENTAL EVALUATION OF EXISTING MODELS OF THE EXTENSOR MECHANISM CALLS FOR NOVEL DATA-DRIVEN MODELS

<sup>1</sup>Manish U. Kurse, <sup>2</sup>Hod Lipson and <sup>1</sup>Francisco J. Valero-Cuevas

<sup>1</sup>University of Southern California, Los Angeles, CA

<sup>2</sup>Cornell University, Ithaca, NY

email: [kurse@usc.edu](mailto:kurse@usc.edu) web: <http://bbdl.usc.edu>

## INTRODUCTION

The functional role of the components of the extensor mechanism to finger function has been debated for decades. While several computational models have been suggested over the years, the normative model developed by An et al. 1979 [1] remains the most comprehensive 3D anatomical model of the index finger to date. Though this model has been used in multiple studies (Eg. [2]), it has not been rigorously validated with experimental data. The model assumes simple bowstringing of all tendons with joint rotation, and a constant force distribution within the different bands of the extensor mechanism (i.e., independent of joint posture). Both assumptions are contrary to experimental observations. Valero-Cuevas et al. in 1998 [4] emphasized the importance of including changes in force distribution through the extensor mechanism with finger posture. They modified a constant moment arm model proposed by An et al, 1983 [3] to include changes in force distribution through the extensor mechanism with posture. However, neither of these models has been validated with experimental data consisting of force transmissions from tendons to the fingertip. In this paper, we evaluate the normative model of the index finger as well as the constant moment arm models described in An et al, 1983 and Valero-Cuevas et al. 1998, with experimental data collected from a cadaveric index finger in multiple postures.

## METHODS

We actuated the seven tendons of the index finger (*flexor digitorum profundus* (FDP), *flexor digitorum superficialis* (FDS), *extensor indicis* (EI), *extensor digitorum communis* (EDC), *first lumbrical* (LUM), *first dorsal interosseous* (FDI), and *first palmar interosseous* (FPI)) of a fresh-frozen cadaveric hand

using dc motors controlled by a National Instruments PXI real-time control system (Fig. 1). All possible combinations of ‘low’ (2N) and ‘high’ (10N) tendon tensions were applied to the cadaveric specimen at random while we recorded the corresponding fingertip forces and torques using a 6 DOF load cell attached to the fingertip. This procedure was repeated at three different postures, P1 (fully flexed), P2 (tap) and P3 (extended).

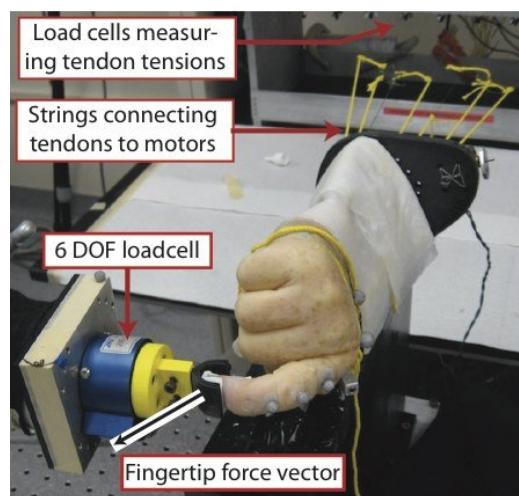


**Figure.1** Experimental setup used to collect fingertip force data from cadaveric specimens.

The experimental action matrix transforming tendon tensions to fingertip forces was regressed in each posture (mean  $R^2 = 0.99$ ). This experimental action matrix was compared against the matrices predicted for those same postures by each of the three models. For the An et al. 1979 model, the moment arm matrix at each finger posture was calculated in MATLAB as described in [1] and using equations for force distribution through the extensor mechanism described in [5]. The action matrix was calculated by multiplying the inverse transpose of the Jacobian, with the moment arm matrix [4]. Similar action matrices were determined for the An et al, 1983 and Valero-Cuevas et al., 1998 models.

All moment arm matrices were scaled to the length of the middle phalanx to reduce the effect of inter-subject variability [1]. Each column of the action matrix (an action vector) represents the fingertip force resulting from 1N tension applied to the corresponding tendon. The robustness of the models to variations in moment arm values was also tested by applying  $\pm 10\%$  uniformly distributed noise to the moment arm matrices in the three models.

## RESULTS AND DISCUSSION

Fig. 2 shows the changes in magnitude and direction of each tendon's action vector as the finger shifts from fully flexed (P1) to a more extended posture (P3). The changes for all models and experimental data (in black) are relative to P1. In general, the magnitude changes in the three

changes in direction for tendons other than EI and EDC (sagittal plane) and LUM, FDI and FPI (radio-ular plane) also do not match with corresponding changes in experimental data. The directional errors for the EI and EDC in the radio-ular plane can be neglected because the components of their action vectors in this plane are small.

Perturbing the moment arms of the three models by  $\pm 10\%$  demonstrates that they can be extremely sensitive to parameter values; especially the flexors (FDP and FDS) and the extensors (EDC, EI that are important contributors to the extensor mechanism), which see  $30^\circ$ - $40^\circ$  change in fingertip force direction and  $\sim 50\%$  change in magnitude. This lack of robustness is a major flaw of models to predict finger mechanics, and calls for better data-driven subject-specific finger models.

## CONCLUSIONS

Our experimental evaluation of the existing models of the index finger reveal that, in general, they do not capture the physics of the system and are functionally inaccurate. More detailed and accurate representations of the topology and parameters of the extensor mechanism, inferred from experimental data, are necessary to develop reliable biomechanical models to understand motor control of manipulation and changes upon damage.

## REFERENCES

1. An KN, et al. J Biomech 12, 775-788, 1979.
2. Harding DC, et al. J Biomech 26,1403-1412, 1993.
3. An KN, et al. J Biomech 16, 419-425, 1983.
4. Valero-Cuevas FJ, et al. J Biomech 31, 693-703, 1998.
5. Chao EY, et al. J Biomech 104, 255-272, 1978.

## ACKNOWLEDGMENTS

This material is based upon work supported by NSF Grants EFRI-COPN 0836042 and NIH Grants AR050520 and AR052345 to FVC.

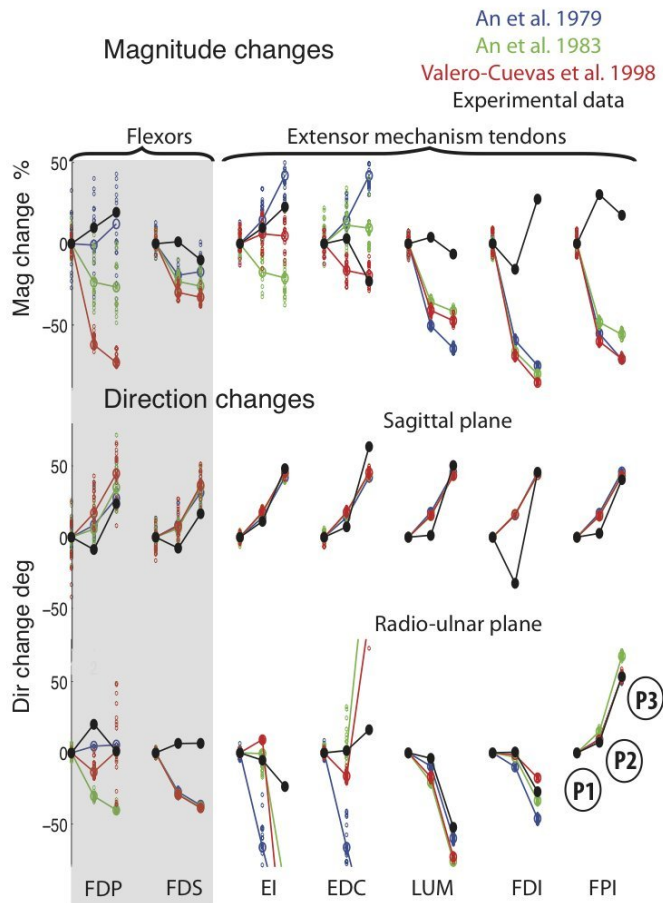


**Figure 2.** Comparison of magnitude and direction changes of fingertip force vector resulting from 1N tendon tension in models and experimental data as the finger shifts from a fully flexed (P1) to a more extended posture (P3).

models disagree with the experimental data, and amongst themselves in several important cases. The

# BIOMECHANICS TO BRAIN: UNRAVELING THE COMPLEX NEURAL CONNECTIVITY OF MULTI-MUSCLE CONTROL

Jason J. Kutch

University of Southern California, Los Angeles, CA, USA  
email: [kutch@usc.edu](mailto:kutch@usc.edu), web: [bbdl.usc.edu](http://bbdl.usc.edu)

## INTRODUCTION

Understanding how the CNS orchestrates the activity in hundreds of muscles to successfully control the human body is a long-standing problem that has generated both scientific and clinical interest [1-3]. The issue is how the CNS selects a muscle coordination pattern from an infinite set of options [4], and how it plausibly implements this pattern in neural connectivity.

Research on this problem has been dominated by the idea that the CNS can not activate a large number of muscles to perform functional tasks before it combines the muscles into a small number of groups, referred to as muscle synergies [5-7]. However, my research has shown that index finger muscles are not controlled using synergies [8], that certain synergies are biomechanically mandated rather than neurally-chosen [9], and that experimentally-observed muscle synergies during movement and force production may reflect a mixture of biomechanical and neural constraints [10].

Here, I propose that complexity in neural structures for multi-muscle control, including the genesis of muscle synergies, results not from a principle of reducing the number of degrees-of-freedom to be controlled, but from the biomechanical need to represent posture-dependent changes in muscle action across multiple joints. I prove this by showing that simple neural connectivity schemes without muscle synergies can readily learn to control large numbers of muscles, but that the resulting networks are not effective at controlling the limb if the posture changes.

## METHODS

Our biomechanical analysis of neural connectivity relies on understanding the transformation of muscle force to endpoint force, and how this transformation changes with posture. We used cadaveric hands to directly measure the transformation from muscle force to index fingertip force (the *action matrix*), as

in prior work [11], for all 7 tendons controlling the index finger (FDS, FDP, EI, EDC, FDI, FPI, LUM) (Figure 1A). We measured the action matrix for a variety of index finger postures in two specimens.

To ensure our results generalized to systems with many more muscles, we assembled a sagittal plane model of the human leg using anthropometric measures [12] and moment arms for 44 muscles [13] (Figure 1B). A posture-dependent action matrix was calculated using standard techniques [14].

We inferred the most basic network necessary to transform neural representations of desired endpoint force into the muscle forces necessary to achieve the desired endpoint forces. This network contains weighted connections between the components of the desired endpoint force and the motor pool of each muscle controlling the limb. The appropriate weights were learned using a simple gradient descent algorithm attempting to minimize the combined cost of making errors in endpoint forces and using too much energy, defined to be the sum of squared muscle forces. We evaluated how well a network generalized by learning the connection strengths at one posture, and attempting to have the network generate the correct endpoint forces at a different posture. This analysis was performed for both the cadaveric measurements and the leg model.

## RESULTS AND DISCUSSION

We found that, not unexpectedly, networks with random (naive) connections generated large errors between the desired and actual endpoint force (Figure 1C). However, we found, surprisingly, that a simple learning algorithm could mature the connection strengths in this network to correctly activate the muscles to produce the desired endpoint forces with minimum muscle effort (Figure 1D). Unfortunately, the mature network for one posture could not produce the desired endpoint forces in a different posture (Figure 1E). We observed this lack of generalization across posture for both the leg model, and the

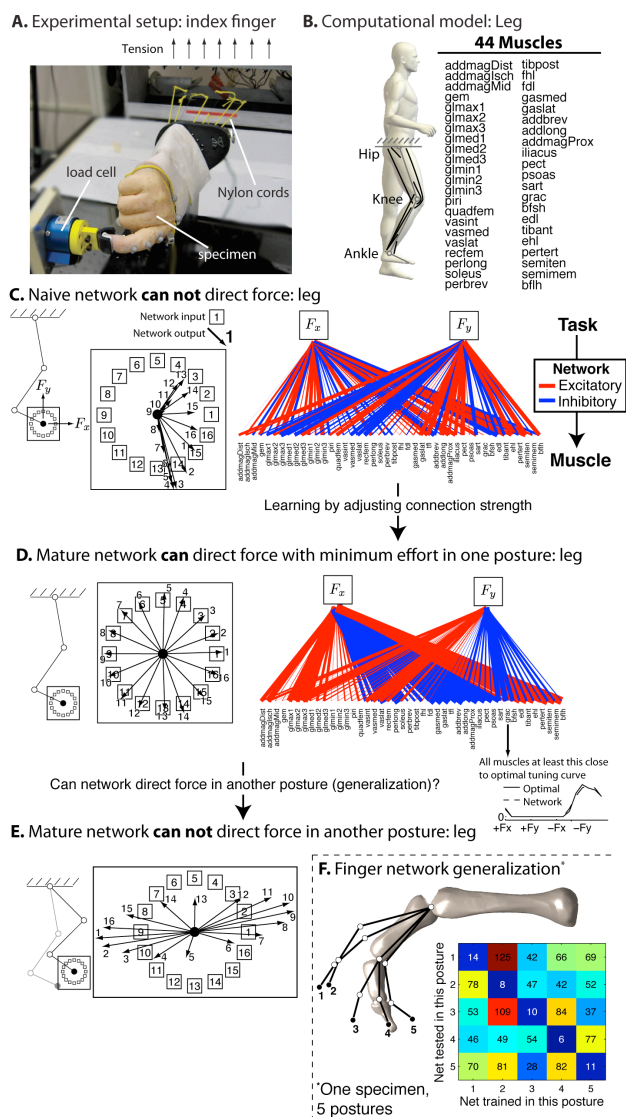


**Figure 1.** Muscles can be activated by simple networks, but these networks do not generalize across posture. Please see text.

cadaveric measurements, where errors in output force could be 125% or more in both specimens (Figure 1F).

Our current understanding of the neural connectivity that drives multi-muscle control is dominated by the notion that the brain must simplify the highly-redundant musculature into task-relevant groups [7]. This is believed to be accomplished by functional units called muscle synergies, perhaps encoded in the spinal cord [15], that act as an intermediary between task goals and muscle activations. Here we have shown that the intermediary of muscle synergies is not necessary from the standpoint of simplification - desired endpoint forces can be mapped directly to the force required in each of a large number

of muscles, and the appropriate connection strengths in this mapping can be learned with simple rules.

These results open a new direction in multi-muscle control research, because muscle synergies, as intermediaries between task-level and muscle-level commands, could be re-interpreted as the necessary elements to perform posture-dependent switching. The results of this study can be used to formulate new hypotheses about the nature of multi-muscle control networks, motivated by an understanding what neural structures are biomechanically mandated.

## ACKNOWLEDGEMENTS

We would like to thank hand surgeons V.R. Hentz, C. Leclercq, I. Fassola, and N. Lightdale for their assistance preparing the cadaveric specimens. Thanks to F.J. Valero-Cuevas and J.M. Inouye for helpful discussions. This work was supported by NSF grant EFRI-COPN 0836042 and NIH grant AR050520 to F.J. Valero-Cuevas.

## REFERENCES

- Buchanan, T.S., et al., *Journal of Neurophysiology*, 1986. **56**(5): p. 1225-1241.
- Cheung, V.C.K., et al., *Proceedings of the National Academy of Sciences*, 2009. **106**(46): p. 19563.
- Dewald, J.P., et al., *Brain*, 1995. **118 ( Pt 2)**: p. 495-510.
- Bernstein, N.A., *The Co-ordination and Regulation of Movements*. 1967, Oxford: Pergamon Press.
- Ting, L.H. and J.M. Macpherson, *Journal of Neurophysiology*, 2005. **93**(1): p. 609-613.
- d'Avella, A., P. Saltiel, and E. Bizzi, *Nature Neuroscience*, 2003. **6**(3): p. 300-308.
- Tresch, M.C. and A. Jarc, *Current Opinion in Neurobiology*, 2009. **19**(6): p. 601-607.
- Kutch, J.J., et al., *J Neurophysiol*, 2008. **100**(5): p. 2455-71.
- Kutch, J.J. and F.J. Valero-Cuevas, *Journal of Biomechanics*, In Press, 2011.
- Kutch, J.J. and F.J. Valero-Cuevas, In review, 2011.
- Valero-Cuevas, F.J., J.D. Towles, and V.R. Hentz, *J Biomech*, 2000. **33**(12): p. 1601-9.
- Winter, D.A., *Biomechanics and motor control of human movement*. 2009: Wiley.
- Arnold, E.M., et al., *Annals of Biomedical Engineering*, 2010: p. 1-11.
- Valero-Cuevas, F.J., *Progress in Motor Control*, 2005: p. 619-633.
- Saltiel, P., et al., *Journal of Neurophysiology*, 2001. **85**(2): p. 605-619.

# A CONTINUOUS METHOD TO QUANTIFY STRESS-STRAIN BEHAVIOR OF BIOLOGIC MATERIALS

<sup>1</sup>Laurel Kuxhaus, <sup>1</sup>Charles A. Weisenbach, <sup>2</sup>Mark Carl Miller, and <sup>3</sup>Martin L. Tanaka

<sup>1</sup>Clarkson University, Potsdam, NY, USA

<sup>2</sup>Allegheny General Hospital, Pittsburgh, PA, USA

<sup>3</sup>Western Carolina University, Cullowhee, NC, USA

email: lkuxhaus@clarkson.edu web: <http://people.clarkson.edu/~lkuxhaus/>

## INTRODUCTION

Mathematical models of biologic structures provide opportunities to understand complex interactions and simulate treatment outcomes. Accurate estimates of the material properties of biologic soft tissues are critical to the fidelity of these models. Biologic soft tissues have a nonlinear mechanical behavior characterized by an exponential toe region followed by a linear elastic region [1-4]. Traditionally, two curves are independently fit to a set of data [5]. Thus, the two portions of the modeled stress-strain curves may not exhibit both  $C^0$  and  $C^1$  continuity, and could inaccurately estimate the true material properties.

Here, a Continuous Method (CM) is introduced that enforces continuity in both the stress-strain curve and its derivative by optimizing the fit for both regions simultaneously. Its performance is evaluated and compared to the traditional Piecewise Method (PM).

## METHODS

Both the traditional PM and the CM were implemented via custom MATLAB® (The MathWorks, Natick, MA) code. Both methods were used to analyze two data sets: ideal data and measured stress-strain data.

*Piecewise Method (PM)* -- The PM employs a linear curve fit to the high-strain end of the stress-strain data. Data is included in the linear region until the  $R^2$  of the fitted line dips below an *a priori* determined threshold value ( $R^2_{\text{cutoff}} = 0.99$  in this work) [5]. The remaining lower strain points are fitted with an exponential curve [3].

*Continuous Method (CM)* -- A mathematical model that contains an exponential region and a linear region maintains a continuous elastic modulus  $E$  by defining the slope of the linear portion as the slope of the stress-strain curve at the transition point  $(p, q)$  between the exponential and linear regions. That is,

$$\sigma = \begin{cases} A(e^{B\varepsilon} - 1) & \forall \varepsilon \leq p \\ E_{(p,q)}(\varepsilon - p) + q & \forall \varepsilon > p \end{cases}$$

where  $E(p, q)$  is the elastic modulus at point  $(p, q)$ .

The optimal parameters values for  $A$ ,  $B$ , and  $p$  are computed by minimizing the mean square error ( $MSE$ ). This yields the least-squares error between the modeled function and the experimental data. The optimization *simultaneously fits the exponential section and linear section*, and the location of the transition point,  $p$ , is included in the optimization.

*Data Sets* -- The ideal data set used an exponential curve that smoothly transitioned to a line,

$$\sigma = \begin{cases} 0.200(e^{35.0\varepsilon} - 1) & \forall \varepsilon \leq 0.10 \\ 232(\varepsilon - 0.10) + 6.42 & \forall \varepsilon > 0.10 \end{cases}$$

The curve had  $C^0$  and  $C^1$  continuity and a known transition point at  $(0.10, 6.42)$ . The measured data was collected from a sample of porcine lateral meniscus undergoing tensile testing.

## RESULTS AND DISCUSSION

*Ideal Data* -- The PM generated a stress-strain curve with a discontinuity of 3.03 MPa at the transition point, or 319% of the actual stress magnitude at this location (Figure 1). The discontinuity in its derivative resulted in a modulus increase from 25.7 MPa to 206 MPa at the transition. The estimates for parameters  $A$  and  $B$  had high errors (Table 1). However, the error in estimating the elastic modulus was lower, 11.2%.

The PM was also inaccurate at estimating the location of the actual transition point, underestimating the both stress and strain (Table 1).

In contrast, the CM generated an unbroken curve through the transition point (Figure 1) and without discontinuity in modulus. The parameters A and B were estimated within 7.00% and 2.57% of the known values, and the elastic modulus, E, within 0.431%. The location of the transition point was within 2% of the known strain and stress.

*Measured Data* -- Application of the PM resulted in a discontinuity of 1.9 MPa at the transition. The model closely approximated the measured data in the exponential region, but it deviated from the actual measured data points in the linear region (Figure 2). The CM yielded a curve that more closely tracks the measured data points and had a MSE over 20 times lower that obtained using the Piecewise Method (Table 2).

**CONCLUSIONS**

The CM dramatically reduced errors in estimating the parameters A, B, E, p, and q when applied to the ideal data with known solutions. When applied to measured data without a known solution, the CM had a much better fit indicated by the reduced MSE. The PM yielded discontinuities in both the stress strain curves and the modulus. In contrast, the CM resulted in a continuous curve and modulus.

The Continuous Method may be a more accurate way to estimate material parameters of soft biological tissues. A key element of the Continuous Method is to simultaneously solve a problem that had historically been solved sequentially. Using this simultaneous approach may broadly impact the fields of engineering modeling and biomechanics.

**REFERENCES**

- 1.Fung YC. *Am J Physiol*, **213**, 1532-1544, 1967.
- 2.Haut RC and Little RW. *J Biomech*, **5**, 423-30, 1972.
- 3.Woo SL. *Biorheology*, **19**, 385-396, 1982.
4. Stabile KJ et al. *Arthrosc*, **26**, 936-948, 2010.
- 5.Voycheck CA, et al. *ASME SBC*, Marco Island, FL, USA 2008.

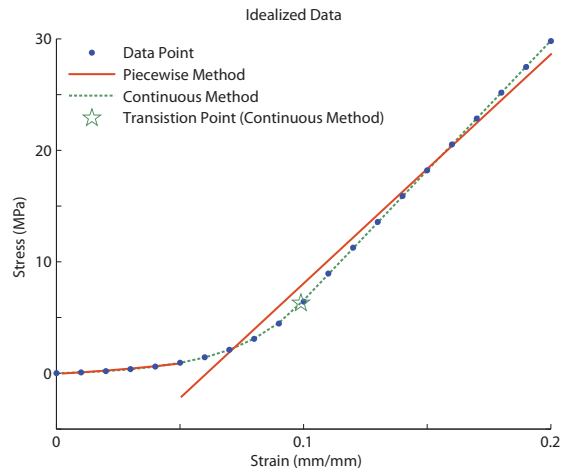


**Figure 1: Ideal Data Set**

**Table 1: Ideal Data Results (Percent Error).**

|                     | A (MPa)      | B           | E (MPa)    | p            | q (MPa)       | MSE    |
|---------------------|--------------|-------------|------------|--------------|---------------|--------|
| <b>Known</b>        | 0.2          | 35          | 232        | 0.1          | 6.42          | --     |
| <b>Piece. Meth.</b> | 0.947 (374%) | 13.7 (61%)  | 206 (11%)  | 0.05 (50%)   | -0.585 (109%) | 1.09   |
| <b>Cont. Meth.</b>  | 0.186 (7.0%) | 35.9 (2.6%) | 233 (0.4%) | 0.099 (1.1%) | 6.3 (1.9%)    | 0.0015 |

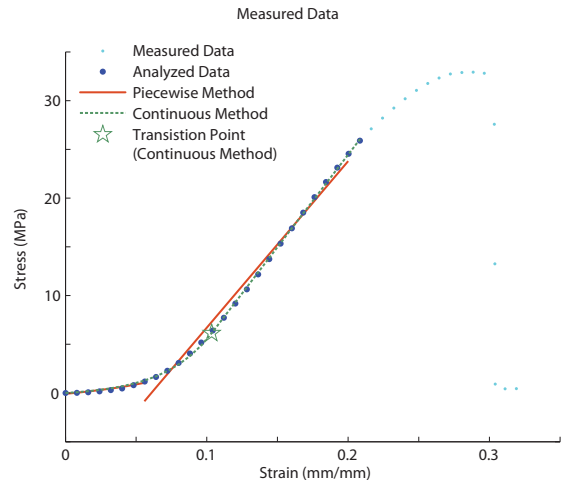


**Figure 2: Measured Data Set**

**Table 2: Measured Data Results**

|                     | A (MPa) | B    | E (MPa) | p      | q (MPa) | MSE   |
|---------------------|---------|------|---------|--------|---------|-------|
| <b>Piece. Meth.</b> | 0.882   | 14.8 | 171     | 0.0561 | 0.0419  | 0.46  |
| <b>Cont. Meth.</b>  | 0.307   | 29.4 | 190     | 0.103  | 6.14    | 0.021 |

**ACKNOWLEDGEMENTS**

The authors thank Mr. Nikolaj Vest, Dr. Melvin Leok, and the Wake Forest University Department of Orthopaedic Surgery.

# A FINITE ELEMENT SIMULATION OF ANTERIOR CRUCIATE LIGAMENT RECONSTRUCTION WITH A PATELLA TENDON GRAFT

<sup>1</sup>Tae-Hyun Kwon, <sup>2</sup>Megan Schroeder and <sup>1,2</sup>Yasin Dhafer

<sup>1</sup>Rehabilitation Institute of Chicago, Chicago, IL, USA

<sup>2</sup>Northwestern University, Evanston, IL, USA

E-mail: t-kwon@northwestern.edu

## INTRODUCTION

The outcome of an anterior cruciate ligament (ACL) reconstruction surgery is dependent on several factors including the type and source of graft, pretension levels, tunnel position and orientation, knee flexion angle at the time of graft fixation, and the method of fixation. Unfortunately, few previously reported finite element (FE) based simulations of the ACL reconstruction procedure incorporate the collective changes associated with the surgery. Thus, in this study, we have employed a previously developed FE knee model [1] that was effectively cross examined against experimental data reported by other investigators. The model was modified to incorporate key surgical parameters associated with an ACL reconstruction procedure. To examine the efficacy of the ACL reconstruction simulation framework, model outputs were tested against experimentally reported tibial internal rotation under passive flexion [2]. The in-situ graft force computed under a 130 N anterior load applied at the tibia was compared to the corresponding force reported by Li and colleagues under the same loading conditions [3].

## METHODS

A detailed description of the model can be found elsewhere [1]; briefly, a three dimensional FE model was created that include bones, articular cartilages, menisci, ligaments, and tendons. Frictionless contact with finite sliding was assumed for the contact surfaces. The joint connective tissues were described with a transversely hyperelastic model, which was calibrated using reported experimental data [1].

A tibial tunnel of 9 mm diameter was initiated at the center of ACL insertion and was oriented with an angle of 20° anteriorly in the sagittal plane and 30° medially in the coronal plane through the tibia [4]. The femoral tunnel was positioned at the posterosuperior aspect of the lateral femoral condyle and oriented 25° anteriorly in the sagittal plane and 15° medially in the coronal plane [4]. The geometry of the graft was excised from the middle one third of the patella tendon (PT) (Fig. 1(a)). The material properties of the graft were the same as the PT. Bone plugs were considered to be linear elastic,  $E = 14,220$  MPa and  $\nu = 0.3$  [5].

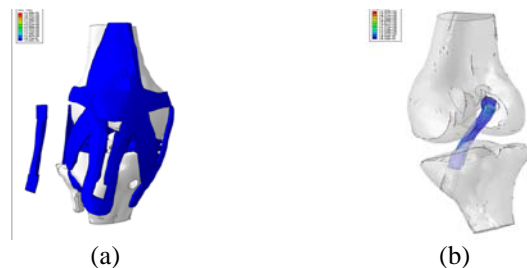


**Figure 1:** (a) FE knee model with a PT graft (b) graft position, fixation, and pretension with other components masked (Max. Von Mises stress of 10 MPa).

One of the important factors that influence the success of an ACL reconstruction is the level of graft pretension. Several authors have studied the effect of different graft tensioning ranging from 0 to 60 N, but the optimal graft tension is not well defined. Thus, 20 N graft pretension was applied with the knee at 20° of flexion [2]. The graft was placed through the tibial and femoral tunnels. The graft pretension was applied by pulling the trapezoidal bone plugs of the graft through the tibial tunnel. The graft fixation was modeled by kinematic

coupling between the bone plugs and tunnels to represent a screw fixation method (Fig 1(b)).

In order to examine the model performance, simulations were conducted to emulate the *in vivo* passive flexion experimental paradigm described by van Kampen and Huijkes [2]. The model was simulated by passively flexing the knee from zero to 90°. While the flexion angle was prescribed, the remaining five degrees-of-freedom were left unconstrained. In this study, we compared the computed tibial internal rotation angle to previous reports [2]. To test the kinetic predictions of the model, the in-situ graft force computed under a 130 N anterior load applied at the tibia was compared to the corresponding force reported by Li and colleagues [3]. The in-situ graft forces, one of the key metrics for the success of the procedure, were computed at discrete flexion angles of 0°, 15°, 30°, 60°, and 90°. In these FE simulations, the graft pretension was adjusted to 90 N to match with experimental setup.

## RESULTS AND DISCUSSION

Von Mises stress patterns in the ACL reconstructed knee are shown at flexion angles up to 90° (Fig. 2).

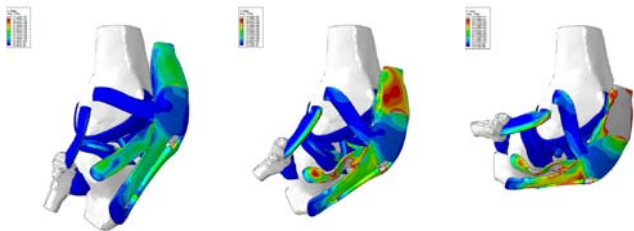


**Figure 2:** ACL reconstructed knee during passive flexion simulations (Max. Von Mises stress 10MPa).

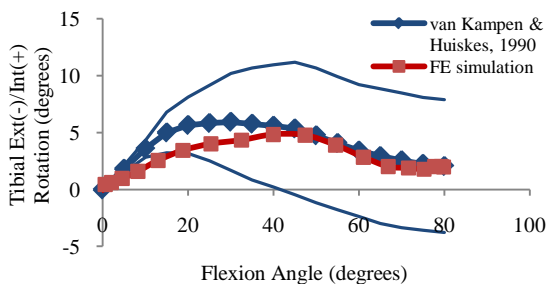


**Figure 3:** Tibia external(-)/internal(+) rotation as a function of flexion angle.

Figure 3 shows the internal rotation of the tibia during the passive flexion simulation. The simulation results show a similar trend and falls within the range of the reported experimental data.

Figure 4 illustrates the in-situ graft as a function of the flexion angle. The model-based estimates of the force peaked at 30° of the flexion and dropped thereafter. The experimental data showed a similar non-monotonic trend, with the exception that the peak occurred at 15° of flexion.

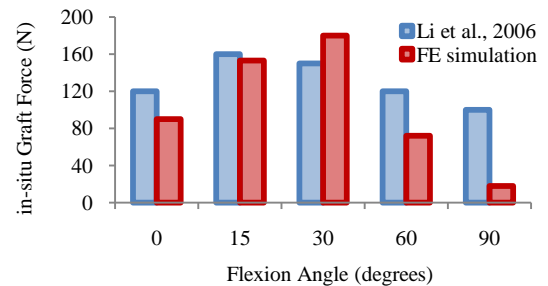


**Figure 4:** In-situ force of the graft under 130 N anterior tibial load at discrete flexion angles.

## CONCLUSIONS

This study investigated a computational framework that emulates the ACL reconstruction procedure. Key surgical parameters were incorporated including graft pretensioning, tunnel morphology, bone plugs, and bone plug fixation. The inclusion of these parameters will facilitate future examinations of the relative contributions of these parameters to the post-surgical intrinsic mechanics of the joint.

## REFERENCES

1. Dhaher YY, et al. *J Biomech* **43**, 3118-3125, 2010.
2. van Kampen A, et al. *J Orthop Res* **8**, 372-382, 1990.
3. Li G, et al. *Acta Orthop* **77**, 267-274, 2006.
4. Vergis A, et al. *J Arth Rel Surgery* **11**, 312-321, 1995.
5. Peña E, et al. *Clin Biomech* **20**, 498-507, 2005.

## ACKNOWLEDGEMENTS

This work was supported by DOD #DR080326; NSF #0966535 & 0966742; and NIH NIAMS #R01-AR049837.

# MOMENT ARMS OF MIDDLE DELTOID AND ROTATOR CUFF WITH ALTERATIONS IN GLENOID AND HUMERAL HEAD INCLINATION

Joseph E. Langenderfer, Nolan R. Faber  
Central Michigan University, Mt. Pleasant, MI  
email: [j.langend@cmich.edu](mailto:j.langend@cmich.edu)

## INTRODUCTION

Computational [1,2] and experimental studies [3] have found increased deltoid abduction moment arm with reverse shoulder arthroplasty when compared to anatomic shoulders [1,3] and natural prostheses [2]. Similarly, rotator cuff abduction moment arms are decreased when the humeral implant is positioned superiorly [4]. Despite marked variability in glenoid [5] and humeral head inclinations [6], their effects on muscle moment arms have not been previously measured. The objective of this study was to measure glenohumeral scapular plane abduction moment arms of rotator cuff and deltoid for normal shoulders and with altered glenoid and humeral head inclinations.

## METHODS

Embalmed cadaver shoulders (N=10) were abducted in the scapular plane while data were collected with a Qualisys Oqus 6 camera motion analysis system from markers attached to the specimen and weights attached to cords sutured to muscle-tendons (Figure 1). Sample size was determined with moment arm variance (S.D.=5 mm) from [7] and a desire to detect a mean difference in moment arms of 3.3 mm ( $\alpha=0.05$ ,  $\beta=0.20$ ). Specimens were tested initially with an anatomic glenoid and humeral head, and then a glenoid or humeral head osteotomy was performed and specimens were retested. Osteotomy order was randomly determined. The glenoid was osteotomized 5mm medially from the articular surface and a 10° plastic wedge was inserted to incline the glenoid inferiorly. A similar osteotomy and wedge altered humeral head inclination both superiorly and inferiorly. The 10° wedge approximates three standard deviations of inclination variability for glenoid [5] (S.D.=3.2-4.4°) and humeral head, e.g. [6] (S.D.=2.9-3.6°).

After testing the initial inclined condition, the glenoid or humeral head was repositioned to restore normal anatomy, and the other conditions were tested. Pilot testing of repositioning on two specimens resulted in moment arms within 0.5 mm of anatomic moment arms.



**Figure 1:** Instrumentation with specimen. Kinematics and tendon excursions measured with markers on scapula, humerus and weights attached to cords sutured to tendons.

Moment arms were calculated by differentiating the tendon excursion vs. joint angle relationships [3,4]. For each muscle, the effects of abduction angle and glenoid (and humeral head separately) inclination on moment arms were analyzed with a two-way analysis of variance (ANOVA).

## RESULTS

Inclining the glenoid 10° inferiorly tended to cause an increase in supraspinatus moment arm (5.3 and 1.6 mm, 22% and 6%) at 0 and 10° of abduction. Similarly, for middle deltoid during the initial 40° of abduction, there was a tendency for the moment arm to be increased up to 6.7 mm (or 34%). However, these differences were not statistically significant. Downward glenoid inclination caused

significant (but small) changes in infraspinatus and subscapularis moment arms (both  $p < 0.02$ ) that varied with abduction angle (Figure 2).

Middle deltoid moment arm increased on average 13.9 mm and 10.5 mm over the initial 10° abduction for increased and decreased humeral head inclination, respectively (both  $p < 0.05$ ) (Figure 3). For supraspinatus, there was a trend toward an increased moment arm for the initial phase of abduction, but the change was not significant. Altering humeral head inclination resulted in significant changes in moment arms for infraspinatus ( $p < 0.02$ ) and subscapularis ( $p < 0.01$ ); these changes varied with abduction angle and were generally smaller than middle deltoid or supraspinatus.

## DISCUSSION

Computational studies of single specimens have found increases in moment arms of middle deltoid [8] and supraspinatus [9] with an inferiorly oriented glenoid. This study, which decreased glenoid inclination by approximately 3 S.D. of measured variability, found similar trends, but the results were non-significant. Moment arms for these muscles are likely most influenced by medial-lateral position of the muscle-tendon insertion relative to joint center of rotation [3], and superior-inferior humeral head location [4], respectively. Increases were found for middle deltoid moment arms when humeral head inclination was altered inferiorly and superiorly, suggesting that both procedures medialized center of rotation in a manner similar to reverse shoulder arthroplasty [3]. Taken together, these results indicate that supraspinatus moment arm is more likely influenced by inferior-superior insertion on the greater tubercle, the position of the humeral head relative to the insertion [4], and head diameter as the tendon wraps around the head, rather than inclination of articular surfaces. These results have implications for understanding variations in inclination angle and component placement in healthy subjects and arthroplasty patients, respectively.

## REFERENCES

1. Terrier A, et al. *JBJS* **90-B**, 751-756, 2008.

2. Masjedi M and Johnson GR, *Proc. IMechE, Part H: J Engin Med* **224**, 1039-49, 2010.
3. Ackland DC, et al. *JBJS* **92-A**, 1221-1230, 2010.
4. Nyffeler RW, et al. *JBJS* **86-A**, 575-580, 2004.
5. Churchill RS, et al. *JBJS* **10**, 327-332, 2001.
6. Hertel R, et al. *JBJS* **11**, 331-338, 2002.
7. Hughes RE, et al. *J Biomech* **31**, 157-160, 1998.
8. Terrier A, et al. *JSES* **18**, 360-365, 2009.
9. Langenderfer JE, et al. *Proceedings of ASB*, State College, PA, 2009.

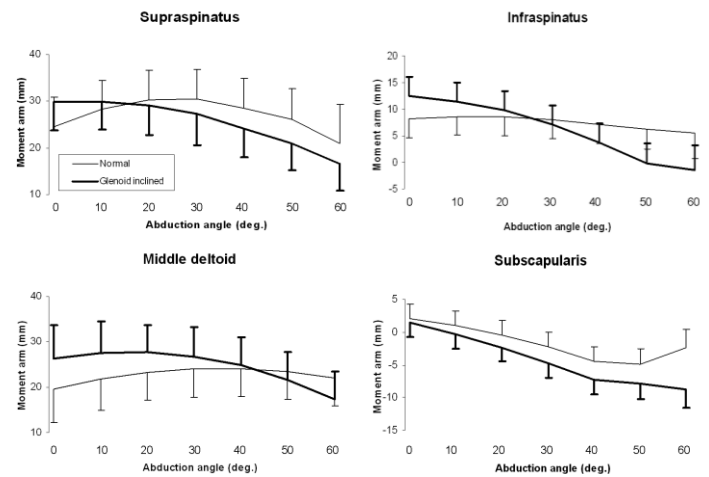


**Figure 2:** Scapular plane abduction moment arms (mean +/- S.D.) for normal and glenoid inclined 10° inferiorly.

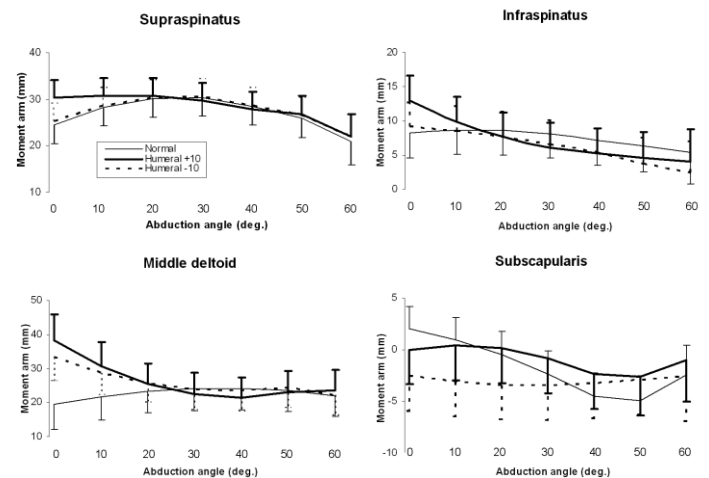


**Figure 3:** Scapular plane abduction moment arms (mean +/- S.D.) for normal, humeral head inclined 10° superiorly (+10) and 10° inferiorly (-10).

## ACKNOWLEDGEMENTS

This work was supported via the Central Michigan University President's Research Investment Fund.

# COMPARING FILTER CUTOFF FREQUENCY EFFECTS ON LOWER EXTREMITY JOINT MOMENTS CALCULATED FOR USE IN MUSCULOSKELETAL MODELING

Walter Laughlin, Joshua Weinhandl and Kristian O'Connor

University of Wisconsin-Milwaukee, Milwaukee, WI, USA  
email: laughlin@uwm.edu web: [www.chs.uwm.edu/neuromechanics](http://www.chs.uwm.edu/neuromechanics)

## INTRODUCTION

A recent investigation into joint moments during high impact activities such as running and jumping has suggested that the traditional inverse dynamic method of calculating knee joint moments induces high frequency errors into this calculation due to the inaccuracy of calculated segment accelerations from experimental position data [1]. Bisseling & Hof suggested that using the same cutoff frequencies to filter the kinematics and force plate data will reduce the high frequency peaks in the force plate data and result in a more gradual rise of the knee moment which is suggested to be more realistic than the fast transient peaks seen in much of the running and jumping literature.

The recent development and implementation of three-dimensional musculoskeletal models [2,3,4] into investigations of such dynamic movements has presented an alternative method of calculating joint moments. Such models input experimental kinematics and force plate data into a residual reduction algorithm (RRA) which computes joint torques necessary to drive a dynamic subject-specific model to follow experimental kinematics. However, no study has currently investigated the differences between the traditional inverse dynamics method of calculating joint moments and the joint moments calculated by the RRA. Therefore, the purpose of this study was to examine the differences in lower extremity joint moment profiles during single-leg landings as calculated by traditional inverse dynamics and the RRA using traditional (12/50) and suggested (20/20) filter cutoffs for the kinematics and force plate data.

## METHODS

Fifteen physically active females (mass =  $63.2 \pm 8.2$  kg), free from musculoskeletal injury volunteered to perform five single-leg drop landings from a 37 cm box. Three-dimensional kinematic data were collected using a ten-camera Motion Analysis Eagle system (200 Hz), and force data were collected with an AMTI force platform (1000 Hz). Kinematic and kinetic data were used as inputs into a subject specific three-dimensional musculoskeletal model (Figure 1) [2,3,4].

Since the purpose of this investigation was to compare joint moments using different methods of calculation and filtering rates the following data processing was conducted. Joint moments were calculated using traditional inverse dynamics as well as using an RRA approach. Kinematics and force plate data were filtered with traditional filtering rates (12 Hz and 50 Hz, respectively) as well as at cutoffs suggested by Bisseling & Hof (20 Hz for both) [1].

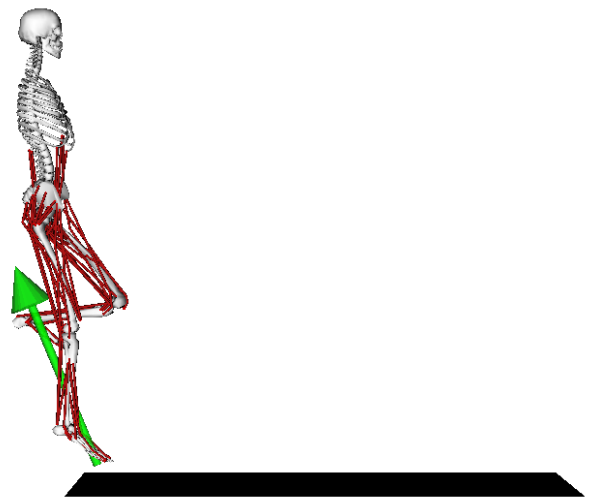


**Figure 1.** 19 Degree-of-freedom, 92 actuator musculoskeletal model

## RESULTS AND DISCUSSION

The hip, knee and ankle joint moments (Figure 2) are presented from 100 ms prior to initial contact (IC) to 200 ms following IC. When kinematic and force plate data were filtered at 12/50, there seems to be overall agreement between the RRA and inverse dynamics calculated joint moments. Although the hip moment calculated by the RRA does reach a larger extension moment following IC, there are few other differences between these profiles noted. The RRA calculation of joint moments at 12/50 is comparable to those calculated by traditional inverse dynamics.

However, 20/20 filtering led to substantial discrepancies between the inverse dynamics and RRA approaches. There are evident differences in the profiles of the hip and knee joint moments calculated by the RRA and traditional inverse dynamics when filtering at 20/20 (Figure 2). The knee moment calculated using traditional inverse dynamics follows those previously reported in during landing [1]. Even when both kinematics and force plate data were filtered 20 Hz, the RRA reintroduces the knee flexor moment immediately following IC which has previously been suggested to be due to high frequency components of force plate data [1].

## CONCLUSIONS

Bisseling & Hof [1] suggested that the frequency mismatch of a 12/50 approach introduced joint

moment artifacts. However, the RRA approach retains those characteristics even when the frequency contents are matched. The most significant consequence of the 20/20 approach is to reduce the anterior-posterior oscillations of the GRF at impact. The RRA attempts to minimize the dynamic inconsistencies introduced by errors in the measured kinematics and kinetics. It accomplishes this by adjusting measured kinematics and segment inertial characteristics such that Newton's laws are satisfied within a set tolerance. Surprisingly, the optimal solution to minimize residuals was to retain the rapid moment oscillations at the knee and hip. A follow-up study to re-examine the accelerometer-based contributions to joint kinetics of Bisseling & Hof [1] is planned to identify the cause of these discrepancies.

## REFERENCES

1. Bisseling R.W. & Hof A.L. *J Biomech* **39**, 2438-2444, 2006.
2. Thelen, D.G. & Anderson, F.C. *J Biomech*, **39**, 1107-15, 2006.
3. Delp, S.L. et al. *IEEE Trans. Biomed. Eng.*, **37**, 757-67, 1990.
4. Thelen, D.G. et al. *J. Biomech*, **36**, 321-28, 2003.

## ACKNOWLEDGEMENTS

UWM College of Health Sciences Student Research Grant

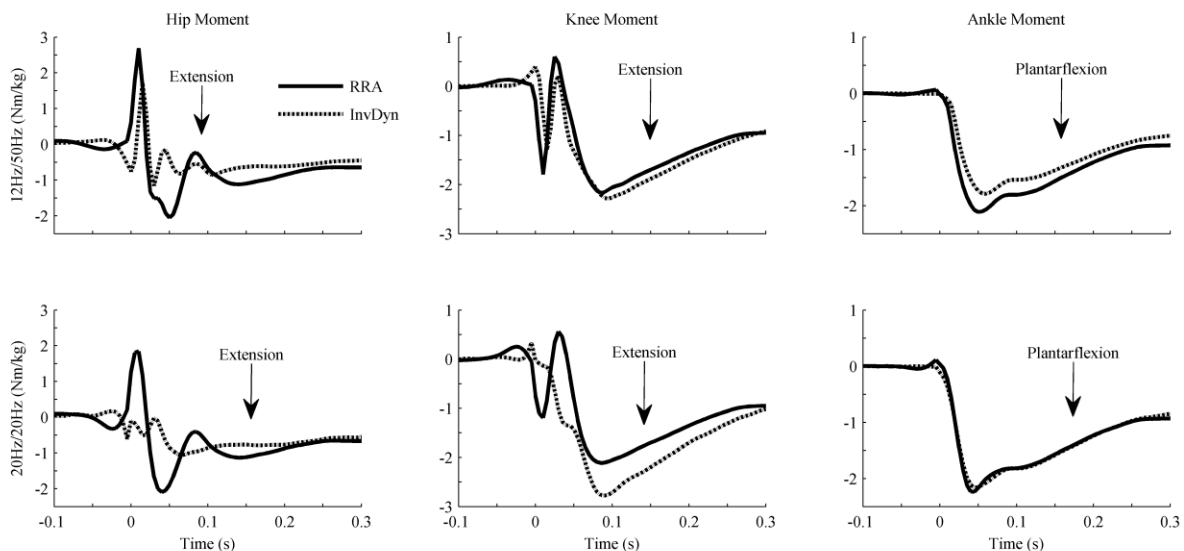


**Figure 2:** Hip, knee and ankle group mean joint moments. Zero time represents initial ground contact.

# EFFECTS OF TOWING A WEIGHTED SLED WITH DIFFERENT LOADS AND ATTACHMENT POINTS ON LOWER LIMB MOMENTS

Michael Lawrence, Erin Hartigan, Chunhao Tu

University of New England, Portland, ME, USA  
email: mlawrence3@une.edu

## INTRODUCTION

The strength and conditioning community uses resisted running and walking to increase lower extremity strength while simulating an athletic task. Several different methods are used to add resistance to the body during gait, including parachutes and weighted clothing. Towing a sled is a popular method since the resistance can be readily altered and used for both running and walking. While positive adaptations to running while towing a sled have been observed [1-2], the lower-extremity kinetics of walking while towing a heavily weighted sled are unknown.

Sprinting while pulling a sled with relatively light weights [13-16% of body weight (BW)] may provide an adequate stimulus without compromising sprint mechanics [3], with 20% BW being the greatest load tested [4]. Whether walking while towing a sled at relatively light and heavy loads alters walking kinetics differently is of interest. The addition of a greater load would in theory produce similar benefits as progressing loads during resistance exercise, such as muscular recruitment and strength.

The two most common methods of attaching the sled to the person while walking are with straps held over the shoulder and with a belt or strap attached at the waist. It is conceivable that the placement of the sled attachment may alter resultant joint moments. A load that is much larger than optimal may completely alter mechanics[4]. However, the alterations in mechanics found in these studies may be due to the decrease in velocity which occurred at greater loads, not the loads themselves. Determining the magnitude of joint moment differences while pulling sleds of different weights while controlling for gait speed will eliminate the effects of gait velocity.

The purposes of this study are to determine how lower extremity biomechanics differ: 1) when different percentages of body weight are towed for each condition and 2) when the sled is attached at the waist compared to the shoulder. Peak knee flexion (PKF) was chosen as the time point of interest due to the aberrant joint moments seen at this time in subjects after anterior cruciate ligament rupture[5] and reconstruction[6]

Five conditions were compared: 20% body weight load (BWL) attached at the shoulder (S20); 50% BWL attached at the shoulder (S50); 20% BWL attached at the waist (W20); 50% BWL attached at the waist (W50); and normal walking (0%BWL due to no sled). We hypothesized that hip, knee, and ankle moments at PKF will be greater in the conditions with heavier loads than those with lighter loads. We also hypothesized that the hip moment at PKF will be greater during conditions in which the sled is attached at the shoulder than when attached to the waist.

## METHODS

12 healthy, uninjured subjects (8 males; 4 females), aged  $21.5 \pm 2.1$  years, were recruited for this study. Lower extremity motion during stance phase of gait was tracked using a cluster marker set.

Subjects completed the 5 conditions: normal walking; S20; S50; W20; and W50. After walking, the order of towing conditions was randomized. Walking speed was set at 1.3 m/s for all conditions and was controlled using a Brower laser timing device [7]. Trials were collected bilaterally, but for this investigation only the dominant side was analyzed. Dominance was determined as the foot used to kick a ball; every subject was right limb dominant. Five stance phases of each condition

were analyzed and the mean joint moments at PKF were calculated. Sleds were towed over an indoor rubber track (Super X, All Sports Enterprises). Kinematic data were collected with 8 Qualisys Oqus Series-3 cameras set at 60Hz and kinetic data were collected by two AMTI BP400600 force plates (Watertown, MA) at 2400Hz. Visual 3D (C-motion, Germantown, MD) was used to apply a Butterworth filter with a cutoff of 6Hz to kinematic data and analog data was filtered with a Butterworth filter with cutoff of 50Hz, as determined by retaining 95% of signal power through a fast Fourier transformation. Inverse dynamics were used to calculate external joint moments at the PKF angle during the stance phase of gait which were normalized to body mass.

A repeated measures ANOVA was used to answer the first hypothesis (joint moment differences against load) with post-hoc paired t-tests calculated if a significant difference was found. For the second hypothesis, paired t-tests were used to determine whether hip moments were greater at the shoulder vs. waist attachment. Statistical analysis was performed using SYSTAT 11 (SYSTAT, Chicago, IL) ( $\alpha=0.05$ ).

## RESULTS AND DISCUSSION

Joint moments per condition are given in Table 1. Only knee flexion moments at the shoulder towing condition significantly increased as load increased. Knee flexion moments during waist towing showed a similar pattern with insignificant results.

Our second hypothesis was supported. Greater hip extension moments were found with attachment at the shoulder conditions for the light (S20 vs. W20:  $p<0.001$ ) and heavy (S50 vs. W50:  $p<0.001$ ) conditions.

Even though attachment at the shoulder produced a greater hip extension moment than attachment at the waist, normal walking produced a moment similar to the greatest moment produced by any sled condition. This is surprising as it was expected that greater moments would be required to counteract the heavier loads. Furthermore, moments at the hip and ankle decreased or remained the same as load increased when pulling a sled. It may be that gait is altered by sled towing to an extent that PKF is not a valid point of comparison. Through visual inspection of the data, the PKF instance appears to be occurring earlier in the stance phase when towing a sled. Therefore future studies should compare moment impulse or peak moments rather than moments at a specific kinematic point.

## REFERENCES

1. Cissik, J., Means and methods of speed training, part I. *Strength Cond J*, 2004. **26**(4): p. 24-29.
2. Faccioni, A., Assisted and resisted methods for speed development: part 2. *Mod Athl Coach*, 1994. **32**: p. 8-12.
3. Alcaraz, P.E., et al., Effects of three types of resisted sprint training devices on the kinematics of sprinting at maximum velocity. *J Strength Cond Res*, 2008. **22**(3): p. 890-7.
4. Cronin, J., et al., Effects of weighted vests and sled towing on sprint kinematics. *Sports Biomech*, 2008. **7**(2): p. 160-72.
5. Rudolph, K.S., et al., Dynamic stability in the anterior cruciate ligament deficient knee. *Knee Surg Sports Traumatol Arthrosc*, 2001. **9**(2):62-71.
6. Lewek, M., et al., The effect of insufficient quadriceps strength on gait after anterior cruciate ligament reconstruction. *Clin Biomech* (Bristol, Avon), 2002. **17**(1): p. 56-63.
7. Bastien, G.J., et al., Effect of load and speed on the energetic cost of human walking. *Eur J Appl Physiol*, 2005. **94**(1-2): p. 76-83.

**Table 1:** External Joint Moments (Nm/kg) at peak knee flexion angle

|      | Hip (Ext -)               | Knee (Ext +)               | Ankle (Plantar flexion -)  |
|------|---------------------------|----------------------------|----------------------------|
| Walk | -0.11 ± 0.05              | -0.03 ± 0.01               | -0.95 ± 0.19               |
| S20  | -0.13 ± 0.07              | -0.05 ± 0.01*              | -0.74 ± 0.20*              |
| S50  | -0.07 ± 0.05 <sup>†</sup> | -0.07 ± 0.01* <sup>†</sup> | -0.88 ± 0.21 <sup>†</sup>  |
| W20  | -0.05 ± 0.08*             | -0.03 ± 0.01               | -0.68 ± 0.18*              |
| W50  | 0.04 ± 0.05* <sup>†</sup> | -0.05 ± 0.01* <sup>†</sup> | -0.52 ± 0.14* <sup>†</sup> |

\*significantly different than walking condition

<sup>†</sup> significantly different than 20%BWL

## Derivation of the Equation of Motion for the Alveolar Spring-Hinge Model

<sup>1</sup>Youngmin Park, <sup>1</sup>Dohyun Kim, <sup>1</sup>Jong-Hoon Ahn, <sup>1</sup>Jongshill Lee and <sup>1</sup>In Young Kim

<sup>1</sup>Department of Biomedical Engineering, Hanyang University, Seoul, Republic of Korea  
email: [youngmin@bme.hanyang.ac.kr](mailto:youngmin@bme.hanyang.ac.kr)

### INTRODUCTION

The alveolar structure is one of the most complicated structures in the living body. Recently, a four-dimensional model of the alveolar structure has been constructed by grounding pulmonary morphogenesis[1]. In the model, the alveolar deformation is modeled by a combination of springs and hinges. Morphometric characteristics of the model during ventilation are well consistent with the previous experimental reports. However, when one tries to use it as a building block of simulating a lung deformation or modeling the loss of lung recoil such as in emphysema, it doesn't provide any necessary information with regard to dynamic behavior. By approximating it as a torsional harmonic oscillator[2], we derive the equation of motion for alveolar dynamics and calculate the natural frequency of vibration.

### METHODS AND RESULTS

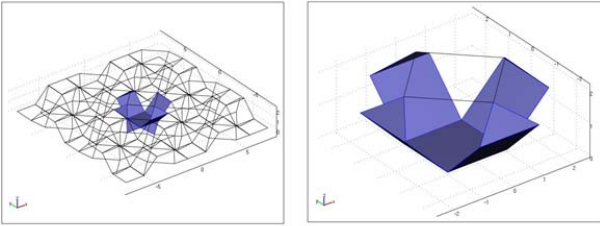


**Fig 1: The spring-hinge model for (a) alveoli (b) a single alveolus**

The spring-hinge model is composed by a square primary septum, four square hinges, four triangular secondary septa, and four springs, as shown in figure 1. The primary septum makes a bottom of each alveolus. Hinges are links between the primary septum and secondary septa. And a secondary septum is orthogonally attached to each hinge. Two adjacent secondary septa are connected by springs. A synchronous motion of the alveolar structure depends on the hinge angle, which ranges from 90°

to 135°. When the four end points of the secondary septa converge into a point, the hinge angle becomes 90°. It would become 135° in the case of figure 1.

Let us consider the dynamics of the single alveolar system in terms of an angle  $\theta$ . The angle is set to zero when the hinge angle is 112.5°. Ignoring a translational motion, we can write the kinetic energy as the sum of rotational kinetic energies:  $T = 4 \times \left(\frac{1}{2}I\dot{\theta}^2\right)$ , where  $I$  is the moment of inertia in each part. The potential energy is written as  $U = 4 \times \left(\frac{1}{2}\kappa_t\theta^2\right) + 4 \times \left(\frac{1}{2} \cdot \frac{1}{2}\kappa_t\theta^2\right)$ , where  $\kappa_t$  is a coefficient of the torsion spring and is assumed to be constant. The first term describes the potential energy of intra-springs within the alveolus and the second term describes the potential energy of inter-springs with other alveoli. Then we get the following Lagrange's equation:

$$2I\ddot{\theta} + 3\kappa_t\theta = 0.$$

Now let us calculate the moment of inertia  $I$ . We regard the lengths of edges of primary septa, hinges and hypotenuses of secondary septa are all 1. The moment of inertia is separated with the moment of inertia of a hinge and the moment of inertia of a secondary septum. We set the edge between a hinge and a primary septum as the axis of the rotation. From the axis we could calculate the moment of inertia of a hinge attached to the axis and the moment of inertia of a secondary septum attached to the other end of the hinge. The moment of inertia of a hinge  $I_h$  :  $I_h = \int_0^1 \int_{-\frac{1}{2}}^{\frac{1}{2}} y^2 \sigma dx dy = \frac{1}{3} \sigma$ . The moment of inertia of a secondary septum  $I_s$  :  $I_s = \int_0^{\frac{1}{2}} \int_{z-\frac{1}{2}}^{-z+\frac{1}{2}} (\sqrt{1+z^2})^2 \sigma dx dz = \frac{25}{69} \sigma$ . The

moment of inertia :  $I = I_h + I_s = \frac{19}{32}\sigma$ . Then we get the equation of motion for a single alveolar model:

$$19\sigma\ddot{\theta} + 12\kappa_t\theta = 0.$$

Because we expect the motion to be oscillatory, we attempt a solution of the form

$$\theta(t) = \theta_0 e^{i(\omega t + \delta)},$$

where  $\theta_0 = \frac{\pi}{8}$  because hinge angles are assumed to be  $135^\circ$  at the maximum expansion and  $90^\circ$  at the minimum volume. Substituting the expression for the displacement into the equation of motion, we find the natural frequency

$$\omega_0 = \sqrt{\frac{12\kappa_t}{19\sigma}}.$$

Next, we add a torque  $\tau(t)$  acting along the  $\theta$ -direction and consider a viscous damping force. The equation of motion becomes

$$\ddot{\theta} + 2\beta\dot{\theta} + \omega_0^2\theta = \tau,$$

where  $\beta$  is a damping constant. The simplest case of driven oscillation is that in which an external driving torque varying harmonically with time is applied to the alveolar model:  $\tau(t) = \tau_0 \cos(\omega t)$ . Then we get a general solution:  $\theta = \theta_c + \theta_p$

We denote a complementary solution ( $\theta_c$ ) and a particular solution ( $\theta_p$ ) like below:

$$\theta_c(t) = e^{-\beta t} \left[ \tau_1 \exp\left(\sqrt{\beta^2 - \omega_0^2}t\right) + \tau_2 \exp\left(-\sqrt{\beta^2 - \omega_0^2}t\right) \right]$$

$$\theta_p(t) = D \cos(\omega t - \delta)$$

Substituting  $\theta_p(t)$  in  $\ddot{\theta} + 2\beta\dot{\theta} + \omega_0^2\theta = \tau_0 \cos(\omega t)$ , we obtain  $\tan\delta = \frac{2\omega\beta}{\omega_0^2 - \omega^2}$ ,  $D = \frac{\tau_0}{\sqrt{(\omega_0^2 - \omega^2)^2 + 4\omega^2\beta^2}}$ .

The term  $\theta_c(t)$  represents transient effects. Effects of  $\theta_c(t)$  are damped out with time. The term  $\theta_p(t)$  represents the steady-state effects. We could calculate a resonance frequency ( $\omega_R$ ) that makes the

amplitude  $D$  maximize. We set  $\left. \frac{dD}{d\omega} \right|_{\omega=\omega_R} = 0$ , and obtain :

$$\Omega_R = \sqrt{\omega_0^2 - 2\beta^2} = \sqrt{\frac{12\kappa_t}{19\sigma} - 2\beta^2}$$

$$\approx \sqrt{\frac{12\kappa_t}{19\sigma}}. \quad (\text{when } \beta \text{ is negligible})$$

## DISCUSSION

In our approach, we made two big assumptions with regard to a spring constant. The springs correspond to elastin fibers at alveolar mouths and, in fact, the fibers exhibit viscoelastic properties. Thus, in the case that viscosity is negligibly small, our model is applicable. Besides, we used the torsion spring instead of a linear spring in order to obtain the closed-form solution. Nevertheless, our results are qualitatively meaningful. The square of the natural frequency or the resonance frequency is approximately proportional to a spring constant at  $\theta \approx 0$ .

## CONCLUSIONS

While the spring-hinge model only describes the alveolar structures and their morphometric characteristics, we have calculated the Lagrangian dynamics of the model. To be precise, we have viewed it as a torsional harmonic oscillator and derived the equation of motion and its natural frequency. Besides, we've considered a damping effect and an external torque.

## REFERENCES

1. Kitaoka H, et al. *J Physiol Sci* **57**, 175-185, 2007.
2. Thornton ST, Marion JB. *Classical Dynamics of Particles and Systems*, Thomson Learning, 2004.

## ACKNOWLEDGEMENTS

This work was supported by the Research fund of Survivability Technology Defense Research Center of Agency for Defense Development of Korea (No. UD090090GD).

# Association between Functional Hip Abductor Strength and Hip Joint Kinematics and Kinetics During a Dynamic Uni-pedal Drop Landing Task

Szu-Ping Lee and Christopher Powers

University of Southern California, Los Angeles, CA, USA  
email:szupingl@usc.edu web:http://pt2.usc.edu/labs/mbrl/index.html

## INTRODUCTION

Diminished hip muscle performance has been shown by several clinical studies to be associated with lower extremity injury.[1-6] Among the hip muscles, the abductors have long been considered the most important as this muscle group provides dynamic hip stability and is an essential stabilizer of the pelvis, particularly during uni-pedal stance.[7] Excessive hip adduction has been recognized as potential contributing factor to a number of lower extremity injuries, including patellofemoral pain, iliotibial band syndrome and non-contact ACL injuries. However, biomechanical evidence regarding the association between hip abductor muscle performance and hip joint mechanics during dynamic activities was very limited.

The purpose of the current study was to investigate the relationship between hip abductor muscle performance and hip joint biomechanics during the deceleration phase of a uni-pedal drop landing task.

## METHODS

Twenty-three subjects (9 male and 14 female, mean age =  $30.9 \pm 4.2$  years) participated in this study. All subjects were recreationally active and have no concurrent lower extremity injuries, pain or history of surgery to the legs or the lower back. Hip abductor muscle performance was tested using a previously described functional weight-bearing method.[8] Briefly, testing was performed with the subject in  $50^\circ$  knee flexion and  $30^\circ$  hip flexion with feet parallel and shoulder-width apart (Fig. 1). This joint position was chosen because most non-contact lower extremity injuries were believed to occur during the early deceleration phase of stance when the hip and knee joints are moderately flexed.



Figure 1: Functional Hip Abductor Performance Assessment

Hip abductor force production was measured using a strain gauge (Omega Engineering, Inc., USA, sampling frequency = 1000Hz) connected to a non-stretchable fabric belt wrapping around the distal ends of the femurs. The belt is positioned around the thigh, 5 cm proximal to the lateral epicondyles. Care was taken to ensure that the strain gauge was in series with the belt, parallel to the line of force application. The subjects were instructed to push as hard and fast as they can on cue, and maintain the maximal effort for 5 seconds. The peak force was recorded and normalized to each subject's bodyweight.

The drop landing task was performed from an elevated position 30.5 cm off the ground. The goal of the task was to jump from this elevated position and to "stick the landing" on one leg. The subjects were instructed to keep the arms folded in front of the body to minimize the effect of compensatory arm movements (Fig.2).



Figure 2: Uni-pedal Drop Landing Task

Lower extremity kinematic and kinetic data were collected using a 11-camera motion system (Qualisys, Sweden, sampling frequency = 250Hz) and a force platform (AMTI, USA, sampling frequency = 1500Hz). Range of frontal plane angular motion and the average hip abductor moment during the deceleration phase of landing were the independent variables of interest. The deceleration phase was defined as from the initial contact to the point when the sacrum marker was at its lowest position. The hip abductor joint moment was normalized to each subject's bodyweight.

The association between normalized peak hip abductor force and range of hip frontal angular motion, and average hip abductor moment were assessed using linear regression models. The significance level was set at  $p = 0.05$  (two-tailed).

## RESULTS AND DISCUSSION

During the deceleration phase of landing, the normalized hip abductor strength was significantly correlated with range of hip frontal angular motion ( $R^2 = 0.20$ ,  $p = 0.03$ , Fig. 3) and the average hip abductor moment ( $R^2 = 0.45$ ,  $p < 0.001$ , Fig. 4). The negative correlation between hip abductor strength and frontal plane hip joint motions indicates that individuals with diminished hip abductor strength exhibited increased hip joint excursion. Conversely the positive correlation between hip abductor strength and the hip abductor force indicates that stronger individuals generated greater abductor moments during landing.

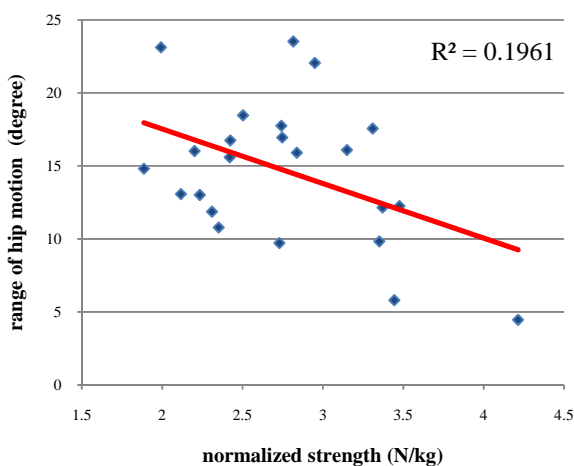


**Figure 3:** Correlation of hip abductor strength and range of the hip frontal motion during the deceleration phase of landing.

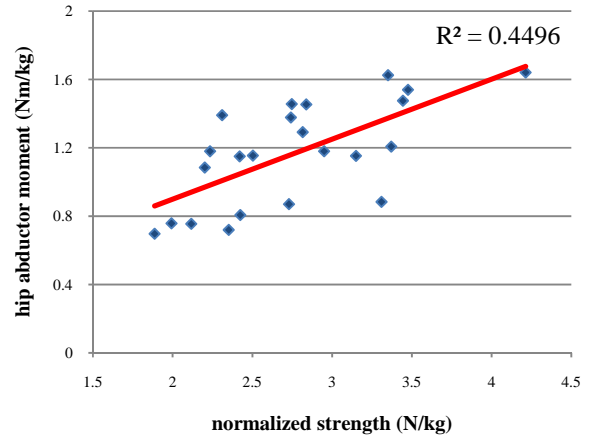


**Figure 4:** Correlation of hip abductor strength and average hip abductor moment during the deceleration phase of landing

## CONCLUSIONS

The hip abductor muscles are important in regulating hip frontal plane joint motion as well as providing stability to the pelvis and trunk. The findings from our study suggested that hip abductor strength is significantly associated with the hip joint kinematics and kinetics during a uni-pedal drop landing task. Our findings suggest that hip abductor strengthening may be indicated in persons with altered hip joint mechanics.

## REFERENCES

1. Powers, CM., *J Orthop Sports Phys Ther*, 2003. **33**(11): 639-46.
2. Souza, RB. and CM. Powers, *J Orthop Sports Phys Ther*, 2009. **39**(1): 12-9.
3. Souza, RB. and CM. Powers, *Am J Sports Med*, 2009. **37**(3): 579-87.
4. Leetun, DT., et al., *Med Sci Sports Exerc*, 2004. **36**(6): 926-34.
5. Ireland, ML., et al., *J Orthop Sports Phys Ther*, 2003. **33**(11): 671-6.
6. Cichanowski, HR., et al., *Med Sci Sports Exerc*, 2007. **39**(8): 1227-32.
7. Inman, V.T., *J Bone Joint Surg*, 1947. **29**(3): 607-619.
8. Lee, S.-P. and C.M. Powers, *Proceedings of University of Southern California Research Day*, 2010.

## ACKNOWLEDGEMENTS

This study is partially supported by the International Society of Biomechanics Student Dissertation Award

# Prediction of Frontal Plane Hip & Ankle Kinematics during Uni-pedal Stance Using a Dual-Segment, Center of Pressure-Based Postural Model

Szu-Ping Lee and Christopher Powers

University of Southern California, Los Angeles, CA, USA  
email:szupingl@usc.edu web:http://pt2.usc.edu/labs/mbrl/index.html

## INTRODUCTION

The coordinated actions of the hip and ankle are essential in maintaining postural stability. Specifically, the ankle and hip movement strategies work together to produce adaptable postural responses to accommodate magnitudes of postural perturbation from different directions.[1] The single-segment “ankle strategy” has been proposed as the preferred response to perturbations of smaller magnitude, while the double-segment “hip strategy” was considered to be more suitable for larger postural adjustments.[2, 3] The spatial orientation of the two joints largely determines the location of the body center of mass. This is particularly apparent in the frontal plane, as the hip and ankle (subtalar joint) are the only lower extremity joints allowing the frontal plane degrees of freedom. Understanding how hip & ankle movement contributes to the maintenance of postural stability is important, as recent clinical studies have found that persons with abnormal hip joint control demonstrate increased risk of lower extremity.[4]

The validity of a sagittal postural model has been demonstrated.[5] However a postural model describing the frontal plane hip-ankle coordinated movement pattern, which is believe to be more related to ankle injury, is currently not available. The purpose of the current study is to develop and validate a postural model that predicts the hip and ankle frontal kinematics during uni-pedal standing using the excursion of the center of pressure time-series as an input variable.

## METHODS

The spatial location of the body center of mass was estimated with anthropometric parameters and center of pressure location time-series as described by Caron et al.[6] The proposed model predicts the

hip and ankle joint motions based on the concept that the system center of mass is the sum of its segments. The model consists of two primary segments: 1) head, arm, trunk as one segment (HAT) and 2) the stance leg. The two segments are connected at the hip, and the stance leg segment is connected to a foot segment fixed to the ground. (Fig. 1)

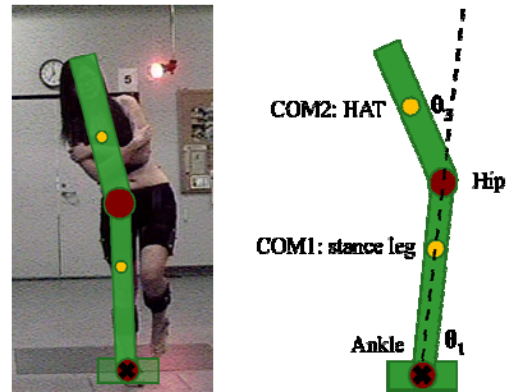


Figure 1: Segmental representation of the postural model

**M:** segment mass relative to body mass

**L:** segment length relative to height

**K:** distance from the segment distal end to the COM relative to L

Segmental COM positions (with respect to ankle joint center as origin):

COM1( $X_1$ ,  $Y_1$ ):

$$X_1 = L_1 * K_1 * \cos(\theta_1)$$

$$Y_1 = L_1 * K_1 * \sin(\theta_1)$$

COM2( $X_2$ ,  $Y_2$ ):

$$X_2 = L_1 * \cos(\theta_1) + L_2 * K_2 * \cos(\theta_1 + \theta_2)$$

$$Y_2 = L_1 * \sin(\theta_1) + L_2 * K_2 * \sin(\theta_1 + \theta_2)$$

Model-based body COM position ( $X$ ,  $Y$ ):

$$X = M_1 * L_1 * K_1 * \cos(\theta_1) + M_2 * (L_1 * \cos(\theta_1) + L_2 * K_2 * \cos(\theta_1 + \theta_2)) + M_0 * X_0$$

$$Y = M_1 * L_1 * K_1 * \sin(\theta_1) + M_2 * (L_1 * \sin(\theta_1) + L_2 * K_2 * \sin(\theta_1 + \theta_2)) + M_0 * Y_0$$

To simplify we introduce:

$$A_1: K_1 * L_1 * M_1 + M_2 * L_1$$

$$A_2: K_2 * L_2 * M_2$$

Then the hip-trunk angle  $\theta_2$  can be expressed as:

$$\cos \theta_2 = \frac{X^2 + Y^2 - A1^2 - A2^2}{2 \cdot A1 \cdot A2}$$

Possible solutions for  $\theta_2$ :

$$\theta_{21} = \text{ArcTan}(\sqrt{1 - (\cos \theta_2)^2}; \cos \theta_2) \text{ or}$$

$$\theta_{22} = \text{ArcTan}(-\sqrt{1 - (\cos \theta_2)^2}; \cos \theta_2)$$

Similarly the possible solutions of ankle angle  $\theta_1$ :

$$\theta_{11} = \text{ArcTan}(\sin \theta_{11}; \cos \theta_{11}) \text{ or}$$

$$\theta_{12} = \text{ArcTan}(\sin \theta_{12}; \cos \theta_{12})$$

To select the optimal hip-ankle angles solution, two criteria were considered:

1. COM position must be reachable given the computed joint angles
2. Hip & ankle joint angular trajectories must be continuous

To validate the model, the model-computed ankle and hip joint kinematics (frontal plane) were compared to video-based measurements of the hip and ankle joint angles obtained from 2 subjects performing 20 seconds of uni-pedal standing. The center of pressure location was obtained using a force platform (AMTI, sampling rate = 250Hz). Frontal plane hip and ankle joint kinematics are captured using a 11-camera digital system (Qualisys®, sampling rate = 250Hz).

## RESULTS AND DISCUSSION

As illustrated in Figures 2 and 3, the model was capable of predicting hip and ankle joint motions to high degrees of accuracy (mean prediction error: hip =  $0.23 \pm 0.01^\circ$ , ankle =  $0.49 \pm 0.15^\circ$ ).

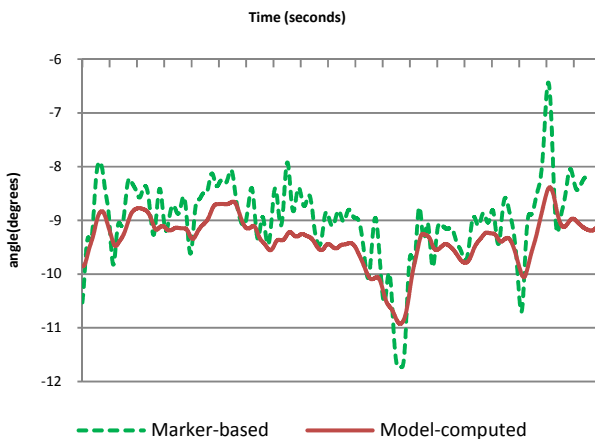


Figure 2: Comparison of model-computed to marker-based ankle joint angle

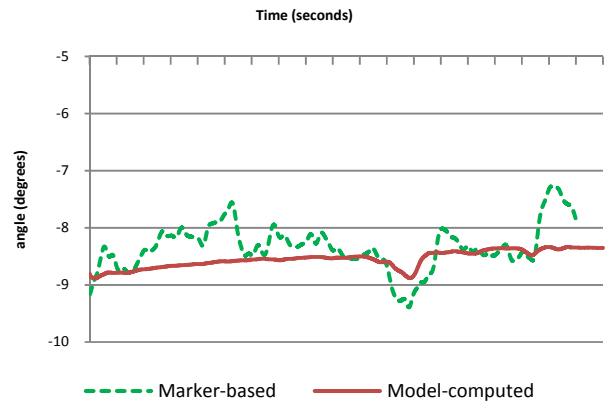


Figure 3: Comparison of model-computed to marker-based hip joint angle

## CONCLUSIONS

Frontal plane hip and ankle joint kinematics were accurately predicted by the proposed modeling approach using only the center of pressure as an input. This highlights the premise that the sway of the body and the orientation of the body segments in the frontal plane during a uni-pedal stance are regulated by the coordinated movements between the hip and ankle. The goal of this postural control strategy is to align the segmental centers of mass to achieve systemic equilibrium by adjusting the orientations of the hip and ankle joints in the frontal plane. Our findings provide support for the concept of an integrated hip-ankle balance strategy during uni-pedal stance.

## REFERENCES

1. Nashner, LM. and G. McCollum, *Behav Brain Sci*, 1985. **8**(1): 135-150.
2. Runge, CF., et al., *Gait Posture*, 1999. **10**(2): 161-70.
3. Gribble, PA. and J. Hertel, *J Electromyogr Kinesiol*, 2004. **14**(6): 641-6.
4. Friel, K., et al., *J Athl Train*, 2006. **41**(1): 74-8.
5. Colobert, B., et al., *Clin Biomech (Bristol, Avon)*, 2006. **21**(4): 427-34.
6. Caron, O., B. Faure, and Y. Breniere, *J Biomech*, 1997. **30**(11-12): 1169-71.

## ACKNOWLEDGEMENTS

This study is partially supported by the International Society of Biomechanics Student Dissertation Award

# USE OF A JUDO BREAK-FALL TECHNIQUE DURING A LATERAL FALL

<sup>1</sup>Stacey Lehman and <sup>2</sup>Kurt DeGoede

<sup>1</sup>Department of Biology, <sup>2</sup>Department of Physics and Engineering  
Elizabethtown College, Elizabethtown, PA. USA  
email: [degoedek@etown.edu](mailto:degoedek@etown.edu)

## INTRODUCTION

The current annual cost of falls, including direct medical expenses and lost work time due to injury and death, is almost 50 billion dollars [1]. One way to combat the expenses and injuries due to falling is to develop a safe falling technique. There appear to be two major factors that affect how severe a fall related injury will be: the peak forces the body receives on impact and the resistance of the bodily tissues to injury caused by these forces. People have some control over the former to reduce the severity of a fall [1]. The configuration of a person's body during the descent phase of a fall affects the magnitude of the forces he or she will experience upon impact.

A previous study showed that both males and females with martial arts experience could perform a judo slap fall from the knees to reduce the impact velocity of the hip and shoulder by performing a slap fall [2]. Although this experiment demonstrated the effectiveness of the slap fall technique to reduce both the hip and shoulder impact forces in those trained in the martial arts, it did not address the ability of untrained individuals to successfully utilize the technique. These current experiments built on the Sabick study to determine if untrained females could perform a similar fall intervention and if the intervention could significantly reduce hip impact force [2].

## METHODS

The experimental set-up consisted of two Pasco force platforms bolted to a piece of laboratory countertop 18 inches apart from center to center. The force platform set up was then bolted to the floor. A wooden platform 72 in x 96 in x 2.5 in was constructed with an opening of 15 in x 33 in to accommodate the force platforms. Two gym mats were placed side by side on top of the platform. The

position of the force platforms was outlined on the mats with duct tape. Crosshairs around the targets, a T-shaped starting mark, and hand targets on the upper cross hairs were also placed on the mat with duct tape. The subjects for this study were 10 female college students, ages 18 to 22, who had no previous martial arts experience. The subjects performed 10 falls in a random order: 5 falls with no intervention and 5 falls with the modified judo technique. Subjects received verbal instructions and saw video demonstrations of both fall types.

Falls without an intervention were performed by kneeling on the mat at the designated location with the shoulders, hips, and knees aligned and the arms folded across the chest. The subject self-initiated a fall by tipping from the knees when given a verbal command. The modified judo fall was performed by kneeling on the mat at the designated location with the shoulders, hips, and knees aligned and the non-dominant arm folded across the chest. The subject self-initiated a fall by tipped from the knees when given a verbal command. The subjects attempted to use their dominant arm to rotate onto their back by aiming their hand towards the designated target.

Additionally, video cameras were mounted on the ceiling and the wall to record subjects' falls. The ceiling camera was used to determine if the subjects fell within the targets. The wall camera was used to determine how much the subjects rotated during the falls. Subjects wore a belt with evenly spaced reflective markers to assess rotation. Data Studio was used to collect force data from the force platforms through a Pasco Xplorer GLX. The data was sampled at a rate of 2000 Hz. The maximum hip impact from each subject was normalized to body weight. Falls were discarded if the subject's hip or shoulder fell outside the target. No comparisons could be made from the shoulder impact because the shoulder tended to miss the target with the modified judo fall. The average

normalized hip impact was calculated for the falls with and without the intervention for each subject. A paired t-test was then performed to determine if the modified judo technique had a significant effect on hip impact.

## RESULTS AND DISCUSSION

Out of the 10 subjects tested, eight could perform the modified judo roll to varying degrees. Subject 2 was eliminated because she used her arm to completely arrest her fall. Subject 9 was eliminated because she did not attempt to use her arm to roll during the fall. Out of the eight subjects tested, seven experienced a lower average impact with the judo roll technique. Subject 10 was the only person who experienced a higher impact force with the intervention. These data are shown in Figure 1.

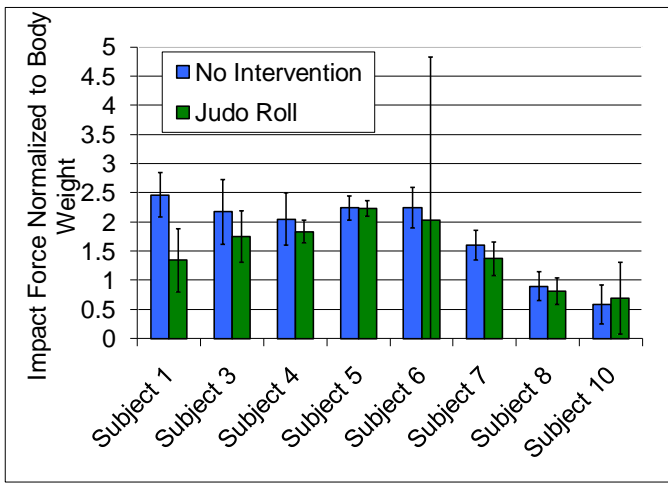


**Figure 1:** Average hip impact forces for falls. Error bars represent uncertainty calculated by  $S_m \cdot t$  value.

Although all but one subject experienced a decrease with the fall intervention, only Subject 1 experienced a significant decrease in hip impact force. The uncertainty for Subject 6's judo roll fall is so large because only two of her five roll falls were able to be used for the analysis. In the other three falls, her hand was too far from the target site to make a valid comparison of the fall techniques.

The average difference between the two falls was 0.27 body weights. A paired t-test was performed on these data to determine if this value was significant. The calculated p value was 0.08. The subject to subject variability in peak force was likely due to the self initiated fall protocol.

## CONCLUSIONS

Although this study did not conclusively show that the modified judo fall significantly reduced hip impact force, it did indicate its potential usefulness. The majority of subjects could perform the intervention without any previous martial arts training. Additionally, nearly all of the subjects who could perform the intervention saw a decrease in hip impact velocity. One subject was able to significantly reduce hip impact velocity ( $p=0.002$ ).

The paired t-test result did not indicate a significant difference between the two falls. However, data was only available from eight subjects. A difference of 0.27 body weights may become significant with the testing of more subjects. This difference represents a 15% reduction in the hip impact force similar to that observed in the previous study [2]. Thus, this study needs to be continued to validly assess the efficacy of the intervention.

A future direction for this study could also include more extensive training in the judo fall intervention. Training could include practice falls with coaching before the trials begin. Because individuals can decrease hip impact force with no training, they may be able to more significantly decrease impact with some small degree of training. Another future experiment could address the ability of subjects to use the roll technique to rotate onto their backside before impact. Instead of aiming to decrease the impact force, this technique would shift the impact from the hip to areas that have more tissue coverage and can better absorb the impact. Subjects in this study were generally not able to rotate before impact, possibly because the descent time is very short when falling from the knees. This type of protocol may have to be performed from a standing position.

## REFERENCES

1. DeGoede K.M., et. al. (2003). *J Biomechanics*, 36, 1043-1053.
2. Sabick M.B., et. al. (1999). *J Biomechanics*, 32, 993-998.

# A TIME-EFFICIENT METHOD FOR ANALYZING BONE STRAIN WITH LARGE SUBJECT POOLS

<sup>1</sup>Daniel Leib, <sup>1</sup>Eric Dugan and <sup>2</sup>Henry Wang

<sup>1</sup>Boise State University, Boise, ID, USA

<sup>2</sup>Ball State University, Muncie, IN, USA

email: [danleib@boisestate.edu](mailto:danleib@boisestate.edu) web: <http://coen.boisestate.edu/COBR/>

## INTRODUCTION

Bone strain is a useful measurement when investigating overuse injuries such as stress fracture [1]. *In-vivo* data for bone strain is difficult to obtain due to the invasiveness of surgical procedures and even when such studies can be conducted, interpretation of data from implanted strain staples and gauges is non-trivial [2].

Due to the difficulties in measuring *in-vivo* strain there has been some momentum in utilizing numerical modeling methods to investigate strain. Finite element modeling (FEM) has been used in past investigations in conjunction with mechanical testing of cadaver specimens to investigate certain aspects of bone stress and strain. This methodology is quite time consuming computationally, however, and can be difficult to use in conjunction with subject-specific kinematic and kinetic data, thus limiting its application in investigations requiring large subject pools.

Recent work has been done to overcome the computational time and de-coupling of FEM inputs by Al Nazer and Klodowski using a flexible body in conjunction with a subject-specific musculoskeletal model [3]. The data and methods presented in these papers still suffer from limitations of small sample size and using simulation-generated ground reaction forces, however, and do not present methods to manage large sets of data.

It is the purpose of this paper to present a time-efficient methodology of calculating bone strain utilizing subject-specific tibial geometry and material properties derived from computed tomography (CT) scans and musculoskeletal models driven by experimental kinematic and kinetic inputs. Data and computational times from a single

subject and gait trial will be presented as an example of how this methodology can be used with implications for automation across large cohorts.

## METHODS

A representative subject from a larger study on tibial stress fracture was used to describe this process. All experimental procedures were approved by the University's Institutional Review Board and the subject signed an informed consent form. The subject was a 21 year old male.

CT scans were collected for the entire length of the tibia using a GE Light Speed VCT (General Electric, USA). Images were segmented in Mimics 12.1 (Materialise, Belgium), a surface mesh automatically generated, and a 3mm<sup>3</sup> solid hexahedral mesh generated from that surface mesh using MD MARC 2008 (MSC.Software, Santa Ana, CA). An automated custom MATLAB routine was used to assign material density and elastic modulus to each individual element of the mesh based on the average Hounsfield unit value of the pixels contained within each element; this process was automated across the full cohort for the larger study as well. Six hundred material properties were used in this assignment with 300 each being considered cortical bone [4] and 300 cancellous [5].

Motion capture data were collected using a cluster-based marker set at 120Hz while the subject walked at 1.67m/s on an in-line AMTI force instrumented treadmill collecting analog data at 2400Hz.

A scaled lower-body model was built using LifeMOD 2008.2805 (Lifemodeler, San Clamete, CA) based on the subject characteristics [6]. Twenty three muscles were then added to the right leg [7]. The tibia constructed in MARC was then exported

and manually aligned in the musculoskeletal model using digitized landmarks. Relative locations of relevant attachment sites were then exported and applied to the FEM tibia in MARC using an automated Python script and a Craig-Bampton modal analysis performed with 6 degrees of freedom applied to each “joint” node. This process was automated using the MD ADAMS command language and references to text files containing subject characteristics and tibia node numbers.

An inverse-kinematic (IK) trial was performed using experimental trajectory data to set kinematic goals for muscle and joint controllers and then the modal neutral file imported to align with three known points in the musculoskeletal model. The rationale for using an MNF is described more fully in [8]. A forward dynamic simulation was then performed using inverse-kinematic results as targets and experimental ground reaction forces applied. Strains were then calculated using the Durability plug-in for MD ADAMS/View (MSC.Software, Santa Ana, CA). This IK through strain calculation process was automated using the MD ADAMS command language and automated across the larger cohort using MATLAB and the Windows command line.

## RESULTS AND DISCUSSION

Strain and strain rate data generated by the model fall well within expected values for gait. An example stride of strain data is shown in Figure 1 and results summarized in Table 1.

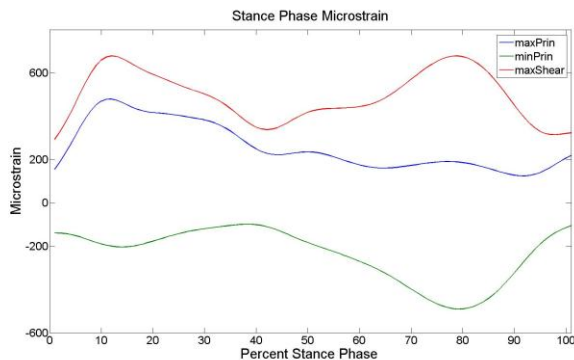


Figure 1: A representative stance phase of strain data.

|                    | Strain Magnitude (Microstrain) |          |           | Strain Rate (Microstrain/s) |            |                |
|--------------------|--------------------------------|----------|-----------|-----------------------------|------------|----------------|
|                    | Max Prin                       | Min Prin | Max Shear | Max P Rate                  | Min P Rate | Max Shear Rate |
| Lanyon et al       | 395                            | -434     | 829       | Not reported                | -4000      | Not reported   |
| Burr et al         | 437                            | -544     | 871       | 11006                       | -7183      | 16162          |
| Milgrom et al      | 840                            | -454     | 1183      | 3955                        | -3306      | 10303          |
| Al Nazer et al     | 305                            | -645     | 948       | 4000                        | -7000      | 10000          |
| Present Simulation | 490                            | -515     | 725       | 6608                        | -2804      | 7305           |

Table 1: Summary of strain results compared to previous studies

The methods utilized in this study are time efficient and highly automatable. User interaction is required through software only to segment CT images (though this is largely automated), select nodes for which to compute strain data, and to orient the tibia model within the musculoskeletal model. These tasks collectively take less than one hour per subject for an experienced operator. Simulation times for this method were easily manageable for large groups, taking only 5.5 minutes per 5 seconds of gait. Calculation of strains in Durability took only 0.5 seconds per node for a 5 second gait trial. With well-planned software automation utilizing scripting capabilities of MARC, LifeMOD, and MATLAB, large volumes of data can be handled reasonably for strain studies requiring large sample sizes.

## REFERENCES

1. Milgrom C. *Musculoskeletal Fatigue and Stress Fractures*, CRC Press, 2001.
2. Burr DB, et al. *Bone*, **18**, 405-10, 1996.
3. Al Nazer R, et al. *Comput Methods Biomech Biomed Engin*, **1**, 2011.
4. Snyder SM and Schneider E. *J Orthop Res*, **9**, 422-31, 1991.
5. Linde F. *Dan Med Bull*, **41**, 119-38, 1994.
6. Huaining C, et al. *Proceedings of the 1996 Fifteenth Southern Biomedical Engineering Conference*, 251-254, 1996.
7. Delp S, et al. *IEEE Trans Biomed Eng*, **54**, 1940-50, 2007.
8. Al Nazer R, et al. *Multibody System Dynamics*, **20**, 287-306, 2008.

## ACKNOWLEDGEMENTS

Funding source: US ARMY #W81XWH-08-1-0587

# DOES TESTER EXPERIENCE INFLUENCE THE RELIABILITY OF 3D-GAIT ANALYSIS? A COMPARISON OF THE FUNCTIONAL AND PREDICTIVE APPROACHES

<sup>1</sup>Ryan J. Leigh, <sup>1</sup>Michael B. Pohl, <sup>1</sup>Chandra H. Lloyd <sup>1</sup>Reed Ferber  
<sup>1</sup>The University of Calgary, Calgary, AB, Canada  
Email: [rleigh@ucalgary.ca](mailto:rleigh@ucalgary.ca); web: <http://www.runninginjuryclinic.org>

## INTRODUCTION:

Anatomical marker placement reliability is an important consideration in 3D gait analysis given its influence on defining joint centers, anatomical coordinate systems (ACSs), and ultimately the resulting joint kinematic outputs. It has been postulated that gait kinematic reliability could be improved using a functional (FUN) method compared to a manual marker placement approach (MAN) [1,2]. This seems logical given that FUN methods would be less reliant on precise anatomical marker placement. However, two studies have reported minor or no differences in gait kinematic reliability when comparing FUN and MAN methods [1,2]. The authors in both studies speculated that similar reliability between the two techniques may have been due to the use of experienced testers. Specifically, an experienced tester may be able to locate anatomical landmarks with greater precision than a novice tester. Therefore, the purpose of the study was to determine whether tester experience influences the reliability of gait kinematics when using a FUN or MAN method. It was hypothesized that: 1) the experienced tester (EXP) would demonstrate greater within-tester reliability using the MAN technique compared to the novice (NOV) tester; 2) EXP and NOV testers would demonstrate similar reliability using the FUN technique; 3) Between-tester reliability would be greater in the FUN method compared to MAN.

## METHODS:

Prior to the reliability testing, a four-part training session was conducted by the EXP tester (8 years gait analysis experience) with the intended purpose of training the NOV tester (physical therapist with no gait analysis experience) on anatomical marker placement. After completion of the training, 10 subjects (6F, 4M, 23±3 years of age) visited the lab on two occasions separated by a minimum of two days. During each visit to the lab, subjects underwent two gait analyses performed by

each tester. Testers were only present during their own data collections. Reflective markers were placed on anatomical landmarks and technical marker clusters were placed on the pelvis, thigh, shank, and foot for tracking purposes. Following a standing calibration trial and removal of anatomical markers, functional movements of the hip and knee were performed [2]. Subjects then walked on a treadmill while kinematic data was collected for five consecutive footfalls. Using Visual 3D software, two custom models were developed for the MAN and FUN methods. The MAN model used anatomical markers to predict the hip and knee joint centers, which were then used to create segmental ACSs. In the FUN approach, the hip and knee joint centers together with the flexion-extension axis of rotation for the knee were defined functionally [3]. The within- (both testers) and between-tester gait kinematic reliability of the FUN and MAN techniques was estimated for the hip and knee in the x, y, and z planes using root mean square error (RMS). RMS provides an estimate of the absolute offset of curves between days by calculating the angular difference between two corresponding points on curves of similar shape [2].

## RESULTS AND DISCUSSION:

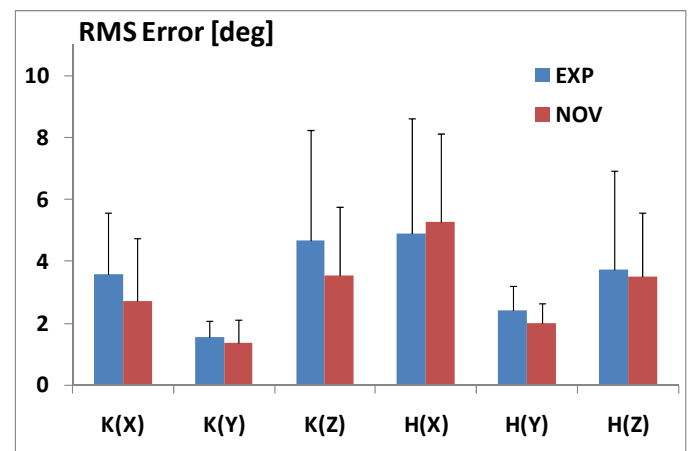


**Figure 1:** Within-tester RMS values (mean, sd) using the MAN method for the hip (H) and knee (K) in the sagittal (x), frontal (y), and transverse (z) planes.

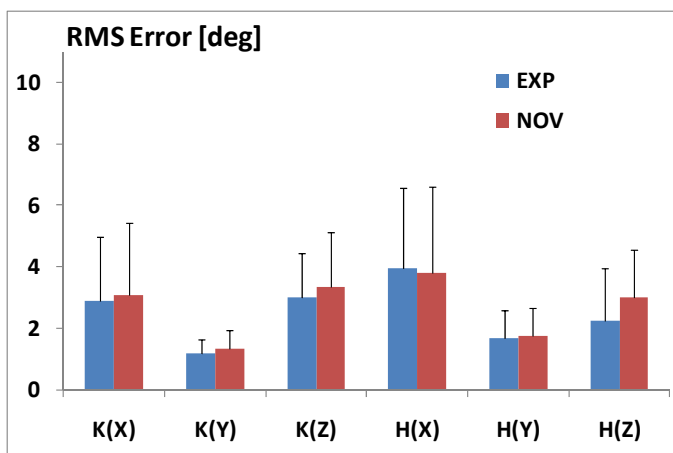


**Figure 2:** Within-tester RMS values (mean, sd) using the FUN method for the knee (H) and hip (K) in the sagittal (x), frontal (y), and transverse (z) planes.

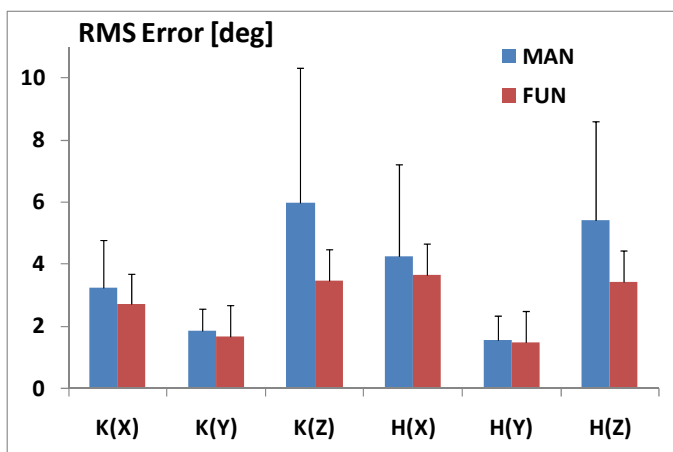


**Figure 3:** Between-tester RMS (mean, sd) across the knee (K) and hip (H) in the sagittal (x), frontal (y), and transverse (z) planes for FUN and MAN.

Contrary to our first hypothesis, within-tester RMS values were not statistically different between the EXP and NOV testers when using the MAN approach (Figure 1). It was expected that the EXP tester would show improved within-tester reliability as compared to the NOV tester using the MAN technique given the experienced tester's previous experience in placing anatomical markers. This was

not observed in the RMS measures across any plane of movement in the hip or knee. The similarity in reliability using the MAN technique may be attributable to the inexperienced tester having four years' experience as a physical therapist and thus familiarity in anatomical land-marking within a clinical setting.

Given its reduced reliance on anatomical marker placement, the FUN technique was expected to produce similar reliability findings for each tester. Supporting this hypothesis, the FUN method resulted in similar RMS error values in the EXP and NOV testers (Figure 2).

Between-tester reliability was improved in both the hip and knee across all planes of movement using the FUN method as compared to the MAN method (Figure 3). This was particularly evident in the transverse plane where RMS values were over 2° lower in the FUN method. However, the differences between the two methods were still of a small enough magnitude to have questionable significance to the practicing clinician.

## CONCLUSIONS

Tester experience does not seem to influence the within-tester reliability of 3D gait analysis regardless of whether a FUN or MAN approach is utilized. The FUN method does appear to improve between-tester reliability in the transverse plane but the observed improvement was small.

## REFERENCES

1. Besier et al. *J Biomech*, 36, 1159-68, 2003.
2. Pohl et al. *Gait & Posture* 34, 559-63, 2010.
3. Schwartz et al. *J Biomech*, 38, 107-16, 2005.

## ACKNOWLEDGEMENTS

Funding was provided by Alberta Innovates:Health Solutions. The authors would like to thank Talia Webber for her assistance with data processing.



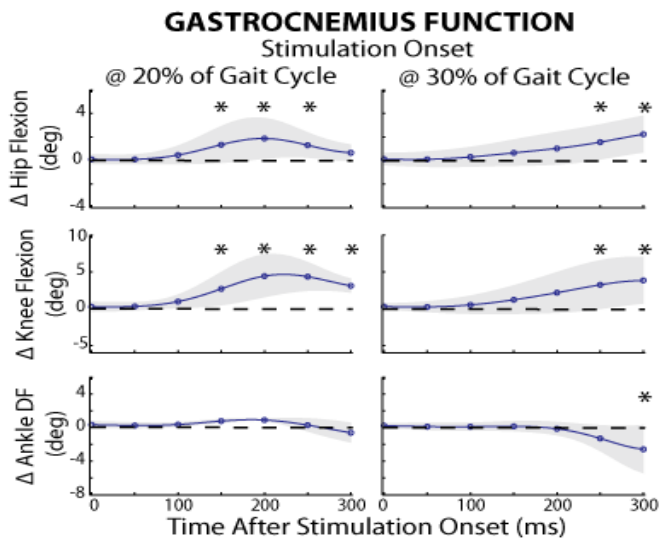


**Figure 2:** Changes in hip, knee, and ankle angles induced by gastrocnemius stimulation (\* $p < 0.05$ ).

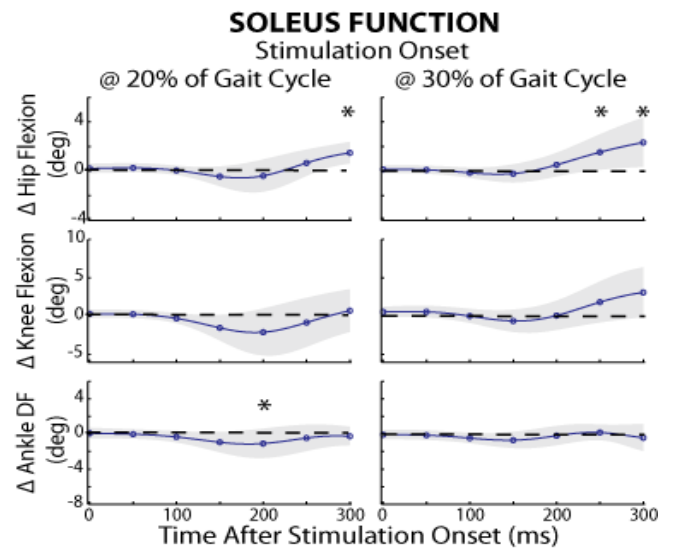


**Figure 3:** Changes in hip, knee, and ankle angles induced by soleus stimulation (\* $p < 0.05$ ).

## RESULTS AND DISCUSSION

*Gastrocnemius (Fig. 2):* The gastrocnemius induced hip flexion and knee flexion when stimulated at 20% or 30% of the gait cycle. The gastrocnemius did not alter the ankle angle when stimulated early, though there was trend toward dorsiflexion. Gastrocnemius stimulation at 30% of the gait cycle induced late ankle plantarflexion.

*Soleus (Fig. 3):* There was a strong tendency toward the soleus inducing hip and knee extension in response to early stimulation, though the effect was not significant. Early soleus stimulation did induce a significant shift toward ankle plantarflexion. Stimulation of the soleus at 30% of the gait cycle induced significant hip flexion and a tendency toward knee flexion, though these effects were seen substantially later.

Our results show distinct roles of the gastrocnemius and soleus during the stance phase of gait. Consistent with our hypothesis, early gastrocnemius activity did induce hip and knee flexion. While there was no significant effect at the ankle, there was a tendency toward the gastrocnemius inducing ankle dorsiflexion as has been reported previously [3]. In contrast, early soleus activity induced ankle plantarflexion and a strong trend toward early hip and knee extension. These latter results may become significant as we add subject numbers. We note that the induced motions due to early

stimulation were all seen within 150-200 ms after stimulation onset, likely reflecting the direct results of induced muscle forces. In contrast, the motion induced in response to later stimulation (30% gait cycle) resulted in significant changes in motion much later, at ~250-300 ms after onset. This would correspond to the pre- and early-swing phases of gait, and could reflect the stimulation inducing an earlier toe-off.

## CONCLUSION

We conclude that the gastrocnemius and soleus induce opposing motion at the hip, knee, and ankle during the stance phase of normal gait. The observations support the idea [1,2] that early ankle plantarflexion in stance, i.e. dynamic equinus, may indicate involvement of the soleus.

## REFERENCES

1. Perry J, et al. *J Bone Joint Surg Am.* **56**, 511-520, 1974.
2. Svehlík M, et al. *Arch Phys Med Rehabil* **91**, 1897-1903, 2010.
3. Stewart C, et al. *Gait and Posture* **26**, 482-488, 2007.
4. Neptune RR, et al. *J Biomech* **34**, 1387-1398, 2001.

## ACKNOWLEDGEMENTS

NIH AR057136, NIH T90 DK070079, NIH 1UL1RR025011, James McCarthy MD

# ALTERED WALKING PERFORMANCE DURING SIMULTANEOUS COGNITIVE TASKS

<sup>1</sup>Amy L. Lenz, <sup>2</sup>Christopher I. Higginson and <sup>1</sup>Jill S. Higginson

<sup>1</sup>University of Delaware, Newark, DE, USA

<sup>2</sup>Loyola University Maryland, Baltimore, MD, USA

email: allenz@udel.edu

## INTRODUCTION

Postural control during motor tasks may be influenced by simultaneous performance of cognitive tasks such as numerical verbal tasks and obstacle crossing [1,2]. Dual task walking is of particular concern in older adults due to the increased risk of falling with age [3]. Previous studies have explored interactions between cognitive function and walking characteristics (e.g. gait velocity, stride length, cadence) [4-6]. Variations in kinematic and kinetic parameters during walking have not previously been reported. The objective of this study was to explore kinematics and kinetics of walking during simultaneous performance of cognitive tasks. We tested the hypothesis that cognitive tasks would alter hip, knee and ankle joint angles, anterior/posterior ground reaction forces and vertical force at heel contact. Furthermore, we expected that changes in gait parameters would be more prominent during fast speed walking relative to walking at self-selected speed.

## METHODS

Five healthy young adults (24±4y, 1.75±0.09m, 72.67±11.05kg) participated in this IRB approved study following written informed consent. Subjects performed eight 120s walking trials on a split-belt instrumented treadmill (Bertec Corp, Columbus, OH), four at a preferred speed (1.13±0.08m/s) and four at a fast speed (120% of preferred speed). During each test, three different cognitive tests were performed. The tests included Paced Auditory Serial Addition Test (PASAT), Symbol Digit Modalities Test (SDMT), and a cellular phone dialing task (Phone) in randomized trial order. The PASAT is a demanding working memory task in which participants add two adjacent single digits presented in an auditory series. The SDMT is a

measure of cognitive processing speed in which participants rapidly state the number matched with a simple geometric symbol according to a key. The Phone task was designed as an ecologically valid experimental measure of attention in which participants dial nine-digit telephone numbers that are presented visually. Additionally, for each speed condition, a baseline trial was collected of walking without simultaneous cognitive tasks.

Whole body kinematics were recorded using a passive motion capture system (Motion Analysis, Santa Rosa, CA), and Visual3D (C-Motion, Germantown, MD) was used to compute joint angles and analyze the vertical and anterior/posterior (AP) ground reaction forces (GRF). All components of analysis were evaluated for the last five gait cycles of each trial. Statistical analysis was performed using paired t-tests comparing walking during each dual task with baseline walking at both speeds.

## RESULTS AND DISCUSSION

Self-selected speed trials including the PASAT task illustrated a significant increase in peak hip extension, decrease in peak hip flexion, decrease in peak knee flexion during stance, and decrease in peak plantarflexion ( $p < 0.05$ ). A significant ( $p = 0.022$ ) decrease in peak hip flexion for self-selected speed during SDMT task was also reported and an ( $p = 0.024$ ) increase in peak ankle plantarflexion occurred for the phone task at self-selected speed. During the fast PASAT condition, a significant ( $p = 0.015$ ) decrease of peak vertical GRF at heel strike was observed.

Walking kinematics in healthy young adults appears to mainly be disturbed when challenged by only the most demanding of cognitive tasks (PASAT). While vertical force exhibited a significant change

during the fast PASAT condition, changes in kinematic parameters only neared significance. Our results currently display minimal influence on walking control while using a phone in this young subject population. Although the t-test is robust to violations of the assumption of normality, more subjects are necessary to draw firm conclusions about this population. Further investigation of the influence of cognition on walking kinematics and kinetics in an older adult group may prove to have greater changes relevant to risk of falling. Plus, it is possible that our participants' performance on the various cognitive tasks was impacted by dual task walking (i.e., they prioritized walking) and will be assessed separately.

## CONCLUSIONS

Although small differences of questionable clinical significance were observed while simultaneously performing cognitive tasks during walking in the young healthy subject population, older adults may have more difficulty with safely multitasking. The potential to identify gait parameters that may be

influenced by cognitive multitasking during walking can have implications for preventing falls in older adults.

## REFERENCES

1. Woollacott M, Shumway-Cook A. *Gait Posture* **16**, 1-14, 2002.
2. Catena RD, et al. *Gait Posture* **25**, 406-411, 2007.
3. Alexander NB, Hausdorff JM. *J Gerontology* **63A**, 1325-1328, 2008.
4. Priest AW, et al. *J NeuroEng Rehab* **5**, 29-37, 2008.
5. Bock O, et al. *IEEE Engr Med & Bio* **8**, 23-28, 2008.
6. Plummer-D'Amato P, et al. *Gait Posture* **27**, 683-688, 2008.
7. Srygley JM, et al. *Brain Research* **1253**, 92-99, 2009.

## ACKNOWLEDGEMENTS

NIH NS055383

# SARCOMERE BEHAVIOUR IN MYOFIBRILS DURING LOCAL DEACTIVATION

Tim Leonard and Walter Herzog  
Faculty of Kinesiology  
University of Calgary, Calgary, Alberta, Canada  
email: [leonard@ucalgary.ca](mailto:leonard@ucalgary.ca) web: [www.ucalgary.ca/knes](http://www.ucalgary.ca/knes)

## INTRODUCTION

One of the principle determinants of force production in muscle is its length, or more precisely the amount of actin and myosin filament overlap within the sarcomere. This property, the so-called force-length relationship, has three regions: an ascending, a plateau and a descending region [1]. Injury to skeletal muscle is thought to occur when individual sarcomeres are pulled beyond actin-myosin filament overlap by the development of sarcomere length non-uniformities during contraction. This condition results when longer/weaker individual sarcomeres (on the descending region of the force-length relationship) are not able to generate equivalent forces to their shorter/stronger neighbours and so are forcibly elongated and “pop” [2]. Non-uniformities on the descending limb of the force-length relationship are expected because of the “unstable” nature of this region [3]. However, recent evidence suggests that the descending region is neither unstable nor do actively stretched sarcomeres become weaker with stretching [4], thereby questioning the idea of “popping” sarcomeres. To date, there is no direct experimental evidence for the development of non-uniformities in force or the popping of sarcomeres on the descending limb of the force-length relationship. We developed a first ever experimental setup using single myofibrils, where selected sarcomeres can be deactivated (weakened) while simultaneously measuring the effect of such weakening on sarcomere lengths and force in the myofibril preparation.

## METHODS

A myofibril preparation has the advantage that all sarcomeres support the same force due to their in-series arrangement and the length of each sarcomere (SL) can be determined by direct observation.

Myofibrils are activated or relaxed by adding the appropriate solution. In order to produce SL non-uniformities, we selectively deactivated mid-myofibril sarcomeres in an otherwise fully activated myofibril and measured the associated changes in sarcomere lengths and myofibril force. This method has been used previously on a much larger structural scale, using rat cardiac trabeculae [5]. Rabbit psoas myofibrils were prepared [4] and the plateau region [2.2 to 2.43  $\mu\text{m}$ ] identified [4]. Force was measured using cantilevers (132 nN/ $\mu\text{m}$ )[6]. Activating (pCa 3.5) and relaxing solutions (pCa 8) were used [4] and the tubes for introducing the jet of relaxing solution aimed at the mid-sarcomeres had an orifice opening of 3-5  $\mu\text{m}$ . Experiments were performed at 20-22 °C. Forces were expressed as stresses so that different experiments can be directly compared. Figure 1 shows a generic representation of the experimental setup.

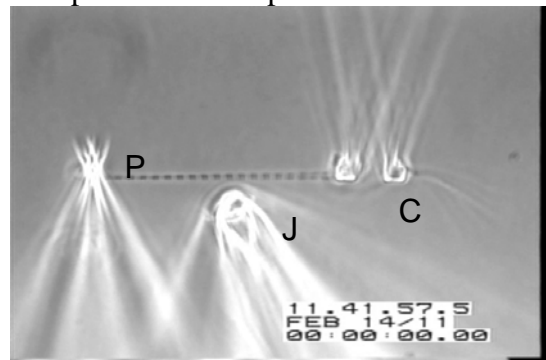


**Figure 1.** Experimental setup showing the motor controlled pipette (P) for adjusting myofibril length, the jet tube (J) for introducing the relaxing solution to the centre of the preparation, and the cantilever pair (C), with the myofibril attached to one lever and the reference lever left undisturbed. The myofibril has a diameter of approximately 1  $\mu\text{m}$ .

## RESULTS AND DISCUSSION

We show results from a myofibril with 16 serially arranged sarcomeres. The myofibril was activated at

a mean sarcomere length of 2.3  $\mu\text{m}$  and produced a stress of 104  $\text{nN}/\mu\text{m}^2$ . Figure 2 shows the individual SL for the tested myofibril, before and after the deactivation of sarcomeres 3-10, counting from the left of the myofibril. It can be seen that the deactivated sarcomeres all elongate, while sarcomeres 1 and 2 and sarcomeres 11 through 16 all shorten in response to the intervention. Force measured at the cantilever remained constant even though 8 central sarcomeres were deactivated. The sarcomeres on either side of the deactivated sarcomeres remained active and shortened until a new length and force equilibrium was reached for the myofibril. The total specimen length remained unchanged (37.5 $\mu\text{m}$ ) for the fully activated and the locally deactivated test.

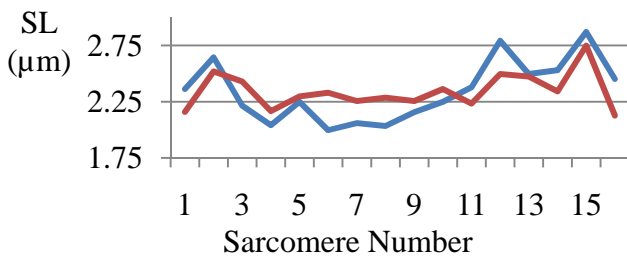


**Figure 2.** Individual sarcomere length versus sarcomere position in the myofibril. Full activation (blue) and activation with local deactivation (red). Sarcomere 1 is at the left side of the preparation and sarcomere 16 is attached to the cantilever on the right.

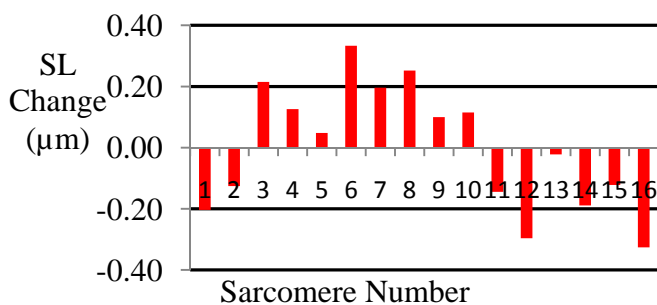


**Figure 3.** Change in SL after the introduction of the relaxing solution to the central region of the myofibril. Sarcomeres 3-10 lengthen but do not “pop”.

A summary of SL changes for the two test conditions is shown in Figure 3.

Traditionally, and in the frame work of the sarcomere length non-uniformity theory, weak sarcomeres are thought to “pop” and only be

restrained by passive forces at very long ( $\gg 4.0\mu\text{m}$ ) sarcomere lengths. However, when introducing severe weakness in multiple sarcomeres in the middle of myofibrils by deactivating them, force is retained at essentially unchanged levels, and sarcomere lengths readjustments are small and well within the range below 4.0 $\mu\text{m}$ . These results question the validity of the sarcomere length non-uniformity [2] and instability [3] theories and suggest that long (weak) sarcomeres on the descending limb of the force-length relationship are stabilized by means other than cross-bridges. In view of recent results in our lab [7], we suggest that titin not only provides stability to active sarcomeres on the descending limb of the force-length relationship, but also prevents “popping”, and therefore loss of force and injury, to sarcomeres in myofibrils even if excitation, and thus active force, in these sarcomeres is completely inhibited.

## CONCLUSION

This study demonstrates that deactivation of previously activated sarcomeres does not result in sarcomere popping, injury to the myofibril or appreciable loss in force. We hypothesize that titin plays a stabilizing role in active sarcomeres that persists even in the event of excitation failure, thus providing a powerful mechanism for preventing injury and instability in muscle.

## REFERENCES

1. Gordon et al., *J. Physiol* **184**, 170-192, 1966.
2. Morgan and Proske. *Clin Exp Pharm Physiol* **31**, 541-545, 2004.
3. A. V. Hill. *Proc R Soc B* **141**, 104-117, 1953.
4. Joumaa et al. *Proc R Soc B* **275**, 1411-1419, 2008.
5. Wakayama et al. *Circ Res* **96**, 1266-1273, 2005.
6. Fauver et al. *IEEE Biomed Eng* **45**, 891-898, 1988.
7. Leonard et al. *AJP-Cell* **299**, 14-20, 2010.

## ACKNOWLEDGEMENTS

Funding was provided by CIHR, NSERC, the Canada Research Chair Program. The cantilevers were fabricated at the University of Calgary AMIF and the NanoFabrication Facility of Cornell University.

# MULTI-FUNCTIONAL USE OF THE ELONGATE HIND FOOT OF THE ZEBRA-TAILED LIZARD DURING RUNNING ON DIFFERENT SUBSTRATES

<sup>1</sup>Chen Li\*, <sup>2</sup>S. Tonia Hsieh, <sup>3</sup>Paul B. Umbanhowar, and <sup>1</sup>Daniel I. Goldman

<sup>1</sup>Georgia Institute of Technology, Atlanta, GA, USA

<sup>2</sup>Temple University, Philadelphia, PA, USA

<sup>3</sup>Northwestern University, Evanston, IL, USA

\*email: [chen.li@gatech.edu](mailto:chen.li@gatech.edu) web: <http://www.prism.gatech.edu/~gth686r/>

## INTRODUCTION

In many organisms, the kinematics and dynamics measured during running on level, rigid, non-slip ground (such as tracks and treadmills) [1] can be represented by the SLIP model [2]. The mechanics by which cursorial animals run over diverse terrain is less understood. To discover how organisms control their movement in more complex environments (such as sand, rubble, and debris), we must understand how feet interact with such terrain. This is a challenge in part due to difficulty observing and modeling foot-ground interaction.

The zebra-tailed lizard, *Callisaurus draconoides* (~ 10 cm, ~ 10 g, Fig. 1a), is a desert generalist and runs rapidly across a diversity of substrates ranging from hard ground to loose sand [3]. Compared to its close relatives, it has the most elongate hind foot (Fig. 1b) and runs the fastest (~ 5 m/s) [4]. Elongation of distal limb segments is thought to enhance running capacity, but the mechanism is not known. In this study, we examine the mechanics of foot-ground interaction in the zebra-tailed lizard during running on hard ground and loose sand to reveal principles of multi-functional foot use which contributes to high locomotor performance.

## METHODS

To mimic a hard substrate, we used a wood board bonded with sandpaper. Our granular substrate was glass beads with properties comparable to dry desert sand (~ 0.3 mm,  $\rho = 2.5 \times 10^3 \text{ kg/m}^3$ ) as a granular substrate. A fluidized bed trackway [5] prepared sand into loosely packed, repeatable initial states. Two high speed cameras obtained dorsal and lateral views at 500 frame/s (Fig. 1c, black setup). High-contrast markers were placed on the joints including neck, center of mass (COM), pelvis, hip, knee, ankle, end, middle, and tip of toe. Kinematics from 2-D videos were reconstructed into 3-D by direct

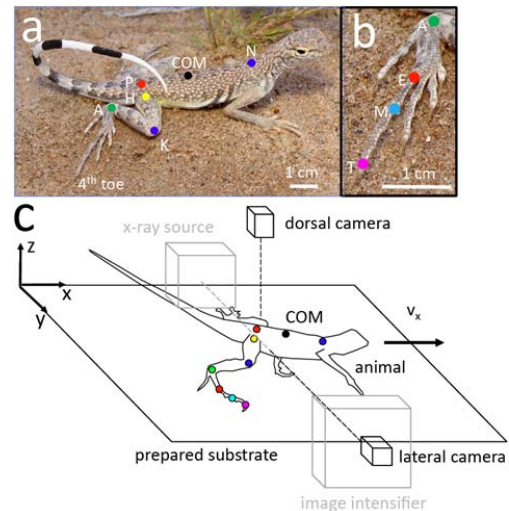


**Figure 1:** Subject animal and experimental setup.

linear transformation. To capture subsurface foot interaction with sand, we used x-ray high speed video (Fig. 1c, black and gray setup). Due to high absorption of x-ray by glass beads, poppy seeds (~ 1 mm,  $\rho = 1.0 \times 10^3 \text{ kg/m}^3$ ) were used, since they have similar penetration resistance as glass beads (~  $10^5 \text{ N/m}^3$ ). We verified that this caused no significant change to our major findings. Opaque markers were bonded to the joints for enhanced contrast. We dissected the hindlimb of a specimen to reveal foot anatomy, and studied the granular physics relevant to the foot-ground interaction using simple intruders like plates and disks.

## RESULTS AND DISCUSSION

For the animals tested, the body length (SVL) is  $6.9 \pm 2.0 \text{ cm}$ , body weight  $9.7 \pm 1.8 \text{ g}$ . The lizards display similar whole body kinematics ( $t$ -test,  $P > 0.05$ ) during running both hard ground and sand: at similar velocity ( $1.51 \pm 0.23 \text{ m/s}$  vs.  $1.42 \pm 0.27 \text{ m/s}$ ), they use similar stride frequency ( $9.0 \pm 1.3 \text{ Hz}$  vs.  $9.3 \pm 1.8 \text{ Hz}$ ) and duty factor ( $0.42 \pm 0.06$  vs.  $0.37 \pm 0.04$ ). On both substrates, the center of mass falls during landing and rises during push off, in accord with the SLIP model [2].

Differences occur in trunk, limb, and particularly hind foot kinematics. On hard ground, the hind foot mainly functions as an energy-saving spring (Fig. 2). The foot touches down (TD) in a digitigrade posture, straight and pointing downwards ( $14 \pm 5^\circ$  relative to the surface). During stance, the toe tip stays fixed on the ground, while the long foot curls into a c-shape (hyperextension). The foot becomes straight briefly after takeoff (TO), and then bends in the opposite direction (flexion) during swing (Fig. 2a). This pattern is quantified by foot curvature  $\kappa = 1/R$  (Fig. 2b; 2c, solid curve).

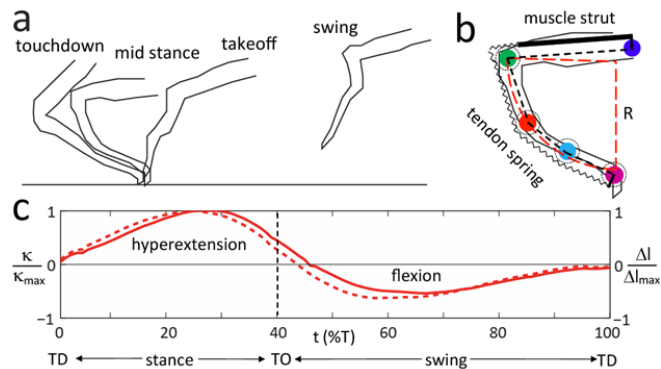


**Figure 2:** The hind foot functions as an energy-saving spring on hard ground (N = 7 for 3 animals).

Dissection reveals tendons on both the dorsal and ventral sides of the hind foot, which originate and insert on the lower leg muscles and digit tips. Inspired by foot anatomy and muscle physiology [1], we propose a mechanical model to explain hind foot mechanics during stance on hard ground (Fig. 2b): (1) rigid segments represent the foot skeleton, free to rotate about joints in a plane; (2) a rigid strut models the lower leg muscles which contract isometrically and transmit forces; (3) a linear spring models the foot tendons, which lengthen and recoil to store and return energy, in response to ground reaction force. Tendon deformation  $\Delta l$  calculated geometrically from the model shows a similar pattern to  $\kappa$  (Fig. 2c, dashed curve).

On sand, the hind foot functions instead mainly as a force-generating paddle (Fig. 3). X-ray lateral video (Fig. 3a,b) shows that during stance the hind foot interacts with the granular substrate in four stages (Fig. 3c), each governed by different intrusion physics. In stage (1), the foot impacts sand rapidly ( $\sim 1$  m/s) in a plantigrade posture (nearly parallel to the surface:  $5 \pm 3^\circ$ , different from on hard ground,  $t$ -test,  $P < 0.05$ ); impact force dominates [6] and quickly stops the foot (within  $3 \pm 1$  ms). In stage (2), the foot penetrates vertically downward slowly

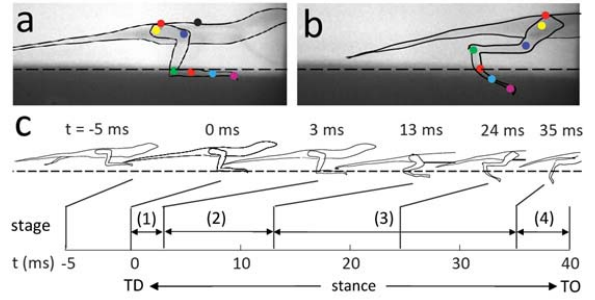


**Figure 3:** The hind foot functions as a force-generating paddle on sand (N = 7 for 4 animals).

( $\sim 0.1$  m/s); vertical penetration force dominates [5], decelerates and stops the COM downward motion. In stage (3), the foot rotates downward and backward ( $< 0.5$  m/s); rotational force dominates [7] and accelerates the COM upward and forward. In stage (4), the foot retracts upward and forward rapidly ( $\sim 1$  m/s) and quickly (within  $5 \pm 2$  ms), during which there is little force.

The foot-ground interaction appears similar to that of the basilisk lizard running on water [8] but the physics is different: For basilisks running on water, thrust is generated mainly by slapping and stroking the foot rapidly ( $\sim 1$  m/s) using the inertia of the water. For zebra-tailed lizard running on sand, the inertia of the grains is relatively small, and thrust is dominated by penetration and rotation forces which increase with granular pressure and foot depth [5,7].

The elongate hind foot enhances the zebra-tailed lizard's ability to run over both substrates. On hard ground, the thin, long foot tendons enhances the capacity for energy storage and return, because by using longer, thinner foot tendons,  $k_{\text{tendon}} \sim l/r^2$  becomes smaller and  $\Delta E_{\text{elastic}} = \frac{1}{2} F_{\text{max}}^2 / k_{\text{tendon}}$  larger. On sand, the relative light weight ( $\sim 0.1$  g) and large area ( $\sim 1$  cm<sup>2</sup>) of the foot helps establish ground engagement, generate thrust, and reduce drag [5,7].

## REFERENCES

- Alexander RM. *Principles of Animal Locomotion*, Princeton Univ. Press, 2003.
- Blickhan R. *J. Biomech.* **22**, 1217-1227, 1989.
- Korff WL & McHenry MJ. *JEB* **214**, 122-130, 2011.
- Irschick D & Jayne B. *JEB* **202**, 1047-1065, 1999.
- Li C, et al. *PNAS* **106**, 3029-3034, 2009.
- Goldman DI & Umbanhowar PB. *Phys. Rev. E* **77**, 1-14, 2008.
- Li C, et al. *Exp. Mechanics* **50**, 1383-1393, 2010.
- Glasheen J & McMahon T. *Nature* **380**, 340-341, 1996.

# COMPARING SURFACE-MARKER BASED AND X-RAY BASED KNEE JOINT KINEMATICS DURING FUNCTIONAL ACTIVITIES

<sup>1</sup>Kang Li, <sup>2</sup>Snehal Shetye, <sup>2</sup>Scott Tashman, and <sup>2</sup>Xudong Zhang

<sup>1</sup>Department of Industrial & Systems Engineering, Rutgers University, Piscataway, NJ, USA

<sup>2</sup>Department of Orthopaedic Surgery, University of Pittsburgh, Pittsburgh, PA, USA

email: [xuz9@pitt.edu](mailto:xuz9@pitt.edu)

## INTRODUCTION

A recently developed open-source platform, OpenSim [1], provides a cost-effective way to create sophisticated musculoskeletal biomechanical models and simulations. More and more in vivo biomechanical studies [2] are utilizing this platform to derive joint kinematics, to estimate neuromuscular responses, and to understand the cause and effect relationship in musculoskeletal dynamics. Most studies using OpenSim as the modeling tool relied on surface-marker based motion capture systems to acquire 3D trajectories of the surface markers attached to body segments, and estimated the in vivo skeletal kinematics from the acquired trajectories with an inverse kinematics algorithm embedded in the OpenSim. While such an approach is easy to use, it is unknown how reliable the calculated kinematics would be, and to what extent the inherent artifacts could affect the conclusions of a simulation (e.g., joint loading or muscle force responses), particularly when used to study the effect of injury on joint mechanics. In this study, we conducted a comparative study to quantify the effect of soft tissue artifacts on knee joint kinematics within OpenSim. We used the kinematics measured by a dynamic stereo-radiography (DSX) system as the “gold standard.”

## METHODS

Two subjects with unilateral, isolated grade II PCL instability performed three activities including standing, level running, and stair ascent. Level running was performed on dual-belt treadmill (Bertec, Inc.) at 2.5 m/s. Stair ascent was completed on a custom-made three-step stairway (run: 11.5 inches, rise: 7.75 inches). Five trials from each subject were selected for the subsequent analysis: two trials of level running (one from the non-injured

limb and one from the injured), and two trials of stair ascent (one from the non-injured limb and one from the injured), and one standing trial (from the non-injured limb)

Dynamic stereo radiography (DSX) images were collected at 150 Hz for running, 100 Hz for stair ascent. High-resolution CT scans were used to reconstruct 3D bone models. A model-based tracking technique [3] was employed to perform 2D to 3D registration, determining the 3D bone position and DSX-based tibiofemoral kinematics.

Reflective markers were placed on the body landmarks of each subject as specified by the Vicon Plug-in Gait Marker Set [4]. The upper body markers were excluded in the placement or data analysis. An 8-camera Vicon MX motion capture system was used to capture the marker trajectories at a sampling frequency of 100Hz. The surface-marker-based tibiofemoral kinematics was derived using the inverse kinematics algorithm in OpenSim [1]. Note that the inverse kinematics algorithm was applied to a recently developed OpenSim model [2] so that the derived kinematics were defined comparable to X-ray-based kinematics. We compared the two types of kinematics by examining the root mean square differences between them.

## RESULTS AND DISCUSSION

Significant differences were observed between surface-marker based and X-ray based knee joint kinematics (e.g. Figure 1-2). The mean ( $\pm$ standard deviation) of the root-mean-square (RMS) values for the pair-wise difference were listed in Table 1.

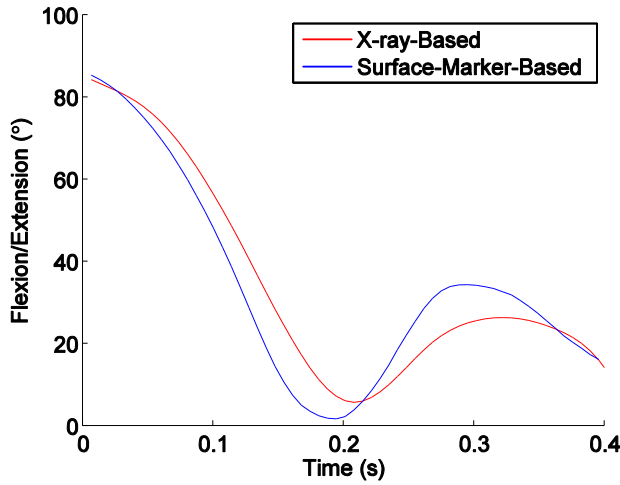


**Figure 1:** Knee flexion/extension angular profile of a running trial.

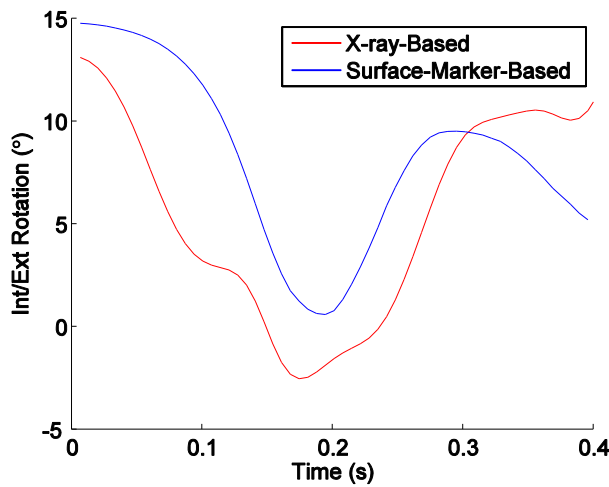


**Figure 2:** Knee internal/external rotation angular profile of a running trial.

These results suggested that the accuracy of surface-marker based joint kinematics derived by

OpenSim was questionable. Dynamic stereo radiography (DSX) can capture skeletal kinematics with superb accuracy but can only focus on one body region at a time. Therefore, a method integrating both surface-marker based kinematics and X-ray based kinematics is favorable so that both the holistic whole-body response and more detailed joint mechanical responses can be examined simultaneously.

## REFERENCES

1. Delp, S.L., et al., *OpenSim: open-source software to create and analyze dynamic simulations of movement*. IEEE Trans Biomed Eng, 2007. **54**(11): p. 1940-50.
2. Arnold, E.M., et al., *A model of the lower limb for analysis of human movement*. Ann Biomed Eng, 2010. **38**(2): p. 269-79.
3. Anderst, W., et al., *Validation of three-dimensional model-based tibio-femoral tracking during running*. Med Eng Phys, 2009. **31**(1): p. 10-6.
4. Davis, R., et al., *A gait analysis data collection and reduction technique*. Human Movement Science, 1991. **10**(5): p. 575-587.

## ACKNOWLEDGEMENTS

This work was supported in part by the NFL Charities and NIH/NIAMS (3R01AR046387-10S1).

**Table 1:** Mean ( $\pm$ SD) RMS difference between surface-marker and X-ray-based knee joint kinematics.

| Kinematics                                 | Activities    |                |                |                |               |
|--|---------------|----------------|----------------|----------------|---------------|
|  | Standing      | Running        |                | Stair Ascent   |               |
|  |               | Injured Knee   | In-tact Knee   | Injured Knee   | In-tact Knee  |
| <b>Flexion/Extension (°)</b>               | 9.8 $\pm$ 7.4 | 9.9 $\pm$ 2.8  | 7.5 $\pm$ 0.1  | 4.5 $\pm$ 3.2  | 3.6 $\pm$ 0.4 |
| <b>Abduction/Adduction(°)</b>              | 1.2 $\pm$ 0.4 | 1.9 $\pm$ 1.0  | 2.0 $\pm$ 0.0  | 2.6 $\pm$ 2.2  | 2.7 $\pm$ 0.6 |
| <b>Internal/External Rotation(°)</b>       | 6.3 $\pm$ 1.8 | 6.95 $\pm$ 4.5 | 7.7 $\pm$ 4.4  | 6.9 $\pm$ 4.7  | 5.6 $\pm$ 2.1 |
| <b>Anterior-Posterior Translation (mm)</b> | 3.7 $\pm$ 3.8 | 9.4 $\pm$ 1.3  | 10.5 $\pm$ 1.4 | 11.6 $\pm$ 0.8 | 9.8 $\pm$ 1.5 |
| <b>Medial-Lateral Translation (mm)</b>     | 9.5 $\pm$ 9.8 | 3.0 $\pm$ 0.1  | 2.1 $\pm$ 0.1  | 1.3 $\pm$ 0.4  | 0.8 $\pm$ 0.6 |

# IS HUMERAL MOTION MORE ACCURATE USING DATA FROM FOREARM AND SCAPULAR SENSORS?

Yin-Liang Lin and Andrew Karduna

University of Oregon, Eugene, OR, USA

email: [yinliang@uoregon.edu](mailto:yinliang@uoregon.edu) web: <http://biomechanics.uoregon.edu/obl/>

## INTRODUCTION

The measurement of three-dimensional humeral kinematics is important for the investigation of upper extremity biomechanics. Humeral motion is commonly measured by placing an electromagnetic sensor on the humerus itself. However, it has been demonstrated that the sensor on the humerus underrepresents the internal/external rotation of the humeral bone [1]. One potential reason may be due to soft tissue artifact. The active or passive soft tissue around the humerus may result in relative displacement between the sensor and the humerus. This problem could be avoided by using a sensor placed on forearm, while utilizing the 2<sup>nd</sup> option of the humeral coordinate system in the ISB proposed standard [2,3]. The humeral motion then could be estimated from the sensors on the forearm and scapula. There is less soft tissue around the forearm than that around humerus. That may decrease the error in humeral motion measurement. The purpose of the study is to compare the accuracy of humeral and elbow motion measurements with sensors on the humerus and forearm.

## METHODS

Six healthy subjects (5 female and 1 male, 19 – 25 years old) were tested. Static humeral elevation and elbow flexion angles were measured with a digital protractor (Macklanburg, OK, USA) and a magnetic tracking device (Polhemus Fastrak, Colchester, VT). The protractor was considered as the gold standard to test the accuracy of the magnetic tracking device. The magnetic sensors were attached on the sternum, scapula, humerus, and forearm. For the humeral method, the sensor on the humerus was used to measure the humeral orientations. For the forearm method, three virtual markers were generated in the calibration procedure to estimate humeral orientations: humeral joint center with respect to the

scapular sensor, elbow joint center and wrist joint center with respect to the forearm sensor. The scapular sensor and the forearm sensor therefore could be used to measure the humeral orientations.

The test protocol included dynamic and static parts. In the dynamic part, the kinematic data of the humerus and elbow were collected only with the magnetic device. The subject performed two motions: humeral elevation in the scapular plane (1), and elbow flexion at 0° of humeral elevation (2). The elbow was splinted in full extension during humeral elevation. The humerus was restrained against the lateral side of trunk with a bandage during elbow flexion. Root mean square (rms) errors were calculated for the elbow flexion angles during humeral elevation and for humeral elevation angles during elbow flexion.

For the static trials, the protractor was also used to measure the humeral and elbow angles. Kinematic data of the humerus and elbow were recorded with the magnetic device at the following positions, as defined by the protractor: 30°, 60°, 90°, and 120° of humeral elevation in the scapular plane (1), full elbow extension and 90° of elbow flexion with the arm at the side (2), and 0° and 90° of humeral external rotation with 90° of humeral elevation in scapular plane (3). The ranges were computed between the positions recorded by the magnetic device (30° ~ 60°, 60° ~ 90°, and 90° ~ 120° of the humeral elevation, 0° ~ 90° of the elbow and humeral external rotation). The three ranges of the humeral elevation (30° ~ 60°, 60° ~ 90°, and 90° ~ 120°) were then averaged.

## RESULTS AND DISCUSSION

The root mean square errors for the dynamic tasks are shown in Table 1. The elbow flexion angles during humeral elevation and the humeral elevation

angles during elbow flexion should be constant. For the forearm method, the rms errors were low for both elbow angles and humeral angles.

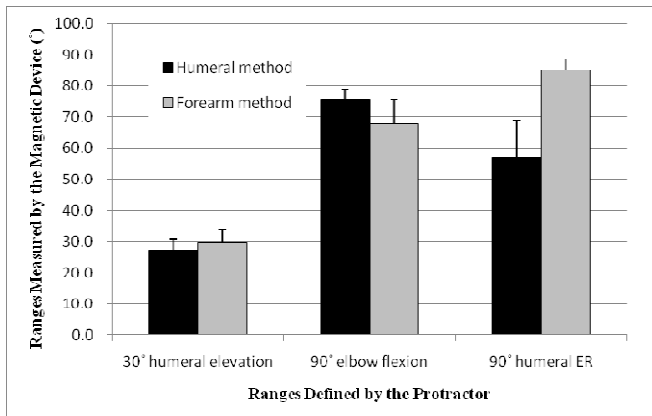


**Figure 1:** The ranges of 30° humeral elevation, 90° elbow flexion, and 90° humeral external rotation were defined by the protractor and measured by using the magnetic device. Both the humeral method and the forearm method are shown.

The ranges of humeral elevation, elbow flexion, humeral external rotation for the static conditions are shown in Figure 1. The range of motion was defined by the protractor. For the humeral elevation trials, the ranges between each position defined by the protractor were 30°. The ranges of both the humeral and forearm methods were close to 30°. In

the elbow flexion trial, the ranges were 90°. Both the humeral and the forearm method tended to underestimate the range of elbow flexion. In the humeral external rotation trial, the ranges were 90°. The humeral method tended to underrepresent the humeral external rotation. That may result from the soft tissue artifact. The relative displacement occurred between the sensor and the humeral bone during humeral rotation.

## CONCLUSIONS

The sensor placed on the forearm may be able to accurately measure the humeral motion and position. Compared the method with the sensor placed on the humerus, the forearm sensor may offer more accurate representation of the humeral internal/external rotation. Therefore, placing the sensors on the scapula and the forearm may be a better option for the measurement of the humeral motion, especially for the humeral internal/external rotation.

## REFERENCES

1. Ludewig PM, et al. *J Appl Biomech* **18**, 163-170, 2002.
2. Schmidt R, et al. *J Biomech* **32**, 615-621, 1999.
3. Cutti AG, et al. *Gait Posture* **21**, 341-349, 2005

**Table 1:** Root-mean-square (RMS) errors for elbow flexion angles during humeral elevation and for humeral elevation angles during elbow flexion

|                | RMS errors of elbow flexion angles | RMS errors of humeral elevation angles |
|----------------|------------------------------------|--|
| Humeral method | 5.8                                | 0.9                                    |
| Forearm method | 2.2                                | 1.3                                    |

# ACL CROSS-SECTIONAL AREA AND MEDIAL TIBIAL PLATEAU GEOMETRY PROVIDE INSIGHTS ON THE GENDER DIFFERENCE IN PEAK ACL STRAIN

David B. Lipps, Youkeun Oh, Edward M. Wojtys, and James A. Ashton-Miller

University of Michigan, Ann Arbor, MI, USA  
email: [dlipps@umich.edu](mailto:dlipps@umich.edu) web: <http://me.engin.umich.edu/brl>

## INTRODUCTION

Individuals with repeated anterior cruciate ligament (ACL) injuries have a larger lateral tibial slope (LTS) and smaller medial tibial depth (MTD) when compared to uninjured and single injured controls [1]. We have shown that females have a 95% greater peak anteromedial bundle (AM-) ACL relative strain than size-matched males during a simulated pivot landing [2]. That study showed ACL cross-sectional area (CSA), determined with magnetic resonance imaging (MRI), was the primary predictor of ACL strain during a simulated pivot landing. Our goal was to perform a secondary analysis on this data set to determine if the geometry of the medial and lateral tibial plateau can further explain why females have increased ACL strain, and ultimately, risk of ACL injury.

## METHODS

Sixteen height- and weight- matched cadaver lower extremities (8 male, 8 female; mean (SD) age: 61 (17) years; weight: 70 (5) kg; height: 173 (8) cm) were dissected and tested using a modified Withrow testing apparatus [3] capable of applying a dynamic impulsive two-times body weight compressive load combined with a 52 Nm knee flexion moment and 17.5 Nm internal tibial torque. The muscle tendons of the quadriceps, hamstrings, and gastrocnemius muscles were pre-tensioned to place the knee at 15 degrees flexion prior to each trial. The *in vivo* quadriceps response to stretch, along with a 20% gender difference in quadriceps stiffness, was modeled with a novel bi-linear quadriceps spring. A DVRT sensor on the distal 3<sup>rd</sup> of the AM bundle of the ACL measured AM-ACL relative strain.

Prior to impact testing, the knee was placed in a 3T MRI scanner to acquire T2-weighted images. The images were analyzed with OsiriX (v3.7.1) to

determine lateral tibial slope [4] and ACL cross-sectional area at 30% ligament length from tibial insertion. After determining the center of articulation, the medial tibial plateau was traced from the most anterior point to the most posterior point along the subchondral bone line. This trace was input into MATLAB (2009b, The Mathworks, Natick, MA), fitted with a 9<sup>th</sup> degree polynomial, was rotated so a line connecting the most proximal anterior and posterior points of the medial tibial plateau would have zero slope. We identified the peak medial tibial depth (MTD), the MTD location relative to the most anterior (0%) and posterior points (100%) on the plateau, and the peak anterior slope of the medial tibial plateau (A-MTP slope). Using SPSS 19 (IBM Corp., Somers, NY), a stepwise multiple linear regression compared peak AM-ACL relative strain to gender, ACL CSA, LTS, MTD, MTD location, and A-MTP slope. Independent t-tests were performed on the dropped factors to determine if a significant gender difference existed ( $p < 0.05$ ).

## RESULTS AND DISCUSSION

Multiple linear regression found ACL CSA (standardized  $\beta = -0.629$ ,  $p = 0.003$ ), MTD ( $\beta = -0.954$ ,  $p = 0.011$ ), and A-MTP slope ( $\beta = -0.899$ ,  $p = 0.014$ ) to be significant predictors ( $R^2 = 0.714$  for all knees,  $R^2 = 0.762$  for female knees only) of peak AM-ACL relative strain during a simulated pivot landing. Gender, LTS, and MTD location were dropped from the stepwise regression model. T-tests found no gender difference in LTS (Table 1,  $p = 0.676$ ), but did find a significant gender difference in MTD location ( $p = 0.011$ ).

Females had nearly double the peak AM-ACL relative strain of size-matched males [2]. While gender was not a significant factor within our regression model, it is still an important factor in

determining the amount of ACL strain because females had a smaller ACL CSA, smaller MTD, and shallower A-MTP (Table 1).

The more posterior MTD location and shallow A-MTP slope found in female knees will result in greater internal tibial rotation than male knees under a given internal tibial torque. We have previously identified internal tibial torque as the worst-case dynamic knee loading for the ACL [5]. Therefore, the medial tibial plateau geometry in females is contributing to their increased ACL strain.

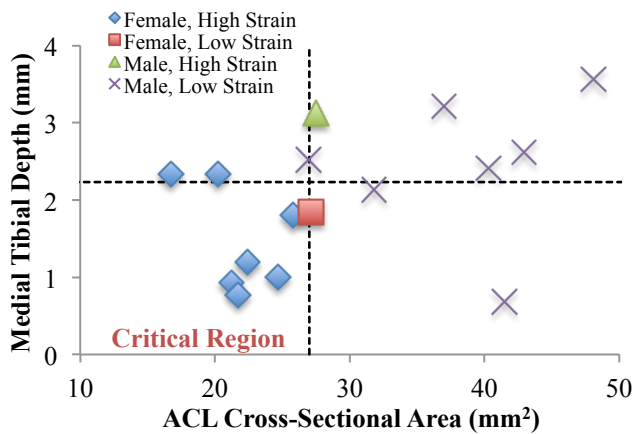


**Figure 1:** MTD vs. ACL CSA for male and female knees. Dashed lines indicate median MTD and CSA, ‘high strain’ is defined as peak AM-ACL relative strain greater than the median strain, and ‘low strain’ is lower than the median strain.

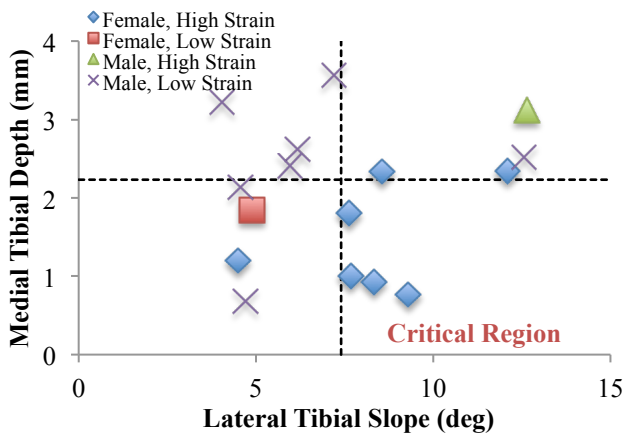


**Figure 2:** MTD vs. LTS for male and female knees. Dashed lines indicate median MTD and LTS.

A closer look at the data identifies a critical MTD-ACL CSA region (Fig. 1). The knees with ACL strain greater than the median appear to have an ACL CSA and MTD lower than their median values. Furthermore, only female knees lie within this critical region, suggesting that female knees may be more prone to higher ACL strain due to their knee morphology.

Low MTD – high LTS has previously been identified as a critical region for ACL injured subjects [1,4]. We investigated this relationship despite the lack of LTS in our regression model (Fig. 2). Very few knees appear to fall in this critical region; however, the knees that fall in this region are female.

Increasing the sample size may create a significant gender factor in the regression model and clarify the effect of LTS on ACL strain.

## CONCLUSIONS

A smaller ACL CSA, smaller MTD, and shallower A-MTP slope helps explain 76% of the variance in AM-ACL relative strain in female knees.

## REFERENCES

1. Hashemi J, et al. *Proceedings of ORS’11*, Abstract 342. Long Beach, CA, USA, 2011.
2. Lipps DB, et al. *Proceedings of AOSSM’11*, San Diego, CA, USA, 2011.
3. Oh Y, et al. *J Bone Joint Surg.* **93**, 372-380, 2011.
4. Hashemi J, et al. *Am J Sports Med.* **38**, 54-62, 2010.
5. Oh Y, et al. *Proceedings of AOSSM’11*, San Diego, CA, USA, 2011.

## ACKNOWLEDGEMENTS

The contributions of Scott McLean, Ashley Brower, Charles Roehm, Suzan Rohrer, and Dr. Catherine Brandon, and funding from PHS R01 AR 054821 and an NDSEG Fellowship (DBL).

**Table 1:** Mean  $\pm$  SD peak AM-ACL strain, ACL cross-sectional area, and medial/lateral tibial plateau geometry

|               | Peak AM-ACL<br>Relative Strain (%) | ACL CSA<br>(mm <sup>2</sup> ) | MTD<br>(mm)   | Peak A-MTP<br>slope | MTD Location<br>(%) | LTS<br>(deg)  |
|---------------|------------------------------------|-------------------------------|---------------|---------------------|---------------------|---------------|
| <b>Female</b> | 6.2 $\pm$ 2.5                      | 22.5 $\pm$ 3.3                | 1.5 $\pm$ 0.6 | -0.2 $\pm$ 0.1      | 58.6 $\pm$ 12.1     | 7.9 $\pm$ 2.4 |
| <b>Male</b>   | 3.4 $\pm$ 2.1                      | 37.0 $\pm$ 7.6                | 2.5 $\pm$ 0.9 | -0.3 $\pm$ 0.1      | 41.9 $\pm$ 8.0      | 7.2 $\pm$ 3.5 |

# Kinematic Variability of the Trunk is Related to Shoulder Variability During Wheelchair Propulsion

Jessica Longworth and Karen Troy

Department of Kinesiology and Nutrition, University of Illinois at Chicago, Chicago, IL, USA  
email: jlongw3@uic.edu web: <http://www.uic.edu/ahs/biomechanics>

## INTRODUCTION

A high incidence of upper extremity pathology, specifically for the shoulder complex, is reported for manual wheelchair users [1]. Contributing factors include continuous repetitive movements and loading, muscle imbalance, and malalignment of the limbs [1]. Larger propulsive forces, which are associated with larger shoulder sagittal flexion and internal rotation moments, have been linked to a higher prevalence of shoulder pathology [1]. A high-level spinal cord injury, generally accompanied by upper limb involvement and low trunk stability, is also associated with an increased number of shoulder disorders [2]. Given the adjacent locations of the trunk and shoulder within the kinetic chain, kinematics of one would be expected to affect the kinematics of the other. A more complete understanding of how shoulder and trunk motions are coupled during wheelchair propulsion may provide additional insights regarding musculoskeletal repetitive injuries.

The purpose of this study was to determine the relationship between cycle-to-cycle variability in trunk and shoulder kinematics. We hypothesized that larger cycle-to-cycle variability in trunk motion would be associated with larger cycle-to-cycle variability in shoulder motion, and that individuals with higher-level spinal cord injury would have larger cycle-to-cycle variability in trunk kinematics.

## METHODS

Twelve subjects (8 males, age:  $37 \pm 13$  yrs, height:  $1.7 \pm 0.1$  m, mass:  $83 \pm 17$  kg, years of wheelchair use:  $10 \pm 6$  yrs) who use a manual wheelchair as a primary means of mobility were recruited for this institutionally approved study. All subjects gave written informed consent prior to their participation. A three-dimensional motion capture system operating at 120 Hz (Motion Analysis, Santa Rosa, CA) was used to collect kinematic data. Reflective markers were placed on the trunk and upper extremities of each subject [3, 4]. Subjects propelled their manual wheelchair at a constant

velocity on a set of wheelchair rollers (McClain, USA) for two minutes. A trial completed by each subject at a fixed speed between 2.0 and 3.0 km/h was selected for data analysis.

Angles of the trunk and right upper extremity were calculated using custom-written software [4]. Shoulder kinematics were calculated by referencing the humerus to the trunk, as described in the ISB reporting standards [3]. Trunk flexion, lateral flexion, and rotation, and shoulder external rotation, plane of elevation, and elevation angle were analyzed. The data from each subject were divided into propulsion cycles that started and ended at the beginning of the push phase. Phase planes were plotted for each of the variables (Figure 1) and the centroid locations of the phase planes were calculated for each propulsion cycle.

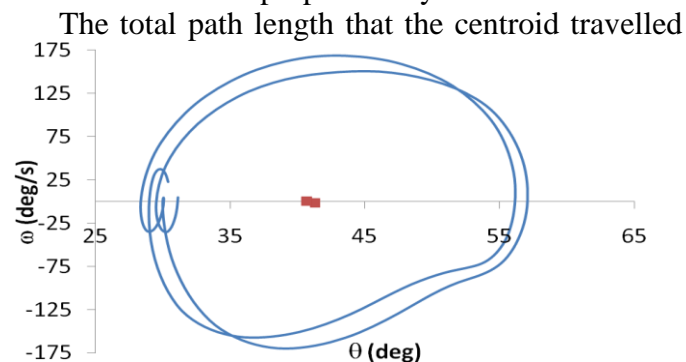


**Figure 1** Phase plane for two cycles of shoulder elevation angle and angular velocity. Square symbols indicate centroid locations for each cycle.

during consecutive propulsion cycles, divided by the total number of analyzed cycles ( $87 \pm 27$ ), was calculated. The resulting quantity was the mean distance the centroid traveled between consecutive cycles. A larger path length corresponded to larger variability [5]. Pearson's correlations were used to test the hypothesis that trunk variability is associated with shoulder variability.

Subjects were classified as having either good or poor trunk control based on two independent criteria: (1) by injury level, or (2) by centroid path length of trunk flexion/extension. In the first method, subjects with an injury level at or above the

fourth thoracic vertebra, and those diagnosed with multiple sclerosis, were assigned to the poor trunk control group and remaining subjects were assigned to the good trunk control group. In the second method, those with below-median trunk flexion path lengths were assigned to the good trunk control group, while those with above-median path lengths were assigned to the poor trunk control group. For both classification methods, Student's t-tests were used to compare trunk and shoulder variability (i.e. centroid path lengths) and ranges of motion (ROM; maximum – minimum values) in the two groups. A p-value less than 0.05 was considered statistically significant for all tests.

## RESULTS AND DISCUSSION

Seven of the nine possible combinations of trunk and shoulder path-length variables were significantly correlated with one another (Table 1). Trunk extension and shoulder elevation variability had the closest relationship (Figure 2). When subjects were classified into good/poor trunk control groups based on median trunk flexion path length, the good trunk control group had greater shoulder external rotation ROM ( $78 \pm 20^\circ$  vs.  $51 \pm 21^\circ$ ,  $p=0.047$ ) and plane of elevation ROM ( $84 \pm 19^\circ$  vs.  $54 \pm 22^\circ$ ,  $p=0.028$ ). In contrast, when subjects were classified according to injury level there were no significant differences between groups in any variable.

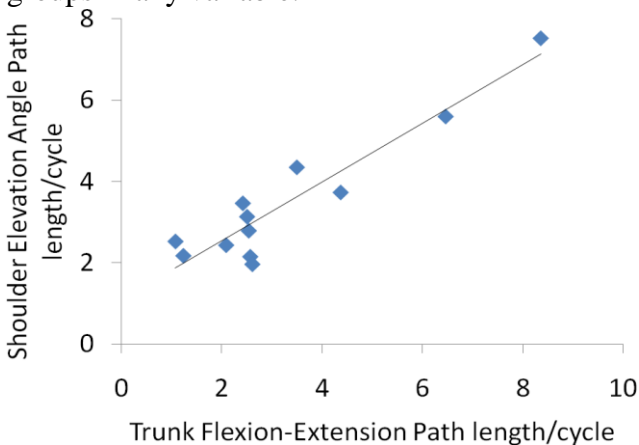


**Figure 2** Relationship between trunk and shoulder centroid path lengths

The absence of a difference between injury level groups may be due to the low demand of propulsion conditions; a speed that all subjects were able to execute was selected, and propulsion was over a smooth (roller) surface without an incline. During low-demand tasks, even subjects with relatively high injury levels may be able to compensate for lack of muscle enervation through changes in

**Table 1** Correlations between trunk and shoulder centroid path lengths

|                         | Trunk flex/ext              | Trunk lateral flex          | Trunk rotation             |
|-------------------------|-----------------------------|-----------------------------|----------------------------|
| Shoulder elevation      | $r = 0.938$<br>$p < 0.0001$ | $r = 0.875$<br>$p < 0.0001$ | $r = 0.585$<br>$p = 0.046$ |
| Shoulder ext. rotation  | $r = 0.669$<br>$p = 0.017$  | $r = 0.576$<br>$p = 0.050$  | $r = 0.745$<br>$p = 0.005$ |
| Shoulder plane of elev. | $r = 0.017$<br>$p = 0.959$  | $r = -0.104$<br>$p = 0.748$ | $r = 0.602$<br>$p = 0.038$ |

coordination or by having greater strength. A low-level injury, generally linked to better trunk control, is associated with a lower prevalence of shoulder pathology [2]. In our study, ROM was significantly larger for individuals with smaller trunk variability, suggesting that ROM is an important factor for individuals who propel with greater trunk control.

The extent that propulsion cycle consistency is related to shoulder pathology is still unknown. The current functional interpretations of variability differ. Some suggest that high variability allows the individual to adapt to different environmental conditions potentially reducing the risk for injury, while others suggest that decreased variability is a protective mechanism against the progression of injury [5]. The potential cause of these discrepancies may be that methods of quantifying variability differ between studies. If high cycle-to-cycle variability in shoulder kinematics were linked to the development of shoulder pathology, then interventions that improved trunk control and increased shoulder ROM during propulsion might be helpful.

## CONCLUSIONS

Our hypothesis that larger cycle-to-cycle variability in trunk motion would be associated with larger cycle-to-cycle variability in shoulder motion was supported. When subjects were classified according to trunk control, larger trunk variability was associated with smaller shoulder ROM. This relationship was absent when subjects were classified according to injury level. The relationship between musculoskeletal variability and pathology should be investigated to determine if interventions could assist with injury prevention.

## REFERENCES

1. Mercer JL, et al. *Clin Biomech* **21**, 781-789, 2006.
2. Sinnott KA, et al. *Spinal Cord* **38**, 748-753, 2000.
3. Wu G, et al. *J Biomech* **38**, 981-992, 2005.
4. Troy KL. *Disabil Rehabil AT* **6(1)**, 22-28, 2011.
5. DiBerardino LA, et al. *Clin Biomech* **25**, 552-556, 2010.

# BALANCE DURING ROTATIONS IN DANCE

<sup>1</sup>Melanie Lott, <sup>2</sup>Kenneth Laws

<sup>1</sup>Bryn Mawr College, Bryn Mawr, PA, USA

<sup>2</sup>Dickinson College, Carlisle, PA, USA

email: [mcluss@brynmawr.edu](mailto:mcluss@brynmawr.edu)

## INTRODUCTION

Dance educators encourage their students to keep their bodies strong, but slightly relaxed, while balancing in a static position, such as on the ball of one foot. This allows the dancer to make slight adjustments to correct for small perturbations from equilibrium. Studies have shown that dancers have significantly faster response times when adjusting for an imbalance than non-dancers and that they perform better on standard balance tests [1,2]. This evidence supports the notion that dancers have a strong sense of overall balance in a static pose. How does the situation change, however, when the dancer is rotating in a pirouette?

Pirouettes, or turns on one foot, are one of the most common movements in all forms of dance. Currently, dance educators teach dancers to attempt to achieve a balanced position at the onset of rotation and rigidly maintain the body configuration, as opposed to correcting an imbalance with small adjustments during the turn. Many, even advanced, dancers have significant difficulty performing more than a two or three turn pirouette before losing balance, despite continued trial and error efforts to improve. This observation suggests it may be more difficult than dance teachers realize to perform a many turn pirouette without making adjustments during the turn.

In this study we performed a theoretical analysis to determine how close to equilibrium a dancer must begin the turn to successfully perform more than a triple pirouette without making any adjustments.

## METHODS

A theoretical model of a dancer in standard pirouette position (Figure 1) was created to understand the mechanics of toppling during a

pirouette. Body segment parameters (mass, length, radii of gyration) were based on anatomical data as reported in de Leva [3]. The model was used to determine the moment of inertia tensor for two hypothetical dancers: a small, female dancer (45 kg, 1.5 m) and a tall, male dancer (77 kg, 1.9 m). The inertia tensor (in a global coordinate system (GCS) with the origin on the ground at the supporting foot) was determined from the principal radii of gyration of the body segments (in the local coordinate system (LCS) with the origin at the segment's center of mass). This is accomplished with a similarity transformation to rotate the LCS so that it is parallel to the GCS and then an application of the parallel axis theorem.

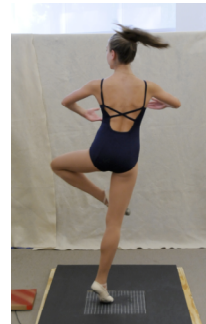


**Figure 1:** A dancer performing a pirouette. The relative positions and orientations of the segments for the model are based on this configuration.

The principal moments (eigenvalues) of the inertia tensor were found, and the rigid body equation of motion for the dancer toppling around an axis of rotation in the plane of the floor was numerically solved. The topple angle,  $\theta$ , (defined as the angle between the vertical and a line from the pivot point to the body's center of mass) as a function of time was then determined.

When dancers reach a large  $\theta$  during a pirouette, they compensate by either hopping the supporting

foot in an attempt to regain balance or landing the turn. This hopping movement is not accepted in the dance community, and is thus characterized as “unsuccessful.” The angle at which dancers feel inclined to hop, denoted as  $\theta_{\max}$ , was determined experimentally. Nine intermediate to advanced ballet dancers (8 female, 1 male;  $16 \pm 2.3$  yrs) participated after giving informed consent (parental consent was given when appropriate). The dancers performed pirouettes while being videotaped from four different angles. A video analysis was performed to determine the position of the dancer’s center of mass and supporting foot location and (therefore  $\theta_{\max}$ ) immediately preceding a hop. One pirouette with a hop was analyzed per dancer.

## RESULTS AND DISCUSSION

The principal moments of inertia (Table 1) demonstrate that the dancer is remarkably symmetric (two equal moments). Because the saggital and transverse moments are equal, the dancer has the same inertia around any topple axis of rotation. The inertia about the spin (longitudinal) axis is less than 1% of the topple inertia.

**Table 1:** Principal moments of inertia of the dancer in pirouette position.

|        | Saggital $I$<br>( $\text{kg}\cdot\text{m}^2$ ) | Transverse $I$<br>( $\text{kg}\cdot\text{m}^2$ ) | Longitudinal $I$<br>( $\text{kg}\cdot\text{m}^2$ ) |
|--------|--|--|--|
| Female | $55.3 \pm 5.1$                                 | $55.3 \pm 4.4$                                   | $0.534 \pm 0.043$                                  |
| Male   | $153 \pm 12.2$                                 | $153 \pm 10.5$                                   | $1.34 \pm 0.11$                                    |

The topple angle as a function time for the dancer under the influence of gravity was numerically solved for three different initial topple angles ( $\theta_i = 0.1^\circ$ ,  $1^\circ$ , or  $3^\circ$ ), assuming that the dancer’s initial topple speed,  $d\theta/dt$ , was zero (Figure 2).

From the video analysis,  $\theta_{\max}$  was found to be  $9.3 \pm 1.9^\circ$ . If a dancer’s body begins the turn displaced only one degree from vertical, it was found that she/he topples to  $\theta_{\max}$  after 1.14s (female) or 1.07s (large, male). For typical rotation rates ( $\sim 2$  rev/sec), these dancers would “fall out” of a pirouette (and be forced to hop or land) after little more than two rotations. For an initial  $\theta$  of a mere  $0.1^\circ$ , a dancer would be able to perform a four-turn pirouette before the need to hop. Even for a very generous assumption that a dancer could potentially

recover from a  $\theta_{\max}$  as large as  $20^\circ$  (the maximum in Figure 2), the dancer would only be able to squeeze in a little more than an extra half of a turn.

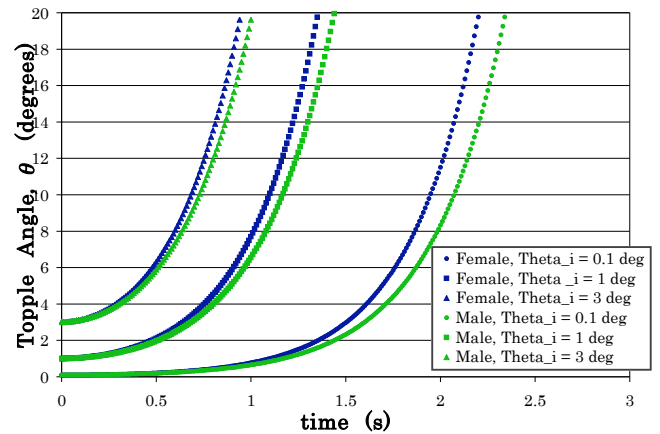


**Figure 1:** Toppole angle from vertical as a function of time for three different initial angles.

## CONCLUSIONS

These results demonstrate the difficulty of achieving many rotations in a pirouette when the body is held rigidly. To perform more than a triple pirouette without adjusting for an imbalance, a dancer would need to begin the turn with his/her body less than one degree displaced from the vertical. This type of accuracy is difficult to achieve; thus, to consistently perform more than a triple pirouette, dancers should be taught strategies for regaining balance while turning. An experimental study is underway to determine what adjustment strategies successfully lead to more balanced pirouettes.

## REFERENCES

1. Simmons R. *Int J Neurosci*, **115**, 1193-1203, 2005.
2. Crotts et al. *J Orthop Sports Phys Ther*, **23**, 12-17, 1996.
3. De Leva P. *J Biomech*, **29**, 1223-1230, 1996.

## ACKNOWLEDGEMENTS

We thank Alan Hiline and the Central Pennsylvania Youth Ballet for their help with the recruitment of dancers and Glenna Clifton, Lydia Marks, and Graceanne Ruggiero for their help with data collection.

# EFFECTS OF LOCOMOTOR TASK AND MARKER PLACEMENT ON MINIMUM FOOT CLEARANCE

<sup>123</sup>Kari Loverro, <sup>3</sup>Nicole Greaves, and <sup>3</sup>Kate Hamel

<sup>1</sup>U.S. Army Natick Soldier Research Development and Engineering Center Natick, MA USA

<sup>2</sup>Oak Ridge Institute for Science and Education (ORISE), Belcamp, MD 21017

<sup>3</sup>Department of Kinesiology, San Francisco State University San Francisco, CA USA

email: hamelk@sfsu.edu

## INTRODUCTION

Falls are the leading cause of unintentional injuries in almost every age group [1], with tripping over an object identified as the leading cause of falls in older adults [2]. Over the last 20 years there has been extensive research on minimum foot clearance (MFC) in both young and older adults during overground walking, obstacle crossing, level changes, and stair negotiation – the primary locomotor tasks during which trips and slips often occur.

The results of these studies have yielded a wide range of MFC results both within and across locomotor tasks. This may be due to the lack of standard MFC measurement methods or/and poor consideration of marker placement for different tasks. The purpose of this study was to compare minimum foot clearance across the primary locomotor tasks during which falls often occur using multiple points on the surface of the shoe. The primary aims were to: 1) examine the difference in overall MFC across all tasks for both leading and trailing limbs; 2) examine the differences between the leading and trailing limbs within each task; 3) determine which region of the shoe experienced the majority of minimum clearances for each task; and 4) determine whether or not the use of minimum toe clearance overestimates the overall MFC.

## METHODS

Ten healthy young adults (6 female, 4 male 24.5±2.9yrs) participated in the study. Participants completed three trials of nine locomotor tasks: single large obstacle (SOB) crossing (17x91x3.5cm (h x w x d)), double large obstacle crossing (first=1OB and second=2OB) (spaced 1.5m apart), single small (threshold-height) obstacle (TOB)

crossing (1.3x91x3.5 cm) a tape (zero-height) obstacle (TAPE) crossing (0x91x3.5cm, stair ascent (AST), stair descent (DST) (7 steps with a rise/run 17/26cm), up level change (ULV), down level change (DLV) (obstacle h x w w/a 3.5m landing) and level overground (OG) walking. Participants were asked to walk at a self-selected pace.

Each participant wore the same model of shoes with five reflective tracking markers attached to the upper of each shoe and 72 points virtually digitized on the bottom, front and rear portions of the shoe. All obstacles, stairs, and level changes were also digitized in the global coordinate system. An 8 camera VICON® MX motion capture system was used to track the markers and a custom model in Visual 3D® 4.75.11 was used to visualize virtual markers and calculate MFC. 3D distances were calculated from each point on the shoe to each region of the obstacle, step or stair. Minimums were calculated for each region of the shoe (5 regions- toe, fore, mid, rear and heel) and overall MFC for both lead and trail limbs. Location of the overall minimum among the 72 virtual points on the shoe was recorded.

Three factor, mixed model ANOVAs were used to analyze the effects of task and trial order on MFC of both the lead and trail limbs. Additional two-way ANOVAs were used to test for differences between the lead and trail limb MFC within each task. Tukey's HSDs were used for post-hoc analysis

## RESULTS AND DISCUSSION

There was a significant main effect of task for both the leading and trailing limbs ( $p < .001$ ). Lead limb MFC was smallest in the overground walking condition (0.4±0.2cm) and largest in the large obstacle crossing conditions (Fig. 1). There was no

significant difference in lead limb MFC between single or double large obstacle crossing conditions. Overall lead limb MFC was reduced with decreasing obstacle height (SOB>TOB>TAPE), but the TAPE MFC was significantly larger than overground walking. There was no significant difference in lead limb MFC between crossing an obstacle (SOB) and going up a level change (ULV) of the same height. MFC going up a level change is larger than MFC ascending stairs of the same height (AST1-7) and larger than going down a level change (DLV). There were no significant differences in MFC between going down a level change (DLV) and going down stairs (DST7-2) except for the last stair (DST1). MFC during DLV and DST was equivalent to the MFC during zero height obstacle crossing (TAPE).

significantly larger than trail limb MFC when going up a level change and when ascending the top stair (AST7). There were no significant differences between the lead and trail limb MFC during mid-stair ascent (AST2-6).

Nearly all lead limb MFCs and ~50% of all trail limb MFCs during obstacle crossing occurred in the rear and heel regions of the shoe. For stair and level change ascent, the lead limb MFC primarily occurred in the toe - midfoot regions while the trail limb MFC was nearly always located in the toe region. When descending the stairs, the MFC always occurred in the rearfoot and heel regions while during level change descent, the MFC occurrences were spread throughout all shoe regions. During overground walking over 80% of MFCs occurred in the rearfoot region of the shoe.

In fact, use of the MFC from just the toe region of the shoe overestimated the actual MFC anywhere between 33-126% for lead limb obstacle crossing, 28% and 50% for ULV and DLV lead limb MFC respectively, 76-409% for stair descent and 128% for overground walking. For the lead MFC during stair ascent and all trail limb MFC however, the toe region MFC was adequate (0-5.75% overestimation of overall MFC).

These results indicate that marker placements typically used for MFC research (marker on toe, virtual marker on sole of toe, etc.), do not provide the actual minimum foot clearance for most tasks and use of these marker placements may affect MFC results – especially when comparing across locomotor tasks. Further research is needed utilizing this methodology to examine MFC in young and older adults during these high risk locomotor tasks to determine if, as previously reported, there are minimal age-related changes in MFC, or if the lack of differences in previous studies was due to methodological inadequacies.

## REFERENCES

1. (2007). *NCIPC Injury Report*. CDC.
2. Berg et al. (1997). *Age Ageing* **26**(4): 261-268.

## ACKNOWLEDGEMENTS

Funded by NIH grant #1R21AG025865

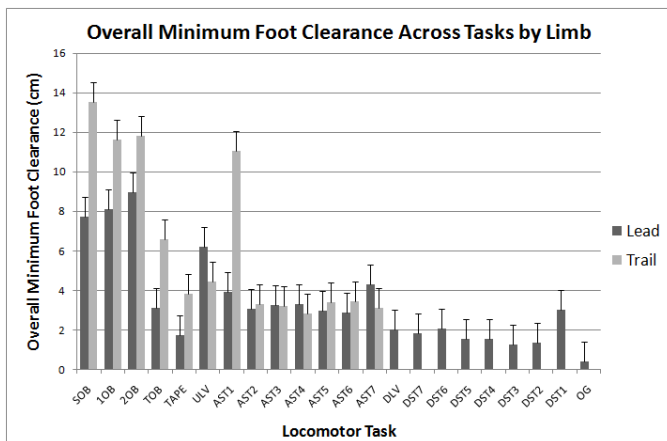


**Figure 1:** Overall minimum foot clearance for each task and each limb.

There was no significant difference in trail limb MFC between single or double large obstacle crossing conditions or between large obstacle crossing and negotiating the first stair during stair ascent (AST1). Overall trail limb MFC was reduced with decreasing obstacle height (SOB>TOB>TAPE). The overall MFC of the trail limb during TAPE crossing was equal to the MFC going up a level change and up all stairs (AST 2-7) except the first stair.

When comparing the lead limb MFC to the trail limb MFC within a task, the trail limb MFC was significantly larger than lead limb clearance for all obstacle conditions and the bottom step (AST1) during stair ascent. Lead limb MFC was

# BILATERAL THREE-DIMENSIONAL WRIST VELOCITY DURING ACTIVITIES OF DAILY LIVING: TOWARDS GENERATING NORMATIVE UPPER LIMB KINEMATIC PROFILES

<sup>1</sup>Tea Lulic, <sup>1</sup>Aneesha Sravanapudi, <sup>1</sup>David A. Gonzalez, <sup>1</sup>Clark R. Dickerson, and <sup>1</sup>Eric A. Roy

<sup>1</sup>University of Waterloo, Waterloo, ON, CA

E-mail: [tlulic@uwaterloo.ca](mailto:tlulic@uwaterloo.ca)

## INTRODUCTION

Normative quantitative kinematic and kinetic profiles exist for lower limbs during gait [1]. However, the complexity of neuromuscular control of the upper limb has made it difficult to create similar quantitative kinematic profiles for the upper limbs during activities of daily living (ADLs). This lack of objective measures to quantify upper extremity movement limits description of neurological impairments [2].

Some of these impairments (e.g. apraxia) affect the motor functioning of the non-preferred limb (left hand). Neuropsychological assessment of apraxic patients relies primarily on qualitative analyses of gross movement characteristics from Waterloo-Sunnybrook Apraxia Battery (WatAB), based on location, posture, action, plane and orientation of the upper limb and the hand [3]. Also, to assess apraxia, patients are required to perform gestures and ADLs with their left hand because the disorder affects the left hand, but the assessment neglects to take this into consideration. Due to this, it is difficult to differentiate whether movements of the limb are because the patients are using their non-dominant hand or due to the disorder itself.

These considerations make it critical to develop bilateral normative kinematic profiles for healthy persons. Once achieved, these will provide a basis for comparing and understanding impaired kinematics observed in patients with apraxia [4,5], which will enable more objective initial diagnoses and rehabilitation evaluation. The purposes of this study were to examine bilateral differences in pantomime versus tool use in the production of gestures during ADLs through three-dimensional kinematic analyses.

## METHODS

The upper limb and trunk movement of ten healthy (no history of musculoskeletal or neurological conditions) right-handed participants (5M, 5F) were captured via a motion

capture system (Vicon, Colorado, USA) during the performance of different tasks included in the WatAB [3]. Forty-five reflective markers were placed on anatomical landmarks of the upper limbs and trunk, in accordance with International Society of Biomechanics (ISB) recommendations [8]. In addition, four markers were placed on the thumb, five on the index, middle, ring, and little fingers and four on the dorsal hand. Markers were also affixed to the manual objects used.

Participants performed two tasks: 1) pantomiming a gesture (e.g. slicing a piece of bread with an imaginary knife); and 2) gesturing using a physical tool. All data was sampled at 100 Hz. Task performances were block randomized by limb, with all gestures performed by both limbs. Three consecutive trials for each movement were completed. All tasks were completed at a self-selected pace.

Raw kinematic data was processed to derive assessment measures by dual low-pass Butterworth filtering at 8 Hz. Wrist velocities were calculated from the midpoint of the two markers on the dorsal hand, just distal to the wrist. Peak velocities from the three trials of each task were averaged to determine average peak velocity. A two factor (task type: pantomime or tool, and limb) repeated measures ANOVA was performed to assess their influence on peak velocities, with significance set at  $p < 0.05$ .

## RESULTS

Higher peak velocities were observed in the non-preferred limb (left hand) in comparison to the preferred limb (right hand) in both, the cup and the knife conditions (Fig. 1) (cup:  $F = 6.95$ ,  $p < 0.0137$ ; knife:  $F = 4.95$ ,  $p < 0.0346$ ).

Further, higher peak velocities existed for the cup condition during pantomime tasks in comparison to the tool use (forward transport:  $F = 4.63$ ,  $p < 0.04$ ; backward transport:  $F = 4.61$ ,  $p < 0.04$ ; medial movement:  $F = 8.37$ ,  $p < 0.01$ ).

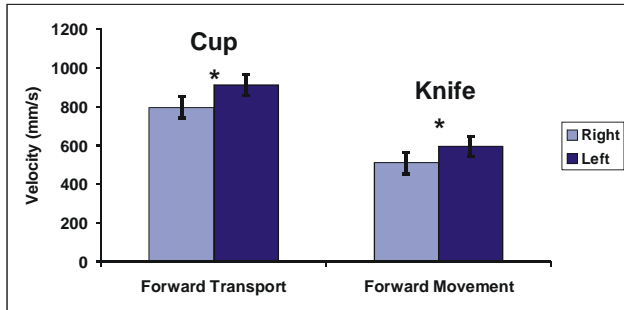


**Figure 1:** Average peak velocity hand differences for the preferred and non-preferred limb for the forward transport in the cup condition (towards body) and forward movement in the knife condition (away from body). Asterisks indicate significant differences between limbs.

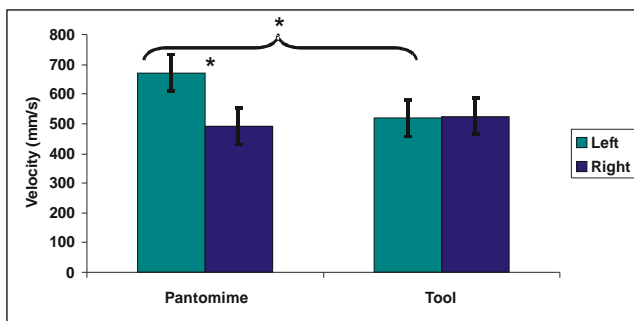


**Figure 2:** Interaction effects between the handedness and the pantomime vs. tool use during tasks. Asterisks indicate significant differences across conditions.

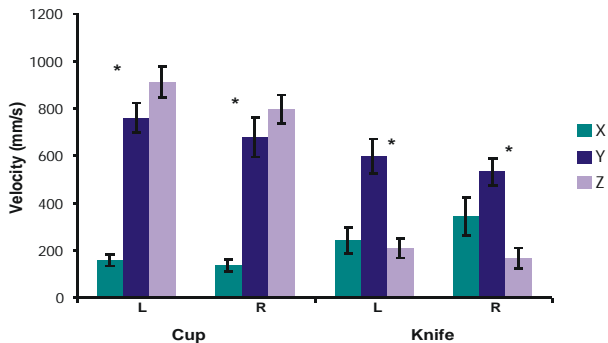


**Figure 3:** Bilateral peak velocities for cup and knife conditions for both limbs in three directions (X = medial/lateral; Y = forward/backward; Z = up/down). Asterisks indicate significant differences between axes.

However, while higher peak velocities occurred for the pantomime task than tool use in the non-preferred limb ( $F=5.65$ ,  $p<0.0248$ ), this difference was absent in the preferred limb. Also, which hand the tool was used with did not make a difference (Fig. 2).

Higher peak velocities for both conditions occurred in the primary movement direction movement ( $F = 234.86$ ,  $p<0.0001$ ) (Fig. 3).

## DISCUSSION

These results suggest manual performance asymmetries influence ADL performance in healthy persons. Although manipulation of tools reportedly improves movement effectiveness for both hands [4], which is suggested to be related to somaesthetic cues received from the tool, this study supports this only for the non-preferred hand. However, the addition of a tool lowered average peak velocities in both limbs for some conditions (e.g. cup) in this study, consistent with earlier reports [4].

Further, primary planes of movement can be defined based on peak wrist velocities. As the highest peak velocities for the cup condition occurred in the Z and Y directions, ZY is designated the plane of movement; for the knife condition, the highest peak velocities existed in the Y and X directions, making YX the plane of movement. This planarity of movement data enables identification of out-of-plane movements frequently identified in apraxic patients [9].

The ultimate purpose of this work is the generation of normative kinematic profiles of task performance by healthy individuals. These can then be compared with those of patients with disorders such as apraxia, in order to both diagnose and assess rehabilitative effectiveness.

## REFERENCES

1. Winter, DA. *Hum Mov Sci*, **3**, 51-76, 1984.
2. Kontaxis, A., et al., *Clin Biomech*, **24**, 246-253, 2009.
3. Roy, EA, et al., 1998 (available from Dr. E. Roy, Department of Kinesiology, University of Waterloo, Waterloo, Ontario, Canada, N2L 3G1)
4. Heath, M., et al., *Laterality*. **7** (2), 2002.
5. Roy, EA, *Manual Assymetries in Motor Performance*, Amsterdam: Elsevier Science Publishers, 1996.
6. Solway, S, et al., *The DASH Outcome Measure User's Manual*, Institute for Work and Health, 2002.
7. Steenhuis, RE, et al., *J Clin Exp Neuropsychol*, **12** (6), 1990.
8. Wu, et al., *J Biomech*, **38**, 2005.
9. Pozner, et al., *Brain*, **118**, 1995.

# DYNAMIC COORDINATION OF LEG MUSCULATURE IS ASSOCIATED WITH AGILITY IN HIGH SCHOOL SOCCER ATHLETES

<sup>1</sup>Mark Lyle, <sup>1</sup>Liang-Ching Tsai, <sup>1,2</sup>Francisco Valero-Cuevas, <sup>1,3</sup>Robert Gregor and <sup>1</sup>Christopher Powers

<sup>1</sup>Division of Biokinesiology & Physical Therapy

<sup>2</sup>Department of Biomedical Engineering, Viterbi School of Engineering  
University of Southern California, Los Angeles, CA, USA

<sup>3</sup>School of Applied Physiology, Georgia Tech University, Atlanta, GA, USA  
email: mlyle@usc.edu web: <http://pt.usc.edu/labs/mbrl>

## INTRODUCTION

Dynamic maneuvers involving rapid whole-body deceleration and change in direction are essential in many sports, but also commonly cause injuries. Because such maneuvers require dynamic interactions among muscles to control momentum and stabilize joints, appropriate dynamic coordination may be critical to athletic performance and to mitigate the risk of injury. Measures of maximal jump height and muscle strength have been studied as potential indicators of agility, but they have only shown modest correlation at best with various agility tasks [1]. Therefore, here we investigate the association of dynamic lower extremity coordination with agility. Recently, we developed a lower extremity coordination test (LEC-test) that is highly reliable and is independent of muscle strength (a lower extremity version of the Strength-Dexterity Test [2,3]). Here we tested whether or not LEC-test performance (as opposed to strength) is associated with agility.

## METHODS

Sixteen high school soccer athletes (8 female, 8 male) participated in this study. First, maximal muscle torques during isometric hip extension, knee extension, and knee flexion were measured using a Humac Norm Dynamometer [CSMi, Stoughton, MA]. Participants then performed the LEC-test, which is a dynamic contact control task that requires participants to compress a helical compression spring with the foot (Fig 1, [2,3]). Subjects were instructed to slowly compress the spring so as to achieve and sustain the highest possible vertical compression force during 16-second trials while provided with visual force

feedback. The compression force was considered to be “sustained” if the coefficient of variation was  $\leq 10\%$ . Because the spring becomes more unstable with increased compression, the highest force sustained is representative of maximal coordination [3]. The maximal compressive force held during the 16-second trial was determined by a 10-second moving average. The average maximal compressive force from the best 3 out of 25 trials was used for statistical analysis.



**Figure 1:** Lower extremity coordination test

Agility was assessed by having participants complete a hopping sequence using their dominant leg with arms akimbo. Four target positions were marked on a force plate (1.2 x 1.2 m) 30 cm anterior, posterior, right, and left of a center position (Fig 2). Participants were instructed to hop as quickly and accurately as possible to each target and then back to the center moving in a clockwise direction for 2 complete cycles. The time to complete the task was determined by the vertical ground reaction force. The average of the best 3 of 6 trials was considered agility performance. Following the agility test, participants’ maximal height achieved during a countermovement vertical jump was recorded.

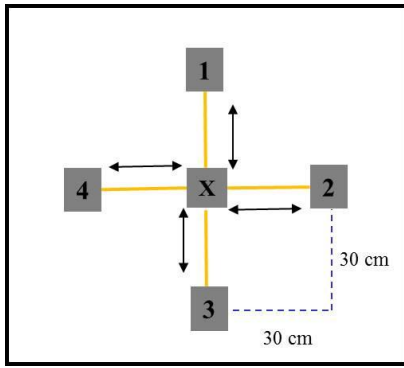


**Figure 2:** Single-leg agility hopping sequence

The dependent variable was the time to complete the agility test, while the independent variables included the maximal compressive force held during the LEC-test, maximal muscle torques (normalized to body mass), and the maximum vertical jump height. Multiple linear regression models were used to examine the association between agility performance and each independent variable while controlling for the potential influence of gender.

## RESULTS AND DISCUSSION

Agility vs. LEC-test performance is plotted in Figure 3, and a significant correlation ( $r=-0.82$ ,  $p<0.001$ , Table 1) is seen after controlling for gender. This indicates that better dynamical coordination of leg musculature to control the instability of the spring was associated with faster times to complete the agility task.

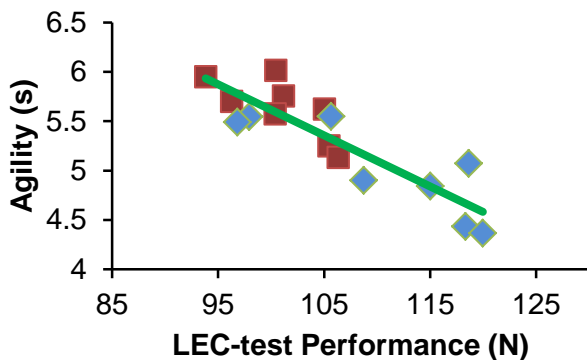


**Figure 3:** Association between agility and LEC-test performance. Red squares and blue diamonds are female and male athletes, respectively.

In contrast, lower extremity strength and vertical jump height were not significantly correlated with agility performance after controlling for gender

( $p>>0.05$ , Table 1). These findings indicate that strength was not a critical determinant for successful performance on the agility task even though the single leg hopping sequence requires significant lower extremity muscular effort. Therefore the LEC-test, as is also seen in the upper extremity [4], assesses an experimental construct that reveals a dimension of dynamic function that is independent of leg strength and power, but informative of agility. As such, this study is the first to identify a strong association between dynamic coordination of leg musculature and agility.

**Table 1.** Partial correlations between agility performance and each independent variable after controlling for gender.

|                        | Partial correlation, r | p      |
|------------------------|------------------------|--------|
| LEC-test               | -0.82                  | <0.001 |
| Vertical Jump Height   | -0.34                  | 0.22   |
| Hip Extensor Strength  | -0.26                  | 0.35   |
| Knee Extensor Strength | 0.24                   | 0.39   |
| Knee Flexor Strength   | 0.05                   | 0.86   |

## CONCLUSIONS

This study provides preliminary evidence that lower extremity coordination as assessed by the LEC-test may provide useful information about the sensorimotor integration required for sudden deceleration and change of direction. Given that most sports injuries occur during rapid transition maneuvers, the LEC-test may have important implications for predicting the risk of non-contact lower extremity injury. This work now enables the framing of hypotheses regarding dynamic muscle coordination during rapid maneuvers. In addition, future research is needed to examine how these factors are associated with the risk of injury.

## REFERENCES

1. Brughelli M, et al. *Sports Med* **38**, 1045-1063, 2008.
2. Lyle MA, et al. *ASB Annual Conference '09*, University Park, PA, USA, 2009.
3. Valero-Cuevas FJ, et al. *J Biomech.* **36**, 265-270, 2003.
4. Vollmer B, et al. *Dev Med Child Neurol.* **52**, 948-954, 2010

## ACKNOWLEDGEMENTS

This study was supported by the Foundation for Physical Therapy (PODS II).

# FASCICLE LENGTH CHANGES IN DENERVATED FELINE SOLEUS DURING WALKING

<sup>1</sup>Huub Maas, <sup>2,3</sup>Robert J. Gregor and <sup>2</sup>Boris I. Prilutsky

<sup>1</sup>Research Institute MOVE, VU University Amsterdam, Netherlands

<sup>2</sup>School of Applied Physiology, Georgia Institute of Technology, Atlanta, GA, USA

<sup>3</sup>Division of Biokinesiology and Physical Therapy, University of Southern California  
Los Angeles, CA, USA

email: [h.maas@vu.nl](mailto:h.maas@vu.nl) web: <http://www.move.vu.nl/members/huub-maas/>

## INTRODUCTION

Nerve transection and its subsequent surgical repair involves a paralytic phase followed by a recovery phase in which regenerating motoneuron axons re-occupy motor endplates in the reinnervated muscle. In the paralytic phase, the affected muscles are not excited, which makes them prone to atrophy [1]. It has been shown that denervation induced atrophy can be suppressed by repetitive stretching in rat soleus muscle [2]. On the other hand, excessive lengthening may cause muscle fiber damage. However, data on muscle length changes in denervated muscles is not available.

The aim of the present study was to investigate the effects of paralyzing cat lateral gastrocnemius (LG) and soleus (SO) muscles on muscle fascicle length changes in SO during walking on a level and sloped surfaces (i.e., +50% and -50%).

## METHODS

First, cats (n=2) were trained to walk on a Plexiglas enclosed walkway. Under aseptic conditions and using isoflurane anesthesia, SO muscle of the right hindlimb was surgically instrumented with EMG electrodes and sonomicrometry crystals [see 3 for details]. One pair of piezoelectric crystals (2 mm, Sonometrics) was implanted near the origin and insertion of a muscle fascicle in the midregion of the muscle belly. A pair of Teflon-insulated multi-stranded stainless steel wires was implanted near the site of muscle fascicle length measurement.

After collecting baseline data, the nerves of LG and SO muscles within the same hindlimb were transected and immediately rejoined using fibrin glue. Denervation was verified in the operating

room by electrical stimulation of the tibial nerve proximal to the cut.

Data were collected prior to and 1–2 weeks after surgical nerve cut and repair, when LG and SO muscles were in a state of paralysis and could not actively contribute to movement control (there was no EMG activity in these muscles). SO fascicle length, hindlimb joint position data (Vicon) and ground reaction forces (Bertec force plate) were collected during walking in each of the three slope conditions. SO muscle-tendon unit (MTU) lengths were calculated using ankle angle kinematics and a geometric model. All data were time normalized with respect to stance or swing duration. Walking cycles within a narrow range of stance durations (~150 ms) were selected to minimize effects of walking speed. This resulted in 4-12 step cycles for all conditions in each cat.

## RESULTS AND DISCUSSION

For all three walking conditions, MTU length changes of SO 1–2 weeks following LG-SO denervation were substantially different from the same measures obtained before denervation (Fig. 1, left). The magnitude of MTU stretch in the beginning of stance was increased and longer absolute MTU lengths were observed throughout the walking cycle after denervation. These results are similar to previously reported MTU length changes of the intact, synergistic medial gastrocnemius (MG) muscle [4].

In contrast, only minor changes in SO fascicle length were found following paralysis of two main ankle extensors, especially during stance (Fig. 1, right). It should be noted that no EMG activity was observed in the denervated SO muscle. Therefore, substantially lower forces are expected to be exerted

through its distal tendon during stance and, hence, the magnitude of tendon lengthening will be decreased. This means that a greater part of MTU length changes must be taken up by the muscle fascicles. The finding that fascicle length changes are similar between intact and denervated SO, even with enhanced MTU length changes, suggests that other mechanisms are involved. One potential mechanism could be mechanical interactions, mediated by epimuscular myofascial pathways [5], with the intact and highly active [see 4, 6] ankle plantar flexors.

## CONCLUSIONS

We conclude that muscle fascicles of paralyzed muscles following selective peripheral nerve injury may still undergo substantial lengthening and shortening excursions. However, fascicle lengthening of denervated SO in the beginning of stance was smaller than expected from a passive independent muscle actuator.

## REFERENCES

1. Foehring RC, et al. *J Neurophysiol* **55**, 947-965, 1986.
2. Agata N, et al. *Muscle Nerve* **39**, 456-462, 2009.
3. Maas H, et al. *J Appl Physiol* **106**, 1169-1180, 2009.
4. Maas H, et al. *Exp Brain Res* **203**, 681-692, 2010.
5. Maas H, Sandercock TG. *J Biomed Biotechnol* doi:10.1155/2010/575672, 2010.
6. Prilutsky et al *Cells Tissues Organs* **in press**

## ACKNOWLEDGEMENTS

Bradley J. Farrell and Drs. Margarita Bulgakova, Emma F. Hodson-Tole and Art English. Supported by NIH grants HD-032571 and NS-048844. The Center for Human Movement Studies at Georgia Tech.

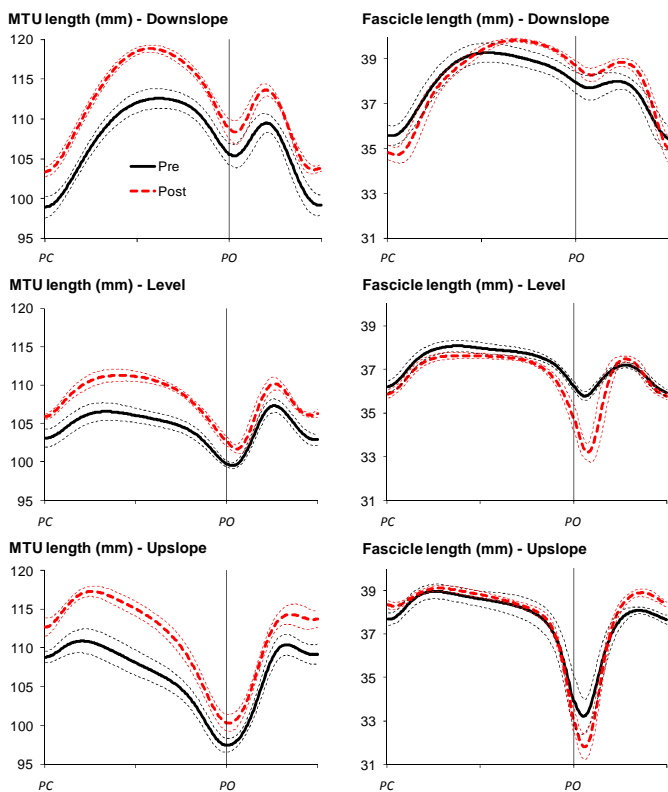


**Figure 1:** Mean ( $\pm$ SD) muscle-tendon unit (MTU) and muscle fascicle length of SO during typical walking cycles for all three walking conditions prior to (pre) and 2 weeks after denervation of LG and SO (post) in Cat #1. Similar data were found for Cat #2. PC, paw contact. PO, paw lift-off.

# THE MECHANICAL EFFECT OF RAT FCU MUSCLE AFTER TENDON TRANSFER

Huub Maas and Peter A. Huijing

Research Institute MOVE, VU University Amsterdam, Netherlands  
email: [h.maas@vu.nl](mailto:h.maas@vu.nl) web: <http://www.move.vu.nl/members/huub-maas/>

## INTRODUCTION

Agonist-to-antagonist tendon transfers are performed to improve gait or upper extremity function in individuals with severe disabilities. In 1997, Riewald and Delp [1] reported that rectus femoris muscle (RF), transferred from its extensor to a flexor site of the knee, still generated a knee extension moment if stimulated intramuscularly. This has been explained by the transmission of RF forces to the patella via epimuscular myofascial pathways [2].

It should be noted that RF moment was assessed in 90° knee flexion exclusively. Different joint angles involve different muscle-tendon complex lengths and relative positions of transferred RF and neighboring knee flexors and extensors. We have shown that the extent and direction of epimuscular myofascial loads is dependent on the relative position of muscle bellies [3]. If the knee is extended, the knee flexors will lengthen and the knee extensors will shorten. At full knee extension, not the knee extensors, but the knee flexors are expected to attract force generated by RF.

The purpose of this study was to test the hypothesis that after agonist-to-antagonist tendon transfer the direction (i.e., flexion or extension) of the muscle's joint moment is dependent on joint angle.

## METHODS

In deeply anesthetized Wistar rats ( $n=3$ ), the distal tendon and distal half of the muscle belly of *m. flexor carpi ulnaris* (FCU) was dissected free and transferred to the distal tendons of *m. extensor carpi radialis brevis* and longus ( $ECR_{B/L}$ ).

Five weeks after the surgery, wrist angle-moment characteristics of transferred and control ( $n=4$ ) FCU were assessed. The skin was resected from the

shoulder to the wrist and a pair of copper electrodes was inserted in the muscle belly. The right forelimb was secured rigidly to the experimental setup (Fig. 1). Wrist joint moments exerted upon excitation of FCU (100 Hz) were measured for different positions of the wrist joint (from 48° flexion to 43° extension). Active moments were calculated by subtracting passive moment from total moment at equal wrist angle.

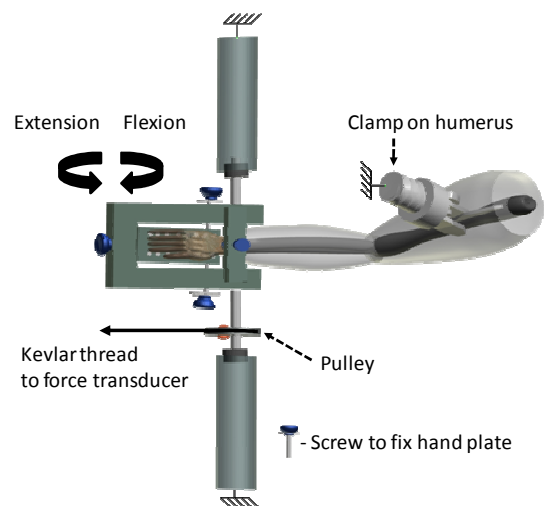


**Figure 1:** Schematic drawing of experimental setup.

## RESULTS AND DISCUSSION

As expected, excitation of control FCU resulted in a flexor moment at all wrist angles tested (Fig. 2A). FCU wrist moment was minimal in maximally flexed position, corresponding to its lowest muscle-tendon complex length, and increased with progressive wrist extension (i.e., FCU lengthening). In addition, FCU wrist moment approached a maximal value at 22° extension (i.e., the highest extension angle tested). In this wrist position, FCU flexor moment was  $2.9 \pm 0.8$  mNm.

According to the new muscle-tendon path and insertion (i.e.,  $ECR_{B/L}$  insertion), transferred FCU muscle is expected to generate an extensor moment

at the wrist. In contrast, we found the mechanical effect of transferred FCU to be bidirectional (Fig. 2B). FCU muscle contraction yielded an extensor moment in flexed positions of the wrist (maximal value between 0.39 and 1.37 mNm). In contrast, FCU activity yielded a flexor moment if the wrist was extended (maximal value between 0.28 and 1.34 mNm).

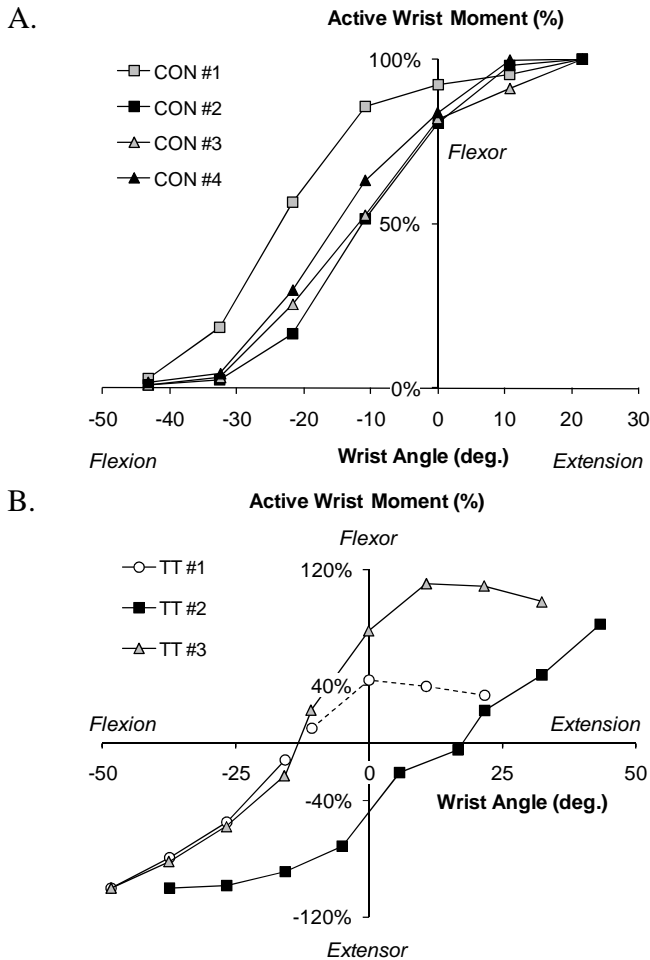


**Figure 2:** Wrist angle-normalized wrist moment characteristics of FCU muscle. (A) control FCU. (B) transferred FCU. Dotted line for rat TT #1 connects data collected following disruption of the FCU insertion. Moments of control muscles were normalized with respect to maximal wrist flexion moment. Moments of transferred muscles were normalized with respect to maximal wrist extension moment.

These results indicate that the mechanical effect of a muscle after recovery from tendon transfer surgery is not exclusively determined by its new muscle-tendon path and insertion. As hypothesized, the mechanical effect of the transferred muscle was dependent on joint angle. Tendon transfer changed the mechanical effect of FCU from wrist flexion to wrist extension, but in flexed wrist positions only.

The bidirectionality of transferred FCU is explained by epimuscular myofascial force transmission. The mechanical linkage between FCU and surrounding muscles was likely provided by connective and scar tissue at muscle belly and tendon boundaries.

## CONCLUSIONS

To the best of our knowledge, this is the first time that a bidirectional mechanical effect of a transferred muscle has been described.

Our results are phenomenologically comparable to previously reported effects of RF transfer in humans [1], i.e. FCU function was unchanged in extended wrist positions. In addition, the data suggest that transferred RF may have generated a knee flexion moment in more extended positions of the knee. Therefore, we conclude that for an accurate evaluation of muscle function following tendon transfer it is necessary to assess its mechanical effect at a range of joint angles.

## REFERENCES

1. Riewald SA, Delp SL. *Dev Med Child Neurol* **39**, 99-105, 1997.
2. Huijing PA. *J Biomech* **32**, 329-345, 1999.
3. Maas H, et al. *J Biomech* **37**: 99-110, 2004.

## ACKNOWLEDGEMENTS

Supported by the European Community's Seventh Framework Programme Grant MIRG-CT-2007-203846.

# EFFECT OF DECISION MAKING ON LANDING MECHANICS IN WOMEN AND MEN

<sup>1</sup>Melissa A. Mache, <sup>2</sup>Mark A. Hoffman and <sup>2</sup>Michael J. Pavol

<sup>1</sup>California State University, Chico, CA, USA

<sup>2</sup>Oregon State University, Corvallis, OR, USA  
email: mmache@csuchico.edu

## INTRODUCTION

ACL injuries have serious consequences, leading to extensive research towards their prevention. Biomechanical factors are considered to be among the most important contributors to ACL injury, yet they are still not fully understood [1]. Given that athletes must frequently modify their movement patterns to maneuver in a dynamic sports environment, a relevant issue is whether decision making influences the biomechanical risk factors for ACL injury. Findings to date suggest that decision making increases the risk of ACL injury during cutting tasks [2]. However, 2-footed landing tasks had not been similarly studied. Of particular interest is whether decision making may differentially affect women and men, as women experience ACL ruptures at a 2- to 8-fold greater rate than men in matched sports [3]. This study thus investigated whether decision making during 2-footed landing tasks would affect biomechanical factors associated with ACL injury, and whether these effects would differ between tasks or sexes.

## METHODS

Twenty-nine young adults ( $22 \pm 3$  yrs; 13 women) with recent experience in jumping activities and no history of knee injury gave their informed consent to participate. Women had to have had a regular menstrual cycle for the previous 3 months, unless they were using a contraceptive that interfered with menstruation. Regularly menstruating women were tested within days 3-5 after starting menstruation.

Data were collected during 3 randomized blocks of trials: 7 preplanned drop landings, 7 preplanned drop-jumps, and a block of 14 randomized decision-making trials consisting of 7 drop landings and 7 drop-jumps. Participants began each trial suspended in the air, hanging stilly by the hands from an

overhead bar while looking straight ahead at a panel with 2 indicator lights. The bar was located above 2 force plates (Bertec) and adjusted so the participant dropped 20% of their body height. In each trial, the participant released the bar and landed with one foot on each force plate. For drop landings, participants were to maintain their balance on landing. For drop-jumps, participants were to jump up immediately on landing and touch the overhead bar. In preplanned trials, participants knew prior to releasing the bar which task they were to perform. In decision-making trials, participants initiated the drop and, about 250 ms before ground contact, were directed by one of the indicator lights which task to perform. Timing of the light was controlled by a force sensor on the bar and LabView (National Instruments).

A set of 33 reflective markers on the participant was filmed by a motion capture system (Vicon) at 120 Hz as ground reaction forces were collected at 1080 Hz. The data were low-pass filtered at 15 Hz and used to compute lower extremity joint angles and internal joint moments in 3-D (Vicon BodyBuilder).

Knee angles at initial ground contact and peak knee angles and moments during landing (i.e., from initial ground contact to peak hip or knee flexion, whichever occurred later) were analyzed for the dominant limb. Values were averaged across trials. Effects of decision making, task, and sex on the dependent variables were tested using 3-way, repeated-measures ANOVA. Significant interaction effects were explored using 2-way ANOVA or t-tests, as appropriate. The alpha level was 0.05 for the ANOVA and 0.025 for all post-hoc analyses.

## RESULTS AND DISCUSSION

Independent of task and sex, participants exhibited  $1.5^\circ$  greater peak external rotation and  $1.0^\circ$  lesser peak internal rotation at the knee under decision-

making compared to preplanned conditions. Both sexes also exhibited smaller peak knee extension moments under decision-making conditions for both tasks (Table 1). These effects of decision making may be indicative of lesser ACL loading [4]. Smaller knee extension moments in combination with external rotation at the knee could act to unload the ACL. Smaller knee internal rotation angles could also result in lesser ACL loading.

Some effects of decision making on knee mechanics were task-dependent (Table 1). Of note, most of the between-task differences seen under preplanned conditions disappeared when decision making was required. Individuals tended to modify their drop-jump technique in the decision-making condition towards their drop landing technique. This was true for knee flexion and abduction at initial ground contact and, in men, peak knee abduction moments.

For drop-jumps, the task-dependent effects of decision making had seemingly adverse effects on landing posture. Specifically, in the decision-making condition, women and men performed drop-jumps with lesser knee flexion and greater knee abduction (or lesser adduction) at initial ground contact and with greater peak knee abduction angles (Table 1). These effects of decision making may result in a relative increase in ACL loading during drop-jumps [4], consistent with the findings of similar studies of cutting tasks [2]. However, the task-independent effects of decision making noted earlier may be acting concurrently to reduce ACL loading. The net effect on loading is thus unknown.

Interacting effects of decision making and sex were found for peak knee extension, abduction, and external rotation moments (Table 1), with men but not women exhibiting smaller external rotation moments under decision-making conditions. These results support the hypothesis that women and men may be differentially affected by decision making during the performance of 2-footed landing tasks.

## CONCLUSIONS

Under decision-making conditions, women and men seem to prepare to perform a drop landing as the default task, in that they perform drop-jumps with greater similarity to drop landings. This may have adverse effects on ACL loading during a drop-jump. There is also evidence that decision making affects women and men differently during 2-footed landing tasks. Yet, under decision-making conditions, both sexes make task-independent changes to their landing mechanics that could act to reduce ACL loading. As a net result, the performance of drop landings and drop-jumps under decision-making conditions may be no more dangerous to the ACL than performing preplanned drop landings.

## REFERENCES

- 1.Griffin LY, et al. *Am J Sports Med* **34**, 1512-1532, 2006.
- 2.Besier TF, et al. *Med Sci Sports Exerc* **33**, 1176-1181, 2001.
- 3.Agel J, et al. *Am J Sports Med* **33**, 524-530, 2005.
- 4.Markolf KL, et al. *J Orthop Res* **13**, 930-935, 1995.

**Table 1:** Knee biomechanical variables as a function of condition, task, and sex (Mean  $\pm$  SD).

| Variable (units)                     | Task | Men                         |                              | Women                       |                              |
|--------------------------------------|------|-----------------------------|------------------------------|-----------------------------|------------------------------|
|                                      |      | Preplanned                  | Decision Making              | Preplanned                  | Decision Making              |
| Flexion Angle at IC (°)              | DL   | 17.2 $\pm$ 5.3              | 16.1 $\pm$ 5.1               | 18.1 $\pm$ 4.6              | 16.7 $\pm$ 3.8               |
|                                      | DJ   | 21.8 $\pm$ 6.3 <sup>†</sup> | 16.0 $\pm$ 5.3*              | 21.2 $\pm$ 4.5 <sup>†</sup> | 17.0 $\pm$ 4.1*              |
| Abduction Angle at IC (°)            | DL   | -1.1 $\pm$ 2.8              | -0.9 $\pm$ 2.6               | -0.2 $\pm$ 2.4              | 0.0 $\pm$ 2.3                |
|                                      | DJ   | -1.9 $\pm$ 3.2 <sup>†</sup> | -0.8 $\pm$ 2.6*              | -0.7 $\pm$ 2.9 <sup>†</sup> | 0.1 $\pm$ 2.3*               |
| Peak Abduction Angle (°)             | DL   | -0.8 $\pm$ 3.2              | -0.4 $\pm$ 3.1               | 0.8 $\pm$ 3.8               | 1.1 $\pm$ 3.7                |
|                                      | DJ   | -1.4 $\pm$ 3.3              | -0.2 $\pm$ 3.1* <sup>†</sup> | 0.8 $\pm$ 4.8               | 1.6 $\pm$ 3.8* <sup>†</sup>  |
| Peak Extension Moment<br>(% bw x bh) | DL   | 10.1 $\pm$ 1.4              | 9.3 $\pm$ 1.5*               | 10.0 $\pm$ 1.9              | 9.1 $\pm$ 2.8*               |
|                                      | DJ   | 12.7 $\pm$ 3.9 <sup>†</sup> | 10.9 $\pm$ 2.7* <sup>†</sup> | 10.3 $\pm$ 2.0 <sup>†</sup> | 10.1 $\pm$ 1.2* <sup>†</sup> |
| Peak Abduction Moment<br>(% bw x bh) | DL   | 2.0 $\pm$ 1.3               | 2.1 $\pm$ 1.1                | 1.5 $\pm$ 0.9               | 1.2 $\pm$ 0.7                |
|                                      | DJ   | 2.5 $\pm$ 1.3 <sup>†</sup>  | 2.1 $\pm$ 1.1                | 1.3 $\pm$ 1.0 <sup>‡</sup>  | 1.3 $\pm$ 0.8 <sup>‡</sup>   |

IC = initial ground contact; DL = Drop Landing; DJ = Drop-Jump; bw = body weight; bh = body height;

\* p < 0.05 vs. Preplanned; <sup>†</sup> p < 0.05 vs. Drop Landing; <sup>‡</sup> p < 0.05 vs. Men

# COMPARING KNEE JOINT KINEMATICS, KINETICS AND CUMULATIVE LOAD BETWEEN HEALTHY-WEIGHT AND OBESE YOUNG ADULTS

Kathleen F. E. MacLean<sup>1</sup>, Monica R. Maly<sup>2</sup>, Jack P. Callaghan<sup>1</sup>

<sup>1</sup>Department of Kinesiology, University of Waterloo, Waterloo, ON

<sup>2</sup>Department of Rehabilitation Sciences, McMaster University, Hamilton, ON

email: k4maclea@uwaterloo.ca

## INTRODUCTION

Obesity has been identified as a worldwide epidemic [1]. While there are many co-morbidities associated with the condition, one of the most poorly understood is the pathway to musculoskeletal diseases, such as osteoarthritis of the knee [2]. To implement appropriate preventative strategies, it is important to explore how excess body weight is a causal factor for osteoarthritis. The present research compared the kinematics and kinetics of a group of young obese, but otherwise healthy, adults to a group of young, healthy-weight adults, in an attempt to identify mechanical abnormalities at the knee during walking that may predispose the obese to osteoarthritis of the knee.

## METHODS

Sixteen participants recruited from the University of Waterloo population included 8 obese (age 23.5 (3.3) and BMI 35.5 (5.69)) and 8 age, height and sex-matched healthy-weight adults (age 23.5 (2.1) and BMI 23.2 (1.54)). Three-dimensional Optotrak motion capture data (NDI, Waterloo, ON) and a synchronized forceplate (AMTI, Watertown, MA) were used to collect and calculate ground reaction forces and knee joint kinematics and kinetics. Knee motions were tracked by fitting participants with 37 wireless skin markers, placed bilaterally on the lower limbs and posterior pelvis. Participants performed 5 successful trials at three walking speeds of self-selected, 15% faster and 15% slower. Healthy-weight participants walked at an additional “matched” speed condition that matched the self-selected speed of the obese participants. Following the lab procedures, participants wore an accelerometer for seven days to measure physical activity levels through steps per day. Average steps per day were combined with the measure of knee

adduction moment impulse to calculate a cumulative knee adductor load (CKAL) [3]. Analyses were performed between groups on the speeds of fast, self-selected and slow. A separate analysis was conducted on the matched speed condition that compared participant groups walking at the same speed. Frontal, sagittal and transverse plane motions were analyzed. A series of dependent t-tests were performed to determine group differences in the maximum, minimum and range of ground reaction forces, knee angles and knee moments, as well as steps per day, knee adduction moment impulse and CKAL. Moments were not normalized to body mass, which allowed the observation of the absolute effect of excess body mass on knee joint kinetics. A multiple regression analysis was used to determine the effect of dynamic knee alignment on peak knee adduction moment and knee adduction moment impulse.

## RESULTS AND DISCUSSION

Compared to the healthy weight group (1.55m/s (0.18)), the obese group walked at a slower self-selected speed (1.25m/s (0.15)) ( $p=0.013$ ). The obese group also had a greater stance duration (0.68s (0.07)) compared to the healthy-weight group (0.59s (0.06)) ( $p<0.001$ ). The three walking speeds of fast, self-selected and slow did not induce a significant difference in kinematic or kinetic variables. As such, the three walking speeds were used as replicates within each participant for the analysis. The obese group had greater mean peak ground reaction forces in all three planes ( $p<0.05$ ). This difference was found despite a slower self-selected walking speed in the obese group, which would serve to reduce ground reaction forces. A greater maximum abduction angle and smaller minimum knee flexion angle at heel contact was found in the obese group ( $p<0.05$ ). There were no

group differences in the frontal moment peaks or impulse (Figure 1). This was surprising, given that moments were not normalized to body mass.

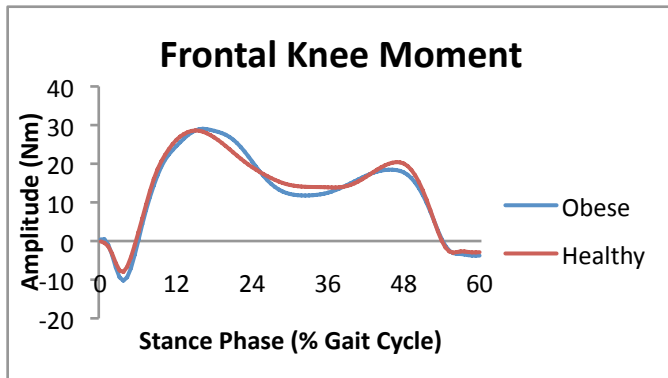


**Figure 1:** Average frontal knee moment waveform for participant groups.

A greater transverse plane peak medial rotation moment was found in the obese group ( $p=0.003$ ). Differences between groups in the ground reaction forces persisted in all three planes at the matched speed ( $p<0.05$ ). However, all knee angle and moment group differences were neutralized at the matched speed condition. Non-significant results from the matched speed condition may have been due to reduced statistical power, being that there were no within participant replicates in this analysis. In some instances, such as the peak frontal and sagittal moments, a greater magnitude of difference between groups was observed at the matched walking speed, with the obese group having greater peak moments. Both participant groups had similar mean daily step counts, which fell well below the recommended 10,000 steps per day. Not only does this suggest comparable physical activity levels between groups, but also that neither group is obtaining daily physical activity levels that will adequately encourage weight-loss or prevent future weight-gain. No significant group differences were found in the CKAL, a consequence of no differences being found between groups in physical activity level and knee adduction moment impulse. Dynamic knee alignment was strongly related to peak knee adduction moment ( $r=0.497$ ) and knee adduction impulse ( $r=0.361$ ). Two obese participants presented with atypical frontal plane moments and were identified as statistical outliers (Figure 2). Both participants had knee alignments of  $10^\circ$  valgus. This alignment reduced the knee

adduction moment magnitude in both obese participants by shifting load away from the medial compartment of the knee joint.

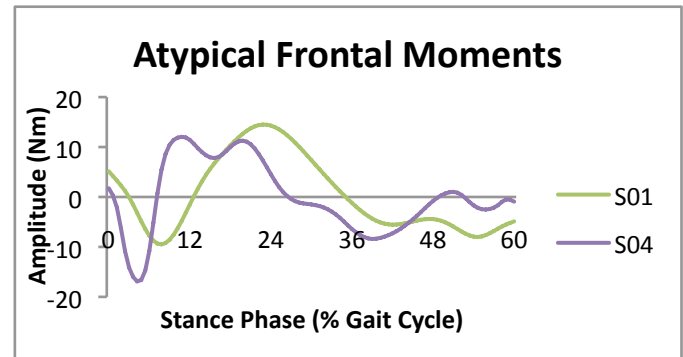


**Figure 2:** Atypical frontal knee moment waveform found in two obese participants, S01 and S04.

Their data were removed and analyses were rerun as a reduced data set. With the reduced data set, the obese group had greater knee adduction moment impulse and CKAL ( $p<0.05$ ). No group differences in the peak frontal moment magnitude were found for the reduced data set. Therefore, the greatest contributing factor to group differences in the knee adduction moment impulse (and resulting CKAL) was likely the increased stance duration in the obese group, which increased the time domain of the moment impulse.

## CONCLUSIONS

Young adults with healthy knees who are obese may modify their gait in an effort to reduce medial knee joint compartment loading through greater knee abduction, medial knee rotation and a slower walking speed. While they are successful in doing this, the ramifications of gait modifications on long-term musculoskeletal health remain unknown. Furthermore, despite the employment of these gait alterations, obese young adults may still expose their knees to a greater daily cumulative load. These compensations and cumulative load may increase risk of osteoarthritis of the knee.

## REFERENCES

1. Caballero, B. *Epidemiol Rev*, **29**, 1-5, 2007
2. Messier, S. P. *Rheum Dis Clin North Am*, **34**(3), 713-729, 2008.
3. Robbins, S. M. K. et al., *Gait & Posture*, **30**, 2009

# ALTERED NEUROMUSCULAR CONTROL AFTER ANTERIOR CRUCIATE LIGAMENT INJURY

Toran D. MacLeod, Kurt Manal, Lynn Snyder-Mackler and Thomas S. Buchanan

University of Delaware, Newark, DE, USA  
email: [macleod@udel.edu](mailto:macleod@udel.edu), web: <http://www.cber.udel.edu/>

## INTRODUCTION

While many studies have examined the movement dysfunction that persists after anterior cruciate ligament (ACL) injury, few studies have investigated the underlying neuromuscular control. Our lab has demonstrated that the muscles about the ACL injured knee contract more globally and less specifically during a single joint seated target-matching task. Global muscle co-contraction can increase tibiofemoral contact forces and increase chance for osteoarthritis. However, activities of daily living are more commonly performed while standing and controlling multiple joints than during the seated task, but we know little about how the ACL injured limb is controlled while standing. Therefore, the purpose of this study was to investigate the neuromuscular control used by ACL injured subjects in comparison to controls during a standing target-matching task. We hypothesized that the muscles of the ACL injured limb would demonstrate less specificity of activation than matched controls.

## METHODS

Fourteen subjects volunteered to participate in this study. Seven (3 females, 4 males; mean age  $23.6 \pm 7.8$  years) had sustained complete, isolated ACL ruptures within 6 months of testing. The remaining 7 subjects (3 females, 4 males; mean age  $23.9 \pm 3.8$  years) were limb, gender, and activity matched participants with no history of knee injuries. All subjects were regular participants ( $>50$  hours/year) in high level sports that require quick changes in direction (e.g., basketball, rugby, soccer).

The experiment required that subjects stand with their bare feet on two force platforms (a separate force platform was used for each foot). One foot was randomly selected to perform the mobilizer task first. The subject received visual feedback of the shear forces on the force platform of the

mobilizer foot, via the movements of a circular cursor. A projector was used to display the cursor on a screen in front of the subject. The cursor moved in the up-down-medial-lateral plane of the screen, corresponding to forward-backward-medial-lateral shear forces from the mobilizer foot. The subject's goal in the experimental protocol was to use the mobilizing foot to position the circular cursor over a narrow target that consisted of two concentric circles. Subjects were required to hold the cursor within the narrow target for 0.5 seconds before the trial was considered successful. The subject was given no visual feedback of the forces produced by the other foot, called the stabilizer. Targets appeared on at a time and in a random order at one of 18 positions (located at  $20^\circ$  increments of a circle in the forward-backward-medial-lateral plane). Seventy-two targets were performed bilaterally (both feet performed the mobilizer task). A force of 30% of the maximum forward or backward shear force, whichever was greater (collected prior to trials), was required to move the cursor in to each target.

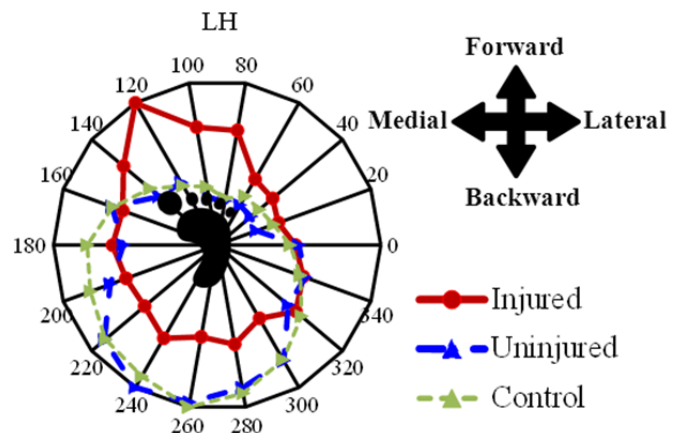


**Figure 1:** Stabilizer limb LH EMG Polar plot with respect force direction demonstrates that the LH of the injured limb was most active in the forwards direction while their uninjured limb and matched controls were most active backwards (plotted in the coordinate system of the right limb).

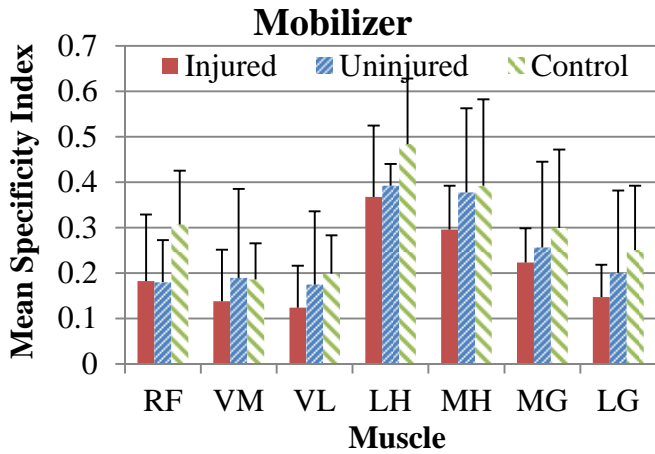


**Figure 2:** For the mobilizer task, mean muscle specificity indices of the Injured limbs tended to be less than either their own uninjured limbs or matched controls.

Electromyography (EMG) of 7 muscles, of both legs, was collected from the rectus femoris (RF), vastus medialis (VM), vastus lateralis (VL), lateral hamstrings (LH), medial hamstrings (MH), medial gastrocnemius (MG), lateral gastrocnemius (LG) during the final 0.5 second the cursor was located within each target using surface electrodes. The data were full wave rectified, averaged, and normalized using maximum EMG data collected prior to the target-matching experiment.

Polar plots were used to display EMG, so that the relative magnitude of muscle activity could be visualized across the 18 force combinations. The directional EMG data for the stabilizer foot were transposed, so that polar plots represent the muscle activity of both the stabilizer and mobilizer under the same external forces. Also, for ease of understanding all polar plots are in the coordinate system of the right limb.

The specificity of muscle utilization was analyzed by calculating a specificity index [1] for each muscle. Vector addition was used to calculate the overall magnitude and direction of muscle activity (EMG) based on the polar plots. The specificity index was calculated by dividing the vector sum by the scalar sum, for a value that ranged between zero and one.

## RESULTS AND DISCUSSION

This is the first time that data have been presented on ACL injured neuromuscular control of a static

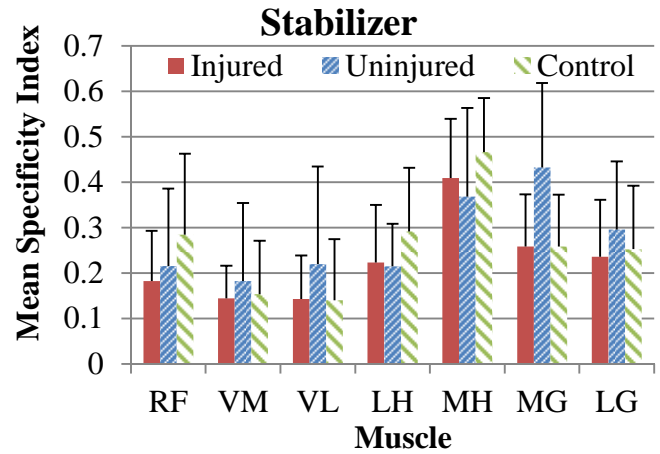


**Figure 3:** For the stabilizer task, mean muscle specificity indices of the Injured limbs tended to be less than either their own uninjured limbs or matched controls for the stabilizer task, especially so for the biarticulate muscles.

isometric standing postural control task. In general the muscles of the ACL injured limb were less well tuned to a particular force direction when compared to either their own uninjured limb, or to matched controls, supporting our initial hypothesis. In contrast to previous findings [1] where the VL was most affected during a seated single joint target-matching task, the biarticulate muscles of both the mobilizer and stabilizer limbs appear to be most affected by ACL injury. Further, the LH was recruited with a pattern of activation while pushing the stabilizer foot in the forwards direction. Perhaps this control strategy was used to resist anterior tibial translation. Support moments have been shown to shift from the knee to the hip of the ACL injured limb, making the hip focused standing target-matching task particularly well suited for examining hip muscle neuromuscular control.

## CONCLUSIONS

We believe that the injured limb of the ACL injured subjects demonstrated diminished neuromuscular control. Further, altered patterns of neuromuscular control may be used in an effort to stabilize the ligament injured knee.

## REFERENCES

1. Williams GN, et al., *Med Sci Sports Exerc*, **36**, 1089-1097, 2004.

Supported by NIH R01-AR046386

# KNEE MECHANICS BEFORE AND AFTER PERTURBATION TRAINING IN SUBJECTS WITH ACL DEFICIENCY

Kurt Manal, Emily Gardinier & Lynn Snyder-Mackler  
University of Delaware, Newark, DE, USA  
email: manal@udel.edu, web: <http://www.dri.udel.edu/>

## INTRODUCTION

Patients with ACL deficiency exhibit truncated knee flexion and a reduced extension moment during the weight acceptance phase of gait [1]. Co-contraction of the hamstrings to dynamically stabilize the knee may be associated with the reduced moment seen in these subjects. Alternatively, the truncated flexion angle may be related subjects using less quadriceps force as the extensors contract eccentrically during weight acceptance. From a rehabilitation perspective it is important to understand why reduced flexion is seen during weight acceptance because it has a direct impact on rehabilitation as therapists attempt to minimize stiff-knee gait prior to surgery.

In this study we investigated the effect of pre-operative perturbation training on the knee extensor moment and flexion angle in a group of ACL deficient subjects. Perturbation training is a therapist assisted protocol designed to improve dynamic stability of the knee[2]. We hypothesized that subjects would use less hamstrings force following perturbation training (ie, they would exhibit a less stiff knee gait) and consequently have a greater knee extension moment and flexion angle compared to their pre-training values.

## METHODS

Seven subjects with acute unilateral ACL rupture participated in this study. All participants were athletes, 18-37 years old and acutely injured (<6 months). Perturbation training consisted of 10 physical therapy sessions administered 2-5 times per week. Stance phase kinematics and kinetics were computed using standard motion analysis methods and analyzed with Visual3D (C-motion, Inc). All subjects walked at a self-selected speed. Electromyography (EMG) was collected for 7

muscles (RF, VL, VM, BFL, ST, MG & LG). EMGs for the BFS and SM were approximated from signals recorded for BFL and ST; VI EMG was assumed to be the average of VM and VL. EMGs were rectified, low pass filtered and normalized to maximum values recorded during maximum efforts. EMG and joint kinematics were input to a modified Hill-type muscle model to estimate individual muscle forces [3]. The quadriceps force was the sum of individual muscle forces for the RF, VL, VM and VI. Similarly, BFL, BFS, SM & ST were summed for the hamstrings. Kinematic & kinetic data for stance were normalized to 100 samples. Moments and forces were normalized to BW\*Ht and BW respectively. Data for both legs were tested and processed in this manner before and after perturbation training.

## RESULTS AND DISCUSSION

Subjects walked at similar speeds ( $\pm 5\%$ ) during pre and post-perturbation testing to minimize potentially confounding effects of walking speed.

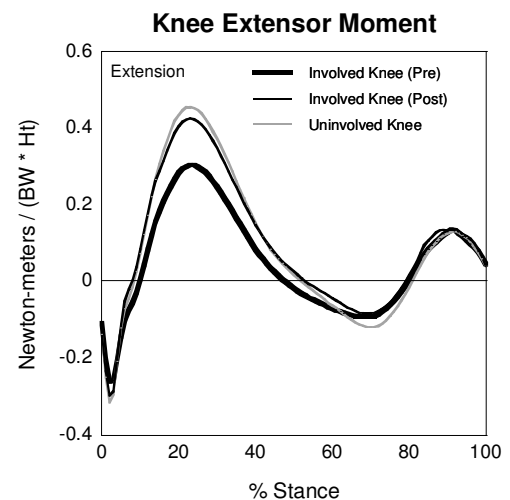


**Figure 1.** Knee extensor moment for the involved knee before and after perturbation training. Note how the Post training Involved knee was similar to the pattern observed for the uninjured limb.

The peak extension moment for the ACL deficient knee was smaller compared to the uninjured leg prior to training. After perturbation training the extension moments were almost identical (Figure 1).

Knee flexion angle increased from  $18.2^{\circ} \pm 5.3^{\circ}$  before training to  $23.5^{\circ} \pm 7.5^{\circ}$  afterwards. This difference was not statistically significant and likely related to our small sample size and relatively large variability. Previous studies with more subjects have reported significant differences as small as 2 degrees [1]. Nonetheless, we did observe a rather large effect size ( $ES=0.78$ ) in flexion angle after perturbation training.

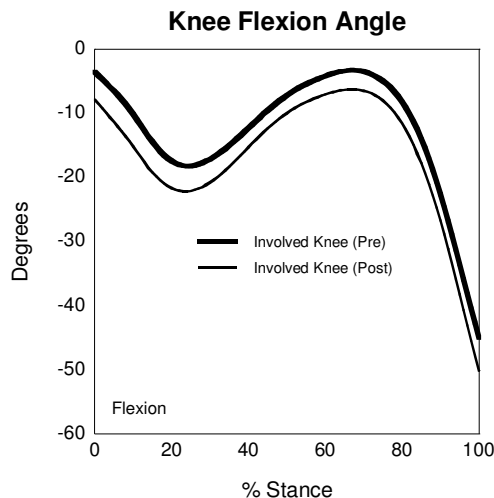


**Figure 2** Knee flexion angle during the stance phase of gait. The angle of interest is the maximum flexion angle within the first 40% of stance.

Ensemble averaged quadriceps and hamstrings forces before and after perturbation training are shown in Figure 3. The model predicted almost identical hamstring forces before and after training which was contrary to our hypothesis. The increase in extension moment observed after training appears to be the result of subjects using more quadriceps force (Figure 3). Peak quadriceps force was significantly greater after training ( $p = 0.03$ ).

This finding was unexpected and raises several interesting observations and questions. Firstly, the increase in quadriceps force suggests a carry-over effect between training and walking. That is, subjects received instruction and feedback during perturbation training only yet positive kinematic

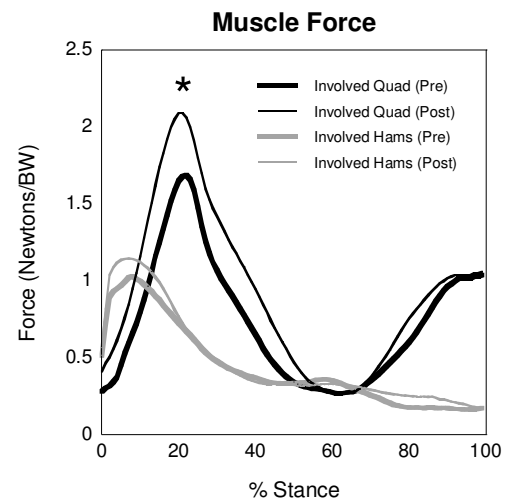


**Figure 3.** Hamstrings force for the ACL deficient knee (ie., Involved) was similar before and after perturbation training. In contrast, note the large difference in peak quadriceps force. \*  $p < 0.05$ .

and kinetic changes were noted during walking. Further, it is unclear why subjects allowed their knee to flex more following perturbation training. We speculate that it may be related to enhanced confidence and reduced fear of giving-way acquired during training. Although our study was not designed to examine this, future work could monitor muscle forces during perturbation training to investigate neuromuscular adaptation that may be occurring.

## CONCLUSIONS

Perturbation training following ACL rupture promotes positive gait adaptations. Increased knee flexion by ACL deficient subjects after perturbation training may reduce joint contact forces during gait. This is clinically relevant since there is a high incidence of knee osteoarthritis following ACL injury.

## REFERENCES

1. Rudolph KS et al. *Knee Surg, Sports Traumatol, Arthrosc* **9**, 62-71, 2001.
2. Chmielewski TL, et al. *J Electromyogr Kinesiol* **12**, 267-74, 2002.
3. Buchanan TS, et al. *J Appl Biomech* **20**, 367-95, 2004.

## ACKNOWLEDGEMENTS

Supported by NIH R01-AR046386 and the Sports Physical Therapy Section Legacy Fund.

# Problem-Based Learning and Interactive White Board Technology Compared to Traditional Lecture for Undergraduate Student Learning in Biomechanics.

<sup>1</sup>David Mandeville, <sup>1</sup>Kimo Ah Yun, <sup>1</sup>Rodney Imamura and <sup>1</sup>Joan Neide

<sup>1</sup>California State University, Sacramento, Sacramento, CA, USA  
email: dmandeville@csus.edu

## INTRODUCTION

Previous studies show that both traditional lecture (TL) and problem based learning (PBL) are effective for student learning of nursing education [1]. While the traditional lecture teaching format is described as teacher centered where facts are simply conveyed from the teacher to the student, PBL is a student centered learning approach in which students work interactively in small groups to solve a problem [2]. PBL challenges students to learn to learn by participating in a group setting to synthesize the new concepts learned in the course with their previous knowledge.

Interactive whiteboards (IWB) are large touch sensitive boards controlled by a computer connected to a digital projector. The IWB allows for increased user interactivity via the ability to: control the computer applications by tapping the board, to write on the board, to use the internet and video to deliver instruction [3]. This technological interactivity is claimed to facilitate more interactive lessons [3]. Although there is increased use of IWB in educational settings, there is a paucity of evidence supporting a positive effect of IWB on students learning or classroom interactions. The use of PBL and IWB has not been reported for undergraduate biomechanics education.

The purpose of this study was to assess the effect of using PBL and IWB on student learning outcomes compared to a traditional lecture format for undergraduate biomechanics.

## METHOD

Eighty-nine total students from 2 successive biomechanics courses were assessed. Students from the initial course were the traditional lecture cohort (TL, n = 44), while the students from the second

course were the problem based learning cohort (PBL, n = 45). The TL teaching method included formal power-point lectures, classroom discussions and laboratory exercises. The PBL teaching method included 3-5 students solving a problem based on the lecture notes, independent study to work on their learning issues, and giving presentations of the solutions. This model was followed for both classroom and laboratory settings. Additionally, each group worked on a laptop connected to an IWB during class sessions. The class room had five IWB so that generally 2 small groups shared an IWB. At every class session, each group would present their solutions using the interactivity features of the IWB. The laboratory did not use IWB and students presented using one laptop and one digital projector.

Both groups had two 50 minute class sessions and one 3 hour laboratory session/week. Each course lasted 15 weeks. Students were assessed using the same set of exams. The set of exams included two midterms and one final. All exams were composed of multiple choice and calculation questions and were graded by the same examiner. Dependent measures include the percentage score for exam 1, exam 2 and exam 3. A mixed ANOVA (SPSS) was used to test for between group and within group differences for exam score,  $\alpha < .05$ .

## RESULTS AND DISCUSSION

The problem based learning cohort scored significantly greater on exam 2 than the traditional lecture cohort ( $P = .05$ , Figure 1, Table 1). Both groups scored significantly lower on exam 3 when compared to their exam 2 scores ( $P < .0001$ , Figure 1, Table 1).

This study was the first to evaluate the use of PBL and IWB to deliver undergraduate biomechanics instruction in a student centered active learning

paradigm. When compared to traditional lecture, the PBL and IWB paradigm resulted in a trend of increased mean exam scores. This positive result may be due to the interactive nature of the small group problem solving and the IWBs.

Inspection of the frequency histograms of the exams indicated a shift towards a negative skew for the PBL group. Thus, it is likely that the increase in the mean PBL score occurred via improved performance by students in the lower score portion of the distribution. Improved exam performance by these students likely was the result of the interactive nature of the PBL and IWB paradigm which brings these students into both the group and the class discussion. Additionally, the IWB may promote improved performance by allowing students to process and display their work in a manner consistent with their individual learning style.

## CONCLUSIONS

This study indicates that students in a PBL and IBW paradigm perform equally or better than their peers in a traditional lecture paradigm for undergraduate biomechanics. Future studies are needed to quantify the effect of both PBL and IWB on student interactions in class as well as additional learning outcome measures.

## REFERENCES

- 1.Lin, CF, et al. A comparison of problem-based learning and conventional teaching.... *Nursing Ethics*, **17**, 373 – 382.
- 2.Lusardi MM, et al. A problem-based learning approach to facilitate evidence-based practice. ... *J Prosthetic and Orthotics*, **14**, 40 - 50, 2002.
- 3.Smith HJ, et al. Interactive white boards: boon or bandwagon?.... *J Computer Assisted Learning*, **21**, 91 - 101, 2005.

**Table 1:** Mean (SD) exam scores for problem based learning students (PBL, n = 45) and traditional lecture students (TL, n = 44) during a 15 week undergraduate biomechanics course.

|     | Exam 1 (%)       | Exam 2 (%)        | Exam 3 (%)         |
|-----|------------------|-------------------|--------------------|
| PBL | 77.84<br>(16.05) | 81.95*<br>(13.14) | 74.84**<br>(11.04) |
| TL  | 72.41<br>(17.63) | 76.41<br>(13.12)  | 71.00**<br>(14.08) |

\*Significant between-group difference,  $P = .05$

\*\*Significant within-group difference,  $P < .0001$

## ACKNOWLEDGEMENTS

This study was made possible by a Pedagogy Enhancement Award, presented by the Center for Teaching and Learning, California State University, Sacramento.

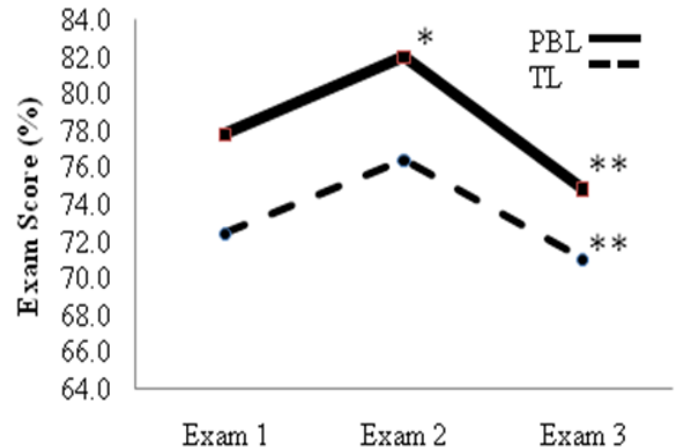


**Figure 1:** Mean exam score (%) for traditional lecture cohort (TL, n = 44) and problem based learning cohort (PBL, n=45) across a 15 week undergraduate biomechanics course. \*Significant between-group difference,  $P = .05$ ; \*\*significant within-group difference,  $P < .0001$ .

# The Effect of Torsion Deformity and Medial Knee Osteoarthritis on Lower Limb Extensor Moments during Gait.

<sup>1</sup>David Mandeville, <sup>2</sup>Sridhar Rachala, <sup>1</sup>Rodney T. Imamura, <sup>2</sup>Mary Bayers-Thering, <sup>2</sup>Ken Krackow

<sup>1</sup>California State University, Sacramento, CA, USA

<sup>2</sup>Kaleida/Buffalo General Hospital Buffalo, NY, USA

email: [dmandeville@csus.edu](mailto:dmandeville@csus.edu)

## INTRODUCTION

Hicks et al. (2007) found across a range of simulated excessive tibial torsion a diminished capacity of gluteus maximus, gluteus medius and the soleus to extend the hip and the knee during the single limb stance of gait. This result was interpreted to be due to altered geometry of bones about the vertical axis and the accompanying deviation of the muscles origins and insertions. The authors studied tibial torsion with respect to the crouched gait of cerebral palsy gait, however, tibial torsion deformity has also been reported for medial knee osteoarthritis (OA) subjects.

Krackow et al., (2011) showed that medial knee OA patients with tibial torsion deformity walked with greater knee varus moments than patients with medial knee OA and healthy controls. However, a kinetic characterization of the effect of tibial torsion on extensor muscle function during gait for knee OA subjects is needed. The total support moment (Ms), defined by (Winter, 1980) as the summation of the net joint moments at the hip, knee, and ankle joints, represents the magnitude of the extensor synergy of the lower extremity during stance phase of gait. This value has been isolated during the first peak vGRF to describe lower limb extensor moment function during the loading response phase of single limb stance for subjects with medial knee OA (Mandeville, 2007).

However, the effects of medial knee OA and tibial torsion on the extensor moments of the lower limb during single limb stance have not been reported. Therefore, the aim of this study was to quantify the effect of torsion deformity on the total moment of support, the hip, knee and ankle moments for patients with medial knee OA and torsion

deformity, medial knee OA patients and healthy controls.

## METHODS

Twenty-four subjects were recruited into 3 groups: end-staged medial KOA with torsion deformity (TKO, n = 6, BMI =  $34.2 \pm 3$  kg/m<sup>2</sup>, age =  $61.8 \pm 8$  yrs.) and without torsion deformity (KOA, n = 8, BMI =  $33.8 \pm 7$  kg/m<sup>2</sup>, age =  $59 \pm 11$  yrs.) and controls (CON, n = 10, BMI =  $28.4 \pm 4$  kg/m<sup>2</sup>, age =  $62.5 \pm 4$  yrs.). Apparent torsion deformity was identified using a long standing lower extremity (LSLE) radiograph. The LSLE was used to classify knee OA disease severity for all subjects based on the Kellgren/Lawrence (K/L) scale; knee OA scores were  $\geq 3$  and controls were  $< 2$ .

The mechanical axis alignment for each study limb was measured by two evaluators (KAK and SRR) using the LSLE. Femoral and tibial torsion was assessed by two evaluators (SRR and DSM) using thin slice computed tomography (CT). A partially loaded-limb CT protocol was used to replicate the tibiofemoral joint angle (10° flexion) during the stance phase of gait. Patients were fitted into a torso harness attached to a foot base plate which was loaded with an axial compression force of approximately 55 N. The feet were secured to the base plate in the toe-out angle determined from an ink and paper gait test. Digital LSLE and CT images were archived and measured using a PC workstation.

Sagittal internal net joint moments were determined using level walking motion analysis involving two force plates and eight-cameras. A Newton/Euler inverse dynamic analysis was used to calculate the internal hip, knee, and ankle joint moments. These net joint moments (normalized to % body weight \*

body height) were extracted at the first peak vertical ground reaction force and summed to present the total moment of support (MS).

Analysis of co-variance using gait velocity as a covariate was used to test for between-group differences for the moment of support, the hip, knee, and ankle joint moments,  $\alpha < .05$ .

## RESULTS AND DISCUSSION

TKO showed a greater moment of support and a greater knee joint moment when compared to both KOA and CON.

These findings represent the kinetic synergy of the involved limb during weight acceptance. When controlling for gait velocity, the adjusted TKO values show a trend of increased extensor output at the hip, knee and ankle joints. Increased extensor output from TKO may be the result of an increased muscular response due to the altered skeletal geometry of the inwardly rotated tibia. Additionally, the increased extensor output may be a result of a stiff knee gait. At the first peak vGRF, knee flexion values were not significantly different between groups, but TKO accepted the body weight with a trend of less knee flexion ( $10.69 \pm 13.29$ ) than KOA ( $16.13 \pm 6.98$ ) and CON ( $14.83 \pm 4.29$ ).

## CONCLUSIONS

Transverse plane deformity of the tibia in combination with the fixed sagittal plane orientation of the knee may increase the extensor demands during weight acceptance for knee OA patients with torsion deformity.

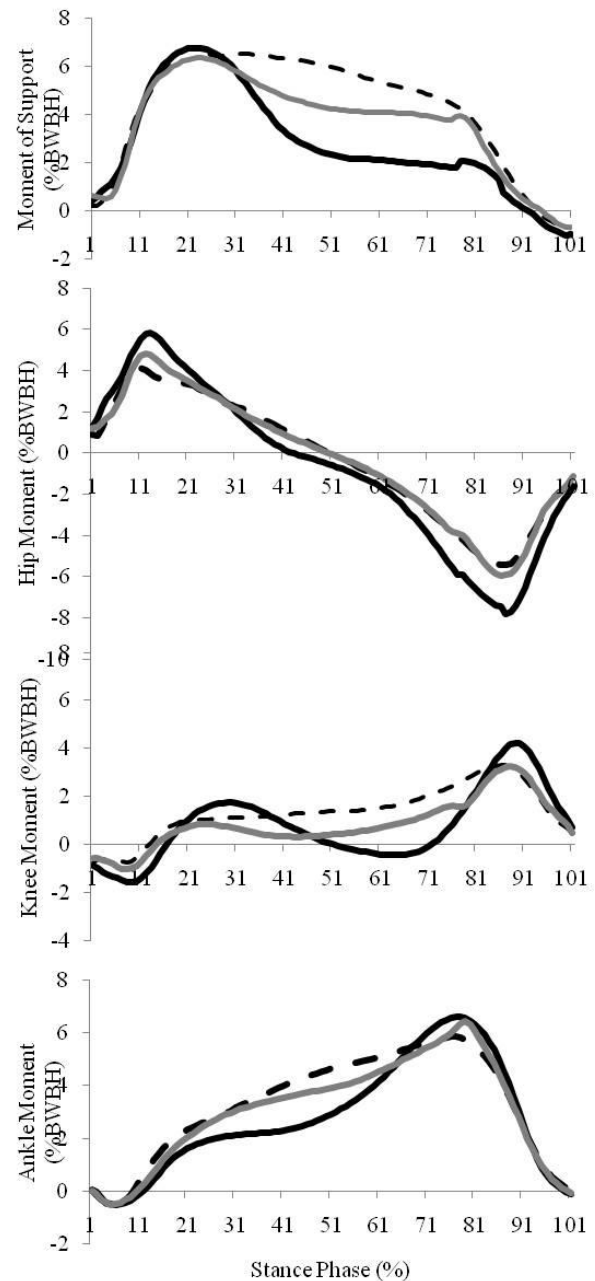


Figure 1. Ensemble curves for net sagittal internal joint moments and moment of support for KOA (gray), TKO (dashed) and CON (black).

Table 1. The estimated means (SE) for the internal sagittal moment of support, hip, knee and ankle moments for patients with medial knee osteoarthritis (KOA), patients with knee OA and torsion deformity (TKO) and healthy controls (CON).

|                              | KOA            | TKO             | CON            |
|------------------------------|----------------|-----------------|----------------|
| Moment of Support<br>(%BWBH) | 6.86<br>(0.57) | 8.90*<br>(0.79) | 5.50<br>(0.57) |
| Hip Moment<br>(%BWBH)        | 2.97<br>(0.37) | 3.24<br>(0.51)  | 2.42<br>(0.37) |
| Knee Moment<br>(%BWBH)       | 1.09<br>(0.30) | 2.57*<br>(0.42) | 1.04<br>(0.30) |
| Ankle Moment<br>(%BWBH)      | 2.81<br>(0.38) | 3.10<br>(0.53)  | 2.03<br>(0.38) |

# MULTI-DIGIT COORDINATION DURING A POURING TASK THAT REQUIRES DYNAMIC STABILITY

Ryan P. Manis and Veronica J. Santos, Ph.D.

Biomechanics Lab, Arizona State University, Tempe, AZ, USA

e-mail: [veronica.santos@asu.edu](mailto:veronica.santos@asu.edu) web: <http://biomechanics.engineering.asu.edu/>

## INTRODUCTION

Prior work on grasping with three or more digits employed pick-and-place tasks to study digit placement and center of mass effects on grip forces [1,2], or used a circular precision grip on the object from above (as when opening a jar lid) [3,4,5]. The pick-and-place tasks did not require purposeful rotation of the grasped object, as is common during activities of daily living. The circular precision grip tasks did not require the subject to counteract gravity during object rotation, as with the two-digit precision grip task in [6], where the “grip axis rotated relative to the field of gravity.”

The goals of this study were to characterize digit responses in a three-fingered grasp for a task that closely relates to an activity of daily living. The pouring task presented here has three key features: (1) perturbations to the grasped object are induced by the subject and are not entirely unexpected, (2) dynamic stability is required for purposefully translating and rotating the grasped object against gravity, and (3) both adduction/abduction and flexion/extension degrees of freedom are required for successful completion of the task.

## METHODS

Data were collected using a protocol approved by the Arizona State University Institutional Review Board. The results presented here are representative of trends observed for five unimpaired subjects (four male, one female, aged 21-23 yrs). Kinematic data were collected using a Vicon motion capture system (200 Hz) with 30 hemispherical retro-reflective markers placed on each subject's dominant hand. Triads of markers were placed on thumb, index finger, and middle finger segments and on the grasped object. Due to marker occlusion during the pouring task, Ascension Flock of Birds

six degree-of-freedom sensors (50Hz) were used on the thumb as well.

Three instrumented test objects were used: one with parallel gripping surfaces as with a water bottle, one with angled gripping surfaces as with a pint glass, and one with a top-heavy shape and a thin stem as with a cocktail glass (Fig. 1). The objects were instrumented with three ATI Nano-17 force/torque load cells (1000 Hz) that were each rigidly attached to independent grip plates and could be easily transferred between test objects. Surface electromyography data were recorded with a Biopac EMG 100C system (1000 Hz) from the pronator teres muscle on the forearm to detect active wrist movement.



**Figure 1:** The three test objects are shown (L-R: parallel, angled, and top-heavy) without the load cells or grip plates attached.

Each subject was instructed to pick up a test object filled with water, pour the water into a receptacle container with a 2cm diameter opening (7" horizontally and 6.5" vertically away) without spilling, and return the test object to the table. The receptacle container was placed on a scale comprised of an ATI Nano-25 force/torque load cell (1000 Hz). Subjects were allowed to select their own digit placements and complete the task at self-selected speeds. Blocks of five trials were used for each test object whose presentation order was

randomized. After these three blocks of trials, each subject was instructed to minimize wrist use and repeat the three blocks of trials using thumb, index, and middle fingers only.

During post-analysis, the finger force/torque data were smoothed using a boxcar moving average having a window of 10 data points (10ms). As in [7], “task subgoals” (e.g., digit-object contact) were defined based on “action phases” (e.g., pour) that comprise the overall task. Initial object contact and final release timepoints were found using fingertip forces normal to the grip plates. Object lift-off and replacement were found using fingertip forces tangential to the grip plates (x-direction). The start and end of pouring were found using scale forces and object kinematics. All trials were synchronized such that “t=0 sec” refers to initial object contact.

## RESULTS AND DISCUSSION

Figure 2 shows each digit’s forces tangential to the grip plate throughout the task, which is subdivided by six task subgoals. The middle finger typically has a higher “lift force” (x-direction) than the index finger for all three test objects.

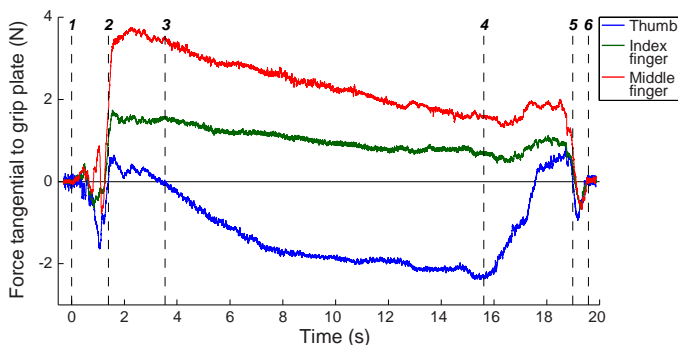


**Figure 2:** Tangential forces for a representative subject (trial 5, parallel grip plates, no wrist constraint). A positive tangential force points towards the top of the test object. Six subgoals are shown: (1) initial contact, (2) object lift-off, (3) start of pouring, (4) end of pouring, (5) object replacement, and (6) release.

Thumb forces in the tangential, x-direction were noticeably different across test objects. For the test objects with parallel and angled grip plates, the thumb initially pushed upwards to lift the object but quickly pushed downwards to help tip the object for pouring (parallel case shown in Fig. 2). However, for the top-heavy test object, the thumb tangential

force remained positive throughout pouring for 4 of 5 subjects, which suggests that the thumb’s role was to hinder over-rotation of the test object.

The effect of test object shape is also evident in the ratios of tangential forces between the index and middle fingers (Fig. 3). For trial 1 of the top-heavy object, the index finger typically applied greater tangential forces than the middle finger. The opposite was true for trial 1 of the object with parallel grip plates. Interestingly, as the trials progressed, the ratio of tangential forces between the index and middle fingers tended towards 0.5.

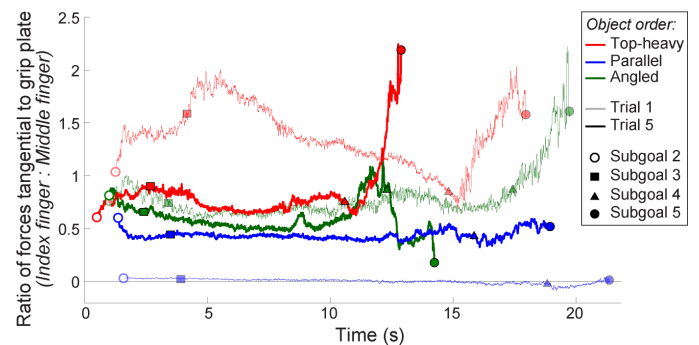


**Figure 3:** Ratio of index to middle finger tangential forces for a representative subject (trials 1 and 5 for each test object, no wrist constraint). The thick blue line corresponds to data from Fig. 2.

Data collection is ongoing, but initial results suggest that multiple grip strategies exist for successful completion of the task. Future work includes the analysis of finger kinematics and digit placement, trial-to-trial adaptation, and effects of the self-imposed wrist constraint as verified by the electromyography data.

## REFERENCES

1. Lukos J, Ansuini C, and Santello M. *J Neurosci.* **27**: 3894-3903, 2007.
2. Niu X, Latash ML, and Zatsiorsky VM. *Exp Brain Res* **194**: 115-129, 2009.
3. Flanagan JR, Burstedt MKO, and Johansson RS. *J Neurophysiol.* **81**, 1706-1717, 1999.
4. Kinoshita H, Murase T, and Bandou T. *Ergonomics* **39**: 1163-1176, 1996.
5. Rácz K and Valero-Cuevas FJ. *Proceedings of NCM’09*, Waikoloa, HI, 2009.
6. Johansson RS, Backlin JL, and Burstedt MKO. *Exp Brain Res* **128**: 20-30, 1999.
7. Flanagan RS, Bowman MC, and Johansson RS. *Curr Opin Neurobiol* **16**: 650-659, 2006.

# Force Sharing Among Fingers During Multi-Finger Pressing in Different Finger Configurations

Joel Martin, Mark L. Latash, and Vladimir M. Zatsiorsky  
Pennsylvania State University, University Park, PA, USA  
email: [jrm496@psu.edu](mailto:jrm496@psu.edu)

## INTRODUCTION

Force sharing among fingers involved in a multi-finger pressing task is a typical example of the motor redundancy problem [1], which have previously been investigated using multi-finger pressing tasks [2, 3, 4]. Previous studies found that during four-finger pressing the I- and M-fingers each contribute approximately 30% of the total force, followed by the R-finger, and lastly the L-finger. It has also been shown that for tasks in which four-fingers increase their force in a ramp-like manner the forces of individual fingers increase in a linear fashion such that the sharing percentages established at the beginning of trials is preserved. The goal of the current study is to investigate finger force sharing in four-finger pressing tasks performed in different finger configurations. Altering finger configuration should result in changes in force sharing due to basic muscle force-length properties [5].

## METHODS

Six subjects participated in the study. All were right handed, in good health, and reported no history of injury or disease affecting function of their upper extremities. Uni-directional force sensors were used to record normal finger forces during the experiment. A custom written LabVIEW program was used to collect the data. The force data were collected at 300 Hz. Data were post-processed using Matlab software.

The experimental procedure consisted of two types of trials. The first type was maximum voluntary contraction (MVC) trials. Subjects were instructed to press as hard as they could with all four fingers, hold the force level for at least a second and then relax. The second type was ramp force production trials. A ramp target force was presented on the screen starting from 0% MVC and going to 60% MVC. The slope of the line was 10% MVC/s.

Subjects were instructed to press with all four-fingers to match the target line. For both the MVC and ramp trials subjects had to perform the task in five different configurations: 1) all fingers FLAT, 2) I-finger raised, 3) M-finger raised, 4) R-finger raised, and 5) L-finger raised. The fingers were raised 2.0 cm in configurations two through four. The MVC trials and ramp trials were performed in separate blocks. Three trials of each condition were performed. Within each block the trials were randomized.

The main point of interest was the sharing pattern of individual fingers forces during the trials. Force sharing percentages of individual finger forces were computed relative to the total force produced at each data point during trials:

$$SH\%_i(t) = \frac{F_i(t)}{F_{TOT}(t)} * 100\%$$

Where  $F_{TOT}(t)$  is the sum of individual finger normal forces and  $F_i(t)$  is the individual finger normal force at time  $t$  ( $i = I, M, R, L$ ).

For the MVC trials the sharing percentages were computed at the time of peak  $F_{TOT}$ . For the ramp trials the sharing percentages were averaged over the entire trial. Ramp trials were visually inspected to ensure that no large oscillations of sharing patterns occurred during the trial (Fig. 1).

Trial sharing percentages were averaged across trials of the same conditions within subjects. The change in individual finger sharing percentages from the FLAT configuration to raised configurations was calculated for each finger using the averaged data. The data presented were then averaged across subjects. Changes in sharing % were averaged in terms of their proximity to the raised finger. Proximity values of 1, 2, and 3 were assigned to fingers that were adjacent to, two

fingers away, or three fingers away from the raised finger, respectively.

Paired t-tests were run to compare the sharing percentage of individual fingers to the FLAT and each raised configuration. A one-way ANOVA was used to test for the effect of PROXIMITY on the change in sharing % of non-raised fingers. Significance was set to  $\alpha = 0.05$ .

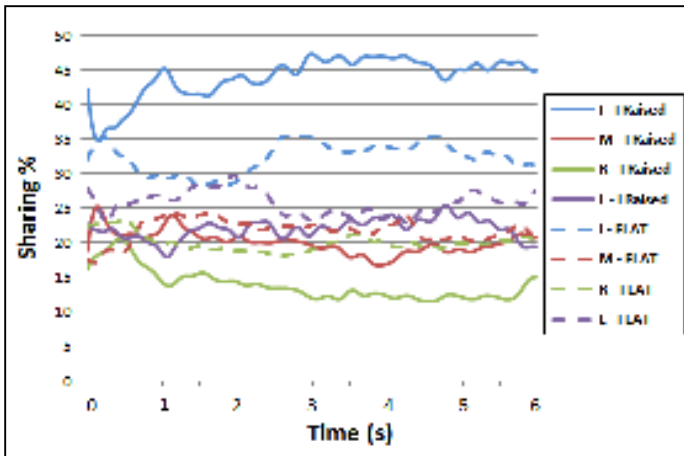
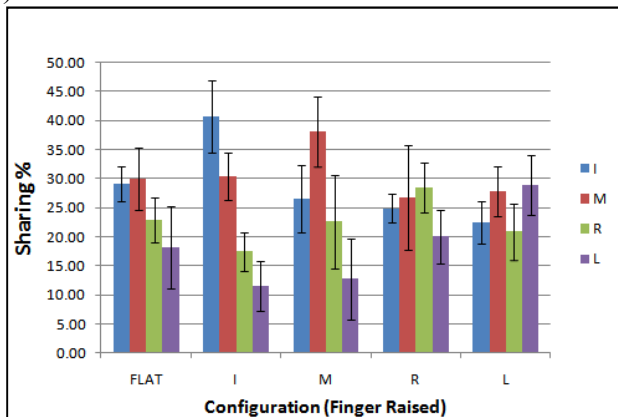


**Figure 1:** Exemplary sharing data from a ramp trial with I-finger raised (solid lines) and trial in the FLAT configuration (dashed lines).

## RESULTS AND DISCUSSION

During both MVC and ramp trials the raised finger showed a substantial increase ( $p < 0.05$ ) in its sharing percentage of the total force (Fig. 2). As a result of the increase in sharing percentage of the raised finger the other fingers showed a drop in sharing percentage, compared to the condition in which none of the fingers were raised.

A)



B)

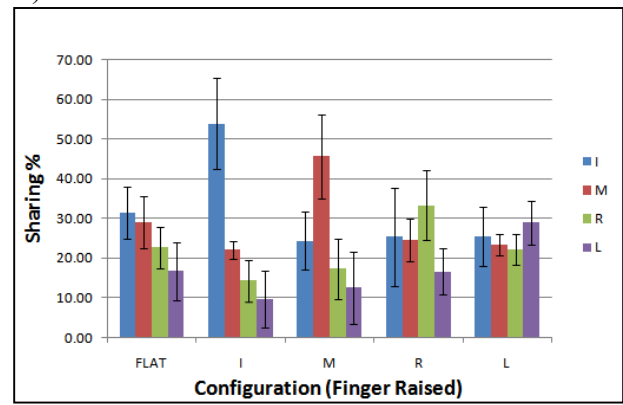


**Figure 2:** Average sharing percentages of individual fingers during: A) MVC trials and B) ramp trials. Error bars are standard error.

The majority of non-raised fingers also showed significant changes in their sharing patterns compared to the FLAT configuration. In five of twelve analyses, non-raised fingers showed a significant change [decrease] in sharing percentage for MVC trials and in nine of twelve analyses, non-raised fingers showed a significant change [decrease] in sharing percentage for ramp trials. One-way ANOVA's showed a significant effect of proximity of non-raised finger to raised finger on the force sharing percent change for MVC trials but not for ramp trials. The general trend, in terms of proximity, was fingers further from the raised finger showed larger decreases in their sharing percentage, compared to the FLAT configuration.

## CONCLUSIONS

The results indicate that the distribution of finger forces in multi-finger tasks is flexible. Raising a finger would increase the length of the muscle tendon unit of that finger which could in turn increase strain on other fingers due to the mechanical connections between fingers. Whether or not the changes in sharing patterns are entirely due to mechanical properties of the tissues in the hand is unknown. This problem can be further examined using optimization and neural network models.

## REFERENCES

1. Bernstein NA, *The co-ordination and regulation of movements*, Oxford Press, 1967.
2. Li ZM, et al. *Exp Brain Res* **119**, 276-286, 1998.
3. Li ZM, et al. *Exp Brain Res* **122**, 71-78, 1998.
4. Zatsiorsky VM, et al. *Biol Cybern* **79**, 1998.
5. Lieber RL. *Dev Med Child Neurol* **28**, 1986.

# **SURVIVORS OF STROKE MAY ACHIEVE CYCLIC REACHING: A BIOMECHANICAL ANALYSIS OF THE HEMIPARETIC AND LESS-AFFECTED UPPER-EXTREMITIES.**

Crystal Massie, Matt Malcolm, and Ray Browning

Colorado State University, Fort Collins, CO, USA  
email: crystal.massie@colostate.edu

## **INTRODUCTION**

Motor control impairments following a stroke impact the ability to generate coordinated reach. Research has demonstrated improvements in the amount of hemiparetic arm use, yet less attention has been devoted to quantifying the quality of use [1]. One potential contribution to the quality of movement is the underlying structure of a reaching task. For example, reaching can be cyclic, i.e. continuous back and forth, or discrete, i.e., defined start and stop. Research on neurologically intact individuals has demonstrated advantages of cyclic reaching including faster movement velocity and smoother trajectories [2]. A key component of cyclic reaching is the ability to produce continuous motion (i.e. not stopping/dwelling on targets). Survivors of stroke, however, often demonstrate segmented movements during forward discrete reaching (i.e. not smooth), and no study has directly addressed the ability to generate cyclic reaching comparing the stroke-affected to the less-affected side. This purpose of this study was to describe cyclic reaching in survivors of stroke in order to evaluate its potential to be incorporated in stroke-rehabilitation interventions aimed at improving the quality of movement.

## **METHODS**

Eight survivors of stroke (5 male; mean age 68.5 years, range 44-86) in the chronic stage of recovery (mean 40 months post-stroke; range 7-82) participated. Subjects met gross and fine-motor criteria for intensive interventions (e.g., ability to extend wrist). Subjects sat comfortably in a chair and were asked to reach between two targets 0.35 m apart (anterior-posterior direction) at a height of 0.71 m (approximate height of a computer desk). The initial starting position was with the shoulder at neutral and the elbow at 90 degrees of flexion.

Subjects were instructed to reach as quickly and as accurately as possible. The pressure sensitive targets were used to quantify beginning/end of reaching cycles. One trial of cyclic reaching (5 cycles) was performed with both the affected and less-affected upper-extremity; order of trials was randomized. A 7-camera Vicon system recorded the motion of the subject's torso and upper extremities. Kinematic data were processed in Visual 3D for outcome measures of interest including:

- time to reach between each target (forward and return, sec),
- peak reach and return velocity (m/sec)
- anterior trunk displacement (m), shoulder range of motion (ROM, degrees), elbow ROM (degrees) during forward reach,
- Movement units during forward reach (number of zero velocity crossings of marker on wrist).

Data were averaged over the 5 reaching cycles and were analyzed with RMANOVA (significance  $p < 0.05$ ).

## **RESULTS AND DISCUSSION**

Subjects reached towards the anterior target significantly faster with the less-affected upper-extremity compared to the stroke-affected side (0.78 sec vs. 1.5 sec,  $p < 0.01$ ), resulting in greater peak velocities (1.0 m/sec vs. 0.64 m/sec,  $p < 0.05$ ). The ability to generate cyclic reaching is considered to be dependent on continuous motion which is evident on velocity profiles. As depicted in Figure 1, the velocity profiles are smooth and continuous when reaching with the less-affected side (i.e., no dwelling on targets); however, corrective submovements are more commonly present when reaching with the stroke-affected side. Figure 1 represents data from two subjects: the subject in panel A is able to generate smooth, continuous motion without dwelling (periods of zero velocity), whereas the subject represented in panel B has

prolonged durations at target contact represented by periods of zero velocity.

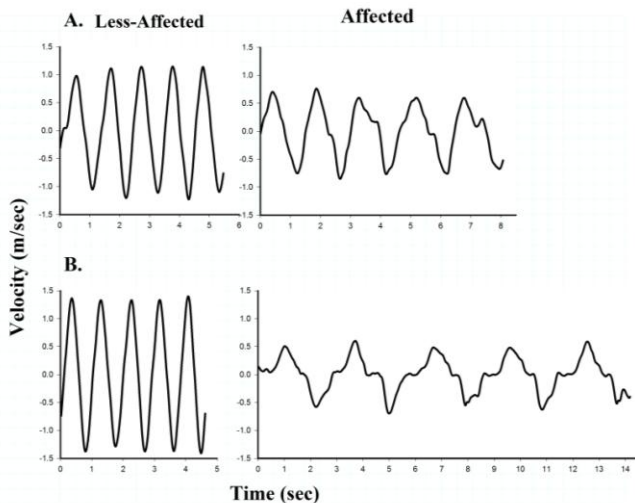


**Figure 1:** Cycling reaching velocity profiles of 2 representative subjects. This figure also depicts longer reaching durations and smaller peak velocities when reaching with the stroke-affected arm. Scales are consistent across panels.

Movement units represent quantification of reaching smoothness (i.e., the number of zero velocity crossings while reaching forward). The absolute number of movement units was significantly less when reaching with the less-affected arm and hand ( $p < 0.01$ ). On average, 16% of the cyclic reaches had secondary movements when reaching with the less-affected arm (i.e., movement correction at target contact) whereas 24% of the reaches had secondary movement with the stroke-affected arm. These observations are consistent with previously reported data [2], suggesting that survivors of stroke may achieve cyclic reaching within a range similar to a neurologically intact population.

As demonstrated in Figure 1, however, the potential exists that not all survivors of stroke can accomplish cyclic reaching (bottom right panel). One reason may be the difficulty extending the elbow during forward reach. As depicted in Figure 2, survivors of stroke utilized an anterior trunk displacement strategy which was observed with decreased shoulder flexion and elbow extension when reaching with the stroke-affected arm compared to the less-affected arm.

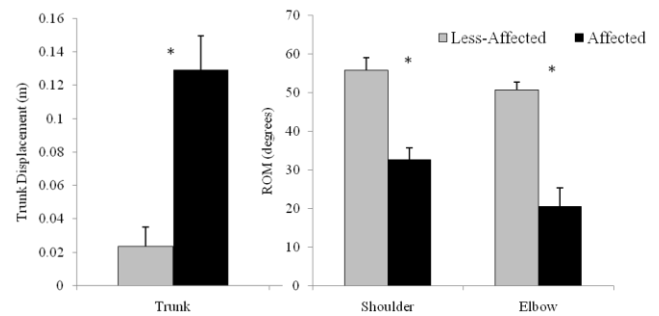


**Figure 2.** Anterior trunk displacement, shoulder ROM, and elbow ROM during forward reach with the less-affected and stroke-affected arm. (Error bars represent SEM; \* indicates  $p < 0.01$ ).

Figure 3 further illustrates the relationship of elbow extension and movement smoothness. Those subjects that demonstrated greater elbow extension had fewer movement units which fell under the spread of movement units when reaching with the less-affected side.

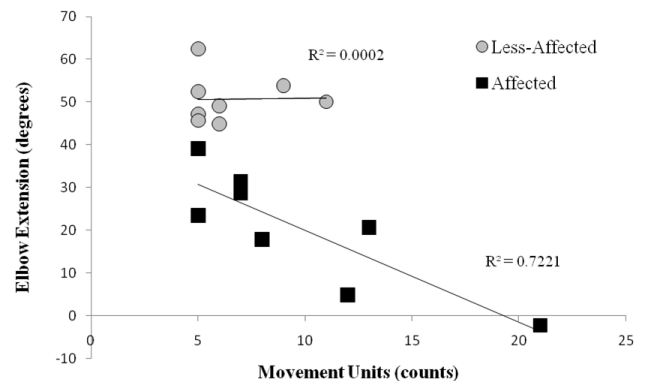


**Figure 3.** Elbow extension is correlated with the number of movement units when reaching with the stroke-affected, but not the less-affected arm.

## CONCLUSIONS

Survivors of stroke may achieve cyclic reaching. The ability, however, may depend on the degree of elbow extension. These findings have implications for incorporating cyclic reaching during interventions.

## REFERENCES

1. Massie C, et al. *Archives of Physical Medicine and Rehabilitation*, 90, 571-579, 2009.
2. Dounskaia N, et al. *Exp Brain Research*, 164, 505-516, 2005.

## ACKNOWLEDGEMENTS

C. Massie is supported by the American Heart Association.

# OBESITY DOES NOT INFLUENCE THE ABILITY OF YOUNG ADULTS TO RECOVER BALANCE FROM A FORWARD FALL WITH A SINGLE STEP

<sup>1</sup>Sara Matrangola, <sup>1</sup>Kerry Costello, and <sup>1</sup>Michael Madigan

<sup>1</sup>Virginia Polytechnic Institute and State University, Blacksburg, VA, USA  
email: [smatrang@vt.edu](mailto:smatrang@vt.edu) web: <http://www.biomechanics.esm.vt.edu>

## INTRODUCTION

Over 33% of US adults, or 72 million, are obese [1]. This total is projected to increase to over 44% by 2020 [2]. Obesity is associated with numerous medical conditions, one of which being an increased risk of falls. For example, obese workers are more likely to experience a fall or multiple falls in the occupational setting [3].

It is possible that the increased risk of falls among the obese may be due to a decreased ability to recover balance after a postural perturbation. Obese individuals exhibit increased postural sway during quiet standing [4] and decreased ability to recover balance using an ankle strategy after perturbations imposing an initial angular velocity on the individual [5]. However, the generalizability of these studies to balance recovery by stepping is unclear. Therefore, the purpose of this study was to investigate the effects of obesity on balance recovery by stepping.

## METHODS

Nineteen male subjects, aged  $21.5 \pm 2.1$  years, participated in this study, including nine obese ( $BMI > 30 \text{ kg/m}^2$ ) and 10 healthy-weight ( $20 < BMI < 25 \text{ kg/m}^2$ ). This study was approved by the Virginia Tech Institutional Review Board, and written consent was obtained from all participants.

Participants were repeatedly exposed to two types of perturbations: position perturbations and velocity perturbations. For position perturbations, participants were released from a static forward lean. This resulted in a perturbation involving an initial displacement of the body center of mass (COM) from its base of support with no initial velocity. Perturbation magnitude was quantified by the force (in percent body weight) in a horizontal

cable used to hold participants in the forward lean. After release from the forward lean, participants attempted to recover balance with a single step of the right foot.

For velocity perturbations, participants stood on a custom-built TRanslatIng Platform (TRIP). The TRIP was pushed at a constant forward velocity until it impacted a rigid stop at the end of a walkway (Figure 1). This resulted in a perturbation involving an initial anteriorly-directed velocity of the body COM relative to the base of support with minimal displacement from an upright standing posture. Perturbation magnitude was quantified by the speed of the TRIP prior to impact. After impact, participants attempted to recover balance with a single step of the right foot.

For each type of perturbation, perturbation magnitude was systematically increased until participants could no longer recover balance using a single step. Participants wore a full body harness for the duration of the experiment to prevent a fall to the ground in the event of an unsuccessful recovery.



**Figure 1.** Photograph of a participant before and after impact of the TRIP during a velocity perturbation trial. An assistant pushed the TRIP and matched speed with a pacing belt.

Whole body kinematics were recorded by placing reflective markers bilaterally over selected anatomical landmarks on the head, arms, trunk, and lower extremities. Marker data were sampled at 100

Hz using a Vicon 460 motion analysis system (Vicon Motion Systems Inc., Lake Forest, CA) and were used to estimate the whole body COM. Whole body COM was calculated using inertial parameter estimate methods by Pavol et al. [6]. The body angle ( $\theta$ ) and body angular velocity ( $\dot{\theta}$ ) were then calculated from a line connecting the non-stepping (i.e. left) ankle to the body COM, and was measured from vertical.

A Wilcoxon Rank-Sum test was used to investigate the effects of obesity on five dependent variables. From the position perturbations,  $\theta_{MAX}$  was the largest initial static lean from which balance could be recovered with a single step (measured from markers immediately before release). From the velocity perturbations,  $\dot{\theta}_{MAX}$ , was the largest body angular velocity immediately after impact from which balance could be recovered with a single step (measured from markers). Liftoff time (i.e. time from perturbation onset to liftoff of stepping toe), step time (i.e. time from perturbation onset to stepping toe contacted the ground), and step length were also compared for each type of perturbation. Statistical analysis was performed using JMP v7 (Cary, North Carolina, USA) with a significance level of  $p \leq 0.05$ .

## RESULTS AND DISCUSSION

There was no difference in  $\theta_{MAX}$  or  $\dot{\theta}_{MAX}$  between healthy-weight and obese participants (Table 1). Additionally, there were no differences in liftoff time, step time, or step length between healthy-weight and obese participants for either type of perturbation.

In our previous study, obesity negatively influenced balance recovery using an ankle strategy only when

perturbations involved an initial angular velocity [5]. It was hypothesized from these results that the increased mass moment of inertia associated with obesity was beneficial for perturbations in which there is limited or no initial velocity, but becomes detrimental as initial velocity increases. In contrast, the current study found no such effect of obesity on balance recovery by stepping. Absolute strength at the hip and knee has been found to be increased in the obese [7]. It is possible that this may help offset the detrimental effects of increased weight and mass-moment of inertia, and would help explain differences in the current study's results compared to the ankle strategy.

## CONCLUSIONS

In conclusion, no differences were found in single step balance recovery ability by stepping between healthy-weight and obese young adults. Additionally, no differences in liftoff time, step time, or step length were found between groups. Future studies will investigate the effects of obesity and aging on recovery after a trip.

## REFERENCES

1. Ogden, C.L., et al. *NCHS Data Brief* 2007.
2. Wang, Y., et al. *Obesity (Silver Spring)* **16**, 2008.
3. Chau, N., et al. *Int Arch Occup Environ Health* **77**, 2004.
4. Handrigan, G., et al. *Int J Obes* 2010.
5. Matrangola, S.L., et al. *Annual Meeting of ASB 2010*, Providence, Rhode Island.
6. Pavol, M.J., et al. *J Biomech* **35**, 2002.
7. Lafortuna, C.L., et al. *Int J Obes (Lond)* **29**, 2005.

## ACKNOWLEDGEMENTS

SLM was supported by a National Defense Science and Engineering Graduate (NDSEG) Fellowship.

**Table 1:** Balance Recovery Measures (no differences found between healthy-weight and obese participants).

|                    | <b>FORWARD LEAN</b>     |                         |                      |                    | <b>TRIP</b>                     |                         |                      |                    |
|--------------------|-------------------------|-------------------------|----------------------|--------------------|---------------------------------|-------------------------|----------------------|--------------------|
|                    | $\theta_{MAX}$<br>(deg) | Liftoff<br>Time<br>(ms) | Step<br>Time<br>(ms) | Step<br>Length (m) | $\dot{\theta}_{MAX}$<br>(deg/s) | Liftoff<br>Time<br>(ms) | Step<br>Time<br>(ms) | Step<br>Length (m) |
| Healthy-<br>Weight | 33.10±2.13              | 169±29                  | 495±30               | 1.19±0.13          | 101.53±14.01                    | 92±20                   | 443±32               | 1.27±0.18          |
| Obese              | 31.46±2.81              | 192±38                  | 517±39               | 1.20±0.11          | 98.71±18.23                     | 88±35                   | 431±24               | 1.21±0.16          |

# OBESITY INCREASES BODY ANGULAR VELOCITY IMMEDIATELY AFTER A TRIP

<sup>1</sup>Sara Matrangola and <sup>1</sup>Michael Madigan

<sup>1</sup>Virginia Polytechnic Institute and State University, Blacksburg, VA, USA  
email: [smatrang@vt.edu](mailto:smatrang@vt.edu) web: <http://www.biomechanics.esm.vt.edu>

## INTRODUCTION

Obesity is a major health concern in the United States (US). It is associated with numerous medical conditions including an increased risk of falls. Falls are the most common cause of hospitalized injuries in the obese (~36% of all injuries) and the cause of a higher proportion of injury-related hospitalization compared to the non-obese [1].

The reason for the increased risk of falls in the obese is unclear. It may be related to alterations in body mass and body segment inertial parameters (BSIPs) associated with obesity making balance recovery after a postural perturbation more challenging than in non-obese individuals. Therefore, the purpose of this study was to investigate the influence of obesity on body kinematics immediately after a perturbation similar to a trip.

## METHODS

The kinematics of the body immediately before the onset of a trip (when the foot during swing impacts an obstacle) can be reasonably modeled as a single segment oriented vertically and translating forward with no angular velocity [2]. Immediately after impact of the foot with the obstacle, the body falls forward and can be reasonably modeled as an inverted pendulum that is pinned and the ground and has a forward angular velocity [2]. The transfer of body linear velocity immediately before the trip to angular velocity immediately after the trip is the focus of this study, as the difficulty of trip recovery likely is related to this body angular velocity.

The impulse momentum-relationship can be used to identify the resulting body angular velocity immediately after a trip [2]. Prior to the trip, the body has a forward velocity  $v$  and no angular velocity. The trip can be approximated by applying

an impulse ( $p$ ) at the base of the body. After the trip, the body forward velocity is zero and the body angular velocity is  $\omega_0$ . Based upon these assumptions, the linear impulse-momentum and angular impulse-momentum equations are:

$$mv = p \qquad I_{ank} \omega_0 = pL_{COM}$$

where  $m$  is the mass of the participant,  $I_{ank}$  is the mass moment of inertia about the ankles, and  $L_{COM}$  is the distance from the ankle (axis of rotation after the trip) to the center of mass (COM). By combining these equations, the ratio of initial angular velocity to initial linear velocity can be expressed as:

$$\frac{\omega_0}{v} = \frac{mL_{COM}}{I_{ank}}$$

It was hypothesized that this ratio would differ between obese and healthy weight adults. To test this hypothesis, nineteen male subjects, aged  $21.5 \pm 2.1$  years, were recruited for this study, including nine obese ( $BMI > 30 \text{ kg/m}^2$ ) and 10 healthy-weight ( $20 < BMI < 25 \text{ kg/m}^2$ ). This study was approved by the Virginia Tech Institutional Review Board, and written consent was obtained from all participants.



**Figure 1.** Participant (a) before and (b) after a TRIP perturbation. An assistant pushed the TRIP and matched speed with a pacing belt.

Participants were repeatedly exposed to anteriorly-directed perturbations by a custom-built TRanslatIng Platform (TRIP). Participants stood on the TRIP, which was accelerated to a constant forward velocity until it impacted a rigid stop connected to a walkway (Figure 1). This imposes an initial anteriorly-directed velocity of the body COM, and results in similar trunk kinematics as

recovery from a trip while walking [3]. After impact, participants attempted to recover balance with a single step of the right foot. Perturbation magnitude (i.e. TRIP speed) was systematically increased until participants could no longer recover balance by using a single step. Also, participants wore a full body harness to prevent a fall to the ground in the event of an unsuccessful recovery.

Whole body kinematics were recorded using a Vicon 460 motion analysis system (Lake Forest, CA, USA). Whole body COM was calculated using inertial parameter estimate methods by Pavol et al. [4]. The body angle ( $\theta$ ) and body angular velocity ( $\omega$ ) were then calculated from a line connecting the non-stepping (i.e. left) ankle to the body COM and was measured from vertical. Using the body angular velocity at perturbation onset ( $\omega_0$ ) and TRIP speed ( $v$ ), the left-hand side of the equation was calculated (*LHS*). Anthropometric measurements and inertial parameter estimates were then used to calculate the right-hand side of the equation (*RHS*) [4, 5].

A t-test was used for all dependent variables to compare between healthy-weight and obese participants. Dependent variables included the average *LHS* (averaged from all successful trials with TRIP speed above 1.5m/s for a participant), the *RHS*,  $L_{COM}$  (normalized to height), and  $I_{ank}$  (absolute and normalized to mass\*height<sup>2</sup>). Additionally, the correlation coefficient was determined between the *LHS* and the *RHS* for each group. Statistical analysis was performed using JMP v7 (Cary, NC, USA) with a significance level of  $p \leq 0.05$ .

## RESULTS AND DISCUSSION

Average group values for all dependent variables are given in Table 1. The *LHS* was 10.1% greater in obese participants compared to healthy-weight ( $p=0.033$ ). The *RHS* was 2.4% higher in obese participants, though these values did not reach statistical significance ( $p=0.171$ ). No differences were found in  $L_{COM}$ . Absolute  $I_{ank}$  was significantly higher in obese participants. Normalized  $I_{ank}$  tended

to be lower in obese participants, though values did not reach statistical significance ( $p=0.135$ ).

Interestingly, the correlation between the *LHS* and the *RHS* is statistically significant for only the healthy-weight participants ( $r = 0.817$ ,  $p=0.004$ ). There was minimal correlation of these variables for obese participants ( $r = -0.076$ ,  $p = 0.847$ ).

First, from calculation of the *LHS*, these results suggest that if a healthy-weight and obese participant were tripped at similar walking speeds, obese participants would have a larger angular velocity of the body about the ankle, increasing the difficulty of recovering from the trip. Second, these results reflect the need for better estimates of BSIPs for obese participants, as seen by the non-significant correlation between the *LHS* and *RHS* in the obese participants.

## CONCLUSIONS

In conclusion, it was found that the ratio of initial linear velocity and initial body angular velocity tends to be larger in obese individuals. This implies that a trip at a similar walking speed would result in a greater body angular velocity in the obese compared to healthy-weight, making trip recovery more difficult. Additionally, more accurate estimates of BSIPs are needed for the obese population.

## REFERENCES

1. Matter, K.C., et al. *Obesity (Silver Spring)* **15**, 2007.
2. van den Bogert, A.J., et al. *J Biomech* **35**, 2002.
3. Caudle, S.K., et al. *Annual Meeting of ASB 2011 [Submitted]*, Long Beach, CA.
4. Pavol, M.J., et al. *J Biomech* **35**, 2002.
5. de Leva, P. *J Biomech* **29**, 1996.

## ACKNOWLEDGEMENTS

SLM was supported by a National Defense Science and Engineering Graduate (NDSEG) Fellowship.

**Table 1:** Dependent variables derived from Eq. 3, \* $p < 0.05$

|                       | <i>LHS</i><br>( $\omega_0/v$ ) | <i>RHS</i><br>( $mL_{COM}/I_{ank}$ ) | $L_{COM}$<br>(normalized) | $I_{ank}$<br>(absolute) | $I_{ank}$<br>(normalized) |
|-----------------------|--------------------------------|--------------------------------------|---------------------------|-------------------------|---------------------------|
| <b>Healthy-Weight</b> | 0.808 ± 0.074 *                | 0.895 ± 0.033                        | 0.537 ± 0.009             | 69.8 ± 8.6 *            | 0.341 ± 0.011             |
| <b>Obese</b>          | 0.890 ± 0.078 *                | 0.916 ± 0.031                        | 0.532 ± 0.009             | 104.2 ± 13.9 *          | 0.333 ± 0.011             |

# The influence of ball mass on youth baseball injury potential: A simulation study

<sup>1,2</sup>Phil Matta, <sup>2</sup>Joseph Myers and <sup>1,2</sup>Gregory Sawicki

<sup>1</sup>North Carolina State University, Raleigh, NC, USA

<sup>2</sup>University of North Carolina, Chapel Hill, NC, USA

email: [pmatta@email.unc.edu](mailto:pmatta@email.unc.edu)

## INTRODUCTION

In order to protect their still developing musculoskeletal system, youth athletes commonly use modified equipment and field sizes compared to their adult counterparts. These modifications are designed to provide protection to the youth player without significantly altering the nature of the game. Youth baseball utilizes smaller fields and different bat materials (i.e. aluminum vs. wood) than the adult game, but surprisingly the baseballs used by both are identical. Previous research has demonstrated that a lightweight baseball limits peak torques on the upper extremity in youth pitchers and may reduce arm injuries [1]. However, a lighter ball, when struck in the same manner, will travel both faster and farther than a standard ball. Pitchers are in the most potential danger as they are positioned only 45 feet from the batter and in a compromised follow through position.

## METHODS

We used a simulation model to compare a lighter ball to a standard ball using (1) the ball exit velocity/reaction time difference for pitchers (2) the difference in pitcher-batted ball impact momentum and (3) the effect of reducing bat-ball coefficient of restitution on exit velocity/reaction time. The simulation included initial conditions for the linear and rotational velocity of the pitched ball, the velocity of the bat at impact, the bat swing angle and the bat-ball undercut distance [2]. These initial conditions were combined with ball and bat properties to determine the linear and rotational velocity of the batted ball, as well as the launch angle of its trajectory at separation. We used the final conditions at separation and a simple aerodynamic model to compute the trajectory of the batted ball.

## RESULTS AND DISCUSSION

Simulations at the mean bat and ball velocity combination (Fig. 1) indicate that a 4-ounce ball (lightweight) reaches a pitcher standing 45 feet away 11% faster (410ms vs. 460ms) than a 5¼-ounce ball (standard). This translates to a 60 millisecond reduction in available reaction time for the pitcher. Even though the lighter ball travels at a higher velocity than the standard ball, the momentum of the ball at a potential impact with the pitcher is 11% less due to the decrease in mass. Finally, decreasing the coefficient of restitution (COR) from the NCAA and MLB standard range of  $0.525 < \text{COR} < 0.550$  to 0.470 decreases the exit velocity of the lightweight batted ball to that of the standard batted ball, decreases the momentum at a potential batted ball-pitcher impact by 22% (Table 1.) and decreases the batted ball range by less than 3 meters (Fig. 2 & Fig. 3).

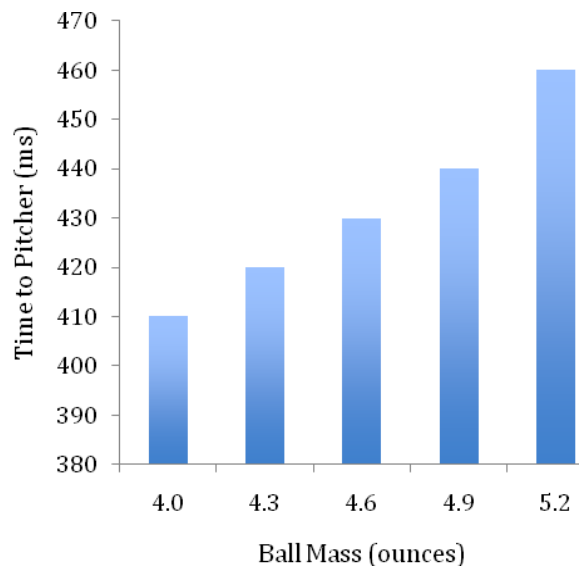


**Figure 1:** Flight time for baseballs with varying mass to reach a pitcher positioned 45 feet away.

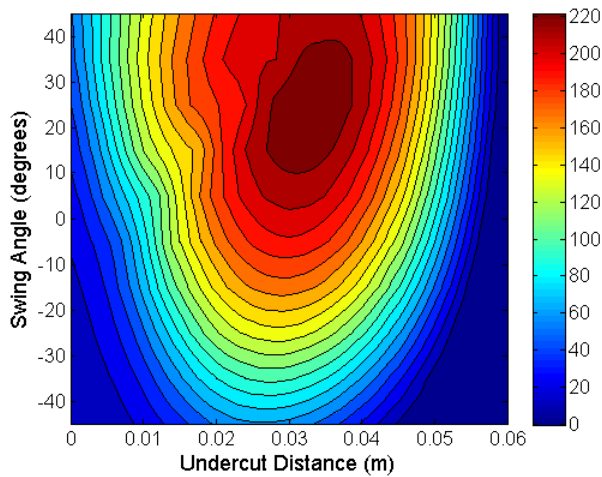


**Figure 2:** Batted ball range (ft) contour for a standard ball.

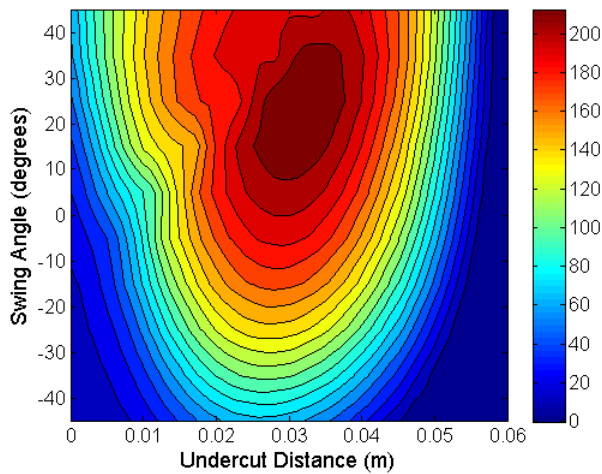


**Figure 3:** Batted ball range (ft) contour for a reduced COR lightweight ball.

## CONCLUSIONS

In summary, the implementation of a lightweight ball in youth baseball would result in an increase in batted ball exit velocity, leaving pitchers with less time to react. However, this added danger is offset by reduced impact momentum in a potential batted ball-pitcher collision. Implementing a lighter ball with a reduced COR may be the optimal adjustment to the game as it reduces the loads on the upper extremity of the pitcher, does not increase the exit velocity of the ball, decreases the impact momentum at a potential batted ball-pitcher collision all without significantly altering the maximum range of batted balls.

In future work, we hope to use the modeling framework presented here to examine changes that could be made to bats and balls in order to scale the game of baseball down, so it can be played in areas with space limitations like urban neighborhood parks. Additionally, we hope to examine if standard clinical measurements of reaction time correlate to a youth pitchers ability to avoid balls that are redirected at them after being struck.

## REFERENCES

1. Fleisig, et al. *Sports Engineering* **9**, 155-163, 2006.
2. Sawicki, et al. *Am J. Phys.* **71**, 1152-1162, 2003.

**Table 1:** Comparison of three balls simulated: (1) Lightweight ball, (2) Standard Ball and (3) Lightweight ball with reduced COR.

| Ball Mass (ounce) | COR  | Exit Velocity (m/s) | Time To Pitcher (ms) | Momentum at Impact (kgm/s) |
|-------------------|------|---------------------|----------------------|----------------------------|
| 4.00              | 0.54 | 34                  | 410                  | 3.68                       |
| 5.25              | 0.54 | 31                  | 460                  | 4.14                       |
| 4.00              | 0.47 | 31                  | 460                  | 3.21                       |

# MUSCLE AND FASCICLE EXCURSIONS IN CHILDREN WITH CEREBRAL PALSY

<sup>1</sup>Sigrun Matthiasdottir, <sup>1</sup>Marlee Hahn, <sup>1</sup>Megan Yaraskavitch, <sup>1</sup>Walter Herzog  
<sup>1</sup>Human Performance Lab, University of Calgary, Canada  
smatthiasdottir@kin.ucalgary.ca

## INTRODUCTION

Cerebral Palsy (CP) is a static lesion in the brain that happens before, during or shortly after birth. It is a non-progressive disorder that leaves children with permanent motor impairments [1]. Many children with CP have spasticity, which is defined as a velocity-dependent resistance of muscles to stretch [2]. Joint contractures often form when spastic muscles become taut and inhibit the full range of motion (ROM) of the joint [3]. Furthermore, children with CP often have weak muscles [1]. The detailed reasons for why muscles become taut remain unknown. It has been suggested in some studies that short fascicle lengths (FL) in spastic muscles cause tightening [4] but other studies do not confirm these findings [5]. There are currently no studies where fascicle excursions were examined for dynamic conditions. The purpose of this study was to measure FL and muscle and fascicle excursions of the medial gastrocnemius (MG) for the full passive ROM of the ankle in children with CP and typically developing (TD) controls.

## METHODS

The experimental group included 8 children with CP between the ages of 8 and 16. The control group included 14 age and sex-matched TD controls. Children with CP were recruited from the Calgary Cerebral Palsy Association and the Cerebral Palsy Association in Alberta. The control group was recruited from the Calgary community. Six of the eight experimental group children had a sex-matched twin sibling that was used for the control group. The children were seated in the chair of a Biodex™ System III dynamometer (Biodex Medical Systems Inc., New York, USA), and their foot was strapped to a footplate. EMG electrodes were placed on the MG and the tibialis anterior muscles. An ultrasound probe (Koninklijke Philips Electronics N.V., The Netherlands) was fixed to the lower leg to visualize the myotendinous (MT) junction first and the mid-belly of the MG muscle second. Torque, ankle angle

and EMG data were collected for four passive trials covering the full ROM of the ankle joint. A common ROM was defined as the range from the lowest maximum dorsiflexion to the lowest maximum plantarflexion found between all subjects. The resting ankle joint angle (RJA) was defined with the leg completely relaxed and was measured. Fascicle lengths and MT displacements were measured from the ultrasound images. In cases where fascicle lengths were not fully visible, trigonometric relationships were used to calculate fascicle lengths from the measured pennation angle ( $\alpha$ ) and muscle thickness ( $T_m$ ) (Figure 1). Non-parametric Mann-Whitney U-statistics ( $\alpha=0.01$ ) were used to test for differences in fascicle lengths, fascicle excursions and muscle excursions between experimental and control group children.

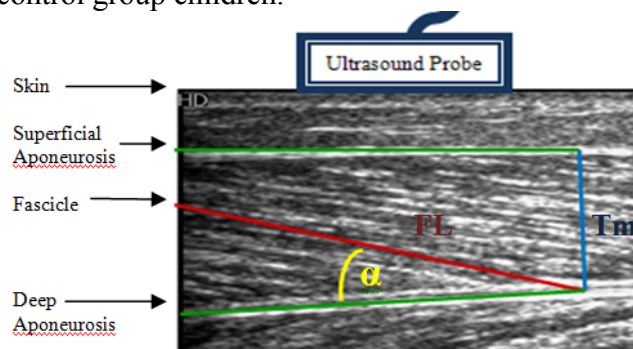


**Figure 1:** FL calculation from an ultrasound image of the MG:  $FL = T_m / \sin(\alpha)$ . Green lines delineate the superficial and deep aponeuroses, blue the muscle thickness ( $T_m$ ), and red the fascicle (FL). Yellow ( $\alpha$ ) defines the pennation angle.

## RESULTS

The common ROM was 87-126°. Fascicle lengths at all ankle angles were shorter for CP children (Figure 2), while fascicle excursions over the common ROM were not significantly different from TD control subjects. However, fascicle excursions as a percent of resting fascicle lengths were significantly greater for CP subjects (Figure 3). Muscle-tendon excursions over the common ROM were greater for control group subjects. Fascicle excursions as a percentage of muscle-tendon excursions were greater in children with CP compared to TD controls.

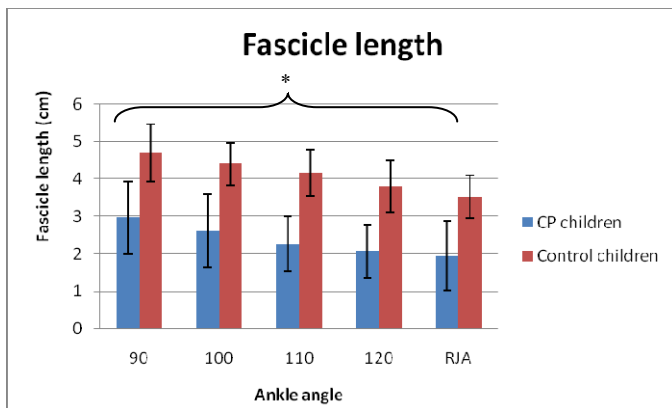


**Figure 2:** Fascicle lengths were shorter for the CP children than control at all ankle angles.

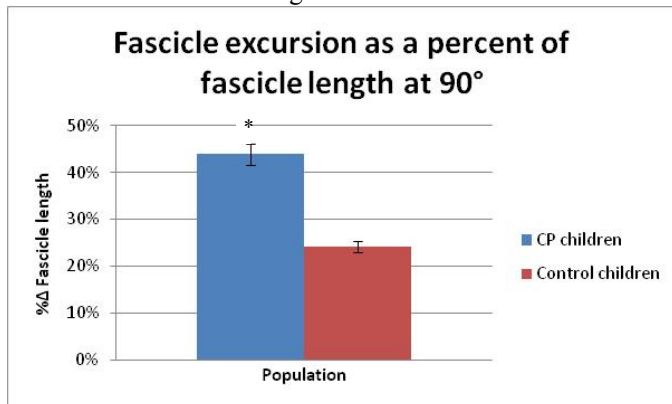


**Figure 3:** Fascicle excursion as a percent of fascicle length at 90° was greater for CP children (44%) than control (24%).

## DISCUSSION

Our results show that fascicle lengths are shorter in children with CP than those in age-matched TD controls and therefore confirm previous results [4]. We also show that fascicle excursions as a percentage of resting fascicle lengths and as a percentage of muscle-tendon excursions are greater in CP children than TD controls over a common ROM. There was no significant difference in absolute fascicle excursions between the groups, but since the fascicles in CP subjects are much shorter, the relative fascicle excursions are greater. The short fascicles and the large relative fascicle excursions imply that the sarcomeres in CP children undergo much greater excursions than in TD controls. It has also been found in static experiments that sarcomere lengths in CP patients are on average much longer than in control subjects for corresponding joint angles [6]. Combined, these results suggest that sarcomeres operate over a greater range and at longer lengths in CP children than in TD age- and sex-matched control subjects. Therefore, it appears that muscle fibres are shorter

and sarcomeres are longer in CP children than controls. This finding has important functional implications for CP patients struggling with strength and joint mobility. First, working at longer than normal sarcomere lengths would likely be associated with sarcomeres operating on the descending limb of the force-length relationship where muscle force is compromised because of lack of actin-myosin filament overlap [7]. Second, at these long sarcomere lengths, and with greater than normal sarcomere excursions during normal movements, passive forces would be increased compared to normal thus restricting full range of joint motion, or at least resisting full motion through passive forces to a greater extent than in TD control children.

## CONCLUSIONS

Our results confirm previous findings that FL are shorter in children with CP compared to TD children. We also show that fascicle excursions relative to fascicle lengths and muscle-tendon excursions are greater in children with CP over a universal ROM. This novel result has important implications for the impairment of function in CP children during everyday movements.

## REFERENCES

1. Campell SK. *Decision Making in Pediatric Neurologic Physical Therapy*. Philadelphia: Churchill Livingstone, e89-97,1999
2. Sanger TD, et al. *Classification and Definition of Disorders Causing Hypertonia in Childhood*. *Paediatrics* 1, e89-97, 2003.
3. Pontén E, et al. *Muscle and Nerve* **36**, 47-54, 2007.
4. Mohagheghi AA, et al. *Developmental Medicine and Child Neurology* **50**, 44-50, 2008.
5. Malaiya R, et al. *Journal of electromyography and Kinesiology* **17**, 657-663, 2007.
6. Friden, I. *Muscle and Nerve* **27**, 157-164, 2003.
7. Gordon et al., *J. Physiol*, **184**, 170-192, 1966.

## ACKNOWLEDGEMENTS

The Canada Research Chair Programme (WH)  
 NSERC CREATE (SM)  
 Calgary Cerebral Palsy Association  
 Calgary Youth Physiotherapy  
 Cerebral Palsy Association in Alberta  
 Alberta Children's Hospital

# MECHANICAL PROPERTIES OF HUMAN CRANIOVERTEBRAL LIGAMENTS

Stephen Mattucci, Duane Cronin, Naveen Chandrashekar, and Jeff Moulton

University of Waterloo, Waterloo, ON, Canada

email: smattucci@uwaterloo.ca

## INTRODUCTION

During physiological motion, cervical spine ligaments limit the range of motion of the neck. However, the integrity of these ligaments can be compromised under excessive loading, specifically during vehicle crash scenarios, which is the leading cause of upper cervical spine injury [1]. Techniques to predict injury, such as the use of finite element models, require accurate mechanical properties, at relevant deformation rates. Currently, there is very limited experimental data for the craniovertebral ligaments connecting the skull to the spine although much of the motion in the neck occurs at this joint, where the structure is very complex, making ligament isolation and testing difficult. The published data are limited to failure force and elongation values at quasi-static rates [2]. The purpose of this study was to investigate the tensile mechanical properties of the craniovertebral ligaments at different deformation rates, to support the development and validation of a detailed cervical spine finite element model.

The study included the tectorial membrane/vertical cruciate/apical/alar ligament complex (TM complex, tested together for modeling purposes), transverse ligament (TL), anterior atlanto-occipital membrane (AAOM), and posterior atlanto-occipital membrane (PAOM).

## METHODS

Sixteen post mortem human subject spines (9 male and 7 female) were tested with an average age of 45 (27-60) years old, height 165 (145-184) cm, and weight 68.4 (36.8-159.1) kg. The spines were kept frozen and then thawed for preparation and testing. Specimens were isolated into bone-ligament-bone complexes, measured, and then potted in a casting resin. Not all ligaments from a given spine could be tested since adjacent ligaments were damaged in the isolation process. Therefore, two spines were required to obtain one of each ligament. For each

spine, the TM complex and TL, or the AAOM and PAOM were isolated for testing.

The TL runs beneath the TM, laterally across the vertebral foramen of C1 (atlas), physiologically keeping the odontoid process in contact with the articular cavity of the anterior tubercle of C1. The Skull-C1-C2 segment was potted at the occiput and C2 vertebra, and the TM complex was carefully tested with the TL in place, so it could then be isolated and tested afterward. The AAOM and PAOM were too wide to fit inside the test fixture grips, so they were carefully separated along the direction of the fibers, without damaging any ligament fibers, into left and right portions for testing.

Tensile tests were performed in an atmospheric chamber at a temperature of  $37 (\pm 1)^\circ\text{C}$  with humidity levels  $>90\%$  to replicate *in vivo* conditions. The ligaments were tested at constant quasi-static ( $0.5\text{s}^{-1}$ ) and high ( $150\text{s}^{-1}$ ) strain rates, which were determined to encompass representative rates for these ligaments in automotive crash scenarios, using an existing detailed cervical spine finite element model [3]. The quasi-static tests were performed using a hydraulic tensile testing fixture and the high strain rate tests were performed using a custom electromagnetic tensile testing fixture. All ligaments underwent a preconditioning phase of 10% strain for 20 cycles prior to being tested to failure.

## RESULTS AND DISCUSSION

Force-elongation curves for the TM complex (Figure 1) include the post-ultimate load response, which shows how the ligaments often fail in a stepwise manner, still supporting load as ligament fibres subsequently fail. There were no significant geometric or property differences between the left and right halves of the AAOM and PAOM, so left/right were grouped together. The plotted values represent half of the entire ligament.

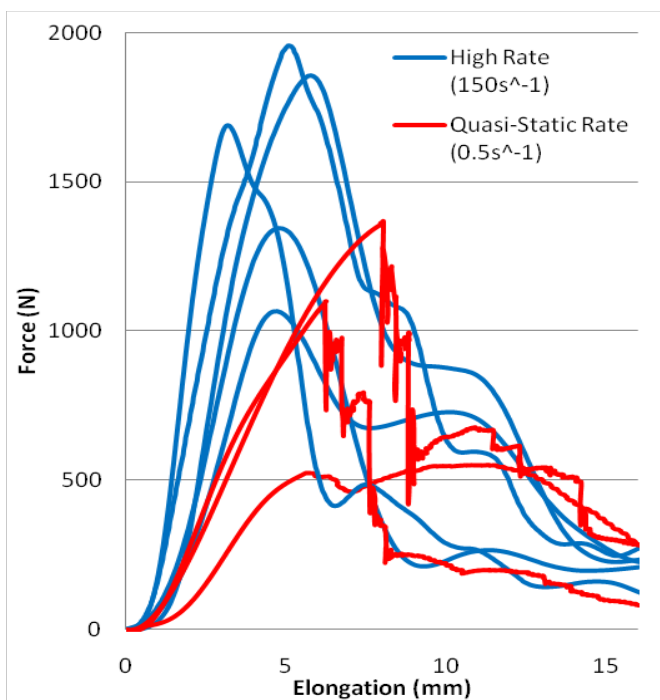


**Figure 1** - Force-Elongation curve of TM complex.

Eight metrics were used to evaluate the response including: failure force, failure elongation, stiffness of linear region, toe region elongation, nominal failure stress, failure strain, modulus, and toe region strain, and reported as average (SD) values (Table 1). All properties were investigated for gender and strain rate effects, those denoted with an asterisk\* were found to be statistically significant at  $p < 0.05$  based on ANOVA.

The significant effects were as follows. The TM complex showed a decrease in failure elongation from 8.55mm (2.57) at quasi-static to 4.71mm (0.96) at high rate, a decrease in failure strain from 0.43 (0.10) at quasi-static to 0.27 (0.04) at high rate, and an increase in stiffness from 219N/mm (51) at quasi-static to 590N/mm (183) at high rate. There was a significant gender effect for the failure force

of the TL, as female ligaments failed at a higher force of 528N (84) compared to male 392N (52). The PAOM had a gender effect for modulus, as the male ligaments had a higher modulus of elasticity 1.63MPa (0.82) than female ligaments of 1.02MPa (0.35).

The results are in agreement with the limited existing data [2], however the measured failure forces were higher and failure elongations smaller, possibly due to the younger age of the samples in this study.

## CONCLUSIONS

This is the first study that has reported detailed data on the tensile properties of young craniovertebral ligaments at different strain rates. The results demonstrate increasing stiffness and decreasing elongation with increasing strain rate for the TM complex. There were no consistent gender effects observed, which could be related to the small sample sizes for these tests. The measured properties are essential for developing response curves for ligaments in detailed finite element models.

## ACKNOWLEDGEMENTS

Global Human Body Model Consortium

## REFERENCES

1. Jackson RS, et al. *J Am Acad Orthop Surg* **10**, 271-280, 2002
2. Myklebust JB, et al. *Spine* **38**, Milwaukee, WI, USA, 1986.
3. Fice J, et. al, *Proceedings of ESV '08*. Stuttgart, Germany, 2009.

**Table 1.** Average measured tensile properties of Craniovertebral ligaments.

| Ligament   | Sample Size | Failure Force (N) | Failure Elongation (mm) | Stiffness (N/mm) | Toe Region (mm) | Failure Stress (MPa) | Failure Strain | Modulus (MPa) | Toe Region Strain |
|------------|-------------|-------------------|-------------------------|------------------|-----------------|----------------------|----------------|---------------|-------------------|
| TM complex | 8           | 1366 (466)        | 6.25 (2.5)†             | 441 (235)†       | 1.9 (0.7)       | 41.3 (12.6)          | 0.33 (0.1)†    | 13.3 (6.6)    | 0.10 (0.03)       |
| TL         | 6           | 460 (97)*         | 5.22 (0.5)              | 184 (35)         | 3.2 (0.8)       | 25.0 (7.3)           | 0.26 (0.04)    | 10.0 (2.6)    | 0.15 (0.04)       |
| AAOM       | 15          | 511 (138)         | 5.91 (1.5)              | 159 (56)         | 2.0 (0.8)       | 6.2 (1.7)            | 0.48 (0.14)    | 1.9 (0.5)     | 0.16 (0.05)       |
| PAOM       | 16          | 173 (63)          | 6.21 (3.3)              | 69 (42)          | 1.7 (0.8)       | 3.6 (1.1)            | 0.45 (0.18)    | 1.4 (0.7)*    | 0.13 (0.07)       |

Statistical significance with respect to gender\* or loading rate†.

# VOLUNTARY CHANGES IN STEP WIDTH AND STEP LENGTH AFFECT STEP-TO-STEP STABILITY DURING HUMAN WALKING

<sup>1</sup>Patricia M. McAndrew Young and <sup>1</sup>Jonathan B. Dingwell

<sup>1</sup>University of Texas at Austin, Austin, TX, USA  
email: mcandrew@mail.utexas.edu

## INTRODUCTION

Changes in step width (SW) and step length (SL), and the variability of these gait parameters, may reflect changes in walking stability, but do not quantify stability (i.e. sensitivity to perturbations) directly [1]. However, increased SW [2] and SL and ST variability [3] do predict increased fall risk.

Hof et al. [4] proposed to use dynamic margins of stability (MOS) to estimate instantaneous stability during walking. MOS relate the extrapolated center of mass (XcoM) to the edge of an individual's base of support (BOS). They are directly related to SW and step time and thus link gait characteristics to mechanical definitions of stability. MOS vary little between walking conditions suggesting that foot placement might be used to maintain a roughly constant mean MOS [5]. Computing only mean MOS across multiple consecutive strides, however, ignores the step-to-step variations in MOS as well as any changes in a given stride that might compensate for events, or stability states, from the previous stride(s).

This study determined if voluntarily adopting wider or shorter steps elicited changes in instantaneous stability. We determined if dynamic step-to-step changes in MOS provided additional insight into *control* of walking stability.

## METHODS

Thirteen healthy young adults completed three 3-minute trials of treadmill walking under each of 6 conditions. Three conditions manipulated step width: normal walking (NO) and walking with wide steps (WI) or narrow steps (NA), and three conditions manipulated step length: normal walking with a metronome (NM) and walking with long (LO) or short (SH) steps. Kinematic data for

the head, trunk, pelvis, arms, legs and feet were collected at 60 Hz using 10 Vicon MX cameras.

Means and standard deviations of step width (SW), length (SL) and stride time (ST) were calculated for each trial. A 14-segment model was used to estimate COM position and velocity. MOS were calculated as the difference between the XcoM and edge of the BOS as in [1].  $MOS_{ap}$  was the perpendicular distance between the XcoM and the line joining the toe markers (Fig. 1A).  $MOS_{ml}$  was the lateral distance between the XcoM and the lateral heel marker of the foot in heelstrike (Fig. 1A). Positive MOS indicate that the XcoM projection is within the BOS. Two-way analyses of variance (condition x subject) were used to assess statistical significance.

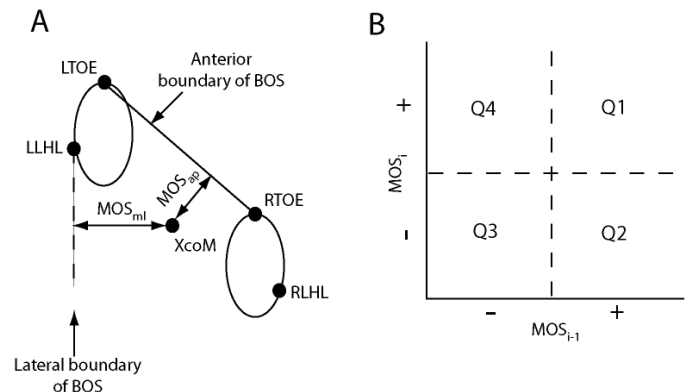


**Figure 1.** (A) Definition of ML and AP margins of stability ( $MOS_{ml}$  and  $MOS_{ap}$ ). LTOE, RTOE, LLHL and RLHL indicate the right and left toe and lateral heel markers. (B) Quadrant definitions for comparisons of stability between steps.

To examine dynamic *step-to-step control* of stability, we quantified the distribution of stability of each step ( $MOS_i$ ) vs. the previous step ( $MOS_{i-1}$ ) in the  $MOS_i$  vs.  $MOS_{i-1}$  plane. Points in quadrants 1 (Q1) and 2 (Q2) indicated stable (+) steps followed

by stable (+) or unstable (-) steps, respectively (Fig. 1B). Points in quadrants 3 (Q3) and 4 (Q4) indicated unstable (-) steps followed by unstable (-) or stable (+) steps, respectively (Fig. 1B).

## RESULTS AND DISCUSSION

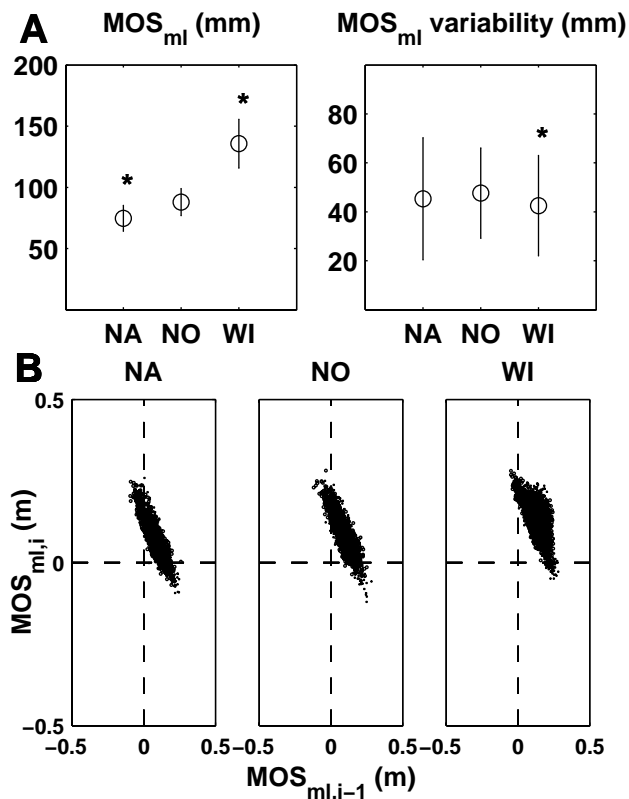


**Figure 2.** (A) Mean and variability of MOS<sub>ml</sub> and MOS<sub>ml</sub> variability for SW manipulations. Error bars indicated standard deviation of the mean. \* indicate significant difference ( $p < 0.05$ ) from NO. (B) MOS<sub>i</sub> vs. MOS<sub>i-1</sub> for NA, NO and WI.

SL manipulations (not shown) yielded no change in mean MOS<sub>ap</sub> or MOS<sub>ap</sub> variability ( $p \geq 0.709$ ). Long steps were associated with increased MOS<sub>ml</sub> and MOS<sub>ml</sub> variability ( $p \leq 0.001$ ). SW manipulations altered mean MOS and MOS variability (Fig. 2A). Walking with narrow steps yielded significant increases in MOS<sub>ap</sub> and decreases in MOS<sub>ml</sub> ( $p < 0.0005$ ). Walking with wider steps had the opposite effect ( $p < 0.0005$ ). Decreased SW has been associated with increased

fall risk [2]. Our results indicate that increasing SW does increase average lateral stability (Fig. 2A).

MOS<sub>i</sub> vs. MOS<sub>i-1</sub> plots demonstrated strong negative linear relationships for MOS<sub>ml</sub> (Fig. 2B). Most stable steps were followed by stable steps (Q1). Strongly stable steps (large MOS<sub>ml</sub>) were sometimes followed by slightly unstable steps (Q2). However, all unstable steps were immediately followed by strongly stable steps (Q4). This relationship was not evident in the mean MOS or MOS variability results (Fig. 2A). The observed relationship supports previous work suggesting ML stability is actively controlled during walking [6].

## CONCLUSIONS

“Cautious” walking is generally associated with wider and/or shorter steps. Voluntarily walking with wider steps increased lateral stability margins. Shorter steps caused no significant changes in MOS<sub>ml</sub>. However, only by examining step-to-step changes in stability (Fig. 2B) do we see how MOS<sub>ml</sub> appears to be directly controlled from each step to the next during walking.

## REFERENCES

1. Kang HG & JB Dingwell (2008) *J Biomech.* 41:2899-2905.
2. Maki, BE (1997) *J Amer Ger Soc*, 45:313-320.
3. Hausdorff, J.M. et al (2001) *Arch Phys Med Rehabil*, 82:1050-1056.
4. Hof AF, et al. (2005) *J Biomech.* 38:1-8, 2005.
5. Rosenblatt NJ & MD Grabiner (2010) *Gait & Posture*. 31:380-384.
6. Bauby & Kuo, AD (2000) *J Biomech* 33:1433-40.

## ACKNOWLEDGEMENTS

Partially supported by an ASB Graduate Student Grant-in-Aid Award (to PMMY) and NIH Grant #1-R21-EB007638-01A1 (to JBD).

# VOLUNTARILY CHANGING STEP WIDTH AND STEP LENGTH AFFECTS DYNAMIC STABILITY OF HUMAN WALKING

<sup>1</sup>Patricia M. McAndrew Young and <sup>1</sup>Jonathan B. Dingwell

<sup>1</sup>University of Texas at Austin, Austin, TX, USA  
email: mcandrew@mail.utexas.edu

## INTRODUCTION

Changes in step width and step length, and their variability in particular, can prospectively indicate increased fall risk [1,2]. However, we do not know how these changes in gait parameters specifically affect an individual's dynamic stability. Measures from nonlinear dynamics, specifically Floquet multipliers (FM) and local divergence exponents (LDE), directly quantify local stability (i.e., response to minute perturbations) during human walking [3,4]. While these measures have demonstrated some promise, they are not intuitively obvious and have not yet been fully validated for clinical use or relevance. The present study determined if simple, voluntary changes in gait characteristics, such as step width and step length, could elicit changes in orbital and local stability of humans during unperturbed treadmill walking.

## METHODS

Fourteen young healthy adults (7 male, 7 female; age, 19 - 28) participated. Participants walked on a motorized treadmill at their preferred walking speed (PWS) and completed three 3-minute walking trials for each of 6 experimental conditions. During the step width (SW) manipulations, subjects walked normally (NO) and then with either wider (WI) or narrower (NA) steps. During the step length (SL) manipulations, subjects walked with in time with a metronome matched to their NO gait (NM) and with either shorter (SH) or longer (LO) steps.

Means and standard deviations of SL, SW and stride times (ST) were calculated for each trial. Additionally, state-spaces were generated using 5-dimensional delay-embedded state spaces of the C7 vertebral marker velocity in the mediolateral (ML), anterior-posterior (AP) and vertical (VT) directions.

To quantify orbital stability of these C7 movements, maximum FM (maxFM) were computed for each time series [4]. If the maxFM had magnitude  $< 1$ , perturbations decayed after successive strides, and the system was orbitally stable. LDE were calculated to quantify short-term and long-term local dynamic stability [3-5]. Larger LDE indicate greater local dynamic instability.

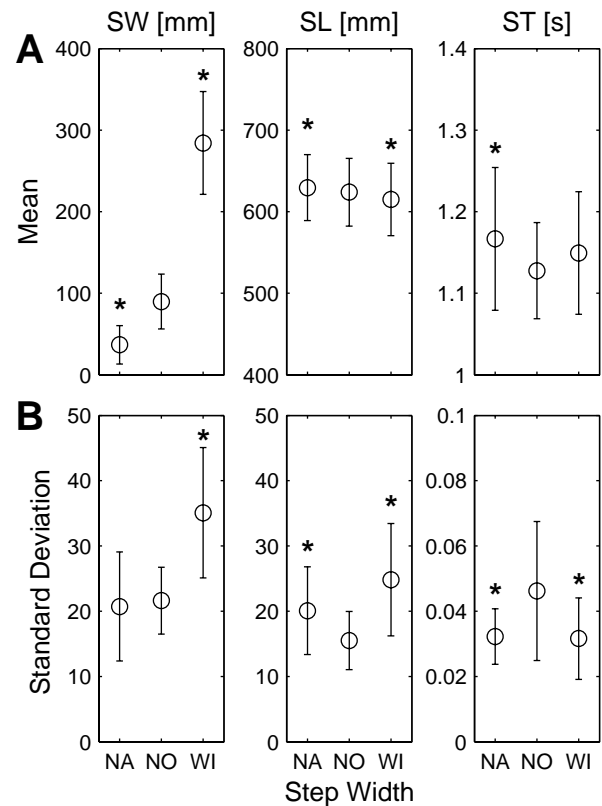


**Figure 1.** (A) Step width (SW), step length (SL) and stride times (ST) and (B) SW, SL and ST variability for the SW manipulations. Error bars are  $\pm 1$  standard deviation. \* indicates  $p < 0.05$ .

Two-way analysis of variance was used to determine differences between gait parameters, variability, maxFM and LDE for the SL and SW manipulations separately.

## RESULTS AND DISCUSSION

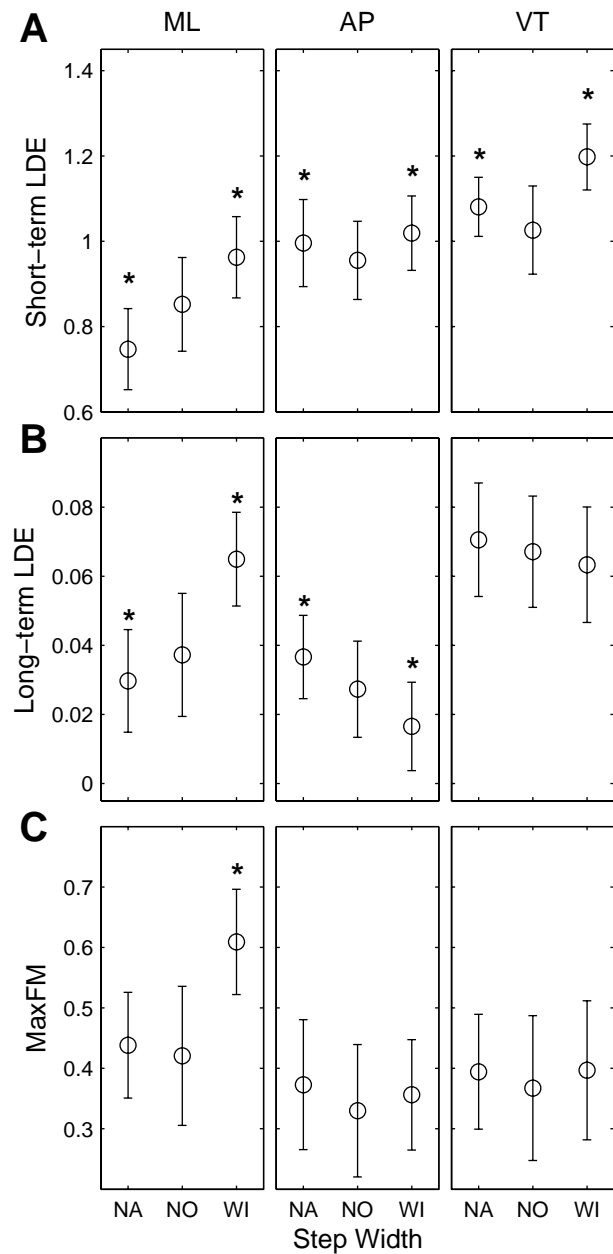


**Figure 2.** (A) Short-term, (B) long-term and (C) orbital stability for the SW manipulations conditions. Error bars are  $\pm 1$  standard deviation. \* indicates  $p < 0.05$ .

When walking with wider or narrower steps, SW were significantly wider and narrower than NO ( $p < 0.001$ ; Fig. 1A), respectively, as expected. SW variability increased significantly when walking with wider steps (Fig. 1B).

When walking with longer or shorter steps (not shown), SL and ST were significantly longer and shorter than NM, respectively ( $p \leq 0.001$ ). SW variability increased when walking with longer or shorter steps ( $p < 0.05$ ). All voluntary changes in gait parameters caused increased SL variability ( $p < 0.001$ ; Fig. 1B).

All voluntary changes in SW caused significant changes in short-term LDE in the ML, AP and VT directions ( $p < 0.05$ ; Fig. 2A) and in long-term LDE in the ML and AP directions ( $p < 0.05$ ; Fig. 2B). Similar trends were observed for the SL manipulations (not shown). Walking with wider (Fig. 2C) or longer (not shown) steps increased lateral maxFM, indicating decreased orbital stability ( $p \leq 0.015$ ).

Our results indicate that simple, voluntary changes in gait do significantly affect an individual's gait variability and their orbital and local stability. Taking wider and longer steps caused decreased orbital stability and long-term LDE in the ML direction. Taking shorter and wider steps caused decreased short-term LDE in the ML direction. All imposed changes in SL and SW resulted significant changes in short-term LDE. Contrary to what we would have anticipated, taking wider steps, at least during the very short-term adaption conditions tested here, led to more unstable movements, rather than to more stable movements. Thus, simply telling individuals with increased fall risk to walk with wider steps may not reduce their fall risk.

## REFERENCES

1. Maki, B.E. (1997) *J Amer Ger Soc*, 45:313-320.
2. Hausdorff, J.M. et al (2001) *Arch Phys Med Rehabil*, 82:1050-1056.
3. Dingwell, J.B. and Cusumano, J.P. (2000) *Chaos*, 10(4):848-863.
4. Kang, H.G. and Dingwell, J.B. (2008) *Journal of Biomechanics*, 41(14):2899-2905.
5. Rosenstein, M. et al. (1993) *Physica D*, 65:117-134.

## ACKNOWLEDGEMENTS

Partially supported by ASB Graduate Student Grant-in-Aid Award (to PMMY) and NIH Grant # 1-R21-EB007638-01A1 (to JBD).

# GROUND REACTION FORCES DURING STAIR ASCENT IN PREGNANT FALLERS AND NON-FALLERS

<sup>1,2</sup>Jean L. McCrory, <sup>2</sup>April J. Chambers, <sup>2,3</sup>Ashi Daftary, and <sup>2</sup>Mark S. Redfern

<sup>1</sup>West Virginia University, Morgantown, WV, USA, <sup>2</sup>University of Pittsburgh, Pittsburgh, PA, USA,

<sup>3</sup>West Penn Allegheny Health System, Pittsburgh, PA, USA

email: [jmccrory@hsc.wvu.edu](mailto:jmccrory@hsc.wvu.edu)

## INTRODUCTION

Falls are a significant risk factor during pregnancy, as over 27% of women fall while pregnant [1, 2]. Falls are a leading cause of trauma-related hospital admissions during pregnancy [3]. Approximately 40% of the falls happen during stair locomotion [1, 2]. Additionally, evidence indicates that pregnant women who fall may have altered neuromuscular control compared to pregnant non-fallers and non-pregnant controls [4, 6].

Ground reaction forces (GRFs) during gait [5, 6] and stair locomotion [7] have been reported for pregnant women. No significant differences in GRFs were noted during gait for women during pregnancy and post-partum [5] or between women in their 2<sup>nd</sup> and 3<sup>rd</sup> trimesters and non-pregnant controls [6]. However, the mediolateral (ML) position of the center of pressure (COP) during the stance phase of gait is shifted laterally during pregnancy [5]. Pregnant fallers in their 3<sup>rd</sup> trimester display a greater ML excursion of the COP during stance than pregnant non-fallers and controls [6]. During stair ascent, women in their 3<sup>rd</sup> trimester demonstrate greater medial and vertical impulses, or area under the GRF curve [7]. Additionally, compared to non-pregnant women, pregnant women in the latter two trimesters display a smaller impact peak and loading rate of the vertical GRF [7].

This study examined GRFs during stair ascent in pregnant fallers, pregnant non-fallers, and non-pregnant controls. We hypothesized that pregnant fallers would demonstrate greater ML GRF magnitudes as well as greater ML excursion of the COP compared to the pregnant non-fallers and non-pregnant control subjects.

## METHODS

Forty one pregnant women (age: 29.5±4.9 yrs, hgt: 1.7±0.7 m, 2<sup>nd</sup> tri. mass: 74.7±12.1 kg, 3<sup>rd</sup> tri. mass: 81.6±11.0 kg) and 40 non-pregnant controls (age: 26.5±6.4 yrs, hgt: 1.7±0.6 m, mass: 66.0±8.9 kg) participated. Data were collected on the pregnant women in the middle of their 2<sup>nd</sup> and 3<sup>rd</sup> trimesters and on the control women in the week following menses.

Informed consent was obtained during the subjects' first visit. At each visit, pregnant subjects were surveyed about their history of falls while pregnant. A fall was defined as a loss of balance such that another part of the body other than a foot touched the ground. Fifteen pregnant subjects were classified as 'fallers' by having at least one fall and 14 as 'non-fallers'. Twelve pregnant subjects withdrew from the study prior to their 3<sup>rd</sup> trimester visit.

Subjects walked at their freely chosen speeds up a four-step staircase during stair ascent. A force plate imbedded in the second stair, but structurally independent of the staircase, was used to collect GRF data (1080 Hz). Kinematic data (120 Hz) were collected from a marker placed on the lumbar spine to determine ascent velocity. Three trials were collected from each subject. All GRF variables were normalized to body weight.

A one-factor ANCOVA was performed between groups (control, pregnant faller, pregnant non-faller) on each of these ML GRF variables: max medial force, time to max medial force, medial impulse, max lateral force, time to max lateral force, and lateral impulse. Stair ascent velocity was a covariate in each statistical analysis. Anteroposterior (AP) GRF variables were also analyzed using ANCOVA: max braking force, time to max braking force,

braking impulse, max propulsive force, time to max propulsive force, and propulsive impulse. An ANCOVA was performed on each of these vertical GRF variables: impact peak, time to impact peak, loading rate, active peak, time to active peak, and impulse. (Bonferroni-corrected  $\alpha = 0.008$ ) An ANCOVA was performed for the ML excursion of the COP during stance and stance time (Bonferroni-corrected  $\alpha = 0.025$ ). Tukey post-hoc tests were performed when appropriate ( $\alpha = 0.05$ ).

## RESULTS AND DISCUSSION

In the ML GRFs, the max medial force was larger in the pregnant fallers compared to the pregnant non-fallers and controls. In the AP GRFs, pregnant fallers displayed a longer time to the max braking force than the pregnant non-fallers and a greater braking impulse than the pregnant non-fallers and controls. Variables that were significantly different between the groups are shown in Table 1. No differences were noted between the pregnant non-fallers and the controls, nor were any differences noted between groups in the vertical GRFs. Additionally, neither stance time ( $p = 0.681$ ) nor the ML excursion of the COP during stance ( $p = 0.743$ ) were different between groups. In the variables that were significant between groups, ascent velocity was not a significant factor.

While not statistically significant, the peak lateral force tended ( $p = 0.072$ ) to be less in the pregnant fallers ( $0.017 \pm 0.004$  BW) than in the pregnant non-fallers ( $0.026 \pm 0.004$  BW) and the controls ( $0.024 \pm 0.004$  BW). Similarly, the medial GRF impulse tended ( $p = 0.072$ ) to be larger in the pregnant fallers ( $-0.035 \pm 0.001$  BW s) than in the pregnant non-fallers ( $-0.031 \pm 0.001$  BW s) and controls ( $-0.028 \pm 0.001$  BW s).

Several differences were noted between pregnant fallers and non-fallers, with fewer differences noted

between pregnant non-fallers and controls. Pregnant fallers may have altered neuromuscular control that increases their risk of falling. In particular, the differences in the ML direction in pregnant fallers may be related to changes in frontal plane control.

If biomechanical alterations were noted in all of the pregnant women, it could be assumed that the falls could have happened purely by the chance encounter of a risk factor for falling, such as a slippery floor, uneven sidewalk, object on the floor, etc. However, pregnant fallers and non-fallers displayed differences in GRFs in our laboratory setting. Additional differences between these pregnant fallers and non-fallers were also noted in other gait and postural stability parameters [4, 6].

## CONCLUSION

Pregnant fallers demonstrated alterations in GRFs during stair ascent compared to pregnant non-fallers and controls. These differences may be indicative of poor control and increased instability.

## REFERENCES

1. Dunning K et al. *Am J Indus Med* **44**; 664-72, 2003
2. Dunning K et al. *Matern Child Health J.* **14**; 720-5, 2010
3. Gardner JG et al. *J Biomech* **38**; 1861-8, 2004.
4. McCrory J et al. *Brit J Obs Gynec* **117**; 954-62, 2010.
5. Lymbery JK and Gilleard W. *J Am Podiatr Med Assoc* **95**; 245-53, 2005.
6. McCrory J et al. *MSSE* **42**; S193, 2010.
7. McCrory J et al. *ACSM*, Denver, CO. 2011.

## ACKNOWLEDGEMENTS

This research was supported by NIOSH K01 OH8548.

Table 1: GRF variables which were different between pregnant fallers (PF, n = 15), pregnant non-fallers (PNF, n = 14) and controls (C, n = 40). Data shown are mean (standard error).

| Variable                 | Control        | Pregnant Non-Fallers | Pregnant Fallers | p-value | Post-hoc    |
|--------------------------|----------------|----------------------|------------------|---------|-------------|
| Time to Braking Peak (s) | 0.137 (0.013)  | 0.107 (0.014)        | 0.171 (0.013)    | 0.001   | PF > PNF    |
| Braking Impulse (BW s)   | -0.006 (0.001) | -0.006 (0.001)       | -0.008 (0.001)   | 0.002   | PF > PNF, C |
| Max Medial Force (BW)    | -0.083 (0.002) | -0.082 (0.002)       | -0.091 (0.002)   | 0.008   | PF > PNF, C |

# Miniaturized Wireless IMU Enables Low-Cost Baseball Pitching Training Aid

<sup>1</sup>Ryan S. McGinnis, <sup>1</sup>Noel C. Perkins, <sup>2</sup>Kevin King

<sup>1</sup>University of Michigan, Ann Arbor, MI, USA

<sup>2</sup>94fifty Sports Technologies, Dublin, OH, USA

email: ryanmcg@umich.edu web: <http://www-personal.umich.edu/~ryanmcg>

## INTRODUCTION

Baseball pitching is one of the most unforgiving positions in sports; one mistake, like a hung curveball or a fastball that tails out over the plate, often results in a run for the opposing team. As a result, there has been considerable research on the free flight behavior of a baseball, and specifically in identifying how a pitcher's input to the ball (i.e. the ball's velocity and angular velocity at release) causes it to break [1-3]. Experiments reveal that the total break of the ball during free flight is proportional to the aerodynamic lift coefficient of the ball [1], is dependent on the seam orientation [1], and is a function of the magnitude of the ball's angular velocity [2]. These studies obtained their experimental data by tracking the position of the baseball in free flight using high speed video analysis systems. This method for data collection is expensive, time consuming, and requires an operator skilled in both the collection and analysis of the data. For these reasons, using high speed video analysis systems in baseball pitcher training is not an option for all but professional baseball programs. However, it is easy to imagine that an inexpensive and non-intrusive method for measuring the velocity, angular velocity, and orientation of the baseball would provide the foundation for an effective training aid for baseball pitching. To this end, we propose a highly miniaturized wireless inertial measurement unit embedded within a baseball (Figs. 1A-B) as a low cost, highly portable and minimally intrusive approach for measuring the baseball's release conditions.

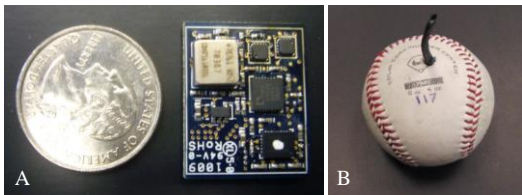


**Figure 1:** The miniaturized wireless IMU (Fig.1A) is embedded within a baseball (Fig.1B). The black “tail” protruding from the baseball is a switch/recharging jack

which, when removed prior to pitching, allows power to flow to the board.

## METHODS

The inertial measurement unit (IMU, Fig. 1A), which provides three-axis sensing of linear acceleration and angular velocity, measures a mere 19 X 24 mm and weighs only 4.5 grams including a small lithium ion battery. The unit transmits data wirelessly using a proprietary RF protocol to a USB-enabled receiver which facilitates data collection on a host (laptop) computer via custom software.

Subjects were instructed to pick the ball off of a tee, come to their set position on the mound, and then throw the ball to the catcher in an otherwise unencumbered manner. This sequence of events is readily identifiable in the example data shown in Fig. 2 where the ball motion is also divided into five distinct phases.

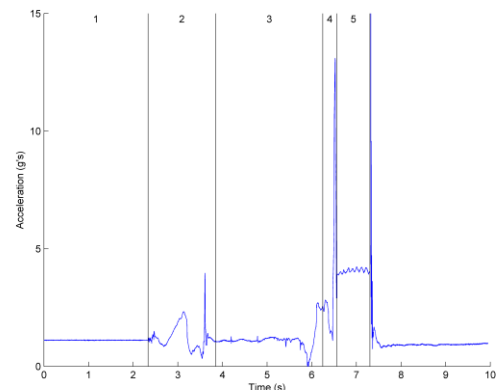


**Figure 2:** Magnitude of the acceleration measured by the IMU embedded in the baseball for a typical trial. The 5 phases of the motion, as defined by our experimental protocol, are also indicated.

Phase 1 corresponds to the ball being at rest in the tee (Accel. Magnitude of 1g) and ends once the ball is picked off the tee by the subject. Phase 2 begins when the subject picks the ball off the tee and ends when the set position is first reached. Phase 3 is the backward portion of the throwing motion, starting at

the start of the set position and ending when the pitcher reaches full arm extension away from the catcher. Phase 4 is then the forward throwing motion starting from the furthest extension position and ending when the ball is released. Finally, phase 5 extends from ball release to impact; the free-flight phase of the ball's motion. These phases were confirmed independently using high-speed video (frame rate of 300 Hz.) which was synchronized with the IMU data using a custom Matlab™ program and using the instant the ball is released as the synchronization event. A video showing the synchronized high-speed video and IMU data is available at <http://www-personal.umich.edu/~ryanmcg/BaseballProject.html>.

As indicated in Fig. 2, it is clear from the acceleration data where the ball is released from the pitcher's hand. At this instant, the IMU provides direct measurement of the baseball's angular velocity and enables the calculation of its linear velocity and the orientation of the seams with respect to the velocity vector (Fig. 3) following the methods outlined in [4,5].

## RESULTS AND DISCUSSION

The difficulty in using an IMU to determine baseball release conditions lies in determining the linear velocity at release, a calculation which relies on integrating inertial sensor data that includes drift error. However, a drift error estimate can be constructed using knowledge of the kinematics of the ball and in doing yield accurate results as illustrated in Fig. 3.

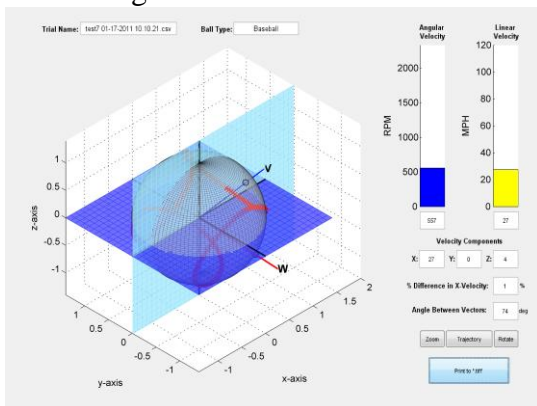


**Figure 3:** Graphic which displays the linear and angular velocity vectors, and the orientation of the ball at release. These values ultimately determine how the ball breaks during free-flight.

The trial whose results are shown in Fig. 3 was a fastball thrown at slow speed so as to avoid exceeding the measurement range of the sensors.

The angular velocity vector's orientation suggests a ball thrown with largely backspin which is consistent with published information about the release conditions of a fastball [3]. The component of the ball's velocity in the direction from the pitcher to catcher is calculated to be within 10% of the value determined by estimating the ball's velocity based on the distance from the point of release to the catcher and the time that the ball is in free-flight.

## CONCLUSIONS

The methods employed in this study enable one to determine a pitched baseball's release conditions using an embedded IMU. Specifically, analysis of the acceleration and angular velocity data provide the 1) ball angular velocity, 2) ball orientation, and 3) ball center linear velocity at the instant of release. For the example shown, these values are consistent with those published for fastballs. Additionally, it is shown that the major component of ball velocity is determined with only a 10% error as compared to an independent measure of that quantity.

This novel training aid will allow pitchers to understand, in a matter of seconds, why their last curveball didn't break or why their fastball tailed out over the plate. It offers an immediate and quantitative analysis of a pitch and should prove valuable in helping pitchers learn to consistently throw effective pitches.

## REFERENCES

1. Alaways LW, et al. *J Sports Sciences* **19**, 349-358, 2001.
2. Alaways LW, et al. *J Applied Biomechanics* **17**, 63-76, 2001.
3. Nathan, AM. *American J Physics* **76**, 119-124, 2008.
4. King KW, et al. *Sensors and Actuators A: Physical* **141**, 619-630, 2008.
5. Simo, JC, et al. *International J Numerical Methods in Eng.* **38**, 1431-1473, 1995.

## ACKNOWLEDGEMENTS

Special thanks to the NSF for funding this project and to Brian Yost, Peter Curran, Jeff Walls, Omar Almagri, and Brian Orr for their willingness to volunteer their throwing motions for analysis.

# THE EFFECT OF INDEPENDENT MANIPULATIONS OF BODY WEIGHT AND MASS ON INSTANTANEOUS METABOLIC POWER DURING WALKING

<sup>1</sup>Craig P. McGowan, <sup>2</sup>Richard R. Neptune and <sup>3</sup>Rodger Kram

<sup>1</sup>University of Idaho, Moscow, ID, USA

<sup>2</sup>The University of Texas at Austin, Austin, TX, USA

<sup>3</sup>University of Colorado at Boulder, Boulder, CO, USA

email: [cpmcgowan@uidaho.edu](mailto:cpmcgowan@uidaho.edu), web: [www.sci.uidaho.edu/McGowanLab/index.htm](http://www.sci.uidaho.edu/McGowanLab/index.htm)

## INTRODUCTION

Walking is composed of multiple mechanical subtasks such as the need for body support and forward propulsion, which each have an associated metabolic cost. A number of studies have examined the relative contribution of specific subtasks to the metabolic cost of walking using experimental manipulations of certain gait parameters [1] or body weight and/or mass [2]. Other studies have used musculoskeletal modeling and forward dynamics simulations to estimate muscle mechanical work [3] and metabolic power [4] throughout the gait cycle. In the present study, we combine these two approaches to examine the relative timing of metabolic power demand of individual leg muscles during walking in response to experimental manipulations of body weight and/or body mass. The goal is to better understand how metabolic energy is expended throughout the gait cycle and to determine the relative energetic costs of body support and forward propulsion. The rationale for this approach is that manipulations of body weight will affect the cost of weight support, whereas manipulations of body mass will affect the cost of forward propulsion.

## METHODS

The experimental data used in this study are a subset of previously collected data [5]. Briefly, subjects walked 1) normally with no manipulation (control), 2) with added trunk loads (increasing both trunk weight and mass: +W&M), 3) with weight support (decreasing weight only: -W), and 4) with a combination of equal added trunk weight and weight support (resulting in increased mass only: +M). Each manipulation was performed at 50% of

the subject's body mass. All trials were performed at 1.3 m/s.

Simulations of the experimental conditions were generated using a previously described 2-D bipedal musculoskeletal model [6] using SIMM (MusculoGraphics, Inc.). The 13 degree-of-freedom rigid segment model consisted of two legs and a trunk that was driven by 25 Hill-type musculotendon actuators per leg. Ground contact was modeled using viscoelastic elements attached to the bottom of each foot. The equations of motion were generated using SD/FAST (PTC).

Instantaneous metabolic power was calculated for each muscle using a model modified from Umberger [4]. The total metabolic power produced by each muscle was determined as the sum of the basal heat rate, activation and maintenance heat rate, shortening heat rate and mechanical work rate. Both activation heat and shortening heat are highly dependent on the percentage of slow and fast fibers being recruited, so we included a fiber type recruitment algorithm based on the "size principle" that for mixed fibered muscles, slow fibers were activated prior to fast fibers. The total metabolic power over the gait cycle was calculated as the sum of all muscles from both legs. Because we do not include an estimate of resting metabolic rate, the total metabolic power is equivalent to net metabolic power measured using indirect calorimetry.

## RESULTS AND DISCUSSION

The simulations emulated well the experimental data for all conditions. Joint angle and ground reaction force data were almost always within two standard deviations of the experimental data, with

average deviations from the experimental data of 3.73 degrees and 0.23 BW, respectively.

Estimates of average net metabolic power for the control simulation (Table 1) agreed well with published values for similar speeds [e.g., 4]. The combination of increased trunk weight and mass resulted in a relative increase in metabolic power of 92%, whereas increased mass alone resulted in a relative increase of 53%. These values are remarkably consistent with a previous experimental study that directly measured relative increases of 98% and 48%, respectively, during similar experimental conditions [2]. While weight support is expected to produce a less than proportional reduction in metabolic power, the -W condition in the present study resulted in a reduction of only 3%, compared to an 11% reduction that was experimentally measured [2].

In general, the +W&M condition produced an increase in metabolic power throughout the gait cycle (Fig. 1). This was largely due to increased metabolic power from the knee extensors (vastii) and ankle plantar flexors (soleus and gastrocnemius) during stance and the hip flexors (iliopsoas) during swing. Increasing body mass alone resulted in a similar pattern of metabolic energy consumption as the control simulation. However, metabolic power was elevated throughout stance, mainly due to relatively small increases in metabolic power by all active muscles. Finally, the -W condition resulted in an overall reduction in metabolic cost throughout stance.

## CONCLUSIONS

The results provide insight into the relative energetic cost associated with the walking subtasks of body support and forward propulsion. Consistent with our rationale, increases (decreases) in body weight resulted in increases (decreases) in metabolic power during early and mid-stance.

**Table 1:** Average metabolic power over the gait cycle.

|                               | Condition |         |        |         |
|-------------------------------|-----------|---------|--------|---------|
|                               | -50%W     | Control | +50%M  | +50%W&M |
| <b>Metabolic power (W/kg)</b> | 2.87      | 2.97    | 4.55   | 5.71    |
| <b>Relative change (%)</b>    | -3.28     | -       | +53.30 | +92.20  |

Increases in body mass resulted in increases metabolic power in late stance when forward propulsion is generated. The changes in metabolic power by individual muscles are generally consistent with the changes in mechanical output by each muscle during similar conditions [6].

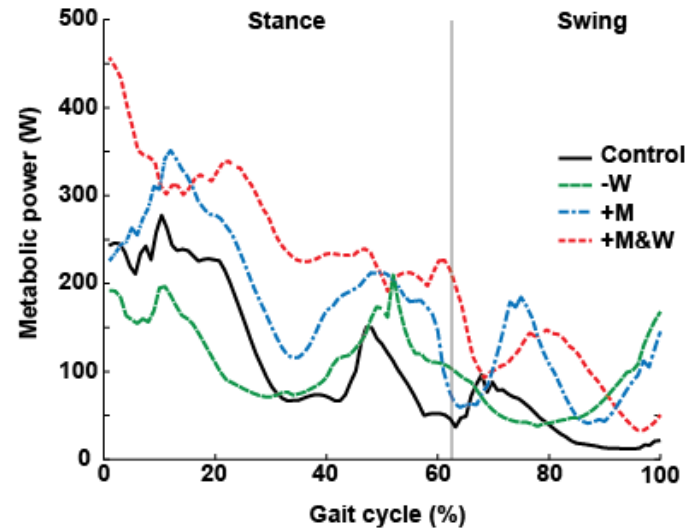


**Figure 1.** A comparison of instantaneous metabolic power from the muscles of one leg during the entire gait cycle across conditions.

## REFERENCES

1. Donelan et al., *J. Exp. Biol.*, **205**, 3717-3727, 2002.
2. Grabowski et al., *J. Appl. Physiol.*, **98**, 579-583, 2005.
3. Neptune et al., *J. Biomech.* **37**, 817-825, 2004.
4. Umberger, *J. R. Soc. Interface*, **7**, 1329-1340, 2010.
5. McGowan et al., *J. Appl. Physiol.*, **105**, 486-494, 2008.
6. McGowan et al., *J. Biomech.*, **42**, 850-856, 2009.

## ACKNOWLEDGEMENTS

This work was supported by NIH grant F32-AR-054245-01.

# NEUROMUSCULAR REGULATION OF REACTION FORCES DURING THE GOLF SWING

J. L. McNitt-Gray<sup>1,2,3</sup>, A. Zaferiou<sup>1</sup>, J. Munaretto<sup>1</sup>, P. S. Requejo<sup>5,2</sup>, and H. Flashner<sup>4</sup>,

<sup>1</sup>Department of Biomedical Engineering, <sup>2</sup>Kinesiology, <sup>3</sup>Biological Sciences

<sup>4</sup>Aerospace and Mechanical Engineering, University of Southern California, Los Angeles, CA

<sup>5</sup>Rehabilitation Engineering, Rancho Los Amigos National Rehabilitation Center, Downey, CA

E-mail: mcnitt@usc.edu

## INTRODUCTION

Regulation of linear and angular momentum during well-practiced goal-directed movements involves control of the total body center of mass trajectory (CM) in relation to the reaction forces generated during contact with the environment[1]. During the golf swing, reaction forces (RF) are generated at each foot, creating moments about the CM that rapidly rotate the body toward the target without compromising balance. During the initial part of the downswing, the RF applied to the target foot (left foot in right handed players) is directed posterior and RF applied to the rear foot (right foot) is directed anterior[2]. Magnitudes of the vertical and anterior posterior components of the target leg RF are reported to be higher than when using a driver as compared to an iron [2,3].

The mechanical objective of the golf swing is to generate club head velocity prior to ball contact so that the ball comes to rest at the intended target. Tension in the muscles during the backswing and the initiation of the downswing is thought to be regulated by controlling hip muscles [4,5]. The purpose of this study is to determine *how* skilled players selectively activate lower extremity muscles to regulate reaction forces and shot distance when using the same club.

During competition, a player often needs to hit a ball into the gap between distances normally achieved with two different clubs. The player must then decide whether to increase the distance using the shorter club (e.g. 7 iron) or reduce distance using the longer club (e.g. 6 iron). In this study, a within-subject design was used to determine how target and rear foot reaction forces are systematically regulated when attempting to reduce ball distance using a 6-iron. We hypothesized that

regulation of shot distance would be controlled the whole body level by selectively modifying the ground reaction forces and that the set of muscles used to regulate force magnitude and direction would remain essentially the same for an individual player to preserve coordinated muscle action in this well-practiced task [4].

## METHODS

Skilled players (n=12; handicap < 5) performed multiple swings using a 6-iron. Each player performed swings as they would normally (N) when using a 6-iron (Taylor Made-adidas Golf) and when reducing shot distance (gap of approximately -10 m between their 6- and 7-irons). Reaction forces at the artificial turf-plate interface plates of the target and rear legs (Kistler, 1200 Hz) and 3D kinematics (110 Hz) of the body and club during the golf swing were simultaneously captured using reflective markers (3D, MATT, Motion Reality, Inc.). Activation of lower extremity muscles were monitored using electromyography using surface electrodes (1x1 cm<sup>2</sup> Konigsberg, Pasadena, CA). Ball velocity and shot distance were estimated using measures from a ball launch monitor (MATT-impact, TMaG). The sound of club-ball contact was recorded using a microphone and sampled with the force-time data to identify the time of ball contact. The trials with the highest player rating for each experimental distance (normal, -10) were used as representative trials for comparison. Resultant horizontal reaction force (RFh) orientation for target and rear legs was expressed as an angle relative to the target line. Moments generated by the target and rear leg RFs about the CM were estimated from the cross product of the position vector from the CM to the center of pressure of the rear and the target legs and the RFh measured for each foot. The magnitude of muscle activation was quantified and compared

within player and within muscle using binned (20ms) root-mean-squared values of filtered EMG (zero-lag fourth-order recursive Butterworth filter at 10-350 Hz) normalized to maximum values obtained during standardized manual muscle tests.

## RESULTS AND DISCUSSION

Effective regulation of shot distance involved control at the whole body level by modifying the magnitude of the target and rear leg reaction forces between normal (N) and -10 conditions. Six of twelve players modified club head speed of the 6-iron between N and -10 conditions by more than 1.8 m/s. Net moments created by the vertical RFs about the anterior-posterior and mediolateral axes passing through the CM acted in opposition to each other; Whereas, both moments created by the RFh about the vertical axis both contributed to body rotation toward the target.

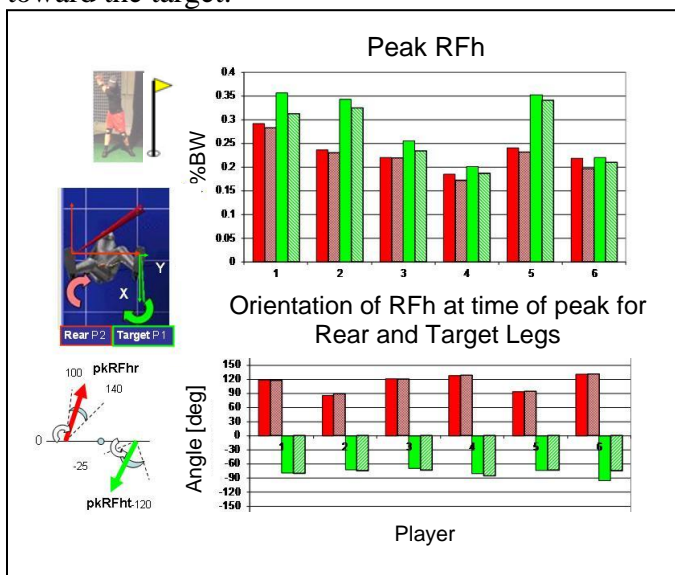


Figure 1. Peak resultant horizontal reaction force magnitude and orientation for target (green) and rear (red) legs for a subset of players that modified ball speed by 1.8 m/s or more. Differences between Normal (dark) and -10 (light) conditions were more pronounced for the target leg than rear leg.

Regulation of RF magnitude between N and -10 trials occurred at essentially the same orientation. Three target leg force-angle regulation patterns were observed: sustained reduction in RFh over a wide angle range, reduction in RFh in a narrow angle range, and reduction in RFh with a shift in orientation. In contrast, modulation in rear leg RFh consistently occurred within a much narrower angle

range unique to each player. Examination of the corresponding muscle activation patterns indicate that muscle activation was selectively modulated between N and -10 trials and the set of muscles involved in regulation varied across players (Figure 2).

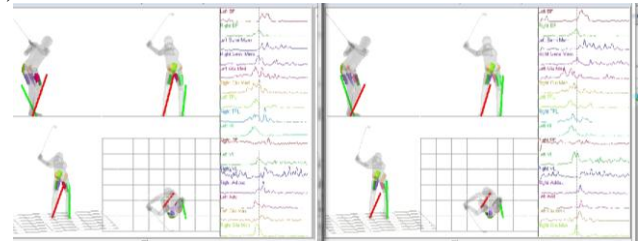


Figure 2. Selective modulation of hip muscles used to regulate reaction forces during early downswing under Normal (left) and -10 (right) conditions for an exemplar player.

## CONCLUSIONS

Subtle yet consistent regulation of reaction forces was observed within player across distances within club. These changes in control associated with a reduction in shot distance were observed as deviations from the remarkably consistent [2] force-time characteristics of each foot under normal conditions. Selective modulation of lower extremity muscle activation was found to be coincident with the player specific RF magnitude modulation range. This common approach for regulation of shot distance is expected to provide multiple advantages from muscle length, coordination, and performance points of view. The player-specific solutions observed, even in this relatively small sample, also emphasizes that there are multiple ways to satisfy the same mechanical objective in well-practiced goal-directed tasks. Understanding how individual players regulate their reaction forces under challenging conditions provides valuable insight for individualizing and facilitating skill acquisition.

## REFERENCES

1. Mathiyakom W, et al. *J. Biomech*, 39, 990-1000, 2006.
2. Williams, K. & Cavanagh, P.R. *MSSE* 15(3), 247-255, 1983.
3. Ball, KA & Best, RJ. *J Sports Sci* 25(7), 757-779, 2007.
4. Hogan, B. (1957). *Five Lessons: The Modern Fundamentals of Golf*, New York, NY: A.S. Barnes & Co.
5. Bechler, J.R., Jobe, F.W., Pink, M., Perry, J. & Ruwe, P.A. (1995). *Clinical JSportsMed*, 5:162-166.

**ACKNOWLEDGEMENTS** partial funding for this research was provided by TaylorMade-adidas Golf. The authors thank David Anderson and Ian Wright for discussions and suggestions during this project.

# COMPARISON OF THREE METHODS FOR MEASUREMENT OF FOOT PROGRESSION ANGLE MAGNITUDE AND ASYMMETRY

Ericka N. Merriwether, Mary K. Hastings, Kathryn L. Bohnert, Karyle Penelton, and David R. Sinacore  
Washington University School of Medicine, St. Louis, MO, USA  
email: [emerriwether@wustl.edu](mailto:emerriwether@wustl.edu)

## INTRODUCTION

The contribution of foot progression angle (FPA) to lower extremity musculoskeletal impairments is the focus of a growing body of orthopedic literature.<sup>1</sup> Symmetry of gait variables is considered one of the characteristics of a normal gait pattern in healthy adults.<sup>2</sup> Development of multi-segment foot models have allowed for the evaluation of foot kinematics during gait to discriminate between normal and pathologic foot function.<sup>3</sup> The purpose of this study is to assess and compare the magnitude and asymmetry of FPA obtained from motion capture with existing validated methods of determining FPA.

## METHODS

**Subjects.** Fourteen healthy subjects (8 F, age=34±15.6 years, height=1.68±0.09 m, weight=71.6±14.4 kg, BMI=25.2±3.2kg/m<sup>2</sup>) volunteered and signed an informed consent approved by the university Institutional Review Board. All data were collected and analyzed by a single experienced tester. **FPA measurement.** **Motion capture.** Bilateral kinematic and kinetic data were collected using an 8-camera video-based motion capture system (Vicon, Los Angeles, CA, USA). Subjects were fitted with 10 mm diameter spherical retro-reflective markers on the bilateral lower extremities. Foot and shank marker placement and segmentation are described by Carson et al (2001)<sup>3</sup>. Subjects performed four barefoot walking trials at a self-selected speed over a 6 m walkway with an embedded force plate (Advanced Medical Technology, Inc., Watertown, MA, USA) to determine force output. **Inked-moleskin method.** During the fourth motion capture walking trial subjects were fitted with pre-cut moleskin shaped like triangles and squares on the plantar surface of the foot. Paper spanning the length of the walkway was placed within the capture volume to allow

simultaneous collection of motion capture and inked-moleskin data. Moleskin pieces were aligned with the center of the heel and 2<sup>nd</sup> metatarsal head landmarks corresponding to two of the foot markers used to define the foot segment (inferior calcaneus--ICAL and distal 2<sup>nd</sup> metatarsal--D2MT). Subjects walked at a self-selected speed. **EMED-ST P-2 pressure platform.** Dynamic plantar pressure distribution was obtained on both feet for three trials of barefoot walking at a self-selected speed over a 3.6m walkway with an embedded pressure distribution platform (Novel Inc., St. Paul, MN, USA). The 2-step method was utilized for the collection of pressure maps.<sup>4</sup> **Data Processing and Analysis.** Kinematic convention for all FPA measurements was to designate external FPA (toe-out) as negative and internal FPA (toe-in) as positive. **Motion capture.** All kinematic data was processed using Visual 3D software (C-motion, Inc., Rockville, MD, USA). The foot was modeled as a single, rigid body segment. FPA was calculated as the magnitude of transverse plane rotation of the foot segment around the local superior-inferior axis at midstance (50% stance). **Inked-moleskin method.** Data were measured and analyzed as described by Boenig (1977)<sup>5</sup>. FPA was measured using 2<sup>o</sup> increment goniometer. The FPA values obtained from the foot step onto the force plate collected from the inked-moleskin and motion capture trial is the comparison used in the analysis. **EMED-ST P-2 pressure platform.** FPA was determined as the measured angle between the line of progression (a line drawn parallel to the printed paper) and a line representing the anterior-posterior bisection of the digitized pressure map of foot plantar surface using a 2<sup>o</sup> increment goniometer. These methods are described by Hastings et al (2010)<sup>6</sup>. FPA asymmetry was defined as the absolute difference between right and left mean FPA values ([RFPA-LFPA]) for each method. Mean FPA and absolute difference values were assessed using a one-way analysis of variance (ANOVA), with post-hoc

testing using least significant difference. Level of association for obtaining mean FPA (right and left) between methods was assessed using Pearson Product Moment coefficient (r).

## RESULTS AND DISCUSSION

**Mean FPA:** There were no significant differences in mean FPA between methods (FPA=-8.8±4.2° to 10.5±4.6°). Methods for determining mean FPA were highly correlated (r=0.74-0.83). Pairwise difference values between the methods are presented in Table 1. **FPA Asymmetry:** All three methods yielded similar side-to-side difference values (p=.661). Pairwise difference values are given in Table 1. All three methods detected a similar difference in right and left FPA, with approximately 64% (9/14) of subjects demonstrating an absolute difference of at least 4 degrees, and 5/14 (36%) exhibiting an absolute difference of at least 6 degrees (Figure 1).

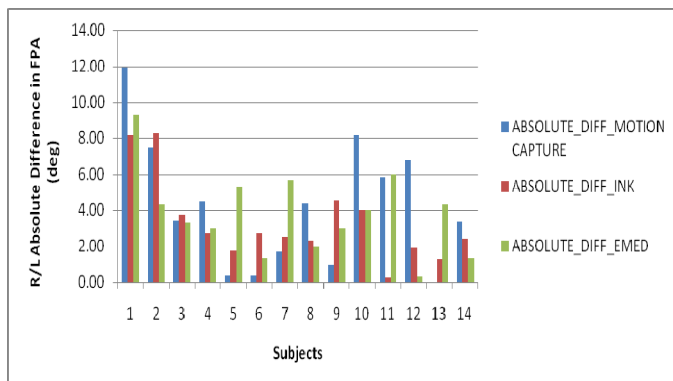


**Figure 1:** Absolute difference in mean FPA values (deg) between right and left for each method.

**Table 1: Pairwise mean differences (degrees) and correlations for mean FPA values between methods**

|                   | Ink/MC            | Ink/EMED           | EMED/MC            | p           |
|-------------------|-------------------|--------------------|--------------------|-------------|
| Mean FPA          | <i>Right</i>      |                    |                    |             |
|                   | 0.97              | 1.36               | 0.39               | .741        |
| Mean FPA          | <i>Left</i>       |                    |                    |             |
|                   | 0.26              | 0.60               | 0.34               | .970        |
| Mean Absolute R/L | 1.51 <sup>+</sup> | 0.78 <sup>++</sup> | 0.43 <sup>++</sup> | .661        |
| <b>r</b>          | <b>0.74</b>       | <b>0.83</b>        | <b>0.77</b>        | <b>.000</b> |

**Ink=Inked moleskin method; MC=motion capture; Mean Absolute R/L=[RFPA-LFPA]**  
<sup>+</sup>: Comparison of FPA values for the foot on the force plate  
<sup>++</sup>: Comparison of FPA values for the foot on the force plate and averaged EMED trials

## CONCLUSIONS

The results of this study suggest that determination of mean FPA and asymmetry in FPA in normal, healthy subjects using motion capture yield similar values to existing validated methods within the precision of the goniometer. In addition, the presence of asymmetry in FPA may be a common characteristic of a normal gait pattern in persons without musculoskeletal pathology. We conclude that motion capture potentially provides a reproducible method of simultaneously assessing FPA characteristics and foot and ankle mechanics.

## REFERENCES

1. Leardini, A. et al. (1999) *Clin Biomech*,14:528-36
2. Olney & Richards (1996) *Gait & Posture*,4: 136-48
3. Carson, MC. et al. (2001) *J Biomech*,34: 1299-1307
4. Meyers-Rice, B et al (1994) *J Am Podiatr Med Assoc*, 84(10): 499-504
5. Boenig, D. (1977) *Phys Ther*, 57(7): 795-798
6. Hastings, MK. et al. (2010) *Gait & Posture*,32: 237-41

## ACKNOWLEDGEMENTS

Funded by NICHD T32 HD 07434-17, American Physical Therapy Association Foundation for Physical Therapy PODS I, K 12 HD 055931, Midwest Stone Institute

# THE INFLUENCE OF HEAD WEIGHT ON THE BIOMECHANICAL RESPONSE OF THE CERVICAL SPINE UNDER APPLIED MOMENTS

<sup>1</sup>Wissal Mesfar, <sup>1</sup>Kodjo Moglo

<sup>1</sup>Royal Military College of Canada, Kingston, ON, Canada

Email: [kodjo.moglo@rmc.ca](mailto:kodjo.moglo@rmc.ca), web: <http://www.rmc.ca>

## INTRODUCTION

Significant research efforts have focused on determining the head and neck complex kinematics and kinetics under various types of loading. The results could be influenced by many factors and parameters such as specimen age, number of segments tested, specimen orientation, loading protocol and biological variation of the tissues. Head weight (HW) parameter is not commonly considered in finite element studies but there exist some studies that did include it [1-4]. All of these studies validated their models based on the same few experimental studies in which the consideration of the compressive load of the head weight or the experimentation devices is not explicitly clear. In this study, we aim to identify the effect of 40 N HW on the biomechanical response of the cervical spine under the extension-flexion moment applied to the centre of mass of the head.

## METHODS

A 3D nonlinear head and neck (HN) complex finite element (FE) model was developed and constructed based on CT scan and MRI images of a 39 year old male. The reconstruction of the head, cervical vertebrae (C1-C7) and the first thoracic vertebra (T1) was based on CT scan images and reconstruction of the intervertebral discs was based on the MRI images. The FE model consists of bony structures and their cartilage facet joints, intervertebral discs and all the ligaments. The non-linear material properties for the ligaments were considered based on the study of Shim et al. [5]. The transverse ligament is modeled as a bundle and all the other ligaments are each modeled by a number of uniaxial elements with non-linear material properties. However, linear and homogenous properties for the annulus and nucleus and the cartilage were used. The bony structures

were considered as rigid due to their greater stiffness to the adjacent soft tissue structures. For stable unconstrained boundary conditions, T1 is fixed while the cervical vertebrae and the head are left free. To study the effect of the head weight under a moment loading, two loading cases were considered. The first one consisted only of the application of the extension-flexion moment to the centre of the mass of the head, while the second one consisted of the application of the same moments in the presence of a 40 N HW. The moment considered in this study ranges from -800 N.mm (extension) to 800 N.mm (flexion).

## RESULTS AND DISCUSSION

The cervical spine vertebrae and the head move anteriorly and distally and flexes under a flexion moment applied to the centre of mass of the head and under the application of 40 N HW with zero moment. The relative angle of flexion is greater in the cephalic cervical levels (C0-C1 and C1-C2) than the caudal vertebrae levels under the pure moment loading case without HW (Figs. 1 and 2). Moreover, under the same absolute moment magnitude of extension or flexion, the relative extension angle is higher than that of the relative flexion angle, respectively. On the other hand, the addition of the 40 N HW increases substantially the flexion angle under the flexion moment and increases the angle of extension under extension moments which are greater than ~200 N.mm. This is due to the fact that the application of 40 N HW induces an initial flexion angle for the whole head and neck complex and the application of extension moment counterbalances this initial flexion moment. The greater relative angles of flexion and extension were computed at C1-C2 and reached 6.7 deg and 12.5 deg under 800 N.mm flexion and extension, respectively. The predicted relative rotations are in good general agreement with the measurements [6,

7]. The trend found under flexion moment is reproduced under the extension moment for the cephalic level and the greater relative extension angle is computed at C1-C2.

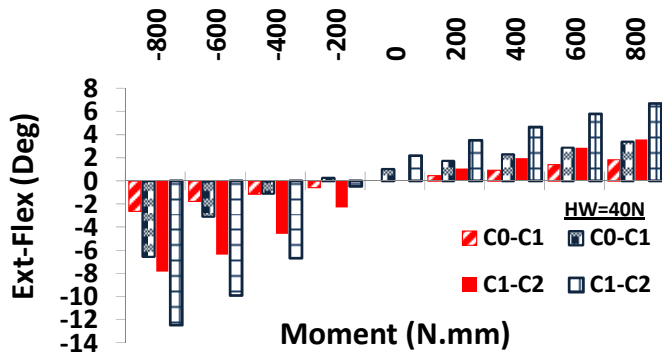


**Figure 1:** The relative extension-flexion angle between the adjacent vertebrae (C0-C1 and C2-C3) at different applied extension and flexion moments.

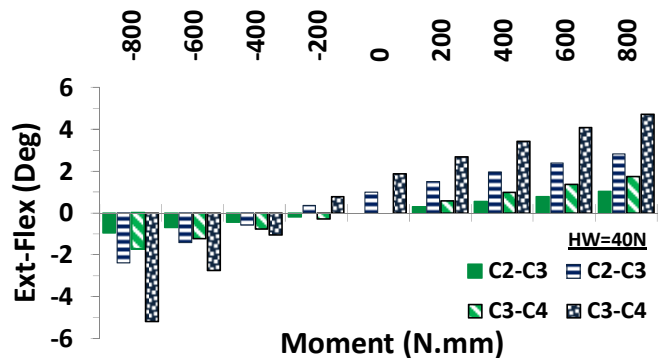


**Figure 2:** The relative extension-flexion angle between the adjacent vertebrae (C2-C3 and C3-C4) at different applied extension and flexion moments.

On the other hand, the contact force (CF) at the facet joints increased with the increase of the applied moment in the case without HW. The addition of the HW increases the CF at the facet joints under the flexion moment; however it increases only beyond ~186 N.mm extension moment for C1-C2 and C2-C3 levels and beyond ~386 N.mm for C0-C1 level. The higher computed CF magnitude was at the level C1-C2 (Fig. 3). Indeed, the CF reaches a maximum of 91 N and 22 N under and 102 N and 38.5 N under 800 N.mm flexion and extension moment and for cases with and without HW, respectively. The results indicate also that the contact force at C2-C3 level is almost nil under the flexion moment for the cases with and without HW. In contrast, the same CF at C2-C3 level increases with the extension moment and reached ~85 N and ~32 N at 800 N.mm extension moment for the cases with and without 40 N HW,

respectively (Fig. 3). Indeed, the facets undergo a widening when the cervical spine flexes and a narrowing in extension which is in good agreement with the observations of Wheeldon et al. [7].

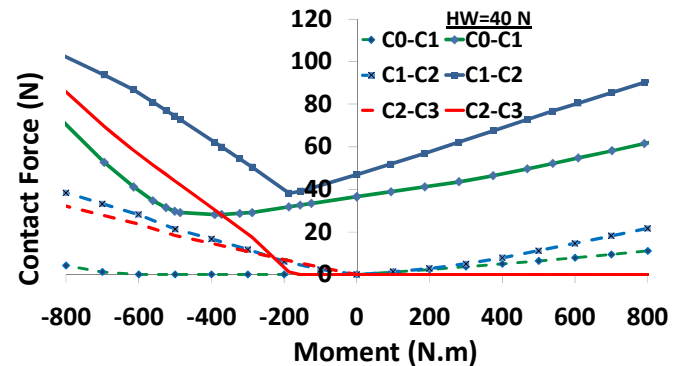


**Figure 3:** The resultant contact force at different applied moments with and without HW=40 N.

## CONCLUSIONS

This study evaluated the effect of the head weight applied to the centre of the mass of the head on the entire response of the joint under extension and flexion moments. The head weight, apart from the compressive load also induces an additional flexion moment due to the existing anterior lever arm. Our predictions show a substantial role of the head weight not only on the kinematics but also on the distribution load of the cervical spine joint. Our findings suggest that the HW is a variable that has a substantial effect on the biomechanical response of the cervical spine and has to be considered when comparing the predictions of the models with the experimental studies.

## REFERENCES

1. del Palomar AP et al. *J Biomech* **41**, 523-31, 2008.
2. Zhang QH et al. *J Biomech* **39**, 189-193, 2006.
3. Tchako A, Sadegh AM. *J Biomech Eng* **131**, p. 051013, 2009.
4. Kallemeyn N et al. *Med Eng Phys* **32**, 482-489, 2010.
6. Panjabi MM. et al. *Spine* **26**, 2692- 2700, 2001.
7. Wheeldon JA et al. *J Biomech* **39**, 375-380. ., 2006.

## ACKNOWLEDGEMENTS

The financial support from the Canadian Dept. of National Defence (DTAES 6) is gratefully acknowledged.

# A NONLINEAR MODEL OF PASSIVE SKELETAL MUSCLE VISCOSITY

<sup>1</sup>Gretchen A. Meyer, <sup>1</sup>Andrew D. McCulloch and <sup>1</sup>Richard L. Lieber

<sup>1</sup>University of California, San Diego and VA San Diego Healthcare System, San Diego, CA  
email: [gmeyer@ucsd.edu](mailto:gmeyer@ucsd.edu) web: <http://muscle.ucsd.edu>

## INTRODUCTION

Skeletal muscle is a composite tissue of contractile and structural proteins, membranes and extracellular matrix that enable both load bearing and force production. Passive properties of muscles have received much less attention than active, however, they are equally vital to proper function. This is easily appreciated when passive properties change due to disuse, disease or injury, leaving patients debilitated. Defining the material properties of load bearing structures in a muscle is a prerequisite for developing therapeutic strategies to improve surgical outcomes, stability and performance.

Current mathematical models of passive muscle viscoelasticity focus on elastic properties and typically characterize viscous properties as linear, despite evidence to suggest sizeable nonlinearity [1, 2]. In this study, stress relaxation tests were performed on single muscle fibers to define the dependence of fiber viscosity with time, strain and strain rate. These data were used to develop a model incorporating viscous nonlinearities, which was shown to more effectively represent fiber behavior over a range of strains and strain rates.

## METHODS

The 5<sup>th</sup> toe of the extensor digitorum longus (EDL) muscle was dissected from mice for mechanical testing. Muscles were skinned overnight in a glycerinated relaxing solution. Single fibers were isolated and mounted in a custom chamber that allowed precise control over specimen length and continuous measurement of passive force. Fibers were loaded to specified strains and allowed to stress-relax for three minutes. Strains were imposed over a range of 10-50% fiber length (FL), at rates from 0.2-200 FL/sec. Care was taken to ensure no plastic deformation occurred. All procedures were

performed in accordance with the NIH Guide for the Use and Care of Laboratory Animals.

Based on experimental data, accurate descriptions of the material behavior of muscle fibers require a viscosity term that is time, strain and strain rate dependent. This complex viscosity was integrated into a single nonlinear element ( $\eta(t, \epsilon, \dot{\epsilon})$ ) in the 3-element Hill model of passive muscle [3] (Eq. 1).

$$\dot{\sigma} + \frac{k_s}{\eta(t, \epsilon, \dot{\epsilon})} \sigma = \frac{k_s k_p}{\eta(t, \epsilon, \dot{\epsilon})} \epsilon + (k_s + k_p) \dot{\epsilon} \quad (1)$$

The strain rate dependence of viscosity was described by equations frequently used in rheology to describe pseudoplasticity, a property observed in these muscle fibers. A linear dependence of viscous parameters on strain was also included based on experimental observations. This ability of the pseudoplastic model to accurately represent fiber stress-relaxation over a range of strains and strain rates was compared with two commonly used models: the 3<sup>rd</sup> order Hill model and the quasi-linear viscoelastic (QLV) model.

## RESULTS AND DISCUSSION

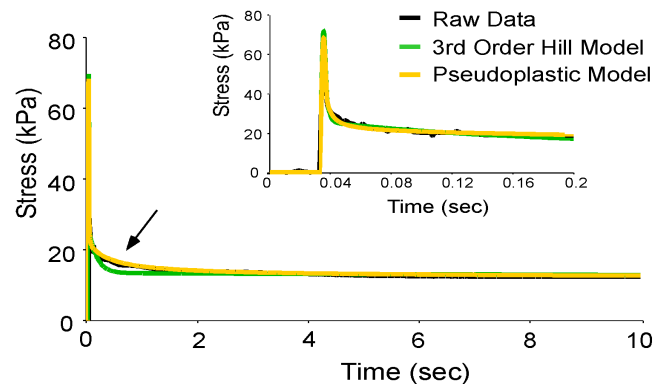


**Figure 1:** The pseudoplastic model better represents muscle fiber stress-relaxation data compared to the 3<sup>rd</sup> order Hill model (arrow).

The pseudoplastic model provided an excellent fit to stress-relaxation tests at super-physiological

strain rates (20 FL/sec) at all strains considered (mean  $r^2=0.99$ ). It outperformed both the 3<sup>rd</sup> order Hill model and the QLV in 71% of the stretches. By representing stress-relaxation as a continuous process rather than with discrete structural elements, it represented the fast phase of relaxation better than the 3<sup>rd</sup> order Hill model (Fig 1).

Structural models such as the 3<sup>rd</sup> order Hill model are highly strain rate sensitive, predicting a large decrease in stress resulting from a decrease in strain rate. Muscle fibers, however, are not very strain rate sensitive, decreasing peak stress by only 8% for a 90% decrease in strain rate. The pseudoplastic model utilizes a strain rate dependent viscosity to describe the strain rate sensitivity of muscle fibers and is thus better able to predict the fiber behavior at 2 FL/sec (Fig 2).

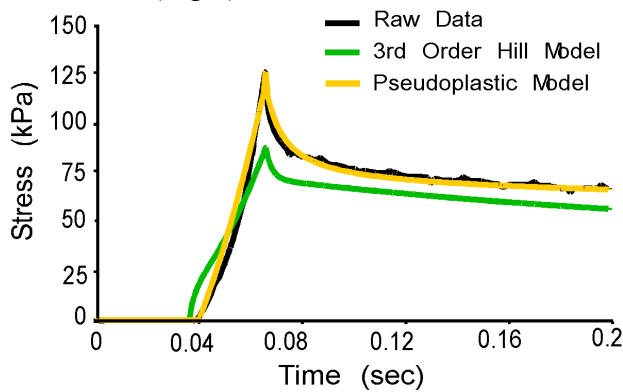


**Figure 2:** The pseudoplastic model more closely predicts fiber behavior at 2 FL/sec with fits based on 20 FL/sec data than the 3<sup>rd</sup> order Hill model and thus better describes its strain rate sensitivity.

The stress relaxation of the fiber showed a clear dependence on the final strain reached. The QLV model assumes that there is no strain dependence in the relaxation function. The pseudoplastic model is

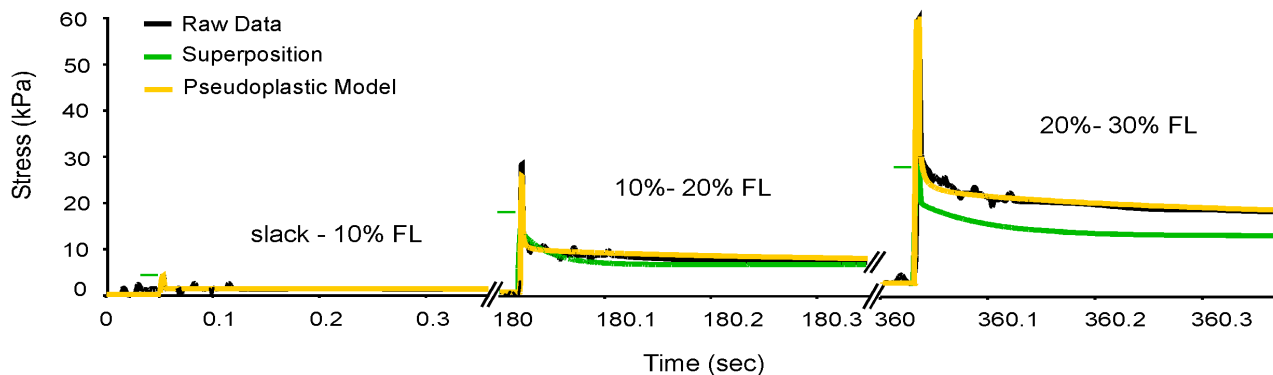


**Figure 3:** Muscle fibers do not obey the principle of superposition as indicated by the fact that in this incremental stress relaxation test, superposition underestimates peak stress by ~50%. The pseudoplastic model can account for this discrepancy with a strain dependent viscosity

able to overcome this limitation by including viscous parameters that are strain dependent. The QLV model also assumes that the material obeys the principle of superposition, which is also a requirement of structural models such as the 3<sup>rd</sup> order Hill model. The superposition prediction of stresses resulting from a series of incremental strains clearly underestimates the peak stress reached by the fiber (Fig 3). However, the pseudoplastic model can explain this discrepancy using strain dependent viscous parameters (Fig 3).

## CONCLUSIONS

These results clearly demonstrate that muscle fiber viscosity is not linear as is typically assumed, but is a more complex function of time, strain and strain rate. The pseudoplastic model developed here to incorporate these nonlinearities was shown to provide an excellent fit to stress relaxation data and to account for the strain rate sensitivity and deviation from superposition observed in the fibers. Many components of muscle fibers have been proposed to contribute to viscosity such as the myoplasm, weakly attached cross-bridges, titin and other cytoskeletal proteins. It remains to be determined the extent to which each of these elements contributes to the nonlinear viscous response, however, these results suggest that linear models of viscosity are inadequate to accurately describe the passive mechanical behavior of muscle.

## REFERENCES

1. Van Loocke et al. *J. Biomech* **41**(7):1555-1566, 2008.
2. Quaia et al. *PLoS One* **4**(8):e6480, 2009.
3. Hill et al. *Proc Roy Soc B*, **126**:136-195, 193

# SKELETAL MUSCLE FIBROSIS IN RESPONSE TO COMPLIANT MUSCLE FIBERS

<sup>1</sup>Gretchen A. Meyer, <sup>1</sup>Lucas R. Smith and <sup>1</sup>Richard L. Lieber

<sup>1</sup>University of California, San Diego and VA San Diego Healthcare System, San Diego, CA  
email: [gmeyer@ucsd.edu](mailto:gmeyer@ucsd.edu) web: <http://muscle.ucsd.edu>

## INTRODUCTION

Muscle fibrosis is a common Orthopaedic problem that results from tissue trauma, degeneration, neurotoxin injection and disuse. However, the interaction between skeletal muscle cells and the components of the extracellular matrix (ECM) that results in development of fibrotic tissue is not well understood. In this study, we have exploited the fact that the skeletal muscle intermediate filament protein desmin alters muscle fiber mechanical properties [1, 2] and show that this change results in the development of whole skeletal muscle fibrosis. Since this occurs in the absence of externally induced damage, this model provides a unique system to study the biology and mechanics of altered mechanical interaction between muscle cells and the ECM.

Desmin forms a mesh-like network around Z-disks and transmits sarcomere force to the ECM. To define both muscle fiber properties and those of the ECM, we measured viscoelastic properties of single muscle fibers and muscle fiber bundles from wildtype (WT) and desmin knockout (DKO) tissue. We also investigated ECM changes at the protein and mRNA levels. To understand the “process” of fibrosis, we compared properties from neonatal time points (postnatal day 10-20), when desmin protein concentration first reaches its mature level, to adulthood (5-7 weeks) when the muscles are mature, to an aged state (12-14 months).

## METHODS

The 5<sup>th</sup> toe of the extensor digitorum longus (EDL) muscle was dissected from WT and DKO mice for mechanical testing (n=5-6 muscles per group). Muscles were skinned overnight and single fibers or bundles (composed of about 20 muscle fibers) were dissected and mounted into a custom designed testing chamber. Passive viscoelastic properties of

the fibers and bundles were derived from an incremental stress relaxation protocol consisting of 10% strain increments applied at 2000%/sec. Stress relaxation data from fibers and bundles were fit to a nonlinear viscoelastic model.

Transcriptional profiles of tibialis anterior muscles from WT and DKO mice were determined using genechip microarray technology and skeletal muscle physiological pathways previously described (3). mRNA was extracted from individual homogenized muscles and processed on Affymetrix 430A 2.0 arrays using standard procedures. Expression of genes involved in ECM regulation and inflammation were quantified. Intramuscular collagen content was quantified by hydroxyproline assay. Data were compared across genotype and time by 2x3 two-way ANOVA and considered significant ( $\alpha$ ) for  $p < 0.05$  and are presented as mean $\pm$ SEM. All procedures were performed in accordance with the NIH Guide for the Use and Care of Laboratory Animals.

## RESULTS AND DISCUSSION

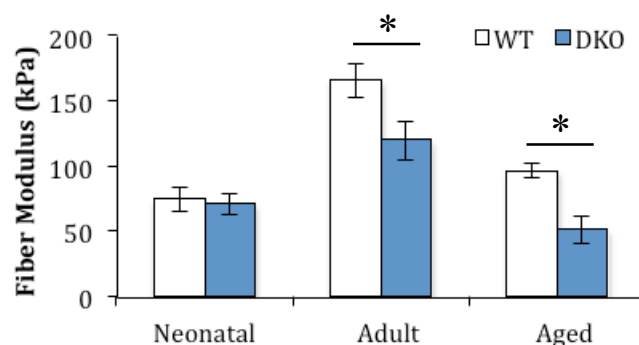


**Figure 1:** DKO single fibers are significantly more compliant in adult and aged muscles but neonatal fibers show no significant effect of genotype.

Fibers from WT and DKO muscles showed no significant differences in elastic or viscous parameters at the neonatal time point. However, by adulthood, fiber modulus was significantly



# EFFECTS OF EXERCISE-INDUCED LOW BACK PAIN ON INTRINSIC TRUNK STIFFNESS

<sup>1,2</sup>Emily Miller, <sup>2</sup>Babak Bazrgari, <sup>1,2</sup>Maury Nussbaum and <sup>1,2</sup>Michael Madigan

<sup>1</sup>Virginia Tech - Wake Forest School of Biomedical Engineering and Sciences, Blacksburg, VA, USA

<sup>2</sup>Virginia Polytechnic Institute and State University, Blacksburg, VA, USA

email: [millerem@vt.edu](mailto:millerem@vt.edu) web: [biomechanics.esm.vt.edu](http://biomechanics.esm.vt.edu)

## INTRODUCTION

Low Back Pain (LBP) is the most significant musculoskeletal health problem in industry [1], accounting for 20% of occupational injury and 40% of worker compensation. Impaired neuromuscular control of the lumbar spine is associated with LBP. Fundamental characteristics of this neuromuscular control include passive tissue properties, active muscle stiffness, and reflex behavior. Any impairment in these characteristics could lead to an insufficient response to a spinal disturbance and cause LBP or injury (e.g. excessive stress or strain in tissues).

Fundamental characteristics of neuromuscular control contribute to what are termed “effective” stiffness and damping in response to a perturbation, with effective stiffness being a combined measure of intrinsic stiffness and a reflex contribution. In an effort to understand the characteristics associated with LBP, studies have compared trunk responses between individuals with and without LBP. For example, following sudden trunk load release, individuals with LBP are reported to have greater effective trunk stiffness and lower effective trunk damping [2], as well as delayed reflex latencies [3], compared to healthy individuals.

Since comparisons between those with and without LBP are susceptible to inter-individual differences, additional insight may be provided by collecting repeated measurements from individuals who experience intermittent LBP. Comparing measures of neuromuscular control between known periods of pain and no pain in these individuals could reveal how/if neuromuscular control changes with the presence of pain, as well as how it differs with individuals who do not suffer from LBP. Additionally, since effective stiffness includes a reflex contribution, determining the intrinsic

stiffness before reflexes occur could be beneficial for the further understanding of LBP. Therefore, the purpose of this study was to investigate effects of exercise-induced LBP on intrinsic stiffness using sudden trunk flexion position perturbations.

## METHODS

Repeated measurements were collected from a local triathlon team, eight males ( $1.83 \pm 4.67$  m,  $72.9 \pm 2.7$  kg) who experience exercise-induced LBP and nine males ( $1.79 \pm 3.15$  m,  $70.8 \pm 7.3$  kg) who do not experience LBP, during known periods of pain and no pain in the LBP group (i.e. 1-2 days and 4-5 days post strenuous training). Participants were seated in a rigid metal frame (Fig. 1), strapped in at the pelvis, and attached to a servomotor (Kollmorgen AKM53K, Radford, VA, USA) via a rigid harness/rod connection at the T8 level. For two trials, the motor applied 12 anterior-posterior perturbations with amplitudes of 10 mm and peak velocities of 0.357 m/s. Perturbations completed within  $\sim 40$  ms, less than typical reflex latencies [4].

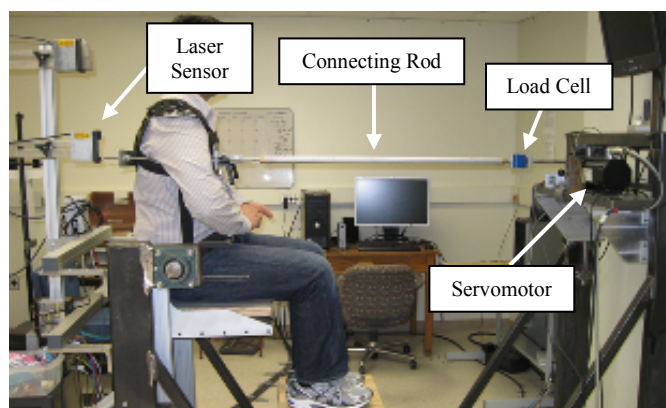


**Figure 1:** Experimental set-up.

During each trial, motor displacement was recorded with a high accuracy encoder on the shaft of the motor. Trunk kinematics were collected with a high accuracy CCD laser displacement sensor (Keyence

LK-G 150, Osaka, Japan) focused on the midline of the dorsal harness just above the rod height. Forces in the rod connecting the motor to the harness were collected with an in-line load cell (Interface SM2000, Scottsdale, AZ, USA). All data was sampled at 1000 Hz and processed with 7<sup>th</sup> order, 10 Hz [5] zero-lag low pass Butterworth filters.

Trunk properties were estimated by modeling the trunk and harness/rod connecting device as a 2DOF system (Fig. 2), with each degree of freedom having parameters of stiffness, damping, and mass [5]. Parameters were determined with a least squares MATLAB<sup>TM</sup> curve fit routine minimizing the difference between estimated and measured forces and using a system of 2<sup>nd</sup> order linear differential equations. Trunk damping, assumed as negligible and indistinguishable for such a quick time period [6], was forced to zero in order to greater represent changes in trunk behavior with those in stiffness.

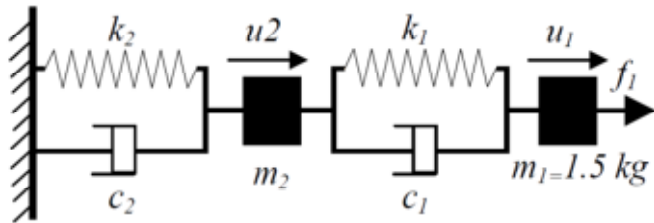


**Figure 2:** 2DOF linear dynamic model of stiffness ( $k$ ), damping ( $c$ ), and mass ( $m$ ) for both the harness/rod connection (1) and the trunk (2). Inputs are displacements from the motor ( $u_1$ ) and laser ( $u_2$ ) along with their 1<sup>st</sup> and 2<sup>nd</sup> derivatives.

To isolate the intrinsic portion of the trunk response, curve fits were restricted to the period of force tension in the load cell during anterior trunk flexion perturbations, visually inspected to occur before reflexes. Intrinsic stiffness was the value corresponding to the best curve fit within the 12 anterior perturbations applied per trial.

Pairwise comparisons using student  $t$ -tests were conducted within a 2-way ANOVA to compare intrinsic stiffness between repeated measurements for both healthy and LBP individuals as well as between healthy and LBP individuals for each repeated measurement. Statistical analyses were conducted using JMP 8 (SAS Software, Cary, NC, USA) and a significance level of  $P \leq 0.05$ .

## RESULTS AND DISCUSSION

Trunk stiffness (Fig. 3) was not different ( $p=0.702$ ) between healthy and LBP participants 1-2 days after exercise, when LBP individuals were experiencing pain. However, trunk stiffness was different ( $p=0.040$ ) between healthy ( $7347 \pm 1561 \text{ kg/s}^2$ ) and LBP participants ( $8728 \pm 801 \text{ kg/s}^2$ ) 4-5 days after exercise, when pain had subsided in the LBP individuals. This is consistent with the significant decrease ( $p=0.002$ ) in trunk stiffness in the healthy participants from the first measurement 1-2 days after exercise ( $9111 \pm 1472 \text{ kg/s}^2$ ). Results suggest rested, healthy individuals exhibit lower trunk stiffness than rested individuals who experience exercise-induced LBP. However, trunk stiffness increases for a few days after exercise in healthy individuals only, not in those with exercise-induced LBP. Therefore, increased stiffness in a rested, pain-free state could indicate a characteristic inherent to the LBP individual.

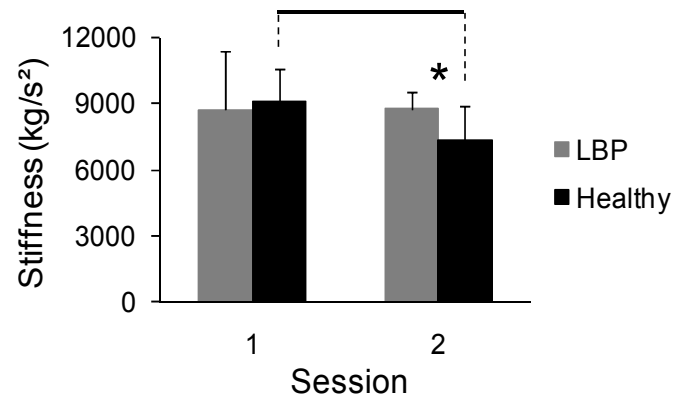


**Figure 3:** Intrinsic stiffness. An asterisk represents a group difference within session, and a line represents a session difference within group.

## REFERENCES

1. Spengler, D.M., et al. *Spine* **11** 241-245, 1986.
2. Hodges, P., et al. *J Biomech* **42** 61-66, 2009.
3. Radebold, A., et al. *Spine* **25** 947-954, 2000.
4. Granata, K.P., et al. *J Biomech* **37** 241-247, 2004.
5. Bazrgari, B., et al. *CMBBE* (in press).
6. Gardner-Morse, M.G. and Stokes, I.A.F. *J Biomech* **34** 457-463, 2001.

## ACKNOWLEDGEMENTS

NIAMS/NIH grant number 2 RO1 AR046111.

# ARE RUNNING AND SPRINTING DIFFERENT GAIT MODES? EVIDENCE FROM FORWARD DYNAMICS SIMULATIONS

Ross H. Miller and Kevin J. Deluzio

Queen's University, Kingston, ON, Canada  
email: [rm111@queensu.ca](mailto:rm111@queensu.ca) web: <http://me.queensu.ca/HMRC>

## INTRODUCTION

Although humans are capable of many different gait modes, we tend to use only two: walking at slow speeds, and running at faster speeds. Walking and running are clearly different gait modes, but it is less clear if very fast running (“sprinting”) is a distinct gait mode from slower running (hereafter referred to as “running”).

Previous research has shown that smoothed surface electromyograms (EMG) from most of the major lower limb muscles can be decomposed as the weighted sums of five common “synergy” signals without loss of information [1]. Further, changes in speed within a gait mode are associated with changes in amplitude (synergy weighting) but no changes in timing (synergy phasing). A distinct shift in the phasing of muscle activity during stance distinguishes walking from running [1,2]. In order for running and sprinting to lie within a common gait mode, their muscle activation synergies should therefore be synchronous, and re-weighting of the synergies should be sufficient for controlling either movement at the neuromuscular level.

Therefore, the purposes of the study were to compare features of muscle activation synergies from running and sprinting, and to determine if adjustments in muscle-specific synergy weighting with no adjustments in timing can control either movement from a common set of synergies. Since muscle activations are not directly accessible and adjustable *in vivo*, we used a computer simulation approach to enable direct access.

## METHODS

Forward dynamics simulations of human running ( $3.6 \text{ m s}^{-1}$ ) and sprinting ( $6.8 \text{ m s}^{-1}$ ) were generated using a 2D bipedal model. Each leg was actuated by nine Hill-based muscle models. Running was simulated by optimizing the muscle excitation signals to minimize the sum of the squared muscle

activation integrals. Sprinting was simulated by maximizing the average horizontal speed.

Nonnegative matrix factorization (NMF) was used to decompose the optimal muscle activations into a set of five “synergies”, or common constitutive signals. NMF is conceptually similar to principal component analysis in that it reduces the dimensionality of the data set, although the new basis is not necessarily orthogonal and the synergy amplitudes are restricted to positive values. The NMF procedure [3] computed the five synergy time series plus  $5 \times 9 = 45$  muscle-specific weighting constants that minimized the root-mean-squared error (RMSE) between the original and NMF-reconstructed muscle activations. Synergies and activations were scaled to 101 equally spaced points over the stride duration. Synergies were compared between running and sprinting by calculating the zero-lag cross correlation, and by the muscles associated with each synergy. A weighting of 0.4 was used as a threshold for association [4]. Finally, the weightings were optimized to reconstruct the muscle activations of one movement as accurately as possible (minimum RMSE) using the synergies of the other movement.

## RESULTS AND DISCUSSION

Both simulations (Fig. 1) reproduced the salient mechanical and energetic features of running and

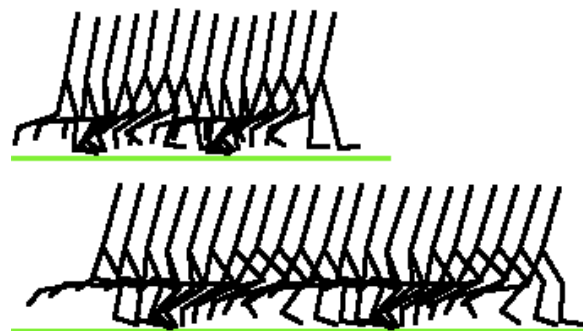


**Figure 1:** Traces of the simulated kinematic states for running (top) and sprinting (bottom).

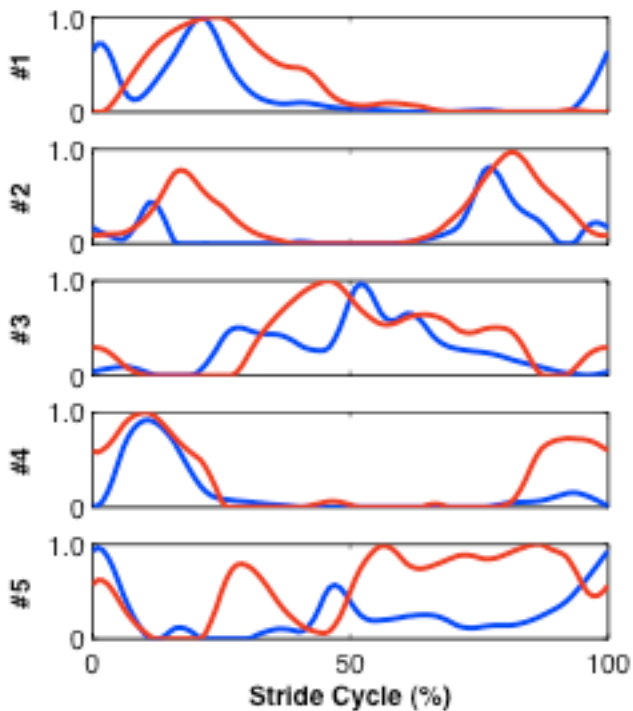


**Figure 2:** Muscle activation synergies throughout the stride cycles for **running** and **sprinting**.

sprinting (speed, stride length and frequency, cost of transport) to within one standard deviation of these same data from a group of 12 adult female runners. The timing of the muscle activations compared well with smoothed EMG data from the human subjects (average cross correlation = 0.58). The NMF procedure reconstructed the optimal muscle activations with an average RMSE of 2% for running and 4% for sprinting. Figure 2 compares the synergies for running and sprinting, while Table 1 lists the muscles associated with each synergy for each movement. Cross correlations between running and sprinting synergies were high for the first four synergies (0.61-0.77) but low for the fifth synergy (0.05). Both movements had a plantarflexors synergy (soleus and gastrocnemius) but the muscles associated with the other four synergies were generally unsimilar between running

**Table 1:** Muscle with weightings greater than 0.4 for each of the five synergies. ‘None’ means muscle weightings were below 0.4 in all synergies.

|             | <b>Running</b> | <b>Sprinting</b> |
|-------------|----------------|------------------|
| <b>#1</b>   | SOL, GAS       | SOL, GAS         |
| <b>#2</b>   | VAS            | GLU, VAS         |
| <b>#3</b>   | ILP            | ILP, BF, TA,     |
| <b>#4</b>   | GLU, VAS, SOL  | GLU, BF, HAM     |
| <b>#5</b>   | HAM            | ILP, RF          |
| <b>None</b> | BF, TA         | --               |

and sprinting, and had at most one common muscle. When the muscle-specific weightings were optimized to reconstruct the original muscle activations using the synergies from the other movement (i.e. sprinting synergies for running), the average RMSEs were 9% for running and 19% for sprinting. Both simulations tripped (clipped the ground with the swing foot before completing a stride) when using these activations. When the weightings as well as the phase shifts of the synergies were re-optimized, the average RMSEs were 4% for running and 7% for sprinting, and both simulations completed a stride at speeds within a standard deviation of the average speeds of the human subjects. Since walking and running are distinguished by a difference in synergy phasing [1], this result suggests that running and sprinting can also be considered different gait modes on the basis of muscle activation synergies.

## CONCLUSION

Characteristics of muscle activation synergies as revealed by NMF differed between running and sprinting, similarly to previously reported differences between walking and running [1]. The simulations were unable to complete a full stride using the synergies from the other movement without adjustments in synergy phasing.

These results suggest that running and sprinting are different gait modes, as are walking and running. Since the biomechanical distinctions between walking and running (double support phase; kinetic and potential energy phasing) do not distinguish between running and sprinting, the distinction may appear at the neural level (e.g. muscle coordination strategies and criteria for optimal performance) rather than the musculoskeletal level. The results have implications in the development of low-dimensional control schemes for forward dynamics simulations as well as theories on human locomotor control.

## REFERENCES

1. Cappellini et al. *J Neurophys* **95**, 3426-3437, 2006.
2. Gazendam & Hof. *Gait Posture* **25**, 604-614, 2007.
3. Tresch et al. *Nat Neurosci* **2**, 162-167, 1999.
4. Neptune et al. *J Biomech* **42**, 1282-1287, 2009.

# VIRTUAL AGING OF THE MUSCULAR SYSTEM AND ITS EFFECTS ON RUNNING BIOMECHANICS

Ross H. Miller, Brian R. Umberger, Jane A. Kent-Braun, and Graham E. Caldwell

University of Massachusetts, Amherst, MA, USA  
email: [rm111@queensu.ca](mailto:rm111@queensu.ca) web: <http://www.umass.edu/sphhs/kinesiology>

## INTRODUCTION

Young and older runners differ on a number of biomechanical factors related to their running gaits. When matched for speed, older runners exhibit shorter stride lengths, limited knee ranges of motion, and larger vertical impact peaks [1]. Aging is also related to changes in the mechanical properties of muscles [2]. In addition, older runners are more prone to calf and hamstrings injuries, and less prone to knee injuries [3].

It is likely that age, muscular properties, and running biomechanics interact to influence the internal loading environment of older runners, and consequently their injury patterns. While muscular properties are often implicated in running injuries, most of the current evidence is inferential. Direct links are difficult to establish with experiments on human runners because muscular properties cannot be manipulated in a timely and well-controlled fashion. Longitudinal studies are limited by the prohibitively long time periods required, and cross-sectional studies can be complicated by numerous confounding variables. A viable solution in these cases is to use computer simulations, which can provide direction control over the manipulation of muscular properties.

Therefore, the purpose of the study was to determine if differences in muscular properties can explain age-related differences in lower limb running biomechanics and internal loading at the calf, hamstrings, and knee. We hypothesized that modifying the muscular properties to represent older adults would (1) induce running biomechanics characteristic of older adults and (2) increase the loading of hamstrings and calf muscles and reduce the loading of the knee joint. We also hypothesized that strengthening the hamstrings and calf muscles in the older simulation would reduce their loading.

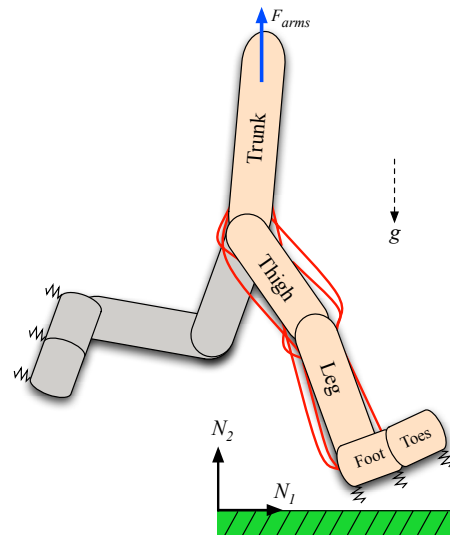


**Figure 1:** Diagram of the musculoskeletal model.

## METHODS

Running was simulated using a 2D forward dynamics model (Fig. 1). Each leg (thigh, shank, foot, toes) was actuated by nine Hill-based muscle models. Numerical optimization was used to generate three separate simulations of one stride of running by minimizing the sum of the squared muscle activation integrals. During model development we found that this criterion generated more realistic simulations than other economy-related criteria.

In simulation #1 (“Young”), muscle model parameters were defined from a series of isovelocity joint strength tests performed on a group of 12 young adults. Specifically, parameters defining the isometric strength and power capabilities of the muscles were optimized to replicate experimental joint torque-time profiles as accurately as possible. In simulation #2 (“Older”), the muscle model parameters were adjusted according to comparisons between young and older adults in the literature. For all muscles, maximum isometric strength was

decreased by 30%, the proportion of fast-twitch fibers was reduced by 20%, maximum shortening velocity was reduced by 20%, maximum shortening velocity was reduced by 20%, and the passive range of motion at the hip was reduced by  $8^\circ$  in flexion and  $13^\circ$  in extension. Decreasing the maximum isometric strength also reduced the absolute stiffness of the muscle series elastic elements. In simulation #3, the Older simulation was repeated with the maximum isometric strengths of hamstrings, gastrocnemius, and soleus returned to their Young values. Other parameters were retained at their Older values. In each simulation, the optimization started from an initial guess that tracked the joint angles and ground reaction forces (GRF) from the young subjects over one stride to within 1.3 standard deviations on average. Penalty functions encouraged solutions with periodic kinematic states and low passive joint moments. Body weight (BW) was 598 N for all simulations.

## RESULTS AND DISCUSSION

The Young and Older simulations ran at nearly the same speed ( $3.64$  and  $3.67 \text{ m s}^{-1}$ , respectively) with similar metabolic costs of transport ( $4.44$  and  $4.49 \text{ J m}^{-1} \text{ kg}^{-1}$ ). The Older simulation used a 6% shorter stride length, a 7% higher stride frequency, and performed 22% less mechanical work on its center of mass. The Older simulation had a smaller knee angle range of motion (Fig. 2) in both stance ( $-14^\circ$ ) and swing ( $-29^\circ$ ), a greater vertical GRF impact peak ( $+0.7 \text{ BW}$ ) and a greater vertical loading rate ( $+28 \text{ BW s}^{-1}$ ). These findings are similar to studies that compared young and older runners [1,4].

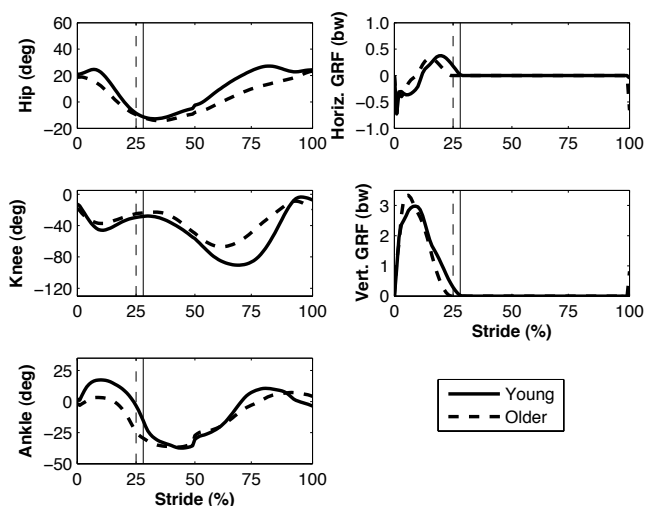


**Figure 2:** Joint angles (left) and GRF components (right) for Young (—) and Older (---) simulations.

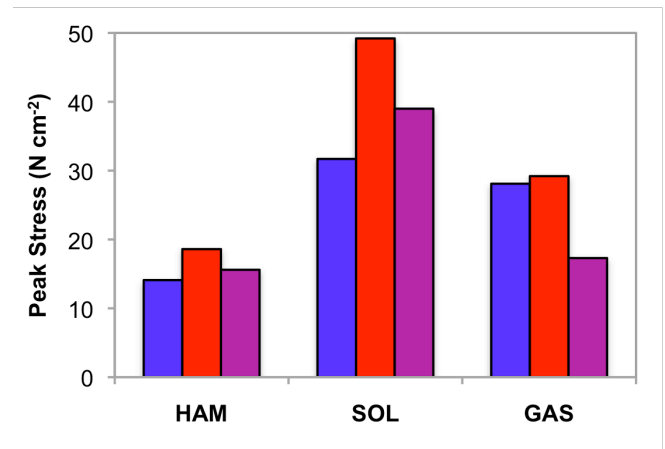


**Figure 3:** Peak muscle stresses for HAMstrings, SOLeus, and GASTrocneMIus from the Young, Older, and Older (strong) simulations.

Compared with the Young case, peak stresses in the Older hamstrings, soleus, and gastrocnemius muscle models (Fig. 3) were 32, 56, and 4% higher. Peak axial knee joint contact force was 40% lower ( $12.7$  to  $7.6 \text{ BW}$ ). When these three muscles were strengthened to their Young values, peak stresses decreased by 16, 21, and 41%. Peak stresses of other muscles increased by 3% on average, and the peak axial knee joint contact force increased by 16% ( $7.6$  to  $8.8 \text{ BW}$ ).

## CONCLUSIONS

Age-related adjustments in muscular properties induced changes in running biomechanics characteristic of differences observed in young and older runners [1,4]. The results suggest direct links between muscle mechanical properties, running biomechanics, and the mechanical loading of injury-prone structures. Older runners may benefit from strengthening the hamstrings and calves to avoid injury, although this hypothesis has not been tested clinically. The simulation approach provides a framework for evaluating theories on muscular properties, preferred movement patterns, and musculoskeletal loading.

## REFERENCES

1. Bus SA. *MSSE* **35**, 1167-1175, 2003.
2. Narici MV et al. *Scand J Med Sci Sports* **15**, 392-401, 2005.
3. McKean KA et al. *Clin J Sports Med* **16**, 149-154, 2006.
4. Cavagna GA et al. *Proc R Soc B* **275**, 411-418, 2008.

# INVESTIGATING THE INFLUENCE OF OBESITY ON GAIT USING SUPPORT VECTOR MACHINE ANALYSIS

<sup>1</sup>Clare E. Milner, <sup>1</sup>Joseph McBride, <sup>2</sup>Julia A. Freedman and <sup>1</sup>Xiaopeng Zhao

<sup>1</sup>University of Tennessee, Knoxville, TN, USA

<sup>2</sup>University of Massachusetts, Amherst, MA, USA

email: [milner@utk.edu](mailto:milner@utk.edu); [xzhao9@utk.edu](mailto:xzhao9@utk.edu)

## INTRODUCTION

As the prevalence of obesity continues to increase at the population level, there is increasing concern about the impact of co-morbidities such as osteoarthritis. Osteoarthritis is a loading-related disease and its development and progression have been linked to excess body weight [1]. Changes in gait biomechanics, particularly at the knee, have been associated with increasing osteoarthritis severity in older adults. Differences in knee flexion excursion, peak knee flexion, peak knee adduction, peak external knee flexion moment, and peak external knee adduction moment have been reported [2,3]. However, it should be noted that these differences in knee variables with osteoarthritis were found in older adults. As the proportion of young people who are obese also rises, it is important to investigate the risk of osteoarthritis development at a younger age. This may be linked to patterns of knee biomechanics during gait. Simple statistical comparisons of discrete knee variables among young adults grouped by body mass index (BMI) found no differences among the groups in a previous report from our study [4]. Any relationship between knee biomechanics and osteoarthritis risk may be more complex in younger adults. Therefore, the purpose of this study was to further examine potential differences in knee biomechanics during gait among normal BMI, overweight, and obese young adults, using support vector machines [5], which are a group of pattern recognition and classification techniques.

## METHODS

Healthy young adults aged between 18 and 35 years with BMI ranging from normal to obese were recruited. All procedures were approved by the Institutional Review Board prior to commencing the

study. All participants provided written informed consent to participate. Groups were determined by BMI, with 10 participants in the normal BMI group (N: BMI 18 – 24.9), 10 overweight (OW: BMI 25 – 29.9), and 10 obese, 9 obese at preferred walking velocity (OB: BMI  $\geq$  30). Gait data were collected using standard three-dimensional motion capture techniques. Participants' lower extremities were instrumented with retroreflective markers and they wore standard laboratory footwear. Marker trajectory data were collected at 120Hz using an optoelectronic motion capture system. Ground reaction force data were collected using force platforms sampling at 1200Hz and synchronized with the motion capture system. Walking velocity was monitored using photoelectric cells and a timer. Participants walked at both their preferred velocity (N:  $1.44 \pm 0.16$ m/s; OW:  $1.35 \pm 0.13$ m/s; OB:  $1.21 \pm 0.13$ m/s) and at a fixed velocity of 1.00m/s ( $\pm$  5%), which is a typical walking velocity of older adults with knee osteoarthritis. Data were processed using standard joint coordinate system and inverse dynamics techniques via commercially available software. Data from five trials at each velocity were extracted from the stance phase: knee flexion excursion, peak knee flexion angle, peak knee flexion moment, peak knee adduction angle, and peak knee adduction moment. Data from the trials were averaged for each participant. Support vector machines were trained to discriminate between N and OW, N and OB, and OW and OB groups. Leave-one-out cross validation was conducted to verify the accuracy of discrimination.

## RESULTS AND DISCUSSION

Support vector machines were able to successfully predict group membership for the N and OB groups. Peak knee flexion moment and peak knee adduction angle were the distinguishing variables. Using data

for the right knee, the combination of these two variables predicted N and OB group membership with 95% accuracy at preferred walking velocity (Figure 1) and 90% accuracy at 1m/s. The same pair of variables was able to predict membership of the N and OB groups for the left knee, with less accuracy 90% at preferred walking velocity and 85% at 1m/s (Figure 2). Membership of the OW group could not be predicted as well using this variable combination.

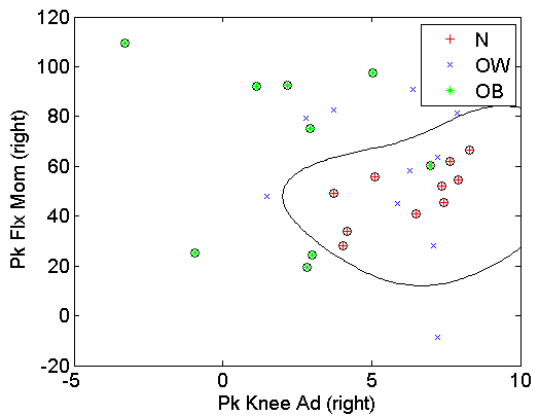


**Figure 1:** Support vector machines identified members of normal and obese groups at preferred walking velocity with 95% accuracy using right knee flexion moment and knee adduction angle.

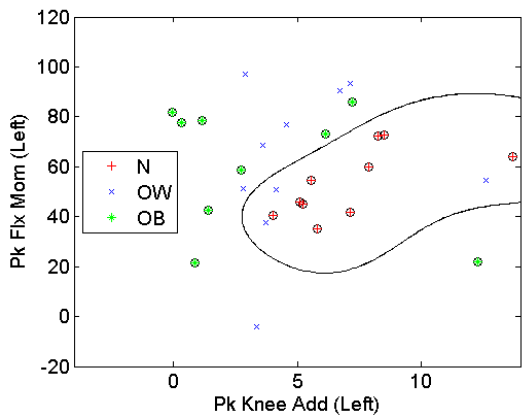


**Figure 2:** Support vector machines identified members of normal and obese groups at preferred walking velocity with 90% accuracy using left knee flexion moment and knee adduction angle.

All of the participants in this study were healthy young adults who had not been diagnosed with knee osteoarthritis. The purpose of the study was to explore whether support vector machine analysis was able to predict BMI group membership using gait variables associated with knee osteoarthritis. A

main feature of the reported analysis is the clustering of normal weight participants with similar or higher peak knee adduction angle than the obese participants. This is contrary to expectations that obese participants would tend to have greater peak knee adduction angle. Furthermore, knee flexion moment has a smaller range in the normal BMI group compared to the obese group. Similar patterns are evident for the left side. As is the nature of a cross-sectional study, it is unknown which, if any, participants will go on to develop knee osteoarthritis in the future. However, there is a higher prevalence of obesity in candidates for total knee arthroplasty, the end-stage treatment for knee osteoarthritis, compared to the general population. This relationship highlights the association between obesity and osteoarthritis [6]. It would be interesting to further investigate whether these associations lead to a greater risk of future development of osteoarthritis in obese young adults.

## CONCLUSIONS

Using classification techniques based on support vector machines, we found that normal and obese BMI groups show different patterns in their knee biomechanics during gait. In particular, the obese group is characterized by a wide range of peak knee flexion moment values, some similar to the normal weight group and some higher. Similarly, there is a large overlap in peak knee adduction angles between the groups, with several obese participants exhibiting lower peak angles than those with a normal BMI.

## REFERENCES

- 1.Cooper C, et al. *Arth Rheum* **43**, 995-1000, 2000.
- 2.Kaufman KR, et al. *J Biomech* **34**, 907-915, 2001.
- 3.Astephen JL & DeLuzio KJ. *Clin Biomech* **20**, 209-217, 2005.
- 4.Freedman, JA, et al. *Med Sci Sports Exerc*, in press.
- 5.Cristianini N & Shawe-Taylor J. *An Introduction to Support Vector Machines and Other Kernel-Based Learning Methods*, 2000.
- 6.Fehring TK, et al. *J Arthroplasty* **22**, 71-76, 2007.

# MARKERLESS TRACKING ERROR OF A BI-PLANAR X-RAY MOTION CAPTURE SYSTEM

<sup>1</sup>Daniel L. Miranda, <sup>2</sup>Joel B. Schwartz, <sup>2</sup>Megan M. Dawson, <sup>2</sup>Braden C. Fleming, and <sup>2</sup>Joseph J. Crisco

<sup>1</sup>Brown University and <sup>2</sup>Department of Orthopaedics, The Warren Alpert Medical School of Brown University and Rhode Island Hospital, Providence, RI, USA

email: Daniel\_Miranda@Brown.edu, web: <http://www.brownbiomechanics.org>

## INTRODUCTION

Three-dimensional (3-D) skeletal motion capture technology, such as X-ray Reconstruction of Moving Morphology (XROMM; Brown University, Providence, RI), currently employs a combination of bi-planar x-ray video and computed tomography (CT) to track dynamic 3-D skeletal movement *in vivo* with high accuracy [1]. Current tracking algorithms can be classified as marker-based tracking or markerless tracking. The invasive nature of marker-based tracking limits its applicability for studying *in vivo* human joint motion. Markerless tracking eliminates implantation of markers and uses tracking algorithms designed to match 3-D bone volumes to the bi-planar x-ray videos. Employing this technology to obtain quantitative data on human joint motion requires an understanding of its systematic error, herein referred to as “kinematic error”.

The purpose of this study was to evaluate the kinematic error of a bi-planar x-ray motion capture system using a markerless tracking algorithm under static and dynamic motion conditions.

## METHODS

The bi-planar XROMM facility consists of two Varian model G-1086 x-ray tubes, two EMD Technologies model EPS 45-80 pulsed x-ray generators, two 16” Dunlee model TH9447QXH590 image intensifiers (IIs), and two Phantom v9.1 high-speed digital video cameras. The resolution of the imaging chain is approximately 2 line pairs/mm. Markerless XROMM uses an auto-registration algorithm based on the work of You et al. [2] and Bey et al. [3] to recover the 3-D pose of the bones from the bi-planar x-ray videos using a clinical CT scan.

Static error was evaluated by translating and rotating a set of human cadaver bones (distal femur, distal radius, and distal ulna) by known increments with high precision linear (RT-3 Series; Newmark

Systems, Mission Viejo, CA) and rotary (NB4 Series; Newmark Systems) positioning stages with accuracies of 0.001 mm and 0.002° (Fig. 1A).

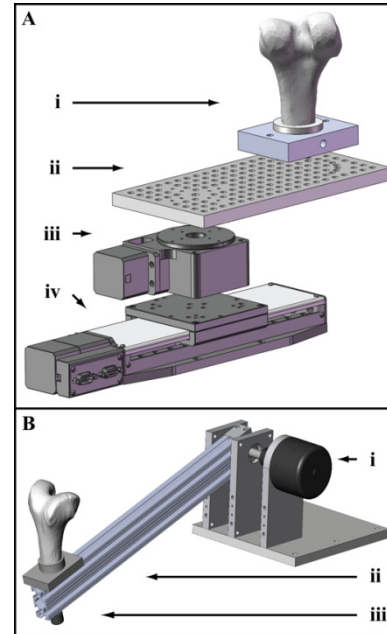


**Figure. 1:** A. Static accuracy testing jig including the specimen (i), mount plate (ii), rotary stage (iii), and linear stage (iv). The static stage assembly was rigidly fixed to a concrete pedestal for all static testing. B. Dynamic accuracy testing jig including the ADT (i), pendulum arm (ii), and rubber impact bumper (iii). The specimen displayed in A.i is attached to the far end of the pendulum arm. The pendulum arm is able to spin along the same axis as the mechanical axis of the ADT. The dynamic testing apparatus was rigidly fixed to a concrete pedestal. During testing, the rubber bumper impacted the concrete pedestal.

For each bone specimen, twenty trials of 15 linear motion steps (0.000, 0.001, 0.010, 0.100, 1.000, 10.000, 10.100, 25.000, 25.100, 50.000, 50.100, 75.000, 75.100, 100.000, and 100.100 mm) and 15 rotational motion steps (0, 0.002, 0.010, 0.100, 1.000, 10.000, 10.100, 25.000, 25.100, 50.000, 50.100, 75.000, 75.100, 100.000, and 100.100°) were performed. A reference position for the linear and rotational tests was determined at 0.000 mm and 0.000°, respectively.

Dynamic error was evaluated using the specimens previously described. A pendulum was fabricated using a high precision ( $\pm 0.06^\circ$ ) angular displacement transducer (ADT; Series 600 Angular Displacement Transducer, Trans-Tek Incorporated, Ellington, CT) (Fig. 1B).

Five pendulum drop trials were performed for each trial where the pendulum arm was accelerated from rest. As the arm fell, it entered the field of view and impacted a concrete pedestal. The motion

of the arm and attached specimen were recorded. Additionally, an average reference position for each specimen was determined by collecting a stationary trial at the final resting position.

The x-ray tube voltage and current were set at 70 kVp and 200 mA and the source to image distance (SID) was set to ~140 cm. For all static testing, the XROMM system recorded in pulsed (4 ms) x-ray generation mode at 60 frames-per-second (fps). During dynamic testing, the XROMM system recorded in continuous x-ray generation mode at 250 fps. Each high-speed video camera was shuttered between 1/1300 and 1/2000 s depending on the specimen.

Kinematic error, defined as the difference between the measured rigid body motion (XROMM) and the true value of the parameter being measured (stages or ADT), was determined for every static and dynamic data point. These data are summarized using sample median, 25-75 percentile, and range statistics. Additionally, absolute error data are summarized using sample mean and standard deviation (SD) statistics.

## RESULTS

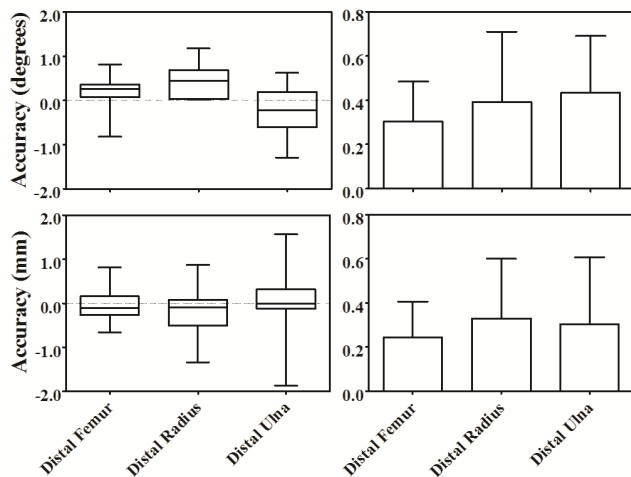


**Figure 2:** Left column Box and whiskers rotational (top) and linear (bottom) plot displaying range, 25-75 percentile, and median static error for each specimen. Right column Mean (+1 SD) rotational (top) and linear (bottom) absolute static error for each specimen.

The overall mean static rotational absolute error was estimated to be  $0.30 \pm 0.18^\circ$ ,  $0.39 \pm 0.32^\circ$ , and  $0.44 \pm 0.26^\circ$  for the distal femur, distal radius, and distal ulna, respectively (Fig. 2). The overall mean static linear absolute error was estimated to be  $0.25 \pm 0.16\text{mm}$ ,  $0.33 \pm 0.27\text{mm}$ , and  $0.30 \pm 0.30\text{mm}$  for the distal femur, distal radius, and distal ulna, respectively (Fig. 2).

The overall mean dynamic error was estimated to be  $0.14 \pm 0.09^\circ$ ,  $0.10 \pm 0.09^\circ$ , and  $0.14 \pm 0.12^\circ$  for

the distal femur, distal radius, and distal ulna, respectively (Fig. 3).

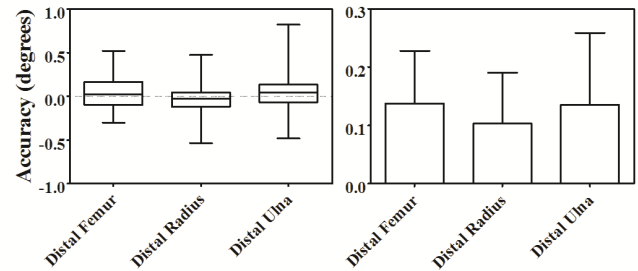


**Figure 3:** Left column Box and whiskers plot displaying range, 25-75 percentile, and median dynamic error for each specimen. Right column Mean (+1 SD) absolute dynamic error for each specimen.

## DISCUSSION

Understanding the systematic error of individual bi-planar x-ray motion capture systems is important for understanding each system's capabilities. Creating a method for quantifying error allows investigators to more easily determine study specific limitations. We determined that the overall dynamic error for the system lies between  $0.1^\circ$  and  $0.15^\circ$ , under the given testing conditions. We unexpectedly observed worse error for the static testing protocol as compared to the dynamic testing protocol. We postulate that is a result of the initial-guess position required as input to the markerless tracking algorithm. During static testing, each frame (or trial) is tracked independent of the previous and succeeding trial. During dynamic testing, each frame uses position information from the previous (or succeeding) frame to determine the bone position at the current frame.

Overall, these results are consistent with those of other 3-D skeletal motion capture technologies [3]. The markerless XROMM system that combines bi-planar x-ray video and CT data for measuring dynamic 3-D *in vivo* skeletal motion will permit novel, non-invasive studies on human joint function during dynamic tasks. Studies quantifying systematic error are critical first steps.

## REFERENCES

1. Brainerd EL, et al. *J Exp Zool A Ecol Genet Physiol.* **313**(5), 262-79, 2010.
2. You BM, et al. *IEEE Trans Med Imaging.* **20**(6), 514-25, 2001.
3. Bey MG, et al. *J Biomech Eng.* **128**(4), 604-9, 2006.

## ACKNOWLEDGEMENTS

This study was funded by the W.M. Keck Foundation.

# TO WHAT EXTENT CAN POSTURE-RELATED CHANGES IN CORTICOMOTOR EXCITABILITY BE EXPLAINED BY MUSCLE BIOMECHANICS?

<sup>1,2</sup>Jeremy P.M. Mogk, <sup>1,3</sup>Lynn M. Rogers, <sup>1,2,3,4</sup>Wendy M. Murray,  
<sup>1,2,3</sup>Eric J. Perreault, and <sup>1,2,5</sup>James W. Stinear

<sup>1</sup>SMPP, Rehabilitation Institute of Chicago, <sup>2</sup>Dept of Physical Medicine & Rehabilitation, and <sup>3</sup>Dept of Biomedical Engineering, Northwestern University, <sup>4</sup>Edward Hines, Jr. VA Hospital, <sup>5</sup>Dept Sport & Exercise Science, University of Auckland,

email: [j-mogk@northwestern.edu](mailto:j-mogk@northwestern.edu), <http://www.smpp.northwestern.edu/research/arms/index.html>

## INTRODUCTION

The excitability of motor pathways is task-dependent and is, in part, modulated by posture. For example, corticomotor excitability of a muscle tends to increase at joint angles that place that muscle at shorter lengths [1, 2]. To date, posture-dependent excitability has only been examined for changes in position of a single joint. How motor pathways respond to postural changes that involve multiple joints remains unclear.

We used transcranial magnetic stimulation (TMS) to examine the effects of upper limb posture on excitability of the posterior deltoid (PD) and biceps brachii (BIC). We hypothesized that the excitability of the multiarticular BIC would increase in all postural combinations that shorten the BIC (i.e. flexed elbow or shoulder, or supinated forearm), while the excitability of the uniarticular PD would be primarily impacted by shoulder position.

## METHODS

Excitability of the corticospinal pathways projecting to the PD and BIC muscles was assessed in twelve healthy subjects (3 females and 9 males; mean age  $26.5 \pm 3.3$  years) using TMS delivered when the muscles were at rest. Single-pulse TMS was delivered to the contralateral motor cortex using a figure-of-eight coil. All stimuli were applied at the location where the largest peak-to-peak amplitude MEP was evoked in the BIC using the lowest stimulation intensity. During experimental trials, the stimulus intensity was set at 120% of resting threshold of the BIC, as determined when the arm was hanging relaxed by the side of the body. Surface electromyography was used to monitor muscle activity prior to each stimulus and record the responses evoked in the PD and BIC muscles.

During experimental trials, the stimulator delivered 20 stimuli at a rate of 0.2 Hz.

Changes in corticomotor excitability of the BIC and PD muscles were quantified by the changes in MEP amplitude across a total of fifteen arm postures. Subjects were seated with their dominant arm fully supported in each of seven primary upper limb postures (Fig. 1). These included three “reference” postures (side, lap, and chair) and four “functional” postures (forward, horizontal, and overhead reach, and pressure relief). Additionally, three forearm postures (full pronation, neutral, and full supination) were examined in each functional posture. Significant differences in MEP amplitudes associated with changes in posture were evaluated using a separate ANOVA for each muscle.

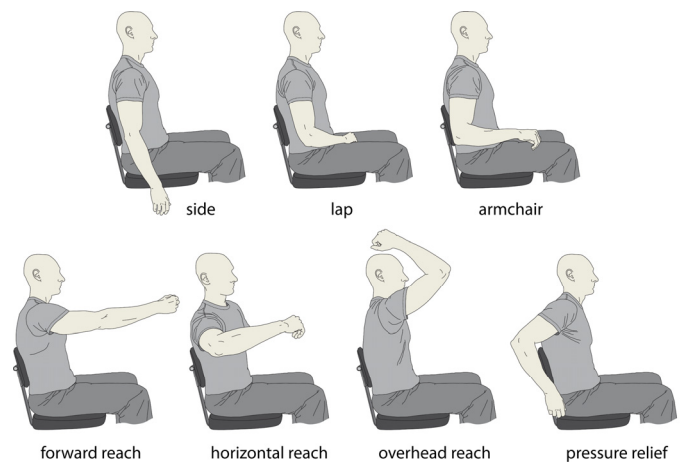


**Figure 1.** Reference and functional postures examined. All TMS-evoked responses were normalized to those elicited in the side posture.

We used a biomechanical model of the upper limb [3] to determine the posture-related changes in muscle fiber lengths in each posture. Note that BIC length changes as a function of shoulder, elbow and forearm posture, while PD fiber length changes only with shoulder posture.

## RESULTS AND DISCUSSION

In general, corticomotor excitability of the BIC and PD was greater in postures where each target muscle was shorter (Fig. 2). For example, relative to the side posture, BIC excitability increased in all postures ( $p < 0.01$  for all postures except forward reach); the musculoskeletal model indicated that side posture was associated with the longest BIC length. Shortening of the BIC from pronation to supination also increased excitability within each functional posture ( $p < 0.0025$ ). Similarly, PD excitability was greater in pressure relief compared to the side posture ( $p = 0.00003$ ). Pressure relief was the only functional posture where PD length was shorter than the reference posture.

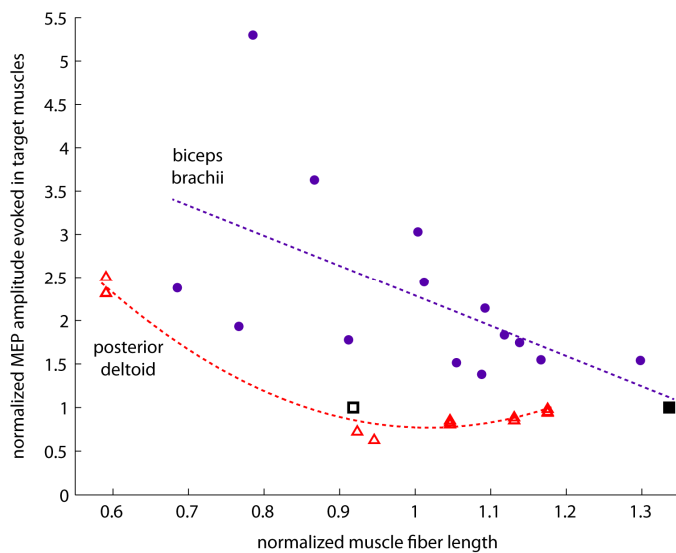


**Figure 2.** Mean responses evoked in the PD (open triangles) and BIC (filled circles) as a function of posture-related changes in muscle length. Black squares signify responses recorded in the side posture, to which all MEP amplitudes were normalized.

Supporting the arm with a flexed elbow (lap and chair) increased the BIC excitability relative to the arm hanging at the side ( $p < 0.005$ ), as would be predicted from decreases in muscle length (Fig. 3). However, PD excitability decreased from the side to both lap and chair postures (36% and 26%, respectively;  $p < 0.0001$ ) despite similar muscle length in all 3 reference postures. A previous study described a similar result, where distal muscle excitability changed when proximal joint posture was altered, but target muscle length remained constant [4]. Biomechanically, elbow posture could impact shoulder muscle excitability via length-related changes to the multiarticular BIC and long

head of the triceps. For example, changes in length of the BIC will alter the passive properties about the forearm, elbow and shoulder joints. Relative to the side posture, excitability of the uniarticular PD changed to a greater extent when it shortened (pressure relief) than when its length remained constant (lap and chair).

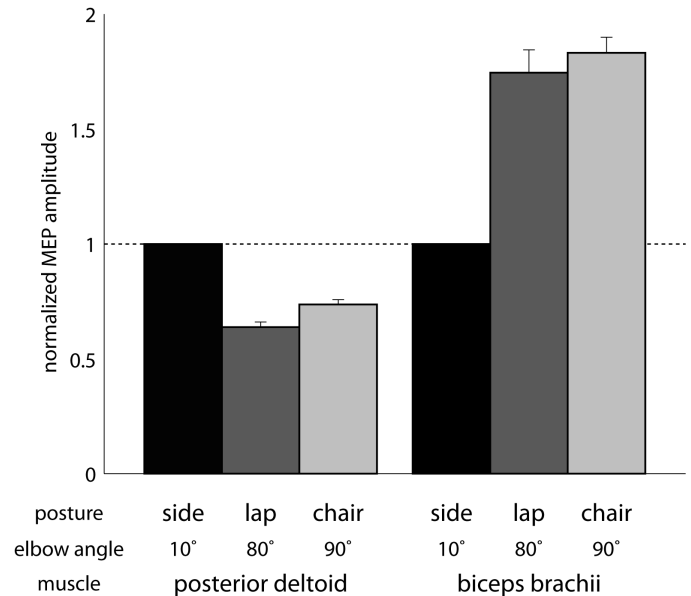


**Figure 3.** Mean responses evoked in the PD and BIC muscles in each of the three reference postures examined. Error bars represent standard error of the mean.

## CONCLUSIONS

Identifying postures that either facilitate or suppress the excitability of specific muscles carries utility for training of muscle recruitment and coordination patterns during rehabilitation. Posture-related modulation of muscle excitability of these two muscles, in particular, may be important for understanding each muscle's potential for motor learning following tendon transfer to restore elbow extension following cervical spinal cord injury.

## REFERENCES

1. Lewis GN, et al. *Brain Res* **900**, 282-294, 2001.
2. Renner CI, et al. *Stroke* **37**, 2076-2080, 2006.
3. Holzbaur KR, et al. *Ann Biomed Eng* **33**, 829-840, 2005.
4. Ginanneschi F, et al. *Exp Brain Res* **161**, 374-385, 2005.

## ACKNOWLEDGEMENTS

This work was supported by the Craig H. Nielsen Foundation (84054).

# EFFECTS OF BIFURCATION ANGLE ON THE WALL SHEAR STRESS IN STENOSED CORONARY ARTERY BIFURCATION

<sup>1</sup>Marjan Molavi Zarandi, <sup>1</sup>Rosaire Mongrain and <sup>2</sup>Olivier F. Bertrand

<sup>1</sup>McGill University, Montreal, Qc, Canada

<sup>2</sup>Laval University, Laval, Qc, Canada

email: [marjan.molavizarandi@mail.mcgill.ca](mailto:marjan.molavizarandi@mail.mcgill.ca) web: <http://www.mcgill.ca/mecheng>

## INTRODUCTION

From clinical practice, it is known that coronary artery bifurcations are regions where the flow is strongly perturbed, and is prone to the development of atherosclerotic lesions. Coronary bifurcation lesions have always represented a major challenge for percutaneous treatment. Part of this challenge is related to the variety of coronary lesions located at bifurcation which present wide range of anatomical morphologies. Investigation of blood flow hemodynamics and shear forces are of great importance in understanding the regions of lesion formation and development. Wall Shear Stress (WSS) is the most important flow related factor in the development of atherosclerosis in arterial branches. Evidences show that changes in bifurcation angles alters the flow conditions and changes the magnitude of WSS within the vessel [1]. It is believed that critical bifurcation angles might create low shear regions that could influence the development of coronary atherosclerosis [2]. In this study, a two dimensional numerical analysis of blood flow in the threshold stenoses of 50% in coronary artery bifurcation is performed for seven different lesion types classified by Medina *et al.* [3]. The effects of bifurcation angle on the WSS distributions on the inner and outer walls of side branch are investigated.

## METHODS

A comprehensive hemodynamic analysis was carried out to obtain the WSS distribution on the walls of stenosed coronary artery bifurcation. The geometrical model corresponds to the bifurcation between left anterior descending artery and a side branch. Figure 1 shows the geometrical model of the bifurcation (main branch proximal (I), main branch distal (II) and side branch (III)) as well as

the lesion locations according to Medina lesion classification.

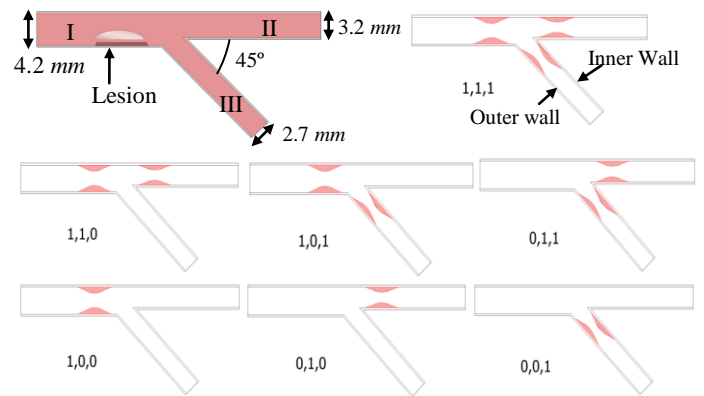


**Figure 1:** Geometrical model and Medina lesion classification of coronary artery bifurcation.

Numerical simulation of blood flow was performed for two bifurcation angles ( $45^\circ$  and  $75^\circ$  which correspond to the anatomical range) to investigate the effect of side branch angle on WSS distribution in stenosed arteries. For the study of blood flow, we assumed that blood can be represented by an incompressible fluid which is governed by the momentum and continuity equation:

$$\rho \left( \frac{\partial u}{\partial t} + u \cdot \nabla u \right) = -\nabla p + \nabla \cdot \eta (\nabla u + (\nabla u)^T) \quad (1)$$

and the continuity equation:

$$\nabla \cdot u = 0 \quad (2)$$

where,  $\rho$  denotes the density of the fluid ( $Kg/m^3$ ),  $u$  the velocity vector ( $m/s$ ),  $p$  the pressure ( $Pa$ ) and  $\eta$  the viscosity of fluid ( $Pa.s$ ). The shear rate ( $\dot{\gamma}$ ), for two dimensions is defined by equation:

$$\dot{\gamma} = \sqrt{\frac{1}{2} \left( \left( 2 \frac{\partial u}{\partial x} \right)^2 + 2 \left( \frac{\partial u}{\partial y} + \frac{\partial v}{\partial x} \right)^2 + \left( 2 \frac{\partial v}{\partial y} \right)^2 \right)} \quad (3)$$

where  $u, v$  are the velocity vectors.

To solve the governing equations, a set of boundary conditions is required. The maximum velocity varies between  $24 \text{ cm/s}$  and  $46 \text{ cm/s}$  [4]. Velocity

variations were obtained from blood flow rate during the cardiac cycle [4]. At the walls, the velocity obeyed the no-slip condition and at the outlet of main branch distal and side branch, a stress-free condition was considered. The Newtonian blood properties in this model are blood viscosity  $\mu_{\infty} = 0.035 \text{ mPa}\cdot\text{s}$ , and blood density  $\rho = 1060 \text{ Kg/m}^3$  respectively [5].

## RESULTS AND DISCUSSION

We investigated the WSS distribution in all seven types of the Medina classification for  $45^\circ$  and  $75^\circ$  branch angles. Figure 2 shows the WSS distributions on the outer wall of side branch for (1, 1, 1) type of Medina classification in a cardiac cycle.

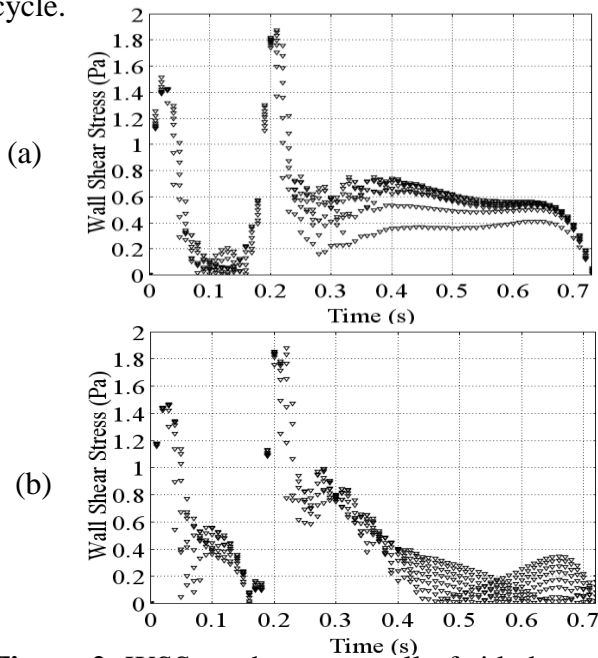


**Figure 2:** WSS on the outer wall of side branch for  $45^\circ$  (a) and  $75^\circ$  (b) branch angles.

WSS on the outer walls of side branch of all types of Medina classification for  $45^\circ$  and  $75^\circ$  branch angles are shown in Figure 3.

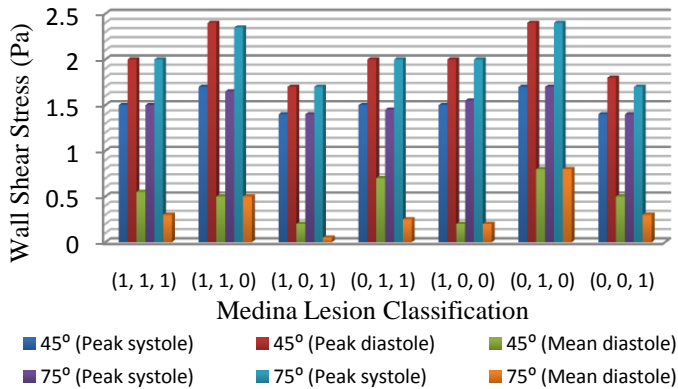


**Figure 3:** WSS on the outer wall of side branch.

Magnitudes of WSS on the inner wall of side branch in the stenosed artery with bifurcation branch angles of  $45^\circ$  and  $75^\circ$  of all types of Medina classification are presented in Figure 4.

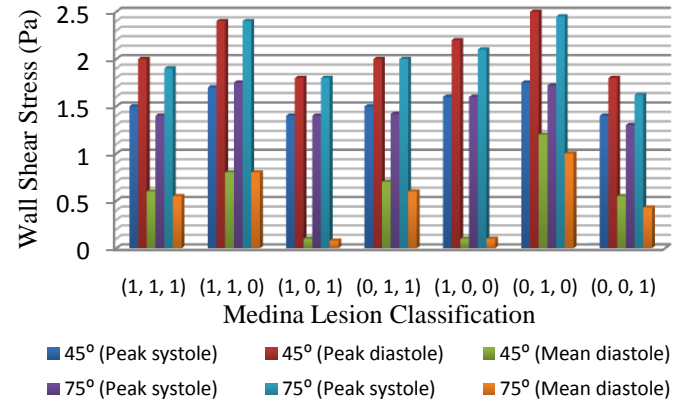


**Figure 4:** WSS on the inner wall of side branch.

Comparison of the values of WSS in three regions of cardiac cycle showed that the significant changes in WSS magnitude for  $45^\circ$  and  $75^\circ$  bifurcation angles appears at the mean diastolic period of a cardiac cycle.

## CONCLUSIONS

We studied the effect of side branch angle on the WSS values in side branch when the entire vessel was subjected to atherosclerosis. Magnitudes of WSS values were obtained for various lesion locations according to Medina classification. By investigating the distribution WSS on the inner and outer walls of side branch for  $45^\circ$  and  $75^\circ$  bifurcation angles, it was found that higher branch angle creates lower magnitudes of WSS on the vessel walls which could be more problematic. The lower magnitudes of WSS on the side branch walls appeared at mean diastolic period of a cardiac cycle with  $75^\circ$  branch angle. It is interesting to note that, the conventional Medina lesion classification doesn't take in to account the bifurcation angel.

## REFERENCES

- 1.Soulis, et al. *J Biomech* **39**, 742-749, 2004.
- 2.Ikeda U, et al. *Jpn Heart J* **32**, 627–33, 1991.
- 3.Medina A, et al. *Rev Esp Cardiol* **59**, 183-184, 2006.
- 4.Faik I, et al. *J Biomedical materials* **2**, 28–37, 2007.
- 5.Benard N, et al. *Annals of biomedical engineering* **34**(8), 1259–1271, 2006.

# 3D ORIENTATION OF THE DISTAL PHALANGES OF THE THUMB AND INDEX FINGER DURING PINCH

Tracy Mondello, Mathieu Domalain, Zong-Ming Li

Departments of Biomedical Engineering, Physical Medicine and Rehabilitation, and Orthopaedic Surgery, Cleveland Clinic, Cleveland, OH. Email: liz4@ccf.org

## INTRODUCTION

Precision pinch plays an important role in hand function and is essential for many every day tasks. It requires accurate coordination as the thumb opposes the index finger. Thumb opposition is a complex motion that results from coordination of several joints moving in multiple planes<sup>1</sup>. Methods exist to describe thumb opposition independently of the fingers<sup>2-4</sup> despite the fact that the primary role of opposition is to coordinate with other fingers. Thumb-finger coordination is the critical part to achieving an accurate pinch. Several studies focused on the location of digit tips<sup>5</sup> or joint angle variability<sup>3</sup> but a good method to describe the relative orientation of the thumb and index finger distal phalanges is still lacking. The knowledge of the relative orientation is crucial to fully describe the coordination between the two digits and might be helpful to quantify kinematic impairment caused by hand disorders. However, finger kinematic studies face the challenge of tracking small segments which exaggerates misalignment errors and skin movement artifacts<sup>6</sup>. Therefore, the purpose of this study was to present a method that utilizes a Digit Alignment Device (DAD) to virtually track the nail coordinate system to describe the relative orientation of the thumb and index finger distal phalanges during pinch.

## METHODS

Experimental Devices. Marker clusters consisting of 3 reflecting markers (4 mm in diameter) attached via a thin rod to an acrylic nail plate (Figure 1) were used to track the 3D motion of the thumb and index finger distal phalanges. The marker clusters easily attached to the finger nail with double sided tape. During the static trial the DAD was used to establish the relationship between the virtual nail coordinate system and the cluster. The device

consisted of a rectangular block (11 cm × 5 cm × 3.5cm) with 8 markers used to define the orientation of the distal phalanges' anatomy. Markers 1, 3 and 2, 4 were aligned with the longitudinal axis of the device. The thumb and index finger were placed onto the lateral side and top of the device, respectively, aligning the fingers with a longitudinal line on the center of the device. Using this device allowed the markers to be spread out on a flat surface avoiding out of plane misalignment (Figure 1).

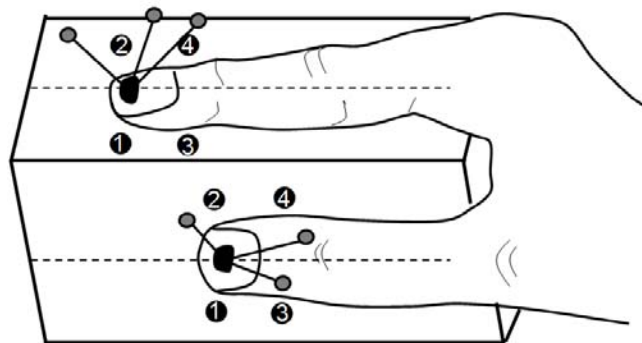


**Figure 1:** Static trial set-up to establish virtual nail coordinate systems

Coordinate System Definitions. The origin of the virtual nail coordinate system was located on the center of the nail surface. The x axis was oriented from the midpoint of markers 3 and 4 to the midpoint of markers 1 and 2 and defined the longitudinal axis of the finger. The z axis was defined as the vector perpendicular to the x axis and was oriented to the right. The y axis was orthogonal to the x and z axes as determined by the right hand rule (Figure 2). An arbitrary technical coordinate system was defined from each marker cluster as its orientation does not have any importance. The coordinate system of the marker cluster was then transformed into the virtual coordinate system of the nail (Figure 2).

**Experimental Procedure.** To illustrate the proposed method, we analyzed the precision pinch of one subject. During the dynamic trial, the virtual nail coordinate systems were tracked with the marker clusters. The subject performed 50 cycles at a pace of 1 Hz with the eyes closed. A marker-based motion analysis system (Vicon, Oxford, UK) was used to capture digit motion data. The pinch cycle began with the thumb and index finger at maximum aperture and ended at pulp contact.

**Data Analysis.** Biomechanical analysis software (Visual 3D, C-Motion Germantown, MD) was used to carry out the kinematic analysis and orientation of the thumb relative to the index finger was described using Euler angle notation yaw (rotation around y), pitch (rotation around z') and roll (rotation around x''). Mean  $\pm$  standard deviation of amplitude of rotations during movement and orientation at timing of pulp contact was calculated.

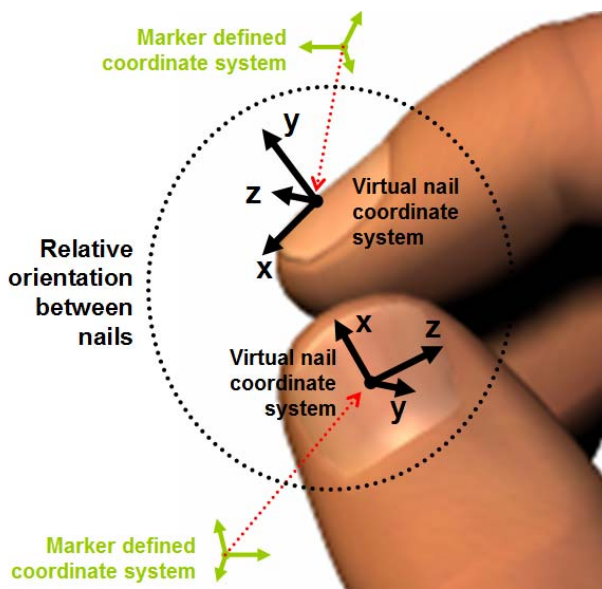


**Figure 2:** Coordinate systems relationship

## RESULTS

Throughout the closing phase of the pinch cycle, the thumb rotates around the index finger y axis (yaw)  $99.6^\circ \pm 6.9^\circ$ . It rotates  $62.0^\circ \pm 6.6^\circ$  and  $104.7^\circ \pm 5.9^\circ$  around the z' (pitch) and x'' (roll) axes respectively (Figure 3). At pulp contact, the thumb distal phalange was orientated with a yaw of  $33.2^\circ \pm 3.1^\circ$ , a pitch of  $32.4^\circ \pm 2.6^\circ$ , and a roll of  $-149.2^\circ \pm 2.2^\circ$  relative to the index finger distal phalange.

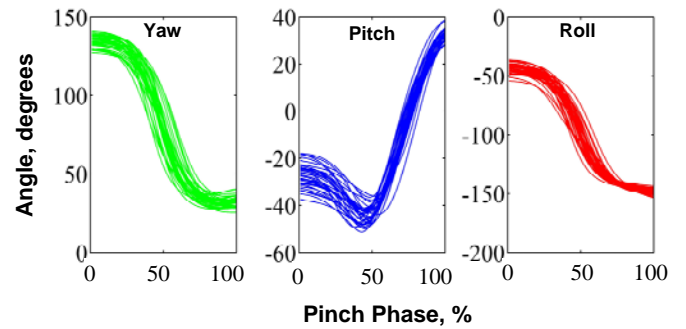


**Figure 3:** Yaw, pitch and roll angles for the closing phase of repetitive pinch cycles

## DISCUSSION

Previous studies investigated thumb opposition as an independent motion, tracking only the thumb tip rotation, joint angle ranges of motion and coordination among the joints<sup>1-4</sup>. This study proposes a new method to investigate the thumb and index finger relative orientation during precision pinch. Specifically we developed a Digit Alignment Device (DAD) that overcomes the limitation associated with the small scale of the digits and avoids skin movement artifact and marker misalignment errors. Furthermore, we propose to describe the orientation of the digits' distal segment the way it is usually done with attached segments. The sequence used here (yaw, pitch and roll), allowed us to avoid any particularities generally encountered with inappropriate choice of rotation order. This method takes advantage of the nail, which is a unique feature of the digits and accurately represents the underlying skeleton<sup>2</sup>, to track the virtual nail coordinate system. The ease of use and limited number of markers needed make this method useful for tracking the small segments of the hand.

## REFERENCES

1. Li ZM, et al. *J Biomech* **40**, 502-510, 2007.
2. Coert JH, et al. *J Orthop Res* **21**,1151-1155, 2003.
3. Cole KJ, et al. *J Neurophys* **55**, 1407-1423, 1986
4. Cooney WP, et al. *J Hand Surg[Am]* **9**, 777-786, 1984.
5. Yokogawa R, et al., *J Biomed Eng* **126**, 212-219, 2004.
6. Murgia A, et al. *Clin Biomech* **19**, 248-254, 2004.

# KINEMATIC MODEL FOR TOTAL KNEE REPLACEMENT SURGICAL TRAINING AND PLANING

Piyawan Moonjaita, Jackrit Suthakorn\*

Department of Biomedical Engineering,  
Center for Biomedical and Robotic Technology  
Mahidol University, Thailand  
email: piyawan@bartlab.org,

\*Corresponding Author: egjst@mahidol.ac.th website: www.bartlab.org

## INTRODUCTION

Total knee replacement (TKR) is an important orthopedic surgery to repair patient's knee for relieving their pain from arthristis; such as, osteoarthritis, rheumatoid arthritis, and traumatic arthritis. TKR is required for patients with significant knee pain from several reasons, such as, to restore the normal mechanical axis alignment of leg [1], pain free and patients able to walk normally [2]. Traditional TKR requires skillful surgeon in order to plan and operate the surgery properly to recover the patient's lower-limb normal activities. Surgeon is required to perform bone cutting and surfacing on femur and tibia to fit the geometrical shape of knee implants. Positioning and orientating of the knee implants is critical for post-operative results [3].

This study is to develop a flexible kinematic model for pre-operative training and planning purpose in TKR surgery. The kinematic model aims to use for demonstrating the post-operative results based on 1) hip-knee-foot angle alignment, 2) intramedullary canal's axis, 3) anatomical landmarks (e.g. medial and lateral femoral condyle, medial and lateral femoral epicondyle and tibia tuberosity), 4) traditional TKR procedures and 5) most orientation error in TKR surgical practices. The study is separated into several stages, which are: kinematic model development, TKR simulations, graphical user interface (GUI) and result displaying and error assessment reporting system. The study compares simulate results from normal and TKR cases. The TKR cases include Case 1: well-aligned TKR case, Case 2: error in orientation about intramedullary canal's axis, Case 3: error in orientation about patella's axis, and Case 4: combination error in

orientation about both intramedullary canal's axis and patella's axis using Euler angle. The kinematic model can accommodate various knee implants due to its kinematic algorithm and input parameter system. The study is a part of research on "TKR surgical navigation system with high flexibility and low learning curve."

## METHODS

### *System Overview*

We have developed a CIS System [4], the project is TKR surgical navigation system with high flexibility and low learning curve, it is base on numerical modeling which can flexible to any prosthesis's models and sizes. The overall system are composed of four parts; 1) Pre-modeling of knee and prosthesis kinematics, 2) Real-time data acquisition processes, 3) Optical tracking system, 4) Graphic User Interface (GUI). Figure 1: shows diagram of the overall system.

In part of Pre-modeling of knee and prosthesis kinematics is the kinematics analysis and algorithms development, which generate the workspace, path planning and flexible kinematics model of cutting shapes on femur and tibia to fit with various popular knee prosthesis.

So, this CIS system is not base on data storage. The algorithm part will retrieve the information of prosthesis dimensions from part 2: the real-time data acquisition process. Then, the algorithm will generate the prosthesis model and path planning and communicate to the surgeon via GUI during perform the task. The optical tracking system is used for indicate the pose (position and orientation) of knee bones and surgical instruments to display

the relationship between each object in the work space.

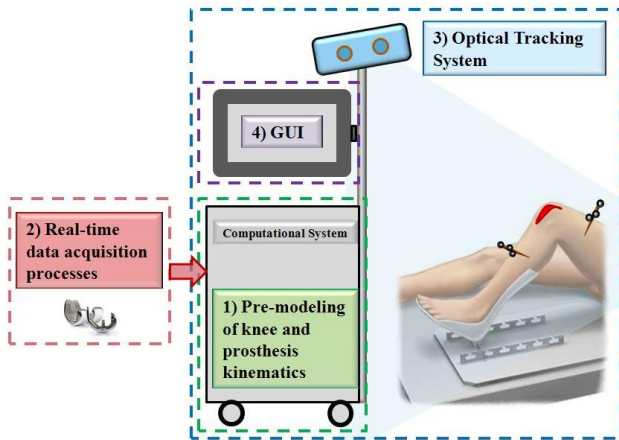


Figure 1: diagram of the TKR surgical navigation system with high flexibility and low learning curve

This study is the first phase of our system, which is the kinematics analysis of knee and knee prosthesis and demonstrate the post-operative result.

### *Kinematics Analysis*

Kinematics is the science of motion which treats motion without regard to the force that causes it [5]. These would involve with the description to specify attributes of various objects. There are positions, orientations and frame is an entity which contains both position and orientations. In this section, describes the kinematics analysis of two objectives which are knee kinematics and knee prosthesis kinematics.

### *Knee Kinematics Analysis*

The human knee is the largest and the most complex joint in the body, which is the interaction between three bones. There are patella, femur and tibia that can be clarified into two structure of joint motion: the tibio-femoral joint (between tibia and femur), the patello-femoral joint (between patella and femur). The greatest range of motion of knee appears in the sagittal plane is occurred by tibio-femoral joint, where the range from full extension to full flexion of the knee from 0 to approximately 140 degrees [6]. In the knee kinematics analysis section, we studied the kinematics in 3-Dimensional (3D) of the normal knee, and analyze the kinematics of implanted knee.

To describe the relative motion between two rigid bodies (femur and tibia) in 3D. Two Cartesian

coordinate systems were assigned to each bone as the bone's representative frame, the femur's frame was fixed as the reference body to tibia, while tibia move relatively. Figure 2: shows an illustration of kinematics of normal knee. Firstly, the sagittal plane was considered, the flexion-extension in the tibio-femoral joint of normal knee is similar as tibia rotates about a revolute joint or about X-axis. The articular surface between circular surface of femoral condyle and flat surface of tibia cause the sliding motion (translation along Z-axis) during knee flexion but not much because the restriction of the anterior and posterior cruciate ligaments. In front plane, medial-lateral translation (translation along X-axis) and upper-lower translation (translation along Y-axis) show a few displacement because the restriction of medial and lateral collateral ligament, and also abduction-adduction (rotation about Z-axis) in a fully extended knee almost no abduction or adduction. In transverse plane, there is internal-external rotation of tibia (rotation about Y-axis) during knee flexion (rotation about X-axis) because the medial femoral condyle is longer than the lateral femoral condyle.

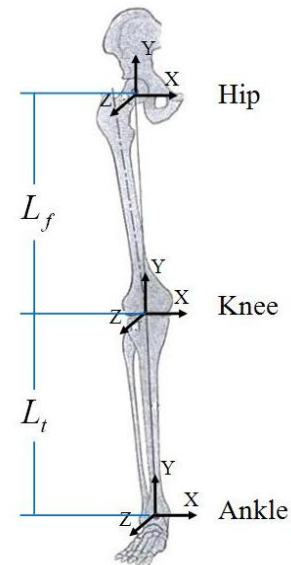


Figure 2: Frame assignment on mechanical axis alignment of leg

In the study kinematics of total knee replacement systems reported that the implanted knee kinematics are not return normal characteristic to those of the normal knee, which depending on the prostheses models [7-8]. Therefore, the main goal of the TKR surgery is to restores the normal mechanical axis and to treats the disease. For that reason this work has developed a numeric model for knee kinematics after TKR surgery to simulate the dislocation of

prosthesis that will cause the abnormal mechanical axis of the knee compare to the proper implantation that will returns the normal mechanical axis for the knee.

To demonstrate the kinematics of implanted knee, three Cartesian coordinate systems was assigned to locate at the center of hip, center of knee and center of ankle to represent the mechanical axis. The characteristic of each frame coordinate can be described by homogeneous transform matrix  $H$ . It can be regarded purely as a construction used to cast the rotation and translation of the general transform into a single matrix form. Where the rotation describes the orientation and the translation describes the position.

At the beginning of analysis, hip is assigned to be fixed as base reference. Then knee's frame is move relative to hip, the description of knee's frame relative to hip's frame is

$${}_{Knee}^{Hip}H = \begin{bmatrix} {}_{Knee}^{Hip}R & {}_{Knee}^{Hip}\vec{P} \\ \hline 0 & 0 & 0 & 1 \end{bmatrix}$$

Where vector  $P$  is the displacement along  $Y$ -axis equal to length of femur ( $L_f$ )

$${}_{Knee}^{Hip}\vec{P} = \begin{bmatrix} x \\ y - L_f \\ z \end{bmatrix}$$

Here,  $R$  is an orthogonal matrix will represent the orientation of the femoral implant. So the parameter of  $R$  is always described by three successive rotations about the coordinate axes. The sequence of rotations was chosen to be the orientation of prosthesis first, after that flexion path motion on tibia will represent the prosthesis orientation. It can be described by Euler angles, start with knee's frame. Then rotate it about  $X$  principal axes by an angle  $\theta_x$ , then rotate about  $Y$  axes by an angle  $\theta_y$ , and the rotate about  $Z$  axes by an angle  $\theta_z$ . Then the rotation matrix takes on the familiar form of planar rotations:

$$R_x(\theta) = \begin{bmatrix} 1 & 0 & 0 \\ 0 & c\theta & -s\theta \\ 0 & s\theta & c\theta \end{bmatrix}$$

$$R_y(\theta) = \begin{bmatrix} c\theta & 0 & s\theta \\ 0 & 1 & 0 \\ -s\theta & 0 & c\theta \end{bmatrix}$$

$$R_z(\theta) = \begin{bmatrix} c\theta & -s\theta & 0 \\ s\theta & c\theta & 0 \\ 0 & 0 & 1 \end{bmatrix}$$

For angle  $\theta_x, \theta_y$  and  $\theta_z$ , abbreviating  $\sin(\theta_x) = s\theta_x, \cos(\theta_x) = c\theta_x$  and so on, rotation matrix  $R$  is define as

$${}_{Knee}^{Hip}R = R_x(\theta_x)R_y(\theta_y)R_z(\theta_z) = \begin{bmatrix} c\theta_x c\theta_y & c\theta_x s\theta_y s\theta_z - s\theta_x c\theta_z & c\theta_x s\theta_y c\theta_z + s\theta_x s\theta_z \\ s\theta_x c\theta_y & s\theta_x s\theta_y s\theta_z + c\theta_x c\theta_z & s\theta_x s\theta_y c\theta_z + c\theta_x s\theta_z \\ -s\theta_y & c\theta_y s\theta_z & c\theta_y c\theta_z \end{bmatrix}$$

Then, the ankle frame can be defined in the similar way as

$${}_{Ankle}^{Knee}H = \begin{bmatrix} I_3 & {}_{Ankle}^{Knee}\vec{P} \\ \hline 0 & 0 & 0 & 1 \end{bmatrix}$$

Where vector  $P$  is the displacement along  $Y$ -axis equal to length of Tibia in the same way as femur length, and  $I$  is an identity matrix setup here since the ankle was no rotation respect to the knee.

$${}_{Ankle}^{Knee}\vec{P} = \begin{bmatrix} x \\ y - L_t \\ z \end{bmatrix}$$

### Knee Prosthesis Kinematics Analysis

The kinematics of femoral prosthesis components was analyzed first, which start at the major plane  $Fil$ -plane. This plane is the most important among others because during the intra-operative procedure, this plane is cut first and marked as reference for the next plane. The procedure depends on the experience of surgeon to perform this step by insert intramedullary rod guidance into the femoral canal of the patient's femur, where respect to the anatomical landmarks of the knee. Figure 3 shows the alignment of distal femoral cutting instrument. At the guidance's head end is attached with first plane cutting block as having a slot to guide the cutting saw. Generally, the conventional procedure performs each step of TKR surgery without accuracy feedback checking. Therefore, the first plane cutting is the critical step to indicate the finished quality of TKR surgery. Figure 4 shows the relationship between each plane of knee prosthesis.

The prosthesis' planes have features as the geometry shape, which can be determined the relationship between plane by using kinematics analysis. The study of forward kinematics is the static geometrical was applied to compute position and orientation of each plane. In the same way of knee analysis, five Cartesian coordinate system were assigned to each plane as the plane's reference frame, and two major frames were assigned as the femoral prosthesis reference at the center of curvature and another being as the matching frame to the center of knee.

Begin at plane 1 is represented the characteristic by Fi1-frame, the origin of frame indicated the position and the direction of three unit vector describe the orientation of the frame. Fi1-frame was fixed as base reference or others plane. Then, the description of plane 2 (Fi2-frame) was respect to plane 1 by translate along Y and Z-axis with vector  ${}^1_2\vec{p}$  and rotate about X-axis with angle  $\theta_2$ , the homogeneous transform of plane 2 respect to plane 1 is

$${}^{Fi1}_{Fi2}H = \begin{bmatrix} R_x(\theta_2) & & & {}^1_2\vec{p} \\ \hline 0 & 0 & 0 & 1 \end{bmatrix}$$

Where vector  ${}^1_2\vec{p}$  is the displacement from plane 1 to plane 2 in Y and Z-axis can be computed by apply sine and cosine rules.

$${}^1_2\vec{p} = \begin{bmatrix} x_1 \\ y_1 + l_2/2 * \sin(\theta_2) \\ z_1 - l_1/2 - l_2/2 * \cos(\theta_2) \end{bmatrix}$$

The remaining planes can be described as like as plane 2, which respect to plane 1. So, the femoral prosthesis will have four homogeneous transform matrix to describe each plane as  ${}^{Fi1}_{Fi2}H, {}^{Fi1}_{Fi3}H, {}^{Fi1}_{Fi4}H, {}^{Fi1}_{Fi5}H$  and  ${}^{Fi2}_{Fi3}H$

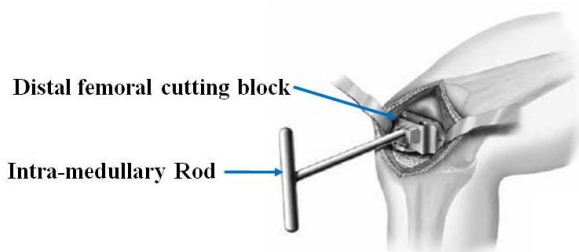


**Figure 3:** Alignment of distal femoral cutting instruments

The others two major frames were assigned as the femoral prosthesis frame and match frame to the center of knee. The femoral prosthesis frame can be defined as the center of Both frames were placed in the same orientation as plane 1, for the position define as translate up and down along Y-axis. The curvature of the prosthesis as shown in the Figure4 The other one is the frame to match with the center of knee frame.

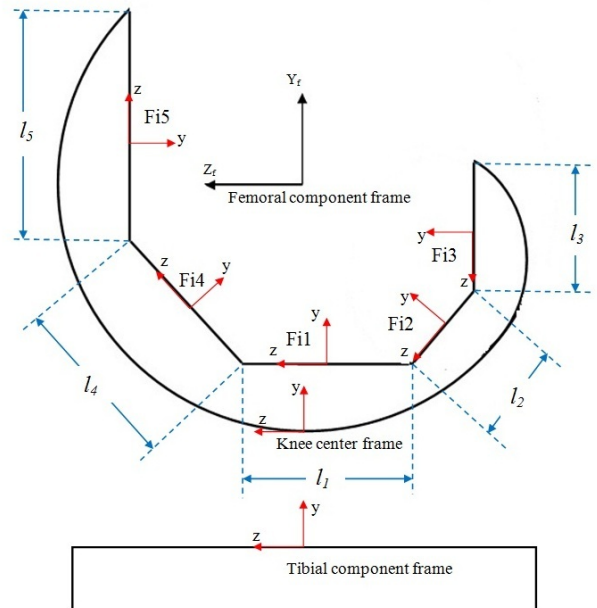


**Figure 4:** Shows the relationship between each plane of knee prosthesis.

On the tibia bone, cutting surface is the single flat plane, which should relate to the femoral cutting plane. A Cartesian coordinate system was assigned to the tibial component as the cutting plane reference, which the origin placed on the center point of the prosthesis and the orientation should parallel with plane 1 on the femoral component.

All information of the feature of prosthesis will be retrieved from the data acquisition process by using laser scanner. Therefore all parameters of our model can be modified the value depends on the shape of prosthesis.

### Kinematics Simulation

The kinematics analysis of implanted knee and prosthesis components was found in the previous section, which can be described the relationship between each body by homogeneous transform. The two modules of kinematics equations are 1)

mechanical alignment module, and 2) kinematics of prosthesis module were combined to simulate the leg alignment and motion after TKR surgery. Ideally, this simulation system is the part of TKR navigation system, which should show the virtual graphic of leg and prosthesis to guide the surgeon when insert the intra-medullary rod. So, surgeon can be able to adjust and find the proper position and orientation of the insertion.

This study is the first phase to analyze the kinematics and model the equations of leg and prosthesis, which will display the normal mechanical alignment compare to 3 pattern of implanted dislocation. 1) location error about Y-axis 10 degrees, 2) location error about Z-axis 10 degrees, and 3) location error about Y-axis and Z-axis 10 degree each.

The model of normal alignment was assigned as reference, then prosthesis models will be placed into the knee frame with each error pattern and show the result of mechanical alignment when fully extended knee and tibia flexion in every 10 degree up to 130 degree. The center point of knee flexion was located at the center of femoral component frame, which the model constructed cylinders for the lateral and medial femoral condyle [9].

## RESULTS AND DISCUSSION

Three cases of simulation display their post-operative result error in the mechanical axis alignment. There are 1) The normal mechanical axis alignment 2) error in orientation about Z-axis, the intramedullary rod was not aligned on femoral anatomical axis, 3) error in orientation about Y-axis, the intramedullary rod's head was not aligned on the medial-lateral femoral epicondyle line, 4) combination error in orientation about both intramedullary orientation using Euler angle. The results were shown in front view and sagittal view to display the mechanical axis angle (hip-knee-ankle angle) error and path motion of tibia bone, while being stand full extension and then flexion 10 degree for each step up to 130 degree.

The simulation in case 2 compare to case 1 shows that at full extension the angle of hip-knee-ankle was show the abnormal mechanical axis alignment in varus/valgus character and change as a linear while being flexion. Figure 5: shows the result of

error when Intra-medullary rod was not aligned on femoral anatomical axis.

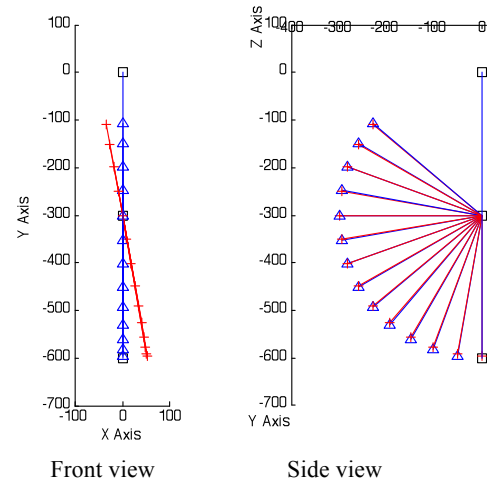


**Figure 5:** Result of error when intramedullary rod was not aligned on femoral anatomical axis

The simulation in 3 compare to case 1 shows that at full extension the angle of hip-knee-ankle was show the normal mechanical axis alignment in front view, and change as a circular while being flexion. Figure 6: shows the result of error when intramedullary rod was not aligned on medial-lateral femoral epicondyle line.

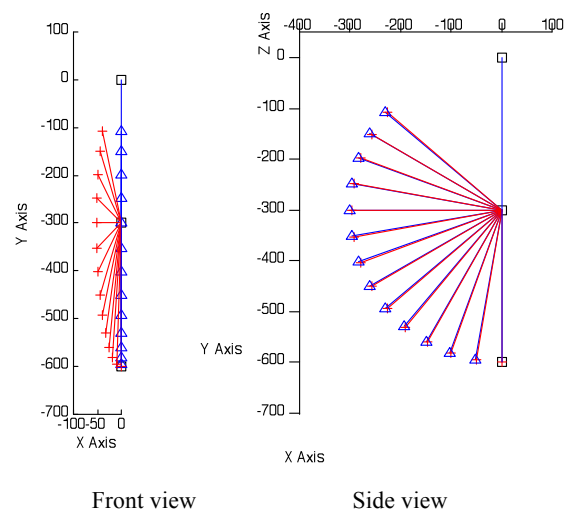


**Figure 6:** Result of error when intramedullary rod was not aligned on medial-lateral femoral epicondyle line.

The simulation in case 4 compare to case 1 shows that at full extension the angle of hip-knee-ankle was show the abnormal mechanical axis alignment

in varus/valgus character, and change as a circular while being flexion. Figure 7: shows the result of error when intramedullary rod was not aligned on both femoral mechanical axis and medial-lateral femoral epicondyle line.

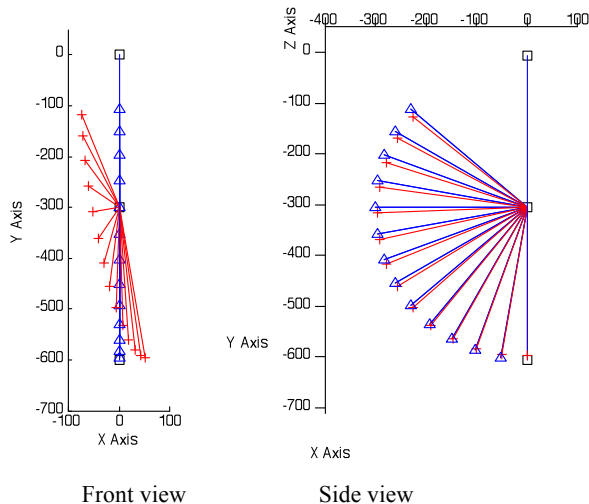


**Figure 7:** Result of error when intramedullary rod was not aligned on both femoral mechanical axis and medial-lateral femoral epicondyle line.

## CONCLUSIONS

A 3-Dimensional kinematics model for simulate and display post-operative results were developed. The kinematics model was based on hip-knee-ankle angle alignment axis, intramedullary rod's axis and anatomical landmarks. Three comparison error cases in total knee replacement surgical practices were explored: (1) TKR with error in orientation about intramedullary canal's axis, (2) TKR with error in orientation about patella's axis, and (3) TKR with combination errors in orientation about both intramedullary canal's axis and patella's axis using Euler angle. The results can display mis-aligned lower-limb system after poor TKR surgical

practice. The effect of mis-alignment would cause a long-term problem for body's postural activities.

## REFERENCES

- 1.J.B. Stiehl, W.H. Konermann & R.G. Haaker, *Navigation and robotics in total joint and spine surgery* (Springer, 2004)
- 2.C.J.M. van Loon, M.A. Wisse, M.C. de Waal Malefijt, R.H. Jansen & R.P.H. Veth, The kinematic total knee arthroplasty: A 10-to 15-year follow up and survival analysis, *Arch Orthop Trauma Surg*, 120, 2000, 48-52.
- 3.R. Hart, M. Janecek, A. Charker & P. Bucek, Total knee arthroplasty implanted with and without kinematic navigation, *International Orthopaedics (SICOT)*, 27, 2003, 366-369.
- 4.Russell H. Taylor, *Computer-Integrated Surgery: technology and clinical applications* (The MIT press, 1995)
- 5.John J. Craig, *Introduction to robotics: mechanics and control 2<sup>nd</sup> ed.* (Addison-Wesley Publishing Company, 1995)
- 6.Victor H' Frankel, Margareta Nordin, *Basic Biomechanics of the Skeletal System* (Lea & Febiger)
- 7.P. Schlepckow, Three-dimensional kinematics of total knee replacement systems, *Archives of Orthopaedic and trauma surgery*, 111, 1992, 204-209
- 8.F.F. Buechel, M.J. Pappas, New jersey integrated total knee replacement system: biomechanical analysis and clinical evaluation of 918 cases. Silver Spring, Maryland, 11 July 1984.
- 9.R. Von Eisenhart-Rothe, T. Vogl, K.-H. Englmeier and H. Graichen, A new in vivo technique for determination of femoro-tibia and femoro-patellar 3D kinematics in total knee arthroplasty, *Journal of Biomechanics*, 4, 2007, 3079-3088.

# Muscle Forces During Single-Leg Jump Landing

<sup>1</sup>Kristin D. Morgan, <sup>2</sup>Cyril J. Donnelly, and <sup>1</sup>Jeffrey A. Reinbolt

<sup>1</sup>University of Tennessee, Knoxville, TN, USA

<sup>2</sup>The University of Western Australia, Perth, Western Australia, AUS

email: [kmorga12@utk.edu](mailto:kmorga12@utk.edu) web: <http://rrg.utk.edu>

## INTRODUCTION

Over 200,000 anterior cruciate ligament (ACL) injuries occur in the United States every year [1, 2] and these injuries often occur in sports where dynamic movements, such as jump landings, place high loads on the ACL ligament [3,4]. Small knee flexion angles, increased knee valgus moments, and anterior tibia translation contribute to ACL injury during landing [5-7]. Muscle forces impact changes in these knee kinematics and kinetics.

There are several methods to evaluate muscle contributions to dynamic knee movements with high risk for injury. Some have analyzed various roles that muscles play in landing biomechanics by evaluating muscle activity recordings such as electromyography (EMG) and co-contraction indices [7]. However, muscle activity does not provide a muscle's relative contribution to the movement, but computer simulations may provide additional insights [8]. For example, algorithms (e.g., computed muscle control) can estimate muscle forces required for the desired movement given kinematic and kinetic data [9].

In this study, we used computed muscle control (CMC) to estimate forces for muscles crossing the knee joint during single-leg jump landing. Identifying muscle contributions to landings may provide researchers with better understanding of landing biomechanics and injury prevention.

## METHODS

We used experimental kinematic and kinetic data collected at the University of Western Australia to study the effectiveness of balance and technique training. One athlete from this study was selected and a subject-specific simulation was created for this subject in OpenSim (Fig. 1).

A subject-specific simulation of single-leg jump landing was created by using the following four steps. First, a generic musculoskeletal model was scaled to the size of the subject by specifying mass properties and segment dimensions obtained from experimental exams and marker data [10]. Second, inverse kinematics was used to derive the joint angles from the marker data obtained during jump landing. Third, simulated kinematic errors were minimized (RMS < 1.5N) to be dynamically consistent with experimental ground reaction forces by using the residual reduction algorithm. Fourth, CMC was used to estimate muscle excitations during jump landing. Associated forces for muscles crossing the knee joint required were recorded. These muscle forces were normalized with respect to maximum vastus lateralis muscle force during the simulation, similar to Besier, et al. [11].

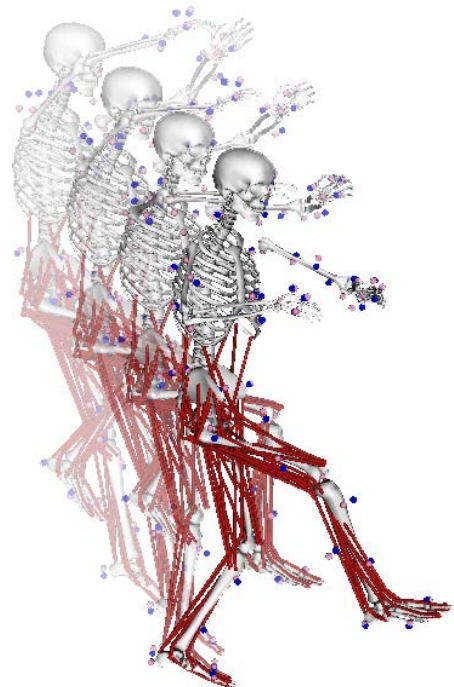


**Figure 1:** Series of images for a subject-specific simulation during single-leg jump landing using a musculoskeletal model with 37 degrees of freedom and 94 muscle-tendon actuators.

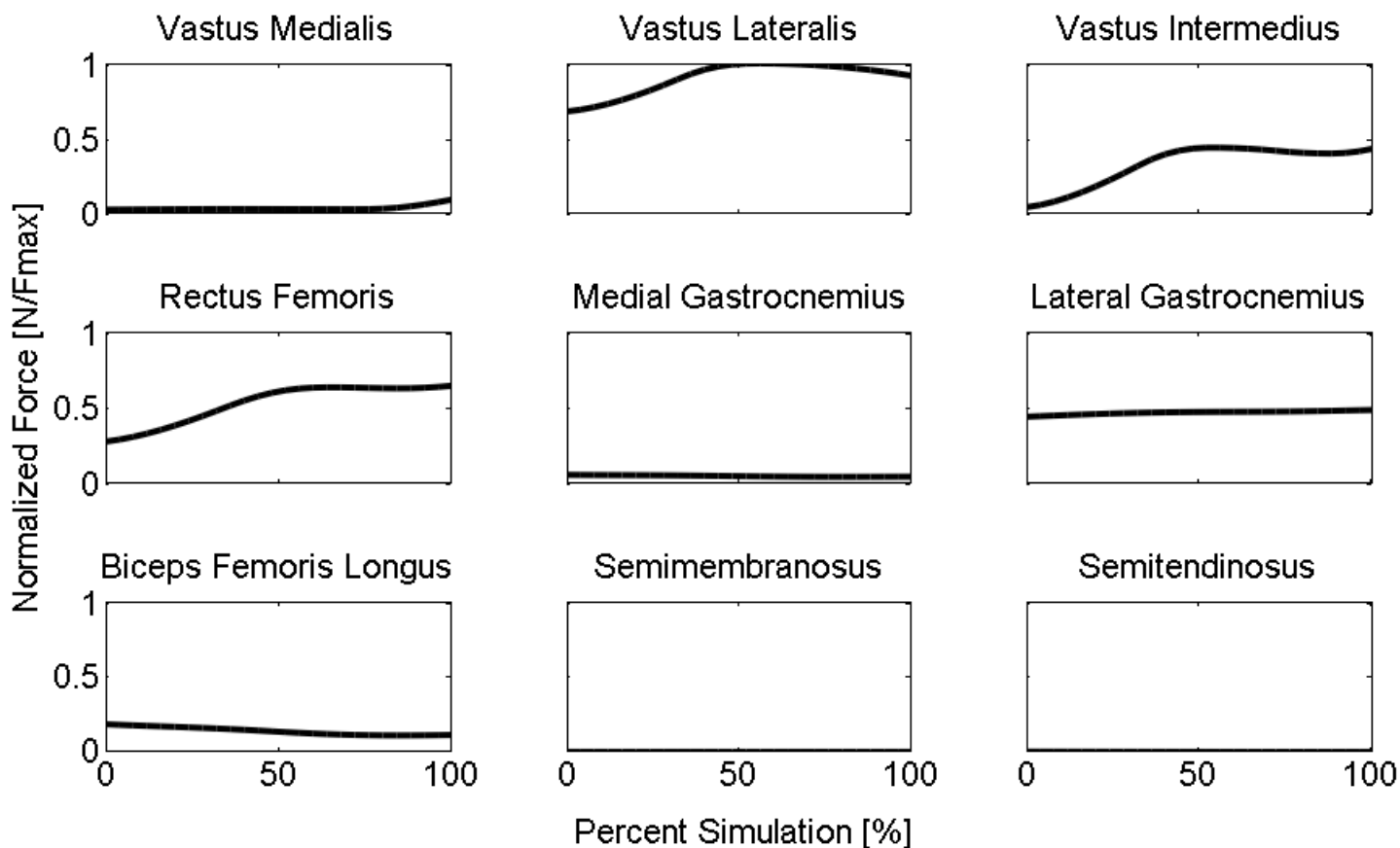


**Figure 2:** Forces for muscles crossing the knee joint normalized by maximum vastus lateralis force ( $F_{max}$ ) during single-leg jump landing

## RESULTS AND DISCUSSION

Muscle contributions during single-leg jump landing resulted in a variation of normalized forces for muscles crossing the knee joint (Fig. 2). Vastus lateralis had the largest muscle force contribution. Normalizing the muscle forces with respect to the vastus lateralis muscle illustrated relative muscle contributions to single-leg jump landing. Our results are consistent with others showing lateral gastrocnemius had increased activity during landing [12]. Our findings for individual muscle forces add to previous work which combined these muscles into two synergistic groups [7].

## CONCLUSIONS

Unlike EMG data for limited muscles, computer simulation provides information about several individual muscle force contributions to a dynamic movement. Future work will analyze additional subjects to determine if the trends reported here are truly representative of muscle force contributions in single-leg jump landings.

## REFERENCES

1. Arendt E and Dick R. *Am J Sports Med* **23**, 694-701, 1995.
2. DeMorat G, et al. *Am J Sports Med* **32**, 477-83, 2004.
3. Ekegren CL, et al. *J Orthop Sports Phys Ther* **39**, 665-74, 2009.
4. Hewett TE, et al. *Am J Sports Med* **24**, 765-73, 1996.
5. Hagood S, et al. *Am J Sports Med* **18**, 182-7, 1990.
6. Walla DJ, et al. *Am J Sports Med* **9**, 13-34, 1985.
7. Podraza JT and SC White. *The Knee* **17**, 291-5, 2010.
8. Anderson FC, et al. *Diagnosis and Management of Movement Abnormalities in Cerebral Palsy*, Cambridge Press, 2005.
9. Thelen DG, et al. *J Biomech* **36**, 321-8, 2003.
10. Hamner SR, et al. *J Biomech* **43**, 2709-16, 2010.
11. Besier TF, et al. *J Biomech* **42**, 898-905, 2009.
12. Wikstrom EA, et al. *J Med Sci Sports* **18**, 55-61, 2008.

# STATIC AND DYNAMIC OPTIMIZATION SOLUTIONS FOR WHEELCHAIR PROPULSION

<sup>1</sup>Melissa M. Morrow, <sup>2</sup>Jeffery W. Rankin, <sup>3</sup>Richard R. Neptune and <sup>1</sup>Kenton R. Kaufman

<sup>1</sup>Mayo Clinic, Rochester, MN, USA, <sup>2</sup>The Royal Veterinary College, University of London, UK,

<sup>3</sup>The University of Texas, Austin, TX, USA, email: kaufman.kenton@mayo.edu

web: mayoresearch.mayo.edu/biomechanics, www.me.utexas.edu/~neptune

## INTRODUCTION

Both static [1] and dynamic [2] optimization techniques have been used with upper extremity (UE) models to investigate manual wheelchair propulsion biomechanics. A major advantage of static optimization is its low computational cost. However, the method is time-independent, which is criticized as lacking physiological rationale. Conversely, dynamic optimization can implement the underlying physiological, time-dependent nature of the musculature, but use is limited due to the high computational requirements. Anderson and Pandy [3] investigated the necessity of complex forward dynamics techniques to model the lower extremity during gait and found that muscle force predictions between static and dynamic approaches were practically equivalent. However, a similar investigation during UE movement tasks has not been explored. The UE model comparison may differ from the lower extremity due to its increased range of motion and increased complexity of the musculature. Therefore, the purpose of this study was to compare the UE muscle force predictions provided by static and dynamic optimization approaches for the push phase of wheelchair propulsion. In addition, both models were compared with EMG [4] to assess prediction accuracy.

## METHODS

Both UE musculoskeletal models were developed in SIMM with associated muscle properties and origin/insertion sites based on the work by Holzbaur et al. [5]. The static optimization model consisted of the humerus, trunk, scapula and 18 musculotendon units [1]. The dynamic model included the elbow and wrist and 8 additional musculotendon units [2].

Experimental data were obtained from 12 experienced manual wheelchair users (10 men, 2 women) with an average age of 32 years. Testing

was conducted on a custom-built wheelchair treadmill while subjects propelled their own wheelchair at a self-selected speed.

The dynamic approach used a global optimization algorithm to identify the muscle excitation patterns that minimized the difference between simulation and experimentally measured push phase data. Cost function quantities included UE joint kinematics and three-dimensional handrim forces and a muscle stress term (force/max. isometric force) to help minimize co-contraction. The group average muscle moment arms and net joint moments from the dynamic solution were used as input into the static optimization. The predicted muscle forces were constrained to produce the muscular joint moments. Two optimal criteria were tested: (1) minimize muscle activation squared, summed across all muscles and (2) minimize the muscle stress cubed, summed across all muscles.

To compare the static and dynamic optimization solutions, the root mean square error (RMSE) was determined for each muscle and then averaged across muscles to yield a global RMSE for each optimization approach. In addition, peak forces for the shoulder rotator cuff and prime movers were identified for comparison and differences with experimental EMG data for both solutions were assessed.

## RESULTS AND DISCUSSION

The global RSME values (Table 1) show good agreement between the static and dynamic solutions. The static cost function based on stress compared moderately better to the dynamic solution (10 % Fmax) than did the cost function based on activation (11 % Fmax). This may be partially explained by the fact that the dynamic optimization had a stress component in the cost function, which would be similar to minimizing stress in the static

routine. Neither cost function in the static optimization did well in predicting the dynamic force output of the middle deltoid, infraspinatus, teres minor, coracobrachialis or triceps long head.

In general, the dynamic routine predicted larger peak forces of the prime movers and rotator cuff muscles than either of the static solutions (Fig. 1). The only exception was the supraspinatus, wherein both static solutions predicted a larger peak force. The overall diminished peaks may be a result of the lack of musculotendon dynamics in the static routine. The reduced activity of the triceps and biceps in the static solution may be attributed to the lack of an elbow in the static model, as elbow flexors/extensor activity during the push phase is likely necessary to satisfy the propulsion demands placed on the elbow rather than the shoulder.

The RMSE values between the solutions and EMG data (Table 2) showed moderate agreement with global error magnitudes for all solutions within 20%. The static stress cost function had the best agreement with EMG (15 % Max). The supraspinatus and pectoralis major had poor agreement with EMG in both approaches, which may be due to the muscle moment arm estimates.

Because much of the clinical focus in the manual wheelchair population is given to the rotator cuff, the differences shown here between the

| Muscles       | D vs. SA    | D vs. SS    |
|---------------|-------------|-------------|
| A Delt        | 6.4         | 7.1         |
| M Delt        | 26.4        | 25.7        |
| P Delt        | 1.7         | 1.0         |
| Supra         | 5.5         | 5.9         |
| Infra         | 22.2        | 17.6        |
| Subs          | 5.9         | 10.6        |
| T Min         | 22.4        | 21.7        |
| T Maj         | 1.4         | 2.9         |
| Pec Maj C     | 3.9         | 3.6         |
| Pec Maj SU    | 9.8         | 9.5         |
| Pec Maj SL    | 4.6         | 4.2         |
| Lat Dor U     | 9.7         | 8.7         |
| Lat Dor M     | 4.9         | 3.1         |
| Lat Dor L     | 12.7        | 11.6        |
| Coroco        | 20.7        | 22.1        |
| Tri L         | 23.7        | 18.6        |
| Bic L         | 11.1        | 8.1         |
| Bic S         | 4.1         | 3.8         |
| <b>GLOBAL</b> | <b>11.0</b> | <b>10.3</b> |

| Muscles       | D           | SA          | SS          |
|---------------|-------------|-------------|-------------|
| A Delt        | 10.1        | 9.0         | 9.7         |
| M Delt        | 17.0        | 18.8        | 18.6        |
| P Delt        | 13.8        | 13.7        | 13.1        |
| Supra         | 31.7        | 27.2        | 26.6        |
| Infra         | 27.3        | 15.2        | 16.4        |
| Subs          | 13.6        | 16.5        | 12.6        |
| Pec Maj SU    | 31.0        | 26.0        | 25.7        |
| Tri L         | 16.6        | 8.2         | 4.7         |
| Bic L         | 5.6         | 11.8        | 10.2        |
| <b>GLOBAL</b> | <b>18.5</b> | <b>16.3</b> | <b>15.3</b> |

models and EMG deserve further investigation. The limitations of comparing muscle force predictions to EMG are well documented. However, no other feasible evaluation exists to make comparisons regarding the timing of muscle force generation.

## CONCLUSIONS

The dynamic and static routines had good overall agreement, although they did not compare as well as Anderson and Pandy showed during walking [3]. The discrete peak force data highlight considerable differences in the rotator cuff and large prime mover shoulder musculature (Fig. 1). In addition, comparisons between the solutions and EMG showed differences in the rotator cuff musculature which require further investigation.

## REFERENCES

1. Morrow MM, et al. *J Biomech* **43**, 2487-92, 2010.
2. Rankin JR, et al. *J Biomech* **43**, 2771-9, 2010.
3. Anderson FC and Pandy MG. *J Biomech* **34**, 153-61, 2001.
4. Mulroy SJ et al. *Arch Phys Med* **77**, 187-93, 1996.
5. Holzbaur KR et al. *Ann Biomed Eng* **33**, 829-40, 2005.

## ACKNOWLEDGMENTS

Funding partially provided by NIH R01 HD048781, R01 HD053732, and 5T32 HD007447.

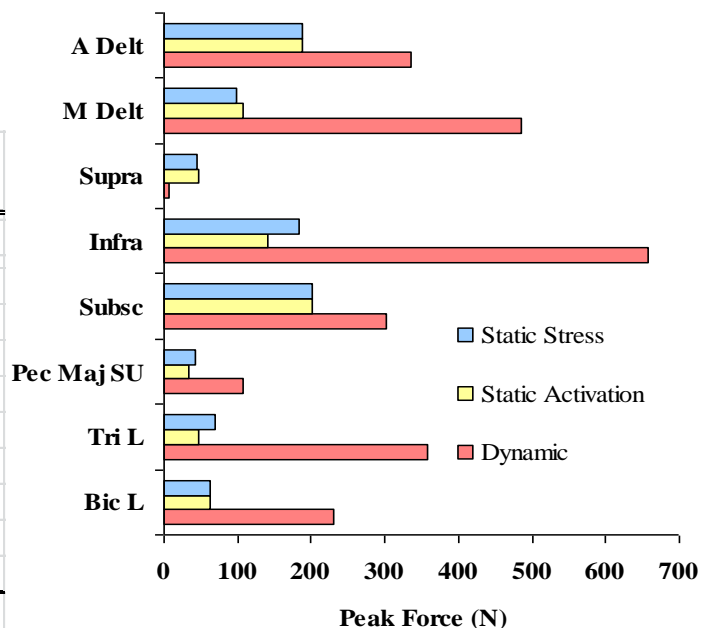


**Figure 1.** Peak muscle forces during push phase

D: Dynamic; SA: Static Activation; SS: Static Stress

# ROLES OF CUTANEOUS SENSATION AND GLOVES WITH DIFFERENT COEFFICIENTS OF FRICTION ON FALL RECOVERY DURING SIMULATED LADDER FALLS

Binal Motawar, Pilwon Hur and Na Jin Seo

University of Wisconsin-Milwaukee, Milwaukee, WI, USA

email: [bmotawar@uwm.edu](mailto:bmotawar@uwm.edu) web: <https://pantherfile.uwm.edu/seon/www/>

## INTRODUCTION

Falling from a ladder is a common injury among industry workers [1, 2]. Hands are the only means available to arrest a fall once it has been initiated. Knowledge on how people detect and respond to a ladder fall with the upper limb is currently limited. In addition, whether gloves affect the hand's detection and response for a fall is unknown. Such knowledge is necessary to design interventions to reduce ladder fall injuries. The objective of this study was to determine the time course of a fall event (i.e., changes in hand force, rung position, upper limb muscle activities) in response to a sudden upward loading of the rung, simulating a ladder fall. In addition, the effect of gloves with different coefficients of friction (COF) on a person's detection and response time was examined.

## METHODS

Thirteen right-handed young adults (9 males and 4 females with the mean age of  $25 \pm 5$  years) with no history of neuromuscular disorders volunteered for this study. Subjects sat on a chair with the non-dominant left hand holding an overhead aluminum rung (3.8 cm in diameter) (Fig 1).

The initial upper limb position was approximately  $160^\circ$  shoulder flexion with no abduction or adduction and  $10^\circ$  elbow flexion. Subjects held the rung with no extra effort at the beginning of a trial. A sudden upward load was applied to the rung at a random time via drop of a weight that was connected to the rung through a cable and pulleys. The weight was set to be each subject's 10% of maximal pull strength. Subjects were instructed to stop the rung from moving up. This rung perturbation trial was repeated three times for each of three glove conditions (polyester glove with COF = 0.33, bare hand with COF = 0.56, and latex glove with COF = 1.1 against aluminum). All subjects were able to stop the rung for all trials.

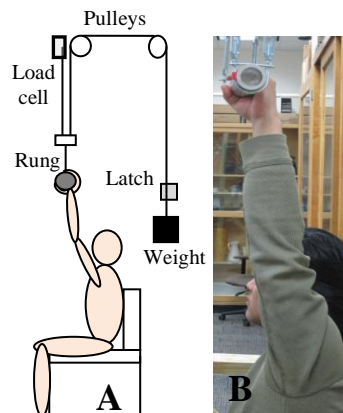


**Figure1:** A. Arrangement of the rung and weight in the experimental layout. B. Upper limb position in the beginning of each trial.

Hand force, rung vertical position, and muscle activities were recorded during each trial. Hand force was recorded using a load cell connected to the rung. The rung's vertical position and the latch opening for a weight drop were recorded using Optotrak 3D Investigator Motion Capture System (NDI, Waterloo, ON, Canada). Muscle activities for flexor digitorum superficialis, flexor carpi ulnaris, extensor digitorum communis, biceps, triceps, deltoid, pectoralis major and latissimus dorsi were recorded using bipolar surface EMG electrodes (Bortec Biomedical Ltd., Calgary, Alberta, Canada). These muscles were selected for their important role in moving and stabilizing the upper limb.

The time course of a typical trial is shown in Fig 2. Times at which (1) hand force started increasing, (2) the rung started moving up, (3) the rung stopped moving, and (4) muscle EMG started increasing were determined relative to the weight drop (Fig 2). The hand force increase was determined to have occurred when the slope of the force curve exceeded 0.030 N/s. The rung movement was determined to have occurred when the velocity of the rung exceeded 0.001 cm/s. The rung was determined to have been stabilized when the rung's velocity reached zero. Increased muscle EMG was determined by visual examination. The earliest EMG increase among the 8 muscles determined the muscle reaction time.

Repeated measures ANOVA determined the differences in mean times for hand force increase,

muscle reaction, rung movement start, and rung stabilization. Four repeated measure ANOVA determined if the within-subject factor of glove affected the times of hand force increase, muscle reaction, rung movement start and stabilization.

## RESULTS

A typical time course entailed 1) hand force increase (41 ms after weight drop), followed by 2) muscle reaction (101 ms), 3) vertical rung movement (116 ms), and 4) stabilization of the rung (461 ms) (Table 1) ( $p < .05$ ). The mean times for hand force increase, muscle reaction, and rung movement initiation did not significantly differ by glove ( $p > .05$ ). The mean rung stabilization time significantly varied by glove ( $p < .05$ ).

## DISCUSSION

The time course of the simulated fall event indicates that people detected the rung perturbation through the increase in hand force (i.e., rung resisted by the upper limb weight) and then they increased muscle activities. The rung movement (and thus associated joint movement) did not occur until after the muscle activities increased, suggesting that the cutaneous sensation was the cue available for people to react to the perturbation, rather than proprioception.

This muscle reaction time was not dependent on the glove condition, possibly because the cutaneous sensation detecting the skin pressure was not affected by the glove layer. However, the glove condition was important for stabilizing the rung. Specifically, the rung stabilization time decreased with increasing COF glove condition. People took the longest time in stabilizing the rung while wearing the lowest-friction polyester glove, probably because a low-friction condition requires a greater grip force to resist the rung slippage out of the hand, compared to a high-friction condition.

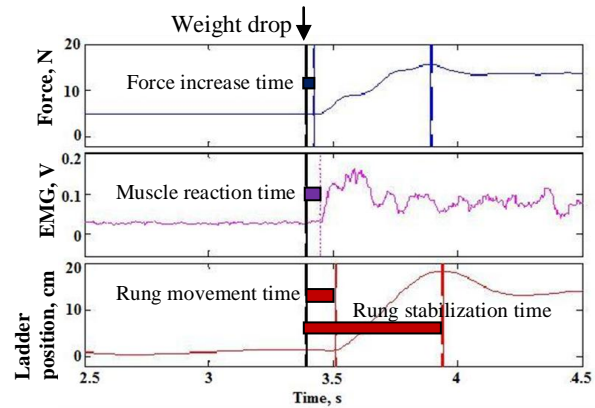


**Figure 2:** Time course of a simulated ladder fall by a sudden loading of the rung. Hand force (top), flexor carpi ulnaris muscle's RMS EMG (middle), and rung displacement (bottom) are shown.

## CONCLUSIONS

The study demonstrated that cutaneous sensation for finger pressure is the first cue available for people to react to a simulated ladder fall. The study also demonstrated that the glove frictional condition can significantly affect a person's ability to stabilize a rung in a timely manner. For functional applications, low-friction gloves such as polyester gloves may hamper a person's ability to recover from a ladder fall and thus may not be advisable. A future study may determine if enhanced cutaneous sensation such as via stochastic resonance may enable a person to detect and respond to a ladder fall faster. Future studies may also include the vestibular input's contribution to fall detection.

## REFERENCES

1. BLS, *Census of fatal occupational injuries summary*, BLS. 2005: Washington.
2. BLS, *Fatal occupational injuries by event or exposure, 2008-2009*, BLS. 2009.

## ACKNOWLEDGMENTS

National Institute of Occupational Safety and Health, University of Illinois at Chicago

**Table 1:** Mean (SD) times for changes in force, rung position, and muscle activity for the 3 glove conditions

|  | Polyester glove | Bare hand      | Latex glove    | <i>p</i> -value |
|--|-----------------|----------------|----------------|-----------------|
| Coefficient of friction against aluminum | 0.33            | 0.56           | 1.1            |                 |
| Hand force increase time (ms)            | 34.29 (5.06)    | 49.48 (10.29)  | 37.97 (7.23)   | >.05            |
| Muscle reaction time (ms)                | 88.13 (7.46)    | 111.69 (13.08) | 102.10 (5.67)  | >.05            |
| Rung movement time (ms)                  | 124.36 (24.28)  | 116.92 (16.53) | 122.82 (19.04) | >.05            |
| Rung stabilization time (ms)             | 483.97 (77.61)  | 456.15 (87.6)  | 455.26 (77.21) | <.05            |

# THE EFFECTS OF BALANCE TRAINING ON OBSTACLE CROSSING IN OLDER ADULTS

Brittney C. Muir, Shirley Rietdyk, Jeffery M. Haddad, Jessica M. Seaman, and Michel J. H. Heijnen

Purdue University, West Lafayette, IN, USA

email: [muir@purdue.edu](mailto:muir@purdue.edu)

## INTRODUCTION

In order to maintain a safe margin of error when stepping over an obstacle, older adults often adopt a higher toe clearance [1]. The increased toe clearance leads to increased instability due to a higher center of mass. These age related gait changes put older adults at an increased risk of falling. The most important fall prevention activity an older adult can perform is exercise [2].

Wobble board (WB) training, a mainstay of physical therapy intervention, has shown improvements in standing balance and tandem walking [3], but the effects on obstacle avoidance during gait are unknown. A new training device, the Biodex Balance System (Biodex Medical Systems, Shirley, NY) couples an unstable platform with visual feedback. Biodex training with typically aging adults has not shown significant improvements in balance [e.g., 4]. To our knowledge, no research has examined the effects of Biodex training on gait characteristics.

This study has two objectives. First, to examine if balance training while standing on an unstable surface will result in improvements in obstacle crossing in older adults. Second, to examine the differential effects of WB training versus Biodex training on obstacle crossing behavior in older adults.

## METHODS

A training group (N=18) was recruited from a local continuing care retirement community (CCRC). This group was age, gender and activity level matched into two sub groups: the WB group (N=9,  $81.7 \pm 7.6$  years) and the Biodex group (N=9,  $80.4 \pm 6.7$  years). A third group, a control group (N=19,  $81.9 \pm 5.6$  years), was also recruited.

The training groups completed 20 min of training three times per week for six weeks. Two assessments were conducted: pre-training and post-training (for the control group, the two assessments were six weeks apart to match the time interval of the training groups). The assessment consisted of testing plantarflexor strength, an ankle position matching task, obstacle height estimate, and obstructed and unobstructed gait. This abstract will focus on the obstructed gait trials.

The gait task required subjects to initiate gait, step over an obstacle at 1.5 m, and continue walking (total path length was 3.2 m). Six randomized trials were completed per obstacle size (no obstacle, 1 cm, 10 cm, and 20 cm). IREDs were placed bilaterally on the fifth metatarsal, heel, lateral malleolus, knee joint, greater trochanter, shoulder and on the right temple. IRED position data were collected with an Optotrak (NDI, Waterloo, Canada) at 60 Hz. Position data were filtered with a fourth-order zero-phase-shift low-pass Butterworth filter at 8 Hz. Gait speed, lead foot and trail foot toe clearance (TC) and stride length (SL) were calculated using MatLab (MathWorks inc., Natick, MA). A three-way mixed between- and within-subject repeated measures ANOVA was conducted using SAS (SAS Institute, Cary, NC).

## RESULTS AND DISCUSSION

A significant obstacle size by time by group interaction was found for both lead TC ( $p=0.02$ ) and trail TC ( $p<0.001$ ). Lead TC decreased for all three groups indicating that the improvements were due to practice with the task, not from the training intervention. The 1 cm and 20 cm obstacles showed no changes in trail TC for all three groups. However, trail TC decreased for the 10 cm obstacle for both training groups, but the control group did not change (Figure 1a). The trail limb is not visible during obstacle crossing, so the subject must rely on

proprioceptive information to clear the obstacle. The change in trail TC provides support for the idea that training improved proprioception, consistent with conclusions of previous research with the Biodex [5]. However, both training groups decreased trail TC similarly indicating that WB training was as effective as Biodex training. It should be noted that only one obstacle height showed this effect. Additional research needs to be completed to fully examine changes in proprioception.

A significant time by group interaction was found for lead SL ( $p=0.005$ ), trail SL ( $p=0.003$ ) and gait speed ( $p<0.001$ ). The WB and Biodex groups both exhibited increased lead and trail limb SL (Figure 1b). Neither lead nor trail SL changed for the control group, indicating that the increased SL was not due to familiarity with the task. Increased gait speed (Figure 1c) was observed for the WB and Biodex groups but not for the control group.

The observed changes in TC, SL, and gait speed indicate that training while standing on an unstable surface led to changes in gait characteristics while stepping over obstacles. This indicates that gait training was not necessary to result in changes in gait; training while standing on an unstable platform was sufficient. Overall, the participants appeared to become less cautious in their gait, taking larger, faster steps that were closer to the top of the obstacle. These changes may reflect improved balance, but they may also reflect improved

confidence without an associated change in balance. Further research should assess balance confidence.

Since both training groups improved the same amount, the common feature of the two training systems, the unstable platform, appears to be the relevant factor for obstacle avoidance. The visual feedback of the Biodex system does not appear to provide any incremental advantage during a six-week intervention.

## CONCLUSIONS

Standing balance training on both the WB and the Biodex resulted in gait changes during obstacle crossing. WB and Biodex training affected adaptive gait similarly, indicating that Biodex balance training did not provide additional benefit beyond traditional WB training.

## REFERENCES

1. Patla AE, et al. *J Exp Psychol* **17**, 603-634, 1991.
2. NIH. <http://nihseniorhealth.gov/fallk/toc.html>. 2008.
3. Nordt WE, et al. *Am J Orthop* **28**, 447-450, 1999.
4. Hinman MR. *J Geriatr Phys Ther* **25**, 10-20, 2002.
5. Malliou P, et al. *JBMR* **17**, 101-104, 2004.

## ACKNOWLEDGEMENTS

We would like to thank the participants, University Place, the students who helped with training and the Center on Aging and the Life Course at Purdue University.

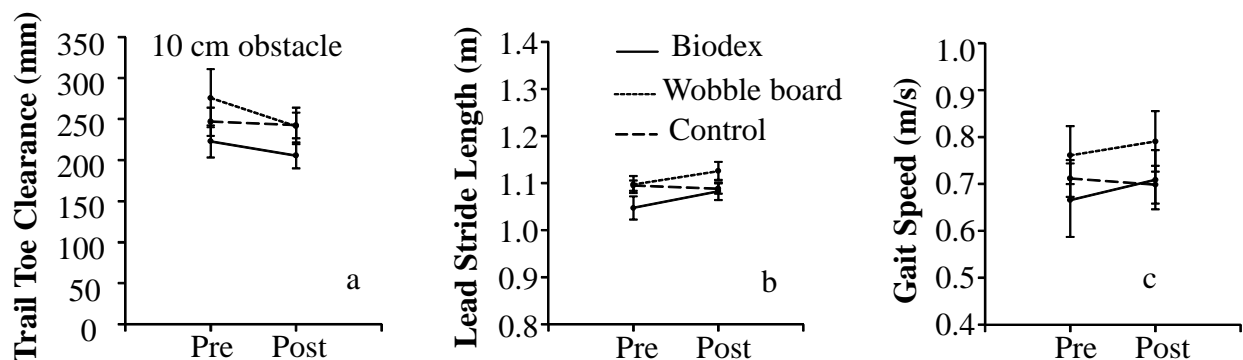


**Figure 1:** Changes in trail toe clearance (a), lead stride length (b), and gait speed (c) with training. Obstacle size by time by group interaction found for trail toe clearance, but only the 10cm obstacle results are shown. Time by group interactions were found for lead toe clearance and gait speed.

# EFFECTS OF DECEPTIVE BEHAVIOR ON BIOMECHANICAL MEASURES OF STANDING POSTURE

Darren S. Mullin, Gregory W. King, Reza R. Derakshani and Christopher T. Lovelace

University of Missouri-Kansas City, Kansas City, MO, USA  
email: [dsmdkc@mail.umkc.edu](mailto:dsmdkc@mail.umkc.edu) web: <http://sce.umkc.edu>

## INTRODUCTION

Accurate deception detection is a very desirable goal with potential applications in many fields including homeland security, counter-terrorism, security screening, and credibility assessment. Currently used deception detection techniques often involve physiological changes associated with deception, and include thermal scanning, polygraph testing, voice stress analysis, and brain activity analysis [1]. However, these techniques are intrusive as they often require sensors to be attached to the body, preventing them from being used for deception detection in their natural environments. Video-based deception detection is an alternative to physiologically-based measures. However, video techniques are prone to image processing errors in real world scenarios, are difficult to use in terms of data reduction and feature extraction, and can be insensitive to small or occluded movements.

We used computerized static posturography (CSP) in order to overcome the limitations of video-based deception detection. CSP involves analysis of the center of pressure (COP). The COP is defined as the intersection of the body's net vertical force with the support surface [2]. We hypothesized that deceptive participants, compared to truthful would exhibit varied COP patterns when responding to interview questions.

## METHODS

**Participants.** Sixty-eight young adults were recruited for this study after providing written consent prior to testing. Data collection was successful for fifty-one of these participants. The remaining trials were unsuccessful due to an unexpected computer lag during data capture. All of the participants were in good health and were able to comply with the requirements of the study.

Participants were randomly assigned to either a control group (CG) or an experimental group (EG).

**Procedure.** Participants were instructed to pack a bag with various items. In addition to items that were identical between the CG and EG groups (socks, shoes, shirts and jeans), the CG was required to pack "control" items (cookies, sunglasses and a travel-size container of mouthwash), while the EG was required to pack "prohibited" items (pocket knife, bottle of rubbing alcohol and cigars). The EG was instructed not to reveal that they were carrying any prohibited items during the testing that followed. After packing the bag each participant was instructed to stand on a force plate by an automated, computer-generated interviewer. Once the subject was standing on the force plate, the interviewer asked a series of questions about the contents of the bag. Although numerous questions were asked, analysis for the present study only focused on the biomechanical response to one question: "Just to be sure that you are not carrying any restricted items, please tell me each item that is in your bag".

**Measurements.** Force and moment data were captured continuously at a rate of 1000 Hz by a single force plate (AMTI, Watertown, MA, USA). Interviewer and participant audio data were captured from the interview PC's audio output and from a wireless microphone attached to the participant's clothing, respectively. Audio data were captured continuously at a rate of 8000 Hz using LABVIEW 2010 (National Instruments, Austin, TX).

**Data Processing.** Outcome measures included COP displacement, velocity, sway, and the total pathlength. Calculation of outcome measures was done between the offset of the interviewer’s question and the offset of the participant’s verbal response (both based on captured audio data). All data were processed with MATLAB R2009a (The MathWorks, Natick, MA, USA).

**Statistical Analysis.** Statistical analysis was performed with SPSS 18 (SPSS, Inc., Chicago, IL, USA). Independent samples t-tests were performed to identify significant differences between groups. Comparisons with p-values  $\leq 0.05$  were considered to be statistically significant.

**RESULTS AND DISCUSSION**

The t-tests revealed a deception-related decrease in mean velocity and pathlength for the EG when compared to the CG. These results are shown graphically in Figures 1-3.

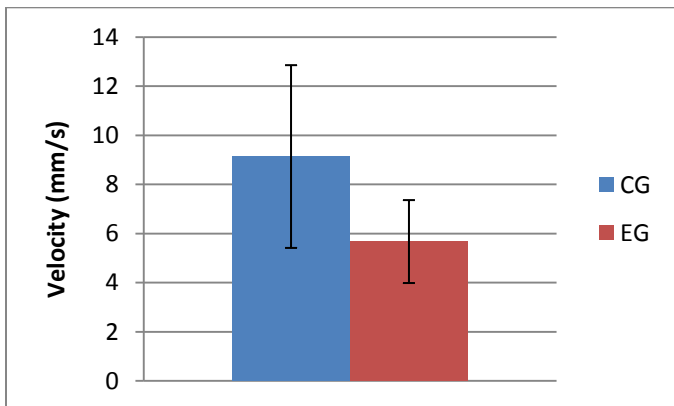


**Figure 1:** Mean COP Velocity (p < 0.0001)

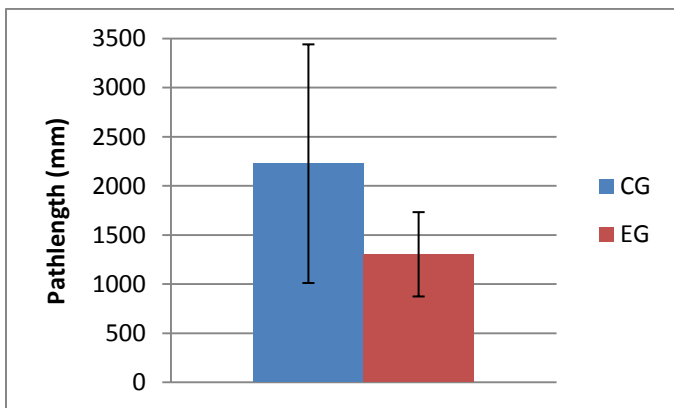


**Figure 2:** COP Pathlength (p < 0.001)

The deception-related decrease in COP mean velocity and pathlength indicates that people “freeze” when being deceptive. These findings are consistent with previous studies [3], which identified decreased body movement during deception, an effect thought to be related to an increased cognitive load. Another explanation that has been proposed is that reduced body movement is an attempt to control one’s behavior. Liars may believe that movements will give their lie away, and they will intentionally avoid movements that are not essential. This results in an unusual amount of rigidity, suppressing non-essential movements that are normally made during quiet stance [4].

**CONCLUSIONS**

This study demonstrates the potential for CSP to detect deception. A decrease in COP mean velocity and pathlength were found to be good indicators of deception. CSP has the potential to detect deception in more natural environments, which has been a major limitation of previously used techniques. As a result of this study we believe that further investigation into CSP-based detection of deception is merited.

**REFERENCES**

- 1.Chen H, et al. *Intelligence and Security Informatics* **135**, 425-441, 2008
- 2.Murray MP, et al. *J Appl Physiol.* **23**, 831-838, 1967
- 3.Eckman P, et al. *J of Communication.* **22**, 1972
- 4.Riggio R, et al. *Applications of Non-Verbal Communication*, 67-70, 2005

**ACKNOWLEDGEMENTS**

We gratefully acknowledge the help of Adam Bruetsch and Liz Duval for their assistance with participant testing. This work was supported by a grant from the Center for Identification Technology Research, a National Science Foundation Industry/University Cooperative Research Center.

# **Biomechanics of the shoulder joint during manual wheelchair propulsion in persons with paraplegia**

Sara Mulroy, Philip Requejo, Puja Ruparel, Patricia Hatchet, Lisa Lighthall Haubert, Valerie Eberly,  
\*Carmen Muller-Karger

Pathokinesiology Laboratory, Rancho Los Amigos National Rehabilitation Center, Downey, CA, USA

\*Department of Mechanical Engineering, Simon Bolivar University, Caracas, Venezuela

Email: smulroy@dhs.lacounty.gov

## **INTRODUCTION**

The prevalence of shoulder pain is increased after spinal cord injury (SCI) negatively impacting independence and quality of life.<sup>1,2</sup> Rotator cuff tendonitis and tears are the most common diagnoses for those with shoulder pain after SCI.<sup>3</sup> This pathology has been attributed to repetitive upper extremity (UE) weight bearing activities including manual wheelchair propulsion (WCP).<sup>4</sup> In small retrospective pilot study we identified that the vertical component of the shoulder joint reaction force during WCP was significantly greater in persons with paraplegia who eventually developed shoulder joint pain over a 10 to 12 year follow-up period compared to those who remained pain-free. Despite a similar velocity, those who developed pain had higher vertical shoulder joint forces (figures 1 and 2) and increased intensity of shoulder muscle activity (figure 3) during the push phase of WCP. Vertically directed forces on the humerus would tend to impinge subacromial structures without sufficient counterbalancing muscular control. The increased intensity of muscle activity would present a greater potential for fatigue in the shoulder muscles. Weakness or fatigue in these muscle groups would reduce the capacity to respond to the high shoulder forces and protect the glenohumeral joint during prolonged WCP. In our current research we are conducting a prospective, longitudinal study to identify factors that predict development of shoulder joint pain over time after SCI. In this presentation we will discuss the stroke parameters of WCP that are correlated with the magnitude of the vertical shoulder joint reaction force. The long term goal is to identify variables that could be altered to reduce vertical shoulder forces during WCP and prevent the onset of shoulder pain after SCI.

## **METHODS**

Volunteers were recruited from the outpatient clinics at Rancho Los Amigos National Rehabilitation Center. Participants included 223 individuals with paraplegia who were free of shoulder pain and who used a manual wheelchair at least 50% of the time for community mobility. The average age of participants was 33 years and time since injury 9 years. The biomechanics of the upper extremities were recorded for each participant during three conditions (free, fast, inclined) of WCP on a stationary ergometer. Hand forces from an instrumented handrim (SmartWheel) were collected (200Hz) along with 3-D kinematic (CODA, 100Hz) data from bilateral upper extremities, trunk and wheels. Temporal-spatial propulsion characteristics, including speed, cadence, cycle length, and push-phase duration were calculated. Upper extremity kinematics and hand force data from multiple propulsion cycles were used to determine shoulder net joint forces and moments. All spatial data were normalized to 100% of the propulsion cycle and the peak upward shoulder force and components of the shoulder moments during the push phase were determined. The angles of initial and final hand contact on the pushrim were determined from the motion of the upper extremity and the wheel. Additionally, the horizontal distance from the center of the shoulder joint to the axle of the rear wheel during the push phase of WCP was identified from the motion markers.

## **STATISTICAL ANALYSIS**

Significant predictors of the peak and average vertical (superior) shoulder joint reaction force during the push phase of WCP will be identified with regression analysis. Potential independent variables will include cadence, cycle length, push percent of the cycle, angle of initial hand contact, arc of hand contact, horizontal distance between

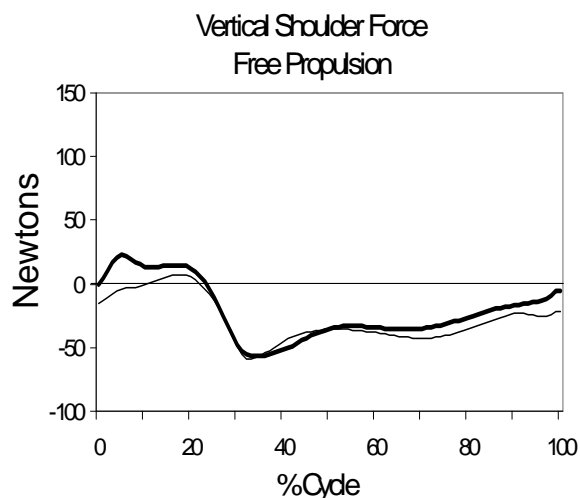


**Figure 1.** Mean vertical shoulder joint reaction force during FREE propulsion. Thick line=painful group; Thin line=asymptomatic.

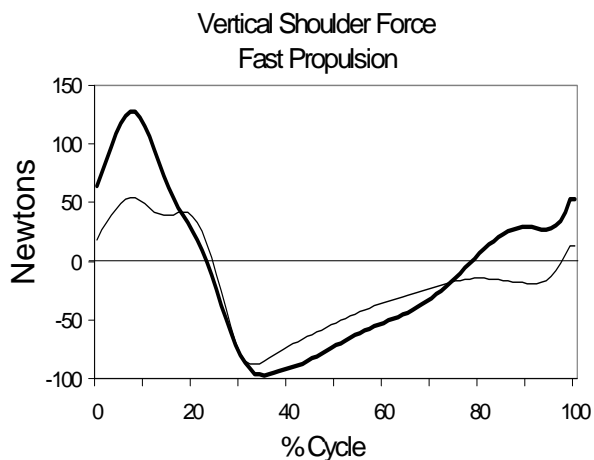


**Figure 2.** Mean vertical shoulder joint reaction force during FAST propulsion. Thick line=painful group; Thin line=asymptomatic.

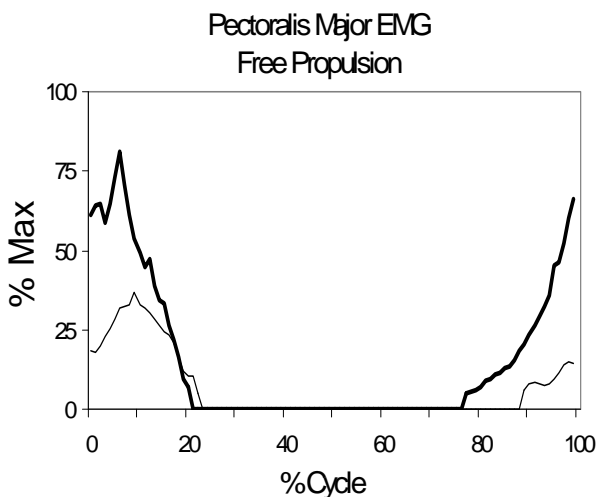


**Figure 3.** Sternal pectoralis major EMG during FREE propulsion. Thick line=painful group; Thin line=asymptomatic.

shoulder joint and rear wheel axle. Separate analyses will be conducted for each of the three propulsion conditions. Propulsion velocity will be explored as a covariate.

### HYPOTHESIS

The vertical shoulder joint force during WCP will be related to the participant's pattern of force application to the push rim. Specifically higher vertical shoulder joint forces will be predicted by higher cadence in free and fast propulsion, shorter cycle length in incline propulsion, a more forward location of the push arc, and a more anterior location of the shoulder joint center relative to the rear wheel axle.

### DISCUSSION

The superiorly directed shoulder forces during the weight-bearing push phase of WCP are the forces that increase the potential for subacromial impingement. Determining the propulsion characteristics that influence the magnitude of the vertical forces at the shoulder during WCP may help identify causative factors of chronic shoulder pain, and therefore assist with preventative efforts to avoid and/or reduce pain.

### ACKNOWLEDGEMENTS:

Funded by NIH grant R01 HD049774

### REFERENCES:

1. Sie, I. H., Waters, R. L., Adkins, R. H., and Gellman, H.: Upper extremity pain in the postrehabilitation spinal cord injured patient. *Arch. Phys. Med. Rehabil.* 73:44-48, 1992.
2. Gutierrez DD, Thompson L, Kemp B, Mulroy SJ. The relationship of shoulder pain intensity to quality of life, physical activity, and community participation in persons with paraplegia. *J Spinal Cord Med.* 2007;30:251-255.
3. Escobedo, E. M., Hunter, J. C., Hollister, M. C., Patten, R. M., and Goldstein, B.: MR imaging of rotator cuff tears in individuals with paraplegia. *Am. J. Roent.* 168: 919-923, 1997.
4. Dalyan M. Cardenas DD, Gerard B. Upper extremity pain after spinal cord injury. *Spinal Cord.* 1999;37:191-195.

# RECONFIGURATION OF THE UPPER EXTREMITY RELATIVE TO THE PUSH RIM AFFECTS LOAD DISTRIBUTION DURING WHEELCHAIR PROPULSION

<sup>1</sup>Joseph M. Munaretto, <sup>1,2,3</sup>Jill L. McNitt-Gray, <sup>4</sup>Henryk Flashner, and <sup>1,5</sup>Philip S. Requejo

<sup>1</sup>Department of Biomedical Engineering, <sup>2</sup>Kinesiology, <sup>3</sup>Biological Sciences

<sup>4</sup>Aerospace and Mechanical Engineering, University of Southern California, Los Angeles, CA

<sup>5</sup>Rehabilitation Engineering, Rancho Los Amigos National Rehabilitation Center, Downey, CA

<sup>1</sup>University of Southern California, Los Angeles, CA, USA

[munarett@usc.edu](mailto:munarett@usc.edu)

## INTRODUCTION

Repetitive loading during manual wheelchair propulsion (WCP) is associated with overuse-related injury of upper extremity (UE) [1]. Redirection of the hand / rim reaction force (RF) relative to the upper extremity segments provides a means to redistribute mechanical load across joints away from areas at risk [2,3]. Reconfiguration of the UE relative to the pushrim was hypothesized to influence how redirection of the RF redistributes load without a decrement in performance.

## METHODS

One wheelchair user with spinal cord injury (SCI) volunteered to participate in this study in accordance with the Institutional Review Board at the Rancho Los Amigos National Rehabilitation Center, Downey, CA. The participant performed self-selected speed wheelchair propulsions for 10 seconds. Reflective markers were used to monitor the 3D motion of the hand, forearm, upper arm, trunk, and wheel segments (VICON, 50 Hz) and 3D hand / pushrim force was collected (SmartWheel 2500 Hz). The markers and upper extremity model to estimate wrist, elbow, and shoulder joint centers followed methods described in [4].

A 2D inverse dynamic model, incorporating subject-specific experimental tangential force and kinematic data, was used to determine the sensitivity of UE loading to shoulder/pushrim distance and wrist placement during WCP. We assume the shoulder is in a constant position as determined by its average position during the push cycle. Forearm and upper arm lengths are determined as averages of the distances between elbow / wrist and shoulder / elbow centers of rotation in 3D during the push phase. The model is then restricted to 2D by assuming shoulder, elbow, and wrist are in sagittal plane. Given the

shoulder/axle distance and wrist angle at time  $t$ , configuration of the forearm and upper arm can be determined (using the law of Cosines) at time  $t$  that agrees with the static constraints of forearm and upper arm segment length (Equation 1&2, Figure 1).

$$\theta_E = \cos^{-1} \frac{L_{SW}^2 - L_U^2 - L_F^2}{-2L_U L_F} \quad (1)$$

$$\theta_F = \tan^{-1} \left( \frac{y_S - y_W}{x_S - x_W} \right) + \theta_E \quad (2)$$

Mechanical loading was characterized by elbow net joint moment (NJM) and shoulder NJM over a range of RF directions. RF direction was systematically varied by maintaining the tangential component of the RF and varying the magnitude of the radial component.

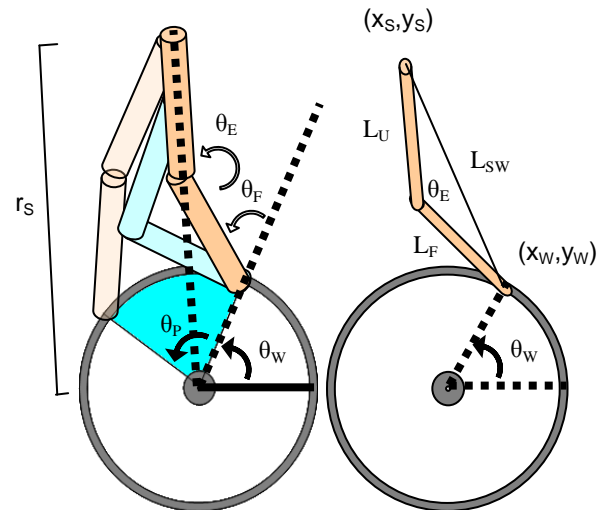


**Figure 1:** 2D model of modifications in UE configurations associated with changes in shoulder distance relative to wheel axle. Distance between shoulder and wheel axle ( $r_s$ ) and push range ( $\theta_p$ ) are modified to give shoulder and wrist coordinates. Law of Cosines is used to determine UE segment orientations

## RESULTS AND DISCUSSION

As forearm angle increases, minimum elbow and shoulder NJMs will occur at increasingly tangential RF directions (Figure 2). Minimum shoulder NJMs occur at more radial RF directions than minimum elbow NJMs. At low forearm angles, RFs that keep moment arms small on the forearm and upper arm are more radially directed and have relatively large magnitudes. As forearm angle relative to pushrim increases, RF directions shift more tangentially and have lower force magnitudes which can allow NJMs of both joints to decrease.

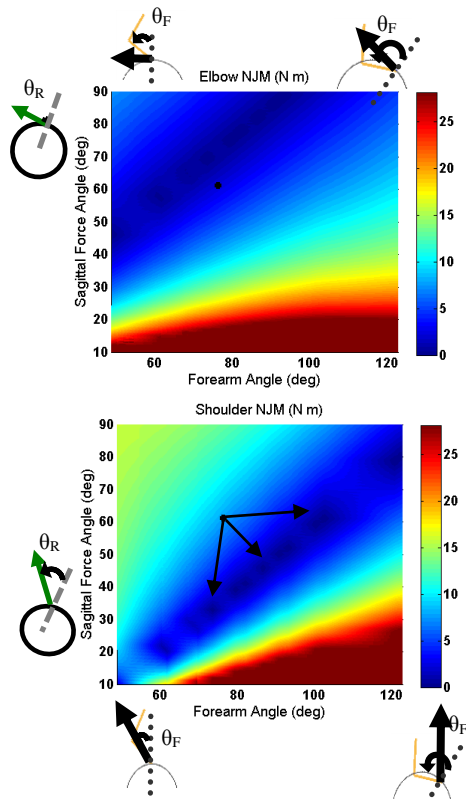


**Figure 2:** Elbow, shoulder, and total NJM and axial shoulder NJF (at time of peak force) in relation to RF direction  $\theta_R$  and forearm angle  $\theta_F$  relative to pushrim when elbow angle  $\theta_E$  is kept constant. The effect of RF direction is dependent on forearm angle. Larger forearm angles shift low moment areas (blue) to more tangential RF directions. Black dot represents location of experimental results within solution space.

As elbow angle increases, there is no change in effect of RF redirection on elbow NJM. RF direction associated with minimal shoulder NJM shifted from  $15^\circ$  to  $40^\circ$  relative to the radial direction (Figure 3). The difference in RF directions which minimize elbow and shoulder NJM decreases with increasing elbow angle. Since forearm orientation relative to the pushrim did not change, there were no changes in how  $r \times RF$  alters elbow NJM. Increasing elbow angle rotates the upper arm

into closer alignment with the forearm. RFs directed through or close to the forearm reduce the moment arm when acting on the upper arm.

## CONCLUSIONS

These simulation results provide mechanically based information to guide clinical interventions that aim to maintain WCP performance and redistribute load by modifying RF direction, seat configuration and hand/rim interaction.

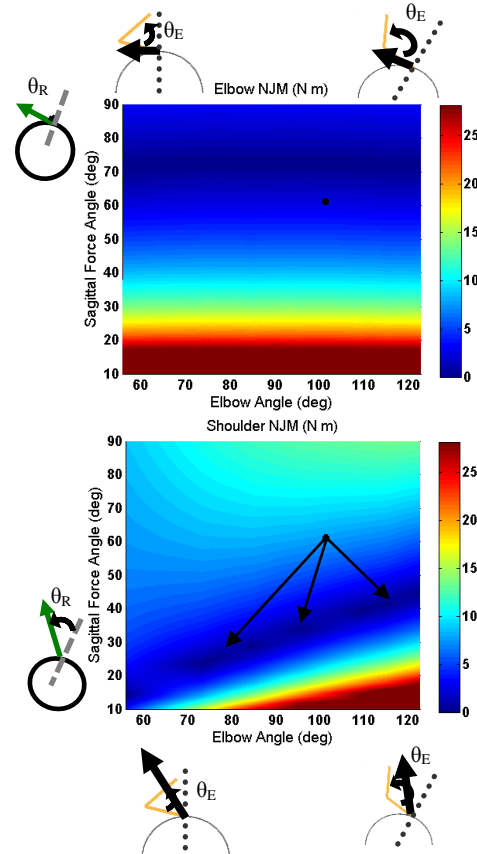


**Figure 3:** Elbow, shoulder, total NJM, and axial shoulder NJF at the time of peak force in relation to RF direction  $\theta_R$  and elbow angle  $\theta_E$  when the forearm angle  $\theta_F$  relative to pushrim is kept constant. The effect of RF direction is dependent on elbow angle. Larger elbow angles shift low shoulder moment areas to more tangential RF directions. Black dot represents location of experimental results within solution space.

## REFERENCES

1. Finley, MA et al. *J of Rehab Res & Dev*, 41(3), 395-402, 2004
2. Munaretto JM, et al. *Proceedings of ASB'09*, State College, PA, 2009.
3. Rankin, JW et al. *J of Biomech*, 2011.
3. Rao SS, et al. *IEEE Trans Rehabil Eng*, 4, 152-60, 1996

## ACKNOWLEDGEMENTS

Rancho Los Amigos National Rehabilitation Center and the USC Biomechanics Research Lab.

# THE EFFECTS OF AGING ON THE METABOLIC COST OF SUPPORTING BODY WEIGHT DURING WALKING

Sarah A. Musolf and Justus D. Ortega

Humboldt State University, Arcata, CA, USA  
email: jdo1@humboldt.edu web: www.humboldt.edu/~jdo1

## INTRODUCTION

Elderly adults consume more metabolic energy for walking than young adults across a range of speeds (1), yet the reason for the greater metabolic cost is unclear. During walking, the muscles of the body consume metabolic energy to generate force to support body weight. Previous walking studies that have measured changes in metabolic cost in response to simulated reduced gravity have shown that the cost of generating muscle force to support body weight accounts for as much as 28-33% of the total metabolic cost of walking (2, 3).

Changes in lower limb posture during the stance phase of walking directly affect the cost of generating muscle force to support body weight. Changes in limb posture affect muscle forces by altering the mechanical advantage for muscle force production (4). For example, by increasing flexion at the hip, knee and ankle joints by approximately 20% during walking, the mechanical advantage of the stance limb muscles decrease and the metabolic cost of walking increases by nearly two-fold (5).

Prior research has shown that elderly adults tend to walk with greater anterior tilt of the pelvis and greater flexion at the hip, knee and ankle joints (6, 7). These increases in flexion of the lower limb joints during the stance phase likely increase the metabolic energy consumed by the active stance limb muscles due to a reduction in their mechanical advantage. In this study, we examined how force generation to support body weight contributes to the cost of walking in young and elderly adults. It is hypothesized that body weight support incurs a substantially greater metabolic cost in elderly adults than young adults.

## METHODS

Twelve healthy young ( $26 \pm 4$  yrs, mean  $\pm$  SD) and twelve healthy elderly ( $75 \pm 4$  yrs) adults walked on a motorized treadmill at an intermediate speed of  $1.3 \text{ m s}^{-1}$  at four levels of body weight support (0%, 25%, 50%, and 75% of body weight). Prior to the walking trials, subjects performed a standing resting metabolic rate trial. Each trial lasted seven minutes followed by five minutes rest. For each trial, we determined net metabolic cost and lower limb kinematics.

We provided weight support by applying a nearly constant upward force to the pelvis and torso near the center of mass using a custom built harness and elastic pulley system (Figure 1) as described by Griffin et al. (8).

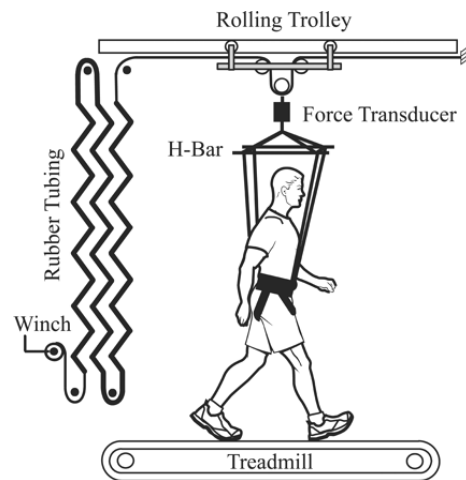


**Figure 1:** Weight support apparatus (adapted from Grabowski et al. 2005).

Metabolic cost was determined using indirect calorimetry (9) during minutes 4-6 of each treadmill trial. We calculated net metabolic cost by subtracting standing metabolic power from gross metabolic power and dividing by body mass.

We determined bilateral hip, knee and ankle joint kinematics for a 20-second period during the last two minutes of each trial using a 100 Hz 6-camera digital motion capture system (Vicon, Centennial, CO, USA). Sagittal plane joint angles were determined for the stance phase of each leg and averaged for ten strides of each walking trial.

## RESULTS AND DISCUSSION

Weight support reduced the rate of metabolic energy consumption to a greater extent in elderly subjects compared to young subjects ( $P < 0.0001$ ; Fig. 2). Without weight support, elderly subjects consumed metabolic energy 15% faster per kilogram of body mass ( $W \text{ kg}^{-1}$ ) than young subjects ( $P < 0.0001$ ; Table 1). As weight support increased, metabolic energy consumption decreased in both young and elderly adults ( $P < 0.0001$ ).

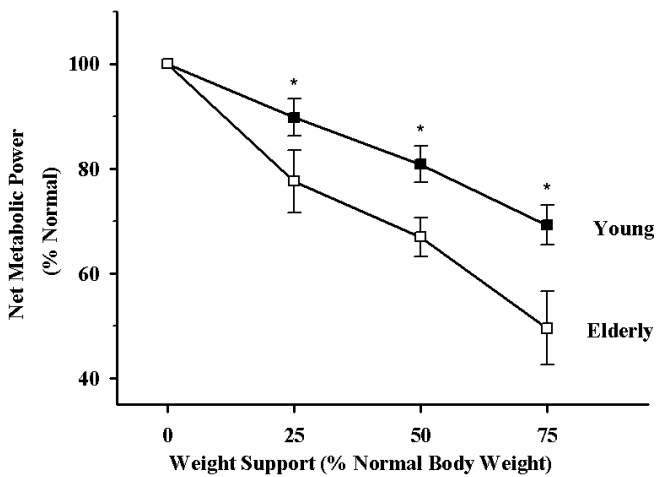


**Figure 2:** Net Metabolic Power as a function of Weight Support. Asterisk indicates significant differences from normal walking ( $P < 0.05$ ).

Weight support decreased metabolic energy consumption more in elderly adults compared to young adults ( $P < 0.0001$ ). Across the range of weight support, metabolic energy consumption decreased an average 50% (SD 7) in older adults,

whereas metabolic energy consumption only decreased by an average 31% (SD 8) in young adults.

Although elderly subjects used a faster step frequency and spent a shorter portion of the gait cycle in single limb support compared to young subjects, our kinematic analysis revealed that elderly subjects only tended to use a more flexed lower limb posture during the stance phase of walking compared to young adults (Table 1).

## CONCLUSION

The results of our study support the hypothesis that elderly adults have a greater cost of generating force to support body weight compared to young adults. Moreover, our results suggest body weight support comprises as much as 50% of the net metabolic cost of walking in elderly adults. Thus, the high metabolic cost of walking in elderly adults is likely due in part to a greater metabolic cost of generating muscle force for supporting body weight.

## REFERENCES

1. Martin PE, et al. *Journal of Applied Physiology*, **73**, 200-206, 1992.
2. Farley CT and TA McMahon. *Journal of Applied Physiology*, **73**, 2709-2712, 1992.
3. Grabowski A, et al. *Journal of Applied Physiology*, **98**, 579-83, 2005.
4. Biewener AA, et al. *Journal of Applied Physiology*, **97**, 2266-2274, 2004.
5. Ortega JD and CT Farley. *Journal of Applied Physiology*, **99**, 2099-2107, 2005.
6. Murray MP, et al. *Journal of Gerontology*, **24**, 169-178, 1969.
7. Judge JO, et al. *Clinics in Geriatric Medicine*, **12**, 659-678, 1996.
8. Griffin TM, et al. *Journal of Applied Physiology*, **86**, 383-390, 1999.
9. Brockway JM. *Human Nutrition: Clinical Nutrition*, **41** 463-471, 1987.

**Table 1:** Baseline energetics and average stance phase kinematics of walking in young and elderly adults.

|         | Net Metabolic Cost (Watts/kg) | Step Frequency (Hz) | Ankle Dorsiflexion (degrees) | Knee Flexion (degrees) | Hip Flexion (degrees) |
|---------|-------------------------------|---------------------|------------------------------|------------------------|-----------------------|
| Young   | 3.88 ± 0.47                   | 1.84                | 12.42                        | 12.26                  | 25.47                 |
| Elderly | 3.39 ± 0.23                   | 2.07                | 13.57                        | 19.40                  | 31.33                 |
| P-value | <0.0001                       | 0.011               | 0.080                        | 0.051                  | 0.073                 |

# RELATIONSHIP BETWEEN MOVEMENT SPEED AND REGULARITY OF MOVEMENT IN PARKINSON'S DISEASE

<sup>1</sup>Anburaj Muthumani, <sup>1</sup>Douglas Powell, <sup>2</sup>Hani Haider, <sup>1</sup>A. Joseph Threlkeld and <sup>1</sup>Ruiping Xia

<sup>1</sup>Creighton University, Omaha, NE, USA

<sup>2</sup>University of Nebraska Medical Center, Omaha, NE, USA

Email: [ruipingxia@creighton.edu](mailto:ruipingxia@creighton.edu) Web: <http://rehablab.creighton.edu>

## INTRODUCTION

Parkinson's disease (PD) is a progressive degenerative disorder of the central nervous system. Bradykinesia is one of the cardinal symptoms of PD and it is used to describe the slowness of movement. Patients with PD also exhibit impaired ability to adjust to movement. Previous reports indicate that the use of anti-PD medication by people with PD produces an increase in movement speed [1, 2] but the regularity of movement decreases. The decrease in regularity may reflect the person's improved ability to selectively adjust the movement after medication [3].

Approximate entropy (ApEn) is one technique used to quantify the regularity of biological signals [4]. In this study, ApEn was used to quantify the regularity of the voluntary wrist movement. There has been no previous investigation of the association between bradykinesia and regularity of the movement pattern. The objective of this study was to examine the relationship between movement speed and regularity of the wrist movement.

## METHODS

Seven patients (3 Males, 4 females;  $63.42 \pm 8.25$  years of age) with idiopathic PD participated in this study. The protocol was approved by the Institutional Review Board at Creighton University in Omaha, Nebraska and written informed consent was obtained from each subject prior to participation. Each subject was seated in an adjustable chair with the hand of the most affected side placed in a manipulandum and the wrist centered over the axis of rotation. The manipulandum was free to rotate horizontally approximately 180 degrees over a fixed base. The subjects' elbow was positioned at  $120^\circ$  and the forearm in the neutral

rotation [Figure 1]. The subject's trunk was strapped to the chair to minimize movement during the course of experiment.

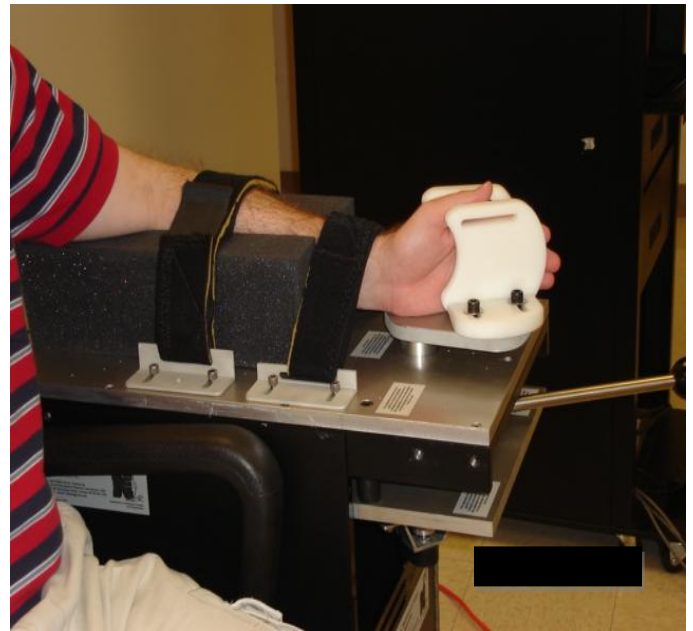


**Figure 1:** Experimental setup for measuring voluntary movement of the wrist flexion and extension

Subjects were first tested in the Off-medication state (OFF-MED) defined as 12 hours after the last dose of anti-PD medication. Each subject's wrist was positioned at his or her maximum extended position. The subject then performed repetitive voluntary reciprocal wrist flexion and extension movements. Subjects were instructed to move his or her hand as quickly as possible through the maximum range of motion for a period of 10 sec. Two trials were collected. Each subject then resumed his or her usual dose of anti-PD medication, and the testing was repeated approximately one hour later in the On-Medication state (ON-MED). Joint position was recorded using

an encoder (SC904 series, PacSci, CA, US). Joint torque was measured with a torque transducer (TRT-200, Transducer Tech, US). The position signal was sampled at 100 Hz.

ApEn was calculated based on the position signal. Typically, ApEn values range between zero and two [4, 5]. A more regular or consistent pattern of movement yields a lower ApEn value. Bradykinesia was quantified by measuring the number of cycles (NOC) of movement and the ability to adjust movement is quantified by measuring regularity. One cycle of movement was defined as the voluntary completion of one flexion and one extension movement. NOC of movement was calculated by counting the number of completed flexion/extension cycles. Pearson's correlation coefficient was used to examine the relationship between number of cycles of movement and ApEn values.

## RESULTS AND DISCUSSION

The NOC during Off-Med ( $9.44 \pm 3.32$ ) was smaller than the NOC during On-Med ( $10.44 \pm 2.98$ ). The ApEn value was lower during Off-Med ( $0.590 \pm 0.188$ ) than the On-Med ( $0.737 \pm 0.279$ ) state. Figure 2 illustrates the correlation between the ApEn and NOC of movement in the Off-Med and On-Med states, respectively. There was a strong correlation between NOC and ApEn during Off-Med ( $r = 0.962$ ) and On-Med ( $r = 0.977$ ) states.

Increased NOC during On-Med compared to Off-Med showed that movement speed increased with anti-PD medication. Lower ApEn values during Off-Med confirm more regularity of wrist movement, while higher ApEn during On-Med state confirm more irregularity of wrist movement. The unique finding of this study was the strong correlation between NOC and ApEn, suggesting that regularity of wrist movement decreased as the speed of wrist movement increased.

## CONCLUSION

The strong correlation between NOC and ApEn indicates that faster wrist movement was associated with decreased regularity regardless of medication state. Anti-PD medication improved movement speed and decreased movement regularity, implying improved functional adaptability of the wrist

motion. However, the influence of anti-PD medication and movement speed on functional adaptability of the wrist remains to be tested.

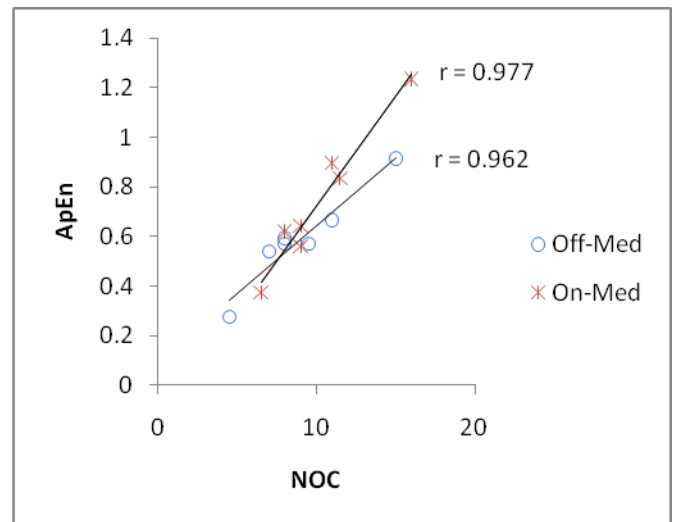


**Figure 2:** Correlation between Number of cycles of movement and ApEn value

## REFERENCES

1. Vaillancourt et al. *Brain* **127**, 491-504, 2004
2. Robichaud et al. *Movement disorders* **17**, 950-960
3. Hanson et al. *Abstract of Society for Neuroscience*, San Diego, CA, USA, 2010
4. Pincus S. M. *Application of nonlinear dynamics to developmental process modeling*, Lawrence Erlbaum Assoc., 1997
5. Myers et al. *J Surgical Research* **164**, 6-12, 2010

## ACKNOWLEDGEMENTS

This study was funded by Faculty Development Fund, School of Pharmacy and Health Professions, Creighton University, Omaha Nebraska, USA. Authors would like to thank Matija Radovic and Andrea Benes for the diligent work in data processing.

# RELATIONSHIP BETWEEN NEURAL-REFLEX TORQUE AND MUSCLE REFLEX RESPONSE IN PARKINSONIAN RIGIDITY

Anburaj Muthumani, Douglas Powell, Nicholas Hanson, Lauren Kremer, Lindsey Wagner, A. Joseph Threlkeld, Ruiping Xia

Creighton University, Omaha, NE, USA

Email: [ruipingxia@creighton.edu](mailto:ruipingxia@creighton.edu) Web: <http://rehablab.creighton.edu>

## INTRODUCTION

Parkinson's disease (PD) is a progressive neurodegenerative disorder. Rigidity is one of the most disabling symptoms of PD and is defined as an increase in resistance to a passive movement persistent through the entire range of motion. Rigidity is quantified by measuring the imposed torque resistance about the joint being examined. Evidence has indicated that both neural component and non-neural component contribute to rigidity [1,2]. The neural component refers to increased reflex responses to passive stretch of the muscle. The non-neural component refers to altered mechanical properties of the passive tissues and muscle fibers.

System Identification and Modeling Approach (SIMA) is one technique used to differentiate between neural and non-neural components associated with increased muscle tone. SIMA technique has previously been used to quantify the two components in healthy individuals, subjects with stroke [3] or spinal cord injury [4]. In this study, SIMA was applied to quantify the neural and non-neural components in parkinsonian rigidity. Given that neural component of torque resistance is mainly attributed to muscle reflex response, we hypothesize that a strong correlation exists between the neural component and reflex response. The purpose of this study was to examine the relationship between neural component and magnitude of muscular reflex response measured by EMG, and to compare with the relationship between non-neural component and magnitude of EMG in subjects with PD. Another objective was to assess the validity of the SIMA technique in differentiating the neural and non-neural components associated with PD.

## METHODS

Nine patients with idiopathic PD participated in this study. Informed consent was obtained from each subject and was approved by the Institutional Review Board of Creighton University in Omaha Nebraska. A servomotor housed in a custom-built apparatus generated passive wrist flexion and extension movements in controlled patterns. In this study, a pseudorandom binary sequence (PRBS) waveform was chosen to characterize dynamic features of the reflex components.

Subjects were tested in the Off-medication (12 hours after the anti-PD medication) and On-Medication (approximately one hour after taking medicine). Each subject was seated in an adjustable chair with the wrist of the most affected hand placed in a manipulandum connected to the motor shaft. The subject's elbow was positioned at an angle of  $120^\circ$ . Each subject's wrist was kept in a neutral position. The passive movement was applied in a PRBS waveform pattern to impose joint displacement of  $5^\circ (\pm 2.5^\circ)$  at a constant velocity of  $200\%$  in the Off-medication and On-medication conditions. Each condition lasted approximately 15 seconds, and three trials were collected for each condition.

Joint position was recorded using an encoder (SC904 series, PacSci, CA, US). Joint torque was measured with a torque transducer (TRT-200, Transducer Tech, US). Surface electromyography (EMG) electrodes were placed over the belly of the wrist flexor muscles (flexor carpi radialis, flexor carpi ulnaris and flexor digitorum superficialis) and extensor muscles (extensor carpi radialis longus and brevis, extensor carpi ulnaris and extensor digitorum communis) using differential surface electrodes (Delsys Inc., MA, US). The position

signal was sampled at 100 Hz and torque was sampled at 1 kHz. EMGs were amplified and band pass filtered (10 - 450 Hz) before being sampled at 1 kHz per channel.

SIMA was applied to the joint position and torque signals to separate neural and non-neural components, using the parallel-cascade structure [Figure 1]. The non-neural component ( $TQ_I$ ) is the torque calculated by using mechanical properties of the joint, and neural component ( $TQ_R$ ) is the torque calculated with the combination of mechanical properties and changes in muscle activation [3-6].

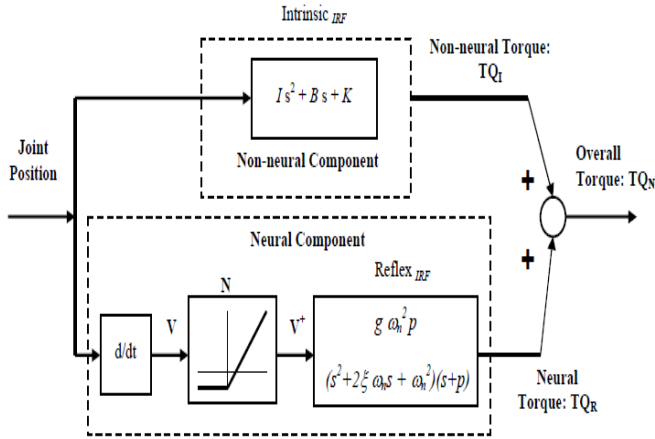


**Figure 1:** Parallel cascade structure of neural and non-neural pathways

The net torque ( $TQ_N$ ), measured experimentally, is given by

$$TQ_N = TQ_I + TQ_R$$

$TQ_I$  was estimated in terms of a linear, dynamic IRF, relating position, and torque. The length of this IRF was fixed at a value less than the reflex delay to prevent torques due to neural component influencing the estimate.  $TQ_R$  was estimated as a pathway comprising a differentiator, a static non-linearity (N), and linear dynamics (Reflex<sub>IRF</sub>), using a Hammerstein identification method [5].

EMG signals were low pass filtered at 20 Hz. Magnitude of EMG activity of the stretched muscles was defined as the sum of the reflex response of stretched muscles. The duration of reflex response was selected between 50 ms and 110 ms after the onset of each movement. Reflex response was calculated as the integrated EMG over the duration of the reflex response and was

normalized to background EMG prior to movement onset. Pearson's correlation coefficient was performed to examine the relationship between EMG activity and neural component of torque resistance, and between EMG activity and non-neural component.

## RESULTS AND DISCUSSION

Table 1 lists the correlation coefficients between the  $TQ_R$  and EMG activity, and between  $TQ_I$  and EMG in the OFF-MED and ON-MED states, respectively. The correlation is stronger between  $TQ_R$  and EMG activity than between the  $TQ_I$  and EMG activity.

**Table 1:** Correlation coefficient between neural torque, non-neural torque and EMG activity

| Correlation coefficient ( r ) |         | Torque           |                      |
|-------------------------------|---------|------------------|----------------------|
|                               |         | Neural component | Non-neural component |
| EMG activity                  | OFF-MED | 0.614            | 0.472                |
|                               | ON-MED  | 0.125            | 0.101                |

The results support our hypothesis that muscular reflex response is correlated with neural component. The correlation is stronger in the OFF-MED than in the ON-MED state. Furthermore, data obtained from the study provide useful information to validate the SIMA technique in differentiating the neural from the non-neural components associated with parkinsonian rigidity.

## REFERENCES

- 1.R.G. Lee et al. *Can. J. Neurol. Sci.* **2**, 285-293, Aug.1975.
- 2.V. Dietz et al. *Brain* **104**, 431-449, 1981
3. L. Galiana et al. *Exp Brain Res.* **165-4**, 422- 434
- 4.M.M. Mirbagheri et al. *Exp Brain Res.* **141**:446-459, 2001
- 5.E. Kearney et al. *IEEE T Bio-Med Eng.* **44**; 493-504, 1997
- 6.R. Xia et al. *Proc of the 4<sup>th</sup> Int. Conf on Bio-info, Bio-med Eng.*, DOI: 10.1109/icbbe.2010.5514861, 2010.

## ACKNOWLEDGEMENT

This study was funded in part by the National Institutes of Health under grant R15-HD061022 and in part under Health Future Foundation, Creighton University, Omaha, NE, USA.

# RECRUITMENT OF MUSCULATURE DURING EXTENSION FROM FULL TRUNK FLEXION IS ALTERED IN PEOPLE WHO DEVELOP LOW BACK PAIN DURING PROLONGED STANDING

Erika Nelson-Wong<sup>1</sup>, Brendan Alex<sup>1</sup>, David Csepe<sup>1</sup>, Denver Lancaster<sup>1</sup>, and Jack P. Callaghan<sup>2</sup>

<sup>1</sup>Regis University, School of Physical Therapy, Denver, CO, USA

<sup>2</sup>University of Waterloo, Waterloo, ON, Canada

email: [enelsonw@regis.edu](mailto:enelsonw@regis.edu)

## INTRODUCTION

Altered muscle activation patterns during lumbar flexion and extension movements have been previously reported in people with clinical low back pain (LBP). A period of electromyographic silence of the lumbar extensors at peak lumbar flexion has been observed in healthy subjects and has been termed the flexion relaxation response. Impairment of this response, shown as a decrease in relaxation has been observed in patients with LBP [1,2]. McGorry et al. [3] found that activation order of the extensor musculature at initiation of extension from a flexed posture progressed from caudal to cephalic in healthy subjects. Previous work aimed at identification of predisposing factors for LBP development during a standing exposure in previously asymptomatic people, showed that people who developed LBP during standing had significantly greater relaxation of the gluteus maximus muscles compared to their non-pain developing counterparts [4]. The purpose of the present study was to investigate differences in extensor muscle recruitment during the return to stand (RTS) phase of standing full flexion between this same sample of pain developers (PD) and non-pain developers (NPD).

## METHODS

These analyses were conducted on data collected as part of a larger study at the University of Waterloo. Forty-three participants (22 male, 21 female) with no previous history of LBP had surface electromyography (EMG) collected from 3 bilateral trunk and hip muscles, including thoracic erector spinae (TES), lumbar erector spinae (LES) and gluteus maximus (GMax). Participants performed standing full flexion trials prior to a 2 hour standing exposure. Visual Analog Scale (VAS) for LBP was

completed every 15 minutes during the 2 hours of standing. Participants were categorized as PD/NPD based on a cutoff threshold of > 10 mm on VAS. EMG data were windowed to isolate the RTS phase of the full flexion movement. Cross-correlation analyses were performed on the linear enveloped data to determine phase relationships (phase lag at peak correlation) between GMax, LES, and TES muscles. Data were entered into the cross-correlation equation such that a +ve phase lag indicated the first-listed muscle in a pair was activated first and a -ve phase lag indicated the first-listed muscle in a pair was activated second. Paired t-tests were performed on phase lag data for right/left muscle pairs, and when no differences were found ( $p > 0.05$ ) these data were averaged to yield a single measure for the muscle group. Phase lag data were entered into a 2-way ANOVA with factors of PD/NPD group and gender with significance criterion set at  $p < 0.05$ .

## RESULTS AND DISCUSSION

Twenty-six and 17 participants were classified as NPD and PD respectively. There were no significant differences detected between left/right muscle pairs, therefore symmetry was assumed. NPD individuals demonstrated the previously reported pattern of caudal to cephalic muscle recruitment during RTS. PD individuals demonstrated the opposite pattern of activation, with cephalic muscles being activated prior to more caudal muscles (Figure 1).

There was a main effect of PD/NPD group for phase lag between LES and GMax ( $F_{1,39} = 5.22, p = 0.03$ ), with PD activating GMax prior to LES (mean lag =  $+ 0.038 \pm 0.33$  s) compared with NPD, where LES was activated prior to GMax (mean lag =  $- 0.196 \pm 0.33$  s) (Figure 1). There were no

significant differences between NPD/PD groups detected for phase lag between the other muscle pairs (TES-LES, TES-GMax).

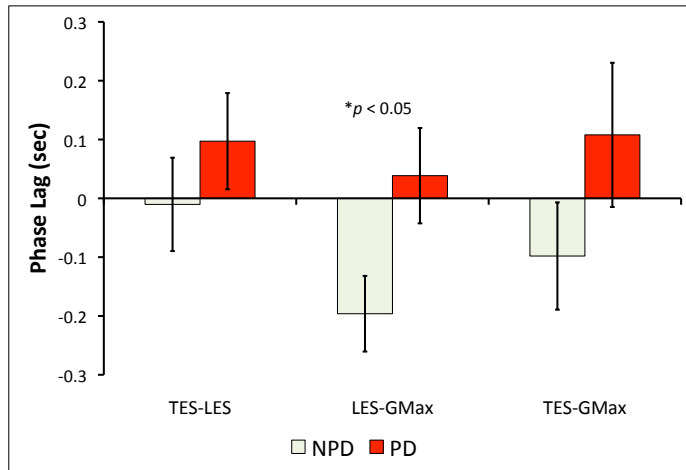


**Figure 1.** NPD individuals activated more caudal muscles prior to more cephalic muscles, or a bottom up pattern, during RTS, while PD showed the reverse pattern. The PD group activated GMax significantly later than LES during RTS ( $p < 0.05$ ).

There was also a main effect of gender for phase lag between TES and GMax ( $F_{1,39} = 4.42, p = 0.04$ ) with females activating TES prior to GMax (mean lag =  $-0.123 \pm 0.46$  s), and males activating GMax prior to TES (mean lag =  $+0.085 \pm 0.50$  s) (Figure 2). There were no significant differences between genders detected for phase lag between the other muscle pairs (TES-LES, LES-GMax). There were no significant interactions between PD/NPD group and gender.

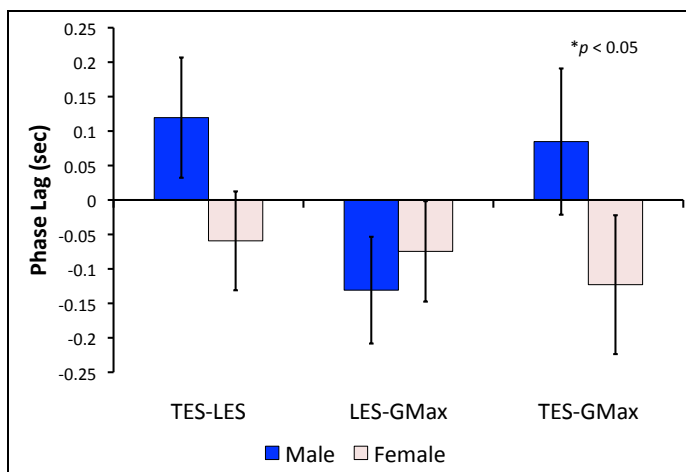


**Figure 2.** There were significant gender differences in activation of extensor musculature during return to stand for the TES-GMax pair with males activating the TES prior to GMax and females demonstrating the opposite sequence.

## CONCLUSIONS

Individuals predisposed to LBP during standing demonstrated a reverse pattern of extensor muscle activation to accomplish return to stand from lumbar forward flexion compared with individuals who did not develop LBP during standing. This was significant for the LES-GMax pair, with PD individuals having delayed activation of the GMax. It is of interest that these individuals had no history of clinical LBP. Alterations in muscle activity have been found previously in people who are predisposed to LBP development during the functional task of standing, leading the authors to hypothesize that these individuals may constitute a sub-clinical group who could be at future risk for LBP development. This provides further support for altered baseline muscle activation patterns as predictive factors for identification of individuals at-risk for LBP development.

## REFERENCES

1. Paquet et al., *Spine*, **19**, 596-603, 1994.
2. Dankaerts et al., *Spine*, **31**, 2017-2023, 2006.
3. McGorry et al., *Spine*, **26**, 418-425, 2001.
4. Nelson-Wong E. & Callaghan J.P., *J Electromyogr & Kinesiol*, **20**, 256-263, 2010.

## ACKNOWLEDGEMENTS

Dr. Erika Nelson-Wong was supported by the Foundation for Physical Therapy with a PODS II Doctoral Scholarship.

# INSIGHT INTO WHEELCHAIR BIOMECHANICS USING MUSCULOSKELETAL MODELING AND SIMULATION TECHNIQUES

<sup>1</sup>Richard R. Neptune, <sup>2</sup>Jeffery W. Rankin and <sup>3</sup>W. Mark Richter

<sup>1</sup>Department of Mechanical Engineering, The University of Texas at Austin, Austin, TX, USA

<sup>2</sup>The Royal Veterinary College, University of London, UK

<sup>3</sup>MAX Mobility, LLC, Antioch, TN, USA

email: [rneptune@mail.utexas.edu](mailto:rneptune@mail.utexas.edu); web: [www.me.utexas.edu/~neptune](http://www.me.utexas.edu/~neptune)

## INTRODUCTION

Manual wheelchair propulsion places considerable physical demand on the upper extremity and is one of the primary activities associated with the high prevalence of upper extremity overuse injuries and pain among wheelchair users [1]. As a result, recent efforts have focused on determining how various propulsion techniques influence upper extremity demand during propulsion [2, 3]. We have directed our efforts towards using modeling and simulation techniques to gain insight into how individual muscles contribute to the mechanical energetics of propulsion and whether improving mechanical efficiency by altering the ratio of tangential to total handrim force (i.e. fraction of effective force, FEF) holds promise for reducing upper extremity demand.

## METHODS

To perform these analyses, an upper extremity musculoskeletal model based on the work of Holzbaur et al. [4] was used to generate forward dynamics simulations of wheelchair propulsion (Fig. 1). The model consisted of six rotational degrees of freedom representing the joints of the upper extremity and trunk lean and 26 Hill-type musculotendon actuators representing the major muscle groups crossing the elbow and shoulder joints. A dynamic optimization algorithm identified muscle excitation patterns to produce different simulations that (1) emulated normal wheelchair mechanics (i.e. nominal), (2) maximized FEF and (3) minimized FEF. In all three simulations, the optimization algorithm minimized differences between the simulation and experimentally collected joint kinematics and handrim forces. The

FEF simulations added average FEF to the cost function to be maximized and minimized.

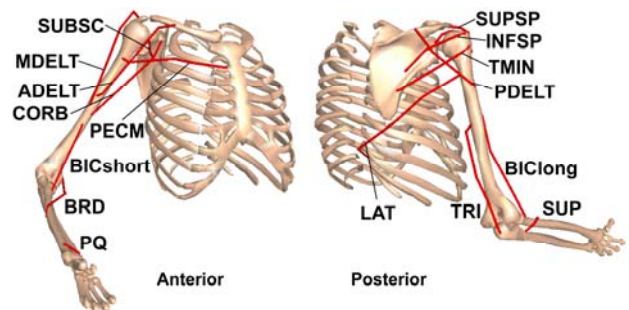


**Figure 1:** Musculoskeletal model used in the wheelchair propulsion simulations. The model had 6 degrees of freedom consisting of trunk lean, shoulder elevation plane, shoulder elevation angle (thoracohumeral angle), shoulder internal-external rotation, elbow flexion-extension and forearm rotation (pronation-supination).

Following the optimization, the nominal simulation was used to determine individual muscle contributions to the mechanical power of each body segment and the external handrim power using a segment power analysis [5]. Muscle contributions to the upper arm, forearm and hand segment powers were combined into a single arm power value. The mechanical power generated, absorbed or transferred by each muscle was determined during the push (handrim power generation) and recovery (arm relocation) regions of the stroke. To assess the influence of FEF on upper extremity demand, individual muscle stress and mechanical work was quantified for all three simulations (i.e., at different values of FEF). Muscle stress was calculated as the percentage of maximum isometric force generated by each muscle at every time step and average and maximum values were determined. Total, positive and negative muscle work was quantified by integrating the positive and negative musculotendon power over the stroke.

## RESULTS AND DISCUSSION

Net positive muscle power was delivered to the handrim over the entire push phase (Fig. 2; dotted line positive). The majority of the power was delivered directly to the handrim (Fig. 2; dotted and solid lines similar), although some power was transferred from the arm to the handrim during the second half of the push phase (Fig. 2; dashed line negative, dotted line > solid line at ~21-34% stroke). During the recovery phase, muscle contributions to arm power alternated between absorption and delivery (Fig. 2; sign of dashed line alternates) in order to reposition the arm for the subsequent push.

Analyzing individual muscle power data revealed that muscles contribute to either push (i.e. deliver mechanical power to the handrim) or recovery (i.e. reposition the arm) subtasks, with the shoulder flexors being the primary contributors to the push and the shoulder extensors being the primary contributors to the recovery. In addition, significant activity from the shoulder muscles was required during the transition between push and recovery, which resulted in increased co-contraction and upper extremity demand.

Simulations maximizing and minimizing FEF had increased average muscle stresses (23% and 112%) and total muscle work (28% and 71%) relative to a nominal FEF simulation. The maximal FEF simulation also shifted muscle use from elbow muscles to those crossing the shoulder (e.g. rotator cuff muscles), which placed greater demand on shoulder muscles during propulsion.

## CONCLUSIONS

The modeling and simulation framework used in these studies provided insight into how individual muscles contribute to the mechanical energetics of wheelchair propulsion and whether altering FEF holds promise for reducing upper extremity demand. Each study has important implications for improving rehabilitation outcomes. For example, strengthening the shoulder flexors and promoting propulsion techniques that improve phase transition mechanics have much potential to reduce upper extremity demand. Also, the optimal FEF value

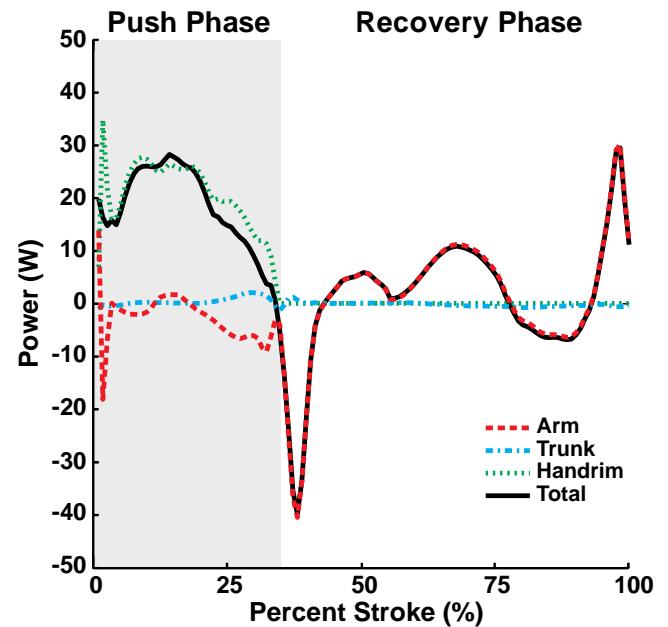


**Figure 2:** Net muscle contributions to segment power during the push and recovery phases. Individual segment powers were combined into four groups for analysis: Arm (upper arm, forearm and hand segments, dashed line), Trunk (trunk, scapula and clavicle, dash-dot line), Handrim (external handrim power, dotted line) and Total (sum of all segments, solid line).

appears to balance increasing push force effectiveness to increase mechanical efficiency with minimizing upper extremity demand. Thus, care should be taken in using force effectiveness as a metric to reduce upper extremity demand.

## REFERENCES

1. Sie IH, et al. *Arch Phys Med Rehabil*, 73, 44-48, 1992.
2. de Groot S, et al. *Clin Biomech*, 23, 434-41, 2008.
3. Rice I, et al. *J Spinal Cord Med* 33, 33-42, 2010.
4. Holzbaur KR, et al. *Ann Biomed Eng* 33, 829-840, 2005.
5. Fregly BJ, et al. *J Biomech* 29, 81-90, 1996.

## ACKNOWLEDGEMENTS

This work was supported by NIH grant R01 HD053732. The contents are solely the responsibility of the authors and do not necessarily represent the official views of the NIH or NICHD.

# IDENTIFYING FACTORS THAT AFFECT CHANGES IN PEAK ACHILLES TENDON STRAIN OVER 6 MONTHS IN YOUTH 10-14 YEARS OLD

<sup>1</sup>Jennifer Neugebauer and <sup>1,2</sup>David A. Hawkins

University of California, Davis, Davis, CA, USA

<sup>1</sup>Biomedical Engineering Graduate Group, <sup>2</sup>Department of Neurobiology, Physiology, and Behavior  
email: dahawkins@ucdavis.edu

## INTRODUCTION

As youth experience periods of rapid height velocity, the Achilles tendon (AT) material and structural properties may change. These changes occur in response to both intrinsic (e.g. sex, age, maturation) and extrinsic (e.g. physical activity, movement mechanics, body weight) factors [1,2]. To date, temporal changes in youth AT structural and material properties have not been characterized. The purpose of this study was to quantify changes over 6 months in peak AT strain developed during a ramped isometric maximum plantar flexion (IMPF) and identify factors that may explain these changes. We hypothesized that peak AT strain during an IMPF would increase over 6 months in youth. We further hypothesized that the increased strain could be explained by an increase in muscle strength that occurs without a temporally matched increase in material and/or structural properties of the AT.

## METHODS

Eight girls ( $11.4 \pm 0.8$  years) and eight boys ( $13.6 \pm 0.5$  years) were tested at the start of the study (0 months (mos)) and the end of the study (6 mos). These age ranges represent the primary growth years [3]. Age, body mass, height, and shank length were recorded. Growth rate was calculated as the difference in height between the end and start of the study. Physical activity was assessed monthly using the Physical Activity Questionnaire (PAQ).

Subjects performed a ramped IMPF effort over five seconds with the knee flexed at ninety degrees in a water bath chamber (Figure 1). A force transducer and lever system were used to quantify IMPF torque. A dual probe ultrasound system (US) was used to quantify AT length. Force and ultrasound data were collected simultaneously.

Three trials with the greatest IMPF torque were analyzed. The calcaneus-tendon (CT) and the

gastrocnemius-tendon (GT) junctions were digitized from images obtained from the distal and proximal US probes, respectively (Figure 1). AT rest length was calculated from the known distance between probes and the relative locations of the digitized CT and GT junctions with muscles relaxed. Peak AT deformation was calculated as the change in AT length from rest to IMPF. Peak AT deformation was divided by AT rest length to calculate peak AT strain. AT force was calculated by dividing IMPF torque by the AT moment arm length. Lastly, the ratio of percent change of AT rest length to percent change of shank length from month 0 to month 6 was calculated (AT:shank).

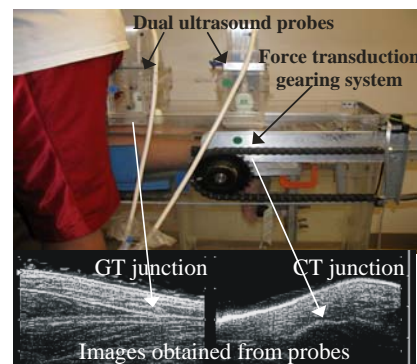


**Figure 1.** Water bath and dual-probe US testing.

Differences in peak AT strain, peak AT force, and AT rest length at 0 mos and 6 mos were determined using repeated measures ANOVA. Significance was defined at  $p < 0.05$  (R, R Foundation for Statistical Computing, Austria). Differences in height, shank length, and PAQ were determined using repeated measures t-tests. Mixed effects linear regressions (to account for repeated measures) were used to identify factors that significantly effected changes in AT strain. The proposed model included peak AT force, sex, AT:shank, and physical activity level as fixed effects.

## RESULTS AND DISCUSSION

The purpose of this study was two-fold: (1) to assess if peak AT strain changed over 6 months, and

(2) to identify factors that may explain the differences in peak AT strain. Increased strain was hypothesized to result from an increase in muscle strength that occurs without a temporally matched change in material and/or structural properties of the AT. We expected the shank growth rate to be faster than AT growth rate, leading to chronic tension in the AT. This would cause the AT to operate over a stiffer portion of its force-length curve and therefore strain less during IMPF. However, we hypothesized that the muscle strength gains would result in greater deformation of the AT and therefore greater strain. We also hypothesized that sex and physical activity levels would influence AT material properties and peak strain.

Peak AT strain increased during the study ( $p < 0.01$ ) (Figure 2). Physical activity levels (Average PAQ  $2.34 \pm 0.34$ ) and the ratio of AT length to shank length did not differ over the course of the study or between sexes ( $48.0 \pm 6\%$  to  $48.3 \pm 4.7\%$ ). Height was significantly different between the start and end of the study, but growth rate did not differ between sexes (Males:  $162.2 \pm 7.5$  to  $165.6 \pm 7.0$  cm; Females:  $149.2 \pm 8.0$  to  $153.2 \pm 7.8$  cm). Peak AT forces increased significantly over the course of the study, but were not different between sexes (790.3 to 884.7 N; standard deviations not reported because of repeated measures).

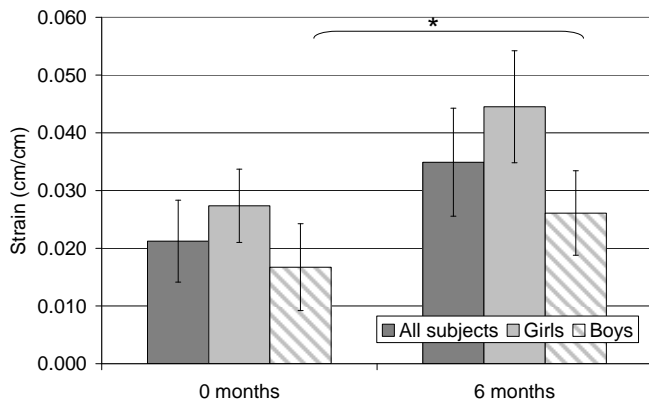


**Figure 2:** Peak AT strain for all subjects (\*,  $p < 0.01$ ) as well as boys and girls at start (0 months) and end of study (6 months).

Of the factors targeted to explain changes in peak AT strain, only sex was marginally significant ( $p = 0.054$ ). Peak AT forces, AT growth relative to shank growth, physical activity, and growth rate were not significant factors in explaining the increase in peak AT strain.

Increased peak AT strain was hypothesized to be due to increased muscle strength which would lead to greater tendon deformation during IMPF. Tendon material properties were expected to be delayed in adapting to the concurrent bone growth and muscle strength gains, leading to a chronic tension in the AT, evidenced by increased rest length and increased force in the AT with no muscle activation. Although AT force increased significantly over the course of the study, it was not significant in explaining the increased AT strain. Additionally, while the rest length of the AT increased significantly during the study, the force in the AT with no muscle activation did not change significantly. This suggests that the tendon was not under chronic load and lengthened to match bone lengthening, as further supported by the comparable ratios of AT length to shank length over the course of the study. Physical activity levels and calf circumference were both unchanged during the study, suggesting that increased strength resulted from changes in neural control or lower leg composition.

The results of this study suggest that increases in peak AT strain are not explained by increased AT force, growth rate, physical activity, or asynchronous changes in AT and shank length. Increases in peak AT strain differed for girls and boys suggesting a sex specific adaptation in the AT over the course of the study. These data represent 16 of 53 subjects enrolled in the study and with a larger data pool, further insight will be gained into the factors investigated. Future studies investigating hormone levels concurrent with tendon properties over a longer time of growth (1-3 years) would provide further insight into the adaptation of AT properties in youth.

## REFERENCES

1. Emery CA. Clin J Sport Med **13**, 256-68, 2003.
2. Frank JB, et al. J Am Acad Orthop Surg **15**, 356-66, 2007.
3. Berkey CS, et al. Stat Med **12**, 403-14, 1993.

## ACKNOWLEDGEMENTS

Many thanks to Katie Reinhardt for digitizing the ultrasound images and to Rosa Ferris and Kelsey Collins for their help with data collection.

# WRIST KINEMATICS FOLLOWING SCAPHOID-EXCISION FOUR CORNER FUSION

<sup>1,3,4</sup>Jennifer A. Nichols, <sup>4,5</sup>Michael S. Bednar, <sup>5</sup>Ajay K. Balamam,  
<sup>4,5</sup>Robert M. Havey, and <sup>1,2,3,4</sup>Wendy M. Murray

Departments of <sup>1</sup>Biomedical Engineering and <sup>2</sup>PM&R, Northwestern University, Chicago, IL

<sup>3</sup>SMPP, Rehabilitation Institute of Chicago, Chicago, IL

<sup>4</sup>Edward Hines Jr. VA Hospital, Hines, IL; <sup>5</sup>Loyola University Medical Center, Maywood, IL  
email: [jnichols@u.northwestern.edu](mailto:jnichols@u.northwestern.edu) web: <http://www.smpp.northwestern.edu/Murray/index.shtml>

## INTRODUCTION

In the United States, approximately 1 in 7 people suffer from wrist arthritis [1]. Patients with wrist arthritis experience severe pain. One of the most reliable ways to reduce pain is surgical intervention. One operation that is commonly used to treat wrist osteoarthritis is scaphoid-excision four corner fusion (SE4CF) [2]. During SE4CF, the scaphoid is removed and the lunate, triquetrum, capitate, and hamate are fused together. Fusion eliminates motion between the carpal rows and creates a wrist joint in which motion occurs between the radius and a single, rigid block of carpal bones.

Despite its success in relieving pain, SE4CF results in a permanent decrease in wrist range of motion and grip strength compared to the nonimpaired wrist [2]. The ability to maintain wrist extension, in particular, is essential for hand function. For example, maximum grip force is produced when the wrist is extended [3]. Additionally, many activities, such as opening a jar or picking up small objects, are more difficult if wrist extension is impaired [4].

We hypothesize that changes in wrist kinematics induced by SE4CF limit wrist extension. In this study, we simulated SE4CF to evaluate if geometric alterations imposed by the surgical reconstruction influence the capacity to maintain wrist extension.

## METHODS

We developed a kinematic model of the wrist following SE4CF by adapting a validated model of the upper limb [5]. To our knowledge, wrist kinematics following SE4CF have not been quantified. Importantly, experimental measurements in the nonimpaired cadaveric wrist [6] describe the overall motion of the wrist as being distributed

across the radiocarpal joint (defined by the motion of the lunate relative to the radius) and the midcarpal joint (defined by the motion of the capitate relative to the lunate). Because SE4CF removes motion at the midcarpal joint and does not directly disturb the articulation between the radius and the lunate, we assumed that the kinematics of the nonimpaired radiocarpal joint define wrist motion following SE4CF.

To evaluate the implications of SE4CF for maintaining an extended wrist, we calculated the torque necessary to maintain 30° wrist extension using the SE4CF model and compared it to the torque necessary to maintain that position for the nonimpaired model. 30° wrist extension was defined as a 30° angle between the long axes of the third metacarpal and radius. This definition enabled us to replicate an identical posture in the two kinematic models, and is comparable to measurements in clinical assessments. The mass of the hand was defined to be consistent with a 50<sup>th</sup> percentile male [7], and the limb was positioned such that gravity opposed wrist extension.

To enable direct comparisons between wrist torques calculated from models with different axes of rotation, the torques resulting from our simulations were decomposed into components about a standard reference frame (Fig. 1). In this reference frame, x is the radial-ulnar axis, y is the proximal-distal axis and z is the palmar-dorsal axis.



**Figure 1.** Standard reference frame, aligned with radius.

Finally, to test our assumption that wrist motion following SE4CF is determined by the kinematics

of the nonimpaired radiocarpal joint, we performed SE4CF in a single cadaveric specimen and measured the axes of rotation using a motion capture system (Optotrack 3020, Northern Digital Inc.). Following surgical reconstruction, we measured the position of the third metacarpal relative to the radius during passive motion of the wrist. A total of 5 trials incorporating flexion-extension, deviation, circumduction, the dart thrower's motion, and the reverse dart thrower's motion were collected. Data were input into a two-tiered optimization algorithm that was developed to calculate the axes of rotation of the nonimpaired wrist [8]. At least 5 initial guesses were processed for each trial. Convergence was sensitive to the initial guess; the mean axes of rotation were calculated from 7 optimization runs that converged and had a maximum residual less than 0.7.

## RESULTS AND DISCUSSION

Our simulations suggest that the magnitude of the torque necessary to maintain 30° wrist extension under static conditions increases with SE4CF (Fig. 2). The component of the torque about the radial-ulnar axis increased by 40 percent, while the component acting about the palmar-dorsal axis increased by 51 percent.

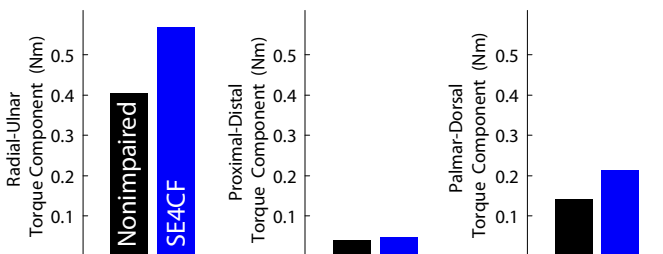


**Figure 2.** Magnitudes of the components of the torque necessary to maintain an extended wrist posture for the nonimpaired (black bars) and SE4CF (blue bars) models.

The increase in torque magnitude is directly related to the simulated axes of rotation. In the nonimpaired radiocarpal joint, the lunate ulnarly deviates (i.e., rotates about the palmar-dorsal axis) during wrist extension; motion at the midcarpal joint decouples

the motion of the lunate from hand motion [6]. Because fusion eliminates motion at the midcarpal joint, the SE4CF model requires a larger torque to achieve the “decoupling” between ulnar deviation and wrist extension.

The orientation of the flexion-extension axis simulated in the SE4CF model fell within the variability of the results from the 7 optimization runs; the orientation of the deviation axis did not (Table 1). Although the data from this specimen suggests that the motion of the lunate relative to the radius is affected by the surgery, the relatively large radial-ulnar component of the deviation axis suggests coupling between deviation and flexion-extension following midcarpal fusion.

## CONCLUSIONS

Surgical simulation of the SE4CF demonstrates that kinematic changes imposed by surgical intervention can substantially influence the torque necessary to maintain wrist extension. This has implications for wrist and hand function, which are known to be limited post-operatively.

## REFERENCES

- Lakshamanan, et al., <<http://emedicine.medscape.com/article/1245097-overview>>, 2010
- Bain & Watts, *J Hand Surg* **35A**, 719-25, 2010
- O’Driscoll et al., *J Hand Surg* **17A**, 169-77, 1992
- Adams, et al. *J Hand Surg* **28A**, 898-903, 2003
- Holzbaur, et al. *Ann Biomed Eng.* **33**, 829-40, 2005
- Ruby, et al. *J Hand Surg* **13A**, 1-10, 1988
- McConville et al. *Technical Report AFAMRL-TR-80-119*, 1980
- Sommer & Miller. *J Biomech Eng.* **102**, 311-17, 1980

## ACKNOWLEDGEMENTS

We would like to acknowledge our funding sources (NIH R01 HD046774, 5T32 HD007418-18, and the Searle Funds of the Chicago Community Trust) and Medcure for donation of the cadaveric specimen. Data was collected at the Musculoskeletal Biomechanics Laboratory at Edward Hines Jr. VA Hospital with assistance from Dongkeun Lee and Vikram Darbhe.

**Table 1. Orientation of Wrist Axes of Rotation\***

| Axis              | SE4CF      | Radial-Ulnar (x) | Proximal-Distal (y) | Palmar-Dorsal (z) |
|-------------------|------------|------------------|---------------------|-------------------|
| Flexion/Extension | Model      | 0.956            | -0.252              | 0.147             |
|                   | Experiment | 0.992 ± 0.056    | -0.099 ± 0.285      | 0.081 ± 0.150     |
| Deviation         | Model      | -0.819           | -0.136              | -0.557            |
|                   | Experiment | 0.478 ± 0.460    | 0.336 ± 0.325       | -0.812 ± 0.169    |

\*Mean and standard deviations are reported for the experimental results for the 7 optimization runs that converged.

# Validation of a real-time markerless tracking system for clinical gait analysis - ad hoc results -

<sup>1</sup>Kai Daniel Oberländer, <sup>1</sup>Gert-Peter Brüggemann

Institute of Biomechanics and Orthopaedics, German Sport University Cologne, Germany  
email: k.oberlaender@dshs-koeln.de

## INTRODUCTION

Gait analysis in clinical applications is generally carried out using a retro-reflective marker based (MB) approach with reconstruction and calculations of a subject's 3-dimensional kinematics and kinetics in the laboratory space. An expert spends a considerable amount of time identifying anatomical landmarks by palpation and attaching markers on the skin. For this purpose, participants are often asked to remove their clothing, resulting in an uncomfortable situation. Motion analysis techniques, which are less time consuming, contactless, require fewer skills, and do not disturb the subject, would be favorable in clinical applications. Several markerless (ML) tracking techniques have been recently presented and may play an important role in addressing this topic [1, 2]. In order to identify the applicability and accuracy of an ML-tracking in clinical gait analysis, we compare a state-of-the-art ML-system with both an MB approach and the internal sensor output of a knee joint prosthesis, by simultaneously acquiring the same walking path.

## METHODS

A male subject with a left-leg prosthesis (Genium, Otto Bock, Germany) participated in the study. The subject walked at a self-selected speed over a distance of 6 m. In order to get relevant information, fifteen gait cycles of the subject's left leg were analyzed. Kinematic data for the MB-system were recorded using a 12 infrared camera system operating at 100 Hz (VICON™, Oxford, UK). For the ML-system category, we selected BioStage (Organic Motion Inc., NYC, USA) due to its commercial availability for clinical application. Post-processing was carried out using The MotionMonitor® (IST, Inc., Chicago, USA). The internal sensors of the Genium leg prostheses (GE)

operate at 50 Hz and measure kinematic and kinetic parameters. Joint angle calculations for the MB-System were performed using a self-devised optimized soft tissue deformation model for lower extremities, realized in MATLAB (xxx,xxx,xxx) [3]. The BioStage system uses an internal full body model, based on simulated joint constraints. Its kinematic output was analyzed with The MotionMonitor® software by using the same angle conventions as in the MB-model. The GE-system measures the knee flexion angle with internal sensors and exports the data via WiFi. To ensure comparable results of the systems, all joint angles were normalized to a static reference. Synchronization was realized by heel-strike events, using forceplate information in the MB- and ML-systems as well as reported force data of the GE-system. Gait cycles were normalized to 100%. For a simplified notation, we define two sets:

$$\mathbf{J} = \{\text{ankle joint, knee joint, hip joint}\}$$
$$\mathbf{S} = \{\text{MB, ML, GE}\}$$

The average joint angles over the 15 gait cycles were calculated as follows:

$${}^u\alpha^k = 15^{-1} * \sum_{j=1}^{15} {}^u\beta_j^k \quad \text{with } k \in \mathbf{J}; u \in \mathbf{S}$$

where the subscript  $j$  refers to the  $j^{\text{th}}$  gait cycle of the joint angle  $\beta$ . In order to account for the offsets between two systems the absolute difference of the mean value of the average angles ( ${}^u\alpha^k$ ) were calculated:

$$\Delta^{u,v}\alpha^k = |{}^u\alpha^k - {}^v\alpha^k| \quad \text{with } u, v \in \mathbf{S}; u \neq v; k \in \mathbf{J}$$

In order to quantify the differences between the systems we calculated the root mean square deviation (RMSD) as well as the normalized root mean square deviation (nRMSD):

$${}^{u,v}\text{RMSD}^k = \sqrt{\frac{\sum_{i=1}^n ({}^u\alpha_i^k - {}^v\alpha_i^k)^2}{n}}$$

$${}^{u,v}\text{nRMSD}^k = {}^{u,v}\text{RMSD}^k * (\max({}^u\alpha_i^k) - \min({}^v\alpha_i^k))^{-1}$$

where the subscript  $i$  refers to the  $i^{\text{th}}$  frame. Pattern differences between the systems were quantified with Spearman's correlation coefficient:

$${}^{u,v}\rho^k = \text{spear}({}^u\alpha^k, {}^v\alpha^k)$$

where  $\text{spear}$  is a symbolic for the entire equation.

## RESULTS AND DISCUSSION

The average sagittal joint angles of the lower extremity during the gait cycles, estimated by the MB-, ML-system, and the GE- system for the knee joint, are reported in Fig. 1. The absolute difference of the mean value ( $\Delta\alpha$ ), the RMSD, the nRMSD and Spearman's  $\rho$  are reported in Tab. 1. The results indicate a good alignment of the ML-system compared to the MB-system as well as to the GE-system for the hip (nRMSD=0.04) and knee flexion (nRMSD=0.05). During the stance phase the ankle angle comparison showed a similar movement pattern, to the exception of an overshoot in the ML-system of approximately  $5^\circ$  in the first maximum

and minimum, compared to the MB-system. In the swing phase the ML-system showed a divergent pattern compared to the ankle angle results of the MB-system.

## CONCLUSIONS

In this report, we presented ad-hoc results of our validation study to identify the applicability and accuracy of a ML-system for clinical gait analysis. The results indicate that ML-systems may play an important role to address the above described restrictions of MB-systems due to a good alignment of the hip and knee angle results. Further investigation is needed to identify secondary plane kinematics.

## REFERENCES

1. Corazza S., et al *Annals of Biomedical Engineering* **34**:1019–29, 2006
2. Chu C.W. *Proc of IEEE Computer Society Conference on Computer Vision and Pattern Recognition*, Madison, USA, 2003
3. Oberländer K.D., et al *IFMBE Proc of 15. Nordic-Baltic Conference on Biomedical Engineering and Medical Physics*, Aalborg, Denmark, 2011

**Table 1:** Root mean square derivation (RMSD), normalized RMSD (nRMSD), absolute difference of the mean values ( $\Delta\alpha$ ) and Spearman's correlation coefficient ( $\rho$ ) are reported between results of the three systems.

|                | MB vs. ML   |            |           | GE vs. ML  | GE vs. MB  |
|----------------|-------------|------------|-----------|------------|------------|
|                | ankle angle | knee angle | hip angle | knee angle | knee angle |
| $\Delta\alpha$ | 0.26        | 0.9        | 0.6       | 0.9        | 0.0        |
| RMSD           | 2.5         | 3.4        | 1.9       | 3.4        | 1.0        |
| nRMSD          | 0.19        | 0.05       | 0.04      | 0.05       | 0.01       |
| $\rho$         | 0.89        | 0.93       | 1.00      | 0.94       | 1.00       |

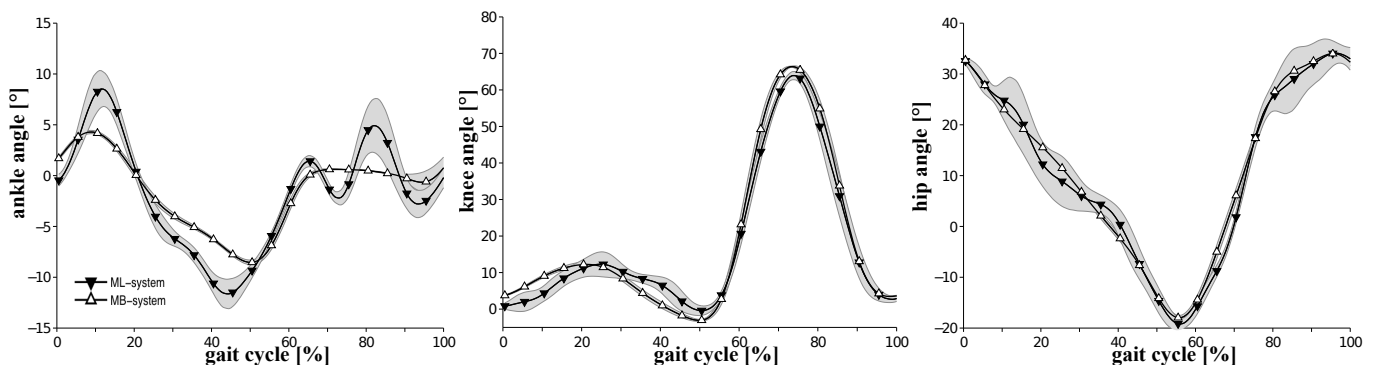


**Figure 1:** Average joint angles of 15 gait cycles for the lower extremity normalized to 100 %. (A: ankle angle; B: knee angle; C: hip angle; shadowed: standard deviation)

# MOTION ANALYSIS OF SIMULATED MINIMALLY INVASIVE SURGERY

<sup>1</sup>Ikechukwu Ohu, <sup>1</sup>Sohyung Cho, <sup>2</sup>Michael Awad and <sup>2</sup>Brent Matthews

<sup>1</sup>Industrial and Manufacturing Engineering, Southern Illinois University, Edwardsville, IL, USA

<sup>2</sup>Department of Surgery, School of Medicine, Washington University, St. Louis, MO, USA

Email: [scho@siue.edu](mailto:scho@siue.edu)

## INTRODUCTION

Surgical training and evaluation for minimally invasive surgery (MIS) have traditionally been an interactive and relatively slow process in which interns and junior residents perform operations under the supervision of faculty surgeons [1]. This training paradigm for MIS lacks objective means of quantifying and assessing surgical skills [2] and is unsustainable in the long run because it is still not well understood how surgeons learn and adapt to the unusual perceptual motor relationship in MIS. This study focuses on the relationship between surgeons' ability to orchestrate different body parts and surgical skill. Specifically, a novel model of real-time measures of surgical skill that can be dynamically updated during surgical exercises is developed and tested. This model that provides trainee with real-time feedback information on their performance can be used for improving quality of MIS training.

## METHODS

In this study, seven (7) subjects performed a surgical exercise (FLS intracorporeal suturing) using laparoscopic instruments on which a 3-dimensional motion sensor was attached. Each subject performed same surgical exercise with three (3) trials. The motion sensor was used to collect surgical motions in terms of roll, pitch and yaw angle, referred to as Euler angles. The collected data was then analyzed by using two well known tools based on complexity theory: (i) time-delay plot and (ii) Hurst exponent. The experimental setup consists of the following equipment:

- Bench-top laparoscopy trainer
- Laparoscopic tools
- Motion sensor kit (Xsens Technology®)
- An endoscope (for visual feedback during the MIS procedure)

## RESULTS AND DISCUSSION

As one of primary analysis tools, time delay plot was used to capture the topology of surgical motions focusing on the chaotic behavior in the surgical exercise. Figures 1 to 3 represent time-delay plots of roll angles for the first, second and third trial, respectively. It can be observed from the figures that there is a clear reduction in the range of the roll angles from the first to the third trial. For more details about reduction, refer to Table 1 that summarizes changes in swing angle and bandwidth of Euler angles for seven subjects. Here, swing angle represents the range of angles and bandwidth quantifies the thickness of diagonal band looking like time-delay plot. It is conjectured from the analysis of the plots that reduction in swing angle and bandwidth is caused by learning experience throughout three trials. It is expected that subjects try to minimize unnecessary movements using laparoscopic tools as the experience builds up.

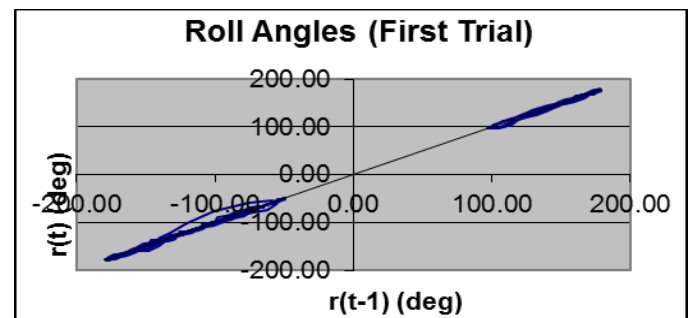


Figure 1: Time-delay plot of roll angles (1<sup>st</sup> trial).

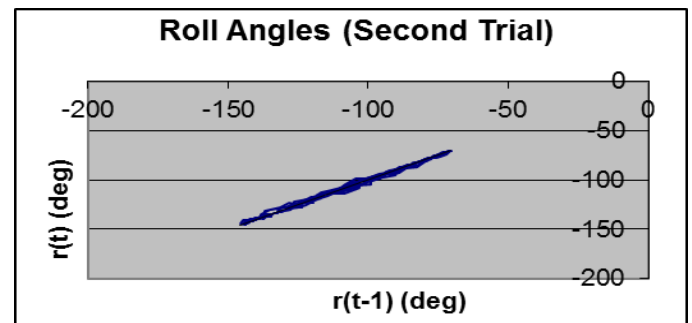
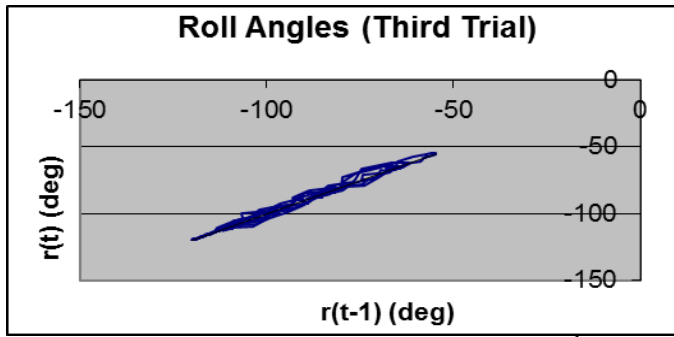
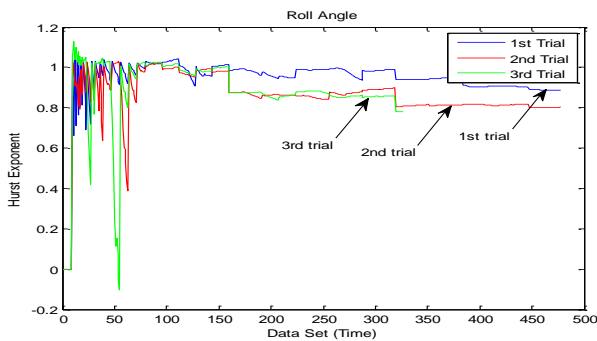


Figure 2: Time-delay plot of roll angles (2<sup>nd</sup> trial).



**Figure 3:** Time-delay plot of roll angles (3<sup>rd</sup> trial).

As another analysis tool, plots of Hurst exponents were used to capture significant differences in the degree of chaos during performing an identical surgical exercise as the number of trials increases. Figures 4, 5 and 6 show the real-time changes in Hurst exponents for roll, pitch and yaw angle, respectively. Figures clearly show the degree of chaos represented by Hurst exponents decreases as the experience builds up.



**Figure 4:** Real-time changes in Hurst exponent (roll angle)

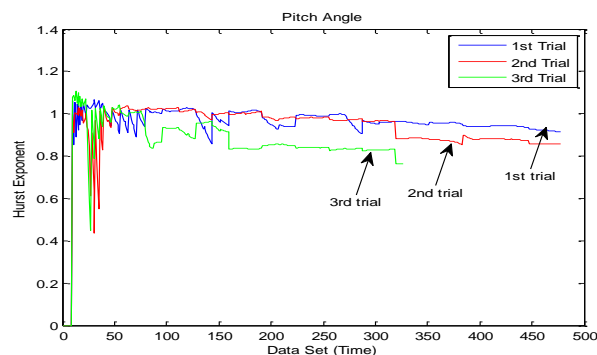


**Figure 5:** Real-time changes in Hurst exponent (pitch angle)

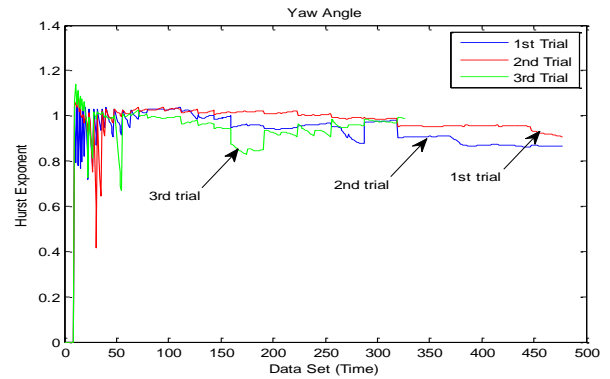


**Figure 6:** Real-time changes in Hurst exponent (yaw angle)

## CONCLUSIONS

The use of a time-delay plot with Hurst exponent as described in this study provides a novel method for assessing improvements in trainee movement efficiency during performance of laparoscopic tasks. These measures can be incorporated into low-cost surgical simulators that provide real-time, active feedback to learners. Ongoing studies are being performed to test the validity and reliability of this methodology.

## REFERENCES

1. Dankelman J, Wentink M, Stassen H. Human reliability and training in minimally invasive surgery. *Minimally Invasive Therapy & Allied Technologies* [serial online]. July 2003;12(3/4):129. Available from: Academic Search Complete, Ipswich, MA. Accessed March 2, 2011.
2. Salgado, J., Grantcharov, T., Pappasavas, P., Gagne, D., & Caushaj, P. (2009). Technical skills assessment as part of the selection process for a fellowship in minimally invasive surgery. *Surgical Endoscopy*, 23(3), 641-644. doi:10.1007/s00464-008-0033-7

**Table 1:** Average Swing Angles and Bandwidths of the Time Delay Plots for the Euler Angles

|           | ROLL        |          |          |           |          |          | PITCH       |          |          |           |          |          | YAW         |          |          |           |          |          |
|-----------|-------------|----------|----------|-----------|----------|----------|-------------|----------|----------|-----------|----------|----------|-------------|----------|----------|-----------|----------|----------|
|           | SWING ANGLE |          |          | BANDWIDTH |          |          | SWING ANGLE |          |          | BANDWIDTH |          |          | SWING ANGLE |          |          | BANDWIDTH |          |          |
| TRIALS    | 1           | 2        | 3        | 1         | 2        | 3        | 1           | 2        | 3        | 1         | 2        | 3        | 1           | 2        | 3        | 1         | 2        | 3        |
| MEAN      | 335.0555    | 262.5553 | 279.3327 | 22.57631  | 16.14939 | 15.78411 | 33.47501    | 30.21322 | 26.56483 | 9.390671  | 4.644257 | 6.087929 | 145.8256    | 136.4921 | 131.0265 | 11.84903  | 6.2334   | 7.215871 |
| AVE. DEV. | 147.5416    | 139.2499 | 131.228  | 9.541245  | 5.841673 | 9.651763 | 12.44155    | 7.289826 | 7.291545 | 5.754082  | 1.451392 | 4.144261 | 103.5162    | 106.9703 | 107.9637 | 8.137649  | 1.550857 | 2.529567 |

# RELATIONSHIP BETWEEN TORSO ROTATION AND GLUTEAL MUSCLE GROUP ACTIVATION IN BASEBALL AND SOFTBALL CATCHERS: SKELETALLY IMMATURE AND MATURE

Gretchen Oliver, Hillary Plummer and Priscilla Dwelly

University of Arkansas, Fayetteville, AR, USA  
email: [goliver@uark.edu](mailto:goliver@uark.edu)

## INTRODUCTION

Emphasis in the literature has begun to focus on the torso, and its role in dynamic human movement. When considering the anatomy of the lumbopelvic-hip complex, the torso is included. Lumbopelvic and torso efficient movement allows for optimal transfer of forces from the lower extremity to the upper extremity. In dynamic movement, it is imperative that one has proximal stability for distal mobility. It is the pelvis and torso that allow for the stable foundation for distal movement, specifically the gluteal muscle group which supplies the foundation for the pelvis and torso positioning.

It is known that as a part of the kinetic chain, the activations of the gluteal muscle group will affect the more distal segments of the lumbopelvic-hip complex [1]. However, the true dynamic manner of gluteal muscle activation and torso rotation has yet to be thoroughly researched. Furthermore, it is not known to what degree the gluteal muscle group is activated in the overhead throwing motion of a catcher throwing down to second base.

Overuse injuries as a consequence of physiological fatigue from repetitive stress and tissue adaptations that ultimately results in mechanical adaptations. With the rise in youth and adolescent throwing injuries, examination of the immature skeleton and its process of maturation are of concern. By understanding the muscle activation of the gluteal muscle group as well as torso kinematics in skeletally immature and mature catchers, pathomechanics may be identified in attempt to prevent injury. Therefore, the purpose of this study was to quantitatively analyze torso kinematics and gluteal muscle activations as well as the relationship between torso kinematics and gluteal activation from the position of shoulder maximum external rotation (MER) to ball release (BR) in skeletally

immature and mature catchers as they throw down to second base.

## METHODS

Forty-six competitively active baseball and softball catchers volunteered to participate. There were no differences between baseball and softball catchers on years of experience or age. Participants were divided into two categories of skeletally immature and mature. From the 46 participants we selected the youngest 10 participants ( $10 \pm 9$  yrs;  $144.3 \pm 10.3$  cm;  $38.7 \pm 10.8$  kg) and described them as skeletally immature and oldest 10 participants ( $18 \pm 2.4$  yrs;  $169.9 \pm 8$  cm;  $74.9 \pm 11.8$  kg) and described them as skeletally mature. All testing protocols were approved by the University's Institutional Review Board.

Location of bilateral gluteus maximus and medius were identified through palpation. Adhesive 3M Red-Dot bipolar (Al/AgCl) disk (6cm) surface electrodes were attached over the muscle bellies and positioned parallel to muscle fibers. Manual muscle tests were then conducted to establish baseline reading for each participant's maximum voluntary isometric contraction (MVIC) to within all sEMG data could be compared.

All sEMG data were transmitted to The MotionMonitor<sup>TM</sup> (Innovative Sports Training, Chicago, IL) through a Noraxon Myopac 1400L (Noraxon, USA, Inc, Scottsdale, AZ) eight channel amplifier. Signals were full wave rectified and smoothed based on the smoothing algorithms of root mean squared at windows of 1000ms, sampling at a rate of 1000 Hz and notch filtered at frequencies of 59.5 Hz and 60.5 Hz respectively.

In addition to sEMG data, kinematic data were collected using a series of 10 electromagnetic

sensors that were attached at the following locations: torso at C7; pelvis at S1; distal, posterior aspect of throwing and non-throwing humerus; distal, posterior aspect of throwing and non-throwing forearm; distal, posterior aspect of throwing and non-throwing side upper leg; and distal, posterior aspect of throwing and non-throwing side lower leg.

Participants then were given an unlimited time to warm-up. For collection, participants were pitched five fastballs from a pitcher located regulation distance. The participant was to catch the pitched ball and then throw down to second base in attempt to throw out a stealing base runner.

Data were analyzed at the events of foot contact (FC), MER, BR, and maximum shoulder internal rotation (MIR).

## RESULTS AND DISCUSSION

Means of sEMG (Figures 1-2) and torso kinematics are presented (Figure 3). Pearson product moment correlations revealed significant relationships between right gluteus maximus ( $r=.66, p=.004$ ), medius ( $r=-.57, p=.02$ ) and left gluteus maximus ( $r=.67, p=.003$ ) and torso rotation in skeletally immature catchers. While no significant relationships existed between the torso rotation and gluteal activation in the skeletally mature catchers.

## CONCLUSIONS

Data reveal although there were significant relationships between gluteal activation and torso rotation in immature catchers, it is speculated that they rotated their torso early in the throwing motion based on the quantitative kinematic torso data. In addition, the lack of relationship between torso rotation and gluteal activation, in the mature catchers identify the lack of posterior chain utilization in the throwing motion. Lack of torso control as evident of early rotation, as well as lack of total kinetic chain sequencing ultimately results in more emphasis placed on the upper extremity. With more performance emphasis placed on the upper extremity, injury propensity could possible increase. These data are the first to be reported for catchers, thus further research is needed to verify these data as well as identify injury implications.

## REFERENCES

1. Putnam, CA. *J Biomech* 26, S125-135, 1993.

## ACKNOWLEDGMENTS

The authors would like to acknowledge the financial support of the University of Arkansas Women's Giving Circle.

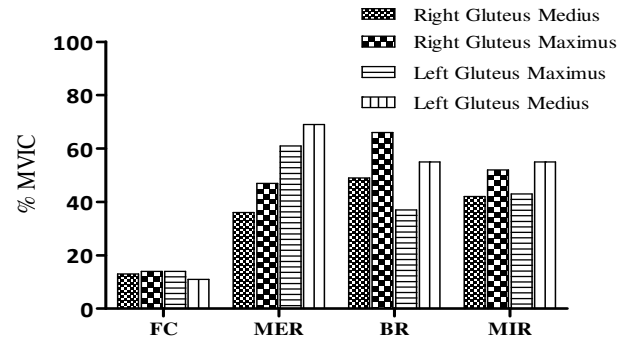


**Figure1.** Skeletally immature muscle activation represented as mean %MVIC for each throwing phase.

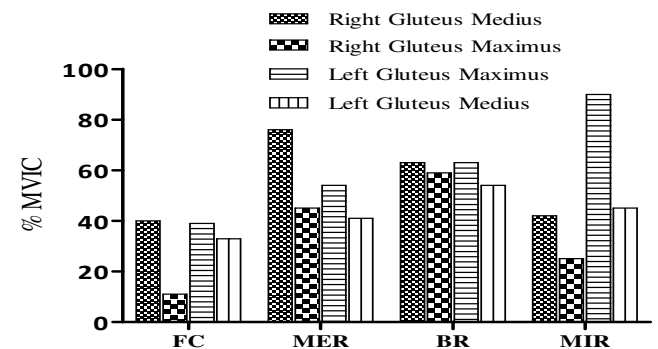


**Figure2.** Skeletally mature muscle activation represented as mean %MVIC for each throwing phase.

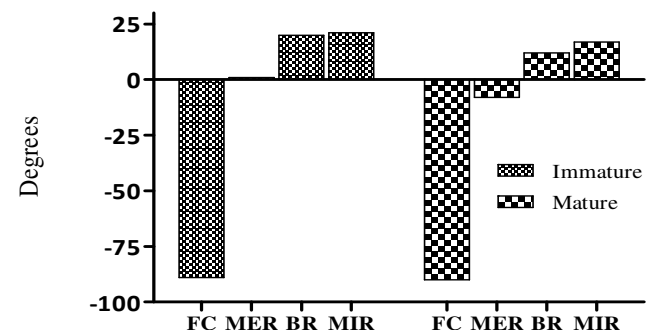


**Figure3.** Torso axial rotation in skeletally immature and mature catchers.

# EFFECT OF PRIOR TESTING ON THE PLANTAR SOFT TISSUE SHEAR PROPERTIES

<sup>1,2</sup>Shruti Pai, <sup>1,2</sup>Paul T. Vawter, and <sup>1,2,3</sup>William R. Ledoux

<sup>1</sup>VA RR&D Center of Excellence for Limb Loss Prevention and Prosthetic Engineering, Seattle, WA  
<sup>2</sup>Mechanical Engineering and <sup>3</sup>Orthopaedics and Sports Medicine, University of Washington, Seattle, WA  
email: wrledoux@u.washington.edu, web: www.amputation.research.va.gov

## INTRODUCTION

Plantar ulceration in the presence of diabetes can lead to amputation of the affected limb [1]. An estimated 15% of all diabetic individuals will develop a foot ulcer during their lifetime [2], affecting 3.6 out of 24 million diabetic Americans [3]. Developing treatments that can reduce plantar ulceration requires first understanding the disease induced tissue property changes under relevant plantar loading, i.e., compression and shear. Towards this effect, our group has to date evaluated diabetic changes in the compressive [4,5] as well as histomorphological [6] properties of the plantar soft tissue from paired cadaveric feet. Further, we intend to conduct shear tests on the specimens previously tested in compression to obtain the corresponding shear properties. However, it is unclear whether these previously tested specimens would provide representative or true shear properties since prior testing may have altered the tissue to an unknown extent. Hence, the purpose of this study was to test the effect of prior testing on the plantar soft tissue shear properties by comparing the results of paired specimens; one previously untested and one previously compression tested.

## METHODS

Plantar tissue specimens (n=8) were obtained from three fresh frozen non-diabetic older cadaveric feet (donors were  $77 \pm 4$  yrs and  $53 \pm 12$  kg). Paired specimens were obtained from the calcaneus and in one foot from the lateral midfoot as well. The tissue was dissected free from the underlying muscle and bone, punched into cylindrical specimens (19.1mm diameter), and further dissected from the skin to maintain *in vivo* thickness. One specimen from each pair was tested in unconfined compression using triangle waves at several frequencies and a ramp and hold per previous methods [4,5] while the other

specimen remained untested. Both specimens were frozen in preparation for shear testing.

The frozen specimens were re-punched (reduced to a 12.7mm diameter to prevent load cell overload) and cut (to prevent buckling) using a custom guillotine to a uniform initial thickness ( $4.40 \pm 0.25$ mm). Specimens were then placed in an environmental chamber at 100% humidity and 35°C and adhered to the shear tester platens (Mach-1, Biomomentum, Laval, QC) using cyanoacrylate. Since tissue properties are most relevant under biomechanically realistic loading, a static compressive strain of 45% was applied prior to shearing the tissue to emulate *in vivo* combined loading patterns. The target shear displacement was calculated as 147% of compressed thickness (81% of initial thickness) based on an estimated *in vivo* shear strain of 55.7° using fluoroscope images of barefoot running for an adult male [7]. The static compression was immediately followed by 14 triangle waves (to allow for preconditioning) at each frequency of 1, 2, and 3Hz and a 0.25s ramp and 300s hold to the target shear displacement.

The triangle data were used to examine nonlinear elastic parameters including peak stress, initial, toe, and final moduli, and energy loss. The relaxation force data were used to quantify several viscoelastic parameters (not fit coefficients due to limitations of current models for the plantar soft tissue and since the fitting process is a potential source of error [5]). These parameters include curve slopes to quantify the relaxation rate at three time intervals, initial (t = 0 to 0.5s), mid (t = 10 to 15s), and end (t = 290 to 300s) and the normalized curve area to compare relative total relaxation. A two-sample t-test (two-tailed,  $\alpha = 0.05$ ) was used to determine the association between test groups (untested vs. compression tested) for all parameters (over all frequencies for the nonlinear elastic parameters).

## RESULTS AND DISCUSSION

Overall, the shear results for all specimens were quite variable as seen by large standard deviations (Tables 1 and 2). This variability appears to be donor based as specimens from two feet yielded opposite nonlinear elastic trends between test groups (Fig. 1, previously untested specimens yielded higher peak stress for A yet lower peak stress for B compared to compression tested ones).

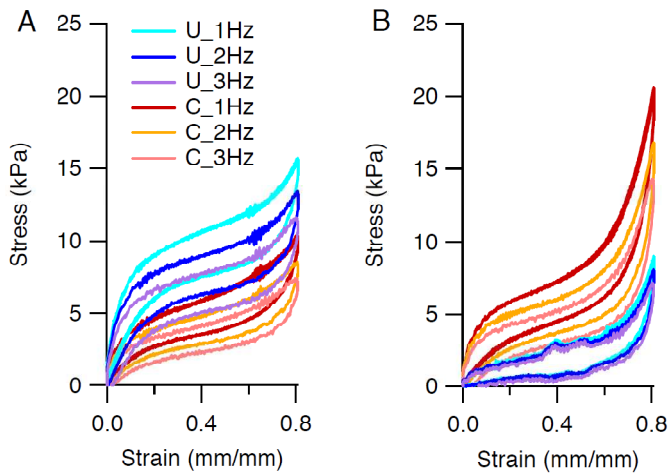


**Figure 1:** Sample stress-strain hysteresis curves showing variability between specimens from two different feet (A vs. B). U= previously untested, C= compression tested.

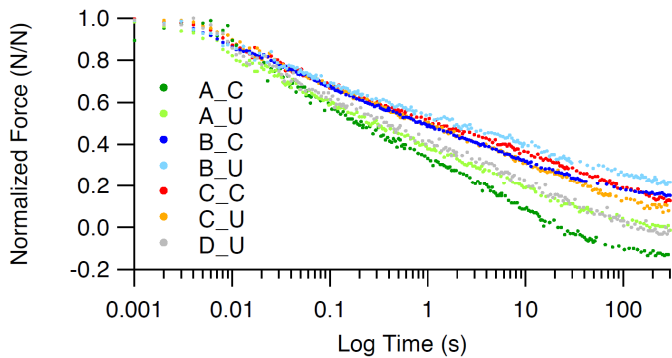


**Figure 2:** Stress relaxation curves for all four paired specimens. U= previously untested, C= compression tested. Note: D\_C was omitted due to excessive noise in data.

Comparison of both nonlinear elastic and

viscoelastic parameters between test groups revealed similar values (Fig 2, Tables 1 and 2). Thus, it appears that prior testing in compression has little effect on the plantar soft tissue properties.

**Table 2:** Mean [SD] viscoelastic shear data parameters obtained from stress relaxation curves.

| Parameter             | U              | C             | p*   |
|-----------------------|----------------|---------------|------|
| Peak stress (kPa)     | 4.5 [1.4]      | 6.1 [3.1]     | 0.44 |
| Initial slope (kPa/s) | -25 [6]        | -33 [16]      | 0.53 |
| Middle slope (kPa/s)  | -0.04 [0.01]   | -0.04 [0.02]  | 0.86 |
| End slope (kPa/s)     | -0.004 [0.004] | 0.001 [0.004] | 0.13 |
| Normalized area (s)   | 35 [31]        | 29 [48]       | 0.86 |

U= previously untested, C= compression tested, \*p<0.05 for two-sample t-test. Note: one compression tested specimen was omitted due to excessive noise in data.

Limitations of this study are that frequency test order was not randomized thereby confounding any trends between frequencies. Further, peak stress was less for the relaxation data compared to the hysteresis data, possibly due to insufficient recovery time between test types. Finally, specimen orientation (anterior/posterior vs. medial/lateral) was not controlled which possibly contributed to variability of the data.

## REFERENCES

1. Van Schie CH, *Int J LE Wnds* 4(3), 160-70, 2005
2. Palumbo PJ, *Diabetes in America*, 401-408, 1995
3. CDCP, *Nat Diab Fact Sheet* Atlanta, GA: 2007
4. Pai S, *J Biomech* 43(9), 1754-1760, 2010
5. Pai S, *Ann Biomed Eng*, epub 2011
6. Wang Y-N, *Foot Ankle Int*, in press 2011
7. De Clercq D, *J Biomech* 27(10), 1213-1222, 1994

## ACKNOWLEDGEMENTS

This work was partially supported by VA RR&D grant A4843C and NIH grant 1R01 DK75633-03.

**Table 1:** Mean [SD] nonlinear elastic shear data parameters obtained from stress-strain hysteresis curves.

| Parameter             | 1Hz     |         | 2Hz     |         | 3Hz     |         | All frequencies |         | p*   |
|-----------------------|---------|---------|---------|---------|---------|---------|-----------------|---------|------|
|                       | U       | C       | U       | U       | C       | C       | U               | C       |      |
| Peak stress (kPa)     | 10 [4]  | 11 [6]  | 9 [3]   | 9 [3]   | 10 [5]  | 10 [5]  | 9 [3]           | 10 [5]  | 0.60 |
| Initial modulus (kPa) | 52 [47] | 55 [24] | 56 [49] | 58 [51] | 61 [32] | 58 [27] | 58 [51]         | 61 [32] | 0.87 |
| Toe modulus (kPa)     | 6 [2]   | 6 [2]   | 5 [1]   | 5 [2]   | 5 [2]   | 5 [2]   | 5 [2]           | 5 [2]   | 0.93 |
| Final modulus (kPa)   | 24 [10] | 28 [21] | 22 [9]  | 22 [8]  | 25 [18] | 26 [21] | 22 [8]          | 25 [18] | 0.56 |
| Energy loss (%)       | 45 [10] | 40 [11] | 47 [10] | 48 [10] | 43 [10] | 42 [11] | 48 [10]         | 43 [10] | 0.22 |

U= previously untested, C= compression tested, \*p<0.05 for two-sample t-test.

# KNEE EXTENSOR AND FLEXOR TORQUE – ANGLE – ANGULAR VELOCITY PROFILES FROM MAXIMAL VOLUNTARY AND ELECTRICALLY STIMULATED EFFORTS

<sup>1</sup>Matthew T.G. Pain, <sup>1</sup>Jinwoo Kim, <sup>1</sup>Fraser Young, and <sup>2</sup>Stephanie Forrester

<sup>1</sup>Sports Biomechanics and Motor Control Research Group, Loughborough University, UK

<sup>2</sup>Sports Technology Research Group, Loughborough University, UK

email: m.t.g.pain@lboro.ac.uk, web: www.lboro.ac.uk/departments/ssehs/org

## INTRODUCTION

The tetanic force – velocity relationship in isolated muscle fibres follows a well established profile characterised by an eccentric force plateau at approximately 1.5 – 1.9 times the isometric value, and a hyperbolic decay in force with increasing shortening velocity [3,4]. *In vivo* measurements of maximum voluntary (MVC) force – velocity show differences to the *in vitro* tetanic profile, with eccentric forces not increasing much above isometric and tending to decline with increasing lengthening velocity [1,6]. Using transcutaneous electrical stimulation to supplement maximum voluntary contractions increases eccentric knee extension torque to above MVC, but has no significant effect on concentric torque [1,6]. Constant stimulation levels that produce 40 – 60% of MVC were used by Dudley et al. [1] to reproduce a torque – velocity profile that was similar to the *in vitro* tetanic profile; the eccentric torque plateaued at 1.4 times the isometric value and did not drop off at higher eccentric velocities. Pain and Forrester [5] used a wider range of knees extension velocities and looked at correcting the torque – velocity profile using normalized, wavelet transformed EMG, and found that the theoretical maximum eccentric was 1.6 times isometric.

The aim of this study was to determine maximal voluntary and electrically evoked torque – angle – angular velocity profiles for the knee extensors and flexors in a group of healthy males.

## METHODS

Fourteen male subjects (age  $23 \pm 2$  yrs, body mass  $77 \pm 7$  kg, height  $178 \pm 6$  cm) gave informed consent. A set protocol was completed on an

isovelocity dynamometer (Con-Trex, CMV AG, Switzerland). The protocol consisted of maximal voluntary and sub-maximally stimulated eccentric and concentric knee extension and flexion series at constant angular velocities ( $\pm 100, 200, 300, 400$  and  $50^\circ/s$ ) through a range of motion from  $100$  to  $5^\circ$  for quadriceps and  $5$  to  $90^\circ$  for hamstrings. Isometric torque was measured at 5 angles equally distributed across the range of motion. To determine more accurate joint angular velocities, trials at  $200$  and  $400^\circ/s$  for each subject were videoed at  $200$  fps to calculate joint-crank angle offsets, and extrapolated to the other velocity trials.

Transcutaneous electrical stimulation of the quadriceps and hamstrings was achieved using a stimulator (DS7AH, Digitimer Ltd., UK) that produced square wave impulse trains of single pulse duration  $100 \mu s$  at  $50$  Hz. Two carbon-rubber electrodes ( $140 \text{ mm} \times 100 \text{ mm}$ ; Electro-Medical Supplies, Greenham, UK) were taped over the RF, VL and VM or the hamstrings. Stimulation began at a current of  $40 \text{ mA}$  and increased in steps of between  $10$  and  $30 \text{ mA}$  until the desired level of torque was achieved. Dynamometer and stimulator data were recorded simultaneously with Spike2 software. Evoked extensor torques were set at  $\sim 35\%$ , and flexors at  $\sim 20\%$  of MVC.

Peak isometric torque was compared to the peak eccentric torque (Ecc/Iso) for the different muscle groups and conditions on a per subject basis. Due to the poor quality of the voluntary eccentric data the single highest average eccentric value from a velocity trial, irrespective of whether it was a high or low velocity trial, was used and called the raw method. Due to the inherent noise and reliability issues with dynamometer testing, subject specific data sets for each condition and muscle group were

further analysed in Matlab using the protocol of Forrester et al. [2] to produce torque – angle – angular velocity profiles which better describe the underlying physiological performances and called the fitted method. Group data for Ecc/Iso were compared between conditions, but not across methods, using a paired t-test ( $P < 0.05$ ) for both the raw data and fitted data.

## RESULTS AND DISCUSSION

Adjusting the crank data to joint data was essential as the initial and range of angles and angular velocities could differ by  $\sim 15^\circ$ ,  $\sim 20^\circ$  and up to  $\sim 50^\circ/s$  respectively, thus preventing serious errors in determining the torque – angle – angular velocity data points. There were no major fatigue effects (retest values between 0 and 9% drop with the norm being  $<5\%$ ). As can be seen in Figure 1 the raw data for the evoked trials appears to follow the *in vitro* tetanic pattern much more closely than the voluntary trials. As in earlier studies the voluntary eccentric torques dropped off with increasing velocity, and this occurred for both extensors and flexors. The mean Ecc/Iso values for voluntary activation and electrically evoked trials are presented in Table 1. There was no significant difference between the extensor and flexor Ecc/Iso values for voluntary activation but there was for the evoked condition with flexors less than extensors.

At the highest eccentric velocities, where torque has not previously been measured, the voluntary drop off became increasingly rapid. This meant that the maximum voluntary eccentric torques typically occurred at  $-50$  or  $-100^\circ/s$  and were more variable than those determined from the fitted method. The effect of this can be seen in the standard deviation values in Table 1. Given the ranges and variability of the raw data it was considered that the fitted method gave a more consistent and reliable set of results with regard to determining Ecc/Iso. For the evoked extensors an Ecc/Iso of 1.61 was almost identical to the EMG corrected value found in Pain and Forrester [5] for the knee extensors. Both the evoked flexor and extensor values were higher than those reported by Dudley [1]. This may be unsurprising for two reasons: in this case torque was measured at much higher eccentric velocities; and the fitting procedure also gives an extrapolated eccentric maximum value. Our values fall more in line with the *in vitro* tetanic values in the literature.

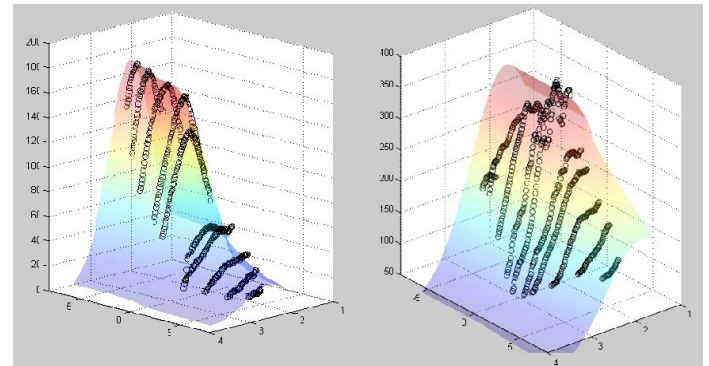


**Figure 1.** Torque (NM) - angle (rad) - velocity (rad/s) knee extensor data for one subject. Parameter surfaces, in colour, fitted to evoked (left graph) and voluntary (right graph) raw torque data shown by black circles.

**Table 1.** Ecc/Iso ratios - group mean and SD for flexors and extensors, voluntary and evoked.

\*  $\Rightarrow P < 0.05$ .

|        |      | Knee extensors |        | Knee flexors |        |
|--------|------|----------------|--------|--------------|--------|
|        |      | Voluntary      | Evoked | Voluntary    | Evoked |
| Raw    | Mean | 0.96           | 1.84*  | 1.01         | 1.48*  |
|        | SD   | 0.11           | 0.38   | 0.17         | 0.25   |
| Fitted | Mean | 1.11           | 1.61*  | 1.06         | 1.50*  |
|        | SD   | 0.09           | 0.08   | 0.03         | 0.22   |

## CONCLUSIONS

Electrically evoked Ecc/Iso ratios in the knee extensors and flexors were 1.61 and 1.50, respectively, with the extensor value found here higher than previously measured across lower velocity ranges [1].

## REFERENCES

- Dudley GA et al. *Journal of Applied Physiology*. **69**; 2215–2221, 1990.
- Forrester SE et al. *Journal of Biomechanics*. DOI: 10.1016/j.jbiomech.2010.11.024.
- Harry JD et al. *Biophysical Journal*. **57**; 201–208, 1990.
- Hill AV. *Proceedings of the Royal Society of London. Series B*. **126**; 135–142, 1938.
- Pain MTG and Forrester SE. *Journal of Biomechanics*. **42**; 1598–1603, 2009.
- Westing SH et al. *Acta Physiologica Scandinavica*. **140**; 17–22, 1990.

# VASTUS LATERALIS:VASTUS MEDIALIS ACTIVATION RATIO CORRELATES WITH VASTUS MEDIALIS ACTIVATION DELAY AND PATELLAR MALTRACKING IN PATELLOFEMORAL PAIN PATIENTS

<sup>1</sup>Saikat Pal, <sup>2</sup>Thor Besier, <sup>1</sup>Christine Draper, <sup>1</sup>Michael Fredericson,

<sup>1</sup>Garry Gold, <sup>1,3</sup>Gary Beaupre, and <sup>1</sup>Scott Delp

<sup>1</sup>Stanford University, Stanford, CA; <sup>2</sup>University of Auckland, NZ; <sup>3</sup>VA PAHCS, Palo Alto, CA

email: [spal5@stanford.edu](mailto:spal5@stanford.edu)

## INTRODUCTION

Vasti muscle activation imbalance is considered a common cause for patellar maltracking in patellofemoral pain (PFP) subjects. Vasti activation imbalance can be evaluated by measuring vastus medialis (VM) activation delay compared to vastus lateralis (VL) activation [1], and normalized VL:VM activation ratio [2]. Measurement of VM activation delay during functional tasks such as walking or running requires synchronization of electromyography (EMG) data with joint kinematics and ground reaction forces (GRF) [1]. These measurements are impractical in most clinical settings. However, VL:VM activation ratio can be obtained by simply placing surface electrodes on a patient while performing the functional tasks during clinical evaluation, and may be a surrogate measure for VM activation delay. The **first aim** of this study was to investigate the relationship between VL:VM activation ratio and VM activation delay in PFP subjects and pain-free controls. Next, evidence relating VL:VM activation ratio to patellar maltracking is sparse. The **second aim** was to investigate the relationship between VL:VM activation ratio and patellar maltracking measured under upright, weightbearing conditions.

## METHODS

We recruited 54 subjects; 39 (18M, 21F) had chronic PFP (> 3 months) but no prior surgery or knee injuries and 15 (7M, 8F) served as pain-free controls. All subjects were between 18-42 years of age, and there were no statistical differences in age, height or weight between gender-specific controls and PFP subjects. The PFP subjects were diagnosed by an experienced clinician.

We measured VL:VM activation ratio and VM activation delay in all subjects during walking at self-selected speeds in a gait laboratory (Fig. 1A).

All subjects performed a minimum of three trials. Acquired EMG activity, lower-limb kinematics, and GRF data were synchronized. Vasti activation onsets during the swing phase prior to heel strike were determined using a threshold function. A muscle was determined to be “on” if its EMG signal exceeded the greater of 3 standard deviations of its resting EMG value or 2% of the larger peak activation between the VM and VL muscles [1]. Vastus medialis activation delay was calculated as the difference between the VL and VM activation onset times; VL:VM activation ratio was determined from peak normalized activity over the entire gait cycle.

All subjects were classified into normal tracking and maltracking groups based on their patellar tilt and bisect offset measures obtained from weightbearing magnetic resonance imaging (MRI) (Fig. 1B) [1]. Images were obtained using a 0.5T Signa SP open-MRI scanner (GE Healthcare) fit with a backrest to stabilize a subject in an upright position (knee flexed  $\sim 5^\circ$ ). An oblique-axial plane image intersecting the center of the patella and the most posterior points of the femoral condyles was

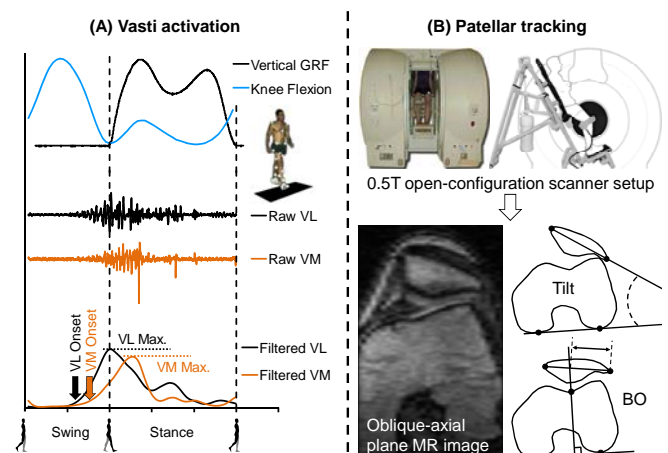


**Figure 1:** Measurement of (A) VM activation delay relative to VL activation, and VL:VM activation ratio, & (B) patellar tracking measures, tilt & bisect offset (BO), during an upright, weightbearing squat.

identified from the MRI volume. Patellar tilt is a measure of the angle between the patella and the posterior femoral condyles. Bisect offset is a measure of the medial-lateral position of the patella relative to the femur. A gender-specific classification using a non-Gaussian Weibull distribution with 75% confidence intervals was used to determine thresholds for patellar maltracking. A subject was classified as a maltracker if his/her patellar tilt or bisect offset value was in the highest quartile of measured population data [1].

## RESULTS

VL:VM activation ratio displayed a significant relationship with VM activation delay in PFP subjects classified as maltrackers (Fig. 2). There were no correlations between VL:VM activation ratio and VM activation delay in the pain-free controls, all PFP subjects grouped together, and PFP subjects classified as normal trackers.

VL:VM activation ratio displayed a significant relationship with patellar tilt in PFP subjects classified as maltrackers (Fig. 3). There were no correlations between VL:VM activation ratio and patellar tracking measures in the pain-free controls, all PFP subjects grouped together, and PFP subjects classified as normal trackers.

## CONCLUSIONS

The results of this study suggest that VL:VM activation ratio may be a surrogate measure for VM activation delay in PFP subjects classified as maltrackers. This study demonstrates a significant relationship between VL:VM activation ratio and

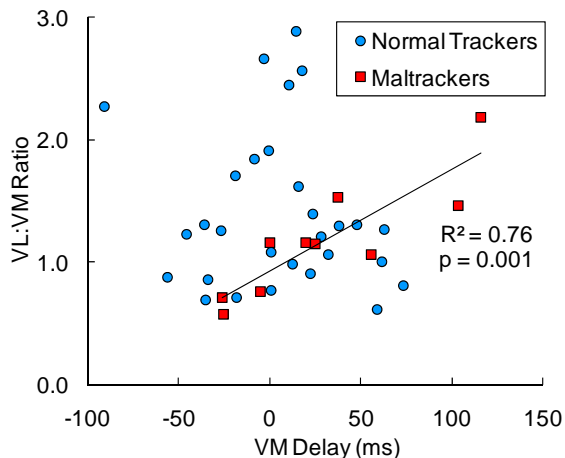


**Figure 2:** Relationship between VM activation delay and VL:VM activation ratio in PFP subjects classified as normal trackers and maltrackers.

patellar tilt in maltracking PFP subjects, providing evidence in support of the role of vasti activation imbalance on patellar maltracking. In PFP subjects classified as normal trackers, there were no clear relationships between VL:VM activation ratio and VM activation delay, or patellar tracking measures. A possible explanation is that vasti activation imbalance is one of several factors affecting patellar tracking. It is plausible that in normal tracking subjects, increased joint conformity [3] and well-functioning PF ligaments minimize the effects of vasti activation imbalance on patellar tracking.

Although we have identified a cost-effective method for diagnosing vasti activation imbalance, the classification of subjects is based on open-MRI, which is expensive and available in few clinics. We are evaluating alternate imaging modalities that are both accurate and cost-effective to classify subjects as part of standard clinical assessment.

This study has the potential for broad clinical impact. Accurate diagnosis of vasti activation imbalance and patellar maltracking during clinical assessment will help identify patients who will most benefit from interventions treating these mechanisms of PFP, such as VM strengthening and EMG biofeedback training.

## REFERENCES

1. Pal S, et al., *Am J Sports Med* 39, 590-8, 2011
2. Powers CM, *Phys Ther* 80, 956-64, 2000
3. Wu SH, et al., *J Rehabil Med* 40, 381-6, 2008

## ACKNOWLEDGEMENTS

VA R&D Service (#A2592R), NIH (EB005790-05)

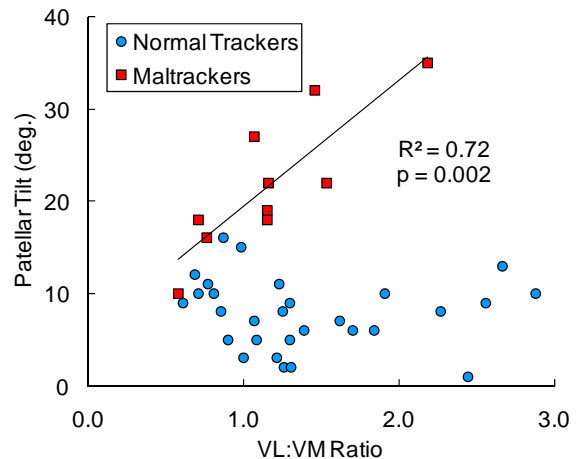


**Figure 3:** Relationship between VL:VM activation ratio and patellar tilt in PFP subjects classified as normal trackers and maltrackers.

# Kinematic methods for determining gait events during level and slope walking in the cat

Annette Pantall and Boris I. Prilutsky

Georgia Institute of Technology, Center for Human Movement Studies, Atlanta, GA, USA  
email: [annette.pantall@ap.gatech.edu](mailto:annette.pantall@ap.gatech.edu) web: <http://www.ap.gatech.edu/Prilutsky/>

## INTRODUCTION

Analysis of gait generally requires that the gait data are temporally segmented into cycles. The gold standard for determining time events for partitioning the data is based on the ground reaction forces (GRF) recorded from force plates. However, this method limits the number of cycles available for analysis. Estimating timing events from kinematic data increases that number. Kinematically derived gait event times have been obtained from visual inspection of the motion capture data [4, 5] or by application of algorithms that automatically determine the timing events from limb displacement, velocity or acceleration.

The advantage of using an algorithm over visual inspection methods is that it is time efficient and eliminates error due to inter-examiner variability. Algorithms to determine gait timing events have been applied to human kinematic data for both treadmill and overground walking [1-3]. In quadrupeds, there is limited description of similar kinematically based algorithms. Observation of video frames is a commonly used method in this subject group [4, 5]. It is not known how locomotor conditions (speed and slope) and gait pathology affect accuracy of determining timing events.

This study aimed to investigate the effectiveness of different algorithms applied to kinematic data to determine gait timing events in feline gait, compared to GRF derived events. Additionally, the effect of different subjects, different slope conditions and measurement times pre- and post nerve surgery on the timing events was assessed.

## METHODS

All experimental and surgical procedures were approved by the Institutional Animal Care and Use Committee. For the purpose of this study, three

female adult cats were investigated. Each cat was trained to walk along level, upslope (+26°) and downslope (-27°) walkway with embedded force plates. Prior to recordings, small retroreflective markers were placed on the anatomical landmarks of the right hindlimb. In this study we focused on the position of the marker over the greater trochanter (GT) and the 5<sup>th</sup> metatarsophalangeal (MTP) joint. A 6-camera motion capture system (Vicon Motion Systems, UK, USA) recorded the marker positions at a sampling rate of 120 Hz. The ground reaction forces were recorded by three force plates at 360 Hz (Bertec Corporation, Columbus, OH, USA). As part of a larger study, the three cats all had nerves supplying two of the ankle extensors of their right hindlimb cut and repaired under sterile conditions and isoflurane anesthesia [6, 7]. Each cat had multiple walking trials recorded before and after surgery several times a week for at least 16 weeks.

Trials immediately prior to surgery, approximately 2 weeks post-, 6 weeks post- and 12 weeks post-surgery were analysed. All analysis was carried out in the Matlab environment. Firstly, 'gold standard' timings for paw-contact and paw-off were identified when the GRF rose above and fell below 0.5 N respectively (Fig 1a). Only stance phases with durations between 300-700 ms were considered. Four different methods plus a fifth method for paw-off were then applied to the filtered (zero-lag 2<sup>nd</sup> order critically damped filter, 10 Hz cut-off) kinematic data to determine paw-contact and paw-off, modified from algorithms for human gait [1-3]:

**Method 1.** Timing of maximum (paw-contact) or minimum (paw-off) MTP horizontal displacement relative to GT (DIFFx) (Fig 1b).

**Method 2.** Timing of MTP horizontal velocity (Vx) crossing a threshold of 0.18 m/s (Fig 1c).

**Method 3.** Timing of minimum (paw-contact) or maximum (paw-off) MTP vertical velocity ( $V_z$ ) (Fig 1d).

**Method 4.** Timing of local maxima in vertical acceleration ( $A_z$ ) of MTP (Fig 1e).

**Method 5.** Timing of maximum in horizontal acceleration ( $A_x$ ) of MTP (Fig 1f).

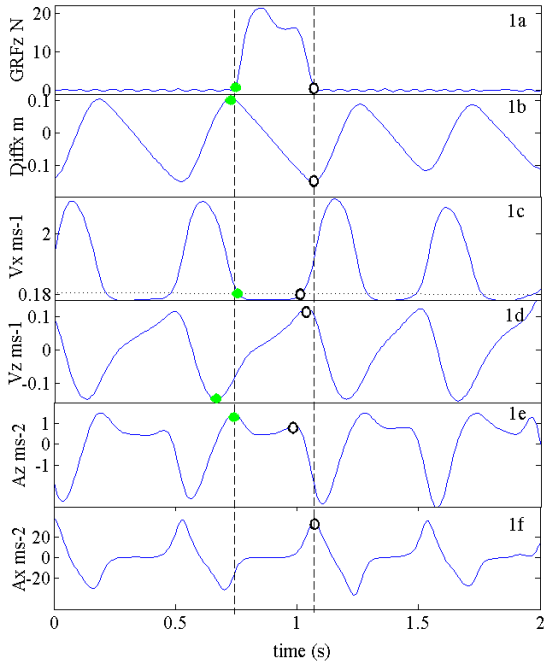


**Figure 1:** Vertical ground reaction force and five kinematic variables for a typical level walking trial. ● - paw-contact. ○ - paw-off.

## RESULTS AND DISCUSSION

A total of 792 step cycles were analyzed. There was a significant difference in the timing of paw-contact and paw-off determined from kinematics and ground reaction forces ( $p < 0.01$ ). There were significant effects of subjects, slope conditions and the time after surgery on the difference ( $p < 0.01$ ).

For paw-contact, Method 1 produced the smallest SD across all cats and measurement dates (Fig 2). The mean time difference between Method 1 and the GRF derived events however was 0.014 s. For slope conditions, Method 1 resulted in the smallest SD (0.011 s) for downslope, with Method 2 yielding the lowest SDs for both upslope (0.012 s) and level (0.011 s) conditions. Paw-contact determined by Method 1 was 0.016 s behind for downslope and upslope, and 0.025s behind for level. The algorithm with the greatest error over all cats, slope conditions and measuring dates was Method 4 (timing of vertical acceleration peaks), with the error  $-0.086 \pm 0.035$  s.

For paw-off, Method 1 produced the lowest SD (0.009 s) and lowest mean difference (0.005 s ahead of GRF paw-off) over all subjects, slope conditions and measurement dates. Mean systematic error was different for both subject and slope condition, with Subject C and upslope having the greatest errors of 0.009 s ahead of GRF timings. Similar SDs of the errors were found between times of measurements, 0.008 s pre-surgery and 0.009 s at 12 weeks. The mean systematic error in paw-off timing increased from +0.002 s pre-surgery to +0.005 s at 12 weeks after surgery. Method 4 produced the highest SD for subject, slope condition and measurement date, with an overall error of  $-0.008 \pm 0.014$  s.

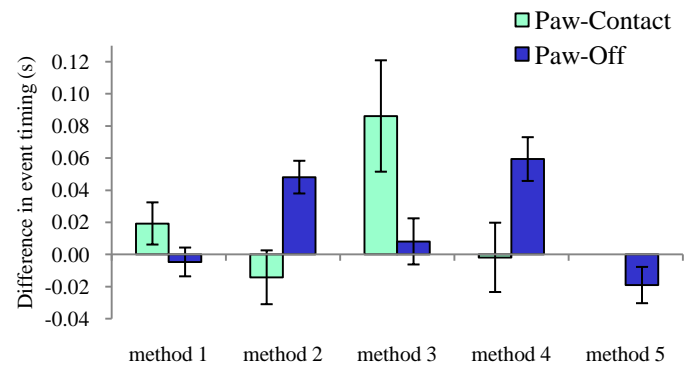


**Figure 2:** Mean difference in timing for paw-contact and paw-off compared to GRF derived timings for five kinematic algorithms.  $n=792$ .

Overall, Method 1 for both paw-contact and paw-off provided timing with the lowest SD or random error. This algorithm differs from the other four, in that it assesses the difference between two marker positions as opposed to the position of one marker relative to the laboratory co-ordinate system. In conclusion, one can determine the timing of events consistently using kinematics, although adjustments must be made to account for the systematic error.

## REFERENCES

1. De Witt JK. *J Biomech* **43**, 3067-3069, 2010.
2. O'Connor CM, et al. *Gait Posture* **25**, 469-474, 2007.
3. Hreljac A, et al. *J Biomech* **33**, 783-786, 2000.
4. Barriere G, et al. *J Neurophysiol* **104**, 1119-1133, 2010.
5. Thota AK, et al. *J Neurotrauma* **22**, 442-465, 2005.
6. Maas et al., *Exp Brain Res*, **181**, 377-393, 2007.
7. Prilutsky et al., *Cells Tissue Organs*, 2011 (In Press).

# ARE KNEE AND HIP JOINT MOTIONS AFFECTED BY A NEWLY DESIGNED CURVED-BOTTOM SHOE DURING LEVEL-WALKING?

Max R. Paquette, Songning Zhang, Clare E. Milner, Carolyn Westlake, Lucas Baumgartner, Erin Byrd

Biomechanics/Sports Medicine Lab, The University of Tennessee, Knoxville, TN, USA  
email: [mpaquett@utk.edu](mailto:mpaquett@utk.edu), web: [web.utk.edu/~sals/resources/biomechanics\\_laboratory.html](http://web.utk.edu/~sals/resources/biomechanics_laboratory.html)

## INTRODUCTION

Curved-bottom shoes (CB) such as MBT have garnered considerable interest in the footwear consumer market and footwear research [1,2,3,4]. Considerable kinematic and kinetic gait changes when wearing CB shoes have been reported at the ankle joint [2,3,4]. However, results from the literature on alterations at the knee and hip joints are not very consistent. *Reductions* in sagittal plane knee and hip peak angle and range of motion (ROM) during stance have been reported in middle-aged males and females [2]. In contrast, another study showed *increases* in peak hip extension in CB shoes during walking [4]. Nigg et al. [3] reported *no changes* in hip and knee kinematics and kinetics in CB shoes during walking. In addition, lower limb muscle activation in mid-stance, measured using electromyography (EMG), shows increased activation in knee extensors (vastus lateralis, vastus medialis, and rectus femoris) in CB compared to control shoes [1,2]. However, significant changes in knee and hip muscle activation were not observed in a separate study [3]. Therefore, the main objectives of this study were to compare a *newly designed* CB shoe (SH2: Active Balance™) with a control shoe (SH1: Glacier) on sagittal and frontal plane knee and hip kinematics and kinetics, and EMG of knee and hip flexor and extensor muscles during level walking at two different speeds.

## METHODS

Fifteen healthy males (age:  $41.1 \pm 4.6$  yrs, height:  $1.77 \pm 0.7$  m, mass:  $83.2 \pm 11.5$  kg) participated in this study. Before the start of experimental testing, participants were asked to walk in SH2 for 10 minutes in an indoor hallway to adapt to the shoes. A seven-camera motion analysis system (240 Hz, Vicon Motion Analysis) was used to obtain three-dimensional (3D) kinematic data while participants walked in the lab. Reflective anatomical and tracking markers were placed on the pelvis, the

right foot, ankle, leg, knee, and thigh. One force platform (1200 Hz, AMTI) was used to measure ground reaction forces (GRF) under the right foot. An EMG system (1200 Hz, Noraxon USA, Inc.) was used to monitor the long head of biceps femoris (BF) and rectus femoris (RF). Each participant performed five successful walking trials in each of the four testing conditions: walking at 1.3 m/s and 1.8 m/s wearing a flat-bottomed control shoe (SH1) and a curve-bottomed testing shoe (SH2). The shoe and speed conditions were randomized independently. All participants were given practice trials prior to each condition. Visual3D software suite (C-Motion, Inc.) was used to obtain the 3D kinematic and kinetic computations for the knee and hip joint and EMG measurement values. Joint moments were computed as internal moments. A right-hand rule was used to establish the 3D kinematics/kinetics conventions. The band-pass filtered EMG signals (20 and 450 Hz) were full-wave rectified and smoothed with a root-mean-square (RMS) filter. EMG signals were normalized to the maximum RMS value of the control shoe during walking at normal speed. The normalized EMG signals were then integrated (IEMG) from heel-strike (HS) to toe-off (TO) during the stance phase. A two-way (Shoe x Speed) repeated measures analysis of variance (ANOVA) was used to detect any differences between the two shoes and two speeds for each variable of interest (18.0, SPSS). Post hoc comparisons were performed using paired t-tests. The significance level was set at 0.05.

## RESULTS AND DISCUSSION

Both knee flexion and hip extension ROMs at the fast speed were greater than the normal speed. The hip mid-stance adduction ROM was greater for SH2 compared to the control shoe, and the fast walking speed induced a greater adduction ROM than the normal speed (Table 1). The increased hip mid-stance adduction ROM may be the result of dynamic coupling in response to greater ankle

eversion ROM in SH2 reported in our other abstract (Zhang et al., ASB 2011).

The joint kinetic results showed that the early stance peak knee extension moment (Mmt\_Ex) had a significant shoe and speed interaction and speed main effect (Table 1). The post hoc comparisons demonstrated that SH2 had greater early stance peak knee extension moment at the fast speed compared to SH1 and, greater peak extensor moment at fast speed compared to normal speed for both shoes. The late stance peak knee flexion moment (Mnt\_FL) was significantly smaller for SH2 compared to the control shoe and, at the normal walking speed compared to the fast speed. Early stance hip peak extension and late stance peak flexion moments showed no shoe main effect. These peak moments were significantly greater at the fast speed. The peak knee abduction moment (Mmt\_Abd) was not different between the shoes but greater in the fast walking speed compared to normal speed (Table 1). The peak hip mid-stance abduction moment, however, was greater in SH2 compared to control shoe and, at fast speed compared to normal speed. This greater peak abduction moment in SH2 follows our finding of increased hip mid-stance adduction ROM as hip abductor muscles must activate eccentrically to produce an abductor moment at the hip to counteract the larger hip adductor range of motion. The RF IEMG values were significantly smaller for SH2 compared to the control shoe and at the fast speed compared to normal speed (Figure 1). The EMG values in the current study were integrated for the entire stance period. Therefore, it may be difficult to associate the IEMG with instantaneous kinetic variables when interpreting the results. However, even with greater early stance peak extensor moment, previous research only found higher knee extensor (vastus lateralis) activation in mid and late

stance in obese males during walking in CB shoes [1]. The BF results did not show any significant difference between the shoes and speeds.

## CONCLUSION

The increased hip adduction ROM in the newly designed Active Balance appears to be the result of dynamic coupling from increased ankle eversion ROM and, counteracted by an increased peak hip abductor moment. The Active Balance also increased peak knee extensor (fast speed only) and flexor moment compared to the control shoe, which could be associated with increased knee extensor involvement. The results seem to suggest that the curved sole of the Active Balance alters frontal plane hip ROM and moment as well as sagittal plane knee moment.

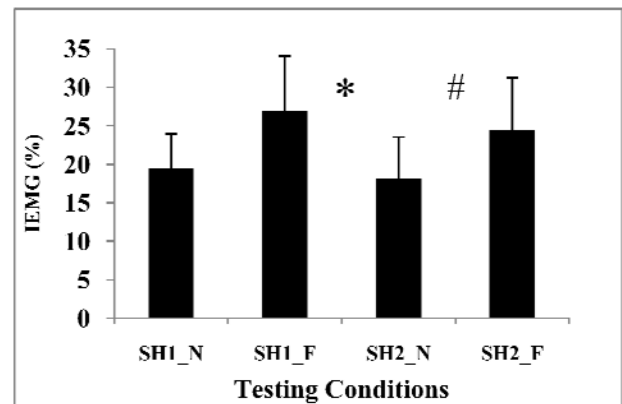


Figure 1. IEMG of rectus femoris in stance.

## ACKNOWLEDGEMENT

This study was sponsored by Genesco, Inc.

## REFERENCES

1. Buchecker et al. *Scan J Med Sci Sp Epub*, 2010.
2. Romkes et al. *Clin Biomech* **21**, 75-81, 2006.
3. Nigg et al. *Clin Biomech* **21**, 82-88, 2006.
4. Myers et al. *Gait Posture* **24**, 323-330, 2006.

Table 1. Knee and hip kinematics and kinetics variables: mean ± STD.

| Cond  | Hip Angle (Deg)       | Knee Moment (Nm/kg)        |                      | Hip Moment (Nm/kg)    |
|-------|-----------------------|----------------------------|----------------------|-----------------------|
|       | ROM_Add <sup>*#</sup> | Mmt_Ex <sup>&amp;#</sup>   | Mmt_FL <sup>*#</sup> | Mmt_Abd <sup>*#</sup> |
| SH1_N | 5.24±1.83             | 0.611±0.237                | -0.229±0.129         | -0.839±0.134          |
| SH1_F | 7.36±2.21             | 1.012±0.315 <sup>\$</sup>  | -0.254±0.136         | -0.982±0.131          |
| SH2_N | 6.23±1.90             | 0.578±0.211                | -0.164±0.125         | -0.877±0.112          |
| SH2_F | 8.01±2.36             | 1.083±0.250 <sup>!\$</sup> | -0.202±0.133         | -1.049±0.148          |

N: Normal speed, F: Fast speed. \*: Shoe main effect; #: Speed main effect; &: Interaction of shoe and speed; !: Difference between shoes at same speed; \$: Difference between speeds for same shoe.

# EFFECT OF TIME NORMALIZING GAIT DATA ON THE CONDITION SIGNATURE OF LOWER LIMB JOINT MOTIONS

Kiwon Park, Emily A. Morris and Elizabeth T. Hsiao-Wecksler

University of Illinois at Urbana-Champaign, Urbana, IL, USA

email: [kpark31@illinois.edu](mailto:kpark31@illinois.edu) web: <http://www.mechse.illinois.edu/research/hsiao-wecksler/>

## INTRODUCTION

A new gait analysis method (Condition Signature analysis) has recently been developed with the intention of providing greater quantitative insight into the complex and coupled nature of human movement [1]. Specifically, this method allows for the examination of pairwise coupling relationships over multiple joints or body segments. In this study, we focus on bilateral lower limb joints. Condition Signature analysis uses the cross-correlation function to compare the shape and timing of time-series gait data for a given pairing, e.g., right hip angle vs. left knee angle as functions of gait cycle – however any time-series gait data can be used: joint angular velocity, muscle moments, segment position, etc. For each cross-correlation, the maximum cross-correlation value (maxCC) and phase shift (PS) at maxCC are recorded for the given comparison pairing. Ultimately, changes in maxCC and PS values are used to examine modifications in coupling behaviors between different test conditions or test populations (case vs. control). Since this technique relies on the shape and timing of the input data, the structure of the time-series gait data may have an impact on the outcome of this method.

Average time series data are often adjusted to 0-100% gait cycle. However, this approach generally ignores timing variability in movement patterns, both between and within gait cycles. Thus, averaged movement data may express reduced peak values and increased standard deviations due to inter- and intra-cycle variability in timing [2]. To address these deficiencies, we have found piecewise linear length normalization (PLLN) to be a preferable technique for removing timing variability between discrete points of interest throughout the gait cycle [2,3]. PLLN is essentially curve registration that compresses or expands the time axis of a cycle to be-aligned with a target data set. Alignments are

done using linear interpolation between specified points of interest along the gait cycle.

In this paper, we examine how the use of PLLN affects the outcome of Condition Signature analysis. We use gait data from a controlled experiment with two conditions (normal healthy control and severely restricted knee flexion).

## METHODS

Previously collected gait data from 20 healthy male subjects ( $23 \pm 2$  yrs) were used [4]. Subjects walked for three minutes on a treadmill at a self-selected speed determined while wearing a knee brace. Two conditions were tested: (1) normal (non-braced) walking, and (2) walking with a brace that locked the right knee in full extension (DonJoy, Vista, CA; #81099). Kinematic data were collected from a six-camera motion capture system (Vicon, Oxford, UK; Datastation 460; 120 Hz). Twelve joint parameters (ankle, knee, and hip flexion/extension angular positions and velocities) were determined from a 10 gait cycle window over each walking trial. This window was examined after at least the first 25 gait cycles of walking.

For PLLN, the gait cycle was divided into five subphase pieces identified from six gait events [3]: (i) loading response: ipsilateral heel strike (IHS<sup>1</sup>) to contralateral limb toe-off (CTO<sup>1</sup>), (ii) mid-stance: CTO<sup>1</sup> to limb alignment (LA, i.e., bilateral hip and knee alignment), (iii) terminal-stance: LA to contralateral heel strike (CHS<sup>1</sup>), (iv) pre-swing: CHS<sup>1</sup> to ipsilateral toe-off (ITO<sup>1</sup>), and (v) swing: ITO<sup>1</sup> to IHS<sup>2</sup>. Average timings, in % gait cycle, were determined for each gait event for both conditions. These average timings were then used to align individual and average unbraced and braced cycles by the PLLN method. Therefore, for each subject, two different averaged time-series data (pre-PLLN and post-PLLN) were determined for

the 12 joint variables. To perform condition signature analysis, temporal cross-correlations were computed for each pair of variables, excluding the autocorrelation. These were done for each subject across both test conditions (unbraced and knee braced) and both averaging conditions (pre- and post-PLLN). For each subject, test condition and averaging condition, the maxCC and PS values are placed into a 12×12 “characteristic matrix” with rows and columns labeled by the twelve joint variables, such that the entries below the diagonal contained the maxCC value for the corresponding pair and the entries above the diagonal contained PS. To assess changes in maxCC and PS between test conditions (unbraced vs. braced), a paired t-test was performed at each corresponding cell across all subjects. A “condition signature” diagram, a color-coded comparison matrix, was then created by coloring black those cells for which a significant difference ( $p < 0.01$ ) was found between the two test conditions, and white those cells with no significant difference (Fig. 1). Condition signature diagrams were created from the gait data pre- and post-PLLN. To assess whether PLLN affected condition signature outcomes, the number of cells with disparate statistical conclusions (i.e., different coloring) were summed.

## RESULTS AND DISCUSSION

Right knee bracing resulted in noticeable time and magnitude changes from normal unbraced motion in right knee joint angular displacement and velocity. Other joints and their coupling relationship to the remaining joints also experienced significant changes. This compensation behavior is evident by the large number of black cells found in the condition signature diagrams (Fig. 1). Recall that black cells suggest that the coupling behavior between the given variable pairings changed significantly between the test conditions (unbraced vs. braced).

Time normalization (or temporal alignment) had a modest effect on the outcome of the condition signatures. Ten cells were identified as being different between pre- and post-PLLN condition signature diagrams (Fig. 1 a-b). Those ten different cells were associated with all six joints (left and right hip, knee, and ankle joints). Temporal alignment using PLLN caused changes in timing of joint angle data which resulted in changes in six

cells of the phase shifts. Although PLLN only affected temporal adjustment, four cells in the maximal cross-correlation values were different from pre-PLLN condition.

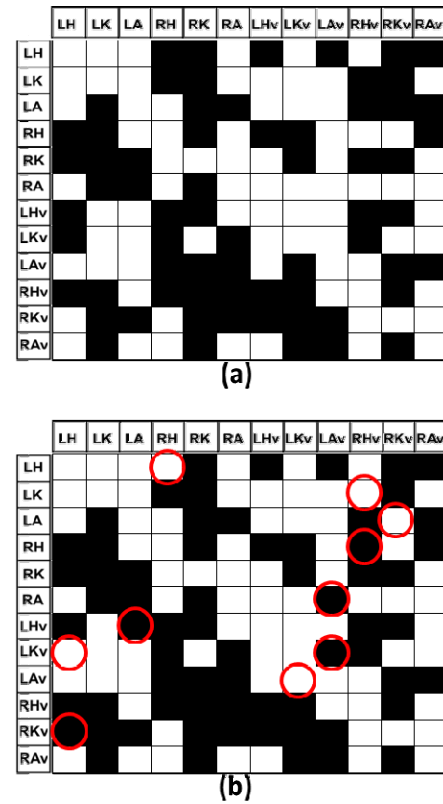


**Figure 1:** Condition signature diagrams (a) pre-PLLN (b) post-PLLN. Red circles in indicate cells for which coupling behavior conclusion changed as a consequence of PLLN adjustment of the time-series gait data.

## CONCLUSIONS

This work investigated the effect of aligning time series data using PLLN over several gait cycles on the results of Condition Signature analysis. Applying PLLN to the time series data resulted in modest changes in the condition signature. These results suggest that choice in averaging methods of gait data might not affect the results obtained from this gait assessment tool.

## REFERENCES

1. Park K, et al. *ASB'10*, Providence, RI, August, 2010
2. Helwig N, et al. *Journal of Biomechanics* **44**:561-566, 2011
3. Morris E, et al. *ASB'10*, Providence, RI, August, 2010
4. DiBerardino, L.A., et al., *Clin Biomech*, 2010. 25(6):552-6.

## ACKNOWLEDGEMENTS

This work was supported by funding from NSF grant # 0727083, and University of Illinois Campus Research Board.

# EFFECTS OF SUBTHALAMIC NUCLEUS DEEP BRAIN STIMULATION ON PARKINSONIAN GAIT BEHAVIOR

Kiwon Park<sup>1</sup>, Srikant Vallabhajosula<sup>2</sup>, Ryan Roemmich<sup>3</sup>, Luke Jungles<sup>1</sup>, Christopher J. Hass<sup>3</sup> and Elizabeth T. Hsiao-Wecksler<sup>1</sup>

<sup>1</sup>University of Illinois at Urbana-Champaign, Urbana, IL, USA

<sup>2</sup>University of Nebraska at Omaha, Omaha, NE, USA

<sup>3</sup>University of Florida, Gainesville, FL, USA

email: [kpark31@illinois.edu](mailto:kpark31@illinois.edu) web: <http://www.mechse.illinois.edu/research/hsiao-wecksler/>

## INTRODUCTION

Deep brain stimulation (DBS) of subthalamic nucleus (STN) has been used to mitigate cardinal symptoms of Parkinson's disease (PD) such as tremor, rigidity, and bradykinesia. Mixed results have been found as to whether DBS leads to improved or sustained gait performance [1]. Recently, Vallabhajosula et al. [2] have examined 18 PD patients with bilateral STN-DBS implants. Using traditional gait analysis parameters, they found that only overground gait speed was significantly different between test conditions when the stimulator was switched OFF or ON. New gait analysis methods have recently been developed with the intention of providing greater quantitative insight into the complex and coupled nature of human movement. Specifically, these methods characterize regions or periods of deviation in joint movement and symmetry [3,4], quantify the complexity & variability of cyclic shapes (i.e., phase space portraits) [5], and identify coupling of multiple joint movements [6]. In the current study, we apply these new gait analysis methods to the PD gait data of Vallabhajosula et al. to assess whether these methods can provide better insight into detecting changes in gait behavior as a consequence of STN-DBS.

## METHODS

Eighteen individuals with idiopathic PD, who had bilateral STN-DBS at least six months, prior to testing were recruited for participation (3 females, 15 males, mean age 62±9 years, mean duration of disease 13±4 years, Hoehn & Yahr score 2 or greater when off medication). Antiparkinsonian medication and DBS stimulation was inactivated 12 hours prior to data collection. After familiarization with the treadmill, participants walked for three

minutes at their self-selected comfortable pace. The DBS stimulators were then turned on and after a short rest, participants again walked on the treadmill for three minutes. The protocol was approved by the university's institutional review board and informed consent was received for each participant. Kinematics of walking were captured using a motion capture system (Vicon Nexus, Oxford, UK; 120Hz). Ankle, knee, and hip flexion/extension angular positions and velocities were determined for a 20 gait cycle window over each walking trial. This window was examined after at least the first 25 gait cycles of walking. To provide comparison of PD gait in both OFF and ON DBS conditions, these data were compared to previously collected gait data from 20 healthy young male control subjects (23 ± 2 years) that walked on a treadmill at their self-selected speed for three minutes. Gait kinematics were captured on a motion capture system (Vicon, Workstation 460, Oxford, UK; 120 Hz) [5].

Regions of Deviation analysis [3,4] was used to examine changes in movement behavior over the gait cycle due to DBS use. This method compared the test conditions (ON vs. OFF, ON vs. healthy control, and OFF vs. healthy control) and examined differences in joint angular position as a function of gait cycle for individual joints or symmetry between bilateral joint pairs. For each comparison, individual joint or symmetry, t-tests ( $\alpha = 0.05$ ) were conducted for three parameters: peak value, peak timing, and integral of absolute difference values over full gait cycle.

To examine changes in the complexity & variability of phase portrait shapes of joint position vs. velocity, the method of DiBerardino et al. [5] was

used. This technique quantifies the complexity of the phase portrait shape by determining the maximum number of Fourier harmonics necessary to reproduce the near-elliptical phase portrait shape with 99.9% accuracy. Inter-cycle variability was determined by examining the movement (drift and swept area) of the phase portrait centroid over the 20 cycles. Paired t-tests ( $\alpha = 0.05$ ) were used to test for difference in complexity and variability measures between ON and OFF DBS.

Condition Signature analysis [6] was used to examine coupling between 12 joint movements (bilateral ankle, knee and hip angular positions and velocities). Temporal cross-correlation compared the timing and shape of these time-series gait parameters. This method utilized changes in maximum cross-correlation (maxCC) value and phase shift at maxCC between ipsilateral and contralateral joint parameter pairs to examine coupling and coordination patterns between conditions (ON vs. OFF, ON vs. healthy control, and OFF vs. control). For each condition, paired t-tests ( $\alpha = 0.05$ ) were used to compare differences in maxCC or phase shift of each joint parameter pairing. These comparisons created 132 parameter coupling cells within a condition signature diagram.

In this report, preliminary results from six subjects (1 female, 5 males, mean age  $63 \pm 10$  years, mean duration of disease  $11 \pm 3$  years) are presented.

## RESULTS AND DISCUSSION

Similar to previous reports evaluating only spatiotemporal gait variables, none of these analysis methods found any significant difference due to STN-DBS use, i.e., there were no significant differences in lower limb joint movements with respect to either healthy normal control behavior nor between the two stimulator settings for the PD group.

Regions of Deviation analysis found that there were no significant differences in symmetry and individual joint regions of deviation between ON vs. OFF, ON vs. healthy control, or OFF vs. control. Further, the use of STN-DBS did not significantly change the complexity & variability of lower extremity joint variables (Table 1). Finally, there were only seven significant changes out of 132 joint couplings between ON and OFF-DBS conditions. In the comparison with healthy controls, the condition signatures for ON and OFF-DBS conditions had 25 and 26 significant changes in joint couplings, respectively. The results from these analyses indicate that joint movement, symmetry, and coupling characteristics during gait of the PD group were similar under both conditions.

## CONCLUSIONS

These results suggest that STN-DBS intervention does not necessarily affect continuous gait behavior among persons with PD. Analysis of the remaining 12 subjects is necessary to substantiate these preliminary observations.

## REFERENCES

1. St. George, R.J. et al. *Neurology* 2010;75: 1292-9.
2. Vallabhajosula, S. et al. (in preparation)
3. Shorter, K.A., et al., *Clin Biomech*, 2008. 23(4): 459-67.
4. DiBerardino, L.A., et al., *Proceedings of 34<sup>th</sup> ASB*, Providence, RI, 2010.
5. DiBerardino, L.A., et al., *Clin Biomech*, 2010. 25(6):552-6.
6. Park, K., et al., *Proceedings of 34<sup>th</sup> ASB*, Providence, RI, 2010.

## ACKNOWLEDGEMENTS

This work was supported by funding from NSF grant # 0727083 (ETHW), University of Illinois Campus Research Board (ETHW, KP), and National Parkinson's foundation Center for Excellence at UF.

**Table 1:** Mean (and standard deviation) values of complexity and variability measures for lower extremity joint variables

| Joint Angle |       | Complexity [# harmonics] |          | Area            |                 | Drift         |               |
|-------------|-------|--------------------------|----------|-----------------|-----------------|---------------|---------------|
|             |       | OFF-DBS                  | ON-DBS   | OFF-DBS         | ON-DBS          | OFF-DBS       | ON-DBS        |
| Hip         | Left  | 166 (25)                 | 176 (39) | 0.0188 (0.0138) | 0.0256 (0.0294) | 1.198 (0.492) | 1.419 (0.801) |
|             | Right | 165 (14)                 | 164 (12) | 0.0163 (0.0123) | 0.0239 (0.0303) | 1.088 (0.464) | 1.305 (0.694) |
| Knee        | Left  | 181 (23)                 | 173 (33) | 0.0146 (0.0050) | 0.0267 (0.0119) | 1.017 (0.234) | 1.535 (0.694) |
|             | Right | 171 (28)                 | 165 (16) | 0.0161 (0.0095) | 0.0255 (0.0120) | 0.964 (0.288) | 1.33 (0.283)  |
| Ankle       | Left  | 241 (15)                 | 231 (25) | 0.0139 (0.0141) | 0.0319 (0.0526) | 1.213 (0.750) | 1.457 (1.152) |
|             | Right | 248 (25)                 | 233 (24) | 0.0134 (0.0159) | 0.016 (0.0136)  | 1.144 (0.825) | 1.301 (0.661) |

# SKELTAL MUSCLE STIFFNESS ACROSS THE ADULT LIFESPAN OF THE RAT

Laura Pauwels, Kyrstin Eklund, Ryan Breighner and Zachary Domire

Texas Tech University, Lubbock, TX, USA

email: [zachary.domire@ttu.edu](mailto:zachary.domire@ttu.edu) web:

<http://www.depts.ttu.edu/hess/content/faculty/facultypage/zdomire.php>

## INTRODUCTION

A common complaint associated with aging is the feeling of being “stiff”. Stiffening of skeletal muscle likely contributes to this subjectively defined sensation. There are two primary sources for passive tension in a muscle (Prado et al 2005), the intracellular titin and the extracellular matrix (ECM). It is known that elderly muscle has higher collagen content (Kovanen 1989) and increased cross-linking between collagen fibers (Kovanen and Suominen 1988) in the ECM. These changes should result in significant increases in passive stiffness of the muscle.

In vitro animal studies have demonstrated a slight increase in muscle modulus in elderly animals (Kovanen and Suominen 1988). The development of magnetic resonance elastography has allowed a more direct in vivo measure of material properties. An investigation using elastography revealed a subgroup of elderly individuals who had passive muscle stiffness far outside the normal range (Domire et al., 2009).

The purpose of this study is to determine the relationship between age and skeletal muscle stiffness by performing in vitro material testing on rats spread throughout the adult lifespan.

## METHODS

The EDL from 25 adult, male FBN-F1 rats between 6 and 37 months old were tested for this study. The average life expectancy for this strain is 32 months. The muscle was removed immediately following sacrifice and was tested within one hour.

Measurements were taken using a custom built tensile tester. Muscle samples were positioned with approximately 25% of the muscle belly length in

each clamp. The specimen was lengthened until a resistive force was developed. The gauge length was measured in this position and used as  $l_0$ . In this position, the width and depth of the muscle was measured with calipers accurate to 0.1mm. The cross-sectional area (CSA) was estimated as an ellipse. Tensile testing was then conducted to failure at a rate of 2cm/min.

Force and length data were filtered using a 3<sup>rd</sup> order butterworth, low-pass filter with a cutoff of 0.5Hz. Following filtering, force and length were normalized to CSA and  $l_0$  allowing stress to be plotted against strain (Figure 1). The slope (E) of the roughly linear region was calculated, as well as the ultimate stress ( $U\sigma$ ).

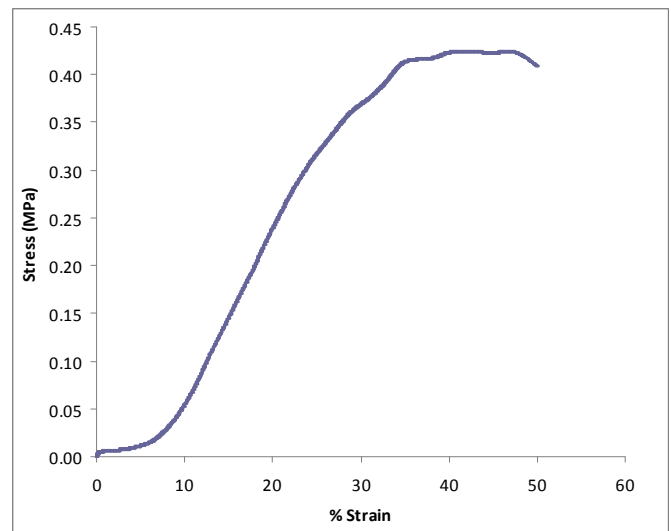
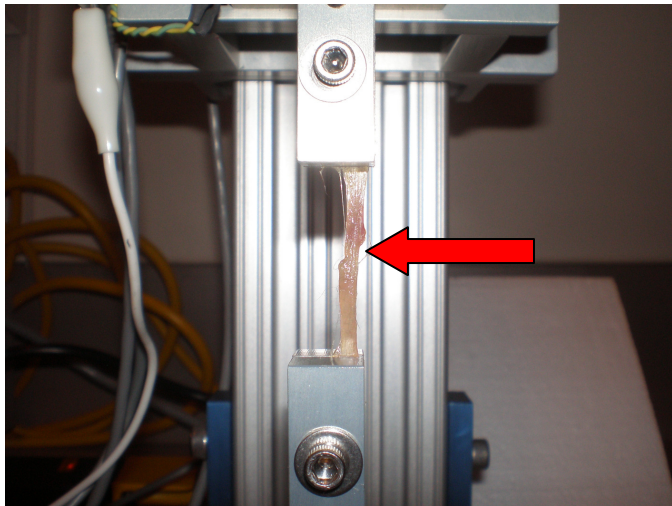


Figure 1: A typical stress strain plot

## RESULTS AND DISCUSSION

Failure of the specimens generally occurred in the middle third of the muscle belly (Figure 2). From inspection of the specimens following failure, it appears that failure typically originated at the interface of aponeurosis and muscle fibers.



**Figure 2:** A typical failure location

Elderly rats were found to have a significantly ( $p \leq 0.05$ ) smaller CSA and larger elastic modulus than younger rats. No difference was found in ultimate stress (Table 1).

**Table 1:** Results for young and old rats

| Age (m.)  | CSA (mm <sup>2</sup> ) | U $\sigma$ (MPa) | E (MPa)       |
|-----------|------------------------|------------------|---------------|
| <30       | 8.9 $\pm$ 1.5          | 0.33 $\pm$ 0.08  | 1.3 $\pm$ 4.1 |
| $\geq 30$ | 7.4 $\pm$ 1.3          | 0.39 $\pm$ 0.09  | 2.5 $\pm$ 1.8 |

Closer inspection of the elastic modulus data reveals an interesting pattern (Figure 3). Approximately half of the elderly specimens had moduli within the normal range and approximately half fell outside this range. One specimen fell well outside this range. It should be noted that, if this data point were removed, the p-value would actually decrease, making difference more detectable as a result of decreased variance in the elderly group.

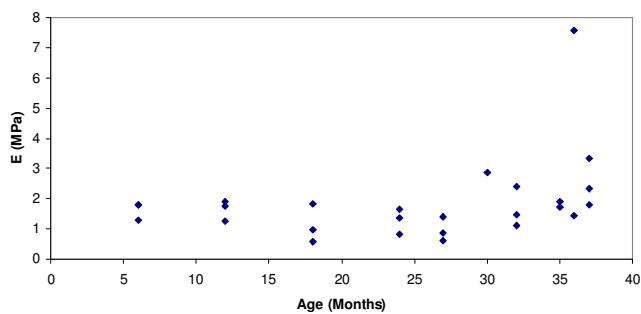


**Figure 3:** Elastic modulus plotted against age

A likely mechanism by which elderly muscle may become stiffer is through the accumulation of advanced glycation end-products (AGE's). It is well established that AGE's accumulate on collagen with

increased age (Paul and Bailey, 1996). The result is the formation of non-enzymatically regulated cross-links between collagen fibers and an increase in tissue stiffness (Reddy 2004). It has previously been shown that AGE's accumulate in elderly muscle tissue (Snow et al., 2007).

It is known that aged muscle cannot respond to exercise as effectively as younger muscle (Jozsi et al., 2000) and that following exercise gene expression of several muscle growth factors is also reduced (Dennis et al., 2008). A possible mechanism for this is that stiffening of ECM impairs mechanotransduction (Goldspink and Harridge 2004). Given equal external stimuli, a stiff ECM would result in aged muscle experiencing reduced strain in the muscle fibers, thereby reducing the signaling to adapt to that stimuli. This may be a major contributor to age related sarcopenia.

## CONCLUSIONS

The results of this study mirrored results from a previous in vivo human study (Domire et al., 2009) showing the elderly are prone to stiffening of muscle tissue. However, this only appears in roughly half the elderly population. If this stiffening is found to have clinical implications, an appropriate screening tool to identify these individuals needs to be identified.

## REFERENCES

1. Dennis RA, et al. *Physiol Genomics* **32**, 393-400, 2008.
2. Domire ZJ, et al. *J Appl Biomech* **25**, 93-7, 2009.
3. Goldspink G and Harridge SD. *Exp Gerontol* **39**, 1433-8, 2004.
4. Jozsi AC et al. *Mech Ageing Dev* **120**, 45-56, 2000.
5. Kovanen V. *Acta Physiol Scand Suppl* **577**, 1-56, 1989.
6. Kovanen V and Suominen H. *Compr Gerontol A* **2**, 18-23, 1988.
7. Paul RG and Bailey AJ *Int J Biochem Cell Biol* **28**, 1297-310, 1996.
8. Prado LG et al. *J Gen Physiol* **126**, 461-80, 2005.
9. Reddy GK. *Exp Diabetes Res* **5**, 143-53, 2004.
10. Snow LM et al. *J Gerontol A Biol Sci Med Sci* **62**, 1204-10, 2007.

# PARETIC MUSCLE WORK IS INCREASED IN PRE-SWING DURING HEMIPARETIC WALKING

<sup>1</sup>Carrie L. Peterson, <sup>2,3</sup>Steven A. Kautz and <sup>4</sup>Richard R. Neptune

<sup>1</sup>Rehabilitation Institute of Chicago, Chicago, IL, USA

<sup>2</sup>Ralph H Johnson VA Medical Center, <sup>3</sup>Medical University of South Carolina, Charleston, SC, USA

<sup>4</sup>The University of Texas at Austin, Austin, TX, USA

email: [cpeterson@ric.org](mailto:cpeterson@ric.org), web: <http://www.me.utexas.edu/~neptune>

## INTRODUCTION

Muscle mechanical work, a quantity that cannot be directly measured during walking, is likely affected by abnormalities observed in hemiparetic walking. Increased co-contraction between antagonist muscles and increased reliance on muscles that contribute to medial-lateral stability in hemiparetic subjects each can result in increased mechanical work without a corresponding increase in walking speed. A simulation analysis of nondisabled walking found that musculotendon (i.e., muscle fiber and in-series tendon) work was consistent with metabolic cost estimates during each region of the gait cycle (Umberger, 2010). Since musculotendon work may partly explain the increased metabolic cost of walking in hemiparetic subjects compared to nondisabled controls at matched speeds (Zamparo et al., 1995), understanding differences in musculotendon work between hemiparetic and nondisabled subjects may provide insight into the energetic cost of hemiparetic walking.

The purpose of this study was to use musculoskeletal modeling and simulation analyses to compare individual musculotendon work generated by representative hemiparetic subjects classified according to functional walking status (i.e., limited community = 0.4-0.8 m/s and community walkers = > 0.8 m/s) to a representative speed and age-matched control subject. Musculotendon work was analyzed at two speeds because metabolic cost is more increased compared to speed-matched controls for hemiparetic walkers with slower self-selected speeds than for hemiparetic walkers with faster self-selected speeds (Zamparo et al., 1995). As a first step in understanding differences between the hemiparetic and control subjects, the paretic leg pre-swing phase was analyzed because many abnormalities secondary

to stroke that limit walking speed occur during this important double support phase of the gait cycle.

## METHODS

Experimental data were collected from 51 hemiparetic subjects walking at self-selected speeds and 21 nondisabled elderly subjects walking at self-selected and slow speeds on a split-belt instrumented treadmill as part of a larger study. From this data set, we selected a representative subject from the limited community walker (age = 53 years, self-selected treadmill speed = 0.45 m/s) and community walker (age = 60 years, self-selected treadmill speed = 0.9 m/s) functional groups and an age matched control subject (female, age = 59 years) walking at speeds of 0.6 and 1.0 m/s for the simulation analyses.

A previously described 3D musculoskeletal model (Peterson et al., 2010) with 23 degrees-of-freedom was developed using SIMM. The model was driven by 43 Hill-type musculotendon actuators per leg with muscle contraction dynamics governed by Hill-type properties and activation dynamics modeled using a nonlinear first-order differential equation. Forward dynamics simulations from paretic mid-stance to paretic toe-off (right leg for control simulations) were generated using a simulated annealing optimization algorithm that varied the muscle excitation patterns until the difference between simulated and experimentally measured walking data and total muscle stress (muscle force divided by muscle cross-sectional area summed across all 86 muscles) was minimized. Net MT, fiber and tendon work were computed by integrating the corresponding power over the paretic (ipsilateral for control) pre-swing phase. Positive and negative work were computed by integrating the positive and negative portions of the power trajectories over pre-

swing and summed (i.e., positive work plus absolute value of negative work) to determine the total MT, fiber and tendon work.

## RESULTS AND DISCUSSION

Simulated joint angles and normalized ground reaction forces emulated well the experimental data with an average error of 1.77 degrees and 2.89 %BW, respectively. The right leg of the control simulations are referred to as the ipsilateral leg for comparison with the paretic leg.

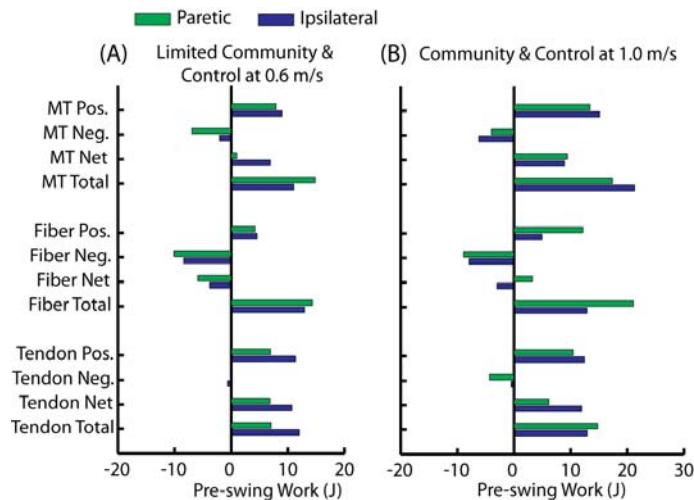


**Figure 1:** Musculotendon (MT), muscle fiber, and tendon work done by all paretic (ipsilateral for control) muscles during pre-swing for the limited community (A) and community hemiparetic walkers (B) compared to the speed-matched control.

For the limited community walker, net MT work by the paretic leg was decreased relative to the ipsilateral leg of the control subject walking at 0.6 m/s (Fig. 1A), which was consistent with a previous experimental study that found decreased net paretic joint moment work during paretic pre-swing compared to speed-matched controls (Chen and Patten, 2008). However, total paretic fiber work was increased (Fig. 1A). More fiber work was done by the paretic muscles of the limited community walker to achieve a similar speed, largely due to decreased paretic plantar flexor activation. While soleus and gastrocnemius recovered the most elastic energy (i.e., positive tendon work) among the paretic muscles for the limited community walker, they recovered much less energy than the control plantar flexors. Because tendon is a passive tissue that uses little metabolic energy, the limited community

walker's decreased ability to exploit elastic energy recovery via the paretic ankle plantar flexors would increase their metabolic cost of walking compared to the speed-matched control.

For the community walker, net paretic MT work was similar to the ipsilateral leg of the control subject (Fig. 1B). However, total paretic fiber work was increased (Fig. 1B) as the paretic hip abductors and adductors did more positive fiber work and paretic gastrocnemius did more positive fiber work while recovering less elastic energy compared to the control.

## CONCLUSIONS

Total paretic fiber work was increased in both the limited community and community hemiparetic walkers compared to the age-matched control subject walking at similar speeds. Increased fiber work in the limited community walker was primarily related to decreased fiber and tendon work by the paretic plantar flexors requiring compensatory work by other muscles. Increased fiber work in the community walker was primarily related to increased work by the paretic hip abductors and adductors. Thus, if the hemiparetic and control subjects were to perform work with the same mechanical efficiency, the hemiparetic walkers would expend more metabolic energy during pre-swing. These results may partly explain why hemiparetic walkers have an increased metabolic cost compared to nondisabled walkers at matched speeds.

## REFERENCES

1. Umberger BR. *J R Soc Interface* **7**, 1329-40, 2010.
2. Zamparo P, et al. *Scand J Med Sci Sports* **5**, 348-52, 1995.
3. Peterson CL, et al. *J Biomech*, **43**, 2348-55, 2010.
4. Chen G and Patten C. *J Biomech*, **41**, 877-83, 2008.

## ACKNOWLEDGEMENTS

This work was funded by NIH grant RO1 HD46820 and the Rehabilitation Research & Development Service of the VA.

# ALTERATIONS IN HIP AND PELVIS KINEMATICS DURING RUNNING IN PERSONS WITH FEMOROACETABULAR IMPINGEMENT

<sup>1</sup>Jennifer Peterson, <sup>2</sup>Brian Giordano, <sup>1</sup>John Meyer, <sup>3</sup>Jason Snibbe, and <sup>1</sup>Christopher Powers

<sup>1</sup>Division of Biokinesiology & Physical Therapy, University of Southern California, Los Angeles, CA

<sup>2</sup>Division of Sports Medicine, University of Rochester, Rochester, NY

<sup>3</sup>Beverly Hills Orthopedic Group, Los Angeles, CA

email: [petersjj@usc.edu](mailto:petersjj@usc.edu)

## INTRODUCTION

Femoroacetabular impingement (FAI) is defined as abutment of the femoral head or neck with the acetabulum and has been shown to be a precursor to hip osteoarthritis and labral pathology.[1] To date, the majority of research in this area has focused on the morphologic features of the femoral head/neck and/or acetabulum that may predispose an individual to impingement. However, previous studies indicate that many individuals with radiographic signs consistent with FAI are asymptomatic, suggesting that other factors likely play a role in this condition.[2,3]

It has been suggested that there are kinematic contributions to the development of FAI. A previous study found decreased total sagittal pelvis range of motion during a maximum depth squat in individuals with FAI, but did not find differences in peak pelvis or hip angles [4]. Another study evaluating gait mechanics in this population reported decreased peak hip abduction and decreased total frontal plane pelvis motion, but no other differences in pelvis or hip kinematics. [5] It is possible that greater kinematic differences may be present between individuals with and without FAI during more challenging tasks. For example, a case report evaluating running and jumping tasks in an individual with FAI suggested that excessive hip adduction and internal rotation while the hip is flexing may result in impingement.[6]

The purpose of this study was to compare hip and pelvis kinematics in individuals diagnosed with FAI and control subjects during running. We hypothesized that individuals with FAI would exhibit greater peak hip flexion and peak anterior

pelvis tilt during the stance phase of running. Furthermore, we hypothesized that FAI subjects would demonstrate increased peak hip adduction and internal rotation.

## METHODS

Over ground running was performed by 8 subjects with radiographically confirmed FAI (5 female, 3 male) and 8 control subjects (4 female, 4 male). Kinematic data were collected at 250 Hz using a Qualysis Motion Capture System (Qualysis, Inc., Gottenberg, Sweden). ATMI force plates (Model #OR6-6-1, Newton, MA) were utilized to define the stance phase of running.

Reflective markers and clusters were placed to define and track the lower extremity and pelvis. The pelvis segment was defined using bilateral iliac crest and greater trochanter markers. Each subject performed 3 successful over ground running trials. A trial was deemed acceptable if the involved foot for FAI subjects or the matched foot for control subjects landed completely on the force at a predetermined speed of 3.8 m/s ( $\pm 5\%$ ). The dependent variables of interest included peak pelvis anterior tilt (relative to the lab coordinate system), peak hip flexion, peak hip adduction, and peak hip internal rotation during stance phase of running. Variables were compared between groups using independent t-tests ( $\alpha = 0.05$ ).

## RESULTS AND DISCUSSION

During the stance phase of running the FAI group demonstrated decreased peak hip flexion compared to control subjects ( $32.1 \pm 4.7^\circ$  vs.  $38.0 \pm 5.3^\circ$ ,  $p=0.019$ ) (Figure 1) and decreased peak pelvis

anterior tilt ( $10.4 \pm 3.3^\circ$  vs.  $13.7 \pm 4.0$ ,  $p=0.046$ ) (Figure 2). There were no statistically significant differences in peak hip adduction ( $10.0 \pm 6.1^\circ$  vs.  $11.2 \pm 4.4^\circ$ ,  $p=0.44$ ) or peak hip internal rotation ( $8.1 \pm 5.8^\circ$  vs.  $8.8 \pm 8.3^\circ$ ,  $p=0.483$ ).

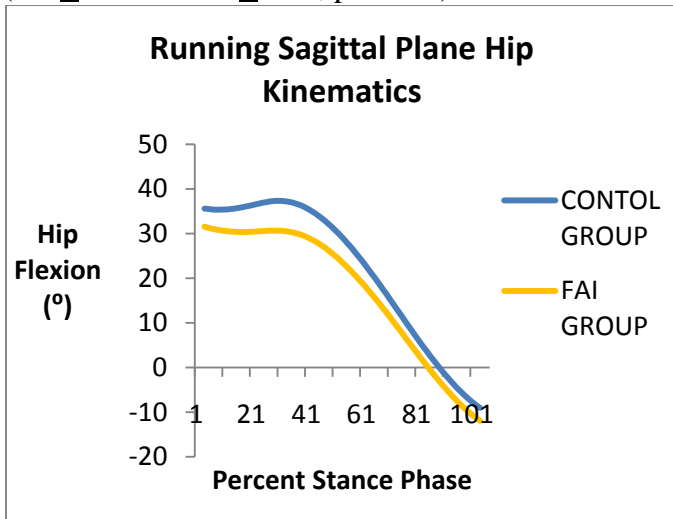


**Figure 1** The ensemble average sagittal hip kinematics time-series curve

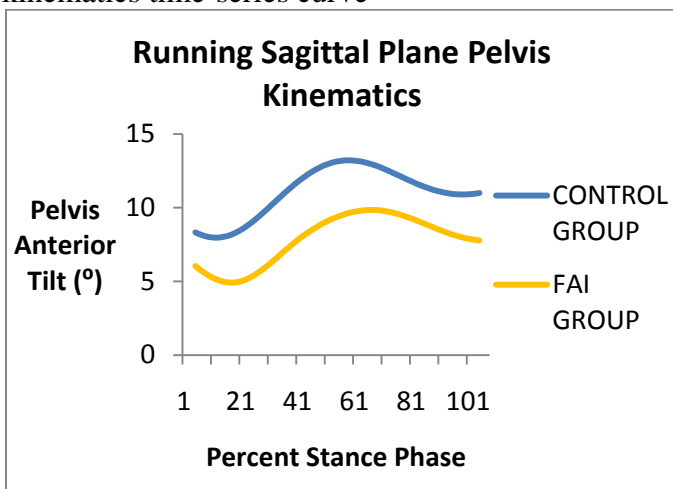


**Figure 2** The ensemble average sagittal pelvis kinematics time-series curve

We anticipated that individuals with FAI would demonstrate increased peak hip flexion, adduction, and internal rotation, as well as greater peak pelvis anterior tilt. Our hypothesis was based on the belief that individuals with FAI may have developed this pathology secondary to abnormal hip and pelvis kinematics.

Contrary to our hypothesis, we found that individuals with FAI presented with decreased peak hip flexion and anterior pelvic tilt and no differences in peak hip adduction or internal rotation. We believe that the sagittal plane differences represent a compensatory strategy to

avoid impingement. However, as all individuals in the FAI group had ongoing complaints of pain, it is impossible to establish a cause and effect relationship.

Our finding of decreased peak pelvis anterior tilt in the FAI group during running is consistent with previous reports of decreased total sagittal pelvis range of motion during squatting in individuals with FAI.[4] Contrary to previous reports of differences in frontal and/or transverse plane hip kinematics during gait, running and jumping in persons with FAI, [5,6] we found no differences in hip frontal or transverse plane motions during running. Additional research is necessary to determine the effect of the observed kinematics at the joint level.

## CONCLUSIONS

Our study found that individuals with FAI demonstrated decreased peak hip flexion and pelvis anterior tilt and no differences in hip frontal and transverse plane kinematics. We believe that the reduction in hip flexion may be a compensatory strategy to avoid approaching impingement during a dynamic task involving high joint forces.

## REFERENCES

1. Beck M, et al. *J Bone Joint Surg Br*, **87** (7), 1012-1018, 2005.
2. Allen D, et al. *J Bone Joint Surg Br*, **91** (5), 589-594, 2009.
3. Kang AC, et al. *Am J Sports Med*, **38** (6), 1160-1165, 2010.
4. Lamontagne M, et al. *Clin Orthop Relat Res*, **467**, 645-650.
5. Kennedy MJ, et al. *Gait Posture*, **30**, 41-44, 2009.
6. Austin A, et al. *JOSPT*, **38** (9), 558-565, 2008.

# Quantitative Comparison of Knee Joint Angles and Moments between Two Different Marker Representations of the Proximal Shank

<sup>1</sup>Daniel J. Petit, <sup>2</sup>John D. Willson, and <sup>1</sup>Joaquin A. Barrios

<sup>1</sup>University of Dayton, Dayton, OH, USA

<sup>2</sup>University of Wisconsin-La Crosse, La Crosse, WI, USA

E-mail: [petitdaj@notes.udayton.edu](mailto:petitdaj@notes.udayton.edu)

## INTRODUCTION

Highly variable marker set configurations are used for instrumented gait analysis [1,2]. Simpler sets are attractive options, but as a result are often less accurate representations of true anatomy. Germane to much work is the representation of the knee joint. Two current methods for defining the proximal end of the shank are to either 1) use shared femoral condyle markers that also define the distal thigh or 2) to apply two independent markers over the proximal tibial plateaus. The exact consequences for choosing to use tibial plateau markers to represent the proximal shank are not entirely understood.

Therefore, the purpose of this study was to compare knee joint angles and moments during walking and running using the aforementioned two knee joint marker configurations. We expected that differences in knee joint mechanics may be revealed.

## METHODS

Two data sets were used in this study, collected by different investigators in separate laboratories. The first data set were of 15 individuals (13 males and 2 females age  $24.0 \pm 3.7$  yrs) with asymptomatic varus knee alignment performing level walking [3]. Average height, mass, and BMI of the data set were  $1.74 \pm 0.08$  m,  $69.1 \pm 9.9$  kg, and  $22.7 \pm 2.2$  kg/m<sup>2</sup> respectively. The second set (15 females,  $20.7 \pm 1.2$  yrs) were taken from healthy individuals while running. Average height, mass and BMI for this subset were  $1.67 \pm 0.07$  m,  $61.4 \pm 9.3$  kg, and  $22.0 \pm 1.8$  kg/m<sup>2</sup>.

Both marker sets were applied simultaneously on the test subjects. Anatomical markers were placed over the iliac crests, greater trochanters, femoral condyles, tibial plateaus, malleoli, first and fifth

metatarsal heads, and distal aspect of the shoe. Tracking markers were placed over the anterior superior iliac spines, L5-S1 interspinous space, a cluster of three on the rearfoot, and two shell-mounted clusters of four markers on the distal posterior shank and distal posterolateral thigh. Subjects walked at 1.5 m/s ( $\pm 5\%$ ) or ran at 3.7 m/s ( $\pm 5\%$ ) until five acceptable dynamic trials had been captured.

3D marker trajectories were captured by an 8 camera Vicon (walking) or Motion Analysis (running) systems at 120Hz. Force data were acquired by Bertec force plates at 1080 Hz. All trials were processed using Visual3D (C-Motion, Germantown, MD) and custom LabVIEW (National Instruments Corporation, Austin, TX) software.

Data processing scripts were identical for both marker sets, however the model used to generate knee angles and moments was different as a result of using either the femoral condyles (2 marker set) or tibial plateaus (4 marker set) to define the proximal shank. For each marker set, peak joint angles (X-Y-Z) and moments (expressed as external moments in the shank coordinate system) were extracted from the individual non-normalized trials during stance-phase intervals of interest in the gait cycle. These values were then averaged within the marker set conditions and compared using paired t-tests ( $p \leq 0.05$ ).

## RESULTS AND DISCUSSION

Statically, knee angles during standing calibration trials (Table 1) were significantly more extended ( $p < 0.001$ ) and more adducted ( $p < 0.001$ ) in the 4 marker set for both data sets.

In walking, peak knee joint flexion (Table 2) after weight acceptance was less ( $p < 0.03$ ) and peak knee

adduction (Table 1) in the first half of stance was greater ( $p < 0.001$ ) in the 4 marker set. Peak knee flexion moment after weight acceptance was less ( $p < 0.001$ ) in the 4 marker set, which also saw a greater ( $p < 0.001$ ) peak internal rotation moment in the second half of stance (Table 2). Although not significant ( $p = 0.07$ ), a greater peak knee adduction moment was seen with 4 markers. Interestingly, the exact same parameters in the running data set were also statistically different (Table 2).

**Table 1:** Standing Calibration Knee Ang. (W=walk R=run)

|               | 2 Markers   | 4 Markers   | p      |
|---------------|-------------|-------------|--------|
| Knee Ext. (W) | 4.08 ± 4.50 | 4.99 ± 4.83 | <0.001 |
| Knee Add. (W) | 4.15 ± 2.23 | 5.53 ± 2.23 | <0.001 |
| Knee IR (W)   | 4.30 ± 3.27 | 3.47 ± 4.91 | 0.261  |
| Knee Ext. (R) | 1.51±6.67   | 3.15±6.62   | <0.001 |
| Knee Add. (R) | -0.32±2.34  | 0.37±2.70   | <0.001 |
| Knee IR (R)   | 4.31±7.51   | 4.59±8.35   | 0.776  |

Knee joint moments were significantly impacted. We observed a significantly decreased flexion moment, significantly increased internal rotation moment and nearly significantly increased knee adduction moment in both data sets. One possible explanation for these differences is that they may be the result of changes in how the shank segment coordinate system has been defined in the two models, previously reported in other work to have significant impact on moment data [4]. Additionally, these differences could be a result of a shortening of the shank. This decrease in length of the shank changes the inertial properties associated with the shank segment of the model, thus altering parameters used in the calculation of joint moments.

Knee angles throughout the gait cycle do not appear to be as uniformly affected across axes as knee moments, but we still saw a significant reduction in knee flexion and increase in knee adduction. Comparing 3D knee angles at standing calibration to the dynamic trials, it appears that a four marker

representation of the knee imposes an offset on the data evident at the standing calibration. This offset appears to be carried forward, on a similar order of magnitude (1-2 degrees), into the dynamic data. Waveform characteristics appeared largely unchanged. As there is no accepted gold standard to reference when evaluating such data, we suggest that the four marker model is theoretically superior because of more accurate anatomical representation of the shank, as well as allowing for independent translations and rotations of the shank relative to the thigh.

## CONCLUSIONS

Shared markers to define the distal thigh and proximal shank resulted in greater knee flexion and lesser adduction angles as well as greater external knee flexor moments during both walking and running in two independent samples. Researchers should be aware of the impact a chosen marker set could have on the collected data. They should also be cautious when comparing results determined through the use of two differing marker sets, keeping in mind how segment coordinate systems have been determined and the subsequent impact on joint angle and moment calculations. Based on our interpretation of these findings, we recommend utilizing proximal tibial plateau markers in addition to femoral condyle markers at the knee.

## REFERENCES

1. Ferrari A, et al. *Gait & Posture* **28**, 207-216, 2008.
2. Collins TD, et al. *Gait & Posture* **30**, 173-180, 2009.
3. Barrios J, et al. *J Orthop Res* **27**, 1414-1419, 2009.
4. Manal K, et al. *Gait & Posture* **15**, 10-17, 2002.

**Table 2:** Knee angles and moments at discrete points in gait cycle; walking on top, running on bottom

| Angles                         | 2 markers    | 4 markers    | p-value | Moments                | 2 markers    | 4 markers    | p-value |
|--------------------------------|--------------|--------------|---------|------------------------|--------------|--------------|---------|
| Peak Knee Flexion after WA     | 20.68 ± 5.92 | 19.48 ± 5.25 | 0.022   | Peak Knee Flex. Moment | 0.48 ± 0.15  | 0.41 ± .12   | <0.001  |
| Peak Knee Adduction (1st half) | 3.76 ± 2.88  | 5.12 ± 3.53  | <0.001  | Peak Knee Add. Moment  | 0.38 ± 0.07  | 0.39 ± 0.06  | 0.072   |
| Peak Knee IR (2nd half)        | 15.43 ± 8.43 | 15.12 ± 8.43 | 0.819   | Peak Knee IR Moment    | 0.11 ± 0.03  | 0.13 ± 0.03  | <0.001  |
| Peak Knee Flexion after WA     | 44.65 ± 5.41 | 42.99 ± 5.28 | <0.001  | Peak Knee Flex Moment  | 1.60 ± 0.26  | 1.27 ± 0.24  | <0.001  |
| Peak Knee Adduction (1st half) | -1.10 ± 5.43 | -0.43 ± 5.51 | <0.001  | Peak Knee Add. Moment  | 0.599 ± 0.27 | 0.561 ± 0.21 | 0.167   |
| Peak Knee IR (2nd half)        | 5.93 ± 7.76  | 6.30 ± 7.23  | 0.714   | Peak Knee IR Moment    | 0.09 ± 0.06  | 0.10 ± 0.06  | <0.001  |

# AGE-RELATED CHANGES IN MOTOR ADAPTATION TO NOVEL DYNAMICS

<sup>1,2</sup>Alison Pienciak and <sup>1</sup>Alaa Ahmed

<sup>1</sup>Neuromechanics Laboratory, Integrative Physiology, University of Colorado, Boulder, CO, USA

<sup>2</sup>Mechanical Engineering, University of Colorado, Boulder, CO, USA

email: [alison.pienciak@colorado.edu](mailto:alison.pienciak@colorado.edu) | web: [http://spot.colorado.edu/~alaa/neuro\\_lab/](http://spot.colorado.edu/~alaa/neuro_lab/)

## INTRODUCTION

Skilled movement relies on our ability to learn and adapt internal models of our bodies and the environment [1]. Older adults move less accurately and efficiently than young adults [2,3]; we hypothesize that this may indicate an impaired ability to learn novel internal models.

We used an experimental paradigm testing motor adaptation of reaching movements to novel dynamics that has been well-characterized in young adults, but not in older adults. We tested whether older adults showed impaired movement adaptation, and further, whether they showed impaired internal model learning, as compared to young adults.

## METHODS

6 young (YA,  $25.3 \pm 3.1$  years old) and 6 old (OA,  $73.0 \pm 7.2$  years old) right-handed, healthy subjects made straight-ahead planar reaching movements to a target while seated and grasping the handle of a force-generating robotic arm (InMotion2 Shoulder-Elbow Robot, Interactive Motion Technologies Inc.) (Fig. 1A). The protocol was 400 trials long, separated into three segments: baseline (trials 1-100; null field, robot forces off), learning (101-350; force field), and washout (351-400; null field). The force field was a velocity-dependent curl field (Fig. 1B). In addition to null and field trials, 1 trial per batch (5 trials) was randomly chosen as a catch trial, in which a force channel restricted handle movement to a straight-line path to the target and measured force exerted into the channel. Movement error and force learning were quantified and compared between groups at 5 phases: late baseline, early learning, late learning, early washout, and late washout (Fig. 1C). For each of these phases, data were averaged over 2 batches (8 non-catch trials or 2 catch trials).

Movement error for each trial was quantified as the maximum absolute value of the perpendicular deviation from a straight-line path between the start

and target positions. Force learning was quantified as "catch force" on each catch trial as the time integral of the force exerted into the channel. Over the learning phase, movement error and catch force data were separately fit to an exponential curve for each subject to determine error reduction and force learning rates, respectively.

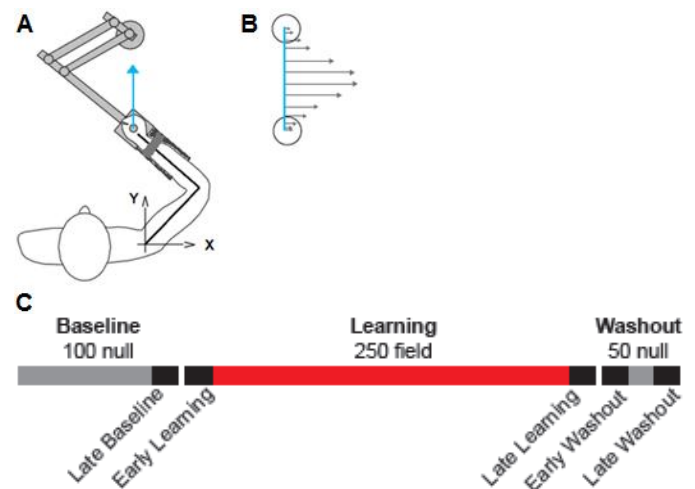


**Figure 1:** A: Robot setup. B: Sample force profile encountered on force field trials. C: Protocol.

EMG data was collected, using a wireless electrode system (Trigno Wireless System, DelSys Inc.), for 3 agonist-antagonist muscle pairs acting about the elbow and shoulder joints: 2 shoulder muscles (pectoralis major and posterior deltoid), 2 biarticular muscles (biceps brachii and triceps long head), and 2 elbow muscles (brachioradialis and triceps lateral head). Data for each muscle was normalized by mean resting activity (recorded prior to movement onset). For each pair, coactivation was quantified per trial as the root-mean square value of the time-trace of minimum normalized activity matched by both muscles throughout the movement.

## RESULTS AND DISCUSSION

At the end of the baseline phase, movement error was significantly higher for OA than for YA ( $p=0.004$ ); otherwise, we found no significant

differences in error between groups. We found that both groups reduced their error over the learning phase to similar extents and at similar rates (Fig. 2).

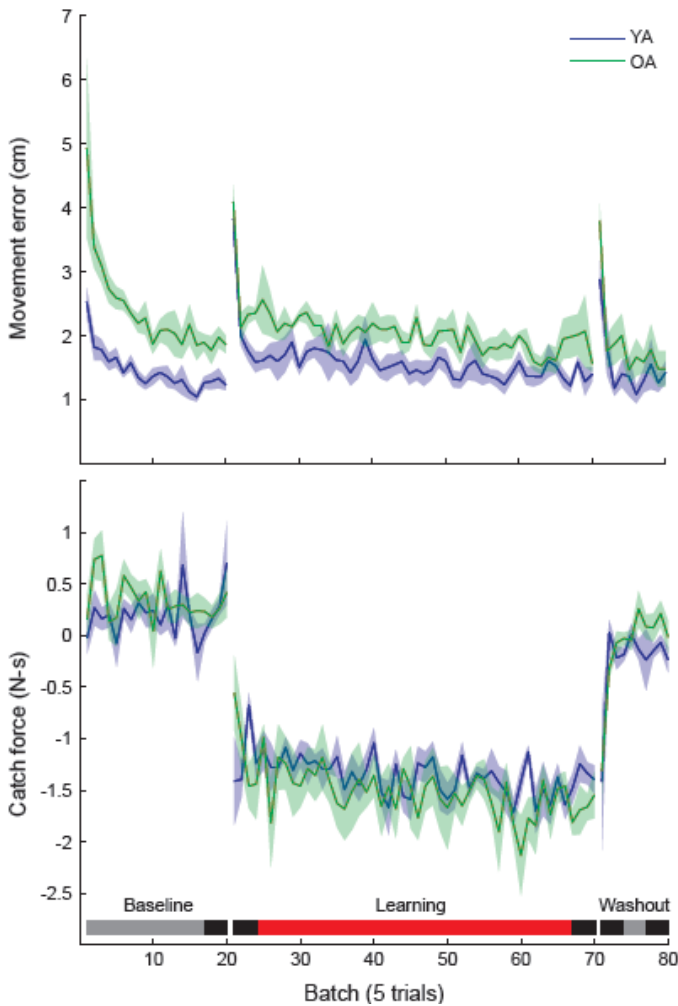


**Figure 2:** Top: Movement error per batch (averaged over 5 trials, excluding catch trials). Bottom: Catch force per batch (1 catch trial per batch). Plots show group mean (solid line; YA blue, OA green)  $\pm$  standard error (shading).

We found no significant differences in catch force between groups at any phase, indicating that they learned the forces to similar extents. However, the OA group showed a significantly slower force learning rate than the YA group ( $p=0.035$ ). This agrees with results from a visuomotor adaptation study which found that older adults adapt more slowly than the young [4].

The OA group also showed a greater increase in shoulder joint coactivation (pectoralis major and posterior deltoid) from late baseline to early learning ( $p=0.069$ ) (Fig. 3), which may help to explain the discrepancy between error and force

learning rates; i.e., the OA group's greater increase in shoulder coactivation could help to reduce error quickly while force learning occurs more slowly. Overall, no statistically significant differences in coactivation were found between groups.

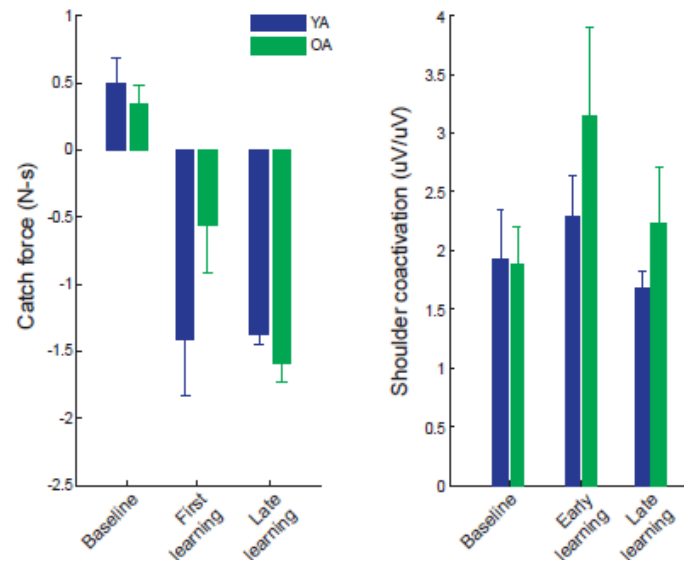


**Figure 3:** Left: Catch force for late baseline phase, first catch trial in early learning phase, and late learning phase. Right: Shoulder coactivation for late baseline phase, early learning phase, and late learning phase. Plots show group mean (bar; YA blue, OA green) with standard error.

## CONCLUSIONS

The older adults reduced their movement error to the same extent and as quickly as the young adults, and they learned the novel dynamics to the same extent. However, they learned the novel dynamics more slowly than the young. This may be explained by the older adults' greater increase in shoulder joint coactivation at the start of learning.

## REFERENCES

1. Shadmehr R, Mussa-Ivaldi FA. *J Neurosci* **14**, 3208-3224, 1994.
2. Darling WG, et al. *Neurobiol Aging* **10**, 149-157, 1989.
3. Seidler-Dobrin RD, et al. *Motor Control* **2**, 314-330, 1998.
4. Fernandez-Ruiz J, et al. *Cognitive Brain Res* **9**, 223-226, 2000.

## ACKNOWLEDGEMENTS

Thanks to HJH for technical assistance. This work was partially funded by a UCB JFD Award.

# CENTER OF PRESSURE TRAJECTORY DIFFERENCES BETWEEN SHOD AND BAREFOOT RUNNING

<sup>1</sup>Eric Pisciotta, <sup>1</sup>James Becker, <sup>3</sup>Komsak Sinsurin, <sup>2</sup>Stan James, <sup>1</sup>Louis Osternig, and <sup>1</sup>Li-Shan Chou

<sup>1</sup>Department of Human Physiology, University of Oregon, <sup>2</sup>Slocum Center for Orthopedics and Sports Medicine, Eugene, OR, USA; <sup>3</sup>Faculty of Physical Therapy, Mahidol University, Thailand  
email: [chou@uoregon.edu](mailto:chou@uoregon.edu); web: <http://biomechanics.uoregon.edu/MAL/>

## INTRODUCTION

While kinematic and kinetic differences between shod and barefoot running have been heavily investigated [1], one area which has not been examined is how the trajectory of the center of pressure (COP) changes between these two conditions. Since the COP trajectory has been shown to be a valid tool for assessing foot function and injury risk [2, 3] understanding how it changes from shod to barefoot running could help clarify the relative injury risks associated with each condition. The COP characteristics most often examined include the anterior-posterior (AP) and medial-lateral (ML) excursions and velocities, as well as the relative locations of the COP at specific instants during stance. To date, one underutilized characteristic is the variability in the above parameters. Reduced variability in the positioning of the COP may concentrate loading under specific anatomic structures, which over time may play a role in the development of repetitive stress injuries, though this has not been reported in the literature.

Therefore, the purposes of this study were to quantify changes in the position of the COP relative to the foot during stance, examine changes in the AP and ML excursions of the COP, quantify changes in the variability of the COP trajectory from shod to barefoot conditions in a group of habitually shod recreational runners.

## METHODS

Ten habitually shod, recreational runners (mean age  $32.4 \pm 4.1$  years) currently running at least 20 miles per week were assessed. Subjects ran continuous laps around a 25 meter track in the laboratory under both shod and barefoot conditions. Whole body motion data were collected at 200 Hz using an 8

camera motion capture system (Motion Analysis Corp.) Ground reaction forces were recorded at 1000 Hz by three force plates (AMTI) located in series along the 5 meter capture region. Subjects ran at a self selected speed approximating their normal training run pace.

The COP trajectory was calculated for all trials with a clean force plate strike. At each instant the COP location was referenced to the anatomic coordinate system of the foot. The orientation of this coordinate system was established when the foot was flat on the ground with the AP axis aligning with the long axis of the foot and the superior-inferior axis being perpendicular to the floor. The foot ML axis was orthogonal to the other two, and pointed laterally for both the left and right feet. Since the origin for both feet was set at the heel marker, the COP positions were subsequently described relative to this point.

Average AP and ML position of the COP relative to the heel marker at each instant, for each foot, was calculated along with standard deviations in both the AP and ML directions, in increments of 10% stance (Figure 1). The AP and ML positions and standard deviations were compared between shod and barefoot running at foot strike, 60% stance, and toe off using 2x3 repeated measures ANOVAs. AP and ML excursions from foot contact to toe off were compared between shod and barefoot running using paired *t* tests. Each foot was analyzed separately.

## RESULTS AND DISCUSSION

The COP was located significantly more medially at all time points in the barefoot condition compared to the shod condition (Figures 2 & 3). In the AP direction, the COP was located more anterior at foot

contact in the barefoot condition compared to the shod condition. However, there was not a difference in the AP location at 60% stance or toe off between conditions (Figure 3).

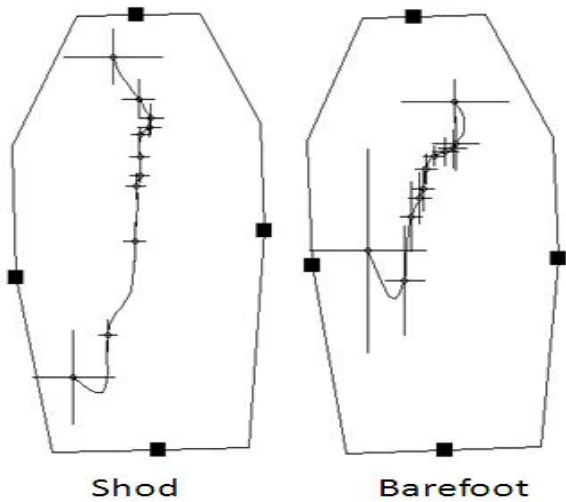


Figure 1. Representative plots of the COP trajectory (from a left foot) and its variability (standard deviation of the average COP location in the AP and ML directions, respectively). t of one subject are shown.

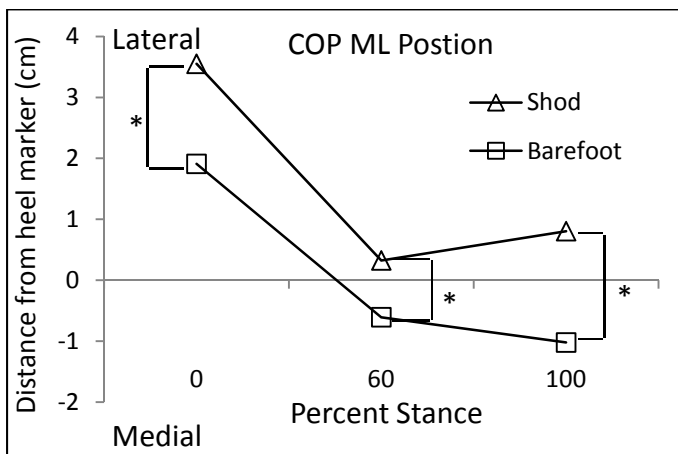


Figure 2. Changes in the COP ML positioning relative to the heel marker. \* indicates significant differences between conditions ( $p < .05$ ).

Variability in the location of the COP showed significant main effects for percent stance, but no main effects for shod and barefoot conditions, in both the AP and ML directions. Both directions showed higher variability at initial foot contact and at toe off and smaller variability through midstance.

The COP excursions showed significant differences between shod and barefoot conditions for only the AP direction, not the ML direction (Table 1).

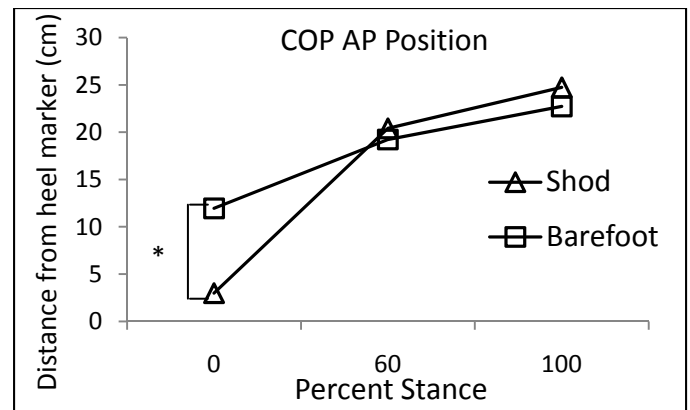


Figure 3. Changes in the COP AP positioning relative to the heel marker. \* indicates significant differences between conditions ( $p < .05$ ).

Table 1. Changes in COP AP and ML excursions. \* indicates significant differences ( $p < .05$ ).

|                       | Shod                    | Barefoot                 |
|-----------------------|-------------------------|--------------------------|
| COP AP excursion (cm) | 21.75<br>( $\pm 2.81$ ) | 10.38*<br>( $\pm 5.73$ ) |
| COP ML excursion (cm) | 2.78<br>( $\pm 1.96$ )  | 2.81<br>( $\pm 1.56$ )   |

## CONCLUSIONS

Compared to shod running, the trajectory of the COP during barefoot running is marked by a more medial location under the foot throughout stance, a more anterior position at initial contact, and reduced AP excursion. That there are no differences in variability of the COP trajectory or ML excursions suggests, apart from the initial contact position, the dynamics of foot roll over are similar between shod and barefoot running. However, the few COP differences which were observed in this study are similar to COP characteristics which have previously been shown to be related to injury [3, 4]. Therefore future studies should examine how or if these changes may be related to injury risk during barefoot running.

## REFERENCES

1. Nigg, B. *Footwear Science*, **1**, 73-79, 2009.
2. De Cock, A. et al. *Gait & Posture*, **27**, 669-675, 2008.
3. Willems, T. et al. *Gait & Posture*, **23**, 91-98, 2006.
4. Van Ginckel, A. et al. *Gait & Posture*, **29**, 387-391, 2009.

# QUANTITATIVE DESCRIPTION OF THROWING FROM THE KNEES IN BASEBALL AND SOFTBALL CATCHERS

Hillary A. Plummer & Gretchen D. Oliver

University of Arkansas, Fayetteville, AR, USA

Email: hplummer@uark.edu

## INTRODUCTION

Baseball and softball are popular sports in which many athletes choose to participate, and understanding proper throwing mechanics is essential for injury prevention. The throwing mechanics of catchers throwing down to second base have yet to be examined thoroughly in the literature. Catchers have the option of throwing down to second from either their stance or knees in order to throw out a stealing runner. In attempt to improve ball release time many catchers will throw down to second base from their knees. Throwing from the knees eliminates the use of the lower extremity which may affect force transfer up the kinetic chain, possibly resulting in decreased torso rotation and increased shoulder and elbow stress. Improper timing or sequential segment movement while throwing from the knees may place the throwing athlete at an increased risk of injury which may explain the increased occurrence of shoulder injuries in youth. Thus, it was the purpose of this study to examine shoulder and torso kinematics in catchers throwing to second base from their knees.

## METHODS

A randomized control trial was implemented in a controlled laboratory setting. Baseball and softball catchers ( $n=29$ ;  $15.2\pm 3.5$  years;  $165.4\pm 12.8$  cm;  $66.4\pm 17.2$  kg) reported for testing prior to engaging in resistance training or any vigorous activity that day. All of the catchers were right handed. Testing protocols were approved by the University's Institutional Review Board.

Kinematic and kinetic data were collected using The MotionMonitor<sup>TM</sup> motion capture system (Innovative Sports Training, Chicago IL) at a rate of 1000Hz. Prior to completing test trials, participants had a series of ten electromagnetic sensors attached at the following locations: (1) the medial aspect of

the torso at C7 [1]; (2) medial aspect of the pelvis at S1 [1]; (3) the distal/posterior aspect of the throwing humerus; (4) the distal/posterior aspect of the throwing forearm; (5) the distal/posterior aspect of the non-throwing humerus; (6) the distal/posterior aspect of the non-throwing forearm; (7) distal/posterior aspect of stride leg femur; (8) distal/posterior aspect of stride leg fibula; (9) distal/posterior aspect of non stride leg femur; and (10) distal/posterior aspect of non stride leg fibula. Sensors were affixed to the skin using double sided tape and secured using flexible hypoallergenic athletic tape. An eleventh sensor was attached to a wooden stylus and used to digitize the palpated position of the bony landmarks. A segment link model was developed through digitization of joint centers for the ankle, knee, hip, shoulder, T12-L1, and C7-T1. The spinal column was defined as the digitized space between the associated spinous processes, as the ankle and knee were defined as the midpoints of the digitized malleoli, and femoral condyles, while by virtue of the least-squares method, the hip and shoulder joint centers were defined.

Participants were given an unlimited time to warm-up. Following warm-up participants were instructed to catch a pitched ball and throw down to second base, simulating a game setting where a runner was attempting to steal second base. Each participant had five fastballs pitched to them in which they caught and threw down to second from their knees. A position player covered second base and only those throws that he/she was able to catch without stepping off the base were recorded. Those data from the fastest throw down to second were selected for detailed analysis. Ball velocity was determined by JUGS radar gun (OpticsPlanet, Inc., Northbrook, IL) positioned behind the pitcher and directed towards second base. Descriptive kinematic data of the trunk and shoulder for the fastest throw to

second base were calculated at the instances of foot contact (FC), maximum external rotation (MER), ball release (BR), and maximum internal rotation (MIR).

## RESULTS AND DISCUSSION

Trunk and shoulder kinematics are depicted in Figure 1. As catchers throw from their knees, the amount of trunk flexion present is greatest at maximum external rotation and decreases until they are in an upright position at maximum internal rotation. At foot contact the trunk is positioned flexed toward the right and then gradually flexes to the left throughout the throwing motion where it finally reaches its greatest value at maximum internal rotation. Trunk axial rotation was greatest at foot contact, the point at which the catcher attempted to rotate towards second base. Shoulder plane of elevation displayed slight extension at MER and then moved into forward flexion at BR and on into MIR. Shoulder elevation, or abduction of the humerus, gradually increased from the start of the motion until reaching a mean maximal angle of 88° at the point of maximum external rotation. It is interesting to note, that when throwing from the knees, catchers do not reach the optimal shoulder elevation of 90°. Following the peak of shoulder elevation, at maximum external rotation, the elevation of the shoulder then decreases. The

shoulder is in an externally rotated position at foot contact and continues to externally rotate until it reached MER.

## CONCLUSIONS

This study successfully described the kinematics of throwing from the knees in catchers. Understanding the kinematics of throwing can lead to the identification of potentially harmful pathomechanics in catchers. The inability for catcher to reach optimal shoulder elevation may lead to additional stresses being placed on the shoulder and elbow and eventually cause injury. To our knowledge, this is the first study to examine the kinematics of catchers throwing from their knees and more studies are needed to validate our results. Future research should be directed towards determining how the throwing mechanics of catchers relates to the kinematics observed in baseball pitchers.

## REFERENCES

1. Myers, JB, et al. *Am J Sports Med* **33**: 263-271, 2005.

## ACKNOWLEDGEMENTS

The authors would like to acknowledge University of Arkansas Women's Giving Circle for their financial support.

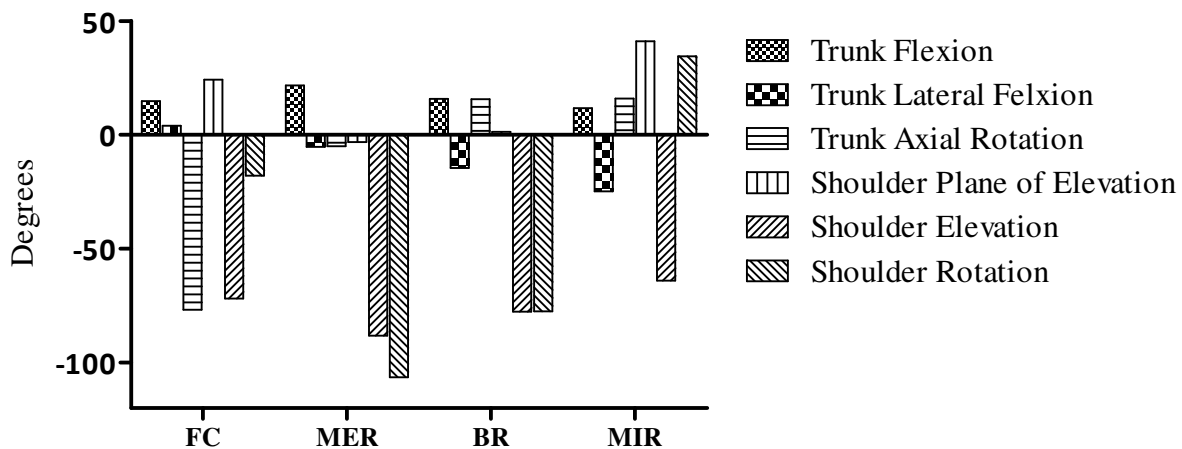


**Figure 1.** Trunk and shoulder kinematic variables at each event mark.

Trunk flexion (-) is flexion; Trunk lateral flexion (+) is to the right for a right handed thrower. Trunk axial rotation (-) is to the right; Shoulder plane of elevation 0= abduction and 90=forward flexion; shoulder elevation 0=full abduction while -90 = 90 degrees abduction; and shoulder rotation (+) is internal rotation while (-) is external rotation.

# THE ROLE OF EXPERIMENTALLY INDUCED HIP ABDUCTOR MUSCLE STRENGTH DEFICITS ON FRONTAL PLANE BIOMECHANICS DURING GAIT

<sup>1</sup>Michael Pohl, <sup>1</sup>Karen Kendall, <sup>1</sup>Preston Wiley, <sup>1</sup>Chirag Patel, <sup>1</sup>Carolyn Emery and <sup>1</sup>Reed Ferber

<sup>1</sup>University of Calgary, Calgary, AB, CANADA

email: [mbpohl@ucalgary.ca](mailto:mbpohl@ucalgary.ca) web: <http://www.runninginjuryclinic.org>

## INTRODUCTION

Knee osteoarthritis (OA) is one of the most common joint diseases, with the majority of OA related changes being observed in the medial tibiofemoral compartment. Biomechanical changes in gait have been observed in patients with medial compartment knee OA (MC-KOA). In particular, the external knee adduction moment (KAM) has been linked with the presence, severity and progression of MC-KOA [1, 2].

It has been speculated that muscular strength of the hip abductors plays an important role in the progression of MC-KOA [1,3]. Indeed, greater internal hip adduction moments during gait have been associated with a reduced likelihood of MC-KOA progression [3]. The link between reduced hip abductor function and knee joint loading during gait was recently explored by injecting a pain-inducing solution into the gluteus medius [4]. Although the injection was successful in reducing hip abductor muscular activation, it resulted in an unexpected drop in the KAM. However, it remains unclear whether the gait adaptations observed post-injection were simply an analgesic gait response to pain.

An alternative method to reduce the force output of muscles is to perform a nerve block injection. This has the advantage of not inducing pain-related gait adaptations. Therefore, this study aimed to reduce hip abductor muscular strength in healthy subjects via a nerve block injection and observe subsequent alterations in gait. Specifically, it was hypothesised that the external KAM would be greater following the nerve block procedure. A secondary hypothesis was that alterations in hip adduction moment along with contralateral pelvic drop hip adduction angles would also be observed.

## METHODS

Eight healthy male subjects with no lower extremity pathology participated (age:  $27\pm 6$ , mass:  $76\pm 10$  kg). Subjects underwent hip abductor

strength testing and a three-dimensional gait analysis both prior to (PRE) and following (POST) a unilateral superior gluteal nerve block procedure. Hip abductor strength was assessed using isometric maximal voluntary contractions (MVCs). Subjects were positioned in a side lying pose with the hip abducted against a fixed strap so that the thigh was horizontal to the surface. A force dynamometer was placed between the thigh and strap to measure force output. Over-ground gait analysis data were collected using a motion analysis system and force plate. Reflective markers were placed on the lower extremity with the position of each marker on the skin accurately marked using an ink stamp. Following a standing trial kinematic and kinetic gait data were collected for 5 trials of the right limb.

The gluteal nerve block procedure involved an ultrasound guided lidocaine injection performed on the right side. Following the injection hip abductor MVCs were collected. The reflective markers which had been removed for the nerve block procedure were then replaced on the ink stamps and a second gait analysis was conducted.

The mean of each subject's 3 MVC trials was taken and normalised by body mass. Three-dimensional joint angles were calculated along with inverse dynamics to estimate external joint moments during gait. Wilcoxon signed-rank tests were used to compare PRE and POST values for the following variables during the stance phase: first peak knee adduction moment (PKAM1), second peak knee adduction moment (PKAM2), hip adduction moment (HAM) at the instance of PKAM1, contralateral pelvic drop angle (PelvDrop) at the instance of PKAM1, hip adduction angle (HipAdd) at the instance of PKAM1.

## RESULTS AND DISCUSSION

Following the nerve block procedure the group mean hip abductor strength decreased from a PRE value of 3.50 ( $\pm 1.05$ ) to a POST value of 1.86

( $\pm 0.66$ ) N/kg. This corresponded to 45% drop in MVC strength. The individual drops in MVC strength are illustrated in Figure 1. Walking speed as indicated by stance time was similar between PRE and POST.

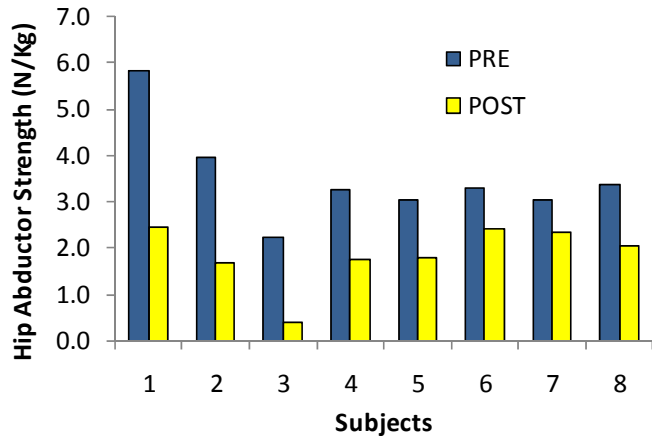


**Figure 1:** PRE and POST hip strength values.

A comparison between the PRE and POST kinematic and kinetic variables are presented in Table 1. It was hypothesized that decreased force output of the hip abductors would lead to subsequent increases in the knee adduction moment. However, despite large reductions in hip abductor strength following the nerve block procedure, there was no change in either PKAM1 or PKAM2. In contrast to the findings of the present study, Henrikson et al. [4] reported a decrease in knee adduction moment following reduced hip abductor activation. However, the reduced muscle activation in the afore-mentioned study was achieved by inducing pain in the hip abductors so the changes in gait may have been an antalgic gait response to pain. Given that reduced hip strength was not pain-induced in the present study, it is likely that the observed gait pattern was more representative of reduced strength as opposed to hip pain.

The present study also found no significant changes in hip adduction moment, contralateral pelvic drop or hip adduction following the nerve block (Table 1). On a similar note, Bennel and

colleagues [5] investigated the relationship between hip strength and hip/knee biomechanics by increasing abductor strength using rehabilitation. They found no biomechanical changes at the hip/knee in knee OA patients following the rehabilitation program. Thus, the relationship between hip strength with hip/ knee biomechanics remains unclear. One possibility is that the decrement in force output of the hip abductors was insufficient to induce changes in walking, given that only submaximal strength is required during this activity. Secondly, it may be that other muscles compensated to control hip and knee motion. Thirdly, subjects may have adopted biomechanical changes proximal to the pelvis, such as ipsilateral trunk lean. Finally, this study may not have been sufficiently powered to detect clinically relevant changes in knee moments. A small sample size was used due to the invasive nature of the protocol.

## CONCLUSIONS

Within the limitations of this preliminary study it can be concluded that a 45% drop in force output of the hip abductor muscle group did not alter the external knee adduction moment. Further, no alterations in hip adduction moment, hip adduction or contralateral pelvic drop were associated with reduced hip abductor strength.

## REFERENCES

1. Mundermann A, et al. *Arthr Rheum* **52**, 2835-44, 2005.
2. Miyazaki T, et al. *Ann Rheum Dis* **61**, 617-22, 2002.
3. Chang A, et al. *Arthr Rheum* **52**, 3515-19, 2005.
4. Henrikson M, et al. *J Biomech* **42**, 1236-40, 2009.
5. Bennel K, et al. *Osteoarthr Cart* **18**, 621-25, 2010.

## ACKNOWLEDGEMENTS

We gratefully acknowledge the assistance of Craig Mathison in collecting the data and Dr. Janet Ronsky for the use of her laboratory. Funding was provided by Alberta Innovates-Health Solutions and the Workers Compensation Board – Alberta.

**Table 1:** Mean ( $\pm$ SD) values for kinetic and kinematic variable of interest. Joint moments are expressed as a percentage of body weight and height (%BW\*ht). Comparisons are made using Wilcoxon signed-rank tests.

|                | PKAM1<br>(%BW*ht)               | PKAM2<br>(%BW*ht)               | HAM<br>(%BW*ht)                 | PelvDrop<br>(°)                 | HipAdd<br>(°)                   | Stance Time<br>(Secs)             |
|----------------|---------------------------------|---------------------------------|---------------------------------|---------------------------------|---------------------------------|-----------------------------------|
| <b>PRE</b>     | <b>3.0 <math>\pm</math> 1.1</b> | <b>2.7 <math>\pm</math> 0.6</b> | <b>4.7 <math>\pm</math> 1.0</b> | <b>1.7 <math>\pm</math> 2.7</b> | <b>3.5 <math>\pm</math> 3.7</b> | <b>0.66 <math>\pm</math> 0.04</b> |
| <b>POST</b>    | <b>2.9 <math>\pm</math> 1.0</b> | <b>2.7 <math>\pm</math> 0.5</b> | <b>4.5 <math>\pm</math> 1.0</b> | <b>1.3 <math>\pm</math> 2.5</b> | <b>3.2 <math>\pm</math> 3.4</b> | <b>0.65 <math>\pm</math> 0.04</b> |
| <b>Z score</b> | <b>-0.65</b>                    | <b>-0.14</b>                    | <b>-1.54</b>                    | <b>-0.63</b>                    | <b>-0.70</b>                    | <b>-1.26</b>                      |
| <b>p-value</b> | <b>0.33</b>                     | <b>0.50</b>                     | <b>0.08</b>                     | <b>0.29</b>                     | <b>0.26</b>                     | <b>0.23</b>                       |

# LACK OF MODULATION OF MAXIMUM PINCH FORCE DEPENDING ON GRIP SURFACE IN STROKE SURVIVORS

Chiranan Pounds, Leah Enders, and Na Jin Seo

University of Wisconsin-Milwaukee, Milwaukee, WI, USA  
email: [seon@uwm.edu](mailto:seon@uwm.edu) web: <https://pantherfile.uwm.edu/seon/www/>

## INTRODUCTION

Pinch grip is used in many daily activities, such as picking up small objects, tying shoelaces, and writing. Our previous study [1] demonstrated that grip surface friction affected maximum pinch force in healthy individuals. Maximum pinch force was 13% greater when people gripped the high-friction rubber surface compared to the low-friction paper surface. Pinch force variance during sustained maximum pinch was 50% less for the rubber surface than for the paper surface. Thus, it appears that healthy people sense the slipperiness of the grip surface and reduce maximum pinch force when gripping the paper surface than the rubber surface.

People who have had a stroke often experience loss of sensation. Thus, they may not sense the grip surface differences and may not modulate maximum pinch force for varying grip surface friction as healthy people do. This study was performed to investigate whether grip surface friction does not affect maximum pinch force in stroke survivors due to their reduced sensation. It was hypothesized that increasing grip surface friction is associated with increased maximum pinch force and decreased pinch force variance in stroke survivors for the nonparetic hand, but not for the paretic hand.

## METHODS

Eleven stroke subjects were seated with the forearm resting on a table. They performed maximum isometric pinch grip exertions (between the tips of the thumb and index finger) for 5 seconds on two fixed parallel flat surfaces (Figure 1). Two types of surfaces – smooth rubber and paper – were tested to simulate high-friction and low-friction surfaces, respectively (coefficient of friction = 0.9 between

rubber and skin [2] and 0.3 between paper and skin [3]. Each grip surface was connected to a load cell (Nano17, Mini40; ATI Industrial Automation, Inc.; Apex, NC) that measured pinch force (in the direction perpendicular to the grip surface) for the thumb and index finger separately.



**Figure 1:** Subjects gripped two fixed parallel flat surfaces covered either with high-friction rubber or with low-friction paper.

Both hands (paretic and nonparetic) were tested with each surface condition twice for a total of eight grip exertions per subject. The two flat surfaces were separated by a distance of 3.8 cm for both rubber and paper conditions. The maximum pinch force for each finger was determined as the mean pinch force across a two-second period during which the mean pinch force for the two fingers was the highest. Pinch force variance in that period was also computed for each finger.

Analysis of variance (ANOVA) was performed to determine whether maximum pinch force was significantly affected by the grip surface (paper, rubber), hand (paretic, nonparetic), finger (thumb, index), and their second-order interactions. Another ANOVA was performed to determine if pinch force variance was affected by the same factors. The *p*-value of .05 was considered significant. In case no significance is found for grip surface, statistical power was computed.

## RESULTS AND DISCUSSION

The maximum pinch force was 1.7 times greater for the nonparetic than for the paretic hand ( $p < .05$ ). However, the maximum pinch force did not change for grip surface nor the interaction between grip surface and hand ( $p > .05$ , Figure 2). It indicates that modulation of maximum pinch force depending on grip surface lacked for both paretic and nonparetic hands. The power for this statistical test was 0.9, indicating that the probability of making type II error was only 0.1. The pinch force variance did not change for grip surface, hand, nor the interaction between grip surface and hand ( $p > .05$ , Figure 3). Therefore, the data did not support the hypotheses.

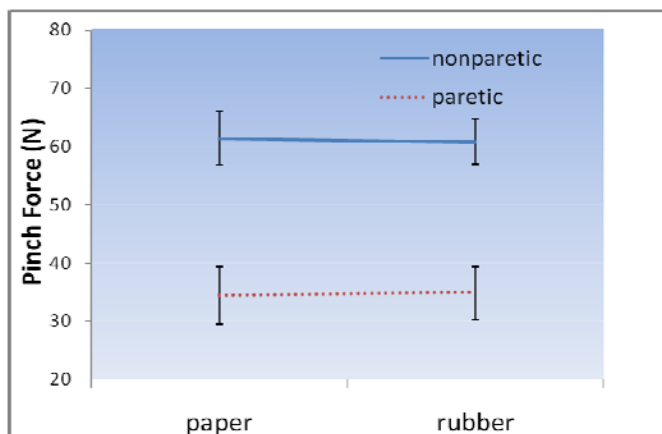


**Figure 2:** Mean  $\pm$  standard error maximum pinch force for the two grip surfaces in the paretic and nonparetic hands.

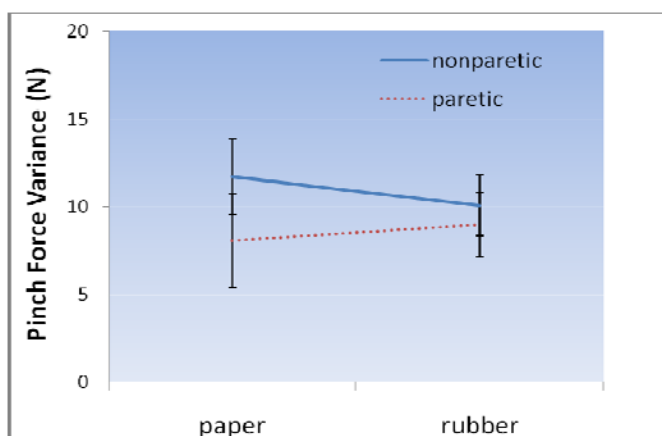


**Figure 3:** Mean  $\pm$  standard error pinch force variance for the two grip surfaces in the paretic and nonparetic hands.

## CONCLUSIONS

Previously, we demonstrated that healthy persons modulate maximum pinch force depending on the grip surface [1]. In the present study, we found that unlike healthy persons, stroke survivors do not modulate their maximum pinch force depending on the grip surface for both the paretic and nonparetic hands. Nine out of eleven stroke subjects had sensory deficit on their fingertip pads, as determined by the monofilament test [4]. Thus, it was expected that stroke survivors may not be able to sense the different grip surfaces with the paretic fingers. The lack of modulation in maximum pinch force for the nonparetic hand may be related to bilateral deficit following stroke, especially for fine skilled movements [5].

This finding has significant implications in rehabilitation as well as ergonomics. In occupational therapy settings, daily objects such as forks and spoons are modified in shape and contact surfaces to accommodate persons with disability in the hand. High-friction rubber surfaces are often used in these modified daily objects to provide better coupling between the hand and grasped object. The present study suggests that stroke survivors may not fully utilize the benefit of high frictional coupling between the hand and grasped object for both the paretic and nonparetic hands. Future studies may examine if sensory enhancement techniques such as tendon vibrations or cutaneous stimulations may improve stroke survivors' ability to sense different grip surfaces and modulate maximum pinch force generation.

## REFERENCES

- 1.Engel AK, et al. *The 34th Annual Meeting of the American Society of Biomechanics*, 2010.
- 2.Seo NJ, et al. *Ergonomics*, **52**, 609-16, 2009.
- 3.Buchholz B, et al. *Ergonomics* **31**, 317-25, 1988.
- 4.Massy-Westropp N. *J Hand Ther* **15**, 48-52, 2002.
- 5.Noskin O, et al. *J Neurol Neurosurg Psychiatry*, **79**, 401-6, 2008.

## ACKNOWLEDGEMENTS

This project was funded by the University of Wisconsin-Milwaukee Research Growth Initiative.

# VELOCITY DEPENDENCY OF PARKINSONIAN RIGIDITY ASSESSED AT THE WRIST JOINT

<sup>1</sup>Douglas Powell, <sup>1</sup>Anburaj Muthumani, <sup>2</sup>Nicholas J. Hanson, <sup>1</sup>A. Joseph Threlkeld and <sup>1</sup>Rui-Ping Xia

<sup>1</sup>Creighton University, Omaha, NE, USA

<sup>2</sup>The Ohio State University, Columbus, OH, USA

email: [douglaspowell@creighton.edu](mailto:douglaspowell@creighton.edu)

## INTRODUCTION

Rigidity is a cardinal symptom of Parkinson's disease (PD). It is central in the diagnosis of PD and in assessing the efficacy of therapeutic interventions. Parkinsonian rigidity has been attributed to neural and non-neural mechanisms [1]. The neural mechanisms of rigidity include enhanced reflex responses to stretch [2] and shortening [3] while the non-neural mechanisms include changes in the mechanical properties of passive tissues including the tendon and connective tissues [4].

While the general mechanisms underlying parkinsonian rigidity have been determined, their characteristics have not been well explored. Parkinsonian rigidity has been characterized as being velocity-independent while spasticity is velocity-dependent. However, there is evidence of a positive relationship between velocity and rigidity in people with PD [5]. PD-associated rigidity has also been shown to be asymmetrical with greater rigidity present in the wrist flexors compared to extensors [6]. Therefore, the purpose of the current study was to directly investigate the relationship between rigidity and movement velocity in people with PD. It was hypothesized that greater velocities of passive movement would be associated with increased rigidity. Due to the previously described asymmetrical presentation of rigidity in PD, it was further hypothesized that rigidity would be greater in the extension movement compared to flexion movement. It was further hypothesized that medication would significantly decrease rigidity.

## METHODS

Twenty subjects (9M; 11F) with idiopathic onset PD participated in the current study. Subjects were between 30 yrs and 75 yrs of age ( $64.0 \pm 8.9$ ),

receiving treatment with dopaminergic medication, had clinical rigidity ( $\geq 2$ ) and had minimal tremor ( $\leq 1$ ) when medication was withdrawn. Subjects were excluded if they had cognitive impairments that prevented informed consent, understanding instructions or providing adequate feedback.

Subjects were seated in a height-adjustable chair while their shoulder and forearm were secured in a neutral position and the elbow was placed in mid-flexion. Subjects were instructed to relax while his or her wrist was moved through a  $60^\circ$  arc of motion at a constant velocity of  $50^\circ/\text{s}$  (SLOW) or  $280^\circ/\text{s}$  (FAST). A strain gauge (1000 Hz, Pacific Instruments) and emulated encoder (100 Hz, Pacific Instruments) were used to measure torque and position, respectively. The servo-motor was controlled by custom software (Labview 2009). Subjects were first tested after a 12-hour withdrawal from medication (OFF-MED) and tested again 30 to 60 minutes after administration of their normal dose of dopaminergic medication (ON-MED).



**Figure 1.** Illustration of experimental set up for data collection.

MatLab (MatLab 2010) was used to quantify rigidity by calculating work scores during the imposed flexion and extension movements (Fig. 1). Work score was defined as the integral of torque with respect to position. A 2x2x2 (medication x direction x velocity) repeated measures ANOVA

was used to determine the effects of medication, movement direction and movement velocity as well as interactions between these variables. Alpha level was set at  $p < 0.05$ .

## RESULTS AND DISCUSSION

Measures of total rigidity were significantly higher in the FAST compared to SLOW condition ( $p < 0.001$ ). When the flexion and extension components of total rigidity were examined, the FAST velocity was associated with greater rigidity in both the flexion ( $p < 0.001$ ) and extension components ( $p < 0.001$ ). The flexion component was associated with significantly greater rigidity than the extension component ( $p = 0.003$ ). Dopaminergic medication did not significantly affect the total ( $p = 0.314$ ), flexion ( $p = 0.272$ ) or extension work scores ( $p = 0.772$ ).

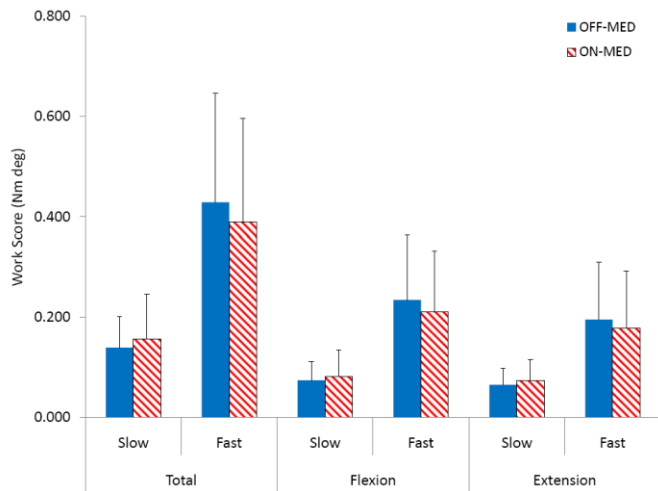


**Figure 2:** Comparison of total, flexion and extension work scores in the OFF-MED (solid) and ON-MED (diagonal) conditions during the imposed flexion and extension movements at FAST and SLOW velocities.

These data demonstrate that parkinsonian rigidity is velocity dependent. The current findings are

clinically relevant as subjective clinical rigidity assessments utilize manual manipulations of the joints in upper and lower extremities and do not employ standardized movement velocities. The current data suggest that the velocity with which the patient's limb is moved directly modulates rigidity. The neural pathways responsible for rigidity have not been determined and much remains unknown. The contribution of the long-latency stretch reflex to rigidity has been implicated as a central component [2]; however, it likely does not act in isolation.

## CONCLUSIONS

Parkinsonian rigidity is velocity-dependent. Future research should investigate the pathways responsible for the effect of velocity on rigidity.

## REFERENCES

1. Dietz, V. et al. *Brain*, **104**:431 – 49, 1981.
2. Tatton, W.G. and Lee, R.G. *Brain Res*, **100** (3), 671-6, 1975.
3. Berardelli *J Neurol Neurosurg Psychiat*, **46**: 45-53, 1983.
4. Watts, RL et al. *J Neurol Neurosurg Psychiat*, **49**, 1177-1181, 1986.
5. Xia, R. et al. *Clin Neurophys*, **120**:1400-1407, 2009.
6. Xia, R. et al. *Clin Neurophys*, **117**:2302-2307, 2006.

## ACKNOWLEDGEMENTS

This study was funded by the National Institutes of Health under Grants R15-HD061022 and R15-HD061022-S1. The authors would like to thank Lauren Kremer and Lindsey Wagner for their diligent work in data processing and Dr. Xiang Fang for conducting the statistical analysis.

# THE DIFFERENT TASK DEMANDS OF A DROP LAND AND SIDE-STEP CUT

Kristamarie A. Pratt, Susan M. Sigward

Jacquelin Perry Musculoskeletal Biomechanics Research Laboratory

Division of Biokinesiology and Physical Therapy

University of Southern California, Los Angeles, CA, USA

email: kristamp@usc.edu, web: www.usc.edu/go/mbrl

## INTRODUCTION

Altered hip and knee mechanics during deceleration of landing and cutting tasks are thought to contribute to greater frontal plane loading of the knee. This is of concern as increased frontal plane moments are associated with greater risk for noncontact anterior cruciate ligament (ACL) injuries [1]. Differences between landing and cutting with respect stance limb (double versus single) and direction of deceleration (vertical versus horizontal) suggest that deceleration strategies may differ as well. The strategies may result in a difference in knee frontal plane loading mechanisms. An understanding of the demands of these high risk tasks is important for the development of effective strategies to reduce knee frontal plane loading.

Therefore, the purpose of this investigation was to compare hip and knee kinematics and kinetics between a double limb landing task and a single limb cutting task. We hypothesize that the sagittal plane contribution to landing would be greater than cutting and that the frontal and transverse plane contributions to cutting would be greater than landing.

## METHODS

Ten healthy, females athletes (ages 19-21yrs, height 166.0±6.2cm, weight 63.8±6.6 kg) with no history of previous knee injury participated. Subjects performed drop land (LAND) and side-step cutting (SCUT) tasks. For the LAND, subjects dropped from a 36 cm platform landing on both feet on force plates before performing a maximum vertical jump. For the SCUT, subjects ran at 4.5-5.5m/s, for 7 meters contacted their dominant foot on the force plate and changed direction to the opposite side at a 45° angle.

Three-dimensional kinematics (8 camera Vicon motion analysis system, 250 Hz), ground reaction forces (AMTI force platforms, 1500Hz) and anthropometrics were used to quantify six degree-of-freedom hip and knee kinematics and kinetics (inverse dynamics) in all three planes (Visual3D™, C-Motion, Inc., Rockville, MD, USA).

Data were analyzed during deceleration of LAND and SCUT defined as the time between force plate contact and maximum knee flexion. To characterize the contributions from each plane average angles, peak moments, average power, and the percent contribution of each plane with respect to average power were determined in all three planes at the knee and hip. Average joint power was computed as the average of the absolute value of the scalar product of angular velocity and net joint moment. Three trials were averaged.

Separate 2 X 3 (task x plane) repeated measures ANOVAs were performed on the above variables. Post hoc testing (t-tests) was performed for significant interactions. Significance set at  $P \leq 0.05$ .

## RESULTS AND DISCUSSION

A significant interaction of plane and task was found for hip and knee average angles. Sagittal plane angles were greater than frontal and transverse plane angles at both joints during LAND and SCUT. When compared to SCUT, average hip ( $p < 0.00$ ) and knee ( $p < 0.00$ ) flexion angles were larger during LAND. Hip transverse angles were greater during the SCUT than LAND ( $p = 0.009$ ).

A significant main effect of plane was noted for hip and knee peak moments. Sagittal plane moments were greater than frontal and transverse moments during LAND ( $p = 0.001$  &  $0.00$ , respectively) and SCUT ( $p < 0.00$  &  $0.00$ , respectively). No main effect for task and no interaction were found.

A significant main effect of plane was found for hip and knee average power; sagittal powers were greater than frontal and transverse powers for both joints during LAND ( $p < 0.00$  &  $0.00$ , respectively) and SCUT ( $p < 0.00$  &  $0.00$ , respectively). A significant interaction between plane and task was noted at the hip. Compared to LAND, SCUT had smaller hip sagittal power ( $p = 0.02$ ) and greater hip frontal power ( $p < 0.01$ ).

When considering the percent contribution of each plane to the total average power during deceleration smaller sagittal and larger frontal plane contributions from the hip and knee were noted in SCUT when compared to LAND (Figure 1). Additionally, the contribution of knee transverse and frontal power was greater in SCUT compared to LAND.

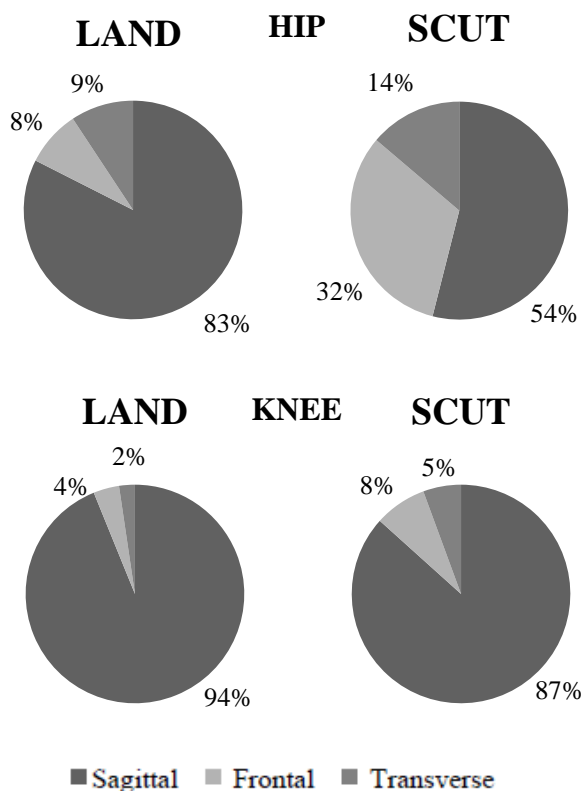


**Figure 1.** Percent contribution from sagittal, frontal and transverse planes to the total power at the hip and knee during deceleration of LAND and SCUT. Significant differences between LAND and SCUT for all planes.

The results of this study indicate that the sagittal plane was the primary contributor to deceleration strategies for both tasks. When compared to the frontal and transverse planes, sagittal plane kinematics and kinetics were greater at both joints during LAND and SCUT. This is not surprising given the greater available hip and knee range of motion in the sagittal plane.

While the sagittal plane was predominate, its contribution to deceleration appeared to be larger during LAND. Subjects exhibited greater hip and knee angles and hip average power in the sagittal plane LAND when compared to SCUT. This suggests that sagittal plane loading is a more effective mechanism for a double limb task that requires vertical deceleration.

Differences in frontal and transverse planes between tasks were seen primarily at the hip. Individuals performed SCUT with greater average hip rotation and exhibited greater hip frontal power compared to LAND. These data suggest that utilization of frontal and transverse planes facilitate horizontal deceleration and redirection during single limb stance. However, these differences did not seem to translate to the knee as no differences between tasks were noted in frontal plane risk factors for ACL injury (knee frontal plane peak moments and average angles).

## CONCLUSIONS

Despite the differences in deceleration strategies, frontal plane risk factors for ACL injury appear to be similar between tasks. However, based on the differences in deceleration strategies it is likely that mechanisms of frontal plane loading at the knee differ. Further work is needed to understand the contributions to frontal plane loading during high risk tasks.

## REFERENCES

- Hewett TE, et al. *Am J Sports Med* **33**, 492-501, 2005

# EFFECTS OF INCREASING INERTIA ON SIDESTEP CUTTING TURNS

<sup>1</sup>Mu Qiao, <sup>1</sup>Brian Brown, <sup>2</sup>Carolyn Westlake and <sup>3</sup>Devin L. Jindrich  
 Kinesiology Program, ASU College of Nursing & Health Innovation<sup>1</sup>  
<sup>2</sup>Department of Kinesiology, University of Tennessee  
 School of Life Sciences<sup>3</sup>, Arizona State University  
 email: devin.jindrich@asu.edu, web: <http://www.limblab.org>

## INTRODUCTION

Previous studies have shown that a simple model can predict the horizontal-plane forces during cutting maneuvers by assuming that body orientation must align with center of mass (COM) movement direction at the end of the turn[1]. Behaviorally, the model predicts that humans could match body orientation to movement direction change by adjusting foot placement at touch down (TD) relative to the COM, changing fore-aft (braking) force, or changing stance period. It was hypothesized that braking forces prevent over-rotation during cutting turns. A second study hypothesized that ostriches use smaller braking forces in part due to higher body inertias about the vertical (yaw) axis ( $I_{zz}$ ) that reduced body rotation[2]. Based on the simple model, we predicted that increasing rotational inertia 3-4 times would result in braking forces being reduced to zero, and tested this prediction by measuring forces and kinematics during running cuts with a custom-built harness to increase  $I_{zz}$ .

## METHODS

A custom-built harness was used to change body yaw moment of inertia by adding balanced weights both anterior and posterior to the COM (Figure 1).



**Figure 1.** Harness used to change  $I_{zz}$ .

Seven participants (age =  $22.5 \pm 1.5$  yrs; body weight (bw) =  $68.2 \pm 4.0$  kg; body height (bh) =  $174.9 \pm 4.2$  cm, mean  $\pm$  std) ran at  $2.79 \pm 0.26$  m s<sup>-1</sup> and performed 5 left 45° side step cutting turns with different mass and yaw moment of inertia increment combinations ( $M0\%I1$  (control), mass increased

15% and body inertia by 3-fold:  $M15\%I3$ ,  $M15\%I3.5$ ,  $M17\%I3.5$ , and  $M17\%I4$ ).

We used a VICON® 3-D motion tracking system and two stationary force platforms (400mm  $\times$  600mm) embedded in the ground to record GRF.  $I_{zz}$  of each participant was determined using standard regression equations accounting for both body mass and height[3]. The COM location was estimated as the middle point between left and right greater trochanter markers (LGT, RGT), and body orientation as the vector connecting LGT and RGT.

The model (Fig. 2) assumes that an individual approaches touchdown (TD) at a horizontal speed of  $V$  and makes a turn that changes COM velocity angle by  $\theta_d$  within a stance duration of  $\tau$ . Relative to the COM the foot 1) is placed a distance of  $P_p$  in the medio-lateral (ML) direction and generates a half-sine shaped ML force with peak of  $F_{pmax}$  and 2) a distance of  $P_{AEP,imd}$  in the anterior-posterior (AP) direction, and generates a full sine wave (peak  $\alpha$ ) and half-sine shaped braking force (peak  $\beta$ )[1]. The “leg effectiveness number” ( $\epsilon$ ) is defined as the body rotation angle  $\theta_p$  that would occur without the braking forces ( $\beta$ ), relative to  $\theta_d$  (Eq. 1).

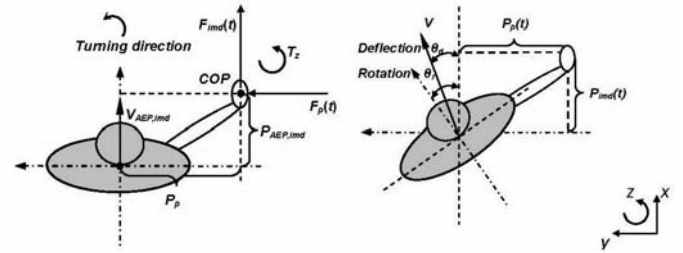


**Figure 2.** Body during TD (left) and turning (right).

$$\epsilon = \frac{\theta_p}{\theta_d} = \frac{MV\tau}{2I} \left( P_{AEP,imd} - \frac{4V\tau}{\pi^2} \right) \quad (1)$$

$$F_{hmax} = \frac{\pi I (1 - \epsilon) \theta_d}{\tau^2 P_p} \quad (2)$$

An  $\epsilon$  of 1 has been interpreted to suggest that braking forces are not necessary to prevent under- or over-rotation.  $\epsilon$  can also be used to predict the peak braking force ( $F_{hmax}$ ) using Eq. 2. Foot placement was the average COP location.

## RESULTS AND DISCUSSION

Contrary to our prediction, braking force ( $\beta$ ) did not decrease significantly with increases to rotational inertia. Instead, consistent initial body rotation and rotational speeds required  $\beta$  in all conditions. Decreased  $\beta$  required to prevent over-rotation due to lateral forces were offset by increased forces required to overcome initial body angle and speed.

Leg effective numbers decreased significantly by 39.5%, 58.0%, 58.7%, and 66.4% from *M15%I2* to *M17%I3* compared to *M0%I1* (Fig. 3), suggesting that lateral turning forces could cause appropriate body rotation without  $\beta$ .

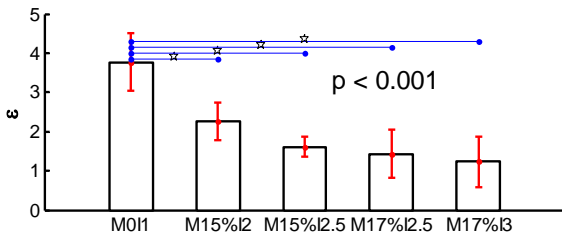


**Figure 3.** Leg effective number ( $\epsilon$ ) across tasks.

$\beta$  did not decrease significantly from *M0%I1* to *M17%I4* (Fig. 4,  $p = 0.59$ ) as hypothesized.

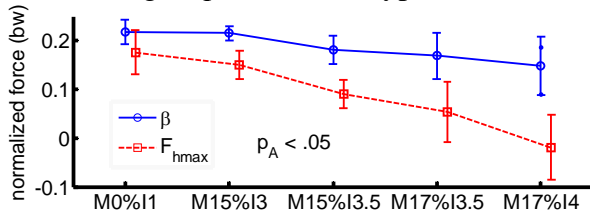


**Figure 4:** Predicted ( $F_{hmax}$ ) and measured ( $\beta$ ) braking forces in all conditions.

In all conditions, although the angle caused by ML force ( $\theta_{Fp}$ ) decreased,  $\beta$  were necessary to overcome initial rotational speed ( $\omega$ ). The angle caused by  $\omega\tau$  was of comparable magnitude to net body rotation ( $\theta_r$ ) in all conditions (Fig. 5). The difference between  $\theta_r$  and ( $\omega\tau + \theta_{Fp}$ ) was accounted for by  $\beta$ .

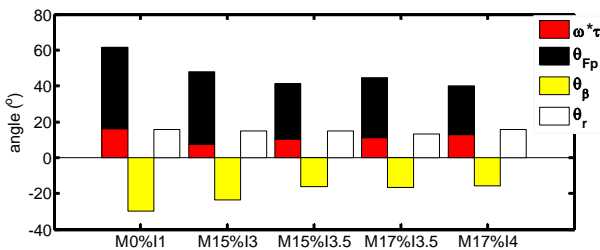


**Figure 5.** Body rotation ( $\theta_r$ ), and its components.

Initial body angle ( $\theta_i$ ) also contributed to body rotation and required  $\beta$  (Fig. 6).

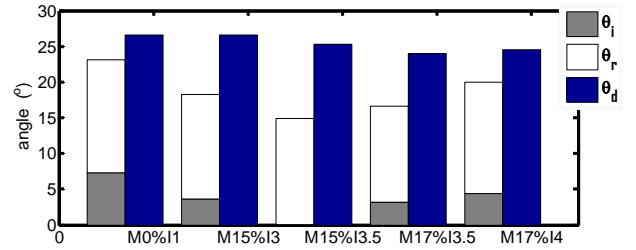


**Figure 6.** Components of body angle at the end of stance compared to movement deflection angle.

The hypothesis that braking force should decrease was rejected. This was due to the invalidity of two assumptions of the model: (1) that body rotation angle ( $\theta_r$ ) should match COM speed deflection angle ( $\theta_d$ ), and (2) that the body rotational angular speed ( $\omega$ ) at the beginning of turning is zero.

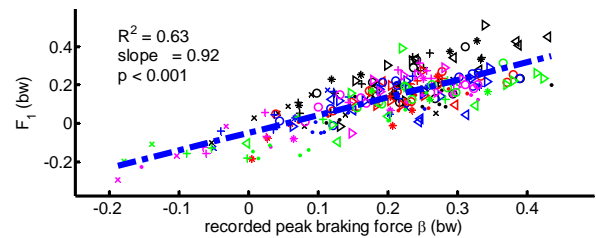


**Figure 7:** Predicted ( $F_1$ ) vs. measured ( $\beta$ ) braking force. Individual participants are indicated by different symbols. Different tasks are different colors, *M0%I1* black, *M15%I3* red, *M15%I3.5* blue, *M17%I3.5* magenta, and *M17%I4* green.

However, by adding additional item  $\omega\tau/\theta_d$  and  $\theta_r/\theta_d$  to Eq 2 accounting for the violation of model assumption a new prediction model (Eq 3) predicted braking force  $F_1$  closer to  $\beta$  in Figure 7.

$$F_1 = \frac{\pi I [(1 - \epsilon) + (\theta_r + \omega\tau)/\theta_d - 1] \theta_d}{\tau^2 P_p} \quad (3)$$

## CONCLUSIONS

Braking forces reflect not only the requirements to prevent over-rotation due to ML turning forces, but also to initial angle and rotational speed.

## REFERENCES

1. Jindrlich, D.L., T.F. Besier, and D.G. Lloyd. J. Biomech., 2006. 39(9): p. 1611-1620.
2. Jindrlich, D.L., et al. J Exp Biol, 2007. 210 (Pt 8): p. 1378-90.
3. Huston, R.L., Passerello, Chris. E., The Mechanics of Human Body Motion. Oxford Science Publications, 1982.

# Force-based Index Finger Biomechanical Model

<sup>1</sup>Dan Qiu and <sup>1,2</sup>Derek G. Kamper

<sup>1</sup>Illinois Institute of Technology, Chicago, IL, USA

<sup>2</sup>Rehabilitation Institute of Chicago, Chicago, IL, USA

email: [dqiu1@iit.edu](mailto:dqiu1@iit.edu) web: <http://handlab.iit.edu>

## INTRODUCTION

Human biomechanics is complex, with a number of muscles impacting the movement of even one joint. In order to make the study of biomechanics more tractable, a “moment arm-based model” is often employed in which each muscle force is mapped to a corresponding joint torque [1]. While this method has proven quite effective for representing certain joints, it has some potential shortcomings for multi-articular musculotendon units, such as those of the hand. Indeed, a “force-based model”, which mapped musculotendon forces directly to the index finger segments, yielded a more accurate forward dynamics simulation than a moment arm-based model [2].

We sought to extend that force-based model to three dimensions. For this study, the model was used to simulate the isometric fingertip force generated under loading of flexor digitorum profundus (FDP). The predicted force directions were compared with the results of muscle stimulation experiments performed in vivo with human subjects [3]. Agreement with the experimental data was substantially better for the force-based model than for a moment arm-based model developed for comparison.

## METHODS

In our force-based model, the index finger is represented as a system of bones, joints and musculotendons within the Simulink SimMechanics environment (MathWorks, Natick, MA). The three phalanges are modeled as simple solid cylinders. The three anatomical joints, metacarpophalangeal (MCP), proximal interphalangeal (PIP) and distal interphalangeal (DIP), are represented with four revolute joints to simulate MCP flexion/extension, MCP abduction/adduction, PIP flexion/extension

and DIP flexion/extension. The two degrees-of-freedom of the MCP joint were represented with two consecutive, intersecting but non-orthogonal revolute joints [4].

In accordance with a previous study, the musculotendon units are represented in our model as inelastic strings with insertions onto the bone segments [5]. The force within the virtual string (string elements are not available in the SimMechanics toolbox), is calculated mathematically at each time step and applied to the segments of interest as an external force. Anatomical pulleys, such as the annular ligaments, and sites of tendon wrapping around the bone are modeled as bodies attached to the finger segments with height but no mass. The force normal to the virtual pulley is then applied to the finger phalanges in the model. Tendons wrap around a virtual sphere at each joint. Passive joint torques are included to account for static and dynamic passive torques [5]. The finger segment dimensions and pulley positions were measured in cadaver specimens.

The model was used to simulate isometric force generation at the fingertip in response to loading of the FDP tendon at 5 N. This level of loading yielded fingertip force vectors similar in magnitude to those evoked by stimulation of FDP. Nine postures across the index finger working space were tested (Table 1). The predicted forces were compared with those obtained from experiments involving in vivo stimulation of FDP with intramuscular electrodes at these same postures [3]. A moment arm model was also built to compare its ability in predicting static fingertip force direction [1].

## RESULTS AND DISCUSSION

Predicted fingertip force direction was far superior for the force-based model than with the moment

arm-based model. In terms of absolute angle, the mean (standard deviation) error in force direction for the force-based model was  $8^\circ (\pm 6^\circ)$  across all 9 postures (Table 1). In accordance with the experimental results, the force direction shifts from more proximal to more palmar when the IP joints are flexed. In contrast, the error was  $90^\circ (\pm 37^\circ)$  for the moment arm-based model (Fig. 1). The relationship with IP angle does not match the experimental data (Table 1). It should be noted that the force-based model predicted a slightly greater directional change of the fingertip force vector for changes in IP posture than the experimental data.

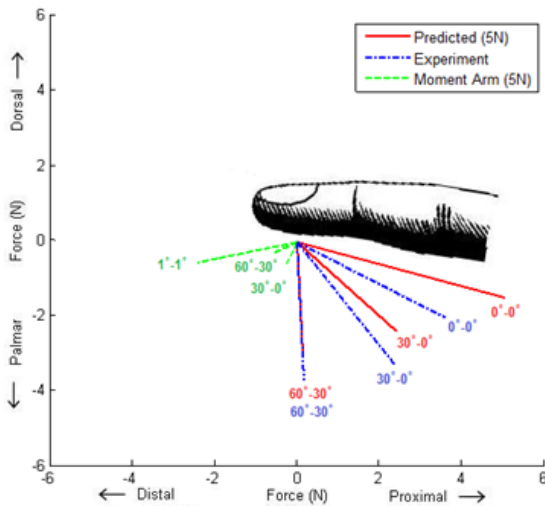


**Figure 1.** Predicted fingertip force compared with in vivo experiment data during FDP loading. In this series of tests, MCP joint are fixed at  $30^\circ$ , while PIP-DIP joints changed across  $0^\circ-0^\circ$ ,  $30^\circ-0^\circ$  and  $60^\circ-30^\circ$ . FDP is under a loading of 5N.

Importantly, the force-based model also permits simulation of any physiological joint angle. The

moment arm-based model, however, creates singularities in the transposed Jacobian matrix and cannot obtain a unique end point force solution when the DIP and PIP angles are both  $0^\circ$  angles. The force-based model does not have such algebraic uncertainty.

## CONCLUSIONS

The force-based model realistically described flexor force transmission within the index finger. Simulation of isometric loading yielded results similar to those obtained from in vivo muscle stimulation. In the future, further validation will be performed with cadaver specimens and for loading of all of the index finger muscles. A corresponding thumb model is underway.

## REFERENCES

1. Valero-Cuevas FJ, et al. *J Biomech* 31(8): 693-703.
2. Lee SW, Kamper DG. *IEEE Transactions on Biomedical Engineering* 56(9):2253-62.
3. Kamper DG, et al. *Clinical Biomechanics* 21:361-369.
4. Brand PW, Hollister AM. *Clinical Mechanics of the Hand*, Mosby, 1999
5. Kamper DG, et al. *J Biomech* 35(12): 1581-1589.

## ACKNOWLEDGEMENTS

This research was supported by NINDS of the National Institutes of Health (1R01NS052369).

**Table 1.** Comparison of predicted fingertip forces for FDP muscle activation

| Joint Angles |            |            | Experiment |              | MA model    |              | Force-based model |              |
|--------------|------------|------------|------------|--------------|-------------|--------------|-------------------|--------------|
| MCP          | PIP        | DIP        | Angle*     | Magnitude(N) | Angle*      | Magnitude(N) | Angle*            | Magnitude(N) |
| $0^\circ$    | $0^{***}$  | $0^{***}$  | $33^\circ$ | 3.09         | $168^\circ$ | 2.55         | $14^\circ$        | 5.25         |
| $0^\circ$    | $30^\circ$ | $0^\circ$  | $48^\circ$ | 4.59         | $113^\circ$ | 0.63         | $38^\circ$        | 3.85         |
| $0^\circ$    | $60^\circ$ | $30^\circ$ | $87^\circ$ | 4.22         | $154^\circ$ | 0.70         | $83^\circ$        | 3.14         |
| $30^\circ$   | $0^{***}$  | $0^{***}$  | $29^\circ$ | 4.21         | $168^\circ$ | 2.55         | $16^\circ$        | 5.36         |
| $30^\circ$   | $30^\circ$ | $0^\circ$  | $53^\circ$ | 4.08         | $113^\circ$ | 0.63         | $44^\circ$        | 3.45         |
| $30^\circ$   | $60^\circ$ | $30^\circ$ | $87^\circ$ | 3.71         | $154^\circ$ | 0.70         | $87^\circ$        | 2.96         |
| $60^\circ$   | $0^{***}$  | $0^{***}$  | $27^\circ$ | 4.87         | $168^\circ$ | 2.55         | $23^\circ$        | 4.32         |
| $60^\circ$   | $30^\circ$ | $0^\circ$  | $45^\circ$ | 3.26         | $113^\circ$ | 0.63         | $54^\circ$        | 2.95         |
| $60^\circ$   | $60^\circ$ | $30^\circ$ | $88^\circ$ | 2.83         | $154^\circ$ | 0.70         | $95^\circ$        | 2.76         |

\*The angle is measured from a proximal direction reference vector (respected to distal phalanx) to the force vector.

\*\*To avoid a singularity posture, the moment arm model simulations were run with (DIP $^\circ$ ,PIP $^\circ$ ) joint angles of ( $1^\circ, 1^\circ$ ) instead of ( $0^\circ, 0^\circ$ ).

# PRENATAL MOTOR DEVELOPMENT AFFECTS OBSERVED MOTOR BEHAVIOR FOR DIFFERENT INCUBATION PERIODS IN DOMESTIC CHICK

Kornelius Rácz<sup>1\*</sup>, Anil Sindhurakar<sup>2\*</sup>, Nina S. Bradley<sup>2,3</sup> and Francisco J. Valero-Cuevas<sup>1,3</sup>

<sup>1</sup>Department of Biomedical Engineering, <sup>2</sup>Systems Biology and Diseases, <sup>3</sup>Division of Physical Therapy and Biokinesiology, University of Southern California, Los Angeles, CA, USA. \*Equal contribution.

Email: {sindhura, raths}@usc.edu

## INTRODUCTION

The length of incubation and thus, the time to hatch, significantly vary in chick embryos (*Gallus gallus*) with light exposure conditions. Continuous incubation in the dark throughout embryogenesis (24D) delays hatching by 1-2 days (~5-10% of total gestation), as compared to incubation in daily periodic light (12 hours of light, 12L) or continuous bright light (24L). Do such light-induced changes during prenatal development impact postnatal motor skill? Our null hypothesis is that, regardless of incubation conditions, chicks adapt and hatch equally ready to cope with the postnatal environment. In agreement with this, a recent study of global gait parameters found no differences in body weight, leg length or locomotor competence across these 3 conditions [1]. However, unconstrained overground locomotion is a highly variable behavior, and the global gait parameters may not have been sufficiently sensitive to detect group differences, if they existed. Thus, in this study we investigate postural control of sway during quiet stance, by examining center of pressure (COP) dynamics, as a more sensitive measure of motor skill [2]. Our results identify significant differences across incubation conditions for several postural metrics, suggesting that length of incubation impacts motor behavior on the day of hatching.

## METHODS

To investigate COP dynamics during quiet stance, we trained chicks on the day of hatching to stand on a custom-designed force plate (Fig. 1), positioned on a 6-axis force transducer (ATI Nano17, Apex, NC). Hatchlings stood quietly on the force plate for 30 s per trial for a minimum of 3 trials (N=30 chicks, 10 chicks per light condition). All procedures were approved by the USC IACUC.

We extracted the 2-dimensional COP data (Fig.2) and analyzed parameters commonly investigated in postural control studies: mean sway velocity (MV), mean sway angle (SW), and mean distance from COP centroid (MD) [2]:

$$MV = \sum_{n=1}^{N-1} |X[n+1] - X[n]| / T$$

$$SW = 1/2T \sum_{n=1}^{N-1} |X_1[n+1]X_2[n] - X_1[n]X_2[n+1]|$$

$$MD = 1/N \sum_{n=1}^N [X_1[n]^2 + X_2[n]^2]^{1/2}$$

where T is the trial length and X[n] are the 2-dimensional coordinates at the n-th sample. Moreover, we computed the variance percentage explained by the anterior-posterior/medio-lateral (AP/ML) directions as well as the ratio of these variances. Next, we separated deterministic components, possibly related to a control strategy, from stochastic components, i.e. the noisiness of the system and looked for differences across conditions [3]. For this purpose, we fitted a 2<sup>nd</sup> order function V(x) to the data's state space [ X,  $\dot{X}$  ] according to

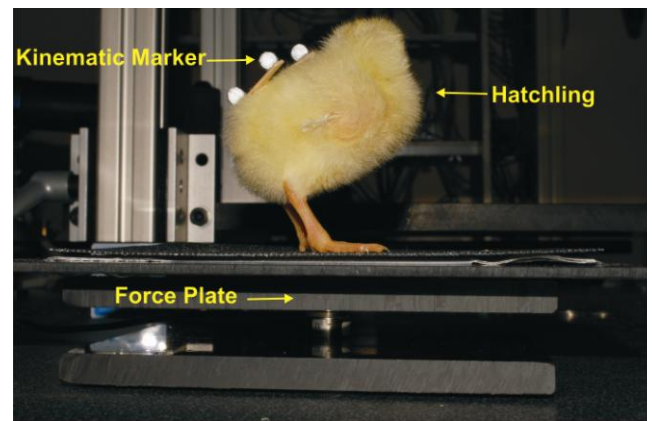


**Figure 1:** Experimental setup. A hatchling performing a quiet stance trial on the force plate.

the potential function formulation  $F = -dV/dx$ , i.e., the force applied to a particle is proportional to the value of a potential function  $V(x)$  [4]. Finally, we fitted a 2<sup>nd</sup> order function to the data's state-dependent variance  $\text{VAR}(X|X = x)$  in a sufficiently large neighborhood of a sample data point  $x$  [2]. The potential function  $V(x)$  quantifies the tendency of a stable system to return to a stable fix point, in this case the COP centroid, for a given displacement,  $dx$ . On the other hand, the conditional variance quantifies the state-dependent variability of the COP dynamics.

## RESULTS AND DISCUSSION

Postural control of sway, as measured by COP dynamics, differed significantly across the 3 incubation conditions with respect to sway velocity, sway area and average distances from the mean COP. All measures were largest for chicks experiencing the longest incubation period (24D condition) and smallest for chicks experiencing the shortest incubation period (24L condition). Also, the proportions of COP variance along the AP and ML directions were largest in the 24D group, while the ratios of these proportions were similar across conditions. This suggests that largest sway area positively varied with length of incubation. However, a similarly shaped COP ellipse was found across all chicks. Other metrics such as total number of turns during postural sway, total length of COP path and mean frequency of sway in AP direction did not vary with length of incubation induced by light conditions.

Regarding the deterministic vs. stochastic analysis, we found that chicks with the largest state-dependent accelerations were associated with longer incubation condition (24D). The findings indicate hatchlings in this group executed larger corrective efforts against COP divergence. Further, we found that these chicks also exhibited the largest state-dependent variability, suggesting a relatively stronger random or noise component.

## CONCLUSIONS

In contrast to the findings of our earlier gait study, we find that quiet stance in chicks is affected by length of incubation, evidence that leads us to reject the null hypothesis. We see higher sway velocity,

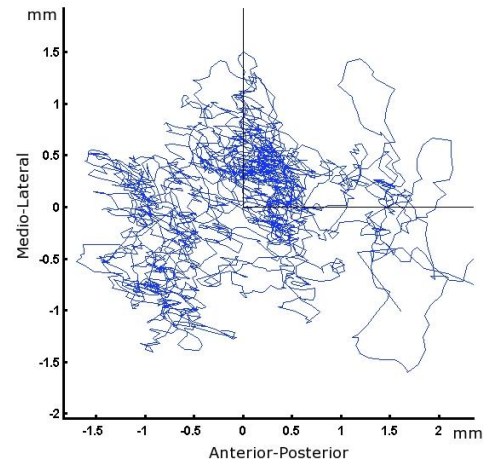


**Figure 2:** COP displacement in ML and AP directions for postural sway in a 24L hatchling.

larger sway area and longer average distances from mean COP in chicks with the longest incubation period (24D). These animals developed a noisier postural system, while exhibiting the strongest tendency to return to a stable fixed-point, possibly to cope with the increased noise level. Larger sway measures are typically associated with inferior postural control following nervous system lesions [5]. Thus, whether or not these differences reflect developmental adaptations in sensorimotor function requires further investigation. Moreover, our results suggest the next set of experiments in which the application of external perturbations during quiet stance tests postural stability. This would be a direct test of whether or not sensorimotor function is impacted by incubation period.

## REFERENCES

1. Sindhurakar A and Bradley NS. *Dev Psychobiol*, **52**, 802-8011, 2010.
2. Prieto TE, et al. *IEEE Trans Biomed Eng*, **43**, 956-966, 1996.
3. Gottschall J, et al. *Physics Letters A*, **373**, 8-9: 811-816, 2009.
4. Strogatz SH. *Nonlinear Dynamics and Chaos*. Westview Press, 1994.
5. Murray MP, et al. *J Bone Joint Surg Am*, **57**, 510-516, 1975.

## ACKNOWLEDGEMENTS

This work was supported in part by NIH HD053367, AR050520 and NSF EFRI 083604.

# SIMULATIONS OF OPTIMAL REWEIGHTING OF MUSCLE COORDINATION REVEAL IMPORTANT BENEFITS OF MUSCLE REDUNDANCY

Kornelius Rácz<sup>1</sup> and Francisco J. Valero-Cuevas<sup>1,2</sup>

<sup>1</sup>Department of Biomedical Engineering, <sup>2</sup>Division of Biokinesiology and Physical Therapy,  
University of Southern California, Los Angeles, CA, USA  
email: raths@usc.edu web: http://bbdl.usc.edu

## INTRODUCTION

For many decades, a dominant view in the motor control research community has been that the nervous system somehow needs to cope with the presumed computational challenge of selecting a muscle activation pattern from a seemingly infinite amount of patterns that give rise to the same endpoint forces [1]. Others have proposed that redundancy offers benefits, such as potentially enabling the preservation of muscle synergies under fatigue [2]. We, on the other hand, propose that instead of adhering to synergistic muscle activations, the central nervous system could take advantage of redundancy to explore the solution space: by dynamical reweighting of muscle activation patterns a (static force production in this case) task could be performed successfully for a longer period of time than by adhering to a same or synergistic pattern. However, the nature and benefits of such dynamical reweighting of muscle activation are not known.

## METHODS

We created a model of isometric three-finger grasps actuated by 21 muscles of the three fingers. The relationship  $\vec{f}(t) = J^{-T} R F_0(t) \vec{a}(t)$  describes the mapping from muscle activations to endpoint forces:  $\vec{a}(t)$  represents the time-varying vector of muscle activations, between 0 and 1, and  $\vec{f}(t)$  the 6-dimensional grasp wrench (3 force and 3 moment components) applied to a grasped object. The matrix  $F_0(t)$  is diagonal and scales the muscle activations with respect to their maximal force generating capabilities. The matrix  $R$  maps the muscle forces to joint torques [4,5], while the transposed inverse Jacobian  $J^{-T}$ , which is posture-dependent, maps the joint torques to the object wrench. To compute  $J^{-T}$ , we based the posture parameter values on [3], and described the fatigue

dynamics of the  $i$ -th muscle by:

$$\text{Fatigue rate: } \frac{df_{0_i}}{dt} = -\frac{1}{t_{fat}} a_i(t) f_{0_i}(t)$$

where the  $f_{0_i}(t)$  are the entries of the matrix  $F_0(t)$ .

Hence, the fatigue dynamics directly affects the ability of muscles to generate force. Their fatigue rate is proportional to their activation level and a fatigue time constant  $t_{fat}$ . Because we focus on activity-dependent fatigue rates, recovery dynamics are not included at this point. We computed the optimal schedule of reweighting of muscle activation as minimizing the quadratic cost

$$Cost_{dynamic} = (F - F_0)^2$$

i.e., maintaining a constant sum of normal forces applied by the three fingers, while minimizing tangential components [3]. In [6] we describe how 20% MVC is a sufficiently low force magnitude such that no one muscle is necessary for the task. The initial coordination pattern  $\vec{a}(0)^*$  minimized the sum of squared muscle activations. This optimal coordination pattern was also the one adhered to when reweighting was not allowed. Its cost function

$$Cost_{proportion} = \left( \frac{\sum_i \vec{a}(t)}{\sum_i \vec{a}(0)^*} \right)^2$$

aims to keep constant the relative activation weights of muscles, i.e. the direction of the vector in activation space, while allowing an overall increase in activation in response to fatiguing. This was the conclusion in [3]. Lastly, we considered

$$Cost_{proportion\&magnitude} = (\vec{a}(t) - \vec{a}(0)^*)^2$$

which in addition to the previous strategy, also aims to keep constant the activation vector magnitude. We used the GPOPS optimal control algorithm, in its MATLAB implementation, to find the optimal muscle activation schedule (i.e., time history of muscle activations) that optimizes each of the 3 cost

functions. Due to computational constraints, we set the fatigue time constant to 1 s and the time horizon to 15 s, and, for now, restricted ourselves to optimizing the activation schedule in the index finger only, assuming that the other 2 fingers produce the necessary force to meet the task conditions. Lastly, we compared the overall force reserves across the three strategies. This suffices for a rigorous initial comparison across these neural control strategies.

## RESULTS AND DISCUSSION

We tracked the relative contributions of individual muscles to overall muscle activation (Figure 1).

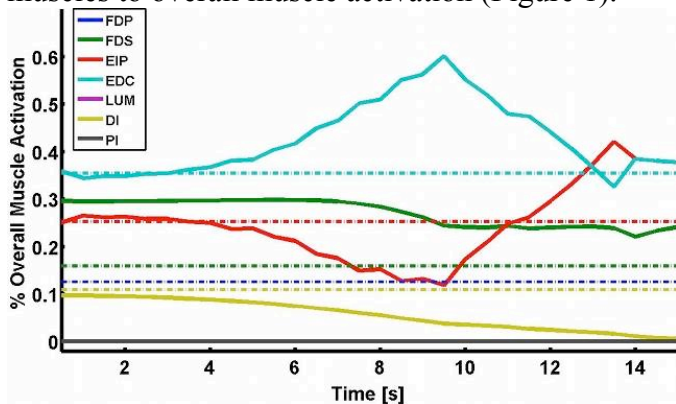


**Figure 1:** Index muscle activations as proportions of overall activation (solid lines: dynamic reweighting strategy, broken lines: rigid strategies). While several muscles hardly contribute, EDC takes over EIP's role initially, later they reverse.

Figure 2 quantifies the fatigue state of index finger musculature over time for all three strategies.

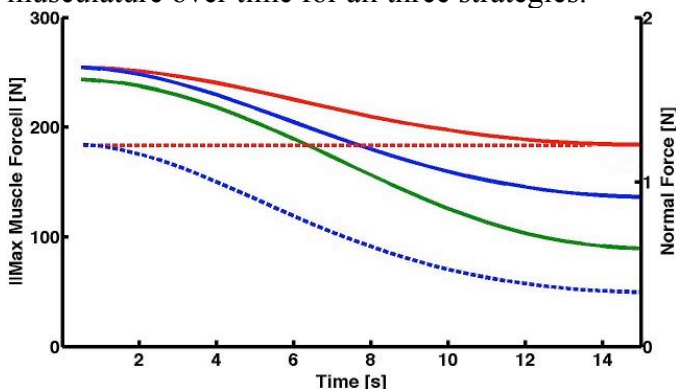


**Figure 2:** Force generating capability for three different muscle activation schedules (solid lines, left y-axis): dynamical (red), constant proportions (blue) and constant proportions and overall magnitude (green). Dashed lines show the index endpoint normal force (right y-axis) generated by each strategy. Note that the most rigid strategy fails quickly, while the other two (red dashed line) maintain the required normal force.

We see that, after 15 s, the dynamical reweighting strategy retains 25 % and 40 % greater force reserves, respectively, compared to the rigid approaches, the latter of which actually fails to produce the required endpoint force.

## CONCLUSIONS

While benefits have been attributed to muscle redundancy, to our knowledge this is the first work to show at the level of optimal coordination that dynamical reweighting provides greater specific functional benefits. Our results suggest that isometric force tasks, subject to very simple fatigue dynamics, can be executed with significantly less expenditure and possibly for a longer time, if the nervous system takes advantage of muscular redundancy by dynamically reweighting the activation magnitudes of muscles, thus traversing the solution space of activation patterns that fulfill the task. Importantly, we show that adhering to a specific, or even synergy-associated or synergy-constrained, activation pattern proves to be functionally detrimental in the presence of fatigue dynamics. Having the ability to dynamically change muscle activation patterns, while generating equivalent forces, possibly outweighs the presumed computational disadvantage of selecting muscle activation patterns.

## REFERENCES

- 1.N. Bernstein, *The Coordination and Regulation of Movements*, Pergamon Press, New York (1967).
- 2.F. Danion, M.L. Latash, Z.M.Li, V.M. Zatsiorsky. *J Physiol* 523(2): 523-532 (2000).
- 3.A. Danna-Dos Santos et al. 104(6): 3576-3587 (2010).
- 4.F.J. Valero-Cuevas, F.E. Zajac, C.B. Burgar, *J Biomechanics* 31(8): 693-704 (1998).
- 5.F.J. Valero-Cuevas, M.E. Johanson, J.D. Towles, *J Biomechanics* 36(7): 1019-1030 (2003).
- 6.K. Rácz, J.J. Kutch, Valero-Cuevas FJ. *Proc. 21th Annual Meeting of the Soc. for the Neural Control of Movement, San Juan, Puerto Rico* (2011).
- 7.A.V. Rao, *ACM Trans Math Softw* 37(2): 1-39 (2010).

## ACKNOWLEDGEMENTS

NIH AR050520, AR052345, NSF EFRI-COPN 0836042 and NIDRR RERC 84-133E2008-8 grants to FVC have supported this work.

# EMG-driven Muscle Activations Tune Post-Stroke Computed Muscle Control Simulations

John W. Ramsay, Thomas S. Buchanan, Jill S. Higginson

Center for Biomedical Engineering Research  
Delaware Rehabilitation Institute  
University of Delaware, Newark, DE, USA  
Email: jramsay@udel.edu

## INTRODUCTION

OpenSim is an open-source musculoskeletal modeling program that uses computed muscle control (CMC) to estimate muscle excitation patterns during a particular task [1,2]. CMC determines the excitations by minimizing the weighted sum of muscle forces while reproducing the desired kinematics. With this approach, estimates of muscle excitations in populations with known muscle activation impairment (i.e., stroke) may not be accurate without proper input signals representative of the neural impairment.

An EMG-driven forward dynamic model that uses signals of neural command from electromyography (EMG) to predict muscle activations during a desired task has been developed [3]. Through a process of muscle activation dynamics and muscle contraction dynamics, muscle forces are determined.

The purpose of this study was to use surface EMG signals to tune a post-stroke computed muscle control simulation by constraining muscle excitations in OpenSim to optimized muscle activation patterns. We expected that by using EMGs we would get different and more reasonable predictions of individual muscle activations and muscle forces than by using CMC alone..

## METHODS

Three dimensional kinematic and kinetic data were collected using a split-belt treadmill for one post-stroke hemiparetic subject (48 yrs, right paretic) and processed in Visual 3D (C-Motion Inc., Bethesda, MD). Subject-specific anthropometric scaling parameters and motion data for one gait cycle was exported by Visual3D and input into OpenSim v.

1.8.1. Net joint ankle moments were calculated using inverse dynamics in Visual 3D for input to the EMG-driven model.

A musculoskeletal model with generic muscle parameters, 23 DOFs and 70 muscles was used in OpenSim [1]. Individual ankle muscle moment arms and musculotendon lengths were calculated based on the subject's kinematics and used as input into the EMG-driven model. CMC was used to estimate ankle muscle excitations and activations during the trial [2].

Raw EMG was also collected during gait analysis. We recorded the medial gastrocnemius (MG), lateral gastrocnemius (LG), soleus (SOL), and tibialis anterior (TA). All were taken from the paretic side. Individual muscle EMG were high-pass filtered, fullwave rectified, and low-pass filtered [3]. Each EMG was normalized to the subject's maximum EMG during data collection and used as input to the EMG-driven model. The model determined the muscle activations required to achieve the desired joint moments by minimizing the error between the model joint moment and moment computed by inverse dynamics and by optimizing subject-specific muscle activation and contraction dynamic parameters [3].

Muscle activations from the EMG-driven model (Figure 1a) were then used to constrain the muscle excitations calculated by CMC. First, all four muscles were constrained and the muscle forces were calculated. Secondly, two arbitrarily chosen muscles (SOL, LG) were constrained to the EMG-driven activations while CMC estimated the remaining activations. Output muscle forces for each condition were then compared.

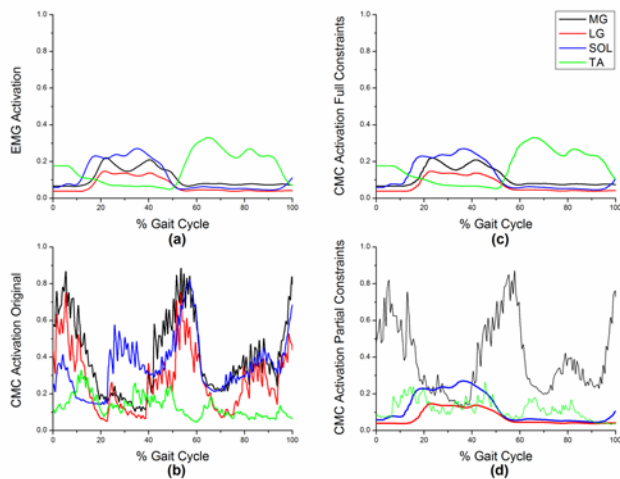


**Figure 1.** Individual muscle activations (a) EMG-driven model (b) CMC, unconstrained (c) CMC, all four muscles constrained (d) CMC, LG and SOL constrained.

## RESULTS AND DISCUSSION

The EMG-driven model calculated muscle activations between 0 and 0.4. Such a low range suggests neural impairment for these paretic muscles. Without constraining any muscle excitations in OpenSim, muscle activation predictions fluctuated between 0.0 and 0.8, with most of the activation occurring over 0.4 (Figure 1b). As a result, muscle forces were almost double that of the EMG-driven model forces (Figure 2a,b). In neurologically impaired populations such as stroke, this activation range is likely to be unrealistic and the muscle forces may not be accurate.

When all muscle excitations were constrained in CMC to the activations from the EMG-driven model (Figure 1c), muscle forces began to resemble those from the EMG-driven model (Figure 2c), within 300 N.

Constraining the LG and SOL resulted in both the activations and muscle forces for MG and TA to revert back to similar patterns of the original CMC estimation (Figure 1d, 2d). While this was not expected, it may be due to the cost function used in CMC. Changing the cost function to minimize the

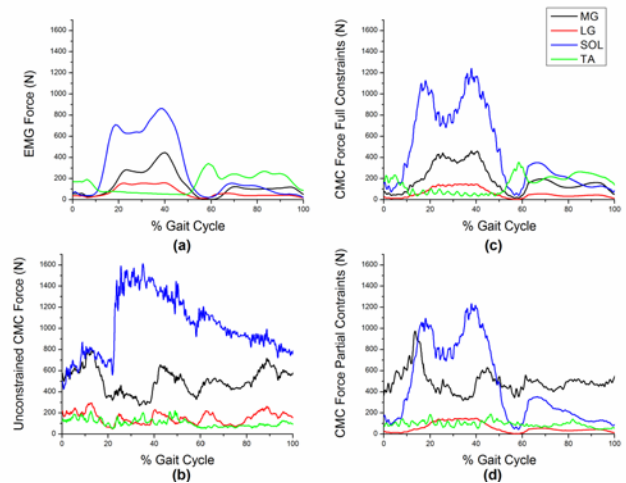


**Figure 2.** Individual muscle forces (a) EMG-driven model (b) CMC, unconstrained (c) CMC, all four muscles constrained (d) CMC, LG and SOL constrained.

activations may produce results closer to the EMG-driven model.

## CONCLUSIONS

For this particular stroke subject, CMC produced inaccurate muscle activations when unconstrained during gait. Using EMGs to tune a computed muscle control simulation can be beneficial and advantageous when simulating gait in subjects with impaired muscle control such as stroke. This indicates that combining EMG-driven modeling with CMC gives biomechanical models the unique ability to account for the unusual muscle activation patterns observed in patients with neuromuscular impairments, thereby giving more reasonable muscle force predictions.

## REFERENCES

1. Delp SL, et al. *IEEE Trans Biomed Engn.* **54**, 1940-1950, 2007.
2. Thelen DG, et al. *J Biomech.* **36**, 321-328, 2003.
3. Buchanan TS, et al. *J Appl Biomech.* **20**, 367-395, 2004.

## ACKNOWLEDGEMENTS

We appreciate data collection by Erin Helm, and funding sources NIH NS055383 and AR046386.

# Automated methods for determination of 3D muscle fascicle orientation in human muscle using free hand ultrasound

Manku Rana and James M. Wakeling

Department of Biomedical Physiology and Kinesiology, SFU Burnaby, B.C Canada  
email:mrana@sfu.ca

## INTRODUCTION

Muscle architecture is a major determinant of mechanical function of skeletal muscle. Muscle fascicle orientation is an important architectural parameter affecting the muscle properties. Most previous studies on muscle architecture have been in 2D and the importance of 3<sup>rd</sup> dimension is not much explored. Further, the 3D orientation of the whole muscle may be regionalized and is not uniform across the whole muscle. In order to study the 3D fascicle orientation across the muscle, we need to develop reliable methods to obtain the same.

In this study, we present the methods that we have developed and validated to determine the 3D muscle architecture using 2D ultrasound and a 3D position tracker system.

## METHODS

### *Data collection and processing*

In order to obtain 3D muscle fascicle orientation, we collected 2D images using a linear ultrasound probe (Echoblaster, Telemed, LT) in B mode that was attached to a rigid body position sensor set up made up of three optotrak markers (Certus, Optotrak, NDI, Ontario). The position sensor provided the position and orientation of the probe in three dimensions. The probe was moved in a sweeping motion while scanning the calf muscle in a water tank, with scan times lasting for 2 mins for the whole calf muscle. 2D fascicle orientations were determined at each pixel in the image plane using the methods described previously [1]. The pixels in the image were transformed to voxels and 2D orientations to 3D direction cosines in 3D lab space using the probe position and orientation in lab space. This involved two transformations (a) from image plane to the position sensor frame of reference (b) from position sensor to the lab frame of reference  $T_p^c$ , represented by the following equation

$$C(x, y, z) = T_p^c T_i^p(su, sv, 0)$$

where  $C(x, y, z)$  is a point in lab frame of reference,  $(u, v)$  is a point in image plane,  $s$  represents the scale between pixels and the actual distance.  $T_p^c$  is calculated using the position and orientation information of rigid body from rigid body frame of reference to lab frame of reference.  $T_i^p$  is the unknown transformation matrix and was calculated by calibrating the ultrasound probe using a two wire method [2]. The 2D fascicle orientations in the image plane were transformed to 3D direction cosines in lab space using the above. From the direction cosine values we calculated mean pennation angle relative to deep aponeurosis and mean length of the fascicles from belly region to compare with previously reported values.

Due to the nature of the sweeping motion of the probe, multiple sweeps over same region result in more than one pixel (from different images) belonging to a particular voxel. We have to choose from multiple pixels belonging to same voxel, based on the fascicle structure in the image. From a view point perpendicular to the fascicle planes, fascicles appear like long lines in the image. At an oblique plane, the fascicles would appear as dots and the orientation information cannot be obtained from there. The pattern in the image lies between these two extremes. We selected the pixels for a particular voxel using the wavelet convolution number. A pixel with greater convolution value matches the spatial frequency of line like pattern in the local region around the pixel with the special frequency expected from that region of image.

### *Validation*

The methods to determine 3D muscle fascicle orientation were validated by testing them on a physical phantom. The phantom was made with horse hair stacked parallel to each other in ten layers 2mm apart. The hair ends were digitized using an optotrak

stylus to determine the orientation of hair in space. The phantom was immersed in water and scanned from different positions and orientations of the probe with the scanning protocol identical to the one used for scanning the muscles. The images were processed using the above methods to obtain 3D orientation of the hair strands as direction cosines.

## RESULTS AND DISCUSSION

The muscle fascicle orientation was represented as direction cosines in 3D and plotted as small vectors in the space as a vector field (fig 1). We tracked a few representative fascicles for visualization. Fig 1 shows the vector grid from different views. View 1 is along the fascicles planes and we can see the planes running along the muscle and the fascicles pennating in the plane which can be viewed from a perpendicular viewpoint as in view 2. The measured pennation angle (12.27 °) and fascicle length (50.4 mm) from direction cosines lie within the range of previously reported values 11.3 - 16.7 ° and 41.6 – 74.0 mm respectively [3,4].

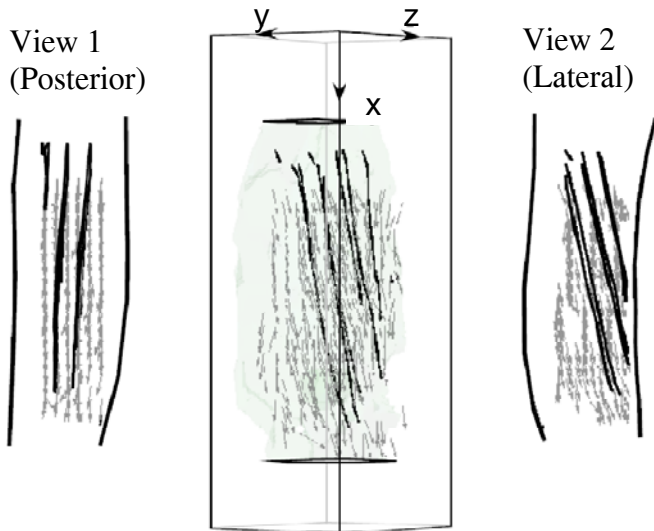


**Figure 1:** Representation of fascicle orientations in 3D, and projections of the image in two perpendicular planes.

The errors in the direction cosines from the validation procedure are shown in table 1. The error was calculated as the difference in each component of the direction cosines as measured from the methods and from phantom digitization. The mean error in predicting the orientation value was less than 0.5 degrees in the three co-ordinate planes for the physical phantom. It has to be considered that this

error is not solely from the automated methods described above rather phantom digitization also contributes to this error. Some part of the standard deviation in the results can be explained from the fact that the orientation of hair were obtained by digitizing the ends of the strands of the hair in the top layer. In a few images, hairs were seen bent and joined together which shows that not all hair stayed at the same orientation in the water.

To the best of our knowledge, there are no previous methods available to quantify 3D muscle fascicle orientations in the whole muscle using ultrasound and our methods are novel. DT-MRI has been used to study muscle architecture in 3D but has not been successfully used for contracting muscle due long scan times of 15 mins. Due to the short scan times our methods can be used to determine muscle fascicle orientation in an active muscle.

## CONCLUSIONS

Our methods can be used to determine *in vivo* muscle fascicle orientation in 3D. The methods provide a tool to quantify the regionalization of fascicle orientation in the muscle and study the change of 3D fascicle architecture in contracting muscle. Having reliable methods to quantify the architecture in 3D will enable to test the importance of the third dimension in the relation to muscle architecture and function.

## REFERENCES

1. Rana M, et al. *J Biomech* **42**(13), 2068-2073, 2009.
2. Dandekar S, et al. *Ultrasound Med Biol* **31**(8), 1083-1093, 2005.
3. Maganaris CN, et al. *J Appl Physiol* **93**(6), 2089-2094, 2002.
4. Martin DC, et al. *J Anat* **199**(Pt 4), 429-434, 2001.

**Table 1:** Error in direction cosines in the three co-ordinate planes

| Plane | Mean error (°) | Std Dev (°) |
|-------|----------------|-------------|
| yz    | -0.32          | 2.81        |
| xz    | -0.41          | 2.21        |
| xy    | 0.05           | 2.11        |

# DEPENDENCY OF SPATIOTEMPORAL CHARACTERISTICS OF HEAD STABILIZATION ON VISUAL AND INERTIAL STIMULATION

Mobin Rastgar Agah, Kurosh Darvish, W. Geoffrey Wright, and Emily Keshner

Temple University, Philadelphia, PA, USA

email: [kdarvish@temple.edu](mailto:kdarvish@temple.edu)

web: [www.temple.edu/engineering/research/labs/tbl](http://www.temple.edu/engineering/research/labs/tbl)

## INTRODUCTION

Falls are a leading cause of injury in older adults. Interaction of visual, vestibular and somatosensory input controls the spatial orientation of the body and a mis-match among these inputs can lead to a faulty perception of body position and motion and cause postural instability. The role of these sensory systems in head control makes the head a good prototype of the whole body to study the effect of conflicting sensory inputs on postural stability [1].

The visual system is more sensitive to retinal slip velocity than acceleration while the vestibular system is more sensitive to accelerations. These neurophysiological properties were employed to investigate the effect of conflicting inputs to these sensory systems in order to determine if both postural control (i.e. head stabilization) and spatial perception are similarly affected by a conflict in these sensory systems [2]. Since the dominance of these sensory systems depends on the velocity and acceleration of the motion, the amplitude and frequency of a periodic passive motion together with changes in the visual depth of field were manipulated. Thus, our goal was to study the spatiotemporal effect of discordant visual and vestibular inputs on head stabilization and visual perception during dynamic visual-inertial stimulation. The relationship between visual to inertial motion directions were manipulated using realistic visual virtual environments.

## METHODS

For detecting the movement of the head in three directions of roll, pitch and yaw, three uni-axial gyroscopes (ADXR623 and ADXR624, Analog Device, Inc.) were attached in an orthogonal array on a light-weight helmet. A mini-camera (203CA-1, Pine Computer, CA) was also attached on top of the

helmet to provide the visual input for the subjects through a head mounted display (HMD) (I-glasses HR920-3D, 920,000 Pixels per LCD, i-O Display Systems, Sacramento, CA).

Twelve subjects (3 females, 9 males, age 22 to 32 yrs) participated in this study. The light-weight helmet was firmly secured on the head of subjects seated on a race car seat (Corbeau, Sandy, UT). Using a 5-point harness system the trunk was comfortably fixed while the head was free to move in all directions. The seat was mounted on a sled allowing passive anterior-posterior (A-P) translation of the subject on a track (WIESEL<sup>TM</sup> SPEEDLine®WH120). The movement of the sled was controlled by a programmable modular drive system (MDS) (Control Techniques Drives Inc.).

Sinusoidal signals at 4 different frequencies of 0.1, 0.2, 0.5 and 1.1 Hz were generated and used as the input signal of the MDS to move the subjects. Each trial included 5 cycles and the amplitudes of sinusoidal input at different frequencies were chosen for overlapping peak acceleration or overlapping peak velocity as shown in Table 1. For each frequency, subjects were exposed to 4 different visual conditions in random sequence: 1- Backward (BW), camera was pointed in the posterior direction, 2- Eyes closed (EC), no input to the HMD, 3- Eyes open (EO), camera was pointed in the anterior direction, 4- Sideways (SW), camera was pointed in the lateral direction parallel to the subject's interaural axis. To test the effect of depth of field on the stability of head in the SW condition, half of the subjects were randomly chosen to see a deep field of view while the rest experienced a shallow field of view. The test was conducted 3 times for each frequency-visual condition and gyroscope signals were processed and recorded at a sampling rate of 1000 Hz.

As a first approximation the head movement was considered a linear response to the inertial

input. To obtain the linear response, the first and last cycles were discarded and a least square sine fit regression was used to evaluate the amplitude and phase of the angular velocities of the head in roll, pitch and yaw axes. Typical curve fits are shown in Figure 1.

**Table 1** – Conditions of sled inertial input

| Freq (Hz) | Amp. (m) | $a_{max}$ (g) | $v_{max}$ (m/s) |
|-----------|----------|---------------|-----------------|
| 0.1       | 1.500    | 0.06          | 0.94            |
| 0.2       | 0.750    | 0.12          | 0.94            |
| 0.5       | 0.120    | 0.12          | 0.38            |
| 1.1       | 0.024    | 0.12          | 0.17            |

## RESULTS AND DISCUSSION

There was a main effect of inertial condition on amplitude for all axes of head motion ( $p < .0000$ ) and a shift ( $F_{6,9} = 248.9$ ,  $p < .0000$ ) from phase lead to phase lag of head pitch with increasing frequency ( $121^\circ$ ,  $127^\circ$ ,  $83^\circ$ , and  $-32^\circ$ , respectively). A main effect of visual input on head pitch ( $F_{3,33} = 4.8$ ,  $p = 0.007$ ) was due to the absence of vision (EC). An interaction effect between inertial and visual input on head yaw occurred in SW ( $F_{9,99} = 2.03$ ,  $p = 0.04$ ). Also in SW when comparing deep and shallow depth of field, a significant interaction of depth of field and inertia on amplitude ( $F_{6,60} = 4.55$ ,  $p < 0.001$ ) and phase ( $F_{2,5} = 6.9$ ,  $p = 0.03$ ) of head yaw occurred especially during high peak velocity conditions.

## CONCLUSIONS

In summary, frequency affects head pitch despite matched inertia (i.e.  $a_{max}$ ). Visual effects were mostly washed out by the inertial dominance. However, in SW, visual effects were pronounced in the high velocity ( $v_{max} = 0.94$ ) conditions. Moreover, the absence of visual input (EC) had a highly significant effect on the feed-forward processing needed to stabilize the head as suggested by the higher gains of head pitch. The visual effect seen in SW suggest that sideways visual flow can organize lateral cervical responses despite being discordant with A/P inertial input, however its effects are dependent on the velocity and spatial density of visual content.

The relevance of virtual reality technology as a useful application is evident by its current use in both cognitive and physical rehabilitation. It is well-suited for creating situations of dual-task expectations and creating challenging contexts which include visual-vestibular stimulation and

discordance. Such discordance, however, is not unusual, in that it occurs for any passenger whose visual frame of reference is fixed, limited, or obscured from seeing outside the vehicle, such as in the backseat of a car, on a bus, airplane, tank, or below deck on a boat. With a clear relevance to real-world behavior, we plan to use dynamic visual-inertial inputs during tasks performed in a virtual environment to gain a greater understanding of the dissociable and overlapping processes for sensorimotor adaptation underlying both postural and upper extremity motor control.

## REFERENCES

1. Pozzo T, et al. *Exp Brain Res* **82**, 97-106, 1990.
2. Wright WG, et al. *J Vestibular Res* **15**, 185-195, 2005.

## ACKNOWLEDGEMENTS

The support for this work was partially provided by a Seed Grant from Temple University.

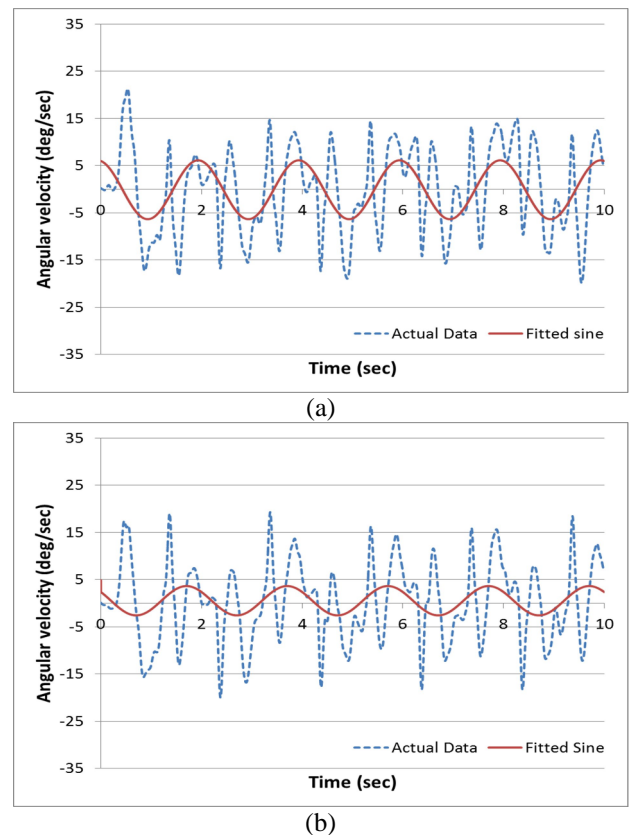


**Figure 1:** Typical fitted sine curves compared to actual angular velocity of the head pitch at 0.5 Hz for one subject (#6) (a) Eyes Closed (EC), (b) Eyes Open (EO).

# WIRELESS MULTI-CHANNEL DEVICE TO CAPTURE DYNAMICS OF COMPLEX SENSORIMOTOR TASKS

Alexander Reyes and Francisco J. Valero-Cuevas

University of Southern California, Los Angeles, CA, USA

email: [reyesale@usc.edu](mailto:reyesale@usc.edu) web: [http://http://bbdl.usc.edu/](http://bbdl.usc.edu/)

## INTRODUCTION

Wearable wireless systems are found in many of today's laboratories to acquire biological or sensor data. However, these systems tend to cater to one type of signal such as EMG or accelerations, have few channels, require specialized wireless protocols, or are bulky and expensive. We describe the design of a novel, low-cost wireless data transmission system that can be used with any Bluetooth-capable computer running Matlab. Consisting of off-the-shelf components, this device provides an inexpensive and reliable means of streaming data a large number of sensors for collection and processing. In addition to being versatile and easy to use, the device adds a level of safety by isolating users from wired power sources. The first use of the device is part of a project to quantify dexterity using the strength-dexterity test [1] and to use force and acceleration data to drive characters, vehicles, etc. in a gaming environment as a means to enhance rehabilitation.

## METHODS

### *Data acquisition and telemetry details*

A user-defined analog low-pass filter is applied to each single-ended analog input channel and digitized using a PIC microcontroller running at 30MHz (Fig. 1). Each 12-bit sample is stored in two 8-bit buffers. The two-byte serial transmission scheme for a single sample is shown in Fig. 2. The four remaining bits contain the channel address to ensure that each sample is stored in the correct location at the receiver. Additionally, start (low) and stop (high) bits are included to ensure invalid data is discarded. These bits indicate to the receiver when a new byte is incoming and when it is complete.

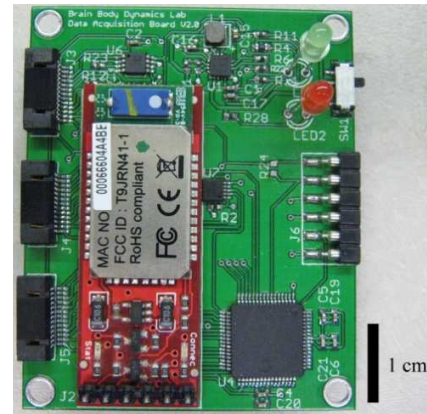


**Figure 1:** Wireless data acquisition system circuit board measuring 4.57 x 5.59 cm (image to scale). 16 single-ended data acquisition channels with 12-bit resolution, Bluetooth wireless link and 2.88 kHz maximal sampling rate per channel when sampling from all 16 channels; 46 kHz for a single channel.

The Bluetooth module (Roving Networks, Los Gatos, CA) can achieve stable transmission rates as high as 921,600 bps. This transmission rate is shared among all channels in use, all of which sample at the same rate. As a result, a maximal sampling frequency per channel is established and given by  $f_{s_{max}} = 46080/N$  (Hz/channel), where N is the number of channels being used. High sampling frequencies are possible even when recording from several channels. For a single channel, the maximal sampling rate is about 46 kHz and 2.88 kHz when sampling from all 16 channels.

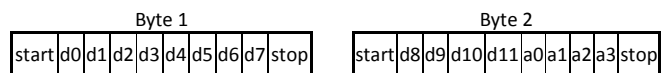


**Figure 2:** Serial communication arrangement for sampled data. 12 data bits and 4 address bits.

### Data collection

To begin data acquisition, the user need only attach the appropriate miniature connectors for the sensors and pair the device to a Bluetooth-enabled computer running Matlab. At the start of data collection, an indication signal is sent to the device to wake it up from a low-power sleep mode. After a user-defined collection time, communication terminates and the device re-enters sleep mode. The data stream is decoded according to channel address and displayed using Matlab.

### Additional salient features

The circuit board is contained within a wearable rectangular enclosure measuring 5.08 x 5.84 x 1.27 cm, making the device smaller than an average cell phone. The device uses a low-profile 3.7 Li-ion rechargeable battery (1000mAh). The board layout was optimized to have direct signal traces with fewer vias and restricted component placement to one side of the board. Two LEDs indicate status: green when the device is on and red when the rechargeable battery is low. Preliminary tests show that with a few hours of use every day, the device can operate for two weeks without the need to recharge the battery.

## RESULTS AND DISCUSSION

Fig. 3 shows five channels of data sampled at 400 Hz for 5 seconds. Channels 0 and 1 show force data applied by the forefinger and thumb, respectively, to the load cells attached at the ends of a spring during compression. Sudden drops in voltage indicate when the fingers lost contact after buckling. Channels 2 through 4 show accelerations in the x, y and z directions as an accelerometer was moved around in space. Here, the accelerometer was not attached to the spring and merely shows that the device is capable of capturing data without signal degradation or inaccurate decoding over a wireless channel. Overall, the data show that it is possible to capture rapid dynamical changes when collecting data from various sensors. All data were collected using a PC laptop running Windows 7, Matlab 2010b and Realterm 2.0.0.70.

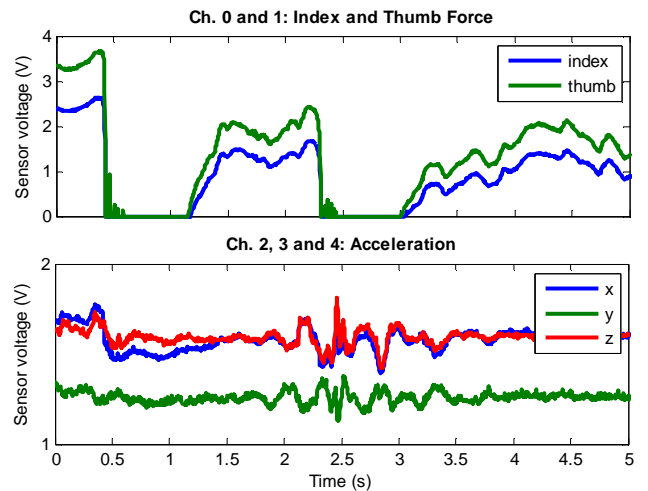


**Figure 3:** Sample of captured dynamical high resolution data.

Overall, the device is easy to use, wearable, low-power and costs approximately \$150. Within a few minutes, users can begin capturing and viewing data. Although the device was created to capture data from a specific array of sensors, it can be tailored to collect analog data from a wide variety of sensors and electrodes, including high frequency signals such as EMG. Currently, the user interface is being updated to increase user capabilities and provide a more aesthetically pleasing look.

Potential clinical uses for this system include data capture for strength-dexterity testing, quantification of dexterity in children and elderly, a means of providing inputs to controllers for rehabilitation gaming, and validation of treatments for individuals with neurological disorders affecting dexterity and manipulation.

## REFERENCES

1. Valero-Cuevas FJ, et al. *J Biomech* **36**, 265-275, 2003.

## ACKNOWLEDGEMENTS

This work is funded in part by grants EFRI-COPN 0836042 and OPTT-RERC 84-133E2008-8 to FVC. We thank Gary Lin for his assistance in the development of the data collection software.

# AN INSTRUMENTED SPLIT-BELT TREADMILL SYSTEM USING COMMERCIAL PARTS

<sup>1</sup>Kari Rich, <sup>2</sup>John Prince, <sup>3</sup>Mu Qiao and <sup>4</sup>Devin L. Jindrich

<sup>1</sup>School of Biological Health Systems Engineering

<sup>2</sup>Dept. of Physics Instrument Shop

<sup>3</sup>Kinesiology, School of Nursing & Health Innovation

<sup>4</sup>School of Life Sciences

Arizona State University

email: devin.jindrich@asu.edu, web: <http://www.limblab.org/>

## INTRODUCTION

Instrumented and split-belt treadmills are useful for investigating the biomechanics and motor control of locomotion [1,2]. Several instrumented, split-belt treadmills (ISBTs) are commercially available or have been custom-built. However, both types of ISBTs are often prohibitively expensive for laboratories. Here we describe a procedure by which relatively inexpensive, commercially-available treadmills were modified to develop a semi-custom ISBT.

## METHODS

Our system is based on light-duty treadmills made by Landice, Inc. (<http://www.landice.com>). The L8 chassis features a 22" x 63" belt surface, thin aluminum frame and compact 4-HP motor. Placed side-by-side, two L8 treadmills could be used as a split-belt system with a belt gap of approximately 2 cm.

To achieve a narrower belt gap, we made several modifications to the treadmill frame. First, we custom built one side of each frame. This replaced the roller mounts and tensioning systems, and provided support for the deck (Fig. 1).

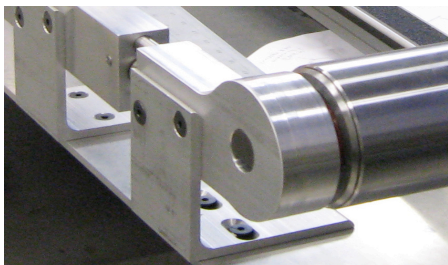


**Figure 1:** Modified inside frame and roller mount assembly.

Inside supports of the treadmills were then staggered, leaving a belt gap of approximately 0.5 cm (Fig.2).

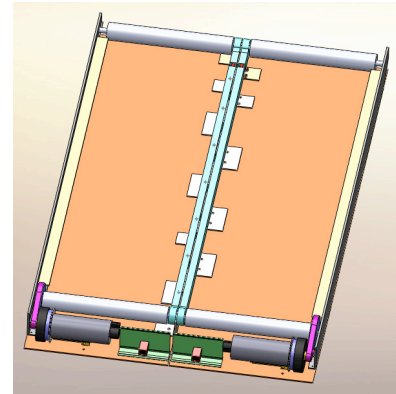


**Figure 2:** Staggered supports for treadmill allow belt gap of approximately 0.5 cm.

Modification of the frames required moving the motor and belt assembly of one treadmill. The new design necessitates that one motor spin in reverse.

To independently record forces from each treadmills, it was necessary to reduce the weight and increase the stiffness. We replaced the heavy decks with lightweight 0.75" thick aluminum honeycomb panels purchased from Paneltec Corp., (<http://www.panelteccorp.com/>) (Fig. 3). The base of each treadmill was replaced with a 0.125" aluminum plate and stiffened with U-channel braces.



**Figure 3:** Treadmills placed side-by-side. The belt and motor of the left treadmill have been removed to expose the rollers and light-weight deck.

Each light-weight deck is mounted on two force transducers (75E20S4-M125-EF mFS-1325L eFS-500L; JR3, Inc.), that are in turn mounted on 0.75" thick aluminum plates. Each force transducer is capable of measuring six degrees of freedom, giving us 12 channels of force and moment information from each treadmill.

The treadmill motors are equipped with optical speed sensors and are controlled by servo motor control boards (ANTA Electric, Inc. and ESI Electronic Products). These boards use pulse-width modulation of a 10 volt signal, at a frequency of 16 kHz to drive the motors. The speed sensors complete a feedback loop and provide better speed control.

Using a custom-developed LabVIEW program and a National Instruments data acquisition device, we are able to control the speed of each treadmill motor separately, and simultaneously record 24 channels of force information. This data can then be analyzed using MATLAB.

## RESULTS AND DISCUSSION

Preliminary tests demonstrate that the system is capable of measuring forces associated with human locomotion (Fig. 4 and Fig. 5). Further, the system has a natural frequency of approximately 19.91 Hz, with a 95% confidence interval of +/-0.27 Hz (Fig. 6).

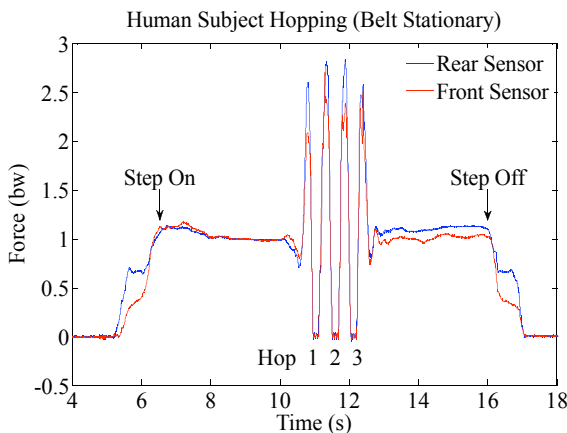


**Figure 4:** Forces associated with a hopping, normalized to body weight.

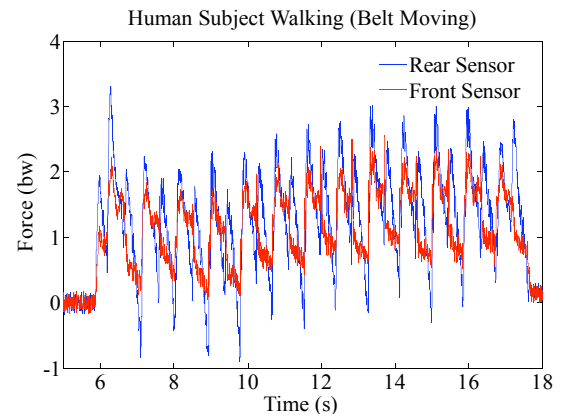


**Figure 5:** Forces associated with walking, normalized to body weight.

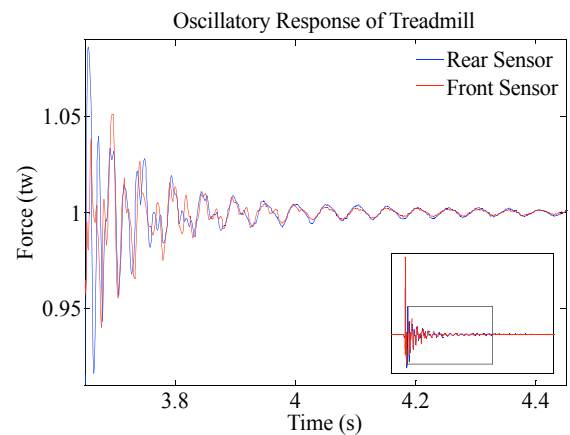


**Figure 6:** Free vibration of the treadmill, normalized to bare treadmill weight.

## CONCLUSIONS

Relatively minor modifications to commercially available treadmills can result in an economic, semi-custom split-belt treadmill system with a belt gap of only 0.5 cm. Additional modifications and the incorporation of force sensors allows for sensitive force measurements that can be used for locomotion and maneuverability analysis.

## REFERENCES

1. Kram, R., et al., *J Appl Physiol*, 1998. 85(2): p. 764-9.
2. Reisman, D.S., A.J. Bastian, and S.M. Morton, *Phys Ther*, 2010. 90(20): p. 187-95.

## ACKNOWLEDGEMENTS

We gratefully acknowledge Jinger Gootschall for her help with the treadmill design.

# KNEE OSTEOARTHRITIS RESULTS IN ASYMMETRIC JOINT MOMENT DISTRIBUTION DURING GAIT

<sup>1</sup>Tyler Richardson and <sup>1,2</sup>Jill S. Higginson

<sup>1</sup>Biomechanics and Movement Science Program, University of Delaware, Newark, DE, USA

<sup>2</sup>Department of Mechanical Engineering, University of Delaware, Newark, DE, USA  
email: higginson@udel.edu

## INTRODUCTION

The prevalence and adverse effects of knee osteoarthritis (OA) are well documented [1]. It has been shown that individuals with knee OA exhibit abnormal kinetic and kinematic gait patterns [2]. While individual joint moments at the hip, knee, and ankle have often been examined during gait, few studies have investigated the intersegmental coordination and distribution of lower extremity joint moments. The total support moment has been shown to be a reliable method of measuring the kinetic synergy of the lower extremity [3]. While many knee OA studies have examined the affected limb, very few have evaluated the contralateral unaffected limb and the degree of symmetry [4]. The objective of our study was to investigate the symmetry of gait in persons with knee OA by examining the magnitude and distribution amongst joints of the peak total support moment between the affected and unaffected limbs. We hypothesized that the magnitude of the peak total support moment would be similar between limbs, but the distribution amongst joints would be asymmetric with the affected limb exhibiting reduced knee loading.

## METHODS

Subjects were recruited locally and gave written informed consent to participate in the study. Twenty-three healthy subjects (age:  $58.9 \pm 10.1$  yrs, BMI:  $26.3 \pm 4.5$ , K-L grade  $\leq 1$ ) and 23 knee OA subjects (age:  $61.6 \pm 8.6$  yrs, BMI:  $28.9 \pm 4.4$ , K-L grade  $\geq 2$ ) were analyzed. The affected limb was determined to be the more painful knee which also had an equal or greater K-L grade than the contralateral knee. Subjects walked at their self-selected walking speed on an instrumented, split-belt treadmill with dual force plates (Bertec Corp., Columbus, OH, USA). Three-dimensional

kinematics were measured using an eight camera Motion Analysis reflective marker system (Santa Rosa, CA, USA). Marker data was processed using a 4<sup>th</sup> order, phase corrected, Butterworth filter with a cutoff frequency of 6 Hz (Cortex 1.0, Motion Analysis Corp.). Inverse dynamics were calculated using Orthotrak 6.3.4 (Motion Analysis) and all kinetic data was normalized to the individual's body mass. All gait cycles for each subject were time normalized to 101 points and then averaged for each variable. Total support moment was calculated as the summation of the hip, knee, and ankle internal extensor moments for each time step [4,5]. Peak total support moment and relative joint contributions at the corresponding time step were used to evaluate differences in total support moment. In order to investigate within group statistical differences in peak total support moment and individual joint contributions between limbs, separate repeated measures ANOVAs were used. For between group comparisons, separate ANCOVAs with speed as a covariate were used. All statistical tests were performed using SPSS software version 18 (Chicago, IL, USA).

## RESULTS AND DISCUSSION

In the healthy group, no significant differences were found between limbs for peak total support moment ( $p=0.474$ ), hip contribution ( $p=0.197$ ), knee contribution ( $p=0.550$ ), or ankle contribution ( $p=0.782$ ) (Fig. 1) (Table 1). This result is evidence of interlimb symmetry in healthy individuals. The peak total support moment and hip contribution for the knee OA group were not significantly different between the affected and unaffected limbs ( $p=0.157$  and  $p=0.386$  respectively) (Fig. 1) (Table 1). The knee OA group exhibited significant differences at the knee ( $p=0.016$ ) and ankle ( $p=0.015$ ) (Fig. 1) (Table 1). This suggests interlimb asymmetry exists

at the knee and ankle in individuals with knee OA. The results of the ANCOVAs comparing the OA unaffected limb with healthy limbs did not show significant differences in total support moment ( $p=0.547$ ), or hip ( $p=0.679$ ), knee ( $p=0.807$ ), or ankle ( $p=0.840$ ) contributions.

**Table 1:** Means and standard deviations for peak total support moment and individual joint contributions for the affected and unaffected limb of each group.

| Group  | TSM (Nm/kg) | Hip (%)     | Knee (%)    | Ankle (%)   |
|--------|-------------|-------------|-------------|-------------|
| H-Aff  | 1.21 ± 0.31 | 36.9 ± 18.3 | 48.9 ± 21.3 | 14.2 ± 15.2 |
| H-UnA  | 1.19 ± 0.27 | 33.7 ± 19.3 | 51.2 ± 20.2 | 15.1 ± 13.7 |
| OA-Aff | 1.24 ± 0.45 | 29.4 ± 16.8 | 34.2 ± 19.6 | 36.4 ± 20.2 |
| OA-UnA | 1.16 ± 0.38 | 26.6 ± 19.2 | 48.9 ± 22.1 | 24.5 ± 9.0  |

**Peak Total Support Moment and Individual Joint Contributions**

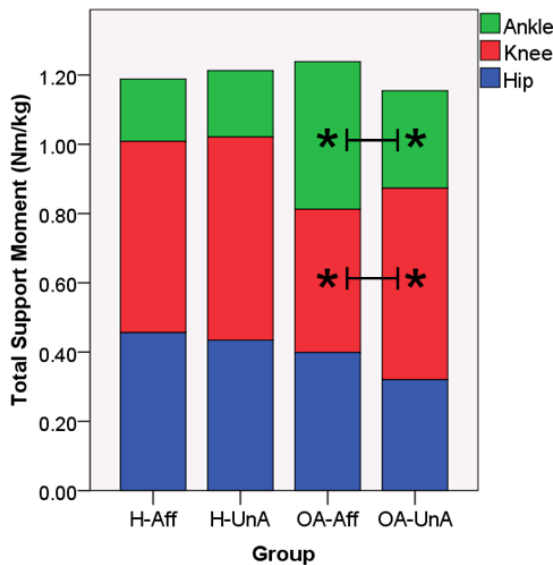


**Figure 1:** Total support moment and individual joint contributions by group. \*'s:  $p < 0.05$ .

We observed redistribution of loading amongst joints within the OA affected limb, although the overall peak total support moment is similar to the unaffected limb. Consequently, this suggests that when the loading of the affected knee joint is reduced, the displaced loading is not shifted to the unaffected limb, but rather to the ipsilateral ankle joint. This is evidence of interlimb asymmetry with respect to joint moment distribution.

Self-selected walking speed was used for analysis in an effort to understand the most common loading strategy specific to each subject. The use of ANCOVAs with speed as a covariate statistically accounted for the significant difference in walking speed between groups. One limitation of this study

was that the OA group was non-homogenous, meaning both unilateral and bilateral OA subjects were used.

While our results demonstrate that redistribution of joint contributions to the peak total support moment is a quality of OA gait, it is not clear as to whether this is a governing control strategy or a consequence of one of many other known compensatory strategies. Several of the gait strategies and qualities of individuals with OA such as decreased knee excursion [2], increased adduction moment [2], decreased walking speed [2,4], and decreased quadriceps strength [6] could be responsible for causing interlimb redistribution of joint moments. In future research we plan to analyze the kinematics, quadriceps strength, and spatiotemporal parameters in order to better understand the mechanisms of this compensatory joint moment redistribution.

## CONCLUSIONS

Although peak total support moments are similar, individuals with knee OA exhibit interlimb asymmetry by significantly reducing knee and increasing ankle contributions in their affected limb. The unaffected OA limb is not significantly different from that of healthy individuals. Further research will be conducted to provide a more complete understanding of this asymmetric compensatory mechanism and will hopefully provide insight into disease progression.

## REFERENCES

1. Buckwalter JA. *Clinical Orthop & Related Research* **427S**, S6-S15, 2004.
2. Astephen JL. *J Orthop Res* **26**, 332-341, 2008.
3. Flanagan SP. *J Appl Biomech* **21**, 181-188, 2005.
4. Zeni JA, Higginson JS. *Knee*, 2010.
5. Winter DA. *J Biomech* **13**, 923-927, 1980
6. Lewek MD. *J Orthop Res* **22**, 110-115, 2004.

## ACKNOWLEDGEMENTS

This study was completed thanks to the help of Dr. Joseph Zeni Jr., Andrew Kubinski MS, Dr. John McDonald, and funding from NIH P20-RR16458.

# Biofeedback Propulsion Training

W. Mark Richter, Ph.D.

MAX Mobility, LLC, Antioch, Tennessee, USA  
email: mark@max-mobility.com, web: www.max-mobility.com

## INTRODUCTION

In a continuing effort to reduce the high prevalence of upper limb (UL) pain in manual wheelchair users [1], we have been working towards the development of training strategies to help improve the efficiency of wheelchair propulsion. This work has involved the development of an instrumented wheelchair wheel with real-time biofeedback, and several studies [2,3] of the equipment and techniques that will hopefully lead to better propulsion, less UL pain, and a higher quality of life.

## METHODS

Biofeedback System: The path to better wheelchair propulsion began with the development of new instrumentation. The OptiPush Biofeedback System was designed to measure three-dimensional forces and moments applied to the handrim, and provide push-by-push feedback on 10 propulsion variables: braking torque, push cadence, contact angle, impact, peak force, peak torque, power output, push distance, smoothness



**Figure 1:** OptiPush wheel.

and speed. The OptiPush Wheel is composed of a customized wheelchair wheel, anodized handrim, 3 aluminum beams, and an Instrumentation Module (Fig. 1), which houses the sensors and electrical components of the device, namely a 6 degree-of-freedom load cell, rotary encoder, and Bluetooth module. Data received by a designated computer are recorded at 200 Hz and filtered with a 4th order Butterworth digital low-pass filter with a 20-Hz cutoff frequency. Conditioned forces, torques and

wheel angles are used to compute the biofeedback variables. Each variable can be displayed in a bar graph with a running average of the last 5 strokes. A target value can be set to help reach or maintain a desired value. For cadence, an auditory beep is also available for cadence. A validation study, which has been submitted for publication, was conducted to establish OptiPush measurement accuracy.

Biofeedback Training: As an initial step towards developing propulsion training guidelines, we studied the effects of single variable biofeedback. Thirty-one manual wheelchair users were enrolled in the study. Their rear wheels were replaced with an OptiPush wheel on the right side and a weighted wheel on the left side. Subjects were secured to a motor-driven treadmill, which was set to match his/her average overground speed and power output. An 1-minute normal propulsion trial was captured, then, one variable at a time, subjects were shown feedback of braking moment, cadence, contact angle, peak force, push distance, and smoothness. They were asked to make a maximum improvement for all variables and a targeted 10% improvement for cadence, contact angle, peak force, and push distance. Subjects were also asked to push with each of the other 3 identified stroke patterns [4].

The differences between each subject's normal propulsion trial and the biofeedback and stroke pattern trials were analyzed with Wilcoxin signed-rank tests and a pair of one way ANOVAs, respectively. Data from this study were also used to compare overground propulsion and treadmill propulsion. Paired t-tests were used to analyze the differences in the values of each propulsion variable for the overground and treadmill conditions.

## RESULTS AND DISCUSSION

OptiPush Validation: The OptiPush was able to accurately measure wheel angle (0.02% error),

wheel speed (0.06% error), and handrim loads. The maximum errors in static force and torque were 3.80% and 2.05%, respectively. Dynamic measurements of planar forces ( $F_x$  and  $F_y$ ) and axle torque also had low error (-0.96 N to 0.83 N for force and 0.10 Nm to 0.14 Nm for torque) and were highly correlated ( $r > .986$ ) with expected values.

**Treadmill Propulsion:** Compared to overground propulsion, the handrim kinetics ( $N = 28$ ) resulting from treadmill propulsion were similar and highly correlated. Contact angle, peak force, average force, and peak axle moment differed by 1.6% or less across the two conditions. While not significant, power output and cadence tended to be slightly higher for the treadmill condition (3.5% and 3.6%, respectively), due to limitations in adjusting the treadmill grade. Based on these results, a motor-driven treadmill can serve as a valid substitute for overground wheelchair propulsion [2].

**Effects of Single Variable Biofeedback:** For 9 of the 11 conditions, subjects were able to significantly improve the value of the biofeedback variable [3]. For the 10% conditions, subjects exhibited good control over cadence, push distance, and contact angle, with deviations within 1% of the targets. On the other hand, subjects had difficulty making changes to peak force and smoothness.

Targeting one variable at a time had both positive and negative cross-variable effects. Most notable was the trade-off between peak force and cadence. Efforts to minimize cadence, and push distance, led to significant changes in all outcome variables, including a 153-173% increase in peak force. Maximizing contact angle also led to a significant 34% increase in peak force. The only biofeedback variable that led to a decrease in peak force was peak force, which had no significant indirect effects, but produced a 20% increase in cadence. To help wheelchair users make more significant reductions in peak force, we have redesigned the

biofeedback display to show force throughout the stroke for each 3 degrees of contact angle (Fig. 2).



**Figure 2:** Redesigned biofeedback display.

**Effects of Stroke Pattern:** Though still under analysis, the results of the stroke pattern testing suggest that the semi-circular (SC) and double-loop (DL) stroke patterns lead to beneficial handrim biomechanics. When using either pattern, subjects ( $N = 25$ ) had the longest contact angles, lowest cadence values, and the smallest braking moments. Subjects also had the lowest UL muscle activity with the DL pattern. While the DL pattern had the highest peak force (60.7 N) of any pattern, this is attributed to a low cadence (0.75 Hz), further highlighting the trade-off between force and cadence.

Future work will include testing the effects of multi-variable biofeedback and optimum seat position on propulsion biomechanics, and establishing guidelines for balancing peak force and cadence values.

## REFERENCES

1. Sie IH, et al. *Arch Phys Med Rehabil* **73**, 44-48, 1992.
2. Kwarcia AM, et al. *Spinal Cord* **49**, 457-462, 2010.
3. Richter WM, et al. *Arch Phys Med Rehabil* **92**, 572-577, 2011.
4. Boninger ML, et al. *Arch Phys Med Rehabil* **83**, 718-723, 2002.

**Table 1:** Direct and indirect effects of four key conditions from the single variable biofeedback study [3].

| Variable      | Minimize Cadence | Maximize Cont. Angle | Minimize Peak Force | Maximize Push Dist. |
|---------------|------------------|----------------------|---------------------|---------------------|
| Cadence       | -64 (14)*        | -30 (21)†            | 20 (33)             | -67 (12)†           |
| Contact Angle | 25 (27)†         | 31 (22)*             | -7 (15)             | 26 (21)†            |
| Peak Force    | 154 (87)†        | 34 (42)†             | -11 (17)*           | 173 (112)†          |
| Push Distance | 221 (119)†       | 65 (76)†             | -11 (19)            | 255 (136)*          |

\* Significant ( $p < .005$ ) direct change, and † significant ( $p < .0008$ ) indirect change from normal propulsion.

# FOOT TYPE AND FALLS IN OLDER ADULTS: THE FRAMINGHAM FOOT STUDY

Jody L. Riskowski<sup>1,2</sup>, Thomas J. Hagedorn<sup>1</sup>, Alyssa B. Dufour<sup>1,3</sup>, Virginia A. Casey<sup>1</sup>,  
Marian T. Hannan<sup>1,2</sup>

<sup>1</sup>Institute of Aging Research, Hebrew SeniorLife, Boston, MA, 02131; <sup>2</sup>Harvard Medical School, Boston, MA, 02115; <sup>3</sup>Boston University School of Public Health, Boston, MA, 02118

## INTRODUCTION

Falls occur in 28-33% of the US older adult population [1,2]. Although the causes of falls are multifactorial, few studies [e.g., 3,4] have investigated foot type and fall risk, despite it being the main or only base of support. Therefore, the purpose of this study was to evaluate foot type and fall risk in a population-based study of older adults.

## METHODS

This study included participants in the Framingham Foot Study [5] who had a valid standing and walking plantar pressure scan of each foot. Plantar pressure scans in which the foot was near the edge and/or a portion of the foot appeared missing were not included.

Foot pressure scans were collected using Tekscan Matscan (Tekscan Inc, Boston, MA; resolution = 1.4 sensels/cm<sup>2</sup>; 40 Hz). Participants walked barefoot at a self-selected pace across a 3.5m walkway, using the two-step method [6]. Based on the vertical ground reaction force generated, the dominant foot was defined as the limb generating the greater propulsive force during walking. Footprints were masked using Novel Automask software (Novel GmbH, Munich, Germany).

Foot type was assessed using two methods: Modified Arch Index (MAI) [7] and Arch Index (AI) [8]. MAI is calculated by dividing the pressure of the middle third of the foot by the total foot pressure, not including the toes. MAI was shown to be inversely correlated with navicular height, meaning that higher values reflect lower arches [7]. AI is the ratio of the midfoot area to the area of the foot, not including the toes. AI has shown an inverse relationship with navicular drop [8].

For both the MAI and AI, the cut-points for foot type were gender-specific and based on the quartiles. The highest 25% of the values considered “Low Arch” and the lowest 25% of the values considered “High Arch.” The middle 50% was the referent.

Symmetry between the feet for the MAI and AI was determined using the symmetry index (SI) [9].

Mathematically, SI is:

$$SI = \frac{x_1 - x_2}{0.5(x_1 + x_2)} * 100$$

with “X” representing peak pressure MAI or AI. The subscript “1” represents the dominant limb. The SI values were also broken down by gender-specific quartiles. The highest 25% considered “Positive Asymmetry” and the lowest 25% “Negative Asymmetry.” The middle 50% was the referent.

Falls were based on participant response to whether or not he or she had fallen in the past year (yes/no).

Gender-specific logistic regression models were used to examine foot type and fall risk relative to the referent (rectus foot). A second model adjusted for age and body mass index (BMI). Statistical analyses were performed using SAS (version 9.2, SAS Institute Inc, Cary, NC).

## RESULTS

There were 2131 participants. There were 954 men (age: 66.0 ± 9.9 years; BMI: 27.7 ± 6.0 kg/m<sup>2</sup>) and 1177 women (age: 65.6 ± 10.6 years; BMI: 28.7 ± 4.6 kg/m<sup>2</sup>). There were 236 men (14.8%) and 456 (22.7%) women who stated they had fallen in the past year. The high and low arch cut-points for men and women were similar (Table 1).

**Table 1:** Cut-points for high and low arch in the dominant (Dom) and non-dominant (NDom) foot and symmetry values.

|                        | Men     |        | Women   |        |
|------------------------|---------|--------|---------|--------|
|                        | Dom     | NDom   | Dom     | NDom   |
| MAI High Arch          | <0.071  | <0.063 | <0.065  | <0.060 |
| MAI Low Arch           | >0.156  | >0.154 | >0.156  | >0.151 |
| MAI Positive Asymmetry | > 37.1  |        | > 47.8  |        |
| MAI Negative Asymmetry | < -26.7 |        | < -24.4 |        |
| AI High Arch           | <0.201  | <0.189 | <0.178  | <0.171 |
| AI Low Arch            | >0.246  | >0.249 | >0.223  | >0.236 |
| AI Positive Asymmetry  | > 12.4  |        | >13.9   |        |
| AI Negative Asymmetry  | < -18.6 |        | < -16.0 |        |

The unadjusted odds ratio in men showed a high arch, defined by MAI, decreasing fall likelihood by 57% (Table 2), with a similar OR in the adjusted model. Conversely in women low arch defined by MAI was linked to 22% reduced likelihood of falls in the adjusted model. Fall risk was also affected by foot type asymmetry.

## DISCUSSION & CONCLUSIONS

Both the unadjusted (clinically relevant) and adjusted (biologic mechanism relevant) models showed an association between foot type and falls

**Table 2:** Odds ratio (OR) with 95% confidence intervals for the association of falls and foot type of the dominant limb only. \* adjusted OR for age and BMI

|                        | Unadjusted OR     |                   | Adjusted* OR      |                   |
|------------------------|-------------------|-------------------|-------------------|-------------------|
|                        | Men               | Women             | Men               | Women             |
| MAI Rectus             | 1.00              | 1.00              | 1.00              | 1.00              |
| MAI High Arch          | 0.43 (0.25, 0.74) | 0.95 (0.69, 1.34) | 0.46 (0.29, 0.75) | 0.90 (0.81, 1.21) |
| MAI Low Arch           | 1.33 (0.88, 2.00) | 1.08 (0.78, 1.37) | 1.27 (0.92, 1.77) | 0.78 (0.68, 0.96) |
| MAI Referent           | 1.00              | 1.00              | 1.00              | 1.00              |
| MAI Positive Asymmetry | 1.43 (0.95, 2.15) | 0.99 (0.72, 1.36) | 1.27 (0.99, 1.55) | 0.90 (0.68, 1.26) |
| MAI Negative Asymmetry | 0.52 (0.31, 0.88) | 0.82 (0.59, 1.15) | 0.67 (0.41, 0.98) | 0.81 (0.51, 1.08) |
| AI Rectus              | 1.00              | 1.00              | 1.00              | 1.00              |
| AI High Arch           | 1.07 (0.77, 1.21) | 0.94 (0.71, 1.26) | 1.16 (0.67, 1.31) | 0.78 (0.68, 1.02) |
| AI Low Arch            | 1.42 (0.98, 2.08) | 1.01 (0.76, 1.35) | 1.37 (0.94, 1.63) | 1.11 (0.68, 1.67) |
| AI Referent            | 1.00              | 1.00              | 1.00              | 1.00              |
| AI Positive Asymmetry  | 1.03 (0.70, 1.51) | 1.28 (0.95, 1.73) | 1.13 (0.70, 1.51) | 1.01 (0.89, 1.54) |
| AI Negative Asymmetry  | 1.09 (0.78, 1.58) | 1.84 (1.40, 2.42) | 1.02 (0.78, 1.58) | 1.78 (1.31, 2.18) |

in men and women. This work is in agreement with previous work that suggested foot function affects fall risk [10]. Future studies should examine foot type and its role in balance and gait to understand how foot type influences fall risk in risk in older adult populations.

## REFERENCES

1. Prudham D & Evans JG. *Age Aging* **10**, 141-146, 1981.
2. Stevens JA, et al. *J Safety Res* **39**, 345-349. 2008.
3. Mickle KJ, et al. *Clin Biomech* **24**, 787-791, 2009.
4. Menz HB, et al. *J Gerontol A Biol Sci Med Sci* **61**, 866-870, 2006.
5. Dufour AB, et al. *Arthritis Rheum* **61**, 1352-1358, 2009.
6. McPoil TG, et al. *J Am Podiatr Med Assoc* **89**, 495-501, 1999.
7. Chu WC, et al. *IEEE Trans Biomed Eng* **42**, 1088-1093, 1992.
8. Cavanagh PR & Rodgers MM. *J Biomech* **20**, 547-551, 1997.
9. Robinson RO, et al. *J Manipulative Physiol Ther* **10**, 172-176, 1987.
10. Mickle KL, et al. *J Am Geriatr Soc* **58**, 1936-40, 2010

## ACKNOWLEDGEMENTS

NIH-NIAMS RO1-AR047853, NIH-T32 - AG023480.



# FORCE RUNNING WHEEL FOR MEASURING INDIVIDUAL LIMB FORCES IN MICE DURING SPONTANEOUS LOCOMOTION

<sup>1</sup>Grahm Roach, <sup>2</sup>Mangesh Edke and <sup>1</sup>Timothy M. Griffin

<sup>1</sup>Oklahoma Medical Research Foundation, Oklahoma City, OK, USA

<sup>2</sup>University of Oklahoma, Norman, OK, USA

email: [Tim-Griffin@omrf.org](mailto:Tim-Griffin@omrf.org) web: <http://omrf.org/research-faculty/scientists-3/griffin-timothy-m/>

## INTRODUCTION

Running wheels are widely used, especially with transgenic mouse models, to study basic mechanisms of how the musculoskeletal system adapts to increased running activity. Knowledge of the individual limb forces generated during wheel running may provide important mechanistic insight into musculoskeletal and neuromuscular function. Our goal was to construct a low-resistance running wheel for measuring the normal and tangential reaction forces applied to the wheel by an individual limb of spontaneously running mice. We tested our device by measuring the hindlimb reaction forces in control and diet-induced obese mice.

## METHODS

An 11.5 cm diameter stainless steel running wheel (Mini Mitter) was modified to allow placement of a strain-gage instrumented rung (Fig. 1). A strain gage (Vishay) was applied to both sides of four strain sensitive surfaces in a half bridge configuration to measure forces applied in the normal and tangential directions. Four strain channels were measured by completing a modified wheatstone bridge on the running wheel, passing the bridge leads through a slip ring (Michigan Scientific), and recording the bridge measurements with a high-speed bridge measurement module from National Instruments (NI 9237). An optical encoder was secured to the end of the axle opposite the slip ring to monitor wheel angular position. Ventral and sagittal plane video data were collected at 125 Hz with a high-speed camera and a 45° angled mirror. Video was collected during the dark light cycle using an infra-red light source. Strain, wheel angle, and video data were collected using a custom-written LabVIEW program whenever strain values exceeded a pre-set strain-threshold event trigger.

36 wk old male C57BL/6J mice fed either a control (10% kcal fat) or high-fat (60% kcal fat) diet for 30 wks were housed overnight in a custom-designed cage with the force running wheel (N=3 control, N=3 high-fat). Mice had been housed with standard running wheels for 10 wks prior to measurements. All procedures were approved by the Institutional Animal Care and Use Committee.

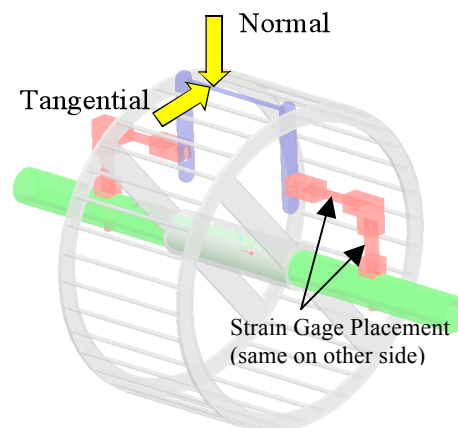


**Figure 1:** Force running wheel with strain-gage instrumented rung, optimized to minimize cross-talk and maximize strain at gage location.

## RESULTS AND DISCUSSION

Strain output varied linearly in the normal and tangential directions with applied loads of up to 70 g ( $r^2 > 0.99$  for both directions). Strain output for a given load was dependent on position for the normal but not tangential component. Foot position data from video images were used to correct for this position dependence. Crosstalk was 38% and 1.5%, for the normal and tangential components, respectively. The higher degree of crosstalk for the normal component resulted in approximately a 6% maximal error in normal force measurements based on the observed peak tangential forces being only 1/6 the normal force values (Table 1). Normal and

tangential strain output varied with wheel angular position by 101mN and 70mN, respectively, due to the effect of gravity on the instrumented rung. We applied an angle-dependent correction factor to account for these gravitational errors. The natural frequencies of the normal and tangential components were 193 Hz and 68 Hz, respectively. Additional low-magnitude strain noise was observed at 60 Hz during wheel rotation. A power spectrum analysis of the normal and tangential forces applied by running mice showed that nearly all frequency components were lower than 35Hz; therefore, we filtered all strain data with a low-pass butterworth filter at 45Hz.

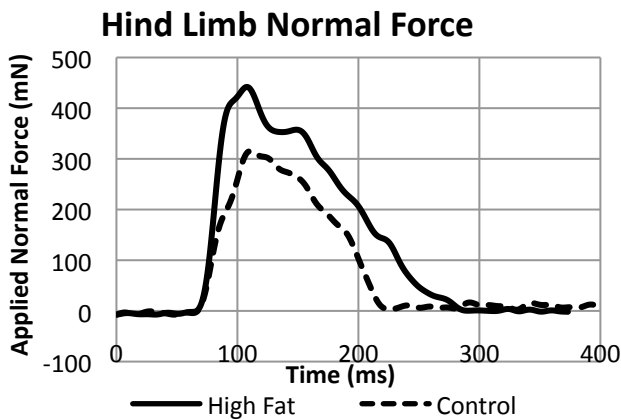


**Figure 2:** Sample trace of the normal reaction forces during steady-speed running from a control (28.9g) and diet-induced obese (50.5g) mouse.

Over the course of a night of data collection, each animal generated over 1000 force events. Each event captured 2.5 seconds of strain data (10 kHz), encoder data (10 kHz), and image data (125 Hz). In our preliminary analysis of these records, 4 hindlimb events per animal were selected for further analysis based on the following: 1) a consistent wheel rotational velocity, 2) a steady gait pattern for two strides before and after the force event, and 3) foot placement only on the instrumented rung. Control mice applied an average peak normal force of 355mN (115 % body weight, BW), about 6-fold

greater than the average peak tangential forces (Table 1). High-fat mice generated greater absolute peak forces compared to control mice (Figure 2). However, when normalized to BW, peak normal forces were significantly less in high-fat animals (Table 1).

## CONCLUSIONS

Peak normal hindlimb forces generated during wheel running are greater than those observed during overground locomotion (1), suggesting that the biomechanics of wheel running may be significantly different from overground locomotion. These findings are intriguing since we have previously reported few kinematic differences between wheel and overground running (2). Measuring individual limb reaction forces during spontaneous wheel running may provide a more sensitive method of quantifying changes in gait behavior that reflect musculoskeletal pathology, as with diet-induced obesity and osteoarthritis (1).

## REFERENCES

1. **Griffin TM, Fermor B, Huebner, J, et al.** Diet-induced obesity differentially regulates behavioral, biomechanical, and molecular risk factors for osteoarthritis in mice. *Arthritis Res Therapy*. 12:R130. 2010.
2. **Costello KE, Guilak F, Setton LA, Griffin TM.** Locomotor activity and gait in aged mice deficient for type IX collagen. *J Appl Physiol* 109: 211-218, 2010

## ACKNOWLEDGEMENTS

We thank Steve Baker, Neil Castelino, Farsh Guilak, and Andrew Schmidt for their assistance in earlier stages of the project. Support from OMRF and the Oklahoma Center for the Advancement of Science and Technology.

**Table 1:** Effect of diet on peak normal and tangential wheel reaction forces by the hindlimb of running mice.

| Diet            | BW          | Peak Normal Forces |             | Peak Tangential Forces |            |
|-----------------|-------------|--------------------|-------------|------------------------|------------|
|                 | (g)         | (mN)               | (% BW)      | (mN)                   | (%BW)      |
| <b>Control</b>  | 29.7 ± 0.9  | 335 ± 17           | 115.2 ± 5.7 | 56.7 ± 12              | 19.6 ± 4.4 |
| <b>High-Fat</b> | 50.0 ± 0.8* | 452 ± 3*           | 92.2 ± 1.0* | 73.9 ± 18              | 15.1 ± 3.9 |

Body weight (BW). Values are mean ± SEM. \*p<0.05 versus control value (Mann-Whitney U-test).

# Controlling Compliance: Feed-forward Stimulation Pattern Influences Elastic Tuning During Cyclic Muscle-Tendon Contractions

<sup>1</sup>Benjamin D. Robertson, <sup>1</sup>Gregory S. Sawicki

<sup>1</sup>UNC-Chapel Hill/NC State University  
Joint Department of Biomedical Engineering  
email: bdrober3@ncsu.edu

## INTRODUCTION

Years of research on the mechanics and energetics of locomotion have established that compliant tissues (i.e. tendon and aponeurosis) are crucial in shaping efficient and stable locomotion. When muscle-tendon (MT) interaction dynamics are optimally ‘tuned’, series elastic tissues stretch and recoil accounting for much of the overall MT length change (Figure 1). Maximizing elastic energy storage allows in-series muscles to remain nearly isometric, reducing metabolic demand with little effect on overall MT power output (Roberts et al., 2011). While the benefits of an optimally ‘tuned’ MT interaction are clear, the role of the nervous system in coordinating the timing and magnitude of muscle stimulation to optimize elastic energy storage and return is unclear. We hypothesize that stimulating a compliant muscle-tendon system at its passive resonant frequency will (1) maximize MTU force generation (2) minimize muscle contractile work and (3) maximize elastic energy storage and return. The combination of these outcomes would indicate an optimally tuned muscle-tendon control strategy.

## METHODS

To investigate the effect that feed-forward neural control has on mechanical energetics (i.e. force and power production) we developed a simple mathematical model of a compliant muscle-tendon unit (MTU). The model includes a Hill-type muscle, or contractile element (CE) in series with a Hookean tendon-spring, or series elastic element (SEE) (Zajac, 1989) operating across a lever on a mass under constant gravitational force. We based our initial muscle ( $\tau_{act}=0.03$  s,  $\tau_{deact}=0.09$  s,  $F_{max}=65$  N,  $V_{max}=0.12$  m/s,  $l_0=0.01$  m,  $k_{CE}=7000$  N/m) and tendon ( $k_{SEE}=7000$  N/m,  $l_{slack}=0.07$  m) properties on data collected from bullfrog plantaris muscle-tendon units. We chose parameters for the load (mass=0.1 kg, in/out lever arm ratio = 0.1) to

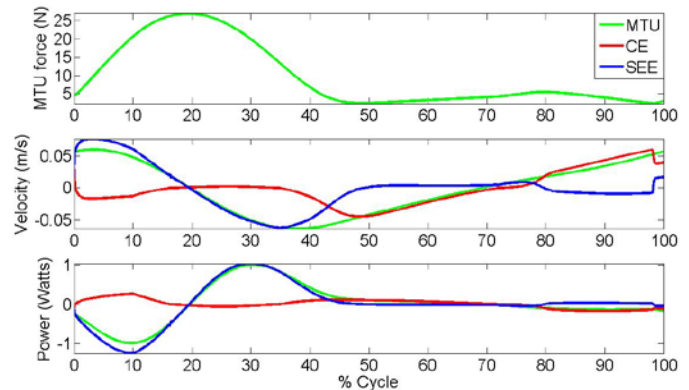


**Figure 1.** Force, velocity, and power generated during a single cycle with a stimulation of 100% and a period of 3Hz. Stimulation is from 0-10% of the cycle. Note significant elastic energy storage and return in the SEE.

get a resonant natural frequency,  $\omega_n \approx 2.5$  Hz, for the passive system without muscle activation. This simple model should scale well with muscle-tendon dynamics at distal joints of the lower-limb (e.g. ankle) of a wide range of terrestrial animals, including humans. To drive active muscle force generation we used a feed-forward neural control signal with no reflex feedback. This was achieved by stimulating the modeled muscle-tendon system over a range of amplitudes (20-100%) and driving frequencies about  $\omega_n$  (2.0-4.0 Hz). By varying these parameters, we were able to systematically investigate the role that feed-forward neural control plays in effective energy storage and return in the SEE of a simple, compliant muscle-tendon system.

## RESULTS

Every control strategy (i.e. amplitude + frequency combination) we used exhibited stable, periodic behavior after a short transient. A sample output showing MT dynamics from a single steady cycle with 100% stimulation at 3 Hz can be seen in Figure 1.

We decided on two key factors for determining the effectiveness of different neural control strategies. The first was average positive

mechanical power generated over a stimulation cycle. In particular we examined how overall MTU power generation was distributed between individual components - the muscle (CE) and the series elastic tissues (SEE) (Figure 2). We consider small ratios of CE to total MTU average positive power to be an important indicator of system efficiency for a given frequency of stimulation. We found that maximum MTU and CE average power outputs occurred at the lower stimulation frequencies (Figure 2). Furthermore, the ratio of muscular (CE) to overall MTU positive power output was minimized at a value of  $\sim 20\%$  over a range of driving frequencies spanning  $\sim 2.6-3.0$  Hz.

The second key factor we examined was peak force generated by the *active* component of the contractile element over a cycle. As was expected, peak active force increased in proportion with stimulation amplitudes for all frequencies (Figure 3.). Active force generation depends on several well-known properties of muscle, including the force-length-velocity relationships that are accounted for in this model. In line with these properties, peak active force occurred when the muscle was at optimal length ( $\sim l_0$ ) and velocity ( $\sim 0$ ) at the time of stimulation onset. As can clearly be seen in Figure 3, this occurred at  $\sim 3$  Hz.

## DISCUSSION/CONCLUSIONS

From our investigation of feed-forward neural control strategies, several important conclusions can

be drawn. First, contrary to our hypotheses, maximal force and minimal contractile element positive work did not occur at the resonant frequency of our passive system (2.5 Hz), but at a range of frequencies above it. This is likely due to the non-linear contribution of active muscle to the overall stiffness of the system during dynamic contractions. Secondly, while *overall* MTU power output scaled well with stimulation amplitude, it had little effect on *within* MTU dynamics. Finally, while lower frequencies produced higher overall MTU power outputs, they required large amounts of work from muscular (CE) components and had minimal contribution from SEE's. This is in stark contrast to the bandwidth of tuned frequencies, where  $\sim 80\%$  of positive power is produced by SEE recoil.

Future work will extend the model to include feedback pathways, and consider how optimal force generation/power production is influenced by both passive and active parallel mechanical assistance. This may provide insight into how feed-forward and feed-back control signals are modulated to re-tune MTU force/power generation when mechanical assistance is present.

## REFERENCES

1. Roberts TJ, Azizi, E. *J Exp Biol.* **214**, 353-361, 2011.
2. Zajac FE. *Crit. Rev. Biomed. Eng.* **17(4)**, 358-411, 1989.

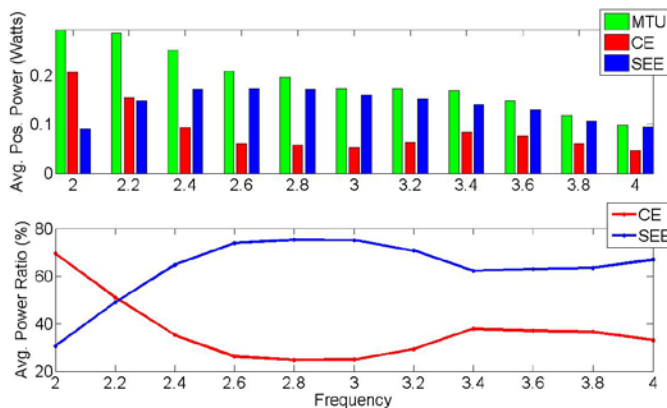


**Figure 2.** Graphs of (top, bars) average positive power output of the muscle-tendon unit (MTU), contractile element (CE), and series elastic element (SEE) and (bottom, lines) Power Ratios -  $CE/(CE+SEE)$  and  $SEE/(CE+SEE)$  versus stimulation frequency calculated over a single contractile cycle.

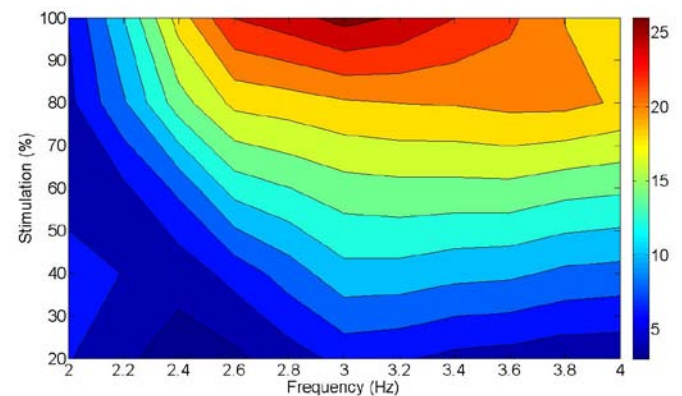


**Figure 3.** Contours of peak *active* contribution to contractile element force (Newtons) as a function of both magnitude and frequency of muscle stimulation. Note that peak active muscle force occurs when stimulated well above the natural frequency of the passive system ( $\sim 2.5$  Hz).

# POSTURAL RESPONSES TO TRANSLATIONAL AND ROTATIONAL PERTURBATIONS IN YOUNG AND OLDER ADULTS

Jennica L Roche and Mark S Redfern

University of Pittsburgh, Pittsburgh, PA, USA  
Email: JLR59@pitt.edu Web: <http://www.odar.pitt.edu/hmbl/>

## INTRODUCTION

Balance control is a complex sensorimotor process that is influenced by aging. Aging is known to impact sensation, reaction time, motor capabilities, and cognition, all of which are known to impact balance [1, 2]. However, the interaction of these factors in postural reactions to perturbations is not clear. The goal of this research is to determine the relationship between sensation of postural perturbations and motor outputs for different types of perturbations in young and older adults.

In this experiment, two types of postural perturbations were presented (toes-up rotations and posterior translations); separately and then mixed together within the same trial. Toes-up rotations require a dorsiflexion motor response to maintain balance. Posterior translations require a plantar flexion motor response. However, the two postural perturbations were designed to initiate a comparable stretch in the plantar flexors. Thus, within the experiment there were two perturbations that create similar initial sensory signals, but require opposing motor responses.

The purpose of this study was to explore the relationship between sensory inputs and motor outputs when the perturbation is known, and when the perturbations are unknown requiring a decision for proper response.

## METHODS

Fifteen young, healthy adults between the ages of 21 and 35 ( $24.3 \pm 2.5$ ) and 12 older, healthy adults between the ages of 70 and 85 ( $75.6 \pm 3.7$ ) were recruited. The groups were not significantly different in height or weight (Y:  $67.5 \pm 4.0$ in O:  $66.5 \pm 3.8$ in; Y:  $159.3 \pm 31.8$ lbs O:  $176.7 \pm 32.9$ lbs). All subjects were screened to be free of

musculoskeletal, neurologic, and vestibular disease. Subjects experienced two types of platform perturbations: rapid toes-up rotations of  $3.4^\circ$  and posterior translations of 4cm. Both perturbations were generated as a sigmoidal position profile with maximum velocities at 18 degrees/s and 24 cm/s respectively. The rotation and translation perturbations were designed to elicit the same amount of stretch in the subjects' ankle plantar flexors while requiring opposite motor responses to maintain balance.

Testing occurred over three separate days with at least 24 hours between each visit. Subjects stood on a dynamic posturography platform (NeuroCom Inc., Clackamas, OR), with ankles aligned to the axis of rotation of the platform. Each test day consisted of three blocks, each containing 16 perturbations. The blocks were presented in the following order: toes-up rotation, posterior translation, and a mixed block containing randomized mixture of rotations and translations. These blocks were performed in the beginning of the testing days as a part of a larger study.

Center of pressure (COP) was recorded and onset latency was found. Onset latency was defined as the time between the start of the perturbation and the initiation of a significant change in the slope of the COP. This COP initiation is created by the first active ankle torque, thus it reflects the onset of active force generation in response to the perturbation [3]. Operationally, COP initiation was determined as the first peak (minimum for rotation) in the second derivative of the COP time series preceding the maximum of the first derivative of COP; this was confirmed by visual inspection.

## RESULTS AND DISCUSSION

Analysis was performed using a three-way mixed ANOVA comprised of the following independent variables: age group (young, old), block type (single perturbation, mixed), and perturbation type (translation, rotation). Age, block type, perturbation and the interaction between block type and perturbation were all found to be significant (Table 1).

**Table 1:** ANOVA results

| Effect                          | P-Value |
|---------------------------------|---------|
| Age                             | 0.046*  |
| Block Type                      | <0.001* |
| Perturbation                    | <0.001* |
| Age x Block Type                | 0.083   |
| Age x Perturbation              | 0.425   |
| Block Type x Perturbation       | 0.014*  |
| Age x Perturbation x Block Type | 0.114   |

\* indicates significance ( $p < 0.05$ )

Overall, the young group reacted approximately 13ms faster than the older group (Figure 1). This effect was seen equally through the block types and perturbation types (i.e. no interaction effect). Between the perturbation types, an increased delay in the older group of 10 and 16ms was observed on average for the rotation and translation trials respectively.

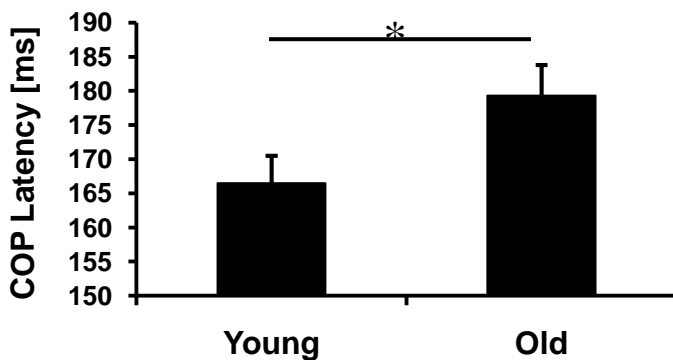


**Figure 1:** Mean latencies (+ s.e.) for young and older subjects. The difference of about 13ms was significant ( $\alpha < 0.05$ ).

Though the perturbations both elicited stretch in the ankle plantar flexors, the time of the motor responses were significantly different. On average,

the COP latency of the rotation trials was 210ms, while the translation trials exhibited a latency of 136ms.

The main effect of block and the interaction of block  $\times$  perturbation reflect only a significant difference between rotation trials of single perturbation blocks when compared to those of the mixed block (Figure 2). The between-subject, least squares difference was approximately 10ms. The translation latencies were not significantly different between block types.

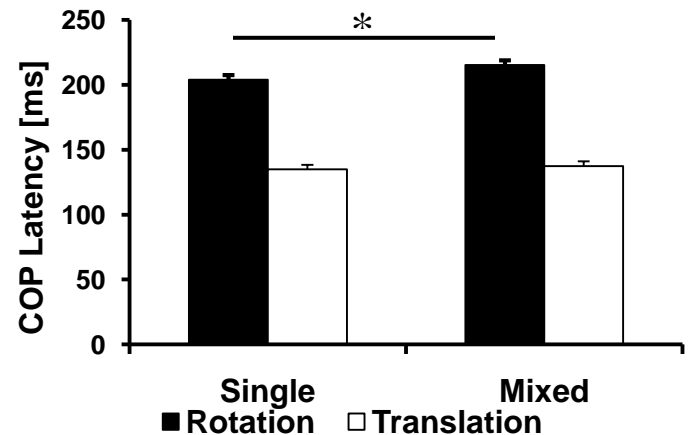


**Figure 2:** Mean latencies (+s.e.) for block types stratified by condition. Rotation latencies were significantly different ( $\alpha < 0.05$ ) between block type, while the translation latencies were not.

## CONCLUSIONS

Overall, older subjects displayed a longer COP latency, indicating a delay in the sensorimotor loop of otherwise healthy adults. The increased delay in the rotation trials of the mixed blocks may be due to an increase in decision processing during the mixed trials. Interestingly, there was no increase in delay time for translational trials of the mixed blocks, suggesting that the response to the translational trials was the primary motor response program. This effect was consistent across the two groups. .

## REFERENCES

- 1.Redfern MS, et al. *J Gerontol Biol Sci* **57**, B298-B303, 2002.
- 2.Doumas M, et al. *Exp Brain Res* **187**, 275–281, 2008.
- 3.Peterka RJ, et al. *J Vestibul Res-Equil* **1**, 87-96, 1990.

# RUNNERS WITH ANTERIOR KNEE PAIN UTILIZE A GREATER PERCENTAGE OF THEIR AVAILABLE PRONATION RANGE OF MOTION

<sup>1,2</sup>Pedro Rodrigues, <sup>1,2</sup>Trampas TenBroek and <sup>2</sup>Joseph Hamill

<sup>1</sup>New Balance Sports Research Lab, Boston, MA, USA

<sup>2</sup>University of Massachusetts, Amherst, MA, USA

email: pedro.rodrigues@newbalance.com

## INTRODUCTION

“Excessive” pronation has been associated with a number of lower extremity injuries including anterior knee pain (AKP) [1]. While this injury paradigm is widely accepted, biomechanical studies often fail to demonstrate pronation differences between injured and healthy runners [2]. Conversely, orthotics used to limit pronation have been shown to effectively reduce pain and improve function in those with AKP [3]. This discrepancy indicates that biomechanical studies may not be evaluating pronation in the right context.

The word “excessive” implies that a threshold has been exceeded. Traditionally, this threshold has been calculated using the means and standard deviations reported in the literature [4], not an individual-specific threshold such as the joint’s available range of motion (ROM). For example, a runner displaying 18° of dynamic ankle joint complex (AJC) eversion would likely be classified as having “excessive” pronation using a traditional definition. However, if this runner had 23° of eversion ROM, the AJC would not likely interpret 18° of dynamic eversion as “excessive” because it still has an eversion buffer of 5°. Therefore, from the joint’s perspective it may be more pertinent to define “excessive” using its available ROM.

This theory has been evaluated by Engsberg et al. [5], who compared dynamic AJC eversion in healthy runners to their available active ROM. These authors found that runners displaying greater quantities of dynamic AJC eversion also exceeded their ROM boundary by an average of 8.4°. However, this study is limited in that only active, not passive ROM was measured, and therefore the joint’s full ROM may not have been captured. Additionally, only healthy runners were evaluated,

and consequently, the association with injury is unknown. Therefore, the purpose of this study was to 1) evaluate the eversion buffer of injured and healthy runners using the AJC’s passive ROM and 2) to evaluate traditional pronation variables to the eversion buffer. It is hypothesized that injured and healthy runners will demonstrate similar pronation profiles; however, injured runners will exhibit a significantly smaller eversion buffers.

## METHODS

Thirteen healthy (6 male, 7 female, 33.2 ± 8.6 years, 1.7 ± 0.1m, 64.9 ± 11.9 kg) and twelve runners with AKP (3 male, 9 female, 30.8 ± 6.0 years, 1.6 ± 0.1m, 61.9 ± 8.1 kg) completed the study. All subjects were running 8+ miles per week for 6 months, utilized a heel-strike foot fall pattern and had no history of lower extremity surgery. Additionally runners were required to be training in neutral shoes and not using orthotics.

Passive eversion ROM was collected using a custom built ROM device (Figure 1) and a motion capture system (Qualisys, Sweden). The AJC was passively everted using a 10 N\*m torque in six pre-defined sagittal plane positions. The joint’s position was captured using retro-reflective markers placed on the lower leg and calcaneus. Three trials in each sagittal plane position were averaged and interpolated to create the eversion ROM boundary.

A barefoot standing calibration was performed to define the thigh, lower leg and calcaneal segments using markers placed on bilateral greater trochanters, medial/lateral knee, medial/lateral malleoli, sustentaculum tali, peroneal tubercle and a calcaneal tracking cluster. Subjects ran (2.9 m/s) in a neutral running shoe with a modified heel counter to allow the calcaneal tracking cluster to be

directly attached to the calcaneus and remain fixed during both ROM and running trials. Dynamic lower extremity kinematics were captured (200 Hz) using marker clusters attached to the lateral thigh, lateral leg and calcaneus.

Kinematic data were analyzed in Visual 3D (C-Motion, Germantown, MD). Marker trajectories were smoothed using a 12 Hz fourth order low pass Butterworth filter. Right handed local coordinate systems were created for each segment. Joint angles were calculated using Cardan angles with an X-y-z rotation sequence. Angles were analyzed during stance, with touchdown (TD) defined as the minimum vertical position of a marker placed on the posterior lateral aspect of the midsole and push-off at peak knee extension [6]. Traditional pronation variables included the AJC's position at TD, peak eversion, and eversion ROM. In addition, the minimum distance from the eversion boundary during stance was calculated (eversion buffer). Statistical differences were determined using a one-way ANOVA ( $\alpha = 0.05$ ).

## RESULTS AND DISCUSSION

No significant differences in traditional pronation variables were present between healthy and injured runners (Table 1). Conversely, injured runners had significantly smaller eversion buffers indicating they used a greater percentage of their available passive eversion ROM. This reduced eversion buffer was in large part due to injured runners having less eversion ROM, particularly at 10° and 20° of dorsiflexion (p-value 0.11, 0.06).

**Table 1.**

|                | Ev Buffer   | TD   | Peak Ev | ROM   |
|----------------|-------------|------|---------|-------|
| <b>Healthy</b> | -8.83       | 3.37 | -8      | 11.36 |
| <b>Injured</b> | -4.15       | 3.38 | -8.14   | 11.52 |
| <b>p-value</b> | <b>0.02</b> | 0.99 | 0.99    | 0.92  |

These findings suggest that where the AJC functions relative to its available passive ROM may be a better indicator of those at risk for injury than traditional pronation related variables. It is feasible that a smaller buffer could reduce the ability of the AJC to adapt to changes in the running terrain. As a result, proximal joints not designed to accommodate for these terrain changes may be required to, increasing their risk of injury. Additionally, this finding could explain the discrepancies between

orthotic and biomechanical studies. While both groups demonstrate a similar amount of eversion, those with AKP had smaller eversion buffers. It is reasonable to assume orthotics increase this buffer by limiting eversion, and subsequently improve AKP.

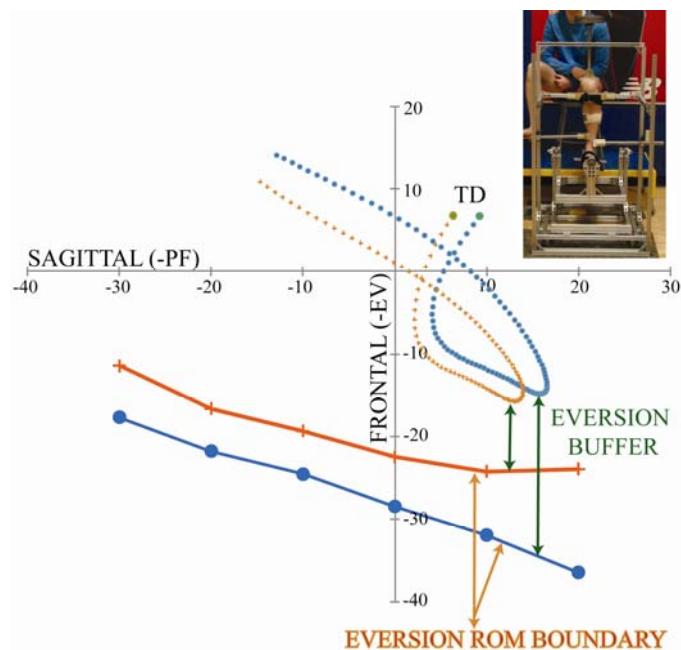


**Figure 1.** ROM device (top right). Dynamic AJC motion was evaluated relative to the passive eversion ROM. Healthy (●) and injured (+) runners demonstrated similar frontal plane movement profiles, however injured subjects had significantly smaller eversion buffers.

## CONCLUSIONS

The percentage of eversion ROM utilized when running may be a better indicator of those at risk for injury than traditional pronation variables.

1. Lun V, et al. *Br J Sports Med* **38**, 576-580, 2004.
2. Duffey M J, et al. *Med Sci Sports Exerc* **32**, 1825-1832, 2000.
3. Saxena A, et al. *J Am Podiatr Med Assoc* **93**, 264-271, 2003.
4. McClay I, et al. *J Appl Biomech* **83**, 109-124, 1997.
5. Engsborg J, et al. *Med Sci Sports Exerc* **28**, 299-304, 1996.
6. Fellin R, et al. *Proceeding from ASB '07*, Palo Alto, CA, 2007.



# LOWER EXTREMITY JOINT MOMENT ASYMMETRY DURING SPLIT-BELT TREADMILL WALKING

Ryan Roemmich and Chris Hass  
University of Florida, Gainesville, FL, USA  
email: rroemmich@ufl.edu

## INTRODUCTION

Several diseased populations, including stroke and Parkinson's disease (PD), are characterized by asymmetric motor deficits. Asymmetry in important gait-related variables have been described in these populations, including diminished ability to generate sufficient propulsive forces on the side most affected by disease or neurologic insult. Diminished unilateral lower extremity joint moment production has also been described in persons post-stroke [1] and with PD [2].

During split-belt treadmill walking (SBTW), the lower limbs each walk at a different speed simultaneously, thus externally altering symmetry patterns in the walker's gait. Consequently, SBTW has been utilized to rehabilitate gait asymmetries. Acute SBTW has been shown to temporarily restore symmetry in step length and double-limb support time in persons post-stroke [3]. However, the potential for SBTW to similarly rehabilitate asymmetry of joint moment production remains unknown. Therefore, in this study, we have investigated changes in peak sagittal joint moment production in the hip, knee, and ankle bilaterally during acute SBTW as compared to normal, tied-belt treadmill walking in healthy young adults.

## METHODS

Twelve participants (age  $22.6 \pm 3.6$  yr,  $167.6 \pm 8.9$  cm,  $62.8 \pm 9.5$  kg, 6 male, 6 female) participated in this study. None of the participants had ever walked on a split-belt treadmill prior to participation in this study. Additionally, all participants were free of lower-extremity orthopedic injury for at least one year.

Sixteen passive reflective markers were attached to the lower body in accordance with the Vicon Plug-in-Gait marker system. Kinematic data, time-

synchronized to the kinetic collection, were collected using a 7-camera motion capture system (Vicon Nexus, Oxford, UK) collecting at 120Hz. Force plate data from the instrumented treadmill (Bertec Corporation, Columbus, OH) were collected at 960 Hz.

Initially, participants began by walking on an instrumented split-belt treadmill while both belts moved together at the same speed. The speed was gradually increased until the participants reported being at the "fastest speed they felt comfortable walking for 15 minutes". This speed was set as the "fast" walking speed, while 50% of this speed was designated as the "slow" walking speed. Participants then walked for two minutes at the "slow" speed and two minutes at the "fast" speed, followed by a two-minute washout period at the "slow" speed. The last 30 seconds of the first "slow" speed trial, the "fast" speed trial, and the "split" trial were collected.

At the conclusion of the washout period, the belt under the nondominant leg was sped up to the "fast" speed while the belt under the contralateral leg remained at the "slow" speed. Participants walked under these conditions for 10 minutes. Following this "split" condition, participants were given 5 additional minutes with both belts at the "slow" speed to eliminate any after effects of the SBTW.

Lower extremity sagittal joint moments were calculated using inverse dynamics techniques. Change scores were calculated by comparing the magnitudes of the peak joint moments produced during SBTW and the average of the peak joint moments produced during the "slow" and "fast" trials.

$$\% \text{ Change} = \left( \left( \frac{\text{moment}_{\text{split}}}{\frac{\text{moment}_{\text{fast}} + \text{moment}_{\text{slow}}}{2}} \right) - 1 \right) \times 100\%$$

Paired samples t-tests were run on the change scores in peak sagittal ankle angle production between limbs during SBTW.

## RESULTS AND DISCUSSION

Analysis of the peak sagittal joint moments during SBTW showed that the “fast” limb ankle produced a significantly higher torque than the “slow” limb ankle at push-off ( $p < .001$ , figures below).

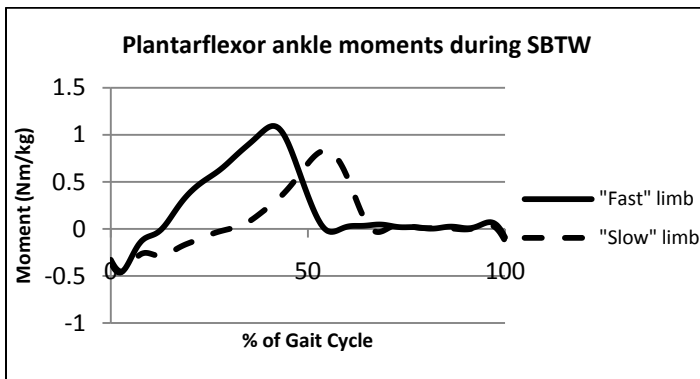


**Figure 1:** Representative sample plantarflexor ankle moment production during SBTW normalized to 100% of gait cycle.

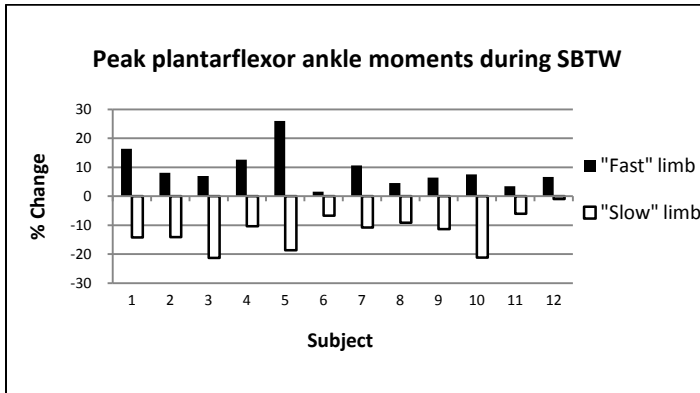


**Figure 2:** Change scores in peak sagittal ankle moment production during SBTW (mean fast limb peak plantarflexor moment change =  $9.26 \pm 6.62\%$ , mean slow limb peak plantarflexor moment change =  $-12.05 \pm 6.19\%$ ).

Interestingly, the change in peak flexion/extension moments of the knee and hip were not significantly different between the “fast” and “slow” limbs during SBTW. These results suggest that SBTW places a greater demand on the ankle of the “fast” limb, requiring the walker to generate a stronger plantarflexor torque.

## CONCLUSIONS

While walking on an instrumented split-belt treadmill, all subjects produced a larger sagittal plantarflexor joint torque in the “fast” limb ankle when compared to the contralateral limb. This information may be useful in rehabilitating asymmetries in gait in populations, such as stroke, in which the ability to generate plantarflexor torque is diminished unilaterally.

## REFERENCES

1. Allen JL, Kautz SA, and Neptune RR. Step length asymmetry is representative of compensatory mechanisms used in post-stroke hemiparetic walking. *Gait & Posture*, In press, 2011.
2. Johnsen EL, Mogensen PH, Sunde NA, and Ostergaard K. Improved asymmetry of gait in Parkinson's disease with DBS: Gait and postural instability in Parkinson's disease treated with bilateral deep brain stimulation in the subthalamic nucleus. *Movement Disorders* **24**, 588-595, 2009.
3. Reisman DS, Wityk R, Silver K, and Bastian AJ. Locomotor adaptation on a split-belt treadmill can improve walking symmetry post-stroke. *Brain* **130**, 1861-1872, 2007.

# CHANGES IN EFFORT DISTRIBUTION OF AMERICAN COLLEGIATE TRIPLE JUMPERS DURING THE COURSE OF A SEASON

<sup>1</sup>Braden Romer, <sup>2</sup>Dean Johnson, <sup>2</sup>Terrieha Romer,  
<sup>3</sup>Amanda Sinclair, and <sup>1</sup>Wendi Weimar

<sup>1</sup>Auburn University, Auburn, AL, USA

<sup>2</sup>Northwestern State University, Natchitoches, LA, USA

<sup>3</sup>University of Colorado at Colorado Springs, Colorado Springs, CO, USA  
email: bhr0002@tigermail.auburn.edu

## INTRODUCTION

The triple jump is considered to be a far more technically and physically demanding event than the long jump due, in part, to the three distinct phases of contact which contribute to total jump length. The success of an individual in the triple jump is largely dependent on the manner in which effort is distributed across the three phases [1]. Though a mixture of phase-dominant techniques are utilized by athletes, researchers have hypothesized that jump-dominant techniques are superior to hop dominant-techniques; however, initial increases in actual jump length may result from increasing the relative contribution of the hop phase, followed by increases in jump phase length [2]. Based on this hypothesis, it would appear that less developed athletes would exhibit greater hop-dominance; however, very little literature exists on the effort distribution of collegiate triple jumpers or how effort distributions are altered by development [1, 2, 3]. Therefore, the purpose of this research was to investigate the effort distribution of collegiate triple jumpers over the course of a typical competition season.

## METHODS

Six male participants were filmed while competing in two separate NCAA division-one meets during the 2010 outdoor track and field season. Participants were filmed with a high-speed digital camera (Casio EX-FH20 Exilim, Casio America, Dover, NJ) operating at 210 Hz at an early season and late season meet. Digital video of all legal trials was digitized on HU-M-AN, Version 6.0 2D (HMA Technology, Guelph, ON, Canada) to determine the longest and shortest actual jumps.

The longest and shortest legal jumps from each competition were further digitized to determine the phase lengths and the horizontal and vertical velocities at takeoff of each phase. Pearson-r correlation analyses were completed to determine relationships with the aforementioned variables to actual jump distances. Phase dominance was accepted as a greater than 2% difference between the largest phase and the next largest phase [2]. A 2 (time) x 2 (length) repeated measures ANOVA, with follow-up t-tests, was employed to determine if a significant difference ( $p < 0.05$ ) existed between the time of season filmed and the performance during each session.

## RESULTS AND DISCUSSION

There was a main effect for jumps in both the initial ( $p = 0.039$ ) and the final ( $p = 0.004$ ) filming sessions, indicating there was a significant difference between the longest and shortest jumps at both competitions (Table 1). A significant difference was also noted between the longest final jump and the shortest initial jump ( $p = 0.008$ ). Though actual jump lengths were meaningfully longer during the final filming session, the difference between the longest total jumps approached, but did not reach, significance. There was a significant difference in step length ( $p = 0.005$ ) and horizontal velocity ( $p = 0.029$ ) between the longest initial and shortest initial jumps, but not at the final competition. A significant difference was also noted between the hop lengths ( $p = 0.037$ ) of the longest final and shortest final jumps. Finally, there was a significant difference between the jump phase length ( $p = 0.043$ ) of the longest final and shortest initial jumps.

A significant positive correlation ( $r = 0.99$ ,  $p < 0.001$ ) existed between official jump distance and actual jump distance. Balanced and hop-dominant techniques were just as effective in actual jump length (14.83m each), while the jump-dominant technique yielded the shortest result (14.38m). The horizontal and vertical velocities of the participants displayed similar relationships between filming sessions. Horizontal velocity during takeoff of the hop phase was notably, though not significantly, higher later in the season ( $8.55 \text{ ms}^{-1}$  and  $8.89 \text{ ms}^{-1}$ ). The participants exhibited less vertical velocity during the takeoff of the step ( $2.30 \text{ ms}^{-1}$  and  $2.15 \text{ ms}^{-1}$ , respectively) and jump phases ( $3.49 \text{ ms}^{-1}$  and  $2.73 \text{ ms}^{-1}$ , respectively) as the season progressed. Of interest are the similar horizontal velocities during the hop phase for the longest initial jump and the shortest final jump ( $8.55 \text{ ms}^{-1}$  and  $8.61 \text{ ms}^{-1}$ , respectively), which are considerably higher than the shortest initial jump ( $8.18 \text{ ms}^{-1}$ ). Furthermore, the participants exhibited much lower vertical velocities during the hop phase for the longest initial jump and the longest final jump ( $3.01 \text{ ms}^{-1}$  and  $3.05 \text{ ms}^{-1}$ , respectively) than the shortest initial jump ( $3.48 \text{ ms}^{-1}$ ).

## CONCLUSIONS

This project endeavored to understand the changes in effort distributions of collegiate triple jumpers over the course of a season. The difference in certain variables may have been too small to reach statistical significance, yet may have meaningful

consequences for athletes and coaches. For example, it appears that over-hopping does have a negative effect on step length and overall jump length; however, the source of over-hopping appears to be important. Early in the season, athletes were attempting to increase hop length, and thereby jump length, by increasing the vertical velocity at the takeoff of the hop. However, forces upon landing may have been too large, resulting in a decreased step and total jump length. As the season progressed, athletes achieved longer hop lengths by increasing the horizontal velocity at the takeoff of the hop, without a detriment to step or total jump length. Finally, as the athletes' development progressed, additional increases in total jump length did result from increases in the length of the jump phase.

## REFERENCES

1. Yu B, et al. *J Biomech*, **29**, 1283-1289, 1996.
2. Hay J G. *Journal of Applied Biomechanics*, **15**, 36-51, 1999.
3. Miller J A, et al. *International Journal of Sport Biomechanics*, **2**, 272-288, 1986.

## ACKNOWLEDGEMENTS

The authors would like to thank the athletes, their member schools, the University of Louisiana at Lafayette, Louisiana State University at Baton Rouge, and Northwestern State University of Louisiana for their participation in this study.

**Table 1:** Official, Actual, and Phase Distances for the Longest and Shortest Jumps

|                         | Official Distance <sup>1</sup>  | Actual Distance <sup>1</sup> | Hop Distance <sup>1</sup>    | Hop Pct <sup>2</sup> | Step Distance <sup>1</sup>   | Step Pct <sup>2</sup> | Jump Distance <sup>1</sup>   | Jump Pct <sup>2</sup> |
|-------------------------|---------------------------------|------------------------------|------------------------------|----------------------|------------------------------|-----------------------|------------------------------|-----------------------|
| <b>Longest Initial</b>  | 14.43 <sup>a</sup><br>(±0.33)   | 14.63<br>(±0.31)             | 5.13<br>(±0.30)              | 35.02%<br>(±1.30%)   | 4.51 <sup>d</sup><br>(±0.17) | 30.84%<br>(±0.89%)    | 4.99<br>(±0.18)              | 34.13%<br>(±1.66%)    |
| <b>Longest Final</b>    | 14.83 <sup>b,c</sup><br>(±0.45) | 14.96<br>(±0.50)             | 5.42 <sup>e</sup><br>(±0.22) | 36.24%<br>(±2.06%)   | 4.43<br>(±0.57)              | 29.56%<br>(±3.28%)    | 5.11 <sup>f</sup><br>(±0.30) | 34.19%<br>(±1.82%)    |
| <b>Shortest Initial</b> | 13.46 <sup>a,c</sup><br>(±0.98) | 13.62<br>(±1.03)             | 5.21<br>(±0.41)              | 38.27%<br>(±1.99%)   | 4.12 <sup>d</sup><br>(±0.18) | 30.37%<br>(±2.32%)    | 4.29 <sup>f</sup><br>(±0.73) | 31.36%<br>(±3.64%)    |
| <b>Shortest Final</b>   | 14.24 <sup>b</sup><br>(±0.33)   | 14.37<br>(±0.33)             | 5.12 <sup>e</sup><br>(±0.08) | 35.64%<br>(±0.87%)   | 4.39<br>(±0.47)              | 30.54%<br>(±2.66%)    | 4.85<br>(±0.23)              | 33.82%<br>(±2.13%)    |

Values are reported in a Mean (± SD) format

<sup>1</sup>Distances are reported in meters

<sup>2</sup>Phase percentages are reported as a percentage of actual jump length

a, b, c, d, e, and f Items are significantly different

# Ground Reaction Forces & Joint Moments in Habitual versus Converted Forefoot Strike Runners

<sup>1</sup>Brandon D. Rooney and <sup>1</sup>Timothy R. Derrick, PhD.

<sup>1</sup>Iowa State University, Ames, IA, USA  
email: bdrooney@iastate.edu web: <http://www.kin.hs.iastate.edu/>

## INTRODUCTION

Limited research has been conducted comparing rearfoot strike (RFS) and mid/forefoot strike (FFS) runners. This is, in part, due to the limited number of FFS runners. However, Hasegawa et al. (2007) found 38% of the top 50 runners at the 15km mark of half marathon exhibited FFS pattern, whereas only 21% of the last 48 runners exhibited FFS pattern. Therefore, elite runners appear to have a greater tendency to run with FFS pattern. Also with increasing minimalist footwear trends in running, a FFS pattern may become more common [3].

Williams et al. (2000) proposed a mechanical link between joints, allowing for habitual RFS runners to convert to FFS patterns. This would provide a larger pool of participants for a FFS vs. RFS comparison. Williams et al. (2000) found few differences for kinematic and kinetic variables between habitual and converted FFS runners. The purpose of this study is to provide additional insight into the ability of converted FFS runners to represent habitual FFS runners.

## METHODS

Fifteen FFS and 15 RFS competitive long distance runners were recruited. The study was approved by the Iowa State Institutional Review Board. Participants were provided the same brand and model of running shoes. Participants performed a 5 minute warm up on a treadmill at a self-selected speed; this speed was used for the over-ground running trials. Then 21 retro-reflective markers were placed on the right leg and shoe, pelvis, and trunk.

Position data were recorded at 200Hz during a static trial and two over-ground running conditions (Vicon MX, Vicon, Centennial, CO, USA). For the running trials, participants ran down a 30m runway

and were instructed to strike either of two adjacent force platforms (AMTI, Watertown, MA), 2000Hz, with their right foot. Speed was monitored for each trial.

Heel strike index (HSI) was calculated as the average center of pressure under the foot for the first five data points of stance and was reported as a percentage of the foot length from the heel. Participants were instructed to run naturally with no mention of strike pattern as the HSI was calculated. Participants were placed in the converted FFS group if their HSI was less than 33.3% and in the habitual FFS group if their HSI was greater than 33.3%. Converted FFS subjects were then instructed to run with a forefoot strike pattern and allowed to practice until they felt comfortable and were able run with a consistent FFS. Habitual FFS subjects continued to run normally. Ten acceptable trials were collected.

Data analysis was performed in Matlab (7.9.0, R2009b). Vaughn et al. (1992) equations were used to determine segment masses, center of mass, and moment of inertia. Joint moments were calculated using a Cardan rotational sequence of flex/ext-add/abd-int/ext rotation. Independent measures t-tests were performed between habitual and converted FFS groups.

## RESULTS

The FFS and RFS groups were both composed of 12 males and 3 females. The groups were not significantly different for age ( $21.3 \pm 2.1$ yr), body mass ( $64.70 \pm 8.10$  kg), height ( $1.78 \pm 0.08$  m), and mileage ( $61.8 \pm 21.2$  mi/wk) ( $p > 0.05$ ). The mean running velocities for the FFS and RFS groups were  $4.39 \pm 0.24$  and  $4.25 \pm 0.27$  m/s, respectively ( $p = 0.079$ ). The stance time was not significantly different between groups ( $p = 0.147$ ). The mean HSI for the habitual FFS group was  $63.8 \pm 7.3\%$ ,

and for the converted FFS group it was  $68.6 \pm 6.8\%$  ( $p = 0.087$ ).

The habitual and converted groups showed similar ground reaction force (GRF) patterns (Fig. 1). Both groups demonstrated a bimodal braking force in the AP GRF, as described by Cavanagh and Lafortune (1980). However, the converted FFS group had significantly decreased peak vertical and braking AP GRF and rate of loading (ROL) (Table 1). The peak plantar flexor, knee and hip extensor moments were less in the converted FFS group, but the knee extensor was the only statistically significant difference (Table 1).

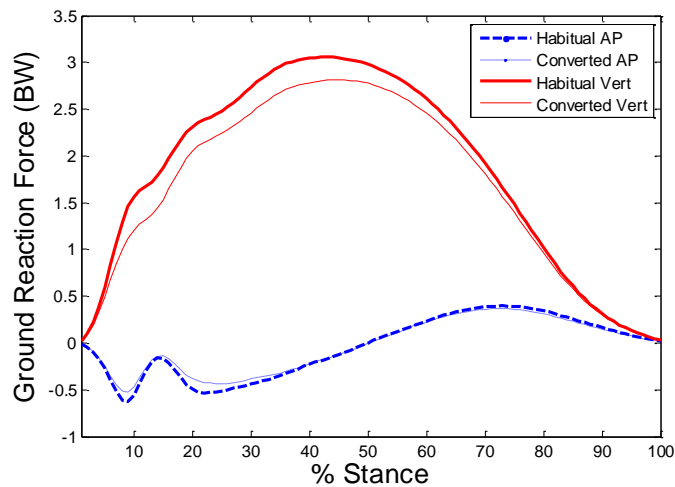


**Figure 1:** Ensemble curves of GRF for Habitual and Converted FFS groups. Positive values indicate vertical and anterior directed forces.

## DISCUSSION

Williams et al. found vertical GRF and plantarflexion moments to be significantly decreased in the converted FFS group. They also found that most of the variables were decreased in the converted group even if it was not statistically different. These previous findings are consistent with our results. However, there were more statistically significant differences in this study and all the kinetic variables were decreased in the converted group. The decreased magnitude of GRF and joint moments may be due to the novelty of the strike pattern and may disappear with further practice.

This study found that converted FFS runners demonstrate similar patterns to habitual FFS runner. However, there should be caution when using RFS runners to represent FFS because of the decreased magnitudes of the GRF and joint moments.

## REFERENCES

1. Cavanagh PR & Lafortune MA. *J Biomech* **13(5)**, 397-406, 1980.
2. Haegawa H, et al. *J. Strength & Conditioning Res* **21(3)**, 888-893, 2007.
3. Lieberman DE, et al. *Nature* **463**, 531-535, 2010.
4. Vaughan CL, et al. *Dynamics of human gait*. Human Kinetics, Champaign, IL.1992.
5. Williams DS, et al. *J Appl Biomech* **16**, 210-218, 2000.

**Table 1:** Mean and standard deviation of peak GRF and sagittal internal joint moments for habitual and converted FFS runners. Positive values represent vertical and anterior GRF, plantar flexor and extensor moments. † = significantly different from habitual FFS ( $p < 0.01$ ), \* =  $p < 0.05$ .

| Variables              | Habitual FFS       | Converted FFS            | p-value |
|------------------------|--------------------|--------------------------|---------|
| Vertical GRF (BW)      | $3.10 \pm 0.22$    | $2.83 \pm 0.22^\dagger$  | 0.005   |
| Vertical ROL (BW/s)    | $131.34 \pm 35.10$ | $103.74 \pm 33.97^*$     | 0.023   |
| AP Breaking GRF 1 (BW) | $-0.65 \pm 0.15$   | $-0.55 \pm 0.15^*$       | 0.050   |
| AP Breaking GRF 2 (BW) | $-0.55 \pm 0.07$   | $-0.46 \pm 0.07^\dagger$ | 0.0005  |
| Ankle Moment (BWm)     | $0.38 \pm 0.03$    | $0.36 \pm 0.04$          | 0.303   |
| Knee Moment (BWm)      | $0.31 \pm 0.07$    | $0.26 \pm 0.04^*$        | 0.038   |
| Hip Moment (BWm)       | $0.38 \pm 0.06$    | $0.32 \pm 0.09$          | 0.118   |

## EFFECT OF FOOTWEAR ON BALANCE

William Rose<sup>1</sup>, Bradley Bowser<sup>1</sup>, Robert McGrath<sup>1</sup>, Jillian Salerno<sup>1</sup>, Joshua Wallace<sup>1</sup>, Irene Davis<sup>2</sup>

<sup>1</sup>University of Delaware, Newark, DE, USA

<sup>2</sup>Harvard Medical School, Boston, MA, USA

email: [rosewc@udel.edu](mailto:rosewc@udel.edu)

### INTRODUCTION

Barefoot and minimal footwear running have become increasingly popular. Barefoot advocates claim that running injuries may be reduced when running in little or no footwear. It has been suggested that this is due, in part, to improved postural stability when shoes are shed, as static and dynamic balance depends on cutaneous and proprioceptive inputs from the feet. Shinohara and Gribble [1] studied balance with 5-toed socks compared to conventional socks and bare feet. They used the time-to-boundary method to assess standing single-leg balance. They found that static balance was compromised in both sock conditions.

Running is a dynamic activity comprised of sequential, single leg landings. If single leg stance balance can be influenced by socks, it is possible that dynamic stability may be compromised by footwear. Therefore, the purpose of this study was to compare measures of dynamic stability during single leg landings across three footwear conditions. We expected that balance would significantly improve as footwear was reduced due to more accurate, unfiltered cutaneous inputs from the foot. Specifically, we hypothesized that balance would be worst in running shoes, better in minimal footwear and best when barefoot.

### METHODS

Eighteen healthy subjects (14 male, 4 female) participated in the study. Subjects were free of injury at the time of the study. All were habitual wearers of Vibram Five-Fingers shoes. Data were collected in a single visit to the lab by each subject, in three footwear conditions: barefoot (BF), wearing their own Vibram Five-Fingers (V5), and wearing Nike Pegasus running shoes (RS), supplied by the investigators, as shown in Fig.1 The footwear order

was randomized across participants. Dynamic balance was assessed by a jump landing protocol. Each subject balanced briefly on their dominant (preferred for kicking) leg on a 10 cm high platform positioned 70 cm from the edge of a force plate. They then jumped, with eyes open, onto the center of the force plate, landing on the non-dominant leg, typically used for stability. Subjects were instructed to stand quietly and motionless on the landing leg for 10 seconds after landing. There was a rest period between jumps. Force plate data were collected at 1000 Hz during and for 10 seconds after landing. Each subject completed 5 jumps with each type of footwear, for a total of 15 jumps.



**Figure 1.** Dynamic balance was assessed in bare feet, Vibram Five Fingers, and Nike Pegasus running shoes.

The medial-lateral, anterior-posterior, and vertical components, and the total dynamic postural stability index, were computed for each landing, using a three-second window beginning at the time of landing [3]. Specifically, we computed the square root of the mean squared deviation of force from the baseline value for three seconds beginning at the time of landing, as shown in Figure 2. The baseline value was zero for anterior-posterior and medial-lateral stability indices (APSI and MLSI), and was equal to body weight for the vertical stability index

(VSI). The total dynamic postural stability index (DPSI) was computed as

$$DPSI = \sqrt{APSI^2 + MLSI^2 + VSI^2} .$$

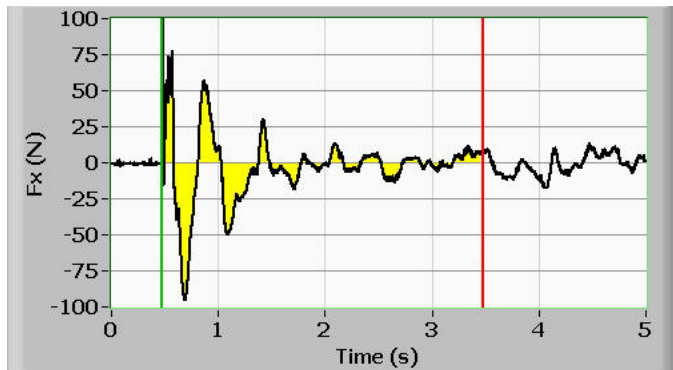


**Figure 2:** MLSI was computed as the square root of the mean squared medial-lateral force, for three seconds after landing. This time window is shown by the shaded region between the green and red cursors, in the plot of medial-lateral force above. APSI and VSI were computed similarly.

APSI, MLSI, VSI, and DPSI were computed for five jump landings in each individual in each type of footwear. One way analysis of variance with repeated measures was used to test the hypothesis that dynamic postural stability was affected by the type of footwear. Pairwise post-hoc testing was done with the Tukey test.

## RESULTS AND DISCUSSION

Mean values,  $\pm$  standard error of the mean of all four indices, are shown in Table 1. The medial-lateral, vertical, and total stability indices were significantly different between conditions (ANOVA,  $p < 0.05$ ). A strong trend was seen in the anterior-posterior stability index ( $p = 0.057$ ). Therefore, post-hoc pairwise tests were conducted on all variables. Results indicated that APSI, MLSI, VSI, and DPSI were all significantly lower (Tukey test,  $p < 0.05$ ) in bare feet than in standard running shoes. In addition, MLSI was significantly lower in BF versus V5 condition.

Our results support those of Shinohara and Gribble who found that static balance was best in bare feet [1]. For three of the four variables, instability increased between BF and V5, and between V5 and RS. This is likely due to the increasing filtering of sensory input that results from additional material between the foot and the ground. It is interesting to

note that DPSI, representing the composite stability measure, exhibited the greatest differences between footwear conditions.

| Footwear                         | Index                |                      |                      |                      |
|----------------------------------|----------------------|----------------------|----------------------|----------------------|
|                                  | APSI                 | MLSI                 | VSI                  | DPSI                 |
| Barefoot (BF)                    | 0.019<br>$\pm 0.001$ | 0.144<br>$\pm 0.003$ | 0.212<br>$\pm 0.009$ | 0.258<br>$\pm 0.008$ |
| Vibram Five Fingers (V5)         | 0.021<br>$\pm 0.001$ | 0.148<br>$\pm 0.003$ | 0.223<br>$\pm 0.011$ | 0.269<br>$\pm 0.010$ |
| Standard Running Shoes (RS)      | 0.022<br>$\pm 0.001$ | 0.147<br>$\pm 0.002$ | 0.227<br>$\pm 0.009$ | 0.272<br>$\pm 0.009$ |
| p (ANOVA)                        | 0.057                | 0.014                | 0.039                | 0.023                |
| Significant pairwise differences | BF<RS                | BF<V5, BF<RS         | BF<RS                | BF<RS                |

**Table 1:** Dynamic postural stability indices in different types of footwear. Mean  $\pm$  SEM.  $n = 18$ .

## CONCLUSIONS

The results of this study indicate that dynamic balance assessed during a single-leg jump landing task is better in bare feet than in standard running shoes, and is not significantly different between Vibrams and standard running shoes. These results are consistent with the hypothesis that filtering or masking of sensory input by footwear can affect dynamic postural stability.

## REFERENCES

1. Shinohara J, Gribble P. Five-Toed Socks Decrease Static Postural Control Among Healthy individuals as Measured with Time-To-Boundary Analysis. *Am Soc Biomech Annual Meeting*, 2009.
2. Hertel J, Olmsted-Kramer LC. Deficits in time-to-boundary measures of postural control with chronic ankle instability. *Gait Posture* **25**: 33-39, 2007.
3. Wikstrom EA, Tillman MD, Smith AN, Borsa PA. A New Force-Plate Technology Measure of Dynamic Postural Stability: The Dynamic Postural Stability Index. *J Athl Train* **40**: 305-309, 2005.

# STRIDE LENGTH INFLUENCES LOWER EXTREMITY COUPLING DURING WALKING

Elizabeth M. Russell<sup>1</sup> & Joseph Hamill<sup>2</sup>

<sup>1</sup> Andrews-Paulos Research and Education Institute, Gulf Breeze, FL, USA

<sup>2</sup> University of Massachusetts, Amherst, MA, USA

email: erussell.kin@gmail.com

## INTRODUCTION

The timing, or coupling, between joint rotations has been shown to be a useful tool for understanding injury etiology. A number of research studies have investigated the kinematic coupling between the foot and leg. Foot eversion/inversion is coupled with leg internal/external rotation at the subtalar joint, which functions like a mitered hinge. During running, cross correlations between these two motions remain relatively high during the stance phase, regardless of running speed (1). During walking at a comfortable speed, however, cross correlations are relatively lower (1), indicating less coupled motion between the segments. Long strides have been shown to have greater implications for various injuries (2) but it remains unclear if the coupling patterns are affected by stride length (SL). The purpose of this study was to investigate the coupled motions of the foot and leg during a range of stride lengths. We hypothesized that longer strides would show less coupled motion between the segments than shorter strides.

## METHODS

Twelve female subjects with no history of lower extremity injury participated in this study (Table 1). Subjects walked on a treadmill while speed was increased and decreased until preferred speed (PS) was identified three consecutive times. Preferred stride frequency (PSF) was recorded by averaging the number of strides counted each minute during a three minute period. Preferred SL (PSL) was then calculated.

| Age (yrs)     | Height (m)     | BMI (kg/m <sup>2</sup> ) | PS (m/s)     | PSF (strides/min) |
|---------------|----------------|--------------------------|--------------|-------------------|
| 20.9<br>(1.8) | 1.65<br>(0.07) | 22.1<br>(1.5)            | 1.4<br>(0.1) | 59<br>(3.4)       |

**Table 1.** Average subject characteristics (standard deviation)

Markers were placed on anatomical landmarks of the right lower extremity and subjects walked on the treadmill at the PS at  $\pm 0\%$ ,  $\pm 5\%$ ,  $\pm 10\%$ ,  $\pm 15\%$ , and  $\pm 20\%$  of the PSL (order randomized) for three minutes. SF was paced to the beat of a metronome. (Note: With speed constant, decreases in SL are associated with increases in SF.) Kinematic marker locations were recorded (240 Hz) during the final 20 seconds of walking using an eight-camera Qualisys system. Kinematic data were low-pass filtered (8Hz) and frontal plane foot and transverse plane leg segment angles were calculated in Visual 3D software. The stance phase between heel strike and toe-off was identified by the maximal displacements of the toe marker relative to the sacral marker along the direction of forward progression.

Zero-lag, cross-correlation coefficients ( $r$ ) of foot frontal plane motion and transverse plane leg motion were calculated during the stance phase of walking (3). Fisher's Z-scores (4) were calculated and used in an ANOVA and post-hoc analyses. Alpha was set at  $p < 0.05$ .

## RESULTS

Cross-correlation coefficients significantly and progressively decreased as SL increased (longer, slower strides) (Figure 1). Figure 2 shows significant differences among SL conditions.

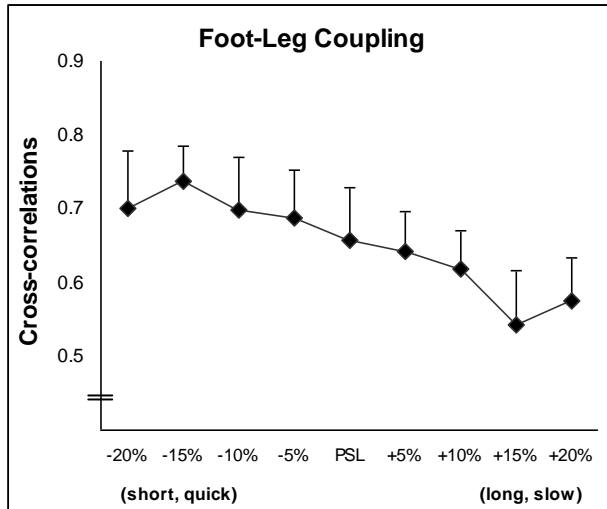


**Figure 1.** Average cross-correlation coefficients and standard error bars for foot-leg coupling at each SF condition. Note that the y-axis scale does not begin at zero.

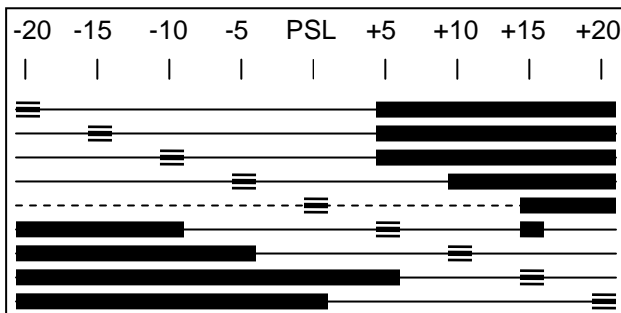


**Figure 2.** Significant differences. Bold, hashed squares indicate the above listed SL condition and the black horizontal bars indicate the SL conditions from which it is significantly different ( $p < 0.05$ ). The baseline measure (PSL) is indicated by the horizontal dashed line.

## DISCUSSION

The SL-SF combination influenced the coupled motions of foot eversion/inversion with leg internal/external rotation. Shorter, quicker strides had a greater the degree of kinematic coupling between the foot and leg than longer, slower strides. It may be that the faster movements of the lower extremity necessitated a more tightly-coupled, synergistic relationship between the foot and leg. Conversely, the longer time in contact with the ground and

slower movements during the increased SL conditions may have provided greater opportunities for deviations from this coupled relationship. At either end of the range of SL-SF combinations ( $\pm 20\%$  PSF) the correlation coefficients deviated from the general trend. This result is likely due to the difficulties many of the subjects experienced maintaining the greatest SL-SF deviations. It remains unknown if SL or SF was the primary influence on the progressive changes in foot-leg coupling and future research will investigate this question.

The coupled relationship of these foot and leg rotations has been shown to be lower in walking than in running; however, cross correlations in this study were greater than in previous reports (1). This is likely due to the fact that subjects were shod in the present study and barefoot in previous reports.

It is possible that incorporating lags into correlation calculations could have yielded greater values, however, with strong kinematic coupling, phase shifts should not be present between angular displacement curves.

## CONCLUSIONS

Taking long, slow strides significantly decreases the coupled relationship between frontal plane foot and transverse plane leg rotations. This finding may have implications for lower extremity soft tissue injury. Future research will identify the independent effects of SL and SF on coupling relationships.

## REFERENCES

1. Pohl MB, et al. *Gait & Posture* **25**: 295-302, 2007.
2. Hamill J, et al. *Hum Mov Sci* **14**: 45-60, 1999.
3. Li L. *J Electromyogr Kinesiol* **9**: 385-389, 1999.
4. Derrick TR & Thomas JM. *Innovative Analyses of Human Movement*. Ch. 7, 2004.

# ALTERED STAIR CLIMBING MECHANICS IN SUBJECTS WITH FEMOROACETABULAR IMPINGEMENT

<sup>1,2</sup>Jonathan Rylander, <sup>3</sup>Beatrice Shu, <sup>1</sup>Jessica Asay, <sup>3</sup>Marc Safran, <sup>1,2,3</sup>Thomas Andriacchi

<sup>1</sup>Veterans Affairs Bone and Joint RR&D, Palo Alto, CA, USA

<sup>2</sup>Stanford University, Stanford, CA, USA

<sup>3</sup>Stanford School of Medicine, Stanford, CA, USA

email: rylandjh@stanford.edu

## INTRODUCTION

Femoroacetabular Impingement (FAI) is defined by the femoral head or neck abutting the acetabular rim and often causing decreased range of motion, pain at extreme ranges of motion, and damage to bone and soft tissue which can lead to early onset osteoarthritis [1,2]. FAI classically impairs hip motion and analyzing functional changes in activities of daily living can provide insight into the pathomechanics of the disease. While abnormal hip kinematics during level walking in individuals with FAI has been reported [3,4], there is little information on more strenuous activities such as stair climbing. The purpose of this study was to determine what functional changes occur in individuals with FAI during stair climbing, an activity which requires increased hip range of motion. This study will address the following hypotheses:

Hypothesis 1: Subjects with FAI will have adapted kinematics in the pelvis and hip to reduce the extreme ranges of motion encountered during stair climbing when compared with healthy controls.

Hypothesis 2: FAI subjects will have secondary kinematic and kinetic adaptations in the trunk, knee, and ankle that will compensate for the reduction of extreme ranges of motion in the hip.

## METHODS

Kinematics and kinetics were gathered for 17 FAI (10M, 7F, 34.6±9.8 y.o., 26.0±4.6 BMI) and 17 healthy matched control subjects (10M, 7F, 36.0±10.2 y.o., 26.9±5.0 BMI) as they ascended two 20 cm stairs without rails at self selected normal speed. IRB approved informed consent was obtained for all subjects. FAI subjects were diagnosed based on plain radiograph and MRI and were unilaterally symptomatic. The healthy controls were matched for age, gender, and BMI and were categorized “healthy” based on self-

reported lack of hip pain or injury history; controls were not specifically screened for FAI. A 9 camera opto-electronic system (120 Hz; Qualisys) and a force plate (120 Hz; Bertec Corporation) located under the first stair were used in this analysis. Each subject performed three trials per leg. The point cluster marking technique used for this study can be seen in Figure 1.

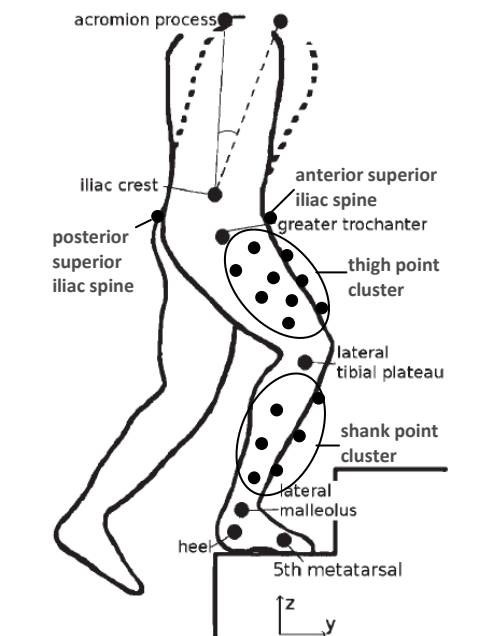


**Figure 1:** Marker setup with trunk flexion angle (adjusted from Asay et al 2009 [5])

Inverse dynamics was used to calculate kinematic and kinetic data for the ankle, knee, and hip. Trunk flexion was also calculated. Inter-group differences were analyzed using a student's t-test ( $\alpha=0.05$ ). Bonferroni adjustments for multiple comparisons were applied for posthoc comparison between groups.

## RESULTS AND DISCUSSION

A significant difference was found in the pelvic rotation and hip internal rotation as well as sagittal plane range of motion at the hip and trunk, knee,

and ankle flexion angles between the affected side in FAI subjects when compared with controls (Table 1).

**Table 1:** Means (standard deviation) for FAI Affected Side and Controls.

|   | FAI Affected | Controls  | p-value (adjusted alpha) |
|---|--------------|-----------|--------------------------|
| Sagittal plane hip range of motion (°)    | 56.8(5.6)    | 63.4(6.1) | 0.004(0.008)             |
| Hip internal rotation (°)                 | 4.2(2.7)     | 8.9(4.9)  | 0.002(0.008)             |
| Pelvic rotation range of motion (°)       | 19.1(5.0)    | 9.7(1.8)  | 0.0001(0.008)            |
| Maximum trunk flexion (°)                 | 10.2(4.8)    | 6.7(2.2)  | 0.011 (0.025)            |
| Terminal stance knee flexion (°)          | 13.8(5.2)    | 9.2(3.5)  | 0.005(0.013)             |
| Terminal stance ankle plantar flexion (°) | 11.7(8.1)    | 17.9(5.2) | 0.012(0.013)             |
| Peak knee flexion moment (%Bw*Ht)         | 4.9(2.5)     | 6.7(1.1)  | 0.011(0.013)             |

Hypothesis 1 was supported by the results; significant decreases in sagittal plane hip range of motion and internal rotation between the femur and pelvis were observed between FAI subjects' affected side when compared with controls (Table 1). A significant increase in pelvic rotation was also observed on the affected side when compared with controls. This increased pelvic rotation could explain the reduced sagittal plane hip range of motion as well as internal rotation of the femur relative to the pelvis, both painful motions that access the damaged area of an individual with FAI. Although not reported in the table, a significant increase in pelvic rotation, decrease in internal rotation, and decrease in hip sagittal plane range of motion were also observed on the asymptomatic side when compared with controls. Since these modified motions occurred on the asymptomatic side, these results suggests that additional factors to pain, such as physical impingement, could also be responsible for the altered motion.

Hypothesis 2 was also supported by the results; a significant reduction in trunk flexion, toe-off knee flexion angle, toe-off ankle plantar flexion angle, and knee flexion moment were observed in individuals with FAI when compared with controls (Table 1). A significant increase in the trunk flexion

on the affected side without a significant difference in sagittal plane pelvic tilt suggests that this increase in trunk flexion occurred in the spine and not at the pelvis. Along with the reduced peak knee flexion moment occurring at midstance, the significant decrease in knee and ankle plantar flexion angles, observed during terminal stance phase, suggests an offloading of the joints and a reduction in the activation of the extensor muscles. These observations could indicate possible muscle weakness that is accessed during this more strenuous activity of daily living.

## CONCLUSIONS

The altered mechanics during stair climbing associated with FAI suggests several interpretations including adaptation to: reduce pain, reduce physical impingement, overcome muscle weakness, or a combination of these factors. These altered mechanics include a decrease in internal hip rotation and hip flexion, two positions which commonly result in impingement, potentially caused by an increase in pelvic rotation. This functional modification decreases the overall hip range of motion an individual with FAI would need in order to perform the more strenuous stair climbing activity and would likely unload the damaged and painful area on the affected limb. An increase in trunk flexion and rotation in the spine were also observed, both of which could help explain the common complaint of lower back pain experienced in individuals with FAI. Additionally, trunk flexion and pelvic rotation with a reduced knee flexion moment along with a reduction in hip, knee, and ankle flexion at terminal stance could indicate a weakness in the hip extensors. Stair climbing is a more strenuous activity of daily living that requires additional muscle strength and hip range of motion than walking and is thus a good activity to evaluate the functional adaptations associated with FAI.

## REFERENCES

1. Beaulé, P et al. *J Orth Res.* 2005; **23**:1286- 92.
2. Ganz, R et al. *Clin Orthop Relat Res.* 2003; **417**:112-120.
3. Rylander, J et al. *ORS 56<sup>th</sup> Annual Meeting N Orleans*; Poster #1921.
4. Kennedy, J et al. *Gait and Pos.* 2009; **30**: 41-44.
5. Asay, J et al. *J Orth Res.* 2009; **27**: 325-329

Parisa Saboori and Ali Sadegh

Dept. of Mech. Eng., The City College of the City University of New York, USA

email: [psaboori@gc.cuny.edu](mailto:psaboori@gc.cuny.edu), and [sadegh@me.ccny.cuny.edu](mailto:sadegh@me.ccny.cuny.edu)

## INTRODUCTION

The interface between the brain and the skull consists of three fibrous tissue layers, dura mater, arachnoid and pia mater, known as the meninges, and strands of collagen tissues connecting the arachnoid to the pia mater, known as trabeculae. The space between the arachnoid and pia mater, known as subarachnoid space (SAS), is filled with cerebrospinal fluid (CSF) which stabilizes the shape and the position of the brain during head movements or an impact, see Fig. 1.

Traumatic brain injury (TBI), which is mainly due to automotive accidents, contact sports or fall, is a major public health problem, especially among male young people. TBI usually happens if a sudden trauma to the head causes damage to the brain or when an object penetrates into the skull and enters the brain tissue. Symptoms of a TBI can be mild, moderate, or severe, depending on the extent of the damage to the brain.

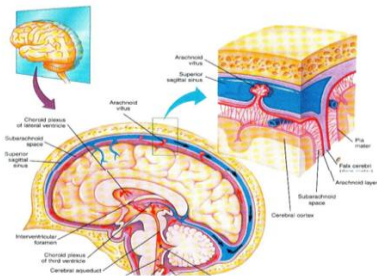


Figure 1- Schematic diagram of head/brain anatomy

It has been shown that subarachnoid space (SAS) trabeculae plays an important role in damping and reducing the relative movement of the brain with respect to the skull, thereby reducing traumatic brain injuries, (Zoghi & Sadegh 2009 and 2010). Several models have been created to predict different types of head injuries. In these models the space between the skull and the brain, i.e., the meningeal layers including the cerebrospinal fluid (CSF) and the subarachnoid space (SAS) have been over simplified as a soft elastic materials having the

bulk modulus of water and very low shear modulus, or in some cases as water only, Kleiven, (2003) and Trosseille, et al., (1992). These over simplification could lead to inaccurate results.

The architecture and material properties of SAS is not well known in the literature. A few studies (e.g. Xin Jin et al. (2008) and Zhang et al. (2001)) have reported a wide range the elastic modulus of trabeculae up to three orders of magnitudes. The preliminary histology study of the trabeculae reveals that it is a collagen based structure. In addition, the effect of the SAS trabeculae on transferring load or impact to the brain has not been fully established. This is due to the fact that the trabeculae have complex architecture and thus the interaction between CSF and the trabeculae (solid-fluid interaction) is very difficult to model. Only the architecture of the trabeculae of the human spinal cord have been studied, Alcolado, et.al. (1987) and Frederickson (1991).

In this paper the mechanotransduction of the external load through the trabeculae in the subarachnoid space (SAS) to the brain was investigated. This has been accomplished by employing the results of our animal studies, i.e. the histology and architecture of trabeculae, and by creating local models consist of a trabecula.

## AIM 1: THE ARCHITECTURE OF THE SAS TRABECULAE

The objective of our animal study was to investigate the architecture of the SAS trabeculae, which has not been addressed in the literature. The first step was to fix and solidify the subarachnoid space and the trabeculae while the animal is alive. Note that as soon as the animal dies the subarachnoid space collapses since the CSF, which is separating the pia mater and the arachnoid, is quickly drained. To preserve this subarachnoid space, pre-fixative solution PBS (Phosphate buffered saline) were injected to the left ventricle of anesthetized Sprague-Dawley (SD) rats (weighting

250-300g and 2 to 3 months old), followed by the fixative solution (glutaraldehyde + formaldehyde). After a few minutes through the blood circulation, the blood vessels of the SAS were solidified. Then the animals were sacrificed and several tissue samples from different regions of the brain were prepared for the Scanning Electron Microscopy (SME). Samples of SEM results are shown in Fig. 2.

The results of this experimental study revealed that approximately 70% of trabecula architecture consists of single trabecula that is bundled with so many collagen fibers. These trabeculae are generally shaped as a tree, each having a stem and branches. The experimental results further reveal that the stem of the majority of the trabeculae were attached to the pia mater and the branches were attached to the arachnoid.

**AIM 2: LOCAL MODELS OF SINGLE TRABECULA**

To have a better understanding of the effect of the trabecular architecture and their orientations on transferring loads or impacts to the brain two basic models of trabeculae, i.e., one with a upright tree-like shaped and the other with an inverted tree-like shaped, were analyzed. The models are shown in Fig. 3a and b. The reason for the two configurations of Figs. 3 is that we need to understand if there is any preference of the original structure to reverted shape and if the trabecula structure has any effect on transferring the load to the brain. This is an important question since it affects the global models of the head and the brain biomechanics. Using fluid elements and proper boundary conditions and loading, the models were analyzed by ABAQUS.

The results of the analysis of the models revealed that the strain, displacement and stress field of the upright tree-like shaped reverted structure is less than that of the inverted one, as shown in Fig.4 a, and b. Note that TBI and concussions occur due to the excessive strain in the brain (approximately more than 15 to 20 percent).

**CONCLUSION**

Our animal studied revealed that a trabecula consists of a bundle of very thin collagen fibers braided together, and as they reach to the pia mater they spread out and merge to the pia mater. That is the trabeculae are configured as an upright tree-like shaped from the brain toward the skull, where their branches are attached to the arachnoid and the stem is attached to the pia mater. The results of the FE

modeling revealed that the natural upright orientation of the trabecula creates less strain in the brain when the head is subjected to external loads, and thereby damps the impact. That is, the upright trabeculae provide more protection for the brain tissue when the head is subjected to a load.

The result of this study will lead to accurately modeling of the SAS and thereby determining the strain in the brain.

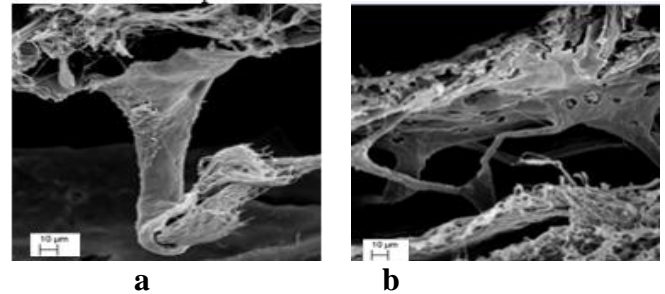


Figure 2. SEM images of SAS showing branching the trabeculae into the arachnoid a: single trabecula connecting pia to arachnoid. b: (zoom out) of the SAS depicting the trabeculae.

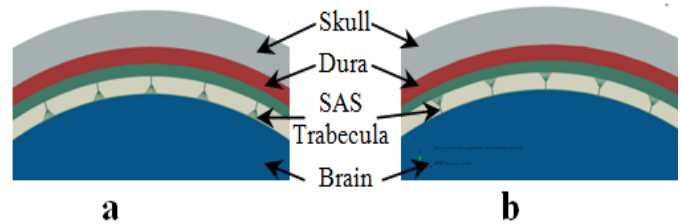


Figure 3. FE models, a: original model of SAS trabeculae, b: reversed model of SAS trabeculae

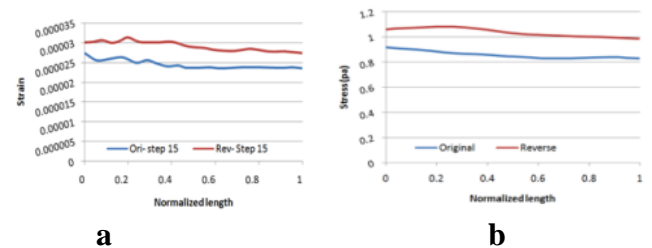


Figure 4. a) Strain, and b) Stress comparison between original and reverted structure of SAS trabeculae. ( Blue is upright tree-like shaped upright trabeculae-Red is reverted shape

**REFERENCE:**

1. Alcolado, et al. (1988) *Neuropath. & applied neurobiology* **14**:1-17
2. Kleiven, S., (2003), *Journal of Neurotrauma*, **20**(4):365-379
3. Killer et al. (2003) *Br J ophthalmol* **2003**; **87**:777-781
4. Trosseille X., et al., (1992), *Stapp*, **36**:922527
5. Zhang et al. (2001) *Stapp Car Crash Conf*, **45**: 2001-22-0017.
- 6- Zoghi and Sadegh (2010) *Int. J. of Bio.Eng. and Tech.* Vol. **4** No. **3**,
- 7- Zoghi, & Sadegh., (2009) *Int. J. of CMBE* vol. **12**, **1**, pp1-12,
- 8- Xin Jin et al. (2008) *J of Neurotrauma* **12** (4) , pp. 689-695.

# KINEMATIC AND KINETIC DIFFERENCES BETWEEN SHOD AND BAREFOOT RUNNING

Sachithra Samarawickrame, Rami Hashish and George Salem

University of Southern California, Los Angeles, CA, USA  
email: [ssamaraw@usc.edu](mailto:ssamaraw@usc.edu) web: [www.pt2.usc.edu/labs/mbrl](http://www.pt2.usc.edu/labs/mbrl)

## INTRODUCTION

Transitioning from shod to barefoot running is becoming increasingly popular among recreational and competitive distance runners. Thus, we believe the merits of barefoot running should be evaluated based on the changes it induces in habitually shod distance runners. To date, however, there is inconclusive scientific evidence of this activity's benefits and/or risks. Available data on overground barefoot running is constrained by speed [1] or limited to a comparison in the sagittal plane between different subject groups [2]. The purpose of this preliminary study was to expand on previous findings by examining sagittal and frontal plane kinematic and kinetic differences in ankle dynamics between shod and barefoot conditions in habitually shod individuals running overground at self-selected speeds.

## METHODS

In this investigation, two female and one male habitually shod runners (Ages 40,34,26 years and BMI 20.4, 22.4, 23.1 kg/m<sup>2</sup> respectively) performed overground running at their self-selected speeds; shod and then barefoot. Each subject completed 6-8 trials in each condition. All subjects had a history of running a minimum of 12 km per week and reported no significant injuries over the preceding 12 months. Kinematic data were recorded using an 8-camera Qualisys motion capture system (Gothenburg, Sweden) at 250 Hz. The foot was modeled as a rigid segment and tracked using a dorsal marker cluster plate. Kinematic data were low pass filtered at 6 Hz and averaged over the available number of trials (6-8). Three-dimensional kinetics were recorded from AMTI force platforms (Watertown, MA) at 1500 Hz. Data is reported for the dominant lower limb of each subject. Standard inverse dynamics methods were used in the moment

calculations. Foot contact was defined at a minimum of 20 N vertical ground reaction force and stance phase is reported after normalizing to 100 data points.

## RESULTS AND DISCUSSION

### *Foot/ankle kinematics*

The average speeds for shod and barefoot running were 4.26 ms<sup>-1</sup> and 4.23 ms<sup>-1</sup> respectively. In the sagittal plane, all three subjects demonstrated a shift from a rear-foot strike to a forefoot strike in the barefoot condition (change in angle at footstrike 115-340%, effect size (ES): 7.8) (Fig. 1).

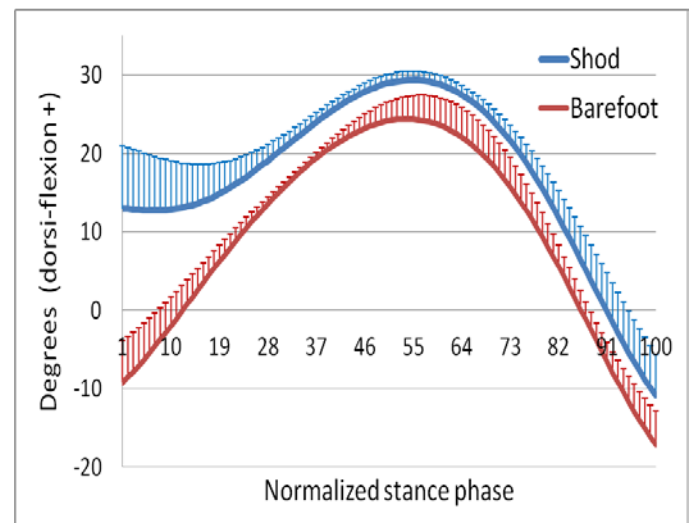


**Figure 1:** Mean+1SD ensemble sagittal plane kinematics of the ankle during stance phase.

In the frontal plane, there was a relative increase in the inversion angle at footstrike in the barefoot condition (120-667%, ES: 3.4) (Fig. 2). However, the peak eversion angle was similar between the two conditions, and thus the change in the total range of motion was not as large (-1 to 25%, ES: 0.4).

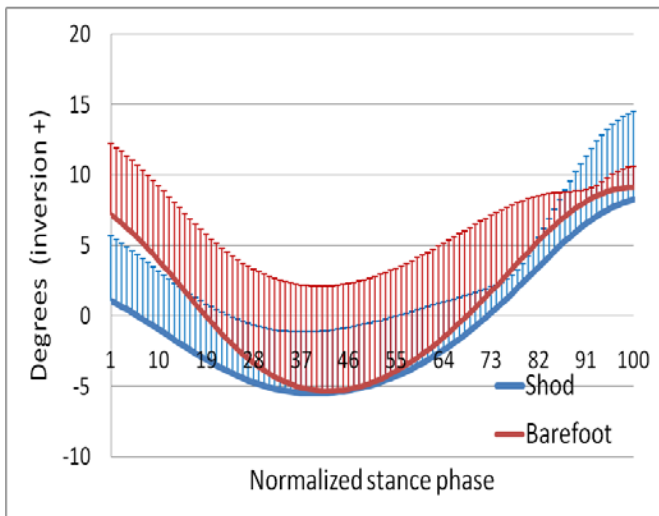


**Figure 2:** Mean+1SD ensemble frontal plane kinematics of the ankle during stance phase.

### Foot/ankle kinetics

In the sagittal plane, barefoot running eliminated the initial dorsiflexor moment observed in the shod condition (Fig. 3). The total impulse demonstrated an increase of 20-23% (ES: 8.0).

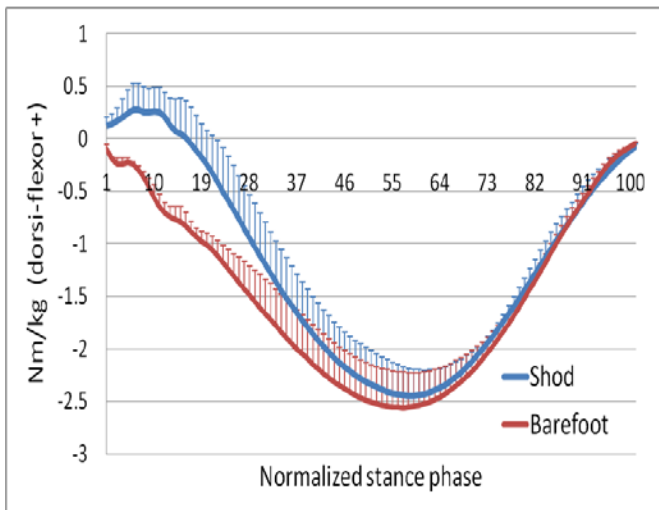


**Figure 3:** Mean+1SD ensemble sagittal plane kinetics of the ankle during stance phase.

Frontal plane kinetics demonstrated an increase in the peak invertor moment in the barefoot condition (Fig. 4). This translated to a 9-92% increase in the impulse (ES: 1.4).

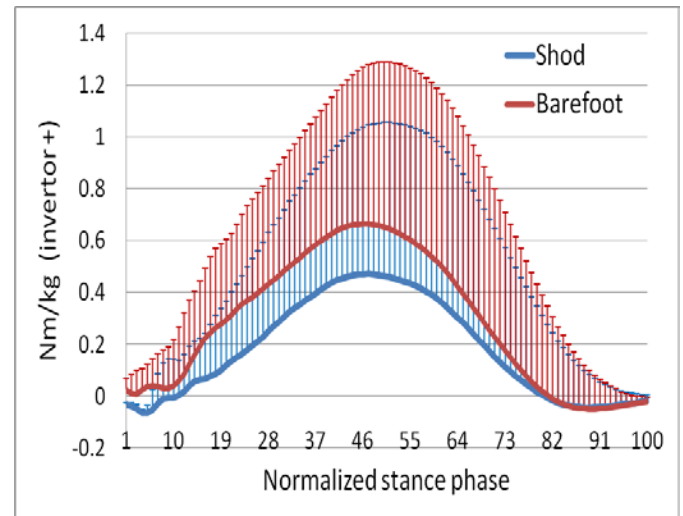


**Figure 4:** Mean+1SD ensemble frontal plane kinetics of the ankle during stance phase.

### CONCLUSIONS

These results demonstrate immediate differences between shod and barefoot overground running in both sagittal and frontal plane foot/ankle dynamics when running at self-selected speeds in habitually shod distance runners. The changes that occur when switching from shod to barefoot running will dictate the new demands that are placed on the foot and ankle musculoskeletal and tendinous structures. These new demands may lead to beneficial effects such as strengthening of muscles and/or detrimental effects through repetitive overloading of muscles, tendons and bones. These preliminary data should inform the design of expanded studies and ultimately the prescription of safe and effective training protocols for persons transitioning from shod to barefoot running.

### REFERENCES

1. De Wit B, et al. *Journal of Biomechanics*, **33**, 269-278, 2000.
2. Lieberman DE, et al. *Nature* **463**, 531-535, 2010.

### ACKNOWLEDGEMENTS

We gratefully acknowledge Dr. Sean Yu for his guidance during data processing.

# TRANSDUCER AND BASE COMPLIANCE ALTER THE IN SITU 6 DOF FORCE MEASURED FROM MUSCLE DURING AN ISOMETRIC CONTRACTION IN A MULTI-JOINT LIMB

<sup>1</sup>Thomas G. Sandercock, <sup>2</sup>Sang Hoon Yeo, <sup>2</sup>Dinesh. K. Pai, and  
<sup>1</sup>Matthew. C. Tresch

<sup>1</sup>Northwestern University, Chicago, IL, USA  
<sup>2</sup>University of British Columbia, Vancouver, BC, Canada  
email: [t-sandercock@northwestern.edu](mailto:t-sandercock@northwestern.edu)

## INTRODUCTION

Verifying the action of a muscle in a detailed musculo-skeletal model is difficult. In situ isometric measurements are a possible solution. We have recently performed this type of experiment in the rat hindlimb (Yeo et al.2011). We immobilized the pelvis of the animal and rigidly attached the tibia to a 6-axis force transducer. Individual muscles were stimulated and the resulting forces and moments were recorded. Typically limbs are modeled as chains of rigid bodies, but in the very common case of fixing the end point to a force transducer, the limb is over-constrained with 6 force constraints. Surprisingly, when we used the standard Jacobian representation and Moore-Penrose pseudo inverse, we were able to obtain a reasonable fit to the data provided the moment data was scaled by  $10^2$ . When we released a degree of freedom at the force transducer, in both the experiments and in the model, so that the number of degrees of freedom of the leg matched the number of constraints, the measured forces and moments were well explained with the model.

In this study we examine these issues further, clarifying how imperfect skeletal fixation and compliance in the connection of the skeleton to the force transducer can alter the measured force and moments.

## METHODS

We assume the bones of the skeleton are rigid bodies and they are linked by joints that determine the position of the limb segments relative to each other (Delp and Loan 2000). Muscles can span the joints and are assumed to exert torque on each of

the joints they span. In order to relate these torques to the resulting endpoint forces and moments, we extended this analysis by adding: 1) a base compliance; 2) passive compliances around the joints; and 3) complaint connections to the force transducer. See Figure 1. Base compliance was modeled by adding 3 translational dof coupled to an elasticity at the hip. We then developed the relationship between joint torques and endpoint forces including these compliances. Our analysis shows that inclusion of these compliances provides a well defined solution for endpoint forces given joint torques, even in the case when the limb is over-constrained.

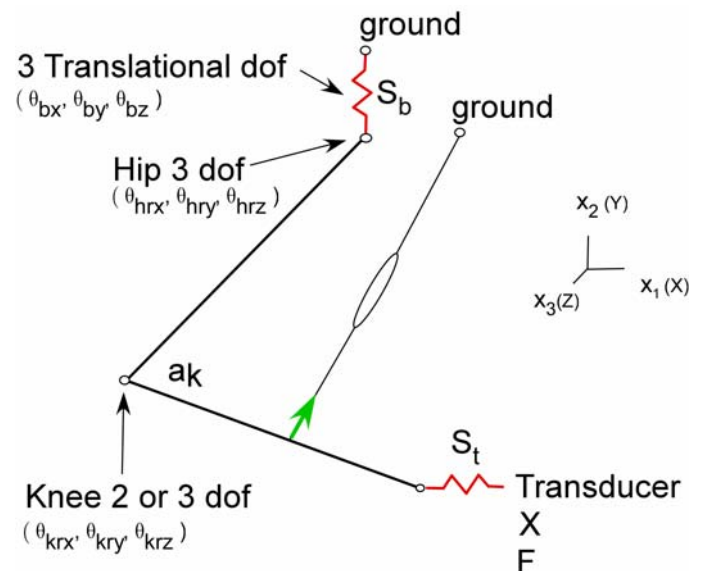


**Figure 1:** Schematic representation of the rat hindlimb.

To illustrate these results, we considered the action of gracilis posticus in the rat hindlimb (Yeo et al. 2011). Numeric results were compared using

different model assumptions: different joint dof, varying base compliance, varying transducer compliance, and varying passive joint compliance. The effects of passive elastic forces and additional dof in the leg joints are not presented here.

## RESULTS AND DISCUSSION

Our analytic results show that when the dof of the limb are exactly matched to the dof restrained at the transducer, neither base compliance nor transducer compliance affects the measured end point generalized force. (This assumes movement is small enough that the limb configuration has not substantially changed.) However, if an additional constraint is added at the transducer, the measured force depends on the comparative stiffness of each axis of the force transducer. Furthermore, when the stiffness of the base is approximately equal to or less than that of the transducer, base stiffness dramatically alters the force.

Numeric computations demonstrate these results (Figure 2). In the over-constrained case force depends on the relative stiffness of the transducer. Row D shows that as the moment axes of the force transducer become more compliant than the translation axes, the measured forces look like the exactly constrained force column. This may explain why similar forces were measured if the exact and over constrained case in Yeo et al (2011).

## CONCLUSIONS

These results suggest it is difficult to measure in vivo isometric force when a single muscle is stimulated. Fixing a limb segment rigidly to a 6 axis force transducer will always involve the above issues. In special cases, where a limb has 5 dof or less, a specially designed attachment to a force transducer, one that releases some of the dof, will mitigate these problems. Unless the dof of the limb are exactly matched to the dof restrained at the force transducer, base and transducer compliance alter the measured force.

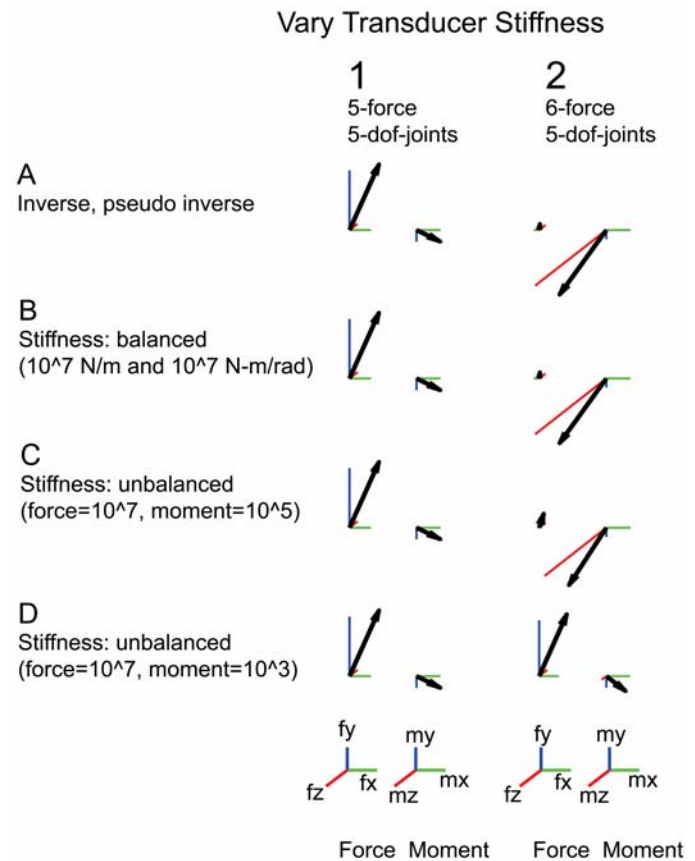


**Figure 2:** Generalized end point force (a vector for each force and moment) computed using different model assumptions, at a single limb position. The limb and muscle position are shown in Figure 1. Base compliance is zero. Column 1 shows the matched dof-joints and dof-force-restraint case. Column 2 shows an additional force constraint—rotation around the z axis. Row A shows force from the standard Jacobian formulation. Rows B to D show force resulting from varying transducer compliance.

## REFERENCES

1. Delp SL, and Loan JP. *Comput. Biol. Med.* 25: 21-34, 1995.
2. Yeo SH, Mullens C, Sandercock TG, Pai DK, and Tresch MC. *J Expt Biol*: 214, 735-746, 2011.

## ACKNOWLEDGEMENTS

Supported by: NIH NAIMS R01AR053608 and NIH NINDS R21NS061208

# GLENOHUMERAL JOINT FORCE ESTIMATIONS DURING SHOULDER EXERTIONS USING FORWARD DYNAMICS SIMULATIONS

Kotaro Sasaki

Boise State University, Boise, ID, USA  
email: kosasaki@boisestate.edu

## INTRODUCTION

Understanding how glenohumeral (GH) joint forces are developed during shoulder exertions has important clinical implications for prevention, treatment and rehabilitation strategies for shoulder joint injuries. Several studies have attempted to estimate GH joint forces and shoulder muscle forces using musculoskeletal models and simulations (e.g., [1, 2]). However, little work has been done to examine whether obtained forces indeed represented actual forces developed in the GH joint. Validating estimated GH joint forces is important because *in vivo* measurements are extremely invasive and expensive [3]. Therefore, the objective of this study was to develop muscle-actuated forward dynamics simulations of shoulder exertions to compare the GH joint forces estimated in the simulations with those forces during the same shoulder exertions reported in a previous *in vivo* study [4].

## METHODS

Subject-specific muscle-actuated forward dynamics simulations were developed using OpenSim [5] to emulate two types of shoulder exertions reported in the study by Bergmann et al. (45-degree shoulder abduction and 90-degree shoulder flexion with a 2kg weight held in the right hand, [4]). The upper-limb musculoskeletal model used in the simulations was based on a previously published model [6]. The model consisted of the thorax, right clavicle, scapula, humerus, radius, ulna and hand, with 13 degrees-of-freedom (thorax translations and rotations, elevation angle, shoulder elevation, shoulder rotation, elbow flexion, forearm pronation, wrist deviation and wrist flexion). The mass and moment of inertia for each segment were determined using anthropometric data obtained from the subject in this study [7, 8]. A total of 30

musculotendon actuators crossing the glenohumeral and elbow joints [6] were included in the model. The thorax segment was controlled by three forces and three couple moments applied to the segment. The wrist was controlled primarily by the torques applied to the joint. A downward force of 19.62 N was applied to the center of the hand segment. GH joint forces were computed as the sum of all forces applied to the joint.

Experimental data were collected from a male subject who was free of musculoskeletal injuries in the upper limbs (age 43 years old, height 170 cm, body mass 60 kg). Reflective markers representing anatomical landmarks in the thorax, clavicle, scapula and humerus [9] and additional markers for the forearm and hand were attached to capture the kinematics of shoulder exertions at 250 Hz (Vicon 460 with seven cameras, Oxford, UK). Surface EMG data (Free EMG 300, BTS, Milan, Italy) were collected at 1500 Hz from eight muscles (pectoralis major, anterior, middle and posterior deltoids, biceps, long and lateral heads of triceps and latissimus dorsi). After a warm-up, the subject performed 45-degree right shoulder abduction (ABD-45) and 90-degree right shoulder flexion (FLX-90) three times with an interval of 30 seconds, in an upright standing posture with a 2kg-dumbbell held in the right hand. Each performance was completed in approximately eight seconds [4]. The kinematic data were low-pass filtered at 6 Hz. EMG linear envelopes were generated by processing the EMG data using a 20-400 Hz band-pass filter, full rectification and a 10 Hz low-pass filter.

## RESULTS AND DISCUSSION

The forward dynamics simulations accurately regenerated the experimental kinematics, with the maximum root mean square error being less than

0.4 degrees in all joint angles and trials (Fig. 1a, b).

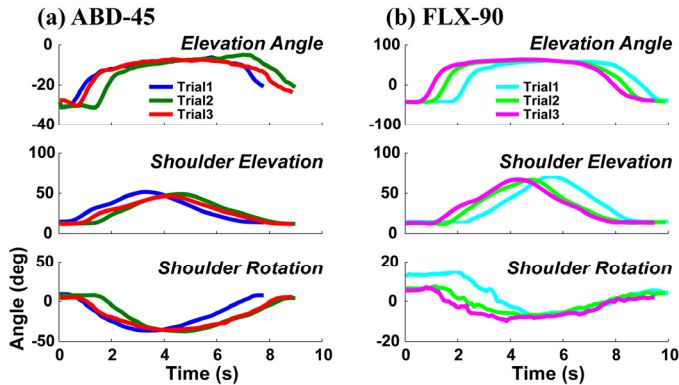


**Figure 1:** Shoulder kinematics during (a) ABD-45 and (b) FLX-90 for each trial. The experimental kinematics and simulation results were virtually identical.

The muscle excitation patterns also matched well the EMG linear envelopes (Fig. 2).

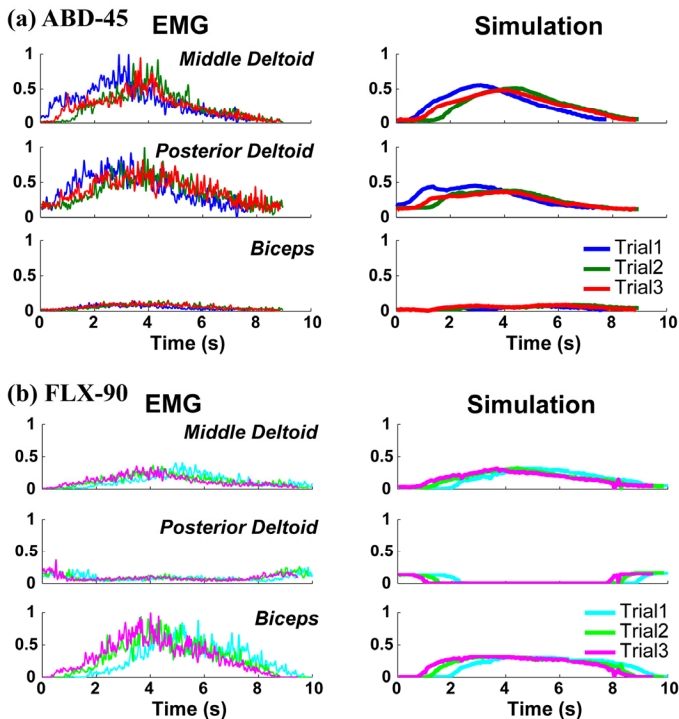


**Figure 2:** EMG from three muscles and corresponding muscle excitation patterns in the simulations: (a) ABD-45 and (b) FLX-90. For each muscle, EMG was normalized to its maximum value during all six trials.

The averaged maximum GH resultant forces of three trials during ABD-45 and FLX-90 were 910 N and 1630 N, respectively (Fig. 3a, b). These values were ~5% higher in ABD-45 and ~30% higher in FLX-90 than the previous *in vivo* measurements of 863 N and 1255 N, respectively [4].

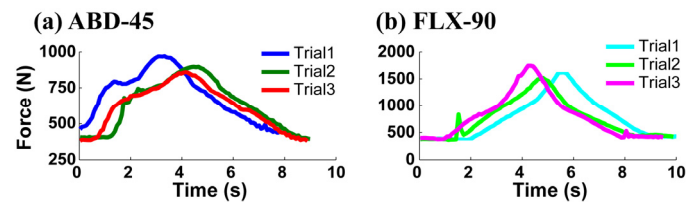


**Figure 3:** GH resultant forces during (a) ABD-45 and (b) FLX-90 for each trial.

The overall patterns of GH resultant joint forces (Fig. 3a, b) were similar to the *in vivo* data [4], although the forces during the initial and final phases of the shoulder exertions appeared higher. These higher forces were primarily due to the forces generated in the rotator cuff muscles. Because complete kinematic data were not provided in the *in vivo* study [4], direct comparisons of GH joint forces may be difficult. For example, the shoulder was in a slightly abducted position during the initial and final phases in the present study (Fig. 1: Shoulder Elevation). Further analyses are required to examine the influence of kinematics on GH joint forces. One limitation is that the prescribed scapula motion in the model [6] could influence the force generation in muscles crossing the GH joint, and therefore, GH joint forces [10]. Also, the translations of the humerus head occurring during shoulder exertions in general were neglected. Future studies need to examine these influences. In summary, subject-specific forward dynamics simulations emulating two shoulder exertions were successfully generated. Although computed GH joint forces were somewhat higher than those reported in a previous *in vivo* study [4], the forward dynamics simulation approach appears promising for investigating GH joint forces during shoulder exertions.

## REFERENCES

1. van der Helm FCT. *J Biomech*, **27**, 527-550, 1994.
2. Morrow M, et al. *J Biomech* **43**, 2487-2492, 2010.
3. Westerhoff P, et al. *Med Eng Phys* **31**, 207-213, 2009.
4. Bergmann G, et al. *J Biomech* **40**, 2139-2149, 2007.
5. Delp SL, et al. *IEEE Trans Biomed Eng* **54**, 1940-1950, 2007.
6. Holzbaur K, *Ann Biome Eng* **33**, 829-840, 2005.
7. de Leva P, *J Biomech* **29**, 1223-1230, 1996.
8. Hinrichs RN, *J Biomech* **18**, 621-624, 1985.
9. de Groot JH, *Clin Biomech* **12**, 461-472, 1997.
10. Mesjedi and Johnson, *Proceedings of IMechE (Part H) J Eng in Med* **225**, 38-47, 2010.

# DOES KNEE EXTENSOR MUSCLE IMBALANCE CAUSE CHANGES IN PATELLAR TRACKING?

Andrew Sawatsky, Tim Leonard, Walter Herzog

University Of Calgary  
email: [asawatsky@kin.ucalgary.ca](mailto:asawatsky@kin.ucalgary.ca)

## INTRODUCTION

Patellofemoral pain syndrome (PFPS) is one of the most common knee disorder seen by clinicians. The main region of pain is the lateral aspect of the patellofemoral joint. Force imbalance in the knee extensor muscles has been associated with changes in patellofemoral tracking [1] and is suspected to cause PFPS. Weakness of the vastus medialis (VM) relative to the vastus lateralis (VL) is the usual imbalance associated with PFPS. The fibers of VM are aligned about 50° from the femoral axis and this structural arrangement has been thought to pull the patella medially while VL has been assumed to provide the corresponding lateral balance [2].

A commonly used treatment for PFPS is exercises directed at increasing VM strength to balance the medial-lateral tensions. Although the idea that muscle imbalance between VM and VL causes maltracking of the patella, has intuitive appeal and anecdotal support, it has not been tested in an intact knee loaded by muscular contraction.

The purpose of this study was to create an animal model of quadriceps muscle imbalance and to test the effect of VM weakness, and thus VM/VL imbalance, on patellar tracking. Muscle imbalance was produced by eliminating the action of VM by cutting it in mid-belly. We hypothesised that transection of VM causes a medial-lateral knee extensor imbalance causing the patella to shift laterally in the femoral groove.

## METHODS

All experiments were performed on knees (n=9) of skeletally mature New Zealand White rabbits (mass 4.8-5.7kg). Patellar tracking was recorded with a high speed camera at 200Hz and a spatial resolution of 80µm.

Two markers were placed on the patella via a bone screw and two further markers on the femur via bone pins, to record frontal plane movements of the patella relative to the femur. The hip and knee of the rabbits were fixed in a stereotaxic frame, while the tibia was attached to a lever arm connected to a motor allowing for knee extensions and flexions at controlled speeds. Movements of the patella relative to the femur were recorded for passive and active concentric and eccentric knee extensor contractions, before and after VM transection.

Knee extensor activation was produced through femoral nerve stimulation using a nerve cuff-type electrode. All contractions were performed at maximal levels of stimulation and a frequency of 40Hz. All (passive and active, concentric and eccentric) tests were executed at an angular speed of 40°/s moving from 30° to 90° of knee flexion. Patellar tracking was recorded with the knee joint and VM intact and then again following VM transection.

## RESULTS AND DISCUSSION

The primary result of this study was that patellar tracking was not affected by VM ablation (Figure 1). This result suggests that even the biggest possible muscle imbalance of the knee extensor complex (zero force in the VM) did not affect the medial-lateral tracking of the patella. This result is in stark contrast to findings by Goh et al. (1995) who suggested, in human cadaveric knees, using wires and pulleys to load the patellofemoral joint, that simulated weakness of the VM caused immediate and pronounced shifts of the patella to the lateral edge of the femoral groove. There are several reasons why our results may differ from those obtained in the literature, but the most compelling appears to be that we measured patellar

tracking using the actual, intact muscles to produce force through nerve stimulation, rather than an artificial loading apparatus which, by design, makes assumptions on how muscles act on the patella. However, our results are consistent with previous observations in the rabbit knee that demonstrated that “isometric” contractions of the knee extensors also did not produce the “expected” lateral shift of the patella in the femoral groove following VM ablation [4].

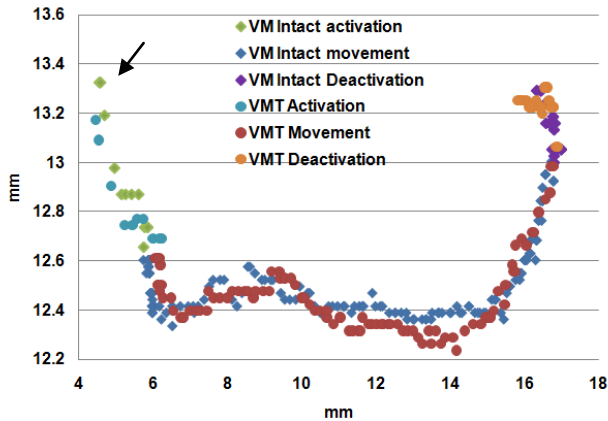


**Figure 1** Exemplar result of patellar tracking before and after VM transection for concentric conditions. The distances shown are measured relative to the origin of an inertial reference system with origin at the medial femoral condyle. The movement starts at the top-left (arrow) with the muscles relaxed. Upon activation, there is a distinct, medial shift of the patella, which is reversed upon deactivation. The patellar tracking before and after VM ablation is virtually identical with differences that are within the resolution of our system.

Patellar tracking, however, was greatly affected by activation of the muscles. The patellae in all experiments tracked more laterally along the femoral groove for passive concentric and eccentric contractions, compared to the corresponding active contractions (Figure 2). Activation, always caused a medial shift of the patella, and when activation was absent in the passive trials, the patella always moved along a lateral path during knee extension and flexion.

Concentric and eccentric active contractions also produced different patellar tracking patterns, but these were less systematic than those observed between the passive and active trials and need further quantification (Figure 2). However, it appears that in general, eccentric contractions might cause a greater medial shift of the patella than concentric contractions. Therefore, if lateral tracking of the patella is implicated in PFPS, as has

been suggested in the literature, and has been thought to occur with VM weakness, then eccentric contractions should be the least likely to cause PFPS syndrome.

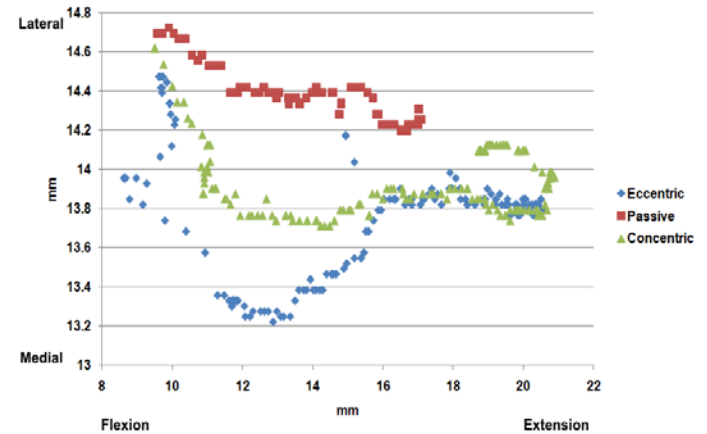


**Figure 2** Exemplar results of patellar tracking for a passive movement, an active eccentric and an active concentric movement with the VM intact. The distances shown are measured relative to an inertial reference system with origin at the medial femoral condyle. Note the medial shift of the patella for the active compared to the passive movements and for the eccentric compared to the concentric movement.

## CONCLUSIONS

VM weakness does not produce changes in patellar tracking in the rabbit knee. This result may have important clinical implications for PFPS in humans, and challenges a long-held clinical paradigm.

## Reference List

1. N. A. Wilson, J. M. Press, J. L. Koh, R. W. Hendrix, L. Q. Zhang, *J Bone Joint Surg Am* **91**, 558-566, 2009.
2. F. J. Lieb, J. Perry, *J Bone Joint Surg Am* **50**, 1535-1548, 1968.
3. J. C. Goh, P. Y. Lee, K. Bose, *J Bone Joint Surg Br.* **77**, 225-231, 1995.
4. Sawatsky, et al. *Proceedings of NACOB'08*, Ann Arbor, MI, USA, 2008.

## ACKNOWLEDGEMENTS

CIHR, the Canada Research Chair Programme in Molecular and Cellular Biomechanics and the AHFMR Team Grant on OA.

# INCREMENTAL TRAINING: REDUCING CHALLENGES TO BALANCE CONTROL WHILE LEARNING A NOVEL LOCOMOTOR TASK

<sup>1,2</sup>Andrew Sawers, <sup>1,3</sup>Michael Hahn

<sup>1</sup>RR&D Center of Excellence Department of Veterans Affairs, <sup>2</sup>Departments of Rehabilitation Medicine, and <sup>3</sup>Mechanical Engineering, University of Washington, Seattle, WA USA  
email: [sawera@u.washington.edu](mailto:sawera@u.washington.edu)

## INTRODUCTION

Conventional motor learning strategies advocate increasing the difficulty of physical practice to augment the size of performance errors during the Acquisition phase in order to enhance motor learning [1]. Alternatively, studies using upper extremity [2] and visuomotor tasks [3] have shown that incrementally increasing task difficulty minimizes performance errors while maintaining a level of learning equivalent to that observed with larger performance errors. While yet untested, this suggests that incremental training could be applied to locomotor rehabilitation where larger performance errors are likely to pose challenges to balance control and increase the risk of falls.

This study sought to determine whether incremental training principles could be applied to learning a novel locomotor task in an effort to reduce training related challenges to balance control without compromising how well the task was learned.

## METHODS

Following 20 minutes of treadmill acclimation at a controlled walking speed (0.7 m/s), healthy young adults were asked to walk on a split-belt treadmill (Bertec; Columbus, OH) where the dominant leg moves at twice the speed as the non-dominant leg (2:1 walking) [4]. This novel locomotor task was introduced using either a single abrupt acceleration of the dominant limb belt (sudden training; large error), after which 2:1 walking was practiced for ~720 strides, or a constant incremental acceleration of the dominant limb belt until 2:1 walking was achieved over ~700 strides (incremental training; small error). Twenty additional strides of 2:1 walking were then performed by the incremental cohort (total practice during acquisition ~ 720

strides per cohort). After a one-hour rest, both cohorts completed a retention test, performing the same 2:1 walking task for ~ 300 strides, using a sudden introduction. Full-body marker data were collected at 120 Hz using a 12-camera digital motion capture system (Vicon; Oxford, UK) throughout the protocol. Whole-body center of mass (COM) position was calculated using a 15-segment weighted sum approach. Balance control was evaluated using an established metric, the frontal plane COM-ankle inclination angle [5]. Values during Acquisition and Retention phases were compared to those over the last 20 strides of treadmill acclimation to identify challenges to balance control. Motor learning was evaluated as the number of strides required during Retention phase to achieve a sagittal plane whole-limb orientation (WLO) angle equivalent to that attained over the last 20 strides of the Acquisition phase. WLO is the angle formed by a vector from the hip to the fifth metatarsal with respect to vertical [6]. It has been established as a descriptive metric of whole-limb function during locomotion [7]. Differences in balance control and motor learning (retention) between sudden and incremental training cohorts were assessed using discrete values from the dominant (fast) leg at contralateral toe-off.

## RESULTS AND DISCUSSION

Preliminary data (n = 2 per cohort) reveal that a similar number of strides were required during retention (incremental=1, sudden=5) to achieve the level of locomotor performance that was attained over the last 20 strides of acquisition (as defined by WLO). Similar to findings from previous non-locomotor studies, these results suggest that incremental training may promote equivalent if not superior learning of locomotor tasks when compared to sudden training of the same task.

Notable differences in frontal plane COM-ankle inclination angles during both acquisition and retention were observed between the two strategies (Figure 1). Sudden training resulted in a substantially higher percentage of strides whose inclination angles were above or below a  $\pm 2SD$  target window created from the last 20 strides of acclimation (Table 1). This was particularly obvious during retention (Figure 1). The magnitude of those angles which exceeded the target window was also larger among the sudden training cohort (Table 1).

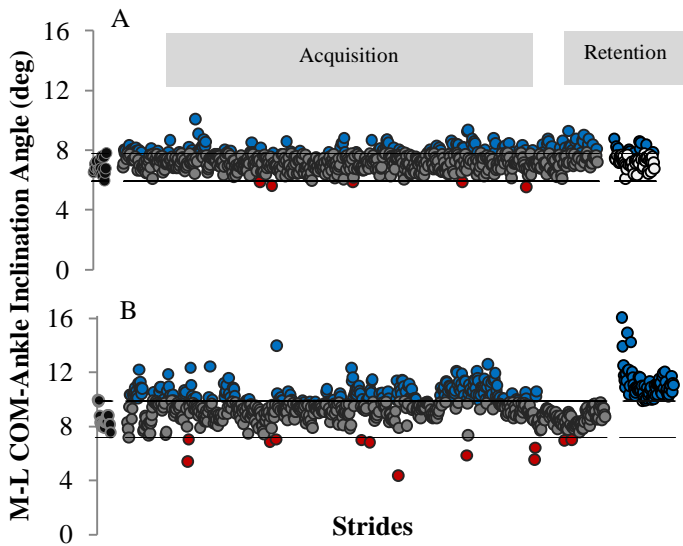


**Figure 1:** Frontal plane COM–ankle inclination angle of the leading limb at contralateral toe off for one incremental (A) and one sudden (B) subject. Incremental training had fewer values above (●) and below (●) the target window (black lines) created from the mean  $\pm 2SD$  of the last 20 strides of acclimation (●).

These differences in inclination angle during sudden and incremental training suggest an increased challenge to balance control for the sudden cohort. During strides where the inclination angle was below the target window, the COM was approaching the lateral border of support, placing the subject at greater risk for a loss of balance and possible fall than during 1:1 walking (acclimation).

Inclination angles above the target window were generally due to an increased lateral positioning of the foot rather than a reduction in horizontal COM excursion. While an increased inclination angle and wider base of support may represent a more guarded response to maintain balance, it requires an increased horizontal COM velocity to facilitate weight transfer between limbs. Inability to control this increased COM velocity as weight is transferred may place subjects at risk for a loss of balance and possible fall. The most striking result is the notable increase in inclination angle adopted and maintained by the sudden but not the incremental cohort throughout retention. The need to respond to the abrupt change in task demand (2:1 walking) and to maintain balance at all cost, may have prevented the sudden cohort from developing a more suitable strategy to maintain balance control.

## CONCLUSIONS

These preliminary results support the notion that incremental training may reduce training related challenges to balance control without compromising how well the locomotor task is learned. Current efforts are directed towards processing newly collected data and identifying further benefits of an incremental training strategy. Future efforts will be directed towards developing clinical applications.

## REFERENCES

- Schmidt R. *Motor Control and Learning*, Human Kinetics, 2005.
- Crisimagna-Hemminger SE et al. *J Neurophysiol* **103**, 2275-2284, 2010.
- Klassen J et al. *Exp Brain Res* **164**, 250-259, 2005.
- Reisman et al. *J Neurophysiol* **94**, 2403-2415, 2005.
- Chen CJ, et al. *Gait and Posture* **31**, 391-393, 2010.
- Bosco et al. *J Neurophysiol* **76**, 715-726, 1996.
- Chang YH, et al. *J Exp Biol* **212**, 3511-3521, 2009.

**Table 1:** Frontal plane challenge to balance control during Acquisition and Retention phases.

| Cohorts            | % of Strides Above $\pm 2SD$ Window | Mean Additional Inclination Above $\pm 2 SD$ Window (°) | Max Additional Value Above $\pm 2 SD$ Window (°) | % of Strides Below $\pm 2SD$ Window | Mean Additional Inclination Below $\pm 2 SD$ Window (°) | Max Additional Value Below $\pm 2 SD$ Window (°) |
|--------------------|-------------------------------------|---|--|-------------------------------------|---|--|
| <b>Acquisition</b> |                                     |   |  |                                     |   |  |
| <b>Sudden</b>      | 29 %                                | 0.76  | 4.09   | 1.8%                                | 0.762   | 2.82   |
| <b>Incremental</b> | 19 %                                | 0.40  | 2.28   | 0.7%                                | 0.153   | 0.37   |
| <b>Retention</b>   |                                     |   |  |                                     |   |  |
| <b>Sudden</b>      | 100 %                               | 1.22  | 6.20   | N/A                                 | N/A   | N/A  |
| <b>Incremental</b> | 19 %                                | 0.40  | 0.98   | N/A                                 | N/A   | N/A  |

# META-ANALYSIS TO PREDICT METABOLIC COST AS A FUNCTION OF WALKING SPEED AND ADDED MASS AT DIFFERENT BODY LOCATIONS

Eliran Scherzter and Raziel Riemer

Ben-Gurion University of the Negev, Beer-Sheva, Israel  
email: rriemer@bgu.ac.il

## INTRODUCTION

The metabolic cost of carrying an additional mass at different locations on the body relates to many areas, such as ergonomics, the military, obesity, and the design of prosthetic and powered exoskeletons devices. It was found that the most important factors that affect change in energy expenditure are the speed of locomotion [1,2], the magnitude of the additional mass[2], and the location of the additional mass on the body [1,2,3]. It was suggested that metabolic cost increases linearly as the speed increases [4], and that it also increases linearly as the mass carried is increased [2]. However, other researchers depicted these relations as nonlinear [5]. Further, to the best of our knowledge the combined effect of the weight speed has not been studied. Yet for practical applications it is important to be able to predict the metabolic cost for any given combination of speed and mass, which has not been possible from previous studies. Therefore, in this study we aim to model the change in metabolic cost as a function of walking speed and the additional mass, at three body locations: the back, the knee, and the ankle. This has been done by a meta-analysis of previous published studies.

## METHODS

To investigate the relations between metabolic cost, speed, and added mass location, we combined data from 14 different studies (back [4,6,7,8,9,10,11,12], knee[ 2,13,14], and ankle [ 1,2,15,16]). Note that for the ankle we also used added mass on the foot, for the knee added mass in the lower section of the thigh, and for the back added mass in all of the back locations. All the results reported in the studies were converted to the following units: weight in kg, speed in km/h, and metabolic cost in Watt/kg. We expected that since the data were gathered from many different studies and labs, there would be differences between the results, even for the same

experimental conditions, due to changes in lab equipment. Therefore, there is a need for a model that takes into account two types of variances: within the experiments and between the experiments. Thus, the statistical method of Linear Mixed Model (LMM) was used. The LMM model assumes a linear relation between the dependent variable and the independent variables, and that error  $\epsilon$  is normally distributed,  $\epsilon \sim N(0, \sigma^2)$ . From our preliminary analyses for the metabolic cost (the dependent variable) and the speed and mass (independent variables), it seems that these assumptions do not hold true. Therefore the Box-Cox power transformation method [17] was used to find a power transformation that changes the relation into a linear one. The mathematical representation after the transformation is:

$$f(y_{ij}) = \beta_0 + \beta_1 * \text{speed}_{ij} + \beta_2 * \text{weight}_{ij} + \beta_3 * \text{weight}_{ij} * \text{speed}_{ij} + \gamma_j + \epsilon_{ij} \quad (1)$$

Where  $f(y_{ij})$  is the function that represent the Box-Cox transformation,  $y$  is the metabolic cost of the  $i_{th}$  measurement of the  $j_{th}$  experiment,  $\beta_0$  is the intercept,  $\beta_{1,2,3}$  is the coefficients,  $\gamma$  is the random effect of the  $j_{th}$  experiments, and  $\epsilon$  is the random error of the  $i_{th}$  measurement within the  $j_{th}$  experiment.

In order to obtain the equations that best represent the published data from the literature, we applied the above procedure. The ankle data are composed of 16 data points. The added mass and speed ranges were 0-6kg and 3.2-6.4km/h, respectively. The knee data are composed of 7 data points. The added mass and speed range were 0-2.82kg and 4.5-5.4km/h, respectively. The back data are composed of 67 data points. The added mass and speed range were 0-33.8kg and 2.4-7.2km/h, respectively. The quality of the model was evaluated with  $R^2$  and a 3D graph depicting the metabolic cost equation in relation to the collected data.

## RESULTS

The statistical analysis yielded an equation that relates walking speed and added mass at the back, knee, and ankle to the metabolic cost. For all three locations the variance between experiments was 2 to 10 times larger than the variance within experiments. This justifies the choice of the LMM. For the ankle and back the equation's coefficients were found to be significant with the p-value < 0.05. However, for the knee equation the coefficients were marginally significant, with p-values of 0.1, 0.12, and 0.05 for  $\beta_0$ ,  $\beta_1$ ,  $\beta_2$ , respectively.

The equation for each of the body locations are presented in Table 1. A visual comparison of the models and the data points shows a good fit, with the  $R^2$  values relatively high (Figures 1, 2, and 3).

**Table 1:** metabolic cost equations for each of the three locations

| location | Metabolic cost [W/kg]                                   | # |
|----------|---|---|
| Ankle    | $(0.658+0.306*\text{speed}+0.131*\text{weight})^2$      | 2 |
| Knee     | $(0.01-0.002*\text{speed}-0.0002*\text{weight})^{-1/3}$ | 3 |
| Back     | $(1.14+0.22*\text{speed}+0.021*\text{weight})^2$        | 4 |

Note: speed of walking [km/h], and weight [kg].

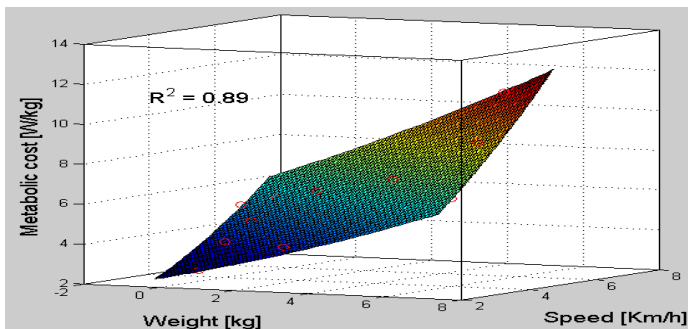


**Figure 1:** Ankle fitted equation (equation 2) is represents as a plane and the data points are in red

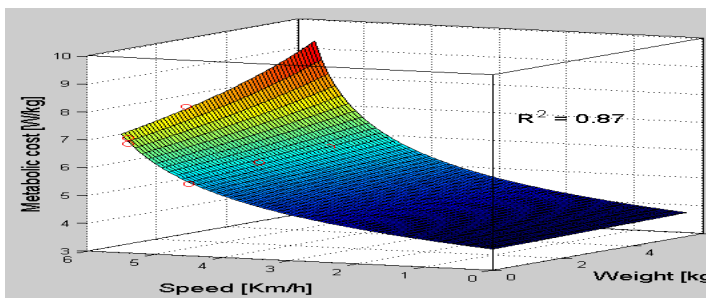


**Figure 2:** Knee fitted equation (equation 3) is represents as a plane and the data points are in red

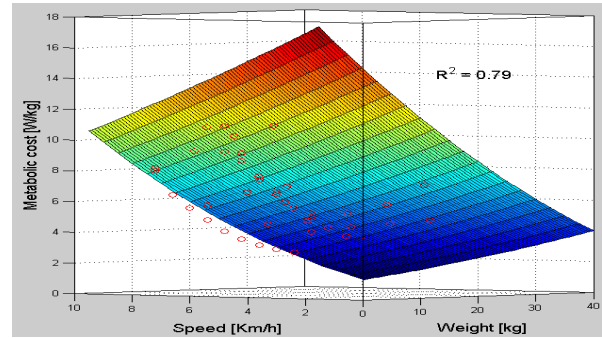


**Figure 3:** Back fitted equation (equation 4) is represents as a plane and the data points are in red

## CONCLUSIONS

In this meta-analysis an LMM and a Box-Cox transformation were used to obtain equations that best describe the changes in metabolic cost as a function of walking speed and added mass, at three different locations (back, knee, and ankle). This is an improvement over previous studies that only consider one factor at a time (i.e., speed or mass). The main limitation of this research: Most of the data is from experiments performed on males, and therefore the accuracy of prediction for females is unknown.

For the knee, there are a small number of data points, and there is a need for more experimental results. The results of this study have many implications for areas such as changes in the metabolic cost of hikers, obesity, and the effect of protective clothing, such as for fire fighters.

## REFERENCES

1. Soul R.G., Goldman R.F. J Appl Physiol 27, 687-690, 1969.
2. Kram R et al. J Med Sci Sports Exerc, 39, 515-525, 2007.
3. Stuempfle K., et al. Ergonomics, 47,784-789, 2004.
4. Epstein Y. et al. J Appl Physiol 46, 317-324, 1981.
5. Daijro A. et al. Ergonomics, 39,392-398, 2007.
6. Mayles W.S. et al. Eur J App Physiol 42, 125-131, 1979.
7. Watson J.C. et al. J of Hum Evol 54, 675-683, 2008.
8. Duggan A. et al. Ergonomics 35, 417-426, 1992
9. Lloyd R. & Cook B. J Appl Physiol 81, 486-492, 2000
10. Daijro A,et al, et al. Appl. Ergon. 35, 329-335. 2004.
11. Legg S.J. Ergonomics 35, 1063-1068, 1992
12. Kram R. J. Appl Physiol 95, 172-183, 2003.
13. Donelan J, et al. Science 319, 808-809, 2008.
14. Martin P. Med Sci Sports Exerc 37, 649-656, 2004.
15. Legg S.J & Mahanty A. Ergonomics 29, 433-438, 1986.
16. Miller J.F. J Applied Physiol 62, 1497-1501, 1987.
17. Box G., Cox D. J Royal Statistical Soc, B 26, 211-252 1964.

# Time to Contact Measures Demonstrate Modulation of Postural Stability during a Lower Extremity Dynamic Movement Task

<sup>1</sup>Sarah Schloemer, <sup>2</sup>Joshua Cotter, <sup>1</sup>Steve Jamison, and <sup>1</sup>Ajit Chaudhari

<sup>1</sup>Ohio State University, Columbus, OH, USA

<sup>2</sup>University of California at Irvine, Irvine, CA, USA

email: chaudhari.2@osu.edu

## INTRODUCTION

Traditional measures of postural stability rely on averaged center of pressure (CoP) motion over an extended period of quiet standing, making it difficult to draw conclusions from these tests to the dynamic situations that individuals experience in daily life. Moreover, these measures may not be sensitive enough to discriminate between healthy individuals or between the later stages of recovery and lower-extremity injury, when the goal of rehabilitation is to restore symmetry.

Unlike traditional measures of postural stability, postural time to contact (TtC) provides a measure of the time for the CoP to contact a stability boundary defined by the base of support, given its instantaneous trajectory. By tracking CoP changes over time, TtC allows for detection of instantaneous modifications in postural stability during dynamic tasks [1].

Previous studies have analyzed TtC during quiet single leg stance [2, 3] and a dynamic upper extremity task [1]. However, no study has used TtC to evaluate postural stability during dynamic lower extremity movement. Therefore, the purpose of this study was to determine the changes in postural stability that occur during the Star Excursion Balance Test (SEBT) [4] using TtC analysis.

## METHODS

Eight 3D motion capture cameras (Vicon, Los Angeles, CA) and one force plate (Bertec, Columbus, OH) were used to calculate the position of the feet and the CoP of 47 athletes (39M/8F,  $22.9 \pm 4.96$  yrs,  $13.9 \pm 0.8$  kg,  $1.75 \pm 0.09$  m) as they performed the SEBT. Prior to testing, all subjects provided IRB-approved informed consent. Subjects

performed the SEBT barefoot in three directions, anterior (ANT), posterolateral (POL) and posteromedial (POM). After 4 practice trials in each direction per leg, nine valid trials per direction per stance leg were recorded for TtC calculations. A trial was valid if the subject kept hands on hips and the heel of the stance foot flat on the floor.

TtC was calculated in MATLAB based on equations developed by Slobounov et al. [5]. The base of support was defined by markers on the big toe, lateral malleolus, medial malleolus, and heel of the subject's stance foot (Figure 1).

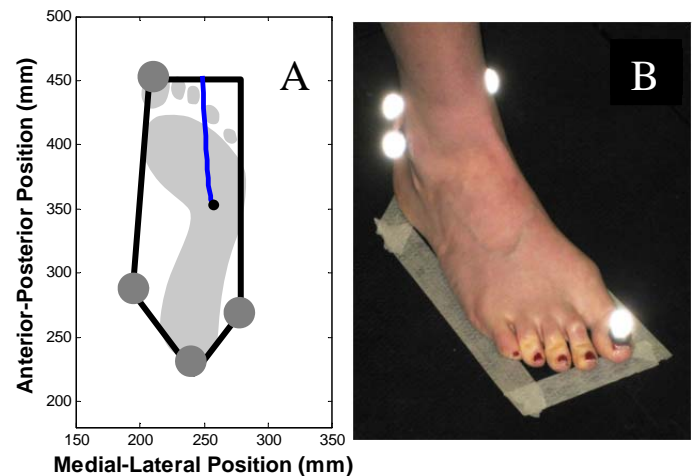


**Figure 1:** A) Base of support for the right foot showing a sample trajectory from the instantaneous center of pressure. B) Right foot with the 4 markers used to define the base of support.

For each trial, the time between toe off and toe touch was divided into five epochs of equal duration. Toe off was defined as the point at which the subject's reaching foot was completely off the force plate and movement was initiated. Toe touch was the first moment the subject's reaching toe made contact with the floor. TtC was averaged over each epoch. To evaluate differences in TtC an unbalanced 3-way mixed effects ANOVA was used

including subject as a random effect and epoch, side, and epoch\*side interaction as fixed effects, with post-hoc Tukey's HSD comparisons ( $\alpha=0.05$ ) to compare individual epochs to each other.

## RESULTS AND DISCUSSION

Epoch was a significant main effect ( $p<0.001$ ). TtC for Epochs 2, 3, 4, and 5 were significantly different from each other ( $p<0.01$ ), but Epoch 1 and Epoch 3 were not significantly different. TtC decreased from Epoch 1 to Epoch 2, and then increased between each of the next three epochs (Figure 2). The TtC of the left leg was significantly higher (more stable) than the TtC of the right leg ( $p<0.001$ ) (Figure 2). The interaction between side and epoch was also significant ( $p<0.05$ ).

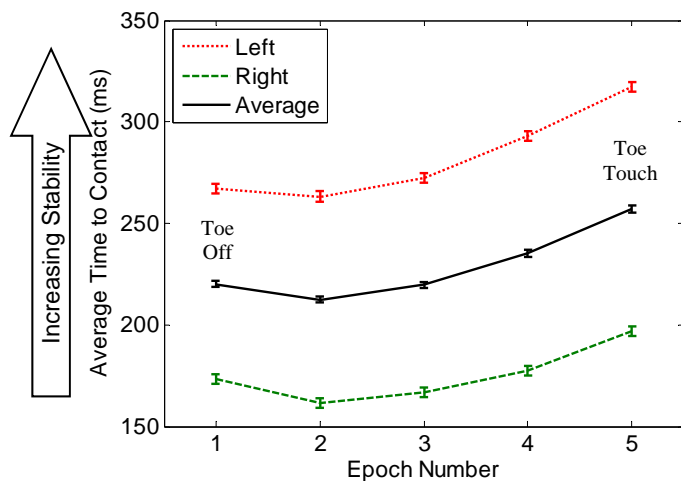


**Figure 2:** Average time to contact (TtC) during the SEBT for left stance, right stance, and the average of the two. Error bars indicate the 95% confidence intervals of the means.

This study is the first to our knowledge to demonstrate that healthy individuals modulate their postural stability during dynamic lower extremity tasks. Haddad et al. observed a similar TtC pattern when measuring changes in TtC during a precision fitting task where the participants picked a block off a table and then pushed it through a hole with their hand while standing comfortably on a force plate with both feet [1]. The initial decrease in TtC is associated with a decrease in postural stability. This period of less stability may be associated with less need for the subject to maintain strict postural stability while the reaching foot is held close to the body. The progressive increase in TtC from Epoch

2 to Epoch 5 represents a progressive increase in postural stability as the subject's reach foot nears the point of toe touch. These results suggest that the task becomes progressively more difficult, both due to the requirement to touch the toe at a single point without applying any weight and because the reaching foot is being extended further from the body.

This study also observed that subjects exercised greater postural stability on their left leg. Reach distance asymmetries with the SEBT have previously been associated with increased injury risk [4]. Further research is necessary to evaluate the utility of this test in identifying side-to-side asymmetries. Side to side differences in TtC could potentially indicate increased risk for injury.

## CONCLUSION

TtC may prove to be a useful tool to examine neurological or orthopedic pathologies in the future, because it quantifies instantaneous postural stability through more challenging tasks than traditional quiet standing protocols, which may increase its ability to discriminate between subtle differences in pathology. Future studies should evaluate the efficacy of using TtC analysis during the SEBT in individuals following acute injury to monitor rehabilitation and evaluate side to side asymmetries, as well as during other single-leg lower extremity tasks to better understand balance deficits in individuals with neuropathologies such as Parkinson's Disease or stroke.

## REFERENCES

1. Haddad JM, et al. *Gait Posture*, **32**, 592-596, 2010.
2. Hertel J, et al. *Gait Posture*, **25**, 33-39, 2007.
3. Hertel J, et al. *J Appl Biomech*, **22**, 67-73, 2006.
4. Plisky PJ, et al. *J Orthop Sports Phys Ther* **36**, 911-919, 2006.
5. Slobounov SM, et al. *J Mot Behav*, **29**, 263-281, 1997.

## ACKNOWLEDGEMENTS

Partial funding for this study was provided by Makkar Athletics, Inc.

# COMPENSATORY MUSCLE CONTROL STRATEGIES WHEN WALKING WITH A CUSTOMIZED PD-AFO

<sup>1</sup>Elisa S. Schrank, <sup>1</sup>Jill S. Higginson and <sup>2</sup>Steven J. Stanhope

Departments of <sup>1</sup>Mechanical Engineering and <sup>2</sup>Kinesiology and Applied Physiology  
University of Delaware, Newark, DE, USA  
email: [schranke@udel.edu](mailto:schranke@udel.edu)

## INTRODUCTION

Passive-dynamic ankle-foot orthoses (PD-AFOs) use the rotational stiffness of the brace to provide plantarflexor assistance during the stance phase of gait, controlling the tibia as it rotates over the stationary foot. We have developed a novel customization and manufacturing framework for such PD-AFOs and demonstrated the feasibility of rapidly fabricating these fit-customized braces [1]. While the rotational stiffness of these PD-AFOs can be experimentally determined, the optimal stiffness is unknown due to the lack of understanding of how the stiffness influences the compensatory control strategy used when walking in a PD-AFO.

There are a multitude of compensatory control strategies that can be used to walk in a customized PD-AFO. For example, a pure substitution paradigm may be employed where the PD-AFO stiffness directly replaces function of the uniaxial plantarflexors. In other words, the contribution of these plantarflexors to the ankle joint moment decreases by the same amount as is contributed by the PD-AFO stiffness, resulting in no change to the ankle joint moment.

The compensatory strategy employed by the body when walking with a customized PD-AFO of a specific stiffness is currently unknown. Therefore, this study aimed to use a combination of experimental and simulation techniques to identify the compensatory muscle control strategy used when walking in a customized PD-AFO with a known stiffness in order to better understand the mechanisms used to walk with PD-AFOs.

## METHODS

*Experimental Data:* Torso, pelvis and bilateral lower extremity movement analysis data were collected as a healthy subject (age: 24 yrs, height: 1.62m, mass: 63.6 kg) walked overground in two

conditions: without and with a customized PD-AFO. The PD-AFO was customized for and worn on the subject's right leg. The subject wore shoes bilaterally in the normal condition and on the contralateral limb in the AFO condition. Kinematics of the PD-AFO cuff were recorded separately from the shank in the AFO condition. Kinematic and kinetic data were filtered at 6 Hz and 25 Hz, respectively, using a zero-lag low-pass Butterworth filter. The right ankle angles and joint moments during right stance were calculated using an inverse kinematics approach in Visual 3D (C-Motion Inc., Germantown, MD, USA), and these data were compared between the normal and AFO conditions.

*Musculoskeletal Models and Simulations:* In OpenSim, a lower-extremity musculoskeletal model, with 23 degrees of freedom and 54 muscle actuators, was scaled the subject's anthropometric measurements [2].

The characteristics of the customized PD-AFO were incorporated into the normal musculoskeletal model for the AFO condition. This PD-AFO-integrated model added two bodies, a footplate and a strut-cuff, to the right lower leg (Fig. 1). The footplate body was welded to the calcaneus. The strut-cuff body was connected to the tibia via a custom joint that only allowed translation of this body along the tibia's longitudinal axis. The two bodies were connected at their origins, the ankle joint center, by a six degree of freedom (DOF) bushing force, which mimicked a spring with user-prescribed passive stiffness values for each DOF. The stiffness for the dorsi/plantarflexion DOF was set to 3.0 Nm/deg to match the stiffness of the customized PD-AFO used in the experimental AFO condition. All other rotational and translational DOFs of the bushing force were set to zero, as the other DOFs were controlled by joint definitions and the PD-AFO strut-cuff body experimental kinematics.



**Figure 1:** PD-AFO-integrated model.

Using OpenSim v. 2.0.2, a quasi-static forward dynamic simulation tracked experimental gait data under the normal and AFO conditions with the corresponding (normal or PD-AFO-integrated) musculoskeletal model. Predicted muscle activity that drove the simulations was calculated through a computed muscle control optimization scheme [3]. Simulated and experimental right ankle angles were compared to assess tracking of the experimental kinematics. Right medial gastrocnemius (MGAS) and soleus (SOL) activations were examined during right stance for both conditions. Additionally, MGAS, SOL and bushing force moments about the right ankle were examined for the AFO condition.

## RESULTS AND DISCUSSION

The subject walked with a decreased ankle range of motion (Fig. 2a) and showed a premature increase in the plantarflexion moment (Fig. 2b) during the AFO condition. Both simulations successfully tracked the experimental ankle kinematics (Fig. 2a).

The simulation predicted that PD-AFO stiffness substitutes for all SOL activity during stance (Fig. 3a). However, the compensatory strategy was not a pure substitution paradigm, as the ankle joint moment differed between the two conditions (Fig. 2b). Furthermore, these changes in net ankle joint moment could not be account for entirely by the PD-AFO stiffness. The bushing force provided an ankle moment proportional to the degree of ankle dorsiflexion, supplying a constant moment during midstance and only accounting for 11% of the peak plantarflexion moment (Fig. 3b). Instead, the ankle moment changes were primarily reflected in altered MGAS activity in the AFO condition (Fig. 3a).

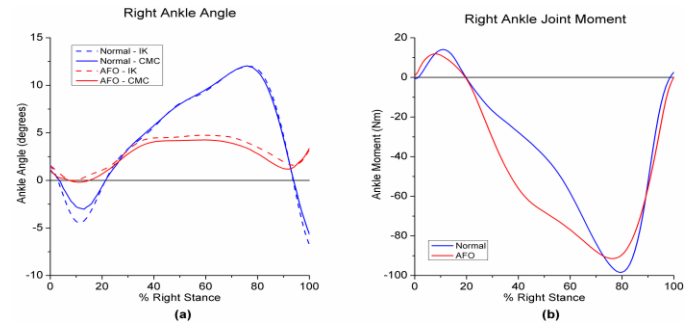


**Figure 2:** Ankle angle and moment. (a) No plantarflexion and reduced dorsiflexion with AFO. (b) Altered ankle moment in AFO condition.

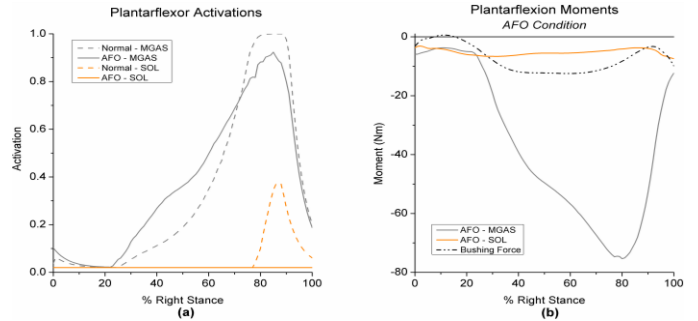


**Figure 3:** Activations and plantarflexion moments. (a) Early MGAS activity burst with reduced peak activation and no SOL activity with AFO. (b) MGAS primary contributor to ankle joint moment.

## CONCLUSIONS

These results indicated that, for this subject, a PD-AFO with a stiffness of 3.0 Nm/deg induced a complex compensatory muscle control strategy involving changes in both joint kinematics and muscle function. Future work will aim to identify the compensatory strategies that arise when walking in customized PD-AFOs with a range of stiffness values in order to gain insight into the spectrum of compensatory mechanisms. Ultimately, this approach may enable optimization of the PD-AFO design to achieve enhanced function for patients with a range of impairments.

## REFERENCES

1. Schrank ES and Stanhope SJ. *J Rehabil Res Dev* **48**, 31-42, 2011.
2. Delp SL, et al. *IEEE Trans Biomed Eng* **54**, 1940-1950, 2007.
3. Thelen DG and Anderson FC. *J Biomech* **39**, 1107-1115, 2006.

## ACKNOWLEDGEMENTS

This material is based upon work supported under a National Science Foundation Graduate Research Fellowship.

# SPATIOTEMPORAL CONTACT PROPERTIES OF THE TIBIOFEMORAL JOINT FOLLOWING ACL-RECONSTRUCTION

<sup>1</sup>Megan Schroeder, <sup>2</sup>Tae-Hyun Kwon and <sup>1,2</sup>Yasin Dhaher

<sup>1</sup>Northwestern University, Evanston, IL, USA

<sup>2</sup>Rehabilitation Institute of Chicago, Chicago, IL, USA

email: [mbarryschroeder@u.northwestern.edu](mailto:mbarryschroeder@u.northwestern.edu)

## INTRODUCTION

Following injury to the anterior cruciate ligament (ACL) of the knee, surgical reconstruction (ACL-R) is often indicated for patients seeking a return to high levels of physical activity. Despite short-term success in restoring stability and improving function, this procedure does not offer protection against early-onset joint degeneration and the development of osteoarthritis in this population [1]. Secondary to the initial trauma, this outcome may in part be mediated by increased or abnormal contact stresses in the joint post-reconstruction, which may be attributable to both surgical (graft type, tensioning level, attachment site), and patient-specific (joint geometry, muscle activation patterns) parameters. In this study, we sought to explore one such factor – the influence of patella tendon (PT) graft properties on tibiofemoral (TF) cartilage contact patterns.

## METHODS

An anatomically representative finite element (FE) model of the knee joint was created (Fig. 1a); a detailed description of the development process can be found elsewhere [2].

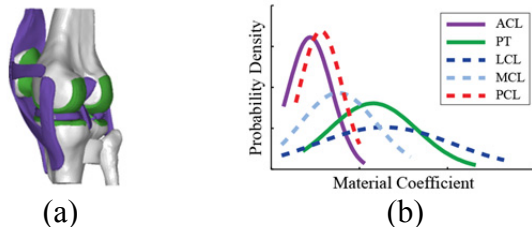


**Figure 1:** (a) FE model; (b) ranges of material coefficients reported for various knee ligaments.

Two separate series of simulations were performed to represent a normal knee and a reconstructed knee. ACL-R with a PT graft was modeled by

adjusting the material properties of the ACL to match the properties of the native PT. Because of the wide variability in soft tissue properties reported, the simulations were carried out using a probabilistic approach [2]. A random selection of material coefficients was selected from the reported ranges for each ligament (Fig. 1b), and a total of 50 simulations were run for each series. In both series, normal muscle and ground reaction forces from the load acceptance phase of gait were used as inputs to the model [3]. Kinematics were not imposed.

## RESULTS AND DISCUSSION

One of the primary goals of rehabilitation following ACL-R is to restore normal kinematics [4]. When comparing the reconstructed to the normal joint, our model predicted almost no difference in flexion angle, a significant ( $p < 0.05$ ) increase in internal rotation, and little variation in varus/valgus (Fig. 2). ACL deficiency has been shown to result in increased internal rotation at the knee [5], and our results suggest that ACL-R with a PT graft does not adequately control that range of motion, thus altering the internal mechanics of the joint.

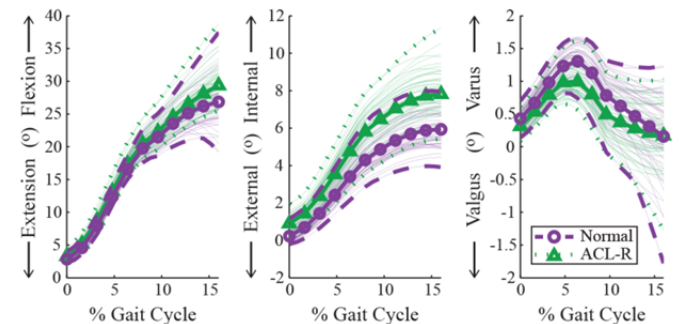


**Figure 2:** Tibiofemoral kinematics (rotational degrees of freedom) as a function of the gait cycle. Individual simulations are represented by thin traces; the mean and overall range for each series is emphasized, as indicated in the legend.

It has been reported that even small changes in these secondary rotational degrees of freedom could lead to substantial differences in stresses applied to the supporting structures [1]. In particular, when we considered the contact pressure on the surface of the tibia cartilage not covered by the menisci (Fig. 3), we observed significant changes following ACL-R.

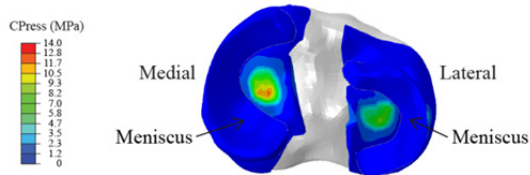


**Figure 3:** General contact pressure pattern on the surface of the tibia cartilage.

The maximum magnitude of the contact pressure on the medial tibia cartilage post-reconstruction was significantly ( $p < 0.05$ ) higher than normal during the latter half of the load acceptance phase, but remained relatively unchanged on the lateral cartilage (Fig. 4). Despite this apparent increase on the medial cartilage, the maximum magnitude after reconstruction was not as high as the contact pressure of the normal knee at heel strike (0% of the gait cycle). Therefore, it is likely that changes in the magnitude of contact stress may not adequately explain the increased rate of cartilage degeneration.

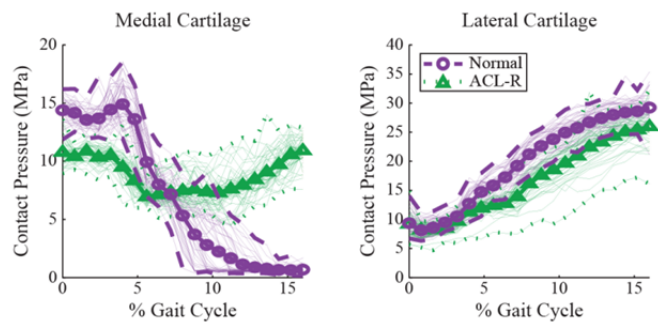


**Figure 4:** Maximum magnitude of contact pressure on the tibia cartilage as a function of the gait cycle.

The side-to-side (medial/lateral) location of the contact pressure on both the medial and lateral tibia cartilage was significantly different throughout the entire load acceptance phase (Fig. 5), results which seem to indicate a more generalized shift in cartilage contact patterns following reconstruction with a PT graft. These alterations could lead to more rapid degeneration of the joint, as areas of

cartilage which are unaccustomed to bearing these loads have to pick up the additional burden [5].

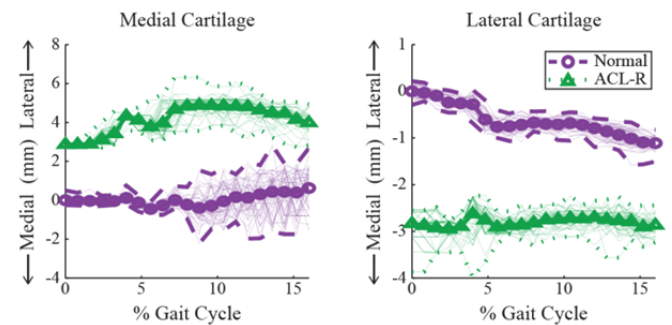


**Figure 5:** Relative position in the medial/lateral direction of the average contact pressure on the tibia cartilage as a function of the gait cycle.

## CONCLUSIONS

Our modeling framework suggests that PT graft stiffness may contribute to changes in the spatiotemporal contact properties of the TF joint and lead to more rapid cartilage degeneration. To reflect one of the goals of rehabilitation following ACL-R, a key assumption in this study was that the muscle activation patterns were restored to their pre-injury state. However, these patterns appear to be suboptimal given the surgically mediated changes to the joint. It remains to be seen if training protocols can be adapted to alter these patterns in favor of restoring normal contact characteristics.

## REFERENCES

1. Tashman S, et al. *Clin Orthop Relat Res* **454**, 66-73, 2007.
2. Barry MJ, et al. *Conf Proc IEEE Eng Med Biol Soc* **2010**, 5440-5443, 2010.
3. Besier TF, et al. *J Biomech* **42**, 898-905, 2009.
4. Andersson D, et al. *Arthroscopy* **25**, 653-685, 2009.
5. Andriacchi TP, et al. *Ann Biomed Eng* **32**, 447-457, 2004.

## ACKNOWLEDGEMENTS

This work has been supported by a Doctoral Dissertation award from the Arthritis Foundation, the DOD #DR080326, NSF #0966535/0966742, and NIH NIAMS R01 AR049837.

# MINIMUM TOE CLEARANCE ADAPTATIONS TO FLOOR SURFACE IRREGULARITY AND GAIT SPEED IN OLDER ADULTS

<sup>1</sup>Brian Schulz, <sup>1</sup>Stephanie Hart-Hughes, and <sup>1</sup>Tatjana Bulat

<sup>1</sup>VA HSR&D/RR&D Center of Excellence in Maximizing Rehabilitation Outcomes,  
James A. Haley VA Hospital, Tampa, Florida, USA  
email: [Brian.Schulz@va.gov](mailto:Brian.Schulz@va.gov)

## INTRODUCTION

Toe speed during gait generally nears its maximum while its height reaches a local minima halfway through swing phase. Trips are thought to frequently occur at these local minima (minimum toe clearance or MTC events) and trip risk has been quantified using the minimum distance between the toe and ground here (MTC) [1]. Previous work has shown age to have little to no effect on MTC [2], but overground MTC on surfaces with obstacles has never before been evaluated in older adults.

## METHODS

Unimpaired younger (7 male, 7 female, age=26±5) and older (7 male, age=73±7) subjects each traversed a 4.88m walkway 4 times at slow, preferred, and fast speeds across surfaces with no obstacles, visible obstacles, and hidden obstacles. Both surfaces with obstacles had the same random obstacle configuration. Shoe and body segment motions were tracked using passive markers and MTC and kinematics calculated using previously-described methods [3]. Also as per these methods [3], MTC events were defined to occur at a point in the swing phase where the following criteria were met: 1) The minimum toe clearance was at a local minima (value is less than that for preceding or following two frames), 2) Toe segment centroid speed (mean speed of the four toe markers) was within the upper quartile for that step, and 3) The minimum toe clearance was lower than the minimum heel clearance. If these criteria were met by more than one point per gait cycle (common on surfaces with obstacles), then the point with the smaller MTC value was used. SAS was used for all statistical analyses and main effects were considered significant at  $p < 0.014$  after Bonferroni corrections for multiple statistical tests.

## RESULTS AND DISCUSSION

Older subjects had similar MTC values as younger subjects (Older=22.7±12.5mm & Young=20.0±9.4), but they adapted the shape of their minimum toe clearance time histories more markedly to the presence of obstacles (see Fig. 1 for exemplar data). This resulted in a smaller percentage of valid MTC events (MTC event occurrence) for the same number of opportunities in older subjects (Fig. 2,  $p=0.0006$ ). The only other significant age effect was a 12° greater downward head tilt in the older subjects ( $p=0.001$ ) to look at obstacles on the floor. All other effects were similar to those for younger subjects [3]. All MTC and kinematic variables tested significantly increased with faster instructed gait speed except the likelihood of MTC event occurrence (local minima in minimum toe clearance trajectory when foot is in upper quartile of speed). MTC events were less frequent on surfaces with obstacles (80% vs. 98% for no obstacles). MTC values, when present, were doubled by the presence of visible obstacles (23.9±8.1mm vs. 10.4±5.3mm) and further increased to 28.3±8.2mm when these obstacles were hidden (all comparisons  $p < 0.0001$ ). Ankle dorsiflexion and knee and hip flexion angles at MTC all significantly increased (Table 1,  $p < 0.0001$ ) with flooring surfaces challenge, but foot segment angles were not affected by flooring surface.

## CONCLUSIONS

Younger and older subjects adapt similarly to changes flooring surface and instructed gait speed. The greater head tilt and reduced frequency of minimum toe clearance event occurrence in the older subjects may indicate less confidence in gait across these surfaces and greater caution, despite the similarities in MTC values and joint kinematics.

## REFERENCES

1. Winter DA. *Physical Therapy*, 72(1), 45-6, 1992.
2. Barrett RS, et al. *Gait Posture* 32, 429-35, 2010.
3. Schulz BW, et al. *J Biomech*, **In Press**, 2011.

## ACKNOWLEDGEMENTS

VA RR&D Career Development Award (E4941W). We thank Wendy Kimmel, Pradeep Ambati, & Scott Barnett for their assistance.

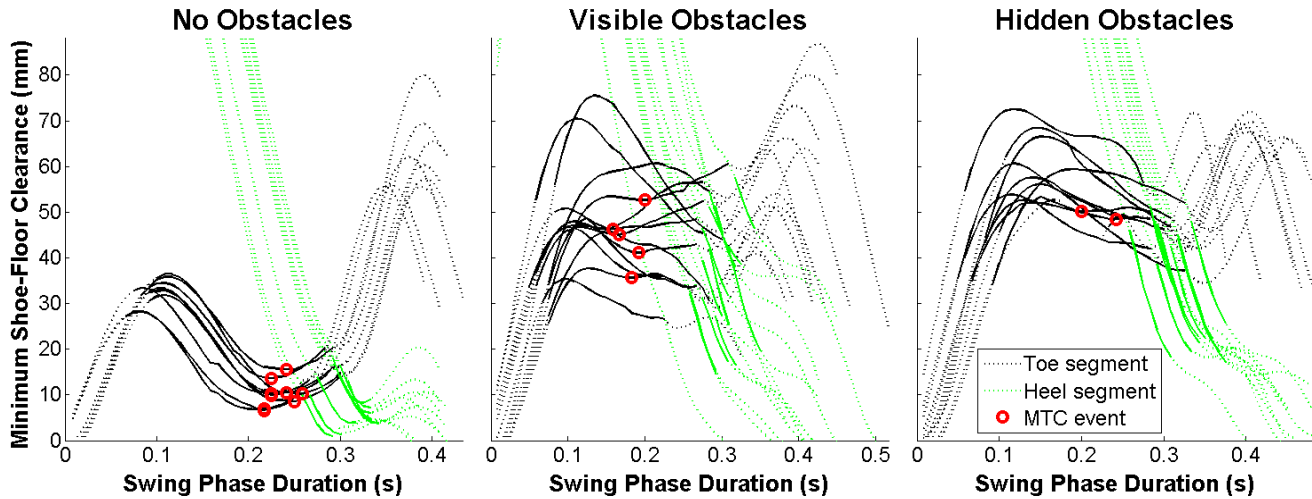


**Figure 1:** Traces of minimum distances from toe (black) and heel (green) shoe segments to floor surface across the swing phase of gait by surface condition. All viable gait cycles of the left foot of a single subject walking at preferred speed shown. Solid lines indicate trace that is closest to floor surface (including obstacles if present) during upper quartile of toe centroid speed. Minimum toe clearance (MTC) events circled in red.

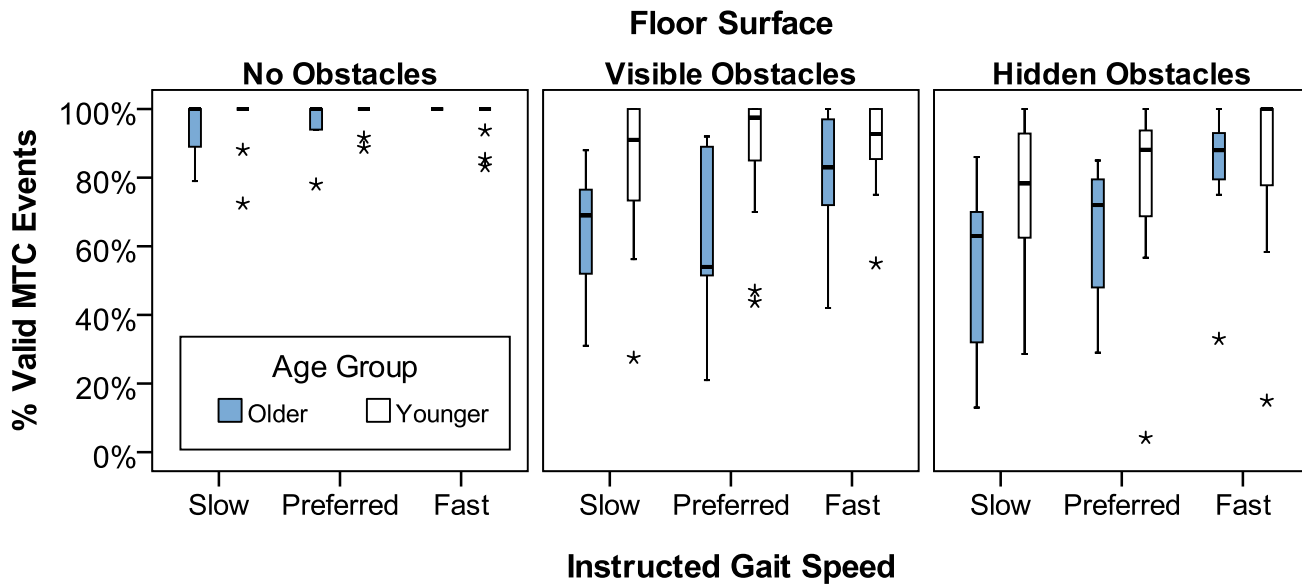


**Figure 2:** Error bar plot of percentage of valid MTC events by age group, floor surface, & instructed gait speed. \* indicate outlier points (>3intraquartile range from the median).

**Table 1: Mean (SD) of all dependent variables tested using repeated-measures linear mixed models by floor surface and instructed gait speed.**

| Dependent Variable                    | No Obstacles Floor Surface |             |             | Visible Obstacles Floor Surface |             |             | Hidden Obstacles Floor Surface |             |             |
|---------------------------------------|----------------------------|-------------|-------------|---------------------------------|-------------|-------------|--------------------------------|-------------|-------------|
|                                       | Slow                       | Preferred   | Fast        | Slow                            | Preferred   | Fast        | Slow                           | Preferred   | Fast        |
| Actual gait speed (% Leg Length/s) *  | 1.12 (0.30)                | 1.55 (0.28) | 2.56 (0.47) | 1.07 (0.28)                     | 1.47 (0.28) | 2.39 (0.44) | 1.08 (0.26)                    | 1.52 (0.29) | 2.32 (0.43) |
| Number of valid swing phases *        | 23.8 (5.2)                 | 18.8 (3.2)  | 13.6 (3.2)  | 23.5 (6.9)                      | 18.9 (5.1)  | 13.3 (3.5)  | 23.8 (7.0)                     | 18.5 (4.2)  | 13.6 (3.4)  |
| Number of MTC events * †              | 22.8 (4.9)                 | 18.2 (3.0)  | 13.4 (3.4)  | 17.0 (5.8)                      | 14.2 (4.6)  | 11.4 (3.1)  | 15.5 (6.7)                     | 13.1 (4.7)  | 11.1 (3.8)  |
| % of swing phases with MTC events † ‡ | 95.6 %                     | 97.5 %      | 98.2 %      | 75.3 %                          | 79.5 %      | 86.7 %      | 68.6 %                         | 74.1 %      | 83.7 %      |
| MTC to flooring surface (mm) * †      | 8.22 (4.6)                 | 9.5 (4.1)   | 13.5 (5.6)  | 20.9 (7.5)                      | 23.5 (6.7)  | 27.4 (9.0)  | 23.5 (5.1)                     | 26.4 (5.8)  | 30.4 (8.5)  |
| Foot segment angle at MTC (deg) *     | -38.4 (7.4)                | -41.5 (6.4) | -48.2 (6.0) | -40.2 (7.4)                     | -42.9 (5.4) | -46.5 (7.6) | -39.0 (7.5)                    | -44.1 (6.8) | -46.3 (6.6) |
| Ankle dorsiflexion at MTC (deg) * †   | 2.4 (3.9)                  | 1.6 (2.8)   | 4.3 (3.5)   | 4.1 (4.5)                       | 3.6 (3.8)   | 5.0 (4.4)   | 6.2 (4.1)                      | 5.7 (2.6)   | 6.6 (2.6)   |
| Knee flexion at MTC (deg) * †         | 48.8 (8.7)                 | 52.7 (7.8)  | 60.9 (6.5)  | 55.8 (10.0)                     | 59.5 (6.7)  | 65.1 (8.7)  | 55.8 (10.0)                    | 61.1 (8.8)  | 65.5 (7.7)  |
| Hip flexion at MTC (deg) * †          | 40.1 (8.6)                 | 42.5 (9.1)  | 44.7 (10.2) | 43.6 (8.9)                      | 54.8 (10.6) | 49.1 (10.2) | 45.2 (9.6)                     | 47.2 (10.3) | 51.3 (11.3) |

Notes: No foot, gender, or interaction effects were significant. Please refer to the text for effects of age and post-hoc multiple comparisons.

Significant main effects indicated by \* for instructed gait speed ( $p < 0.0001$ ), † for floor surface ( $p < 0.0001$ ), and ‡ for age group ( $p = 0.0006$ ).

# 3-D TARSAL KINEMATICS ACQUIRED USING BI-PLANAR VIDEOfLUOROSCOPY AND A SIMPLE STATIC GAIT SIMULATOR

Joel B. Schwartz, Megan M. Dawson, Brad D. Blankenhorn, Jason T. Bariteau,  
Michael J. Rainbow, Christopher W. DiGiovanni and Douglas C. Moore

Bioengineering Laboratory, Department of Orthopaedics, Brown University, Providence, RI, USA  
email: douglas\_moore@brown.edu, web: <http://www.brownbiomechanics.org>

## INTRODUCTION

Three-dimensional (3D) foot bone kinematics are challenging to measure due to the inaccessibility of the individual tarsal bones. A handful of studies have been performed using x-ray marker-based stereoradiogrammetry or through-skin bone pins [1,2], however, the invasiveness of these techniques makes their use difficult to justify.

Bi-planar videofluoroscopy offers a promising technique for measuring foot bone kinematics *in vivo*. In this abstract we report a simple gait simulator designed to be used with a bi-planar videofluoroscopy system. The system was developed for use with simple *in vitro* biomechanical studies, and to generate data that could be used to validate the development of markerless registration techniques for future *in vivo* biomechanical analysis.

## METHODS

The simulator was designed to facilitate positioning of the shank and foot in nine separate positions distributed evenly (as a function of time) along the stance phase of normal gait. Shank position was constrained by foot contact with a radiolucent carbon fiber base plate and the anterior/posterior and vertical position of the head of the fibula [3,4], which was defined by a machined track (Fig. 1) that profiled fibular head height from heel contact to 90% of the stance phase [3]. An F-Scan System (Tekscan, South Boston, MA) was used to record the pressure distribution between the feet and the base plate. The track was adjusted above the carbon fiber platform and locked in place to exert approximately ~35 kg in compression (roughly 50% of body weight) as measured by the F-Scan. This magnitude provided reasonable loading given the confines of the

apparatus, based on the work of Hurschler et al [5]. Tendon loading was accomplished with dead weights, applied through low-friction cable assemblies. Individual tendon loads at each position were based on EMG data from the literature [4].

The simulator was evaluated with three fresh-frozen cadaver right feet (1 male, 2 female, age  $72.3 \pm 7.4$  yrs). Specimen preparation involved dissection and preparation of the seven extrinsic foot tendons (Achilles (calcaneal), tibialis posterior, flexor digitorum longus, flexor hallucis longus, combined peroneus longus and brevis, tibialis anterior, and combined extensor digitorum longus and extensor hallucis longus), potting of the proximal tibia and fibula such that the height between the lateral maleolus and the center of the machined track was 34 cm, and implantation of  $\geq 3$  1.0 mm dia. tantalum beads into the tibia, fibula, talus, calcaneus, navicular, cuboid, medial cuneiform, and first, third, and fifth metatarsals.

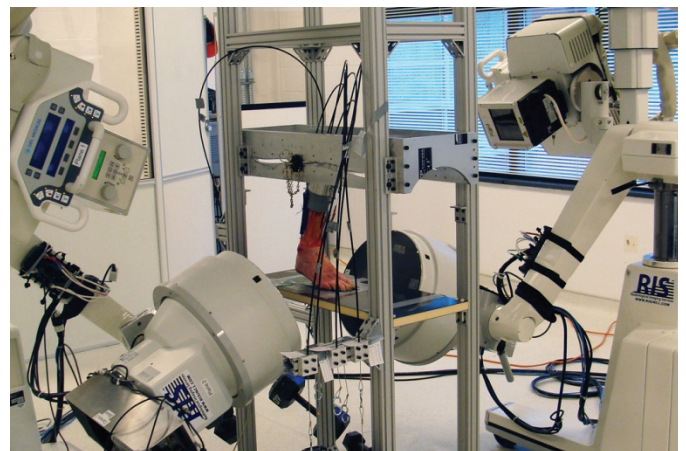


**Figure 1:** Apparatus within the XROMM system, with 2 x-rays oblique to the lateral aspect of the foot.

The specimens were imaged at each position using a bi-planar videofluoroscopy system (XROMM; Brown University, Providence, RI). The resolution of the imaging chain was approximately

2 line pairs/mm [6]. Marker tracking and rigid body transforms for each of the tracked bones were generated using custom written Matlab code (XRayProject, xromm.org). Digital models of the bones (and marker bead) in each specimen were generated from CT acquired at a voxel resolution of  $\sim 0.6 \text{ mm} \times \sim 0.6 \text{ mm} \times 0.625 \text{ mm}$ . Kinematic analysis was performed in the context of a right-handed anatomical coordinate system based on axes that passed through the medial and lateral malleoli and the first inertial axis (long-axis) of the tibia. For a reference position, we used “foot flat” which occurred at position 2 (12% stance). We measured ankle dorsi/plantar flexion by tracking the talus relative to the tibia in our anatomical coordinate system. Finally, we compared our results to previously published *in vivo* kinematics measured with skin markers [3].

## RESULTS AND DISCUSSION

The ground reaction force calculated from pressure data showed a biphasic pattern characteristic of the stance phase of the gait cycle (Fig. 2). The magnitude of the ground reaction force at “foot flat” approximated our targeted amount, roughly one half of that observed *in vivo* [3,5]. However, we found that our peak forces occurred approximately 10% earlier in the stance phase compared to *in vivo* results [3]. The first peak corresponds with our “foot flat” position.

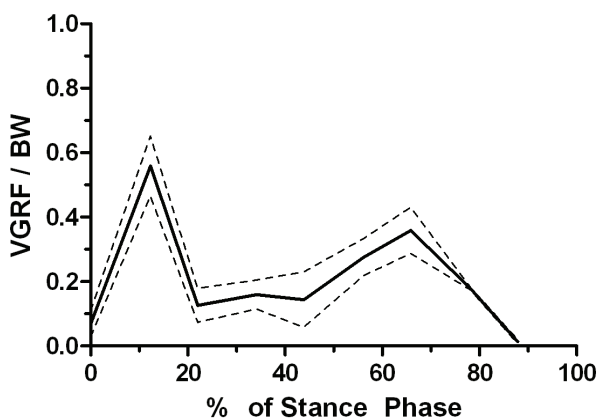


**Figure 2:** Vertical Ground Reaction Force (VGRF) as a percentage of body weight (BW, 70 kg). Mean and standard deviation (SD) demonstrate relative consistency between subjects.

Ankle dorsi/plantar flexion was consistent between subjects and mimics a typical ankle dorsi/plantar flexion pattern (Fig. 3).

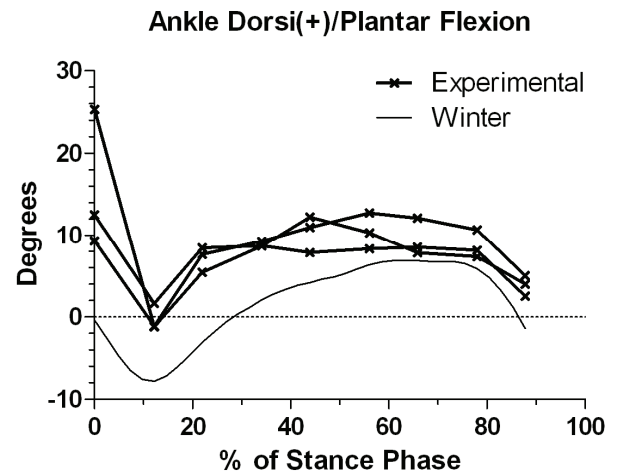


**Figure 3:** Experimental ankle dorsiflexion (+) and plantar flexion (-) of the talus with respect to the tibia plotted against *in vivo* measurements reported by Winter [3].

## CONCLUSIONS

In this abstract we report a simple static gait simulator that is used with a bi-planar x-ray system to measure foot bone kinematics. Through the nine simulated positions, the vertical ground reaction force and ankle dorsi/plantar flexion was similar to literature-reported patterns of normal gait. Our preliminary results suggest the system will be appropriate for simple *in vitro* biomechanical studies, and to generate data that could be used to validate the development of markerless registration techniques.

## REFERENCES

1. Lundberg A, et al. *J Bone Joint Surg*, **71**, 94-99, 1989.
2. Nester C, et al. *J Biomech*, **40**, 3412-3423, 2007.
3. Winter DA. *Biomechanics and Motor Control of Human Movement*, John Wiley & Sons, Inc., 1990.
4. Sharkey, et al. *Clin Biomech*, **13**, 420-433, 1998.
5. Hirschler, et al. *Foot Ankle Int*, **24**(8), 614-622, 2003.
6. Brainerd EL, et al. *J Exp Zool A Ecol Genet Physiol*. **313**(5), 262-79, 2010.

## ACKNOWLEDGEMENTS

This study was supported by a grant from the AOFAS and the Department of Orthopaedics.

# IDENTIFICATION AND IMPROVEMENT OF DIFFICULT HAND GRIP MOVEMENT COMPONENTS FOR STROKE SURVIVORS USING THE BOX AND BLOCK TEST

Jerome O. Scott, Alek R. Brandenburg, Brett M. Allard, and Na Jin Seo

University of Wisconsin-Milwaukee, Milwaukee, WI, USA  
email: [seon@uwm.edu](mailto:seon@uwm.edu) web: <https://pantherfile.uwm.edu/seon/www/>

## INTRODUCTION

The leading cause of long-term disability in the US is stroke [1]. The disability is most prevalent in the hand and arm, impairing hand grip-and-release function [2-4]. The objectives of this study were (i) to identify difficult movement components during grip-and-release for stroke survivors and (ii) to determine if grip-and-release performance can improve by increasing frictional coupling between the fingers and gripped objects. Specifically, two hypotheses were tested: (i) The most difficult movement component during grip-and-release for the paretic hand compared to the nonparetic hand is grasping a block to initiate lift-off; (ii) Modifying object or finger surfaces with high-friction materials enhances grip-and-release function.

## METHODS

Six chronic stroke survivors participated (2 male and 4 female, age = 39 to 74 with a mean of 55 years). People with coexisting medical issues were not recruited. All subjects signed the consent form.

Subjects' hand grip-and-release performance was quantified by the Box and Block Test (BBT) (Sammons Preston, Bollingbrook, IL) [5]. The BBT quantifies hand function as the number of blocks that a person moves from one box to another in 60 seconds as fast as s/he can (Fig.1). To identify movement components that take particularly long for the paretic compared to the nonparetic hand, all BBT was videotaped. Motion-time analysis was performed by analyzing videos frame by frame using Quick-Time (Apple Inc., Cupertino, CA). Movements associated with the BBT were broken down to 6 movement components as follows.

(i) “Hand Closing” begins one frame prior to the first frame where the fingers start closing about the

metacarpophalangeal joint. (ii) “Contact-to-lift” begins on the frame when fingers have made contact with the block. (iii) “Transport” begins on the frame the block was lifted off the floor of the box. (iv) “Release” begins on the frame at which the block has left contact with the fingers for the first time and is in free-fall. (v) “Return” begins on the frame in which the hand begins moving back to the first box. (vi) “Reaching” begins on the frame in which the hand is over the barrier. Each frame was counted for a single movement component (no overlap).

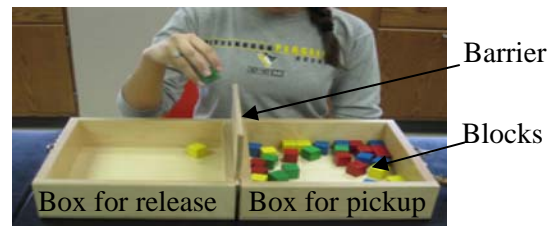


**Figure 1:** BBT is an assessment of hand function.

To determine the effect of frictional coupling between the fingers and blocks on stroke survivors' grip-and-release performance, the BBT score was obtained for four frictional conditions: (i) bare finger against standard painted wooden blocks with coefficient of friction (COF) = 0.6, (ii) bare finger against paper-covered blocks with COF = 0.5, (3) bare finger against rubber-covered blocks with COF = 1.1, and (4) the thumb and index finger wearing the rubber thimbles against standard painted wooden blocks with COF = 0.7 [6-9], tested only for the paretic hand. The BBT for each hand and frictional condition was repeated two times.

To test the first hypothesis, repeated measures ANOVA was performed to determine if mean time spent in each movement component significantly varied for hand (paretic vs. nonparetic), movement component, frictional condition, and their second-order interactions. For the second hypothesis,

another ANOVA was performed to determine if the BBT score significantly varied for hand, frictional condition, and their second-order interaction. Pairwise comparison was additionally performed to evaluate differences among individual conditions.

## RESULTS

The mean movement time was 31% longer for the paretic than for the nonparetic hand (movement components pooled;  $p < .01$ ). The paretic hand took particularly longer to achieve the “Contact-to-lift” and “Reaching” movements, compared to the nonparetic hand (Fig. 2;  $p < .01$  for the interaction between hand and movement component). Mean movement times for the two components were 50% longer for the paretic than for the nonparetic hand.

The mean BBT score was 17% higher for the nonparetic than for the paretic hand ( $p < .01$ ). The mean BBT score significantly changed with frictional conditions ( $p < .01$ ). Specifically, the BBT score was 12% higher for the rubber-covered blocks against fingers than for the wooden blocks (Fig. 3;  $p < .01$  for pairwise comparison). The higher score for the rubber-covered blocks was related to reduced time spent for the “Contact-to-lift” movement (Fig. 4). The interaction between hand and surface was not found significant ( $p > .05$ ).

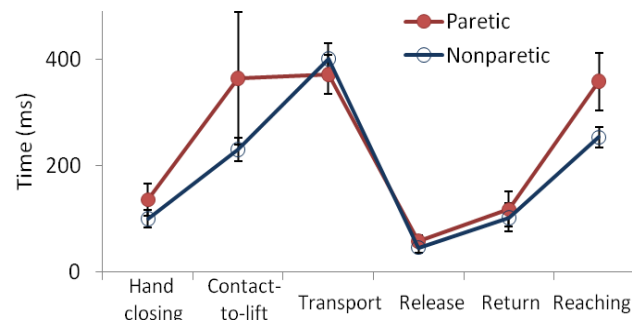


**Figure 2:** Mean  $\pm$  SE time (ms) for each movement component for the paretic vs. nonparetic hands.

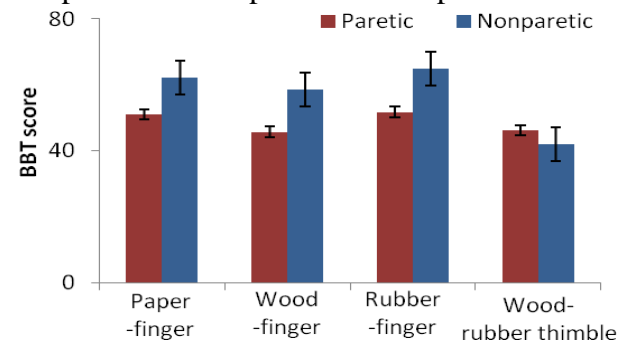


**Figure 3:** Mean  $\pm$  SE BBT score for four frictional conditions for the paretic vs. nonparetic hands.

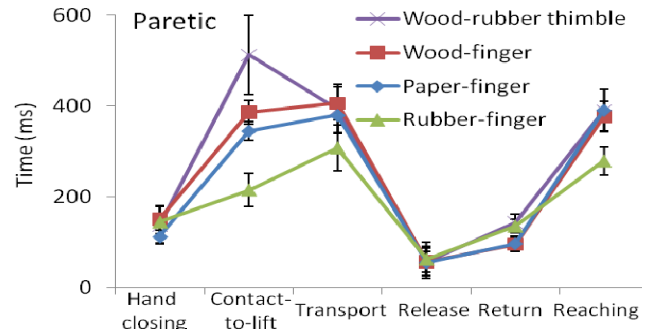


**Figure 4:** Mean  $\pm$  SE movement time (ms) for the four frictional conditions for the paretic hand.

## DISCUSSION

The “Contact-to-lift” and “Reaching” movements took particularly long for the paretic than for the nonparetic hand. Development of assistive devices and therapies may focus on those movement components. Considerable increase of the object surface friction improved a person's grip-and-release function, by shortening the time for the “Contact-to-lift”. Thus, modifying daily objects with high-friction surface may help hand function. Use of rubber thimbles appears to hinder grip-and-release movements, both mechanically and by reducing cutaneous sensations. The present study provides information that can be used to improve hand motor functions in persons with stroke.

## REFERENCES

- Lloyd-Jones D, et al. *Circulation* **119**, 480-6, 2009.
- Woodson AM. In: Trombly CA, Ed. *Occupational Therapy for Physical Dysfunction*, Lippincott, Williams & Wilkins, 2002.
- Kamper DG, et al. *Muscle Nerve* **28**, 309-18, 2003.
- Verbunt JA, et al. *BMC Neurology* **8**, 7, 2008.
- Desrosiers J, et al. *Arch Phys Med Rehabil* **75**, 751-5, 1994.
- Bullinger HJ, et al. *Germany: Federal Institute for Occupational Safety and Accident*, 1979.
- Buchholz B, et al. *Ergonomics* **31**, 317-25, 1988.
- Seo NJ, Armstrong TJ, *Ergonomics* **52**, 609-16, 2009.
- Blau PJ and Dekker M, *Friction Science and Technology (Mechanical Engineering Series)*. Taylor & Francis Group, 1995.

## ACKNOWLEDGEMENTS

University of Wisconsin-Milwaukee

# RADIOLUCENT COMPOSITES PROVIDING HIGH RESISTANCE AGAINST STERILIZATION DECOMPOSITION

<sup>1</sup>Radek Sedláček, <sup>1,2</sup>Tomáš Suchý, <sup>1</sup>Miroslav Sochor, <sup>2</sup>Karel Balík, <sup>2</sup>Zbyněk Sucharda and <sup>3</sup>Jan Beneš

<sup>1</sup>Laboratory of Biomechanics, CTU in Prague, Fac. of Mechanical Eng., Prague 6, Czech Republic

<sup>2</sup>Institute of Rock Structure and Mechanics ASCR, v.v.i., Prague 8, Czech Republic

<sup>3</sup>MEDIN, Inc., Nové Město na Moravě, Czech Republic

email: [radek.sedlacek@fs.cvut.cz](mailto:radek.sedlacek@fs.cvut.cz) web: <http://www.biomechanics.cz/>

## INTRODUCTION

There are nowadays numerous materials available for use in constructing various medical devices, including surgical intra-operative guides and instrumentations, and screening equipment accessories. Traditionally, metallic materials such as stainless steel and titanium alloys have been used in the construction of medical devices. They exhibit suitable physical and chemical properties and are compatible with widely-used sterilization techniques. The metallic elements have a sufficiently high atomic number to be effectively opaque to X-rays. Metals containing iron are however magnetic, which distorts the images obtained by MRI [1]. Accurate intra-operative imaging is vital in surgery in order to achieve precise reduction of fractures, precise placement of implants or screws and correct positioning of osteotomies [2, 3], as small changes in component positioning can lead to significant changes in post-operative performance [4]. Insufficient radiolucency of metal alloys can be resolved by the application of non-metallic materials. Composite materials can be turned toward radiolucent structural materials and materials providing mechanical performance and mechanical properties competitive with the properties of some metals. Another important property of medical devices is their mechanical, shape and chemical stability after repeated sterilization without any sign of degradation [1]. The development of novel materials for use in medical devices necessarily encompasses an assessment of the effects of a range of commercially available sterilization processes.

The aim of this study was to prepare an advanced composite material with suitable mechanical

and radiolucent properties and structural stability after repeated sterilization by commonly-used techniques.

## METHODS

Composites based on carbon T300 fibers (plain weave fabrics, Toray, Japan) and/or polyetheretherketon (Porcher Industrie, France) and polyphenylenesulfide (TenCate, Holland) were prepared. T300/polyetheretherketon (PEEK) was cured under a pressure of 0.08 MPa at 395°C. T300/polyphenylenesulfide (PPS) was cured under a pressure of 1.0 MPa at 310°C.

Mechanical properties were measured before (A) and after 1 (B1) and after 30 (B30) sterilization process periods. The steam sterilization (134°C, 304 kPa, 10 min) in the autoclave (Sterident, Prodenta, CZ) was used for this purpose. The ultimate strength in bending and the modulus of elasticity in bending in the direction of the fiber axis were determined by a four-point and three-point bending set-up using the Inspekt 100 HT material tester (Hagewald & Peschke, Germany), in accordance with ISO 14125.

The intensity of X-rays transmitted through studied composites was measured (80 kV, 2 mA, 1000 ms). On the basis of the Beer-Lambert law, the transmissivity was calculated for each sample. Finally, the linear absorption coefficients ( $\mu$  [ $\text{mm}^{-1}$ ]) were calculated. Since the absorption coefficient is not influenced by sample thickness (it is influenced mainly by material properties) it was possible to assess and compare the radiolucency of each studied material. The transmissivity was measured by Shado-o-Box<sup>TM</sup> 4K (Rad-Icon Imaging, USA). The X-ray Tubehousing ISOVOLT 420/5 (Agfa

NDT Pantak Seifert, Germany) was used as a X-ray source. In order to make a comparison with the real environment (radiolucency of human bone), the control material was added to the analyses performed. An aluminum control sample was used. An X-ray analysis of the Al sample was performed, and the transparency of its various thicknesses was compared with the transparency of the human humerus (see Fig. 1). For this purpose, a densitometer was used for single point measurements of the optical densities of X-ray films (Densoquick 2, PEHA, Germany). The suitable radiolucency was found in the case of Al control sample thicknesses up to 3 mm, and the highest rate was for part 1 mm in thickness.

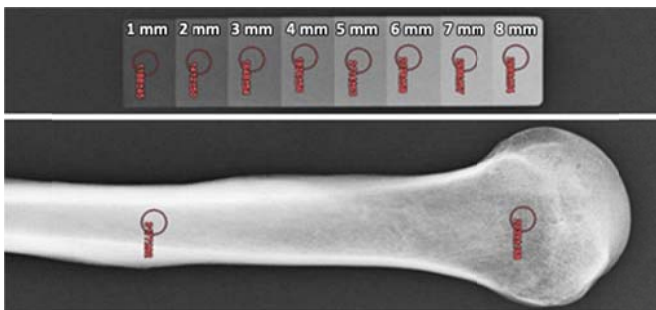


**Figure 1:** An example of the optical densities of an X-ray film measurement.

## RESULTS AND DISCUSSION

The flexural properties after multiple sterilizations were tested and compared with those of the corresponding unsterilized samples (Fig. 2 and 3).

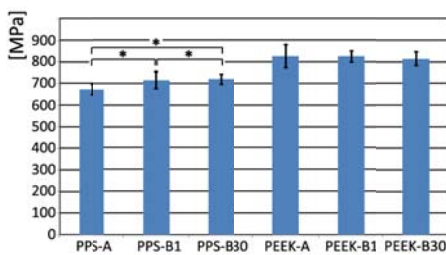


**Figure 2:** Ultimate strength in bending (\* denotes stat. sig. differences, Newman-Keuls, 0.05).

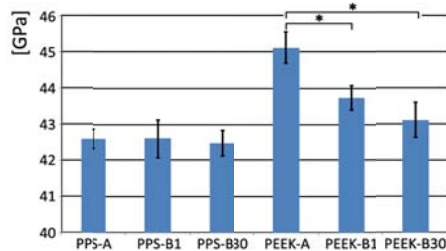


**Figure 3:** Modulus of elasticity in bending (\* denotes stat. sig. differences, Mann-Whitney, 0.05).

The modulus of elasticity in bending is influenced by multiple sterilizations only in the case of T300/PEEK composite (PEEK). The inexpressive decrease in modulus is equal to approx. 3 - 4% after 30 sterilization cycles. In the case of ultimate strength in bending, no decrease occurred. From this point of view we can state that no weakening of the reinforcement-matrix bond occurred.

The X-ray analysis results are summarized in Figure 4. Both composites are sufficiently radiolucent, and both displayed lower linear absorption coefficient values than the Al control sample.

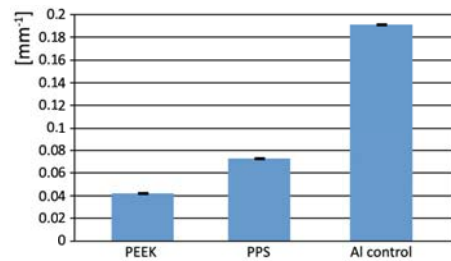


**Figure 4:** Linear absorption (all values display stat. significant differences, Mann-Whitney, 0.05).

## CONCLUSIONS

Our analyses show that both composites are good candidates for application as radiolucent materials providing resistance against sterilization decomposition. It will be necessary to increase the number of applied sterilization processes and perform further physical properties analyses before the materials can be recommended for application.

## REFERENCES

- [1] Ramakrishna S, et al. *An Introduction to Biocomposites*, Imperial College Press, 2004.
- [2] Norris BL, et al. *J Orthop Trauma* **13**, 414-417, 1999.
- [3] Routt Jr ML, et al. *Clin Orthop Relat Res* **375**, 15-29, 2000.
- [4] Siston RA, et al. *J Biomech* **40**, 728-735, 2007.

## ACKNOWLEDGEMENTS

This study was supported by the Czech Science Foundation under project No. P108/10/1457, and by Ministry of Education project Transdisciplinary Research in Biomedical Engineering II., No. MSM 6840770012.

# EXPERIMENTAL KNEE JOINT PAIN AFFECTS CERTAIN RUNNING KINEMATICS

Matthew Kirk Seeley, Jihong Park, Daniel King, and J. Ty Hopkins

Brigham Young University, Provo, UT, USA  
email: matt\_seeley@byu.edu web: biomech.byu.edu

## INTRODUCTION

Scientists have estimated that knee pathology will affect half of Americans who reach the age of 85 [1]; related annual costs are approaching twenty billion dollars. Knee pain is a primary symptom that limits function for individuals who suffer from knee pathology. The effects of knee joint pain on movement mechanics, independent of other knee pathology factors, are unclear. Researchers have reported that knee joint pain can independently alter lower-extremity muscle activation patterns and mechanics [2]. If knee pain independently alters movement mechanics, it may also predispose patients to chronic knee disease. For example, as tibiofemoral articular cartilage health depends upon appropriate knee joint load, altered load may promote knee joint degradation.

The purpose of this study was to evaluate the effect of experimental knee joint pain on running kinematics, in order to clarify the independent role of knee pain on movement mechanics. We hypothesized that experimental knee joint pain would alter lower-extremity running kinematics.

## METHODS

Twelve able-bodied subjects gave informed consent and participated in this study (6 males, 6 females; age =  $23 \pm 3$  yrs; height =  $1.73 \pm 0.09$  m; mass =  $75 \pm 14$  kg). Subjects completed three data collection sessions. Each session corresponded to a different experimental condition (control, sham, and pain) and was separated by two days. For each session, reflective markers were first applied to subjects in order to facilitate motion analysis. Subjects then performed the *pretreatment* running trials. These trials and all subsequently mentioned running trials consisted of a brief warm-up and a 30-s running period at a standardized speed on a treadmill. Next, for the control session only, subjects performed the

*treatment* and *post-treatment* running trials. For the pain and sham sessions, hypertonic or isotonic saline (5% or 0.9% sodium chloride, respectively) were infused into the right infrapatellar fat pad (infusion rate =  $0.3 \text{ ml}\cdot\text{min}^{-1}$ ) via a 20-gage flexible catheter. During these infusions, subjects performed the treatment running trials (for the pain and sham sessions). The catheter was then removed and subjects performed the post-treatment running trials. For all sessions, subject-perceived pain was evaluated every two minutes using a 10-cm visual analog scale. Motion data for all running trials were collected using six digital video cameras (100 Hz). Coordinate data were tracked using VICON Nexus and exported into Visual 3D, where data were smoothed and used to calculate three-dimensional hip, knee, and ankle angles. Three-dimensional joint angles throughout stance were calculated, exported to MATLAB, and the dependent variables were then determined using custom algorithms.

Two-factor repeated measures ANOVAs were used to evaluate the influence of the two independent variables (condition: control, sham, and pain; and time: pretreatment, treatment, and post-treatment) on nine kinematic variables (Table 1) and subject-perceived pain. Tukeys *post hoc* comparisons were used to determine the nature of any detected condition  $\times$  time interactions. All significance levels were set to 0.05.

## RESULTS AND DISCUSSION

Condition  $\times$  time interactions were detected for two kinematic variables: peak hip adduction ( $p = 0.014$ ) and peak plantarflexion ( $p = 0.026$ ) angle (Table 1). For the pain condition only, peak hip adduction angle was 14% less for treatment trials than for pretreatment trials (Effect Size = -0.52) and 12% less for post-treatment trials (Effect Size = -0.37). Similarly, for the pain condition only, peak plantarflexion angle was 10% less for treatment

trials than for pretreatment trials (Effect Size = -0.59) and 11% less than for post-treatment trials (Effect Size = -0.52). Additionally, as was expected, a condition  $\times$  time interaction existed for subject-perceived pain ( $p < 0.001$ ). For the pain condition only, subject-perceived pain was significantly greater for treatment trials ( $4.2 \pm 1.9$  cm) than for pretreatment ( $0.0 \pm 0.0$  cm) and post-treatment ( $0.3 \pm 0.3$  cm) trials.

The results confirmed our hypothesis and demonstrated that experimental knee joint pain independently influences certain running kinematics (hip adduction and plantarflexion angles). The observed decrease for hip adduction fits with a previous report of decreased hip adduction for runners with patellofemoral pain [2]. Like runners with patellofemoral pain, our subjects may have rotated the trunk in the direction of the involved leg (reducing hip adduction angle) in an attempt to decrease pain and gluteus medius requirements during stance. Although the idea that patellofemoral pain results from gluteus medius weakness is commonly accepted, perhaps it is patellofemoral pain, due to other factors, that may partially cause gluteus medius weakness via some sort of arthrogenic muscle inhibition. The reduced plantarflexion angle, due to experimental knee joint pain, could be related to an attempted reduction of tibiofemoral joint reaction forces; the gastrocnemius is the largest contributor to tibiofemoral reaction forces during late stance [3].

As this approach to studying independent effects of knee pain is novel, some issues remain unclear. We are unsure how closely pain experienced by our subjects resembles clinical knee pain. However, scientists who have studied the physiological characteristics of experimental knee pain, due to hypertonic saline, have reported pain characteristics that are similar to clinical musculoskeletal pain.

## CONCLUSIONS

Knee pathology and corresponding joint pain are significant problems, yet the independent effects of knee pain on movement mechanics are unclear. The major findings of this study are that peak hip adduction and peak plantarflexion angle during the stance phase of running are significantly reduced as a result of experimental knee joint pain.

## REFERENCES

1. Murphy L, et al. *Arthritis Rheum* **59**, 1207-1213, 2008.
2. Henriksen HM, et al. *Arthritis Care Res* **62**, 501-509, 2010.
3. Dierks TA, et al. *J Orthop Sports Phys Ther* **38**, 448-456, 2008.
4. Sasaki K, et al. *J Biomech* **43**, 2780-2784, 2010.

## ACKNOWLEDGEMENTS

We acknowledge the Brigham Young University Gerontology Program for funding this study.

**Table 1:** Means and standard deviations for control, sham, and pain conditions. Condition  $\times$  time interactions were not detected for control or sham conditions, so values were averaged across time (pretreatment, treatment, and post-treatment). Asterisks indicate a condition  $\times$  time interaction and between-time difference for the pain condition.

|                                | Control         | Sham            | Pain            |                 |                 |
|--------------------------------|-----------------|-----------------|-----------------|-----------------|-----------------|
|                                |                 |                 | Pretreatment    | Treatment       | Post-treatment  |
| Peak Hip Extension Angle       | -14.3 $\pm$ 5.8 | -16.1 $\pm$ 3.7 | -16.7 $\pm$ 3.7 | -15.9 $\pm$ 5.3 | -18.2 $\pm$ 4.6 |
| Peak Hip Flexion Angle         | 31.5 $\pm$ 4.1  | 29.2 $\pm$ 4.0  | 29.3 $\pm$ 3.6  | 27.8 $\pm$ 4.2  | 27.5 $\pm$ 4.8  |
| Peak Hip Adduction Angle*      | 12.7 $\pm$ 4.5  | 12.3 $\pm$ 5.1  | 14.3 $\pm$ 3.3  | 12.3 $\pm$ 4.4  | 13.9 $\pm$ 4.2  |
| Heel Strike Knee Flexion Angle | 8.9 $\pm$ 7.0   | 8.1 $\pm$ 5.4   | 8.6 $\pm$ 5.9   | 8.7 $\pm$ 6.9   | 8.5 $\pm$ 7.5   |
| Peak Knee Flexion Angle        | 41.0 $\pm$ 4.4  | 39.4 $\pm$ 3.8  | 38.2 $\pm$ 4.4  | 37.4 $\pm$ 5.3  | 38.5 $\pm$ 5.2  |
| Peak Knee Adduction Angle      | 0.9 $\pm$ 1.9   | 0.8 $\pm$ 3.9   | 1.1 $\pm$ 2.2   | 1.8 $\pm$ 2.7   | 2.0 $\pm$ 2.8   |
| Peak Dorsiflexion Angle        | -13.8 $\pm$ 2.9 | -14.4 $\pm$ 2.9 | -14.3 $\pm$ 3.6 | -13.3 $\pm$ 4.0 | -14.7 $\pm$ 5.2 |
| Peak Plantarflexion Angle*     | 35.8 $\pm$ 6.4  | 34.9 $\pm$ 5.6  | 35.9 $\pm$ 4.8  | 32.3 $\pm$ 7.5  | 36.1 $\pm$ 7.0  |
| Stance Time                    | 0.35 $\pm$ 0.06 | 0.38 $\pm$ 0.05 | 0.38 $\pm$ 0.06 | 0.38 $\pm$ 0.05 | 0.39 $\pm$ 0.05 |

# QUANTITATIVE EVALUATION OF ROTATIONAL KNEE JOINT STABILITY USING A MECHANICAL ‘PIVOT SHIFT’ DEVICE

<sup>1</sup>Mark Sena, <sup>2</sup>Dezba Coughlin, <sup>2</sup>Jeffrey Lotz and <sup>2</sup>Brian Feeley

<sup>1</sup>UC Berkeley - UCSF Graduate Program in Bioengineering, San Francisco, CA, USA

<sup>2</sup>University California San Francisco, San Francisco, CA, USA

email: [feeleyb@orthosurg.ucsf.edu](mailto:feeleyb@orthosurg.ucsf.edu)

## INTRODUCTION

Anterior cruciate ligament (ACL) injury is a common occurrence in many sports, with up to 135,000 ACL injuries leading to over 95,000 reconstructions per year in the United States<sup>1</sup>. The ACL is a two-bundle ligament that stabilizes against anterior displacement (AD) and internal rotation (IR) of the tibia. Currently, the manual ‘pivot shift’ test is the most specific knee stability examination for diagnosis of ACL injuries<sup>2</sup>. It is performed by applying internal and valgus torque along with an axial load to the joint. A positive ‘pivot’ (consisting of tibial AD and IR followed by a rapid reduction, or ‘clunk’) is a strong predictor of osteoarthritis risk, patient-reported instability, and poor long-term patient outcome<sup>3, 4</sup>. Unfortunately, the test is semi-quantitative and difficult to perform reproducibly.

We have developed a novel device that mimics the clinical pivot shift test through the application of standardized dynamic loads by a constant-tension spring. It reliably induces the characteristic ‘pivot’ event in an ACL-deficient knee. In this work, we compare the 3D rotational and translational kinematics of tibiofemoral motion during manual and mechanized pivot shift tests for both intact and ACL-deficient knees. We hypothesized that the mechanical pivot shift device (MPSD) allows for more sensitive detection of deficiencies in rotational knee stability in comparison to a manual test.

## METHODS

Fresh-frozen full lower limb specimens (n=2) were sectioned, potted, and mounted on a hinged testing base. To replicate iliotibial (IT) band tension, a 4.5 kg weight was suspended from cord sutured to the isolated IT band. Kinematic trajectories were recorded using the Optotrak® navigation system

(<1° and <1mm resolution). Coordinate frames for the femur and tibia rigid bodies were defined using anatomical landmarks. Carbon fiber rods were attached separately to the lateral side of the tibia and femur using a surgical external fixation system. Finally, a constant-tension (48N) spring was attached between the rods. For each mechanized test the examiner gently supported the distal tibia from underneath, raised it, and then lowered it into flexion. Throughout knee flexion the MPSD applies the axial load and internal/valgus torque needed to replicate a manual pivot shift test.

For each specimen, manual and mechanized pivot shift tests (with and without IT tension) were performed in triplicate by an experienced knee surgeon. Manual and MPSD tests were performed in intact, followed by ACL-deficient knee states. For each test, knee joint configuration was recorded using the Optotrak system and represented in MATLAB (as a function of flexion angle  $\theta$ ) by a set of tibial translations  $T(\theta)=[T_x, T_y, T_z]$  and rotations  $R(\theta)=[R_\psi, R_\phi]$  of the tibia relative to a full-extension reference configuration. Maximum internal tibial rotation ( $IR_{max}$ ), maximum anterior displacement ( $AD_{max}$ ), and posterior tibial velocity (PTV) were employed as joint stability metrics.

## RESULTS AND DISCUSSION

The MPSD was successful in mimicking the IR, AD, and PTV trajectories of a manual pivot shift maneuver performed by an experienced clinician (Fig. 1). In ACL-deficient knees, the tibia first became subluxed (AD and IR) at a knee flexion angle of  $17\pm 1^\circ$ . At an angle of  $35\pm 2^\circ$  the tibia was then rapidly reduced, exhibiting peak posterior tibial (PTV) near 70 mm/s. Intact knees became only slightly subluxed, and did not exhibit rapid tibial reduction. Although IT tension was needed to

generate a positive pivot in ACL-deficient knees using the manual tests, such tension was not a requirement when using the MPSD.

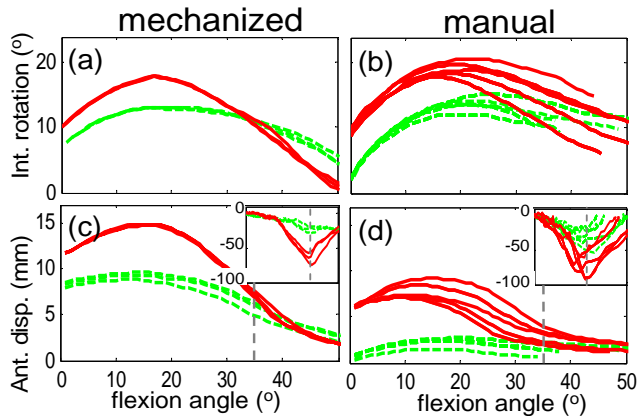


**Figure 1:** Intact (---) and ACL deficient (—) pivot shift trajectories for the MPSD (n=3, left) and manual test (n=5, right) for a single knee. IR (top), AD (bottom), and PTV (inset), versus knee flexion angle. A clanking ‘pivot’ occurred at ~35° (:).

Both the manual and MPSD tests demonstrated increased  $IR_{max}$ ,  $AD_{max}$ , and PTV following ACL transection (Fig. 2), however the coefficient of variation ( $c_v = \sigma/\mu$ ) was significantly less for the MPSD metrics (mean  $c_v = 0.028$ ) in comparison to the manual metrics (mean  $c_v = 0.16$ ). When comparing matched right and left knees using the device,  $IR_{max}$  and  $AD_{max}$  differed by less than 1.5° and 2 mm in either the intact or ACL-deficient state. These results demonstrate the capacity of the MPSD to produce a realistic pivot shift in an unstable knee with a high degree of reproducibility.

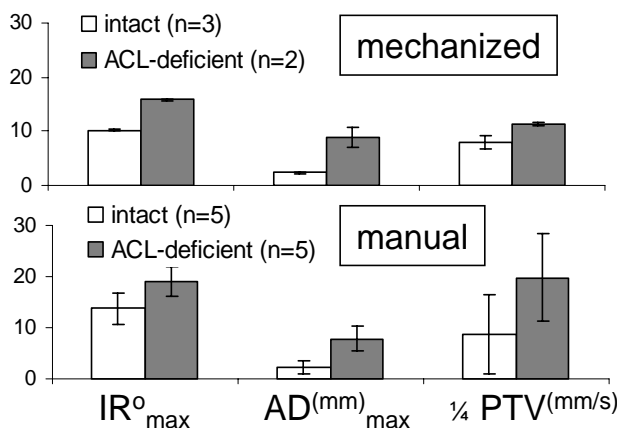


**Figure 2:**  $IR_{max}$ ,  $AD_{max}$ , and PTV values from MPSD tests (top), and manual maneuvers (bottom), for both intact (□) and ACL-deficient (■) knees. Error bars represent 99% confidence intervals.

Logistic regression procedures (JMP; version 7.0) were used to relate the categorical knee state (intact or ACL deficient) to continuous measurements ( $IR_{max}$ ,  $AD_{max}$ , PTV; n=5 tests each from 2 knees) made during the mechanical pivot shift test. Univariate analysis demonstrated that  $IR_{max}$  was the most predictive of ACL condition and explained 40% of the variance ( $R^2 = 0.41$ ,  $p = 0.0001$ ). The knee state was predicted with complete accuracy when the logistic regression included two variables,  $IR_{max}$  and PTV ( $R^2 = 1$ ,  $p = 0.0001$ ). These data suggest that measurements made using the MPSD are sensitive to ACL condition and provide valuable clinical information.

## CONCLUSIONS

The purpose of this study was to evaluate a novel mechanized pivot shift apparatus and analysis system for quantitative assessment of rotational knee stability under controlled laboratory conditions. The testing apparatus facilitated reproducible application of dynamic forces and moments to the knee during a simulated pivot shift, while the data-acquisition system recorded 3D tibio-femoral motion. Our results support the hypothesis that the MPSD allows for more sensitive detection of deficiencies in rotational knee stability in comparison to the manual test.

Development of a standardized rotational knee stability evaluation will be vital in determining the consequences of graded soft tissue defects of the knee joint, or the effects of different ACL reconstruction techniques, on rotational stability. Diagnostic kinematic signatures specific to certain injuries will enhance our current understanding of knee biomechanics, and may ultimately help improve clinical outcomes through in vitro optimization of surgical techniques.

## REFERENCES

- Steiner, M. E., *Sports Med Arthrosc* 2009, 17 (4), 247-251.
- Prins, M., *Aust J Physiother* 2006, 52 (1), 66.
- Shelbourne, K. D.; Benner, R. W., *J Knee Surg* 2009, 22 (3), 187-90.
- Leitze, Z.; Losee, R. E.; Jokl, P.; Johnson, T. R.; Feagin, J. A., *Clin Orthop Relat Res* 2005, (436), 229-36.

# IMPACT FORCES WHEN STEPPING OFF MOVING RAILROAD EQUIPMENT

Elaine R. Serina, Ph.D., and Kirsten White

Talas Engineering, Inc.  
email: [eserina@talasinc.com](mailto:eserina@talasinc.com), web: [www.talasinc.com](http://www.talasinc.com)

## INTRODUCTION

Getting on and off moving railcars and locomotives is a practice that has been used throughout the railroad industry. Employees ride on moving equipment for transport during their job duties, and dismount at speeds less than 10 mph. The technique begins with the individual on the side of the equipment, facing it, with both feet on the lowest step and both hands holding the ladder. The trailing foot is lowered, and that leg is angled towards the direction of travel. The individual then steps down to the ground and releases his hands and leading foot. Upon landing, the body is upright and the individual continues his gait generally in the direction of travel.

Cumulative trauma injuries have been claimed by railroad employees as a result of this practice. To date, no published studies have investigated the forces on the body from getting off moving equipment or vehicles. The purpose of this study is to characterize the movement of, and forces on the body, when stepping down off a moving railcar and locomotive, and draw comparisons to the forces on the body when performing various other activities.

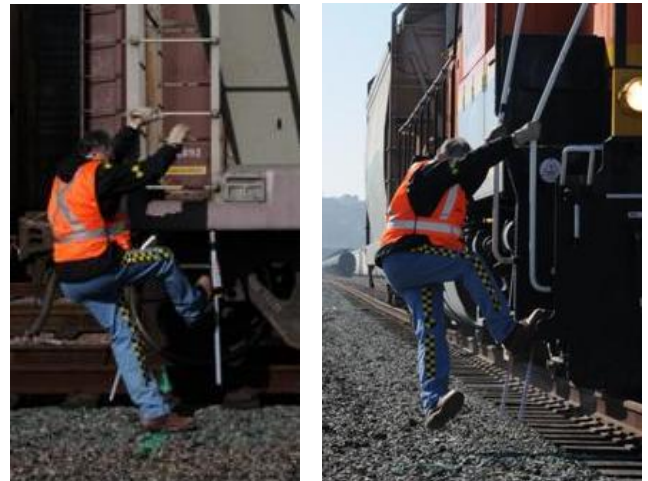
## METHODS

A series of 22 dynamic tests were conducted at speeds ranging from 1 to 10 mph. A 1965 GP39-3 locomotive engine (2300 hp) was coupled to a railcar (hopper). Tests were conducted in a railroad yard in an area where the ground was level, and the walking surface was composed of small gravel and rocks (known as yard ballast).

During each test a male subject (6', 195 lb) familiar with the technique for getting off moving equipment rode on the equipment and stepped down at the designated location. In 16 tests he stepped off from the bottom step of the ladder on the side of the

railcar, a distance of 26½ inches (Fig. 1). In 6 tests he stepped off from the bottom step of the locomotive front stairs, a distance of 26 inches (Fig. 2). The subject also stepped off stationary equipment 6 times and performed many daily activities.

A tri-axial accelerometer (Measurement Specialties) was mounted with double-sided body tape and medical tape to the subject's lower back, at the height of the umbilicus. Acceleration data was recorded at 10,000 Hz (GMH Engineering DataBRICK) and low-pass filtered in post processing with a cutoff of 30 Hz. Overall body motion and railcar speed were captured with two video cameras (30 fps) and one high speed camera (120-240 fps).



**Figures 1, 2:** Stepping down from railcar ladder (side view) and locomotive steps (front view).  
Direction of travel is to the subject's right.

## RESULTS AND DISCUSSION

Acceleration data was reduced to vertical and horizontal components, and the resultant was calculated (Fig. 3). Results were similar for the railcar and locomotive tests so the data was combined for analysis. It was noted that the highest peak accelerations often did not occur with the landing step.

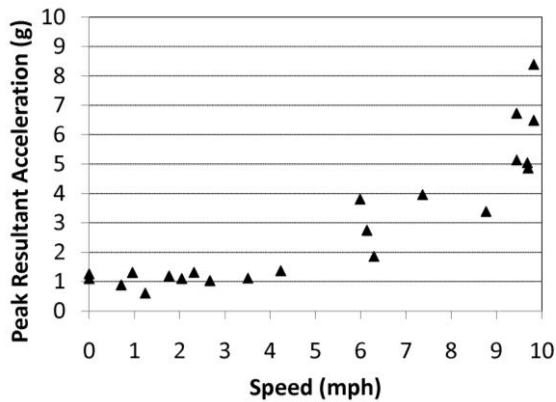


**Figure 3:** Peak resultant acceleration by speed.

Cadence was calculated for each test, and was compared to walking (1.7 steps/s) and jogging (2.4 steps/s). After dismounting the equipment, the subject took a number of steps before reaching a steady state walking cadence (Fig. 4).

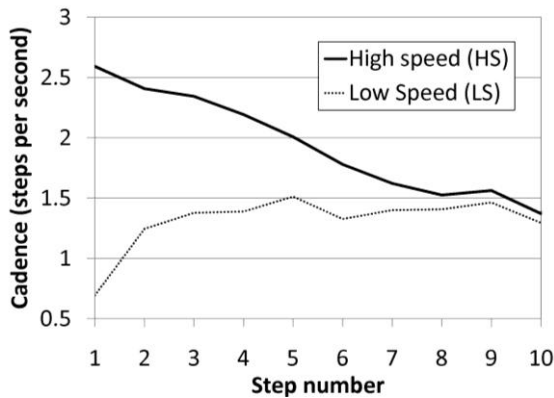


**Figure 4:** Cadence step by step for representative HS and LS tests.

Body forces and technique were influenced by equipment speed. The results fell into two groups: equipment speeds less than 5 mph (lower speeds=LS) and greater than 5 mph (higher speeds=HS). In the LS group, the subject increased his cadence in less than 4 steps to reach a steady state walking cadence. Peak accelerations were relatively constant with equipment speed, and were comparable to stepping off stationary equipment. In the HS group, peak accelerations increased with speed. The subject's cadence was initially greater than jogging then slowed to steady state walking in more steps than in the LS tests. At the higher speeds the subject aligned his trailing foot parallel to the direction of travel and had increased dorsiflexion in preparation for the initial ground contact. In all but one test the leading foot remained on the equipment until after the trailing foot had touched the ground.

Vertical body forces were examined as research has determined that compression is a significant load experienced by the intervertebral disc [1]. In the LS group, peak vertical accelerations ranged from 0.6 to 1.3 g and often occurred after steady state cadence was reached. In the HS group, the peak vertical acceleration occurred within the first four steps in each test, and ranged from 1.6 to 7.7 g. We hypothesize that the peak vertical forces in the HS tests were due to decelerating the body to a walking speed, rather than to the initial landing. These forces are not excessive.

The body forces measured when stepping off moving equipment were comparable to those during the daily activities tested. Not surprisingly, the LS peak resultant accelerations were similar to those while walking on asphalt (1.6 g) or ballast (1.7 g), since they often occurred once steady state walking was reached. The HS peak resultant accelerations were comparable to those during jumping forward (8.3 g), vertical jumping (6.6 g), jogging on asphalt (5.8 g), and jumping jacks (4.4 g). Peak vertical forces were comparable to those measured when exiting commercial tractors, trailers, and trucks [2].

This study demonstrated the effective use of a body-mounted tri-axial accelerometer to characterize this dynamic event. While force plates have been used in studies of dismounting vehicles, they cannot capture the steps that occur after the initial landing.

## CONCLUSIONS

The forces on the body when stepping off moving railroad equipment are not excessive and are comparable to those during daily activities and exiting commercial vehicles. At railroad equipment speeds of 0 to 5 mph, the peak accelerations on the body are similar to normal walking. At 5 to 10 mph, the peak accelerations increase with speed. These findings may be useful to future studies of stepping off moving vehicles and stepping onto moving platforms.

## REFERENCES

1. Adams MA and Dolan P *Clin Biomech* **10**, 03-19, 1995.
2. Fathallah FA and Cotnam JP *Appl Ergo* **31**, 25-33, 2000.

# POSTURAL TRAINING IN A NON-THREATENING ENVIRONMENT RESULTS IN LIMITED TRANSFER DURING INDUCED POSTURAL ANXIETY

K. David Sessford, Jon Doan, Daniel Weeks and Lesley Brown,

University of Lethbridge, Lethbridge, AB, Canada  
email: [david.sessford@uleth.ca](mailto:david.sessford@uleth.ca) web: <http://people.uleth.ca/~l.brown>

## INTRODUCTION

Falling among the elderly is a problem that results in injury, loss of independence, premature death, and affects over 3.7 million North Americans annually [1]. Rehabilitation and reintegration efforts from falling episodes lead to significant economic consequences [1]. Although the causes of falls are multifaceted, falls most commonly occur in response to unpredictable challenges and environmental contexts. In an effort to manage the risk, frequency, and consequences of fall episodes, clinicians have integrated pre-emptive training into therapeutic interventions in developing strategies for balance remediation and improvement [2]. Recent research has demonstrated that both the young and the elderly maintain a capacity for practice-related improvements in postural control during unpredictable balance challenges [3]. Fear and anxiety however, are known to interfere with practice effects [4], an outcome that may compromise the efficacy of any training effort dedicated to improving the strategies of postural adaptation. To test this possibility, this study investigated whether the capacity to use an acquired adaptation strategy to preserve postural control is influenced by the presence of anxiety. To impose anxiety we introduced an increased possibility of experiencing a fall episode within the training environment.

## METHODS

Twenty younger adults ( $22.0 \pm 2.7$  yrs; 13 females) participated in a dynamic, unpredictable postural learning task, defined by Acquisition (day one), and Retention and Transfer assessments (day two). Participants stood on a platform that translated to a maximum amplitude of  $\pm 8$  cm at 0.5 Hz in a sinusoidal fashion of a seemingly random pattern for 45 s. The first and last 15 s of each trial consisted

of random amplitudes, but the amplitudes of the translations during the middle 15 s were identical between each trial (Fig. 1). Participants were not informed and did not indicate any awareness of this between trial repetition. Training consisted of 36 trials administered in six blocks of six trials with a three minute break between blocks (day one). Three Retention and three Transfer assessments using the same trial structure were administered on day 2.

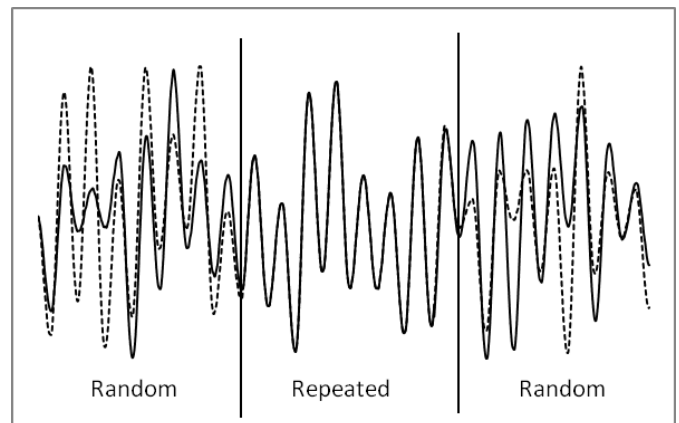


**Figure 1:** Overlaid sinusoidal translations of two example trials (solid & dashed). The middle 15 s segment is identical for each trial, while the first and last segments are random.

Participants were divided into two groups differentiated by training environment. Group one trained in non-threatening conditions while the second group trained in a balance threatening environment. Threat to balance was induced by performance of the task whilst standing with each foot on a wooden pedestal (41 cm long x 13 cm wide x 10 cm high). The starting condition of threat on day two was counterbalanced within each group.

Anxiety was inferred by physiological arousal and measured by the change in Galvanic Skin Conductance (GSC) between the non-threatening and threatening conditions. Learning was assessed by the change in performance scores between the first Acquisition trial and the first Retention trial.

The capacity to use an acquired adaptation strategy was assessed by differences in postural control between Retention and Transfer assessments. Performance was determined by the dampening of the movement of the center of mass (COM) in space [5] during the 15s repeated segment during each trial. Performance was calculated from the 95% probability ellipse that encompassed the excursions of the COM in the horizontal plane.

Anxiety and performance differences between groups in the Acquisition, Retention and Transfer phases were ascertained independently through mixed design ANOVAs with post-hoc follow up of paired t-tests. Alpha was set at 0.05.

## RESULTS AND DISCUSSION

A three way interaction (condition x group x trial) was observed ( $p = 0.05$ ) for anxiety, indicating that training differentially affected the anxious response in differing environmental contexts. Post hoc follow up suggested that this difference was driven by the response in the first balance threatening trial, where subjects who trained in a non-threatening environment exhibited higher anxiety ( $p = 0.05$ ; Fig. 2).

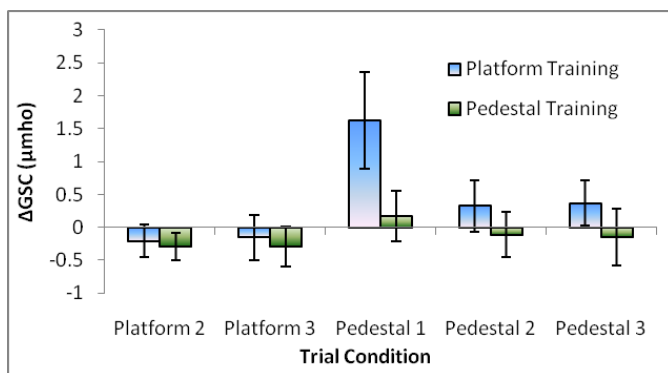


**Figure 2:** Change in GSC between platform and pedestal trained groups on day two using the first platform trial as a baseline.

Learning was the same regardless of training environment (trial x group;  $p = 0.67$ ), and both groups exhibited improved postural performance scores between the first Acquisition trial and the first Retention trial ( $p = 0.011$ ). Analysis of the ability to use acquired postural strategies within an anxious environment was limited to the first trials of the Retention and Transfer assessments, as subjects exhibited the greatest anxious responses in these trials. Different training environments resulted in

different postural performance scores (condition x group;  $p = 0.033$ ), whereby those who trained in a threatening environment showed no difference in postural performance between the Retention and Transfer assessments. Post-hoc follow up however, revealed that subjects who trained in a non-threatening environment exhibited less dampening when on the pedestal than on the platform ( $p = 0.05$ ; Fig. 3). This finding may suggest that transfer of acquired protective adaptation for controlling balance was limited in an anxious environment.

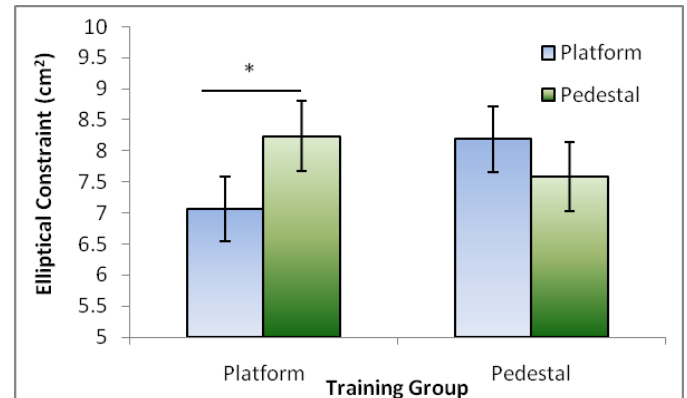


**Figure 3:** Dampening of the COM during repeated, dynamic perturbations for. Lower indicates better performance.

## CONCLUSIONS

Anxiety influenced the ability to use an acquired postural adaptation. Subjects without prior training within a balance threatening environment exhibited a reduced ability to stabilize the COM when anxious. This outcome suggests that acquired balance strategies may be less accessible when anxiety is present. Our findings carry implication toward the consideration of the emotional responses to environmental and situational contexts in the design of balance remediation protocols.

## REFERENCES

1. Shumway-Cook A, et al. *Phys Ther* **89**, 324-332, 2009.
2. Nagy EA, et al. *Eur J Appl Physiol* **100**, 97-104, 2007.
3. Van Ooteghem K, et al. *Exp Brain Res* **199**, 185-193, 2009.
4. Oudejans RRD, et al. *Q J Exp Psychol* **62**, 1631-1647, 2009.
5. Buchanan JJ, et al. *J Neurophysiol* **81**, 2325-2339, 1999.

# ANKLE AND KNEE MUSCLE CO-CONTRACTION DIFFERENCES IN TRANS-TIBIAL AMPUTEE RESIDUAL AND INTACT LIMBS AND MATCHED CONTROLS DURING GAIT

<sup>1,2</sup>Mahyo Seyedali, <sup>1,3</sup>David Morgenroth, <sup>1,3</sup>Joseph Czerniecki, and <sup>1,2</sup>Michael Hahn

<sup>1</sup>RR&D Center of Excellence, Department of Veterans Affairs; Departments of <sup>2</sup>Mechanical Engineering and <sup>3</sup>Rehabilitation Medicine, University of Washington, Seattle, WA, USA  
email: [mehahn@u.washington.edu](mailto:mehahn@u.washington.edu) web: <http://www.amputation.research.va.gov/>

## INTRODUCTION

Myoelectric control of upper extremity powered prostheses have been used clinically for many years, however this approach has not been fully developed for lower extremity prosthetic devices. A variety of external mode control switches have been developed for commercially available lower extremity powered prostheses. More recent innovations have utilized voluntary activation of residual muscles to switch modes of a novel prosthetic foot/ankle between level-ground and stair descent ambulation [1]. Although not a continuous control, it provides evidence that residual limb myosignal can be used as a control input. Proximal lower extremity muscle activation has been shown to be effective in estimation of gait phase [2] which provides further evidence of the utility of a myoelectric controller. However a recent study has reported unique knee muscle co-contraction patterns in trans-tibial amputees [3]. Further, initial findings indicate that co-contraction of residual ankle muscles may be greater during specific phases of gait [4]. Differences in co-contraction between the residual and intact limbs of trans-tibial amputees and those of controls, and the effect of walking speed on co-contraction needs to be analyzed to account for any confounding effects that co-contraction may have on myoelectric control.

The purpose of this study was to analyze activation and co-contraction patterns of two ankle muscles, Tibialis Anterior (TA) and Medial Gastrocnemius (MG), and two knee muscles, Vastus Lateralis (VL) and Biceps Femoris (BF) during three speeds of gait. It was hypothesized that residual limbs would have greater ankle co-contraction than intact and control limbs. It was also hypothesized knee co-contraction would be different among all limbs. Lastly it was hypothesized that co-contraction would be affected by walking speed.

## METHODS

Fourteen individuals participated in this study, nine of which were unilateral transtibial amputees and five were matched control subjects (pooled sample:  $52 \pm 13$  years;  $1.82 \pm 0.54$  m;  $86.7 \pm 12$  kg). The protocol was approved by the Institutional Review Board. Written informed consent was obtained prior to participation. Surface electromyography (EMG) was used to record muscle activation at 1200Hz. Signals from the TA, MG, VL and BF for the prosthetic, intact and controls limbs were recorded using disposable wet-gel neonatal passive electrodes in a bi-polar single differential configuration. Foot marker trajectories in combination with ground reaction forces were used to determine gait cycle events. All subjects walked on their prescribed prosthetic components. Five trials were collected at three different speeds; self-selected walking speed (SSWS), 10% slower than SSWS, and 10% faster than SSWS.

Initial signal processing involved a band-pass filter (10-500Hz), a high pass filter (cutoff at 50Hz) to remove motion artifact, and a notch filter to remove power line noise from the signal. The signal was then full-wave rectified, and low-pass filtered to result in a linear envelope, from which all subsequent calculations were made. Muscle activations were normalized to each subject's maximum magnitude during their fast walking trials. Signals were also time normalized to gait cycle. Co-contraction area (CCA) during various phases of gait was quantified as the ratio between integrated antagonist signal and integrated agonist signal. Tables 1 and 2 list agonist and antagonist designations for each phase of gait analyzed. Agonist was defined as the muscle group that is most active in controlling the function required during a particular phase. A two-factor ANOVA was used to test each hypothesis.



# OPTIMAL CONTROL AND FORWARD DYNAMICS OF PERIODIC FOREARM MOTIONS USING FOURIER SERIES FOR MUSCLE EXCITATIONS

Mohammad Sharif Shourijeh, John J. McPhee, and Nasser L. Azad

Systems Design Engineering Department, University of Waterloo, Waterloo, ON, Canada  
email: [msharifs@uwaterloo.ca](mailto:msharifs@uwaterloo.ca) web: <http://real.uwaterloo.ca/people/msharifs.htm>

## INTRODUCTION

Dynamic musculoskeletal models are well-established tools to simulate, predict, and analyze human movements. Furthermore, although forward dynamics studies are slow and time consuming due to forward integrations, they are preferred over inverse dynamics models due to being predictive. A forward dynamics musculoskeletal simulation often involves solving an optimal control problem (OCP). In this paper, a model for the forward dynamic simulation of a forearm performing a periodic motion is presented. Using a new parameterization function based on Fourier series for the muscle excitation patterns, the OCP is converted to an optimization problem, which is solved for the optimal motion and muscle excitations.

## METHODS

The presented skeletal model consists of forearm and hand while the wrist angle is assumed to be constant. Thus the only degree of freedom (DOF) is due to the elbow revolute joint. Four muscles are considered in the model: Brachioradialis (BRD), Brachialis (BRA), Biceps (BIC), and Triceps (TRI). Muscle models are of the three-element Hill type. All muscle activation and contraction dynamic equations and parameters are according to [1]. Additionally, muscle moment arms are based on the model presented by [2].

The model is supposed to move from a rest position where the elbow angle is zero,  $\theta(0)=0$  and  $\dot{\theta}(0)=0$ . The upper arm is kept fixed vertically beside the body during the forearm motion.

The model is indeterminate since the number of muscle actuators is greater than the DOF of the dynamic system. Therefore to reach a unique solution, the system dynamics are forced to satisfy an extra criterion, an objective function within an

optimization procedure. The platform for such simulations would be the following OCP:

$$\min J = \sum_{j=1}^4 \int_0^T a_j^2 dt \quad (1)$$

with the system dynamics  $\dot{x}(t) = f(x(t), u(t), t)$  and subject to imposed nonlinear (NL) constraints. In equation 1, the objective functional  $J$  is a time-integral of a quadratic function of activation states,  $a$ , in which index  $j$  refers to the muscle number.  $x$  is the state vector and the control signal  $u$  is the muscle excitation. The principal constraints are those on muscle excitations as follows:

$$0 \leq u_j \leq 1$$

Furthermore, two additional restrictions are imposed on the system motion as follows:

$$\theta(T/2) = \theta_{\max} \text{ and } 0 \leq \theta \leq \theta_{\max}$$

where  $\theta$  is the elbow flexion angle and  $T$  is the motion period that is assumed to be 2 seconds. The last constraint on motion assures elbow angle not to hyperextend and not to go beyond an upper bound. Also, the forearm would be fully flexed at the middle of the motion interval.  $\theta_{\max}$  is assumed to be  $2\pi/3$  which is approximately how far an elbow can flex [2]. In addition,  $\theta(T) = 0$  and  $\dot{\theta}(T) = 0$  are added as constraints to guarantee the periodicity of the motion.

To solve this OCP, it can be converted to a NL optimization problem by using parametric pattern functions as the control inputs, the neural excitations [4]. Fourier series (FS) terms are chosen here to approximate the excitation signals where these functions consist of the first  $K$  terms of a FS as follows:

$$u_j(t) = A_0 + \sum_{k=1}^K [A_k \sin(\frac{2\pi kt}{T}) + B_k \cos(\frac{2\pi kt}{T})] \quad (2)$$

where  $K$  is assumed to be 5 according to [3]. As a result, excitation signals would be periodic that

would give the required periodic motion. The optimization algorithm seeks the optimal set of coefficients for excitation parameterized functions to minimize the objective functional and satisfy the constraints mentioned above. At each iteration of optimization, after forming the excitation functions, system dynamics is integrated to find the relevant state vector of that iteration. Given the initial angle and angular velocity of forearm, the system dynamics is a set of initial value problems rather than the general case in OCPs where two-point boundary value problems are involved.

The resulting NL optimization problem is solved using the *Sequential Quadratic Programming* algorithm implemented in *fmincon* function in MATLAB®.

## RESULTS AND DISCUSSION

Results of this simulation are presented in Fig. 1, for the optimal motion and muscle excitations of the forearm model. As depicted, the motion is periodic and has satisfied the additional imposed constraints on the motion. The motion has started from the rest position when elbow is fully extended ( $\theta = 0$ ), touched the maximum flexion ( $\theta = 120^\circ$ ) and returned to the initial position.

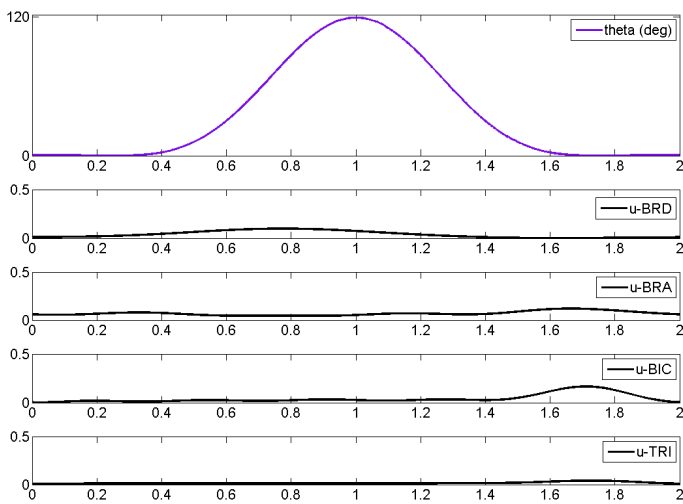


**Figure 1:** Results of forearm motion followed by excitations of BRD, BRA, BIC, and TRI muscles, respectively.

The excitation results have satisfied the corresponding necessary constraints and also are periodic due to the assumed parametric pattern. As shown, the only extensor muscle (TRI) is rarely active during the course of motion which can be

justified due to gravity. In contrast, all three flexor muscles are more active, which can be explained by the need to drive the forearm against gravitational force. The small values of muscle excitations can be related to the fact that the forearm performed the motion freely, i.e. in absence of any external load other than its weight. At the end of the period, a small amount of co-contraction is observed; although it apparently increases the objective function value, it is required to satisfy the dynamic constraints of the system.

A convergence study was performed by running the optimization problem using several different initial guesses to confirm the globality of the results.

A separate study was also done by increasing  $K$  to 6 to investigate the corresponding effects on the values of cost function and system dynamics. Using  $K=6$  made no significant change in the results, but increased the simulation time considerably.

## CONCLUSIONS

Optimal control problems can be converted to NL optimization problems using parametric pattern functions for the control signals. Choosing a suitable pattern function depends on the conditions of the problem, such as periodicity. FS-based functions are smooth and periodic which can approximate the neural excitations in periodic movements. The number of FS terms utilized for each control input can be debatable and definitely depends on the type of movement and might be determined by having tentative before-hand information about the corresponding excitation signals.

## REFERENCES

1. Thelen DG, et al. *ASME J Biomechanical Engineering* **125**, 70-77, 2003
2. Murray WM, et al. *J Biomechanics* **28-5**, 513-525, 1995
3. Peasgood M, et al. *ASME J Computational and Nonlinear Dynamics*, **2**, 65-72, 2007
4. Sharif Shourijeh M, et al. *Canadian Society of Biomechanics Conference*, Kingston, ON, Canada 2010

## ACKNOWLEDGEMENTS

The authors wish to acknowledge NSERC for funding support of this study.

# LOSS OF VASTI MEDIALIS FUNCTION ALTERS IN VIVO KNEE JOINT KINEMATICS: IMPLICATIONS FOR PATELLOFEMORAL PAIN SYNDROME

Frances T. Sheehan, Abrahm J. Behnam, Bhushan S. Borotikar, and Katharine E. Alter  
Rehabilitation Medicine Department, CC, NIH, Bethesda, Maryland, USA email: [fsheehan@cc.nih.gov](mailto:fsheehan@cc.nih.gov)

## INTRODUCTION

Patellofemoral (PF) pain syndrome (PFPS) is one of the most common problems of the knee. A widely accepted theory in regards to the source of PF pain is that a force imbalance around the knee leads to PF static malalignment and dynamic maltracking. In turn, this causes elevated joint contact stresses, which ultimately results in PF pain. The source of this force imbalance is still open to debate with some postulating the cause to be delayed timing or loss of strength in the vasti medialis (VM) or an imbalance in the passive structures [1]. Yet, numerous studies refute these claims as well [2]. Since muscle force cannot be measured directly, without highly invasive techniques, previous studies have relied on electromyography (EMG). Yet, an earlier study demonstrated that in patients with PFPS the assumptions required to estimate muscle force from EMG may not be valid [3]. Thus, the purpose of this study was to determine how a loss of force in the VM alters the dynamic control of 3D *in vivo* PF and tibiofemoral (TF) kinematics during a volitional extension task.

## METHODS

To date, 18 asymptomatic females with no history of knee pain, trauma, surgery, or contraindications to magnetic resonance (MR) imaging have been enrolled in this IRB approved study. During the first visit, subjects provided signed consent, had a clinical knee joint evaluation (Q-angle, laxity, etc), and a history and physical was performed. Next, subjects were placed supine in an MR imager (3.0 T, Philips Medical Systems, Best, NL). For the dynamic scanning, the knee was bent and supported on a cushioned block. A customized coil holder held a pair of flex coils medial and lateral to the knee. The subjects were asked to cyclically flex and extend their knee while a dynamic cine-phase contrast (CPC) MR image set (x,y,z velocity and anatomic images frames) was acquired [4]. Dynamic cine images (anatomic images only) were also acquired, to establish anatomical coordinate

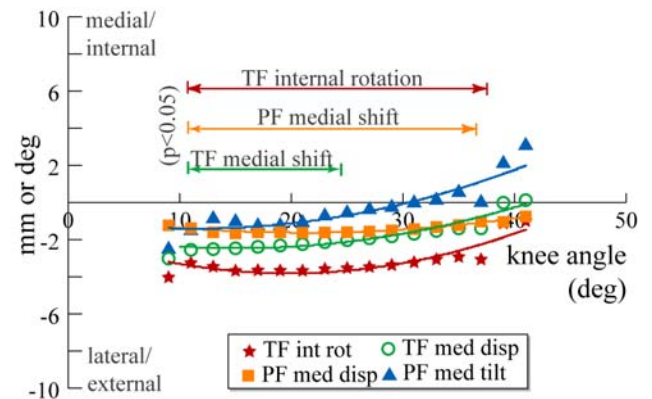


**Figure 2:** Post-injection differences in axial plane kinematics. A 2<sup>nd</sup> order polynomial is fit to the data. For clarity symbols are provided at 2° KA increments. The KA ranges where significant differences were found post-injection are shown using double arrow lines.

systems. With the knee in full extension, high resolution 3D static images were acquired and read by a radiologist. The scanning protocol was saved on the scanner so that the identical dynamic scanning parameters could be used for the second visit. If the data acquired revealed the presence of a valid exclusion criteria, the subject was removed from the study (n=5), if not, the subject was asked to return within a week (n=13, age=28.6±9.8years, height=165.3 ±7.7cm, mass= 58.9±7.3kg).

For the second visit, scanning began immediately after administering a motor branch block to the VM. A single physician performed all nerve blocks. Using ultrasound (US) guidance and electrical stimulation, the femoral nerve motor branch to the VM was localized and then 3 cc of 1% lidocaine was injected. Evaluation of the effectiveness of the block was assessed by absence of visible twitch (visual surface inspection and B mode US) with percutaneous electrical stimulation of the motor nerve. An absence of a twitch response upon stimulation indicated a complete or near complete block of the VM. The absence of VM contraction was also confirmed in a similar manner while the subject performed a maximal isometric quadriceps contraction. If the twitch response was not ablated (n=6),

the procedure was repeated at a second site with up to 2 cc of 1% lidocaine. Immediately following the muscle block, the volunteer was transported to the MR scanner by wheelchair. The coil holder was returned to the same location within the scanner. Using reference marks on both the coil holder and the skin over the subject's knee, the subject was placed in as similar a position as possible to the first exam. All dynamic scanning occurred within 20 minutes of completing the muscle block. Lidocaine has a minimum effective period of 1 hour.

The PF and TF kinematics, both pre- and post-injection (*pre-I* and *post-I*) were quantified through integration of the CPC data. All kinematic data were interpolated to single knee angle (KA) increments. The *pre-I* and *post-I* kinematics were compared using paired Students' t-test. Correlations between the change in kinematics post-injection and the pre-injection kinematics were quantified at the KA of maximum post-injection change in PF medial shift (KA = 15°).

## RESULTS AND DISCUSSION

*Post-I*, the patella shifted lateral (Figure 1, max = 1.7±1.7mm,  $p=0.004$ , KA=15°), whereas the tibia rotated externally (max=3.7°±3.5°,  $p=0.003$  KA=15°) and shifted laterally (max=2.6±2.5mm,  $p=0.04$ , KA=12°). These changes were 4.1-4.7 times greater than the average subject repeatability [4]. An insignificant trend of PF lateral tilt was seen *Post-I*. *Post-I* PF lateral shift was correlated with *pre-I* PF superior displacement ( $r=0.48$ ) and valgus rotation ( $r=0.59$ ). TF external rotation and lateral shift were not correlated with any *pre-I* kinematics, but were correlated with each other ( $r=0.81$ ).

The loss in VM function produced kinematics changes that mirrored the difference in axial plane kinematics seen between patients diagnosed with PFPS and controls [5]. Even though the muscle block likely produced a greater loss in VM strength than that experienced by patients with PFPS, the *Post-I* changes in PF lateral shift was only 59% of the differences between the PFPS and controls cohorts. Yet, the PFPS cohort also demonstrated increased PF superior displacement, flexion, valgus, and TF external rotation. Thus, the loss in VM function cannot explain all the kinematics changes in PFPS cohort and it is most likely that VM weakness is a major factor in, but not the sole source of, PF maltracking.

The kinematic changes seen *post-I* are best related to PFPS, in the context of patient subgroups (e.g., lateral and non-lateral maltrackers [6]). Lateral maltrackers, demonstrate increased PF lateral and superior shift, lateral tilt, flexion, valgus rotation, and TF internal rotation. Results from the current study indicate that the loss of VM function accounts for a portion of this lateral shift and tilt. An increase in ligament laxity would likely increase this shift and rotation, as well as increase the patellar ligament length. An increase in ligament length leads to patella alta, reducing the influence of the femoral groove on PF kinematics; and increasing PF lateral shift, lateral tilt, and valgus rotation. Therefore, a combination of VM weakness and generalized ligament laxity would account for the kinematics variations in the lateral maltracking group, potentially leading to PF pain.

The non-lateral maltrackers demonstrated increased PF flexion and increased TF internal rotation only. As demonstrated previously [7], the higher lateral femoral sulcus combined with a normative PF superior shift in the non-lateral maltrackers prevents lateral PF shift. Thus, in this subgroup, a loss of VM strength would likely be compensated for by increased contact force between the lateral femoral sulcus and the patella, resulting in PF pain.

## CONCLUSIONS

In the current study, a loss of VM function led to increased lateral PF shift and external TF rotation. This supports the fact that the VM exerts a medially directed force on the patella [8] and an internal rotation moment on the tibia via the patellar tendon. Combining these results with past results pertaining to kinematics and bone shape alterations in patients with PFPS supports two paths to PFPS in two kinematically unique subgroups. Future work is required to provide further evidence to the validity of these paths.

## REFERENCES

1. Lin, YF, et al. *Am J Sports Med* **36**,741-6, 2008.
2. Malone T, et al. *C Sport Med* **21**, 349-62, 2002.
3. *Skeletal Muscle Mechanics: From Mechanism to Function*, (ed. Herzog), 2000, p. 343-363.
4. Behnam AJ, et al. *J Biomech* **44**, 193-197, 2011.
5. Sheehan FT, et al. *JOR* **27**, 561-70, 2009.
6. Sheehan FT, et al. *CORR* **468**, 266-75, 2009.
7. Harbaugh CM, et al. *JOR* **28**, 865-72, 2010.
8. Wilson NA, et al. *J Biomech* **43**, 2106-13, 2010.



# DYNAMIC SAGITTAL-PLANE TRUNK CONTROL DURING ACL-INJURY

Frances T. Sheehan<sup>1</sup>, William Sipprell<sup>1</sup>, Barry P. Boden<sup>2</sup>

<sup>1</sup>Rehab Medicine Department, CC, NIH, Bethesda, MD; <sup>2</sup>The Orthopaedic Center, Rockville, MD

email: [fsheehan@cc.nih.gov](mailto:fsheehan@cc.nih.gov)

## INTRODUCTION

ACL-injuries typically occur in active healthy young adults, involve expensive intervention with long recoveries, and result in many athletes losing knee function and quality of life [1]. For these reasons a sustained and extensive research effort has been put forth to identify the risk factors associated with ACL-injuries as a first step in trying to prevent them [2]. ACL-injury and prevention literature tends to focus on the lower limb, yet more recent work has focused on trunk orientation and control. In a descriptive videotape study, it was shown that athletes who sustained an ACL-injury were leaning backwards at the time of injury [3]. To date, no quantitative studies have confirmed this. Therefore, this study tested the hypothesis that the distance from the center-of-mass to the base-of-support (COM\_BOS) was larger at the time of ground contact for athletes performing non-contact, one-legged, landing maneuvers that resulted in an ACL-injury (provocative position), as compared athletes performing a similar maneuver that did not result in an ACL-injury (safe position). In addition, the hypothesis that limb angle was larger, but trunk angle was no different, in the provocative, as compared to the safe, landing position was also tested. Since female athletes tend to injure their ACL more frequently than their male counterparts [4] a tertiary hypothesis was tested: COM\_BOS and limb angle were larger in the female as compared to the male athletes.

## METHODS

Movie captures of 20 athletes performing a non-contact, one-legged, landing maneuver, resulting in a torn ACL were compared to matched movie captures of 20 athletes performing a similar maneuver that did not result in an ACL-injury (controls). Matching was based on gender (13F and 7M per group) and sport (10 basketball, 2 soccer, 3 football and 3 handball per group). For each movie, the frame when the foot contacted the ground

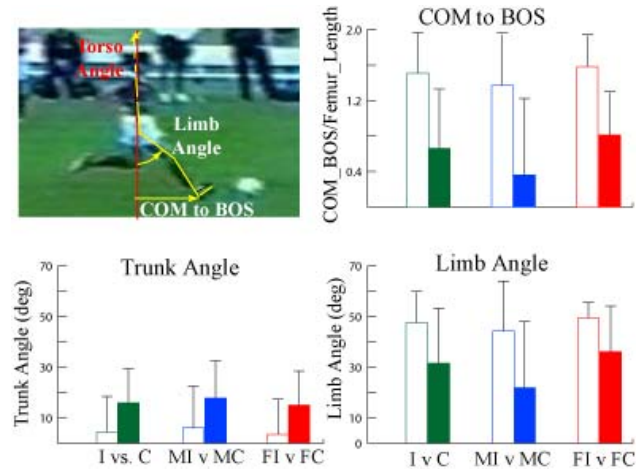


**Figure 1: Top Left:** An ACL-injury subject with measures of interest superimposed. I = injured C= Controls, M = males, F= Females.

(initial contact) was captured and stored for analysis in ImageJ (NIH, Bethesda, MD).

The COM was defined as the center of an ellipse delineating the athlete's trunk (Fig 1). The BOS was defined as the center of the line of contact between the shoe and the floor at initial contact. To account for small variations in camera angle across images, perpendicular lines on the field of play (e.g., the key in basketball) were used to denote the anterior and medial directions relative to the athlete. The COM\_BOS (in pixels) was then taken along the anterior/posterior direction. Since the camera magnification factor varied across images and the conversion from pixels to mm was not available, the COM\_BOS was normalized by femur length, which was measured from the identical image as the COM\_BOS. This scaling accounted for the variations in magnification factors and subject height, along with the slight variations in camera angle relative to the athlete across subjects. Two angles were also measured. The trunk relative to gravity ( $\text{trunk}_G$ ) angle was defined as the angle from the vertical to the centerline of the trunk. The limb relative to gravity ( $\text{limb}_G$ ) angle was defined as the angle between the vertical and the thigh

(represented as the line from the center of the knee joint to the center of the hip joint).

A 2x2 ANOVA was used to assess main and interaction effects of injury\_status and gender on three variables (COM\_BOS, limb<sub>G</sub> angle, and trunk<sub>G</sub> angle). A discriminant analysis determined if any single variable could distinguish injury\_status. A  $p$ -value < 0.05 was considered significant.

## RESULTS AND DISCUSSION

Injury\_status was a significant main effect for COM\_BOS, limb<sub>G</sub> angle, and torso<sub>G</sub> angle, but gender was not, and there were no interaction effects. The COM\_BOS was greater in the ACL-injured population ( $\Delta=0.86$ ,  $p < 0.001$ , Fig 3). If an average height of 177.8 cm (5' 10") and a femur length of  $0.245 \times \text{height}$  [6] is assumed for both groups, then on average, the COM was 37.5 cm more posterior relative to the BOS in the subjects who sustained an ACL-injury as compared to those that did not. The limb<sub>G</sub> angle was greater ( $\Delta=16.4^\circ$ ,  $p=0.004$ ) and the trunk<sub>G</sub> angle was smaller ( $\Delta=11.6^\circ$ ,  $p=0.016$ ) in the ACL-injured, as compared to the control, population. Interestingly, the same trends existed if each sport was evaluated separately, but due to power issues, significant differences were only found for basketball. The similarities across gender likely indicate that a large COM\_BOS during a one-legged landing is a risk factor that transcends gender.

The value of COM\_BOS discriminated between athletes who sustained an ACL-injury and athletes that did not with 80% accuracy (Fig 2, Wilks' Lambda,  $p < 0.001$ ), demonstrating that improper positioning of the body's COM is a likely risk factor for ACL-injury, but that it also likely works in conjunction with other factors to cause injury. No control subject landed with the COM\_BOS greater than 1.6, thus the COM\_BOS is likely a primary mechanism of ACL-injury when the COM\_BOS is large. In the range of 1.2-1.6 ACL-injury both occurred and did not occur. In this range the posterior position of the trunk is a minor factor and it combines with other factors in order to result in injury. When the trunk is positioned close to the base of support (COM\_BOS < 1.2) ACL-injury did not occur, with one exception. In this range the location of the COM\_BOS is not a critical factor and other factors are the most likely cause of injury.

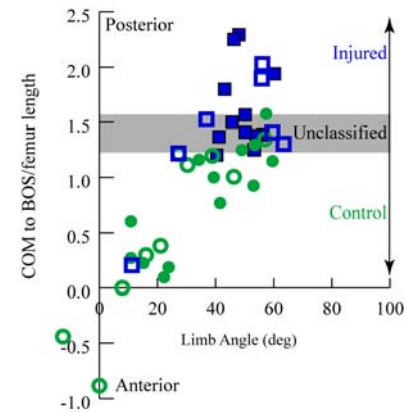


**Figure 1:** Blue squares: ACL-injury, green circles: controls, hollow symbols: Males, & filled symbols: females control group are represented by green circles. COM\_BOS could predict membership in a group to within 80% accuracy (1 injured and 7 controls were misclassified).

## CONCLUSIONS

This study demonstrates that having the COM far posterior to the BOS at initial ground contact is a likely risk factor for noncontact ACL-injury. Landing in an unstable posture may contribute to the ACL-injury by lowering the level of impulsive force required to buckle the leg and cause an ACL tear. These results may be useful in screening athletes who are at risk for ACL-injury and for implementing prevention programs that train athletes to keep the foot closer to the body when landing. Further, training athletes to fall safely when landing with the COM far posterior to the BOS, instead of counteracting this posture, may help prevent ACL-injuries. Future studies are needed to determine if neuromuscular interventions focused on improving core stability and positioning can help reduce the incidence of ACL-injuries.

## REFERENCES

1. Swirtun LR, et al., *Scand J Med Sci Sports* **18**, 318-24, 2008
2. Alentorn-Geli, E, et al., *Knee Surg Sports Traumatol Arthrosc.* **17**, 705-29, 2009.
3. Boden BP, et al. *Orthopedics* **23**. 573-8, 2000.
4. Arendt E, et al., *AJSM.* **23**, 694-701, 1995.
5. Boden BP, et al., *AJSM*, 2009. **37**, 252-9.
6. Winter DA. *Biomechanics and Motor Control of Human Movement* 4ed. 59, 2005
7. Willson JD, et al., *J Am Acad Orthop Surg*, 2005. **13**, 316-25.

# RAMP ANGLE, NOT FINAL PLATEAU HEIGHT, DETERMINES HILL WALKING TRANSITION STRATEGIES

Riley C. Sheehan and Jinger S. Gottschall

The Department of Kinesiology, The Pennsylvania State University  
University Park, PA, USA

email: [rcs241@psu.edu](mailto:rcs241@psu.edu) web: <http://biomechanics.psu.edu/nml/>

## INTRODUCTION

Walking individuals often encounter hills of different angles and final plateau heights in their everyday lives. These people are able to safely traverse the changing environment and seamlessly transition between the different terrains. When walking up a hill, it is necessary to increase propulsion. This demand for a larger positive force results in a greater propulsive impulse ( $Prop_{Imp}$ ), a greater moment about the knee ( $Knee_{Mom}$ ), and a greater lateral gastrocnemius activity in late stance ( $LG_{Stance}$ ) compared to level walking [1,2,3]. The magnitude of these modifications correlates with ramp angle [3].

Just as walking strategies change when traversing hills with various angles, there is also a change in the transition strategies when taking the first step onto a hill. We, as well as Prentice and colleagues, found that when individuals transition from a level to a hill surface, they employ unique walking strategies in anticipation of the upcoming change in terrain [4,5]. More specifically, propulsive impulse was 10% less and lateral gastrocnemius activity was 15% greater from the 15° to the 23° ramp with the same final plateau height [5].

Our testing apparatus consisted of 2 ramps, each a different fixed length. Thus, in order to evaluate hill transition strategies at various angles, we could maintain a constant final plateau height or utilize a single ramp length that yielded different plateau heights. During data collection of this original study, the participants often inquired about the steep ramp angle or the high final plateau height, which caused us to contemplate how walking individuals devise a transition strategy. Therefore, the goal of the current study was to determine what factor, ramp angle or final plateau height, individuals

prioritize to choose their transition strategy. Based on the findings that gait patterns differ with angle, we hypothesized that  $Prop_{Imp}$ ,  $Knee_{Mom}$ , and  $LG_{Stance}$  would be greater with increased angle, but not with increased final plateau height.

## METHODS

Ten healthy, college students (5 male, 5 female) completed level walking and 3 ramp walking conditions a 15° ramp to a 65cm high plateau (15Low), a 23° ramp to a 65cm high plateau (23Low), and a 23° ramp to a 95cm plateau (23High). We collected force, kinematic, and EMG data for the stance phase on a force plate for the stride just prior to the transition onto the ramp from the level walkway. Markers were placed bilaterally on the joint centers of the legs and inverse dynamics were used to calculate joint moments. We averaged 5 trials for each condition of every participant. The variables were normalized to the values obtained during level walking to allow comparison between participants. We used a series of paired t-tests to compare the transition strategies for the same angle and different height conditions (23Low and 23High), in addition to the strategies for the different angle and same height conditions (15Low and 23Low). Significance was defined as a  $p < 0.05$ .

## RESULTS AND DISCUSSION

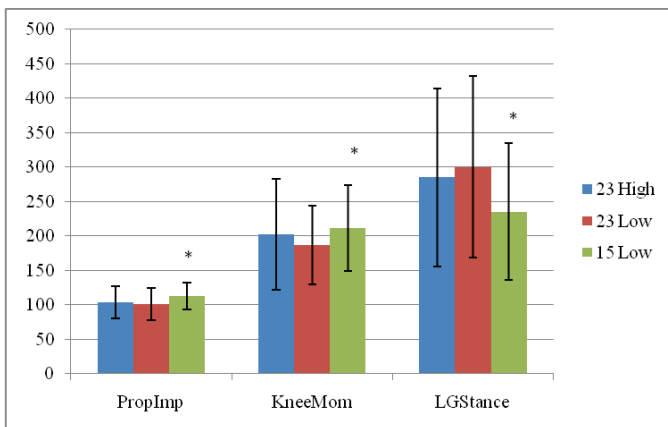
Our hypothesis was supported as  $Prop_{Imp}$ ,  $Knee_{Mom}$ , and  $LG_{Stance}$  were greater with ramp angle, but not final plateau height. While there was no significant difference for plateau height,  $Prop_{Imp}$  was 11% greater for 15Low than 23Low ( $p < 0.05$ , Figure/Table 1). Similarly,  $Knee_{Mom}$  increased 24% from 23° to 15°, but showed no difference between

65cm and 95cm plateaus ( $p < 0.05$ , Table 1 and Figure 1). Additionally,  $LG_{Stance}$  during 15Low was 65% less than 23Low ( $p < 0.05$ ). Together, these results suggest that it is the angle of the ramp, not the final plateau height, that determines the hill walking transition strategy.

**Table 1:** Mean  $\pm$  standard deviation for all values are reported as percent of level walking. **Bold** values indicate a significant difference from 23Low.

| Variable      | 23High        | 23Low         | 15Low               |
|---------------|---------------|---------------|---------------------|
| PropImp       | 104 $\pm$ 23  | 102 $\pm$ 24  | <b>113</b> $\pm$ 19 |
| KneeMom       | 202 $\pm$ 80  | 187 $\pm$ 57  | <b>211</b> $\pm$ 62 |
| $LG_{Stance}$ | 285 $\pm$ 130 | 300 $\pm$ 132 | <b>235</b> $\pm$ 99 |

**Figure 1:** Comparison of the means of 23High and 23Low (height difference) and 15Low and 23Low (angle difference) for propulsive impulse (PropImp), knee moment in late stance (KneeMom), and lateral gastrocnemius activity in late stance ( $LG_{Stance}$ ). An asterisks indicates significantly different from 23Low.



The main difference between the walking strategies of different ramp angles is the propulsive demands. Our results suggest that when transitioning onto the 15° ramp, participants generate greater forward propulsion through greater knee moments, rather than increased LG activity compared to the 23° ramp.

The interpretation that participants would use angle information to determine the appropriate transition strategy fits with previous literature. Marigold and Patla [6] showed that when participants were traversing uneven terrain, their gaze fixated on the terrain transitions, rather than on the terrain changes themselves. Additionally, Proffitt et al demonstrated

that humans are capable of accurately estimating hill angles from a distance [7]. These findings, coupled with the fact that transition strides are an accurate anticipation of the demands of the new surfaces, support our results that transition strategies are dependent upon ramp angle [8]. Walking individuals accurately estimate the angle of the ramp, with the ability to anticipate the new demands for a smooth and safe transition.

## CONCLUSIONS

In summary, walking individuals prioritize ramp angle, not final plateau height, when devising a transition strategy. This suggests that individuals who may have a limited ability to see or judge angles, may not be able to choose appropriate transition strategies and could potentially experience an increased fall risk. Furthermore, these findings could influence building choices, where a long, shallow ramp might be more appropriate for a specific population than a shorter, steep ramp to traverse the same height.

## REFERENCES

1. Kuster M, et al. *Clin Biomech* **10**, 79-84, 1995.
2. Lay AN, et al. *J Biomech* **40**, 1276-85, 2007.
3. Lay AN, et al. *J Biomech* **39**, 1621-8, 2006.
4. Prentice, et al. *Gait and Posture* **20**, 255-265, 2004.
5. Sheehan RS & Gottschall JS, *J Appl Biomech*, in review.
6. Marigold DS & Patla AE, *Neuroscience* **144**, 302-13, 2007.
7. Proffitt DR, et al. *Psychol Sci* **12**, 418-23, 2001.
8. Sheehan RS & Gottschall JS, *J Electromyography Kinesiol*, in press.

# DYNAMIC EFFECT OF LACROSSE STICK SHAPE ON BALL SPEED DURING THROWING

<sup>1</sup>Alison L. Sheets and <sup>2</sup>Mont Hubbard

<sup>1</sup>The Ohio State University, Columbus, OH, USA

<sup>2</sup>University of California, Davis, CA, USA

email: [sheets.203@osu.edu](mailto:sheets.203@osu.edu)

## INTRODUCTION

The sport of lacrosse is played with a solid rubber ball that can be caught, held and thrown with a net strung inside of a head and attached to a long-handled stick (Fig. 1). Lacrosse was originally played by Native Americans as a part of ceremonial rituals, a way to train for war, or a method for settling disputes between tribes. In the modern game, teams of 10 players attempt to score by shooting the ball into the opposing team's 6ft x 6ft goal. Although the rules and purpose for playing have taken many forms over the centuries, the equipment remained largely unchanged until the mid 1950's. At this time, the popularity of lacrosse began steadily increasing. It is currently the fastest growing sport in the United States [1].



**Figure 1:** Examples of new, plastic lacrosse head shape, and older wooden design  
([www.southswellsports.com](http://www.southswellsports.com))

In response to the surge in popularity, there have been fundamental changes to lacrosse stick design. The most notable change was the replacement of wooden stick heads with plastic ones in the men's and women's games in 1966 and 1997, respectively. The use of plastic decreased the variability between sticks, decreased manufacturing time and cost, and increased durability. More recently, stick head designs have been customized to increase shot speed, throwing distance and ball retention capabilities. Now there are hundreds of stick heads with subtle geometric variations (Fig. 1).

Stick head design significantly affects shot speed [2,3] but exactly how the ball and stick head interact is unclear. The ball speed at release is significantly faster than the tip of the stick and the velocity direction varies by as much as 0.31 rad [3]. This indicates that net curvature is an important factor to include in the interaction between the ball and stick.

The goal of this study was to create a lacrosse head model and throwing simulation that can be used to systematically investigate the effect of stick head geometry on throwing speed and direction. This tool could be used by the governing bodies of lacrosse to attempt to reduce player injury risk by developing more stringent requirements for approved stick head designs. This is a concern because the very fast shot speed has caused fatal injuries in the men's game, and has necessitated the addition of protective eye-wear to the women's game.

## METHODS

A generalized planar lacrosse stick model was developed and used to propel a one-degree-of-freedom ball that was 0.065m in diameter and weighed 0.1465 kg (Fig. 2). The stick was initially positioned at a 30° angle from vertical at rest. From this position it rotated with linearly increasing angular acceleration  $\alpha=3500 \cdot t$  rad/s<sup>2</sup> around a fixed point 0.1405 m behind, 0.1015 m above the distal end of shaft. This point was an experimentally measured instant center at ball release [3].

Four experimentally measured points defined the geometry and depth of the net in the stick head (Fig. 2). Depth was measured by placing a ball in the net at numerous locations and applying a load to the ball. This defined a rigid envelope that the ball rolls on, which incorporates the non-rigid movement of the net. From these points, the radius from the

center of the stick head face to the surface of the net was defined as a piecewise function of  $\theta$  with a continuous slope:

$$R(\theta) = \begin{cases} -0.403\theta^2 - 1.565\theta - 1.383 & -1.21 \leq \theta < -0.98 \\ -0.065 / \cos \theta & \text{if } -0.98 \leq \theta < -0.15 \\ 0.027\theta^2 + 0.170\theta + 0.334 & -0.15 \leq \theta < 1.57 \end{cases}$$

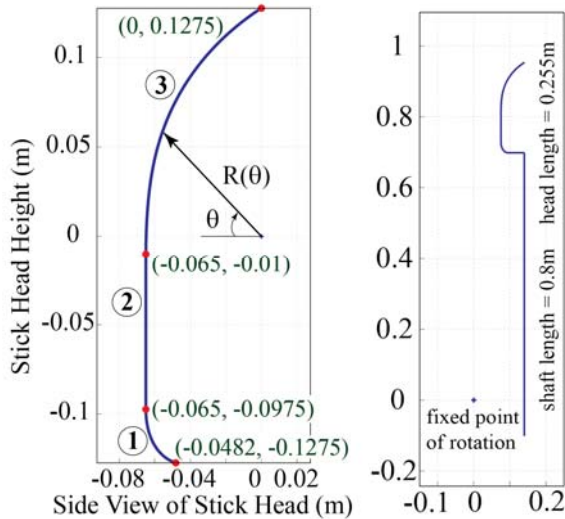


**Figure 2:** Side view of stick head (left) and whole stick including shaft (right)

The ball was assumed to roll without slipping on the stick head surface. The state variables of the system were  $\theta$ , the angle to the ball center from a line passing perpendicularly through the center of the stick face, and  $\dot{\theta}$ . Ball release was defined to be when the ball had rolled past the stick tip,  $\theta > 1.57$ .

## RESULTS AND DISCUSSION

Ball speed at release, 19.02 m/s, exceeded the speed of the tip of the stick (Fig. 3) and was similar to speeds measured for high-level, female collegiate players, 18.8 m/s-19.7 m/s [3]. The ball velocity was primarily in the horizontal direction, 19.25 m/s, with a small downward component, -2.4 m/s.

Additionally, there was a very small angle, 0.015 rad, between the directions of the velocity vectors of the ball and stick tip. This is smaller than the experimentally measured differences of 0.23-0.31 rad [3]. It is likely the simulated differences in velocity direction would increase with a more realistic model of the ball-stick interaction just prior to release. The model described in this paper

defines release velocity as the state of the ball when the contact point reaches the tip of the stick. Actually, before the contact force becomes zero and the ball leaves the stick, it continues to rotate about the very small radius of the stick tip. During this short additional contact period, the stick tip velocity would continue rapidly changing direction, since it is rotating about a fixed point, while the ball velocity is not constrained in this way. The marginally longer contact time would also slightly increase ball speed at release.

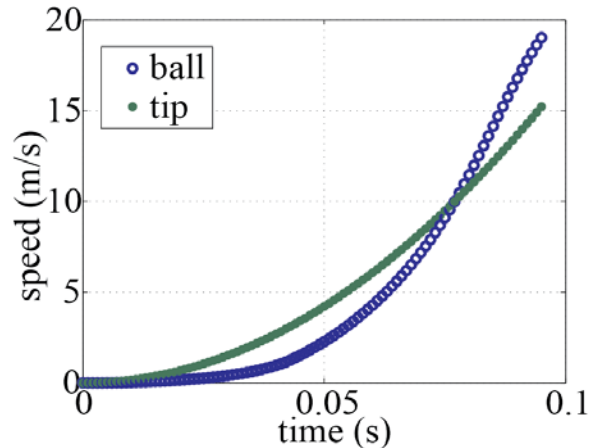


**Figure 3:** Ball speed exceeds that of the stick tip at ball release

This study describes a method for modeling the complex geometry of a lacrosse stick head by defining a radius from the center of the head to the net as a piecewise function. The dynamic model was able to reproduce characteristics of experimentally measured ball velocities, and will be used to investigate the effects of surface geometry on throwing speed and technique.

## REFERENCES

1. Sterenson S. *2007 US Lacrosse Participation Survey*. 2008.
2. Livingston LA. *J Science and Medicine in Sport* **9**, 299-303, 2006.
3. Crisco JJ, et al. *J Applied Biomech*, **25**, 184-191, 2009.

## ACKNOWLEDGEMENTS

The OSU Department of Mechanical Engineering provided the support for this study.

# INCORPORATION OF DYNAMIC X-RAY BASED KNEE KINEMATICS IMPROVES QUADRICEPS FORCE PREDICTION IN MUSCULOSKELETAL MODELING

<sup>1</sup>Snehal Shetye, <sup>2</sup>Kang Li, <sup>1</sup>Scott Tashman, <sup>1</sup>Christopher Harner, <sup>1</sup>Xudong Zhang

<sup>1</sup>University of Pittsburgh, Pittsburgh, PA, USA

<sup>2</sup>Rutgers, The State University of New Jersey, New Brunswick, NJ, USA  
email: xuz9@pitt.edu

## INTRODUCTION

Surface-based systems are most commonly used for measuring subject-specific whole-body kinematics. Whole body musculoskeletal modeling software tools such as OpenSim [1] and AnyBody have successfully used the resulting data coupled with ground reaction forces for creating forward dynamic simulations of human movements. However, surface-based kinematics data are afflicted with significant skin motion artifact, and may not be able to capture subtle but important joint kinematics differences or changes. A recently developed dynamic stereo X-ray (DSX) system can measure in vivo joint kinematics with high accuracy [2], but only for one body region at a time. The purpose of this study was to evaluate whether the incorporation of DSX-based knee joint kinematics data into surface-based whole-body kinematics data can improve the muscle force prediction by a forward dynamic simulation tool (OpenSim).

## METHODS

Two decline walking (15°) trials of a patient with a lateral meniscectomy were used for this study. The whole-body kinematics were acquired using a 8-camera surface-based motion capture system (VICON) at 100Hz, while the knee joint kinematics were obtained using a custom-designed DSX system also at 100Hz. Ground reaction force (GRF) was measured by force plates embedded in a dual-belt treadmill. EMG data were collected from 7 muscles: vastus medialis (VM), rectus femoris (RF), vastus lateralis (VL), biceps femoris (BF), semimembranosus (SM), tibialis anterior (TA), and medial gastrocnemius (GA). Both GRF and EMG data were collected with a sampling frequency of 1000Hz. All EMG data were post-processed starting with a high-pass filter with a cutoff frequency of

20Hz followed by rectification. The data were then low-pass filtered with a frequency of 5Hz. A 24-DOF 92-muscle biodynamical model was developed in OpenSim, and made patient-specific by incorporating first the surface-based whole-body kinematic data. Two forward dynamic simulations were then created, one with the default OpenSim knee joint kinematics (where rotations and translations are cubic spline functions of knee flexion angle) and one with patient-specific DSX-based knee joint kinematics. In both, the whole-body joint positioning was done through inverse kinematics using the surface marker data; a residual reduction algorithm resolved the dynamic inconsistencies inherent in the model. Forces in all 92 muscles were predicted in both simulation models using the computed muscle control (CMC) algorithm provided in OpenSim [3].

## RESULTS AND DISCUSSION

A comparison of muscle force predictions for VM, VL and RF by the default model and the DSX-incorporated model is provided in Figure 1a & 1b. Overall, the magnitudes of the quadriceps muscle forces predicted were lower for the DSX-incorporated model. The muscle force distributions were also considerably different, with the default model predicting a higher contribution by RF immediately after heel strike.

Figure 1c depicts the EMG patterns obtained for RF, VL and VM. A strong correlation was observed between the EMG patterns and muscle force predictions by the DSX-incorporated model (Figure 1b). The model with the default knee kinematics (Figure 1a) failed to correctly predict the force distribution within the quadriceps muscle group. These results indicate that accurate joint kinematics is critical for making correct muscle force

predictions by a musculoskeletal dynamic model. Muscle force predictions by models that employ only surface-based kinematics data should be interpreted with caution.

## CONCLUSIONS

Subject-specific musculoskeletal models were created by combining whole-body surface marker data and DSX-based knee joint kinematics data. Comparison of muscle force predictions with and without incorporating the DSX-based kinematic data revealed major differences. Muscle force predictions by the DSX-incorporated model better correlated with corresponding EMG measurements.

## REFERENCES

1. Delp SL, et al. *IEEE Trans. Biomedical Engineering*, **54**, 1940-1948, 2007.
2. Tashman S, et al. *J Biomech Eng*, **125**, 238-245, 2003.
3. Thelen DG et al. *J Biomech*, **36**, 321-328, 2003.

## ACKNOWLEDGEMENTS

The authors would like to acknowledge NIH grants (3R01AR046387-10S1 & 1R03AR059939-01) and Tim Dorn at University of Melbourne for the freely available GaitExtractToolbox for OpenSim.

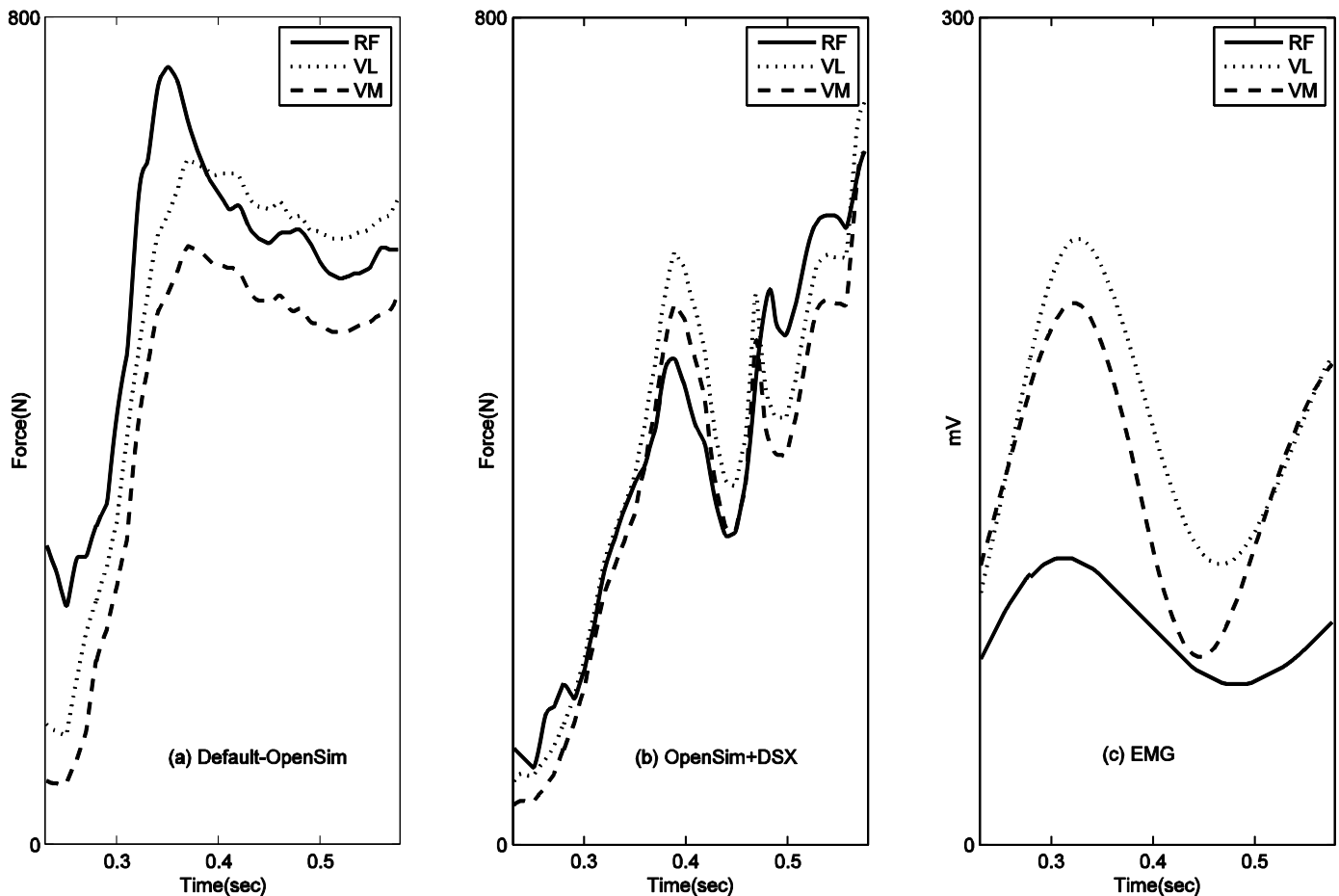


**Figure 1:** Muscle force predictions by musculoskeletal dynamic models with the default (a) and DSX-incorporated (b) kinematics, and the corresponding EMG data (c).

# THE HUMAN SPLENIUS CAPITIS MUSCLE IS PRIMARILY A HEAD-NECK ROTATOR

<sup>1,2</sup>Gunter P. Siegmund, <sup>3</sup>Anita N. Vasavada and <sup>2</sup>Jean-Sébastien Blouin

<sup>1</sup>MEA Forensic Engineers & Scientists, Richmond, BC, Canada

<sup>2</sup>School of Human Kinetics, University of British Columbia, Vancouver, BC, Canada

<sup>3</sup>Washington State University, Pullman, WA, USA

email: [gunter.siegmund@meaforensic.com](mailto:gunter.siegmund@meaforensic.com)

## INTRODUCTION

In most individuals, the tuning curve of the human splenius capitis muscle (SPL) exhibits a preferred activation towards the ipsilateral postero-lateral direction (i.e., extension and lateral bending) during isometric contractions of the head and neck in the neutral posture [1,2]. In some individuals, however, the preferred direction of SPL is towards the ipsilateral antero-lateral direction (i.e., flexion and lateral bending) [2,3]. Possible explanations for these latter data include functional compartmentalization of SPL and the presence of a confounding axial moment during testing. The goal of this study was to examine the activation patterns of the splenius capitis muscle under controlled conditions of flexion/extension and axial moments in order to better determine its role in generating neck moments and to assess whether SPL exhibits behavior consistent with compartmentalization.

## METHODS

Six subjects (3F, 3M) performed two blocks of isometric neck muscle contractions with their head and neck in a neutral posture. In one block, subjects generated a combined flexion moment and right axial rotation moment in three different orders: a) flexion moment first, followed by axial moment, b) axial moment first, followed by flexion moment, and c) both moments simultaneously (Figure 1A). The other block was similar, but an extension moment replaced the flexion moment (Figure 1B). Reaction forces and moments were measured using a 6-axis load cell via a tight-fitting helmet. Subjects were provided real-time visual feedback of the anteroposterior and mediolateral forces they applied to the helmet in the horizontal plane, and the axial moment they generated about the vertical axis. The flexion and extension contractions were at 15% of

the flexion maximum voluntary contraction (MVC); the axial moment was at 15% of the axial moment MVC. All six conditions were repeated 3 times, and both the condition order within a block and the block order within a subject were randomized.

Fine-wire electrodes were placed under ultrasound guidance at four locations approximately equally spaced between the medial and lateral borders of the right SPL muscle (SPL 1 through SPL 4) at the C4 level. EMG and load cell data were acquired at 2kHz. Root-mean-square (RMS) EMG was calculated using a 500 ms window and the force and moment data were low-pass filtered at 5 Hz. Plots of RMS EMG versus flexion/extension force and axial moment were generated to examine the behavior of SPL in the four electrodes (Figure 1).

## RESULTS AND DISCUSSION

SPL was active in all subjects during each condition. Peak activation levels were greater during the extension condition than during the flexion condition in SPL 2, 3 and 4 (paired t-test,  $p < 0.05$ ), but not in SPL 1 ( $p = 0.054$ ). There were no significant differences in the RMS EMG levels at the end of the contractions (i.e., at 15% force and moment) between the three order-of-contraction conditions (ANOVA,  $p = 0.94$ ).

The muscle activity measured at all four electrodes exhibited a similar pattern. RMS EMG amplitude increased linearly with right axial moment (columns 1 and 3 in the lower panels of Figure 1), but did not vary with either flexion or extension force (columns 2 and 4 in the lower panels of Figure 1). This pattern indicates that SPL is primarily an axial rotator, and not an extensor, of the head and neck at the contraction levels used in this study.

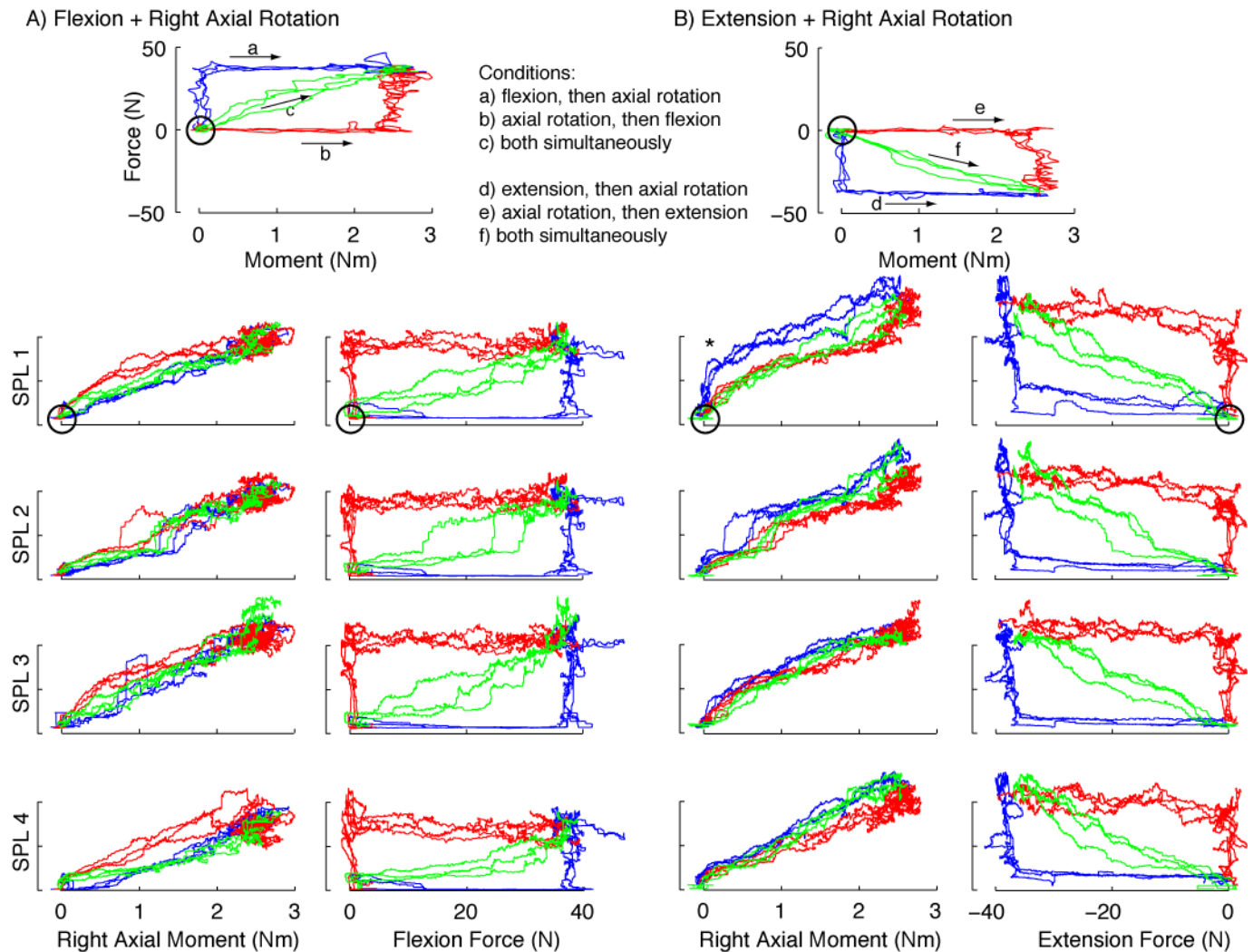


**Figure 1:** Exemplar force, axial moment and RMS EMG data for the flexion conditions (A) and extension conditions (B) for the medial to lateral electrodes (SPL 1 to SPL 4). Blue traces show three repetitions of conditions a and d (force first, then axial moment); red traces show conditions b and e (axial moment first, then force); and green traces show conditions c and f (force and moment simultaneously). The circles indicate the starting point of the contraction.

Activity in the medial electrode (SPL 1) increased slightly with forces during the extension task for the exemplar subject shown in Figure 1 (see blue traces marked with an asterisk in column 3). This behavior suggests the more vertical fibers of SPL near its medial border may behave differently than its more lateral fibers, and may be evidence of compartmentalization in SPL. This pattern was not present, however, in all subjects.

## CONCLUSIONS

The human SPL muscle is primarily an axial rotator of the head and neck, and behaves relatively consistently across its width. SPL is not strongly compartmentalized, but some subjects exhibited minor evidence of non-uniformity across the four wire locations tested here.

## REFERENCES

1. Vasavada AN, et al. *Exp Brain Res* **147**, 437-448, 2002.
2. Blouin JS, et al. *J Neurophysiol* **98**, 920-928, 2007.
3. Keshner EA et al. *Exp Brain Res* **75**, 335-344, 1989.

## ACKNOWLEDGEMENTS

Funding: National Skeletal Muscle Research Center (ANV), Natural Sciences and Engineering Research Council of Canada (GPS, JSB), and Canada Foundation for Innovation, Canadian Institutes of Health Research, Canadian Chiropractic Research Foundation & Michael Smith Foundation for Health Research (JSB). We also thank Robyn Newell.

# EFFECT OF INCLINE ON WALKING MECHANICS, ENERGETICS AND NEUROMUSCULAR CONTROL

<sup>1</sup>Amy Silder, <sup>1</sup>Scott Delp and <sup>2</sup>Thor Besier

<sup>1</sup>Stanford University, Stanford, CA, USA

<sup>2</sup>University of Auckland, Auckland, New Zealand

Email: silder@stanford.edu

## INTRODUCTION

Identifying the relationship between mechanical work and metabolic cost is essential to improve our understanding of the mechanisms by which humans select various gait patterns. In recent years, muscle models have been refined to account for energy consumption [1,2] and used in conjunction with whole body simulations to estimate the metabolic cost of normal human walking [2,3]. Yet, our knowledge of different locomotion patterns, such as walking up an incline, is limited, primarily due to a lack of comprehensive experimental data. Such data would provide the foundation for deciphering the mechanical determinants of energetic cost. The purpose of this study was to systematically evaluate lower extremity kinematics, kinetics, muscle activities, and energetics as a function of surface incline.

## METHODS

Thirteen healthy subjects ( $35\pm 8$ y,  $68\pm 12$ kg,  $1.77\pm 0.10$ m) provided informed consent to participate in this study. Each subject completed three five-minute walking trials on a split belt instrumented treadmill (Bertec Corp.) at surface inclines of 0%, 5% and 10%. Subjects completed each trial at his/her preferred level ground walking speed ( $1.28\pm 0.12$ m/s). Steady-state oxygen uptake was measured (K4b2, COSMED) and analyzed during the final minute of each condition.

Whole body kinematics (100Hz) and ground reaction forces (GRFs) (2000Hz) were measured over five strides using an eight-camera motion capture system (Vicon). A 31-degree of freedom whole body model was scaled to the size and mass of each subject [4]. A global optimization inverse kinematics routine was used to compute lower extremity joint angles. Inverse dynamics was then used to compute lower extremity joint moments and powers.

Muscle activities were measured on the left limb from the soleus, medial gastrocnemius, tibialis anterior,

vastus medialis, vastus lateralis, rectus femoris, and the medial and lateral hamstrings. Electromyographic (EMG) signals were band-pass filtered (30-500Hz) and full wave rectified. Root mean square (RMS) activities were computed from the average signal across five gait cycles.

Oxygen consumption, spatiotemporal, kinematic, kinetic, and EMG data were compared across inclines using a one-way repeated measures ANOVA with significance set at  $p < 0.05$ .

## RESULTS

Oxygen consumption increased  $40\pm 8\%$  (0 to 5%) and  $31\pm 6\%$  (5 to 10%) with each increase in incline ( $p < 0.01$ ). No significant changes in stride length, stride frequency, or the magnitude of peak GRFs were detected. Peak hip flexion angle, stance and swing phase knee flexion angles and ankle plantarflexion angle all increased with incline ( $p < 0.01$ ) (Fig. 1).

During the first half of stance, the peak hip extension moment and power increased an average of  $\sim 16\%$  and  $\sim 65\%$  between 0% and 10% incline, respectively ( $p < 0.01$ ). At this same time, the peak knee extension moment decreased  $\sim 30\%$  between 0% and 10% incline ( $p < 0.01$ ) (Fig. 1). During the second half of stance, the knee flexion moment increased  $\sim 58\%$  across inclines ( $p < 0.01$ ). Knee power absorption and generation both increased with incline ( $p < 0.01$ ). Smaller, though significant changes were measured at the ankle, with the peak plantarflexion moment and power generation increasing  $\sim 14\%$  and  $\sim 25\%$ , respectively, from 0% to 10% incline ( $p < 0.01$ ) (Fig. 1).

RMS muscle activity increased with incline for the soleus, gastrocnemius, and medial and lateral hamstrings ( $p < 0.05$ ). All other muscles showed small, but insignificant increases in activity as incline increased.

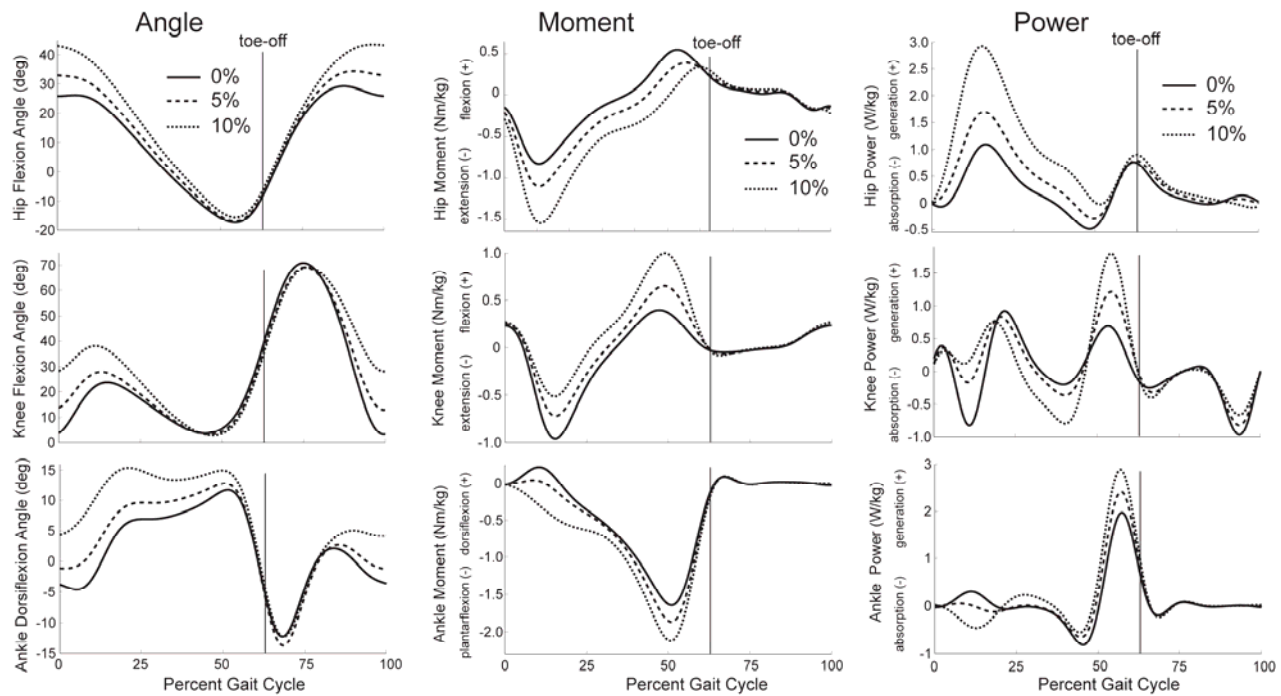


**Figure 1.** Ensemble averaged sagittal joint angles, moments and powers averaged across five gait cycles, normalized to body weight.

## DISCUSSION

Similar to observations made during inclined running, walking up an incline resulted a change in hip and knee joint function [5]. Although joint angles were similar approaching toe-off, increased incline resulted in a more anteriorly directed GRF, thereby dramatically altering joint moments. Most notably, the hip extensors took on a dominant role, with greater hip power generation as incline increased. The knee flexion moment increased throughout stance phase, and when coupled with a greater range of motion, energy absorption during the first half of stance and power production during the second half of stance both increased. These findings were supported by increased hamstring muscle activity.

Numerous factors contribute to the ~84% increase in oxygen consumption between 0% and 10% incline. A complete understanding of the interaction between the mechanical and metabolic changes cannot be inferred with an experimental approach alone [2]. Nevertheless, several observations can be made from the data presented here. In particular, the ankle plantarflexors have been shown to be the primary contributors to forward progression during level walking [2,6]. With increasing incline, we observed relatively larger changes in hip and knee power generation, compared to the ankle. Given that peak hip extension angles were similar across incline and elastic energy contributions at the hip derive primarily from stretching the hip flexors during late stance [7],

the proximal shift in power likely results in less passive energy storage and return, compared to level walking. Furthermore, larger angular excursions across all joints necessitate higher average musculotendon velocities and therefore create the potential for higher energetic costs.

In conclusion, we have presented comprehensive data describing how incline alters neuromuscular control, energetic cost, and lower extremity joint kinematics and kinetics. Musculoskeletal modeling simulations using these data will aid in our understanding of how specific muscles contribute to these observed changes in joint kinetics and the increased energy cost of inclined walking.

## REFERENCES

1. Umberger BR, et al., *Comput Methods Biomech. Biomed. Engin.* **6**, 99-111, 2003.
2. Anderson FC, et al., *Human Walking*, Williams and Williams, 2006.
3. Umberger BR, et al., *J R Soc Interface* **7**, 1329-40, 2010.
4. Delp SL, et al., *IEEE Trans Biomed Eng* **37**, 757-67, 1990.
5. Devita P, et al., *J Biomech* **36**, 1632-1641, 2008.
6. Liu MQ, et al., *J Biomech* **41**, 3243-52, 2008.
7. Whittington B, et al., *Gait Posture* **27**, 628-34, 2008

## ACKNOWLEDGEMENTS

Department of Defense (#1004-001), Deans Postdoctoral Fellowship (Stanford University), Hyper Wear LLC.

# TRUNK NEUROMUSCULAR CONTROL IS REDUCED IN PATIENTS WITH CLINICAL LUMBAR INSTABILITY

Sheri Silfies, Marco Cannella, Won Sung, Peemongkon Wattananon, and Rupal Mehta

Drexel University, Rehabilitation Sciences Spine Research Lab, Philadelphia, PA, USA

email: [silfies@drexel.edu](mailto:silfies@drexel.edu) web: [http://www.drexel.edu/cnhp/rehab\\_sciences](http://www.drexel.edu/cnhp/rehab_sciences)

## INTRODUCTION

Altered trunk neuromuscular control is a proposed underlying mechanism of pain generation for a subgroup of patients with non-specific mechanical low back pain (MLBP). Testing paradigms that can detect altered control and determine treatment efficacy of widely used motor control exercises are critical to advancing treatment of MLBP. The purposes of this study were to 1) establish the test-retest reliability of volitional trunk control parameters using a paradigm of seated balance on an unstable surface, and 2) evaluate differences in isolated trunk control between patients with MLBP attributed to clinical lumbar instability and healthy matched subjects.

## METHODS

A testing apparatus was designed to isolate trunk control by minimizing the contribution of the lower extremities.<sup>1</sup> Subjects sat on seat with a hemisphere mounted underneath (Fig. 1). The seat created an unstable surface thereby requiring active trunk control to maintain an upright seated posture. The seating system itself was balanced and adjustable to allow the location of the hemisphere and starting posture to be the same for each subject. Limits of stability were tested by having participants actively tilt the chair moving their center of pressure (COP) from a center target (average static balance position) along 8 different lines (0°, 45°, 90°, 135°, 180°, 225°, 270°, 315°) that were visible on a computer screen. Participants also completed static balance trials with instructions to maintain balance with as little movement as possible. Following a practice trial, participants completed 3, 60 s balance trials with eyes open (EO) and closed (EC). Force data were collected at 2400 Hz, filtered (piecewise-linear), down sampled (400 Hz) and COP time series were calculated. Task performance was

examined using limits of stability (LOS (mm)), root mean square displacement (RMS (mm)), maximal displacement (MAX (mm)), path length (TOT (mm)), mean velocity (MVEL (mm/s)), and a 95% confidence ellipse area (CEA (mm<sup>2</sup>)).<sup>2</sup>

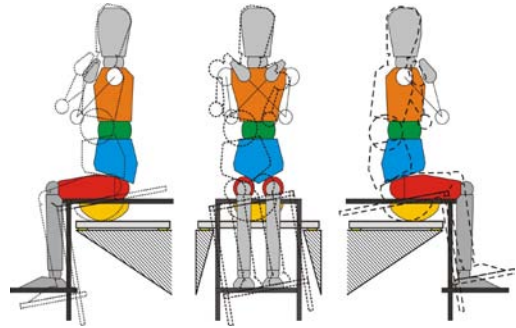


**Figure 1:** Subject position used for the seated paradigm. Sagittal plane motion (flexion/ extension) is represented by the x-direction and frontal plane motion (lateral bending right and left) by the y-direction.

Patients (n = 17, 12 female, age  $35 \pm 14$ ) with sub-acute MLBP (NPRS  $6/10 \pm 2$ ; Oswestry  $22 \pm 6\%$ ) attributed to clinical instability, and age, gender and trunk length matched healthy controls (n = 17, 12 female, age  $36 \pm 14$ ) were tested. Measurement stability was established by testing healthy subjects on two occasions 8-weeks apart and analyzed using ICCs<sub>(2,3)</sub>. Group differences were assessed using MANOVA for LOS and mixed-model ANOVA (Group, Condition (EO, EC)) for static balance. Alpha was set at .05.

## RESULTS

Across all measures, test-retest reliability ranges (8-week apart) were ICCs<sub>(2,3)</sub> (.80 to .94), SEM ( .49 mm to  $159 \text{ mm}^2$ ) and  $\text{MDC}_{90}$  (1.2 mm to  $371 \text{ mm}^2$ ). Seated LOS were not significantly different between the groups ( $F_{(1,8)} = .28$ ;  $p = .97$ ); Fig. 2).

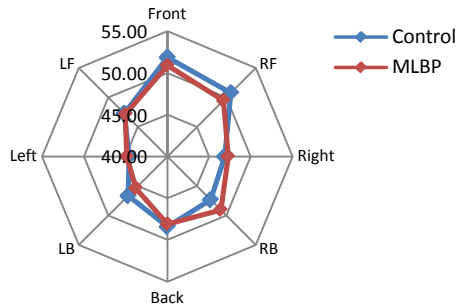


**Figure 2:** Limits of stability (millimeters) presented as group means per direction.

For static balance, the main effect of group revealed that the MLBP group demonstrated less control (MAX<sub>y</sub>) and greater position variability (RMS<sub>y</sub>) in the frontal plane. There was also a significant main effect for condition across all variables with decreased postural control in the EC condition. However, the main effects were qualified by significant interactions representing decreased trunk control in the MLBP group in the EC condition for all variables in the y-direction (Fig. 3). These differences exceeded our MDC<sub>90</sub> values.

## DISCUSSION AND CONCLUSIONS

These seated postural control variables demonstrate sufficient precision and appear to be sensitive to trunk control performance. SEM and MDC<sub>90</sub> values will allow determination of true changes following an 8- week intervention. The subjects with MLBP demonstrated greater difficulty maintaining trunk control only when visual input was removed. This was particularly true for frontal plane control and may represent altered spinal proprioception in this subgroup of MLBP patients. This testing paradigm isolates trunk control and provides a method to assess the efficacy of interventions designed to enhance trunk neuromuscular control and stability.

## REFERENCES

1. Radebold, et al. *Spine*. 2001;**26**(7):724-30.
2. Preito, et al. *IEEE Trans Biomed Eng*, 1996; **43**:956-66.

## ACKNOWLEDGEMENTS

This study was supported in part the by the National Institutes of Health (NICHD, K01HD53632).

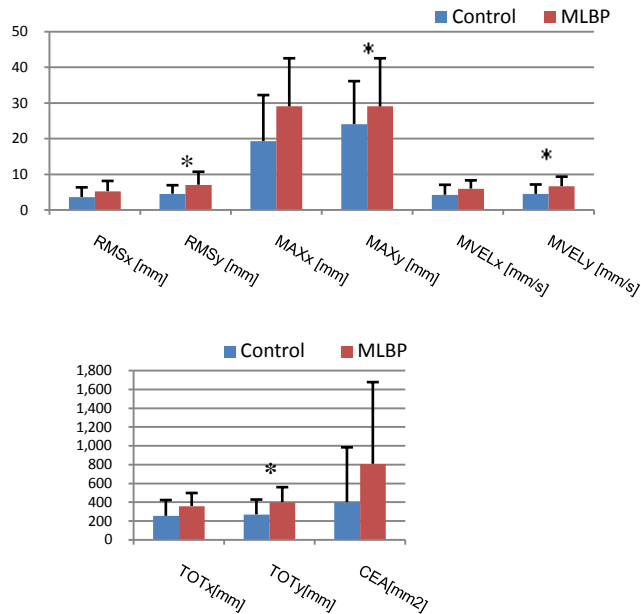


**Figure 3:** Group means ± standard deviations for all variables in the eyes closed (EC) condition. The asterisks represent a significant difference between groups ( $p \leq .025$ ).

# WHOLE-BODY ANGULAR MOMENTUM WHILE WALKING ON SLOPED SURFACES

<sup>1</sup>Anne K. Silverman, <sup>2</sup>Jason M. Wilken, <sup>2</sup>Emily H. Sinitski and <sup>3</sup>Richard R. Neptune

<sup>1</sup>Division of Engineering, Colorado School of Mines, Golden, CO, USA

<sup>2</sup>Center for the Intrepid, Department of Orthopedics and Rehabilitation, Brooke Army Medical Center, Ft. Sam Houston, TX, USA

<sup>3</sup>Department of Mechanical Engineering, The University of Texas at Austin, Austin, TX, USA  
email: asilverm@mines.edu

## INTRODUCTION

Walking on sloped surfaces occurs frequently in daily living activities and the risk of slip-related falls increases on slopes [1]. The regulation of whole-body angular momentum is critical to maintaining dynamic balance during level walking and necessary to recover from trips and prevent falls [2]. However, how angular momentum varies while walking on a slope is not known. Changes in foot placement, body segment kinematics and ground reaction forces (GRFs) while walking on a slope all influence the angular momentum profile. Muscles are the primary mechanism to regulate angular momentum [3] and generate net joint moments that have been shown to change with different slope conditions [4]. The purpose of this study was to analyze 3D angular momentum during inclined and declined walking over a range of slope angles. We tested the hypothesis that the range of angular momentum would be different in sloped walking relative to level walking, and that these differences would be related to specific changes in the joint moment profiles.

## METHODS

Thirty able-bodied subjects walked at a fixed speed up and down a 16-foot walkway at four randomly-ordered slope angles: 0, 5, 10 and 15 degrees (seven total conditions). 3D kinematic and GRF data were collected at 120 and 1200 Hz, respectively. An inverse dynamics model was used to find the center-of-mass (COM) location and velocity of each segment including the head, torso, pelvis, upper arms, lower arms, thighs, shanks and feet. Whole-body angular momentum (H) about the COM was determined as:

$$\vec{H} = \sum_{i=1}^n [(\vec{r}_i^{COM} - \vec{r}_{body}^{COM}) \times m_i(\vec{v}_i^{COM} - \vec{v}_{body}^{COM}) + I_i \vec{\omega}_i]$$

where  $\vec{r}_i^{COM}$ ,  $\vec{v}_i^{COM}$  and  $\vec{\omega}_i$  are the position, velocity and angular velocity vectors of the  $i$ -th segment's COM,  $\vec{r}_{body}^{COM}$  and  $\vec{v}_{body}^{COM}$  are the position and velocity vectors of the body COM,  $m_i$  and  $I_i$  are the mass and moment of inertia of each segment, and  $n$  is the number of segments.

The angular momentum was normalized by body mass (kg), walking speed (m/s) and body height (m) and expressed as a percentage of the left leg gait cycle. The range of each angular momentum component, defined as the peak-to-peak value, was compared across incline conditions using a one-factor ANOVA. When a significant main effect was found, pairwise comparisons using a Bonferroni adjustment were performed to determine which conditions were significantly different from level walking ( $\alpha=0.05$ ). Pearson correlation analyses were then performed between the range of angular momentum and peak joint moments in each component direction.

## RESULTS AND DISCUSSION

There were significant main effects in the range of angular momentum for all three components ( $p<0.001$ , Fig. 1). In addition, several peak joint moments were correlated with the range of angular momentum.

*In the frontal plane*, range of H for all incline conditions had a significantly greater range compared to level walking ( $p<0.001$ ), but there were no significant differences for the decline conditions. The range was most strongly correlated with the first peak abduction moment at the hip ( $r=0.526$ ,  $p<0.001$ ,  $n=210$ ) and knee ( $r=0.503$ ,  $p<0.001$ ,  $n=210$ ).

In the transverse plane, the range of H was smaller than level walking for all decline conditions ( $p \leq 0.004$ ) and was only significantly larger than level walking for the 15 degree incline condition ( $p = 0.012$ ). The peak hip external moment ( $r = -0.282$ ,  $p < 0.001$ ,  $n = 210$ ) and knee moment ( $r = -0.461$ ,  $p < 0.001$ ,  $n = 210$ ) in late stance had the strongest correlations with the range of H.

In the sagittal plane, all conditions were significantly different from level walking ( $p \leq 0.004$ ), with a smaller range for declined walking and a larger range for inclined walking. The peak ankle plantar flexor moment ( $r = 0.665$ ,  $p < 0.001$ ,  $n = 210$ ), hip extensor moment ( $r = -0.588$ ,  $p < 0.001$ ,  $n = 210$ ) and knee moment in late stance ( $r = -0.611$ ,  $p < 0.001$ ,  $n = 210$ ) all had strong correlations with the range of H.

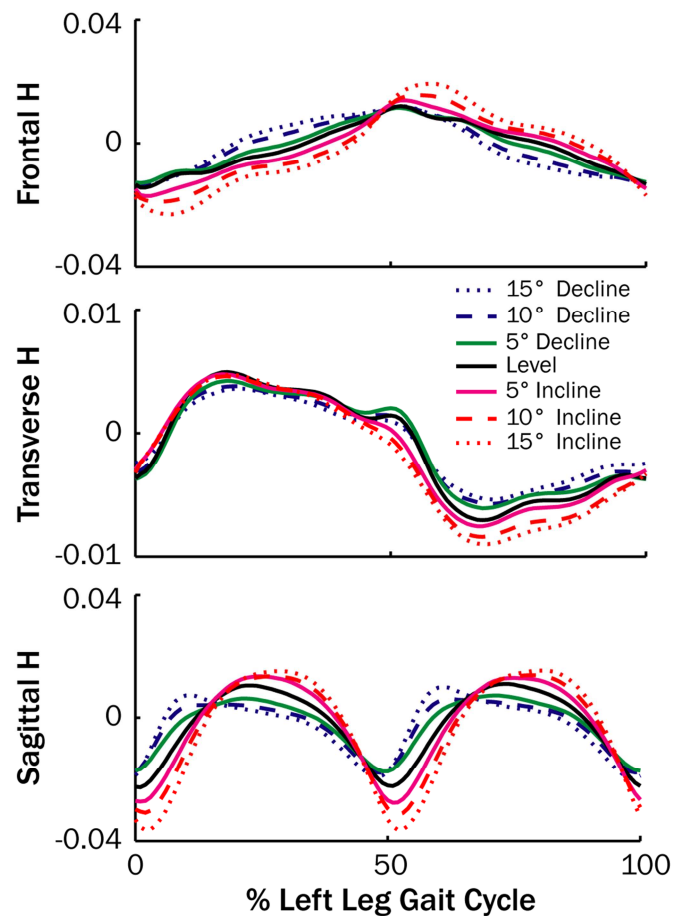


**Figure 1:** Normalized 3D angular momentum (H) trajectory across slope conditions.

The peak knee moments in the sagittal and transverse planes are of particular interest because the moment transitioned from positive (extensor and

internal) in the decline conditions to negative (flexor and external) in the incline conditions, which is consistent with previous work [4].

Previous simulation work has shown the gluteus medius is a major contributor to the hip abduction moment and medial acceleration of the body COM [5]. The vasti are also a large contributor to medial COM acceleration [5], which will affect the frontal and transverse angular momentum. The correlation of the sagittal angular momentum with the ankle plantar flexor moment is supported by previous simulation results showing the soleus and gastrocnemius contribute to negative and positive angular momentum in late stance, respectively [3]. In addition, the hamstrings and gluteus maximus contribute to the hip extensor moment and positive angular momentum in early stance in the sagittal plane [3]. Thus, increased contributions from these muscles on sloped surfaces would influence the range of angular momentum.

## CONCLUSIONS

These results suggest that able-bodied subjects actively regulate angular momentum differently while walking on sloped surfaces compared to level ground. The greatest differences occurred in the frontal and sagittal planes. In general, the range of angular momentum was larger for inclined walking compared to level walking, and similar or smaller for declined walking compared to level walking. Walking down a slope increases the risk of slips and falls compared to walking up a slope due to differences shear forces developed on the bottom of the foot [1]. Thus, it appears that individuals more tightly control angular momentum while walking down a slope to help prevent a slip or fall.

## REFERENCES

1. Redfern, MS, et al. *Ergonomics* **44**, 1138-1166, 2001.
2. Pijnappels M, et al. *J Biomech* **37**, 1811-1818, 2004.
3. Neptune, RR, et al. *J Biomech* **41**, 6-12, 2011.
4. Lay, AN, et al. *J Biomech* **39**, 1621-1628, 2006.
5. Pandy, MG, et al. *J Biomech* **43**, 2055-2064, 2010.

# BIOMECHANICS OF SIT TO STAND AND STAND TO SIT FROM HIGH AND LOW CHAIR AFTER TOTAL HIP ARTHROPLASTY IN OBESE SUBJECTS

<sup>1</sup>Bhupinder Singh, <sup>2</sup>Thomas D Brown, <sup>3</sup>John J. Callaghan, <sup>1</sup>John H. Yack

<sup>1</sup>Program in Physical Therapy & Rehabilitation Sciences  
<sup>2</sup>Orthopaedic Biomechanics Laboratory, <sup>3</sup>Department of Orthopaedic Surgery  
UNIVERSITY OF IOWA, IA, USA  
Email: bhupindersingh@uiowa.edu

## INTRODUCTION

The sit to stand (SitTS) movement, a prerequisite in many activities of daily living, becomes more difficult to perform with age, obesity, and after Total Hip Arthroplasty (THA), a common surgical procedure. SitTS movement has been extensively investigated but the studies on different chair heights are limited (1, 2). Using a lower seat height increases hip extensor moments in healthy normal weight subjects (3), but no studies have been done to see the effect of low chair height in THA subjects. Furthermore, most of the studies include only the sit to stand part and not the complete cycle until the subjects sit back down. Burnett (4) reported similar peak hip flexion and moments during SitTS and stand to sit (StandTS) activity in normal subjects, but no study has looked at StandTS in THA subjects.

The purpose of study is to analyze kinetics during SitTS and StandTS from high and low chair height. We hypothesize that peak hip extensor moments during SitTS will be higher for low chair height as compared to high chair and will be similar during SitTS and StandTS activity.

## METHODS

Seven patients with unilateral hip replacement, aged between 50-70 years, mean BMI 34.9 kg/m<sup>2</sup> (range 30.5-40.8) were recruited for the study along with 14 age matched control obese subjects; mean BMI 37 kg/m<sup>2</sup>). The study was approved by the local institutional review board. Marker triads were placed on the pelvis, trunk and bilaterally on the thigh, leg, and foot. Three dimensional kinematic data (Optotrak) and Ground reaction force data

(Kistler) were collected at 60 Hz and 300 Hz, and filtered at 6 Hz and 10 Hz, respectively.

Participants were asked to cross their arms over their chests during SitTS task. Foot position was self-selected as they stood from a standard chair (46 cm high) and a low-height chair (38 cm high) and returned to the seated position at their preferred speed. The average of five SitTS trials was used to assess kinetic data. The initiation and end of the SitTS movement was differentiated by vertical pelvic velocity.

## DATA ANALYSIS

Visual 3D software (C-Motion) was used for processing and the moments were normalized to body mass. Repeated measures One Way Analysis of Variance (ANOVA) was performed to compare three dimensional peak hip moments at 6 weeks, 6 months and 1 year post operatively. Paired t-tests were used to determine significant differences. SPSS 17.0 was used for analysis with p-value <0.05.

## RESULTS AND DISCUSSION

Sagittal plane peak hip extensor moments for SitTS-L (1.13±0.26) were higher during SitTS-L (1.09 ±0.20) for the control subjects. However the peak hip extensor moments during SitTS-H (1.13 ±0.16) were found to be similar to SitTS-L (1.20 ±0.20) for obese THA subjects at 6 months after surgery. (p-value 0.90) (Fig.1). This may be attributed to greater asymmetry in loading during SitTS-L as compared to SitTS-H. Asymmetric limb loading resulting in decreased hip moments at operated hip has been shown during SitTS in THA subjects. The heavier subjects may have less

flexibility when it comes to loading the involved side given the huge amount of weight that has to be moved.

also similar during SitTS and StandTS motion (See table 1).

Therefore, SitTS and StandTS motion has symmetrical hip and knee kinetics, suggesting similar joint stresses while sitting back from a standing position. Considering these findings, emphasis should also be given to StandTS activity while analyzing THA subjects.

## CONCLUSIONS

The results of the study show that normalized peak hip extensor moments for obese THA subjects at 6 months after surgery were similar for SitTS-H and SitTS-L whereas their normal obese counterparts show greater peak moment during SitTS-L.

The SitTS and StandTS motion exert similar moments at hip and knee in obese THA population, indicating the need of analyzing the joint stresses while sitting back from a standing position in addition to the normal sit to stand activity.

## REFERENCES:

1. Janssen WGM, et al. Phys Ther, 82, 866-879, 2002.
2. Schenkman M, et al., Phys. Ther. **70**:638-648, 1990.
3. Jason Gillette, Proceedings of ASB 2010.
4. David Burnett, Proceedings of ASB 2010.

## ACKNOWLEDGEMENTS:

Department of Veterans Affairs-ICVMC

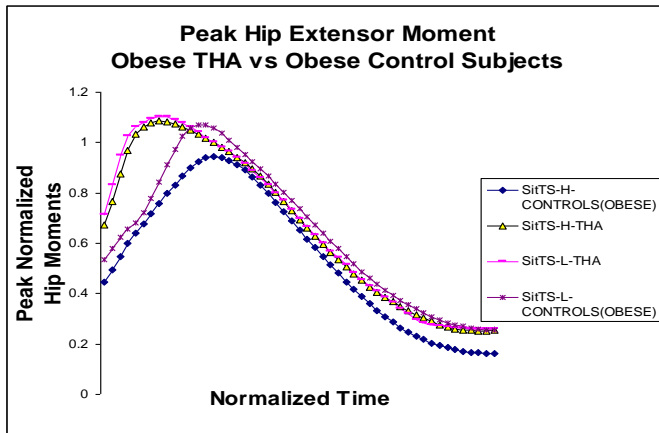


**Figure 1: Mean ensemble average graph showing the peak hip extensor moments from High (SitTS-H) and Low chair height (SitTS-L) for 7 Obese THA patients, relative to the obese control subjects.**

The peak knee extensor moments were found to be greater in SitTS-L than in SitTS-H, although not significant. It can be one of the modifications in THA subjects to protect the operated hip by putting same load on hip and more on the knees to accommodate for the higher load experienced during SitTS-L.

For StandTS, the peak hip moment for obese THA subjects at 6 months for SitTS-H (1.13+/-0.16) was similar to StandTS-H (1.02 +/- 0.19) (p-value 0.38). following similar trend found in normal healthy subjects. (Burnett,2010). The Knee moments were

| PEAK MOMENTS IN THA (OBESE)      |             |             |             |             |             |             |
|----------------------------------|-------------|-------------|-------------|-------------|-------------|-------------|
|                                  | 6 WEEKS     |             | 6 MONTHS    |             | 1 YEAR      |             |
|                                  | HIP         | KNEE        | HIP         | KNEE        | HIP         | KNEE        |
| SitTS-H                          | 0.98 (0.16) | 0.54 (0.38) | 1.13 (0.16) | 0.59 (0.15) | 1.08 (0.15) | 0.60 (0.18) |
| SitTS-L                          | 0.95(0.40)  | 0.61(0.41)  | 1.20 (0.20) | 0.65 (0.75) | 1.11 (0.10) | 0.57 (0.34) |
| StandTS-H                        | 1.05 (0.24) | 0.58(0.52)  | 1.02 (0.19) | 0.57 (0.16) | 1.03 (0.14) | 0.56 (0.17) |
| PEAK MOMENTS IN CONTROLS (OBESE) |             |             |             |             |             |             |
|                                  | HIP         |             | KNEE        |             |             |             |
| SitTS-H                          | 1.09 (0.20) |             | 0.67 (0.13) |             |             |             |
| SitTS-L                          | 1.13 (0.26) |             | 0.68 (0.10) |             |             |             |

**Table 1: Peak hip and knee extensor moments during SitTS and StandTS from High and Low chair height in obese THA subjects at 6 weeks, 6 months and 1 year after THA and obese controls.**

# AFFECT OF WEIGHT AND TYPE OF JACKHAMMER ON VIBRATION AND GRIP PRESSURE

<sup>1</sup>Gurjeet Singh, <sup>1,2</sup>Naira Campbell-Kyureghyan, <sup>2</sup>Daniel Strobel, and <sup>1,2</sup>Karen Cooper

<sup>1</sup>Department of Industrial Engineering, University of Wisconsin-Milwaukee, Milwaukee, WI, USA

<sup>2</sup>CARGI, University of Wisconsin-Milwaukee, Milwaukee, WI, USA

email: [campbeln@uwm.edu](mailto:campbeln@uwm.edu) web: <http://cargi.uwm.edu>

## INTRODUCTION

Every day construction workers utilize jackhammers to break concrete, asphalt, and various other hard surfaces. The jackhammer operator faces several risks for injury, including exposure to vibration. Prolonged vibration exposure to the hand and forearm can cause hand arm vibration syndrome (HAVS) [1], leading to potentially disabling numbness, tingling, and pain.

Previous studies investigated the relationship between the application of force and transmitted vibration [2]. When the grip forces exerted on the tool handle increase, the transmission of vibration into the hand from the tool also increases [3]. Research by Pyykkoö et al. [4] identified grip force, frequency and magnitude of handle vibration as important factors with respect to the vibration transmitted to the hand, and consequently in the development of HAVS. It was found that if grip strength increases then the vibration also increases with the cube root of the grip pressure [4]. Tool manufacturers have recently developed lighter weight jackhammer designs intended to reduce the required grip and push forces during operation. However, the effect of the new jackhammer designs on grip pressure and the resulting vibrations are currently unknown.

Therefore, the objectives of this study were to compare the measured vibration and grip pressure **1)** between conventional (90 lb) and light weight (60 lb) jackhammers, **2)** between different pavement type/thickness combinations, and **3)** between pneumatic and hydraulic (60 lb & 90 lb) jackhammers

## METHODS

*Design*-The experimental design included the “breaking” of a 3’x3’ square of four different pavement type/thickness combinations: 4” and 6” thick asphalt and concrete. Five commercially available jackhammers were tested: 1-60 lb

hydraulic, 1-90 lb hydraulic, 2-60 lb pneumatic and 1-90 lb pneumatic. Four subjects consented to participate in this study, which was approved by the UWM IRB. Each subject was asked to “break” each pavement type using each jackhammer.

*Equipment*-An accelerometer was attached to the jackhammer handle (NexGen Ergonomics, sampling frequency 2500 Hz) while another accelerometer (Delsys TRIGNO wireless, sampling frequency 296 Hz) was attached at the subject’s left hand. A pressure-sensing glove (Vista Medical, FSA Glove, sampling frequency 5 Hz), comprised of 24 individual sensors, collected hand grip pressure for the subject’s right hand.

*Analysis*-The vibration data was analyzed using the VATS software (NexGen Ergonomics Inc, Pointe Claire, Quebec, Canada) using the ISO 5349 standard for hand arm vibration. The vibration data for the jackhammer handle was smoothed by a moving window RMS technique. The data was filtered using a 2<sup>nd</sup> order Butterworth filter with a low band cut off frequency of 4 Hz using Hanning window size of 1024 data values. A Fast Fourier Transform was performed and 1/3 octave band analysis was conducted. The ISO 5349 weighting factor was applied in each principal axis and the resultant is a single aRMS (aRMS<sub>JH</sub>) value. Similarly, the aRMS was calculated for hand vibration (aRMS<sub>wrist</sub>). The difference in vibration ( $\Delta$ RMS) was calculated using:

$$\Delta\text{RMS} = \text{aRMS}_{\text{JH}} - \text{aRMS}_{\text{wrist}}$$

A customized Matlab™ algorithm was used to analyze the grip pressure results. For each of the 24 sensors a RMS value was computed and those values were summed to obtain total grip pressure in psi during the trial.

The  $\Delta$ RMS and grip pressure (psi) were compared across the 60lb and 90lb jackhammers, and the four pavement type/thickness combinations. Pearson correlation was calculated for vibration at the

handle to the grip pressure measured between the pneumatic and hydraulic jackhammers.

## RESULTS AND DISCUSSION

**Jackhammer Weight** – The average hand grip pressure for 60 lb and 90 lb jackhammers was 50.6 and 58.1 psi respectively for subject 4 (Figure 1). The differences in vibration between the jackhammer handle and the hand were 4.4 m/s<sup>2</sup> and 4.2 m/s<sup>2</sup> for the 60 and 90 lb jackhammers respectively, also for Subject 4. Similar results were obtained for the other subjects. The 90 lb jackhammers required higher grip pressure during operation, leading to smaller differences between the handle and hand vibrations. That is, higher grip pressure leads to greater transmission of vibration into the hand, as was found in similar research on chain saws [5].

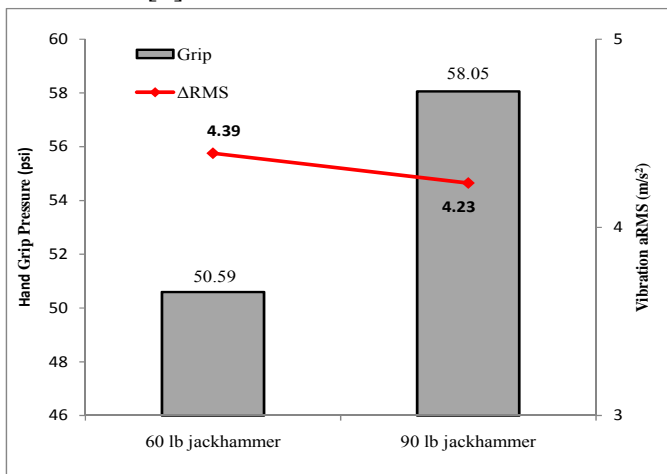


**Figure 1:** Comparison of hand grip pressure and difference in vibration ( $\Delta$ RMS) between jackhammer weights for Subject 4.

**Pavement Type/Thickness** – Grip pressure increased with pavement thickness and was higher for asphalt pavements than for concrete for Subject 4 (Figure 2). Conversely, the vibration difference between the handle and the hand decreases with increasing thickness and is greater for concrete than for asphalt. Similar results were obtained for the other subjects. Overall, the grip pressure and vibration transmission variation is greater across the pavement types/thicknesses than between the different jackhammer weights.

**Power Source** – Grip pressure averaged 52.7 psi for hydraulic jackhammers and 51.4 psi for pneumatic jackhammers. Similarly, the  $\Delta$ RMS for the hydraulic and pneumatic jackhammers was found to be 4.5 and 3.5 m/s<sup>2</sup> respectively.

The Pearson correlation coefficient between grip pressure and handle vibration was 0.39 for pneumatic powered jackhammers and -0.56 for hydraulic powered jackhammers. The correlation of 0.39 indicate a medium correlation between grip pressure and vibration data for pneumatic jackhammers, whereas the -0.56 indicates a stronger negative correlation and negative interaction effect between grip pressure and vibration data for hydraulic jackhammers.

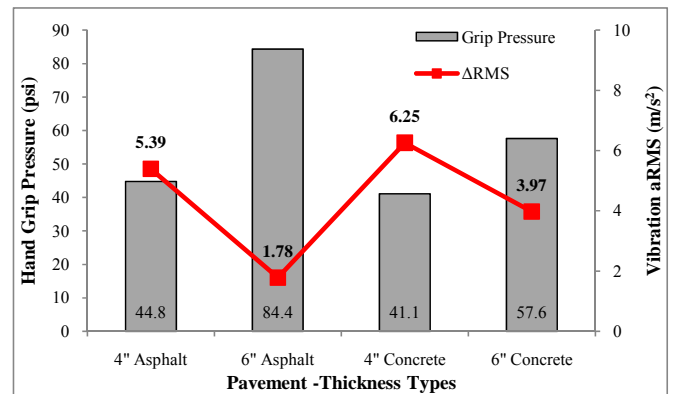


**Figure 2:** Comparison of hand grip pressure and difference in vibration ( $\Delta$ RMS) across the difference pavement-thickness types for Subject 4.

## CONCLUSIONS

The results of this study indicate that differences in both grip strength and vibration transmission to the hand are affected by jackhammer weight and type. The increase in vibration transmission with increasing grip strength is in agreement with previous studies. Further, the pavement type/thickness had a greater effect on both grip strength and vibration transmission than did the jackhammer characteristics. Further investigation is required to determine the potential benefits of 60lb and 90lb jackhammer including additional factors such as job completion time and muscle activity.

## REFERENCES

- Gemne G, Taylor W. *J Low Freq Noise Vib.* **55**, 185-9, 1983.
- Welcome D, et al. *Int J Ind Ergo*, **34** (6), 507-18, 2004.
- Hartung E, Dupius, Scheffer M. *Int. Arch. Occup. Environ. Health*, **64**, 463-7, 1993.
- Pyykö I, et al. *Scan. J. Work Environ & Health*, **2**, 87-95, 1976.
- Naslund U. *The vibration syndrome*. W. Taylor (ed.), Academic Press, London, 1974.

# THE EFFECT OF PERTURBATION MAGNITUDE ON WALKING STABILITY DURING VISUAL AND PLATFORM PERTURBATIONS

<sup>1</sup>Emily H. Sinitski, <sup>1,2</sup>Kevin Terry, <sup>1</sup>Jason M. Wilken and <sup>2</sup>Jonathan B. Dingwell

<sup>1</sup>Department of Orthopedics and Rehabilitation, Center for the Intrepid,  
Brooke Army Medical Center, Ft. Sam Houston, TX, USA

<sup>2</sup>University of Texas at Austin, Austin, TX, USA

E-mail: jason.wilken@us.army.mil

## INTRODUCTION

External perturbations applied to the walking surface or visual field can challenge an individual's ability to maintain stability during walking. Accurately quantifying and predicting changes in stability during walking will further our understanding of how individuals respond to challenges encountered during daily life, and guide the development of assessments for individuals at increased risk of falling. Orbital and local stability measures have demonstrated that they are able to detect changes associated with age [1], pathology [2], and the application of external perturbations [3]. Orbital and local stability quantify how system trajectories respond (diverge or converge) to perturbations *between* (orbital) or *within* (local) consecutive strides [4]. This study was the first to investigate how orbital and local stability change in response to continuous medial-lateral visual and surface perturbations of different amplitudes.

## METHODS

Eleven healthy individuals participated after giving written informed consent. Participants walked at normalized speeds on a 2m x 3m treadmill embedded in a 4m movable platform in a virtual environment (CAREN) with a scene projected 300° around the participant. Participants completed a 6-min acclimation period followed by two 3-min trials of walking with either no perturbations (NP) or one of 3 platform perturbation amplitudes (P1 - P3), or one of 5 visual perturbation amplitudes (V1 - V5). All perturbations were applied as pseudo-random translations in the medial-lateral direction [3]. A marker on the C7 vertebra was tracked at 60 Hz using a 24-camera Vicon system. Orbital stability was quantified by calculating maximum Floquet

multipliers (maxFM) [4]. Local stability was quantified by calculating divergence exponents (short-term,  $\lambda_s^*$  and long-term,  $\lambda_L^*$ ) [2, 4]. These measures were calculated using a 5-dimensional delay-embedded state space of C7 medial-lateral velocity with a time delay of  $\tau = 30$  samples. One-way repeated measures ANOVAs were used to determine statistical differences between amplitudes.

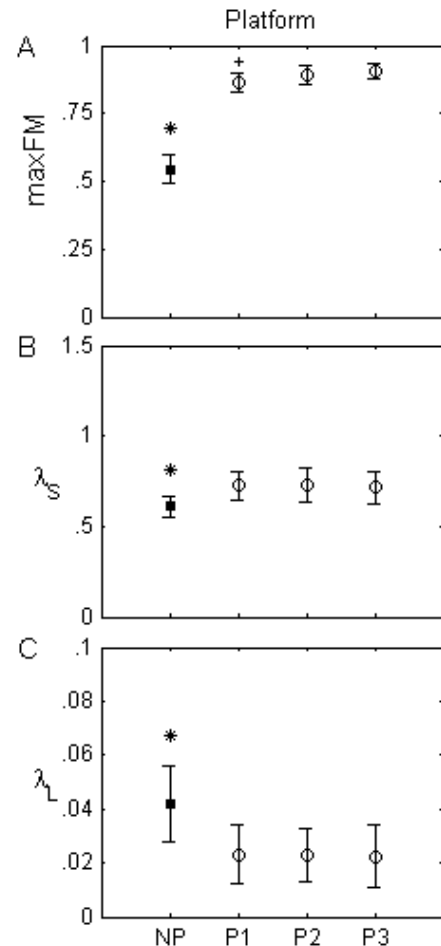


**Figure 1.** Dynamic walking stability (mean  $\pm$  SD) for *platform* perturbations: (A) maxFM, (B)  $\lambda_s^*$  and (C)  $\lambda_L^*$ . The \* indicates significantly different from perturbed walking. The + indicates significantly different from all other amplitudes.

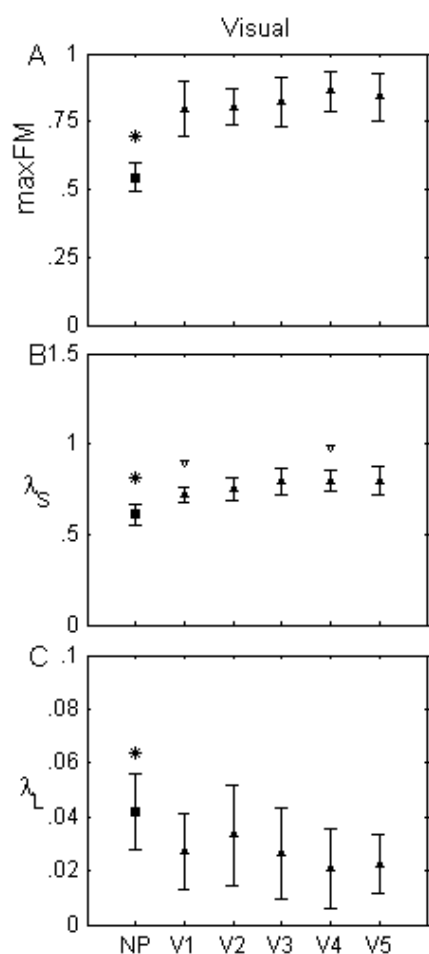


**Figure 2.** Dynamic walking stability (mean  $\pm$  SD) for *visual* perturbations: (A) maxFM, (B)  $\lambda_s^*$  and (C)  $\lambda_L^*$ . The \* indicates significantly different from perturbed walking. The  $\nabla$  indicates significant differences between amplitudes V1 and V4.

## RESULTS and DISCUSSION

For *platform* perturbations (Fig. 1), subjects exhibited increased maxFM and  $\lambda_s^*$ , and decreased  $\lambda_L^*$  ( $p \leq 0.001$ ) relative to NP. As platform perturbation amplitude increased above P1, maxFM also significantly increased, suggesting subjects were more orbitally unstable with increasing amplitude (P1 vs P2,  $p \leq 0.008$ ; P1 vs P3,  $p \leq 0.001$ ). Increasing platform perturbation amplitude did not significantly change local stability.

For *visual* perturbations (Fig. 2), subjects exhibited increased maxFM and  $\lambda_s^*$ , and decreased  $\lambda_L^*$  ( $p \leq 0.001$ ) relative to NP. Increasing visual perturbation

amplitude did not significantly change maxFM or  $\lambda_L^*$ , but  $\lambda_s^*$  was significantly different between visual perturbation amplitudes V1 and V4 ( $p \leq 0.022$ ).

Consistent with a previous study [3], we observed an increase in orbital and short-term local instability for platform and visual perturbed walking compared to unperturbed walking. Only maxFM showed a consistent increase as platform perturbation amplitude increased. Conversely, orbital and local stability varied inconsistently as visual perturbation amplitude increased. The decreases in  $\lambda_L^*$  were also consistent with the relative changes in the *shapes* of the local divergence curves discussed by McAndrew et al. [3].

## CONCLUSIONS

These findings demonstrate that dynamic stability measures can be used to detect differences between unperturbed and perturbed walking, but may have more limited ability to detect differences associated with different visual perturbation amplitudes used in this study. It is possible that beyond a given perturbation magnitude, a ceiling effect occurs and subject response is no longer affected.

## REFERENCES

1. Granata, K.P. & Lockhart, T.E., (2008) *J Electromyogr and Kines* **18** (2): 172-178.
2. Dingwell, J.B. & Cusumano, J.P., (2000) *Chaos* **10** (4): 848-863.
3. McAndrew, P.M., Wilken, J.M., & Dingwell, J.B., (2011) *J Biomech* **44** (4): 644-649.
4. Dingwell, J.B. & Kang, H.G., (2007) *J Biomech Eng* **129** (4): 586-593.

## ACKNOWLEDGMENTS

Supported by Grant 1-R01-HD059844 from the National Institutes of Health (NICHD).

The view(s) expressed herein are those of the author(s) and do not reflect the official policy or position of Brooke Army Medical Center, the U.S. Army Medical Department, the U.S. Army Office of the Surgeon General, the Department of the Army, Department of Defense or the U.S. Government.

# INTERRATER AND INTRARATER RELIABILITY OF THE FUNCTIONAL MOVEMENT SCREEN

<sup>1</sup>Craig Smith, <sup>1</sup>Nicole Chimera, <sup>1</sup>Nik Wright, and <sup>1</sup>Meghan Warren

<sup>1</sup>Northern Arizona University, Flagstaff, AZ, USA  
email: cs773@nau.edu web: www.nau.edu

## INTRODUCTION

The Functional Movement Screen (FMS) is a series of 7 fundamental movements scored using a 4 point ordinal scale (3-0) to examine the risk of injury based on total score (21-0) and/or side to side asymmetry [1]. The movements include deep squat, hurdle step, inline lunge, shoulder mobility, active straight leg raise, trunk stability pushup, and rotational stability. Asymmetry is noted in 5 movements performed bilaterally: hurdle step, inline lunge, shoulder mobility, active straight leg raise, and rotational stability. The score for the FMS is determined by specific criteria for each movement [1] with a 1 indicating inability to perform the movement, 2 corresponding to performing the movement with compensation, and 3 corresponding to the ability to correctly complete the movement without compensation. If there is pain during any portion of the movement or pain with a clearing test, a score of 0 is given [1].

The FMS has been described as an injury predictor with a score below 14 associated with an increased risk of serious injury in professional football players [2]. Since musculoskeletal injury is an inherent risk for anyone involved in athletics, a screening system that is able to assess injury risk due to aberrant movement patterns is critical. Currently two previous interrater reliability studies for the FMS using the standard scoring system have been published [3,4] and one also investigated intrarater reliability [4]. Minick et al. [3] used video and tested the ability of two expert and two novice raters' scores based on anterior and lateral viewpoints. The use of video with set viewpoints does not represent administration or scoring of an actual FMS that requires the clinician to move and see from multiple viewpoints during a single trial, especially for lunge and rotary stability tests [3]. Teyhan et al. [4] used only novice raters (n=8) to determine inter and intrarater reliability which did

not allow for comparison with experienced or certified FMS raters. Despite the stated limitations, the previous studies demonstrated high [3] to good [4] interrater reliability and moderate intrarater reliability [4].

Therefore, the purpose of this study was to test the interrater and intrarater reliability of the FMS following a single two hour education session with raters of different educational background and experience levels with FMS administration in healthy, injury-free men and women.

## METHODS

To determine the interrater and intrarater reliability of the FMS, four raters observed the participants complete the FMS using the standard instructions on two separate days (7 days apart). At the beginning of the study a two hour training session was conducted using materials from the creators of the FMS [1]. This session was led by a non-certified, but experienced FMS tester and covered the 7 movements, the 3 clearing tests, the verbal instructions, and scoring criteria.

The four raters included a certified FMS tester (Rater 1); an entry-level physical therapy student who had completed over 100 FMS tests, but was not certified (Rater 2); a faculty member in Athletic Training with a PhD in Biomechanics & Movement Science, but no previous experience with FMS (Rater 3); and an entry-level physical therapy student with no previous experience with FMS (Rater 4).

Data to calculate intra- and inter-rater reliability of the FMS was collected in a convenience sample of 19 healthy, injury-free men (n = 10) and women (n = 9).

The instructions for the screen were taken from the standardized protocol from the most recent FMS text [1]. These instructions were recorded on audio with pictures taken for each setup and starting position. The audio and pictures were combined into videos that were shown to each participant before the movement was performed.

Each participant began each session with a 5 minute warm-up on a stationary bicycle. After warming up, the tibial tuberosity height and hand length from the longest finger to the distal crease of the wrist were measured by all four raters. The measurements of Rater 2 were randomly selected to be used during all testing sessions for setting hurdle height, the distance between the feet on the inline lunge, and scoring for the shoulder mobility.

The participant was instructed to listen to the videos, assume the proper starting position, and repeat the movement 3 times. After the last movement, the video for the next movement in the FMS was played. At the conclusion of the first testing, the participants were instructed to return the following week for retesting with the same shoes. The participants were also instructed not to practice any of the movements between the two testing sessions to limit a learning effect in movement patterns. The same procedure was followed for the second testing to determine intrarater reliability; interrater reliability was computed for both testing sessions.

Descriptive statistics were calculated as means with standard deviation for normal interval data and medians with range or percent for non-normal or categorical data. Intra-class correlation coefficients (ICC) from an analysis of variance (ANOVA) were calculated to determine by intra- and interrater reliability. All analyses were completed using SAS, Version 9.2.

**Table 1:** Intra-class correlation coefficients for intra-rater reliability

| Rater Number | Rater Description   | ICC  |
|--------------|---|------|
| 1            | Certified FMS tester  | 0.81 |
| 2            | Physical therapy student. Non-certified, experienced FMS tester           | 0.90 |
| 3            | Athletic Training Faculty member. Non-certified, inexperienced FMS tester | 0.91 |
| 4            | Physical therapy student. Non-certified, inexperienced FMS tester         | 0.88 |

## RESULTS AND DISCUSSION

The sample included 9 women and 10 men and was aged (median [range]) 26 [22-41] years and overall was normal weight (body mass index  $24.0 \pm 2.9$  kg/m<sup>2</sup>). The overall FMS scores ranged from 11 to 17 with a mean  $\pm$  SD of  $14.3 \pm 1.7$  (using testing session number 1 and Rater 3 as an example). Overall, inter-rater reliability was good for session one (ICC = 0.89) and for session two (ICC = 0.87). Additionally, there was 100% agreement with the 3 clearing tests amongst all of the raters. Intra-rater reliability was acceptable to good for each rater (Table 1).

Contrary to expectations, the certified FMS rater had the lowest intrarater ICC. While this rater demonstrated acceptable intrarater reliability (ICC=0.81), certification did not improve this reliability. Further, the most consistent rater had no previous FMS experience but did have the most education and experience in movement analysis (Rater 3). Therefore intrarater reliability with the FMS may be increased with more structured education and experience in movement analysis.

## CONCLUSIONS

In this small study of injury free men and women the results show the FMS could be accurately scored by people with a varying degree of experience with the FMS. Also, a single two-hour training session was sufficient for reliable scoring.

## REFERENCES

1. Cook G. *Movement*, On Target Publications, 2010.
2. Kiesel K, et al. *NAJSPT* **2**, 147-158, 2007.
3. Minick K, et al. *J Strength Cond Res* **24**, 479-486, 2010.
4. Teyhan D, et al. *US Army Med Dep J* **Jul-Sep**, 71, 2010.

# RELATIONSHIPS BETWEEN QUIET STANDING AND LIMITS OF STABILITY ASSESSMENTS IN CANCER SURVIVORS

Jeremy D. Smith<sup>1</sup>, Abigail L. Carpenter<sup>1</sup>, Gary D. Heise<sup>1</sup>, Chris P. Repka<sup>1</sup>, & John H. Challis<sup>2</sup>

<sup>1</sup>Rocky Mountain Cancer Rehabilitation Institute, University of Northern Colorado, Greeley, CO

<sup>2</sup>The Pennsylvania State University, University Park, PA

email: jeremy.smith@unco.edu

## INTRODUCTION

Common side effects of chemotherapy and radiation treatments in cancer survivors include peripheral neuropathy and vestibular dysfunction. These side effects can lead to a loss of balance, increasing the risk of falling. However, balance and posture in a cancer population has received little to no attention in the research literature. Previous results in a cancer population demonstrate that traditional center of pressure (COP) based measures during quiet standing are sensitive to changes in surface and vision conditions [1,2].

Research has suggested that quiet standing assessments are not associated with an ability to recover balance after a balance perturbation [3,4,5]. In cancer survivors who exhibit deficits in posture and balance it is important to understand whether quiet standing assessments alone are enough to identify individuals who may be at a greater risk of falling. Limits of stability (LOS) tests are another means of assessing postural stability. In these assessments, an individual's willingness to approach the stability boundary is assessed by quantifying how far a person is willing to displace his or her COP in both anterior/posterior (AP) and medial/lateral (ML) directions. LOS, however, typically require the availability of some type of harness system to provide support in case of a loss of balance during the assessment. These harness systems may not be available in a clinical setting.

Thus, the purpose of this study was to determine whether measures from LOS and quiet standing assessments are related and essentially provide practitioners with the same information. It was hypothesized that more demanding tasks during quiet standing (e.g., standing on a foam surface with eyes closed) would exhibit higher correlation

coefficients with LOS measures given the increased fluctuations of the COP during these types of assessments.

## METHODS

Quiet standing was measured in cancer survivors ( $n=11$ ; mass =  $75.6 \pm 22.1$  kg; height =  $1.60 \pm 0.05$  m; age =  $56 \pm 14$  years) during four different conditions. For quiet standing assessments, participants stood on a rigid surface with eyes open (RSEO), a rigid surface with eyes closed (RSEC), a compliant surface with eyes open (CSEO), and a compliant surface with eyes closed (CSEC). In addition, participants performed a LOS assessment that involved individuals leaning forward, backward, left, and right as far as possible without losing their balance. Participants were instructed to use an ankle only strategy to perform the movements, and when movements at the other joints were observed, the test was repeated. Figure 1 presents an example stabilogram for each condition.

Force data were sampled at 1000 Hz for 30 s during all assessments. Traditional COP based measures of postural steadiness were calculated in accordance with previous literature [6]. Time-to-boundary measures were also included and were based on previous literature [7]. A lower TTB is indicative of lower postural steadiness given that less time would be available for individuals to recover from a perturbation to their balance.

Root-mean-squares (RMS) of the AP and ML COP, total excursion of the AP and ML COP, mean velocity of the AP and ML COP, 95% confidence ellipse area, mean frequency of AP and ML COP, 95% power frequency of the AP and ML COP, fractal dimension of the confidence ellipse, and absolute minimum TTB were investigated.

COP measures were correlated between LOS assessments and each of the quiet standing assessments. For a two-tailed test, the critical r-value for determining statistical significance was 0.60 ( $n = 11$ ;  $\alpha = 0.05$ ).

## RESULTS AND DISCUSSION

A total of 52 correlations (13 COP measures x 4 contrasts) were analyzed and only two were statistically significant: RMS distance of the ML COP (RSEO) and LOS ( $r = 0.61$ ); mean frequency of the ML COP (CSEO) and LOS ( $r = 0.60$ ).

The lack of correlation between static assessments and LOS, a dynamic assessment, is consistent with previous results in the literature. Mackey and Robinovitch reported that postural steadiness during quiet stance was not related to the ability to recover balance from a maximum lean test [3]. Maki et al [4] found that quiet standing measures did not correlate with induced sway during force platform translations. Owings et al. [5] concluded that postural steadiness during quiet standing was independent of the ability to recover balance after a tethered release and after an unexpected trip. Others [3] have suggested that the lack of correlation between static and dynamic postural assessments may be due to differences in control strategies between the two tasks. Our results agree with this

interpretation and suggest that the control strategy during quiet stance was different than the control strategy during the LOS assessment. Both quiet standing and some form of dynamic assessment (e.g., LOS) should be used to assess postural steadiness in cancer survivors.

## CONCLUSIONS

Our hypothesis that more demanding tasks during quiet standing would exhibit higher correlation coefficients with LOS measures was rejected. COP measures during LOS assessments and quiet standing appear to be independent of each other.

## REFERENCES

- [1] Carpenter, A et al. (2011). ACSM abstract C-38-Posture/Balance, Denver, CO.
- [2] Smith, J et al. (2011). ACSM abstract C-38-Posture/Balance, Denver, CO.
- [3] Mackey, D & Robinovitch, S (2005). *Clinical Biomech*, 20, 776-783.
- [4] Maki, B et al. (1990). *J Am Geriatr Soc*, 39, 1-9.
- [5] Owings, T et al. (2000). *J Am Geriatr Soc*, 48, 42-50.
- [6] Prieto, T et al. (1991). *IEEE Trans Biomed Engin*, 43, 956-966.
- [7] Slobounov, S et al. (1998). *J Gerontol A Biol Sci Med Sci*. 53, B71-8.

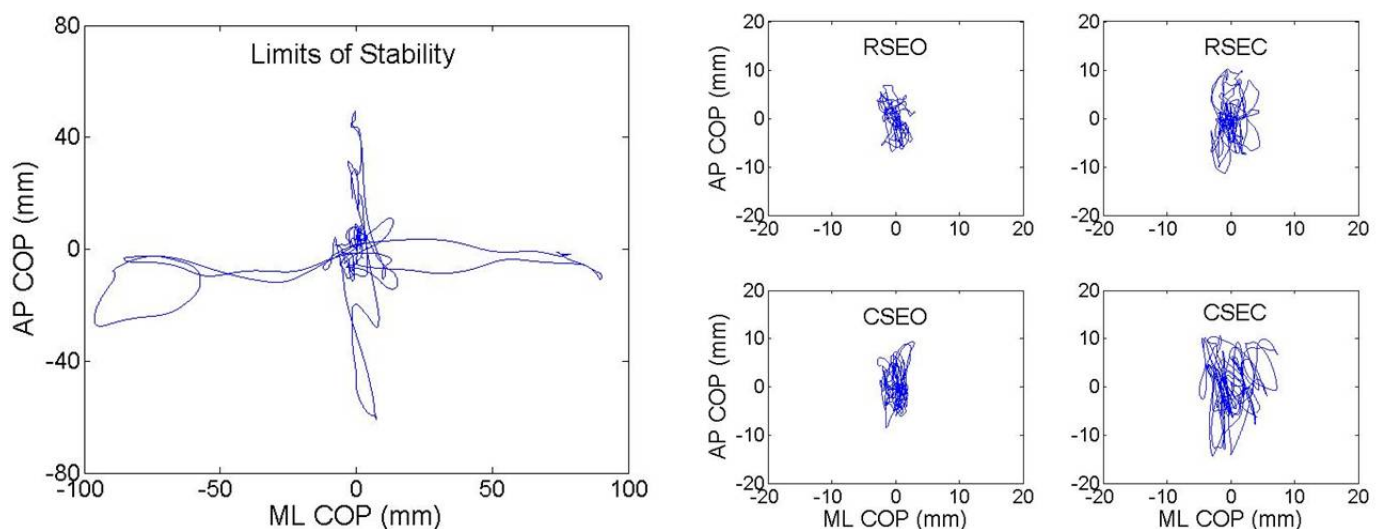


**Figure 1.** Stabilograms of the LOS (left panel), RSEO (top, middle panel), RSEC (top, right panel), CSEO (bottom, middle panel), and CSEC (bottom, left panel) conditions. These data are from one participant that was chosen at random to illustrate the characteristic differences in COP trajectories during the five tests.

# Mechanical Properties of Muscle in Hamstring Contractures of Children with Spastic Cerebral Palsy

<sup>1</sup>Lucas R. Smith, <sup>1</sup>Ki S. Lee, <sup>1</sup>J. Austin Carr, <sup>1</sup>Samuel R. Ward, <sup>2</sup>Henry C. Chambers, <sup>1</sup>Richard L. Lieber

<sup>1</sup>University of California and V.A. Medical Center, San Diego

<sup>2</sup>Rady Children's Hospital, San Diego, CA

email: rlieber@ucsd.edu web: <http://muscle.ucsd.edu>

## INTRODUCTION

Children with spastic cerebral palsy (CP) often develop hamstring contractures; however, the mechanism of contracture formation is not known. Contractures represent a resistance of muscle to increased length, but the structural elements responsible for increased stiffness are not known [1]. Previous work showed that single fibers from “contractured” muscle tissue has increased passive stiffness that could lead to the overall increased stiffness of the muscle [2]. Interestingly, the opposite result was observed when scaled to bundles of muscle fibers, as bundles from typically developing (TD) children were stiffer than contractured bundles [3]. Unfortunately, these samples were compared across a variety of muscles, which may have confounded the results. To avoid potential complications associated with comparing among different muscles, the purpose of the current study was to investigate passive mechanical properties of two specific hamstring muscles involved in gait—gracilis (GR) and semitendinosus (ST).

Despite new therapies, current best practices are unable to prevent contractures. Further understanding of the mechanism of contracture and the elements responsible for them could lead to new therapies to prevent contracture development and improve muscle function.

## METHODS

Biopsies were obtained during hamstring lengthening surgery for patients with CP and from the hamstring autograft used in ACL reconstruction surgery for TD patients. All procedures were performed with full IRB approval from UCSD.

Biopsies were removed and placed directly into a glycerol relaxing solution. Single fibers were dissected in chilled relaxing solution and transferred to a loading chamber at room temperature. The fiber was attached to a force transducer on one end and a motor arm on the other end. Muscle fiber sarcomere length was measured by laser diffraction and monitored using a photodiode. Fiber length was set to the minimum length that produced measurable force. The motor stretched the fiber in approximately 0.25  $\mu\text{m}$  sarcomere length increments. Force was continuously measured over 2 minute time interval while the fiber underwent stress-relaxation. Stretches were repeated  $\sim 10$  times. Fibers stress vs. sarcomere length curves were linearly fit. Fiber bundles were measured in the same way as single fibers but with a quadratic

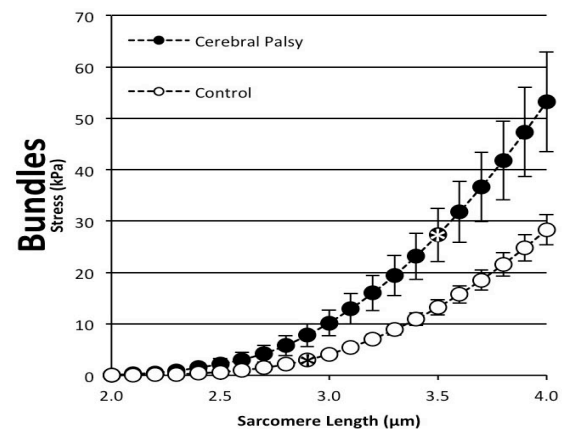


**Figure 1:** Average stress vs sarcomere length fits of gracilis bundles. CP bundles are stiffer at longer sarcomere lengths. (\*) in vivo sarcomere length. stress-strain fit (Fig. 1).

Single fibers were homogenized in sodium dodecyl sulfate-vertical agarose gel electrophoresis (SDS-VAGE) sample buffer used in gel electrophoresis [4] to determine titin size. Titin mass was calculated by regression based on three standard lanes.

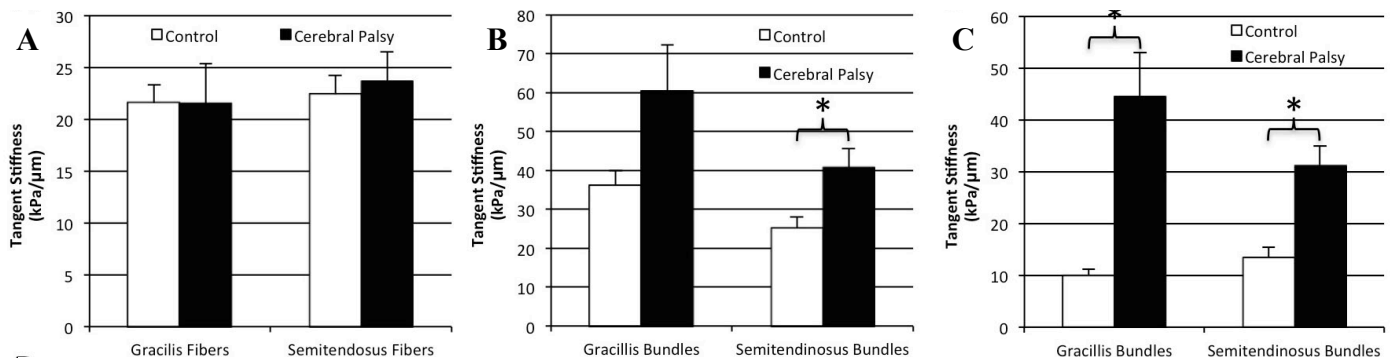


**Figure 2:** Tangent stiffness measures of fibers (A), bundles (B, C) from fits at a sarcomere length of 4.0 μm (A,B) or at the *in vivo* sarcomere length measured at 90° of hip and knee flexion (C). CP fibers are not significantly stiffer than controls, but CP bundles are stiffer and the stiffness difference is greatly enhanced at *in vivo* sarcomere lengths.

Sarcomere lengths were determined *in vivo* using specialized biopsy clamps. After the muscle was exposed the leg was placed in 90° of hip and knee flexion and the biopsy clamp was engaged. The clamped biopsy was then freed and placed in a fixing solution for 3 days. Sarcomere length was determined by laser diffraction after fixation.

## RESULTS

To compare stiffness across samples and muscles, tangent stiffness at a sarcomere length of 4.0 μm was calculated (Fig. 2A, 2B). A 3-way ANOVA was run with specimen scale, muscle, and condition with significant main effects ( $p < 0.05$ ). There was also a significant condition by scale interaction, suggesting a CP-dependent difference in bundle properties. *Post Hoc* tests demonstrated that, in contrast to previous studies in the upper extremity [2], stress was equal between control and contractured fibers at all sarcomere lengths for both gracilis and semitendinosus muscles (Fig. 2A). However, when fiber bundles were considered,

contractured muscle was stiffer than control muscle ( $p < 0.05$ ). Sarcomere strain experienced by the muscle *in vivo* was also investigated. At a position of 90° of hip and knee flexion CP muscles had significantly longer sarcomere lengths than predicted by model data for controls (Fig. 3). This means that bundles *in vivo* at the same joint configuration would produce much larger stiffness for CP (Fig. 2C). Titin molecular weight has been linked to passive stiffness of skeletal muscle fibers [5]. However, there was no significant difference in titin molecular weight between CP and control fibers in either muscle tested (CP: 3784±27 kDa; TD: 3747±21 kDa).

## DISCUSSION

These results demonstrate that the passive mechanics of gracilis and semitendinosus muscle cells themselves are not altered in contracture, but that the ECM connecting fibers together is altered and becomes stiffer in CP muscle. Because fiber bundles have a non-linear stress strain relationship, this difference becomes more pronounced at greater sarcomere lengths. This is compounded by the fact that CP muscles have longer sarcomere lengths *in vivo*. These results implicate a major role of the ECM in the increased passive stiffness in joint contracture, rather than titin mechanics.

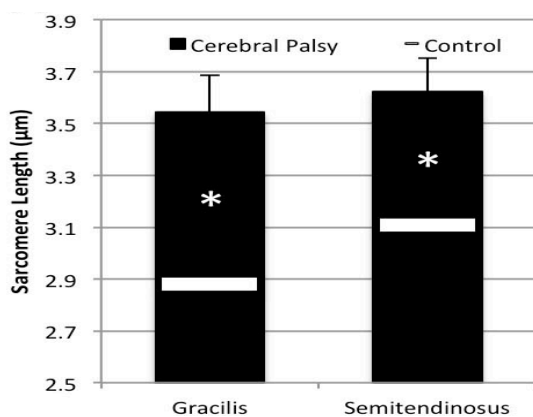


**Figure 3:** *In vivo* sarcomere length measured with biopsy clamps at 90° hip and knee flexion. Control lines are from model predictions.

## REFERENCES

1. Foran et al. *Dev Med Child Neurol.* **47**:713-717, 2005.
2. Fridén and Lieber. *Muscle Nerve.* **27**:157-164, 2003.
3. Lieber et al. *Muscle Nerve.* **28**:464-471, 2003.
4. Warren et al. *Electrophoresis.* **24**:1695-1702, 2003.
5. Prado et al. *J Gen Physiol.* **126**:461-480, 2005.

# THE EFFECT OF WHOLE BODY VIBRATION ON PROPRIOCEPTION IN LUMBAR SPINE

<sup>2</sup>Amy Solc, <sup>1</sup>Neha Chopra, <sup>1</sup>Sylvain Grenier

<sup>1</sup>Laurentian University, Sudbury, Ontario, CDN

<sup>2</sup>McMaster University, Hamilton, Ontario, CDN

email: [sgrenier@laurentian.ca](mailto:sgrenier@laurentian.ca)

## Introduction

Whole-body vibration has long been linked to low back pain (Okunribido et al. 2007; Lis et al., 2007). This may be related to diminished quality of afferent information from mechanoreceptors sent to the central nervous system, making the resulting muscle response inefficient. Whole body vibration has been found to cause fatigue in the back, perhaps making muscles less reactive (Okunribido et al. 2007). There are many different methods to test proprioception, depending on which aspects of proprioception are being measured. This study uses velocity following and velocity replication tasks to test proprioception.

## Methods

Seven female subjects were exposed to two sessions; 45 minutes of static sitting, and 45 minutes of whole-body vibration at a magnitude of 0.8 m/s/s, randomly applied on different days. Two different proprioceptive tasks were performed before and after the exposure to the two seated conditions. For velocity following task, subjects were exposed to passive movement starting in extended position and subjects were asked to follow along with four different speeds (10, 20, 30, 45 deg/s) in random order providing as little resistance as possible. Torque production was a measure of error in this case. For velocity replication task, subjects were exposed to passive movement starting in flexed position with speed randomly chosen. Subjects were then asked to replicate previous speed through range of motion. The difference in speed was the measure of error in this case. Both tests were repeated twice in random order.

## Results

The seated condition or vibration exposure had no significant effect on the velocity replication (figure 1) or “following” (figure 2) tasks. Significant differences were found in the speed of motion, type of movement and interaction between the two for the “following” tasks. As the speed increased the absolute torque error decreased for both seated conditions (figure 3). Flexion movement was more difficult to follow at lower speeds. Significant differences were found in the speed, and pre/post tests for the replication tasks. Movements were more difficult to follow at higher speeds for both seated conditions (figure 1). “Following” before the exposure was better than “following” after exposure for both seated conditions (figure 3). Subjects could reproduce velocities with less error at slower speeds (figure 1) but they could “follow” velocities with less error at faster speeds (figure 2).

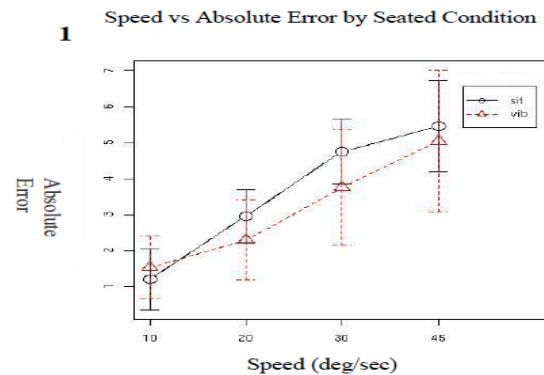


Figure 1: There was no difference in speed replication error when comparing vibration exposure and sitting.

Speed vs Average Torque by Seated Condition

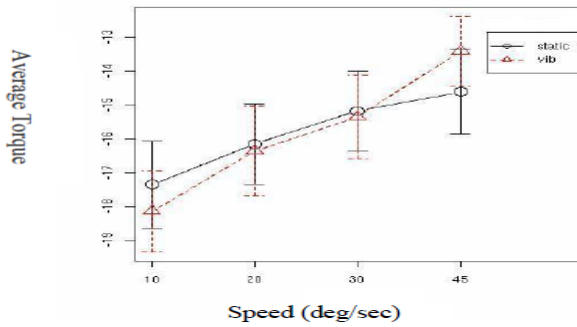


Figure 2: There was no difference between vibrations exposure and sitting in error during following tasks.

Speed vs Average Torque by Pre/Post Test

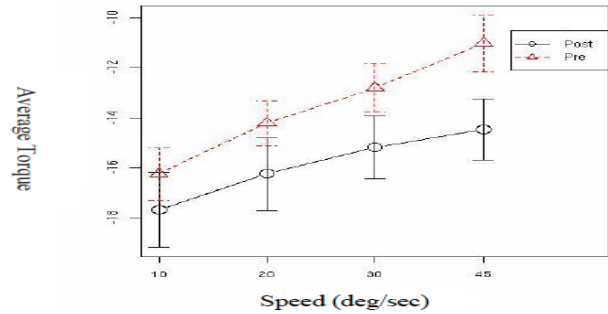


Figure 3: Following the Biodex was more difficult at lower speeds and after vibration exposure. The pre-post difference was greater at higher speeds.

**Discussion and Conclusion:** Whole-body vibration did not have an effect on the proprioceptive system's ability to follow or match a velocity of movement (figure 4). Evidence suggests that the brain uses internal models to plan and perform smooth and accurate movement with feed forward and feedback control. Two types of internal models are known- Forward models and Inverse models. Forward model by feedback error learning mechanism can execute slow movements accurately (Miall and Wolpert, 1996). Fast movements cannot be executed solely under feedback control, due to the delay in loops, thus inverse dynamics model controlled through motor learning is viable for fast movements (Kawato, 1999). These results support the presence of internal models in the cerebellum and movements can thus be coordinated in dynamic environments by motor learning and adapting the internal model.

2 Pre/Post Test vs Absolute Error by Seated Condition

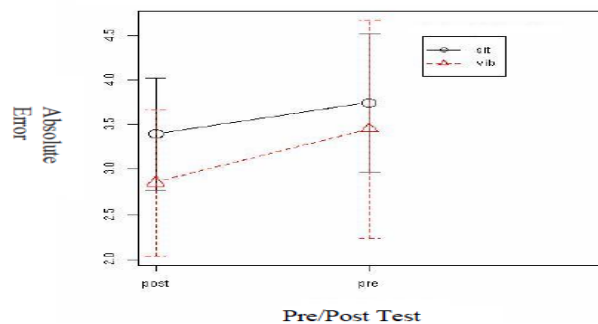


Figure 4: Vibration exposure resulted in reduced speed replication errors. In both cases the error decreased after exposure.

## REFERENCES

- Okunribido et al. (2007): Appl. Ergon. 38 (2007), pp. 29–38.
- Lis et al. (2007): Eur. Spine J. 16 (2007), pp. 283–298.
- Miall and Wolpert (1996): Neural Networks. 9 (8) (1996), pp. 1265-1279.
- Kawato (1999): Current Opinion in Neurobiology 9 (1999), pp. 718-727.



instantaneous ankle position and the virtual ankle path, as well as functional electrical stimulation to ankle muscles to help with toe clearance during swing and ankle push-off the late stance. Target templates of ankle path were created for training that were based on stroke subjects' pre-training baseline data and healthy elderly subjects' data at the same walking speed.

Kinematic data from the right leg were collected while subjects walked with the leg exoskeleton. To quantify the deviation between stroke subjects' actual ankle path to the virtual ankle path derived from that of healthy controls, we computed the area enclosed between the two during the swing phase before and after 5-day training. Subjects' preferred over-ground walking speeds were also recorded.

## RESULTS AND DISCUSSION

Both the stroke survivors showed improvements in walking patterns after 5 days of training. Preferred over ground walking speeds increased slightly for both subjects (S1: 0.81  $\rightarrow$  0.86 m/s; S2: 0.7  $\rightarrow$  0.76 m/s).

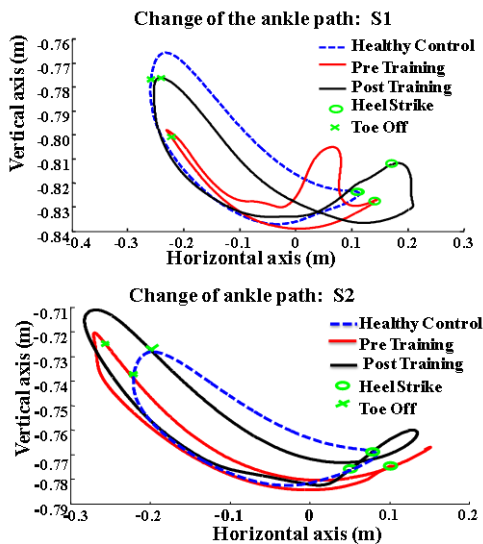


**Figure 2:** Change in the ankle path of subjects 1 (upper panel) and 2 (lower panel) with training.

Both the subjects walked with an ankle path closer to healthy subjects' ankle path by the end of one week of training (Fig.2), evidenced by a smaller computed area between the paths compared to the pre-training baseline. The computed area of subject

one was 105 cm<sup>2</sup> before training and 57 cm<sup>2</sup> after training. The computed area of subject two was reduced from 71 cm<sup>2</sup> to 52 cm<sup>2</sup>.

Increased total joint range of motion during swing phase in treadmill walking was also demonstrated after the training compared to the baseline. For subject one, the total hip joint excursion increased from 17° to 24° during swing phase, total knee joint excursion increased from 15° to 45° and total ankle joint excursion increased from 7° to 27°. For subject two, the total hip joint excursion increased from 17° to 19°, knee joint excursion increased from 6° to 12° during swing phase of the gait cycle and ankle joint excursion increased from 4° to 7° during swing phase of the gait cycle.

## CONCLUSIONS

Both stroke survivors in this preliminary study showed improvements in their walking patterns after receiving only five training sessions. Gait speed changed in the desired direction but less than the typically reported minimal detectable difference. These results suggest that robotic gait training emphasizing error-enhancement may have potential to improve walking capacity in the long-term for chronic stroke survivors. Future work is to conduct a relatively long-term training protocol with this robotic error-enhancement paradigm and to compare the changes in walking ability for stroke survivors receiving error-enhancement to those receiving assist-as needed robotic training. This will allow us to identify the training strategy that best facilitates improved walking ability after stroke.

## REFERENCES

1. Dhamoon et al. Stroke, 2009.
2. R. Riener et al., IEEE Trans Neural Syst Rehabil Eng, 2005.
3. Emken and Reinkensmeyer. IEEE Transactions on Neural Systems and Rehabilitation Engineering, 2005.
4. Banala et al. IEEE International Conference on Robotics and Automation, 2007.

## ACKNOWLEDGEMENTS

Supported by NIH grant HD038582

# THE EFFECTS OF ANKLE BRACING ON JOINT MOMENTS AND LOADING RATES DURING JUMP LANDING TASKS

Elizabeth D. Stafford and Jason C. Gillette  
Iowa State University, Ames IA, USA  
email: [estaffo1@iastate.edu](mailto:estaffo1@iastate.edu)

## INTRODUCTION

Ankle sprain is the most common injury in sports [1]. However, the question of whether or not prophylactic ankle bracing is effective at preventing sprains is still a topic of much debate. Given that tibial internal and external rotation are coupled with pronation and supination of the foot in weight bearing [2], the impact of short and long term bracing at the ankle on muscle firing patterns, loading patterns, and kinematics at the knee and the hip are important considerations. Richards et al. (2002) found that ankle inversion moments during landing from a spike jump were a significant predictor of patellar tendinopathy in male volleyball players [3]. Santos et al. (2004) assessed two rotation tasks, one with arms (ball catching task) and one without (target touching), while subjects were wearing ankle braces in single leg stance [4]. Their findings indicated that when wearing the ankle brace, the subjects demonstrated decreased trunk rotation during the ball catching task and increased knee axial rotation during the target touching task. Increased axial rotation at the knee may put the knee joint at higher risk for injury during forceful trunk rotations when the ankle is braced.

The purpose of the current study was to investigate the effect of functional fatigue on lower extremity response to jump landing tasks with and without a semi-rigid ankle brace. Suboptimal positioning when landing from a jump is a common mechanism of injury for ankle sprain and anterior cruciate ligament (ACL) injuries. It was expected that knee and hip joint rotations would be affected by restricting ankle inversion/eversion with a brace. Therefore, it was hypothesized that knee and hip frontal plane moments and loading rates would be greater in the braced condition than the unbraced condition. It was also hypothesized that these joint moments would further increase in the braced condition when the subjects were fatigued.

## METHODS

Ten individuals (2 males/8 females, age  $22\pm 1$  years, height  $1.71\pm 0.10$  m, mass  $73.4\pm 26.6$  kg) participated in the study. Breg Ultra FullCourt ankle braces were used since they are worn by this institution's volleyball team. For the pre-fatigue tests, participants performed 2 trials of forward and backward jumps starting on both feet and landing on one foot only. The jumps were performed to the left and right sides starting at a  $45^\circ$  angle to the force platform. The jumps were performed in both the braced and unbraced conditions for a total of 16 pre-fatigue and 16 post fatigue trials. Two force platforms (AMTI) were used, along with an 8 camera motion capture system (Vicon). Joint moments at the knee and the hip were calculated during the jump landing using inverse dynamics. The jump landing was defined to occur when the vertical ground reaction force exceeded 50 N to when it returned to body weight after the landing impact. Loading rates were determined by taking the first central difference of the joint moments and analyzing values that were increasing in magnitude. Ankle joint moments were not included because their meaning would be unclear during bracing.

After finishing the pre-fatigue testing, participants completed a fatigue protocol while wearing the ankle braces. The fatigue protocol included the Southeast Missouri agility drill (SEMO) and use of a Bosu, cones, and hurdles. Participants averaged a score of 15 on the Borg scale of perceived exertion at the end of the fatigue protocol, indicating that they had worked "hard". Multivariate ANOVA was performed to assess whether joint moments and loading rates were dependent upon bracing, type of jump, fatigue, and their interactions (SPSS). When significant main effects were found, differences between braced vs. unbraced, forward vs. backward jumps, and non-fatigued vs. fatigue conditions were tested with univariate ANOVA. Significance was set at  $p < 0.05$ .

## RESULTS AND DISCUSSION

Peak joint moments and loading rates were dependent upon bracing and type of jump ( $p < 0.01$ ). Joint moments and loading rates were not dependent upon fatigue or any interactions between comparisons.

**Bracing (Table1):** Peak hip flexion and hip adduction moments were significantly higher in the braced than in the unbraced condition ( $p < 0.04$ ). In addition, peak knee extension, knee flexion, knee varus, and hip flexion loading rates were significantly higher in the braced condition ( $p < 0.04$ ). The most striking differences were the increases in hip adduction moments ( $p < 0.02$ ) and knee extension loading rates ( $p < 0.01$ ) when braced.

**Type of Jump:** Peak knee flexion, hip extension, and hip abduction moments were significantly higher in the forward jump than in the backward jump direction ( $p < 0.01$ ). In addition, peak knee extension, knee flexion, hip extension, hip flexion, and hip abduction loading rates were significantly higher in the forward jump ( $p < 0.04$ ). In contrast, peak knee varus, knee valgus, and hip adduction moments were significantly higher in the backward jump than in the forward jump ( $p < 0.03$ ). Hip adduction loading rates were also significantly higher in the backward jump ( $p < 0.01$ ). The most distinct differences were the increases in hip abduction moments ( $p < 0.01$ ) and hip abduction loading rates ( $p < 0.01$ ) with the forward jumps.

The first hypothesis that knee and hip frontal plane moments and loading rates would increase with ankle bracing was partially supported. Hip adduction moments and knee varus loading rates significantly increased with bracing, indicating the value of examining both moments and loading rates. The second hypothesis that knee and hip frontal plane moments would further increase with fatigue

was not supported. There were no significant differences due to fatigue, although this observation may be due to an ineffective fatigue protocol or due to test movements that were not challenging enough to detect changes.

There were numerous significant differences in joint moments and loading rates when comparing backward and forward jumps. Fundamental kinetic differences between these types of jumps were demonstrated by significantly higher hip abduction moments and loading rates during forward jumps ( $p < 0.01$ ) and significantly higher hip adduction moments and loading rates during backward jumps ( $p < 0.01$ ). Although there were no significant interactions, common main effects of bracing and type of jump indicate that knee extension, knee flexion, and hip flexion loading rates during braced forward jumps and hip adduction moments during backward jumps merit further study with a larger sample size.

## CONCLUSIONS

Overall, individuals displayed increased hip joint moments and knee joint loading rates during jump landings when wearing an ankle brace. Forward and backward jumps were kinetically different, which would support testing and potentially training with both types of jumps if a target movement involves multidirectional jumping.

## REFERENCES

1. Safran MR, et al. *Med Sci Sports Exerc*, **31**, S429-437, 1999.
2. Neumann DA. *Kinesiology of the musculoskeletal system: foundations for physical rehabilitation*, 2002.
3. Richards DP, et al. *Clin J Sport Med*, **12**, 266-272, 2002.
4. Santos MJ, et al. *Clin Biomech*, **19**, 964-971, 2004.

**Table 1:** The effects of bracing on joint moments and loading rates (average  $\pm$  SD).

| Condition | Hip Flexion Moment (N·m/kg) | Hip Adduction Moment (N·m/kg) | Knee Extension Loading Rate (N·m/kg·s) | Knee Flexion Loading Rate (N·m/kg·s) | Knee Varus Loading Rate (N·m/kg·s) | Hip Flexion Loading Rate (N·m/kg·s) |
|-----------|-----------------------------|-------------------------------|--|--------------------------------------|------------------------------------|-------------------------------------|
| Braced    | 1.30 $\pm$ 0.57*            | 0.44 $\pm$ 0.22*              | 73.2 $\pm$ 27.6*                       | 64.6 $\pm$ 41.6*                     | 33.4 $\pm$ 15.6*                   | 110.7 $\pm$ 57.7*                   |
| Unbraced  | 1.05 $\pm$ 0.43             | 0.33 $\pm$ 0.18               | 59.6 $\pm$ 18.4                        | 49.4 $\pm$ 27.4                      | 27.2 $\pm$ 9.3                     | 85.6 $\pm$ 38.5                     |

\* Braced > Unbraced ( $p < 0.04$ )

# GENDER DIFFERENCES IN LOWER EXTREMITY BIOMECHANICS DURING LANDING ARE ASSOCIATED WITH HIP AND KNEE EXTENSOR STRENGTH

<sup>1</sup>Kristen M. Stearns and <sup>1</sup>Christopher M. Powers

<sup>1</sup>University of Southern California, Los Angeles, CA, USA

email: [kristen.stearns@gmail.com](mailto:kristen.stearns@gmail.com)

## INTRODUCTION

Female athletes sustain a higher number of ACL injuries when compared to their male counterparts [1]. While the cause of this gender bias is unknown, it is thought that females demonstrate a specific biomechanical profile during sports specific maneuvers that may place them at increased risk for injury. For example, it has been shown that females tend to exhibit greater knee extensor moments relative to hip extensor moments, and exhibit greater knee valgus moments and angles when compared to males [2,3]. In addition, females tend to absorb more energy at the knee when compared to males during the deceleration phase of landing. In contrast, males tend to absorb more energy at the hip relative to the knee [4].

It has been suggested that weakness of the hip musculature may underlie the biomechanical strategy observed in female athletes during the performance of athletic tasks [5]. Specifically, diminished strength of the hip extensors relative to the knee extensors may place increased reliance on the knee musculature to control deceleration of the center of mass during landing. As such, we propose that an inter-limb muscle imbalance between hip and knee extensors may contribute to the “at risk” movement pattern observed in female athletes.

The purpose of this study was to evaluate the role of hip and knee extensor muscle performance on hip and knee biomechanics during landing in male and female athletes. We hypothesized that when compared to males, females would demonstrate greater knee extensor strength relative to the hip extensors and that this strength ratio would be associated with the sagittal plane moment distribution between the hip and knee during a double-leg drop-jump task.

## METHODS

Twenty-six recreational athletes (13 males and 13 females) between the ages of 18 and 25 participated in this study. Each participant was free from lower extremity pathology or previous injury and participated in 2 data collection sessions: 1) biomechanical analysis of a double-leg drop-jump task from a 36cm platform, and 2) isometric strength testing of the hip and knee extensors. Data were obtained from the dominant lower extremity, defined as the leg with which the subject would prefer to kick a ball and land on during a single-leg jump.

For the double-leg drop-jump task, lower extremity kinematics and ground reaction forces were collected using a 10-camera Qualisys Motion Capture System (250 HZ) and 2 floor-embedded AMTI force plates (1500 Hz). Average hip and knee extensor moments were calculated over the first 200 ms of the drop land task. Moments were calculated using inverse dynamics and are reported as internal moments, normalized to body mass. The average hip and knee extensor moment values were used to calculate the knee/hip extensor moment ratio. A ratio  $>1$  indicated that the knee extensor moment was greater in magnitude than the hip extensor moment, while a ratio  $<1$  indicated that the hip extensor moment was greater in magnitude than the knee extensor moment.

For the isometric strength testing, subjects performed 3 maximum isometric contractions of 5 seconds duration for both hip and knee extension. The peak isometric torque produced during the best repetition for each muscle group was identified and then used to calculate the knee/hip extensor strength ratio. A strength ratio  $>1$  indicated that knee extensor muscle strength was greater in magnitude than hip extensor muscle strength, while a ratio  $<1$

indicated that hip extensor muscle strength was greater in magnitude than knee extensor muscle strength.

Average hip and knee joint moments, peak hip and knee extensor muscle torques, and moment and strength ratios were compared between males and females using independent samples t-tests (one-tailed,  $p < 0.05$ ). Pearson's correlations were used to assess the relationship between the moment ratio and the strength ratio during the double-leg drop-jump task (one-tailed,  $p < 0.05$ ).

## RESULTS AND DISCUSSION

Although there were no significant differences in average knee or hip extensor moments between groups, females exhibited a trend towards higher knee extensor moments, and lower hip extensor moments compared to males (Table 1). However, females had a significantly higher knee to hip extensor moment ratio compared to males during the deceleration phase of the drop-jump ( $p = 0.01$ ; Table 1).

On average, females exhibited significantly lower peak isometric strength of the hip extensors ( $p = 0.0002$ ) and knee extensors ( $p = 0.003$ ) compared to males (Table 2). In addition, females had a higher knee to hip strength ratio compared to males ( $p = 0.03$ ; Table 2).

Pearson's correlation revealed a significant positive association between the knee/hip strength ratio and the knee/hip moment ratio during landing ( $R = 0.42$ ,  $p = 0.02$ ). The positive relationship indicated that individuals with greater knee extensor strength,

relative to hip extensor strength, generated greater knee moments relative to the hip during the deceleration phase of landing.

## CONCLUSIONS

The tendency of females to utilize greater knee moments relative to the hip during landing (i.e. knee strategy) has been proposed a potential risk factor with respect to ACL injury. The results of our study suggest that an intra-limb strength imbalance between the knee and hip extensors may underlie this biomechanical tendency. More specifically, weakness of the hip extensors relative to the knee extensors may explain why females tend to generate lower hip moments relative to knee moments during landing, as compared to males. As such, training programs aimed at improving hip muscle performance may be important consideration in decreasing the 'at risk' biomechanical profile observed in female athletes.

## REFERENCES

1. Agel J, et al. *Am J Sports Med* **33**, 524-530, 2005.
2. McLean SG, et al. *Clin Biomech* **20**, 863-870, 2005.
3. Sigward S, et al. *Scand J Med Sci Sports Ex* (epub ahead of print), 2011.
4. Decker MJ, et al. *Clin Biomech* **18**, 662-669, 2003.
5. Jacobs C, et al. *J Sport Rehab* **14**, 346-355, 2005.

## ACKNOWLEDGEMENTS

This research was supported in part by the Foundation for Physical Therapy.

**Table 1:** Comparison of the hip and knee extensor moments and moment ratio during the drop-jump task (\* indicates significant difference between groups).

|                | Average Knee Extensor Moment (Nm/kg) | Average Hip Extensor Moment (Nm/kg) | Knee/Hip Moment Ratio |
|----------------|--------------------------------------|-------------------------------------|-----------------------|
| <b>Males</b>   | 1.10 ± 0.2                           | 0.92 ± 0.2                          | 1.24 ± 0.3            |
| <b>Females</b> | 1.20 ± 0.2                           | 0.77 ± 0.3                          | <b>1.83 ± 0.8*</b>    |

**Table 2:** Comparison of peak isometric hip and knee extensor strength and the strength ratio between males and females (\* indicates significant difference between groups).

|                | Knee Extensor Strength (Nm/kg) | Hip Extensor Strength (Nm/kg) | Knee/Hip Strength Ratio |
|----------------|--------------------------------|-------------------------------|-------------------------|
| <b>Males</b>   | 3.7 ± 0.6                      | 4.4 ± 1.0                     | 0.88 ± 0.2              |
| <b>Females</b> | <b>3.0 ± 0.5*</b>              | <b>2.8 ± 0.8*</b>             | <b>1.09 ± 0.3*</b>      |

# ESTIMATION OF CURVATURE FEATURE USING A BIOMIMETIC TACTILE SENSOR

<sup>1</sup>Zhe Su, <sup>1</sup>Yao Li, and <sup>1</sup>Gerald E. Loeb

<sup>1</sup> University of Southern California, Los Angeles, CA, USA  
Email: [szhe.bme@gmail.com](mailto:szhe.bme@gmail.com) web: <http://mddf.usc.edu/>

## INTRODUCTION

Human's sense of touch is rich in the amount of information it can acquire simultaneously. Unlike vision, haptic sensing can extract information about many attributes of an object: shape, mass, volume, rigidity, texture, and temperature etc. A variety of technologies have been used in tactile sensors, but commercially available tactile sensors tend to be limited to relatively coarse arrays of normal force sensors based on compression of elastic materials. In fact, most of the commercially available robotic and prosthetic hands are not supplied with any tactile sensing.

Many technologies are difficult to apply to the curved, deformable "skin" that facilitates grip and few are able to resist damage in the electromechanically hostile environments in which hands are often used (moisture, grit, sharp edges, etc). One promising new candidate is the BioTac®, a biomimetically designed, multimodal array that provides most of the dynamic range of human tactile sensing for location, magnitude and vector direction of contact forces, micro-vibrations associated with slip and textures, and thermal flux resulting from contact with objects that differ in thermal effusivity(Figure.1), [1, 2, 3].

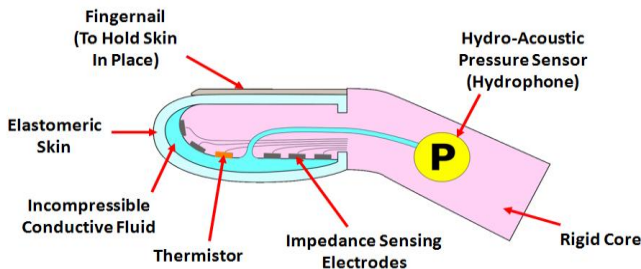


**Figure 1:** Schematic diagram of the BioTAC® biomimetic tactile sensor.

The mechanism of implementing these sensing modalities are: measurement of normal and shear forces detected by changes in impedance between electrodes as fluid pathways deform, detection of

slip-related microvibration which propagate through the skin and fluid and are detected by the hydro-acoustic pressure sensor, and thermal properties as detected by a thermistor capable of detecting heat flow between the preheated core and contacted objects.

Phillips and Johnson [4] showed that SA-I mechanoreceptors embedded in the skin of fingertips are particularly sensitive to spatial details for example: points edges, corners and different radius of curvatures. Psychological experiments also show that human are able to differentiate several forms of spatial pattern independent of contact force [5, 6]. To replicate this dedicated spatial feature extraction scheme, we designed a novel algorithm to facilitate the radius of curvature estimation on a BioTac® sensor.

Just like human fingers, the most sensitive region of our tactile sensors is located on the tip. We used the impedance signals from this cluster of four electrodes (*E7, E8, E9, and E10*) (Figure. 2) to characterize the spatial features from contacted object.

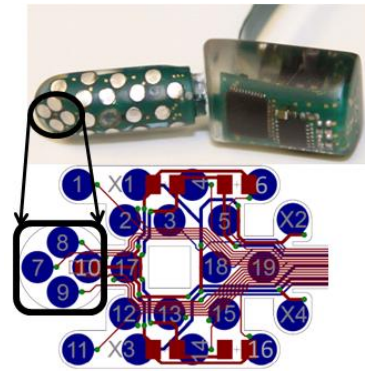


**Figure 2:** Electrodes array distribution of the tactile sensor corresponding to different spatial features.

## MODELS

In this work, we used a BioTAC® fingertip tactile sensor to probe an object. The radius of curvature is estimated from the deformation pattern detected by the pair of electrodes (*E7/E10* or *E8/E9* in Figure 2)

at the contact surface. The fingertip of BioTac® sensor is modeled as one quarter of a circle, which has a radius of  $R$ . The probed object is assumed rigid, frictionless, and circular with unknown radius  $r$ . The radius of the object can then be estimated from the measurable deformation at the BioTac® sensor. The indentation distance of deformation is define as  $d$  and tangential contact points are  $A$  and  $C$ . The angle between  $OA$  and  $OC$  is  $\theta$ , where  $O$  is the origin of the fingertip, (Figure. 3).

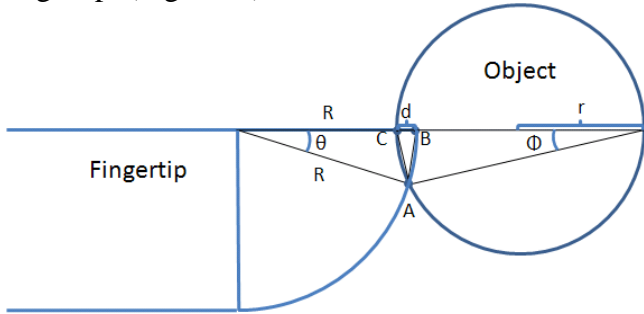


**Figure 3:** Schematic of mathematical model for radius of curvature estimation in the plane space.

We begin with deriving the geometric properties of the deformation at the BioTac® fingertip.

$$|AB| = 2R\sin\frac{\theta}{2} \quad (1)$$

$$|BC| = d \quad (2)$$

$$|AC| = d^2 + 4R(R-d)\sin^2\frac{\theta}{2} \quad (3)$$

$$\cos\angle ACB = \frac{d-2R\sin^2\frac{\theta}{2}}{\sqrt{d^2+4R(R-d)\sin^2\frac{\theta}{2}}} \quad (4)$$

$$\cos\angle ACB = \frac{|AC|}{2r} \quad (5)$$

The analytical solution for estimating the unknown object's radius of curvature is obtained.

$$r = \frac{d^2+4R(R-d)\sin^2\frac{\theta}{2}}{2(d-2R\sin^2\frac{\theta}{2})} \quad (6)$$

## RESULTS

The analytical solution indicates that estimating radius  $r$  depends on three variables:  $R$  and  $\theta$  are initially designed in the BioTac® tactile sensor, indentation  $d$  is measured by the distributed electrode array (Figure. 2). We have tested various radii of curvature by our designed estimation model, and the results are depicted in Figure 4.

The parameter  $\theta$  defines the effective contact area between the sensor and object; it is designed and built in BioTac®. We could predict the radius of curvature by only measuring the indentation distance  $d$ . initial contact point of the fingertip is labeled by red line in

the left circle, and the dotted lines are estimated radius for various objects.

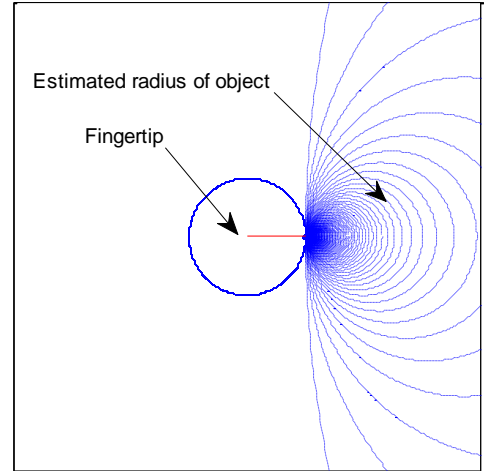


**Figure 4:** Simulation results for radius estimation.

## DISCUSSION AND FUTURE WORK

Human fingers tend to have the best discrimination for the objects with similar radius as the fingertip. The developed BioTac® sensor along with the estimation algorithm provides us a platform to further analysis of the sensitivity of human fingertip.

Biological tactile sensors in the skin of fingertip are relatively noisy. Thus, we plan to implement a probabilistic model, Gaussian Mixture Model (GMM) [7], to account for the noise in this proposed estimation model. We have found that GMM model is effective at extracting three dimensional force vectors [3]. Some other important spatial features (edges, corners, etc.) have also been successfully characterized on the GMM model.

## REFERENCES

- 1.N. Wettels, V. J. Santos, R. S. Johansson and G. E. Loeb, *Advanced Robotics*, 22(7), 829-849, 2008.
- 2.C. H. Lin, T. W. Erickson, J. A. Fishel, N. Wettels, G. E. Loeb, *IEEE Intl Conf on Robotics and Biomimetics*, 2009.
- 3.Wettels N., Fishel J.A., Su Z., Lin C.H., Loeb G.E., *Intl Conf on Humanoid Robots*, 2009.
- 4.Philips, J. R., Johnson, K. O. *Journal of Neurophysiology*, 46, 1192-2003, 1981.
- 5.Goodwin, A. W., John K. T., and Marceglia A. H. *Experimental Brain Research*, 86, 663-672,1991.
- 6.Goodwin, A. W., Wheat, H. E. *Somatosensory and Motor Research*, 9, 339-344, 1992.
- 7.G. MaLachlan and D. Peel. "Finite Mixture Models" Wiley, 2000.

# MOVING MUSCLE POINTS PROVIDE ACCURATE CURVED MUSCLE PATHS IN A MODEL OF THE CERVICAL SPINE

Bethany Suderman and Anita Vasavada

Washington State University, Pullman, WA, USA

email: [bethsuderman@wsu.edu](mailto:bethsuderman@wsu.edu)

## INTRODUCTION

Modeling muscle paths accurately in the cervical spine is challenging. Currently there are several common modeling methods for muscle paths; straight lines from origin to insertion [1], curved paths which wrap over objects [2], or (curved) paths consisting of straight line segments connecting via points fixed to bones [1, 3]. Modeled curved muscle paths have improved accuracy from modeled straight paths when compared to anatomic paths; however, they do not often take into consideration deformation of soft tissue with posture.

A recent improvement in musculoskeletal modeling is the development of moving muscle points. These points are similar to fixed via points but are not statically fixed within one body or segment. Using these points to model muscle paths will allow for curvature of paths to adapt to deformations in soft tissue as the neck rotates from one position to the next. We hypothesize that modeling moving muscle point paths in the neck during sagittal plane motion will provide more anatomically accurate muscle paths than paths modeled with fixed via points.

## METHODS

Subject-specific models of two approximate 50<sup>th</sup> percentile male subjects were created from axial and sagittal magnetic resonance images (MRI) in 5 sagittal plane head and neck postures;  $-30^\circ$  (flexion) to  $30^\circ$  (extension) in  $15^\circ$  increments. Vertebral body coordinate systems were determined by digitizing the corners of each vertebral body on sagittal scans. The origin was the average of all four corners. Axes of the bodies were determined as follows: y – vector connecting mid-point of upper and lower plates pointing cephalad, x – perpendicular to y axis in the mid sagittal plane passing through the origin, and z – cross product of x and y axes [4] (Fig. 1).

Anatomic muscle paths were determined by the centroid of the cross-sectional area traced on consecutive axial slices for all neck muscles in MRI scans of the different postures. Muscle centroid paths were smoothed using a cubic b-spline curve. Models were developed in OpenSim [5].

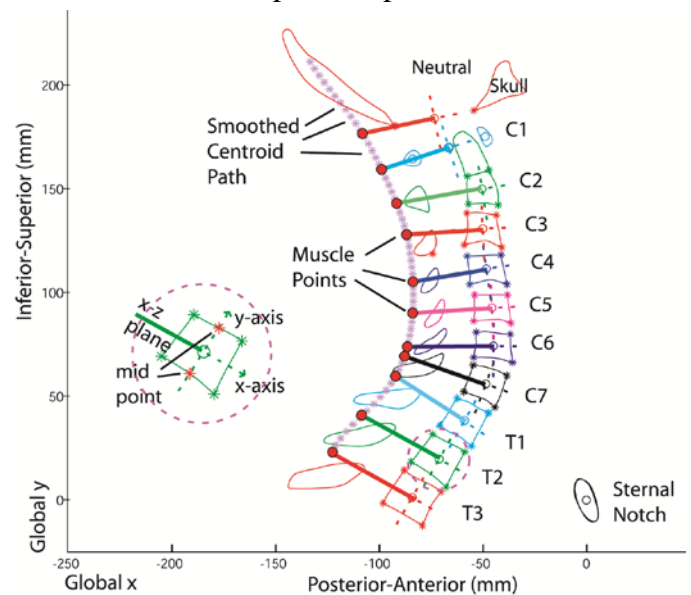


**Figure 1:** 2D representation of vertebral body coordinate systems, smoothed centroid muscle path (\* – light) and modeled muscle points (o – dark) for the semispinalis capitis muscle in the neutral posture.

Modeled muscle points were determined for each muscle path as the intersection of the x-z plane of each vertebral body's coordinate system (Skull, C1 – T3) with the smoothed centroid path for all postures (Fig. 1). Fixed via point paths were defined by the muscle points determined in the neutral posture only. Moving muscle point paths were represented by muscle points determined in all 5 postures. Because the moving muscle points changed with posture, the trajectories of each x and z coordinate with respect to the vertebral bodies were smoothed using a cubic (polynomial) fit over all 5 postures. Muscle points were connected by straight line segments to form the modeled curved path (Fig. 2).

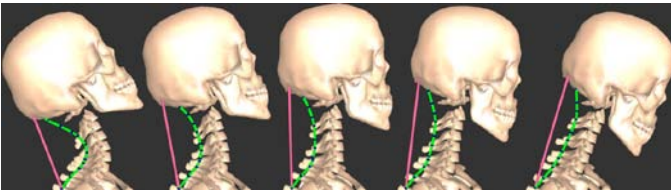


**Figure 2:** Model of the semispinalis capitis moving muscle point and straight path in 5 postures. From left to right: 30° and 15° extension, neutral, 15° and 30° flexion. Dark points on the curved path represent muscle points. The OpenSim model was imported into SIMM for visualization of muscle points.

To determine the anatomical accuracy of the modeled paths an error metric (EM) was defined that described the deviation of the modeled paths (moving muscle point, fixed via point or straight) from the smoothed centroid path at each centroid global y-value [2]. Percent improvement was calculated to compare EM of the modeled curved paths (moving muscle point or fixed via point) to EM of the modeled straight path, assuming the straight path was the worst possible modeled path.

## RESULTS AND DISCUSSION

Error metric values for each muscle and posture were found to be significantly different among all modeled paths ( $p < 0.01$ , one-way repeated measures ANOVA). Moving muscle point paths had significantly lower EM values than fixed via point paths ( $p < 0.01$ , paired t-test). Moving muscle point paths also provided a larger mean improvement than fixed via point paths [ $68.0\% \pm 19.5\%$  (SD) vs.  $50.6\% \pm 37.1\%$ ] when compared to straight paths for both subjects over all muscles (Fig. 3).

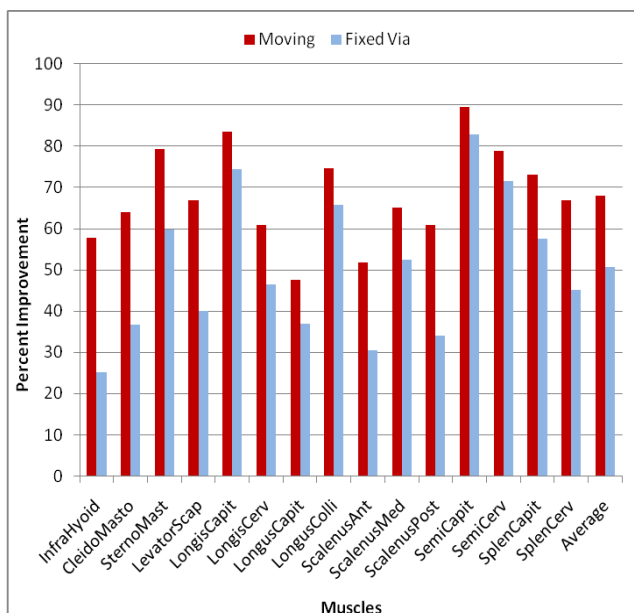


**Figure 3:** Mean percent improvement in EM of moving muscle and fixed via point paths compared to straight paths averaged for both subjects over all postures.

In a similar study by Vasavada et al. [2], curved muscle paths using one wrapping surface were determined for the Sternocleidomastoid (sternal head, SM) and Semispinalis Capitis (SeC). Error metric was also calculated between each wrapped path and centroid path. For both of these muscles the moving muscle point path provided a larger percent improvement in sagittal plane motion than the wrapped paths for subjects 1 and 2 respectively; SM [73.6% & 85.0% vs. 24.3%] and SeC [86.4% & 92.8% vs. 73.6%].

The moving muscle point method provides accurate muscle paths over a range of postures because it utilizes the centroid path over a range of postures, not just the neutral position. However, this required the acquisition of MRI scans of anatomic muscle paths over multiple postures. A limitation of this model is that moving muscle points were determined in sagittal plane postures only. To accurately represent postures out of the sagittal plane, MRI scans would need to be acquired in other postures (axial rotation and lateral bending).

## CONCLUSIONS

In this study we hypothesized that moving muscle points would provide more anatomically accurate modeled muscle paths than fixed via points. Our results indicate that moving muscle points are vital when describing the changes in distance from the x-z plane of a vertebral body coordinate system to the smoothed centroid path in each posture. The results support the hypothesis and suggest that the moving muscle point method should be used rather than the fixed via point to model muscle paths accurately.

## REFERENCES

1. Vasavada A, et al. *SPINE* **23**, 412-421, 1998.
2. Vasavada A, et al. *J Biomech* **41**, 1450-57, 2008.
3. Kruidhof J, & Pandy M. *Comp Methods Biomech and Biomed Engr* **9**, 343-352, 2006.
4. Siegler S, et al. *J Biomech* **35**, 543-548, 2002.
5. Delp S, et al. *Biomed Engr IEEE Trans* **54**, 1940-1950, 2007.

## ACKNOWLEDGEMENTS

Supported by NSF (CBET #0748303) and the National Center for Skeletal Muscle Research. We would also like to thank the University of British Columbia (UBC) MRI Research Centre.

# THE EFFECT OF SHOULDER POSITION ON SCAPULAR KINEMATICS IN A TRADITIONAL PUSH-UP

David N. Suprak, Jennifer A. Donegan, Gabriel L. Morales, and Joseph R. Stroschein

Western Washington University, Bellingham, WA, USA  
email: [David.Suprak@wwu.edu](mailto:David.Suprak@wwu.edu)

## INTRODUCTION

The push-up is a common exercise used recreationally for strength improvements as well as in the rehabilitation of upper extremity disorders. Much of the past research into the potential efficacy of the push-up has focused on muscle activation levels and forces encountered in different push-up variants, while very little has examined the kinematic patterns exhibited in these exercises.

Activation levels of the scapular stabilizing muscles during push-up variations have been shown to depend on hand placement and joint angles during execution [1, 2]. The modified (knees down) push-up and push-up with a plus appear to promote a favorable upper trapezius/serratus anterior (UT/SA) activation ratio [3], while the wall push-up results in greater activation of the UT compared to that of the SA [4]. The degree of scapular stabilizer activation appears to be related to a complex interplay between the weight-bearing demand of the exercise and the degree of arm elevation during execution [5]. However, we have very little knowledge about the motion exhibited by the scapula during these exercises. This information would be especially useful in the rehabilitation setting, in which appropriate shoulder mechanics for restoration of health relies on proper positioning of the scapula during corrective exercises. The purpose of this study was to examine the effect of shoulder elevation on 3D scapular kinematics in a traditional push-up exercise.

## METHODS

Eight healthy subjects (4 males, 4 females, age  $21.38 \pm 1.19$  yrs.) participated in the study. Following a standardized warm-up for both arms, subjects removed shirts (females wore sports bras) for instrumentation and digitization. Kinematic data were collected via the Polhemus Fastrak magnetic tracking system, with receivers on the thorax, and

the dominant side ulna (proximal to the styloid) and scapula (via a custom-machined tracker) (Figure 1).

Following digitization of bony landmarks, subjects assumed a push-up position with their hands positioned so the middle finger was directly below the acromion process. The hand position was marked with tape on the floor to standardize placement across conditions. A 10-cm wood block was positioned on the floor such that it contacted the middle of the chest at the bottom of the push-up movement.

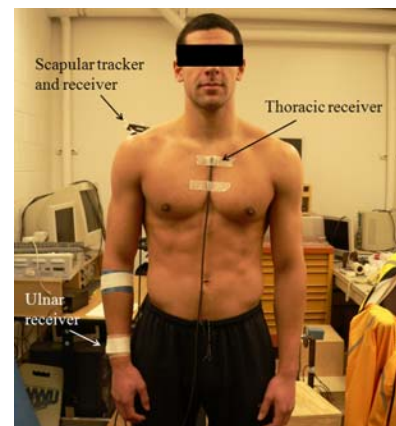


**Figure 1:** Experimental Set-up.

Subjects practiced push-ups with their shoulders in a self-selected (SS) position, with the shoulders adducted so the elbows were at the side upon descent (AS), and elevated to approximately 90° abduction (E) upon descent. Subjects performed three repetitions of each condition to a 4-second count (2 seconds down, 2 seconds up). Once familiarized with the procedures, subjects performed the three shoulder position conditions in a random order.

During the concentric phase in each condition, mean scapular orientations (posterior tilt, upward rotation, and external rotation) for the three repetitions were examined across the largest common elbow extension range of motion (ROM) for all subjects (105° - 40°).

## RESULTS AND DISCUSSION

There was no significant shoulder position by elbow flexion interaction effect on scapular posterior tilt (PT) ( $F[26, 182] = .966, p = .516$ ) (Figure 2). There was also no significant main effect of elbow flexion on PT ( $F[13, 182] = .487, p = .927$ ). However, PT was significantly affected by shoulder position ( $F[2, 182] = 22.96, p < .001$ ). Pairwise comparisons indicated PT was greater in both the SS and AS conditions ( $p = .01$  and  $p = .001$ , respectively), when compared to the E condition. However, no significant difference was found in PT between the SS and AS conditions ( $p = .122$ ).

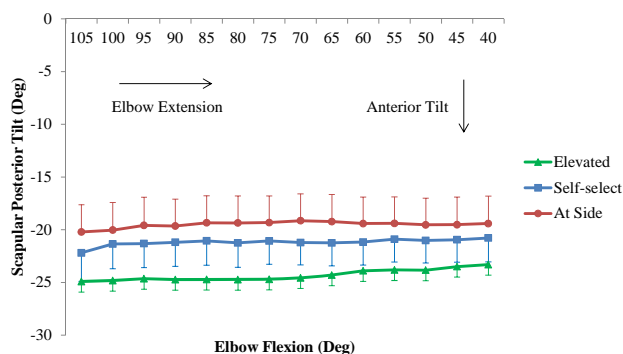


**Figure 2:** Scapular posterior tilt (mean  $\pm$  SEM) across elbow flexion angle for each shoulder position condition.

There was a significant shoulder position by elbow flexion interaction effect on upward rotation (UR) ( $F[26, 156] = 12.62, p < .001$ ). Figure 3 indicates that UR was highest in the AS condition, while it decreased consistently in both the SS and E conditions.

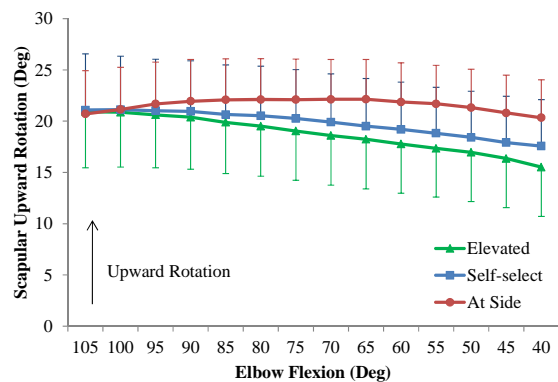


**Figure 3:** Scapular upward rotation (mean  $\pm$  SEM) across elbow flexion angle for each shoulder position condition.

There was a significant shoulder position by elbow flexion interaction effect on scapular external rotation (ER) ( $F[3.49, 24.45] = 2.94, p = .046$ ). Figure 4 indicates that, although the scapula internally rotated during the push-up in all three conditions, this pattern was more pronounced in the E condition.

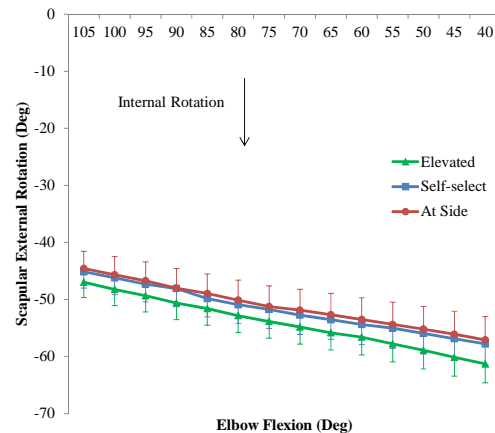


**Figure 4:** Scapular external rotation (mean  $\pm$  SEM) across elbow flexion angle for each shoulder position condition.

## CONCLUSIONS

The current data indicates that, during a traditional push-up, greater degrees of shoulder elevation may result in less PT across the concentric ROM, as well as decreasing UR and ER. These observations may be related to more favorable activation patterns of scapular stabilizing muscles with decreased shoulder elevation. However, muscle activation was not monitored in this study, and this hypothesis should be examined in the future. Practitioners may avoid elevated positions when prescribing these exercises in the rehabilitation of shoulder pathologies.

## REFERENCES

1. Cogley, RM, et al. *J Strength Cond Res* **19**, 628-633, 2005.
2. Decker, MJ, et al. *Am J Sports Med* **27**, 784-791, 1999.
3. Ludewig, PM, et al. *Am J Sports Med* **32**, 484-493, 2004.
4. de Oliveira, AS, et al. *J Electromyogr Kinesiol* **18**, 472-479, 2008.
5. Suprak, DN, et al. *J Strength Cond Res* **25**, 497-503, 2011.



# Energy Expenditure and Muscular Activation Patterns through Active Sitting on Compliant Surfaces

Rachel Surowiec, Henry Wang, Andrea Hite and D. Clark Dickin  
Biomechanics Laboratory – Ball State University, Muncie, IN, USA  
email: rksurowiec@bsu.edu

## INTRODUCTION

Modifications to various sitting surfaces have been made as a means to influence muscle recruitment levels and potentially influence energy expenditure through increased instability [1]. Replacing an office chair with an exercise ball or an air cushion may be helpful in increasing activity in the workplace [2]. However, the effects of sitting on an air cushion on energy expenditure and levels of muscle activation have not been quantified.

Active sitting is a concept that applies primarily to sitting surfaces that allow movement. The premise of active sitting is to permit or encourage the seated occupant to move [3]. Although active sitting can be performed on a stability ball or on an air cushion placed on a chair, it is not generally considered suitable to use a stability ball as a seating surface in many situations (e.g., at the office, in waiting areas). As such the purpose of the study is twofold, first to determine the levels of caloric expenditure using a direct measure of metabolic function and secondly to compare levels of muscle activity between an active sitting cushion, a stability ball and a firm sitting surface.

## METHODS

Eleven healthy female subjects (age=  $20 \pm 1.8$  yrs; height= $167.27 \pm 6.48$  cm; weight= $67.14 \pm 9.22$  kg) were recruited for the study. All subjects had a body mass index (BMI) of less than  $30 \text{ kg/m}^2$ . All subjects were able to sit for three, 10-minute sessions while maintaining an upright posture. Additionally, each participant completed an informed consent document outlining the experiment that was approved by a university Institutional Review Board.

To determine the level of muscular activity and metabolic cost of active sitting, three different task conditions were measured. The three tasks included 1) sitting on a flat surface, 2) sitting on an Automatic Abs air cushion (Licensing Services

International, Philadelphia, Pennsylvania) and 3) sitting on a stability ball (Power Systems Inc, Knoxville, Tennessee). The three conditions were assigned in random order and each lasted 10-minutes with a 5-minute break between conditions to permit a rest period and to prepare for the next sitting condition. All conditions were performed within the same day with the entire session lasting approximately 90 minutes.

Muscle activity was measured at one minute intervals throughout each 10-minute condition for a period of 10 seconds using a Delsys EMG system (Delsys Bagnoli Desktop EMG System, Boston, Massachusetts). Each subject had 6 pairs of surface EMG electrodes (Delsys DE-2.1 Single Differential EMG Electrode, Boston, Massachusetts) (inter-electrode distance: 1cm) attached to the external oblique, rectus abdominus, erector spinae, adductor longus, soleus, and tibialis anterior on both the right and left side of the body. The EMG signals were amplified (gain=1000, CMRR >92dB) and were collected at 2400 Hz. VICON Workstation 5.0 (Vicon, Denver, Colorado) was used to capture the raw EMG signals. Root-mean-square (RMS) was calculated for each muscle for the 10, 10-second trials taken during each 10-minute sitting condition using a custom C++ program.

Energy expenditure was measured via open-circuit direct calorimetry using a Parvomedics (Sandy, Utah) metabolic cart. Heart rate was measured using a heart rate monitor (Polar Electro Inc. Lake Success, New York) and transmitted to a receiver on the metabolic cart. Average energy expenditure was calculated based on the rates of oxygen consumption and carbon dioxide production during the three, 10-minute sitting tasks with sampling occurring every 30 seconds.

Using measures of direct calorimetry the effect of sitting surface (i.e. stability ball, cushion, flat) on energy expenditure, a one-way RM-ANOVA was

performed. To assess the effect of sitting surface on muscular activity a  $6 \times 3$  (Muscle  $\times$  Surface) RM-ANOVA was used. Follow-up pairwise comparisons were performed, where appropriate. For all tests the significance level was set at  $P \leq 0.05$ .

## RESULTS AND DISCUSSION

**Energy Expenditure:** Mean values for the measure of energy expenditure (collected at 30 second intervals over the course of ten minutes of sitting) were  $12.64 \pm 1.69$ ;  $12.55 \pm 2.11$ ;  $11.45 \pm 2.42$  kcal for the ball, cushion and flat surface, respectively, which resulted in significant differences between the three surfaces ( $P=0.02$ ). Follow-up comparisons revealed that caloric expenditure on the flat surface was less than either the ball ( $P=0.01$ ) or the cushion ( $P=0.03$ ) with no significant difference between the ball and cushion ( $P=0.84$ ).

**Muscle activation:** Measures of muscle activation revealed a significant effect for surface ( $P=0.001$ ) and muscle ( $P<0.001$ ). However, the higher-order interaction effect of surface and muscle was also significant ( $P=0.001$ ), indicating that the individual muscles were impacted differently by the various sitting surfaces. **Figure 1** illustrates the interactive effect in that the upper body musculature (i.e. rectus abdominus, external obliques, erector spinae) were not impacted differently by the three sitting surfaces, while, lower body musculature (i.e. adductor longus, soleus, tibialis anterior) demonstrated differential effects across the three sitting surfaces.

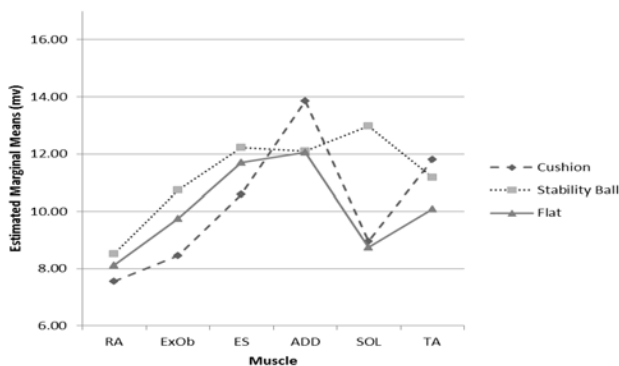


**Figure 1:** Mean EMG data for the six muscles tested on the three sitting surfaces. The figure illustrates the significant Muscle  $\times$  Surface interaction revealed in the lower body musculature.

The cushion demonstrated increased levels of activation for the adductor when compared to the ball and flat conditions while the soleus resulted in higher activation levels for the ball over either the cushion or the firm surface. Finally, both the ball and cushion demonstrated increased activation over the flat surface for the tibialis anterior muscle.

The findings from this study demonstrated an increase in caloric expenditure as well as increased muscle activation in certain muscles when sitting on an exercise ball or an air cushion over that of a flat non-compliant surface. This finding suggests that sitting on a stability ball or air cushion does promote “active” sitting involving frequent postural adjustments that increase caloric expenditure likely through the measured increases in muscular activity. Although sitting on an exercise ball or an air cushion expended more calories than the non-compliant flat surface, there was difference between the two compliant surfaces tested.

## CONCLUSIONS

The findings from this study demonstrated increased energy expenditure and increased levels of muscle activation when sitting on a compliant surface over a firm and stationary surface. These results extend findings from studies using an exercise ball to suggest that similar results can be achieved using a more discreet sitting alternative to a large air-filled ball. Although the difference in caloric expenditure was relatively small over the course of the 10 minutes of sitting, the cumulative level becomes considerable when extrapolated over the course of the average work day and beyond.

## REFERENCES

1. Gregory DE, et al. *Human Factors*, 48(1), 142-153, 2006.
2. Kingma I, et al. *Applied Ergonomics*, 40(2), 199-205, 2009.
3. McGill SM, et al. *Clinical Biomechanics*, 21(4), 353-360, 2006.

# VARIATIONS IN POSTUROGRAPHY TESTING METHODS: EFFECT OF TALKING, VISUAL FIXATION, AND TIME ON PLATE ON SWAY MEASUREMENTS

Erin Sutton, Deborah Kinor, Christopher Denzinger, Alexander Jules and Kimberly Edginton Bigelow

University of Dayton, Dayton, OH, USA

email: [Kimberly.Bigelow@udayton.edu](mailto:Kimberly.Bigelow@udayton.edu) web: <http://academic.udayton.edu/~ewsl>

## INTRODUCTION

Posturography, the measurement of postural stability using a force plate, has demonstrated potential to identify individuals with vestibular and balance problems, neurological disorders, high risk of falls, and susceptibility to sports-related injuries [1]. However debate over the clinical utility of posturography continues, in part due to significant variations in testing methods which may affect the conclusions drawn [1,2]. Previous efforts to standardize posturography methods have focused on more explicit variations in testing, such as feet placement, the number and duration of trials, and which postural measures to report [3,4]. Although these findings were a step toward reducing the more obvious variations in testing procedure, little information exists on the more implicit variations that occur within the clinical setting.

In a step toward creating standardized methods for posturography, this study examined three variations in testing methods that have previously received limited attention: the effect of a subject talking during the test, the time on the balance plate before initiation of data collection, and the presence or absence of a visual fixation point.

## METHODS

Thirty healthy young adults participated in this study (22 female, 8 male; mean age  $21.4 \pm 1.4$  years; mean height  $170.1 \pm 8.7$  cm; mean weight  $74.1 \pm 14.5$  kg). A Design of Experiments methodology was utilized to test the three independent variables of interest. Each of these factors was analyzed at two levels: Present (+) and Absent (-). For those trials where Factor A, Subject Talking, was present (+), the researcher asked the subject to: "Please state your birth date including the year" approximately 15 seconds into data

collection and the subject responded. For those trials where the same factor was absent (-), no question was asked and the subject remained quiet throughout testing. For trials where Factor B, Time On the Balance Plate, was present (+), the data collection did not begin until 30 seconds after the subject stepped onto the plate. When this time was absent (-), the subjects stepped onto the plate and the researcher began testing quickly, normally within 5 seconds. For those trials where Factor C, Visual Fixation, was present (+), a scenic poster was placed on the wall at subject eye level. When this poster was absent (-), subjects were instructed to look straight ahead at the beige painted wall.

Tests were run for all possible factor/level combinations. This resulted in a total of eight trials per subject, where each factor, at each level, was present a total of four times. For all trials, subjects stood barefoot on a force plate (Bertec Corp., Model BP5050) while wearing a harness connected to a safety structure. Subjects were instructed to stand comfortably, remaining as still and as quiet as they could, and looking straight ahead with eyes open, arms at their side. Anterior-posterior (A/P) and medial-lateral (M/L) center of pressure data was collected for 60 seconds at 1000 Hz for each trial. Between trials subjects stepped off the plate, and after four trials all subjects were given a 2 minute break. From the center of pressure data A/P Sway Range, M/L Sway Range, Mean Sway Velocity, and M/L Mean Sway Velocity were calculated. A multivariate analysis of variance (MANOVA) was conducted to determine the statistical significance of the interactions and main effects of these three factors ( $p < 0.05$ ).

## RESULTS AND DISCUSSION

Figure 1 shows the mean A/P and M/L sway ranges for each factor at each level.

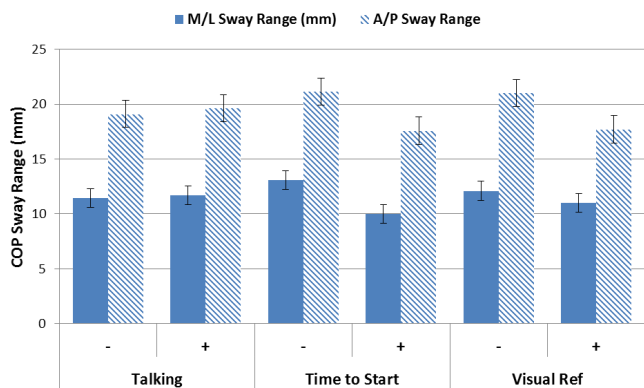


**Figure 1:** Mean M/L and A/P Sway Ranges when each factor is either absent (-) or present (+), with errors bars representing the 95% confidence intervals.

Statistical analysis revealed that there were no interactions between variables, allowing the main effects of the three factors to be examined. Table 1 shows the p-values for each of the sway measures.

**Table 1:** P-values for Main Effects, with statistically significant ( $p < 0.05$ ) denoted with \*

|                   | Talking | Time Prior to Start | Visual Fixation |
|-------------------|---------|---------------------|-----------------|
| M/L Sway Range    | 0.677   | 0.000*              | 0.079           |
| A/P Sway Range    | 0.550   | 0.000*              | 0.000*          |
| Mean Velocity     | 0.063   | 0.000*              | 0.000*          |
| M/L Sway Velocity | 0.546   | 0.000*              | 0.000*          |

Results indicate that when the subject talks briefly during testing, postural sway measurements are not significantly affected. This is notable, as it was observed that while talking, some subjects also moved their head or motioned with their hands, actions initially believed to likely affect postural sway measurements. These findings suggest that should an individual briefly talk or move during quiet standing balance tests, it may not be necessary to discard the trial. However the observed power for the analysis on this factor was low (less than 0.50), indicating the need for significantly more subjects to confirm this particular conclusion.

Results show that the presence of a visual target to fixate on significantly reduced A/P Sway Range ( $p=0.000$ ), Velocity ( $p=0.000$ ), and M/L Velocity ( $p=0.009$ ). Though having subjects fixate on a black, circular-shaped target is common, artwork was used in this study to mimic a typical clinical

environment. In this study, subjects were not explicitly instructed to look at the poster during the test, but results indicate most did. This suggests that hanging artwork in clinical exam rooms used for balance testing may have the unintended consequence of masking subtle postural instability by reducing sway, while also having a potential benefit in rehabilitation settings, where patients may achieve stabilized balance through purposefully gazing at artwork.

The presence of a “stabilization period” prior to the initiation of data collection strongly affected postural sway results, with all four sway measures significantly reduced ( $p = 0.000$  for all). The observed powers were all above 0.95, indicating sufficient number of subjects to draw this conclusion. This suggests that, as proposed by others [2], individuals take a short period of time to “settle” and that posturography reporting should only occur after this point.

Future work is now needed to relate the findings of this study to the ability to discriminate healthy individuals from those with compromised balance so that standards to improve clinical utility can be proposed.

## CONCLUSIONS

Providing subjects with time to stabilize prior to data collection and artwork to look at during testing both significantly reduce postural instability. Brief periods of talking do not appear to influence sway, but additional subjects are needed to confirm.

## REFERENCES

1. Visser JE, et al. *Clin Neurophysiol* **119**, 2424-2436, 2008.
2. International Society of Posturography. *Agressologie* **24**, 321-326, 1983.
3. McIlroy, WE, Maki BE. *Clin Biomech* **12**, 66-70, 1997
4. Carpenter MG, et al. *Gait Posture* **13**, 35-40, 2001.

## ACKNOWLEDGEMENTS

The authors would like to acknowledge Dr. Wiebke Diestelkamp, and research assistants Julia Schaeffer, Melissa Taylor, and Martin Piskiewicz.

# A UNIFIED DEFORMABLE SEGMENT MODEL OF THE COMBINED ANKLE-FOOT SYSTEM THAT DOES WORK

<sup>1</sup>Kota Z. Takahashi, <sup>1</sup>Alexander R. Razzook, <sup>1</sup>Lakisha D. Guinn, <sup>1</sup>Elisa S. Schrank, <sup>2</sup>Thomas M. Kepple, and <sup>1</sup>Steven J. Stanhope

<sup>1</sup>University of Delaware, Newark, DE, USA

<sup>2</sup>C-Motion Inc., Germantown, MD, USA

email: [ktaka@udel.edu](mailto:ktaka@udel.edu)

web: <http://www.udel.edu/kaap/research/biomechanicslab.html>

## INTRODUCTION

The field of lower limb prosthetics has continuously evolved, producing novel prosthetic ankle-foot components (PAFCs) that attempt to restore the mechanical capabilities of the natural ankle-foot complex (NAFC) [1]. However, as contemporary designs have emerged, the biomechanical models used to analyze the PAFCs have lagged behind. Traditionally, biomechanical analyses have combined principles of rigid body mechanics and inverse dynamics to model the human limb as a series of rigid body segments joined together via mechanical joints. In contrast, numerous PAFC designs, such as the 'energy-storing' PAFCs, are deformable objects by design, and hardly represent the assumptions grounded in the existing anatomically relevant (AR) models. Therefore, traditional biomechanical analyses may be inadequate for directly comparing the functions of PAFCs and NAFCs during gait.

Segmental power analysis is a valuable method for revealing the total energy flow of a segment, and is ideal for exploring the energy transfer mechanisms between adjacent segments [2]. However, traditional segmental power techniques require isolating the individual segments (i.e. shank and foot), complicating its applicability for PAFCs that contain non-articulated components. A viable alternative is to model the lower leg as a unified deformable (UD) segment, and quantify the total mechanical power of the UD ankle-foot system. Therefore, the goals of this study are to: 1) develop a novel method of the UD segmental power analysis, and 2) validate the new UD model by comparing its results to the AR model in normal gait, in which the AR method quantifies the sum of all mechanical power distal to the shank.

## METHODS

Eleven healthy subjects (ages 20-29, height 1.63-1.83m and weight 59.5-132.5 kg) participated in instrumented gait analysis, while walking at a targeted scaled walking velocity of 0.8 body heights/second. Kinematic data were collected using a six camera-based motion capturing system (Motion Analysis Corp., Santa Rosa, CA), and kinetic data were collected from four strain gauge force platforms (AMTI, Watertown, MA). Data were analyzed using Visual3D software (C-Motion Inc., Germantown, MD). The total power of the AR system ( $P_{AR}$ ) was calculated as the sum of the power at the distal shank and the total foot segmental power, or equivalently, the sum of the total ankle joint power ( $P_{ank}$ ) and the distal foot power ( $P_{ftd}$ ):

$$P_{AR} = P_{ank} + P_{ftd} \quad (1)$$

where the  $P_{ank}$  is the summation of power due to the dot product of the ankle joint force ( $F_{jt}$ ) and the joint translational velocity ( $\Delta v$ ), and power due to the dot product of the ankle joint moment ( $M_{jt}$ ) and the joint angular velocity ( $\omega_{jt}$ ) [3],

$$P_{ank} = F_{jt} \cdot \Delta v + M_{jt} \cdot \omega_{jt} \quad (2)$$

and  $P_{ftd}$  is the summation of power due to the dot product of the distal ground reaction force ( $F_{grf}$ ) and the distal foot translational velocity ( $v_{ftd}$ ), and power due to the dot product of the distal free moment ( $M_{free}$ ) and the foot angular velocity ( $\omega_{ft}$ ) [4]:

$$P_{ftd} = F_{grf} \cdot v_{ftd} + M_{free} \cdot \omega_{ft} \quad (3)$$

The total power of the UD segment ( $P_{UD}$ ) was calculated as the sum of two distal power terms:

$$P_{UD} = F_{grf} \cdot v_{UDd} + M_{free} \cdot \omega_{sh} \quad (4)$$

where  $F_{grf}$  and  $M_{free}$  are the the ground reaction force and the free moment from the force platform,  $\omega_{sh}$  is the angular velocity of the shank, and  $v_{UDd}$  is the distal translational velocity of the UD segment, computed by:

$$v_{UDd} = v_{cm} + (\omega_{sh} \times r_d) \quad (5)$$

where  $v_{cm}$  is the linear velocity of the center of mass of the shank, and  $r_d$  is the vector from the center of mass of the shank to the center of pressure (COP) location.

The agreement between  $P_{AR}$  and  $P_{UD}$  were assessed by comparing the peak powers, and the total positive and negative work, as well as computing the total difference between the two estimates during stance.

## RESULTS AND DISCUSSION

The percent difference between  $P_{AR}$  and  $P_{UD}$  for the average total peak powers was 0.37%. The total positive work, and total negative work differed by 0.33% and 5.04%, respectively (Table 1). The difference between the  $P_{AR}$  and  $P_{UD}$  measures were more pronounced during early and late stance (Figure 1), which can be attributed to the contribution of powers due to inertial factors of the foot segment as it moves independently of the shank. Analytically, the UD model neglects the inertial properties of the foot. Since inertial factors may minimally influence the estimates of ankle joint forces and moments [5], the  $P_{UD}$  can closely approximate the measures obtained from the  $P_{AR}$ .

Although the UD model does not directly assess the motion of the foot segment, the analysis can capture the deformation profiles of the UD segment through the displacement of the COP within the shank's coordinate system. This displacement of the COP can induce energy flow into or out of the segment. Since the PAFCs during stance have been shown to undergo COP excursions in the shank's coordinate system [6], the UD model is expected to accurately quantify the total energy flow of the PAFCs without the necessity to identify the foot kinematics and inertial contributions.

## CONCLUSIONS

The AR model was used as the 'gold standard' for capturing the total power of the combined ankle and

foot in normal gait, while the UD model attempted to capture the total power by analyzing the ankle-foot system as a single deformable segment. The results indicated that  $P_{UD}$  estimates showed very close agreement with the  $P_{AR}$  for majority of stance. Because the UD model does not require the precise isolation of 'shank' and 'foot' segments, the analysis may be an ideal technique for characterizing the total energy flow of PAFCs during gait, and may facilitate direct comparisons to natural ankle-foot systems.

## REFERENCES

1. Verslyus R, et al. *Disabil Rehabil Assist Technol.* **4**, 65-75, 2009
2. Prince F, et al. *IEEE Trans. Rehabil. Eng.* **2**, 247-255, 1994.
3. Buczek FL, et al. *J Biomech* **27**, 1447-1457, 1994.
4. Siegel KL, et al. *J Biomech* **29**, 823-827, 1996.
5. Wells RP. *Bull Prosthet Res*, **18**, 15-19, 1981.
6. Hansen AH, et al. *Disabil Rehabil*, **32**, 2201-9, 2010

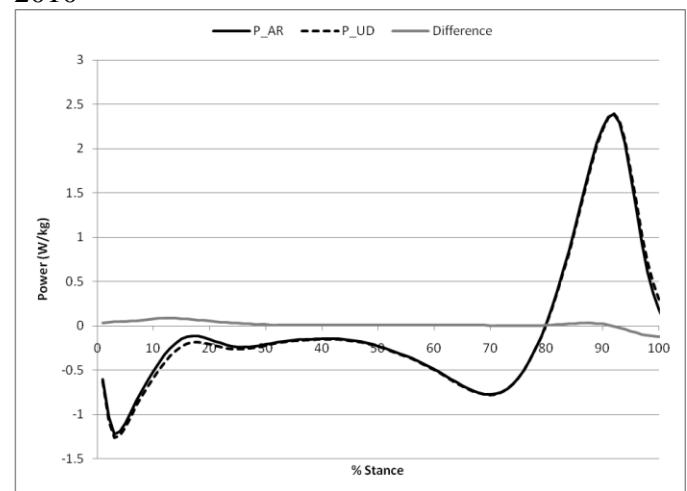


**Figure 1:** The average total powers of the  $P_{AR}$  (solid line) and  $P_{UD}$  (dashed line), as well as the difference (gray line) between the two estimates during stance.

**Table 1:** Means and Std of peak power, total negative and positive work for  $P_{AR}$  and  $P_{UD}$ .

|              | Peak Power (W/kg) | Total Pos Work (J/kg) | Total Neg Work (J/kg) |
|--------------|-------------------|-----------------------|-----------------------|
| $P_{AR}$     | 2.485             | 0.173                 | -0.198                |
| std          | 0.449             | 0.036                 | 0.049                 |
| $P_{UD}$     | 2.476             | 0.174                 | -0.207                |
| std          | 0.461             | 0.034                 | 0.046                 |
| % Difference | 0.37              | 0.33                  | 5.04                  |

# THE INFLUENCE OF SAGITTAL-PLANE TRUNK POSTURE ON PATELLOFEMORAL JOINT STRESS DURING RUNNING

<sup>1</sup>Sharon Hsiang-Ling Teng, <sup>1</sup>Kai-Yu Ho and <sup>1</sup>Christopher M Powers

<sup>1</sup>University of Southern California, Los Angeles, CA, USA  
email: [hsianglt@usc.edu](mailto:hsianglt@usc.edu), web: <http://pt2.usc.edu/labs/mbrl/>

## INTRODUCTION

Patellofemoral pain (PFP) is one of the most common knee joint problems among runners [1]. A commonly accepted cause of PFP is elevated patellofemoral joint (PFJ) stress [2]. As stress is defined as force per unit area, elevated stress could occur as a result of an increase in the PFJ reaction force and/or a decrease in contact area. In turn, an increase in the PFJ reaction force could occur with an increase in the knee flexion angle and/or an increase in the knee extensor moment.

Recent literature suggests that sagittal plane trunk posture can have a significant influence on knee joint kinematics and quadriceps muscle activation during landing [3]. Therefore, modifying sagittal plane trunk posture may be a potential strategy to alter PFJ stress during running. As such, the purpose of this study was to investigate whether alteration of sagittal plane trunk posture would lead to changes in lower-extremity biomechanics and PFJ stress during overground running. We hypothesized that increased trunk flexion would result in a reduction in PFJ stress. Conversely, we hypothesized that running with a more erect posture would increase PFJ stress.

## METHODS

To date, 5 asymptomatic individuals (2 females, 3 males) have participated in this study. Three-dimensional trunk and knee kinematics and the ground reaction force data were collected at 250 Hz and 1250 Hz respectively (Qualysis, Gothenburg, Sweden; AMTI force plate, Watertown, MA) while subjects ran overground at a velocity of 3.4 m/s. Data were obtained under 3 conditions: preferred posture (Preferred), flexed trunk posture (Flexed) and extended trunk posture (Extended). The trunk segment was defined by markers placed on bilateral

acromioclavicular joints and the highest point of the iliac crests. Trunk orientation was calculated relative to the pelvis. Trunk and knee flexion angles as well as knee extensor moment during the stance phase of running were computed by Visual 3D™ software.

A previously described biomechanical model was used to estimate PFJ stress [2]. The model input variables included subject specific parameters (i.e. knee joint kinematics, net knee joint moment) and data from the literature (i.e. knee moment arms, quadriceps force/patella ligament force ratios and joint contact area). The model outputs were PFJ reaction force and PFJ stress. Variables of interest consisted of peak PFJ stress and the PFJ reaction force, as well as the trunk and knee flexion angles and knee extensor moment at the time of peak PFJ stress. The Friedman tests with post-hoc Wilcoxon Signed Rank test were used to compare differences in PFJ stress and PFJ reaction force among the 3 trunk conditions.

## RESULTS AND DISCUSSION

Peak PFJ stresses for each condition are shown in Figure 1. PFJ reaction force, trunk and knee flexion angles and knee extensor moment at the time of peak stress occurred are reported in Figure 2 and Table 1. Significant differences in PFJ stress and reaction force among the 3 trunk conditions were observed ( $P = 0.041$ ). Post-hoc analysis indicated a significant difference between the Flexed and Extended conditions ( $P = 0.043$ ). On average, a 13% decrease in both PFJ stress and reaction force was observed between the Flexed and Extended conditions. The reduction of peak stress in Flexed condition was accompanied by a  $9.5^\circ$  increase in trunk flexion, a  $1.3^\circ$  increase in knee flexion and a 0.45 Nm/kg decrease in the knee extensor moment compared to the Extended condition (Table 1).

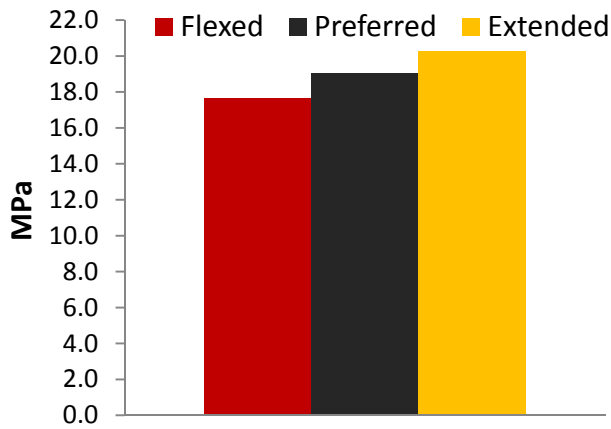


**Figure 1:** The effect of trunk orientation on peak patellofemoral joint stress during the stance phase of running.

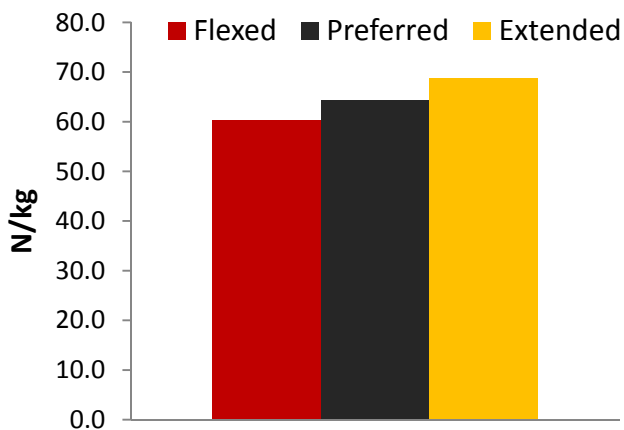


**Figure 2:** The effect of trunk orientation on patellofemoral joint reaction force (at the time of peak stress) during the stance phase of running.

Our results indicate that a slight increase in trunk flexion (9.5°) can lead to a significant decrease in PFJ stress during running. Conversely, running with a more erect trunk resulted in elevated PFJ stress. The primary contributor to the change in PFJ stress with trunk orientation was a change in the PFJ reaction force. In turn, the change in the PFJ reaction force was driven by a change in the knee extensor moment as opposed to a change in the knee angle. This is logical as a slight change in trunk orientations can have a significant effect on the location of the center of mass and, therefore, the knee moment.

## CONCLUSIONS

This is the first study to demonstrate the influence of sagittal plane trunk posture on PFJ stress during running. Our data suggest that running with a forward trunk posture can result in decreased PFJ stress. In turn, running with a backward trunk posture can lead to increased PFJ stress. Future studies need to be conducted to determine whether changes in trunk postures can reduce PFP in symptomatic runners.

## REFERENCES

1. Taunton JE, et al. *Br J Sports Med* **36**, 95-101, 2002.
2. Heino BJ, et al. *Med Sci Sports Exerc* **34**, 1582-93. 2002.
3. Blackburn JT, et al. *Clin Biomech* **23**, 313-19, 2008

**Table 1:** Trunk and knee kinematics and knee kinetics at the time of peak PFJ stress.

|                                      | Trunk posture (N=5) |            |            |
|--------------------------------------|---------------------|------------|------------|
|                                      | Flexed              | Preferred  | Extended   |
| <b>Trunk flexion angle (degrees)</b> | 12.1 ± 5.7          | 6.3 ± 6.5  | 2.5 ± 6.3  |
| <b>Knee flexion angle (degrees)</b>  | 45.8 ± 6.9          | 45.0 ± 7.9 | 44.5 ± 7.4 |
| <b>Knee extensor moment* (Nm/kg)</b> | 2.7 ± 0.3           | 3.0 ± 0.4  | 3.2 ± 0.4  |

\*normalized by subject's body weight

# KINEMATIC CHANGES IN CONTRALATERAL KNEE DURING TRAINING WITH REAL-TIME BIOFEEDBACK IN WOMEN WITH KNEE HYPEREXTENSION

Patricia Teran-Yengle and John H. Jack  
University of Iowa, Iowa City, IA, USA  
Email: [patricia-teranyengle@uiowa.edu](mailto:patricia-teranyengle@uiowa.edu)

## INTRODUCTION

Knee hyperextension is thought to be associated with increased stress to the posterior joint capsule of the knee [1] and anterior cruciate ligament (ACL) [2] and increased contact stress on the anterior compartment of the tibial-femoral joint [3]. Abnormal stress to these tissues can be detrimental to the knee joint [4]. Compared to men, women demonstrate greater incidences of knee hyperextension [5]. A recent study aimed at correcting knee sagittal alignment in women with asymptomatic knee hyperextension showed significant reduction of extension patterns after a six-session treadmill training intervention using real-time kinematic feedback [6]. Results of knee hyperextension study also reported tendency of training program to influence kinematic changes on contralateral knee. The purpose of this study was to investigate sagittal plane kinematic changes in contralateral knee during treadmill training in women with asymptomatic knee hyperextension.

## METHODS

Ten healthy women, ages 18 to 39 years, with asymptomatic knee hyperextension underwent a three-week (6 sessions) treadmill gait retraining program. Clinical measures of knee hyperextension greater than 5° were used as the inclusion criteria. Participants underwent a physical and gait evaluation. The physical evaluation assessed muscular strength and passive range of motion in each subject's lower limbs using standard techniques. The gait evaluation was conducted along an 8 m walkway using a three-dimensional motion analysis system (Optotrak, NDI; Kistler) with subjects walking at their self-selected (SS) speed and at 3 mph. Three non-collinear infrared markers were used to track each of the following body segments: feet, legs, thighs, and pelvis. Marker coordinate data was collected at 60 Hz and

filtered at 6 Hz. An anatomical model was created by digitizing standard bony landmarks to define the axes of each of the seven body segments. Gait data was processed using Visual 3D software (C-Motion). After the initial evaluation, subjects participated in a three-session supervised treadmill training. Each training session lasted one hour and consisted of three eight-minute sessions with three-minute rest periods in between training sessions. Real-time biofeedback (Visual 3D) was provided on a computer screen placed on a table (150 cm in height) about 1m in front of subject. Participants received real-time biofeedback for the knee that showed the greater degree of knee extension (involved knee) during the initial over-ground gait evaluation. Treadmill gait data were collected, without feedback, at the beginning (pretraining) and end (posttraining) of each training session. A final over-ground gait evaluation, following initial evaluation protocol, was performed at the end of the three weeks of training.

## RESULTS AND DISCUSSION

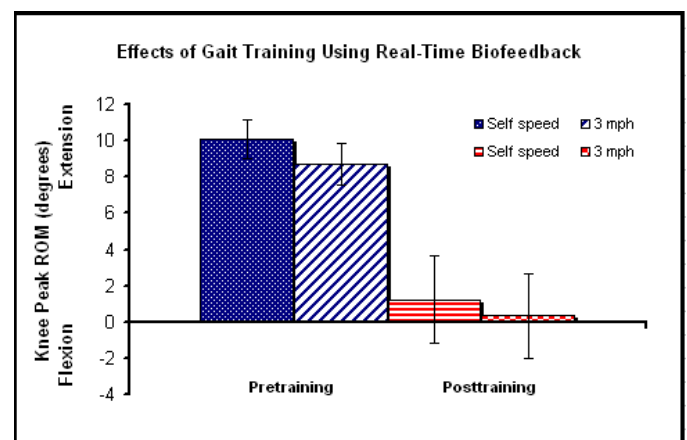


**Figure 1:** Peak knee extension at initial and final gait evaluations. Treadmill gait retraining intervention, using real-time biofeedback, significantly reduced knee hyperextension patterns during over ground walking at self-selected (SS) ( $p < 0.01$ ) and 3 mph ( $p < 0.01$ ).

Ten women (age  $27.5 \pm 5$ ; weight  $58 \pm 7$  Kg; height  $1.6 \pm 0.1$  m) took part in this study. Initial muscular testing showed normal values for knee extensors ( $142 \pm 11$  N), and flexors ( $111 \pm 16$  N). The passive range of motion showed  $8 \pm 1.7^\circ$  (from  $5^\circ$  to  $12^\circ$ ) of knee extension. Initial gait evaluation showed that six subjects had greater knee extension in their left knee. Maximum knee extension occurred at initial contact in 6 subjects and at toe-off in 4 subjects. A paired T-test showed significant evidence that treadmill gait retraining intervention using real-time

over ground walking at self selected speed and 3mph. When working on correcting the knee hyperextension patterns in the involved knee, subjects demonstrated simultaneous reduction in peak knee extension in the less involved knee. Improvements in decreasing knee hyperextension during walking may help to relieve constant stress in the knee joint. The present study showed that knee sagittal plane kinematics, in trained and contralateral knee, can be influenced with dynamic gait training using real-time biofeedback.

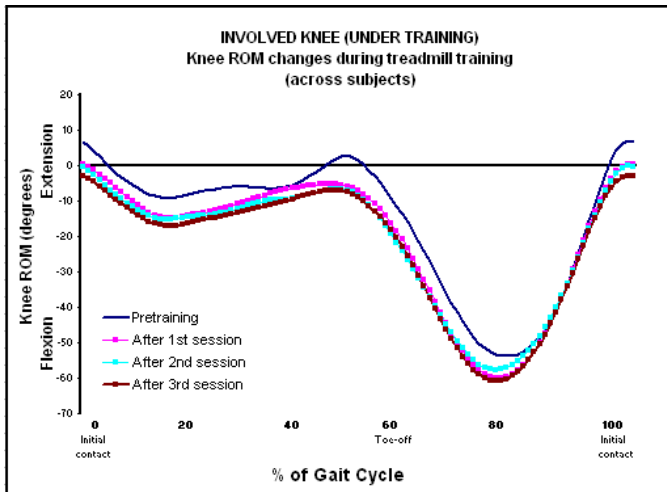


**Figure 2:** Average data across subjects showing kinematic changes (sagittal plane) in involved knee during treadmill training.

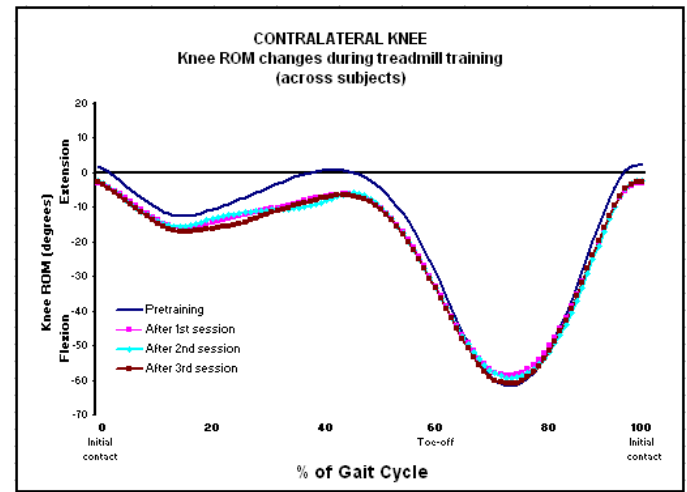


**Figure 3:** Average data across subjects showing kinematic changes (sagittal plane) in the contralateral knee during treadmill training.

biofeedback reduced hyperextension pattern in involved knee (Fig. 1) at self-selected speed and 3mph. The greatest reduction of knee extension pattern, in the involved knee, occurred after the first training session (Fig. 2). Figure 3 shows the kinematic changes on the contralateral knee during the three treadmill sessions. A paired T-test showed significant reduction of knee extension patterns in the contralateral knee during the first training session.

## CONCLUSIONS

The results of this study indicate that participants showed decreased knee hyperextension patterns during treadmill gait retraining intervention using real-time biofeedback. Subjects showed greatest improvement in decreasing knee hyperextension during the first treadmill training session. Subjects demonstrated gradual improvements that continued over the three-week training program. Gained proficiency, controlling knee hyperextension patterns during treadmill training, was evident for

## REFERENCES

1. Oatis CA. Kinesiology.: Mechanics & Pathomechanics of human movement (2004).
2. Senter, C., & Hame, S. L. (2006). Biomechanical analysis of tibial torque and knee flexion angle *Sports Medicine (Auckland, N.Z.)*, 36(8), 635-641.
3. Nisell R et al (1986). Joint Forces in Extension of the Knee *Acta Orthop Scand* (57); p. 41- 46.
4. Sharma L. et al. (2008). *Arthritis & Rheumatism*, 58(6), 1716-1726.
5. Medina McKeon J M et al. (2009). Sex Differences and Representative Values for 6 Lower Extremity Alignment Measures. *Journal of Athletic Training*, 44(3); p.249-55.
6. Teran-Yengle P et al. (*Proceedings of ASB 2010*, Providence, Rhode Island, USA, 2010).

## ACKNOWLEDGEMENTS

This study was supported by the Graduate Program in Physical Therapy and Rehabilitation Science at the University of Iowa.

# CHANGES IN LOCOMOTOR ADAPTATIONS AND AFTEREFFECTS IN CONTROL AND SPINAL CORD INJURY POPULATIONS FOLLOWING SWING PHASE RESISTANCE

M. Thajchayapong<sup>1</sup>, B.D. Schmit<sup>2,4</sup>, T.G. Hornby<sup>3,4</sup>

<sup>1</sup>Dept of Mechanical Engineering, Northwestern University, Evanston, IL, <sup>2</sup>Dept of Biomedical Engineering, Marquette University, Milwaukee, WI, <sup>3</sup>Dept of Physical Therapy, University of Illinois at Chicago, Chicago, IL, <sup>4</sup>Dept of Physical Medicine and Rehabilitation, Northwestern University, Chicago, IL

## INTRODUCTION

Providing perturbations to the limbs is intended to alter sensory inputs associated with walking and potentially improve walking recovery. Our previous study using swing phase assistance in control population showed that selected muscle activity and gait kinematics are altered during and following swing phase assistance in control population. However, the effects of swing-phase assistance on locomotor behaviors of individuals with neurological injury are still unclear. Additionally, data suggests that swing-phase resistance may generate motor adaptations which may augment performance in impaired patients (Lam et al., *Neurorehabil Neural Repair*. 2008 22: 438-446). Accordingly, the purpose of the present study was to investigate alterations in lower extremity kinematics and muscle activity during and following application of posteriorly directed external swing resistance (ESR) during treadmill walking in control and spinal cord injury (SCI) individuals. Preliminary data indicated that gait parameters such as walking speed and specific walking instruction can contribute to alterations of kinematics outcomes.

## METHODS

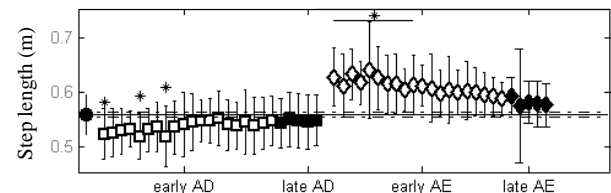
A device was adapted with permission from Gottschall and Kram (Gottschall JS and Kram R. 2005). We applied a pulling force of approximately 5% body weight (BW) above the knee during treadmill walking in 10 and 11 subjects from control and SCI group, respectively. Electromyographic activity of six lower extremity muscles and hip kinematics were collected from both legs during constant treadmill walking. Three-dimensional kinematic data were collected using a 6-camera video system and 21 reflective markers on

the lower limbs placed over pre-determined anatomical landmarks.

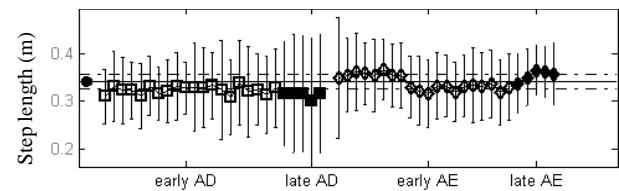
## RESULTS AND DISCUSSION

### Control group

A) 4 kmph : no instruction

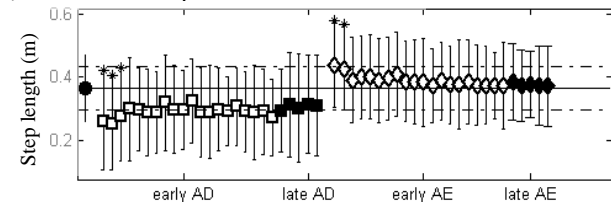


B) Matched averaged SCI speed, 2.1 kmph : no instruction



### SCI group

C) Self-selected speed: no instruction



D) Self-selected speed: with instruction

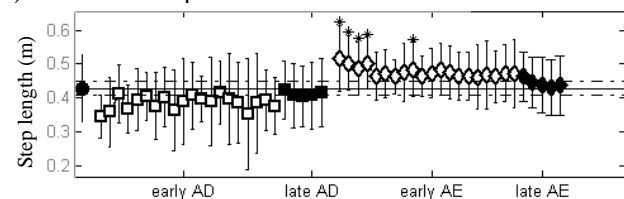


**Figure 1:** Changes in step length in control group during early adaptation (AD), late AD, early aftereffect (AE) and late AE. Data from BL conditions (filled circles), the 1<sup>st</sup> 20 steps (early AD; open squares), and minutes 2, 4, 6, 8, 10 (late AD; filled squares) during ESR application, and

following removal of ESR during the early AE (open diamonds), and late AE (filled diamonds) period. Significant differences from BL marked by asterisk (\*). Adaptation or aftereffects was defined to be completed at 95% of steady state (dashed line). Control subjects walked at 4 kmph (A) demonstrated “negative aftereffects” following exposure to ESR ( $P=0.002$ ) while small changes in both adaptation and aftereffects were shown when the same group of subjects walked at 2.1 kmph (B). SCI subjects walked at their self-selected speed without (C) or with (D) instruction. Walking without instruction resulted in no adjustment to BL level after repetitive stepping with ESR and showed small negative aftereffects. With instruction to resist the perturbation, adjustment to BL during late AD was found as well as significantly negative aftereffects. Slower walking speed in control group walking without instruction showed similar early AE adaptive behavior (feedback control) found in SCI group walking without instruction (compare A and C). However, when the instruction was given in SCI group, early AE adaptive behavior (feedforward control) was found to be consistent with those found in control group walking at faster speed without instruction.

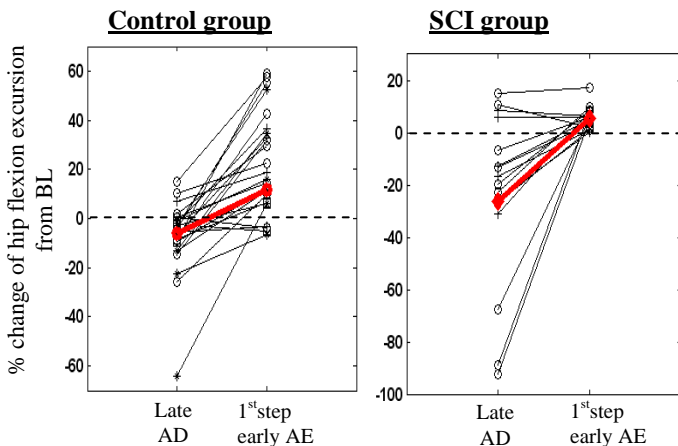


**Figure 2:** Percentage changes in peak hip flexion excursion from BL to late AD and the 1<sup>st</sup> step early AE periods of individual subjects from all testing sessions of each group and its average (red line). Changes are more evident in SCI group due to substantial reduction of hip flexion excursion in AD period. Less aftereffect behavior was found when there was no adaptation in late AD (i.e. SCI group)

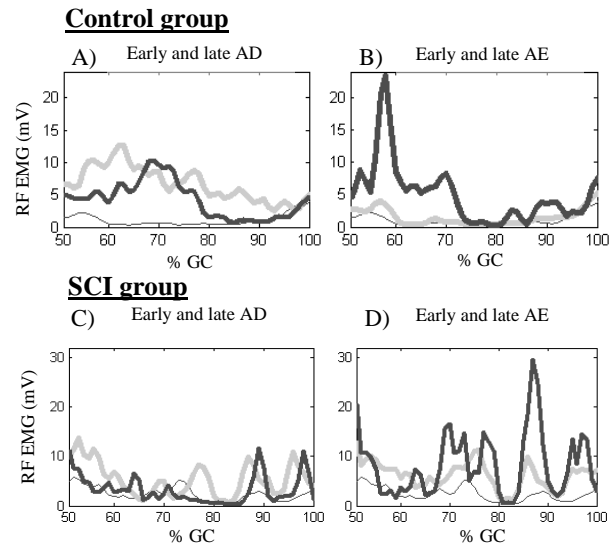


**Figure 3:** Changes in RF activity during BL conditions (thin light line), at the 1<sup>st</sup> step of application/removal of ESR (dark thick line), and during the 10<sup>th</sup> minute of application/removal ESR (thick light line) from a single subject selected from control (A-B) and SCI (C-D) group. Analysis of RF activity during 50-75% of the gait cycle was performed. RF activity was increased following ESR application and stayed increased throughout the adaptation period corresponded to an effort to complete stepping affected by ESR. Control and SCI subjects increased RF activity further immediately following the removal of ESR. No significantly different among testing sessions in both groups.

## CONCLUSIONS

We concluded that subjects from both groups used different control strategies responding to the effects of the external perturbation. Feedforward command was involved in adaptive strategy used in control group. On the other hand, SCI group seemed to modify their walking by “reacting” to the change of environment and there was no learning involved (feedback control). But with specific walking instruction, SCI subject showed the potential of using feedforward mechanism for their adaptive strategy. Walking speed and numbers of practiced stepping also should be considered as parameters that can alter kinematics outcomes.

## REFERENCES

1. Lam et al., *Neurorehabil Neural Repair*. 2008 22: 438-446 Gardner JG, et al. *J Biomech* **38**, 1861-1868, 2004.
2. Gottschall and Kram, *J Appl Physiol*. 2005 99:23-30.

# ULTRASONOGRAPHIC INVESTIGATION OF HAND MUSCLE ATROPHY IN STROKE SURVIVORS

<sup>1</sup>Kristen Triandafilou and <sup>1,2</sup>Derek Kamper

<sup>1</sup>Sensory Motor Performance Program, Rehabilitation Institute of Chicago, Chicago, IL, USA

<sup>2</sup>Department of Biomedical Engineering, Illinois Institute of Technology, Chicago, IL, USA

email: [k-triandafilou@northwestern.edu](mailto:k-triandafilou@northwestern.edu) web: <http://smpp.northwestern.edu/research/hand.html>

## INTRODUCTION

Contralesional limb weakness is a common finding in stroke survivors. Strength deficits in the hands can be especially profound, with losses of greater than 75% [1,2]. While excessive coactivation and an inability to fully activate these muscles contribute to this weakness, muscle atrophy may also play a role. Indeed, atrophy in the hemiparetic leg has been described (initially via needle biopsy [3] or cadaveric specimens and more recently using imaging techniques [4]). However, paretic muscles of the upper extremity, particularly those controlling the hand, have not been studied in detail. These muscles may be particularly susceptible to changes following stroke due to the heavy cortical innervation of their motoneurons. Additionally, deficits appear to be non-uniform, with greater loss in finger extension than flexion. Thus the goal of this study was to quantify the extent of muscle atrophy in index finger musculature *in vivo* by means of ultrasonography. It was hypothesized that finger intrinsic and extensor muscle would atrophy to a greater extent than flexor muscle based on clinically observed reductions in fine motor control, individuation and extension force.

## METHODS

Twenty-five subjects with severe hand impairment, classified as Stage 2 or 3 on the Stage of Hand component of the Chedoke-McMaster Stroke Assessment [5], participated. All stroke survivors had chronic hemiparesis resulting from a stroke incurred 2-4 years prior. Ten healthy, age-matched controls were included in this study to gauge the extent to which muscle size varies between the dominant and non-dominant side for the upper extremity. All participants were between 45 and 65 years of age.

Muscle component definition of index finger muscles such as flexor digitorum superficialis

(FDS), flexor digitorum profundus (FDP), and extensor digitorum communis (EDC) with imaging modalities with poor time resolution, such as magnetic resonance imaging, is very difficult. Thus, ultrasonography was employed to non-invasively measure the geometry of the muscles controlling the index finger. Utilizing the advantageous real-time feedback, localization of the proper muscle/muscle compartment was conducted by viewing the displacement of muscle fibers in response to isolated muscle contraction or imposed movement of the joint(s). The musculoskeletal transducer probe was positioned over the muscle belly and adjusted to determine the maximal muscle parameter of interest for each of the muscles of the index finger: first compartments of FDS, FDP, and EDC, extensor indicis (EI), first dorsal interosseous (FDI), first palmar interosseous (FPI), and lumbrical (LUM).

Two different muscle parameters were evaluated: peak cross-sectional area (CSA) and thickness, in the anatomical transverse and sagittal planes, respectively. CSA was estimated assuming an elliptical configuration for each muscle. While CSA provides a more complete description of atrophy, muscle thickness was often more accurately measured due to enhanced image quality. Ultrasound images were saved as movie segments and analyzed offline in MATLAB (Fig. 1).

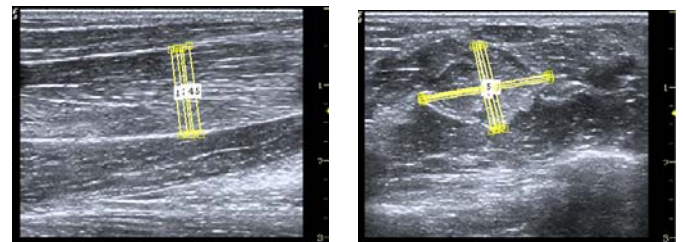


**Figure 1:** MATLAB GUI for offline measurements/estimation of muscle thickness (left) and CSA (right) of the first compartment of FDS.

For each measured parameter and group, a MANOVA was performed (SPSS Inc., Chicago, IL)

to explore the impact muscle type and non-dominance/paresis had on the output. If significance resulted, additional post-hoc RMANOVA analyses were performed. A Bonferroni correction for multiple comparisons was implemented ( $\alpha = 0.05$ ).

## RESULTS AND DISCUSSION

As expected, paretic muscle size was significantly reduced (Wilks' lambda < 0.001) for the stroke group. For the control group, hand dominance did not significantly affect muscle size (Wilks' lambda = 0.411) and the muscle size was not significantly different between the dominant hand (Control) and the non-paretic hand (Stroke) for muscle thickness ( $p = 0.112$ ) or CSA ( $p = 0.639$ ). Overall, the data showed an average decrease of  $15 \pm 4\%$  in muscle CSA of the paretic limb compared to the non-paretic limb for this stroke population whereas the age-matched control group demonstrated only a non-significant  $6 \pm 2\%$  decrease in CSA of the non-dominant limb compared to the dominant limb. Thus, the true deficit in the stroke group was only 10%. In comparison, measured flexion force deficits were found to be over 83% and extension force deficits were 88% in this stroke population.

Decreased muscle CSA was evident in all muscles of the paretic index finger for the stroke group, but surprisingly, there was no significant difference in the relative atrophy of the different muscles. The muscles most noticeably impacted, in fact, were FDS and FDP, which exhibited size reductions of 21% and 19%, respectively, on the paretic as compared to the non-paretic side. The decreases observed for the extrinsic extensor muscles EI (17%) and EDC (12%) and the intrinsic muscles FPI (13%) and LUM (15%) were smaller, although not significantly. Interestingly, the atrophy observed in the intrinsic FDI muscle (9%) was less than half of that of FDS (Fig. 2). Hence, muscle atrophy could not account for the relatively greater deficits in force generation in certain directions.

Paretic muscle thickness attenuation was also detected in all muscles investigated of the Stroke group. Thickness of the extrinsic flexors was reduced by 8% in FDS and 12% in FDP, while thickness of the extrinsic extensor muscles was diminished by 11% in EI and 10% in EDC, and that

of the intrinsic muscles by 6% in FDI, 11% in FPI, and 15% in LUM. Once again, the degree of muscle atrophy in FDI was least. Similarly to CSA, we observed an average decrease of  $11 \pm 2\%$  in muscle thickness in the paretic limb compared to the non-paretic limb, with the control group presenting less than a  $1 \pm 4\%$  decrease in muscle thickness of the non-dominant limb compared to the dominant limb. Thus, muscle thickness appears to be a reasonable indicator of muscle atrophy, and is fairly easily measured with ultrasonography.

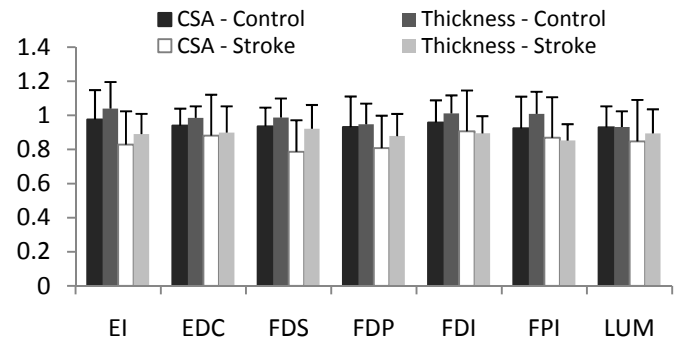


**Figure 2:** Normalized muscle peak CSA and thickness. Paretic normalized to non-paretic side (Stroke) and non-dominant normalized to dominant side (Control). Error bars represent SD of the mean.

## CONCLUSIONS

Although muscle atrophy was detected in the paretic limb following stroke, it is not explanative of the marked impairment seen in this stroke population. Admittedly, other alterations in muscle morphology may contribute to the emergent muscle weakness post-stroke. Fatty infiltrations and changes in fiber structure have been identified in lower limb musculature following stroke. These potential alterations may warrant future examination in upper extremity musculature.

## REFERENCES

1. Cruz EG, et al. *Brain* **128**, 1112-1121, 2005.
2. Triandafilou KM, et al. *J Neurophys*, [In Revision].
3. Dattola R, et al. *Eur Neurol* **33**, 109-114, 1993.
4. Klein CS, et al. *J Appl Physiol* **109**, 1337-1346, 2010.
5. Gowland C, et al. *Stroke* **24**, 58-63, 1993.

## ACKNOWLEDGEMENTS

Supported by NIH NINDS (R01 NS052369), the Coleman Foundation and the Achievement Rewards for College Scientists (ARCS) Foundation.

# TYPING STYLE AFFECTS ARM KINETICS, KINEMATICS AND MUSCLE ACTIVATION

<sup>1</sup>Matthieu Trudeau, <sup>1</sup>Krishna Asundi and <sup>1,2</sup>Jack Dennerlein

<sup>1</sup>Harvard School of Public Health, <sup>2</sup>Harvard Medical School, Boston, MA, USA  
email: [mtrudeau@hsph.harvard.edu](mailto:mtrudeau@hsph.harvard.edu)

## INTRODUCTION

Many different typing styles exist in the workplace. The common typing styles are “two-finger” typing and touch-typing. Two-fingered typists use a maximum of two fingers per hand and often look at the keyboard. Touch-typists use all fingers of both hands and infrequently look at the keyboard. Ergonomic interventions lean towards “relaxed” touch typing methods [1,2]; however, typing styles have not been quantified through biomechanical measures. This study aims to determine the effects of two different typing styles on posture, joint torque, and muscle activity in the upper extremity. These findings inform prevention efforts with reduced biomechanical loading, thus possibly reducing the risk of developing musculoskeletal disorders (MSDs).

## METHODS

Two groups of participants were recruited according to their typing style: 15 two-fingered typists (11 men, 4 women, mean age 44 years old) and 16 touch-typists (7 men, 9 women, mean age 39 years old). Participants completed a typing task consisting of transcribing text into a word processing document. Two minutes of force and kinematic data were collected after some practice time.

Three-dimensional (3-D) kinematics of the right upper extremity were recorded using an active-marker infrared motion analysis system (Optotrak Certus System, Northern Digital, Ontario, CAN). Typing force was measured by a 6-axis force-torque transducer (ATI Industrial Automation, model Gamma, SI-65-5.5, Apex, NC, USA) underneath the right-hand side of a split keyboard, and electromyographic (EMG) activity from eight muscles of the arm was recorded during the task

(DE-2.1 Single Differential Electrode; Delsys, Boston, MA, USA).

All joint angles were calculated with respect to a neutral posture in which the elbow was flexed 90° and the forearm was pronated 180° relative to the anatomical position. A 3-D multi-segment inverse dynamic model [3,4] calculated net torques for the right wrist, elbow and shoulder joints. Root mean square (RMS) EMG signals were normalized to maximum voluntary contractions.

Summary statistics were calculated for the upper extremity 3-D postural and joint torque data. Angle and torque variation was calculated as the standard deviations averaged across participants. Distance from the keyboard was calculated as the horizontal distance between the right acromion and the front of the keyboard. These biomechanical parameters were averaged across the whole trial (2 minutes). For the muscle activity data, the 10th, 50th and 90th percentiles provided metrics in the distribution-EMG signal amplitude.

Sample t-tests were used to determine the effect of typing style on the biomechanical parameters ( $\alpha = 0.05$ ).

## RESULTS AND DISCUSSION

Touch typists had significantly higher shoulder internal rotation angle and wrist ulnar deviation (Table 1), which might be explained by the fact that they sat significantly closer to the keyboard compared to two-fingered typists (32.8 (1.3)cm vs. 28.2 (0.9)cm respectively). Two-fingered typists had significantly higher variation for shoulder rotation and flexion angles (Table 1).

Two-fingered typists had generally higher total joint torques and total torque variation compared to

touch-typists, with wrist total torque and torque variation being significantly different between the two groups (Table 1). More specifically, the two-fingered typists had significantly higher wrist RMS torque in flexion/extension (0.28 (0.02)Nm vs. 0.19 (0.02)Nm respectively) and in rotation (0.29 (0.04)Nm vs. 0.20 (0.02)Nm respectively), and significantly higher shoulder torque variation in flexion/extension (0.46 (0.05)Nm vs. 0.32 (0.04)Nm respectively), rotation (0.29 (0.04)Nm vs. 0.20 (0.02)Nm respectively), as well as in add/abduction (0.21 (0.02)Nm vs. 0.14 (0.01)Nm respectively). All other RMS torques and torque variations were not significantly different between the two groups. These results suggest that joint loads are different between the two typing styles in terms of frequency and magnitude.

The 10<sup>th</sup> percentile value of EMG amplitude for the anterior deltoid muscle was significantly greater for two-finger typists ( $p = 0.047$ ), which means that static shoulder muscle loading was higher for two-finger typists compared to touch-typists.

## CONCLUSIONS

Two-finger typists had larger dynamic loading and increased variability in joint torques and postures compared to touch typists. These differences suggest that injury mechanisms for the upper extremity associated with computer work may be different for the two typing styles.

## REFERENCES

- 1.Kilbom A., Persson J. *Ergonomics*. **30**: 273-279, 1987.
- 2.Pascarelli EF, Kella JJ. *Journal of Occupational Medicine*, **35**: 522-532, 1993.
- 3.Kingma I, et al., *Journal of Biomechanics*. **29(5)**: 693-704, 1996.
- 4.Kuo P, et al., *Journal of Biomechanics*. **39(16)**: 2934-2942, 2006.

## ACKNOWLEDGEMENTS

This study was funded in part by NIOSH R01 OH008373, and the NIOSH ERC at Harvard University-grant (T42 OH008416-05).

**Table 1:** Across subject mean (s.e.) joint angles and angle variation (s.e.) for two-fingered typists (Finger) and touch-typists (Touch).

|                       | Flexion            |                    | Internal rotation   |                     | Abduction           |                     |
|-----------------------|--------------------|--------------------|---------------------|---------------------|---------------------|---------------------|
|                       | Finger             | Touch              | Finger              | Touch               | Finger              | Touch               |
| <b>Shoulder</b>       |                    |                    |                     |                     |                     |                     |
| mean angle (deg)      | -2.84 (1.66)       | -2.20 (1.09)       | <b>19.43 (1.37)</b> | <b>26.14 (1.84)</b> | -7.21 (0.89)        | -6.88 (1.21)        |
| angle variation (deg) | <b>2.51 (0.32)</b> | <b>1.52 (0.24)</b> | <b>4.21 (0.47)</b>  | <b>1.80 (0.17)</b>  | 1.14 (0.16)         | 0.83 (0.09)         |
| <b>Elbow</b>          |                    |                    |                     |                     |                     |                     |
| mean angle (deg)      | -7.53 (1.20)       | -4.94 (1.49)       | 8.61 (1.91)         | 4.11 (2.18)         | -                   | -                   |
| angle variation (deg) | 1.97 (0.42)        | 1.44 (0.12)        | 2.85 (0.26)         | 2.75 (0.21)         | -                   | -                   |
| <b>Wrist</b>          |                    |                    |                     |                     |                     |                     |
| mean angle (deg)      | -25.20 (2.11)      | -20.04 (2.28)      | -                   | -                   | <b>13.83 (1.29)</b> | <b>19.13 (1.47)</b> |
| angle variation (deg) | 6.25 (0.36)        | 5.54 (0.34)        | -                   | -                   | 3.25 (0.26)         | 3.16 (0.31)         |

\*Negative angles mean that the angle is in the opposite direction from that stated in the column heading (ex: negative shoulder flexion is extension). Statistically significant differences between the two groups are in bold.

**Table 2:** Across subject mean (s.e.) total joint torques and total torque variation (s.e.) for two-fingered typists (finger) and touch-typists (touch). Statistically significant differences between the two groups are in bold.

|                             | Finger             | Touch              |
|-----------------------------|--------------------|--------------------|
| <b>Shoulder</b>             |                    |                    |
| mean total torque (Nm)      | 2.05 (0.69)        | 1.20 (0.40)        |
| total torque variation (Nm) | 1.42 (0.54)        | 0.60 (0.17)        |
| <b>Elbow</b>                |                    |                    |
| mean total torque (Nm)      | 0.35 (0.11)        | 0.19 (0.07)        |
| total torque variation (Nm) | 0.22 (0.05)        | 0.11 (0.03)        |
| <b>Wrist</b>                |                    |                    |
| mean total torque (Nm)      | <b>0.01 (0.00)</b> | <b>0.00 (0.00)</b> |
| total torque variation (Nm) | 0.00 (0.00)        | 0.00 (0.00)        |

# EFFECTS OF A FATIGUING RUN ON LOWER EXTREMITY MECHANICS IN FEMALE RUNNERS

Carrie A. Truebenbach, Jennifer Earl-Boehm, Wendy Huddleston, Ann Swartz & Kristian M. O'Connor

Department of Human Movement Sciences  
University of Wisconsin-Milwaukee, Milwaukee, WI, USA  
email: [catrueb@uwm.edu](mailto:catrueb@uwm.edu) web: [www.chs.uwm.edu/neuromechanics](http://www.chs.uwm.edu/neuromechanics)

## INTRODUCTION

The ability to continue running injury-free is an accepted goal for competitive athletes. The majority of runners, however, pursue running as a recreational activity. In fact many engage in this form of physical activity to minimize the risks, and potentially deleterious effects of increasingly common cardiovascular disease. To reduce the potential for time away from activity due to injury, modifiable factors need to be identified, in order to design preventative interventions. Due to the repetitive stresses that occur during running, an individual's mechanics may pose a risk factor for injury. At-risk movement patterns in runners may be best identified under conditions that closely approximate the state of the neuromuscular system during effort. Specifically, inducing general fatigue, within a laboratory setting, could replicate the state condition present when a musculoskeletal overuse injury is likely to occur. In recent years, there is a growing body of literature examining runners under some form of fatigue condition [1,2,3] Additionally, prospective work is beginning to identify mechanics present in injured compared with control populations [4]. Hip and knee frontal and transverse plane mechanics, in particular have been linked to injury risk [4]. The purpose of this study was to examine whether mechanical changes are apparent in healthy female runners, following a fatiguing run.

## METHODS

Participants were 12 female rearfoot strike runners, aged 20-36 years old. Participants ran at least 10 miles per week, and injury-free for at least the previous 3 months. Data were obtained during two testing sessions. At session 1, participants completed maximal metabolic testing ( $\text{VO}_2 \text{ max}$

test) on a treadmill. The speed at which a participant achieved ventilatory threshold (VT) during the testing was utilized to establish the speed for the prolonged run during session 2. At session 2, kinetic and kinematic data were obtained before and after a 30-minute run at VT. Metabolic data were monitored during the run with an open circuit spirometry metabolic measurement system (TrueOne 2400). End tidal carbon dioxide pressure ( $\text{P}_{\text{ETCO}_2}$ ) was assessed to provide a physiological marker of fatigue [3]. Measurements were completed as participants ran across an AMTI force plate (sampling rate of 1000 Hz) at 3.6 m/s. Kinematics were collected with a 7-camera Motion Analysis Eagle System at a sampling rate of 200 Hz. Participants performed five trials pre- and post-exercise.

The dependent variables were touchdown angle (TD), range of motion (ROM - defined as TD to peak), and peak joint moment for the hip and knee in the frontal and transverse planes.  $\text{P}_{\text{ETCO}_2}$  at the beginning and end of the 30 minute run served as another dependent variable. Differences between pre- and post-exercise in the kinematic, kinetic, and physiological dependent variables were assessed with one-tailed paired t-tests. An alpha level of  $p < .05$  was utilized for all analyses.

## RESULTS AND DISCUSSION

Runners completed the 30 minute run at an average of  $3.5 \pm 0.4$  m/s. General fatigue was achieved by all participants as evidenced by a significant decrease of  $11.3 \pm 4.9\%$  ( $p < .05$ ) in  $\text{P}_{\text{ETCO}_2}$  from minute 1 to 30 of the run.

No significant differences were detected with respect to TD angles (Table 1). Hip and knee transverse plane ROM both demonstrated

significant differences following the fatigue run. Greater hip external rotation range of motion (ER) was present as well as greater internal rotation range of motion (IR) at the knee. There was also a significant decrease in the transverse plane hip IR moment following the fatigue run (Figure 1).

## CONCLUSIONS

The findings in this study demonstrate kinematic and kinetic changes in a healthy sample of female runners following a run that induced general fatigue.  $P_{ET}CO_2$  has previously been used as a physiological marker of fatigue during running, and the results in this study suggest a degradation in general neuromuscular function. The increase in knee IR ROM is consistent with findings of other researchers studying a fatigue condition in healthy female runners [1]. It is also consistent with a potential risk of injury to the iliotibial band syndrome as reported in a prospective running injury study [4]. Findings in the present study suggest that proximal transverse plane changes may necessitate a response at the knee. This is evidenced by a decrease in hip IR moment, along with an increase in hip ER ROM, with fatigue (Figure 1). One may expect an increase in the hip IR moment as a response to increased ER motion at the hip in a healthy cohort. The dynamic patterns in the current research may be indicative of an in-plane mechanism to reduce tissue strain during an effort. The fact that all fatigue-related mechanical changes took place in the transverse plane may also reflect the need for greater control of motion in this plane. The control strategies may be best directed at control of the hip.

**Table 1.** Group mean (SD) hip and knee dependent variables. Positive TD and moment values are adduction and internal rotation

|                          |         |       | Pre         | Post        |
|--------------------------|---------|-------|-------------|-------------|
| <b>TD</b><br>(°)         | Frontal | Hip   | 3.3 (4.4)   | 4.4 (3.0)   |
|                          |         | Knee  | 0.92 (2.8)  | 1.0 (3.0)   |
|                          | Trans   | Hip   | 2.0 (4.8)   | 2.7 (3.9)   |
|                          |         | Knee  | -5.8 (5.6)  | -6.0 (3.8)  |
| <b>ROM</b><br>(°)        | Frontal | Hip   | 7.2 (3.4)   | 6.2 (2.2)   |
|                          |         | Knee  | 2.8 (1.8)   | 2.7 (1.5)   |
|                          | Trans   | Hip*  | 6.2 (3.8)   | 7.4 (4.0)   |
|                          |         | Knee* | 10.1 (3.0)  | 11.6 (4.1)  |
| <b>Moment</b><br>(Nm/kg) | Frontal | Hip   | -1.9 (.25)  | -1.9 (.29)  |
|                          |         | Knee  | -1.0 (.31)  | -0.98 (.26) |
|                          | Trans   | Hip*  | 0.49 (.11)  | 0.47 (.13)  |
|                          |         | Knee  | -0.13 (.05) | -0.14 (.06) |

\* $p < .05$

## REFERENCES

1. Dierks TA, et al. *J Biomech* **43**, 2993-2998, 2010.
2. Mizrahi J, et al. *Ann Biomed Eng* **28**, 463-469, 2000.
3. Voloshin A, et al. *Clin Biomech*, **13**, 513-520, 1998.
4. Noehren B, et al. *Clin Biomech*, **22**, 951-956, 2007.

## ACKNOWLEDGEMENTS

College of Health Sciences Student Research Grant

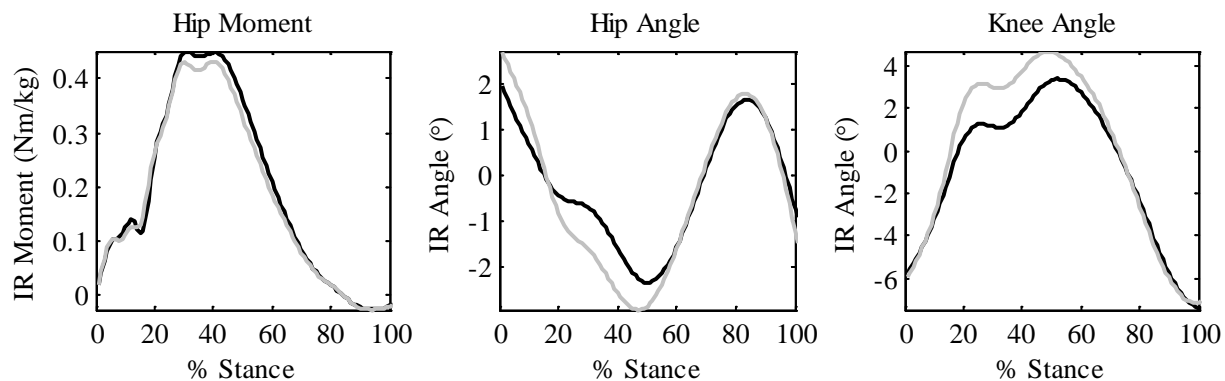


**Figure 1:** Group mean transverse plane hip moment, and hip and knee angles. Positive represents internal rotation. Black lines represent pre-run, and gray lines represent post-run mechanics.

# INCREASED TIBIOFEMORAL COMPRESSIVE LOADS IN FEMALES WHO HAVE UNDERGONE ANTERIOR CRUCIATE LIGAMENT RECONSTRUCTION

<sup>1</sup>Liang-Ching Tsai, <sup>2</sup>Scott G. McLean, <sup>1</sup>Patrick M. Colletti and <sup>1</sup>Christopher M. Powers

<sup>1</sup>University of Southern California, CA, USA

<sup>2</sup>University of Michigan, MI, USA

email: [liangcht@usc.edu](mailto:liangcht@usc.edu), web: <http://pt.usc.edu/labs/mbrl/>

## INTRODUCTION

Individuals who have undergone anterior cruciate ligament reconstruction (ACLR) have been shown to have a higher risk of developing knee osteoarthritis (OA) [1]. The elevated risk of knee OA may be associated with an increase in knee joint compressive load resulting from an altered neuromuscular strategy (i.e., increased muscle co-contraction, decreased knee flexion) that has been observed in this population [2]. The purpose of this study was to examine whether females who have undergone ACLR demonstrate greater tibiofemoral compression due to greater co-contraction when compared to healthy females.

## METHODS

Ten females who have previously undergone ACLR formed the experimental group, while 10 females without a history of ACLR served as the control group (Table 1). Subjects participated in 2 data collection sessions: 1) magnetic resonance imaging (MRI) assessment; and 2) biomechanical testing of a single-leg drop-land task. Data collected from the 2 testing sessions were used as input variables for a subject-specific electromyography (EMG) driven model to quantify tibiofemoral compression during landing. The input variables of the model included MRI-measured muscle volumes and patella tendon orientation as well as lower extremity kinematics and muscle activation (see below for details).

Sagittal and axial MR images of the lower extremity were obtained using a 3T MRI system. For each muscle used in the model, the cross sectional area was measured on each axial image to calculate the total muscle volume. The total volume was combined with the pennation angle, fiber length,

and specific tension [3, 4] to calculate the maximum isometric muscle force for each muscle. The angle formed by the patella tendon and medial tibial plateau was measured from the sagittal MR images at 0, 15, 30, 45, and 60° of knee flexion. A linear regression curve fitting procedure was used to estimate the angle from 0 to 120° of knee flexion.

Lower extremity kinematics and ground reaction forces (GRF) during landing were recorded using a motion analysis system (250 Hz) and force platform (1500 Hz). Muscle activation levels were recorded from the vastus lateralis (VL), vastus medialis (VM), rectus femoris (RF), semitendinosus (ST), biceps femoris long head (BFL), medial (MG) and lateral gastrocnemius (LG) using surface EMG. For each muscle group, 3 maximum voluntary isometric contractions (MVIC) were collected. Raw EMG data were band-pass filtered (35-500 Hz), smoothed (6-Hz low-pass), and normalized to the maximum EMG value recorded either from the MVIC or drop-land tasks. Activation of the vastus intermedius (VI) was estimated as the average of the VM and VL EMG. Biceps femoris short head (BFS) and semimembranosus (SM) were assumed to have the same activation as BFL and ST, respectively. A 40-ms electromechanical delay was used to adjust the time difference between EMG and force output [5]. To quantify the level of co-contraction between the knee flexor and extensor muscles, a co-contraction index (CCI) was calculated for each subject.

SIMM software was used to create a generic anatomical knee joint model [3] that included 10 musculotendon actuators: VL, VI, VM, RF, ST, SM, BFL, BFS, MG, and LG. The estimated maximum isometric forces (derived from MRI-measured muscle volumes) and patella tendon orientation were incorporated into the generic

SIMM knee model for each subject. The calculated muscle force vectors were combined with the weight of the lower leg, GRF, and the linear acceleration of the lower leg to estimate the tibiofemoral compressive force during landing.

The primary dependent variable of interest was the peak tibiofemoral compressive force during the deceleration phase of the drop-land task. Secondary analyses were performed to test for differences in the CCI and peak knee flexion between groups. Between-group differences were examined using independent t-tests (significance level:  $p \leq 0.05$ ).

**Table 1:** Subject characteristics of the ACLR and control groups.

|                            | ACLR        | Control     | p value |
|----------------------------|-------------|-------------|---------|
| Age (year)                 | 25.3 ± 2.4  | 24.9 ± 1.7  | 0.67    |
| Mass (kg)                  | 60.3 ± 6.7  | 60.5 ± 5.5  | 0.97    |
| Height (cm)                | 164.2 ± 8.5 | 167.1 ± 4.5 | 0.36    |
| Time Post Surgery (months) | 36.2 ± 18.5 | N/A         |         |

## RESULTS AND DISCUSSION

The ensemble average curves of the tibiofemoral compressive force for the 2 groups are shown in Figure 1. The ACLR group exhibited significantly greater peak tibiofemoral compressive forces than the control group ( $97.3 \pm 8.0$  vs.  $88.8 \pm 9.8$  N·kg<sup>-1</sup>,  $p = 0.025$ ; Table 2). On average, the ACLR group also demonstrated a significantly greater CCI value as well as a reduction in the peak knee flexion angle when compared to the control group (Table 2).

The strategy of increased muscle co-contraction is thought to be a protective mechanism to decrease the anterior tibia shear loads. However, our findings

suggest that this neuromuscular pattern may contribute to elevated compressive loads on the tibiofemoral joint. Excessive compressive loads have been shown to negatively impact articular cartilage health [6]. Therefore, it stands to reason that the high risk of knee OA in persons post-ACLR may result, in part, from the elevated joint compression associated with increased muscle co-contraction. As such, reducing co-contraction through neuromuscular retraining may be beneficial to decrease tibiofemoral loading in this population.

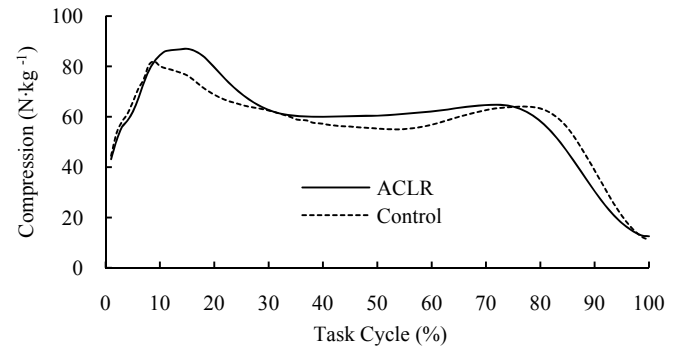


**Figure 1:** The ensemble average time-series curves of the tibiofemoral compressive force for the ACLR group (solid line) and the control group (dashed line) during the single-leg drop-land task.

## REFERENCES

1. Pinczewski LA, et al. *Am J Sports Med* **35**, 564-574, 2007.
2. Ortiz A, et al. *Am J Sports Med* **36**, 149-157, 2008.
3. Delp SL, et al. *IEEE Trans Biomed Eng* **37**, 757-767, 1990.
4. Friederich JA and Brand RA. *J Biomech* **23**, 91-95, 1990.
5. Lloyd DG and Besier TF. *J Biomech* **36**, 765-776, 2003.
6. Clements KM, et al. *Osteoarthr Cartil* **9**, 499-507, 2001.

**Table 2:** The peak tibiofemoral compressive force, co-contraction index, and peak knee flexion angle during the deceleration phase of the single-leg drop-land task. Values are mean ± SD.

|  | ACLR (n = 10) | Control (n = 10) | p value |
|--|---------------|------------------|---------|
| Peak Compression (N·kg <sup>-1</sup> ) | 97.3 ± 8.0    | 88.8 ± 9.8       | 0.025   |
| Co-contraction Index                   | 0.28 ± 0.10   | 0.18 ± 0.05      | 0.004   |
| Peak Knee Flexion (degrees)            | 67.6 ± 8.8    | 79.1 ± 10.9      | 0.009   |

# MAMMALIAN MUSCLE MODEL FOR PREDICTING FORCE AND ENERGETICS DURING PHYSIOLOGICAL BEHAVIORS

<sup>1</sup>George A. Tsianos, <sup>2</sup>Cedric Rustin and <sup>1</sup>Gerald E. Loeb

<sup>1</sup>University of Southern California, CA, USA

<sup>2</sup>University of Mons, Mons, Belgium

email: [tsianos@usc.edu](mailto:tsianos@usc.edu) web: <http://mddf.usc.edu>

## INTRODUCTION

Muscles convert metabolic energy into mechanical work. A computational model of muscle would ideally compute both effects efficiently for the entire range of muscle activation and kinematic conditions (force and length). Estimating metabolic energy is particularly important as it is a teleologically appealing criterion of task performance. There are empirical data supporting it for locomotion and reaching but it is difficult to measure or model. Instead, cost functions in models that employ optimal control principles usually include estimates of muscle recruitment, stress or work that may differ greatly from energy consumption depending on factors such as sarcomere velocity and fiber type.

## METHODS

We have extended the original Virtual Muscle™ algorithm [1] to predict energy consumption for both slow and fast twitch muscle fiber types, partitioned according to the activation process ( $E_a$ ), cross-bridge cycling ( $E_{xb}$ ) and ATP/PCr recovery ( $E_{recovery}$ ). Because the terms of these functions correspond to identifiable physiological processes, their coefficients can be estimated directly from the types of experiments that are usually performed and extrapolated to dynamic conditions of natural motor behaviors. We also implemented a new approach to lumped modeling of the gradually recruited and frequency modulated motor units comprising each fiber type, which greatly reduced computational time.

To validate the energetics model for a wide range of physiological conditions, we simulated a maximal cycling ergometry task [2], having a duration of three minutes. Our model of the musculoskeletal

system consisted of two segments (thigh and shank plus foot) linked by a hinge joint at the knee. The knee was actuated by two muscle elements representing the rectus femoris and vasti muscles. Muscles were controlled in a "bang-bang" fashion, which is typical for tasks requiring maximal effort [3].

We computed initial energy consumption and force production for a model of human biceps longus (40% Slow-twitch, 60% Fast-twitch) to illustrate the emergent behavior of the force and energy formulations.

## RESULTS AND DISCUSSION

Validation results are plotted in Fig. 1. The model computed the energy consumed in phase with the exercise ( $E_{initial}$ ), which is related to ATP/PCr consumption and the delayed energy ( $E_{recovery}$ ) related to ATP/PCr recovery. The model captures remarkably well the dynamics of energy consumption and the total amount consumed (model: 35,000J; experiment: 30,000-40,000J; integral of curves in Fig. 1).

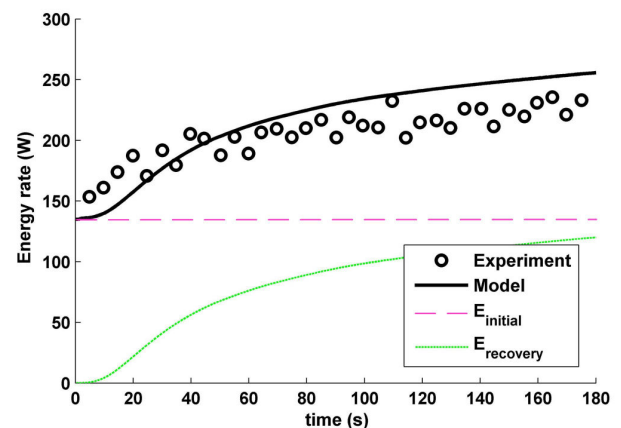


**Figure 1:** Validation results for a dynamic knee extension task.

The initial energy consumption and force production for the biceps model is plotted in Fig. 2 as a function of fascicle velocity from -6 to +3 rest lengths per second ( $L_0/s$ ). These two results are approximately inversely related for a family of curves for neural drive in 20% steps from 0 to maximal voluntary contraction (Fig. 2). Maximal force of  $\sim 840N$  (140% of maximal isometric force) occurs for stretching velocities greater than  $1L_0/s$  when energy consumption is  $\sim 40W$ . Maximal energy consumption of  $\sim 330W$  occurs near  $V_{max}$  ( $\sim 6L_0/s$ ), when force drops to zero. Energy consumption per unit isometric force rises from  $0.1W/N$  at 40% drive (all slow-twitch fibers) to  $0.2W/N$  at 100% drive.

It is evident from Fig. 2 that force and energy measures are vastly different and they will probably lead to different neural strategies when they are incorporated into an optimization algorithm's cost function. A cost function based on muscle force (or related parameters such as torque, stress etc.), for example, would lead to preferential recruitment of muscles that are shortening, whereas a cost function based on energy would lead to recruitment of muscles that are lengthening. This is particularly relevant for tasks like locomotion where subjects tend to recruit muscles during their lengthening phase to improve energetic economy of the movement.

## CONCLUSIONS

Given the accuracy of the model and its structure based on physiological processes, it should be possible to add effects such as fatigue and disuse atrophy. Such conditions result in a variety of experimentally characterized changes regarding calcium kinetics, cross-bridge cycling and glucose and glycogen metabolism. Such models would greatly extend the analysis of disabilities, which is now mostly limited to EMG and inverse dynamic analysis of recorded motion.

The emergent behavior of the model also has significant implications for studies of optimal motor control and development of rehabilitation strategies because its trends were quite different from traditional estimates of energy (e.g. activation, force, stress, work etc.).

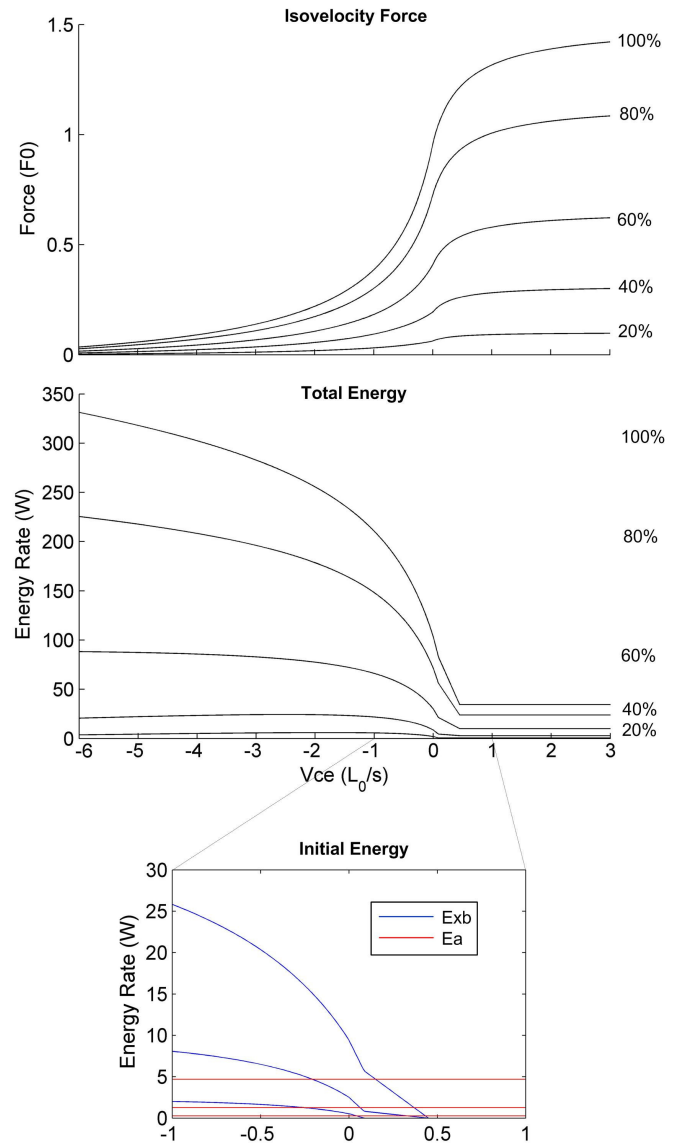


**Figure 2:** Emergent behavior of energetics and force formulations.

## REFERENCES

1. Cheng E et al. *J Neurosci Methods* **101**, 117-130 2000.
2. Gonzalez-Alonso J et al. *J Physiol* **524**, 603-615 2000.
3. Pandy MG and Zajac FE. *J Biomech* **24**, 1-10 1991.

## ACKNOWLEDGEMENTS

G. A. Tsianos was supported by the Myronis Fellowship Foundation and the DARPA REPAIR Program.

## A Sub-Maximal Treadmill Protocol to Assess VO<sub>2</sub>

Kirsten Tulchin MS and Kelly Jeans MS

Texas Scottish Rite Hospital for Children, Dallas, TX, USA  
email: kirsten.tulchin@tsrh.org web: <http://www.tsrhc.org>

### INTRODUCTION

Maximal VO<sub>2</sub> testing is often used as a measure of physical fitness and represents the maximum amount of oxygen that a subject can utilize during exercise. These graded exercise tests can be difficult to administer in patient populations. In particular, the successful completion of such protocols is challenging in pediatric patients where reaching a maximum may be compromised by cooperation and effort. Sub-maximal tests have been used in the past and are based on the assumption that there is a linear relationship between heart rate and oxygen consumption as the workload increases. A new sub-maximal treadmill VO<sub>2</sub> protocol was developed for use in pediatric populations, and was designed as a walking only protocol (no running) for safety purposes. The purpose of this study was to assess the repeatability of this protocol in predicting VO<sub>2</sub> max in healthy adults.

### METHODS

The TSRHC VO<sub>2</sub> treadmill protocol is a graded exercise test with each workload stage lasting three minutes. Raises in workload are obtained first by an increase in walking speed in 0.5mph increments. Treadmill speed is increased until the subject was unable (self-reported) to continue the test walking at a faster speed. Once this maximum treadmill speed is reached, all following workload increases consist of raising the incline in 3% grade increments. When used as a sub-maximal test, the protocol is completed when 1) the subject reaches 85% of age-predicted heart rate maximum (220-age) [1]; 2) subject discontinues the test for exhaustion, discomfort, or pain; or 3) subject completes the 15% grade on the treadmill at their maximum walking speed. For the purpose of this study, all participants were pushed further in an effort to achieve a truly maximal oxygen consumption test,

however the 15% is the maximum grade of the treadmill used.

Seven healthy adult subjects (4 males, 3 females) were assessed using the TSRHC VO<sub>2</sub> treadmill protocol. All subjects completed the protocol twice, a minimum of 7 days apart. VO<sub>2</sub> was measured using a COSMED K4B2 telemeter portable unit (Chicago, IL) and heart rate was assessed using a POLAR chest strap.

All subjects began the test with a 5 minute seated rest period. Prior to the start of the treadmill protocol, all subjects completed a 5 minute overground walk around a 40m track to determine a self-selected walking speed (SSW). This test was used as a warm-up prior to the start of the treadmill protocol, and served to determine each subject's preferred walking speed, rounded to the nearest 0.5 mph.

The initial treadmill workload was completed at 0% grade at a walking speed 0.5mph *slower* than the subject's overground SSW speed. Three minutes of recording was done for each workload, and the last minute was used for analysis of oxygen consumption rate (normalized to body weight) and heart rate. Thirty seconds prior to the end of the stage, the subject was asked to rate their perceived exertion (RPE) using the Borg RPE Scale [2].

A linear regression between heart rate and VO<sub>2</sub> was calculated across stages to predict maximal VO<sub>2</sub> at age-predicted heart rate maximum for each subject and each testing session using 1) all stages completed (VO<sub>2</sub>\_ALL) and 2) all stages up to 85% HR max (VO<sub>2</sub>\_85%). This was compared to the maximal oxygen consumption rate (VO<sub>2</sub>\_TEST) reached during the test. The subject was assumed to have reached a maximal VO<sub>2</sub> effort if they achieved ALL of the following conditions 1) a minimum of 85% age-predicted HR max, 2) RPE of 17 and 3)

respiratory exchange ratio (volume of carbon dioxide produced divided by volume of oxygen consumed) of 1.20.

## RESULTS AND DISCUSSION

The average day to day difference in maximal oxygen consumption (VO<sub>2</sub>\_TEST) was 3.75 ± 2.75 ml/kg/min (9.7 ± 6.8%). However it should be noted that only 4 subjects achieved a true VO<sub>2</sub> maximum test based on the criteria listed above. Since the protocol was designed to be sub-maximal, this was not a surprising finding. Therefore, a better assessment of the protocol was to compare the predicted VO<sub>2</sub> max based on stages up to 85% (VO<sub>2</sub>\_85%, where the test would typically have been stopped) with the predicted VO<sub>2</sub> max based on all stages completed (VO<sub>2</sub>\_ALL) (Figure1)

The day to day difference in the predicted VO<sub>2</sub>\_85% was 3.1 ± 2.4 ml/kg/min (7.2 ± 5.1%

range 0.8 to 15.5%). The average difference in predicted VO<sub>2</sub>max using the two methods (VO<sub>2</sub>\_85% vs. VO<sub>2</sub>\_ALL) was 1.74 ± 1.42 ml/kg/min (range 0.00 to 3.89 ml/kg/min). This corresponds to a difference of 4.1 ± 3.5% in VO<sub>2</sub>max.

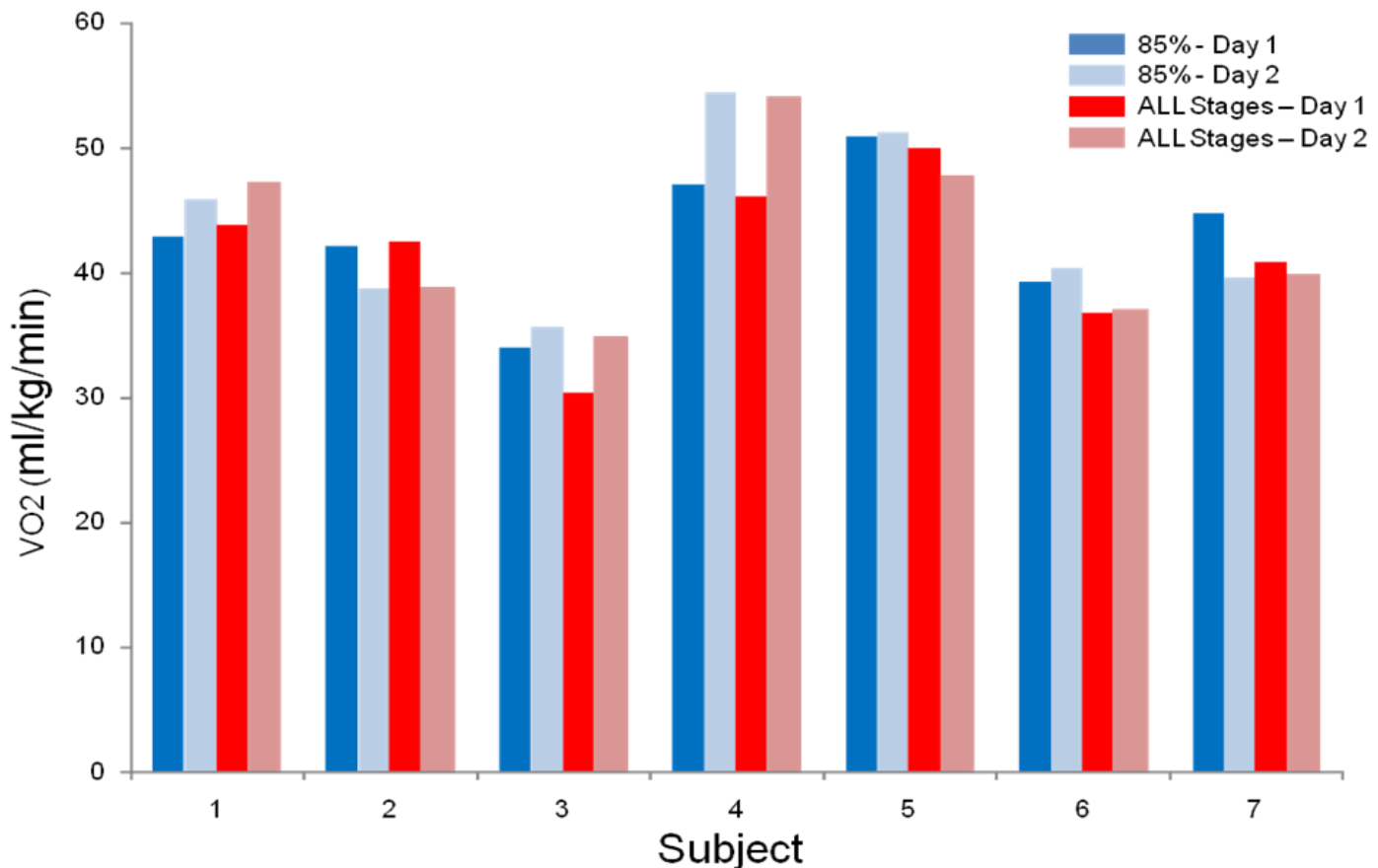
## CONCLUSIONS

The TSRHC sub-maximal VO<sub>2</sub> treadmill protocol is a reliable method to predict maximal oxygen consumption in healthy adults. Further work needs to be conducted to test and apply this protocol in healthy children and in patients with movement disorders or disabilities.

## REFERENCES

1. Jackson AS *Med. Sci. Sports Exerc* **39**(5), 822-829, 2007.
2. Borg, GA. *Med. Sci. Sports Exerc* **14**, 377-381, 1982.

**Table 1:** Individual results are presented for predicted VO<sub>2</sub> max a) with all stages (RED) and stages up to 85% age-predicted HR max (BLUE) for two testing sessions 1 week apart.



# A MODEL OF CHIMPANZEE HINDLIMB MUSCULOSKELETAL GEOMETRY

<sup>1</sup>Brian R. Umberger, <sup>2</sup>Matthew C. O'Neill, <sup>2</sup>Susan G. Larson, <sup>2</sup>Brigitte Demes and <sup>2</sup>Jack T. Stern Jr.

<sup>1</sup>University of Massachusetts Amherst, Amherst, MA, USA

<sup>2</sup>Stony Brook University School of Medicine, Stony Brook, NY, USA  
email: umberger@kin.umass.edu web: <http://www.umass.edu/locomotion>

## INTRODUCTION

Musculoskeletal models have become common tools for studying the biomechanics, energetics, and control of locomotion. Several models of the human musculoskeletal system have been developed [e.g., 1, 2]; however, few comparable models exist for other species. The chimpanzee is a facultative biped and our closest living relative, and has long provided important context for understanding the evolution of bipedal locomotion in humans. Yet, surprisingly little is known about how chimpanzees are able to move bipedally. A musculoskeletal model for simulating chimpanzee locomotion would therefore be a valuable tool for understanding the general principles that govern two-legged locomotion, and may provide insights as to the origins and evolution of bipedalism.

Here, we describe the initial development of a chimpanzee musculoskeletal model, focusing on the musculoskeletal geometry. Moment arms predicted by the model are compared with published moment arm functions, and we present an initial application demonstrating how the model can be used to study the effects of morphology on locomotor function. Specifically, we examined hip muscle moment arms to better understand why chimpanzees use a crouched gait when walking bipedally.

## METHODS

We created a 3D musculoskeletal model of the chimpanzee (*Pan troglodytes*) hindlimb in SIMM<sup>®</sup> (Fig. 1). Model skeletal elements were generated by CT scanning a pelvis, femur, patella, tibia, fibula, tarsals, metatarsals, and phalanges from an adult skeleton. The hip was modeled as a spherical joint between the pelvis and femur. The knee joint had one rotational degree of freedom, coupled to translation of the tibia relative to the femur and

translation and rotation of the patella relative to the tibia. The talocrural joint was modeled as a revolute joint between the tibia/fibula and talus, with the rotational axis running between the medial and lateral malleoli. The first tarsometatarsal joint and the metatarsophalangeal joints of the second through fifth digits were also treated as revolute joints, with the axes determined from congruence of the adjoining skeletal elements.

The model included 35 muscle-tendon units. Muscles with broad attachments were represented by multiple compartments, resulting in 45 individual muscle-tendon pathways. Origin and insertion locations were estimated from markings on the scanned bones and from reference to published muscle maps. Via points and wrapping surfaces were used where necessary to keep muscle paths from passing through bones or other muscles, and to redirect muscle lines-of-action where they passed around anatomical structures.

The quality of our reconstruction of musculoskeletal geometry was evaluated by comparing muscle moment arms predicted by the model with published flexion/extension moment arm functions determined experimentally in a chimpanzee cadaver [4]. We further investigated the moment arms of muscles acting about the hip joint to determine the ranges of hip flexion over which muscles are capable of generating moments for balancing the body above the support limb in single-limb stance.

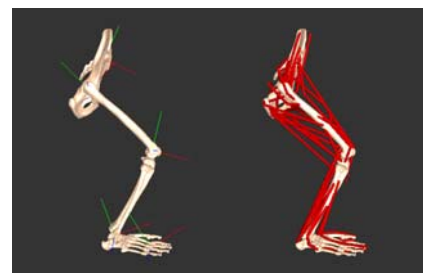


**Figure 1:** Chimpanzee musculoskeletal model.

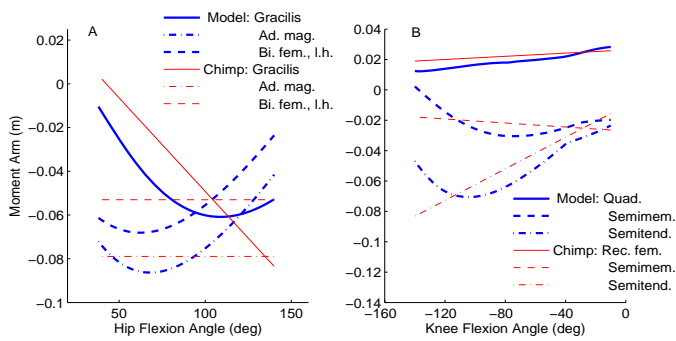


**Figure 2:** Moment arms predicted by the model (blue/thick) compared with experimental moment arm functions from the literature [4] (red/thin).

## RESULTS AND DISCUSSION

The moment arms predicted by the model were generally in good agreement with published moment arm functions [4]. For some muscles, there was good correspondence in both magnitude and slope over much of the joint angle range (e.g., quadriceps, Fig. 2B). For other muscles, the model predicted the proper average magnitude, but included higher-order features not present in the experimental functions (e.g., biceps femoris, Fig. 2A). Specifying the path for muscles with broad areas of attachment or complex arrangements always involves simplifications. Thus, to further evaluate model performance we are analyzing the sensitivity of model predictions to the assumptions made in specifying muscle path parameters.

Walking bipedally requires activation of muscles capable of helping support the body in single-limb stance. In humans, this role is served in large part by gluteus medius via abduction [1]. With the hip joint fully extended in the chimpanzee model, gluteus medius has a robust hip abduction moment arm (Fig. 3A). However, in this posture, gluteus medius also has a hip flexor moment arm, and the hamstrings hip extension moment arm is severely compromised (Fig. 3B), precluding these muscles from contributing meaningfully to support or propulsion. Flexing the hip improves hip extension moment arms (Fig. 3B). However, with the hip flexed, a medial rotation moment, rather than an abduction moment, is needed to balance the trunk at the hip [3]. This role can also be served by gluteus medius (Fig 3A). Therefore, the morphological differences between humans and chimpanzees at the

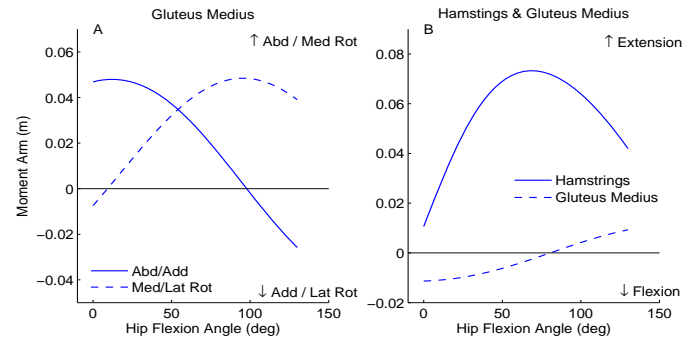


**Figure 3:** Gluteus medius and hamstrings moment arms. Each curve is the mean of three muscles or muscle compartments.

hip joint seem to be associated with generating hip extension moments with a fully extended hip, rather than frontal plane balance mechanisms. The ability of gluteus medius to generate moments that would help balance the body about the stance limb hip joint in the chimpanzee is independent of hip flexion angle, though via two different actions (Fig. 3A). This role of gluteus medius appears to be conserved across the great apes [3].

## CONCLUSIONS

The model of musculoskeletal geometry reported here represents an important first step in the development of a fully dynamic model for simulating chimpanzee locomotion. Analysis of hip joint muscles indicates that the flexed hip posture used by chimpanzees provides muscles with the necessary leverage to contribute to both support and propulsion of the body during bipedal locomotion.

## REFERENCES

1. Anderson FC & Pandy MG. *Gait Posture* **17**, 159-169, 2003.
2. Arnold EM, et al. *Ann Biomed Eng* **38**, 269-279, 2010.
3. Stern JT & Susman RL. *Am J Phys Anthropol* **55**, 153-166, 1981.
4. Thorpe SK, et al. *Am J Phys Anthropol* **110**, 179-199, 1999.

## ACKNOWLEDGEMENTS

The American Museum of Natural History kindly provided the skeletal materials. Supported by NSF BCS-0935321 and NSF BCS-0935327.

# FRONTAL JOINT DYNAMICS WHEN INITIATING STAIR ASCENT WITH AND WITHOUT GAIT SPEED

<sup>1</sup>Srikant Vallabhajosula, <sup>1</sup>Jennifer M. Yentes, <sup>1</sup>Chi-Wei Tan, <sup>1,2</sup>Ka-Chun Siu, <sup>1,2</sup>Nicholas Stergiou

<sup>1</sup>Nebraska Biomechanics Core Facility, University of Nebraska at Omaha, Omaha, NE

<sup>2</sup>College of Public Health, University of Nebraska Medical Center, Omaha, NE

Email: svallabhajosula@unomaha.edu web: <http://biomech.unomaha.edu/>

## INTRODUCTION

Stair negotiation is a challenging activity of daily living for certain populations. More than two-thirds of people aged 65 years or above experience falls yearly and about 18% of these falls have been attributed to stair negotiation. Interestingly, previous research focused on stair ascent initiation exclusively directly in front of the staircase. However, initiating stair ascent farther away from the stairs could allow participants to achieve a more natural gait speed before the transition phase from level walking to stepping onto the staircase. This is actually the case many times when we negotiate stairs (for example at home or in a mall). Intuitively, initiating stair ascent in front of the staircase would require more effort than initiating from farther away because of the lack of momentum thereby influencing the magnitudes of joint moments. However, this is currently unknown. Previous literature reported mostly on joint moments in the sagittal plane. However, the importance of understanding the biomechanical demands of stair ascent in the frontal plane has been previously documented [1,2,3]. Therefore, the objective of this research was to determine joint moments in the frontal plane when one begins stair ascent after achieving a comfortable gait speed compared to beginning stair ascent from a static position directly in front of the stairs. We hypothesized that the joint moments during stair negotiation will be different between the two conditions. Additionally, these differences will appear in consecutive ipsilateral footfalls on the stairs.

## METHODS

Ten healthy young adults (3 females; 26.4±3.7y; 76.2±13.6kg; 1.78±0.08m) ascended a four step

custom-built staircase (angle of staircase rise = 32.73°) five times under two conditions: starting from farther away (C1) and starting in front of the staircase (C2). Kinematics (Motion Analysis System, Santa Rosa CA; 60 Hz) and kinetics (AMTI, Watertown, MA; 600 Hz) were collected. Force platforms were embedded in the first and the third stair treads. Calculation of joint moments was accomplished using a custom Matlab (MathWorks Inc., Natick, MA) program. Peak abduction and adduction moments at the ankle, knee and hip joints were calculated through group means for each condition. A repeated 2 (conditions 1 vs 2) by 2 (steps 1 vs 2) ANOVA was performed using the SPSS software (SPSS Inc., Chicago, IL). The  $\alpha$ -value was set at 0.05.

## RESULTS AND DISCUSSION

The subjects produced greater peak knee abduction moment ( $P = 0.014$ ) and peak hip abduction moment ( $P = 0.006$ ) during early stance phase after foot-strike when initiating stair ascent starting from farther away (Fig. 1). In addition, the subjects produced greater peak ankle ( $P = 0.007$ ), knee ( $P < 0.001$ ) and hip abduction moments ( $P < 0.001$ ) while traversing the second step in comparison with the first step (Fig. 2). There were no significant interactions. The joint moment profiles and values in the current study were similar to the ones reported in the literature [1,2]. The three lower-extremity joints largely experienced abduction moments throughout the stance phase (Fig. 3). One plausible reason is the passage of the ground reaction force vector medially with respect to the joint centers [2]. The magnitude of the abduction moment at the ankle joint was minimal when compared to the other two joints. The greater peak knee abduction moment when starting from farther away shows that the lateral portions of the knee

experience higher levels of stress. Nadeau et al. (2003) mentioned that during stair negotiation, the hip abductors influence lateral pelvic obliquity to control the contralateral leg swing [1]. Greater hip abduction moment when approaching the staircase with a gait speed (Fig. 1) and when negotiating a higher ipsilateral step (Fig. 2) indicates an increased activity of the ipsilateral hip abductors. This increased activity could help to avoid contact of the contralateral limb with the intermediate step by counteracting the pelvic drop on the contralateral side [1,2].

## CONCLUSION

Results from the present study show that the knee and hip joints experience greater abduction moments in the frontal plane. This happened especially when initiating stair ascent from farther away. This could be an important finding in the literature concerning people with weaker hip abductors. These people may not be able to generate sufficient moments to counteract the pelvic drop on the contralateral side possibly resulting in a mechanically inefficient stair ascend. This could also be particularly relevant when starting from farther away and when encountering higher steps during stair ascent. Results of the present study also add an important methodological finding that researchers should be concerned about the position that they use to start stair ascend.

## REFERENCES

1. Nadeau S, et al. Clin Biomech **18(10)**, 950-959, 2003.
2. Kirkwood RN, et al. Phys. Ther. **79**, 360-370, 1999.
3. Andriacchi TP et al., J. Bone Joint Surg., **62-A**, 749-757

## ACKNOWLEDGEMENTS

Funding provided by the National Institute on Disability and Rehabilitation Research (Grant No. H133G080023), National Institute of Health (Grant No. 1R011AG034995-01A1) and the Nebraska Research Initiative.

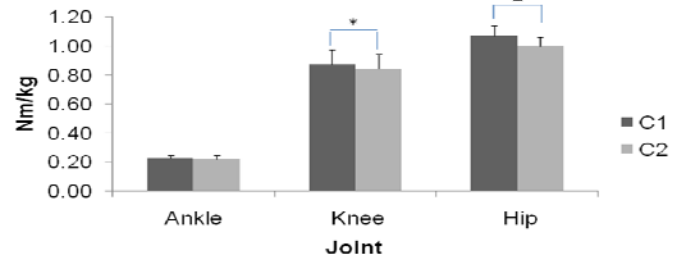


**Figure 1:** Peak abduction moments at the three lower-extremity joints; C1 – Condition 1 (Starting from farther away); C2 – Condition 2 (Starting from front); \*Significant condition main effect ( $P < 0.05$ )

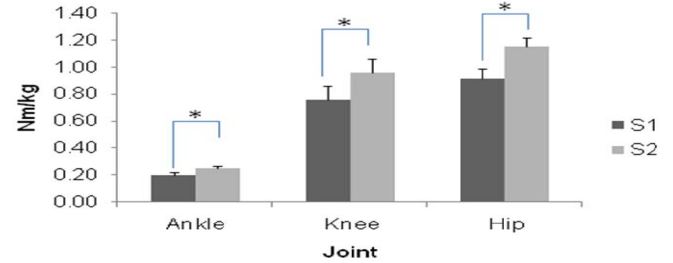


**Figure 2:** Peak abduction moments at the three lower-extremity joints; S1 – First ipsilateral step; S2 – Second ipsilateral step; \*Significant step main effect ( $P < 0.05$ )

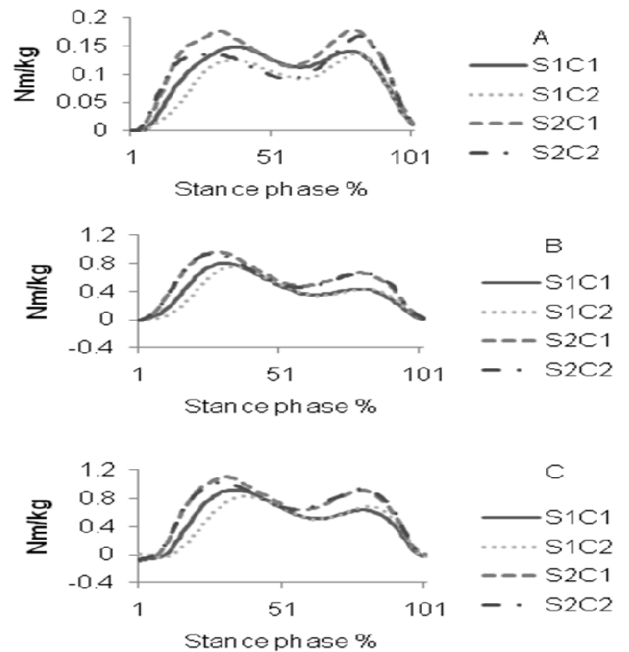


**Figure 3:** Ensemble curves representing frontal plane joint moments of A) Ankle B) Knee and C) Hip during stair ascent. S1 – Step 1; S2 – Step 2; C1 – Starting from farther away; C2 – Starting from front; Positive and increasing ordinate values represent the abduction of all joints.

## UPPER LIMB MUSCLE VOLUME AND STRENGTH, AND THEIR RELATIONSHIP IN OLDER ADULTS

<sup>1</sup>Meghan E. Vidt, <sup>1</sup>Melissa Daly, <sup>3,4</sup>Michael E. Miller, <sup>3,4</sup>Cralen C. Davis, <sup>1,2</sup>Anthony P. Marsh and  
<sup>1</sup>Katherine R. Saul

<sup>1</sup>Virginia Tech – Wake Forest University School of Biomedical Engineering and Sciences

<sup>2</sup>Department of Health and Exercise Science, Wake Forest University, Winston-Salem, NC USA

<sup>3</sup>Department of Biostatistical Sciences, Wake Forest University, Winston-Salem, NC

<sup>4</sup>WFU School of Medicine, Department of Public Health Sciences, Winston-Salem, NC

email: mvidt@wfubmc.edu, web: <http://www.sbes.vt.edu/kholzbau/MoBL/index.html>

### INTRODUCTION

Aging leads to a progressive decline of the neuromuscular system that includes loss of skeletal muscle mass, declines in muscle force, decreased neural activation and a diminished quality of contractile proteins [1,2]. It has been suggested that the degree of atrophy and the force-generating capability of muscle may differ for different functional groups of muscles with age, though evidence in the upper limb is limited [3]. The relationship between muscle volume and strength in the upper limb has been established for young adults (age 24-37y) [4,5]. However, this relationship has not been examined in an older cohort and it is not known whether the relationship between these measurements differ among the major functional groups of the upper limb of older adults (age $\geq$ 65). Changes in the distribution of muscle volume among functional groups in the upper limb and the relationship between muscle volume and joint strength may have important functional consequences in older adults who may struggle to perform daily upper limb self-care tasks.

The objective was to (1) measure muscle volume and isometric joint moment-generating capacity at the shoulder, elbow, and wrist in a single group of older adults (N=18), (2) characterize the relationship between muscle volume and isometric joint moment for the major functional groups in the upper limb, and (3) compare these relationships to those previously assessed in young adults [4,5].

### METHODS

Eighteen ostensibly healthy older adults were evaluated (10M, 8F; 75.1 $\pm$ 4.3y; 75.7 $\pm$ 12.2kg; 169.8 $\pm$ 9.4cm); all gave written informed consent. For each subject, muscle volume and isometric joint moment were measured on the dominant arm.

Subjects were imaged with a 1.5 T MRI scanner (GE Healthcare, Milwaukee, WI) using 3D spoiled gradient imaging sequences. The body coil was used to obtain images of the muscles crossing the shoulder and arm (scan time ~16 min). A flexed-array long bone coil (Invivo, Orlando, FL) was used to obtain images of muscles crossing the elbow and wrist in two successive scans (scan time ~22 min).

The MR images were manually segmented (3D Doctor, Able Software Corp., Lexington, MA) to produce a three-dimensional reconstruction of the 32 muscles crossing the glenohumeral joint, elbow, forearm, and wrist. Muscles were assigned to functional groups according to each muscle's primary action. Functional group volume was calculated as the sum of individual muscle volumes within the group; total upper limb muscle volume was the sum of all muscle volumes. Volume fraction was calculated by determining the functional group volumes as a percent of total upper limb volume.

Maximum isometric joint moment-generating capacity was measured at the wrist (flexion, extension), elbow (flexion, extension) and shoulder (abduction, adduction) joints using a KIN-COM dynamometer (Isokinetic International, Harrison, TN). Measurements were compared to those reported previously for the same postures in young adults [4,5]. A generalized linear model, accounting for gender, height, body mass, and functional group volume was used to assess volume and strength differences between young and older adults. We used pair-wise comparisons to assess strength distribution across joints ( $p\leq 0.0125$ ), mixed model ANCOVA to assess strength differences between age groups, accounting for gender, ( $p\leq 0.0167$ ), and linear regression to assess the relationship between joint moment and functional group volume ( $p\leq 0.05$ ).

## RESULTS AND DISCUSSION

On average, total muscle volume for the older adults was 16.5% less than total upper limb volume for young adults. With the exception of wrist extensors, all functional groups for older adults had significantly less ( $p < 0.027$ ) volume than young adults (Figure 1). When converted to volume fraction, shoulder adductors ( $p = 0.008$ ) still had significantly reduced volume fraction compared to young adults, while wrist extensors were significantly increased ( $p < 0.001$ ).

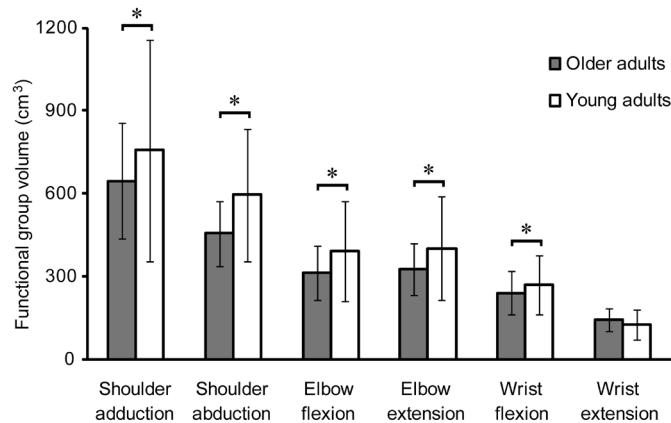


**Figure 1:** Muscle volume by functional group for older (grey) and young (white) adults.

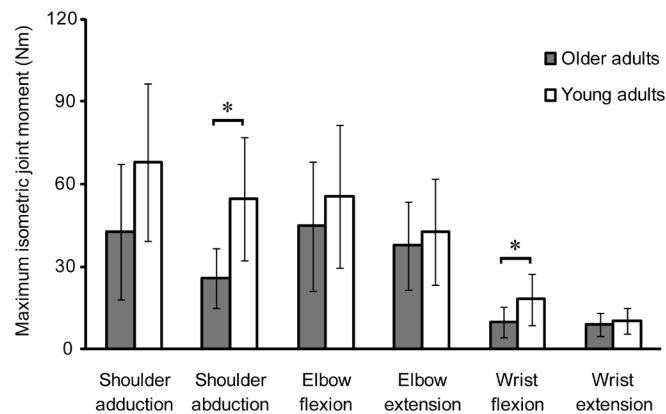


**Figure 2:** Isometric joint moment for older (grey) and young (white) adults.

Older adults also demonstrated decreased isometric joint moments across all functional groups compared to young adults (Figure 2), with significant differences for shoulder abductors ( $p < 0.001$ ) and wrist flexors ( $p < 0.001$ ). Using mixed model ANCOVA, the age difference in strength was significantly greater for shoulder abduction versus wrist flexion ( $p = 0.003$ ) and shoulder adduction versus wrist extension ( $p = 0.0144$ ). While young adults were consistently strongest at the shoulder, older adults were consistently strongest at the elbow, indicating a change in the relative strength

among functional groups. Although muscle volume remained a significant linear predictor ( $p < 0.025$ ) of joint moment in older adults, only  $41.4 \pm 10.9\%$  of the variation in moment was accounted for by volume, compared to  $81.0 \pm 10.8\%$  in the young adults. In addition, there was a reduction in shoulder abduction strength produced by a given volume of muscle in the older adult subjects, indicating a reduction in muscle force-generating capacity.

In older adults, we have detected reduced muscle volumes that are consistent with sarcopenia, and reduced strength, which is in line with previous reports of increased connective tissue, decreased neural drive, and diminished quality of contractile proteins [1,2]. At the shoulder, the decreased strength in older adults is associated with significantly greater reductions in muscle volume compared to young adults. We have also expanded upon the findings of Klein et al. [3], demonstrating changes in strength and volume that differ by functional group.

## CONCLUSIONS

We conclude that with age, upper limb muscle volume and isometric joint moment-generating capacity are reduced in older adults, with marked deficits at the shoulder. Although both volume and joint moment were lower for the older adults, muscle volume remained a significant predictor of joint moment across all joints in the upper limb. These data provide a foundation for exploring functional deficits in older adults both from an experimental perspective and as a resource for developing simulation-based analyses that better reflect the strength and muscle characteristics of older adults.

## REFERENCES

1. Jones, EJ, et al. *Sports Med* **38**, 987-94, 2008.
2. Clark, BC and Manini, TM. *Curr Opin Clin Nutr Metab Care* **95**, 139-59, 2010.
3. Klein, CS, et al. *J Appl Physiol*. **91**, 1341-9, 2001.
4. Holzbaur KR, et al. *J Biomech* **40**, 742-9, 2007.
5. Holzbaur KR, et al. *J Biomech* **40**, 2442-9, 2007.

## ACKNOWLEDGEMENTS

WFU Science Research Fund, WFU Cross-Campus Collaborative Research Fund, WFU Claude D. Pepper Older Americans Independence Center (P30-AG21332), Center for Biomolecular Imaging of WFU School of Medicine.

# OPTIMIZATION OF SHIFT LEVER POSITION

<sup>1</sup>Miloslav Vilimek, <sup>1</sup>Zdenek Horak and <sup>2</sup>Kubovy Petr

<sup>1</sup>Czech Technical University in Prague, Prague, Czech Republic

<sup>2</sup>Charles University in Prague, Prague, Czech Republic

email: [miloslav.vilimek@fs.cvut.cz](mailto:miloslav.vilimek@fs.cvut.cz) web: <http://www.biomechanics.cz>

## INTRODUCTION

This paper presents relation between position of car shift lever and muscular activity of upper extremity during manually shift control. The purpose of this study was to find as optimum as possible position of shift lever so that it was user comfortable. This investigation was aimed at cars with manual transmission.

## METHODS

Each person have own specific style for shifting, but good set up of steering wheel, seat and shift lever handle position can bring comfortable car driving.

Investigation was based on assumption, that the length at which the maximum active force can muscle produce is called the optimal muscle length. In this position can muscle produce active force more easily than in shortened or extended position. If we will solve optimization task for minimum error of optimum muscle length for each upper extremity muscle during shifting, we can find optimum position from muscle function point of view.

First, the 3D movement of right upper extremity was experimentally measured simultaneously with collection of main upper extremity actuators EMG's. The observed upper extremity muscles were BRD - brachioradialis, BICL biceps brachii long head, BICS – biceps brachii short head, BRA - brachialis, TRIMed – triceps brachii medial head, TRILat - triceps brachii lateral head, TRILong - triceps brachii long head, DLT - deltoideus. Used car for experimental investigation included manual transmission with five forward gears and one reverse speed. Each specimen had own set up for the driver's seat and steering wheel. We use

parameter “shifting position” for evaluation this position between specimens. This parameter was calculated as ratio of elbow angle when specimen has hand on a steering wheel and when specimen has hand on a shift gear handle. Specimens were instructed so that subsequently shift speed gears from neutral to fifth gear, then subsequently back to neutral and then to reverse and back to neutral gear. 3D kinematic parameters were collected by Qualisys motion capture system and EMG's were collected by 16 channel EMG system (Motion Lab Systems, Inc.).

Second, the musculoskeletal model of upper extremity was developed. The OpenSim software was used for design the upper extremity model, Figure 1. Muscle parameters (PCSA, optimum muscle length, tendon slack length) were taken from literature [1]. The anthropometric data for each specimen were experimentally obtained from MRI. The musculoskeletal model was scaled for each specimen.

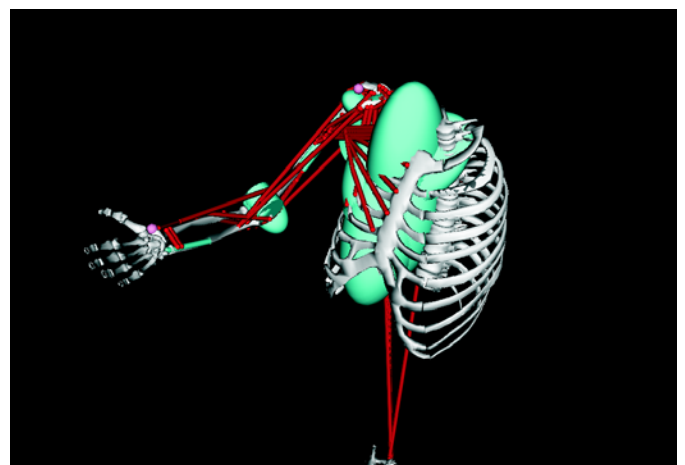


**Figure 1:** The OpenSim musculoskeletal model of upper extremity used in presented study.

The kinematic data were input into the musculoskeletal model of upper extremity. By the OpenSim musculoskeletal model were calculated

muscle lengths of main actuators during gear shifting. These calculated muscle lengths during gear shifting were compared with optimum muscle lengths and operating range of muscle fiber length. Normalized operating range of muscle length was taken from literature [1], and is described in Table 1.

Table 1: Optimum muscle length and operating range of muscle length of observed upper extremity muscles.

| Muscle  | Operating range of muscle fiber length (normalized) | Optimum muscle length [cm] |
|---------|---|----------------------------|
| BRD     | 0.55÷1.10   | 27.03                      |
| BICL    | 0.30÷1.25   | 14.22                      |
| BICS    | 0.20÷1.30   | 14.22                      |
| BRA     | 0.50÷1.15   | 10.28                      |
| TRIMed  | 0.35÷1.40   | 8.77                       |
| TRILat  | 0.50÷1.40   | 8.77                       |
| TRILong | 0.55÷1.40   | 8.77                       |
| DLT     | 0.50÷1.40   | 12.8                       |

Next step was developing the optimization routine for calculation the new shift lever handle position. Optimization routine reflects the optimum muscle length and minimum muscle force production. For muscle force estimation was used Hill type EMG-driven muscle model [2,3]. Initial movements used to optimization routine were experimentally collected kinematic data during gear shifting. Experimental set up is evident from Figure 2.



Figure 2: EMG and kinematic data collection during gear shifting.

## RESULTS AND DISCUSSION

Main result from this investigation was the new three dimensional position of shift bar and shift handle position of used car. This new position was calculated based on data from 8 specimens.

From EMG's was detected that during pushing the shift gear handle Deltoideus shows a main activity of all muscles. In opposite, during pulling the handle to the body, the main activity showed in elbow flexors. Was experimentally shown, gear shifting is in any case an active movement. From investigated muscles results interesting finding, that elbow flexors have during shifting normalized muscle length greater than 1 and elbow extensors less than 1. From the normalized muscle lengths would be better placed the shift lever handle more closely to the driver's body, so that the elbow angle would be about 100 degrees. In this case will be extensors lengthened and flexors shortened and will be close to the optimum muscle length. Next practical finding was that the least "popular" movement is shifting the gears at arm's length and moving the hand on steering wheel. In every cases, the Deltoideus is most stressed muscle.

Considering the experiments and calculations, we can say two general findings which can help the shifting operations. First, is suitable to have steering wheel and shift lever handle in the similar length from the driver's shoulder, so that the movements in elbow joint will be minimalized. From the results was observed that the main muscle activity was collected during moving the hand between shift lever handle and steering wheel. Second, it would be comfortable to have the elbow angle in position about 100 degrees.

## REFERENCES

1. Gardner BA, et al. *Ann Biomed Eng* **31**, 207-220, 2003.
2. Lloyd, DG, et al. *J Biomech* **36**, 765-776, 2003.
3. Vilimek M. *Acta Bioeng Biomech.* **9**, 41-47, 2007.

## ACKNOWLEDGEMENTS

This research study was supported by grant MSM 6840770012.

# EFFECT OF STRAIN GAUGE SIZE AND PLACEMENT DURING THE MOUSE AXIAL ULNAR LOADING PROTOCOL CALIBRATION

<sup>1</sup>David W. Wagner and <sup>1</sup>Gary S. Beaupre

<sup>1</sup>Bone & Joint Center of Excellence, VA Palo Alto Health Care System, Palo Alto, CA  
email: [dwwagner@va51.stanford.edu](mailto:dwwagner@va51.stanford.edu) web: <http://www.rehab.research.va.gov/cent/paloalto.html>

## INTRODUCTION

Understanding the mechanisms of bone mechanobiology has benefitted from the use of animal models in which controlled loading protocols can be used to test bone adaptation hypotheses in-vivo. In particular, the axial ulnar loading protocol is a popular model [1,2]. The axial ulna loading protocol facilitates the direct manipulation of applied force magnitude, duration, and frequency. A key initial step in any study utilizing this protocol is a load-strain calibration experiment using a uniaxial strain gauge attached at the medial diaphysis, typically using five sacrificed animals and loading those limbs in the same manner as will be done in live animals. Some of these calibration experiments in the literature show significant variability in the strain values among animals. Two questions that have not been adequately examined are 1) how sensitive is the measured strain to small differences (e.g., 250 microns) in the placement of the strain gauge, and 2) what is the effect of gauge size on the magnitude of measurable strain?

## METHODS

The methods used here were similar to those described previously [3]. Briefly, the left forelimb of a C57BL/6 strain mouse was scanned with a Scanco vivaCT 40 microCT scanner. The voxels in the model were down sampled by a factor of two, resulting in 21.0  $\mu\text{m}$  voxels. A direct voxel to hex element conversion was performed to create the FE model and was solved using the Scanco FE software (v1.15b). The elastic modulus and Poisson's ratio of the bone elements were 13.3 GPa and 0.3, respectively. The ulna model had 1,166,563 nodes and 1,063,357 elements and was subjected to a 1 Newton axially oriented force (Figure 1).

Uniaxial strain along the longitudinal axis was calculated for each node. The nodal strains along the ulna surface can be interpreted as an 'idealized' gauge strain with a gauge size equal to the element size of the FE model (0.021 mm x 0.021mm). In a second model, an active gauge area of 0.51 x 0.38 mm<sup>2</sup> (Figure 1), which represents the size of a commonly used uniaxial strain gauge (EA-06-015DJ-120, Vishay), was used [2]. The equivalent 'Vishay' gauge strain was calculated by averaging the surface nodal strains within the active gauge area. A similar investigation was performed with a smaller active gauge area of 0.1524 x 1.27 mm<sup>2</sup>, corresponding to the gauge size of a semiconductor bar gauge (SS-080-050-500P-S1, Micron Instruments) and is referred to here as the 'semiconductor' model.

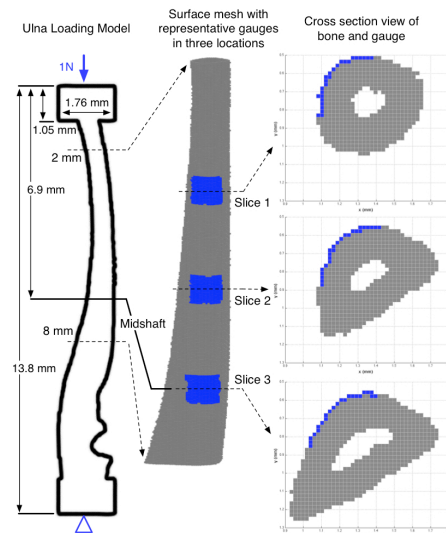


**Figure 1:** Ulna model and active gauge area for the Vishay gauge at three axial slice locations.

## RESULTS AND DISCUSSION

Uniaxial nodal strain for three representative axial slice locations is presented for three unique strain gauge sizes. Additionally, to simulate a small error in gauge placement, we present the results of an analysis in which the Vishay gauge location

corresponding to the location of peak strain for the axial slices (Fig. 1) was perturbed in four directions: distal, proximal, circumferential clockwise (CW), and counterclockwise (CCW). All perturbations in gauge placement were 250 microns in magnitude (e.g. approximately half of the Vishay gauge active width or about 2.5 times the thickness of standard printer paper) and calculated as the distance along the bone surface.

The effect of gauge size on peak strain measurement for the three selected axial slices is presented in Table 1. The Vishay and semiconductor gauges underestimated the idealized peak strain by an average of 25% and 16%, respectively. The results of the perturbation analysis for the Vishay gauge size are presented in Table 2. Perturbations of the gauge position along the longitudinal axis resulted in a maximum decrease of 116  $\mu\epsilon$  at slice 2 for a perturbation in the proximal direction. The counter-clockwise circumferential perturbations resulted in the largest deviation from the unperturbed Vishay model with the smallest absolute change of 737  $\mu\epsilon$  occurring for slice 3 and the largest magnitude change of 1046  $\mu\epsilon$  occurring for slice 2.

**Table 1:** Peak strains at three representative axial slices for the different gauge models (Fig. 1).

|                | <b>Ideal<br/>(<math>\mu\epsilon</math>)</b> | <b>Vishay<br/>(<math>\mu\epsilon</math> / % of ideal)</b> | <b>Semiconductor<br/>(<math>\mu\epsilon</math> / % of ideal)</b> |
|----------------|---|---|--|
| <b>Slice 1</b> | -3526                                       | -2624 / 74.4%   | -3040 / 86.2%  |
| <b>Slice 2</b> | -3642                                       | -2806 / 77.0%   | -3079 / 84.5%  |
| <b>Slice 3</b> | -3122                                       | -2334 / 74.8%   | -2530 / 81.0%  |

The purpose of this study was to quantify the sensitivity in peak longitudinal strain associated with direct measurement limitations related to strain gauge size and placement position for the axial ulnar loading technique of the mouse forelimb. The relative importance of the results presented here may be best interpreted in the context of reported bone formation and response to induced strain. Lee et al. [1] reported an approximate increase in the periosteal bone formation rate ( $\mu\text{m}^2/\mu\text{m}$  per day)

from 0.5 to 2.8 for CD1 mice resulting from a change in induced peak strain from 2000  $\mu\epsilon$  to 3000  $\mu\epsilon$ . Lee et al. also observed a change from a lamellar to a mixed woven/lamellar response with the same increase of induced peak strain indicating a potential damage response. In the results presented here, a relatively small change in circumferential gauge placement (250 microns Counter-CW) resulted in a strain gauge reading nearly 40% lower than the true, peak strain value at certain slice locations. In the context of the induced strains used by Lee et al., such a perturbation would result in a larger change in peak strain than the 1000  $\mu\epsilon$  increase reported to induce a change from a lamellar to a mixed woven/lamellar response.

Considering the sensitivity of bone response (magnitude and response type) to strain magnitude, accurately quantifying the induced strain during the calibration procedure is critical to interpreting the results of the axial ulnar loading protocol and to better understanding the mechanisms driving a particular mechanistic response. The results presented here, particularly the underestimation of peak strain associated with available strain gauges and the high degree of sensitivity of measured strain to gauge placement circumferentially about the longitudinal axis, suggest that additional consideration must be afforded how specimens are reliably calibrated such that the desired strain level at a particular location of interest is accurately interpreted.

## REFERENCES

1. Lee KCL, et al. *Bone* **31**, 562-569, 2002.
2. Robling AG, et al. *Bone* **31**, 407-412, 2002.
3. Wagner DW, et al. *Proceedings of ORS 2011*, Long Beach, CA, USA, 2011.

## ACKNOWLEDGEMENTS

We would like to thank Derek Lindsey and Alesha Castillo. Supported by the Dept of Veterans Affairs, Rehab R&D Service (Proj. A6816R).

**Table 2:** Vishay model perturbations for the peak strain locations of three representative axial slices (Fig. 1).

|                           | <b>No Perturbation<br/>(<math>\mu\epsilon</math>)</b> | <b>Distal*<br/>(<math>\mu\epsilon</math> / % diff.)</b> | <b>Proximal<br/>(<math>\mu\epsilon</math> / % diff.)</b> | <b>Clockwise (CW)<br/>(<math>\mu\epsilon</math> / % diff.)</b> | <b>Counter-CW<br/>(<math>\mu\epsilon</math> / % diff.)</b> |
|---------------------------|---|---|--|--|--|
| <b>Slice 1</b>            | -2621   | -2664 / 2%  | -2615 / 0%   | -1959 / -25%   | -1626 / -38%   |
| <b>Slice 2</b>            | -2806   | -2881 / 3%  | -2690 / -4%  | -1987 / -29%   | -1760 / -37%   |
| <b>Slice 3 (Midshaft)</b> | -2334   | -2392 / 2%  | -2220 / -5%  | -1841 / -21%   | -1597 / -32%   |

\*All perturbations result in a 250 micron change in position of the Vishay gauge along the direction listed.

# INFLUENCES OF LOAD CARRIAGE AND FATIGUE ON LOWER EXTREMITY KINETICS DURING WALKING

<sup>1</sup> He Wang, <sup>1</sup>Jeff Frame, <sup>1</sup>Elicia Ozimek, <sup>2</sup>Cara Reedstrom, <sup>2</sup>Daniel Leib, and <sup>2</sup>Eric Dugan,  
<sup>1</sup>Ball State University, <sup>2</sup>Boise State University  
email: hwang2@bsu.edu

## INTRODUCTION

Military personnel are commonly afflicted by lower extremity overuse injuries such as knee pain and stress fractures [1, 2]. Walking with heavy loads is an inevitable part of the military training and during the twelve-weeks of basic training, the combined running and walking distance could exceed 200 miles [1]. Therefore, military personnel commonly face physical challenges comprised of load carriage and muscle fatigue.

Load carriage has been found to alter gait kinematics [3]. Specifically, there are increases of pelvic anterior tilt, hip flexion, and knee flexion angles at heel strike [3, 4]. Ground reaction forces and ground reaction loading rates are also increased during loaded walking [3, 5]. Muscle fatigue has also been found to alter running kinematics with increases of hip and knee angles at heel strike [6, 7]. During fatigued walking, vertical ground reaction force and loading rate are found to increase [8]. Further, fatigued muscles' ability to attenuate impact loading is decreased [9].

Thus, under the influences of load carriage and muscle fatigue, the lower extremities are exposed to increased ground reaction impact forces with increased loading rate during walking. The risk of lower extremity injury may be increased. However, it is yet to be determined if the lower extremity joint kinetics are altered as a result of load carriage and muscle fatigue. Analyzing lower extremity joint kinetics during loaded and fatigued walking will broaden our knowledge on the potential causes for development of lower limb injuries during military training.

The purpose of the study was to investigate the lower extremity joint kinetics during loaded and fatigued walking. As the vertical ground reaction force and loading rate are increased during weight

acceptance, it is expected that the lower extremity joint kinetics will be altered to accommodate the increased external impact loading.

## METHODS

Eighteen healthy male subjects (age:  $21 \pm 2$  yr.; body mass:  $79 \pm 11$  kg; body height:  $181 \pm 4$  cm) participated in the study. Subjects wore military boots and participated in a fatiguing protocol which involved a series of metered step-ups and heel raises while wearing a 16 kg rucksack. Subjects performed the following tasks in sequence: 5-min unloaded walking; 5-min loaded walking with a 32 kg rucksack; Fatiguing protocol; 5-min loaded walking with a 32 kg rucksack under fatigue; 5-min unloaded walking under fatigue. All walking tasks were performed at 1.67 m/s on a force instrumented treadmill (AMTI). A 15-camera system (VICON) was used to track reflective markers placed on the human body at 120 Hz. Ground reaction forces were collected at 2400 Hz. Visual 3D (C-Motion) was used to calculate lower extremity joint kinetics. The following variables were analyzed: peak knee and hip extensor moments and peak knee and hip joint powers during weight acceptance of walking. Two-way repeated measures ANOVAs were performed. Load carriage and fatigue were the independent factors.  $\alpha = 0.05$ .

## RESULTS AND DISCUSSION

No interactions were found between load carriage and fatigue ( $P > 0.05$ ). Load carriage led to significant increases of knee and hip extensor moments, knee and hip joint powers ( $P < 0.001$ ) (Table 1). Fatigue did not lead to changes in knee extensor moment and knee joint power ( $P > 0.05$ ) but resulted in significant increases of hip extensor moment and hip joint power ( $P < 0.01$ ) (Table 1).

In this study, we found the knee extensor moment increases as a partial mechanism to absorb the increased ground impact forces during loaded walking. Therefore, during long-distance loaded walking, it is possible that the increased knee power absorption along with high magnitudes of impact forces could expose the military recruits to increases of overuse knee injuries. We also found the hip joint exhibited increased extensor moment and joint power magnitude during weight acceptance. As increased pelvic anterior tilt is associated with load carriage [4], the increased hip extensor moment may be used to decelerate the increased pelvic anterior tilt at heel strike.

During fatigued walking, the hip extensor moment and power increase during weight acceptance. The increased hip extensor moment may be used to stabilize the pelvis and elevate the center of mass. Also, the increased hip extensor moment can help stabilize the femur and prevent knee flexion during weight acceptance. Interestingly, Fatigue does not lead to alteration of knee extensor moment and knee power absorption during weight acceptance. Thus, the increased vertical ground reaction force during fatigued walking may be attenuated by lower leg bone structures such as the tibia.

In summary, during weight acceptance, load carriage leads to alterations of knee and hip joint

kinetics; Fatigue leads to alterations of hip kinetics. The altered lower extremity joint kinetics associated with load carriage and fatigue may be related to the high incidence of lower extremity overuse injuries in the military.

## REFERENCES

1. Jones, B.H., et al. *Exercise & Sport Sciences Rev.* **17**: 379-322,1989.
2. Knapik, J. *Military Medicine* **169**: 45-53, 2004.
3. Kinoshita, H., *Ergonomics* **28**: 1347-1362, 1985.
4. Birrell, S., et al. *Ergonomics* **52**(10): 1298-1304, 2009.
5. Wang, H., et al., *Proceeding of ASB*, Providence, RI. 2010.
6. Derrick, T., et al., *Med. Sci. Sports Exerc.* **34** (6): 998-1002, 2002.
7. Mizrahi, M.B., et al., *Hum. Mov. Sci.* **19**: 139-151, 2000.
8. Wang, H., et al., *Med. Sci. Sports Exerc.* **42**(5) S192, 2010.
9. Voloshin, A., et al., *Clin. Biomech.* **13**: 515-520, 1998.

## ACKNOWLEDGEMENTS

Funding source: US ARMY #W81XWH-08-1-0587

**Table 1:** Means and SDs of Peak knee and hip extensor moments and peak knee and hip joint powers during weight acceptance of walking.

| Variables                      | Unloaded and Unfatigued | Loaded and Unfatigued | Loaded and Fatigued | Unloaded and Fatigued |
|--------------------------------|-------------------------|-----------------------|---------------------|-----------------------|
| Knee extensor moment (Nm/kg)*  | 0.88 (0.20)             | 1.61 (0.37)           | 1.63 (0.42)         | 0.90 (0.25)           |
| Hip extensor moment (Nm/kg)* # | 1.54 (0.41)             | 2.26 (0.42)           | 2.38 (0.42)         | 1.85 (0.48)           |
| Knee joint power (W/kg)*       | -1.34 (0.37)            | -2.65 (1.40)          | -2.76 (1.06)        | -1.39 (0.54)          |
| Hip joint power (W/kg)* #      | 1.03 (0.36)             | 1.69 (0.61)           | 1.97 (0.64)         | 1.47 (0.49)           |

Note. \* indicates significant difference between loaded and unloaded walking conditions ( $P < 0.00$ ); # indicates significant difference between fatigued and unfatigued walking conditions ( $P < 0.01$ ).

# A MARKER SET-INDEPENDENT APPROACH TO JOINT TRANSLATION MEASUREMENT OF THE KNEE DURING WALKING

Hongsheng Wang, +Nigel Zheng

University of North Carolina at Charlotte, Charlotte, NC, USA  
email: [nzheng@uncc.edu](mailto:nzheng@uncc.edu) <http://coe.uncc.edu/~nzheng>

## INTRODUCTION

Skin marker-based motion analysis has been widely used for understanding in vivo locomotion and pathological disorders of human musculoskeletal system in biomechanics research and clinical application. Since the knee joint translation is expressed as the displacement of pre-selected reference point on the femur relative to the tibia local coordinate system (LCS), the translation measurement is highly dependent on the selections of the reference point. In conventional motion analysis, they are often determined based on the marker set, which results in the marker dependent knee translation measurement (MDKT). Unfortunately, the location of bony landmarks which mostly are determined by palpation has limited accuracy and consistency which propagate to poor prediction of knee translation. In this study, we studied the sensitivity of knee translation measurement in response to the selection of different reference points. A marker set-independent approach (MIKT) was developed for the purpose of finding the optimal reference point for much smaller variances in knee joint translation measurements.

## METHODS

Thirty healthy subjects (12 females, height  $1.72 \pm 0.10$  m, weight  $66.4 \pm 12.9$  kg) with no lower extremity injuries or functional disorders were recruited following an Institutional Review Board approved protocol. Eighty retro-reflective markers were placed on lower limbs following a previous reported protocol [1] (Fig. 1A). A static trial was recorded at neutral standing, which was taken as the reference posture. Ten level walking trials were collected from each subject using motion capture system (FX 40, VICON, Oxford UK). Three trials were randomly picked out for representing the

subject. All ten trials from one subject were used for within-subject variance analysis.

Both femur and tibia LCSs were defined at a neutral posture (T-pose): the tibia origin was located at the midpoint of medial and lateral edges of tibial plateau. Both LCSs were defined base on markers placed on bony landmark as previously reported (Fig. 1B) [2].

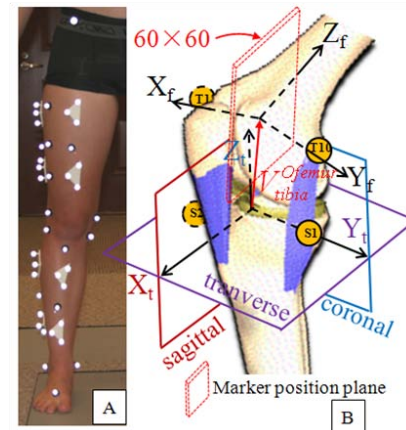


**Figure 1:** A: marker placement protocol; B: local coordinate system of tibia and femur at a dynamic instant.  $V_{tibia}^{Ofemur}$ : the position vector of femur origin in tibia LCS.

In MDKT, the reference point was selected as the origin of the femur LCS. Knee joint translation was determined as the displacement of reference point in the tibia LCS (change of position vector  $V_{tibia}^{Ofemur}$ ). The reference point was selected in different positions, changing from 10 – 70 mm in superior direction of the origin of the tibia LCS, and -30 – 30 mm in anteroposterior (AP) direction, with step of 3 mm in both directions (Fig. 2). The 3D knee joint motion was determined according to a previously reported study [3]. In MIKT, the reference point was selected when the knee joint translation in AP direction was minimized during the stance phase. The reference point was constrained in a position

plane of 60mm×60mm (in sagittal plane) with the center at the origin of the femur LCS (Fig. 1B). A MATLAB (MathWorks Inc., Natick, MA, USA) program was developed to find the optimal reference point by using Levenberg-Marquardt algorithm (Fletcher’s version).

## RESULTS AND DISCUSSION

For MDKT, the range of knee joint AP translation was changing with the origin definition of the femur LCS at T-pose. For a typical walking trial, the knee joint AP translation range during standing phase varied from 7 mm to 27 mm (Fig. 2). AP translation was very sensitive to the superior/inferior (Z-value) position of pre-selected reference point at T-pose, whereas it was relatively less sensitive to the anterior/posterior (X-value) position. For MIKT, the optimal reference point was found at [-5, 0, 50] in the tibia LCS, which had 7 mm range of AP translation.

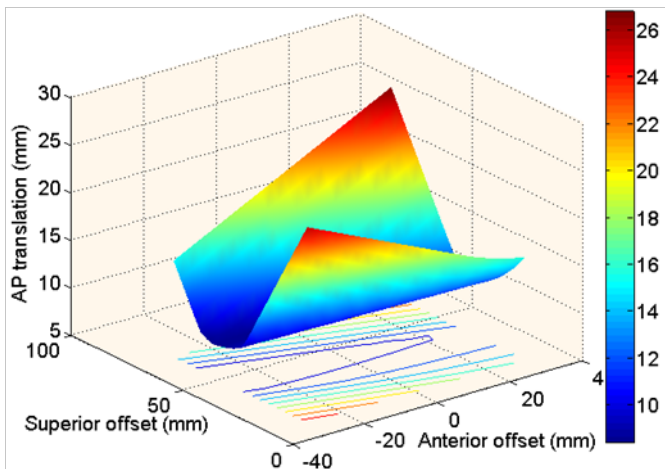


**Figure 2:** Range of knee joint AP translation during stance phase at different pre-selected reference points. Superior and anterior offsets were the position of pre-selected reference points in tibia LCS.

Compared with the AP translation using MDKT where the femur origin was defined at 20 mm above the tibia origin ([0, 0, 20] in tibia LCS), the average magnitude of AP translation from 30 subjects was reduced from 25.1 mm using MDKT to 11.1 mm using MIKT, an over 50% reduction (Table 1). The AP translation in this study was closer to the average excursion (12.4 mm) of femur medial (17.4 mm) and lateral (7.4 mm) condyles on tibia plateau from a previous dual fluoroscopic study [4]. The

standard derivation of bilateral differences (left - right) for AP translation using MIKT was smaller than those using MDKT (Table 1). Both the AP translation and variances among 10 trials from a subject were significantly less using MIKT than those using MDKT.

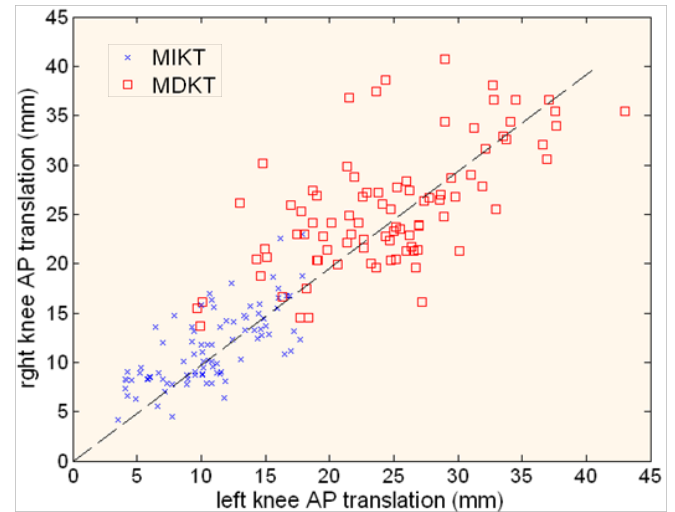


**Figure 3:** Cross plot of the range of knee joint translation in AP direction during stance phase between two legs.

**Table 1:** Means±SD of the ranges of knee AP translations and bilateral difference (left – right, BilaDiff) during stance phase.

|                |          | MDKT     | MIKT     |
|----------------|----------|----------|----------|
| all subject    | Range    | 25.1±5.9 | 11.1±3.5 |
|                | BilaDiff | -1.1±5.5 | -0.7±2.9 |
| within-subject | Range    | 19.6±1.8 | 13.0±0.5 |
|                | BilaDiff | -0.6±1.9 | 1.7±1.0  |

## REFERENCES

- 1.Wang H and Zheng N. *Int J Sports Med* **31**, 742-746, 2010.
- 2.Wang H and Zheng N. *J Biomech Eng* **132**, 124502, 2010.
- 3.Veldpaus FE et al. *J Biomech* **21**, 45-54, 1988.

## ACKNOWLEDGEMENTS

This work was supported, in part, by funds provided by the University of North Carolina at Charlotte. The authors would like to thank Bo Gao, PhD., Bing Xiao, M.S., Jeff Thousand for data collection and reduction.

# BIOMECHANICAL DEMANDS OF THERAPEUTIC HATHA YOGA POSES IN OLDER ADULTS: MODIFIED CHAIR AND DOWNWARD FACING DOG

<sup>1</sup>Man-Ying Wang, <sup>1</sup>Shin-Yuan Yu, <sup>1</sup>Rami Hashish, <sup>1</sup>Sachithra Samarawickrame, <sup>1</sup>Michelle Haines, <sup>1</sup>Lauren Mulwitz, <sup>2</sup>Leslie Kazadi, <sup>3</sup>Gail Greendale, and <sup>1</sup>George Salem

<sup>1</sup>University of Southern California, Los Angeles, CA, USA

<sup>2</sup>Westside Yoga Therapy Clinic, Los Angeles, CA, USA

<sup>3</sup>University of California at Los Angeles, Los Angeles, CA, USA

email: [mwang@usc.edu](mailto:mwang@usc.edu) web: <http://pt.usc.edu/mbrl>

## INTRODUCTION

Yoga has become one of the most commonly used complementary and alternative medicine therapies in the United States. Based on the National Health Survey, yoga participation jumped 40% from 1997 to 2002 and the total population who participated in yoga in the past 12 months reached 13.2 million in 2007 (Barnes, 2004; Barnes, 2008). Chair (CH) and downward facing dog (DFD) are two of the most frequently practiced yoga poses and props such as a wall, chair, and/or blocks are often used to modify the poses in order to maintain proper alignment of the body, especially for those who have limited strength and flexibility, such as older adults. However, the poses performed with props have never been examined biomechanically and no information regarding the musculoskeletal demands of these activities has been reported. The purpose of this investigation was to characterize and compare the kinematics and kinetics of the modified CH and DFD poses, performed with a wall.

## METHODS

Twenty-four independent older adults ( $70.8 \pm 4.1$  yrs) participated in a 32-week Hatha yoga program, twice per week. Baseline biomechanical measurements were taken after 2 weeks of introductory classes, where the subjects practiced the yoga poses. The program was designed to improve strength, flexibility, and balance for older adults and was led by a yoga instructor, experienced in teaching seniors. At the baseline visit, subjects performed the poses while instrumented for biomechanical analysis. Reflective markers and tracking marker plates were placed on subject's bony landmarks (head, trunk, pelvis, upper extremities, and lower extremities (LE)) to define each body segment. Subjects then went through breathing exercises, a short warm-up session, and

then performed the yoga poses while guided by the yoga instructor. During data collection, a plexiglas wall was used for support (Fig. 1). To perform the modified CH, subjects stood with their back approximately one step distance from the wall, their feet hip-width apart, and a block held between their inner thighs. The subjects then brought their arms overhead, while flexing their knees and hips to a self-selected maximum depth, where they could safely and statically hold the pose while completing a full breath. The subjects then returned to the starting position. To perform the modified DFD, the subject stood approximately a forearm's length from the wall with their feet hip-width apart, and their hands placed on the wall at the level of their shoulders. They then stepped back as far as safely possible from the wall while extending their elbows, flexing their shoulders, and flexing at their hips. Their hands remained in contact with the wall at all times. They were instructed to hold the position during a full breath, while keeping their elbows extended and their spine in a neutral position (Fig. 2). They then returned to their starting position.

Whole-body kinematic data were collected using an 11-camera motion capture system at 60 Hz (Qualisys; Gothenburg, Sweden). Ground reaction forces were recorded through force platforms at 1560 Hz (model #OR6-6-1000, AMTI, Watertown, MA). Joint moments at the hip, knee and ankle, in the sagittal and frontal planes, were calculated using standard inverse dynamic techniques. Two successful trials were collected for each pose and the average joint moments and angles produced over the 2 trials were computed. Baseline data from the dominant limb are reported here.

Paired t-tests were used to test for differences in LE joint angles and moments between the 2 poses. Cohen's effect sizes (*d*) are provided.

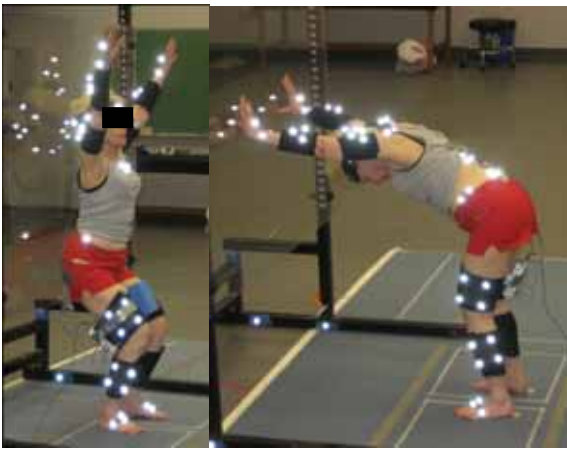


**Figure 1 & 2:** Modified CH (left) and DFD (right) poses performed with a plexiglas wall.

## RESULTS AND DISCUSSION

There were statistically significant differences in sagittal plane joint angles at the hip ( $d = -1.93$ ) and knee ( $d = 2.15$ ) between CH and DFD ( $p < 0.001$ , Table 1). Knee abduction angle was also significantly greater in DFD than CH ( $p < 0.01$ ,  $d = -0.53$ ). Both poses had statistically significantly different moment profiles at the hip, knee, and ankle in the sagittal plane ( $p < 0.01$ ,  $d = 1.58$ ,  $-2.72$ , and  $1.08$ , respectively; Fig. 3) and frontal plane ( $p < 0.001$ ,  $d = 2.5$ ,  $7.57$ , and  $-1.67$ , respectively; Fig. 4). Both DFD and CH generated extensor moments at the hip and ankle. Conversely, at the knee, CH generated an extensor moment while DFD generated a flexor moment. This finding suggests that CH should be selected over DFD when the goal is the strengthening of the quadriceps. In the frontal plane, CH produced abductor moments at all three LE joints, whereas DFD produced adductor moments at the hip and knee. The results suggest that CH may be more effective in training the hip abductors whereas DFD may be more effective in training peroneal muscles - important muscle groups for maintaining balance in older adults. Although both poses generated potentially unfavorable frontal plane moments at the knee, the magnitude was greater during performance of the

DFD. These findings should be considered when using these poses in seniors with knee OA.

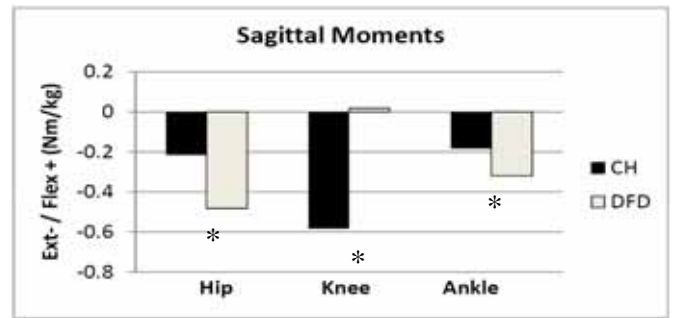


**Figure 3:** LE joint moments in the sagittal plane during CH and DFD poses. \* $p < 0.01$ .

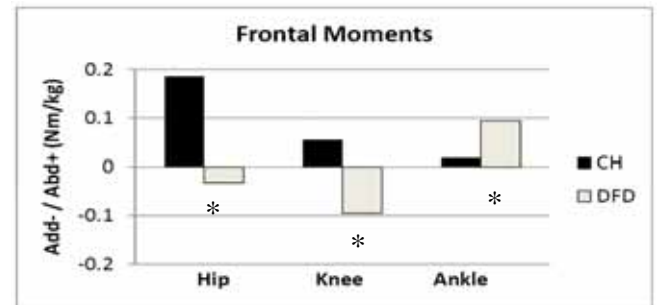


**Figure 4:** LE joint moments in the frontal plane during CH and DFD poses. \* $p < 0.001$ .

## CONCLUSIONS

Both DFD and CH appear to be effective at targeting the extensor muscles of the hip and ankle. To strengthen the quadriceps, CH may be more appropriate than DFD. Both CH and DFD appear to target important muscle groups for balance training (CH targeting the hip abductors and DFD targeting the peroneal muscles). DFD may be more detrimental to the knee joint as compared to CH in those who have knee problems.

## REFERENCES

1. Barnes PM, et al. *Adv Data* **27**, 1-19, 2004.
2. Barnes PM, et al. *Natl Health Stat Report* **12**, 1-24, 2008.

## ACKNOWLEDGEMENTS

Supported by NIH Grant ROI –AT004869-01

**Table 1:** Lower-extremity joint angles during modified CH and DFD poses

| Joint Angle (deg) | CH          |             |            | DFD          |                        |            |
|-------------------|-------------|-------------|------------|--------------|------------------------|------------|
|                   | Hip         | Knee        | Ankle      | Hip          | Knee                   | Ankle      |
| Flex (+)/Ext (-)  | 50.8 ± 15.8 | 54.7 ± 13.1 | 13.7 ± 6.4 | 83.1 ± 17.6* | 26.1 ± 13.5*           | 12.6 ± 6.4 |
| Abd (+)/Add (-)   | -0.2 ± 4.1  | 1.3 ± 5.4   | 3.0 ± 4.7  | -1.1 ± 5.6   | 4.0 ± 4.8 <sup>#</sup> | 3.6 ± 3.6  |

\*Significantly different between CH and DFD ( $p < 0.001$ ). <sup>#</sup>Significantly different between CH and DFD ( $p < 0.01$ )

# EFFECTS OF WHOLE-BODY VIBRATION TRAINING ON DYNAMIC POSTURAL STABILITY IN ELDERLY ADULTS

<sup>1</sup>Yen-Ting Wang, <sup>2</sup>Wei-Hsiu Lin, <sup>3</sup>Jun-Dar Lin, and <sup>2,3</sup>Alex J. Y. Lee

<sup>1</sup>National Taiwan Sport University, TaoYuan, Taiwan

<sup>2</sup>National ChiaYi University, ChiaYi, TAIWAN

<sup>3</sup>National HsinChu University of Education, HsinChu, TAIWAN

email: [jylee@nhcue.edu.tw](mailto:jylee@nhcue.edu.tw)

## INTRODUCTION

Ageing is associated with the deterioration of the neuromuscular and sensorimotor function, which might affect physical activities and postural stability (PS) during the daily life. Among these functional disability, falls are the major problem for both the elderly and broader community, resulting fractures to the upper limb, lower limb, hip, head, and trunk. PS has been defined as the ability to maintain an upright posture in a weight carrying position without falling and to keep the center of gravity within the limits of the base of support. It is also defined as the act of maintaining, achieving, or restoring a state of balance during any postural disturbance or physical activity [1, 2].

Whole-body vibration (WBV) is a new biophysical modality to provide systemic vibration signals for mechanical stimulation and has recently emerged as an exercise intervention that can have positive effects on the neural, muscular and skeletal systems. WBV exercise involves standing on a platform that oscillates at a particular frequency and amplitude, which activating muscle contractions via stimulation of sensory receptors. WBV was reported to improve the neuromuscular performance such as the 5-Chair Stands test, the Timed Up and Go test, and the Tinetti test in community-dwelling older adults [3]. To date, most investigations have reported acute WBV effects in young adults, but chronic WBV effects on PS in older adults are relatively unknown. Therefore, the purpose of this study was to examine the effects of an 8-week WBV exercise program on dynamic PS in the elders.

## METHODS

Twenty-two elderly people with normal ability of movement were recruited and randomized as the WBV group (13 elders, Age:  $67 \pm 6$  yrs; Ht:  $162 \pm 6$  cm; Mass:  $63 \pm 8$  kg), and the control group (9 elders, Age:  $70 \pm 8$  yrs; Ht:  $159 \pm 8$  cm; Mass:  $64 \pm 10$  kg). Participants were excluded if their activity habit had changed during the study period. The study was approved by the ethics committee of the university, and informed consent was obtained from all the participants before enrollment into the study.

Participants in the WBV group were asked to receive a WBV exercise 3 times a week for 8 weeks in bare feet throughout the study. The WBV was performed on a vertical vibration device with amplitude of low, 2.5 or high, 5 mm and frequency of 30 to 45 Hz. The amplitude and frequency were controlled by adjusting the setting from the top panel, with the larger the number, the greater the acceleration. Participants performed static and dynamic knee-extensor exercises on the vibration platform: squat, deep squat, wide stance squat, one-legged squat, and lunge.

Training volume increased systematically over the training period by increasing the duration of one vibration session, the number of series of one exercise, or the number of different exercises. Training intensity was increased by shortening the rest periods or by changing the execution form of the exercises from predominantly two-legged to one-legged exercises. The duration of the WBV program was a maximum of 30 minutes, which included warm up (10 min) and cool down (5 min). During the training, all participants were under direct supervision by the same instructor and were instructed on how to perform each exercise.

The PS was assessed by the Biodex Stability System (Biodex Medical System, NY) which uses a circular platform that is free to move in the anterior-posterior and medial-lateral axes simultaneously. The BBS calculates three different parameters according to the direction of the deviations from the horizontal plane; total stability index (OSI), anterior-posterior index (API) and medial-lateral index (MLI). The stability of the platform can be varied by adjusting the level of resistance given by the springs under the platform. In this study, subjects were bare footed and tested on a bipedal stance at levels 2 representing unstable situations.

One-way ANCOVA (pretest as covariate) were used to analyze the differences between groups on PS parameters: OSI, API and MLI, after WBV. The level of significance difference was set at  $p < .05$ . Statistical analyses were conducted in Statistical Package for Social Science for Microsoft Windows, version 12.0 (SPSS Inc, Chicago, Ill, US).

## RESULTS AND DISCUSSION

After 8 weeks of training, the improvements of PS in the WBV group was significantly greater than that in the control group, implying that the WBV group showed significant decreased the OSI, API, and MLI in post-test than pretest (Fig. 1, \* represented significant differences between groups).

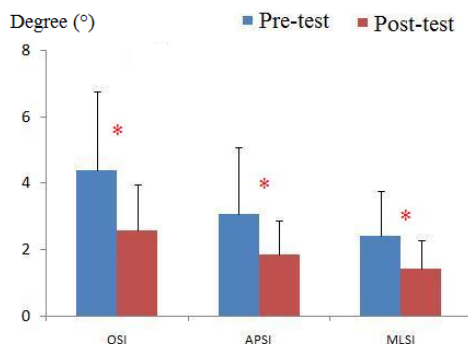


**Figure 1:** PS Performance in the WBVT group before and after training at Level 2

This study demonstrated the positive effect of WBV in PS which showed that significant improve the performance of unstable dynamic conditions in the elders. The repetitive vibration might be a rearrangement of balance control strategies, which results in improvement of PS after regular WBV. The findings of this study showed significant improvements in the indices of PS (OSI, API and

MLI) after training in the WBV group in the level 2, unstable testing condition, which in agree with the results of authors who studied the positive effects of vibration in patients' balance [4,5]. This might be due to positive effects of WBV on muscle strength, improved synchronization of firing of the motor units and improved co-contraction of synergist muscles, which could bring about better PS strategies during the unstable condition [6].

It was suggested that WBV can stimulate the exteroceptive receptors on the sole of the foot (Merkel, Meissner, and Ruffini receptors), that lead to physiological changes at numerous levels including stimulation of skin receptors, muscle spindles, joint mechanoreceptors, and changes in neurotransmitter which can improve PS and neuromuscular control. Furthermore, mechanistic findings indicate that WBV induces underlying neural and muscular changes, such as stimulation of human spindle endings, and changes in biogenic amines, which should help to enhance the balancing ability. Moreover, in this study it was noted that WBV was a very pleasant experience for all participants, and the acceptance of the program by participants of the WBV group was encouraging.

## CONCLUSIONS

Eight-week WBV can improve the dynamic PS in the elders, not only in the medial-lateral directions, but also in the anterior-posterior directions during unstable condition.

## REFERENCES

- 1.Lee AJY & Lin WH. *J Appli Biomech* **23**, 173-179, 2007.
- 2.Lee AJY & Lin WH. *Clin Biomech* **23**, 1065-1072, 2008.
- 3.Furness TP & Maschette WE. *J Strength Cond Res* **23**, 1508-1513, 2009.
- 4.Bogaerts et al. *Gait Posture* **26**, 309-316, 2007.
- 5.Schuhfried et al. *Clin Rehabil* **19**, 834-842, 2005.
- 6.Van Nes et al. *Am J Phys Med Rehabil* **83**, 867-873, 2005.

## ACKNOWLEDGEMENTS

Supported by grants from National Science Committee, Executive Yuan, TAIWAN, R.O.C.



# AN IMPROVED METHOD FOR INFERRING STABILITY AND OTHER DYNAMICAL INFORMATION FROM NEARLY-PERIODIC NOISY HUMAN LOCOMOTION DATA

<sup>1</sup>Yang Wang, and <sup>2</sup>Manoj Srinivasan

<sup>1</sup>The Ohio State University, Columbus, OH, USA

<sup>2</sup>The Ohio State University, Columbus, OH, USA

email: [wang.1513@osu.edu](mailto:wang.1513@osu.edu), [srinivasan.88@osu.edu](mailto:srinivasan.88@osu.edu) web: <http://movement.osu.edu>

## INTRODUCTION

The broad purpose of this research is to develop data-driven analysis techniques and rigorously determine dynamic stability (e.g., eigenvalues of the return map) from experiment data, identify a mathematical model for human body. We present an improved least-squares-based technique that determine eigenvalues of the linearized stride-to-stride Poincare map from noisy human or animal locomotion data, or more generally, motion near the limit cycle of a dynamical system. The key idea is to use data at a large number of “Poincare sections” (see below for explanation) all around the periodic orbit.

There is a long history of linear time-series analysis techniques for inferring linear discrete-time dynamical systems from noisy data (ARMA, ARMAX, etc) in the statistics literature. Here, our objective is to adapt these ideas to the analysis of locomotion data. In particular, we wish to identify the “Poincare map”, among other things. Roughly, a Poincare map is the function relating the state of the system from one cycle to the next cycle, at roughly the same phase of the cycle (say defined by some even like heel-strike or toe-off). Hurmuzlu [1] appears to have been the first to infer a Poincare map from purely experimental locomotion data. He used a state-event-based Poincare section and used data from lots of strides to find the best-fit linear transformation (in the sense of minimizing least-squares residual) from one stride to the next. And the least square algorithm is used for the statistic consideration. Revzen [2] recently presented an alternate technique that used a data-derived phase for Poincare sections, and also used a least-squares technique for deriving the Poincare map from one stride to the next. Both these methods have the property that if different Poincare sections are used,

one obtains different eigenvalues for the linearized Poincare maps (because of noise and how noise propagates through the system). Our method avoids this undesirable feature.

## METHODS

The Steady human locomotion, say on a treadmill or on solid ground, is only roughly periodic. Every step is similar to, but slightly different from every other step. One hypothesis is that these slight differences between individual steps are due to the fact that muscle forces are “noisy” and there are small uncertainties in the nervous system’s knowledge of the external world, including the external forces. In particular, we assume that this kinematic and kinetic step-to-step variability in gait can be modeled as the motion near a periodic orbit (also called a limit cycle) of a continuous dynamical system, excited by noise-like terms (which could be due to noisy environment, noisy sensing, or noisy muscle forces). Once this assumption has been made, we can derive a local dynamical model of the dynamical system purely from noisy experimental locomotion data (namely, motion-captured kinematics of a few major segments).

Here we present an improved method that, by construction, has the property that the eigenvalues from different Poincare sections are identical, based on two simple ideas: (1) Instead of considering exactly one Poincare section, we consider a large number of Poincare sections all around the limit cycle. (2) Instead of deriving the map from one stride to the next, we instead simultaneously derive (all) the maps from one section to the next; the net map for one stride is obtained by composing the individual maps. We prove that this “multiple sections” method is more accurate (in the sense of error covariance of the eigenvalues) than the “single

section” method in the context of some simple discrete dynamical systems with Gaussian additive noise.

## RESULTS AND DISCUSSION

Before we apply this new method to locomotion data whose detailed properties we do not know (except from the data itself), we validate the method by considering a model system with a periodic orbit and external noise, and whose properties are completely known (so we can check the answers). In particular, we consider the Van der Pol oscillator with random force:

$$\ddot{x} - c(1 - x^2)\dot{x} + x = f(t)$$

where  $f(t)$  is random piecewise external force. As we know, Van Der Pol oscillator would perform perfect periodic response when there is no external force (i.e.  $f(t) = 0$ ). The stability of such periodic response can be evaluated by computing eigenvalue of the Poincare map. However, the response will be non-periodic when the noisy force is applied as shown in Fig.1(a) – the gray oval-shaped band is actually 1000 cycles of the noisy response. Fig 1(a) also shows the intersection of these cycles with six Poincare sections, defined by three lines through the origin. Fig.1(b) shows the change of mean values of eigenvalues when the number of Poincare sections increase. The variance (error) in the eigenvalues is shown in Fig.1(c), and we see that the error decreases with the number. The traditional method is to use one section. One section is not good enough (high variance) and too many sections is bad too (high bias). We find an optimal number of sections, where the estimate of stability is quite reliable with no bias and small variance.

## CONCLUSIONS

The multiple sections method is overall more robust than the single section method because all the locomotion data is used in the inference, rather than just at a single section (so high local noise cannot affect it too much). Also, the multiple sections approach naturally derives dynamical information all around the limit cycle, which would be useful in understanding or interpreting decay of state-dependent perturbations. We will soon be applying these techniques to analyzing human walking and running data.

Note: A shorter no-figures version of this abstract was submitted to the Dynamic Walking Conference 2011.

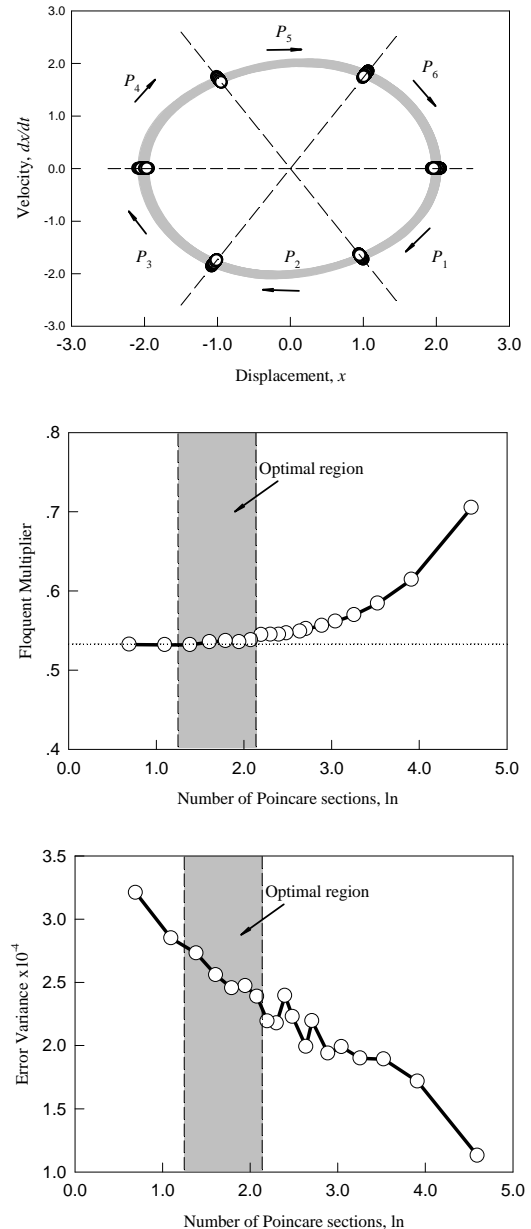


Fig.1 (a) noisy Van Der Pol oscillator with 6 Poicare section, (b) mean eigenvalues with different sections used for multiple Poincare mapping; c) the variance of eigenvalues with different sections used for multiple Poincare

## REFERENCES

- 1.Hurmuzlu Y. and Basdogan C. *J Biomech Engg.*, 116, 30-36, 1994.
- 2.Revzen S. *presentation in Conference of Dynamic Walking*, MIT, Boston, 2010.
- 3.Revzen S. and Guckenheimer J. *Phy Rev E*, 78, 051907, 2008.
- 4.Dingwell J. B, et al. *J Biomech Engg* 123, 27-32, 2000.

# ALTERATIONS IN GENE EXPRESSION DUE TO DIFFERING MAGNITUDES OF CYCLIC COMPRESSIVE LOADS IN HEALTHY SKELETAL MUSCLE

Christine Waters, Esther Dupont-Versteedgen, and Timothy A. Butterfield  
University of Kentucky, Lexington, KY, USA

Email: [chris.waters24@gmail.com](mailto:chris.waters24@gmail.com) Website: [http://www.mc.uky.edu/athletic\\_training/butterfield](http://www.mc.uky.edu/athletic_training/butterfield)

## INTRODUCTION

According to the CDC, Complementary and Alternative Medicine (CAM) therapies are highly popularized and sought after for numerous musculoskeletal disorders, which were one of the leading causes of injury from 2004 to 2007. These therapies often require out-of-pocket costs having potential to exceed those paid towards traditional family practitioners, and in 2007 were estimated at \$33.9 billion in the United States. Although Massage therapy is one of the most common CAM treatments, little is known regarding its efficacy. Previous investigations regarding the physiological effects of cyclic compressive load (CCL as an analogue of massage) have demonstrated strong *in vivo* evidence of its effectiveness at facilitating functional recovery and attenuating the inflammatory process following eccentric exercise [1]. Recently, we have shown that the magnitude of applied CCL is an excellent predictor of cellular infiltration in healthy skeletal muscle [2], which suggests an optimal magnitude of load for positive immunomodulating effects. Therefore, the purpose of this study was to uncover potential clusters of mechanosensitive genes that exhibit load dependent expression in skeletal muscle, to provide pathways of interest for future studies in mechanotransduction and massage.

## METHODS

Our custom fabricated CCL device (CCLD) has the ability to quantify compressive loads to soft tissues during cyclic motions, from a range of 1.4N to 100N [3]. Calibration of the device was performed prior to the application using equation 1, which accounts for the stiffness of the two springs ( $k$ ) and the weight ( $mg$ ) of the chassis assembly. Strain gage calibration confirmed the linearity of the

$$\text{Eq. 1 } F(Y(t)) = 2k(y_0+y(t))-mg-F_s$$

output voltage ( $R^2 > 0.99$ ) through a range greater than required for our protocol.

The length of the left tibialis anterior (TA) muscle of male Wister rats was subjected to 30 min bout of CCL over four consecutive days, using one of three pre-determined loads: 1.4N, 4.5N, and 11N. Twenty-four hours following the final bout, muscle tissue was harvested and stored at  $-80^\circ\text{C}$  for further analysis.

RNA isolation was performed in accordance with TotallyRNA kit protocol (Ambion Incorporated). Once isolated, RNA samples were subjected to agilent analysis on RNA Nano Chips (Agilent Technologies) using Agilent Bioanalyzer 2100 Technologies Software (Agilent Technologies). Samples obtaining  $\geq 8.0$  level of integrity were frozen and sent for analysis at The Microarray Core Facility at the University of Kentucky. Data from the microarray were processed using Command and Expression Console software (Affymetrix). Output generated was further analyzed using Partek software (Partek Incorporated). ANOVA ( $p < 0.01$  significance) was run, after chips were normalized using Robust Multichip Average, to compare treatment groups. Two sample Student's  $t$ -tests ( $p < 0.05$ ) were used to determine 494 differentially expressed genes.

The 494 genes of interest were entered online into DAVID for gene ontology. Using the 'Functional Annotation' tool, the genes were clustered into 84 functional groups using high stringency. Of the 84 functional groups, 15 met acceptable enrichment scores of  $\geq 1.3$ . One cluster of particular interest, apoptosis, fell just below the 1.3 cut off (1.24), but was included in our analysis for a total of 16 clusters.

## RESULTS AND DISCUSSION

Eighty-one different genes comprised the 16 clusters, with multiple genes displaying redundancy across functional clusters. Each cluster was exhaustively analyzed for genes that were highly related to multiple clusters. Two genes, Cd74 and Similar to 60kD heat shock protein, were expressed in 9 of the 16 functional clusters. Major histocompatibility complex was expressed in 8 clusters.

Five clusters representing the immune response were combined to give an overall representation of 16 functional clusters. (Figure 1)

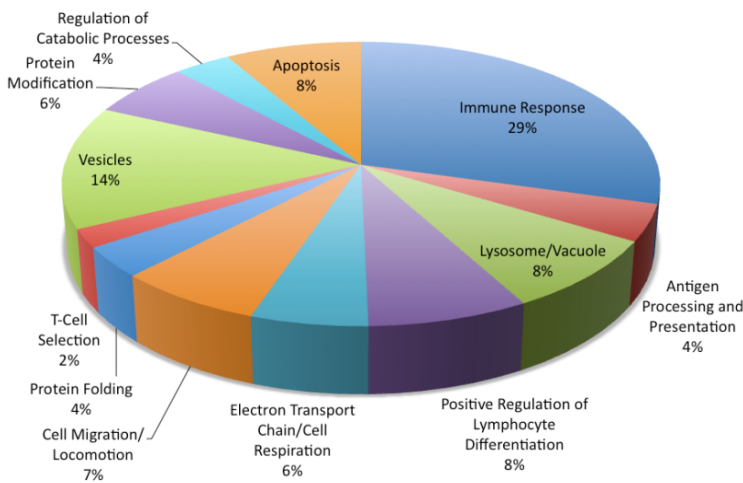


**Figure 1:** Representing the distribution of 16 functional annotated clusters obtained from DAVID.

The largest functional cluster consisted of genes related to the activation or regulation of the immune response. A majority of which increased in relative expression with increased magnitude of load (Table 1). This agrees with our recent investigation showing varying levels of monocyte infiltration dependent to magnitude of load [2].

Of particular interest is the cluster representing apoptotic signaling events. It has recently been hypothesized that the apoptotic signaling of neutrophils may play a large role in the phenotype change from one subpopulation of macrophages to another (ED1+ to ED2+) [4]. Switch in phenotype

change coincides with the transition from the inflammatory T1 to the T2 cytokine pathway, representing repair and regeneration. The ability of an ED1+ macrophage to consume an apoptotic neutrophil before it is lysed, promotes this “switch” [5]. The apoptosis cluster consisted of 12 genes, the majority of which displayed an increase in relative expression with increasing magnitude of applied compressive load (Table 1).

## CONCLUSIONS

The influence of mechanical loading on signaling pathway specificity has been demonstrated previously *in vitro* [6]. To our knowledge this is the first study to show the mechanical influences of a compressive load influencing gene expression. Having the ability to mimic a commonly performed manual therapy has given us the opportunity to investigate these mechanisms in an *in vivo* model. Though the cellular response to mechanical stimuli is complex, we have identified load dependent mechanosensitive genes that potentially govern immunomodulation in response to massage. Further mechanistic studies regarding the efficacy of massage are needed to determine specific intervention strategies for CAM therapy applications.

## REFERENCES

1. Butterfield, et al. *Med Sci Sports Exerc.* **40**, 1289-1296, 2008.
2. Waters, et al. *Proceedings of NATA '11*, New Orleans, LA, USA, 2011.
3. Cunningham, et al. *Proceedings of ASB '10*, Baltimore, MD, USA, 2010.
4. Tidball, et al. *AM J Physiol Regul Integr Comp Physiol.* **289**, R1173-1187, 2010.
5. Fadok, et al. *J Immunol.* **166**, 6847-6854, 2001
6. Hornberger, et al. *Am J Physiol Cell Physiol.* **288**, C185-194, 2005.

## ACKNOWLEDGEMENTS

Supported by UK CHS Pilot Funds Program

**Table 1:** Relative Gene Expression with increased magnitude of compressive load (ML: Moderate Load 4.5N). Asterisk (\*) indicates inclusion of redundant genes

| Cluster          | Increased Expression with ML | Decreased Expression with ML | No Change in Expression with ML |
|------------------|------------------------------|------------------------------|---------------------------------|
| Immune Response* | 26/42 (62%)                  | 8/42 (19%)                   | 8/42 (19%)                      |
| Apoptosis        | 10/12 (83%)                  | 1/12 (8%)                    | 1/12 (8%)                       |

# EFFECT OF CYCLIC COMPRESSIVE LOADING ON ED1+ AND ED2+ MACROPHAGES IN HEALTHY SKELETAL MUSCLE IN VIVO

Christine Waters, Esther Dupont-Versteedgen, and Timothy A. Butterfield

University of Kentucky, Lexington KY, USA

Email: [chris.waters24@gmail.com](mailto:chris.waters24@gmail.com) Web: [http://www.mc.uky.edu/athletic\\_training/butterfield](http://www.mc.uky.edu/athletic_training/butterfield)

## INTRODUCTION

Mechanotransduction has been shown to have significant effects on the specificity of cellular signaling in muscle tissue *in vitro* [1]. Butterfield 2008 demonstrated cyclic compressive load (CCL) applied to an eccentrically exercised muscle, results in an attenuated inflammatory response, rapid recovery of force production, and function when compared to non-compressed tissue [2]. Recently our lab investigated the effects of CCL on healthy muscle tissue and found that cellular infiltration is directly correlated with the magnitude of load applied to the tissue ( $R^2 = .99$ ), showing a potentially beneficial immunomodulatory effect with a lower magnitude load [3]. Analogous to massage, CCL *in vivo*, has proven to be a useful tool, identifying the cellular response on the physiological level. Monocytes, such as macrophages, are of particular interest as the “switch” in phenotype from ED1+ to ED2+ macrophage is a critical event. This marks cessation of the inflammatory response, and commences the transition into the repair, and regeneration phase. Therefore the purpose of this study was to quantify macrophage subpopulations in response to compressive loading in health skeletal muscle.

## METHODS

Our custom fabricated CCL device (CCLD) has the ability to quantify compressive loads to soft tissues during cyclic motions, from a range of 1.4N to 100N [4]. The device was calibrated prior to the application using equation 1. Utilizing the principal of a Hookean Spring, (k) accounts for stiffness, and the weight (mg) of the chassis assembly. Strain gage calibration confirmed linearity of output voltage ( $R^2 > 0.99$ ) through a range greater than required for our protocol.

$$\text{Eq. 1 } F(Y(t)) = 2k(y_0 + y(t)) - mg - F_s$$

The length of the left tibialis anterior (TA) muscle of male Wistar rats was subjected to 30 min bout of CCL over four consecutive days, using one of three pre-determined loads: 1.4N (LL), 4.5N (ML), 11N (HL), and 0N (C). Twenty-four hours following the final bout, muscle tissue was harvested and stored at  $-80^\circ\text{C}$  for further analysis.

Four  $8\mu\text{m}$  sections (taken every fifth section of good quality) of muscle tissue was cut on a Cryostat set at  $-25^\circ\text{C}$ , and placed on a Superfrost® Plus Microscope Slide (Fisher Scientific), using O.C.T Embedding Medium (Tissue-Tek- Sakura). Tissue underwent immunohistochemistry staining for the identification of ED1+ (Mouse anti-Rat CD68 1:100-Serotec) and ED2+ (Mouse anti-Rat CD163 1:100-Serotec) macrophages. Both staining protocols included TSA Amplification (Fluorescein Tyramide Reagent System-Perkin Elmer) following peroxidase secondary treatment (ImmPRESSReagent-Vector Labs). Finally, sections were stained with Dapi for the identification of nuclei.

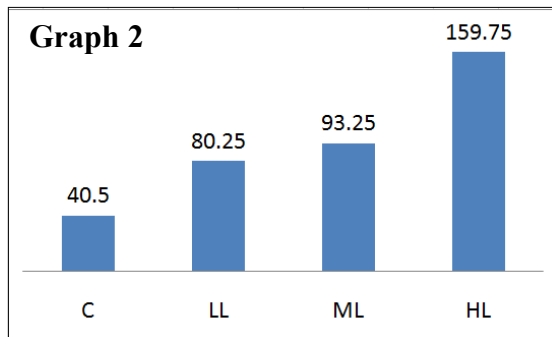
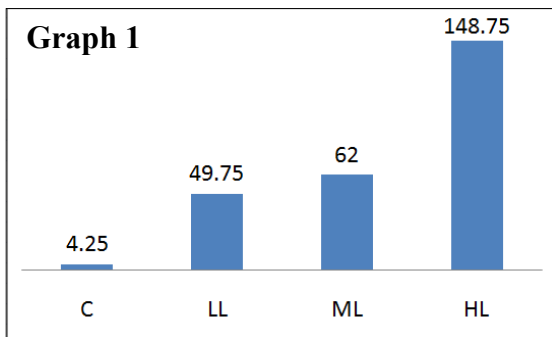
Tissue images were obtained using a ZeissAxio Imager M1 microscope (Carl Zeiss Microimaging). Two pictures of a randomly selected field, were taken at 200x magnification from each section yielding 4 images of ED1+ and ED+2 macrophages per slide (8 total images per slide). Stereological point counting techniques were utilized to quantify macrophage subpopulations per  $0.16\text{mm}^2$  area. ANOVA analysis ( $p \leq 0.05$ ) was performed using IBM SPSS statistical software.

## RESULTS AND DISCUSSION

Four one-way ANOVAs were performed to compare the differences between load and cellular infiltration for the massaged right limb (RL) and the non-massaged left limb (LeL), for both ED1+ and

ED2+ subpopulations respectively. No significant differences were found between groups in the LeL. However, a significant difference ( $p=.012$ ) was found in ED2+ between groups in the RL. A highly significant difference was found in ED2+ between groups in the RL as well. Post-hoc comparisons was used to determine difference between specific groups (**Table 1**).

Student's Paired T-tests, comparing ED1+RL vs ED1+LeL (per load) and ED2+RL vs ED1+LeL (per load), resulted in significant differences only between the high load of each ( $p=.005$  for both).



**Graphs 1 and 2:** Demonstrating load dependency responses of ED1+ (Graph 1) and ED2+ (Graph 2) in relation to magnitude of load (compared to control (C) tissue).

As demonstrated by **Graphs 1 and 2**, there is a noticeable influence of magnitude in regards to the amount of infiltrating macrophages. ED2+, also known as 'resident' macrophages are naturally higher than ED1+ as they are already present in the tissue. No differences were seen between the LL and ML in both analyses, which suggests that

compressive load at low and moderate levels may be attenuating the inflammatory response. As demonstrated by the data (**Table 1**), and graphs, application of a high compressive load exacerbates the inflammatory response. Increased levels of ED1+ macrophages at four days past initial bout, would suggest increased levels of edema and tissue necrosis.

Student's Paired T-test analysis compared massaged limb (RL) to the non-massaged (LeL), and showed only a highly significant difference for the HL in both ED1+ and ED2+. With no significant difference between RL and LeL in either the ML or LL, this suggests that LL and ML somewhat resemble healthy tissue. These two loads may potentially represent an optimal operating range, physiologically beneficial in the modulation of the immune response.

## CONCLUSIONS

Our preliminary results suggest an optimal range for the application of compressive load to healthy skeletal muscle. Further analysis absent of confounding effects, is needed to better target specific signaling pathways modified by mechanical loading. Identification of these pathways may lead to significant information regarding the practice of massage therapy.

## REFERENCES

1. Hornberger, et al. *Am J Physiol Cell Physiol.* **288**, C185-194, 2005.
2. Butterfield, et al. *Med Sci Sports Exerc.* **40**, 1289-1296, 2008.
3. Waters, et al. *Proceedings of NATA '11*, New Orleans, LA, USA, 2011
4. Cunningham, et al. *Proceedings of ASB '10*, Baltimore, MD, USA, 2010.

## ACKNOWLEDGEMENTS

Supported by NIH NCCAM R01AT004922 (TMB)

**Table 1:** Post-hoc comparisons demonstrating the differences between groups in accordance to load magnitude.

| Macrophage | HL vs. LL | HL vs. Mod | HL vs. C | LL vs. M | LL vs. C | Mod vs. C |
|------------|-----------|------------|----------|----------|----------|-----------|
| ED1+       | $p=.003$  | $p=.007$   | $p=.001$ | $p=.673$ | $p=.254$ | $p=.144$  |
| ED2+       | $p=.003$  | $p=0.11$   | $p=.013$ | $p=.584$ | $p=.979$ | $p=.673$  |

# INTER-RATER RELIABILITY OF RATING KINEMATIC PLOTS OF FORWARD BEND MOVEMENT PATTERNS

Peemongkon Wattananon, Won Sung, Scott Biely, Sheri Silfies and Marco Cannella

Drexel University, Rehabilitation Sciences Spine Research Lab, Philadelphia, PA, USA

email: [pw86@drexel.edu](mailto:pw86@drexel.edu) web: [http://www.drexel.edu/cnhp/rehab\\_sciences](http://www.drexel.edu/cnhp/rehab_sciences)

## INTRODUCTION

The presence of aberrant movement patterns during active forward bending is one criterion used to identify patients who would benefit from trunk stabilization exercises.<sup>1</sup> These aberrant patterns represent altered coordination among spinal segments. Tracking 3D-kinematics in conjunction with a dynamical systems approach to data analysis can be utilized to represent the contribution and inter-segment coordination of the pelvis, lumbar and thoracic spine to quantify segment coordination and pattern stability.<sup>2</sup> However, the operational definitions of these aberrant patterns and the reliability of rating kinematic plots of trunk movement have not been established.

## METHODS

Twenty-one participants (8 men, 13 women; mean age  $40 \pm 7$ ) were recruited from 2 orthopedic outpatient physical therapy clinics. Participants included individuals with current low back pain ( $n=8$ ), previous episode of low back pain ( $n=4$ ), and no history of low back pain ( $n=9$ ). Kinematic data from the femur, pelvis, lumbar and thoracic segments were recorded using an electromagnetic tracking device (Polhemus, Inc.) during simultaneous clinical observation of 6 repetitions of an active forward bend task. Standard clinical operational definitions for aberrant patterns were used (Table 1.).

Euler angles were derived from the kinematic data and resampled to 100 data points across the task. The following plots were created: 1) angle-angle plots of each segment in frontal and transverse planes vs. total sagittal plane (Fig. 1a), 2) phase plane plots (sagittal angular motion vs. velocity) for each segment (Fig. 1b), 3) sagittal plane angle-angle plots of the lumbar spine vs. pelvis (Fig. 1c). Angle-

angle and phase plane plots ( $n=120$ ; subject  $\times$  repetitions) were rated as either normal or aberrant by 2 independent raters who were blinded to subject group and clinical ratings of forward bend motion.

McNemar's tests were used to determine marginal homogeneity between the raters and Kappa statistics were used to determine inter-rater reliability of ratings based on kinematic algorithms.

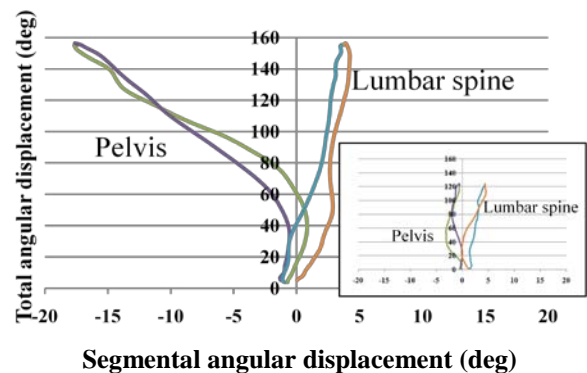


**Figure 1a:** Example of out-of-plane motion of the pelvic segment (green line forward bend, purple return) in this frontal plane angle-angle plot. Deviation defined as segment moved  $> 5^\circ$  from sagittal plane within the first 2/3 of total motion. Insert represents normal movement pattern.

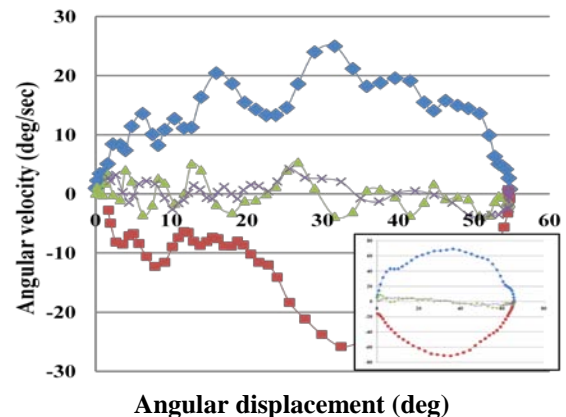


**Figure 1b:** Example of judder (shaking) in a lumbar segment phase plane plot represented by 1) sudden increases and decreases in instantaneous change in angular velocity (green line) and 2) fluctuations in angular velocity with relatively low segment velocity  $\leq 20^\circ/s$  (blue line) during forward bend. Insert represents a normal pattern of control.

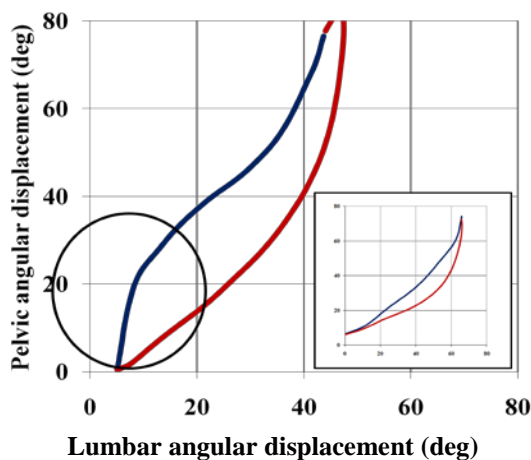


**Figure 1c:** Example of an angle-angle plot of aberrant lumbar spine and pelvis/hip coordination during forward (blue) and return (red) motion. Reversal defined as hip motion > lumbar in first 1/3<sup>rd</sup> of movement (circle). Insert represents normal lumbopelvic coordination pattern.

## RESULTS

McNemar's tests were non-significant between raters for the number of trials rated aberrant or normal for each type of movement pattern. Inter-rater reliability of kinematic plot ratings was substantial to almost perfect <sup>3</sup> (Table 2).

## DISCUSSION AND CONCLUSIONS

These findings indicate that the measurements obtained, operational definitions, and methods for representing trunk coordination and control have adequate inter-rater reliability. This will allow comparison of clinical observations to kinematic data and provide a first step toward better understanding which trunk segments contribute to these aberrant patterns and their underlying mechanisms.

## REFERENCES

1. Hicks GE, et al. *Arch Phys Med Rehabil.* 2005;**86**(9):1753-62.
2. Kurz MJ, Stergiou N. *Applied dynamic system theory for the analysis of movement.* 2004;93-119
3. Sim J, Wright CC. *Phys Ther.* 2005;**85**(3):257-68

## ACKNOWLEDGEMENTS

This study was supported in part the by Orthopaedic Section, American Physical Therapy Association.

**Table 1:** Operational definitions of aberrant movement patterns during standing trunk flexion and extension.

| Aberrant Pattern                            | Clinical Observation Operational Definition  |
|---|--|
| <b>Out-of-Plane (DEV)</b>                   | Movement away from the sagittal plane during flexion or extension including either transverse rotations and/or lateral flexion motion.   |
| <b>Judder (JUD)</b>                         | <i>Shaking:</i> trembling seen either in the paravertebral muscles during forward bending or return.<br><i>Quick out-of-plane:</i> momentary deviation away from the sagittal plane of motion.<br><i>Sudden deceleration and acceleration:</i> any stop or deceleration in motion followed by an acceleration of motion. |
| <b>Reversal of Lumbopelvic Rhythm (LPR)</b> | Hip motion > lumbar spine motion during the first 1/3 <sup>rd</sup> and/or lumbar motion > hip motion during the last 1/3 <sup>rd</sup> of the movement.   |

**Table 2:** Marginal frequency and inter-rater agreement for movement patterns during standing trunk flexion and extension.

| Aberrant Patterns | McNemar's Test         | Percentage Agreement | Kappa (95% CI) |
|-------------------|------------------------|----------------------|----------------|
| DEV               | $\chi^2=3.50; p = .06$ | 83                   | .74 (.60-.81)  |
| JUD               | $\chi^2=0.18; p= .68$  | 81                   | .62 (.46-.74)  |
| LPR               | $\chi^2=0; p = 1.00$   | 94                   | .88 (.77-.94)  |

# IMAGE SEGMENTATION AND REGISTRATION ALGORITHM FOR QUANTIFICATION OF RIB MORPHOLOGY ACROSS AGES AND GENDERS

<sup>1,2</sup>Ashley A. Weaver, <sup>1,2</sup>Joel D. Stitzel

<sup>1</sup>Virginia Tech – Wake Forest University Center for Injury Biomechanics, Winston-Salem, NC, USA

<sup>2</sup>Wake Forest University School of Medicine, Winston-Salem, NC, USA

email: [asweaver@wfubmc.edu](mailto:asweaver@wfubmc.edu) web: [www.cib.vt.edu](http://www.cib.vt.edu)

## INTRODUCTION

Adults 65 years of age and older currently constitute more than 12% of the total population and the elderly population is projected to reach nearly 20% by 2030 [1]. Previous studies have shown that skeletal and physiological resilience decline with age, resulting in a decreased ability to withstand traumatic insults [2,3]. In the current study, an algorithm was developed to collect rib landmark data and quantify age and gender-specific variations in the thoracic skeletal morphology. These variations will be used to generate a parametric thoracic model for injury prediction.

## METHODS

A minimum of 10 normal chest CT scans for each gender were collected from a radiological database for the following ages: newborns, 3, 6, and 9 month, and 1, 3, and 6 year olds. Beginning with 10 year olds, a minimum of 10 CT scans for each gender were collected by decade up to age 100.

Image segmentation and subsequent image registration was used to collect homologous landmark data from the ribs. A semi-automated method was used to segment each rib and create a mask and three-dimensional (3D) model. An atlas was created from segmentation of a normal chest CT scan of an average male. The atlas contains 24 ribs with over 100 landmark points on each rib. For every subject in the study, each segmented rib was registered with the corresponding rib in the atlas. Rigid, affine, and non-rigid, non-linear transformations were used in the registration algorithm to morph the atlas to the rib of each subject (Fig. 1, Steps 1 and 2). Following the registration, the landmark points on each rib have been transformed to the subject-specific coordinate

system of the CT scan (Fig. 1, Step 3). Effectively, this allows for collection of homologous rib landmarks across subjects of all ages. Geometric morphometrics, particularly the Procrustes superimposition method, can then be used to analyze the landmark data to formulate age and gender-specific shape and size variation functions.

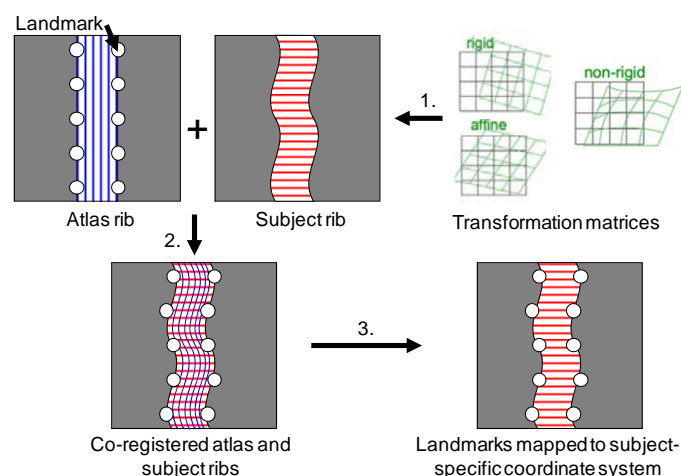


**Figure 1:** Simplified image registration process.

## RESULTS AND DISCUSSION

An example of the registration algorithm results is provided in Fig. 2. The left fourth rib from a 16 year old male (“subject rib”) was registered with the left fourth rib of the average male (“atlas rib”). The rigid transformation (Fig. 2, Step 1) translates and rotates the atlas rib to align three landmarks on the atlas rib with those on the subject rib. The affine transformation (Fig. 2, Step 2) applies translation, rotation, scaling, and shearing operations to morph the atlas rib to the subject rib. In the final step, a non-rigid, non-linear transformation is applied to morph the atlas rib to the subject rib (Fig. 2, Step 3).

To quantify the robustness of the image registration, differences in the 3D models of the registered atlas

and subject ribs were compared. Acceptable ranges of deviation were related to scan resolution and set to the maximum voxel length of the scan, 0.74 mm. The color bar in Fig. 3 illustrates the deviations in millimeters between the two models. Over 99% of the deviations fell within the acceptable range (-0.74 to 0.74 mm). The average deviations in the positive and negative directions were 0.194 and -0.138 mm, respectively with a standard deviation of 0.222 mm. The maximum deviations in the positive and negative directions were 1.208 and -3.109 mm, but occurred in localized regions on the rib and accounted for less than 1% of the overall deviations.

## CONCLUSIONS

The image segmentation and registration algorithm developed was used to collect extensive homologous landmark data from the ribs of over 320 subjects aged 0-100 years. The algorithm improves on the previous methods of measuring rib geometry by utilizing the full 3D information in the scan to collect landmarks [4,5]. The algorithm uses rigid, affine, and non-rigid, non-linear transformations to morph segmented ribs from different subjects to a rib atlas. The collected landmarks will be analyzed to formulate age and gender-specific shape and size variation functions and generate a parametric finite element model of the rib cage. Results of this study will lead to an improved understanding of the complex relationship between thoracic geometry, age, gender, and injury risk.



**Figure 3:** Deviation analysis results.

## REFERENCES

1. U.S. Census Bureau, *Public Information Office*, 2008.
2. Burstein AH, et al. *J Bone Joint Surg Am* **58**, 82-86, 1976.
3. Zioupos P, et al. *Bone* **22**, 57-66, 1998.
4. Gayzik FS, et al. *J Biomech* **41**, 1545-54, 2008.
5. Kent R, et al. *Stapp Car Crash J* **49**, 231-49, 2005.

## ACKNOWLEDGEMENTS

Funding was provided by the National Highway Traffic Safety Administration and the National Science Foundation Graduate Research Fellowship Program. Thanks to Dr. Chris Wyatt, Haiyong Xu, and students of the Center for Injury Biomechanics for their assistance with this study.

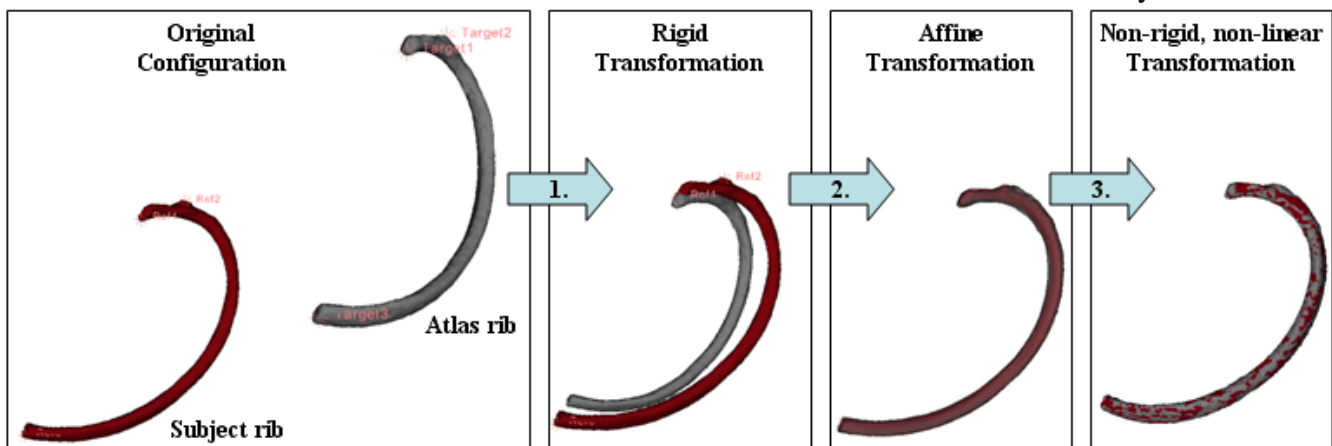


**Figure 2:** Image registration example. 1) Rigid transformation applied to align three landmarks on the atlas rib with three landmarks on the subject rib. 2) Affine transformation applied. 3) Non-rigid, non-linear transformation applied.

# **A BIOMECHANICAL MODEL OF THE RAT HINDLIMB: MODELING WITH STRANDS AND SUBJECT-SPECIFIC REGISTRATION**

<sup>1</sup>Qi Wei, <sup>1</sup>Anthony Jarc, <sup>2</sup>Sang Hoon Yeo, <sup>1</sup>T. G. Sandercock, <sup>1</sup>Matthew C. Tresch, <sup>2</sup>Dinesh K. Pai

<sup>1</sup>Northwestern University, Evanston, IL, USA

<sup>2</sup>University of British Columbia, Vancouver, BC, Canada

email: pai@cs.ubc.ca

## **INTRODUCTION**

A three-dimensional neuro-musculoskeletal model of the rat hindlimb was developed, which simulates muscle actions and dynamic movement of the hindlimb. The goals of the study were to use this computational model to study the biomechanical consequences of muscle actions and to quantitatively assess characteristics of complex musculoskeletal systems through model-based simulation against experimental observations.

The model has several distinctive features. Muscles and tendons were represented by strands, which are novel musculotendon primitives [1] and are able to model curved paths. In order to simulate complex interactions between musculotendons and the skeleton, the model utilizes features of the strand framework such as sliding and force transmission along general constraints, which are hard to simulate with previous models. Given target motion trajectory of the skeletons, the simulator can calculate muscle innervations that drive the skeletons to produce the desired motion. Dynamic movement can be simulated at interactive rates. Unlike some of the existing biomechanical simulators, this strand-based model does not lump muscle masses with bone segments but associates distributed mass with each strand, which avoids one source of errors in dynamic simulation [2].

## **METHODS**

As a first step, a generic musculoskeletal model of the rat hindlimb was built. Each muscle (tendon) was modeled by a strand, which utilizes a B-Spline curve to represent its geometric path and is associated with mass as well as experimental tissue constitutive models. Instead of using several connected line segments to represent a curved muscle, a single strand is sufficient to depict axial muscle path realistically. Multiple strands can be joined to model one muscle, which is useful to simulate muscles with broad attachments or with complex architectures. Strands model longitudinal

actions such as generated forces and nonuniform strains. The kinematic characteristics of the rat hindlimb model including the bone geometries, muscle attachment locations, and joint centers were based on measurements reported in [3]. The hip was modeled as a ball joint and the knee was modeled as a universal joint. Individual muscle maximum isometric forces were taken from the OpenSIM model from the same group [3]; PCSAs in [4] were used to compute muscle masses.

While the generic model defines a normative computational representation of the rat hindlimb musculoskeletal system, it can be customized to study a specific subject from which empirical data is obtained. The kinematic configuration of the skeleton was tracked using a Vicon motion capture system (Vicon, Los Angeles, CA). Distinctive bony landmarks were identified and their 3D locations were determined by a pointer device with infrared retroreflective markers. Corresponding landmarks were labeled on the computer skeleton models. The template model was registered to the Vicon marker data to minimize the error between the virtual and experimental bony landmark positions. While the skeletons were straightforward to transform, curved muscle and tendon strands were not, as they were not defined simply by the origins and insertions. The proposed solution was to utilize simulation of the whole model from the generic model posture to the target posture, applying an inverse dynamics innervation solver [1]. The musculotendon strands were transformed directly during the inverse simulation. The resulting registered model provided the kinematic configuration consistent with the empirical condition, and thus could be used for subject-specific and quantitative study while combining with experimental data.

## **RESULTS AND DISCUSSION**

As an example of the utility of using strands, we can model the common quadriceps tendon as a

single strand, rather than as separate elements, which implements the knee extensor mechanism in a physiologically more realistic way. The extensor quadriceps femoris muscles (RF, VL, VM, and VI) were represented by four contractile muscle strands. Their distal ends connected to a tendon strand which inserted on the tuberosity of the tibia and modeled the quadriceps and patellar tendons. This common tendon strand slid on top of the patellar surface; the interaction force between the tendon and femur can be quantitatively analyzed as a function of joint angles, which is potentially useful for studying movement disorders. As Figure 1 shows, simultaneous innervation of four quadriceps muscles extends the knee and also flexes the hip.

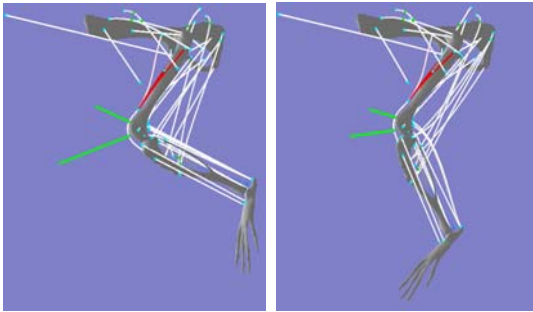


**Figure 1:** Simulation of knee extensor mechanism by innervating the quadriceps. Forces transmitted between the common tendon and the femur are shown as green line segments.

The model performs both forward and inverse dynamic simulation. Figure 2 demonstrates the inversely computed muscle innervations that enable the corresponding muscles to extend the hip by 20 degrees. As expected, hamstring and relevant hip muscles were associated with relatively higher innervations to generate the desired movement. The innervation solver was also used to register the generic model to the specific subject posture; the registration error was less than 2mm.

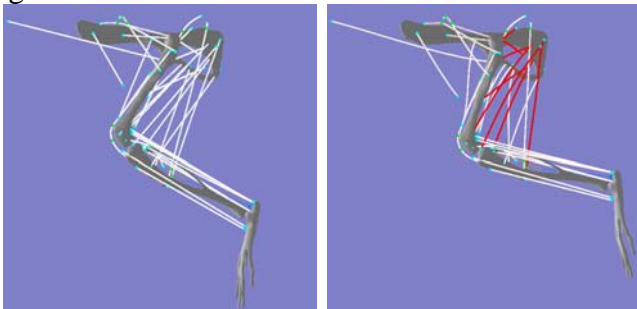


**Figure 2:** Inversely estimated muscle innervations to extend the hip by 20 degrees.

An effective approach to validate a musculoskeletal model is to evaluate muscle actions characterized

by experimental end point forces. Forces predicted by the model were compared to forces measured by the force transducer fixed near the ankle using the protocol in [5]. The generic model was registered to match the Vicon kinematic data. To emulate the experiment, a 1-DOF hinge joint (allowing rotation about the mediolateral axis) was placed at the corresponding position and the joint reaction force was calculated. The end point force predicted by the model with stimulated posterior head of biceps femoris (BFp) was consistent with the empirical data at this posture, shown in Figure 3(a). Origin and insertion locations of BFp were based on the optimized values in [5]. Similarly, predicted force from simulating abductor magnus (AM) also agrees with the measured force (see Figure 3(b)). Such analysis can be extended to various muscles to determine functional muscle attachments and to investigate coupled actions of multiple muscles.

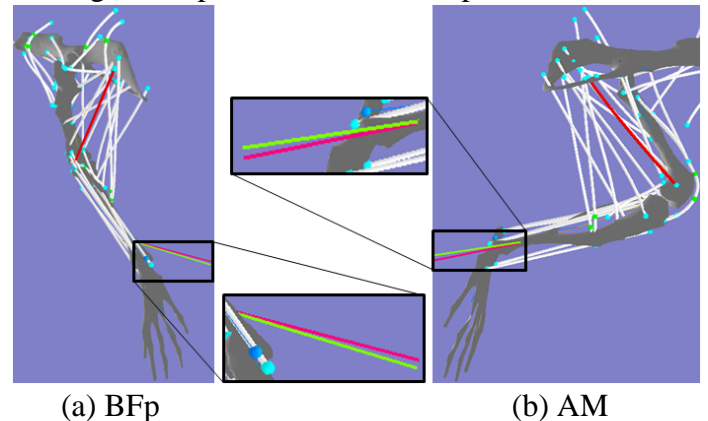


**Figure 3:** Comparison of predicted end point forces of stimulated (a) BFP and (b) AM to in situ measurement of muscle actions. Force vectors were normalized. Red segments – measured forces; green segments – predicted forces.

## CONCLUSIONS

A computational model of the rat hindlimb musculoskeletal system was presented. The model can be utilized to evaluate muscle actions against empirical data and to simulate dynamic locomotion.

## REFERENCES

1. Sueda S, et al. *ACM Trans. Graph.* **27:3**, 2008.
2. Pai DK, *J Biomech* **43**, 2093-2098, 2010.
3. Johnson WL, et al. *J Biomech* **41**, 610-619, 2008.
4. Eng GM, et al. *J Exp Biol* **211**, 2366-2345, 2008.
5. Yeo S-H, et al. *J Exp Biol* **214**, 735-746, 2011.

## ACKNOWLEDGEMENTS

Supported by NIH 5R01AR053608-04

# KINETICS AND KINEMATICS OF SWIMMING PUSH-OFF STRATEGIES

<sup>1</sup>Wendi H. Weimar, <sup>1</sup>Andrea M. Sumner, <sup>1</sup>Jay Patel, <sup>1</sup>Braden Romer, <sup>1</sup>John Fox, <sup>1</sup>James Snead & <sup>2</sup>Justin F. Shroyer

<sup>1</sup>Auburn University, Auburn, AL, USA

<sup>2</sup>University of Louisiana at Lafayette, Lafayette, LA, USA  
email: weimawh@auburn.edu

## INTRODUCTION

It has been suggested that the turn in swimming comprises as much as 20.5% of a 50m race [1]. With such a large proportion of the race occurring during the turns it is surprising that more attention is not being directed to this area, particularly in the area of force production. Observation of the flip-turn indicates that the push off movement is like that associated with the vertical jump, but without a counter movement. However, since it is readily accepted that a counter movement does improve the height of a vertical jump, why do more swimmers not utilize this motion as part of the push-off strategy. Particularly in light of the findings that the fastest swimmers tend to tuck further away from the wall with the legs more extended at contact [2]. Therefore the purpose of this project was to investigate the forces and velocities produced by different push-off strategies executed on a dry land sled. Specifically, what forces, impulses and velocities at 2.5 m away from the wall are developed as a result of four push-off strategies.

## METHODS

A dryland training sled, on a railing system, was developed for this project. In addition an underwater force platform (AMTI OR6-WP-1000, Watertown, MA) was affixed to the wall at the end of the railing system. An elastic band was affixed to the sled and provided the propulsion of the sled toward the force platform for all dynamic trials. Two Canon GL2 cameras were utilized in this study. One was used to verify knee angles at wall contact and one was used determine velocity of the sled/swimmer at 2.5 m from the wall. The video data were digitized using the Ariel Performance

Analysis System (APAS) (Ariel Dynamics Inc., Trabuco Canyon, CA) and followed standard techniques.

Nineteen Master or Professional Swimmers served as participants (males=11, females=5; age = 25.9 yrs (10.3); height = 69.39 in (4.15); weight = 159.36 lbs (29.11) and years swimming = 18 (10.8)). The participants were instructed to lie supine on the sled and assume the appropriate knee angles for the four push-off strategies employed and were asked to push forcefully off of the wall. For Strategy 1–Dynamic 90 (D90), the sled was pulled a distance equivalent to 2 leg lengths of the participant, away from the wall, stretching the elastic band. Once released, the sled moved toward the wall, and the participants were asked to let the wall flex the knees to 90 degrees before forcefully pushing off of the wall. Foam blocks were affixed to the knees of the participant as a kinesthetic marker to initiate the push. For Strategy 2–Dynamic quick (DQ), the sled was pulled a distance equivalent to 2 leg lengths of the participant, away from the wall, stretching the elastic band. Once released, the sled moved toward the wall, and the participants were asked to push off the wall forcefully, in the shortest time possible. Strategy 3- Static 90 (S90) required that the participants be positioned immediately in front of the force platform with the knees at 90 degrees. The participants were asked to use both feet to push off forcefully. Strategy 4 – Static 1-2 (S12) required that the participants be positioned immediately in front of the force platform with the knees at 90 degrees and the participants were asked to push forcefully with the dominant leg first and then the non-dominant leg.

Statistical procedures were calculated by PASW software (Version 18.0; SPSS Inc., Chicago,

Illinois, USA), and statistical significance was determined by a p value less than 0.05.

## RESULTS AND DISCUSSION

The results indicate that the peak force for each strategy was significantly different, with the exception of D90 & S90 (the two 90 deg strategies). All strategies yielded a significantly different impulse, and all velocities were significantly different with the exception of DQ & S90. DQ yielded the greatest peak force but the second largest impulse and the second largest velocity. D90 yielded the second largest peak force but the largest impulse and the largest velocity. S90 yielded the next largest peak force and impulse, but the second largest velocity. S12 yielded the smallest values for all three variables (Figures 1 & 2).

The results of the present study imply that the largest forces do not produce the greatest velocities at a position 2.5 m from the wall. It is hypothesized that this will be more pronounced during water trials as the drag force will be more detrimental to this velocity. The next step in this line of research is to move this project to the water and consider not only the forces and velocities, but also the time it takes to cover specified distances. For it is possible that a push-off strategy could produce the largest

impulse and velocities but result in longer times, if the time spent at the wall is too long and the drag force is too large.

## CONCLUSIONS

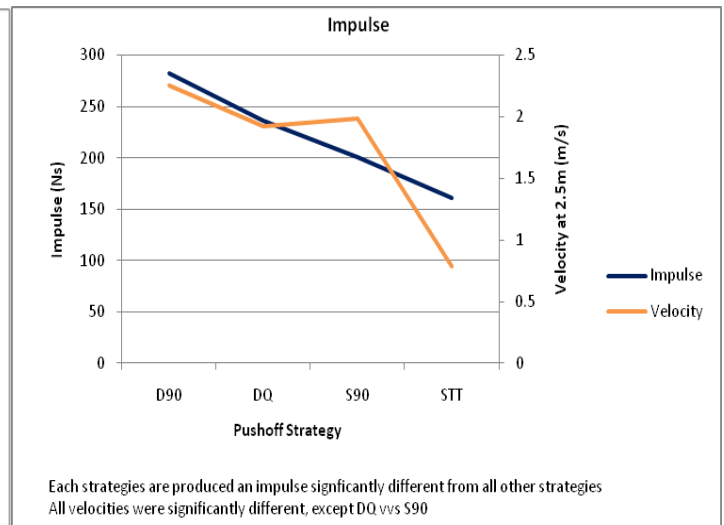
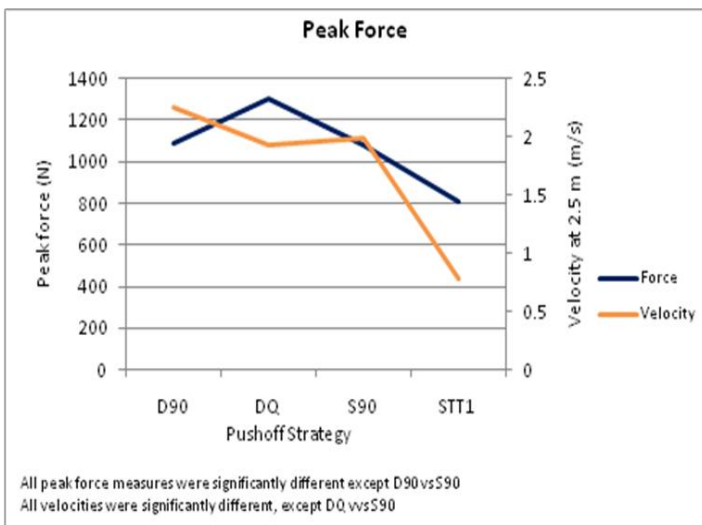
The results suggest that, on land, the inclusion of a counter movement did yield a larger impulse as well as the largest velocity. These findings indicate that a counter movement should be included in the push-off method of the flip-turn.

## REFERENCES

1. Thayer, A. L. & Hay, J. G. (1984). Motivating start and turn improvement. *Swimming Technique*, 20(4), 17-20.
2. Cossor, J. M., Blanksby, B. A., & Elliott, B. C. (1999). The influence of plyometric training on the freestyle tumble turn. *Journal of Science and Medicine in Sport* 2 (2): 106-116.

## ACKNOWLEDGEMENTS

The authors would like to thank the coaching and support staff of the Auburn University Swimming and Diving Team as well as the Auburn Masters Swimming Program.



# AN OPTIMIZATION ALGORITHM TO IMPROVE COMPUTED MUSCLE CONTROL

Joshua T. Weinhandl, Walter A. Laughlin, and Kristian M. O'Connor

University of Wisconsin-Milwaukee, Milwaukee, WI, USA  
 email: [weinhan2@uwm.edu](mailto:weinhan2@uwm.edu), web: [www.chs.uwm.edu/neuromechanics](http://www.chs.uwm.edu/neuromechanics)

## INTRODUCTION

Advances in computational power and modeling techniques have enabled large-scale subject-specific musculoskeletal models that can produce realistic simulations much more complex than those produce just 10 years ago. Specifically, computed muscle control has become a popular choice because of its availability within OpenSim [1] and its ability to generate a muscle-driven simulation in a only a few minutes [2,3]. However, producing a reasonable simulation often takes several days of “trial and error” to find the appropriate input parameters that minimize kinematic tracking errors and the residual forces/torques needed to balance Newton’s equations of motion.

In this study, we used optimization to minimize the kinematic errors and residuals by adjusting input parameters for computed muscle control. Our goal was to determine optimal input parameters that produce a simulation which closely tracks experimental data of single leg landing with limited residuals. We hypothesized that the optimization would produce a simulation with comparable results to standard inverse dynamics, and within less time than the optimization routine proposed by Reinbolt & Donnelly [4].

## METHODS

Three dimensional kinematic and force plate data were collected from one physically active female (23 years; 65.6 kg; 1.76 m) performing a single-leg

drop landing from a 37 cm box. A subject-specific musculoskeletal model was then generated in OpenSim [1] consisting of 19 degrees-of-freedom (*dof*), driven by 19 actuators. The position and orientation of the pelvis relative to the ground was defined with 6-*dof*. The head, arms and torso was represented as a rigid segment connected with the pelvis by 3-*dof*. Each hip was modeled as a 3-*dof* ball-and-socket joint, while each knee and ankle was modeled as a 1-*dof* revolute joint. Computed muscle control was then implemented to produce a forward dynamic simulation generally consistent with the experimentally measured kinematics. To minimize the kinematic errors and residuals, optimal computed muscle control input parameters were found using two optimization algorithms.

The first algorithm (Equation 1) found a set of acceleration weights ( $w_q$ ) that minimized cubed root-mean-square (*rms*) error between the experimental and simulated kinematics ( $q^{err}$ ) of the pelvis, uniformly weighted ( $W_K=2$ ;  $W_L=4$ ) cubed *rms*  $q^{err}$  over the remaining *dof*, and cubed *rms* magnitude of the residuals ( $R$ ).

The second algorithm, proposed by Reinbolt & Donnelly [4] (Equation 2), found an optimal set of acceleration weights ( $w_q$ ), maximum residuals ( $R^{max}$ ), and maximum joint torques ( $T^{max}$ ) that minimized uniformly weighted ( $W_{pelvis}$ , 1000) squared  $q^{err}$  of the pelvis, squared  $q^{err}$  over the remaining *dof*, uniformly weighted ( $W_R$ , 500) squared residuals, and squared joint torques ( $T$ ).

$$\min_{w_q} \left[ \sum_{i=1}^6 (rms(q_i^{err}))^3 + \sum_{i=7}^{nq-3} \left( \frac{rms(q_i^{err})}{W_K} \right)^3 + \sum_{i=nq-2}^{nq} \left( \frac{rms(q_i^{err})}{W_L} \right)^3 + \sum_{j=1}^6 (rms(R_j))^3 \right] \quad (1)$$

$$\min_{w_q, R^{max}, T^{max}} \left[ \sum_{i=1}^{nf} \left( W_{pelvis} \sum_{j=1}^6 (q_{ij}^{err})^2 + \sum_{j=7}^{nq} (q_{ij}^{err})^2 + W_R \sum_{k=1}^6 R_{ik}^2 + \sum_{l=1}^{nT} T_{il}^2 \right) \right] \quad (2)$$

## RESULTS AND DISCUSSION

Optimal input parameters for computed muscle control were found using both algorithms such that the simulations produced joint torques that closely matched those calculated using standard inverse dynamics (Figure 1). Additionally, the experimental data was closely tracked (Figure 2a) by both methods with the largest *rms* error being lumbar rotation at  $\sim 2^\circ$ .

Both methods also resulted in functionally small residual. The optimal input parameters found using our algorithm yielded *rms* residuals less than 1.3N and 2.3Nm. Comparatively, the Reinbolt & Donnelly [4] algorithm resulted in *rms* residuals less than 0.3N and 1.3Nm.

As for total time required to generate each simulation, our optimization algorithm converged approximately 6 times faster than the Reinbolt & Donnelly [4] algorithm. This was due to limiting the number of design variables to the set of acceleration weights, effectively cutting the inputs to the algorithm in half.

## CONCLUSIONS

Improving computed muscle control through optimization allows researchers to produce reasonable simulations in less time and with increased accuracy than when determining input parameters by hand.

Furthermore, by reducing the number of design variables in the optimization problem we were able to greatly reduce the time necessary to generate a simulation which closely tracks experimental data and minimizes the residual forces/torques needed to balance Newton's equations of motion.

## REFERENCES

- [1] Thelen et al. *J Biomech.* **36**:321-8. 2003
- [2] Thelen & Anderson. *J Biomech.* **39**:1107-15. 2006
- [3] Delp et al. *IEEE Trans Biomed Eng.* **54**:1940-50. 2007.
- [4] Reinbolt & Donnelly. *3D Analysis of Human Movement*. San Francisco, CA. July 14-16, 2010.

## ACKNOWLEDGEMENTS

UWM College of Health Sciences Student Research Grant.

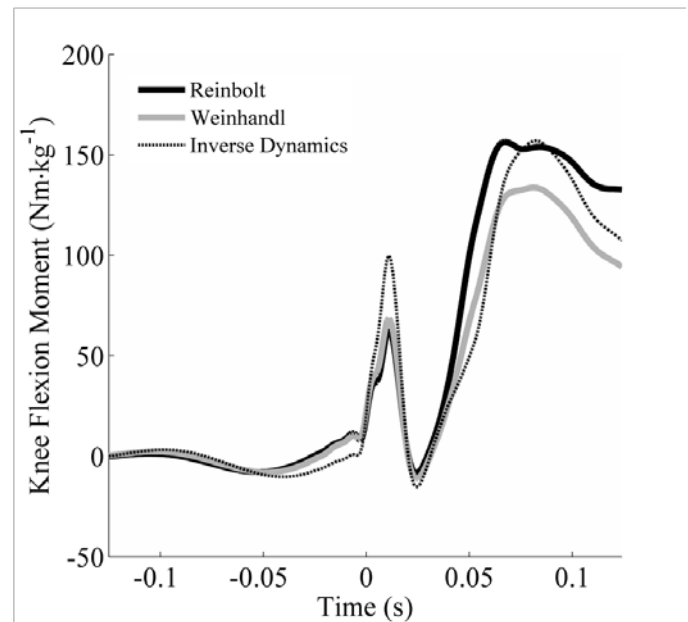


**Figure 1.** Knee joint torque calculated using the Reinbolt & Donnelly [4] algorithm (solid black line), our algorithm (solid grey line), and standard inverse dynamics (dashed black line).

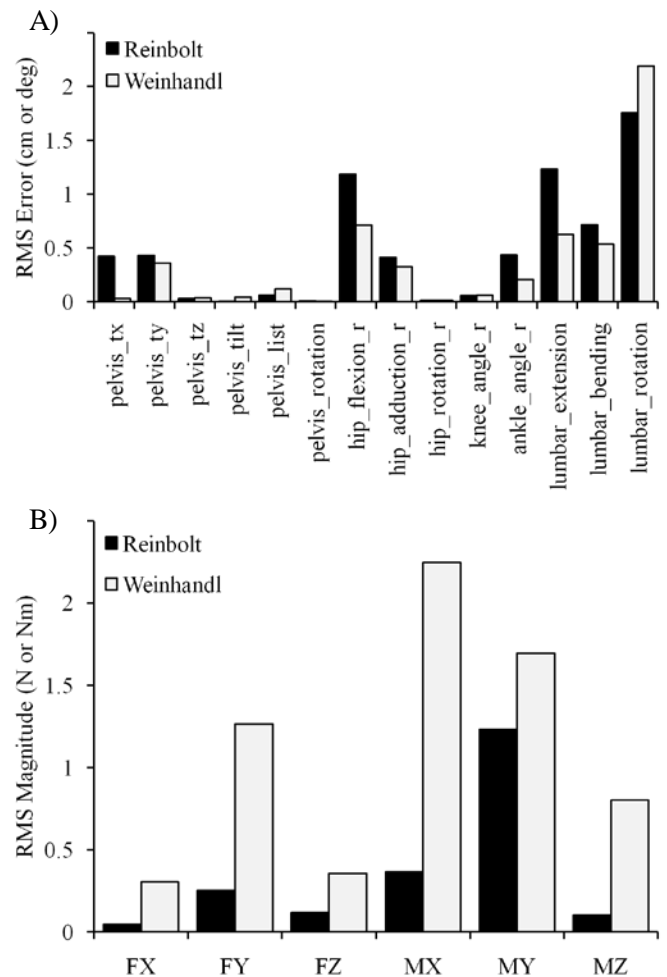


**Figure 2.** A) Kinematic tracking error and B) residual forces/torques using the Reinbolt & Donnelly [4] algorithm (black bars), and our algorithm (white bars).

# A NOVEL TECHNIQUE FOR MEASUREMENT OF ULNAR COLLATERAL LIGAMENT STRAIN

<sup>1</sup>Charles A. Weisenbach, <sup>1</sup>Justin G. Rosch, <sup>1</sup>Nicole C. Corbiere, <sup>2</sup>Mandy L. Cowgill, <sup>3</sup>Mark Carl Miller, and <sup>1</sup>Laurel Kuxhaus

<sup>1</sup> Clarkson University, Potsdam, NY, USA

<sup>2</sup> Wright State University, Dayton, OH, USA

<sup>3</sup> Allegheny General Hospital, Pittsburgh, PA, USA

email: lkuxhaus@clarkson.edu web: <http://people.clarkson.edu/~lkuxhaus/>

## INTRODUCTION

Models of ligament material properties are essential to develop new reconstructive surgical techniques and improve post-surgery patient performance [1]. The ulnar collateral ligaments of the elbow have been studied, but convincing estimates of *in vivo* strains during multi-directional loading have not been reported [2]. A fixture to load ligaments multi-directionally in a uniaxial load frame was developed. This fixture permits the elbow flexion angle and loading direction to be easily varied, resulting in physiological realistic loading directions. A better understanding of how tissues behave *in vivo* will be obtained with the ability to test the same specimens in multiple positions. The method is demonstrated with the lateral ulnar collateral ligament (LUCL).

## METHODS

*Fixture Design* - To test the sample at varying flexion angles a custom fixture was built (Fig. 1). The potted ends can rotate 90° in 15° increments to permit rotation relative to loading direction. The fixture rides along a lockable 2-degree-of-freedom sled to permit precise positioning in a load frame.

*Demonstration of Use* - A fresh-frozen cadaver elbow (F, 68 yrs, right) was dissected to reveal the LUCL. The radius, ulna, and humerus were potted in polymethylmethacrylate. Cyanoacrylate adhesive attached 7 markers (brass spheres, 1 mm diameter, coated in black paint) to the LUCL. The specimen was secured in the fixture and inserted into the load frame (Bionix 858, MTS, Eden Prairie, MN).

To ensure that the ligament was truly slack before

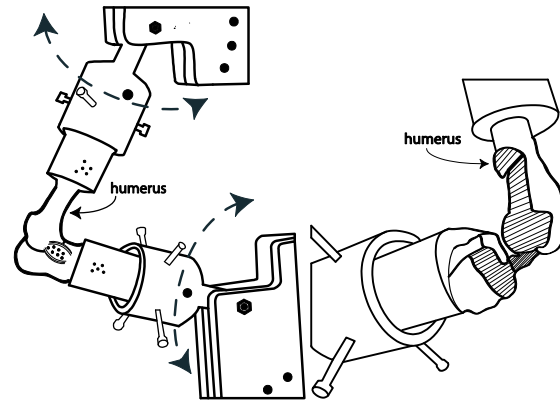


**Fig. 1:** Sketch of fixture (a) and elbow osteotomy (b).

loading, an osteotomy was performed to remove portions of the radius, ulna, and the medial condyle of the humerus (Fig. 1b). Thus the joint could be easily compressed to create a slack LUCL. After preconditioning the ligament three times at a displacement of 2.5 mm, it was stretched a total of 5 mm at a rate of 1.66 mm/s. Marker position was recorded using a two-camera SpicaTek (SpicaTechnology, Maui, HI) motion analysis system at 20 Hz. Measurements were taken with the elbow in two positions: Position 1 (flexion angle of 90°; humerus at 45° to the loading direction), and Position 2 (flexion angle of 105°; humerus at 15° to the loading direction).

To compute strain ( $\epsilon = \Delta L / L_0$ ) the length,  $L$ , and physiologic slack length,  $L_0$ , were computed. All data was filtered with a fourth order Butterworth filter at a cutoff frequency of 12 Hz. Custom MATLAB® (The MathWorks, Natick, MA) code computed the change in distance between all pairs of markers ( $\Delta L$ ) over time. Given that the ligament was known to be slack (due to the osteotomy) when loading began, the change in  $\Delta L$  for a given pair of markers over time showed a distinct change in the

slope at the point where the ligament began to carry load, clearly identifying  $L_0$  [3] (Fig. 2). This method to estimate  $L_0$  was used to compute the strain between all pairs of markers.

## RESULTS AND DISCUSSION

Examples of computed strain are shown in Figs. 3 and 4. Fig. 3 shows the strain as computed from the data shown in Fig. 2, with the elbow in Position 1. Fig. 4 shows additional results from the same ligament in Position 2. Measurements from two different pairs of markers during the same collection are shown. Note that the strain behavior is different between the two positions (Fig. 3 compared to Fig. 4), but consistent within each position regardless of marker pair used (Fig.4).

The results illustrate the feasibility of the novel fixture and osteotomy technique to effectively measure ligament strain with loads applied in varying directions. The clear change in intra-marker distance when loaded from a known slack condition indicates the ability of this method to identify a suitable slack length ( $L_0$ ) for use in strain computations. The strain computed between different marker pairs on the same ligament are in agreement, suggesting an accurate measurement. The differences observed between Position 1 and Position 2 suggests that loading direction may dramatically influence strain behavior of elbow ligaments.

Future work will include measuring strain at the same elbow flexion angles while varying loading direction, and will evaluate the effects of loading directions on ligament material properties. For example, studies of medial ulnar collateral ligament failure may reveal the importance of loading direction and emphasize the placement of the graft relative to common loading directions in surgery.

## CONCLUSIONS

In conclusion, this method for measuring elbow ligament strain permits easy adjustment of elbow position and loading direction relative to the ligament. Application of this technique to other soft tissues will provide more accurate estimates of the *in vivo* biomechanical properties of these tissues when combined with an appropriate material model.

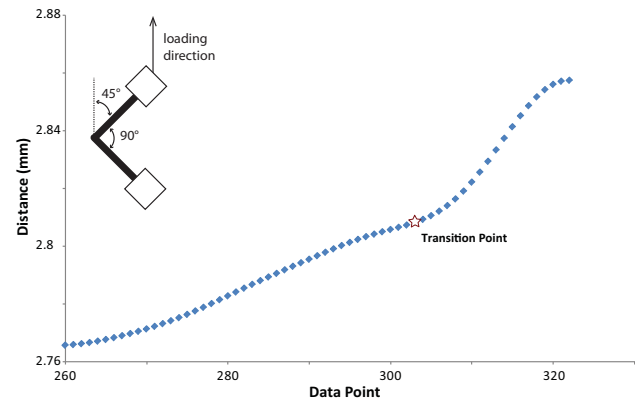


**Fig. 2:** Intra-marker distance example.

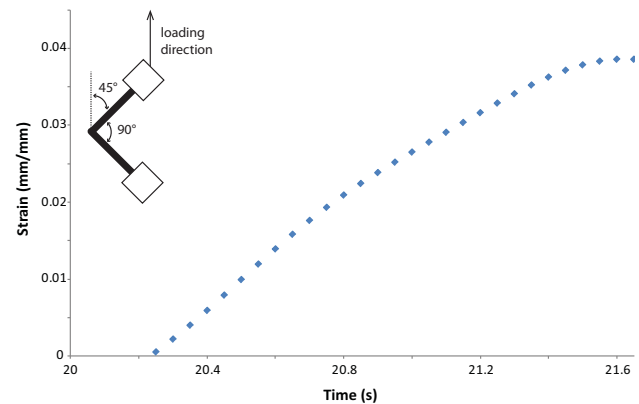


**Fig. 3:** Strain for Position 1.

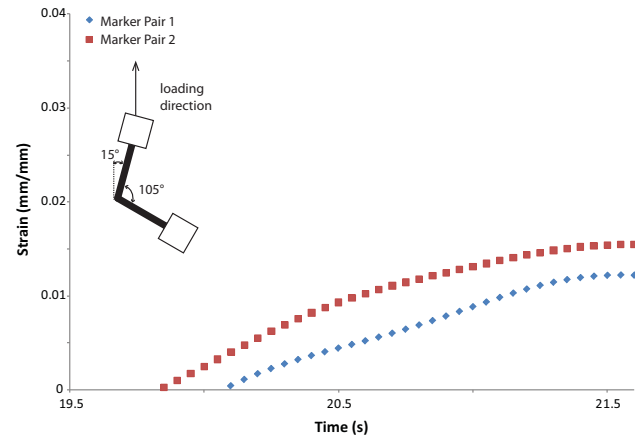


**Fig. 4:** Strain for Position 2.

## REFERENCES

1. DeVita R, et al. *Biomech Model Mechanobiol* **6**, 189-197, 2007.
2. Takigawa N, et al. *J Hand Surg Br* **30**, 143-147, 2005.
3. Brogdon ML et al. *ICMMB*, Pittsburgh, PA, USA, 2008.

## ACKNOWLEDGEMENTS

The authors thank Amin Mohaghegh and Sunghwan Kim for their technical assistance.

# CHANGES IN FOOT BONY MOTION UNDER DIFFERENT LOADING CONDITIONS USING A CADAVERIC ROBOTIC GAIT SIMULATOR

<sup>1</sup>Eric C. Whittaker, <sup>1,2</sup>Patrick M. Aubin, and <sup>1,3,4</sup>William R. Ledoux

<sup>1</sup>VA RR&D Center of Excellence for Limb Loss Prevention and Prosthetic Engineering, Seattle, WA  
Departments of <sup>2</sup>Electrical Engineering, <sup>3</sup>Orthopaedics & Sports Medicine, and <sup>4</sup>Mechanical Engineering,  
University of Washington, Seattle, WA

Email: wrledoux@u.washington.edu, web: <http://www.amputation.research.va.gov/>

## INTRODUCTION

Cadaveric gait simulation is a useful tool for exploring a wide variety of invasive biomechanics questions such as the effect of a surgery on foot bone kinematics. Frail cadaveric specimens however have made testing at reduced body weight (BW) a common practice [1,2]. While *in vivo* foot kinematics are known to be sensitive to the different loading conditions (e.g., slow running vs. walking) [3] the effect of reduced BW on *in vitro* foot kinematics is unknown. Understanding how foot kinematics change *in vitro* under different loads may provide additional insight into the limitations of cadaveric gait simulators and ultimately enhance our understanding of *in vivo* foot function and strategies to treat or correct pathologic conditions.

Our group has developed a robotic gait simulator (RGS, Figure 1) that can produce biomechanically realistic ground reaction forces (GRFs), muscle tendon forces, and foot bone kinematics [4,5]. Previously, we have reported the foot bone kinematics resulting from GRFs scaled to 75% BW [5]. As part of the same data set, we also performed simulations at 50% BW. Using a ten-segment foot model and the RGS, the goal of this study was to compare the kinematics of cadaveric walking simulations performed at 50% BW and 75% BW. Identifying differences or similarities will provide a better understanding of the effects of scaled loading conditions on foot bony motion.

## METHODS

Six neutrally aligned cadaveric specimens were tested, each with nine extrinsic tendons attached to force-controlled tendon actuators driven by muscle forces prescribed from *in vivo* EMG or directly measured data [4,5]. The prescribed motion of the

6-degree of freedom RGS was based on average *in vivo* tibia-to-ground kinematics from 10 healthy subjects [4]. Vertical GRF (vGRF) was scaled to 50% of the donor's BW. vGRF was maintained with fuzzy logic real time control of the Achilles (Ach) and tibialis anterior (TA) tendon forces, and closed loop iterative fuzzy logic control of the force plate position. Three stance phase trials were performed for each foot, with duration of 2.7 sec (four times slower than *in vivo* stance). This process was repeated with the vGRF scaled to 75% BW.

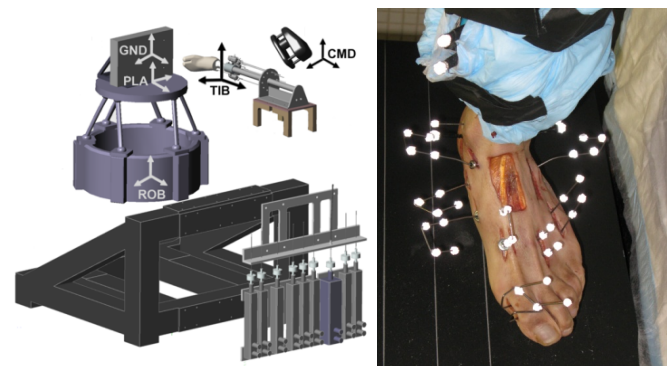


Figure 1: RGS schematic and fully instrumented specimen

A previously described foot model [4,5] (Figure 1) was used to capture individual foot bone motion. The model consisted of the following ten segments: tibia/fibula (TIB), talus (TAL), calcaneus (CALC), navicular (NAV), cuboid (CUB), medial cuneiform (CUB), first (MET1), third (MET3), and fifth (MET5) metatarsals, and the proximal phalanx (HAL). Anatomical coordinate systems were created from either retro-reflective markers attached to each bone at specific locations with bone pins or digitized with a stylus wand and tracked with arbitrarily placed quad marker clusters. Kinematic data was collected with a six-camera Vicon MX system. Linear mixed effects regression models were used to test for differences in range of motion (ROM) by body weight (50% vs. 75%) for 12

angles (joints or kinematic relationships) of interest. To assess the effect of BW on ROM for all angles together, linear mixed effects models were carried out combining all angles (51) into one model.

## RESULTS AND DISCUSSION

Kinetic data was very similar between 50% BW and 75% BW. GRF root mean square (RMS) error for 50% BW was 5.1%, 3.7%, and 1.8% BW for superior/inferior, anterior/posterior, and medial/lateral directions, respectively. For 75% BW, the RMS errors were only slightly larger, at 5.9%, 4.0%, and 3.6% BW. Muscle tendon force tracking RMS error was also nearly similar, at 3.6N for 50% BW and 3.9 N for 75% BW.

Statistical analysis of the kinematic ROM data (Table 1) revealed that six of the 12 angles of interest showed significant differences ( $p < 0.05$ ) between the two loading conditions. There was a clear trend of larger ROM for the 75% BW data. Average difference between 50% and 75% for these 12 angles was  $2.3 \pm 1.7^\circ$ . When assessing the “All Angles” data set, average ROM for 75% BW was systematically higher than that for 50% BW ( $p < .0001$ ), although the magnitude of the difference was small ( $1.2 \pm 0.2^\circ$ ).

Five of the six significant angles included the talus, indicating that it may become increasingly mobile under larger loads. Similarly, the first ray experienced a greater range of motion at higher loads as evidenced by MET1 wrt TAL (read, first metatarsal with respect to talus) (Figure 2, Table 1) and HAL wrt MET1 (Table 1). Based on these data and the complicated anatomy of the foot, it is evident that there is not a uniform change in kinematics across all joints with increasing load. The kinematic changes were small ( $< 3^\circ$ ) for most

joints; however, the temporal characteristics of the kinematics were very similar between loading conditions (Figure 2). These data help pinpoint the joints that are the most mobile, and quantify their motion under varying loads.

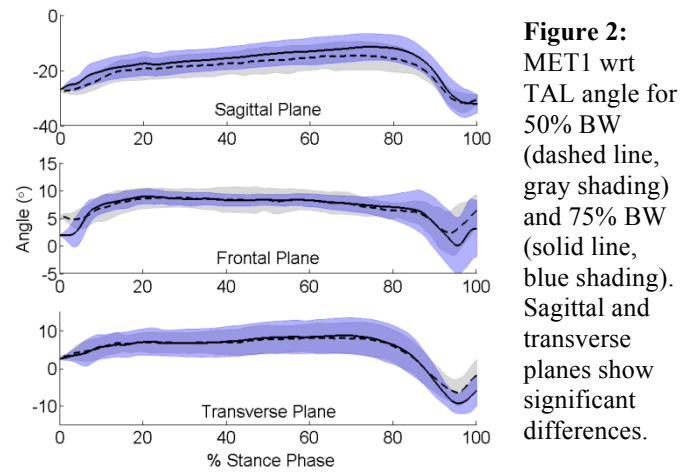


**Figure 2:** MET1 wrt TAL angle for 50% BW (dashed line, gray shading) and 75% BW (solid line, blue shading). Sagittal and transverse planes show significant differences.

## CONCLUSIONS

By scaling the GRFs during cadaveric gait simulation to 50% BW instead of 75% BW, there is a slight underestimation of the ROM of the joints of the foot. However, the kinematic differences are minimal and likely within the variability of current *in vivo* foot models.

## REFERENCES

1. Nester CJ, et al. *J Biomech.* **40**, 2007.
2. Hurschler C, et al. *Foot & Ankle Int.* **24**, 2003.
3. Arndt A, et al. *J Biomech.* **40**(12), 2007.
4. Aubin PM. Dissertation, U. of Washington, 2011.
5. Whittaker E, et al. *Gait Posture.* In press, 2011.

## ACKNOWLEDGEMENTS

This work was funded in part by the VA RR&D, grants A3923 and A4843C.

**Table 1:** Range of motion data [standard error] for 12 kinematic relationships and “All Angle” data set

| Angle (°)                            | 50% BW     | 75% BW     | $\Delta$ from 50-75% | p-value           | Angle (°)               | 50% BW     | 75% BW     | $\Delta$ from 50-75% | p-value       |
|--------------------------------------|------------|------------|----------------------|-------------------|-------------------------|------------|------------|----------------------|---------------|
| <b>Sagittal Plane</b>                |            |            |                      |                   | <b>Frontal Plane</b>    |            |            |                      |               |
| CALC wrt TIB                         | 22.0 [3.0] | 23.6 [2.9] | 1.6 [0.8]            | .057              | CALC wrt TIB            | 8.2 [0.9]  | 9.2 [1.3]  | 1.0 [0.6]            | .11           |
| TAL wrt TIB                          | 22.5 [2.0] | 23.2 [1.9] | 0.7 [0.7]            | .3                | CALC wrt TAL            | 7.1 [0.7]  | 8.6 [1.1]  | 1.4 [0.5]            | <b>.016*</b>  |
| NAV wrt TAL                          | 8.4 [1.8]  | 9.6 [1.9]  | 1.2 [0.7]            | .094              | NAV wrt TAL             | 15.9 [1.9] | 18.8 [2.1] | 2.9 [0.8]            | <b>.0056*</b> |
| CUN wrt NAV                          | 11.0 [1.2] | 12.2 [0.9] | 1.2 [0.6]            | .062              | <b>Transverse Plane</b> |            |            |                      |               |
| MET1 wrt TAL                         | 18.9 [2.6] | 22.6 [2.7] | 3.7 [0.6]            | <b>.0002*</b>     | CALC wrt TAL            | 5.4 [0.7]  | 6.2 [0.9]  | 0.8 [0.4]            | .086          |
| HAL wrt MET1                         | 55.2 [3.0] | 61.9 [2.8] | 6.7 [1.9]            | <b>.0061*</b>     | NAV wrt TAL             | 12.2 [1.7] | 14.9 [2.4] | 2.7 [0.9]            | <b>.014*</b>  |
| <b>All Angles (all three planes)</b> |            |            | 1.2 [0.2]            | <b>&lt;.0001*</b> | MET1 wrt TAL            | 16.3 [1.3] | 19.4 [1.6] | 3.1 [0.9]            | <b>.0059*</b> |

# Joint Specific Toy Controller for Pediatric Upper Extremity Rehabilitation

Bethany J. Wilcox<sup>1</sup>, Karen Kerman<sup>2</sup>, Joseph J. Crisco<sup>1</sup>

<sup>1</sup>Bioengineering Laboratory, Department of Orthopaedics, Brown University, Providence RI, USA

<sup>2</sup>Department of Pediatrics, Hasbro Children's Hospital, Providence RI, USA

email: joseph\_crisco@brown.edu web: <http://www.brownbiomechanics.org>

## INTRODUCTION

Cerebral palsy (CP) is non-progressive neuromotor impairment that affects approximately 3.6 out of every 1,000 children in the United States<sup>1</sup>. Wrist flexor muscles are profoundly affected in most children with hemiplegic CP and are one of the major targets of physical and occupational therapy (PT/OT) efforts to increase function.

Our objective was to design a toy controller that requires specific joint movements for toy play and targets the affected muscle groups. Design requirements include low cost, adjustability for children of all levels of function and the ability to record all play activity, including usage and joint motion data. Our approach capitalizes on the highly motivational, primary learning avenue for children – toy play. The premise of this project is that increased therapy in the form of toy play, targeted to the affected muscle groups along with the possibility of neurofeedback, will improve functional recovery.

## METHODS

The toy controllers (Figure 1) consist of three main components; the cuffs for the hand and forearm, the Motion Sensing Unit (MSU), and the Joint Control Unit (JCU). The throttle (forward/reverse) is controlled by wrist flexion/extension. Features of the toy controllers include: remote control of commercially available toys, sensing of targeted relative joint motion, configurable range and gain setting for sensed joint motion, and data logging of joint motion during play.

Each controller consists of two cuffs, one that engages the hand while the other engages the forearm. Cuffs in current design are fabricated with a substructure of a malleable alloy and covered with

two-layers of expanded polyethylene foam, making them light-weight and fully conformable to any size wrist and forearm, left or right.

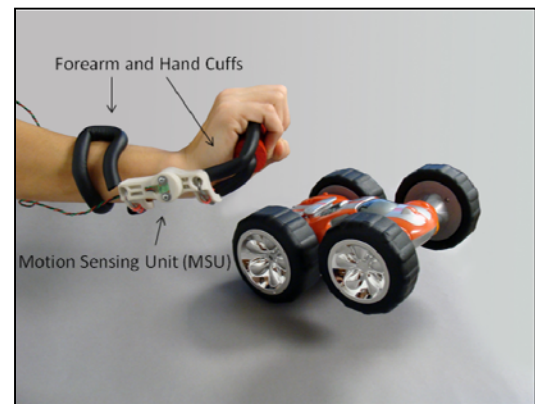


**Figure 1:** Toy controller (wrist flexion/extension controls forward/backward) with readily available and relatively inexpensive (< \$30.00) RC car. The cuffs' malleable alloy readily permits sizing to a wide variety of children. The Joint Control Unit (JCU), not shown, is housed in a small pack worn around the waist.

The MSU is the structural component that connects the hand and forearm cuffs and provides a platform for the joint motion sensor. The motion sensor in the current design is a single axis 10 kilohm potentiometer (Taiwan Alpha Electronic Co., Taiwan) with a range of 315 degrees of rotation.

The JCU receives and processes input from the MSU sensor, transmits toy commands, and data logs play activity. Specific minimum, maximum and gains are adjustable for each user. The frequency of the transmitter is 27MHz. The controller is powered by four AA rechargeable alkaline batteries and after several minutes of non-use the controller automatically powers down to save battery life. The data logging capabilities of the controller are important in quantifying “usage” or “dosage” and establishing efficacy. The

controllers have a high-speed USB interface (virtual serial port) for data logging and configuration. The event data logging system utilizes a real-time clock for timestamps could log up to 64Mb of data. Programming of the JCU is accomplished through a GUI interface (written in Labview, National Instruments, Austin, Texas) designed to be user-friendly for therapists and caregivers. Features of the user interface include the ability to set range of motion (ROM), minimum and maximum position, time threshold to trigger play action, and the ability to download and save play activity data.

The toy controllers were designed to control commercially available remote control (RC) toys in order to maximize child engagement, whereas the child could be playing with the same toy as their peers. The Bounceback Racer (Hasbro Toys, Pawtucket, RI) was selected as the RC toy for this effort because it possesses the appropriate degrees of freedom (1, forward/reverse) and it has the ability to flip itself over if the car encounters any obstacles.

Toy controllers were evaluated at Hasbro Children's Hospital Pediatric Rehabilitation Center (Providence, RI). Feedback from both occupational and physical therapists was crucial in the design effort. IRB approval was obtained in order to allow children with and without hemiplegic CP, ages 5-12 to use the toy controller and provide feedback.

## RESULTS AND DISCUSSION

The purpose of this study was to design and develop toy controllers that are specifically designed to provide neuromuscular upper extremity therapy, specifically to the wrist. Design criteria were successfully met and included: remote control of commercially available toys, sensing of targeted relative joint motion, configurable range and gain setting for sensed joint motion, and data logging of joint motion during play.

The controllers were evaluated by PT's, OT's, and children (ages 5-12) with and without hemiplegic CP. The children were successfully able to control and play with the remote control car. Individual gain and range settings were set for each child. This adjustability allows for children of varying levels of

function to play with the toy, and allows adjustments to an individual's setting as functional improvement occurs. The cuffs were flexible enough to adjust to children with different wrist sizes and varying contractures. The kinematic data (Figure 2), provided by the data logging capabilities of the toy controller, may provide a better framework for guiding therapeutic interventions to improve functional abilities. Moving forward, this usage and kinematic data will be used to evaluate the efficacy of the toy controllers, where functional improvement will be evaluated quantitatively using a battery of standard measures of upper limb function including: the Pediatric Evaluation of Disability Inventory (PEDI), the Modified Ashworth Scale (MAS), the Shriners Hospital for Children Upper Extremity Evaluation (SHUEE), and the Assisting Hand Assessment (AHA).

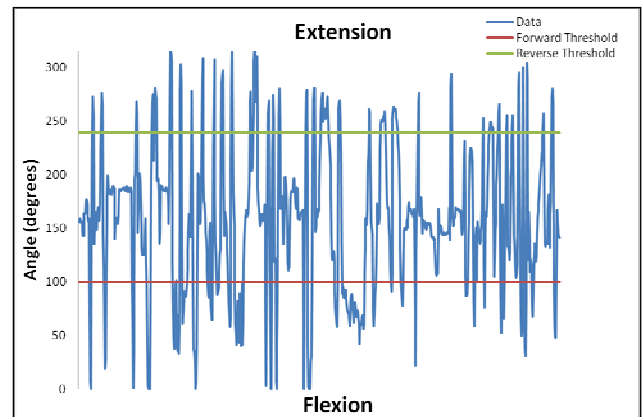


**Figure 2:** Data from approx. 5 minutes of play with toy controller. Displayed is flexion/extension (wrist relative joint angle) data in degrees. Child's individual extension reverse throttle and flexion forward throttle thresholds (green and red reference lines) are displayed.

We propose that these home-based, cost effective, joint specific toy controllers will be engaging rehabilitative devices that could potentially enhance treatment, promote neuroplasticity, and improve functional recovery for children with hemiplegic cerebral palsy and other movement disorders.

## REFERENCES

1. Boyle CA, et al. *Pediatrics*. Mar 1994; 93(3):399-403.

# LONGITUDINAL CHANGES IN MUSCLE STRENGTH, FLEXIBILITY AND KNEE LAXITY DURING PUBERTY IN GIRLS

Catherine Y Wild, Julie R Steele and Bridget J Munro

Biomechanics Research Laboratory, University of Wollongong, Australia  
email: [cw418@uowmail.edu.au](mailto:cw418@uowmail.edu.au); web: [www.uow.edu.au/health/brl](http://www.uow.edu.au/health/brl)

## INTRODUCTION

From the onset of puberty, females are at a greater risk of sustaining a non-contact anterior cruciate ligament (ACL) rupture than males [1]. One factor commonly associated with greater ACL injury risk is increased passive knee laxity and the accompanying decrease in knee joint stability [2]. Females tend to display fluctuations in knee laxity across the menstrual cycle [3] as well as greater anterior knee laxity compared to their male counterparts [2]. However, how knee laxity changes at the onset of puberty and throughout the adolescent growth spurt is relatively unknown.

Rapid and differential timing of segment growth around the time of peak height velocity (PHV; peak growth in height) alters the moment of inertia of an individual's limbs, in turn, requiring greater strength to perform movement tasks [4]. Although boys display a defined 'spurt' in the development of quadriceps strength after PHV, this trend is not apparent in girls [5]. As the hamstring muscles work in synergy with the ACL by imparting a posterior drawer force to the tibia [6], any changes in hamstring strength during the growth spurt are vital to understand risk factors for ACL injuries in this adolescent population. Therefore, this study aimed to investigate changes in lower limb muscular strength, flexibility and anterior knee laxity throughout the adolescent growth spurt in pubescent girls, with implications for ACL injuries.

## METHODS

Thirty-five healthy girls (10-13 years), confirmed as Tanner Stage II of pubertal development [7] and 4-6 months from their PHV, determined using a gender-specific multiple regression equation [8], volunteered to participate in the study. Participants were tested in the laboratory four times over 12

months, based around the timing of their PHV (Figure 1). Each participant's height and mass were also tracked monthly in their homes to determine the precise timing of their PHV.

During each laboratory testing session, participant height, mass and lower limb anthropometrics were measured. Passive anterior knee laxity was quantified for each participant's dominant lower limb using the Dynamic Cruciate Tester (DCT; Smith & Nephews Richards, Australia), with the knee flexed between 20-30° [2]. Force (N)/displacement (mm) curves were plotted to determine changes in knee laxity throughout the growth spurt. Goniometric measurements of the knee and hip were also performed to determine changes in flexibility of the hamstrings, quadriceps and iliopsoas muscles over time. Concentric and eccentric strength of the quadriceps and hamstring muscles were assessed using an isokinetic dynamometer (KinCom, Chattanooga Inc., USA) at 180°.s<sup>-1</sup>. Peak torque was recorded and normalized to body mass (Nm.kg<sup>-1</sup>) to determine changes in lower limb strength throughout the growth spurt.

A linear mixed model design was used to determine any significant ( $p \leq 0.05$ ) main effects of time on the dependent variables, controlling for growth variables as covariates. *Post-hoc* comparisons were performed using a *t*-test with a Bonferroni adjustment.

## RESULTS AND DISCUSSION

A significant main effect of time ( $p < 0.001$ ) on PHV was found, such that the participants grew significantly faster during Test 2 compared to the other test sessions (Figure 1). Although the participants were growing more rapidly at the time of Test 2, no significant main effect of time on iliopsoas ( $p = 0.302$ ) or quadriceps ( $p = 0.394$ )

flexibility was evident. However, a significant ( $p = 0.05$ ) increase in hamstring flexibility was found from Test 1 to 4.

A significant ( $p = 0.005$ ) main effect of time on passive knee laxity was displayed. *Post-hoc* analyses revealed a significant increase in passive knee laxity from Test 1 to 2 ( $p = 0.008$ ), as well as from Test 1 to 3 ( $p = 0.046$ ; Figure 1). It is postulated that greater knee joint laxity may lead to a decrease in knee joint stability, increasing the likelihood of rupture [2]. This suggests that girls may be at an increased risk of ACL injury at the time they are experiencing their PHV.

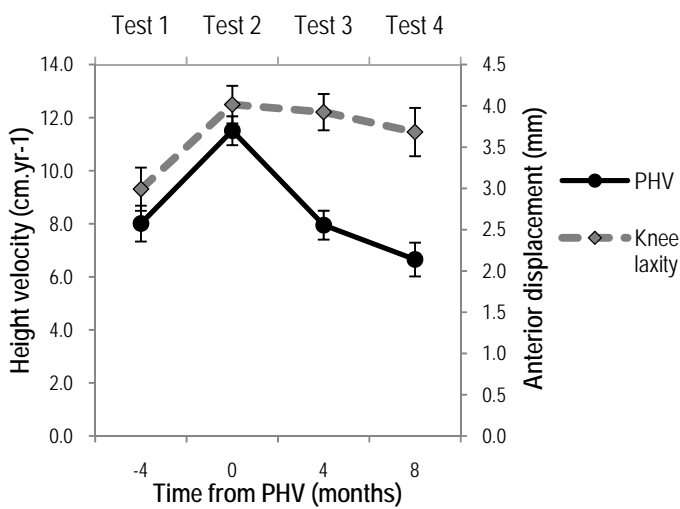


**Figure 1:** Means ± SE for peak height velocity (PHV) and passive knee laxity over 12 months.

The participants displayed no change in either concentric or eccentric hamstring strength over time (Table 1). However, a significant effect of time on concentric quadriceps strength was evident, whereby *post-hoc* analyses revealed a significant strength increase from Test 1 to 4 (Table 1). Contracting the quadriceps during dynamic movements increases anterior tibial translation, placing greater strain on the ACL. We speculate that, during the adolescent growth spurt, the

hamstring muscles might be less proficient when acting synergistically with the ACL against the stronger quadriceps contractions when performing dynamic movements. This may potentially place girls at a greater risk of sustaining an ACL injury during the adolescent growth spurt, although further research is warranted to support this notion.

## CONCLUSIONS

From the time of PHV participants displayed significantly increased passive knee laxity accompanied by a significant increase in quadriceps strength over time, with no subsequent increase in hamstring strength. It is postulated that this strength imbalance combined with increased knee laxity may increase the risk of ACL injury at the time of PHV.

## ACKNOWLEDGEMENTS

We thank the University of Wollongong and ASICS Oceania for providing funding for this research.

## REFERENCES

1. Shea KG, et al. *J Pediatr Orthoped* **24**, 623-628, 2004.
2. Myer GD, et al. *Am J Sport Med* **36**, 1073-1080, 2008.
3. Heitz NA, et al. *J Athl Training* **34**, 144-149, 1999.
4. Hawkins D, et al. *Med Sci Sport Exer* **33**, 1701-1707, 2001.
5. Parker DF, et al. *Ann Hum Biol* **17**, 199-211, 1990.
6. Cowling EJ, et al. *J Electromyogr Kines* **11**, 263-268, 2001.
7. Taylor SJC, et al. *Paediatr Perinat Ep* **15**, 88-94, 2001.
8. Mirwald RL, et al. *Med Sci Sport Exer* **34**, 689-694, 2002.

**Table 1:** Means ± SE and *p*-values for changes in peak concentric and eccentric hamstring and quadriceps torque, normalized to body mass, over time.

| Torque (Nm.kg <sup>-1</sup> ) | Test 1<br>(n = 22) | Test 2<br>(n = 35) | Test 3<br>(n = 32) | Test 4<br>(n = 16) | <i>p</i> -value |
|-------------------------------|--------------------|--------------------|--------------------|--------------------|-----------------|
| <b>Concentric hamstring</b>   | 0.779 ± 0.054      | 0.772 ± 0.042      | 0.759 ± 0.044      | 0.774 ± 0.062      | 0.991           |
| <b>Eccentric hamstring</b>    | 1.476 ± 0.077      | 1.290 ± 0.063      | 1.261 ± 0.066      | 1.292 ± 0.088      | 0.086           |
| <b>Concentric quadriceps</b>  | 0.953 ± 0.062      | 0.995 ± 0.051      | 1.086 ± 0.054      | 1.181 ± 0.072      | 0.034*          |
| <b>Eccentric quadriceps</b>   | 2.239 ± 0.117      | 2.047 ± 0.096      | 2.042 ± 0.101      | 2.315 ± 0.138      | 0.142           |

\*Significant increase in strength from Test 1 to 4 ( $p = 0.05$ ).

# LOADING PATTERNS DURING A STEP TASK IN INDIVIDUALS WITH KNEE OSTEOARTHRITIS

<sup>1</sup>Joshua D. Winters, <sup>2</sup>Deepak Kumar and <sup>1</sup>Katherine S. Rudolph

<sup>1</sup>University of Delaware, Newark, DE, USA

<sup>2</sup>University of California at San Francisco, San Francisco, CA, USA

email: [jwinters@udel.edu](mailto:jwinters@udel.edu)

## INTRODUCTION

Dynamic loading patterns and kinematic changes during walking influence the initiation and progression of osteoarthritis (OA) of the knee [1]. Peak external knee adduction moment (PkKAM) has become the hallmark measure of dynamic loading in medial compartment knee OA because it is highly correlated with progression and severity of knee OA. However other measures of knee loading may provide insight into the influence of movement patterns on onset and progress of the disease.

The rate at which loading occurs plays an important role in the deformation and degradation of cartilage [2] so the rates at which the knee joint is loaded during functional activities may be very important in the progression or severity of knee OA. Both load magnitude and load duration are important variables that define the wear conditions of a joint [3] and combining these into a single variable, impulse, may more accurately describe the loading patterns experienced in a specific joint during a particular task.

Normal walking is the most commonly performed activity of daily living (ADLs) however, the degree of knee loading required during level walking is low compared to other activities of daily living. Mundermann et al. (2008) analyzed data from a person with an instrumented total knee prosthesis and found that peak total compressive forces at the knee were highest during stair ascent and descent compared to walking, squatting, sit to stand from a chair, and during a golf swing [4]. Examining compensation strategies used to minimize loading patterns placed on the knee during a stepping task, will allow for a more complete understanding of the role of dynamic loading and mechanics in people with knee OA.

## METHODS

26 individuals (13 OA and 13 healthy matched controls) completed multiple trials of a step up and over task. A wooden step (with a height of approximately 20 cm) was fastened to a force platform and the participants were instructed to step up onto the step with one limb, traverse across the step and land with the contralateral limb as shown in Figure 1).

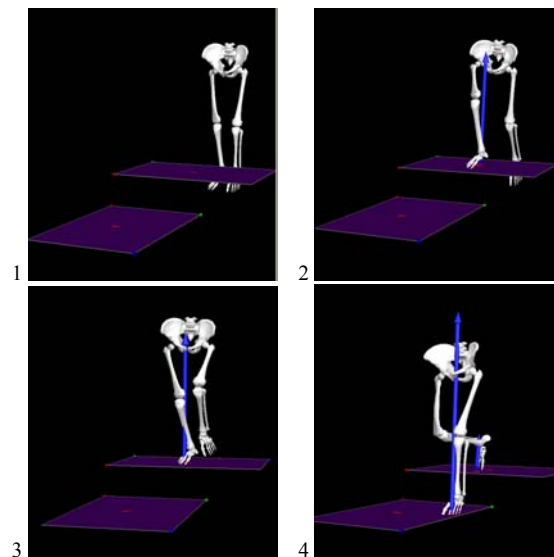


**Figure 1:** This diagram illustrates the step task from start of the step up (2) with the right limb (4) to landing with the left limb.

An 8 camera Vicon system (Lake Forest, CA) was used to collect the kinematic data (120 Hz) and 2 Bertec force platforms (Bertec Corp, Worthington, OH) were used to collect the kinetic data during the step tasks (1080 Hz). Visual 3D (C-Motion Inc., Germantown, MD) was used to calculate kinematics and kinetics using inverse dynamics. Average loading rates were calculated using the 1<sup>st</sup> derivative of the ground reaction force (VGRF) from initial

contact (IC) to peak VGRF. Peak instantaneous loading rates were calculated as the peak 1<sup>st</sup> derivative VGRF value between IC and peak VGRF. Loading impulses, the integral of the VGRF signal, were calculated from IC to peak VGRF. All loading values were normalized to body weight (BW). Independent-samples t-tests were used to evaluate differences between the OA and healthy controls. An analysis of covariance was also performed, with the velocity of the pelvis center of mass (COM) during the landing phase as the covariate. Differences were considered statistically significant when  $p \leq 0.05$ .

## RESULTS AND DISCUSSION

Lower average loading rates ( $t = -3.013$ ,  $p = 0.008$ ), peak instantaneous loading ( $t = -2.396$ ,  $p = 0.029$ ), and peak VGRF normalized to body weight ( $t = -3.187$ ,  $p = 0.004$ ) were observed in the OA subjects compared to the healthy controls (Table 1). However, no difference in the VGRF loading impulse was observed ( $t = .245$ ,  $p = 0.808$ ).

The OA group had significantly smaller knee flexion excursions during the landing than healthy controls ( $t = -5.060$ ,  $p = .000$ ) and the velocity of the pelvis center of mass was slower in the OA group during the landing phase ( $t = -5.05$ ,  $p = 0.000$ ). None of the previously mentioned loading measures (average loading rate, peak instantaneous, or peak VGRF) remained significant when velocity of the pelvis COM was used as a covariate ( $F = 0.074$ ,  $p = 0.788$ ,  $F = 0.599$ ,  $p = 0.447$ , and  $F = 0.055$ ,  $p = 0.816$  respectively).

## CONCLUSIONS

The movement strategy involving slowed descent from the step that was used by the OA subjects resulted in significantly lower valued of both

loading rates (average and instantaneous) as well as the peak normalized VGRF during landing despite having a stiffened knee during landing. The decreased velocity while lowering the pelvis was mostly controlled eccentrically by the quadriceps of the limb on the step indicating the importance of understanding the role of muscle involvement in compensation strategies used in knee OA. Assessing the different types of loading patterns encountered by the knee during common activities of daily living and examining the strategies used to minimize these loading patterns will allow for more effective intervention strategies for knee OA that would be more individualized to each specific patient.

Lower peak VGRF values along with lower loading rates increasing the duration of the loading in OA and higher peak GRF values and higher loading rates decreasing the duration of the loading in the healthy controls allowed for similar loading impulse values. These results indicate the importance of analyzing the loading rates and peaks separately along with the impulse so that specific patterns are not over looked.

## REFERENCES

1. Andriacchi TP, et al. *J Bone Joint Surg Am* **91**, 95-101, 2009.
2. Radin EL. *J Rheumatol* **32**, 1136-1138, 2005.
3. Thorp LE, et al. *Arthritis Rheum* **54**, 3842-3849, 2006
4. Mundermann A, et al. *J Orthop Res* **26**, 1167-1172, 2008.

## ACKNOWLEDGEMENTS

Funded By: NIH P20 RR16458, NIH S10RR022396, ACR REF Health Professional Graduate Student Research Preceptorship

**Table 1:** Group means and standard deviations of significant loading variables

| Group                   | Average Loading Rate | Peak Impact   | Peak VGRF  | GRF Loading Impulse | Landing Velocity Pelvis |
|-------------------------|----------------------|---------------|------------|---------------------|-------------------------|
|                         | BWs/sec              | BWs/sec       | BWs        |                     | m/s                     |
| <b>Knee OA</b>          | 17.53 ± 4.91         | 35.85 ± 12.96 | 1.75 ± .22 | .088 ± .029         | .70 ± .11               |
| <b>Healthy Controls</b> | 27.12 ± 10.37        | 56.74 ± 28.64 | 2.09 ± .33 | .086 ± .021         | .89 ± .09               |
| <b>p value</b>          | p=0.008              | p=0.029       | p=0.004    | p=0.808             | p=0.000                 |

# SCALING OF PASSIVE TENSION IN SKELETAL MUSCLE

<sup>1</sup>Taylor M. Winters, <sup>1</sup>Mitsuhiko Takahashi, <sup>1</sup>Richard L. Lieber, and <sup>1</sup>Samuel R. Ward

<sup>1</sup>University of California: San Diego, San Diego, CA, USA  
email: [srward@ucsd.edu](mailto:srward@ucsd.edu) web: <http://muscle.ucsd.edu>

## INTRODUCTION

Skeletal muscle passive tension is altered in a number of pathological conditions, such as cerebral palsy, peripheral nerve injury, and tenotomy. Passive tension is often considered to arise from the passive stretching of the megadalton-sized protein titin. Magid and Law [1] demonstrated that passive tension scaled with the size of the specimen, indicating that the source of passive load-bearing in muscle was within the normal myofibrillar structure. Furthermore, titin molecular weight was later shown to be inversely correlated with the stiffness of the specimen [2].

Despite these claims, several studies have demonstrated that the extracellular matrix is responsible for a large percentage of the passive load-bearing. Collagen content, isoform distribution, and crosslinking have all been shown to play important roles in passive tension [2,3]. Furthermore, the contribution of these proteins has been shown to be strain-dependent [4]. Thus, it is unclear which structural proteins are responsible for passive load-bearing as a function of strain and muscle tissue size scale (i.e., fibers, bundles, fascicles, whole muscle).

## METHODS

Passive stress-strain curves were measured across size scales for the tibialis anterior (TA), extensor digitorum longus (EDL), and extensor digitorum II (EDII) muscles of New Zealand White rabbits. To examine passive tension scaling, single fibers, fiber bundles (approximately 15 fibers), fascicles (250-300 fibers), and whole muscles (10k-30k fibers) were evaluated.

A mid-line incision was made on the rabbit hindlimb, and the distal tendon was transected and clamped to a servo-motor at the muscle-tendon

junction (Fig. 1). The muscle was passively stretched, and the stress at a given strain was measured after three minutes of stress relaxation. The smaller size scales (single fibers, fiber bundles, and fascicles) were sutured to a force transducer on one end and a motor arm on the other (Fig. 1). Sarcomere length was measured by laser diffraction, and specimens were stretched in 0.25  $\mu\text{m}$ /sarcomere increments. The stress-relaxed force was normalized to specimen cross-sectional area, and length was normalized to slack length.

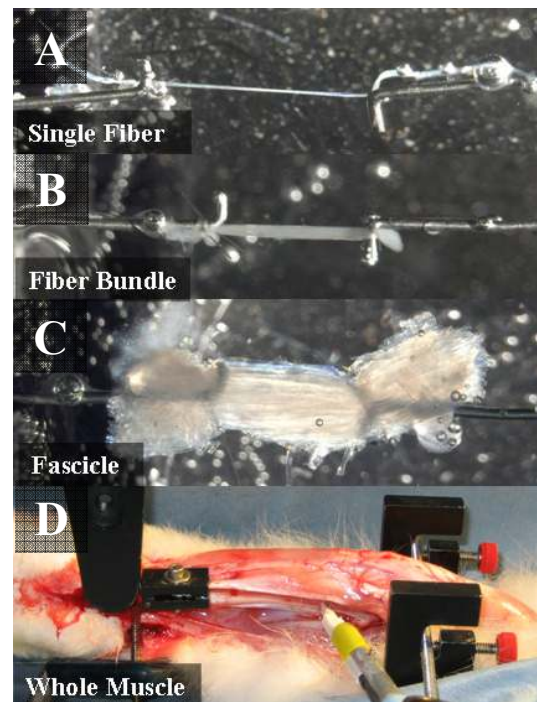


**Figure 1:** Experimental set-up for single fibers (A), fiber bundles (B), fascicles (C), and whole muscles (D).

To obtain results that are pertinent to *in vivo* function, the *in vivo* sarcomere length range was determined for each muscle by fixing two rabbit hindlimbs at the extremes of plantarflexion and dorsiflexion and then measuring the corresponding muscle and sarcomere lengths. At 90% of this *in*

*in vivo* range, the tangent modulus of the stress-strain curve was obtained.

To examine the relationship between titin and collagen and passive tension, titin gels and hydroxyproline assays were used to measure titin molecular weight and the collagen content (% wet weight) of each muscle, respectively. Titin assays were obtained from bundle-sized samples, and hydroxyproline assays were obtained from whole muscle-sized samples. Tangent moduli were then correlated with protein isoform/content to characterize important structures involved in passive load-bearing.

## RESULTS AND DISCUSSION

Passive tension was significantly different between muscles at the fascicle level, and this result was magnified at the whole muscle level. However, Single fiber and fiber bundle data were not significantly different among muscles (Fig. 2). The changes in passive tension were muscle specific, as shown by the disproportionate increases in passive tension for the EDII muscle (Fig. 2).

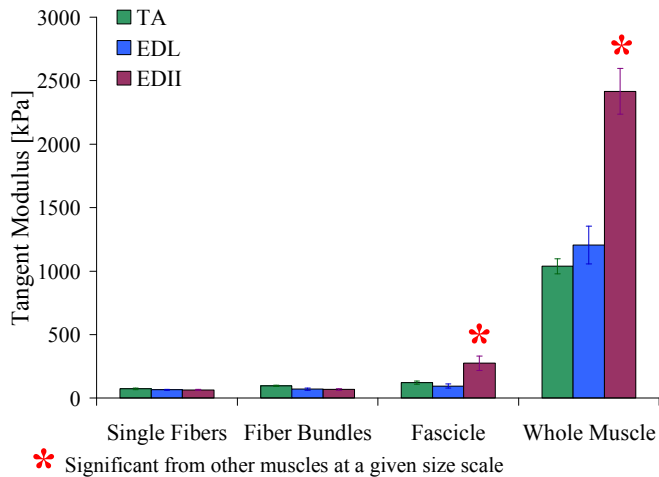


**Figure 2:** Passive tension tangent modulus for the TA, EDL, and EDII across four specimen size scales.

Titin size was inversely correlated with tangent modulus at the fiber bundle scale ( $r^2 = 0.97$ ; Fig. 3), and collagen content was correlated with modulus at the whole muscle scale ( $r^2 = 0.99$ ; Fig. 4). However, titin size was not correlated with tangent modulus at larger size scales (fascicles:  $r^2 = 0.36$ ; whole muscles:  $r^2 = 0.60$ ). These relationships must be interpreted with caution because the variations in

titin isoform and collagen content are limited in the current study. The addition of muscles with a wider range of protein isoforms/concentrations is needed to test this idea more rigorously.

These data suggest that intracellular components (e.g., titin) may be mechanically important at size scales that have limited extracellular matrix, but at larger size scales (with more extracellular matrix component), collagen content may become the main determinant of passive tension.

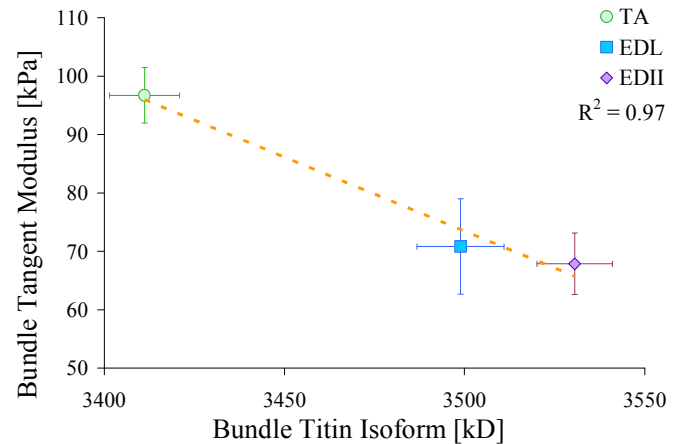


**Figure 3:** Relationship between titin isoform and tangent modulus at the bundle level.

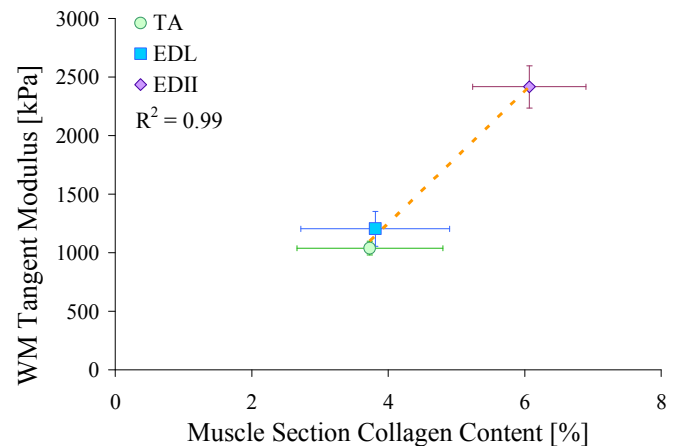


**Figure 4:** Relationship between collagen content and tangent modulus at the whole muscle level.

## REFERENCES

- Magid A, et al. *Science* **230**, 1280-1282, 1985.
- Prado LG, et al. *J Gen Physiol* **126**, 461-480, 2005
- Kovanen V, et al. *J Biomech* **17**, 725-735, 1984
- Granzier HL, et al. *Biophys J* **68**, 1027-1044, 199

# EVALUATING A BIOMECHANICAL MODEL OF THE THUMB FOR SIMULATION OF BOTH INDIVIDUAL AND COORDINATED MUSCLE ACTIONS

<sup>1,3</sup>Sarah J. Wohlman and <sup>1,2,3,4</sup>Wendy M. Murray

Departments of <sup>1</sup>Biomedical Engineering and <sup>2</sup>PM&R, Northwestern University, Chicago, IL

<sup>3</sup>SMPP, Rehabilitation Institute of Chicago, Chicago, IL; <sup>4</sup>Edward Hines Jr. VA Hospital, Hines, IL

email: [sarah.wohlman@u.northwestern.edu](mailto:sarah.wohlman@u.northwestern.edu) web: <http://www.smpp.northwestern.edu/Murray/index.shtml>

## INTRODUCTION

In terms of the forces produced at the thumb-tip, state-of-the-art biomechanical models of the thumb do not replicate either the maximum pinch forces produced via coordinated muscle actions [1] or the magnitudes of forces produced by individual muscles [2]. For example, Valero-Cuevas et al. [1] developed a biomechanical model of the thumb to calculate forces produced by the coordinated action of all thumb muscles. When simulation results were compared to experimental measurements of forces produced by nonimpaired subjects during maximum effort, the model was found to be four times weaker than subjects [1]. In contrast, Goehler and Murray [2] simulated the force produced by each of the four extrinsic muscles individually and compared model results to measurements from cadaveric muscles that were loaded with a known weight, one at a time [2]. The model implemented in this second study yielded endpoint forces that were, on average, approximately 60% larger than the forces measured in cadavers.

The biomechanical models evaluated in these two studies differed from each other. In particular, Valero-Cuevas et al. [1] concluded that an oversimplified representation of the kinematics contributed to underestimation of the forces produced by human subjects. As a result, Goehler and Murray implemented a model [3] that better reflected experimental kinematics [7]. In this study, we augment the thumb model utilized by Goehler and Murray to include the intrinsic muscles of the thumb in order to investigate the feasibility of accurately simulating both individual and coordinated muscle actions.

## METHODS

To evaluate how effectively we could simulate the forces produced at the thumb-tip by individual muscles, muscle-tendon paths of the 5 intrinsic muscles were added to an existing model of the upper limb, which already includes the four

extrinsic muscles and has been validated and described previously [2, 3]. In addition, we incorporated an extensor hood as described by Valero-Cuevas et al. [1]. We then used the principle of virtual work to relate the joint torques produced by a given muscle to the resulting force at a point of interest on the distal phalanx:

$$\bar{F} = \left( J J^T \right)^{-1} J \bar{L}_{MA} f_{muscle}, \quad (1)$$

where  $\bar{F}$  is the 3x1 endpoint force vector;  $J$  the 3x4 Jacobian matrix;  $\bar{L}_{MA}$  the 4x1 muscle moment arm vector [4]; and  $f_{muscle}$  the given force of the muscle of interest. We specified the magnitude of a given muscle force to replicate the load applied to that muscle in experimental cadaveric studies [5]. The load corresponded to 30% of maximum isometric force-generating capacity, as determined from muscle cross-sectional areas measured in cadaveric specimens [5]. For each muscle, one simulation was run to estimate the force produced in a lateral pinch posture (Table 1) and one simulation was run in an opposition pinch posture.

**Table 1. Joint angles\***

| <i>Joint</i>  | <i>Pinch</i>   |                   |
|---------------|----------------|-------------------|
|               | <b>Lateral</b> | <b>Opposition</b> |
| CMC flexion   | -20°           | -20°              |
| CMC abduction | -25°           | -20°              |
| MCP flexion   | 45°            | 10°               |
| IP flexion    | 10°            | 45°               |

\*Positive angles indicate flexion or abduction.

To evaluate how effectively we could simulate the forces produced by nonimpaired subjects during maximum effort, we replicated simulations described by Valero-Cuevas et al. [1]. In these simulations, we implemented linear programming to identify activation levels for each of the 9 muscles in the augmented model. We solved for the activation patterns that maximized force magnitude in five distinct directions (Fig. 1), given the constraints described in the previous study [1]. Specifically, the magnitude of the force components

in the directions perpendicular to the desired direction were constrained to be  $<17\%$  of the maximum magnitude and the torque was  $\leq 0.05$  Nm. All five force directions were simulated in both the lateral and opposition pinch postures.

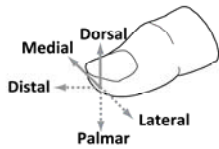


**Figure 1.** Force directions at the thumb-tip.

The sensitivity of the estimated forces to variability in model parameters was evaluated via Monte Carlo simulation. Linear programming was used to find the activation levels that produced maximum forces in each of 5000 iterations. These simulations varied the parameter values for muscle moment arms [4] and maximum isometric forces in a normal distribution based on experimental variability. Maximum isometric forces were determined from muscle volumes measured via imaging [6].

## RESULTS AND DISCUSSION

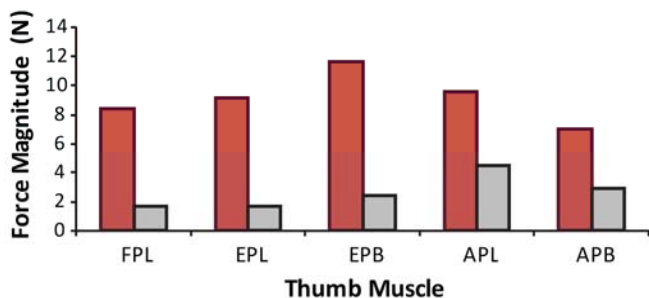


**Figure 2.** Magnitude of the forces produced by the individual intrinsic muscles in the lateral pinch posture. Simulation results are indicated in red, experimental data [5] are shown in gray.

The forces produced at the thumb-tip by the individual intrinsic muscles were overestimated. Despite simulating muscle forces identical to the load applied experimentally, the endpoint forces simulated with the model were, on average, 2.9 times larger than the forces measured experimentally in lateral pinch (Fig. 2) and 2.5 times larger in opposition pinch. Inclusion of the extensor hood had minimal effect on individual muscle forces. These results suggest that the average values of moment arms of the thumb muscles described in the literature did not accurately reflect the moment arms of the thumb muscles in the experimental endpoint force study.

In contrast, simulations using the same biomechanical model yielded comparable forces in

magnitude to those produced by nonimpaired subjects [1]. When model parameters identical to those used to generate Figure 2 were implemented, our model did not overestimate the human subjects data. In addition, mean force magnitudes calculated from the 5000 Monte Carlo simulations fell within 1 standard deviation of the experimental results in 3 of 5 directions for both postures (Fig. 3). When the mean force magnitudes from the simulations did not fall within experimental variability, the model predicted larger forces than the data. In lateral pinch, palmar forces could not be predicted accurately without the extensor hood.

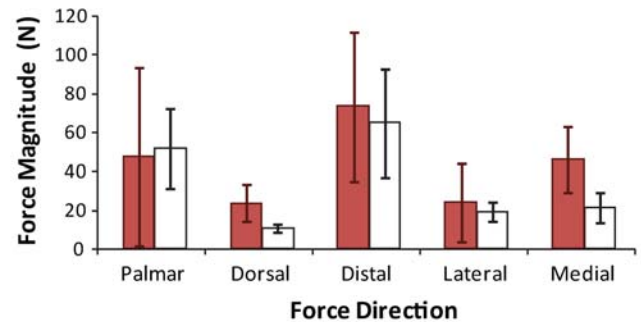


**Figure 3.** Force magnitudes produced in the lateral pinch posture during coordinated muscle action. Simulation results are indicated in red, experimental data [1] are shown in white. Error bars indicate  $\pm 1$  standard deviation from the mean.

## CONCLUSIONS

We were able to simulate force magnitudes comparable to those produced by human subjects using Monte Carlo simulations that explored the full range of variability in musculoskeletal parameters. However, endpoint forces produced by individual muscles were substantially overestimated when the same model incorporated average moment arms values described in the literature [4]. Given the sensitivity of the model to musculoskeletal geometry, further quantitative studies describing moment arms of the thumb muscles are warranted.

## REFERENCES

1. Valero-Cuevas, et al. *J Biomech* **36**, 1019-30, 2003.
2. Goehler & Murray, *J Biomech* **43**, 1553-59, 2010.
3. Holzbaur, et al. *Ann Biomed Eng* **33**, 829-40, 2005.
4. Smutz, et al. *J Biomech* **31**, 565-70, 1998.
5. Pearlman, et al. *J Orthop Res* **22**, 306-12, 2004.
6. Holzbaur, et al. *J Orthop Res* **40**, 742-49, 2007.
7. Hollister, et al. *J Orthop Res* **10**, 454-60, 1992.

## ACKNOWLEDGEMENTS

We thank Joe Towles for helpful discussions regarding implementation of the extensor hood. This work was funded by NIH R01 HD046774.

# INVESTIGATION ON INDIVIDUAL COLLAGEN FIBRILS OF OSTEOARTHRITIC CARTILAGE WITH ATOMIC FORCE MICROSCOPY

<sup>1</sup>Cheuk-Bun Wu, <sup>1</sup>Bin Tang, <sup>2</sup>Chun-yi Wen, <sup>2</sup>William Weijia Lu, <sup>2</sup>Chun-Hoi Yan, <sup>2</sup>Kwong-yuen Chiu

<sup>1</sup> Department of Mechanical Engineering,

<sup>2</sup> Department of Orthopaedics and Traumatology, Li Ka Shing Faculty of Medicine,  
The University of Hong Kong, Pokfulam, HKSAR

Email: [bennywu\\_abest@yahoo.com.hk](mailto:bennywu_abest@yahoo.com.hk)

## INTRODUCTION

It is believed that the degradation of articular cartilage in Osteoarthritis (OA) initiates from the molecular scale to the structure level [1]. Individual collagen fibril, as a major component of articular cartilage, its change in nanomechanical properties becomes an important indicator in the OA process. In this study, the nanomechanical properties of single collagen fibrils with different grades of osteoarthritis were examined with AFM nanoindentations. A novel protocol which can correct for the viscoelastic effects and calibrate the spring and tip constants accurately was employed [2], it was found that with the progressing of OA, the individual collagen fibrils became stiffer.

## METHODS

### Sample preparation

The fresh specimens of articular cartilage were collected with informed consent from postmenopausal women, who underwent arthroplasty due to the end-stage of osteoarthritis (OA) or hip fracture. The fresh specimens were cryo-sectioned with 50 $\mu$ m layer. Afterward, all the specimens were embedded on glass slip and dehydrated with alcohol with same protocol and store at 4°C before indentation tests.

### Experimental detail

The atomic force microscope (AFM) used in this study is Solver Pro47 SPM supplied by NT-MDT company, Russia. The tips used for the indentation is NSG20 tip supplied by the same company, with nominal tip radius smaller than 10 nm. The collagen fibrils were located by AFM imaging under tapping mode. Cartilage layers from 5%, 30%, 70% & 95% of total thickness were selected for AFM nanoindentation. A total of twenty indentations were

performed for each layer of the specimens under ambient condition with indentation depth around 20 nm.

### Analysis method

In this study, the rate jump protocol was employed to analyze the DFL and height data obtained from the AFM indentation tests [2]. The protocol enables the tip-cantilever properties to be calibrated and the viscoelastic effects during the indentation tests to be well addressed. The key equation is

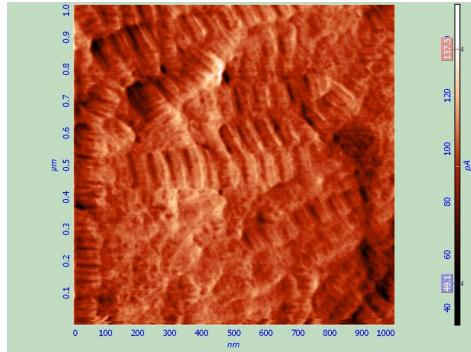
$$\frac{\Delta\dot{\delta}}{\Delta\dot{D}} = A\left(1 + \frac{\alpha}{E_r}\right) \quad (1)$$

where  $\Delta\dot{\delta}$  and  $\Delta\dot{D}$  are the height rate jump and the DFL signal rate jump respectively.  $E_r$  is the reduced modulus,  $A$  is the cantilever sensitivity and  $\alpha$  is a constant represent the tip-cantilever property. By analyzing the DFL-Height curves of AFM indentation tests performed on two samples with known reduced modulus (in this study, a PP and a fused quartz sample were used), the cantilever sensitivity  $A$  and the tip-cantilever constant  $\alpha$  can be determined. The calibrated  $A$  and  $\alpha$  then can be used to calculate the reduced modulus of collagen fibril based on the experimental data of performed indentation tests.

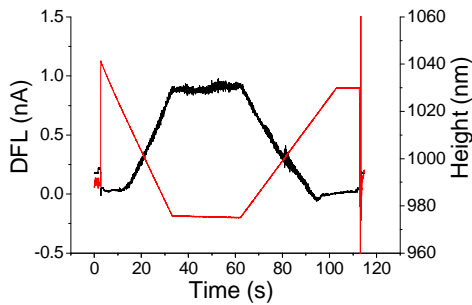
## RESULTS AND DISCUSSION

Fig. 1 shows typical AFM image of collagen fibrils, the high resolution of image enables the indentation tests to be performed on the collagen fibrils precisely. Fig. 2 shows the typical DFL and height signals obtained. Table 1 is the average Young's moduli measured from indentation tests performed on all samples (Poisson's ratio of collagen fibrils are taken

to be 0.3). As the increasing of OA grade, the cartilage suffered from severer OA and the thickness decreased. The results from OA1 to 3 show that the Young's modulus of individual collagen fibrils on the upper and the bottom layer are higher than those in the middle layers.



**Figure 1:** Typical AFM image of collagen fibrils (1  $\mu\text{m} \times 1 \mu\text{m}$ )



**Figure 2:** Typical DFL and Height curves obtained from AFM indentation tests performed on collagen fibrils

## CONCLUSION

The Young's modulus of individual collagen fibrils of cartilage is compatible with the data previously reported. Our findings firstly addressed that individual collagen fibrils are mechanically deteriorated from the top and bottom of the osteoarthritic cartilage. The weakened middle layer of OA cartilage might contribute to the progression of articular cartilage erosion.

## REFERENCE

1. Stolz M. et al. *Nat Nanotechnol.* 2009 4(3):186-92
2. Ngan and Tang. *J. Mat. Res.* 2009 24(3):853-862

## ACKNOWLEDGEMENT

This study was supported by University Seeding Fund (Ref No. HKU10400853).

**Table 1.** Average Young's modulus measured from all samples.

| Thickness                           |     | Young's modulus (GPa), Mean $\pm$ S.E.M |                 |                 |                 |                 |
|-------------------------------------|-----|---|-----------------|-----------------|-----------------|-----------------|
|                                     |     | OP (n=20)                               | OA1 (n=20)      | OA2 (n=18)      | OA3 (n=18)      | OA4 (n=18)      |
| Cartilage<br>$\updownarrow$<br>Bone | 5%  | 2.26 $\pm$ 0.31                         | 2.61 $\pm$ 0.18 | 3.31 $\pm$ 0.14 | 3.09 $\pm$ 0.18 | 3.19 $\pm$ 0.18 |
|                                     | 30% | 2.42 $\pm$ 0.14                         | 2.49 $\pm$ 0.15 | 3.10 $\pm$ 0.12 | 2.44 $\pm$ 0.11 | 4.06 $\pm$ 0.19 |
|                                     | 70% | 2.62 $\pm$ 0.14                         | 2.45 $\pm$ 0.12 | 3.35 $\pm$ 0.25 | 2.70 $\pm$ 0.14 | 3.93 $\pm$ 0.24 |
|                                     | 95% | 3.44 $\pm$ 0.21                         | 2.80 $\pm$ 0.12 | 4.17 $\pm$ 0.22 | 5.58 $\pm$ 0.18 | 4.79 $\pm$ 0.23 |
| OA Grade                            |     | Normal                                  | Grade I         | Grade II        | Grade III       | Grade III       |

# JOINT LOADING OF THE THUMB WHILE OPERATING A MECHANICAL PIPETTE – AN INVERSE DYNAMIC ANALYSIS

<sup>1</sup>\*John Z Wu, <sup>1</sup>Erik W. Sinsel, <sup>1</sup>Daniel S. Gloekler, <sup>1</sup>Bryan M. Wimer, <sup>2</sup>Kristin D. Zhao, <sup>2</sup>Kai-Nan An, <sup>1</sup>Frank L. Buczek

<sup>1</sup>National Institute for Occupational Safety and Health, Morgantown, WV, USA. <sup>2</sup>Mayo Clinic, Rochester, MN, USA. \* Email: jwu@cdc.gov

## INTRODUCTION

Thumb-push manual pipettes are commonly used tools in many medical, biological, and chemical laboratories. Epidemiological studies [1] indicate that the use of pipettes is strongly associated with musculoskeletal disorders (MSDs) in the hand and shoulder. Almost 90% of pipette users, who continuously used the pipettes for more than an hour on a daily basis, reported hand and/or elbow disorders [2]. Despite the strong evidence that operation of the thumb-push manual pipette is related to MSDs in the thumb, the biomechanics of the thumb during pipetting have not been quantified. It is not known if the operation of the thumb-push pipette would induce excessive joint torque in the CMC joint, a factor that may potentially cause degeneration of the articulation [3]. The purpose of the current study was to analyze the kinematics and loading in the joints of the thumb during pipetting.

## METHODS

A typical thumb-activated pipette (P300, Pipetman, Gilson, Inc, Middleton, WI, USA) was used in the study (Fig.1A). This type of pipette is actuated by a thumb-push button to extract and to dispense fluid, whereas there is a separate button to eject the disposable tip. One female participant was recruited in the study. The subject first pressed the plunger to the first stop, extracted the sample fluid from the container by releasing the plunger, pointed the tip to

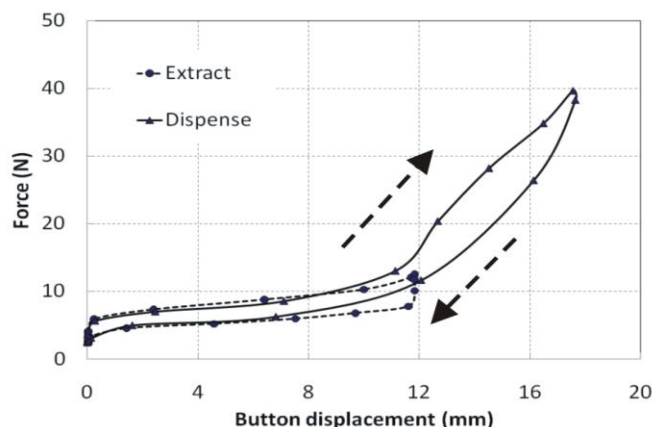


**Figure 2.** Variation in the button displacement and push force during the extraction and dispensing cycles.

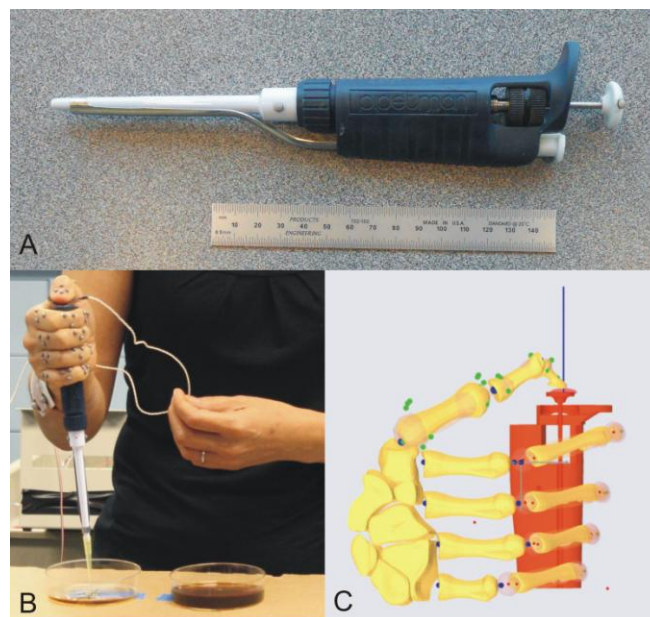


**Figure 1.** Experimental set-up and model. A: The pipette used in the study. B: The subject operating the pipette during the testing. C: The model of pipetting.

a second container, and dispensed the fluid by depressing the plunger to the second stop (Fig. 2B). The subject was instructed to repeat the same procedure 15-20 times in a test session.

In order to measure the plunger press force, a film force sensor (Type C500, Pressure Profile Systems, Inc., Los Angeles, CA) was placed on the top of the plunger button. The relative displacement of the plunger button was measured via two motion markers placed on the plunger press button and the pipette handle. Kinematics for the fingers, hand, and forearm were determined using methods previously described [4]. Retro-reflective markers (4 mm diameter hemispheres) were applied individually on the finger/thumb/hand segments using a thin self-adhesive tape (Fig. 1B). The measurement model consists of 12 finger segments (three segments for each of the four fingers), three thumb segments, a hand, and a forearm, with a total of 55 tracking markers being used to obtain pipetting kinematics. A 14-camera Vicon Nexus system (Oxford Metrics Ltd., Oxford England) provided marker trajectories at 100 Hz, with calibration residuals less than 0.5

mm for a control volume approximately 3 m (wide) x 3 m (long) x 2 m (high).

The hand was modeled as a multi-body linkage system and includes four fingers (index, long, ring, and little finger), thumb, and a palm segment (Fig. 1C). Each of the fingers is comprised of a distal, an intermediate, and a proximal phalange and a metacarpal. The thumb is comprised of a distal and a proximal phalanx, a metacarpal bone, and a trapezium. The metacarpals of the four fingers and the trapezium of the thumb were considered to be fixed to the palm segment. Although the model includes the entire hand, we have analyzed only the biomechanics of the thumb because it is the focus of the current study. The model was developed using the commercial software package AnyBody (v4.0, AnyBody Technology, Aalborg, Denmark). There is only one DOF (degree-of-freedom) for the IP (interphalangeal) joint, i.e., in flexion/extension motion. The MP (metacarpophalangeal) and CMC (carpometacarpal) joints are modeled as spherical joints and have three DOFs.

## RESULTS

Since the extraction and dispensing actions are cyclic in nature, we have summarized all calculation results in terms of task cycle, as researchers traditionally do with gait analysis [5]. An entire work cycle is divided into extraction and dispensing phases. The plunger button stiffness during the extraction and dispensing actions is represented in the slope of the curves of push force versus displacement (Fig. 2). The IP joint moment as a function of the joint angle is shown in Fig. 3A. The joint angle for the extraction is similar to that for the dispensing action; however, the peak joint moment for the dispensing action is about three times that for the extraction. For the MP and CMC joints, the moment in flexion/extension is predominant (Fig. 3B-C). The peak MP joint moment in flexion/extension is approximately 5-7 times of those in adduction-abduction and internal-external rotation (not shown). The peak CMC joint moment in flexion/extension is close to that in adduction-abduction, while approximately four times that in internal-external rotation (not shown).

## DISCUSSION AND CONCLUSIONS

Our results show that the force-displacement curves of the pipette plunger button in loading differ from those in the un-loading process (Fig. 2), which is consistent with a previous study [6]. During the loading process, work is done by the musculoskeletal system to push the plunger, whereas the potential energy stored in the pipette

spring mechanism is given back to the hand system during the unloading process. The joint power absorption during the unloading is mainly caused by the CMC joint that produces resistant flexion moment in the presence of extension; this action controls the speed of the compressed spring returning to its resting length.

## REFERENCES

1. Bjorksten MG, Almy B, Jansson ES. *Appl Ergon* 25 (2) (1994) 88–94.
2. David G, Buckle P. *Appl Ergon* 28 (4) (1997) 257–62.
3. Feldon P, Belsky MR. *Hand Clin* 3 (3) (1987) 429–47.
4. Buczek FL, Sinsel EW, Gloekler DS, Wimer BM, Warren CM, Wu JZ. 2010. Submitted to: *J Biomech*.
5. Winter DA, *Biomechanics and motor control of human movement*, John Wiley and Sons, 2005.
6. Asundi KR, Bach JM, Rempel DM, *Hum Factors* 47 (1) (2005) 67–76.

## DISCLAIMER

The findings and conclusions in this report are those of the authors and do not necessarily represent the official position of the National Institute for Occupational Safety & Health. The mention of trade names, commercial products, or organizations does not imply endorsement by the US Government.

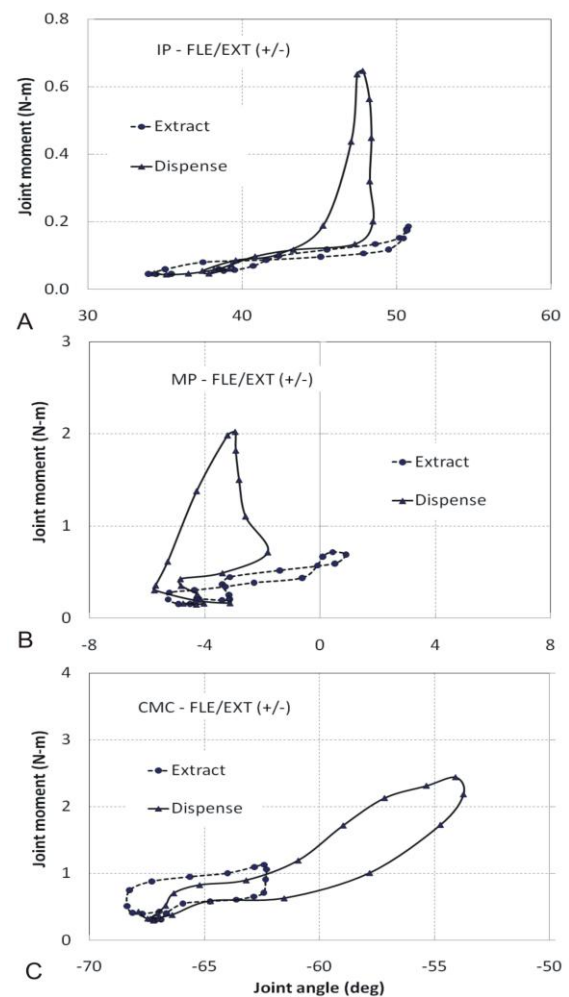


**Figure 3:** Joint moments as a function of joint angles in flexion/extension (+/-) motions during pipetting.

# PASSIVE ELASTIC PROPERTIES OF THE RAT ANKLE

<sup>1</sup>Mengnan (Mary) Wu, <sup>2</sup>Matthew C. Tresch, <sup>3</sup>Dinesh K. Pai, and <sup>4</sup>Thomas G. Sandercock

<sup>1,2,4</sup>Northwestern University, Evanston, IL, USA

<sup>3</sup>University of British Columbia, Vancouver, BC, Canada

Contact email: MengnanWu2012@u.northwestern.edu

## INTRODUCTION

Passive elastic properties of muscles and tendons help create realistic musculoskeletal models and influence postural control. Muscles and tendons are often assumed to be “slack” – contributing zero passive torque – at certain joint angles in simulations [1], but this assumption has not always been verified experimentally. Passive joint properties also create a constant rest posture for the joint. Hooper et al [2] has shown that animals with large ratios of muscle passive force capacity to limb size exhibit constant, gravity-independent leg postures that occur within the range where passive force magnitudes of the flexor and extensor muscles overlap. The current work measured passive elastic torques at the rat ankle, a joint that allows the muscle groups to be easily severed and their relative contributions to ankle torque distinguished. Also, passive properties are especially significant at the rat ankle since a constant rest posture was observed.

Previous studies that measured passive rat hindlimb tension and torque have suggested the importance of extensor (a.k.a. “plantarflexor”) contributions to total passive ankle torque. Gillette and Fell [23] found that the extensors gastrocnemius, soleus, and plantaris contributed 29% of the passive tension of the entire hindlimb. Ochi et al [4] observed a statistical correlation between the passive resistive torque of the ankle joint and the passive tension of the gastrocnemius muscle. However, these studies did not measure joint torques directly and examined only flexion (a.k.a. “dorsiflexion”) positions. They also used behaviorally unrealistic knee postures, and measurements of musculotendon contributions to ankle torques may have been confounded by gravitational forces on the foot. The current study has implemented methodological improvements and measured passive torques across the ankle range of motion.

## METHODS

Passive rat ankle torques were measured before and after cutting the extensors to find over what joint angles they have an effect or go slack. Measurements were taken at five ankle positions, including “zero” position where the foot was orthogonal to the tibia. Joint positions greater than the zero position were considered flexion positions. Flexion torques, which move the foot towards flexion positions, were also greater than zero.

Two female Sprague-Dawley rats were used for the experiments. The animals were anesthetized with ketamine xylazine and the left hindlimb denervated by severing the sciatic and femoral nerves. The protocol was approved by the Northwestern Univ. Institutional Review Board.

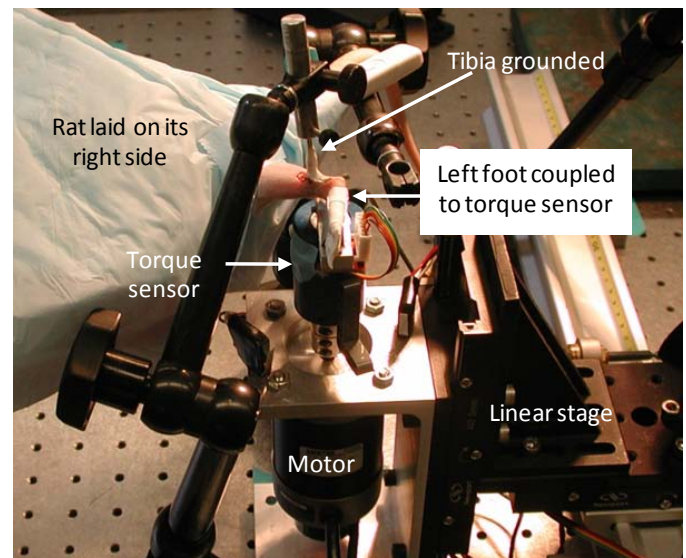


**Figure 1:** Experimental setup. A brushless servo motor (Galil Motion Control) rotated a reaction torque sensor (Interface Force), a coupler to the rat foot, and the foot, all attached rigidly in series. A linear stage allowed precise alignment of the center of rotation of the apparatus with the rat ankle. The ankle was mechanically isolated by fixing the tibia and femur with bone screws with the knee at 90 degrees. The animals were placed so that ankle torques were not affected by gravity.

The experimental apparatus rotated the rat ankle to desired joint positions and measured torque and angular position. The motor controller (Galil Motion Control CDS-3310) was commanded by a host computer that ran the experiment protocol. Torque data was recorded at 10 kHz with a resolution of  $8.33 \times 10^{-5}$  Nm through an external DAQ board (Measurement Computing 1208FS) connected to the host computer. The motor encoder recorded position with a resolution of  $1.57 \times 10^{-3}$  radians at approximately 500 Hz, and position data was synchronized to torque data in post-processing.

The experimental procedure consisted of: 1) stress relaxation at zero position, 2) slow movement at 0.40 radians/s to a non-zero position, 3) stress relaxation at the non-zero position, and 4) slow movement back to zero position. This sequence of events occurred for each of the four non-zero ankle positions. In some sequences, pseudo-random perturbations about a mean ankle position occurred between events 3) and 4), and the data will be used for system identification in the future. The return to zero position ensured that joint torques at each non-zero position had the same history. The presentation of all four non-zero ankle positions was repeated twice for the intact ankle and after the extensors triceps surae and plantaris were severed at the Achilles tendon. Stress relaxations lasted two minutes to allow ankle torques to stabilize, and the last 30 s of data was used to calculate passive torque for that position. The slow movement data was also analyzed and showed similar trends to the stress relaxation data. Future studies will also examine flexor contributions to ankle passive elastic torque.

## RESULTS AND DISCUSSION

A constant, gravity-independent rest posture was observed in the passive rat ankle, and the posture was restored after external perturbations to the foot. The ankle ROM was also much larger in extension than flexion, as measured relative to zero position - where the foot was orthogonal to the tibia.

Passive torques across the range of motion shifted towards greater flexion torque, and the zero-torque ankle position shifted towards flexion after cutting the triceps surae and plantaris (fig. 2). Since extensors exert passive extension torque in flexion positions, the decrease in magnitude of extension torques in flexion positions after tendon cuts is not

surprising. However, the result that flexion torques for extension positions increase in magnitude after tendon cuts shows that triceps surae and plantaris have an effect throughout the range of motion and oppose the action of the flexors in the passive intact ankle. The shift of the zero-torque ankle position towards flexion after tendon cuts further supports that the rest posture of the ankle is created by the balance of flexor and extensor passive torques and not by slack in the muscle groups.

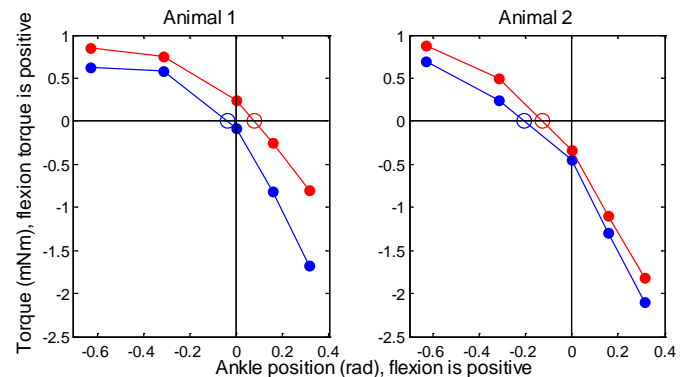


**Figure 2:** Passive ankle torque for ankle intact (blue) and after triceps surae and plantaris were severed (red). Solid markers show data points, circle denotes estimate of equilibrium position, and black lines denote zero torque and zero position.

## CONCLUSIONS

The current study measured passive elastic joint torques across the range of motion for the intact rat ankle and after severing the primary extensors. Passive torques across the range of motion shifted towards greater flexion torque after extensors were severed, showing that extensors exert passive torque across the range of motion. The shift of the zero-torque ankle position towards flexion after cutting extensors is further evidence that the rest posture of the ankle is created by the balance of passive ankle flexion and extension torques. These results challenge the common assumption that muscles and tendons go slack within a joint's range of motion, and support previous work [3] that found a constant rest posture exists in animals with small limb sizes relative to muscle force capacity.

## REFERENCES

1. Kamper DG, et al. *J Biomech* **21**, 361–369, 2002.
2. Hooper SL, et al. *J Neurosci* **29**, 4109–4119, 2009.
3. Gillette PD, et al. *J App Phys* **81**, 724–30, 1996.
4. Ochi E, et al. *J Sports Sci and Med* **6**, 543–548, 2007.

# DO KNEE ECCENTRIC STRENGTH AND KNEE JOINT KINETRICS DIFFER BETWEEN JUMPERS AND NON-JUMPERS IN LANDING ACTIVITIES?

Xie Wu<sup>1</sup>, Songning Zhang<sup>2</sup>, Dongbin Zhang<sup>1</sup> and Chenbin Xie<sup>1</sup>

<sup>1</sup>Sports Performance Research Center, Shanghai University of Sport, Shanghai, China

<sup>2</sup>Biomechanics/Sports Medicine Lab, The University of Tennessee, Knoxville, TN, USA

email: [wuxie1115@yahoo.com.cn](mailto:wuxie1115@yahoo.com.cn), web: <http://ykszyx.sus.edu.cn/sprc/>

## INTRODUCTION

Landing is a common movement task used in investigating impact attenuation and mechanisms of impact related lower extremities injury [1-5]. In the literature, there is limited biomechanical information regarding the relationship between eccentric strength of lower extremities and impact related biomechanics in landing. It is still unclear what roles of lower extremity eccentric strength plays in impact force attenuation during landing activities. Therefore, the main purpose of this study was to investigate the differences of knee eccentric strength and impact related knee biomechanics between jumpers and non-jumpers during step-off landing tasks.

## METHODS

A total of 20 male college swimming athletes (non-jumper) and track and volleyball athletes (jumper) were recruited to participate in the study: 10 jumpers (age: 21.0±1.5 years, height: 185.3±5.2cm & weight: 712.7±66.7N) who received regular training on jumping/landing and lower extremity eccentric strength, and 10 age, height and weight matched non-jumpers (age: 20.2±1.4 years, height: 181.6±4cm & weight: 731.0±64.9N) who rarely received regular training on jumping/landing activities and lower extremity eccentric strength. The concentric and eccentric knee muscle strengths of dominant leg were tested at 60 deg/s on an isokinetic dynamometer (CON-TREX, MJ). The step-off landing trials were tested in a separate testing session. The participant performed five trials in each of four step-off landing conditions: soft and stiff landing from 0.4 m and 0.6 m landing heights. To ensure consistent and reliable landing techniques in the four landing conditions, the maximum knee flexion angle (2D angle) during testing were monitored using these criteria: 95-105 deg and 60-70 deg for soft and stiff landing at 0.4 m, and 100-

110 deg and 65-75 deg for soft and stiff landing at 0.6 m, respectively. All participants wore a pair of standard lab running shoes (ALCE007-4, Li Ning) during landing trials. Anatomical and tracking reflective markers were placed on the pelvis and the dominant side of the lower extremity segments/joints. Three-dimensional kinematic (250 Hz, 8-camera Vicon) and ground reaction force (1250 Hz, Kistler) data were recorded simultaneously. 3D kinematic and kinetic variables were computed using Visual 3D (C-Motion, Inc). A right-hand rule was used to define the conventions of kinematic and kinetic variables. Additional data processing and analyses were performed using customized software (VB\_V3D). A 3-way (group x height x stiffness) mixed design analysis of variance was used to detect group, height and landing stiffness differences for selected 3D variables. A 2-way (group x contraction) mixed design analysis of variance was used to detect group and contraction difference for max knee extension torques. The alpha level was set at 0.05.

## RESULTS AND DISCUSSION

The isokinetic strength result showed that the jumper had significantly greater peak concentric and eccentric knee extension torques compared to the non-jumpers ( $p = 0.002$ , Figure 1). However, the group by contraction interaction was not significant ( $p = 0.063$ ).

No significant group effects were found for the 1<sup>st</sup> or 2<sup>nd</sup> peak vertical ground reaction force (Fz\_Max1 and Fz\_Max2, Table 1). The jumpers had significantly larger knee flexion angle (KA\_On\_X,  $p = 0.017$ ) and abduction angle (KA\_On\_Y,  $p = 0.037$ ) at initial contact and larger maximum knee flexion angle (KA\_X\_Max,  $p = 0.018$ ) compared to the non-jumpers. However, no significant group difference on knee flexion ROM (KA\_X\_ROM) was observed. The jumpers had significantly larger

1<sup>st</sup> peak knee extensor moment (KM\_Max1\_X,  $p = 0.033$ ) and 1<sup>st</sup> peak power (KP\_Min1\_X,  $p = 0.012$ ). In addition, no significant group related interactions were found for those selected variables. As expected, all kinetic variables increased significantly from 0.4 to 0.6 m and from soft to stiff landing whereas significant decreases were observed for knee kinematic variables (Table 1).

Although the knee eccentric strength was different between the groups, no differences on the vertical GRFs during landing were found. These results may be related to the similar knee flexion ROM across four landing conditions between the two groups. This similarity in knee flexion ROMs is more related to the experimental control of the landing stiffness employed in this study and less related to the knee eccentric strength. The jumpers tended to land with the knee in a more flexed position at touchdown. This result may indicate the athletes with more training in jumping and eccentric strength activities positioned the knee joint in a more favorable (flexed) position and pre-stretched the knee extensors to attenuate impact force compared to those athletes lacking jumping and eccentric training experience. As a result the peak knee extensor moment and power were greater for the jumpers compared to the non-jumpers.

## CONCLUSIONS

No differences on the vertical GRFs were found between the two athlete groups although the jumper group had greater eccentric and concentric knee extension strength. However, the more experienced athletes adopted an impact attenuation strategy with

greater knee flexion angle at initial contact that increased pre-stretching of knee extensors and increased peak knee extensor moment and power. It is still unclear whether there would be differences in the landing strategy, impact forces, and impact attenuation related variables if the participants chose their own landing technique during landing activities.

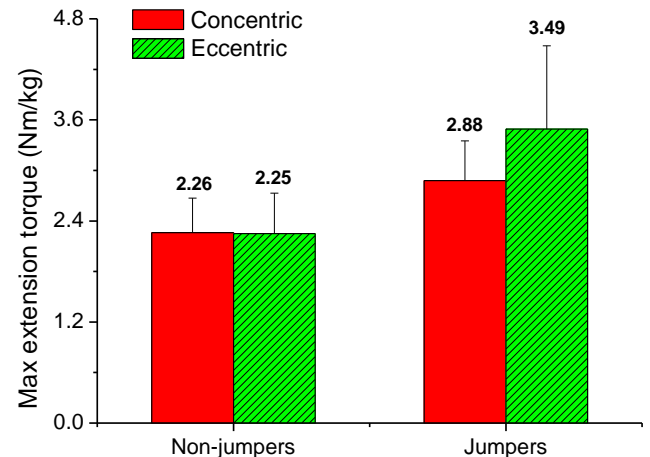


**Figure 1.** Peak concentric and eccentric knee extension torques at 60 deg/s.

## REFERENCES

1. McNitt-Gray. (1993). *J Biomech.*, **26**, 1037-1046.
2. Decker., et al. (2003). *Clin Biomech.*, **18**, 662-669.
3. Bobbert, et al. (1987). *Med. Sci. Sports Exerc.*, **19**, 339-346.
4. Self, et al. (2001). *Med. Sci. Sports Exerc.*, **33**, 1338-1344.
5. Zhang, et al. (2008). *Sports Biomech.*, **7**, 296-309.

**Table 1.** Kinematic and kinetics variables in the four landing tasks: mean  $\pm$  STD.

| Variable                 | Unit    | Non-jumpers     |                 |                  |                 | Jumpers          |                 |                  |                 |
|--------------------------|---------|-----------------|-----------------|------------------|-----------------|------------------|-----------------|------------------|-----------------|
|                          |         | 40soft          | 40stiff         | 60soft           | 60stiff         | 40soft           | 40stiff         | 60soft           | 60stiff         |
| Fz_Max1 <sup>*^</sup>    | (BW)    | 0.89 $\pm$ 0.20 | 1.38 $\pm$ 0.28 | 1.39 $\pm$ 0.32  | 2.01 $\pm$ 0.38 | 0.93 $\pm$ 0.10  | 1.33 $\pm$ 0.28 | 1.31 $\pm$ 0.28  | 1.99 $\pm$ 0.40 |
| Fz_Max2 <sup>*^</sup>    | (BW)    | 3.24 $\pm$ 0.53 | 4.02 $\pm$ 0.80 | 4.03 $\pm$ 0.95  | 4.84 $\pm$ 0.94 | 3.29 $\pm$ 1.29  | 4.66 $\pm$ 1.95 | 3.77 $\pm$ 1.00  | 5.00 $\pm$ 1.68 |
| KA_On_X <sup>*^#</sup>   | (deg)   | -26.3 $\pm$ 3.6 | -16.8 $\pm$ 4.4 | -29.2 $\pm$ 3.3  | -18.4 $\pm$ 4.0 | -32.3 $\pm$ 4.6  | -21.1 $\pm$ 4.0 | -34.1 $\pm$ 7.2  | -21.2 $\pm$ 3.6 |
| KA_On_Y <sup>*^#</sup>   | (deg)   | 2.7 $\pm$ 3.0   | 1.5 $\pm$ 3.4   | 3.0 $\pm$ 3.5    | 1.7 $\pm$ 3.6   | 4.7 $\pm$ 3.6    | 5.0 $\pm$ 3.7   | 6.4 $\pm$ 3.6    | 5.9 $\pm$ 3.1   |
| KA_Max_X <sup>*^#</sup>  | (deg)   | -95.3 $\pm$ 4.6 | -59.2 $\pm$ 4.2 | -101.2 $\pm$ 3.9 | -66.8 $\pm$ 4.8 | -101.2 $\pm$ 5.7 | -64.9 $\pm$ 3.9 | -106.7 $\pm$ 5.6 | -70.1 $\pm$ 4.5 |
| KA_ROM_X <sup>*^</sup>   | (deg)   | -69.0 $\pm$ 5.1 | -42.4 $\pm$ 4.7 | -72.0 $\pm$ 5.3  | -48.4 $\pm$ 6.1 | -68.9 $\pm$ 4.4  | -43.9 $\pm$ 3.6 | -72.6 $\pm$ 6.1  | -48.9 $\pm$ 4.1 |
| KM_Max1_X <sup>*^#</sup> | (Nm/kg) | 1.77 $\pm$ 0.31 | 2.22 $\pm$ 0.43 | 2.78 $\pm$ 0.61  | 3.17 $\pm$ 0.60 | 2.27 $\pm$ 0.60  | 2.91 $\pm$ 0.78 | 3.04 $\pm$ 0.57  | 3.64 $\pm$ 0.83 |
| KP_Min1_X <sup>*^#</sup> | (W/kg)  | -14.9 $\pm$ 2.8 | -17.2 $\pm$ 3.9 | -24.1 $\pm$ 5.9  | -28.7 $\pm$ 7.7 | -21.8 $\pm$ 8.4  | -24.7 $\pm$ 8.4 | -29.9 $\pm$ 6.9  | -36.8 $\pm$ 7.5 |

Note: \*: significant difference on Height, ^: significant difference on Stiffness, #: significant difference on Group.

# VARIABILITY OF GAIT IS DEPENDENT ON DIRECTION OF MOTION

<sup>1,2</sup>Shane R. Wurdeman, <sup>1</sup>Neil B. Huben, and <sup>1,2</sup>Nicholas Stergiou

<sup>1</sup>Nebraska Biomechanics Core Facility, University of Nebraska at Omaha, Omaha, NE, USA

<sup>2</sup>College of Public Health, University of Nebraska Medical Center, Omaha, NE, USA

email: swurdeman@unomaha.edu web: <http://nbcf.unomaha.edu>

## INTRODUCTION

Bipedal gait has been modeled through passive dynamic walkers that are effectively able to ambulate with no active control[1]. However, these walkers are inherently unstable in the mediolateral (ML) direction, leading to the necessity of either passive stabilization with wide feet or hips, or through active stabilization from artificial neural control. The principles behind these walkers have been extended to human walking. Similarly, human walking displays increased uncertainty in the ML direction compared to the anteroposterior (AP) direction[2], typically measured through increased amount of variability. As a result, it has been suggested that ML foot placement during walking requires increased upper motor neuron control whereas AP foot placement is a more passive reflex action generated in the spinal cord[2]. Unfortunately, all studies have utilized walking in the AP direction, an obvious bias as this is the primary direction of human locomotion. However, this would also be consistent with the direction gravity would have the largest effect from its impulse, which for the passive dynamic walker would be the sole source of energy. Thus, it is not entirely clear for walking if the AP and ML direction have truly been partitioned within the neuromuscular system, or whether foot placement in the plane least reliant upon gravity requires increased dependence on active neural control. Therefore, we investigated how altered direction of gait will affect amount of variability in foot placement in the AP and the ML plane.

## METHODS

Sixteen subjects (age: 23.4 yrs  $\pm$  3.3; height: 179.0 cm  $\pm$  7.4; mass: 83.4 kg  $\pm$  15.7) were recruited to perform a lateral stepping gait. Subjects performed a three minute trial on the treadmill while heel and toe reflective marker position were recorded (60 Hz; Motion Analysis Corp., Santa Rosa, CA).

Subjects were initially given a three minute practice period followed by a one minute rest. Subjects were instructed to select the speed at which they felt comfortable ( $0.34 \pm 0.04$  m/s). Further instructions included: keep head up while stepping laterally, not to allow crossover of the legs, nor at any point were both feet to be off the treadmill (i.e. no flight phase). All subjects faced left such that the left leg lagged the right leg. By shifting the plane of motion from AP to ML, gravity is now possibly affecting the ML plane but at the least is no longer contributing to AP motion. The first 100 steps of each trial were analyzed. Foot position was calculated as the middle point of the heel and toe markers for each foot. Dependent measures were the coefficient of variation (CoV) of step length (AP) and step width (ML). Since the altered gait requires different tasks from the right and left leg, the step length and width for each leg were not combined. Thus, Left AP and Left ML were the distance from the right foot to the left foot in the AP and ML planes, respectively, following movement of the left foot and vice versa for the Right AP and Right ML (Figure 1). Significance was tested through 2x2 (plane by leg) fully repeated measures ANOVA.

## RESULTS AND DISCUSSION

The CoV for the AP direction was significantly greater than the ML direction ( $F_{1,15}=340.770$ ,  $p<0.001$ ). There were no differences between the right and left leg CoV measures ( $F_{1,15}=3.968$ ,  $p=0.065$ ) nor any interaction ( $F_{1,15}=0.520$ ,  $p=0.482$ )(Table 1). The results supported our hypothesis; without gravity working in the AP plane, there was a large amount of variability for foot placement as measured through CoV. However, we did not expect such a large difference in CoV between the two planes. Specifically, for each leg, the amount of variability in the AP plane was approximately 7-10 times greater than in the

ML plane which may be the result of the novelty of the task. Regardless of novelty, our results clearly show that the effects of gravity and inertia play a much larger role in the active neural control of gait. It appears that the body's planes (AP and ML) may not be so simply partitioned into the spinal cord and upper motor cortex. These findings are contrary to what has previously been reported in studies comparing variability in the AP and ML directions[2,3]. Bauby et al[2] reported a 79% larger magnitude of variability in the ML direction, although their subjects walked in the AP plane. Similarly, O'Connor et al[3] concluded an increased active neural control of the ML direction based on findings of visual perturbations in the AP and ML direction although their subjects only traversed in the AP direction. Interestingly, standing posture has an increased amount of variability in the AP plane compared to the ML[2,4]. It has been speculated that this is a result of the degrees of freedom in the AP compared to ML plane. This seems to explain the standing posture difference in variability. However, when translating such interpretation to gait, the degrees of freedom are no longer considered and instead reflex actions from the spinal cord are credited with dominating the movement. Our study may offer additional insight into the differences between AP and ML variability in posture and standing. Specifically, it seems that the effect of gravity and inertia has a stronger influence on decreasing the amount of variability in the AP and ML directions than what was previously

assumed and the degrees of freedom available as well as the reflex actions of the spinal cord may not have as strong of an impact.

## CONCLUSIONS

In summary, the directions of movement control are not set but rather it seems that active control is assumed over the direction that is not benefiting from inertia and gravity. The direction orthogonal to the motion will have the least amount of influence from inertia and thus be dependent upon active neural control for correction. Further work should implement increased stress on the lateral stepping task to evoke changes in the amount of variability in the AP and ML plane and thus allowing for sensitivity analysis. Furthermore, the implications of this work should be considered and extended to the elderly that show increased ML variability in gait but also typically decrease their gait speed, and thus decrease inertia[5].

## REFERENCES

1. McGeer T. *J Theor Biol.* 1993 Aug 7;163(3):277-314.
2. Bauby CE, Kuo AD. *J Biomech.* 2000 Nov; 33(11):1433-40.
3. O'Connor SM, Kuo AD. *J Neurophysiol.* 2009 Sep;102(3):1411-9.
4. Winter DA, Prince F, Frank JS, Powell C, Zabjek KF. *J Neurophysiol.* 1996 Jun;75(6):2334-43.
5. Owings TM, Grabiner MD. *Gait Posture.* 2004 Aug;20(1):26-9.

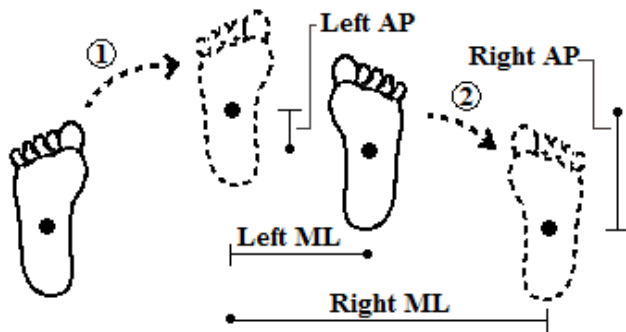


**Figure 1:** Left and right step measures in anteroposterior (AP) and mediolateral (ML) planes. This shows a left step first (1) followed by a right step (2).

**Table 1:** Average coefficient of variation for the step length measures; the anteroposterior (AP) plane had significantly more variability than the mediolateral (ML), reflecting greater uncertainty in foot placement.

|                      | Coefficient of Variation<br>(n=16) |
|----------------------|------------------------------------|
| <b>Left AP Step</b>  | 0.71 ± 0.16                        |
| <b>Right AP Step</b> | 0.73 ± 0.11                        |
| <b>Left ML Step</b>  | 0.06 ± 0.02*                       |
| <b>Right ML Step</b> | 0.10 ± 0.03*                       |

\* Sig.  $p < 0.05$  AP vs. ML

# INFLUENCE OF A FIXED ANKLE ON JOINT MECHANICS AND METABOLIC COST OF WALKING

Clinton J. Wutzke<sup>1</sup>, Gregory S. Sawicki<sup>1,2</sup> and Michael D. Lewek<sup>1</sup>

<sup>1</sup>University of North Carolina at Chapel Hill, Chapel Hill, NC, USA

<sup>2</sup>North Carolina State University, Raleigh, NC, USA

email: cwutzke@med.unc.edu

## INTRODUCTION

Inability to control the ankle muscles can contribute to gait deficits in people post-stroke [1]. Specifically, reduced power generation from the plantarflexors may result in compensatory movement strategies. These strategies may increase reliance on less efficient proximal muscles (e.g. hip) or the non-paretic limb to achieve a functional walking velocity [2]. Such compensations are thought to require greater metabolic energy expenditure and may contribute to reductions in walking endurance [1, 3].

The purpose of this study was to determine the effect of walking with reduced ankle power generation on metabolic cost and the redistribution of mechanical power generation in unimpaired subjects. To model reduced ankle plantarflexion generation, we had subjects walk with a unilaterally fixed ankle. We hypothesized that fixed ankle walking would elicit greater hip mechanical power generation in the braced (i.e. ipsilateral) leg, thereby increasing the net metabolic power demands of the task.

## METHODS

All participants read, understood and signed an IRB approved consent form. Six unimpaired adults (5F, 1M,  $\bar{x}$  age  $23.3 \pm 1.4$  years;  $\bar{x}$  mass  $63.1 \pm 5.9$  kg) completed two treadmill walking conditions at 1.2 m/s (2.7 mph). Subjects wore a lockable ankle brace (Ballert International, LLC, FL; mass = 1.35 kg) on the dominant limb during both conditions. In one condition, subjects walked on the treadmill with the ankle locked in a neutral position (FIXED ankle) while in the other condition subjects walked with the brace unlocked (FREE ankle). Subjects walked for 4 minutes in each condition to achieve 'steady

state' prior to a single 30 second collection of kinematic and kinetic data. A minimum break of 4 minutes was provided between conditions.

A motion capture system (VICON/PEAK, Denver, CO) was used to record three dimensional lower extremity kinematics (120 Hz) and an instrumented split-belt treadmill (Bertec Corp., Columbus OH) recorded ground reaction forces generated by each limb (1080 Hz). Peak positive mechanical power (normalized to body mass, W/kg) at the ankle and hip were calculated using inverse dynamics with Visual 3D software (C-Motion, Germantown, MD). Peak anteriorly-directed ground reaction forces were measured for each step and averaged for each condition. Finally, indirect calorimetry (OxyCon, Yorba Linda, CA) was used to determine mass specific net metabolic power [4].

Non parametric statistics (Wilcoxon sign rank tests) were used to identify differences between limbs and conditions ( $\alpha=0.05$ ).

## RESULTS AND DISCUSSION

The braced limb exhibited a reduced peak ankle plantarflexion angle during the FIXED condition compared to the FREE condition (within limb change:  $p=0.028$ ). Likewise, we observed a between limb change during FIXED ankle walking, with reduced plantarflexion observed in the braced ankle compared to the non-braced ankle (between limbs comparison:  $p=0.028$ ). These results confirm that the brace restricted ankle movement during the FIXED ankle walking condition.

As anticipated, this reduction in ankle angle contributed to a reduction in peak ankle power during FIXED walking compared to FREE walking

( $p=0.028$ ) and the non-braced limb ( $p=0.046$ ) during FIXED walking.

Mass specific net metabolic power did not change between conditions ( $p=0.173$ ; FREE ankle  $3.59 \pm 0.39$  W/kg, FIXED ankle  $3.79 \pm 0.47$  W/kg) (Figure 1).

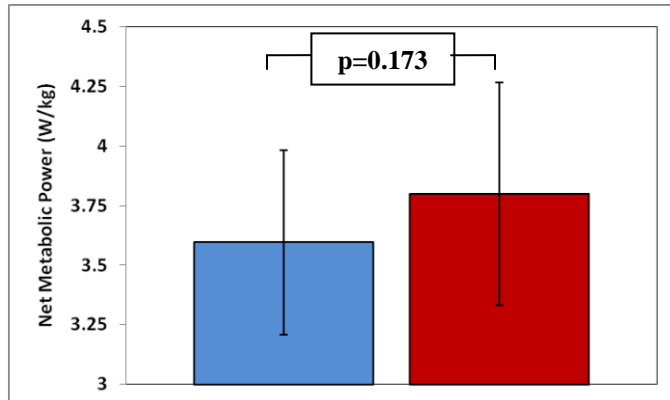


**Figure 1:** Mass specific net metabolic power during FREE (left) and FIXED (right) ankle walking conditions.

Peak hip power was significantly greater in the braced limb during FIXED ankle walking compared to FREE ankle walking ( $p=0.046$ ) (Table 1).

The peak anteriorly directed ground reaction force of the braced limb did not significantly differ between FIXED and FREE ankle walking conditions ( $p=0.173$ ). Peak anteriorly directed ground reaction force was significantly greater however in the non-braced limb compared to the braced limb during the FIXED ankle condition

**Table 1:** Lower extremity ankle and hip kinematic and kinetic measures during free ankle (FREE) and fixed ankle (FIXED) walking conditions.

|                                 | FREE Ankle                  |                         | FIXED Ankle                 |                         |
|---------------------------------|-----------------------------|-------------------------|-----------------------------|-------------------------|
|                                 | Non-Braced<br>Mean $\pm$ SD | Braced<br>Mean $\pm$ SD | Non-Braced<br>Mean $\pm$ SD | Braced<br>Mean $\pm$ SD |
| Peak Ankle Plantarflexion (deg) | 19.92 $\pm$ 2.86            | 9.12 $\pm$ 2.96         | 19.52 $\pm$ 3.47            | 0.44 $\pm$ 3.25*†       |
| Peak Ankle Excursion (deg)      | 27.80 $\pm$ 4.56            | 26.00 $\pm$ 3.17        | 27.44 $\pm$ 5.18            | 13.64 $\pm$ 3.75*†      |
| Peak Ankle Power (W/kg)         | 3.04 $\pm$ 0.55             | 2.84 $\pm$ 0.20         | 2.96 $\pm$ 0.61             | 2.02 $\pm$ 0.47*†       |
| Peak Hip Power (W/kg)           | 0.86 $\pm$ 0.24             | 0.93 $\pm$ 0.18         | 0.89 $\pm$ 0.22             | 1.00 $\pm$ 0.15*        |

\* =  $p < 0.05$  compared to free ankle walking condition.

† =  $p < 0.05$  between limbs in fixed ankle walking condition.

(non-braced limb  $118.51 \pm 17.06$ N, braced limb  $95.24 \pm 7.93$ N;  $p=0.046$ ).

## CONCLUSIONS

As hypothesized, subjects redistributed mechanical power production within the braced limb in order to maintain walking velocity in the FIXED ankle condition. Peak power output from the hip was increased to compensate for reduced peak ankle power.

Contrary to our expectations, the marked trade-off between peak ankle and peak hip mechanical power generation within the braced limb during FIXED ankle walking did not result in significantly elevated net metabolic power. Although we find evidence of redistribution of lower extremity power generation from the relatively efficient ankle muscles to the less efficient hip muscles in the braced limb during FIXED walking, it does not seem to significantly impact the overall metabolic demands of the task. Further mechanical analysis is necessary to further resolve this issue.

## REFERENCES

1. Kesar, TM, et al., *Physical Therapy*, **90**(1), 55-66, 2010
2. Bowden MG, et al, *Stroke*, **37**, 872-876, 2006.
3. Olney SJ, et al, *Gait & Posture*, **4**, 136-148, 1996.
4. Brockway JM. *Hum Nutr Clin Nutr*, **41**:463–471,1987.

# POSTURAL SWAY IN PATIENTS WITH LOW BACK PAIN – ASSOCIATION BETWEEN MEAN SWAY CHARACTERISTICS AND CLINICAL OUTCOMES

<sup>1</sup>Ting Xia, <sup>1</sup>Cynthia Long, <sup>1</sup>Ram Gudavalli, <sup>1</sup>James DeVocht, <sup>2</sup>Edward Owens, <sup>3</sup>David Wilder, <sup>1</sup>Ying Cao, <sup>4</sup>William Meeker and <sup>1</sup>Christine Goertz

<sup>1</sup>Palmer College of Chiropractic – Davenport Campus, Davenport, IA, USA

<sup>2</sup>Northwestern Health Sciences University, Bloomington, MN, USA

<sup>3</sup>University of Iowa, Iowa City, IA, USA

<sup>4</sup>Palmer College of Chiropractic – West Campus, San Jose, CA, USA

email: [ting.xia@palmer.edu](mailto:ting.xia@palmer.edu)

## INTRODUCTION

Low back pain (LBP) has long been recognized as one of the major health problems in the US not only because of its impact on quality of life but also the staggering medical and socioeconomic costs [1]. The pathophysiology of chronic LBP is poorly understood. A majority of LBP cases are idiopathic or non-specific. Previously it was shown that LBP may interfere with postural stability [2]. In general, patients with LBP demonstrate a larger excursion, indicating less ability to regulate their postural stability. However, it is not clear how postural sway varies with the severity of LBP. In the present study this relationship was examined.

The treatment methods for LBP include medication, exercise, manual therapy, and surgery. Spinal manipulation (SM) is a form of manual therapy with moderate clinical effectiveness similar to other non-surgical interventions for acute and chronic LBP. In the present study, two forms of SM, High-Velocity Low-Amplitude (HVLA) side-posture adjustment and Low-Velocity Variable-Amplitude (LVVA) flexion-distraction, were applied to treat patients with sub-acute or chronic LBP. It was hypothesized that the interventions would reduce postural sway due to a decrease in LBP severity.

## METHODS

Participants were eligible if they were 21-54 years old, presented with LBP of at least 4 weeks in duration, scored 6 or above on the Roland Morris Disability Questionnaire (RMDQ), and met diagnostic classification of 1, 2, or 3 of the Quebec Task Force Classification for Spinal Disorders. 192

participants (89 females, 103 males) were randomly assigned to HVLA (N=72), LVVA (N=72), or a wait-list control (N=48), respectively. SM was applied to one or two joints at L4-L5, L5-S1, or sacroiliac joints for 4 intervention visits over 2 weeks.

The mean excursion of the center of pressure in the anterior-posterior (AP) and side-to-side (SS) directions were monitored using a force plate at a sampling rate of 1000 Hz [3]. The participant stood quietly first on a hard surface, i.e. directly on the force plate, and then on a soft surface, i.e. on a 10 cm thick latex foam pad, for a period of 30 seconds, respectively. They were allowed to choose their comfortable stance while blindfolded and in their socking feet. The procedure was repeated twice.

Postural sway, pain (Visual Analog Scale) and RMDQ scores, were obtained at baseline and following the two-week SM intervention. To examine the association between postural sway and pain or RMDQ, a mixed model with repeated measures was applied using the SAS software package. The estimated least-square means and 95% confidence intervals adjusted for sex, age and height were presented for each model. Statistical significance was set at 0.05.

## RESULTS AND DISCUSSION

The mean±SD age and height of the participants were 40±9.4 years old and 172.7±9.7 cm. The mean baseline pain and RMDQ scores were 55.7±20.9 and 9.7±3.2. 62% of the participants had the condition longer than one year. The relationship between the baseline postural sway and pain or

RMDQ are demonstrated by dividing all possible pain (0-100 mm) or RMDQ (0-24) scores into equal segments (Figures 1). There were significant associations between postural sway on the soft surface and LBP severity in both the AP and SS directions at baseline (Table 1). There was a significant association between postural sway on the hard surface and pain in the SS direction.

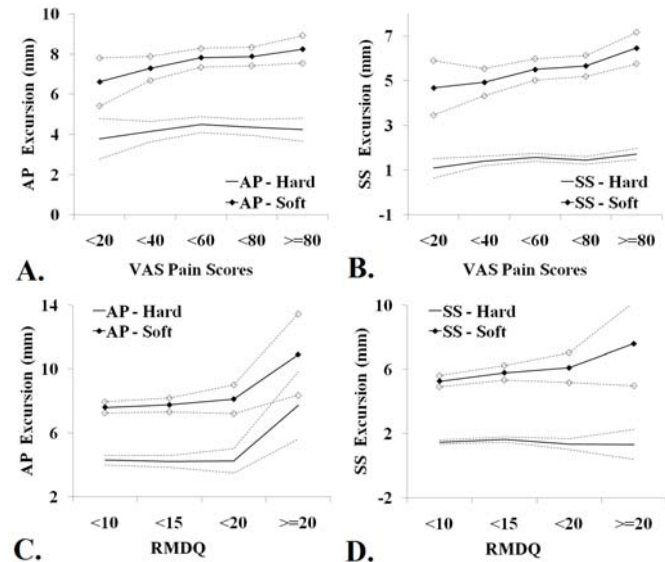


**Figure 1:** The relationship between the model estimated least-square means of postural sway in the anterior-posterior (AP) and the side-to-side (SS) directions and pain (A. and B.) or RMDQ (C. and D.) scores on the hard and soft surfaces at baseline. The dash lines represent 95% confidence intervals.

**Table 1:** p values for the association between postural sway and pain or RMDQ at baseline.

|      | Pain  |       | RMDQ |      |
|------|-------|-------|------|------|
|      | AP    | SS    | AP   | SS   |
| Hard | 0.26  | 0.04  | 0.46 | 0.97 |
| Soft | 0.003 | 0.002 | 0.01 | 0.01 |

The HVLA and LVVA interventions had significant effects ( $p < 0.001$ ) on LBP severity while the wait-list control group did not. Specifically, the mean pain scores dropped  $23.5 \pm 28.1$ ,  $17.8 \pm 25.7$ , and  $6.1 \pm 19.4$ , and the mean RMDQ scores dropped  $4.0 \pm 4.2$ ,  $3.8 \pm 4.1$ , and  $1.0 \pm 3.0$  for three groups, respectively. Table 2 summarizes the adjusted effects of the change in postural sway from baseline to 2 weeks. While the HVLA and LVVA groups had larger mean changes in postural sway than the wait-list group on the soft surface, there were not significant differences between the groups.

## CONCLUSIONS

In the present work we demonstrated significant associations between postural sway and LBP severity at baseline when the participants stood on the soft surface while blindfolded. While there was a significant improvement in LBP severity in patients receiving SM interventions, the decrease in postural sway compared to the control was not significant, suggesting a more complex nature in balance control. It is possible that the two-week SM intervention was not long enough to improve balance control or the SM interventions provided was too restricted compared to normal practice.

## REFERENCES

1. Dagenais S. et al. *Spine J*, **8**, 8-20, 2008.
2. Ruhe A, et al. *Eur Spine J* [Ahead of Print], 2010.
3. Bhattacharya A. et al, *Ann Biomed Eng*, **15**, 533-50, 1987.

## ACKNOWLEDGEMENTS

The present work was supported by NIH Award Numbers 1U19 AT002003 and C06 RR15433-01.

**Table 2:** Effects of interventions (Tx 1: HVLA; 2: LVVA; 3: wait-list) adjusted for decrease ( $\Delta$ , positive if decreasing) in LBP severity: estimated least-square mean  $\Delta$ sway (95% CI) on the hard and the soft surfaces

| Tx   | $\Delta$ Sway (mm) adjusted for $\Delta$ Pain |                     | $\Delta$ Sway (mm) adjusted for $\Delta$ RMDQ |                     |                    |
|------|---|---------------------|---|---------------------|--------------------|
|      | AP  | SS                  | AP  | SS                  |                    |
|      | Hard  |                     |   |                     |                    |
|      | 1   | -0.23 (-0.6, 0.14)  | -0.12 (-0.3, 0.05)                            | -0.15 (-0.51, 0.22) | -0.13 (-0.3, 0.05) |
|      | 2   | -0.11 (-0.46, 0.22) | 0.08 (-0.08, 0.24)                            | -0.06 (0.41, 0.29)  | 0.08 (-0.08, 0.24) |
|      | 3   | -0.22 (-0.71, 0.27) | -0.28 (-0.51, -0.05)                          | -0.25 (-0.78, 0.28) | 0.16 (-0.49, 0.0)  |
| Soft |   |                     |   |                     |                    |
|      | 1   | 0.32 (-0.13, 0.79)  | 0.41 (0.03, 0.79)                             | 0.32 (-0.15, 0.79)  | 0.34 (-0.04, 0.72) |
|      | 2   | 0.31 (-0.13, 0.76)  | 0.56 (0.21, 0.91)                             | 0.20 (-0.2, 0.59)   | 0.59 (0.23, 0.94)  |
|      | 3   | 0.01 (-0.63, 0.64)  | 0.05 (-0.46, 0.55)                            | 0.21 (-0.45, 0.88)  | 0.05 (-0.50, 0.60) |

# Increase Patella Cartilage Stress with Internal Femoral Rotation: Evaluation Using Finite Element Analysis

Nicholas H. Yang<sup>1</sup>, Kai-Yu Ho<sup>1</sup>, Shawn Farrokhi<sup>2</sup>, Christopher M. Powers<sup>1</sup>

<sup>1</sup>University of Southern California, Los Angeles, CA, USA

<sup>2</sup>University of Pittsburgh, Pittsburgh, PA, USA

email: powers@usc.edu, web: <http://pt.usc.edu/labs/mbrl>

## INTRODUCTION

Disorders of the patellofemoral joint (PFJ) are among the most common and clinically challenging conditions encountered in orthopedic practice. Patellofemoral pain (PFP) affects a wide range of individuals, with higher incidence rates among women and those who are physically active.<sup>1</sup> The most commonly cited hypothesis as to the cause of PFP is related to abnormal patella alignment and/or tracking, which increases patellofemoral joint stress and subsequent articular wear.<sup>2</sup> Recent studies have shown that altered PFJ kinematics is the result of abnormal femoral internal rotation as opposed to abnormal patellar motion.<sup>3</sup> Internal rotation of the femur with respect to the patella has been shown to decrease the contact area and increase the stress at the patellofemoral joint in cadaver knees.<sup>4</sup> Using finite element analysis methods, the objective of this study was to compare the hydrostatic pressure at the patella cartilage-bone interface at 15° and 45° of knee flexion at different degrees of internal rotation of the femur.

## METHODS

Subject-specific PFJ geometry of 7 females with PFP was obtained from high-resolution, sagittal plane MR images acquired with a 3.0 T MR scanner (General Electric Healthcare). Weight-bearing PFJ kinematics was acquired using sagittal plane MR sequence while the knee joint was loaded with 25% of body weight at 15 and 45° of knee flexion. Quadriceps muscle morphology was assessed from thigh MR images in coronal and axial planes. For biomechanical testing, lower extremity kinematics were collected using a Vicon (Oxford Metrics LTD.) 8-camera motion analysis system at 60 Hz. Ground reaction forces were recorded at 1560 Hz using 2 AMTI force plates. EMG signals of knee

musculature were recorded at 1560Hz, using pre-amplified, bipolar, surface electrodes (Motion Lab Systems).

Input parameters for the FE model included: 1) joint geometry, 2) weight-bearing PFJ kinematics, and 3) quadriceps muscle forces (Fig. 1). The PFJ geometry was manually segmented on high-resolution MR images and the FE mesh of cartilage and bone was created using a FE pre-processor (Hypermesh, Altair Engineering Inc.). The FE mesh was then registered to the position of each structure in the weight-bearing MR images. To estimate quadriceps forces, a previously described subject specific model of the PFJ was used.<sup>5</sup>

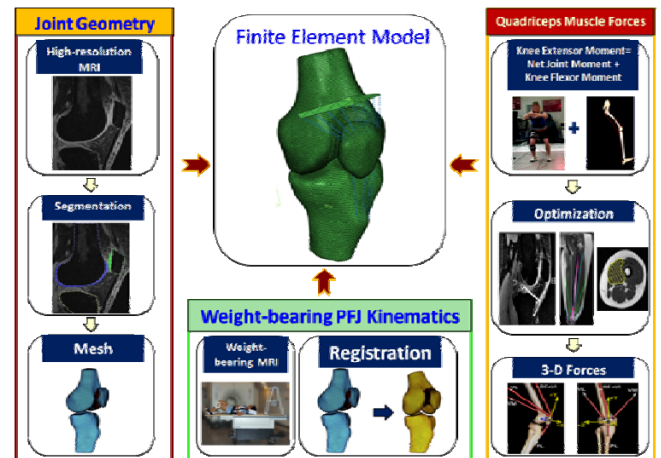


**Figure1:** Pipeline of patellofemoral joint FE model.

A previously described method was used to perform quasi-static loading simulations using a nonlinear FE solver (Abaqus, SIMULIA).<sup>6</sup> Bone was modeled as rigid and the cartilage of the patella and femur was modeled as homogeneous isotropic tetrahedral continuum elements (elastic modulus of 4 MPa and Poisson ratio of 0.47). Quadriceps muscles were divided into 3 functional groups (rectus femoris/vastus intermedius, vastus medialis, and vastus lateralis) made up of 6 equivalent uniaxial

connector elements. Patellar tendon was modeled as six uniaxial, tension-only elements with stiffness of 4334 N/mm. Simulations were performed at 15° and 45° of knee flexion at 0° (neutral), 5° and 10° of internal femoral rotation. Since the soft tissues controlling the rotation of the patellofemoral joint were not included in the current model (i.e., ligaments and peripatellar retinaculum), the 3 rotational degrees of freedom of the patella were constrained.

A mixed model (hip angle x knee angle) analysis of variance (ANOVA) was performed to examine the difference in peak and average hydrostatic pressure of the patella cartilage elements at the cartilage-bone interface. The significance level was set at 0.05.

### RESULTS AND DISCUSSION

Significant group main effects (no interactions) were found for both stress variables of interest (Table 1). When averaged across knee flexion angles, 5° and 10° of femoral internal rotation resulted in significant increases in peak (2.88 MPa and 3.25 MPa vs. 2.14 MPa) and average (1.14 MPa and 1.15 MPa vs. 0.80 MPa) hydrostatic pressure when compared to the neutral position.

Besier et al.<sup>7</sup> has reported that femoral rotation with the knee flexed at 60° increased PFJ stresses in one-third of their subjects. However, when simulating internal rotation, the patella was allowed to move with the femur. Kinematic MRI studies have shown

the patella does not move with the femur as it rotates in weightbearing.<sup>3</sup> Our results agree with conclusions of cadaveric<sup>4</sup> and imaging studies<sup>3</sup> that femoral internal rotation is a contributor of altered patellofemoral joint mechanics in persons with PFP.

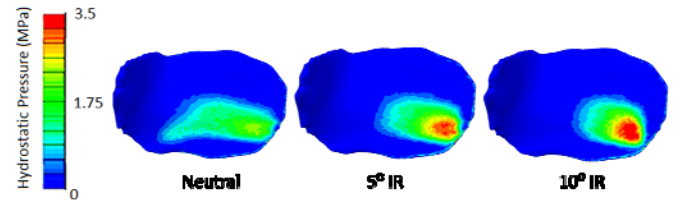


**Figure 2:** Hydrostatic pressure distribution at the patella cartilage-bone interface at knee flexion of 45°.

### REFERENCES

1. Almeida SA, et al. *Med Sci Sports Exerc* **31**, 1807-1812, 1999.
2. Fulkerson JP, et al. *Disorders of the patellofemoral joint*. Lippincott Williams & Wilkins, 2004.
3. Powers CM, et al. *J Orthop Sports Ther* **33**, 677-685, 2003.
4. Lee TQ, et al. *J Orthop Sports Phys Ther* **33**, 686-693, 1994.
5. Chen YJ, et al. *J Appl Biomech*, **26**, 415-423, 2010.
6. Farrokhi S, et al. *Osteoarthr Cartilage*, **19**, 287-294, 2010.
7. Besier TF, et al. *J Orthop Res* **26**, 1627-1635, 2008.

**Table 1:** Peak hydrostatic pressure and average hydrostatic pressure at the cartilage-bone interface at different values of internal rotation of the femur

| Cartilage-Bone Interface |                                 |                                    |
|--------------------------|---------------------------------|------------------------------------|
| Internal Rotation        | Peak Hydrostatic Pressure (MPa) | Average Hydrostatic Pressure (MPa) |
| Neutral                  | 2.14±0.65                       | 0.80±0.19                          |
| 5°                       | 2.88±0.83*                      | 1.14±0.27*                         |
| 10°                      | 3.25±1.03*                      | 1.15±0.29*                         |

Values are presented as mean ± SD. \* indicates a significant difference in hydrostatic pressure from neutral position of femur.

# SPARSE CONTROL OF FORCE DURING HUMAN LOCOMOTION: LESSONS FROM HOPSCOTCH

Jasper T. Yen and Young-Hui Chang

Comparative Neuromechanics Laboratory, Georgia Institute of Technology, Atlanta, GA, USA  
email: [jaspery@gatech.edu](mailto:jaspery@gatech.edu) web: <http://www.ap.gatech.edu/Chang/Lab/CNL/home.html>

## INTRODUCTION

How do we control our legs during locomotion? For hopping and running gaits, the behavior of neuromechanically complex legs can be replaced with a simple linear spring [1]. This suggests that higher levels of the nervous system may only attend to a relatively small number of task-level variables. But, what are these variables? Since end-point leg force determines COM movement dynamics, we tested whether covariation of joint torques acted in concert to stabilize the limb force during bouncing gaits. Previous work showed that forces generated by the leg are stabilized during 1-legged hopping in place [2,3]. Here, we tested the generality of this force-control hypothesis for: (i) 2-legged hopping and (ii) how this force control changed between steady-state hopping versus when subjects were asked to alternate between 1-legged and 2-legged hopping in a hopscotch-like pattern.

## METHODS

Eleven healthy subjects (24.4±3.0yrs, 61.3±7.3kg, 173.2±4.6cm) provided informed consent (Georgia Tech IRB H09036) to hop in place to the beat of a metronome (2.2 Hz). Subjects hopped for three 30-second trials in each of three randomized conditions: (1) on their right leg only; (2) on both legs; and, (3) alternating 2 hops each on 1leg and then 2 legs throughout the trial in a hopscotch fashion. Sagittal plane ankle, knee and hip torques (net muscle moments) were calculated from kinematics (Vicon, UK, 120Hz) and ground reaction forces (AMTI, USA, 1080 Hz). Approximately 150 hops were analyzed for each subject and condition.

We used a previously described [3] hybrid Uncontrolled Manifold and permutation approach to determine if vertical force was controlled through covariation of joint torques. Briefly, for each subject and hopping condition, total joint torque variance across hops was separated into two

components: goal-equivalent variance (GEV) that maintains a consistent force value from hop to hop; and non-goal equivalent variance (NGEV) that contributes to inconsistent forces across hops. We used index of motor abundance (IMA, eq. 1) to quantify and compare the degree of force stabilization across subjects, normalized by the total joint torque variance (TOTV).

For a given time slice of the hop cycle, GEV was found by projecting the 3x3 joint torque covariance matrix onto the null space of a 1x3 matrix. This 1x3 matrix maps joint torques to vertical force and is the dynamically consistent inverse of the Jacobian relating joint angle changes to vertical endpoint position changes. NGEV was found by projecting the covariance matrix again, but onto the range space instead of the null space. The difference of these two projections normalized by total joint torque variance per degree of freedom (TOTV), yields IMA. This procedure was repeated for the same covariation matrix, but with the non-diagonal elements set to zero, which is the equivalent of removing all effects of covariation. This can also be done via creating a second data set through permutating all joint torque combinations of the experimental data set or randomly shuffling the data an infinite number of times. This process yields a quantity of independent variation (InV). CoV is the difference of IMA and InV (eq. 2).

$$\text{IMA} = [\text{GEV}-\text{NGEV}]/\text{TOTV} \quad \text{eq. 1}$$

$$\text{CoV} = \text{IMA} - \text{InV} \quad \text{eq. 2}$$

Therefore, a positive CoV (Student's 1-tailed t-test,  $\alpha=0.005$ ) will indicate that joint torques are covaried to stabilize the force value at a particular time slice across hop cycles.

## RESULTS AND DISCUSSION

The net vertical force trajectory for all hopping conditions followed the typical monophasic pattern, with peak force being reached at mid-stance phase.

The variance of net vertical force, however, showed a local minimum at mid-stance suggesting that peak force was relatively consistent from hop to hop (Fig.1). Interestingly, this is exactly when joint torques are most variable from hop to hop (Fig.1).

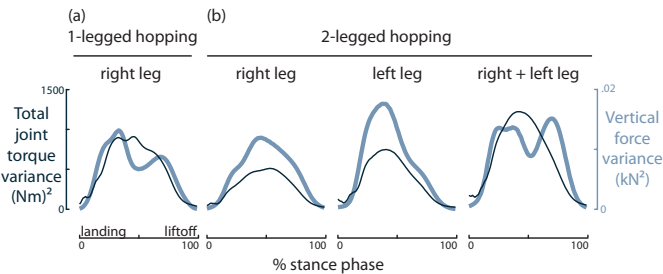


**Figure 1:** Across hops, total joint torque variances (thin black lines) show monophasic trajectories. Vertical force variances (thick blue lines) show biphasic pattern, but only when the net force for the task is considered: (A) right leg force for 1-legged hopping (A), and (B) right+left leg force for 2-legged hopping. Data are from a representative subject.

Peak value of the net force generated on the ground was always stabilized through joint torque covariation. Our metric of joint torque covariation for force stabilization, CoV, was positive only at mid-stance and only when net force applied to the ground was considered (Fig.2). For example, during steady state 1-legged hopping the joint torques of the right leg were covaried to stabilize the peak force generated by the right leg. And, during steady state two-legged hopping joint torques from both legs were covaried to stabilize the net force from both legs. In contrast, individual leg forces during 2-legged hopping were not stabilized indicating that stabilizing each leg's force was not a requirement of the control system. Rather, the implicit task variable for hopping appears to be peak value of the net force generated on the ground, regardless of the number of legs used. This rule for stabilizing the peak value of net vertical force was still observed even when subjects alternated between 1-legged and 2-legged hops during the same trial in a hopscotch-like fashion (Fig.2).

Surprisingly, we found that only the peak force, rather than the entire force trajectory, needs to be stabilized for hopping locomotion to emulate a spring-mass system. In another study, we also found identical results for human treadmill running [4], so it is likely these principles extend to bouncing gaits in general.

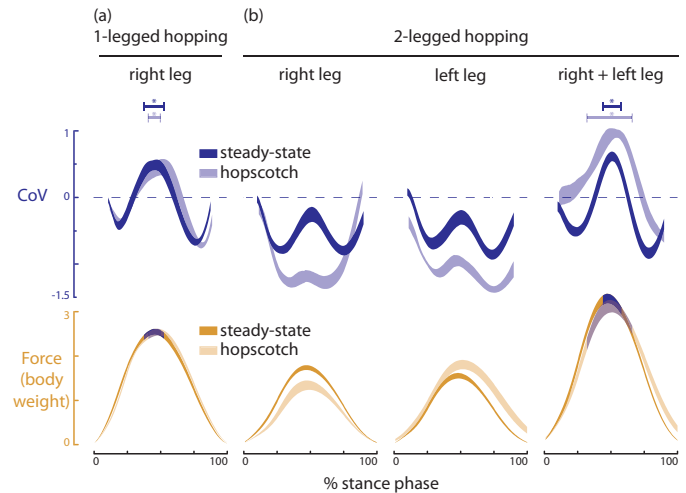


**Figure 2:** CoV (upper) and vertical force (lower) trajectories across subjects plotted for: (A) 1-legged hopping; and (B) 2-legged hopping. Steady state (darker) vs. Hopscotch (lighter) conditions are indicated in the legend. Data are means ( $\pm$ SD) across subjects and analyze the legs individually (right, left) or together (right+left). Horizontal bars and asterisks indicate when  $CoV > 0$  ( $p < 0.005$ ).

Humans coordinated joint torques to counteract natural deviations in order to make peak force consistent from hop to hop. This principle applies whether one is hopping on 1 leg, 2 legs or alternating between the two. Our results also agree with previous findings that 2-, 4-, 6-, and even 8-legged animals coordinate their legs to generate a single force trajectory emulating a spring-mass system [1]. This sparse control of force provides increased computational bandwidth that would be useful for real-time locomotor adjustments to other unexpected tasks such as stepping over obstacles or accommodating changes in surface properties.

## REFERENCES

1. Blickhan R and Full RJ. *J. Comp. Physiol. A*, **173**, 509-517, 1993.
2. Yen JT, et al. *J Exp Brain Res* **196**, 439-451, 2009.
3. Yen JT and Chang YH *J. Roy. Soc. Interface*, **7**, 801-810, 2010.
4. Yen JT. *Doctoral Thesis*, Georgia Institute of Technology, 2011.

## ACKNOWLEDGEMENTS

This work was supported by NSF IGERT and NSF GRFP to J.Y. and NSF BCS-0847325 to Y.H.C.

# Size of Error Affects Retention of Locomotor Adaptation in Human SCI

<sup>1,2</sup>Sheng-Che Yen, <sup>1</sup>Jill Landry and <sup>1,2</sup>Ming Wu\*

<sup>1</sup>Rehabilitation Institute of Chicago, Chicago, IL, USA

<sup>2</sup>Northwestern University, Evanston, IL, USA

\*Email: w-ming@northwestern.edu

## INTRODUCTION

Motor learning is driven by error detection and correction. Previous studies with an arm reaching task have shown that the error size may affect the retention of motor learning [1]. Specifically, when healthy subjects practiced adapting to a force perturbation in a reaching task, the aftereffect persisted longer if the perturbation force was applied in a gradual manner (i.e., causing a small size of error) than in an abrupt manner (i.e., causing a large size of error). However, it remains unclear if such motor learning rules can be generalized to leg movement in locomotor training. The purpose of this study was to determine whether the size of error affects the retention of locomotor adaptation in patients with incomplete spinal cord injury (SCI). We hypothesized that a large size of error caused by a large amount of resistance load may be detrimental to the retention of locomotor adaptation.

## METHODS

Twelve subjects with incomplete SCI (ASIA D) were recruited for this study. They were asked to walk on a treadmill while a controlled swing phase resistance load was applied to the right leg at the ankle using a customized cable-driven robot [2]. The resistance was applied from the late stance to the mid swing phase of gait.

There were 3 randomized testing conditions: light, medium, and heavy resistance loads. The medium resistance load was determined by the maximum load that each subject could comfortably tolerate. The light and heavy resistance loads were then defined as 30% below and above the medium resistance, respectively. Each test condition consisted of three periods, including baseline (1 minute), adaptation (7 minutes), and post-adaptation (2 minutes). In the baseline period, subjects walked

on a treadmill without resistance. In the adaptation period, subjects walked with a controlled resistance load. In the post-adaptation period, the resistance load was unexpectedly released while subjects continued walking on a treadmill.

The ankle trajectory data were recorded using customized position sensors. Electromyographic (EMG) activities of 6 muscles, including the tibialis anterior (TA), medial gastrocnemius (MG), soleus (SO), vastus medialis (VM), rectus femoris (RF), and medial hamstrings (MH) of right leg, were recorded. The stride length of right leg was calculated based on the ankle trajectory data. The EMG data were integrated for the first 30% of swing phase (IEMG data) of gait.

The stride length and IEMG data of each test condition were averaged across the last 20 strides of the baseline period (baseline values). We then calculated the difference between the baseline and the adaptation and post-adaptation values (the first 15 strides of each period). A positive difference indicated an increase in stride length or EMG activity from the baseline. One sample t-test was conducted at the  $\alpha$  level of 0.05 to examine if the difference was significantly different from 0.

## RESULTS AND DISCUSSION

The stride length from a typical subject during the post-adaptation period is presented in Figure 1A. There was an increase in stride length compared to the baseline, i.e., aftereffect, following the load release, for all three loading conditions. However, the retention of the aftereffect during the post-adaptation period varied depending on the loading condition. Subjects showed the longest retention of aftereffect with the medium resistance load. For instance, the stride length was 6 cm greater than the baseline at the first stride, and remained greater than

the baseline over the first 15 strides during the post-adaptation period. In the heavy resistance condition, the subject had a greater stride length at the first stride (i.e., 8 cm greater than the baseline), but the stride length declined rapidly in the following 9 strides. In the light resistance condition, the subject had a modest increase in stride length at the first stride (3 cm greater than the baseline), and the aftereffect was washed out after the 11<sup>th</sup> stride.

Statistical analyses using the group data are showed in Figures 1B, C and D. Significant increases in stride length were observed in 10 out of the first 15 strides during the post-adaptation period in the medium resistance condition (Figure 1B). In contrast, significant increases in stride length were observed in only 2 and 3 out of the first 15 strides during the post-adaptation period in the light (Figure 1C) and heavy (Figure 1D) resistance conditions, respectively.

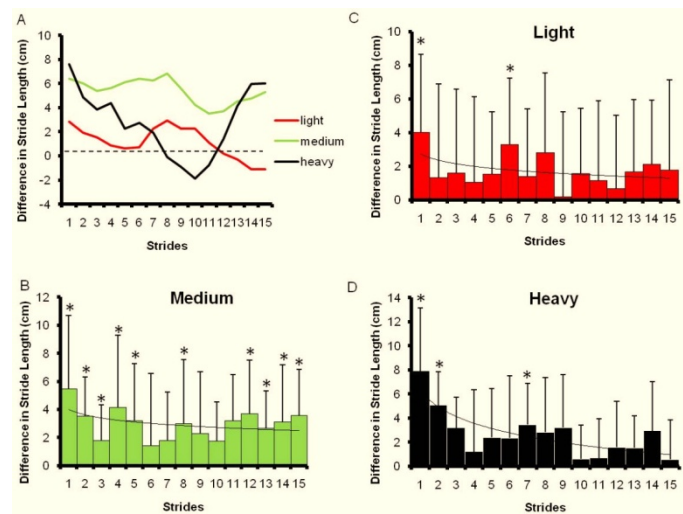


**Figure 1:** The gain in stride length in the first 15 strides during the post-adaptation period. (A) A typical subject's data in all conditions. Data were smoothed using a 3-point moving average technique. (B) Group data in the medium resistance condition. (C) Group data in the light resistance condition. (D) Group data in the heavy resistance condition. \*p < 0.05

Subjects experienced a larger error size in stride length when the resistance load was greater during adaptation period. For instance, the average stride length across the first 15 strides during adaptation period was reduced by  $0.42 \pm 5.8$ ,  $0.16 \pm 6.2$ , and  $0.1 \pm 4.7$  cm for the heavy, medium, and light resistance conditions, respectively. In addition, we

also observed that the swing time duration during the early adaptation period was increased by  $0.032 \pm 0.04$ ,  $0.025 \pm 0.04$  and  $0.015 \pm 0.03$  seconds for the heavy, medium, and light resistance conditions, respectively. Meanwhile, the peak velocity of leg swing was reduced by  $13.48 \pm 23.05$ ,  $10.64 \pm 16.87$  and  $5.49 \pm 12.79$  cm/s for the heavy, medium, and light resistance conditions, respectively.

Due to the larger variability of muscle activity across subjects with incomplete SCI, we did not observe significant changes in the IEMG data during the adaptation and post-adaptation periods for all test conditions.

The size of error during the adaptation period may influence the retention of aftereffect during the post-adaptation period. Specifically, the medium error size in stride length during adaptation was associated with the longest retention of the aftereffect during the post-adaptation period. In contrast, a large error size led to a greater aftereffect during the early post-adaptation period, but declined rapidly. In addition, a small size of error led to a modest amount of aftereffect, and was retained for a short period of time. Thus, it seems that there is an optimal amount of error that is needed to promote a longer retention of motor learning.

## CONCLUSIONS

We examined whether the size of error affects the retention of locomotor learning in patients with incomplete SCI. We observed that errors that are too large or too small are detrimental to the retention of motor learning. These results suggest that a patient-specific optimal amount of error in leg kinematics may be needed to enhance the locomotor training in patients with SCI.

## REFERENCES

1. Criscimagna-Hemminger, et al. *J Neurophysiol* **103**, 2275-2284, 2010.
2. Wu, et al. *Gait & Posture*, **33**: 256-60, 2011.

## ACKNOWLEDGEMENT

This study is supported by Craig H. Neilsen Foundation, #124890 (Wu, M). The authors would like to thank Drs. Brian D. Schmit and T. George Hornby for their helps.

# GAIT IN PATIENTS WITH COPD IS MAINLY AFFECTED IN PROXIMAL MUSCULATURE

<sup>1</sup>Jennifer Yentes, <sup>2</sup>Stephen Rennard and <sup>1,2</sup>Nicholas Stergiou

<sup>1</sup>University of Nebraska at Omaha, Omaha, NE, USA

<sup>2</sup>University of Nebraska Medical Center, Omaha, NE, USA

email: [jmyentes@unmc.edu](mailto:jmyentes@unmc.edu) web: <http://nbcf.unomaha.edu>

## INTRODUCTION

Chronic obstructive pulmonary disease (COPD) is currently the only chronic disease on the rise. In December of 2010, the US Centers for Disease Control ranked COPD as the third leading cause of death [1]. Typically thought of as a lung disease, the effects of COPD are not limited to the lung, however. It is known that patients with COPD exhibit abnormalities in structure and function of skeletal muscle tissue [2,3]. These include muscle fiber type shifting and decreased mitochondrial density and oxidative capacity [2]. These changes have been noted primarily in thigh musculature with little change being documented in shank musculature [3]. Thus, we hypothesized that the abnormalities in skeletal muscle tissue lead to changes in gait patterns in patients with COPD, especially at the hip.

## METHODS

Twenty [10 controls (66.8±6.3 years; FEV1: 1.0±11.1), 10 COPD (64.8±7.8 years; FEV1: 46.2±19.3)] subjects walked at their self-selected pace along a ten meter pathway while kinematics (60 Hz; Motion Analysis Corp.) and kinetics (600 Hz; Kistler Instrument Corp.) were recorded. All subjects underwent a rest condition. Patients with COPD were also subjected to a fatigue condition. The rationale for the fatigue condition was that due to the decreased oxidative capacity and muscle fiber type shifting, further changes in gait may be noted.

For the rest condition, subjects were asked to rest a minimum of one minute between each trial to minimize fatigue. A total of five trials were collected. Patients with COPD then underwent a treadmill protocol to induce fatigue. They were then asked to walk at a self-selected pace at 10% incline until the onset of fatigue or for a maximum of 15

minutes. Subjects then repeated five walkover trials with no rest between trials. Group means from spatio-temporal parameters and peak joint moments during the stance phase were calculated from the patients with COPD in the rest and fatigue condition and were compared to the rest condition of the controls using independent t-tests. Data from the patients with COPD in the rest and fatigue condition were compared using dependent t-tests.

## RESULTS AND DISCUSSION

### Rest Condition

No differences were found between healthy controls and patients with COPD for the spatio-temporal variables. Peak hip extension moment was significantly increased in patients with COPD as compared to healthy controls ( $p=0.012$ ; Figure 1). No significant differences were found for the knee and ankle.

### Fatigue Condition

No differences were found between healthy controls and patients with COPD for spatio-temporal variables. Hip extension moment was significantly increased in patients with COPD as compared to healthy controls ( $p = 0.017$ ) (Figure 1). No significant differences were found for the knee and ankle.

### Rest vs. Fatigue Condition

No significant differences were found in spatio-temporal parameters or peak joint moments in the rest vs. the fatigue condition in patients with COPD.

In accordance with our hypothesis, the hip was the only affected joint. The peak hip extension moment was the only parameter to demonstrate significant differences in both the rest and fatigue conditions. Since only the extensors were affected, this may not be due to the changes in skeletal muscle structure

and function noted previously in proximal tissues. Underlying mechanisms to abnormal skeletal muscle tissue could arise from physical inactivity or peripheral inflammation. The peak hip extension moment in early stance represents the ability to move the body's center of mass forward and upward. It is possible that the subjects with COPD walked with a forward trunk inclination as compared to controls; hence, demonstrating an increased hip extension moment [4]. This strategy may have been adopted because the primary focus of trunk musculature in patients with COPD is on respiratory activity and may not be on movement. However, trunk angle was not measured in this study.

Curiously enough, the peak hip extension moment was not significantly different within the patients with COPD from rest to fatigue condition. It appears that the gait abnormalities in patients with COPD are present even when the subject is well rested and metabolic demand is at its lowest. Another reason for lack of significant differences between the two conditions could have been our fatigue protocol. This protocol was modified from a standard fatigue protocol for peripheral arterial disease [5]. However, the selection of self-selected pace may not be enough to increase metabolic demand.

## CONCLUSIONS

These results provide preliminary evidence that patients with COPD demonstrate an altered gait pattern as compared to controls. In accordance with our hypothesis, these changes are documented at the hip joint and were not seen at the knee or ankle. The use of biomechanical gait analysis allowed us to determine specific adaptations at the hip that are unique in comparison to gait adaptations from other pathologies such as peripheral arterial disease and multiple sclerosis. Further investigations are warranted to clearly identify mechanisms of altered gait patterns in patients with COPD.

## REFERENCES

1. Miniño A, et al. *Natl Vital Stat Rep* **59**, 2010.
2. Allaire J, et al. *Thorax* **59**, 673-678, 2004.
3. Gosker HR, et al. *Eur Respir J* **30**, 73-79, 2007.
4. Leteneur S, et al. *Clin Biomech* **24**, 190-5, 2009.
5. DiBianco R, et al. *Am Heart J* **108**, 1121-7, 1984.

## ACKNOWLEDGEMENTS

Funding provided by American Society of Biomechanics Grant-in-Aid, NASA Nebraska Space Grant Fellowship program and Research Support Fund from the Nebraska Medical Center and the University of Nebraska Medical Center, NIH/NIA 1R011AG034995-01A1 and NIDRR H133G080023.

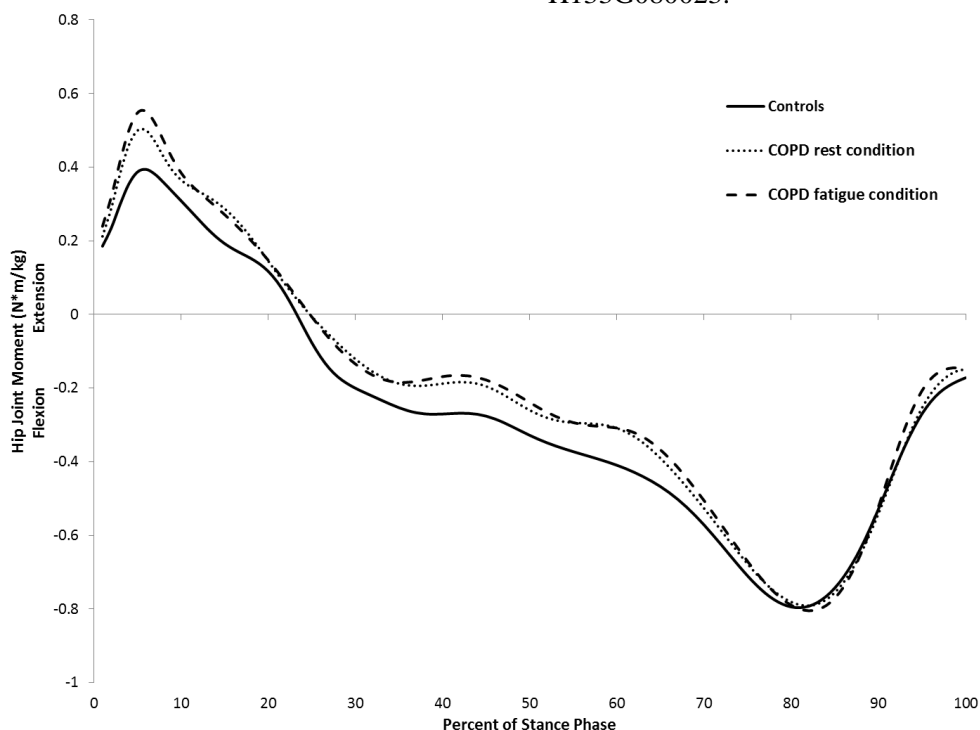


**Figure 1:** Mean ensemble curves for hip joint torques from the stance phase of gait. A positive value indicates extension moment and negative values indicate flexion moment.

# ADAPTATIONS IN JOINT KINETICS OVER CONSECUTIVE STEPS IN STAIR NEGOTIATION

<sup>1</sup>Jennifer Yentes, <sup>2</sup>Srikant Vallabhajosula and <sup>1,2</sup>Nicholas Stergiou

<sup>1</sup>University of Nebraska at Omaha, Omaha, NE, USA

<sup>2</sup>University of Nebraska Medical Center, Omaha, NE, USA

email: jyentes@unomaha.edu web: <http://nbcf.unomaha.edu>

## INTRODUCTION

For over 40 years, biomechanists have worked to understand strategies employed during stair negotiation. Due to limitations in experimental design, stair negotiation has not been completely defined. Typically, stair design has allowed for one to two force platforms to be inserted into the steps of the stairway. These designs would allow for analysis of one step or potentially two consecutive steps from opposite limbs. Further analysis has been done to compare joint kinematics and kinetics from stair negotiation to overground walking. However, we have been unable to find published data on consecutive steps from the same limb during stair negotiation. Therefore, we have developed a unique design that allows collection of three consecutive steps from the same limb, one overground step and two steps during stair ascent. The aims were to investigate adaptations in joint kinematics and kinetics as one approaches the stairway and then continues towards stair ascent.

## METHODS

A custom built four-step stairway was used for this study. The stairway was instrumented with force platforms (AMTI, Watertown, MA; 600 Hz) in the first three steps. The rise and run were set to architectural standards (0.18m and 0.27m, respectively). An additional fourth force platform (Kistler, Amherst, NY; 600 Hz) was mounted into the walkway 0.48 meters in front of the stairway. This allowed for collection of one overground step, and two consecutive steps (step 1 and 3) on the stairway.

Ten healthy subjects (age:  $26.4 \pm 3.7$  years; height:  $1.78 \pm 0.08$  meters; mass:  $76.2 \pm 13.6$  kg) were asked to start from a distance of three meters in

front of the stairway. Starting positions were determined by having the subject approach the stairs so that their right leg would contact the in-ground force platform, first and third step of the stairway. Five trials were collected and analyzed for each subject.

Joint kinematics and kinetics were calculated from 3D marker trajectories (Motion Analysis Corp., Santa Rosa, CA; 60 Hz) and raw data from the force platform using custom MatLab code (Mathworks, Inc., Natick, MA). General linear models were used to compare group means of joint range of motion and discrete points from joint moment and power curves from the overground, step one and step three stance phases of gait using SPSS 18.0 (SPSS, Inc., Chicago, IL).

## RESULTS AND DISCUSSION

Results are presented in Table 1.

Comparing overground to step 1, it appears that the lower limb demonstrates a straighter leg approach with the knee and hip not as flexed when compared to previous results [1]. Hip joint power generation at early stance exhibits a much smaller peak moving quickly into power absorption. Previous overground data demonstrate a much larger peak in power generation at early stance with power generation lasting for roughly the first 50% of the stance phase [1]. During late stance, the knee joint moment remains as a flexion moment whereas previous reports showed that the knee will move into an extension moment at late stance [1]. This is associated with increased knee power generation at approximately 70% of the stance phase followed by reduced knee power absorption in the last 10% of stance phase as compared to published literature [1]. These adaptations are mainly seen at the hip during

early stance and in the knee during late stance. It appears that the hip demonstrates decremented function at early stance and the knee generates an extra boost of energy in late-mid stance. These changes are potentially due to the increased hip and knee flexion that is needed to clear the first step of the stairway.

The current data do demonstrate that adaptations are made from the first step to the second step within the same limb. During early stance, the hip displays increased power generation almost immediately before the knee displays increased power absorption. In addition, the knee demonstrates an increased knee flexion moment at late-mid stance, followed closely by the ankle exhibiting increased plantarflexion moment at late stance. These findings appear to support a redistribution of joint moments and powers. It is known that this is an adaptation seen in level walking in older adults [2] and quite possibly could be demonstrated in young adults

under certain demanding tasks as well. Mechanically, this could also be due to the changes in joint ROM seen during stair ascent. Increased ROM in the hip and knee would allow for increased angular velocity, which is directly associated with power.

## REFERENCES

1. Riener R. *Gait Posture*, **15**, 32-44, 2002.
2. DeVita P & Hortobagyi T. *J App Physiol*, **88**, 1804-1811, 2000.

## ACKNOWLEDGEMENTS

Funding provided by American Society of Biomechanics Grant-in-Aid, NASA Nebraska Space Grant Fellowship program and Research Support Fund from the Nebraska Medical Center and the University of Nebraska Medical Center, NIH/NIA 1R011AG034995-01A1 and NIDRR H133G080023.

**Table 1:** Statistical results reported for joint range of motion and peak discrete points from joint moment and power curves. Results are reported in mean±standard deviation. Main effect and post-hoc p-values are provided.

|                 | Overground   | Step 1       | Step 3       | p-value        | Over –<br>Step 1 | Over –<br>Step 2 | Step 1 –<br>Step 2 |
|-----------------|--------------|--------------|--------------|----------------|------------------|------------------|--------------------|
| Ankle ROM (deg) | 20.2 ± 5.4   | 7.0 ± 2.6    | 4.9 ± 4.2    | < <b>0.001</b> | < <b>0.001</b>   | < <b>0.001</b>   | 0.130              |
| Knee ROM (deg)  | 9.0 ± 4.3    | 42.7 ± 4.3   | 48.2 ± 5.3   | < <b>0.001</b> | < <b>0.001</b>   | < <b>0.001</b>   | <b>0.039</b>       |
| Hip ROM (deg)   | 32.1 ± 3.2   | 46.1 ± 4.2   | 50.1 ± 3.4   | < <b>0.001</b> | < <b>0.001</b>   | < <b>0.001</b>   | <b>0.034</b>       |
| ADM (N/kg) †    | -0.26 ± 0.12 | -0.04 ± 0.03 | -0.07 ± 0.05 | < <b>0.001</b> | < <b>0.001</b>   | < <b>0.001</b>   | 0.091              |
| APM (N/kg)      | 1.6 ± 0.40   | 1.5 ± 0.41   | 1.7 ± 0.45   | <b>0.03</b>    | 0.180            | 0.249            | <b>0.006</b>       |
| KEM (N/kg)      | 0.56 ± 0.15  | 0.27 ± 0.10  | 0.27 ± 0.08  | < <b>0.001</b> | < <b>0.001</b>   | < <b>0.001</b>   | 0.675              |
| KFM (N/kg)      | -0.11 ± 0.07 | -0.30 ± 0.20 | -0.07 ± 0.12 | < <b>0.001</b> | <b>0.012</b>     | 0.308            | < <b>0.001</b>     |
| HEM (N/kg)      | 0.88 ± 0.27  | 0.40 ± 0.16  | 0.38 ± 0.18  | < <b>0.001</b> | < <b>0.001</b>   | < <b>0.001</b>   | 0.781              |
| HFM (N/kg)      | -1.0 ± 0.25  | -0.78 ± 0.26 | -0.75 ± 0.22 | < <b>0.001</b> | <b>0.003</b>     | < <b>0.001</b>   | 0.561              |
| A1 (W/kg) †     | -0.63 ± 0.25 | -0.61 ± 0.19 | -1.0 ± 0.82  | 0.12           |                  |                  |                    |
| A2 (W/kg)       | 3.8 ± 1.1    | 3.4 ± 1.2    | 3.8 ± 1.5    | 0.34           |                  |                  |                    |
| K1 (W/kg) †     | -0.65 ± 0.53 | -0.18 ± 0.13 | -0.25 ± 0.12 | <b>0.020</b>   | <b>0.016</b>     | <b>0.024</b>     | <b>0.014</b>       |
| K2 (W/kg) †     | 0.31 ± 0.31  | 1.8 ± 0.46   | 1.8 ± 0.47   | < <b>0.001</b> | < <b>0.001</b>   | < <b>0.001</b>   | 0.840              |
| K3 (W/kg) †     | -0.38 ± 0.22 | -0.21 ± 0.11 | -0.29 ± 0.11 | 0.15           |                  |                  |                    |
| H1 (W/kg)       | 0.38 ± 0.23  | 0.95 ± 0.47  | 1.2 ± 0.56   | < <b>0.001</b> | <b>0.002</b>     | < <b>0.001</b>   | <b>0.006</b>       |
| H2 (W/kg) †     | -0.53 ± 0.19 | -0.38 ± 0.17 | -0.45 ± 0.59 | 0.56           |                  |                  |                    |
| H3 (W/kg) †     | 0.96 ± 0.30  | 0.23 ± 0.19  | 0.25 ± 0.27  | < <b>0.001</b> | < <b>0.001</b>   | < <b>0.001</b>   | 0.615              |

Note: (†) indicates the variable did not meet the standards of normality. **Joint ROM:** Range of motion is defined as the range from lowest peak to highest peak. **Joint moment:** All values are normalized to body mass in kilograms and height in meters. A positive value for the ankle indicates plantarflexion moment. For the hip and knee, a positive value indicates extension moment. Peak variables used in analysis are Ankle Dorsiflexor Moment (ADM), Ankle Plantarflexor Moment (APM), Knee Extensor Moment (KEM), Knee Flexor Moment (KFM), Hip Extensor Moment (HEM), and Hip Flexor Moment (HFM). **Joint power:** For all joints, a positive value indicates power generation. The peak variables identified for joint powers were: ankle power absorption in mid-stance (A1), ankle power generation in late stance (A2), knee power absorption in early stance (K1), knee power generation in early stance (K2), knee power absorption in late stance (K3), hip power generation in early stance (H1), hip power absorption in mid-stance (H2) and hip power generation in late stance (H3).

# AN EVALUATION OF PHENOMENOLOGICAL MODELS OF THE FORCE-VELOCITY RELATIONSHIP OF SHORTENING MUSCLE

Sang Hoon Yeo<sup>1</sup>, A. Kristopher Lappin<sup>2</sup>, Kiisa C. Nishikawa<sup>3</sup> and Dinesh K. Pai<sup>1</sup>

<sup>1</sup> University of British Columbia, Vancouver, BC, Canada

<sup>2</sup> California State Polytechnic University, Pomona, CA, USA

<sup>3</sup> Northern Arizona University, Flagstaff, AZ, USA

email:shyeo@cs.ubc.ca

## INTRODUCTION

Muscle, as a dynamical system, changes its force with length and velocity. Although there are well established models of its isometric force-length (FL) and force-velocity (FV) relationships, the coupled dynamics of these two relationships is still not clearly understood [4].

Hill's characteristic equation [1] is widely used for describing the apparent viscosity of shortening muscle, and can be written as:

$$(P + a)(V + b) = (P_0 + a)b = \text{const},$$

where  $P$  is the load,  $V$  is the velocity,  $P_0$  is the load in the isometric condition, and  $a$  and  $b$  are considered to be constants. Hill also suggested a dimensionless parameter  $k$  that is consistent over various types of muscle, which is defined as:

$$k = \frac{a}{P_0} = \frac{b}{V_{max}},$$

where  $V_{max}$  is the maximum unloaded velocity.

Please note that the characteristic equation only describes FV behavior at rest length. At different lengths,  $a$ ,  $b$ ,  $V_{max}$  and  $k$  may not be constant since  $P_0$  will be changed due to the FL relationship.

Surprisingly, there are few studies that clarify this problem. An investigation conducted by Abbott and Wilkie [2] showed that  $a$  and  $b$  stay constant for different lengths. Later, Edman revisited this problem using a different method of estimating  $V_{max}$  [3] and showed that  $V_{max}$  is constant over a wide range of sarcomere lengths. Epstein and Herzog [4] (Equation 2.13) proposed an alternative formulation we call the "force scaling model" that keeps  $V_{max}$  constant; this appears to be a common assumption in computer models as well ([6], p. 366).

The goal of this study is to investigate how well these two models predict force-length-velocity dynamics. Rather than measuring initial velocities at different lengths, we try to identify a model that can explain time series data of shortening muscle.

## METHODS

We use load-clamp data from toad (*Bufo alvarius* Girard) depressor mandibulae muscles used by Lappin et al. [5] (Figure 1, black lines). By removing fast oscillatory responses that are thought to be due to elastic recoil of the serial elastic elements, we can extract slow phase responses (Figure 1, red lines). We focus on how length and velocity are coupled in these slow phase responses.

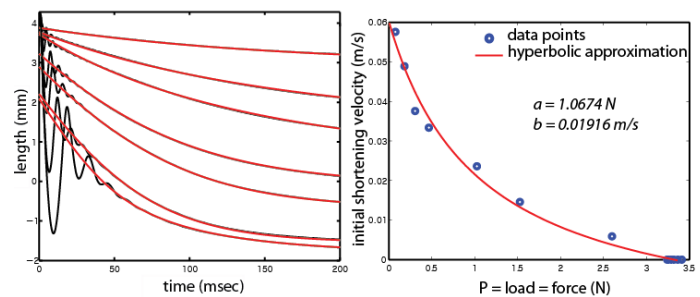


**Figure 1:** (left) Load-clamp data for different external loads (black lines) and estimated slow phase responses (red lines) of the toad DM muscle. (right)  $a$  and  $b$  were estimated from measuring initial shortening velocities vs. loads.

First, we estimate  $a$  and  $b$  using the traditional method that analyzes the relationship between initial velocity and loads. Using these constants, we qualitatively evaluate two models.

When the muscle length is shorter than its rest length and the corresponding isometric force at that length is  $\bar{P}_0 = r P_0$  with  $r < 1$ , we assume that the

parameters  $(a, b, V_{max}, k)$  are changed to  $(\bar{a}, \bar{b}, \bar{V}_{max}, \bar{k})$ . Two predictions above can be summarized as:

**Table 1:** Predictions of FV parameters

| New Constants           | $\bar{a}$ | $\bar{b}$ | $\bar{V}_{max}$ | $\bar{k}$ |
|-------------------------|-----------|-----------|-----------------|-----------|
| Abbott and Wilkie 1953  | $a$       | $b$       | $rV_{max}$      | $k/r$     |
| Force Scaling Model [4] | $ra$      | $b$       | $V_{max}$       | $k$       |

Since  $P$  is given,  $[\bar{a}, \bar{b}]$  are predicted, and  $V$  is measured, we can estimate  $\bar{P}_0 = (P + \bar{a})(V + \bar{b}) / \bar{b} - \bar{a}$  for each measurement within each time series. By plotting  $\bar{P}_0$  with respect to the measured length at a given time, FL can be estimated. If the model is correct, the estimated FLs for different trials should fall on a curve that is expected to look similar to the ascending limb of the muscle's FL curve. Based on a qualitative evaluation of the estimated FL curves, we select a model that gives the best result. After selecting the model, we find the corresponding parameters  $[a, b, V_{max}, k]$  that minimize the estimation error. Finally, the estimated parameters are compared to the results using the traditional method.

## RESULTS AND DISCUSSION

Using FV relationships for two different models, the estimated FL curves are shown in Figure 2.

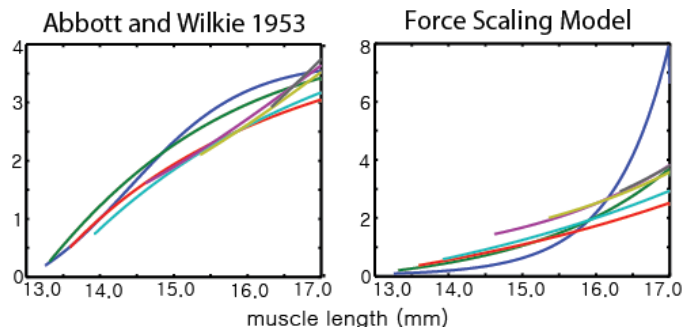


**Figure 2:** Estimation of dynamic FL curves. The measured rest length is 17.0mm. Note the scale difference in y-axis due to the blue outlier of the right figure, corresponding to the fastest shortening.

Abbott and Wilkie's 1953 model gives a reasonable result that shows a linear FL with slightly convex region around the rest length. The force scaling model predicts concave FL relationships and significantly overestimates load for high speed contraction. These preliminary analyses suggest that Abbott and Wilkie's model is a reasonable representation of the FV relationship at varying muscle lengths.

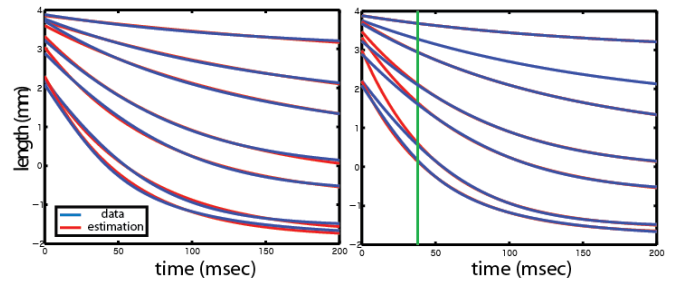


**Figure 3:** (left) Data (blue) and estimation (red) of the slow phase data using Abbott and Wilkie's model. (right) Estimation when initial data are excluded. Estimation starts after green line.

Using Abbott and Wilkie's formulation, values of  $[a, b]$  that minimize the prediction error are found to be  $[0.419N, 0.01m/s]$ . The error does not exceed 6% of the total length change. Surprisingly, these values are about 50% smaller than those predicted using the traditional method. Since our method accounts for the entire time series data (not just the initial velocity), we think that these are more reasonable for use in simulations. We also verified that the qualitative comparison still holds for smaller initial estimates of  $a$  and  $b$ .

Although the result is preliminary and needs more validation, the reason for this discrepancy in FV parameters can be an interesting question. As shown in Figure 3 (right), most of the error is from the initial phase, and the amount of the initial instant shortening (length at  $t=0$ ) is consistently larger than expected. This may indicate that the fast, initial phase of the shortening is affected by a non-cross-bridge component, which is consistent with the interpretation of Lappin et al. [5] of elastic recoil. Considering that  $a$  is related to the heat production of the muscle, the result is also consistent with Hill's original observation that muscle produces remarkably less heat when shortening at higher speeds, suggesting that this un-modeled component may initially power the sarcomere to shorten quickly without ATP hydrolysis.

## REFERENCES

1. Hill AV, *Proc. Roy. Soc. B.* **126** 136-195, 1938.
2. Abbott BC, Wilkie DR, *J. Physiol.* **120**, 214-223, 1953
3. Edman KA, *J. Physiol.* **291**, 143-159, 1979
4. Epstein M, Herzog W, *Wiley* (book), p. 42, 1998
5. Lappin AK, et al. *J Exp Biol* **209**, 2535-2553, 2006
6. Zajac FE, *Crit. Rev. Biomed. Engg.*, 17 (4), 1989

## ACKNOWLEDGEMENTS

This work was supported in part by the Canada Research Chairs program, a CIHR (CRCNS) operating grant, PWIAS, NSERC, and NSF grants IIS-0827688 and NSF IOS-1025806.

# QUANTIFICATION OF SENSORY REWEIGHTING FOR THE DIRECTIONAL MOTION PERCEPTION

Yongwoo Yi and Sukyung Park

Korea Advanced Institute of Science and Technology, Daejeon, Korea  
email: sukyungp@kaist.ac.kr

## INTRODUCTION

The body motion is detected by the multi-sensory organs such as eyes, vestibular organ, and somatosensory system. Obtained multi-sensory cues are then integrated in the central nervous system to perceive the motion. This sensory integration process is adjusted and changed according to various sensory conditions and each sensory state. This sensory reweighting is necessary for postural control. There are, however, few quantitative models to describe the sensory reweighting for motion perception. In this study, we suggested the novel model that quantifies the visual and vestibular sensory reweighting for the motion perception.

## METHODS

We measured perception of directional movement under two different sensory conflict conditions. Nine healthy young volunteers (aged  $23.2 \pm 2.1$ ) were participated. Subjects reported no history of balance disorder, and signed the informed consent form. Subjects were experienced randomly sequenced translational support surface movement of a single sinusoidal acceleration (1mG, 0.1Hz) under various visual conditions. After each translation, subjects verbally reported their perceived direction of motion. Three different visual conditions (eyes closed, eyes open with coherent or reversed vision) were designed to examine the change of the sensory weight under the sensory conflict conditions. Subjects wore the head mounted display (HMD) that displayed coherent or reversed vision based on the tracked head motion.

Collected perceived directional response data was fitted using a sensory reweighting model. The sensory reweighting model consisted of a single inverted pendulum model and an internal model [1, 2]. Since the stimulus was short and smooth

translational movement, we assumed the dominant motion cues would be come from the otolith and vision. The estimation of perceived movement was calculated from sum of the each weighted sensory signal. Sensory error between actual sensory cues and the efferent copy was feed back to the Kalman filter and then used to estimate the perceived motion [3] (Fig. 1).

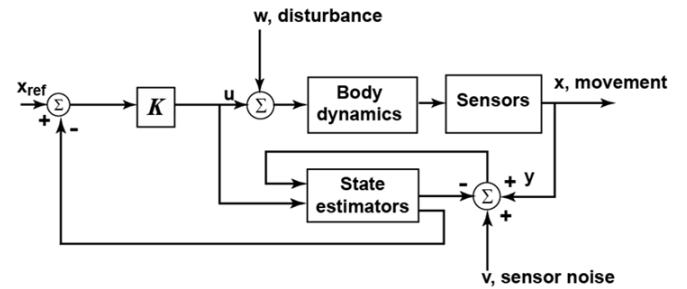


Figure 1: State estimate feedback realization.

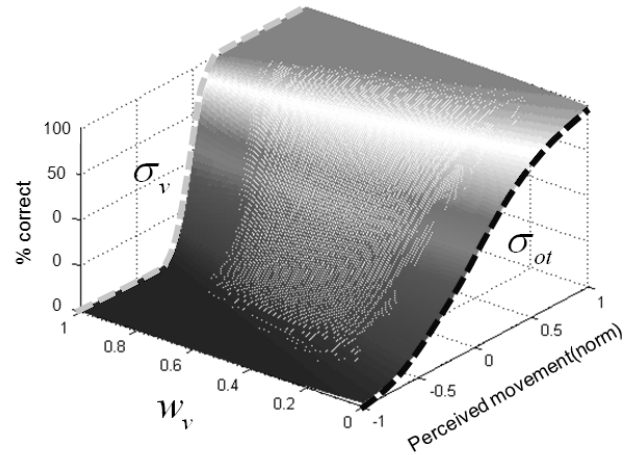
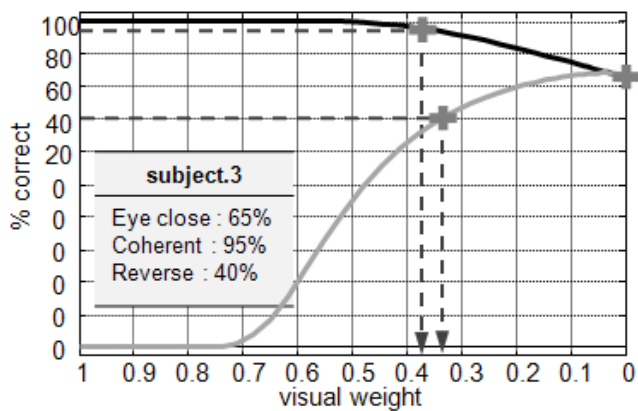


Figure 2: Extended psychometric function. To reflect the visual and otolith sensory characteristics, a sum of the weighted  $\sigma_v$  and  $\sigma_{ot}$  was used for the model parameter.

Estimated direction of motion (i.e. perception) was converted to %-correct response using psychometric function and then compared with empirical data.

Since the simulation model only included otolith and visual cues, the psychometric function had two empirical model parameters ( $\sigma_v, \sigma_{ot}$ ) that determined the overall shape of psychometric function. The probability of correct responses became the function of a perceived distance ( $x$ ) and a visual weight ( $w_v$ ) (Fig. 2). By combining psychometric function and estimated perceived movement, we obtained a relation between the sensory weight and %-correct response (Fig. 3A). Finally, the sensory weight was obtained by matching the empirical %-correct response data to the relation between the sensory weight and %-correct response.



**Figure 3:** A. Relation between the change of sensory weight and correct response under coherent (black) or reversed (grey) visual trial.

## RESULTS AND DISCUSSION

When visual information was reversed from actual head movement, correct perceived directional response was reduced. When subjects did not know the possibility of the sensory conflict condition, they entirely trusted the visual information even in the reversed vision trial (%-correct in coherent trial: 98.8% / reversed trial: 4.7%) (Fig. 4A). On the other hand, reliability for vision cues was consciously reduced when subjects were aware of the sensory conflict (%-correct in coherent trial: 92.2% / reversed trial: 16.1%) From model, we estimated relative sensory weights that matched % correct data. In a coherent sensory condition, the ratio of visual to vestibular sensory weight was calculated as 0.68: 0.32( $\pm 0.13$ ) (Fig. 4B). The visual sensory weight was significantly reduced to 0.46( $\pm 0.05$ ) when the reversed vision was provided ( $p < 0.01$ ). When subjects were aware that the HMD

may provide reversed visual information, a visual weight was significantly reduced even under coherent vision trial ( $p < 0.05$ ). In this case, reduction of visual weight was not significantly changed under sensory conflict condition because visual weight was already consciously decreased.

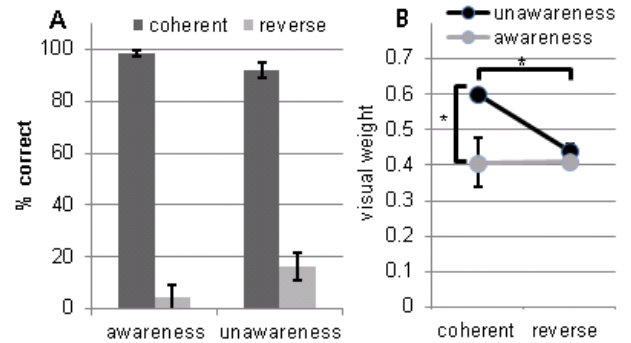


**Figure 4:** a. % correct response under each visual condition with and without aware of the sensory conflict trial. b. Visual sensory weight in each condition. Visual weight was reduced under sensory conflict.

## CONCLUSIONS

We modeled the sensory reweighting for motion perception using the Kalman filter and a psychometric function. Sensory weight was significantly changed under sensory conflict condition. Vision cue plays dominant roles for the perception of the directional movement and the visual weight was reduced under sensory conflict condition. Moreover, awareness of sensory condition could influence the change of sensory weight. This result implies that CNS may adjust sensory weights in an optimal matter to better use of reliable sensory information. Conscious sensory conditions would also affect sensory reweighting.

## REFERENCES

1. Wolpert D. et al. *Science* **269**, 1880-1882, 1995.
2. Kuo A. *J Neural Eng* **2**, S235-S249, 2005.
3. Zupan LH. *Biol Cybern* **86**, 209-230, 2002.

## ACKNOWLEDGEMENTS

This research was supported by the Happy tech. program through the National Research Foundation of Korea (NRF) funded by the Ministry of Education, Science and Technology (#2010-0020488).

# HAMSTRING CONTRIBUTIONS TO KNEE MOTION DURING TERMINAL SWING IN CROUCH GAIT

<sup>1</sup>Jennifer R. Yong, <sup>1</sup>Katherine Steele, <sup>1</sup>Jennifer L. Hicks, <sup>2</sup>Michael S. Schwartz, <sup>1</sup>Scott L. Delp

<sup>1</sup>Stanford University, Stanford, CA, USA

<sup>2</sup>Gillette Children's Specialty Healthcare, St. Paul, MN, USA

email: [jryong@stanford.edu](mailto:jryong@stanford.edu)

## INTRODUCTION

Crouch gait, a gait abnormality characterized by excessive knee flexion during stance, is common in patients with cerebral palsy. Over-activity of the hamstrings during terminal swing is often implicated as a cause of this gait pathology. If an individual is unable to fully extend the knee before foot strike, he or she may not have the strength to extend the knee during stance and will remain in a crouched posture. One current treatment for crouch gait is surgical lengthening of the hamstrings, but this procedure does not always result in improved knee extension. A previous study showed that the hamstrings generate small contributions to knee angular accelerations during terminal swing of normal gait [1]. The goal of this study was to determine if a crouched posture changes the contribution of the hamstrings to knee motion and to evaluate whether the hamstrings contribute substantially to knee flexion accelerations during the terminal swing phase of crouch gait.

## METHODS

Previously reported averaged joint kinematics data of subjects walking in a normal gait (N=83) and in mild (N=89), moderate (N=127) and severe (N=100) crouch gait from Gillette Children's Specialty Healthcare was used to represent typical body positions [2]. Swing phase was assumed to occur during 60 – 100% of the gait cycle. The kinematics data was used to position a musculoskeletal model with 19 degrees of freedom and 92 musculotendon actuators [3] (Fig. 1). We used an induced acceleration analysis to calculate the angular acceleration of the knee generated by 1 N of force in each of the musculotendon actuators.

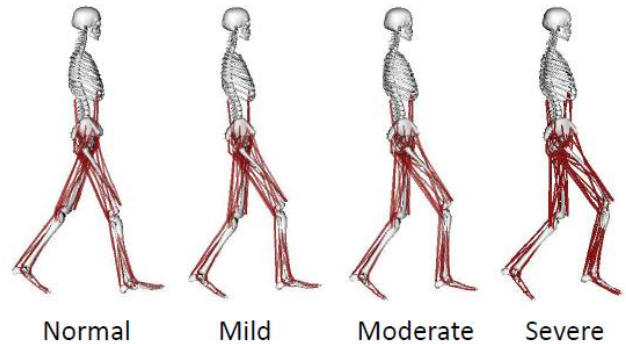


**Figure 1:** Musculoskeletal models during normal gait, mild, moderate and severe crouch gait from averaged kinematics data.

The acceleration generated per newton of force is referred to as the muscle's potential [4].

The angular acceleration of the knee was calculated for each gait pattern by double differentiating measured knee angle data. The swing phase was divided into an extension phase, when the knee experiences extension accelerations, and a subsequent braking phase, when the knee undergoes flexion accelerations [1]. For the purposes of this study, we defined terminal swing as the braking phase. The muscles' potentials were averaged over terminal swing. The primary contributors to knee flexion and extension accelerations on the swing limb were identified and compared to the potentials of the hamstrings for each of the different gait patterns.

## RESULTS AND DISCUSSION

We found that the transition to the braking phase of swing occurs later with more severe crouch. In normal gait, the braking phase of the right knee begins at 83% of the gait cycle, whereas it begins at

89%, 91% and 93% for mild, moderate and severe crouch gait respectively.

The medial hamstring muscles (semimembranosus and semitendinosus) had the potential to generate flexion accelerations at the knee during terminal swing (Fig. 2). For the semitendinosus, the magnitude of the flexion potential increased with increasing crouch severity. For the semimembranosus, we observed the opposite pattern. However, these discrepancies are small since the potentials all have magnitudes between 0.6 and  $2.4^{\circ}/s^2/N$ . In contrast, the biceps femoris long head, a lateral hamstring muscle, had a knee extension potential during terminal swing. The magnitude of these extension potentials decreased with the severity of crouch. Hamstring potentials are somewhat dependent on how degrees of freedom between the pelvis and the torso are modeled; however, the medial hamstrings consistently exhibit a greater knee flexion potential than the biceps femoris long head.

Although the medial hamstrings had flexion potentials in a crouch gait, the magnitudes of the potentials were small relative to other lower extremity muscles (not shown), as has been demonstrated for normal gait [1]. For example, the sartorius muscle, a hip and knee flexor, exhibited the greatest knee flexion potential with values that were an order of magnitude greater than the hamstrings during normal and crouch gait. The range of potentials for the sartorius muscle during terminal swing was  $20 - 27^{\circ}/s^2/N$ . Extension potentials by the vasti muscles were also significantly greater in magnitude. The vasti muscles had extension potentials ranging from  $22^{\circ}/s^2/N$  during terminal swing in severe crouch to  $43^{\circ}/s^2/N$  during normal gait. Thus, although we only calculated the potentials of the lower extremity muscles and not the forces they generated, our results suggest that the hamstrings have a minimal effect on angular knee motion during the terminal swing of crouch gait.

## CONCLUSIONS

Subjects walking in an increasingly severe crouch gait exhibited an increasingly delayed braking phase

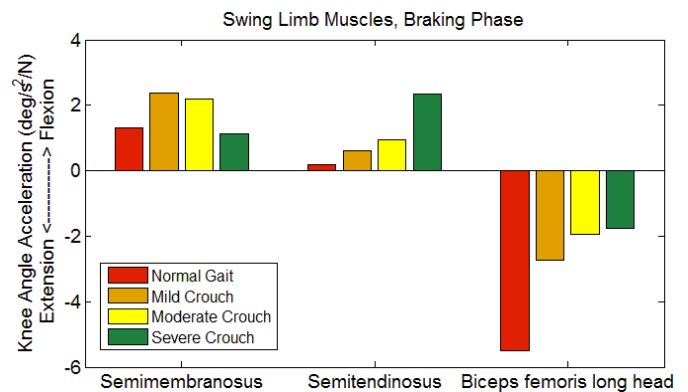


**Figure 2:** Potential of hamstring muscles to accelerate the knee during terminal swing of normal and crouch gait.

during swing. Individuals walking in a crouch gait experience a reduced range of motion and reduced knee extension accelerations during swing, and therefore do not require as much time to slow the angular velocity of their knee before foot strike. The medial hamstrings had flexion potentials during terminal swing, while the lateral biceps femoris long head had extension potentials. This suggests that during corrective surgery, focusing on the medial hamstrings may result in greater improvements in knee kinematics during swing. Although body position affects the hamstrings' ability to contribute to knee angle accelerations, potentials during crouch gait are similar to normal gait. Even in crouched postures, the hamstrings appear to be relatively small contributors to knee motion and would require significant force generation to produce excessive knee flexion in terminal swing. While overactive hamstring muscles may contribute through other mechanisms, such as their ability to decelerate the leg, a crucial next step is identifying how other muscles with larger potentials affect angular knee motion and may potentially contribute to crouch gait.

## REFERENCES

1. Arnold AS, et al. *J Biomech* **40**, 3314-3324, 2007.
2. Hicks JL, et al. *J Biomech* **41**, 960-967, 2008.
3. Delp SL, et al. *IEEE Trans Biomed Eng* **37**, 757-767, 1990.
4. Hamner SR, et al. *J Biomech* **43**, 2709-2716, 2010.

# A TECHNIQUE FOR DYNAMIC MARKER IDENTIFICATION TO LOCATE OCCLUDED ANATOMICAL LANDMARKS

<sup>a</sup>ByungJu Yoo, <sup>a</sup>SungDo Kim and <sup>a</sup>Andrew Merryweather, PhD

<sup>a</sup>University of Utah, Salt Lake City, UT, USA

email: robert.b.yoo@utah.edu web: <http://mech.utah.edu/ergo/>

## INTRODUCTION

Accuracy of anatomical landmark identification through marker placement is critical in biomechanical model creation. Various marker sets have been presented over the years, and have been widely adopted [1]. More recently, markerless systems for biomechanical analyses have been developed [2, 3]. Regardless of the system, there are situations where both techniques currently fail to identify landmarks that are hidden or blocked from the environment, or from assistive devices and equipment that interfere with the identification of body segments. The purpose of this study was to demonstrate the effectiveness of an alternate technique to locate anatomical landmarks on the pelvis, back and shoulders during gait to investigate the effect of being encumbered with a full-frame backpack.

## METHODS

The mathematical equation finding the location vector from two vectors, which are on the same line, is described in Figure 1 and Equation 1.

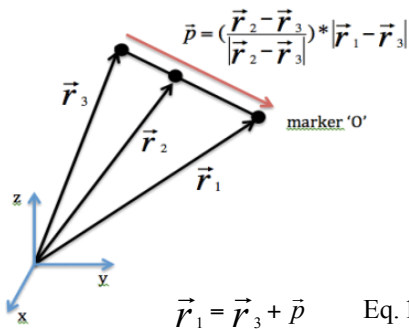


**Figure 1:** Vector notation to calculate the unit vector using two points located on the same line.

Multiplying the unit direction vector by the rod length defines the vector  $p$ . It represents the vector from the marker  $r_3$  to the marker  $r_1$  (Eq. 1).

Marker ‘O’ describes the point where the marker would be placed when not occluded. A similar technique is often used to identify virtual points with other models [4]. To calculate the feasibility and sensitivity of this method during dynamic motion capture, two lightweight, rigid rods were constructed with 3 retro-reflective markers concentrically aligned. Marker ‘O’ was located on one end of the rod, and defined the position of a “virtual” maker being calculated in place of an occluded anatomical landmark using Eq. 1. The lengths of the two rods are 254 mm and 127 mm. The distances between each marker are described in the Figure 2.

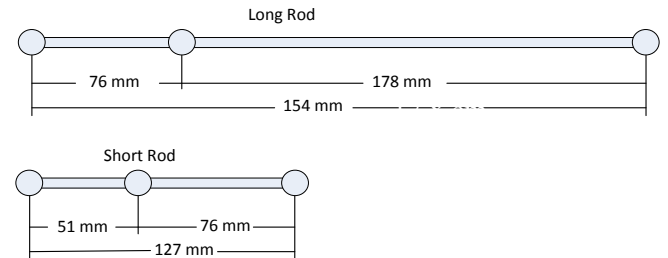


**Figure 2:** Two test rods and their dimensions (diameter of the marker is 1cm).

Marker position data were collected using 11 OptiTrack FLEX:V100R2 cameras and ARENA Motion Capture software (NaturalPoint Inc.) with 100 Hz sampling rate in a 2 x 3 x 2 m<sup>3</sup> capture volume. A single 5 sec trial for each rod was performed by waving the rod through space. A sensitivity analysis to compare the difference between the calculated position of point ‘o’, and the actual position determined from motion capture was conducted using Microsoft Excel for Mac.

## RESULTS AND DISCUSSION

Raw 3D marker coordinate data were conditioned using a quintic spline algorithm. A virtual marker position was calculated from the two other markers on the rod and compared to the measured marker position of the origin for both rods.

The error was defined as a difference between the actual and the virtual marker positions (Table 1). Both rods showed relatively small mean errors, however, the long rod showed a slightly lower mean error. Both rods had R-square values greater than 0.999, indicating near perfect correlation between actual and virtual points. Thus, the origin marker can be accurately determined from the other rod markers if the origin were missing.

**Table 1:** Summary of mean errors (mm) between actual and virtual “origin” markers.

|          | Short  | Long   |
|----------|--------|--------|
| Mean     | 1.15   | 0.22   |
| SD       | 3.81   | 3.00   |
| Range    | 2.4    | 2.4    |
| R-square | 0.9993 | 0.9998 |

Figure 5 illustrates the error for each rod over the 5-second trial. In some regions, such as 1.72 second in the short rod, larger deviations were observed. The sources of these errors directly related to the camera system accuracy, location in the capture volume, and length of the rod.

This method can be widely applied to a research using 3D motion analysis system, especially, under certain circumstances that external objects block anatomical landmarks which are significant for the marker setup for the analysis. Figure 6 shows one example of these circumstances.

Controlling the fixation of the rod to the anatomical landmark, and preventing movement of the end point of the rod are challenges that have to be handled case by case.

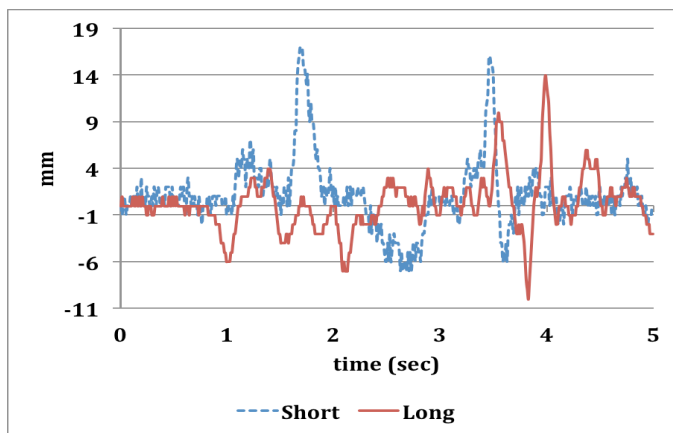


**Figure 5:** Comparison of resultant vectors between the actual and the virtual markers’ centroid.

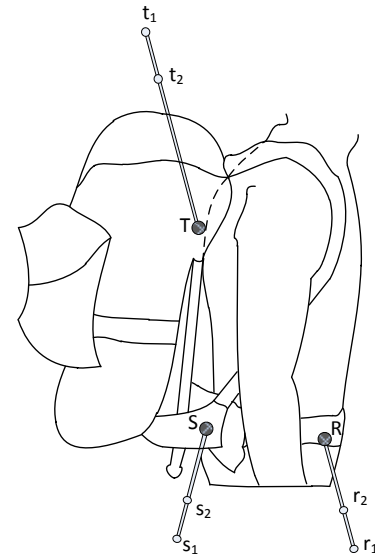


**Figure 6:** Backpack occluding sacrum (S), Trunk (T) and ASIS (R) landmarks. Rods used to define missing points on landmarks.

## CONCLUSIONS

Special cases arise when studying motion when tracking of anatomical landmarks using traditional models and techniques proves difficult, if not impossible. This is particularly challenging when studying participants encumbered by equipment or devices that limit access to these locations. The proposed method addresses this problem by attaching a rod with 2-concentrically aligned markers on a landmark that can be located at a position where no occlusions occur.

This technique demonstrates a relatively simple, straightforward approach to solve the problem of marker placement and model building when anatomical landmarks are not directly accessible.

## REFERENCES

1. Kadaba, M.P., H.K. Ramakrishnan, and M.E. Wootten, *Measurement of lower extremity kinematics during level walking*. J Orthop Res, 1990. 8(3): p. 383-92.
2. Corazza, S., L. Mundermann, and T. Andriacchi, *A framework for the functional identification of joint centers using markerless motion capture, validation for the hip joint*. J Biomech, 2007. 40(15): p. 3510-5.
3. Mundermann, L., S. Corazza, and T.P. Andriacchi, *The evolution of methods for the capture of human movement leading to markerless motion capture for biomechanical applications*. J Neuroeng Rehabil, 2006. 3: p. 6.
4. Startzell, J.K. and P.R. Cavanagh, *A three-dimensional approach to the calculation of foot clearance during locomotion*. Human Movement Science, 1999. 18: p. 603-611.

# CONVENTIONAL WISDOM REGARDING YOGA POSE MODIFICATION MAY NOT BENEFIT HEALTHY OLDER ADULTS: EXAMINING THE MODIFIED TREE POSE

<sup>1</sup>Sean S.-Y. Yu, <sup>1</sup>Man-Ying Wang, <sup>1</sup>Lauren Mulwitz, <sup>1</sup>Michelle Haines, <sup>1</sup>Sachithra Samarawickrame, <sup>1</sup>Rami Hashish, <sup>2</sup>Leslie Kazadi, <sup>3</sup>Gail Greendale and <sup>1</sup>George Salem

<sup>1</sup>University of Southern California, Los Angeles, CA, USA

<sup>2</sup>Westside Yoga Therapy Clinic, USA

<sup>3</sup>University of California, Los Angeles, CA, USA

email: [syyu@ihpnet.usc.edu](mailto:syyu@ihpnet.usc.edu) web: <http://pt2.usc.edu/labs/mbrl>

## INTRODUCTION

Yoga is widely accepted as a beneficial exercise activity for older adults because of its relatively smooth movements and low resistance, and its purported associated improvements in strength, muscular endurance, flexibility, and balance [1, 2]. Conventional wisdom suggests, however, that the traditional poses (asanas) used in older-adult programs should be modified in order to increase senior participation and prevent injury. One pose traditionally incorporated into these programs is the Tree (Vrksasana; Fig. 1a). Common modifications of the pose include the use of a wall for balance (TreeW; Fig. 1b) and placement of the contralateral foot on the floor (TreeWF; Fig. 1c). In this study we sought to better understand the biomechanical demands of the tree pose and its modifications by examining the lower extremity joint moments engendered during their performance by senior participants.

## METHODS

Two male and eight female, healthy older adult participants ( $71.5 \pm 5.0$  yr.) were recruited from the greater Los Angeles area. Participants had limited exposure to Yoga and were free from neurological and musculoskeletal disorders prior to participating in the study.

For the study, a yoga program was specifically developed for older adults and implemented with several traditional Yoga asanas at a beginner's level. In order to become familiar with the poses, the participants practiced yoga under the guidance of an experienced yoga instructor twice weekly for 16 weeks.

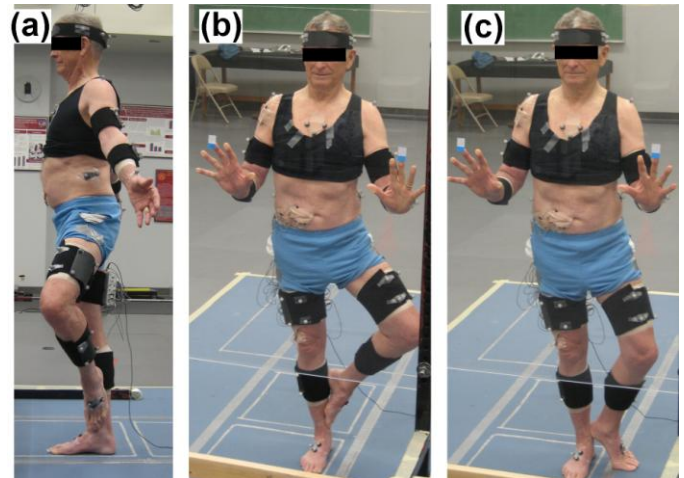


**Figure 1:** Variations of yoga Tree pose. (a) Tree: the traditional Tree pose with single leg stance only; (b) TreeW: single leg stance with lateral support from hands; (c) TreeWF: full support from both feet and hands.

After the yoga sessions, the participants were instrumented for biomechanical analysis in a laboratory setting. Each of the three Tree pose variations were performed with two repetitions while the yoga instructor provided standard positioning and movement cues. Under instructions from the yoga instructor, the participants positioned a pose, held it for a full breathe and then returned to relaxed position. Kinematic and kinetic data were collected over 3 seconds during the static portion of the pose.

Joint moment of force (JMOF) of the dominant knee and hip in the frontal plane, and the support moment [3] were chosen as dependent variables and averaged over the full duration of each trial and both repetitions. They were also normalized by the participant's body weight. Repeated measures ANOVA and Tukey HSD post hoc tests were used

to examine the differences in the outcome variables across variations of the Tree pose.

## RESULTS AND DISCUSSION

The internal moment differences across the Tree variations are illustrated in Fig. 2.

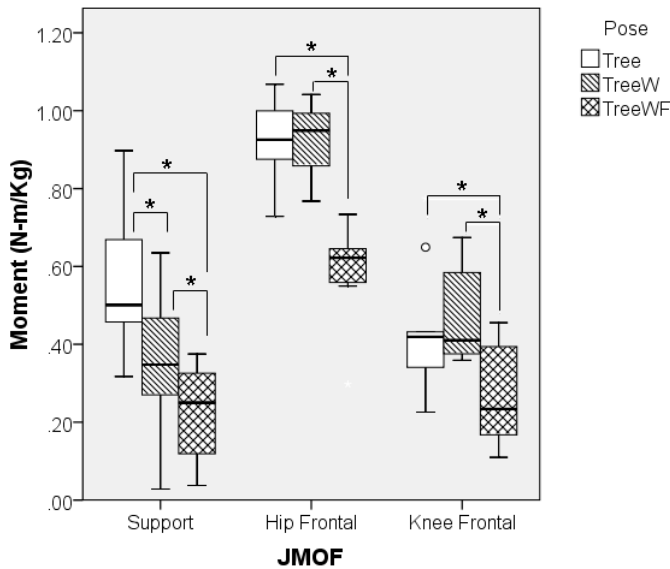


**Figure 2:** Comparison of JMOF for Yoga pose variations –Tree, TreeW, and TreeWF. (\*  $p \leq 0.01$ )

Support moment for the traditional Tree pose was significantly larger than both of its variations (Table 1). In addition, TreeW was also significantly larger than TreeWF. These findings suggest an increasing physical demand from the double support to single-support position (TreeWF to TreeW) and from wall support to unsupported pose (TreeW to Tree).

Surprisingly, the hip abductor moment did not differ between the Tree and TreeW; however, both single-support poses produced a hip abductor moment that was greater than the double-support pose. Thus, it appears the hip abductor moment associated with the two single-support Tree poses is not affected by wall support and both of these forms of the pose are likely to have a similar effect on hip abductor adaptation.

Similarly, the knee abductor moment for the Tree and TreeW were significantly greater than TreeWF. There was no significant difference between Tree and TreeW. Since high knee frontal moments may be detrimental to the knee joint, both single-support Tree poses appear to expose the same risk level of injury and osteoarthritis(OA) [4] in this population, independent of wall support.

## CONCLUSIONS

Traditional perspectives related to the modification of yoga poses may not lead to safer or more effective positions for older practitioners. This study demonstrated that using a wall for support during performance of the Tree does not reduce knee or hip frontal plane moments. With regard to hip strengthening, it is observed that both single-support Tree poses are likely to be equally effective at targeting the hip abductors. Thus, instructors need not insist on a free-standing Tree pose for this training purpose and older adults with balance limitations can be encouraged to use a wall for support. Conversely, using a wall for support in order to reduce the risk of injury or deteriorating OA associated with performance of the Tree pose, is not likely to be helpful. In this case, the double-support Tree variation may be more appropriate, although the effects of this modification on hip abductor adaptations and overall LE strengthening/fatigue resistance, are likely to be reduced.

## REFERENCES

- 1.Haber D. *Gerontologist* **26**(2), 119-121.
- 2.Chen KM, et al. *J Clin Nur* **17**(19), 2634-2646, 2008.
- 3.Winter, DA. *J Biomech* **13**, 923–927, 1980.
- 4.Sharma L, et al. *JAMA* **286**(2), 188-195, 2001

## ACKNOWLEDGEMENTS

Supported by NIH Grant ROI-AT004869-01.

**Table 1:** JMOF and Support Moments Across Tree variations

| JMOF (N-m/Kg)              | Average across subjects |                 |                 | Mean difference $\pm$ Std error |                   |                   |
|----------------------------|-------------------------|-----------------|-----------------|---------------------------------|-------------------|-------------------|
|                            | Tree                    | TreeW           | TreeWF          | Tree-TreeW                      | Tree-TreeWF       | TreeW-TreeWF      |
| <b>Support Moment</b>      | $0.55 \pm 0.19$         | $0.38 \pm 0.23$ | $0.26 \pm 0.20$ | $0.17 \pm 0.04^*$               | $0.29 \pm 0.04^*$ | $0.12 \pm 0.04^*$ |
| <b>Hip Frontal Moment</b>  | $0.92 \pm 0.11$         | $0.93 \pm 0.09$ | $0.59 \pm 0.12$ | $-0.01 \pm 0.04$                | $0.33 \pm 0.04^*$ | $0.34 \pm 0.04^*$ |
| <b>Knee Frontal Moment</b> | $0.44 \pm 0.16$         | $0.47 \pm 0.12$ | $0.27 \pm 0.13$ | $-0.03 \pm 0.03$                | $0.17 \pm 0.03^*$ | $0.20 \pm 0.03^*$ |

\*: The mean difference is significant at  $p < 0.01$ .

# DIFFERENCES IN EXTERNAL KNEE ADDUCTION MOMENT BETWEEN ACL RECONSTRUCTED AND CONTRALATERAL KNEES

<sup>1</sup> Zabala, ME; <sup>1,2</sup> Scanlan, SF; <sup>3</sup> Donahue J; <sup>1,2</sup> Andriacchi, TP

<sup>1</sup> Stanford University, Stanford, CA, <sup>2</sup> VA Palo Alto Health Care System, Palo Alto, CA

<sup>3</sup> Sports Orthopedic & Rehabilitation (SOAR), Redwood City, CA

email: [tandriac@stanford.edu](mailto:tandriac@stanford.edu)

## INTRODUCTION

An increased risk for osteoarthritis (OA) persists even after reconstruction of a ruptured ACL [1]. It has been reported [2] that the failure to restore the normal kinematics of the knee following ACL injury can lead to OA. It has also been reported that ACL reconstructed (ACLR) knees experience a greater magnitude external knee adduction moment (KAM) [3]. This is important since the KAM has been shown to be correlated with the progression and severity of OA in subjects with idiopathic OA [2,4]. A change in loading can possibly attribute to premature clinical OA in ACLR knees.

KAM is the product of the frontal plane ground reaction force (GRF) and the moment arm. Lateral trunk lean has been shown as one mechanism that affects KAM, possibly by changing the length of the moment arm [5].

The purpose of this study was to test for differences in external KAM and possible mechanisms for change. This study tested the hypothesis that there are differences during the stance phase of walking in peak KAM, moment arm in the frontal plane, lateral trunk lean, and GRF for the ACLR knee when using the healthy, contralateral as a control.

## METHODS

Forty-five subjects with unilateral ACL reconstructions and no other history of serious lower limb injury ( $29 \pm 6.3$  yrs, 1.7 m, 73 kg, 22 left legs, 19 females,  $26 \pm 3.4$  mos. past surgery,  $2.24 \pm 1.7$  mos. between injury and surgery, 41 achilles

allograft, 3 patellar tendon autograft, 1 patellar tendon allograft) participated in this study after providing IRB-approved informed consent. Exclusion criteria included the presence of OA or history of other serious ligamentous injury to either lower limb. A 9-camera opto-electronic system and a multi-component force plate were used to record the kinematics and KAM. The frontal plane moment arm, defined as the perpendicular distance from the GRF to the knee joint center, and trunk lean (measured from the lab vertical, positive towards stance limb) was calculated with methods based on previous studies at the time coincident with peak KAM [5]. Subjects performed three trials of walking at their self-selected normal walking speed for each leg. A paired Student's T-test, with an alpha value of 0.05, was used to determine significant differences in ACLR versus contralateral knees.

## RESULTS AND DISCUSSION

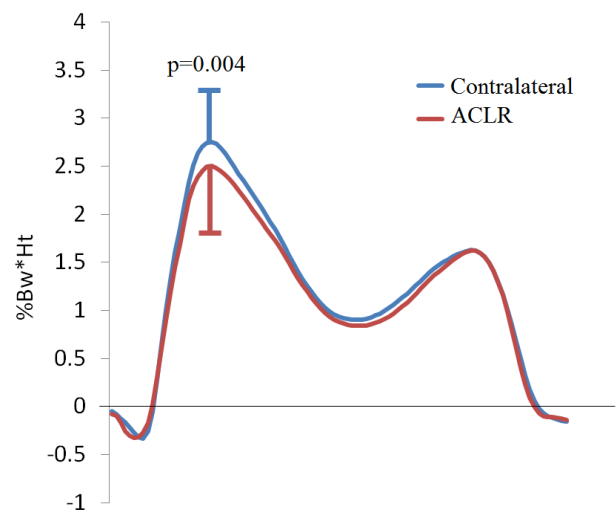


**Figure 1:** External knee adduction moment (KAM) during stance phase of walking

There was a significant reduction in the first peak of KAM of the ACLR knee compared to the healthy contralateral ( $2.50\pm 0.66$ ,  $2.75\pm 0.60$  %Bw\*Ht respectively,  $p=0.004$ , **Fig. 1**) as well as a decrease in frontal plane moment arm length ( $2.43\pm 0.55$ ,  $2.65\pm 0.47$  %Ht,  $p<0.001$ , **Fig. 2**) and an increase in trunk lean ( $2.28\pm 1.76^\circ$ ,  $1.43\pm 1.95^\circ$ ,  $p=0.024$ , **Fig. 2**). These results supported the first part of our hypothesis that there would be differences in KAM, frontal plane moment arm, and lateral trunk lean between ACLR and healthy contralateral knees during stance phase of each respective side. No significant differences were found in the magnitude of the GRF ( $112.1\pm 10.7$ ,  $113.1\pm 9.7\%$  BW,  $p=0.45$ ) which refuted the final part of our hypothesis.

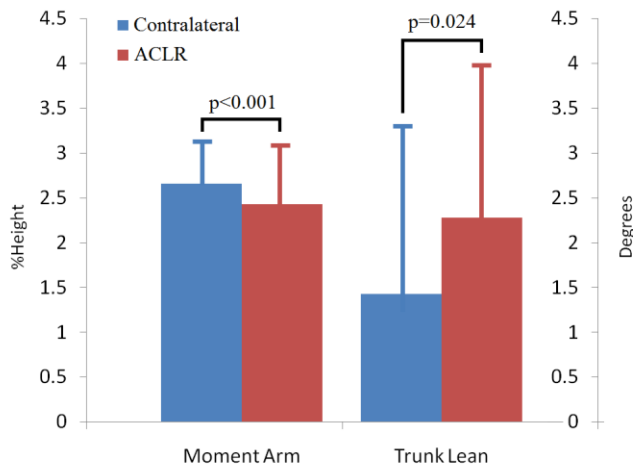


**Figure 2:** Frontal plane moment arm and trunk lean

A reduction in peak KAM of the ACLR knees suggests a load reduction in the medial compartment of the knee. The lower peak KAM seems to be a result of a shorter moment arm which is possibly caused by increased trunk lean. Increased trunk lean can reduce the frontal plane moment arm by shifting the body's center of mass to be more in line with the knee joint center during stance phase.

It is unknown why subjects exhibit an increase in lateral trunk lean towards the affected limb. It is possible that subjects experienced pain near the time of injury and/or surgery and altered their gait

accordingly. This change may have persisted even well past the presence of pain. Subjects may also be attempting to align the body's center of mass and knee joint center in order to counteract lost proprioception or lack of stability due to the injury. Furthermore, the differences might be a result of other unknown compensatory reasons which warrant further investigation.

The results of this study differ from the study by Butler et al. [3] which found an increase in KAM in ACLR knees versus a healthy control population. However, the aforementioned study did not report the presence of OA, meniscal or cartilage damage. Also, subjects were  $5.3\pm 4.4$  yrs past reconstruction. Subjects may have already had progressive OA and exhibited an increase in KAM accordingly [4]. It is possible that individuals may experience a shift from a decreased KAM following ACL reconstruction, to an increased KAM coinciding with the progression of OA.

## CONCLUSION

The most important finding of this study was a difference in KAM of ACLR and healthy contralateral knees. Long term effects of this difference are still unknown. Therefore, future longitudinal studies are needed in order to better understand the effects of a decreased KAM as well as the role of increased lateral trunk lean on long-term joint health.

## REFERENCES

1. Lohmander LS 2004 Arthritis Rheum., 50(10), 3145-3152
2. Andriacchi TP 2009 J Bone Joint Surg Am. 91, 1:95-101
2. Butler 2009 Br J Sports Med 2009;43:366-370
3. Miyazaki T 2002 Ann Rheum Dis; 61:617-622
4. Hunt MA 2008 Osteo & Cart. 16:591-599

# A CURVED-BOTTOM SHOE ALTERS GROUND REACTION FORCES AND ANKLE BIOMECHANICS DURING WALKING

Songning Zhang, Max R. Paquette, Clare E. Milner, Carolyn Westlake, Erin Byrd and Lucas Baumgartner

Biomechanics/Sports Medicine Lab, The University of Tennessee, Knoxville, TN, USA  
email: [szhang@utk.edu](mailto:szhang@utk.edu), web: [web.utk.edu/~sals/resources/biomechanics\\_laboratory.html](http://web.utk.edu/~sals/resources/biomechanics_laboratory.html)

## INTRODUCTION

Over the last decade several studies have investigated the effects of curved-bottom (CB) shoes such as the Masai Barefoot Technology on gait parameters during level-walking. Previous studies on CB shoes show increased ankle dorsiflexion in the early stages of stance [1,2], but reduced in the late stage compared to control shoes [1,3]. However, no changes have been found in frontal plane kinematics in CB shoes [2]. Previous findings also demonstrate that CB shoes reduce early stance dorsiflexor moments, and late stance plantarflexor moments [3]. No significant changes in frontal-plane ankle moments have been reported in CB shoes. In addition, data on center of pressure (COP) displacement and ground reaction forces (GRF) in CB shoes during walking have been rarely reported [4]. Therefore, the main objectives of the study were to compare a *newly designed* CB shoe (SH2: Active Balance™) with a control shoe (SH1: Glacier) on ground reaction forces (GRF), and ankle kinematics and kinetics during level-walking.

## METHODS

Fifteen healthy males (age:  $41.1 \pm 4.6$  yrs, height:  $1.77 \pm 0.7$  m, mass:  $83.2 \pm 11.5$  kg) participated in this study. Before the start of experimental testing, participants were asked to walk in SH2 for 10 minutes in an indoor hallway to get adapted to the shoes. A seven-camera motion analysis system (240 Hz, Vicon Motion Analysis) was used to obtain the three-dimensional (3D) kinematic data. Reflective anatomical and tracking markers were placed on the pelvis, the right foot, ankle, leg, knee, and thigh. One force platform (1200 Hz, AMTI) was used to measure ground reaction forces (GRF) under the right foot. The participant performed five successful walking trials in each of the four testing conditions: walking at 1.3 m/s ( $\pm 5\%$ ) and 1.8 m/s ( $\pm 5\%$ ) wearing SH1 and SH2. The shoe and speed conditions were randomized independently. All

participants were given practice trials prior to each condition. Visual3D software suite (C-Motion, Inc.) was used to obtain the 3D kinematic and kinetic computations of the ankle joint. Joint moments were computed as internal moments. A right-hand rule was used to establish the 3D kinematics/kinetics conventions. A 2 x 2 (Shoe x Speed) repeated measures analysis of variance (ANOVA) was used to detect any differences between the two shoes and two speeds for each variable of interest (18.0, SPSS). Post hoc comparisons were performed using a paired t-test. The significance level was set at 0.05.

## RESULTS AND DISCUSSION

The first peak (F1\_Z) of the vertical ground reaction force (GRF) demonstrated a significant interaction of shoe and speed (Table 1). The post hoc comparison showed that F1\_Z was slightly smaller in SH2 at the normal speed than the control shoe. Also the peak was greater at fast speed compared to normal speed in both shoes. However, the loading rate of this peak (LR\_F1) was significantly greater in SH2 compared to the control shoe. The 2<sup>nd</sup> peak GRF (F2\_Z) during push-off also showed a significant interaction of shoe and speed. The comparison indicated a slightly smaller peak at normal speed compared to fast speed for SH1 and SH2, as well as smaller peaks in SH2 at normal and fast speeds. The mediolateral COP displacement (COP\_ML) was greater in SH2 compared to SH1 (Table 1). The anteroposterior COP movement (COP\_AP) showed a significant interaction of shoe and speed. The post hoc comparisons showed that SH2 had smaller COP\_AP movement than the control shoe at both walking speeds. The COP\_AP movement was significantly greater at fast speed compared to normal speed for both shoes. For SH2, COP\_AP was larger at fast speed compared to normal speed. Our study provides the first reported results on GRF and COP data in curved-bottom shoes during level-walking. The smaller sagittal

plane GRF in the Active Balance compared to SH1 indicate reduced loading and push-off forces on lower limb joints and especially, loading on the ankle plantar/dorsiflexors. The greater COP\_ML indicates greater ML instability in the unstable shoe.

The kinematic results showed smaller plantarflexion range of motion (ROM\_P) for SH2 compared to SH1 and greater ROM of both shoes at the fast speed than the normal speed (Table 2). In addition, the peak dorsiflexion (Max\_D) in late stance was significantly smaller for SH2 and at fast speed, although these differences were small. This result is supported by previous findings [1,3]. The reduction in ROM\_P in SH2 is likely due to the increased heel slope in SH2. Similarly, the increased midfoot-to-toe slope reduces Max\_D in SH2. Finally, results showed greater total stance ankle ROM (ROM\_T, heel strike to toe-off) in SH2 compared to the control shoe and, at fast speed. In the frontal-plane, the ankle joint showed greater eversion ROM (ROM\_E) for SH2 compared to SH1. This greater eversion ROM is related to the greater COP\_ML in SH2.

The early stance peak dorsiflexion moment (Mmt\_D) and late stance peak plantarflexion moment (Mmt\_P) were significantly smaller for SH2 compared to the SH1. These sagittal plane ankle moment reductions are consistent with

previous research [3]. The fast speed induced greater peak sagittal ankle moments compared to normal speed (Table 2). The ankle joint showed greater early stance peak inversion moment (Mmt\_I) in SH2 compared to SH1. The reduced sagittal plane ankle moments signify reductions in plantar and dorsiflexor muscle involvement, while the larger early stance inversion moment indicates greater inverter muscle involvement.

## CONCLUSION

Our results indicate that reduced loading and push-off vertical ground reaction forces observed in the Active Balance seem to be associated with the reductions in early stance dorsiflexor moment and late stance plantarflexor moment. The increased heel and forefoot slopes not only reduced AP COP excursion but also ML COP excursion, thus increasing the inverter moment in early stance.

## ACKNOWLEDGEMENT

This study was sponsored by Genesco, Inc.

## REFERENCES

1. Romkes et al. *Clin Biomech* **21**, 75-81, 2006.
2. Nigg et al. *Clin Biomech* **21**, 82-88, 2006.
3. Myers et al. *Gait Posture* **24**, 323-330, 2006.
4. Stoggl, T., et al. *Clin Biomech*, **25**, 816-822, 2010.

**Table 1.** Ground reaction force and center of pressure variables: mean  $\pm$  STD.

| Cond  | F1_Z <sup>&amp;#</sup><br>(BW) | F2_Z <sup>&amp;*&amp;#</sup><br>(BW) | LR_F1 <sup>*#</sup><br>(BW/s) | COP_ML <sup>*</sup><br>(m) | COP_AP <sup>&amp;*&amp;#</sup><br>(m) |
|-------|--------------------------------|--------------------------------------|-------------------------------|----------------------------|---------------------------------------|
| SH1_N | 1.14 $\pm$ 0.09                | 1.10 $\pm$ 0.04                      | 6.69 $\pm$ 0.91               | -0.037 $\pm$ 0.02          | 0.29 $\pm$ 0.01                       |
| SH1_F | 1.33 $\pm$ 0.12 <sup>\$</sup>  | 1.22 $\pm$ 0.07 <sup>\$</sup>        | 10.05 $\pm$ 1.5               | -0.043 $\pm$ 0.02          | 0.29 $\pm$ 0.01                       |
| SH2_N | 1.10 $\pm$ 0.06 <sup>!</sup>   | 1.08 $\pm$ 0.03 <sup>!</sup>         | 7.58 $\pm$ 1.9                | -0.065 $\pm$ 0.02          | 0.26 $\pm$ 0.02 <sup>!</sup>          |
| SH2_F | 1.35 $\pm$ 0.09 <sup>\$</sup>  | 1.18 $\pm$ 0.07 <sup>!\$</sup>       | 11.43 $\pm$ 1.2               | -0.067 $\pm$ 0.02          | 0.27 $\pm$ 0.01 <sup>!\$</sup>        |

N: Normal speed, F: Fast speed. \*: Shoe main effect; #: Speed main effect; &\*: Interaction of shoe and speed, !: Difference between shoes at same speed; \$: Difference between speeds for same shoe.

**Table 2.** Ankle kinematic and kinetic variables: mean  $\pm$  STD.

| Cond  | Kinematics (Deg)    |                     |                     |                    | Moments (Nm/kg)     |                     |                    |
|-------|---------------------|---------------------|---------------------|--------------------|---------------------|---------------------|--------------------|
|       | Sagittal            |                     |                     | Frontal            | Sagittal            |                     | Frontal            |
|       | ROM_P <sup>*#</sup> | Max_D <sup>*#</sup> | ROM_T <sup>*#</sup> | ROM_E <sup>*</sup> | Mmt_D <sup>*#</sup> | Mmt_P <sup>*#</sup> | Mmt_I <sup>*</sup> |
| SH1_N | -12.2 $\pm$ 1.3     | 9.6 $\pm$ 3.0       | -15.2 $\pm$ 4.0     | -6.4 $\pm$ 2.8     | 0.35 $\pm$ 0.09     | -1.46 $\pm$ 0.12    | 0.12 $\pm$ 0.08    |
| SH1_F | -13.4 $\pm$ 1.7     | 8.1 $\pm$ 3.3       | -20.2 $\pm$ 4.2     | -7.0 $\pm$ 4.2     | 0.51 $\pm$ 0.10     | -1.68 $\pm$ 0.15    | 0.11 $\pm$ 0.06    |
| SH2_N | -8.0 $\pm$ 1.8      | 9.1 $\pm$ 2.9       | -17.8 $\pm$ 3.9     | -8.6 $\pm$ 2.5     | 0.24 $\pm$ 0.07     | -1.41 $\pm$ 0.14    | 0.13 $\pm$ 0.05    |
| SH2_F | -8.7 $\pm$ 1.6      | 7.1 $\pm$ 3.5       | -22.0 $\pm$ 3.5     | -8.5 $\pm$ 1.7     | 0.38 $\pm$ 0.07     | -1.64 $\pm$ 0.15    | 0.15 $\pm$ 0.05    |

# MULTI-DIGIT COORDINATION AND ADAPTATION TO OBJECT MASS DISTRIBUTION IN CARPAL TUNNEL SYNDROME

<sup>1</sup>Wei Zhang, <sup>2</sup>Jamie Johnston, <sup>3</sup>Anthony A. Smith, <sup>3</sup>Mark Ross  
<sup>3</sup>Brandon J. Coakley, <sup>3</sup>Elizabeth A. Gleason, <sup>3</sup>Amylou C. Dueck, <sup>1</sup>Marco Santello

<sup>1</sup>Arizona State University, Tempe, AZ 85287, USA  
<sup>2</sup>University of Calgary, Calgary, AB T2N 1N4, Canada  
<sup>3</sup>Mayo Clinic Hospital, Phoenix, AZ 85054, USA  
email: wzhang70@asu.edu

## INTRODUCTION

In healthy individuals, somatosensory feedback from the fingertips is integrated with voluntary control of hand muscles to ensure successful manipulation (Johansson and Westling 1984). The delicate tuning of hand muscle activity to object properties can be disrupted by neurological and musculo-skeletal diseases, such as Carpal Tunnel Syndrome (CTS). This compression neuropathy of the median nerve results in decreased tactile sensitivity of the thumb, index, middle and lateral half of the ring finger as well as motor deficits (Moberg 1962). CTS poses unique challenges to the central nervous system (CNS) for whole-hand manipulation as it selectively impairs sensorimotor function of a subset of digits. This raises the question of how the CNS integrates sensory information from CTS-affected and non-affected digits with motor commands to finely modulate digit forces to task requirements. The primary objective of this project is to use CTS as a model to improve our understanding of the mechanisms underlying sensorimotor integration responsible for whole-hand grasping as a function of object center of mass (CM).

## METHODS

Fourteen CTS patients (3 males, 11 females) and age- and gender-matched controls participated in the study. Subjects were instructed to grasp, lift, hold, and release a grip device with five digits for 7 consecutive lifts. Five six-component force/torque transducers (F/T, ATI Industrial Automation, Apex, NC) mounted on both sides of the grip device were used to measure three force and three moment-of-force components produced by each digit (Index, I;

Middle, M; Ring, R; Little, L; Thumb, TH, Fig. 1B). An electromagnetic position/orientation tracking sensor (P/O, Polhemus Fastrak, Colchester, VT; 0.075 mm resolution; Fig. 1A) was used to measure object kinematics.

Object CM was changed across blocks of trials by inserting a mass (200 g) into one of the three slots underneath the grip device (Fig. 1): 1) center (Center), 2) thumb side (Thumb), and 3) finger side slot (Finger). CM conditions were presented to the subjects in a counterbalanced order. Subjects were unaware of the object CM on the first trial, but were aware that it would remain the same within the trial block. We measured forces and torques exerted by each digit and object kinematics and analyzed modulation of these variables to object CM at object lift onset (anticipatory control based on previous manipulations) and during object hold (influenced by sensory information acquired during the lift).

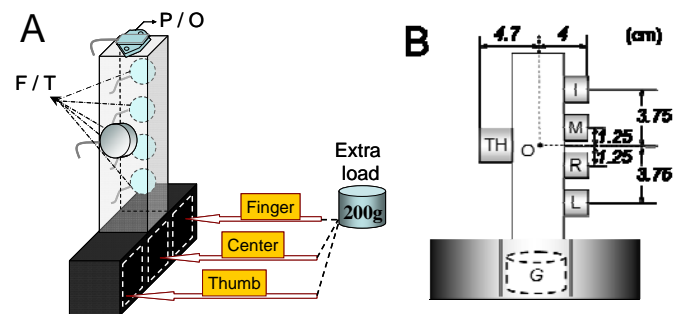


**Figure 1:** (A) Grip device and center of mass (CM) conditions. (B) Dimensions of grip device, front view.

## RESULTS AND DISCUSSION

CTS and controls learned to generate a compensatory moment at object lift onset ( $M_{com}$ ) at similar rates from trial to trial for all CM conditions, and therefore both groups improved their grasp performance by significantly reducing object peak roll after the first lift ( $P < 0.05$ ).

Despite the similar  $M_{com}$  produced by both groups at object lift onset, CTS patients showed different patterns of multi-digit coordination compared with controls at object lift onset and during object hold. Specifically, CTS presented a ‘default’ grip force for all CM conditions which was significantly larger than controls. This also induced non-zero moment of normal force in Center CM condition even though this condition required zero  $M_{com}$  (Fig. 2). In contrast, controls increased grip force in lateral CM conditions (*Thumb* and *Finger*) (Group $\times$ CM interaction effect,  $P < 0.05$ ). In addition, trial-to-trial practice allowed controls to increase tangential moment ( $M_{tan}$ ) contribution to  $M_{com}$ . However, normal moment ( $M_n$ ) was the dominant  $M_{com}$  component in CTS, especially for the *Finger* CM condition (Fig. 2).

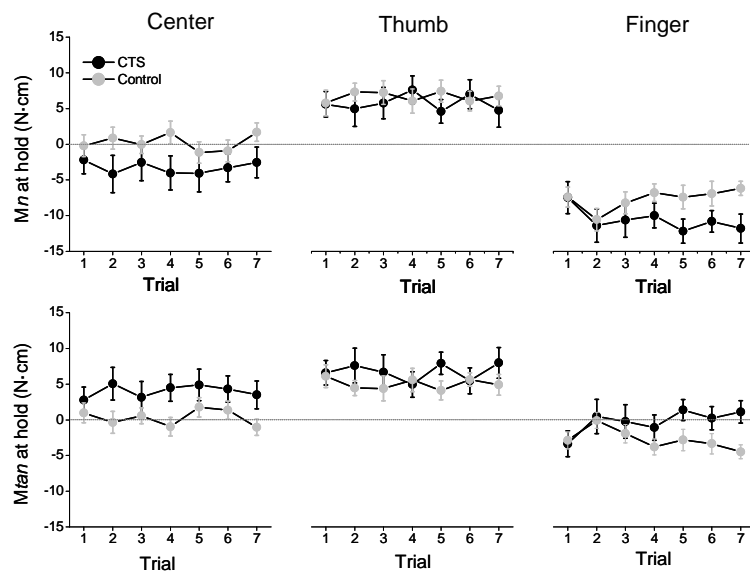


**Figure 2:** Moment of normal force ( $M_n$ , upper panels) and moment of tangential moment ( $M_{tan}$ , bottom panels) during object steady hold by CTS patients and controls.

Our findings indicate that CTS patients have a residual learning ability of anticipatory control to produce a proper moment to counteract an external moment on the object. However, such anticipatory control is not as accurate as controls, as indicated by (a) the lower extent to which grip force was modulated according to different CM conditions and (b) larger within-trial variability of grip force ( $P < 0.05$ ). In addition, CTS-induced sensorimotor deficits affected the ability to accurately modulate the manipulative forces, as indicated by the lack of tangential force modulations.

## CONCLUSIONS

We found that CTS does not affect macroscopic features of grasp control when adapting multi-digit forces to object center of mass. However, patients with CTS exhibited deficits in sensorimotor integration as revealed by the consistent use of excessively large digit forces when zero normal moment was required, higher within-trial digit force variability, and reduced ability in tangential force modulation. Our findings suggest that these behavioral deficits, although subtle, result from subjects’ reduced ability to generate, store, and retrieve accurate sensorimotor memories of previous manipulations, thus preventing them to fully compensate for impaired somatosensory feedback.

## REFERENCES

1. Johansson RS, and Westling G (1984). *Exp Brain Res* **56**: 550-564.
2. Moberg E (1962) *Neurology* **12**: 8-19.

## ACKNOWLEDGEMENTS

This work was supported by grant 1R01 HD057152 from the National Institute of Child and Health Development (NICHD) at the National Institutes of Health (NIH).

# ACCURATE PREDICTION OF NECK MUSCLE VOLUMES USING A TWO-STEP PROCESS

<sup>1</sup>Liying Zheng, <sup>2,3</sup>Gunter Siegmund and <sup>1</sup>Anita Vasavada

<sup>1</sup>Washington State University, Pullman, WA, USA

<sup>2</sup>MEA Forensic Engineers & Scientists, Richmond, BC, Canada

<sup>3</sup>University of British Columbia, Vancouver, BC, Canada

email: liying.zheng@email.wsu.edu

## INTRODUCTION

Neck muscle volume data are needed for most computational neck models because they determine the muscle force. However, the approaches to obtaining neck muscle volume (e.g., cadaveric morphometry data or *in-vivo* MRI data) are expensive and time-consuming. We have previously shown that males and females have significant differences in head and neck geometry and neck strength [1], and it is likely that sex differences are also reflected in neck muscle size. We propose to predict individual neck muscle volumes using a 2-step approach: first by predicting the total neck muscle volume from subject anthropometric data; and then by predicting the individual neck muscle volumes using a fixed volume distribution among subjects. We hypothesized that (1) the total neck muscle volume can be predicted from sex-specific regression equations based on anthropometric data, and (2) the volume distribution of the individual neck muscles among the total neck muscle volume is sex-specific.

## METHODS

Axial proton density-weighted magnetic resonance (MR) images from skull to sternum were obtained from 11 subjects (8 male and 3 female). The subjects' height, weight, neck circumference (NC), neck length (NL) and head circumference (HC) were also measured (Table 1). Sixteen neck muscles were traced on axial slices, and individual neck muscle volumes (IMV) were calculated by integrating area over all slices. Total neck muscle

|   | Age   | Height  | Weight | NC**   | NL     | HC**   |
|---|-------|---------|--------|--------|--------|--------|
| F | 31±11 | 165±5.1 | 68±7.7 | 35±1.3 | 11±0.9 | 56±1.0 |
| M | 32±9  | 175±7.9 | 75±7.2 | 39±1.9 | 12±1.9 | 59±1.4 |

**Table 1.** Subject data. (\*\*Significant differences between males and females;  $p < 0.01$ )

volume (TMV) was the sum of individual neck muscle volumes. Volume distribution for each muscle was defined as  $IMV/TMV$ . Total traced neck volume (NV; also includes non-muscular tissue) was estimated by multiplying the neck area at the C4 level by the traced neck length. Sex differences in volume and distribution were analyzed by unpaired t-tests.

Multivariate regression models were screened to predict total neck muscle volume from among the following potential predictors: sex, height, height<sup>2</sup>, weight, neck circumference (NC), NC<sup>2</sup>, neck length (NL), head circumference (HC), body mass index, height<sup>2</sup>\*weight. A regression model was developed from the data of 10 subjects and validated using the 11<sup>th</sup> subject's data. Individual neck muscle volumes were then calculated from the regression-predicted total neck muscle volume and the individual volume distributions. Coefficient of concordance [2] was used to assess the agreement between the predicted and MRI-estimated muscle volumes.

## RESULTS AND DISCUSSION

Females have significantly lower total neck muscle volumes (TMV) compared to males (45% lower;  $p < 0.05$ ). Total neck volumes (NV), however, are only 11% lower in females ( $p > 0.4$ ). Therefore, females have less muscle per unit volume of the neck compared to males (32% lower;  $p < 0.05$ ).

Regression analysis showed that NC was the best single predictor of total neck muscle volume (adjusted  $R^2 = 0.64$ ). Prediction of total neck muscle volume was improved when sex was added as a predictor (for equations with sex and NC or NC<sup>2</sup> as predictors, adjusted  $R^2 = 0.71$ ). Adding a third predictor (HC) did not significantly improve the

prediction (adjusted  $R^2=0.70$ ). Therefore, total neck muscle volume was predicted by the equation:  $TMV = 357 + 0.313*NC^2 - 156*Sex$ . (Adjusted  $R^2 = 0.71$ ;  $p=0.005$ ; Male: Sex=0, Female: Sex=1).

For most of the muscles, the volume distributions (IMV/TMV) were similar between female and male subjects (Figure 2;  $0.05 < p < 0.9$ ). However, small sex differences ( $< 2.5\%$  volume distribution differences) existed for 3 muscles (semispinalis cervicis + multifidus (traced together), longus capitis and obliquus capitis inferior ( $p<0.05$ )).

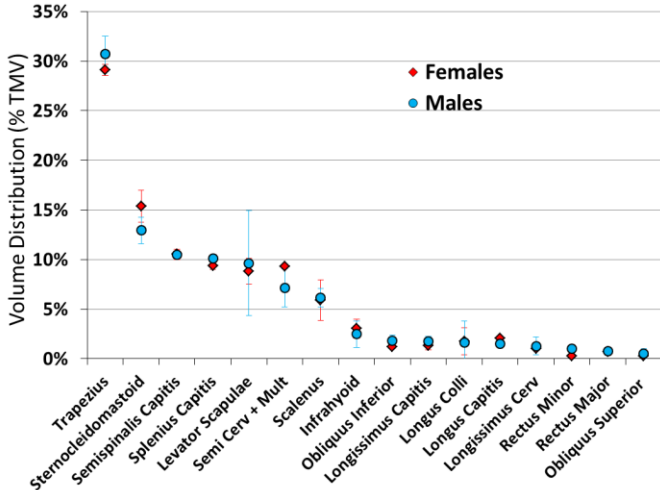


Figure 2. Neck muscle volume distribution (IMV/TMV).

Individual neck muscle volumes were calculated using the volume distribution (average of male and female). Prediction of individual muscle volumes in the 11<sup>th</sup> subject with this two-step process, yielded a coefficient of concordance of 0.98 (Figure 3).

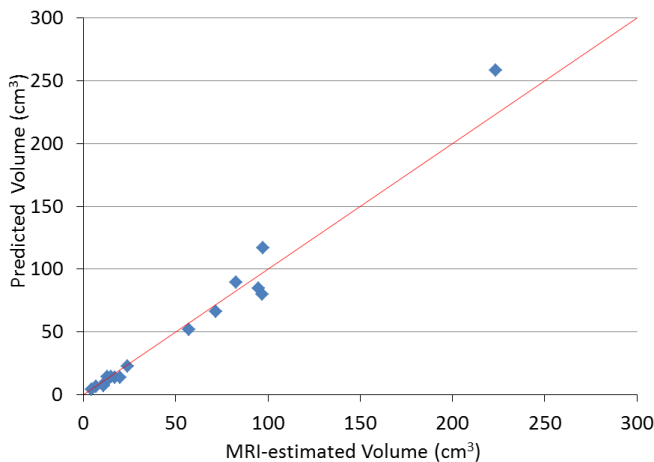


Figure 3. Predicted vs. MRI-estimated neck muscle volumes in a subject that was not used to generate the regression equations. The line is the line of equality: predicted = MRI.

Errors in predicted volume were largest in the largest muscles (trapezius, sternocleidomastoid).

As a percentage, error ranged from 5% to 37% of MRI-estimated volumes, with the largest percent error in the suboccipital muscles.

This two-step approach utilized one regression equation along with average data on muscle volume distribution to predict individual neck muscle volumes. A previous study [3] related muscle volume data from MRI to external measurements using separate regression equations for individual muscles. However, in that study, volumes of only seven neck different neck muscles were predicted, often using different sets of anthropometric parameters. The previous study also did not include sex, which based on our data is an important factor in neck muscle volume.

## CONCLUSIONS

The results supported the first hypothesis that the total neck muscle volume regression equation is sex-specific. We used sex and neck circumference squared to predict total neck muscle volume. For most neck muscles, the data did not support the second hypothesis: the volume distribution of the individual neck muscles among the total neck muscle volume is not sex-specific. Using volume distribution data which were an average of male and female, we predicted muscle volumes that were in high agreement with MRI-estimated volumes. Even though the subject number is relatively low in this study, especially for female subjects, this method produced a model with strong predictive power. This method has an advantage of using only one regression equation and one set of volume distributions to predict volumes of 16 neck muscles.

## REFERENCES

1. Vasavada AN, et al. *J Biomech*, **41**:114-121, 2008.
2. Lin, L I-K. *Biometrics*, **45**(1):255-268, 1989.
3. Burnett A, et al. *J Biomech*, **40**(S2):S314, 2007.

## ACKNOWLEDGEMENTS

Supported by NSF (CBET #0748303), NIH (R01HD053525) through Dr. David Nuckley at University of Minnesota, and the National Center for Skeletal Muscle Research. We also thank Gulsum Ozyigit, Jessica Jahn, and the University of British Columbia (UBC) MRI Research Centre.

# A PILOT STUDY OF BIOMECHANICAL FACTORS AFFECTING UPPER LIMB POSTURE DURING GRASPING, HOLDING, AND PLACING CYLINDRICAL OBJECT

<sup>1</sup>Wei Zhou, <sup>1</sup>Thomas J. Armstrong, <sup>2</sup>Diana M. Wegner, and <sup>1</sup>Matthew P. Reed

<sup>1</sup>University of Michigan, Ann Arbor, MI, USA

<sup>2</sup>General Motors, Warren, MI, USA

email: [wzhousci@umich.edu](mailto:wzhousci@umich.edu)

## INTRODUCTION

A biomechanical analysis was performed to explain upper limb postures during grasping, holding, and placing cylindrical objects. This study is needed for ergonomic design of work equipment and methods to provide workers with sufficient control over objects in object transfer tasks.

We previously showed that self-selected postures used to grasp, hold (approximately eight seconds), and place cylindrical objects are influenced by object weight. Horizontal cylinders varying from 0.34 to 5.44 kg were presented to four males and four females at elbow height. The cylinders were supported at each end such that there was sufficient clearance for the hand to approach and grasp the object from above or beneath (overhand or underhand grips as described by Rosenbaum et al. [1]). We observed that 1) the probability of grasping with an overhand grip (Figure 1a) decreased, while that of an underhand grip (Figure 1b) increased with increasing weight; 2) after grasping, subjects repositioned and held the object primarily using either a hook grip at the side of the body (Figure 1c), an underhand palm grip in front of the body, or a palm grip at shoulder height (Figure 1d); 3) the probability of holding the object using the hook grip decreased while that of the palm grips increased with increasing weight; and 4) the subject placed the object back onto stands using overhand or underhand grips in similar trends as in grasping.

These results are qualitatively consistent with Rosenbaum's theory that posture selection for grasping objects is related to end-state comfort [1]. We propose that comfort and posture behavior can be explained in terms of relative upper limb joint loads (% maximum voluntary joint strength). In this study we estimated and compared the relative

loads that would be produced on the hands, wrists, elbows and shoulders for the postures observed in our previous study.

## METHODS

Major external forces and moments of the upper limb during grasp, hold and place are shown in Figure 1. The load moments at the wrist, elbow, and shoulder joints were estimated using the University of Michigan 3D Static Strength Prediction Program™ (3DSSPP) version 6.0.4 [2] and were compared with the mean population strengths reported by 3DSSPP. The 3DSSPP also considered the contribution of static body weight to the joint load moment. Human figures were scaled by the heights and weights of the eight subjects. The postures (Figure 1) were entered based on estimation from videos.

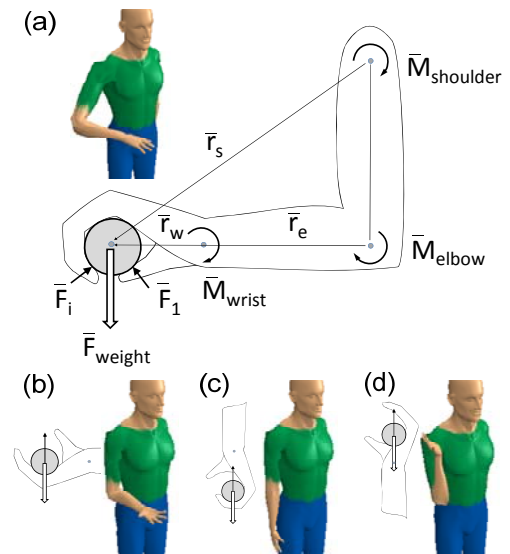


**Figure 1:** External forces and moments on upper limb joints in (a) overhand approach and finger grip; (b) underhand approach and palm grip; (c) holding cylinder at side of body using a hook grip (thigh height); and (d) holding cylinder with a vertical forearm using a palm grip at shoulder height.

The finger load for the overhand grip was estimated using a simplified biomechanical analysis (Figure 1a). The finger placements were computed using a kinematic model scaled for the subjects' hand size and a hand-object contact algorithm [3] for a 70 mm diameter cylinder used in the laboratory study. The contact forces were assumed to be vectors acting perpendicular on the distal phalanges. The weight of the cylinder was assumed to be distributed in proportion to relative finger strengths [4]. The force on the thumb required to achieve static equilibrium was computed. The loads on the fingers and thumb were compared with reported mean pulp pinch strengths [5]. The force exerted in hook grip (Figure 1c) was compared directly with mean strength data for a similar diameter cylindrical grip dynamometer [6]. The contact forces in Figure 1b and 1d were assumed to be vectors acting on the metacarpals; the forces on the fingers were assumed to be negligible compared with those acting on the palm.

## RESULTS AND DISCUSSION

Subjects reached and grasped cylinders less than 1.6 kg using the overhand approach and finger grip (Figure 1a) more than 50% of the time. In this posture, a 1.6 kg load produced an average finger force of 17 N across the subjects, corresponding to 24% and 37% of mean male and female pulp pinch strength, respectively. The average load moments at the wrist, elbow, and shoulder were corresponding to 19%, 8%, and 13% of mean male joint strengths, and 25%, 15%, and 23% of mean female joint strengths, respectively. Subjects used an underhand palm grip for heavier objects (>1.6 kg) more than 50% of the time. As subjects gained control over the cylinder, they shifted to one of the grips shown in Figures 1b-d. The hook grip posture (Figure 1c) was observed more than 50% of the time for holding cylinders with mass less than 3 kg, which produced 29 N of finger load, corresponding to 24% and 40% of mean male and female cylindrical grip strength, respectively. Only traction forces are exerted on the wrist, elbow and shoulder in this posture, so the load moments are negligible. The underhand grip (Figure 1b) was observed from 30% to 40% of the time for holding cylinders more than 3 kg. The posture of palm grip at shoulder height (Figure 1d) was observed more than 50% of the time for cylinders more than 4.5 kg. In the underhand grip the load on the fingers is negligible. Average load moments at the wrist, elbow and shoulder joints

corresponding to 35%, 21%, and 21% of mean male joint strength, and 44%, 41%, and 41% of mean female strength respectively, are computed for a 4.5 kg cylinder. In the palm grip at shoulder height the finger force is negligible, and the moments on the wrist, elbow and shoulder are all low (ranging from 2 to 11% of mean male and from 3 to 17% of mean female joint strength for a 4.5 kg cylinder). After holding the cylinders for about 8 seconds the overhand grip was used more than 50% of the time to return the cylinders with 1.7 kg or less to their starting location. The underhand grip was used more than 50% of the time for heavier cylinders (>1.7 kg).

Grasping objects with overhand and hook grips required the highest relative finger force and was observed only for the lightest objects (<24% mean finger strength of male or 40% of female). Holding objects at the shoulder height with a palm grip minimized relative finger, wrist, elbow, and shoulder loads and was observed for the heaviest objects (wrist, elbow, and shoulder load moments >21% male or 41% female strength).

These results are limited by a small number of subjects and conditions and the use of population strengths versus measured individual strengths. The results support further studies to develop models that use specified load thresholds for predicting work postures for ergonomic application.

## REFERENCES

1. Rosenbaum DA, et al. in *Motor control and learning over the lifespan*, M. Latash, F. Lestienne, Eds. Springer, 2006, 9-25.
2. Chaffin DB, et al. *Occupational Biomechanics*, Wiley-Interscience, 1999.
3. Choi J, et al. 16th congress of the International Ergonomics Association, Maastricht, The Netherlands, 2006.
4. Hazelton FT, et al. *J Biomech* **8**, 301-306, 1975.
5. Imrhan SN, et al. *Hum Factors* **31**, 689-701, 1989.
6. Seo NJ, et al. *J Biomech* **40**, 3236-3243, 2007.

## ACKNOWLEDGEMENTS

This work was supported by General Motors and by the partners of the Human Motion Simulation Laboratory at the University of Michigan.